QA: N

PROBABILISTIC SEISMIC HAZARD ANALYSES FOR FAULT DISPLACEMENT AND VIBRATORY GROUND MOTION AT YUCCA MOUNTAIN, NEVADA

FINAL REPORT VOLUME 1 TEXT

Prepared for the

U.S. Geological Survey

by the

Civilian Radioactive Waste Management System
Management & Operating Contractor

Ivan G. Wong and Carl Stepp
Report Coordinators

A report to the U.S. Department of Energy
that fulfills Level 3 Milestone SP32IM3
WBS Number 1.2.3.2.8.3.6

Prepared in cooperation with the
U.S. Department of Energy under
Interagency Agreement DE-AI08-97NV12033
Contract DE-AC04-94AL8500

Oakland, California
23 September 1998

PROBABILISTIC SEISMIC HAZARD ANALYSIS (PSHA)
FINAL REPORT

TABLE OF CONTENTS

TABLE OF CONTENTS (Continued)

TABLE OF CONTENTS (Continued)

TABLE OF CONTENTS (Continued)

TABLE OF CONTENTS (Continued)

TABLE OF CONTENTS (Continued)

LIST OF APPENDICES

TABLE OF CONTENTS (Continued)

LIST OF TABLES (Follow Sections)

TABLE OF CONTENTS (Continued)

TABLE OF CONTENTS (Continued)

LIST OF FIGURES (Follow Sections)

TABLE OF CONTENTS (Continued)

TABLE OF CONTENTS (Continued)

TABLE OF CONTENTS (Continued)

TABLE OF CONTENTS (Continued)

TABLE OF CONTENTS (Continued)

TABLE OF CONTENTS (Continued)

LIST OF ACRONYMS

AAR	Arabasz, Anderson, Ramelli team
ASM	Ake, Slemmons, McCalpin team
CNWRA	Center for Nuclear Waste Regulatory Analysis
CRWMS	Civilian Radioactive Waste Management System
DOE	U.S. Department of Energy
DSR	Doser, Fridrich, Swan team
EPRI	Electric Power Research Institute
ESF	Exploratory Studies Facility
GM	Ground Motion
IAEA	International Atomic Energy Agency
M_{max}	maximum magnitude
M_w	moment magnitude
M&O	Management and Operating (Contractor)
NRC	U.S. Nuclear Regulatory Commission
NTS	Nevada Test Site
PGA	peak ground acceleration
PSHA	Probabilistic Seismic Hazard Analyses
QA	quality assurance
QARD	Quality Assurance Requirements and Description
RVT	Random Vibration Theory
RYA	Rogers, Yount, Anderson team
SBK	Smith, Bruhn, Knuepfer team
SDO	Smith, de Polo, O'Leary team
SSCs	structures, systems, and components
SSFD	Seismic Source and Fault Displacement
SSHAC	Senior Seismic Hazard Analysis Committee
UHS	uniform hazard spectrum
UNE	underground nuclear explosion
USBR	U.S. Bureau of Reclamation
USGS	U.S. Geological Survey
WCFS	Woodward-Clyde Federal Services

ACKNOWLEDGMENTS

This technical report is the result of many individuals' efforts over the past three plus years beginning in August 1994. We would like to acknowledge the many contributions of the Project participants described in Chapter 1 whose hard work and conscientious efforts are reflected in this report. Many individuals provided us tremendous support in the performance of the project, particularly in the workshop logistics and preparation of the Activity and Final Reports. In particular, we would like to express our gratitude to Sue Penn of Woodward-Clyde Federal Services and Kathryn Hanson and Nancy Iacono of Geomatrix Consultants, Inc. Other individuals who provided valuable assistance included Tom Statton, Jacqueline Bott, Anna Sojourner, Doug Wright, Rein Dillon, Sadako McInerney, Fumiko Goss, Ron Goss, Melinda Lee, Rachel Griener, and Roger Ocampo of Woodward-Clyde; Nick Gregor, consultant; Patricia Sheaffer, Martha Mustard, Bruce Parks, John Stuckless, Tom Chaney, and Dan Soeder of the U.S. Geological Survey; Robin McGuire, John Vlasity, and Katherine Morgan of Risk Engineering, Inc.; John Savino of Golder Associates; John Stamatakos of the CNWRA; and Mary-Margaret Coates.

This project was performed under the auspices of the U.S. Geological Survey with support from the Civilian Radioactive Waste Management System Management and Operating Contractor TRW Environmental Safety Systems, Inc. and DOE under contract DE-AC04-94AL85000. Special thanks to Tim Sullivan of DOE for his advice, guidance, and most of all, patience.

John Whitney
Carl Stepp
Ivan Wong
Richard Quittmeyer

EXECUTIVE SUMMARY

As part of the U.S. Department of Energy's (DOE) evaluation of Yucca Mountain as the site of a potential geologic repository for spent nuclear fuel and high-level radioactive waste, vibratory ground motion and fault displacement hazards were assessed probabilistically. The assessment methodology incorporated expert characterization of seismic sources, surface fault displacement, and ground motion. The experts also quantified estimates of uncertainties in their interpretations. Based on these inputs, hazard was calculated and expressed as the annual frequency at which levels of ground motion or fault displacement will be exceeded. These results form the basis for developing seismic design inputs and provide information on the frequency of occurrence of potentially disruptive events for assessments of long-term performance of a potential repository.

The assessment of seismic hazards relied upon the findings of scientific investigations carried out over the past 20 years or more to study the Yucca Mountain vicinity. Building upon earlier investigations of the Nevada Test Site region, characterization of the Yucca Mountain site has included:

- Evaluation of faults within about 100 km for evidence of Quaternary activity
- Detailed fault-trenching studies of active faults near Yucca Mountain to determine the history and characteristics of past earthquakes
- Monitoring of current seismicity
- Compilation of a catalog of historical and instrumentally recorded earthquakes in the Yucca Mountain region
- Development of a ground motion attenuation relation for extensional tectonic regimes which include the Yucca Mountain region
- Investigation of local site attenuation characteristics
- Numerical modeling of ground motion from scenario earthquakes
- Assessments of the tectonic stress field from hydrofracture measurements and earthquake focal mechanisms
- Collection and analysis of geophysical data to assess tectonic models and identify subsurface faults

- Collection and analysis of data to measure ongoing crustal deformation.

Results of these studies are described in the report "Seismotectonic Framework and Characterization of Faulting at Yucca Mountain, Nevada, (USGS, written communication, 1996). In addition, scientists from the State of Nevada, the Center for Nuclear Waste Regulatory Analyses, and various universities have contributed to the current understanding of the seismotectonic framework for Yucca Mountain. This extensive data base of information formed the basis for the Yucca Mountain seismic hazards analysis.

The probabilistic seismic hazard analysis (PSHA) methodology, which is described in the Topical Report *Methodology to Assess Fault Displacement and Vibratory Ground Motion Hazards at Yucca Mountain, Revision 1* (DOE, written communication, 1997a), allows for the uncertainties inherent in characterizing future ground motions and fault displacements to be explicitly incorporated into the assessment of hazards. By providing information on the annual frequency with which different levels of ground motion or fault displacement will be exceeded, the results support a graded approach to seismic design and provide information needed for performance assessment.

Title 10 of the Code of Federal Regulations, Part 60 defines two events that must be considered in seismic design: Frequency Category 1 and Frequency Category 2 events. In the Topical Report *Preclosure Seismic Design Methodology for a Geologic Repository at Yucca Mountain, Revision 2* (DOE, written communication, 1997b), DOE requires that design for Frequency Category 1 events will use ground motion with an annual frequency of exceedance of 10^{-3} and fault displacements with an annual frequency of exceedance of 10^{-4}. Corresponding values for Frequency Category 2 events are 10^{-4} and 10^{-5} for ground motion and fault displacement, respectively. Although criteria are defined for fault displacement design, the primary approach is to avoid faults capable of significant movement in laying out a repository.

Results of the seismic hazards analysis also support assessment of the long-term performance of a repository at Yucca Mountain. The annual frequencies of exceedance for ground motion and fault displacement provide information on how often the potentially disruptive effects of earthquakes will affect a repository.

Approach to Implementing Probabilistic Seismic Hazards Analyses. Topical Report *Methodology to Assess Fault Displacement and Vibratory Ground Motion Hazards at Yucca Mountain* (DOE, written communication, 1997a) describes DOE's approach to seismic hazard assessment. The approach is generally consistent with state-of-the-practice guidance provided by the Senior Seismic Hazard Analysis Committee (SSHAC, 1997) and the *NRC's Branch Technical Position on the Use of Expert Elicitation in the High-level Radioactive Waste Program* (NRC, 1996).

The PSHA for Yucca Mountain was performed in three strongly integrated parallel activities leading to the determination of fault displacement and vibratory ground motion hazards. The activities were (1) evaluation and characterization of relevant seismic sources including potential for fault displacement; (2) evaluation and characterization of vibratory ground motion attenuation, including effects of earthquake source, wave propagation path, and a rock site; and (3) probabilistic calculation of both fault displacement and vibratory ground motion hazards.

The hazard analyses are based on evaluations of seismic source characteristics, fault displacement, and earthquake ground motions that reflect interpretations of different scientific hypotheses and models using available data. These interpretations include uncertainties due to the inability of data to resolve different hypotheses and models. To evaluate scientific uncertainty, experts were used. Uncertainties were quantified using a logic tree approach in which different interpretations form different branches of a logic tree. Branches are given a weight depending on the expert's evaluation, using the available data, that each branch is the correct interpretation. Using this approach and the Cornell-McGuire formulation of the hazard calculation, uncertainties are propagated through the analysis. The hazard results are presented as mean, median, and fractile hazard curves representing the total uncertainty in input interpretations.

Seismic Source Evaluation and Characterization. Seismic source and fault displacement evaluations were performed by six expert teams (Table ES-1). The evaluations were conducted following a structured elicitation process that included information assimilation and interpretation workshops and individual team elicitations. The process was facilitated by the Seismic Source and Fault Displacement (SSFD) Facilitation Team, which was responsible for

TABLE ES-1
SSFD AND GM EXPERTS

SSFD TEAMS	AFFILIATION
Walter J. Arabasz	University of Utah
R. Ernie Anderson	U.S. Geological Survey
Alan R. Ramelli	Nevada Bureau of Mines & Geology
Jon P. Ake	U.S. Bureau of Reclamation
D. Burton Slemmons	Consultant
James McCalpin	GEO-HAZ Consulting, Inc.
Diane I. Doser	University of Texas, El Paso
Christopher J. Fridrich	U.S. Geological Survey
Frank H. (Bert) Swan	Geomatrix Consultants, Inc.
Albert M. Rogers	GeoRisk Associates, Inc.
James C. Yount	U.S. Geological Survey
Larry W. Anderson	U.S. Bureau of Reclamation
Kenneth D. Smith	University of Nevada, Reno
Ronald Bruhn	University of Utah
Peter L. K. Knuepfer	Binghamton University
Robert B. Smith	University of Utah
Craig dePolo	Nevada Bureau of Mines & Geology
Dennis W. O'Leary	U.S. Geological Survey

GM EXPERTS	AFFILIATION
John G. Anderson	University of Nevada, Reno
David M. Boore	U.S. Geological Survey
Kenneth W. Campbell	EQE International Inc.
Arthur F. McGarr	U.S. Geological Survey
Walter J. Silva	Pacific Engineering & Analysis
Paul G. Somerville	Woodward-Clyde Federal Services
Marianne C. Walck	Sandia National Laboratories

carrying out the technical elicitation and aiding the experts in structuring and quantifying their subjective evaluations. The elicitation process included a total of six workshops and a one-day elicitation meeting with each team. Each SSFD expert team evaluated seismic sources for ground motion and fault displacement hazard computation. The evaluations included alternative interpretations expressing the teams' uncertainties.

Two basic types of seismic sources were considered by the SSFD experts: fault-specific sources and areal source zones. For fault-specific sources, both local and regional faults were considered. Areal source zones are defined to represent zones of distributed seismicity that are not apparently associated with known specific faults. Local faults within a distance of about 20 km were characterized in terms of probability of activity, their geographic locations, rupture lengths, sense of slip, fault dips, and maximum seismogenic depths. The geometric characterization depended on the tectonic model(s) considered by the experts. Approaches used to evaluate the maximum earthquake for faults (maximum magnitude [M_{max}]) were based on empirical relationships between magnitude and the maximum rupture dimensions (e.g., surface rupture length, rupture area, and maximum and average displacement). Earthquake recurrence rates for the faults were described using either recurrence intervals and/or slip rates. Four recurrence models were used depending on the teams' evaluations: characteristic, truncated exponential, modified truncated exponential, and maximum moment.

In the characterization of local faults, alternative faulting behavior and structural models were evaluated by the SSFD expert teams to capture the range of complex rupture patterns and fault interactions. A planar-fault block model was preferred by most teams; linkages along strike or coalescence downdip were considered by all teams. Simultaneous rupture of multiple faults was also included in all of the teams' interpretations. Some teams considered detachment models to constrain the extent and geometry of the local faults while others included the detachment as being itself seismogenic.

Regional faults were evaluated and characterized by all SSFD expert teams using similar approaches. Regional faults are those faults within about 100 km that were evaluated to be capable of generating earthquakes of moment magnitude (M_w) 5 or greater. The number of regional faults included as seismic sources by teams ranged from 11 to 36. This reflects the teams' evaluations regarding the activity of various faults. All teams modeled the regional

faults as planar faults to maximum seismogenic depths with dips depending on the style of faulting (90° for strike-slip faults, 60° or 65° for normal-slip faults). Alternative fault lengths were included to express uncertainty in their mapped lengths.

Seismicity related to volcanic processes, particularly basaltic volcanoes and dike-injection, was explicitly modeled in volcanic source zones by only two teams. Volcanic-related earthquakes were not modeled as a separate source by the other teams, but owing to the low magnitude and frequency of volcanic-related seismicity, were accounted for by the areal source zones.

For areal seismic source zones, the experts defined their boundaries and assessed M_{max} and recurrence. Several teams defined a site areal source zone representing the area where more detailed investigations have been conducted, and thus where the mapping of fault sources is more complete. M_{max} distributions for the areal zones represent uncertainty in the largest random earthquake in the region (associated with the minimum threshold for surface faulting) and/or estimated for a geologic structure that was not explicitly included as a fault-specific seismic source. Earthquake recurrence for the areal zones was derived from the historical seismicity record. Four alternative historical catalogues, which were provided to the SSFD expert teams, were evaluated for completeness, dependent events (e.g., foreshocks and aftershocks) removed, and underground nuclear explosions and other forms of blasting identified. All teams used the truncated exponential recurrence model to estimate earthquake recurrence rates within the areal source zones. Varying treatments of the background seismicity included (1) uniform smoothing of seismicity and (2) nonuniform smoothing using Gaussian kernels having different smoothing distances.

Fault Displacement Characterization. In addition to characterizing seismic sources, the SSFD expert teams also evaluated the potential for surface fault displacement at Yucca Mountain. Fault displacement characterization was carried out for nine locations within the Conceptual Controlled Area boundary. The test locations were defined to span the range of conditions for which fault displacement characterization is needed. They ranged from sites on block-bounding faults to a site in unfaulted rock and included sites on secondary faults and on fractures, both with a series of hypothetical displacement histories. Table ES-3 lists the test locations and their resulting hazard.

The SSFD expert teams developed original approaches to characterize fault displacement potential. These approaches were based primarily on empirical observations of faulting characteristics at Yucca Mountain and in the Basin and Range Province during past earthquakes. Empirical data were fit by statistical models to allow use by the experts.

The potential for fault displacement was categorized as either principal or distributed faulting. Principal faulting is faulting along a main plane (or planes) of crustal weakness that is the locus for release of seismic energy during an earthquake. Where the principal fault rupture extends to the surface, it may be represented by displacement along a single narrow trace or over a zone that is a few to many meters wide. Distributed faulting is rupture that occurs on faults in the vicinity of the principal rupture in response to the principal displacement. Distributed faulting is spatially discontinuous and may occur over a distance of several tens of meters to many kilometers from the principal rupture. A fault that can produce principal rupture may also undergo distributed faulting in response to principal rupture on other faults.

The approaches developed by the SSFD expert teams address characterizing the frequency of displacement events, λ_{DE} and the conditional probability [$P(D>d)$] that, given an event, the observed displacement, D, will be greater than some value of interest, d. Approaches to characterize λ_{DE} divide into two categories: the *displacement approach* and the *earthquake approach*. The displacement approach provides an estimate of the frequency of displacement events directly from observed feature-specific or point-specific observed data. The earthquake approach relates the frequency of slip events to the frequency of earthquakes on the seismic source evaluated for seismic source characterization input to the ground motion hazard assessment.

For distributed faulting, the conditional probability of exceedance, $P(D>d)$, contains two-parts: the variability of slip from event to event, and the variability of slip along strike during a single event. The teams developed several approaches for characterizing the distribution of slip at a location given a principal faulting event.

Principal faulting hazard was assessed for sites located on faults that the SSFD expert teams identified as being seismogenic. The preferred approach for estimating the frequency of displacement events used slip rate divided by the average displacement per event. The expert teams used a number of approaches to evaluate the $P(D>d)$ based on empirical distributions derived from Yucca Mountain trenching data.

To characterize λ_{DE}, the teams used the frequency of earthquakes developed for the ground motion hazard assessment multiplied by the conditional probability that an event produces surface rupture at the site of interest. The along-strike intersection probability was computed using the rupture length estimated from the magnitude of the event randomly located along the fault length. Most teams used an empirical model based on historical ruptures to compute the probability of surface rupture. The preferred approach to assess the conditional probability of exceedance was to define a distribution for the maximum displacement based either on the magnitude or the rupture length of the earthquake. This distribution was convolved with a distribution for the ratio of the displacement to the maximum displacement to compute $P(D>d)$.

The preferred approach to characterize the frequency of displacement events on features subject to only distributed faulting was to use slip rate divided by the average displacement per event. The slip rates were based on the cumulative displacement and slip history. The teams used similar approaches for evaluating the conditional probability of exceedance to those used in the displacement approach for characterizing principal faulting hazard. The empirical distributions used are correlated with a scaling relationship used to estimate the average displacement per event.

The SSFD expert teams displayed the most variability in characterizing distributed faulting potential using the earthquake approach. The basic evaluation of the frequency of earthquakes was derived from the seismic source characterization for ground motion hazard assessment defined by each team. The probability that an earthquake causes slip at the point of interest was assessed in a variety of ways. The preferred approach utilized a logistic regression model based on analyses of the pattern of historical ruptures. The widest variations in approaches were those for assessing the distribution for displacement per event on the distributed ruptures.

Ground Motion Attenuation. Ground motion evaluations were developed using a similar process to that for seismic source and fault displacement characterization. Seven ground motion (GM) experts (Table ES-1) performed the evaluations. The evaluations were conducted following a structured elicitation process, which included information assimilation and interpretation workshops, working meetings, and individual expert elicitations. The process was facilitated by the GM Facilitation Team, which consisted of persons experienced in technical elicitation and in structuring and quantifying experts' subjective evaluations. The elicitation process included three workshops, two working meetings, and a one-day elicitation meeting with each ground motion expert.

The GM experts estimated median ground motion, aleatory uncertainty, and associated epistemic uncertainties for a matrix of earthquake magnitudes, source-to-site distances, and faulting styles and for a suite of spectral frequencies. These estimates were based on empirical and numerical simulation-based models and combinations of conversion factors. The matrix of point estimates consisted of 51 combinations of parameters considered to adequately define attenuation for the seismic sources considered by the SSFD expert teams. The matrix covered the range from M_w 5.0 to 8.0, distances from 1 to 160 km, and strike-slip and normal faulting (both hanging wall and footwall). The range of frequencies for which ground motion was evaluated spans the range of interest for the proposed Yucca Mountain facility: 0.3, 0.5, 1, 2, 5, 10, and 20 Hz in addition to peak ground acceleration (PGA) and peak ground velocity (PGV).

The GM experts' evaluations of point estimates were used as the bases to compute attenuation relations. The regression analysis to develop the attenuation relations was performed by the GM Facilitation Team. Each GM expert defined the distance measure used in the regression analyses for his/her point estimates. Each expert evaluated whether the footwall and hanging wall point estimates were regressed together, as a single normal faulting attenuation equation, or separately, yielding separate models for sites on the hanging wall and footwall. In addition, the experts evaluated the degree of magnitude saturation at close distances. The GM experts also evaluated two special cases, multiple parallel fault rupture and a shallow detachment fault, and developed scaling rules to apply to their models to represent these seismic sources.

Vibratory Ground Motion Hazard Results. Vibratory ground motion hazard was computed at a defined reference rock outcrop having the properties of rock at a depth of 300 m below the ground surface at Yucca Mountain - the waste emplacement depth. Ground motion was computed at this reference location as a control motion for later determination of seismic design bases motions for surface and potential waste-emplacement level (underground) locations.

The reference rock outcrop was defined to have a shear-wave velocity of 1900 m/sec and a median value of kappa (near-surface attenuation parameter) of 0.0186 sec. Based on limited data, this was the best estimate of kappa for the Conceptual Controlled Area available at the time of the study. If ongoing studies of kappa reveal that the median value for the shallow crust beneath the reference rock outcrop is different from 0.0186 sec, the median attenuation models provided by the GM experts can be adjusted using scale factors. Only the median ground motions would be effected. It is also expected that kappa will vary over the Conceptual Controlled Area due to variations in rock properties. This variability has been accounted for by the GM experts in their estimates of uncertainty in their ground motion attenuation relationships.

Based on equally weighted evaluations of the six SSFD expert teams and the seven GM experts, the probabilistic hazard for vibratory ground motion was calculated at the reference rock outcrop for PGA, PGV, and spectral accelerations at frequencies of 0.3, 0.5, 1, 2, 5, 10, and 20 Hz and are expressed in terms of hazard curves. The hazard is also expressed in terms of uniform hazard spectra. PGA, 0.3 and 1.0 Hz spectral acceleration values and PGV are summarized below for the annual exceedance probabilities of 10^{-3} and 10^{-4}.

Table ES-2

MEAN GROUND MOTION HAZARD AT 10^{-3} AND 10^{-4} ANNUAL EXCEEDANCE PROBABILITIES

Frequency (Hz)	Horizontal		Vertical	
	10^{-3}	10^{-4}	10^{-3}	10^{-4}
PGA	0.169g	0.534g	0.112g	0.391g
0.3	0.051g	0.168g	0.029g	0.105g
1.0	0.162g	0.471g	0.073g	0.222g
PGV	15.3 cm/sec	47.6 cm/sec	7.4 cm/sec	23.4 cm/sec

Vibratory Ground Motion Sensitivity Results. Extensive evaluations of the sensitivity of hazard results to evaluated parameters were performed. The earthquake recurrence approach (either slip rates or recurrence intervals) and recurrence models (e.g., characteristic, exponential, or maximum moment) were found to contribute most to uncertainty in the ground motion hazard, at the design basis hazard of 10^{-3} and 10^{-4} per year (Frequency Categories -1 and -2, respectively). M_{max} has a small effect on uncertainty especially for 10 Hz motions, because a large fraction of the hazard at this frequency comes from more frequent moderate-magnitude events. Geometric fault parameters (e.g., rupture lengths, dips, maximum depths) are minor contributors to uncertainty. These parameters have a moderate effect on the locations of earthquakes and on evaluations of M_{max}, but do not affect earthquake recurrence.

Although the SSFD expert teams' results vary somewhat, deaggregation of the mean hazard for an annual exceedance probability of 10^{-4} shows that at high frequencies (e.g., 5 to 10 Hz), ground motions are dominated by earthquakes smaller than M_w 6.5 occurring at distances less than 15 km. The sources of these events are the Paintbrush Canyon - Stagecoach Road and Solitario Canyon faults (or coalesced fault systems including these two faults) and the host areal seismic source zone. Dominant events for low-frequency ground motions, (e.g., 1 to 2 Hz) display a bimodal distribution showing significant contributions to the total hazard from large nearby earthquakes from the same three sources mentioned above and M_w 7 and larger earthquakes beyond distances of 50 km. The latter contribution is due mainly to the relatively higher earthquake recurrence rates for the Death Valley and Furnace Creek faults. Multiple-rupture interpretations involving comparable seismic moment release on more than one fault (i.e., those requiring modification of the attenuation equations) make a small contribution to the

total hazard. Buried strike-slip faults, volcanic seismicity, and seismogenic detachments contribute negligibly to the total hazard. Uncertainty due to team-to-team differences in SSFD expert teams' evaluations is less than a factor of three from lowest to highest team.

The major contributor to epistemic uncertainty in the ground motion hazard is the experts' epistemic uncertainty in ground motion amplitude (within-expert epistemic uncertainty). Expert-to-expert uncertainty is moderate. This is believed to be the result of using a common information base and having elicitation and feedback, which minimized knowledge differences.

Fault Displacement Hazard Results. Probabilistic fault displacement hazard was calculated at nine demonstration sites within the Conceptual Controlled Area. Two of the sites have four hypothetical conditions representative of features encountered within the ESF. The integrated hazard results provide a representation of fault displacement hazard and its uncertainty at the nine sites, based on the interpretations and parameters developed by the six SSFD expert teams. Separate results are obtained for each site in the form of summary hazard curves. Table ES-3 summarizes the mean displacement hazard results for the two design basis annual exceedance probabilities, 10^{-4} and 10^{-5} (Frequency Categories -1 and -2, respectively), at the nine sites.

TABLE ES-3

MEAN DISPLACEMENT HAZARD AT NINE DEMONSTRATION SITES

Site	Location	Mean Displacement (cm) Annual Exceedance Probability	
		10^{-4}	10^{-5}
1	Bow Ridge fault	<0.1	7.8
2	Solitario Canyon fault	<0.1	32
3	Drill Hole Wash fault	<0.1	<0.1
4	Ghost Dance fault	<0.1	<0.1
5	Sundance fault	<0.1	<0.1
6	Unnamed fault west of Dune Wash	<0.1	<0.1
7	100 m east of Solitario Canyon fault		
7a	2-m small fault	<0.1	<0.1
7b	10-cm shear	<0.1	<0.1

Site	Location	Mean Displacement (cm) Annual Exceedance Probability	
		10^{-4}	10^{-5}
7c	fracture	<0.1	<0.1
7d	intact rock	<0.1	<0.1
8	Between Solitario Canyon and Ghost Dance		
8a	2-m small fault	<0.1	<0.1
8b	10-cm shear	<0.1	<0.1
8c	fracture	<0.1	<0.1
8d	intact rock	<0.1	<0.1
9	Midway Valley	<0.1	0.1

With the exception of the block-bounding Bow Ridge and Solitario Canyon faults (sites 1 and 2, respectively), the mean displacements are all 0.1 cm or less at a 10^{-5} annual exceedance probability. For the Bow Ridge and Solitario Canyon faults at 10^{-5} probability, the mean displacements are 7.8 and 32 cm, respectively. Thus, sites not located on a block-bounding fault (i.e, sites on the intrablock faults, other small faults, shear fractures, and intact rock) are assessed to have displacements of 0.1 cm or less for return periods up to 100,000 years.

The fault displacement hazard results display large uncertainty although the hazard levels are quite low. This uncertainty is indicative of the state-of-the-practice in PSHA for fault displacement, which is less mature than PSHA for ground motions. Nonetheless, the results obtained here are considered robust by virtue of the extensive efforts at expert elicitation and feedback, as well as the methodological developments, that were undertaken as part of this study. Sites with the highest fault displacement hazard show uncertainties comparable to those obtained in ground motion PSHA. Sites with low hazard show much higher uncertainties.

There is also a not unexpected correlation between the amount of geologic data available at a site and the uncertainty in the calculated hazard at that site. For sites where there are significant geologic data, the team-to-team uncertainty is less than one order of magnitude. For sites where there are few or no data, the individual team curves span three orders of magnitude. The larger uncertainty at these sites is considered to be due to data uncertainty, i.e., less certain constraints on the team's fault displacement characterization models.

REFERENCES

Senior Seismic Hazard Analysis Committee (SSHAC), 1997, Recommendations for probabilistic seismic hazard analysis: Guidance on uncertainty and use of experts: U.S. Nuclear Regulatory Commission (NRC) NUREG/CR-6372, Washington, DC.

U.S. Nuclear Regulatory Commission, 1996, Branch technical position on the use of expert elicitation in the high-level radioactive waste program: NUREG-1563, Washington, DC.

1.0
INTRODUCTION

The Nuclear Waste Policy Amendments Act of 1982, as amended, assigns to the U.S. Department of Energy (DOE) the responsibility of evaluating Yucca Mountain as a potential geologic repository to site the nation's first permanent disposal facility for spent nuclear fuel and high-level radioactive waste. As part of this effort, two projects related to the seismic performance of the repository have been carried out: (1) probabilistic seismic hazard analyses (PSHA) and (2) the development of seismic design basis parameters. Both projects are being performed jointly by the U.S. Geological Survey (USGS) and the Civilian Radioactive Waste Management System (CRWMS) Management and Operating (M&O) contractor. The USGS has been assigned the primary responsibility for the PSHA Project and Woodward-Clyde Federal Services (WCFS), a member of the M&O Team, has been assigned the task to manage the project. This report describes the PSHA Project. The determination of seismic design basis input is being conducted by a Seismic Design Basis Team under contract to the CRWMS M&O (Risk Engineering, written communication, 1998a).

The PSHA Project was performed in three strongly integrated parallel activities leading to evaluations of fault displacement and vibratory ground motion hazards and to a documentation of the technical bases for these evaluations. The resulting hazards form the basis for determination of seismic design basis inputs for the Yucca Mountain repository structures, systems, and components (SSCs). Seismic design basis covers surface and subsurface SSCs. Both the preclosure and postclosure performance periods of the repository (100 and up to 100,000 years, respectively) were addressed in this project. The activities performed were: (1) evaluation and characterization of seismic sources including the characterization of potential fault displacement; (2) evaluation and characterization of vibratory ground motion attenuation, including earthquake source, wave propagation path, and rock site effects; and (3) computation of hazard results for both fault displacement and vibratory ground motion. This report describes the process followed to carry out the PSHA Project and includes documentation of the interpretations and uncertainties used as input to the hazard calculations for both the seismic source and fault displacement characterization and ground motion characterization.

1.1 PROJECT OBJECTIVES AND SCOPE OF WORK

The overall approach that the DOE has undertaken to address potential seismic hazards at Yucca Mountain is documented in three topical reports: "Methodology to Assess Fault Displacement and Vibratory Ground Motion Hazards at Yucca Mountain" (Topical Report No. 1) (DOE, written communication, 1997a) and "Preclosure Seismic Design Methodology for a Geologic Repository at Yucca Mountain" (Topical Report No. 2) (DOE, written communication, 1997b). Topical Report No. 3 planned for completion later this fiscal year, will document the results of both the PSHA and Seismic Design Basis Projects. The methodology adopted and used in the PSHA Project is described in Topical Report No. 1. The methodology and acceptance criteria used by the DOE to determine the preclosure seismic design of repository SSCs is described in Topical Report No. 2.

The objectives of the PSHA Project are to: (1) evaluate the fault displacement and vibratory ground motion hazards and their uncertainty at the Yucca Mountain site and (2) provide documentation of the technical basis for determining these hazards. The PSHA also provides quantitative hazard results to support an assessment of the potential repository's long-term performance with respect to waste containment and isolation and forms the basis for developing seismic design inputs for the License Application of the potential repository. The hazards results are in the form of annual frequencies of various levels of fault displacement at nine locations within the repository Controlled Area and of vibratory ground motion at a "reference rock outcrop." The reference rock outcrop is defined as free-field ground surface at the elevation of the proposed repository (300 m below the repository ground surface at Point A; Figure 1-1).

The hazard analyses are based on evaluations of seismic source characteristics, earthquake ground motions, and fault displacement that reflect interpretations of different scientific hypotheses and models using available data. These interpretations have associated uncertainties related to the ability of data to resolve different hypotheses and models with certainty. The interpretations described in this study are based on seismological, geological, geophysical, and geotechnical data specific to the Yucca Mountain site and the surrounding region within at least a radius of 100 km. To evaluate scientific uncertainty, seismic source and fault displacement characterizations have been made by six teams of experts, who in composite are expert in the

seismicity, tectonics, and geology of the Yucca Mountain site and region. Ground motion evaluations have been made by seven individuals expert in the generation and attenuation of earthquake ground motions.

Interpretations for hazard assessment have been coordinated and facilitated through a series of workshops. Each workshop was designed to accomplish a specific step in the overall evaluation and to ensure that the relevant data were being appropriately considered and integrated. This process, which for this project is called the elicitation process, was designed to insure that credible hypotheses and models were evaluated and input to the fault displacement and vibratory ground motion hazard assessment.

The seismic hazard computational procedures used for this project produced quantitative assessments of seismic hazard based on input interpretations provided by the experts. Uncertainty in individual interpretations was captured in a logic tree structure as weighted alternatives and propagated through the hazard calculations. Thus the quantification incorporates uncertainty in the hazard due to scientific uncertainty in the input interpretations as well as to random variability in input parameters. The hazard results are presented as mean, median, and fractile hazard curves representing the total uncertainty in input interpretations.

1.2 RELATIONSHIP OF PSHA PROJECT TO PRECLOSURE AND POSTCLOSURE SEISMIC DESIGN BASIS DETERMINATION AND POSTCLOSURE PERFORMANCE ASSESSMENT

The following describes how the PSHA Project results will be used in the development of both preclosure and postclosure seismic design bases and in the assessment of postclosure performance.

1.2.1 Preclosure Seismic Design Basis Determination

The PSHA Project provides the needed information base for determining fault displacement and vibratory ground motion levels appropriate for seismic design of the proposed repository SSCs. The criteria for determining seismic design inputs are described in Topical Report No. 2 (DOE, written communication, 1997b) and will be used together with the PSHA results by the Seismic Design Basis Team to establish the seismic design basis for fault displacement and

ground motions for the proposed repository. The seismic design basis will be documented in a separate report, "Seismic Design Input for a High-Level Waste Repository at Yucca Mountain, Nevada," which is in preparation (Risk Engineering, written communication, 1998a).

In accordance with Topical Report No. 2, seismic design inputs will be developed for Frequency Categories-1 and -2. For vibratory ground motion, the reference annual frequencies of exceedance for these two categories are 10^{-3} and 10^{-4}, respectively, or return periods of 1,000 and 10,000 years. The corresponding annual frequencies (and return periods) for fault displacement are 10^{-4} (10,000 years) and 10^{-5} (100,000 years), respectively.

Vibratory ground motion hazard has been assessed at the reference rock outcrop (Point A; Figure 1-1). As part of the seismic design basis determination now in development, design basis motions in the form of peak values, response spectra, and time histories for acceleration and velocity and for both horizontal and vertical components are being computed at Points B and C (Risk Engineering, written communication, 1998a). Also, peak ground velocity and dynamic strains are being computed at Points B and C and with depth between the ground surface and the repository level. The methodology for determining seismic design basis motions at the proposed locations of the surface facilities, which will be on alluvium in Midway Valley, illustrated by Point D on Figure 1-1, is being described as part of the separate seismic design basis evaluation. Actual computations of the seismic design basis motions for the surface facilities will be completed when the facility design and layout is more mature and the geotechnical properties of the alluvium have been obtained.

The seismic design basis motions will be developed considering four controlling earthquakes: an earthquake controlling high frequencies (5 to 10 Hz) and an earthquake controlling low frequencies (1 to 2 Hz) for the two return periods of 1,000 and 10,000 years. These four controlling earthquakes are derived by de-aggregating the probabilistic hazard as determined in the PSHA Project in terms of mean magnitude $(\overline{M})$, mean distance $(\overline{d})$, and ground motion deviation (ε).

For fault displacement, the principal design criterion provided in Topical Report No. 2 (DOE, written communication, 1997b) is to avoid faults that have the potential for offsets of engineering significance where reasonably feasible. Only in cases, if any, where fault avoidance

is not feasible and for which the potential fault displacement is significant, as quantified by the PSHA, will fault displacement design be implemented in the design of the Yucca Mountain SSCs.

1.2.2 Postclosure Design Evaluation

Vibratory ground motion and fault displacement hazard information developed by the PSHA Project will be used to evaluate the effects of disruptive processes during the postclosure period on repository performance. SSCs important to safety must be designed and constructed to meet postclosure as well as preclosure performance requirements (DOE, written communication, 1997b). The DOE is employing a systems approach, which establishes the life cycle functions of repository SSCs, to ensure that they are designed to meet their performance requirements. Postclosure performance requirements may be controlling for some SSCs for which repetitive ground motion or fault displacementis is important.

An example is the postclosure performance with respect to rockfalls in emplacement drifts. Presently the DOE does not intend to rely on rockfalls not occurring in emplacement drifts for any period of time to meet postclosure performance (DOE, written communication, 1997b). Rather, the DOE intends to evaluate the effects of rockfalls, including incremental effects of repetitive seismic loading, on postclosure performance and, if necessary, design to mitigate their consequences. The seismic hazard curves developed by the PSHA Project will be integrated with consequence curves for this assessment. Other postclosure performance evaluations will make similar use of the PSHA Project results.

Postclosure performance evaluations generally involve integration of hazard curves taking account of uncertainty. The vibratory ground motion and fault displacement hazard curves developed by the PSHA Project contain the necessary information for this evaluation.

1.2.3 Postclosure Performance Assessment

Postclosure Total System Performance Assessment - Viability Assessment (TSPA-VA) will evaluate the effects of spatially and temporally varying processes on waste isolation and containment after the repository system is sealed and closed (CRWMS M&O, written communication, 1997). To accomplish the TSPA-VA, the respository system is divided into a

series of natural spatial component models: the waste package, the engineered barrier system, the host rock, etc. The total system assessment model is constructed by linking the component models of the total system such that the input boundary conditions of each successive component are provided by the output of the preceding one. The base case total system performance is obtained by synthesizing the performance of the various component models.

The TSPA-VA treats vibratory ground motion and fault displacement hazards (together with other disruptive processes) as disruptive events and evaluates the impact (in terms of offsite consequences) on the base case repository system performance of their occurrence. The analysis procedure is essentially similar to any probabilistic seismic risk assessment in which the seismic hazard quantifies initiating event frequencies. The hazard is input as a vector of ground motion values or fault displacement values, and recurrence frequencies. The component model performance analysis converts the initiating event frequencies to component consequence frequencies, which are propagated through succesive component models to the total system performance, to obtain the effect of the hazard on the repository performance. Gauthier et al. (1995) have demonstrated the analysis process and performed preliminary evaluations of the response of repository component models to ground motion hazards. The fault displacement and ground motion hazard results of the PSHA Project will be used directly together with the refined component model response analyses, in subsequent TSPA-VA.

1.3 PREVIOUS STUDIES FOR YUCCA MOUNTAIN

The following briefly summarizes previous studies which are relevant to the probabilistic seismic hazard at Yucca Mountain.

1.3.1 Seismotectonic Studies

Since the late 1970s, Yucca Mountain has been investigated by DOE as a potential geologic repository for the storage of high-level radioactive wastes. As part of a broad interdisciplinary program designed to comprehensively evaluate site suitability, a series of specific studies bearing on the structural geology, tectonic evolution, and seismicity of the Yucca Mountain area and region was undertaken in the mid-1980s to analyze vibratory ground motion and fault displacement hazards that may affect repository design and performance (W.R. Keefer, USGS, written communication, 1996).

The structural geology and deformational and volcanic histories of the southern Great Basin have long been subjects of study since the beginning of the century. A period of extensive geologic and related studies at and near Yucca Mountain began in 1956, when efforts were initiated to investigate the feasibility of underground testing of nuclear devices at the Nevada Test Site, which includes the eastern part of Yucca Mountain. An integrated program of geologic mapping, stratigraphic and hydrologic studies, geophysical surveys, drilling and tunneling, and laboratory analyses of physical and chemical properties of rocks and surficial materials resulted in a large accumulation of new scientific data that provided the basic framework for interpreting the complex geologic and hydrologic conditions of the approximately 3900 km^2 test site area as well as adjoining areas (Eckel, 1968). Geologic mapping of all the 7½-minute quadrangles covering the test site including Yucca Mountain, at a scale of 1:24,000, was largely completed during the 1960's. The accumulated data, discussed in Eckel (1968), were instrumental in the subsequent selection of Yucca Mountain as a potential site for the underground storage of high-level radioactive wastes.

The Site Characterization Plan in 1988 (DOE, written communication, 1988) presented an integrated program of multidisciplinary studies designed to collect, analyze, and interpret the many and varied kinds of data that are considered essential for meeting regulatory, performance, and design requirements for a geologic repository. Since its issuance, the Site Characterization Plan has guided virtually all later investigations at Yucca Mountain, including seismotectonic studies within the Preclosure Tectonics Program (DOE, written communication, 1988), which were designed to develop an understanding of, and to characterize, the tectonic events and processes that could impact the potential repository SSCs.

1.3.2 PSHA Studies

Since the inception of the Yucca Mountain Project, several PSHA studies have been performed. The first analysis by URS/John A. Blume & Associates, Engineers (URS/John A. Blume & Associates, written communication, 1986) evaluated the ground motion hazard at Yucca Mountain for repository conceptual design. In that study, only areal source zones were defined and they were based on the historical earthquake record and limited paleoseismic data. Based on that probabilistic analysis, peak horizontal accelerations of 0.25, 0.40, and 0.65 g were calculated for return periods of 500, 2,000, and 10,000 years.

In a subsequent study, URS/John A. Blume & Associates, (written communication, 1987) evaluated both ground motion and fault displacement hazards to assess the effects of model and parametric uncertainties on the computed hazards. In that analysis, active faults were specifically characterized and modeled based on the available paleoseismic data. A simplified fault model was used to calculate the fault displacement hazard based on a joint probability for surface rupture displacement, length, and rupture radius exceedances together with the fault recurrence models. The calculated probabilistic ground motion hazard was dominated by the Paintbrush Canyon and related faults and by background seismicity and was most sensitive to the relationships between slip rate and fault lengths used in the analysis. The surface fault displacement hazard was calculated for the Paintbrush Canyon fault, and related primary (block-bounding) faults in the site vicinity. The resulting hazard was most sensitive to the assumed slip rate-fault length relations.

In a 1994 study for seismic design of the Exploratory Studies Facility (ESF), the CRWMS M&O performed a PSHA for ground shaking (Quittmeyer *et al.*, WCFS, written communication, 1994; Wong *et al.*, 1996). In that study, 24 Quaternary faults and a background areal zone were included in the analysis. Characterization of seismic sources included consideration of additional paleoseismic data collected as part of the site characterization activities. Four western U.S. empirical ground-motion relationships for rock were used to characterize the ground motion attenuation. The resulting peak horizontal accelerations for return periods of 1,000 and 10,000 years were 0.27 g and 0.66 g, respectively.

In a recent PSHA for the preliminary design of the Waste Handling Building (Wong *et al.*, 1998), the ESF study was updated by incorporating new paleoseismic data, particularly on the local faults, and the extensional regime ground motion attenuation relationship by Spudich *et al.* (1996). The resulting peak horizontal accelerations were 0.16, 0.21, and 0.50 g, for return periods of 500, 1,000, and 10,000 years, respectively. These motions were significantly lower than the ESF values due to the high weight (0.50) assigned to the Spudich *et al.* (1996) relationship (which results in calculated ground motions about 20% lower than California-based attenuation relations) and lower slip rates for the local faults based on more recent paleoseismic data.

In a demonstration project in 1992, Electric Power Research Institute (EPRI) sponsored an expert elicitation PSHA for fault displacement at Yucca Mountain. The objectives were to (1) demonstrate methods for eliciting expert judgment and (2) quantify the uncertainties associated with earthquake and tectonic issues for use in the EPRI High-Level Waste performance assessment.

In addition to these site-specific studies, PSHAs have been performed for hazard mapping on a national and state basis. Since 1948, ground shaking hazard maps have been developed for the entire U.S. that form the basis for the zonation in the Uniform Building Code. In the most recent maps (Frankel *et al.*, 1996), the peak horizontal accelerations for return periods of approximately 500, 1,000, and 2,500 years are about 0.16, 0.19, and 0.29 g, respectively, for the Yucca Mountain site. In a study for the Nevada Department of Transportation, R. Siddharthan *et al.* (written communication, 1993) developed statewide probabilistic hazard maps, which show peak horizontal acceleration values for the Yucca Mountain site of 0.24 g and 0.30 g for return periods of 500 and 1,000 years, respectively. Other PSHAs for vibratory ground motions have been performed for the Nevada Test Site by Rogers *et al.* (1977) and Coats and Murray (1984).

1.4 PROJECT ORGANIZATION

The major components of the project organization included the Principal Investigator, the Project Management Team, Review Panel, technical teams including the facilitation, data management, and calculations teams, and the two expert panels. Team members and experts are shown on Figure 1-2 and in Tables 1-1 to 1-4.

Although not part of the project organization, an important part of the PSHA process was the inclusion of model and data specialists. Specialists participated in the project by providing the expert evaluators with descriptions of their data, models, and interpretations, during workshops and the field trip. These technical specialists and their affiliations are listed in the summaries of the workshops and the field trip (Appendices C and D). At certain workshops, members of both the facilitation teams and evaluation experts also acted as technical specialists advocating a particular model, data set, or interpretation.

Dr. John Whitney was the Principal Investigator for the Project. In this role, he provided overall technical guidance for the work. In addition, he was responsible for implementing the Quality Assurance procedures by which the work was controlled.

1.4.1 Project Management Team

Management of the PSHA Project was provided by the Project Management Team. This team provided overall management of the project, managed the Project Review Panel, advised on technical issues relating to the project, and oversaw the efforts of the four technical teams. They also ensured consistency with regulatory requirements, DOE policies and guidelines, and program needs. They provided logistical and organizational management of the workshops and the preparation of reports. Regarding the latter, the Project Management Team ensured that appropriate project reviews were implemented in a participatory mode (SSHAC, 1997) to achieve completeness and high technical quality, and that project schedules and milestones were met. The team consisted of Dr. Carl Stepp, Project Director, Deputy Project Directors, Mr. Ivan Wong and Dr. Jean Savy, and Dr. Richard Quittmeyer, Senior Scientist responsible for CRWMS M&O geoscience activities.

1.4.2 Review Panel

The Review Panel (Figure 1-2) consisted of four individuals who are experts in the range of disciplines and topics that constitute the assessment of seismic hazards. Each member of the panel was responsible for a specific technical scope of work of the project: Dr. C. Allin Cornell - PSHA methodology and process, Dr. Thomas Hanks - vibratory ground motion, Dr. James N. Brune - seismic source characterization and vibratory ground motion, and Dr. David P. Schwartz - seismic source characterization and fault displacement evaluations. The panel review was fully participatory (SSHAC, 1997). Panel members attended the workshops and meetings relevant to their assigned scope of review; they provided formal review comments and recommendations within their technical scope following each workshop, and reviewed draft reports and prepared comments and recommendations that were reviewed and implemented by the Project Management Team.

1.4.3 Technical Teams

To plan, organize, and lead the technical workshops, facilitate the experts in their interpretations, and perform the required hazard calculations, four technical teams were

assembled: (1) Seismic Source and Fault Displacement (SSFD) Facilitation, (2) Ground Motion (GM) Facilitation, (3) Data Management, and (4) PSHA Calculations (Figure 1-2).

1.4.3.1 Seismic Source and Fault Displacement Facilitation Team. This team facilitated the experts' seismic source and fault displacement evaluations for the hazard analyses. They provided the technical leadership to facilitate interactions and elicit interpretations by the experts. The SSFD Facilitation Team organized, planned, and led all technical workshops related to characterization of seismic sources and evaluations of the potential for fault displacement. Their responsibilities included (1) planning the technical scope, preparing any necessary white-paper documentation of the state-of-the-art, obtaining input and participation in workshops of data, model, or interpretation proponents, and facilitating discussion in the workshops; (2) preparing workshop agendas, conducting the workshops, and writing workshop summary reports; (3) eliciting interpretations of the experts; (4) providing feedback to the experts regarding the hazard results of their interpretations; and (5) preparing an Activity Report to describe the process followed to develop the experts' interpretations and to present the interpretations themselves. The team was led by Dr. Kevin Coppersmith. Other members of this team and their principal responsibilities are listed in Table 1-1.

1.4.3.2 Ground Motion Facilitation Team. This team facilitated the characterization of ground motion attenuation by the GM experts for a suite of parameters that was used in the PSHA. The responsibilities of the GM Facilitation Team were the same as those of the SSFD Facilitation Team. Dr. Norm Abrahamson led this team; other members and their principal responsibilities are listed in Table 1-2.

1.4.3.3 Data Management Team. The Data Management Team provided common data sets to the experts. The team compiled relevant data and provided derivative data products and evaluations as identified by the experts during the data needs workshops. The goal was to eliminate differences in interpretations caused by different data and knowledge bases. The historical earthquake catalog was compiled by the Data Management Team. This team was led by Dr. John Whitney and Ivan Wong and support was provided by the USGS and WCFS personnel (Figure 1-2).

1.4.3.4 PSHA Calculations Team. The PSHA Calculations Team performed both preliminary and final seismic hazard computations. The computed seismic hazard is in the form of seismic hazard curves for (1) a range of spectral periods for vibratory ground motions and (2) for locations representing the range of faulting conditions within the Controlled Area. The team also modified the existing seismic hazards computational code for ground shaking to incorporate the code for calculating the hazard from fault displacement. The team was led by Dr. Gabriel Toro and consisted of staff at Risk Engineering, Inc. (Figure 1-2).

1.4.4 Experts

Scientific interpretations and uncertainty were incorporated into the probabilistic hazard analyses by including multiple evaluations of scientific evaluators with complementary experience and knowledge. These experts evaluated hypotheses, models, and processes using available data, and developed and documented interpretations for input into the PSHA calculations. For the seismic source and fault displacement characterizations, six three-person expert teams performed the interpretations. The aggregate expertise of each group covered the seismic geology, geology, tectonics, seismology, and geophysics of Yucca Mountain and the Basin and Range Province. Each SSFD expert team was responsible for identifying and characterizing the seismic sources significant to Yucca Mountain vibratory ground motions or fault displacement hazards. In addition, each SSFD team provided a characterization of the fault displacement potential for calculation of the fault displacement hazard at locations within the Controlled Area. These teams performed as virtual experts, expressing interpretation uncertainty that represented the teams uncertainty.

For ground motion attenuation characterization, seven individual GM experts provided evaluations for input to the PSHA. Each expert provided ground motion point estimates for a specified range of parameters. The GM experts were selected to cover the two principal approaches to estimating ground motions, empirical and numerical modeling, and included one expert in nuclear explosion ground motions. Tables 1-3 and 1-4 list the SSFD and GM experts, respectively, and their affiliations. Biographies of the experts are provided in Appendix A.

1.5 PROJECT ACTIVITIES

Planning of the PSHA Project by the Project Management Team began in August 1994 with the development of Study Plan 8.3.1.17.3.6 "Probabilistic seismic hazard analysis" and the Project Plan: "Probabilistic analysis of fault displacement and vibratory ground motion and development of seismic design bases for Yucca Mountain." The latter included the seismic design basis activities to insure integration with the PSHA Project. Selection of team members and experts followed in the fall of 1994.

Major activities of the PSHA Project were the workshop elicitation interactions conducted by the facilitation teams. These workshops provided the experts with the expert elicitation methodology, facilitated interaction among the experts, defined the data needed to perform their evaluations, provided a forum for discussing the range of relevant technical issues requiring evaluation, and facilitated the presentation and evaluation of state-of-the-knowledge research as well as proponent models and interpretations. The first workshop was held in April 1995. Due to Yucca Mountain Project funding constraints, the project was suspended in FY96 and resumed in FY97 with the remaining workshops. A thorough discussion of the workshops and the PSHA process as a whole is presented in Chapters 2.0 to 4.0 and 7.0; workshop summaries are in Appendices C and D. A final project meeting to present the results of the PSHA was held in April 1998 (Appendix C). The following briefly describes the general aspects of the three primary activities in the PSHA Project: the seismic source and fault displacement and ground motion characterizations and the hazard calculations.

1.5.1 Seismic Source and Fault Displacement Characterization

The purpose of this activity is to characterize known seismic sources significant to ground shaking and fault displacement hazard at Yucca Mountain. The SSFD expert teams were asked to provide and document in an elicitation summary their interpretations of the location, geometry, probability of activity, maximum magnitude, and recurrence rates of all seismic sources they identified as being significant to Yucca Mountain both in terms of vibratory ground motions and fault displacement. In addition, they were asked to characterize the fault displacement potential of faults and features at nine locations within the Controlled Area, including both primary and distributed faulting.

The process of evaluating and characterizing seismic sources for vibratory ground motion hazard assessment and characterizing potential for fault displacement for fault displacement hazard assessment generally followed the guidance in NUREG/CR-6372, "Recommendations for Probabilistic Seismic Hazard Analyses: Guidance on Uncertainty and Use of Experts" (NRC, 1997a), and in NUREG-1563, "Branch Technical Position on the Use of Expert Elicitation in the High-Level Radioactive Waste Program" (NRC, 1996). The determination of seismic design basis ground motion generally follows the guidance in Regulatory Guide 1.165, "Identification and Characterization of Seismic Sources and Determination of Safe Shutdown Earthquake Ground Motion" (NRC, 1997b), and NUREG-1451, "Staff Technical Position on Investigations to Identify Fault Displacement Hazards and Seismic Hazards at a Geologic Repository" (NRC, 1992). The evaluation and characterization of the potential for fault displacement made use of the guidance in NUREG-1494, "Staff Technical Position on Consideration of Fault Displacement Hazards in Geologic Repository Design" (NRC, 1994).

A very important objective of the SSFD characterization was to identify and assess the uncertainties in seismic source and fault displacement characterization. This aspect of the evaluation was designed to capture uncertainty both in the *models* used to characterize seismic sources, and the *parameter values* used in the models. The experts, who were both from within and outside the Yucca Mountain Project, represented a range of experience and expertise relevant to performing the evaluations. A deliberate process was followed in facilitating interactions among the experts, in training them to express their uncertainties, and in eliciting their interpretations. The resulting evaluations, therefore, provide reasonable assurance that the knowledge and uncertainties about seismic source and fault displacement characterization relevant to PSHA at the Yucca Mountain site has been captured and expressed in the seismic hazard results. The seismic source and fault displacement characterization is described in detail in Chapters 3.0 and 4.0.

1.5.2 Ground Motion Characterization

The goal of this activity was to characterize vibratory ground motion at the proposed repository as a function of ground motion frequency, given an earthquake magnitude and distance. The evaluation of ground motion resulted in ground motion attenuation relations specific to the repository site. The relations include earthquake source, propagation path, and site effects specific to Yucca Mountain. The attenuation relations describe ground motions for the range of

structural response periods required for design of the proposed facility SSCs. Both horizontal and vertical components of motion have been characterized. Like the seismic source and fault displacement characterization, the experts evaluated the uncertainties in ground motion as part of their characterizations.

Ground motion attenuation relationships were characterized for both fault-specific and areal sources. Ground motions resulting from the different styles of faulting (strike-slip, normal, or reverse) were incorporated into the characterization. Thus the seismogenic sources, to a degree, define the technical issues that the ground motion characterization had to address. The ground motion characterization activity thus required coordination with the SSFD Facilitation Team and the PSHA Hazard Calculations Team. A detailed description of the ground motion characterization is contained in Chapters 5.0 and 6.0.

1.5.3 Probabilistic Seismic Hazard Analyses

The PSHA methodology for vibratory ground motions was first developed by Cornell (1968, 1971) and has become standard practice in evaluating seismic hazards. Subsequent to Cornell's work, the basic computational analysis method has changed little, but PSHA methodology has undergone extensive development principally by the U. S. Nuclear Regulatory Commission (NRC) and utilities that operate nuclear power plants. The most extensive and important developments have been structured procedures for quantifying subjective scientific evaluations of seismic sources, source earthquake recurrence characteristics, and ground motion input to seismic hazard assessment. This work has resulted in development of procedures to quantify input interpretations including experts' uncertainty in their evaluations, and a process for conducting PSHA that provides reasonable assurance that scientific and data uncertainties are properly captured and represented in the hazard results. These procedures and their application have undergone extensive review by the NRC and have been accepted for application to determine seismic design bases for nuclear facilities (EPRI, 1988, 1989; NRC, 1988, 1991, 1997a; SSHAC, 1997).

A probabilistic hazard assessment results in calculated annual probabilities that a given level of vibratory ground motion (e.g., peak horizontal acceleration) will be exceeded at a site. The resulting seismic hazard curve is obtained by integrating over all earthquake sources and magnitudes of potential future earthquake occurrence and ground motion variability. The

methodology for assessing fault displacement hazard probabilistically is nearly identical to that for vibratory ground motions--the most important difference being that expert evaluations of fault displacement potential are the inputs to the assessment.

The calculation of ground motion hazard and fault displacement employs similar processes. For ground motion hazard, three basic inputs are required: (1) the identification of relevant seismic sources and characterizations of their source geometries; (2) an evaluation of the rate of earthquake occurrence, recurrence model, and maximum magnitude distribution for each seismic source; and (3) attenuation relationships that provide for the estimation of a specified ground motion parameter as a function of magnitude, source-to-site distance, and when needed, fault type and geometry. Inputs (1) and (2) are developed by SSFD expert teams and (3) by GM experts. For assessing fault displacement hazard, the ground motion attenuation relationships are replaced by relationships that describe the distribution, sense, and amounts of displacement with earthquake occurrence. Potentials for both primary and secondary fault displacement are characterized. Uncertainties in these input evaluations are expressed as alternative interpretations using a logic tree structure. In this study, the probabilistic ground shaking hazard was calculated using a Quality Assurance-approved computer code FRISK 88 version 2.0 developed by Risk Engineering, Inc. (written communication, 1998) For the calculation of the fault displacement hazard, the evaluations provided by the SSFD experts were coded and incorporated into the basic hazard code. Extensive sensitivity analyses were performed and provided to the experts. A detailed description of the calculated results is contained in Chapters 7.0 and 8.0.

1.6 QUALITY ASSURANCE

The PSHA Project was performed under the USGS Quality Assurance Program for the Yucca Mountain Project. DOE's Quality Assurance Requirements and Description document (QARD) (DOE/RW-0333P) provides the QA requirements for the Yucca Mountain Project and the USGS Quality Assurance Program is written to meet applicable requirements of the QARD. The key elements of the program applicable to PSHA were personnel qualifications and training, scientific expert elicitation, software controls, records management, and data management.

Personnel qualifications files consisting of position descriptions, resumes, and verification statements have been collected for members of the Project Management Team, the Review Panel, and the technical teams. Training in expert elicitation and in the applicable procedures was provided via workshops and reading assignments. At the time that the PSHA was performed, the QARD was silent on requirements applicable to scientific expert elicitation; however, the USGS developed a new Quality Management Procedure to include appropriate requirements for scientific expert elicitation. Revision 8 of the QARD, to become effective in June 1998, now includes requirements for scientific expert elicitation based on NUREG-1563, "Branch Technical Position on the Use of Expert Elicitation in the High-Level Radioactive Waste Program" (NRC, 1996). During a QA audit (USGS-ARP-98-01) of the USGS in October 1997, DOE's Office of Quality Assurance compared the USGS procedure, the PSHA Project Plan, and implementation to the NUREG guidance and to the then-draft QARD requirements. The QARD and the NUREG require the experts to document the reasons for any modifications to their interpretations. Within the structured expert elicitation process implemented for this Project, this requirement of the NUREG is considered to be met by the workshop summaries. The summaries contain descriptions of preliminary evaluations by experts. Any additional specific requirement to justify evolving evaluations is considered to have the unacceptable consequence of anchoring and biasing the expert's evaluations. The audit team accepted this position and justification.

Software QA requirements were applicable only to the computer codes for ground shaking and fault displacement hazard developed and modified by Risk Engineering. The Risk Engineering code modifications were required to be verified and the released code placed in the USGS Yucca Mountain Project Branch software configuration management system. Any software used by the experts in developing their interpretations were exempted from the QARD software requirements.

The report and the information required to support the development of Risk Engineering computer codes will be submitted to the CRWMS M&O records processing center. The hazards curves and logic trees will be submitted to the CRWMS M&O technical data base.

1.7 DOCUMENTATION OF PSHA EXPERT EVALUATIONS

The integrity of a PSHA is considered to rest principally on how it is structured and implemented to derive seismic source and ground motion inputs for hazard computation. For performing the Yucca Mountain PSHA, a structured process was adopted to obtain inputs that insured independent evaluations by recognized experts, representing the scientific community's state of knowledge. Evaluations were elicited through a process involving workshops each structured and implemented to achieve a specifically defined step in the overall evaluation (Sections 3.2 and 5.3), and through individual meetings between the facilitation teams and the experts. All workshops and meetings between the facilitation teams and experts were documented by summaries that are part of the basic documentation of the PSHA Project (Appendices C and D).

Two defining principles guided the elicitation process: 1) the experts are evaluators and their combined evaluations represent the informed scientific community's state of knowledge, and 2) the experts themselves are the owners of their independent evaluations. Thus, the elicitation process continually emphasized the role of the experts as independent evaluators responsible for considering proposed hypotheses and models using available data. It also emphasized that the experts themselves were responsible for describing their final evaluations in a summary report that would become part of the PSHA Project documentation.

Preliminary evaluations were developed by the experts and presented, discussed, and documented in the workshops. In recognition of principle (1) and the unacceptable risk of anchoring the interpretations at an immature stage, the experts were not required to provide written descriptions of their preliminary evaluations beyond the presentation materials in the workshops. Based on the experience base developed over the past decade or more in carrying out seismic hazard assessments, requiring specific documentation of experts' preliminary evaluations and specific justification for any change was considered to present an unacceptable risk of anchoring, and thus biasing, the evaluations before completion of the elicitation process. The experts also were provided feedback of hazard results based on their preliminary input evaluations. This feedback activity took place after the experts had completed draft expert summaries that described their input evaluations. These draft summaries are part of the PSHA Project basic documentation. Following the feedback activity, the experts were free to make changes in their evaluations before completing and submitting their final summaries for the

seismic hazard calculations. The experts' final summaries of their interpretations are the final products of their evaluations. These are included in this report as Appendices E and F.

1.8 PROJECT PRODUCTS AND REPORT ORGANIZATION

This PSHA Final Report is a DOE Level 3 milestone. It is comprised of three Activity Reports that describe and summarize the three major project activities. These Activity Reports, which are Level 4 documents, are the "Seismic Source and Fault Displacement Characterization Project" (Geomatrix Consultants, written communication, 1997), "Ground Motion Characterization at Yucca Mountain, Nevada" (N. A. Abrahamson and A. M. Becker, Consultants, written communication, 1997a), and "Probabilistic Seismic Hazard Calculations for Yucca Mountain, Nevada" (Risk Engineering, written communication, 1998c`). In addition, as part of the milestone requirements, for the Final Report, included in Volume 3 are Appendix K "Yucca Mountain Project Records and Data Tracking Information for Data Used and Cited Within the Report," and Appendix L "Milestone SP32IM3 Description/Completion Criteria Compliance Location."

Following this Introduction (Chapter 1.0), there are eight chapters and 11 appendices in the Final PSHA Report. Chapter 2.0 describes the process of selecting the experts and provides a general description of the expert elicitation. Chapters 3.0 and 5.0 describe the facilitation approaches taken in the seismic source and fault displacement and ground motion characterizations, respectively. Chapters 4.0 and 6.0 describe the experts' evaluations of seismic source and fault displacement and ground motion, respectively. The probabilistic methodology used to quantify the ground shaking hazard at Yucca Mountain is presented, and the results along with sensitivity analyses are described, in Chapter 7.0. Chapter 8.0 presents the probabilistic hazard methodology for fault displacement and the results. References cited in the report are contained in Chapter 9.0. Appendix A contains biographies of both the SSFD and GM experts. Data packages distributed to both the SSFD expert teams and GM experts are listed in Appendix B. Appendices C and D contain the workshop summaries including a summary of the final project meeting where the final PSHA results were presented (Appendix C). The expert elicitation summaries are contained in Appendices E and F. Appendix G describes the development of the historical seismicity catalog. The development of the fault displacement hazard parameter distributions is discussed in Appendix H. Appendices I and J

show the results of the attenuation regression analysis and the development of the hypocentral distance-based models for the areal sources, respectively.

TABLE 1-1
SSFD FACILITATION TEAM MEMBERS AND THEIR PRINCIPAL RESPONSIBILITIES

NAME	AFFILIATION	RESPONSIBILITIES
Kevin J. Coppersmith	Geomatrix Consultants, Inc.	Team leader, project planning and methodology development; facilitating workshops; documentation
Susan S. Olig	Woodward-Clyde Federal Services	Workshop and field trip coordination; workshop summaries; documentation
Roseanne C. Perman	Geomatrix Consultants, Inc.	Project planning and methodology development; documentation
Silvio Pezzopane	U.S. Geological Survey	Project planning and methodology development; data synthesis
Peter A. Morris	Applied Decision Analysis, Inc.	Review of project direction; expert elicitation methodologies and training
Robert R. Youngs	Geomatrix Consultants, Inc.	Project planning and methodology development; eliciting and formulating alternative models; documentation of results/sensitivity

Note: Kathryn L. Hanson, Geomatrix Consultants, Inc., assisted with documentation, review, and report preparation.

TABLE 1-2
GM FACILITATION TEAM MEMBERS AND THEIR PRINCIPAL RESPONSIBILITIES

NAME	AFFILIATION	RESPONSIBILITIES
Norm A. Abrahamson	Consultant	Team leader, project planning and methodology development; facilitating workshops; documentation
Ann M. Becker	Woodward-Clyde Federal Services	Project planning and methodology development; workshop summaries; documentation; data synthesis, elicitation
Peter A. Morris	Applied Decision Analysis, Inc.	Review of project direction; expert elicitation methodologies and training

Note: John Schneider was an original member of the Facilitation Team but left the Project in October 1996.

TABLE 1-3
SSFD EXPERTS

NAME	AFFILIATION	EXPERTISE
Jon P. Ake	U.S. Bureau of Reclamation	Seismology
R. Ernest Anderson	U.S. Geological Survey	Regional Geology and Tectonics
Larry W. Anderson	U.S. Bureau of Reclamation	Paleoseismology
Walter J. Arabasz	University of Utah	Seismology
Ronald Bruhn	University of Utah	Regional Geology and Tectonics
Craig dePolo	Nevada Bureau of Mines & Geology	Paleoseismology
Diane I. Doser	University of Texas, El Paso	Seismology
Christopher J. Fridrich	U.S. Geological Survey	Regional Geology and Tectonics
Peter L.K. Knuepfer	Binghamton University	Paleoseismology
Dennis W. O'Leary	U.S. Geological Survey	Regional Geology and Tectonics
James McCalpin	GEO-HAZ Consulting, Inc.	Paleoseismology
Alan R. Ramelli	Nevada Bureau of Mines & Geology	Paleoseismology
Albert M. Rogers	GeoRisk Associates, Inc.	Seismology
D. Burton Slemmons	Woodward-Clyde Federal Services	Regional Geology, Tectonics, and Paleoseismology
Kenneth D. Smith	University of Nevada, Reno	Seismology
Robert B. Smith	University of Utah	Seismology
Frank H. (Bert) Swan	Geomatrix Consultants, Inc.	Paleoseismology
James C. Yount	U.S. Geological Survey	Regional Geology and Tectonics

Note: Peter Knuepfer and Dennis O'Leary replaced Anthony J. Crone, USGS and Christopher M. Menges, USGS, respectively, during the course of the project.

TABLE 1-4
GM EXPERTS

NAME	AFFILIATION
John G. Anderson	University of Nevada, Reno
David M. Boore	U.S. Geological Survey
Kenneth W. Campbell	EQE International Inc.
Arthur F. McGarr	U.S. Geological Survey
Walter J. Silva	Pacific Engineering & Analysis
Paul G. Somerville	Woodward-Clyde Federal Services
Marianne C. Walck	Sandia National Laboratories

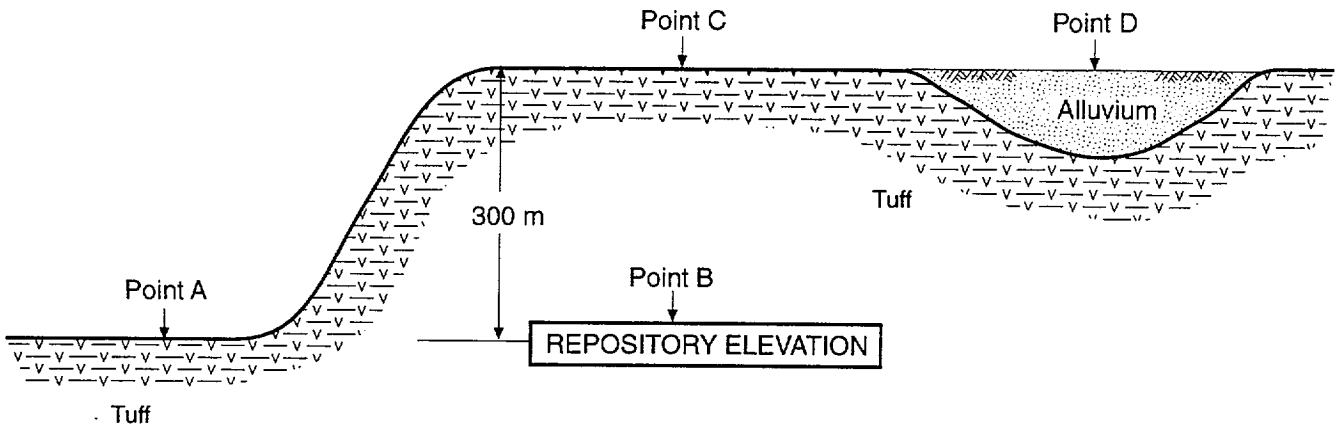

LEGEND

Point A – Reference rock outcrop at repository elevation

Point B – Repository elevation with tuff overburden

Point C – Rock surface

Point D – Soil surface

Figure 1-1 Locations of specified Design Basis Earthquake ground motions

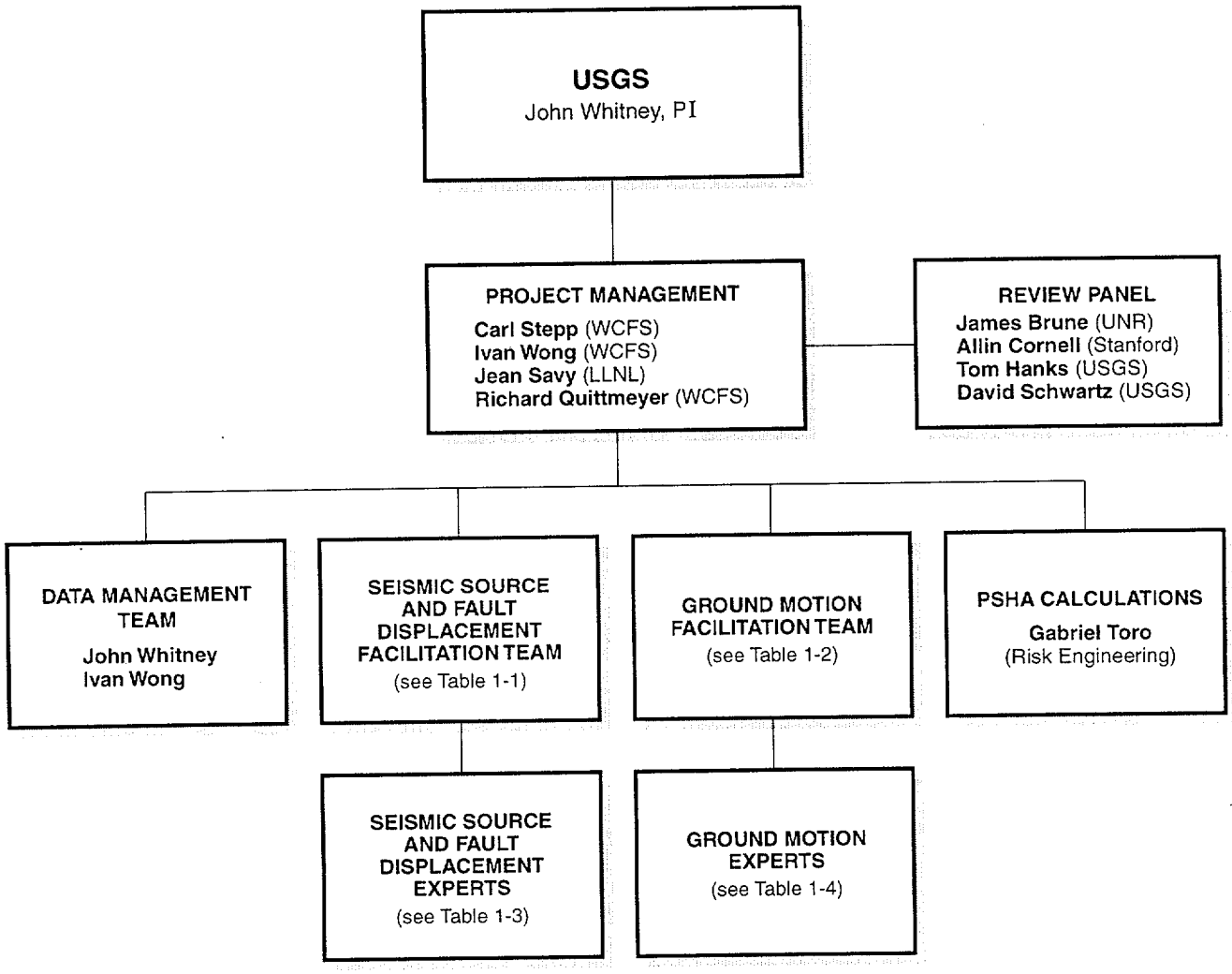

WCFS – Woodward-Clyde Federal Services

LLNL – Lawrence Livermore National Laboratory

UNR – University of Nevada, Reno

USGS – U.S. Geological Survey

Figure 1-2 Project organization

2.0
GENERAL GUIDANCE, OVERVIEW OF EXPERT ELICITATION PROCESS, AND SELECTION OF EXPERTS

This chapter describes the criteria for being an expert, the expert selection process, and the general process followed in eliciting the evaluations of the experts. Experience has shown that to be credible and useful, technical analyses such as those performed for the seismic source, fault displacement, and ground motion characterizations must: (1) be based on sound technical information and interpretations, (2) follow a process that considers all available data, and (3) incorporate uncertainties (SSHAC, 1997). A key mechanism for quantifying uncertainties is the use of multiple expert evaluations.

In the PSHA Project, the term "elicitation" was used in a broad sense to include all of the processes involved in obtaining the technical evaluations of multiple experts. These processes include reviewing available data, debating technical views with colleagues, evaluating the credibility of alternative views, expressing interpretations and uncertainties in interviews, and documenting interpretations. In this sense, the elicitation process began with the first workshops and ended with the finalization of the expert elicitation summaries.

Because of the importance of the entire expert elicitation process, facilitation teams were established at the outset of the project. Facilitation team members had experience in developing guidance for and implementing multiexpert studies and in understanding the technical aspects of the project.

2.1 GUIDANCE REGARDING EXPERT EVALUATIONS

The procedures and approaches for expert elicitation developed through conducting many studies, have been formalized in guidance documents that were followed in this Project. DOE developed guidance for the formal use of expert elicitation by the Yucca Mountain Project (DOE, written communication, 1995), and the NRC staff issued a Branch Technical Position on use of expert elicitation in the high-level waste program (NRC, 1996). Comprehensive guidance on expert elicitation for seismic hazards assessments recently was set forth in a study sponsored by the DOE, the EPRI, and the NRC (SSHAC, 1997).

In this project, multidiscipline, multiexpert teams were used to evaluate seismic sources and fault displacement potential. Individual experts were used in the characterization of ground motion attenuation. Teams were used previously in a large probabilistic evaluation conducted to assess the seismic hazard at 37 commercial nuclear power plant sites in the central and eastern U.S. (EPRI, 1986). In the EPRI study, experts were arranged into six earth science teams, each having a range of expertise required for characterizing seismic sources, including seismology, geophysics, and geology/tectonics. Multiple workshops were held to evaluate technical issues, and each team developed seismic source characterizations, including their associated uncertainties. The technical basis for the assessments was documented in a final report (EPRI, 1986), and the study underwent extensive NRC review (EPRI, 1988). As with the EPRI study, each expert team in the seismic source and fault displacement characterization was expected to function as a virtual expert, expressing their evaluations and uncertainties as an individual expert. Teams were not asked to provide a single consensus evaluation, no more than an individual expert is asked to provide a single estimate. Rather, teams were asked to provide alternative interpretations expressing their range of uncertainties, just as individual experts are asked to provide their expressions of uncertainty.

The Senior Seismic Hazard Analysis Committee (SSHAC, 1997) defines the roles of expert *proponent, evaluator,* and *integrator.* An expert proponent advocates a particular technical hypothesis or interpretation, an expert evaluator considers the support for alternative hypotheses and interpretations in the available data and evaluates the associated uncertainties, and an expert integrator combines the evaluators' alternative interpretations into a composite distribution that includes uncertainties. The expert evaluators forego the role of proponent in making their interpretations and evaluating uncertainties. Proponents of specific hypotheses or interpretations participated as resources and presented their hypotheses or interpretations in workshops. Alternative proponent interpretations were presented to the experts and open scientific debate was facilitated by the integrator. Some expert evaluators also were proponents of a particular hypothesis or interpretation in a workshop.

Expert interactions are a central component of the elicitation process and must be properly facilitated (SSHAC, 1997). Experience from numerous seismic hazard studies has shown

that experts interact frequently in their professional activities, and that workshops serve to provide information and interaction that facilitate their consideration of hypotheses and data and, ultimately, their evaluations and interpretations. Expert interactions in the PSHA Project were facilitated through multiple workshops and, for seismic source and fault displacement characterization, a field trip. Technical challenge and debate of alternative interpretations was the focus of these meetings, which included discussions of preliminary interpretations made by the experts.

The SSHAC (1997) process emphasizes the need to consider at the outset of a project the strategy for integration or aggregation of the experts' evaluations. This project at the outset defined a strategy to combine the evaluations of the experts using equal weights. The key procedural components of the project (ranging from the selection of experts to the dissemination of data sets) were designed to allow the equal-weights strategy to be implemented in a defensible manner. As noted by SSHAC (1997), the goal of a multiexpert evaluation of inputs to a PSHA is to capture and express the range of uncertainty such that the aggregated hazard results represent uncertainty of the informed technical community.

The PSHA Project followed the procedural guidance set forth in the SSHAC (1997) study, both in spirit (e.g., recognition of the importance of facilitated expert interactions) and, as applicable, in details of implementation (e.g., suggestions for conducting workshops and elicitation interviews). For example, the seismic source and fault displacement characterization elicitation was designed in accordance with SSHAC (1997) guidance. The expert teams were informed about and reminded of the need to express the full range of uncertainty, that is, they were asked to express alternative interpretations permitted by the available data weighted by the degree that each was considered to be supported by the data. The NRC Branch Technical Position (NRC, 1996) is generally consistent with the SSHAC guidance, providing the criteria for when expert elicitation should be used and outlining approaches for motivating, eliciting, and documenting expert evaluations. Other documents in the literature provide complimentary approaches to the formal or informal use of expert elicitation (e.g., Meyer and Booker, 1991).

2.2 GENERAL APPROACH

The general approach implemented by the PSHA Project for eliciting the evaluations of the experts is described in this section. The principal steps were:

(1) **Selection of Experts**. The Project Management Team established criteria for the selection of experts (see Section 2.3). These criteria were intended to insure that all the experts had proper professional stature and technical expertise. A list of candidates was developed by the Project Management Team with input from the facilitation team leaders. From this list of candidates, 18 SSFD and 7 GM experts were selected.

(2) **Development of Project Plan.** The Project Management Team developed a Project Plan that outlined the goals and key elements of the project, the scheduling of significant activities such as workshops, and the general topics to be covered by workshops and the field trip. Throughout the project, flexibility was maintained to address additional needs as they arose in order to assure that the project goals were achieved. For example, an additional feedback workshop was implemented to review fault displacement characterization methodologies, and additional feedback teleconferences were held to facilitate the finalization of fault displacement characterization. These additional activities are documented in this report.

(3) **Data Compilation and Dissemination.** The compilation and distribution of pertinent data, including published reference material, began early and continued throughout the project (Appendix B). Before the first workshops, the experts were sent a number of data sets and publications. Important data sets and publications identified during each workshop also were distributed. Experts were provided access, as needed, to all Yucca Mountain data gathered as part of the project and to data gathered by others (for example, the State of Nevada and the Center for Nuclear Waste Regulatory Analyses [CNWRA]).

(4) **Meetings of the Experts.** Structured, facilitated interaction among the experts took place during the workshops (and one field trip for the SSFD experts) and working meetings. The workshops were designed to identify the significant issues, review available data, debate alternative models, and review methods to quantify uncertainties in seismic source and fault displacement and ground motion interpretations. Proponents of particular technical positions provided their interpretations to the experts. Debate and technical challenge of alternative interpretations were facilitated to identify uncertainties. At these meetings, researchers from a variety of organizations engaged in studies relevant to the project, including the USGS, University of Nevada at Reno, Nevada Bureau of Mines and Geology, CNWRA, Lawrence Berkeley National Laboratory, and California Institute of Technology, presented pertinent data sets and alternative models and methods.

(5) **Elicitation Interviews.** One-day elicitation interviews were held between each of the three-member SSFD expert teams, GM experts, and representatives of the facilitation teams. Each expert or expert team provided their preferred and alternative evaluations, expressed their uncertainties, and specified the technical bases for their assessments. The facilitation teams documented the elicitation during the interview. The experts then independently prepared documentation of their evaluations, included as Appendices E and F in this report.

(6) **Feedback of Preliminary Results.** Following the elicitation interviews and the completion of preliminary interpretations, feedback workshops were held. The objectives of these workshops were to review, discuss, and debate the interpretations of each of the experts or expert teams, allowing them to understand the alternative approaches used by others as well as to technically defend their preliminary interpretations. Debate and technical challenge of the interpretations were encouraged to make sure that alternatives were understood and uncertainties were being appropriately incorporated. Facilitation and calculations team members presented preliminary analysis and sensitivity results. At the final workshops, the aggregation process was discussed.

(7) **Finalization of Expert Evaluations.** Following the feedback workshops, the experts revised and refined their interpretations and developed their final elicitation summaries. A series of technical reviews were conducted to insure that the sequence of models, components, and parameters was logical and complete and that the technical bases for the assessments were clearly provided.

(8) **Preparation of Activity Reports.** Activity Reports for seismic source and fault displacement characterization and ground motion characterization were prepared to document the process followed and the expert elicitation summaries.

2.3 SELECTION OF EXPERTS

The selection of experts involved four steps: (1) developing selection criteria, (2) obtaining a list of candidates, (3) selecting and inviting candidates to participate, and (4) for seismic source and fault displacement characterization, dividing the experts into six multidisciplinary teams. A selection panel, formed from members of the Project Management Team and other members of the project including the facilitation team leaders, was responsible for the selection process. The panel included Carl Stepp, John Whitney, Ivan Wong, Tom Hanks, David Schwartz, Silvio Pezzopane, Kevin Coppersmith, and Norm Abrahamson.

Expert selection was based on the following criteria:

- Strong relevant expertise as demonstrated by professional reputation, academic training, experience, and peer-reviewed publications and reports

- Willingness to forsake the role of proponent of any model, hypothesis, or theory and to perform as an impartial expert who considers all hypotheses and theories and evaluates their relative credibility as indicated by the data

- Availability and willingness to commit the time required to perform the evaluations needed to complete the study

- Specific knowledge of the Yucca Mountain area, the Basin and Range Province, or ground motion characterization

- Willingness to participate in a series of open workshops, diligently prepare required evaluations and interpretations, and openly explain and defend technical positions in interactions with other experts participating in the project

- Personal attributes that include strong communications skills, interpersonal skills, flexibility and impartiality, and the ability to explain clearly and succinctly the basis for interpretations and technical positions

The selection panel developed a preliminary list of candidates. Additional candidates were added to the preliminary list to form the final list of candidate experts. Candidates were nominated to capture the needed breadth of scientific expertise and technical knowledge and to obtain a range of organizational representation. Individuals who had expertise in each of three technical areas for seismic source and fault displacement were specifically nominated.

From the candidate list, 18 SSFD experts were initially selected in November 1994. Five of the seismic source and fault displacement candidates who were initially invited to become experts declined, stating schedule conflicts or perceived conflicts of interest. Additional individuals were contacted until the full complement of 18 experts was attained in January 1995.

In addition to the specific selection criteria, an important general requirement for the GM experts was to insure that the range of credible ground motion attenuation relations was represented. To that end, GM experts were selected from individuals knowledgeable in both the empirical approach to ground motions as well as numerical modeling techniques. Also, individuals knowledgeable in technical issues such as near-field source effects, crustal attenuation, path effects, site response, and ground motions from nuclear explosions were sought.

From the candidate list, six GM experts were selected by the panel in November 1994. In advance of their selection, the Project Management Team had concluded that the minimum number of experts necessary to provide diversity of knowledge was six (Geomatrix Consultants, written communication, 1997). A seventh GM expert was added to complete the representation of various ground motion models. All experts were contacted in late November and early December 1994 to determine whether they could participate in the PSHA Project. All seven selected GM experts agreed to participate.

Of the 18 SSFD experts who attended the initial April 1995 workshop, two subsequently resigned. Before the project resumed in October 1996, Dr. Tony Crone informed the Project Management Team that new commitments prevented him from continuing to serve as an expert. The selection panel chose Dr. Peter Knuepfer as a replacement. In early February 1997, the panel replaced Dr. Chris Menges, who withdrew for health reasons, with Dr. Dennis O'Leary. Dr. O'Leary is a member of the USGS Yucca Mountain geologic team and had been an active participant in all the seismic source and fault displacement workshops held to date.

The Project Management Team chose to form expert teams for seismic source and fault displacement characterization in order to incorporate the required scientific disciplines and diversity of knowledge. It was deemed essential that both geologic and seismologic disciplines were represented on the teams. Six three-person teams were formed, consisting of (1) an individual having particular knowledge and expertise about the paleoseismology and Quaternary faulting in the Yucca Mountain area, (2) an individual having particular knowledge and expertise about the regional geology and tectonics of the Yucca Mountain region and/or Basin and Range Province, and (3) an individual having experience or education in seismology and seismicity. The six individuals from each of the three technical areas were selected at random by the SSFD Facilitation Team and combined into teams. The acronyms for each team used in this report are given in order of area of expertise as follows: (1) seismology, (2) regional geology/tectonics, and (3) paleoseismology (e.g., the AAR team is composed of seismologist W. Arabasz, regional geologist E. Anderson, and paleoseismologist A. Ramelli) (see Section 4.3.1.1).

Consistent with the guidance of NUREG-1563 (NRC, 1996), all experts were asked to document any conflicts of interest relating to their roles as evaluators of seismic sources, fault

displacement, and ground motion attenuation for Yucca Mountain. Each expert completed a conflict of interest statement, which is included as part of the records of the PSHA Project. None of the selected experts was precluded from participating in the Project on the basis of conflicts of interest.

3.0
SEISMIC SOURCE AND FAULT DISPLACEMENT CHARACTERIZATION FACILITATION APPROACH

In this chapter, the approach utilized by the SSFD Facilitation Team to elicit interpretations from the SSFD experts is described.

3.1 DATA COMPILATION AND DISSEMINATION

Data compilation and dissemination formed an important aspect of the seismic source and fault displacement characterization process. The goal was to ensure that the evaluations by the SSFD expert teams were based on a knowledge of all available data and existing interpretations in the published and unpublished literature. Initially during 1995, the USGS served as a clearinghouse for requests for and dissemination of data. In subsequent stages of the study, the SSFD Facilitation Team and the Data Management Team were responsible for receiving requests for data and for compiling and disseminating the data to the experts. The data distributed included journal articles, preprints of recently completed work, synthesis reports for Yucca Mountain work, digital data bases such as the fracture data base derived from the line-survey for the ESF, and empirical data compiled from literature. In some cases, compilations of data and simple analyses of the data (e.g., linear regressions) were performed by the SSFD Facilitation Team at the specific request of the expert teams. For example, Silvio Pezzopane conducted a number of analyses of empirical data regarding historical surface ruptures to fulfill requests made by the expert teams. These analyses are documented in the workshop summaries.

3.2 SEISMIC SOURCE AND FAULT DISPLACEMENT WORKSHOPS

The following sections summarize the workshops and field trips conducted during the project (Figure 3-1). These activities were the primary vehicles for expert interaction and review of technical issues. Detailed summaries of the workshops and field trip are provided in Appendix C.

3.2.1 Workshop #1-Data Needs

The Workshop on Data Needs, April 17-19, 1995, was the first of six workshops conducted for the seismic source and fault displacement characterization. The primary goals of the workshop were to identify key technical issues of importance to seismic source characterization and to specify the data required to characterize the seismic sources for vibratory ground motion and fault displacement hazards. Other objectives of the workshop were to provide information to the experts on the overall study, the products to be developed, the project schedule, the roles of various participants, alternative expert roles (evaluators, proponents, specialists), basic approaches to PSHAs and expressing uncertainties, and ground rules regarding communication and interaction throughout the study.

To accomplish these goals, the workshop included a series of presentations and discussion sessions that involved scientists from various organizations. The basic approach of the workshop was to (1) identify technical issues of most significance to seismic hazards at Yucca Mountain, (2) link those issues with the data most relevant to addressing the issues, (3) specify the available relevant data for the Yucca Mountain region, and (4) identify the data required by the experts to characterize seismic sources. During a discussion that followed workshop presentations by several technical specialists, the experts identified the issues deemed most important to characterizing seismic sources at Yucca Mountain. The identification of technical issues was essential for identifying the types of data needed, and to help create a common understanding among the experts of the important elements that directly or indirectly influence future seismic hazards at Yucca Mountain.

The major technical issues identified by the experts during the first workshop included (1) defining candidate seismic sources and associated maximum magnitudes for the background earthquake, (2) choosing recurrence models and weights for fault sources, (3) developing models for fault segmentation and multiple fault ruptures, (4) assessing the effects of triggering on earthquake recurrence, (5) characterizing fault geometry and kinematics, (6) characterizing distributive faulting, (7) assessing nonstationary and temporal clustering of earthquakes, and (8) assessing the importance of volcanic earthquakes and characterizing potential sources of such events. A complete list of the technical issues and required data identified by the experts is included as Table 2 in the workshop summary in Appendix C.

Presentations by specialists on technical issues identified from previous studies of historical seismicity and fault sources at Yucca Mountain were the focus of the first day and a half of the workshop. These were followed by a day and a half of presentations on available and forthcoming data sets for the Yucca Mountain region. Topics included historical seismicity, regional and local faults, geologic mapping (both surficial and bedrock), geochronological, structural, and stratigraphic studies, and a variety of geophysical studies. Presentations were given by Yucca Mountain principal investigators who not only provided reference information for published data, but also offered to provide much of the unpublished data to the experts either through personal communications or the USGS Yucca Mountain Project Branch. Before the workshop, the USGS distributed a large amount of available data and lists of relevant data sources to each expert. A complete list of this material is included as Table 3 of the workshop summary (Appendix C).

3.2.2 Workshop #2-Seismic Hazard Methodologies

The workshop on Seismic Hazard Methodologies, October 16-18, 1996, was conducted after the project resumed following a 1-year hiatus. The purpose of this 2½-day workshop was twofold: (1) to review data that had become available since the project had stopped and (2) to identify and evaluate methods and approaches for characterizing seismic sources in the Yucca Mountain region. The workshop also served as a kickoff meeting for restarting the project, and participants were advised of revisions to the Project Plan and schedule.

The approach during the workshop was to divide seismic source characterization into two parts for vibratory ground motion analysis and fault displacement analysis. These parts were then further subdivided into three components: seismic source location and geometry, maximum earthquake magnitude, and earthquake recurrence assessment. Presentations by a variety of technical specialists, many of them experts, were given on each of these topics, first focusing on available methods for characterization and then describing newly available data. A complete list of the data provided is included as Table 1 in the workshop summary (Appendix C).

3.2.3 Workshop #3-Alternative Models and Interpretations and Field Trip

The workshop on Alternative Models and Interpretations, November 18-21, 1996, was combined with a field trip to Yucca Mountain, Crater Flat, and Bare Mountain. The purpose of the 4-day field trip and workshop was to review and evaluate alternative models, hypotheses, and interpretations that are important to the characterization of seismic sources in the Yucca Mountain region. The agenda for the workshop and field trip was developed with the explicit purpose of juxtaposing alternative ideas and views presented by various proponents. Discussions were facilitated to encourage the experts to probe for a better understanding of the technical bases for each model, to debate and listen to the pros and cons of the alternatives, and to quiz the proponents to better understand the uncertainties associated with each model. Additionally, the field trip enabled the experts to observe both surface and subsurface exposures at many key sites, providing first-hand insights into field data and interpretations. In this way they were able to evaluate the limits on resolution and the uncertainties associated with the field data and interpretations.

Throughout the workshop and field trip, a forum was provided for structured debate. Various scientists, including some experts, assumed the role of proponent in presenting arguments in favor of a particular model or interpretation. The experts were then encouraged to act as evaluators by probing the proponent positions in an effort to better understand the interpretations, the supporting data for each interpretation, and the associated uncertainties.

The field trip included 2½ days of field review and discussion focused on (1) the behavior of faults in the Yucca Mountain vicinity, (2) the nature of faulting in the potential repository block, and (3) the behavior of the Bare Mountain fault. John Whitney coordinated the field trip; individual stops were led by a variety of Yucca Mountain investigators. Numerous excavations and natural exposures were reviewed along many faults, including the Bare Mountain, Crater Flat, Windy Wash, Solitario Canyon, Ghost Dance, Bow Ridge, and Paintbrush Canyon faults. At these stops the principal investigators explained the field relationships, provided interpretations of the displacements, their ages, and recurrence, and expressed their uncertainties. A half-day trip into the ESF provided a subsurface view of faults and fractures in the proposed repository block. Highlights of this trip included exposures of (1) the Bow Ridge fault, (2) small intrablock reverse and normal faults, (3) cooling joints and faults, (4) the Drill Hole Wash fault, and (5) breccia zones.

The workshop discussions entailed presentations and debate centered around five key issues to seismic source and fault displacement characterization: tectonic models, three-dimensional geometry of faults, definition and synchronicity of faulting events, characterization of faulting in the proposed repository block, and maximum background earthquakes. Presentations of proponent positions on the five key issues were followed by debate by the experts. Some of the most extensive discussions focused on (1) the possible existence and character of large, buried strike-slip shear zones and detachment faults, (2) structural models of the subsurface geometry of the Bare Mountain and Yucca Mountain faults, (3) the occurrence of distributive faulting on multiple faults, possibly associated with volcanism, (4) slip rates on the Bare Mountain fault and implications to Yucca Mountain faults, (5) the origin of fracturing events observed in many exposures throughout Yucca Mountain, and (6) the age of youngest activity and Quaternary rates of activity for faults in Tertiary bedrock. A more comprehensive summary of the field trip itinerary and the issues discussed throughout the 4-day session is included in the workshop summary (Appendix C).

3.2.4 Workshop #4-Preliminary Interpretations

The goals of the Preliminary Interpretations Workshop, January 6-8, 1997, were to (1) provide an opportunity for the expert teams to receive feedback from their colleagues by presenting and discussing their preliminary interpretations regarding key issues, (2) train the expert teams in the process of elicitation and the characterization of uncertainty, and (3) present and discuss additional information and interpretations of importance to the study. To accomplish these goals, a series of presentations by the experts and group discussions were conducted. Five key issues were identified: (1) tectonic models, (2) potential seismic sources, (3) maximum magnitudes, (4) earthquake recurrence, and (5) fault displacement methodology. Two expert teams were assigned to present their preliminary interpretations of each issue. These presentations were followed by group discussion of each issue, during which the other teams were given the opportunity to debate the credibility of alternative views and to present their preliminary interpretations.

The focus of the presentations and discussions was on understanding the interpretations, their technical bases, their consistency or inconsistency with data, and the expression of uncertainty. Discussion was facilitated so that each team understood the interpretations of others, including the degree to which an interpretation was supported by earthquake and

faulting models and observed data. The experts could then more knowledgeably reevaluate their own team interpretations. The objective was to help teams prepare for the upcoming elicitation interviews so that interpretations would be well-reasoned, technically supported, and complete. Throughout this 2½-day workshop, the facilitator encouraged the experts to explore the issues thoroughly, ask questions that would help them during the elicitations, and continually keep in mind the characterization of uncertainties.

Also included in the workshop was a half-day elicitation training session conducted by normative expert Peter Morris, along with presentations by technical specialists of additional information on some key issues that were highlighted or outstanding from previous workshops. These included presentations on investigations of the Sundance fault, interpretations of seismic reflection lines and relevant geophysical data in the Yucca Mountain vicinity, the southern extent of Yucca Mountain faults, and the seismogenic potential of known or postulated shallow-dipping normal faults. More details on these presentations and those given by the teams on their preliminary interpretations are included in the workshop summary (Appendix C).

3.2.5 Workshop #5-Feedback

The Feedback Workshop, April 14-16, 1997, occurred after the elicitation interviews (discussed below). The purpose of the workshop was to provide feedback to the expert teams by (1) providing an opportunity for the teams to discuss the first round of their interpretations, (2) allowing each team to understand and ask questions about the interpretations made by other teams, (3) providing information on the derivative products of their first-round assessments (i.e., seismic source characteristics), and (4) providing sensitivity analyses to show the relative impact of various assessments on the calculated results. To accomplish these goals, a series of presentations and group discussions were conducted, with emphasis on facilitated interaction among the experts and feedback from the SFFD Facilitation and PSHA Calculations teams. For each of six key issues, two or three expert teams presented their interpretations, followed by a general discussion that included all of the teams. These six key issues, identified by the SSFD Facilitation Team from the preliminary results, included (1) characterization of areal seismic source zones, (2) geometry of local faults, (3) synchronous ruptures of local faults, (4) maximum magnitudes and recurrence on local faults, (5) characterization of other seismic sources, such as buried strike-

slip shear zones, detachments, volcanic zones, and other buried or postulated structures, and (6) methodologies for evaluating fault displacement.

The focus of the presentations and discussion was on understanding the interpretations of others, their technical bases, consistency with data, and expression of uncertainty. Preliminary results and sensitivity analyses were presented, highlighting the sources and parameters most significant to the analyses.

The specific aspects of the six issues discussed were (1) different approaches for defining and determining M_{max} for areal source zones containing Yucca Mountain (i.e., host zones), (2) processing and analysis of the historical seismicity catalog to estimate earthquake recurrence for host zones, (3) different approaches to determining seismogenic depths, (4) the use of structural and tectonic models to constrain subsurface geometries of local faults and potential buried seismic sources, (5) different approaches to developing models of rupture behavior for local faults, (6) the bases for assessing the potential activity of faults, and (7) different approaches to assessing the amounts and rates of fault slip for smaller (not block-bounding) faults in Tertiary bedrock within the Controlled Area. In regard to the latter, the experts extensively discussed the distinction between seismogenic or principal slip, distributive or secondary slip, and nontectonic slip. A clear and common understanding of this distinction is important, because some faults were included as potential sources of fault displacement, but were determined not to be independent seismogenic sources capable of generating earthquakes in the ground motion assessment.

During the workshop, feedback was also provided from the PSHA Calculations Team regarding preliminary results and sensitivity analyses for the first round of seismic source characterization and ground motion interpretations. Feedback included specific results for five teams' characterization models for the ground motion assessment and for four teams' methods and characterization models for the fault displacement assessment. The PSHA Calculations Team sent preliminary hazard curves and results of sensitivity analyses after the workshop to teams that did not complete their input in time to receive feedback at the workshop. At the end of the Feedback Workshop, a joint session was held with the SSFD experts and the GM experts. The purpose of this joint session was to provide an opportunity for interaction between the two groups of experts, specifically to discuss common issues, ask

questions about each other's interpretations and assessments, highlight any inconsistencies between the seismic source and ground motion characterizations, and come to a better common understanding of the linkages between the two groups' input to the seismic source and fault displacement. For example, a subject of considerable discussion was the geometry of seismogenic sources, especially interpretations that call for the simultaneous rupture of multiple Yucca Mountain faults. In addition, interpretations of earthquake stress drop were discussed. The summary of this workshop includes more detail on these and other issues discussed during the Feedback Workshop (Appendix C).

3.2.6 Workshop #6-Fault Displacement

The Fault Displacement Workshop, June 3, 1997, the final workshop conducted for the seismic source and fault displacement characterization, was designed to provide feedback to the teams on their fault displacement approaches and assessments. The threefold purpose of the 1-day workshop was to (1) review and discuss alternative methods and models for assessing fault displacement, (2) discuss uncertainties in parameter values and models, and (3) facilitate the expert teams' discussion of the pros and cons of alternative approaches, models, and submodels. Prior to the workshop, a "white paper" summarizing the fault displacement evaluation approaches developed by the expert teams was prepared by the SSFD Facilitation Team and distributed to the experts. During the workshop, the approaches taken by each expert team to evaluate displacement at nine demonstration points were reviewed in more detail than at the previous workshop. This was followed by extensive discussion and technical challenge about the strengths and weaknesses of all the approaches, data required to apply them, and uncertainties in model parameters.

The methods used for estimating the frequency of displacement events and the expected displacement per event at locations where faults or fractures are present in Tertiary rocks, but Quaternary paleoseismic data are lacking, were discussed extensively. Discussion also focused on the use of data from historical surface faulting events to develop relations for the likelihood of distributive faulting and the pros and cons of approaches using observed displacements versus those that rely on mechanical models of rock deformation. The experts explained different approaches to characterizing both along-strike and event-to-event variations in displacement. Presentations also were given on newly available information from the ESF, as the tunnel boring machine had completed its excavations since Workshop

#5. More details on these presentations and the fault displacement issues discussed are included in this workshop summary (Appendix C).

3.3 ELICITATION OF SSFD EXPERTS

The elicitation interviews involved a series of activities, which can be grouped into two steps: (1) preparation for the interviews and (2) the elicitation interviews.

3.3.1 Preparation for the Elicitation

Peter Morris of the SSFD Facilitation Team provided elicitation training at Workshop #4. The objectives of the training were to demonstrate how to quantify uncertainties using probabilities, to recognize common cognitive biases and compensate for them, and to present examples of the types of assessments that would be made at the elicitation interview (e.g., continuous variables, discrete hypotheses, and associated weights). The training was designed to help the experts be comfortable with the *process* of elicitation, so that the elicitation interview itself could focus on the *technical issues* of importance to the seismic source and fault displacement characterization.

At Workshop #4, the experts had been informed that the seismic source characterization issues presented would be covered in the elicitation interviews. A memo providing guidance for the characterization of fault displacement was provided to the expert teams before the elicitation interviews. The memo described the alternative approaches available to evaluate fault displacement (earthquake-based approaches that rely on the location, frequency, and size of earthquakes, and displacement-based approaches that evaluate the amount and frequency of displacement directly from displacement observations). In addition, the memo identified nine demonstration points within the Controlled Area that would serve as representative points (representing the range of expected conditions) at which all teams' fault displacement methodologies would have to be operative.

3.3.2 Elicitation Interviews

The elicitations of the expert teams took place in separate 1-day interviews in the San Francisco office of Geomatrix Consultants. The interviews were conducted by members of the SSFD Facilitation Team. Dr. Coppersmith (specialist and normative expert) and Dr.

Youngs (generalist and hazard analyst) attended all of the interviews, Dr. Perman, Ms. Olig, and Dr. Morris (normative expert) attended selected interviews. Drs. Whitney and Toro, and an NRC representative, also attended some interviews to observe the process followed.

All data sets provided or made available to the experts during the project were present during the elicitation. The elicitation interview followed a logical sequence from general to more specific assessments. Alternative models, approaches, and hypotheses were discussed, and the logic structure for the assessments and associated probability distributions were developed. Team members discussed the various issues among themselves and arrived at alternative models and probability distributions that they believed spanned the range of views across their team and across the larger technical community. The SSFD Facilitation Team representatives took written notes of all assessments during the interviews.

3.3.3 Documentation and Review

Documentation of the expert elicitations began with documentation and a summary prepared by the SSFD Facilitation Team representatives during the interviews. Experience on several other expert elicitation projects has shown this approach to be preferable to other documentation methods (e.g., written questionnaires, experts writing their interpretations following the interview, or tape recordings). During the 1-day interview, each expert team was asked to make many assessments, to quantify uncertainties, and to provide the technical bases for their interpretations. By having the SSFD Facilitation Team document and summarize, experts were free to focus on thinking through their answers and thoroughly expressing interpretations. The SSFD Facilitation Team was able to be flexible in the elicitation sequence (i.e., following the logic comfortable to the team) while ensuring that all elements were covered.

Following the interviews, the SSFD Facilitation Team provided each expert team with written documentation of the interview, organized by model component. The experts, in accordance with the requirements of the Project Plan, independently prepared a summary that reflected their interpretations. The summaries prepared by each expert team became the first draft document. This draft was reviewed for logical consistency and completeness and returned to the expert team for revision. The revised summary became a second draft that was reviewed by Dr. Stepp. These reviews were conducted to provide for completeness and

clarity of documentation. The teams responded to any requests for further clarifications, and the summaries were finalized. The elicitation summaries are provided in Appendix E.

3.3.4 Feedback and Sensitivity

Feedback to the experts occurred throughout the seismic source and fault displacement characterization, primarily through interaction among experts. By presenting their evaluations of models and associated interpretations at workshops and in general discussions, the experts both provided and received feedback from their peers on the panel.

More formally, feedback was provided to the experts using several approaches.

- At Workshop #4, the expert teams presented their preliminary interpretations regarding the key technical issues to the other teams. The teams were encouraged to understand the alternative views, their technical bases, and uncertainties.

- At Workshops #5 and #6, which occurred after the elicitation interviews, discussion focused on team interpretations. Discussions included the technical bases for the interpretations, the weights assigned to alternative hypotheses, and expressions of uncertainty in parameter values and alternative models (e.g., logic trees).

- Calculations showing the results of each team's initial interpretations were presented at Workshops #5 and #6. Calculations included maximum magnitude distributions, earthquake recurrence relationships for important seismic sources, calculated seismic hazard curves and dominant contributors, and fault displacement hazard curves and dominant contributors.

- Prior to the finalization of the seismic source and fault displacement models, each team was provided with (1) calculations showing the results of their preliminary interpretations, (2) plots showing the sensitivity of their results to alternative maximum magnitude and recurrence approaches or models, and (3) comparison of the calculated seismic hazard curves for all sources combined for all teams to mean recurrence estimates for individual teams. Conference calls with each of the

teams and members of the SSFD Facilitation Team were conducted to provide clarification and additional feedback. Revisions to the seismic source and fault displacement models based on the feedback provided were incorporated into the final results.

- Members of the SSFD Facilitation Team, Project Management Team, and Review Panel reviewed the written elicitation summaries for clarity, adequacy, and completeness of documentation of the technical basis for the evaluations described in them.

The feedback-revision process required the experts to defend/revise their assessments as considered appropriate and to provide appropriate documentation. In all cases, the experts responded positively to critical reviews of their documentation. The resulting assessments and finalized elicitation summaries reflect the significant effort expended by each expert team.

3.3.5 Aggregation of Expert Assessment

The approach taken to combine, or aggregate, the expert evaluations is equal weighting. This approach was not a default but a goal from the start of the project, a goal the experts were apprised of throughout the project. Accordingly, the proper conditions were created throughout the project to allow for using equal weights (SSHAC, 1997). The actions taken to provide these conditions included:

- Carefully selecting highly qualified experts who represent diverse disciplines and experience

- Establishing and confirming the commitment of each expert to provide the required effort throughout the project

- Identifying available data sets and disseminating them to all experts

- Educating the experts in issues important to seismic source and fault displacement characterization and training the experts in elicitation methodologies and the role of experts as evaluators

- Facilitating interaction among the experts in workshops and field trips to foster a free exchange of data and interpretations and scientific debate with respect to hypotheses and resolution of data

- Providing feedback and sensitivity analyses to the experts

- Providing an opportunity for experts to revise their assessments in light of feedback

It should be noted that, in accordance with the guidance provided by SSHAC (1997), conditions could have been such that different weights would have been necessary. For example, if an expert team had been unwilling or unable to devote the required time and effort to develop a complete assessment and documentation, that team would have been removed from the project.

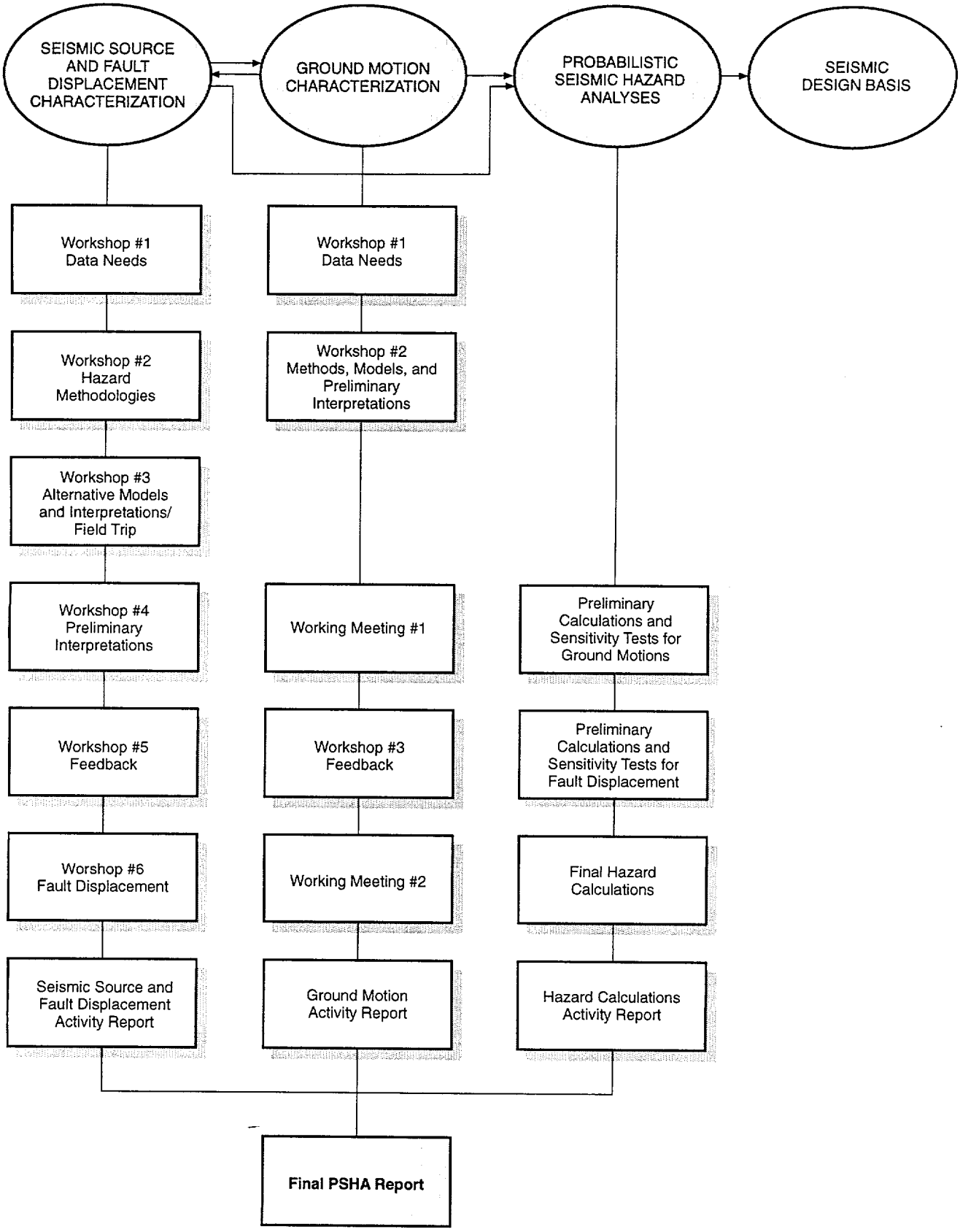

Figure 3-1 Probabilistic Seismic Hazard Analyses Project process for Yucca Mountain

4.0
SEISMIC SOURCE AND FAULT DISPLACEMENT CHARACTERIZATION

This section describes the methodologies used by the expert teams to (1) characterize the sources of potential earthquakes in the vicinity of the Yucca Mountain site for the PSHA for ground shaking hazard and (2) characterize fault displacement hazard within the Controlled Area. Section 4.1 presents the formulations used for seismic source characterization. Section 4.2 presents the formulations used for characterizing fault displacement hazard. The seismic source and fault displacement models developed by the six SSFD expert teams are described in Section 4.3. A detailed description of the PSHA methodology for vibratory ground motions is contained in Section 7.1.

4.1 SEISMIC SOURCE CHARACTERIZATION METHODOLOGY FOR GROUND MOTION HAZARD ASSESSMENT

The role of the SSFD expert teams in the ground motion PSHA is to identify the seismic sources that may produce earthquakes significant to ground motion hazard at the site. Then for each source they are to evaluate the frequency of earthquake occurrence, the maximum earthquake the source can produce, the distribution of earthquake sizes, and the spatial distribution of earthquakes on the source so that the distance to an earthquake of given magnitude can be computed. The methodologies used to assess these characteristics are discussed below.

4.1.1 Logic Trees

The PSHA methodology is formulated to represent the randomness inherent in the natural phenomena of earthquake generation and seismic wave propagation. The randomness in a physical process has come to be called *aleatory* uncertainty (SSHAC, 1997). In all assessments of the effects of rare phenomena, one faces uncertainty in selecting the appropriate models and model parameters because the data are limited and/or there are alternative interpretations of the data. This uncertainty in knowledge has come to be called *epistemic* uncertainty (SSHAC, 1997). The SSFD experts placed a major emphasis on developing a quantitative description of the epistemic uncertainty.

The uncertainty assessment was performed using the *logic tree* methodology. The logic tree formulation for seismic hazard analysis (Kulkarni *et al.*, 1984; Coppersmith and Youngs, 1986; EPRI, 1988; NRC, 1988) involves setting out the sequence of assessments that must be made in order to perform the analysis and then addressing the uncertainties in each assessment sequentially. Thus, it provides a convenient approach for dividing a large, complex assessment into a sequence of smaller, simpler components that can be addressed more easily.

Figure 4-1 shows an example of a logic tree. The logic tree is composed of a series of nodes and branches. Each node represents a state of nature or an input parameter that must be characterized to perform the analysis. Each branch leading from a node represents one possible alternative interpretation of the state of nature or parameter being evaluated. If the variable in question is continuous, it can be discretized at a suitable increment. The branches at each node are intended to represent mutually exclusive and collectively exhaustive states of the input parameter. In practice, a sufficient number of branches are placed at a given node to represent the evaluator's uncertainty in estimating the parameter.

Probabilities are assigned to each branch that represent the expert's evaluation that the branch represents the correct value or state of the input parameter. These probabilities are conditional on the assumption that all the branches leading to that node represent the true state of the preceding parameters. Because they are conditional probabilities for an assumed mutually exclusive and collectively exhaustive set of values, the sum of the conditional probabilities at each node is unity. The probabilities are based on scientific evaluations because the available data are often too limited to allow for objective statistical analysis, and because scientific evaluation is needed to weigh alternative interpretations of the available data. The logic tree simplifies these evaluations, because the uncertainty in each parameter is considered individually, conditional on assumed known states from prior evaluations. The nodes of the logic tree are sequenced to express conditional aspects or dependencies among the parameters and to provide a logical progression of evaluations from general to specific in characterizing the input parameters for PSHA.

The probabilities (relative weights) assigned to the branches at a node of the logic tree represent one of two types of probability assessments. For the first type, the branches at a node define the

range of parameter values; the associated weights define the probability distribution for the parameter. For example, estimates of the slip rate on a fault are uncertain because of uncertainties in the amount of displacement of a particular geologic unit across the fault and the age of the unit. The probability distribution for a parameter value may be characterized in several ways: as a discrete distribution defined by a preferred value and a range of discrete higher and lower values, a cumulative distribution based on scientific evaluations, or by a mean and standard deviation for a specified statistical distribution. Examples of these means of characterization are given below. Continuous distributions can be discretized to form logic tree branches following a number of approaches. Keefer and Bodily (1983) showed that most distributions can be represented reliably by three values: the median estimate (50^{th} percentile), assigned a weight of 0.63, and a higher and lower value, each given weights of 0.185, which represent the 5^{th} and 95^{th} percentiles (± 1.645 standard deviations for a normal distribution). They list other discretization schemes for more points. Another four-point representation of a normal distribution is described in EPRI (1993, Chapter 9). Miller and Rice (1983) present a number of discrete approximations to subjectively defined, continuous cumulative distributions.

In some instances, the uncertainty in assessing parameters can be estimated using formal statistical techniques. In these cases, continuous parameter distributions developed from statistical estimation procedures can be discretized for use in a logic tree formulation. An example of this approach is presented in Section 4.1.3.

A second type of probability assessment, to which logic trees are particularly well suited, is indicating a relative preference for, or degree of belief in, alternative hypotheses. For example, the sense of slip on a fault may be uncertain – two alternatives might be strike-slip or reverse-slip. Based on the pertinent data, a relative preference for these alternatives can be expressed by weights in the logic tree. A very strong preference (i.e., the data strongly support one interpretation over the other) for one alternative over the other usually is represented by weights such as 0.9 and 0.1. If there is no preference (i.e., the data equally support either alternative) for either hypothesis, they are assigned equal weights (0.5 and 0.5 for two hypotheses). Increasing the weight assigned to one alternative from 0.5 to 0.9 (or more) reflects increasing support in the data for that alternative. Because the relative weights ultimately are the result of scientific evaluations based on available information, it is important to document

the data and interpretations that led to the characterization of parameter values and their relative weights so that the process can be reviewed by others.

The example logic tree shown on Figure 4-1 characterizes the uncertainty in assessing the magnitude of paleoearthquakes that have occurred on a fault on the basis of dip-slip offsets observed in a trench placed across the fault. (Such assessments may be one means of characterizing the maximum magnitude [M_{max}] for a seismic source.) There may be multiple sources of uncertainty in the assessment. Stratigraphic relationships in the trench walls may be somewhat ambiguous so that the amount of dip-slip displacement can be estimated only within a factor of two (e.g., 1.0 to 2.0m). One may also be uncertain about the existence of a significant component of lateral slip, which would indicate whether the fault is primarily a normal fault or an oblique-normal fault having a ratio of strike slip to dip slip in the range of 1:1 to 1.5:1. In addition, there is the uncertainty in whether the observed slip is more representative of the maximum slip during the paleoearthquake or the average slip.

The logic tree expresses these uncertainties. The interpretations in the logic tree usually are ordered from general to specific (Figure 4-1). The order of the interpretations, however, is dictated primarily by convenience in dealing with interdependencies in the characterization. For example, the down-dip width of a fault is a function of the thickness of the seismogenic crust and the fault dip. While fault dip may differ from fault to fault in an area, the seismogenic thickness may be the same for all the faults. Therefore, it is more convenient to place the assessment of thickness before the assessment of dip. After the logic tree is constructed, the order of the nodes can be changed. In cases where the interpretation depends on the state of another unknown, then it is placed to the right of that one in the logic tree.

In the example on Figure 4-1, the total amount of fault offset is dependent on whether the fault is a normal fault or an oblique-normal fault. In addition, the evaluation of whether the observed displacement is representative of the maximum or the average displacement may also depend on the style of faulting. The trench may have been placed in an area where the fault scarp was most pronounced, indicative of maximum vertical displacement. However, this may not be the area of maximum slip if the fault is oblique-normal. Because these two interpretations are made more easily given knowledge of the style of faulting, the node for interpretations of the style of faulting is placed first (to the left) in the logic tree. For the example on Figure 4-1, the

evaluation of the assessor is that the interpretation of normal faulting is preferred slightly (0.6) to the interpretation of oblique-normal faulting (0.4). In actual interpretations, the assessor documents the reasons for this evaluation.

Further characterization in the example (Figure 4-1) addresses the amount of displacement. The stratigraphic relationships indicate from 1.0 to 2.0 m of offset. The interpretation of these data may favor displacements in the range of 1.0 to 1.5 m but allow for as much as 2.0 m. Thus, if the fault is a normal fault, the distribution for the observed offset may be specified by three discrete values: 1.0, 1.5, and 2.0 m. The probabilities (relative weights) assigned to these values are 0.4, 0.4, and 0.2, respectively, reflecting that the data more strongly support displacements of 1.0 to 1.5 m.

If the fault is considered an oblique-normal fault, then the observed offsets must be increased to account for unmeasured strike-slip offset to obtain the net slip on the fault plane. The factor of increase is 1.4 for a 1:1 strike-slip/dip-slip ratio, and 1.8 for a 1.5:1 strike-slip/dip-slip ratio. In this example, it is considered twice as likely that the strike-slip to dip-slip ratio is closer to 1:1 than to 1.5:1. Thus the factors are given relative weights of 0.67 and 0.33. The evaluation of the strike-slip to dip-slip ratio is added to the logic tree after the branch for oblique-normal faulting. The evaluation is unnecessary along the normal faulting branch. There the distributions for the amount of net slip are assumed to be equal to those developed for normal faulting multiplied by the appropriate factor.

The final evaluation is whether the observed offsets represent maximum displacements or average displacements. This evaluation is important because separate empirical relationships between magnitude and fault offset are given for maximum and average displacement (e.g., Wells and Coppersmith, 1994). (One could, of course, argue that other interpretations are possible in an exhaustive list of alternatives. It is important that the evaluator considers a sufficiently broad distribution of alternative interpretations to adequately represent the uncertainties in the assessment.) The evaluation of the relative likelihood of the two interpretations is made conditionally on which sense of slip is assumed to be correct—that is, the probability that the observed offset is a maximum given normal faulting is a separate evaluation from the probability that it is a maximum displacement given oblique-normal faulting, and the two probabilities do not have to be equal. In the example the data strongly

support the interpretation that the observed displacements represent maximum (0.8) rather than average (0.2) values if the style of faulting is deemed normal. If the fault is considered oblique-normal, then the maximum and average displacement is considered to be equivocal, and the two alternatives are given equal weight.

Each end branch on the right-hand side of the logic tree (Figure 4-1) specifies one estimate for the magnitude of the paleoearthquake. The magnitude estimate is obtained using the appropriate empirical relationship between fault displacement (either average or maximum) and moment magnitude (M_w) given by Wells and Coppersmith (1994). Their relationships for normal faulting earthquakes were used for the normal style of faulting; their relationships for strike-slip faulting were used for the oblique-normal style of faulting. The resulting magnitudes are listed along the right side of the logic tree. Each magnitude assessment listed on the right-hand side of the logic tree represents a specific set of states of the parameters, and the joint probability of that set is equal to the product of the conditional probabilities assigned to each branch. These probabilities are given in parentheses next to the magnitude assessments. It is possible that two or more end branches may result in the same magnitude estimate (within a specified tolerance), and the joint probabilities can be added together in forming a distribution for the assessed variable. These probabilities are given in parentheses next to the magnitude assessments. The characterization in the logic tree specifies a discrete distribution for the magnitude of the paleoearthquake. This distribution is shown at the right of Figure 4-1 in discrete density and cumulative forms.

The process illustrated above for characterizing magnitude of paleoearthquakes was used to quantitatively express the uncertainty in the seismic source characterization for ground shaking hazard. Each SSFD expert team identified potential seismic sources and then characterized their geometry, M_{max}, frequency of occurrence, and spatial distribution of earthquakes. The scientific uncertainty in all of these evaluations was expressed using the logic tree format. Although it is not necessary that all six teams adopt the same logic tree structure, it was suggested that similar forms be used to facilitate discussion between the teams of the important issues.

Figure 4-2 shows the general structure of a logic tree used to develop the seismic source model to represent faulting within the immediate vicinity of the Yucca Mountain site. The logic tree

begins on the left with consideration of the alternative tectonic/faulting models that may control the number and characteristics of the seismic sources that would be defined for the region. These alternative models may include planar faults extending through the seismogenic crust, a shallow detachment with planar faults above and perhaps a strike-slip source at depth, one or more master faults at depth with coupled surface faults at the surface, or some other model.
The second level of the logic tree expresses the uncertainty in the maximum depth of seismogenic rupture. This is important to the evaluation of M_{max} as well as earthquake recurrence based on fault slip rate .

The next two levels express alternative source configurations for each tectonic model. For example, given the planar fault model, one may have alternative interpretations as to which faults are independent and which faults are coupled. For the detachment model, there may be uncertainty about the depth of the detachment and the underlying driving mechanism. For the master fault, there may be uncertainties about the number of master faults and which of the surface faults are coupled at depth. There may be several levels at this point that express uncertainties in specific attributes of a tectonic/faulting model that are common to all of the seismic sources that will be defined using that model.

At this point, the logic tree lists the individual seismic sources defined by a given tectonic/faulting model and a specific set of model attributes. Here the logic tree branches into subtrees, one subtree for each identified seismic source. We use the convention of a vertical line connecting a series of seismic sources, each with is own subtree, to denote the summation of hazard from multiple sources. No dot is placed at the connecting point, indicating that these are not alternatives but individual, independent sources. The distributions of parameters for each source (defined by the subtree to the right of the source name) are assumed to be independent.

The next level of uncertainty expressed is the likelihood that an individual source is active, that it produces earthquakes in the current tectonic regime. If a source is active, then it is considered a discrete seismic source that contributes to the hazard.

The remaining levels of the logic tree characterize the evaluations of M_{max} and seismicity rate parameters. The approaches that may be used for these evaluations are discussed in Sections 4.1.3 and 4.1.4, respectively.

The logic tree structure shown on Figure 4-2 presents a general framework for representing the uncertainty in defining and characterizing the local seismic sources in the immediate vicinity of the Yucca Mountain block. In addition to these sources, the SSFD expert teams identified and characterized regional sources consisting of specific faults and areal zones of seismicity that cannot be attributed to specific known faults. Figures 4-3 and 4-4 present example logic tree structures used to represent the uncertainties in identifying and characterizing these two types of regional sources.

Figure 4-3 presents an example logic tree structure for the regional fault sources. The first level of the logic tree characterizes interpretations of alternative regional tectonic models that are considered to affect which regional faults are considered potential seismic sources. The logic tree is then expanded into subtrees for each of the individual faults or fault zones considered potential sources. The next level of the logic tree characterizes alternative interpretations of the coupling of individual faults within a particular fault zone or fault system. For example, the evaluator might consider the Furnace Creek and Death Valley faults to be part of a single fault system. They may be a single fault having one set of characteristics, or they may be two separate faults having independent characteristics. The remaining levels of the logic tree characterize the individual fault or fault segment activity, maximum seismogenic depth, M_{max}, and seismicity rate parameters.

Figure 4-4 presents an example logic tree structure for regional areal source zones. Areal source zones are sometimes referred to as "background" sources. Within the framework of this PSHA, areal source zones and background sources are equivalent. Both terms refer to a region where seismicity is not associated with specific geologic structures (faults), but instead is represented by a specified spatial distribution. The first node of the logic tree characterizes alternative approaches for zonation of the region. The alternatives may include defining areal source zones having a uniform spatial density of seismicity, defining areal source zones having a nonuniform spatial density of seismicity, or the spatial smoothing of seismicity without defining specific source zone boundaries. At this point, the logic tree is expanded into subtrees

for each areal source zone. The remaining levels of the logic tree characterize alternative parameters for defining the spatial distribution of seismicity within each zone or within the region, the M_{max}, and the seismicity rate parameters.

4.1.2 Types of Seismic Sources and the Spatial Distribution of Seismicity

Two types of seismic sources were used by the SSFD expert teams, faults and areal source zones. Fault sources are used to represent the occurrence of earthquakes along a known or suspected fault trace or traces. Uncertainty in the definition of fault sources is expressed by considering alternative total lengths, alternative fault dips, and possible linkages with other faults. In addition, an evaluation is made of the probability that a particular fault is active, i.e., the fault produces earthquakes in the current tectonic regime.

Faults were represented in the PSHA by segmented planar features; the fault dip and the minimum and maximum depths of rupture on the fault plane were specified by the SSFD expert teams. Earthquake ruptures typically are considered to occur with equal likelihood at any point on the fault plane, the size of the rupture being specified by an empirical relationship between magnitude and rupture area.

Areal sources represent areas of distributed seismicity that are not apparently associated with specific known faults and, therefore, are considered to be occurring on unidentified and/or unidentifiable faults. Areal source zones may also be used to model the occurrence of earthquakes at great distances from a site when the details of the individual faults are not significant to the hazard assessment. The boundaries of areal zones delineate areas that have relatively uniform seismic potential in terms of earthquake occurrence and maximum earthquake magnitude. Uncertainty in defining areal zones typically was expressed by considering alternative zonations of the region surrounding the Yucca Mountain site.

Two alternative approaches were used by the SSFD expert teams to characterize the spatial distribution of future earthquakes within the areal zones. The first considers that there is equal likelihood of occurrence of earthquakes at all locations within the zone. Under this interpretation the spatial density, $f(x,y)$, of future earthquakes at any point x,y in the areal zone is $1/A_Z$, where A_Z is the area.

The alternative interpretation was nonuniform spatial occurrence expressed by a nonuniform spatial density function for the areal zone using the recorded seismicity estimation of kernel density. This interpretation implies that future seismicity is more likely to occur near where it has in the historical past. This interpretation currently is being used to develop the national seismic hazard maps for the U.S. (Frankel, 1995).

The kernel density estimate of the spatial density function is given by the expression

$$f(x,y) = \frac{\sum_{i=1}^{N} K(d_i,h)}{\iint_Z \sum_{i=1}^{N} K(d_i,h) \cdot dx \cdot dy} \qquad (4\text{-}1)$$

where $K(d_i,h)$ is a kernel density function with characteristic dimension h, and d_i is the distance from point x,y to the i^{th} earthquake in the source zone. The denominator in Equation (4-1) is the integral of the spatial density over the region of the areal zone; this normalizes the kernel density estimate to a proper probability density function.

The SSFD expert teams chose to use a two-dimensional Gaussian kernel function. The form of the kernel function is (Silverman, 1986)

$$K(d_i,h) = \frac{e^{-d_i^2/2h^2}}{2\pi h^2} \qquad (4\text{-}2)$$

The controlling factor in kernel density estimation is the selection of the characteristic dimension h. The SSFD expert teams expressed the uncertainty in defining a nonuniform spatial density by considering various values for h.

4.1.3 Assessment of Maximum Magnitude

The M_{max} for a seismic source represents the largest earthquake for the source, regardless of its frequency of occurrence. Thus, M_{max} defines the upper limit of the earthquake recurrence relationship for the source.

4.1.3.1 Fault-Specific Sources. The approach used to evaluate the M_{max} for a fault source was to estimate the maximum physical dimensions of rupture on the source and use relationships between rupture dimensions and earthquake magnitude to estimate M_{max}. The types of empirical relationships available are magnitude versus rupture length, rupture area, maximum surface displacement, and average surface displacement. Some published empirical relationships include more than one parameter, such as rupture length and slip rate or the product of rupture length and displacement (e.g., Anderson *et al.*, 1996). Estimates of the rupture area and average slip on the fault can also be used to estimate the seismic moment of the maximum event, which then can be converted to M_w using the relationship specified by Hanks and Kanamori (1979). The PSHA was conducted using M_w as the magnitude measure, because this is the scale of choice in ground-motion estimation; all estimates of M_{max} were converted to this scale.

The SSFD expert teams considered multiple sources of uncertainty in estimating M_{max} for fault sources. These include consideration of the (1) relative merit of alternative rupture characteristics for estimating magnitude (such as estimates based on rupture length versus estimates based on maximum displacement), (2) relative merit of alternative published empirical relationships, and (3) uncertainty in estimating the physical dimensions of the maximum rupture on a fault. Figure 4-5 illustrates the approach used to express these uncertainties. In the example, alternative fault widths are assessed by considering a range of permissible maximum depths of rupture and alternative fault dips. Alternative maximum rupture lengths are assessed based on evidence for lasting segmentation points and differences in fault behavior. Alternative empirical relationships are considered: magnitude versus rupture length or rupture area from Wells and Coppersmith (1994), or magnitude versus rupture length and slip rate (Anderson *et al*, 1996). If the Anderson *et al.* (1996) relationship is used, then a distribution of possible fault slip rates is assessed. The example logic tree shown at the top of Figure 4-5 shows only some of the branches to illustrate the various evaluations. The complete logic tree leads to the discrete distribution for M_{max} shown at the bottom of the figure.

4.1.3.2 Areal Source Zones. Different approaches may be used to evaluate the M_{max} for areal zones. In cases where an areal zone is used to model the occurrence of earthquakes at large distances from a site where the details of the individual fault sources are not significant to the

hazard assessment, the M_{max} represents the largest earthquake determined to occur on any of the faults within the areal zone. In cases where areal zones are used to model the occurrence of earthquakes on unknown faults (there may be fault sources within the areal zone that are modeled explicitly as separate sources in the hazard), the M_{max} for the areal zone is determined by the largest fault within the zone that is mapped, or the largest earthquake that is not associated with surface faulting. The size of this fault will depend on the level of detailed mapping of the region and the identification of fault sources. Guidance for this evaluation is provided by studies that examine the frequency at which earthquakes of various magnitudes rupture the surface (e.g., Wells and Coppersmith, 1993; de Polo, 1994; and S. K. Pezzopane and T. E. Dawson, USGS, written communication, 1996). The data sets of de Polo (1994) and S. K. Pezzopane and T. E. Dawson (USGS, written communication, 1996) are specific to the Basin and Range Province.

4.1.4 Assessment of Earthquake Recurrence

Earthquake recurrence relationships for a seismic source describe the frequency at which earthquakes of various magnitudes occur. They are determined by estimating the overall frequency of earthquakes on the source, $\alpha_n(m^0)$, and the relative frequency of earthquakes of various sizes defined by the probability density of earthquake size, $f(m)$, between m^0 (minimum magnitude) and the upperbound magnitude, m^U. Different approaches were used to determine the recurrence relationships for areal source zones and fault sources.

4.1.4.1 Areal Source Zones. The earthquake recurrence relationships for areal zones were determined from the historical seismicity. Appendix G describes the development of the earthquake catalog for the region within 300 km of the Yucca Mountain site. The earthquakes in the catalog are described in terms of a uniform magnitude scale, M_w. The catalog was analyzed to identify dependent events (earthquakes that were aftershocks or foreshocks of larger earthquakes) to produce data sets of earthquakes that can be considered to correspond to a Poisson process. Several alternative methods for identifying dependent events were used to express the uncertainty in the process. The SSFD expert teams used the alternative catalogs (as discussed in Appendix G) to develop alternative recurrence relationships for their areal source zones.

The distribution of earthquake sizes in each areal zone was interpreted to follow the Gutenberg and Richter (1954) exponential recurrence model. Because each source has a defined M_{max}, the truncated exponential magnitude distribution (Cornell and Van Marke, 1969) was used to define the recurrence relationships. The truncated exponential relationship is of the form

$$N(m) = \alpha(m^0)\frac{10^{-b(m-m^0)} - 10^{-b(m^U-m^0)}}{1-10^{-b(m^U-m^0)}} \tag{4-3}$$

where $N(m)$ is the annual frequency of occurrence of earthquakes of magnitude greater than m, and b is the Gutenberg and Richter (1954, 1956) b-value parameter.

The recurrence parameters needed for each areal zone are $\alpha(m^0)$ and b. The maximum likelihood procedure developed by Weichert (1980) was used to estimate these parameters from the historical catalog. The likelihood function used in this study was modified from that presented by Weichert (1980) to allow for variable periods of complete reporting within the boundaries of the source as well as variable magnitude intervals (Johnston *et al.*, 1994). The source zone is divided into subregions in which the catalog is considered to be homogeneous. The procedure then sorts the catalog by size into a number of magnitude intervals of width Δm. For each magnitude interval, $m_i \leq m < m_i+\Delta m$, and for each of the j subregions of the source, the period of complete reporting, t_{ij}, is identified. Given the truncated exponential recurrence model, the expected frequency of occurrence of earthquakes of magnitude $m_i \leq m < m_i+\Delta m$ within the j^{th} subregion is defined as $\lambda_j(m_i)$ and is given by the expression

$$\lambda_j(m_i) = \alpha(m^0)\frac{e^{-\beta(m_i-m^0)} - e^{-\beta(m_i+\Delta m-m^0)}}{1-e^{-\beta(m^U-m^0)}} \cdot A_j \Big/ A_Z \tag{4-4}$$

where $\beta = b \cong \ln(10)$, A_j is the area of the j^{th} subregion, and A_Z is the total area of the source zone. Interpreting the occurrence of earthquakes within the source to be described by a Poisson process, then the likelihood of observing the recorded catalog is given by

$$L\{\alpha(m^0),\beta\} = \prod_i \prod_j \frac{[\lambda_j(m_i)t_{ij}]^{k_{ij}} e^{-\lambda_j(m_i)t_{ij}}}{k_{ij}!} \quad (4\text{-}5)$$

where k_{ij} is the number of earthquakes of magnitude $m_i \leq m < m_i+\Delta m$ that have been recorded in the j^{th} subregion during the period of compete reporting t_{ij}. The maximum likelihood recurrence parameters for the source are found by maximizing L{ $\alpha(m^0)$, β }over $\alpha(m^0)$ and β.

The uncertainty in the recurrence relationships for the regional sources was characterized as follows. Using the asymptotic standard errors in $\alpha(m^0)$ and β computed from the maximum likelihood fit to the data, five values of $a(m^0)$ and five values of b were defined ranging from -2 standard deviations to +2 standard deviations. These were then used to define 25 recurrence relationships (Figure 4-6) that may have generated the observed data. The likelihood that the observed data were a product of the process defined by each of the recurrence relationships was computed using Equation (4-6). These likelihoods were then normalized to define a discrete distribution for the seismicity parameters. The resulting distribution indicates the degree to which the data constrain the recurrence relationship for the source zone and accounts for the correlation between $\alpha(m^0)$ and β. Figure 4-6 shows an example of the resulting distribution in computed earthquake recurrence frequencies, including the uncertainty in M_{max} . An additional level of uncertainty in the recurrence relationship for the areal source zones was consideration of the alternative catalogs of independent earthquakes generated using the alternative declustering methods.

4.1.4.2 Fault-Specific Sources. Two approaches were used to estimate the earthquake recurrence relationships for faults. The first involved estimating the frequency of large-magnitude surface-rupturing earthquakes on the fault either by dating of paleoearthquakes or by dividing an estimate of the fault slip rate by an estimate of the average slip per event. The complete recurrence relationship for the source is then specified by constraining a particular form of an earthquake recurrence model (magnitude distribution function) to pass through the estimated frequency of large events. The second approach was to translate the estimated fault slip rate into seismic moment rate and then partition the moment into earthquakes of various magnitudes according to the magnitude distribution or recurrence model used. Both of these approaches constrain the earthquake recurrence relationship for the fault at the frequency of

magnitudes near the M_{max}. The frequency of smaller-magnitude earthquakes is then extrapolated from this frequency based on the form of the magnitude distribution used.

Several magnitude distribution models were considered by the SSFD expert teams (Figure 4-7). One form is the "characteristic" earthquake magnitude distribution developed by Youngs and Coppersmith (1985). The form of the characteristic magnitude distribution is

$$N(m) = N^e \frac{10^{-b(m-m^o)} - 10^{-b(m^u-\frac{1}{2}-m^o)}}{1-10^{-b(m^u-\frac{1}{2}-m^o)}} + N^c \quad for\ m^o \le m < m^u - \frac{1}{2} \qquad (4\text{-}6)$$

$$N(m) = N^c \frac{m^u - m}{\frac{1}{2}} \quad for\ m^u - \frac{1}{2} \le m < m^u$$

with $$N^e = N^c \frac{1.0 - 10^{-b(m^u-1-m^o)}}{\frac{1}{2} b \ln(10) 10^b 10^{-b(m^u-1-m^o)}}$$

where the terms N^e and N^c represent the rate of exponential and characteristic events, respectively. $N^c = N(m^U\text{-}½)$, the cumulative frequency of characteristic events, and the total seismicity rate equals the sum of the rate for exponential and characteristic events, $\alpha(m^0) = N^e + N^c$. When the rate of large events is specified by the SSFD expert teams, it is assumed to be equal to N^c, and Equation (4-6) is used to define the recurrence relationship. When the recurrence relationship is to be based on slip rate, then the parameters N^e and N^c are given by

$$N^e = \frac{\mu A_f S \left[1 - 10^{-b(m^u-\frac{1}{2}-m^o)}\right]}{M_o(m^u) 10^{-b(m^u-\frac{1}{2}-m^o)} \left[\frac{b \cdot 10^{\frac{-c}{2}}}{c-b} + \frac{b \cdot 10 b(1-10^{\frac{-c}{2}})}{c}\right]} \qquad (4\text{-}7)$$

$$N^C = \frac{\frac{1}{2} b \ln(10) N^e 10^{-b(m^U - \frac{3}{2} - m^O)}}{1 - 10^{-b(m^U - \frac{1}{2} - m^O)}}$$

where μ is the shear modulus of fault zone rock (taken to be 3×10^{11} dyne/cm^2), A_f is the total fault surface area, S is the slip rate, and $M_o(m^U)$ is the seismic moment for the m^U on the fault [$M_o(m)=10^{cm+d}$, with c equal to 1.5 and d equal to 16.1, Hanks and Kanamori (1979)].

The second recurrence model used was the truncated exponential model, Equation (4-3). When the recurrence for the fault is specified to be the recurrence interval for large events, it is interpreted to correspond to the frequency for earthquakes of m^U-½ , $N(m^U$-½), and Equation (4-3) is used to define the recurrence relationship for the source. When the recurrence relationship is to be based on slip rate, then the formulation developed by Anderson (1979) is used:

$$\alpha(m^O) = \frac{(c-b)\mu A_f S[1-10^{-b(m^U-m^O)}]}{b M_O(m^U) 10^{-b(m^U-m^O)}} \qquad (4\text{-}8)$$

Youngs *et al.* (1987) introduced a modification to the standard truncated exponential distribution that was used by one of the SSFD expert teams. The modification considers the upperbound magnitude in the density function to be uniformly distributed over the range of m^U-½ to m^U in a similar fashion to the characteristic earthquake model. The effect is to generalize the upper boundary of the magnitude distribution without altering the general shape of the recurrence relationship. The formulation for the modified truncated exponential is:

$$N(m) = \alpha(m^O)\left[1 - \frac{\left[1-10^{-b(m-m^O)}\right] - \left[\ln(f^U) - \ln(f^i)\right]}{b \cdot \ln(10)/2}\right] \quad for\ m^O \le m < m^U - \frac{1}{2} \qquad (4\text{-}9)$$

$$N(m)=\alpha(m^O)\left[1-\frac{\left[1-10^{-b(m-m^O)}\right]\left[\ln(f^U)-\ln(f^i)\right]}{b\cdot\ln(10)/2}-2(m-m^U)\right] \quad for\ m^U-\frac{1}{2}\le m<m^U$$

$$f^i=10^{b(m^U-\frac{1}{2})}-10^{bm^O}$$

$$f^u=10^{bm^U}-10^{bm^O}$$

$$f^i=10^{bm}-10^{bm^O}$$

If the recurrence relationship for a fault is specified by the frequency of large earthquakes, then it is interpreted to equal the cumulative frequency for earthquakes of magnitude m^U-½, $N(m^U$-½), and Equation (4-9) is used to determine the recurrence relationship for the source. If the recurrence relationship is based on slip rate, then the integral of the event frequency derived from Equation (4-9) times the moment for each event is set equal to the moment rate. As a result, $\alpha(m^0)$ is given by

$$\alpha(m^O)=\frac{6\mu A_f S(c-b)}{\frac{M_o(m^U-\frac{1}{2})}{10^{b(m^U-\frac{1}{2}-m^O)}-1}+\frac{4M_o(m^U-\frac{1}{4})}{10^{b(m^U-\frac{1}{4}-m^O)}-1}+\frac{M_o(m^U)}{10^{b(m^U-m^O)}-1}} \qquad (4\text{-}10)$$

The fourth magnitude distribution model the SSFD expert teams considered is the maximum moment model developed by Wesnousky *et al.* (1983), in which only large earthquakes are assumed to occur on the fault. For this model, the recurrence relationships were specified using Equations (4-6) and (4-7) for the characteristic model with N^e set equal to zero (no exponentially distributed events).

Figure 4-7 compares the shape of the exponential, modified exponential, characteristic, and maximum M_w distributions. Shown on the left are the four distributions developed for an assessed fault m^U of M_w 7.5, with the frequency of events larger than M_w 7 set at one per 5000

years. Shown on the right on Figure 4-7 are the magnitude distributions developed on the basis of a slip rate of 1 mm/yr and a fault area of 1,000 km^2. All the recurrence relationships were developed with a *b*-value of 0.8. As can be seen, the modified truncated exponential distribution is very similar to the truncated exponential distribution. The characteristic magnitude distribution results in about a factor of ten reduction in the frequency of small-magnitude events compared to the exponential model.

Uncertainty in the recurrence relationships for the faults can incorporate alternative recurrence models, alternative methods to constrain the rate of large events (i.e., slip rate versus recurrence interval), uncertainty in the slip rates and recurrence intervals, and alternative *b*-values.

4.2 METHODOLOGY FOR FAULT DISPLACEMENT HAZARD CHARACTERIZATION

At the present time, methodologies for the probabilistic assessment of fault displacement hazard (especially distributed faulting hazard) have not matured to the level of those used for the assessment of ground shaking hazard and there is little relevant literature. As a result, the SSFD expert teams developed a number of original approaches as part of their assessments for the project. These approaches were originated to a significant degree by one of the teams, were discussed in Workshops #4, #5, and #6, and then were refined and modified in the individual team characterizations of fault displacement hazard. The methods are based primarily on empirical observations of the pattern of faulting during earthquakes and on data gathered during studies of the faulting in the Yucca Mountain region. As part of these characterizations, the individual teams developed a number of empirical distributions from data gathered at Yucca Mountain or published in the literature. The SSFD Facilitation Team fit statistical models to these empirical distributions to facilitate numerical calculation of the hazard. Appendix H documents the development of these statistical models.

4.2.1 Principal and Distributed Fault Displacement

The potential for fault rupture within the Controlled Area can be described in terms of two types of fault rupture: *principal faulting* and *distributed faulting*. These are illustrated on Figure 4-8, which shows the surface rupture pattern for the 1959 M_W 7.4 Hebgen Lake earthquake. Principal faulting is the faulting along the main plane (or planes) of crustal weakness

responsible for the release of seismic energy during the earthquake. Where the principal fault rupture extends to the surface, it may be represented by displacement along a single narrow trace or over a zone that is a few to many meters wide. For principal faulting, the faults of concern are those that may produce earthquakes (i.e., are directly related to the primary source of energy release). Repeated large earthquakes on a given fault segment are considered to be produced by repeated principal faulting on the same fault trace or traces, so that faults that are capable of principal rupture can be recognized based on detailed mapping of outcrops and/or in the walls of subsurface excavations (trenches and tunnels).

Distributed faulting is defined as rupture that occurs on other faults in the vicinity of the principal rupture in response to the principal displacement. It is expected that distributed faulting will be discontinuous in nature and occur over a zone that may extend outward several tens of meters to many kilometers from the principal rupture. A fault that can produce principal rupture may also undergo distributed faulting in response to principal rupture on other faults. The extent to which faults that can undergo distributed rupture can be identified depends on the level of detailed mapping but the minimum resolution for detection is generally smaller for distributive faulting than for principal faulting. Interpretation of distributive faulting is more subjective and is, therefore, less certain than for principal faulting.

Both types of faulting are important to the assessment of the fault displacement hazard at the Yucca Mountain site. Figure 4-9 shows the Controlled Area and the nine locations at which the fault displacement methodology is demonstrated. These points were chosen to represent the range of conditions in the Controlled Area. Some of these points lie on faults that may experience principal faulting (the Solitario Canyon fault, the Bow Ridge fault, and possibly some of the intrablock faults) and distributed faulting. The other points are sites of potential distributed faulting. The locations and specific conditions for the nine points are described further in Section 4.3.2. The methodologies described below were developed by the SSFD expert teams to assess the hazard at any location within the Controlled Area, including all of these nine demonstration points.

4.2.2 Basic Formulation

The basic formulation for probabilistic evaluation of the hazard from fault displacement is analogous to that developed for the hazard from ground shaking. The fault displacement PSHA

addresses how frequently it occurs and how large the displacements are. The hazard can be represented probabilistically by a displacement hazard curve that is analogous to ground motion hazard curves. The hazard curve shown on Figure 4-10 represents the hazard at a point within the Controlled Area. It relates the amount of displacement in a *single* event to how often larger displacements occur (i.e., the frequency of exceeding a specified amount of displacement). In the example hazard curve (Figure 4-10), single event displacements larger than 10 cm occur with a frequency of 10^{-4} per year (a return period of 10,000 years); single event displacements larger than 50 cm occur with a frequency of 10^{-5} per year (a return period of 100,000 years). Thus, the hazard curve is a plot of the frequency of exceeding fault displacement value d, designated by $\nu(d)$. This frequency can be computed by the expression:

$$\nu(d) = \lambda_{DE} \cdot P(D > d) \tag{4-11}$$

where λ_{DE} is the frequency at which displacement events occur on the structure located at the point of interest, and $P(D>d)$ is the conditional probability that the displacement in a single event will exceed value d. The SSFD expert teams used different approaches to characterize fault displacement hazard and, thus, different techniques to express these two terms. They also used a variety of data sets to develop the necessary parameters. These approaches and data sets are generally described below. Specific applications of these approaches by each team are described in Section 4.3.2.

The displacement hazard curve can be used to estimate the effective slip rate on the feature of interest. The negative of the slope of the hazard curve, $\partial\, \nu(d)/\partial\, d$, provides the rate density of displacements of amount d. Integrating this over displacement provides an estimate of fault slip rate, SR. Specifically:

$$SR = \int_0^\infty \left[-\partial \nu(d) \Big/ \partial d \times d \right] dd \tag{4-12}$$

4.2.3 Assessment of Scientific Uncertainty

As with the ground motion PSHA methodology, the formulation given by Equation (4-11) represents the randomness in the natural phenomena of earthquake-induced fault displacement

(the aleatory uncertainty). The scientific (epistemic) uncertainty is represented in the process of selecting the appropriate models and model parameters for the fault displacement hazard characterization. The logic tree methodology described in Section 4.1.1 was utilized to characterize the uncertainty in the fault displacement PSHA.

4.2.4 Estimation of Displacement Event Frequency

The approaches for estimating the frequency of displacement events, λ_{DE}, developed by the SSFD expert teams can be divided into two categories. The first, designated the *displacement approach*, provides an estimate of the frequency of displacement events directly from observed feature-specific or point-specific data. The second, designated the *earthquake approach*, involves relating the frequency of slip events to the frequency of earthquakes on the various seismic sources defined by the seismic source characterization models developed in Section 4.3.1. Both approaches are used for assessing the fault displacement hazard for principal faulting and distributed faulting.

4.2.4.1 Displacement Approach. The displacement approach estimates the frequency of displacement events, λ_{DE}, from the information available for the specific feature (point) in question. There are two techniques for direct estimation of λ_{DE}, estimation of recurrence intervals and the use of slip rates.

Recurrence Interval Technique. An example of the recurrence interval technique is the assessment of the frequency of displacement events on a source of principal faulting using paleoearthquake data. The SSFD expert teams used such data to estimate the frequency of surface-rupturing events as part of their seismic source characterization models for the ground shaking hazard. This assessment can be used directly in assessing the frequency of faulting events.

Slip-Rate Technique. Fault slip rate, SR, is a measure of the amount of slip averaged over a time period that encompasses multiple ruptures. If the slip rate and the average slip in a faulting event, $\bar{D}_E$, are known, then λ_{DE} can be estimated by:

$$\lambda_{DE} = SR / \bar{D}_E \qquad (4\text{-}13)$$

Given *SR*, the use of Equation (4-13) requires an estimate of the average slip in an event, $\bar{D}_E$. For some features (typically those that may be the location of principal faulting), this may be assessed directly from trenching data. For other features, the SSFD expert teams developed scaling relationships that relate $\bar{D}_E$ to fault length, L, or cumulative fault displacement, D_{cum}. These are described in the summaries of the models the SSFD expert teams developed for displacement hazard (Section 4.3.2).

The displacement approach does not tie slip events to specific earthquakes, it only evaluates the frequency of slip events. Thus, the displacement approach does not explicitly distinguish between principal and distributed ruptures on a feature.

4.2.4.2 Earthquake Approach. The earthquake approach utilizes the earthquake recurrence models developed for the ground shaking hazard assessment. Each SSFD expert team provided an assessment of the frequency of earthquakes on each seismic source. The occurrence of a slip event (earthquake) on source j may induce slip on the feature (point) of interest, point i. The probability that slip will occur given an event on source j, P_i *(Slip| Event on j)*, can range from 0 to 1.0. The frequency of displacement events at point i, λ_{DE}, is obtained by summing the contributions from all of the seismic sources:

$$\lambda_{DE} = \sum_{j=i}^{n} \lambda_j \,(\text{Events on source } j) \cdot P_i\,(\text{Slip} \mid \text{Event on source } j) \qquad (4\text{-}14)$$

As defined by Equation (4-14), the earthquake approach for assessing the frequency of displacement events consists of two-parts, an evaluation of the opportunity frequency, the frequency of earthquakes, and an evaluation of the probability each opportunity will result in fault slip. Because the earthquake approach is tied directly to the occurrence of earthquakes on various sources, the distinction between principal and distributed faulting events is maintained.

The methods used to evaluate P_i *(Slip/ Event on j)* depend on whether one is considering principal ($j = i$) or distributed faulting ($j \neq i$).

Probability of Slip for Principal Faulting. In this approach the frequency of principal faulting events is assessed using earthquake recurrence models developed for a seismic source. The models define the frequency of various size earthquakes up to the maximum earthquake assessed for the source. In many cases, the recurrence models were developed by specifying the frequency of surface-rupturing earthquakes from trenching data, interpreting these events to be near the maximum earthquake. For these events, P_i *(Slip| Event on i)* is expected to be 1.0. However, earthquakes smaller than the maximum earthquake may not always rupture to the surface or at shallow depths where the repository is to be located (300 m). They also may have rupture lengths that are shorter than the total fault length. The contribution of these events to the fault displacement hazard will depend on their relative frequency compared to the largest events and the likelihood that they will rupture to near the surface and at the point along the fault where the hazard is being evaluated. Two approaches were developed to assess the probability of surface rupture in a principal faulting event, one based on empirical data on the frequency of surface rupture, and one based on the numerical randomization of the depth of rupture on the fault used in the analysis of ground shaking hazard.

Empirical Probability of Principal Faulting Surface Rupture. Wells and Coppersmith (1993), de Polo (1994), and S. K. Pezzopane and T. E. Dawson (USGS, written communication, 1996) present data sets that indicate the frequency at which earthquakes of various magnitudes rupture the surface. The data sets of de Polo (1994) and S. K. Pezzopane and T. E. Dawson (USGS, written communication,. 1996) are specific to the Basin and Range Province. These data can be used to develop an empirical model for P_i *(Slip| Event on i)* as a function of magnitude. For example, Wells and Coppersmith (1993) used a *logistic regression* model to evaluate the probability of surface rupture. The logistic regression model (e.g., Hosmer and Lemeshow, 1989) is a commonly used model for assessing the outcome of a dichotomous variable; in this case, surface rupture either occurs or does not occur. The probability of a positive outcome (the occurrence of principal faulting given the occurrence of the event) is given by the expression

$$P(\text{Rupture}) = \frac{e^{a+bm}}{1+e^{a+bm}} \tag{4-15}$$

where a and b are constants estimated from data (see Appendix H, Section H4.1). Figure 4-11 presents the results of fitting Equation (4-15) to the various data sets presented by S. K.

Pezzopane and T. E. Dawson (USGS, written communication, 1996) for surface rupture as a function of magnitude.

Focal Depth Distribution. Each SSFD team provided an evaluation of the focal depth distribution for earthquakes in the Yucca Mountain region. Using this distribution along with an assessment of the size of earthquake ruptures as a function of magnitude (e.g., an empirical relationship of rupture area as a function of magnitude) and rupture aspect ratio, the distribution for the down-dip location ruptures on a fault was modeled as part of the calculation of the source-to-site distribution in the ground motion hazard analysis. This process can also be used to calculate the frequency at which earthquakes of a given magnitude occurring on a fault are expected to rupture near the surface, thus providing a fault-specific estimate of P (*surface rupture*).

Probability of Intersection Along Strike. The probability that the earthquake rupture will intersect the point of interest along the fault is computed from the distribution for the location of the rupture along the fault. This distribution is computed for each fault as a part of the ground motion hazard assessment by assuming that earthquake ruptures are equally likely to occur anywhere along the fault. The probability of along-strike intersection of the rupture, $P(intersection)$, times the probability of surface rupture provides the probability of principal faulting in the earthquake, that is:

$$P_i(principal\ faulting\ slip | event\ on\ j) = P(surface\ rupture) \times P(intersection) \qquad (4\text{-}16)$$

Probability of Slip for Distributed Faulting. For distributed faulting, P_i (*Slip| Event on j*) expresses the likelihood that slip on an earthquake source some distance r from the feature of interest will trigger slip locally. Several approaches were considered for assessing P_i (*Slip| Event on j*) for distributed faulting.

Analysis of Historical Distributed Ruptures. S. K. Pezzopane and T. E. Dawson (USGS, written communication, 1996) developed a data base of distributed ruptures resulting from historical earthquakes in the western U.S. These data were used to assess the density of distributed ruptures as a function of distance from the principal rupture. The process used was to place a 0.5 km × 0.5 km grid on each map of surface ruptures. The number of grid cells that

contain a secondary rupture divided by the total number of grid cells at a given distance from the principal rupture provides a measure of the frequency or likelihood that a distributed rupture will occur. Figure 4-12 shows a plot of these data segregated by magnitude and by location in the hanging wall block and footwall block of the rupture. The data show a decrease in the likelihood of experiencing distributed rupture with increasing distance from the principal rupture. The data also show clear differences between the hanging wall and footwall sides of the rupture. The size (magnitude) of the earthquake appears to provide some control on the maximum distance distributed rupture has been observed away from the principal faulting.

The probability of occurrence of distributed faulting on a feature located r km from a magnitude m earthquake can be determined from these data using the logistic model.

$$P_i(\text{Slip} \mid \text{Event on } j) = \frac{e^{f(m,r)}}{1+e^{f(m,r)}} \tag{4-17}$$

where $f(m,r)$ represents a suitable function of m and r. The data shown on Figure 4-12 indicate that $f(m,r)$ should account for the effect of being on the hanging wall or foot wall sides of the principal rupture. Appendix H, Section H4.2 presents models fit to these data that were used by the expert teams to assess P_i (*Slip*| *Event on j*) for distributed faulting. This probability is considered an aleatory probability because it defines the likelihood of the occurrence of distributed faulting at a point in a single earthquake.

Slip Tendency. Another approach to estimating the likelihood that a feature will experience distributed faulting is based on characteristics such as feature and orientation. Morris *et al.* (1996) and H. L. McKague *et al.* (CNWRA, written communication, 1996) have performed slip-tendency analyses of faults in the Yucca Mountain region using their orientations with respect to the current stress field. These assessments have been used to either modify P_i (*Slip*| *Event on j*) (i.e., reduce the probability that distributed slip will occur as the orientation of the feature changes from favorable to unfavorable in the present stress regime) or as an assessment of whether the feature can slip at all in response to earthquakes in the present tectonic stress regime.

Another approach to assessing the likelihood that distributed slip could occur on a feature in response to principal faulting on a seismic source involves evaluating the angle between the strike of the principal fault and the strike of the feature under consideration. Section H4.3 of Appendix H presents an analysis of the pattern of distributed ruptures from mapping data developed by S. K. Pezzopane and T. E. Dawson (USGS, written communication, 1996). The relative frequency of rupture orientations with respect to the principal rupture provides an estimate of the likelihood that the feature will slip in response to a principal rupture.

4.2.5 Conditional Probability of Exceedance for Displacement

The conditional probability of exceedance, $P(D>d)$, in Equation 4-11, defines the probability that the amount of displacement occurring at a point during a single displacement event will exceed a specified amount d. The probability can be considered to contain two-parts: the variability of slip from event to event, and the variability of slip along strike during a single event. The first part represents a distribution for the "size" of faulting events and is analogous to an earthquake magnitude distribution model used in the ground shaking hazard analysis. The second part represents the variation of the displacement at a point from the size of the event. This might be considered analogous to the lognormal distribution for peak ground motion about the median value predicted by an attenuation law for a specific magnitude and distance.

The teams developed a variety of approaches for evaluating the distribution of slip at a point in an individual event. Some methods utilize the two-part representation of displacement variability; others combine them into a single distribution function. The various methods are described below as they are applied to principal and distributed faulting. The approaches also differ depending on whether the earthquake or displacement approaches are being used for the assessment.

4.2.5.1 Two-Step Approach for Conditional Probability of Exceedance. The two-part approach for assessing $P(D>d)$ was typically used in the earthquake approach for principal faulting hazard. The size measure used to describe the event was the maximum displacement, *MD*, in an earthquake and was typically assessed using empirical relationships between magnitude and maximum displacement. The value of *MD* in an event was assumed to be distributed according to the empirical regression model, typically lognormal. In some cases, the SSFD expert teams used trenching data to assess *MD* for maximum events on the source.

The second part is an assessment of the variability of slip at a point as a fraction of the maximum displacement in the event. The ASM team analyzed the slip distributions for a number of surface rupturing events. The plot on the left side of Figure 4-13 shows the results in the form of smoothed curves defining the minimum, median, and maximum values of *D/MD* at a point as a function of location along strike. These values, which can be interpreted as representing a low percentile, the median value, and a high percentile for *D/MD*, can be used to construct a cumulative distribution function for *D/MD*. Shown at the right of Figure 4-13 are examples of cumulative distribution functions for *D/MD* at three values of *x/L*, the location of the point along the rupture. These cumulative functions were made by fitting a beta distribution to the percentiles shown by the solid dots on the plot. The beta distribution was selected because it is a very flexible distribution for modeling variables that are defined over a finite range, in this case $0 \le D/MD \le 1$. The beta distribution has the density function

$$f(y) = y^{a-1}(1-y)^{b-1}\frac{\Gamma(a+b)}{\Gamma(a)\Gamma(b)} \tag{4-18}$$

where $\Gamma(\ )$ is the Gamma function. For this application, $y = D/MD$. The cumulative distributions shown on the right of Figure 4-13 were obtained by developing relationships for the parameters a and b as a function of x/L (see Appendix H). The SBK team developed a similar model for the distribution of *D/MD* using numerical simulations of fault rupture patterns (see Appendix H and the SBK elicitation summary in Appendix E).

The conditional probability of exceedance, $P(D>d)$, is then obtained by convolving the distribution for *D/MD* with the distribution for *MD* as a function of the magnitude of the earthquake.

$$P(D > d) = 1 - \int f(MD)\left[\int_0^{d/MD} f(y)\,dy\right] d(MD) \tag{4-19}$$

where $f(MD)$ was typically defined by a lognormal distribution and $f(y)$ is given by Equation (4-18).

4.2.5.2 Single-Step Approach for Conditional Probability of Exceedance. The single step approach for assessing $P(D>d)$ involved developing an empirical distribution for the displacement data collected at Yucca Mountain by normalizing the data from each trench location by a normalizing parameter related to the location where the data were obtained. The resulting distribution of D/D_{norm} were then used to compute $P(D>d)$, given an assessment for D_{norm} at the location of interest. A variety of normalization parameters were developed by the SSFD expert teams, including: the average displacement observed in a trench with multiple displacements, the average or maximum displacement expected for a fault based on its dimension, and the cumulative displacement that has occurred on the feature where the trench was located. These empirical distributions were then fit with statistical models for use in the displacement hazard computation (see Appendix H). Examples of these distributions are shown on Figure 4-14.

4.3 EXPERT TEAM MODELS

The following summarizes the expert team's seismic source characterization and a description of the fault displacement models. Complete expert team elicitation summaries are contained in Appendix E.

4.3.1 Seismic Source Characterization

The previous section describes the type of probabilistic models used to define the spatial location, frequency, and size distribution of earthquakes in the Yucca Mountain region that may generate significant ground motion at the repository. This section describes the seismic source models developed by the SSFD expert teams. Section 4.3.1.1 provides summaries of the individual team models, which are presented in full in each team's elicitation summary in Appendix E. This discussion is followed by a summary in which the assessments of key components of the source characterization models are compared (Section 4.3.1.2).

4.3.1.1 Individual Expert Team Models. The seismic source characterization models for each of the six SSFD teams are summarized in this section using common terminology and format. We do not attempt to summarize the bases for the teams' models, that information is contained in Appendix E. An abbreviated summary of models is given in Table 4-1. Lists of

acronyms used to designate fault sources on various source maps referred to in the following sections are given in Table 4-2. The seismic source characterization developed by each SSFD team is described in terms of local faults in the Yucca Mountain region, regional faults within 100 km of the site, and regional areal source zones. Much of the seismic hazard characterization involves assessing seismicity rates and M_{max} for seismic sources. In was the role of the SSFD Facilitation Team to compute these parameters using the methods and data that the SSFD expert teams specified. The results of these calculations for each team are presented as part of the description of their models. In addition, we employ the expert teams' models to compute the implied rate for future seismicity within 100 km of Yucca Mountain. Figure 4-15 shows the region for which this calculation is made. We present calculated earthquake recurrence rates for local seismic sources, which generally lie within the shaded region at the center of Figure 4-15, the regional faults that lie within a 100-km radius of Yucca Mountain, adjusting for the portions of these faults that may lie outside of this circle, and for those parts of the areal source zones that lie within 100 km of Yucca Mountain. The recurrence rates for the regional faults and the areal zones, as well as the combined recurrence rates for all three types of sources, are compared to the observed seismicity rate within the 100-km circle based on each SSFD team's selection of the appropriate earthquake catalog and catalog completeness periods. Shown on Figure 4-15 are the earthquakes of M_w 5 and larger that have been recorded within the 100-km circle. The choice of a 100 km radius encloses the region containing the seismic sources that will affect the seismic hazard at the Yucca Mountain site.

Arabasz, Anderson, Ramelli (AAR) Team. Tectonic models provide a fundamental framework for the AAR team's seismic source characterization for local sources. Many of their seismic source parameters are dependent on tectonic models, including the geometry of local faults and buried sources, rupture behavioral models for local faults, and the seismogenic potential of hypothesized buried sources. Figure 4-16a and 4-16b show the logic tree that defines the alternative interpretations of local faults developed by the AAR team. These models are based on the inference that the controlling tectonic model for the Crater Flat structural domain is simple shear. Figure 4-16a shows the logic structure for considering alternative models for local faults. The first assessment addresses whether or not a superposed NW-SE dextral shear is manifested as specific structures. If so, three alternative models for these structures are considered: (1) a regional throughgoing dextral shear zone subjacent to Yucca Mountain (Model A), (2) a right-stepping dextral shear zone that produces a pull-apart basin

without an underlying cross-basin fault (Model B), and (3) a right-stepping dextral shear zone that produces a pull-apart basin with an underlying cross-basin fault (Model C). The integral structures in all of these models are buried and/or hypothesized, with the possible exception of the Highway 95 (or Carrara) fault, which may form the southern boundary of the pull-apart basin in Models B and C. The locations of these sources are shown on Figure 4-17. The case with no specific dextral shear source is designated Model D. The Highway 95 fault and the north-bounding fault are assessed to have less than 1.0 probability of being seismogenic.

The possible existence of a local detachment zone was considered, with the likelihood that the detachment exists dependent on the existence of cross-basin shear structures (Figure 4-16a). Although not considered to be seismogenic, the detachment zone controls the down-dip extent of all local faults, except the Bare Mountain fault, and hypothesized buried dextral shear structures. Possible depths for detachments range from 3 km to the maximum thickness of the seismogenic crust. Under the assumption that a detaching layer does not exist, the down-dip extent of the local faults is controlled by the Bare Mountain fault and the thickness of the seismogenic crust.

The AAR team distinguished two parameters for the maximum depth of the seismogenic crust: (1) DMAX1 constrains down-dip extent of fault rupture for calculating rupture area to be used with empirical relations for estimating M_{max} and (2) DMAX2 is the maximum depth of seismogenic rupture during larger earthquakes, in which case rupture area is entered into an equation for seismic moment to estimate M_{max}. DMAX1 was assessed to range from 11 km to 17 km, based on the depth distribution of seismicity in the southern Great Basin, and represents the nominal definition of maximum depth defined in Wells and Coppersmith (1994). DMAX2, ranging from 14 km to 22 km, is based on the assessment that longer ruptures ($\geq$ 25 km) extend below the seismogenic crust into the brittle-ductile transition zone.

Two alternative modes of behavior were assessed for the local fault sources (Figure 4-16b). The first considered the local faults to act as independent sources. Figure 4-18 shows the locations of these faults. Some of these sources were considered to be potentially linked along strike into larger faults (the Paintbrush Canyon-Stagecoach Road system and the Southern, Central, Northern Windy Wash-Fatigue Wash system). The alternative considered that all of the observed normal faults in the Yucca Mountain area coalesce at depth into one to four master

faults (Figure 4-19). In general, coalesced behavior is favored over independent behavior, with the specific weight dependent upon the existence and depth of potential detachments. When the number of coalesced faults is less than four, then it is assumed that large earthquakes produce comparable amounts of slip on parallel fault traces during a single earthquake. Under the assumption of independent fault behavior, the minor faults such as the Ghost Dance, west Dune Wash, and Crater Flat) are assessed to have less than 1.0 probability of being seismogenic.

M_{max} for the local sources was based on empirical relationships between magnitude and rupture length, rupture length and slip rate, rupture area, and on estimation of seismic moment. The assessed distributions for M_{max} are shown on Figure 4-20. The AAR team chose to follow the convention developed by Youngs *et al.* (1987) in developing recurrence relationships for the faults. Following this approach, M_{max} assessed from the various empirical relationships is considered the central value of the characteristic magnitude interval, which is $M_{max} \pm ¼$ magnitude units. The upperbound magnitude of the recurrence relationship, m^U, is thus equal to $M_{max} + ¼$. The magnitudes plotted on Figure 4-20 are m^U.

Earthquake recurrence relationships for the local faults were based on assessments of slip rates and the recurrence intervals of large earthquakes (when data are available for a specific fault), with slip rate slightly favored. Slip rates of individual faults were summed across strike to assess rates for coalesced systems. A characteristic recurrence model was favored over a modified exponential model.

The AAR team identified 19 regional fault sources (Figure 4-21). The potential for two faults to be linked together into a single fault system was considered for the Death Valley and Furnace Creek faults, and for the Amargosa River and Pahrump faults. Preferred dips were generally 65° for normal faults and 90° for strike-slip faults. M_{max} for the regional sources were based on empirical relationships between magnitude and rupture length, rupture length and slip rate, and rupture area. The assessed distributions for M_{max} are shown on Figure 4-22. These values again are $M_{max} + ¼$. Earthquake recurrence relationships for the individual faults were assessed using the approaches outlined above for the local faults.

The AAR team defined regional source zones to account for the potential occurrence of earthquakes on faults not specifically identified as potential sources or unknown faults. Figure

4-23 shows the logic tree that defines the alternative interpretations of regional zones. Three alternatives were considered for defining these zones in which the spatial distribution of seismicity was assessed to be uniform (Figure 4-24). A fourth alternative was to use the kernel density estimation technique (discussed in Section 4.1.2) to define the spatial distribution of earthquakes within 100 km of Yucca Mountain without imposing source zone boundaries. The potential occurrence of volcanic-related earthquakes was addressed by the regional zones.
The M_{max} assessed for the regional zones ranged from M_w 6.6 to 7.3. Because of greater confidence in the identification and characterization of fault sources in the immediate Yucca Mountain vicinity, M_{max} was assessed to range from M_w 6.0 to 6.6 for the areal zone within 20 km of the Yucca Mountain site. The AAR team used the catalog of independent events produced by the declustering method of Veneziano and van Dyck (1985). The recurrence relationships for the individual source zones were estimated using the approach described in Section 4.1.4.1. All earthquakes occurring in the underground nuclear explosion (UNE) zone post-1950 were removed from the recurrence calculation. Figure 4-25 shows the recurrence relationships for each of the regional zones. These relationships were obtained using the maximum likelihood techniques discussed in Section 4.1.4.

The seismic source models developed by the AAR team can be used to calculate earthquake recurrence relationships (Figure 4-26) for the area shown on Figure 4-15. Plot (a) shows the distribution of earthquake frequencies computed using the AAR model for local faults (Figures 4-17 through 4-19). This distribution of earthquake occurrence rates applies to the area approximated by the shaded region around Yucca Mountain shown on Figure 4-15. The AAR local fault model contains about one and one-half orders of magnitude uncertainty in the combined recurrence rate for the local sources.

Plot (b) shows the distribution of earthquake frequencies computed using the AAR model for regional faults (Figure 4-21). Occurrence rates were computed for those portions of the regional faults that lie within 100 km of the Yucca Mountain site. The uncertainty in the recurrence rate for the regional faults is significantly smaller than that for the local faults. It should be noted that for all of the expert team characterizations, the predicted recurrence rates for regional faults are dominated by those estimated for the Death Valley and Furnace Creek faults. Also shown on Plot (b) are the observed frequencies of earthquakes occurring within

100 km of the Yucca Mountain site. Most of the smaller earthquakes are not close to the regional faults.

Plot (c) shows the distribution of earthquake frequencies computed using the AAR model for regional source zones (Figure 4-24). Again, the occurrence rates were computed for those portions of the regional source zones that lie within 100 km of the Yucca Mountain site. The uncertainty in the recurrence rate for the regional sources zones is also significantly smaller than that for the local fault sources. Also shown on Figure 4-26 are the observed frequencies of earthquakes occurring within the same region. (These are the same frequencies as those shown on Plot [b].) The predicted earthquake frequencies for the regional zones are somewhat greater than the observed frequencies because they are based on larger source areas that include regions of higher seismicity rates that lie beyond the 100-km circle.

Plot (d) shows the distribution of earthquake frequencies computed for all the sources in the AAR seismic source model for the region that lies within 100 km of the Yucca Mountain site compared to the observed earthquake frequencies. There is reasonable agreement between the observed and predicted rates for magnitudes of interest to the ground motion hazard assessment.

Ake, Slemmons, McCalpin (ASM) Team. The ASM team incorporates various aspects of planar fault block, detachment, lateral shear, and volcanic-tectonic models into their characterization of the local seismic sources. Figures 4-27a and 4-27b show their logic tree defining the uncertainties in characterizing the local faults. The locations of these faults are shown on Figures 4-28 and 4-29. The ASM team considers the possibility of the existence of a regional detachment underlying Yucca Mountain, although their preferred tectonic model is that the faults are planar to a depth controlled by the brittle-ductile transition and the Bare Mountain fault. The regional detachment has a very low probability (0.01) of being seismogenic and may lie at three alternative depths: 6 km, halfway between 6 km and the brittle-ductile transition (preferred), and at the brittle-ductile transition. The brittle-ductile transition is assessed to lie in the depth range of 12 to 17 km. They also consider the potential for the existence of a buried strike-slip fault, with the probability that it exists dependent on the existence of a regional detachment. The probability that a buried strike-slip fault is seismogenic depends on its minimum depth, which is controlled by the depth of the detachment (Figure 4-27).

The ASM team identified 10 local faults as seismic sources near Yucca Mountain (Figure 4-28). Five of these faults (Bare Mountain, Windy Wash, Solitario Canyon, and Paintbrush Canyon/Stagecoach Road) are termed major, block-bounding faults, and are assessed to be seismogenic. The remaining faults (Northern and Southern Crater Flat, Fatigue Wash, Iron Ridge, and Bow Ridge) are interpreted to be minor or secondary faults and have a probability of being seismogenic less than 1.0.

Two alternative geometries are considered for the local faults: planar and merging down dip. Under the planar assumption, the major faults penetrate to the base of the seismogenic crust and the down-dip extent of the minor faults is controlled by an aspect ratio of 1.5. Under the merging down-dip assumption, the major faults are truncated by the Bare Mountain fault or the detachment (if it exists) and the minor faults merge with the major faults. Three alternative geometries are assessed for this merging system: shallow, intermediate, and deep merging depths.

Two alternative behaviors were considered for the case of merging faults: the principal faults always rupture independently (the preferred model) and sometimes the principal faults rupture simultaneously (Figure 4-27b). Specific fault rupture combinations and the fraction of fault ruptures that are simultaneous ruptures were assessed by the ASM team.

The M_{max} for the local fault sources was assessed using empirical relationships between magnitude and surface rupture length, maximum displacement, rupture length times maximum displacement, average displacement, and rupture area (depending upon the available data). Only combined rupture area was used to assess the magnitude of multiple fault ruptures. The resulting M_{max} probability distributions are shown on Figure 4-30.

The ASM team used the convention of Youngs *et al.* (1987) in developing recurrence relationships for the faults, with the upperbound magnitude of the recurrence relationship, m^u, equal to M_{max} obtained from the empirical relationships plus ¼ magnitude units. The magnitudes plotted on Figure 4-30 are m^U. The rates of seismic activity on the local sources were assessed using fault slip rate and large magnitude earthquake recurrence interval approaches (depending on available data). For the mapped normal faults, the characteristic recurrence model was favored (0.7) with lesser weight given to the truncated exponential (0.2)

and maximum moment (0.1) recurrence models. Only the characteristic recurrence model was used for the detachment and buried strike-slip sources and the simultaneous rupture of multiple faults was assessed to conform to the maximum moment recurrence model.

Figure 4-31 shows the 26 regional fault sources characterized in the ASM seismic source models. With the exception of the Carrara (Highway 95) fault, these faults are assigned a probability of 1.0 of being seismogenic based on paleoseismic evidence. The sources are modeled as planar faults that extend to the depth of the brittle-ductile transition. Generalized dips of 90° for strike-slip faults and 60° for normal faults were used. M_{max} was assessed based on an assessed distribution for maximum surface rupture length. The resulting M_{max} probability distributions are shown on Figure 4-32. Again, these magnitudes are M_{max} + ¼. Rates of seismicity were assessed based on fault slip rate and estimates of the recurrence intervals for surface-rupturing earthquakes. A maximum moment model was strongly favored (0.8) over a characteristic recurrence model (0.2).

The ASM team defined six regional source zones to account for the potential occurrence of earthquakes on faults not specifically identified as potential sources. Figure 4-33 shows the logic tree that defines the alternative interpretations of the regional source zones shown in Figure 4-34. Volcanic-related earthquakes were not modeled as a separate source, but rather were modeled as part of the earthquakes occurring in the areal source zones.

The M_{max} assessed for the regional zones ranged from M_w 6.5 to 7.2. Because of the greater detail of fault investigations and seismic source characterization in the immediate Yucca Mountain vicinity, M_{max} was assessed to range from M_w 6.0 to 6.6 within 50 km of the Yucca Mountain site. The ASM team used the catalogs of independent events produced by the declustering methods of Youngs *et al.* (1987) and Veneziano and van Dyck (1985). The recurrence relationships for the individual source zones were estimated using the approach described in Section 4.1.4.1. All earthquakes occurring in the UNE zone post-1950 were removed from the recurrence calculation. Figure 4-35 shows the recurrence relationships for each of the source zones.

Figure 4-36 shows the distribution for earthquake recurrence predicted by ASM seismic source characterization for local faults, regional faults, regional zones, and all sources

combined compared to the observed frequency of earthquakes occurring within 100 km of the Yucca Mountain site. The ASM local fault model contains about one and one-half orders of magnitude uncertainty in the combined recurrence rates. A significant part of this uncertainty is due to differences between the recurrence rates assessed using fault slip rate and those assessed using paleoseismic recurrence intervals. The uncertainty in the recurrence rate for large earthquakes occurring on the regional faults is much smaller than that for smaller earthquakes because of the range in earthquake recurrence models used by the ASM team. It should be noted that the use of the maximum moment model for regional fault recurrence does not imply a complete absence of smaller-magnitude earthquakes on or in the immediate vicinity of these faults. The fault sources are superimposed on regional source zones. Thus, the use of a maximum moment recurrence model for the regional faults implies that the occurrence rate for smaller earthquakes is no larger on the fault than at other locations within the regional zone. Within 100 km of Yucca Mountain, the predicted earthquake frequencies for the regional zones are somewhat greater than the observed frequencies, because they are based on larger source areas that include regions of higher seismicity that lie beyond the 100-km circle. The predicted occurrence rates from all sources for earthquakes of interest to the hazard assessment generally fall within the uncertainties in the observed rates.

Doser, Fridrich, Swan (DFS) Team. The DFS team does not specifically address tectonic models in developing an overview model for seismic source characterization, but rather uses aspects of various structural models to estimate the location, style of faulting, and down-dip geometry of local fault sources and hypothetical faults near the site. Figure 4-37 shows the logic tree developed by the DFS team to address uncertainties in defining and characterizing the local faults. Two alternative modes of behavior are considered for the local fault sources: (1) independent fault behavior, which is strongly preferred (weight 0.95), and (2) distributed fault behavior (0.05) (Figure 4-37a). The locations of the independent fault sources are shown on Figure 4-38. The Ghost Dance fault is included as a possible independent fault with a low probability of activity (0.05). The distributed fault behavior model allows for simultaneous rupture on subparallel faults, including faults on either side of Yucca Mountain. The pattern of fault rupture given the distributed fault behavior model varies from single to quadruple parallel ruptures depending on the inferred length of fault rupture. Alternative assessments are defined for the total length of distributed faulting (Figure 4-37b) and for the total length of individual

faults (Figure 4-37c). The assessed distributions of maximum rupture length for individual faults depend on the total fault length (Figure 4-37c).

The next assessment in the logic tree addresses the existence of a detachment. The preferred model (weight 0.8) is that the faults are planar to the base of the seismogenic crust (inferred to be at a depth in the range of 12 to 16 km) The alternative model (weight 0.2) is that the Paintbrush Canyon fault becomes listric at depth, forming a detachment. All of the west-dipping faults at Yucca Mountain are assumed to truncate against the east-dipping Bare Mountain fault. Two alternative structural models are used to define the down-dip geometry of the planar faults and a single model is used to define the down-dip geometries for the detachment model. These geometries are shown in the DFS elicitation summary (Appendix E). The detachment model allows for the possibility of a seismogenic detachment, whereby the Paintbrush Canyon/Stagecoach Road fault is modeled as a shallow-dipping seismogenic source that extends beneath the Crater Flat Basin. The detachment model also allows for the possibility of the existence of a buried strike-slip fault of local (weight 0.5) or regional (weight 0.5) extent. Figure 4-39 shows the location of the hypothesized buried strike-slip fault. The three traces indicate alternative locations for the source. Also shown on Figure 4-39 is the location of the hypothesized Highway 95 fault.

The methods used to calculate M_{max} for the local faults were empirical relations between magnitude and rupture length and area. Figure 4-40 shows the resulting M_{max} probability distributions. The DFS team considered the magnitude estimated from the empirical relationships to be the upperbound magnitude of the recurrence relationships, but included an uncertainty of ±¼ magnitude units about these estimates in forming their M_{max} distributions. The recurrence relationships for the local faults were based on estimates of slip rates. Three recurrence models were used for the local faults: exponential, characteristic, and maximum moment, with the characteristic earthquake model preferred (weight 0.6). The weights assigned to the two other models are conditional on the fault behavior model for the local faults. The maximum moment model is given greater weight in the independent rupture model (Figure 4-37c) and a weight equal to the exponential model in the distributed model (Figure 4-37b).

The DFS team included 18 regional faults that are judged to be capable of generating M_w 5 or larger earthquakes and inferred to have had multiple late Quaternary displacements. These sources are shown on Figure 4-41. All these faults are considered active with a probability of 1.0 and are characterized as planar faults extending to the maximum seismogenic depth with dips dependent on the style of faulting (90° for strike-slip faults, 60° for dip-slip faults). M_{max} were calculated using empirical relationships between magnitude and fault rupture lengths and rupture areas. Figure 4-42 shows the resulting M_{max} probability distributions. Earthquake recurrence relationships for the regional sources were based on estimates of fault slip rates. The same three earthquake recurrence models used for the local faults were used for the regional sources.

Figure 4-43 shows the logic tree used to define the uncertainty in characterizing the regional source zones. The DFS team considered two alternative source zone models: Model A (weight 0.2), which consists of one regional zone, and Model B (weight 0.8), which has three regional zones. Figure 4-44 shows the configurations of these regional zones. The spatial distribution of earthquakes within these regional zones is interpreted to either conform to the existing pattern of seismicity, estimated using kernel spatial density estimation, or to be uniform, with the nonuniform pattern preferred.

The M_{max} assessed for the regional source zones ranged from M_w 7.0 to 7.7. Because of the greater detail of fault investigations and seismic source characterization in the immediate Yucca Mountain vicinity, M_{max} was assessed to range from M_w 5.6 to 6.0 within the local zone shown on Figure 4-44. The DFS team used the catalogs of independent events produced by the declustering methods of Youngs *et al.* (1987) and Veneziano and van Dyck (1985). The recurrence relationships for the individual source zones were estimated using the approach described above in Section 4.1.4.1. Earthquakes that occurred in close proximity to the regional faults were assumed to be associated with those sources and were not included in the data used to compute the seismicity rates for the regional zones. Figure 4-45 shows the recurrence relationships for each zone.

Figure 4-46 shows the distribution for earthquake recurrence predicted by the DFS team's seismic source characterization for local faults, regional faults, regional source zones, and all sources combined compared to the observed frequency of earthquakes occurring within 100

km of the Yucca Mountain site. The DFS local fault model contains about one and one-half orders of magnitude uncertainty in the combined recurrence rates. A significant part of this uncertainty is due to differences in predicting the frequency of earthquakes smaller than the maximum based on alternative recurrence models. The uncertainty in the recurrence rate for the regional faults is similar to that for the local faults, and also has a significant component contributed by the alternative recurrence models considered to estimate the frequency of earthquakes smaller than the maximum. Within 100 km of Yucca Mountain, the predicted earthquake frequencies for the regional zones are somewhat higher than the observed frequencies, because they are based in part on larger source areas that include regions of higher seismicity rates that lie beyond the 100-km circle. The predicted occurrence rates from all sources for earthquakes of interest to the hazard assessment generally fall within the uncertainties in the observed rates.

Rogers, Yount, Anderson (RYA) Team. The RYA team states that none of the tectonic models that have been proposed provide a unified explanation of all the available seismic, geologic, and geophysical data for Yucca Mountain and the larger Walker Lane. Therefore, they do not specifically address tectonic models in developing an overview seismic source model. Rather, they use aspects of various structural models to estimate the location, style of faulting, and down-dip geometry of local fault sources and hypothetical faults near the site. Figure 4-47 shows the logic tree used by the RYA team to describe the uncertainty in characterizing the local faults. The basic model is a system of from one to three west-dipping, coalescing faults and the east-dipping Bare Mountain fault (Figure 4-48). The weight assigned to the existence of one, two, or three faults depends upon the thickness of the seismogenic crust, which is assessed to be in the range of 12 to 20 km.

M_{max} for the local faults was estimated using empirical relationships between magnitude and surface rupture length and rupture area. The RYA team considered the magnitude estimated from the empirical relationships to be the upperbound magnitude of the recurrence relationships, but included an uncertainty of ± ½ magnitude units about these estimates in forming their M_{max} distributions. The resulting M_{max} probability distributions are shown on Figure 4-49. Earthquake recurrence rates for the local faults were based on trench recurrence interval data and slip-rate data, with a preference for the slip-rate approach. Characteristic and truncated exponential recurrence models were used. The weight assigned to each model was

dependent on the number of coalescing faults, with increasing preference for the exponential model as the number of independent sources decreased.

The RYA team defined 11 regional faults (Figure 4-50). These faults all are considered active with a probability of 1.0. Regional faults are treated as steeply-dipping planar faults penetrating to the maximum thickness of the seismogenic crust, with dips depending on the style of faulting (90° for strike-slip faults, 60° for normal faults). M_{max} for the regional faults were estimated using empirical relationships between magnitude and surface rupture length, rupture area, and maximum displacement, depending upon the available data. The resulting M_{max} probability distributions are shown on Figure 4-51. Earthquake recurrence relationships for the regional faults were estimated using estimates of fault slip rate . The characteristic and the truncated exponential recurrence models were used, with the characteristic model strongly preferred. In addition, the earthquakes occurring on the regional faults were limited to M_w 6.3 and larger. The occurrence of earthquakes smaller than M_w 6.3 was accounted for by the areal source zones. This approach is based on the concept that earthquakes smaller that M_w 6.3 do not occur on the faults with any greater frequency than elsewhere in the regional source zones.

Figure 4-52 shows the logic tree developed by the RYA team to describe the uncertainty in characterizing regional source zones. The RYA team divided the region within a 100-km radius surrounding Yucca Mountain into three primary seismic source zones with two alternate zonations (Scenarios 1 and 2) used to model a local source (Figure 4-53). The spatial distribution of earthquakes was assessed to be either uniform or nonuniform, with the latter based on a kernel density estimation using historical seismicity.

The M_{max} assigned to each of the areal zones is M_w 6.3 ± 0.3. The recurrence rates for the source zones were estimated by fitting truncated exponential relationships to simulations of the declustered catalogs. The technique used and results are described in the RYA team elicitation summary (Appendix E).

The RYA team also included in their seismic source model a volcanic source that encompasses the area of younger volcanism in the Yucca Mountain region and extends north to include Thirsty Mesa and Buckboard Mesa. They assess the probability that a separate volcanic source

exists to be 0.7. The recurrence rate is based on the estimated return period for volcanic events (assessed to be 2×10^5 years to 2×10^6 years) and M_{max} was assessed to be M_w 5.5.

Figure 4-54 shows the distribution for earthquake recurrence predicted by the RYA team's seismic source characterization for local faults, regional faults, regional source zones, and all sources combined compared to the observed frequency of earthquakes occurring within 100 km of the Yucca Mountain site. The RYA local fault source model contains about one order of magnitude uncertainty in the combined recurrence rates. The uncertainty in the recurrence rate for the regional faults is similar to that for local faults. As discussed above, the regional zones are used to model the occurrence of earthquakes smaller than M_w 6.3 on or near the regional faults. The RYA team used only the recorded earthquakes within 100 km of Yucca Mountain to evaluate the recurrence rate for the regional zones, thus there is good agreement between predicted and observed earthquake frequencies for the regional zones. The predicted occurrence rates for all sources for earthquakes of interest to the hazard assessment generally fall within the uncertainties in observed rates.

Smith, Bruhn, Knuepfer (SBK) Team. The SBK team considered a variety of tectonic models in the development of their seismic source model. Local seismic sources are characterized based on their strongly preferred oblique-rift/planar-fault model, with other tectonic models considered as constraints on source geometry and the potential for existence of hidden seismic sources. In this model, 3-D strain in the Yucca Mountain region is accommodated by normal-slip, strike-slip, and oblique-slip on planar faults. The Bare Mountain (master) and Yucca Mountain (antithetic) faults form a half-graben, whereas the Rock Valley and Highway 95 faults act as accommodation zones. Other potential sources, such as detachment faults, buried dextral shear zones, and volcanic sources related to dike-injection were considered either not to be seismogenic (e.g., detachments) or to be covered by background earthquakes in areal source zones (e.g., buried dextral shear zones and volcanic sources) and, thus, were not explicitly modeled as specific seismic sources.

Figure 4-55 shows the logic tree developed by the SBK team to represent the uncertainty in characterizing the local sources (shown on Figure 4-56). Four alternative behavioral modes were considered for local faults. Independent behavior of the mapped faults was the favored model (weight 0.5). The next most favored behavior mode (weight 0.4) is that the major block-

bounding faults are linked along strike to form independent faults along with the Bare Mountain fault. The two additional, less-likely, modes entail all of the Yucca Mountain faults soling into a detachment between 5 km and the base of the seismogenic zone (0.01), and all of the Yucca Mountain faults coalescing at depth into a master block-bounding fault (0.09). For all four modes of behavior, the possibility of simultaneous rupture events triggered by volcanic activity is considered. The likelihood of this simultaneous rupture event is considered greater for the detachment and coalescing fault behavior modes (0.5) than for the linked and independent modes (0.1). Three alternative geometries that defined the down-dip extent of the Yucca Mountain faults were considered for all four behavior modes.

M_{max} for the local faults was estimated using empirical relationships between magnitude and surface rupture length, rupture area, and maximum displacement, as well as estimates based on evaluation of seismic moment (rupture area times average displacement) and static stress drop. The resulting M_{max} probability distributions are shown on Figure 4-57. The SBK team also used the convention of Youngs *et al.* (1987) in developing recurrence relationships for the faults, with the upperbound magnitude of the recurrence relationship, m^U, equal to M_{max} obtained from the empirical relationships plus ¼ magnitude unit. The magnitudes plotted on Figure 4-57 are m^U. Earthquake recurrence relationships for the local faults were estimated from fault slip rates and recurrence intervals, depending upon the available data. For nonsimultaneous ruptures on coalescing fault and detachment models, slip rates were summed along across-strike transects. Recurrence of simultaneous ruptures was assessed based on recurrence of volcanic eruptions in Crater Flat. The characteristic and truncated exponential recurrence models were used for all but the simultaneous rupture scenarios, with the truncated exponential model generally favored. The maximum moment recurrence model was used for the simultaneous rupture scenarios.

Sixteen regional faults (Figure 4-58) were included with assessed likelihoods of seismogenic activity ranging from 0.01 to 1.0. Regional faults were modeled as independent, planar sources extending to the maximum seismogenic depth (12 to 17 km). Fault dips were based on fault type: 60° for normal, 70° for oblique, and 90° for strike-slip. The SBK team considered the possibility of linked-fault behavior for the Death Valley-Furnace Creek-Fish Lake Valley system of faults. The preferred model is that the four faults, Southern Death Valley, Death Valley, Furnace Creek, and Fish Lake Valley, are independent faults. Approximately 0.05 probability is given to a model with two linked faults, and 0.01 probability is given to a model with all four

faults linked. M_{max} for the regional faults was evaluated using empirical relationships between magnitude and surface rupture length, rupture area, and maximum displacement, as well as estimates based on evaluation of seismic moment. The resulting M_{max} probability distributions are shown on Figure 4-59. Again, these are M_{max} + ¼. Both the slip rate and recurrence interval approaches were used to assess rates of seismic activity with the former being favored, but fault-specific weights were assigned depending on available data. A characteristic recurrence model was favored for range-bounding faults and a truncated exponential model was favored for other fault zones exhibiting distributed faulting on multiple traces.

Figure 4-60 shows the logic tree developed by the SBK team to represent the uncertainty in characterizing the regional source zones. Two alternative zonation models were considered (Figure 4-61): one consisting of three zones and one in which an additional Rock Valley zone is defined. The spatial distribution of seismicity within the source zones was assessed to be uniform.

The M_{max} for regional source zones was assessed to range from M_w 6.2 to 6.6. Because of the greater detail of fault investigations and seismic source characterization in the immediate Yucca Mountain vicinity, M_{max} was assessed to range from M_w 5.6 to 6.2 within the local zone shown on Figure 4-61. The SBK team used the catalogs of independent events produced by the declustering methods of Youngs *et al.* (1987) and Veneziano and van Dyck (1985). The recurrence relationships for the individual source zones were estimated using the approach described above in Section 4.1.4.1. Adjustments for the effects of UNEs were incorporated as an alternative assessment of the recurrence rates. Figure 4-62 shows the recurrence relationships for each of the regional zones.

Figure 4-63 shows the distribution for earthquake recurrence predicted by the SBK team's seismic source characterization for local faults, regional faults, regional source zones, and all sources combined compared to the observed frequency of earthquakes occurring within 100 km of the Yucca Mountain site. The SBK local fault model contains about one order of magnitude uncertainty in the combined recurrence rates. The uncertainty in the recurrence rate for the regional faults is similar to that for the local faults. The SBK team used only the recorded earthquakes within 100 km of Yucca Mountain to evaluate the recurrence rate for the regional zones, thus there is good agreement between predicted and observed earthquake frequencies for

the regional zones. The predicted occurrence rates for all sources for earthquakes of interest to the hazard assessment generally fall within the uncertainties in observed rates.

Smith, de Polo, and O'Leary (SDO) Team. The preferred tectonic model for Yucca Mountain proposed by the SDO team is that of a half-graben partly filled by a collapsed volcanic carapace. They acknowledge that the site region also may be experiencing a component of northwest-directed dextral shear that is either confined to Crater Flat Basin (i.e., the basin itself is becoming distorted because of distributed, regional shear), or less likely, is being accommodated by an external, discrete strike-slip fault. To account for the latter, they assign a relatively high (0.4) probability to a strike-slip fault within or proximal to Crater Flat Basin along the hingeline-Pahrump-Stewart Valley fault zone alignment. They give zero weight to detachment models.

Figure 4-64 shows the logic tree developed by the SDO team to characterize the local faults. The SDO team identified six major faults (Paintbrush Canyon, Stagecoach Road, Solitario Canyon, Iron Ridge, Fatigue Wash, and Windy Wash faults) (Figure 4-65). All of these faults with the exception of the Iron Ridge and Fatigue Wash faults are considered to be "block-bounding" faults, structures that define major tilted panels of the carapace and that probably penetrate to significant seismogenic depth without intersection. Several other faults (Bow Ridge, Ghost Dance, Abandoned Wash, Northern Crater Flat, and Southern Crater Flat faults) might penetrate the carapace, but were deemed not capable of an earthquake larger than the maximum background earthquake (M_w 6.2). Three alternative geometries were defined to represent the interaction between the east-dipping Bare Mountain fault and the west-dipping Yucca Mountain faults. The major faults, as well as the faults that are thought to be confined to the carapace, were included in six individual (single, discrete planes), nine linked (individual planes linked along strike by complex structure) and eight distributed (planes linked across dip) fault rupture scenarios. As indicated on Figure 4-64, these rupture scenarios are not alternatives. All rupture scenarios are assumed to occur. The SDO team established the frequency of rupture on a particular fault, such as Paintbrush Canyon, from paleoseismic data on the occurrence of past ruptures. For each paleoseismic rupture, they evaluated the likelihood that the event corresponded to various rupture scenarios (e.g., rupture of just the northern part of the Paintbrush Canyon fault, versus rupture of all of the Paintbrush Canyon fault, versus rupture of Paintbrush Canyon and Stagecoach Road faults). These assessments for each paleoevent

were used to estimate the relative frequency of the various rupture scenarios for each fault. The product of the relative frequencies for the rupture scenarios times the estimates for frequency of ruptures on the fault provide estimates for the frequency of occurrence of the individual rupture scenarios.

M_{max} for the local faults was evaluated based on empirical relationships between magnitude and surface rupture length, maximum displacement, rupture length times maximum displacement, and rupture area, as well as estimates of seismic moment. The resulting M_{max} probability distributions for local faults are shown on Figure 4-66. The SDO team also used the convention of Youngs *et al.* (1987) in developing recurrence relationships for the faults, with the upperbound magnitude of the recurrence relationship, m^U, equal to M_{max} obtained from the empirical relationships plus ¼ magnitude unit. The magnitudes plotted on Figure 4-66 are m^U. A characteristic recurrence model was favored (0.7) over a truncated exponential model (0.3) for predicting the frequency of smaller events. A minimum magnitude of M_w 6.2 was used in the recurrence assessment for the local sources.

As noted above, the SDO seismic source model includes a buried strike-slip fault source. The hingeline, which appears to represent the structural boundary to a zone of features suggestive of distributed dextral shear deformation, is chosen by the SDO team as the best candidate location for a buried strike-slip fault. This fault is shown as fault T6-SS on Figure 4-67. The preferred (27 km) and minimum (20 km) estimates for fault length are based on the postulated length of the hingeline in the Crater Flat area. They also allow for the possibility that the hingeline represents the northwestern extension of the Pahrump-Stewart Valley fault zone. In this case they infer a maximum length of 120 km. The buried strike-slip fault is treated in a similar fashion to the other regional faults discussed below.

Thirty-six regional faults were characterized as separate fault sources by the SDO team (Figure 4-67). Within 50 km of Yucca Mountain, all identified Quaternary and possible Quaternary faults capable of $M_{max} \geq 6.4 \pm 0.2$ were included. In the distance range of 50 to 100 km from Yucca Mountain, faults of lengths of 20 km or more were included. Two faults that generally lie beyond 100 km, the Panamint Valley fault zone and the Ash Hill fault zone, also were included for their potential long-period ground motion contribution. Of the 36 faults included, 24 are judged to be active with a probability of 1.0, and 12 were judged active with probabilities

ranging from 0.2 to 0.9. Regional faults are modeled as planar fault sources extending to the maximum seismogenic depth (assessed to be in the range of 14 to 19 km) with dips depending on the style of faulting (90° for strike-slip faults, 60° for normal faults).

M_{max} for the regional faults was assessed using empirical relationships between magnitude and surface rupture length, maximum displacement, rupture length times maximum displacement, and slip rate plus rupture length. Fault weights were assigned depending on available data. The resulting M_{max} probability distributions are shown on Figure 4-68. These are also M_{max} + ¼. A recurrence interval approach was used by the SDO team to assess recurrence for regional faults. Specifically, the method used involved estimating average surface displacement from the minimum, preferred, and maximum fault lengths using relationships from Wells and Coppersmith (1994), dividing average displacement per event by slip rate to get a slip accumulation time (average recurrence interval), and inverting this estimate to obtain an annual earthquake occurrence rate. The characteristic recurrence model was favored over the truncated exponential model. A minimum magnitude of M_w 6.2 was used in the recurrence assessment. The occurrence of earthquakes smaller than M_w 6.2 was accounted for by the areal source zones. This approach is based on the concept that earthquakes smaller that M_w 6.2 do not occur on the faults with any greater frequency than elsewhere in the regional source zones.

Figure 4-69 shows the logic tree developed by the SDO team to represent the uncertainty in characterizing the regional source zones. Eight independent source zones were defined. Three of these zones lie within 100 km of the site (Figure 4-70). The spatial distribution of seismicity within the source zones was assessed to be either uniform or spatially varying, based on the observed pattern of recorded seismicity.

The M_{max} for the regional source zones was assessed to be M_w 6.4 ± 0.2. The SDO team used the catalogs of independent events produced by the declustering methods of Youngs *et al.* (1987) and Veneziano and van Dyck (1985), as well as a specific set of aftershock criteria defined by the team. The recurrence relationships for the individual source zones were estimated using the approach described above in Section 4.1.4.1. Figure 4-71 shows the recurrence relationships for each of the source zones.

The SDO team included two volcanic earthquake sources related to basaltic volcanoes and dike-injection (Figure 4-72): one based on the NE alignment of approximately 1-million-year-old volcanic vents across Crater Flat, and a second based on the vent alignment that encompasses the approximately 70-ka-years-old Lathrop Wells volcanic vent. The M_{max} for a volcanic-related earthquake in these zones was assessed to lie in the range of M_w 5.5 to 6.0. A recurrence of two to three volcanic events per million years was used to estimate an activity rate for these zones.

Figure 4-73 shows the distribution for earthquake recurrence predicted by the SDO team's seismic source characterization for local faults, regional faults, regional source zones, and all sources combined compared to the observed frequency of earthquakes occurring within 100 km of the Yucca Mountain site. The SDO local fault source model contains about one order of magnitude uncertainty in the combined recurrence rates. The uncertainty in the recurrence rate for the regional faults is similar to that for the local faults. As discussed above, the regional zones are used to model the occurrence of earthquakes smaller than M_w 6.2 on or near the regional faults. The regional zones defined by the SDO team extended beyond the 100-km-radius circle about Yucca Mountain, but did not include the areas of higher seismicity to the northwest that were included by other teams in their Walker Lane regional source zones. Thus, the SDO team's predicted rate of seismicity for the regional source zones within 100 km of Yucca Mountain are in good agreement with the observed earthquake frequencies for the regional zones. The predicted occurrence rates from all sources for earthquakes of interest to the hazard assessment generally fall within the uncertainties in observed rates.

4.3.1.2 Summary of Expert Seismic Source Characterization Assessments. In this section we summarize the range of interpretations made by the expert teams regarding key components of their seismic source characterization models. This section is organized by the various types of sources included in the models: seismic source zones, regional faults, local faults, and other sources (including buried strike-slip fault sources, seismogenic detachment fault, and volcanic sources). A summary of the key components of each of the source models is provided in Table 4-1.

Areal Source Zones. Areal source zones were defined by all teams to account for background earthquakes that occur on potential buried faults or faults not explicitly included in their model.

Four teams (AAR, DFS, RYA, and SBK) included alternative models in their characterization of the areal zones within a 100-km radius of the Yucca Mountain site. The RYA team's model always includes three zones, but allows for different configurations of the zone that include the site. The other three teams (AAR, DFS, and SBK) considered models that include one to three areal zones. The ASM and SDO teams each presented a single model that included two and three zones, respectively. Four teams (AAR, ASM, DFS, and SDO) define areal zones that extend beyond 100 km of the Yucca Mountain site. Four teams (AAR, ASM, DFS, and SBK) defined a site region or zone solely for assigning a lower M_{max} to the area where more detailed investigations have been conducted and the inventory of fault sources is more complete.

All teams used the truncated exponential model to estimate earthquake recurrence rates within the areal source zones. In regard to processing the catalog, the declustering method of Veneziano and van Dyck (1985) (catalog version 7) and the method of Youngs *et al.* (1987 catalog version 5) were both used by five of the teams, one team (AAR) used only catalog version 7 and one team (SDO) also gave some weight to a third catalog (version 8) based on their own analysis of declustering and completeness. Three of the teams (AAR, ASM, and SBK) made adjustments for UNEs in relevant zones. Varying treatments of the background seismicity were included: (1) uniform smoothing of seismicity was used solely or given significant weight by most of the teams, and (2) nonuniform smoothing using Gaussian kernels having different smoothing distances was included by four teams.

The M_{max} distributions for the areal zones were based on the largest earthquake that could occur in the region either randomly and/or on a geologic structure that was not explicitly included in the seismic source model. As noted above, lower values were included in several models for the local area around the Yucca Mountain site.

Regional Fault Sources. Regional faults were treated in a similar fashion by all six teams. Regional faults were defined by most teams as faults within 100 km that were judged to be capable of generating earthquakes of M_w 5 or greater based primarily on fault length and Quaternary histories of multiple surface fault rupturing earthquakes. Paleoseismic data from Piety (1995) was used by all the teams to identify and characterize potential regional faults. Other sources, such as Anderson *et al.* (1995a, 1995b), H. L. McKague *et al.* (CNRWA, written communication, 1996), W. R. Keefer and S. K. Pezzopane (USGS, written communication,

1996), and Pezzopane (USGS, written communication, 1996) also were used to varying degrees by some of the teams. Many of the faults that H. L. McKague *et al.* (CNWRA, written communication, 1996) consider Type 1 faults were not judged relevant to the hazard analysis and were not included as fault sources by any of the teams because of their short length, distance from Yucca Mountain, and evidence that indicates that many of these faults either have no significant Quaternary displacement or are much shorter than previously thought.

The number of faults included in the seismic source models for the various teams ranged from 11 to as many as 36. This reflects the judgments of the teams regarding the activity of various faults. One team included only faults that were judged to be active with a probability of 1.0, whereas the other five teams also included faults that were judged to be active with probabilities of less than 1.0. All teams modeled the regional faults as simple, planar faults to maximum seismogenic depths with generalized dips depending on the style of faulting (90° for strike-slip faults, 60° or 65° for normal-slip faults). Alternative fault lengths were included for most of the faults by all teams.

A variety of empirical relations were used by the teams to estimate M_{max} for the regional faults. Two teams (ASM and DFS) used only surface rupture length relations, whereas the other four teams incorporated one or more other regression relations based on rupture area, maximum displacement, average displacement, rupture area times maximum displacement, and surface rupture length plus slip rate, depending on available data.

Two general approaches were used to estimate recurrence rates for the regional faults: slip rates and recurrence intervals. Two teams (DFS and RYA) relied strictly on the slip-rate approach, whereas three teams (AAR, ASM, and SBK) used both. The SDO team used only a recurrence interval approach based on dividing the fault slip rate by the displacement for the maximum event. Four different recurrence models were used by the various teams: the characteristic recurrence model was used by all teams with weights ranging from 0.2 to 0.9, four teams used the truncated exponential with weights ranging from 0.1 to 0.3, two teams used a maximum moment model, and one team used a modified exponential.

Local Fault Sources. Varying fault behavioral and structural models were employed by the teams to capture the full range of complex rupture patterns and fault interactions in the

characterization of local faults. A planar fault block model is preferred by most teams, with linkages along strike or coalescence down dip considered by all teams. Simultaneous rupture of multiple faults was included in all models and was variously referred to as simultaneous rupture models (ASM and SBK), synchronous behavior (AAR), distributed behavior (DFS and SDO), and coalescing models (AAR, SBK, and RYA). In general, preferred models for multiple fault rupture included two to four coalescing fault systems. Four teams (ASM, AAR, DFS, and SBK) used detachment models to constrain the extent and geometry of the local faults. Two teams (ASM and DFS) include detachment models in their source model with weights of 0.15 and 0.2, respectively, and use these models to both characterize local faults as well as seismogenic detachment fault sources. In the AAR model, the likelihood of existence of hypothesized, local detachments is dependent on the type of dextral shear structures assumed to be present. The SBK team gave very low weight (0.01) to a model in which the local faults sole into a detachment. The RYA and SDO teams excluded detachments in their source models.

A variety of empirical relations were used by the teams to estimate M_{max} on the local faults. At a minimum, the teams considered rupture length and rupture area relationships. Four teams also considered relationships based on maximum displacement, average displacement, rupture area times maximum displacement, surface rupture length plus slip rate , and seismic moment, depending on available data.

As was done for the regional faults, two general approaches were used to estimate recurrence rates for the local faults: slip rate s and recurrence intervals. Four teams (ASM, AAR, RYA, and SBK) used both approaches with equal weight, or favored the slip-rate approach. The DFS team relied strictly on the slip-rate approach, and the SDO team used only recurrence intervals. Four different recurrence models were used by the various teams: the characteristic recurrence model was used by all teams with weights ranging from 0.2 to 0.9, five teams used the truncated exponential with weights ranging from 0.1 to 0.8, two teams gave weight (0.1 to 0.8) to a maximum moment , and one team used a modified exponential model (weight 0.3).

Buried Strike-Slip Faults. The possibility that dextral shear is being accommodated in the Yucca Mountain region by a buried strike-slip fault was considered by all teams. Four teams included a regional buried strike-slip fault source with low probability. Two teams (AAR and DFS) included throughgoing regional dextral shear zones with fault lengths ranging from 50 to

100 km and 30 to 200 km, respectively. The AAR team included the regional strike-slip fault as part of their throughgoing dextral shear model (0.05). Both the DFS and ASM teams considered the possibility of a buried strike-slip fault source to be conditional upon the existence of a detachment. The ASM team also considered the probability that a buried strike-slip fault was seismogenic conditional upon the depth of the inferred detachment. They used lengths of 25 km (preferred) and 60 km to model their buried fault source. The SDO team included a discrete buried strike-slip fault, but argued that the hypothesized fault would not extend north of the Crater Flat Basin, they also preferred a relatively short length (27 km), but allowed for a longer rupture (120 km) along the Pahrump/Stewart Valley fault zone to the south. Two teams (RYA and SBK) did not explicitly include buried strike-slip fault sources. Although they do not preclude the possibility of a buried fault, they conclude that this source would be incapable of generating an earthquake larger than those associated with their regional source zones.

Seismogenic Detachment Fault Source. As noted previously five teams incorporated detachment models in their treatment of local fault sources. Only two teams (ASM and DFS) explicitly allow for the existence of a seismogenic detachment fault source in their detachment models, which are given low weights (0.15 and 0.2, respectively). In the DFS model, only a local detachment is considered, whereby the Paintbrush Canyon-Stagecoach Road fault system is modeled as a shallow-dipping seismogenic source. The ASM team allows for a larger detachment source (rupture area of 4000 $\forall$ 2000 km^2) in their model, but give very low weight to the possibility of a seismogenic detachment (0.1) given that a detachment exists (0.15).

Volcanic Sources. Seismicity related to volcanic processes, particularly seismicity related to basaltic volcanoes and dike-injection, was explicitly modeled in volcanic source zones by two teams (RYA and SDO). Volcanic-related earthquakes were not modeled as a separate source by the other four teams, but owing to the low magnitude and frequency of volcanic-related seismicity, were accounted for by the areal source zones.

The concept of a volcanic-tectonic earthquake whereby some surface-rupturing earthquakes in Crater Flat Basin are accompanied by dike-injection (i.e., the postulated 70 ka "ash event"), was explicitly modeled by only one team (SBK). All the other teams included the possibility of such an event indirectly as part of their simultaneous rupture models (variously referred to as

synchronous [AAR], distributive behavior [DFS], coalescing fault [RYA] rupture models) but did not necessarily tie it to volcanism.

Predicted Recurrence Relationships. Figures 4-74 through 4-77 compare the predicted mean recurrence rates developed by each team to the combined distribution in recurrence rates over all teams for local faults, regional faults, regional source zones, and all sources combined. The combined distributions were obtained by giving equal weights to the individual team distributions. As was the case for the results presented by each team, the recurrence rate for local sources is for the area approximated by the shaded region on Figure 4-15 and the recurrence rate for the regional faults, regional source zones, and all sources combined is for the region within 100 km of the Yucca Mountain site.

There is approximately an order of magnitude range in the overall uncertainty in recurrence rate for M_w 6 and larger earthquakes on the local faults (Figure 4-74). The range between the mean results for the six teams is about one-half the overall range. The uncertainty in the recurrence rate increases significantly for larger magnitudes, primarily due to differences between the expert teams' assessment of M_{max} for the local faults. Assessments that favor multiple-fault ruptures, the use of displacement-based estimates of M_{max}, and recurrence rates for maximum events based on paleoseismic recurrence intervals tend to produce larger M_{max} and higher overall recurrence rates for the local faults. Assessments that favor the use of M_{max} assessments based on rupture area and recurrence rates based on slip rate tend to produce smaller M_{max} and lower overall recurrence rates. The uncertainty in recurrence rate also increases somewhat for magnitudes less than M_w 6. This increase is due primarily to uncertainty in the form of the recurrence model (truncated exponential versus characteristic versus maximum M_w distributions).

The uncertainty in the recurrence rate for M_w 6 and larger earthquakes on the regional faults (Figure 4-75) is about the same as that for the local faults. However, the uncertainty does not increase for larger magnitudes, because these recurrence rates are controlled by the recurrence for the Death Valley-Furnace Creek system of faults, for which the six teams developed similar characterizations. The very large range in results for smaller magnitudes reflects how the teams characterized the recurrence model (magnitude distribution for the regional sources). The RYA and SDO teams made the assessment that moderate earthquakes would not occur on the

regional faults at a greater rate than predicted for the regional source zones and, thus, limited their recurrence models for the regional faults to earthquakes larger than M_w 6.3 and 6.2, respectively. The occurrence of smaller earthquakes on or near the regional faults was modeled by their regional source zones. The remaining four teams considered truncated exponential, characteristic, and M_w distributions, generally favoring the characteristic model. Thus the large range in recurrence rate for M_w 5 and smaller earthquakes shown on Figure 4-75 is somewhat artificial. The observed rate of earthquakes (Figure 4-75) was not used by any of the teams to characterize the regional faults.

The combined distribution and mean estimates for the individual SSFD teams for recurrence in the regional source zones within 100 km of the Yucca Mountain site is shown on Figure 4-76. The spread in recurrence rates in the M_w 4 to 5.5 range reflects the degree to which the teams based their characterizations on a uniform distribution of seismicity in regional zones that extend beyond the 100-km region. Seismicity zones that included the higher rate of seismicity occurring to the northwest tend to predict higher rates of seismicity than observed in the Yucca Mountain region. This is based on the assumption that larger regions are required to adequately characterize the seismicity rates. The large range in results for magnitudes greater than M_w 6 reflects the differences in how the teams assessed the M_{max} for the regional zones within 100 km of the site. Three teams allowed for the occurrence of earthquakes greater than M_w 7 on sources that were not characterized explicitly as regional or local faults, and three teams considered that the sources of these events were treated explicitly in their characterization of other sources. Thus, the differences between the individual team assessments shown on Figures 4-75 and 4-76 reflect, in part, how each team partitioned the seismic source characterization between regional faults and regional source zones.

Figure 4-77 compares the combined distribution for earthquake recurrence from all seismic sources and the mean results for the six expert team characterizations. There is generally less than an order of magnitude range in uncertainty in the estimation of regional seismicity rates. At smaller magnitudes, the range reflects the differences in how the teams characterize the regional source zones. The overprediction of the observed rate of M_w 4 to 5 earthquakes within 100 km of the site reflects the teams' general assessment that larger regions are needed to characterize the seismicity rates. At larger magnitudes, the assessments from the individual teams lie within the uncertainty in the occurrence rates of earthquakes based on the historical

record. As discussed above, the results shown on Figure 4-77 are for the entire region within 100 km of the Yucca Mountain site. It is expected that the ground motion hazard will be influenced largely (at least for high spectral frequency ground motions) by nearby seismic sources. Thus, the larger uncertainty in recurrence rates for the local sources (Figure 4-74) will have a significant effect on the uncertainty in the ground motion hazard.

4.3.2 Fault Displacement Hazard Characterization Models

The instructions given to the SSFD expert teams were to develop a fault displacement hazard characterization model that could be applied to any location within the Controlled Area at the Yucca Mountain site. To demonstrate the application of these models and to provide an estimate of the fault displacement hazard, nine demonstration points were selected (see Figure 4-9) for fault displacement hazard characterization. The points were selected to represent the expected range of fault displacement hazard conditions within the Controlled Area in terms of the types of features that may be encountered: block-bounding faults with greater than 50 m of cumulative offset that may be seismogenic, mapped intrablock faults with north-south and northwest-southeast strikes having a few to tens of meters of cumulative displacement, and features observed within the ESF that are likely to be encountered within the proposed repository block, ranging from small faults uncorrelated with surface feature to intact rock. The selected points are (Figure 4-9):

Point 1. A location on the Bow Ridge fault where it crosses the ESF. The Bow Ridge fault is a block-bounding fault that has been characterized by the SSFD expert teams as being a potentially seismogenic fault and/or to be part of a seismogenic fault system.

Point 2. A location on the block-bounding Solitario Canyon fault, which has been characterized by the expert teams as one of the longer seismogenic faults within the Yucca Mountain site vicinity.

Point 3. A location on the Drill Hole Wash fault where it crosses the ESF, which is one of the longer of the northwest-striking faults within the Yucca Mountain site vicinity.

Point 4. A location on the Ghost Dance fault, which is one of the longer north-south intrablock faults within the Controlled Area.

Point 5. A location on the Sundance fault within the proposed repository footprint west of the ESF. The Sundance fault is an intermediate size, northwest-trending intrablock fault.

Point 6. A location on a small fault mapped in bedrock on the west side of Dune Wash. This point represents a location on one of the many small north-south-striking intrablock faults that have been mapped at the surface of Yucca Mountain.

Point 7. A location approximately 100 m east of Solitario Canyon at the edge of the proposed repository footprint. Any one of four hypothetical conditions were assumed to exist at this location that are representative of features encountered within the ESF that are not directly correlated with specific features observed at the surface:

(a) A small fault having 2 m of cumulative displacement
(b) A shear having 10 cm of cumulative displacement
(c) A fracture having no measurable cumulative displacement
(d) Intact rock

Point 8. A location within the proposed repository footprint midway between the Solitario Canyon and Ghost Dance faults. The same four hypothetical conditions were assumed to exist here as at Point 7.

Point 9. A location in Midway Valley east of the Bow Ridge fault on an observed fracture having no measurable displacement in Quaternary alluvium.

4.3.2.1 Individual Expert Team Models. The fault displacement hazard assessment models developed by the six SSFD expert teams are described in this section along with how the models are to be applied to the nine demonstration points. Table 4-3 summarizes key points of the fault displacement hazard assessment models for each team. Note that many of the terms and parameters used in this section were previously defined in Section 4.2.

Arabasz, Anderson, Ramelli (AAR) Team. The AAR team's characterization of fault displacement hazard differentiates between those sites that are subject to potential principal faulting hazard and those sites that are subject to distributed faulting hazard.

Characterization for Sites of Potential Principal Faulting Hazard. Figure 4-78 presents the AAR team's logic tree for characterization of sites subject to principal faulting hazard. The AAR team considers both the earthquake and displacement approaches.

Earthquake Approach. In the earthquake approach, two contributions to hazard are included (indicated by the vertical line on the logic tree under sources of hazard): hazard from principal faulting due to the occurrence of earthquakes on the fault and distributed faulting hazard from earthquakes occurring on other seismic sources. The first assessment in the earthquake approach is an evaluation of whether or not the feature can experience principal faulting or distributed faulting, $P(C)$. Because the occurrence of principal faulting requires that the feature in question be seismogenic, $P(C)$ for principal faulting is equal to the probability that the fault is seismogenic, $P(S)$, which was assessed as part of the AAR team's seismic source characterization for the ground motion evaluation (see Section 4.3.1.1). The probability that the feature in question can experience distributed slip, $P(C)$, was assessed based on the orientation of the feature in the present stress regime and evidence for past movement.

The next assessment in the earthquake approach is an evaluation of the frequency of occurrence of earthquakes of various magnitudes on each of the seismic sources. The characterization of earthquake recurrence developed by the AAR team for the ground motion hazard assessment was used directly to define the distributions for earthquake occurrence frequency.

Given the occurrence frequency of earthquakes, the next assessment is the approach for evaluating the probability that slip will occur in a given event. For principal faulting, the AAR team assessed P_i(slip|event on i) using the focal depth randomization for each fault developed for the ground motion hazard assessment. Two alternative empirical models for the size of earthquake ruptures as a function of magnitude were used to develop the rupture depth distribution and the distribution for along-strike location of rupture: one that defines

rupture length as a function of earthquake magnitude and one that defines rupture area as a function of earthquake magnitude. An empirical distribution for aspect ratio was used to evaluate rupture width given rupture length or rupture area. For distributed faulting, the AAR team assessed P_i(slip|event on j) using the logistic regression model based on the mapped density of distributed ruptures. The data and resulting model are shown in Figure H-13c. When evaluating the potential distributed faulting events induced by earthquakes occurring within the regional source zones, it is assumed that the point of interest is equally likely to be located in the hanging wall or footwall of the rupture.

The conditional probability of exceeding a specified displacement, $P(D>d)$, was evaluated using the two-part method defined by Equation (4-19). For principal faulting the AAR team considered three alternative empirical relationships for estimating the maximum displacement *MD*: (1) a published empirical model based on earthquake magnitude, (2) a published empirical model based on rupture length, and (3) an empirical model based on fault rupture length developed by the AAR team from Yucca Mountain data. The location of the point of interest was assessed for each rupture to define the parameter x/L, and the distribution for D/MD was based on the analysis of historical ruptures shown on Figure 4-13. For distributed faulting, an empirical distribution for the ratio of maximum distributed displacement to maximum principal displacement was defined based on published data. This ratio, ranging from 0.2 to 0.7, was used to scale the estimated *MD* for the earthquake source to that for distributed rupture on the fault of interest. The distribution for D/MD shown on Figure H-6 was then used to compute the conditional probability of exceedance assuming $x/L = 0.5$ for the distributed rupture.

Displacement Approach. The displacement approach does not distinguish between principal and distributed ruptures. The first assessment in the logic tree (Figure 4-78) is an evaluation of the probability the feature can slip, $P(C)$. This assessment is the same as the assessment of $P(C)$ in the earthquake approach.

The AAR team uses estimates of fault slip rate and average displacement per event to obtain the frequency of displacement events [Equation (4-13)]. The slip-rate estimates are given by the seismic source characterization model developed by the AAR team. The assessment of the average displacement per event, $\bar{D}_E$, is based on the AAR team's evaluation of the

displacement data from trenching studies at Yucca Mountain. For each trenching site, they made an estimate of the expected maximum displacement in the maximum event, which they denote by MD^{max}. They then normalized the displacement data from the trench by this value and pooled the data from all trenches. The mean of the pooled data for D/MD^{max} is 0.83. The AAR team assesses the average displacement per event by estimating MD^{max} for the fault and then uses the expression $\bar{D}_E = 0.83\ MD^{max}$. In applying this approach, they consider three alternative approaches for estimating MD^{max}. The first is based on maximum rupture length and two alternative empirical relationships between rupture length and maximum slip: a published empirical model and an analysis of Yucca Mountain data performed by the AAR team. The second approach uses a scaling relationship between cumulative bedrock offset and average displacement per event developed by the AAR team. The third approach utilized the team's assessments of maximum displacements estimated from paleoseismic data as part of their seismic source characterization of the faults for the ground motion hazard assessment.

The final part of the displacement approach is the model for the conditional probability of exceedance. The AAR team found that the distribution of D/MD^{max} could be modeled by an exponential distribution (see Figure H-5), and utilized this distribution to assess $P(D>d)$.

Characterization for Sites of Only Potential Distributed Faulting Hazard. Figure 4-79 presents the AAR team's logic tree for characterization of sites subject to only distributed faulting hazard. The AAR team considers both the earthquake and displacement approaches and the hazard characterization model is similar to that for sites of principal faulting hazard (Figure 4-78). The differences between the approaches for hazard characterization at the two types of sites primarily reflect the types of data available.

Earthquake Approach. In the earthquake approach, the first assessment is an evaluation of whether or not the feature can experience distributed faulting, $P(C)$, which is assessed based on the orientation of the feature in the present stress regime. The next assessment in the earthquake approach is an evaluation of the frequency of occurrence of earthquakes of various magnitudes on each of the seismic sources. As was the case for sites subject to principal faulting hazard, the characterization of earthquake recurrence developed by the AAR team for the ground motion hazard assessment was used to define the distributions for

earthquake occurrence frequency. Given the occurrence frequency of earthquakes, the probability that slip will occur in a given event, P_t(slip|event on j), was assessed using the logistic regression model shown on Figure H-13c.

The conditional probability of exceeding a specified displacement, $P(D>d)$, was evaluated using an assessment of the expected maximum slip in the maximum event, MD^{max}, and the exponential distribution for D/MD^{max} discussed above. Two alternative approaches for estimating MD^{max} were considered, one based on the length of the feature and one based on the cumulative offset. If only one of these types of data were known for a feature, the assessment of MD^{max} was based on a single approach.

Displacement Approach. The displacement approach for sites of only distributed faulting hazard parallels that discussed above for principal faulting hazard. The first assessment in the logic tree (Figure 4-79) is an evaluation of the probability the feature can slip, $P(C)$, which is the same as the assessment of $P(C)$ in the earthquake approach.

The frequency of displacement events again is obtained using Equation (4-13). Three alternative approaches are used to estimate slip rate on the feature: (1) one based on assuming uniform slip for the past 11.6 Ma, (2) one assuming uniform slip for the past 3.7 Ma, and (3) one based on a empirical regression model developed by the AAR team relating Quaternary slip rate to cumulative bedrock offset. For the uniform slip approaches, the AAR team assessed the fraction of the cumulative offset that occurred prior to the period of uniform slip and used only the remaining portion of the cumulative slip to compute the slip rate. For example, one assessment is that 84% of the cumulative slip occurred prior to 3.7 Ma. The fault slip rate then is obtained by the expression: $SR = 0.16 \times D_{cum}/3.7$ Ma. The assessment of the average displacement per event, $\bar{D}_E$, likewise is based on the expression $\bar{D}_E = 0.83\ MD^{max}$, with MD^{max} estimated using either fault length or cumulative displacement in the same way as is done for the earthquake approach. The exponential distribution for D/MD^{max} is used to assess $P(D>d)$. Uncertainty in the cumulative displacement was included in the assessment.

Summary of Application of Model to Nine Demonstration Points. The AAR team interprets Points 1, 2, 4, and 6 to lie on faults that are potentially seismogenic and utilizes the logic tree shown on Figure 4-78 to characterize the hazard at these sites. Point 6 is interpreted to lie on a seismic source that they designated as west Dune Wash fault 1 (WD1 on Figure 4-18). The remaining points are interpreted to be subject to distributed faulting hazard only and the logic tree shown on Figure 4-79 is used to characterize hazard at these sites. Considering the hypothetical features at points 7 and 8, they utilize the assumed cumulative displacements of 2 m and 10 cm to Characterize the hazard for conditions (a) and (b), respectively; provide a distribution for the length of a fracture to characterize the hazard at point (c); and make the assessment that the potential fault displacement hazard for a point in intact rock is essentially zero.

Ake, Slemmons, McCalpin Team. The ASM team utilizes the earthquake approach to assess the hazard at all locations within the Controlled Area. Their hazard characterization is developed in terms of principal faulting hazard and distributed faulting hazard.

Principal Faulting Hazard Model. Figure 4-80 presents the logic tree that defines the ASM team's characterization of principal faulting hazard. The first assessment is whether the fault can experience principal faulting. This assessment is equal to the probability that the fault is seismogenic, as defined by the ASM team's seismic source characterization for the ground motion hazard assessment.

Conditional on the fault being seismogenic, the frequency of occurrence of earthquakes of various magnitudes on each of the seismic sources is assessed using the characterization of earthquake recurrence developed by the ASM team for the ground motion hazard assessment. Given the occurrence frequency of earthquakes, the next assessment is the probability that surface displacement will occur in a given event. The ASM team assessed P_i(slip|event on i) [Equation (4-16)] using the empirical logistic regression model for the probability of surface rupture, Equation (4-15). Two alternative empirical relationships were considered for the probability of surface rupture: one based on post-1930 Great Basin earthquakes and one based on earthquakes from the extensional Cordillera (see Figure 4-11).

The conditional probability of exceeding a specified displacement, $P(D>d)$, was evaluated using the two-part method defined by Equation (4-19). The distribution for the maximum displacement in an earthquake, *MD*, was defined using a published empirical model based on earthquake magnitude. The location of the point of interest within the rupture was assessed for each rupture to define the parameter x/L, and the distribution for D/MD was based on the analysis of historical ruptures shown on Figure 4-13.

Distributed Faulting Hazard Model. Figure 4-81 presents the logic tree that defines the ASM team's characterization of distributed faulting hazard. The first assessment is whether the fault can experience slip. This is composed of two assessments. The ASM team categorized the features in the site vicinity into six classes based on their cumulative slip (see Table ASM-9 in Appendix E). For each class of features, an assessment was made of the probability that the feature could undergo slip. The probability the feature can slip was further modified by a factor equal to the cosine of the strike azimuth of the feature, thus reducing the probability that the feature can slip with increasing deviation of its orientation from north-south. The resulting relationship is $P(C) = P(\text{slip}|\text{class})\times\cos(\phi)$, where ϕ is the strike azimuth of the feature of interest.

The frequency of earthquakes on each of the seismic sources that could cause distributed rupture on the feature of interest was assessed using the seismic source characterization developed by the ASM team for the ground motion hazard characterization. The probability that a specific earthquake on source j induces slip on feature i was assessed using a two-part approach:

$$P_i(\text{slip}|\text{earthquake on } j) = P(\text{surface rupture on } j) \times P_i(\text{distributed slip}|r,h) \qquad (4\text{-}20)$$

The first term to the right of the equal sign is the probability that a earthquake on source i will produce surface rupture. This probability is given by the logistic regression model used in the principal faulting hazard characterization, Equation (4-15). The second term is the probability that a surface-rupturing earthquake on source j produces distributed slip on the feature of interest at point i. This probability is assessed using a form of the logistic regression model defined by Equation (4-17). The ASM team developed two alternative relationships that define the likelihood of the occurrence of distributed slip at a point as

functions of distance from the principal rupture and location in the hanging wall (h=1) or footwall (h=0) of the rupture (Figure 4-82). While these relationships are independent of earthquake magnitude, the combined assessment defined by Equation (4-20) depends on the magnitude of the earthquake on source *i* through the probability of principal surface rupture.

The probability defined by Equation (4-20) represents aleatory probability in that it defines the likelihood of distributed slip in an individual earthquake. Epistemic uncertainty in the assessment is represented by the two alternative relationships for the probability of surface rupture and the two alternative relationships for the probability of distributed slip.

The ASM team assesses the distributed faulting displacement as a reduction factor, *RF*, times the principal faulting displacement that occurs on the seismic source at its closest approach to the point of interest. Two approaches are used to define the reduction factor, one based on a displacement potential defined on the basis of an observed ground displacement profile and one based on the relative cumulative slip between the principal fault and the feature of interest.

The displacement potential approach assumes the amount of displacement that can occur decreases with distance from the principal rupture in the same manner as the ground surface displacement decays. The ASM team utilizes the fault-normal geodetic displacement profile for the 1983 Borah Peak earthquake normalized by the displacement at the fault (Figure 4-83) as the basis for defining the net ground surface movement resulting from an earthquake. The normalized displacement profile was fit with the following algebraic expression to provide a relationship for the reduction factor, RF:

$$\begin{aligned} RF &= \varepsilon \times \exp(-0.045 r_n^{1.5}) \text{ for hanging wall} \\ RF &= \varepsilon \times 0.21 \exp(-0.14 r_n) \text{ for footwall} \end{aligned} \qquad (4\text{-}21)$$

where ε is a factor that defines what portion of the displacement potential is realized in an event. The distance term r_n is the distance from the principal rupture normalized to the conditions for the Borah Peak earthquake. The normalizing factor is the crustal depth of the rupture compared to that for the Borah Peak earthquake, such that a decrease in the crustal depth of the rupture decreases the distance extent of the displacement potential. The

resulting relationship is $r_n = r \times 16\text{km}/[w \times \sin(\text{dip})]$, where w is the rupture width of the earthquake.

Parameter ε defines how the displacement potential is distributed among the available structures that could slip in the vicinity of the site of interest. Four alternatives are proposed that are considered to be event-to-event variability in how the displacement potential is distributed. The possibilities include full realization ($\varepsilon = 1.0$), distribution equally among the possible classes of features ($\varepsilon = 0.2$), distribution equally among the estimated number of features of a specific class available ($\varepsilon = 1/N$), or distribution equally among the possible classes of features and the estimated number of features of a specific class ($\varepsilon = 0.2/N$). The expected number of features present, N, is evaluated assuming a power law for feature density, with the relative number of features in two classes proportional to the ratio of their cumulative slip raised to a power of -0.7. The resulting values of N are listed in Table ASM-9 in Appendix E.

The second approach for assessing RF involves identification of the portion of the cumulative displacement on the feature of interest at point i that resulted from earthquakes occurring on source j and using the ratio of this cumulative displacement to the cumulative displacement on earthquake source j to estimate the relative amplitude of displacements in individual events. The term within the summation in Equation (4-14), $\lambda_j \times P_i(\text{slip}|\text{event on } j)$, defines the frequency of earthquakes on source j producing distributed slip on the feature at point i. If all events produce comparable amounts of displacement, then the portion of the cumulative displacement at i that is contributed by source j is given by $\lambda_j \times P_i(\text{slip}|\text{event on } j) / \sum \lambda_j \times P_i(\text{slip}|\text{event on } j)$. However, the displacements induced by various magnitude earthquakes on the various earthquake sources are not equal. To address this, the ASM team makes the assumption that the relative contribution of each source to the cumulative displacement at point i can be estimated from the results of the displacement potential approach. Using Equation (4-12), the displacement hazard curve from each source j is used to obtain an effective slip rate from source j, ESR_j. The ratio of this effective slip rate to the effective slip rate obtained from the total displacement hazard curve from all sources provides a estimate of the contribution of source j to the cumulative slip at point i. Thus, the interpretation developed by the ASM team is that the reduction factor to scale, on average,

the principal rupture displacement occurring on source j to the distributed rupture displacement at point i is given by the expression:

$$RF = \frac{ESR_j}{\sum ESR_j} \times \frac{(D_{cum})_i}{(D_{cum})_j \times P_i(\text{slip}|\text{event on } j)} \qquad (4\text{-}22)$$

In Equation (4-22), the cumulative slip on source j is multiplied by P_i(slip|event on j) to account for the fact that not every principal faulting earthquake on source j that contributed to its cumulative slip also produced distributed slip at point i.

Summary of Application of Model to Nine Demonstration Points. The ASM team interprets Points 1 and 2 to lie on faults that are potentially seismogenic and utilizes the logic tree shown on Figure 4-80 to characterize the hazard at these sites. The remaining points are interpreted to be subject to distributed faulting hazard only and the logic tree shown on Figure 4-81 is used to characterize hazard at these sites. Considering the hypothetical features at Points 7 and 8, they utilize the assumed cumulative displacements of 2 m and 10 cm to characterize the hazard for conditions (a) and (b), respectively; provide an assumed maximum cumulative displacement of 1 cm for a fracture with no measurable offset to characterize the hazard at condition (c); and make the assessment that the potential fault displacement hazard for a point in intact rock is essentially zero.

Doser, Fridrich, Swan Team. The DFS team uses the displacement approach for assessing the hazard at all locations.

Principal and Distributed Faulting Hazard Model. Figure 4-84 shows the logic tree used by the DFS team to characterize fault displacement hazard. The first assessment addresses the probability that the feature of interest can slip in a displacement event, $P(C)$. Features that display evidence of Quaternary movement (typically the block-bounding faults) are assigned a probability of 1.0. North-south-striking intrablock faults are assigned a probability of activity of 0.4 and northwest-southeast-trending faults are assigned a probability of activity of 0.01. Minor faults and shears are assigned a probability of activity of 0.05 to 0.01, depending on proximity to block-bounding faults.

The next two assessments are the approaches for estimating the frequency of slip events and the average displacement per event. The DFS team uses the relationship given in Equation (4-13) in two ways. In one approach, a direct estimate of the frequency of slip events is used together with the slip rate on the feature to calculate the average displacement per event. In the second approach, a direct estimate of the average slip per event together with the slip rate is used to evaluate the frequency of slip events.

Both approaches for estimating slip event frequency and average slip per event require an estimate of the slip rate on the feature. The DFS team considers four alternative approaches for estimating the Quaternary slip rate. The favored approach is the use of paleoseismic data from trenching studies on the feature. The other three approaches estimate the Quaternary slip rate utilizing the cumulative offset of the top of the Tiva Canyon tuff and alternative assumptions for the history of deformation. The first interpretation is that the slip rate has been uniform post-Tiva Canyon and the fault slip rate is $SR=D_{cum(\text{Tiva Canyon})}/12.7\pm1.3$ Ma. The second interpretation is that 80 percent of the post-Tiva Canyon slip occurred prior to deposition of the 11.6±1 Ma Rainier Mesa member of the Timber Mountain tuff and the slip rate has been uniform post-Rainier Mesa, resulting in $SR=0.2D_{cum(\text{Tiva Canyon})}/11.6\pm1$ Ma. The third interpretation is that slip rates have been decreasing through time such that the Quaternary slip rate is in the range of 0.3 to 3.9 percent of the late Miocene slip rate. The late Miocene slip is defined to be the deformation that occurred post-Tiva Canyon and pre-Rainier Mesa and is interpreted to be 80 percent of the post-Tiva Canyon cumulative slip. The resulting relationship for Quaternary slip rate is $SR=RF\times0.8D_{cum(\text{Tiva Canyon})}/1.1\pm0.6$ Ma, where RF is the reduction factor from late Miocene to Quaternary slip rates and ranges from 0.3 to 3.9 percent. If no paleoseismic data are available for a feature, then the DFS team utilizes the three estimates based on the alternative slip history interpretations, giving each equal weight. Uncertainty in the cumulative displacement and age of the units was included in the assessment.

For fractures and unbroken rock, the frequency of displacement events and the average displacement per event are assessed directly. The frequency of events is assessed to lie within a broad range of uncertainty defined from alternative assumptions for the deformation history of Yucca Mountain. The average displacement per event for fractures with no offset

and unbroken rock was assessed on the basis of the level of detection for deformation. The assessments for these features are considered to be upperbound values by the DFS team.

The final part of the displacement hazard model is the evaluation of the conditional probability of exceedance. The DFS team developed a triangular probability distribution for *D/AD* from the trenching data in the Yucca Mountain region (see Appendix E) As described in Section H.2.1, a gamma distribution provides a better fit to the data and the DFS team actually adopted this distribution for hazard computation. The selected distribution is shown on the left-hand side of Figure 4-14. The probability of exceeding a specified value of d is computed using this distribution together with the estimate of the average displacement per event given for the feature ($\overline{D}_E = AD$).

Summary of Application of Model to Nine Demonstration Points. The DFS team interprets Points 1, 2, 4, and 9 to lie on features that have paleoseismic data for slip rate. Slip rates for the remaining points are evaluated solely from the cumulative slip and alternative interpretations of the deformation history. Considering the hypothetical features at Points 7 and 8, they utilize the assumed cumulative displacements of 2 m and 10 cm to characterize the hazard for conditions (a) and (b), respectively, and estimate the average displacement per event and displacement event frequency for fractures and intact rock, conditions (c) and (d).

Rogers, Yount, Anderson Team. The RYA team uses the displacement approach to characterize the hazard at all locations. Their displacement hazard characterization differs depending on whether or not Quaternary paleoseismic data are available for the location of interest.

Displacement Hazard Characterization for Sites with Quaternary Data. Figure 4-85 shows the logic tree used by the RYA team to characterize the displacement data at locations for which Quaternary paleoseismic data are available. The first assessment is the likelihood that the feature of interest can slip in a displacement event, $P(C)$. This probability is assessed based on evidence for recency of slip and the relationship of the feature to the structural elements of Yucca Mountain. Block-bounding faults with evidence of Quaternary movement are assigned $P(C)$=1.0.

The next assessment is the approach used to assess the frequency of displacement events. The RYA team considers two alternatives: the use of direct estimates of the frequency of displacement events from paleoseismic data, and the use of slip rate and Equation (4-13). The distributions for the average displacement per event, the Quaternary slip rate, and direct estimates of the frequency of displacement events are all based on paleoseismic data.

The final assessment is the approach for estimating the conditional probability of exceedance. Two alternatives are considered. The first is the use of the empirical distribution for D/AD developed by the DFS team from Yucca Mountain data. These data were fit with a gamma distribution (see Section H.2.1). The second approach is the distribution for D/MD^{max} developed by the AAR team from Yucca Mountain data. These data were fit by an exponential distribution (see Section H.2.5). The appropriate value of MD^{max} was assessed from paleoseismic data for the feature.

Displacement Hazard Characterization for Sites Without Quaternary Data. Figure 4-86 shows the logic tree used by the RYA team to characterize the displacement data at locations for which no Quaternary paleoseismic data are available. The overall approach parallels are shown on Figure 4-85, except that scaling relationships based on fault length and cumulative displacement are used in place of Quaternary data. The first assessment is the likelihood that the feature of interest can slip in a displacement event, $P(C)$. Intrablock faults with north-south trends are assigned $P(C)$=0.4, and those with northwest-southeast trends are assigned $P(C)$=0.1. Small faults and shears are assigned $P(C)$=0.5 to 0.3.

The frequency of displacement events is assessed using only slip rate and Equation (4-13). The slip rate is assessed based on the cumulative offset of a feature, which is considered to be an uncertain parameter. Three alternative interpretations of the slip history of the faults are considered. The first is that the slip rate has been uniform post deposition of the Tiva Canyon Tuff and the slip rate is given by $SR=D_{cum(\text{Tiva Canyon})}/12.7$ Ma. The second interpretation is that 20 percent of the cumulative deformation on the Yucca Mountain faults occurred after the onset of volcanism in Crater Flat about 3.7 Ma, yielding an estimate of $SR=0.2D_{cum(\text{Tiva Canyon})}/3.7$ Ma. The favored interpretation is that 98 percent of the deformation occurred prior to the Quaternary. The resulting slip-rate estimate is

$SR=0.02D_{cum(\text{Tiva Canyon})}/1.6$ Ma. Uncertainty in the cumulative displacement was included in the assessment.

The next assessment is the average displacement per event. The RYA team considers two alternative scaling relationships developed by the AAR team to be appropriate, one based on the length of the feature and one based on the cumulative offset of the feature. These relationships provide estimates of MD^{max}. The data for D/MD^{max} have a mean value of 0.83 and the RYA team interpreted $\bar{D}_E$ to be equal to 0.83 MD^{max}. If length information is not available for a feature (such as is the case for the hypothetical features at Points 7 and 8), then the assessments are made using only the cumulative offset of the feature.

The final assessment is the approach for estimating the conditional probability of exceedance. The same two alternatives are considered for these sites as were used for sites with Quaternary data (Figure 4-85).

Summary of Application of Model to Nine Demonstration Points. The RYA team interprets Points 1 and 2 to lie on features that have paleoseismic data. Slip rates for the remaining points are evaluated solely from the cumulative slip and alternative interpretations of the deformation history. Considering the hypothetical features at Points 7 and 8, they utilize the assumed cumulative displacements of 2 m and 10 cm to characterize the hazard for conditions (a) and (b), respectively, and interpret the probability of fault slip on a fracture with no measurable offset (c) or in intact rock (d) to be essentially zero.

Smith, Bruhn, Knuepfer Team. The SBK team's characterization of fault displacement hazard differentiates between those sites that are subject to potential principal faulting hazard and those sites that are subject to only distributed faulting hazard.

Characterization for Sites of Potential Principal Faulting Hazard. Figure 4-87 presents the SBK team's logic tree for characterization of sites subject to principal faulting hazard. The SBK team considers both the earthquake and displacement approaches.

Earthquake Approach. In the earthquake approach, two contributions to hazard are included (indicated by the vertical line on the logic tree under sources of hazard): hazard from

principal faulting due to the occurrence of earthquakes on the fault and distributed faulting hazard from earthquakes occurring on other seismic sources. The first assessment in the earthquake approach is an evaluation of whether or not the feature can experience principal faulting, $P(C)$. This is interpreted to be equal to the probability that the fault is seismogenic, $P(S)$, which was assessed as part of the SBK team's seismic source characterization (see Section 4.3.1.1). The SBK team's assessment is that all faults can experience distributed slip.

The next assessment in the earthquake approach is an evaluation of the frequency of occurrence of earthquakes of various magnitudes on each of the seismic sources. The characterization of earthquake recurrence developed by the SBK team for the ground motion hazard assessment was used directly to define the distributions for earthquake occurrence frequency.

Given the occurrence frequency of earthquakes, the next assessment is the approach for assessing the probability that slip will occur in a given event. For principal faulting, the SBK team assessed P_i(slip|event on i) using the logistic regression model, Equation (4-15), to assess the probability that surface rupture occurs, selecting the parameters of the model developed from the data base of 32 post-1930 Great Basin earthquakes (Figure 4-11). The probability of intersection with the site was computed by randomization of the rupture length along the fault.

For distributed faulting, the SBK team developed a two-part approach for assessing P_i(slip|event on j):

$$P_i(\text{Slip} \mid \text{event on } j) = P(\theta) \times F(event) \qquad (4\text{-}23)$$

where $P(\theta)$ is a function of the orientation of the feature of interest at point i and $F(event)$ is a function of the earthquake occurring on source j. Two alternatives were used to evaluate the probability $P(\theta)$. The first utilizes an assessment of the slip tendency of the feature with respect to the present stress regime. The slip tendency analysis indicates that features with a north-south orientation are favorably oriented for slip in the present stress regime. Thus, the SBK team considered $P(\theta)$ for these features to be at or near 1.0, if there was evidence of

Quaternary displacement. Alternative values of $P(\theta)$ were assessed to account for uncertainty in the interpretation. For features oriented in a northwest-southeast direction, the assessed values for $P(\theta)$ were about 0.5. The second approach for assessing $P(\theta)$ utilized the analysis of the distribution for the angle between the strike azimuths of the principal fault rupture and the associated distributed ruptures presented in Section H.4.3. An evaluation of the focal mechanisms for earthquakes in the immediate Yucca Mountain vicinity (see Chapter 7, USGS, written communication, 1996) indicates that the distribution of nodal plane strike azimuths is approximately uniform and an average value of $P(\theta)$ was computed assuming random strike to apply to earthquakes occurring in the areal source zones.

The second term of Equation (4-23) expresses the probability of slip as a function of the earthquake on the seismic source. The SBK used two alternative approaches for assessing this probability. The first approach is the logistic regression model developed from the analysis of the density of distributed faulting in historical ruptures defined by Equation (4-17) and shown on Figure 4-12. The second approach defines the probability of slip as a function of the peak velocity (PV in cm/sec) induced by the earthquake at the site. The relationship developed by the SBK team (see Figure SBK-19 in Appendix E) was fit with the logistic regression model:

$$F(event) = \frac{e^{-7.0+0.14PV}}{1+e^{-7.0+0.14PV}} \qquad (4\text{-}24)$$

The peak velocity induced by the earthquake is estimated using the ground motion models developed for the Yucca Mountain site. The SBK team considers this approach to be valid for underground openings.

The final assessment is the approach for evaluating the conditional probability of exceeding a specified displacement, $P(D>d)$. For principal faulting, this probability was evaluated using the two-part method defined by Equation (4-19). The distribution for MD was defined by a published empirical model based on earthquake magnitude. The location of the point of interest was assessed for each rupture to define the parameter x/L. Two alternatives are considered for the distribution for D/MD. The first is the analysis of data from historical ruptures shown on Figure 4-13. The second is a model developed from numerical

simulations of fault displacements (see Section H.3.2). For distributed faulting, an empirical distribution for D/D_{cum} (see Section H.2.6) is used to evaluate the probability of exceeding a specified displacement.

Displacement Approach. The displacement approach does not distinguish between principal and distributed ruptures (Figure 4-87). The first assessment in the logic tree is an evaluation of the probability the feature can slip, $P(C)$. This assessment is the same as the assessment of $P(C)$ for distributed faulting in the earthquake approach.

The SBK team uses two approaches for estimating the frequency of displacement events. The first method uses a direct estimate of the frequency from paleoseismic data. The second approach uses estimates of fault slip rate and average displacement per event to obtain the frequency of displacement events [Equation (4-13)]. The recurrence rate (inverse of recurrence interval) and slip-rate estimates are given by the seismic source characterization model developed by the SBK team.

The SBK team uses three alternative methods to assess the average displacement per event, $\bar{D}_E$, and the conditional probability of exceedance, $P(D>d)$ that are based on evaluations of the data from Yucca Mountain trenching studies. The first method utilizes the average displacement estimated for paleoearthquakes, designated as AD_{paleo}, to specify $\bar{D}_E$ and uses a distribution for D/AD_{paleo} to compute $P(D>d)$. This distribution is discussed in Appendix H, Section H.2.2. For the second approach, the SBK team used an empirical model between rupture length and average displacement, designated $AD_{F(RL)}$ to develop a distribution for $D/AD_{F(RL)}$ (see Section H.2.3). The mean of this distribution is 1.46 and $\bar{D}_E$ is set equal to $1.46 \times AD_{F(RL)}$. The distribution for $D/AD_{F(RL)}$ is used to compute $P(D>d)$. For the third approach, the SBK team used an empirical model between rupture length and maximum displacement, designated $MD_{F(RL)}$ to develop a distribution for $D/MD_{F(RL)}$ (see Section H.2.4). The mean of this distribution is 0.72 and $\bar{D}_E$ is set equal to $0.72 \times MD_{F(RL)}$. The distribution for $D/MD_{F(RL)}$ is used to compute $P(D>d)$.

Characterization for Sites of Only Potential Distributed Faulting Hazard. Figure 4-88 presents the SBK team's logic tree for characterization of sites subject to only distributed faulting hazard. The SBK team considers both the earthquake and displacement approaches, and the hazard characterization model is similar to that for sites of principal faulting hazard (Figure 4-87). The differences between the approaches for hazard characterization at the two types of sites primarily reflect the different types of data available.

Earthquake Approach. The earthquake approach for sites subject to distributed faulting hazard is identical to that shown on Figure 4-87.

Displacement Approach. The displacement approach for sites of only distributed faulting hazard parallels that discussed above for principal faulting hazard, except that slip rates and average displacements estimated from paleoseismic data are not available and are replaced by scaling relationships utilizing cumulative displacement.

The frequency of displacement events is again obtained using Equation (4-13). Two alternative approaches are used to estimate slip rate on the feature. The first approach is based on the cumulative slip and three alternative interpretations of the history of slip. The first interpretation is uniform slip post-Tiva Canyon. The second interpretation is uniform slip post-Rainier Mesa 11.6 Ma tuff deposition, in which 20 percent of the post-Tiva Canyon deformation has occurred. The third interpretation is that the Quaternary slip rates are 2.1±1.8 percent of the late Miocene slip rates, with the late Miocene rates computed by dividing 80 percent of the post-Tiva Canyon displacement by 0.9 Ma. The second approach for estimating slip rate used by the SBK team involves using the ratio of cumulative slip between the feature of interest and the cumulative slip on those faults with Quaternary slip rate estimates to scale the measured Quaternary slip rates to an estimate for the feature of interest. Uncertainty in the cumulative displacement was included in the assessment.

The SBK team again uses three alternative methods to assess the average displacement per event, $\overline{D}_E$, and the conditional probability of exceedance, $P(D>d)$ that are based on evaluations of the data from Yucca Mountain trenching studies. Two of these are the estimates based on $AD_{F(RL)}$ and $MD_{F(RL)}$ discussed above. For the third approach, the SBK team developed a distribution from the Yucca Mountain data for D/D_{cum} (see Section H.2.6).

The mean of this distribution is 0.00176 and $\bar{D}_E$ is set equal to $0.00176 \times D_{cum}$. The distribution for D/D_{cum} is used to compute $P(D>d)$. If the length of the feature is not known, the SBK team uses only the estimate based on cumulative displacement.

Summary of Application of Model to Nine Demonstration Points. The SBK team interprets Points 1 and 2 to lie on faults that are subject to both principal and distributed faulting hazard and utilizes the logic tree shown on Figure 4-87 to characterize the hazard at these sites. The remaining points are interpreted to be subject to distributed faulting hazard only and the logic tree shown on Figure 4-88 is used to characterize hazard at these sites. Considering the hypothetical features at Points 7 and 8, they utilize the assumed cumulative displacements of 2 m and 10 cm to characterize the hazard for conditions (a) and (b), respectively; provide a distribution for the relative hazard between a fracture, condition (c), and a minor shear, condition (b); and make an estimate of the frequency and amplitude for displacement in intact rock, condition (d).

Smith, de Polo, O'Leary Team. The SDO team's characterization of fault displacement hazard differentiates between those sites that are subject to potential principal faulting hazard and those sites that are subject to only distributed faulting hazard.

Principal Faulting Hazard Model. The SDO team uses the earthquake approach for characterizing the hazard due to principal faulting. Figure 4-89 shows the logic tree that defines their characterization. The frequency of occurrence of earthquakes of various magnitudes on each seismic source are defined by the seismic source characterization model (Section 4.3.1.1). The probability of slip at or near the surface given the occurrence of a magnitude m earthquake is computed using the logistic regression model defined by Equation (4-15). The SDO team uses two alternative data sets to develop the parameters for Equation (4-15): one based on 32 post-1930 Great Basin earthquakes and one based on 47 post-1930 northern Basin and Range earthquakes (Figure 4-11). The probability of intersection of the point of interest is computed by randomizing the location of the rupture length for an earthquake of magnitude m along the fault trace.

The conditional probability of exceeding a specified displacement, $P(D>d)$ for principal faulting was evaluated using two alternative approaches: one based on average displacement,

AD, and one based on maximum displacement, *MD*. The assessment of *AD* and *MD* depended upon the size of the earthquake. For earthquakes of magnitude smaller than the characteristic magnitude (defined as $m \leq m^U$-½), the values of *AD* and *MD* are assessed using an empirical relationship between displacement per event and earthquake magnitude. For the characteristic magnitude earthquakes (m^U-½ $\leq m \leq m^U$) assessments of *AD* and *MD* also are made using the maximum rupture length of the fault and paleoseismic data. Two scaling relationships are used between *AD* and rupture length: a published empirical model and a scaling model developed by the AAR team. In addition, the SDO team utilized the displacement profile for the Solitario Canyon fault presented by Alan Ramelli in Workshop #6 to characterize the average displacement at Point 2. Given an assessment of *AD*, the distribution for *D/AD* developed by the DFS team (Section H.2.1) was used to compute $P(D>d)$. Given an assessment of *MD*, the two-part method defined by Equation (4-19) was used to compute $P(D>d)$. The distribution for *MD* was defined as lognormal using the standard deviation associated with the empirical model. Two alternatives are considered for the distribution for *D/MD*. The first is the analysis of historical ruptures shown on Figure 4-13. The second is a model developed from numerical simulations of fault displacements (see Section H.3.2).

The SDO team also considered the potential for distributed faulting hazard at sites subject to principal faulting hazard. Their earthquake approach for characterizing distributed faulting hazard, discussed below, was used for these sites.

Distributed Faulting Hazard Model. Figure 4-90 presents the SDO team's logic tree for characterization of distributed faulting hazard. The SDO team considers both the earthquake and displacement approaches for sites subject to only distributed faulting hazard and only the earthquake approach for sites subject to both principal and distributed faulting hazard.

Earthquake Approach. The first assessment is the probability that the feature can slip in the present stress regime, $P(C)$. The SDO team's interpretation is that features oriented in a north-south direction (or are interpreted to be seismogenic) are assigned $P(C) = 1.0$. Features oriented in a northwest-southeast direction are assigned $P(C) = 0.8$.

The frequency of earthquakes occurring on each of the seismic sources is defined as part of the SDO team's seismic source characterization for the ground motion hazard assessment. The probability that slip occurs in an individual earthquake was assessed using the two-part approach defined by Equation (4-23) discussed above for the SBK team. The probability $P(\theta)$, was assessed using the analysis of the distribution of angles between the strikes of principal and distributed ruptures presented in Section H.4.3. An evaluation of the focal mechanisms for earthquakes in the immediate Yucca Mountain vicinity (see Chapter 7 of USGS, written communication, 1996) indicates that the distribution of nodal plane strike azimuths is approximately uniform and an average value of $P(\theta)$ was computed assuming random strike to apply to earthquakes occurring in the areal source zones. The probability $F(event)$ was assessed using the logistic regression model developed from the analysis of the density of distributed faulting in historical ruptures defined by Equation (4-17) and shown on Figure H-13c.

The conditional probability of exceedance, $P(D>d)$, was assessed using two approaches. The first approach defined a reduction factor, RF, equal to the ratio of the cumulative displacements on the feature of interest to the cumulative displacement on the earthquake source. The procedures described above for principal faulting were used to assess the distribution for displacement on the earthquake source at its closest approach to the point of interest. The distribution for displacement at the point of interest then is set equal to RF times the distribution on the earthquake source. The second approach utilized empirical observations of the displacement on distributed ruptures normalized to the maximum displacement on the principal rupture. A curve was defined that approximately enveloped these data (see Figure 4-91). This curve is considered to represent the 95^{th} percentile of the distribution of possible displacements on a distributed rupture. For earthquakes occurring in the areal source zones, the conditional probability of exceedance was computed using only the second approach and the assumption that the point of interest was equally likely to lie in the hanging wall or footwall of the rupture.

Displacement Approach. The first assessment in the displacement approach for characterization of distributed faulting hazard is an assessment of whether or not slip can occur, $P(C)$. This assessment is the same as that for the earthquake approach.
The frequency of displacement events is obtained using Equation (4-13). The slip rate on the feature is estimated from the interpretation that from 0.2 to 2.0 percent of the cumulative

post-Tiva Canyon slip has occurred in the Quaternary. The average displacement per event, $\overline{D}_e$, is estimated from the cumulative displacement using two approaches. The first is the scaling relationship developed by the AAR team in which $D_E = 0.83 \times 1.32 \times \beta \times D_{cum}$, where β varies from 1.40×10^{-3} to 1.85×10^{-2}. The second approach is the empirical distribution for D/D_{cum} (see Section H.2.6). The mean of this distribution is 0.00176 and $\overline{D}_e$ is set equal to $0.00176 \times D_{cum}$.

The conditional probability of exceedance, $P(D>d)$, is assessed using two approaches that correlate with those used to assess D_E. If the scaling relationship developed by the AAR team is used, then $P(D>d)$ is assessed using the distribution for D/MD^{max} (see Section H.2.5) with $MD^{max} = D_E/0.83$. If the mean of the empirical distribution for D/D_{cum} presented in Section H.2.6 is used, then the same distribution is used to assess $P(D>d)$.

Summary of Application of Model to Nine Demonstration Points. The SDO team interprets Points 1 and 2 to lie on faults that are subject to both principal and distributed faulting hazard and utilizes the logic tree shown on Figure 4-89 plus the earthquake approach on the logic tree shown on Figure 4-90 to characterize the hazard at these sites. The remaining points are interpreted to be subject to distributed faulting hazard only and the logic tree shown on Figure 4-90 is used to characterize hazard at these sites. Considering the hypothetical features at Points 7 and 8, they utilize the assumed cumulative displacements of 2 m and 10 cm to characterize the hazard for conditions (a) and (b), respectively, and interpret the probability of fault slip on a fracture with no measurable offset, condition (c), or in intact rock, condition (d), to be essentially zero.

4.3.2.2 Summary of Fault Displacement Hazard Characterization Approaches. In this section we summarize the range of interpretations made by the SSFD expert teams regarding their characterization of fault displacement hazard. A summary of the key components of their models is provided in Table 4-3.

Overall Approach for Characterizing Faulting Hazard. In aggregate, the six SSFD expert teams slightly prefer the displacement approach (aggregate weight ~ 0.6) over the earthquake approach for characterizing fault displacement hazard at sites subject to principal faulting and at sites subject to only distributed faulting. For characterizing principal faulting hazard, four

of the teams (ASM, DFS, RYA, and SDO) considered only one approach for characterizing the hazard. Three of the teams (ASM, DFS, and RYA) considered only one approach for characterizing distributed faulting hazard.

Displacement Approach for Principal Faulting Hazard. Principal faulting hazard was assessed for sites located on faults that the SSFD expert teams identified as being seismogenic. The preferred approach for estimating the frequency of displacement events is the use of slip rate divided by the average displacement per event [Equation (4-13)]. The slip rates were primarily based on the teams' seismic source characterization for the ground motion hazard assessment. One team (DFS) included slip-rate estimates based on cumulative displacement and slip history. The alternative approach used was a direct assessment of the frequency of events from the paleoseismic data applied in the seismic source characterization. The average displacement per event was primarily assessed from paleoseismic data for the sources of principal faulting hazard.

The teams used a variety of approaches to evaluate the conditional probability of exceedance. These are based on empirical distributions derived from Yucca Mountain trenching data normalized by various parameters, including the expected maximum displacement in the maximum event, MD^{max}, the average displacement estimated from displacement data, and the average and maximum displacements estimated from the length of the feature.

Earthquake Approach for Principal Faulting Hazard. The approach used for assessing the frequency of displacement events used by all of the teams was to use the frequency of earthquakes developed for the ground motion hazard assessment multiplied by a probability that each event produces rupture at the site of interest. This probability is the product of the probability of surface rupture times the probability of intersection of the rupture along the strike of the fault. The along-strike intersection probability was computed using the rupture length estimated from the magnitude of the event randomly located along the fault length. Most teams used the empirical model based on historical ruptures (Figure 4-11) to compute the probability of surface rupture. The AAR team used randomization of the rupture location over the down-dip width of the fault to compute the probability of surface rupture.

The approach used by most of the teams to assess the conditional probability of exceedance was to define a distribution for the maximum displacement, *MD*, based either on the magnitude or the rupture length of the earthquake. This distribution is then convolved with a distribution for *D/MD* to compute $P(D>d)$. The preferred distribution of *D/MD* is the empirical model developed by the ASM team from data compiled by Wheeler (1989) on historical ruptures. Some weight was given to a model developed by the SBK team from fractal simulations of fault ruptures. The SDO team also gave some weight to using the average displacement per event, *AD*, estimated from magnitude, rupture dimensions, and paleoseismic data together with an empirical distribution for *D/AD*.

Displacement Approach for Distributed Faulting Hazard. The majority of the SSFD expert teams specified that the frequency of displacement events on features subject to only distributed faulting be estimated by slip rate divided by the average displacement per event [Equation (4-13)]. The slip rates were primarily based on the cumulative displacement and slip history, though the AAR team developed a correlation between cumulative displacement and Quaternary slip rate from Yucca Mountain data. The interpretations of the slip histories were similar across all teams. The preferred model is that slip has been decreasing with time and the present-day rate is a small percentage of the late Miocene rate. Low weight was given to a uniform slip history for deformation post-12.7 Ma Tiva Canyon tuff deposition. Somewhat higher weight was given to an intermediate model of uniform slip for a time period that ranged from 3.7 to 11.6 Ma. The average displacement per event for features subject to only distributed faulting hazard was estimated using scaling relationships based on either the length of the feature or the cumulative displacement of the feature. If both length and cumulative displacement are known, then the teams gave nearly equal weights to these two approaches.

The teams used similar approaches for evaluating the conditional probability of exceedance to those used in the displacement approach for characterizing principal faulting hazard. The empirical distributions used are typically correlated with the scaling relationship used to estimate the average displacement per event. For example, if the average displacement per event is to be estimated from the cumulative displacement, then the associated distribution for displacement in a single event is based on D/D_{cum}.

Earthquake Approach for Distributed Faulting Hazard. The SSFD expert teams displayed the most variability in characterizing distributed faulting hazard using the earthquake approach. The basic assessment of the frequency of earthquakes was derived from the seismic source characterization for the ground motion hazard assessment defined by each team. The probability that an earthquake causes slip at the point of interest was assessed in a variety of ways. Most teams utilized the logistic regression model based on analyses of the pattern of historical ruptures (e.g., Figure 4-12). Two of the teams (SBK and SDO) introduced an additional factor based on either the orientation of the feature in the present stress field (slip tendency) or on the angle between the strikes of the feature and the principal rupture. The ASM team introduced a factor that depends on the probability of the earthquake producing principal faulting surface rupture. The SBK team also introduced an approach that is based on the peak velocity induced by the earthquake at the point of interest.

The widest variations in approaches were those for assessing the distribution for displacement per event on the distributed ruptures. Two of the teams (ASM and SDO) used methods defined as a reduction factor, *RF*, times the displacement distribution on the principal rupture. The methods used to assess *RF* were based on (1) the relative cumulative displacement of the feature of interest compared to that of the earthquake source, (2) a scaling relationship defined from the observed ground displacement profile in the 1983 Borah Peak earthquake, and (3) empirical data for the amount of cumulative displacement normalized by the maximum principal faulting displacement. Two other teams (AAR and SBK) used distributions defined by the characteristics of the feature at the point of interest, either length or cumulative displacement. These distributions were the same as those used in the displacement approach.

Application of Models to Nine Demonstration Points. All of the teams considered that Points 1 and 2 are subject to principal faulting hazard. Two of the teams (AAR and DFS) also considered some potential for principal faulting hazard at Point 4 because they had interpreted some probability that the Ghost Dance fault is seismogenic. The AAR team also made the interpretation that Point 6 in Dune Wash lies on their West Dune Wash Number 2 seismic source and may also be subject to principal faulting hazard.

The teams widely varied in their assessments of the probability that distributed faulting could occur in future earthquakes at Points 3 through 9, which are located off of the block bounding faults. These assessment were based on fault orientation, cumulative slip, and structural relationship. The SBK team's interpretation is that all features with some evidence of cumulative displacement are capable of displacement in future earthquakes. The DFS team's interpretation is that for most of these features, the probability that they are capable of displacement in future earthquakes is low. Four of the teams (AAR, ASM, RYA, and SDO) consider that the probability of displacement at a point in intact rock due to the occurrence of a future earthquake is essentially zero.

TABLE 4-1
SUMMARY OF SEISMIC SOURCE CHARACTERIZATION MODELS
Page 1 of 9

Issue	AAR Team	ASM Team	DFS Team	RYA Team	SBK Team	SDO Team
TECTONIC MODELS						
Overall Approach	Viable models based on observations and inferred processes for the Crater Flat structural domain, with simple shear model given full weight (1.0). Superposed NW-SE dextral shear manifested as specific structures (tectonic models A, B, & C) (0.5) or not (tectonic model D) (0.5).	The source model incorporates various aspects of planar block fault (preferred), detachment, lateral shear, and volcanic-tectonic models.	Alternative tectonic and structural models are considered primarily in the characterization of local faults: domino model (0.8) (planar fault); detachment (0.2) (includes hypothetical hidden strike-slip fault of either local or regional extent).	None of the tectonic models presented provides a unified explanation for all the seismic, geologic, and geophysical data. Alternative tectonic and structural models are considered primarily in the characterization of local faults. A coalescing fault model best fits the Yucca Mountain area.	Preferred model: oblique rift-planar faults. 3D strain accommodated on planar, strike-slip, normal, and oblique-slip faults. Rock Valley and Highway 95 faults act as accommodation zones in the rift.	Alternative tectonic and structural models are considered in the characterization of local faults. Preferred model for Crater Flat – Yucca Mountain is a half-graben formed within a larger rift that opens and deepens to the north. Deformation history and structure are associated with carapace effect, clockwise vertical axis rotation, basaltic volcanism, age and behavior of Bare Mountain fault.
Planar Block-Faulting Models	Regional faults are modeled as independent and linked (for selected faults) planar faults to maximum seismogenic depth. Local faults include linked and coalesced models; planar faults to maximum seismogenic depth, to depth of local detachment, or in some cases to a depth constrained by allowable aspect ratio or by intersection with a higher-order fault.	Regional faults are modeled as independent planar faults to maximum seismogenic depth. Local faults—the preferred model is that the faults are planar to a depth controlled by the brittle-ductile transition and the Bare Mountain fault; treated as independent and coalescing faults that merge at depth.	Regional faults are modeled as independent planar faults to maximum seismogenic depth. Local faults—include models of independent (0.95) and distributed (0.05) fault behavior; alternative structural models (domino-planar and detachment-listric) used to constrain downdip geometry and extent.	Bare Mountain and regional faults are modeled as independent planar faults to maximum seismogenic depth. Local faults—planar to listric (1 to 3 coalescing systems).	Regional faults are modeled as independent planar faults to maximum seismogenic depth. Local faults—Yucca Mountain faults are part of a half-graben, with Bare Mountain as the master fault, predominantly normal slip with a left-lateral component.	Regional faults are modeled as independent planar faults to maximum seismogenic depth. Local faults: half-graben model (1) end member—all Yucca Mountain faults are seismogenic, continuous planar faults to maximum seismogenic depth. (2) carapace effect—only major block-bounding faults are through-the-crust seismogenic faults; other intrablock faults are confined to the carapace (i.e., are aseismic) or link to faults having different attitudes and aspect ratios below the unconformity.

TABLE 4-1
SUMMARY OF SEISMIC SOURCE CHARACTERIZATION MODELS

Issue	AAR Team	ASM Team	DFS Team	RYA Team	SBK Team	SDO Team
Shear Models (buried strike-slip faults or fault systems)	Included three alternatives: Model A – Throughgoing regional dextral shear zone (0.05); Model B - right-stepping dextral shear zone that produces a pull-apart basin WITHOUT an underlying cross-basin fault (0.6); and Model C - right-stepping dextral shear zone that produces a pull-apart basin WITH an underlying cross-basin fault (0.35).	Model 1 – Continuous, long (240-km) strike-slip fault zone as proposed by Schweikert considered. Regional (60-km-long) strike-slip fault given low weight. Model 2 – Shorter (25-km), more complex or segmented zone. Assessment of existence of buried strike-slip fault conditional (yes–0.2; no–0.05) on whether or not detachment exists; assessment of the seismogenic potential of the buried strike-slip fault is conditional on the depth of the detachment (shallow–0.8, moderate–0.6, deep–0.0).	Model allows for component of northwest-directed right-lateral strike-slip strain. Hypothetical hidden strike-slip fault source ($P_A = 0.05$) is included in detachment model. Two postulated strike-slip fault sources are included: regional strike-slip fault (0.5) local strike-slip fault (0.5)	None (possibility of local buried source covered by background source).	A buried regional shear zone model is given low weight (0.01); no evidence for a buried strike-slip fault trending northwest across Crater Flat that would result in a earthquake larger than the maximum assigned to the host source zone.	Three sources of dextral shear were evaluated to account for vertical axis rotation at Yucca Mountain: (1) distributed shear (restricted to Crater Flat basin; basin is a discrete domain controlled by local bounding faults); (2) external transcurrent strike-slip fault (passes through the basin, totally hidden); and (3) external strike-slip fault enters basin from southeast (manifested at Yucca Mountain by the N25°W striking "hingeline") and terminates in Crater Flat. Only (1) and (3) are credible modifications to the basic model.
Detachment Models	Regional detachment not viable (0.0), but hypothesized local detachments included, with weights dependent on the type of dextral shear structures assumed to be present. Local detachments not included as specific seismic sources; detachments affect only down-dip fault extent for local fault sources. Depths included for local detachments range from 3 km to the maximum thickness of the seismogenic crust, with 3 to 10 km preferred.	Detachment Model (0.15): Hypothesized detachment affects down-dip geometry and extent of local fault sources; seismogenic detachment is included as possible fault source with very low probability (see below).	Detachment Model (0.2): Hypothesized detachment chiefly affects down-dip geometry and extent of local fault sources; seismogenic detachment is included as possible fault source with very low probability (see below).	Detachments are not explicitly modeled. Possibility that local faults truncate down dip in a detachment or zone of decoupling is included in coalescing fault model.	Hypothesized detachment affects only the down-dip extent of local fault sources.	A seismogenic detachment (modeled as an independent source) was thoroughly considered but could not be substantiated by the available evidence.

TABLE 4-1
SUMMARY OF SEISMIC SOURCE CHARACTERIZATION MODELS
Page 3 of 9

Issue	AAR Team	ASM Team	DFS Team	RYA Team	SBK Team	SDO Team
Volcanic-Tectonic Models ("ash event")	The possibility of simultaneous rupture on subparallel Yucca Mountain faults as postulated for the "ash event" is included in coalesced fault models for local faults.	The possibility that some surface rupturing earthquakes in Crater Flat are accompanied by dike injection (e.g., the 70-ka "ash event") is included in simultaneous rupture models for local faults.	The possibility of simultaneous rupture on subparallel Yucca Mountain faults as postulated for the "ash event" is included in the distributed faulting model for local faults.	The coalescing fault model used to model local faults (see below) would explain the apparent sychroneity of faulting on Yucca Mountain faults (i.e., the 70 ka "ash event").	Explicitly models a simultaneous rupture event (triggered by volcanic event; see Local Fault Model)	Distributed fault models involve simultaneous rupture of local faults that are parallel to each other. Such models would account for volcanism and tectonic faulting as a coupled process.
Thickness of Seismogenic Crust	Dmax1 11 km (0.185) 15 km (0.63) 17 km (0.185) Dmax2 14 km (0.185) 18 km (0.63) 22 km (0.185)	12 (0.1) 15 (0.6) 17 (0.3)	12 (0.6) 14 (0.3) 16 (0.1)	12 km (0.2) 15 km (0.7) 20 km (0.1)	12 (0.3) 15 (0.6) 17 (0.1)	14 km (0.2) 17 km (0.7) 19 km (0.1)
SEISMIC SOURCES						
Seismic Source Zones	Four scenarios: Scenario I w/3 zones (0.3), Scenario II w/2 zones (0.3), Scenario III w/3 zones (0.3), and Scenario IV w/1 zone (0.1). For all scenarios, a host zone (within 20-km radius) is defined only for assigning a lower M_{max}—not for separate recurrence estimate.	Two source zones within 100-km radius of site. A local zone (within 50-km radius) is included that is defined solely for assigning a lower M_{max}.	Model A (0.2) One zone Model B (0.8) Three zones Both models include a local zone that is defined for constraining M_{max} in the area of the detailed site characterization studies.	Three primary source zones within 100 km of site; two alternative configurations to model Zone A (local Yucca Mountain region) and Zone B (the zone surrounding Zone A).	Model A (0.7) 3 zones Model B (0.3) 4 zones Both models include a local zone that is defined solely for assigning a lower M_{max}.	Eight source zones within a 300-km radius of the site were considered initially, but only 3 remained given a filter of radius <100 km.
Seismic Source Zones—Recurrence	Truncated exponential recurrence model (1.0)	Truncated exponential recurrence model (1.0)	Truncated exponential recurrence model (1.0)	Truncated exponential recurrence model (1.0)	Truncated exponential recurrence model (1.0)	Truncated exponential recurrence model (1.0)

TABLE 4-1
SUMMARY OF SEISMIC SOURCE CHARACTERIZATION MODELS

Issue	AAR Team	ASM Team	DFS Team	RYA Team	SBK Team	SDO Team
Seismicity Catalog	300-km radius catalog Version 7 (1.0) Adjustment made for UNEs in relevant source zones.	300-km radius catalog Version 7 (0.7) Version 5 (0.3) Adjustment made for UNEs.	300-km radius catalog Version 7 (0.5) Version 5 (0.5)	100-km radius catalog Version 5 (0.5) Version 7 (0.5)	100-km radius catalog Version 7 (0.3 -0.6) Version 5 (0.4 -0.7) Weights vary depending on source zone. In relevant zones, adjustments made for UNEs weighted (0.4) versus no adjustment (0.6).	300-km radius catalog Version 5 (0.6) Version 7 (0.2) Version 8 (0.2)
Spatial Smoothing Model	For Scenarios I - III: Uniform (1.0). For Scenario IV: h = 5 km (0.25) h = 10 km (0.5) h = 20 km (0.25)	Uniform (1.0)	Model A: h = 10 km (0.25) h = 25 km (0.6) Uniform (0.15) Model B: h = 10 km (0.22) h = 25 km (0.53) Uniform (0.25)	Uniform (0.4); h = 5 km (0.4) h = 15 km (0.2)	Uniform (1.0)	Uniform (0.5) h = 10 km (0.25) h = 20 km (0.25)
Seismic Source Zones—M_{max}	Excluding Host Zone 6.6 (0.3) 6.9 (0.4) 7.3 (0.3) Host Zone (within 20 km) 6.0 (0.3) 6.3 (0.4) 6.6 (0.3)	Walker Lane 6.5 (0.185) 6.8 (0.63) 7.1 (0.185) Basin and Range 6.9 (0.185) 7.2 (0.63) 7.5 (0.185) Site Region (within 50 km) 6.0 (0.185) 6.3 (0.63) 6.6 (0.185)	Model A (not including site vicinity) 7.0 (0.2) 7.3 (0.6) 7.7 (0.2) Model B (not including site vicinity) SW Walker Lane 7.0 (0.2) 7.3 (0.6) 7.7 (0.2) NE Walker Lane and Basin and Range 7.0 (0.2) 7.25 (0.6) 7.5 (0.2) Site Vicinity 5.6 (0.2) 5.8 (0.6) 6.0 (0.2)	6.0 (0.185) 6.3 (0.63) 6.6 (0.185)	Excluding Local Zone: 6.2 (0.2) 6.3 (0.5) 6.4 (0.2) 6.6 (0.1) Local Zone 5.6 (0.2) 6.0 (0.6) 6.2 (0.2)	Within 100 km 6.4 ± 0.2 cumulative lognormal distribution 6.2 (0.03) 6.4 (0.5) 6.6 (0.97 Beyond 100 km: estimated from a correlation of fault length with magnitude for longest fault: in Zones 2 and 3 Ms 7.4 ± 0.2

TABLE 4-1
SUMMARY OF SEISMIC SOURCE CHARACTERIZATION MODELS
Page 5 of 9

Issue	AAR Team	ASM Team	DFS Team	RYA Team	SBK Team	SDO Team
Regional Fault Sources	19 regional fault sources; includes faults with Pa of <1.0; includes two possibly linked fault systems: Death Valley with Furnace Creek (0.8), and Amargosa River with Pahrump (0.1); also includes five faults considered as segmented (max. rupture length < total fault length); included range of rupture lengths for each source. Preferred dips: normal 65° strike-slip 90°	24 regional faults (within 15 to 100 km of site); all fault sources active (1.0); considers alternative total lengths, generalized down-dip geometry (strike-slip 90°, normal 60°).	18 regional fault sources (within 100 km of site vicinity); all fault sources active (1.0); considered alternative total lengths, generalized down-dip geometry (strike-slip 90°, normal-60°).	11 regional fault sources (within 100 km of site); all fault sources active (1.0); includes possibility (0.1) of simultaneous rupture of Death Valley and Furnace Creek faults; includes alternative rupture lengths for 9 faults, generalized down-dip geometry (strike-slip 90°, normal 60°).	16 regional fault sources (within 100 km radius); includes faults with Pa < 1.0; includes range of rupture lengths for each source—for long faults ranges reflect probable rupture segment lengths, assigned dips based on fault type, with preferred values of: strike-slip 90°, normal 60°, and oblique 70°.	36 regional fault sources (24 faults (Pa 1.0), 12 faults (Pa < 1.0); two faults generally outside 100 km (Panamint Valley and Ash Hill fault zone) included; alternative total lengths, generalized down-dip geometry (strike-slip 90°, normal 60°).
Regional Faults—M_{max}	SRL (0.4) RA (0.2) SRL and S (0.4) $M_{max} \pm ¼$ unit, $M_{max} + ¼ = m^u$	SRL (1.0) $M_{max} \pm ¼$ unit, $M_{max} + ¼ = m^u$	SRL (1.0) Alternative rupture segments (SRL) are considered resulting in a range of M_{max} for each fault. $M_{max} \pm ¼$ unit (with some exceptions)	SRL (0.35) RA (0.35) MD (0.3) Or RL (0.5) RA (0.5) depending on available data $M_{max} \pm 0.5$ unit	SRL, RA, MD, AD, and moment approaches; weighted on a fault basis depending on available data. $M_{max} \pm ¼$ unit, $M_{max} + ¼ = m^u$	RL, MD, RL x MD, Slip rate +RL; weighted on a fault basis depending on available data. $M_{max} \pm ¼$ unit, $M_{max} + ¼ = m^u$
Regional Faults—Recurrence Approach	Slip Rate Approach (0.6); Recurrence Interval Approach (0.4) - where data are available. Characteristic (0.7) Modified exponential (0.3) DV –FC Characteristic (1.0) $M_{max} + ¼ = m^u$ b-value 0.80 (0.3), 1.00 (0.4), 1.20 (0.3)	Slip Rate Approach (0.5) Recurrence Interval (0.5) or Slip Rate (1.0) depending on available data. Characteristic (0.2) Maximum moment (0.8) b-value varies from fault to fault.	Slip Rate Approach (1.0) Characteristic (0.6) Maximum moment (0.3) Truncated exponential (0.1) b-value varies from fault to fault.	Slip Rate Approach (1.0) Characteristic (0.9) Truncated exponential(0.1) b-value 1.07 (0.185) 1.12 (0.63) 1.2 (0.185) $M_{min} = 6.3$	Slip Rate and Recurrence Interval Approaches; weights vary from fault to fault depending on available data. Characteristic and truncated exponential models used. Weights vary from fault to fault, with characteristic behavior favored for range-bounding faults, and exponential for zones with multiple distributed traces. b-value varies from fault to fault.	Moment rates (slip rates) Characteristic (0.7) Truncated exponential (0.3) b-value varies from fault to fault. $M_{min} = 6.2$

TABLE 4-1
SUMMARY OF SEISMIC SOURCE CHARACTERIZATION MODELS

Issue	AAR Team	ASM Team	DFS Team	RYA Team	SBK Team	SDO Team
Local Fault Sources	20 individual faults included w/ P[s] 0.1 to 1.0 Synchronous Behavior Approach: (1) Faults rupture independently or are grouped in distributed systems by linkages along strike or coalescence down dip. (2) Likelihood of coalesced behavior is dependent on tectonic model (in general, coalesced behavior strongly favored over independent behavior). (3) Four coalesced models defined with from one to four fault systems. Assigned weights depend on tectonic models, but models having three to four systems are strongly favored. (4) For independent fault behavior, two cases of possibly linked faults are generally favored. Preferred dip 60°. Dominantly normal slip w/ left-lateral component.	Planar Fault Block Model- 5 faults modeled as major block-bounding faults (seismogenic–1.0) 5 faults modeled as minor or secondary faults (probability of being seismogenic—fault, P_A ranges from 0.5 to 0.9). Simultaneous rupture models are based on the probability of linkage at depth (geometric constraints) and temporal overlap inferred from paleoseismic data.	Two Fault Behavioral Models: Distributed (0.05) 9 scenarios Independent (0.95) Two Structural Models: *Domino* model (0.8) (high-angle planar faults to seismogenic depth except where they intersect larger-throw fault); existence of H95 fault not dependent on domino model—considered as an independent source with low probability of being an active seismogenic structure. *Detachment* model (0.2) listric geometry detachment modeled at 6 km depth; includes hidden strike-slip fault sources.	Coalescing Fault Model (1.0) Bare Mountain fault, independent planar fault to seismogenic depths. Yucca Mountain faults are assumed to coalesce down dip at relatively shallow depth (2 to 5 km). Three faults (WW, SC, and PBC) are primary independent seismogenic faults in three-fault system. Coalescing Models: 12 km (0.2) and 15 km (0.7) seismogenic depth: 1-fault system (0.1) 2-fault system (0.5) 3-fault system (0.4) 20 km (0.1) seismogenic depth 1-fault system (0.3) 2-fault system (0.4) 3-fault system (0.3) Planar fault and detachment-decoupled model geometries are considered part of range of behavior for coalesced systems.	Within Crater Flat domain, included 11 individual faults (9 YM, BM, and Hwy 95); excluded 7 mapped faults ($P_A = 0$) based on no or low rates of Quaternary activity (including GD and SD). Model- local faults sole into detachment between 5 km and base of seismogenic zone (0.01). Model- block-bounding faults coalesce at depth either in one or two master faults (0.09) Model (end member) - 4 linked block-bounding faults (0.4) Model (end member) - faults behave independently (0.5) All of the above models include a simultaneous rupture scenario that acts as an additional source; weights on activity vary according to rupture model (0.1 on independent and linked; 0.5 on detachment and coalescing models).	Behavior models included: (1) single-fault (2) linked-fault (3) distributed-fault Single-fault scenarios - 6 major local faults 9 linked-fault scenarios 8 distributed fault scenarios
Local Faults—M_{max}	RLD (for buried structures) or SRL (all others) RA SRL + S Moment Equation	General weights SRL (0.3) SRL x D (0.3) MD (0.15) AD (0.15) RA (0.1)	RL (0.4) RA (0.6) ± 0.25 units	RL (0.5) RA (0.5) ± 0.5 units	SRL, RA, MD, AD, M_o inferred from stress drop; weights vary depending on available data.	RL (0.206) MD (0.104) RL x MD (0.207) RA (0.207) SRL + S (0.069) Seismic Moment (0.207)

TABLE 4-1
SUMMARY OF SEISMIC SOURCE CHARACTERIZATION MODELS
Page 7 of 9

Issue	AAR Team	ASM Team	DFS Team	RYA Team	SBK Team	SDO Team
	Different weights assigned depending on fault length (< or ≥ 25 km), tectonic model, and coalesced behavior model. $M_{max} \pm ¼$ unit, $M_{max} + ¼ = m^u$	Modified on a fault basis depending on available data. $M_{max} \pm ¼$ unit, $M_{max} + ¼ = m^u$			$M_{max} \pm ¼$ unit, $M_{max} + ¼ = m^u$	$M_{max} \pm ¼$ unit, $M_{max} + ¼ = m^u$
Local Faults—Recurrence	Slip-Rate Approach (0.6); Recurrence Interval Approach (0.4) - where data are available. Characteristic (0.7), Modified exponential (0.3) b-value 0.80 (0.3), 1.00 (0.4), 1.20 (0.3)	Slip-Rate Approach (0.5) Recurrence Interval Approach (0.5) Characteristic (0.7) Truncated Exponential (0.2) Maximum moment (0.1)	Slip-Rate Approach (1.0) Independent behavior- Characteristic (0.6) Maximum moment(0.3) Exponential (0.1) Distributed behavior- Characteristic (0.6) Maximum moment(0.2) Exponential (0.2)	Slip-Rate Approach (0.7) Recurrence Interval Approach (0.3) Characteristic and truncated exponential—weights vary depending on coalescing model used.	Slip-Rate Approach (0.7 to 1.0) Recurrence Interval Approach (used where data are available, but given lower weight, 0.2 to 0.3) Both characteristic and truncated exponential models used (weight varies depending on fault model)	Moment Rate (0.33) Average Recurrence Interval (0.33) Interseismic Recurrence Interval (0.33) Characteristic (0.7) Truncated exponential (0.3)
OTHER SOURCES						
Buried Regional Dextral Shear Zone	Included w/ P[s] = 1.0 for Tectonic Model A (0.05). Regional strike-slip fault 50 to 100 km in length Slip Rate 0.05 (0.3) 0.1 (0.4) 0.2 (0.3)	Yes; see above. M_{MAX} M_w 7.1 (0.3) 60-km rupture M_w .6.7 (0.7) 25-km rupture Slip Rate 0.1 mm/yr (0.6) 0.025 mm/yr (0.2) 0.24 mm/yr (0.2)	Includes a hypothetical strike-slip fault of regional or local extent, with low probability (0.05) that it is a seismogenic source. Local strike-slip fault (0.5) 30-km length. Regional strike-slip fault (0.5) 200-km length.	Not included as fault source; possible buried strike-slip fault judged incapable of producing earthquakes larger than the maximum background earthquake or any other source included in the source model.	Not included as fault source; possibility is covered by seismic source zone.	Yes; see above. Fault Length 20 km (minimum) 27 km (preferred) 120 km (maximum) Slip Rate 0.001 (minimum) 0.005 (preferred) 0.02 (maximum)

TABLE 4-1
SUMMARY OF SEISMIC SOURCE CHARACTERIZATION MODELS

Issue	AAR Team	ASM Team	DFS Team	RYA Team	SBK Team	SDO Team
Seismogenic Detachment (modeled as independent source)	No (possibility is covered by areal source zone).	Detachment Model (0.15) Probability—seismogenic (0.01) Depth to detachment 6 km (0.25) (BD-6) / 2- 6 km (0.5) BD (0.25) BD=brittle-ductile transition Maximum magnitude 7.1 (0.15) 7.6 (0.7) 8.0 (0.15) Slip Rate 0.05 mm/yr (0.6) 0.013 mm/yr (0.2) 0.12 mm/yr (0.2) Mean Recurrence 25 kyr (0.15) 75 kyr (0.7) 200 kyr (0.15) Characteristic (1.0)	Yes (Paintbrush Canyon /Stagecoach fault in the detachment model (0.2) is modeled as a shallow-dipping, seismogenic source that extends beneath the Crater Flat Basin).	Possibility of a seismic detachment is excluded.	No (shallow and deeper detachments as active seismogenic structures are given no weight). Hypothesized detachments affect only down-dip fault extent of Yucca Mountain faults; depth is dependent on Bare Mountain fault.	A seismogenic detachment (modeled as an independent source) was thoroughly considered but could not be substantiated by the available evidence.
Volcanic Source Zone (basaltic)	No (possibility is covered by areal source zone).	No (maximum magnitudes for volcanic-related earthquakes are less than M_{max} for fault and background seismic zones, and recurrence rate for volcanic eruptive events is estimated to be insignificant compared to seismicity rates).	No (possibility is covered by seismic source zones).	Yes (0.7) Spatial location (basaltic cones in site vicinity). Preferred return periods 2×10^5 and 2×10^6 $M_{max} = 5.5$.	No (possibility is covered by seismic source zones).	Defines two volcanic sources with probabilities of 0.25 and 0.7. Recurrence—2 to 3 volcanic events per Ma Maximum magnitude distribution for volcanic events: 6.0 ± 0.2 (0.1) 5.8 ± 0.4 (0.6) 5.5 ± 0.3 (0.3)

TABLE 4-1
SUMMARY OF SEISMIC SOURCE CHARACTERIZATION MODELS
Page 9 of 9

Issue	AAR Team	ASM Team	DFS Team	RYA Team	SBK Team	SDO Team
Gravity Fault	Considered distinct from Ash Meadows fault, which is included as a regional fault; accounted for in assessment of M_{max} for background source zones >20 km from site.	Not discussed. Ash Meadows fault is included as regional fault source (probability of activity 1.0).	Amargosa/Gravity (Ash Meadows) fault is included as regional fault source (probability of activity 1.0).	Not discussed. Ash Meadows fault included as regional fault.	Included as potential northern extension of the Ash Meadows fault (0.1).	Characterized as a regional fault source, probability of activity (0.9).
Cross-Basin Fault	Included w/ P[s] = 1 in Tectonic Model C (0.35)	Includes local buried strike-slip fault with low probability (see above); preferred length (25-km) (0.7) based on down-on-east segments along the west side of Crater Flat.	A local hidden strike-slip fault is included with a low probability (P_A = 0.05) in the detachment model for local faults.	Not explicitly included in SSC model; see comment above regarding buried strike-slip faults.	Not included.	Based on evidence for distributed dextral faulting, the hingeline-Pahrump-Stewart Valley fault is characterized as a buried strike-slip fault.
Highway 95 or Carrara Fault	Included w/: P[s] = 0.5 for Tectonic Model A P[s] = 0.8 for Tectonic Models B & C.	Carrara fault characterized as active (P_A = 0.85) regional fault source.	Included with low probability (P_A = 0.1) as a hypothetical regional source.	Not included.	Included as independent fault source (P_A = 0.4).	Highway 95 fault assigned a probability of 0.2 (regional fault source).

TABLE 4-2
ACRONYMS FOR FAULT SOURCES

LOCAL FAULT SOURCES	
AW	Abandoned Wash Fault
BC	Black Cone Fault
BM	Bare Mountain Fault
BWR	Bow Ridge Fault
CF	Crater Flat Fault
CCF	Central Crater Flat Fault
CWW	Central Windy Wash Fault
E-SIDE (ES)	East Side Fault (PC+SR+BWR+MWV+GD+WD1+WD2+EB (Team AAR)
EB	East Busted Butte Fault
ELC	East Lathrop Cone Fault
FW	Fatigue Wash Fault
GD	Ghost Dance Fault
H95	Carrara (Highway 95) Fault
IR	Iron Ridge Fault
MWV	Midway Valley Fault
NCF	Northern Crater Flat Fault
NPC	Northern Paintbrush Canyon Fault
NWW	Northern Windy Wash Fault
PBC	Paintbrush Canyon Fault
SC	Solitario Canyon Fault
SCF	Southern Crater Flat Fault
SPC	Southern Paintbrush Canyon Fault
SR	Stagecoach Road Fault
SWW	Southern Windy Wash Fault
WD1	West Dune Wash Fault #1
WD2	West Dune Wash Fault #2
W-SIDE 1	West Side Fault #1 (SC+IR) (Team AAR)
W-SIDE 2	West Side Fault #2 (WW+FW+CF) (Team AAR)
WW	Windy Wash Fault
WSIDE	West Side Fault (Team RYA)

Table 4-3
SUMMARY OF SSFD EXPERT TEAM FAULT DISPLACEMENT HAZARD CHARACTERIZATIONS
Page 1 of 6

Issue	AAR team	ASM team	DFS team	RYA team	SBK team	SDO team
PRINCIPAL FAULTING APPROACH	Displacement approach [0.67]; Earthquake approach [0.33]	Earthquake approach [1.0]	Displacement approach [1.0]	Displacement approach [1.0]	Displacement approach [0.85-0.9] Earthquake approach [0.1-0.15]	Earthquake approach [1.0]
Displacement Approach for Principal Faulting						
Probability That Principal Faulting Can Occur P(C)	Evaluate P(C) based on probability fault is seismogenic	NA	Evaluate P(C) based on probability fault being seismogenic	Evaluate P(C) based on probability fault is seismogenic	Evaluate P(C) based on probability fault being seismogenic	Evaluate P(C) based on probability fault being seismogenic
Frequency of Displacement Events	Slip rate, (*SR*) [1.0]	NA	$SR/\overline{D}_E$ [0.5]; Recurrence intervals (*RI*) [0.5]	Slip rate [0.2]; Recurrence intervals [0.8]	Slip rate [0.8]; Recurrence intervals [0.2]	NA
Slip Rate (*SR*)	Quaternary slip rates used in SSC model	NA	Paleoseismic data [0.7]; uniform post-Tiva Canyon [0.1]; uniform post-Rainier Mesa [0.1]; decreasing slip rate model [0.1]	Quaternary slip rates used in SSC model	Quaternary paleoseismic data point specific or interpolated	NA
Average Displacement Per Event, $\overline{D}_E$	$\overline{D}_E = 0.83\ MD^{max}$ MD^{max} from fault length [0.3]; D_{cum} [0.3]; paleoseismicity data [0.4]	NA	Paleoseismologic data [0.5]; $SR \times RI$ [0.5]	Paleoseismic data [1.0]	Paleoseismic data [0.8]; From *AD-RL* [0.1]; From *MD-RL* [0.1];	NA
Conditional Probability of Exceedance, *P(D>d)*	Distribution for D/MD^{max} [1.0]	NA	Distribution for *D/AD* [1.0]	Distribution for *D/AD* [0.5]; Distribution for D/MD^{max} [0.5]	D/AD_{paleo} $D/AD_{F(RL)}$ $D/MD_{F(RL)}$ correlated with $\overline{D}_E$	NA

Issue	AAR team	ASM team	DFS team	RYA team	SBK team	SDO team
Earthquake Approach for Principal Faulting						
Probability That Principal Faulting Can Occur, P(C)	P(C) = P(S) from SSC model	P(C) = P(S) from SSC model	NA	NA	P(C) = P(S) from SSC model	P(C) = P(S) from SSC model
Frequency of Earthquakes on Principal Faulting Source	Earthquake frequency from SSC model	Earthquake frequency from SSC model	NA	NA	Earthquake frequency from SSC model	Earthquake frequency from SSC model
Probability of Surface Rupture	Randomization of rupture depth with rupture width based on *RL*/aspect ratio; *RL* specified by magnitude-*RL* [0.5]; magnitude-rupture area [0.5]	Empirical models 32 GB earthquakes [0.5]; 105 EC earthquakes [0.5]	NA	NA	Empirical model 32 GB earthquakes [1.0]	Empirical models 32 GB earthquakes [0.5]; 47 NB&R earthquakes [0.5]

Table 4-3
SUMMARY OF SSFD EXPERT TEAM FAULT DISPLACEMENT HAZARD CHARACTERIZATIONS

Issue	AAR team	ASM team	DFS team	RYA team	SBK team	SDO team
Conditional Probability of Exceedance, *P(D>d)*	Maximum displacement per event, *MD*, from *SRL* [0.33]; M_w [0.33]; and *RLD* [0.34]; *D/MD* from Wheeler data [1.0]	*MD* from M_w [1.0] *D/MD* from Wheeler data [1.0]	NA	NA	*MD* from M_w [1.0] *D/MD* from Wheeler data [0.5]; fractal model [0.5]	*AD* and distribution for *D/AD* [0.5]; *AD* from* M_w [0.2]; *RL* [0.4]; and Paleoseismic data [0.4] *MD* and distribution for *D/MD* [0.5]; *MD* from* M_w [0.2]; *RL* [0.4]; and Paleoseismic data [0.4]; *D/MD* from Wheeler data [0.8], and fractal model [0.2] * for $m<m^U$-½ use only M_w Ramelli curve also was used for Solitario Canyon fault

Table 4-3
SUMMARY OF SSFD EXPERT TEAM FAULT DISPLACEMENT HAZARD CHARACTERIZATIONS

Issue	AAR team	ASM team	DFS team	RYA team	SBK team	SDO team
DISTRIBUTED FAULTING APPROACH	Displacement approach [0.67]; Earthquake approach [0.33]	Earthquake approach [1.0]	Displacement approach [1.0]	Displacement approach [1.0]	Displacement approach [0.8]; Earthquake approach [0.2]	*On Principal Faults–* Earthquake approach [1.0]; *Other Sites–* Displacement approach [0.3, Earthquake approach [0.7]
Earthquake Approach for Distributed Faulting						
Probability of Occurrence P(C)	If capable of principal faulting P(C) = P(S) Otherwise, P(C) based on slip-tendency	Function of the category and orientation of feature, cos(strike azimuth)	NA	NA	P(C)=1.0	Slip tendency [1.0]
Frequency of Earthquakes on Seismic Sources	Earthquake frequency from SSC model	Earthquake frequency from SSC model	NA	NA	Earthquake frequency from SSC model	Earthquake frequency from SSC model
Probability of Slip Per Event, P_i(Slip|Event on j)	Logistic regression of historical faulting data [1.0]	Probability a function of r and hanging wall-footwall location; preferred model [0.6]; upper-bound model [0.4]	NA	NA	$P(\theta)\times F(event)$ $P(\theta)$ based on slip tendency [0.5]; Relative orientation [0.5] $F(event)$ based on logistic regression of historical surface faulting data [0.5], peak velocity [0.5]	$P(\theta)\times F(event)$ $P(\theta)$ based on relative orientation [1.0] $F(event)$ based on logistic regression of historical surface faulting data [1.0]

Table 4-3
SUMMARY OF SSFD EXPERT TEAM FAULT DISPLACEMENT HAZARD CHARACTERIZATIONS

Issue	AAR team	ASM team	DFS team	RYA team	SBK team	SDO team
Conditional Probability of Exceedance, *P(D>d)*	*For site of principal faulting* use principal faulting–distribution times *RF* [1.0] *For other sites–* Distribution of D/MD^{max}; MD^{max} from *RL* [0.5], D_{cum} [0.5]	*RF* times principal faulting distribution; *RF* from Displacement potential [0.7], Relative cumulative displacement [0.3]	NA	NA	D/D_{cum} [1.0]	Distribution for *D/MD* on principal rupture as a function of distance from rupture [0.8], Distribution for *D/MD* on principal rupture times function of relative D_{cum} [0.2]
Displacement Approach for Distributed Faulting						
P(C)	Evaluate P(C) based on orientation.	NA	Evaluate P(C) based on orientation, location, and P(S)	Evaluate P(C) based on orientation, location, and P(S)	P(C)=1.0	Based on slip tendency [1.0]
Frequency of Dstributed Faulting Events	Slip rate [1.0]	NA	$SR/\overline{D}_E$ [0.5], and Recurrence intervals (*RI*) [0.5]	Slip rate [1.0]	Slip rate [1.0]	Slip rate [1.0]
Slip Rate	Uniform post 11.6 Ma [0.1], Uniform post 3.7 Ma [0.3], and 3.26×10^{-5} D_{cum} [0.6]	NA	Uniform post-Tiva Canyon [0.33], Uniform post-Rainier Mesa [0.33], and Decreasing slip rate model [0.34]	D_{cum}/12.7 [0.1], 0.02 D_{cum}/1.6 [0.6], and 0.2 D_{cum}/3.7 [0.3]	Geologic history [0.75] with D_{cum}/12.5 [0.1], 0.2 D_{cum}/11.6 [0.3], and 0.8 D_{cum} x 0.21/0.9 [0.6]; Ratio of cumulative slip to that of block-bounding faults and their slip rates [0.25]	0.02 D_{cum}/1.6Ma [0.3]; 0.006 D_{cum}/1.6Ma [0.4]; 0.002 D_{cum}/1.6Ma [0.3]
Average Displacement Per Event, $\overline{D}_E$	0.83MD^{max} from Length [0.5], D_{cum} [0.5]	NA	Direct estimate [0.5] SR*RI [0.5]	Fault length [0.5] D_{cum} [0.5]	D_{cum} [1.0]	Based on D_{cum} and AAR scaling relationship [0.5]; SBK distribution [0.5]

Table 4-3
SUMMARY OF SSFD EXPERT TEAM FAULT DISPLACEMENT HAZARD CHARACTERIZATIONS

Issue	AAR team	ASM team	DFS team	RYA team	SBK team	SDO team
Conditional Probability of Exceedance, $P(D>d)$	Distribution for D/MD^{max} [1.0]		Distribution for D/AD [1.0]	Distribution for D/AD [0.5] Distribution for D/MD^{max} [0.5] with $MD^{max} = AD/0.83$	Distribution for D/D_{cum} [1.0]	For AAR scaling distribution for D/MD^{max}, for SBK scaling distribution for D/D_{cum}

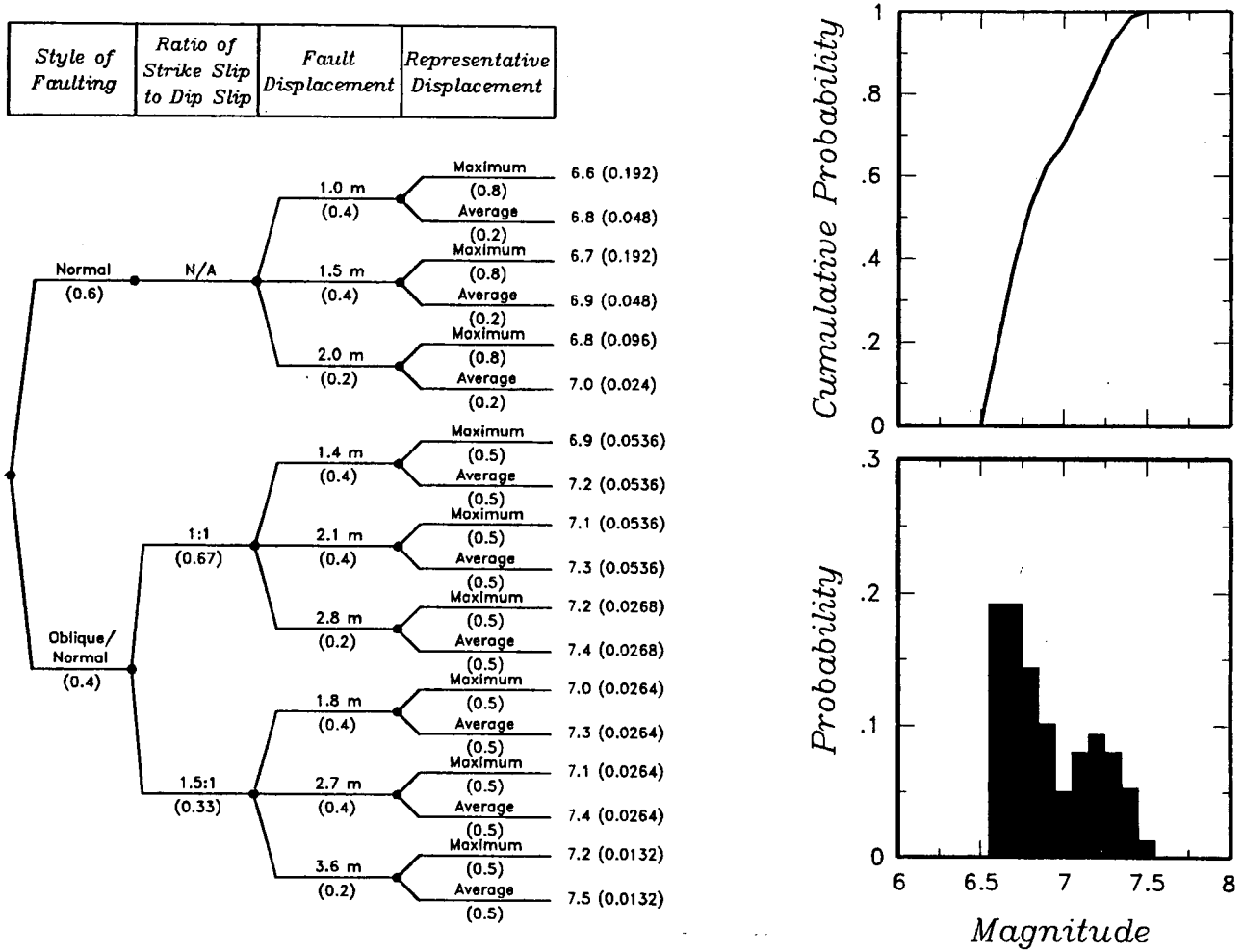

Figure 4-1 Example logic tree and resulting discrete probability distributions for assessing the magnitudes of paleoearthquakes

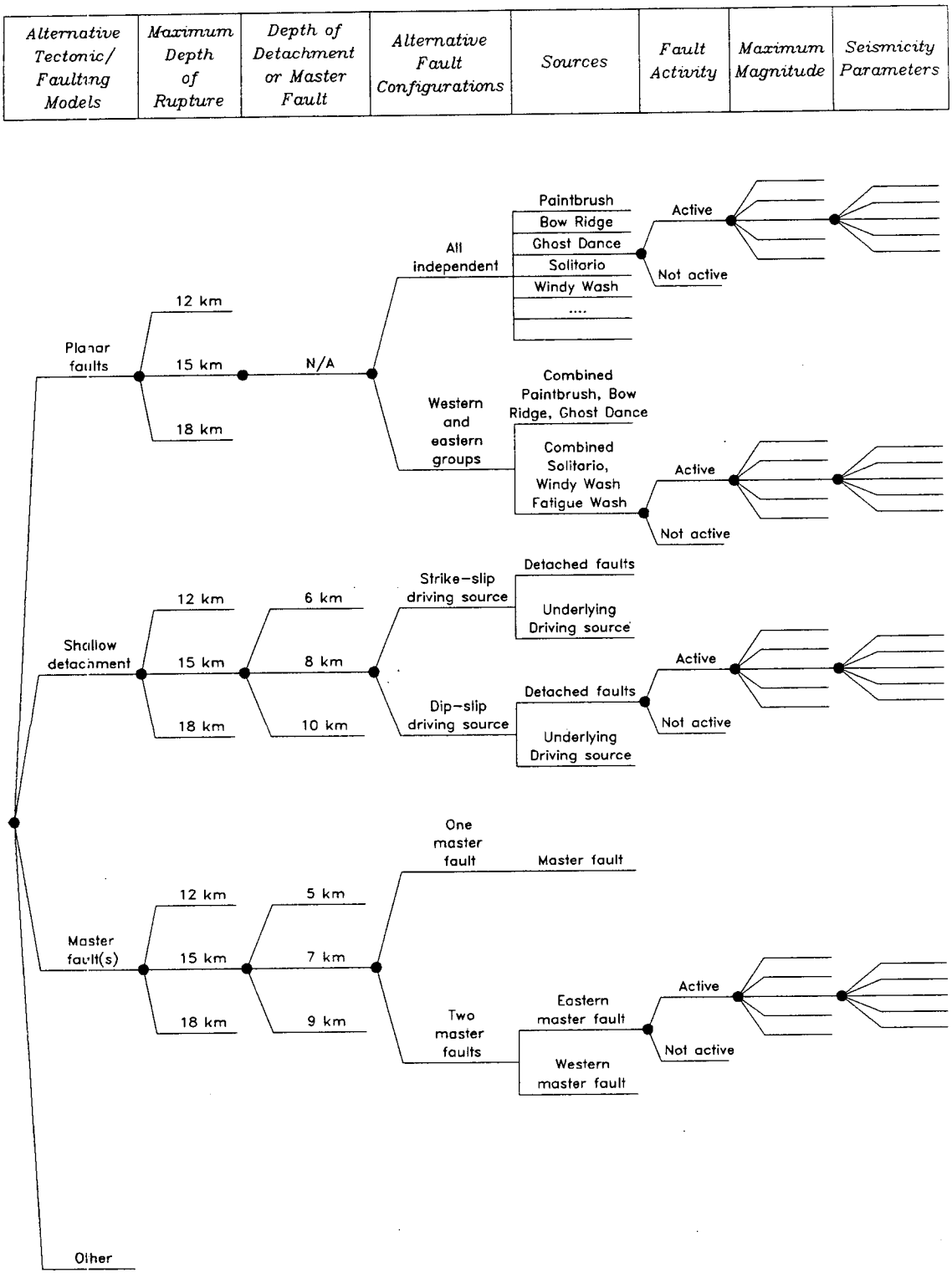

Figure 4-2. Example logic tree for expressing the uncertainty in characterizing local fault sources

TABLE 4-2 (Continued)

REGIONAL FAULT SOURCES	
AH	Ash Hill Fault
AM	Ash Meadows Fault
AR	Amargosa River Fault
BH	Buried Hills Fault
BLR	Belted Range Fault
BM	Bare Mountain Fault
CB	Carpetbag Fault
CS	Cane Spring Fault
DV	Death Valley Fault
EDV	Eastern Death Valley Fault
EM	Emigrant Fault
EN	East Nopah Fault
EPR	East Pintwater Range Fault
ER	Eleana Range Fault
ESR	East Spector Range Fault
EVN	Emigrant Valley North Fault
EVS	Emigrant Valley South Fault
FC	Furnace Creek Fault
FLV	Fish Lake Valley Fault
GM	Grapevine Mountains Fault
GV	Grapevine Fault
H95	Cararra (Highway 95) Fault
HM	Hunter Mountains Fault
JFG	Jackass Flats Gravity Fault
KR	Kawich Range Fault
KW	Keane Wonder Fault
MDV	Middle Death Valley Fault
MM	Mine Mountain Fault
OAK	Oak Springs Fault
OSV	Oasis Valley Fault
PAN	Panamint Valley Fault
PC	Peace Camp Fault
PM1	Pahute Mesa Fault
PRP	Pahrump Fault
RV	Rock Valley Fault
RWBW	Rocket Wash-Beatty Wash Fault
SF	Sarcobatus Flat Fault
SPR	Spotted Range Fault
SPRP	South Pahrump Fault
SSC	South Silent Canyon Fault

TABLE 4-2 (Concluded)

REGIONAL FAULT SOURCES (Cont'd.)	
TOL	Tolicha Pass Fault
TP	Towne Pass Fault
WAH	Wahmonie Fault
WDV	Western Death Valley Fault
WPR	West Pintwater Range Fault
WSM	West Spring Mountains Fault
WSR	West Spector Range Fault
YB	Yucca Butte Fault
YC	Yucca Fault
YCL	Yucca Lake Fault

INFERRED STRIKE-SLIP FAULT SOURCES	
TI-BSS	Team ASM Buried Strike-Slip Fault
T2-HSS	Team DFS Hidden Strike-Slip Fault
T4-CB	Team AAR Cross Basin Fault
T4-PA2	Team AAR North-Bounding Strike-Slip Fault
T4-SS	Team AAR Regional Strike-Slip Fault
T6-SS	Team SDO Strike-Slip Fault

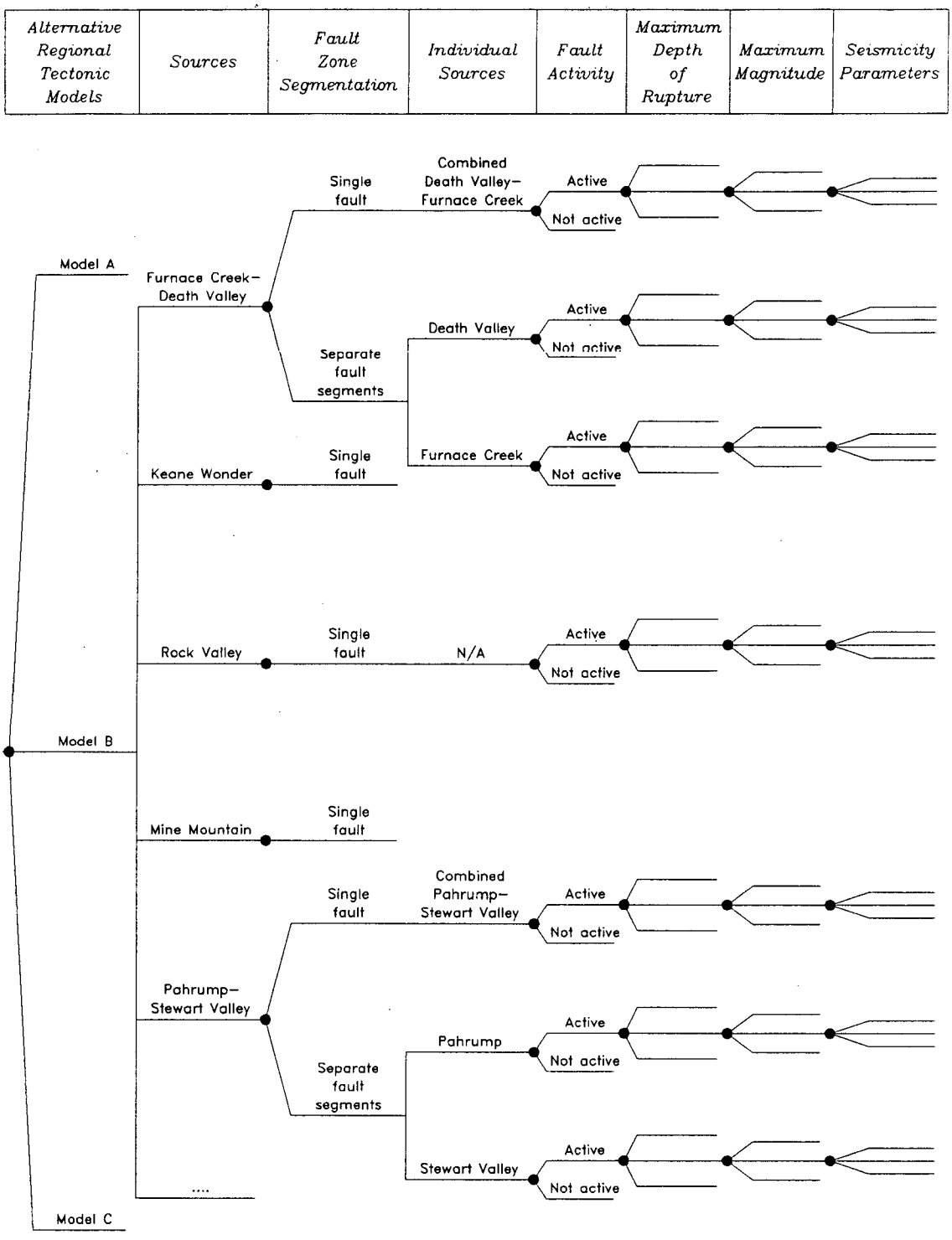

Figure 4-3. Example logic tree for expressing the uncertainty in characterizing regional fault sources

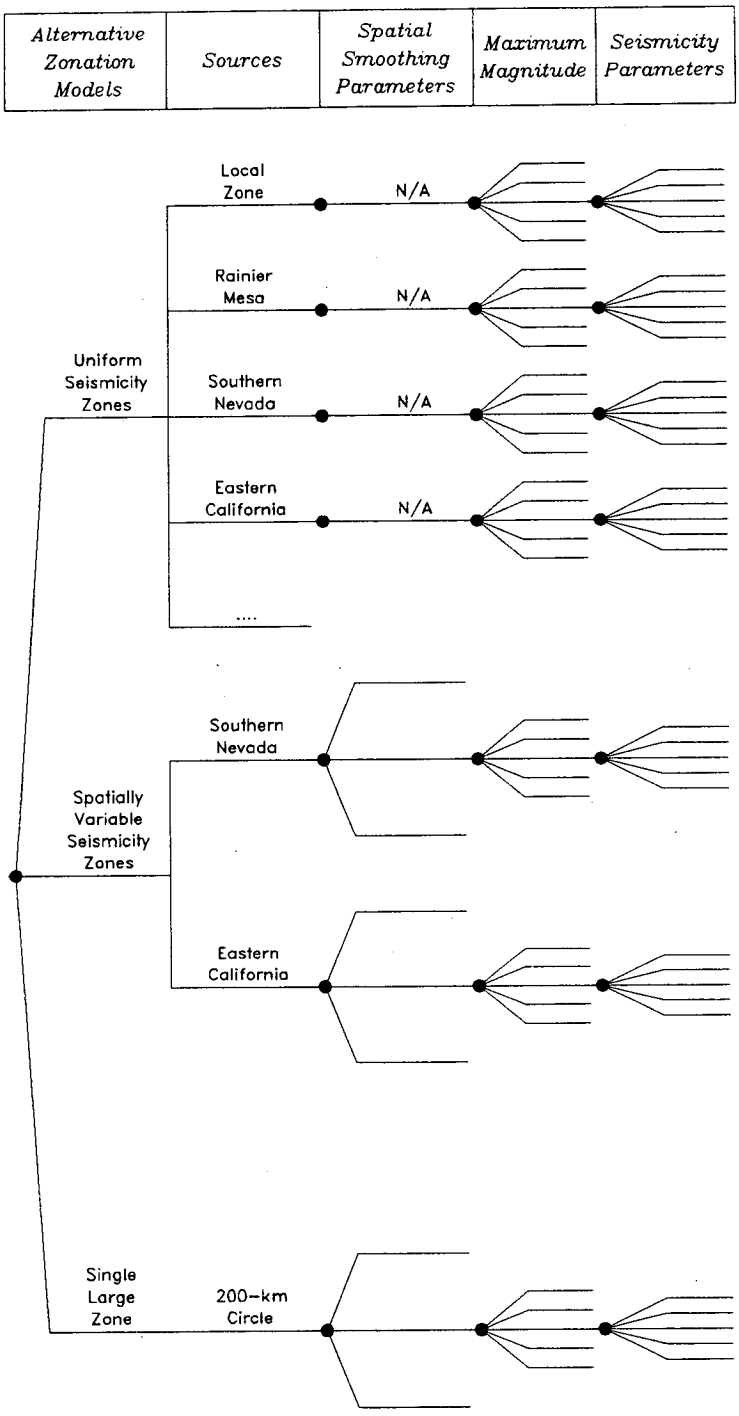

Figure 4-4. Example logic tree for expressing the uncertainty in characterizing regional areal source zones

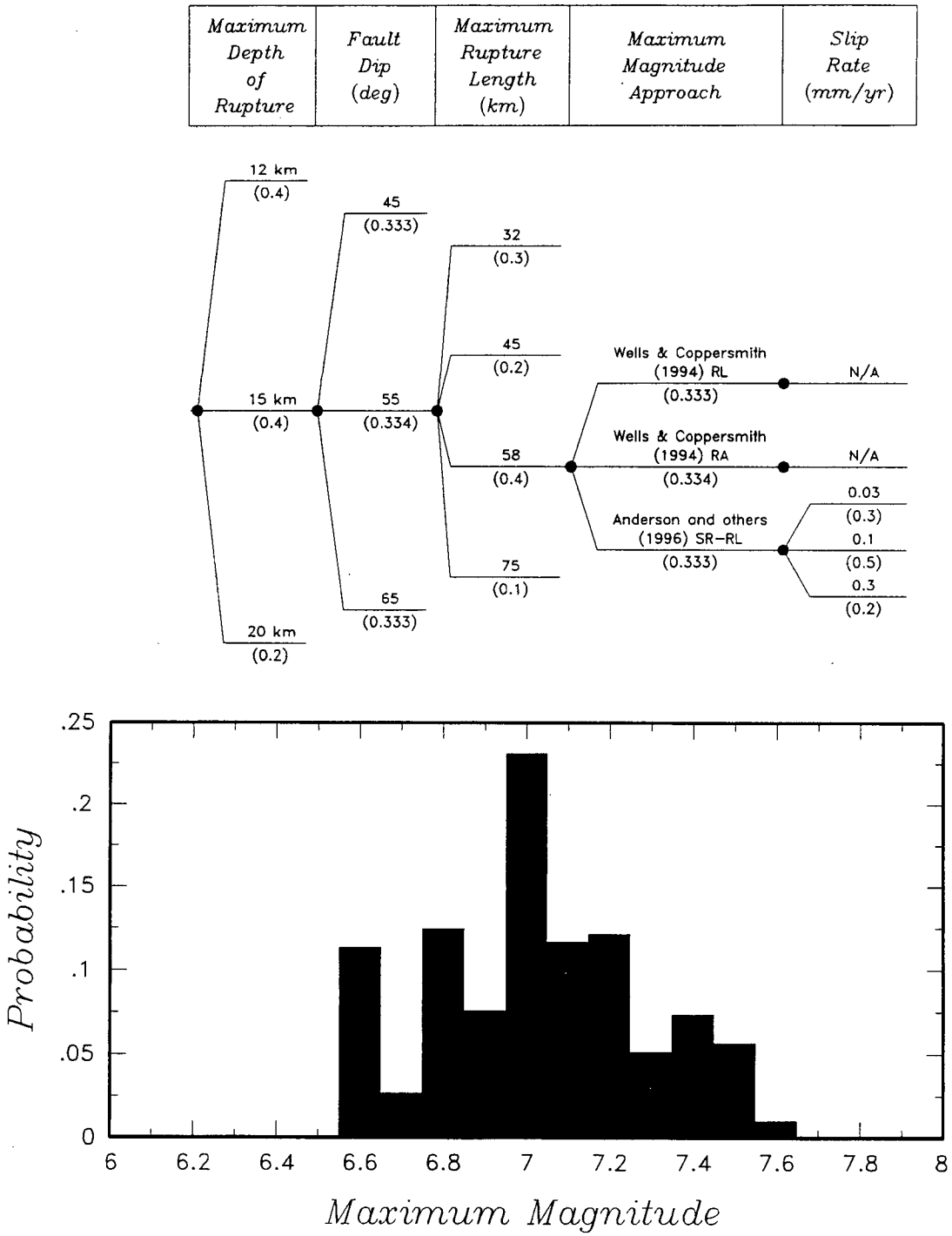

Figure 4-5. Example assessment of maximum magnitude for a fault source. Top, logic tree for uncertainty assessment. Bottom, resulting discrete distribution for maximum magnitude.

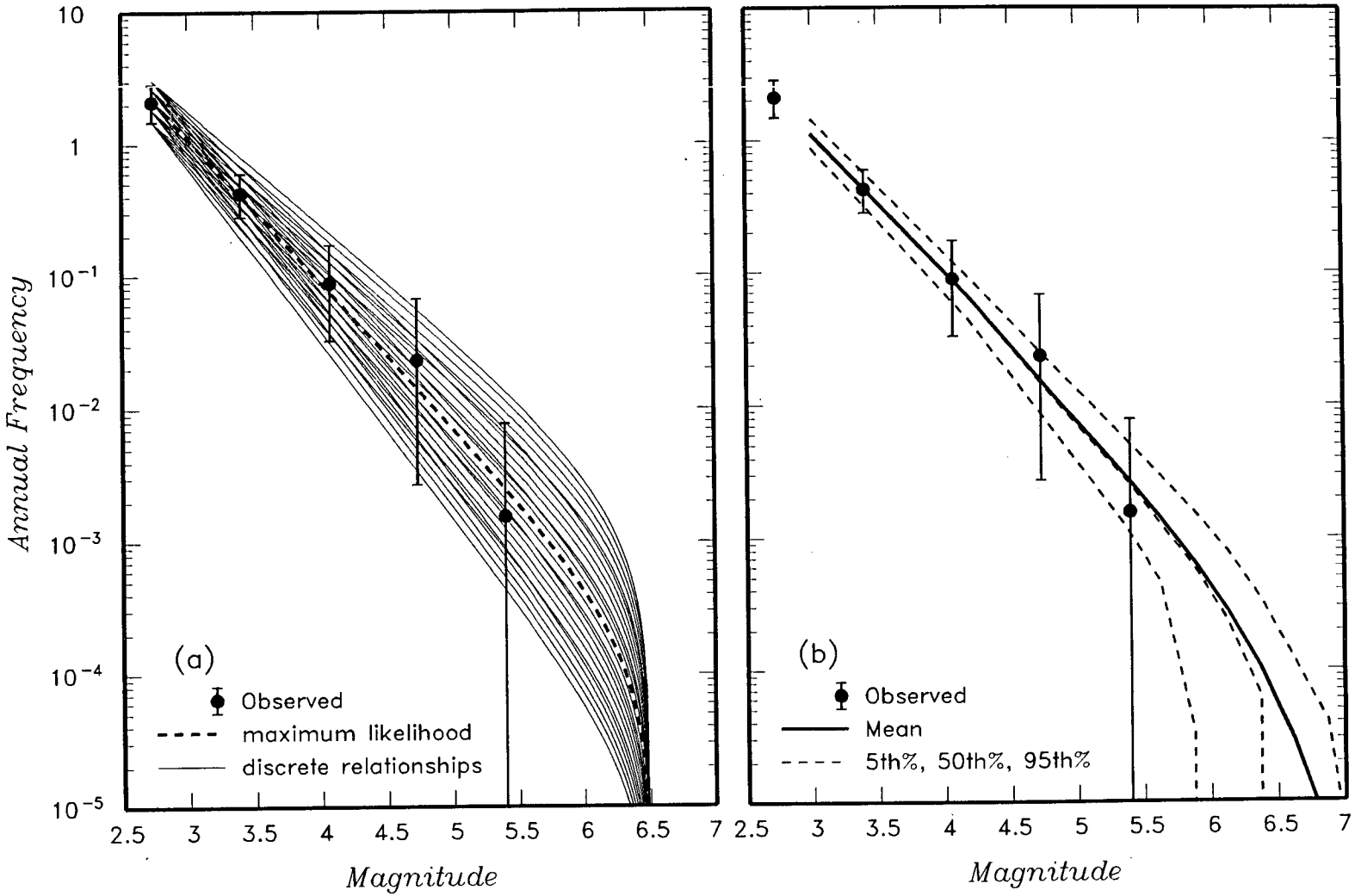

Figure 4-6 Example assessment of the recurrence relationships for an areal source zone. Left, 25 alternative recurrence relationships defined from maximum likelihood fit to observed seismicity. Right, resulting mean and percentile recurrence relationships for source zone.

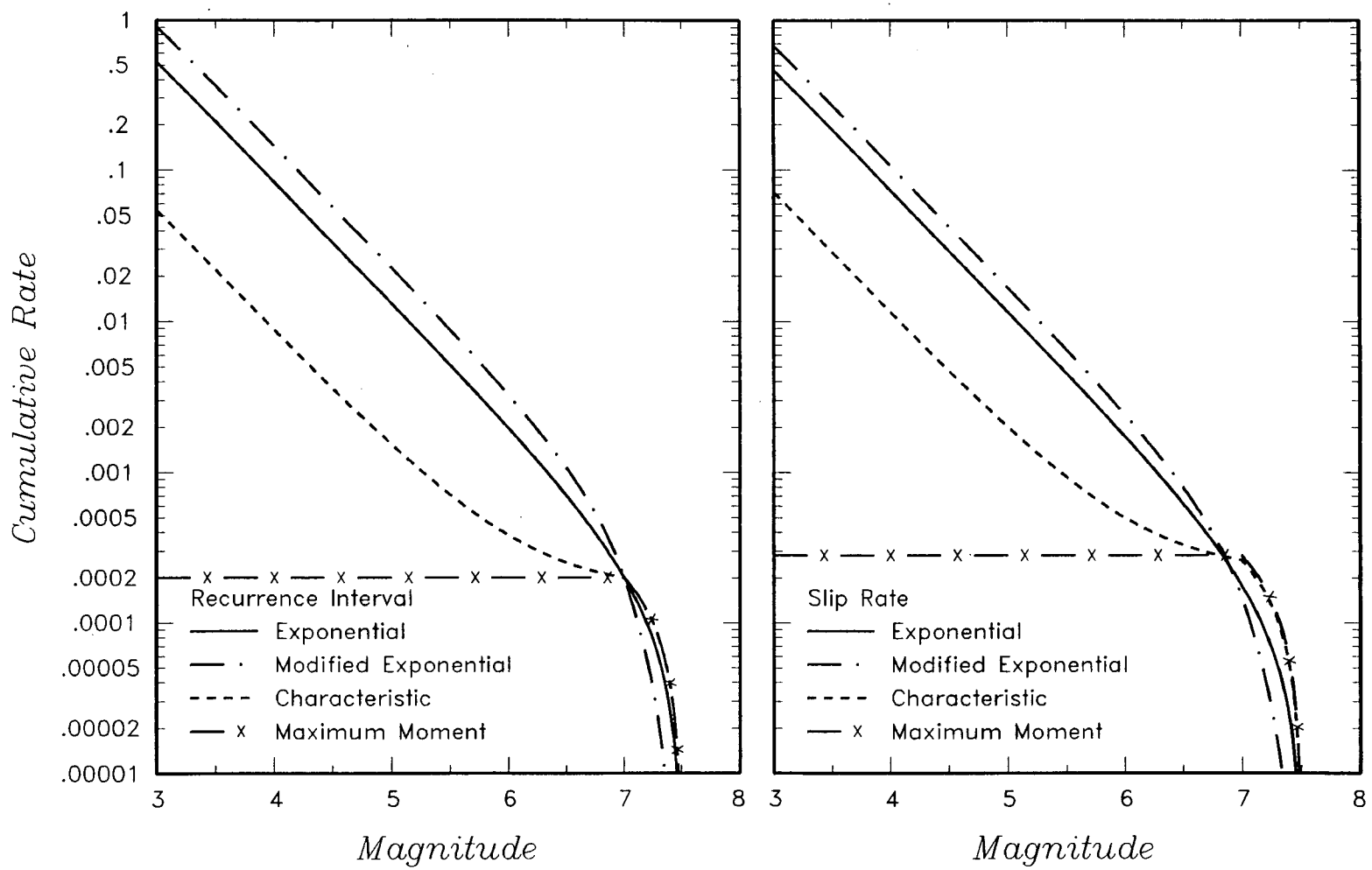

Figure 4-7. Alternative recurrence models constrained by either the recurrence interval for large events (left) or by fault slip rate converted to moment rate (right)

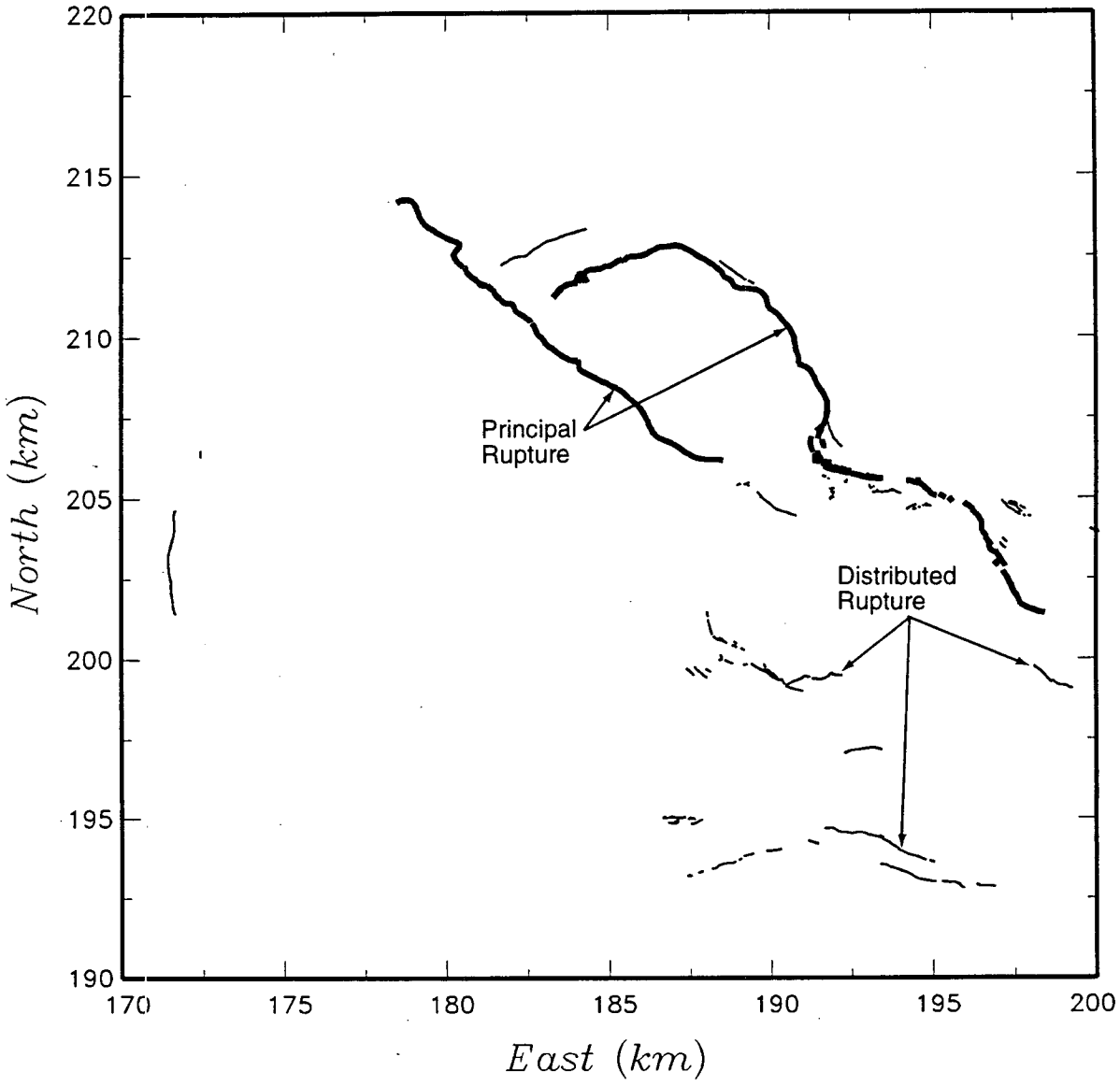

Figure 4-8 Examples of principal and distributed rupture in an earthquake

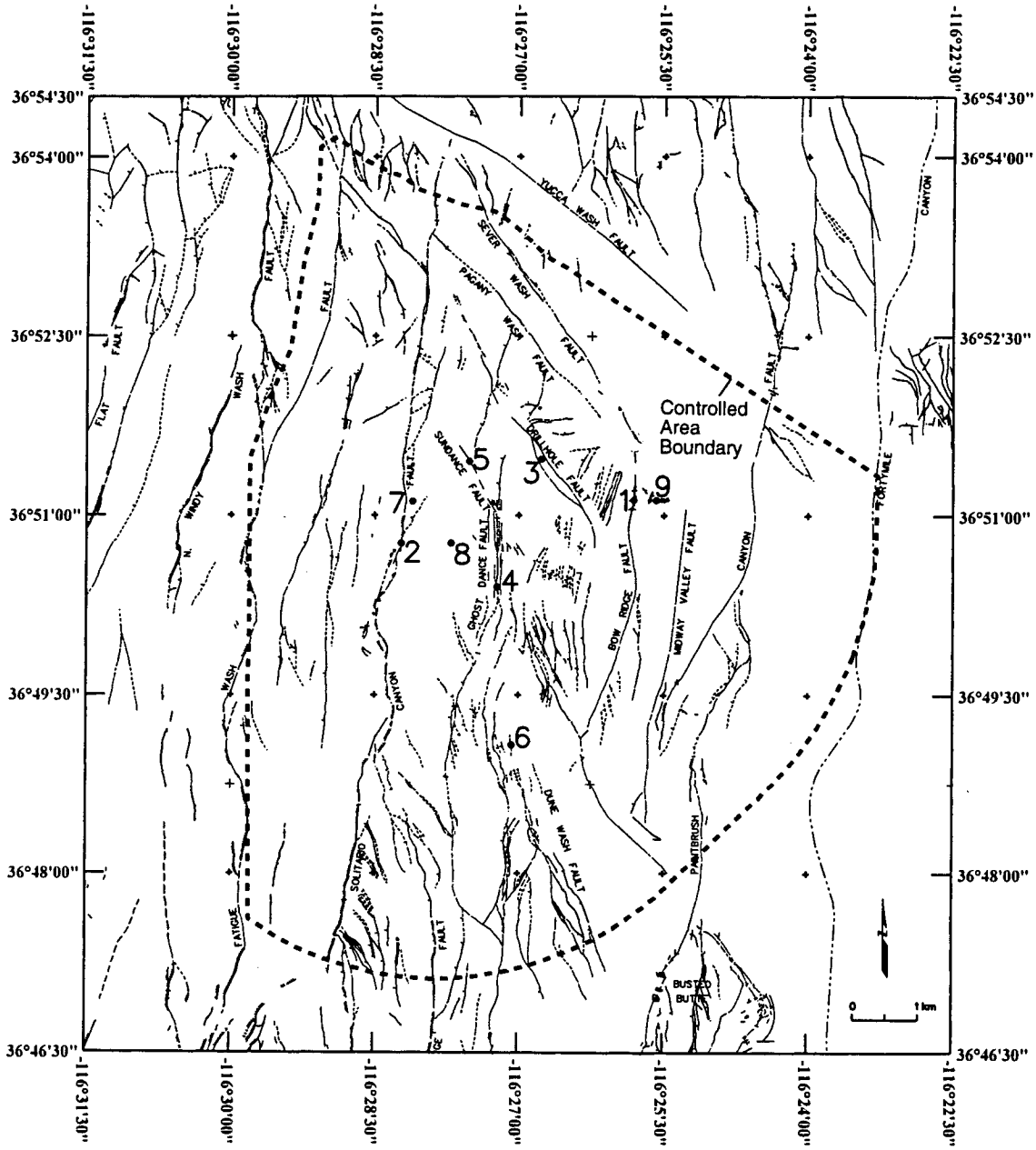

Figure 4-9 Location of nine points for demonstration of fault displacement hazard assessment

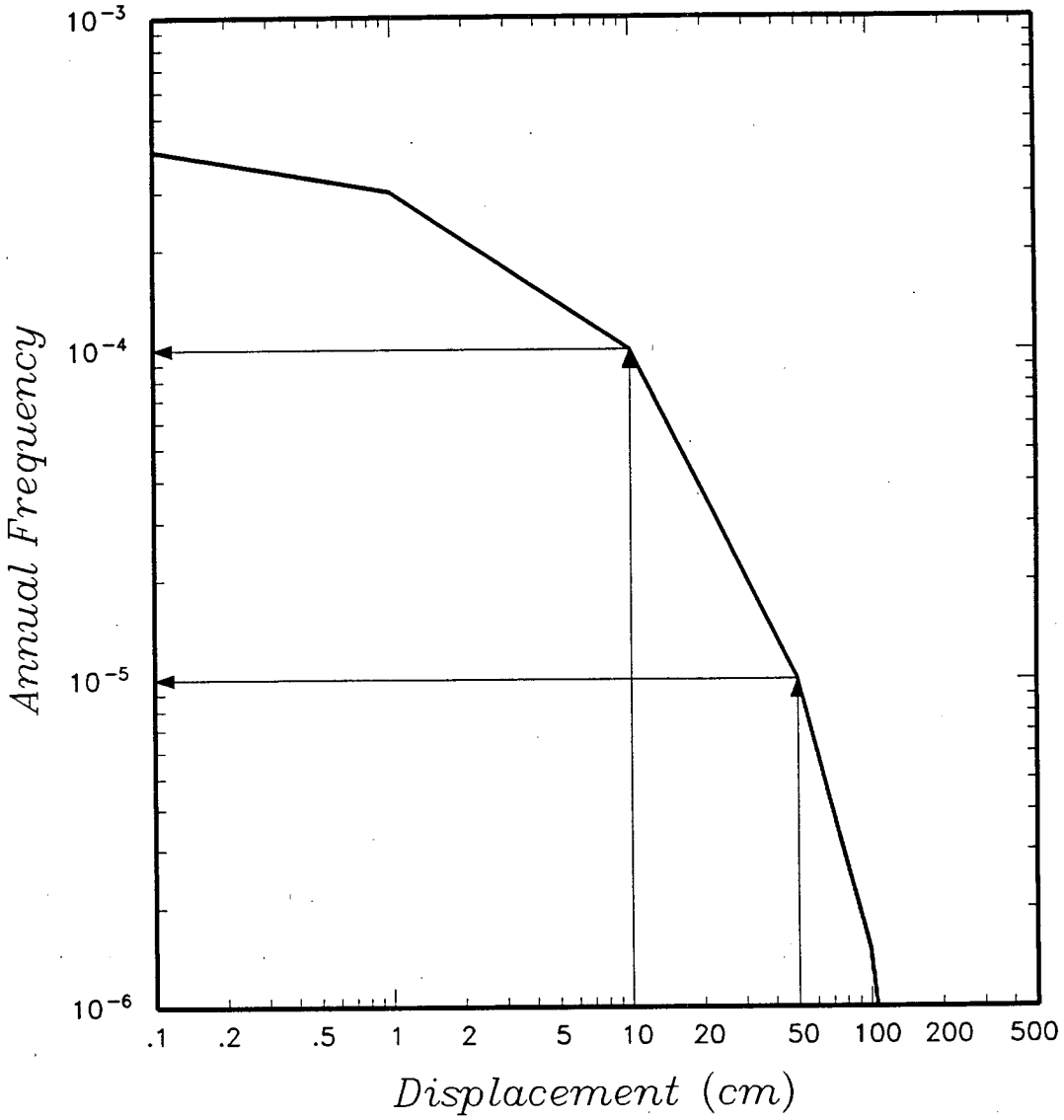

Figure 4-10 Example fault displacement hazard curve

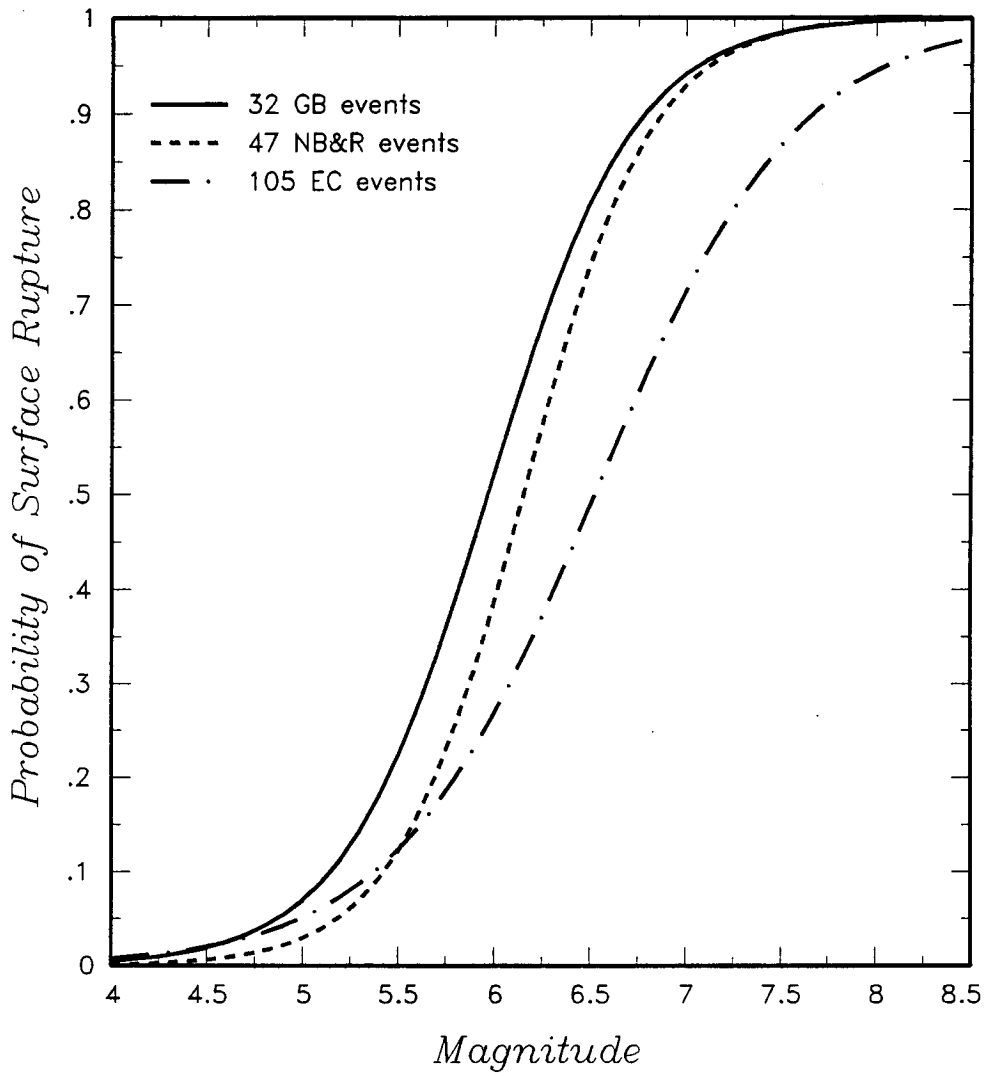

Figure 4-11 Probability of surface rupture as a function of earthquake magnitude computed from various data sets given in S.K. Pezzopane and T.E. Dawson (USGS, written communication, 1996)

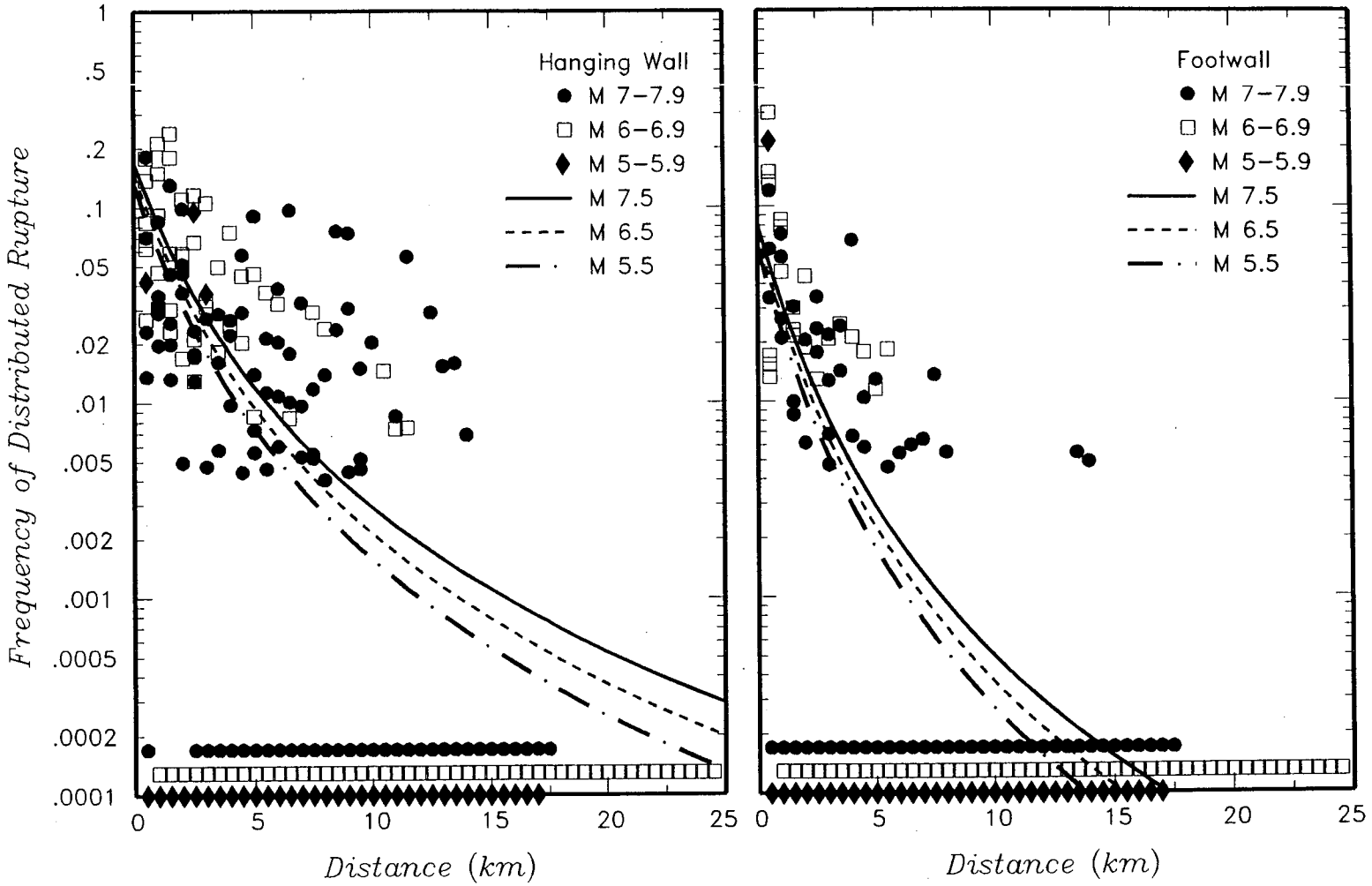

Figure 4-12. Probability of induced distributed slip as a function of distance from the rupture and hanging wall/footwall location computed from the data presented in S.K. Pezzopane and T.E. Dawson (USGS, written communication, 1996). Curves show logistic regression fits to the data.

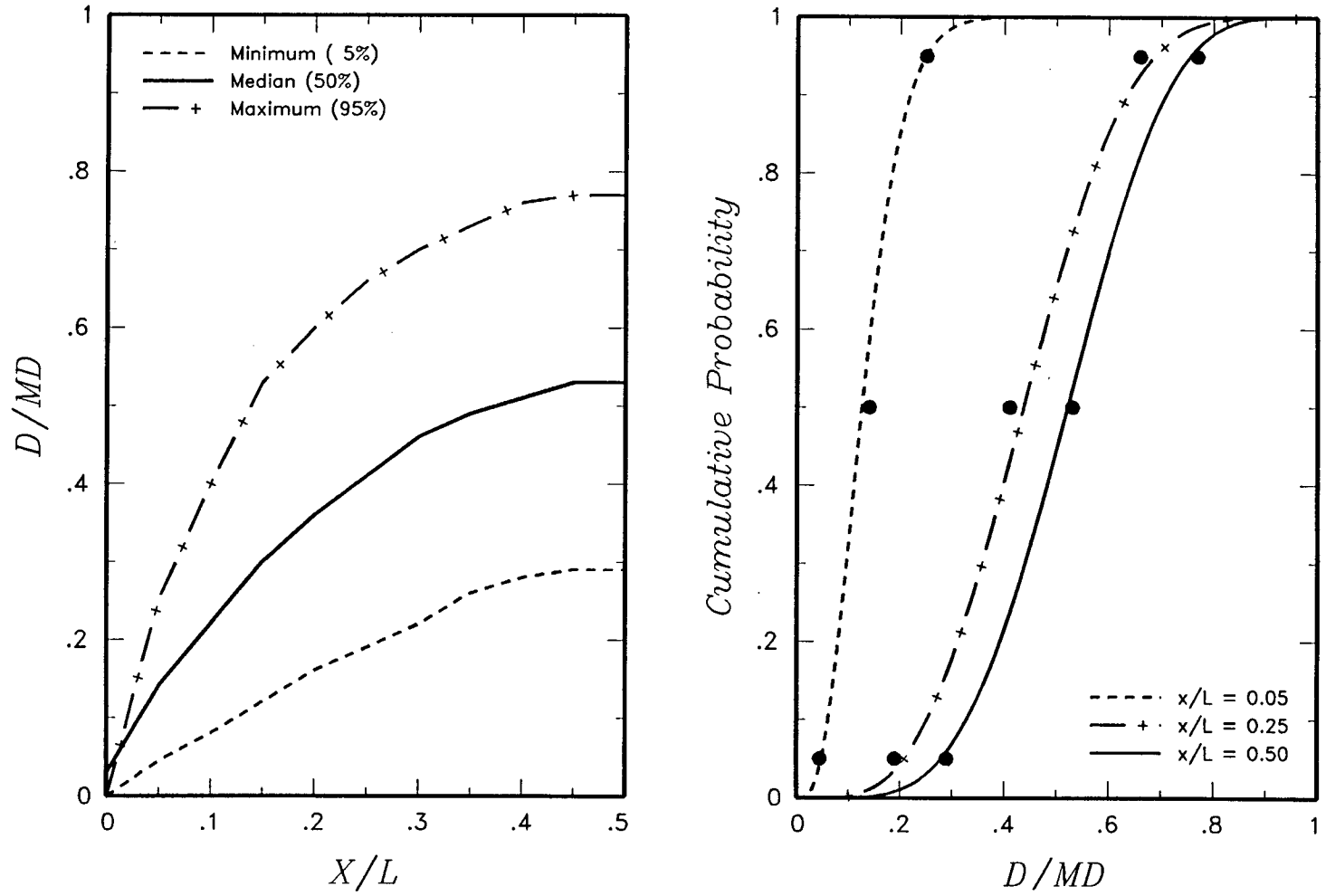

Figure 4-13 Probability distributions for D/MD as a function of location along a principal rupture. Left, smooth curves for minimum, median, and maximum values of D/MD developed by the ASM team from analysis of historical ruptures. Right, Beta distributions fit to the D/MD values at specific values of x/L.

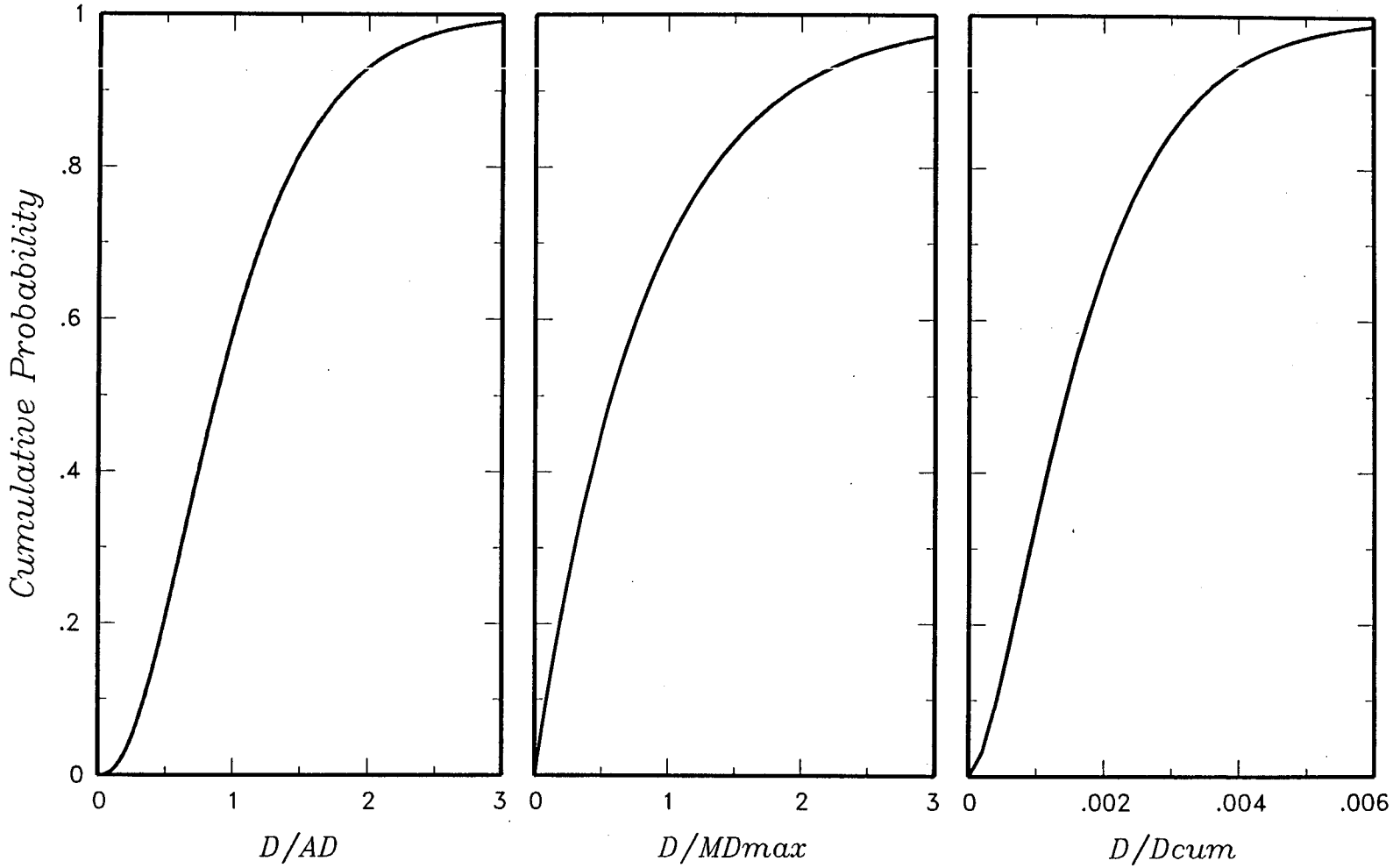

Figure 4-14 Example distributions for computing the conditional probability of exceeding a specific displacement, *d*

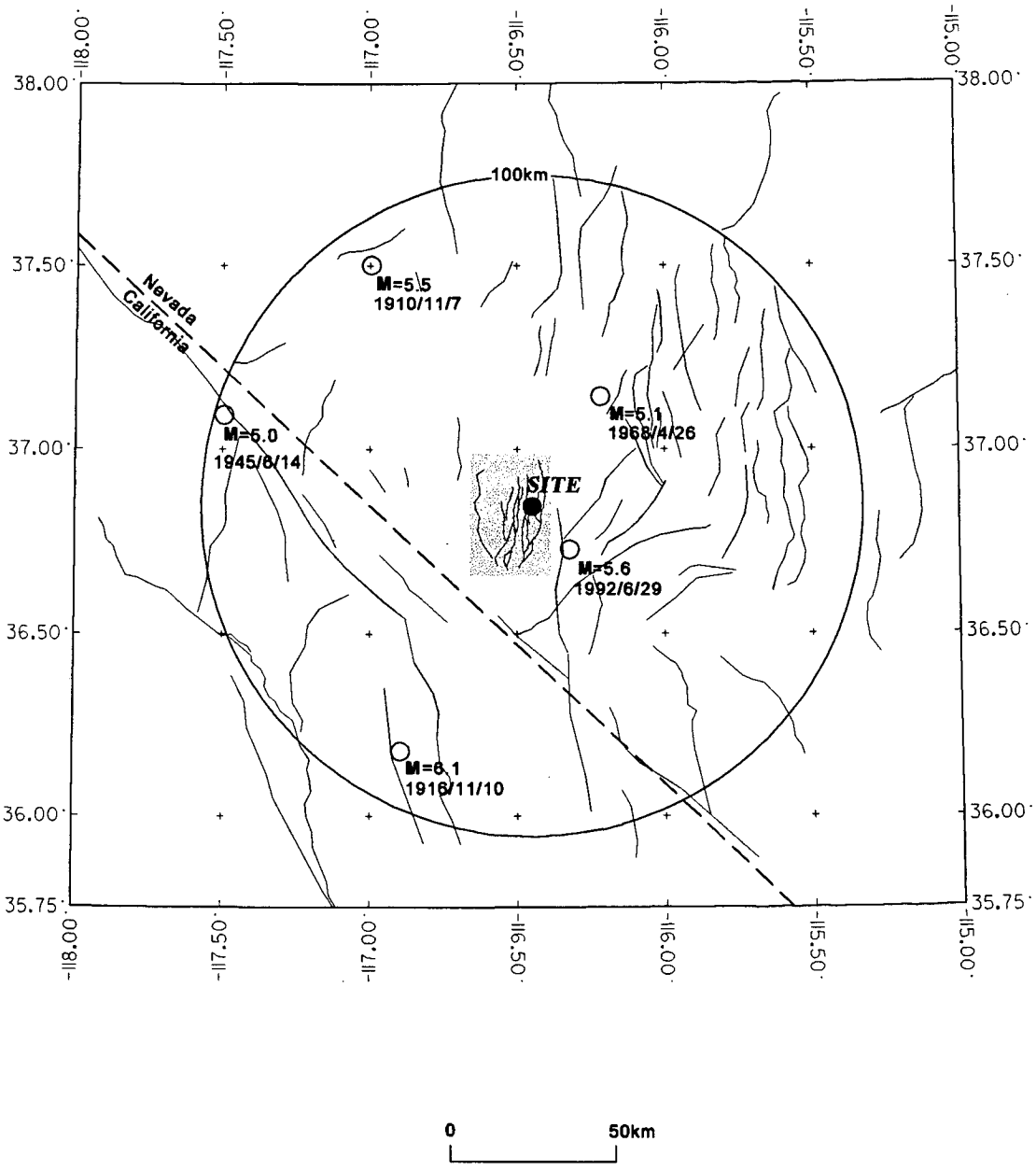

Figure 4-15 Region used for comparison of earthquake recurrence relationships developed from SSFD team models. Also shown are recorded earthquakes of magnitude M_W5 and greater.

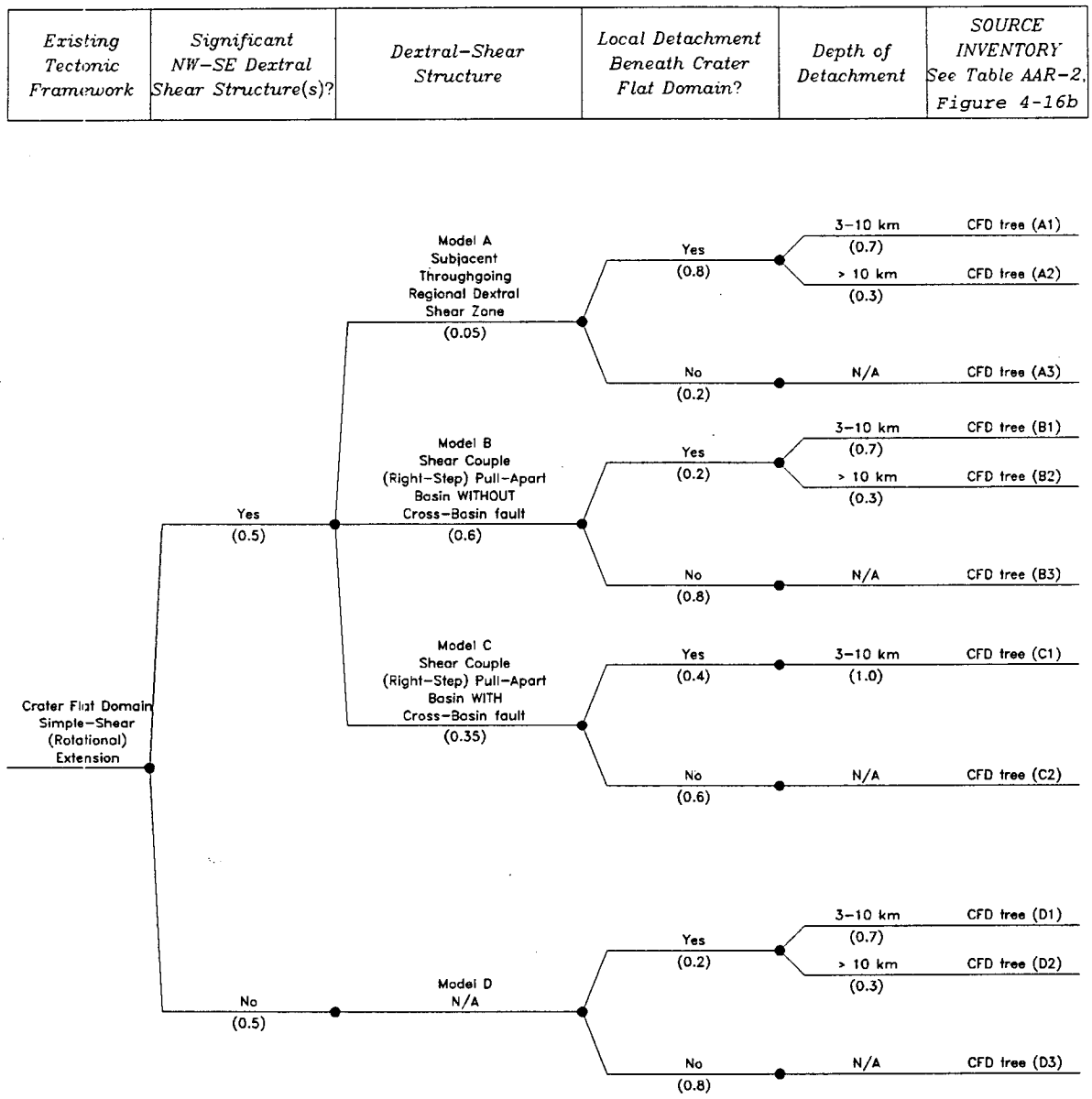

Figure 4-16a Logic tree for local fault source models developed by the AAR team

Crater Flat Domain (CFD) Model	*Behavior*	*Coalesced Behavior*	*Source List*	*Independent Linked Behavior*	*Source List*

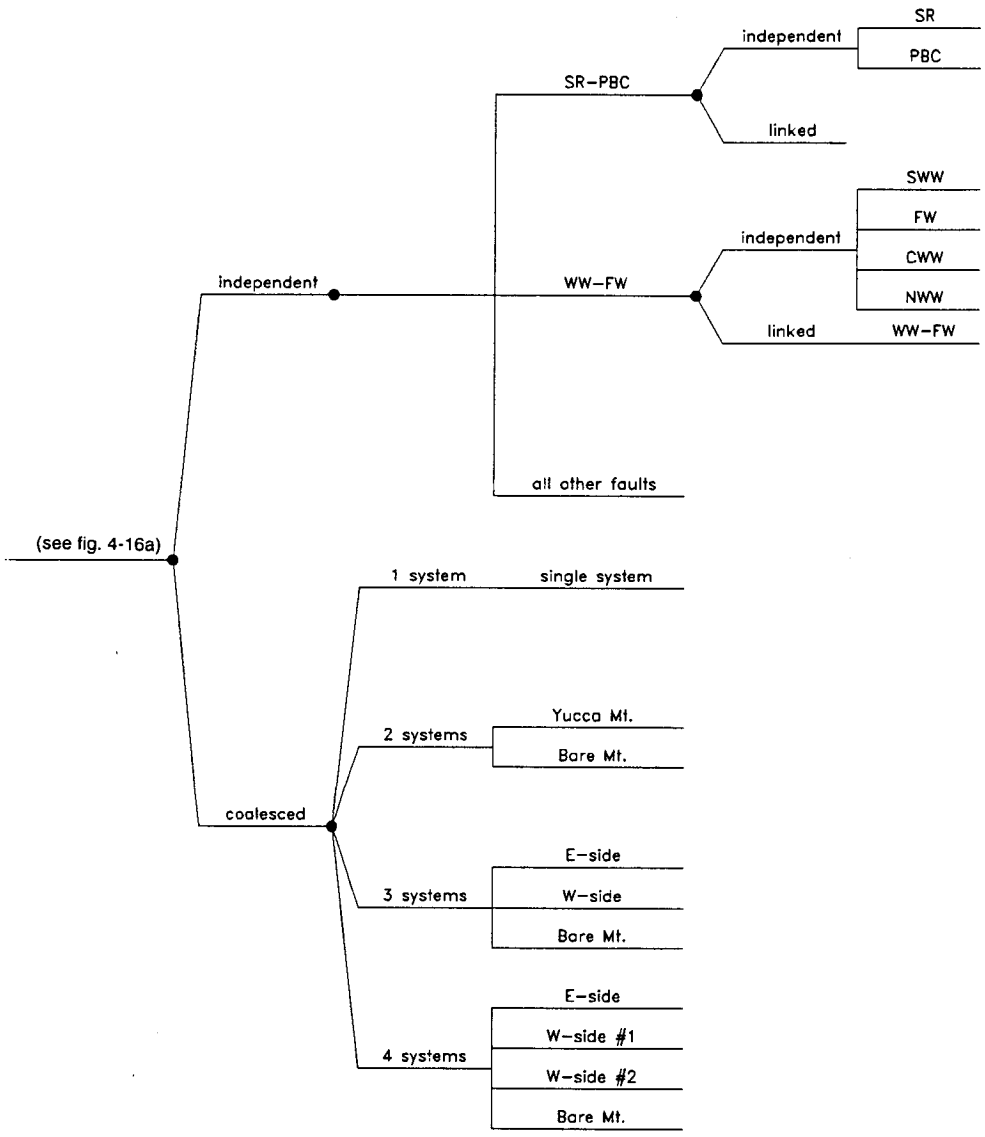

Figure 4-16b Logic tree for local fault source behavior developed by the AAR team

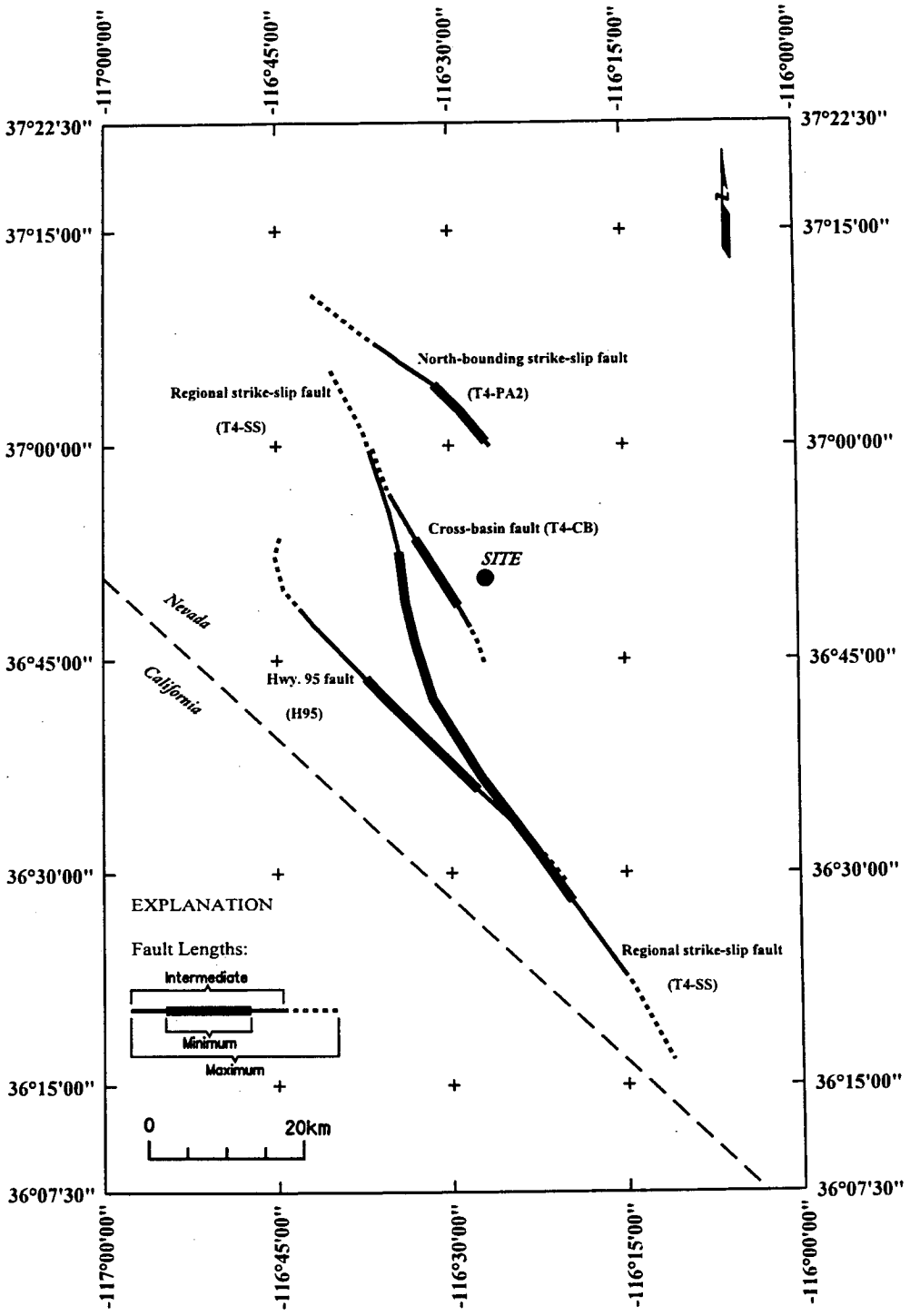

Figure 4-17 Location of AAR team's inferred local dextral shear sources

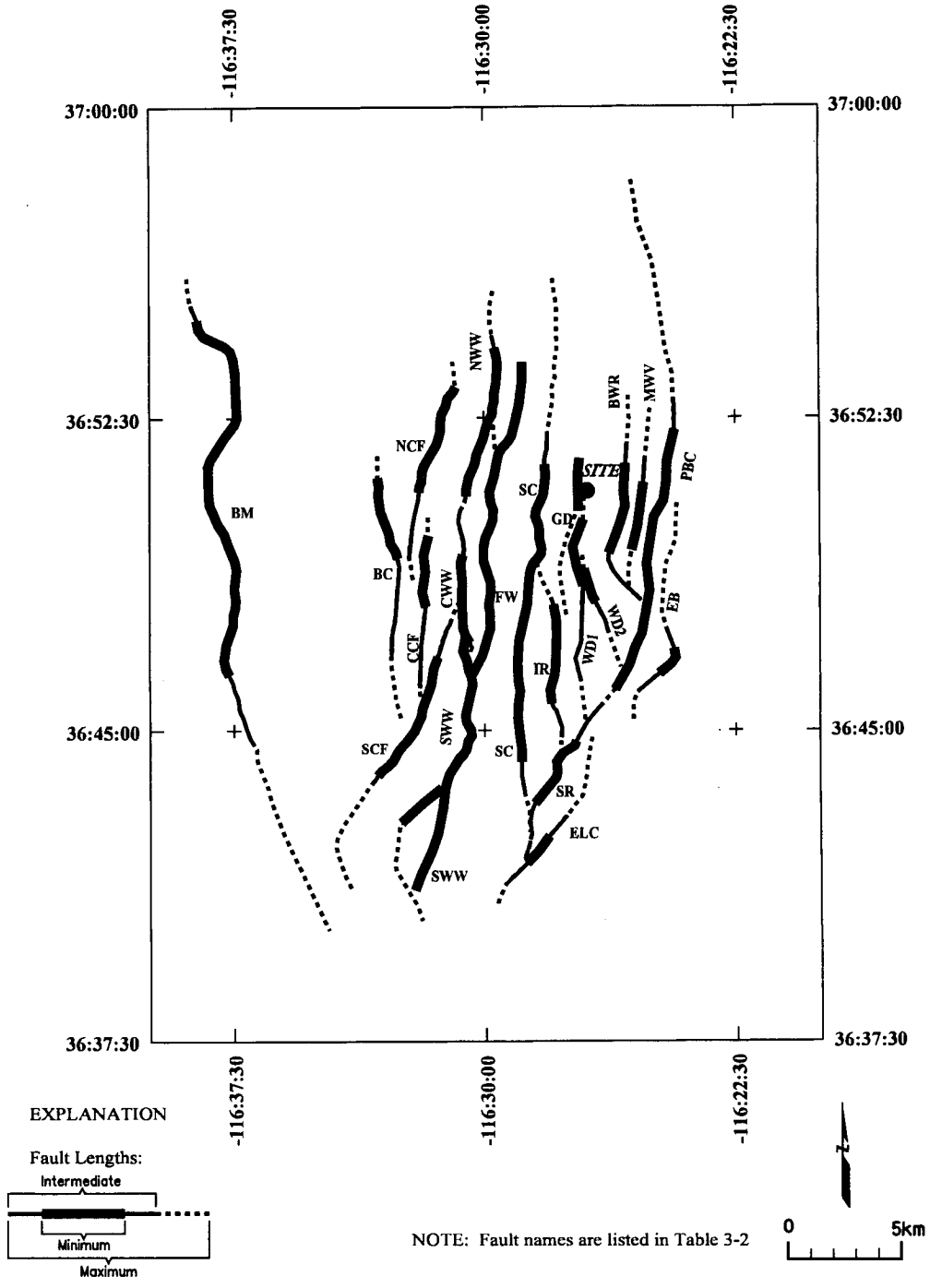

Figure 4-18. Location of local faults considered by the AAR team to be acting as independent sources

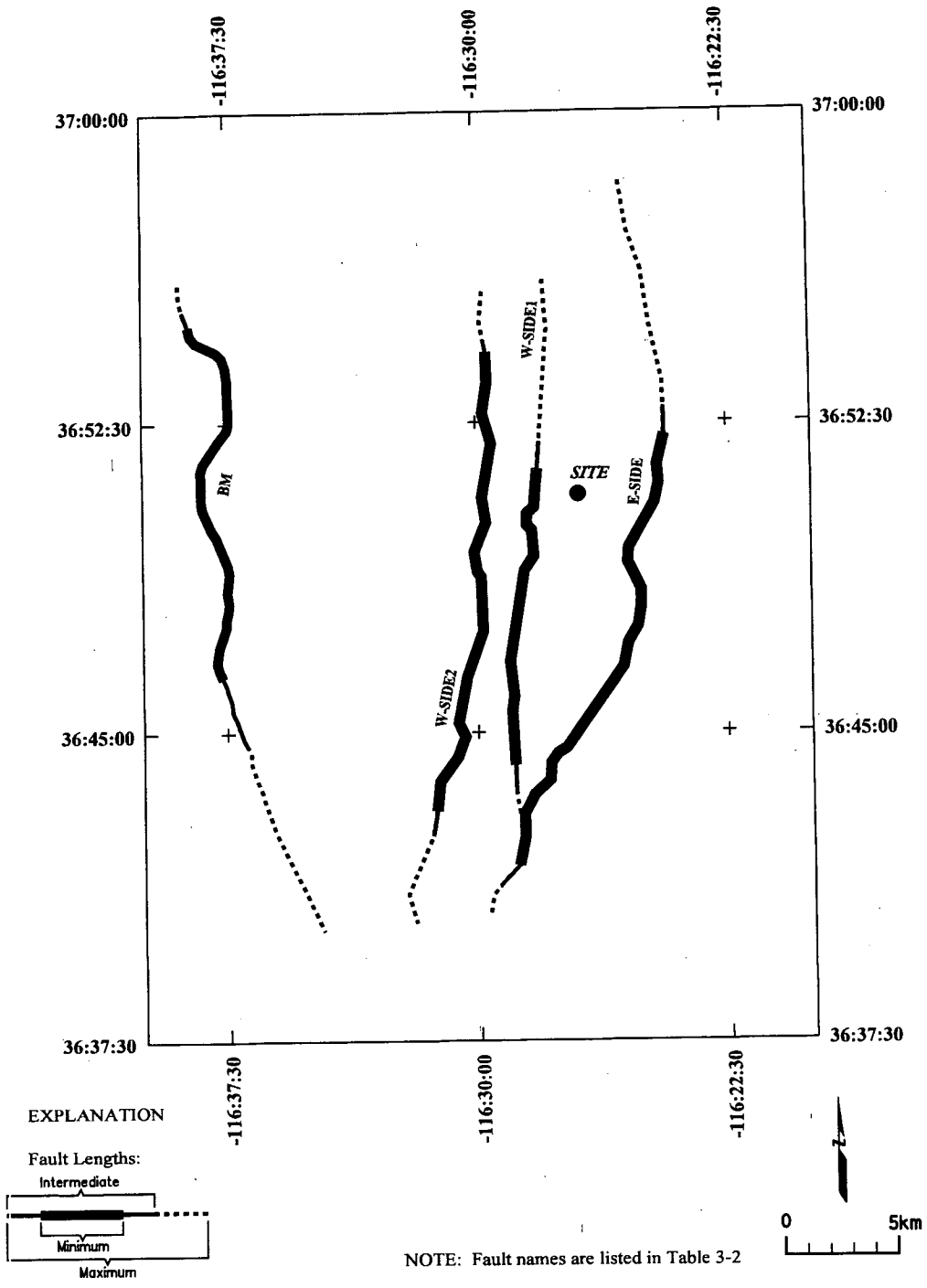

Figure 4-19. Location of coalesced faults considered by the AAR team

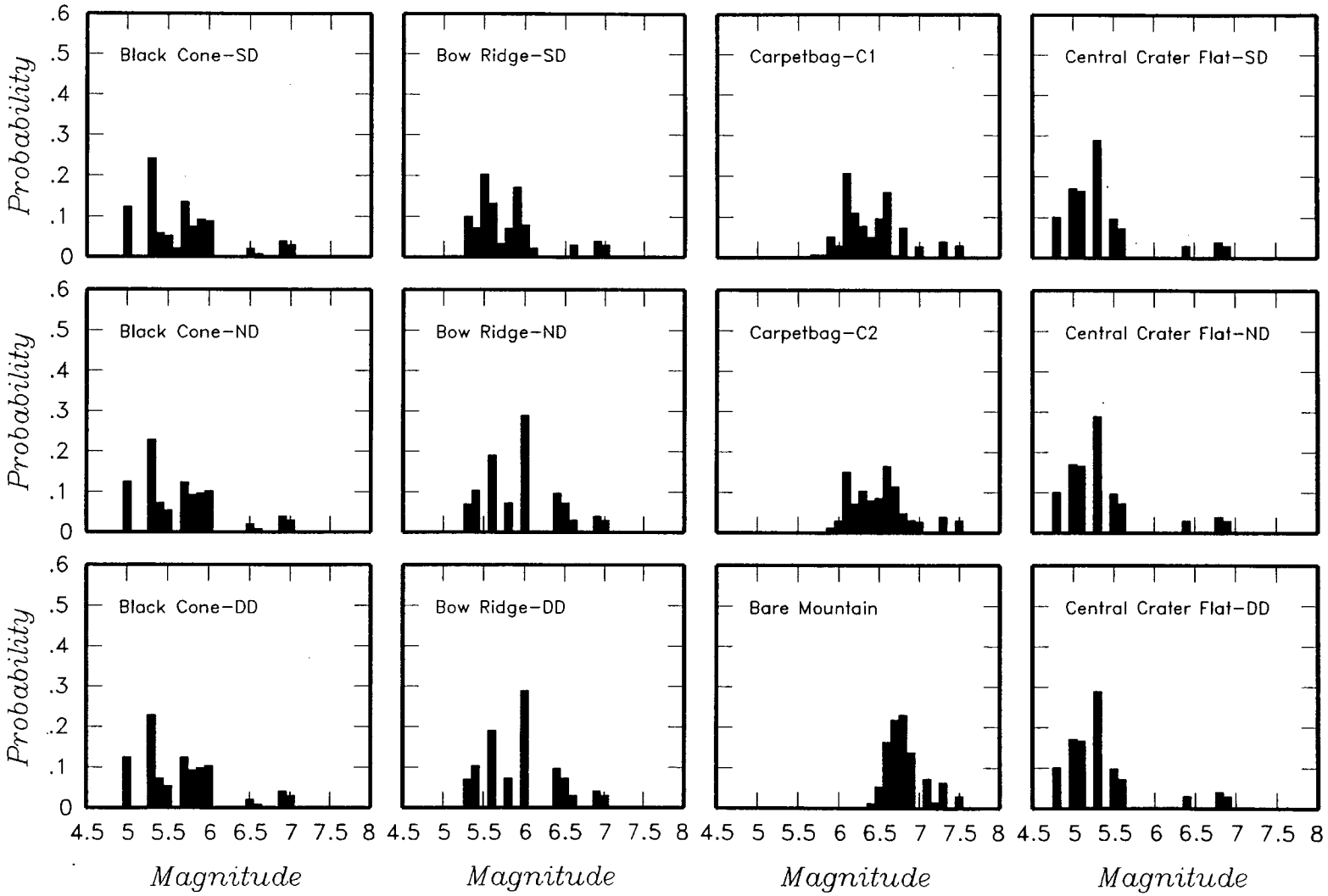

Figure 4-20a. Maximum magnitude distributions for AAR team's local fault sources. A, B, and C and numbers refer to variations of tectonic models A, B, and C; DD–deep detachment, ND–no detachment, SD-shallow detachment, SINGLE–single rupture (BM and YM faults), Single west-side rupture of west-side faults (WS1+WS2), Single Yucca Mountain–coalesced single YM system.

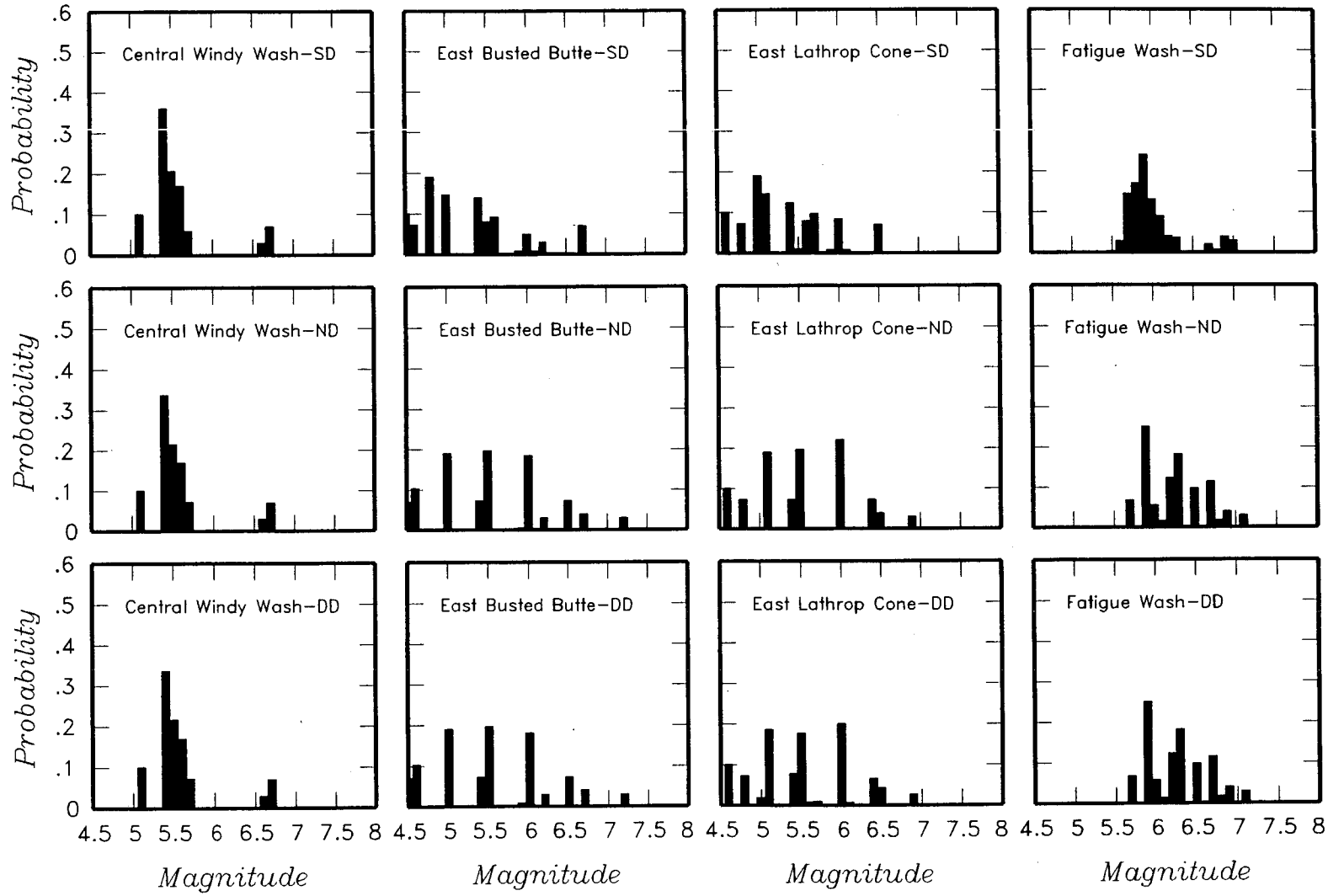

Figure 4-20b. Maximum magnitude distributions for AAR team's local fault sources

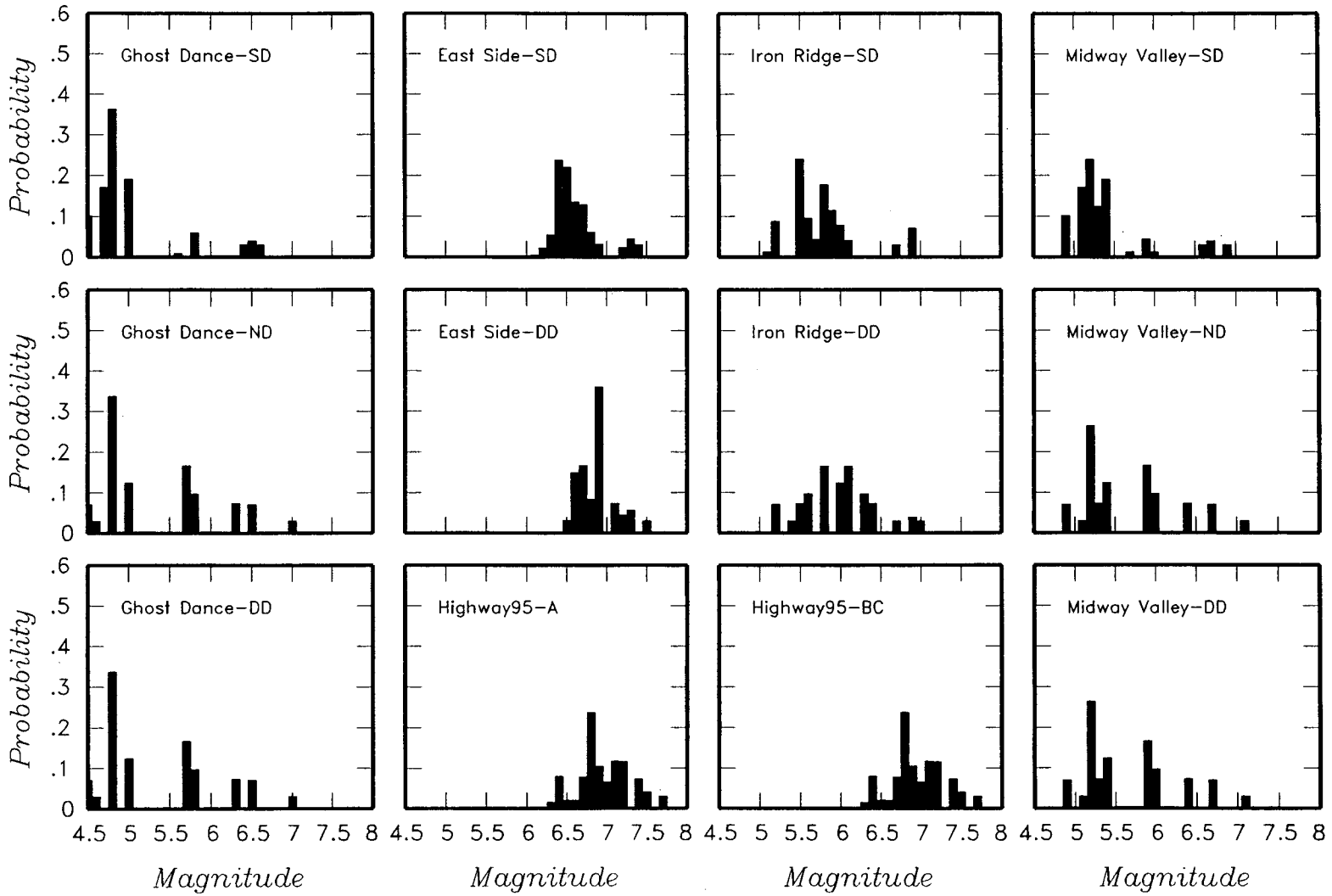

Figure 4-20c. Maximum magnitude distributions for AAR team's local fault sources

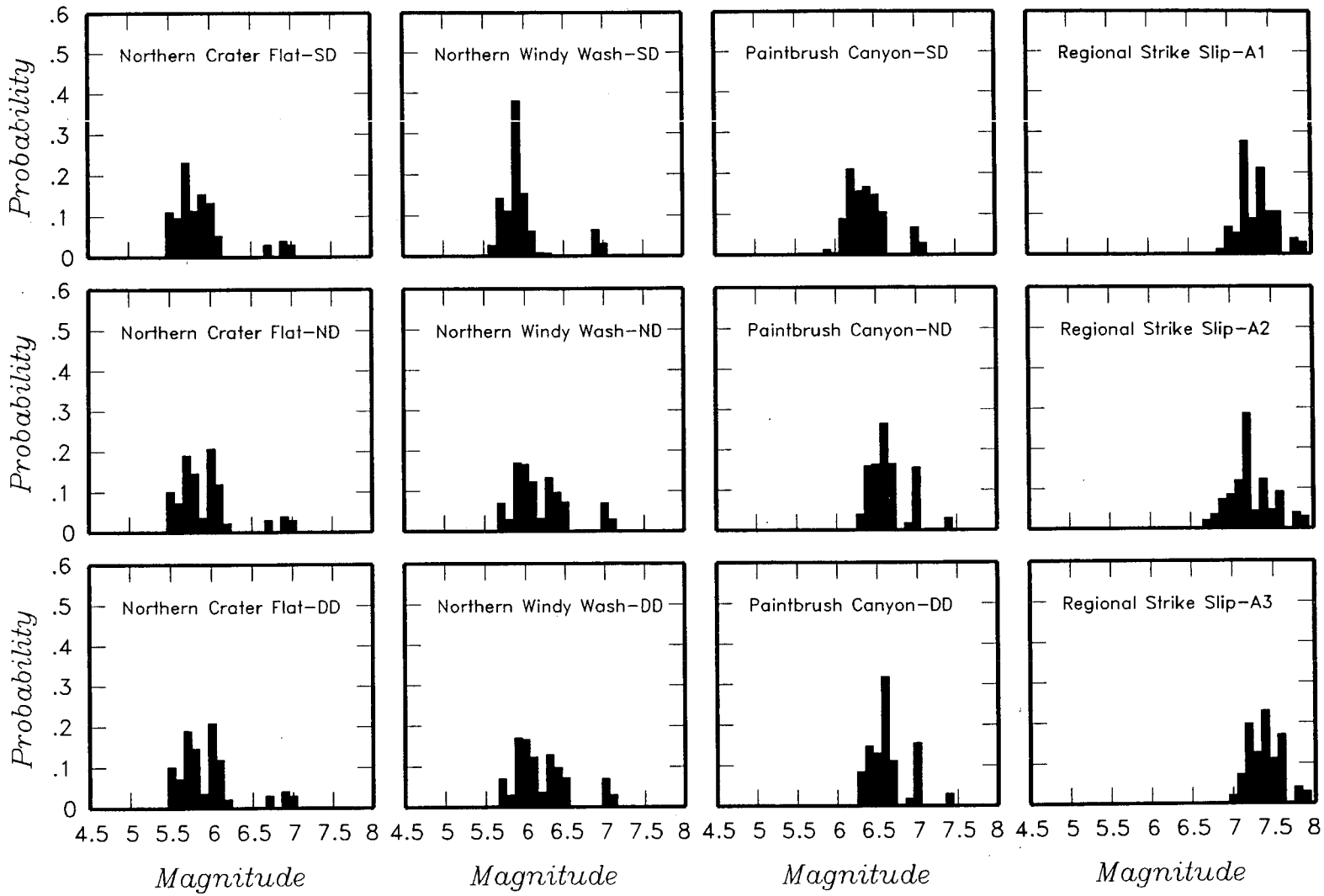

Figure 4-20d. Maximum magnitude distributions for AAR team's local fault sources

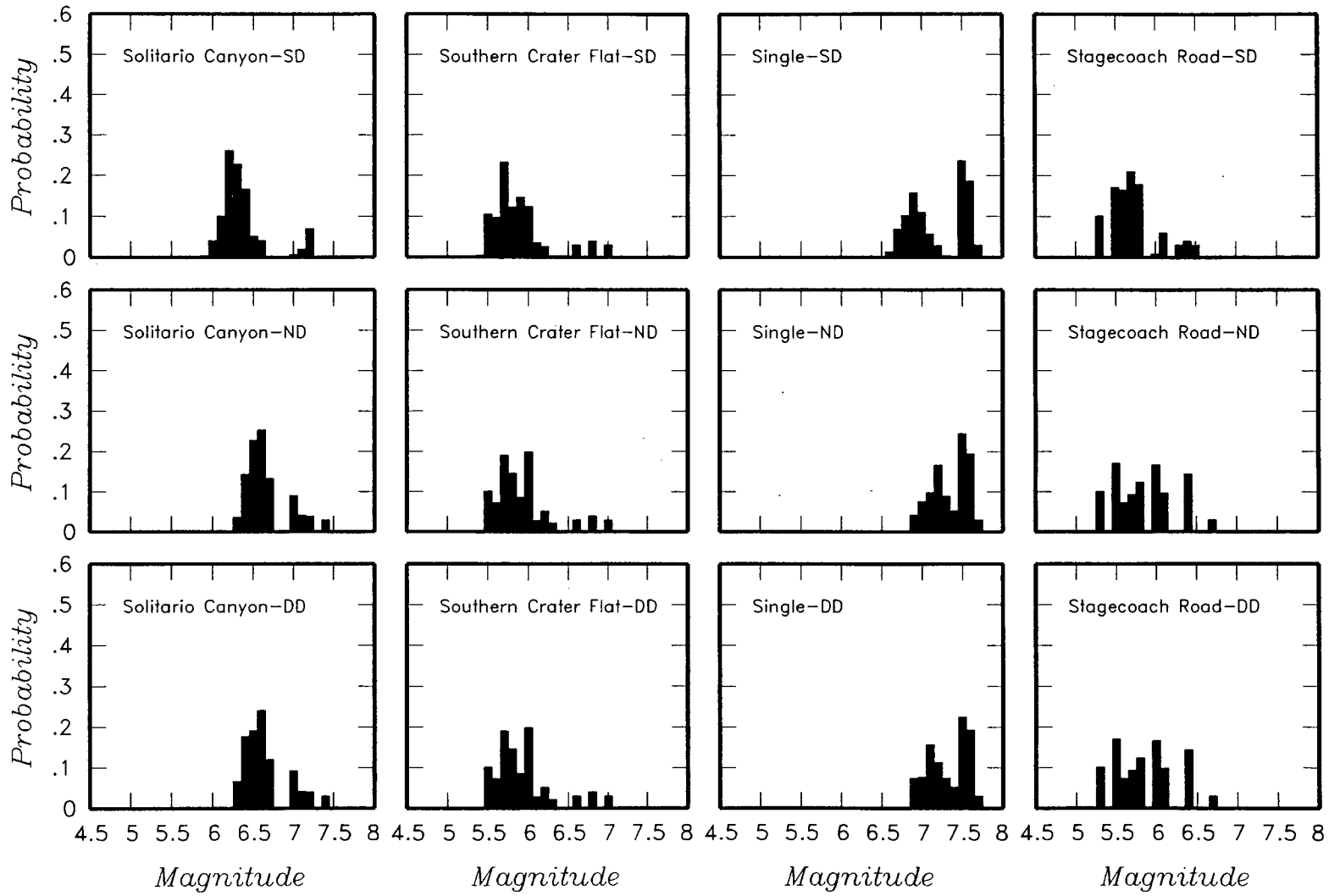

Figure 4-20e. Maximum magnitude distributions for AAR team's local fault sources

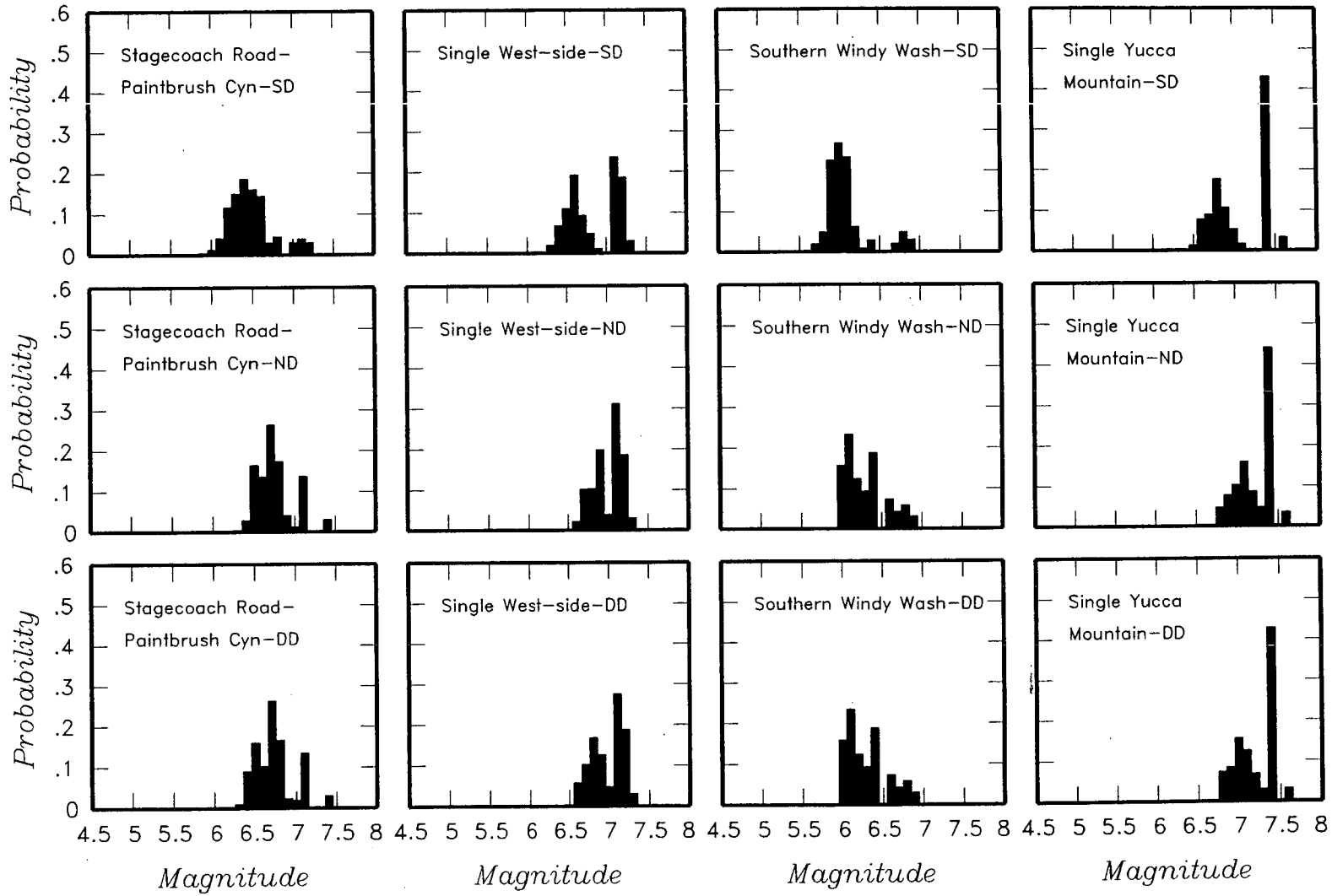

Figure 4-20f. Maximum magnitude distributions for AAR team's local fault sources

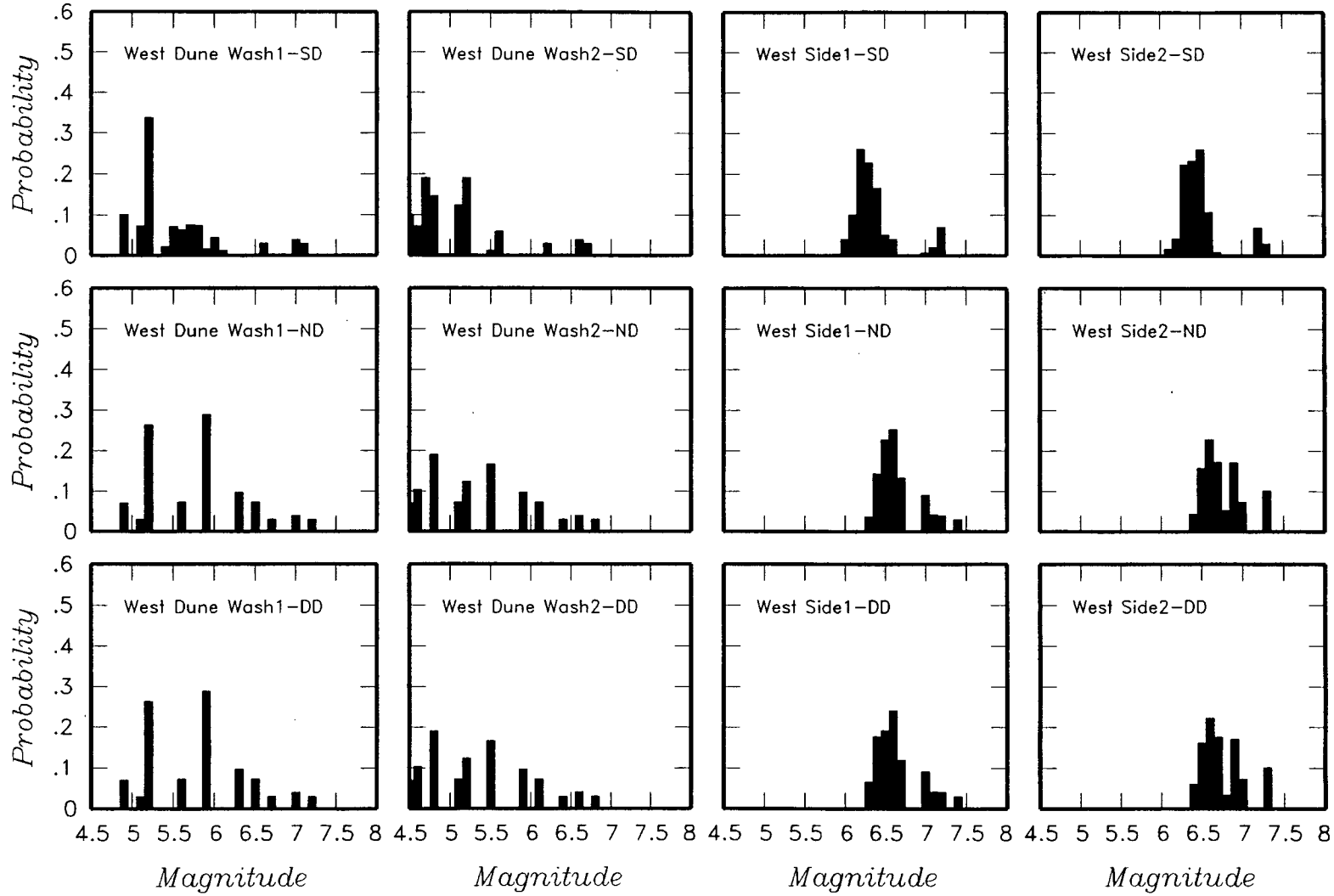

Figure 4-20g. Maximum magnitude distributions for AAR team's local fault sources

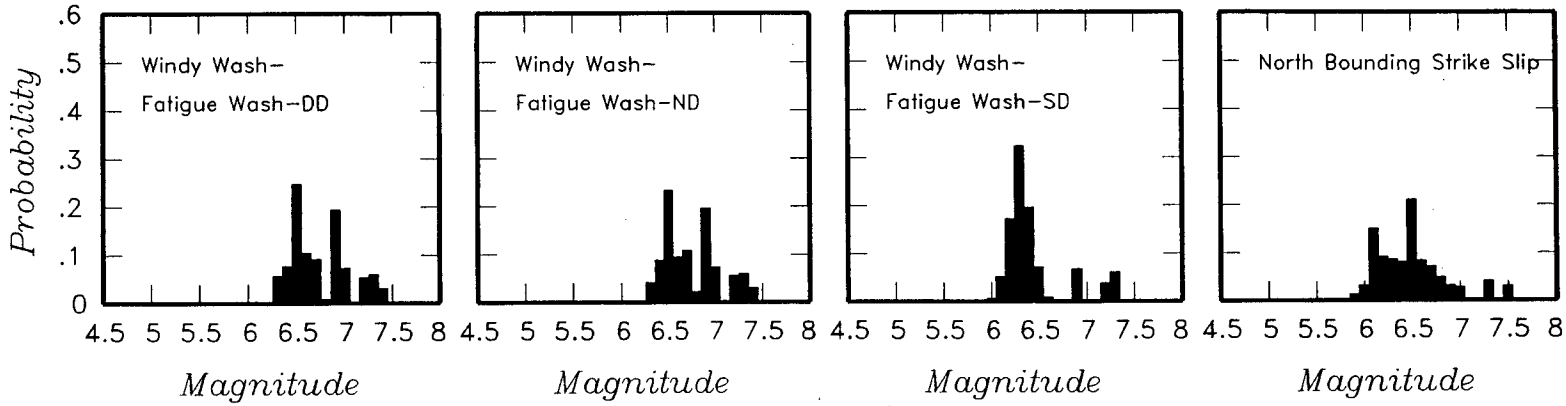

Figure 4-20h. Maximum magnitude distributions for AAR team's local fault sources

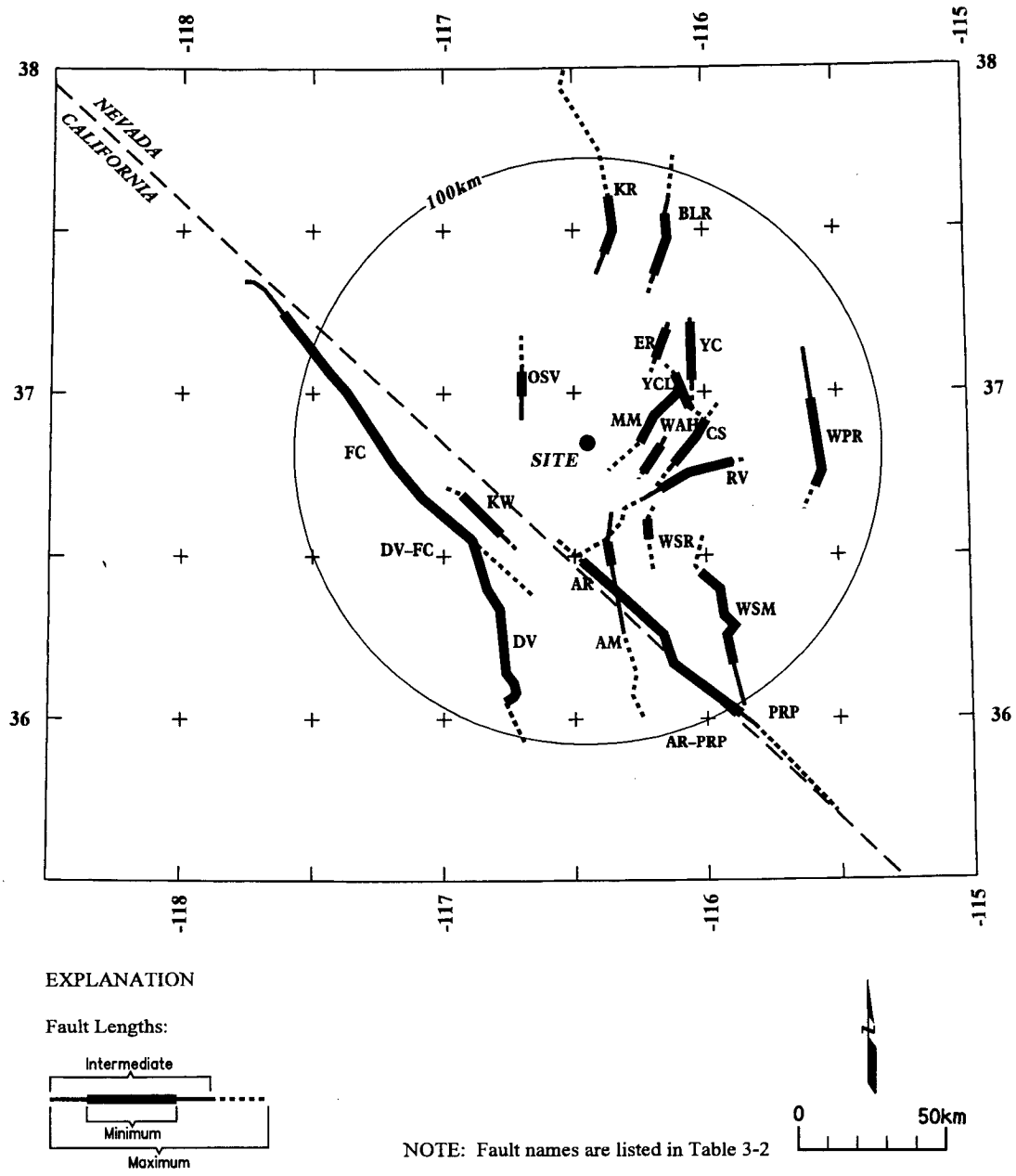

Figure 4-21. Regional fault sources considered by the AAR team

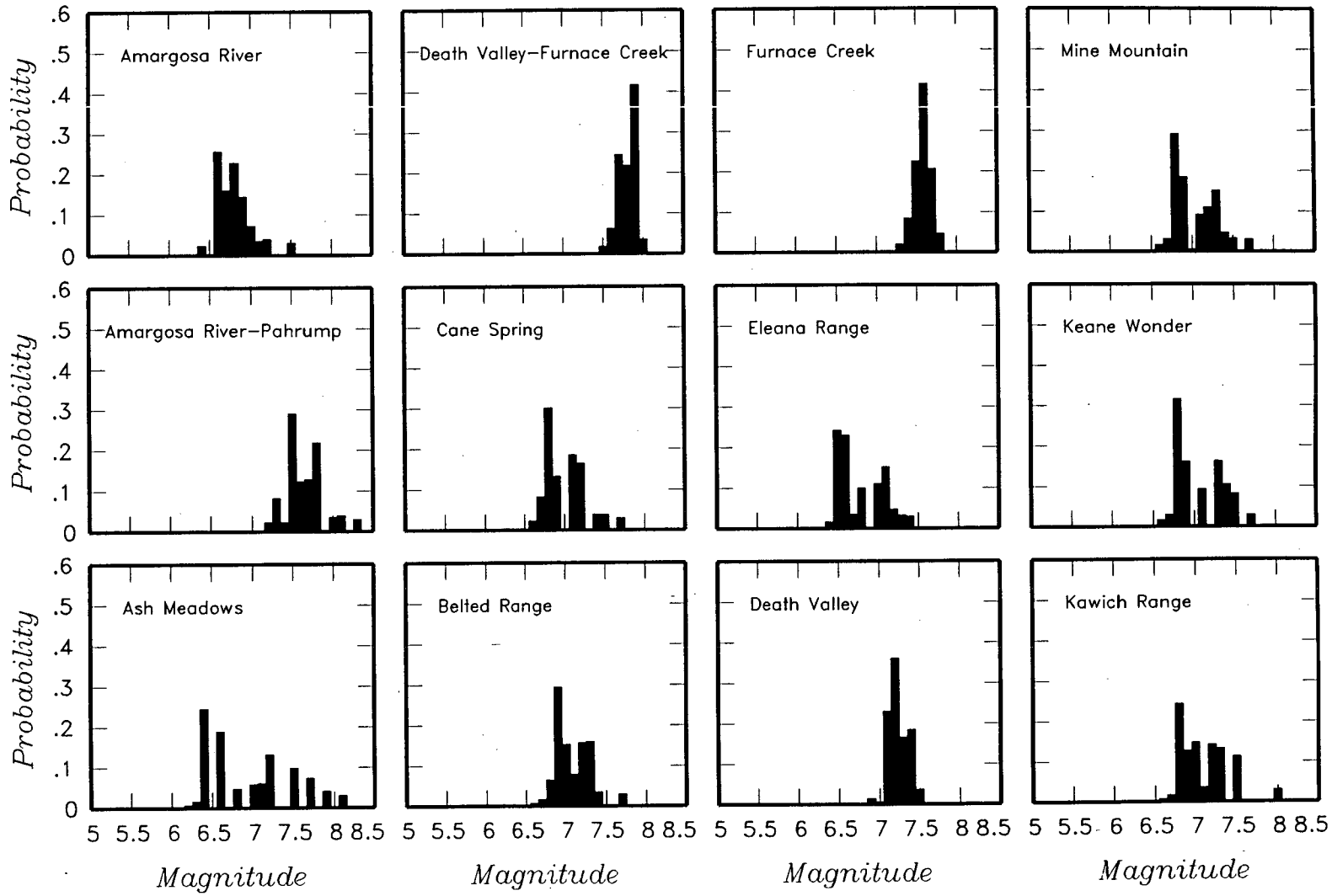

Figure 4-22 Maximum magnitude distributions for AAR team's regional fault sources

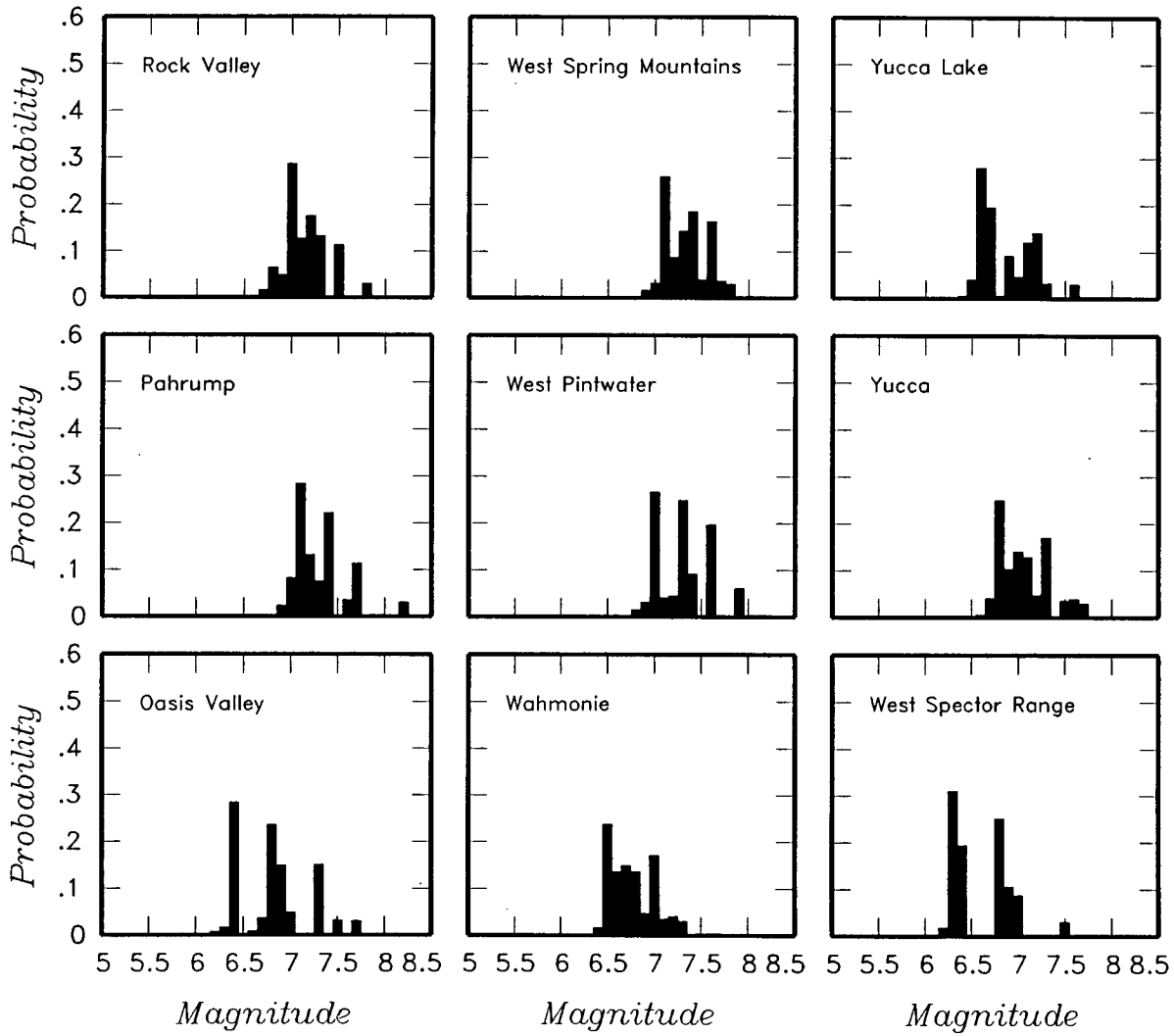

Figure 4-22 (Cont'd.) Maximum magnitude distributions for AAR team's regional fault sources

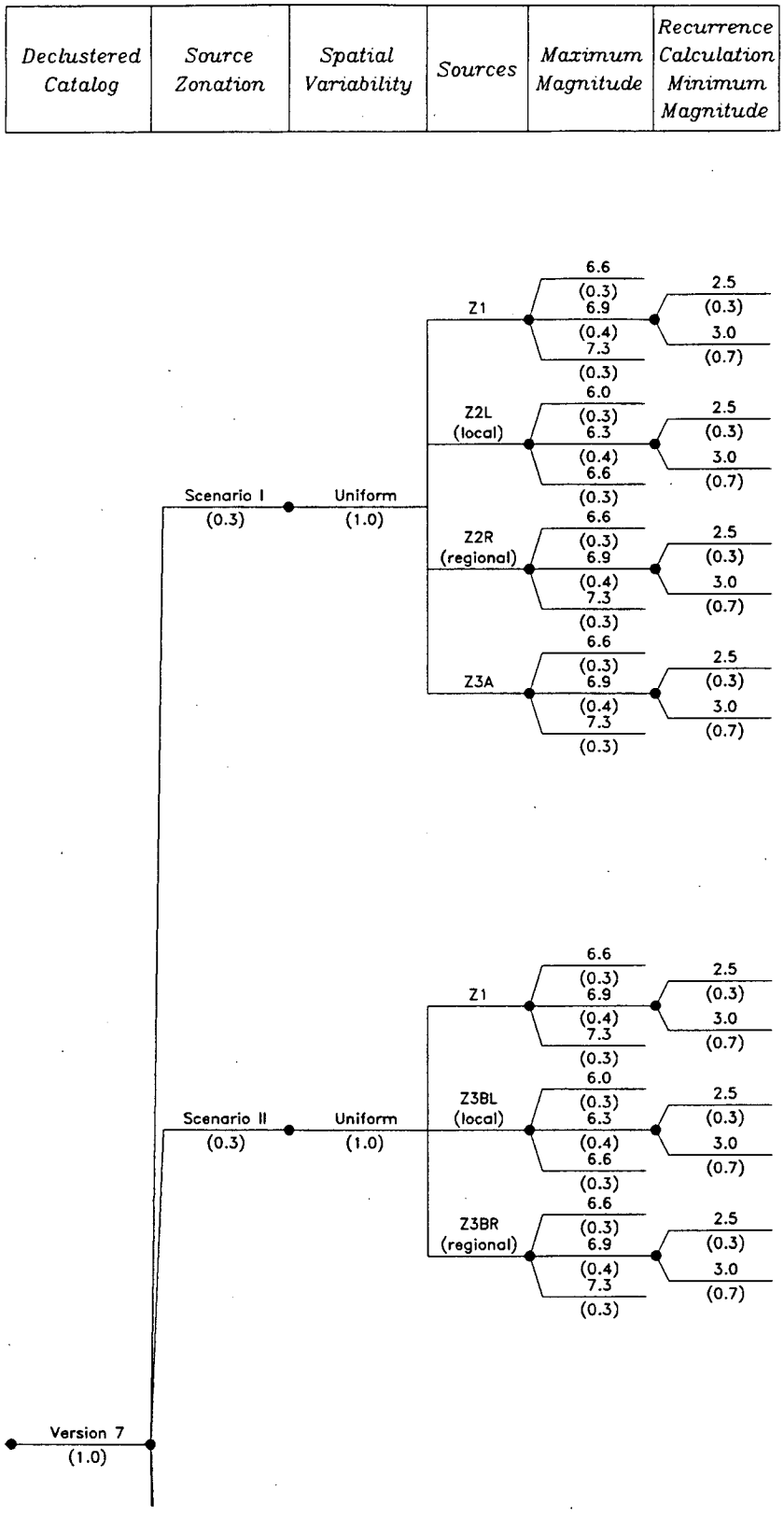

Figure 4-23 Logic tree for regional source zones developed by the AAR team

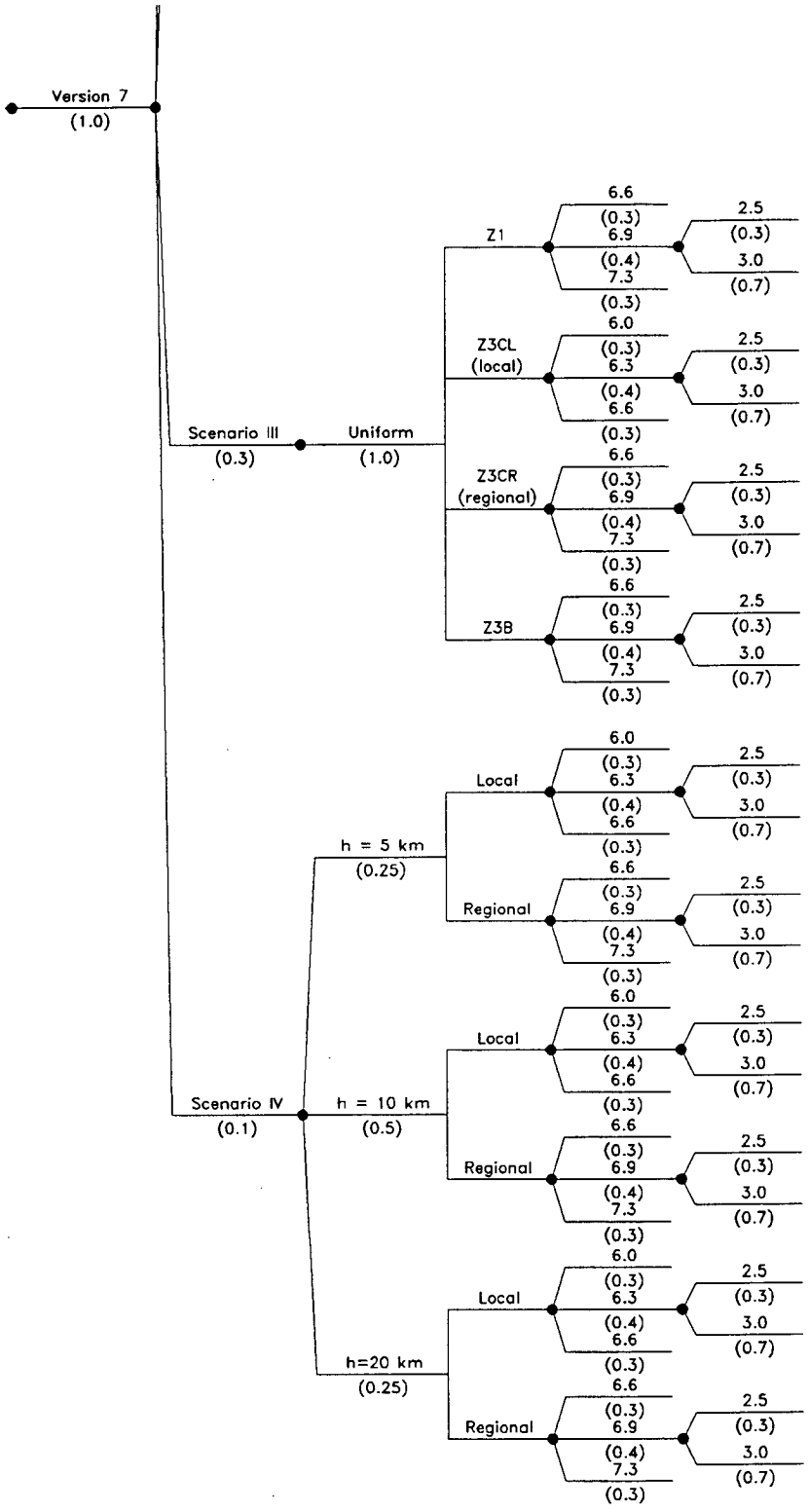

Figure 4-23 (Cont'd.) Logic tree for regional source zones developed by the AAR team

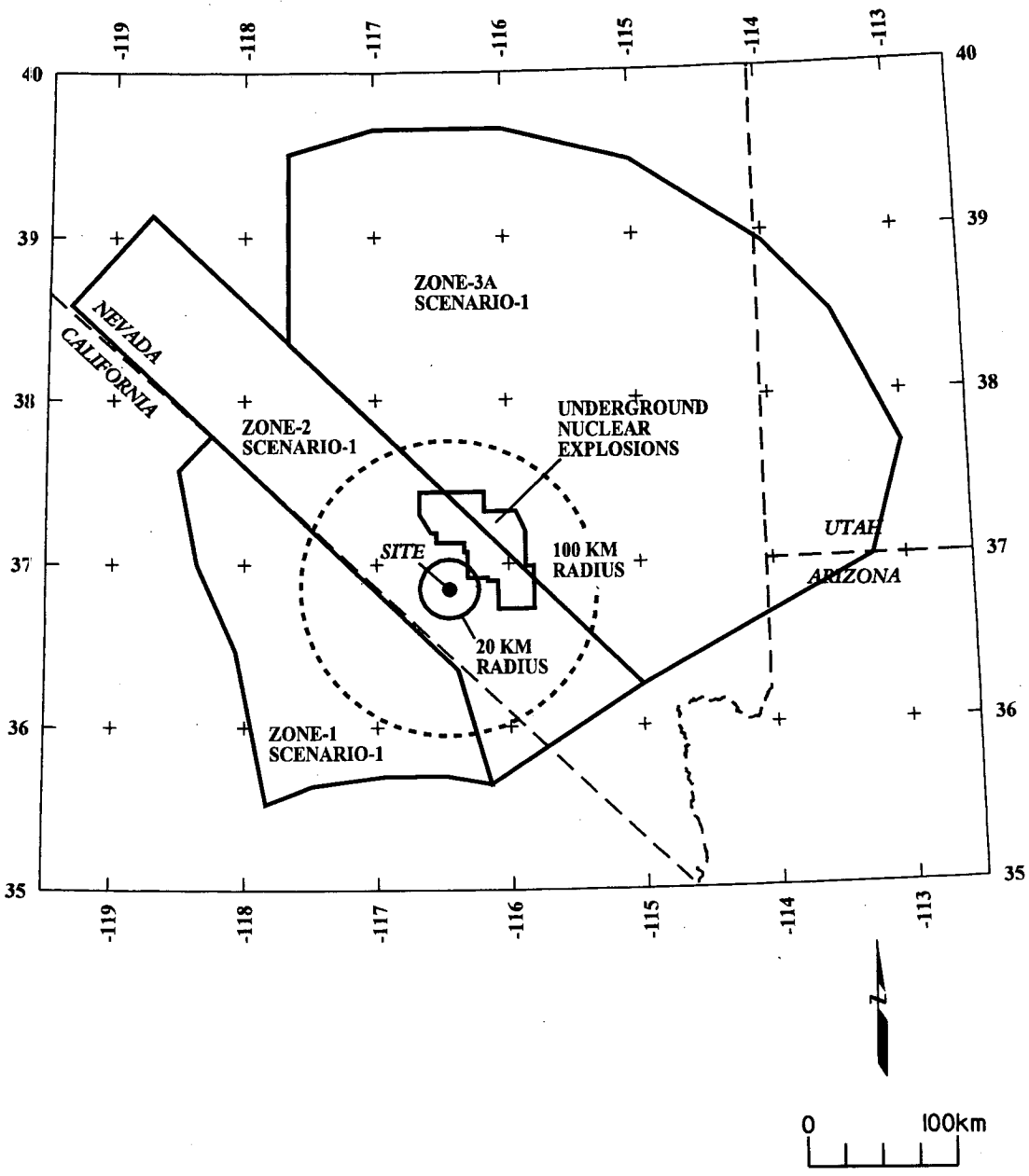

Figure 4-24a. Alternative regional source zone models considered by the AAR team

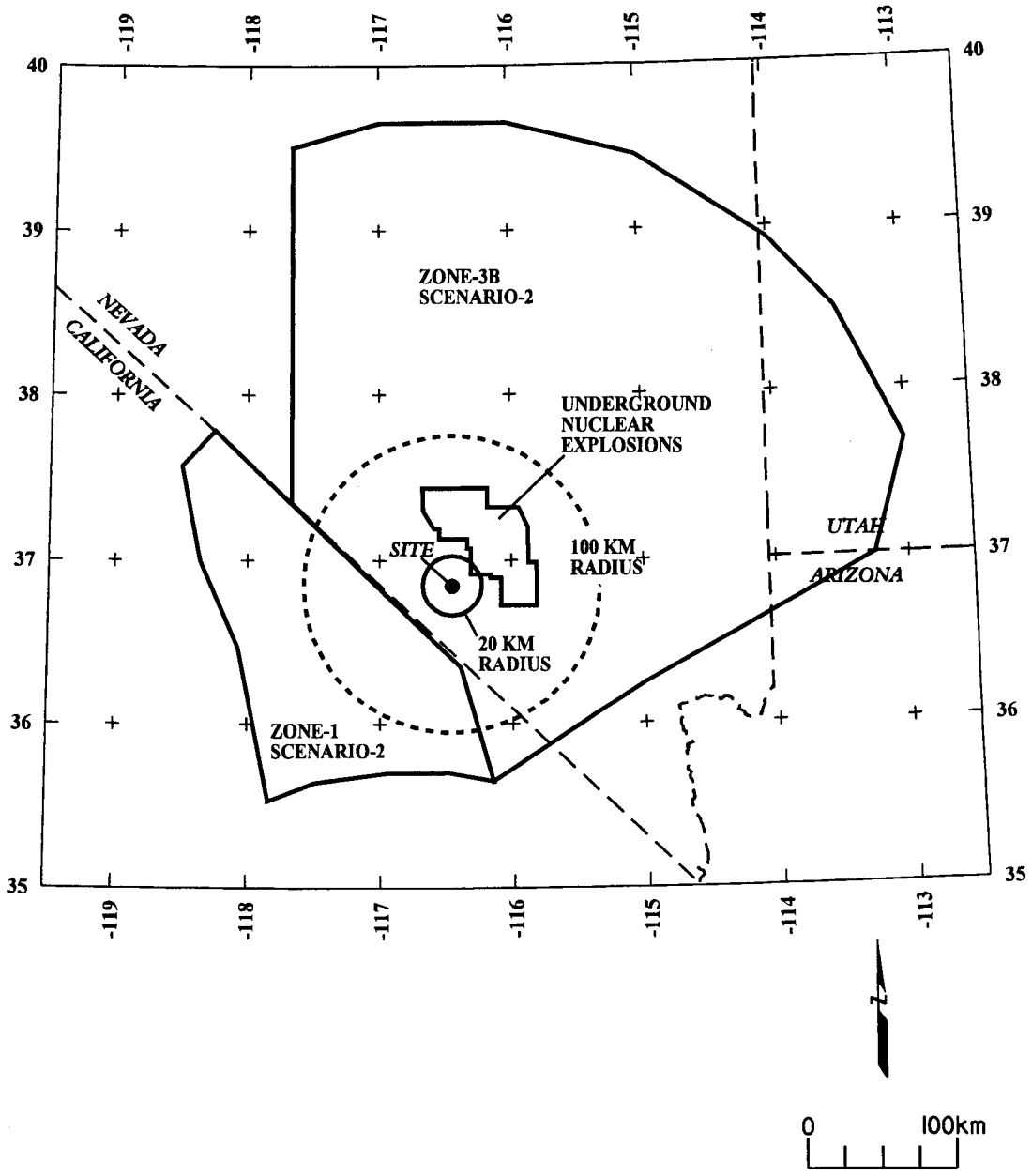

Figure 4-24b. Alternative regional source zone models considered by the AAR team

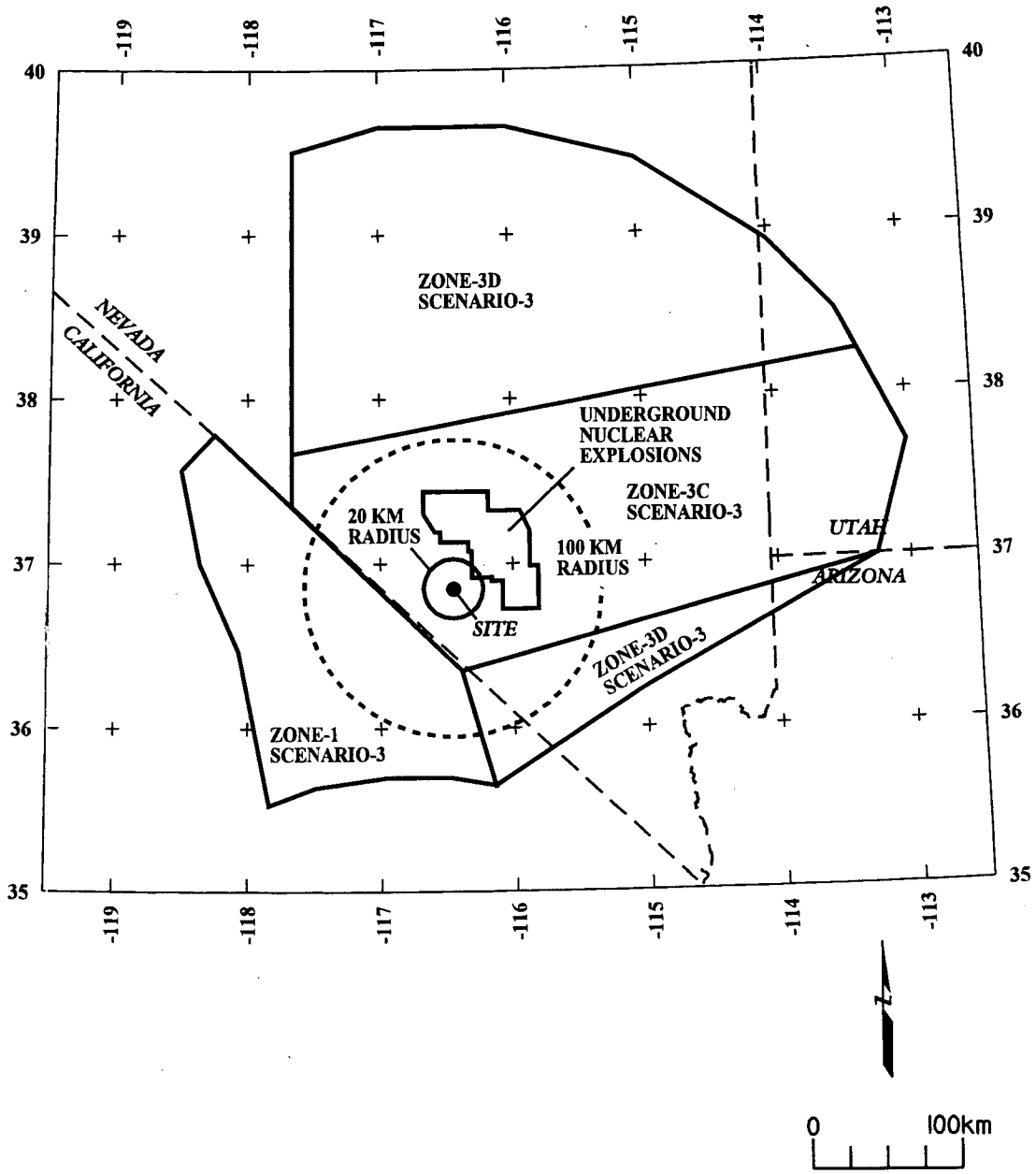

Figure 4-24c. Alternative regional source zone models considered by the AAR team

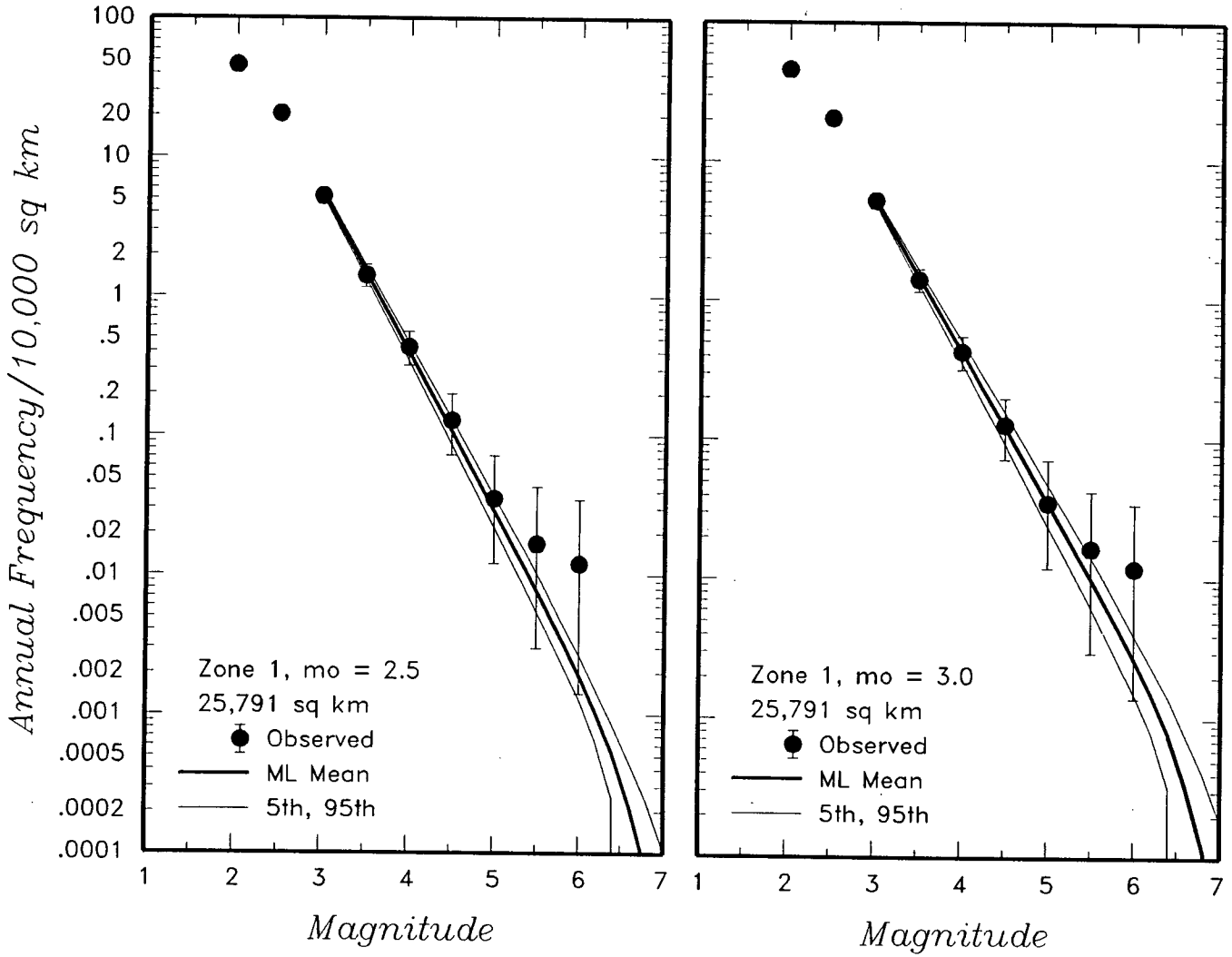

Figure 4-25 Earthquake recurrence relationships for the regional source zones defined by the AAR team. The solid dots with vertical error bars represent the observed data. The thick and thin solid curves are the mean, 5th, and 95th percentiles of the recurrence rates based on the uncertainty in recurrence parameters and maximum magnitude.

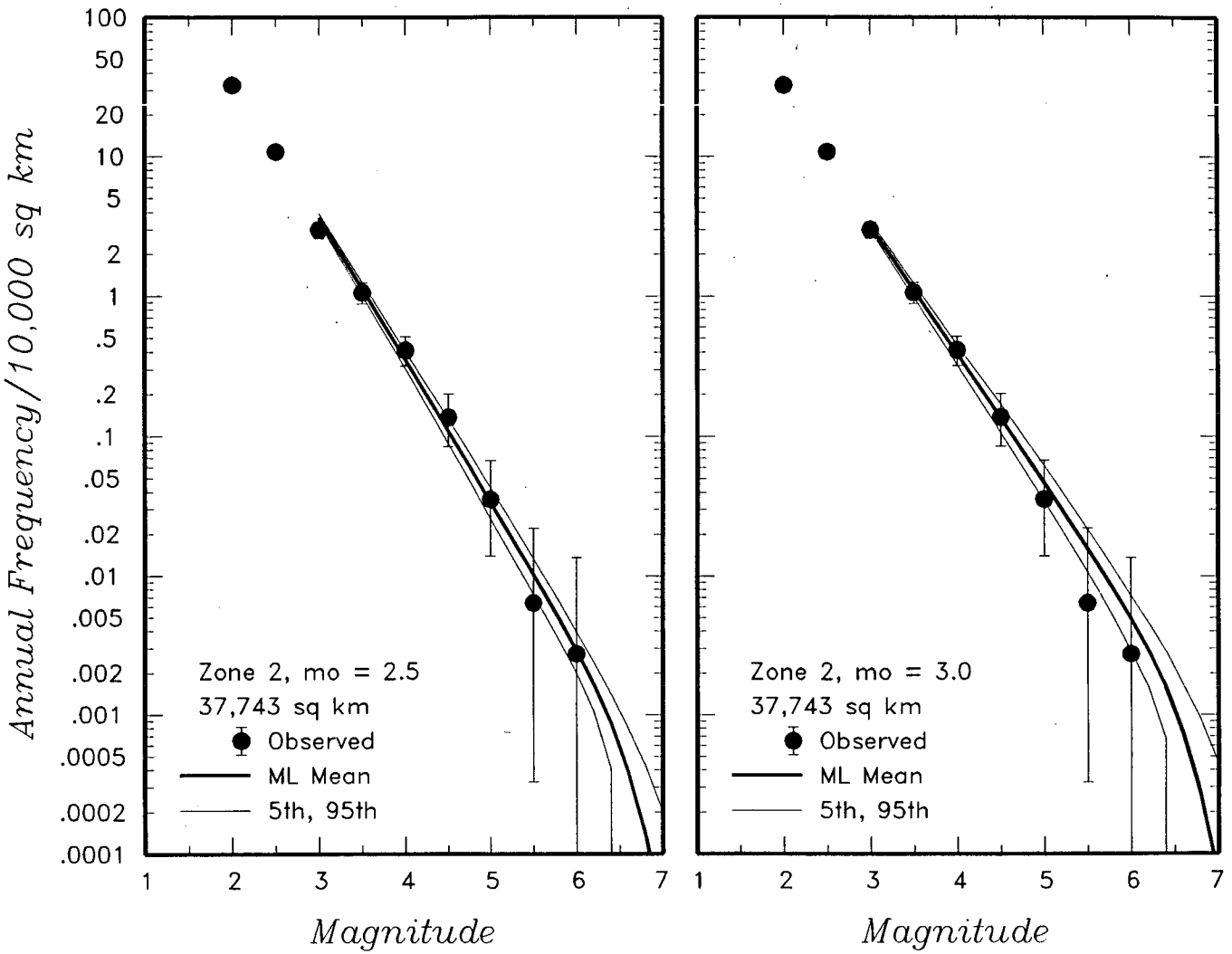

Figure 4-25 (Cont'd.) Earthquake recurrence relationships for the regional source zones defined by the AAR team

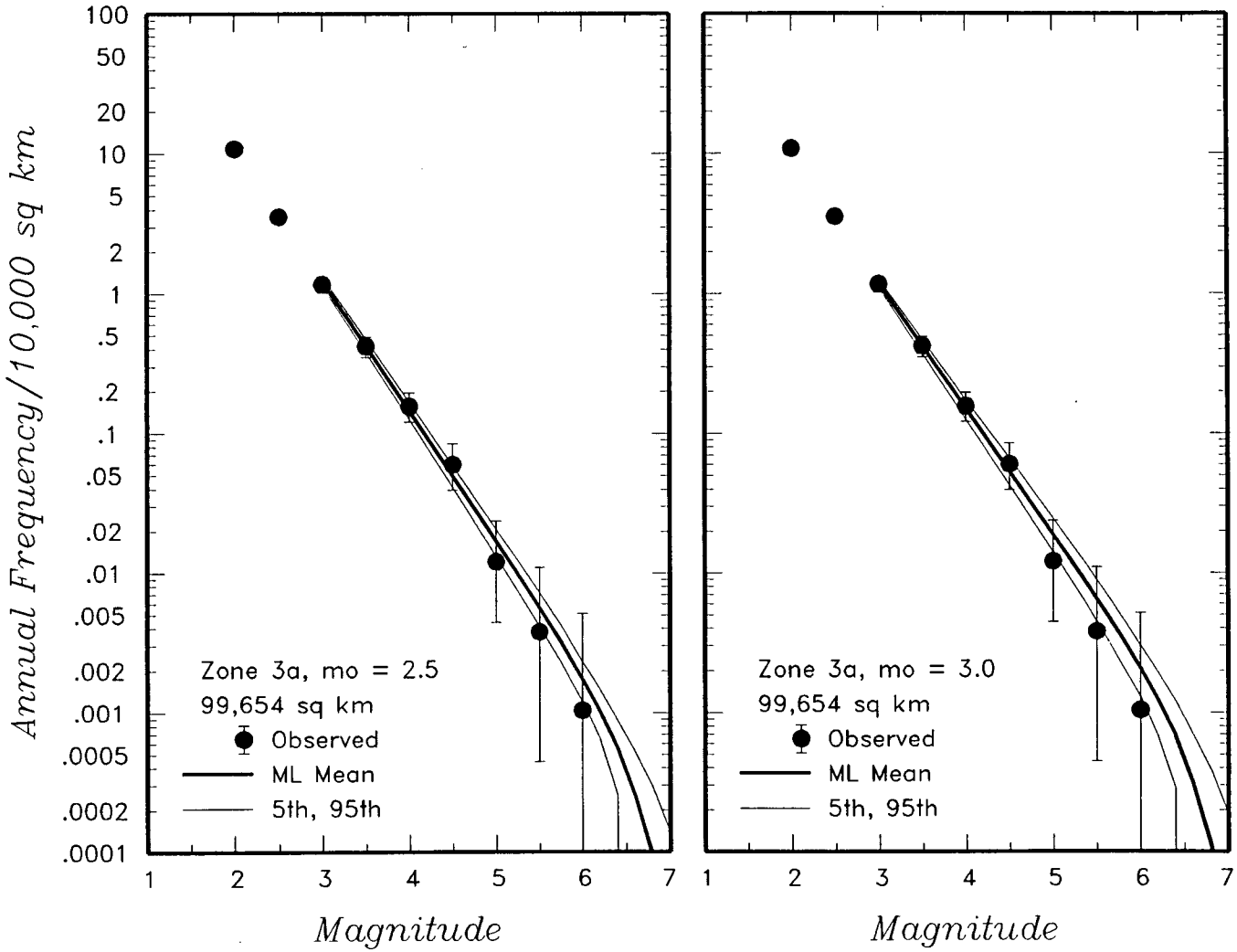

Figure 4-25 (Cont'd.) Earthquake recurrence relationships for the regional source zones defined by the AAR team

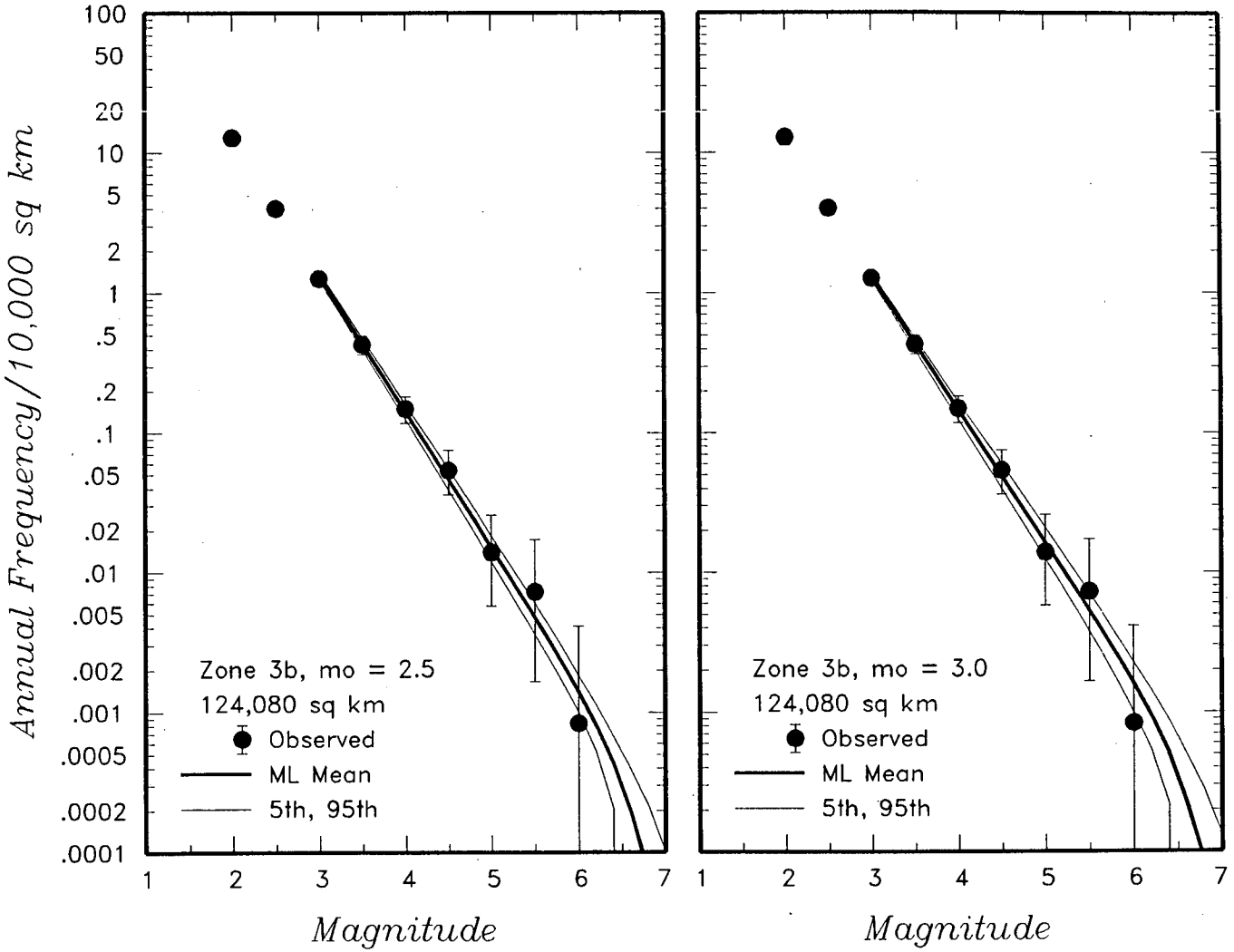

Figure 4-25 (Cont'd.) Earthquake recurrence relationships for the regional source zones defined by the AAR team

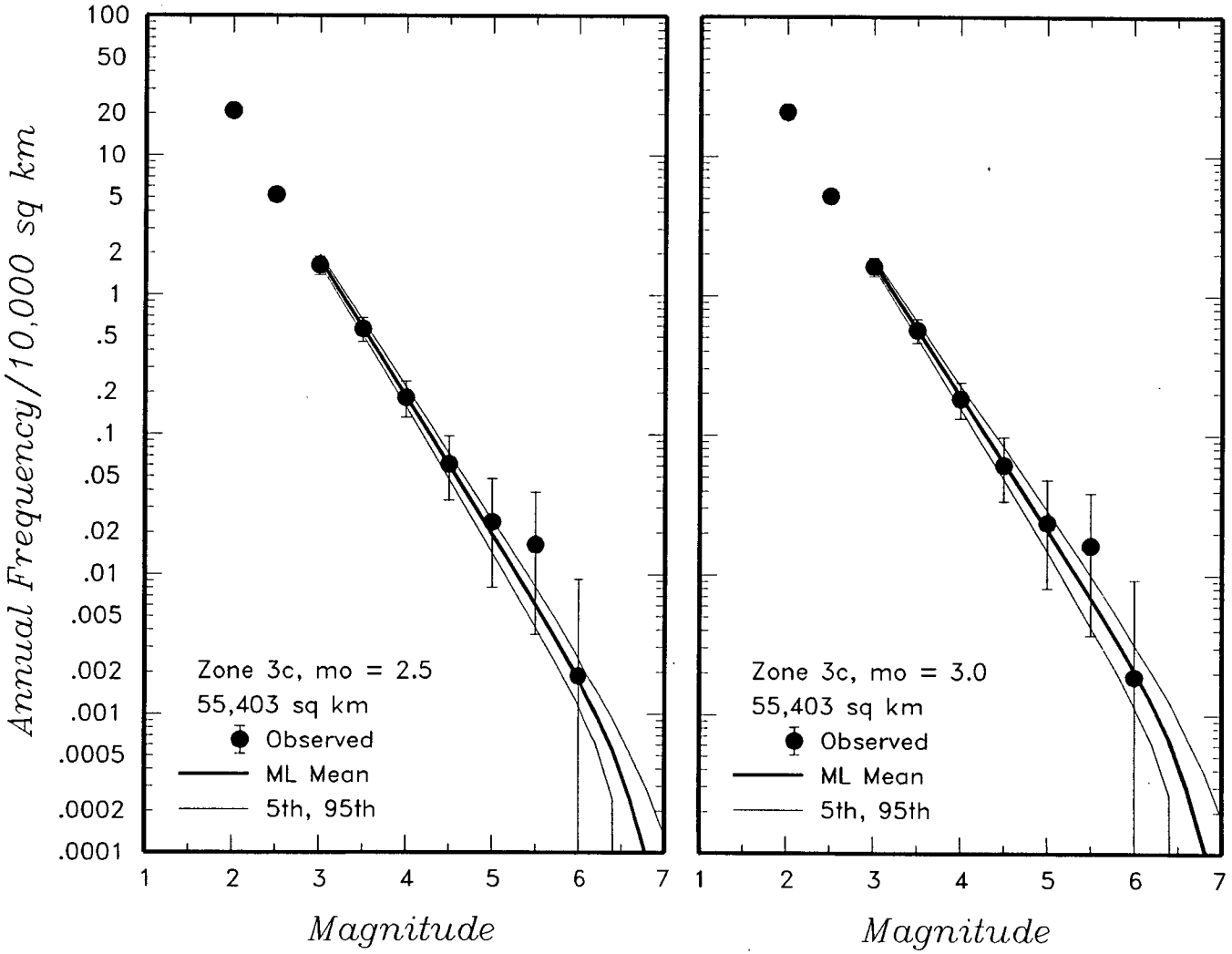

Figure 4-25 (Cont'd.) Earthquake recurrence relationships for the regional source zones defined by the AAR team

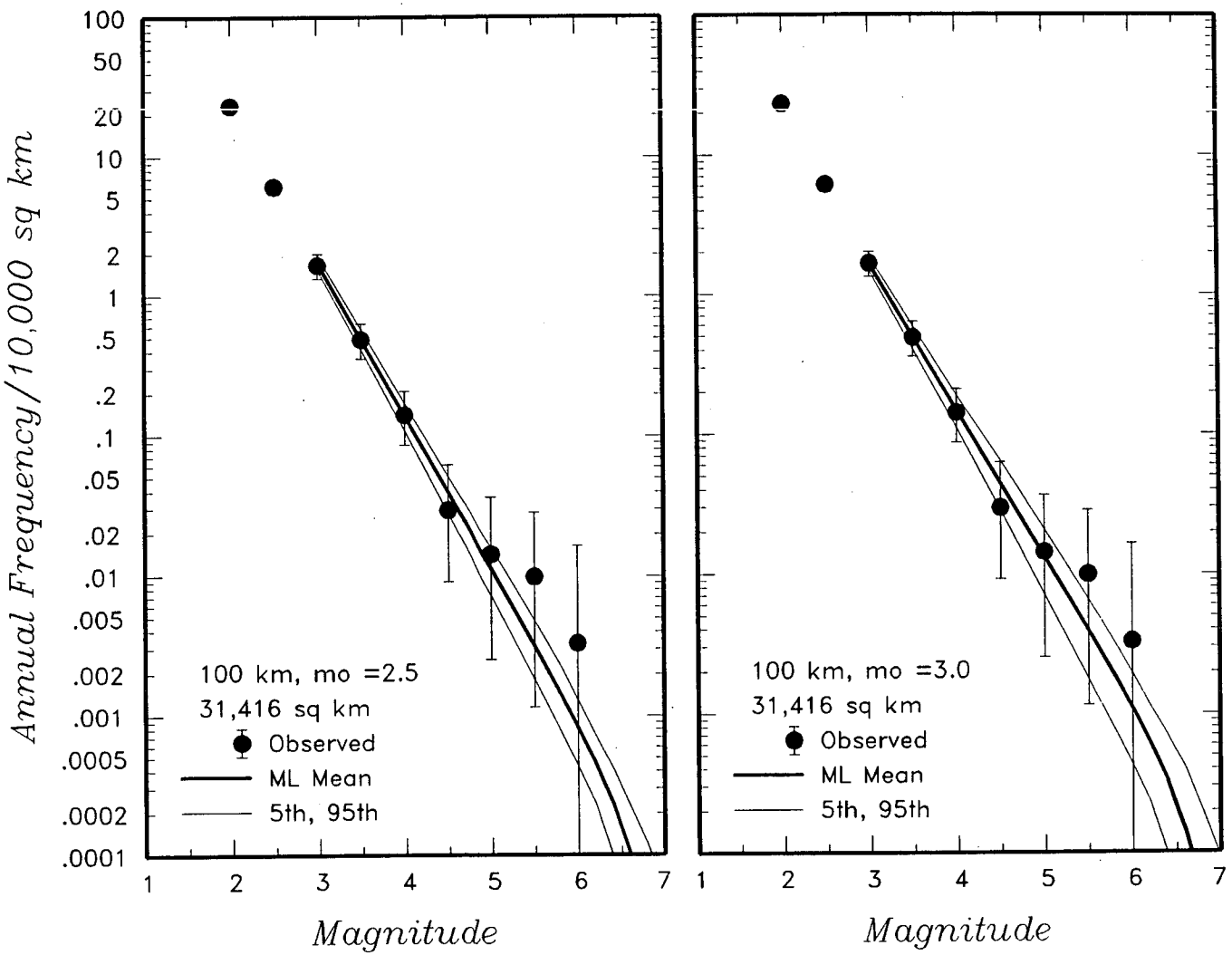

Figure 4-25 (Cont'd.) Earthquake recurrence relationships for the regional source zones defined by the AAR team

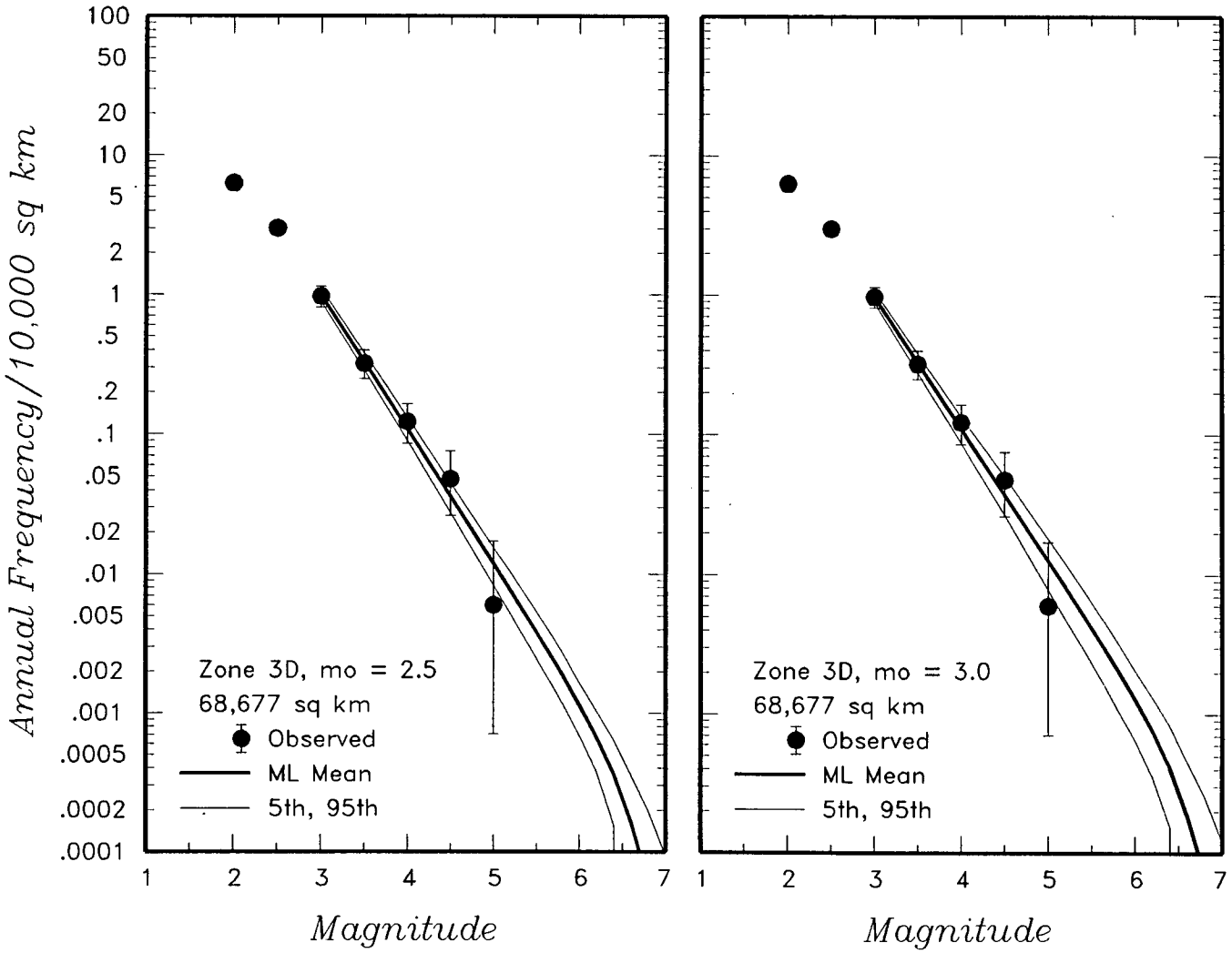

Figure 4-25 (Cont'd.) Earthquake recurrence relationships for the regional source zones defined by the AAR team

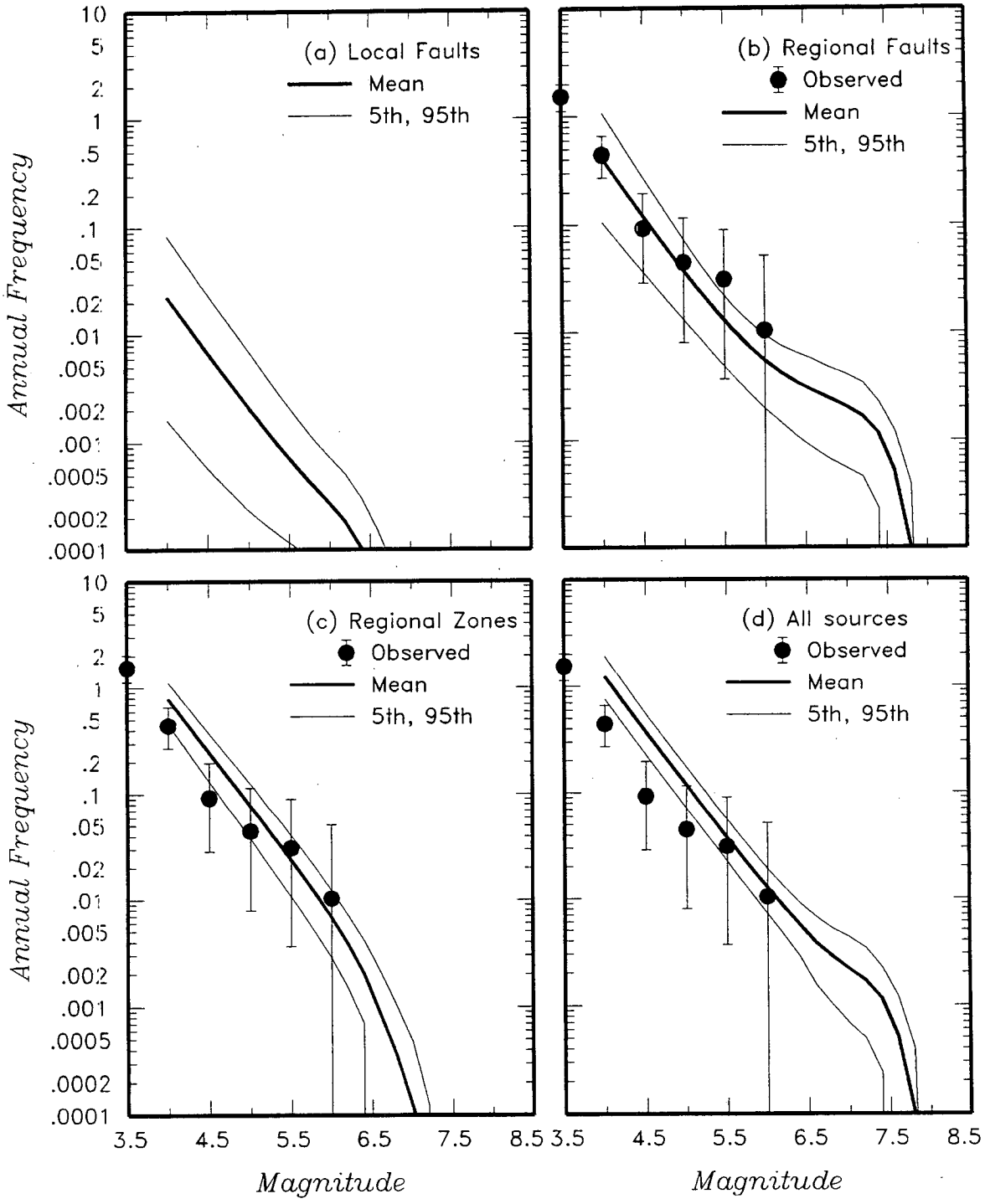

Figure 4-26. Predicted mean, 5th-, and 95th-percentile recurrence rates for (a) local fault sources, (b) regional fault sources, (c) regional source zones, and (d) all sources combined for the AAR team. The solid dots with vertical error bars show the observed frequency of earthquakes occurring within 100 km of the Yucca Mountain site.

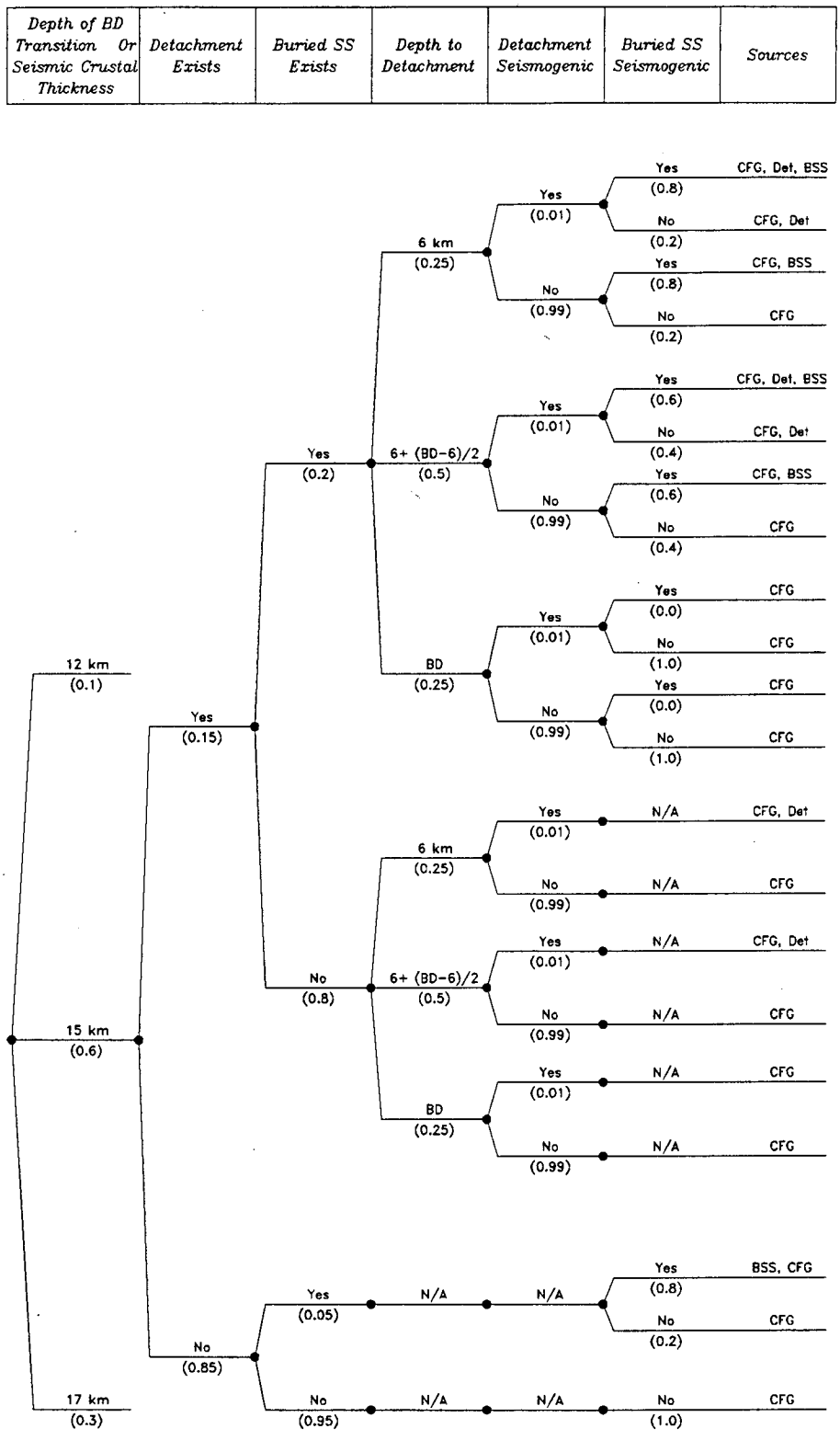

Figure 4-27a Logic tree for local fault sources developed by the ASM team

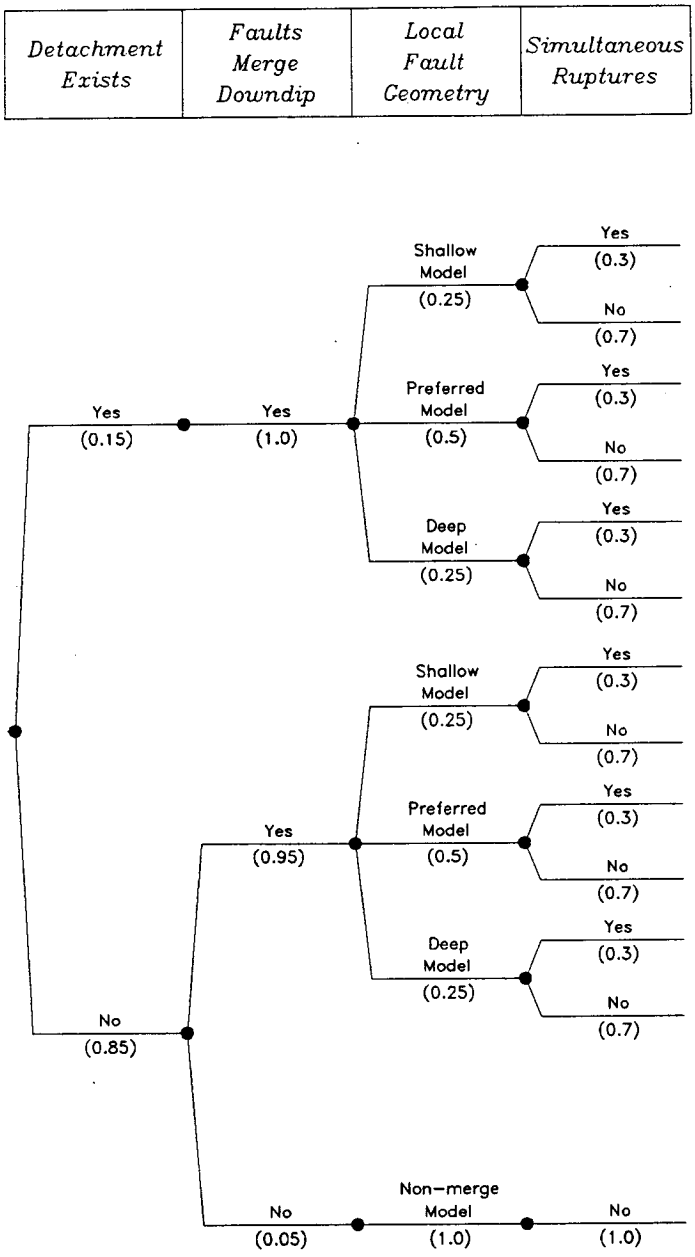

Figure 4-27b Logic tree for rupture behavior of Crater Flat group of faults

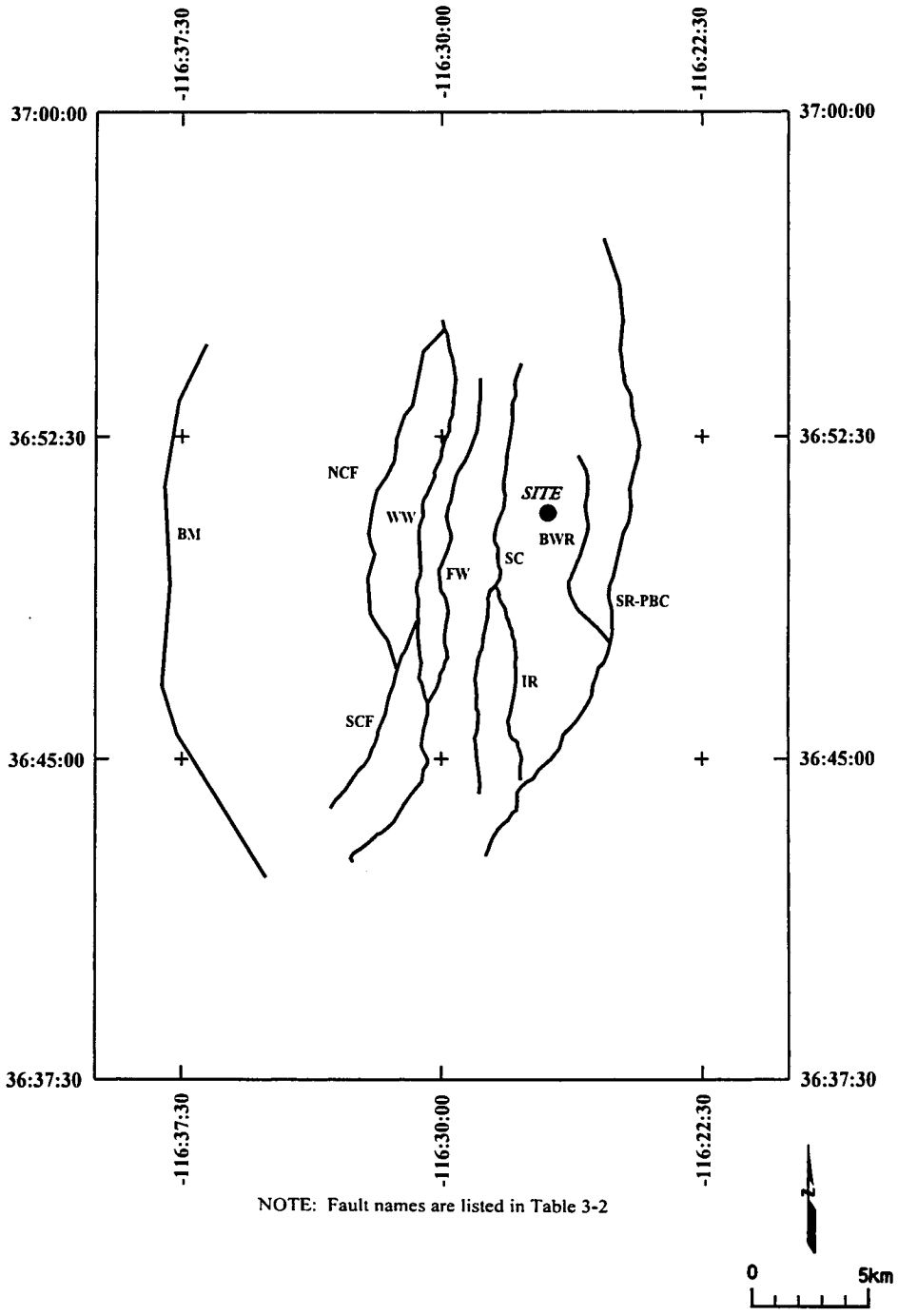

NOTE: Fault names are listed in Table 3-2

Figure 4-28 Location of fault sources considered by the ASM team

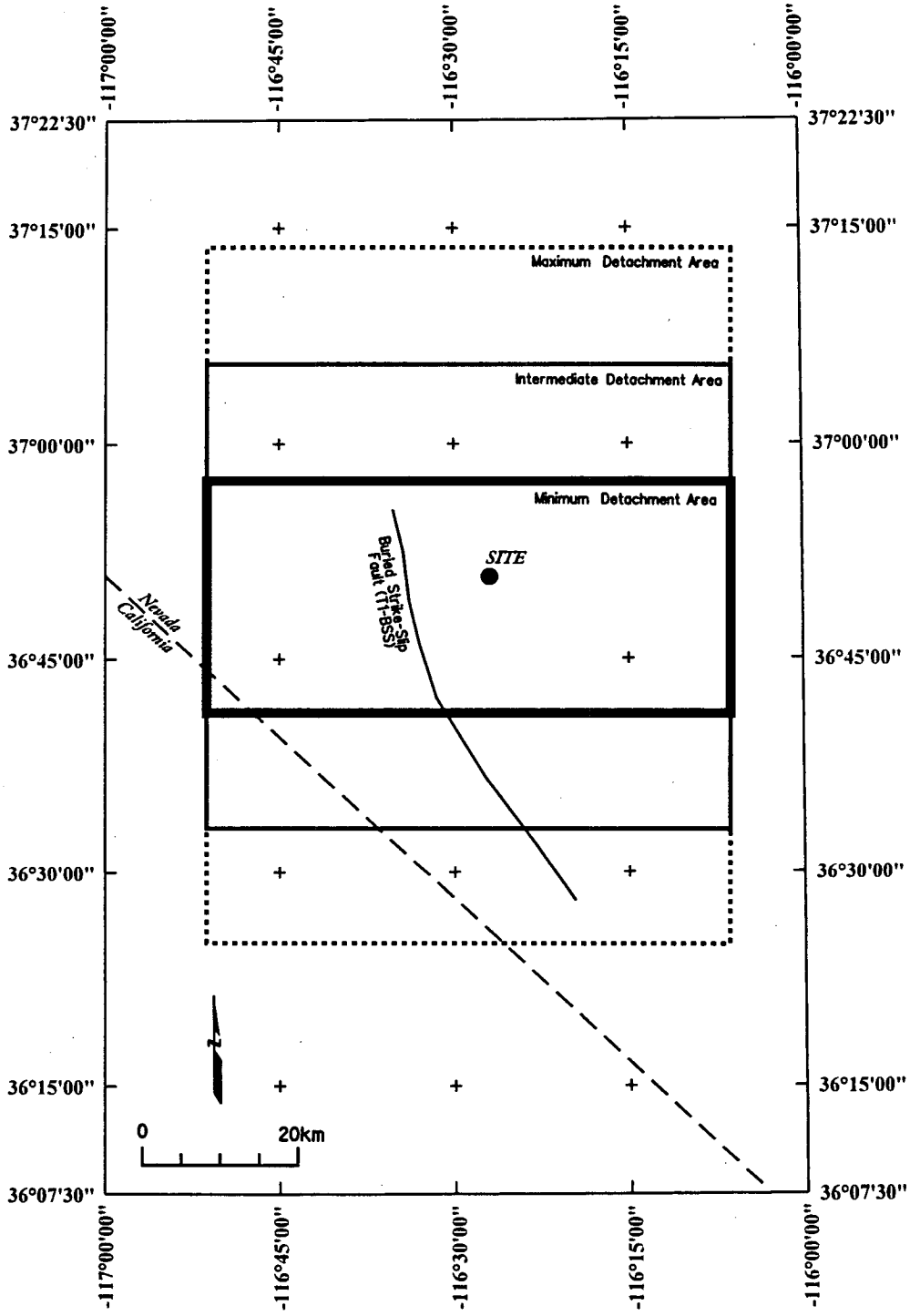

Figure 4-29 Location of hypothetical buried strike-slip and detachment faults in the vicinity of Yucca Mountain included in the ASM seismic source model

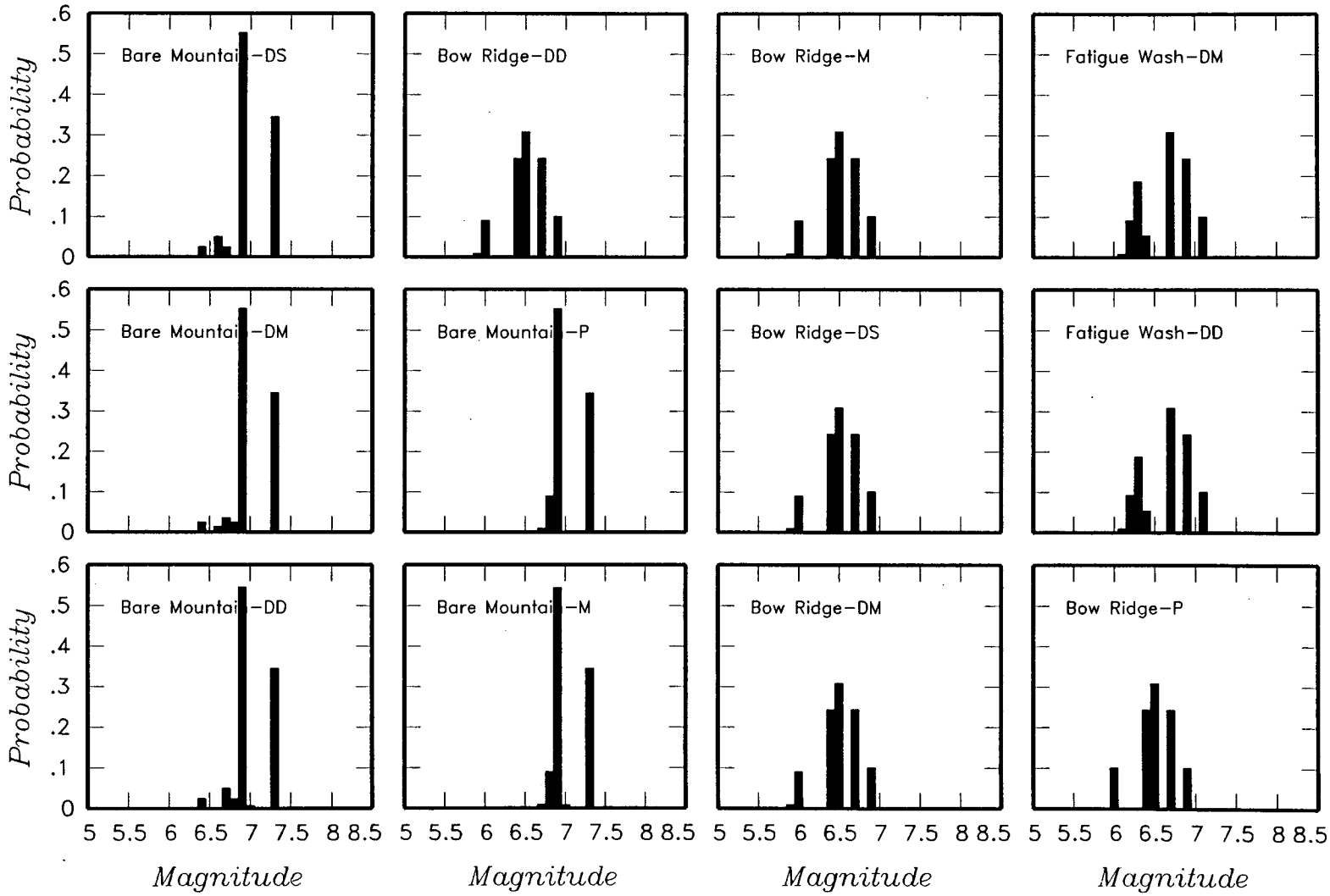

Figure 4-30 Maximum magnitude distributions for ASM team's local fault sources. DS–shallow detachment, DM–preferred detachment, DD–deep detachment; M–merging model, P–planar model; BM–Bare Mountain, W–Windy Wash, SRPBC–Stagecoach Road-Paintbrush Canyon.

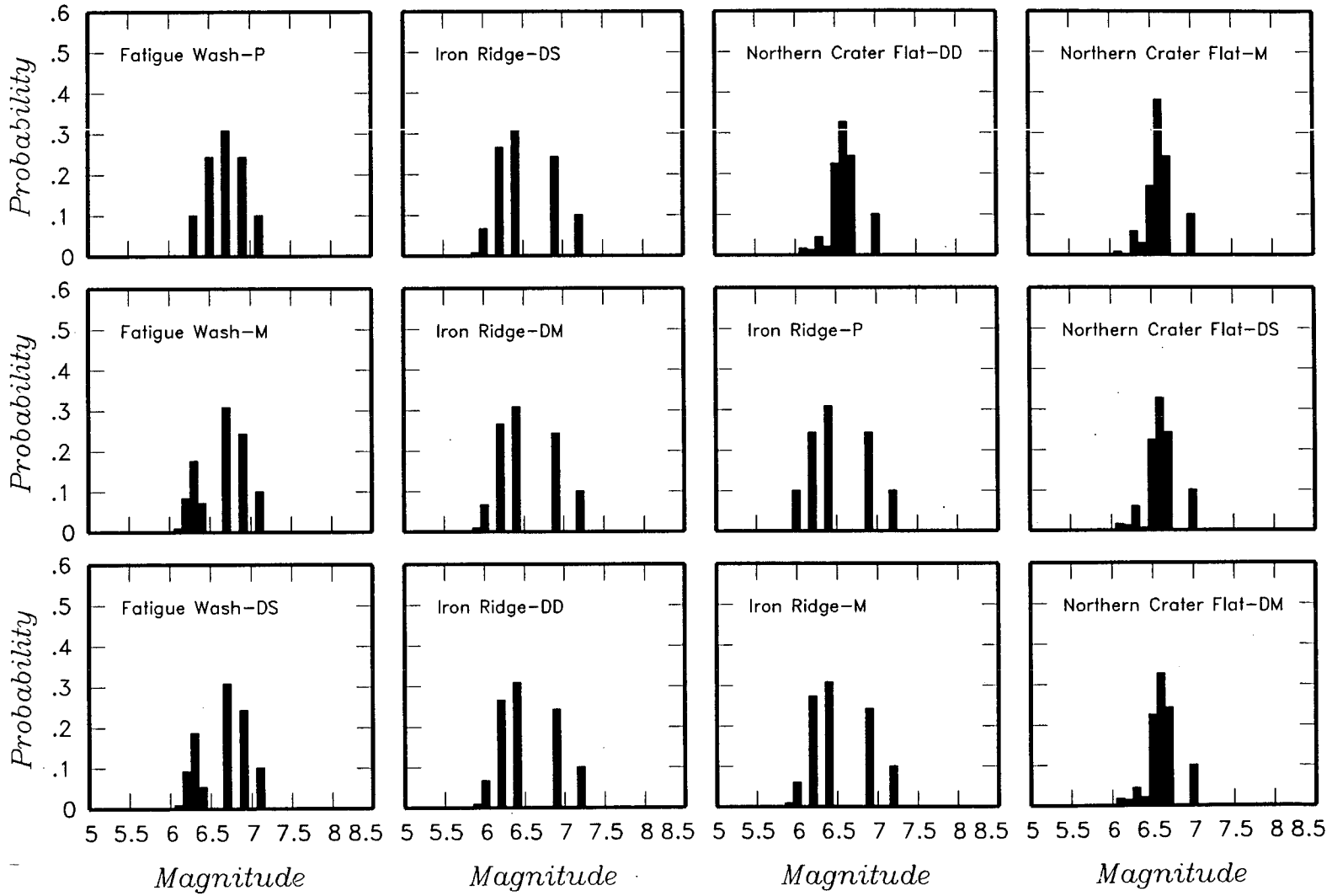

Figure 4-30 (Cont'd.) Maximum magnitude distributions for ASM team's local fault sources

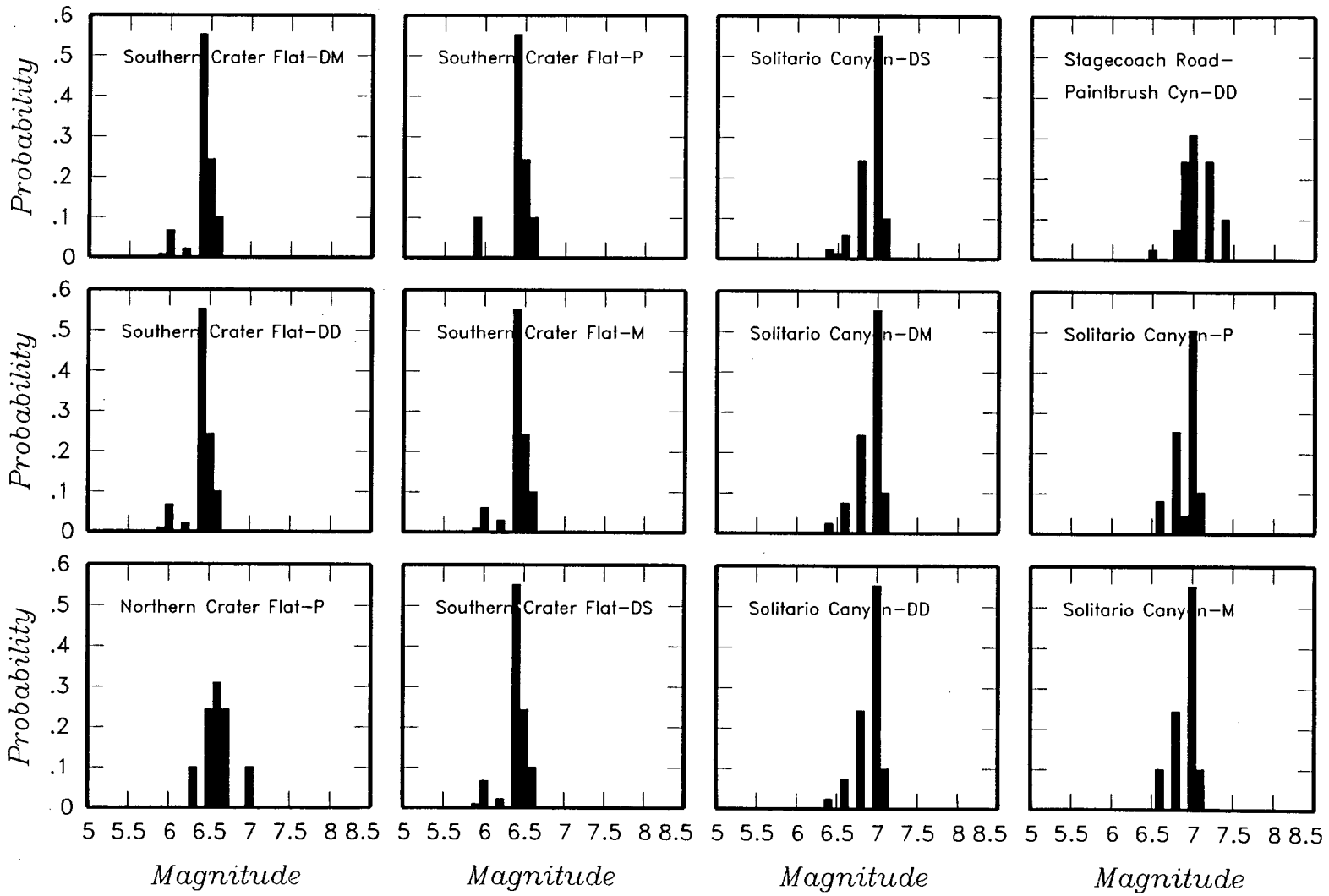

Figure 4-30 (Cont'd.) Maximum magnitude distributions for ASM team's local fault sources

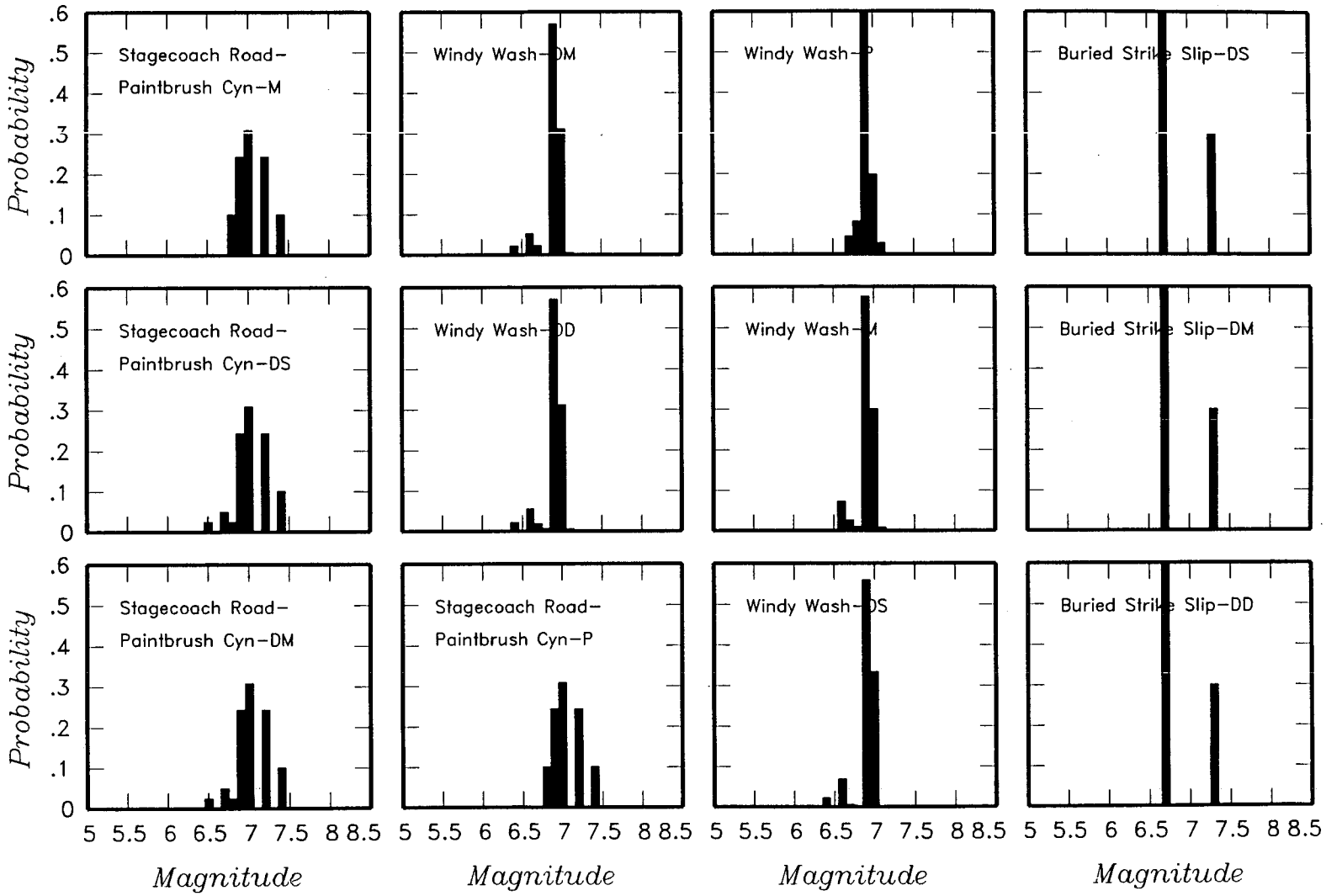

Figure 4-30 (Cont'd.) Maximum magnitude distributions for ASM team's local fault sources

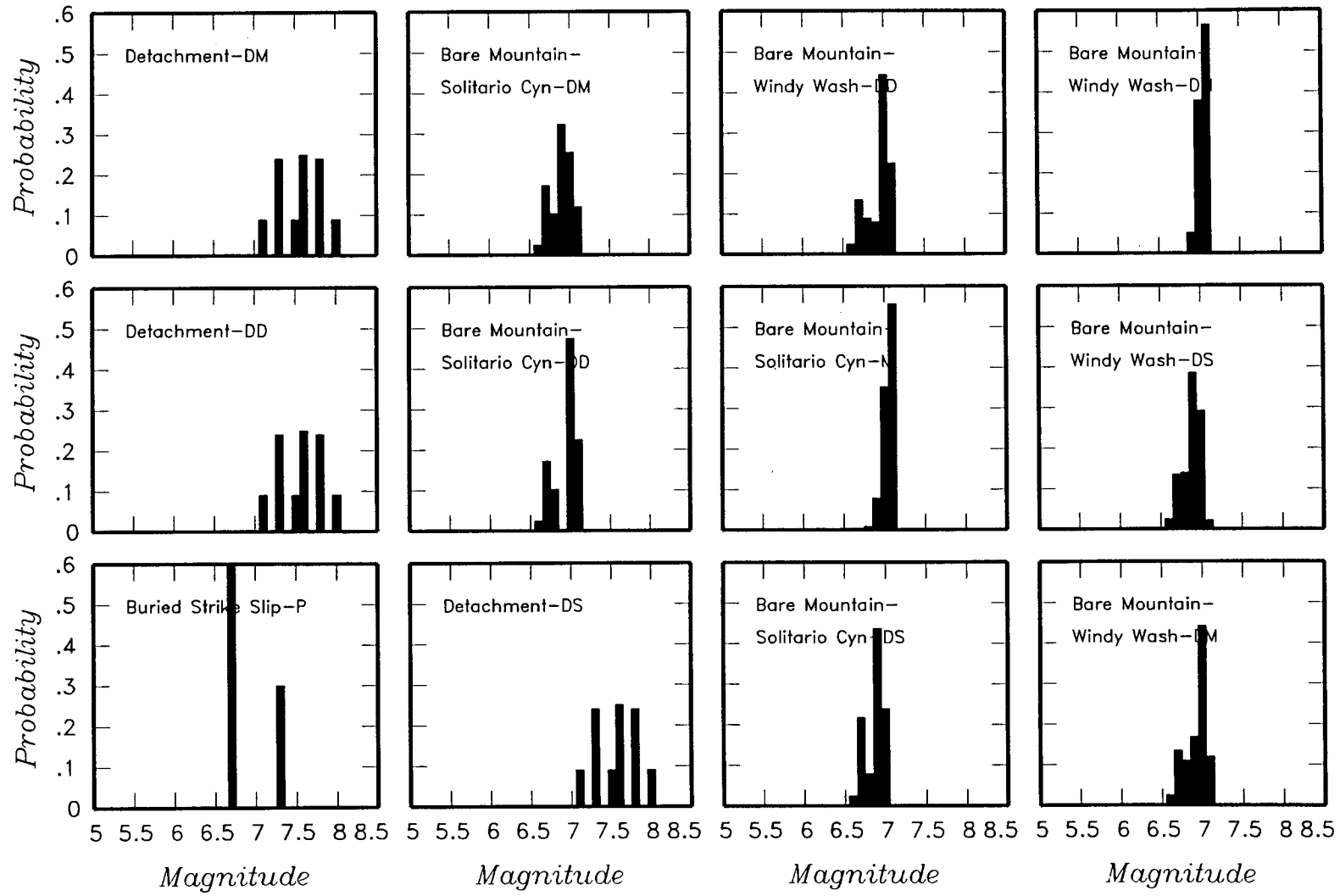

Figure 4-30 (Cont'd.) Maximum magnitude distributions for ASM team's local fault sources

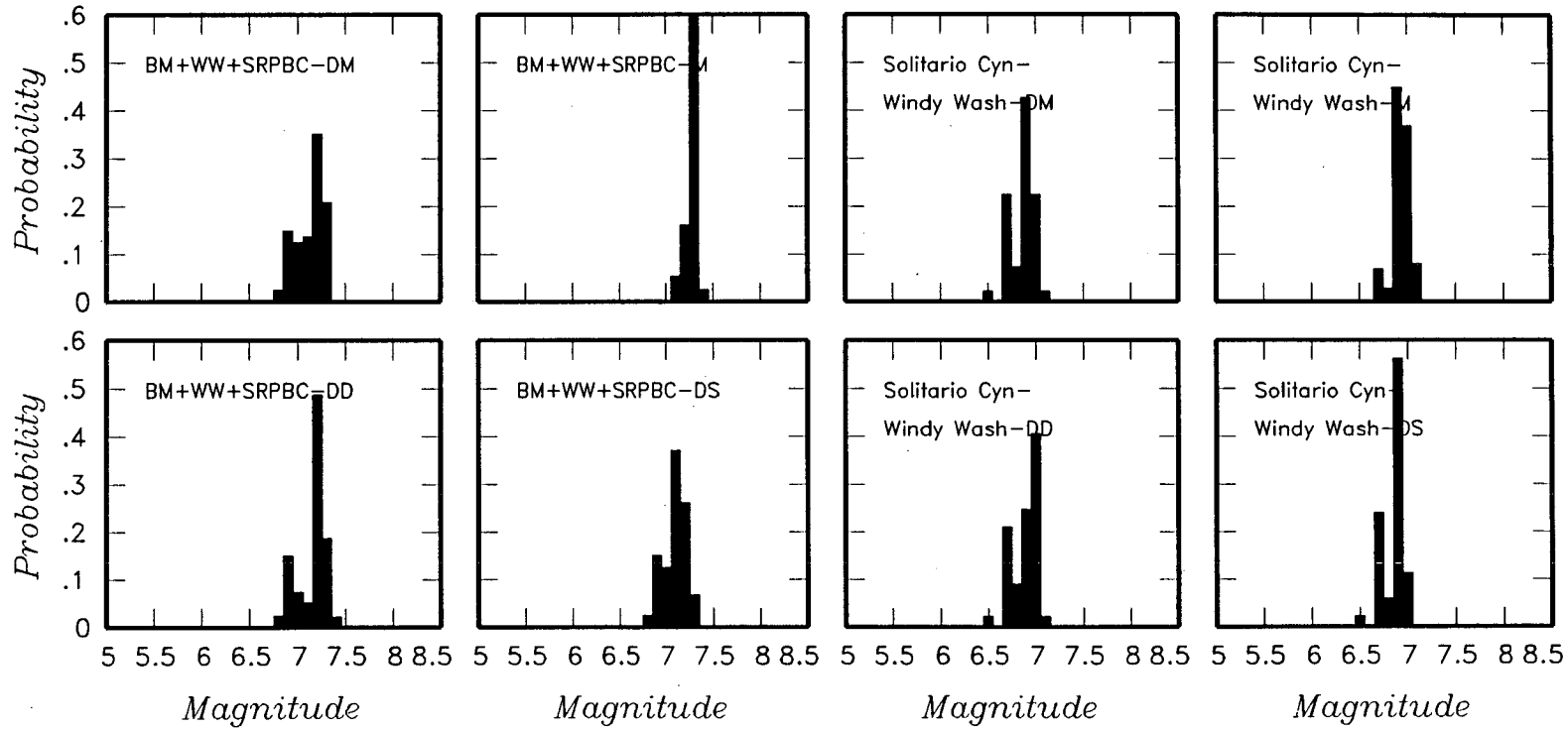

Figure 4-30 (Cont'd.) Maximum magnitude distributions for ASM team's local fault sources

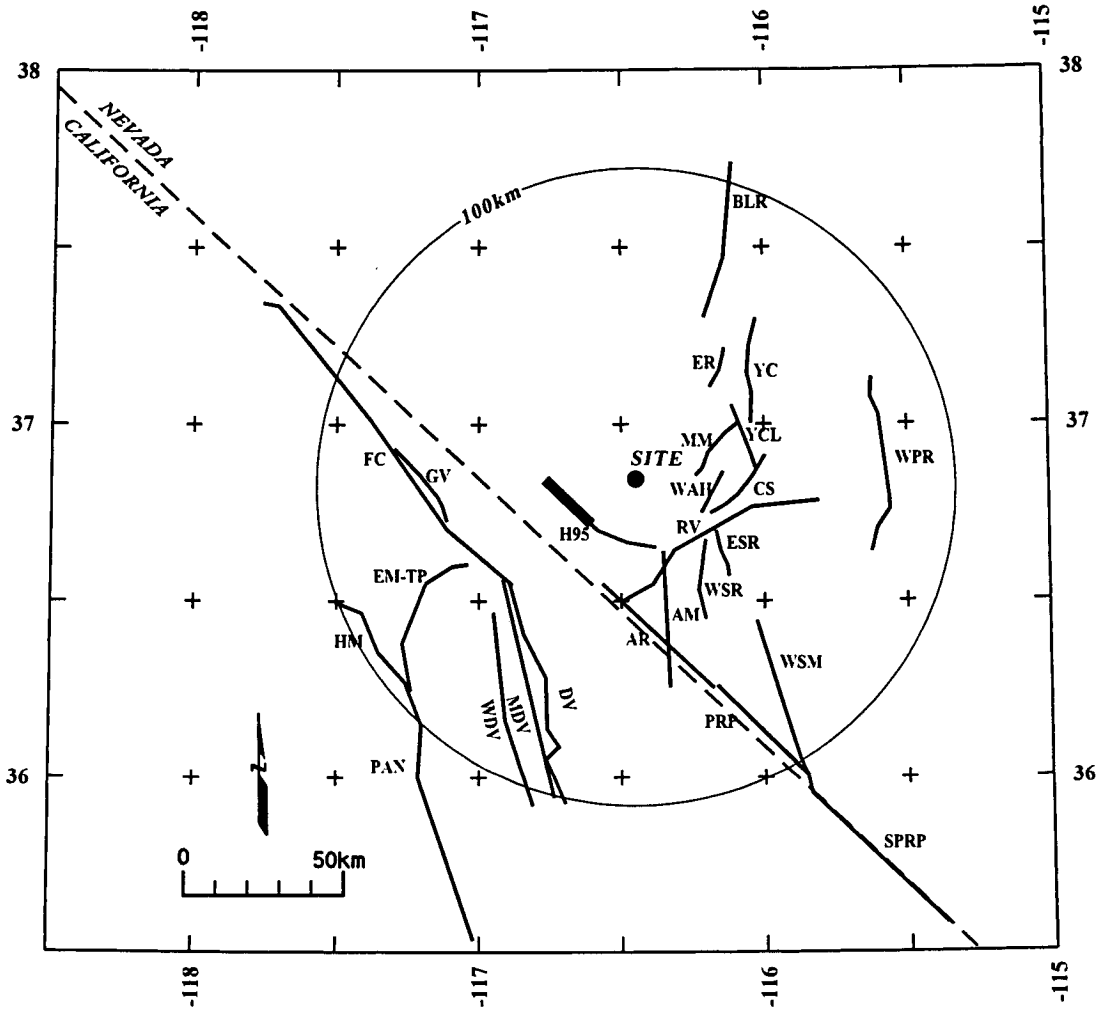

EXPLANATION

NOTE: Fault names are listed in Table 3-2

Fault Lengths:

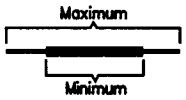

Figure 4-31 Reginal fault sources considered by the ASM team

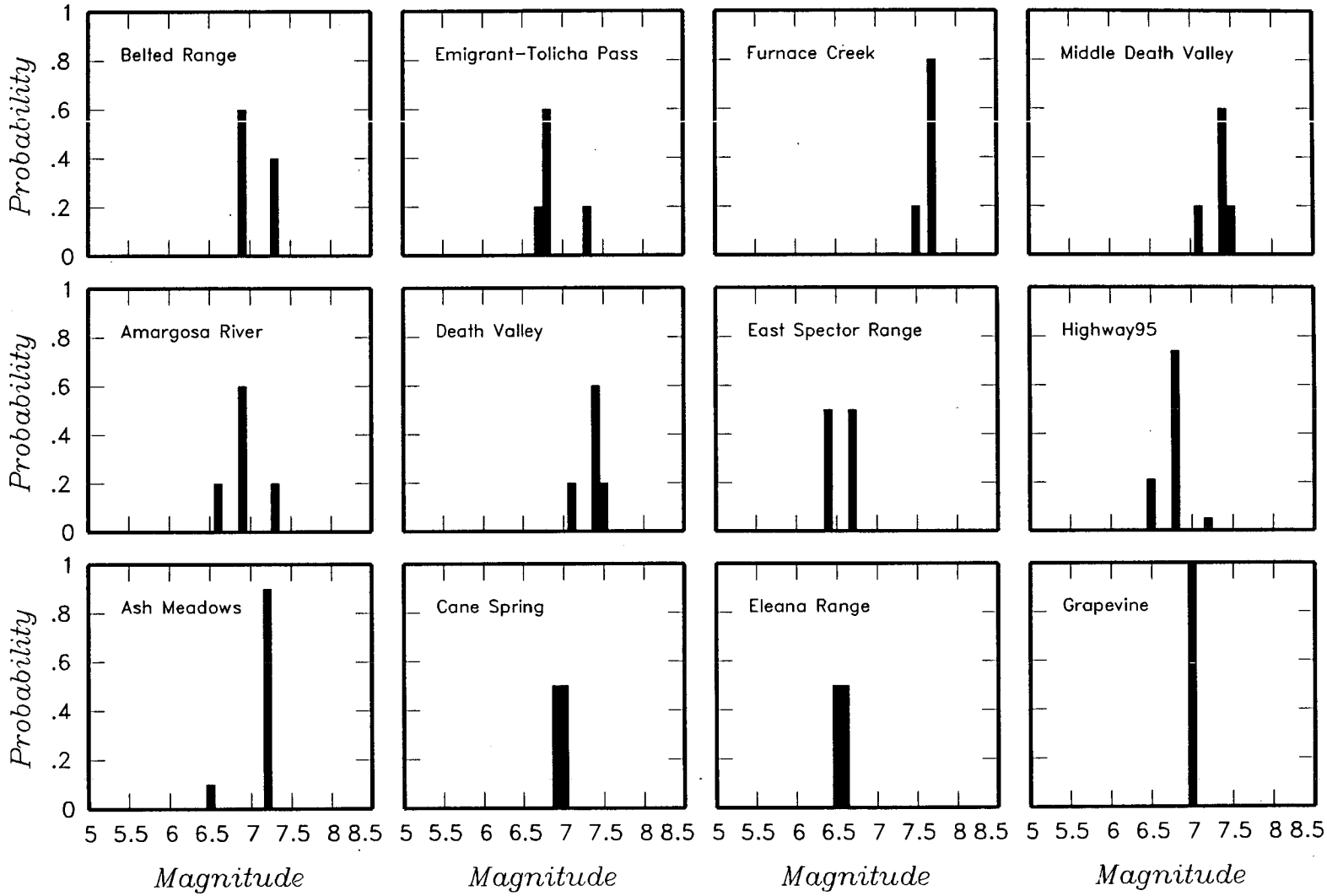

Figure 4-32 Maximum magnitude distributions for ASM team's regional fault sources

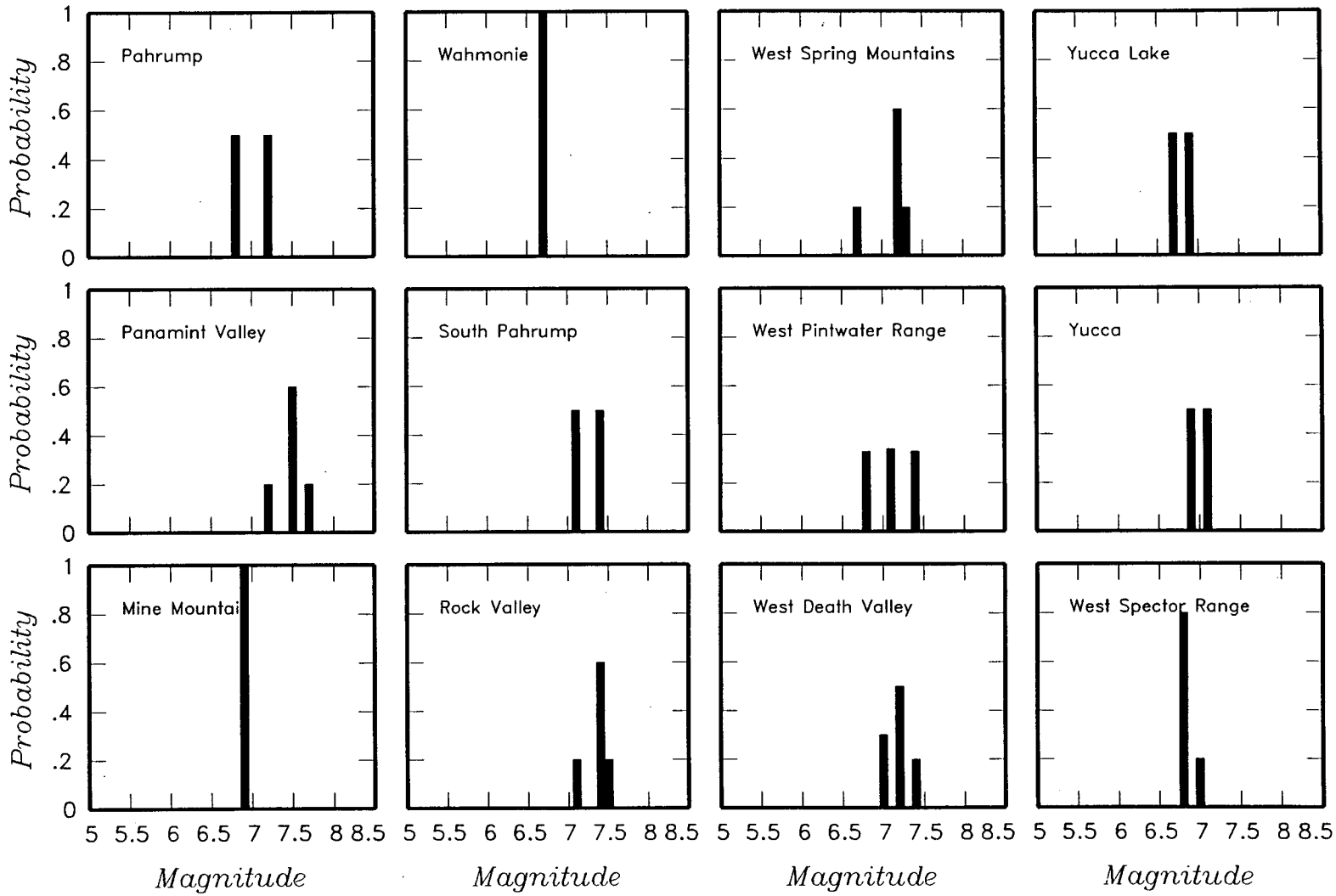

Figure 4-32 (Cont'd.) Maximum magnitude distributions for ASM team's regional fault sources

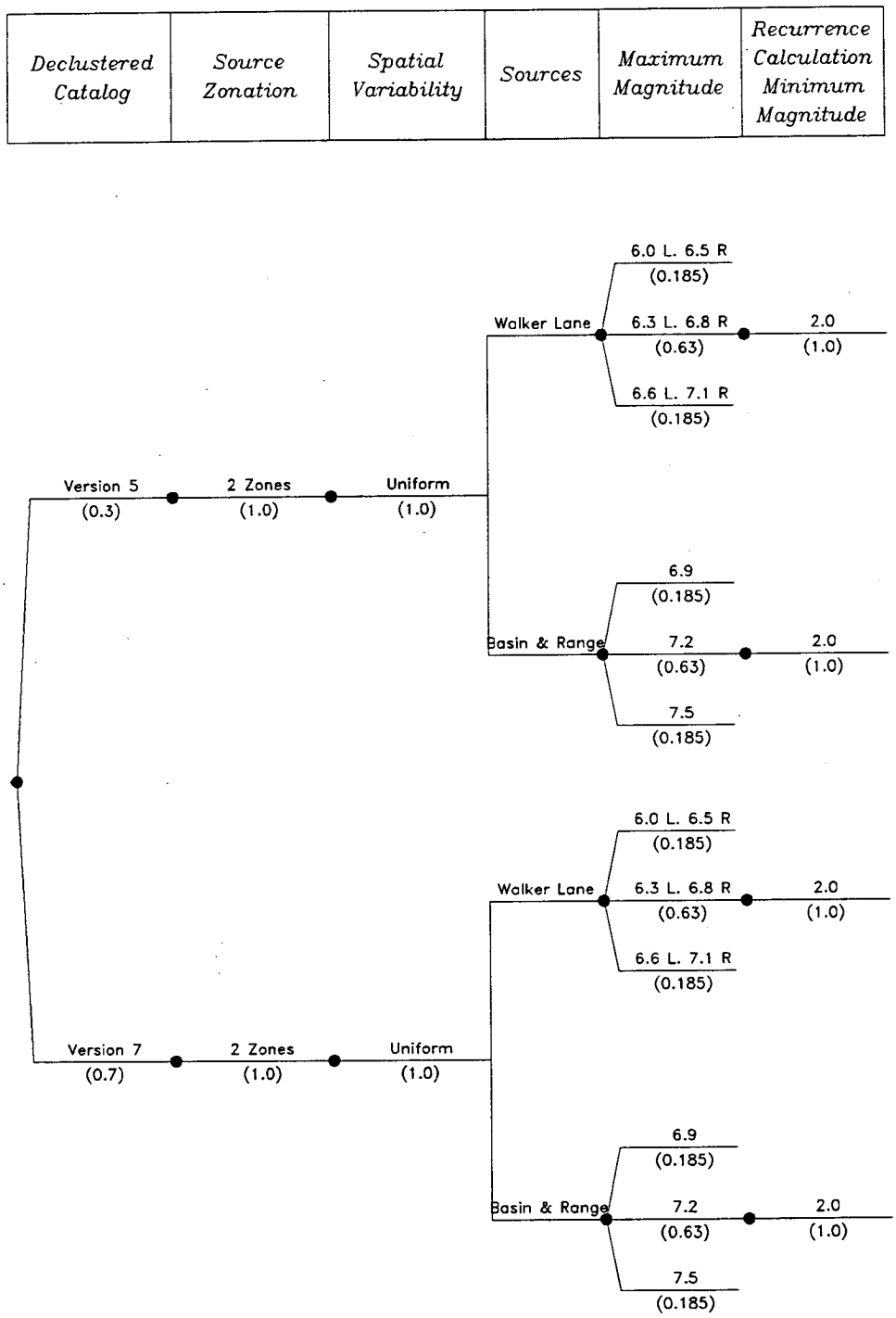

Figure 4-33 Logic tree for regional source zones developed by the ASM team

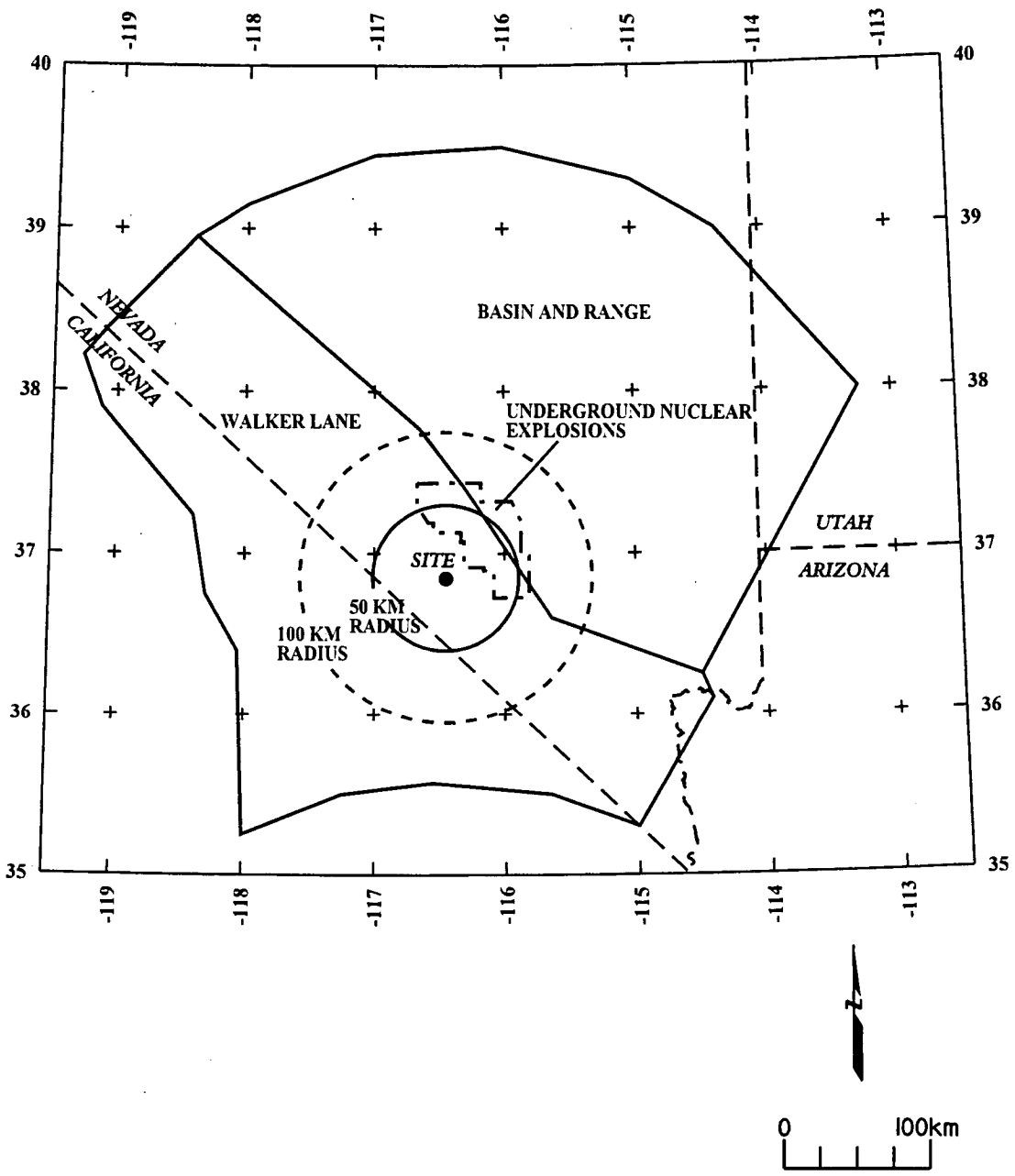

Figure 4-34 Regional source zones considered by the ASM team

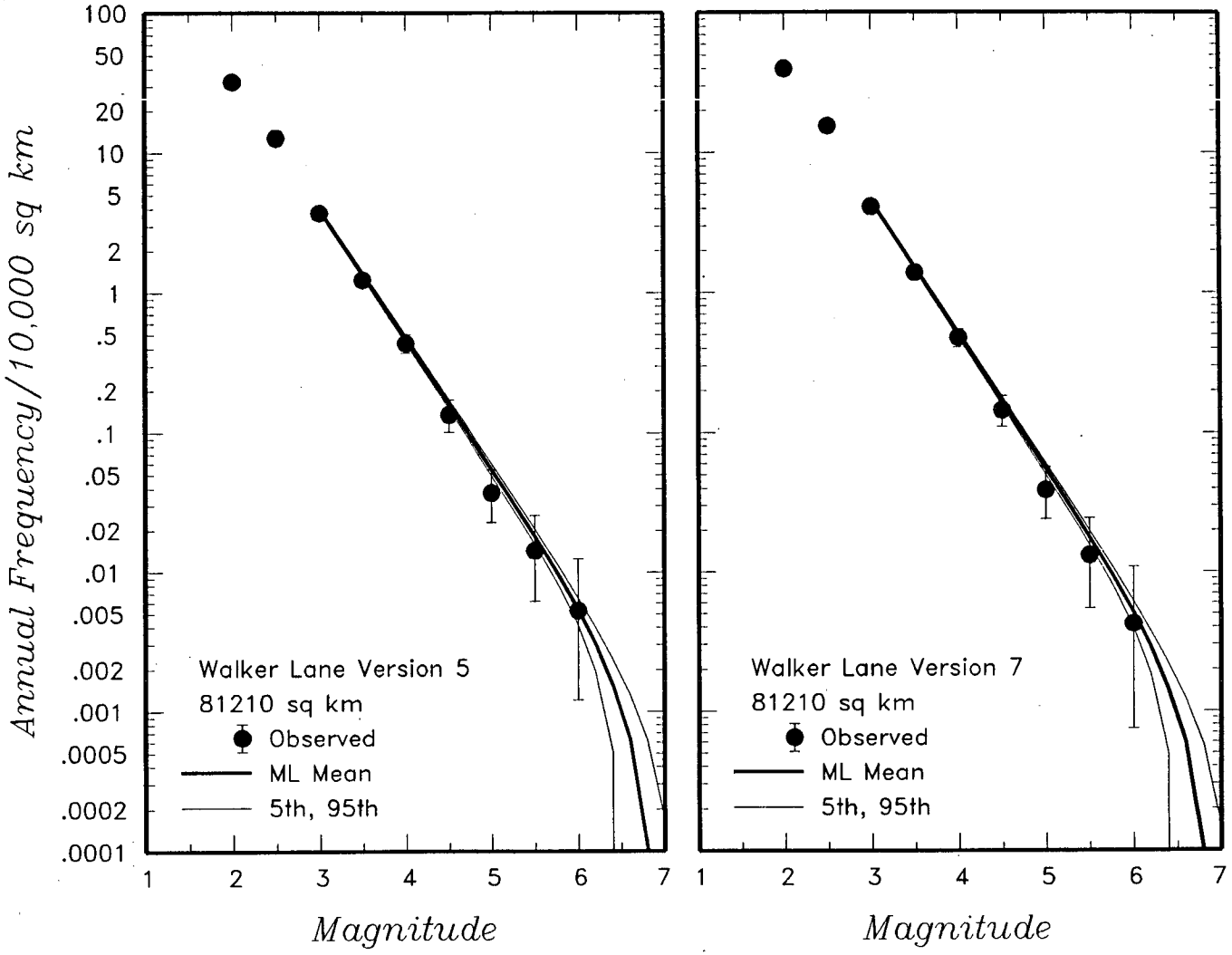

Figure 4-35 Earthquake recurrence relationships for the regional source zones defined by the ASM team. The solid dots with vertical error bars represent the observed data. The thick and thin solid curves are the mean, 5th, and 95th percentiles of the recurrence rates based on the uncertainty in recurrence parameters and maximum magnitude.

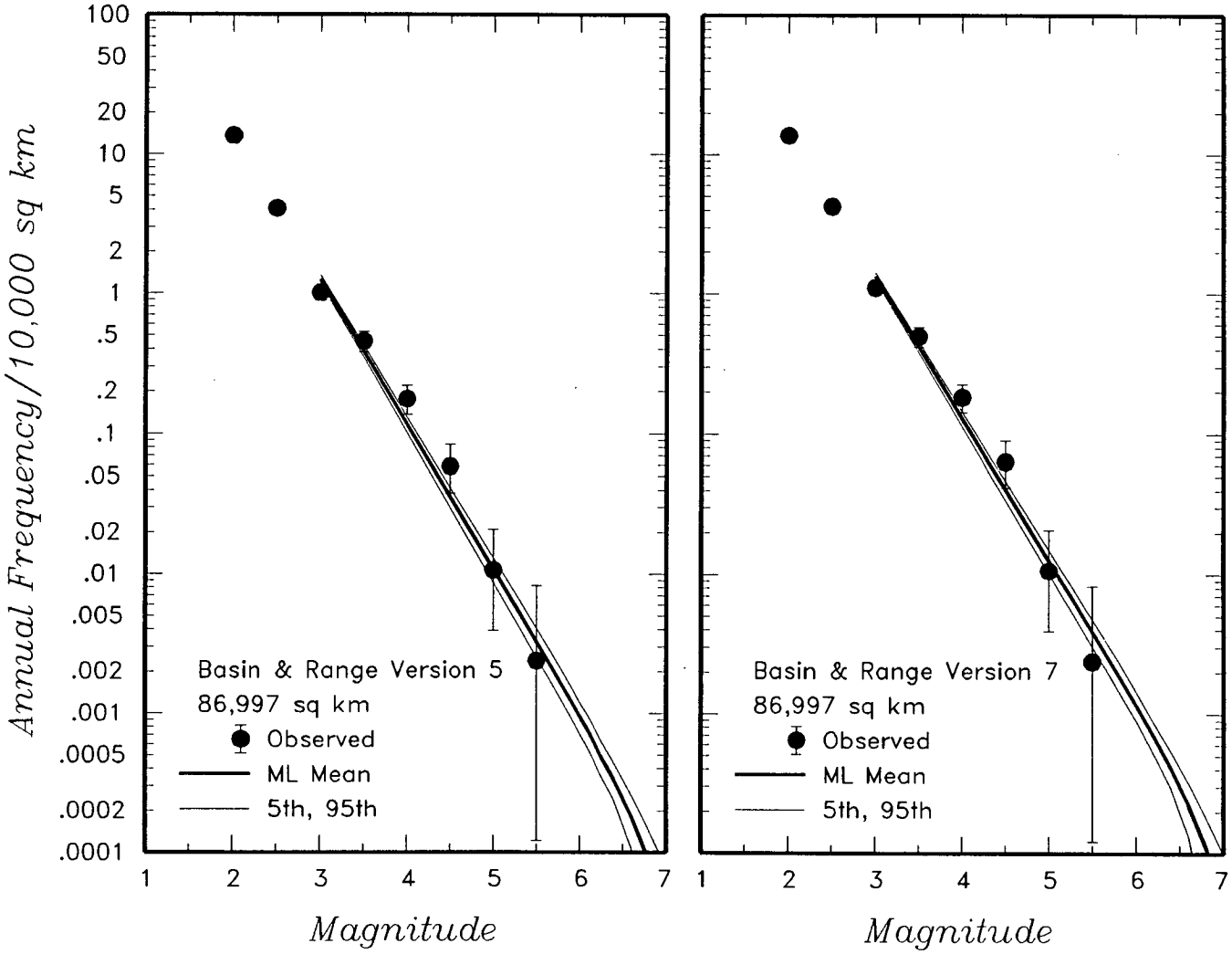

Figure 4-35 (Cont'd.) Earthquake recurrence relationships for the regional source zones defined by the ASM team

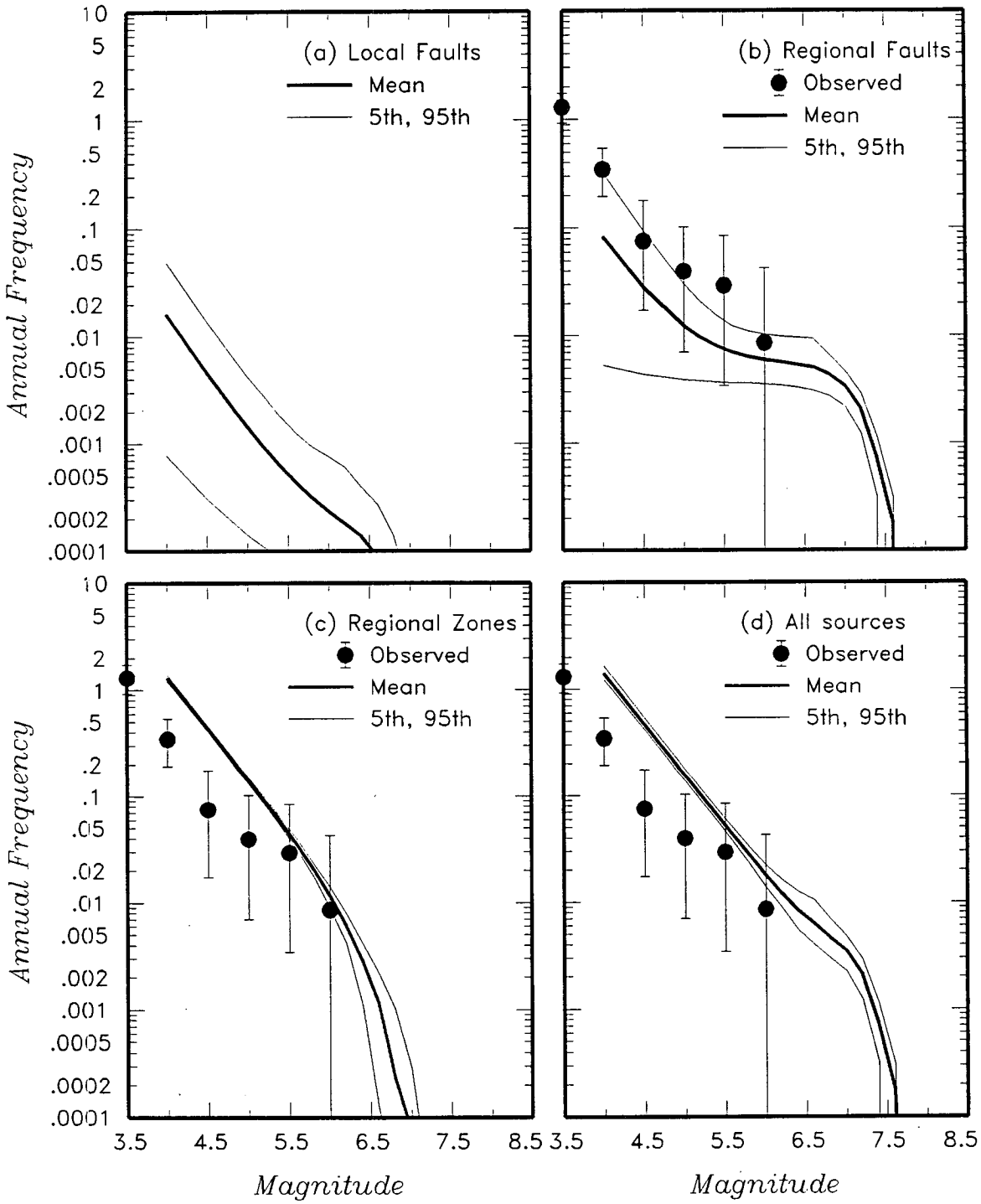

Figure 4-36 Predicted mean, 5th-, and 95th-percentile recurrence rates for (a) local fault sources, (b) regional fault sources, (c) regional source zones, and (d) all sources combined for the ASM team. The solid dots with vertical error bars indicate the observed frequency of earthquakes occurring within 100 km of the Yucca Mountain site.

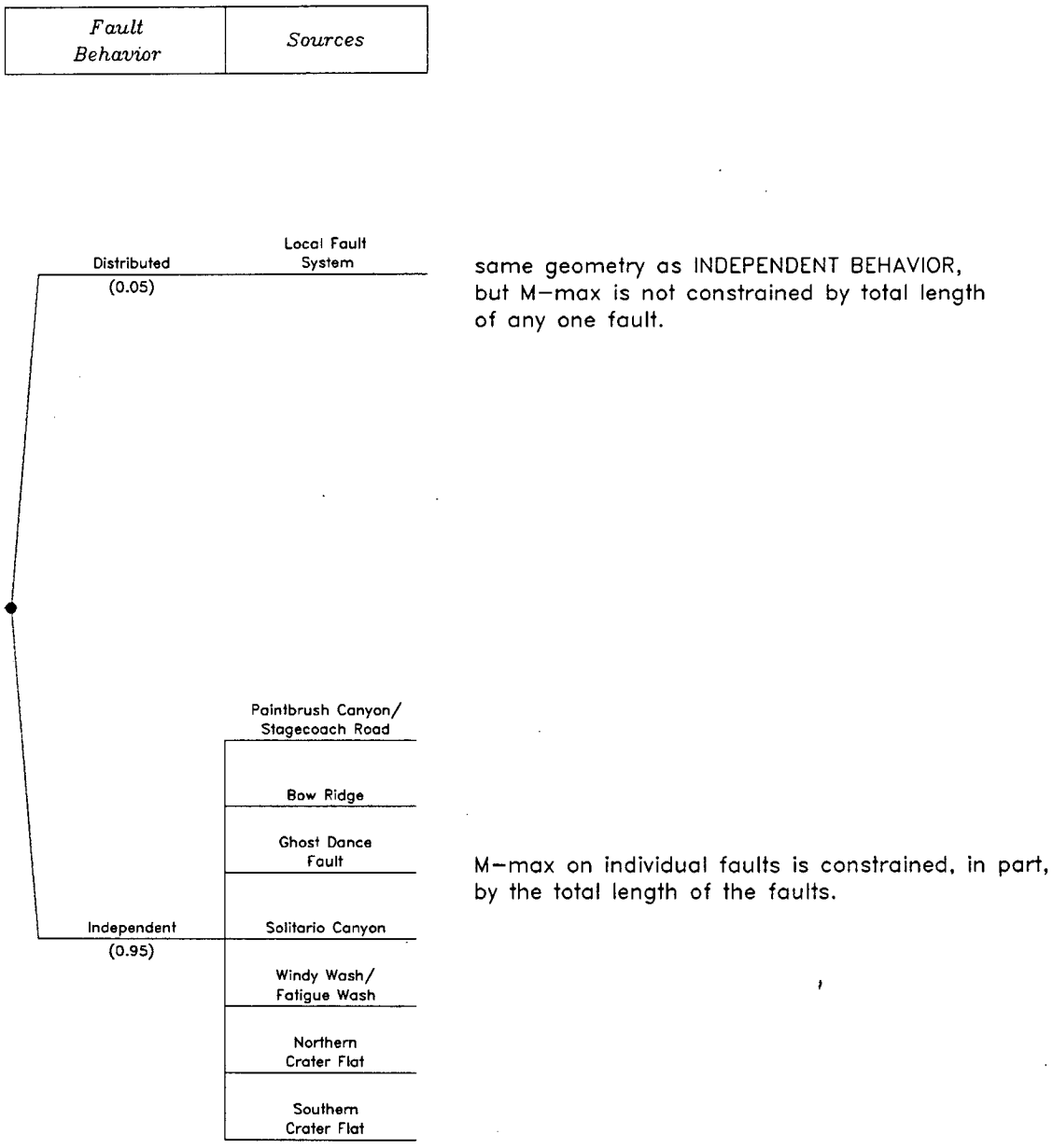

Figure 4-37a Logic tree for local fault sources developed by the DFS team

Seismic Source	Total Fault Length Scenarios	Maximum Rupture Length	Structural Model	Dip/Width	Slip Rate (mm/yr)	Maximum Earthquake Method	Earthquake Recurrence Model

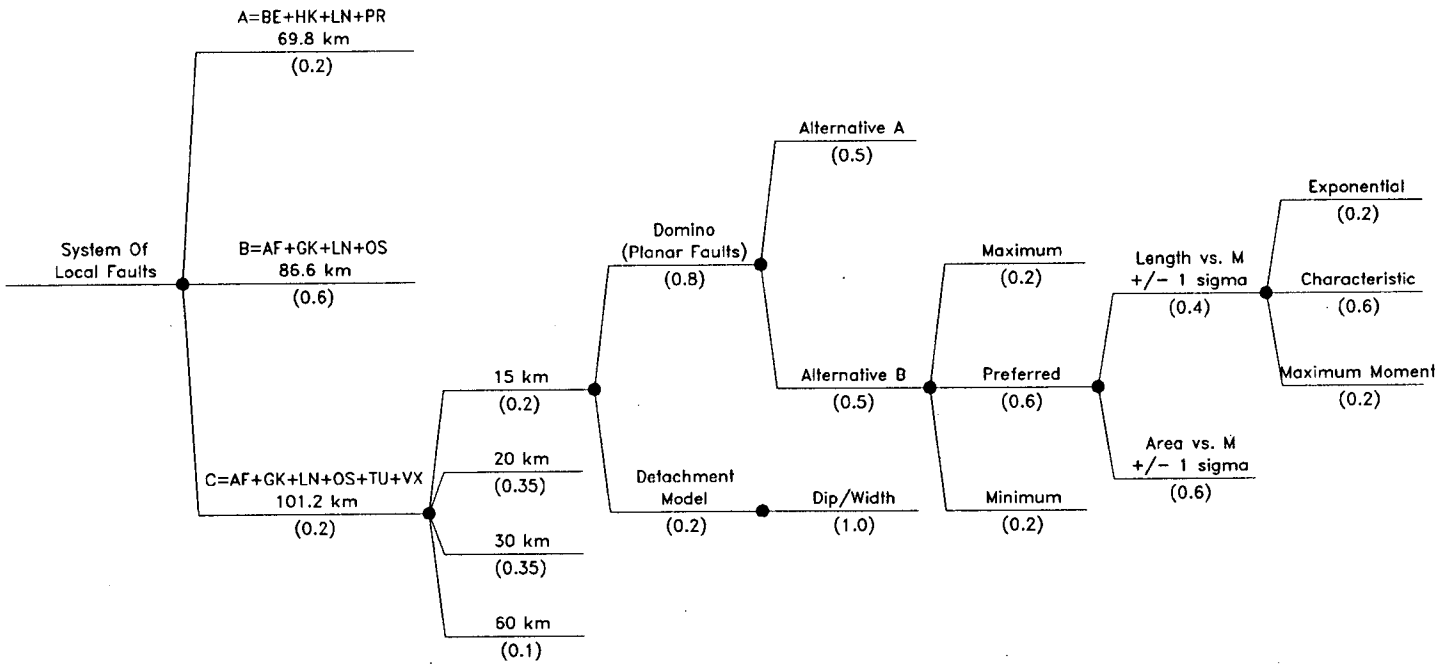

Figure 4-37b Logic tree for local fault source given distributed fault behavior

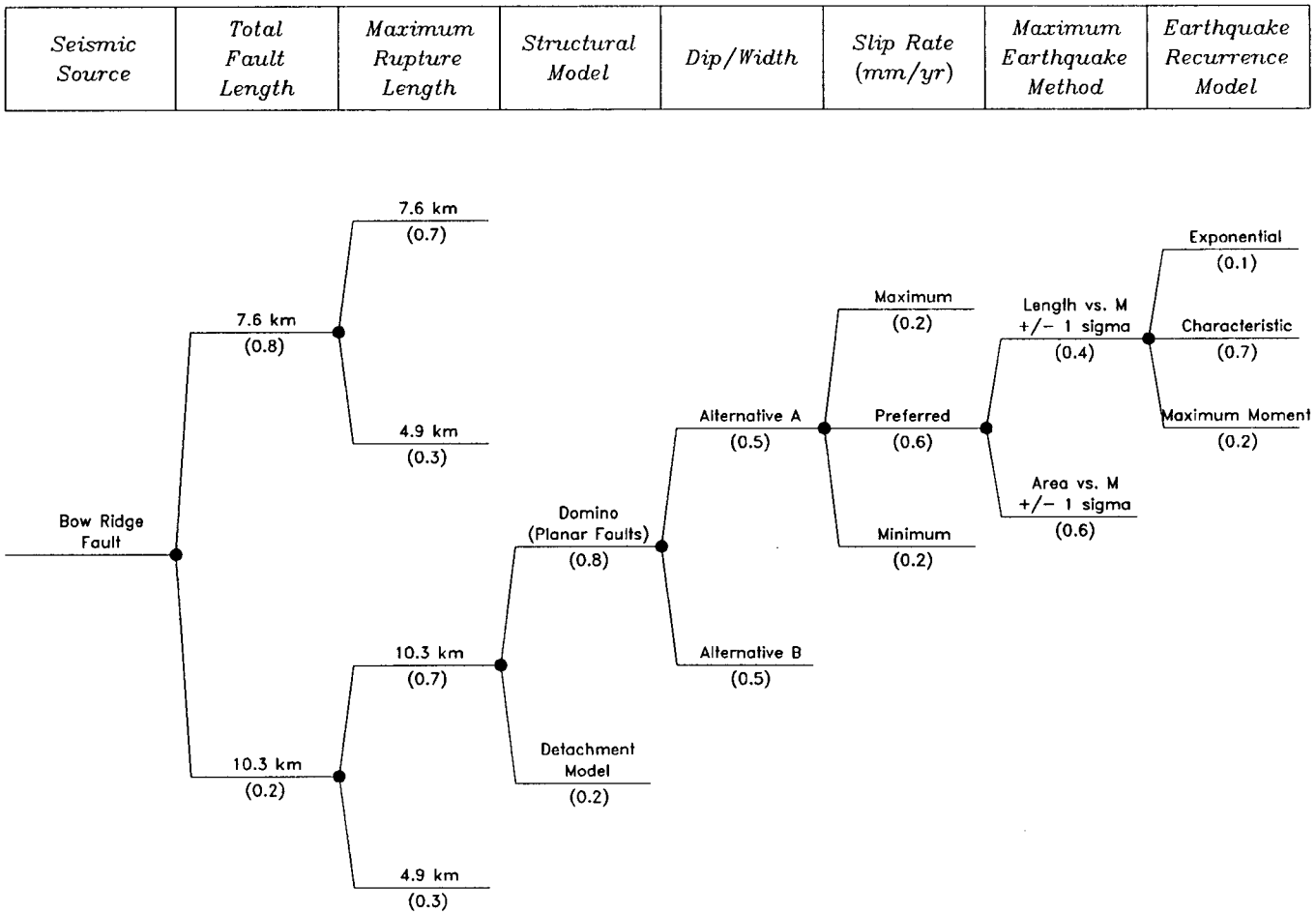

Figure 4-37c Example logic tree for local fault source given independent fault behavior

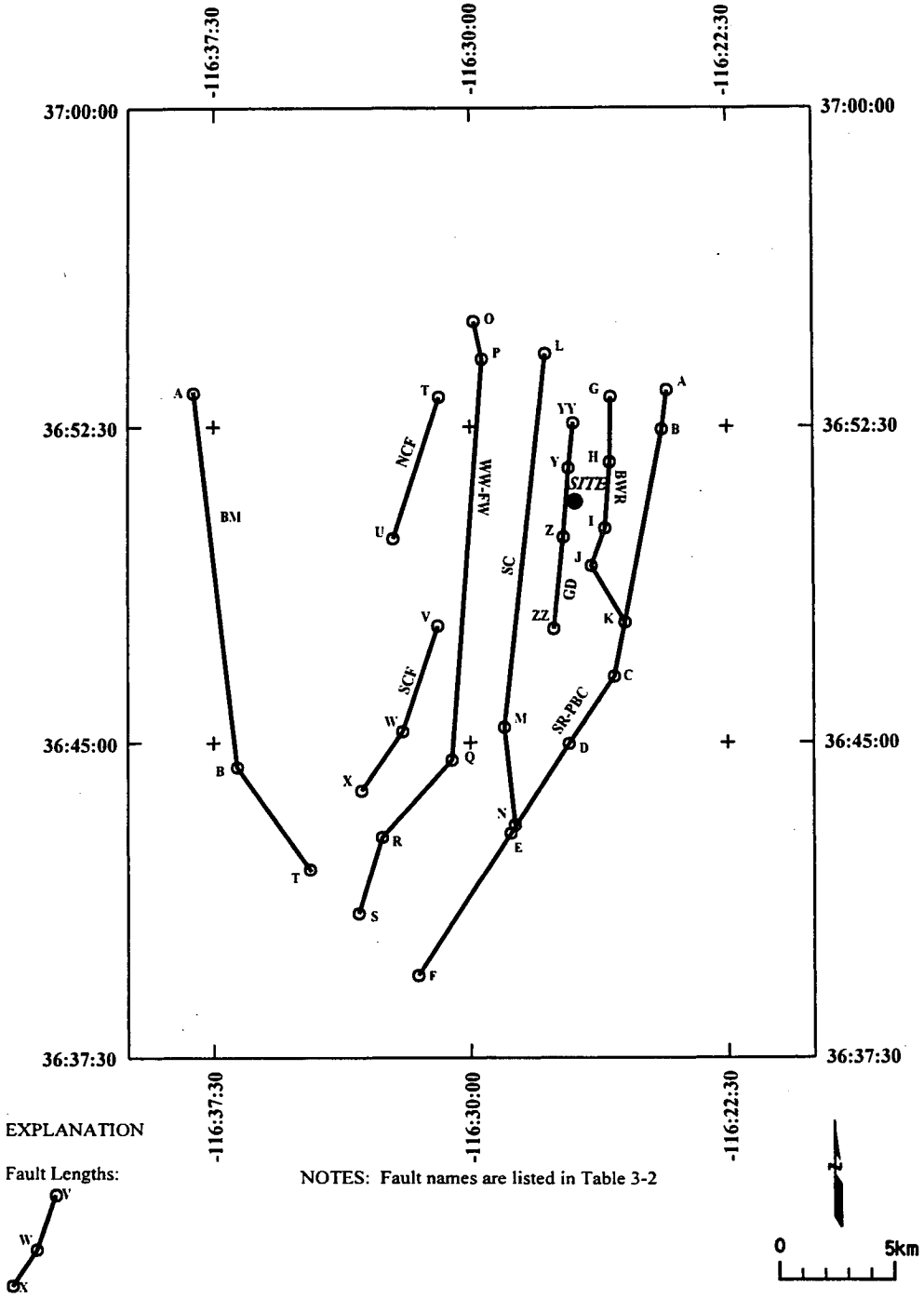

Figure 4-38 Location of local faults considered by the DFS team to be acting as independant sources

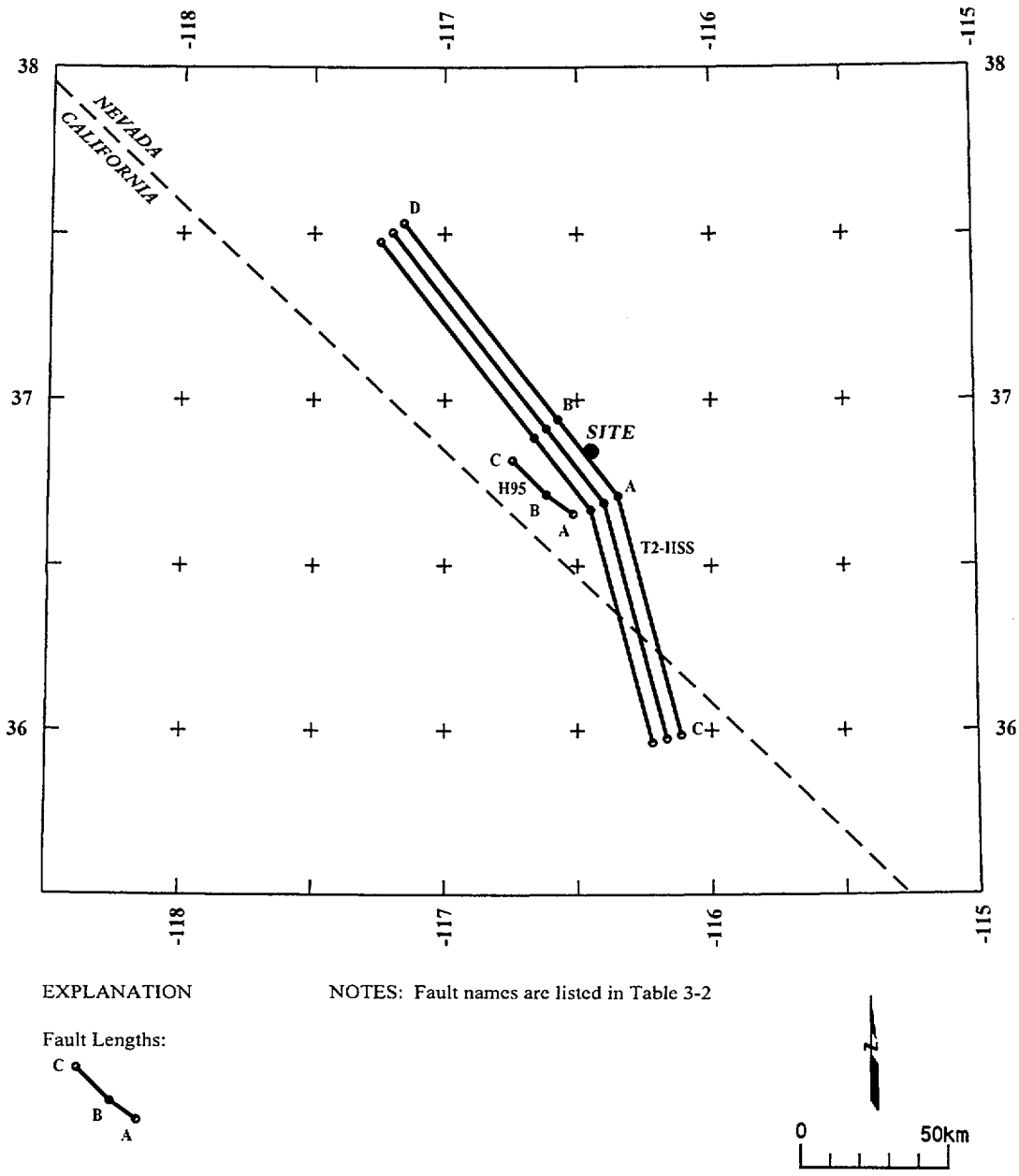

Figure 4-39 Potential locations of DFS team's inferred buried strike-slip sources

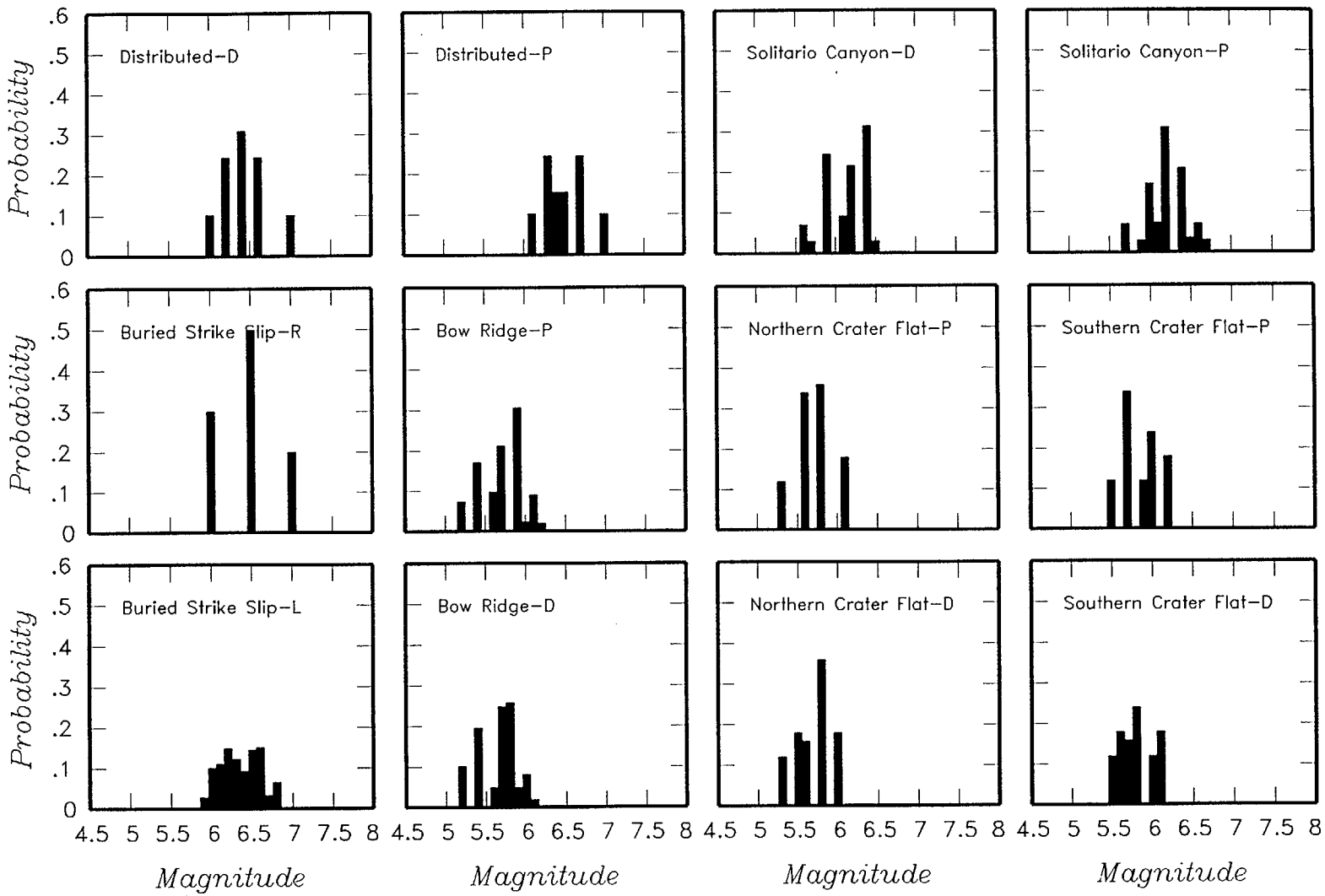

Figure 4-40 Maximum magnitude distributions for DFS team's local fault sources. D–detachment, L–local, R–regional, P–planar.

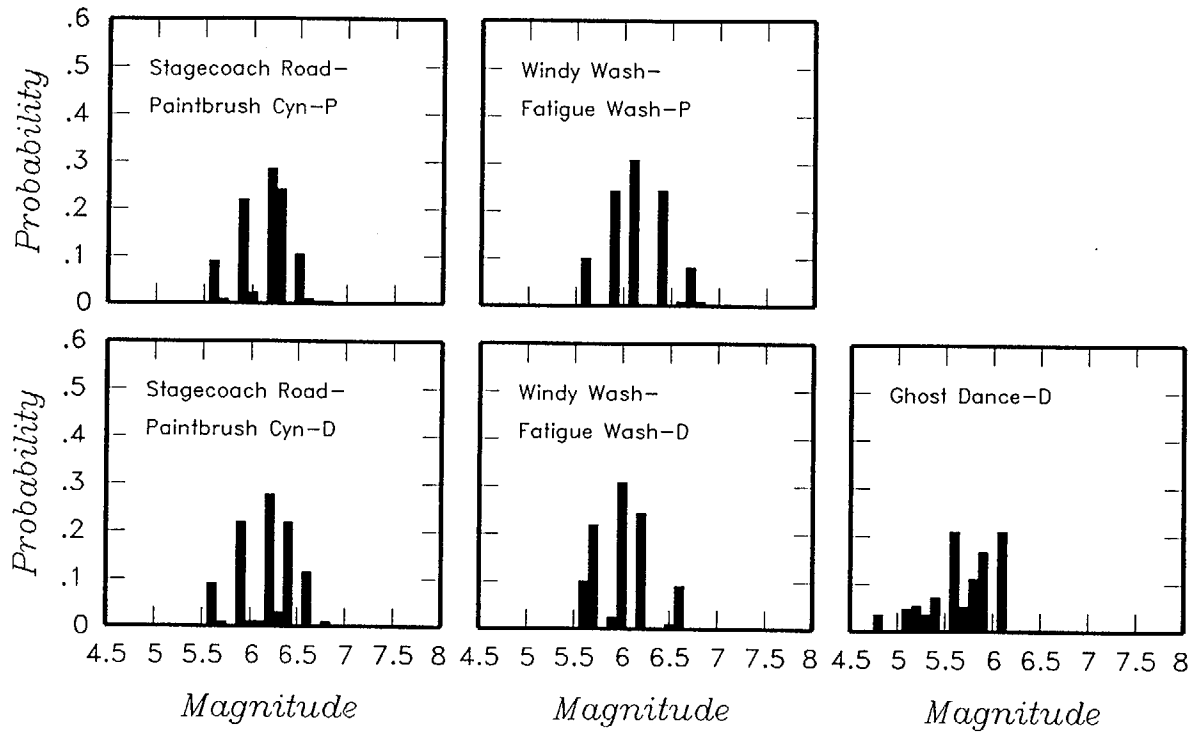

Figure 4-40 (Cont'd.) Maximum magnitude distributions for DFS team's local fault sources

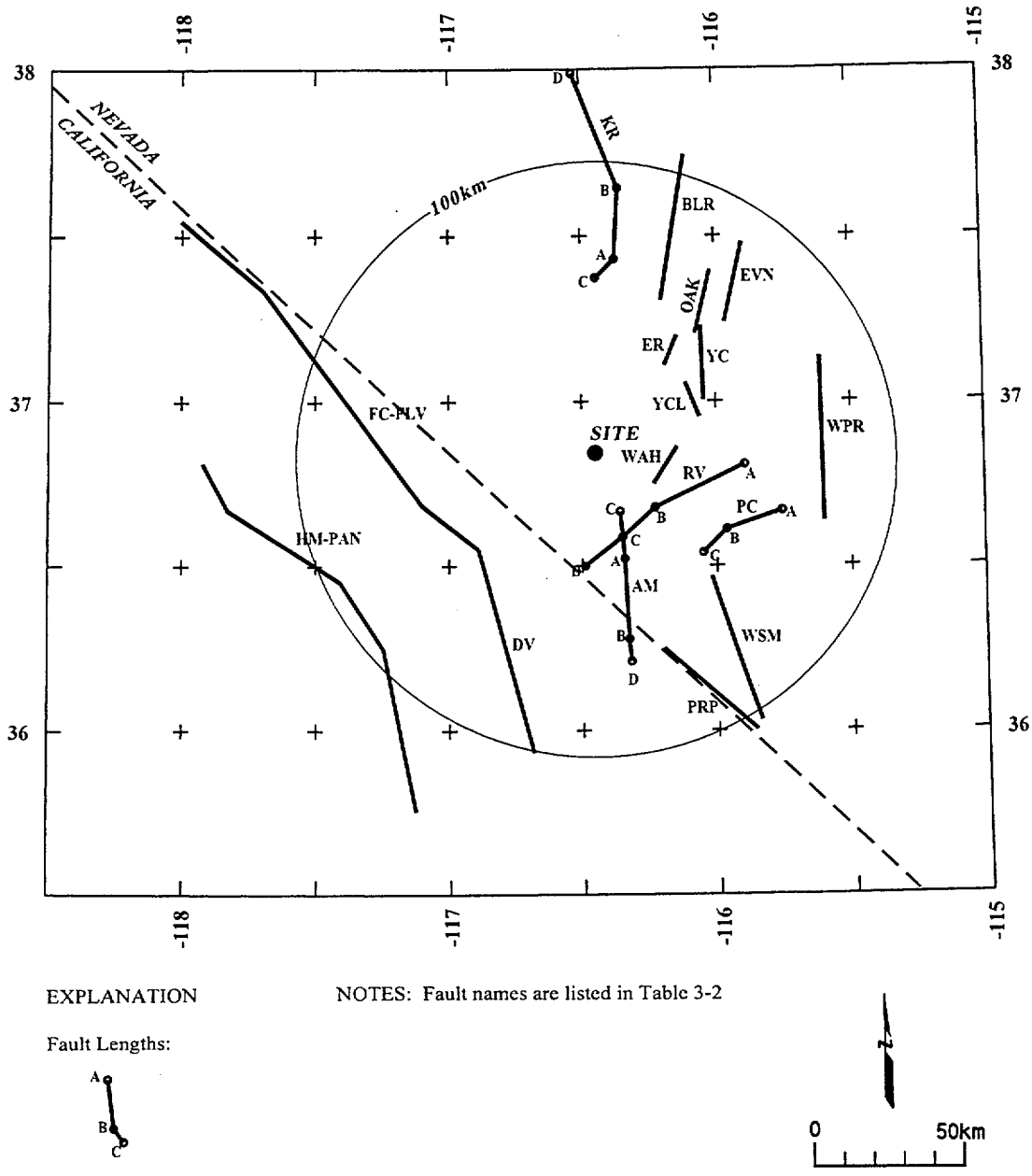

Figure 4-41 Regional fault sources considered by the DFS team

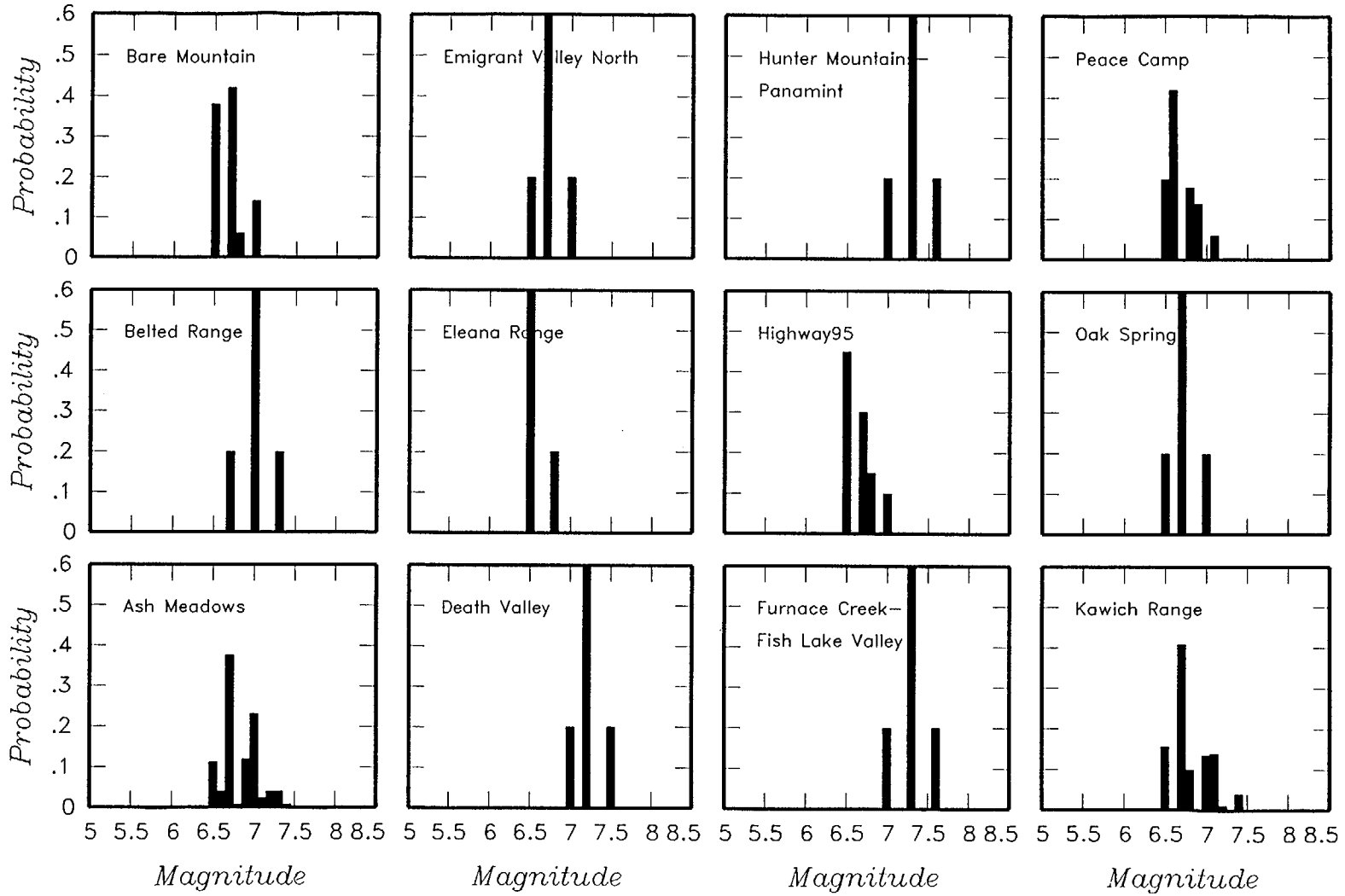

Figure 4-42 Maximum magnitude distributions for DFS team's regional fault sources

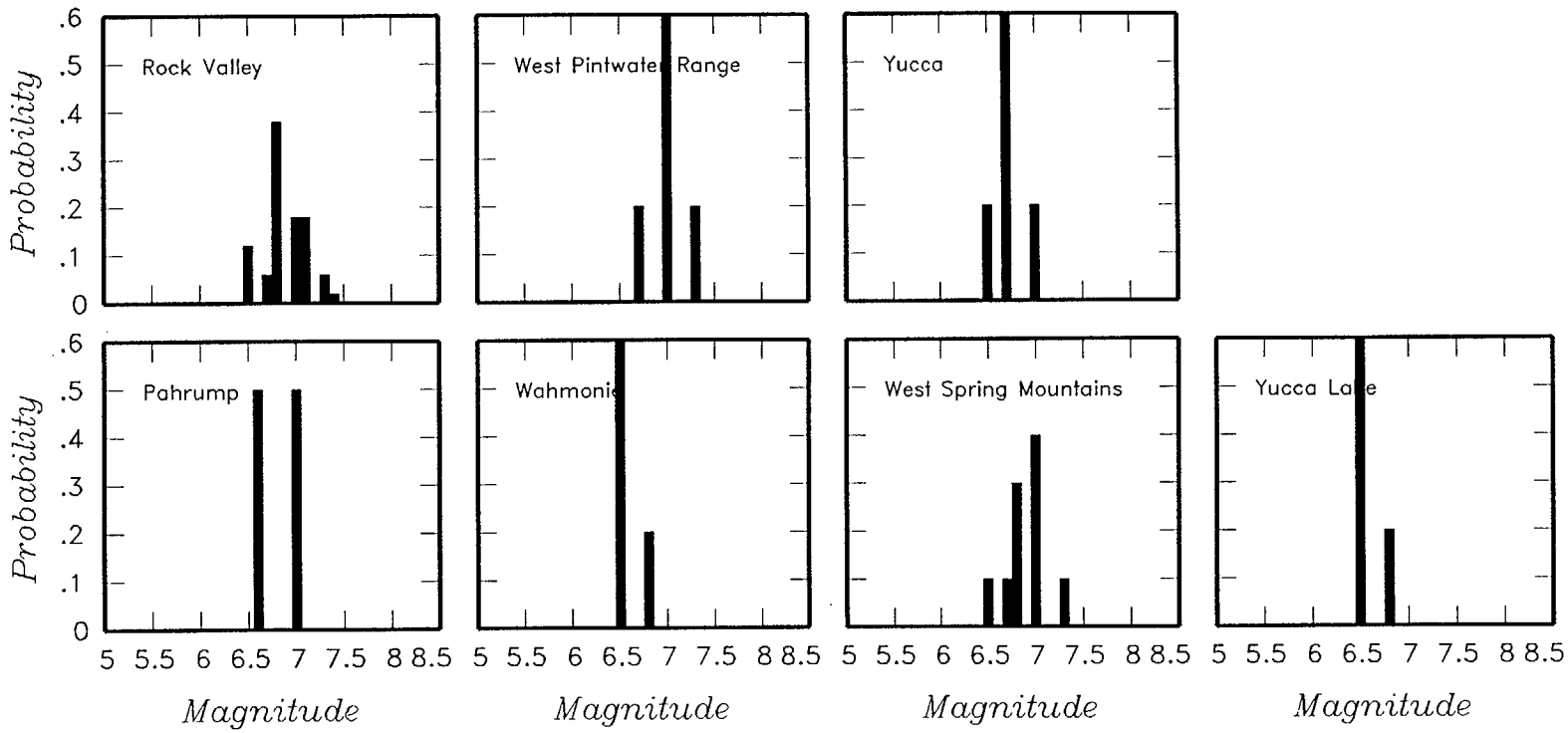

Figure 4-42 (Cont'd.) Maximum magnitude distributions for DFS team's regional fault sources

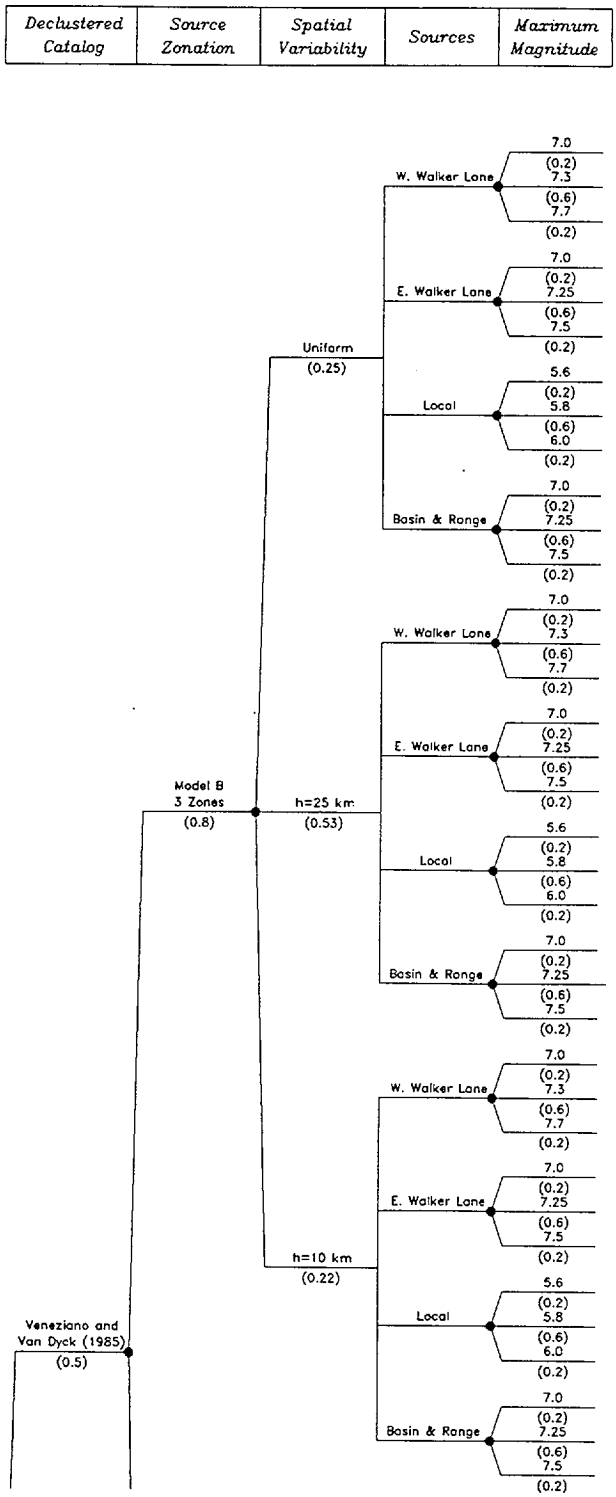

Figure 4-43 Logic tree for regional source zones developed by the DFS team

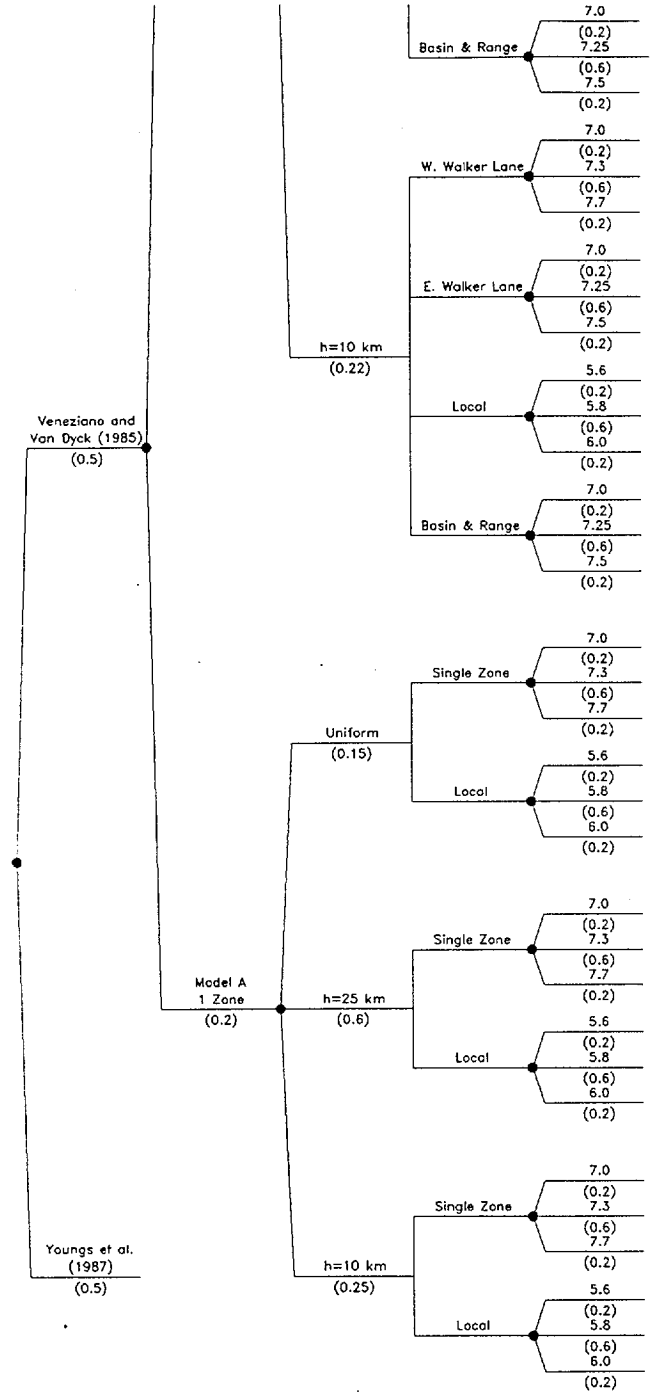

Figure 4-43 (Cont'd.) Logic tree for regional source zones developed by the DFS team

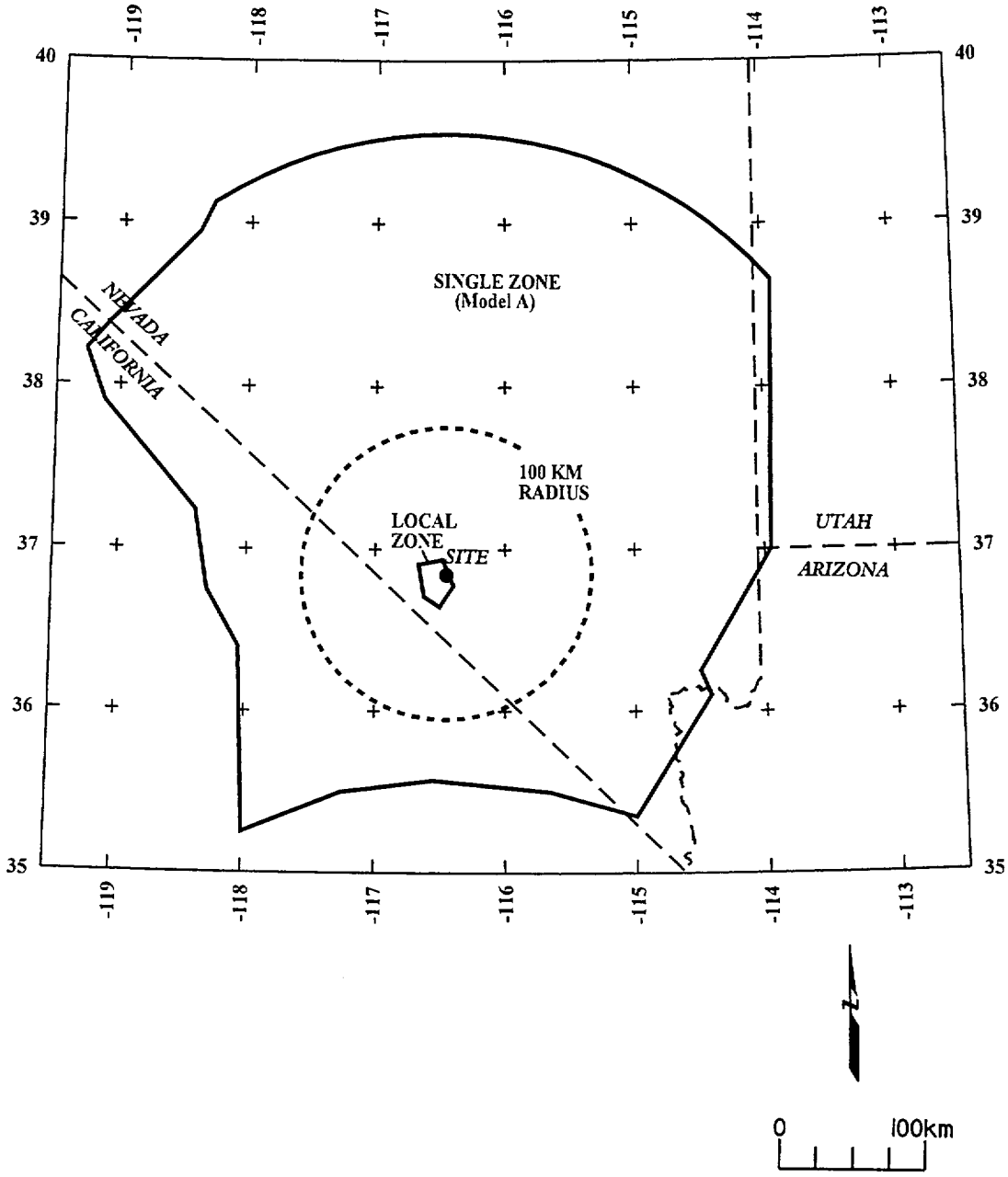

Figure 4-44 Alternative regional source zone models considered by the DFS team

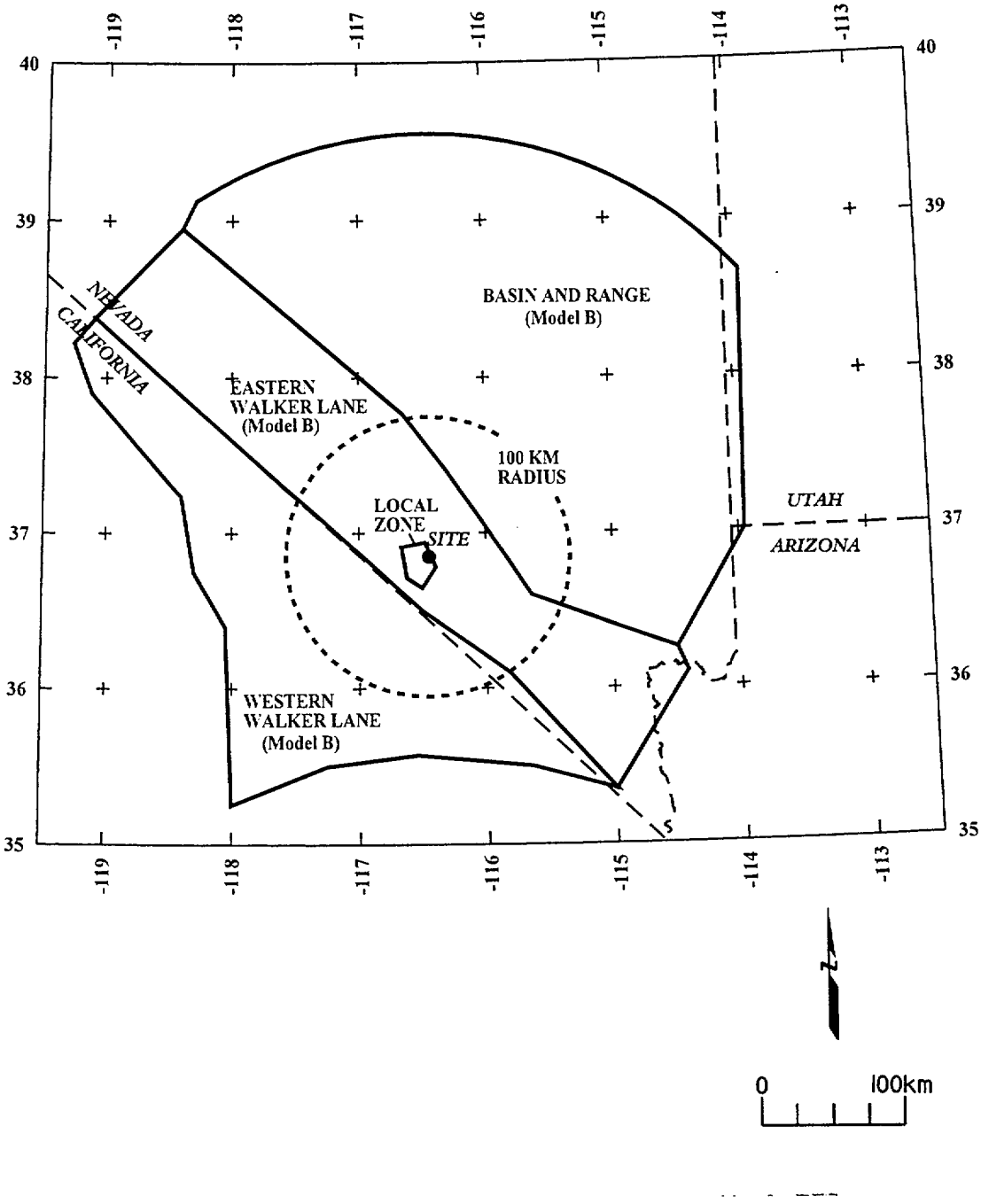

Figure 4-44 (Cont'd.) Alternative regional source zone models considered by the DFS team

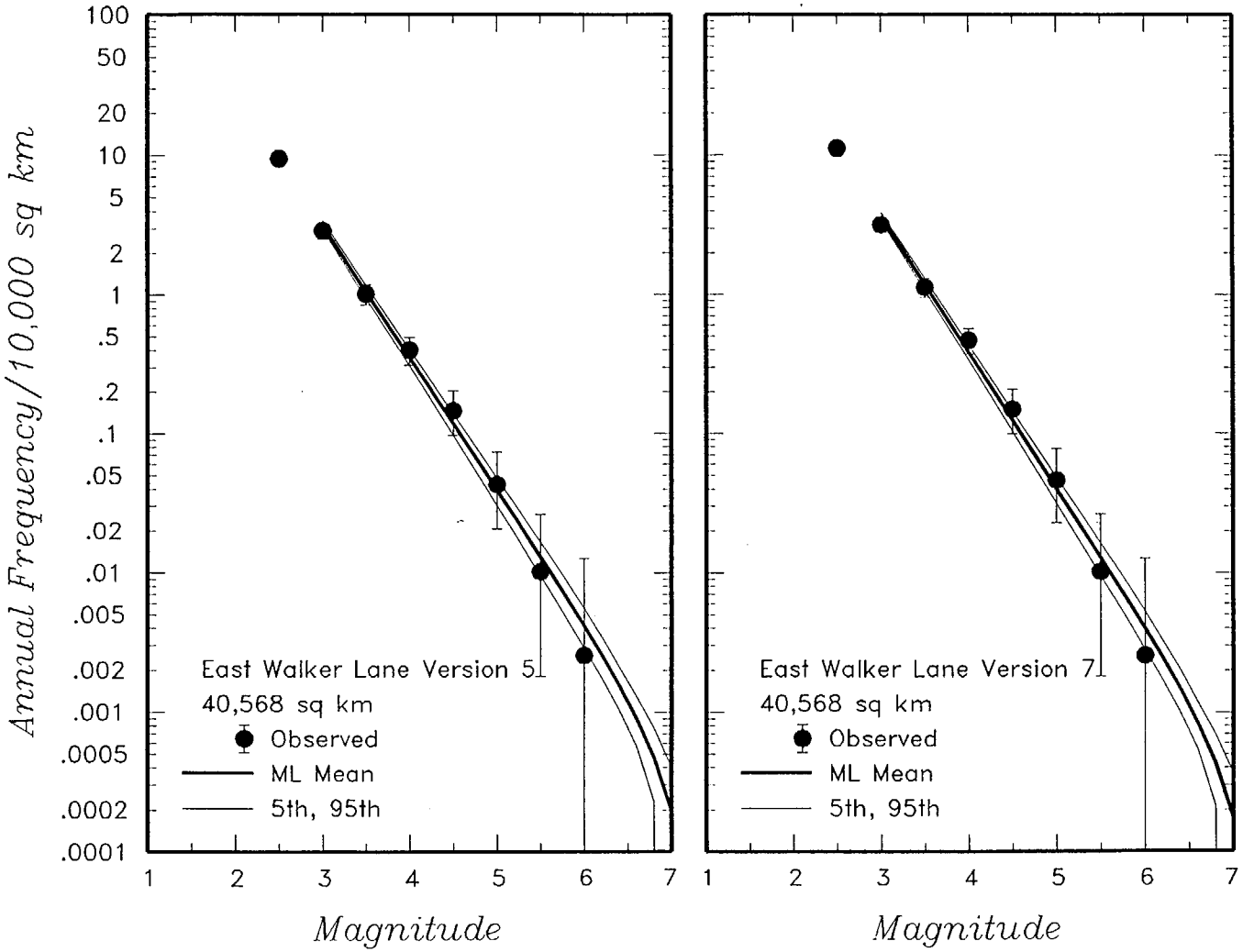

Figure 4-45 Earthquake recurrence relationships for the regional source zones defined by the DFS team. The solid dots with vertical error bars represent the observed data. The thick and thin solid curves are the mean, 5th, and 95th percentiles of the recurrence rates based on the uncertainty in recurrence parameters and maximum magnitude.

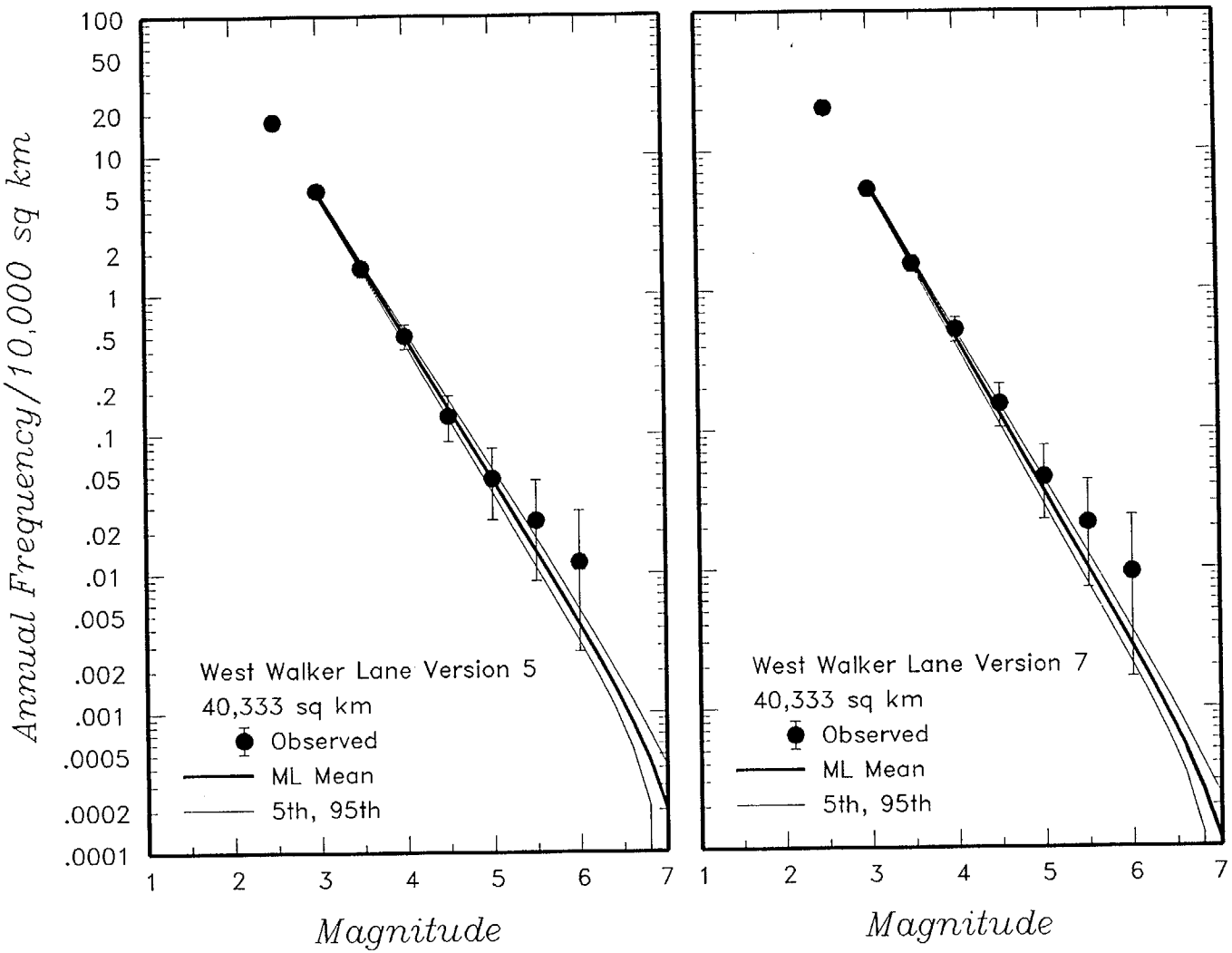

Figure 4-45 (Cont'd.) Earthquake recurrence relationships for the regional source zones defined by the DFS team

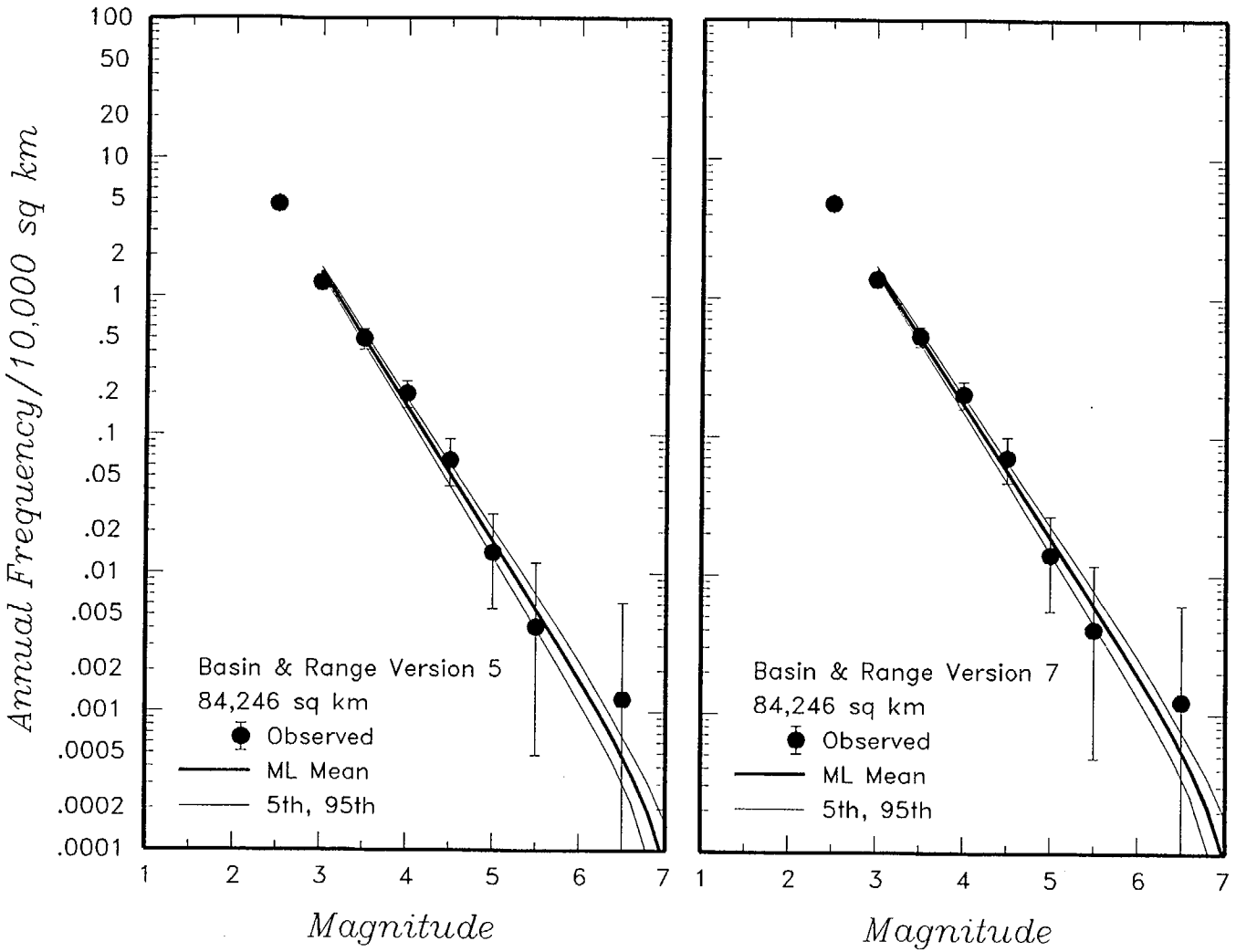

Figure 4-45 (Cont'd.) Earthquake recurrence relationships for the regional source zones defined by the DFS team

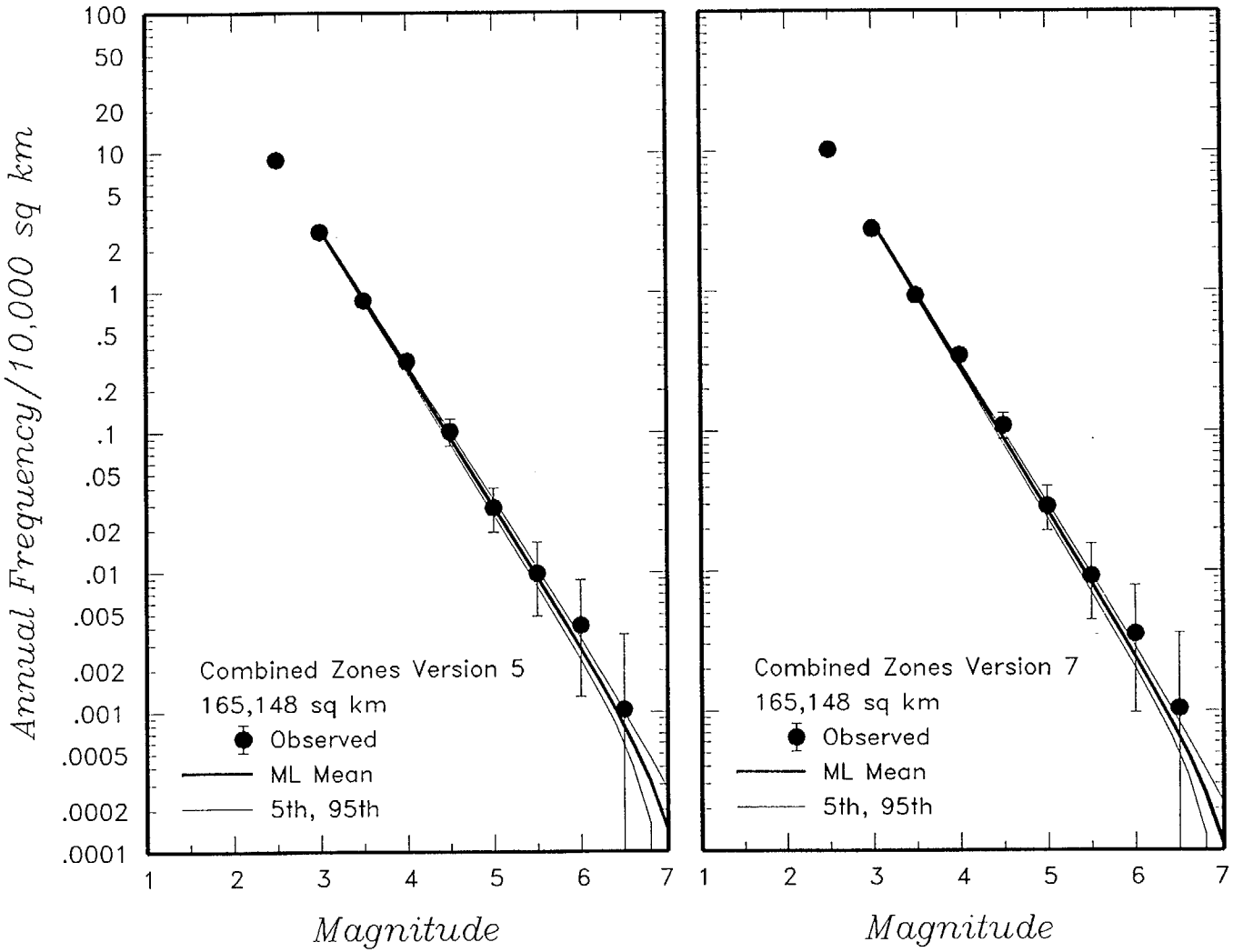

Figure 4-45 (Cont'd.) Earthquake recurrence relationships for the regional source zones defined by the DFS team

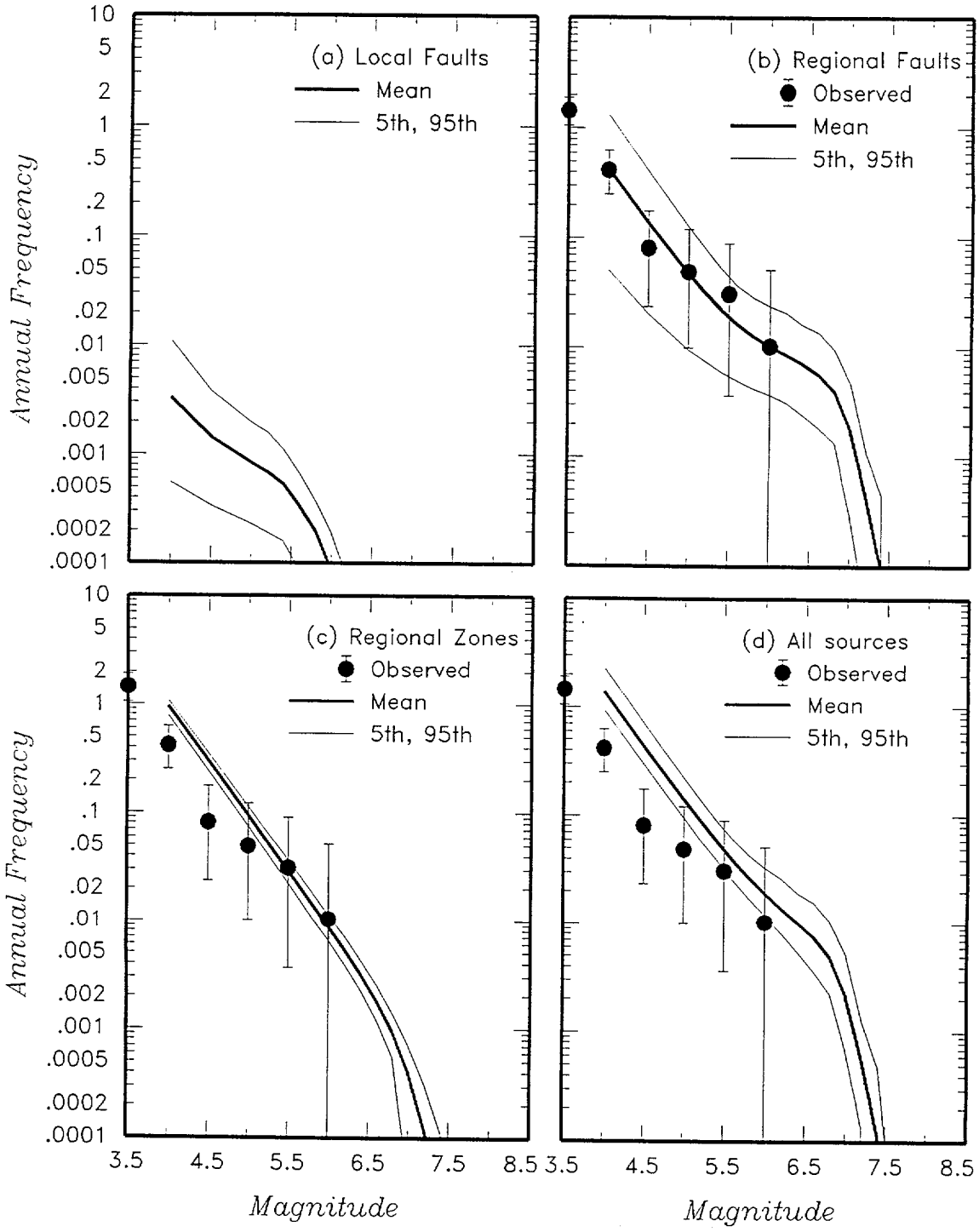

Figure 4-46 Predicted mean, 5th-, and 95th-percentile recurrence rates for (a) local fault sources, (b) regional fault sources, (c) regional source zones, and (d) all sources combined for the DFS team. The solid dots with vertical error bars indicate the observed frequency of earthquakes occurring within 100 km of the Yucca Mountain site.

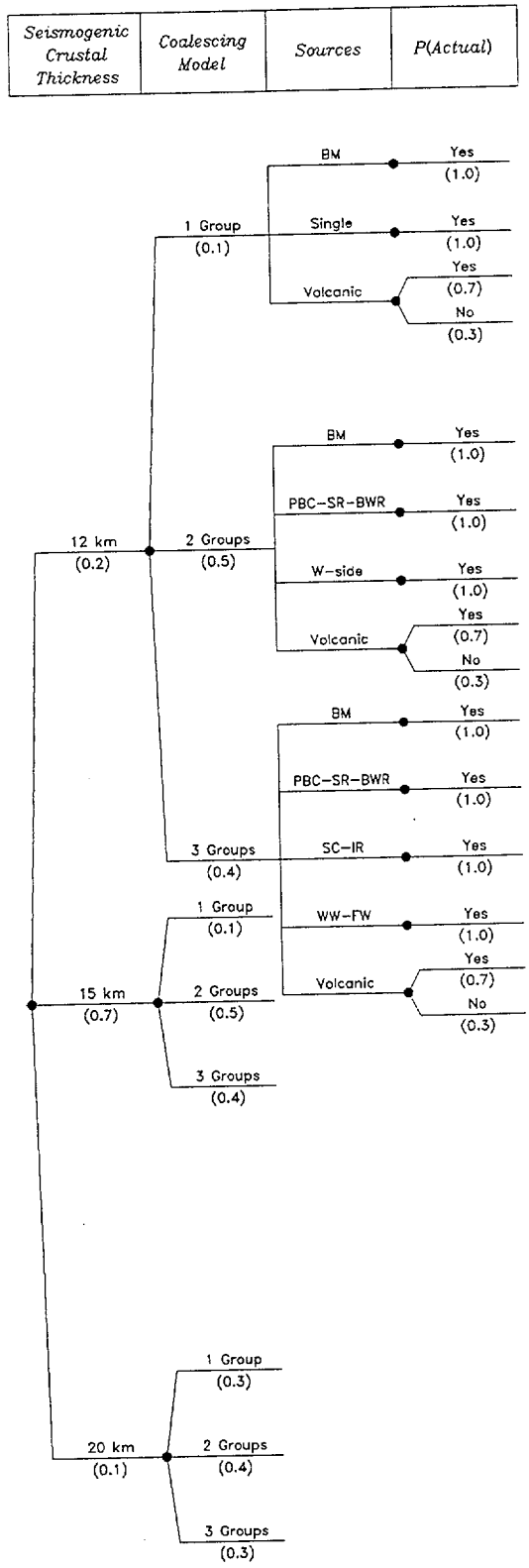

Figure 4-47 Logic tree for local fault sources developed by the RYA team

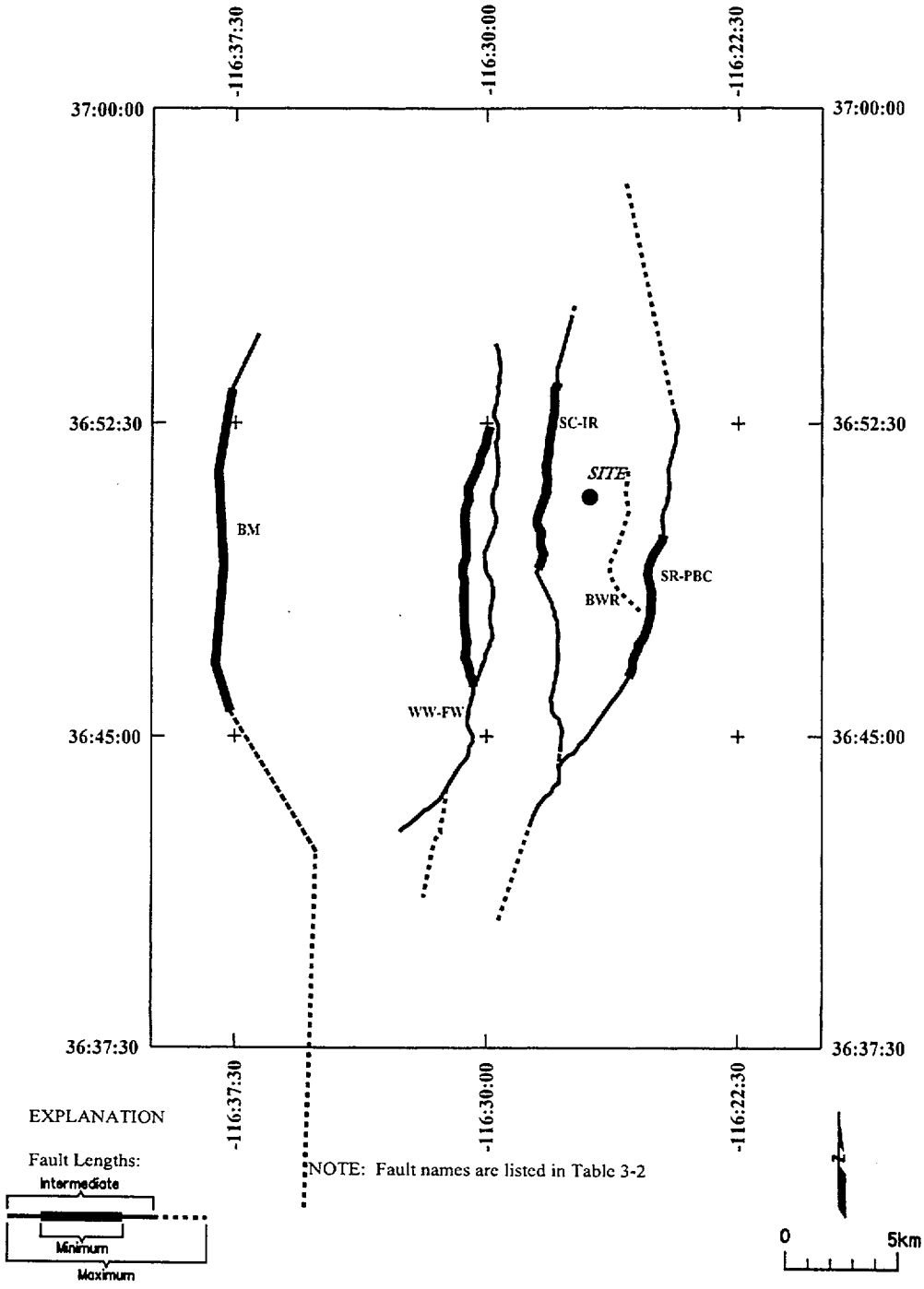

Figure 4-48 Location of local fault sources considered by the RYA team

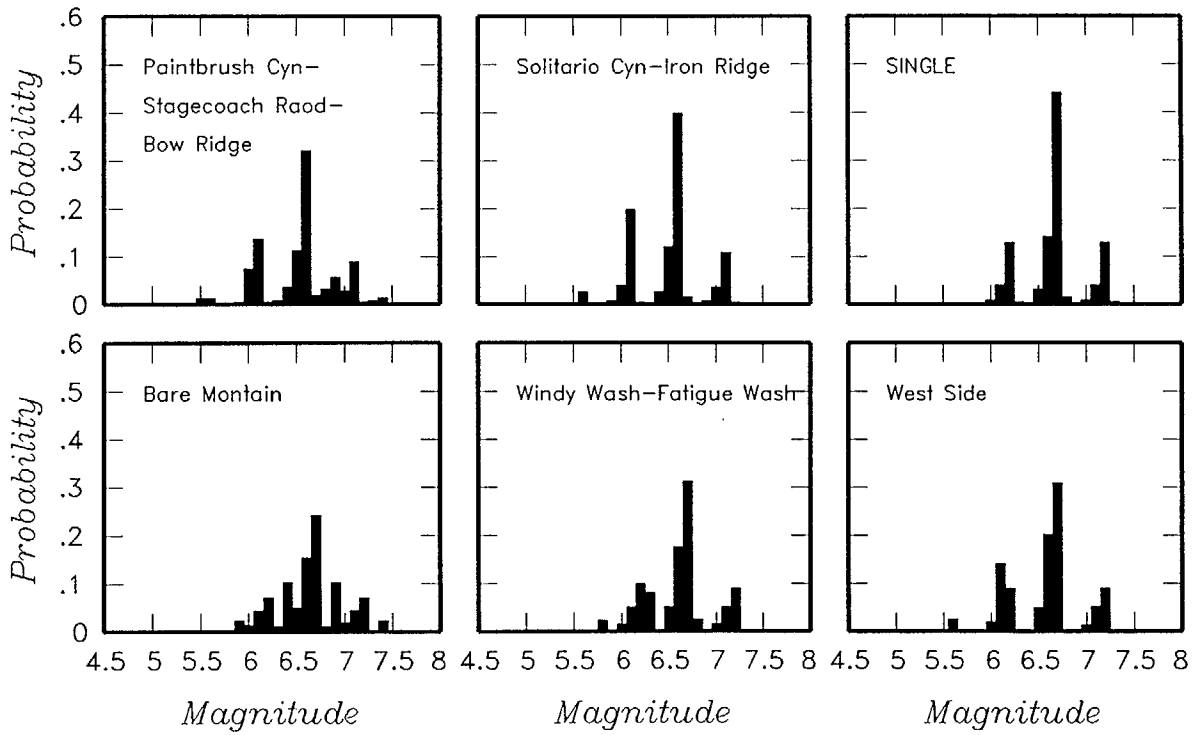

Figure 4-49 Maximum magnitude distributions for RYA team's local fault sources. SINGLE–coalescing source model with single fault system.

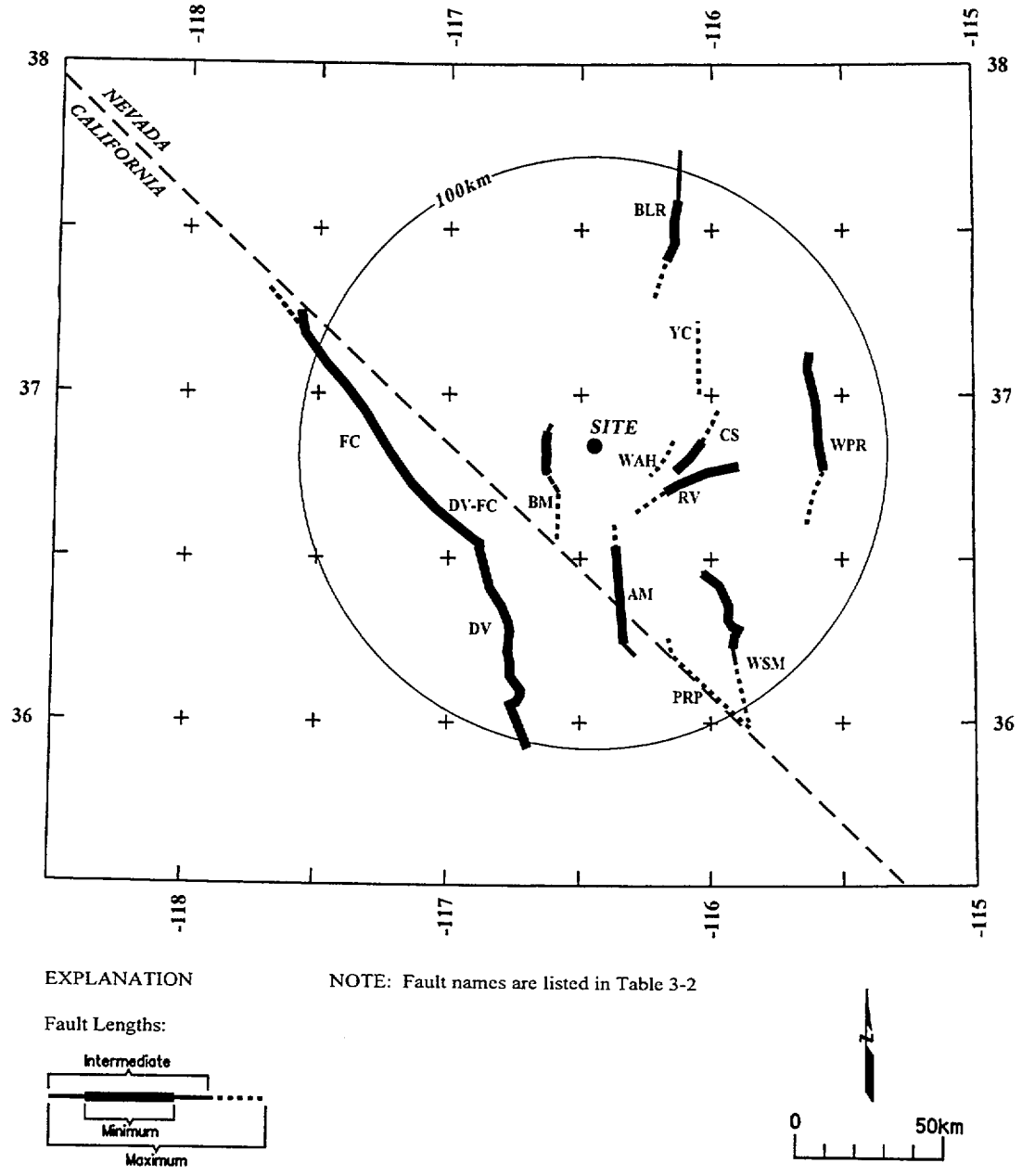

Figure 4-50 Regional fault sources considered by the RYA team

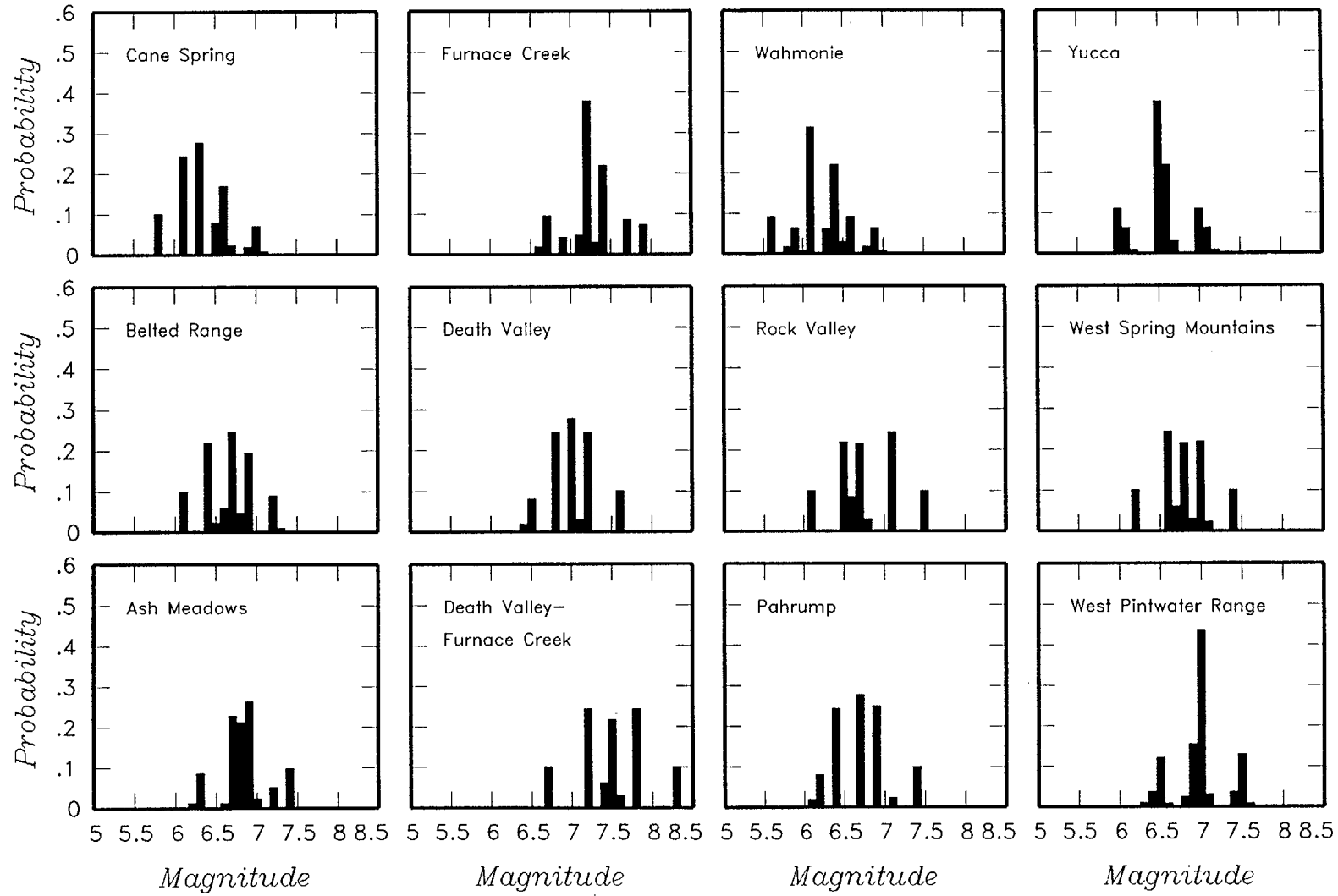

Figure 4-51 Maximum magnitude distributions for RYA team's regional fault sources

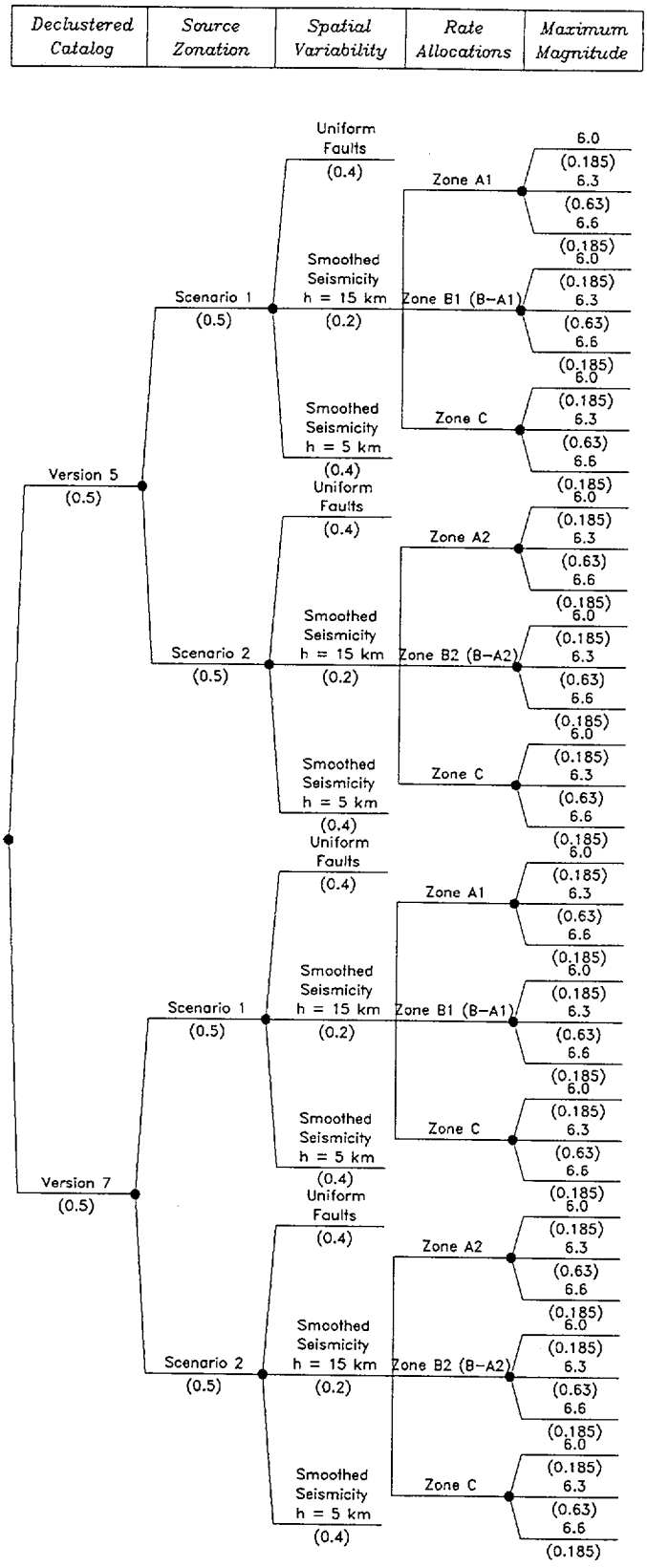

Figure 4-52 Logic tree for regional source zones developed by the RYA team

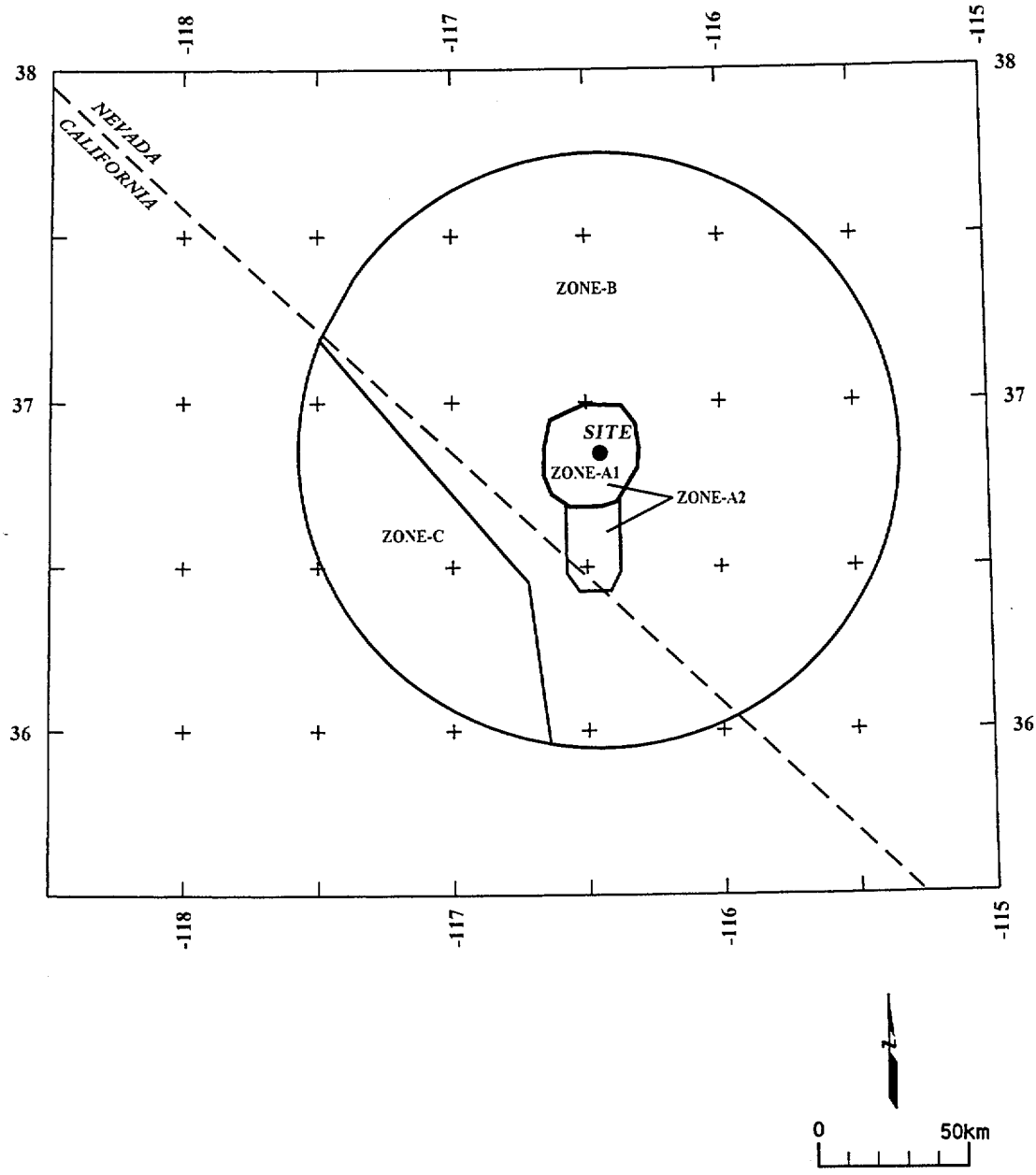

Figure 4-53 Alternative regional source zone models considered by the RYA team

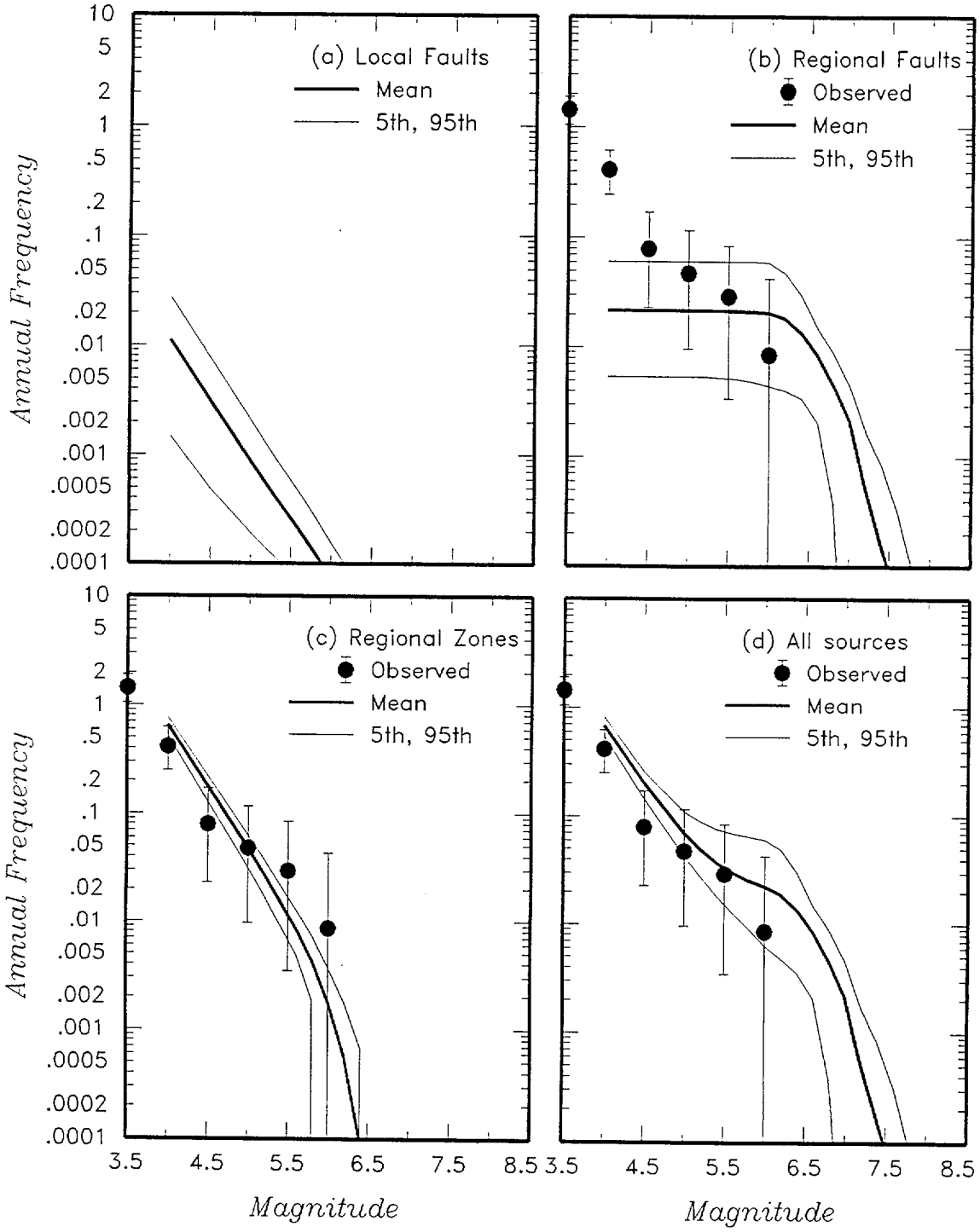

Figure 4-54 Predicted mean, 5th-, and 95th-percentile recurrence rates for (a) local fault sources, (b) regional fault sources, (c) regional source zones, and (d) all sources combined for the RYA team. The solid dots with vertical error bars indicate the observed frequency of earthquakes occurring within 100 km of the Yucca Mountain site.

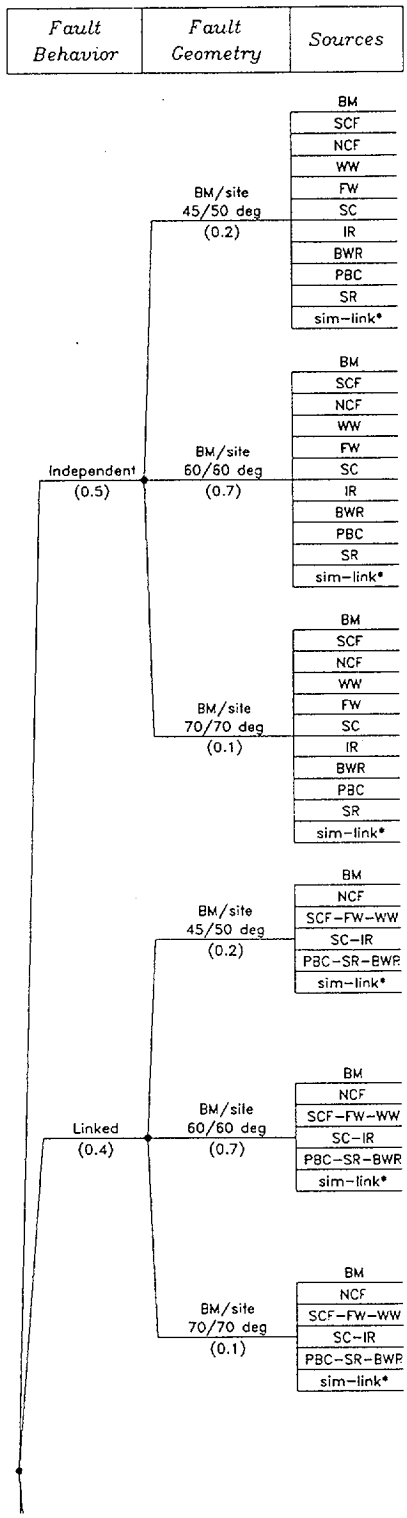

Figure 4-55 Logic tree for local fault sources developed by the SBK team

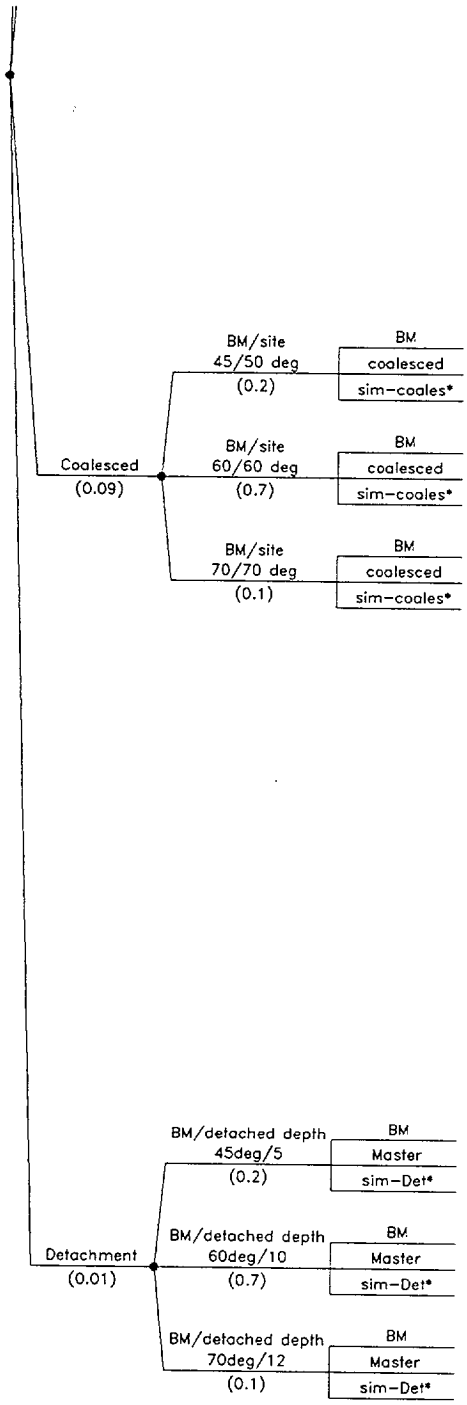

* sim-link, sim-coales and sim-det are synchronous rupture scenarios that act as additional sources of large events

Figure 4-55 (Cont'd.) Logic tree for local fault sources developed by the SBK team

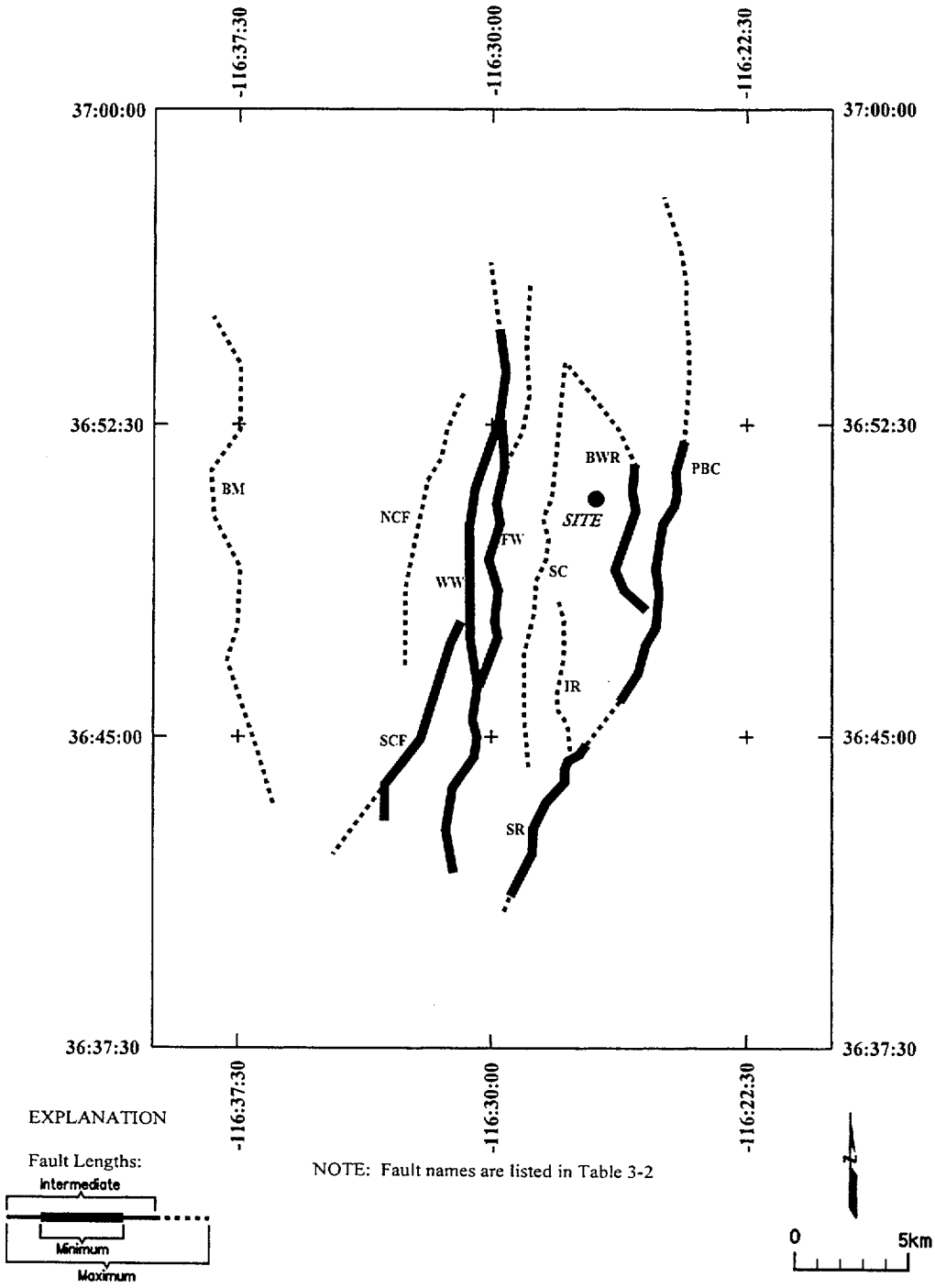

Figure 4-56 Location of local faults characterized by the SBK team

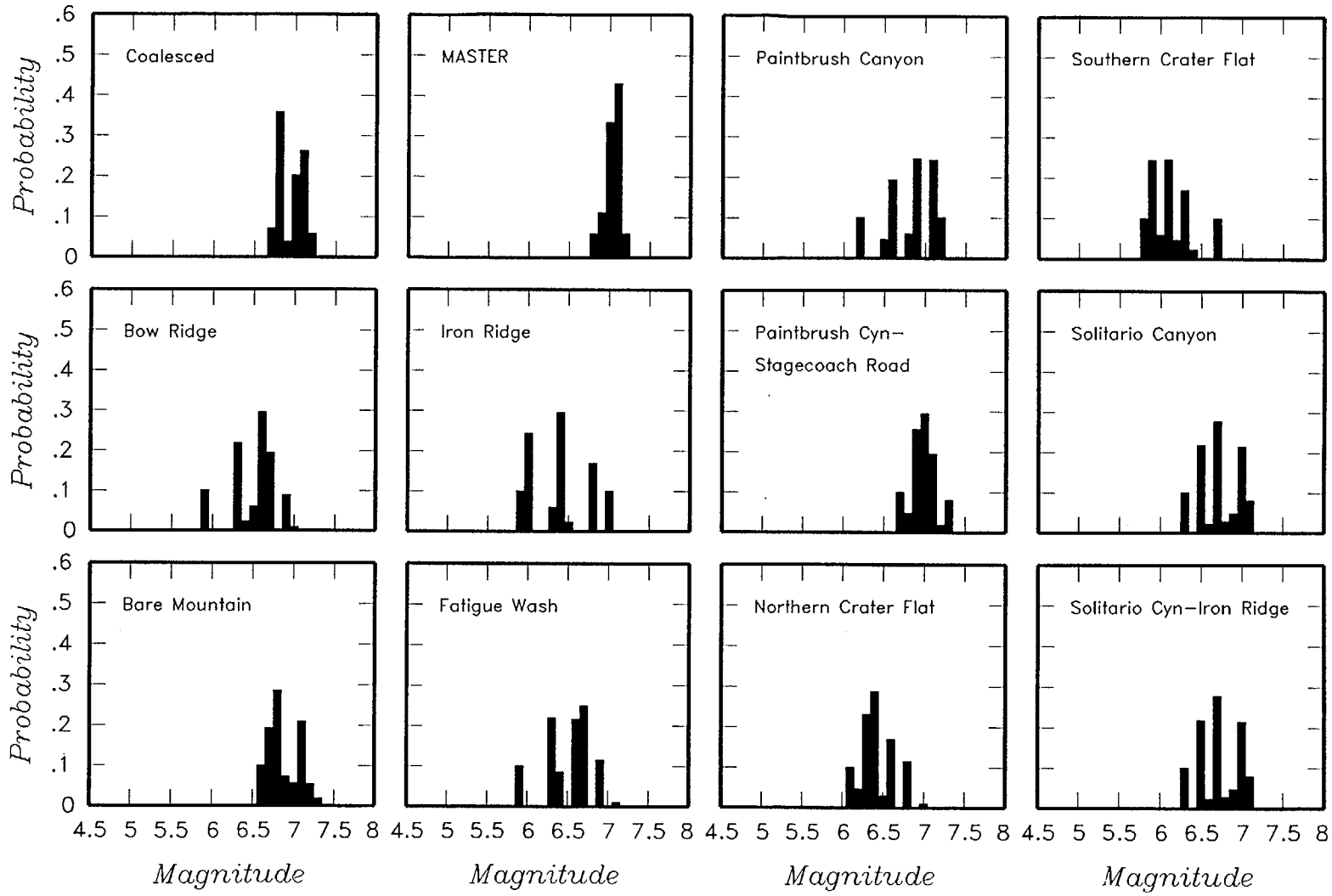

Figure 4-57 Maximum magnitude distributions for SBK team's local fault sources. MASTER–detachment with underlying master fault.

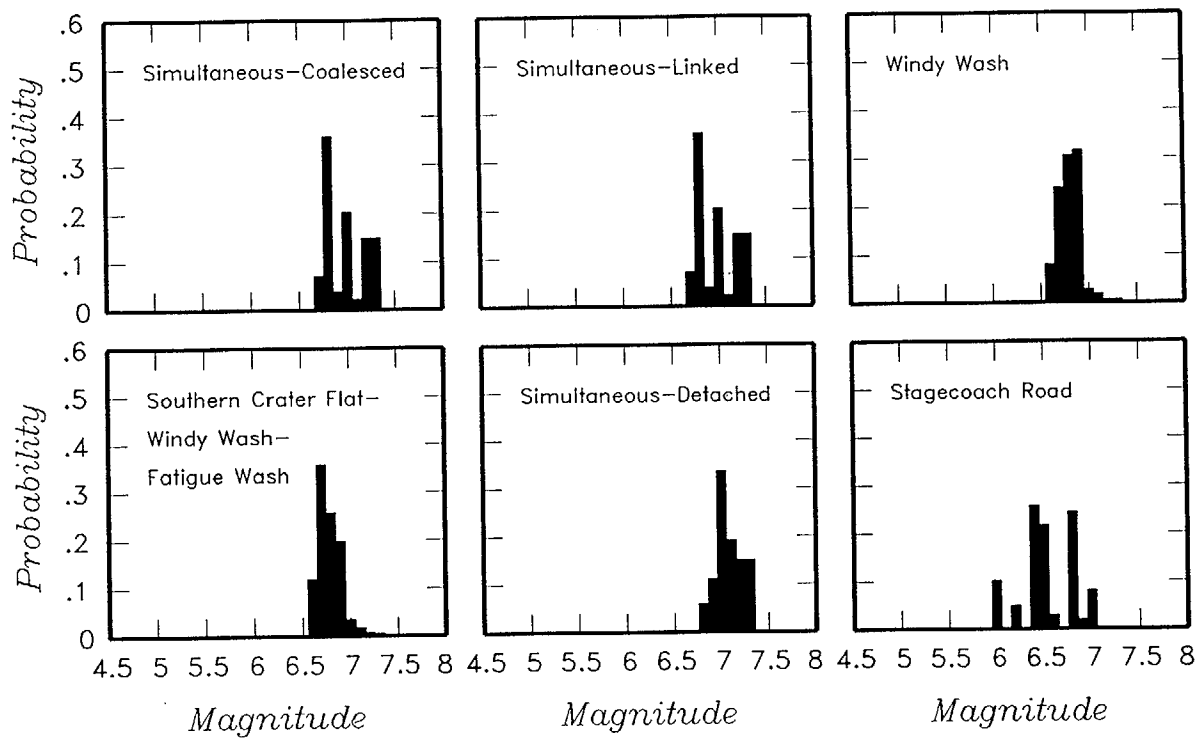

Figure 4-57 (Cont'd.) Maximum magnitude distributions for SBK team's local fault sources. MASTER–detachment with underlying master fault.

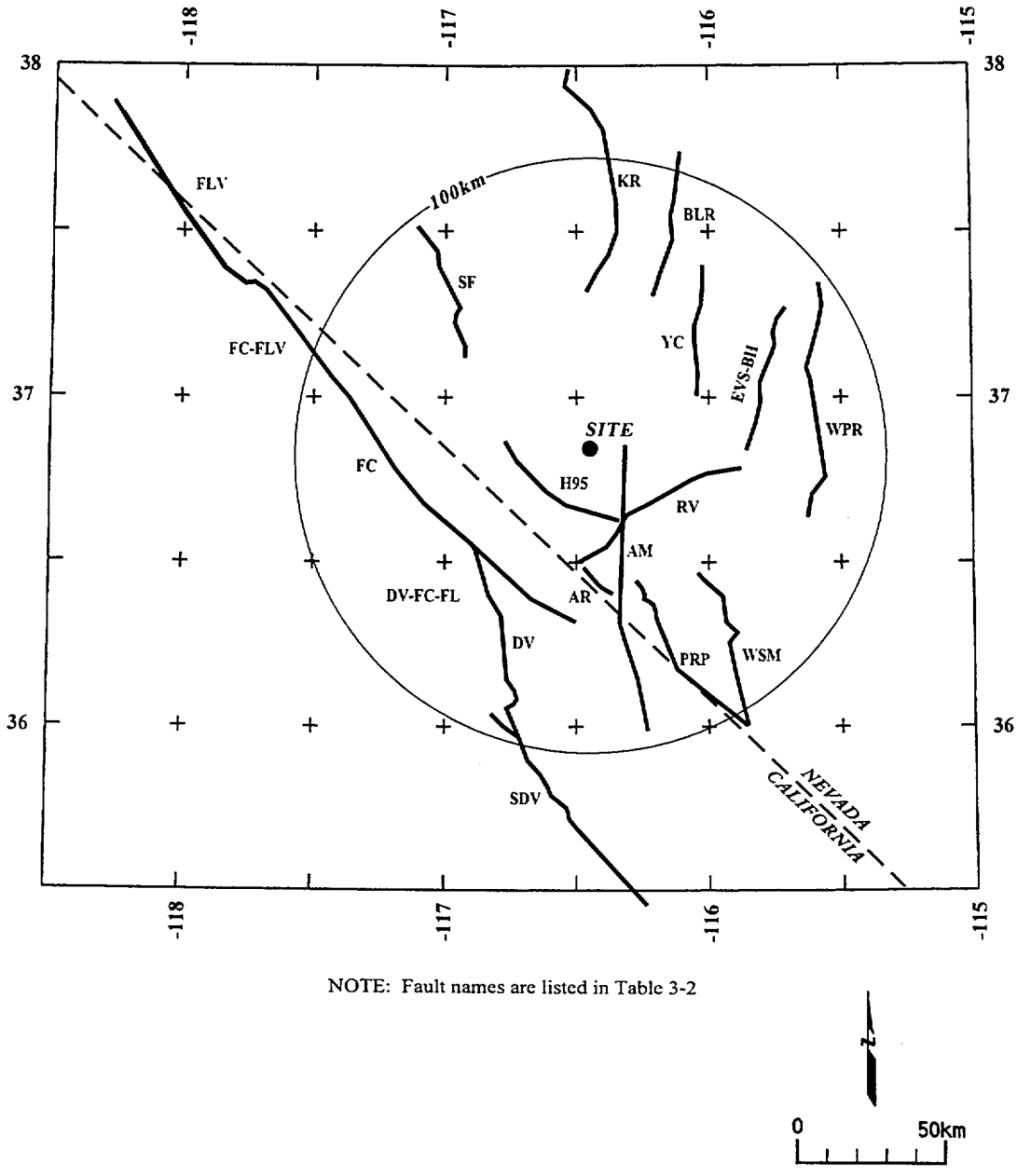

NOTE: Fault names are listed in Table 3-2

Figure 4-58 Regional fault sources characterized by the SBK team

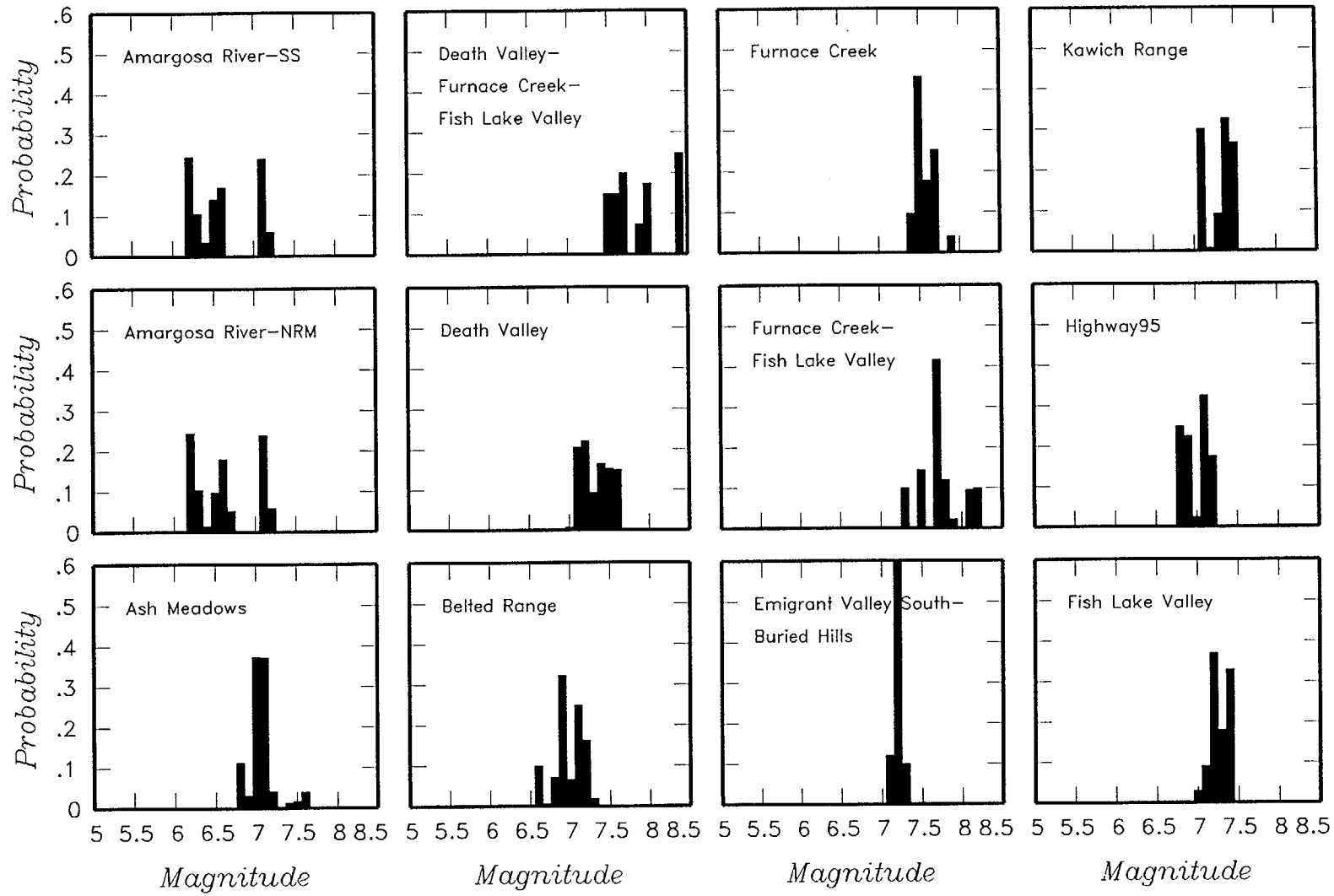

Figure 4-59 Maximum magnitude distributions for SBK team's regional fault sources. SS–strike slip; NRM–normal slip, OBL–oblique slip.

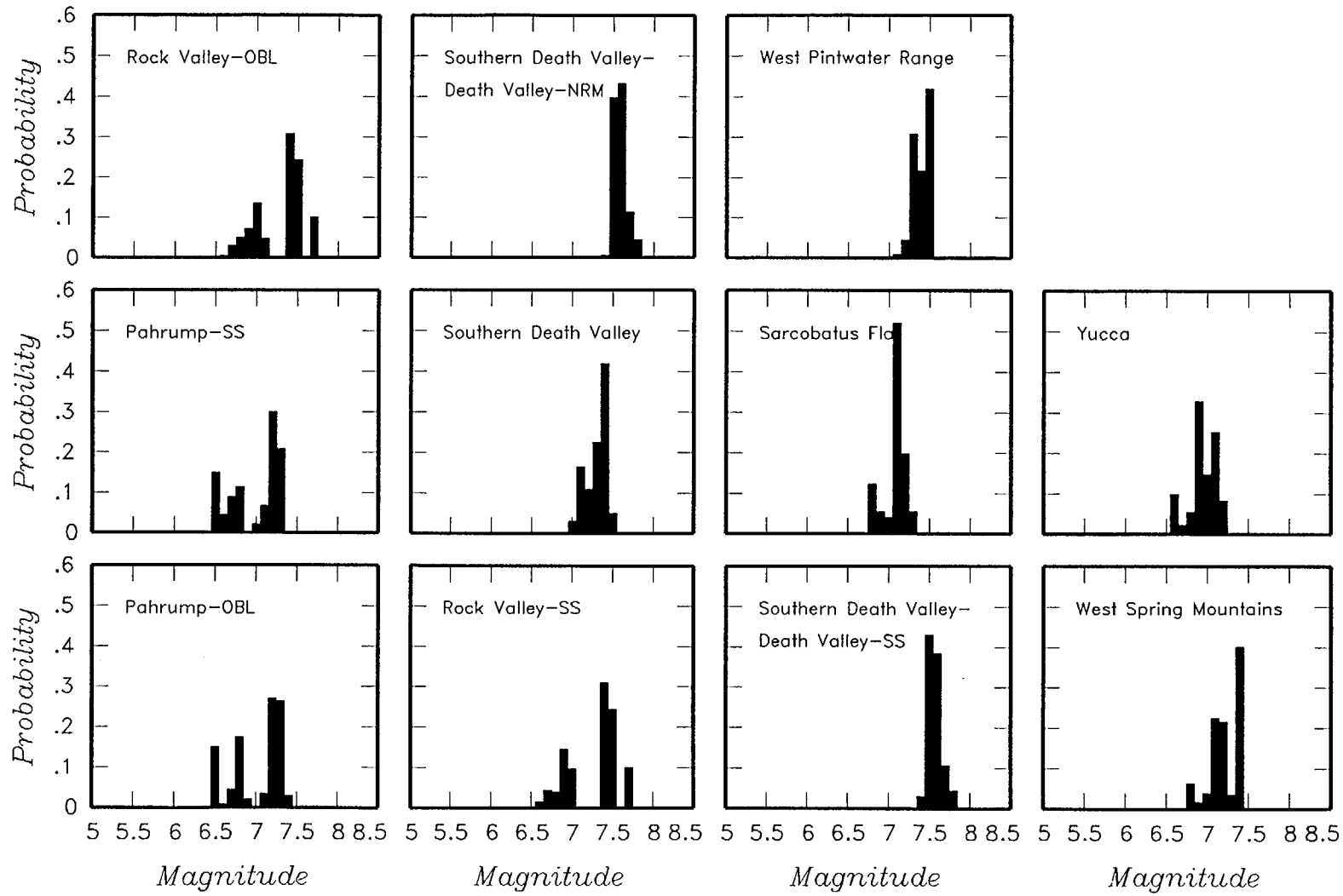

Figure 4-59 (Cont'd.) Maximum magnitude distributions for SBK team's regional fault sources. SS–strike slip; NRM–normal slip, OBL–oblique slip.

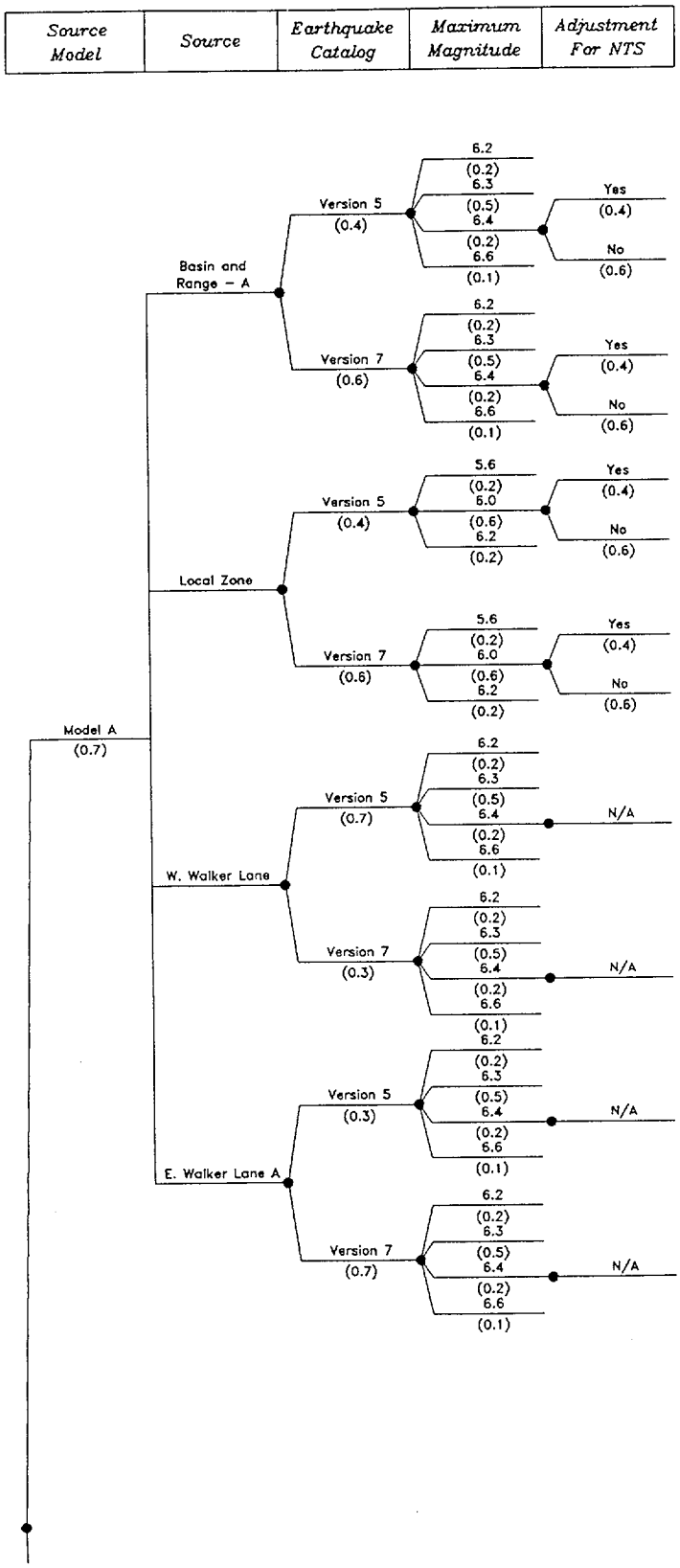

Figure 4-60 Logic tree for regional source zones developed by the SBK team

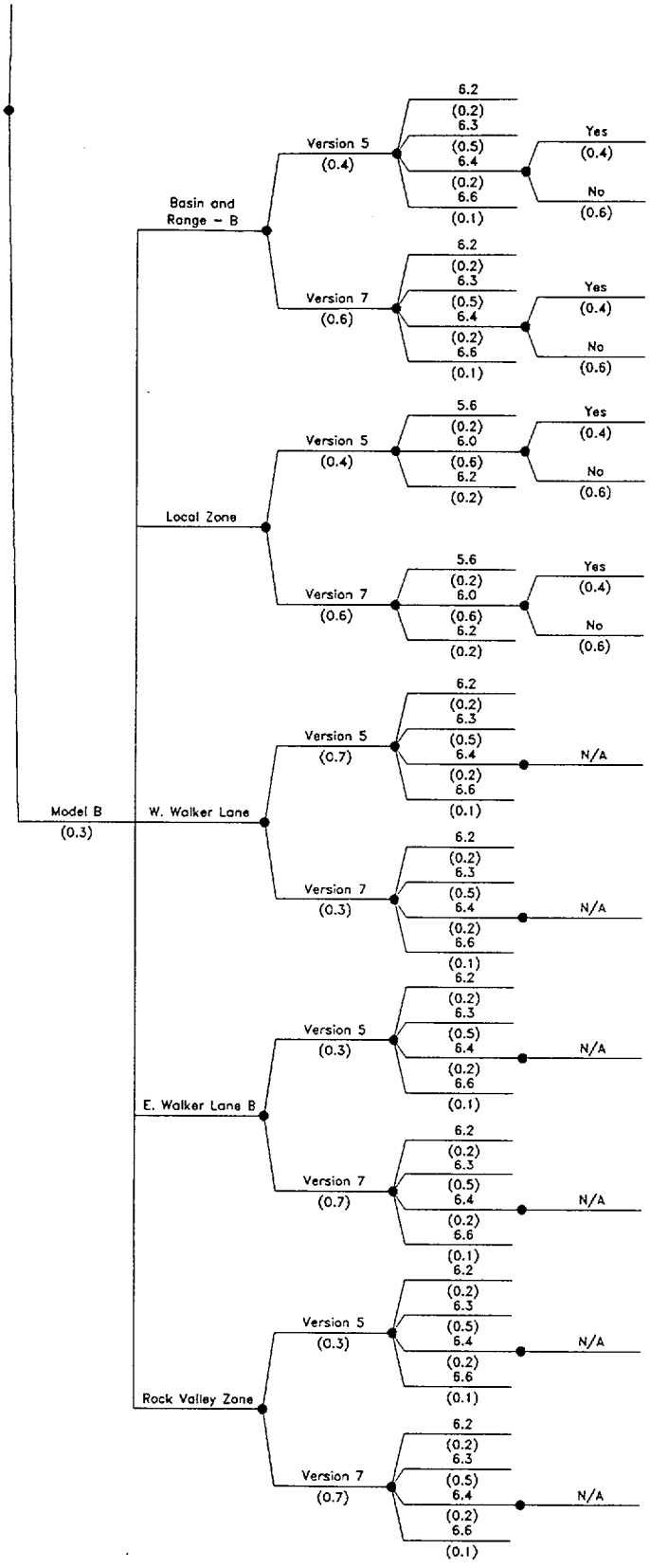

Figure 4-60 (Cont'd.) Logic tree for regional source zones developed by the SBK team

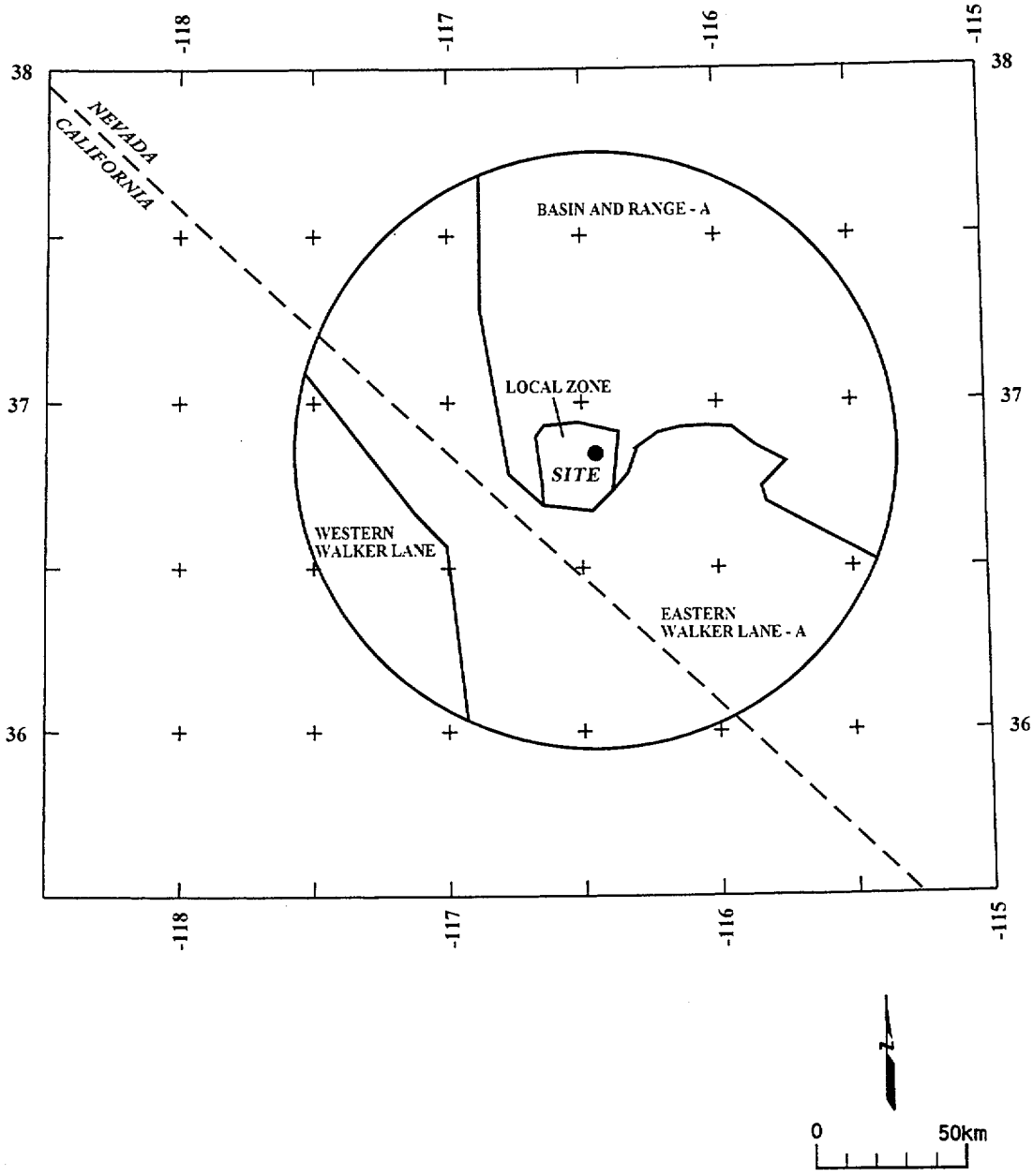

Figure 4-61 Alternative regional source zone models considered by the SBK team

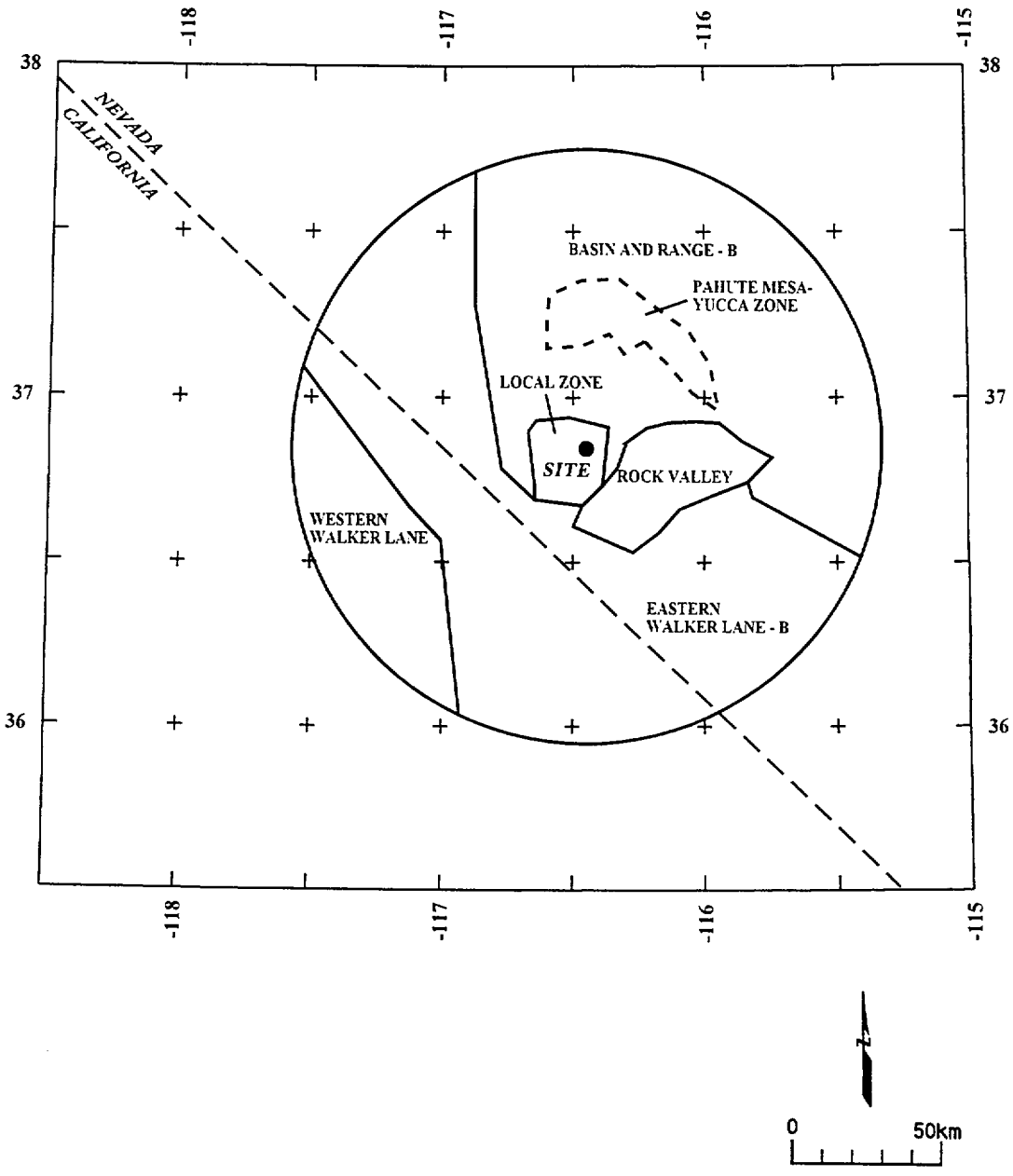

Figure 4-61 (Cont'd.) Alternative regional source zone models considered by the SBK team

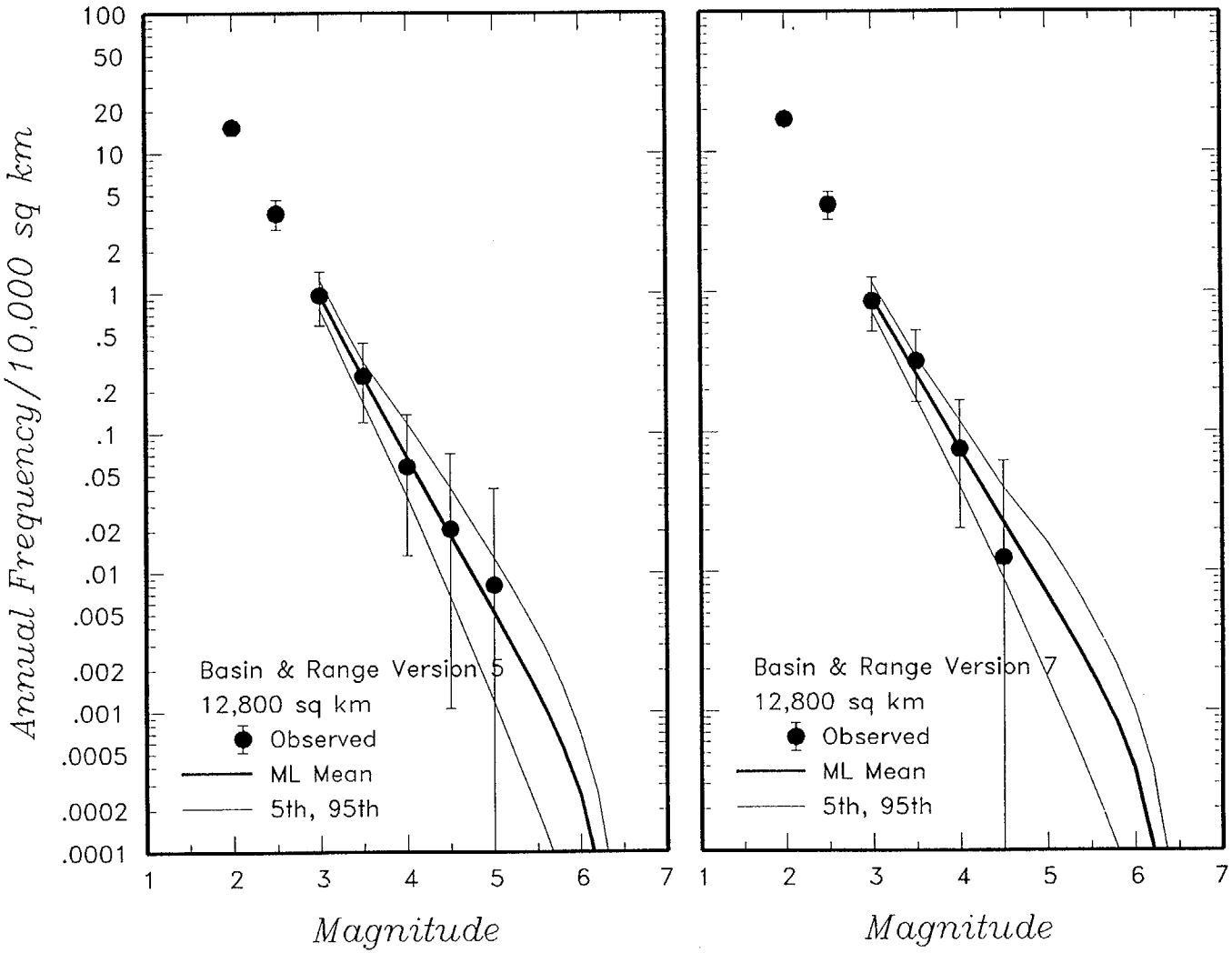

Figure 4-62 Earthquake recurrence relationships for the regional source zones defined by the SBK team. The solid dots with vertical error bars represent the observed data. The thick and thin solid curves are the mean, 5th, and 95th percentiles of the recurrence rates based on the uncertainty in recurrence parameters and maximum magnitude.

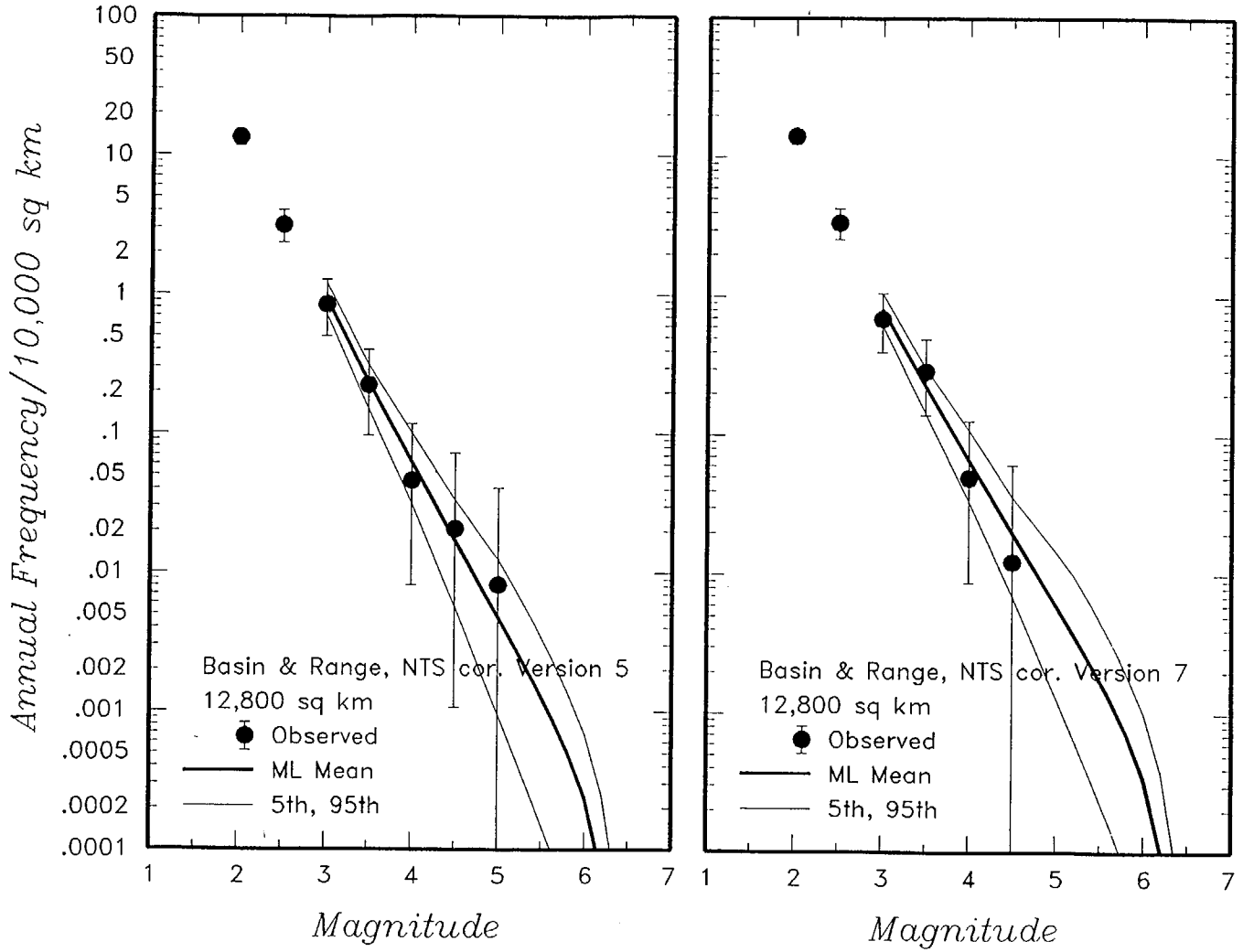

Figure 4-62 (Cont'd.) Earthquake recurrence relationships for the regional source zones defined by the SBK team.

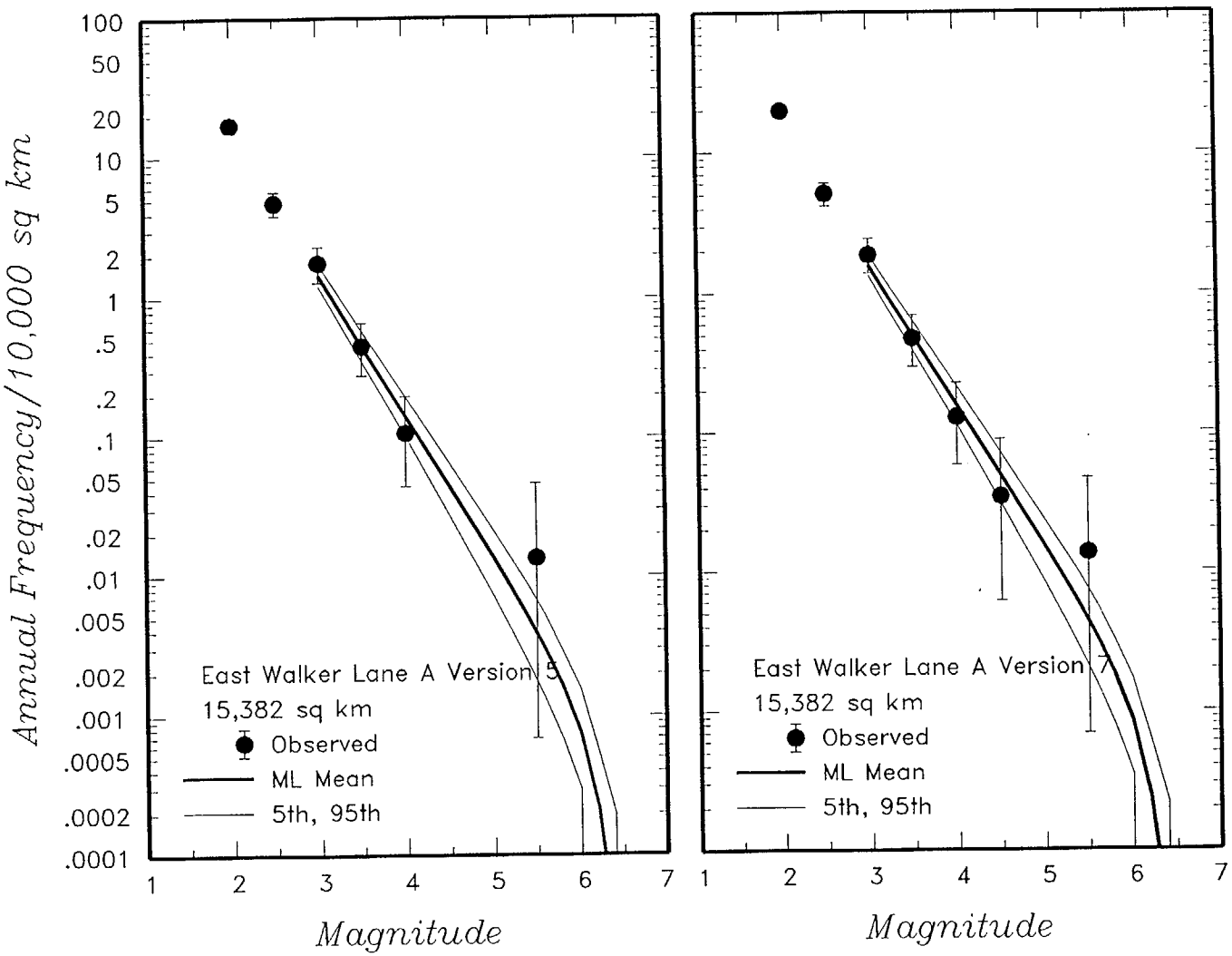

Figure 4-62 (Cont'd.) Earthquake recurrence relationships for the regional source zones defined by the SBK team.

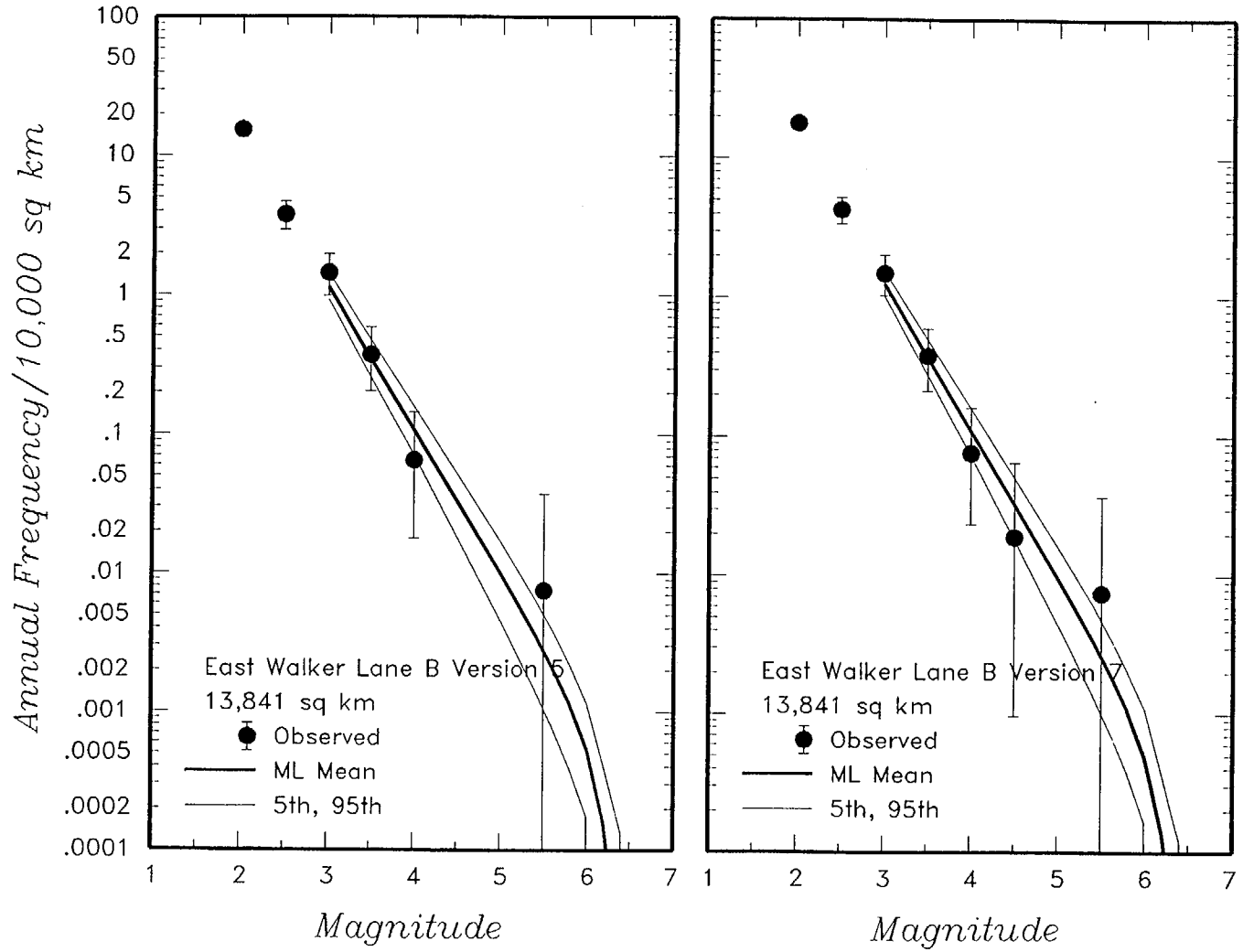

Figure 4-62 (Cont'd.) Earthquake recurrence relationships for the regional source zones defined by the SBK team.

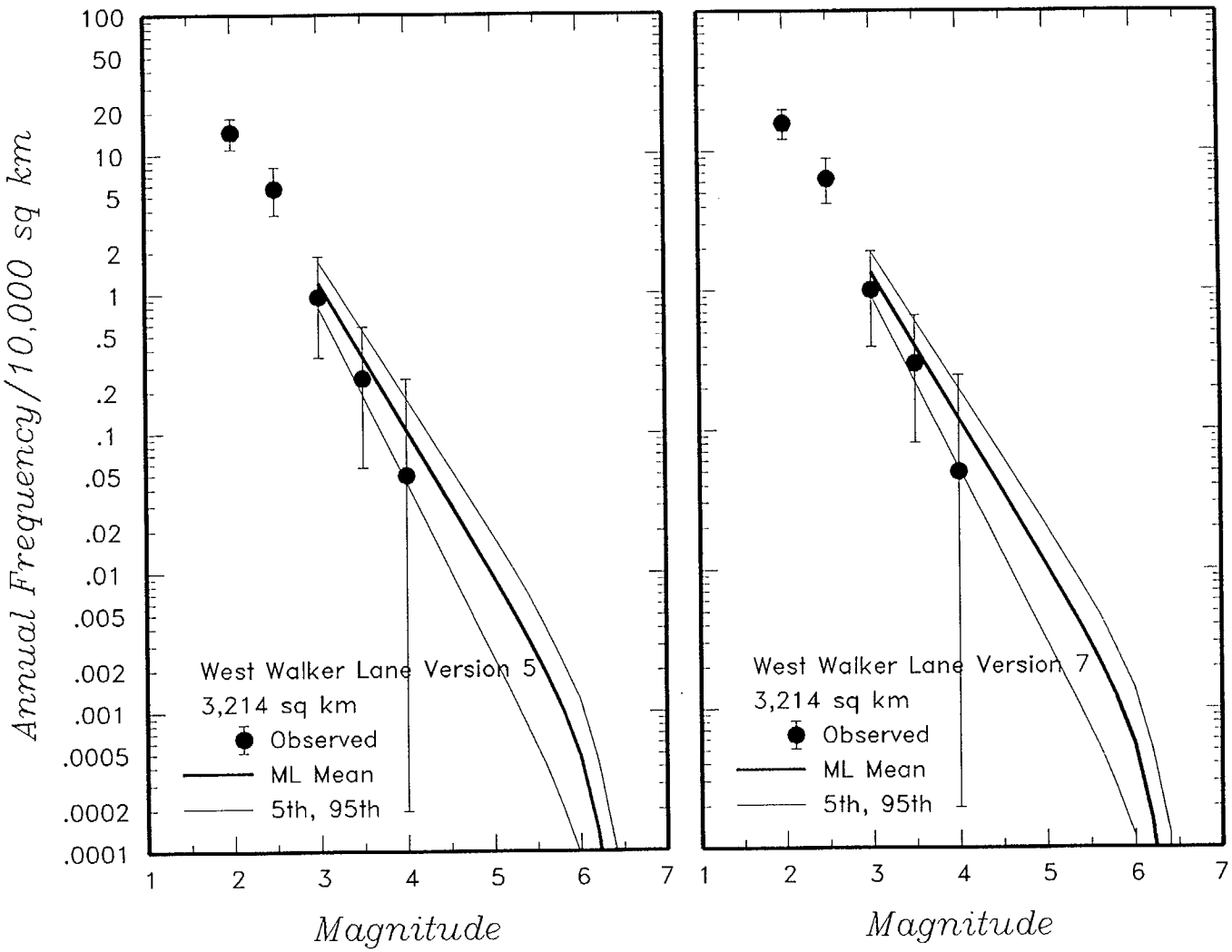

Figure 4-62 (Cont'd.) Earthquake recurrence relationships for the regional source zones defined by the SBK team.

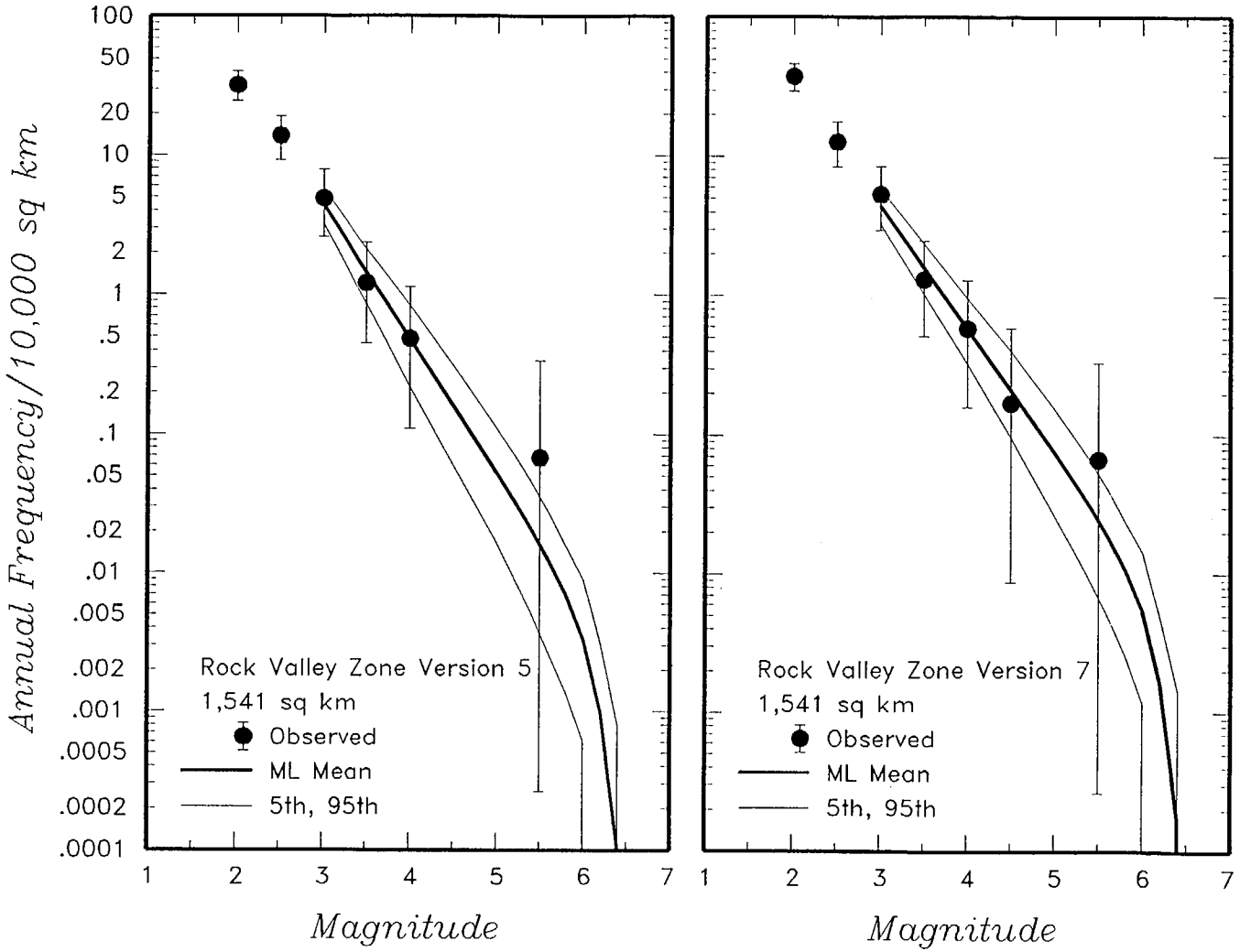

Figure 4-62 (Cont'd.) Earthquake recurrence relationships for the regional source zones defined by the SBK team.

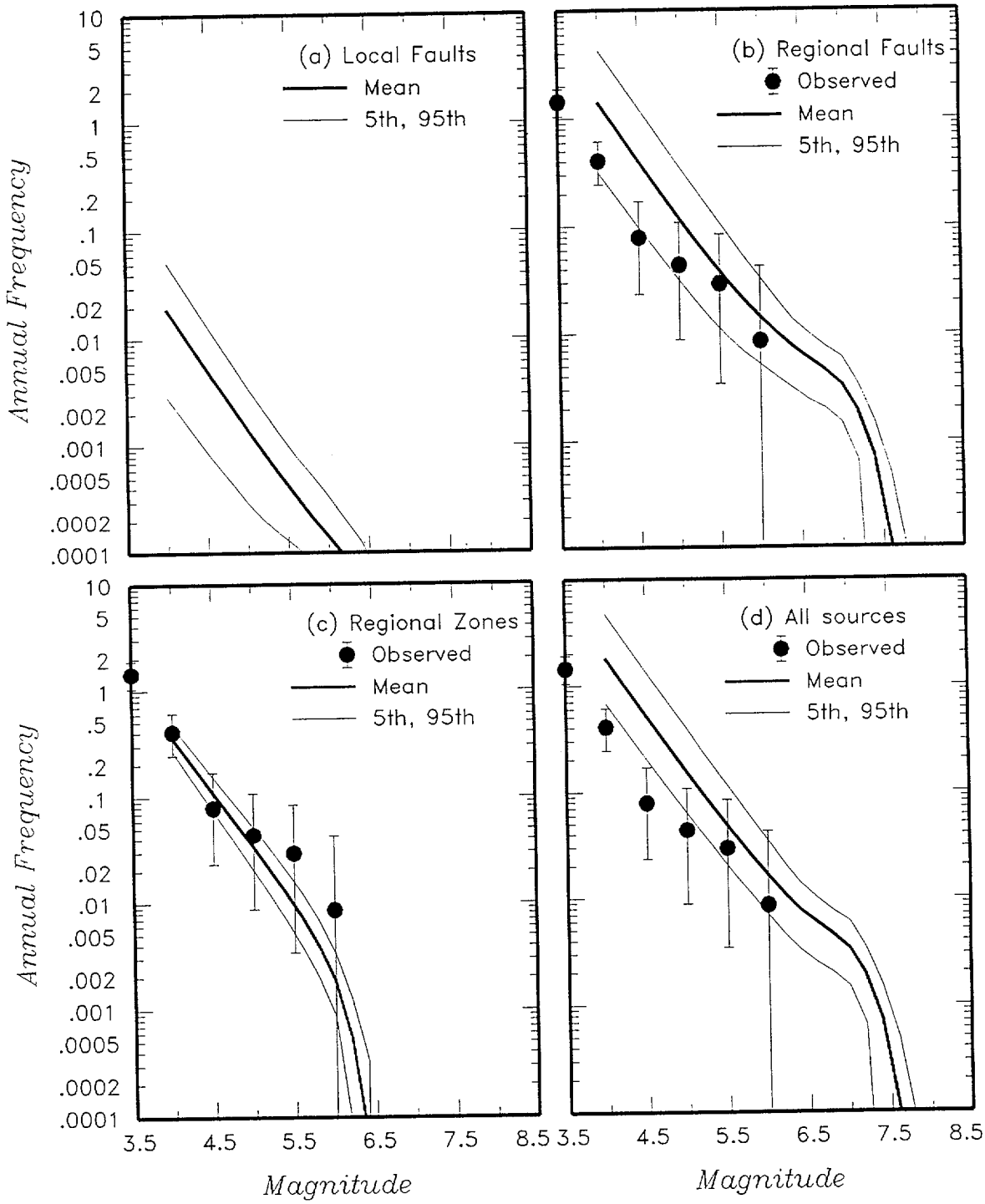

Figure 4-63 Predicted mean, 5th-, and 95th-percentile recurrence rates for (a) local fault sources, (b) regional fault sources, (c) regional source zones, and (d) all sources combined for the SBK team. The solid dots with vertical error bars represent the observed frequency of earthquakes occurring within 100 km of the Yucca Mountain site.

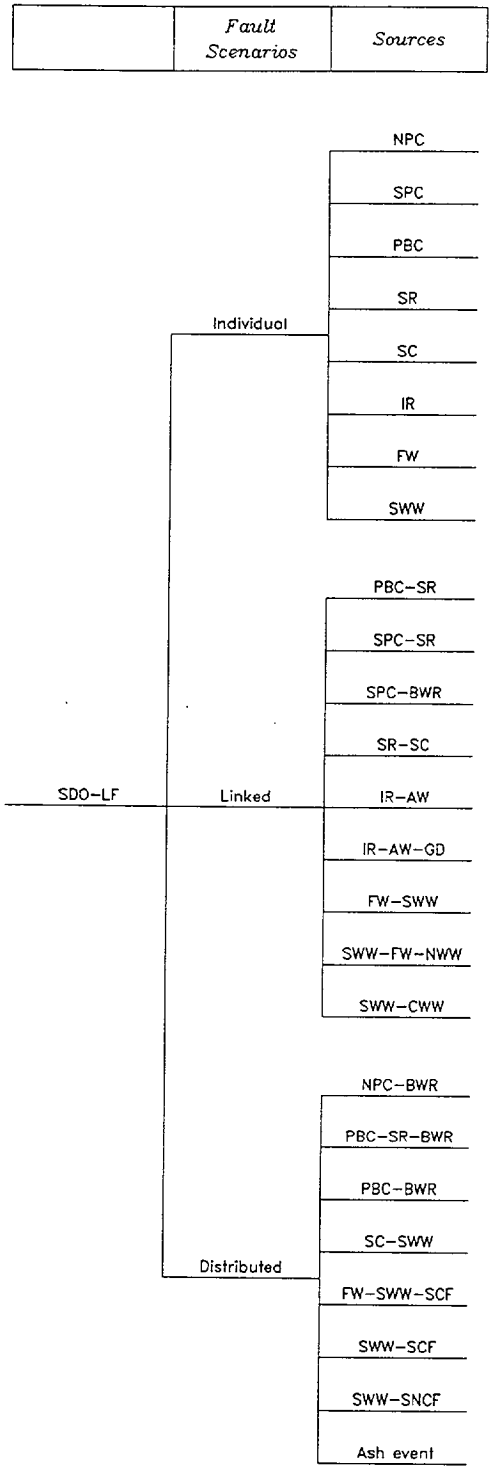

Figure 4-64 Logic tree for local fault sources developed by the SDO team

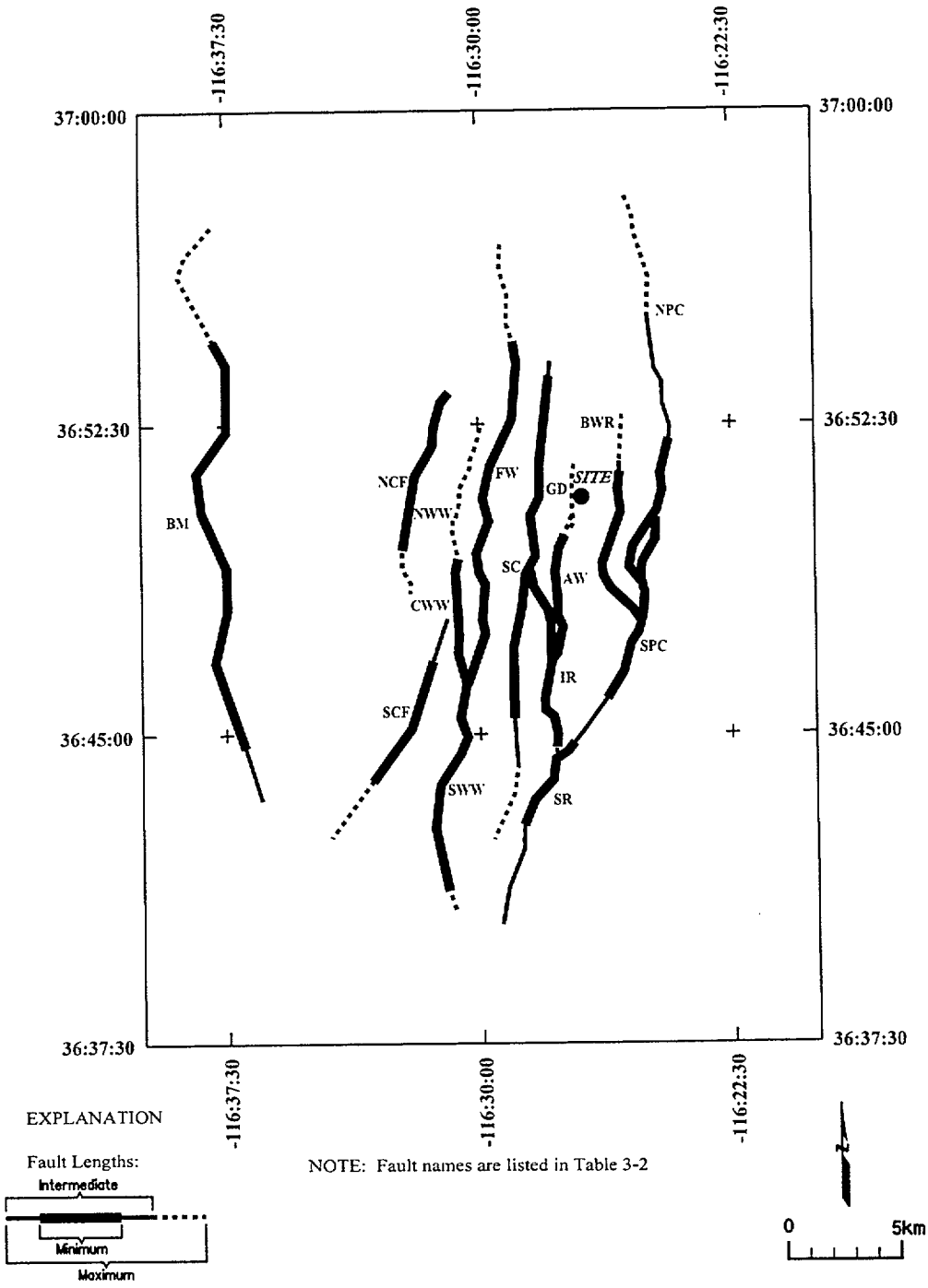

Figure 4-65 Location of local fault sources considered by the SDO team

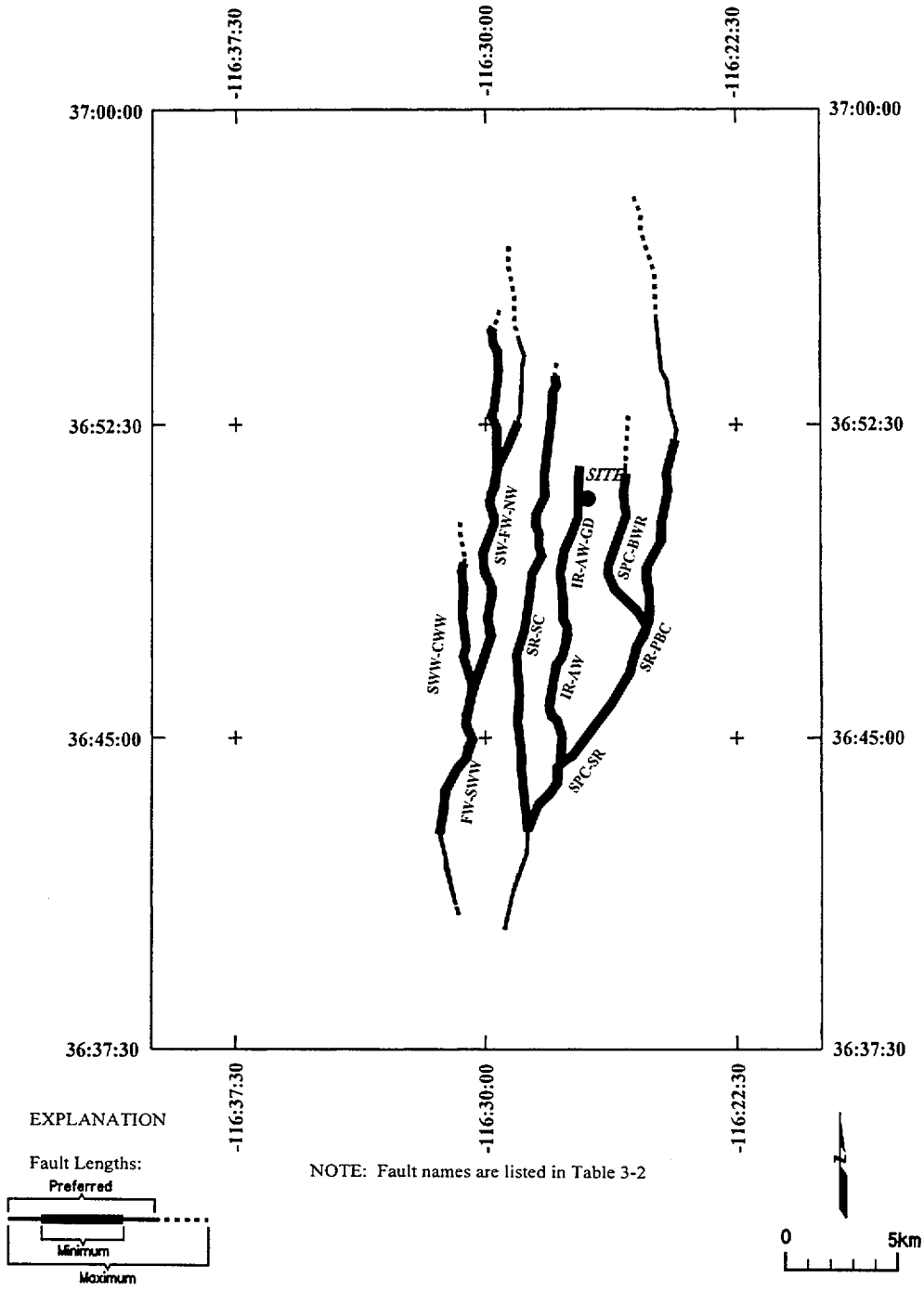

Figure 4-65 (Cont'd.) Location of local fault sources considered by the SDO team

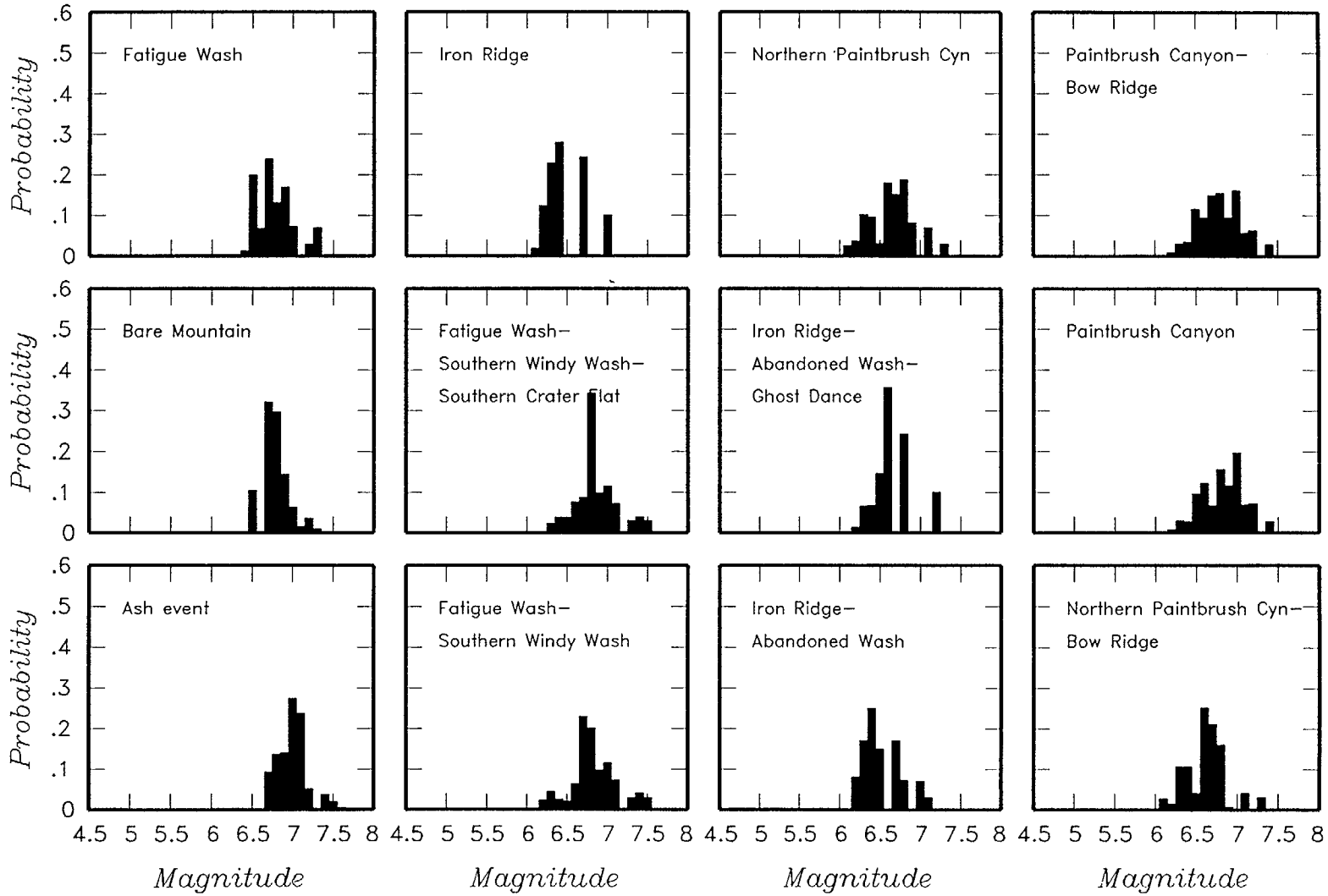

Figure 4-66 Maximum magnitude distributions for SDO team's local fault sources

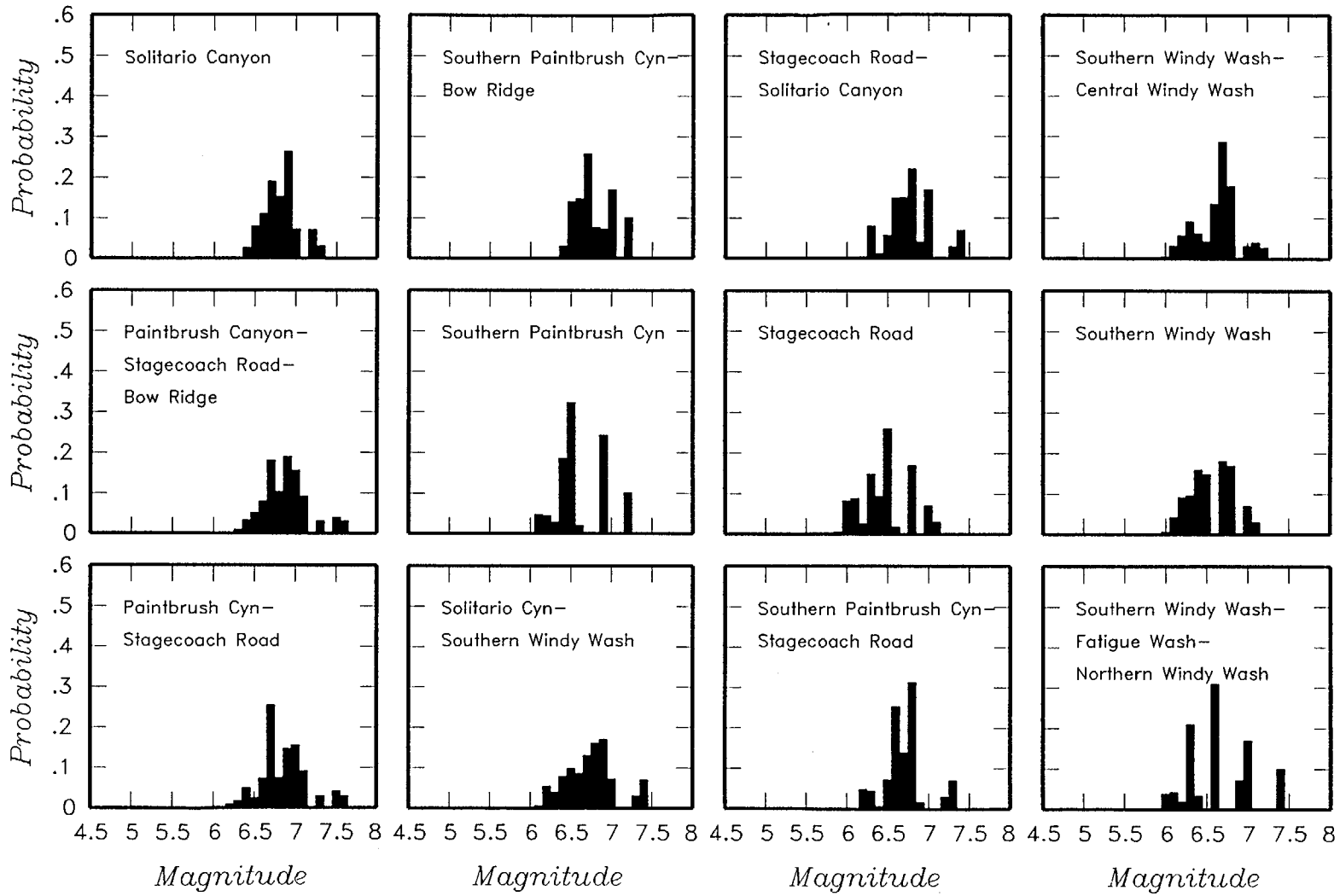

Figure 4-66 (Cont'd.) Maximum magnitude distributions for SDO team's local fault sources

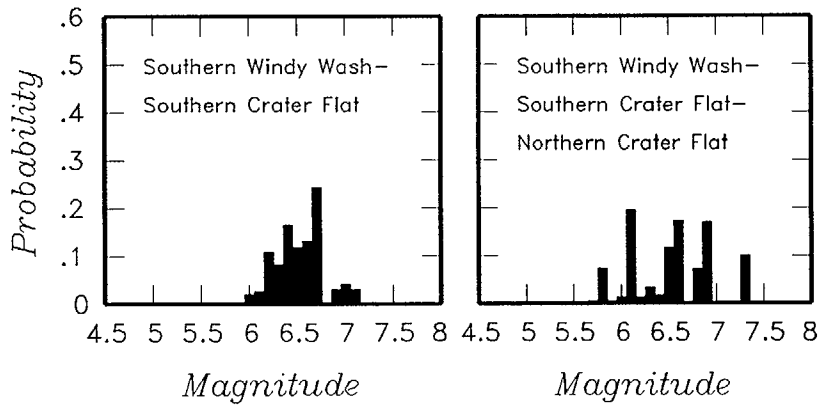

Figure 4-66 (Cont'd.) Maximum magnitude distributions for SDO team's local fault sources

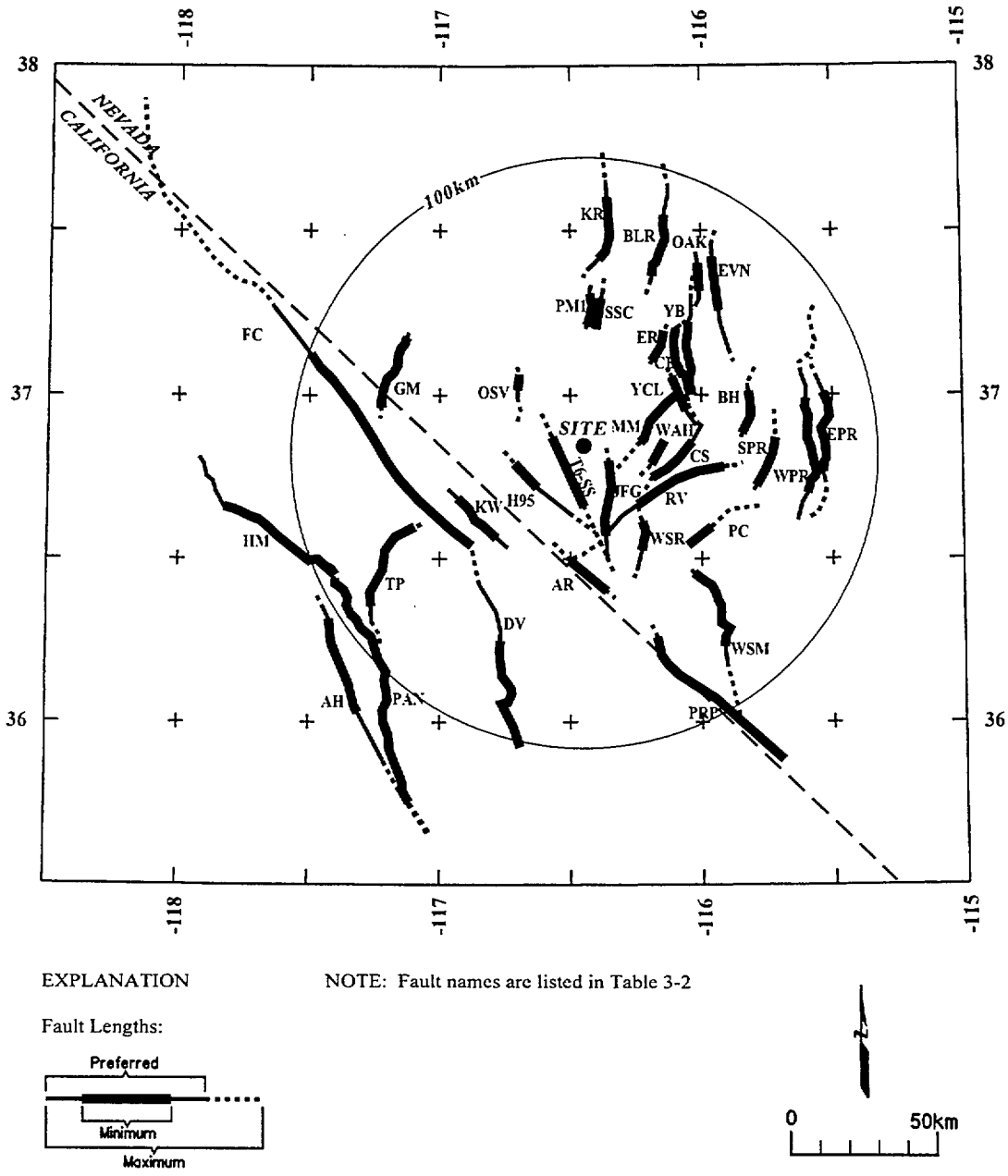

Figure 4-67 Regional fault sources considered by the SDO team

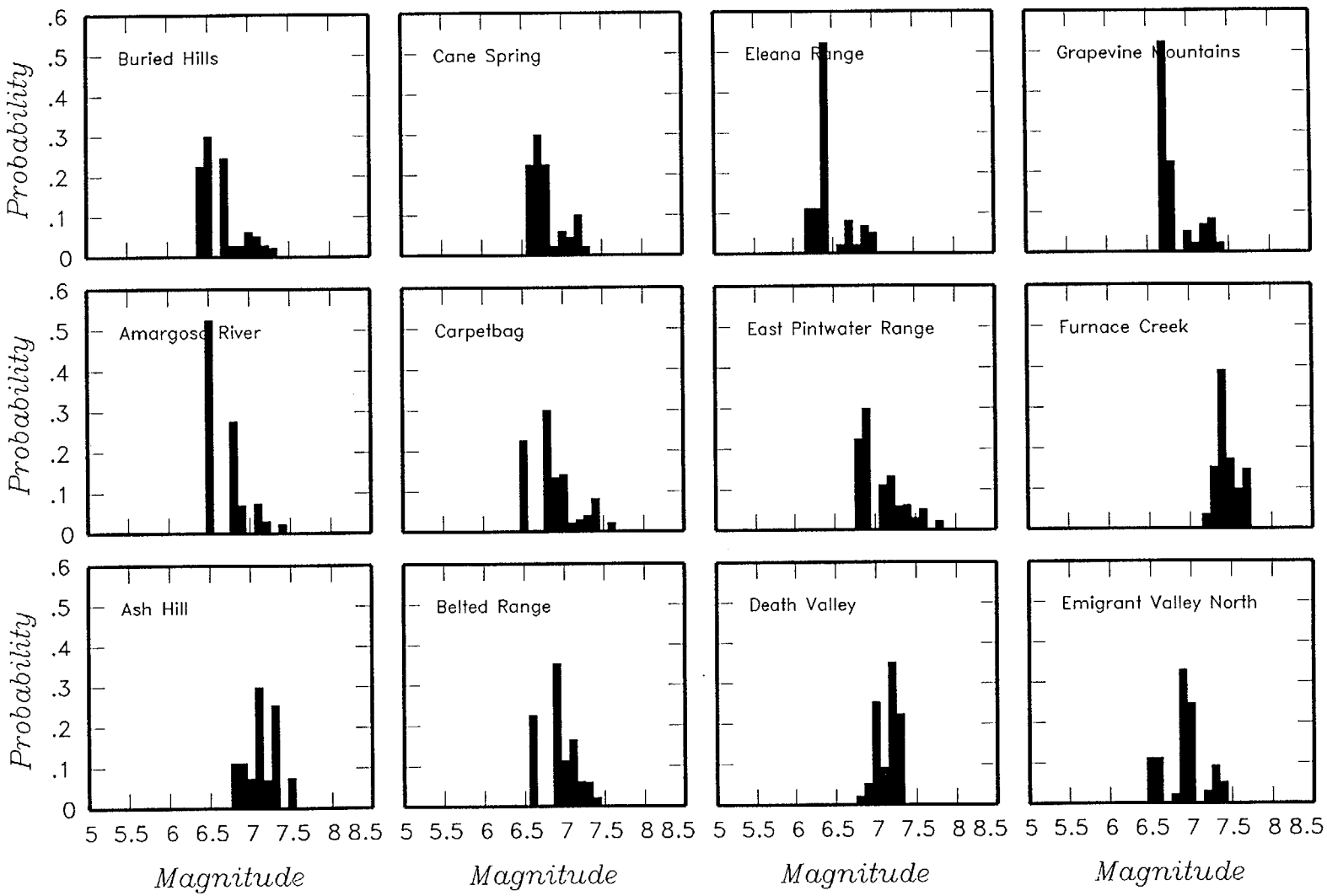

Figure 4-68 Maximum magnitude distributions for SDO team's regional fault sources

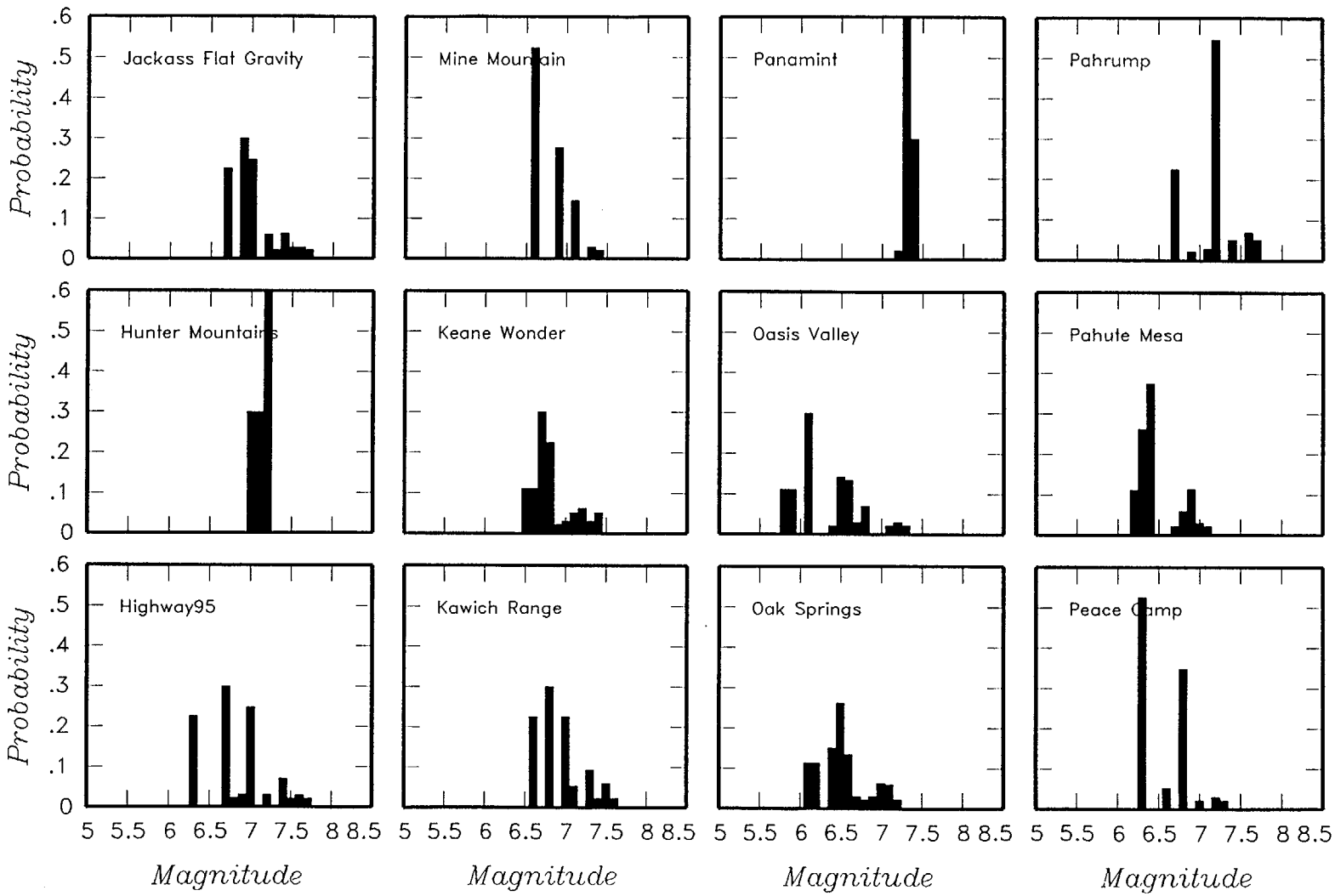

Figure 4-68 (Cont'd.) Maximum magnitude distributions for SDO team's regional fault sources

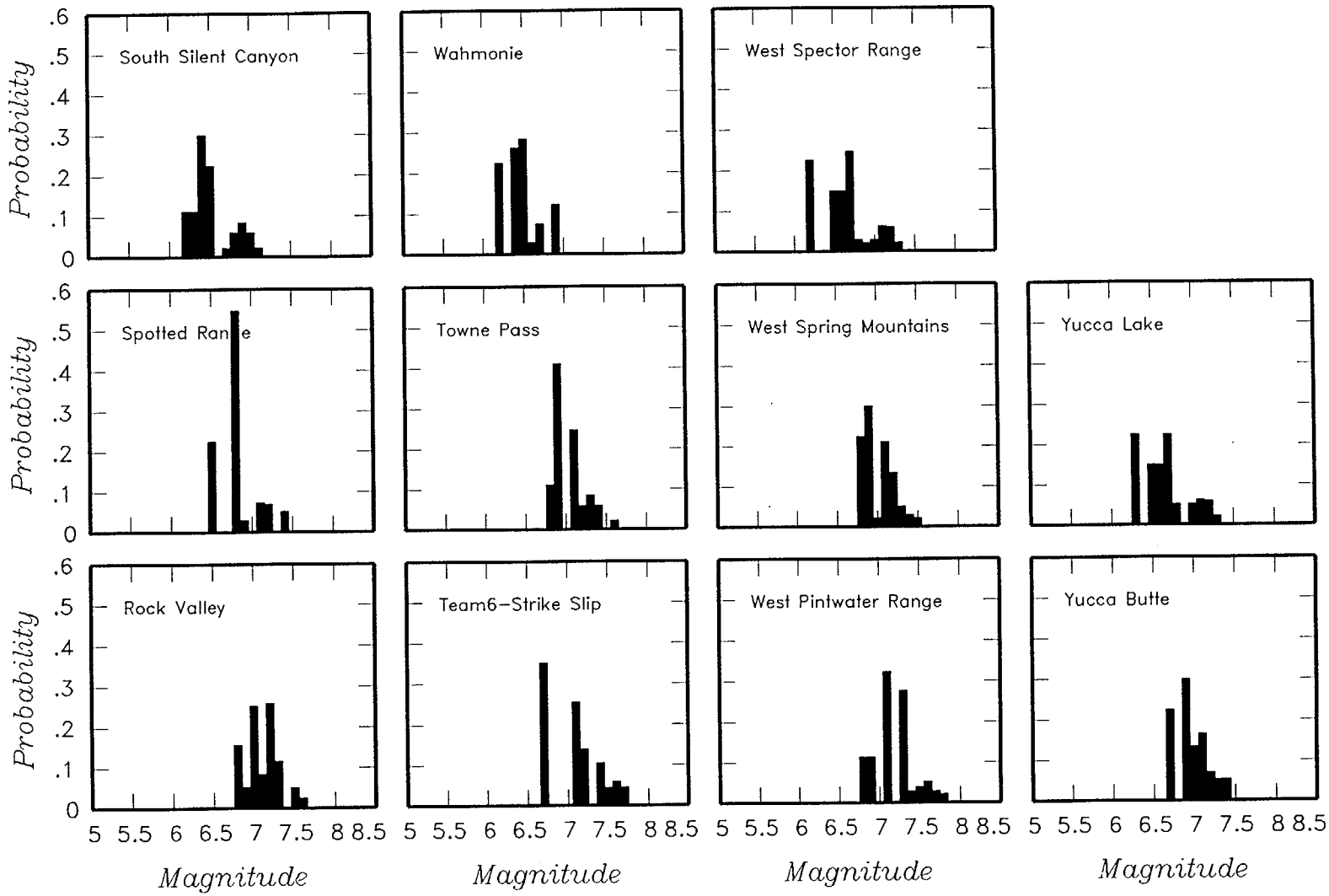

Figure 4-68 (Cont'd.) Maximum magnitude distributions for SDO team's regional fault sources

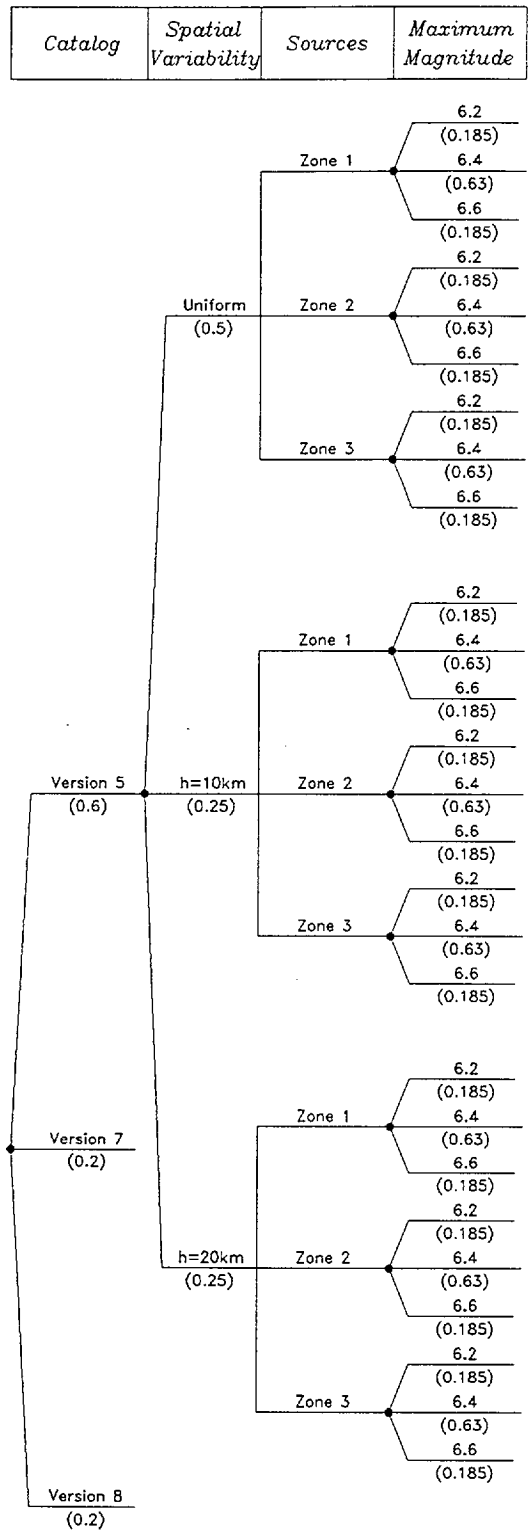

Figure 4-69 Logic tree for regional source zones developed by the SDO team

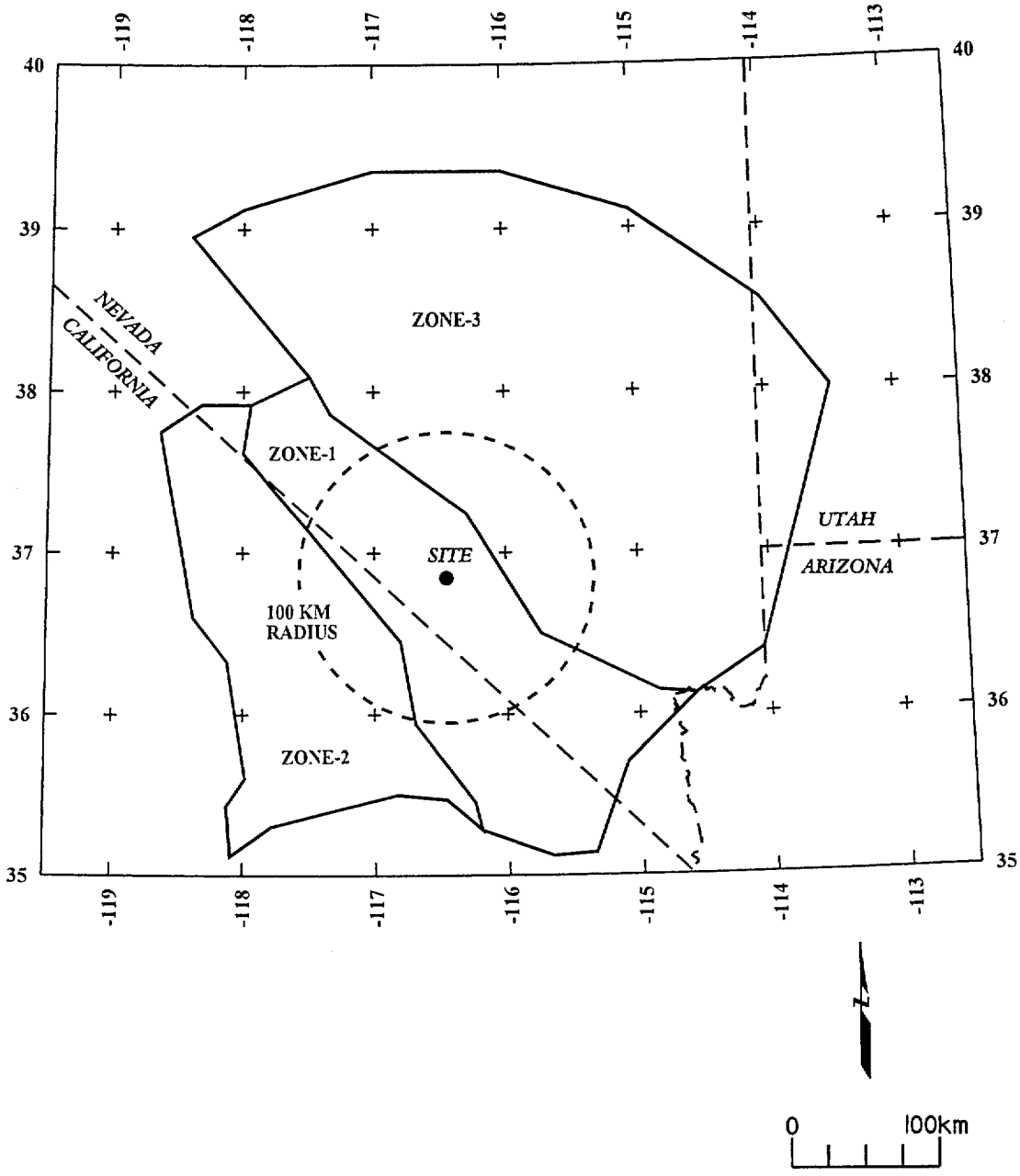

Figure 4-70 Alternative regional source zone models considered by the SDO team

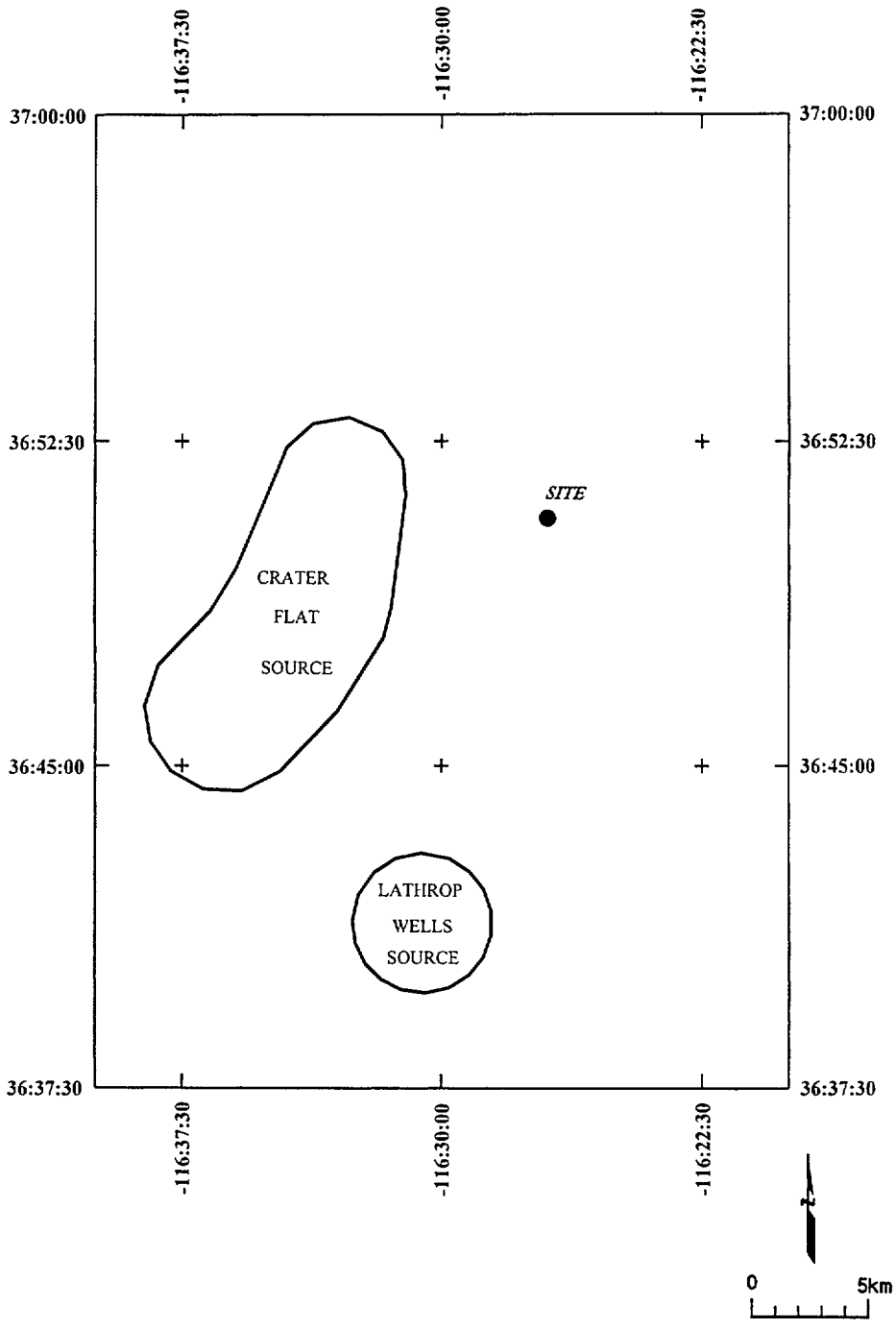

Figure 4-71 Volcanic source zones considered by the SDO team

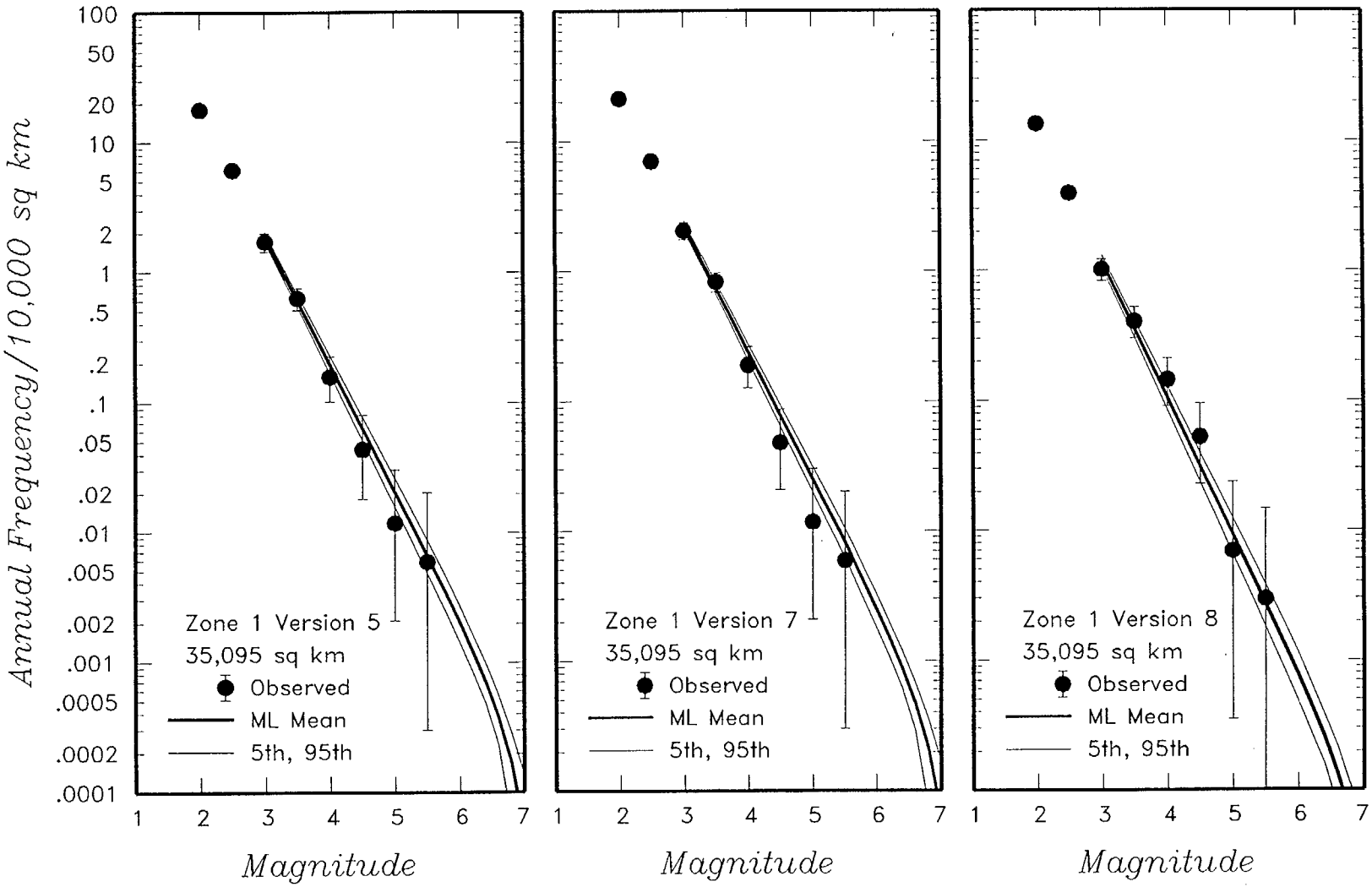

Figure 4-72 Earthquake recurrence relationships for the regional source zones defined by the SDO team. The solid dots with vertical error bars represent the observed data. The thick and thin solid curves are the mean, 5th, and 95th percentiles of the recurrence rates based on the uncertainty in recurrence parameters and maximum magnitude.

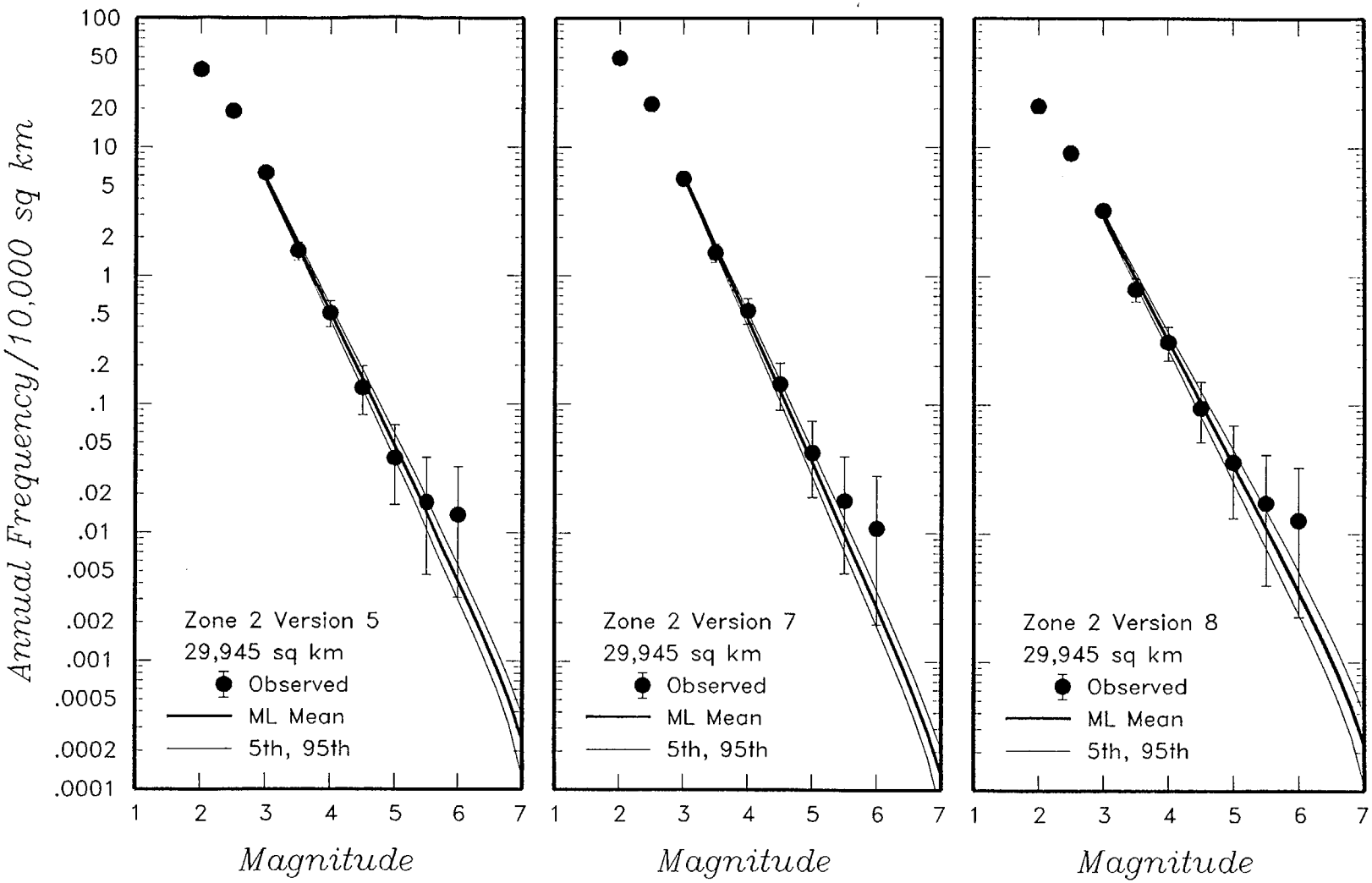

Figure 4-72 (Cont'd.) Earthquake recurrence relationships for the regional source zones defined by the SDO team.

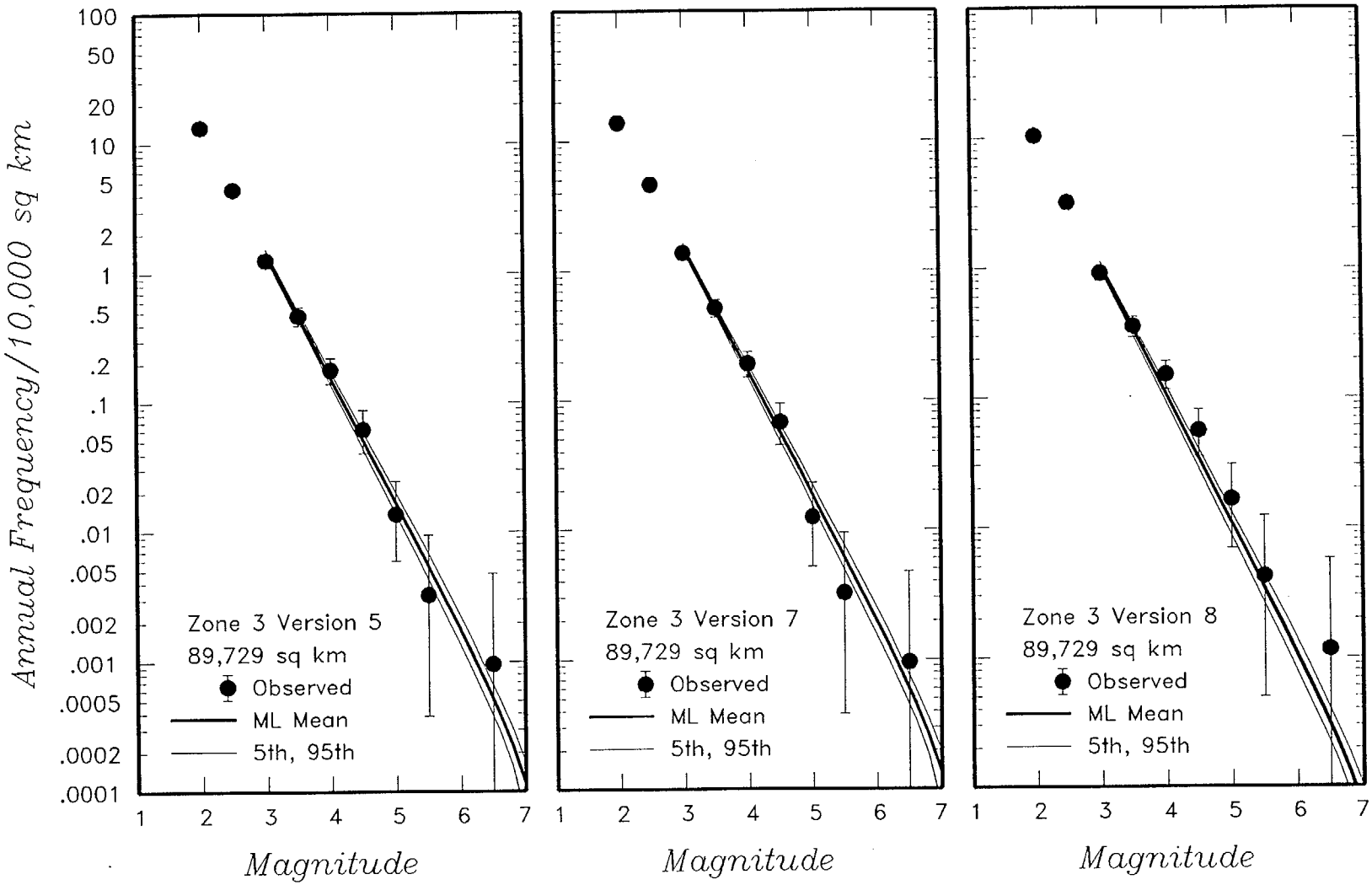

Figure 4-72 (Cont'd.) Earthquake recurrence relationships for the regional source zones defined by the SDO team.

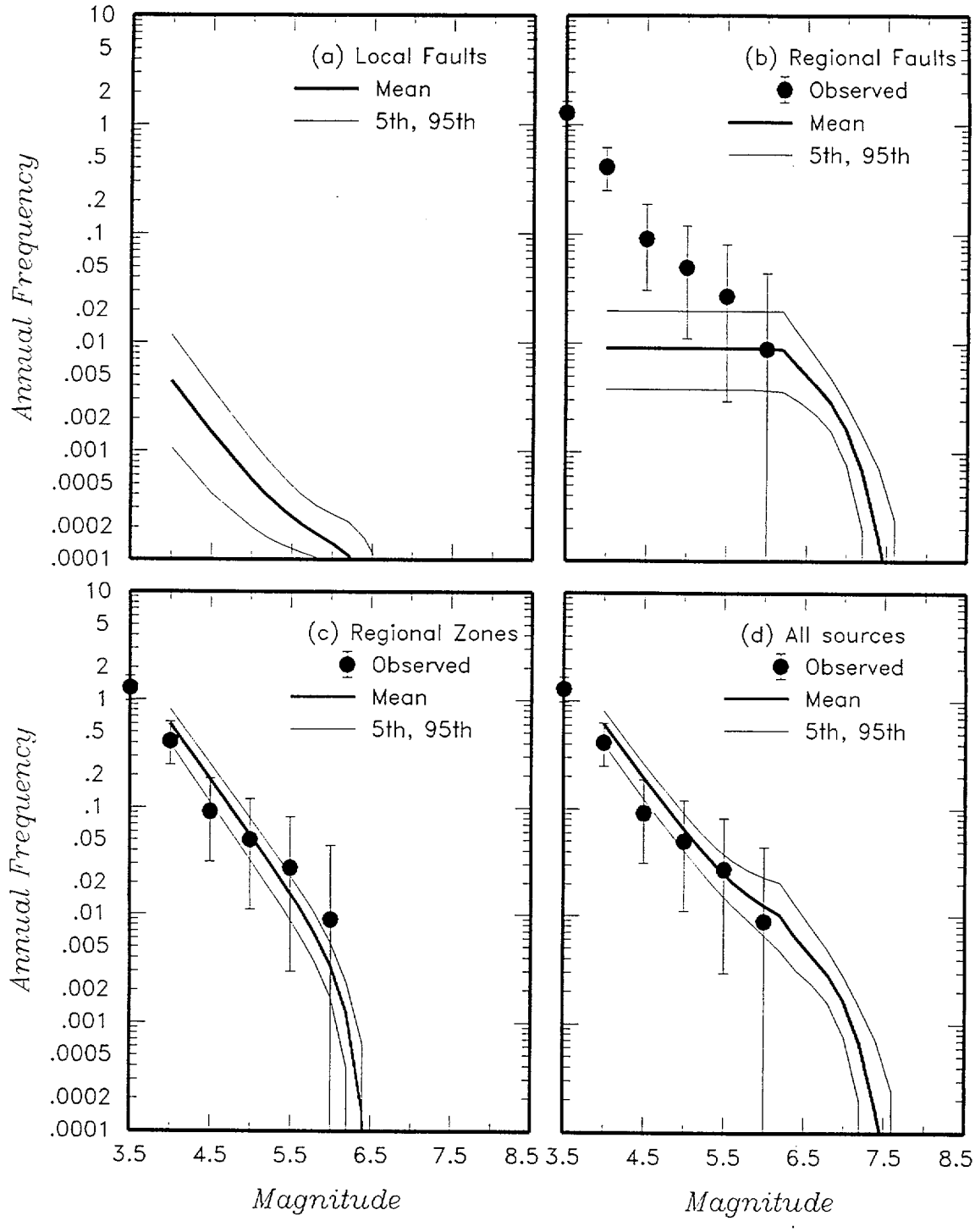

Figure 4-73 Predicted mean, 5th-, and 95th-percentile recurrence rates for (a) local fault sources, (b) regional fault sources, (c) regional source zones, and (d) all sources combined for the SDO team. The solid dots with vertical error bars represent the observed frequency of earthquakes occurring within 100 km of the Yucca Mountain site.

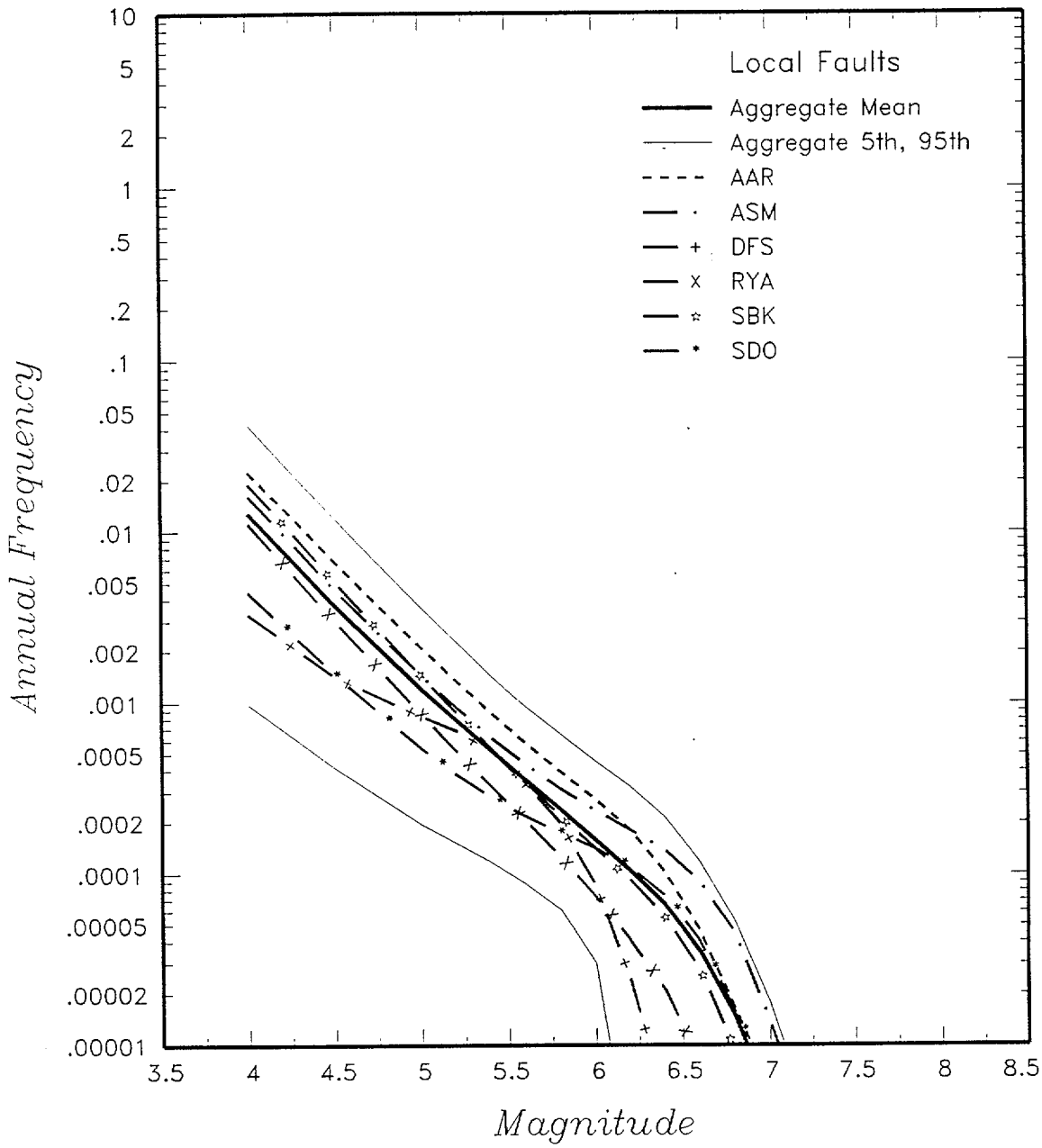

Figure 4-74 Predicted mean, 5th-, and 95th-percentile recurrence rates for local fault sources for all teams combined compared to mean recurrence estimates for individual team.

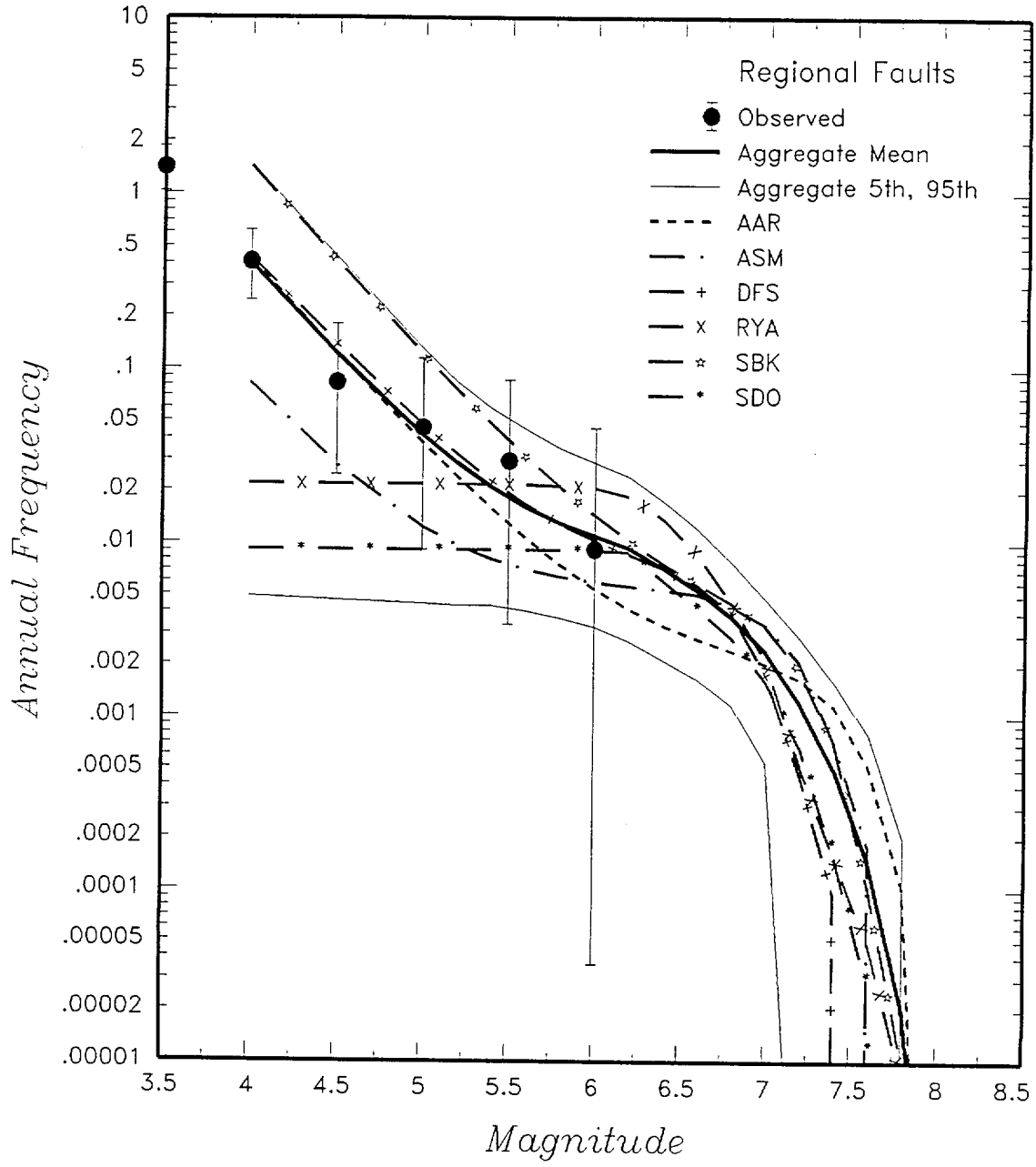

Figure 4-75 Predicted mean, 5th-, and 95th-percentile recurrence rates for regional fault sources for all teams combined compared to mean recurrence estimates for individual teams. The solid dots with vertical error bars represent the observed frequency of earthquakes occurring within 100 km of the Yucca Mountain site.

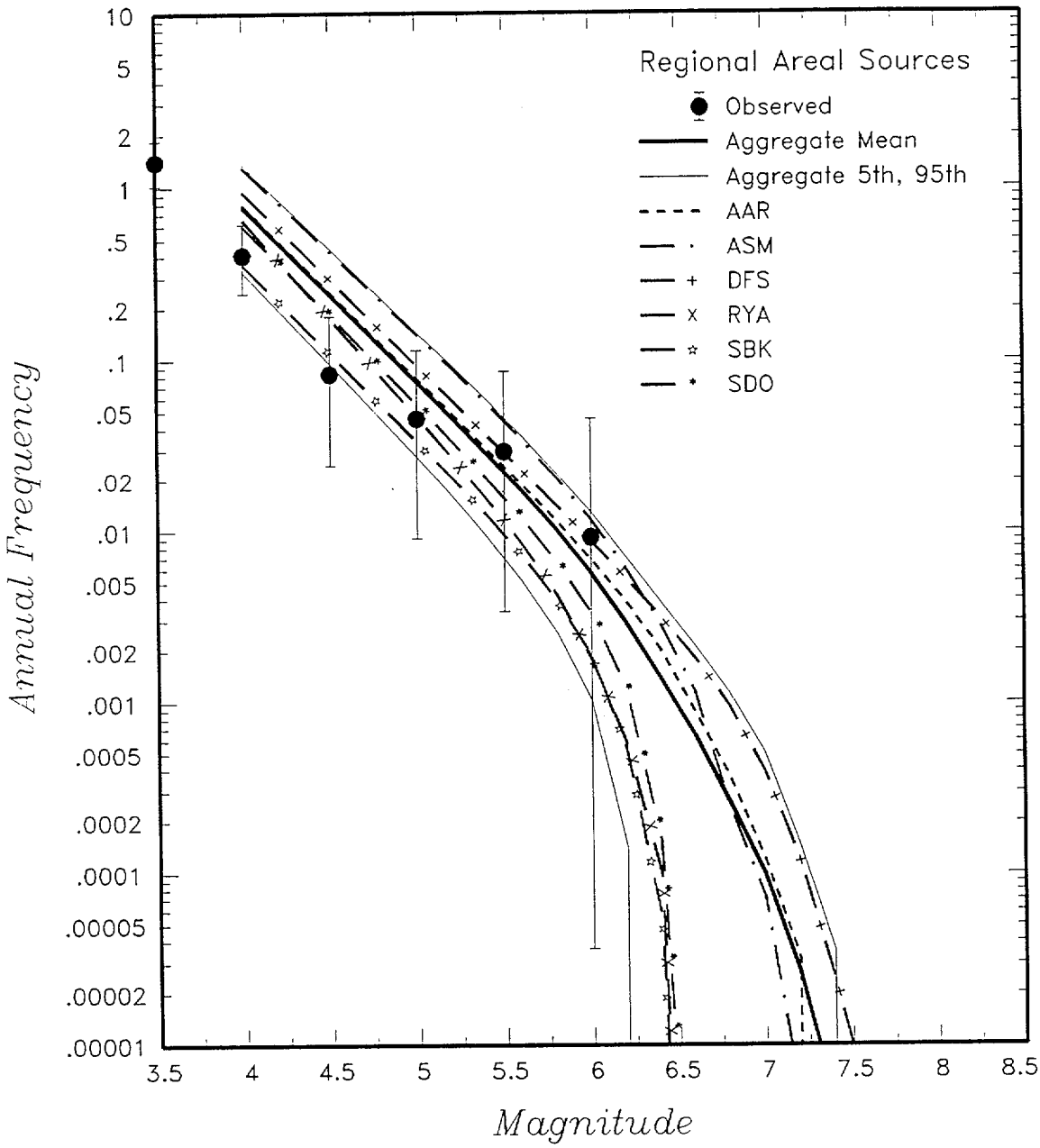

Figure 4-76 Predicted mean, 5th-, and 95th-percentile recurrence rates for regional source zones for all teams combined compared to mean recurrence estimates for individual team. The solid dots with vertical error bars represent the observed frequency of earthquakes occurring within 100 km of the Yucca Mountain site.

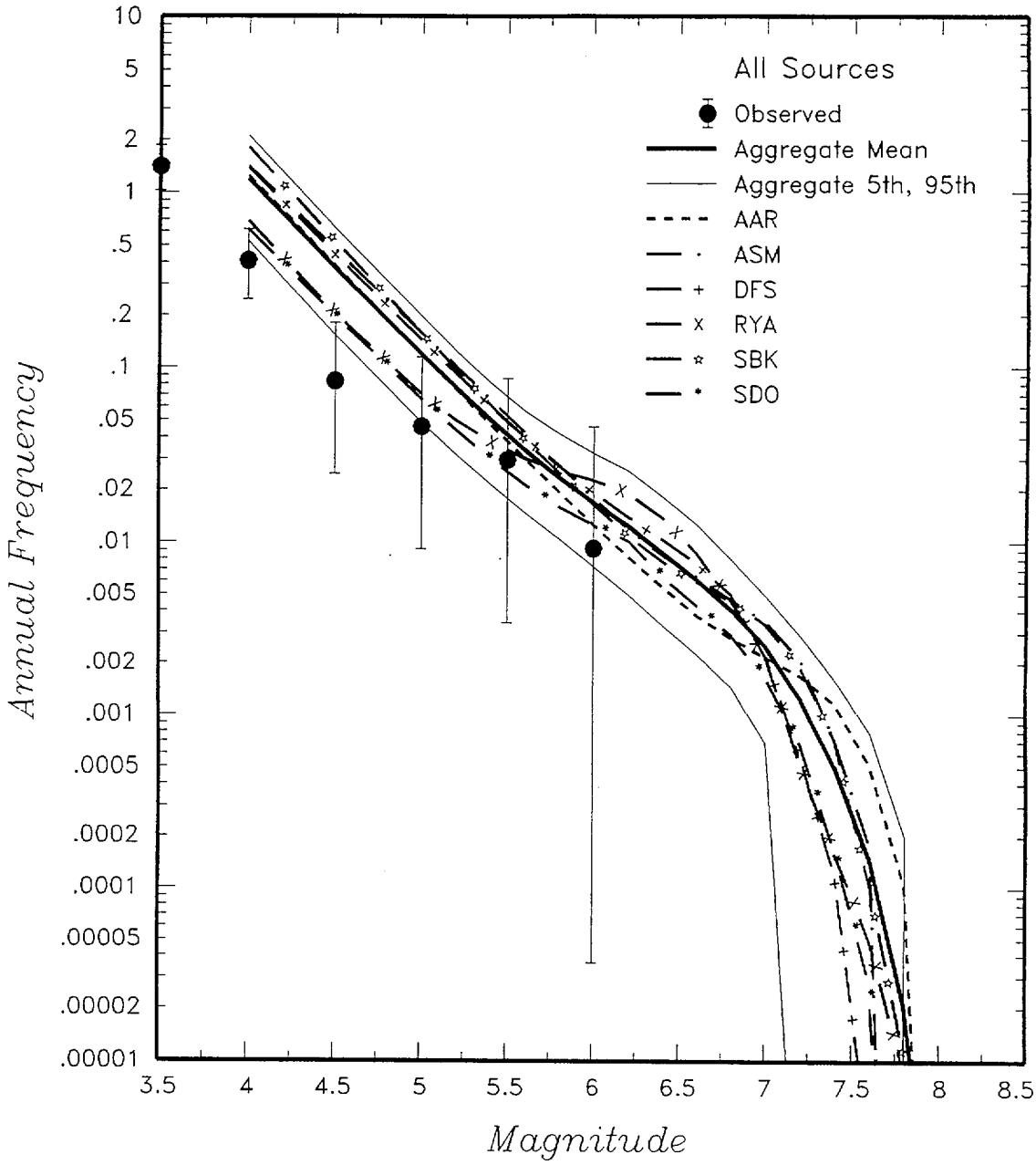

Figure 4-77. Predicted mean, 5th-, and 95th-percentile recurrence rates for all sources combined for all teams combined compared to mean recurrence estimates for individual team. The solid dots with vertical error bars represent the observed frequency of earthquakes occurring within 100 km of the Yucca Mountain site.

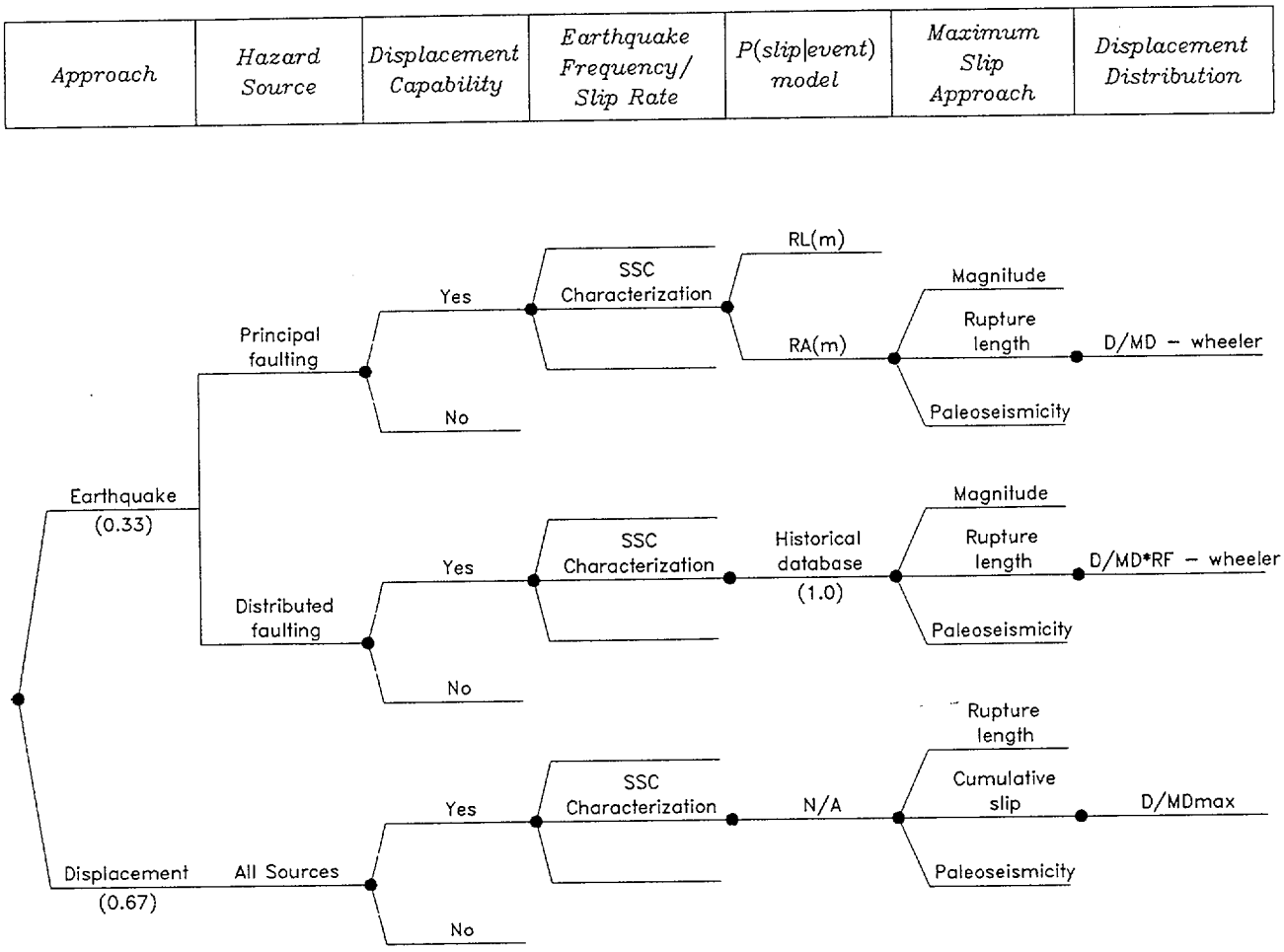

Figure 4-78 Logic tree defining the AAR team's characterization of displacement hazard at sites subject to principal faulting

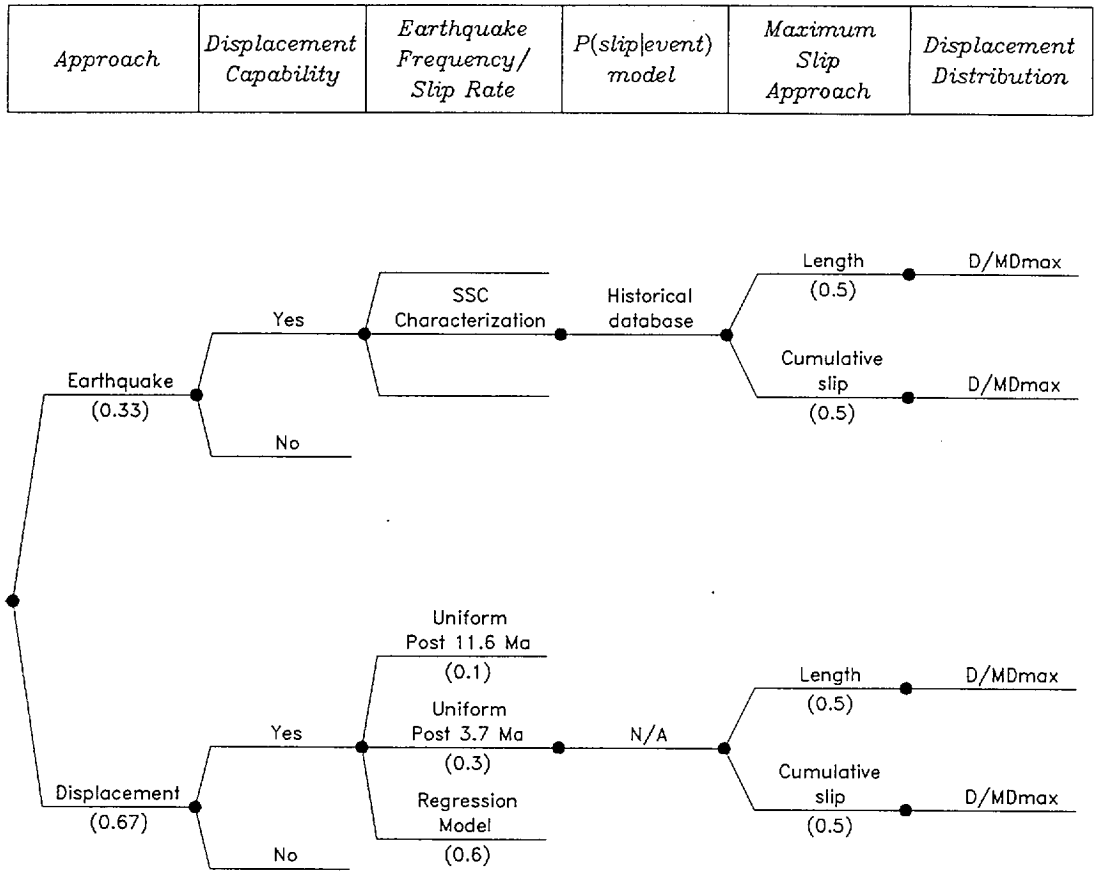

Figure 4-79 Logic tree defining the AAR team's characterization of displacement hazard at sites subject to distributed faulting

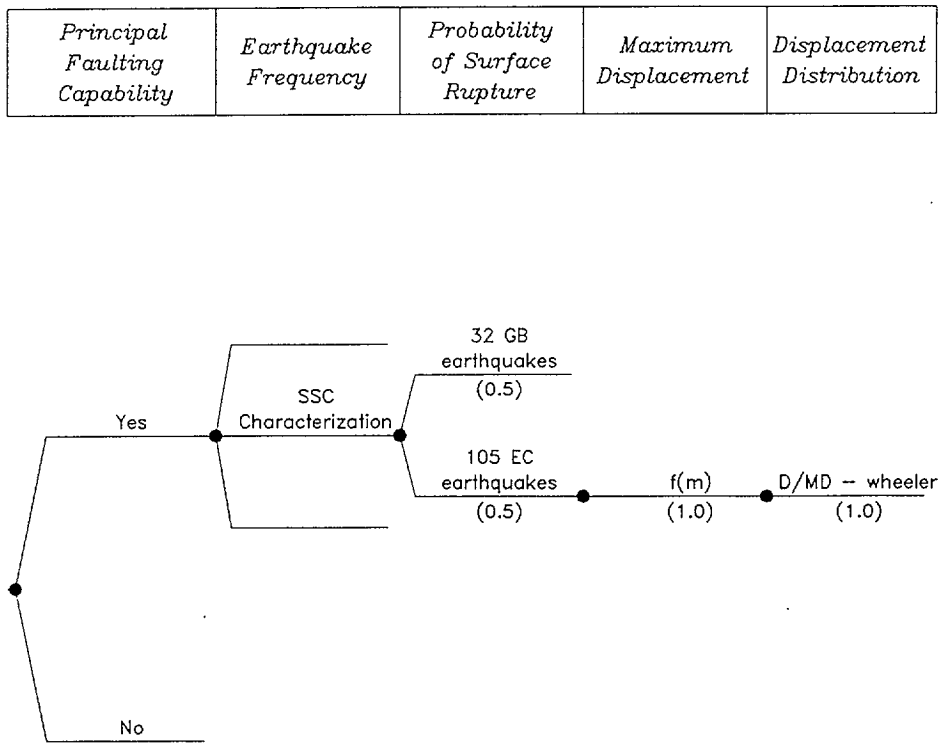

Figure 4-80 Logic tree defining the ASM team's characterization of principal faulting displacement hazard

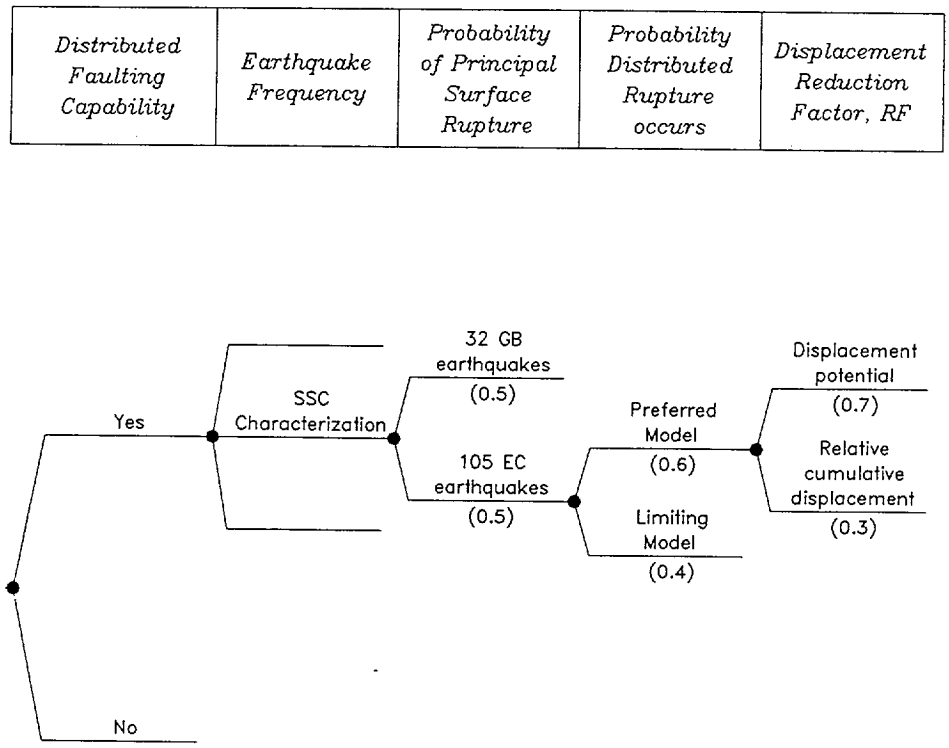

Figure 4-81 Logic tree defining the ASM team's characterization of distributed faulting displacement hazard

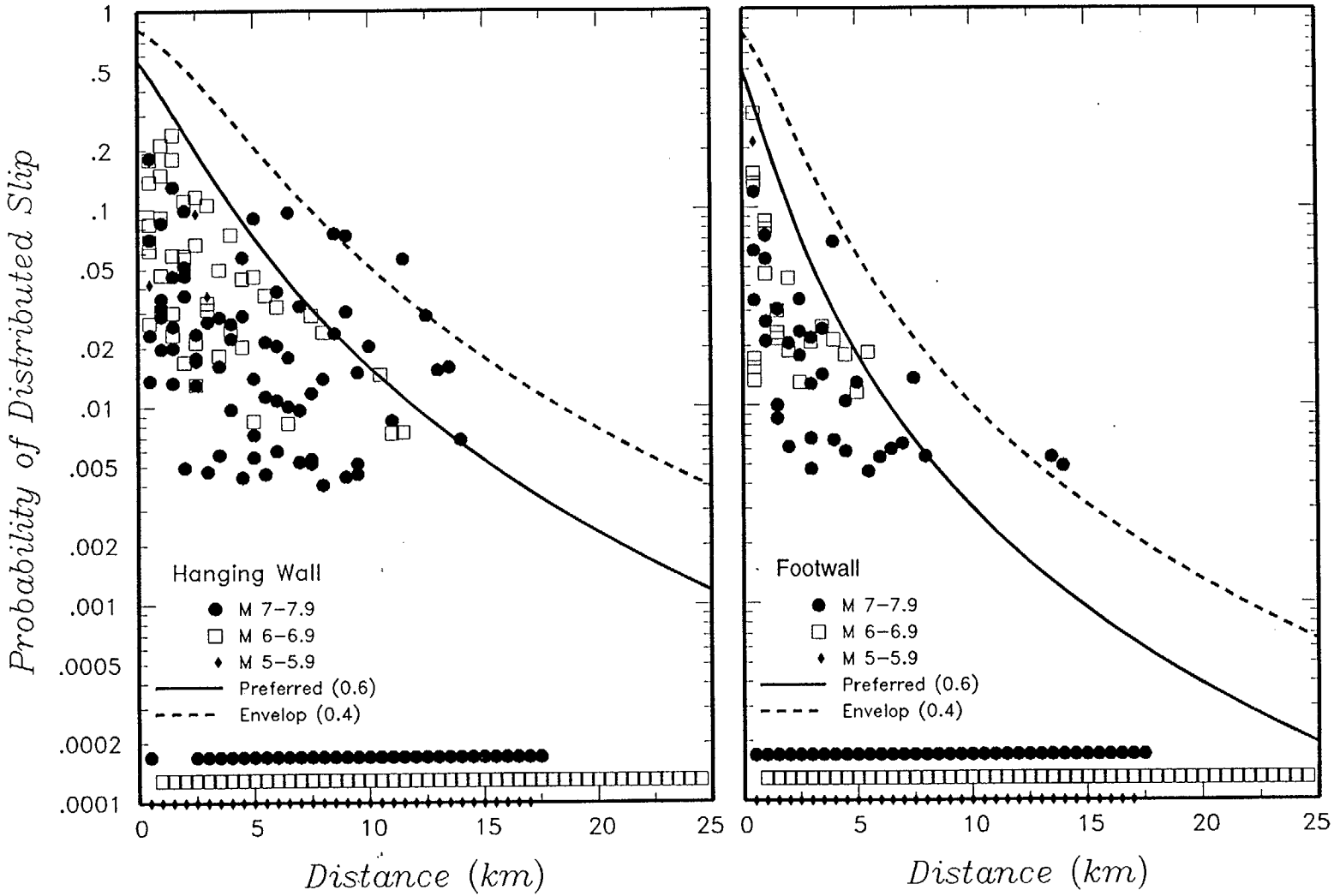

Figure 4-82 Probability of distributed rupture as a function of distance from the principal rupture defined by the ASM team. Data are the same as those presented on Figure H-13b

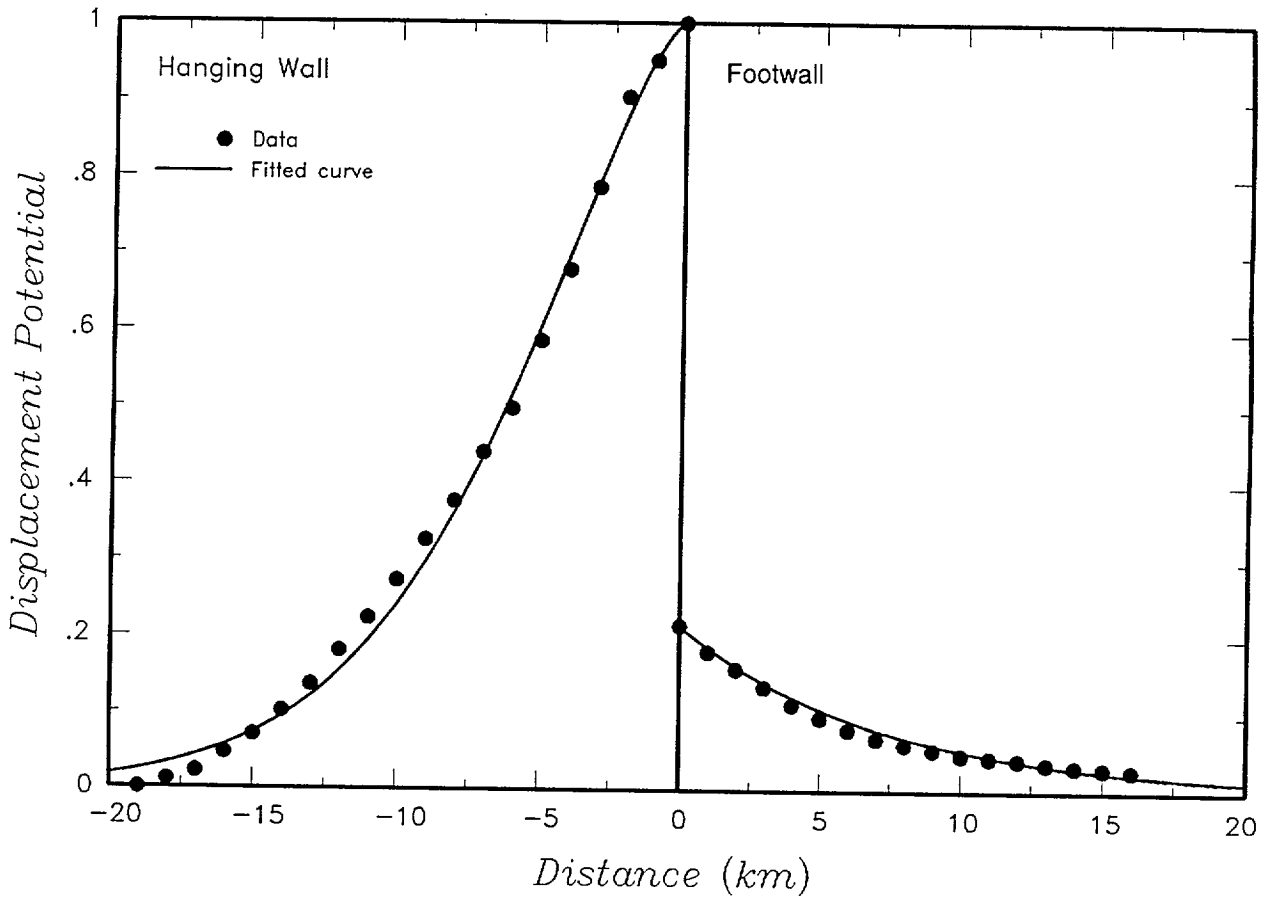

Figure 4-83 Normalized displacement profile for the 1983 Borah Peak, Idaho earthquake used by the ASM team to define the distributed faulting displacement potential

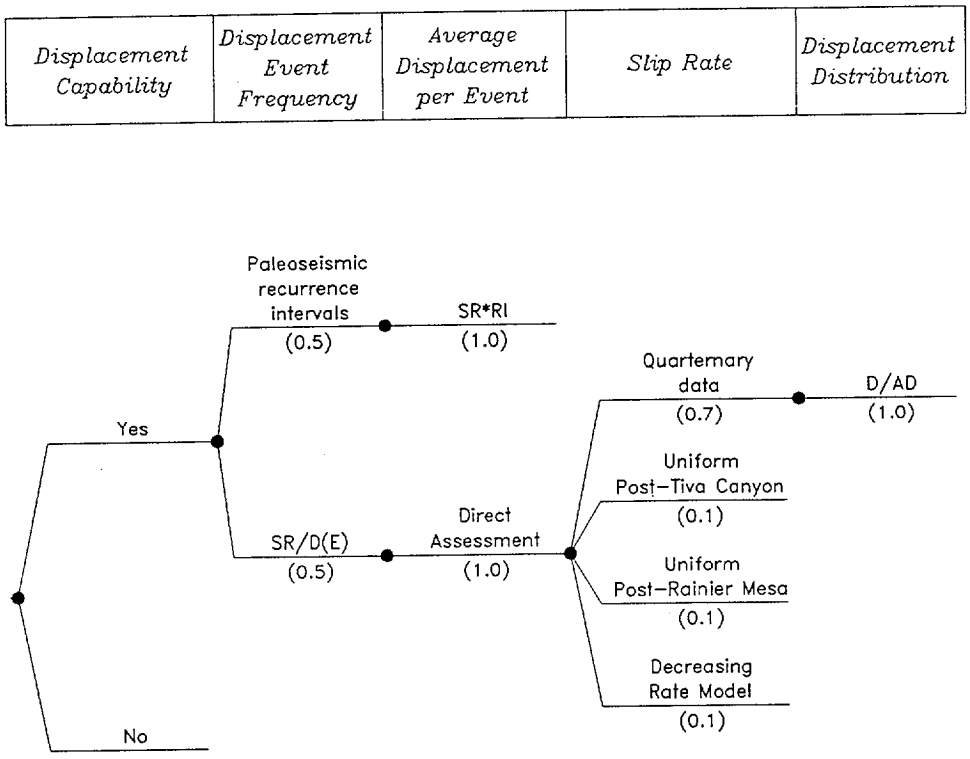

Figure 4-84 Logic tree defining the DFS team's characterization of displacement hazard

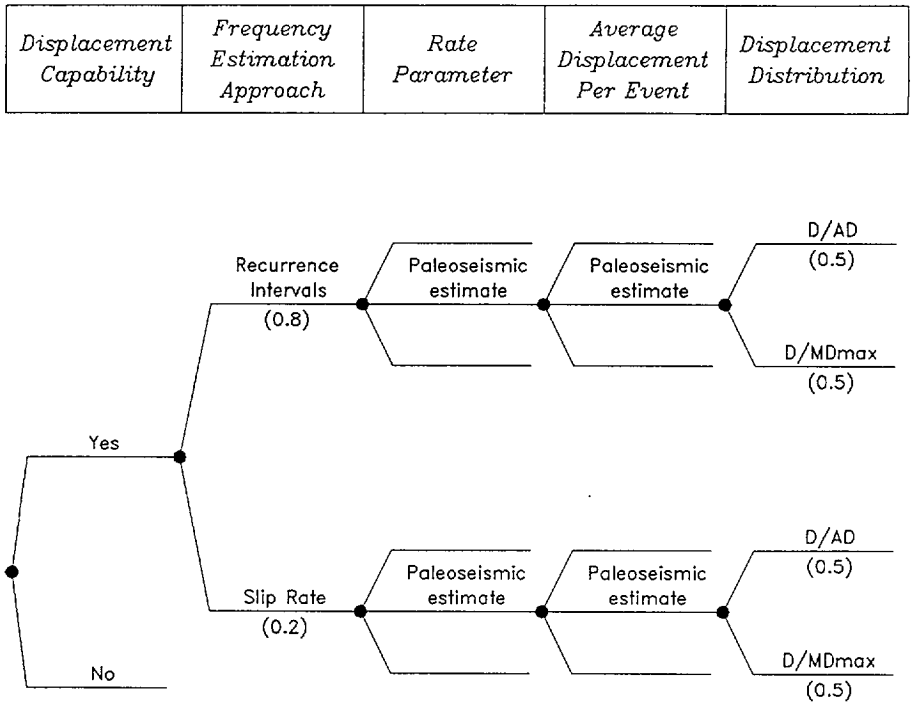

Figure 4-85 Logic tree defining the RYA team's characterization of displacement hazard at sites with Quaternary data for fault displacement

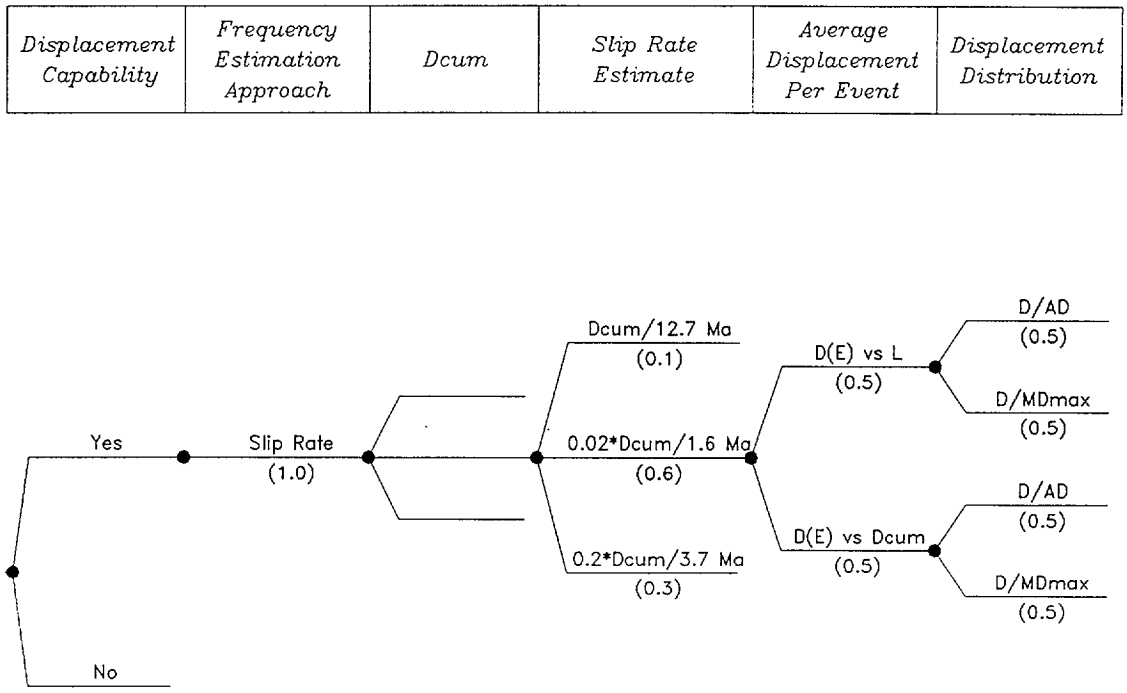

Figure 4-86 Logic tree defining the RYA team's characterization of displacement hazard at sites without Quaternary data for fault displacement

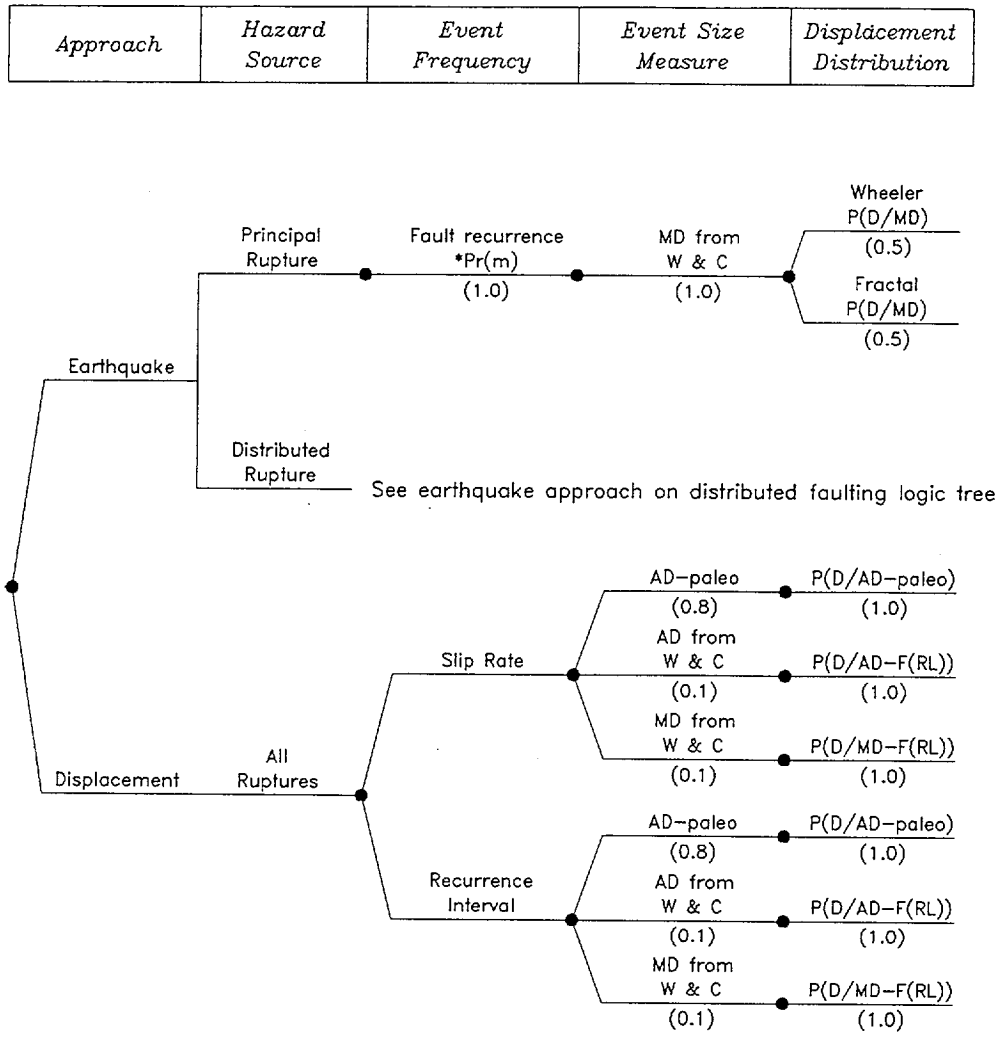

Figure 4-87 Logic tree defining the SBK team's characterization of principal faulting displacement hazard

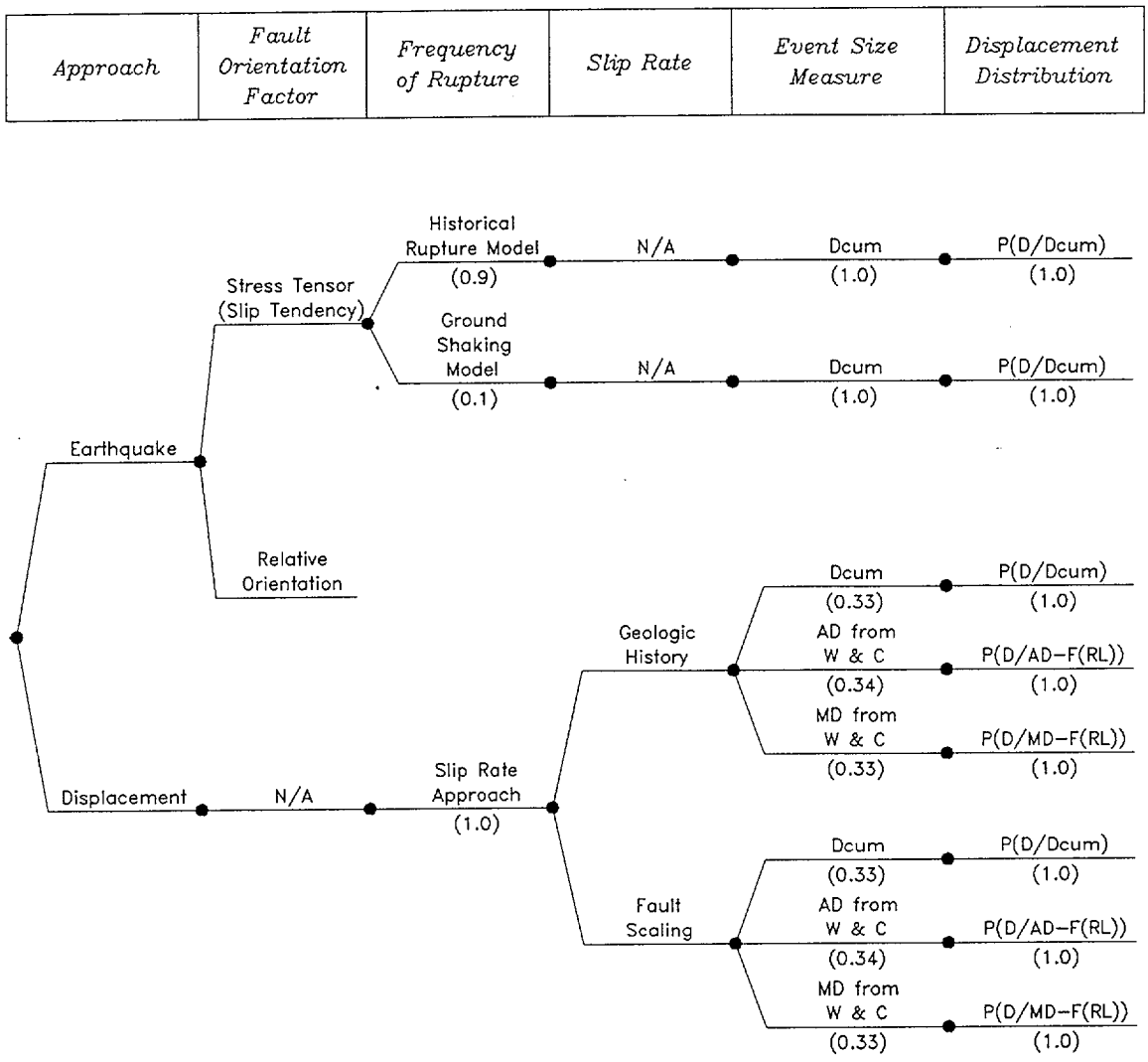

Figure 4-88 Logic tree defining the SBK team's characterization of distributed faulting displacement hazard

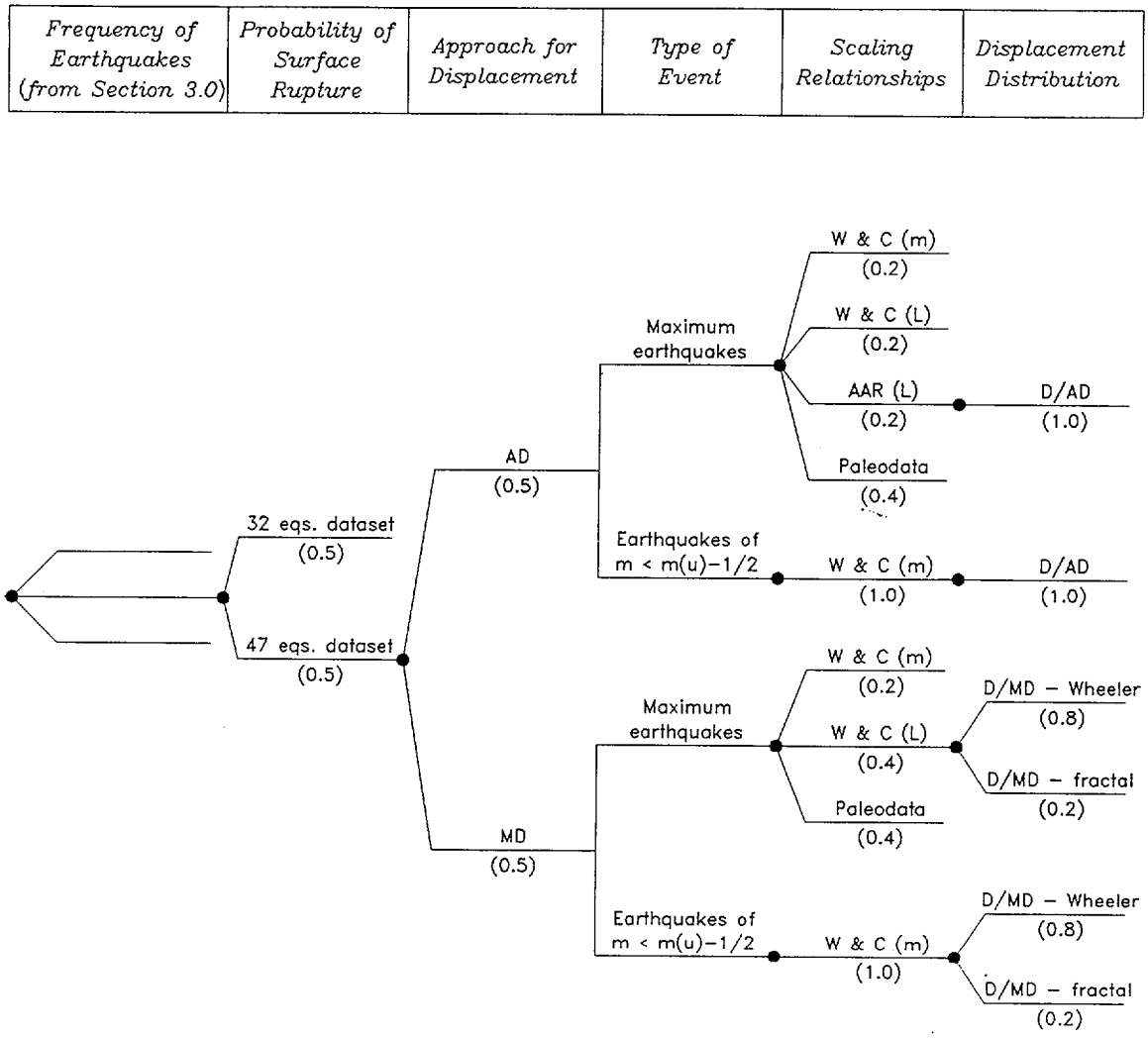

Figure 4-89 Logic tree defining the SDO team's characterization of principal faulting displacement hazard

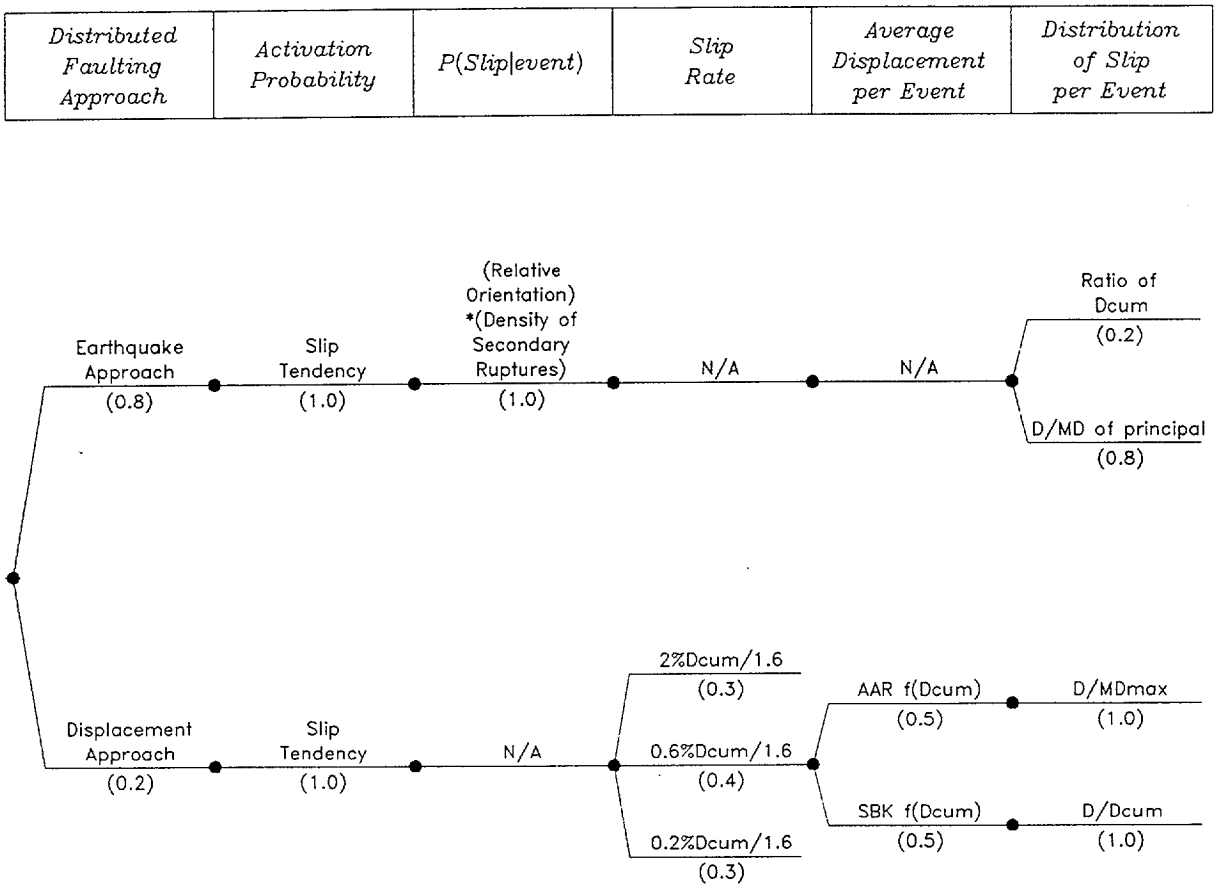

Figure 4-90 Logic tree defining the SDO team's characterization of distributed faulting displacement hazard

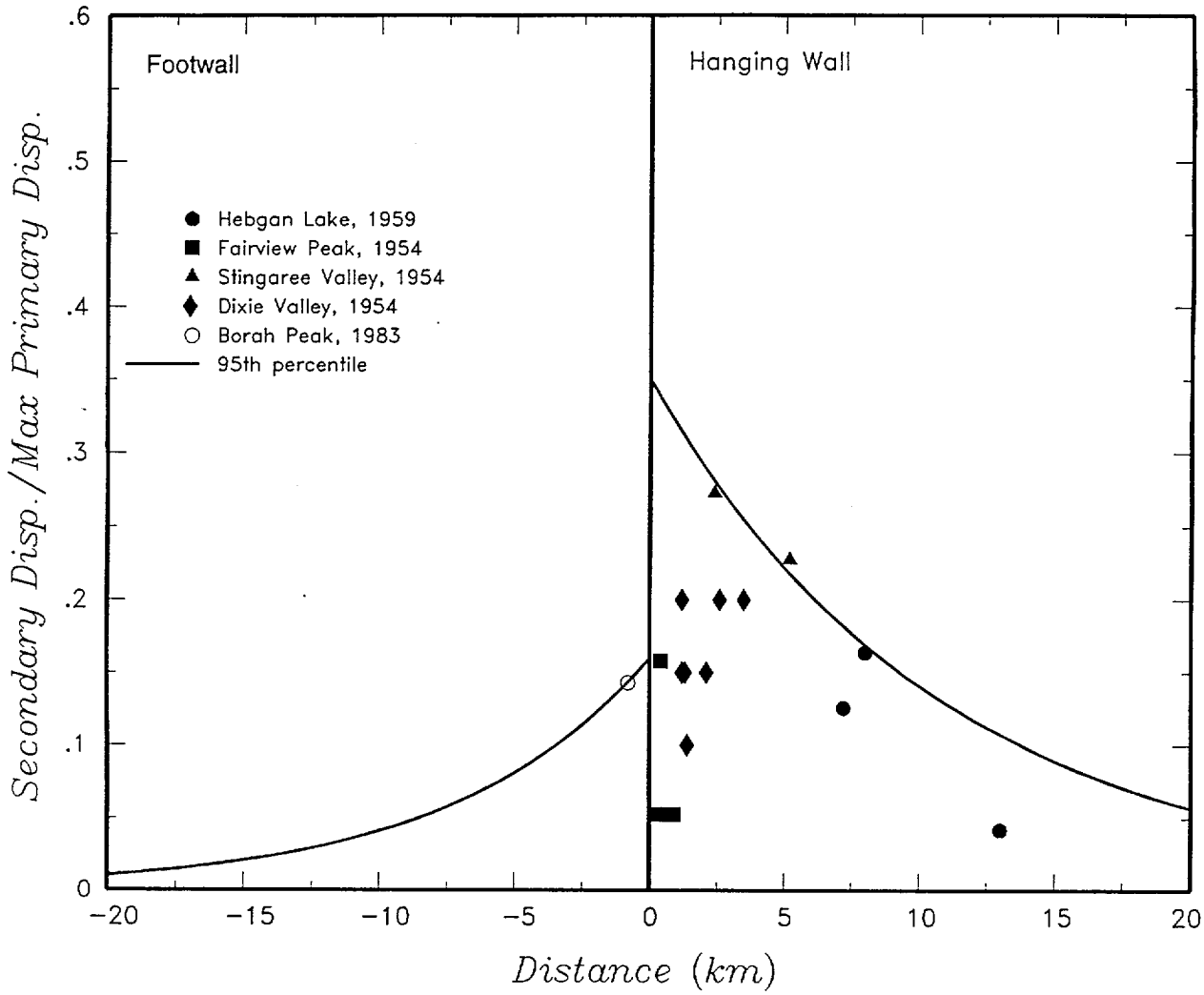

Figure 4-91 Curve defining the 95th percentile of the distribution for displacement on a distributed rupture developed by the SDO team

5.0
GROUND MOTION CHARACTERIZATION FACILITATION APPROACH

The goal of the ground motion characterization was to formulate vibratory ground motion models for input into the PSHA. The description of ground motion in this context consists of ground motion attenuation relations specific to the repository site. The ground motion study has been structured to incorporate the uncertainty in the science of ground motion estimation. A ground motion evaluation necessarily involves interpreting data, existing predictive models, and geologic and geophysical characteristics of Yucca Mountain. These data and the process by which they are synthesized into a predictive model have associated uncertainties. Therefore, fully evaluating uncertainty is an essential element of a comprehensive study. In this chapter, the approach utilized by the GM Facilitation Team to elicit interpretations from the GM experts as well as the experts' methodologies are described.

5.1 EXPERT ELICITATION PROCESS

Development of the expert interpretations was coordinated and facilitated in a series of three technical workshops. Each workshop was designed to accomplish a specific step in the overall process of developing the interpretations in order to ensure that all relevant data and credible interpretations were fully considered by each expert.

The ground motion characterization required coordination with the SSFD Facilitation Team and the PSHA Calculations Team. During the course of the project, the focus of the ground motion activity was tailored to take into account the range of seismic source descriptions identified in that activity. As first envisioned, the relevant sources included normal dip-slip faults and vertical strike-slip faults. Single ruptures of each source were assumed. However, the seismic source characterization activity identified the possibility of multiple ruptures on parallel dipping faults and a possible low-angle detachment surface underlying Yucca Mountain. Consequently, these types of seismic sources were also included in the suite of sources for which ground motion estimates were developed.

Using the various information and data discussed below, the GM experts each developed a series of estimates of ground motion for a defined suite of earthquake magnitudes and distances, fault geometries, and faulting styles. The estimates included the median ground motion and its (aleatory) variability, and the scientific (epistemic) uncertainty on both. These "point estimates" were fitted to yield attenuation equations as a function of all four parameters. The independent variables used in the regression were selected by the expert and the computations were performed by the facilitation team.

Each expert formed his or her interpretations using the information and data presented in three workshops. Additionally, the elicitation process included a formal interview, led by a normative expert, in which each expert presented and defended his or her preliminary point estimates. The facilitator challenged each expert to defend and, as necessary, clarify his or her thought process to ensure that all relevant data and information were evaluated.

As a computational aid, the GM Facilitation Team Leader provided the experts with summaries of proponent model estimates – computed ground motions from numerous empirical attenuation relations and numerical simulations the experts selected for study. All such derivative data are documented in a series of Ground Motion Data Packages, 12 volumes in all. The Data Package volumes are listed in Appendix B.

5.1.1 Compilation and Discussion of Data and Information

To ensure that all experts had equal access to data and information, a key element of the elicitation process was the dissemination of data. Two workshops were organized specifically to facilitate presentation and discussion of the data (Figure 3-1) . Detailed agenda and workshop plans were provided to all participants in advance, copies of all presentation materials were made available during each meeting, and the proceedings were summarized by the GM Facilitation Team. Copies of the workshop summaries are contained in Appendix D.

Workshop #1 - Data Needs held in April 1995 identified the tectonic, geologic, seismologic, and ground motion issues to be evaluated and the primary data sets and derivative products needed to complete the evaluations. This workshop provided the experts a review of the seismologic setting of Yucca Mountain. It allowed the experts to debate the significance of

various technical issues and the data and information available to resolve them. As a result, several data needs identified by the experts were subsequently provided in the project.

Workshop #2 - Methods, Models, and Preliminary Interpretations held in January 1997 focused on methods of characterizing ground motion for the PSHA, new data and derivative analyses, and a review of the point estimate format required for the interpretations. Technical presentations centered on competing empirical attenuation models and results of synthetic modeling. Several of these proponent models were developed for other geographic regions. The experts discussed how to interpret ground motions from other regions and also discussed methods of developing adjustment factors that account for the differences between Yucca Mountain and these regions.

Although discussions of the data and other information were most focused among the experts during the workshops, throughout the project there was a continual informal dialog among the experts themselves and between the experts and the GM Facilitation Team Leader. During informal interaction among the experts, an expert was most often acting as a proponent to resolve questions regarding the application of his specific model. During informal interaction between the experts and the GM Facilitation Team, the experts raised issues that required general clarification by the GM Facilitation Team Leader.

In addition to the workshops, two working meetings were held to discuss the proponent models. These two working meetings addressed issues related to the proponent models and conversion factors that had not been resolved at the workshops. The meetings also provided additional feedback to the experts.

5.1.2 Elicitation Interviews

A formal elicitation interview between the GM Facilitation Team and each expert was held following Workshop #2. The interviews were conducted in accordance with guidelines developed by the SSHAC (1997). The elicitation team (Facilitation Team, Dr. Jean Savy, and Dr. Peter Morris) met prior to the first interview to establish a systematic approach to the questioning to ensure that the first expert would be asked the same questions as the last.
Dr. Abrahamson served as a generalist in all interviews. In the first interview (with Silva), Dr. Morris served as the normative expert. In the next four interviews (Walck, Campbell,

Somerville, and Anderson), Jean Savy served as the normative expert. Dr. Morris was not available during the remaining interviews; based on guidance from Dr. Morris and their previous experience with elicitation interviews, Drs. Savy and Abrahamson conducted the remaining interviews. Dr. Becker documented the interviews.

The interviews were private and uninterrupted. Each expert provided written documentation of the proponent models he deemed relevant to the study and the means by which he formed point estimates from the proponent models. In the interview, each expert was asked to explain the procedures he adopted to obtain median estimates, aleatory uncertainties, and the epistemic uncertainties on both. Each defended his selection of 'relevant' proponent models and also explained on what basis other models were rejected.

The elicitation interview was an important source of feedback for the experts. Inconsistencies in the treatment of uncertainty and use of conversion factors were identified and later corrected by the experts. In advance of the interview, several experts had considered only a limited number of proponent models. They tended to expand the number of models considered following challenges in the elicitation to defend their initial selection. Most importantly, in preparation for the interview, all experts had used weighted averages of the proponent models to develop preliminary estimates. All had also used the concept of classes of models; the weights of the individual models were often selected so that a desired relative weight between the model classes was achieved. As a result of the interviews, a formal dual weighting scheme was adopted by each expert in which the weights were separated into weights for classes of models and weights for models within a class.

A major conclusion following the interviews was that the volume of point estimates ultimately requested could not be managed readily by the experts. The key issue was the effort needed for the computation of the weighted combinations of the proponent model estimates and appropriate adjustment factors on which the experts point estimates were based. To facilitate this effort, the GM Facilitation Team calculated the preliminary ground motion estimates for each expert using weights supplied by the expert. Consequently, a single computer program was developed by the GM Facilitation Team Leader for use by all experts to weight proponent models as a step towards forming their point estimates. This computer program (WT_AVE) was used to compute weighted model values (used as

preliminary point estimates) for each of the experts. This allowed the experts to simply develop weights for the models freeing them to concentrate on evaluating the resulting point estimates. The weighted values were used solely for preliminary computations: the experts were charged to evaluate the preliminary estimates to form their final point estimates.

5.1.3 Feedback and Revision

Feedback for the experts occurred at several different times in addition to the formal Feedback Workshop. At the working meetings, interaction among the experts was significant as they discussed the alternative approaches and proponent models. As mentioned above, the elicitation interviews resulted in significant feedback in terms of identifying inconsistencies and misconceptions by the experts. The experts were also encouraged to discuss the issues among themselves as needed in between the formal workshops and working meetings.

The Feedback Workshop informed the experts of the implications of their preliminary interpretations on the hazard computation. This workshop included a joint session with the SSFD expert teams to facilitate understanding of the technical issues and models each expert had developed. Preliminary hazard results were also presented and the sensitivity of the hazard to various input parameters was assessed. The workshop primarily consisted of discussions of the technical basis for each expert's point estimates and the attenuation equations developed from the expert's interpretations by the GM Facilitation Team. A few selected cases (magnitude, distance, and frequency combinations) were selected for in-depth discussions among the experts. The reasons for the differences in the point estimates for these cases were explored including discussions of the strengths and weaknesses of the proponent models for each case. As part of this discussion, a formal procedure for developing statistical estimates of the epistemic uncertainties was agreed upon. By the conclusion of the workshop, each participant was fully briefed on the technical basis for all other experts' estimates.

An additional working meeting, which provided additional feedback, was held shortly after the Feedback Workshop. This meeting included an exercise to focus the experts on the values of the point estimates and not on the weights given to the models.

Following the Feedback Workshop and working meeting, the experts revised their estimates. The GM Facilitation Team developed revised attenuation models based on the experts' revised estimates. The experts were then given the opportunity to revise their point estimates and/or the functional form of the regression equations. This process was repeated until the experts were satisfied that the regression models adequately characterized their estimates of the ground motion.

5.1.4 Documentation

Each expert documented the reasoning behind his development of the point estimates. This documentation is given in Appendix D. An outline of key sections was provided to each expert to ensure a standardized format was followed in the reports. The GM Facilitation Team first reviewed the documentation for internal consistency and completeness. The reports were then reviewed by the Project Management Team, and finally by the Review Panel.

5.2 REVIEW OF TECHNICAL ISSUES

Yucca Mountain lies within the Basin and Range Province, a regime primarily characterized by extensional crustal stresses. Known late Quaternary faulting within 20 km of the proposed repository is principally normal dip-slip, occurring both with and without an oblique component. Major strike-slip faults, which contribute to the potential ground shaking hazard at the site, have been identified at distances of 25 km and greater.

Ideally, ground motions recorded from earthquakes in the Yucca Mountain region, or at a minimum the Basin and Range Province, should be used to develop attenuation relations for Yucca Mountain; however, strong motion data from these environments are not sufficient to adequately constrain an empirical model. A key issue in characterizing ground motion attenuation at Yucca Mountain was the applicability of standard western U. S. attenuation models to the Basin and Range Province. Empirical attenuation relations commonly applied in the western U.S. are based primarily on recordings from California strike-slip and reverse earthquakes. For example, in the data base used by Sadigh *et al.* (1993), 15% of the earthquakes and less than 2% of the recordings used to develop their attenuation relations are from normal or normal/oblique faulting events. This data distribution is similar for all other

western U.S. attenuation models in common use. Due to the sparse amount of strong motion data recorded from normal faulting earthquakes, separate style-of-faulting factors typically have not been estimated for these types of events. Instead, the normal faulting event data are usually grouped with strike-slip faulting earthquakes because the few recorded normal event strong ground motions had not been found to be statistically different than those predicted for strike-slip events in previous evaluations (Westaway and Smith, 1989).

Further, significant differences may exist in the seismic source, regional crustal, and shallow site properties for Yucca Mountain as compared to the average source, path, and site properties represented in the western U.S. strong motion data set. An issue that the experts addressed was whether, or to what degree, these differences could affect median ground motions or variability in ground motions expected at Yucca Mountain compared to those predicted by those proponent models based primarily on California data.

5.3 GROUND MOTION WORKSHOPS AND MEETINGS

Three workshops and two working meetings on ground motion characterization were held and they are summarized below. The complete workshop summaries are contained in Appendix D.

5.3.1 Workshop #1 - Data Needs

The goal of Workshop #1 was to identify critical data needs requiring additional analyses and, secondarily, to provide site-specific information about ground motion attenuation at Yucca Mountain. The goals of the PSHA and the relevance of the ground motion characterization within the overall PSHA project were presented as background to the experts.

Because incorporation of scientific uncertainty was a key element of the study, the means by which uncertainty is characterized were discussed. Total uncertainty was decomposed as epistemic and aleatory, each of which is partitioned into parametric and modeling variability.

Various technical issues and available seismologic data were presented. Known and suspected Quaternary faults and their characteristics were described. Data on source

parameters, crustal structure, attenuation parameter Q, and site effects were summarized and ranges of stress drops and Q values reported in various studies were noted. The effect of site conditions on spectra using empirical and theoretical data was illustrated. Using theoretical data, the potential influence of the uncertainty in the site properties as compared to the potential influence of the variability of source properties was examined in terms of the resulting variability of the ground motion. Key seismological data include records of the June 29, 1992 Little Skull Mountain main shock and aftershock sequence and the 1993 Rock Valley sequence. The experts were briefed on source focal mechanisms, event locations, and seismograms from this sequence. Estimated values of kappa and site amplification were provided corresponding to several stations in the Yucca Mountain region. Site response effects were examined using UNE data, which indicate strong azimuthal dependence. The data were evaluated for two-dimensional crustal structure to explain the amplification.

Two ongoing Yucca Mountain Project site characterization activities had direct relevance to the ground motion characterization activity. The first was to evaluate empirical vibratory ground motion models for extensional tectonic regimes. Spudich *et al.* (1996) had assembled a worldwide data set from normal and strike-slip faulting in these regions. Their goal was to first evaluate several empirical attenuation relations and, if they did not adequately describe the data, to develop correction factors for the relations or alternatively produce a new relation based on the extensional data (Spudich *et al.*, 1996). The second activity was the ground motion modeling of scenario earthquakes at Yucca Mountain (J. F. Schneider *et al.*, WCFS, written communication, 1996). The activity was aimed at developing ground motion time histories and response spectra for realistic earthquake faulting scenarios. As part of this project, the modeling procedures were calibrated against the Little Skull Mountain records.

Ground motion estimation methods were reviewed including empirical attenuation relations, numerical simulations, and hybrid empirical-numerical schemes. The input required by each model was summarized as well as source parameters that were not well defined at the time at Yucca Mountain.

5.3.1.1 Issues from the Data Needs Workshop.

Throughout Workshop #1, the GM Facilitation Team Leader and experts discussed the technical issues to be resolved and data required for a thorough assessment of ground motions. Six principal issues were identified for further study and were prioritized as to importance by the experts (Table 5-1). Most arose from a lack of detailed information or from a need to further evaluate an available data set.

Issue #1 Site Response. The reference site condition considered at the Data Needs Workshop was for a site located on the top of "typical" tuff at Yuuca Mountain. To develop ground motions for this site condition, the experts require detailed information on the shear-wave velocity and non-linear properties of the shallow tuff at Yucca Mountain (primarily the top 50 m). A preliminary velocity profile for the shallow tuff had been estimated as part of the Scenario Earthquake Modeling Project (J. F. Schneider *et al.*, WCFS, written communication, 1996), but this velocity profile was not well constrained. The available laboratory testing studies to determine the non-linear properties were also not adequate to meet the experts needs. Therefore, the experts requested that additional site data be collected.

Issue #2 Stress Drops for Normal Faulting Earthquakes. The ground motion evaluation presented by Spudich *et al.* (1996) found lower ground motions for earthquakes in extensional regimes than for earthquakes in transpressional regimes. Since the Spudich *et al.* (1996) analysis was based on residuals from attenuation relations, it was not clear that this difference was due to the earthquake source rather than site or path effects. The experts requested that stress drops be computed for the Spudich *et al.* (1996) data set to compare with stress drops for California earthquakes to determine the causes of the ground motion differences.

Issue #3 Shallow Slip. The numerical simulation methods used in the scenario earthquake report do not include significant seismogenic slip in the top few km, although shallow slip has occurred in past earthquakes and can occur on the local faults at Yucca Mountain. The validity of not including seismogenic shallow slip in the numerical simulations was questioned.

Issue #4 Numerical Simulations. Numerical simulations of ground motions at Yucca Mountain were available for the earthquakes considered in the Scenario Earthquake Modeling Project; however, the experts are required to estimate the ground motions for a much larger range of magnitudes and distances than was considered in that study. Therefore, the experts requested that numerical simulations be generated for the full set of events (point estimates) that the experts had considered. Three preferred methodologies were identified by the experts from the six included in the Scenario Earthquake Modeling Project. The selected procedures were those by Zeng and Anderson, Silva, and Somerville. These procedures were selected based on their perceived superior modeling ability as evidenced by comparisons included in the Scenario Earthquake Modeling Project (J. F. Schneider *et al.*, WCFS, written communication, 1996). The experts requested that ground motions based on these three numerical simulation methods be generated.

Issue #5 Regional Q Models. Discrepancies in the literature regarding regional attenuation (Q) were identified; a consistent Q model was required for use by the experts.

Issue #6 2-D and 3-D Effects. Data recorded at Yucca Mountain from UNEs show significant lateral variations indicating strong 2-D and 3-D effects in the wave propagation. The importance of these effects on earthquake ground motions was questioned.

5.3.1.2 Resolution of Data Needs Issues. The site response characteristics specific to Yucca Mountain (Issue 1), the source parameters (stress drops) for earthquakes in the extensional regimes (Issue 2), reported 2-D and 3-D effects on ground motion amplification from UNEs (Issue 6) were resolved by additional evaluations of new or existing data. Yucca Mountain-specific ground motions predicted by numerical ground motion simulations (Issue 4) were requested, which was a furtherance of the Scenario Earthquake Modeling Project (J. F. Schneider *et al.*, WCFS, written communication, 1996).

Issue #1 Site Response. Limited studies to evaluate the shear-wave velocity and non-linear properties of the shallow tuff were conducted. Since these additional studies did not fully define the site properties to the extent required for site-specific application, it was decided to define the reference site condition by removing the top 300 m from the shear-wave velocity

profile used in the Scenario Earthquake Modeling Project. This site condition was called the "reference rock outcrop" in this report.

To define the appropriate kappa for the reference rock outcrop site condition, laboratory studies of the low strain damping of the tuff in the top 300 m were conducted (K. H. Stokoe *et al.*, University of Texas, Austin, written communication, 1998). The low strain damping was found to be very low with an equivalent kappa of 0.0014 sec in the top 300 m. The average kappa for sites at the surface at Yucca Mountain had been previously estimated to be 0.02 sec based on studies of Su *et al.* (1996). Subtracting the kappa in the top 300 m from the surface kappa of Su *et al.* (1996) results in a kappa of 0.0186 sec for the reference rock outcrop.

The reference rock outcrop provided a well defined reference site condition for the experts to estimate their ground motions and allowed the ground motion study to proceed without complete site characterization which was not available. With the change of the reference site condition from the surface of the tuff to the reference rock outcrop, the nonlinear properties of the tuff are not needed for the development of ground motions in this study. In addition, using the reference rock outcrop motion provides a better reference for estimating the motions at the repository depth. Accounting for updates to the ground motion estimates as additional site information becomes available is discussed below in Section 5.7.

Issue #2 Stress drops for Normal Faulting Earthquakes. Median stress drops were computed using the normal-faulting earthquakes in the Spudich *et al.* (1996) worldwide data set and were found to be consistently lower than those for California events, which comprise the majority of the strong ground motion data base used to develop empirical attenuation relations. Ground motion scale factors accounting for the change in stress drop were developed.

Issue #3 Shallow Slip. Additional analyses were conducted using foam rubber modeling to evaluate the effect of ignoring shallow slip. Weak surficial layers were shown to significantly reduce the ground motion from near-surface slip due to increased rise-time. This supports ground motion modeling experience, which consistently shows reduced high-frequency ground motions radiated from shallow slip. In addition, it was also shown that

significant differences in near-fault ground motions for normal and reverse faults are observed in foam rubber models.

The proponents of the numerical models also stated that their models required small amounts of shallow seismogenic slip otherwise they would greatly overpredict observed near fault ground motions. Therefore, the assumption of little or no seismogenic shallow slip is part of the numerical modeling procedure. None of the experts felt that this issue was important for their evaluations of the ground motions from the numerical simulations.

Issue #4 Numerical Simulations. Ground motions for the required point estimates were generated the three requested numerical simulation procedures (Silva, Somerville, and Anderson and Zeng). These procedures focused on the larger magnitude simulations because the models are calibrated for larger magnitude earthquakes and the subevent size for Silva and for Somerville's methods is approximately a M_w 5. Only the Anderson and Zeng procedure was used to generate ground motions for the M_w 5 events since it is applicable to smaller magnitudes (a result of using a range of subevent sizes). The numerical simulations used the revised site condition discussed in Issue #1 above.

Issue #5 Q Model. The basis for the apparent discrepancies in regional attenuation (combined effect of Q and geometrical spreading) (Issue 5) was investigated and resolved. Self-consistent Q and geometrical spreading coefficients were developed.

Issue #6 2-D and 3-D Effects. Observed lateral variations in the ground motions from UNEs recorded at NTS were evaluated. The shallow depths of UNEs result in large surface waves which are strongly affected by lateral variations in the velocity and structure of the shallow crust. However, confined shallow seismic sources such as blasts are unlike large earthquakes which extend to seismogenic depths. The conclusion of the evaluation was that variability in ground motion amplitudes from energy released at typical earthquake depths due to shallow lateral velocity variations in the crust would be much less than that observed in the blast data.

5.3.2 Workshop #2 - Methods, Models, and Preliminary Interpretations

The second workshop was held after a 1-year project hiatus. The primary goals of this workshop were to refamiliarize the experts with the issues, present available models for characterizing ground motions (proponent models), and discuss ways in which elements inherent to the proponent models may differ from conditions at Yucca Mountain. Secondarily, the technical issues raised in Workshop #1 were addressed. The experts also participated in a preliminary ground motion modeling exercise for a postulated earthquake. The exercise was intended to focus the workshop discussions on modeling techniques and highlight issues that were to be resolved in the workshop. Lastly, the range of the magnitude and distance modeling to be covered by the experts' interpretations was specified.

An important change from Workshop #1 was the reference site condition. In Workshop #1, the reference site condition was a site on the surface of the tuff. The reference site condition was redefined as a reference rock outcrop at the ground surface with properties equivalent to the existing conditions at repository level. The reference rock outcrop velocity profile is based on the Yucca Mountain velocity profile from the Scenario Earthquake Modeling Project (J. F. Schneider *et al.*, WCFS, written communication, 1996) with the top 300 m removed. This velocity profile is listed in Table 5-2. This change in the reference site condition was made to facilitate estimation of the ground motion at the depth of the repository using procedures currently being developed for the NRC. Using reference rock outcrop ground motions is the best approach for computing the ground motions at any of the SSC locations (at depth or on the surface).

5.3.2.1 Proponent Models. The balance of Workshop #2 focused on proponent models. The point-source random vibration theory (RVT) model, the hybrid empirical model, models derived from nuclear blast data, the finite source numerical simulation models arising from the Scenario Earthquake Modeling Project, and available empirical models were all presented. During the workshop, the experts added to the list of proponent models they wished to consider in their deliberations. For example, McGarr's (1984) model relating peak ground motions with stress state and focal depth was included. All models ultimately evaluated by the experts are listed in Table 5-3.

The Spudich *et al.* (1996) data base of strong ground motion records in extensional tectonic regimes was presented and these ground motions were compared with existing empirical attenuation relations. The data set contains both strike-slip and normal faulting events from extensional regimes around the world. The study focused on calculating correction factors for empirical relations to better fit the extensional data and on developing a new predictive relation derived from the extensional data. The factors included a bias correction and a standard deviation correction, and many showed a frequency dependence. The new attenuation relations were presented, and as they are based solely on extensional regime data, could be applied at Yucca Mountain without changes to the source.

Although the Yucca Mountain region has not experienced a major earthquake in historic times, the western boundary of the Basin and Range Province has, and clues to ground motion attenuation may be found in studies of the numerous precariously balanced rocks found regionwide. The distance of balanced rocks from historic ruptures, combined with the ground accelerations required to topple these rocks, provide physical evidence of the attenuation of ground motion from an historic earthquake. This information was collated to provide a constraint on ground motion attenuation in the region.

The GM experts presented trial estimates of median ground motion and uncertainties for two postulated M_w 6.5 earthquakes occurring at 10 km distance: one event as a result of strike-slip faulting and the other, normal faulting. The purpose of the exercises was to familiarize the experts with the process and the point estimate format. Several experts only used their own proponent models as their estimates rather than evaluating the suite of alternative credible models. (Consequently, the distinct roles of proponent expert and evaluator expert were again emphasized.) As a result, expert-to-expert variability in estimates was large; the estimates of the median peak ground acceleration varied by about a factor of two for the strike-slip case, up to three for the hanging wall of the normal faulting case, and over three for the footwall.

The experts were presented with the range of earthquake magnitudes, source distances, faulting styles, and fault geometries to be interpreted. They were to develop ground motions as a series of point estimates for 51 specified magnitudes and source - site geometries (Tables 5-4 and 5-5). Both strike-slip faulting on a vertical surface and normal slip on a moderately

dipping fault were to be considered. Horizontal and vertical motions were to be estimated for peak ground acceleration (PGA), peak ground velocity (PGV), and spectral acceleration at frequencies of 0.3, 0.5, 1, 2, 5, 10, and 20 Hz. The experts were to provide the median motion, aleatory variability, and the epistemic uncertainties on both the median and the aleatory variability.

5.3.3 Working Meeting #1

Subsequent to Workshop #2, an interim working meeting was held for the experts at which they were provided with the first of several volumes of documentation of proponent models and the estimates derived from the proponent models. These "Ground Motion Data Packages" (Appendix B) were provided throughout the project as a tool to facilitate the experts' comparisons of their point estimates against the many proponent models and against the estimates of the other experts. Discussions at the working meeting were focused by the GM Facilitation Team Leader on the differences between estimates arising from the various classes of proponent models and also the differences between estimates arising from the various proponent models in each class. For convenience of comparison, classes of models were defined as empirical, finite source numerical, point source (RVT), and blast. These estimation methodologies had been presented previously in the workshops.

5.3.4 Elicitation Interview

In the formal elicitation interviews, each GM expert explained the procedures he/she adopted to obtain estimates of the median (μ), aleatory uncertainty (σ), and the epistemic uncertainties on both (σ_μ, σ_σ). As each expert explained the reasoning for the weights given to each model, it became apparent that all of the experts had included the concept of assigning weights to general classes of models and then assigning separate weights to the models within each class. The underlying logic was a dual weighting scheme with the weight for a model given by the product of the class weight and the model weight, although not all experts formally applied the approach. Once this dual weighting scheme was identified during the interviews, the experts all adopted a formal class/model weighting approach. With this common structure to the model weights, it became much easier to compare the weights used by the experts.

In general, each expert developed weighting schemes for the proponent models, applied the weights, and evaluated the resulting ground motions. In most cases, the weights were not the same for all magnitudes, distances, and frequencies as the experts considered the strengths and weaknesses of each of the classes of models and of the individual models within each class. Two experts included unique aspects in their approaches. Marianne Walck developed a method to identify outlier points among the proponent values and eliminated these from further consideration. John Anderson implemented two weighting schemes, which he then combined to develop his estimates. In the first scheme, he accommodated all relevant proponent models and developed a uniform distribution between the maxima and minima of all of the empirical models. In the second scheme he selected preferred empirical and numerical simulation proponent models.

In all interviews, inconsistencies in the treatment of the aleatory uncertainty (σ) and epistemic uncertainty on the median estimates (σ_m) and on the aleatory uncertainty (σ_σ) were identified. Therefore, the treatment of uncertainty was reviewed and each expert worked out how it should be applied in the context of his estimates.

In order to modify the empirical models to reflect Yucca Mountain repository-depth conditions, several proponent scaling and conversion factors had been provided earlier in the project. While the technical aspects of the development of the conversion factors were well understood, some inconsistencies in the details of their application were identified. Misconceptions were clarified by reviewing the sections in the Ground Motion Data Package that summarized the factors.

Substantial revisions in the experts' point estimates resulted from the interviews, largely the product of clarifying misconceptions, identifying inconsistencies, and formalizing the dual class/model weighting approach. Further, when challenged to defend their use or elimination of each model, in some instances experts identified previously unconscious bias in their approach. The tendency was to expand the number of models considered by each expert.

As a result of the elicitation interviews, many of the differences in the ground motion estimates were identified as not resulting from differences in scientific opinion, but rather

from misconceptions or other inconsistencies. Removal of these unintended differences was one of the main goals of the expert elicitation process.

5.3.5 Workshop #3 - Feedback

To give the GM experts a better understanding of the technical issues of the overall PSHA, a joint session was held with the SSFD experts. In the joint session, preliminary models developed by the experts in the two groups were summarized. Although the SSFD expert teams developed models with numerous fault geometries, the GM experts developed ground motion estimates for a few specified fault geometries. These geometries were taken as representations of 'average' geometries, and the fault geometry variation within a range was incorporated as aleatory uncertainty in the ground motion estimates. Seismic source characteristics that introduce additional uncertainty in the estimates include deviations from the specified geometry, multiple ruptures on parallel faults, and a subhorizontal detachment fault. The latter two cases deviate so far from the average models that special consideration was needed. These special cases were discussed subsequently during the workshop.

Preliminary hazard computations were presented, based on the preliminary models developed by the source characterization teams and the fits based on the preliminary ground motion point estimates. Large magnitude earthquakes on distant faults dominated the hazard at long period and the contribution from faults and areal sources more local to the site dominated at all other periods. Significant hazard arose from multiple ruptures. However, many of the multiple ruptures coalesce at shallow depths. Separate ground motions were not estimated for these cases using numerical simulations because the numerical proponent models consider shallow slip to be nearly aseismic, which is the consensus of expert opinion. However, there were some cases for rupture coalescing at depths of 5 km or more. These cases were evaluated using numerical simulations to develop scaling factors for multiple-rupture scenarios. In general, the preliminary results showed that the largest contribution to uncertainty in the hazard is uncertainty in the ground motion models, emphasizing the importance of proper treatment of uncertainty in the ground motion estimates.

Because the focus of Workshop #3 was feedback and discussion among the experts, all outlined their approach to developing their point estimates. Each of the experts employed a weighting scheme to compute their preliminary point estimates from the proponent models.

Due to the large number of points to be estimated, using a weighted average of the proponent models was the only practical approach to developing the preliminary estimates; however, it was reiterated that the role of the experts is to develop point estimates of the ground motion and not weights for models. The weights are a means of getting preliminary results, but the need for the experts to focus on the resulting ground motions was emphasized.

Using the weights for the median ground motion and aleatory uncertainty was straightforward and well understood by all the experts, but the methodology for computing the epistemic uncertainties (in both μ and σ) was not well understood. In particular, an issue that was raised was how the epistemic uncertainties from the individual proponent models should be combined with the epistemic uncertainties computed from the weighted proponent models. At the workshop, a procedure was agreed upon. This procedure is described in the documentation of the WT_AVE computer program (see Data Package Vol. 1b).

To facilitate comparisons between the individual experts' point estimates, a series of plots of these estimates and the proponent model estimates on which they were based was shown. For a given earthquake magnitude and distance, and at a given response frequency, the proponent model estimates had a bimodal distribution. Empirical estimates were generally tightly grouped separately from the numerical simulation estimates, which were less closely clustered. Because the experts weighted both empirical attenuation relations and numerical simulation proponent estimates, in general their point estimates lay between the two distributions. The experts discussed differences in the numerical proponent models at length to determine if differences in modeling methodology would require further adjustments in the point estimates. This discussion led to further checking of the numerical simulations subsequent to the workshop. These checks identified several errors in the inputs to the finite-fault numerical simulation proponent model calculations. Corrected proponent ground motions for these models were computed and these corrections were explained to the experts and discussed by them at Working Meeting #2, which was held shortly after the Feedback Workshop. After the corrections were made, the bimodal nature of the empirical estimates and the simulations was reduced. In most cases, the distributions overlapped significantly (see Data Package Vols. 2, 7, and 8).

Closure was reached on the study of precarious rocks. At four locations near large historic earthquakes, the motion required to topple the rocks was computed and compared to motions for a M_W 6.5 earthquake estimated by the experts. In general, the expert estimates significantly exceeded the toppling motions suggesting that the estimates were in turn larger than the motions that had actually occurred. However, because the study evaluated only rocks that had not toppled, and not those that had, and because the effects of motion duration, frequency content, and location in a possible shadow zone could not be quantified in the case of the precarious rocks, most of the experts believed that this information could not yet be incorporated in their estimates.

Two seismic sources had been defined by the SSFD expert teams that were significantly different than the strike-slip and normal faulting cases the GM experts had evaluated. The two rupture scenarios were (1) multiple ruptures on parallel faults, perhaps coalescing at depth, and (2) rupture on a low-angle detachment zone with multiple parallel faults near the surface. The multiple rupture scenario was shown to have a large contribution to the preliminary hazard computation for both shallow (3 km) and deeply (8 km) coalescing faults whereas the contribution from a low-angle rupture had little effect. The first scenario was investigated in numerical modeling studies. For the multiple rupture scenario, both the parallel faults and deep coalescing model results suggested that the rate of attenuation was approximately the same whether several faults ruptured or whether only the central fault ruptured. Issues that pertain to estimating these motions were identified as including moment partitioning among the rupture planes, the relative timing of the ruptures, and the distances of each plane to the site. Regarding rupture on a low-angle detachment fault, issues that affected ground motions included the stress drops of the events and the geometry. Because these issues cannot be determined *a priori*, the experts were to address any changes to their point estimates for these scenarios by incorporating additional uncertainty.

At the close of the workshop, experts briefly described potential changes to their weighting schemes applied to the proponent models based on the workshop presentations. None of the experts anticipated major modifications to their procedures, but rather refinements based on closer reevaluations of various proponent models.

5.3.6 Working Meeting #2

A second working meeting was held following the Feedback Workshop. Its first goal was to correct errors identified in checks of the finite source simulations. Inconsistencies in kappa and the crustal model had been uncovered that affected two of the models, and directivity effects were corrected in a third model. Discussions centered on the effect of these modifications on the numerical simulations. The second goal was a training exercise developed to focus the experts on their point estimates as opposed to model weights. They were shown a plot of proponent estimates (median, aleatory uncertainty, and epistemic uncertainties) and each visually formed a preferred composite estimate. This training was effective in drawing their attention to the 'estimates' themselves and not the numerical weights given to the models.

5.4 PROPONENT MODELS

The GM Facilitation Team provided an initial list of candidate proponent models for the experts to consider. The experts added additional models that they wanted to evaluate. The proponent models were separated into classes: empirical attenuation relations, hybrid empirical, point source numerical simulation, finite-fault numerical simulations, and blast models. A complete list of the models is shown in Table 5-3.

The empirical attenuation models are results of regression analyses of empirical strong motion recordings. The models are primarily based on recordings from California earthquakes, but the hybrid model, developed by Campbell, incorporates the conversion factors discussed below directly into the model. The details of the development of this model are given in the Data Package Vol. 1.

The numerical simulations are computer-generated ground motions based on seismological models of the source, path, and site effects. There are two groups of numerical simulations: point source models and finite source models. The point source models are the simplest models with the smallest number of parameters. The point source model (with an omega-squared source) is well understood. The major source of uncertainty is in the selection of the median stress-drop, its aleatory variability, and the epistemic uncertainty in both the median and aleatory variability. To allow each expert freedom to set the stress-drops to the values

that he/she preferred, the results of this proponent model were presented with median stress-drops, aleatory variability of stress-drops, and epistemic uncertainties in both as parameters to be set by each expert.

The finite-source numerical simulation models significantly differ in the model parameters required and in the procedures used to estimate ground motion. These differences can lead to significant variations in the predicted ground motions. Therefore, three different finite fault simulation procedures were used: Zeng and Anderson, Silva, and Somerville. The first two proponents additionally provided results for various alternative modeling cases. Zeng and Anderson presented three alternative models (A, B, and C) for the ground motions from their model. Case A, their base model, used the specified source geometries. Case B used shorter fault rupture lengths for the M_W 7.5 and 8.0 events to reflect the geometric constraints on the fault length determined from faults in the region. Case C used the same fault dimensions as case B, but with nonlinear properties of the shallow tuff (top 12 km) applied to the reference rock outcrop.

Silva presented two models. His base model (Case A) included the spatial variability of ground motion along the length of the fault. The variability was very large for long ruptures because the ground motion estimates off the ends of the fault were lower than elsewhere along the fault length. (This variability was not included in the other two proponent finite fault models.) In an alternative model (Case B) for the large-magnitude events, he computed the median and parametric aleatory variability for a single site located 1/3 of the rupture length from the end of the rupture (consistent with the approach used by the other two finite fault simulation methods). Case B resulted in higher median ground motion estimates and lower variability than Case A.

The blast models are based on empirical recordings from UNEs at NTS. The three blast models include alternative approaches to account for the differences in the source of earthquakes and sources of explosions.

5.4.1 Conversion Models

The ground motions developed in this study are intended to characterize surface shaking at a hypothetical site (reference rock outcrop) with properties the same as those encountered at a depth of 300 m at Yucca Mountain ("YM300"). The faulting styles considered are normal and strike-slip. These conditions are different than those represented by events comprising the data sets used to develop the WUS empirical relations.

A fundamental question that the experts were to address is whether ground motions at Yucca Mountain differ significantly from the motions represented by the data set that forms the basis for empirical models and, if they differ, by how much. Differences could be caused by source effects (extensional versus compressional regimes and normal versus strike-skip faulting), path effects (differences in the regional crustal structure), or site effects (differences in the shallow site properties). The region-and site-specific aspects of the ground motion can be directly incorporated as input for the numerical simulations, but for the empirically based models, proponent conversion factors were developed to account for these differences.
Suites of conversion factors were computed to address the experts' needs. They were developed specifically in this project using the results of (1) numeric finite-fault simulations, (2) stochastic point source simulations, and (3) empirical attenuation relations. Complete summaries of the conversion factors are presented in Data Package Vol. 1. The conversion factors included corrections for

- Source - western U.S. sources to Yucca Mountain extensional sources (values ranging between about 0.35 to 0.9),
- Crust - western U.S. crust to Yucca Mountain crust (ranging between about 0.9 and 1.2),
- Site - reference rock outcrop to Yucca Mountain surface (ranging between about 1.1 and 2.2).

The proponent conversion models for source and crust/site effects considered by the experts are listed in Tables 5-6a and b, respectively. For each proponent model estimate, the experts selected whichever source and crust/site conversions they wished to be applied. If a model did not require a correction term, "no correction" was selected. For example, the numerical

simulations were computed for Yucca Mountain reference rock outcrop conditions so no crust/site correction was needed and none was applied.

An additional issue was that many of the empirical models did not cover the full range of ground motion parameters required in this study. In particular, not all of the empirical models included 20 Hz spectral acceleration, peak velocity, horizontal component-to-component variability, or vertical component ground motions. Therefore scaling rules to estimate these ground motion parameters were also required. These models are listed in Table 5-7a, b, c, and d. Again, the experts selected the appropriate scaling factors for each model. For example, the Boore *et al.* (1994) empirical model does not include 20 Hz estimates. To use this model at 20 Hz, rules for computing it must be specified (e.g., log-log interpolation). If no correction is selected for a model that does not include the desired parameter, then that model is not used in a weighted average (e.g., zero weight).

In Workshops #1 and #2, the experts had requested that the numerical simulations developed in the Scenario Earthquake Project (J. F. Schneider *et al.*, WCFS, written communication, 1996) be reevaluated to encompass the suite of magnitudes and distances needed to characterize attenuation and also to reflect reference rock outcrop (YM300) conditions. They identified three finite fault simulation methods for this additional study (Table 5-4) and the requested computations were made. Results are summarized in Data Package Vols. 1, 1B, and 2. Further, they requested that the stochastic point source/RVT model also be used to develop motions and, consequently, an attenuation model. Synthetics from this model are presented in Data Package Vols. 1 and 2.

5.5 WEIGHTING PROCEDURE

Due to the large volume of estimates required, the experts used numerical weighting of proponent model estimates to develop their initial estimates. The weighting procedure applied two levels of weights. The models were first separated into classes and weights were assigned to each class based on the expert's judgment as to the applicability of each class. Then for each range of magnitude, distance, and fault type, weights were assigned to the models within each class based on the expert's judgment as to the strengths and weaknesses of each model in terms of its applicability to Yucca Mountain. In general, each expert varied

the class and model weights on a case-by-case basis to reflect his or her assessment of the applicability of each model. For example, an expert may have downweighted or eliminated an empirical model outside the magnitude range represented by the data on which the empirical model was based. The weighting procedure produced initial estimates of the median ground motion, aleatory uncertainty, and the epistemic uncertainties on the median and aleatory uncertainty. The proponent models and conversion factors that each expert included in his analysis are summarized in Tables 5-8 and 5-9a through 5-9f.

Plots of the estimates of the ground motion resulting from the weighting procedure were provided to the experts. They reviewed the plots and revised their estimates on a case-by-case basis by either adjusting the weights, setting bounds, or by setting the values of the point estimates themselves. This process was repeated until the experts were satisfied with their estimates. Some experts revised their point estimates only once whereas others made up to five revisions.

5.6 EXPERTS POINT ESTIMATES

The experts estimated median ground motion, aleatory uncertainty, and associated epistemic uncertainties for a matrix of event magnitudes, distances, and faulting styles and at a suite of spectral frequencies. The experts' documentation of their evaluations is included as Appendix F. The information on which these estimates were based includes the many proponent models and combinations of conversion factors. The matrix of point estimates consisted of 51 combinations of parameters, which was judged to adequately define attenuation for the seismic sources considered in the PSHA. The matrix (Tables 5-4, 5-5, and Data Package Vol. 1) covers a range of M_w 5.0 to 8.0, distances from 1 to 160 km, strike-slip and normal faulting, and both hanging wall and footwall for the latter style. These magnitude-distance pairs were selected to provide adequate constraints on the attenuation without burdening the experts. The frequencies were selected to cover the range of interest for all facilities. The range was defined as 0.3 to 20 Hz. As with the magnitude-distance pairs, a minimum number of frequencies needed to adequately describe the spectral shape was used. The frequencies were selected to vary by approximately a factor of two between each frequency. The selected frequencies are: 0.3, 0.5, 1, 2, 5, 10, and 20 Hz plus PGA and PGV.

All proponent data are summarized in Data Package Vols. 1, 1B, and 2. The experts' initial and revised point estimates are contained in a series of Data Package volumes. The proponent data are plotted together with the Revision 1 expert estimates in Data Package Vol. 3 (horizontal) and Vol. 4 (vertical). The experts' Revision 1 estimates are compared in Vol. 5. The proponent data are plotted together with the Revision 2 expert estimates in Data Package Vol. 7 (horizontal) and Vol. 8 (vertical). The experts' Revision 2 estimates are compared in Vol. 9. The final estimates (Revision 3) are compared in Vol. 12.

All point estimates for the 51 cases are plotted in Data Package Vol. 9. Median response spectral values (μ), aleatory variability (σ), epistemic uncertainty on the median (σ_μ), and epistemic uncertainty on the aleatory variability (σ_σ) are plotted for three cases on Figures 5-1 through 5-12. Shown are estimates for a smaller event (M_w 5.8) at moderate distance (20 km) and for a moderate event (M_w 6.5) at close distance (5 km), corresponding to hanging wall sites in normal faulting (Figures 5-1 through 5-8). Estimates for a larger (M_w 7.5), relatively distant (50 km), strike-slip event are also included (Figures 5-9 through 5-12).

The two special faulting scenarios (on parallel multiple faults and on a deep, shallow-dipping detachment surface) were not envisioned when the matrix of cases was developed. In lieu of expanding the case definitions following the Feedback Workshop, the experts evaluated the adjustments to their point estimates needed to model the two scenarios. The adjustments consisted of modifications to the median estimates (μ) and the aleatory uncertainty (σ). Their documentation and the adjustments are also included in Appendix F.

5.7 SITE-SPECIFIC MODIFICATIONS TO THE REFERENCE SITE CONDITION

As discussed in Section 5.3.2, the ground motions were computed for a free-field reference rock outcrop condition with a shear-wave velocity of 1900 m/sec. The shallow velocity at the ground surface above the repository is expected to be less than this reference velocity. For any application, the ground motion estimates for the reference rock outcrop will need to be modified by a transfer function to account for the shallow material. This modification will be needed for both rock and soil sites. Any non-linear response of the tuff or soils will be included in the site response analysis.

5.7.1 Accounting for Updates to Kappa

In addition to accounting for the shallow material in site response analysis, the ground motion evaluations provided by the experts may need to be modified for site-specific application if information from continuing studies of kappa at Yucca Mountain result in modification of the value used. The reference rock outcrop site condition included a median kappa of 0.0186 sec for the material below a shear-wave velocity of 1900 m/sec. This was the best estimate of median kappa for the reference rock outcrop at the time of this study.

The kappa for the reference rock outcrop is an estimate of the median value over the Controlled Area. However, for deriving site-specific ground motions, it may be appropriate to vary kappa over the Controlled Area. The use of the specified kappa of 0.0186 sec does not imply that there is no variability of kappa over the Controlled Area, rather it is the median value. The effect of variability in kappa on the variability of the ground motion has already been accounted for since the experts used estimates of the ground motion variability based on empirical data evaluated from either standard deviations for empirical attenuation relations or modeling uncertainty for numerical simulations. The empirical estimates of ground motion variability account for kappa variability within broad site categories (e.g. rock or deep soil). The variability of the log (kappa) for the strong motion sites within a site category used in either the empirical attenuation relations or validations of the numerical simulations is considered to be similar to the variability of log (kappa) at Yucca Mountain. Thus the effect of kappa variability is already included in the expert's estimates of ground motion standard deviations.

If ongoing studies find that the median kappa for material below 1900 m/sec depth is different from 0.0186 sec, the median attenuation models provided by the experts can be adjusted using scale factors for kappa. Only the median ground motion would be modified.

TABLE 5-1
KEY ISSUES IDENTIFIED AT THE DATA NEEDS WORKSHOP

Issue 1	What are the site response characteristics specific to Yucca Mountain?
Issue 2	What is the range of values of source parameters for earthquakes in this region of the Basin and Range?
Issue 3	What is the explanation for the apparent aseismic slip in the uppermost few kilometers of crust for earthquakes with rupture that reaches the surface?
Issue 4	What is the Yucca Mountain specific ground motion attenuation predicted by various numerical simulation procedures?
Issue 5	What is the basis for apparent discrepancies in the literature regarding regional attenuation (combined effect of Q and geometrical spreading?
Issue 6	What is the explanation for the reported large amplification of motions at Yucca Mountain compared to other NTS sites?

TABLE 5-2
YUCCA MOUNTAIN VELOCITY AND Q PROFILES

LAYER	DEPTH TO TOP (m)	V_S (km/sec)	V_P (km/sec)	DENSITY (g/cm^3)	Q_S	Q_P
1	0	0.6	1.8	1.7	25	80
2	40	1.2	2.5	2.0	40	120
3	80	1.5	2.9	2.3	40	120
4	220	1.9	3.2	2.4	70	150
5	1000	2.1	3.6	2.4	100	200

Source: J. F. Schneider *et al.* (WCFS, written communication, 1996)

TABLE 5-3
MODEL CLASSES AND PROPONENT MODELS

MODEL CLASS	PROPONENT MODELS IN CLASS	USED FOR FINAL ESTIMATES?
Empirical	Abrahamson and Silva (1997)	Yes
	Boore *et al.* (1997) (Vs model)	Yes
	Boore *et al.* (1994) (Class A)	No
	Boore *et al.* (1994) (Class B)	No
	Campbell (1997) (Soft Rock)	Yes
	Campbell (1997) (Hard Rock)	No
	Campbell (1993, 1994)* (Hard Rock)	No
	Campbell (1990, 1994) (Soft Rock)	No
	Campbell (1990) (Soil, Soft Rock)	No
	Idriss (1993) (Rock, Stiff Soil)	No
	Idriss (written comm. 1997) (Rock, Stiff Soil)	Yes
	Joyner and Boore (1988) (Rock)	Yes
	Sadigh *et al.* (1997) (Rock)	Yes
	Sabetta and Pugliese (1996) (Rock)	Yes
	Spudich *et al.* (1996) (Rock)	Yes
	McGarr (1984) (Rock)	Yes
Hybrid Empirical	Campbell (This Study)	Yes
Finite Fault Simulation	Silva (This Study)	Yes
	Somerville (This Study)	Yes
	Zeng and Anderson (This Study)	Yes
Point Source RVT	Silva (This Study)	Yes
Blast	Bennett Model 1 (1995 Scenario Study)	No
	Bennett Model 2 (1995 Scenario Study)	Yes
	Bennett Model 3 (1995 Scenario Study)	No

*Campbell 1994 is Campbell and Borzognia (1994)

TABLE 5-4
POINT ESTIMATE MATRIX

DISTANCE[1]	DEEP FOCUS[2]		SHALLOW FOCUS[2]					
(KM)	M 5.0	5.8	5.0	5.8	6.5	7.0	7.5	8.0
1	SS[3]		SS, HW[3]	SS	SS, HW, FW[3]	SS	SS	
5	SS, HW	HW, FW		HW, FW	SS, HW, FW			
10		SS	SS, HW	SS, HW, FW	SS, HW, FW	SS, HW, FW	SS, HW	
20		HW			SS, HW, FW			
50			SS, HW	SS, HW	SS, HW	SS, HW	SS, HW	SS
100					SS			
160			SS		SS			SS

[1] Horizontal distance from surface expression of fault (up-dip extension).

[2] Shallow focus is centered at 5 km depth; bottom of deep focus rupture is at 14 km depth. See Data Package Vol. 1 for full definitions.

[3] HW refers to hanging wall location in normal faulting, FW to footwall location in normal faulting, and SS to strike-slip faulting.

TABLE 5-5
51 CASE DEFINITIONS FOR POINT ESTIMATES

CASE NO.	MAGNITUDE (M_W)	DEPTH[1]	X-DISTANCE[2] (km)	FAULTING STYLE[3]	R_{RUPT}[4] (km)	R_{JB}[4] (km)	R_{SEIS}[4] (km)
1	5.0	Shallow	1	SS	3.2	1.0	3.2
2	5.0	Shallow	1	HW	3.4	0.9	3.4
3	5.0	Deep	5	SS	11.3	5.0	11.3
4	5.0	Deep	5	HW	10.7	1.1	10.7
5	5.8	Deep	10	SS	12.2	10.0	12.2
6	5.8	Deep	20	HW	17.3	11.9	17.3
7	6.5	Shallow	1	SS	1.0	1.0	3.2
8	6.5	Shallow	1	HW	0.9	0.0	3.1
9	6.5	Shallow	-1	FW	1.0	1.0	4.1
10	6.5	Shallow	5	HW	4.3	0.0	4.4
11	6.5	Shallow	-5	FW	5.0	5.0	7.4
12	6.5	Shallow	50	SS	50.0	50.0	50.1
13	6.5	Shallow	50	HW	44.1	45.3	45.3
14	7.0	Shallow	10	SS	10.0	10.0	10.4
15	7.5	Shallow	50	SS	50.0	50.0	50.1
16	7.5	Shallow	50	HW	44.2	41.9	44.2
17	5.0	Deep	1	SS	10.2	1.0	10.2
18	5.8	Deep	5	HW	7.9	0.0	7.9
19	5.8	Deep	-5	FW	12.4	9.6	12.4
20	5.0	Shallow	10	SS	10.5	10.0	10.5
21	5.0	Shallow	10	HW	8.7	6.1	8.7
22	5.0	Shallow	50	SS	50.1	50.0	50.1
23	5.0	Shallow	50	HW	46.6	46.1	46.6
24	5.0	Shallow	160	SS	160.0	160.0	160.0
25	5.8	Shallow	1	SS	1.8	1.0	3.2
26	5.8	Shallow	5	HW	4.3	0.4	4.4
27	5.8	Shallow	-5	FW	6.4	6.1	7.4
28	5.8	Shallow	10	SS	10.1	10.0	10.4
29	5.8	Shallow	10	HW	8.7	5.4	8.7
30	5.8	Shallow	-10	FW	11.3	11.1	12.1
31	5.8	Shallow	50	SS	50.0	50.0	50.1
32	5.8	Shallow	50	HW	46.1	45.4	46.1
33	6.5	Shallow	5	SS	5.0	5.0	5.8
34	6.5	Shallow	10	SS	10.0	10.0	10.4
35	6.5	Shallow	10	HW	8.7	4.1	8.7
36	6.5	Shallow	-10	FW	10.0	10.0	12.1

TABLE 5-5 (Continued)

CASE NO.	MAGNITUDE (M_W)	DEPTH[1]	X-DISTANCE[2] (km)	FAULTING STYLE[3]	R_{RUPT}[4] (km)	R_{JB}[4] (km)	R_{SEIS}[4] (km)
37	6.5	Shallow	20	SS	20.0	20.0	20.2
38	6.5	Shallow	20	HW	17.3	14.1	17.3
39	6.5	Shallow	-20	FW	20.0	20.0	21.9
40	6.5	Shallow	100	SS	100.0	100.0	100.0
41	6.5	Shallow	160	SS	160.0	160.0	160.0
42	7.0	Shallow	1	SS	1.0	1.0	3.2
43	7.0	Shallow	10	HW	8.7	1.9	8.7
44	7.0	Shallow	-10	FW	10.0	10.0	12.1
45	7.0	Shallow	50	SS	50.0	50.0	50.1
46	7.0	Shallow	50	HW	44.2	41.9	44.2
47	7.5	Shallow	1	SS	1.0	1.0	3.2
48	7.5	Shallow	10	SS	10.0	10.0	10.4
49	7.5	Shallow	10	HW	8.7	1.9	8.7
50	8.0	Shallow	50	SS	50.0	50.0	50.1
51	8.0	Shallow	160	SS	160.0	160.0	160.0

[1] Shallow depth indicates rupture is centered at a depth of 5 km; deep depth indicates the bottom edge of rupture occurs at 14 km depth.

[2] X-distance is the horizontal distance from the surface "trace" of the fault.

[3] HW refers to hanging wall location in normal faulting, FW to footwall location in normal faulting, and SS to strike-slip faulting.

[4] R_{Rupt} is rupture distance, the closest distance from the site to the fault rupture surface; R_{JB} is the Joyner-Boore distance, the closest distance to the surface projection of the rupture surface; R_{Seis} is seismogenic distance, the closest distance to the assumed seismogenic part of the rupture surface, here used as the part of the rupture surface that lies at least 3 km below the ground surface.

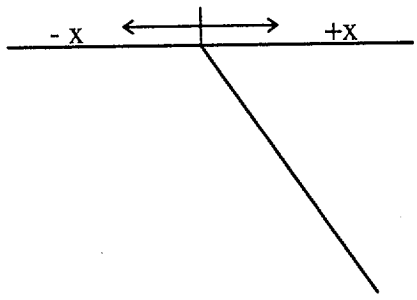

TABLE 5-6a
PROPONENT SOURCE CONVERSION FACTORS

Model #	Model
1	No correction for source
2	Spudich *et al.* (1996) extensional regime scale factors (d<20 km)[1]
3	Spudich *et al.* (1996) extensional regime scale factors (all distances)[1]
4	Campbell point source RVT (this study)[2]
5	Silva point source RVT (this study)[2]
6	Abrahamson and Silva (this study) normal faulting factors (horizontal comp)[3]
7	Abrahamson and Silva (this study) normal faulting factors (vertical comp)[3]
8	1/2 Abrahamson and Silva (this study) normal faulting factors (horizontal comp)[3]
9	1/2 Abrahamson and Silva (this study) normal faulting factors (vertical comp)[3]

[1] Based on the mean residuals of empirical attenuation relations
[2] Based on differences in $\Delta\sigma$ between California and Yucca Mountain (YM)
[3] Based on mean residuals for the Abrahamson and Silva (1997) empirical attenuation relation

TABLE 5-6b
PROPONENT CRUST/SITE CONVERSION FACTORS

Model #	Model
1	No correction for crust/site
2	Campbell point source RVT (this study): CA -> YM Repository outcrop[1]
3	Silva point source RVT (this study): CA -> YM Repository outcrop[1]
4	Silva point source RVT (this study): YM Surface-> YM Repository outcrop[2]
5	Silva finite fault (this study): YM Surface -> YM Repository outcrop[2]

[1] Based on differences in Q, kappa, and velocity profile from California to YM repository outcrop
[2] Based on differences in velocity profile and kappa from YM surface to YM repository outcrop

Note: Conversion factors are completely documented in Data Package Vol. 1.

TABLE 5-7a
PROPONENT VERTICAL/HORIZONTAL RATIO MODELS

Model #	Model
1	No correction
2	Campbell (1997) empirical attenuation
3	Silva (YM point source, this study)
4	Abrahamson & Silva (1997) empirical attenuation
5	Spudich *et al.* (1997) empirical attenuation
6	Sabetta & Pugliese (1996) empirical attenuation
7	Zeng and Anderson finite fault simulation (this study)
8	Somerville finite fault simulation (this study)

TABLE 5-7b
PROPONENT PEAK VELOCITY/SA(F) RATIO MODELS

Model #	Model
1	No correction
2	pgv/pga Campbell (1997) empirical attenuation
3	pgv/pga Silva (YM point source this study)
4	pgv/pga Joyner and Boore (1988) empirical attenuation
5	pgv/pga Sabetta & Pugliese (1996) empirical attenuation
6	pgv/pga Zeng and Anderson finite fault simulation (this study)
7	pgv/pga Somerville finite fault simulation (this study)
8	pgv/ pga Silva finite fault simulation (this study)
9	pgv/Sa(f=1 Hz) Campbell (1997) empirical attenuation
10	pgv/Sa(f=1 Hz) Silva (YM point source this study)
11	pgv/Sa(f=1 Hz) Joyner and Boore (1988) empirical attenuation
12	pgv/Sa(f=1 Hz) Sabetta & Pugliese (1996) empirical attenuation
13	pgv/Sa(f=1 Hz) Zeng and Anderson finite fault (this study)
14	pgv/Sa(f=1 Hz) Somerville finite fault simulation (this study)
15	pgv/Sa(f=1 Hz) Silva finite fault simulation (this study)

Note: Models are completely documented in Data Package Vol. 1.

TABLE 5-7c
PROPONENT HORIZONTAL COMPONENT-TO-COMPONENT VARIABILITY MODELS

Model #	Model
1	No correction
2	Boore *et al.* (1997) empirical attenuation
3	Spudich *et al.* (1996) empirical attenuation

TABLE 5-7d
PROPONENT 20 HZ SPECTRAL ACCELERATION INTERPOLATION MODELS

Model #	Model
1	No correction
2	Average coefficients for pga and 10 Hz
3	log-log interpolation between 33 Hz (pga) and 10 Hz
4	Boore scaling (this study)

Note: Models are completely documented in Data Package Vol. 1.

TABLE 5-8
PROPONENT MODELS USED BY EACH EXPERT

Model Class	Proponent Models In Class	Anderson	Boore	Campbell	McGarr	Silva	Somerville	Walck
Empirical	Abrahamson and Silva (1997)	Yes	Yes	Yes[1]	Yes	Yes	Yes	Yes
	Boore *et al.* (1997) (Vs model)	Yes	Yes	Yes[1]	Yes	Yes	No	Yes
	Campbell (1997) (Soft Rock)	Yes	Yes	Yes[1]	Yes	Yes	Yes	Yes
	Idriss (University of California, Davis, written communication, 1997) (Rock, Stiff Soil)	Yes	Yes	Yes[1]	Yes	No	Yes	Yes
	Joyner and Boore (1988) (Rock)	No	Yes	Yes[1]	Yes	Yes	Yes	Yes
	McGarr (1984) (Rock)	No	Yes	No	Yes	No	No	Yes
	Sadigh *et al.* (1997) (Rock)	Yes	Yes	Yes[1]	Yes	Yes	Yes	Yes
	Sabetta and Pugliese (1996) (Rock)	Yes	No	No	No	No	No	Yes
	Spudich *et al.* (1996) (Rock)	Yes	Yes	Yes[1]	Yes	No	Yes	Yes
Hybrid Empirical	Campbell (This Study)	No	No	Yes	No	No	No	No
Finite Fault Simulation	Silva Case A (This Study)	Yes	Yes	Yes	Yes	Yes	Yes	Yes
	Silva Case B (This Study)	No	No	No	No	No	No	No
	Somerville (This Study)	Yes	Yes	Yes	Yes	Yes	Yes	Yes
	Zeng and Anderson Case A (This Study)	Yes	Yes	Yes	Yes	Yes	Yes	Yes
	Zeng and Anderson Case B (This Study)	Yes	No	No	No	No	No	No
	Zeng and Anderson Case C (This Study)	Yes	No	No	No	No	No	No
Point Source RVT	Silva (This Study)	Yes	Yes	Yes	Yes	Yes	Yes	Yes
Blast	Bennett Model 2 (1995 Scenario Study)	No	No	No	No	No	Yes	Yes

[1]These empirical models are incorporated in the Hybrid Empirical model.

TABLE 5-9a
SOURCE CONVERSION FACTORS USED BY EACH EXPERT

CONVERSION FACTOR	ANDERSON	BOORE	CAMPBELL	MCGARR	SILVA	SOMERVILLE	WALCK
Spudich (d < 20 km)	No	No	No	No	No	No	No
Spudich (all distances)	No	No	No	No	No	No	No
Campbell (point source RVT)	No	No	Yes	No	No	No	Yes
Silva (point source RVT)	No	Yes	No	Yes	No	No	Yes
Abrahamson & Silva (horizontal)	No	No	No	No	No	Yes	No
Abrahamson & Silva (vertical)	No	No	No	No	No	No	No
1/2 Abrahamson & Silva (horizontal)	No	No	No	No	Yes	No	No
1/2 Abrahamson & Silva (vertical)	No	No	No	No	Yes	No	No

TABLE 5-9b
CRUST/SITE CONVERSION FACTORS USED BY EACH EXPERT

CONVERSION FACTOR	ANDERSON	BOORE	CAMPBELL	MCGARR	SILVA	SOMERVILLE	WALCK
Campbell (point source) CA -> YM outcrop	Yes	Yes	Yes	Yes	Yes	Yes	Yes
Silva (point source) CA -> YM outcrop	Yes	No	No	No	No	No	No
Silva (point source) YM surface -> YM outcrop	Yes	No	No	No	No	No	No
Silva (finite fault) YM surface -> YM outcrop	Yes	No	No	No	No	No	No

TABLE 5-9c
VERTICAL/HORIZONTAL RATIO MODELS USED BY EACH EXPERT

RATIO MODEL	ANDERSON	BOORE	CAMPBELL	MCGARR	SILVA	SOMERVILLE	WALCK
Campbell (1997) empirical	No	No	No	No	No	No	Yes
Silva (YM point source)	No	No	Yes	Yes	Yes	No	Yes
Abrahamson and Silva (1997) empirical	No	No	No	No	No	No	No
Spudich *et al.* (1997) empirical	No	No	No	No	No	No	No
Sabetta and Pugliese (1996) empirical	No	No	No	No	No	No	No
Zeng and Anderson finite fault	No	No	No	No	No	No	No
Somerville finite fault	No	No	No	No	No	No	No

TABLE 5-9d
PEAK VELOCITY/SA(F) RATIO MODELS USED BY EACH EXPERT

RATIO MODEL	ANDERSON	BOORE	CAMPBELL	MCGARR	SILVA	SOMERVILLE	WALCK
pgv/pga Campbell (1997) empirical	No	No	No	No	No	No	No
pgv/pga Silva (YM point source)	No	No	No	No	Yes	No	No
pgv/pga Joyner and Boore (1988) empirical	No	No	No	No	No	No	No
pgv/pga Sabetta and Pugliese (1996) empirical	No	No	No	No	No	No	No
pgv/pga Zeng and Anderson finite fault	No	No	No	No	No	No	No
pgv/pga Somerville finite fault	No	No	No	No	No	No	No
pgv/pga Silva finite fault	No	No	No	No	No	No	No
pgv/Sa (f=1Hz) Campbell (1997) empirical	No	No	No	No	No	No	No
pgv/Sa (f=1Hz) Silva (YM point source)	No	Yes	No	No	No	No	No
pgv/Sa (f=1Hz) Joyner and Boore (1988) empirical	No	No	No	No	No	No	No
pgv/Sa (f=1Hz) Sabetta and Pugliese (1996) empirical	No	No	No	No	No	No	No
pgv/Sa (f=1Hz) Zeng and Anderson finite fault	No	No	No	No	No	No	No
pgv/Sa (f=1Hz) Somerville finite fault	No	No	No	No	No	No	No
pgv/Sa (f=1Hz) Silva finite fault	No	No	No	No	No	No	No

TABLE 5-9e
HORIZONTAL COMPONENT-TO-COMPONENT VARIABILITY MODELS USED BY EACH EXPERT

VARIABILITY MODEL	ANDERSON	BOORE	CAMPBELL	MCGARR	SILVA	SOMERVILLE	WALCK
Boore *et al.* (1997) empirical	Yes	Yes	Yes	Yes	Yes	Yes	Yes
Spudich *et al.* (1996) empirical	No	No	No	No	No	No	No

TABLE 5-9f
20 HZ SPECTRAL ACCELERATION INTERPOLATION MODELS USED BY EACH EXPERT

INTERPOLATION MODEL	ANDERSON	BOORE	CAMPBELL	MCGARR	SILVA	SOMERVILLE	WALCK
Average coefficients for pga and 10 Hz	Yes	No	No	Yes	No	No	No
log-log interpolation between 33 Hz (pga) and 10 Hz	No	No	Yes	No	No	No	Yes
Boore scaling (Appendix F)	No	Yes	No	No	Yes	No	Yes

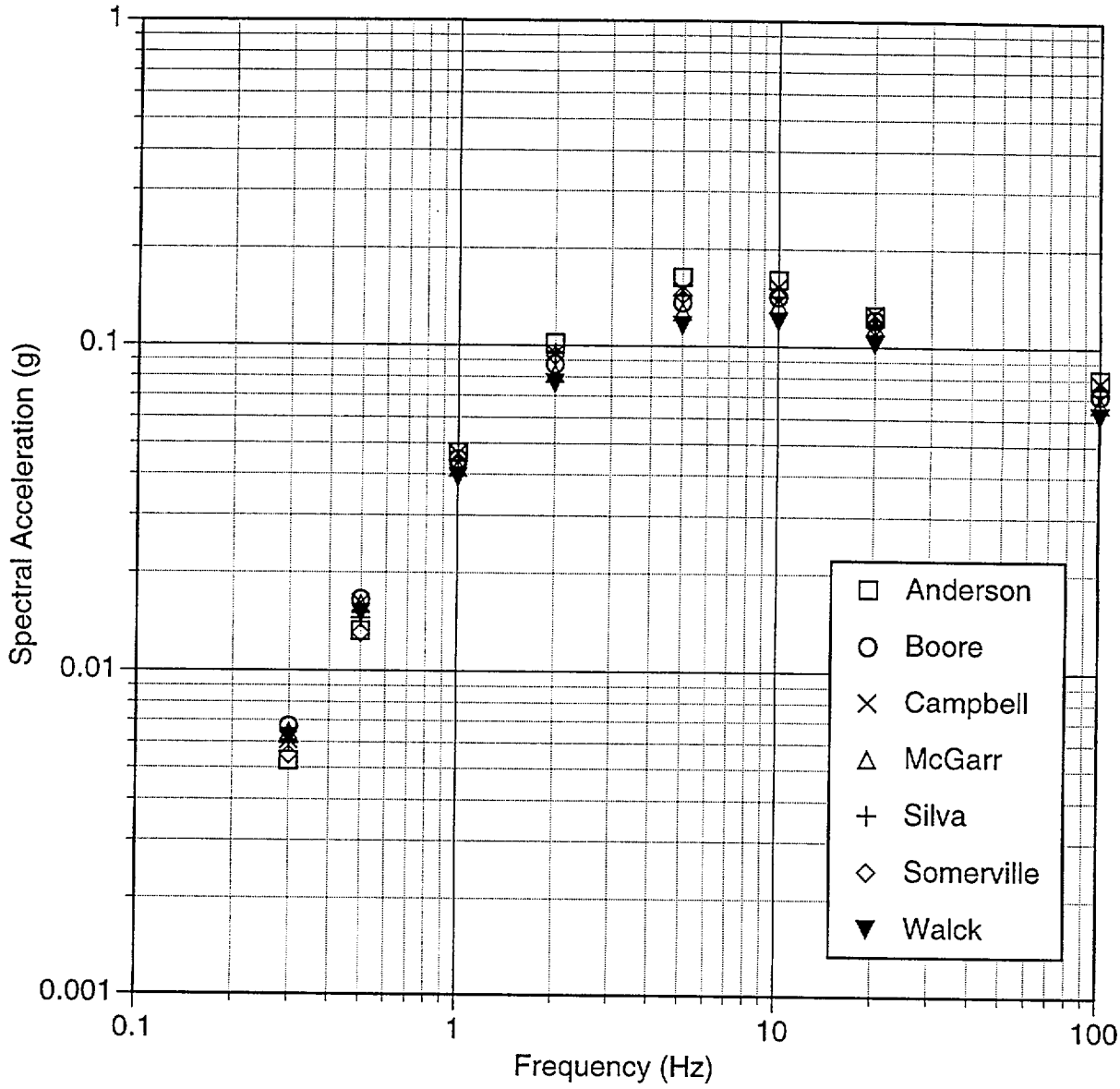

Figure 5-1 Median horizontal ground motion estimates for a M_W 5.8 earthquake at 17 km (rupture distance), normal faulting, hanging wall (Case 6)

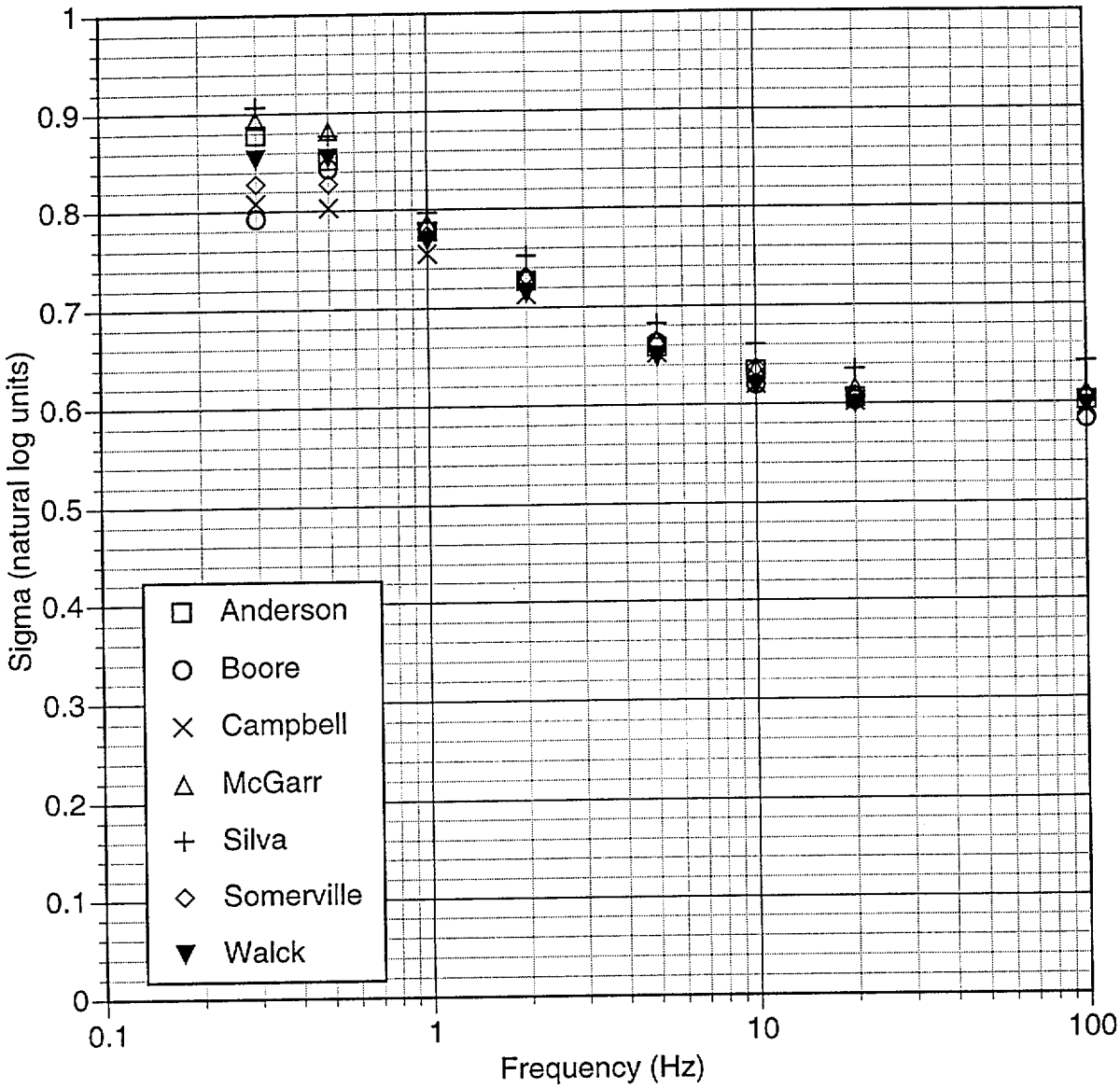

Figure 5-2 Aleatory variability in horizontal ground motion estimates for a M_W 5.8 earthquake at 17 km (rupture distance), normal faulting, hanging wall (Case 6)

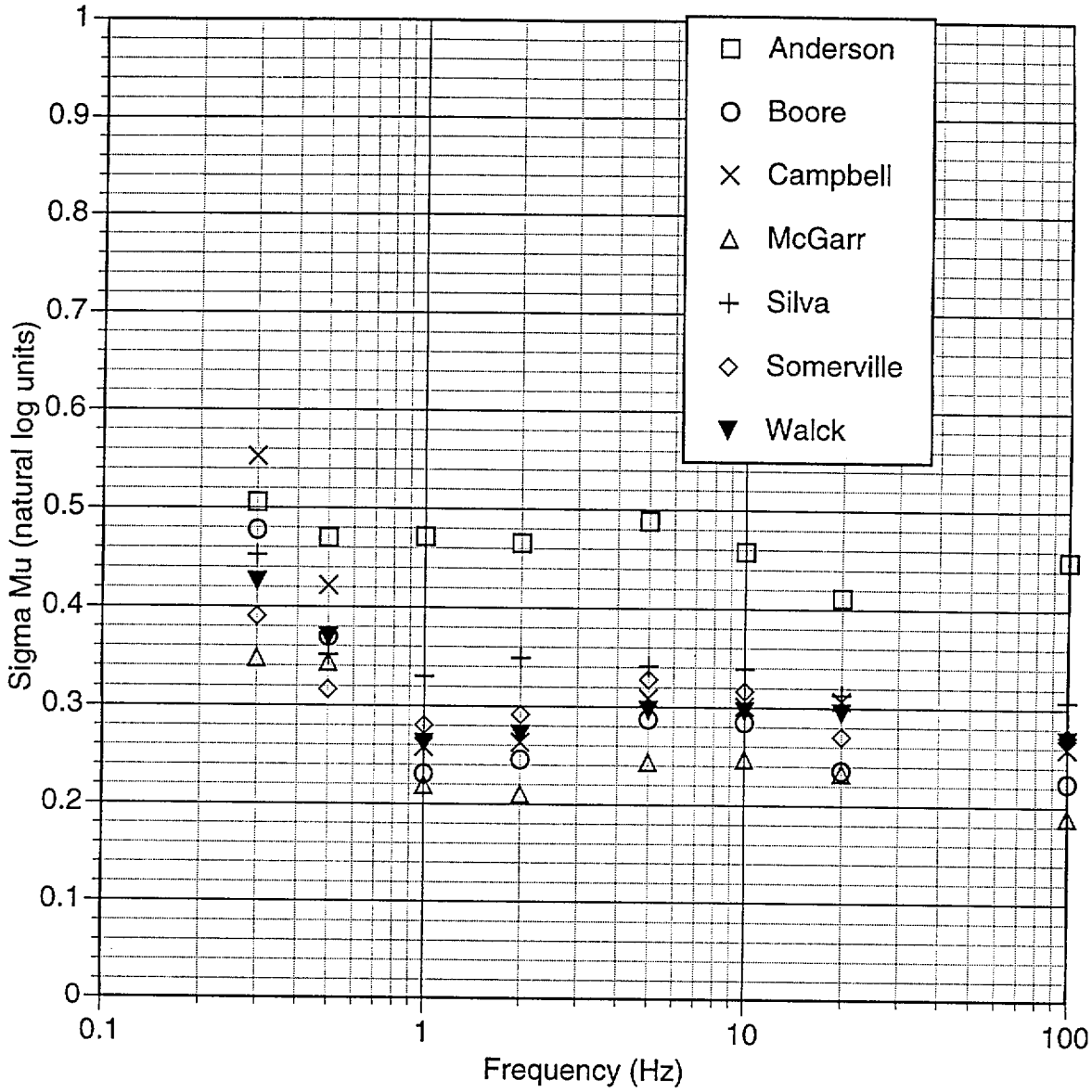

Figure 5-3 Epistemic uncertainty on the median horizontal ground motion estimates for a M_W 5.8 earthquake at 17 km (rupture distance), normal faulting, hanging wall (Case 6)

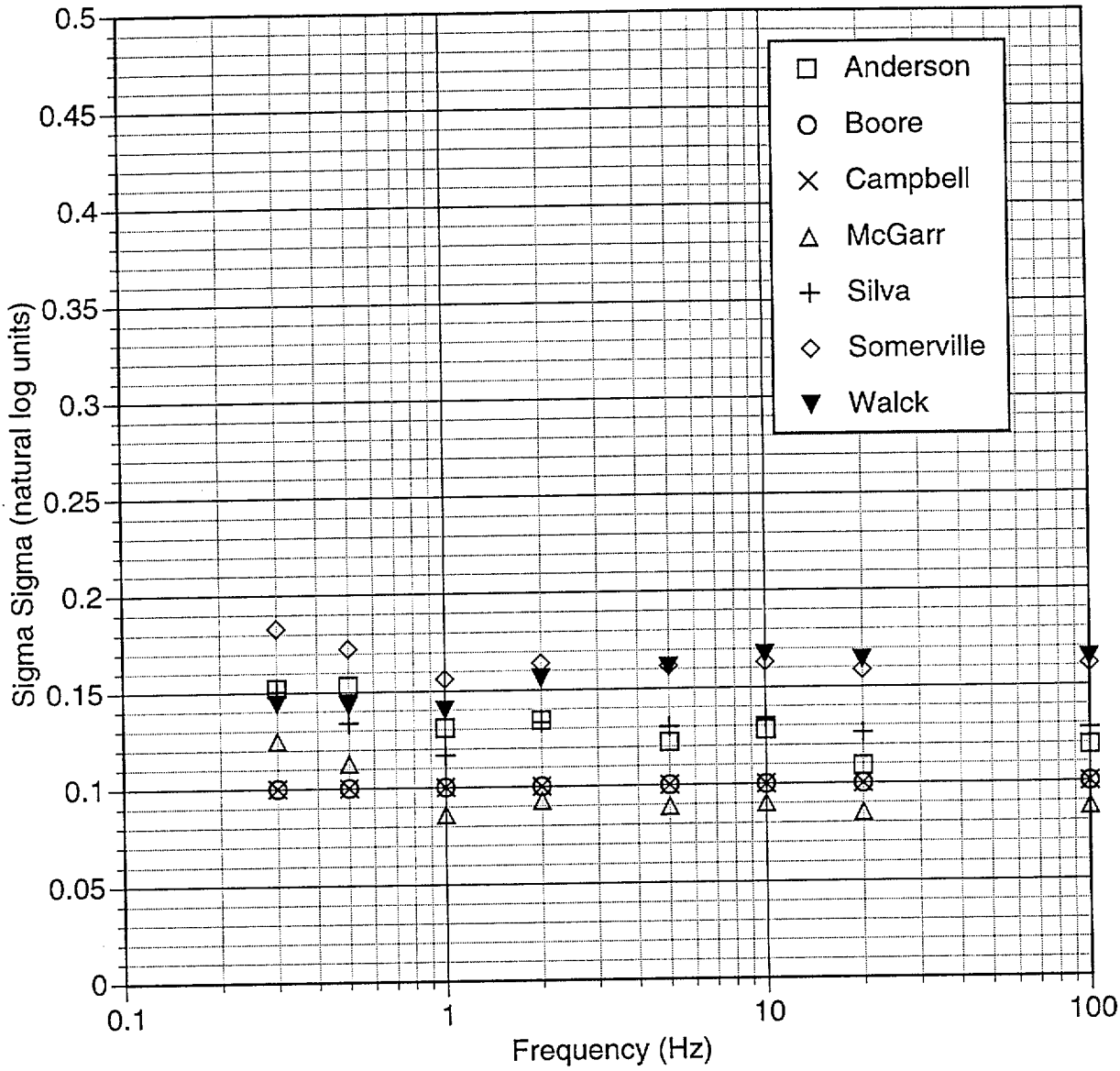

Figure 5-4 Epistemic uncertainty on the aleatory variability of horizontal ground motion estimates for a M_W 5.8 earthquake at 17 km (rupture distance), normal faulting, hanging wall (Case 6)

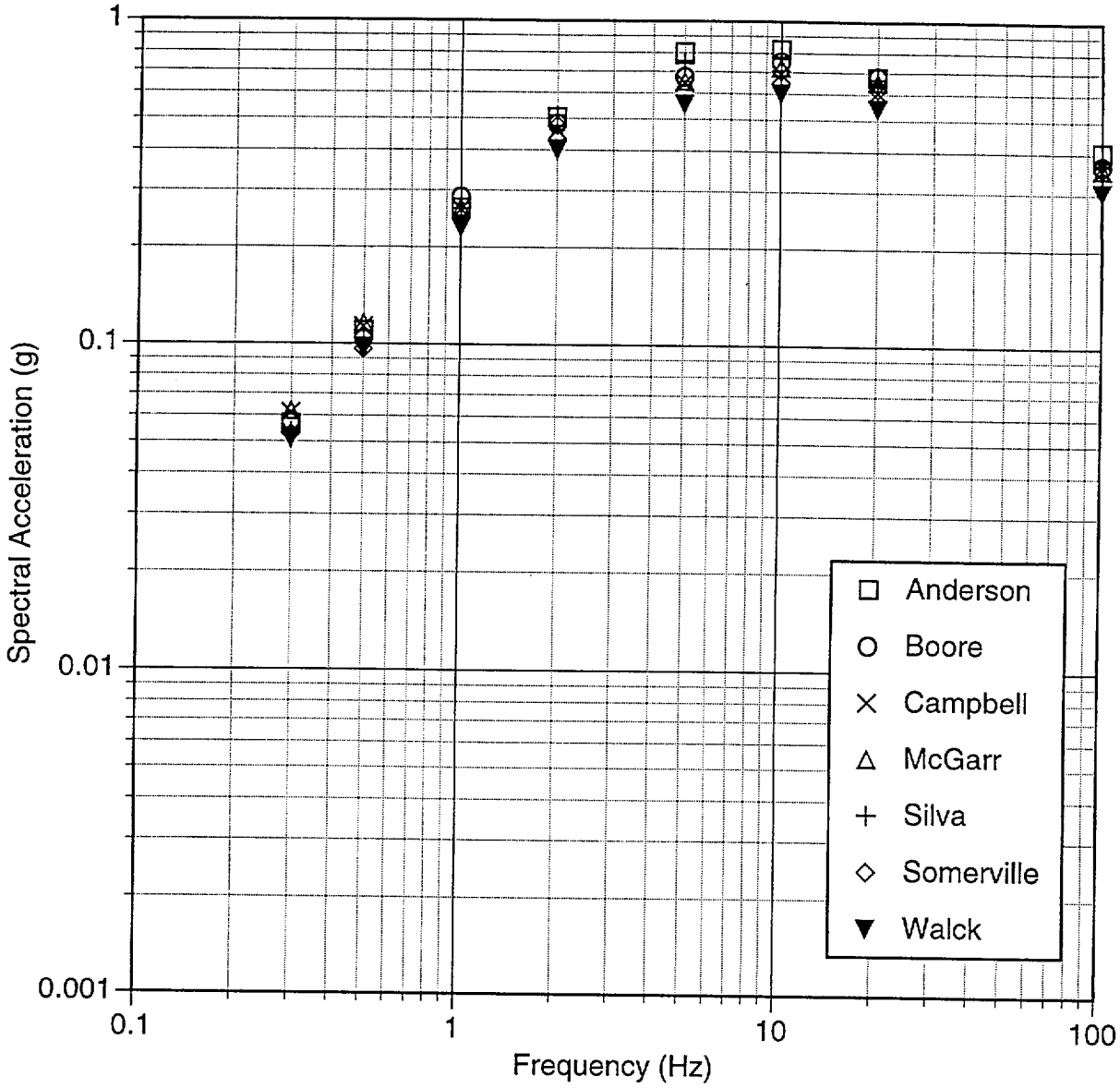

Figure 5-5 Median horizontal ground motion estimates for a M_W 6.5 earthquake at 4 km (rupture distance), normal faulting, hanging wall (Case 10)

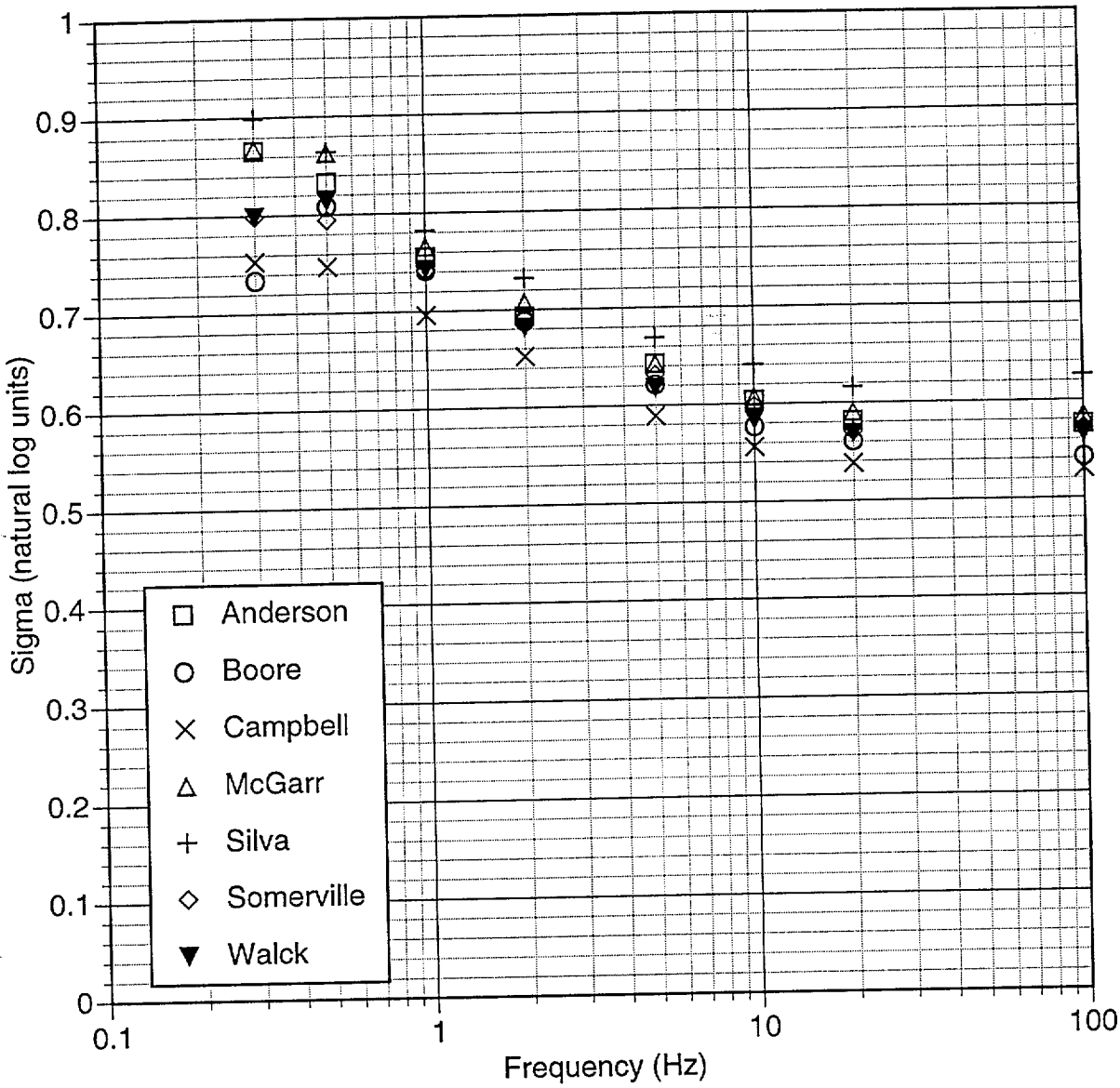

Figure 5-6 Aleatory variability in horizontal ground motion estimates for a M_W 6.5 earthquake at 4 km (rupture distance), normal faulting, hanging wall (Case 10)

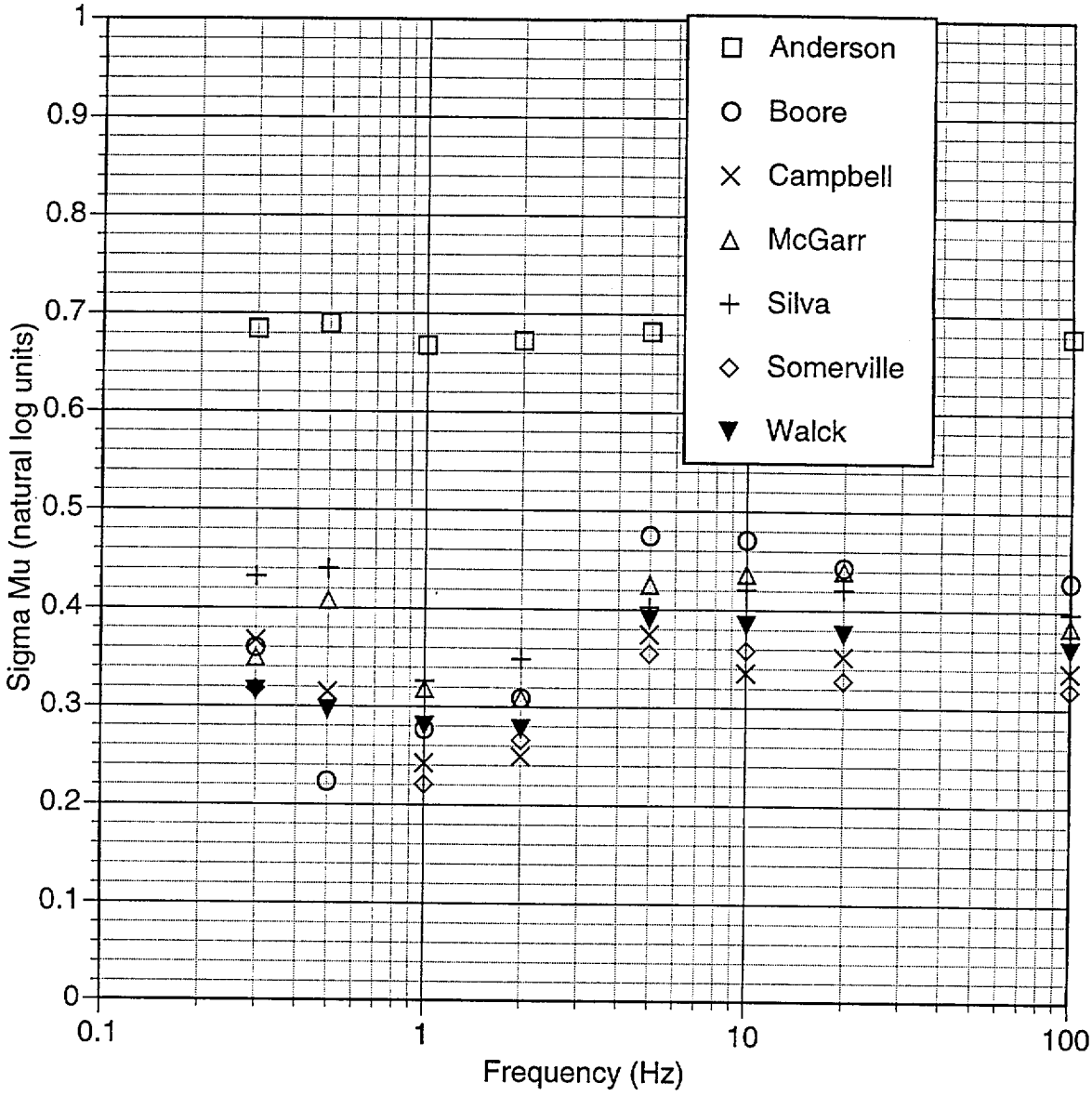

Figure 5-7 Epistemic uncertainty on the median horizontal ground motion estimates for a Mw 6.5 earthquake at 4 km (rupture distance), normal faulting, hanging wall (Case 10)

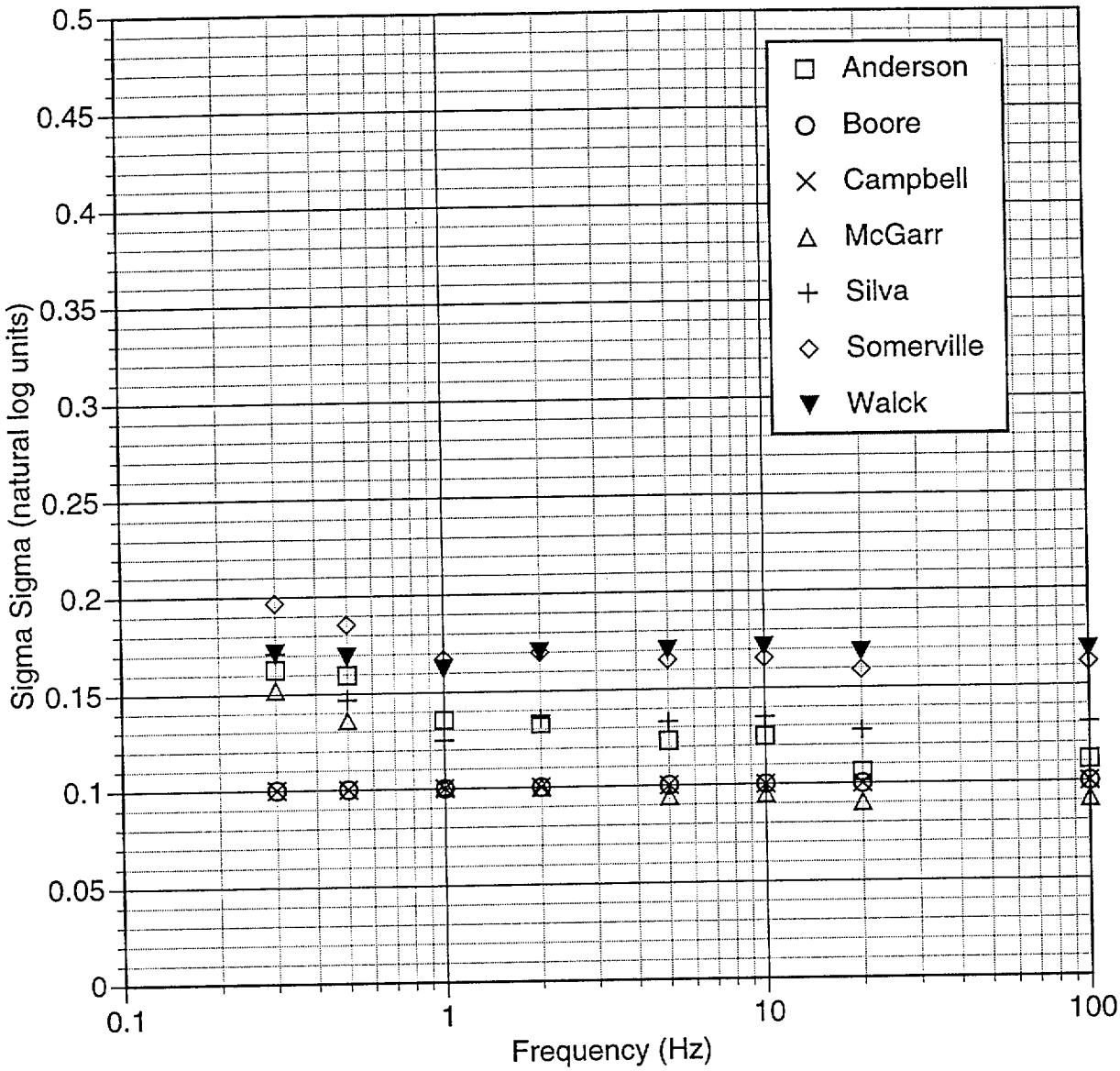

Figure 5-8 Epistemic uncertainty on the aleatory variability of horizontal ground motion estimates for a Mw 6.5 earthquake at 4 km (rupture distance), normal faulting, hanging wall (Case 10)

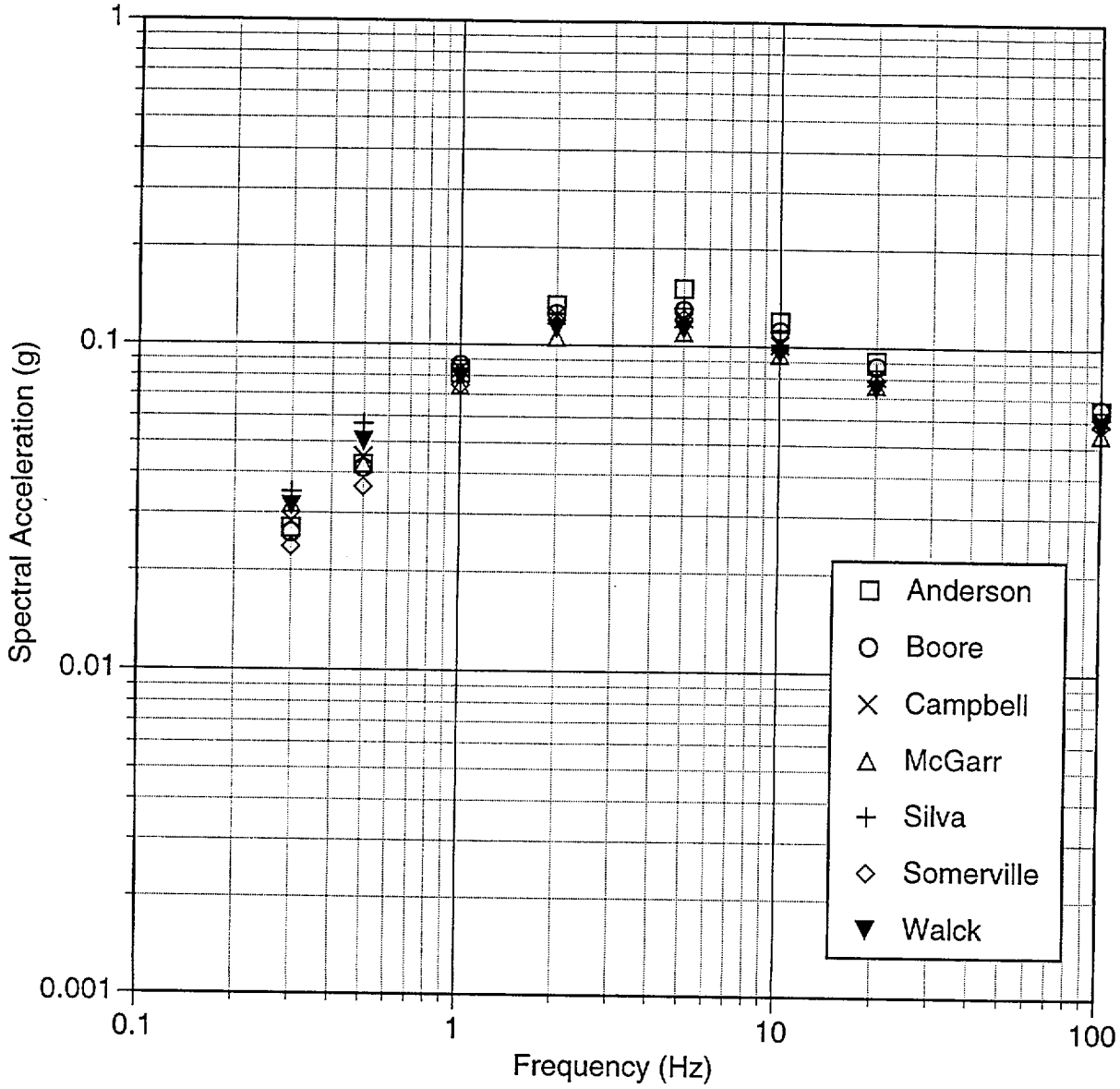

Figure 5-9 Median horizontal ground motion estimates for a M_W 7.5 earthquake at 50 km (rupture distance) strike-slip faulting (Case 15)

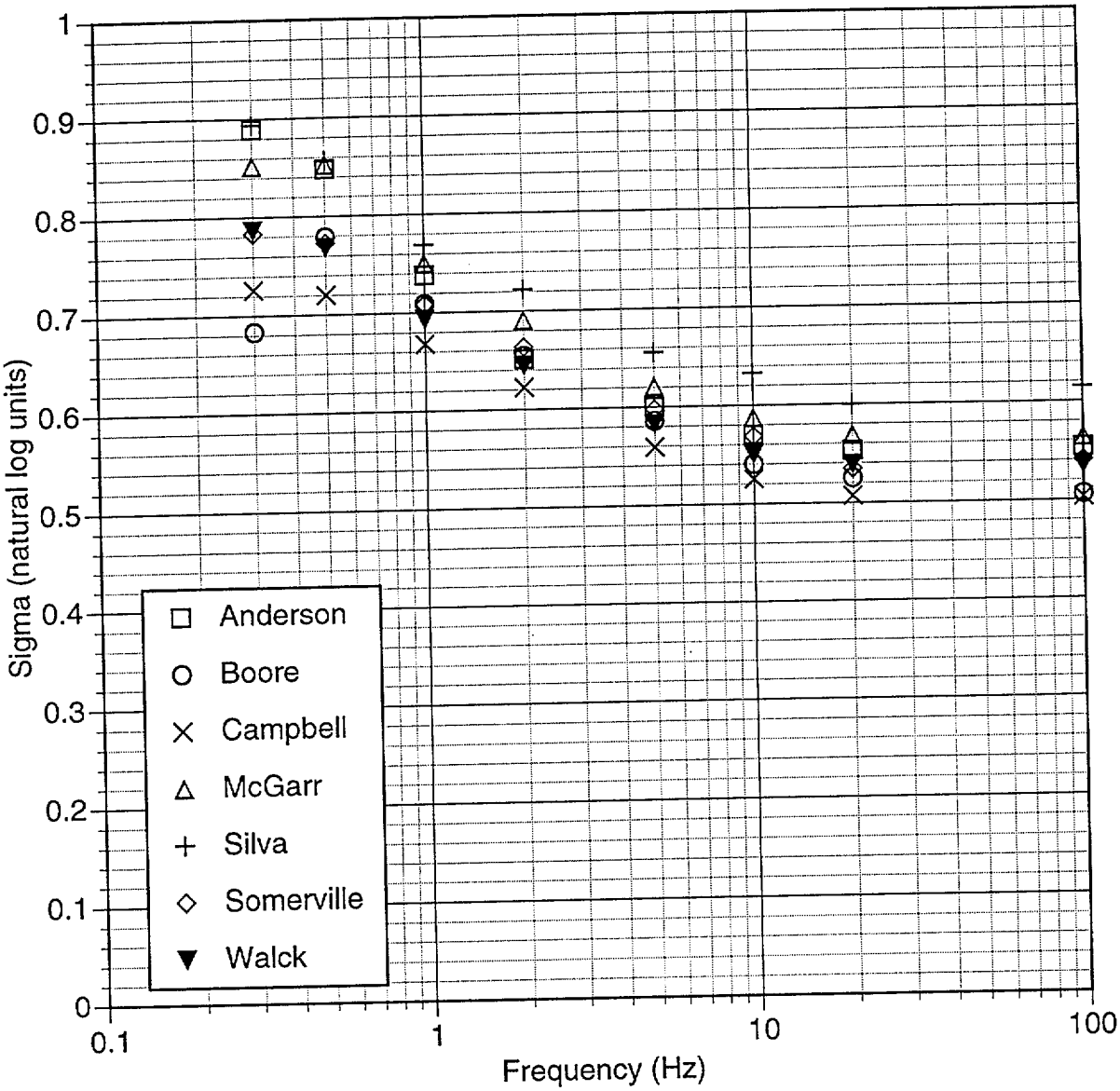

Figure 5-10 Aleatory variability in horizontal ground motion estimates for a Mw 7.5 earthquake at 50 km (rupture distance), strike-slip faulting (Case 15)

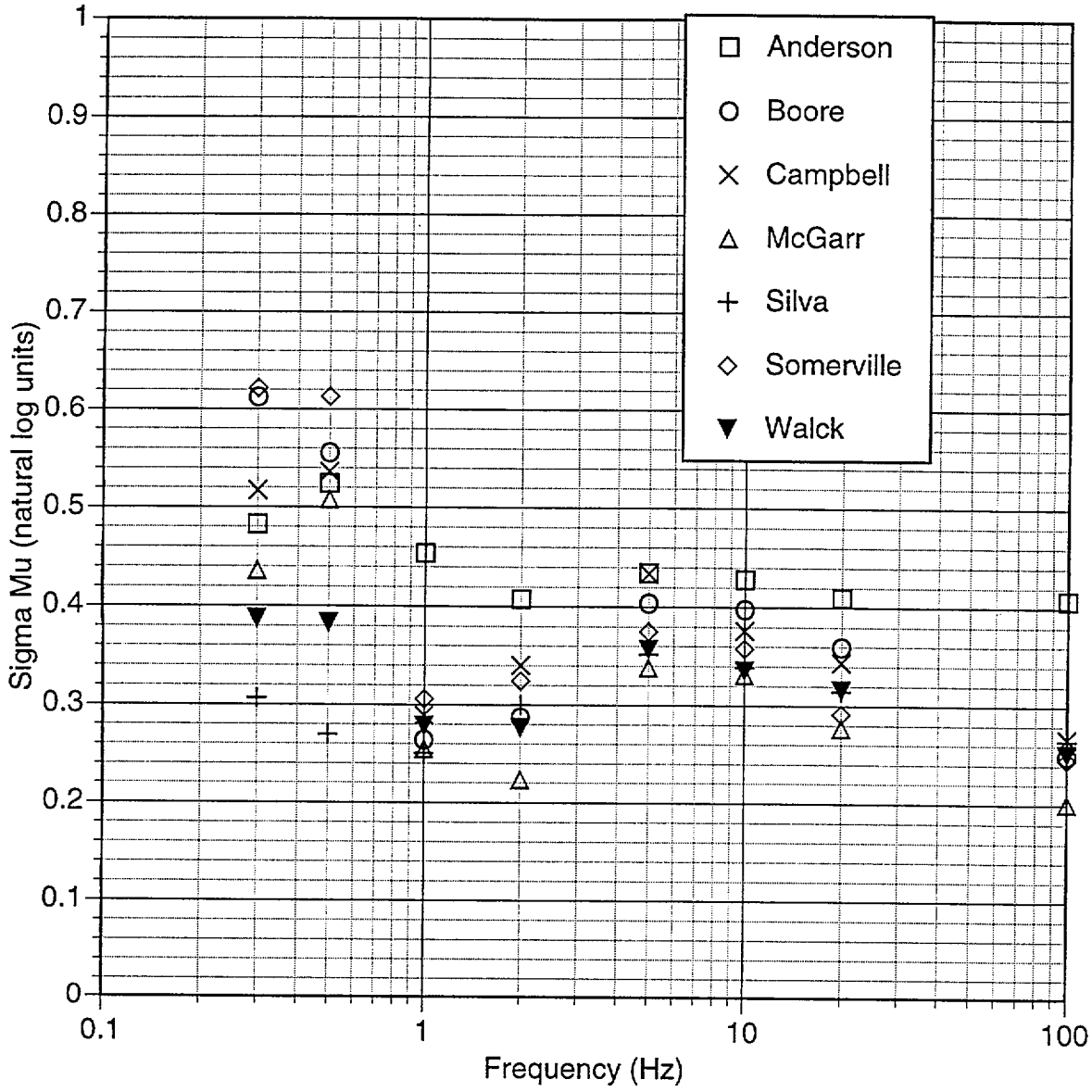

Figure 5-11 Epistemic uncertainty on the median horizontal ground motion estimates for a M_W 7.5 earthquake at 50 km (rupture distance), strike-slip faulting (Case 15)

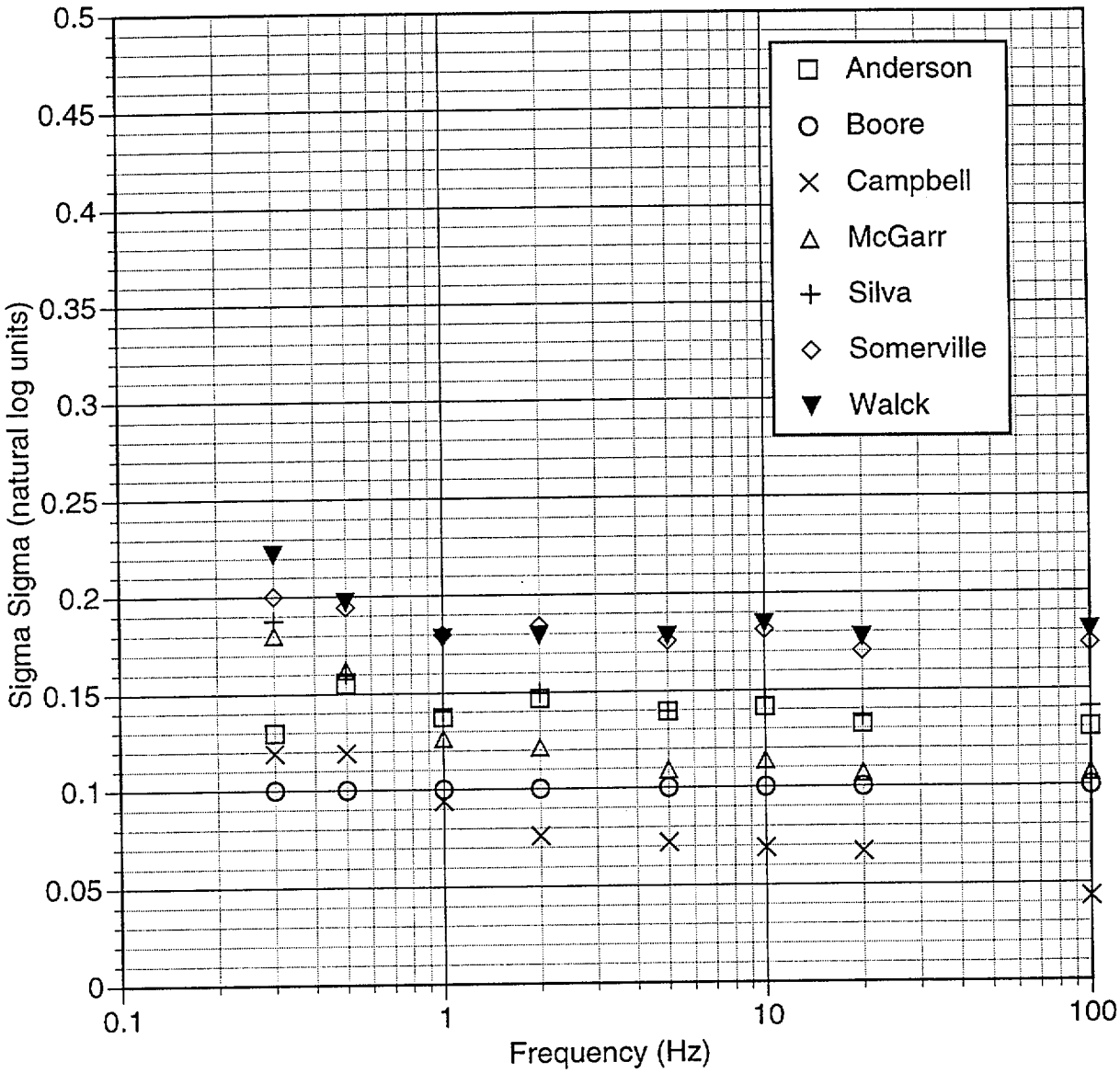

Figure 5-12 Epistemic uncertainty on the aleatory variability of horizontal ground motion estimates for a M_W 7.5 earthquake at 50 km (rupture distance), strike-slip faulting (Case 15)

6.0
GROUND MOTION ATTENUATION RELATIONS

To facilitate the use of the ground motion models in the hazard calculation, the experts' point estimates were parameterized by attenuation relations. The regression analysis to develop the attenuation relations was performed by the GM Facilitation Team. Each expert selected the distance measure used in the regression analyses for his/her point estimates. They chose whether the footwall and hanging wall point estimates were regressed together, resulting in a single normal faulting attenuation equation, or separately, yielding separate models for sites on the hanging wall and footwall. In addition, the experts could constrain the degree of magnitude saturation at close distances.

The experts reviewed the resulting regression models and either approved the models or made revisions to their point estimates or to the functional form used in the regression. This process was repeated until each expert was satisfied with the resulting models and is documented in Data Package Vols. 3 through 12. The final regression results are presented in this chapter.

6.1 REGRESSION MODEL FORM

Based on an examination of the experts' point estimates and with feedback from the experts, general functional forms were selected. Different functional forms were used for the median estimates, the aleatory variability, and the epistemic uncertainties.

The independent variables used in all regressions correspond to:

- M_w Moment magnitude
- R Distance (experts' selected distance measure in km)
- F Mechanism flag (0=strike-slip, 1 = normal)
- W_H Hanging wall flag (1=hanging wall, 0 = not hanging wall)
- W_F Footwall flag (1=footwall, 0=not footwall)

The predicted values for μ are in natural logarithm of g for spectral acceleration and natural logarithm of cm/sec for peak velocity. The σ_{al}, σ_{μ}, and σ_{σ} are all in natural log units. All of

the experts except for Campbell selected "rupture distance," defined as the closest distance from the site to the fault rupture as the distance metric. Campbell selected "seismogenic distance," the closest distance from the site to the assumed seismogenic part of the rupture (herein used as the part of the rupture that is at a depth of least 3 km)

The adopted general forms for the regression model are given below. As noted above, in some instances the experts added constraints to these general forms. These constraints are summarized in Table 6-1.

Median (μ):

For $M < m_1$,

$$\mu = a_1 + a_2(M - m_1) + a_6(8.5 - M)^2 + \left[a_3 + a_5(M - m_1)\right] \cdot \ln\sqrt{R^2 + a_8^2} + a_7 F + a_9 W_H f_1(M,R) + a_{10} W_F f_1(M,R) \quad (6\text{-}1a)$$

For $M \geq m_1$,

$$\mu = a_1 + a_4(M - m_1) + a_6(8.5 - M)^2 + \left[a_3 + a_5(M - m_1)\right] \cdot \ln\sqrt{R^2 + a_8^2} + a_7 F + a_9 W_H f_1(M,R) + a_{10} W_F f_1(M,R) \quad (6\text{-}1b)$$

in which

$$f_1(M,R) = \begin{cases} 0 & \text{for } R \leq x_1 \\ \dfrac{R - x_1}{x_2 - x_1} & x_1 < R < x_2 \\ 1 & x_2 \leq R \leq x_3 \\ \dfrac{x_4 - R}{x_4 - x_3} & x_3 < R < x_4 \\ 0 & \text{for } R \geq x_4 \end{cases} \cdot \begin{cases} 0 & \text{for } M < a_{11} \\ \dfrac{M - a_{11}}{a_{12} - a_{11}} & \text{for } a_{11} \leq M \leq a_{12} \\ 1 & \text{for } M > a_{12} \end{cases} \quad (6\text{-}2)$$

Aleatory Variability (σ_{al}):

For $M < b_4$,

$$\sigma_{al} = b_1 + b_2(M - b_4) \quad (6\text{-}3a)$$

For $M \geq b_4$,

$$\sigma_{al} = b_1 \tag{6-3b}$$

Epistemic Uncertainty in the Median (σ_μ):

$$\sigma_\mu = c_1 + c_2(M - c_6) + c_3 \ln(R+1) + c_4[\ln(R+1)]^2 + c_5 F \tag{6-4}$$

Epistemic Uncertainty in the Aleatory Variability (σ_σ):

For $M < d_4$, $$\sigma_\sigma = d_1 + d_2(M - d_4) \tag{6-5a}$$

For $M \geq d_4$, $$\sigma_\sigma = d_1 \tag{6-5b}$$

6.2 REGRESSION RESULTS

The following values are used for all models and for all periods:

$x_1 = 3$

$x_2 = 8$

$x_3 = 20$

$x_4 = 30$

$m_1 = 6.25$

Coefficients a_j, b_j, c_j, and d_j are listed in Appendix I. The process of fitting the experts' point estimates with a smooth equation leads to additional aleatory variability due to the misfit between the equation and the point estimates. To account for this additional variability, the total aleatory variability is given by the combination of the experts' estimate of the aleatory variability (parameterized by the regression equation as σ_{al}) and the standard deviation of the fit to the median ground motion (listed as Sigma Fit in the Appendix I tables). The total aleatory variability is given by

$$\sigma_{total} = \sqrt{\sigma_{fit}^2 + \sigma_{al}^2} \tag{6-6}$$

Comparisons of the regression model fits and the experts' point estimates are contained in Data Package Vols. 11A through 11G. Examples of the resulting attenuation relations for the

seven experts are compared for peak ground acceleration and for 1 Hz spectral acceleration for two faulting cases: a M_w 6.5 normal earthquake on the hanging wall and a M_w 7.5 strike-slip earthquake. The models for the horizontal component median ground motions are compared on Figures 6-1 through 6-4. These figures show that the range in the median ground motions from these models is generally less than a factor of 1.5. The models for the horizontal component aleatory variability are compared on Figures 6-5 and 6-6 for peak acceleration and spectral acceleration at a period of 1.0 sec. The range in the aleatory variability in the models is generally less than 0.1 natural log unit. The epistemic variability in the median horizontal ground motion is compared on Figures 6-7 to 6-10. The range of the models is generally less than 0.1 natural log units except for Anderson's model, which has much larger values due to his larger estimates of the epistemic uncertainty for the proponent model median estimates. Finally, the epistemic uncertainty in the aleatory variability is shown on Figures` 6-11 to 6-12. The range of these models is generally less than 0.1 natural log unit.

A corresponding set of plots of the models for the vertical component are shown on Figures 613 through 6-24. The vertical median ground motion models tend to be more variable between experts than the horizontal models. This larger variability is due to having fewer vertical proponent models available and much less validation for the numerical simulations. The experts individual estimates of the epistemic uncertainty also tend to be larger for the vertical component than for the horizontal component.

6.3 HYPOCENTRAL-BASED MODELS

The seismic source characterization also includes areal source zones, which are treated as point sources in the hazard calculation. Since the GM expert point estimates and the attenuation relations were developed for closest distance, a conversion factor is needed to make the model applicable to hypocentral distance, which is the relevant distance for areal sources.

The use of hypocentral distance rather than closest distance affects both the median ground motion and the aleatory variability since for a given hypocentral distance, there is a range of possible closest distances. Rather than developing independent attenuation models based on

hypocentral distance, the GM Facilitation Team evaluated the relation between hypocentral distance and rupture distance based on an assumed distribution of hypocenters on the fault plane. Note that this distribution is not the same as the distribution of hypocenters with depth in an earthquake catalog, but rather the distribution of the hypocenters on the rupture plane for a specific rupture dimension. With this relation between hypocentral distance and rupture distance, the uncertainty of the ground motion due to uncertainty in the closest-distance can be directly propagated using standard methods for propagation of errors (see Appendix J).

The adjustments using hypocentral distance are presented as a mapping of the mean rupture distance (as a function of the hypocentral distance and magnitude) and additional aleatory variability. The additional epistemic uncertainty in the median ground motion and aleatory variability due to the uncertainty in the distribution of hypocenters on the rupture plane are also estimated, but they are negligible. The development of these correction factors is given in Appendix J. Here, just the final models are presented.

For a given hypocentral distance H (in km) and magnitude M, the mean rupture distance R (in km) is given by

$$R = \begin{cases} H\left(1 + e_1 + e_2(M-5)\right) + H^2\left(e_3 + e_4(M-5)\right) & \text{for } H \le 30 \text{ km} \\ H + 30\left(e_1 + e_2(M-5)\right) + 900\left(e_3 + e_4(M-5)\right) & \text{for } H > 30 \text{ km} \end{cases} \tag{6-7}$$

in which the estimated coefficients are listed in Table 6-2.

The aleatory variability of the rupture distance as a function of the hypocentral distance and M is given by:

$$\sigma_R(H,M) = \sqrt{\left[\left(e_5 + e_6(M-5)\right)\tanh\left\{H\left(e_7 + e_8(M-5)\right)\right\}\right]^2 + 1.2^2} \tag{6-8}$$

with the coefficients listed in Table 6-2.

The additional aleatory variability in ground motion due to the use of hypocentral distance is given by

$$\sigma_{Hypo} = \left|\frac{\partial Y}{\partial R}\right| \sigma_R(H,M) \tag{6-9}$$

in which Y is the natural log of the ground motion parameter of interest. Ignoring hanging wall and footwall effects, then

$$\frac{\partial Y}{\partial R} = \left(a_3 + a_5(M - 6.25)\right)\frac{R(H,M)}{R^2(H,M) + a_8^2} \tag{6-10}$$

in which a_3, a_5, and a_8 are coefficients in the regression equations for each expert (Appendix I tables). This additional aleatory variability is combined with the total aleatory variability for the experts' models (Equation 6-6) to give the total aleatory variability of ground motion for the hypocentral model:

$$\sigma_{total}^{hypo} = \sqrt{\sigma_{hypo}^2 + \sigma_{total}^2} \tag{6-11}$$

The additional epistemic uncertainties in ground motion for a hypocentral distance model are computed in Appendix J. They are small enough to be neglected.

6.4 SPECIAL CASES

The experts developed scaling rules to apply their ground motion models to the two special cases discussed in Chapter 5.0: rupture of multiple (parallel) faults, and a shallow detachment fault.

6.4.1 Multiple Rupture Case

In the hazard calculation, the multiple rupture case is simplified and approximated by summing the moment of all of the ruptures and using the closest distance of any of the ruptures to the site. The resulting ground motion estimates must be adjusted, however, because using the total moment at the closest distance is not conservative compared to the case of multiple faults rupturing near the site. Multiple ruptures with small magnitude events can produce constructive interference that will result in larger ground motion than would be predicted for a single larger-magnitude event. Therefore, the GM Facilitation Team developed scale factors for the calculated ground motions, based on rules given by each of the experts.

Most of the experts used the concept of random vibration theory to predict the effect of multiple ruptures on ground motion. The main issue is whether the ground motions from the

multiple ruptures are correlated or are independent. In general, the experts considered the ground motions to be independent.

The scale factors for multiple ruptures are the ratios of ground motion as predicted by the experts' rules to the ground motion predicted from the experts' attenuation relations, using the full moment at the closest distance. Each expert's rules for developing the multiple rupture scale factors are given in the experts' documentation in Appendix F.

The scale factors are presented for cases of 2, 3, 4, and 5 faults rupturing simultaneously. The faults are assumed to be separated by 2 to 3 km (between any two faults). The ground motion was evaluated for several locations within 5 km of any of the faults. The average adjustment factors for the median, the aleatory uncertainty, and epistemic uncertainties are listed in Tables 6-3 to 6-9. The experts provided their adjustment factors for the uncertainties in either of two ways: as a scale factor or as an addition (in a square root of the sum of the squares method) to the total.

6.4.2 Detachment Fault Case

The second special case is a low-angle detachment fault with a dip of about 30 degrees. At Workshop #2, this case was presented as a combination of a low-angle detachment and multiple parallel faults that splayed off from the detachment fault. Six of the seven experts addressed the low-angle detachment separately from the multiple parallel faults; Somerville addressed the combined case. The adjustment factors for this case are listed in Tables 6-10 and 6-11. These factors should be applied to the computed ground motions based on the experts' attenuation relations.

TABLE 6-1
CONSTRAINTS ON THE REGRESSION

EXPERT	MEDIAN: INCREASE SATURATION AT SHORT DISTANCES?	MEDIAN: INCLUDE FOOTWALL AND HANGING WALL DIFFERENCES?	σ_μ: MAGNITUDE DEPENDENCE?	σ_μ: DISTANCE DEPENDENCE?
Anderson	Yes	Yes	No	Yes
Boore	No	Yes	Yes	Yes
Campbell	Yes	No	No	Yes
McGarr	Yes	No	No	Yes
Silva	Yes	Yes	No	No
Somerville	No	Yes	Yes	Yes
Walck	Yes	Yes	No	Yes

TABLE 6-2
REGRESSION MODEL COEFFICIENTS FOR THE HYPOCENTRAL-BASED MODELS

COEFFICIENT	ESTIMATE
e_1	-0.207
e_2	-0.323
e_3	0.0058
e_4	0.0059
e_5	1.894
e_6	3.854
e_7	0.0116
e_8	0.0094
e_9	-0.177
e_{10}	0.0055
e_{11}	0.0111

TABLE 6-3
J. G. ANDERSON: MULTIPLE RUPTURE SCENARIO
FACTORS APPLIED TO MEDIAN ESTIMATES

COMPONENT	FREQUENCY (HZ)	MEDIAN 2 FAULTS	MEDIAN 3 FAULTS	MEDIAN 4 FAULTS	MEDIAN 5 FAULTS	FACTOR SIGMA	FACTOR SIGMA-MU	ADDITIONAL SIGMA (SRSS)	ADDITIONAL SIGMA-MU (SRSS)
Horizontal	PGA	1.20	1.31	1.40	1.47	1.0	1.0	-	-
	20.	1.21	1.33	1.42	1.50	1.0	1.0	-	-
	10.	1.20	1.31	1.41	1.48	1.0	1.0	-	-
	5.	1.19	1.30	1.39	1.45	1.0	1.0	-	-
	2.	1.16	1.24	1.31	1.36	1.0	1.0	-	-
	1.	1.13	1.21	1.27	1.32	1.0	1.0	-	-
	0.5	1.09	1.13	1.17	1.21	1.0	1.0	-	-
	0.3	1.05	1.05	1.07	1.08	1.0	1.0	-	-
	PGV	1.13	1.20	1.25	1.29	1.0	1.0	-	-
Vertical	PGA	1.11	1.17	1.21	1.24	1.0	1.0	-	-
	20.	1.11	1.17	1.21	1.24	1.0	1.0	-	-
	10.	1.17	1.27	1.35	1.41	1.0	1.0	-	-
	5.	1.18	1.30	1.39	1.45	1.0	1.0	-	-
	2.	1.14	1.22	1.29	1.35	1.0	1.0	-	-
	1.	1.12	1.18	1.24	1.29	1.0	1.0	-	-
	0.5	1.04	1.04	1.06	1.07	1.0	1.0	-	-
	0.3	1.00	0.98	0.98	0.98	1.0	1.0	-	-
	PGV	1.11	1.16	1.20	1.24	1.0	1.0	-	-

TABLE 6-4
D. M. BOORE: MULTIPLE RUPTURE SCENARIO
FACTORS APPLIED TO MEDIAN ESTIMATES

COMPONENT	FREQUENCY (HZ)	MEDIAN 2 FAULTS	MEDIAN 3 FAULTS	MEDIAN 4 FAULTS	MEDIAN 5 FAULTS	FACTOR SIGMA	FACTOR SIGMA-MU	ADDITIONAL SIGMA (SRSS)	ADDITIONAL SIGMA-MU (SRSS)
Horizontal	PGA	1.25	1.38	1.48	1.55	1.0	1.0	-	-
	20.	1.26	1.38	1.48	1.55	1.0	1.0	-	-
	10.	1.25	1.37	1.47	1.53	1.0	1.0	-	-
	5.	1.24	1.37	1.46	1.53	1.0	1.0	-	-
	2.	1.21	1.31	1.39	1.45	1.0	1.0	-	-
	1.	1.18	1.26	1.33	1.37	1.0	1.0	-	-
	0.5	1.17	1.25	1.31	1.36	1.0	1.0	-	-
	0.3	1.10	1.13	1.16	1.18	1.0	1.0	-	-
	PGV	1.15	1.22	1.26	1.30	1.0	1.0	-	-
Vertical	PGA	1.22	1.33	1.41	1.46	1.0	1.0	-	-
	20.	1.22	1.32	1.4	1.45	1.0	1.0	-	-
	10.	1.22	1.32	1.39	1.44	1.0	1.0	-	-
	5.	1.21	1.31	1.39	1.44	1.0	1.0	-	-
	2.	1.19	1.28	1.35	1.39	1.0	1.0	-	-
	1.	1.17	1.24	1.3	1.34	1.0	1.0	-	-
	0.5	1.13	1.18	1.22	1.25	1.0	1.0	-	-
	0.3	1.09	1.11	1.14	1.16	1.0	1.0	-	-
	PGV	1.15	1.20	1.24	1.27	1.0	1.0	-	-

TABLE 6-5
K. W CAMPBELL: MULTIPLE RUPTURE SCENARIO
FACTORS APPLIED TO MEDIAN ESTIMATES

COMPONENT	FREQUENCY (HZ)	MEDIAN 2 FAULTS	MEDIAN 3 FAULTS	MEDIAN 4 FAULTS	MEDIAN 5 FAULTS	FACTOR SIGMA	FACTOR SIGMA-MU	ADDITIONAL SIGMA (SRSS)	ADDITIONAL SIGMA-MU (SRSS)
Horizontal	PGA	1.0	1.0	1.0	1.0	1.2	1.0	-	-
	20.	1.0	1.0	1.0	1.0	1.2	1.0	-	-
	10.	1.0	1.0	1.0	1.0	1.2	1.0	-	-
	5.	1.0	1.0	1.0	1.0	1.2	1.0	-	-
	2.	1.0	1.0	1.0	1.0	1.2	1.0	-	-
	1.	1.0	1.0	1.0	1.0	1.2	1.0	-	-
	0.5	1.0	1.0	1.0	1.0	1.2	1.0	-	-
	0.3	1.0	1.0	1.0	1.0	1.2	1.0	-	-
	PGV	1.0	1.0	1.0	1.0	1.2	1.0	-	-
Vertical	PGA	1.0	1.0	1.0	1.0	1.2	1.0	-	-
	20.	1.0	1.0	1.0	1.0	1.2	1.0	-	-
	10.	1.0	1.0	1.0	1.0	1.2	1.0	-	-
	5.	1.0	1.0	1.0	1.0	1.2	1.0	-	-
	2.	1.0	1.0	1.0	1.0	1.2	1.0	-	-
	1.	1.0	1.0	1.0	1.0	1.2	1.0	-	-
	0.5	1.0	1.0	1.0	1.0	1.2	1.0	-	-
	0.3	1.0	1.0	1.0	1.0	1.2	1.0	-	-
	PGV	1.0	1.0	1.0	1.0	1.2	1.0	-	-

TABLE 6-6
A. MCGARR MULTIPLE RUPTURE SCENARIO
FACTORS APPLIED TO MEDIAN ESTIMATES

COMPONENT	FREQUENCY (HZ)	MEDIAN 2 FAULTS	MEDIAN 3 FAULTS	MEDIAN 4 FAULTS	MEDIAN 5 FAULTS	FACTOR SIGMA	FACTOR SIGMA-MU	ADDITIONAL SIGMA (SRSS)	ADDITIONAL SIGMA-MU (SRSS)
Horizontal	PGA	1.0	1.0	1.0	1.0	1.2	1.0	-	-
	20.	1.0	1.0	1.0	1.0	1.2	1.0	-	-
	10.	1.0	1.0	1.0	1.0	1.2	1.0	-	-
	5.	1.0	1.0	1.0	1.0	1.2	1.0	-	-
	2.	1.0	1.0	1.0	1.0	1.2	1.0	-	-
	1.	1.0	1.0	1.0	1.0	1.2	1.0	-	-
	0.5	1.0	1.0	1.0	1.0	1.2	1.0	-	-
	0.3	1.0	1.0	1.0	1.0	1.2	1.0	-	-
	PGV	1.0	1.0	1.0	1.0	1.2	1.0	-	-
Vertical	PGA	1.0	1.0	1.0	1.0	1.2	1.0	-	-
	20.	1.0	1.0	1.0	1.0	1.2	1.0	-	-
	10.	1.0	1.0	1.0	1.0	1.2	1.0	-	-
	5.	1.0	1.0	1.0	1.0	1.2	1.0	-	-
	2.	1.0	1.0	1.0	1.0	1.2	1.0	-	-
	1.	1.0	1.0	1.0	1.0	1.2	1.0	-	-
	0.5	1.0	1.0	1.0	1.0	1.2	1.0	-	-
	0.3	1.0	1.0	1.0	1.0	1.2	1.0	-	-
	PGV	1.0	1.0	1.0	1.0	1.2	1.0	-	-

TABLE 6-7
W. J. SILVA: MULTIPLE RUPTURE SCENARIO
FACTORS APPLIED TO MEDIAN ESTIMATES

COMPONENT	FREQUENCY (HZ)	MEDIAN 2 FAULTS	MEDIAN 3 FAULTS	MEDIAN 4 FAULTS	MEDIAN 5 FAULTS	FACTOR SIGMA	FACTOR SIGMA-MU	ADDITIONAL SIGMA (SRSS)	ADDITIONAL SIGMA-MU (SRSS)
Horizontal	PGA	1.29	1.44	1.56	1.66	1.0	1.0	-	-
	20.	1.30	1.46	1.58	1.68	1.0	1.0	-	-
	10.	1.29	1.45	1.57	1.66	1.0	1.0	-	-
	5.	1.29	1.44	1.56	1.65	1.0	1.0	-	-
	2.	1.25	1.39	1.49	1.57	1.0	1.0	-	-
	1.	1.22	1.34	1.43	1.50	1.0	1.0	-	-
	0.5	1.46	1.56	1.64	1.70	1.0	1.0	-	-
	0.3	1.40	1.45	1.50	1.54	1.0	1.0	-	-
	PGV	1.21	1.32	1.40	1.46	1.0	1.0	-	-
Vertical	PGA	1.29	1.45	1.57	1.66	1.0	1.0	-	-
	20.	1.30	1.46	1.58	1.67	1.0	1.0	-	-
	10.	1.29	1.43	1.55	1.63	1.0	1.0	-	-
	5.	1.28	1.43	1.54	1.63	1.0	1.0	-	-
	2.	1.25	1.38	1.48	1.55	1.0	1.0	-	-
	1.	1.22	1.34	1.42	1.49	1.0	1.0	-	-
	0.5	1.45	1.55	1.62	1.69	1.0	1.0	-	-
	0.3	1.39	1.45	1.49	1.51	1.0	1.0	-	-
	PGV	1.22	1.33	1.42	1.48	1.0	1.0	-	-

TABLE 6-8
P. G. SOMERVILLE: MULTIPLE RUPTURE SCENARIO
FACTORS APPLIED TO MEDIAN ESTIMATES

COMPONENT	FREQUENCY (HZ)	MEDIAN 2 FAULTS	MEDIAN 3 FAULTS	MEDIAN 4 FAULTS	MEDIAN 5 FAULTS	FACTOR SIGMA	FACTOR SIGMA-MU	ADDITIONAL SIGMA (SRSS)	ADDITIONAL SIGMA-MU (SRSS)
Horizontal	PGA	1.63	1.63	1.63	1.63	-	-	0.3	0.2
	20.	1.63	1.63	1.63	1.63	-	-	0.3	0.2
	10.	1.63	1.63	1.63	1.63	-	-	0.3	0.2
	5.	1.63	1.63	1.63	1.63	-	-	0.3	0.2
	2.	1.58	1.58	1.58	1.58	-	-	0.3	0.2
	1.	1.5	1.5	1.5	1.5	-	-	0.3	0.2
	0.5	1.5	1.5	1.5	1.5	-	-	0.3	0.2
	0.3	1.5	1.5	1.5	1.5	-	-	0.3	0.2
	PGV	1.5	1.5	1.5	1.5	-	-	0.3	0.2
Vertical	PGA	1.63	1.63	1.63	1.63	-	-	0.3	0.2
	20.	1.63	1.63	1.63	1.63	-	-	0.3	0.2
	10.	1.63	1.63	1.63	1.63	-	-	0.3	0.2
	5.	1.63	1.63	1.63	1.63	-	-	0.3	0.2
	2.	1.58	1.58	1.58	1.58	-	-	0.3	0.2
	1.	1.5	1.5	1.5	1.5	-	-	0.3	0.2
	0.5	1.5	1.5	1.5	1.5	-	-	0.3	0.2
	0.3	1.5	1.5	1.5	1.5	-	-	0.3	0.2
	PGV	1.5	1.5	1.5	1.5	-	-	0.3	0.2

TABLE 6-9
M. C. WALCK: MULTIPLE RUPTURE SCENARIO
FACTORS APPLIED TO MEDIAN ESTIMATES

COMPONENT	FREQUENCY (HZ)	MEDIAN 2 FAULTS	MEDIAN 3 FAULTS	MEDIAN 4 FAULTS	MEDIAN 5 FAULTS	FACTOR SIGMA	FACTOR SIGMA-MU	ADDITIONAL SIGMA (SRSS)	ADDITIONAL SIGMA-MU (SRSS)
Horizontal	PGA	1.28	1.42	1.53	1.61	-	-	0.0	0.1
	20.	1.30	1.45	1.58	1.67	-	-	0.0	0.1
	10.	1.29	1.43	1.55	1.63	-	-	0.0	0.1
	5.	1.27	1.42	1.53	1.61	-	-	0.0	0.1
	2.	1.23	1.35	1.45	1.52	-	-	0.0	0.1
	1.	1.20	1.30	1.38	1.43	-	-	0.0	0.1
	0.5	1.17	1.25	1.31	1.36	-	-	0.0	0.2
	0.3	1.13	1.17	1.22	1.25	-	-	0.0	0.2
	PGV	1.21	1.32	1.40	1.46	-	-	0.0	0.1
Vertical	PGA	1.25	1.37	1.46	1.53	-	-	0.0	0.1
	20.	1.26	1.39	1.48	1.55	-	-	0.0	0.1
	10.	1.26	1.39	1.49	1.56	-	-	0.0	0.1
	5.	1.25	1.38	1.47	1.54	-	-	0.0	0.1
	2.	1.20	1.30	1.38	1.43	-	-	0.0	0.1
	1.	1.18	1.26	1.33	1.37	-	-	0.0	0.1
	0.5	1.14	1.19	1.23	1.26	-	-	0.0	0.2
	0.3	1.09	1.11	1.13	1.14	-	-	0.0	0.2
	PGV	1.20	1.28	1.35	1.40	-	-	0.0	0.1

TABLE 6-10
LOW-ANGLE DETACHMENT FAULT SCENARIO
SCALE FACTORS

EXPERT	MEDIAN SCALE FACTOR	SIGMA-MU SCALE FACTOR	SIGMA SCALE FACTOR	ADDITIONAL SIGMA-MU (SRSS[1])	ADDITIONAL SIGMA (SRSS[1])
Anderson	1.0	1.0	1.0	-	-
Boore	1.0	1.0	1.0	-	-
Campbell (D = depth to bottom of rupture)	1.0 for D < 8 1.0+0.2*(D-8)/7 + 1 for 8<D<15 1.2 for D > 15	1.2	1.2	-	-
McGarr	1.0	1.3	1.0	-	-
Silva	1.0	1.0	1.0	-	-
Somerville[2]	See Table 4-17	-	-	0.3	0.2
Walck	1.0	-	-	0.25	0.0

[1] Square root of the sum of the squares method.

[2] Somerville addressed the case of a low-angle detachment fault combined with multiple parallel faults splaying off of the detachment (as requested). All of the other experts addressed the detachment fault by itself.

TABLE 6-11
ADJUSTMENT FACTORS FOR SIMULTANEOUS RUPTURES ON PARALLEL FAULTS AND A DEEP DETACHMENT SURFACE (SOMERVILLE)

FREQUENCY (HZ)	MEDIAN SCALE FACTOR	ADDITIONAL SIGMA (SRSS[1])	ADDITIONAL SIGMA-MU (SRSS[1])
PGA	1.0	0.3	0.2
20	1.0	0.3	0.2
10	1.0	0.3	0.2
5	1.0	0.3	0.2
2	1.2	0.3	0.2
1	2.2	0.3	0.2
0.5	2.2	0.3	0.2
0.3	1.7	0.3	0.2
PGV	2.2	0.3	0.2

[1] Square root of the sum of the squares method.

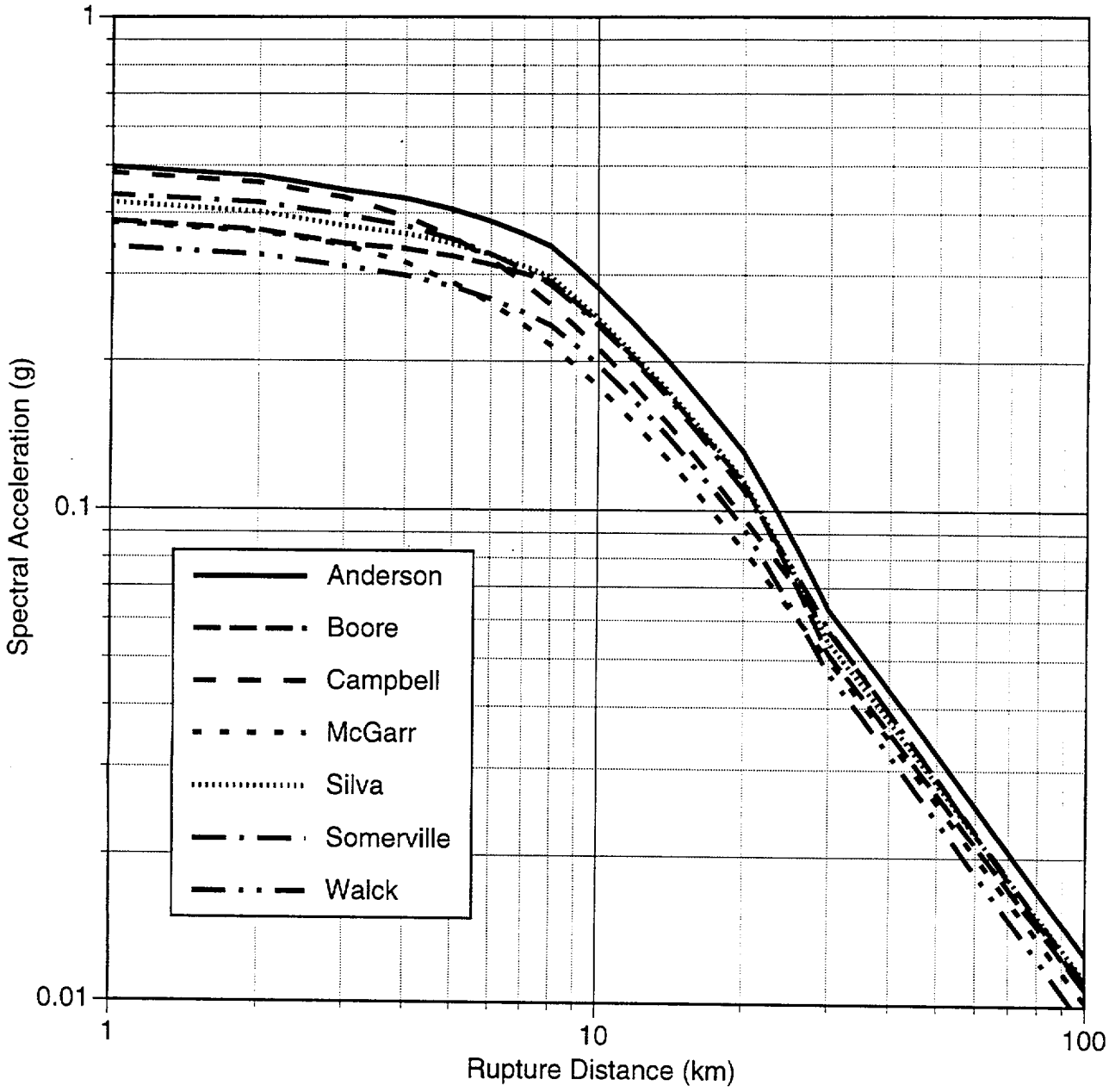

Figure 6-1 Comparison of median attenuation of horizontal PGA for M_W 6.5, normal faulting, hanging wall

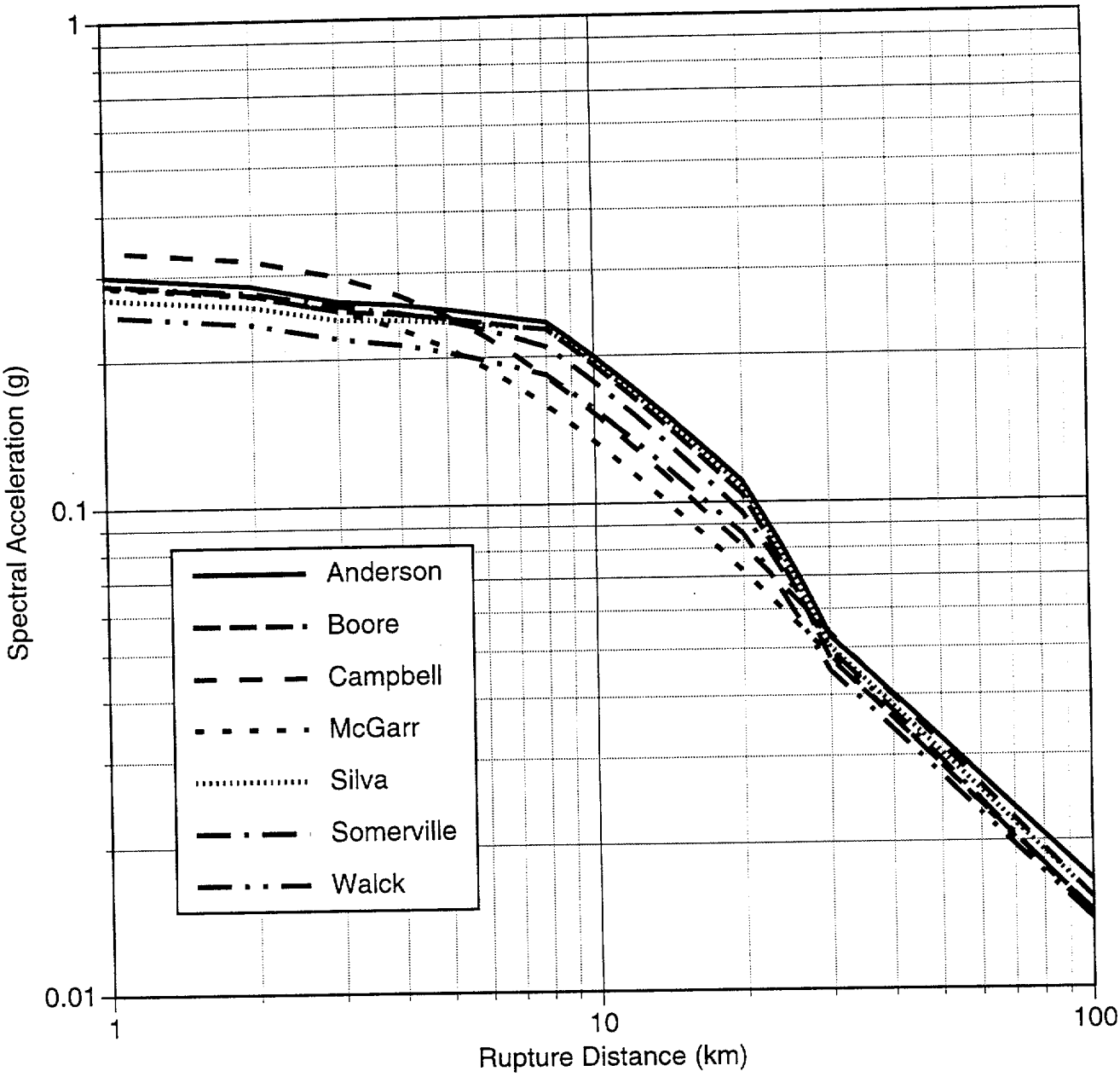

Figure 6-2 Comparison of median attenuation of horizontal spectral acceleration (T = 1.0 sec, 5% damping) for M_W 6.5, normal faulting, hanging wall

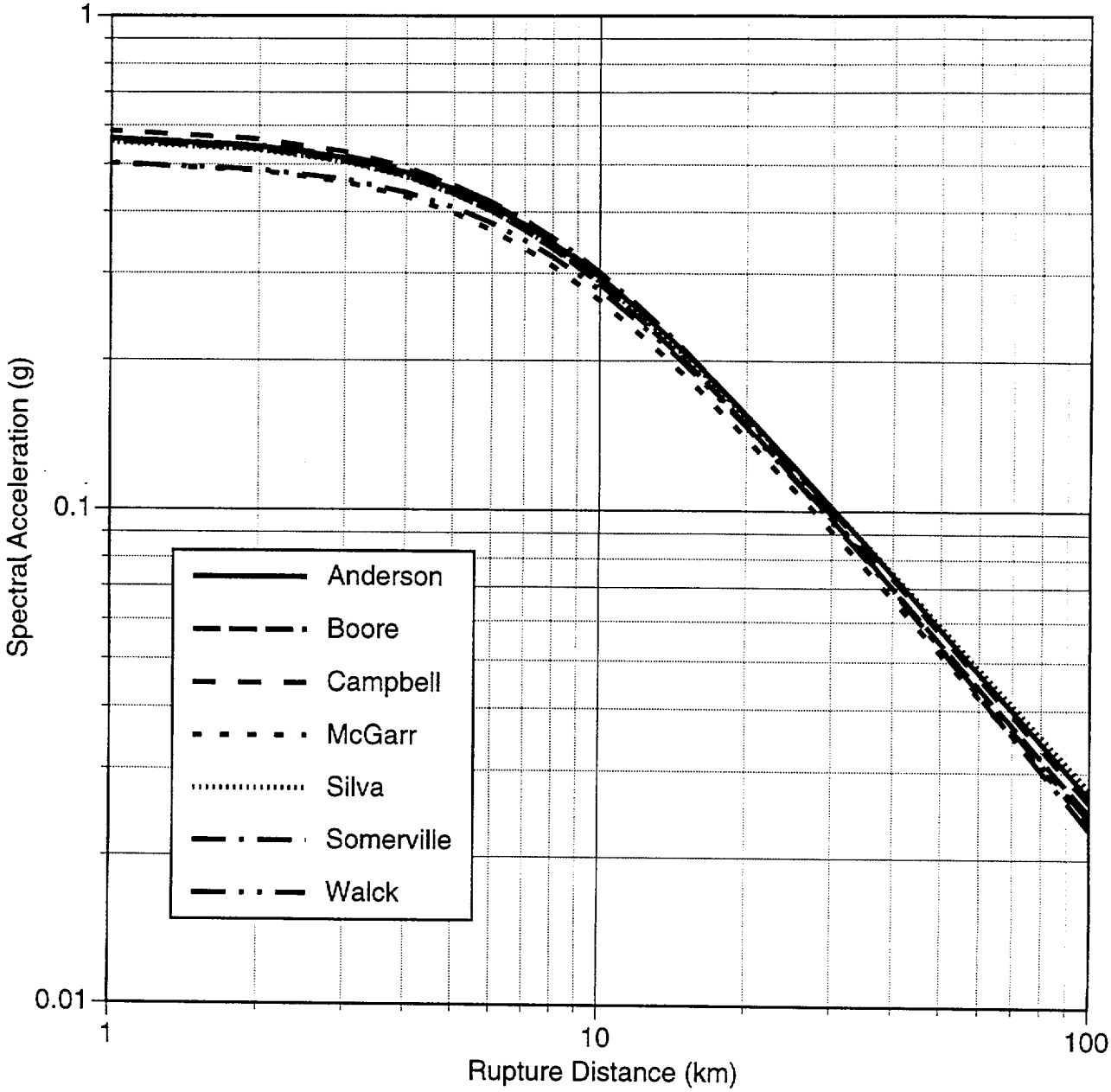

Figure 6-3 Comparison of median attenuation of horizontal PGA for M_W 7.5, strike-slip faulting

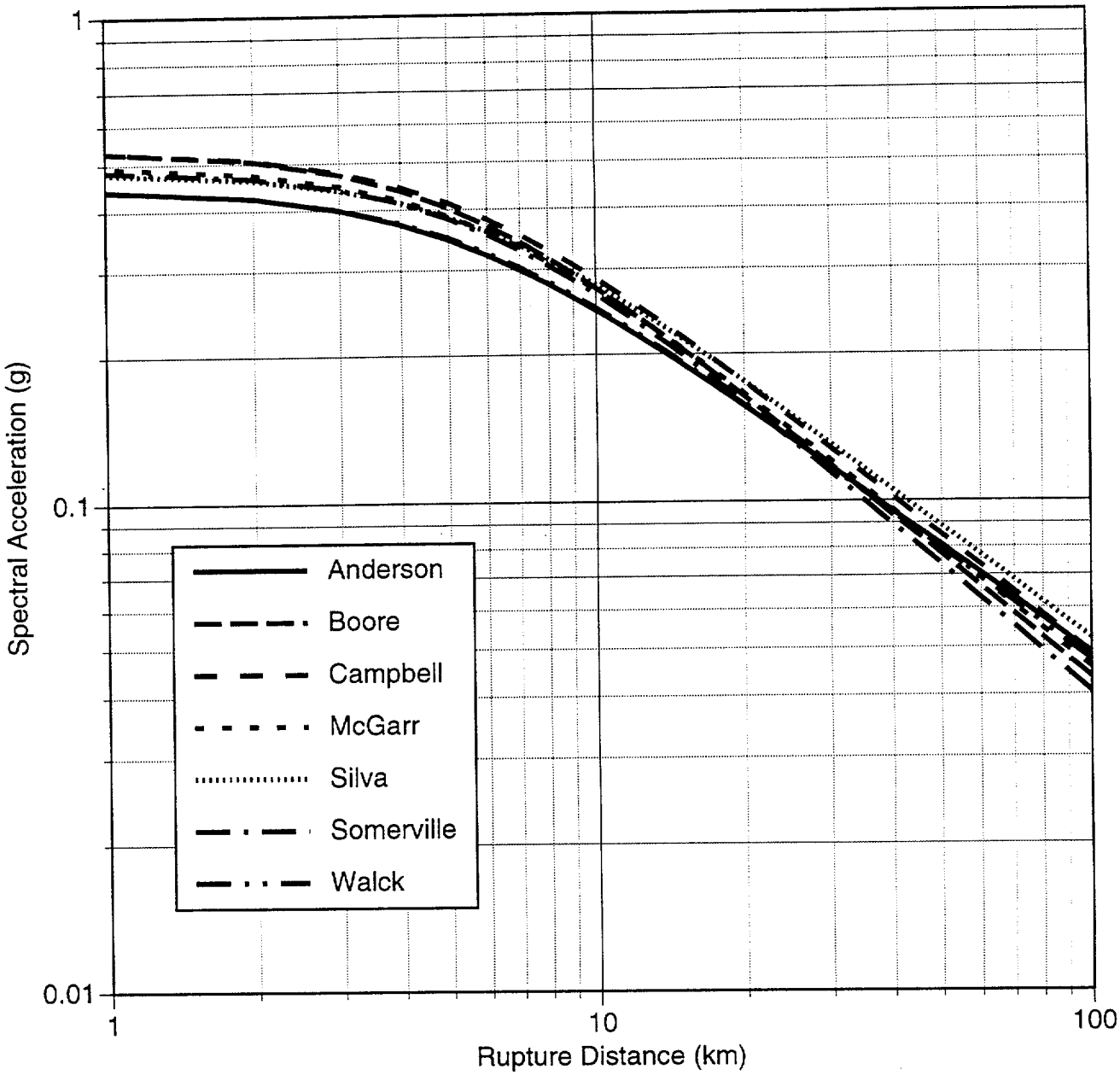

Figure 6-4 Comparison of median attenuation of horizontal spectral acceleration (T = 1.0 sec, 5% damping) for M_W 7.5, strike-slip faulting

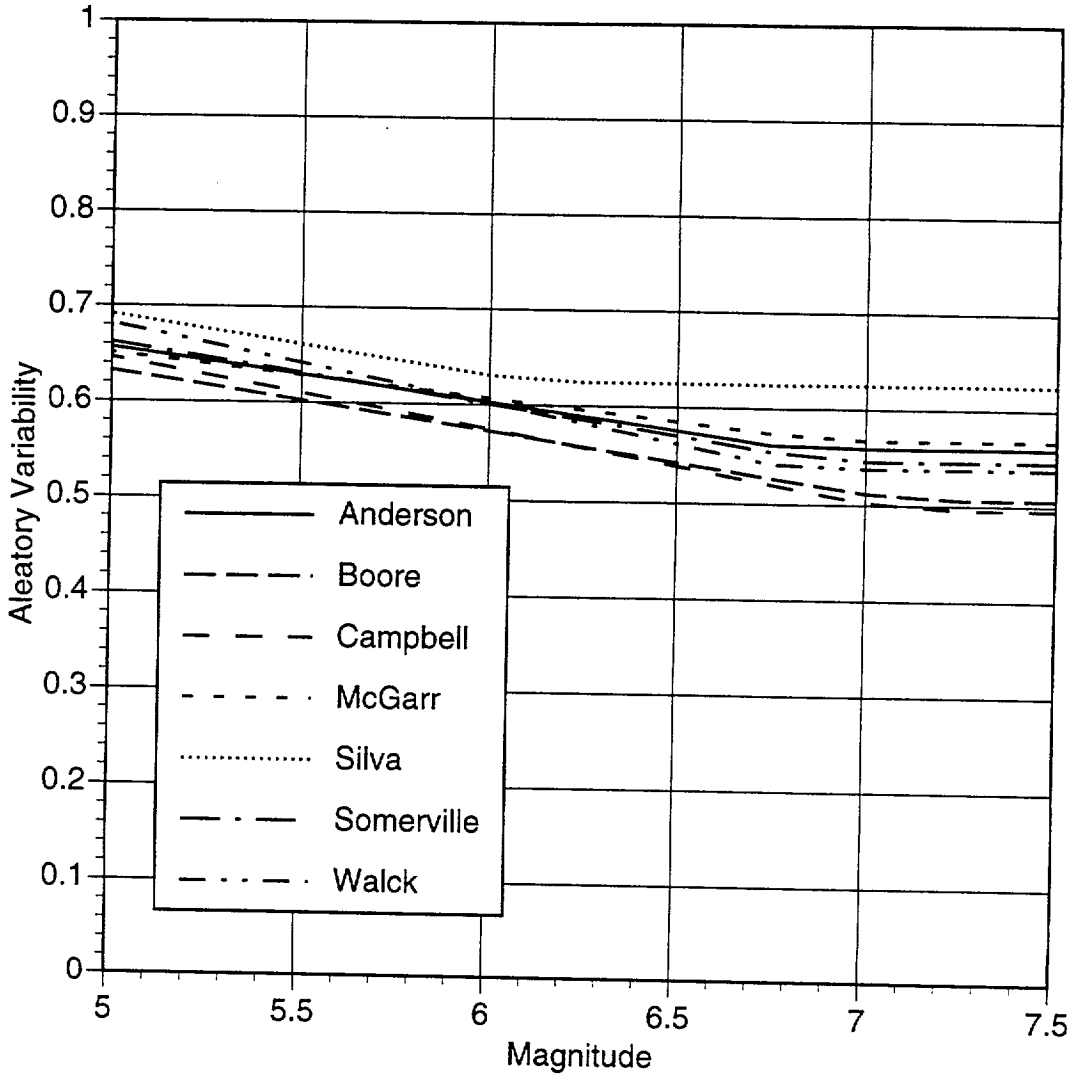

Figure 6-5 Comparison of aleatory variability of horizontal PGA

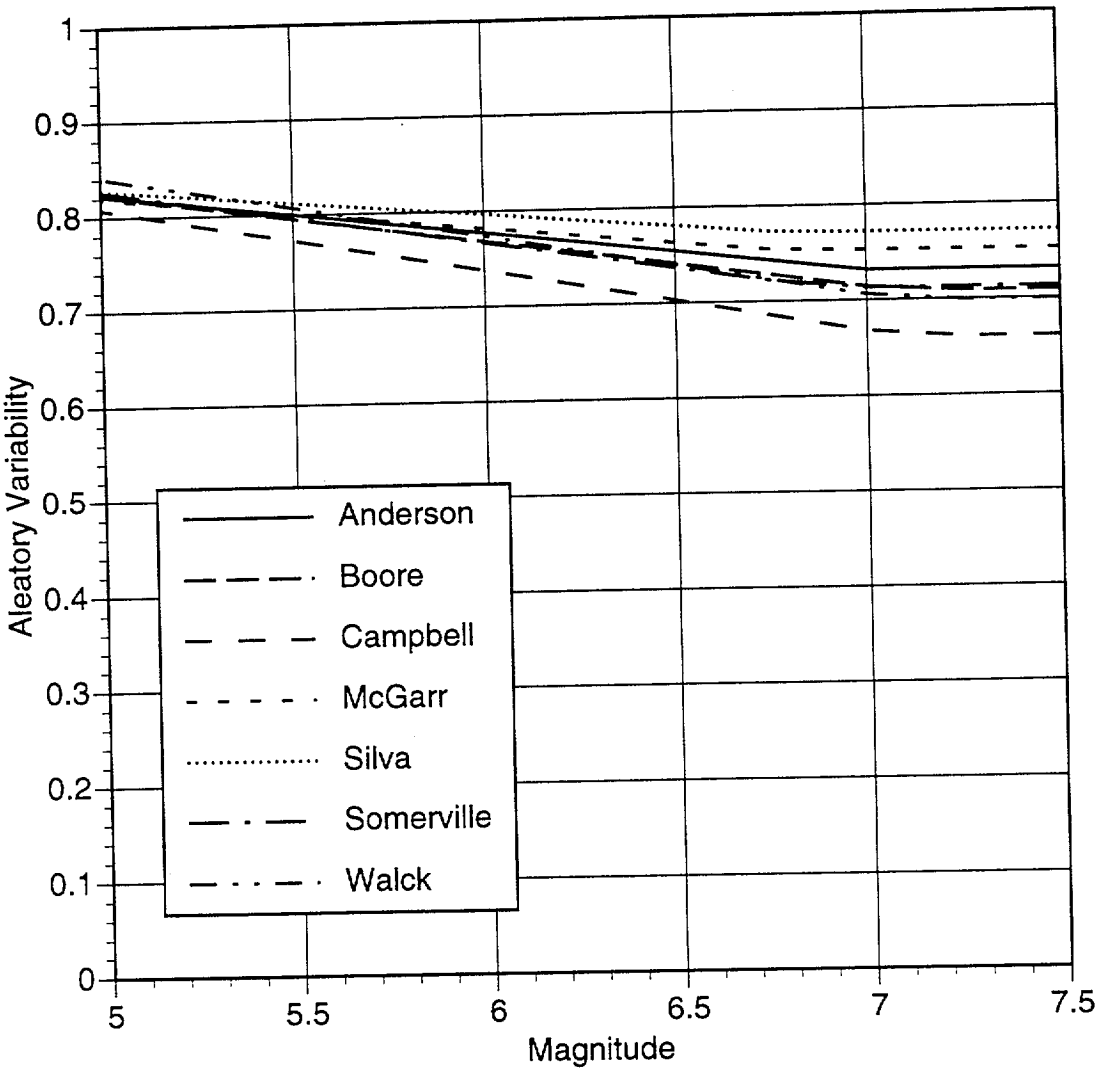

Figure 6-6 Comparison of aleatory variability of 1.0 sec horizontal spectral acceleration (at 5% damping)

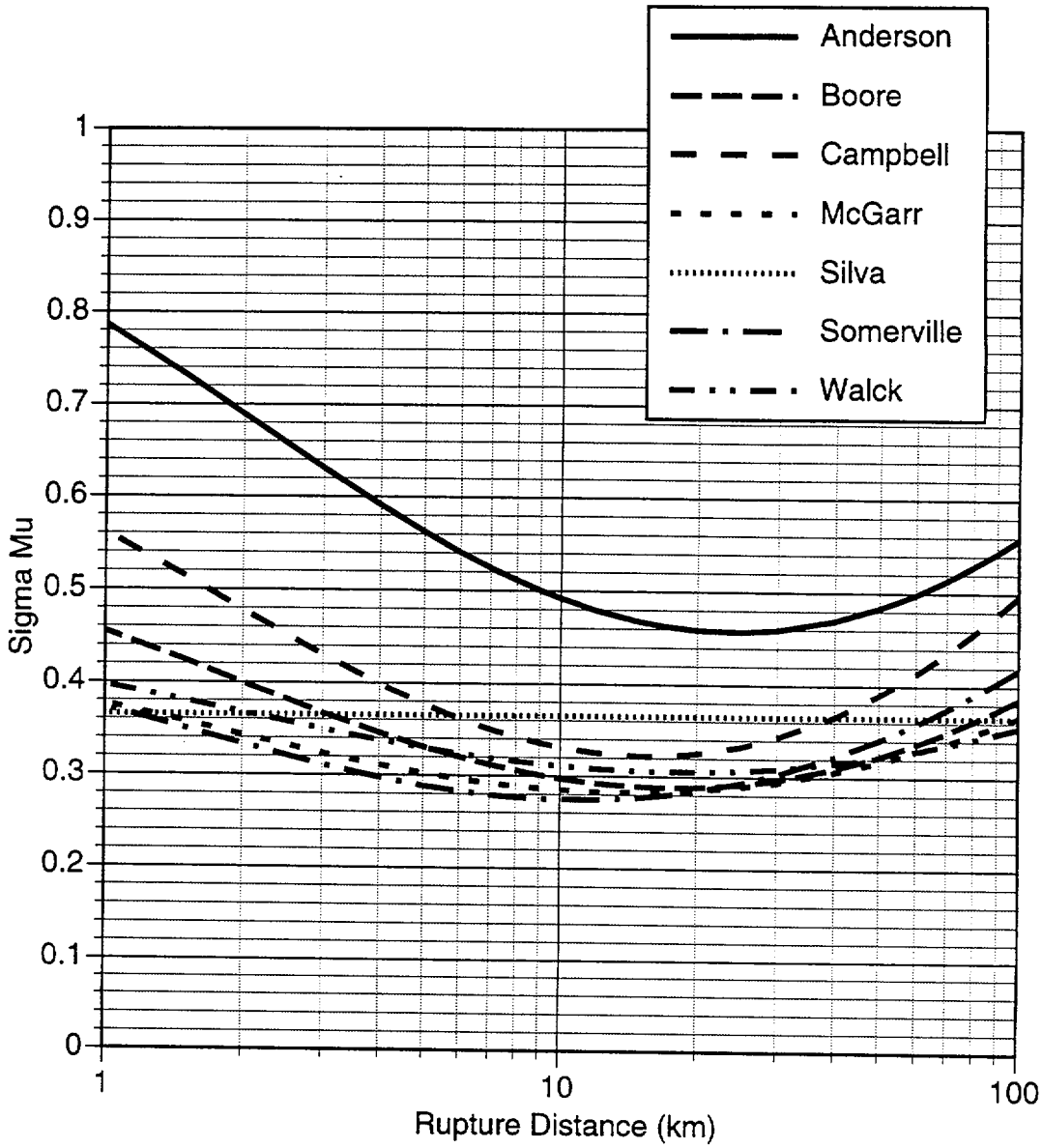

Figure 6-7 Comparison of epistemic uncertainty in the median horizontal PGA for M_W 6.5, normal faulting

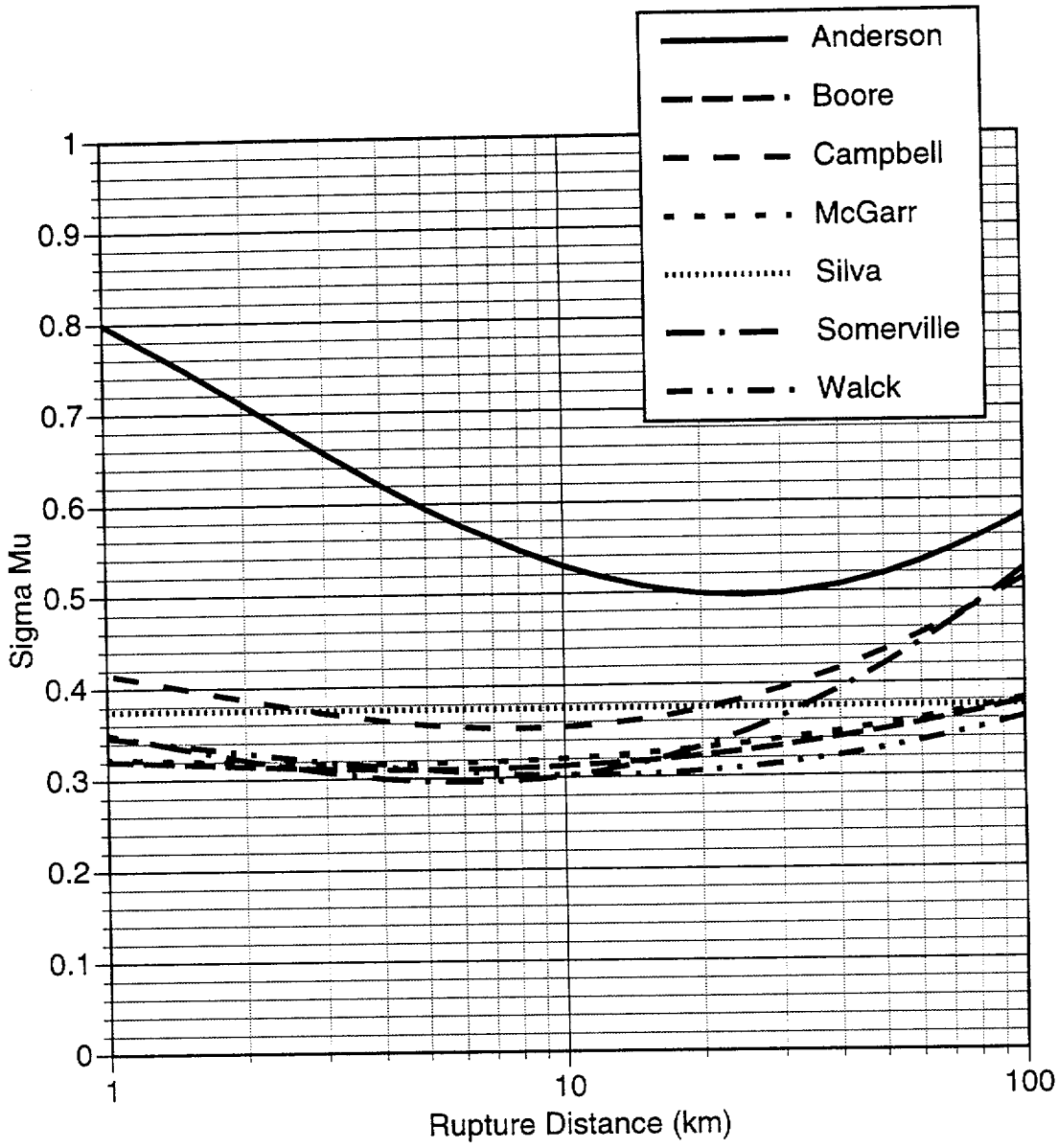

Figure 6-8 Comparison of epistemic uncertainty in the median 1.0 sec horizontal spectral acceleration (at 5% damping) for Mw 6.5, normal faulting

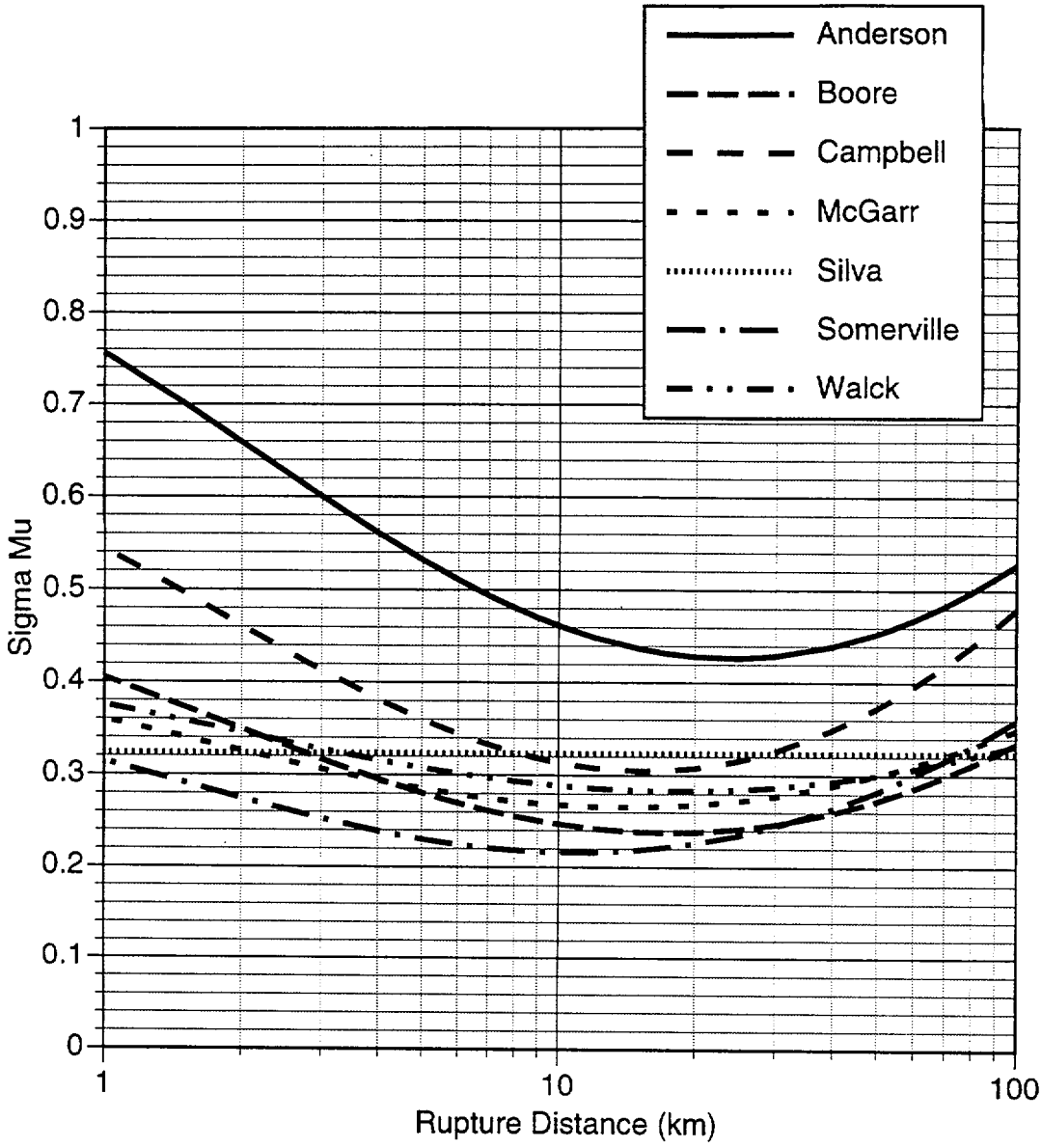

Figure 6-9 Comparison of epistemic uncertainty in the median horizontal PGA for M_W 7.5, normal faulting

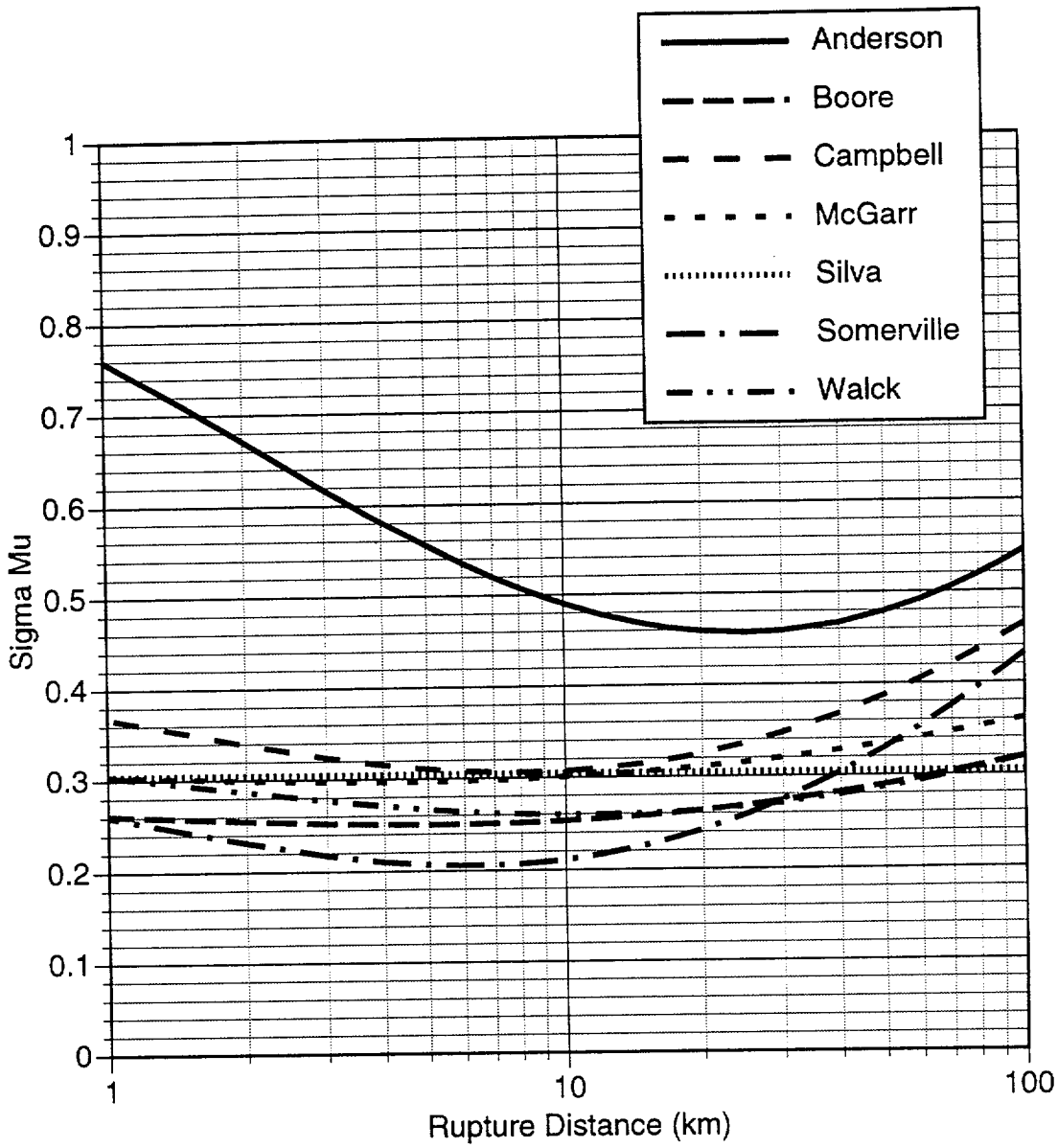

Figure 6-10 Comparison of epistemic uncertainty in the median 1.0 sec horizontal spectral acceleration (at 5% damping) for M_W 7.5, normal faulting

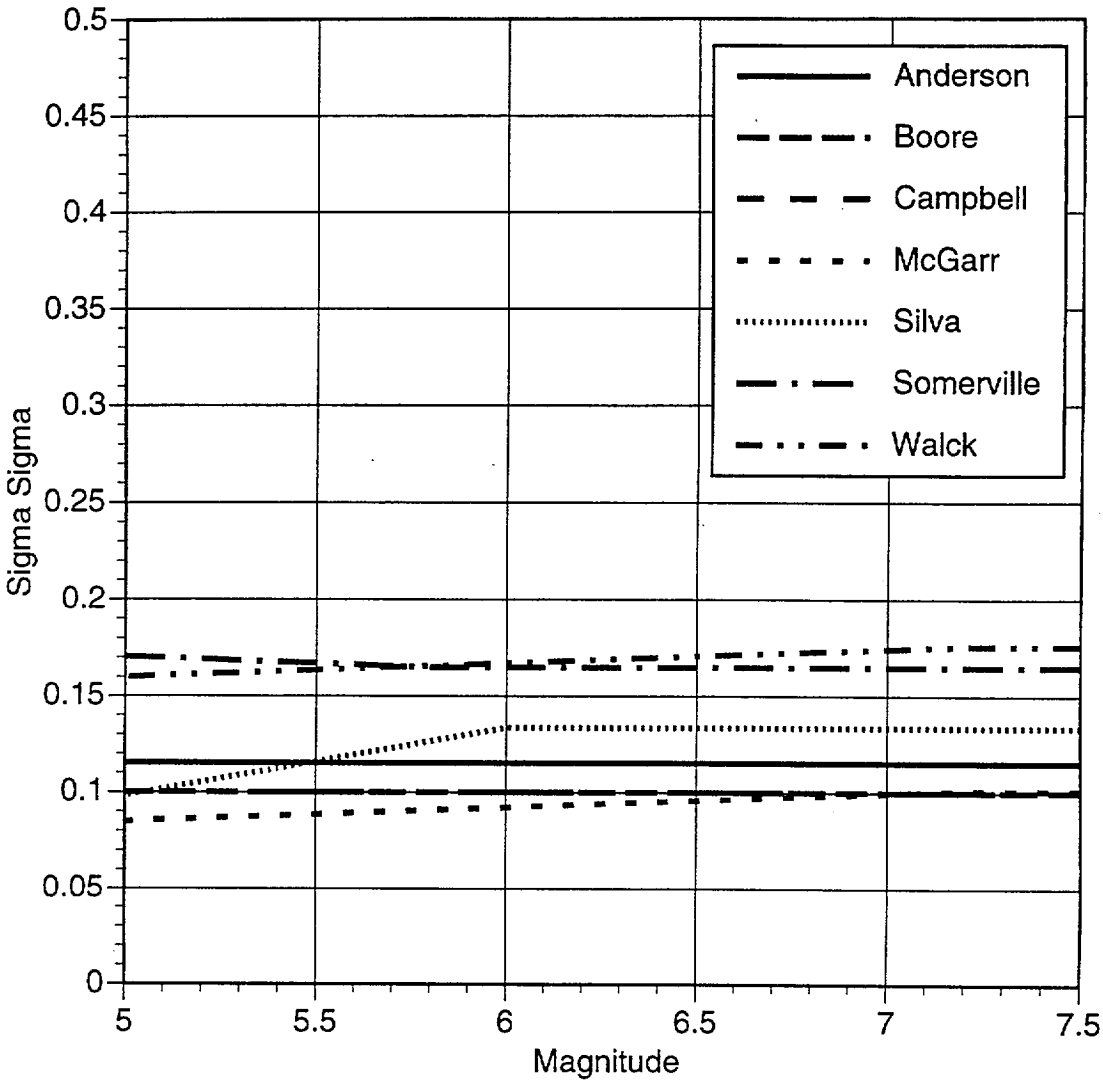

Figure 6-11 Comparison of epistemic uncertainty in the aleatory variability of horizontal PGA.

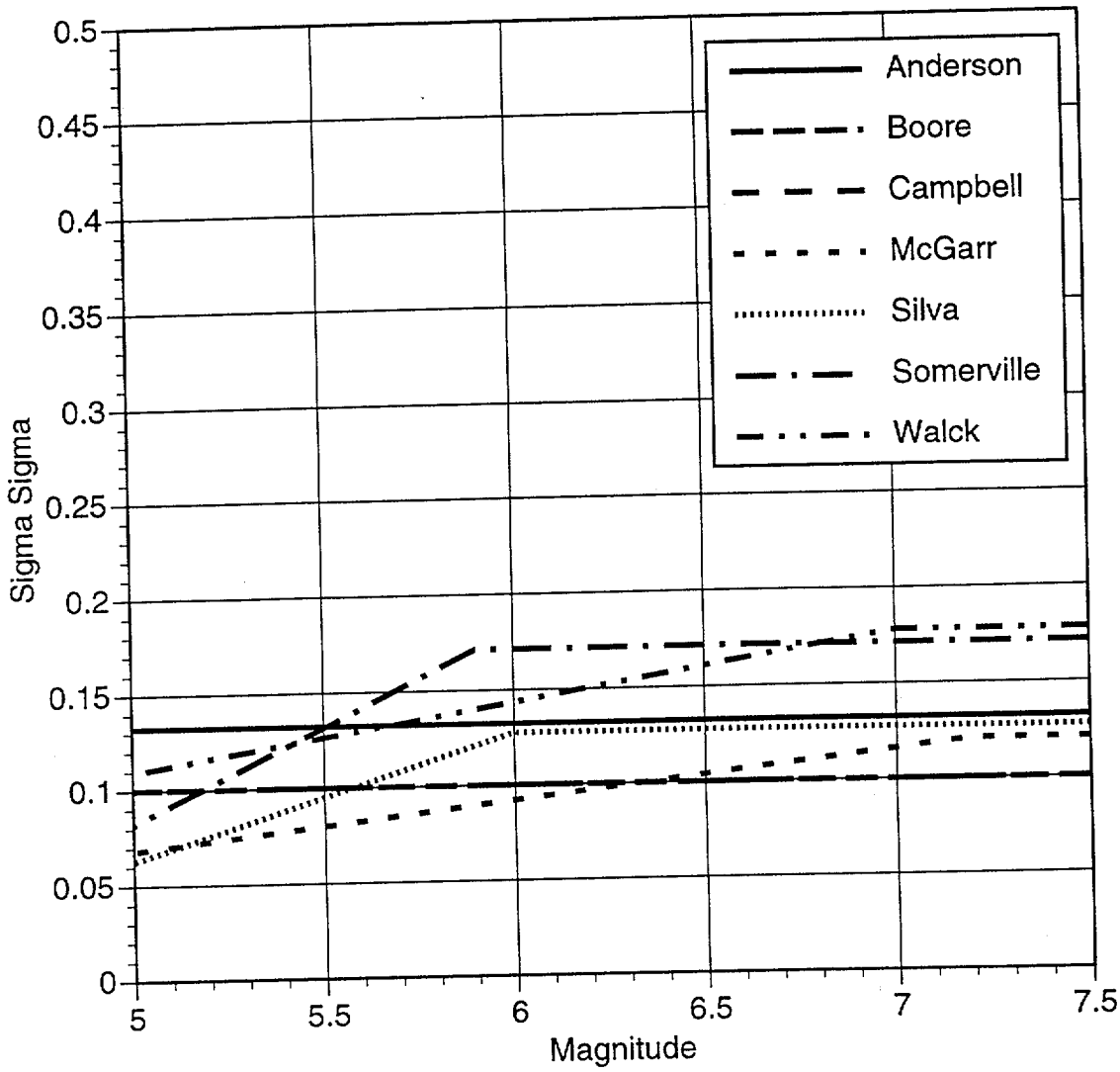

Figure 6-12 Comparison of epistemic uncertainty in the aleatory variability of 1 second horizontal spectral acceleration (5% damping).

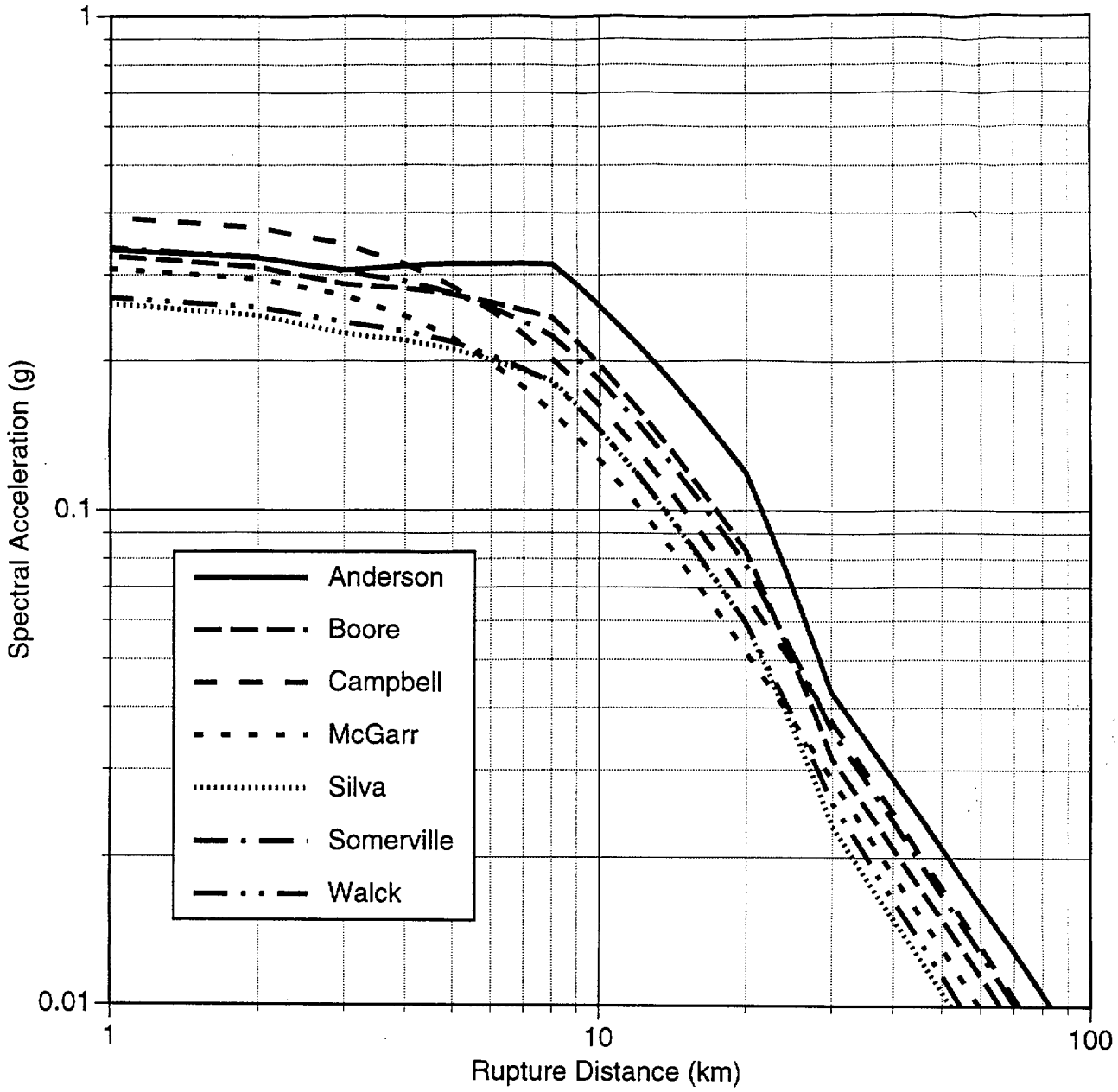

Figure 6-13 Comparison of median attenuation of vertical PGA for M_W 6.5, normal faulting, hanging wall

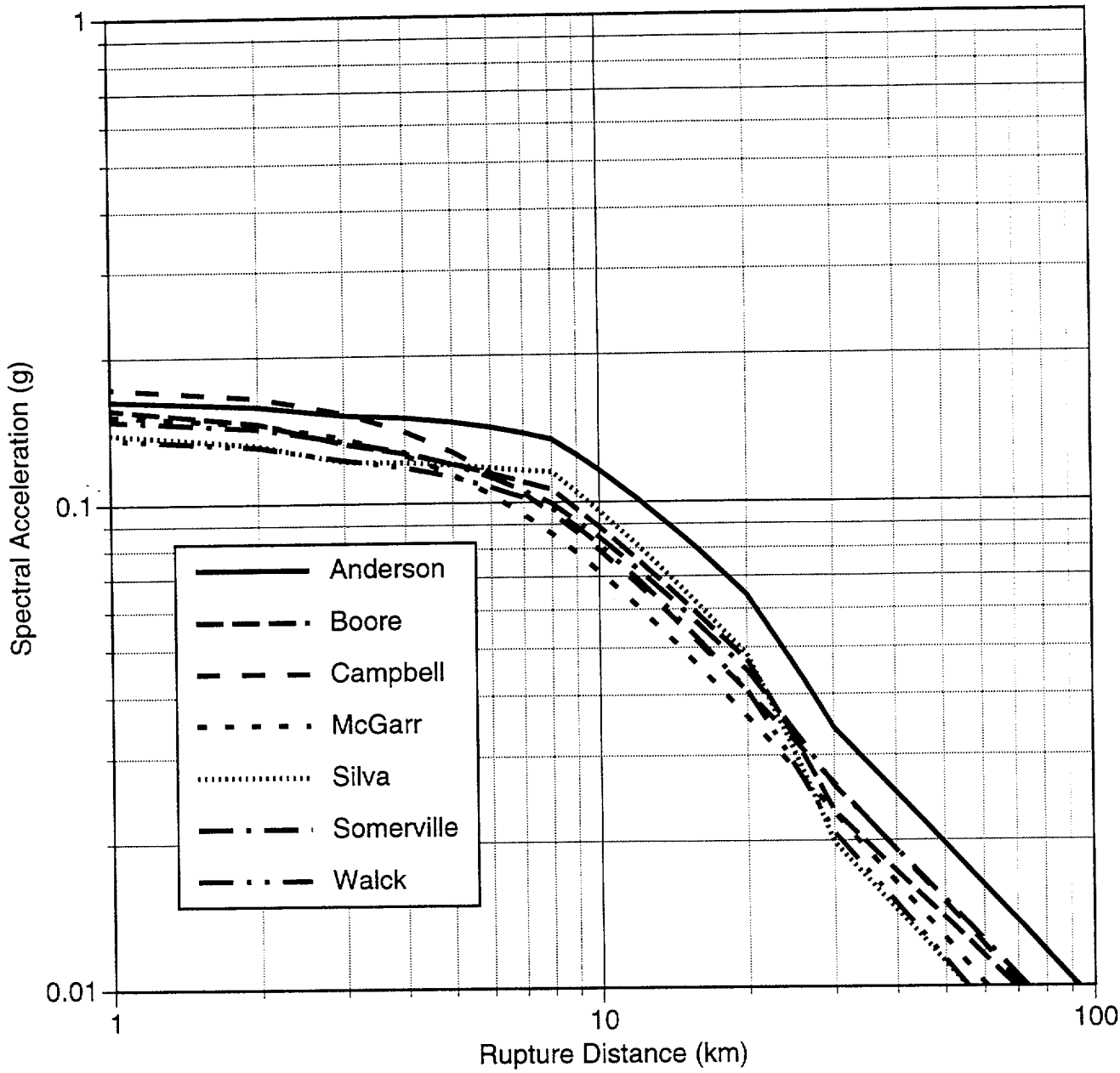

Figure 6-14 Comparison of median attenuation of vertical spectral acceleration (T= 1.0 sec, 5% damping) for M_W 6.5, normal faulting, hanging wall

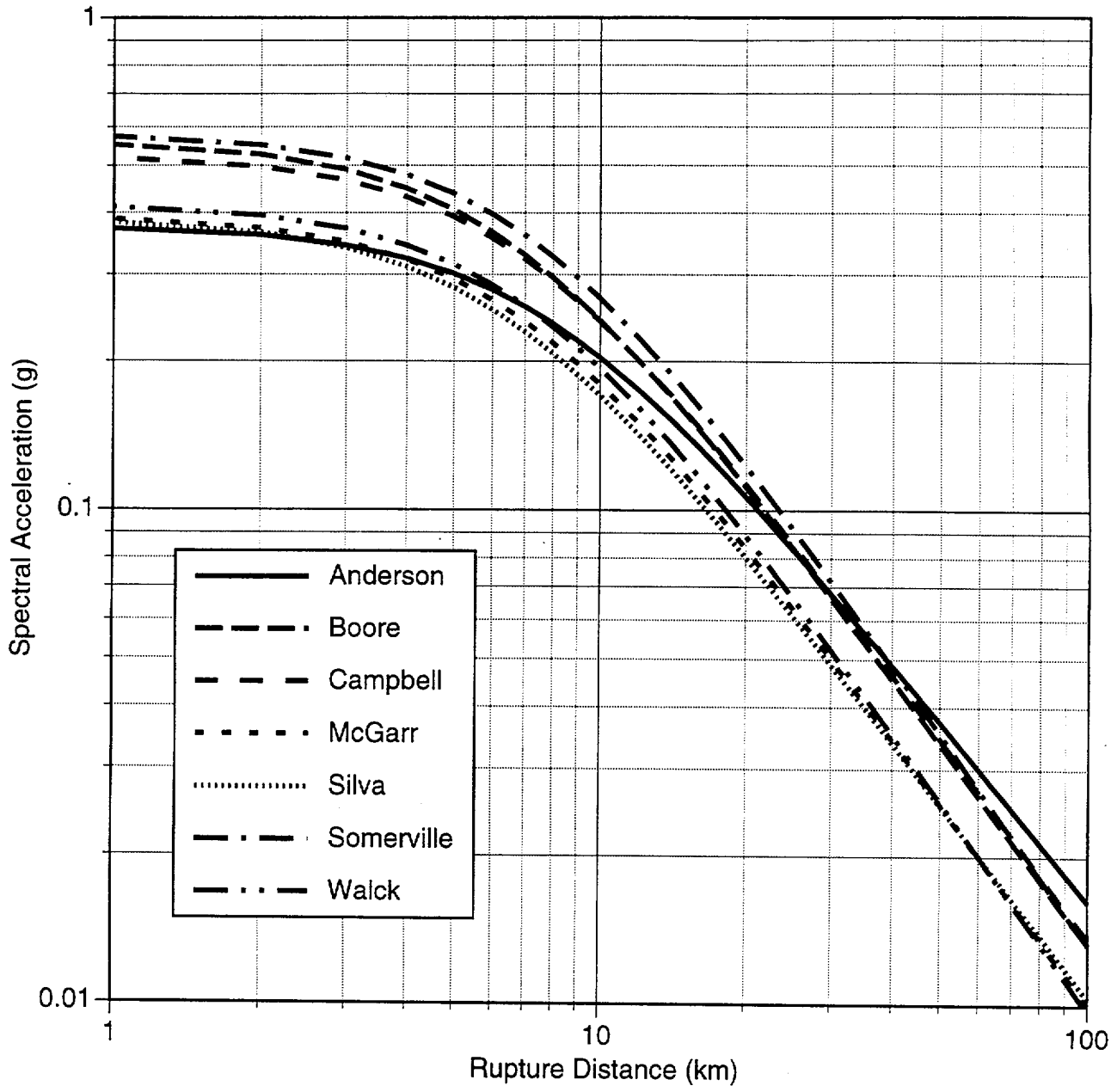

Figure 6-15 Comparison of median attenuation of vertical PGA for M_W 7.5, strike-slip faulting

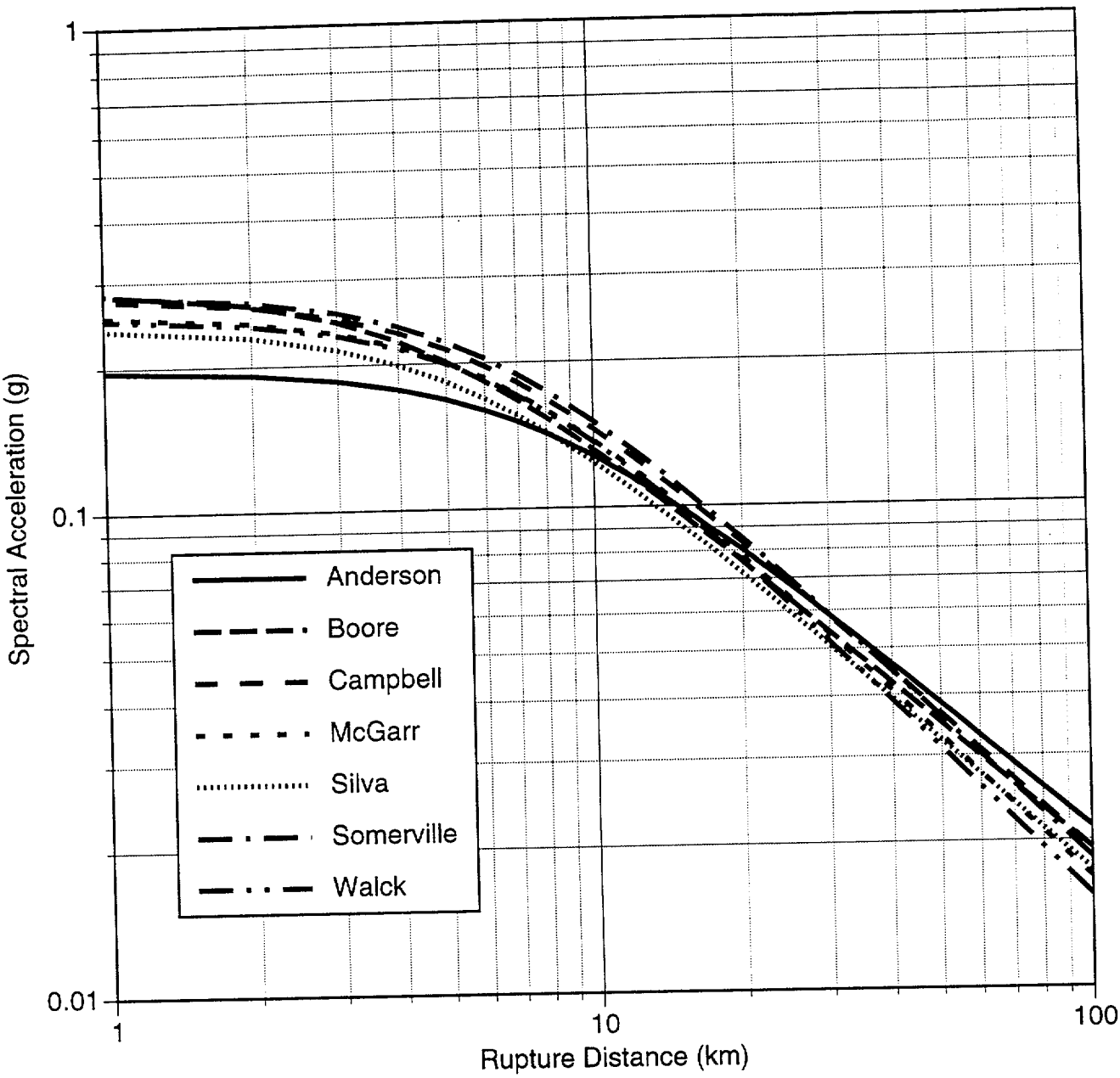

Figure 6-16 Comparison of median attenuation of vertical spectral acceleration (T= 1.0 sec, 5% damping) for M_W 7.5, strike-slip faulting

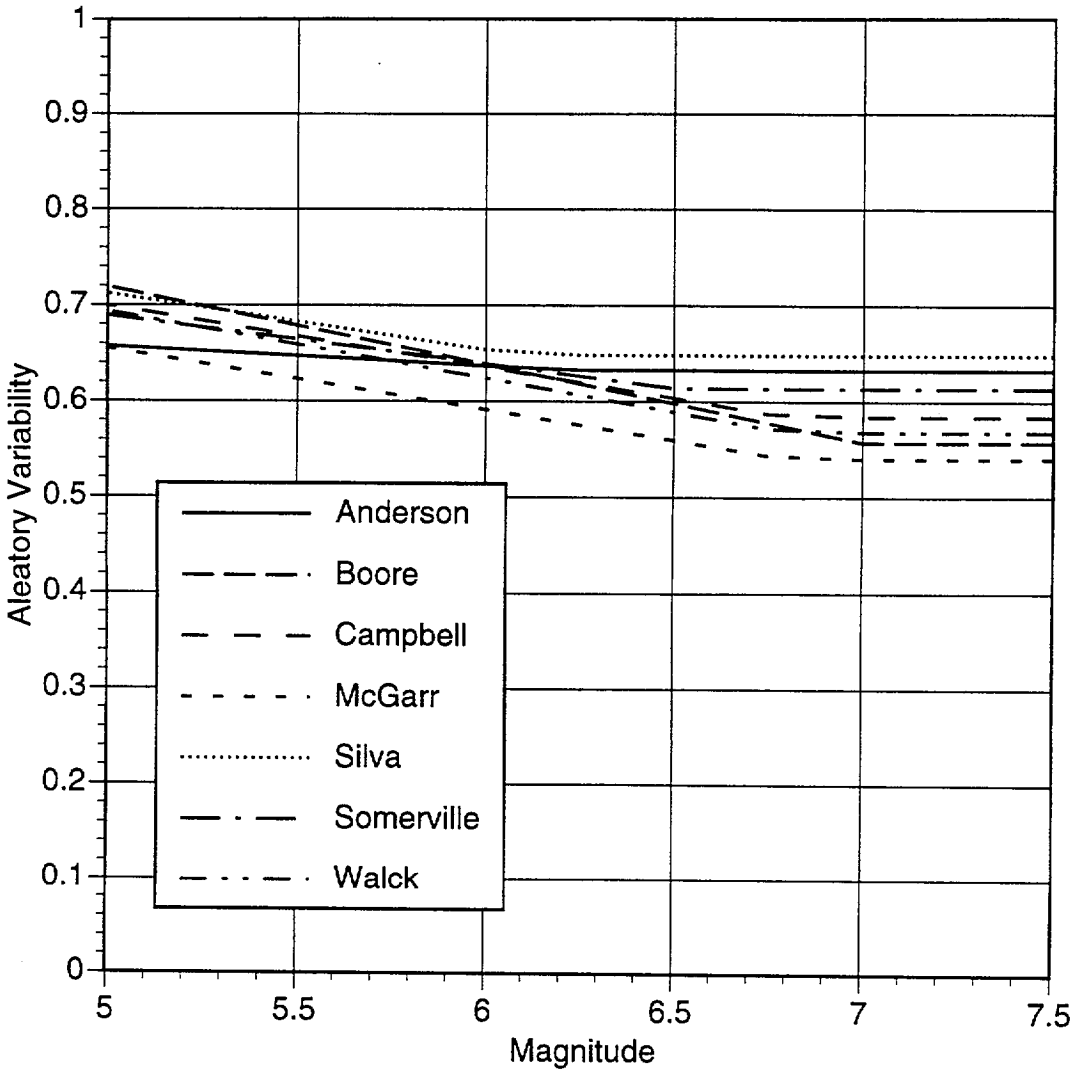

Figure 6-17 Comparison of aleatory variability of vertical PGA

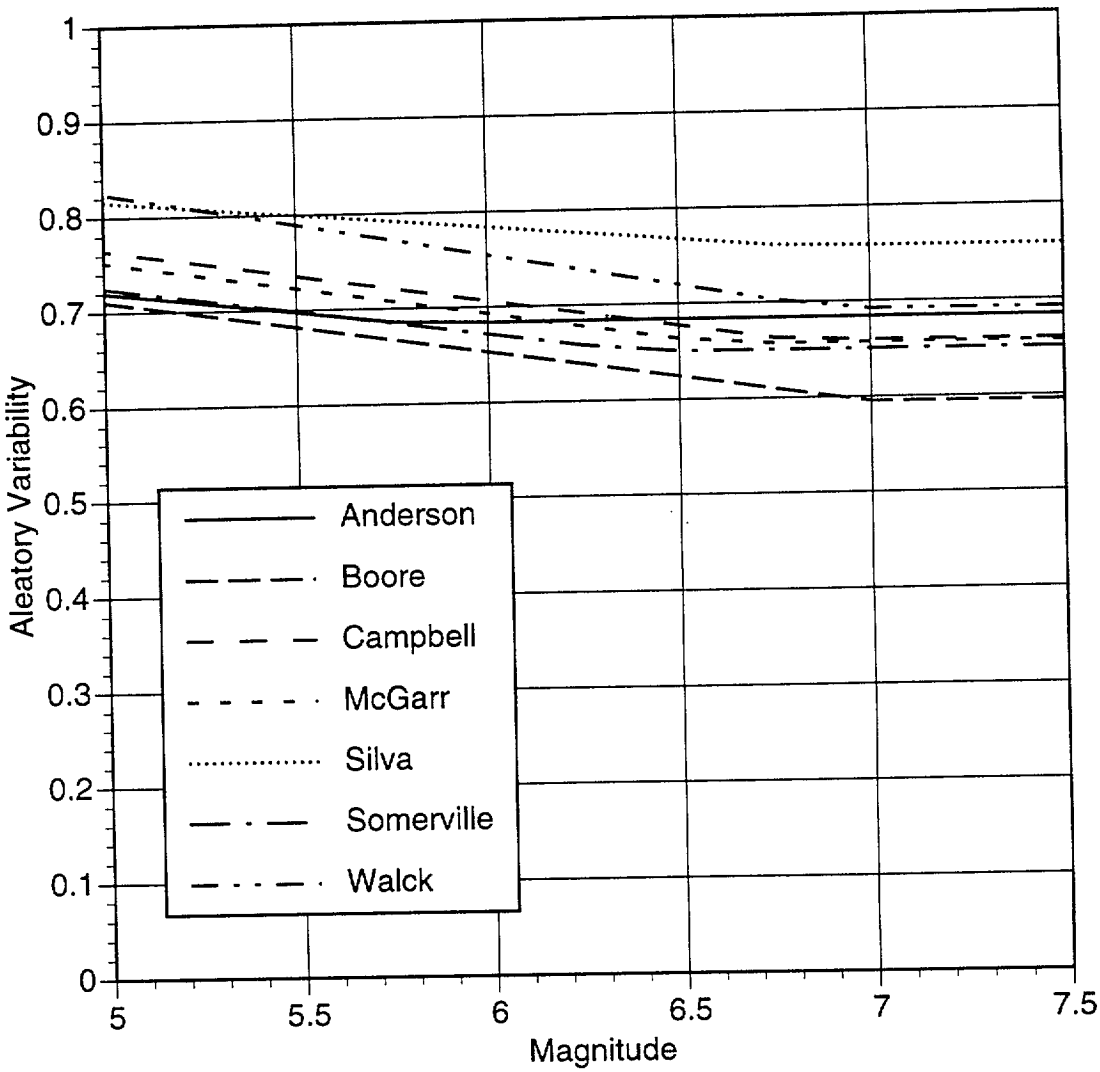

Figure 6-18 Comparison of aleatory variability of 1.0 sec vertical spectral acceleration (at 5% damping)

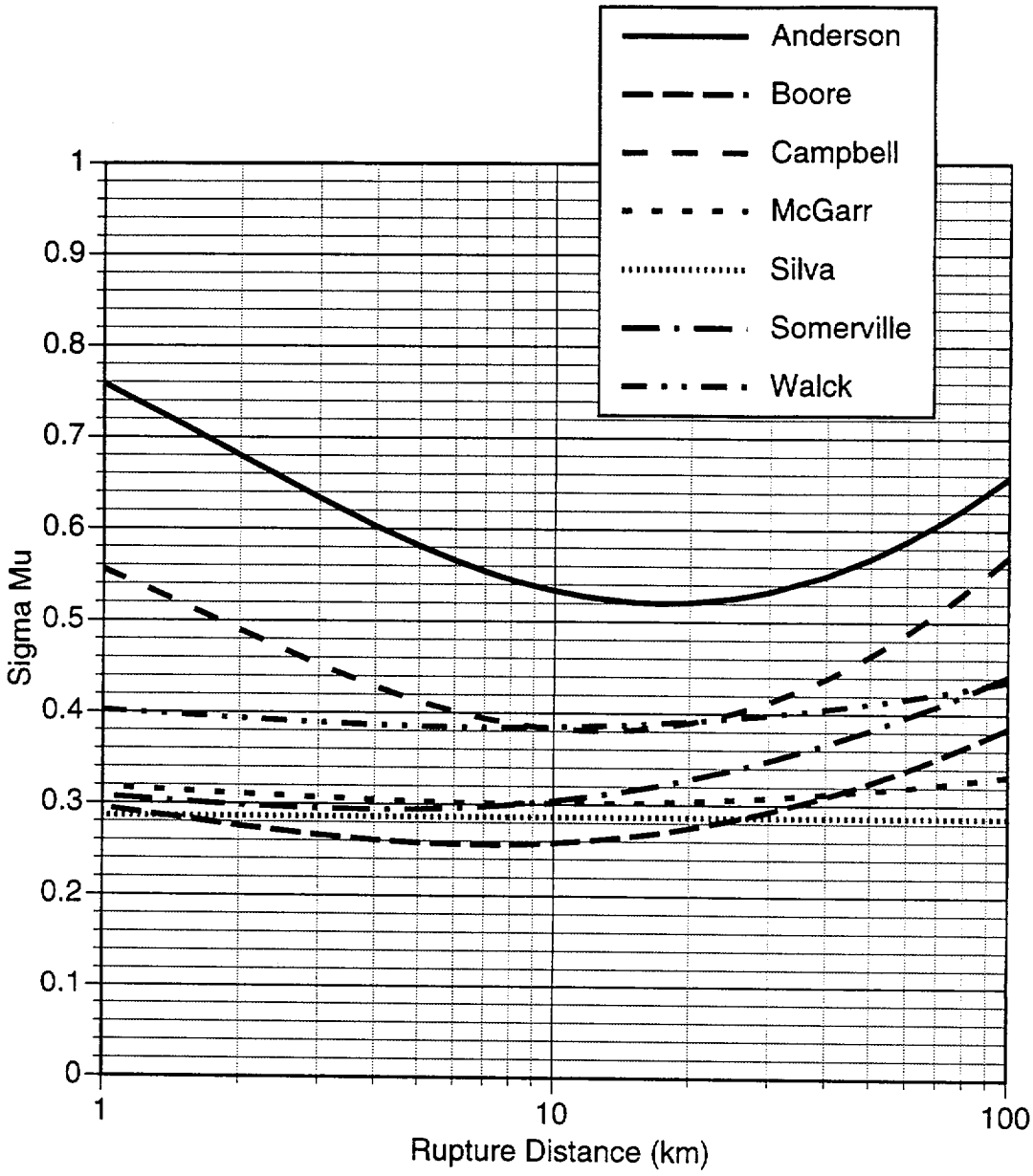

Figure 6-19 Comparison of epistemic uncertainty in the median vertical PGA for M_W 6.5, normal faulting

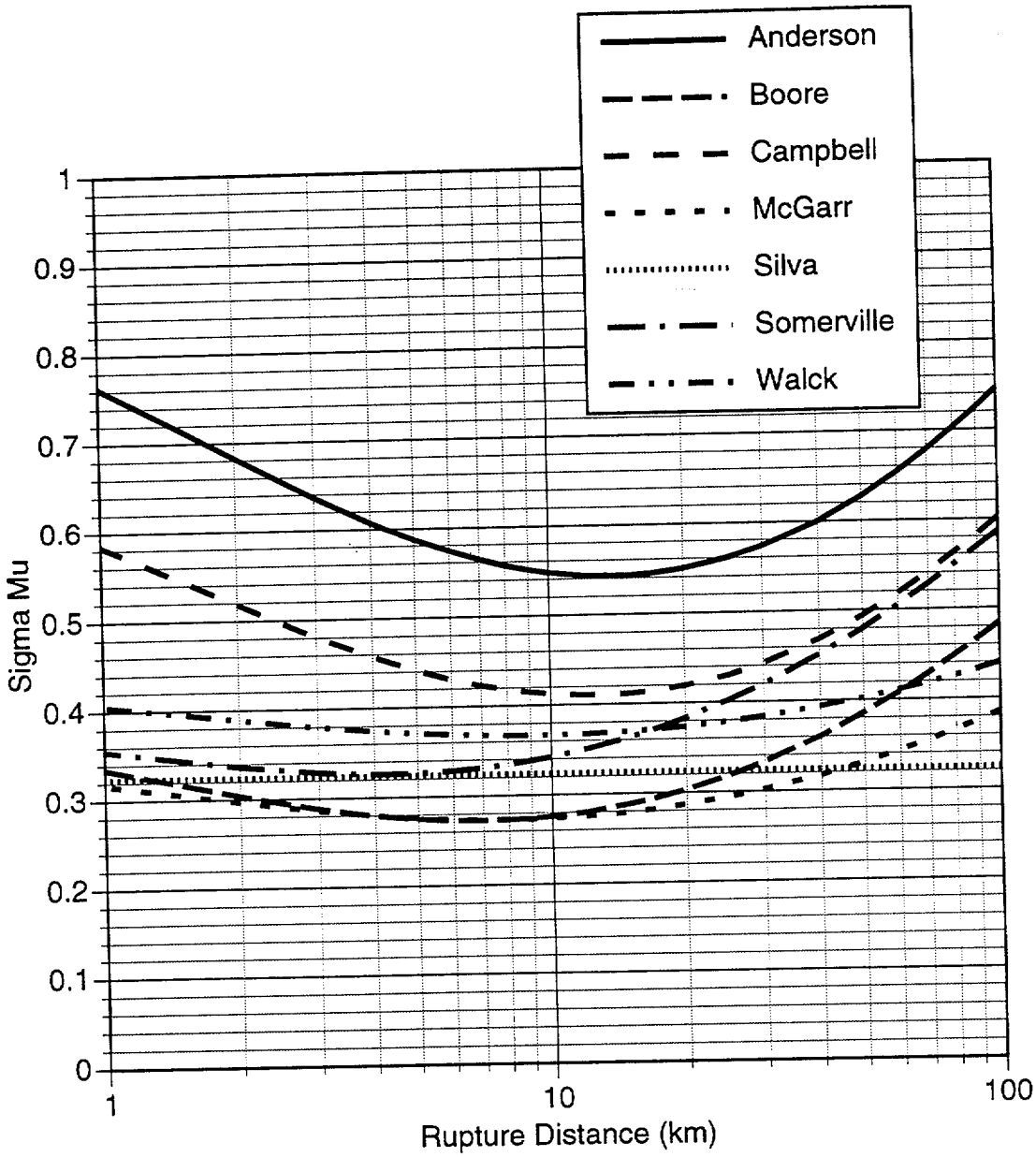

Figure 6-20 Comparison of epistemic uncertainty in the median 1.0 sec vertical spectral acceleration (at 5% damping) for M_W 6.5, normal faulting

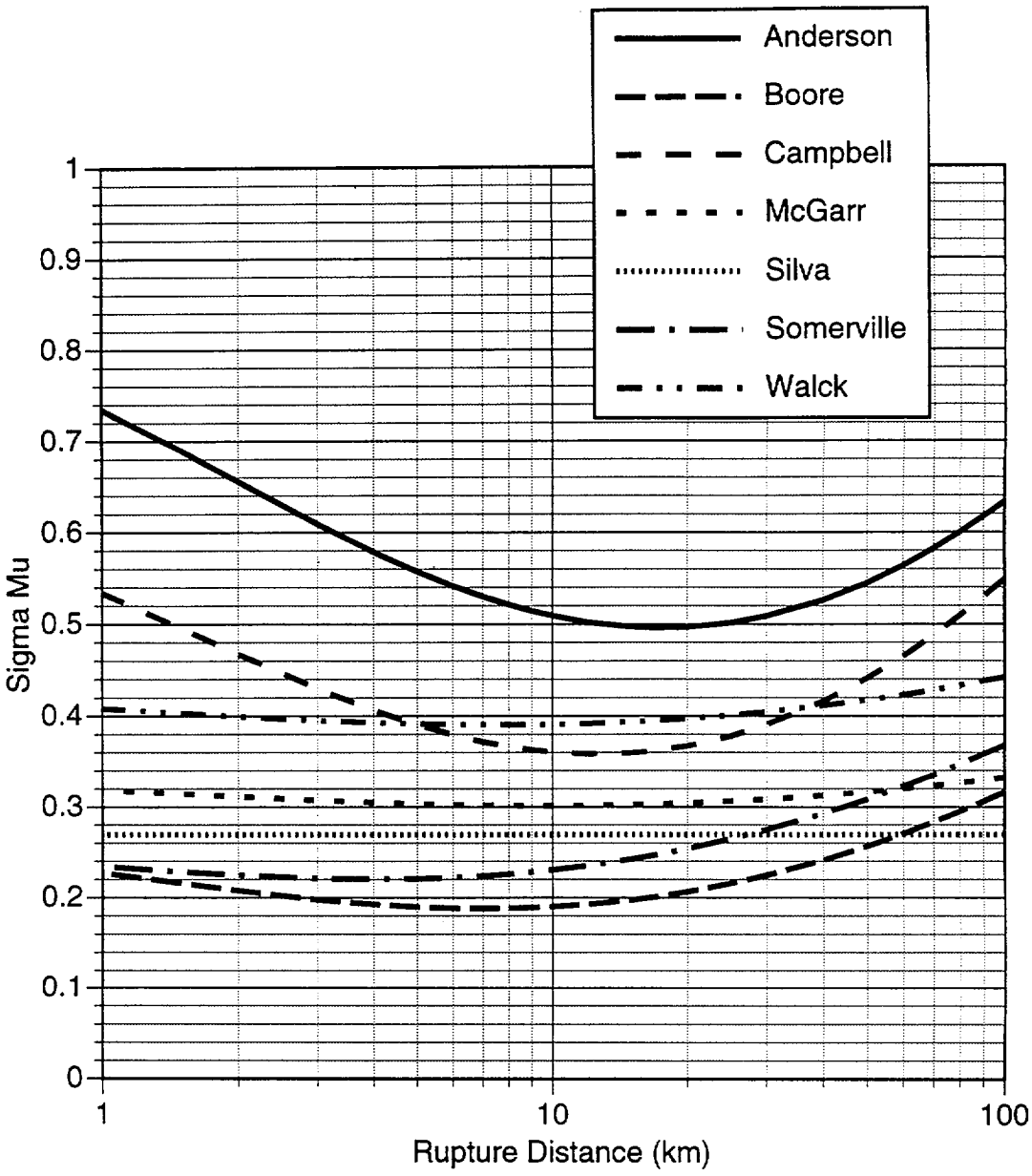

Figure 6-21 Comparison of epistemic uncertainty in the median vertical PGA for M_W 7.5, normal faulting

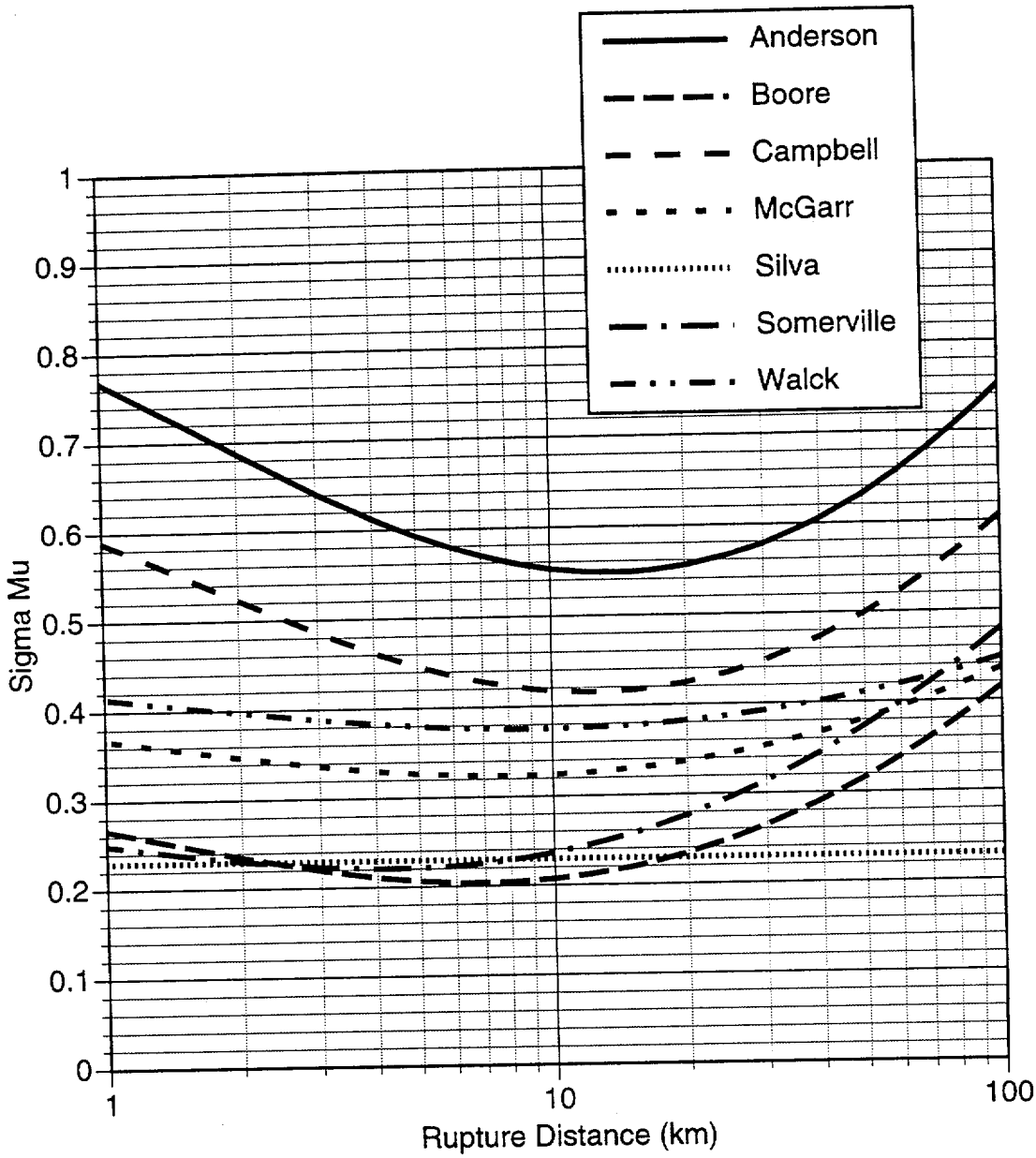

Figure 6-22 Comparison of epistemic uncertainty in the median 1.0 sec vertical spectral acceleration (at 5% damping) for M_W 7.5, normal faulting

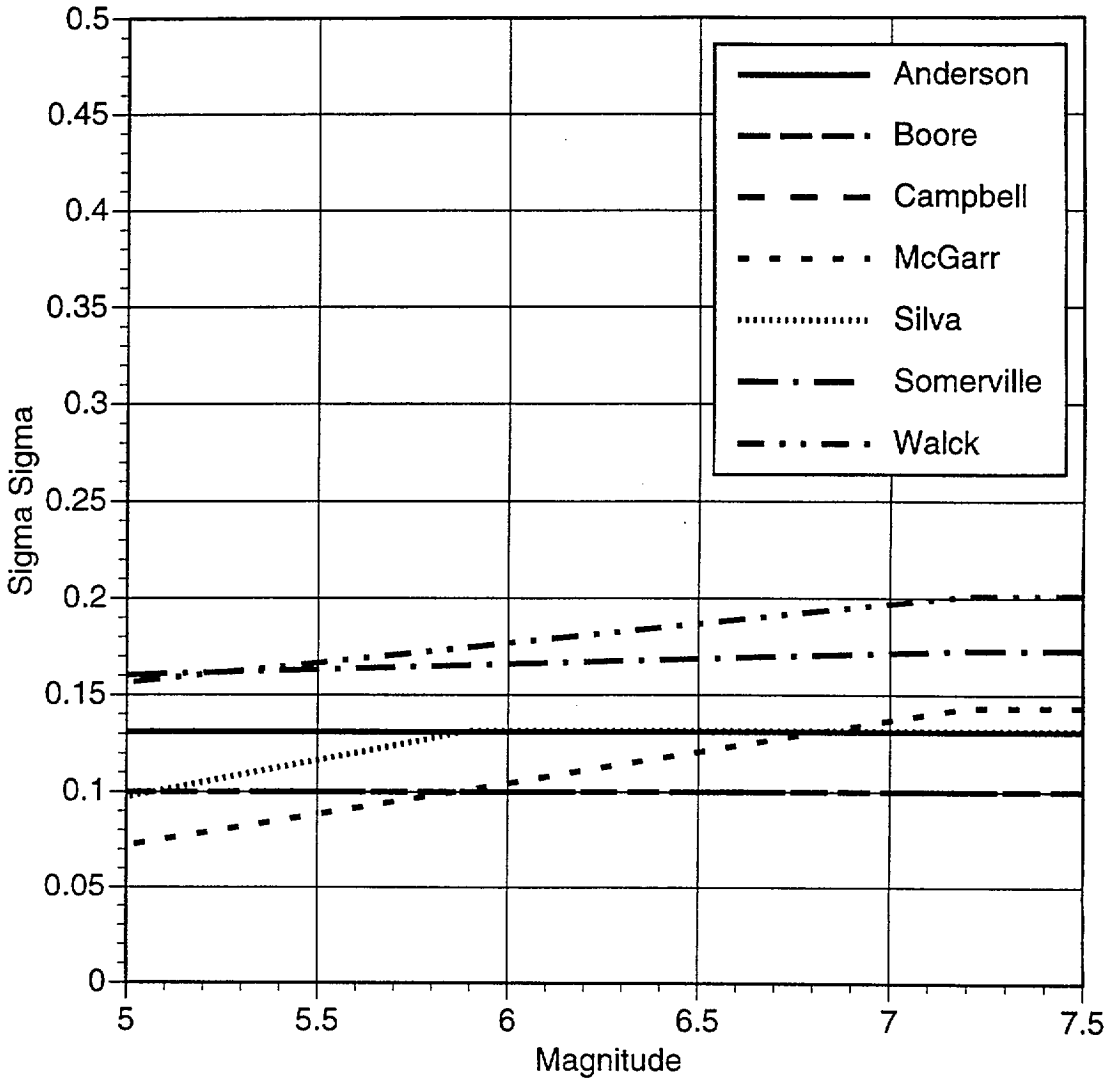

Figure 6-23 Comparison of epistemic uncertainty in the aleatory variability of vertical PGA.

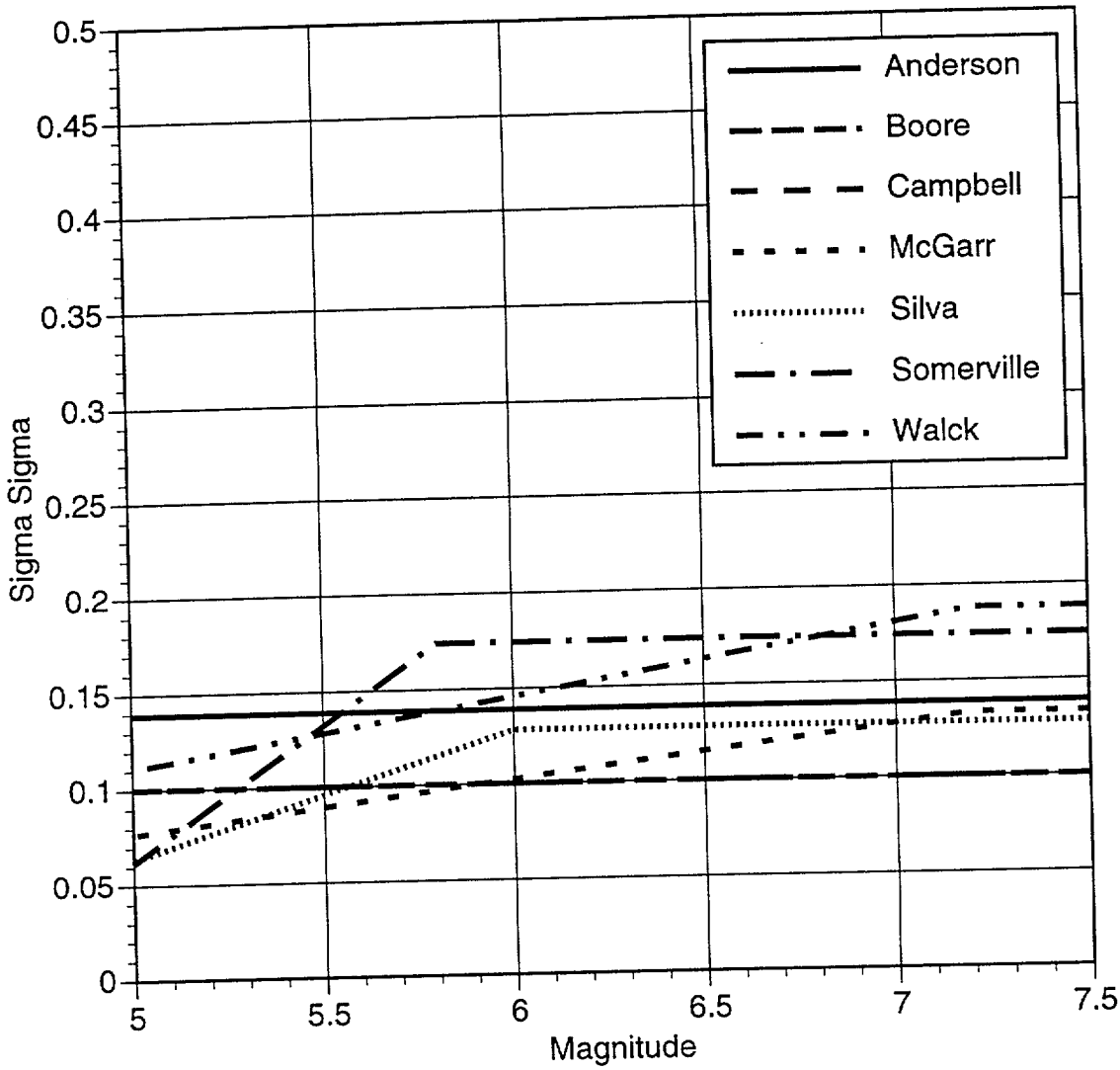

Figure 6-24 Comparison of epistemic uncertainty in the aleatory variability of 1 second vertical spectral acceleration (5% damping).

7.0
PSHA METHODOLOGY AND RESULTS FOR GROUND MOTION HAZARD

This chapter describes the methodology used to perform the PSHA for vibratory ground motion and the resulting calculations for the Yucca Mountain site. Section 7.1 provides an overview of the PSHA approach and introduces some key terms. Section 7.2 provides details about the implementation of the PSHA methodology specifically for the Yucca Mountain site. Section 7.3 presents the seismic hazard results, integrated over all SSFD expert teams and GM experts. Section 7.4 presents sensitivity results divided into three parts: Section 7.4.1, a comparison of hazard results across SSFD expert teams; Section 7.4.2, sensitivity to the alternative models formulated by each SSFD expert team; and Section 7.4.3, sensitivity to GM experts.

The hazard was calculated for reference rock outcrop (Figure 1-1) at the center of the potential repository block between the Solitario Canyon and Ghost Dance faults. The site coordinates are UTM 547.953 km easting, 4077.750 km northing.

7.1 BASIC PSHA MODEL

The methodology to calculate the probabilistic ground motion hazard at a site is well established in the literature (Cornell, 1968, 1971; McGuire, 1976, 1978). Calculation of the hazard requires specification of the following three inputs:

- The geometry of a seismic source (e.g., source i) relative to the site, and a relationship between rupture size and magnitude determine the conditional probability distribution of distance r from the earthquake rupture to the site (given magnitude): $f_{R(i)|M(i)}(r,m)$. The types of sources are faults and areal source zones.

- The mean annual rate of occurrence ν_i and magnitude distribution $f_{M(i)}(m)$ of earthquakes occurring on each source i. This characterization includes the M_{max} that a seismic source can produce. The M_w scale is used in all the final hazard calculations.

- An attenuation relation for the estimation of ground motion amplitude (e.g., peak ground acceleration [PGA] or spectral acceleration) at the site as a function of earthquake magnitude and distance. This characterization includes both an equation for the median amplitude and a standard deviation σ that describes the site-to-site and event-to-event scatter in ground motion amplitude observations for the same magnitude and distance.

These inputs are illustrated on Figure 7-1, Parts a through c. Figure 7-1a shows the geometry of a seismic source and the distance distribution for a given value of magnitude. The distribution of magnitude $f_{M(i)}(m)$ for an areal source is typically specified as the doubly truncated exponential distribution. Seismicity for a source with the exponential magnitude distribution is completely specified by the minimum magnitude m_o and parameters a and b. Parameter a is a measure of seismic activity, b is a measure of relative frequency of large versus small events, and $\log[\nu_i f_{M(i)}(m)]$ is proportional to $-bm$ for $m \leq m_{max}$. Except for truncation effects near M_{max}, this is the well-known Gutenberg-Richter relation. The distribution of magnitude $f_{M(i)}(m)$ for a fault is specified by an exponential distribution, a characteristic distribution (Youngs and Coppersmith, 1985, as illustrated on Figure 2-1b), or a maximum-moment distribution (Wesnousky *et al.*, 1983). The rate information for these three distribution shapes may be specified, respectively, as the rate ν_i, the rate of large earthquakes (magnitude greater than M_{max} - ½), or the slip rate (for faults only).

The ground motion is modeled by an attenuation function, as illustrated on Figure 7-1c. Attenuation functions are usually of the form $ln[A] = f(M,R) + \varepsilon$, where A is ground motion amplitude, M is magnitude, R is distance, and ε is a random variable (with mean zero and standard deviation σ) that represents scatter in $ln[A]$ for the same magnitude and distance. The attenuation function is used to calculate $G_{A|m,r}(a^*) = P[A > a^*|m,r]$: the probability that the ground motion amplitude A is larger than a^*, for a given M and R. The seismic hazard over all sources is calculated as a summation:

$$\nu(a^*) = \sum_i \nu_i \iint_r G_{A^*|m,r}(a^*)\, f_{M(i)}(m) f_{R(i)|M(i)}\, dm\, dr \qquad (7\text{-}1)$$

in which $\nu(a^*)$ is the annual rate of earthquakes that produce amplitudes $A > a^*$ at the site, and the summation is performed over all seismic sources i. The integration on magnitude in Equation 7-1 considers only earthquakes with magnitudes greater than a minimum magnitude m_o, typically taken as M_w 5. Smaller earthquakes are assumed to produce no damage to engineered structures, regardless of the ground motion amplitudes they generate. Thus, both ν and $f_{M(i)}(m)$ are only specified for magnitudes greater than m_o, although smaller magnitudes are considered in the determination of the rate and magnitude distribution.

Equation 7-1 is formulated using the assumption that earthquakes (most particularly, successive earthquakes) are independent in size and location. In all seismic hazard applications, primary interest is focused on computing probabilities for the occurrence of high (rare) ground motions (as a result, the probability of two exceedances in 1 year is negligible). Thus, the quantity on the right side of Equation 7-1, which is the annual rate of earthquakes with amplitude $A > a^*$, is a very good approximation to the probability of exceeding amplitude a^* in one year.

The calculation of hazard from all sources is performed for multiple values of a^*. The result is a hazard curve, which gives the annual probability of exceedance as a function of a^*. This calculation is performed for multiple measures of ground motion amplitude (i.e., PGA and spectral acceleration at multiple frequencies).

7.1.1 Treatment of Uncertainty

The most recent PSHA studies distinguish between two types of uncertainty, namely epistemic and aleatory. Aleatory uncertainty (sometimes called randomness) is probabilistic variability that results from natural physical processes. The size, location, and time of the next earthquake on a fault and the details of the ground motion are examples of quantities considered aleatory. In current practice, these quantities cannot be predicted, even with the collection of additional data. Thus, the aleatory component of uncertainty is irreducible. The second category of uncertainty is epistemic (sometimes called simply uncertainty), which results from imperfect knowledge about earthquakes and their effects. An example of epistemic uncertainty is the shape of the magnitude distribution for a given seismic source. In principle, this uncertainty can be reduced with advances in knowledge and the collection of additional data.

These two types of uncertainty are treated differently in advanced PSHA studies. Integration is carried out over aleatory uncertainties to get a single hazard curve (see Equation 7-1), whereas epistemic uncertainties are expressed by incorporating multiple assumptions, hypotheses, models, or parameter values. These multiple interpretations are propagated through the analysis, resulting in a suite of hazard curves and their associated weights. Results are presented as curves showing statistical summaries (e.g., mean, median, fractiles) of the exceedance probability for each ground motion amplitude. The mean and median hazard curves convey the central tendency of the calculated exceedance probabilities. The separation among fractile curves conveys the net effect of epistemic uncertainty about the source characteristics and ground motion prediction on the calculated exceedance probability.

Epistemic uncertainties are associated with each of the three inputs to the seismic-hazard evaluation. The seismogenic potential of faults and other geologic features is uncertain, as a result of (1) uncertainty about the tectonic regime operating in the region and (2) incomplete knowledge of these geological features. The geometry of these geologic features is also uncertain. Uncertainty in the rate of seismicity is generally divided into uncertainty in M_{max}, uncertainty in the type of magnitude distribution, uncertainty in the rate parameter (i.e., activity rate, rate of large events, or slip rate), and uncertainty in b or other shape parameters of the magnitude distribution $f_{M(i)}(m)$. Finally, the attenuation functions are uncertain, which arises from uncertainty about the dynamic characteristics (source, path, and site effects) of earthquake ground motions in the vicinity of Yucca Mountain. This uncertainty is large because few strong motions have been recorded in the region. Uncertainties in seismic source characterization and ground motion attenuation relations were quantified by considering inputs from six SSFD expert teams and seven GM experts, and by each team's and expert's own assessment of uncertainty.

That is, each SSFD expert team formulated multiple alternative interpretations about the seismogenic characteristics of potential seismic sources, and assigned weights to these hypotheses according to their credibility given the current state of knowledge and the degree to which they are supported by data. Each GM expert applied a similar procedure to alternative interpretations about the source, path, and site characteristics affecting ground motions. The development of these seismic source and ground motion interpretations was described previously in Chapters 4.0, 5.0, and 6.0.

7.2 IMPLEMENTATION OF METHODOLOGY IN THIS STUDY

This section describes the PSHA calculation methodology in more detail, with emphasis on methodological developments that were introduced to represent the specific conditions at Yucca Mountain.

7.2.1 Fault Sources

Fault sources were modeled as planar features and their geometry was represented in three dimensions by a fault trace, a dip angle, and minimum and maximum depths. Earthquakes occurring on these faults are treated as having finite, magnitude-dependent length and width, which are calculated using the Wells and Coppersmith (1994) relationship for subsurface rupture length (all fault types).

Due to the presence of closely spaced parallel local faults, all of the SSFD expert teams included scenarios in which ruptures occur simultaneously on two or more of these faults. The teams specified these seismic sources by indicating the associated faults, their occurrence or slip rates, and their magnitude distributions.

The ASM, RYA, SBK, and SDO expert teams specified the multiple-rupture scenarios as having magnitudes comparable to their M_{max} (i.e., these scenarios have maximum-moment magnitude distributions) and always rupturing all the faults involved. Smaller events on these faults are only considered as part of the respective individual sources, which are not mutually exclusive from the multiple-rupture sources.

The AAR and DFS expert teams specified the multiple-rupture sources as having exponential or characteristic magnitude distributions and being capable of single- as well as multiple-rupture events, depending on their magnitude. Each team specified the range of magnitudes associated with ruptures on one fault, two faults, three faults, etc., for each multiple-rupture scenario. These multiple-rupture sources are therefore mutually exclusive from the corresponding single-rupture fault sources.

For events with multiple ruptures, the rupture length and width on each fault are calculated as $L\ n^{-\alpha}$ and $Wn^{-\alpha}$, respectively, where L is the single-rupture length and W is the single-rupture width given by Wells and Coppersmith (1994), and n is the number of simultaneous ruptures. This equation arises from the assumption that the seismic moment of the multiple-rupture event is divided equally among the various faults and that the stress drop is constant across ruptures and is the same for single-rupture and multiple-rupture events.

The SSFD expert teams specified which simultaneous-rupture sources should be treated as multiple ruptures for the purposes of ground motion evaluation (see below), and which should be treated as single rupture plane events.

The GM experts parameterized ground motion amplitude from multiple-rupture events as a function of the total magnitude of the event, the distance to the closest rupture, and the number of faults that rupture simultaneously. According to some of their interpretations, multiple ruptures affect not only the median amplitude, but also the aleatory and/or the epistemic standard deviations (Section 6.4.1).

7.2.2 Areal Source Zones

Areal source zones are defined by a polygon in latitude-longitude space. In most PSHA studies, areal zones are assumed to have uniform activity rate per unit area (EPRI, 1986; USGS, written communication, 1996, constitute notable exceptions). This study allowed for both uniform and variable rates per unit area. Each SSFD expert team specified the approach to use for each areal zone. If they specified variable seismicity, they also specified the degree of smoothing. The teams could also specify that an areal zone could have both uniform and variable seismicity, or multiple degrees of smoothing, by means of alternative branches in the logic tree. The methodology to calculate variable seismicity utilizes the spatial pattern of historical seismicity within the source, as described in Section 4.1.4.1.

Hypocentral depth is considered explicitly in the hazard integration (as part of the calculation of $f_{R(i)|M(i)}(r;m)$ in Equation 7-1). The SSFD expert teams specified the distribution of hypocentral depth, as well as optional values for the minimum and maximum depths. All distributions specified are well represented by normal distributions.

The depth distributions specified by the SSFD expert teams are assumed to apply to small events (with negligible source dimensions) and are modified for the effect of magnitude-dependent rupture dimensions. The approach followed is described in Appendix J and is summarized below.

The down-dip rupture width for a given magnitude is calculated using the corresponding relationship by Wells and Coppersmith (1994) and projected into a vertical width using a typical dip angle of 70 degrees. The vertical location of the hypocenter is taken as uniformly distributed over the lower 75% of the vertical width. Using this distribution, we calculate the probability that a certain hypocentral depth is realizable, for a given magnitude. This is simply the probability that the top of the rupture is below ground, given hypocentral depth and rupture width. Viewed as a function of depth, this probability has the shape of a ramp. The resulting magnitude-dependent depth distribution is obtained by multiplying the small-event magnitude distribution by the magnitude-dependent probability that each depth is realizable, and then normalizing so that the distribution integrates to unity. The resulting distribution forces the hypocenters of larger events to greater depths. Figure 7-2 illustrates this calculation. This distribution is consistent with the depths on Figure 9-11 of S. K. Pezzopane and T. E. Dawson (USGS, written communication, 1996), which shows focal depths as a function of magnitude for events in the Basin and Range Province.

Because the attenuation equations predict amplitude as a function of magnitude and distance to the rupture, a relationship between hypocentral and rupture distance is required. This relationship takes the form of equations for the conditional mean and standard deviation of rupture distance given magnitude and hypocentral distance (Appendix J). The effect of the conditional standard deviation in rupture distance is to make the aleatory uncertainty given hypocentral distance larger than the aleatory uncertainty given rupture distance, as has been observed in the development of empirical attenuation equations (e.g., Campbell, 1981).

7.2.3 Ground Motion Attenuation

Each GM expert characterized epistemic uncertainty in the median amplitude and the ground motion scatter by means of standard deviations σ_μ and σ_σ, respectively. For the purposes of the PSHA calculations, it is necessary to represent these uncertainties as discrete values of the associated "epistemic" variables ε_μ and ε_σ. Following EPRI (1993) and Toro *et al.* (1997),

ε_μ was discretized into four points at locations $\pm\ 0.74\,\sigma_\mu$ (weight 0.454) and $\pm\,2.33\,\sigma_\mu$ (weight 0.0454) (Figure 7-3). The variable ε_σ was discretized conditionally on σ_μ, as follows. For $\varepsilon_\mu = \pm\ 0.74\,\sigma_\mu$, ε_σ was discretized into three points at 0 (weight 2/3) and $\pm\ 1.73\ \sigma_\sigma$ (weight 1/6 each). For $\varepsilon_\mu = \pm\,2.33\,\sigma_\mu$, ε_σ was discretized into two points at $\pm 1\,\sigma_\sigma$ (weight 0.5 each). Each combination of ε_μ and ε_σ is treated as one attenuation equation in the PSHA calculations. The resulting total number of attenuation equations for all seven experts is 70.

7.2.4 Calculations

Hazard calculations for vibratory ground motions for a single SSFD expert team proceeded in two steps, as follows:

1. Calculation of seismic hazard from each individual source: This calculation was performed for each combination of attenuation equation and seismic source parameters resulting in one hazard curve and one weight for each combination.

2. Calculation of total hazard (i.e., the hazard from all seismic sources) and its epistemic uncertainty. For the calculation of quantities other than the mean hazard, this calculation takes into account the probabilistic dependence introduced by hypotheses in the logic tree that affect more than one source. This calculation considers each possible branch of the overall logic tree (which includes attenuation equations as well as seismic source characteristics). The hazard associated with one branch of the logic tree includes only those sources that are active given that branch and only those source parameters that are consistent with that branch. The result of this calculation is a set of mean and fractile hazard curves. (We compute 11 fractiles in order to carry distribution-shape information into the integration step below.)

Calculation of the integrated hazard (across all SSFD expert teams) was performed by combining the expert teams' mean and fractile hazard curves, giving each team equal weight. The result is a set of integrated mean and fractile hazard curves.

In addition to these main results, deaggregation results calculate and display the contributions of various magnitude-distance-ε combinations to the mean hazard. This information is required

for the selection of the magnitude-distance-ε combinations to use in seismic design. Furthermore, sensitivity results provide insights into the effect of various parameters and assumptions on the calculated seismic hazard and its uncertainty.

7.3 INTEGRATED RESULTS

The integrated results provide a representation of seismic hazard and its uncertainty at the site, based on the interpretations and parameters developed by the six SSFD expert teams and seven GM experts. Separate results are obtained for PGA and spectral accelerations at 0.3, 0.5, 1, 2, 5, 10, and 20 Hz. The results for each ground motion measure are in the form of summary hazard curves. Figures 7-4 through 7-6 show the mean and fractile hazard curves for PGA and for 10- and 1-Hz spectral acceleration. Figures 7-7 and 7-8 show the mean and fractile hazard curves for horizontal and vertical PGVs, respectively. The mean and median hazard curves convey the central tendency of the calculated exceedance probabilities. The separation between the 15th and 85th percentile curves conveys the effect of epistemic uncertainty on the calculated exceedance probability. A large portion of this epistemic uncertainty results from epistemic uncertainty in ground motions, as will be shown in Section 7.4.3. Figure 7-9 shows the uniform hazard spectrum (UHS) for 10^{-4} annual exceedance probability, which is calculated from the spectral acceleration hazard curves (PGA is treated as 100-Hz spectral acceleration for these plots).

Figures 7-10 through 7-13 show analogous hazard curves and spectrum for the vertical component of ground motion. Figure 7-14 shows the horizontal and vertical mean UHS for 10^{-4} annual exceedance probability in a tripartite scale. This scale shows the spectrum in terms of spectral acceleration, spectral velocity, and spectral displacement. Table 7-1 lists the mean UHS values and PGV values for 10^{-3} and 10^{-4} annual exceedance probability, and for both horizontal and vertical motions.

Figures 7-15 and 7-16 show the deaggregation of the mean hazard (for 10^{-4} annual exceedance probability) into magnitude-distance-ε bins, where ε is the difference between the logarithm of the ground motion amplitude and the mean logarithm of ground motion (for that M and R) measured in units of the standard deviation σ of log (ground motion). Figure 7-15 indicates that the 5 to 10-Hz ground motions (and other high-frequency motions as well) are dominated by

events of less than M_w 6.5 at distances less than 15 km. In contrast, ground motions at 1 to 2 Hz (and other low-frequency motions as well) contain a sizable contribution from M_w 7 and greater events at distances beyond 50 km. Results in Section 7.4 will show this contribution is primarily from the Death Valley, Furnace Creek, and Fish Lake Valley faults, which have higher M_{max} and much higher activity rates than the local faults.

7.4 SENSITIVITY RESULTS

Sensitivity results provide insights into the effect of various interpretations and parameters on the calculated seismic hazard and its uncertainty. These results provide insight into the PSHA process. They also provide a consistency check for the experts and analysts.

7.4.1 Comparisons Across SSFD Expert Teams

Figures 7-17 through 7-20 compare the mean hazard curves obtained by the six SSFD expert teams, for PGAs and spectral accelerations at 10, 1, and 0.3 Hz. These results show a reasonable degree of consistency among the mean estimates of the expert teams, with less than a factor of three (in annual exceedance probability) between the lowest and the highest teams. This consistency among experts is likely the result of using a large common information base and of having an elicitation and feedback format that minimizes differences in knowledge or understanding among experts.

7.4.2 Sensitivity Results for Each SSFD Expert Team's Interpretations

Several types of sensitivity results are presented in this section for each SSFD expert team. (AAR, Figures 7-21 through 7-52; ASM, Figures 7-53 through 7-80; DFS, Figures 7-81 through 7-104; RYA, Figures 7-105 through 7-132; SBK, Figures 7-133 through 7-158; and SDO, Figures 7-159 through 7-177). Table 7-2 provides a "road map" for these figures, whereas the following text first describes the results generally, then discusses results specifically for each team. The number and type of figures shown vary somewhat between teams, as each team defined different logic trees and different sources.

The most straightforward type of sensitivity results are obtained by deaggregating the calculated mean hazard into contributions by source group, by individual source, or by magnitude-

distance-ε bins. Six figures of this type are first presented for each SSFD expert team (three for 10-Hz and three for 1 Hz), as follows:

1. Mean seismic hazard by source type (i.e., local faults, local areal zones, and regional faults). The local fault type is subdivided into single-rupture and multiple-rupture fault sources. This subdivision is based on whether the single-rupture or multiple-rupture attenuation equations apply to a fault or faults, as specified by the SSFD expert team. (Recall that the expert teams specified that the multiple-rupture attenuation equations are applicable to some, but not all, the multiple-rupture fault sources.)

2. Dominant seismic sources, based on their contribution to seismic hazard at 1.1g (for 10 Hz) and at 0.5g (for 1 Hz). Each source is labeled to indicate its type.

3. Magnitude-distance-ε deaggregation of the mean hazard for each source type.

Note two important considerations when examining the figures showing dominant sources. First, the contributions shown on these figures are mean contributions. Thus, the contribution of a source may be written as

$$P\,[\text{Source is Active}] \times \text{Mean Hazard given that the Source is Active}$$

Therefore, a source that can produce a high hazard (if active), but with a low probability of activity, will not necessarily show as having a high contribution to the mean hazard. The importance of this source may be seen in the sensitivity to the logic tree branch that controls whether the source is active. Second, the definition of a "source" for the purposes of this and other figures has some limitations. Consider the Solitario Canyon fault as an example and assume that the SSFD expert team is certain that the fault is active. The Solitario Canyon fault may appear by itself in some branches of the logic tree and also as part of a multiple-rupture source in other branches. These and other figures show separate contributions from Solitario Canyon fault (alone) and from the multiple-rupture source.

Next, sensitivity results with respect to interpretations or parameters are presented separately for a variety of seismic sources. They show the effect of each interpretation or parameter on the

calculated seismic hazard from that type of source. Results for the local faults and areal source zones are shown for 10 Hz; results for the regional faults are shown for 1 Hz because these faults are important only at low frequencies. Sensitivities to all global interpretations and parameters (i.e., those that affect more than one seismic source) were calculated and examined; all important sensitivities are shown here. Sensitivities to source parameters were calculated and examined for the two or three most important sources in each type. Typically, only the results for the most important source in each type are shown here. Results for other sources have smaller contributions to the total uncertainty and are not shown.

Sensitivity results with respect to global interpretations are calculated by computing the mean hazard for each interpretation and then comparing the results obtained with the various interpretations. The weights assigned to the various interpretations or branches of the logic tree are also an important element of these comparisons and are shown (in parentheses) on all figures.

Sensitivity results with respect to source parameters are calculated in a different manner. For instance, to investigate the sensitivity to the M_{max} of the Solitario Canyon fault, the following steps are implemented:

1. Compute the combined hazard from all local faults, for all combinations of global and fault parameters.

2. Group these hazard curves into bins defined so that the parameters of all hazard curves in one bin differ only in the M_{max} for the Solitario Canyon fault (i.e., all other parameters used to compute these hazard curves are the same).

3. For each bin, calculate the mean and standard deviation of hazard and create mean $\pm \sigma$ hazard curves.

4. Compute the average of the mean + σ curves over all bins. Do the same for the mean - σ curves. The resulting difference between the mean - σ and mean + σ curves indicates the sensitivity of the results to uncertainty in the M_{max} of the Solitario Canyon fault. If the fault does not appear in all branches of the logic tree, an additional curve (labeled NA) is also shown, corresponding to the mean hazard from those branches of the logic tree where the fault does not appear. (Recall that the Solitario Canyon fault by itself may not appear in all branches of the logic tree, even if the SSFD expert team considers this fault to be active with certainty.)

This approach is more convenient because source parameters may have distributions that vary as a function of the values of other variables in the logic tree. For instance, the distribution of M_{max} has a range of number of magnitudes, a range of values, and different weights, depending on fault length. Other source parameters, such as the recurrence of areal source zones, have up to 25 different (rate,b) pairs. These factors make it difficult to display and interpret these results in the same manner as the global sensitivity results. It is important to emphasize that this approach shows the mean $\pm$ σ effect *on hazard* of the uncertain parameter, not simply the results associated with the mean - σ and mean + σ values of the parameter.

The following discusses sensitivity results specifically by team. This discussion focuses on the amplitudes associated with 10^{-4} annual exceedance probability (1.1 g for 10 Hz, 0.5 g for 1 Hz). When necessary, the discussion includes a brief description of some elements of a team's seismic source characterization.

7.4.2.1 AAR Team

Figures 7-21 and 7-22 show the contributions of the various source types to the mean hazard. For 10 Hz, both the individual local faults and the areal sources are the major contributors to the hazard. For 1 Hz, the individual local faults, the areal zones, and the regional faults contribute similarly to the hazard.

Figures 7-23 and 7-24 show the contributions of the most important individual seismic sources from all source types. The most important local faults are two coalesced fault systems, namely the East-side (all local faults east of Yucca Mountain; active with a probability of 75%), and West-side #2 (all local faults west of Yucca Mountain except the Solitario Canyon and Iron

Ridge faults; active with a probability of 60%). Both of these fault systems involve simultaneous ruptures on multiple faults. The AAR team associated these fault systems with the single-rupture attenuation equations because most of the seismic moment release is postulated to occur on a single-rupture plane. The most important areal zone is Zone 2, which includes the Nevada Walker Lane, the host areal source zone for Scenario 1 (see Section 4.3.1.1). The most important regional fault is the Death Valley-Furnace Creek fault system, which is also the most important contributor to hazard at 1 Hz.

The 10-Hz deaggregation results (Figure 7-25) show that most of the hazard comes from events of M_w 5 to 6.5 at short distances (<15 km occurring on local faults and generally within areal zones). The 1-Hz results (Figure 7-26) show a shift to higher magnitudes for the local faults and areal sources, and a large contribution from regional faults in the 45 to 60 km distance range and magnitudes greater than M_w 7 (associated with the Death Valley-Furnace Creek fault system).

Figures 7-27 through 7-41 show sensitivity results of the AAR local faults for 10-Hz horizontal spectral acceleration. The major nodes in the AAR global logic tree for local faults represent the existence of NW-SE dextral structures, the type of dextral structure, and the existence of a detachment. Additional branches consider detachment depth, the possibility of coalescence, coalescence pattern (i.e., which groups of faults rupture simultaneously), and seismogenic crustal thickness. The probability of coalesced behavior depends on preceding branches of the logic tree, with a high marginal probability of coalescence. The existence and pattern of coalescence are the only nodes to show significant sensitivity. Other branches of the local fault global logic tree show negligible sensitivity. Of the source parameters for the East-side fault system, recurrence model and recurrence (given the recurrence model and recurrence approach) show moderate sensitivity; b-value, rupture length, M_{max}, and recurrence approach show low sensitivity. Similar trends are observed in the sensitivity to the parameters of the West-side fault system (only results for recurrence model are shown here).

Figures 7-42 through 7-46 show sensitivity results for the AAR areal zones and 10-Hz horizontal spectral acceleration. The major nodes in the AAR global logic tree for areal zones represent three scenarios with differing areal zone configurations, and a fourth scenario containing only one areal zone. The first three scenarios use uniform seismicity; the fourth

scenario uses variable seismicity, with four alternative degrees of smoothing. In all scenarios, a portion of the host areal source zone (20-km radius around the site), is assigned a lower M_{max} by the AAR team due to more detailed knowledge of local fault sources. Sensitivity to scenario and to spatial variability is important. Sensitivity to minimum magnitude used in the recurrence calculations, M_{max}, and recurrence is low.

Figures 7-47 through 7-52 show sensitivity results for the AAR regional faults and 1-Hz spectral acceleration. The only regional faults that make any significant contribution to the hazard are Death Valley and Furnace Creek faults, which may be linked (i.e., rupture together, probability 80%) or independent (i.e., rupture separately, probability 20%). Sensitivity to the recurrence of the Death Valley-Furnace Creek fault system is moderate; sensitivity is low for other global and source parameters (i.e., linked vs. independent, fault lengths, sense of slip, recurrence used, dip angles, b-values, and M_{max}).

7.4.2.2 ASM Team

Figures 7-53 and 7-54 show the contributions of the various source types to the mean hazard. For 10 Hz, both the areal source zones and the single-rupture local faults are the major contributors to the hazard. For 1 Hz, the single-rupture local faults, the areal zones, and the regional faults contribute significantly to the hazard.

Figures 7-55 and 7-56 show the contributions of the most important individual seismic sources from all types of sources. The Walker Lane areal source is dominant, both at 10 Hz and 1 Hz, and its contribution is a factor of two or three larger than that of the next source. Important local faults include Stagecoach Road-Paintbrush Canyon and Solitario Canyon faults. Important regional faults include the Furnace Creek and Death Valley faults.

The 10-Hz deaggregation results (Figure 7-57) show that most of the hazard comes from short distances (<15 km), either M_w 5 to 6.5 events from the areal zones or M_w 5 to 7 events on the local faults. The 1-Hz results (Figure 7-58) show a shift to higher magnitudes for the local faults and areal zones, and a large contribution from regional faults in the 45 to 60 km distance range and magnitudes greater than M_w 7 to 7.5 associated with the Furnace Creek and Death Valley faults.

Figures 7-59 through 7-71 show sensitivity results of the ASM local faults for 10-Hz horizontal spectral acceleration. The major nodes in the ASM global logic tree for local faults consider the existence of a detachment and whether the detachment is seismogenic, the existence of a buried strike-slip fault and whether it is seismogenic, whether the faults merge at depth, the occurrence of simultaneous ruptures, the recurrence approach used, and dip angles. The type of recurrence approach (slip rates versus recurrence intervals) and the occurrence of simultaneous ruptures are the only nodes that show significant sensitivity. Of the source parameters of the Stagecoach Road-Paintbrush Canyon fault system, the recurrence model and recurrence (given the recurrence model and recurrence approach) show significant sensitivity.

Figures 7-72 through 7-75 show sensitivity results of the ASM areal zones for 10-Hz horizontal spectral acceleration. The only node in the ASM global logic tree for areal zones corresponds to the choice of alternative seismicity catalogs. The two areal zones (Walker Lane and Basin and Range) use uniform seismicity. Sensitivity to the catalog used is very low. Sensitivity to source parameters of the Walker Lane source (i.e., recurrence and M_{max}) is low. Figure 7-75 shows the sensitivity to the M_{max} of the Walker Lane source for 1-Hz horizontal spectral acceleration. This sensitivity is also low, although somewhat higher than the one for 10 Hz shown on Figure 7-73.

Figures 7-76 through 7-80 show sensitivity results for the ASM regional faults and 1-Hz horizontal spectral acceleration. The only regional faults that make any significant contribution to the hazard are the Furnace Creek and middle Death Valley faults. The global logic tree for regional faults has nodes to represent recurrence model, recurrence approach, b-value, and maximum depth. Sensitivity to all these nodes is low. Sensitivity to recurrence and M_{max} is also low.

7.4.2.3 DFS Team

Figures 7-81 and 7-82 show the contributions of the various source types to the mean hazard. For 10 Hz, both the individual local faults and the areal zones are the major contributors to the hazard. For 1 Hz, the individual local faults and areal zones contribute equally to the hazard; the regional faults contribute slightly less.

Figures 7-83 and 7-84 show the contributions of the most important individual seismic sources from all source types. The most important local faults are the Stagecoach Road-Paintbrush Canyon fault system and the Solitario Canyon fault. The most important areal zone for both 10-Hz and 1-Hz motions is the East Walker Lane for their Model B, which includes a local host areal zone. The most important regional fault is the Death Valley-Furnace Creek fault system, which is a moderate contributor to hazard at 1 Hz.

The 10-Hz deaggregation results (Figure 7-85) show that most of the hazard comes from short distances (<15 km), and M_w 5 to 6.5 events for local faults or M_w 5 to 7 events for areal sources. The 1-Hz results (Figure 7-86) show a shift to higher magnitudes for the local faults and areal zones (with a shift to longer distances in the latter), and a moderate contribution from regional faults in the 45 to 60 km range and M_w 6.5 to 7.5 associated with the Death Valley, Furnace Creek, and Fish Lake Valley faults.

Figures 7-87 through 7-94 show sensitivity results of the DFS local faults for 10-Hz horizontal spectral acceleration. The major nodes in the DFS global logic tree for local faults consider the presence of independent versus multiple-fault ruptures, the subsurface geometry (planar versus detached, with two planar-fault scenarios) and multiple-fault rupture scenarios, the recurrence model, and the b-value. Sensitivity to the presence of multiple-fault ruptures versus independent faulting is important although the multiple branch has low weight, so that the resulting uncertainty is low. Sensitivity to other nodes in the global logic tree is low. Sensitivity to M_{max} and the recurrence of the Stagecoach Road-Paintbrush Canyon fault system is also low.

Figures 7-95 through 7-99 show sensitivity results of the DFS areal zones for 10-Hz horizontal spectral acceleration. The major nodes in the DFS global logic tree for areal zones represent the catalog used, zonation (one model with three source zones, the other with a single zone), and spatial variability and smoothing of seismicity within a source. The host zones included in both models contain a small local portion with a lower M_{max}. The sensitivity to spatial smoothing is low to moderate; all other sensitivities to global parameters are low. Sensitivities to M_{max} and the recurrence are also low.

Figures 7-100 through 7-104 show sensitivity results for the DFS regional faults and 1-Hz horizontal spectral acceleration. The major nodes in the DFS global logic tree for regional faults represent recurrence model, maximum depth, and b-value. Sensitivity to these three quantities is low. Sensitivity to the slip rate of the Death Valley fault is moderate, but the sensitivity to the corresponding M_{max} is low.

7.4.2.4 RYA Team

Figures 7-105 and 7-106 show the contributions of the various source types to the mean hazard. For 10 Hz, the single- and multiple-rupture local faults, together with the areal zones, are the major contributors to the hazard. For 1 Hz, the regional faults contribute the most, but the other source types also have important contributions to seismic hazard.

Figures 7-107 and 7-108 show the contributions of the most important individual seismic sources from all source types. The most important local faults are the Paintbrush Canyon-Stagecoach Road-Bow Ridge and the West-side coalesced fault systems. The latter involves the Solitario Canyon, Iron Ridge, Windy Wash, and Fatigue Wash faults, and is associated with the multiple-rupture attenuation equations. The most important areal source zones are A2 and A1: two alternative geometries for a small host source. The most important regional faults are the Furnace Creek and Death Valley, which are also the two most important contributors to hazard at 1 Hz.

The 10-Hz deaggregation results (Figures 7-109) show that most of the hazard comes from short distances (<15 km) and M_w 5 to 6.5 events for areal sources and M_w 5 to 7.0 events for local faults. The 1-Hz results (Figure 7-110) show a large contribution from regional faults in the 45 to 75 km range and M_w 6.5 to 7.5 associated with the Death Valley and Furnace Creek faults.

Figures 7-111 through 7-121 show sensitivity results of the RYA local faults for 10-Hz horizontal spectral acceleration. The major nodes in the RYA global logic tree for local faults represent maximum fault depth, coalescence model, b-values, fault lengths, and recurrence approach. Sensitivity is significant only for recurrence approach, and moderate for fault lengths. Other sensitivity branches are low. Sensitivity to the source parameters (recurrence model, M_{max}, and recurrence) of the East-side faults, the Paintbrush Canyon-Stagecoach Road-

Bow Ridge fault system is low to moderate. Sensitivity to the M_{max} and recurrence of the West-side fault system is moderate.

Figures 7-122 through 7-126 show sensitivity results of the RYA areal zones for 10-Hz horizontal spectral acceleration. The major nodes in the RYA global logic tree for areal zones represent choice of catalog used, zonation, and spatial smoothing of seismicity (in all but the host source). Sensitivity to all these branches is low. Sensitivity to the M_{max} and the recurrence of A2 zone is also low.

Figures 7-127 through 7-132 show sensitivity results of the RYA regional faults for 1-Hz horizontal spectral acceleration. The major nodes in the RYA global logic tree for regional faults are the configuration of the Death Valley-Furnace Creek fault system (linked or separate), the recurrence model, the maximum fault depth, and the b-value. Sensitivity to all of these branches is low. Sensitivity to the M_{max} and recurrence of the Furnace Creek fault is also low.

7.4.2.5 SBK Team

Figures 7-133 and 7-134 show the contributions of the various source types to the mean hazard. For 10 Hz, the single-rupture local faults are the major contributors to the hazard. For 1 Hz, the regional faults and the single-rupture local faults are the major contributors.

Figures 7-135 and 7-136 show the contributions of the most important individual seismic sources from all source types. The most important local faults are the Paintbrush Canyon-Stagecoach Road and Solitario Canyon faults. The most important areal zone is the Basin and Range zone, which is the host source zone. The most important regional fault is the Furnace Creek fault, which is also the most important contributor to hazard at 1 Hz.

The 10-Hz deaggregation results (Figure 7-137) show that most of the hazard comes from individual local faults; events at short distances (<15 km) and M_w 5 to 7. The 1-Hz results (Figure 7-138) show a large contribution from regional faults in the 45 to 60 km range and M_w 7 to 7.5 (associated with the Death Valley-Furnace Creek-Fish Lake Valley fault system).

Figures 7-139 through 7-146 show sensitivity results of the SBK local faults for 10-Hz horizontal spectral acceleration. The major nodes in the SBK global logic tree for local faults

represent fault behavior (independent, linked, coalesced, or detachment), fault dip, maximum depth, and b-value. Sensitivity to all of these nodes is low. Sensitivity to recurrence approach and recurrence model of the Paintbrush Canyon-Stagecoach Road fault system is moderate to low; sensitivity to other source parameters (M_{max} and recurrence) is low.

Figures 7-147 through 7-151 show sensitivity results of the SBK areal sources for 10-Hz spectral acceleration. The major nodes in the SBK global logic tree for areal zones represent zonation, choice of catalog (treated as independent across source zones), and adjustment for NTS events. Sensitivity to these nodes is low. Sensitivity to source parameters of the Basin and Range zone is moderate for recurrence and low for M_{max}.

Figures 7-152 through 7-158 show sensitivity results for the SBK regional faults and 1-Hz horizontal spectral acceleration. The major nodes in the SBK global logic tree for regional faults represent the rupture behavior of the Death Valley-Furnace Creek-Fish Lake Valley fault system, sense of slip of the Death Valley fault, maximum depth, dip angles, and b-values. Sensitivity is high for the scenario in which all faults in the Death Valley-Furnace Creek-Fish Lake Valley fault system are linked. The resulting contribution to uncertainty is low, however, because the branch associated with this scenario has a very low probability. Sensitivity to other global branches is low. Sensitivity is low for source characteristics of the Furnace Creek fault (i.e., recurrence approach, recurrence model, M_{max}, and recurrence).

7.4.2.6 SDO Team

Figures 7-159 and 7-160 show the contributions of the various source types to the mean hazard. For 10 Hz, both the single-rupture local faults and the areal source zones are the major contributors to the hazard. For 1 Hz, the single-rupture local faults, the areal zones, and the regional faults contribute equally to the hazard.

Figures 7-161 and 7-162 show the contributions of the most important individual seismic sources from all source types. The most important local fault is Solitario Canyon fault. The most important areal zone is Zone 1, the host zone, which represents the Walker Lane. Zone 1 is also the largest contributor to hazard at both 10 Hz and 1 Hz. The most important regional fault is the Furnace Creek fault.

The 10-Hz deaggregation results (Figure 7-163) show that most of the hazard comes from short distances (<15 km) and M_w 5 to 6.5 events for areal zones or M_w 5 to 7 events for local faults. The 1-Hz results (Figure 7-164) show a large contribution from regional faults, with a peak in the 45 to 60 km distance range and M_w 7 to 7.5 associated with the Death Valley and Furnace Creek faults. In addition, regional faults at other distances significantly contribute.

Figures 7-165 through 7-169 show sensitivity results of the SDO local faults for 10-Hz horizontal spectral acceleration. The SDO global logic tree for local faults considers only the b-value. Multiple-rupture scenarios are treated as part of the aleatory model (e.g., over time, some events involve multiple simultaneous ruptures, others involve single ruptures). Sensitivity to b-values is very low. Source parameters for the local faults include maximum depth, recurrence model, M_{max}, and recurrence. Sensitivity to these parameters is shown for the Solitario Canyon fault, and found to be low.

Figures 7-170 through 7-173 show sensitivity results of the SDO areal zones for 10-Hz spectral acceleration. The major nodes in the SDO global logic tree for areal zones represent choice of catalog and spatial variability and smoothing of seismicity within an areal zone. Sensitivity to choice of catalogs is moderate, with Version 8 giving a hazard that is roughly half the hazard from either of the other two catalogs. Sensitivity to spatial variability is low. Sensitivity to the parameters of Zone 1 (i.e., M_{max} and recurrence) is also low.

Figures 7-174 through 7-177 show sensitivity results for the SDO regional faults and 1-Hz horizontal spectral acceleration. The major nodes in the SDO global logic tree for regional faults represent maximum depth, recurrence model, and b-value. Sensitivity to these nodes is low. Source parameters include fault length, M_{max}, and activity rates. Sensitivity to these parameters for the Furnace Creek fault is low.

7.4.2.7 Overall Trends

The sensitivity results for all SSFD expert teams indicate the following general trends:

- Seismic source parameters with a direct effect on activity rates (e.g., recurrence approach [either slip rates or recurrence intervals], and recurrence model [characteristic,

exponential, or maximum moment] are the parameters that contribute the most to uncertainty in seismic hazard, for the exceedance probabilities of interest in this study.

- M_{max} has a small effect on uncertainty for the exceedance probabilities of interest in this study, especially for 10 Hz, because a large fraction of the hazard comes from more frequent moderate-magnitude events.

- Geometric fault parameters (e.g., rupture lengths, dips, maximum depths) are minor contributions to uncertainty. These parameters have a moderate effect on the locations of earthquakes and an effect on M_{max}, but do not affect earthquake frequency. (Fault geometry affects occurrence rates when activity is specified by slip rates. However, the increased activity that results from increased length of a fault that comes near the site [and whose closest approach to the site is the perpendicular distance] will occur away from the site and will have little effect on the hazard)

- Although expert teams vary somewhat, the dominant sources for seismic hazard at 10 Hz are the Paintbrush Canyon-Stagecoach Road and Solitario Canyon faults (or coalesced fault systems including these two faults), and the host areal zone (not necessarily in that order). At 1 Hz, the dominant sources are the Death Valley and Furnace Creek faults and the same three sources mentioned above.

- Multiple-rupture scenarios of the type with comparable seismic moment release on more than one fault (i.e., those requiring modification of the attenuation equations) make a small contribution to the total hazard for five of the six expert teams.

- All expert teams considered the existence of buried strike-slip faults and seismogenic detachments. Several of them explicitly included these sources in their models. The contribution of these sources to the total seismic hazard is negligible primarily because the corresponding branches in the logic tree have low probabilities. This is also true for volcanic sources of seismicity, which were explicitly considered by only two expert teams.

7.4.3 Sensitivity to Ground Motion Experts and Parameters

Figures 7-178 through 7-187 show the sensitivity of the total hazard to the GM experts and their interpretations. These comparisons all use the seismic source interpretations by the ASM team as an example. Results are shown for 10 Hz, 1 Hz, and 0.3 Hz. Three types of figures are shown, as follows:

1. Mean hazard calculated using the interpretations by each GM expert.

2. Mean hazard curves for all values of $\varepsilon_{\mu,}$, the parameter that scales each expert's median prediction to represent the expert's assessment of epistemic uncertainty in the median ground motion. These figures show the contribution of σ_μ to uncertainty in the hazard. σ_μ also has an effect on the mean hazard, because of the skewness of the lognormal distribution of ε_μ.

3. Mean $\pm$ σ curves showing the effect of σ_σ (each expert's assessment of epistemic uncertainty in σ) on the uncertainty in the calculated hazard (see the discussion of this type of sensitivity results in Section 3.3.2). σ_σ also affects the mean hazard, because the calculated seismic hazard is a nonlinear function of σ (with a positive second derivative).

In general, the most important ground motion contributors to uncertainty in the hazard are σ_μ and σ_σ (i.e., within-expert uncertainties), rather than expert-to-expert uncertainties. The moderate expert-to-expert variation is likely the result of using a common information base and of having an elicitation and feedback format that minimizes differences in knowledge and understanding among experts.

Other sensitivity results (not included in this report) indicate that the effect of σ_μ is higher for Anderson, and to a lesser extent for Boore, than for the other GM experts. This is one of the factors that make Anderson's results higher. The effect of σ_σ is more uniform across GM experts.

The importance of σ_σ increases as frequency decreases. This is consistent with the magnitude-distance-ε distributions on Figures 7-15 and 7-16, which show that the contribution from events with $\varepsilon > 2$ is more important for 1 Hz than for 10 Hz.

The total uncertainty due to ground motion issues (i.e., the combined expert-to-expert and within-expert uncertainties) is larger than the uncertainty due to seismic source-characterization issues. This conclusion may be qualitatively confirmed by comparing Figures 7-5 and 7-179. This is a common situation in multiple-expert PSHA studies.

In summary, the major contributor to epistemic uncertainty in seismic hazard is the uncertainty in ground motion amplitude that was expressed by each individual GM expert (within-expert epistemic uncertainty). Additional contributions to epistemic uncertainty arise from moderate differences among the SSFD expert teams and among the GM experts, as well as from the uncertainties expressed by the seismic source logic trees.

TABLE 7-1
MEAN UNIFORM HAZARD SPECTRAL VALUES (g) AND PGV VALUES (cm/sec) FOR REFERENCE ROCK OUTCROP

Freq. (Hz)	Horizontal		Vertical	
	10^{-3}	10^{-4}	10^{-3}	10^{-4}
0.3	0.051	0.168	0.029	0.105
0.5	0.091	0.278	0.046	0.159
1	0.162	0.471	0.073	0.222
2	0.263	0.782	0.130	0.406
5	0.346	1.083	0.200	0.660
10	0.355	1.160	0.250	0.906
20	0.284	0.951	0.225	0.853
PGA	0.169	0.534	0.112	0.391
PGV	15.3	47.6	7.4	23.4

TABLE 7-2
GUIDE TO WITHIN-TEAM SENSITIVITY RESULTS

Figure Numbers	Team	Description
7-21 through 7-22	AAR	Mean hazard by source group
7-23 through 7-24	AAR	Dominant seismic sources
7-25 through 7-26	AAR	M-R- deaggregation by source group
7-27 through 7-34	AAR	Local faults, sens. to global parameters
7-35 through 7-41	AAR	Local faults, sens. to source parameters
7-42 through 7-43	AAR	Area sources, sens. to global parameters
7-44 through 7-46	AAR	Area sources, sens. to source parameters
7-47 through 7-48	AAR	Regional faults, sens. to global parameters
7-49 through 7-52	AAR	Regional faults, sens. to source parameters
7-53 through 7-54	ASM	Mean hazard by source group
7-55 through 7-56	ASM	Dominant seismic sources
7-57 through 7-58	ASM	M-R- deaggregation by source group
7-59 through 7-67	ASM	Local faults, sens. to global parameters
7-68 through 7-71	ASM	Local faults, sens. to source parameters
7-72	ASM	Area sources, sens. to global parameters
7-73 through 7-75	ASM	Area sources, sens. to source parameters
7-76 through 7-78	ASM	Regional faults, sens. to global parameters
7-79 through 7-80	ASM	Regional faults, sens. to source parameters
7-81 through 7-82	DFS	Mean hazard by source group
7-83 through 7-84	DFS	Dominant seismic sources
7-85 through 7-86	DFS	M-R- deaggregation by source group
7-87 through 7-92	DFS	Local faults, sens. to global parameters
7-93 through 7-94	DFS	Local faults, sens. to source parameters
7-95 through 7-97	DFS	Area sources, sens. to global parameters
7-98 through 7-99	DFS	Area sources, sens. to source parameters
7-100 through 7-102	DFS	Regional faults, sens. to global parameters
7-103 through 7-104	DFS	Regional faults, sens. to source parameters

TABLE 7-2 (continued)

Figure Numbers	Team	Description
7-105 through 7-106	RYA	Mean hazard by source group
7-107 through 7-108	RYA	Dominant seismic sources
7-109 through 7-110	RYA	M-R- deaggregation by source group
7-111 through 7-115	RYA	Local faults, sens. to global parameters
7-116 through 7-121	RYA	Local faults, sens. to source parameters
7-122 through 7-124	RYA	Area sources, sens. to global parameters
7-125 through 7-126	RYA	Area sources, sens. to source parameters
7-127 through 7-130	RYA	Regional faults, sens. to global parameters
7-131 through 7-132	RYA	Regional faults, sens. to source parameters
7-133 through 7-134	SBK	Mean hazard by source group
7-135 through 7-136	SBK	Dominant seismic sources
7-137 through 7-138	SBK	M-R- deaggregation by source group
7-139 through 7-142	SBK	Local faults, sens. to global parameters
7-143 through 7-146	SBK	Local faults, sens. to source parameters
7-147 through 7-149	SBK	Area sources, sens. to global parameters
7-150 through 7-151	SBK	Area sources, sens. to source parameters
7-152 through 7-154	SBK	Regional faults, sens. to global parameters
7-155 through 7-158	SBK	Regional faults, sens. to source parameters
7-159 through 7-160	SDO	Mean hazard by source group
7-161 through 7-162	SDO	Dominant seismic sources
7-163 through 7-164	SDO	M-R- deaggregation by source group
7-165	SDO	Local faults, sens. to global parameters
7-166 through 7-169	SDO	Local faults, sens. to source parameters
7-170 through 7-171	SDO	Area sources, sens. to global parameters
7-172 through 7-173	SDO	Area sources, sens. to source parameters
7-174	SDO	Regional faults, sens. to global parameters
7-175 through 7-177	SDO	Regional faults, sens. to source parameters

a) Seismic source i

Earthquake locations in space (and magnitude-dependent rupture dimensions) lead to a distribution of distance $f_{R(i)|M(i)}(r;m)$

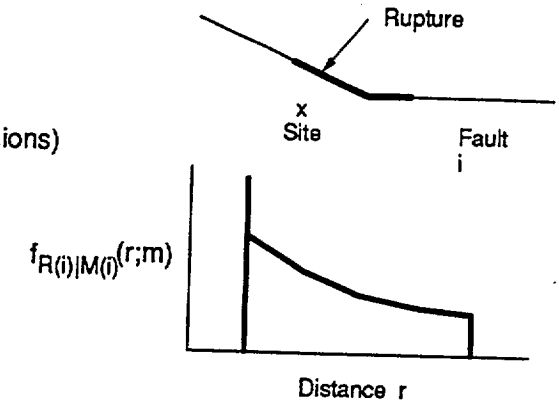

b) Magnitude distribution and rate of occurrence for source i

$f_{M(i)}(m)$, ν_i

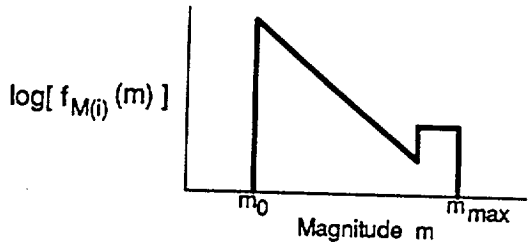

c) Ground-motion attenuation equation

$G_{A|m,r}(a)$

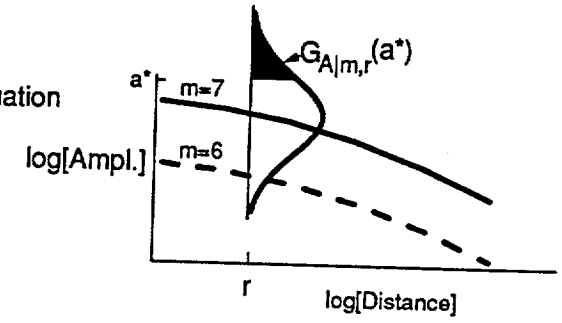

d) Probability analysis: annual exceedence probability

$$\approx \sum_i \nu_i \int_r \int_m G_{A|m,r}(a^*)\, f_{M(i)}(m)\, f_{R(i)|M(i)}(r,m)\, dm\, dr$$

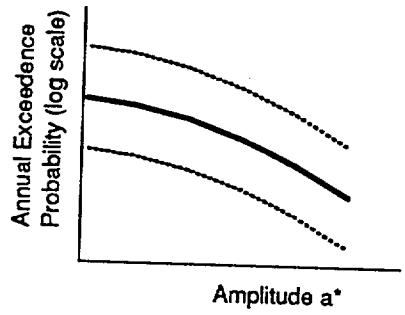

Figure 7-1 Seismic hazard computational model (modified from McGuire and Arabasz, 1990)

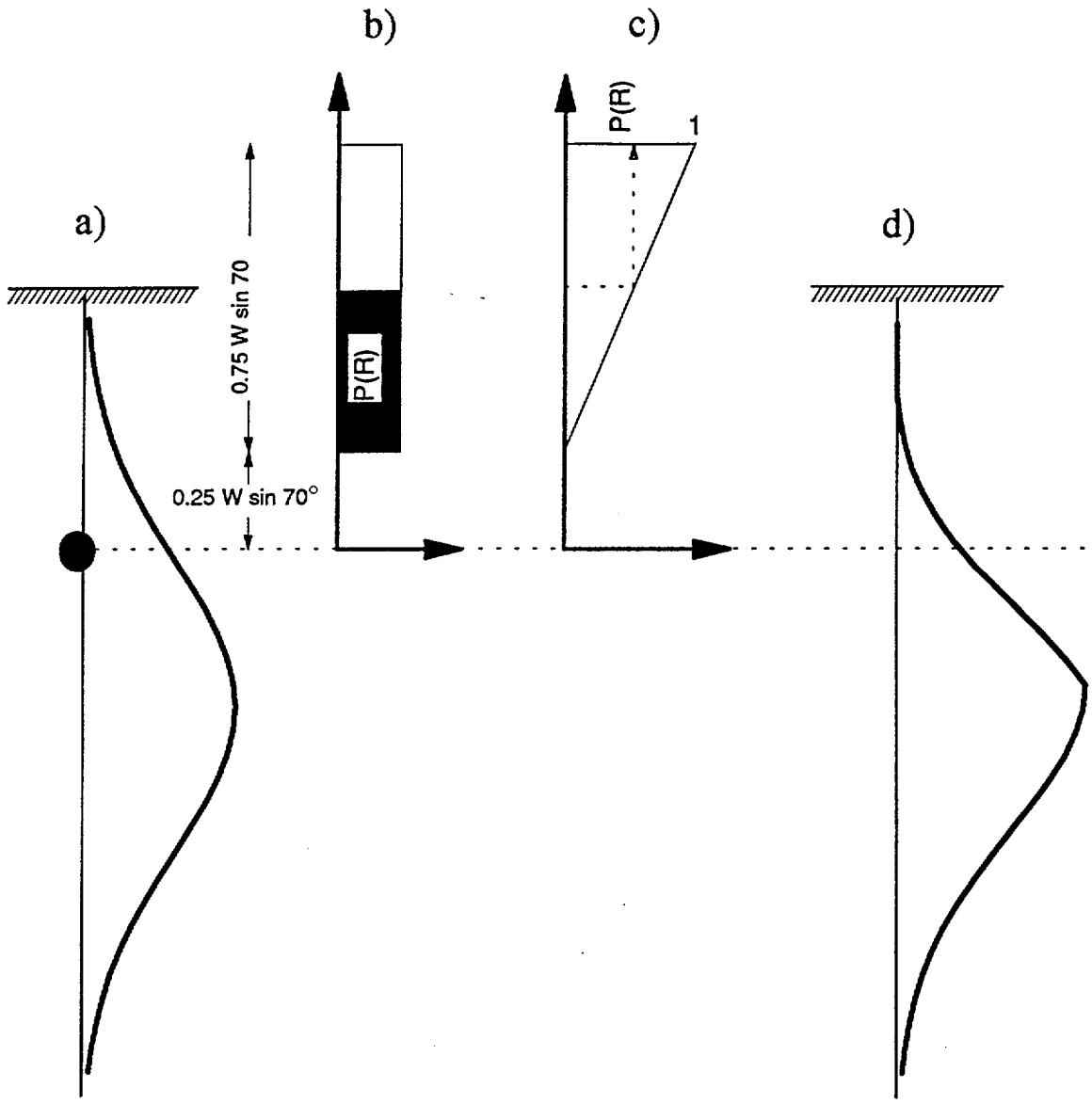

Figure 7-2 Calculation of hypocentral depth distribution for area sources considering the dimensions of the rupture. a) Normal distribution of depth for small events; the solid ellipse indicates a hypothetical hypocentral location. b) probability density function for the location of the top of the rupture. W is the magnitude-dependent rupture width. The probability P(R) that the event is realizable is the probability that the top of the rupture is below the ground surface (the shaded area). c) cumulative distribution function for the location of the top of the rupture, showing P(R). d) Distribution of depth for event with finite width W. This distribution is obtained by multiplying the distribution in (a) by P(R) and normalizing to an area of 1.

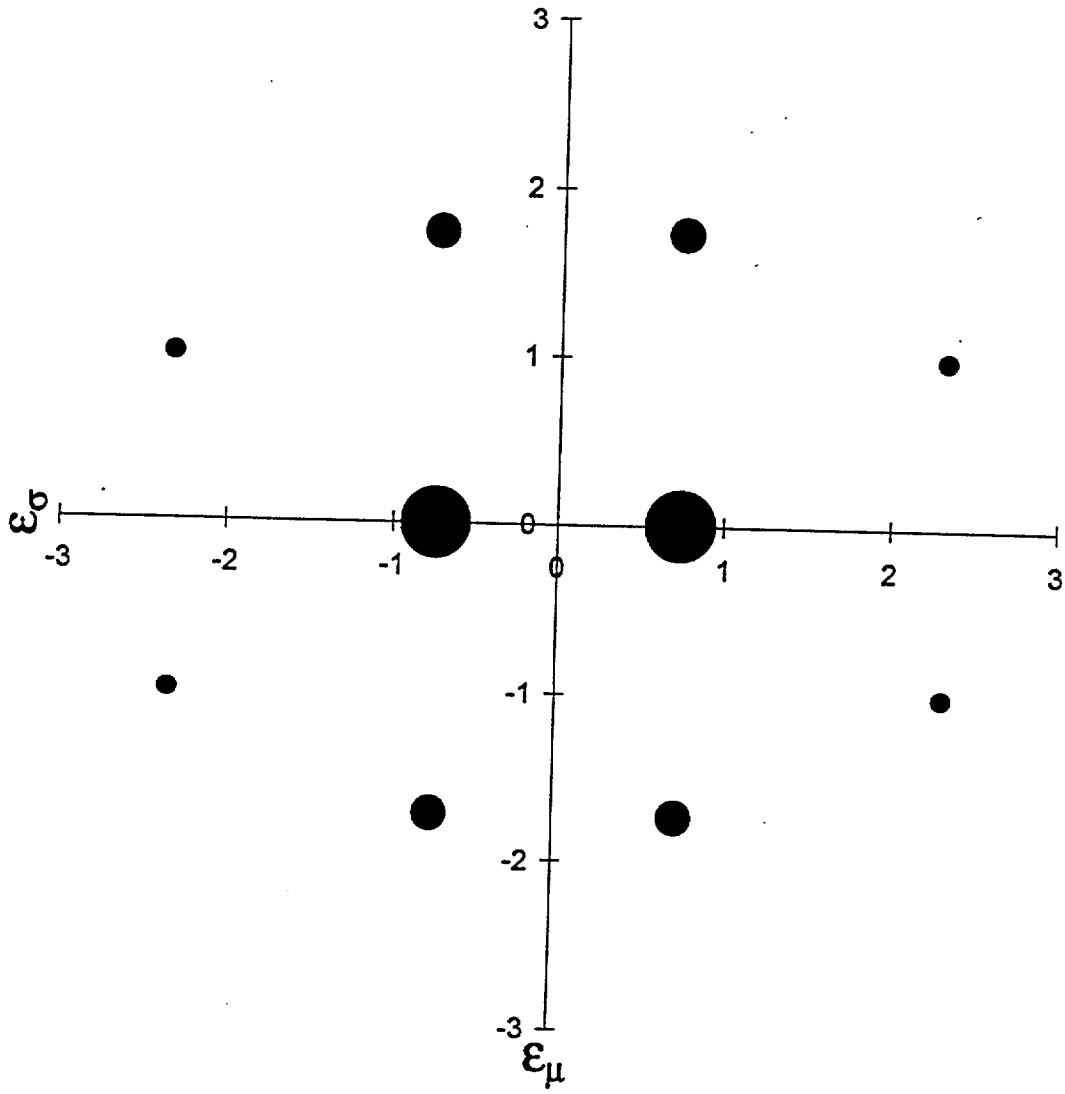

Figure 7-3 Discretization of the joint distribution of ε_μ (horizontal axis) and ε_σ (vertical axis) used to represent within-expert epistemic uncertainty in ground motions. The areas of the circles are proportional to the weights for the corresponding points.

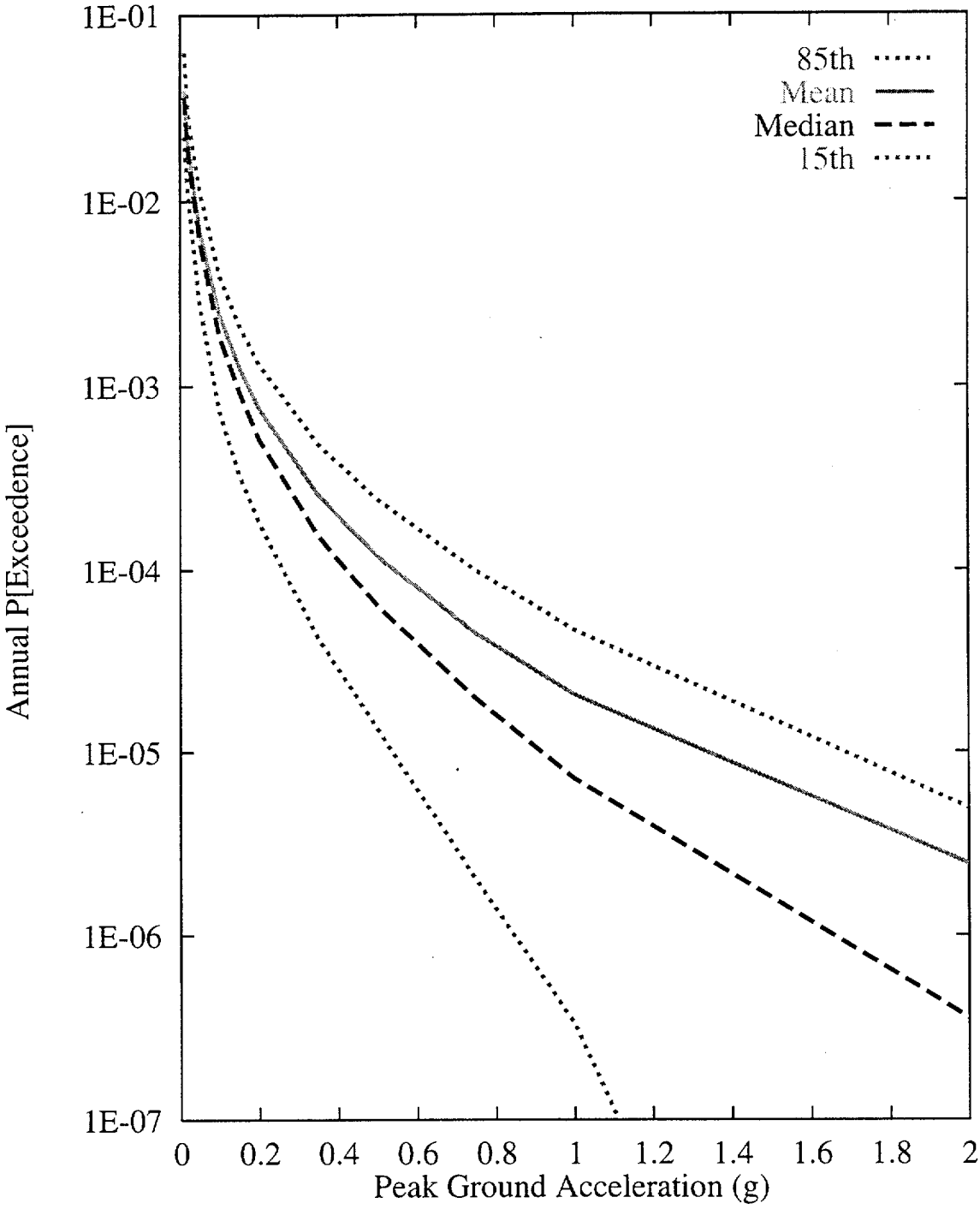

Figure 7-4 Integrated seismic hazard results: summary hazard curves for horizontal PGA

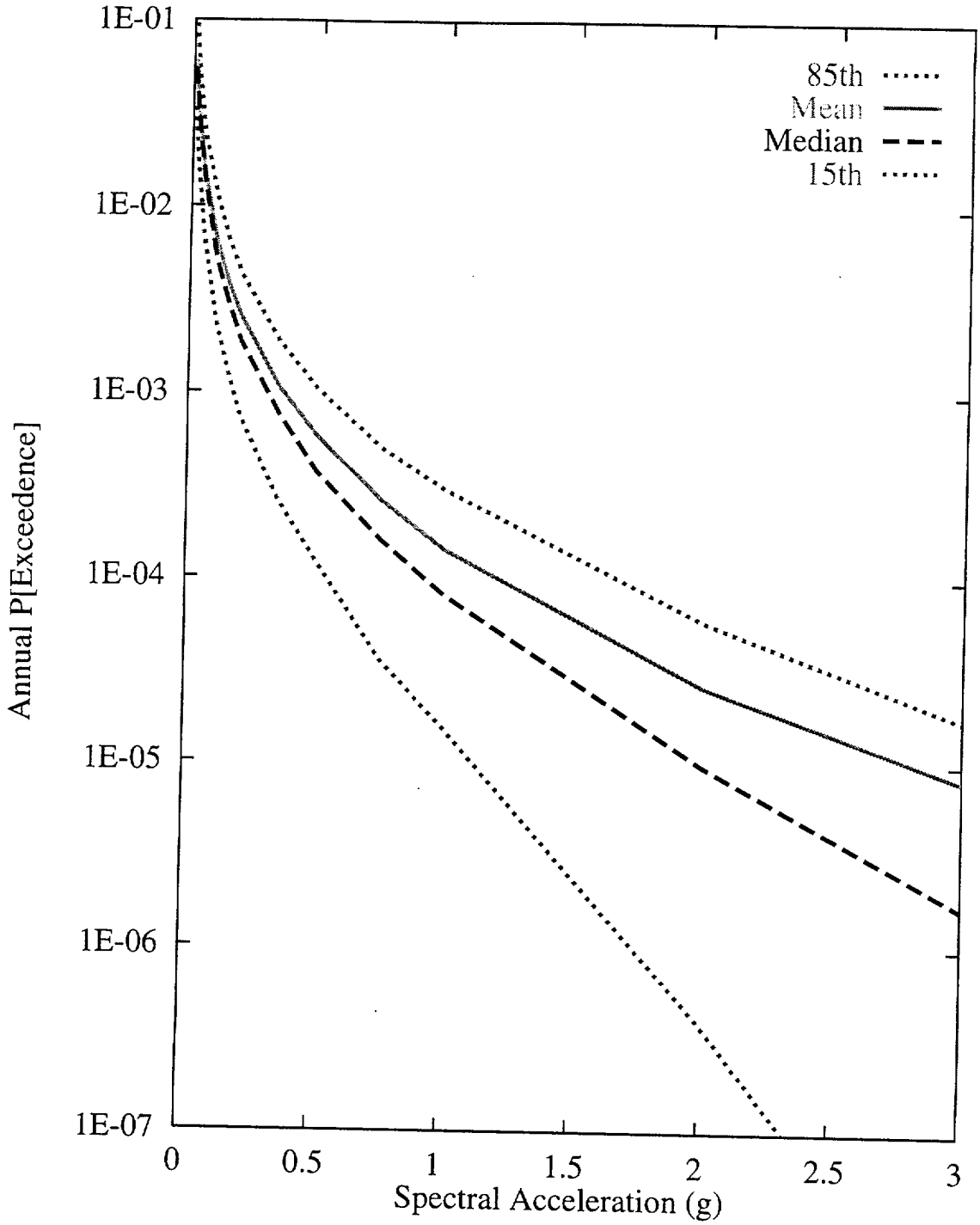

Figure 7-5 Integrated seismic hazard results: summary hazard curves for 10-Hz horizontal spectral acceleration

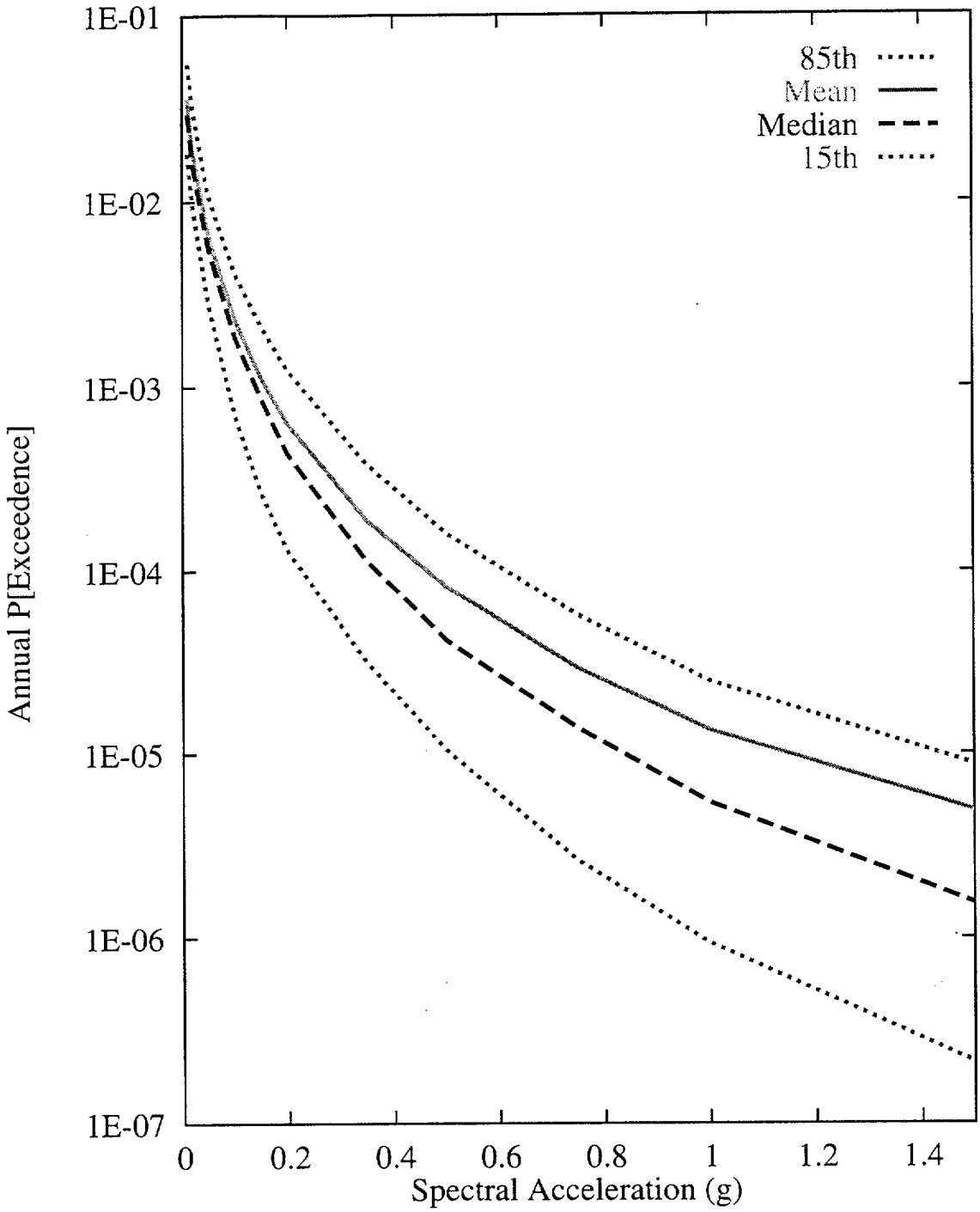

Figure 7-6 Integrated seismic hazard results: summary hazard curves for 1-Hz horizontal spectral acceleration

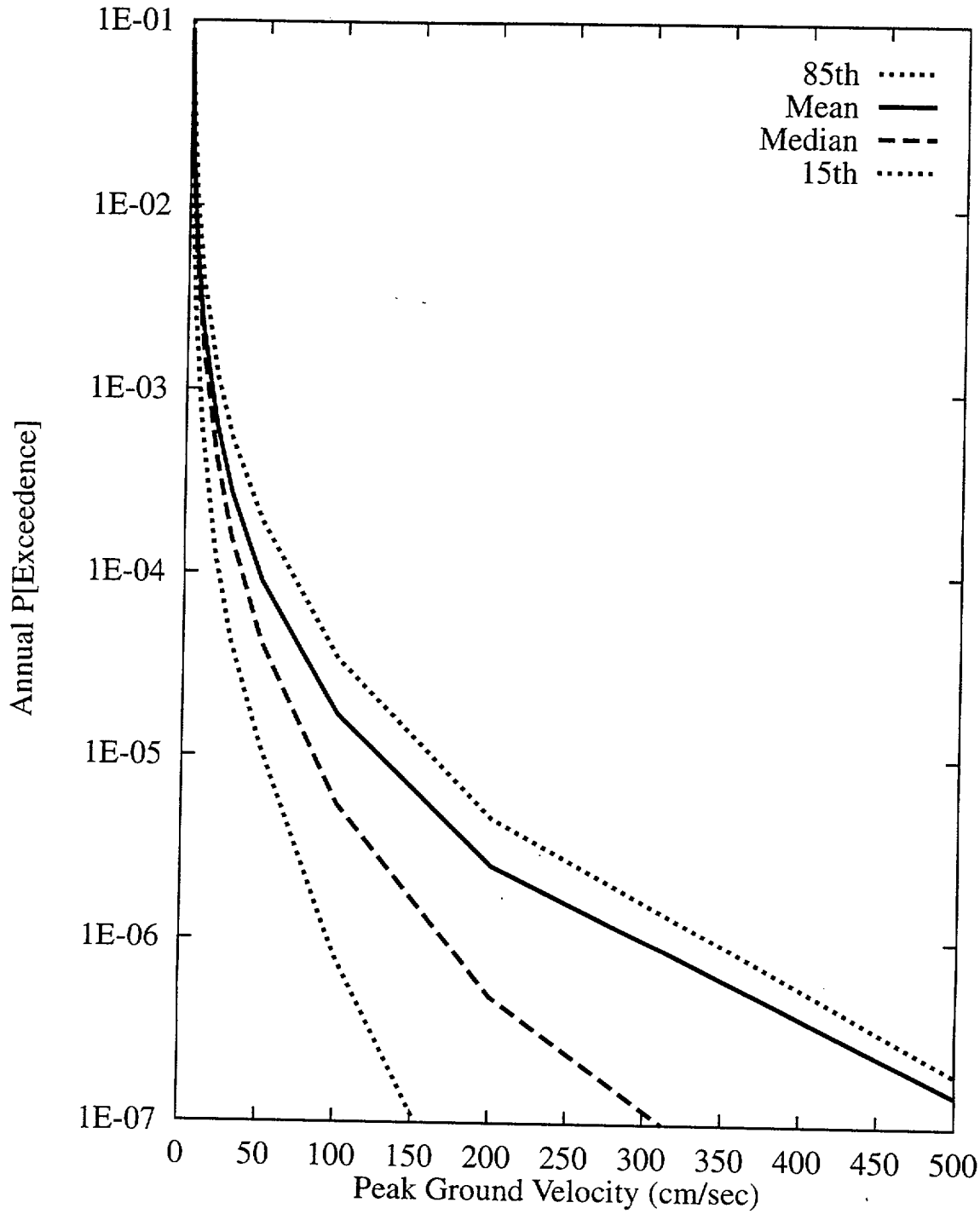

Figure 7-7 Integrated seismic hazard results: summary hazard curves for horizontal PGV

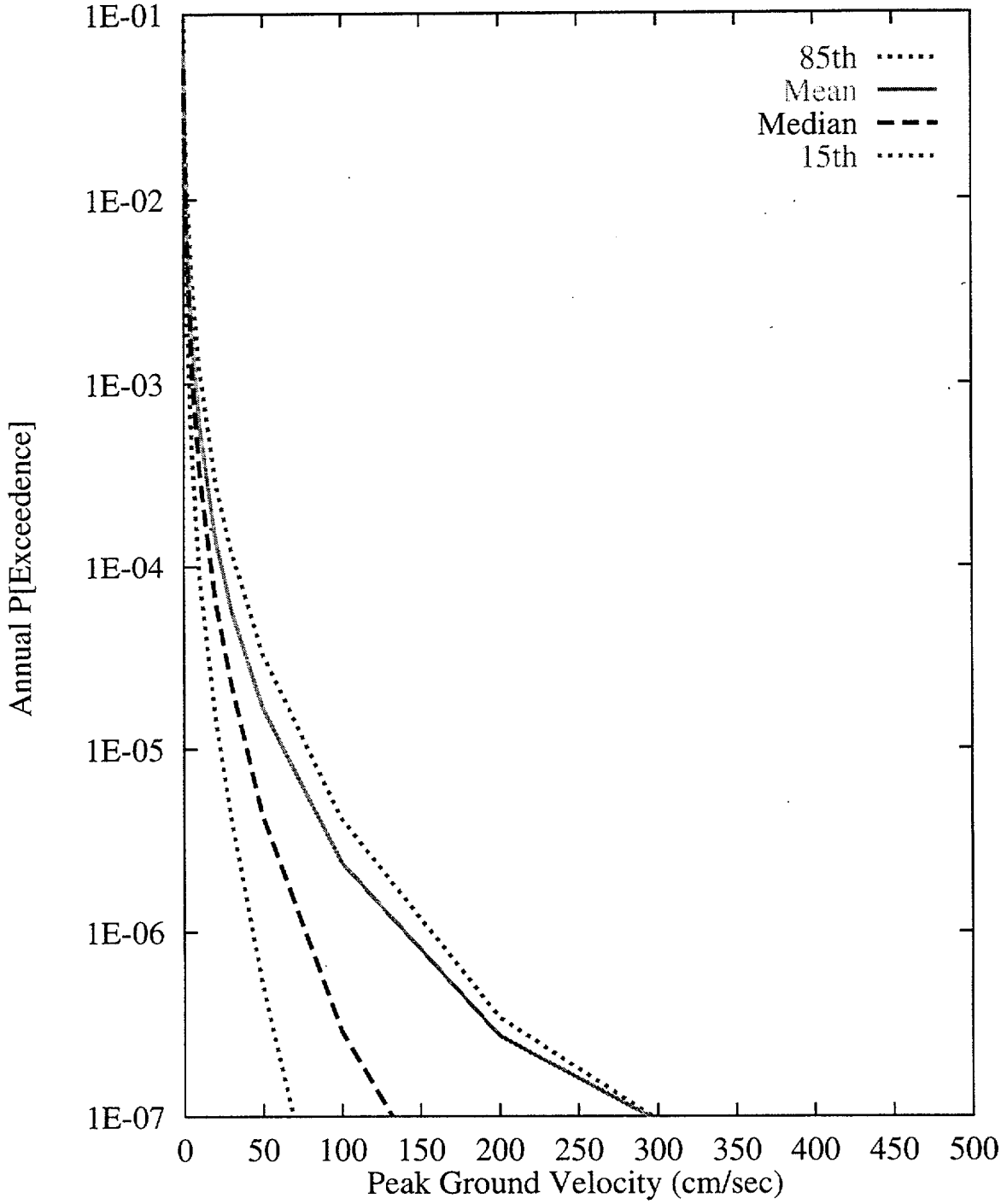

Figure 7-8 Integrated seismic hazard results: summary hazard curves for vertical PGV

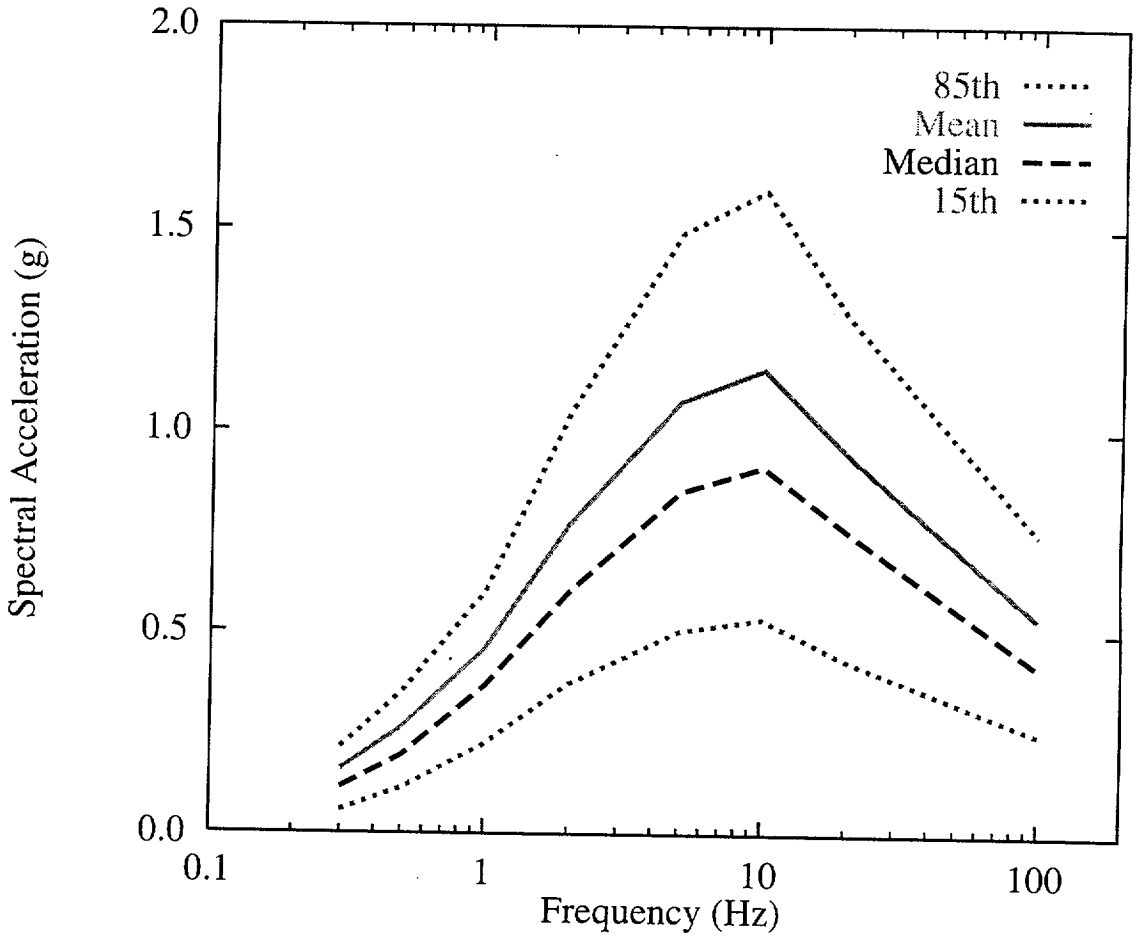

Figure 7-9 Integrated seismic hazard results: horizontal uniform hazard spectrum (UHS) for 10^{-4} exceedence probability

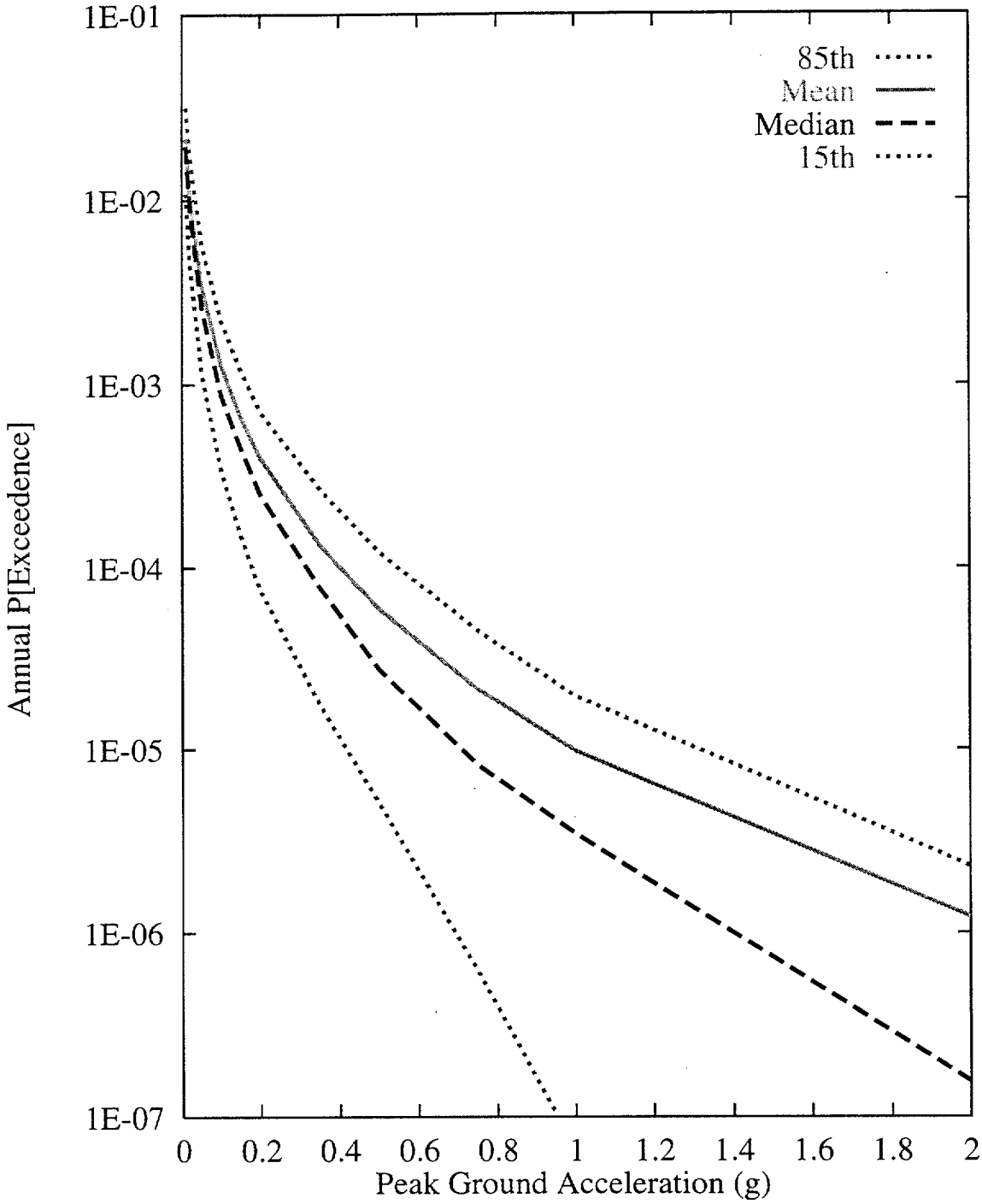

Figure 7-10 Integrated seismic hazard results: summary hazard curves for vertical PGA

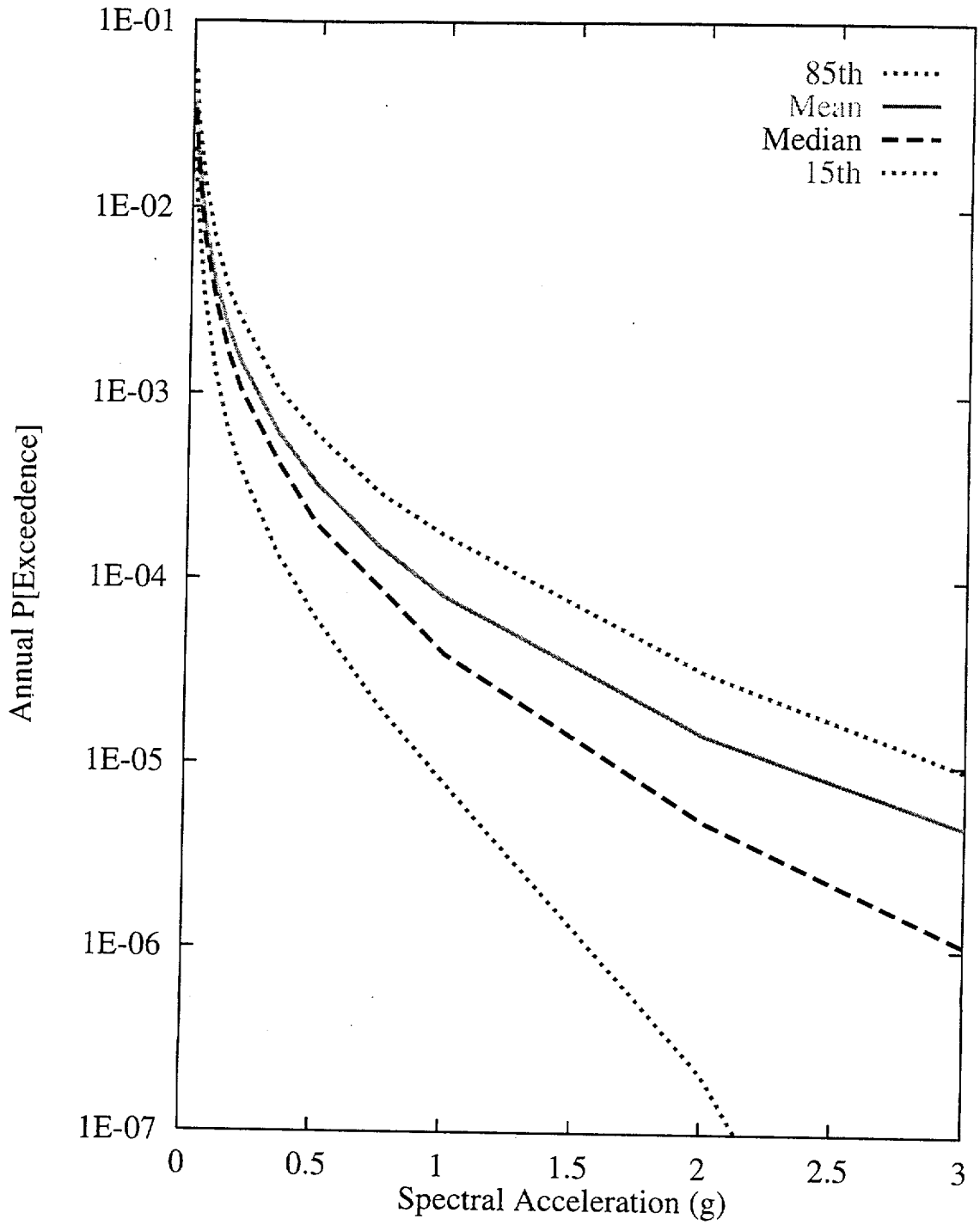

Figure 7-11 Integrated seismic hazard results: summary hazard curves for 10-Hz vertical spectral acceleration

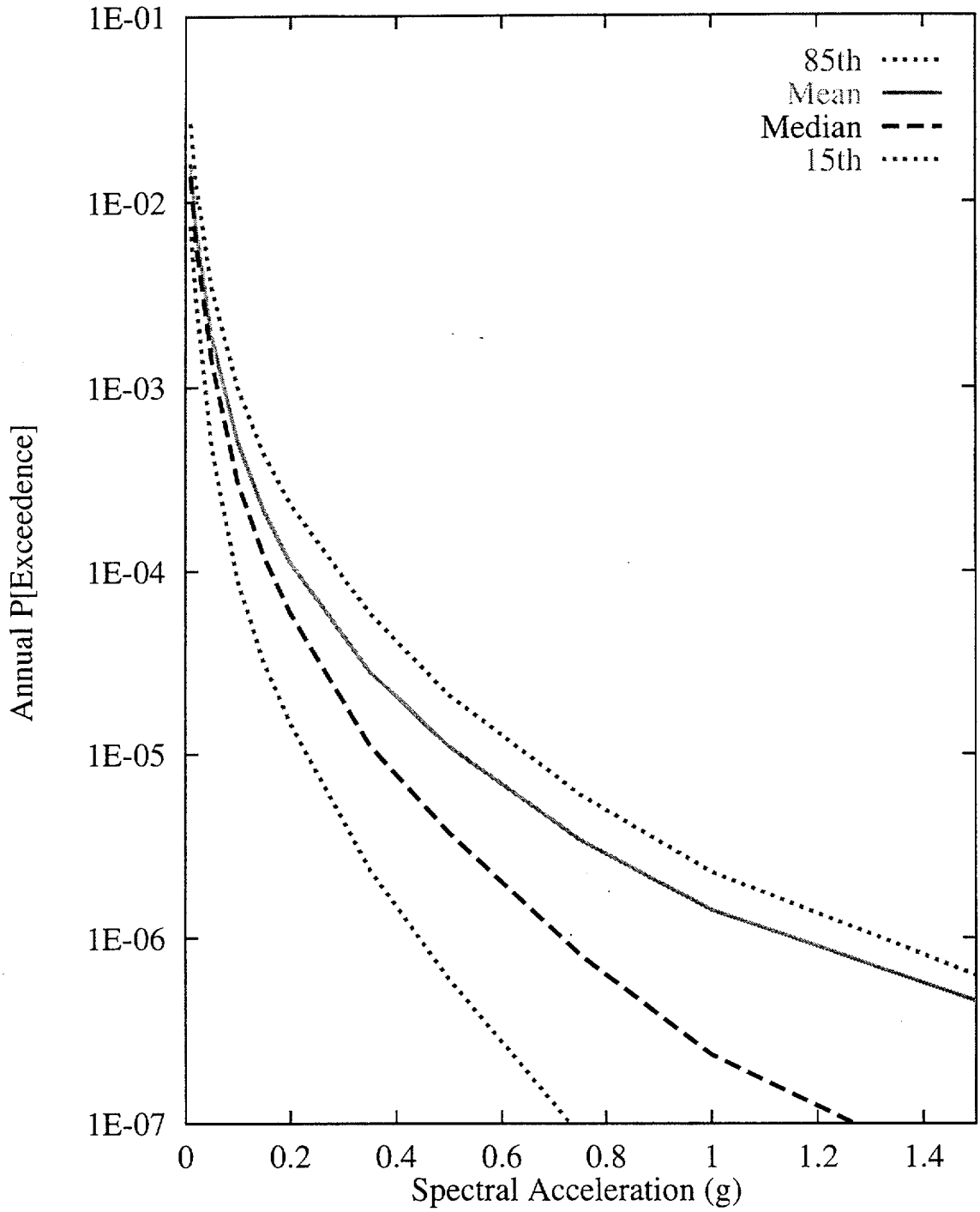

Figure 7-12 Integrated seismic hazard results: summary hazard curves for 1-Hz vertical spectral acceleration

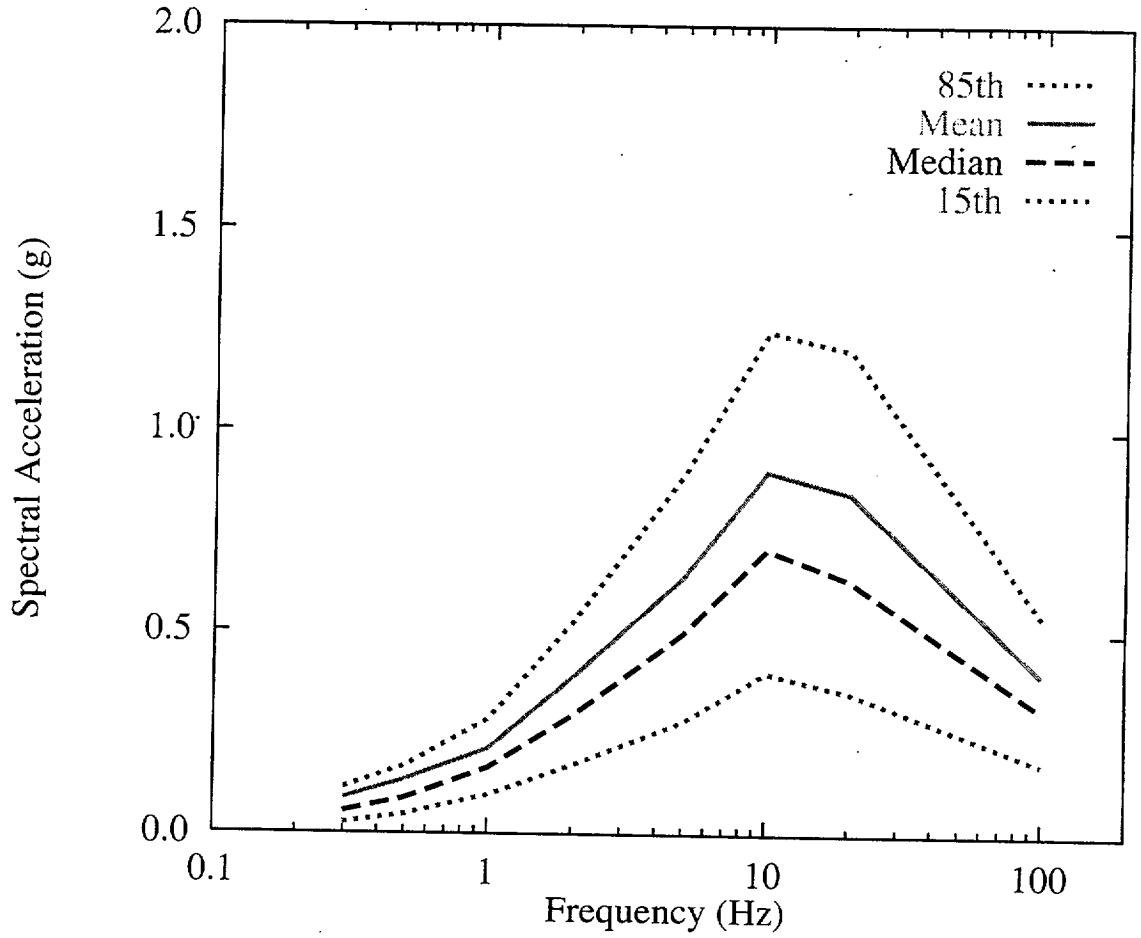

Figure 7-13 Integrated seismic hazard results: vertical uniform hazard spectrum (UHS) for 10^{-4} exceedence probability

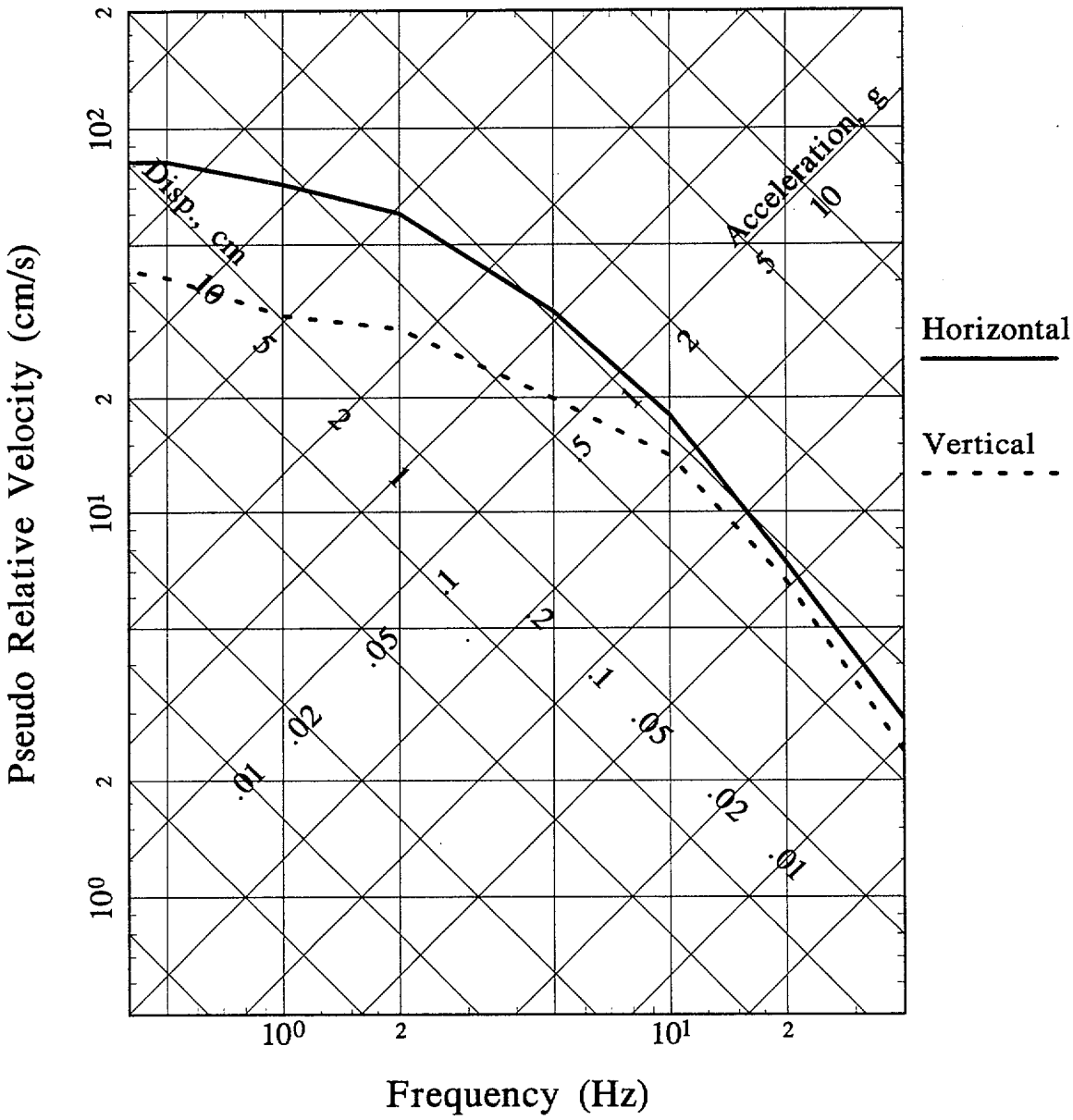

Figure 7-14 Integrated seismic hazard results: uniform hazard spectra for 10^{-4} exceedence probability shown in tripartite scale

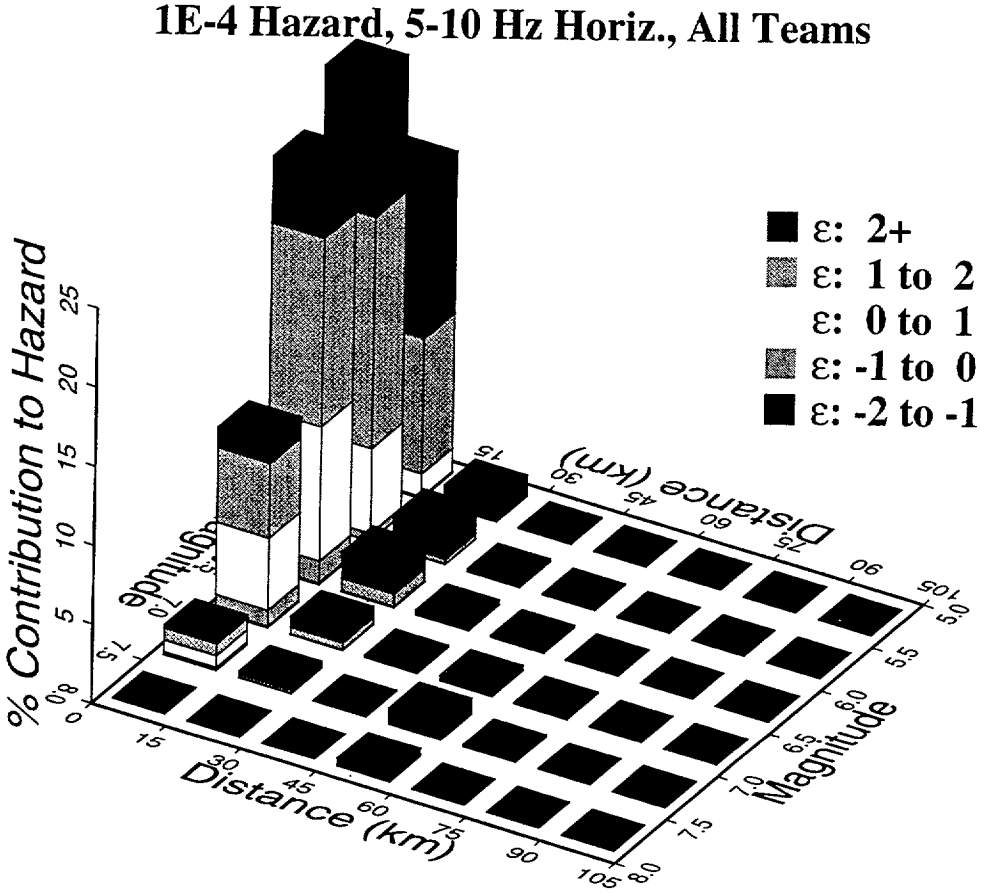

Figure 7-15 Magnitude-distance-epsilon deaggregation of integrated seismic hazard for 5- and 10-Hz horizontal spectral acceleration at 10^{-4} exceedence probability

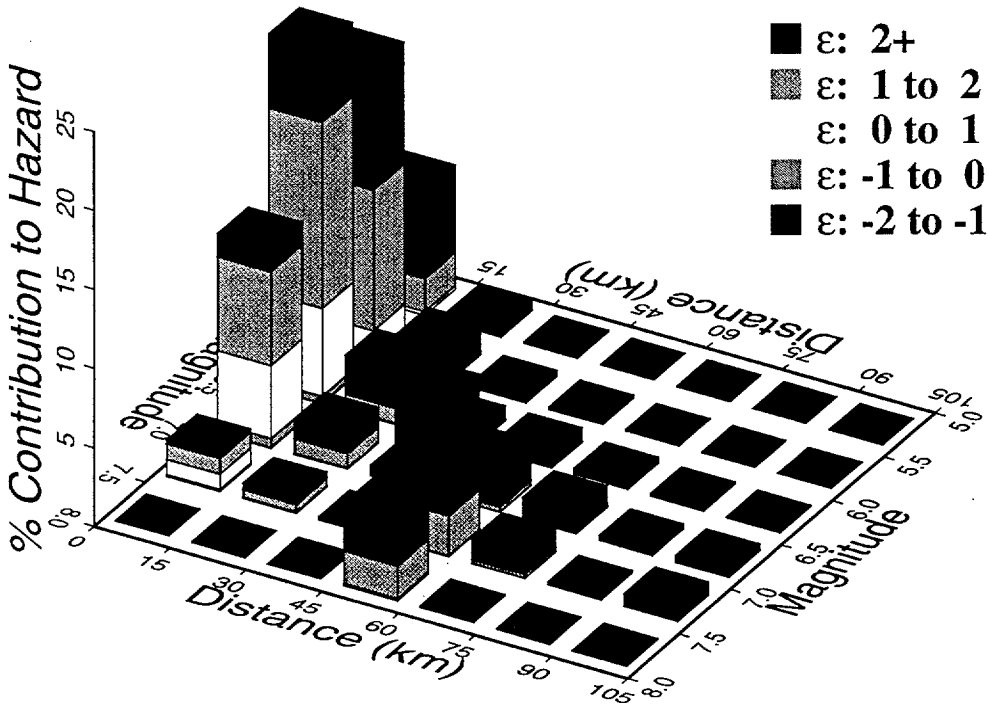

Figure 7-16 Magnitude-distance-epsilon deaggregation of integrated seismic hazard for 1- and 2-Hz horizontal spectral acceleration at 10^{-4} exceedence probability

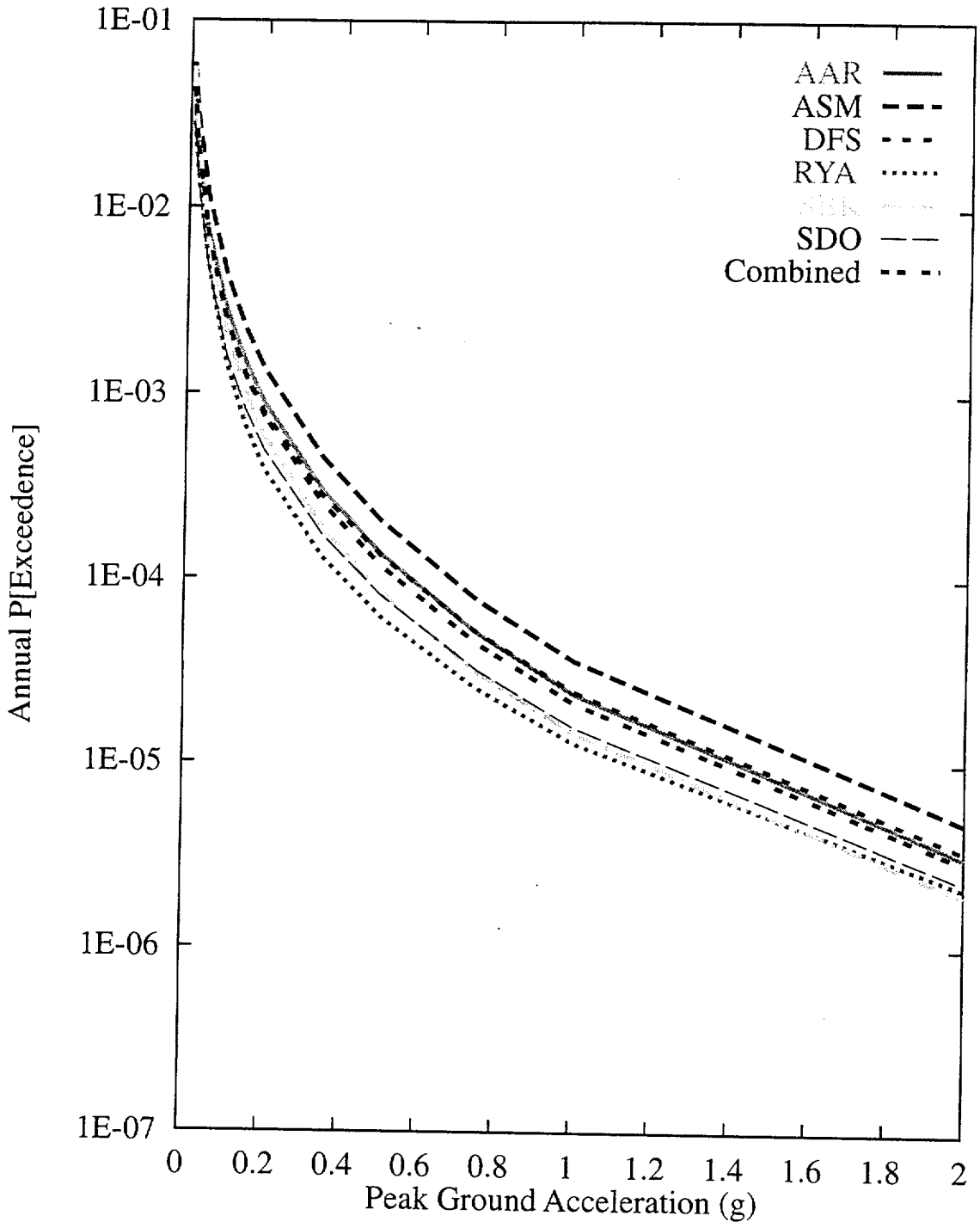

Figure 7-17 Mean hazard by team for horizontal PGA

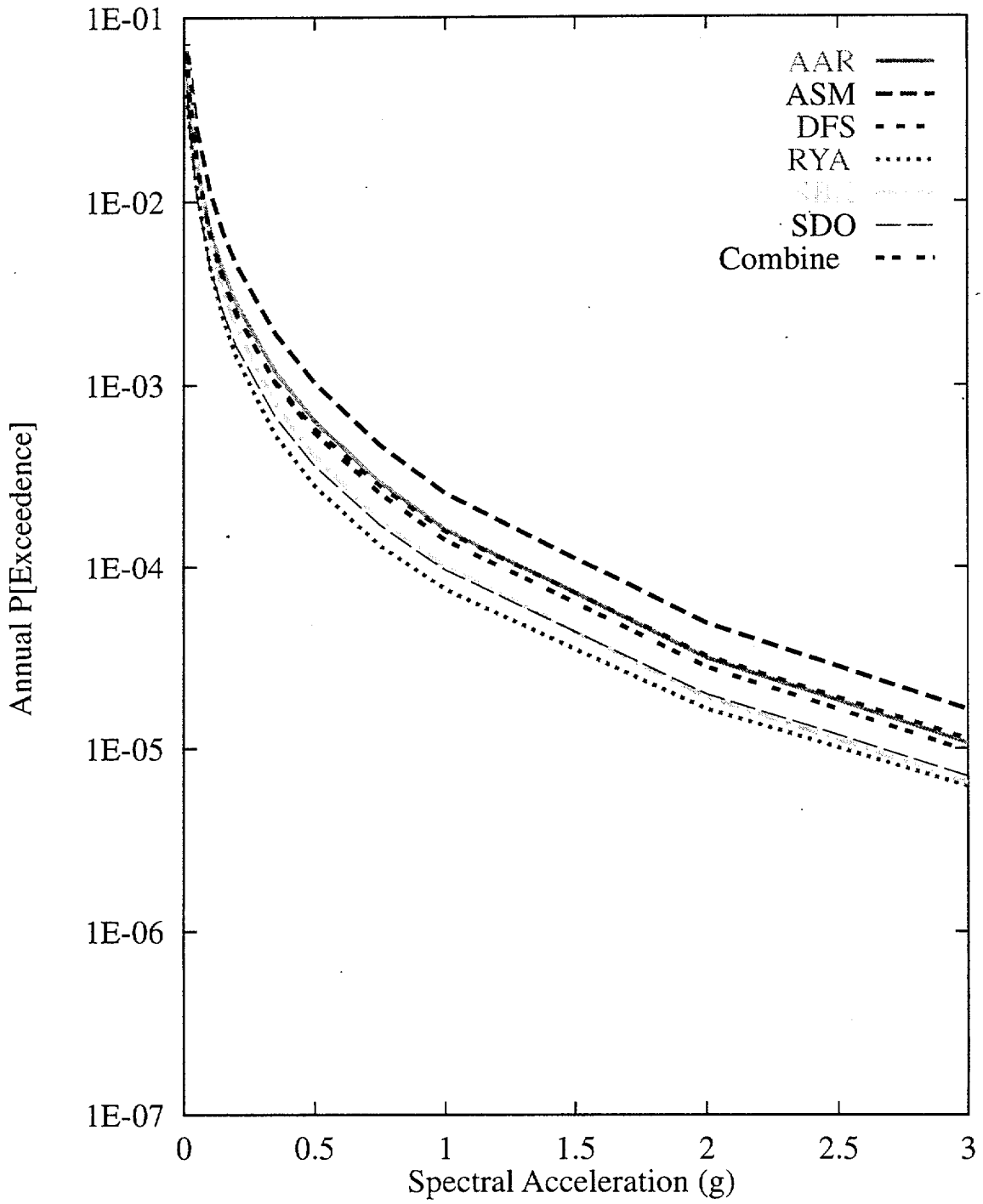

Figure 7-18 Mean hazard by team for 10-Hz horizontal spectral acceleration

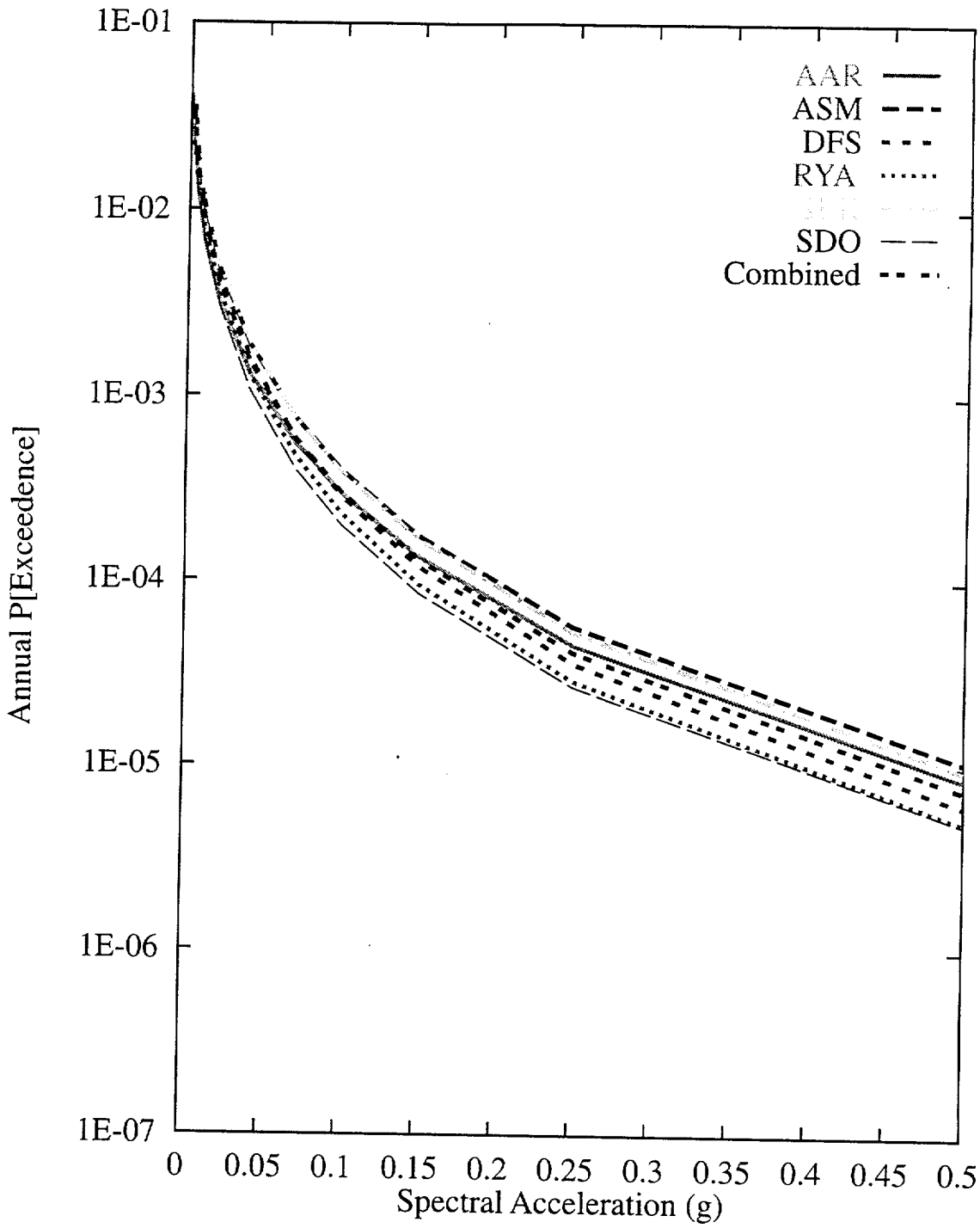

Figure 7-19 Mean hazard by team for 1-Hz horizontal spectral acceleration

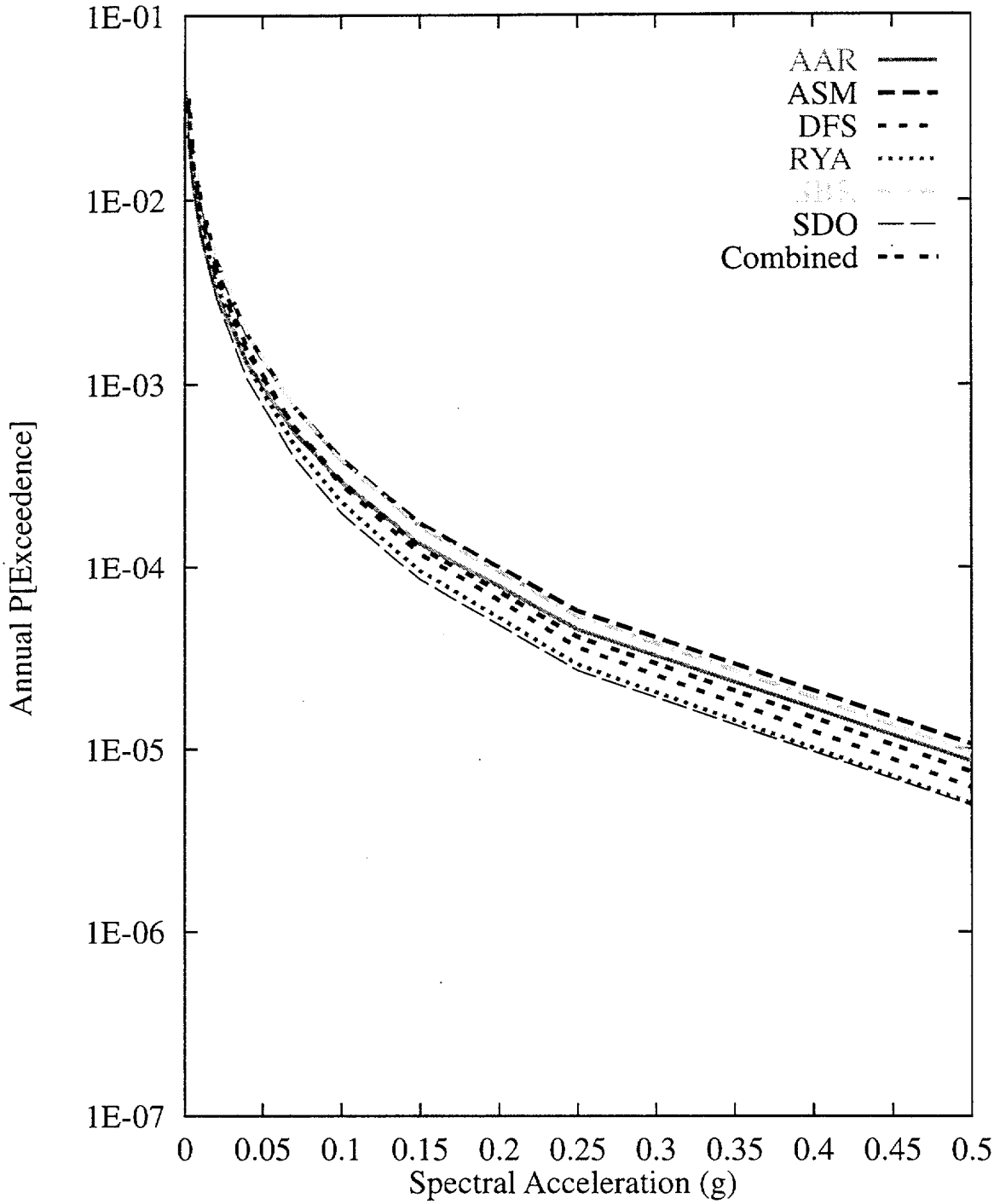

Figure 7-20 Mean hazard by team for 0.3-Hz horizontal spectral acceleration

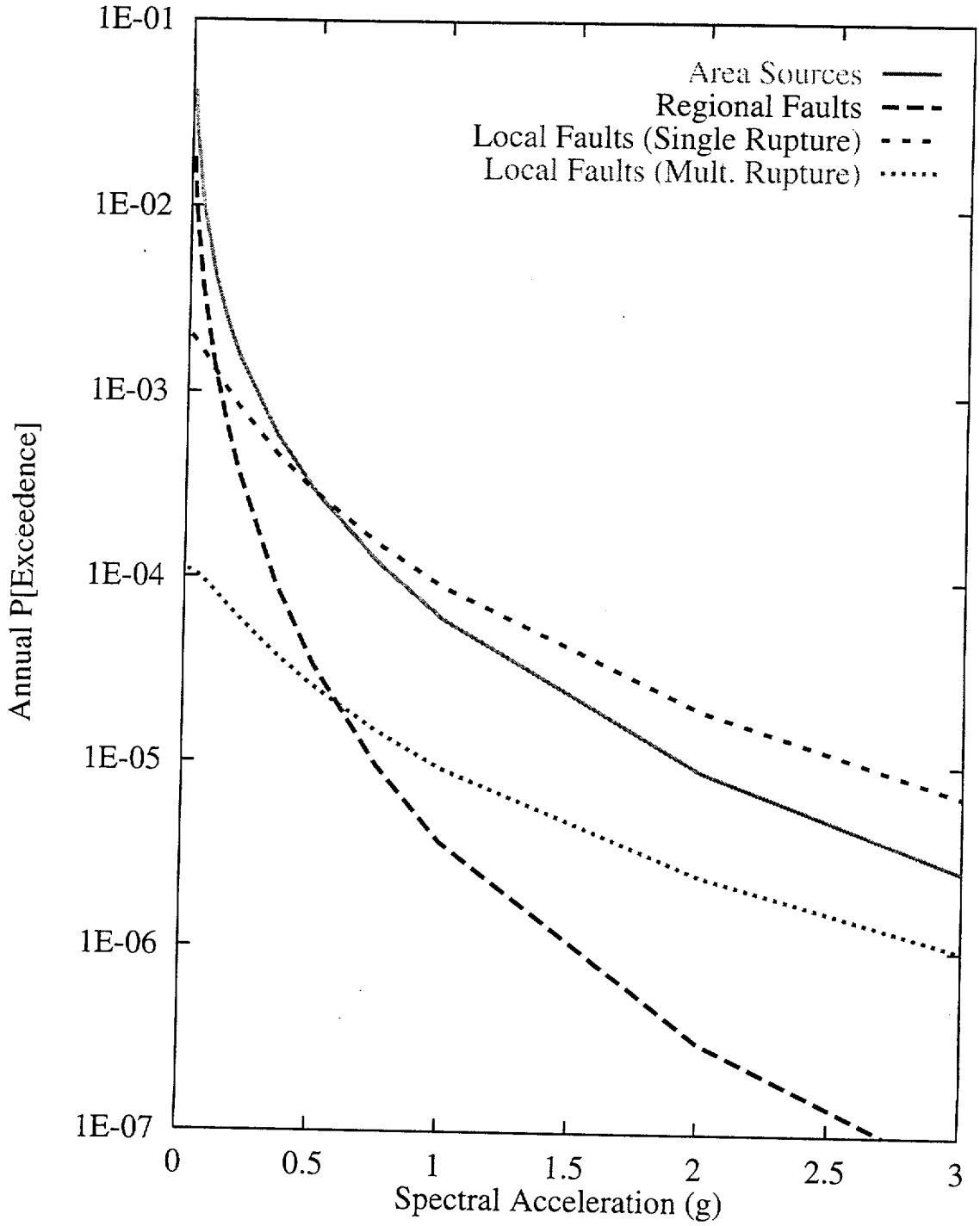

Figure 7-21 Contributions of source type to the mean hazard: AAR team, 10-Hz horizontal spectral acceleration

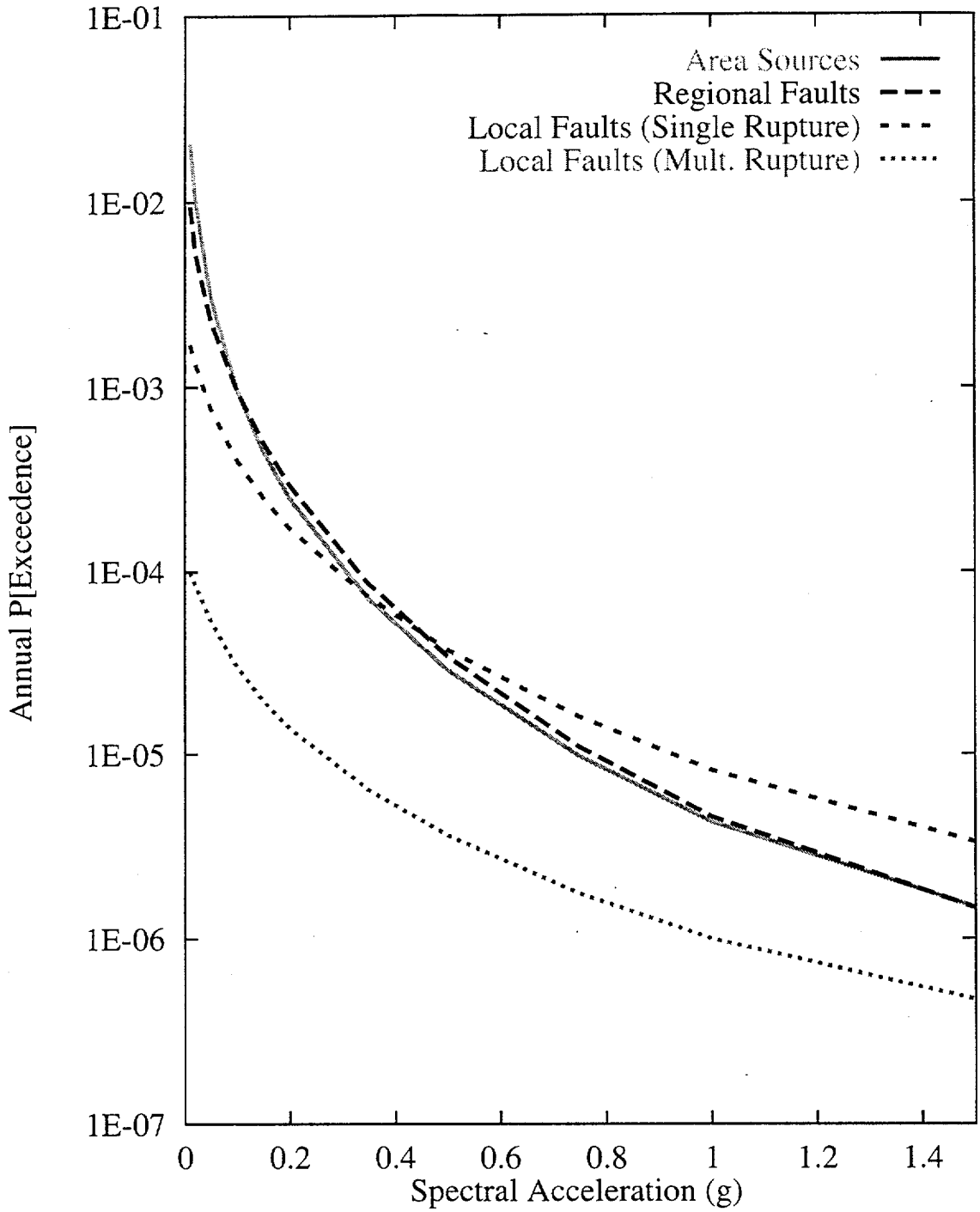

Figure 7-22 Contributions of source type to the mean hazard: AAR team, 1-Hz horizontal spectral acceleration

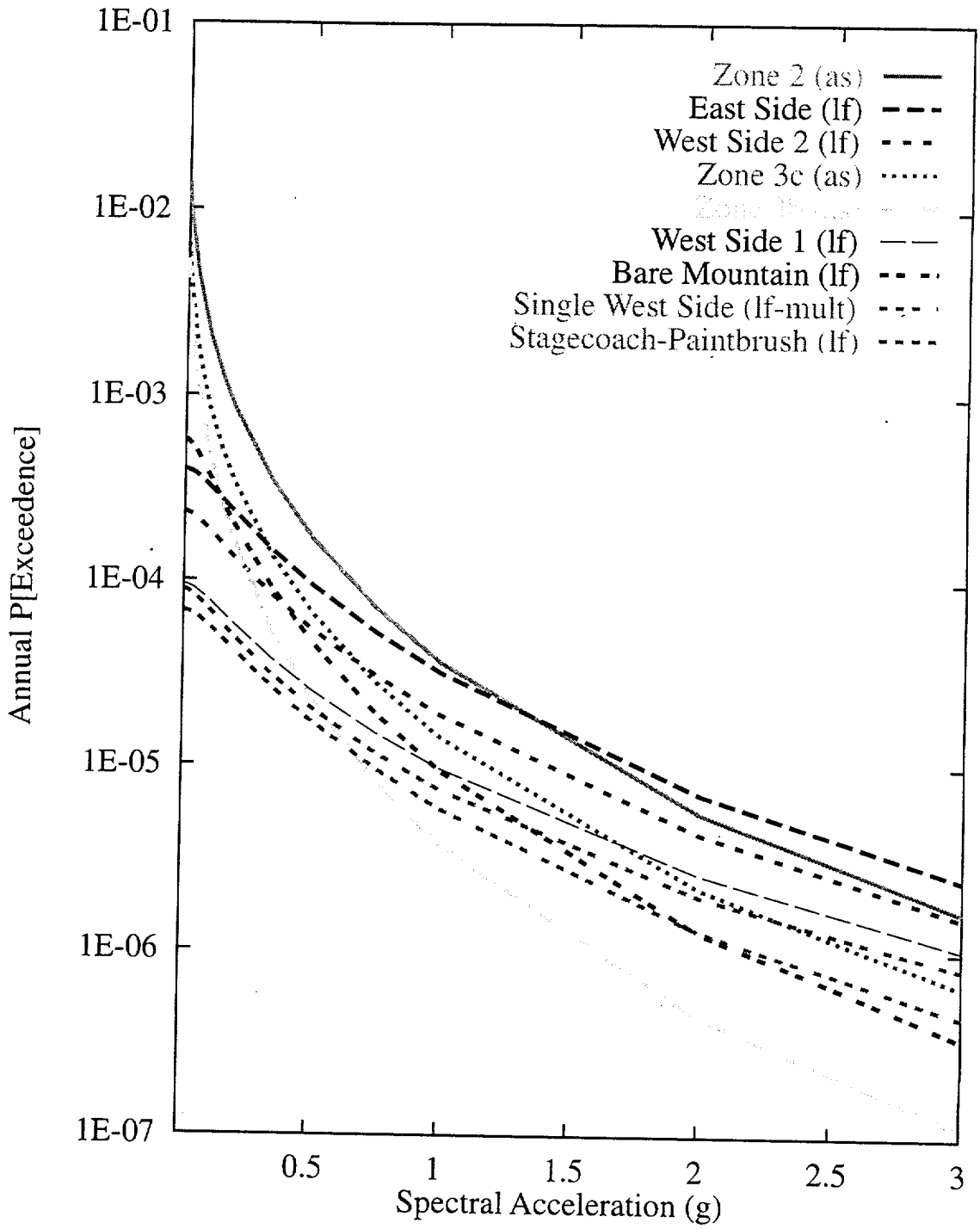

Figure 7-23 Mean seismic hazard from dominant seismic sources: AAR team, 10-Hz horizontal spectral acceleration. Acronyms in parentheses refer to source types: as-area source zone; lf-local fault; and mult-multiple fault rupture.

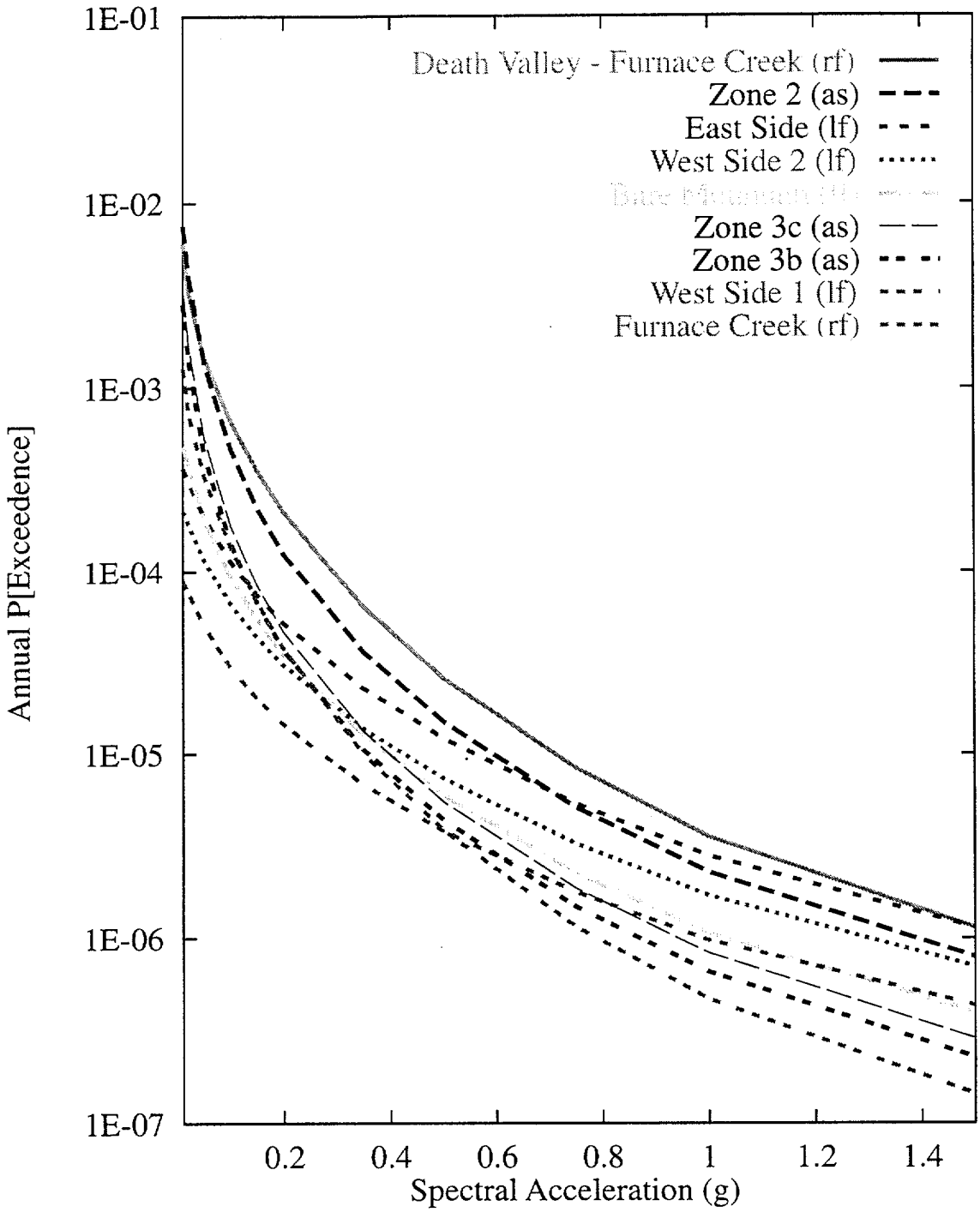

Figure 7-24 Mean seismic hazard from dominant seismic sources: AAR team, 1-Hz horizontal spectral acceleration. Acronyms in parentheses refer to source types: as-area source zone; rf-regional fault; and lf-local fault.

10 Hz, AAR Area Sources

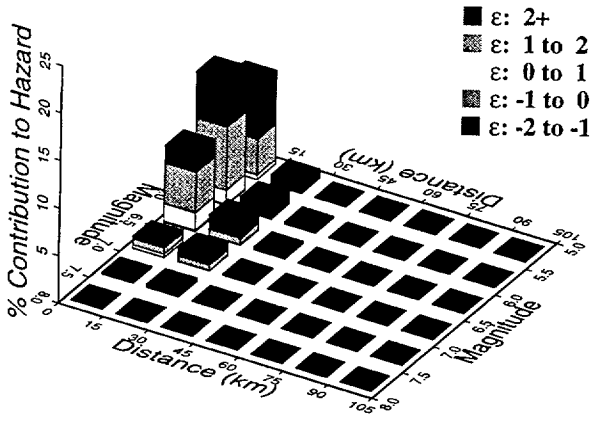

10 Hz, AAR Regional Faults

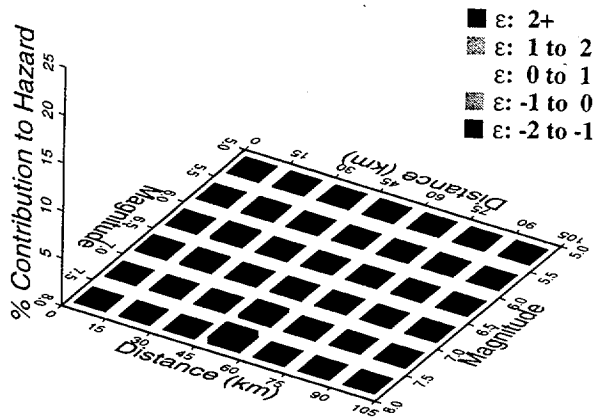

10 Hz, AAR Local Faults (Single)

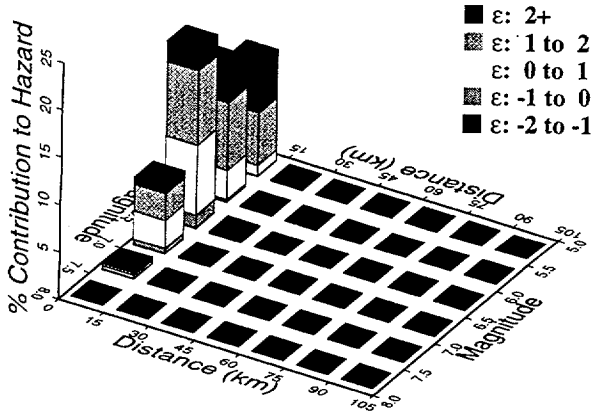

10 Hz, AAR Local Faults (Mult.)

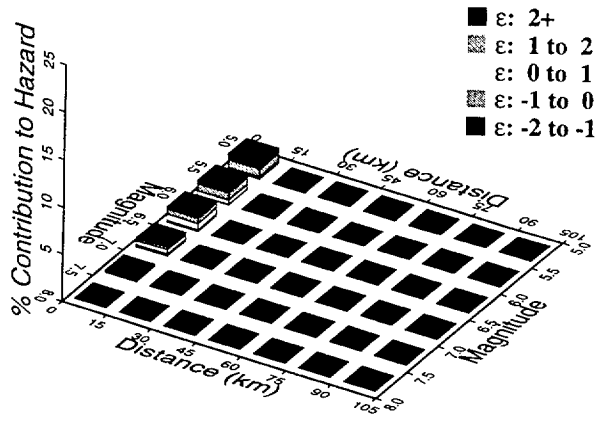

Figure 7-25 Magnitude-distance-epsilon distributions for the four source types: AAR team, 10-Hz horizontal spectral acceleration

1 Hz, AAR Area Sources

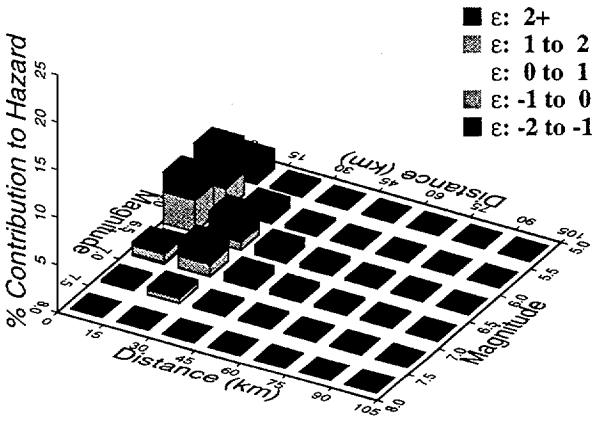

1 Hz, AAR Regional Faults

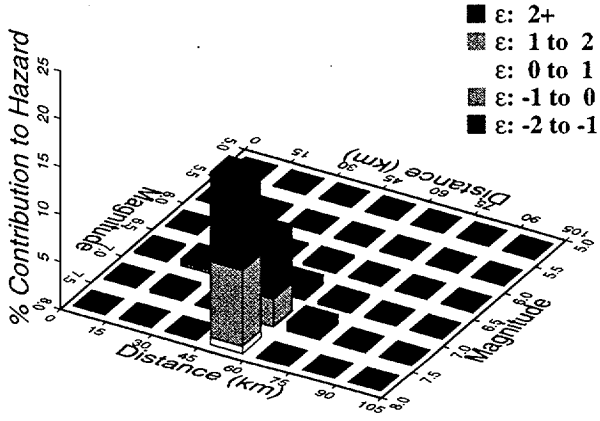

1 Hz, ARR Local Faults (Single)

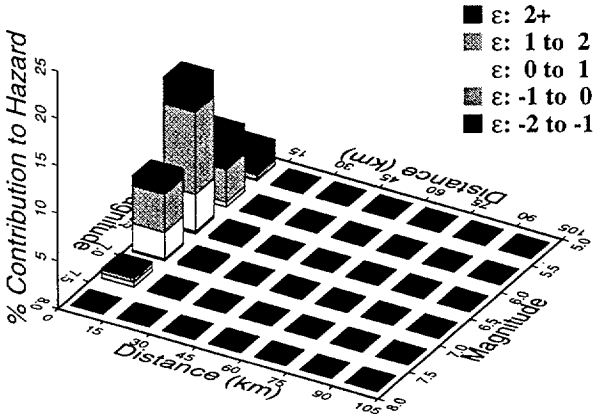

1 Hz, AAR Local Faults (Mult.)

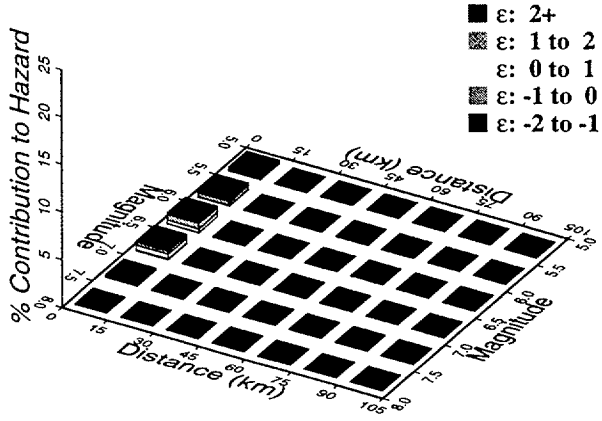

Figure 7-26 Magnitude-distance-epsilon distributions for the four source types: AAR team, 1-Hz horizontal spectral acceleration

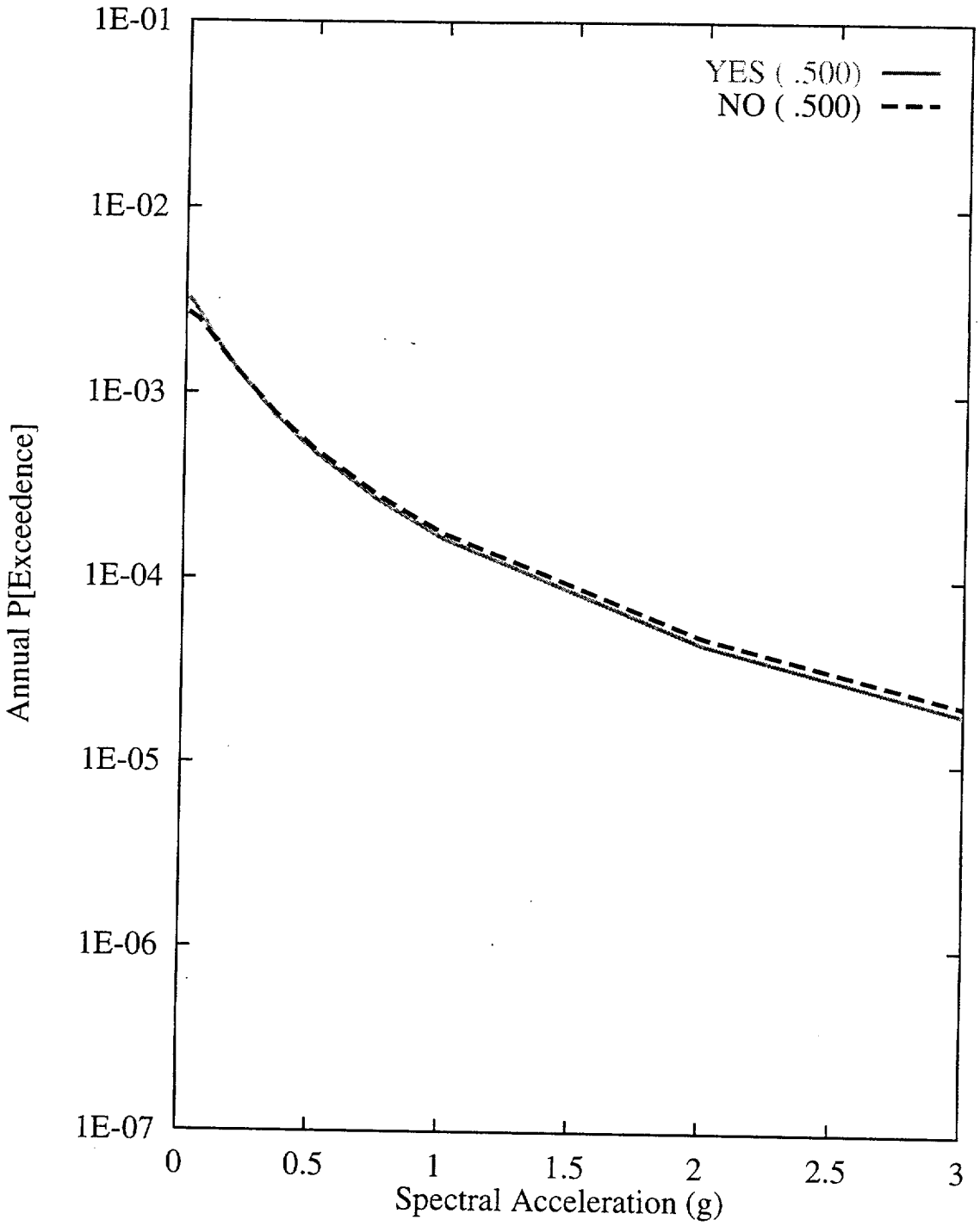

Figure 7-27 Sensitivity of seismic hazard from local faults to presence of dextral shear: AAR team, 10-Hz horizontal spectral acceleration

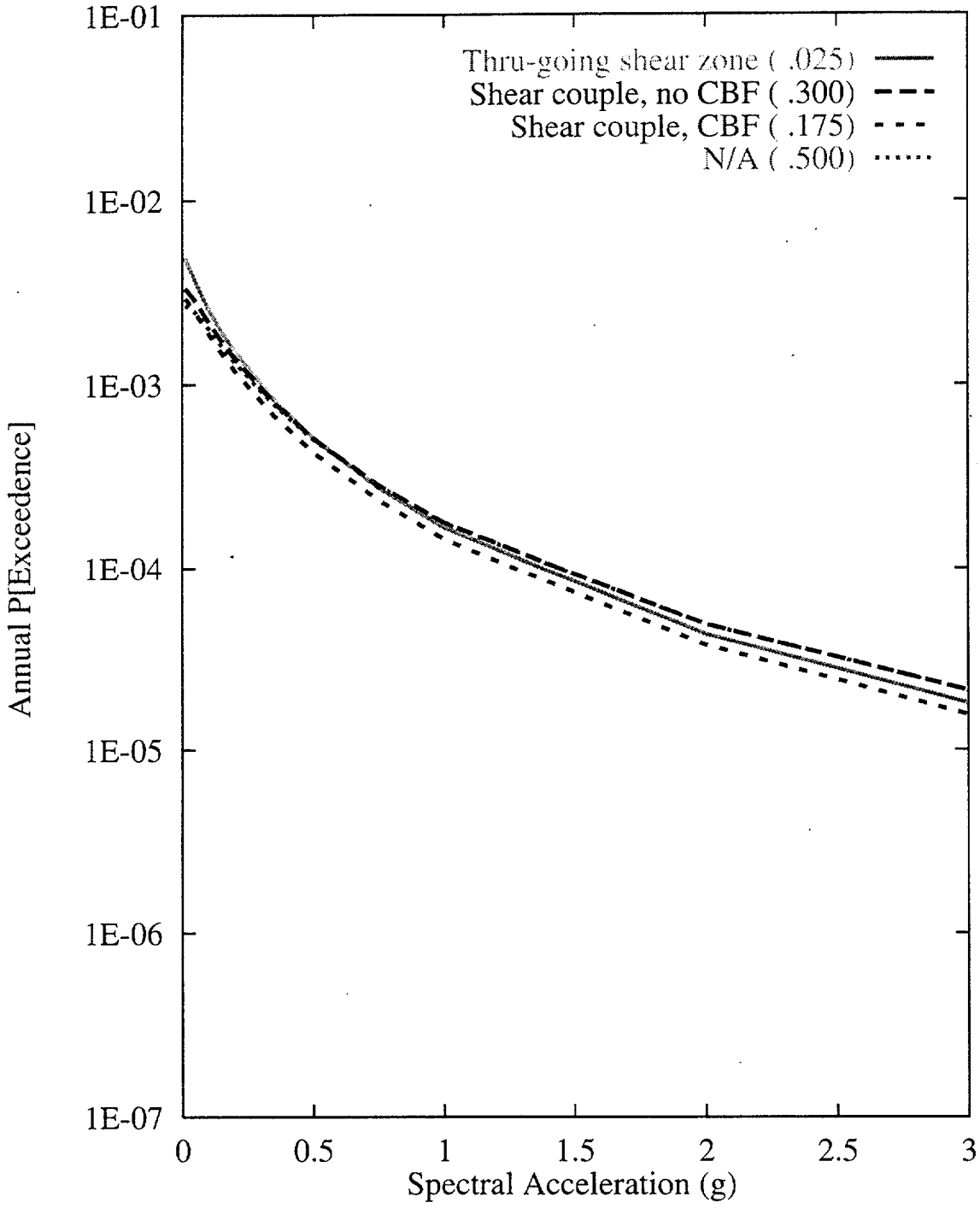

Figure 7-28 Sensitivity of seismic hazard from local faults to type of dextral shear structure: AAR team, 10-Hz horizontal spectral acceleration

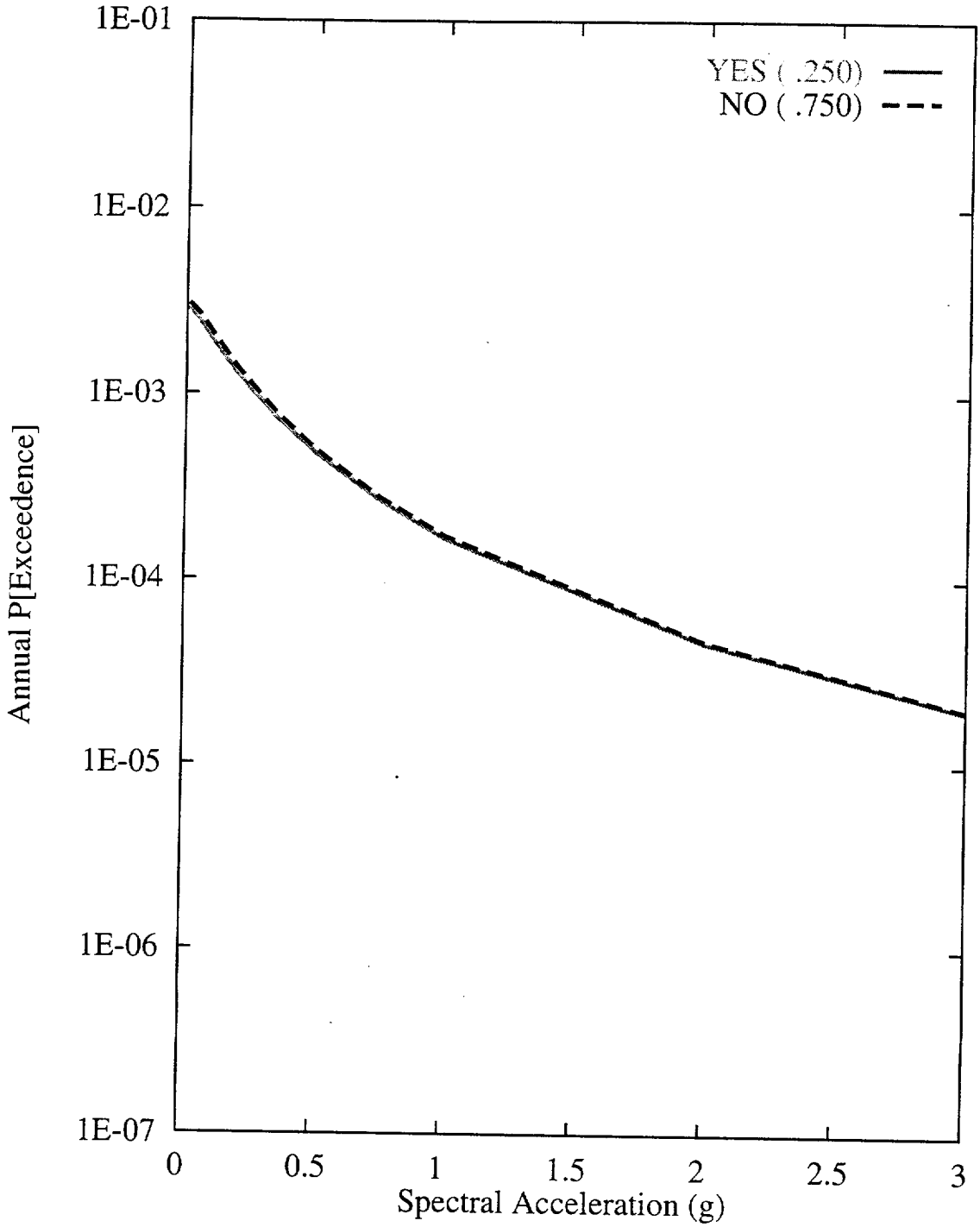

Figure 7-29 Sensitivity of seismic hazard from local faults to existence of local detachment: AAR team, 10-Hz horizontal spectral acceleration

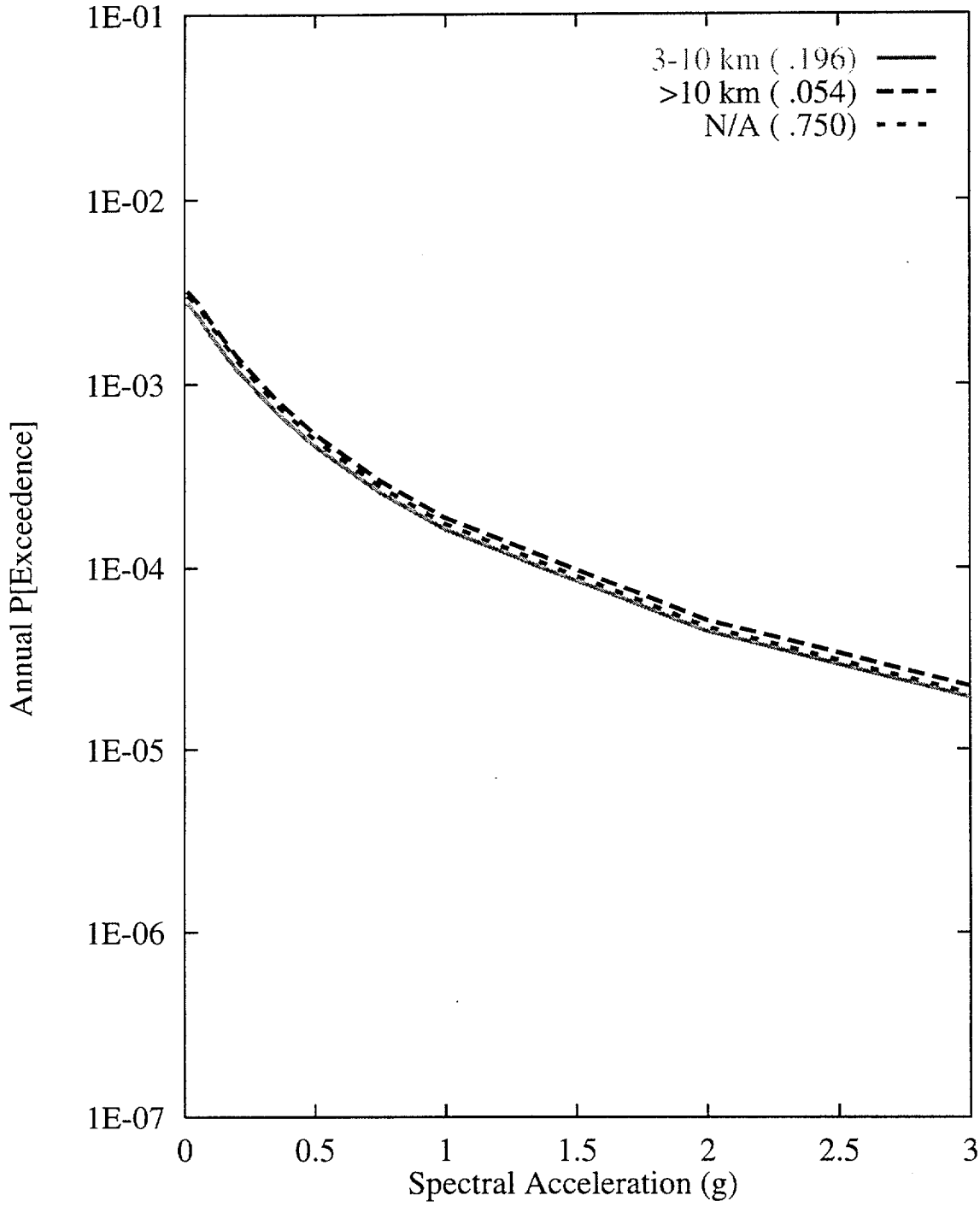

Figure 7-30 Sensitivity of seismic hazard from local faults to detachment depth: AAR team, 10-Hz horizontal spectral acceleration

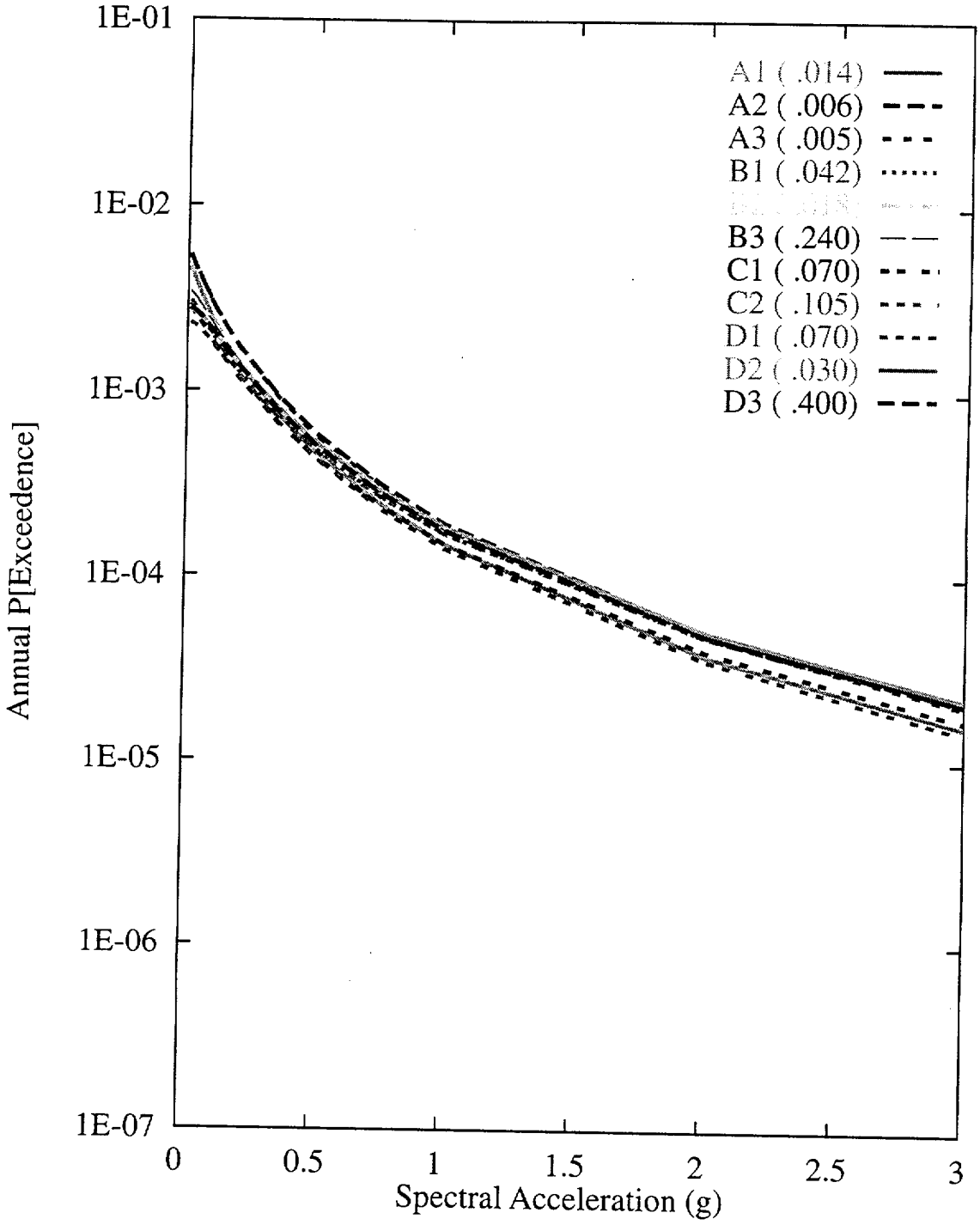

Figure 7-31 Sensitivity of seismic hazard from local faults to local fault scenarios: AAR team, 10-Hz horizontal spectral acceleration

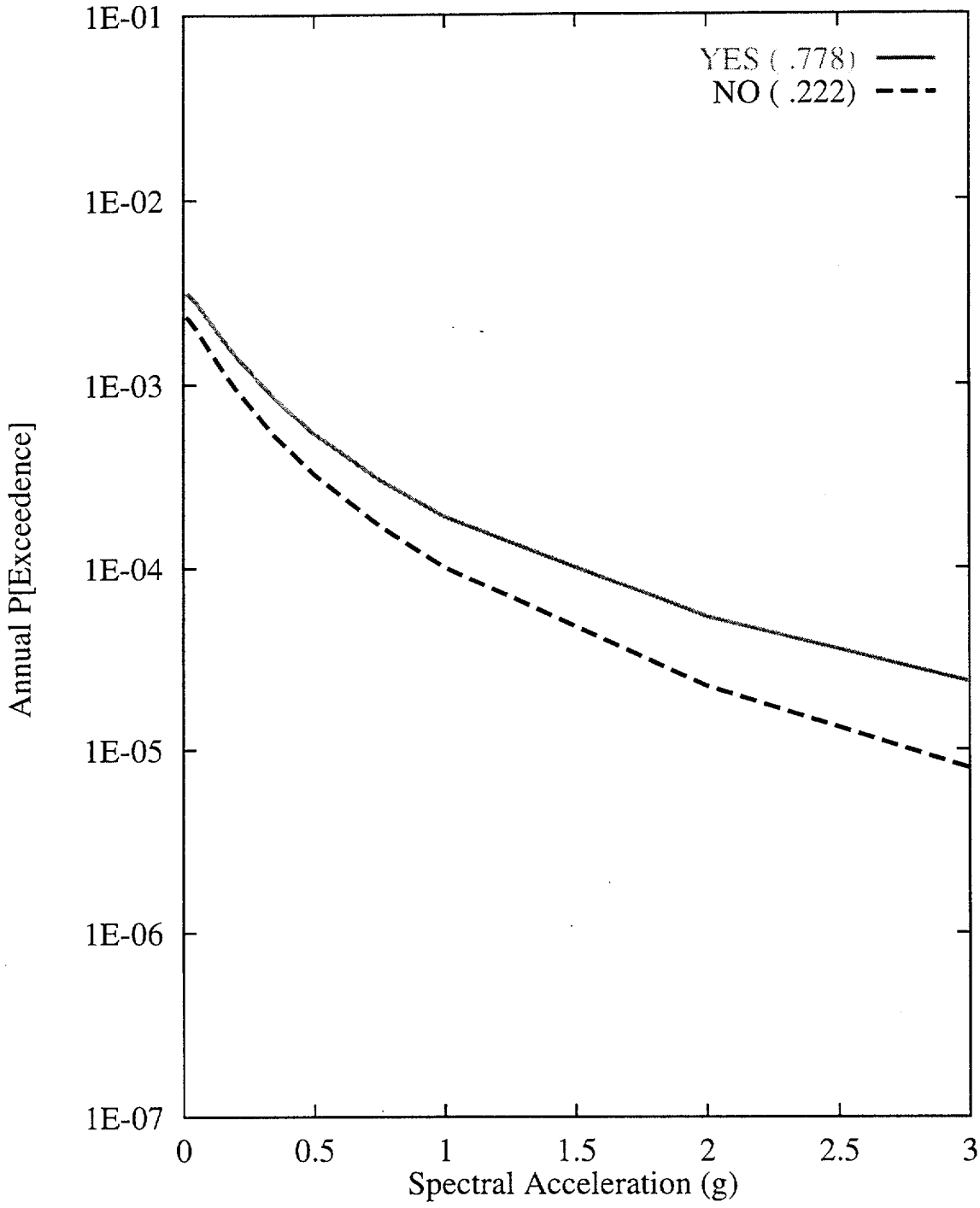

Figure 7-32 Sensitivity of seismic hazard from local faults to presence of coalescence: AAR team, 10-Hz horizontal spectral acceleration

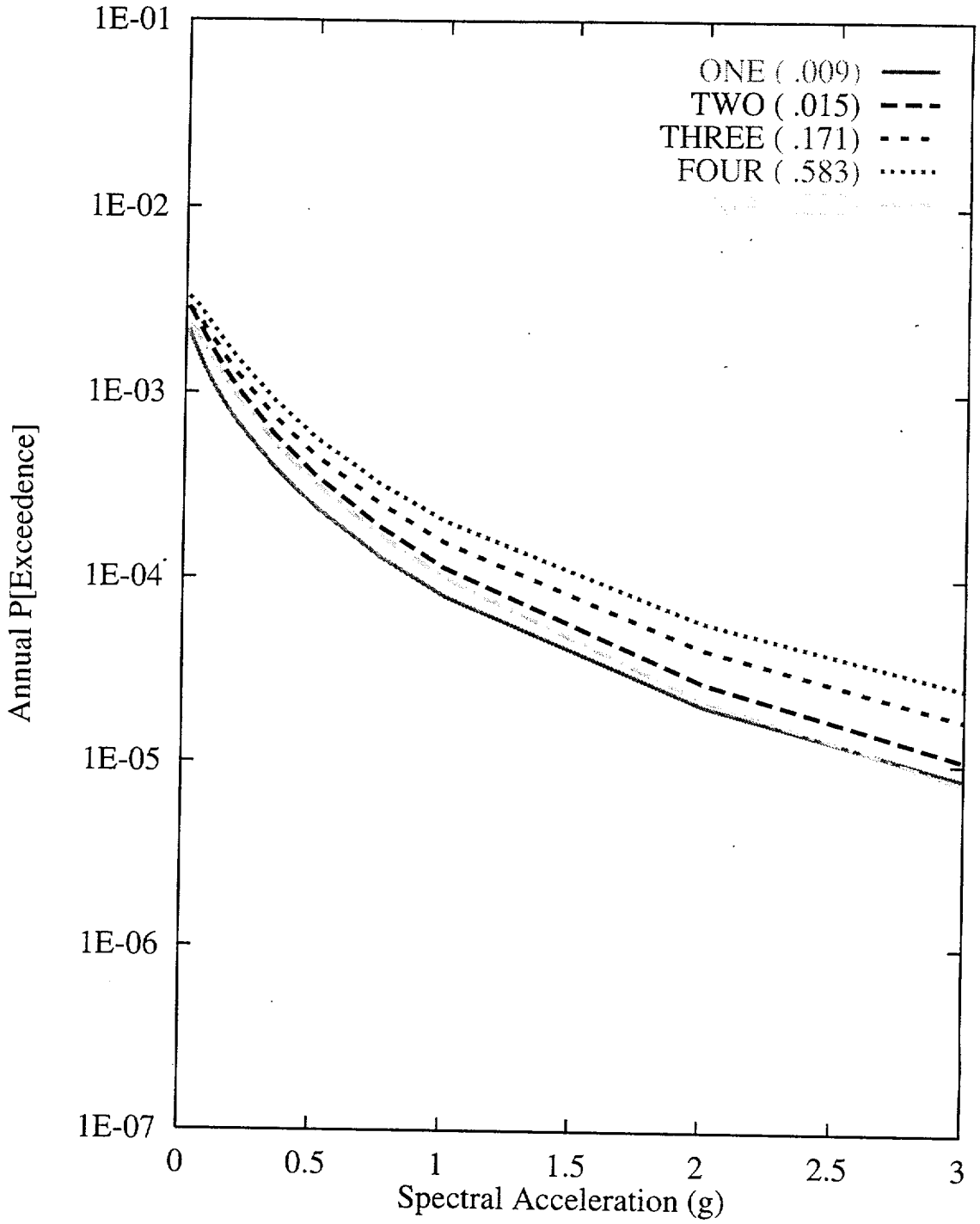

Figure 7-33 Sensitivity of seismic hazard from local faults to type of coalesced behavior: AAR team, 10-Hz horizontal spectral acceleration

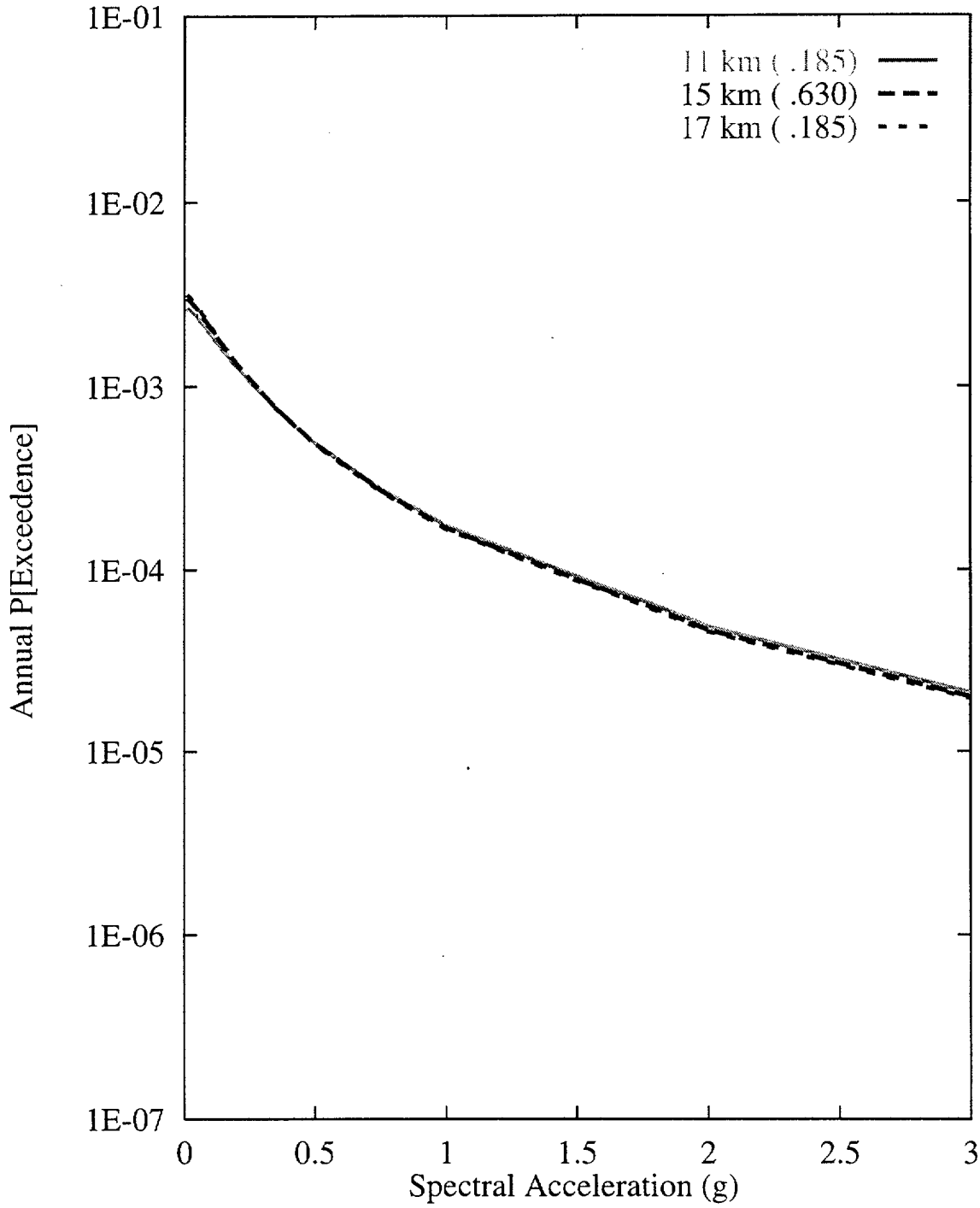

Figure 7-34 Sensitivity of seismic hazard from local faults to maximum fault depth: AAR team, 10-Hz horizontal spectral acceleration

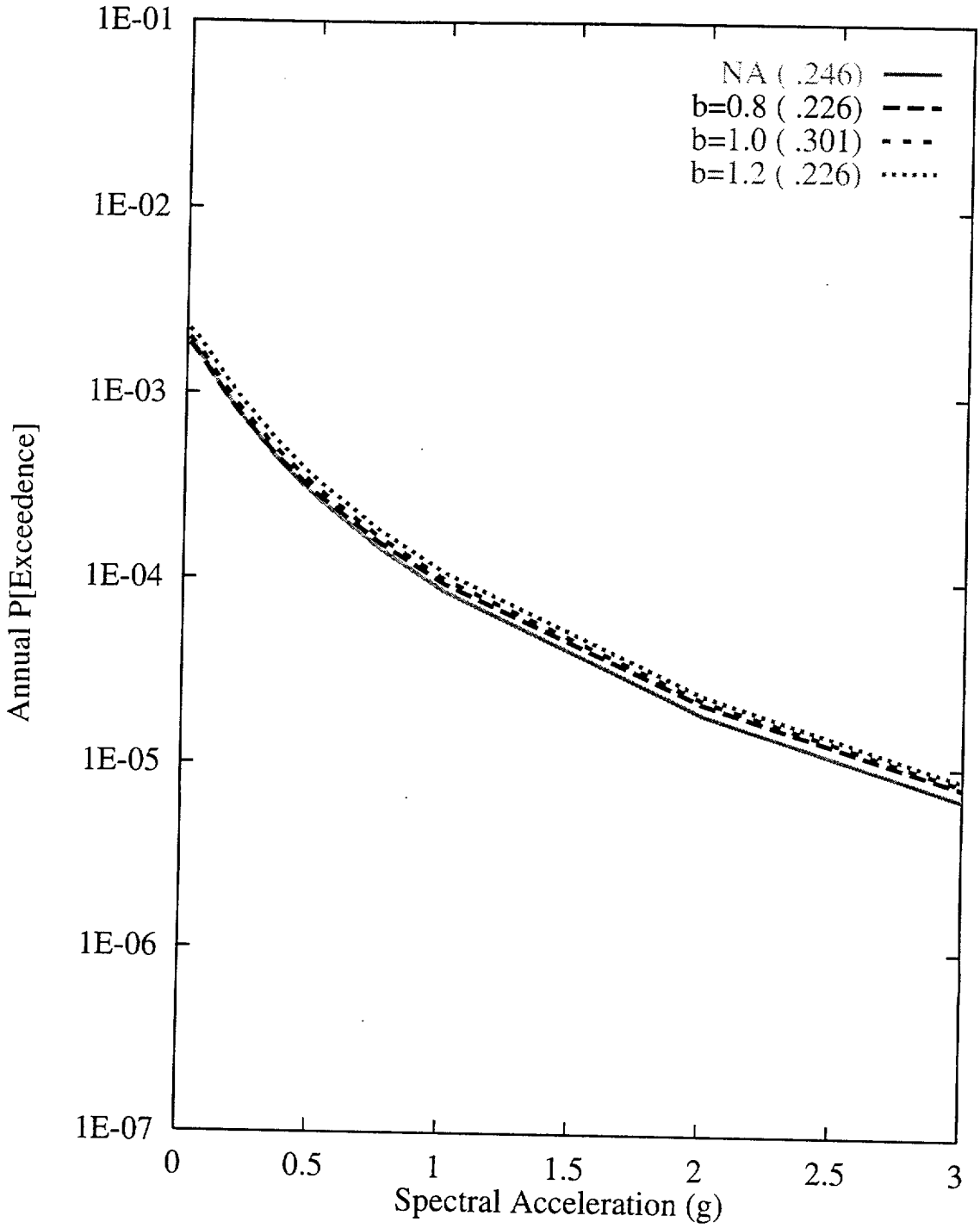

Figure 7-35 Sensitivity of seismic hazard from local faults to b-value of East-side fault system: AAR team, 10-Hz horizontal spectral acceleration

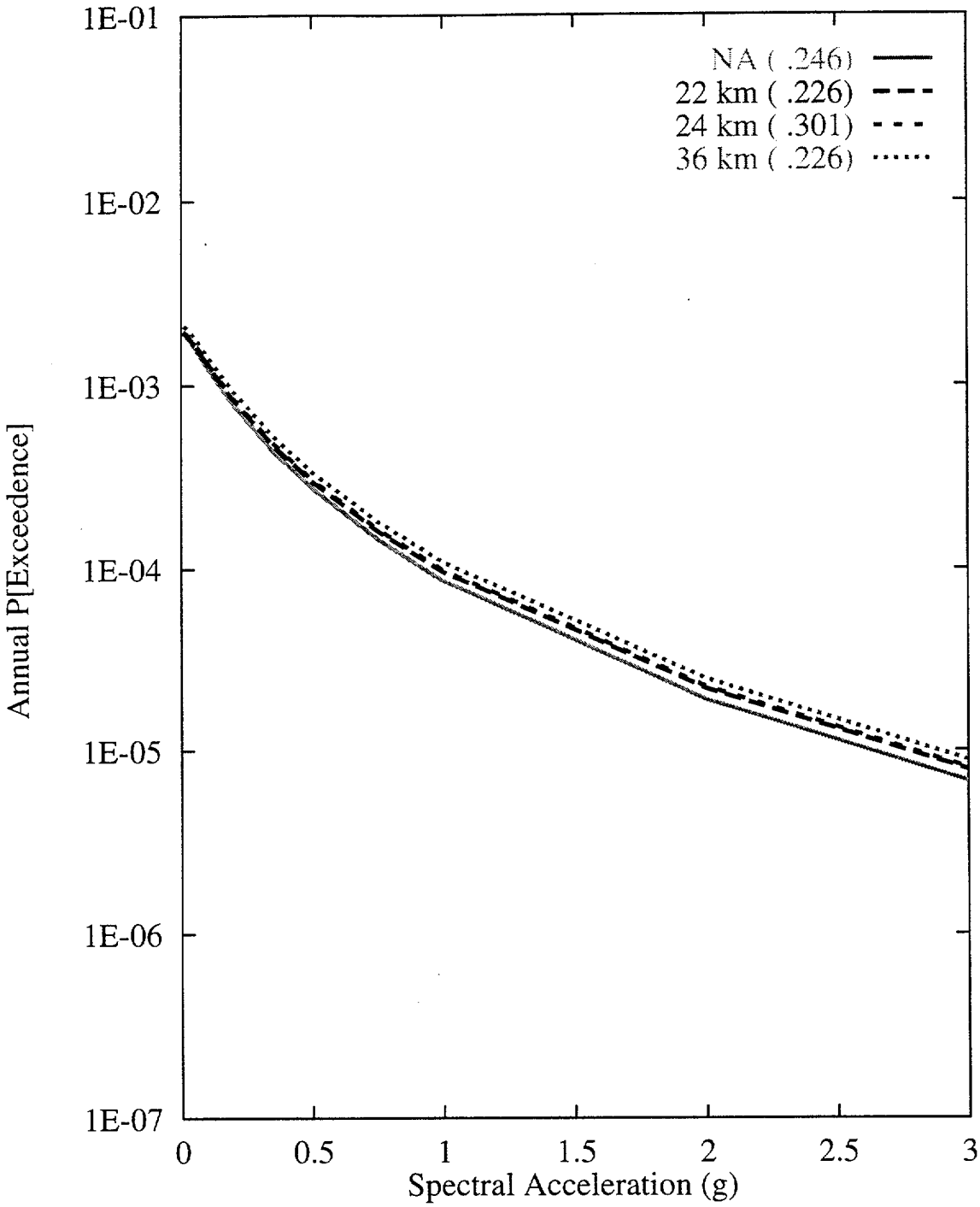

Figure 7-36 Sensitivity of seismic hazard from local faults to length of East-side fault system: AAR team, 10-Hz horizontal spectral acceleration

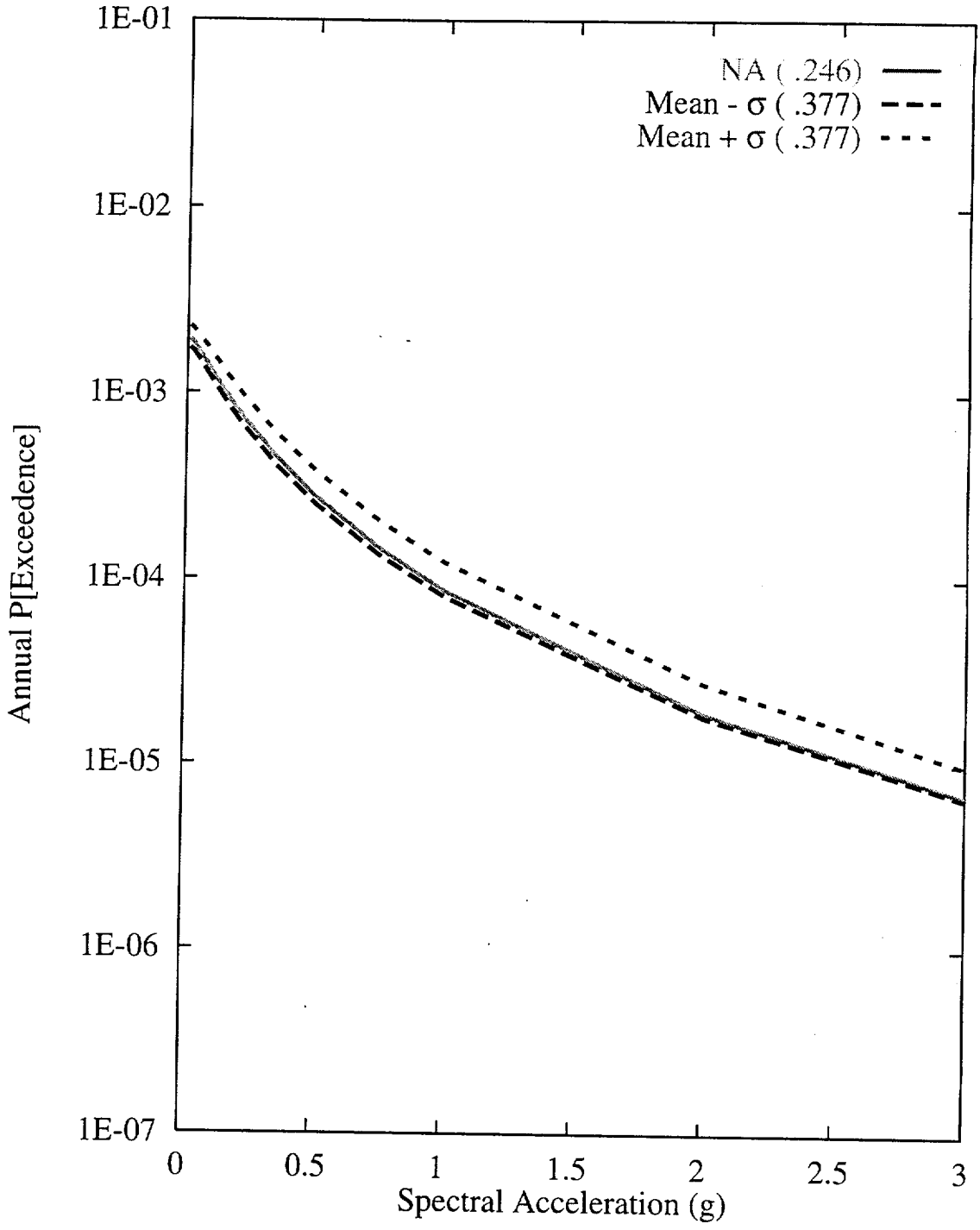

Figure 7-37 Sensitivity of seismic hazard from local faults to Mmax for the East-side fault system: AAR team, 10-Hz horizontal spectral acceleration

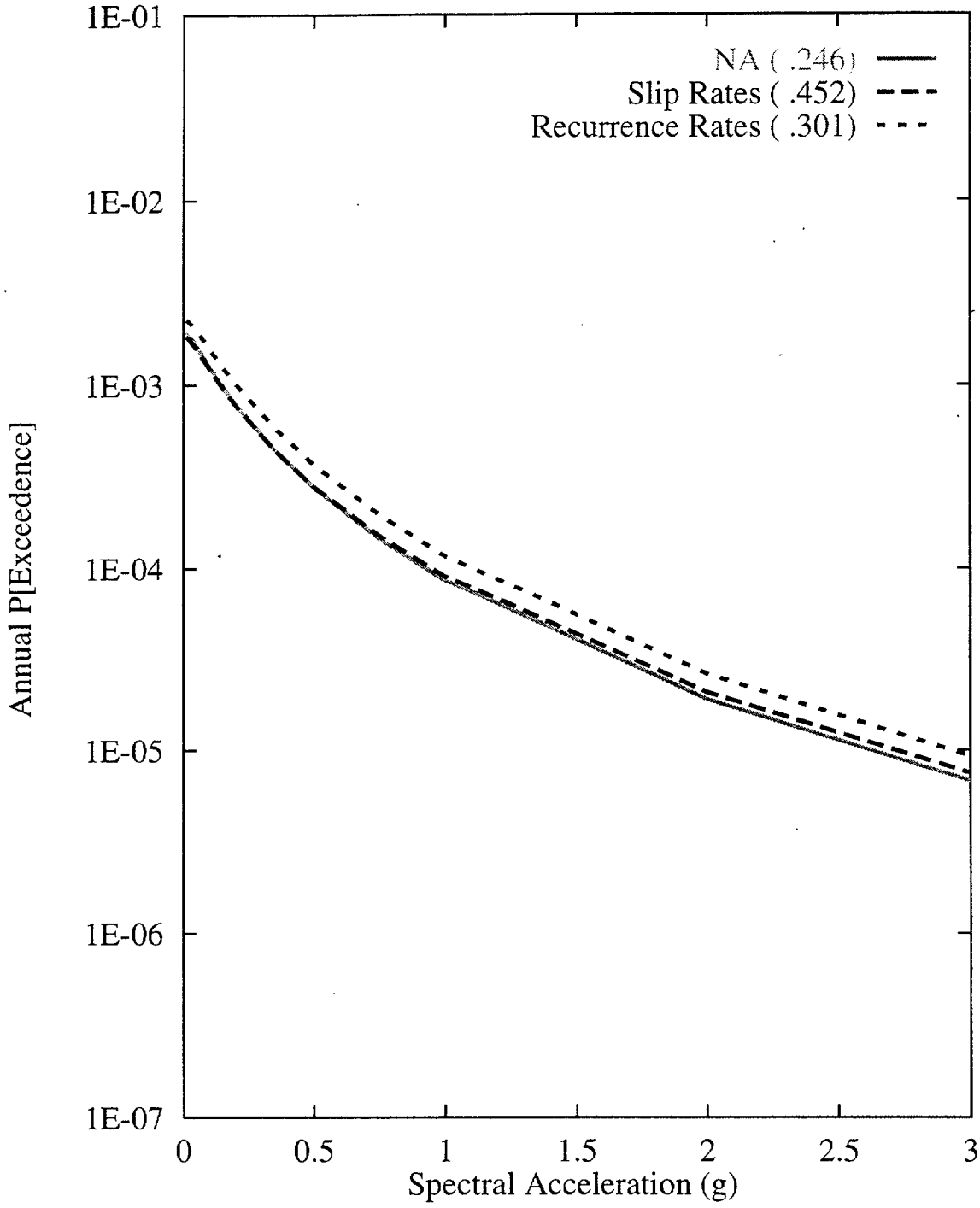

Figure 7-38 Sensitivity of seismic hazard from local faults to recurrence approach for the East-side fault system: AAR team, 10-Hz horizontal spectral acceleration

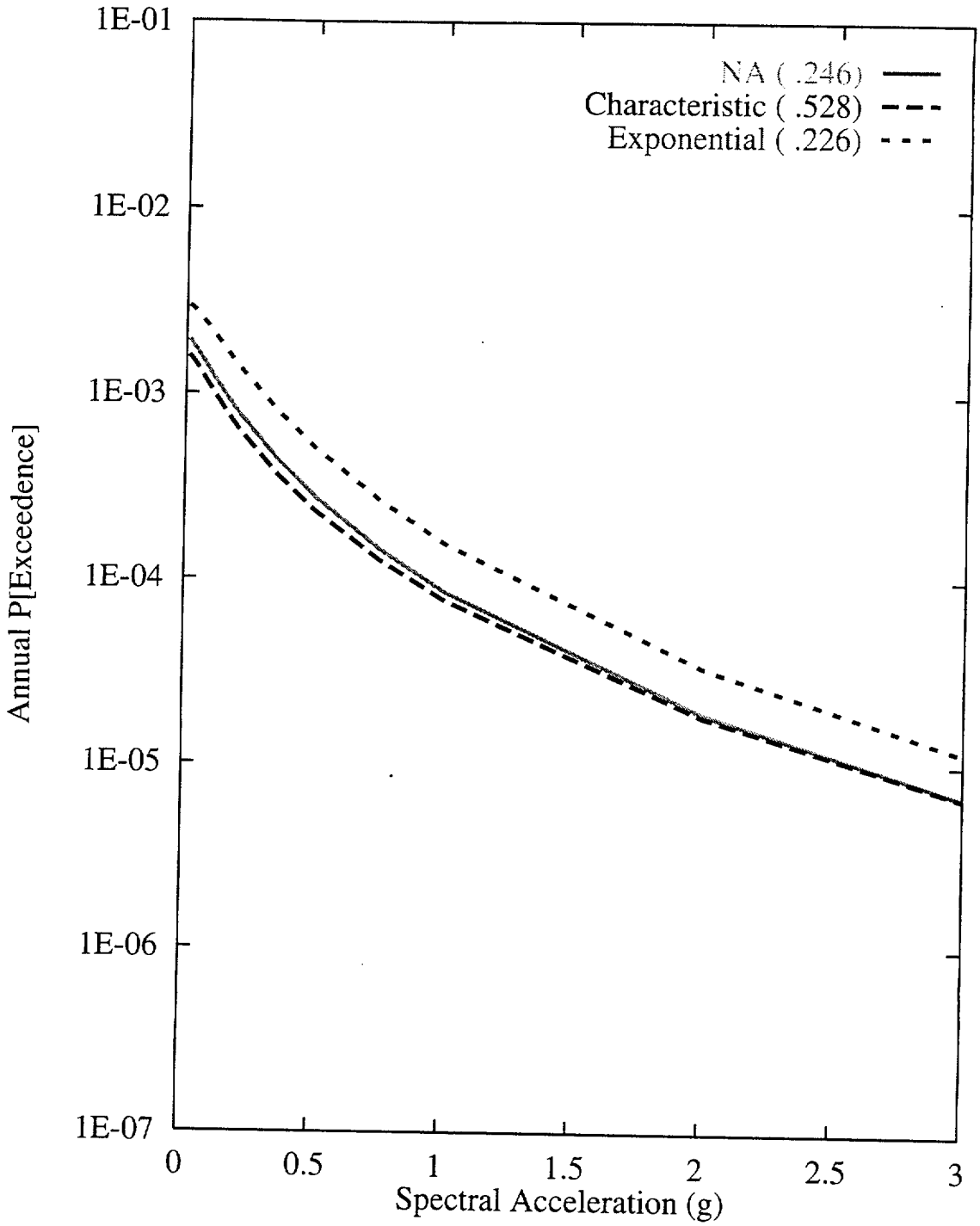

Figure 7-39 Sensitivity of seismic hazard from local faults to recurrence model for the East-side fault system: AAR team, 10-Hz horizontal spectral acceleration

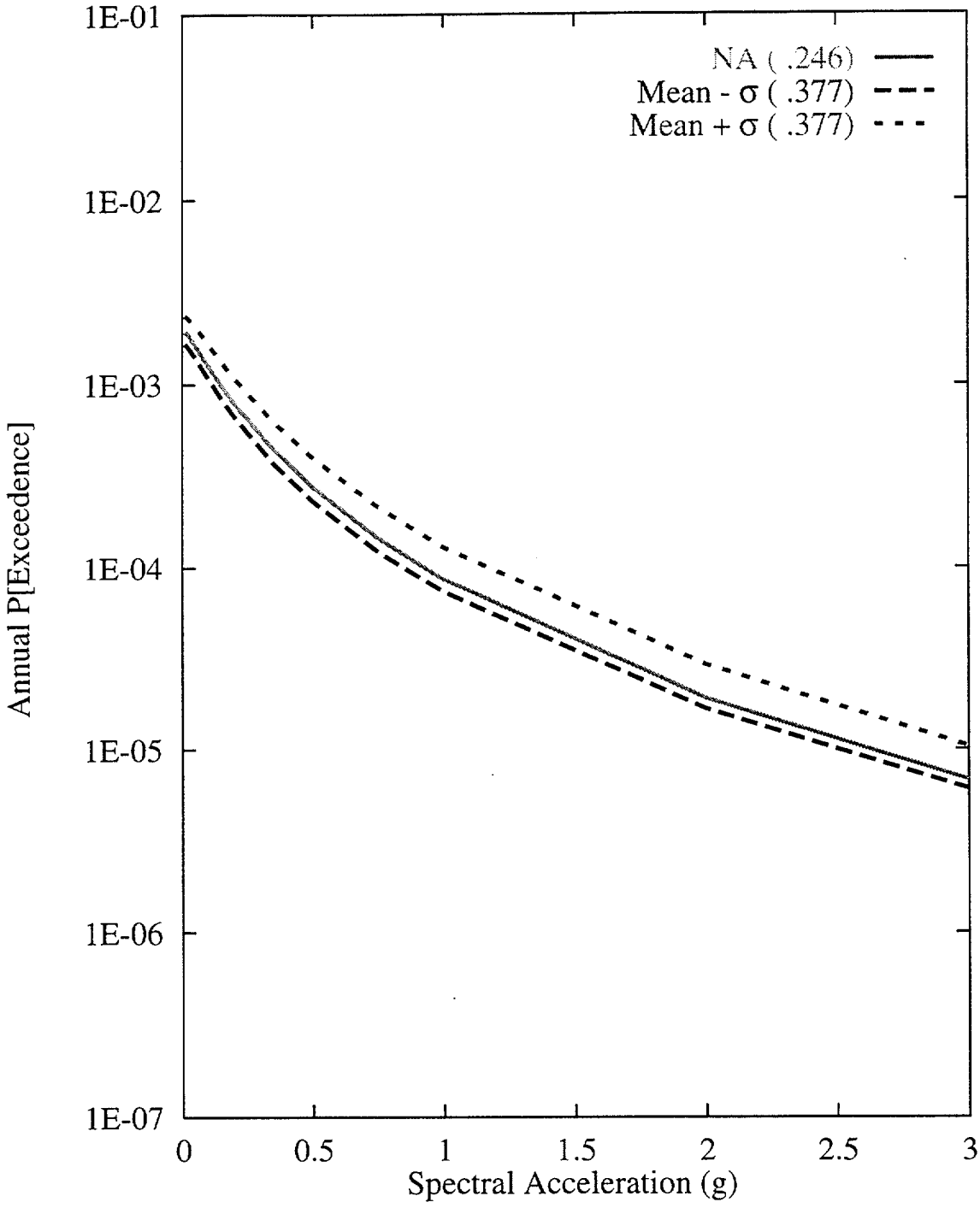

Figure 7-40 Sensitivity of seismic hazard from local faults to recurrence of the East-side fault system: AAR team, 10-Hz horizontal spectral acceleration

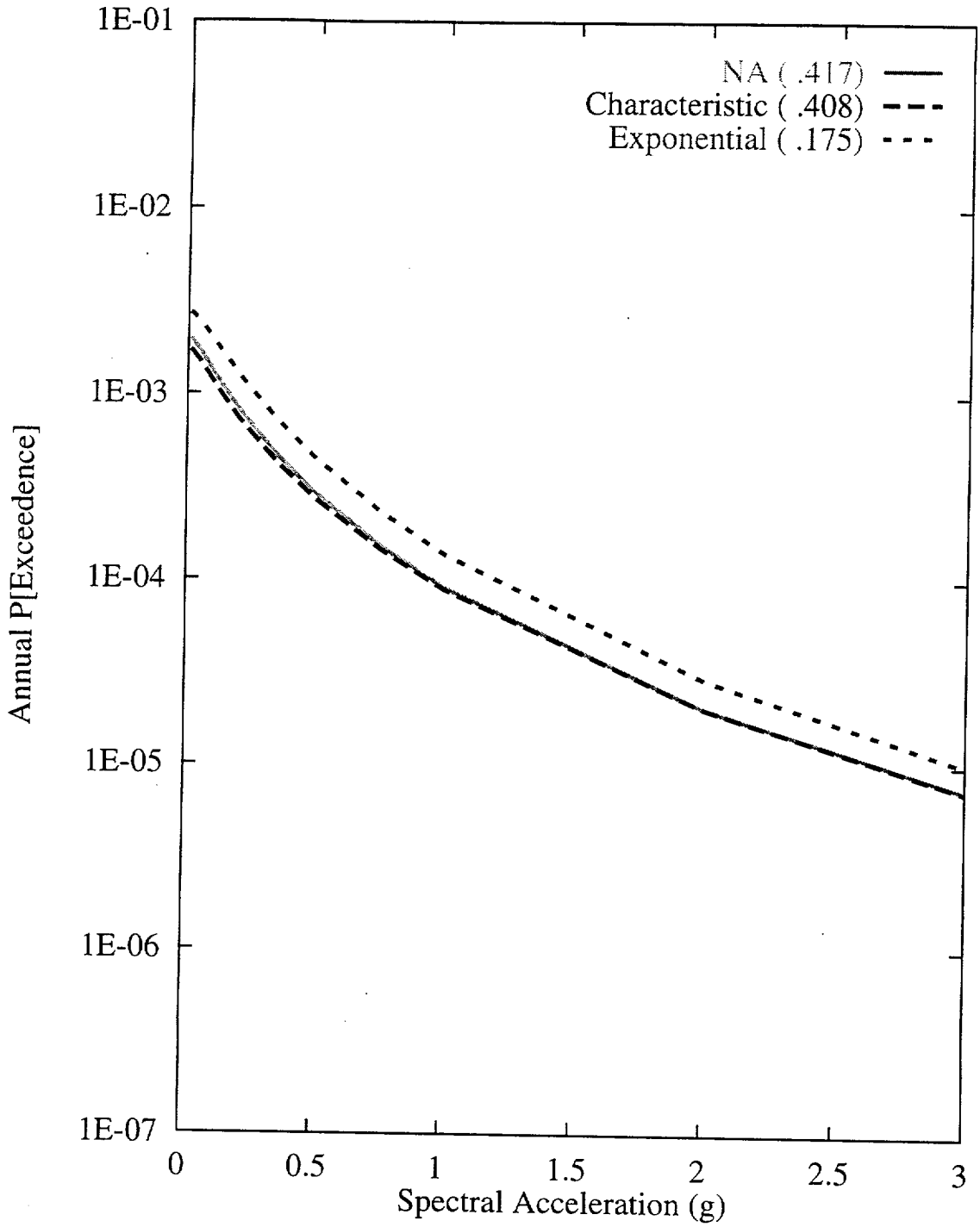

Figure 7-41 Sensitivity of seismic hazard from local faults to recurrence model of the West-side fault system: AAR team, 10-Hz horizontal spectral acceleration

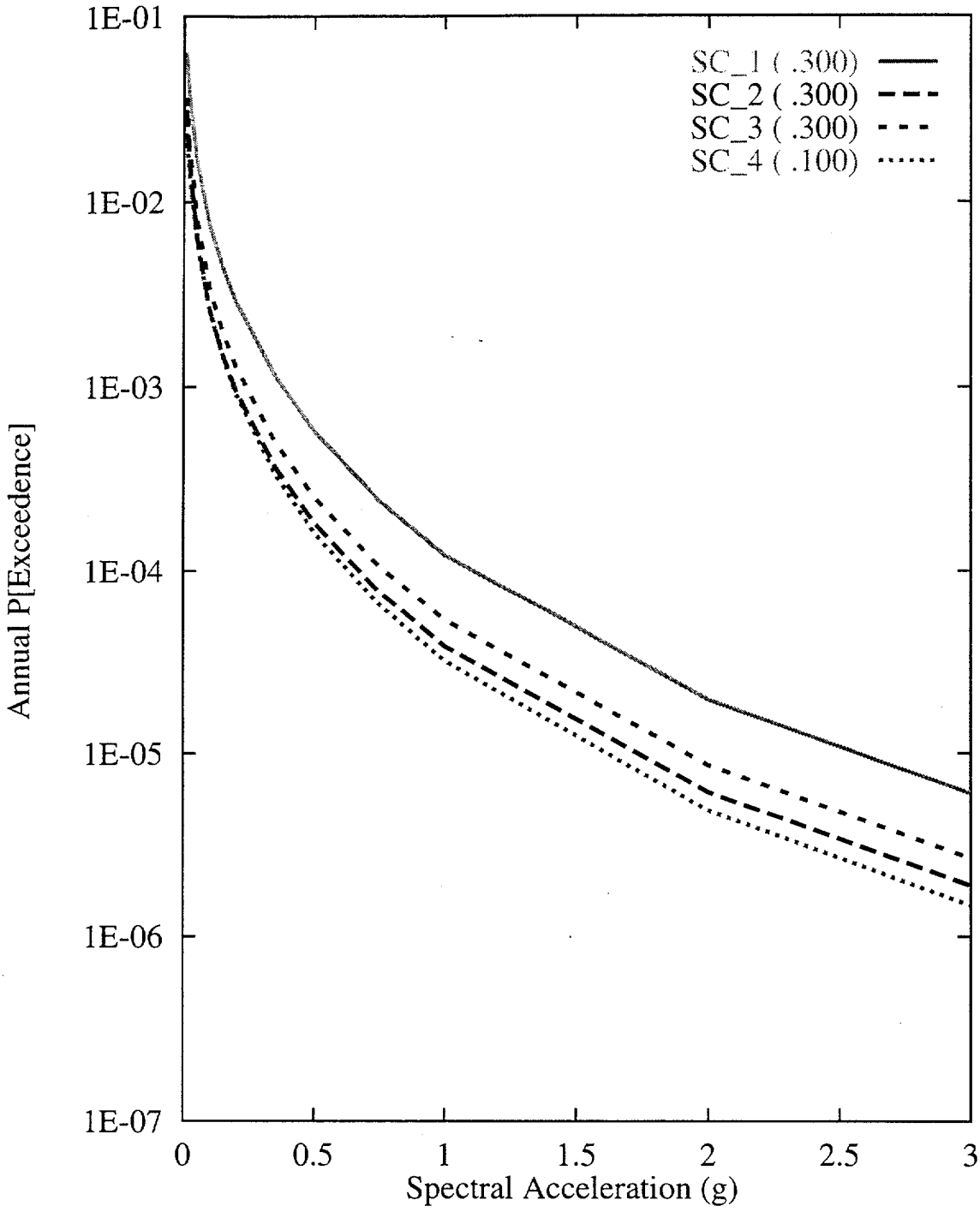

Figure 7-42 Sensitivity of seismic hazard from area source zones to various scenarios (SC) for zonation: AAR team, 10-Hz horizontal spectral acceleration

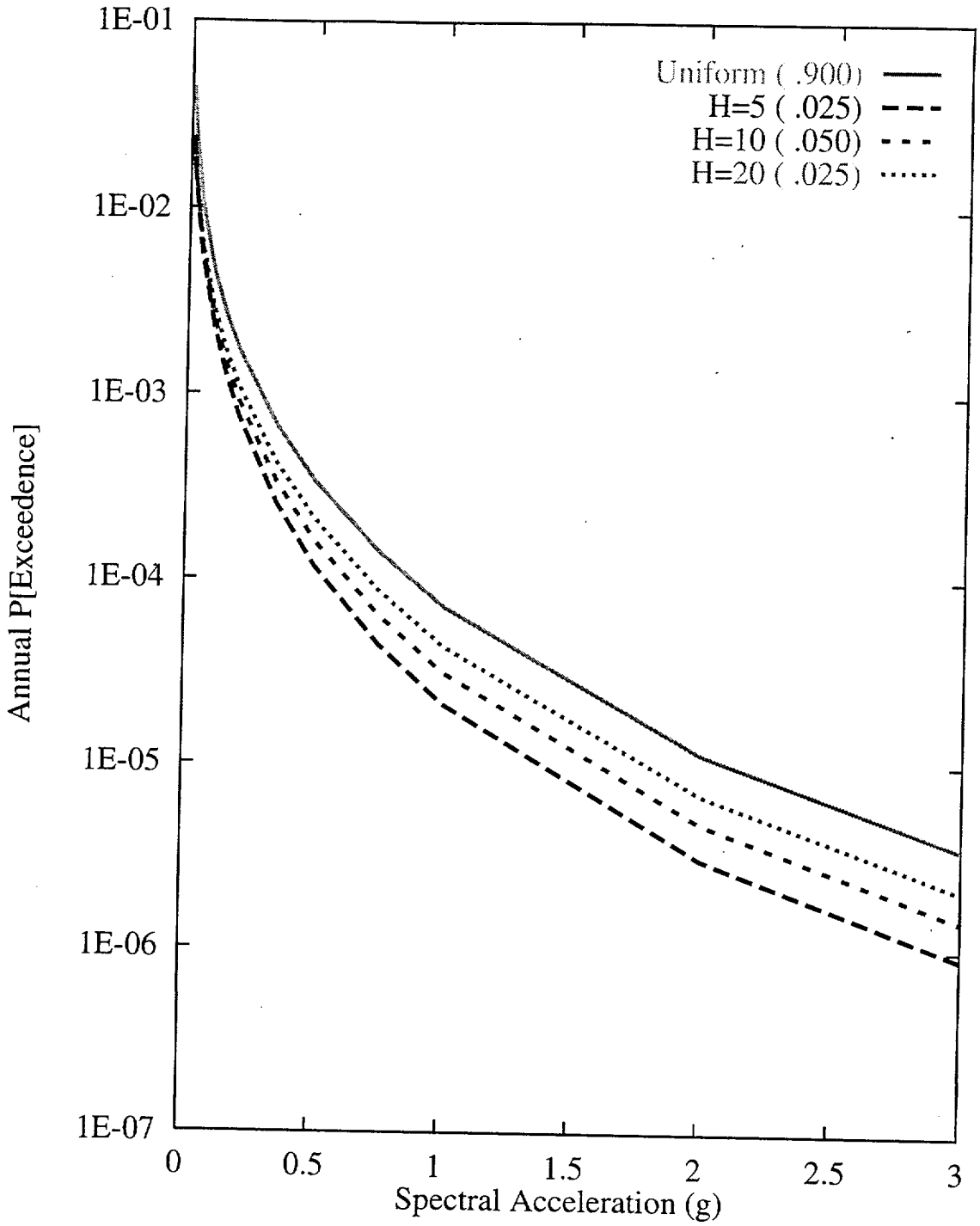

Figure 7-43 Sensitivity of seismic hazard from area source zones to spatial variability and smoothing (H): AAR team, 10-Hz horizontal spectral acceleration

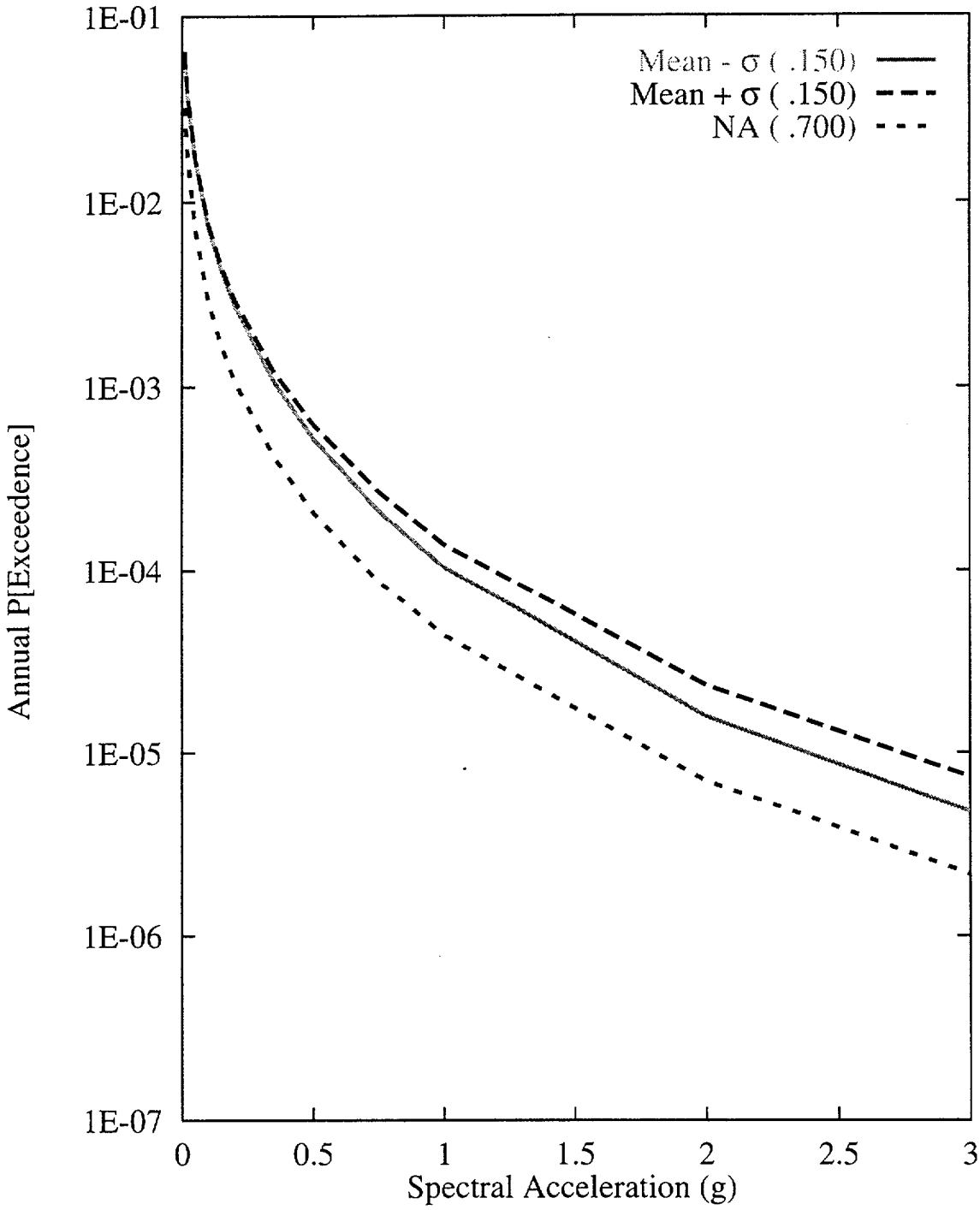

Figure 7-44 Sensitivity of seismic hazard from area source zones to Mmax for the Z2 area source: AAR team, 10-Hz horizontal spectral acceleration

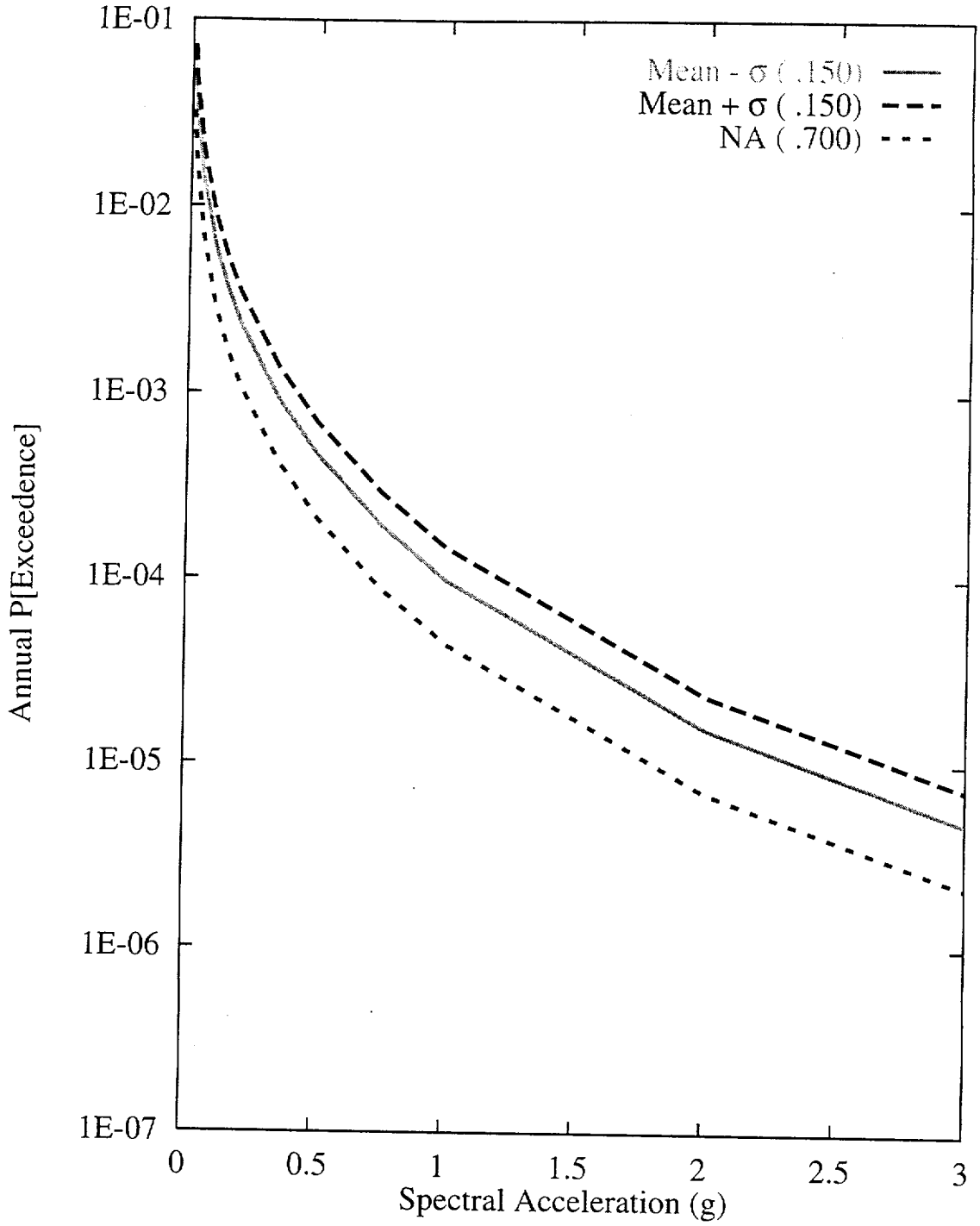

Figure 7-45 Sensitivity of seismic hazard from area source zone to recurrence of the Z2 source zone: AAR team, 10-Hz horizontal spectral acceleration

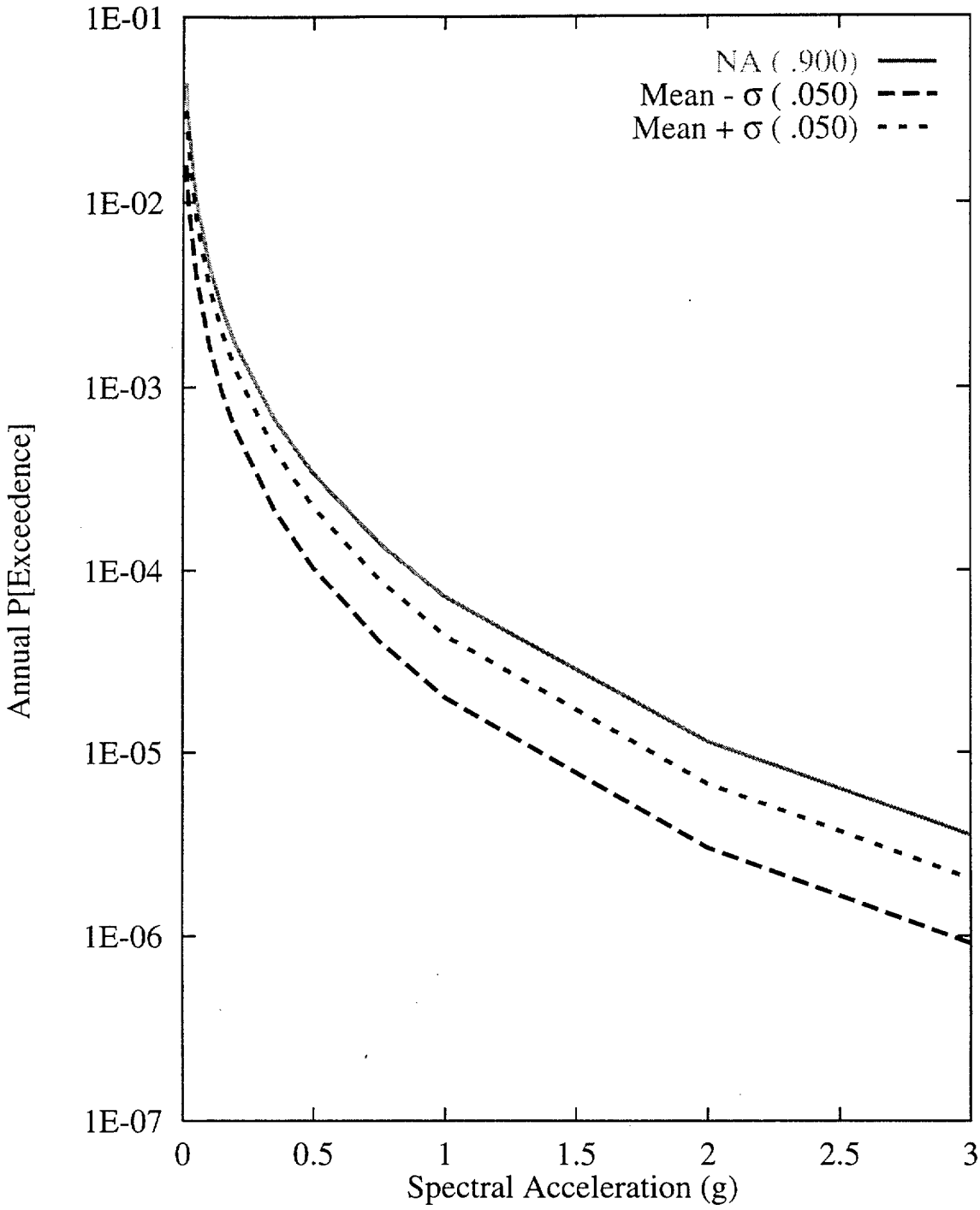

Figure 7-46 Sensitivity of seismic hazard from area source zone to recurrence of the 100-km background zone: AAR team, 10-Hz horizontal spectral acceleration

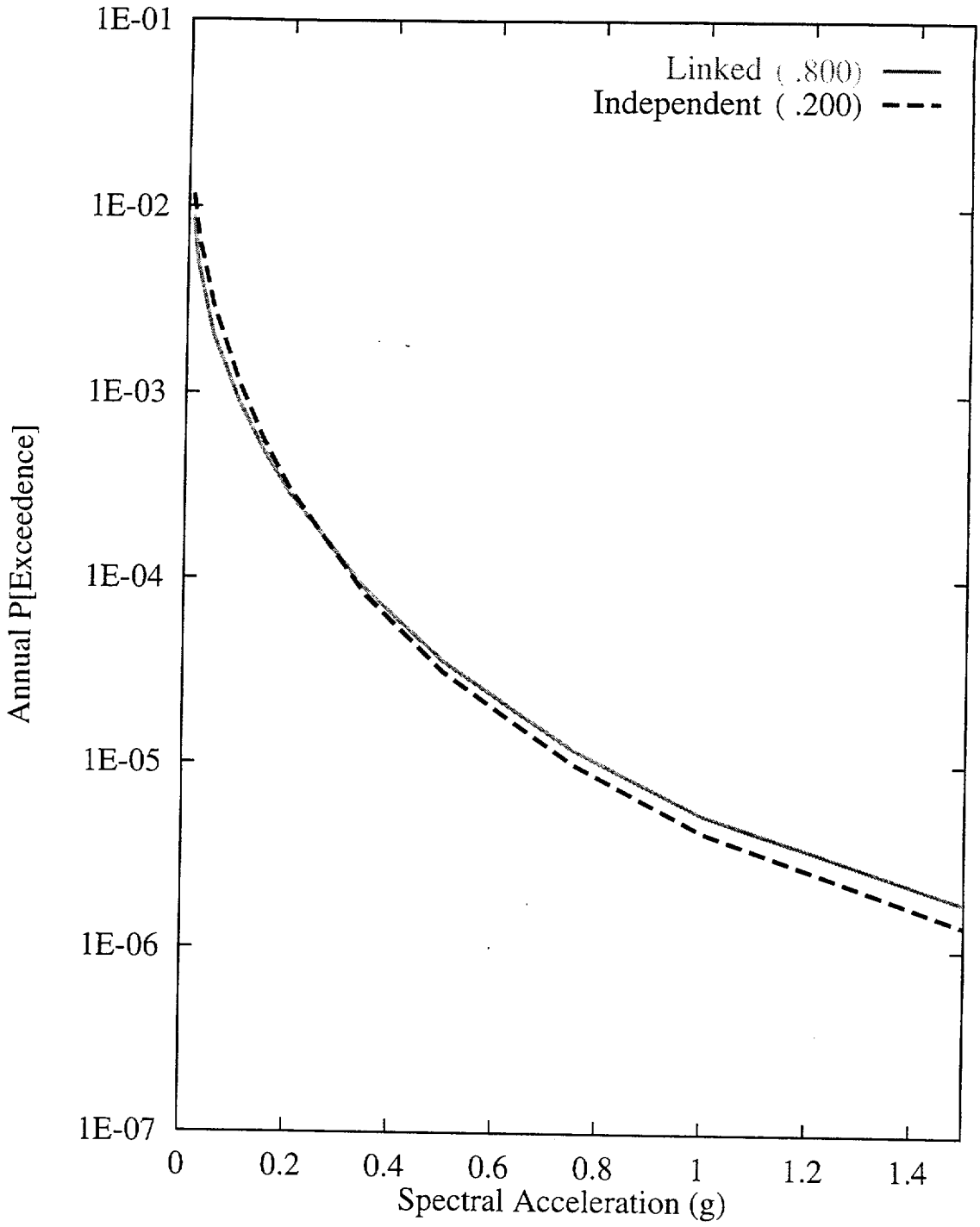

Figure 7-47 Sensitivity of seismic hazard from regional faults to configuration of the Death Valley-Furnace Creek fault system: AAR team, 1-Hz horizontal spectral acceleration

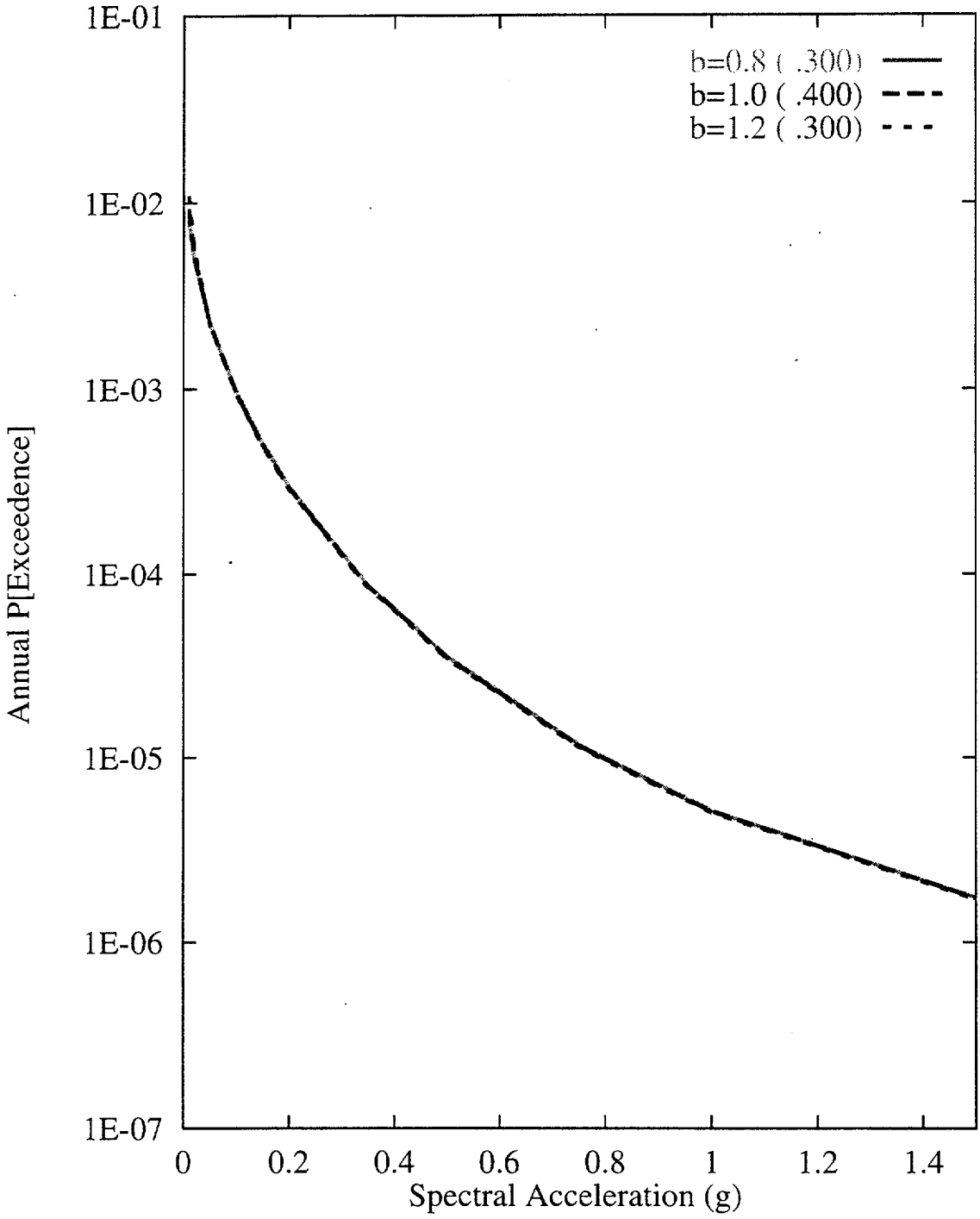

Figure 7-48 Sensitivity of seismic hazard from regional faults to b-values: AAR team, 1-Hz horizontal spectral acceleration

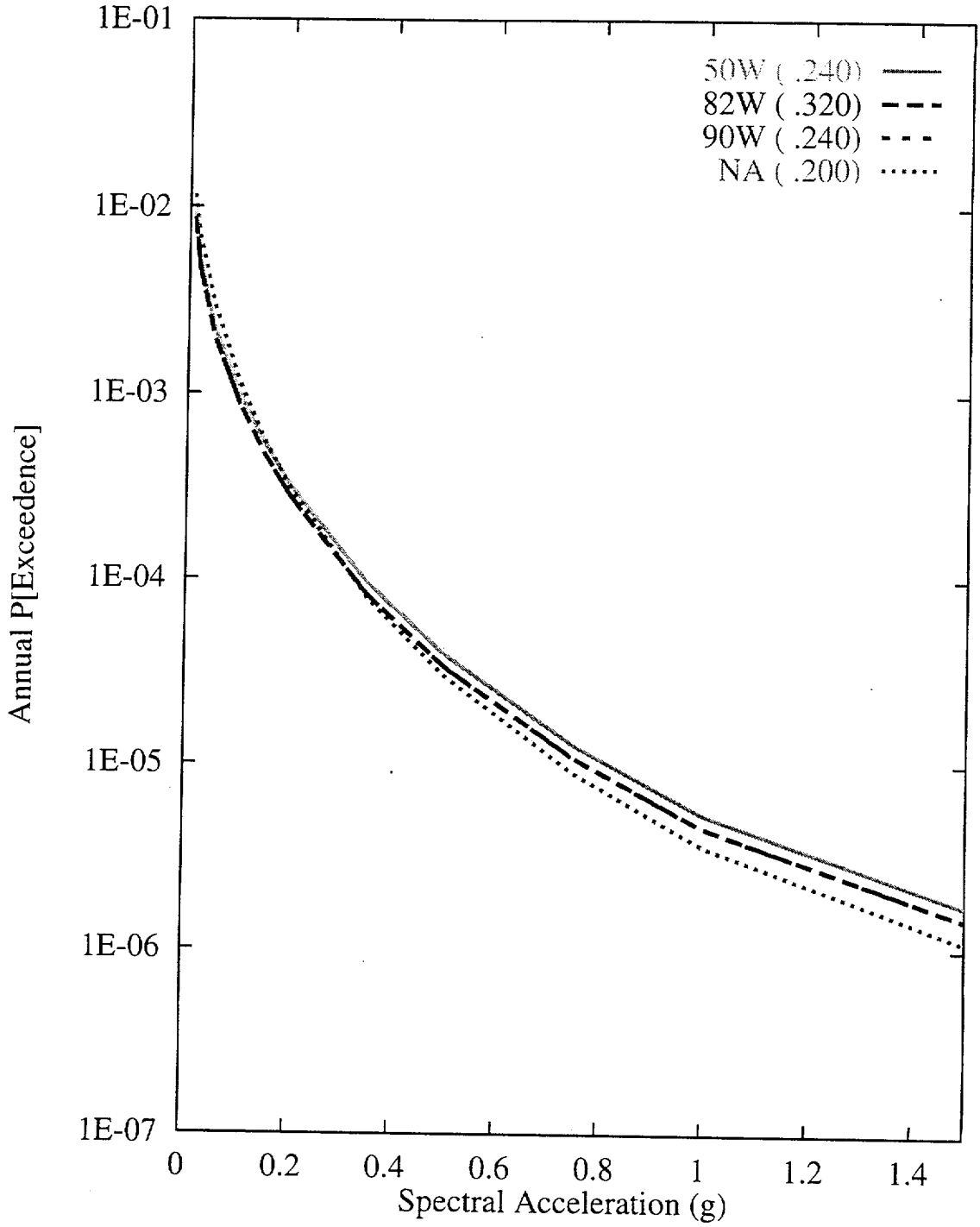

Figure 7-49 Sensitivity of seismic hazard from regional faults to the Death Valley-Furnace Creek fault system: AAR team, 1-Hz horizontal spectral acceleration

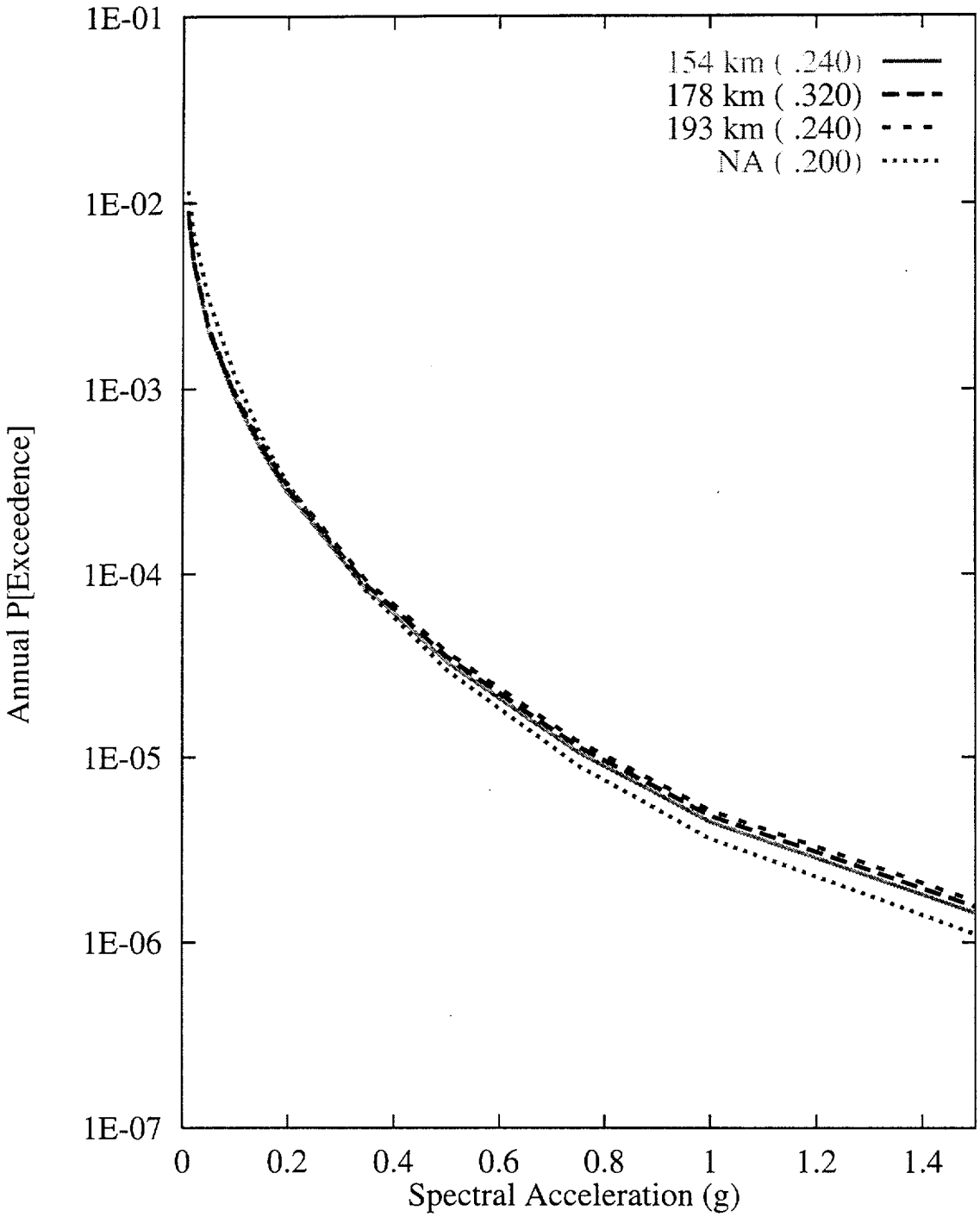

Figure 7-50 Sensitivity of seismic hazard from regional faults to length of the Death Valley-Furnace Creek fault system: AAR team, 1-Hz horizontal spectral acceleration

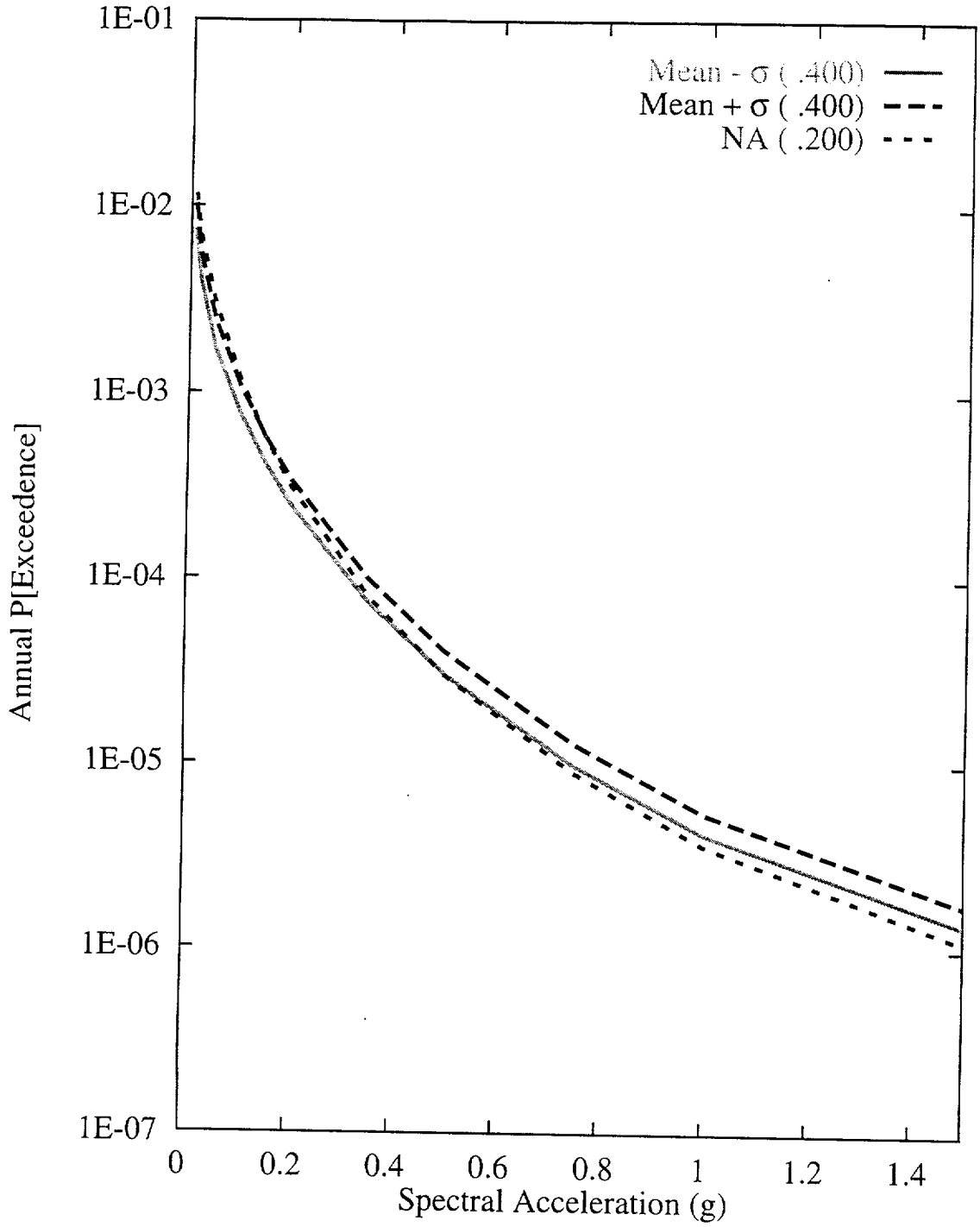

Figure 7-51 Sensitivity of seismic hazard from regional faults to Mmax of the Death Valley-Furnace Creek fault system: AAR team, 1-Hz horizontal spectral acceleration

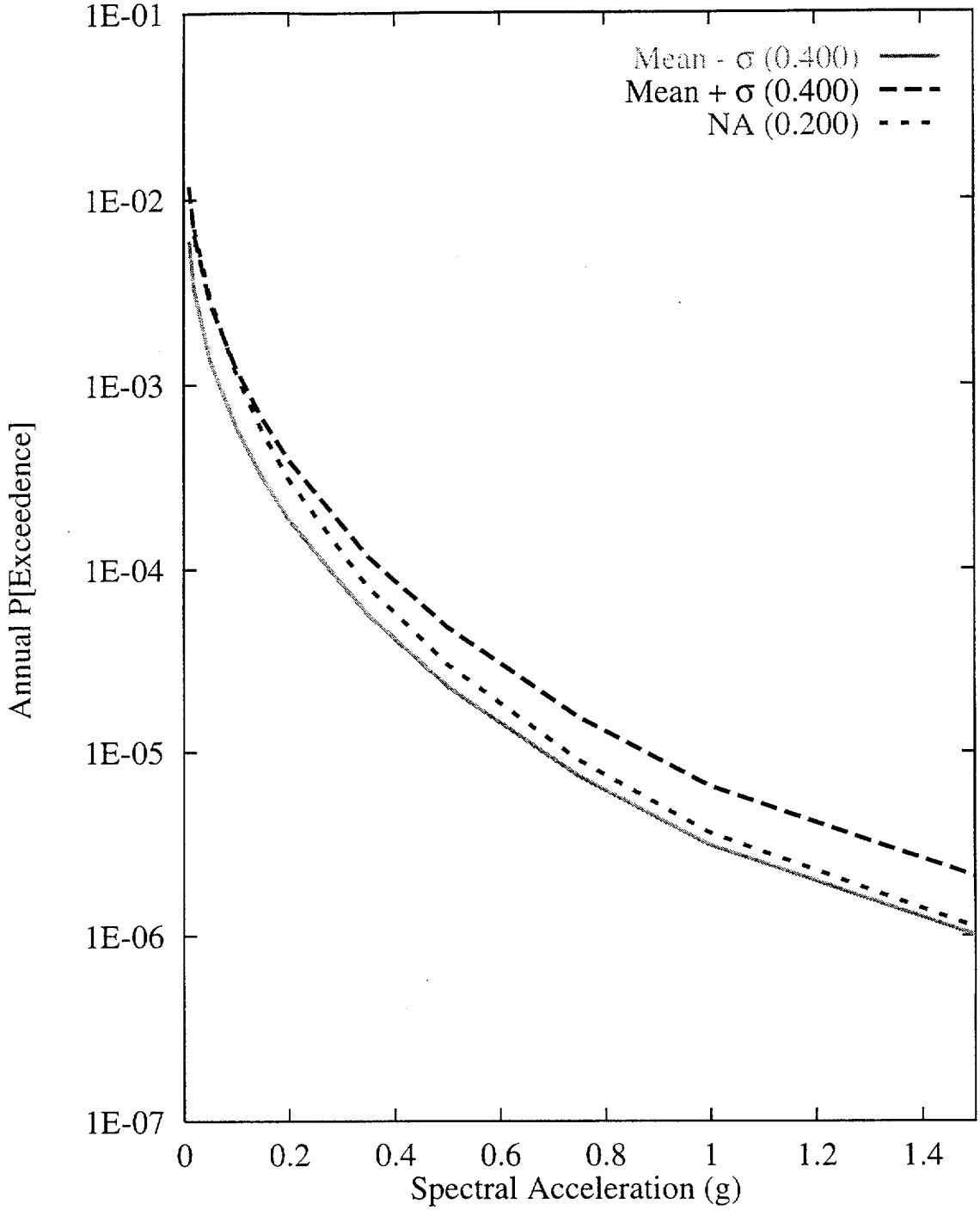

Figure 7-52 Sensitivity of seismic hazard from regional faults to recurrence of the Death Valley-Furnace Creek fault system: AAR team, 1-Hz horizontal spectral acceleration

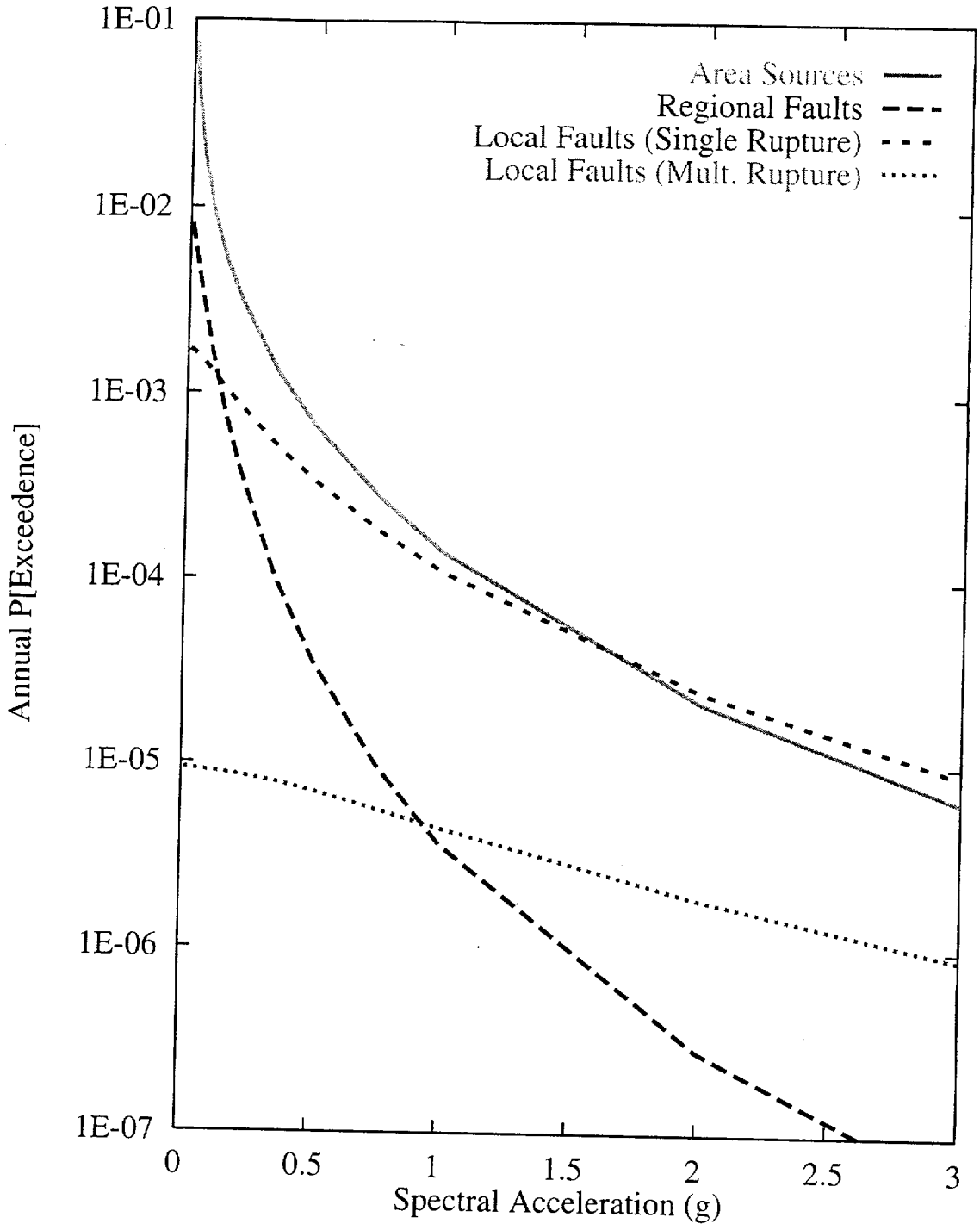

Figure 7-53 Contribution of source type to the mean hazard: ASM team, 10-Hz horizontal spectral acceleration

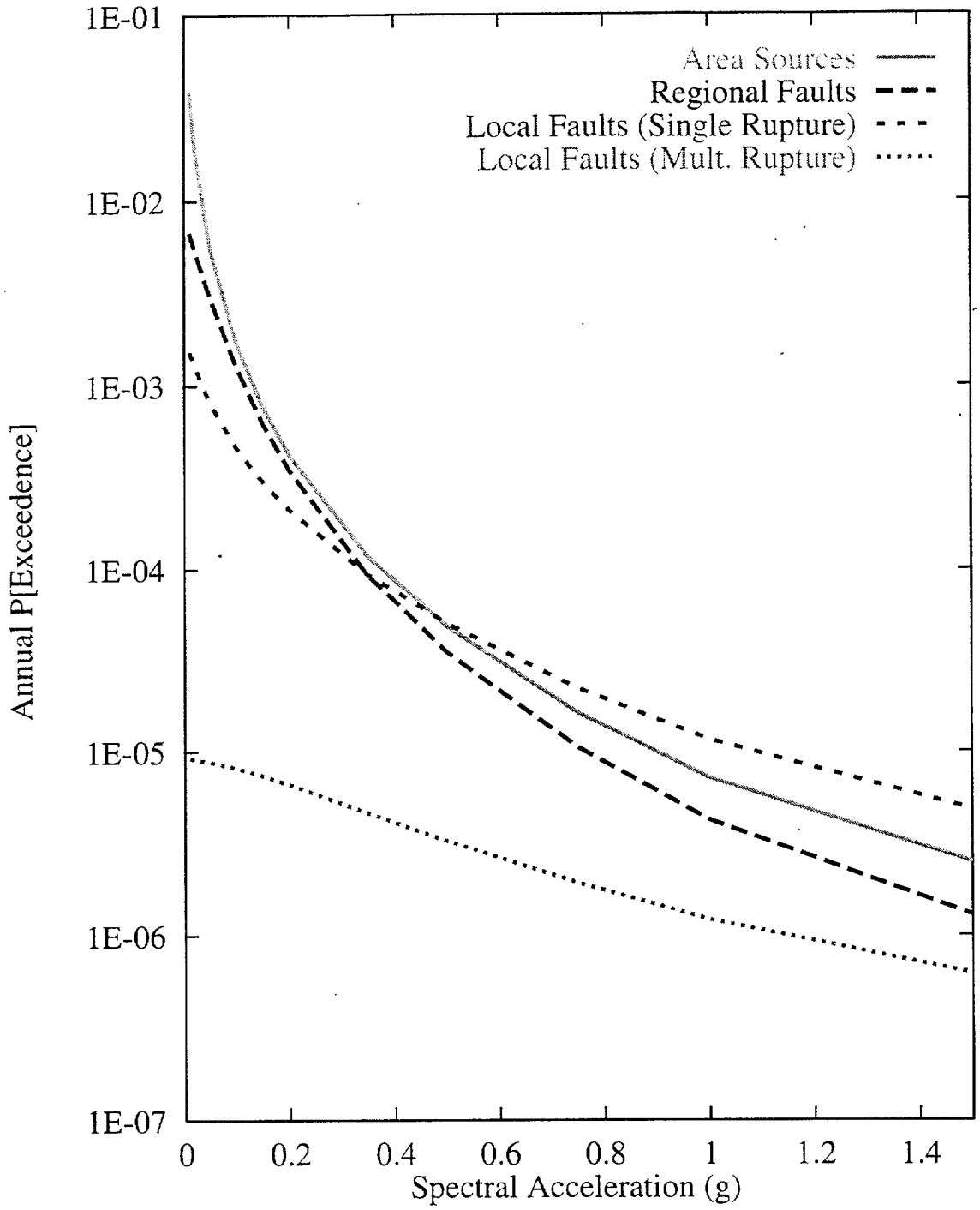

Figure 7-54 Contribution of source type to the mean hazard: ASM team, 1-Hz horizontal spectral acceleration

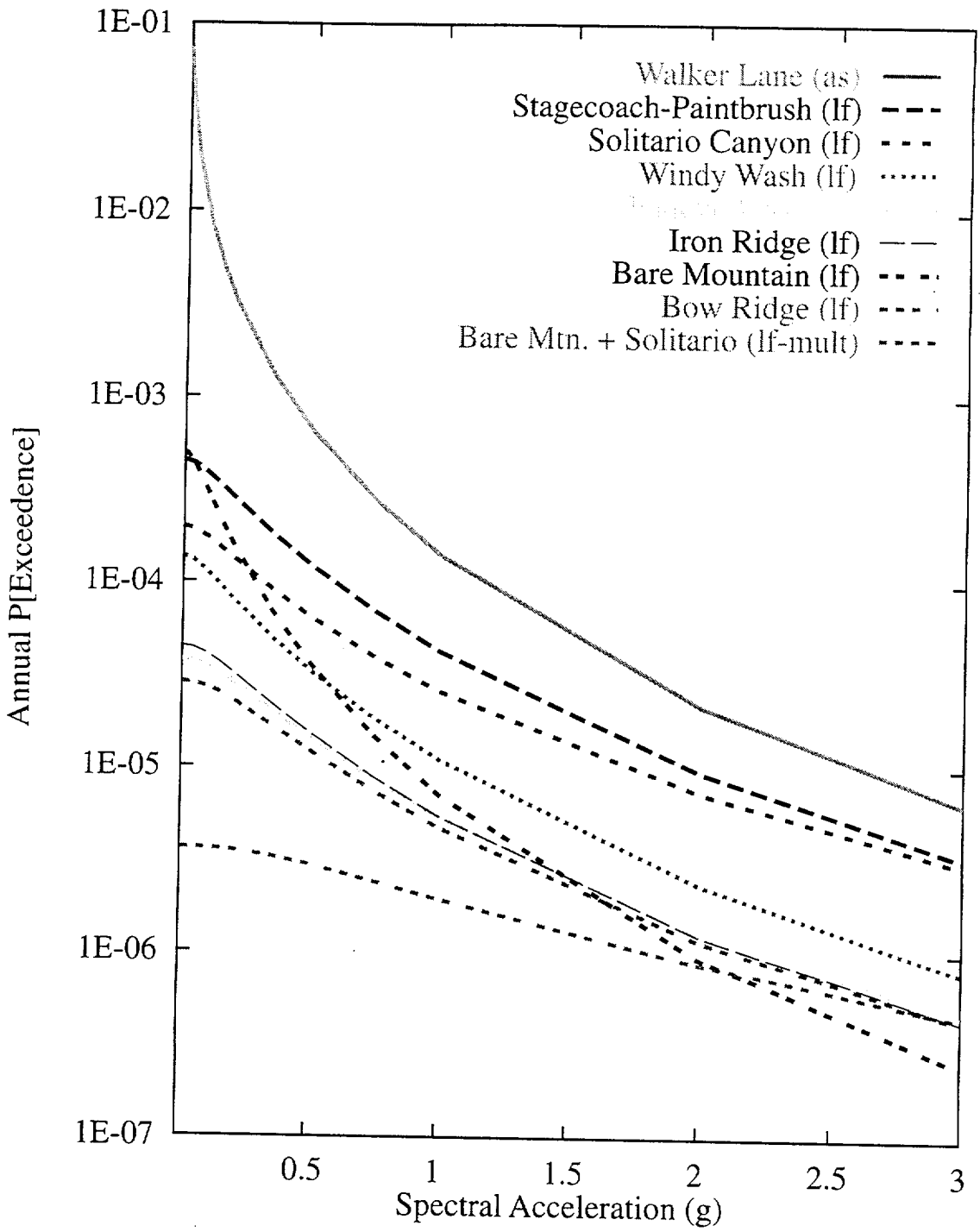

Figure 7-55 Mean seismic hazard from dominant seismic sources: ASM team, 10-Hz horizontal spectral acceleration. Acronyms in parentheses refer to source types: as-area source zone; lf-local fault; and mult-multiple fault rupture.

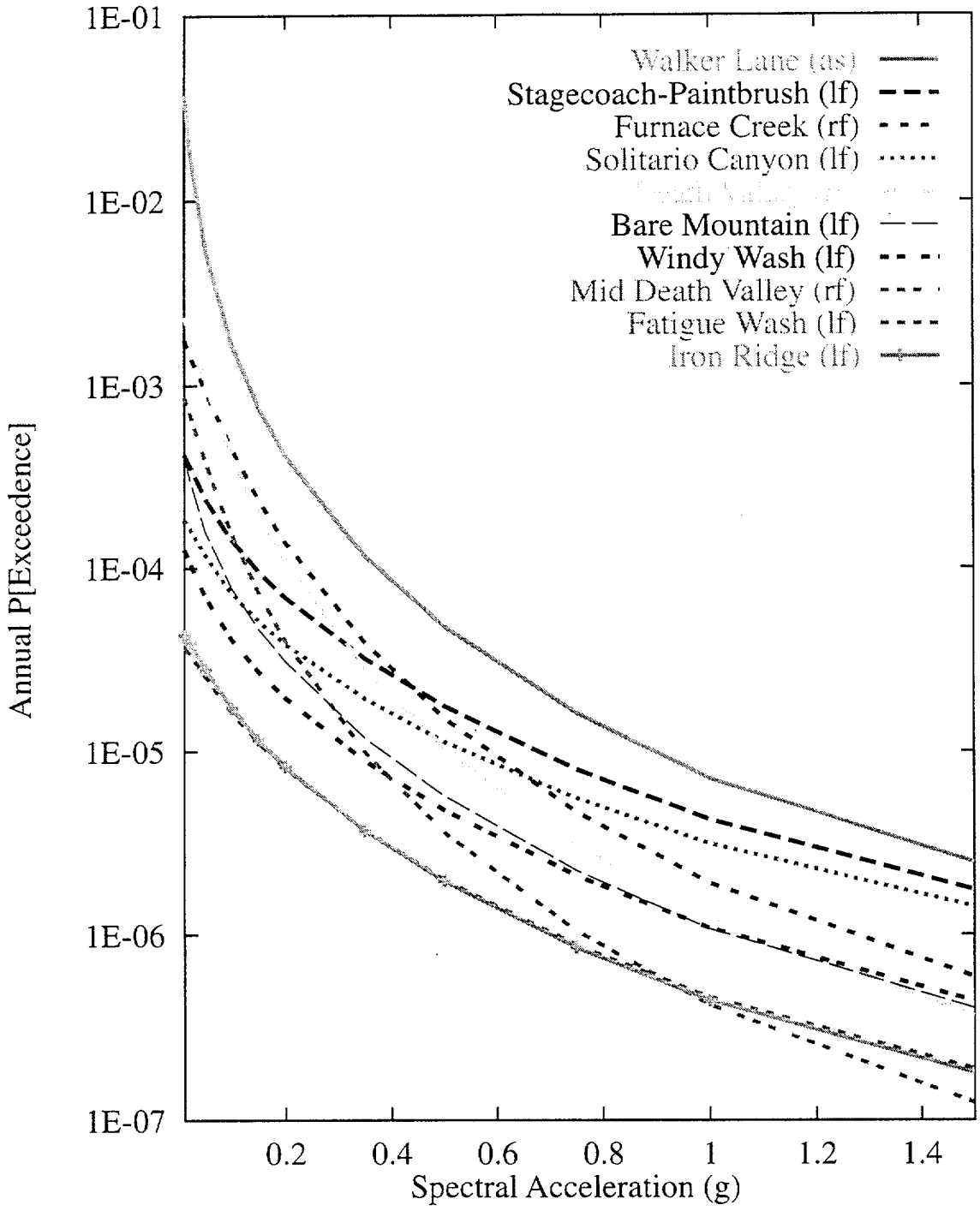

Figure 7-56 Mean seismic hazard from dominant seismic sources: ASM team, 1-Hz horizontal spectral acceleration. Acronyms in parentheses refer to source types: as-area source zone; lf-local fault; and rf-regional fault.

10 Hz, ASM Area Sources

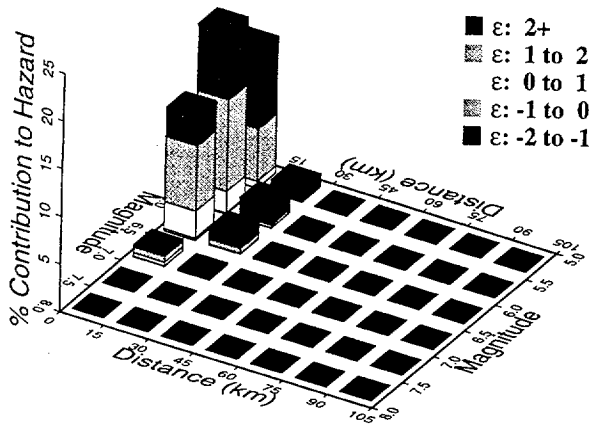

10 Hz, ASM Regional Faults

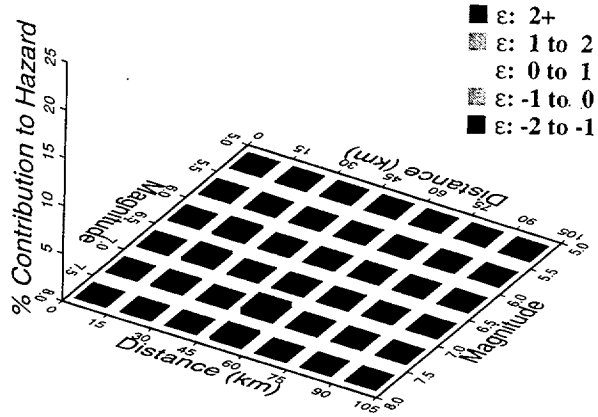

10 Hz, ASM Local Faults (Single)

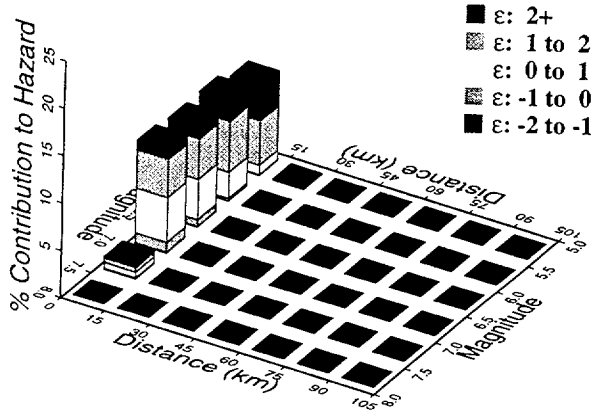

10 Hz, ASM Local Faults (Mult.)

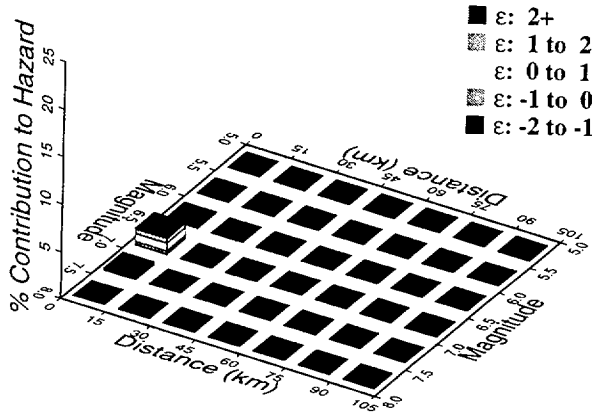

Figure 7-57 Magnitude-distance-epsilon distributions for the four source types: ASM team, 10-Hz horizontal spectral acceleration

1 Hz, ASM Area Sources

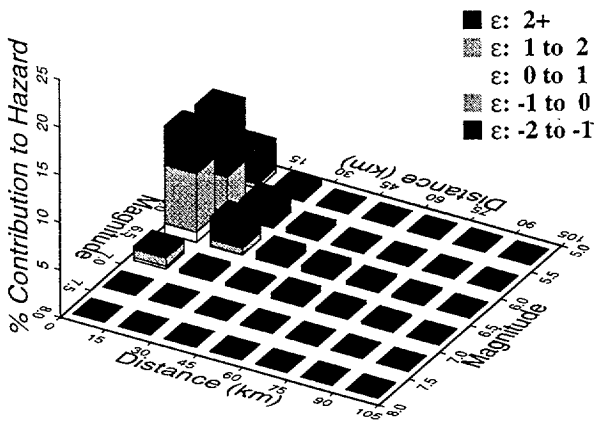

1 Hz, ASM Regional Faults

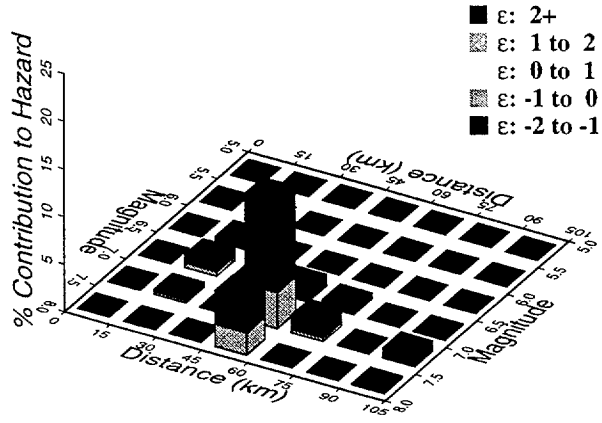

1 Hz, ASM Local Faults (Single)

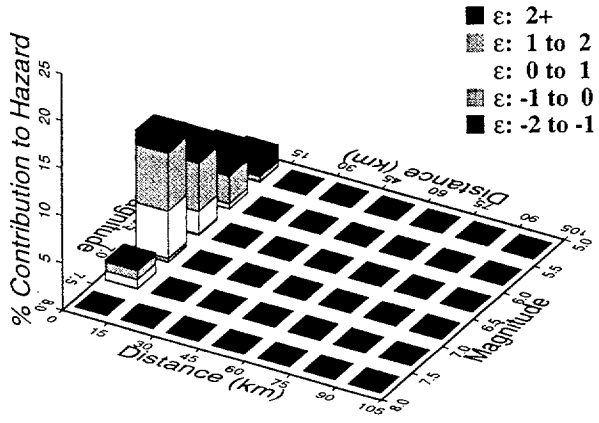

1 Hz, ASM Local Faults (Mult.)

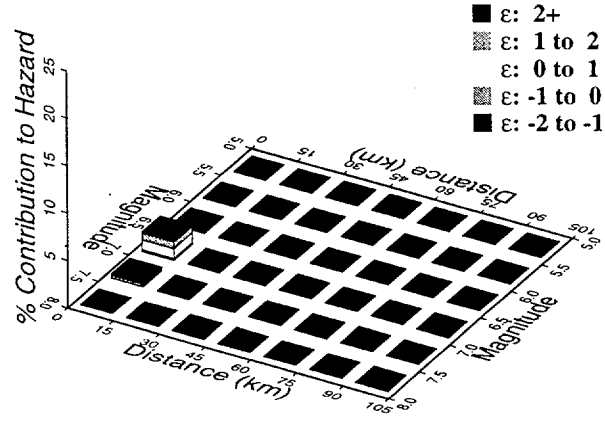

Figure 7-58 Magnitude-distance-epsilon distributions for the four source types: ASM team, 1-Hz horizontal spectral acceleration

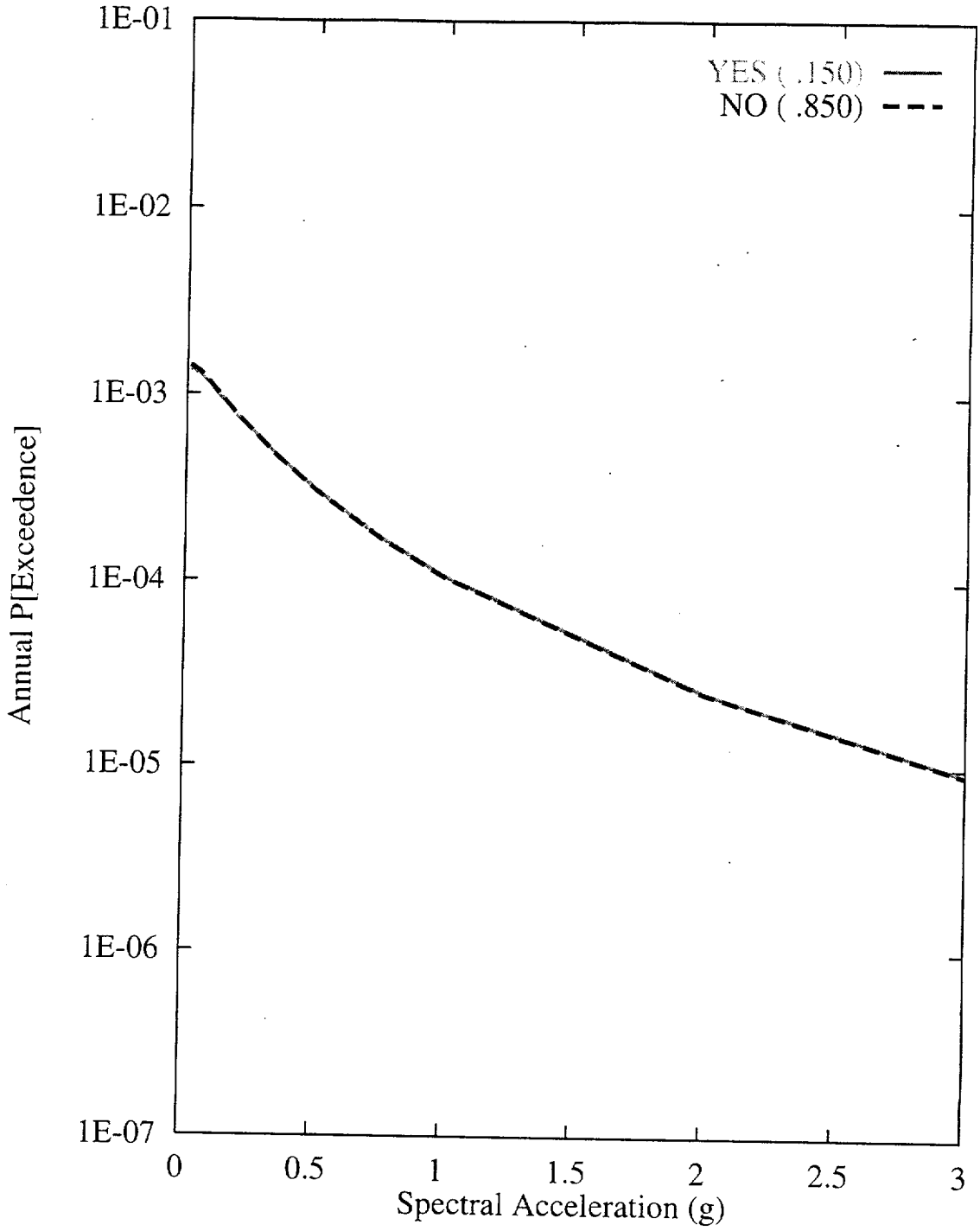

Figure 7-59 Sensitivity of seismic hazard from local faults to existence of detachment: ASM team, 10-Hz horizontal spectral acceleration

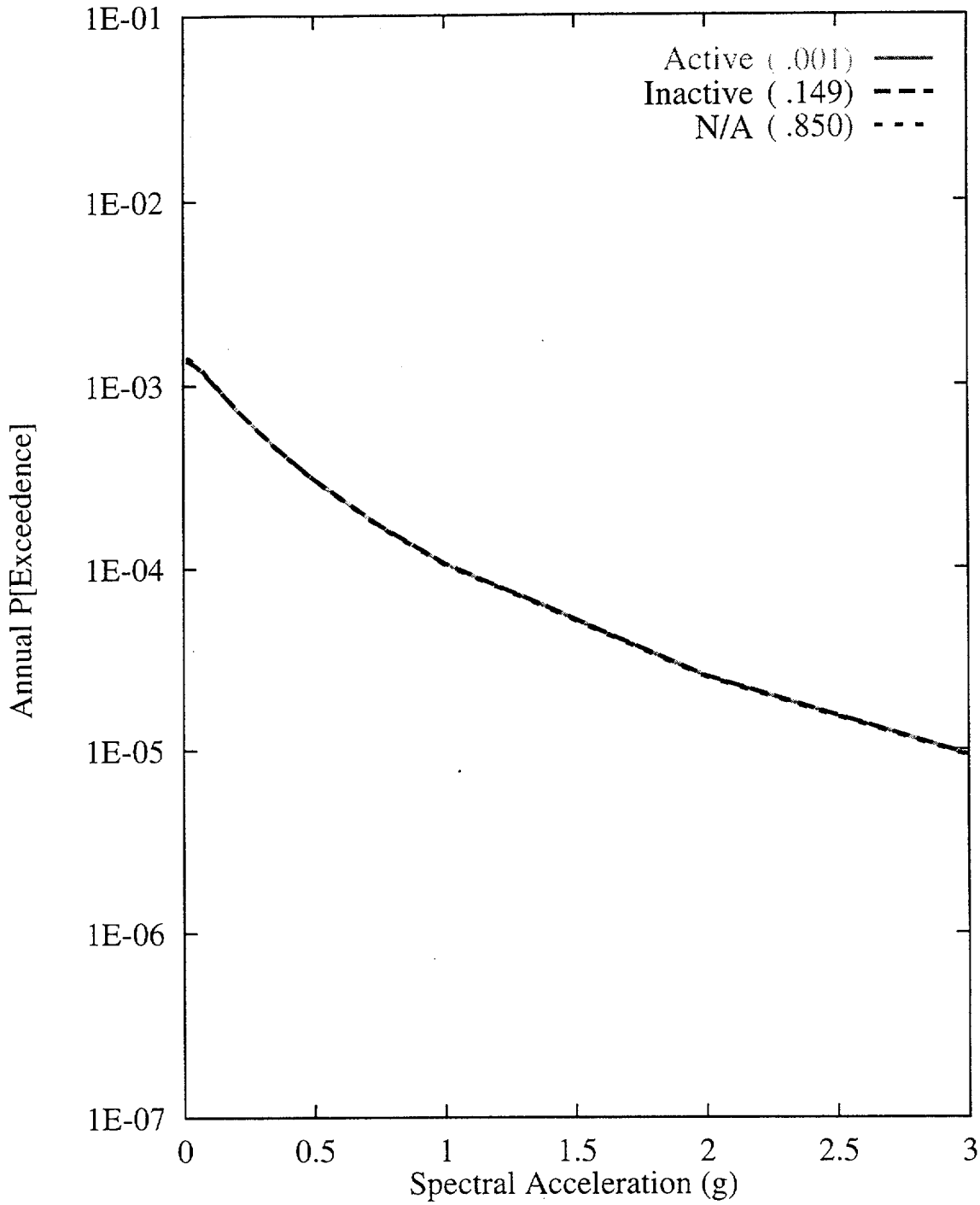

Figure 7-60 Sensitivity of seismic hazard from local faults to activity of datachment: ASM team, 10-Hz horizontal spectral acceleration

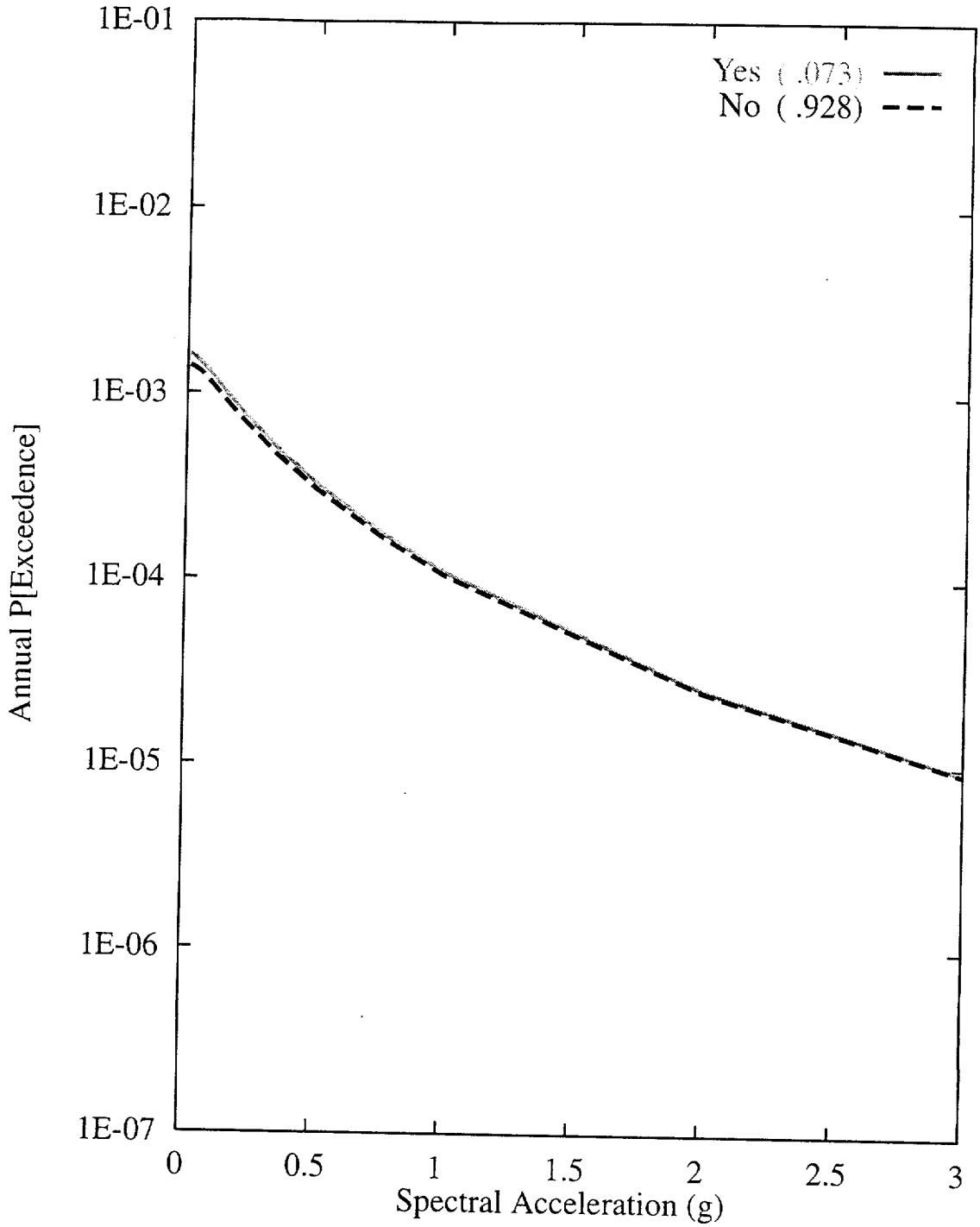

Figure 7-61 Sensitivity of seismic hazard from local faults to existence of buried strike-slip fault: ASM team, 10-Hz horizontal spectral acceleration

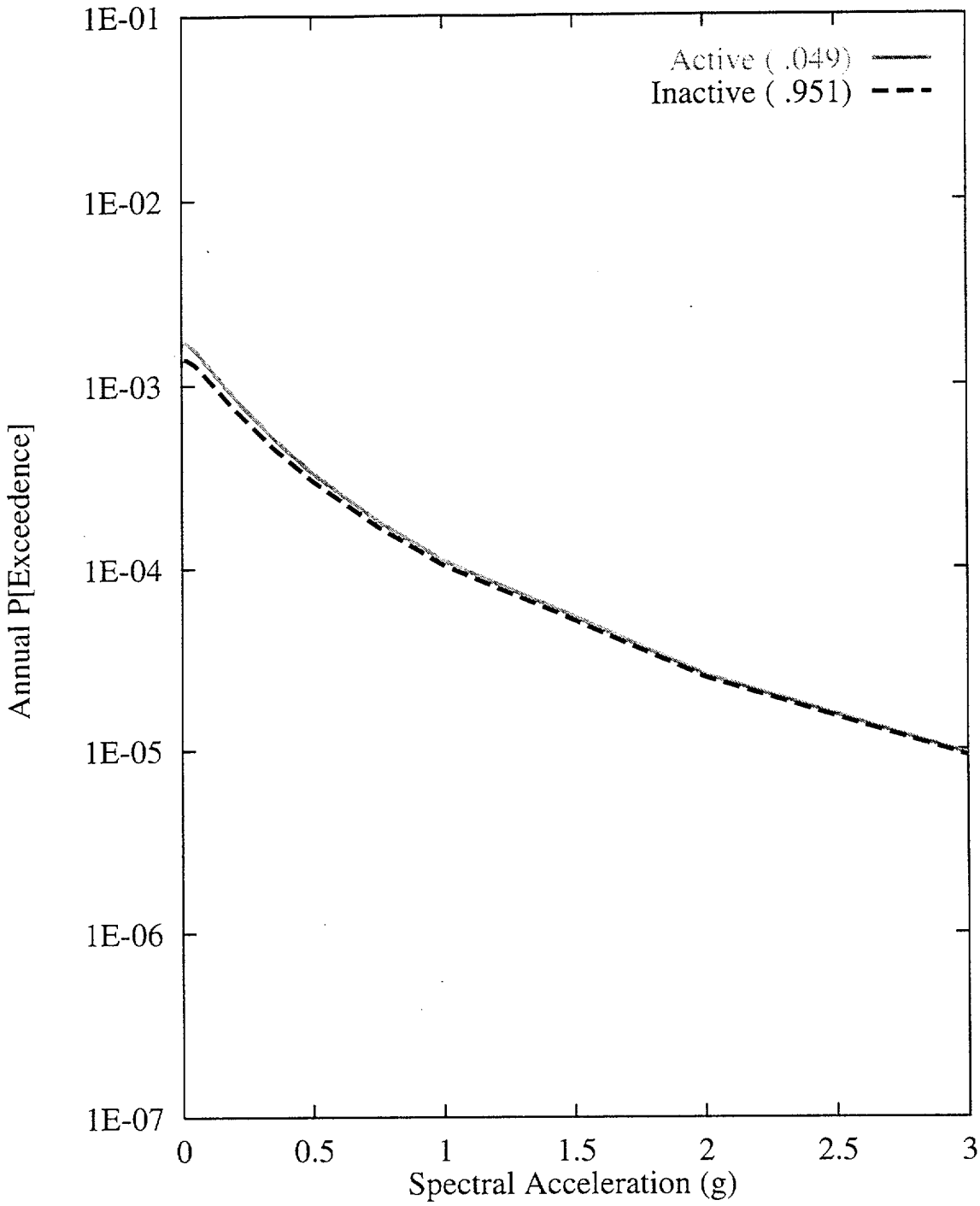

Figure 7-62 Sensitivity of seismic hazard from local faults to activity of buried-strike-slip fault: ASM team, 10-Hz horizontal spectral acceleration

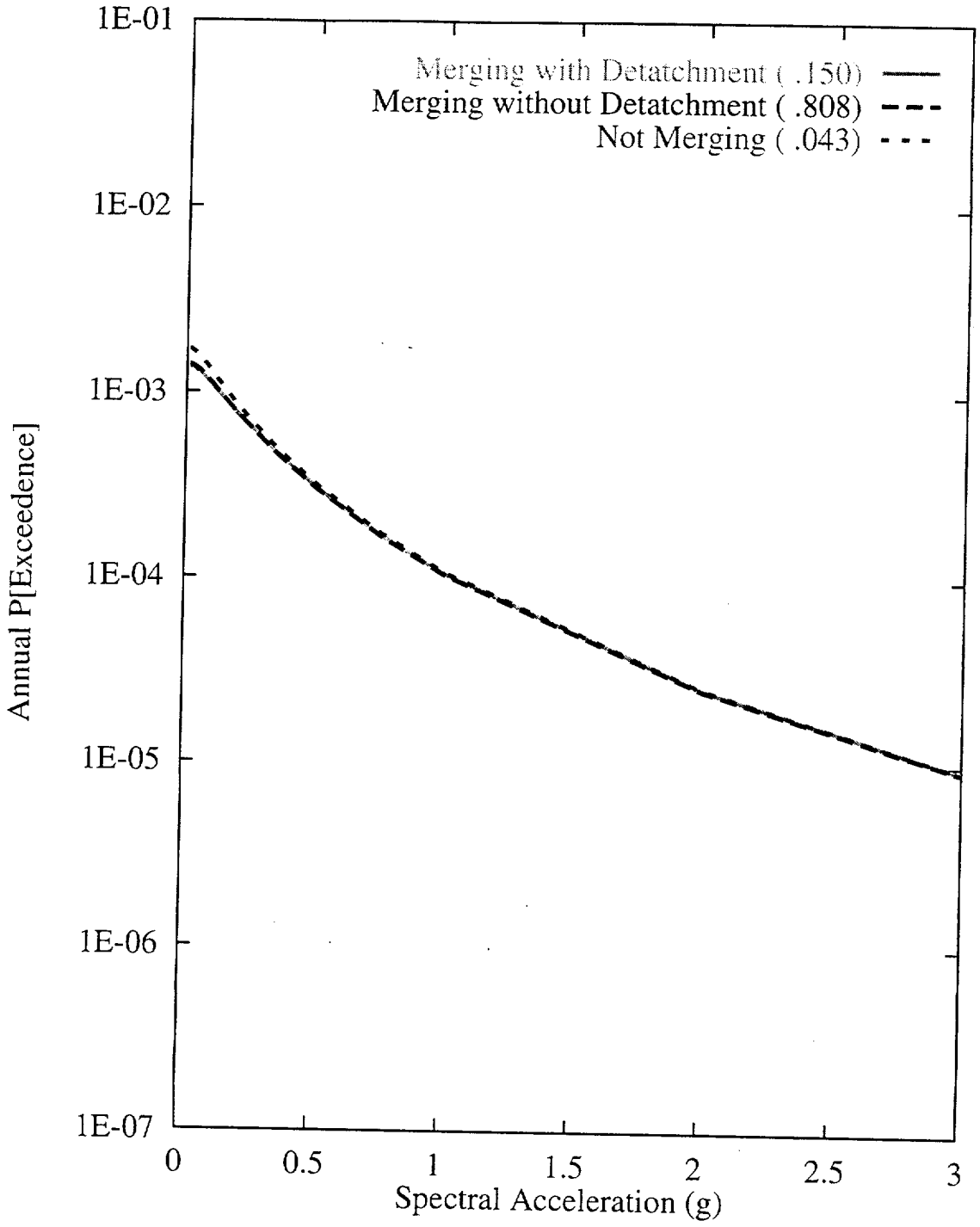

Figure 7-63 Sensitivity of seismic hazard from local faults to down-dip geometry: ASM team, 10-Hz horizontal spectral acceleration

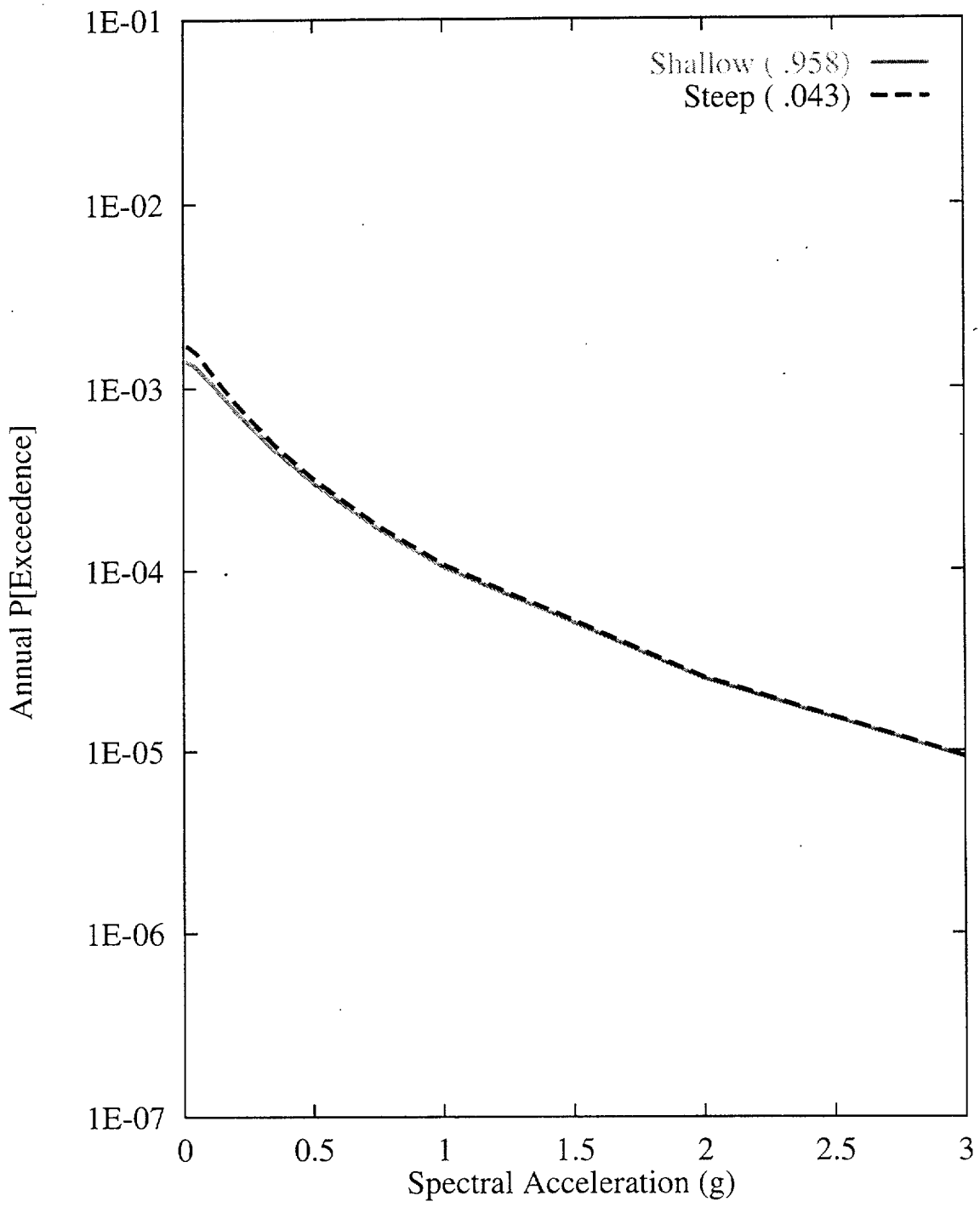

Figure 7-64 Sensitivity of seismic hazard from local faults to fault dip: ASM team, 10-Hz horizontal spectral acceleration

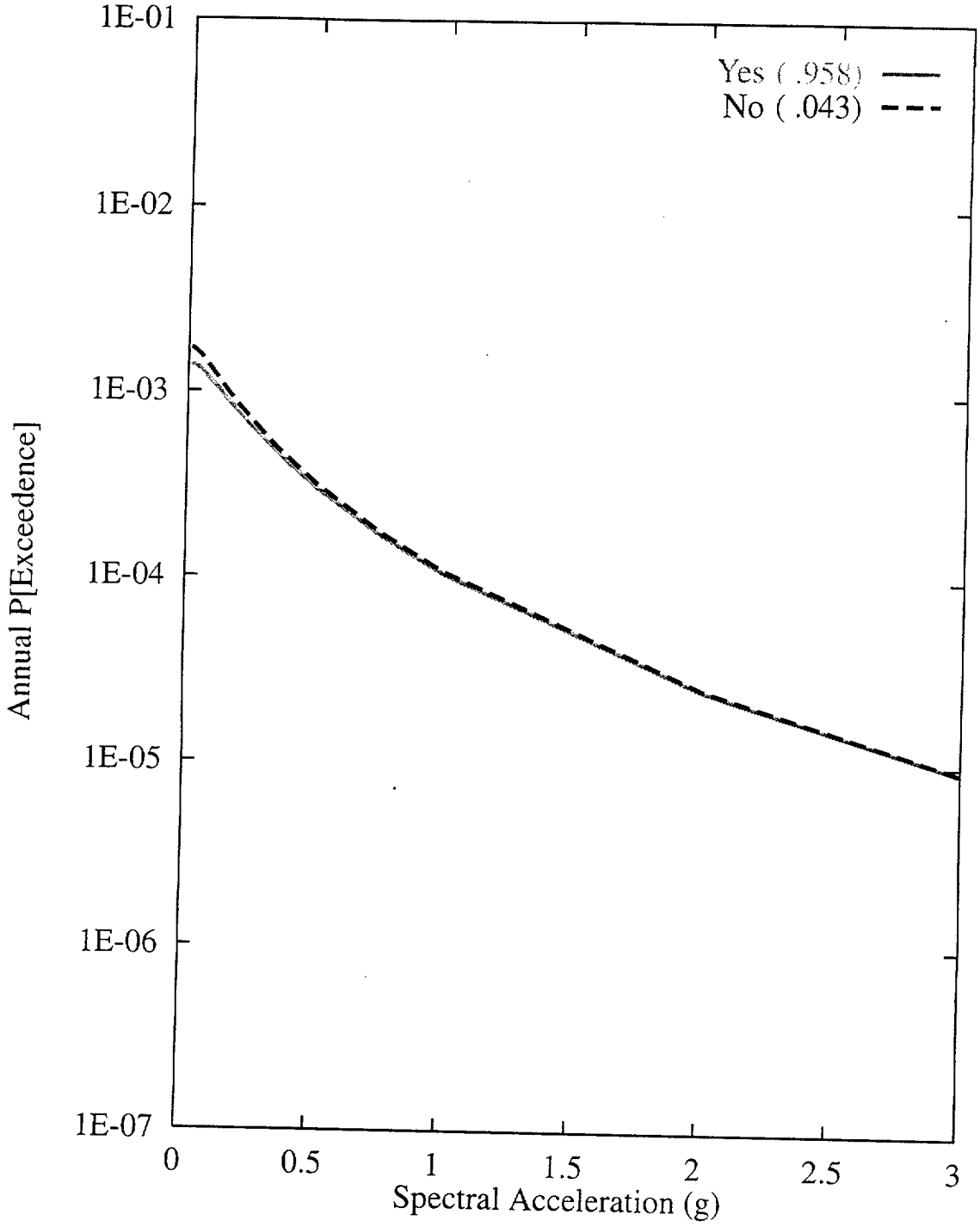

Figure 7-65 Sensitivity of seismic hazard from local faults to fault merging: ASM team, 10-Hz horizontal spectral acceleration

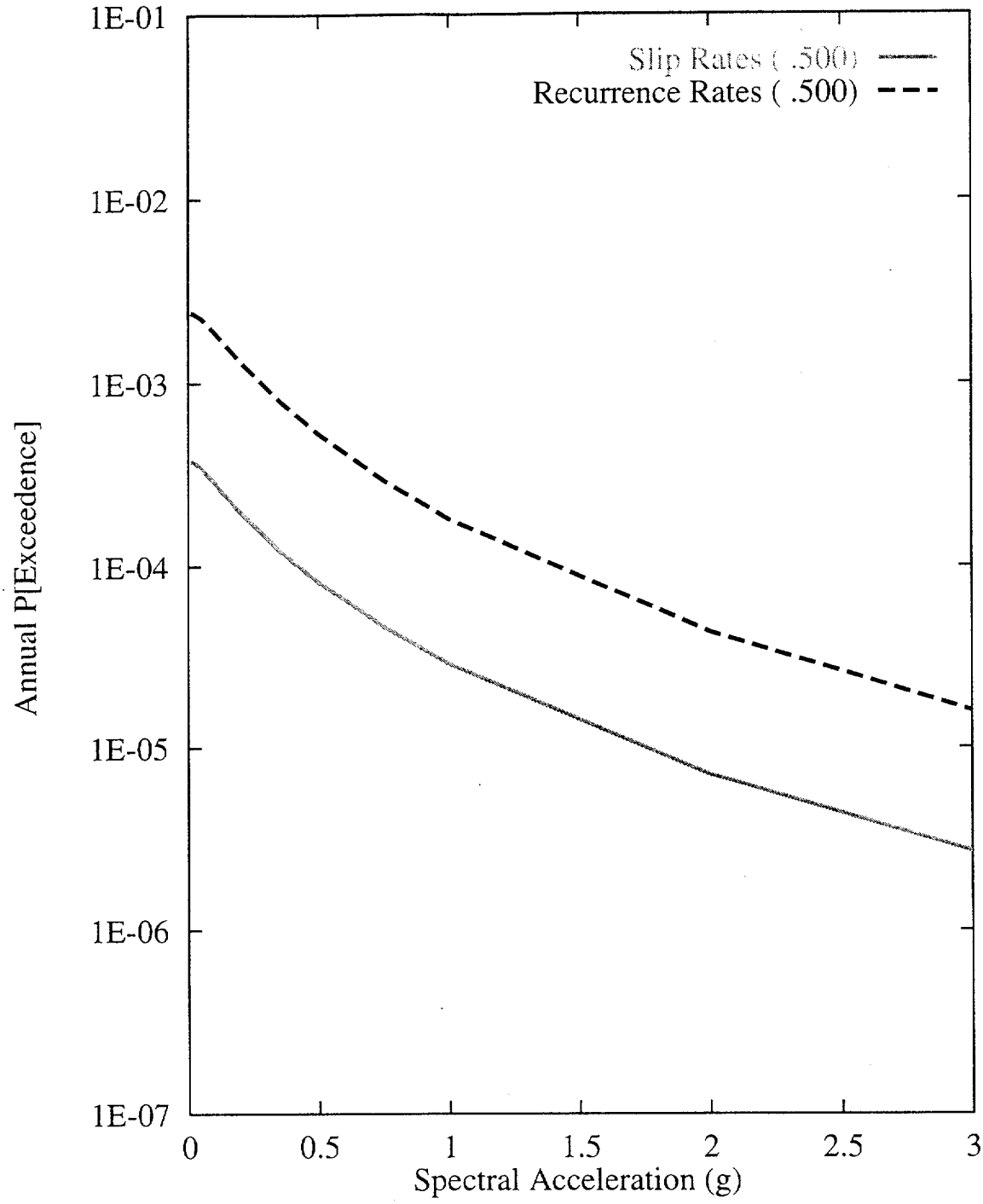

Figure 7-66 Sensitivity of seismic hazard from local faults to recurrence approach: ASM team, 10-Hz horizontal spectral acceleration

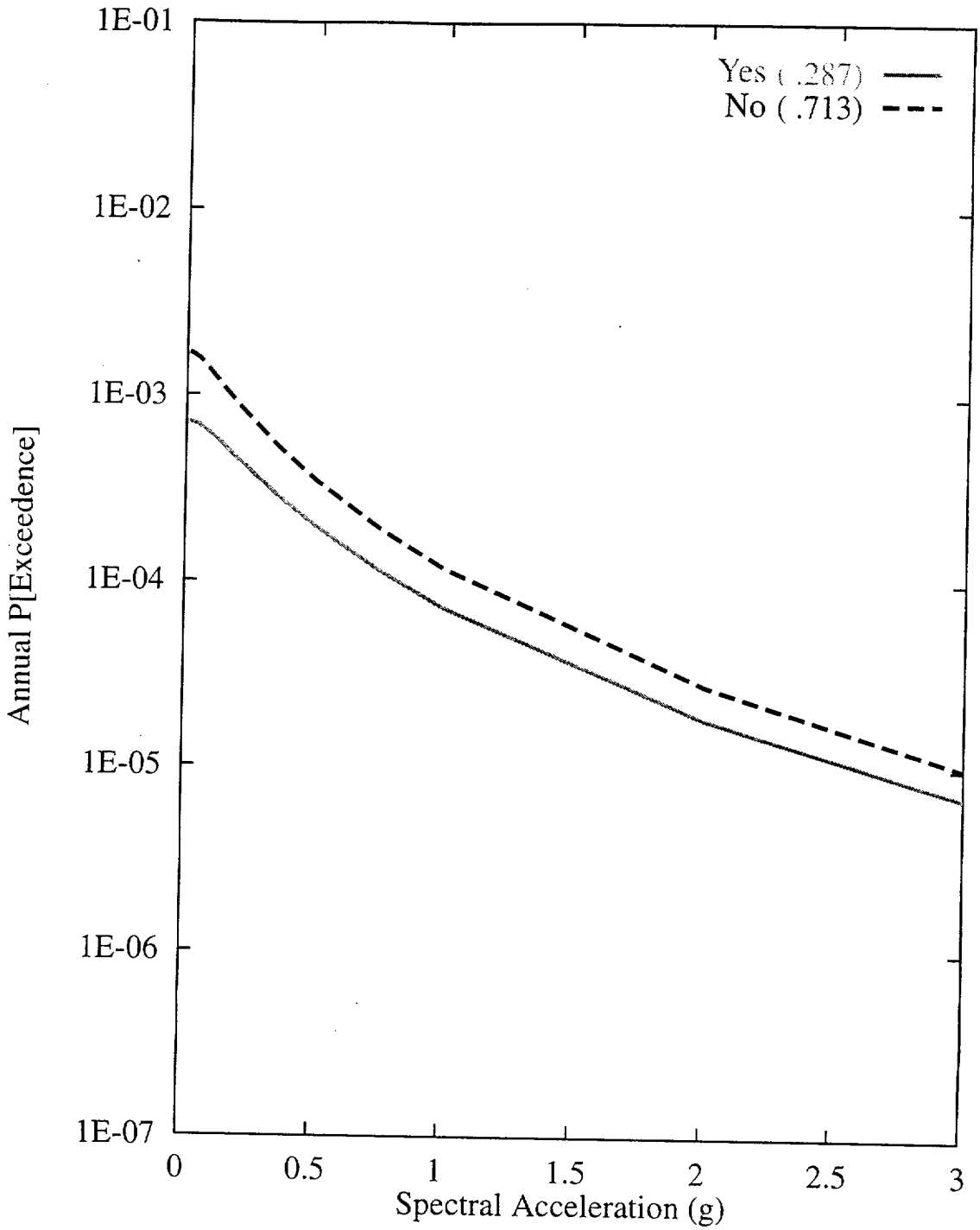

Figure 7-67 Sensitivity of seismic hazard from local faults to simultaneous ruptures: ASM team, 10-Hz horizontal spectral acceleration

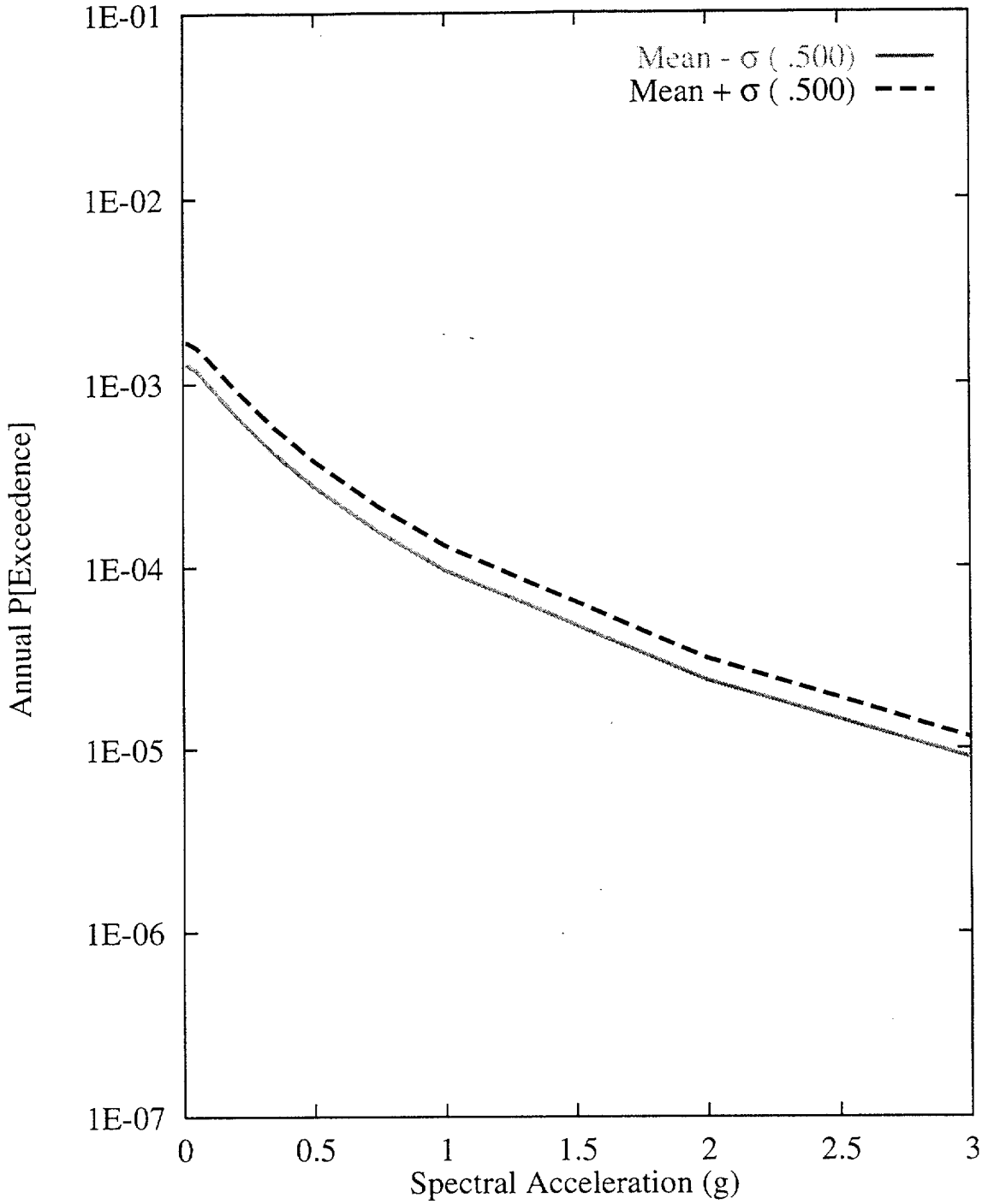

Figure 7-68 Sensitivity of seismic hazard from local faults to Mmax, Stagecoach Road-Paintbrush Canyon faults: ASM team, 10-Hz horizontal spectral acceleration

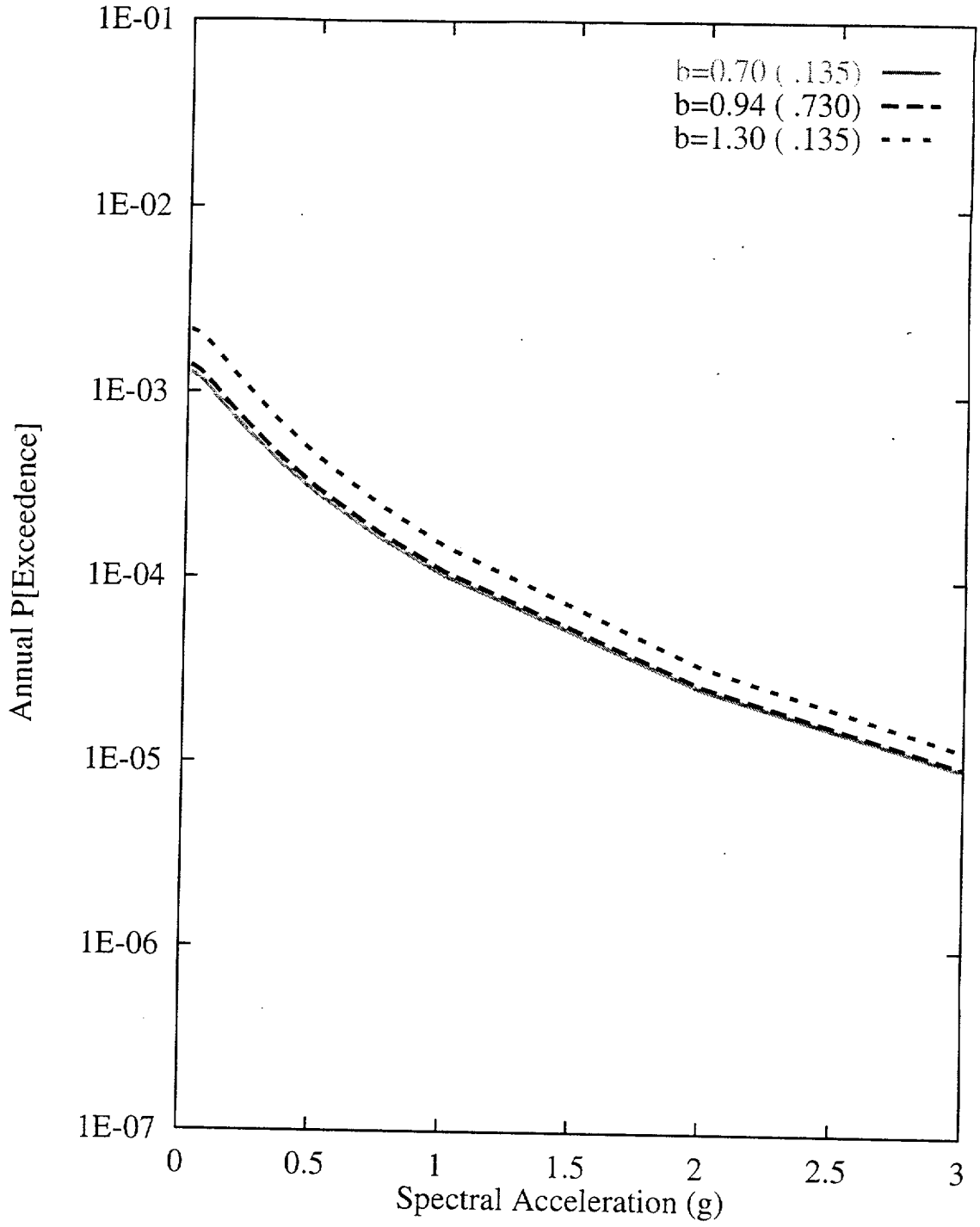

Figure 7-69 Sensitivity of seismic hazard from local faults to b-value, Stagecoach Road-Paintbrush Canyon fault system: ASM team, 10-Hz horizontal spectral acceleration

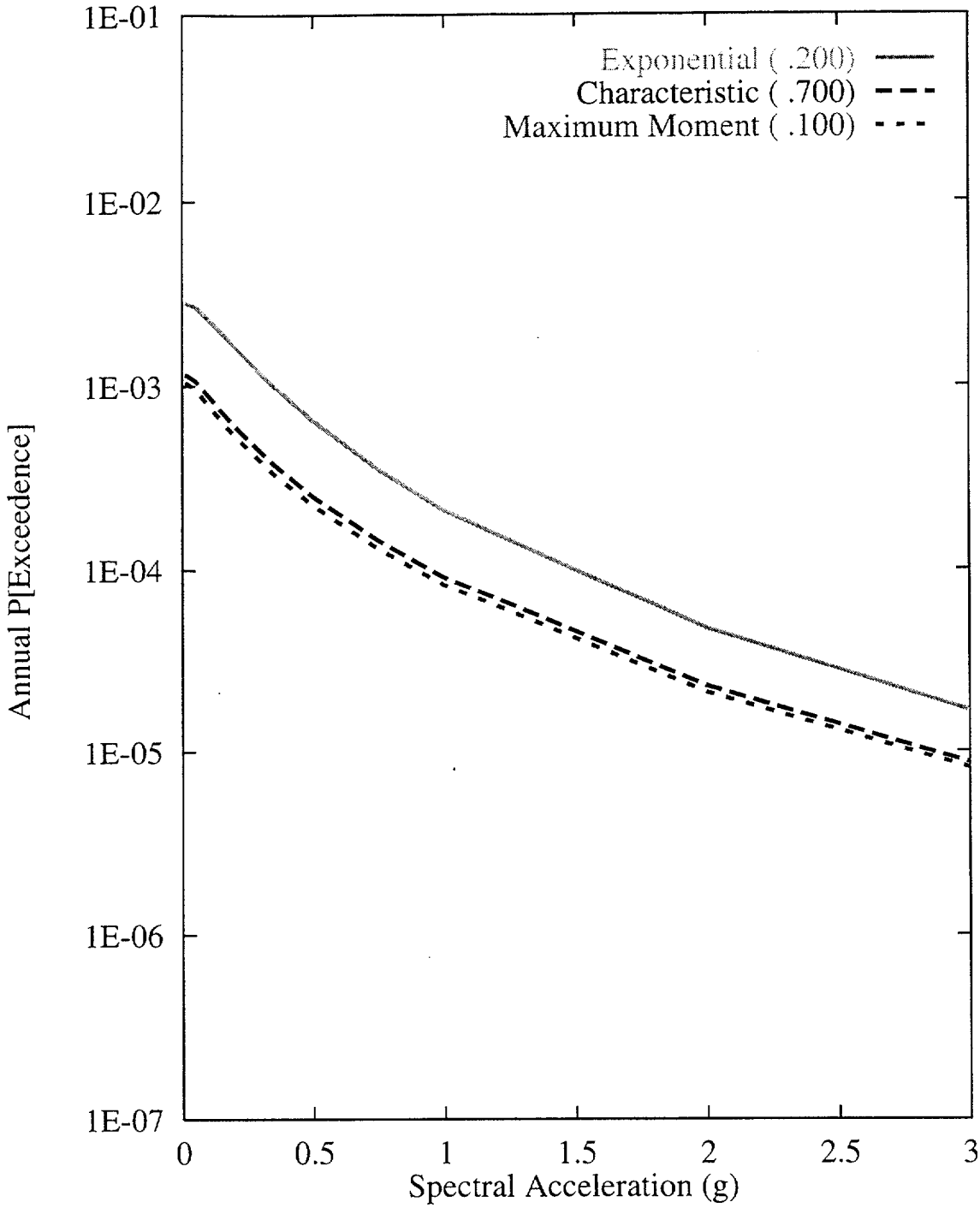

Figure 7-70 Sensitivity of seismic hazard from local faults to recurrence model, Stagecoach Road-Paintbrush Canyon fault system: ASM team, 10-Hz horizontal spectral acceleration

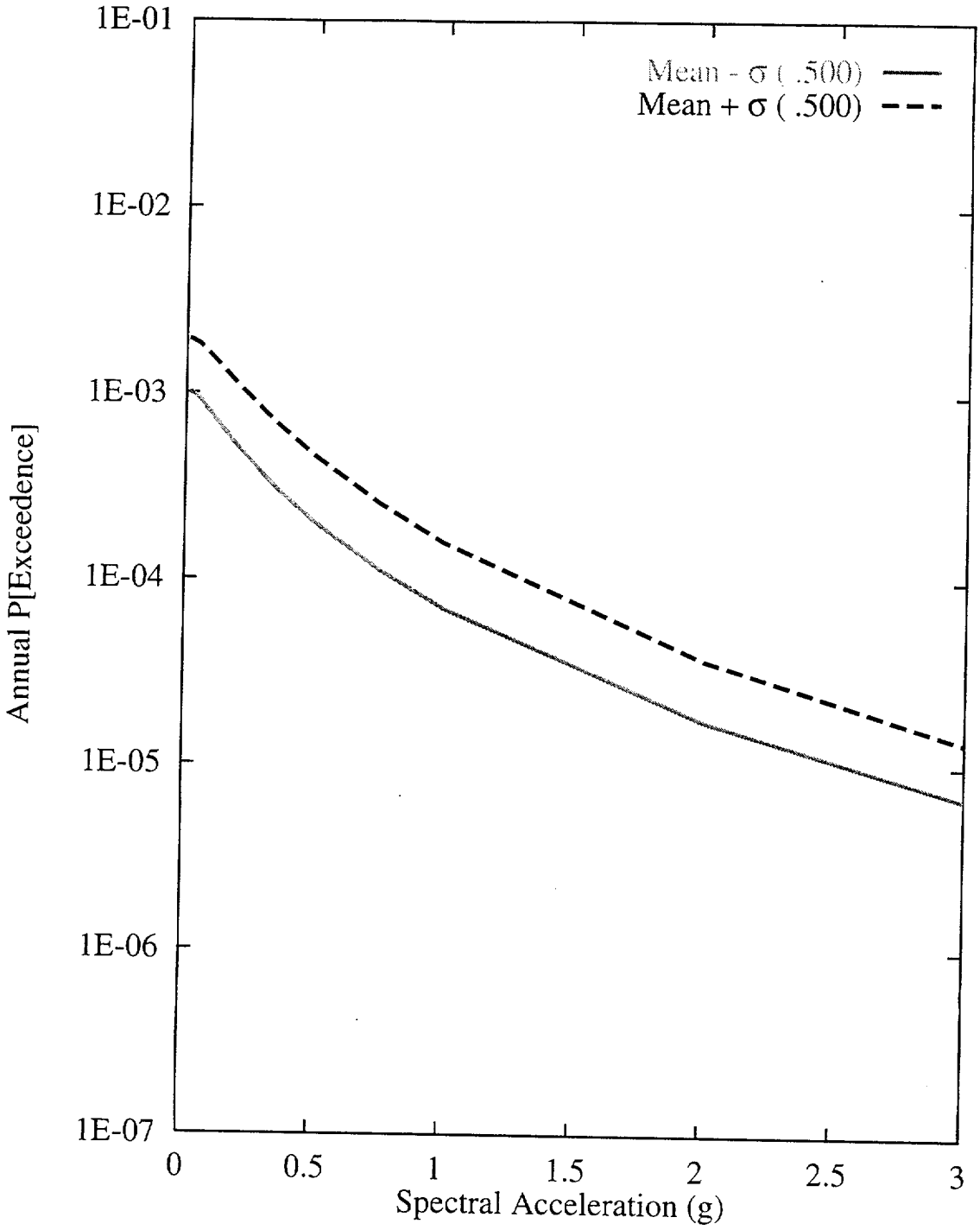

Figure 7-71 Sensitivity of seismic hazard from local faults to recurrence, Stagecoach Road- Paintbrush Canyon fault system: ASM team, 10-Hz horizontal spectral acceleration

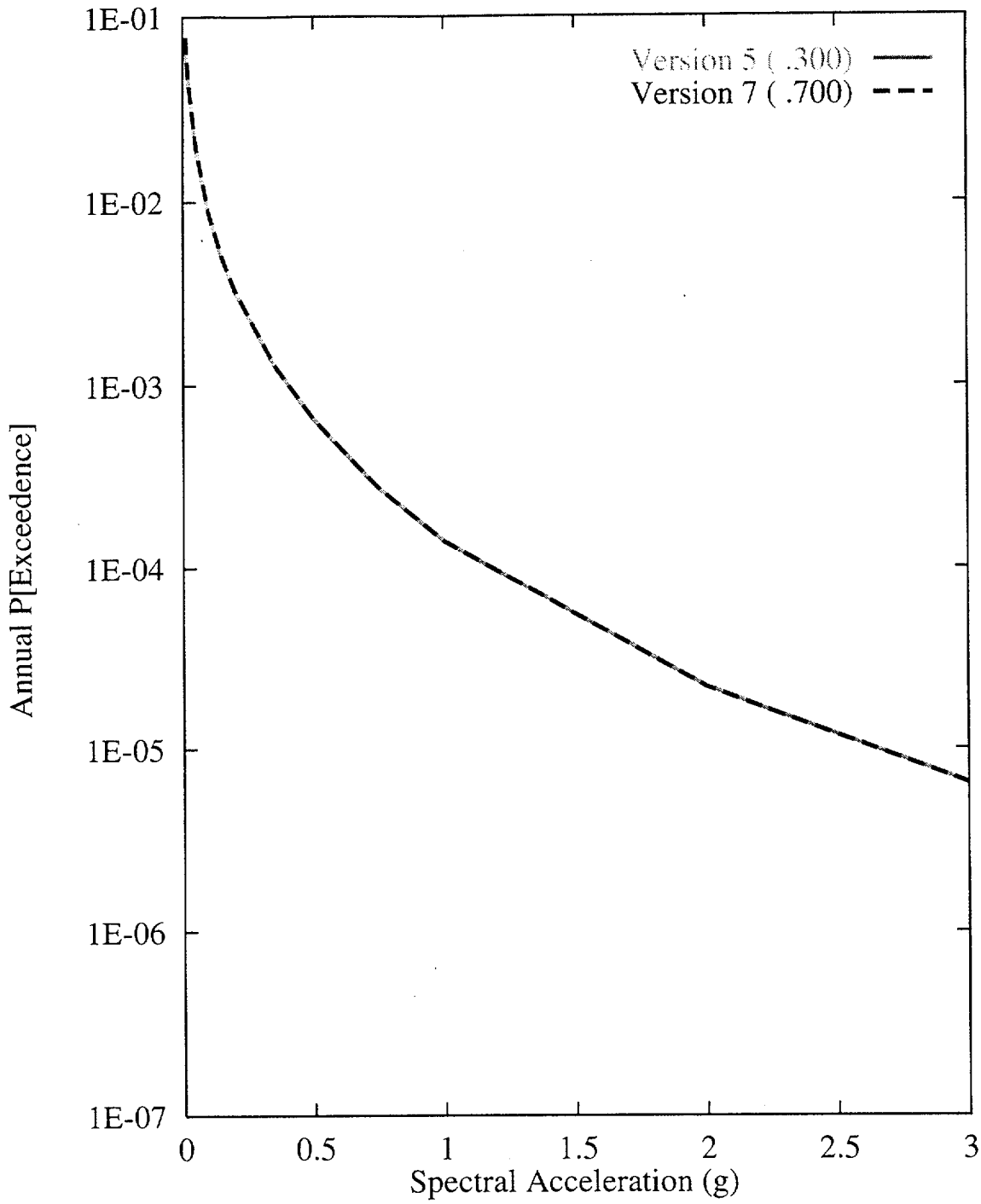

Figure 7-72 Sensitivity of seismic hazard from area zones to choice of seismicity catalog: ASM team, 10-Hz horizontal spectral acceleration

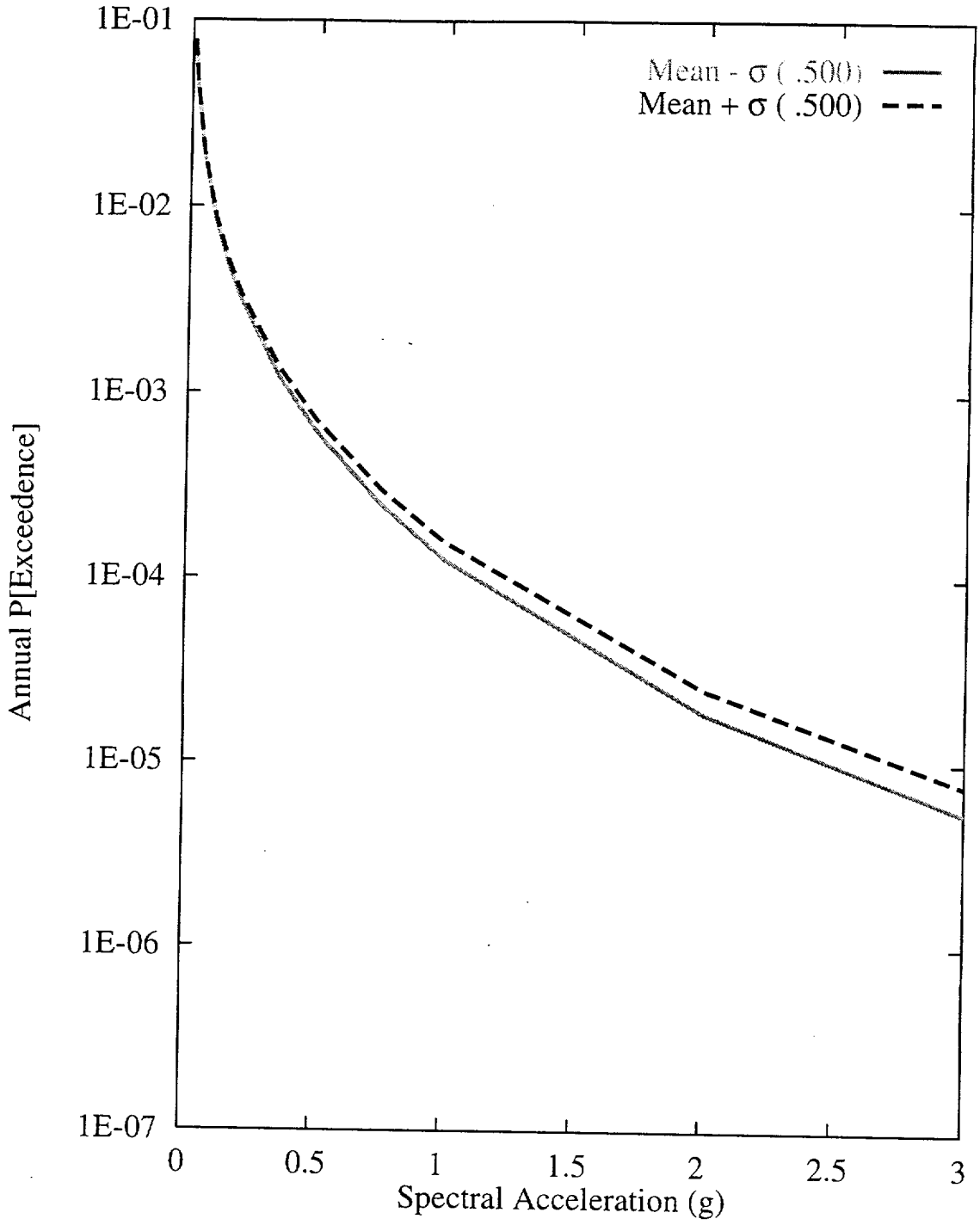

Figure 7-73 Sensitivity of seismic hazard from area zones to Mmax of the Walker Lane local source: ASM team, 10-Hz horizontal spectral acceleration

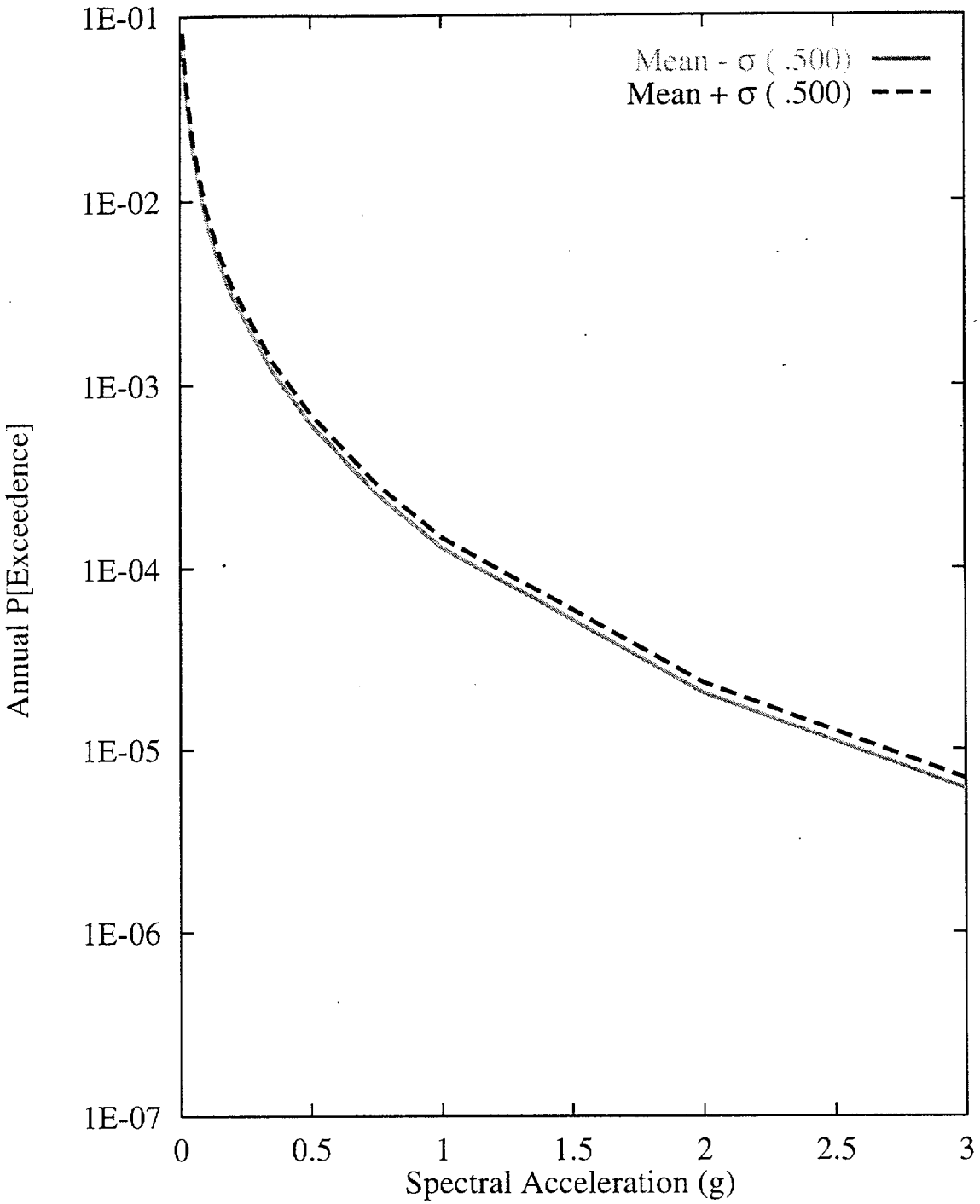

Figure 7-74 Sensitivity of seismic hazard from area zones to recurrence of the Walker Lane local source: ASM team, 10-Hz horizontal spectral acceleration

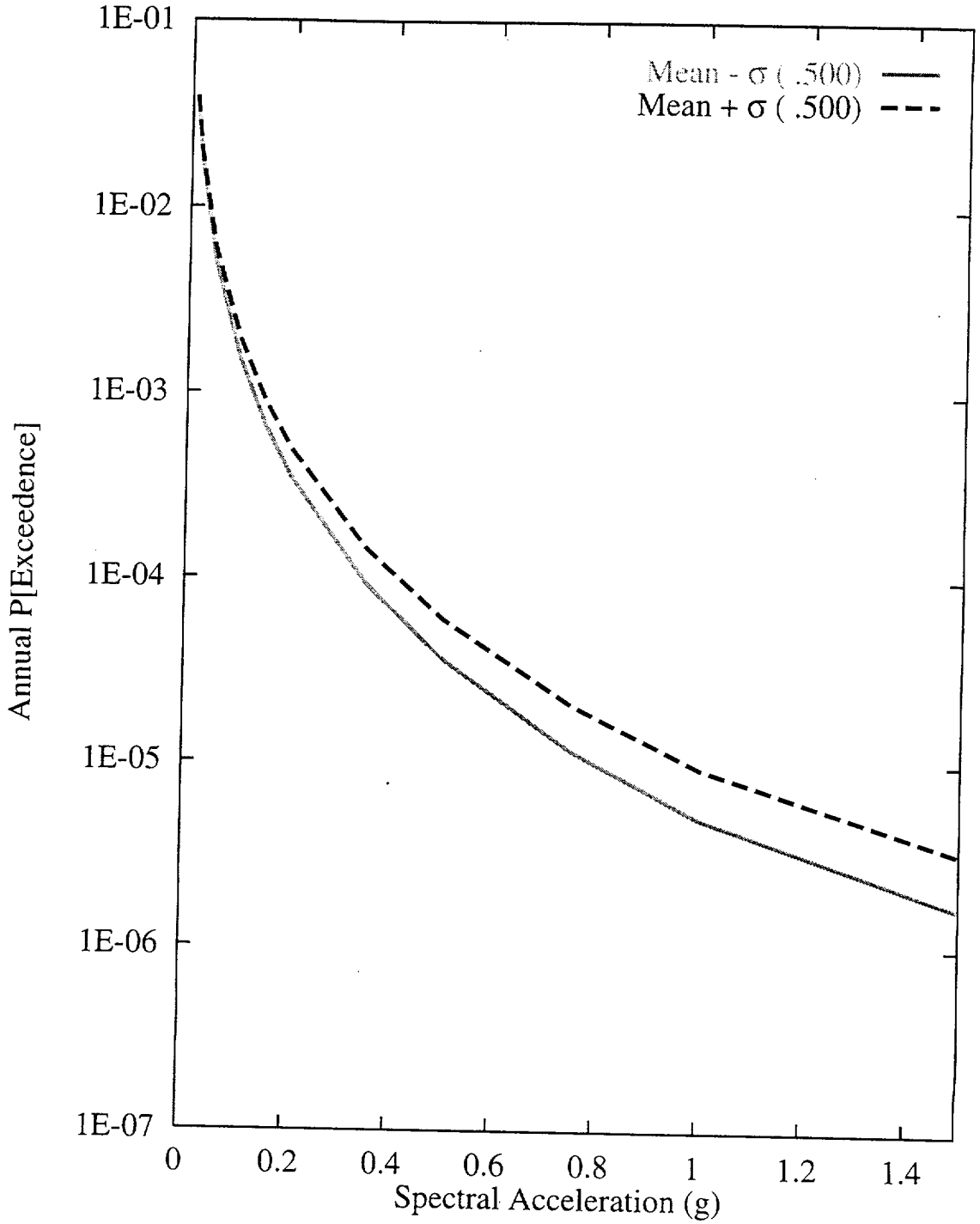

Figure 7-75 Sensitivity of seismic hazard from area zones to Mmax of the Walker Lane local source: ASM team, 1-Hz horizontal spectral acceleration

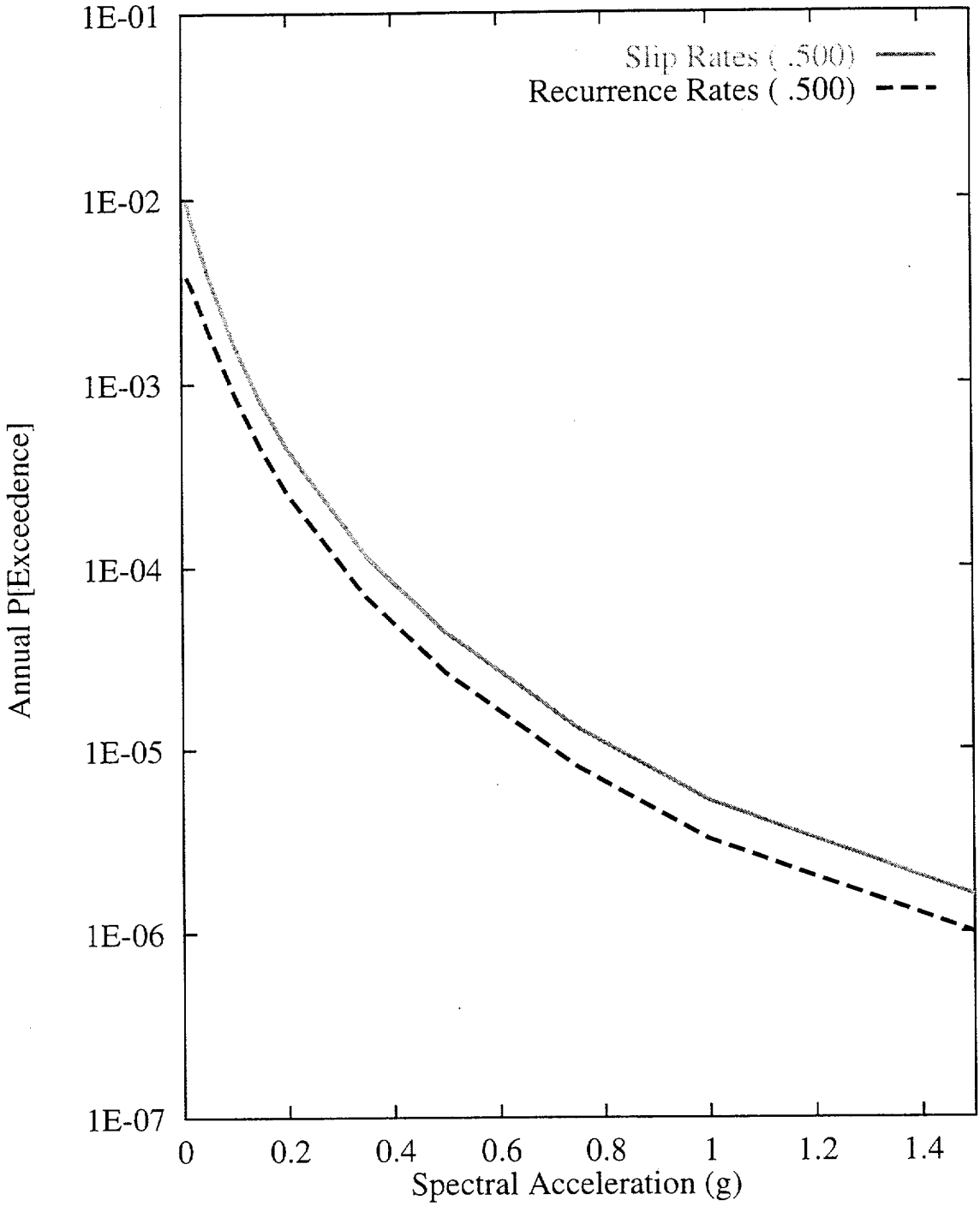

Figure 7-76 Sensitivity of seismic hazard from regional faults to recurrence approach used: ASM team, 1-Hz horizontal spectral acceleration

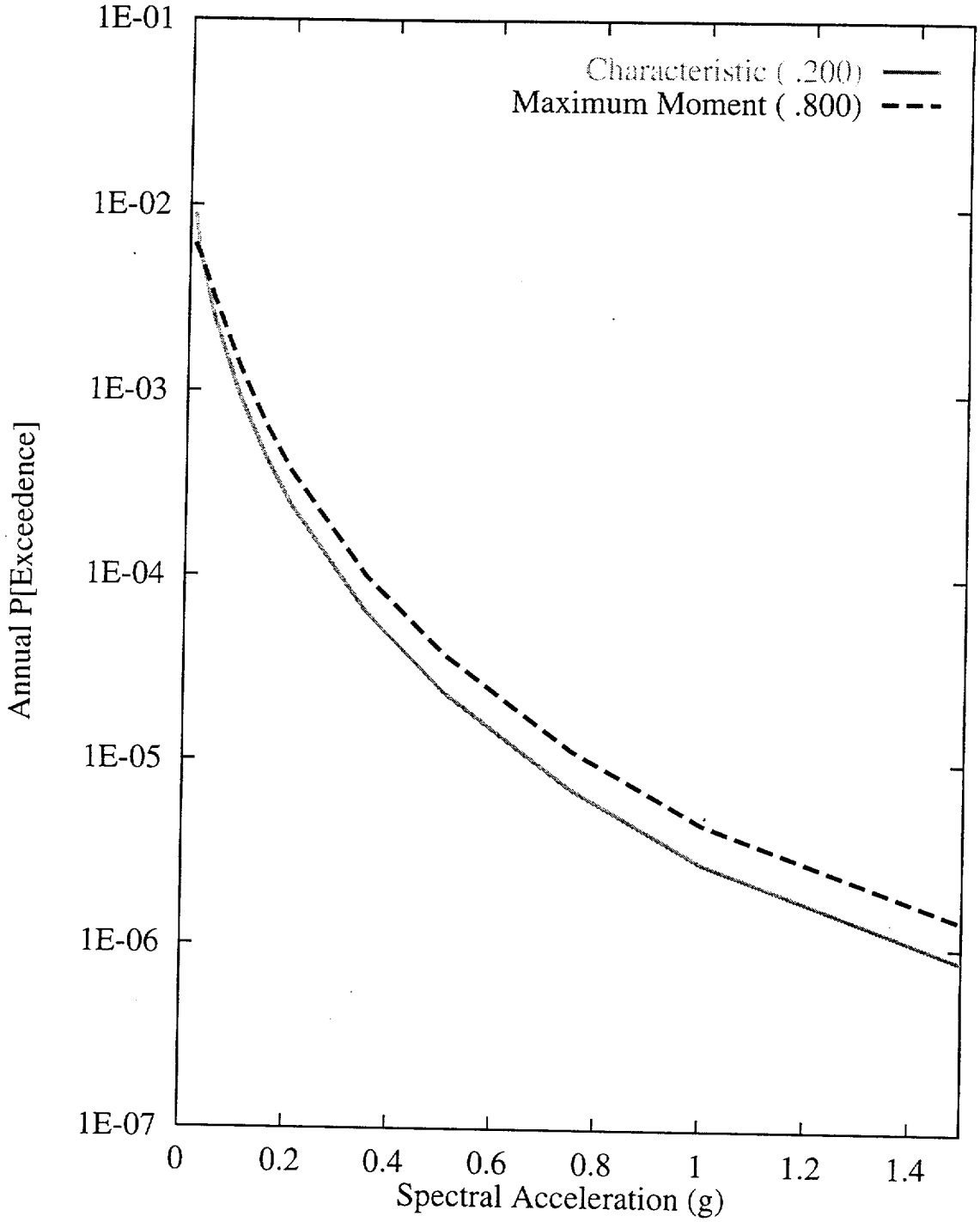

Figure 7-77 Sensitivity of seismic hazard from regional faults to recurrence model: ASM team, 1-Hz horizontal spectral acceleration

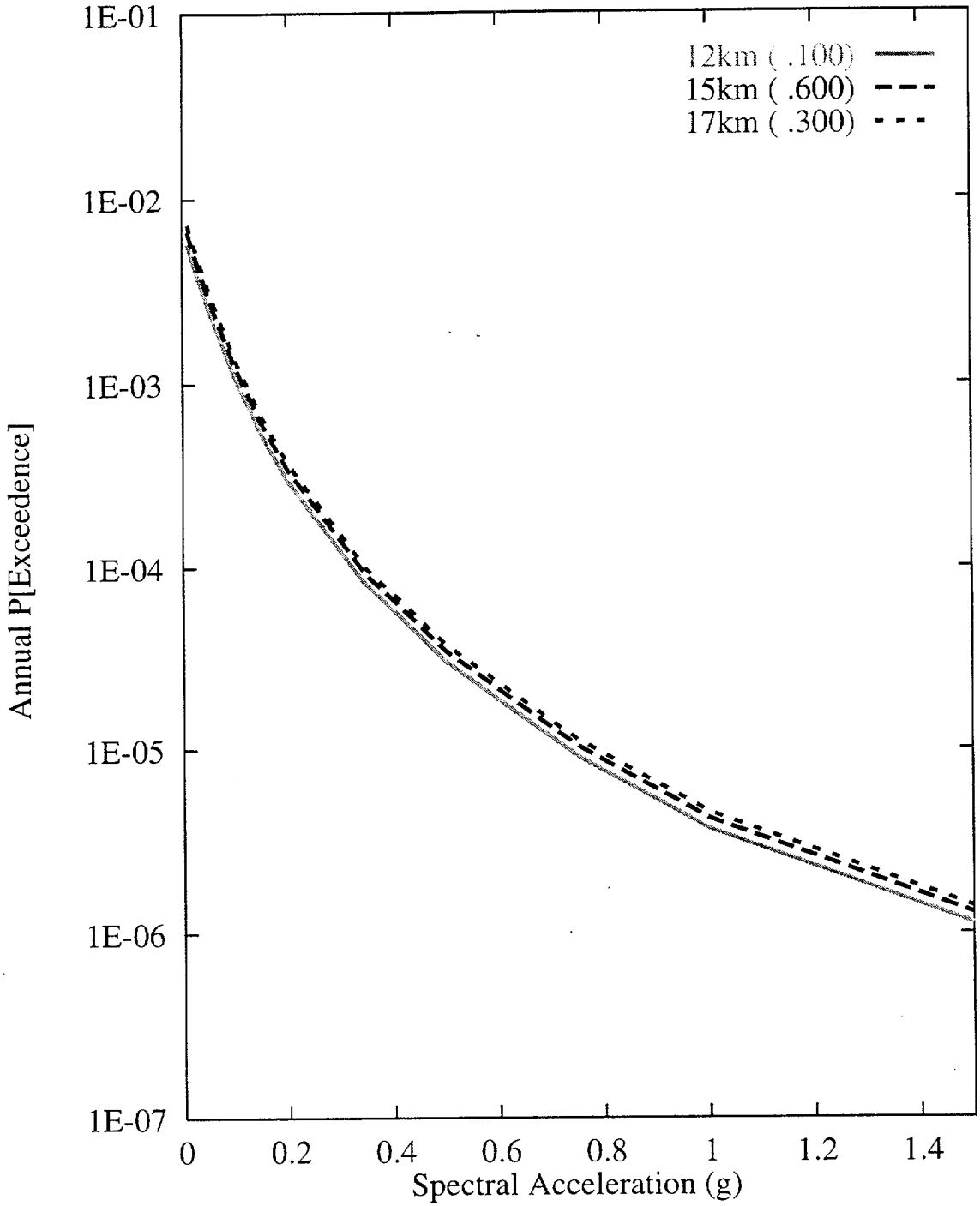

Figure 7-78 Sensitivity of seismic hazard from regional faults to maximum fault depth: ASM team, 1-Hz horizontal spectral acceleration

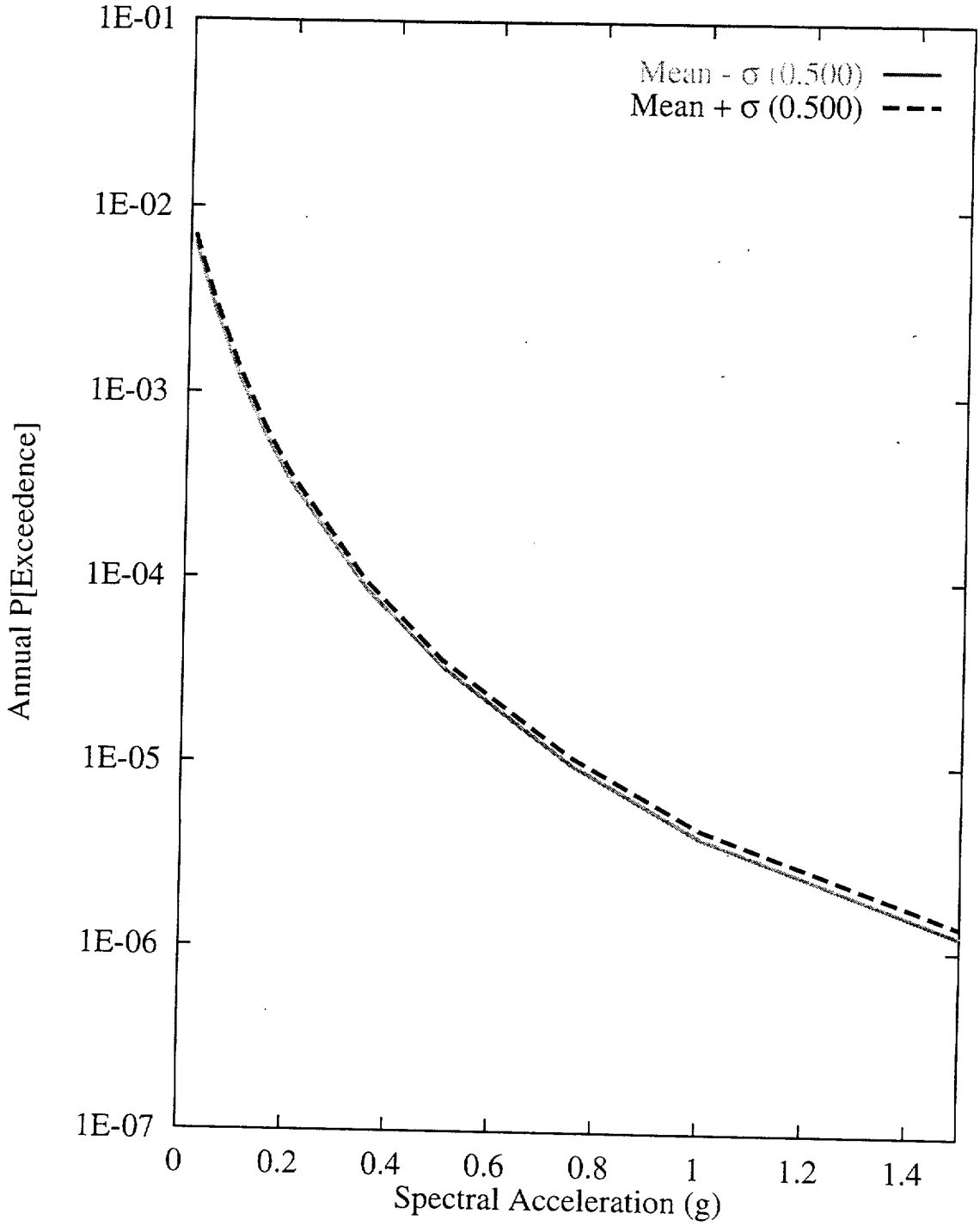

Figure 7-79 Sensitivity of seismic hazard from regional faults to Mmax on the Furnace Creek fault: ASM team, 1-Hz horizontal spectral acceleration

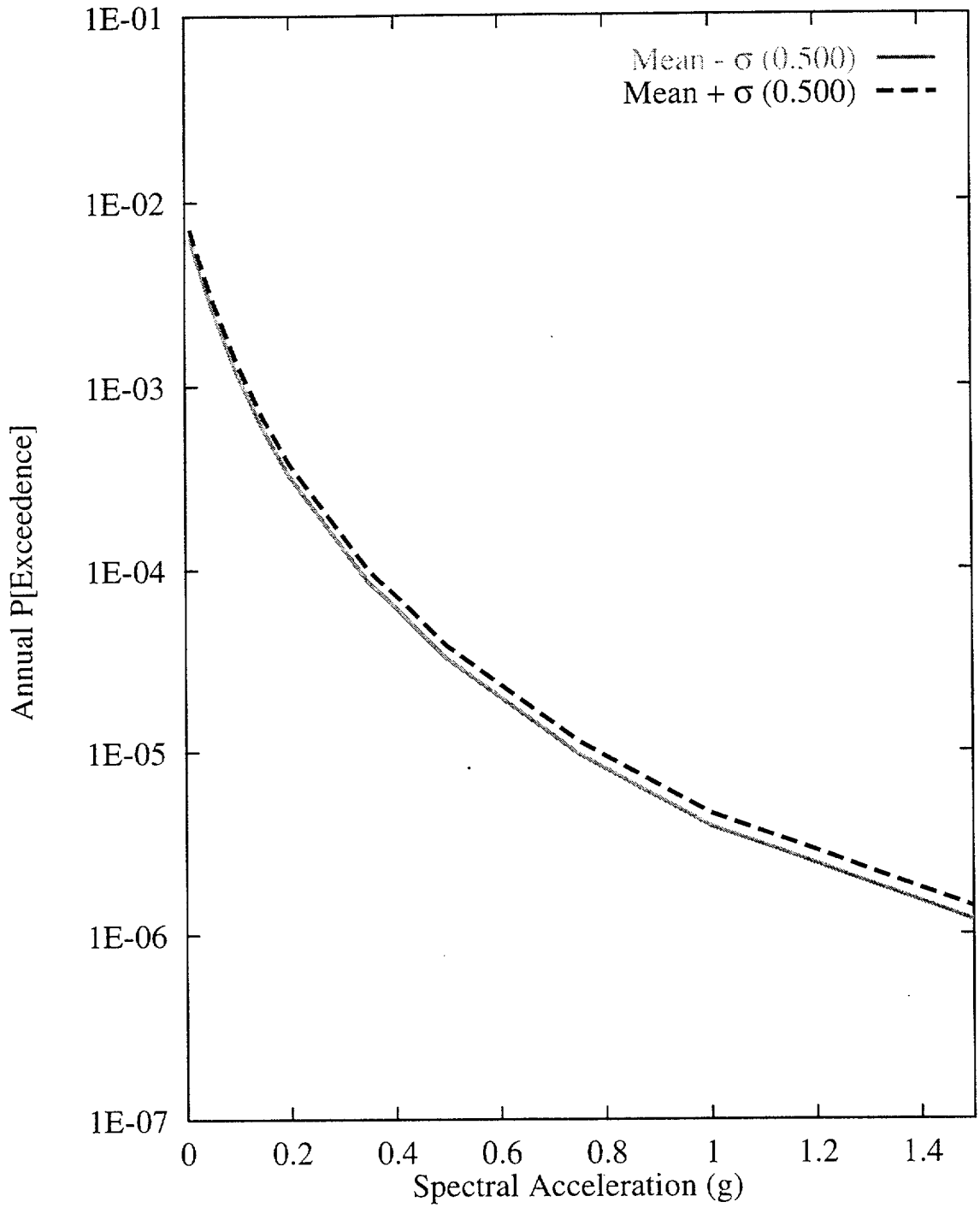

Figure 7-80 Sensitivity of seismic hazard from regional faults to recurrence, Furnace Creek fault: ASM team, 1-Hz horizontal spectral acceleration

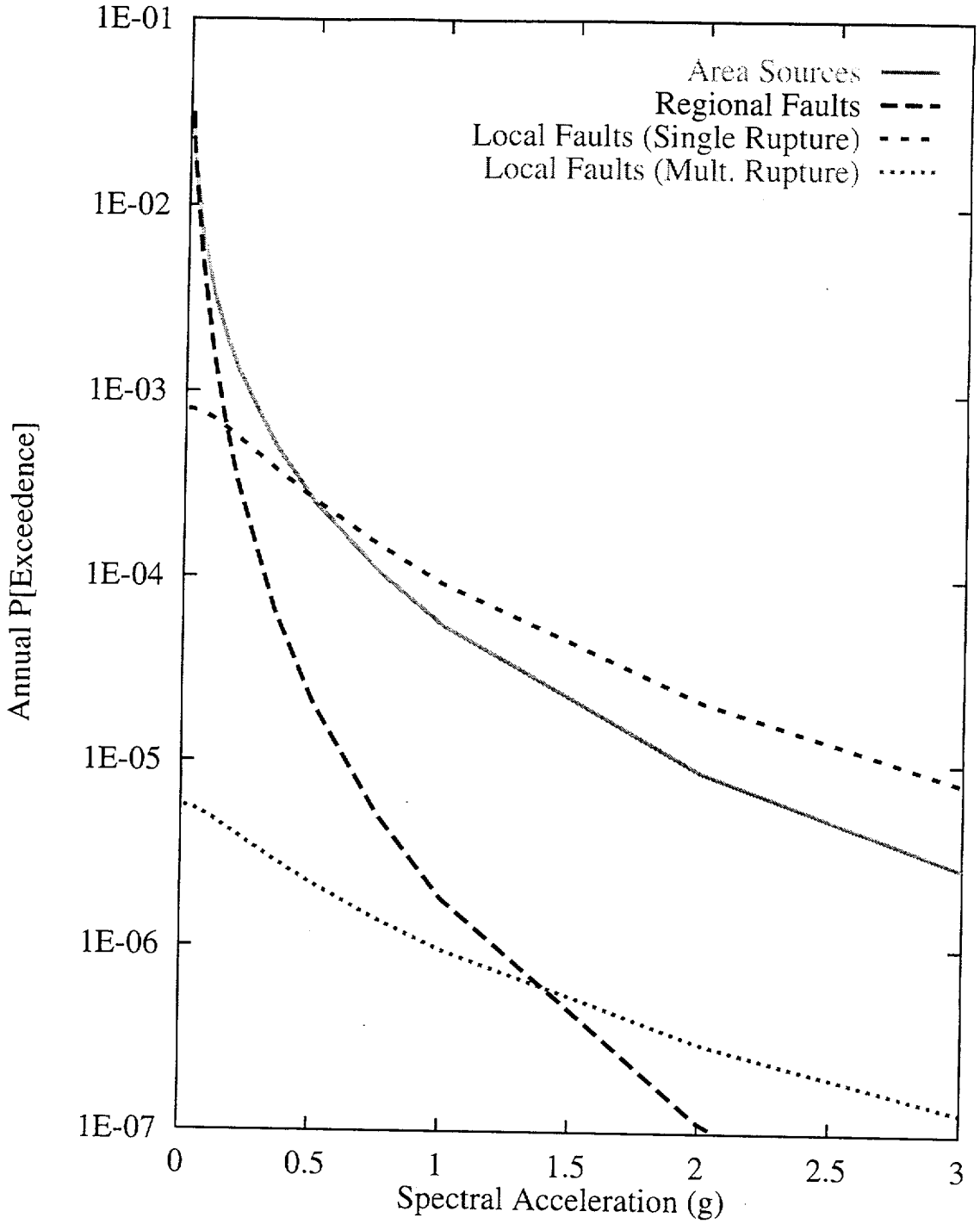

Figure 7-81 Contributions of source types to the mean hazard: DFS team, 10-Hz horizontal spectral acceleration

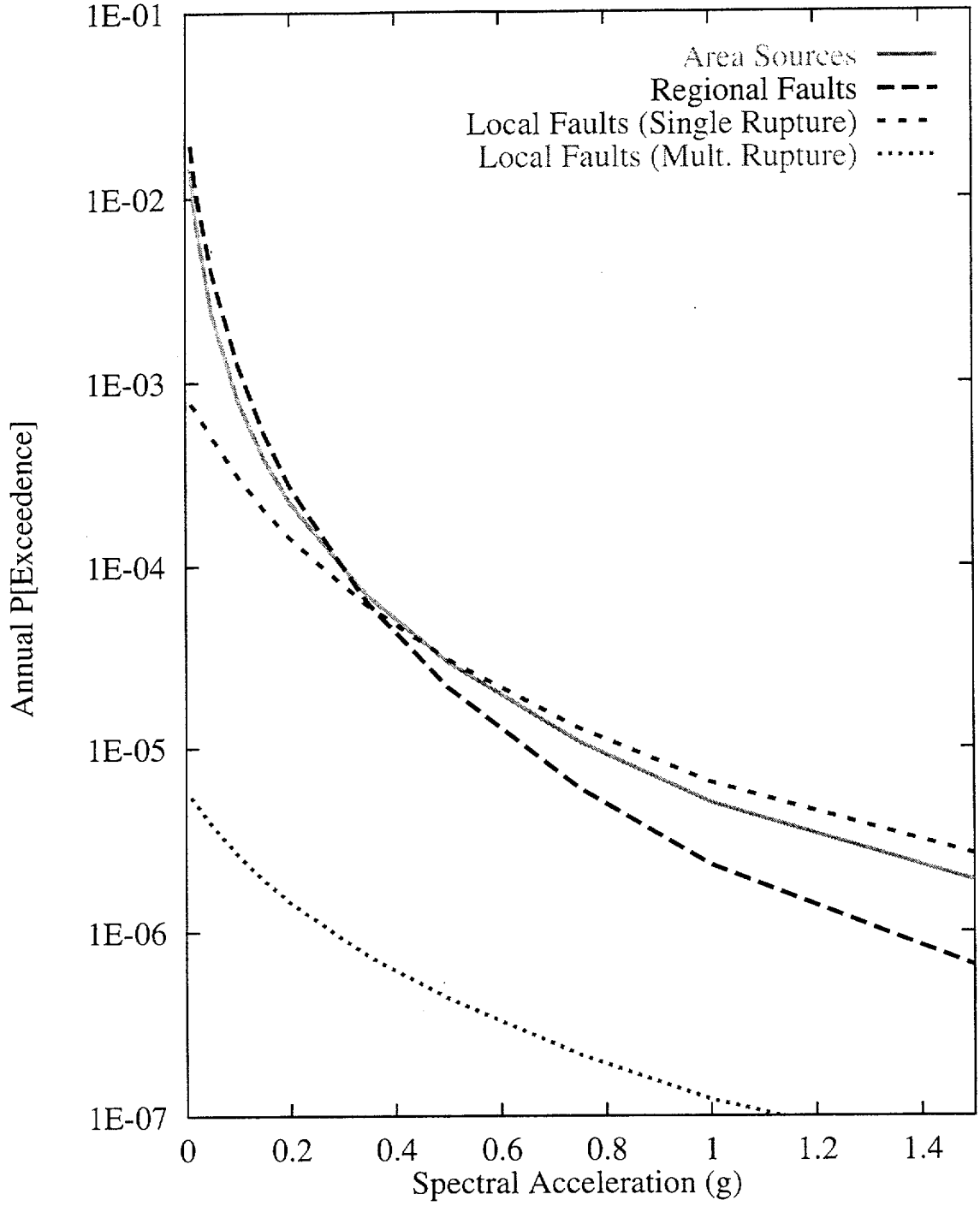

Figure 7-82 Contributions of source types to the mean hazard: DFS team, 1-Hz horizontal spectral acceleration

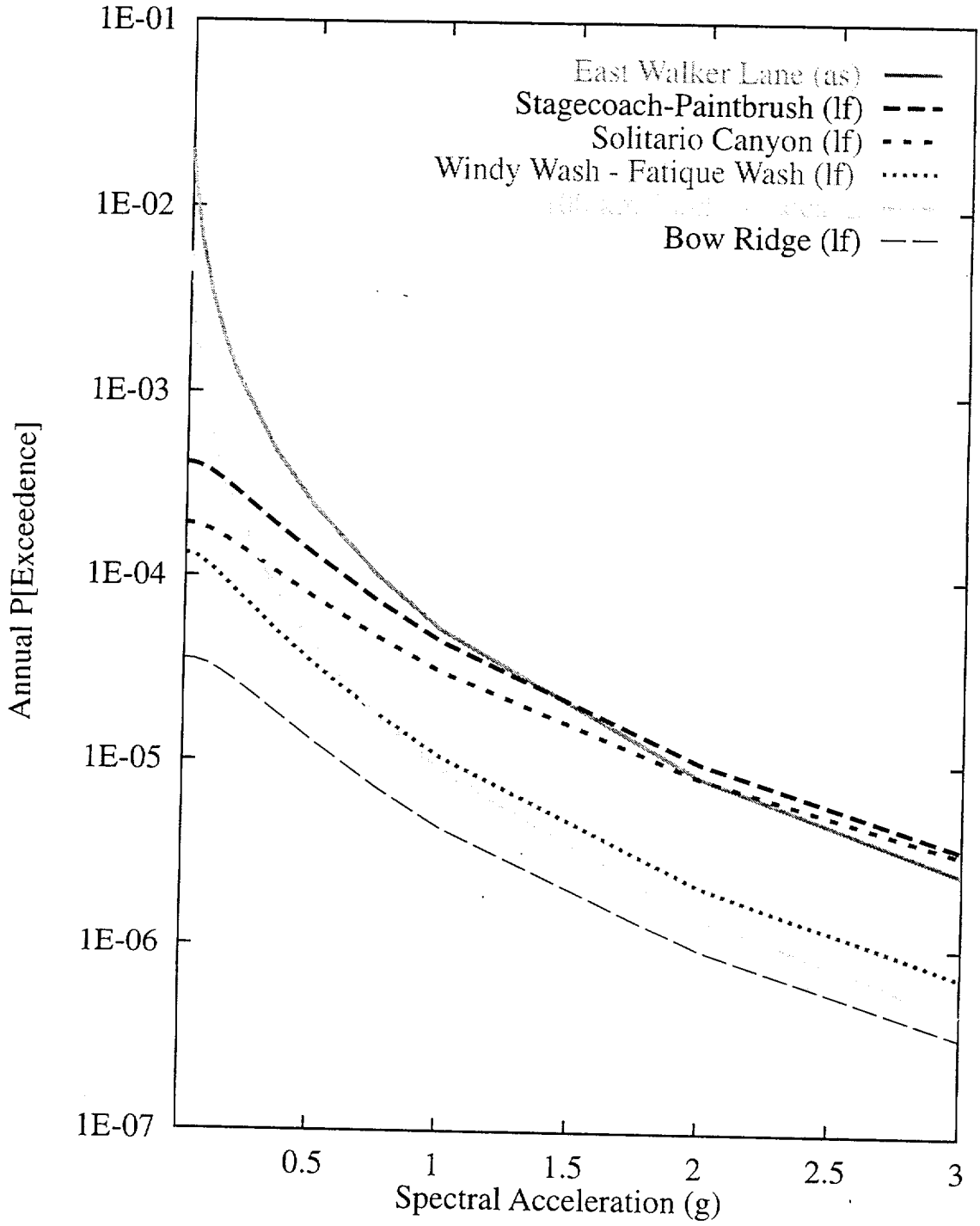

Figure 7-83 Mean seismic hazard from dominant seismic sources: DFS team, 10-Hz horizontal spectral acceleration. Acronyms in parentheses refer to source types: as-area source zone; and lf-local fault.

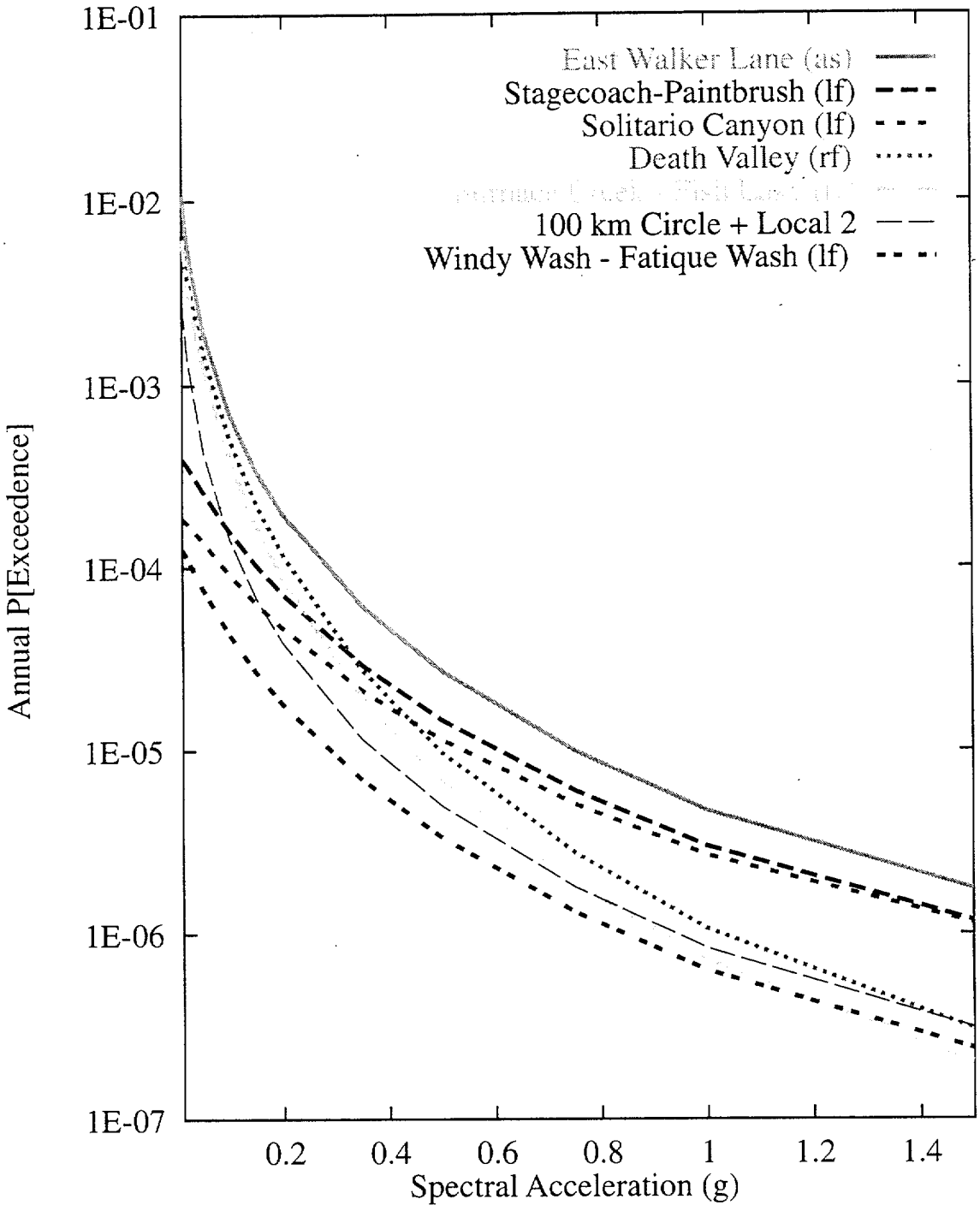

Figure 7-84 Mean seismic hazard from dominant seismic sources: DFS team, 1-Hz horizontal spectral acceleration. Acronyms in parentheses refer to source types: as-area source zone; lf-local fault; and rf-regional fault.

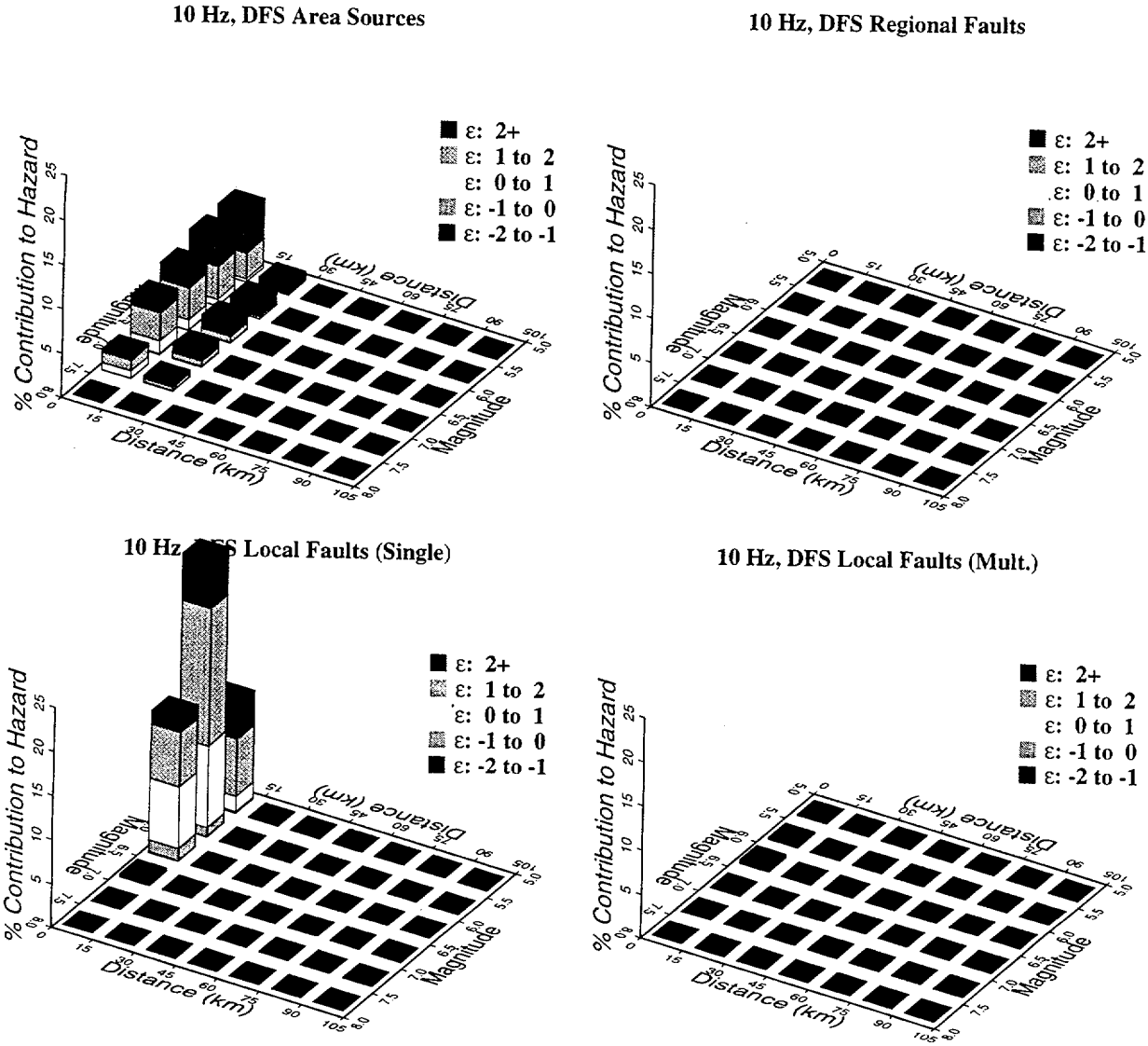

Figure 7-85 Magnitude-distance-epsilon distributions for the four source types: DFS team, 10-Hz horizontal spectral acceleration

1 Hz, DFS Area Sources

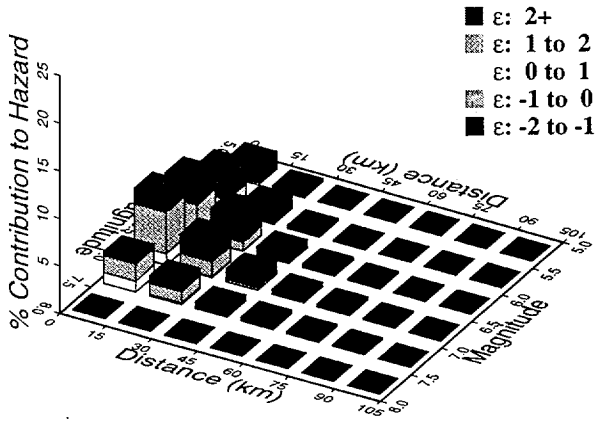

1 Hz, DFS Regional Faults

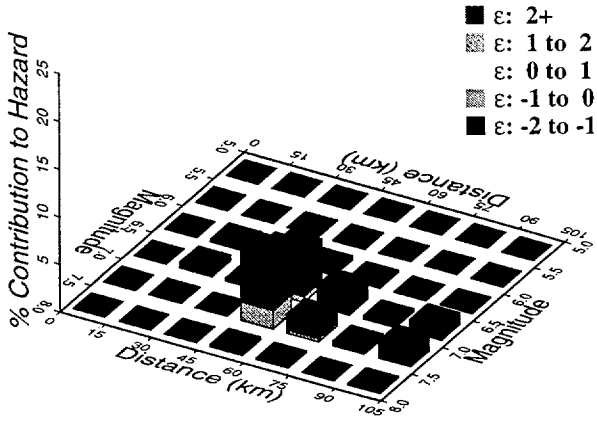

1 Hz, DFS Local Faults (Single)

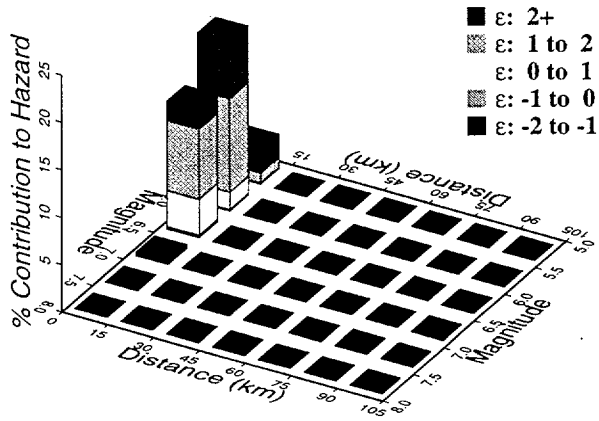

1 Hz, DFS Local Faults (Mult.)

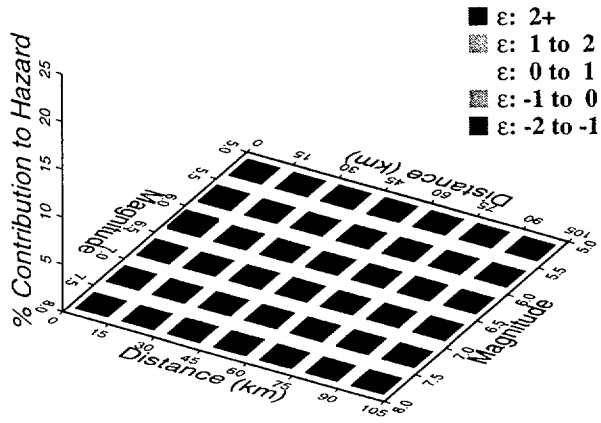

Figure 7-86 Magnitude-distance-epsilon distributions for the four source types: DFS team, 1-Hz horizontal spectral acceleration

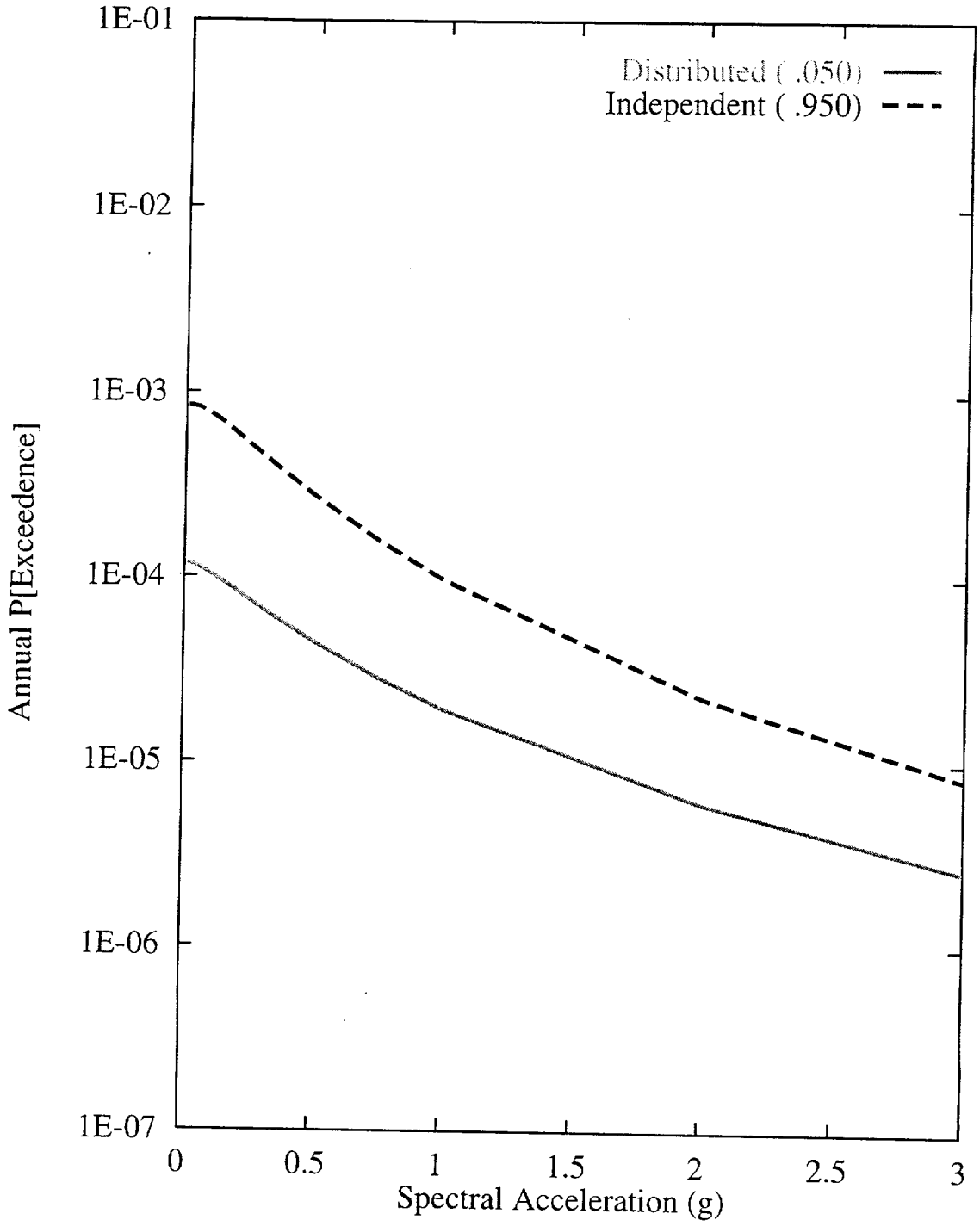

Figure 7-87 Sensitivity of seismic hazard from local faults to presence of distributed versus independent faults: DFS team, 10-Hz horizontal spectral acceleration

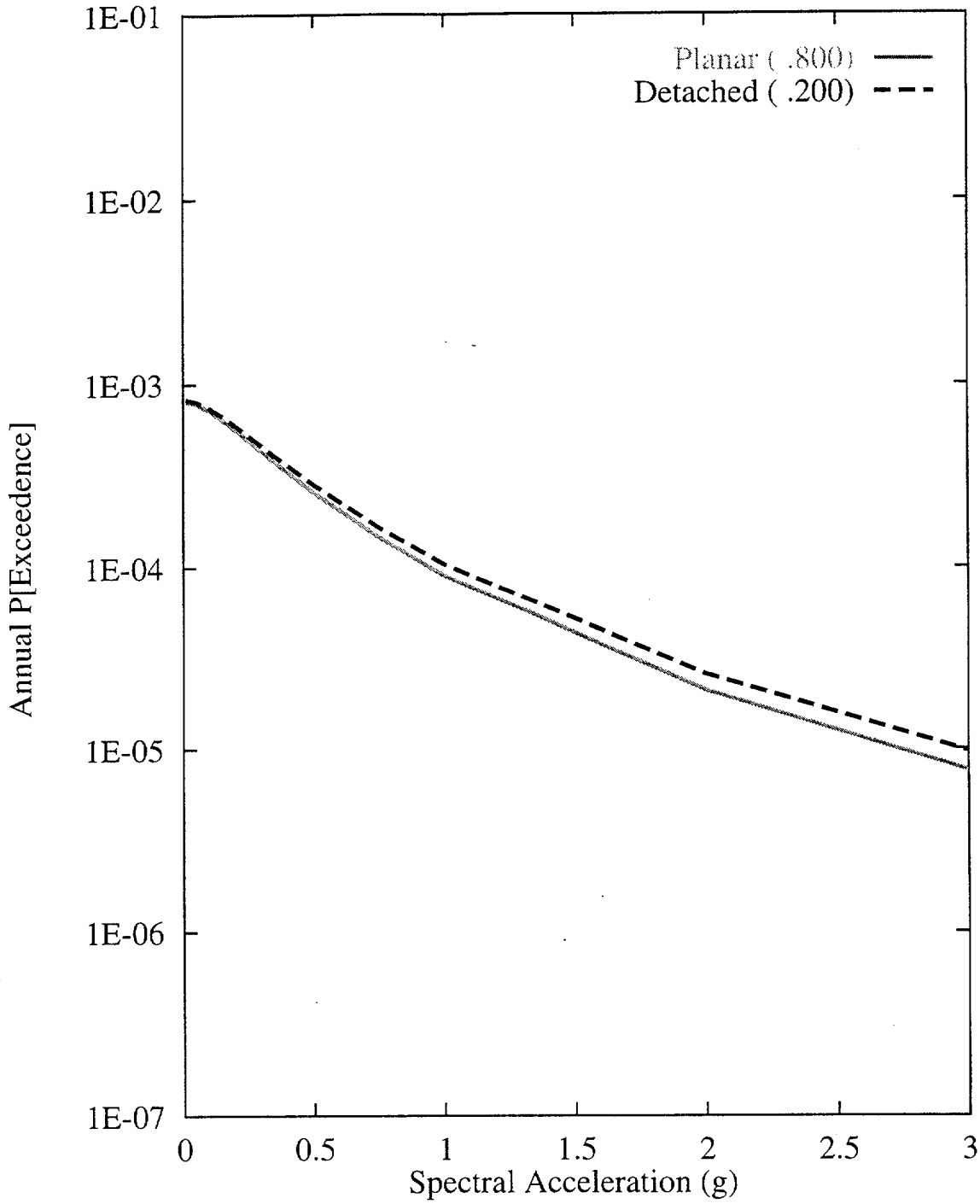

Figure 7-88 Sensitivity of seismic hazard from local faults to subsurface geometry: DFS team, 10-Hz horizontal spectral acceleration

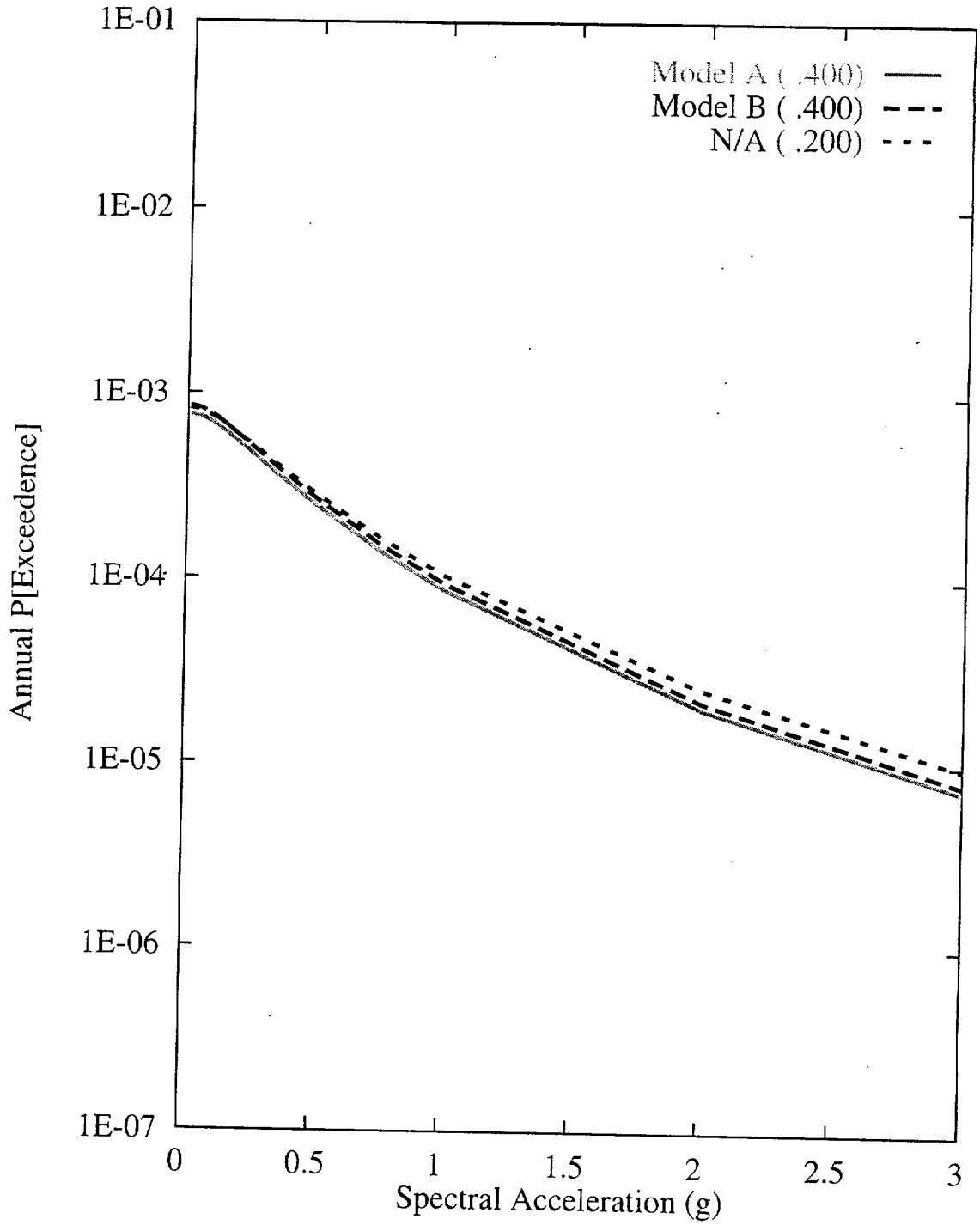

Figure 7-89 Sensitivity of seismic hazard from local faults to fault subsurface geometry for planar faults: DFS team, 10-Hz horizontal spectral acceleration

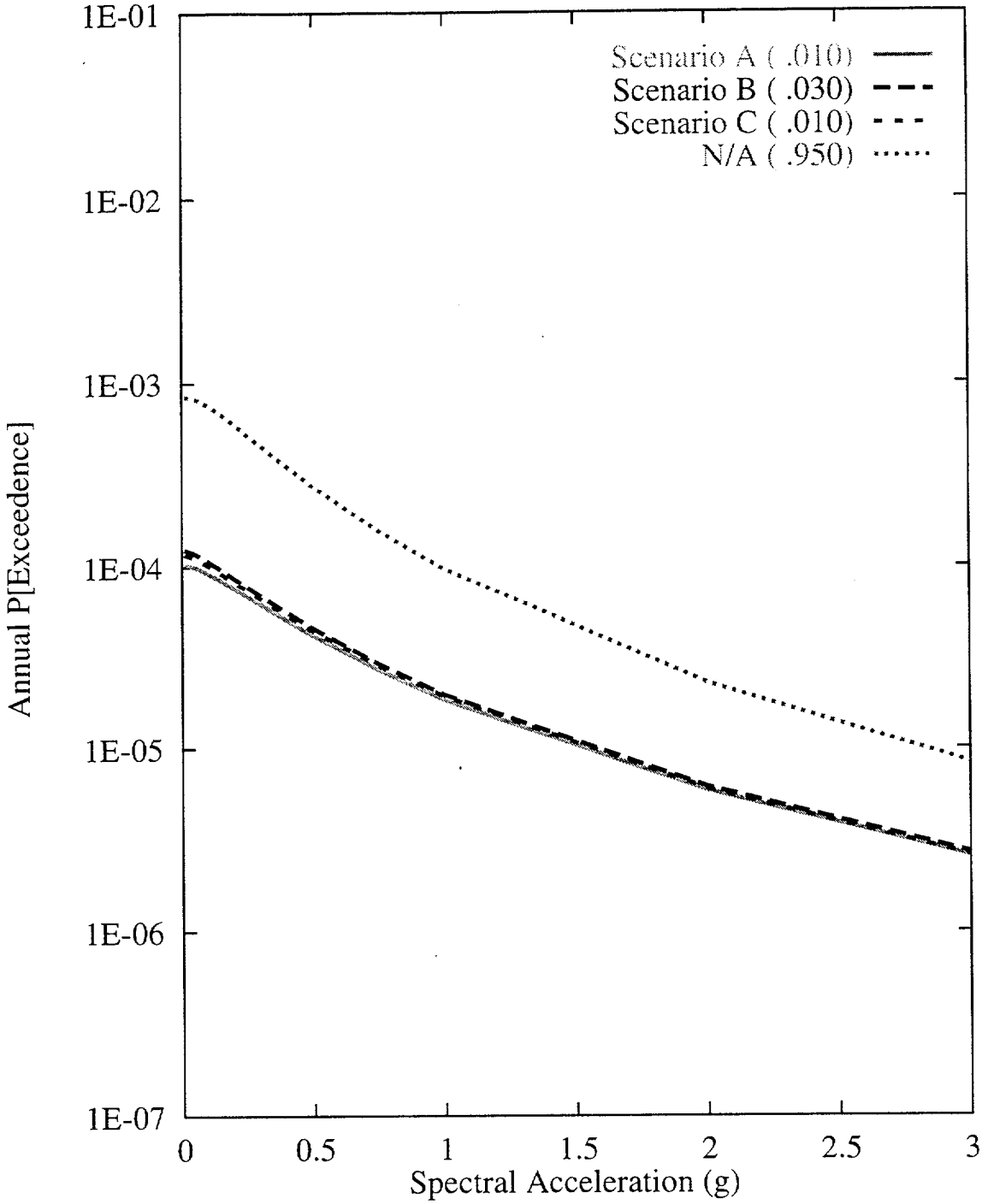

Figure 7-90 Sensitivity of seismic hazard from local faults to multiple-fault rupture scenarios: DFS team, 10-Hz horizontal spectral acceleration

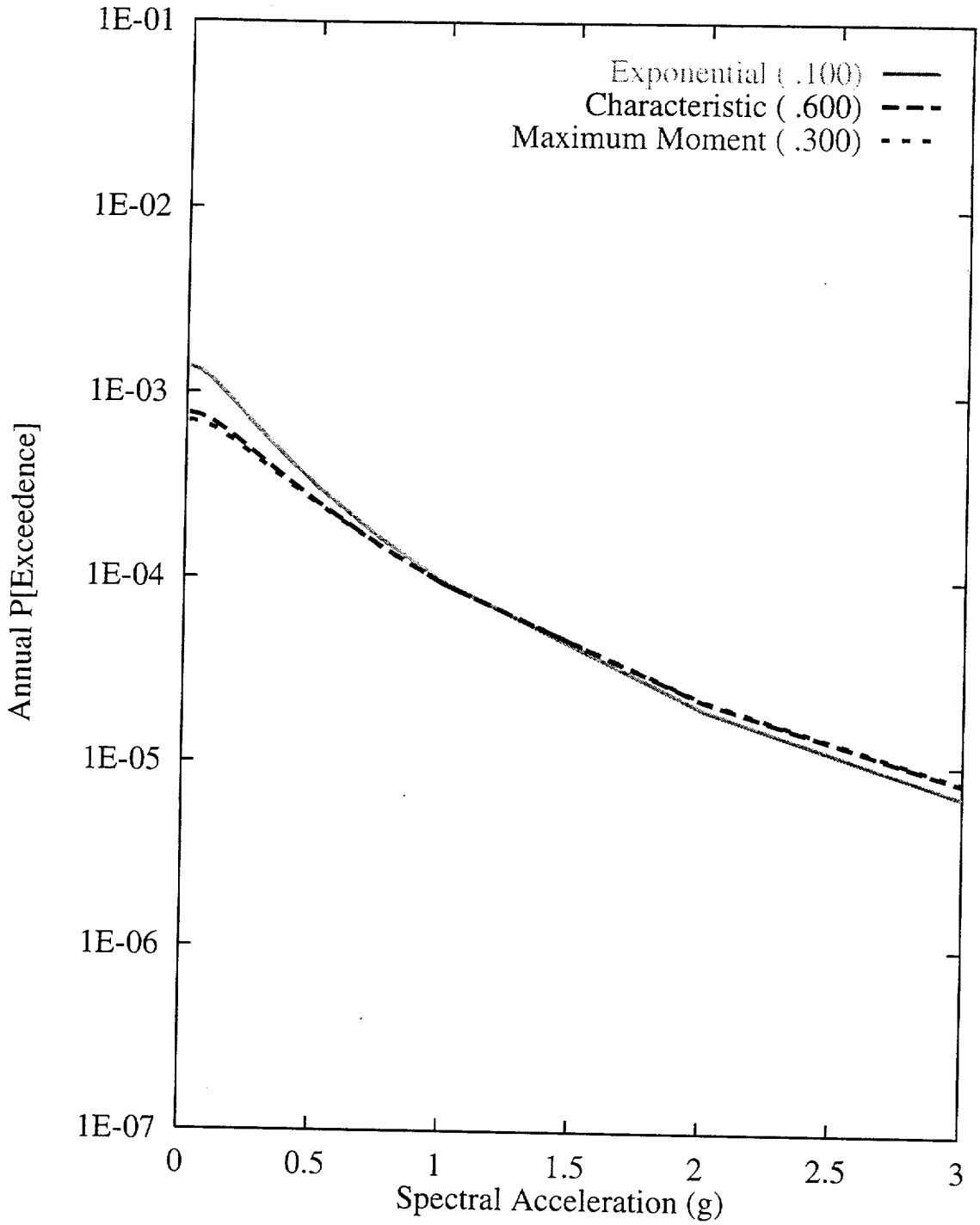

Figure 7-91 Sensitivity of seismic hazard from local faults to recurrence model: DFS team, 10-Hz horizontal spectral acceleration

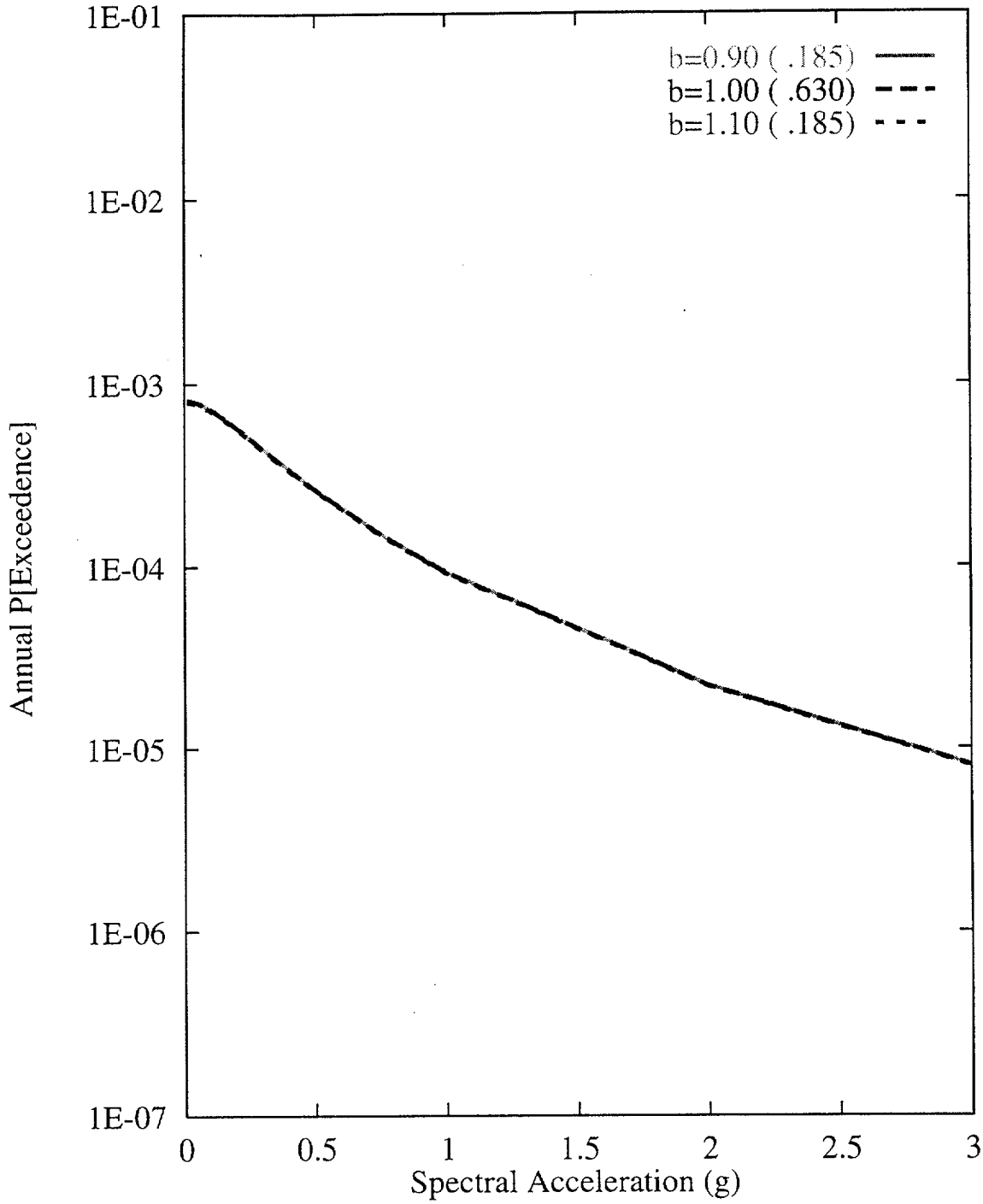

Figure 7-92 Sensitivity of seismic hazard from local faults to b-value: DFS team, 10-Hz horizontal spectral acceleration

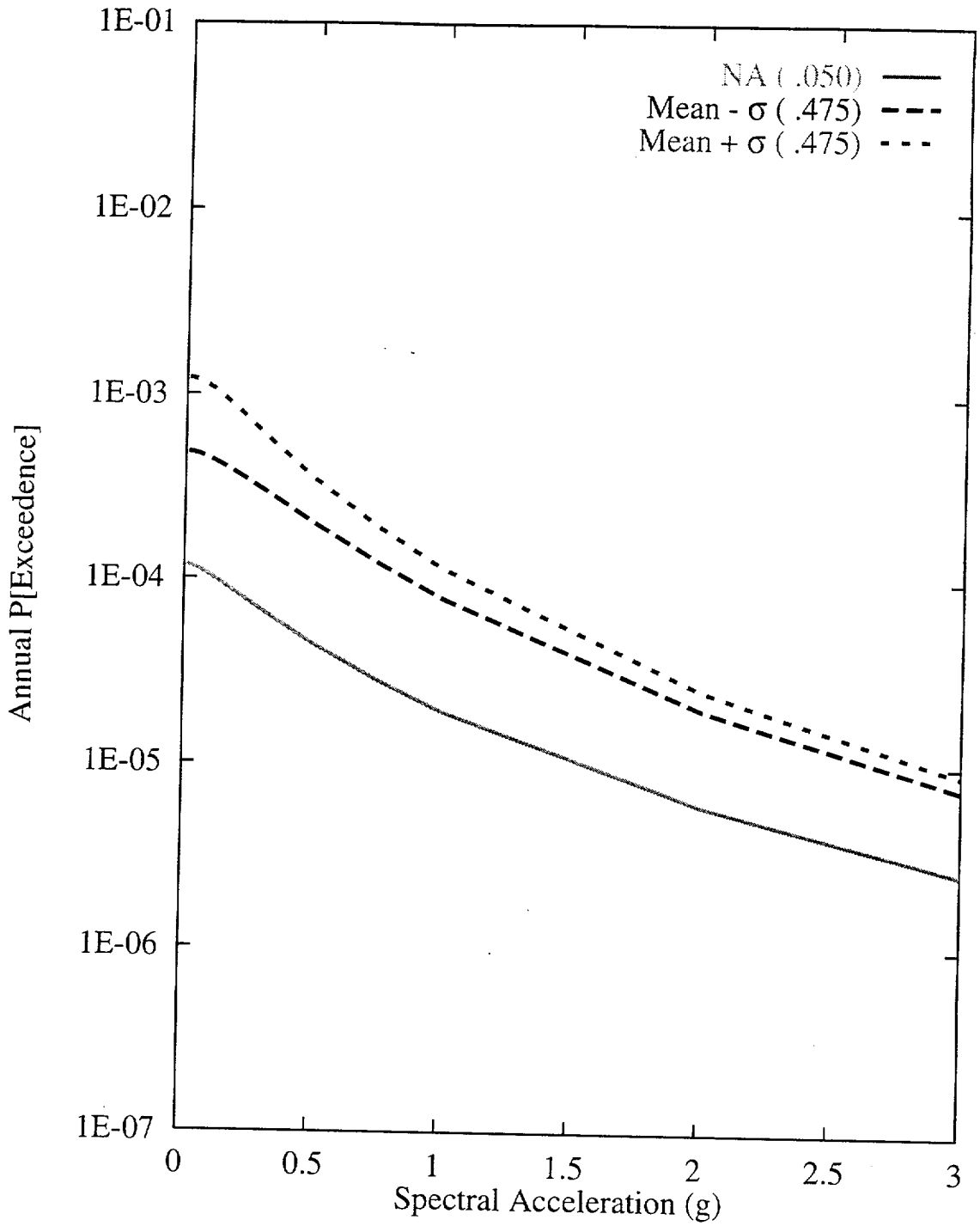

Figure 7-93 Sensitivity of seismic hazard from local faults to Mmax on Stagecoach Road-Paintbrush Canyon fault system: DFS team, 10-Hz horizontal spectral acceleration

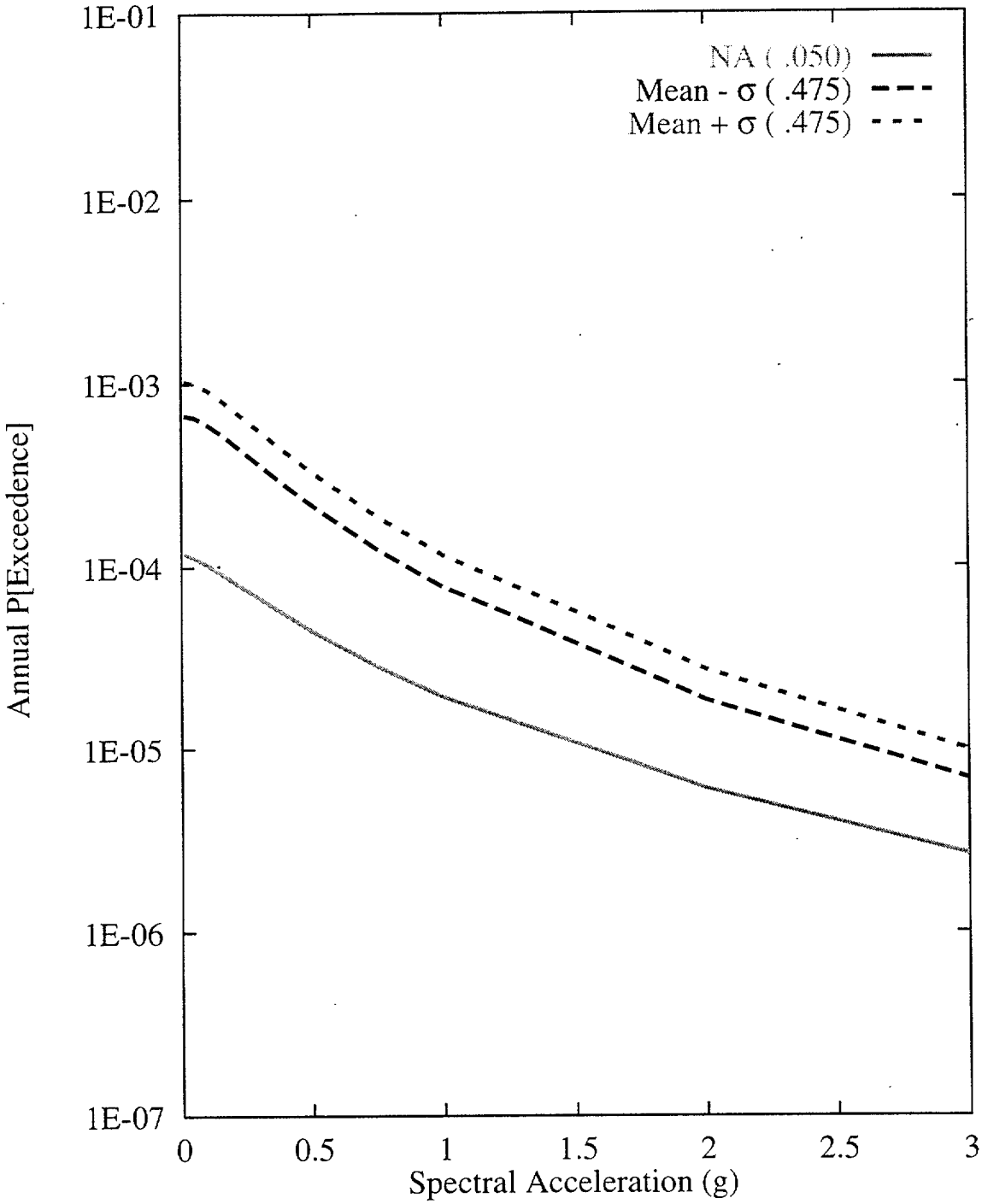

Figure 7-94 Sensitivity of seismic hazard from local faults to recurrence of Stagecoach Road-Paintbrush Canyon fault system: DFS team, 10-Hz horizontal spectral acceleration

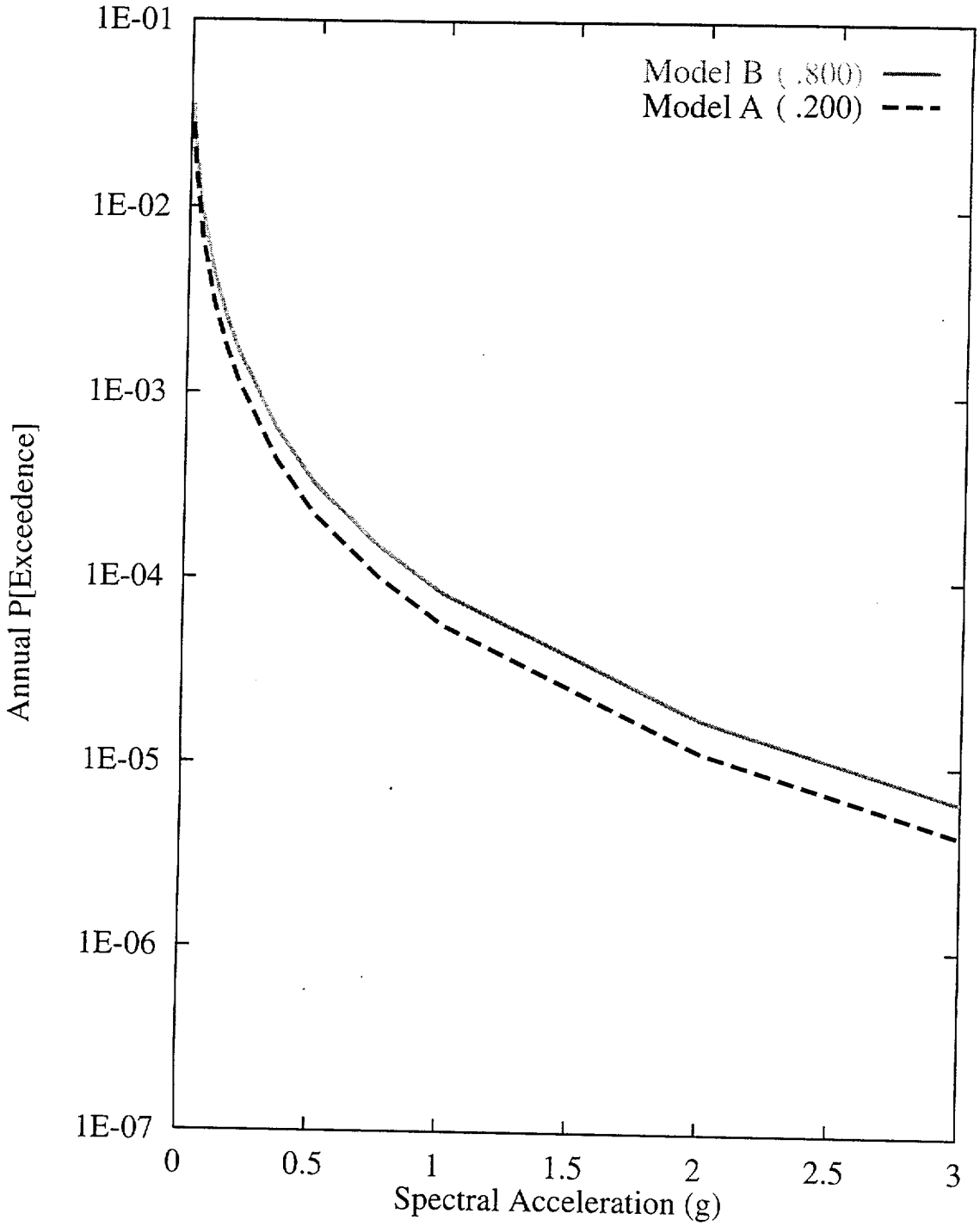

Figure 7-95 Sensitivity of seismic hazard from area zones to zonation: DFS team, 10-Hz horizontal spectral acceleration

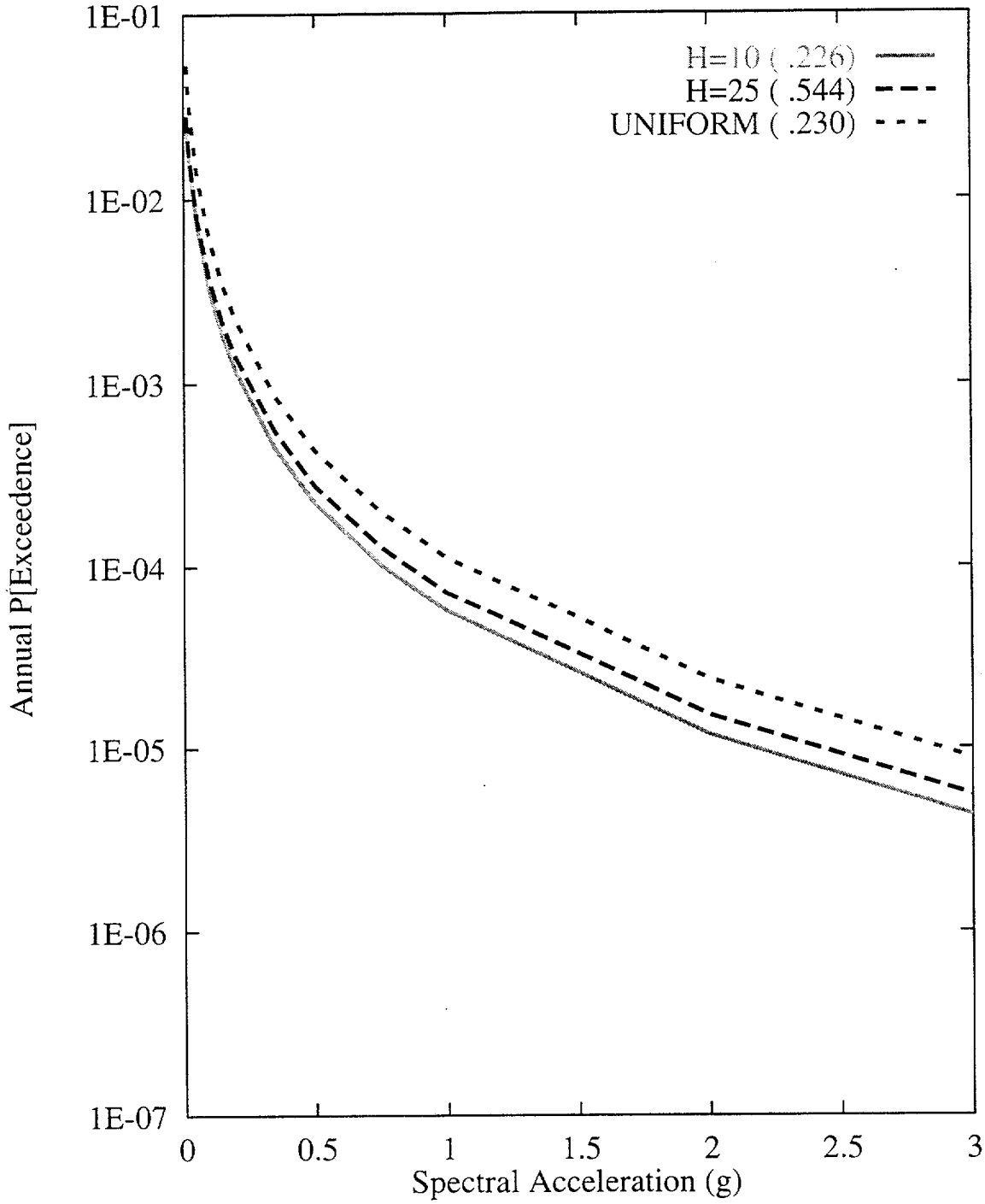

Figure 7-96 Sensitivity of seismic hazard from area zones to spatial variability and smoothing (H) of seismicity: DFS team, 10-Hz horizontal spectral acceleration

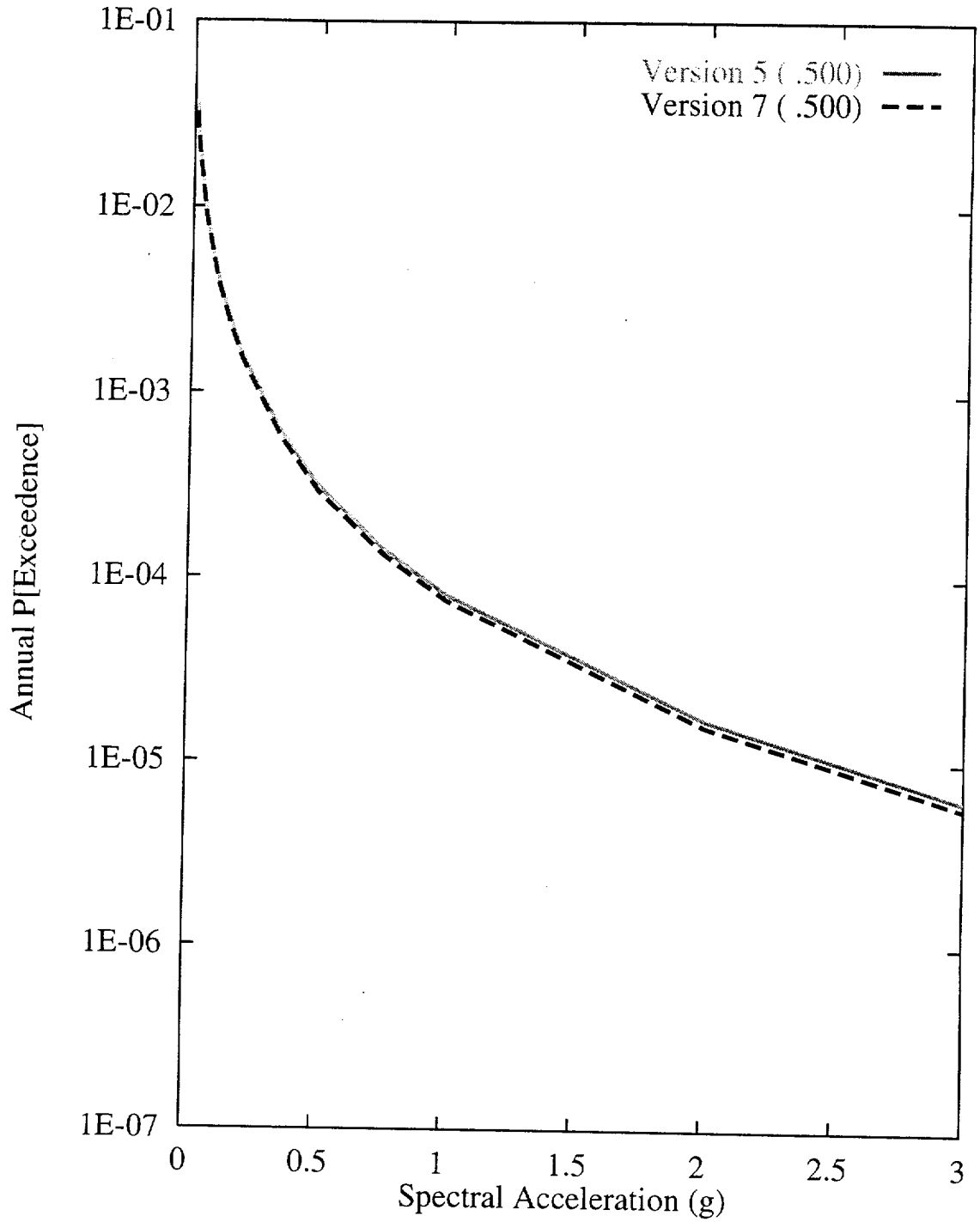

Figure 7-97 Sensitivity of seismic hazard from area zones to choice of seismicity catalog: DFS team, 10-Hz horizontal spectral acceleration

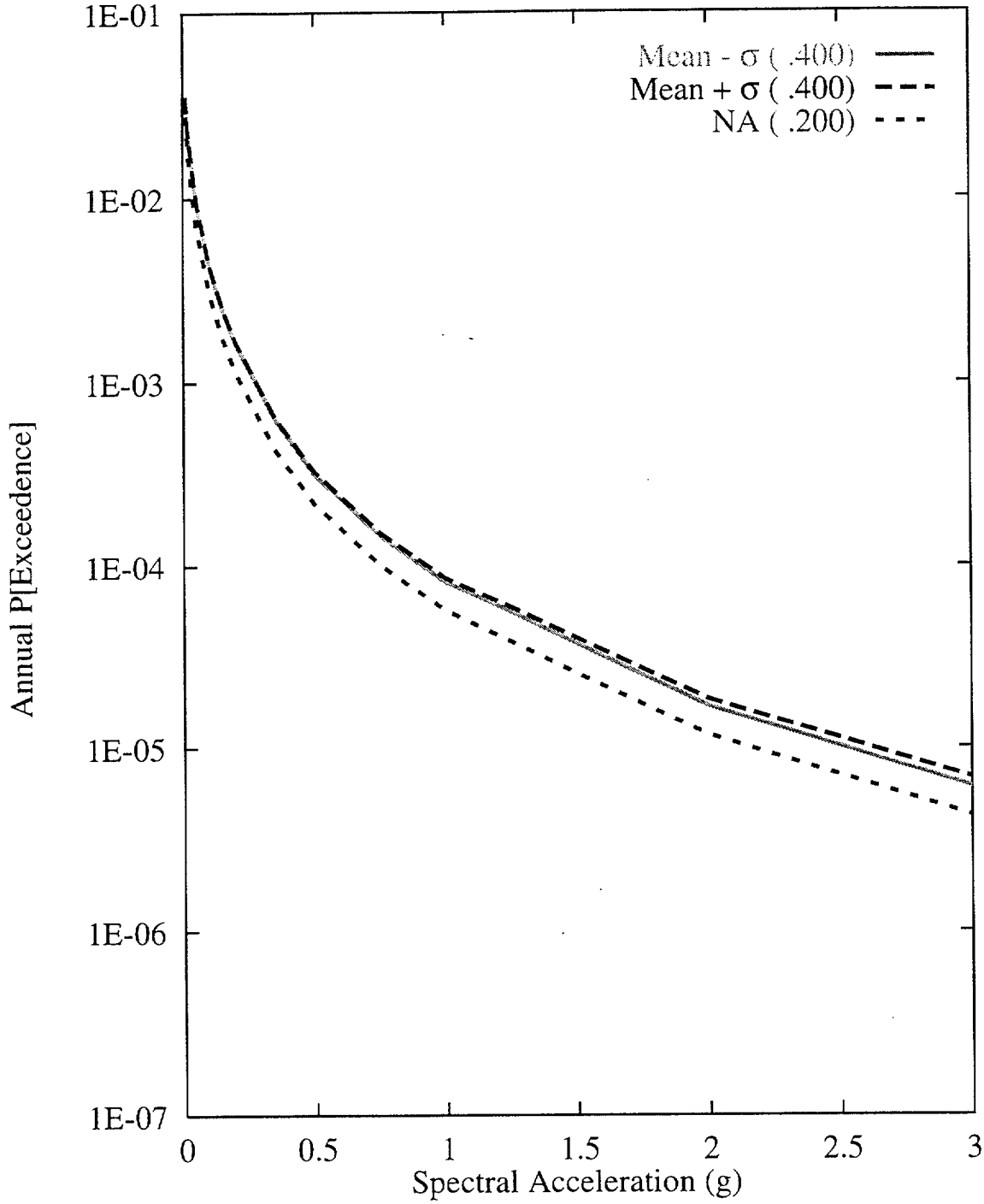

Figure 7-98 Sensitivity of seismic hazard from area zones to Mmax on the East Walker Lane+local seismic source: DFS team, 10-Hz horizontal spectral acceleration

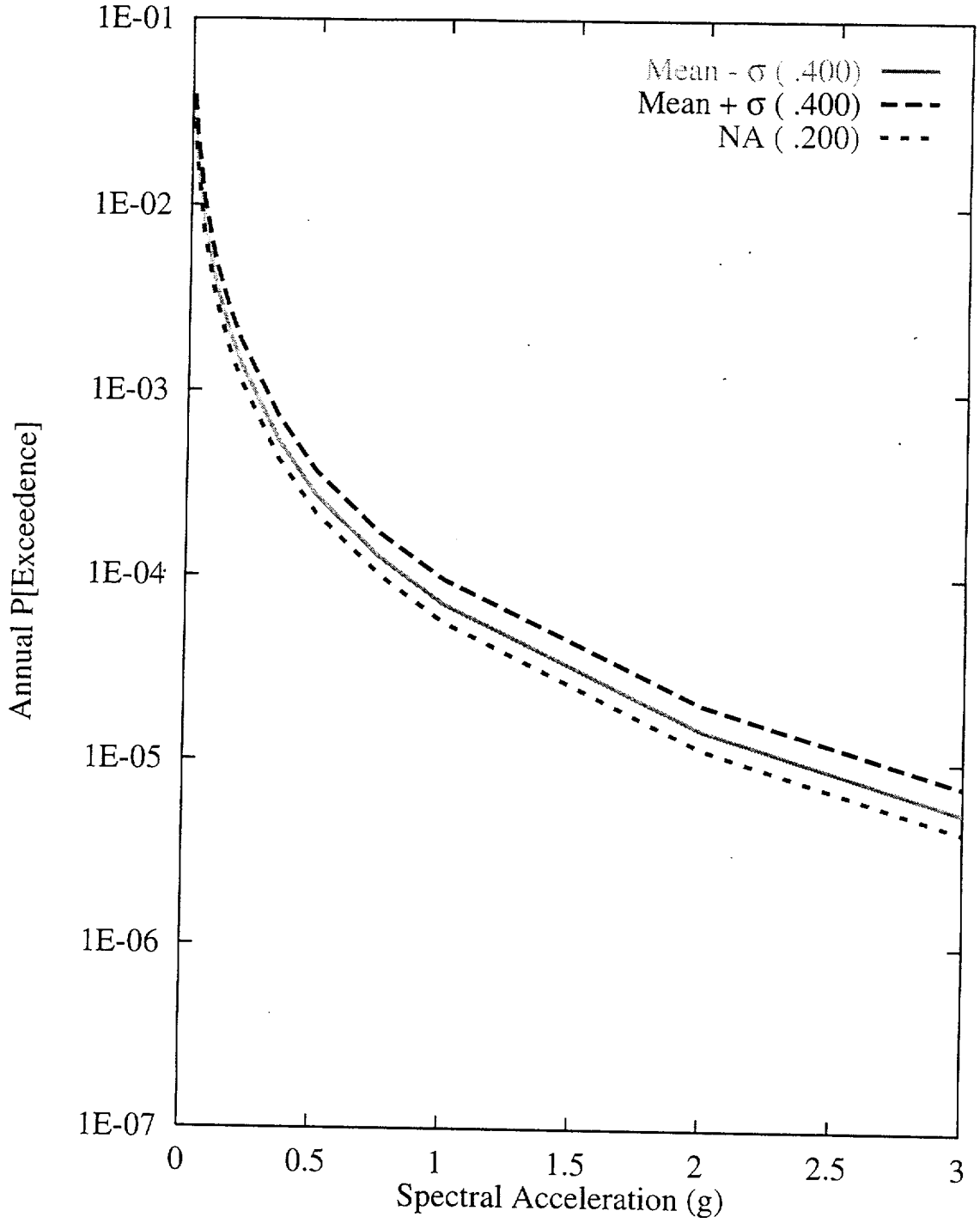

Figure 7-99 Sensitivity of seismic hazard from area zones to recurrence of the East Walker Lane+local seismic source: DFS team, 10-Hz horizontal spectral acceleration

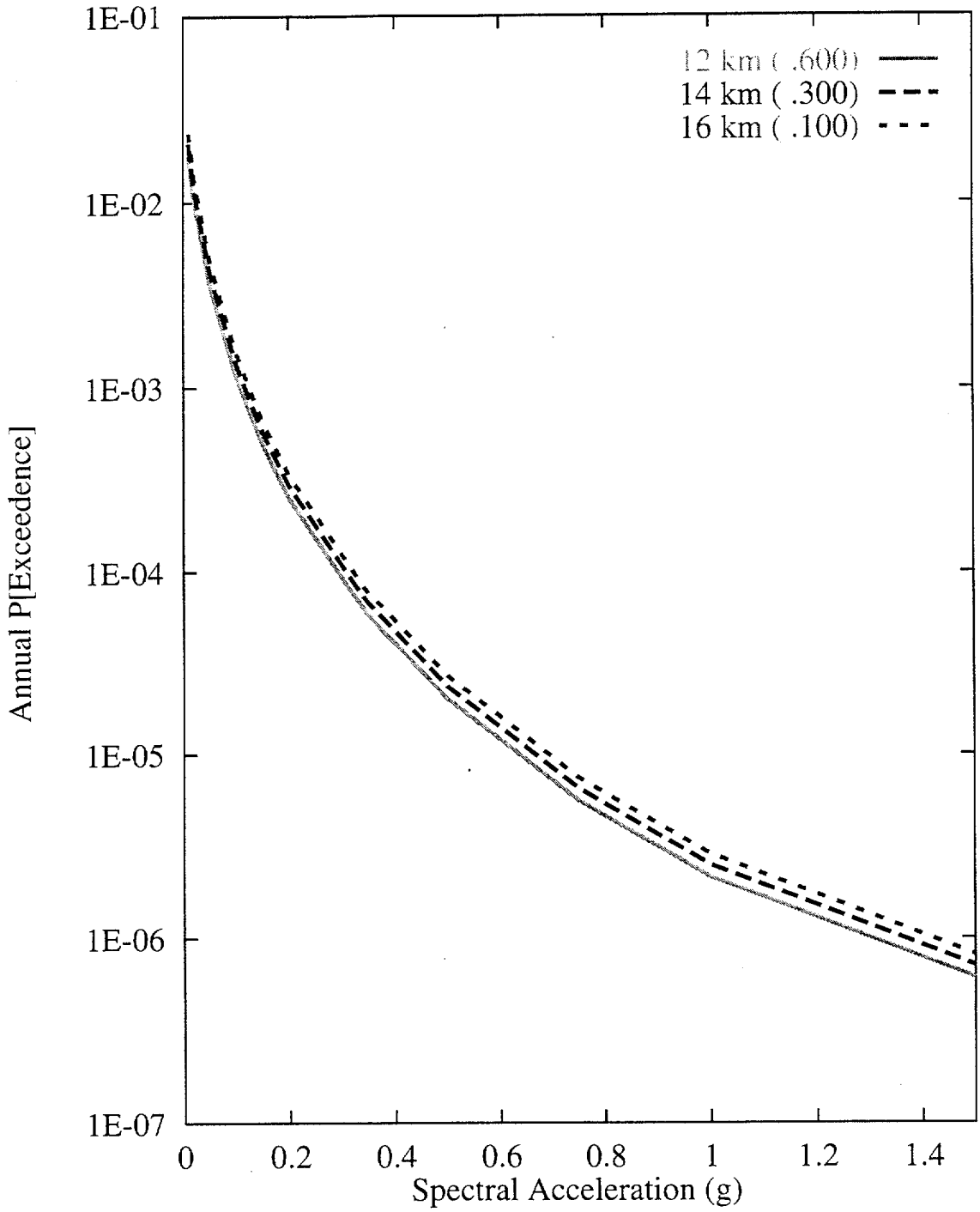

Figure 7-100 Sensitivity of seismic hazard from regional faults to maximum fault depth: DFS team, 1-Hz horizontal spectral acceleration

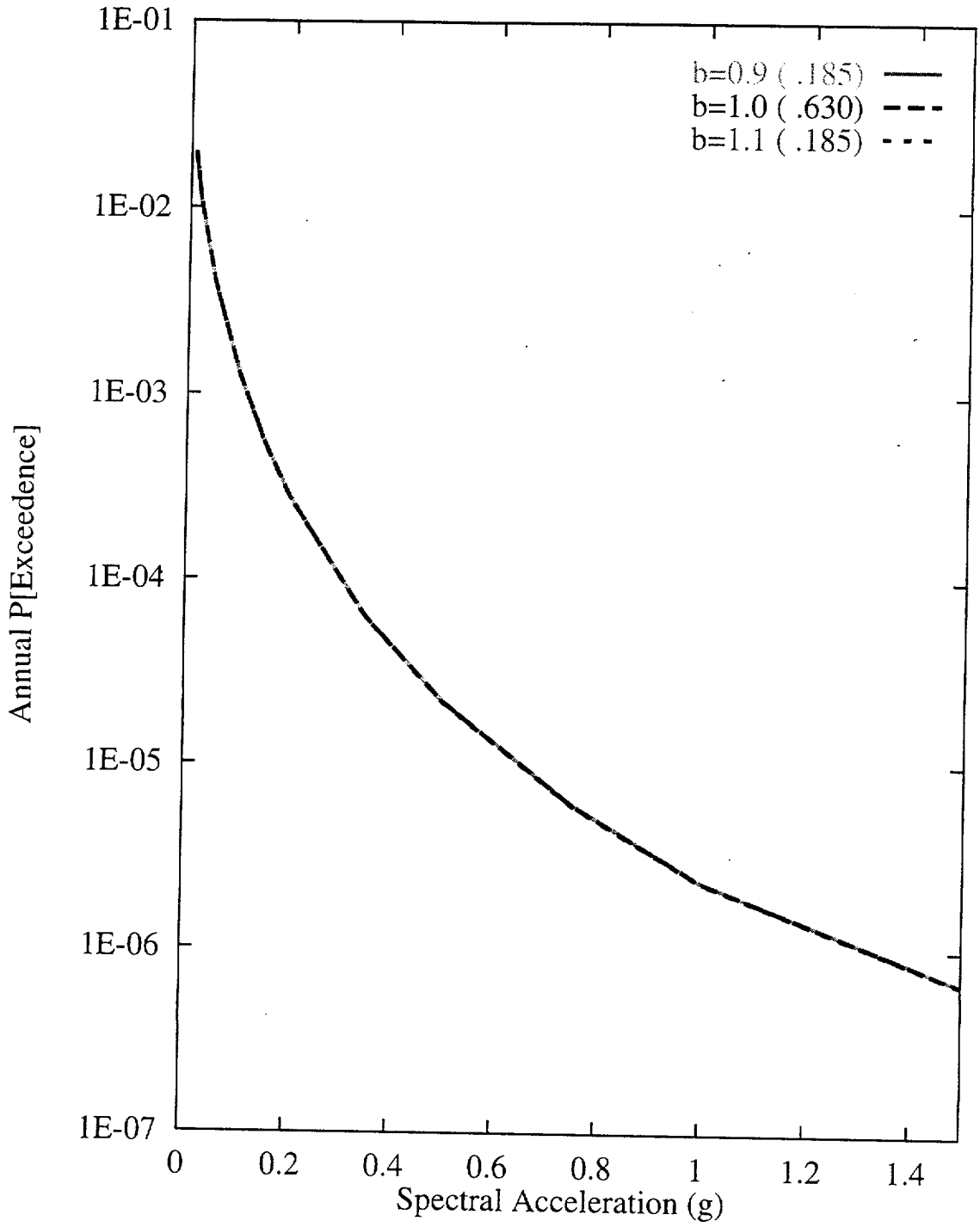

Figure 7-101 Sensitivity of seismic hazard from regional faults to b-values: DFS team, 1-Hz horizontal spectral acceleration

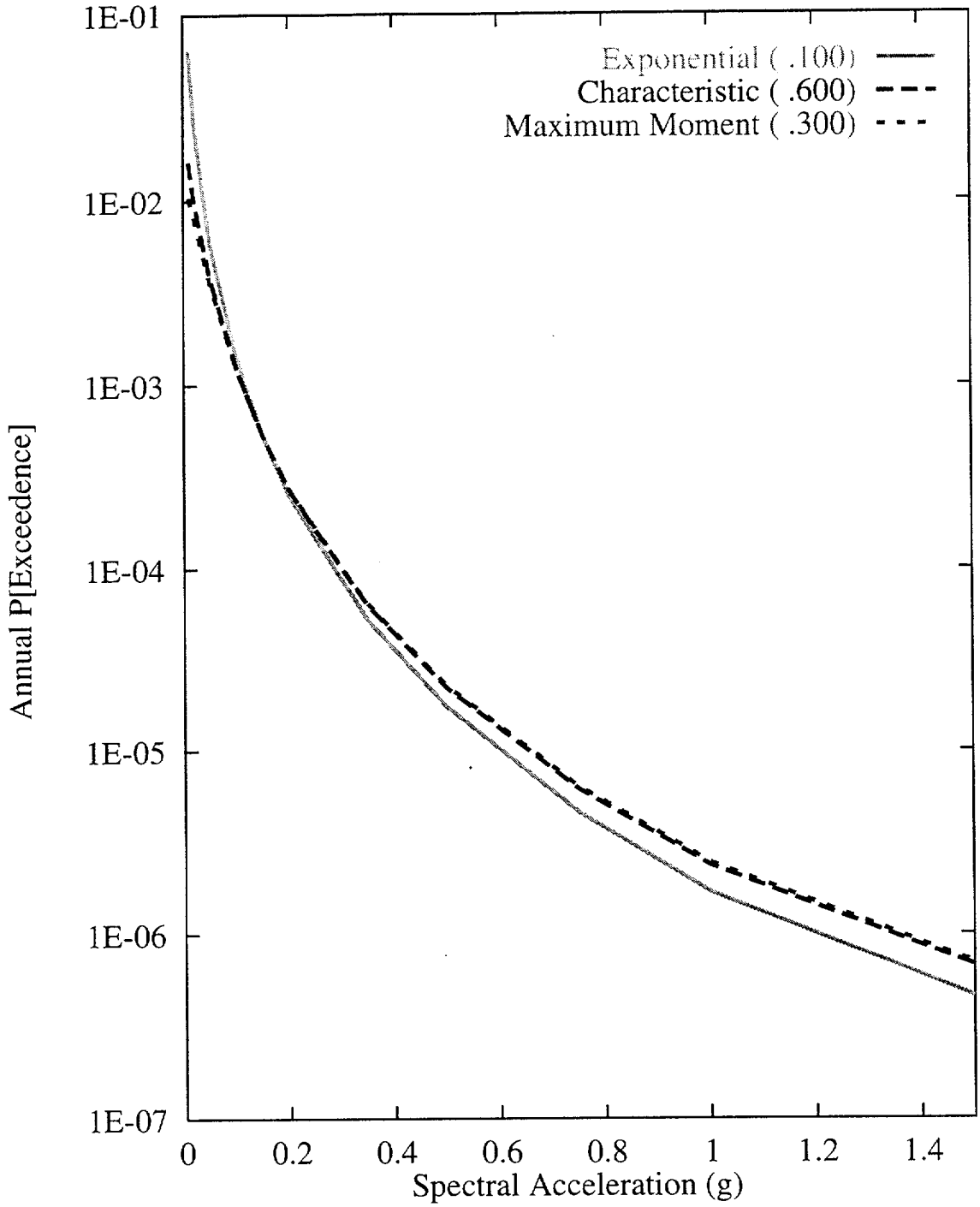

Figure 7-102 Sensitivity of seismic hazard from regional faults to recurrence model: DFS team, 1-Hz horizontal spectral acceleration

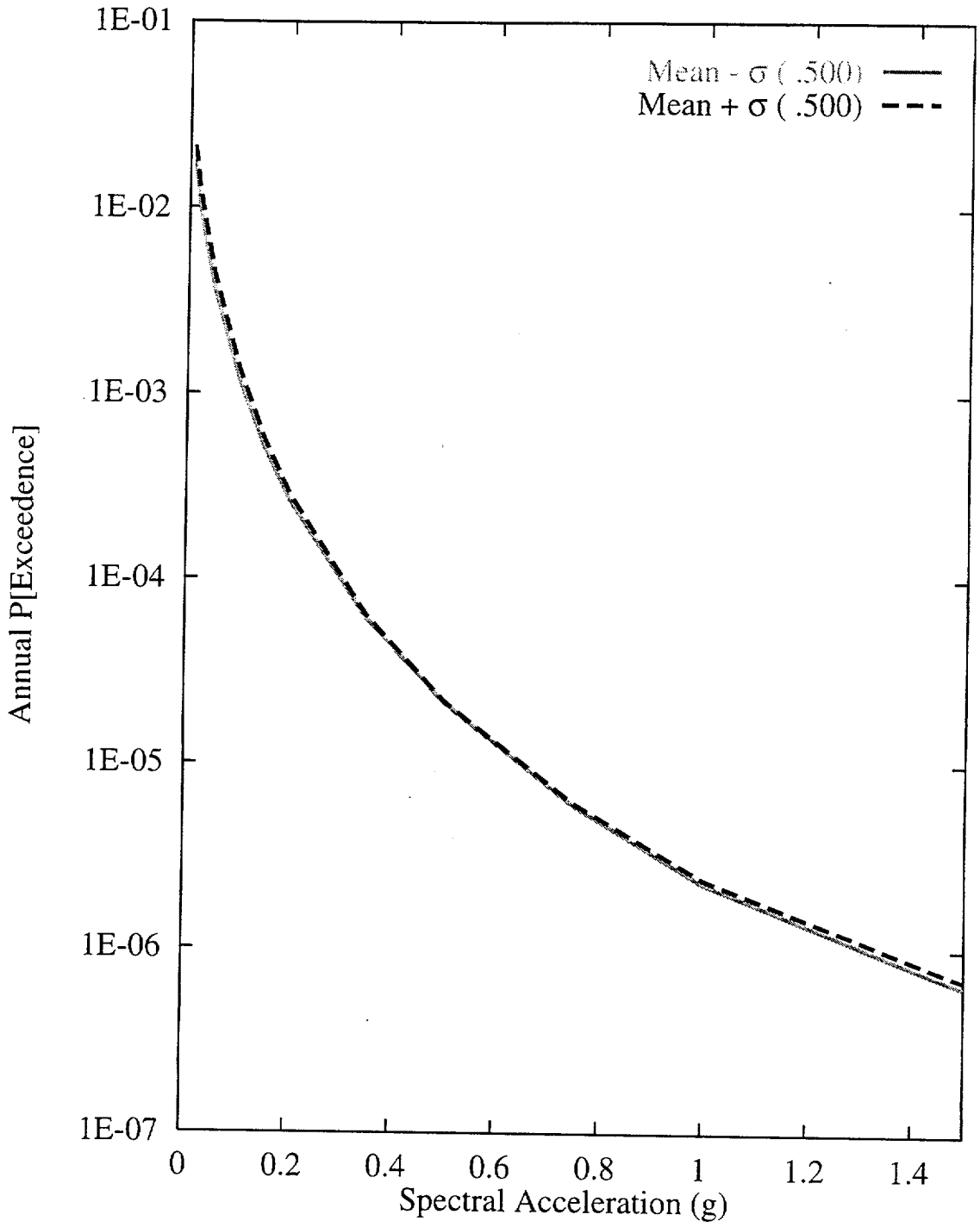

Figure 7-103 Sensitivity of seismic hazard from regional faults to Mmax on the Death Valley fault: DFS team, 1-Hz horizontal spectral acceleration

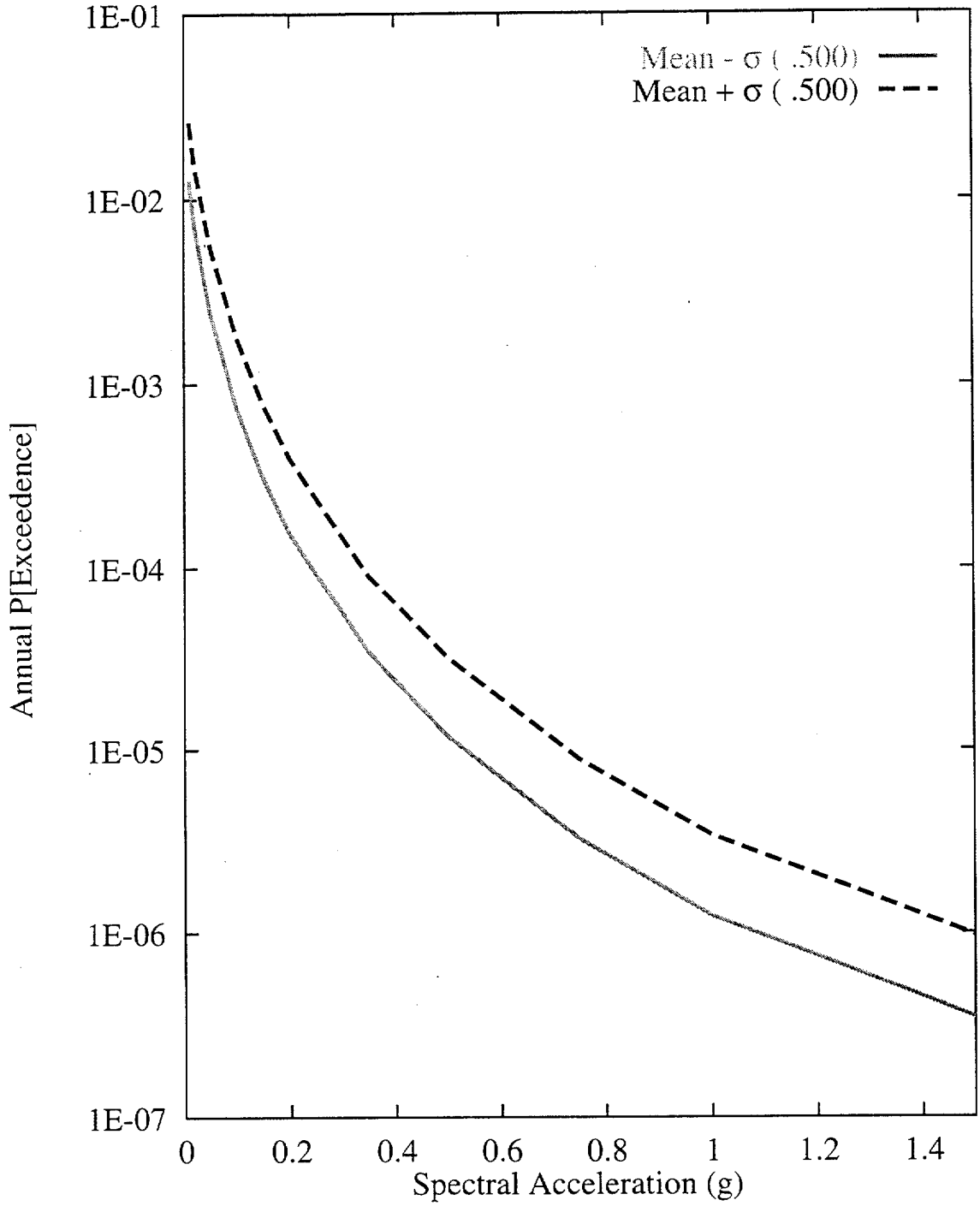

Figure 7-104 Sensitivity of seismic hazard from regional faults to slip rate of the Death Valley fault: DFS team, 1-Hz horizontal spectral acceleration

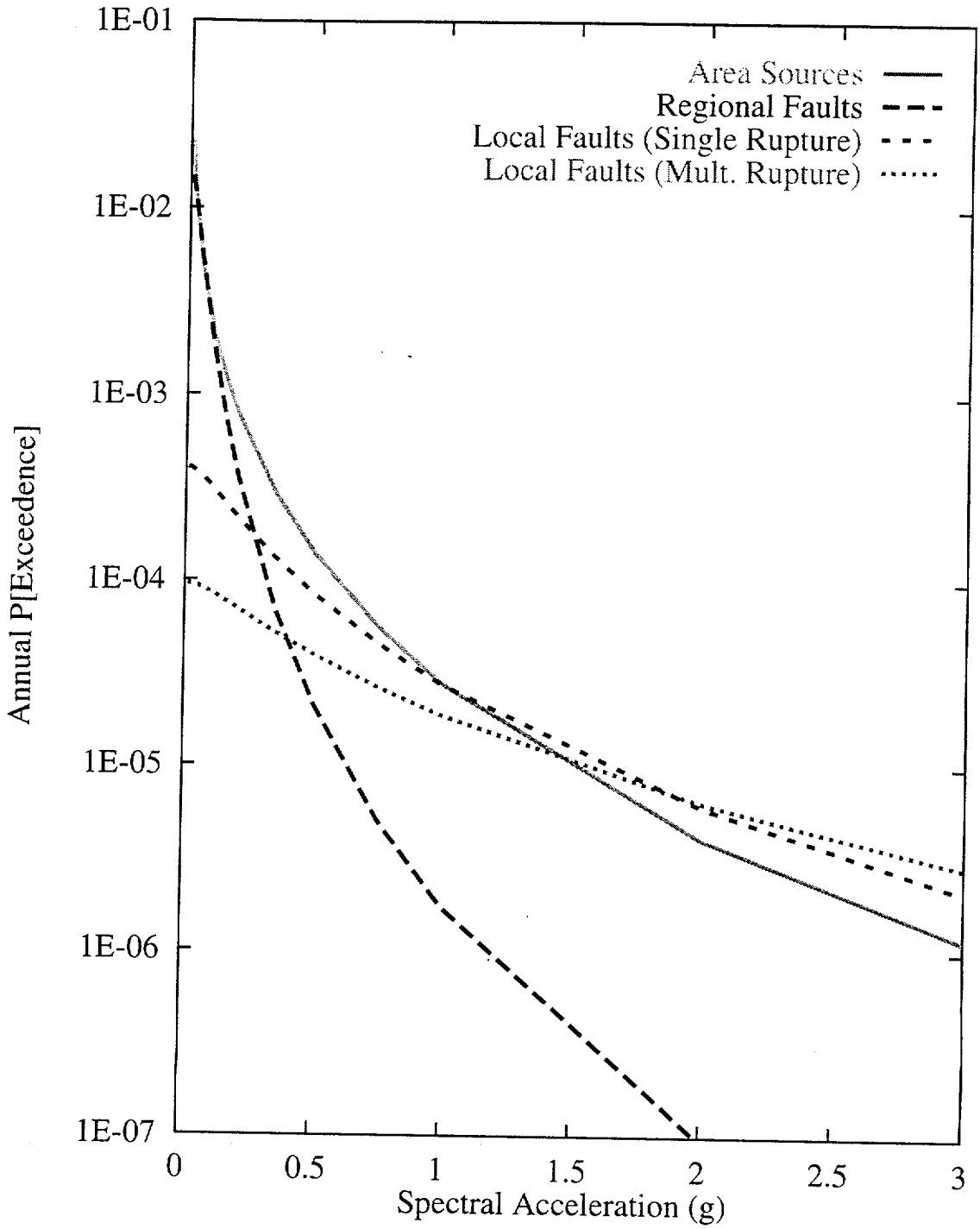

Figure 7-105 Contributions of source types to the mean hazard: RYA team, 10-Hz horizontal spectral acceleration

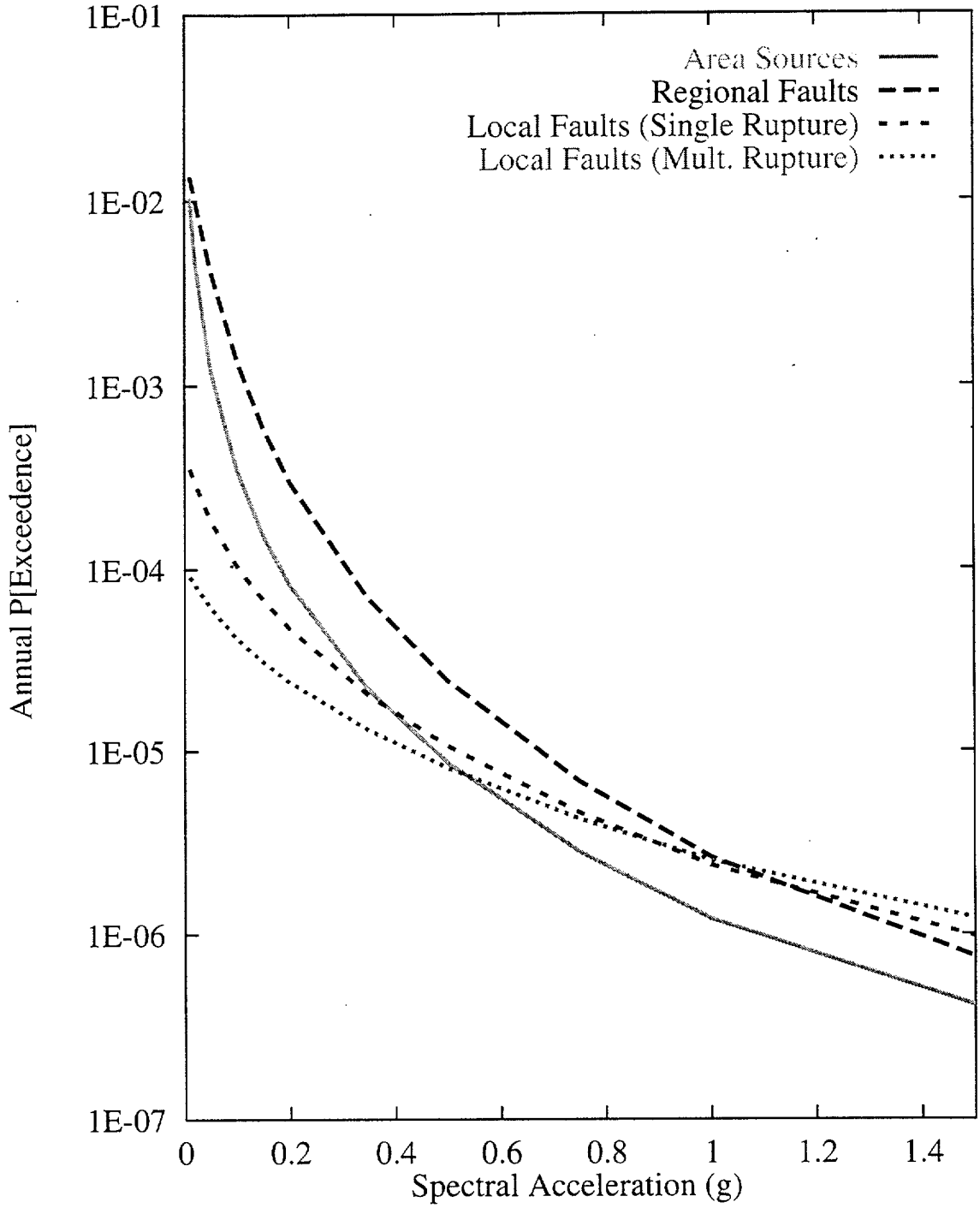

Figure 7-106 Contributions of source types to the mean hazard: RYA team, 1-Hz horizontal spectral acceleration

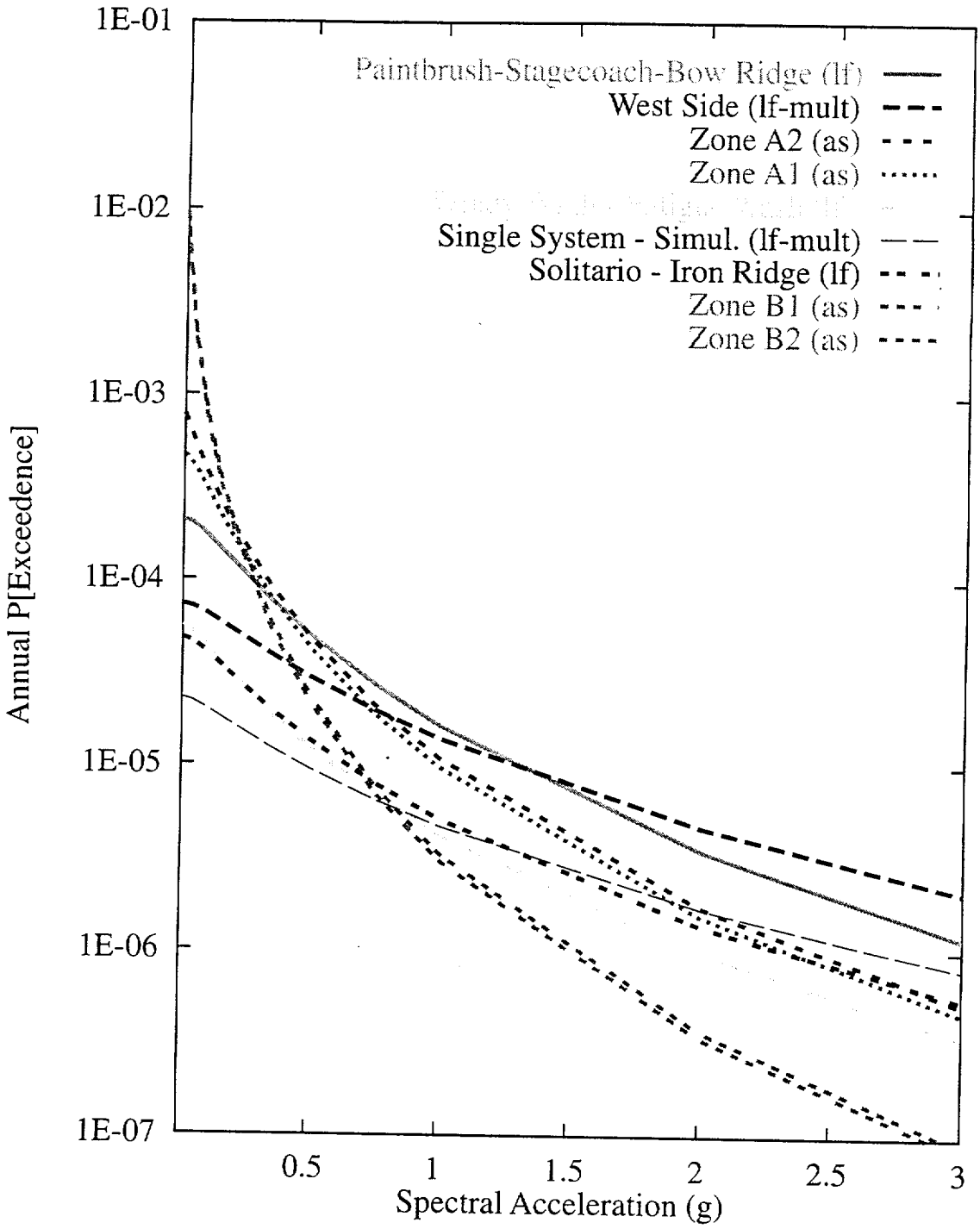

Figure 7-107 Mean seismic hazard from dominant seismic sources: RYA team, 10-Hz horizontal spectral acceleration. Acronyms in parentheses refer to source types: as-area source zone; lf-local fault; and mult-multiple fault.

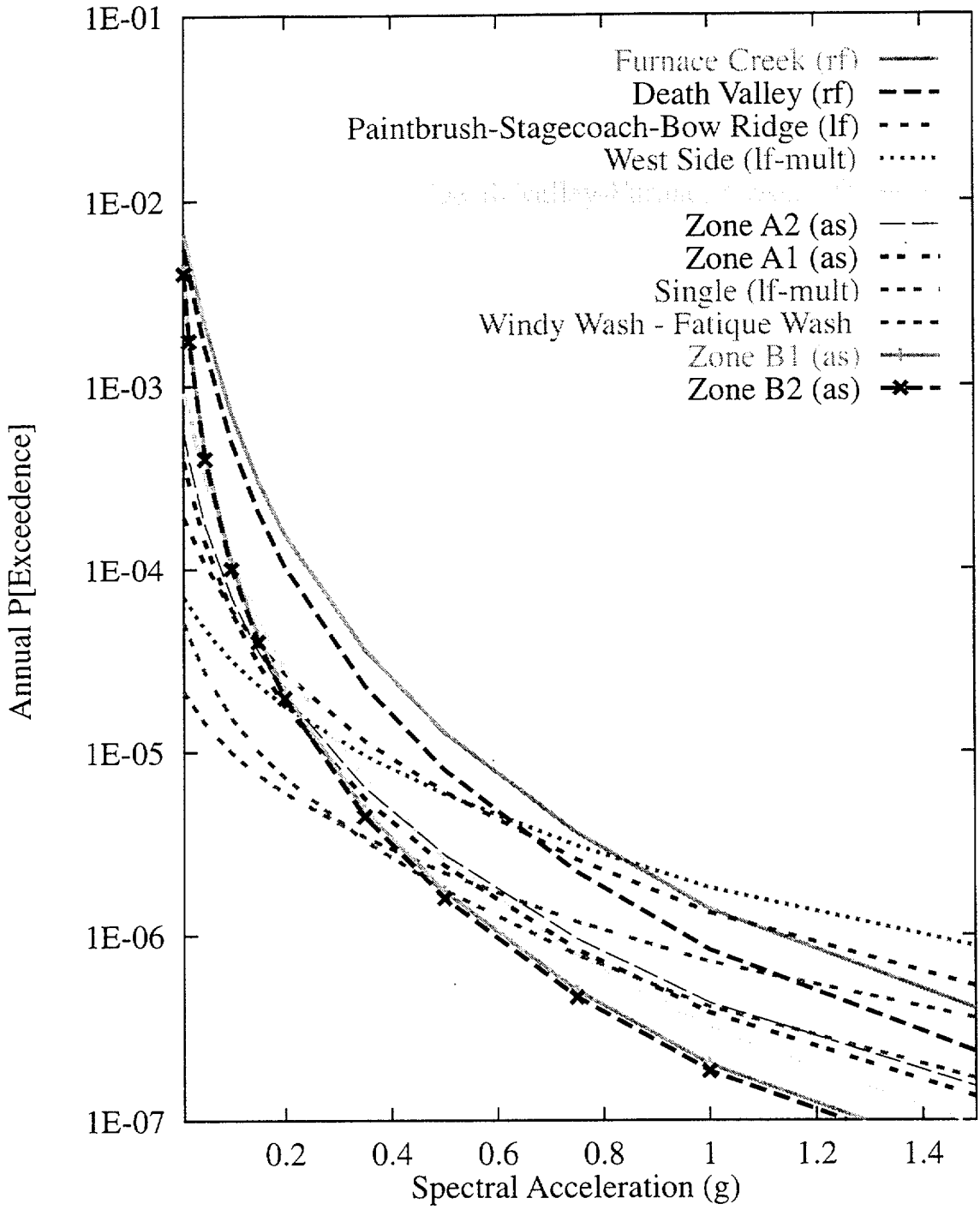

Figure 7-108 Mean seismic hazard from dominant seismic sources: RYA team, 1-Hz horizontal spectral acceleration. Acronyms in parentheses refer to source types: as-area source zone; rf-regional fault; lf-local fault; and mult-multiple fault.

10 Hz, RYA Area Sources

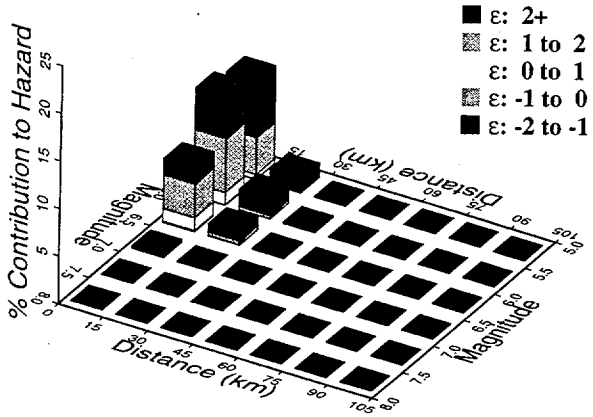

10 Hz, RYA Regional Faults

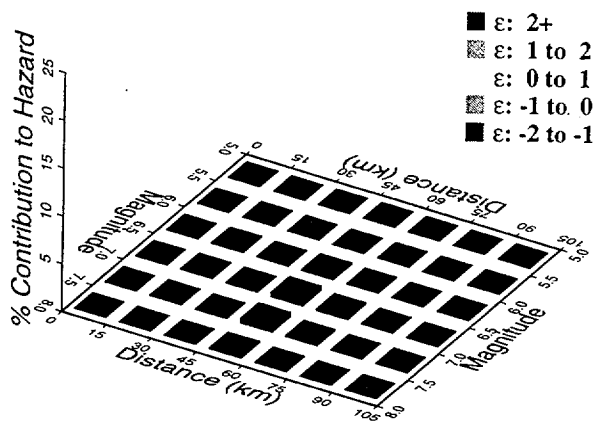

10 Hz, RYA Local Faults (Single)

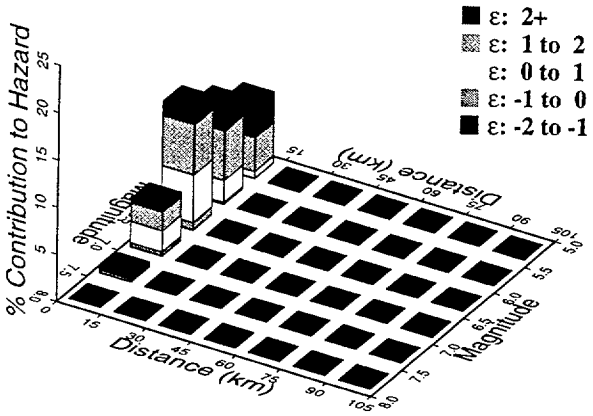

10 Hz, RYA Local Faults (Mult.)

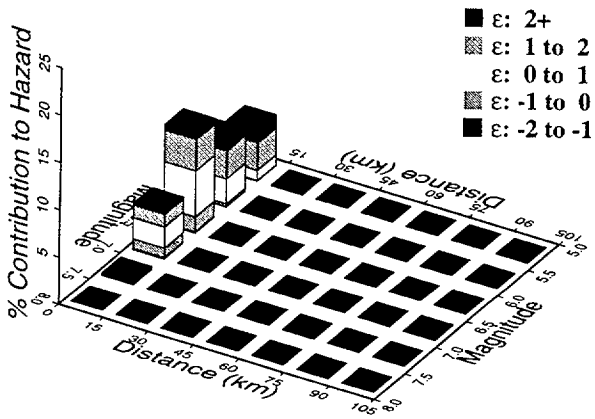

Figure 7-109 Magnitude-distance-epsilon distributions for the four source types: RYA team, 10-Hz horizontal spectral acceleration

1 Hz, RYA Area Sources

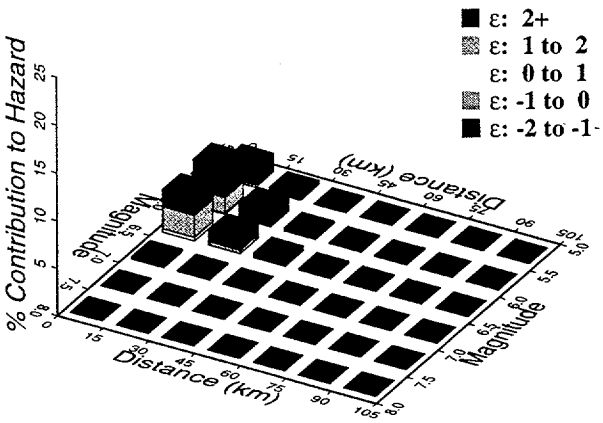

1 Hz, RYA Regional Faults

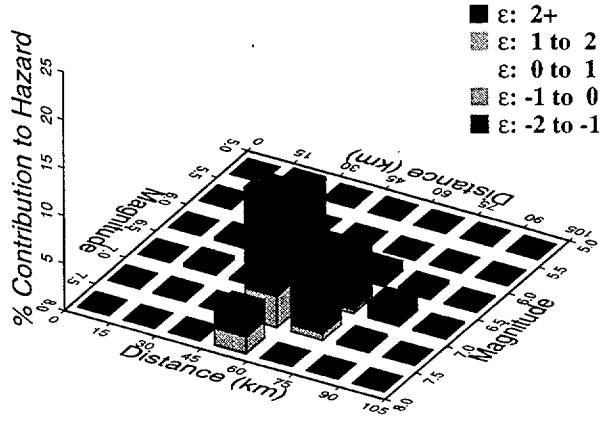

1 Hz, RYA Local Faults (Single)

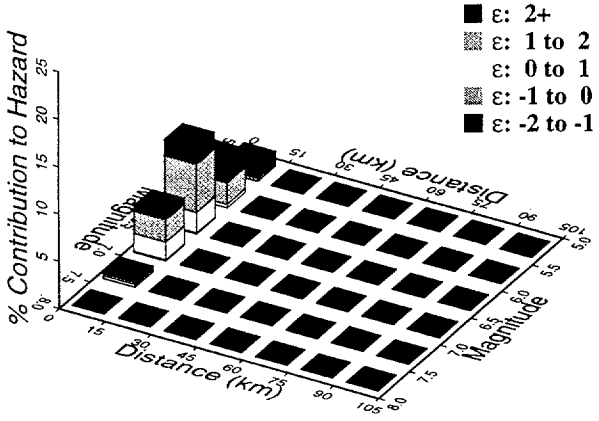

1 Hz, RYA Local Faults (Mult.)

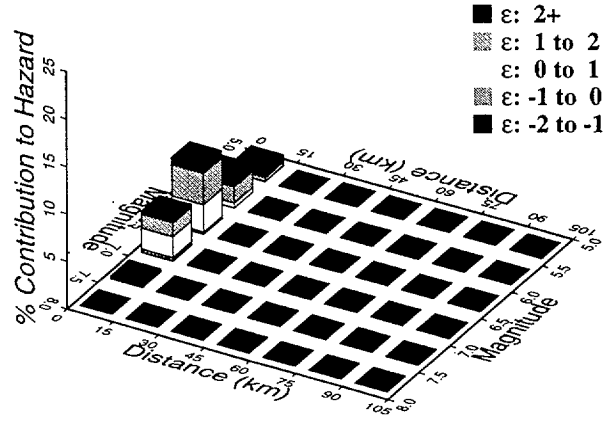

Figure 7-110 Magnitude-distance-epsilon distributions for the four source types: RYA team, 1-Hz horizontal spectral acceleration

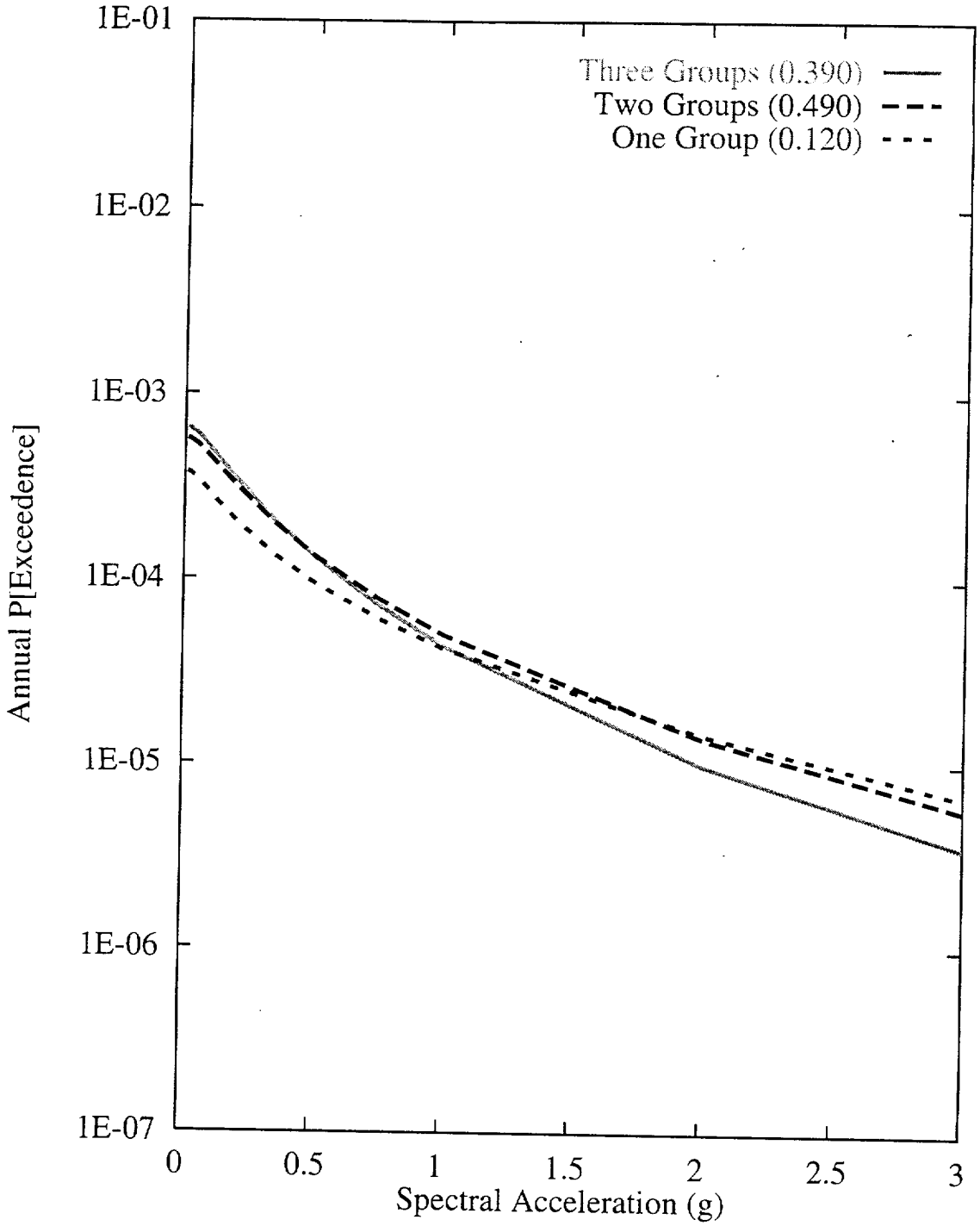

Figure 7-111 Sensitivity of seismic hazard from local faults to coalescence model: RYA team, 10-Hz horizontal spectral acceleration

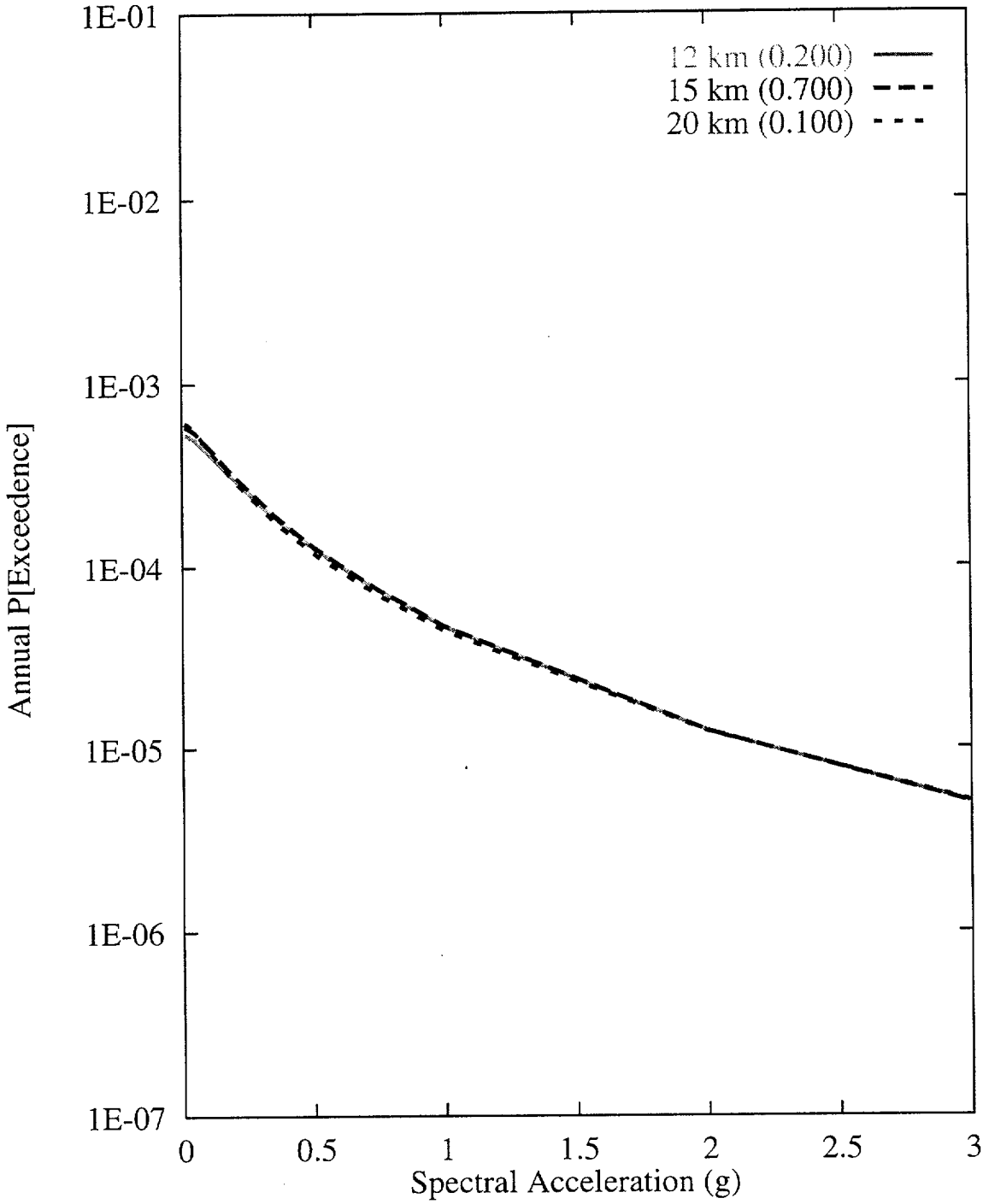

Figure 7-112 Sensitivity of seismic hazard from local faults to maximum fault depth: RYA team, 10-Hz horizontal spectral acceleration

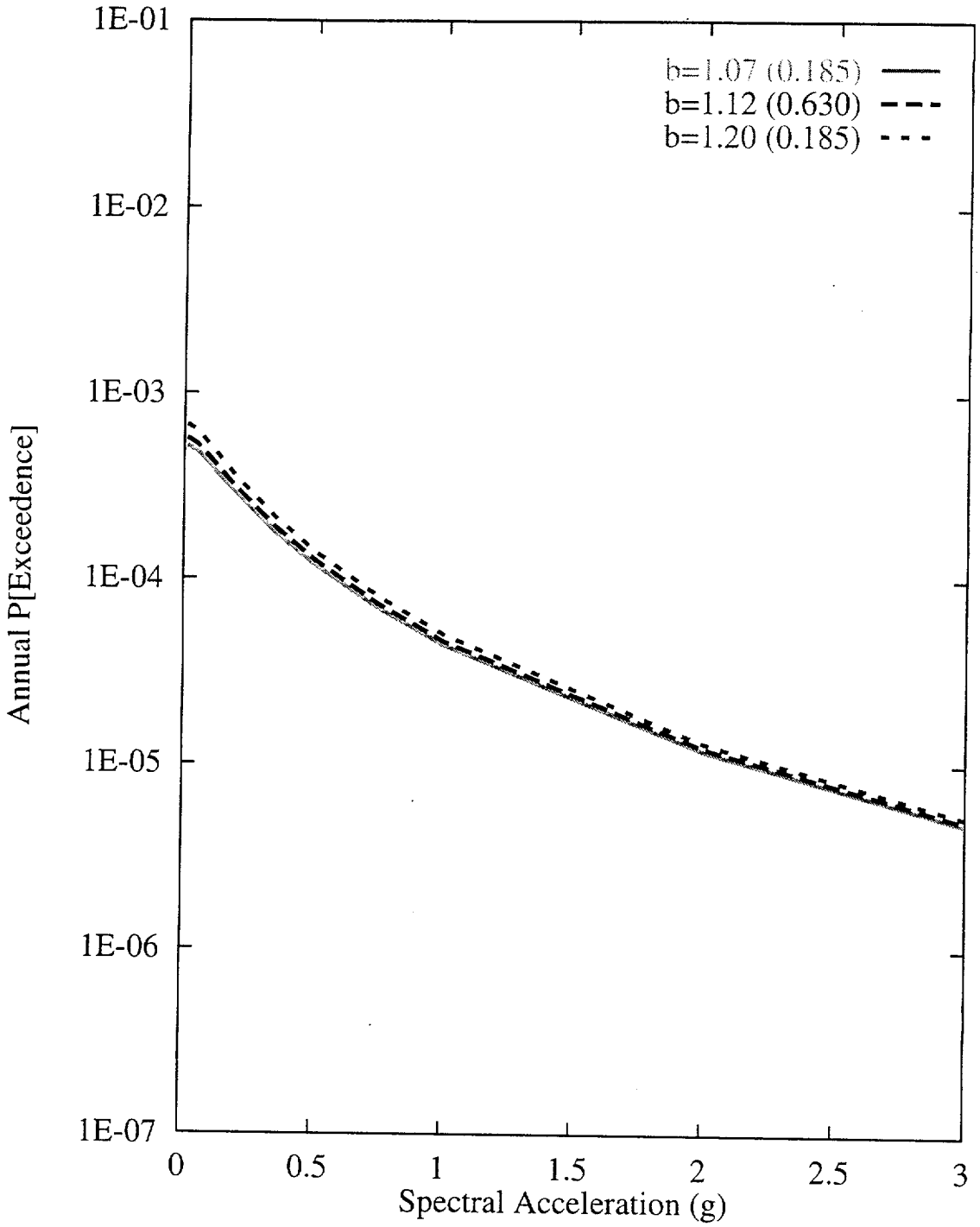

Figure 7-113 Sensitivity of seismic hazard from local faults to b-value: RYA team, 10-Hz horizontal spectral acceleration

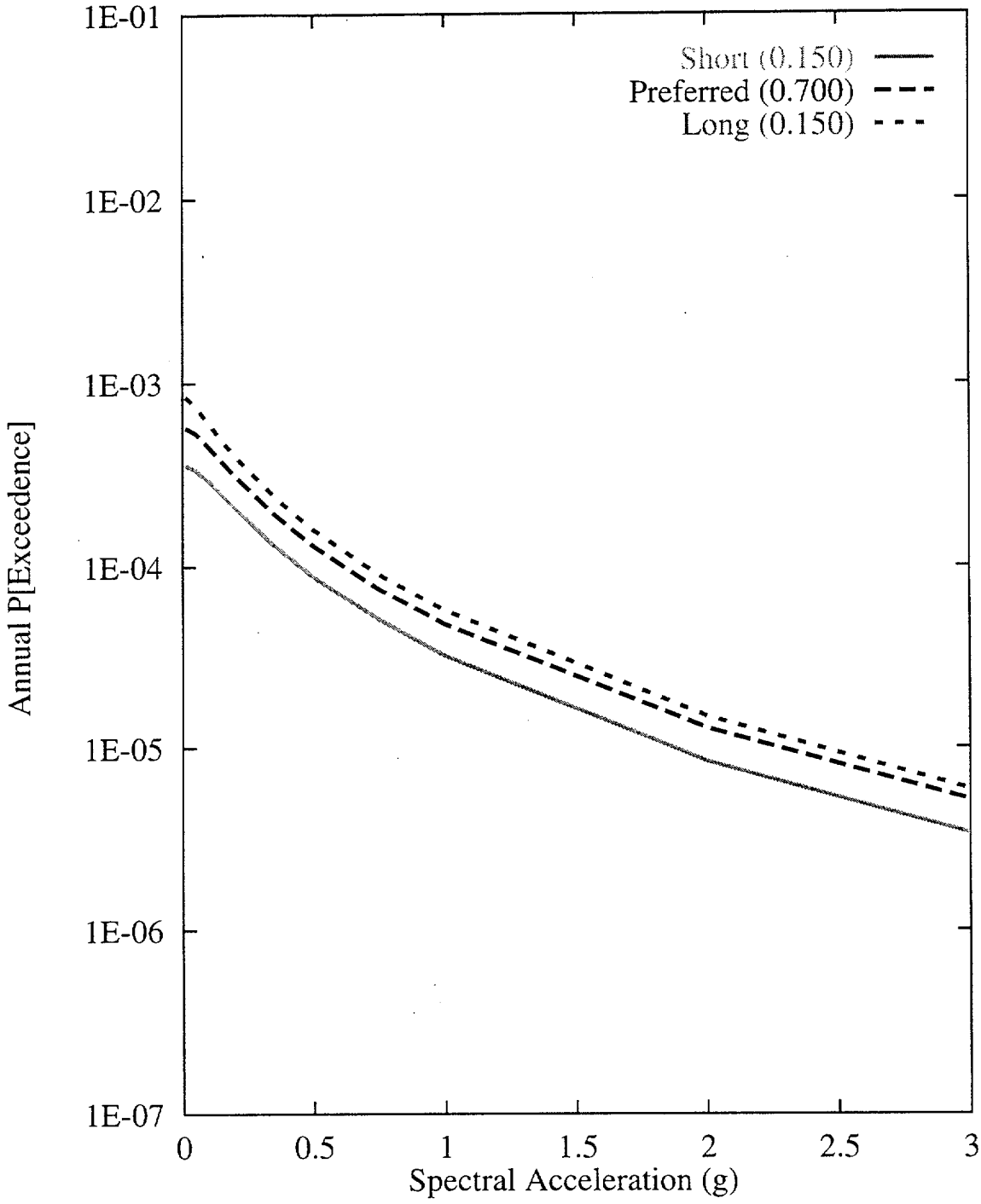

Figure 7-114 Sensitivity of seismic hazard from local faults to fault lengths: RYA team, 10-Hz horizontal spectral acceleration

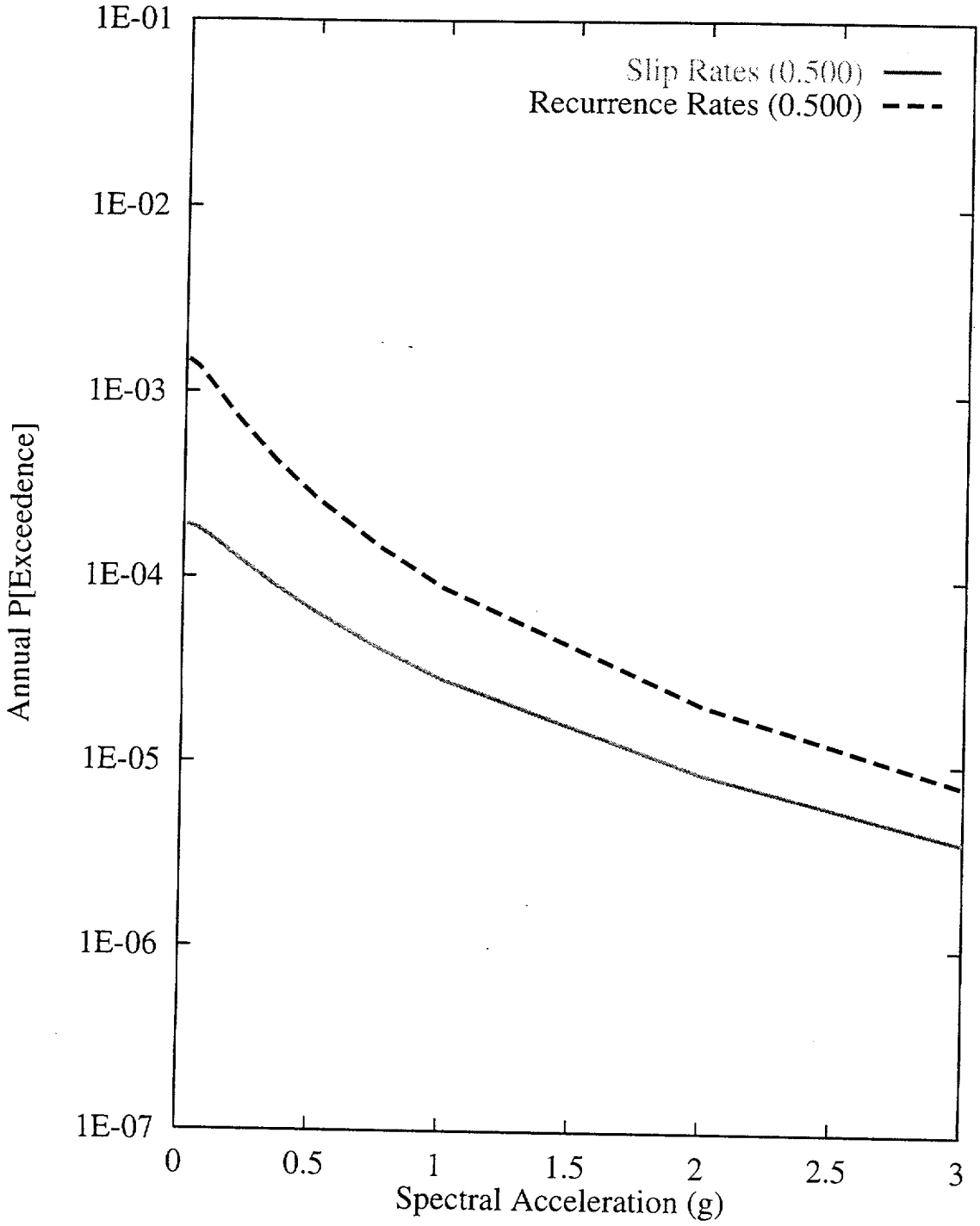

Figure 7-115 Sensitivity of seismic hazard from local faults to recurrence approach used: RYA team, 10-Hz horizontal spectral acceleration

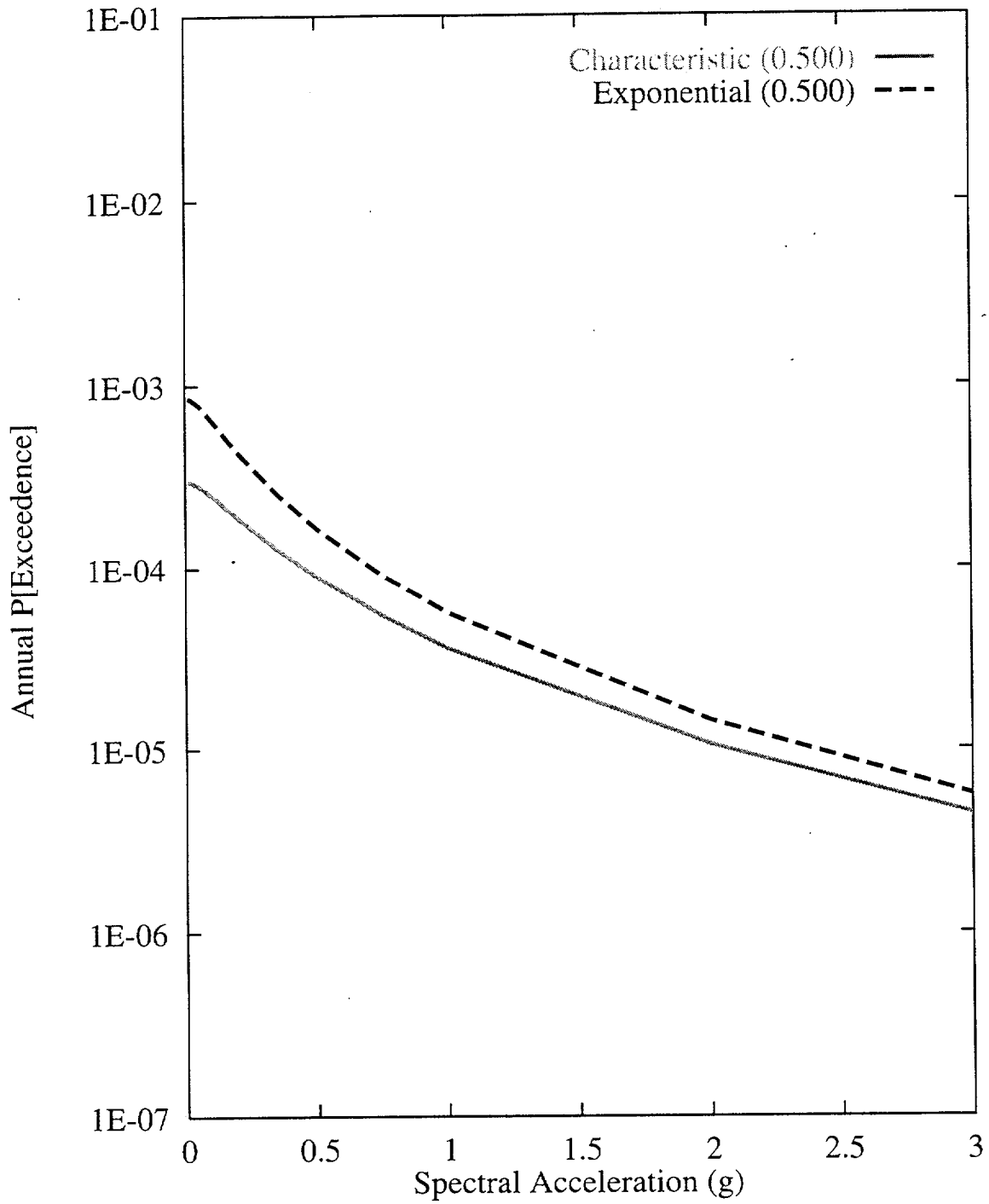

Figure 7-116 Sensitivity of seismic hazard from local faults to recurrence model for the Paintbrush Canyon-Stagecoach Road-Bow Ridge fault system: RYA team, 10-Hz horizontal spectral acceleration

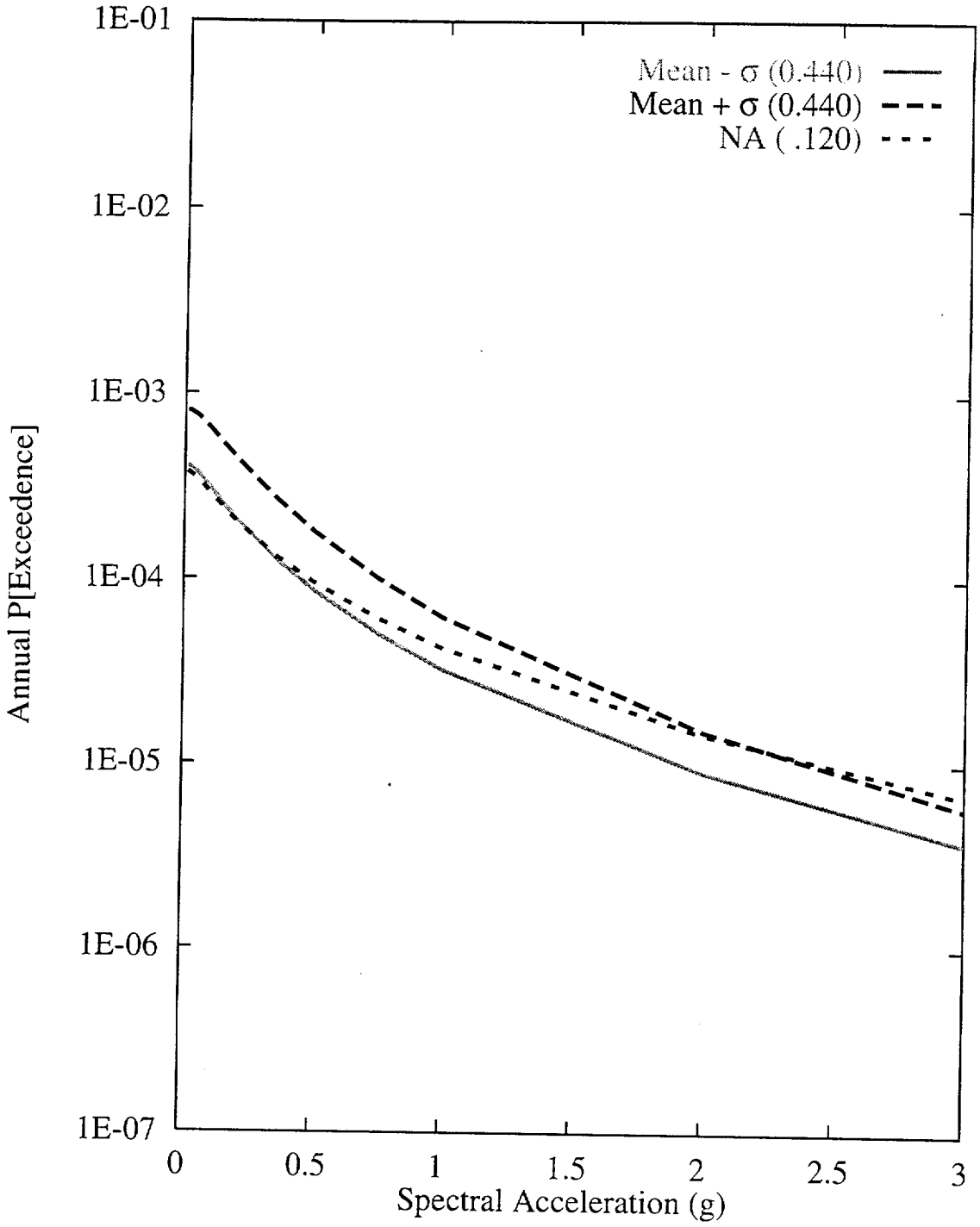

Figure 7-117 Sensitivity of seismic hazard from local faults to M_{max} on the Paintbrush Canyon-Stagecoach Road-Bow Ridge fault system: RYA team, 10-Hz horizontal spectral acceleration

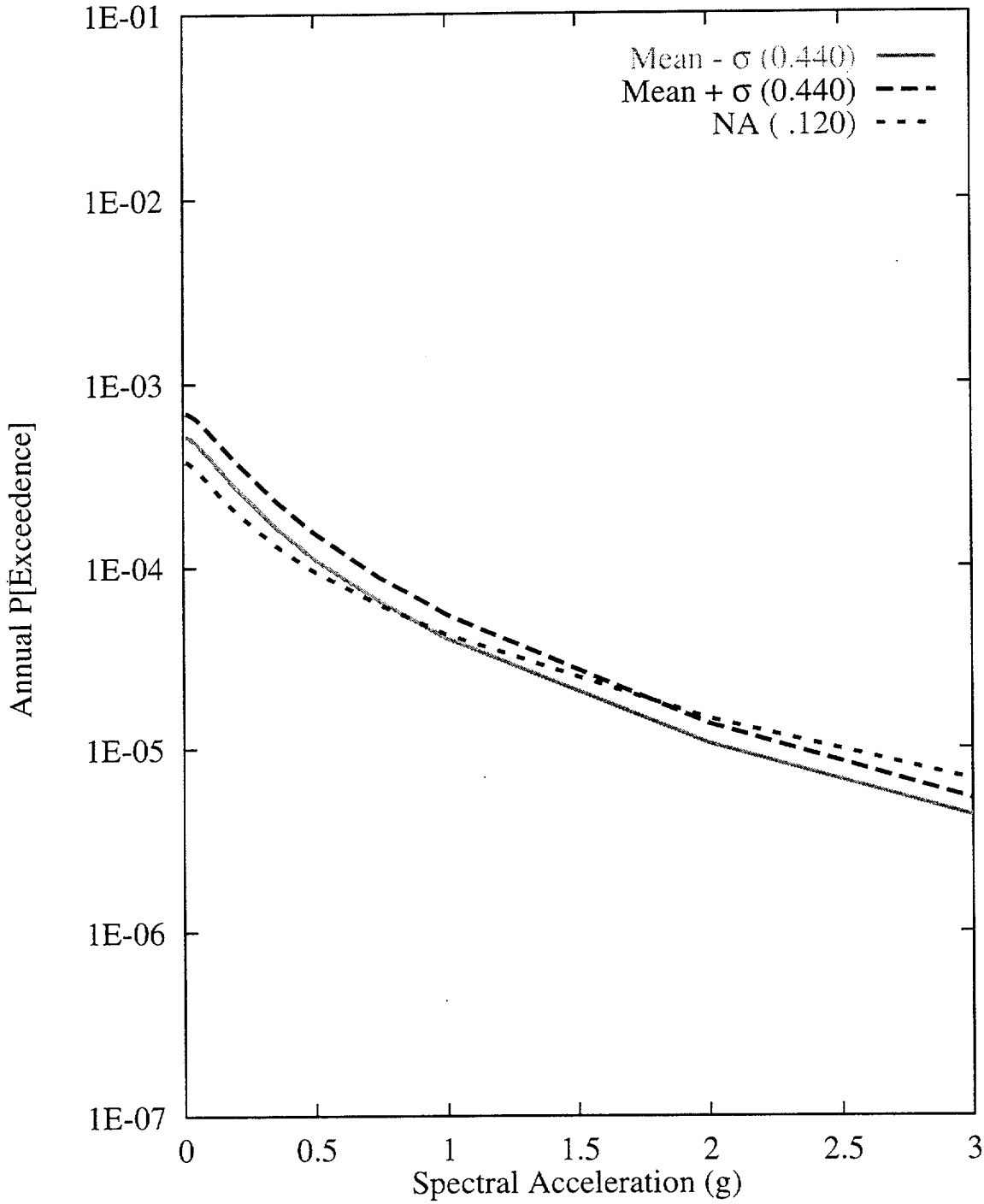

Figure 7-118 Sensitivity of seismic hazard from local faults to recurrence of the Paintbrush Canyon-Stagecoach Road-Bow Ridge fault system: RYA team, 10-Hz horizontal spectral acceleration

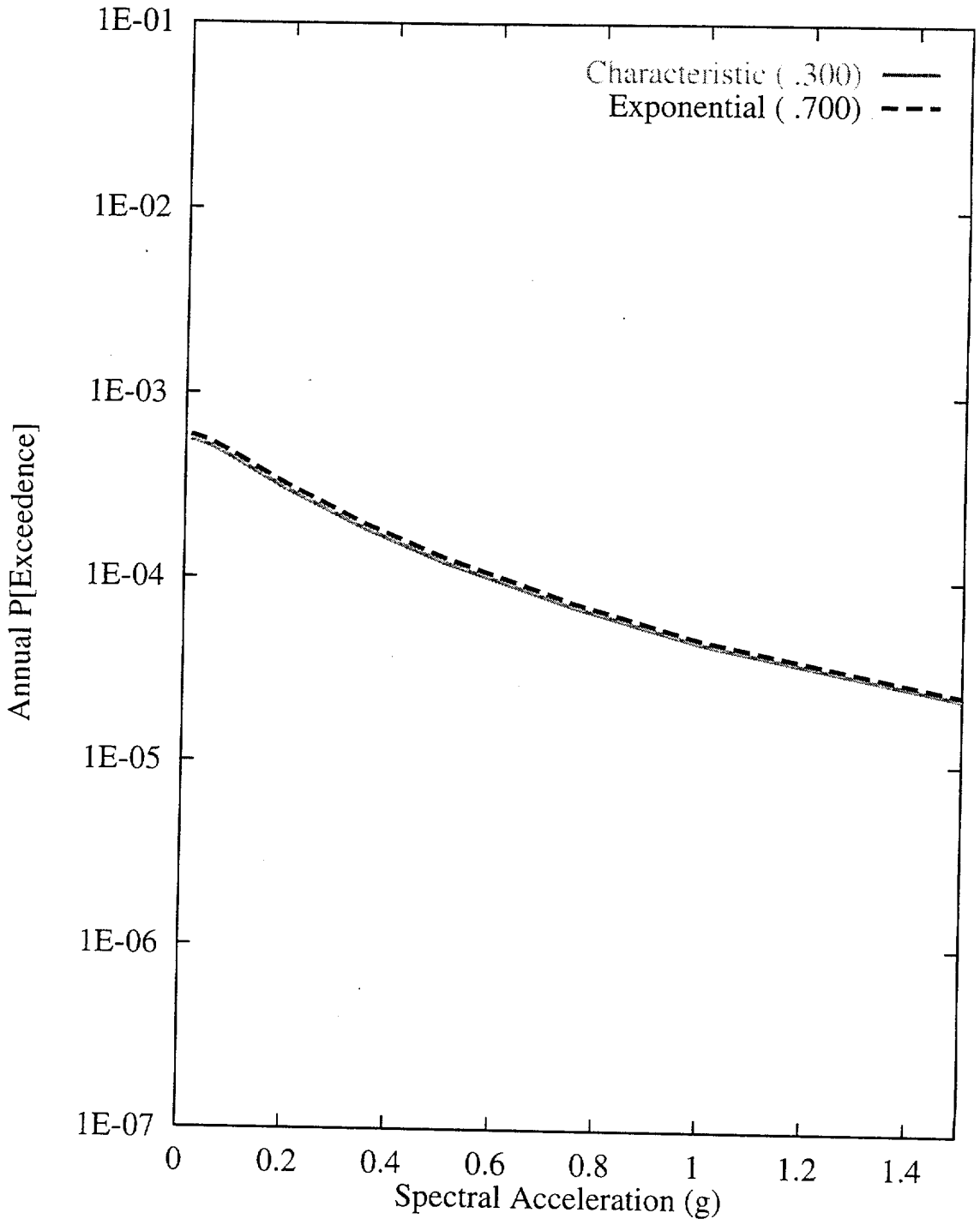

Figure 7-119 Sensitivity of seismic hazard from local faults to recurrence model for the West-side fault system: RYA team, 10-Hz horizontal spectral acceleration

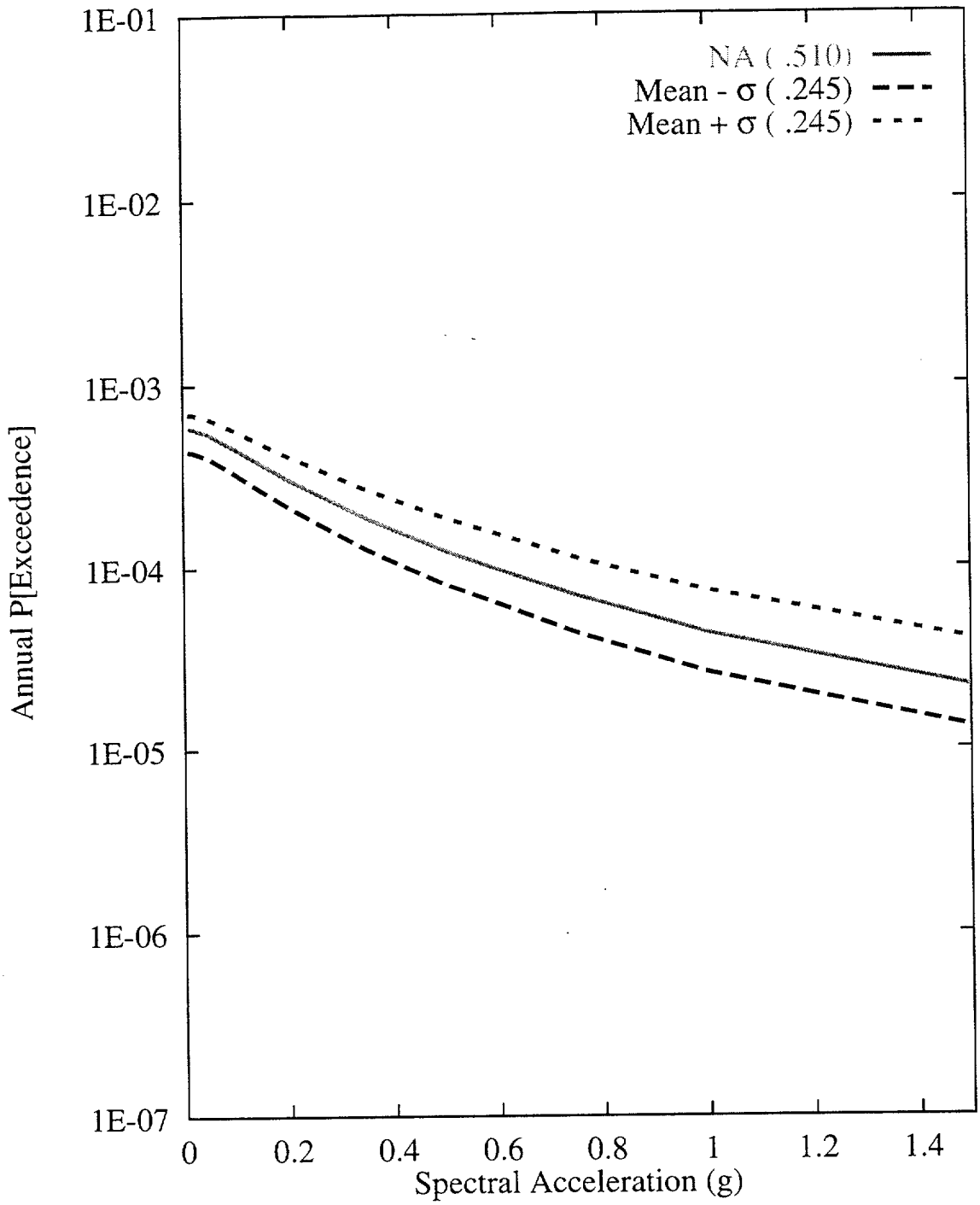

Figure 7-120 Sensitivity of seismic hazard from local faults to Mmax on the West-side fault system: RYA team, 10-Hz horizontal spectral acceleration

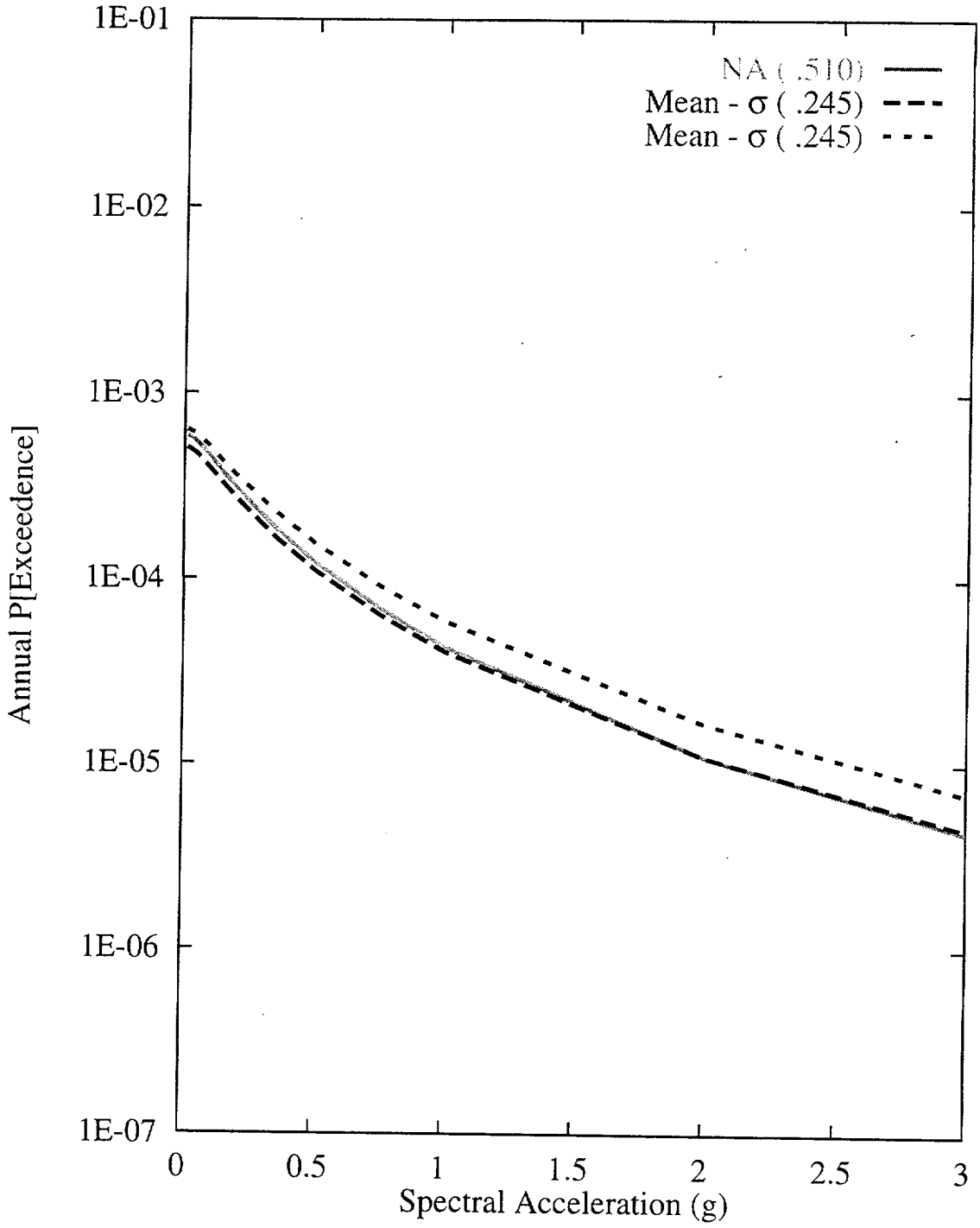

Figure 7-121 Sensitivity of seismic hazard from local faults to recurrence of the West-side fault system: RYA team, 10-Hz horizontal spectral acceleration

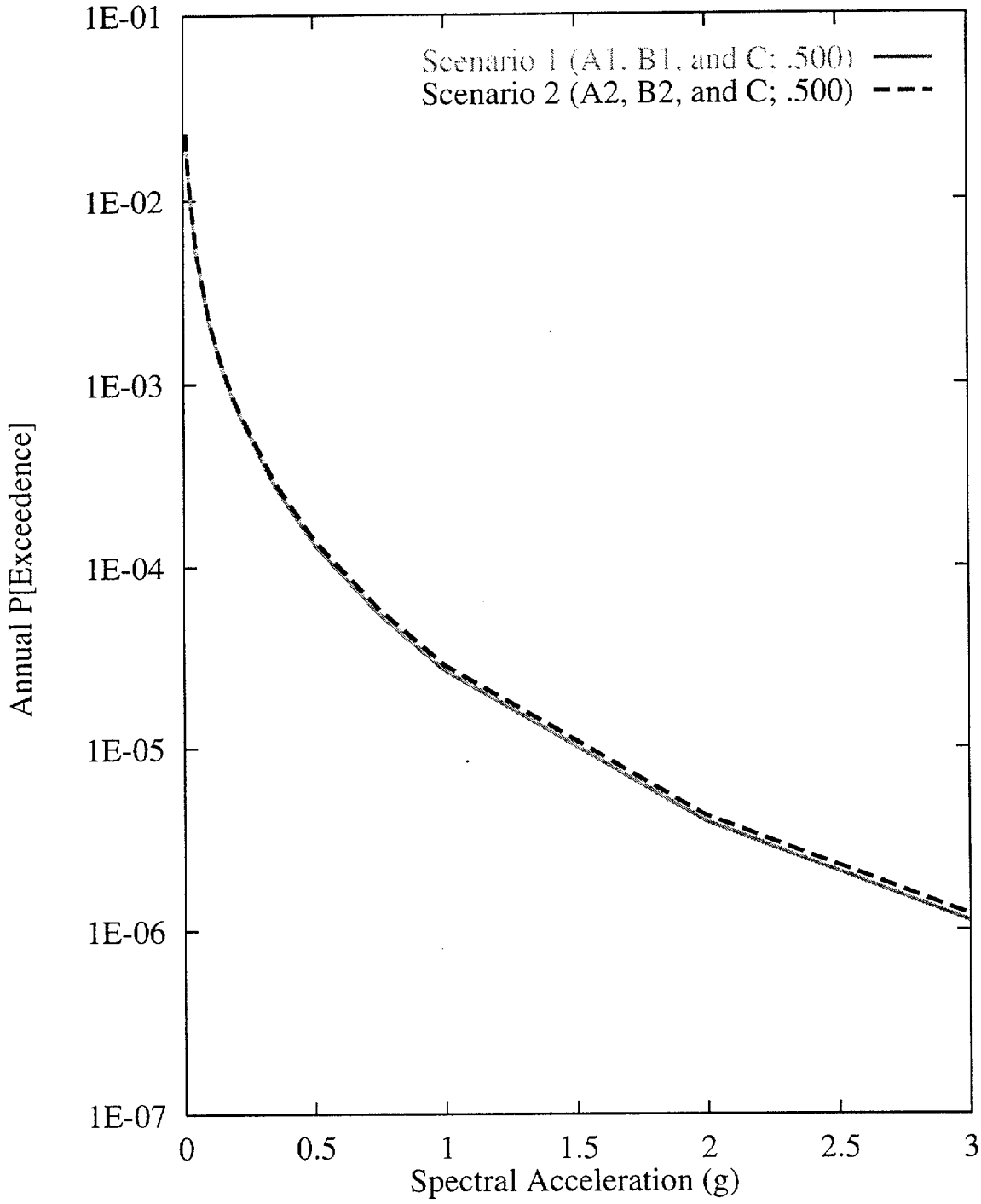

Figure 7-122 Sensitivity of seismic hazard from area zones to alternative zonation scenarios: RYA team, 10-Hz horizontal spectral acceleration

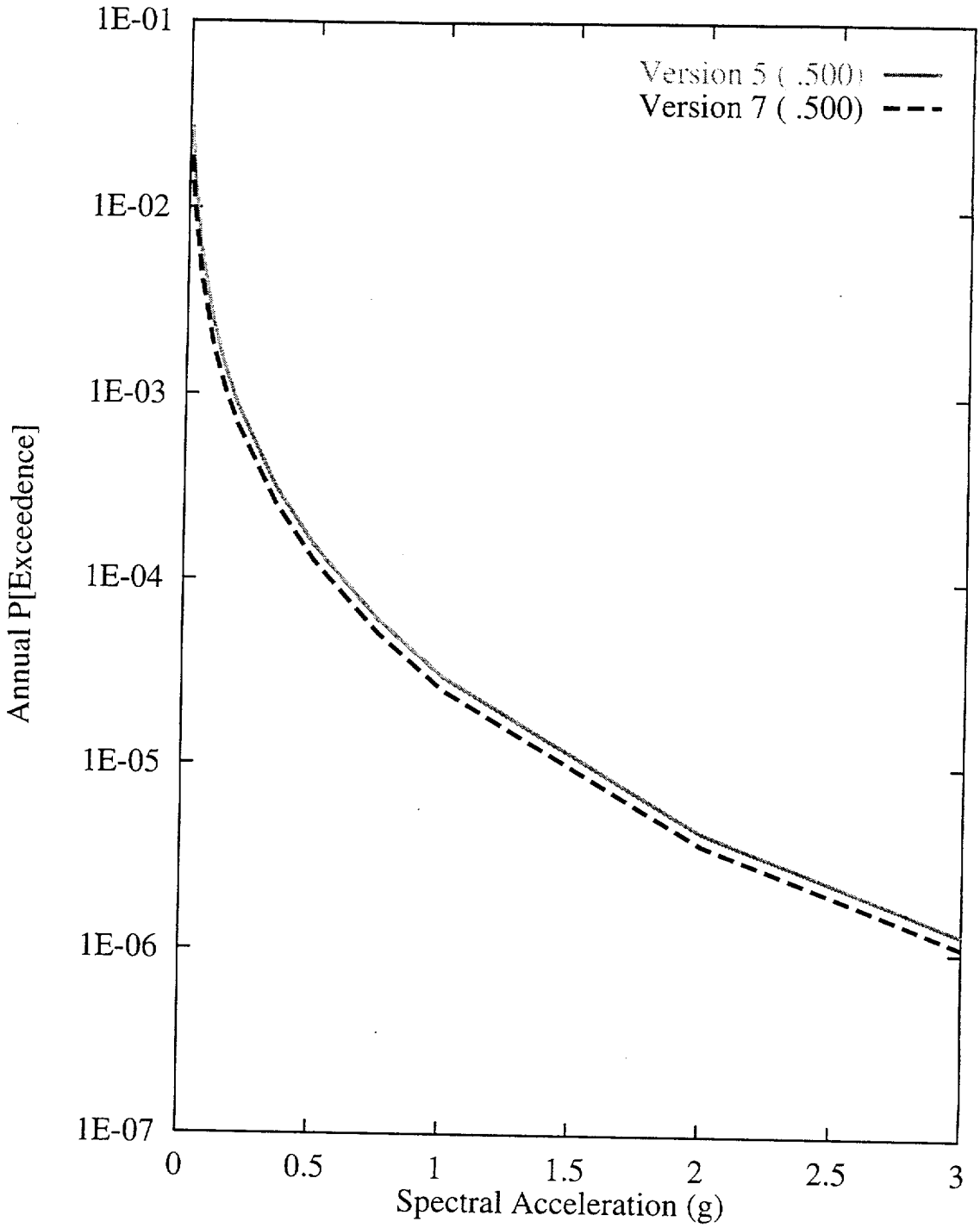

Figure 7-123 Sensitivity of seismic hazard from area zones to choice of seismicity catalog: RYA team, 10-Hz horizontal spectral acceleration

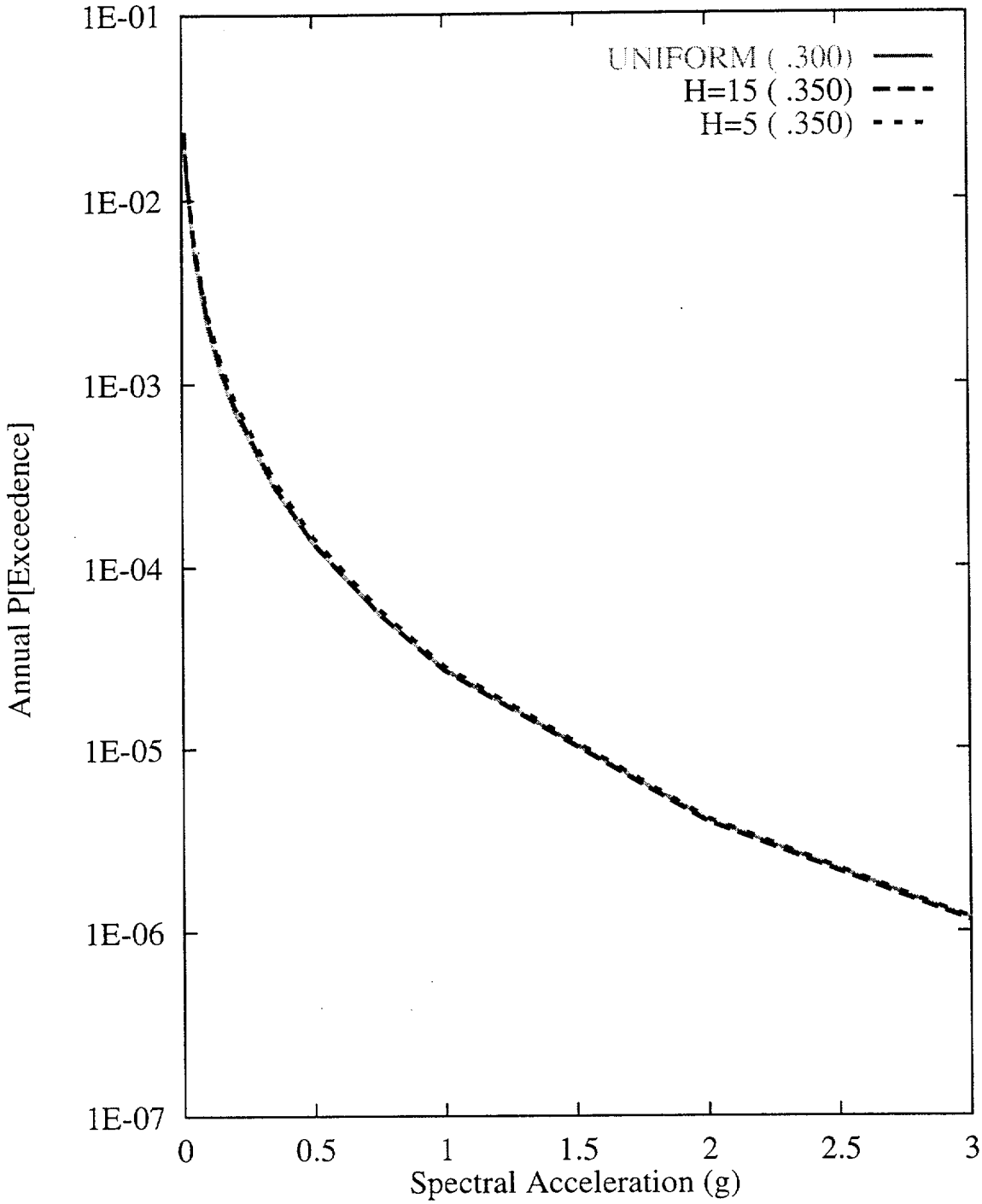

Figure 7-124 Sensitivity of seismic hazard from area zones to spatial variability and smoothing (H): RYA team, 10-Hz horizontal spectral acceleration

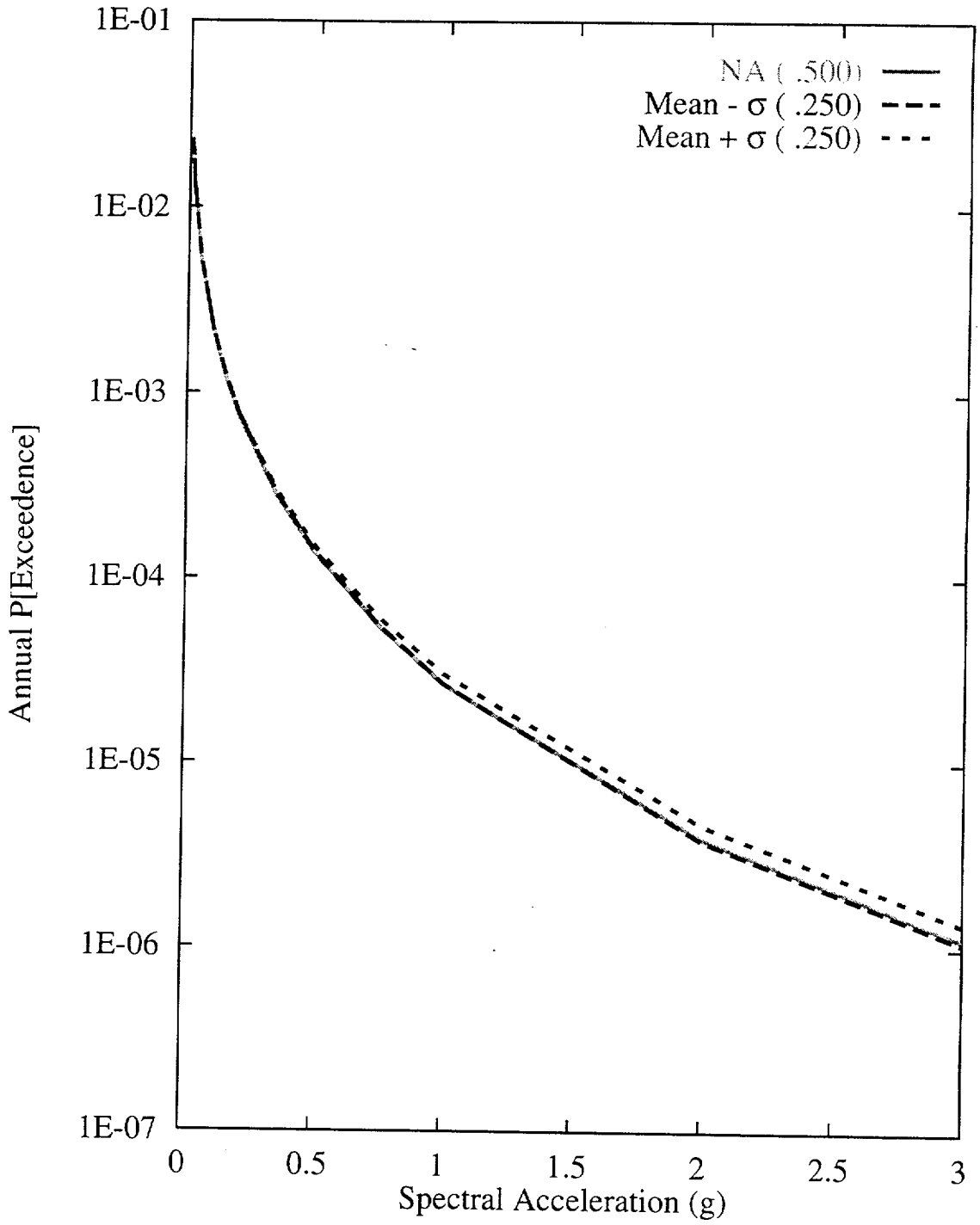

Figure 7-125 Sensitivity of seismic hazard from area zones to M_{max} on source zone A2: RYA team, 10-Hz horizontal spectral acceleration

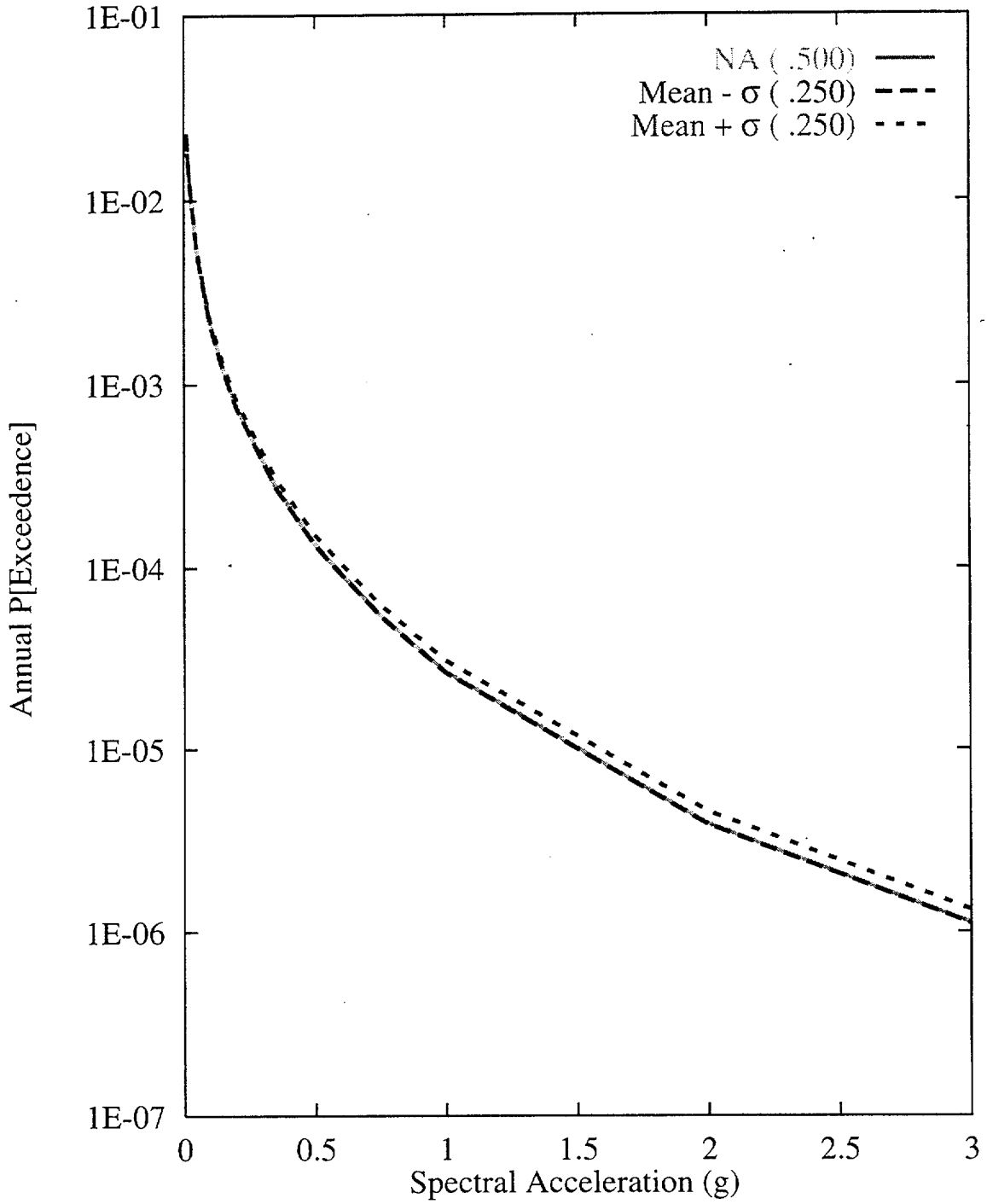

Figure 7-126 Sensitivity of seismic hazard from area zones to recurrence of source zone A2: RYA team, 10-Hz horizontal spectral acceleration

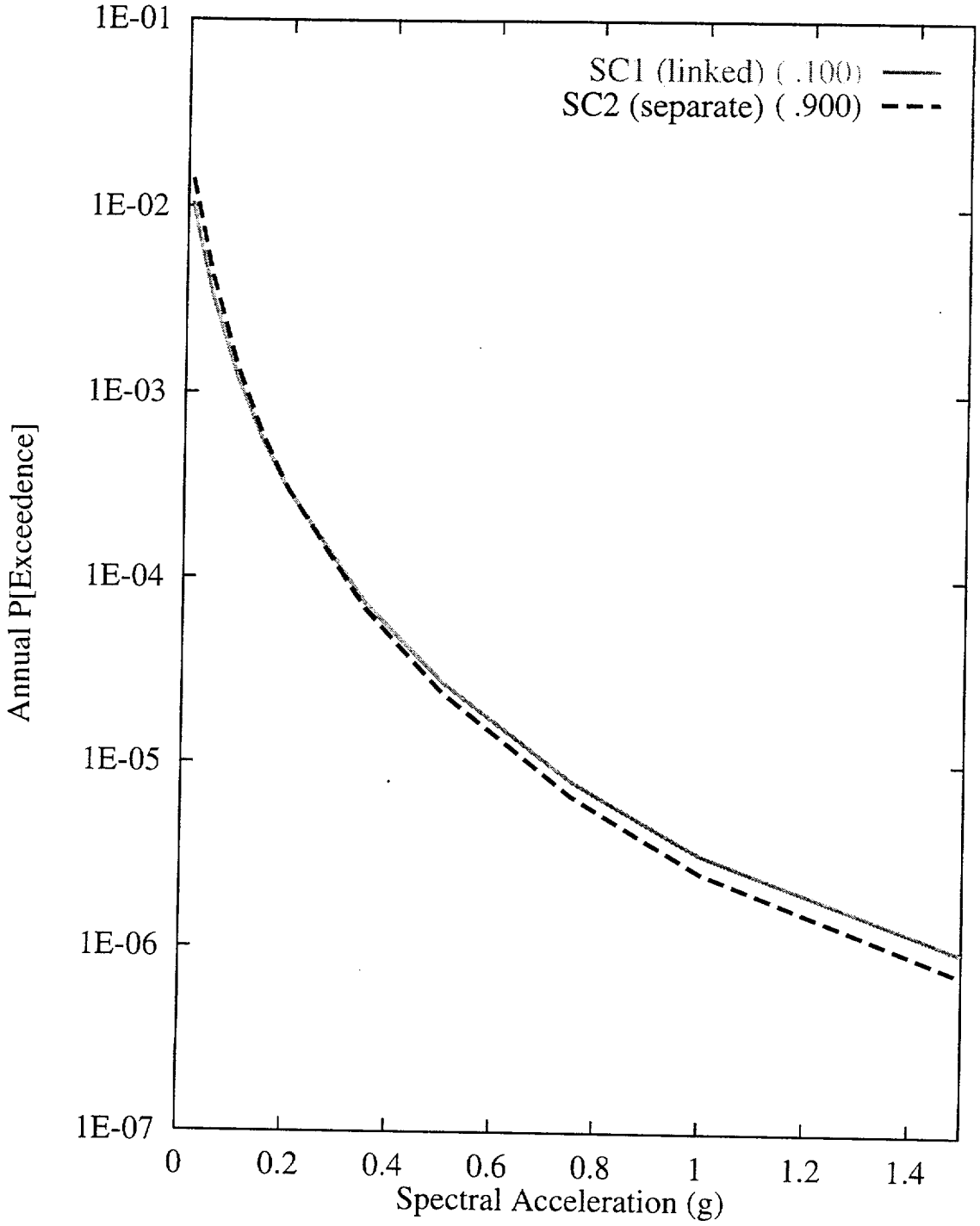

Figure 7-127 Sensitivity of seismic hazard from regional faults to Death Valley-Furnace Creek fault system behavior scenarios: RYA team, 1-Hz horizontal spectral acceleration

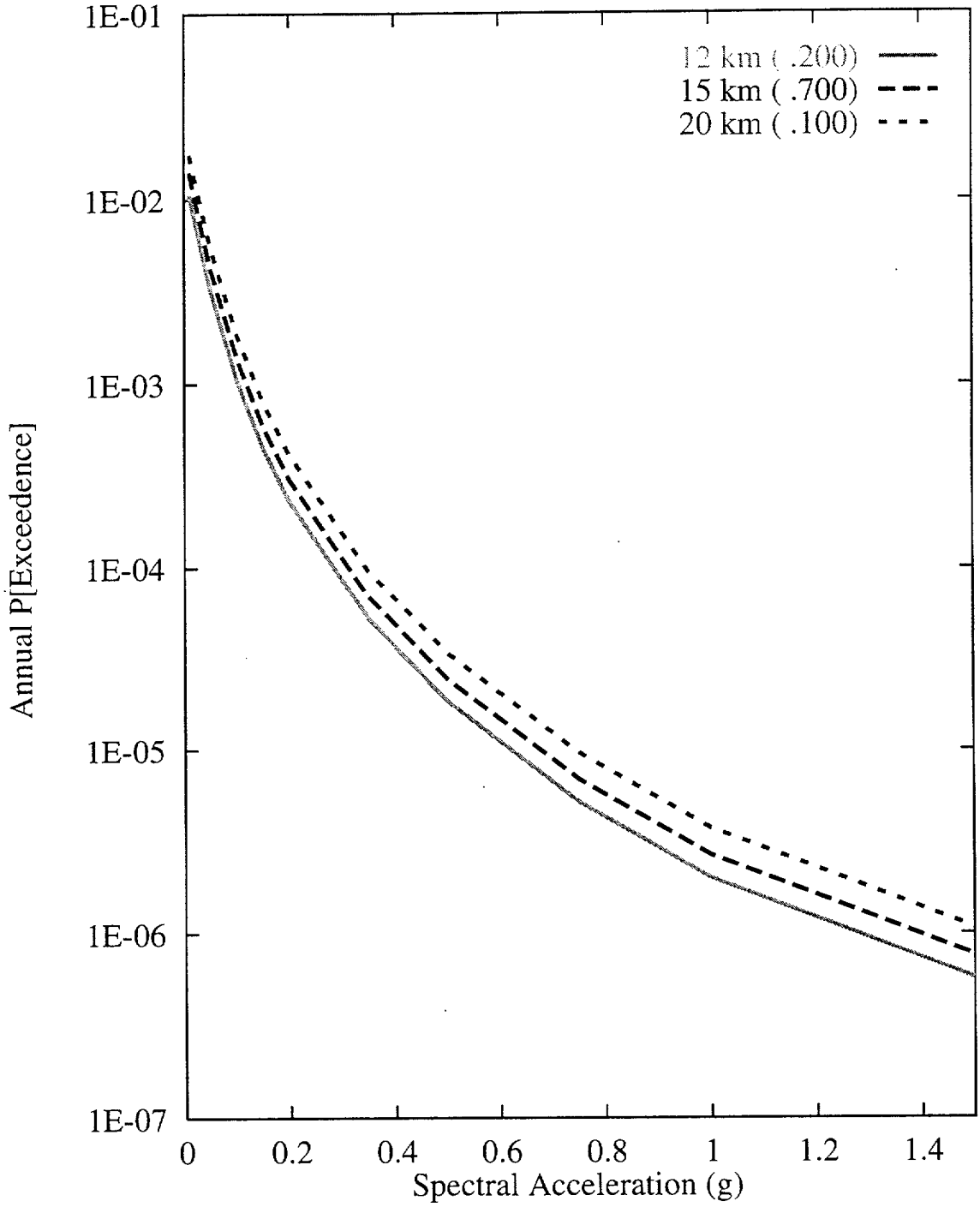

Figure 7-128 Sensitivity of seismic hazard from regional faults to maximum fault depth: RYA team, 1-Hz horizontal spectral acceleration

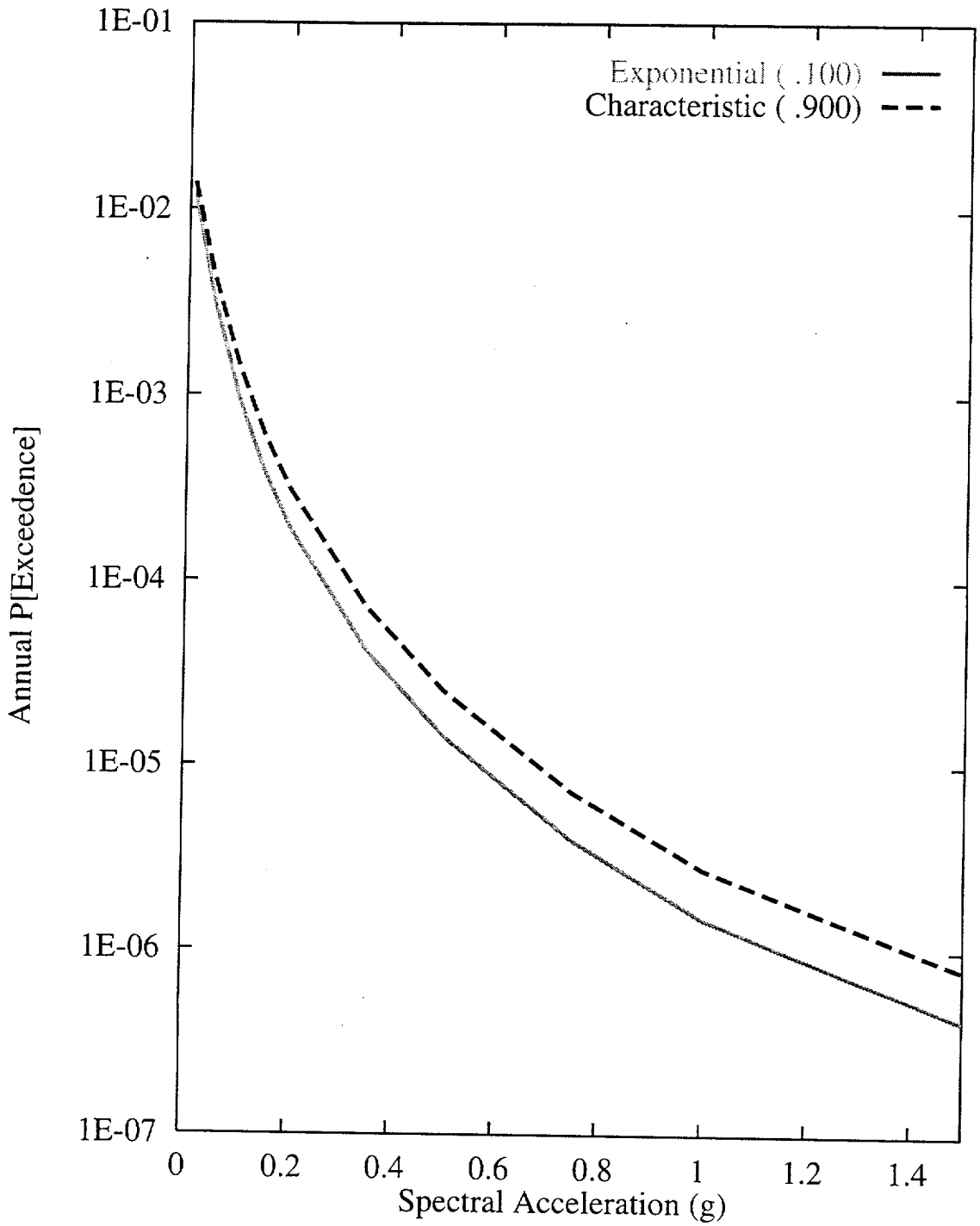

Figure 7-129 Sensitivity of seismic hazard from regional faults to recurrence model: RYA team, 1-Hz horizontal spectral acceleration

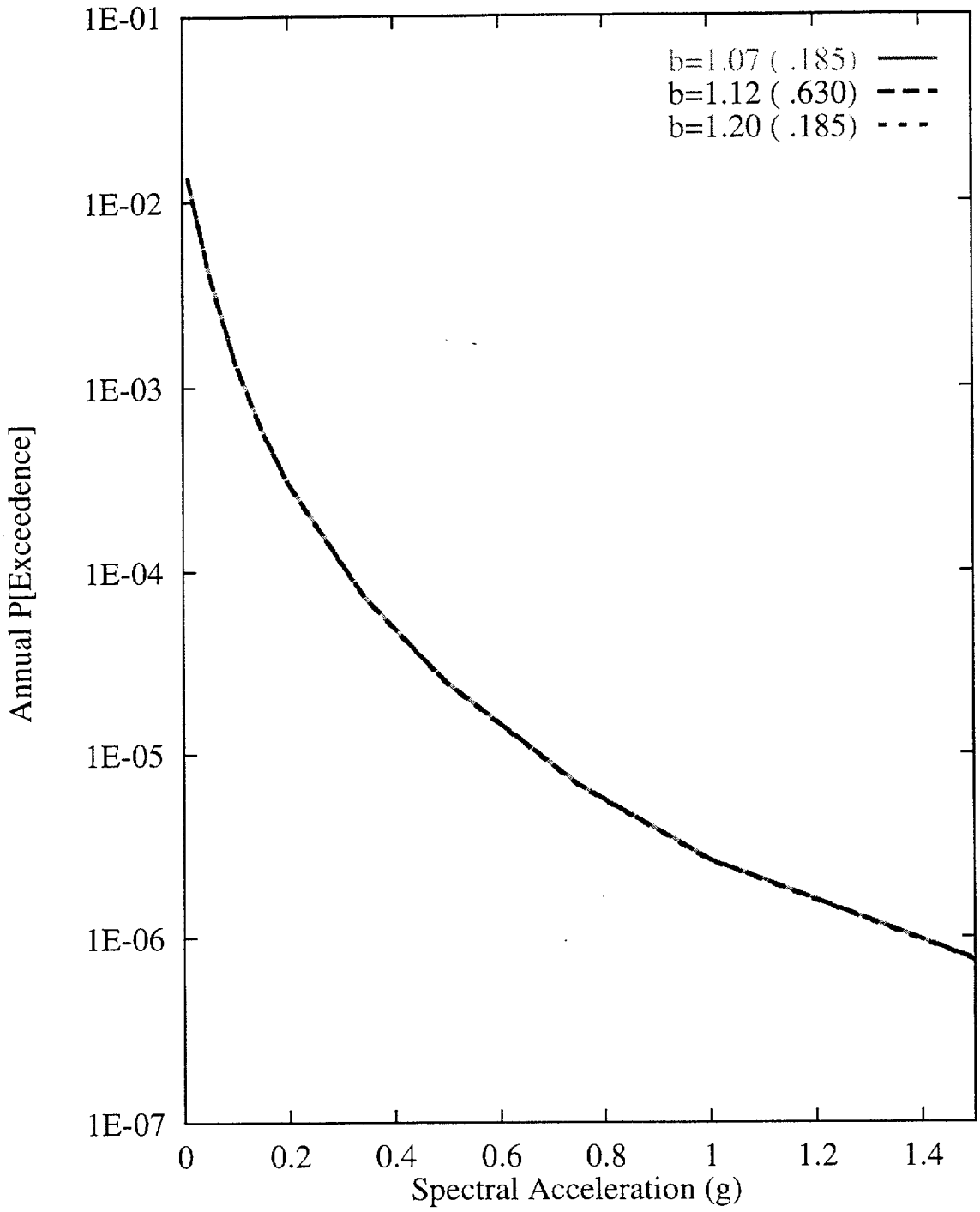

Figure 7-130 Sensitivity of seismic hazard from regional faults to b-value: RYA team, 1-Hz horizontal spectral acceleration

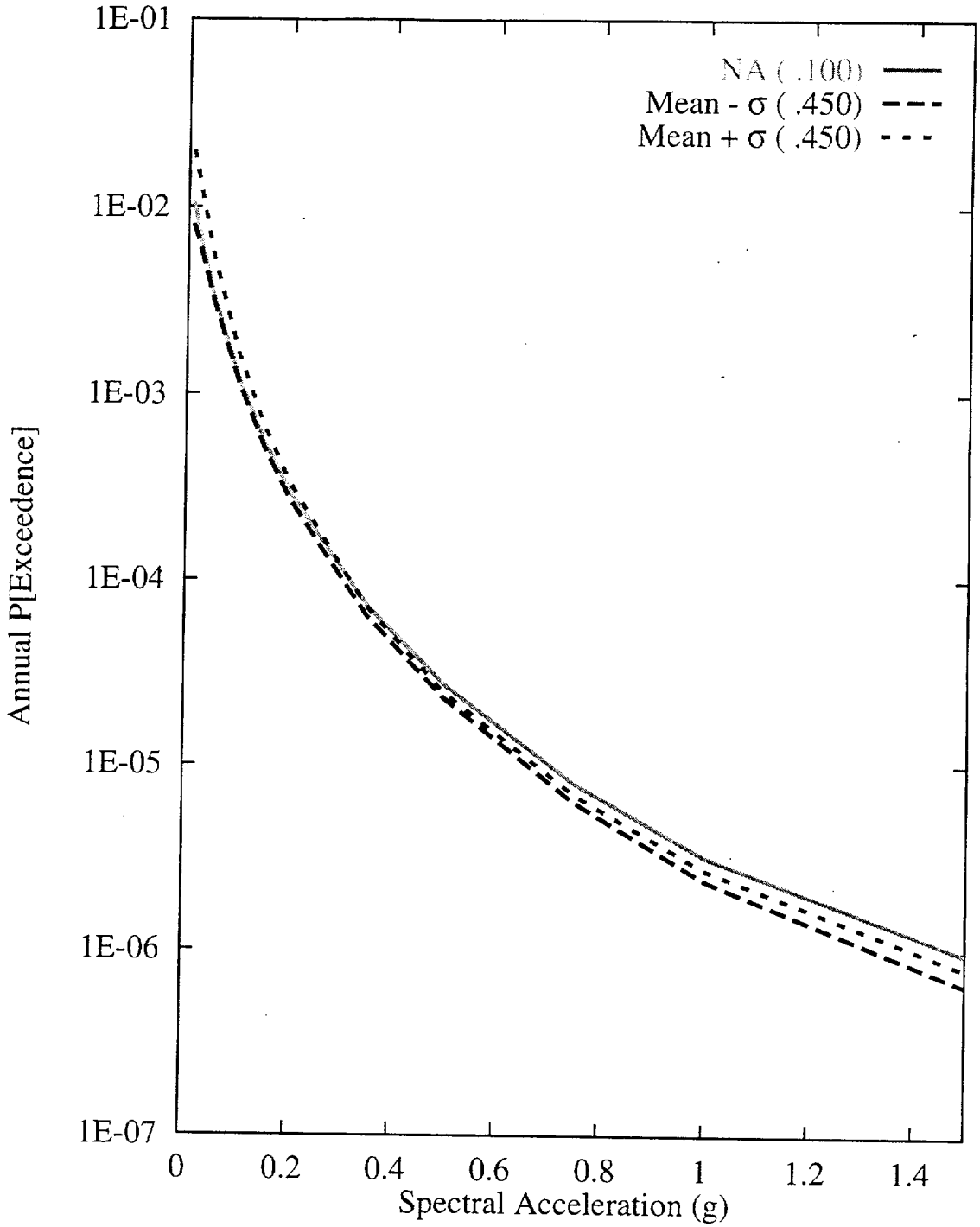

Figure 7-131 Sensitivity of seismic hazard from regional faults to Mmax on the Furnace Creek fault: RYA team, 1-Hz horizontal spectral acceleration

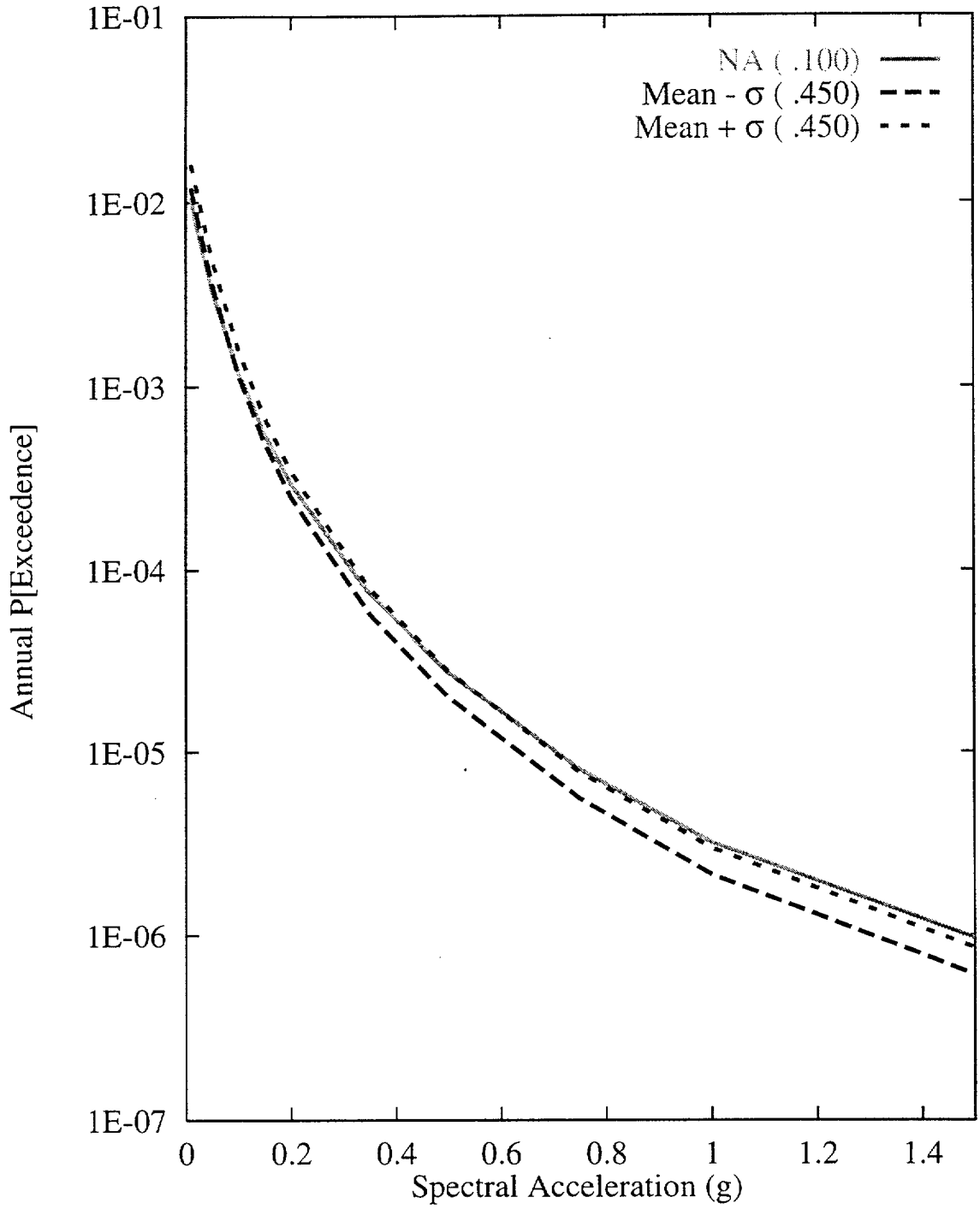

Figure 7-132 Sensitivity of seismic hazard from regional faults to recurrence of Furnace Creek fault: RYA team, 1-Hz horizontal spectral acceleration

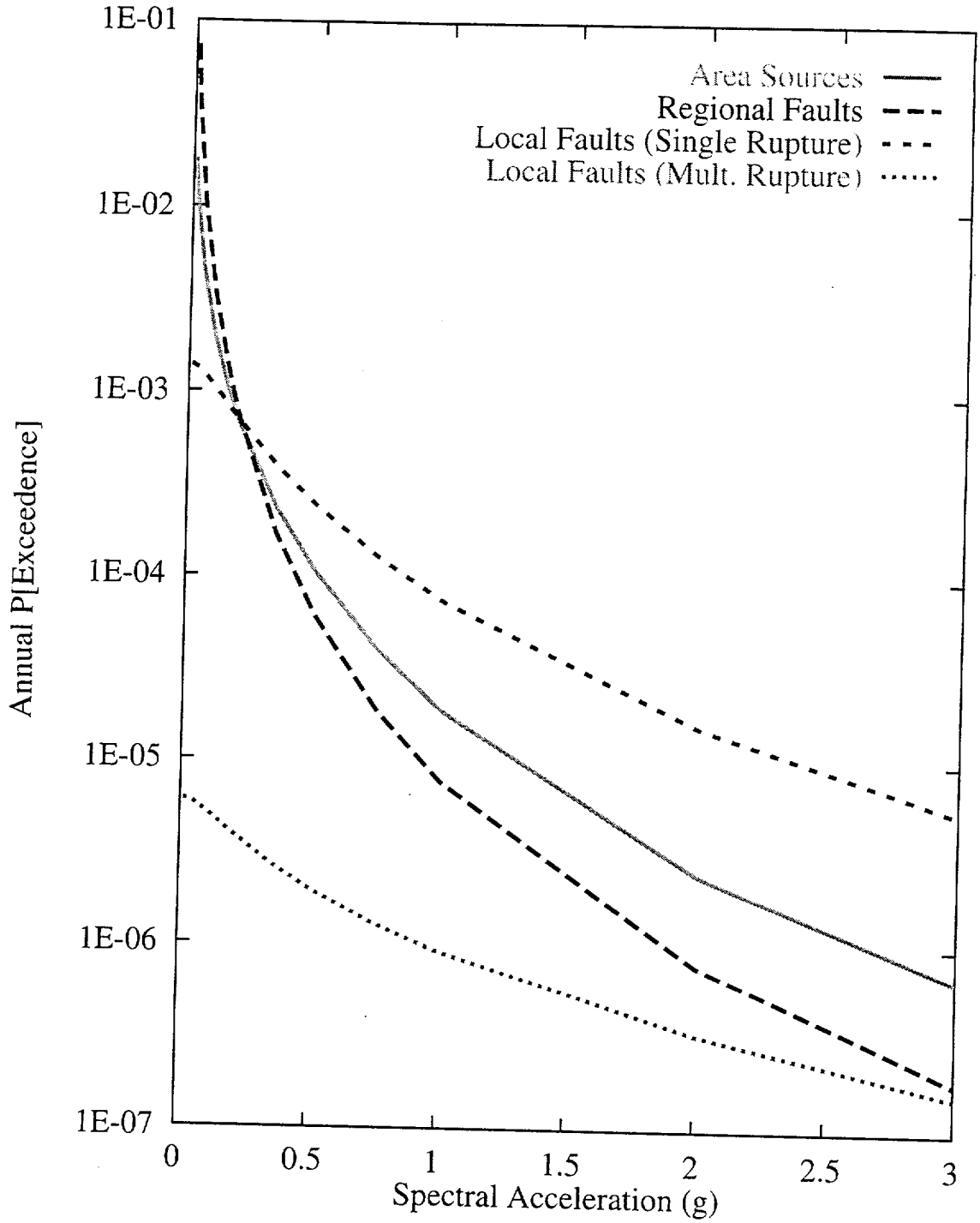

Figure 7-133 Contributions of source types to the mean hazard: SBK team, 10-Hz horizontal spectral acceleration

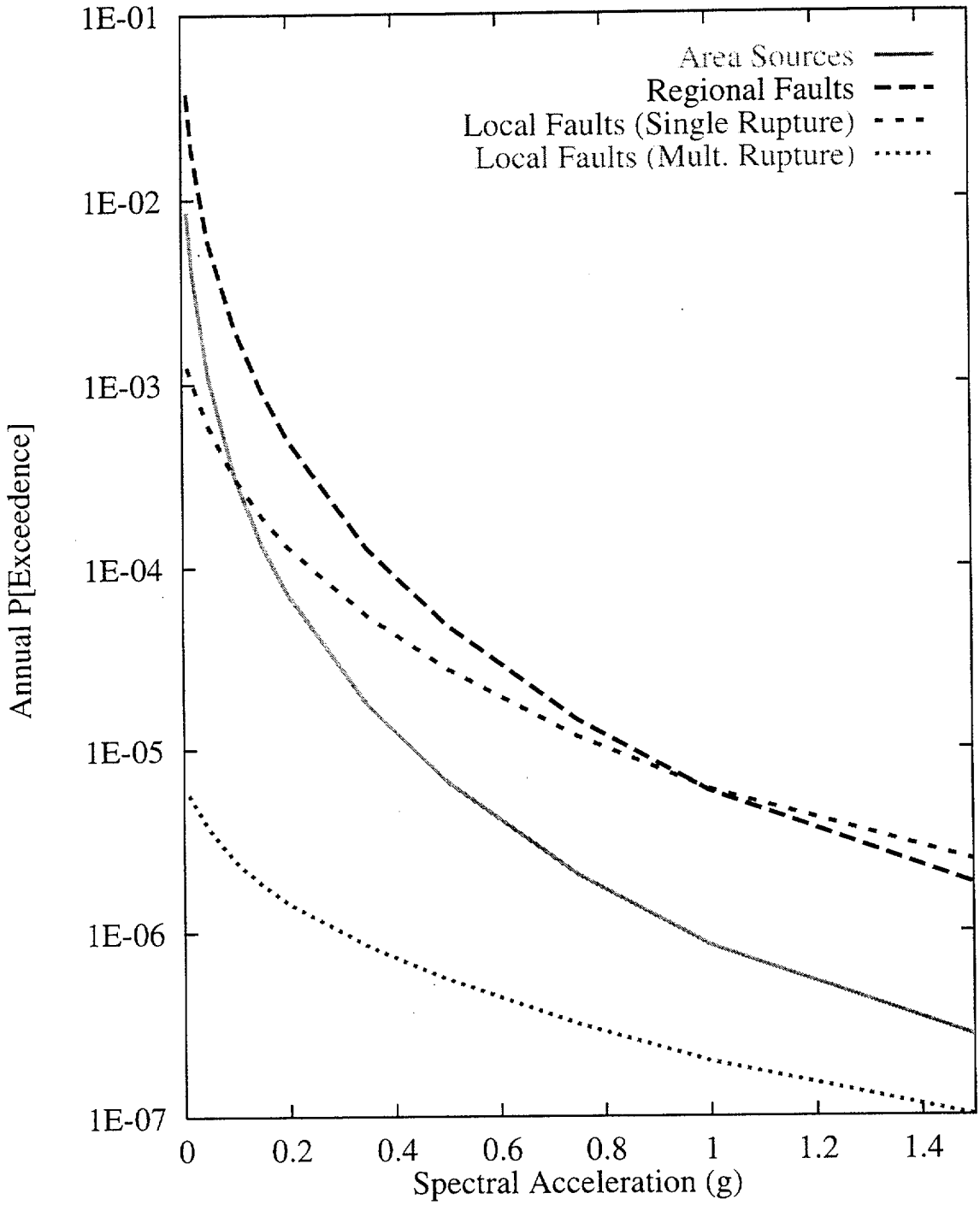

Figure 7-134 Contributions of source types to the mean hazard: SBK team, 1-Hz horizontal spectral acceleration

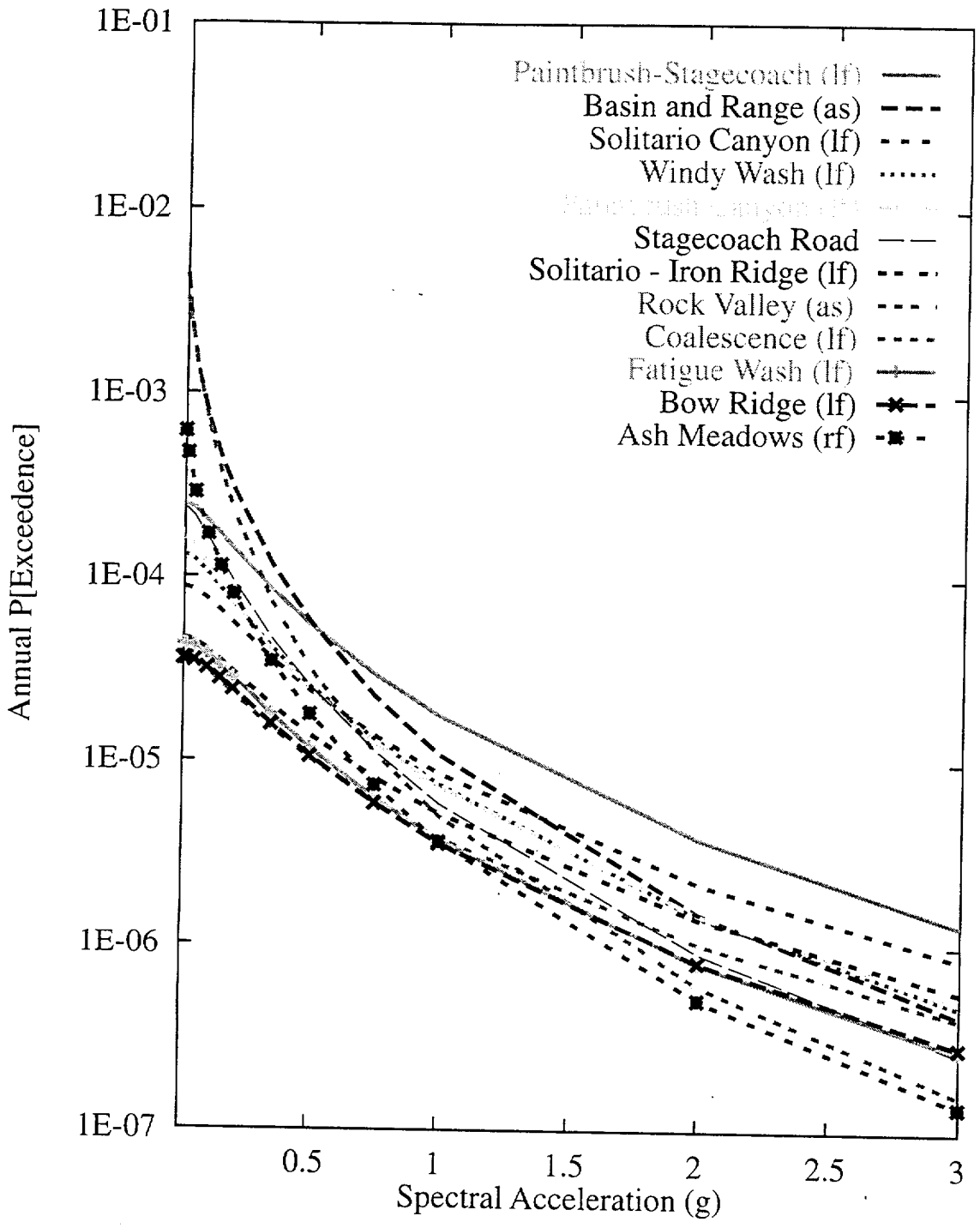

Figure 7-135 Mean seismic hazard from dominant seismic sources: SBK team, 10-Hz horizontal spectral acceleration

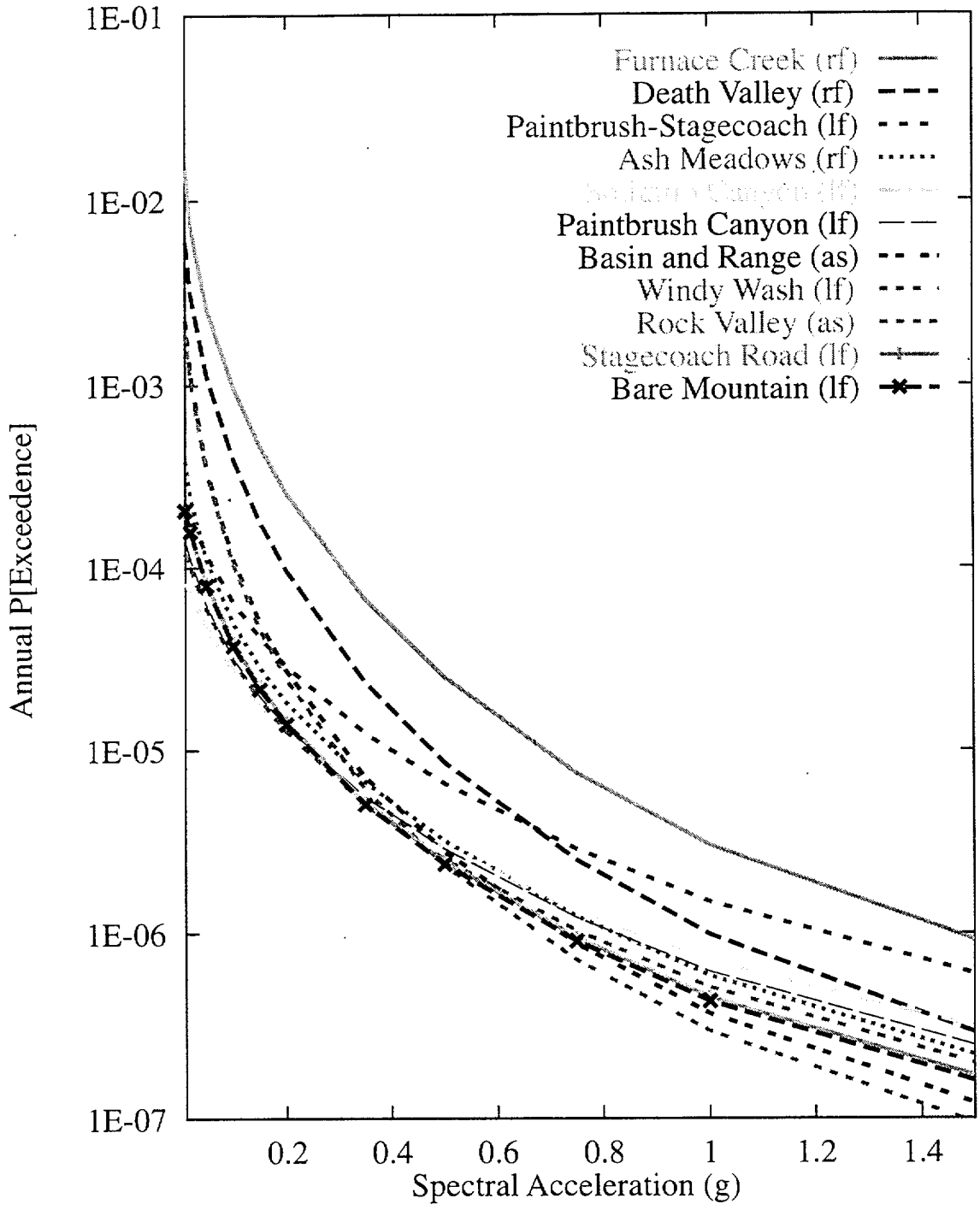

Figure 7-136 Mean seismic hazard from dominant seismic sources: SBK team, 1-Hz horizontal spectral acceleration

10 Hz, SBK Area Sources

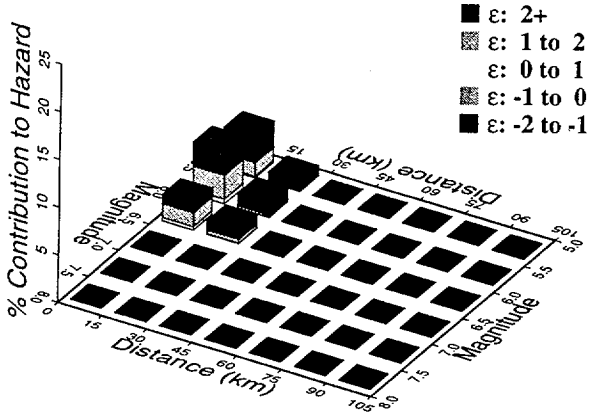

10 Hz, SBK Regional Faults

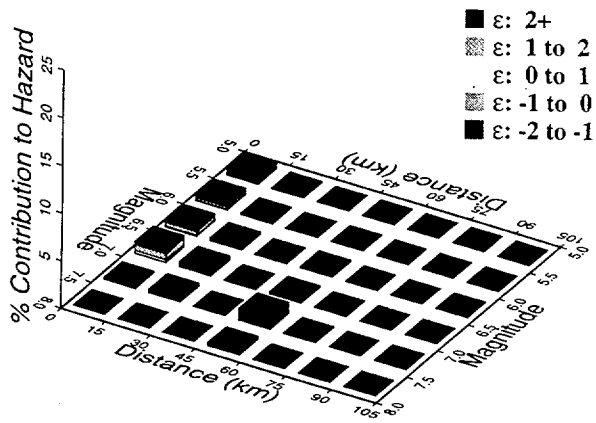

10 Hz, SBK Local Faults (Single)

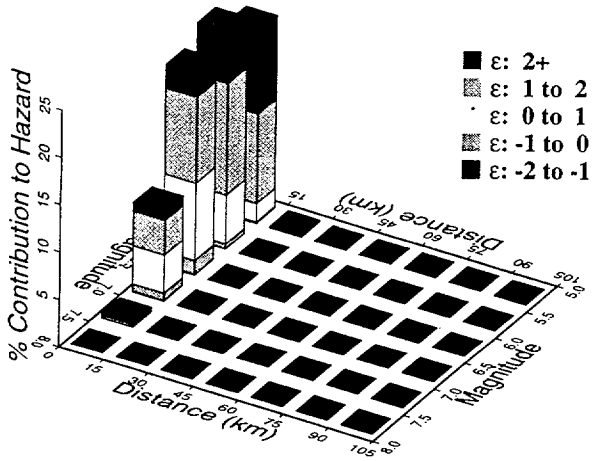

10 Hz, SBK Local Faults (Mult.)

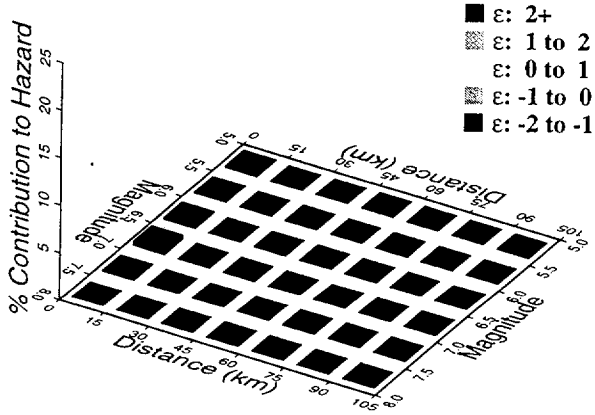

Figure 7-137 Magnitude-distance-epsilon distributions for the four source types: SBK team, 10-Hz horizontal spectral acceleration

1 Hz, SBK Area Sources

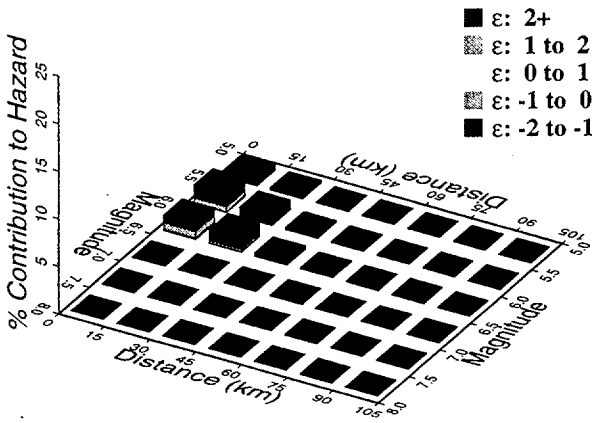

1 Hz, SBK Regional Faults

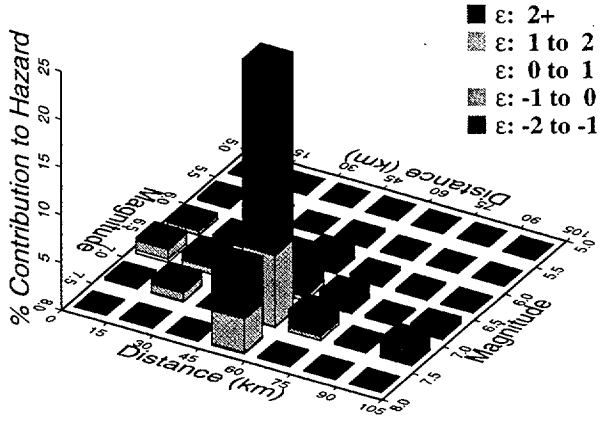

1 Hz, SBK Local Faults (Single)

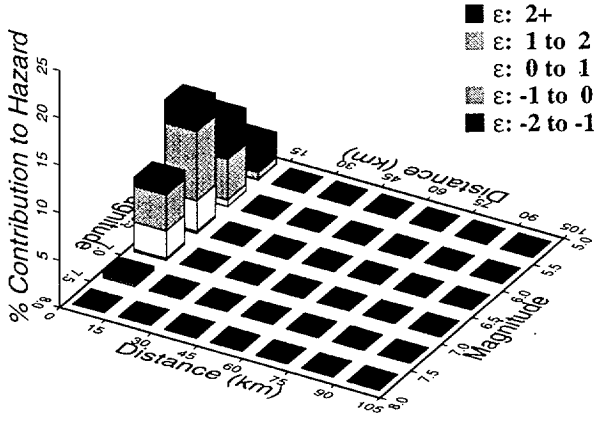

1 Hz, SBK Local Faults (Mult.)

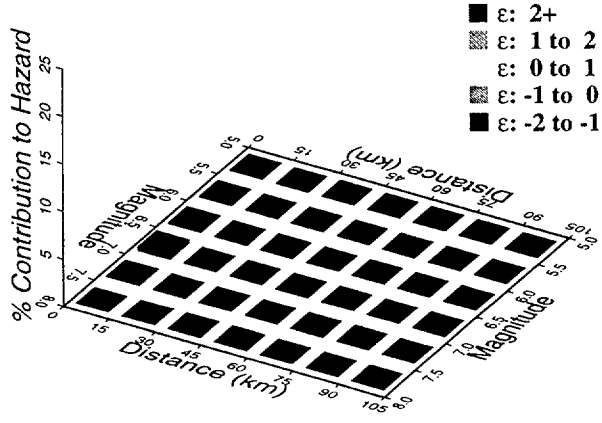

Figure 7-138 Magnitude-distance-epsilon distributions for the four source types: SBK team, 1-Hz horizontal spectral acceleration

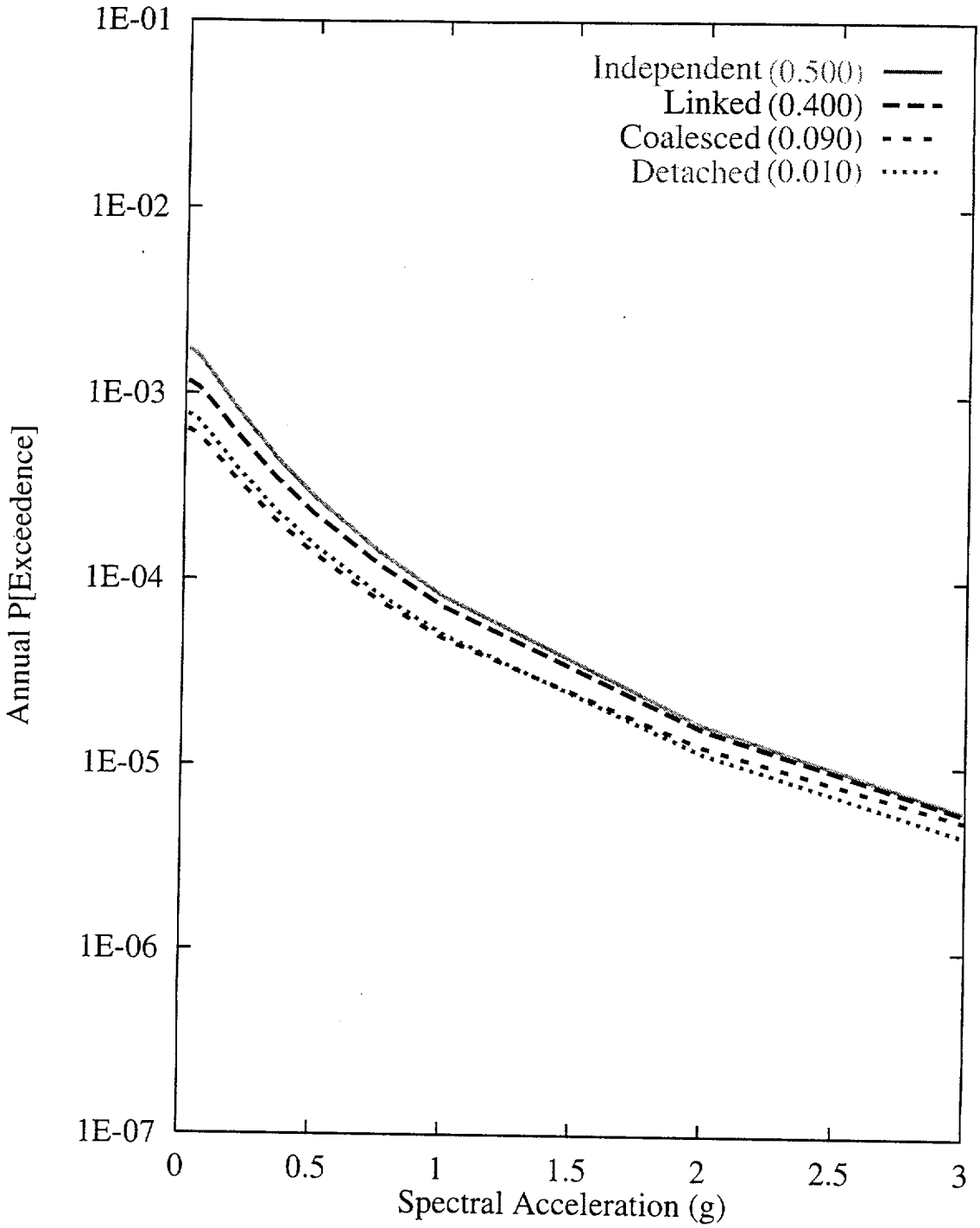

Figure 7-139 Sensitivity of seismic hazard from local faults to behavior of local faults: SBK team, 10-Hz horizontal spectral acceleration

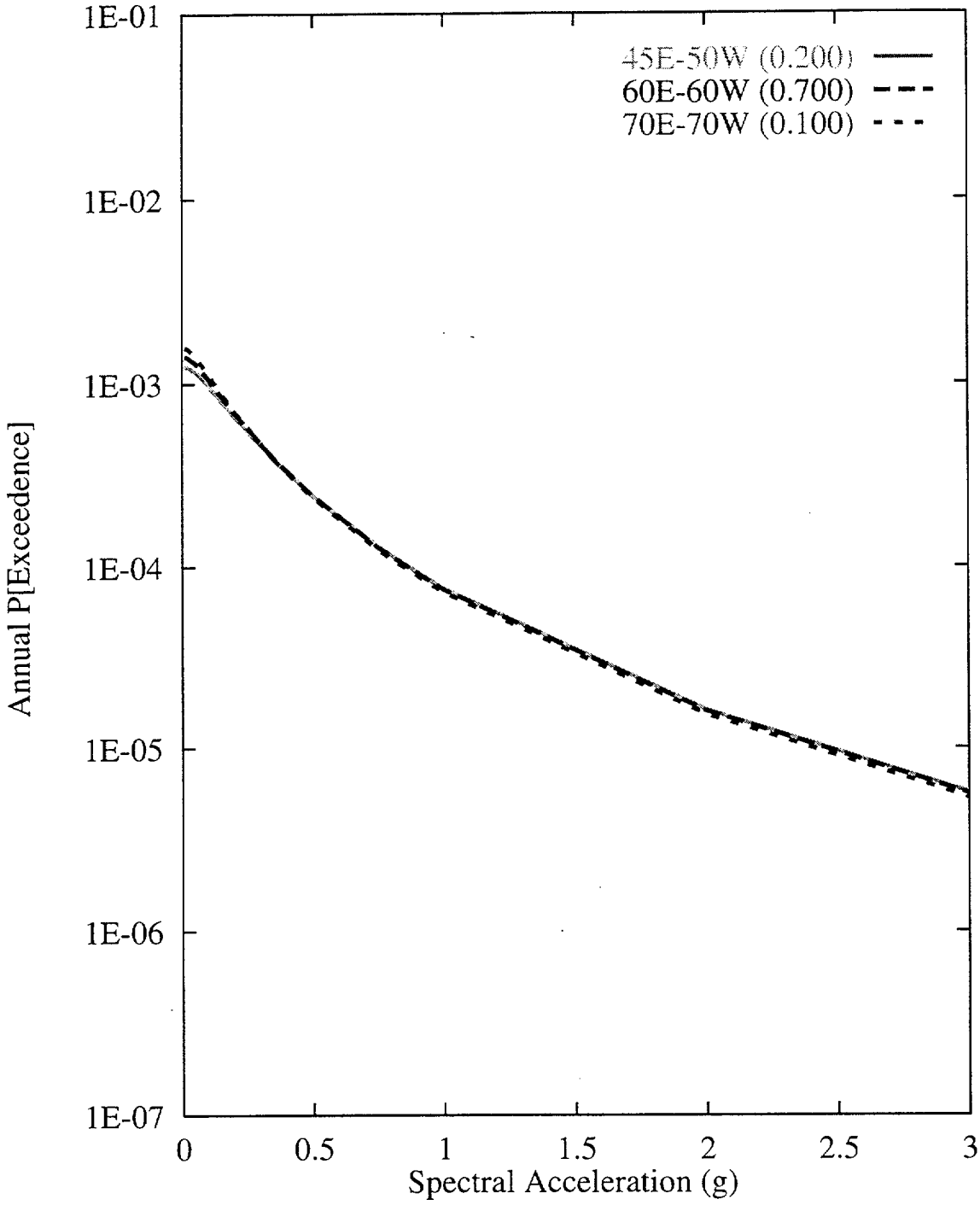

Figure 7-140 Sensitivity of seismic hazard from local faults to fault dip: SBK team, 10-Hz horizontal spectral acceleration

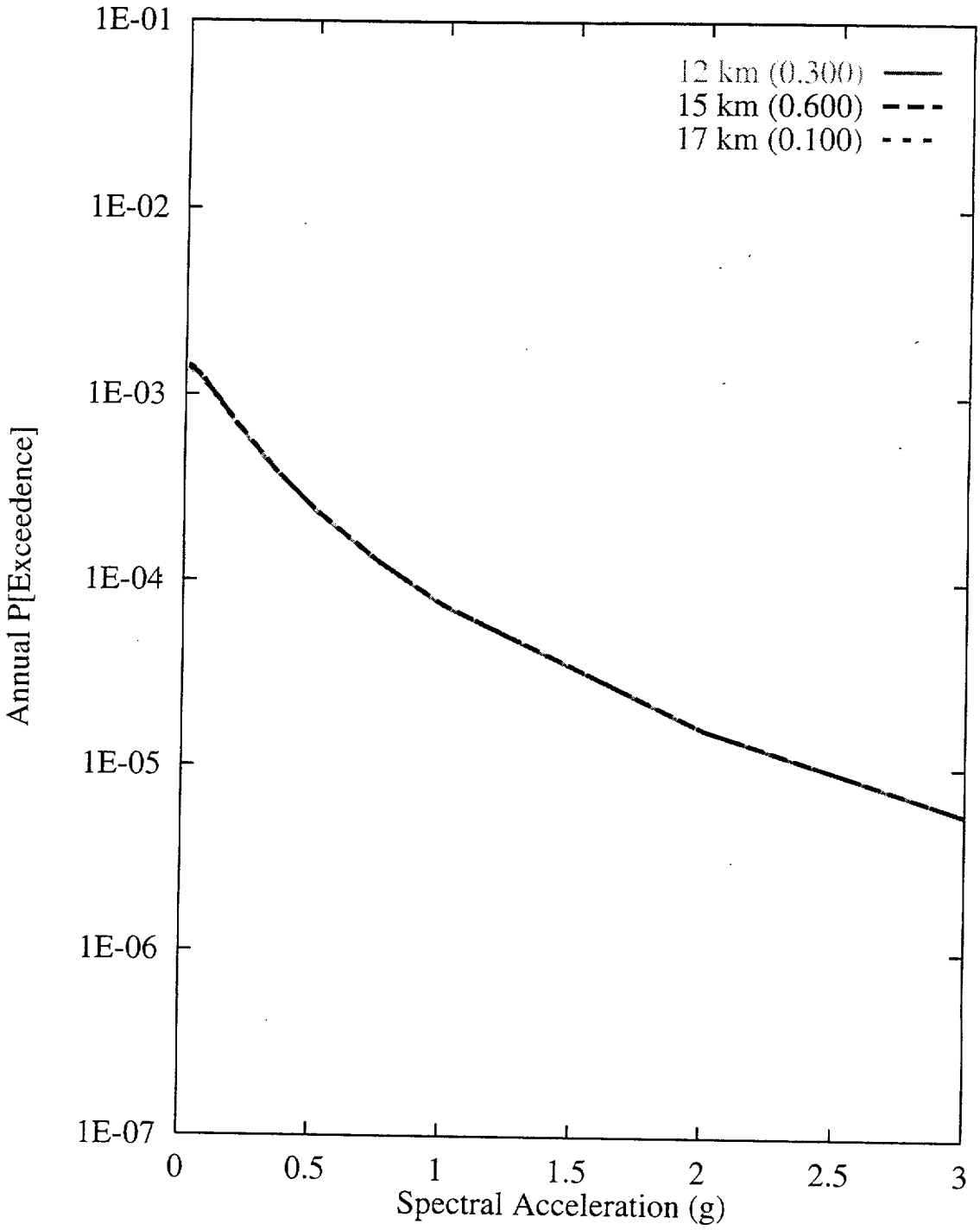

Figure 7-141 Sensitivity of seismic hazard from local faults to maximum fault depth: SBK team, 10-Hz horizontal spectral acceleration

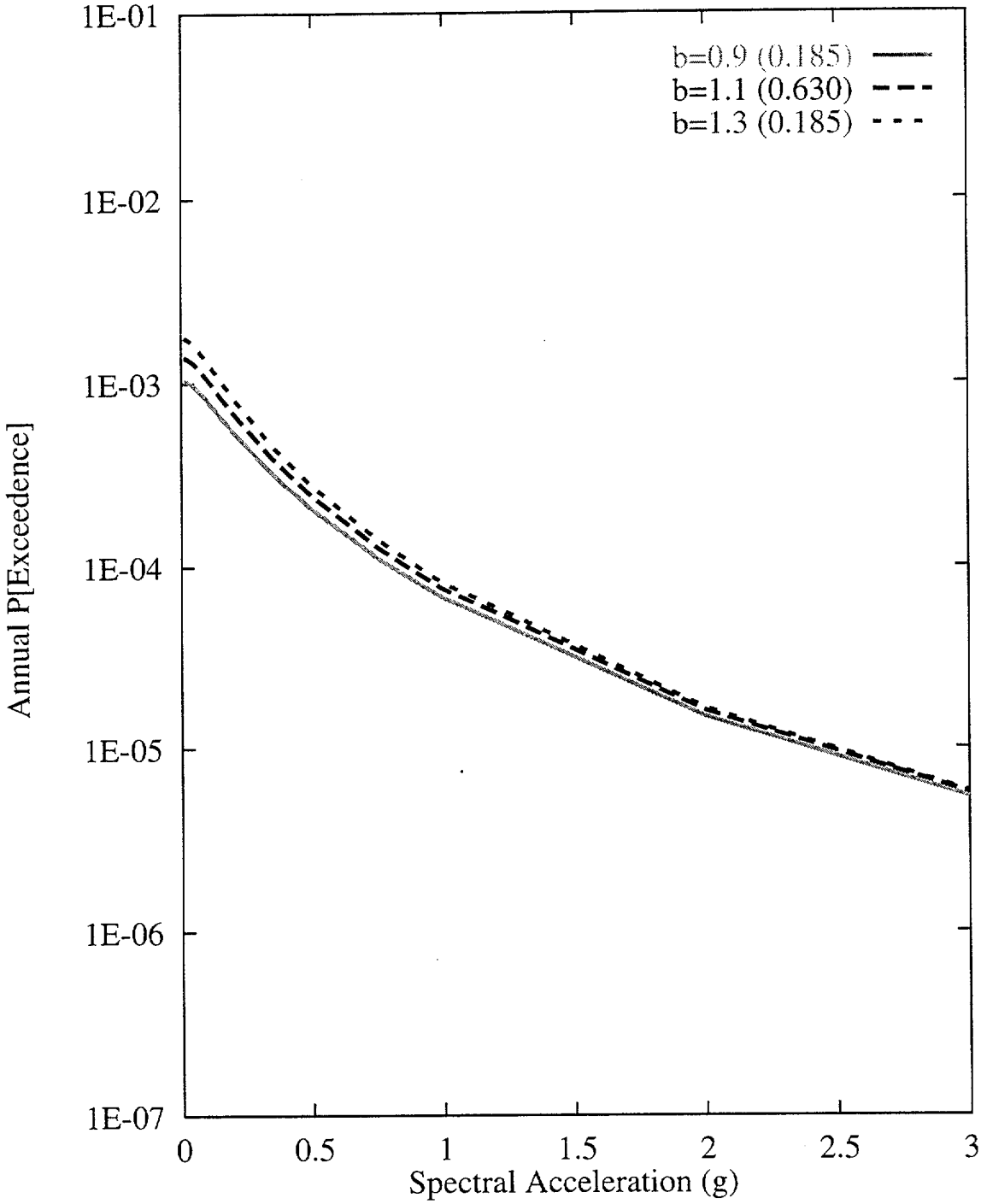

Figure 7-142 Sensitivity of seismic hazard from local faults to b-value: SBK team, 10-Hz horizontal spectral acceleration

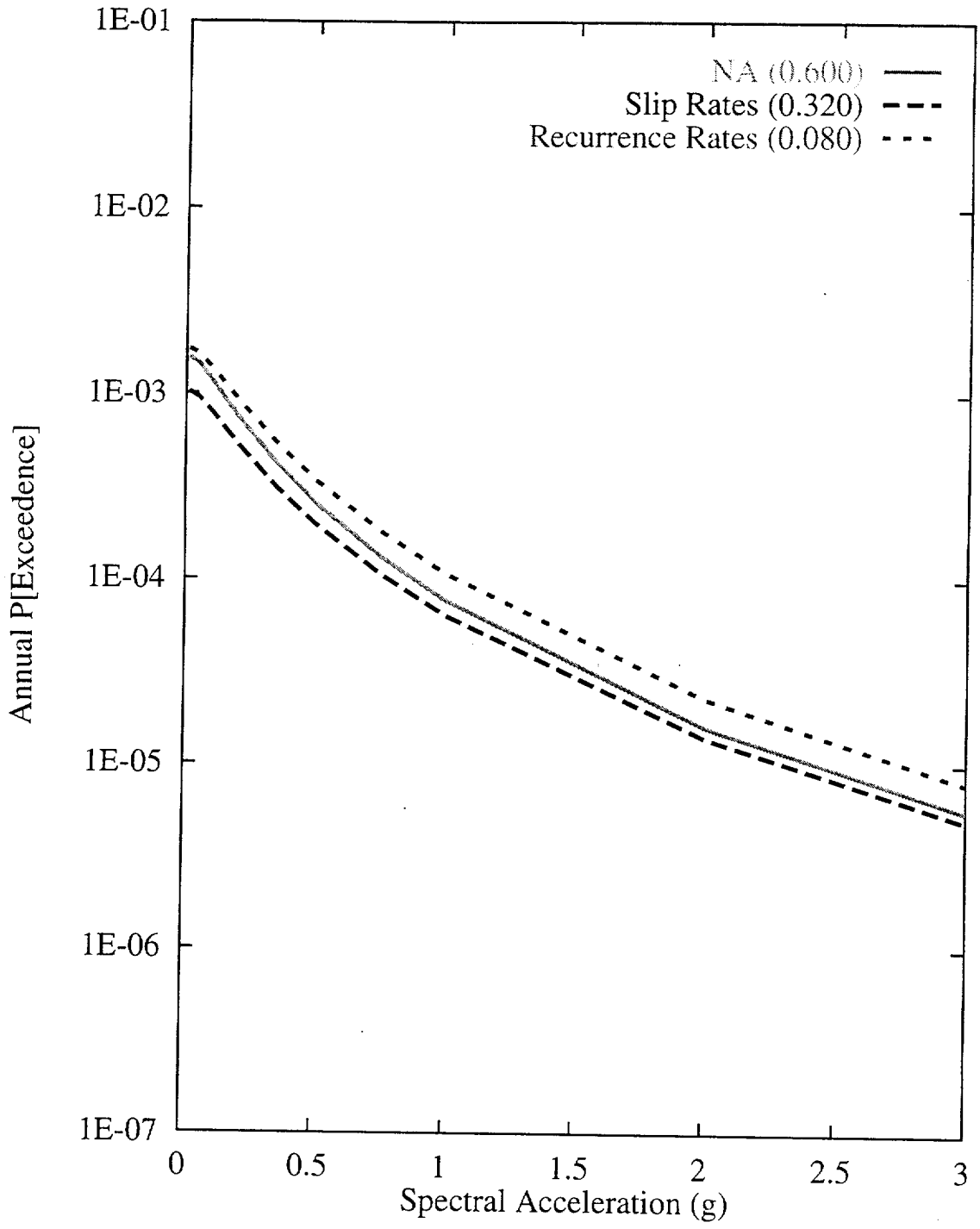

Figure 7-143 Sensitivity of seismic hazard from local faults to recurrence approach for the Paintbrush Canyon-Stagecoach Road fault system: SBK team, 10-Hz horizontal spectral acceleration

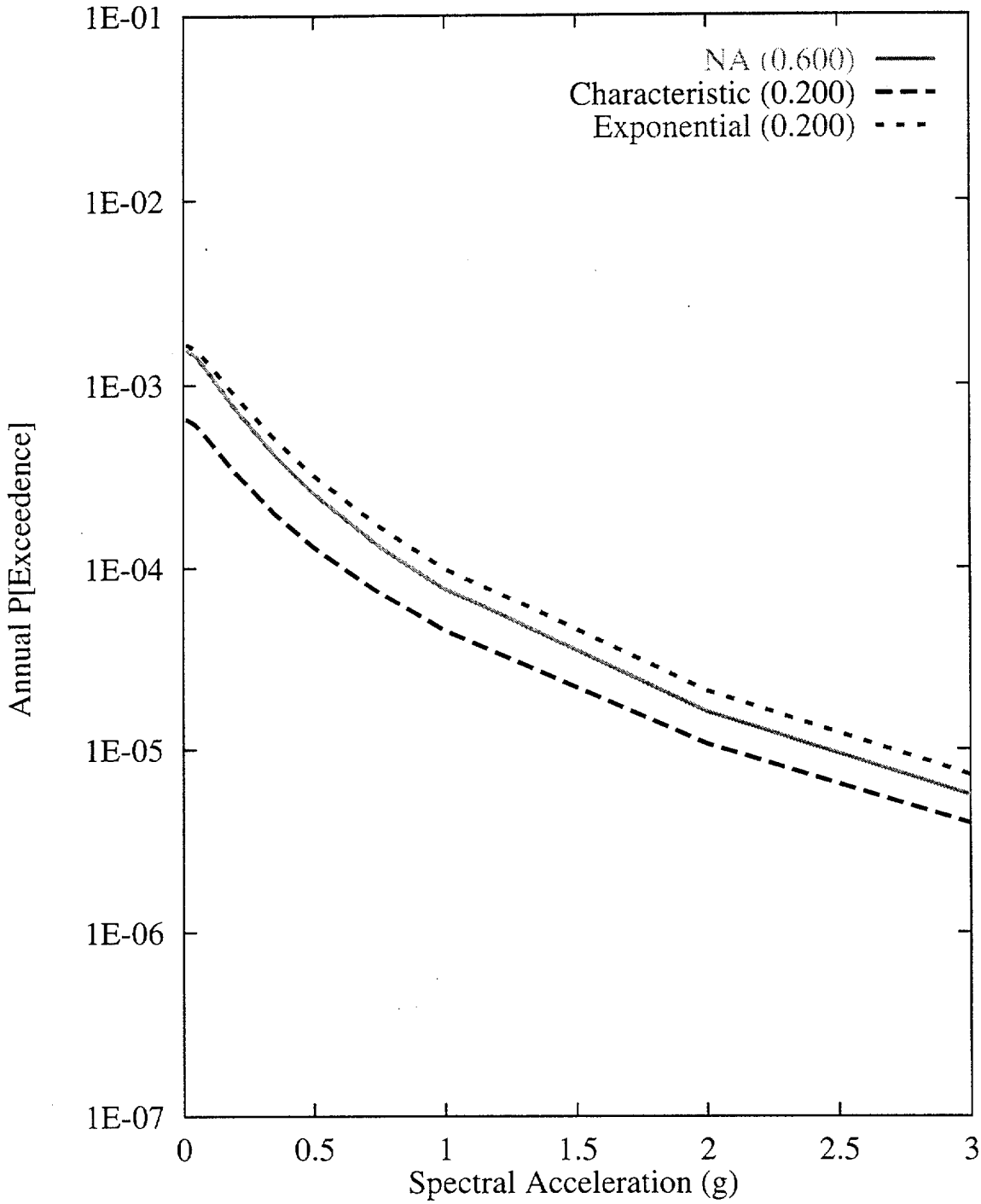

Figure 7-144 Sensitivity of seismic hazard from local faults to recurrence model for the Paintbrush Canyon-Stagecoach Road fault system: SBK team, 10-Hz horizontal spectral acceleration

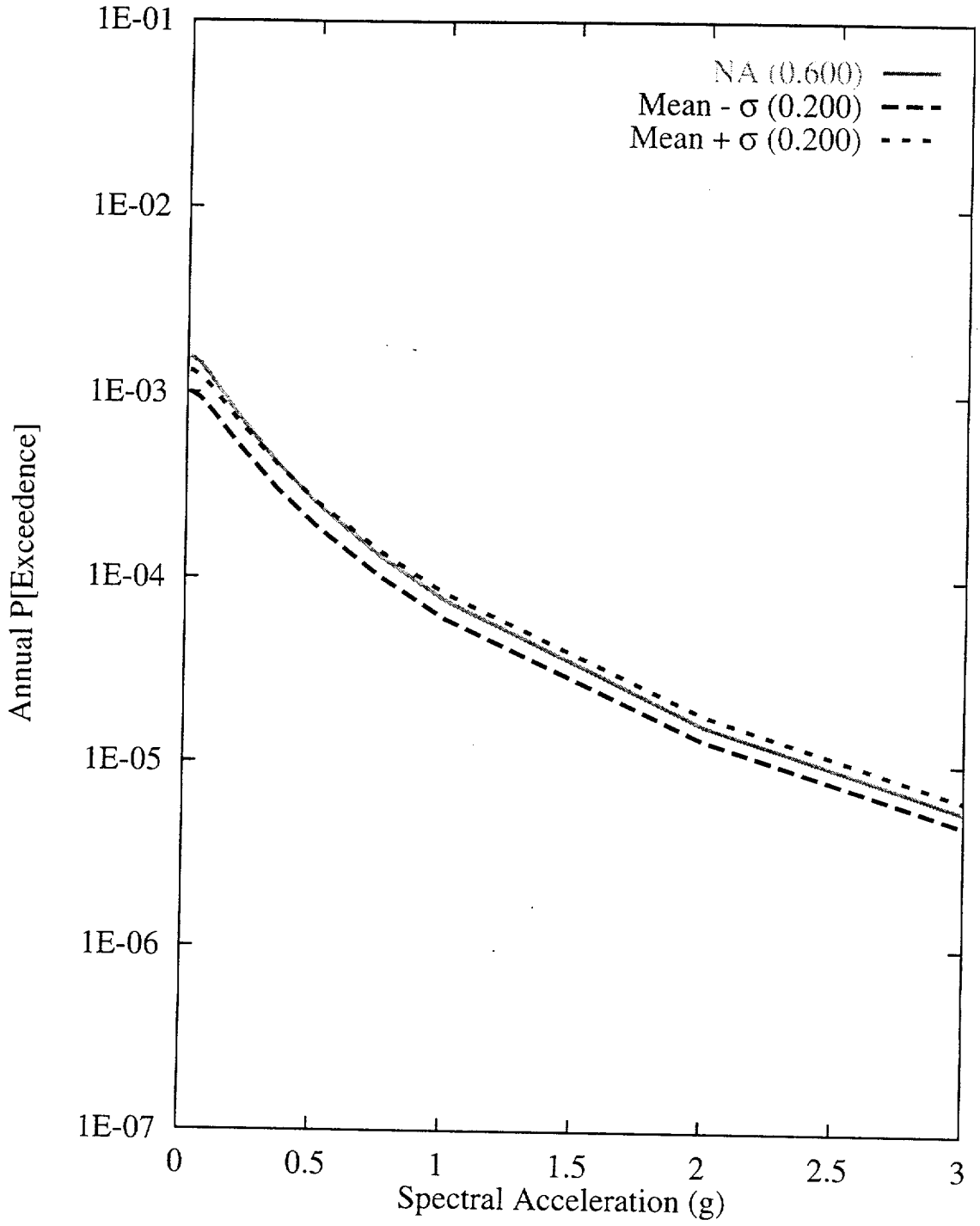

Figure 7-145 Sensitivity of seismic hazard from local faults to Mmax on the Paintbrush Canyon-Stagecoach Road fault system: SBK team, 10-Hz horizontal spectral acceleration

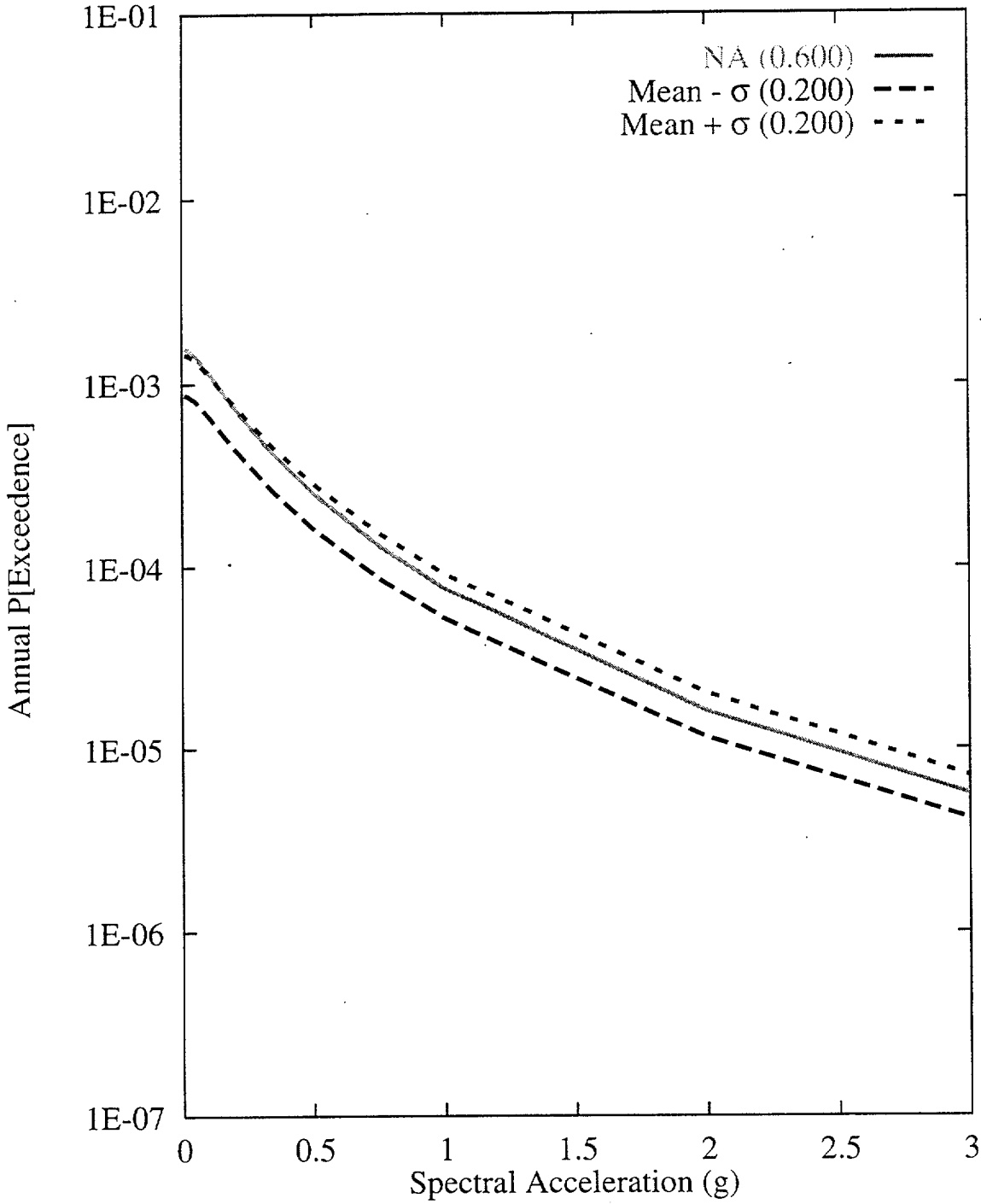

Figure 7-146 Sensitivity of seismic hazard from local faults to recurrence of the Paintbrush Canyon-Stagecoach Road fault system: SBK team, 10-Hz horizontal spectral acceleration

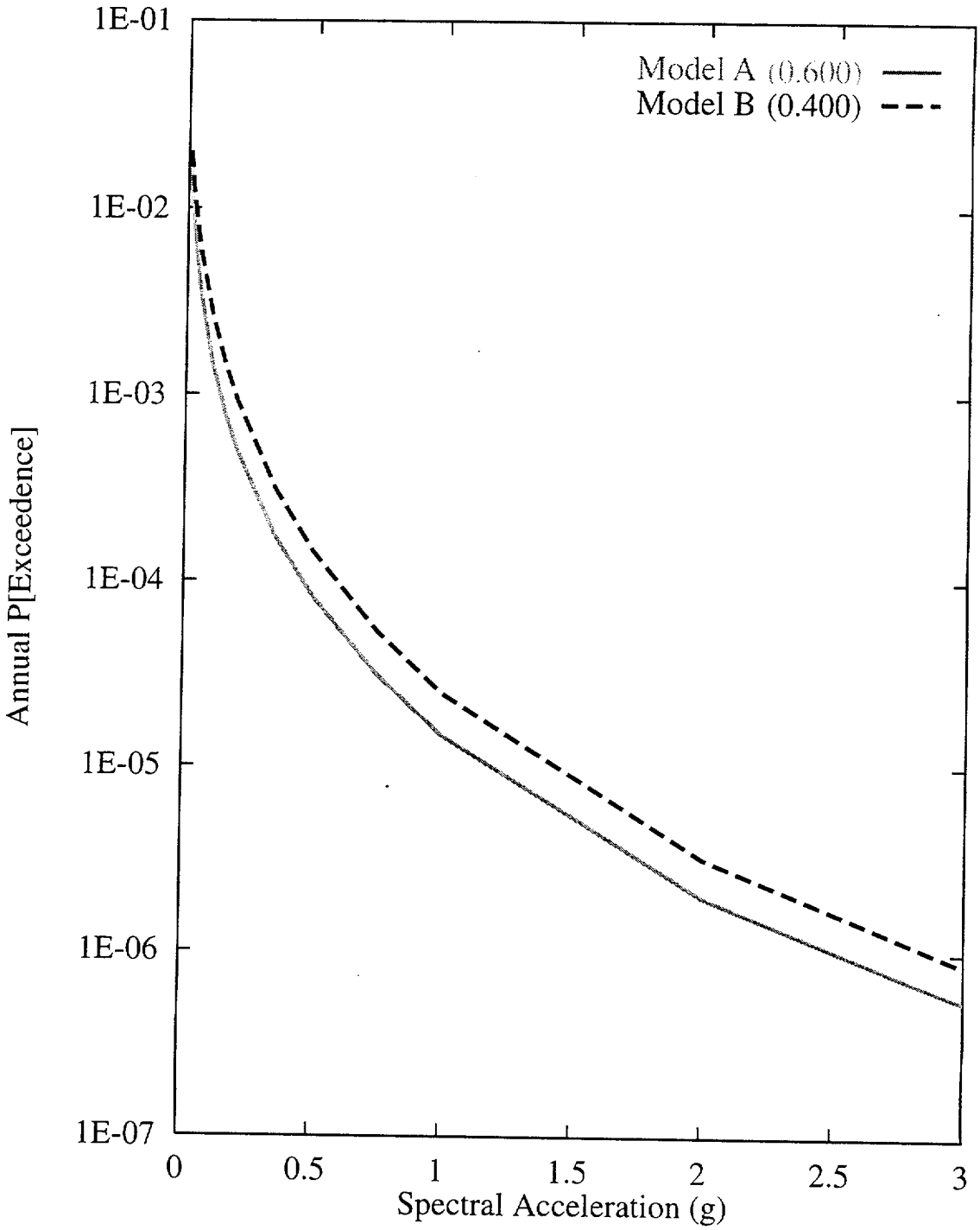

Figure 7-147. Sensitivity of seismic hazard from area zones to zonation: SBK team, 10-Hz horizontal spectral acceleration

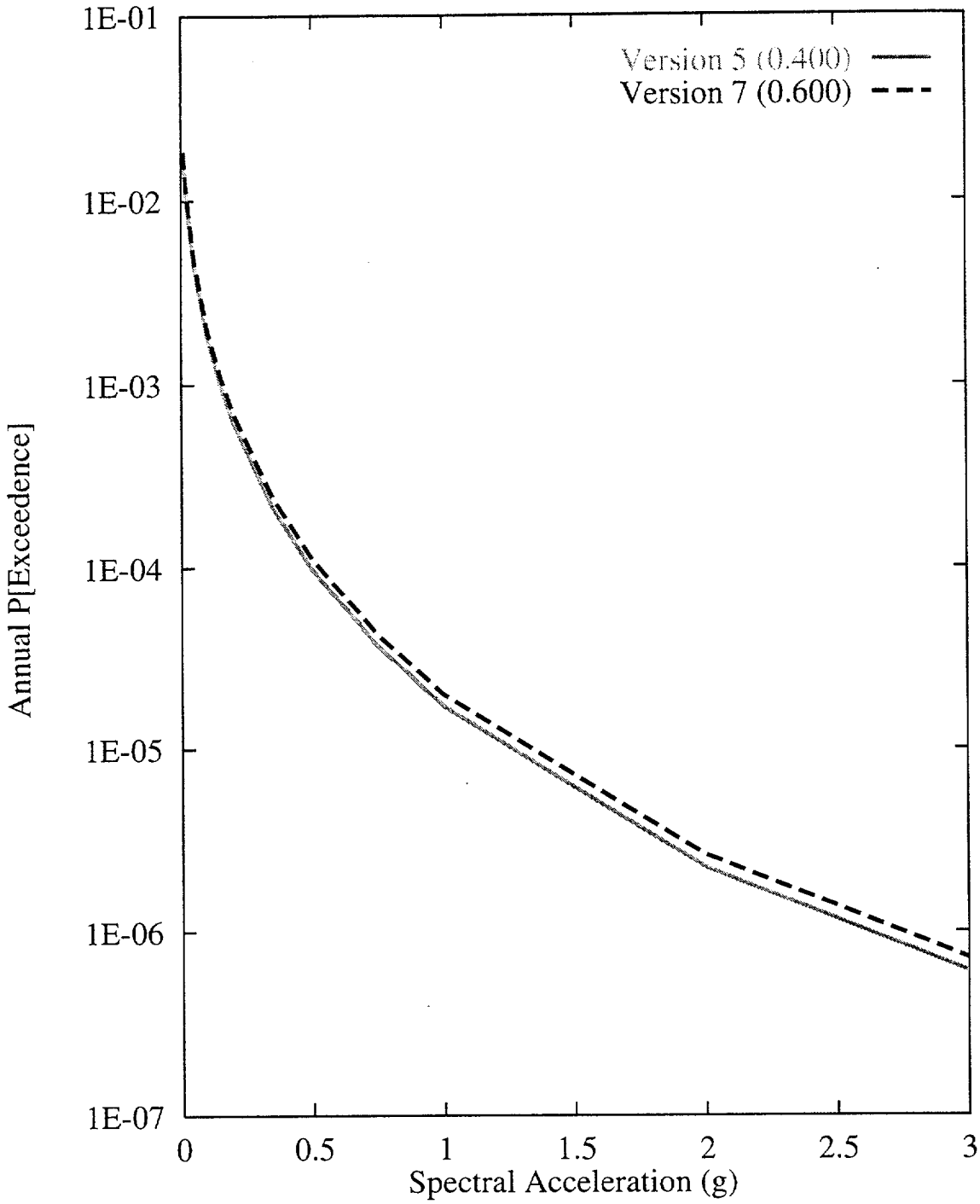

Figure 7-148 Sensitivity of seismic hazard from area zones to choice of seismicity catalog for the Basin and Range zone: SBK team, 10-Hz horizontal spectral acceleration

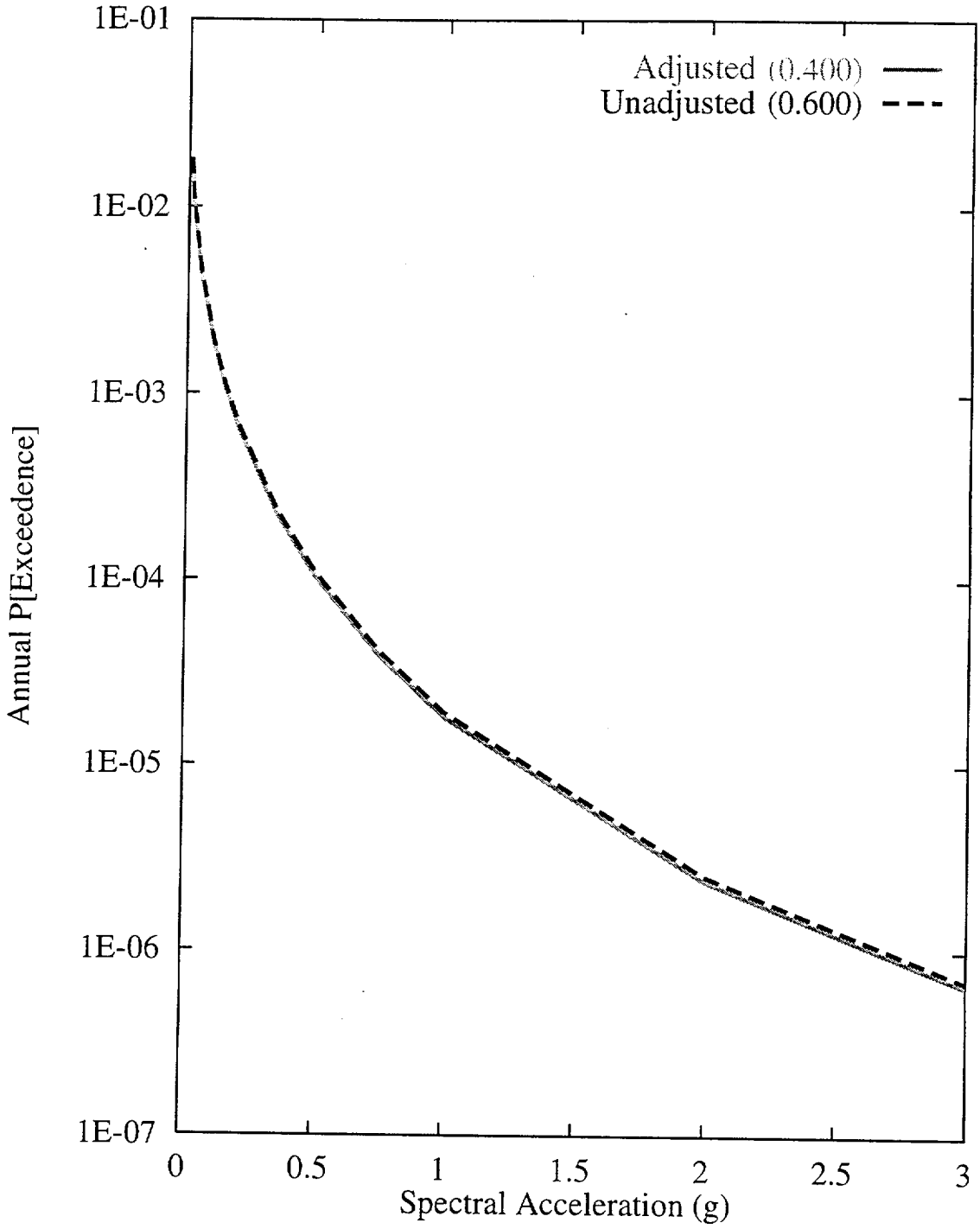

Figure 7-149 Sensitivity of seismic hazard from area zones to adjustment for NTS events: SBK team, 10-Hz horizontal spectral acceleration

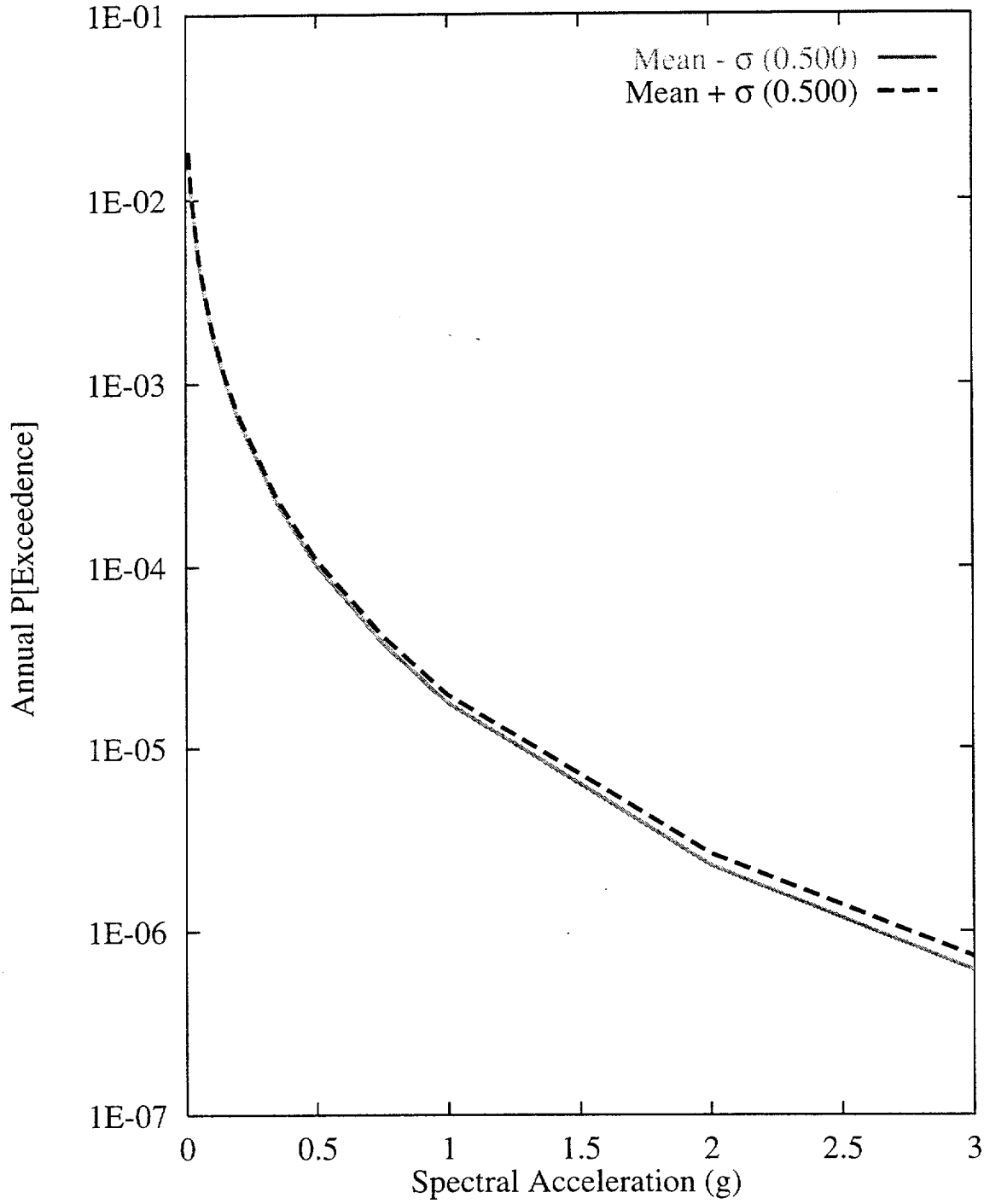

Figure 7-150 Sensitivity of seismic hazard from area zones to Mmax of the Basin and Range zone: SBK team, 10-Hz horizontal spectral acceleration

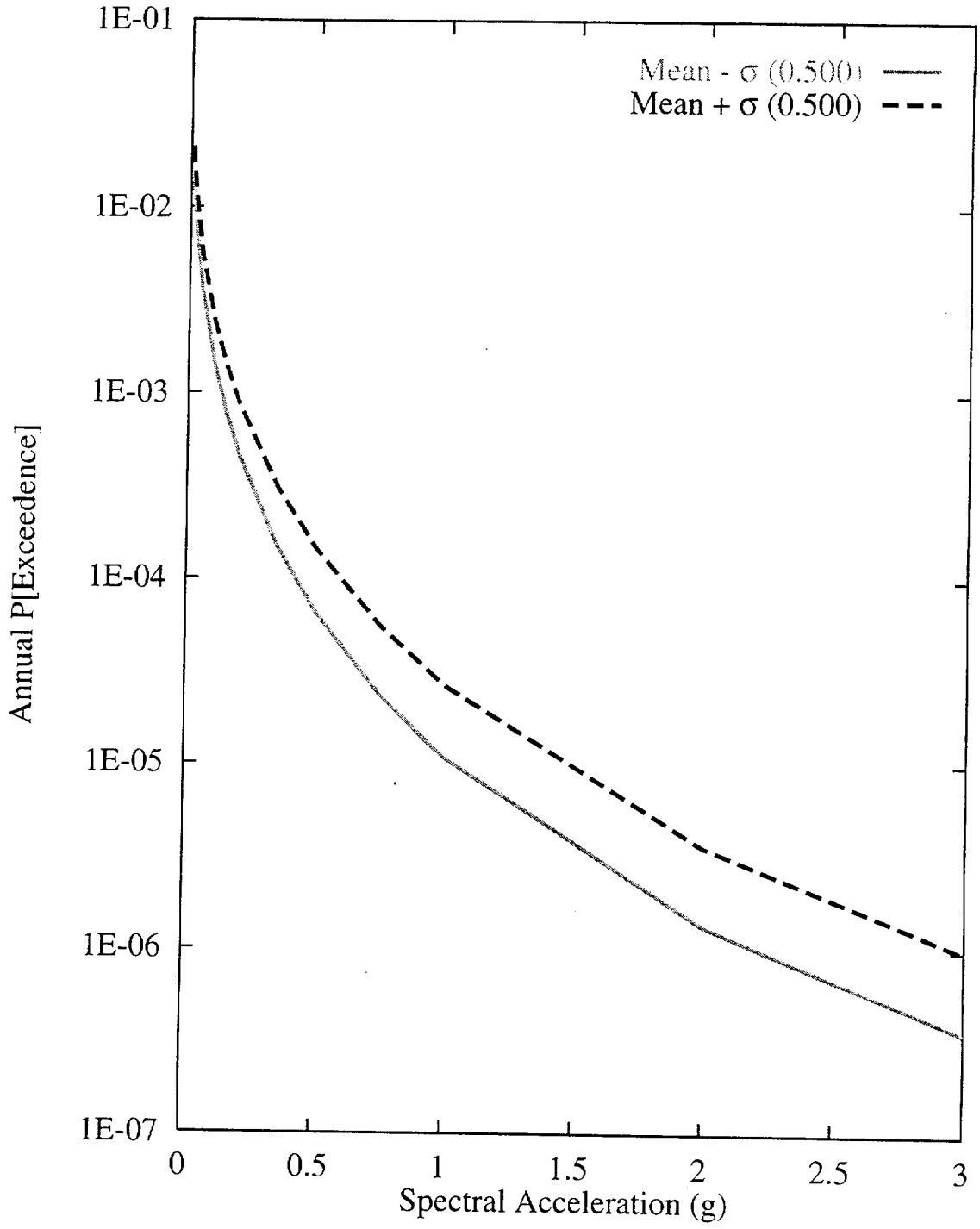

Figure 7-151 Sensitivity of seismic hazard from area zones to recurrence of the Basin and Range zone: SBK team, 10-Hz horizontal spectral acceleration

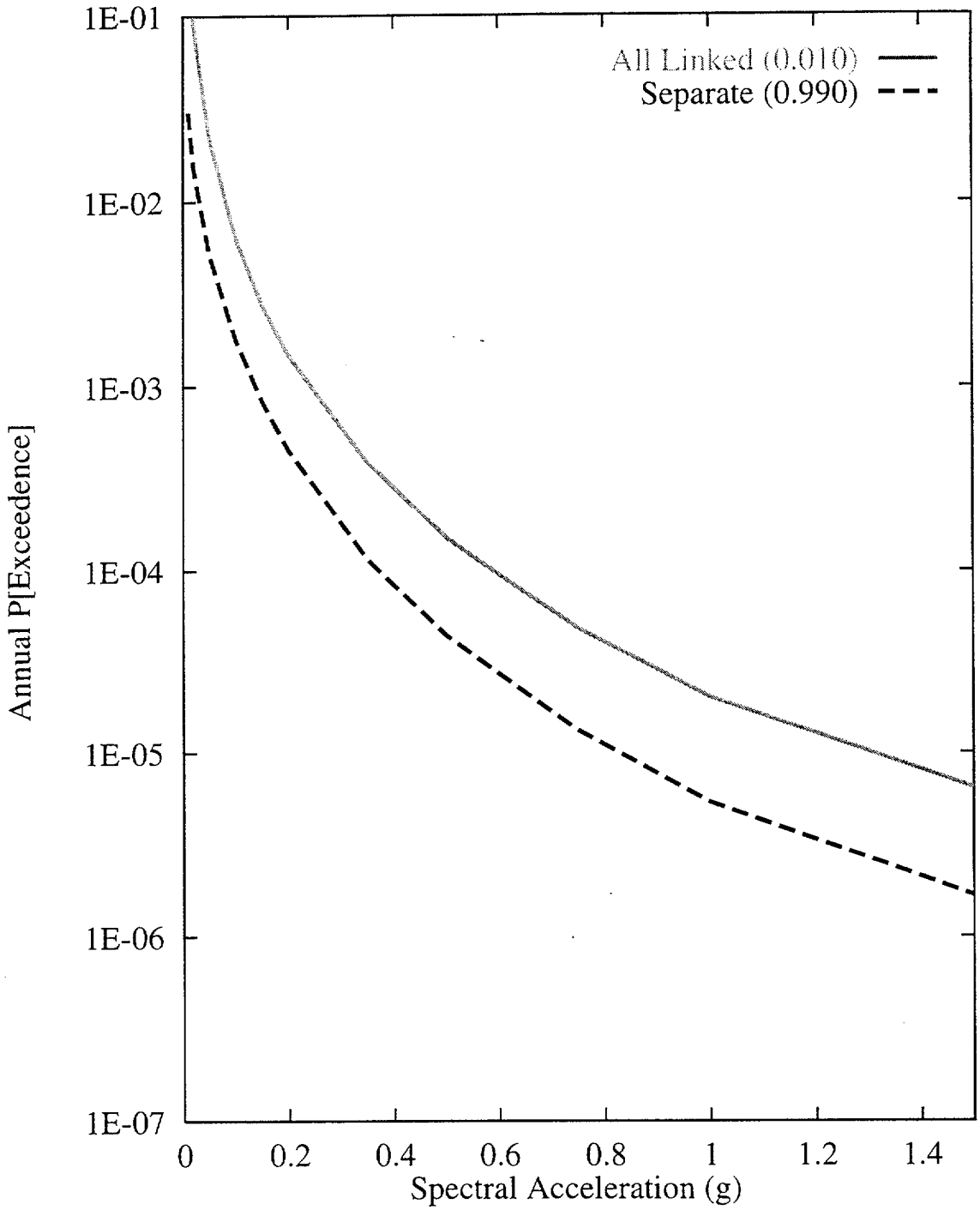

Figure 7-152 Sensitivity of seismic hazard from regional faults to rupture behavior of the Death Valley-Furnace Creek-Fish Lake Valley fault system: SBK team, 1-Hz horizontal spectral acceleration

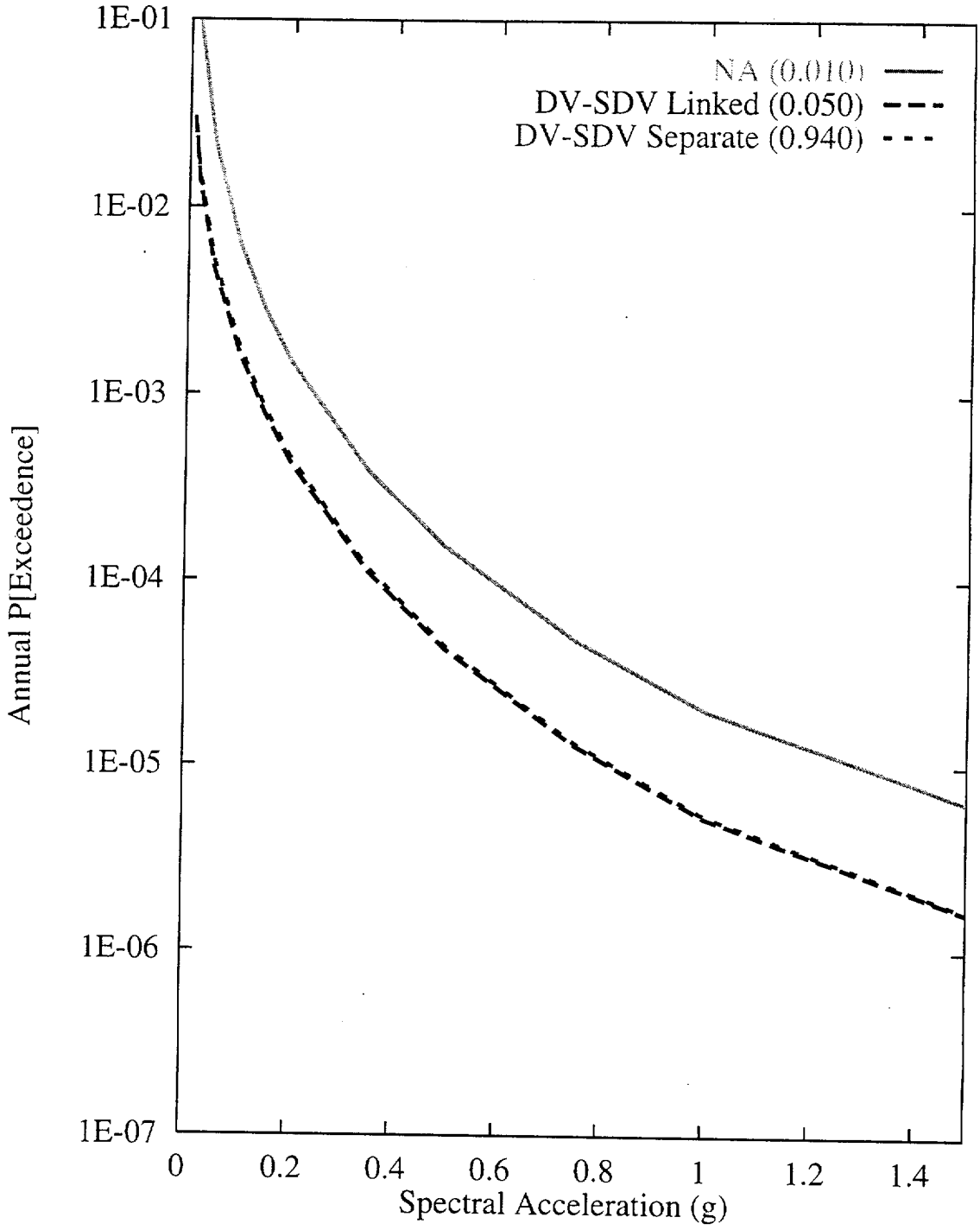

Figure 7-153 Sensitivity of seismic hazard from regional faults to rupture behavior of the Death Valley-southern Death Valley fault system: SBK team, 1-Hz horizontal spectral acceleration

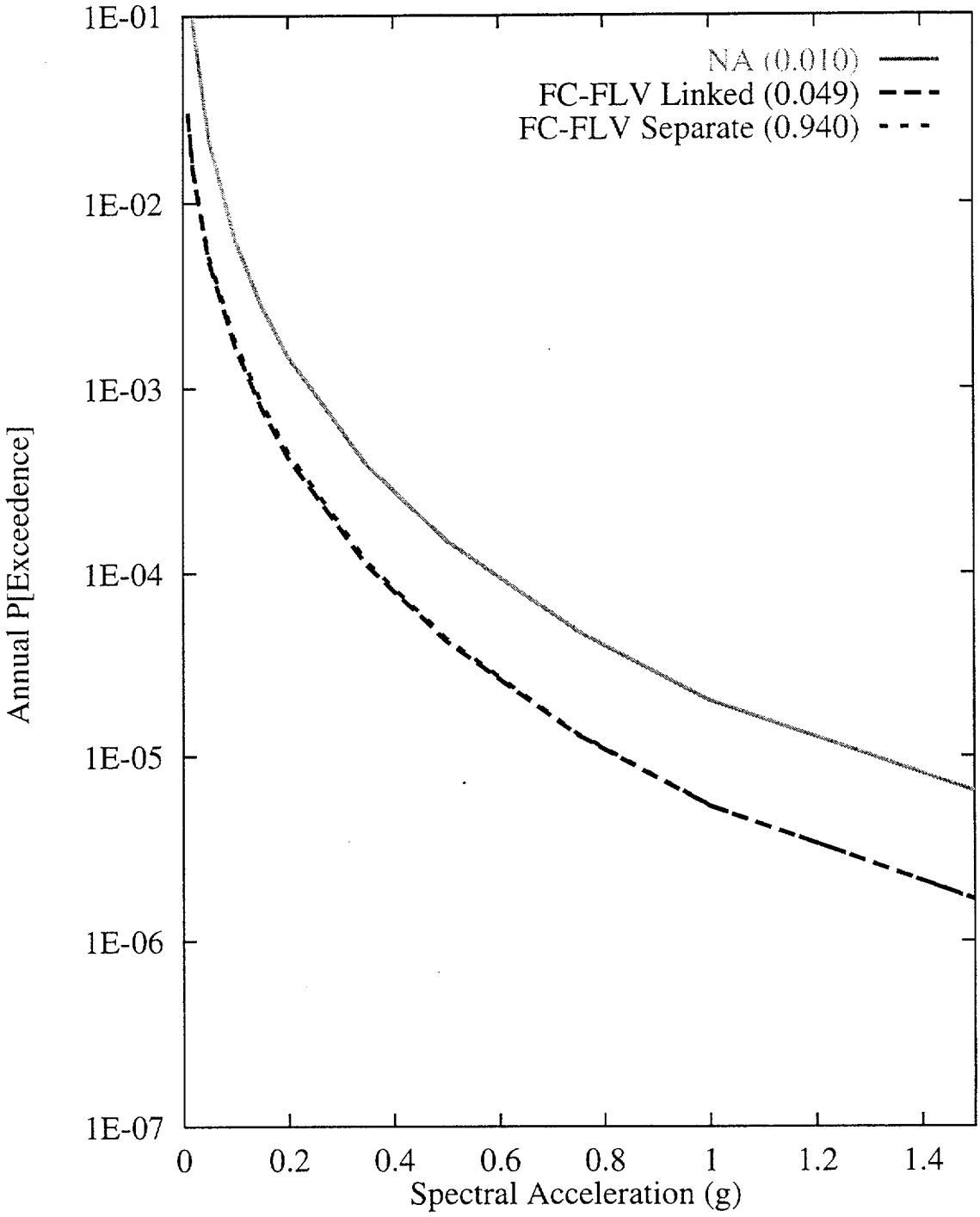

Figure 7-154 Sensitivity of seismic hazard from regional faults to rupture behavior of the Furnace Creek-Fish Lake Valley fault system: SBK team, 1-Hz horizontal spectral acceleration

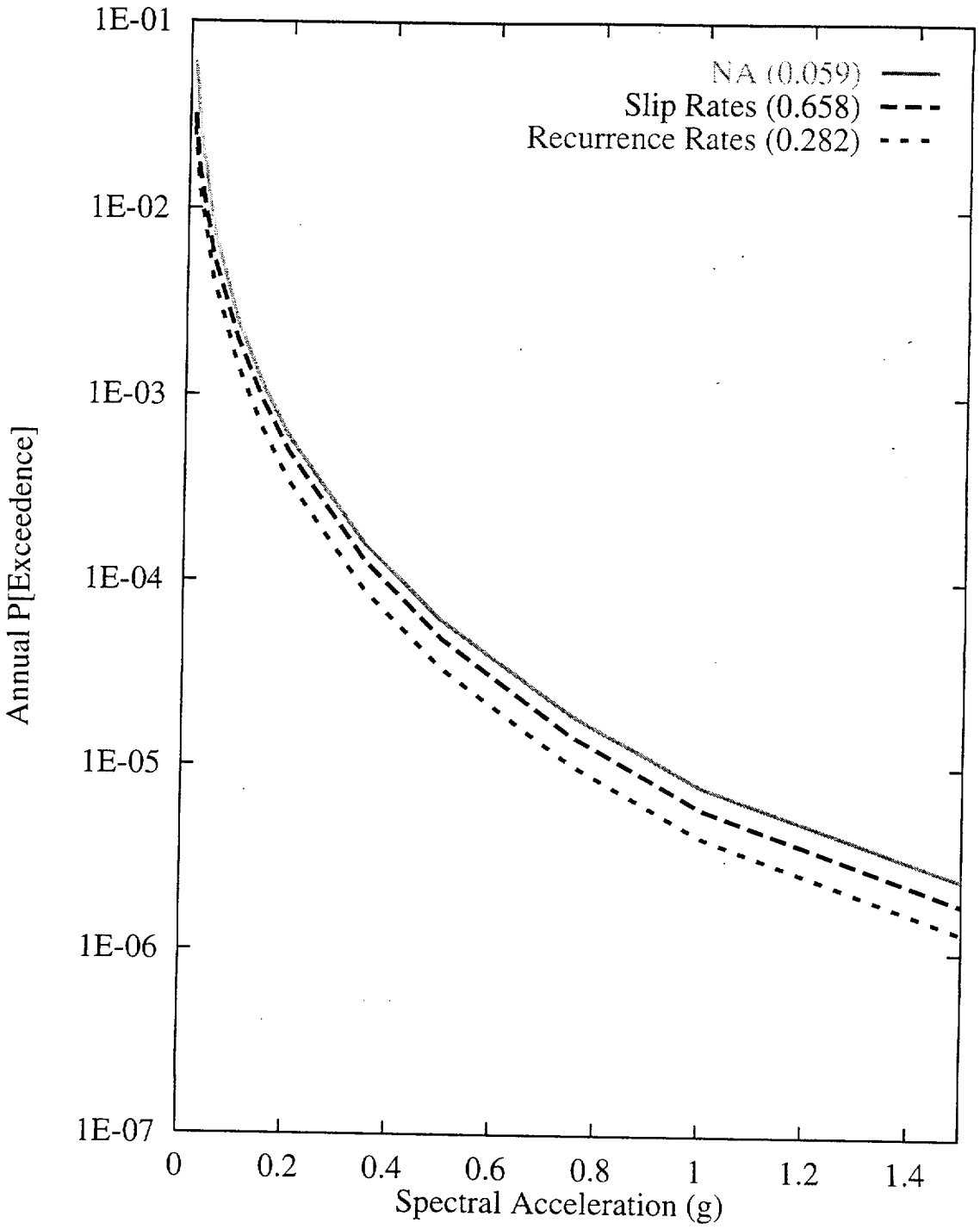

Figure 7-155 Sensitivity of seismic hazard from regional faults to recurrence of the Furnace Creek fault: SBK team, 1-Hz horizontal spectral acceleration

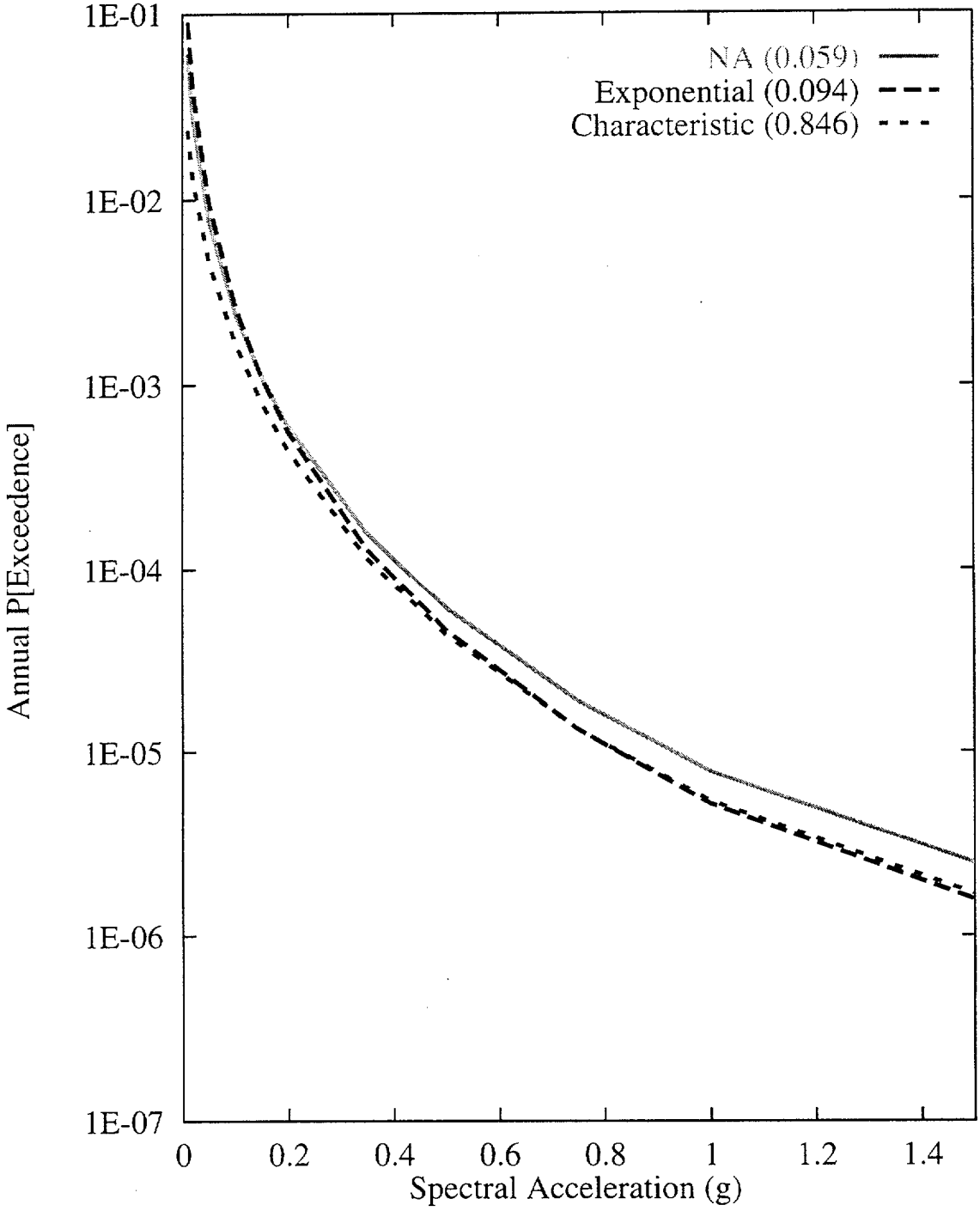

Figure 7-156 Sensitivity of seismic hazard from regional faults to recurrence model of the Furnace Creek fault: SBK team, 1-Hz horizontal spectral acceleration

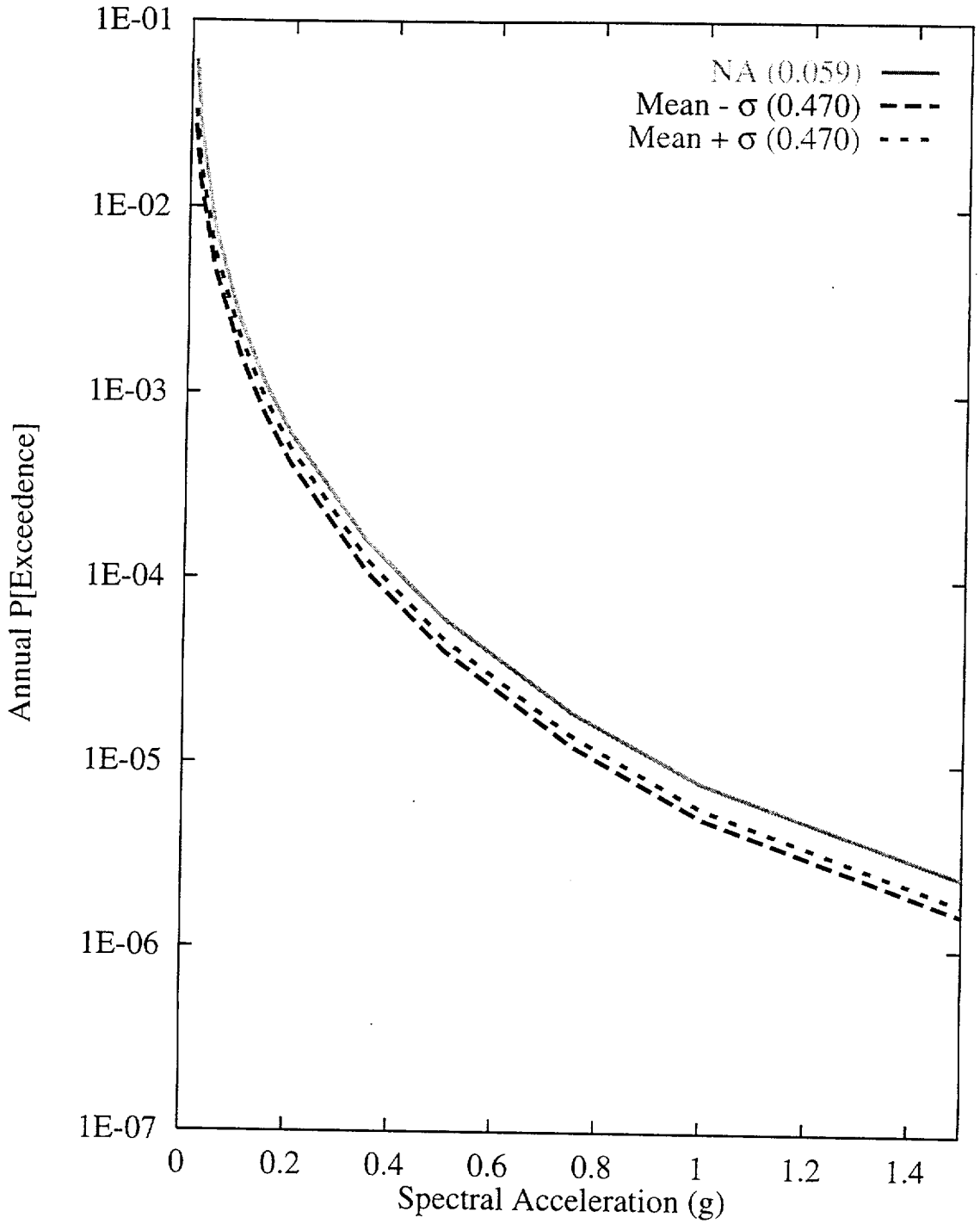

Figure 7-157 Sensitivity of seismic hazard from regional faults to M_{max} on the Furnace Creek fault: SBK team, 1-Hz horizontal spectral acceleration

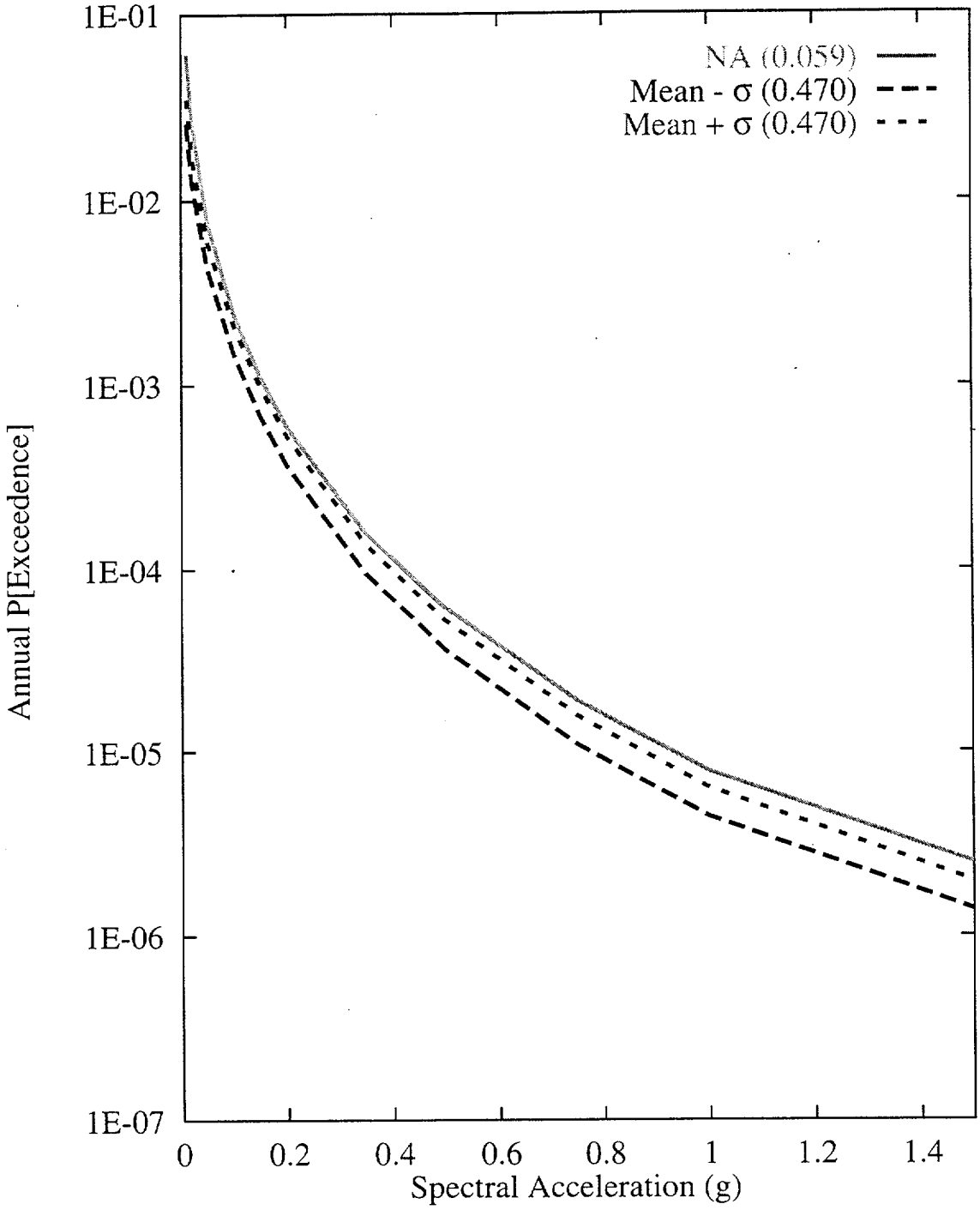

Figure 7-158 Sensitivity of seismic hazard from regional faults to recurrence of the Furnace Creek fault: SBK team, 1-Hz horizontal spectral acceleration

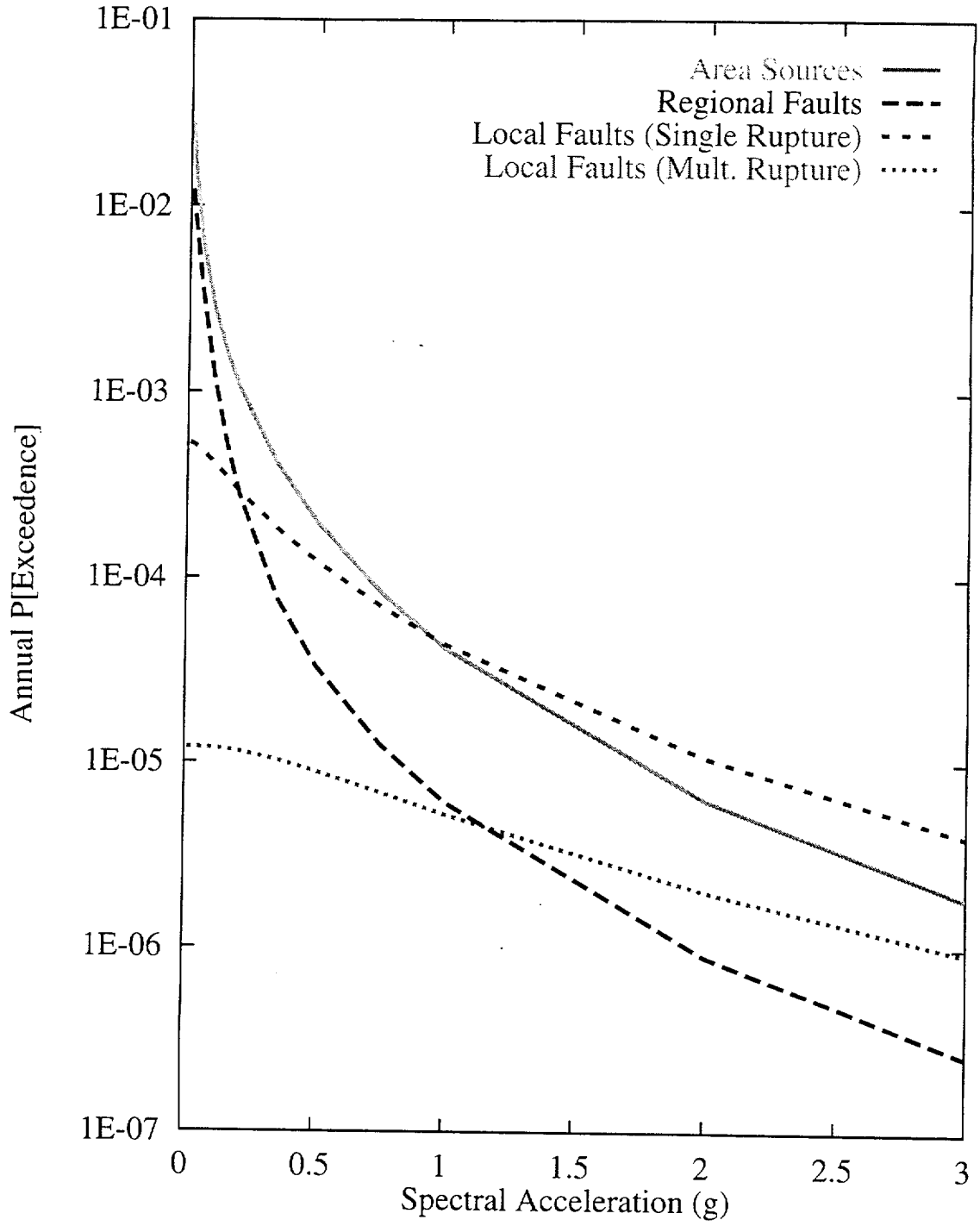

Figure 7-159 Contributions of source types to the mean hazard: SDO team, 10-Hz horizontal spectral acceleration

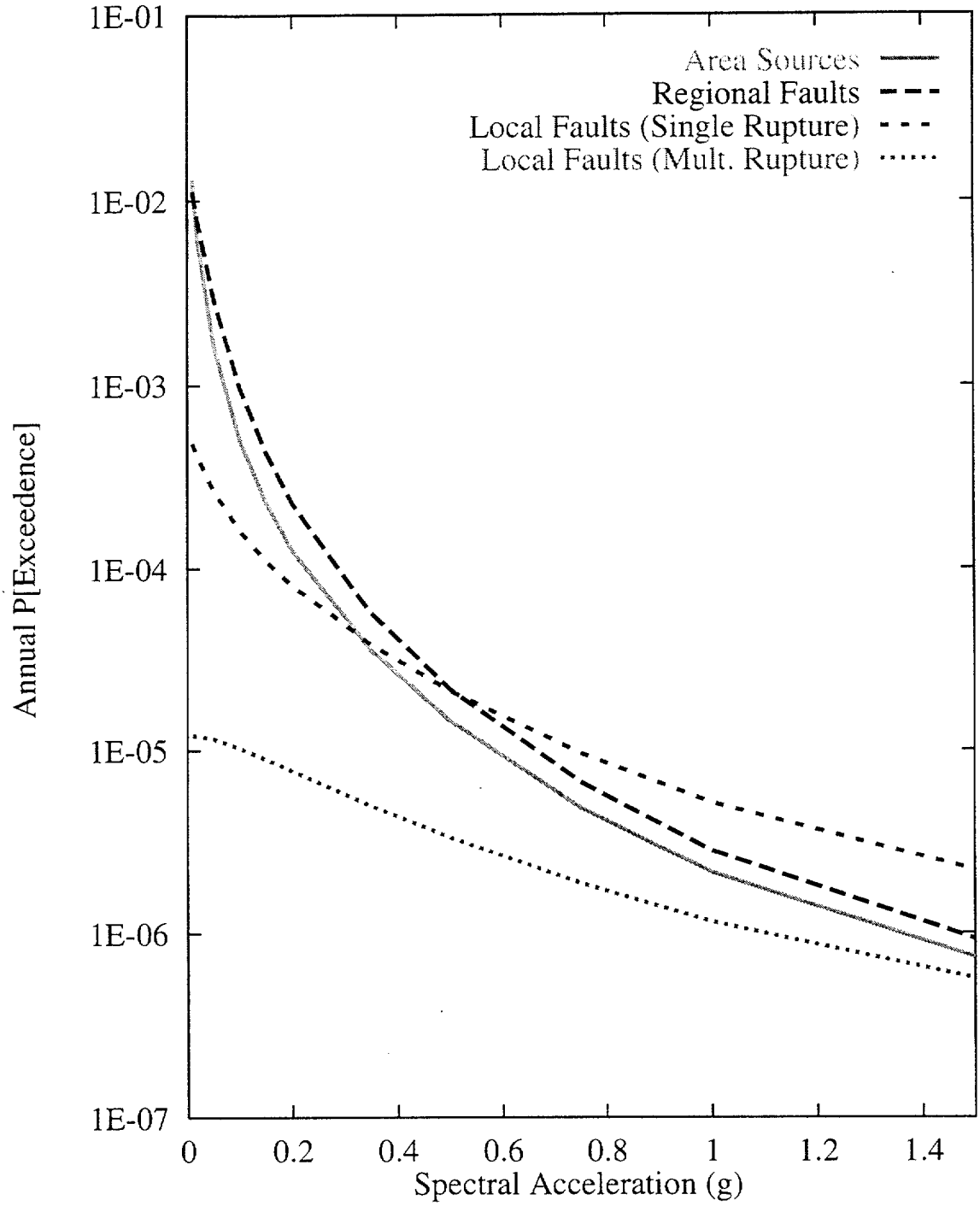

Figure 7-160 Contributions of source types to the mean hazard: SDO team, 1-Hz horizontal spectral acceleration

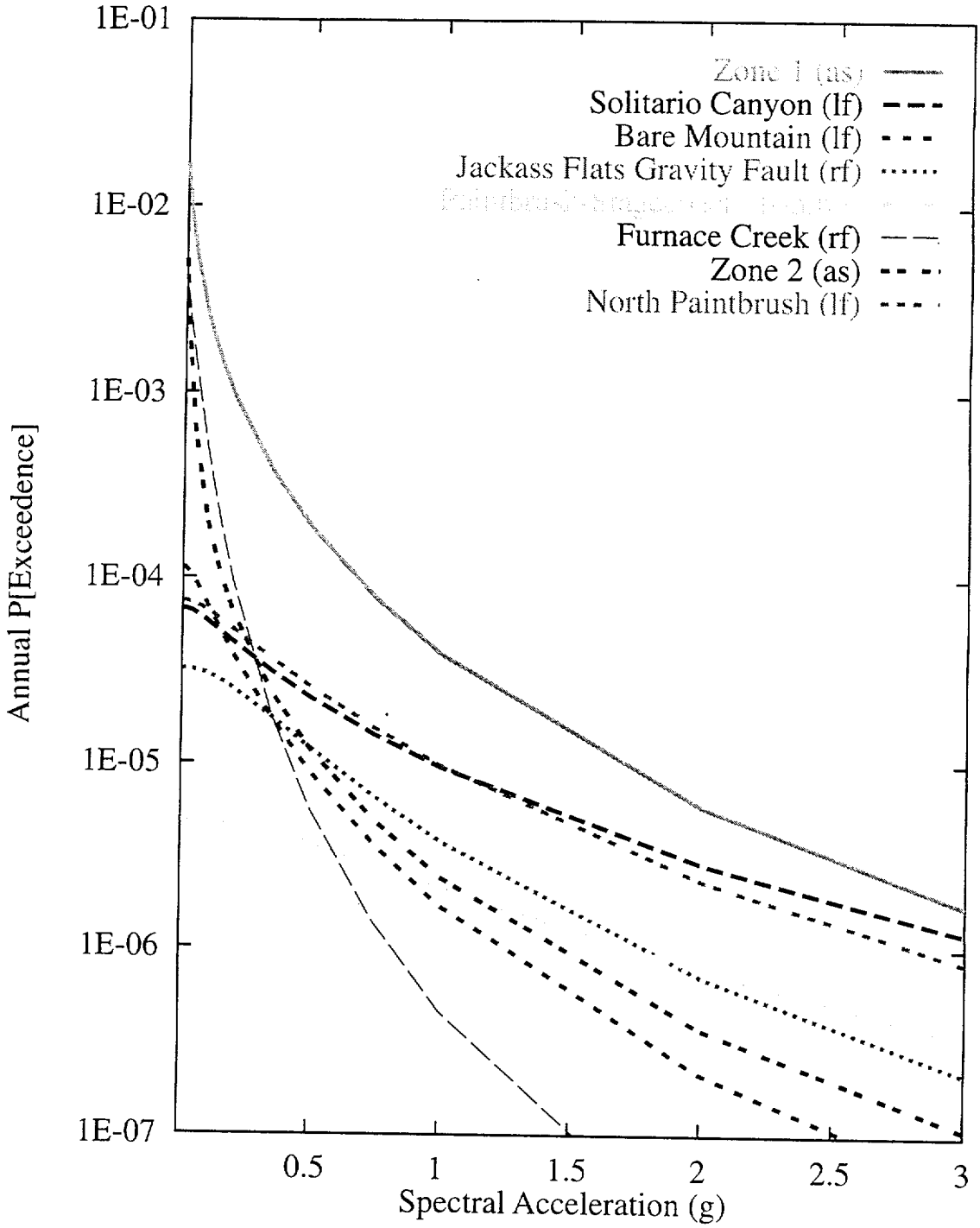

Figure 7-161 Mean seismic hazard from dominant seismic sources: SDO team, 10-Hz horizontal spectral acceleration. Acronyms in parentheses refer to source types: as-area source zone; lf-local fault; rf-regional fault; and mult-multiple fault.

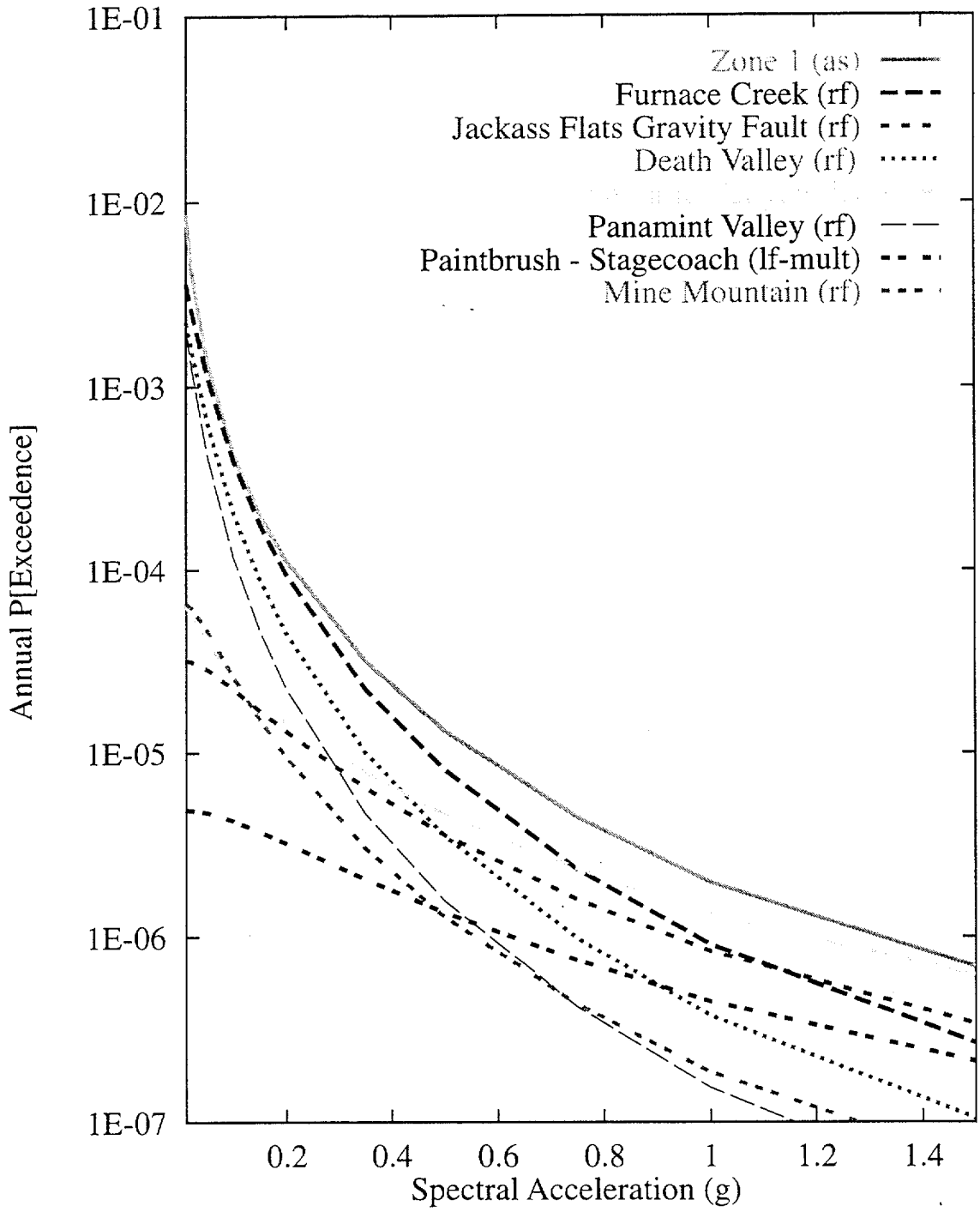

Figure 7-162 Mean seismic hazard from dominant seismic sources: SDO team, 1-Hz horizontal spectral acceleration. Acronyms in parentheses refer to source types: as-area source zone; rf-regional fault; lf-local fault; and mult-multiple fault.

10 Hz, SDO Area Sources

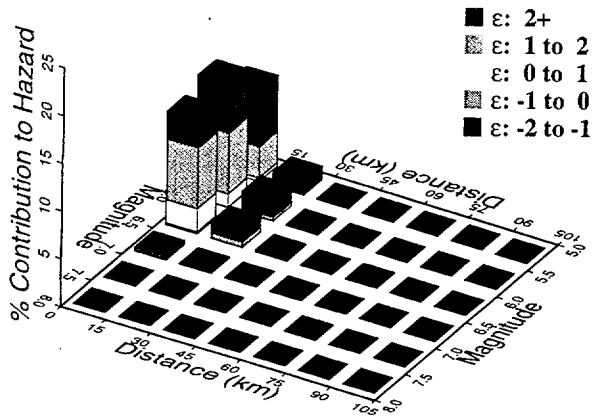

10 Hz, SDO Regional Faults

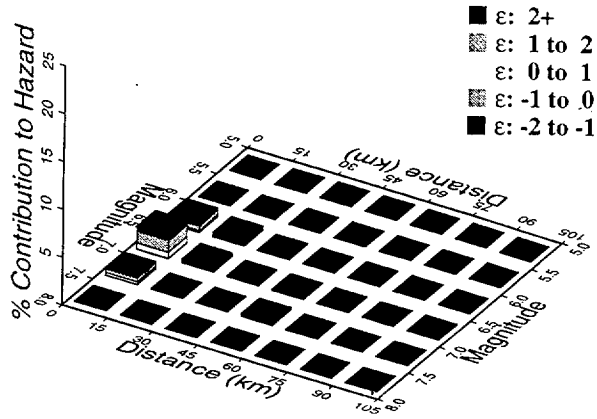

10 Hz, SDO Local Faults (Single)

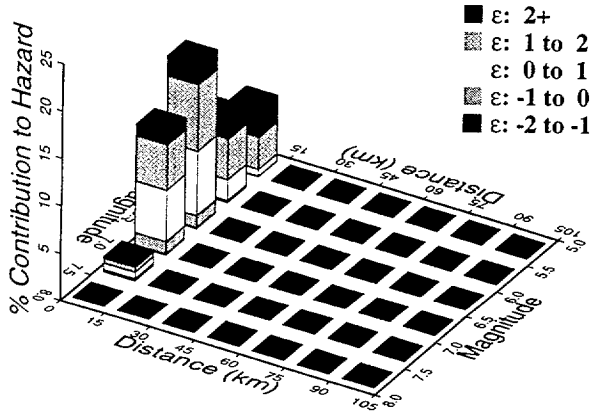

10 Hz, SDO Local Faults (Mult.)

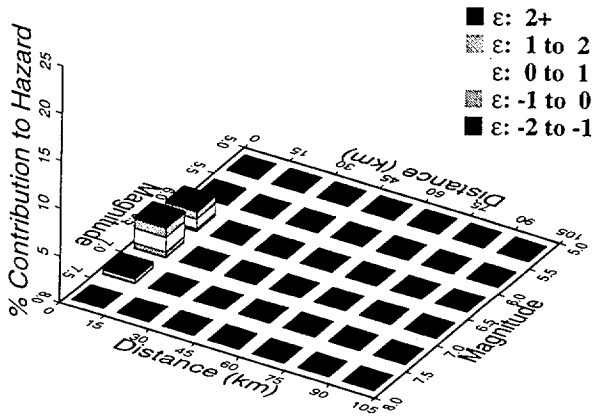

Figure 7-163 Magnitude-distance-epsilon distributions for the four source types: SDO team, 10-Hz horizontal spectral acceleration

1 Hz, SDO Area Sources

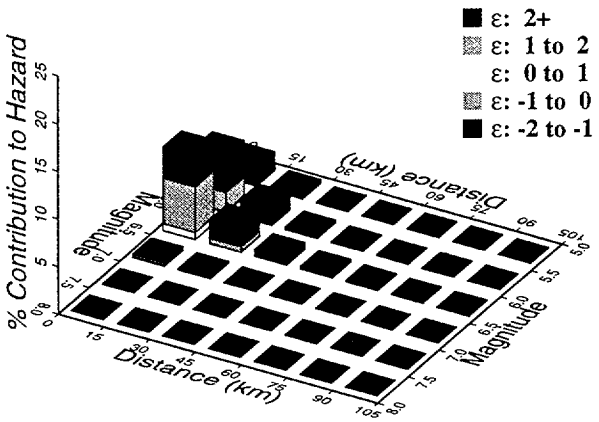

1 Hz, SDO Regional Faults

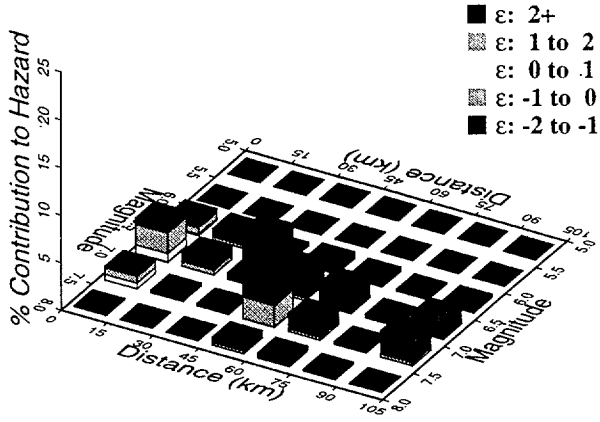

1 Hz, SDO Local Faults (Single)

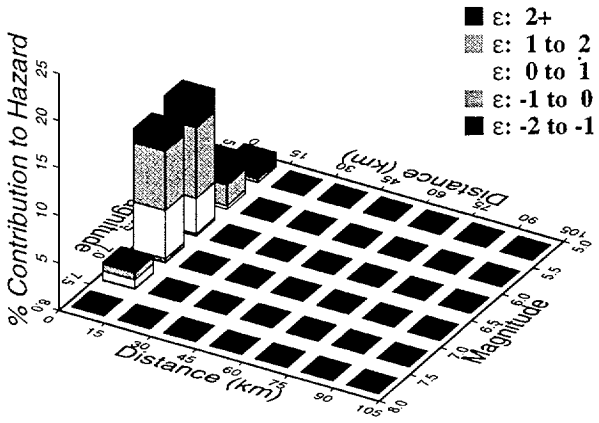

1 Hz, SDO Local Faults (Mult.)

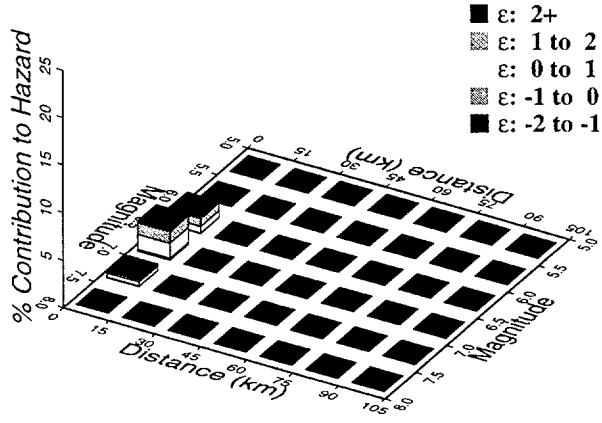

Figure 7-164 Magnitude-distance-epsilon distributions for the four source types: SDO team, 1-Hz horizontal spectral acceleration

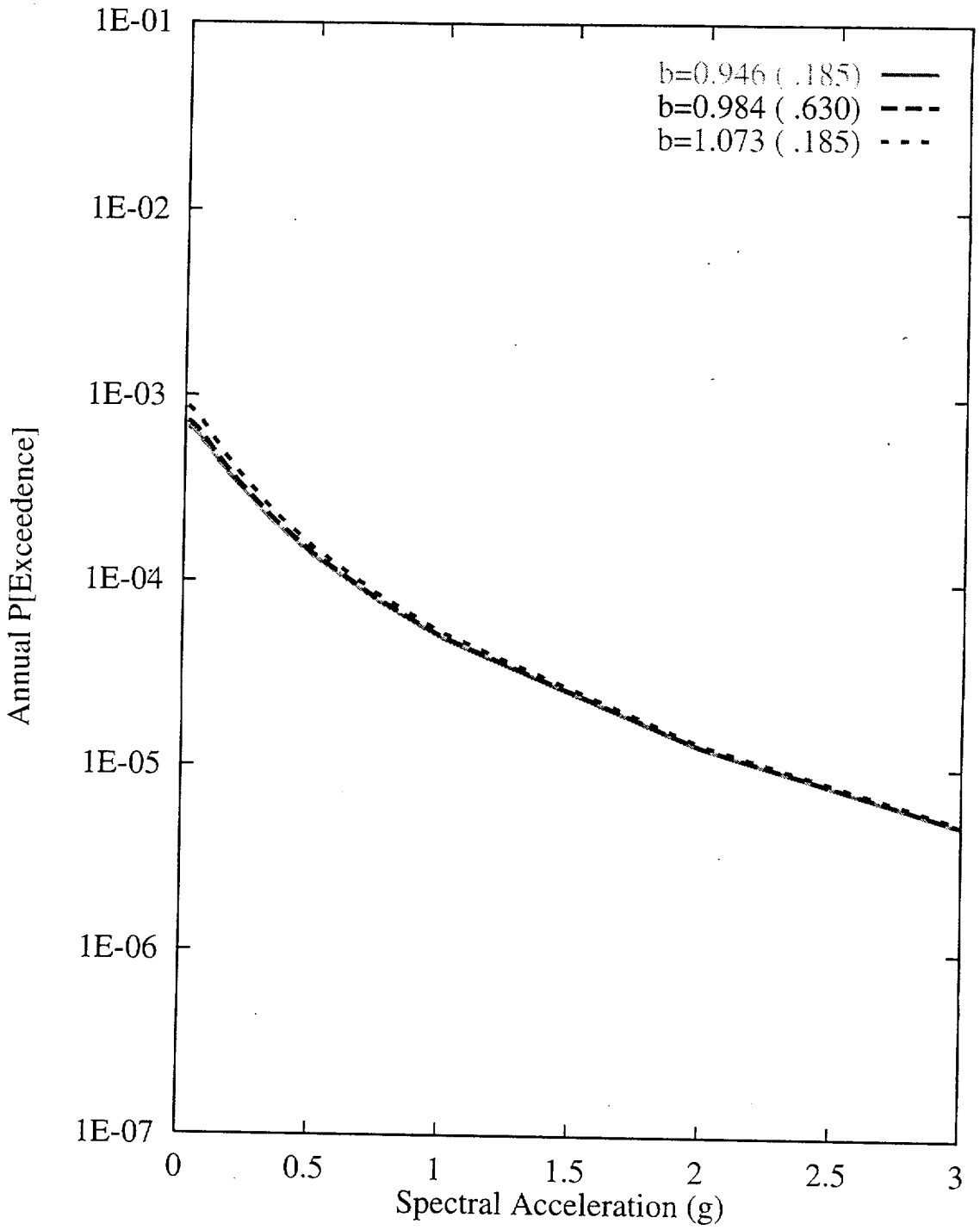

Figure 7-165 Sensitivity of seismic hazard from local faults to b-value: SDO team, 10-Hz horizontal spectral acceleration

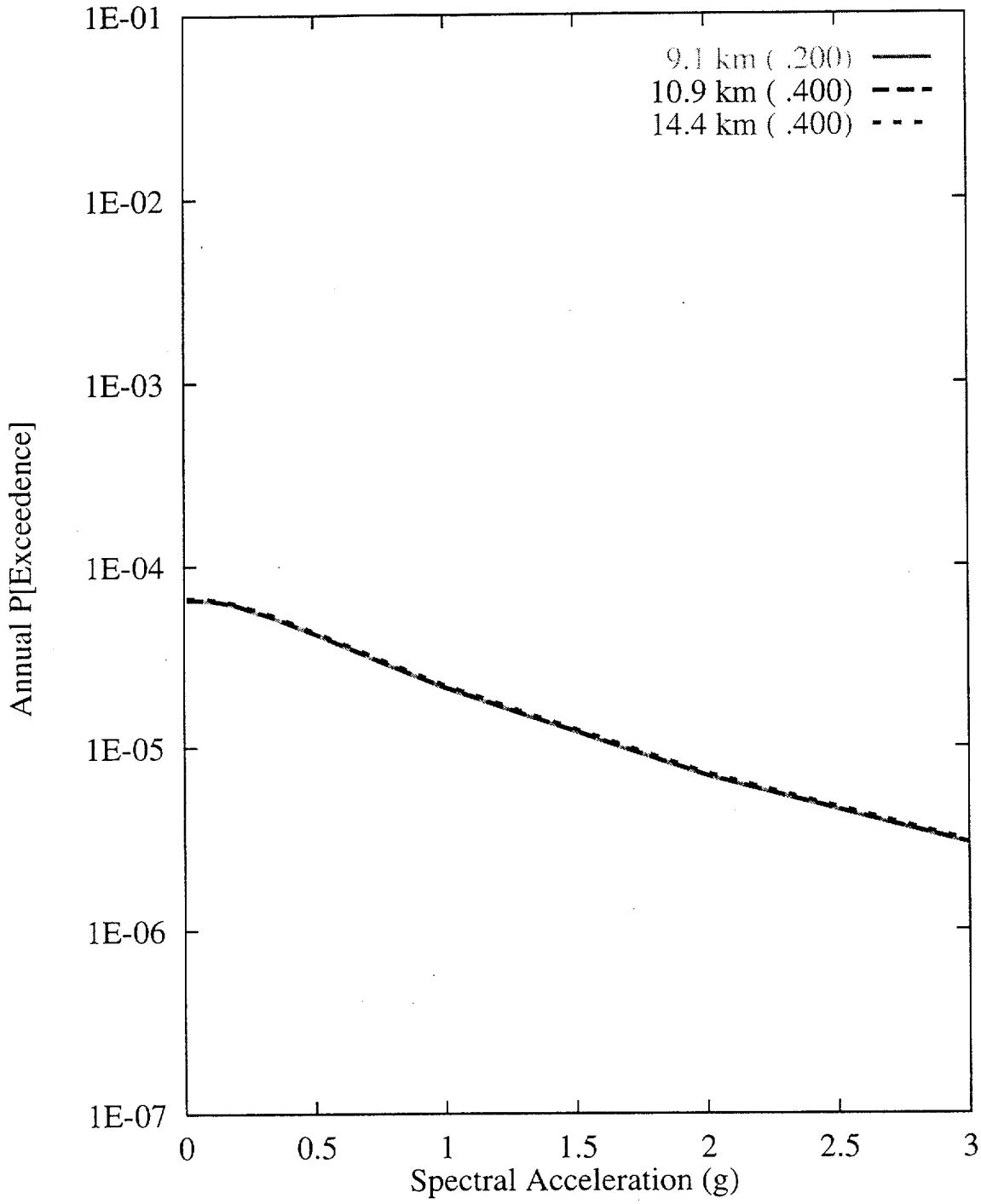

Figure 7-166 Sensitivity of seismic hazard from local faults to maximum depth of the Solitario Canyon fault: SDO team, 10-Hz horizontal spectral acceleration

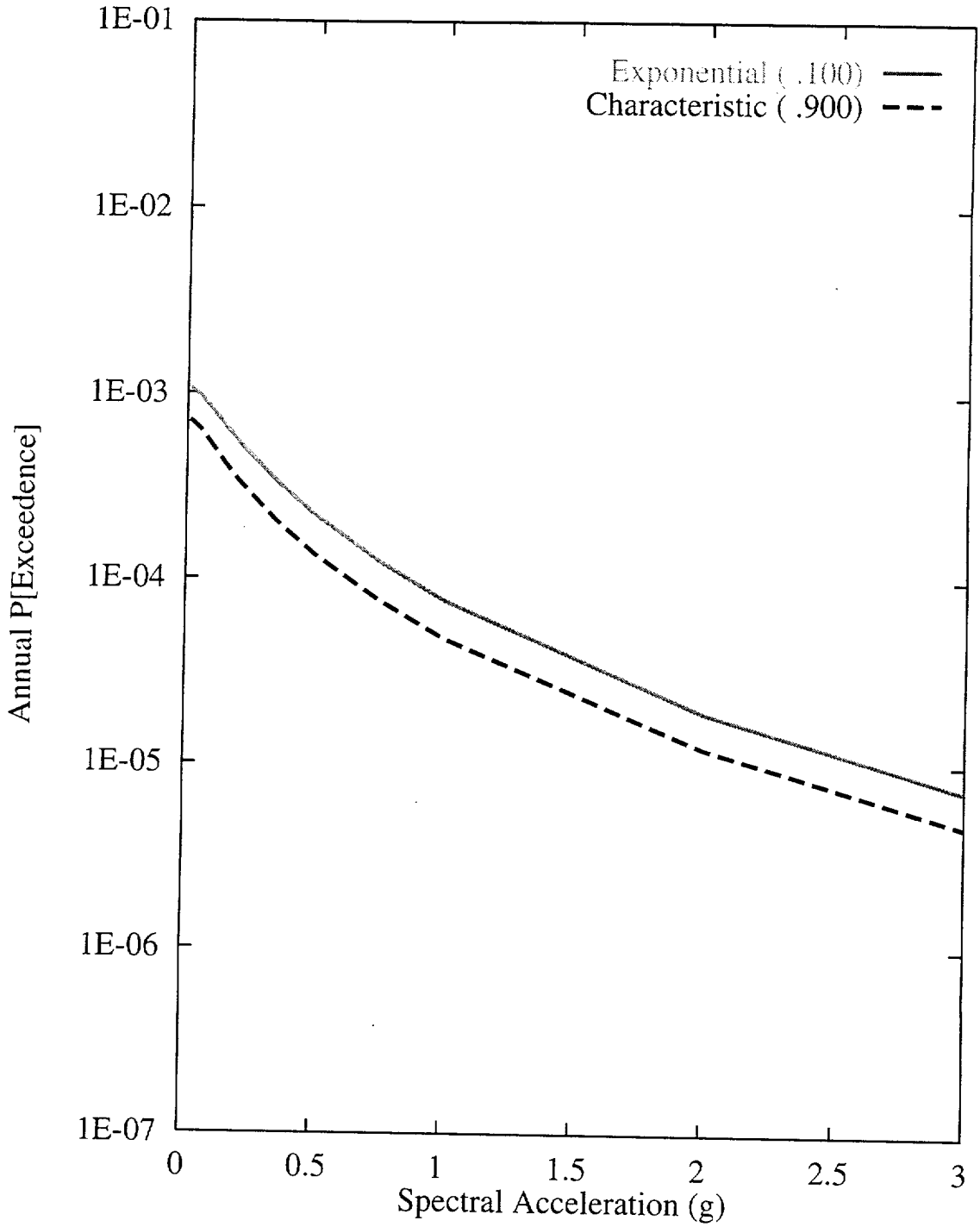

Figure 7-167 Sensitivity of seismic hazard from local faults to recurrence model of the Solitario Canyon fault: SDO team, 10-Hz horizontal spectral acceleration

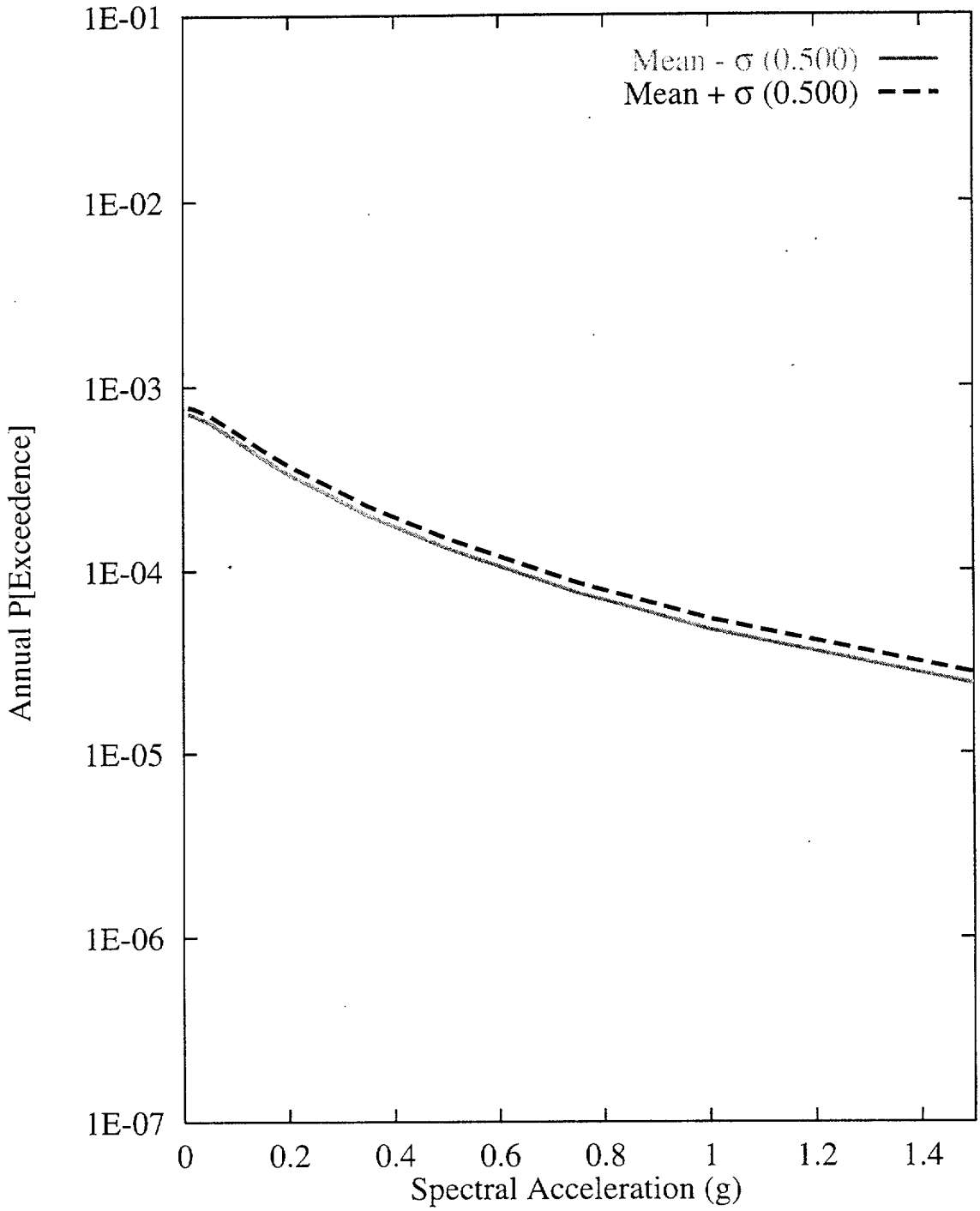

Figure 7-168 Sensitivity of seismic hazard from local faults to Mmax for the Solitario Canyon fault: SDO team, 10-Hz horizontal spectral acceleration

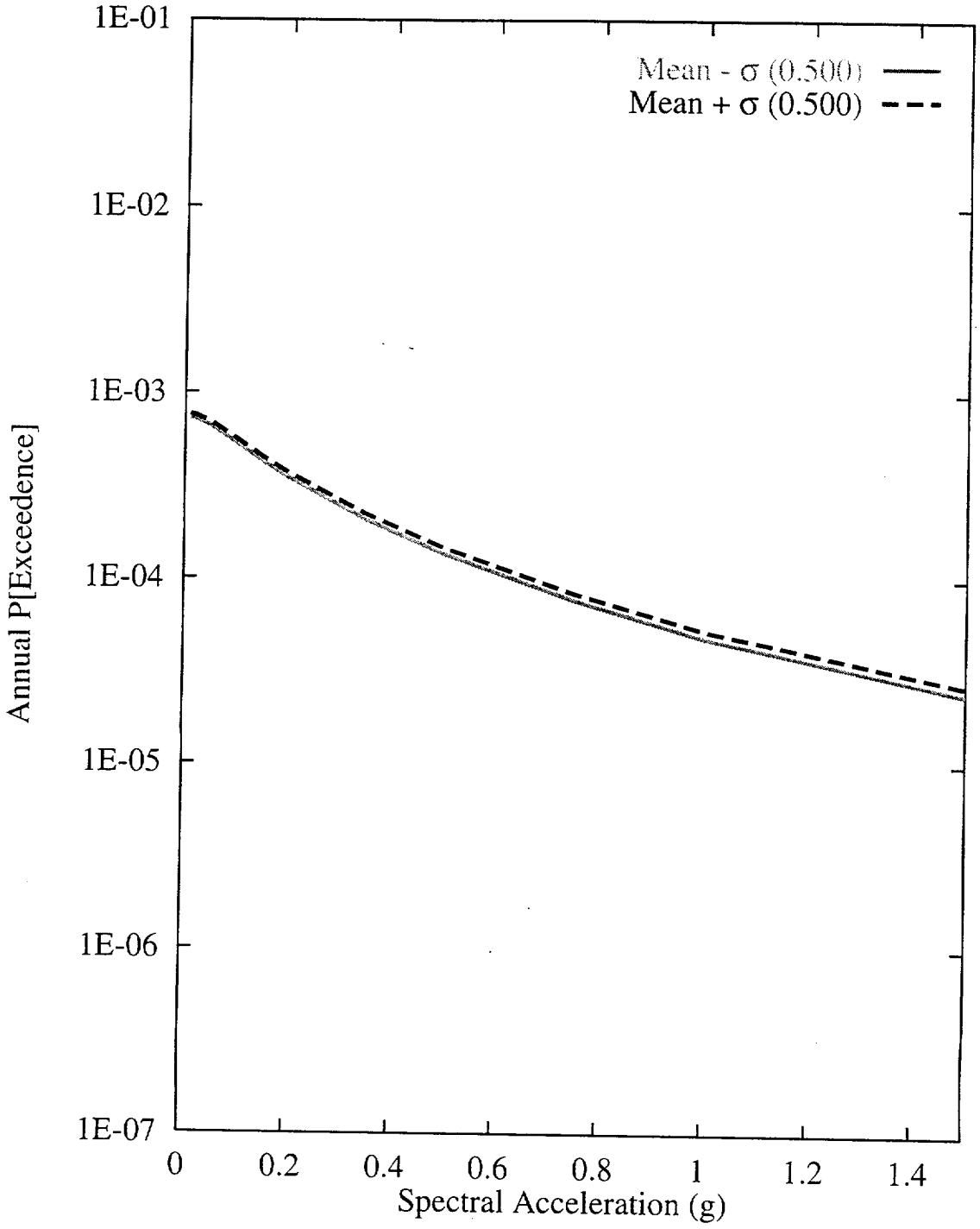

Figure 7-169 Sensitivity of seismic hazard from local faults to recurrence of the Solitario Canyon fault: SDO team, 10-Hz horizontal spectral acceleration

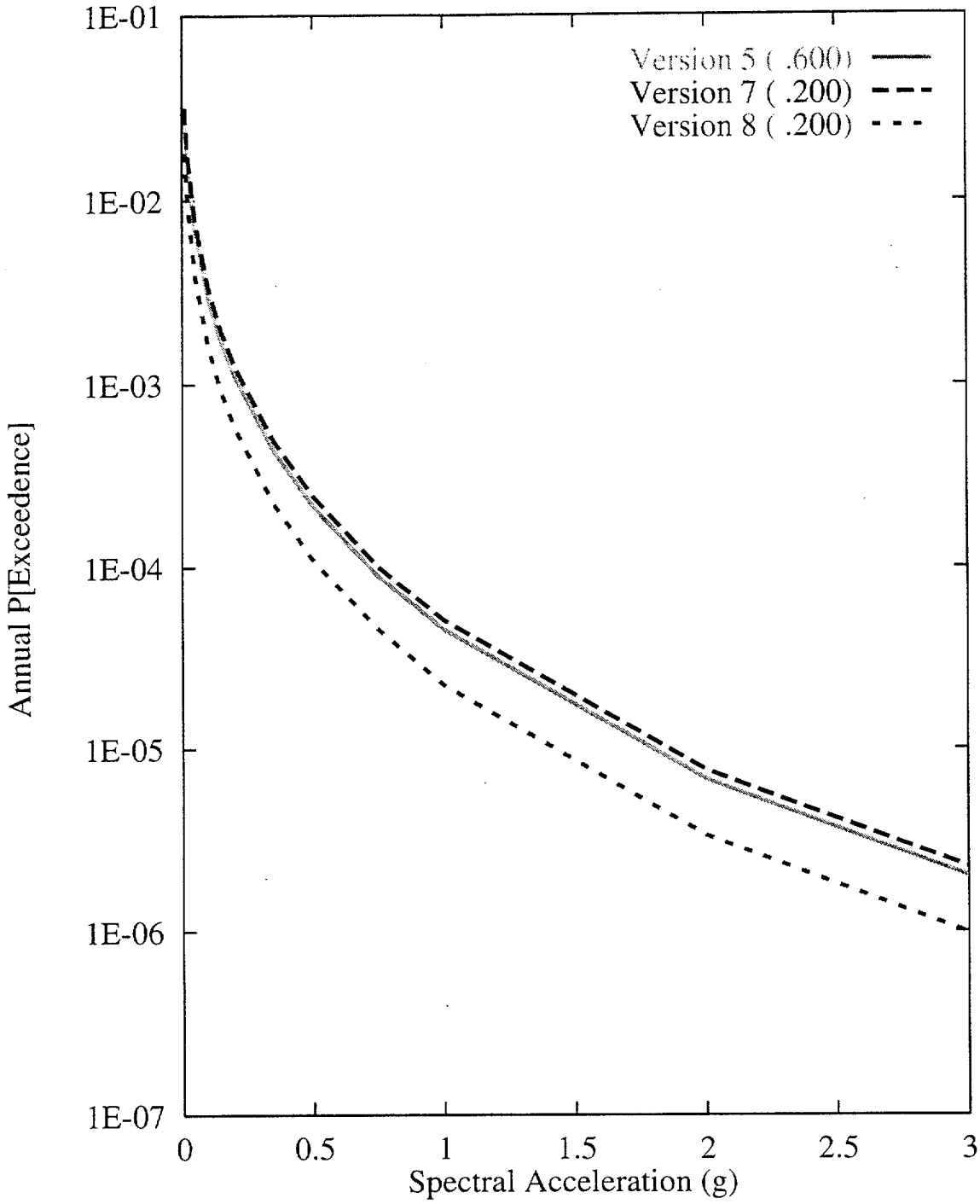

Figure 7-170 Sensitivity of seismic hazard from area zones to choice of seismicity catalog: SDO team, 10-Hz horizontal spectral acceleration

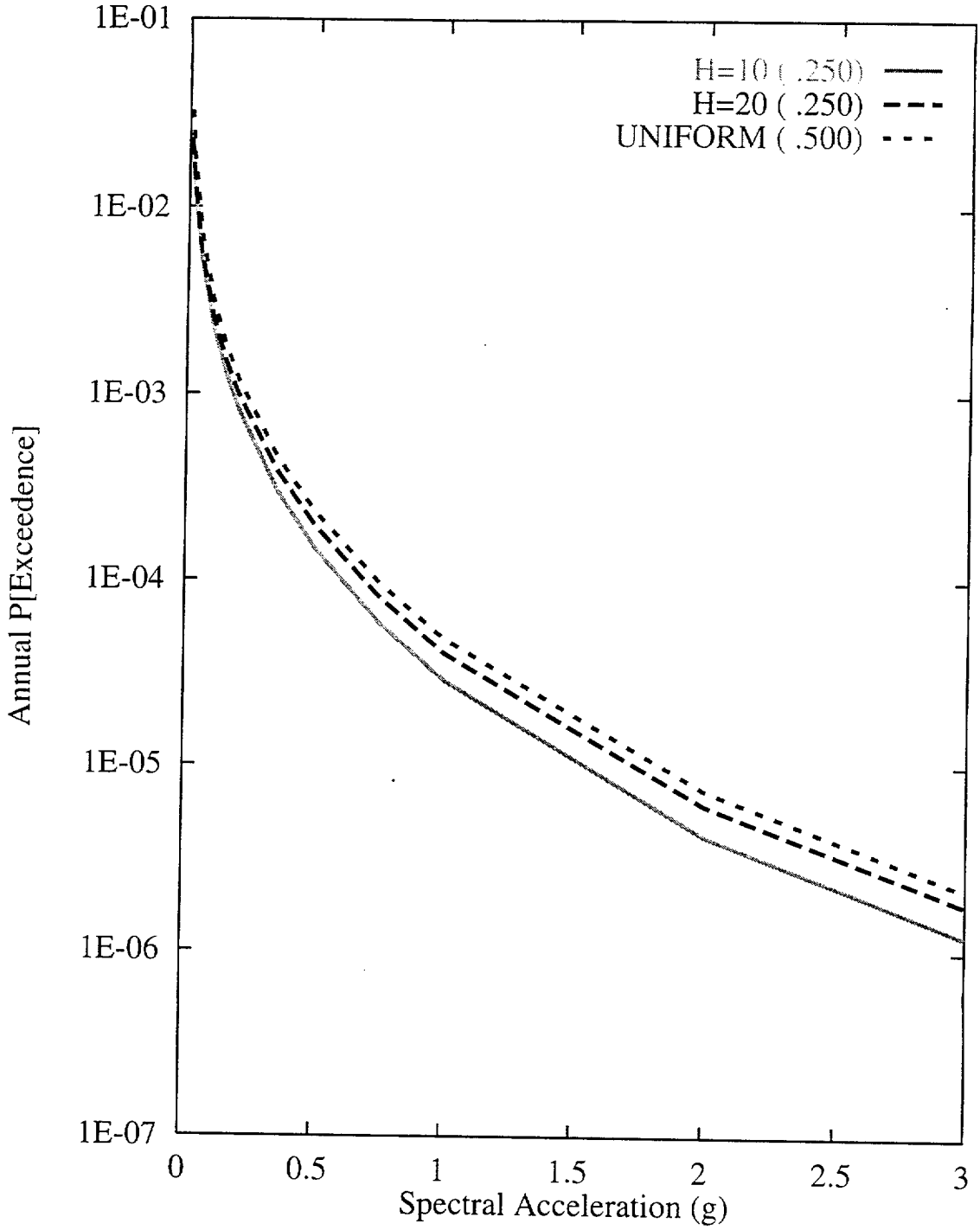

Figure 7-171 Sensitivity of seismic hazard from area zones to spatial variability and smoothing (H) of seismicity: SDO team, 10-Hz horizontal spectral acceleration

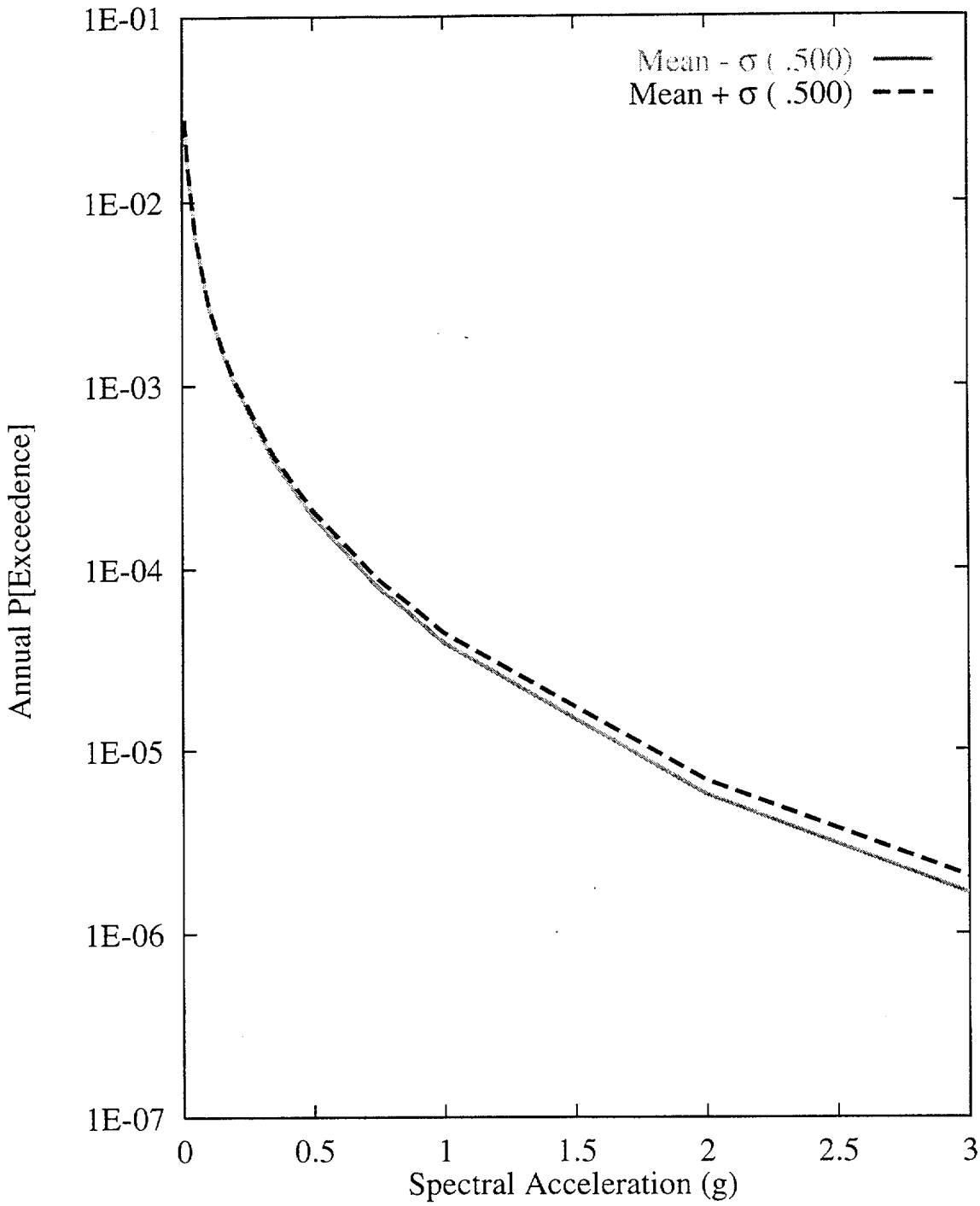

Figure 7-172 Sensitivity of seismic hazard from area zones to Mmax of the Z1 area zone: SDO team, 10-Hz horizontal spectral acceleration

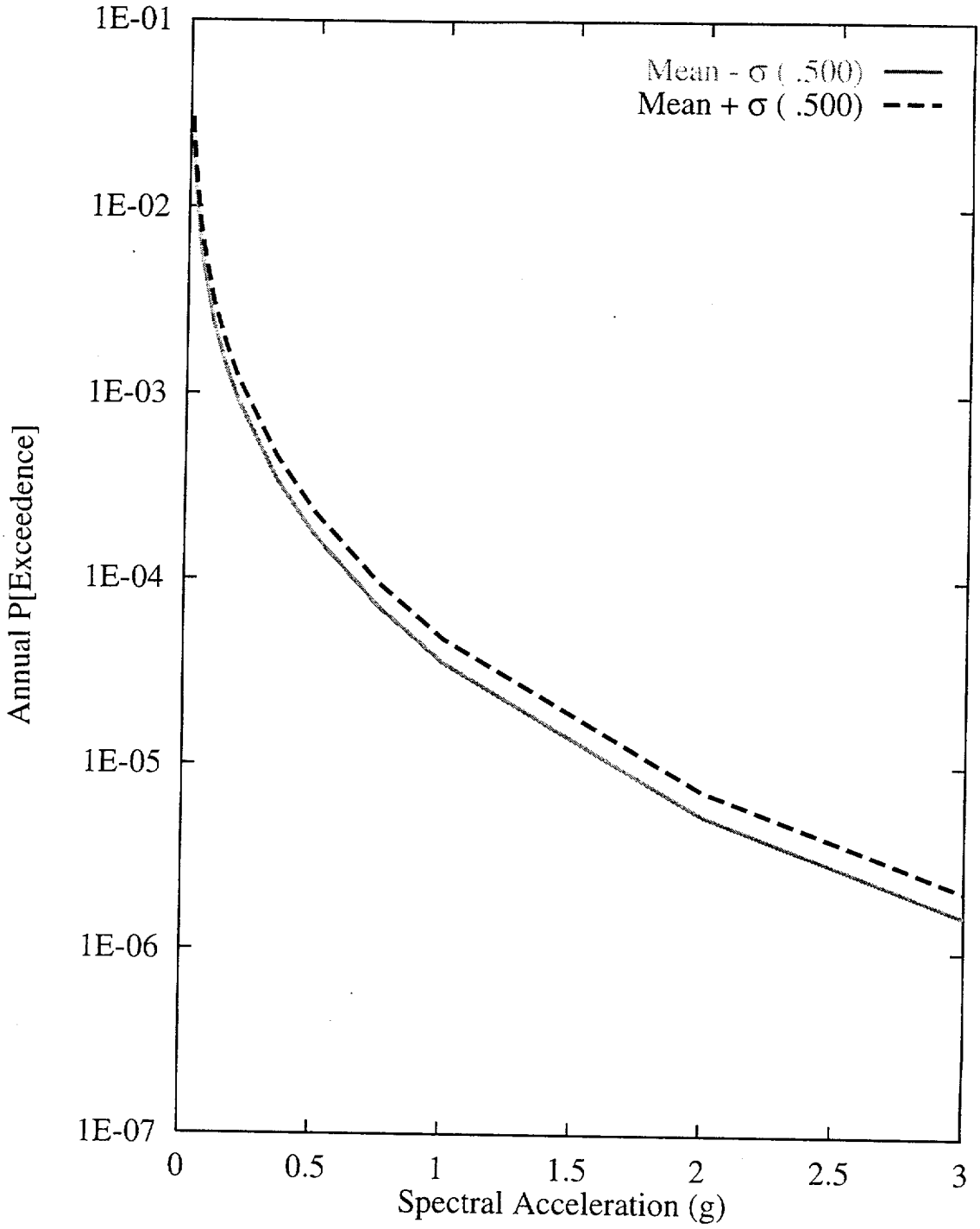

Figure 7-173 Sensitivity of seismic hazard from area zones to recurrence of the Z1 area zone: SDO team, 10-Hz horizontal spectral acceleration

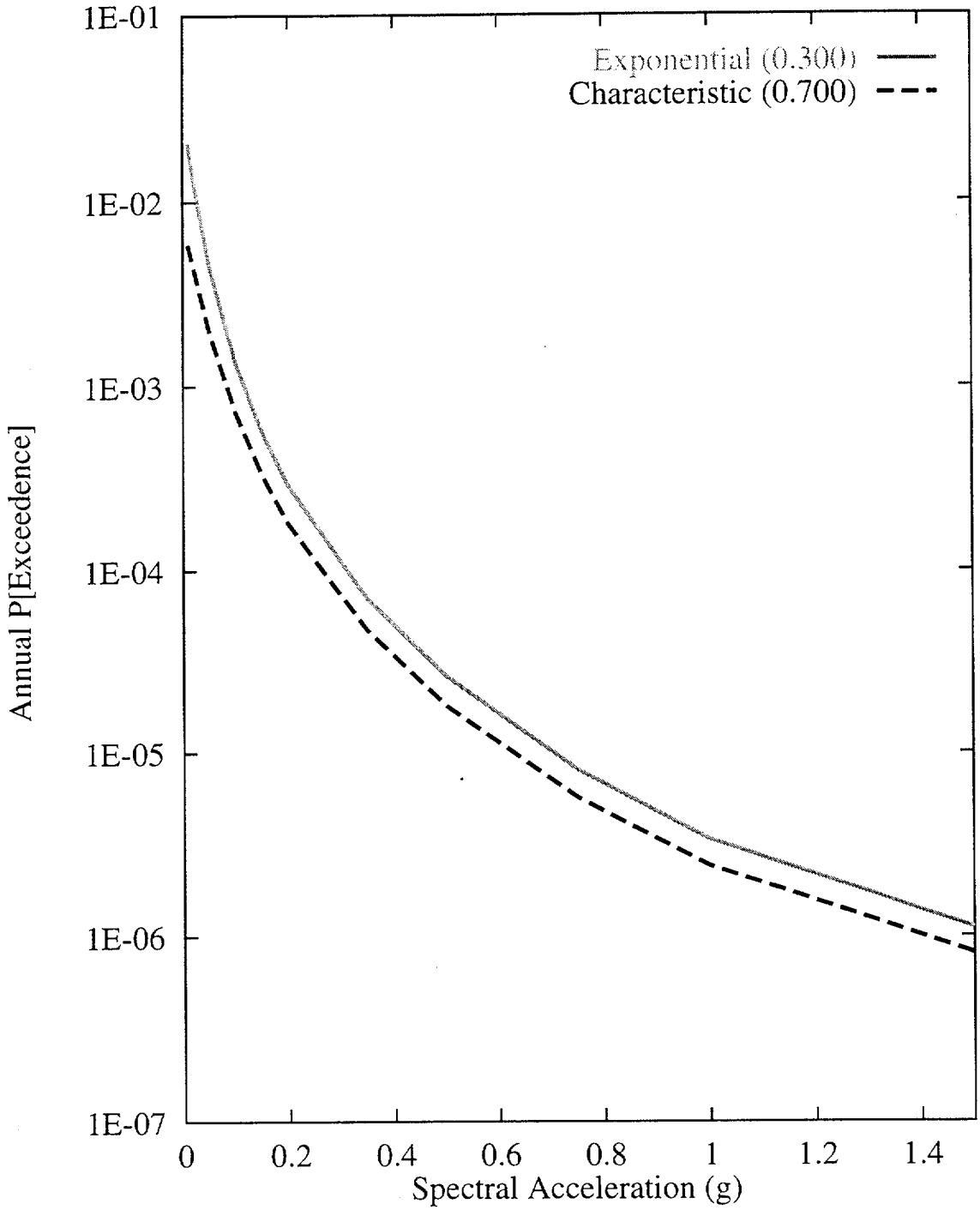

Figure 7-174 Sensitivity of seismic hazard from regional faults to recurrence model: SDO team, 1-Hz horizontal spectral acceleration

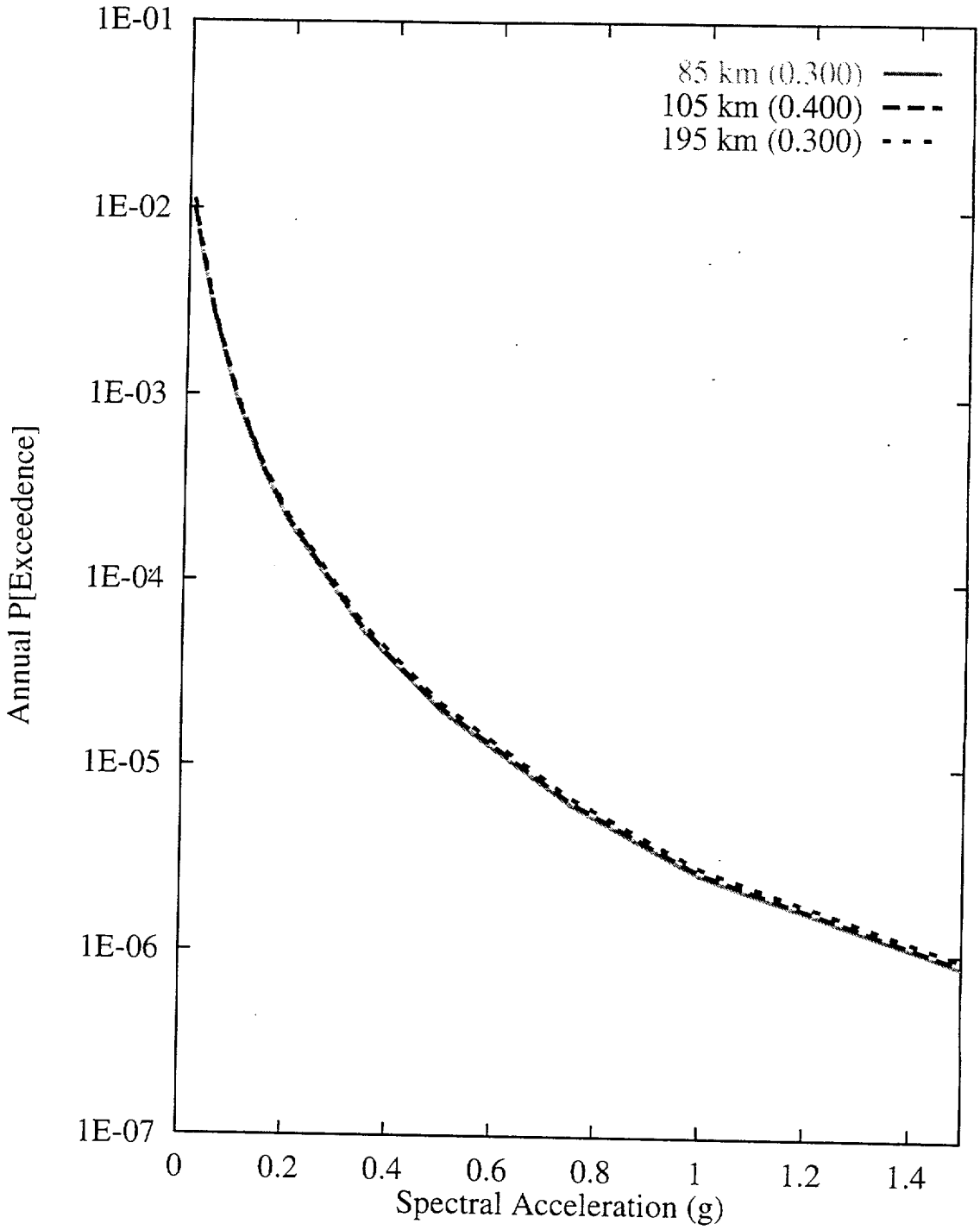

Figure 7-175 Sensitivity of seismic hazard from regional faults to length of the Furnace Creek fault: SDO team, 1-Hz horizontal spectral acceleration

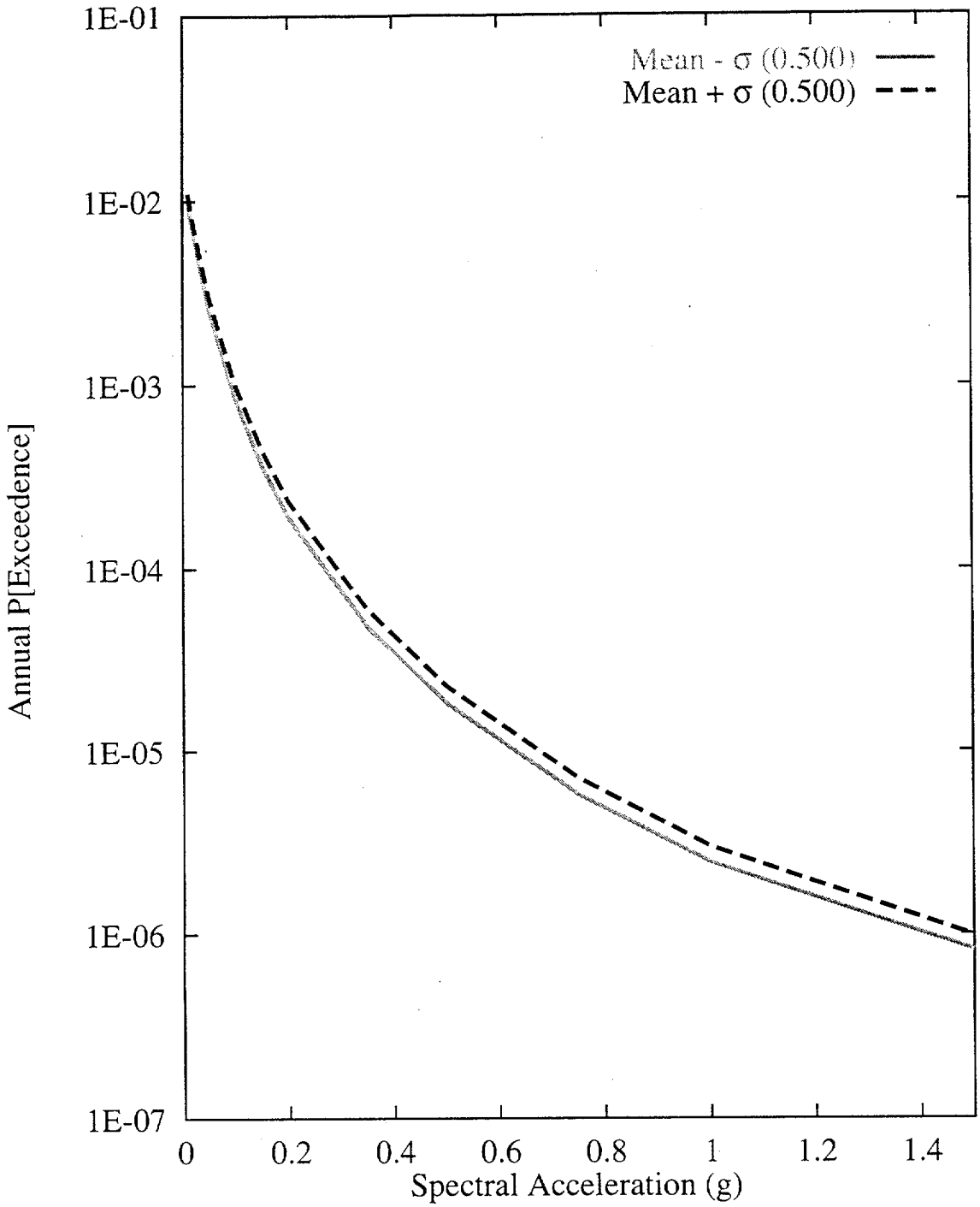

Figure 7-176 Sensitivity of seismic hazard from regional faults to Mmax for the Furnace Creek fault: SDO team, 1-Hz horizontal spectral acceleration

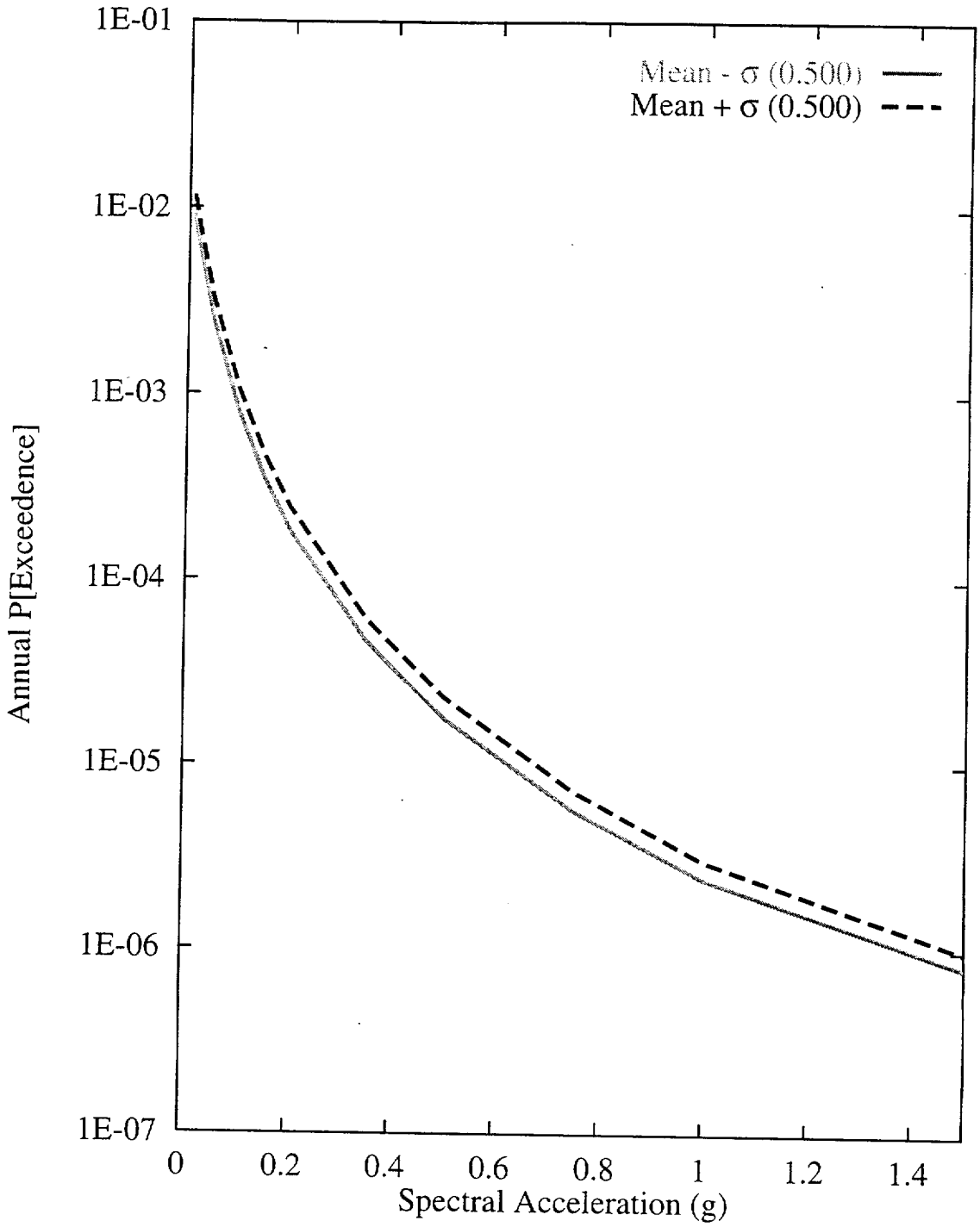

Figure 7-177 Sensitivity of seismic hazard from regional faults to recurrence of the Furnace Creek fault: SDO team, 1-Hz horizontal spectral acceleration

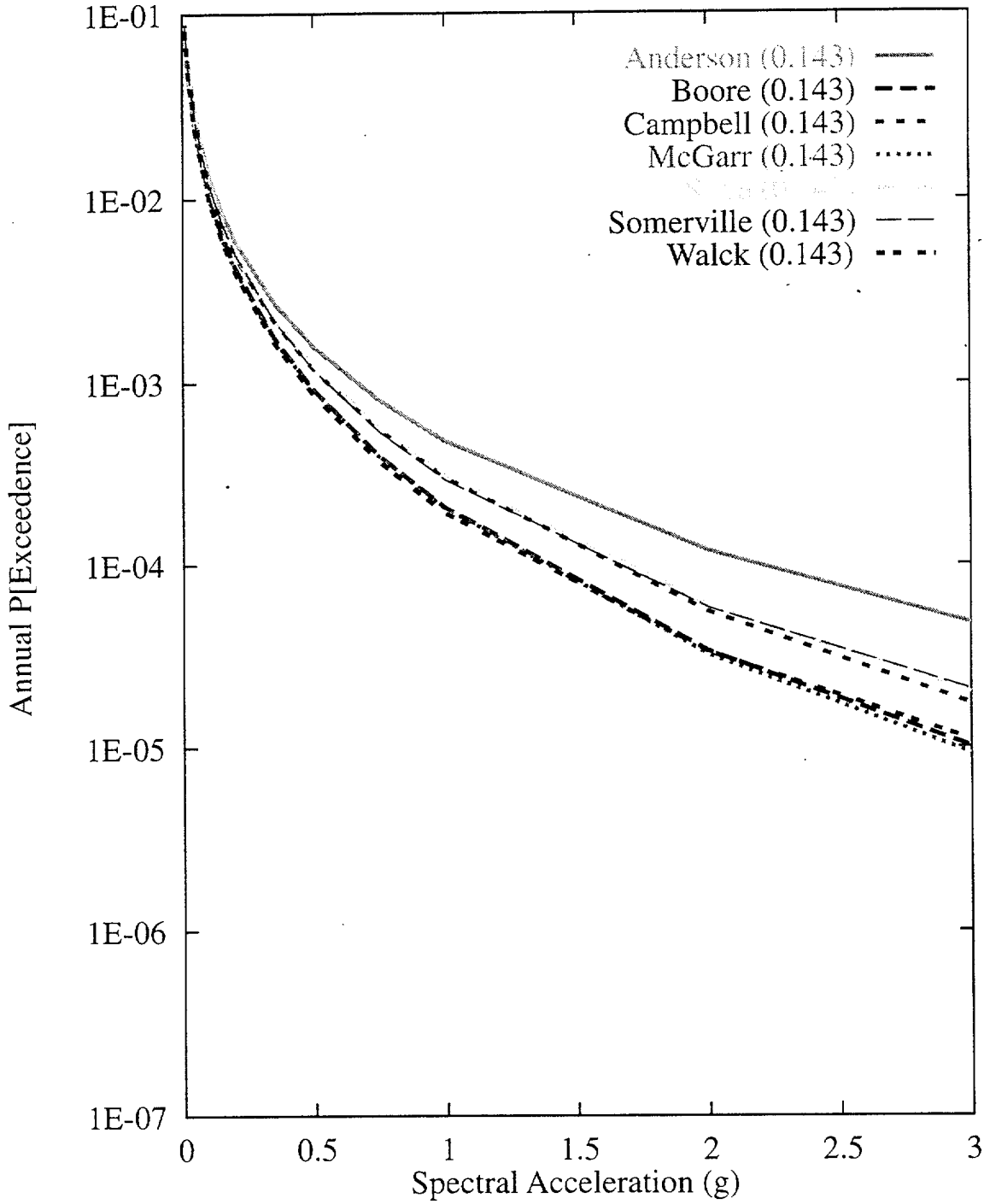

Figure 7-178 Sensitivity of seismic hazard to GM experts: ASM team, 10-Hz horizontal spectral acceleration

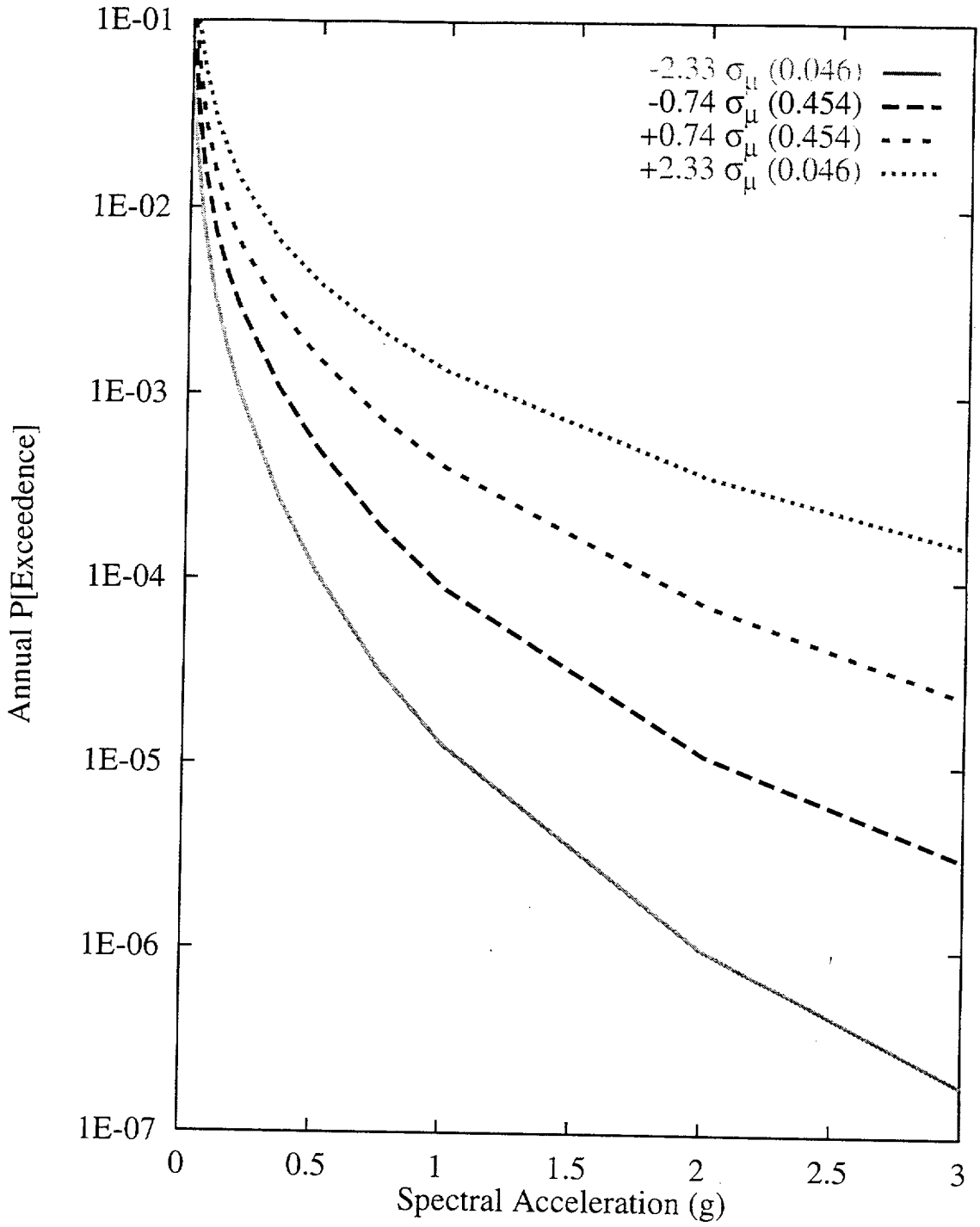

Figure 7-179 Sensitivity of seismic hazard to within-expert epistemic uncertainty in the median ground motion amplitude: ASM team, 10-Hz horizontal spectral acceleration

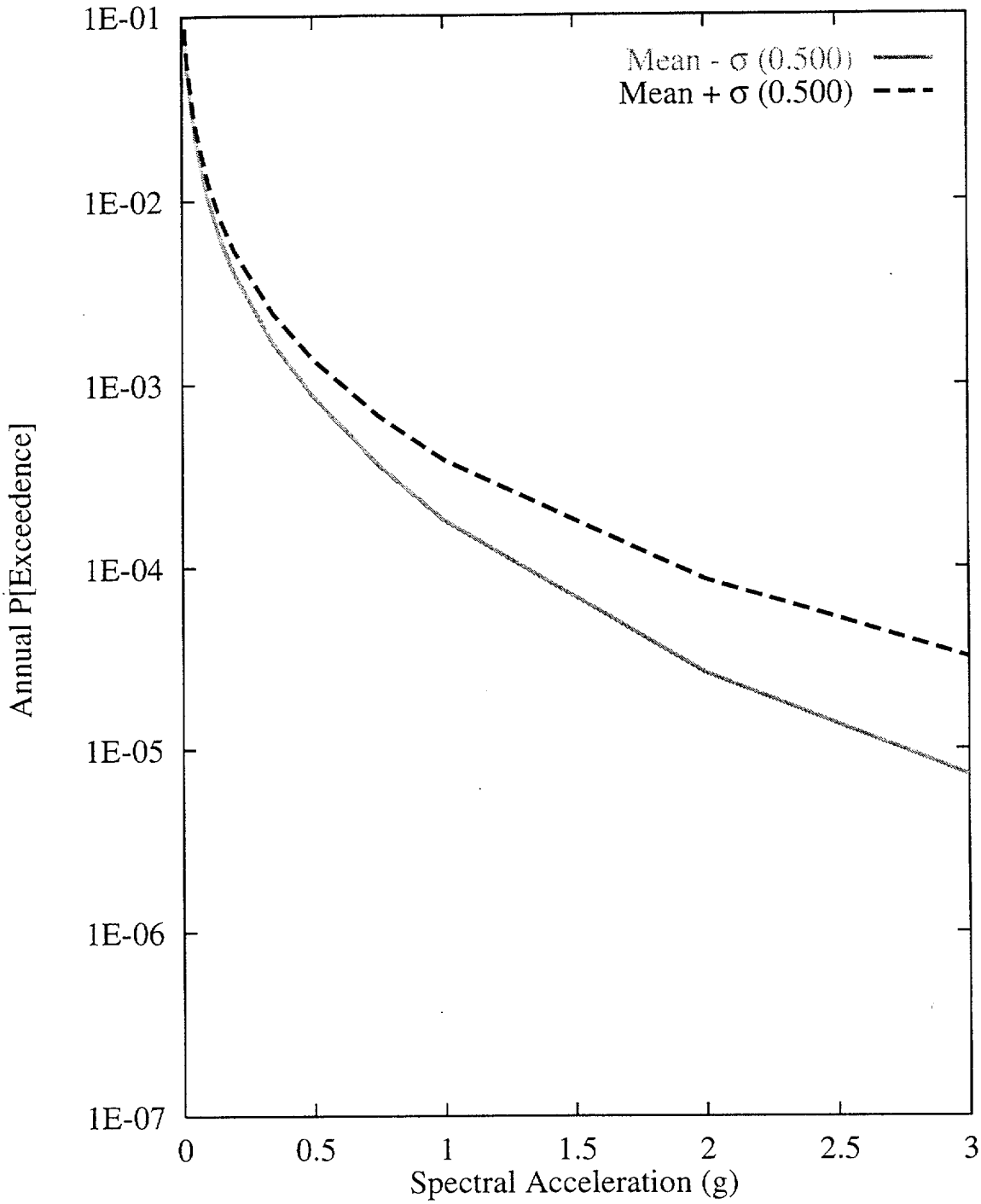

Figure 7-180 Sensitivity of seismic hazard to within-expert epistemic uncertainty in the standard deviation (sigma) of ground motion amplitude: ASM team, 10-Hz horizontal spectral acceleration

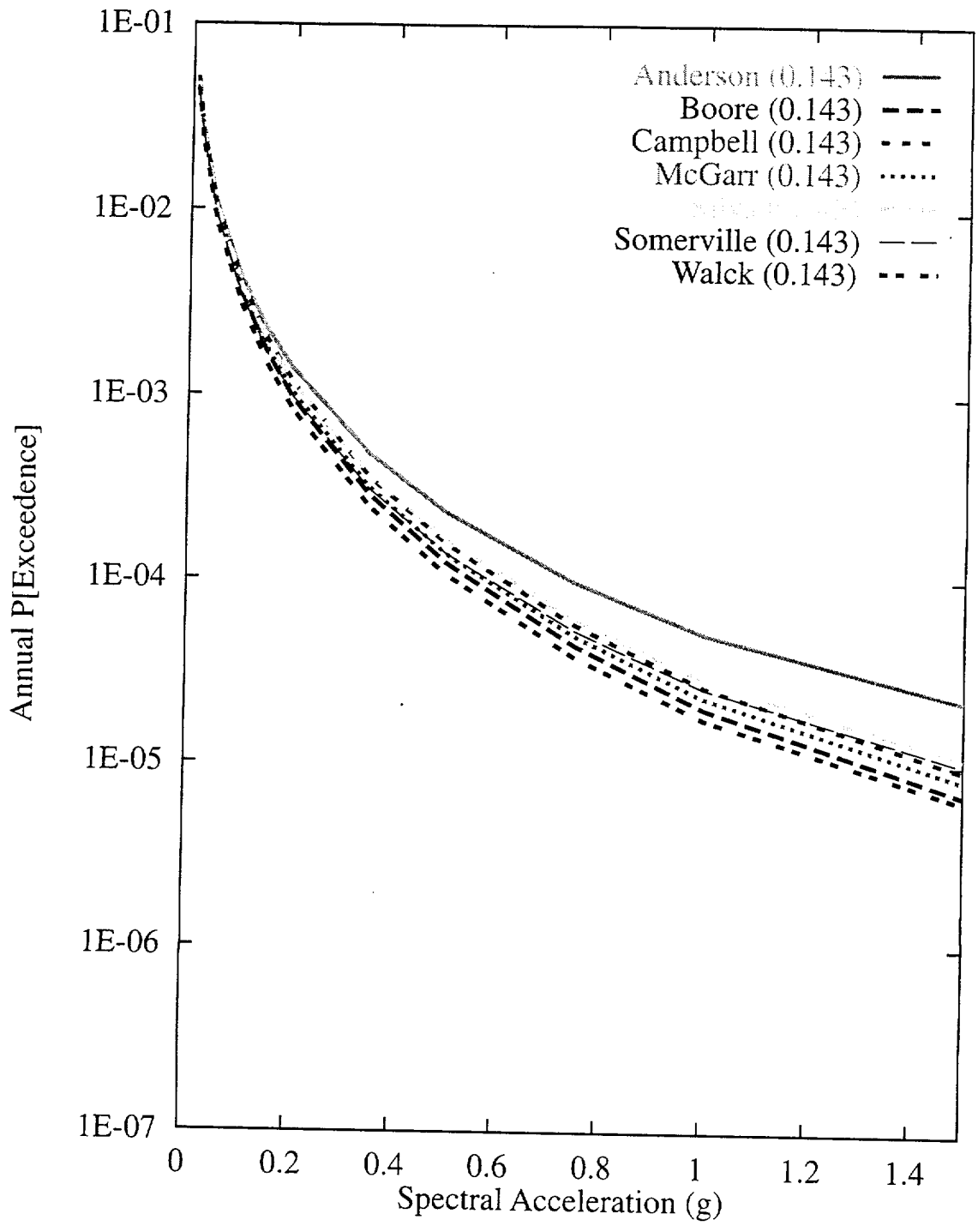

Figure 7-181 Sensitivity of seismic hazard to GM experts: ASM team, 1-Hz horizontal spectral acceleration

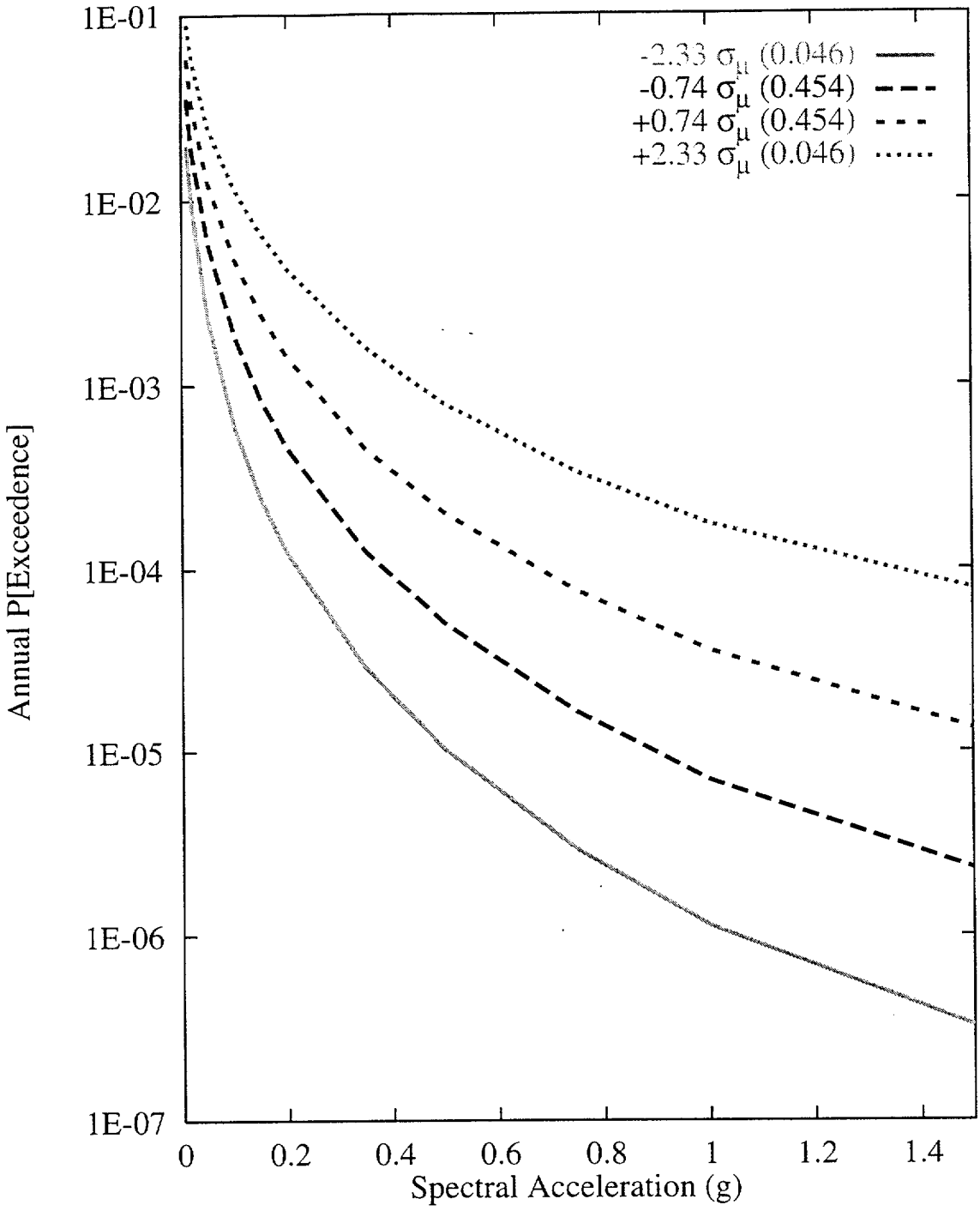

Figure 7-182 Sensitivity of seismic hazard to within-expert epistemic uncertainty in the median ground motion amplitude: ASM team, 1-Hz horizontal spectral acceleration

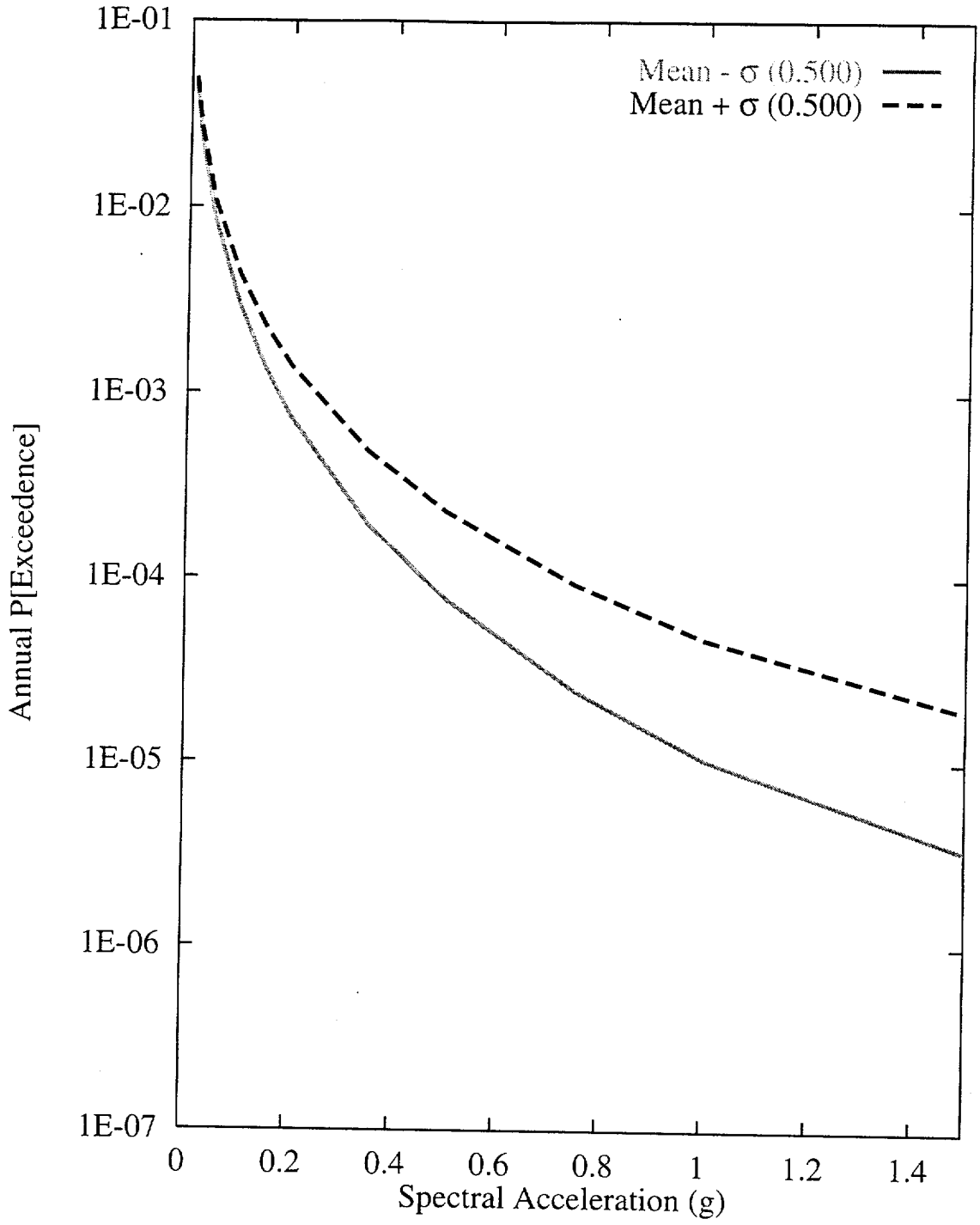

Figure 7-183 Sensitivity of seismic hazard to within-expert epistemic uncertainty in the standard deviation (sigma) of ground motion amplitude: ASM team, 1-Hz horizontal spectral acceleration

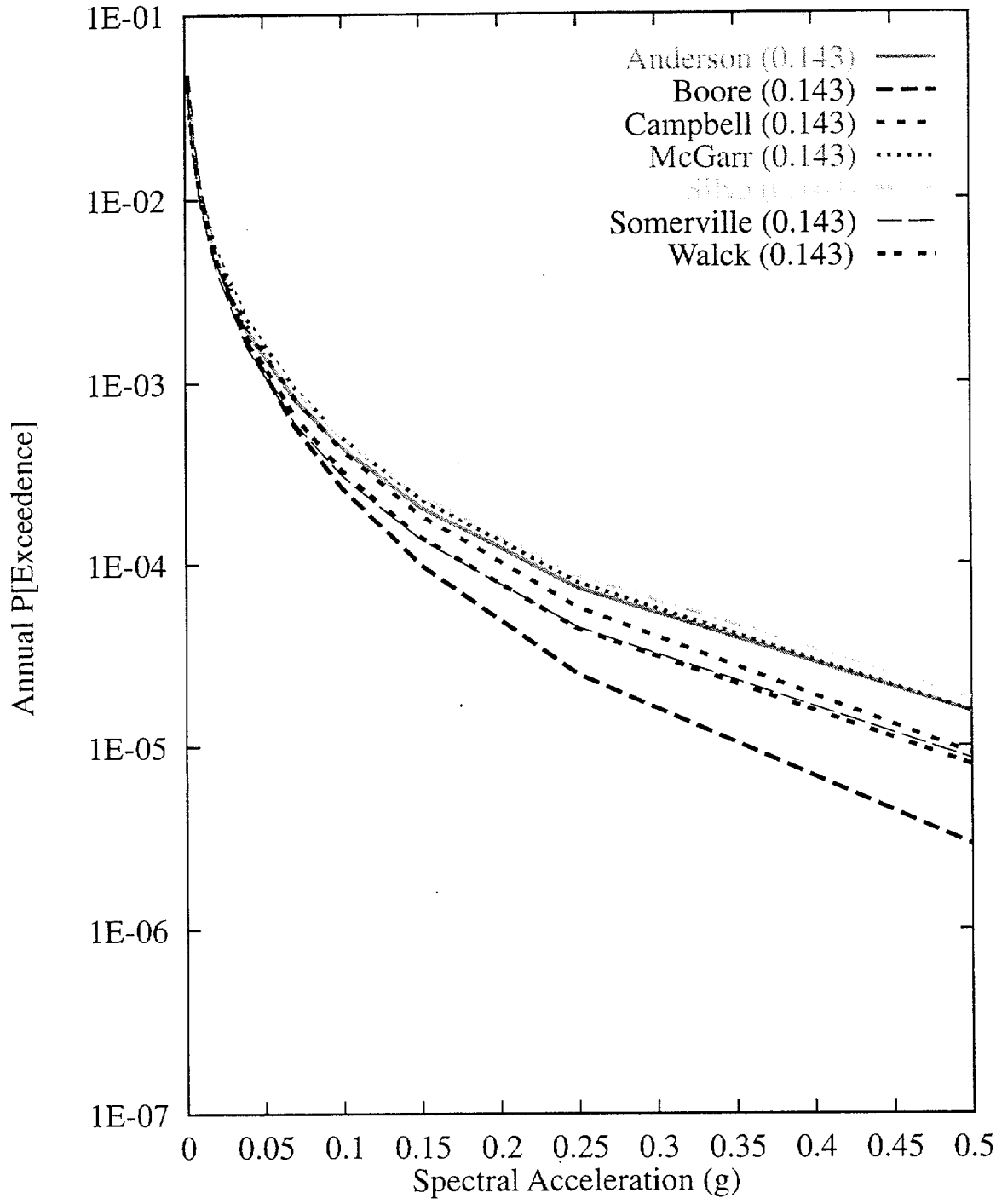

Figure 7-184 Sensitivity of seismic hazard to GM experts:
ASM team, 0.3-Hz horizontal spectral acceleration

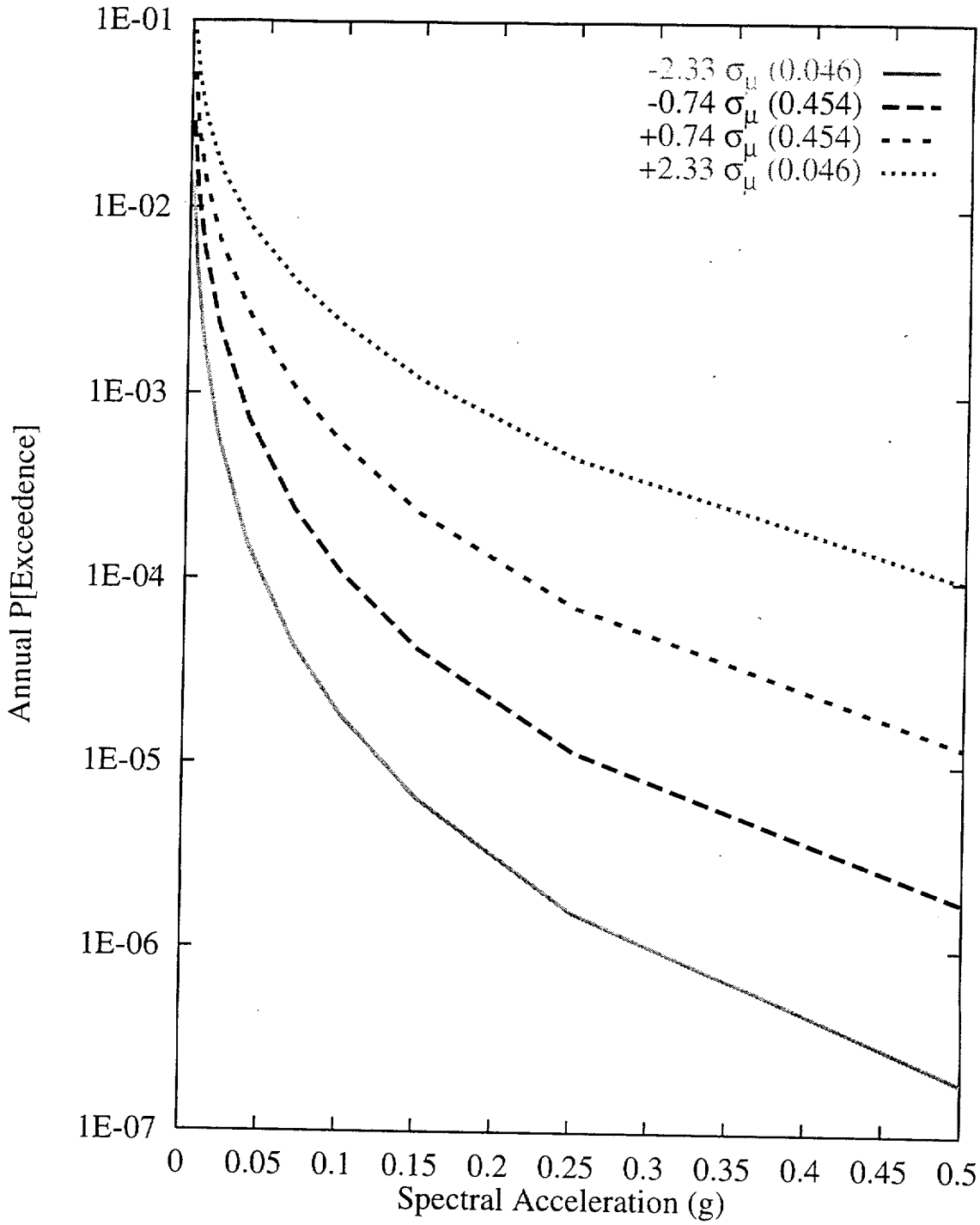

Figure 7-185 Sensitivity of seismic hazard to within-expert epistemic uncertainty in the median ground motion amplitude: ASM team, 0.3-Hz horizontal spectral acceleration

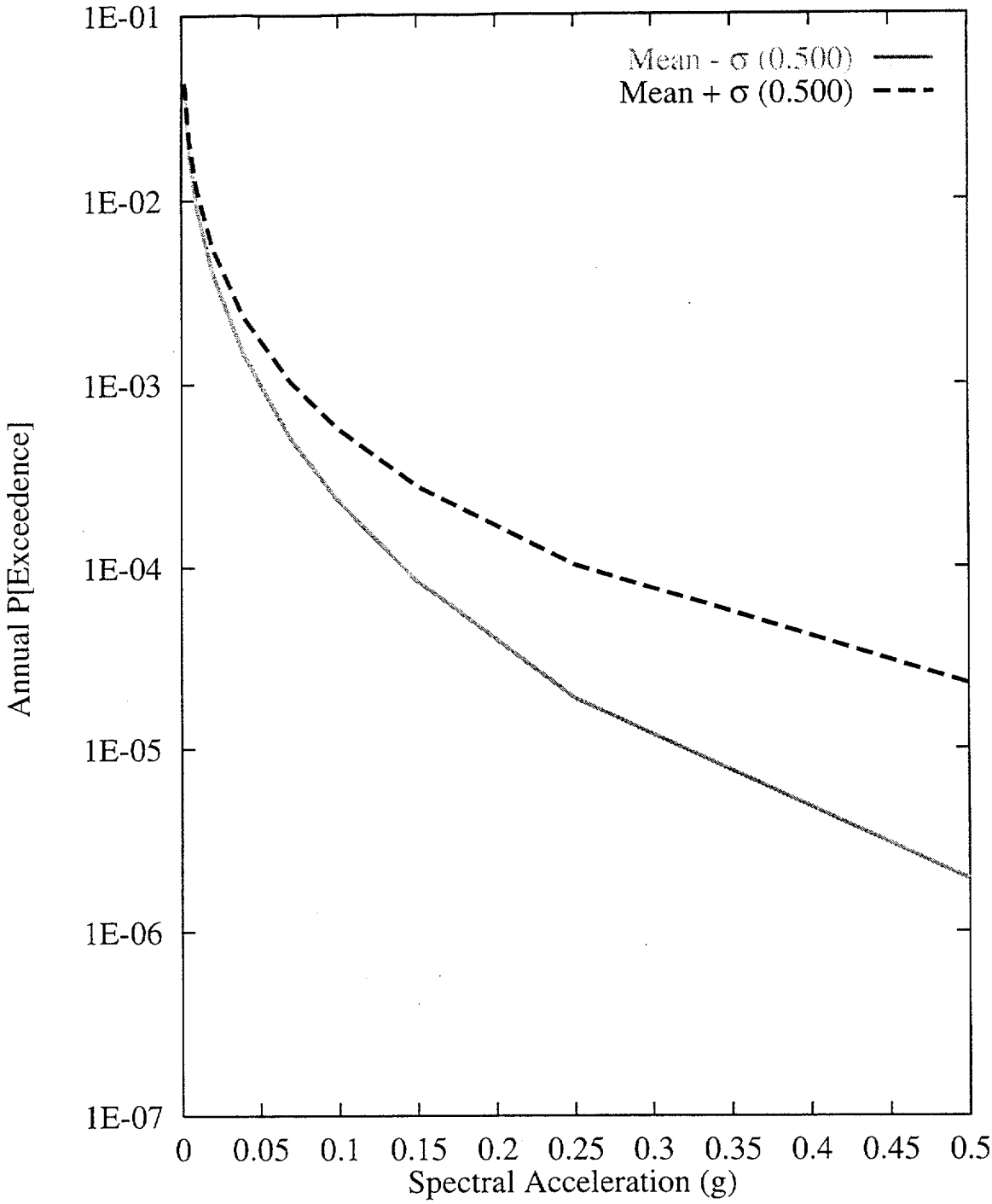

Figure 7-186 Sensitivity of seismic hazard to within-expert epistemic uncertainty in the standard deviation (sigma) of ground motion amplitude: ASM team, 0.3-Hz horizontal spectral acceleration

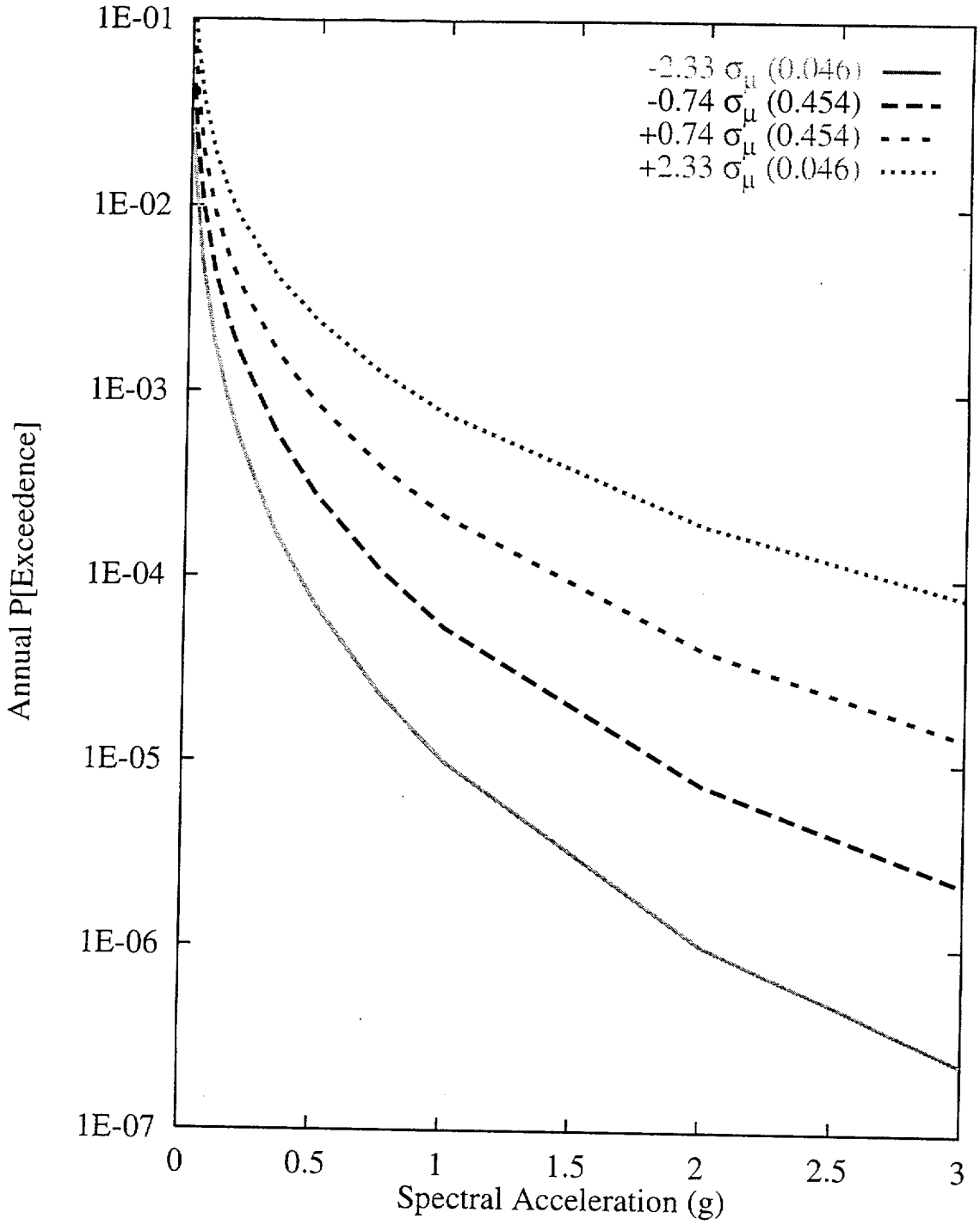

Figure 7-187 Sensitivity of seismic hazard to within-expert epistemic uncertainty in the median ground motion amplitude: ASM team, 10-Hz vertical spectral acceleration

8.0
PSHA METHODOLOGY AND RESULTS FOR FAULT DISPLACEMENT HAZARD

This section describes the methodology used to perform the probabilistic seismic hazard calculations for fault displacement at the Yucca Mountain site and the application of this methodology to nine points (referred to as "sites" in this chapter) within the Controlled Area. Section 8.1 introduces the PSHA methodology for assessing fault displacement hazard. This presentation uses many of the elements and concepts from the ground motion PSHA, which were introduced and described in Chapter 7.0. Section 8.2 presents the results for all nine demonstration sites, including sensitivity analyses.

8.1 PSHA METHODOLOGY FOR FAULT DISPLACEMENT

Fault displacement PSHA results in the probability that the tectonically induced fault displacement at a given site will exceed any value. The site of interest may or may not be on an active fault. Results are in the form of fault displacement hazard curves, which show annual exceedence probability for values of the displacement.

Of the two approaches for fault displacement PSHA described in Section 4.2, the earthquake approach calculates the principal and distributed faulting separately, using different attenuation equations, and then adds them to obtain a total displacement hazard curve. The displacement approach, on the other hand, considers both principal and distributed faulting but does not distinguish between them.

8.1.1 Earthquake Approach

The earthquake approach explicitly considers earthquake magnitudes and locations as intermediate variables in the calculation of fault displacement and uses the same seismic source models (i.e., source geometries and magnitude-recurrence models, and their associated uncertainties) that are used in the ground motion PSHA. The only substantive difference between the earthquake approach for fault displacement PSHA and the ground motion

analysis described in Section 7.0 relates to the attenuation equations. These differences fall into the following two categories:

1. Because both principal and distributed faulting are non-uniformly distributed, there is a probability of no displacement at the site under consideration, given the occurrence of an earthquake in the vicinity of the site. Thus, the attenuation equation is written as the product of two terms: (1) the probability of nonzero displacement given the occurrence of an earthquake of certain characteristics at a given location and (2) the probability that the displacement at the site will exceed a value d*, given non-zero displacement.

2. Both the probability of nonzero displacement and the conditional probability on the amount of displacement depend on a number of quantities besides magnitude and distance. These quantities may be grouped into three categories: (1) geometry of the site relative to the rupture (particularly the along-rupture location x/L defined in Figure 8-1), (2) characteristics of the principal fault (e.g., total length, cumulative displacement), and (3) characteristics of the feature where the site is located (e.g., total length, cumulative displacement).

The resulting attenuation equations for fault displacement are of the form

$$G_D\left(d^* \middle| M, \underline{R}, \underline{X}_{principal}, \underline{X}_{site}\right) = P[D > 0 | M, \underline{R}, \underline{X}_{principal}, \underline{X}_{site}] \times P\left[D > d^* \middle| D > 0, M, \underline{R}, \underline{X}_{principal}, \underline{X}_{site}\right] \quad (8\text{-}1)$$

where $\underline{R}$ represents the location of the rupture relative to the site (not just distance), and $\underline{X}_{principal}$ and $\underline{X}_{site}$ represent characteristics of the principal fault and site (all quantities in $\underline{X}_{principal}$ and $\underline{X}_{site}$ will be represented by $\underline{X}$ for the sake of brevity). Separate attenuation equations are developed for principal and distributed faulting. The attenuation equation for principal faulting is used only in conjunction with the fault where the site is located, if that fault is active. The attenuation equation for distributed faulting is used for all other faults and for the areal source zone containing the site.

The calculation of fault displacement hazard, considering all seismic sources and all earthquake magnitudes, is performed using a modified version of Equation 7-1, namely

$$v(d^*) = \sum_i \nu_i \iint_{\underline{r}\, m} G_D(d^* | m, \underline{r}, \underline{X}) f_{M(i)}(m) f_{\underline{R}_{(i)|M(i)}}(\underline{r}; m)\, dm\, d\underline{r} \qquad (8\text{-}2)$$

where i indicates source number, ν_i is the rate of earthquakes on source i, $f_{M(i)}(m)$ is the probability density function of magnitude, and $f_{\underline{R}_{(i)|M(i)}}(\underline{r}; m)$ is the probability density function of earthquake location (given magnitude). The calculation of fault displacement hazard given by the equation above is performed for multiple values of d^*. The result is a hazard curve, which gives the annual probability of exceedance as a function of d^*.

As in the case of ground motions, the primary interest is focused on computing probabilities for large but rare displacements. As a result, the probability of two or more events with $D > d^*$ in one year is negligible. Thus, the quantity on the right side of Equation 8-2, which is the annual rate of earthquakes with displacement $D > d^*$ is a very good approximation to the probability of exceeding displacement d^* in one year. If the quantity of interest is the maximum single-event fault displacement during a long time period T, one can use the equation $P\,[\,D_{max}\,(T) > d^*] = 1 - exp[-\nu(d^*)T]$. It should be emphasized that these hazard results are applicable to single events. If the quantity of interest is the cumulative displacement from one or more earthquakes over a long time period, which is not the intent in this study, it is necessary to use the theory of compound Poisson processes (Parzen, 1962).

8.1.2 Displacement Approach

The displacement approach uses a direct characterization of the occurrence rate of displacement events at the site and the probability distribution of displacement per event, without using earthquake magnitude and location as intermediate variables. The occurrence rate information may be provided as direct values of the rate λ or in the form of a slip rate SR. Specification of the probability distribution of displacement per event $P\,[D > d^* | \text{event}]$ is in

the form of a scale parameter (such as the average displacement per event $\overline{D}_E$, maximum displacement D_{max}, or cumulative displacement D_{cum}) and information about the shape and spread of the distribution.

Calculation of the fault displacement hazard curve for the displacement approach (under the assumption of rare events discussed above) is straightforward, namely:

$$\nu(d^*) = \lambda \; P[D > d^* | event] \tag{8-3}$$

8.1.3 Treatment of Uncertainty

As with the ground motion PSHA methodology (discussed in Section 7.1), the formulations given above for the earthquake and displacement approaches for the fault displacement PSHA represent the aleatory uncertainty in the natural phenomena of tectonically-induced fault displacement. Mathematically, aleatory uncertainty is represented by the rates and probability distributions in Equations 8-1, 8-2, and 8-3. Epistemic uncertainty is associated with imperfect knowledge about these phenomena. In the earthquake approach, epistemic uncertainty is in the seismic source characterization, the attenuation equations, and the characteristics of the site that affect fault displacement. In the displacement approach, epistemic uncertainty is in the two elements of the model, namely the rate information and the parameters of the displacement per event distribution, as well as in the characteristics of the site that affect fault displacement.

Epistemic uncertainties in seismic source characterization and fault displacement attenuation equations are quantified by considering inputs from the six SSFD expert teams, and by each team's own assessment of epistemic uncertainty. Each expert team selects an approach for fault displacement PSHA (earthquake, displacement, or a weighted combination of both), and then formulates multiple alternative interpretations for the fault displacement attenuation equations (if using the earthquake approach) or for the rate and the distribution of displacement per event (if using the displacement approach). Calculations for the earthquake approach consider each expert team's fault displacement attenuation equations in conjunction with that team's source characterization.

Further details on the fault displacement models developed by the six SSFD expert teams are provided in Sections 4.2 and 4.3.2 and in the expert summaries(Appendix E).

8.1.4 Implementation of Methodology for Fault-Displacement PSHA

In the following, the earthquake and displacement approaches are discussed in the context of the implementation of the PSHA methodology.

8.1.4.1 Earthquake Approach. Calculations for the earthquake approach consider all local faults, as well as the host area source zone(s). The regional faults do not contribute to distributed fault displacement because the distributed displacement attenuation equations decay rapidly with distance, given the models formulated by the SSFD expert teams.

The rate portion of the attenuation equations for principal displacement (i.e., the first term in Equation 8-1) consists of a portion that depends on x/L (i.e., unity for x/L in the interval [0,1], zero otherwise), and a magnitude-dependent portion. The magnitude-dependent portion is a logistic function of magnitude, except for one team that considers the probability distribution of hypocentral depth, the magnitude-dependent rupture width, and the down-dip geometry of the fault. The rate portion of the attenuation equations for fault displacement is a logistic function of magnitude and distance, or peak ground velocity at the site. The rate portion for distributed faulting also includes the probability P[C] that the site is capable of fault displacement. This probability represents epistemic uncertainty (unless it is exactly zero or unity).

The distribution portion of the attenuation equations for principal and distributed displacement (i.e., the second term in Equation 8-1) is specified as an expression for the scale parameter of the distribution (e.g., mean displacement given magnitude, x/L, etc.), and information about the shape and spread of the distribution. For several teams, this expression consists of a product of several random terms. For instance, several teams calculate the principal displacement as the product of the maximum displacement, MD (taken as lognormal, with a median value that depends on magnitude) times a random shape function (which, for a given x/L, takes the form of a beta distribution with parameters that depend on x/L). In all these instances, these products are approximated using lognormal probability

distributions, with medians and coefficients of variation computed using the well-known approximations for products of random variables. The accuracy of all these approximations was tested by comparing the exact and approximate distribution shapes.

There are also situations in which the distribution portion of the attenuation equation for distributed displacement is not a function of the earthquake magnitude or distance, and depends only on some characteristic of the site. This approach constitutes a hybrid between the earthquake and displacement method, where the occurrence portion of the model considers earthquakes, but the distance-distribution portion depends only on the characteristics of the site.

8.1.4.2 Displacement Approach. Although calculation of the hazard curve for this approach does not require integration over magnitudes and distances or summation over seismic sources, a logic tree analysis is required because the expert teams specified multiple alternatives for the various elements of the model and for the characteristics of the site.

8.1.4.3 Models Selected by the SSFD Expert Teams. Each team had the option of using the earthquake approach (chosen by one team), the displacement approach (two teams), and a weighted combination of the two approaches (three teams). The details on each team's approaches are described in Section 4.3.2 and their expert summaries (Appendix E).

8.2 PSHA RESULTS FOR FAULT DISPLACEMENT

The following describes the probabilistic fault displacement hazard calculated at the nine demonstration sites described in Section 4.3.2 and shown in Figure 4-9. Two of the sites have four hypothetical conditions representative of the features encountered within the ESF.

8.2.1 Integrated Results

The integrated results provide a representation of fault displacement hazard and its uncertainty at the nine demonstration sites, based on the interpretations and parameters developed by the six SSFD expert teams. Separate results are obtained for each site in the form of summary hazard curves, which are shown on Figures 8-2 through 8-14. No results

are shown for Sites 7d and 8d because all summary curves for these sites are below an annual exceedance probability of 10^{-8}. Table 8-1 summarizes the mean displacement hazard results for the two annual exceedance probabilities of interest, 10^{-4} and 10^{-5}, at the nine demonstration sites.

With the exception of the block-bounding Bow Ridge and Solitario Canyon faults at 10^{-5} annual exceedance probability, the mean displacements are all less than 0.1 cm. At 10^{-5} probability, the mean displacements are 7.8 and 32 cm, respectively for the two faults (Table 8-1). Thus sites not located on the block-bounding faults such as sites on the intrablock faults, small faults, shear fractures, and intact rock are estimated to undergo displacements of significantly less than 0.1 cm for periods up to 100,000 years.

The mean and median hazard curves indicate the central tendency of the calculated exceedence probabilities. The separation between the 15th- and 85th-percentile curves conveys the effect of epistemic uncertainty on the calculated exceedance probability (note that for some sites the 15th percentile hazard curve, and sometimes the median hazard curve, does not appear on the figure because the entire curve is below 10^{-8} annual exceedance probability). This epistemic uncertainty includes team-to-team, as well as within-team epistemic uncertainty in both the fault displacement models and the source and site characterizations.

The epistemic uncertainty (measured by the distance between the 15^{th} and 85^{th} percentile curves), is higher for sites with no principal faulting, especially for those with the lowest cumulative displacements. Larger epistemic uncertainty at low hazard sites compared to high hazard sites is a common observation when comparing ground motion hazard PSHAs.

In some instances, the mean hazard curve is higher than the 85th percentile hazard curve. This is an indication that the mean hazard is being controlled by an interpretation that has a low weight, but predicts much higher hazard than the majority of the interpretations.

Some of the hazard curves also have a nearly flat portion for low displacements. For instance, Figure 8-3 is nearly flat between 0.1 and 10 cm. This implies that, if there is a

displacement event on Solitario Canyon fault, it is likely to cause a displacement greater than 10 cm.

8.2.2 Comparisons Across Teams

Figures 8-15 through 8-27 show the mean hazard by each team, for all sites except 7d and 8d. Two mean curves are shown for those teams that used two approaches. For Sites 7b, 7c, 8b, and 8c, some teams specified $P[C]=0$, which implies that the hazard is zero. Although these curves are not shown on the figures, they are considered in the calculation of the summary statistics for the site.

Figures 8-15 through 8-27 indicate that variation among the SSFD expert teams is a significant contributor to total uncertainty. Recalling that the differences among the seismic source characterizations by the expert teams were small contributors to uncertainty in the ground motion hazard (Section 7.4.3), we can infer that the large differences among teams seen here are due to differences in the fault displacement models.

8.2.3 Sensitivity Results for Each SSFD Expert Team's Interpretations

Sensitivity results provide insights into the effect of various interpretations and parameters on the calculated seismic hazard and its uncertainty. These results provide insight into the PSHA process. They also provide a consistency check for the experts and analysts.

Sensitivity results are shown for Sites 1 (subject to both principal and distributed faulting) and 7a (subject to distributed faulting only). Several types of results are presented here for each combination of SSFD expert team and approach (earthquake versus fault displacement):

1. Summary hazard curves for that team's approach combination

2. Dominant seismic sources (for the earthquake approach only)

3. Sensitivity to important parameters of the fault displacement attenuation equations (earthquake approach) or to important parameters of the displacement model (displacement approach).

The procedure to generate the sensitivity results is described in Section 7.3.2.

8.2.3.1 AAR Team's Earthquake Approach. Figures 8-28 through 8-31 show the summary hazard curves and dominant seismic sources for Sites 1 and 7a. The most important contributors to hazard at Site 1 are the East-side coalesced system and Areal Source 2 (both contributors to distributed faulting), and the Bow Ridge fault (principal). The most important contributors to hazard at Site 7a are the East-side coalesced system and Areal Source 2.

For Site 1, the alternative displacement attenuation functions have small contributions to epistemic uncertainty. Most of the uncertainty at Site 1 is due to source characterization parameters (not shown), particularly the recurrence parameters for the dominant sources. For Site 7a, parameter beta, which controls the ratio of maximum displacement at the site to maximum displacement on the principal fault, is an important contributor to epistemic uncertainty (Figure 8-32). The AAR earthquake approach for distributed faulting is an example of the hybrid earthquake-displacement approach mentioned earlier. Because the shape of the attenuation equations does not depend on magnitude or distance, the mean hazard curves from all sources have the same shape.

AAR Team's Displacement Approach. Figures 8-33 and 8-34 show the summary hazard curves for Sites 1 and 7a. The hazard curves for the latter site shows a much more rapid drop-off and a slightly higher uncertainty. For Site 1, the most important contributors to uncertainty in the hazard are the cumulative displacement and the slip rate (Figures 8-36 and 8-37). For Site 7a, the most important contributor to uncertainty is parameter beta, which controls the ratio of maximum displacement at the site to maximum displacement on the principal fault (Figure 8-37).

8.2.3.2 ASM Team's Earthquake Approach. Figures 8-38 through 8-41 show the summary hazard curves and dominant seismic sources for Sites 1 and 7a. (The contributions by source on these figures are those obtained using the Borah-Peak reduction factor [70% weight] (Section 4.3.2.1), not the actual mean contributions.) The results for Site 7a show

the effect of truncation at D_{cum}=2 m (Section 4.3.2.1). The most important contributors to hazard at Site 1 are the Stagecoach Road-Paintbrush Canyon (distributed) and Bow Ridge (principal) faults. The most important contributors to hazard at Site 7a are the Solitario Canyon and Stagecoach Road-Paintbrush Canyon faults.

For Site 1, the alternative displacement attenuation functions have small contributions to epistemic uncertainty. Most of the uncertainty at Site 1 is due to source-characterization parameters (not shown), particularly the recurrence parameters for the dominant sources. For Site 7a, the only important uncertainty in the displacement attenuation equations is the model used to scale displacement on the principal fault to distributed displacement at the site (Figure 8-42).

8.2.3.3 DFS Team's Displacement Approach. Figures 8-43 and 8-44 show the summary hazard curves for Sites 1 and 7a. For Site 1, the most important contributors to uncertainty in the hazard are the choice to use the recurrence interval or the average displacement per event $\overline{D}_E$ (both derived from paleoseismic observations; Figure 8-45), the value of $\overline{D}_E$ (Figure 8-46), and the value of the recurrence interval (Figure 8-47). For Site 7a, the most important contributors to uncertainty in the hazard are the capability for fault displacement at the site (Figure 8-48), the value of $\overline{D}_E$ (Figure 8-49), and the value of the recurrence interval (Figure 8-50).

8.2.3.4 RYA Team's Displacement Approach. Figures 8-51 and 8-52 show the summary hazard curves for Sites 1 and 7a. For Site 1, the most important contributors to uncertainty in the hazard are the recurrence interval (Figure 8-53) and the distribution shape (Figure 8-54). For Site 7a, the most important contributors to uncertainty in the hazard are parameter beta (discussed above for AAR and ASM; Figure 8-55), and the expression used in the calculation of slip rates from cumulative displacements (Figure 8-56).

8.2.3.5 SBK Team's Earthquake Approach. Figures 8-57 through 8-60 show the summary hazard curves and dominant seismic sources for Sites 1 and 7a.. The most important contributors to hazard at Site 1 are the Stagecoach Road-Paintbrush Canyon fault and the Basin and Range source zone (both distributed) and the Bow Ridge fault (principal). The

most important contributors to hazard at Site 7a are the Basin and Range source zone and the Stagecoach Road-Paintbrush Canyon and Solitario Canyon faults.

For both Sites 1 and 7a, the alternative displacement attenuation functions have small contributions to epistemic uncertainty. The most important among these is the model for the probability of displacement given an event (not shown), for which SBK uses two models. The first model is a logistic function in terms of magnitude and distance. The second model is a logistic function in terms of the peak ground velocity predicted by the ground motion models. Although the latter model predicts higher hazard, its contribution to epistemic uncertainty is small because it has a weight of only 10%.

SBK Team's Displacement Approach. Figures 8-61 through 8-62 show the summary hazard curves for Sites 1 and 7a. For Site 1, the most important contributors to uncertainty in the hazard are the average displacement per event (Figure 8-63) and the recurrence interval (Figure 8-64). Site 7a has no important contributors to uncertainty in the hazard, as indicated by the tight clustering of the fractile hazard curves on Figure 8-62.

8.2.3.6 SDO Team's Earthquake Approach. Figures 8-65 through 8-68 show the summary hazard curves and dominant seismic sources for Sites 1 and 7a. For both Sites 1 and 7a, the alternative displacement attenuation functions have small contributions to epistemic uncertainty. Source characteristics also have a small contribution to epistemic uncertainty, as indicated by the tight clustering of the fractile hazard curves on Figures 8-65 and 8-66.

SDO Team's Displacement Approach. Figure 8-69 shows the summary hazard curves for Site 7a (no results are shown for Site 1 because SDO does not apply the displacement approach to sites with principal faulting). The most important contributors to uncertainty in the hazard are the ratio beta (Figure 8-70), the procedure to calculate the average displacement per event (Figure 8-71; SDO uses the procedures formulated by the AAR and SBK teams), and the procedure to calculate slip rate from cumulative displacement (Figure 8-72).

8.3 SUMMARY

The results shown here illustrate the wide diversity in approaches used to evaluate fault displacement hazard (Section 4.3.2.1). This diversity is indicative of the state of practice in PSHA for fault displacement, which is less mature than PSHA for ground motions. Nonetheless, the results obtained here are considered robust by virtue of the extensive efforts at expert elicitation and feedback, as well as the methodological developments, that were undertaken as part of this study. In addition, much of the experience in ground motion PSHA can be transferred into fault displacement PSHA. Sites with the highest fault displacement hazard show uncertainties comparable to those obtained in ground motion PSHA. Sites with low hazard show much higher uncertainties.

There is also an interesting, but not unexpected, correlation between the amount of geologic data available at a site and the uncertainty in the calculated hazard at that site. For Sites 1 and 2, where there are significant geologic data, and even for Site 4 where there are some geologic constraints, the scatter among teams is less than one order of magnitude. For Sites 3, 5, 6, 7a, 7b, 8a, and 8b, the individual team curves span three orders of magnitude. These are the sites for which there are little or no data. The calculated hazard for these sites is driven largely by models.

Regarding the latter group of sites, it is important to note that most of the uncertainty relates to the lower portion of the epistemic distribution, as one can verify by noting that the mean and 85th percentile curves are relatively close to each other, whereas the 15th percentile curve is often much lower, if not lower than 10^{-8} (e.g., Figures 8-8 and 8-9). This implies that the experts agree that the hazard at these sites is low or very low, but they do not agree on how low it is.

TABLE 8-1
MEAN DISPLACEMENT HAZARD AT NINE DEMONSTRATION SITES

Site	Location	Mean Displacement (cm) Annual Exceedance Probability 10^{-4}	10^{-5}
1	Bow Ridge fault	<0.1	7.8
2	Solitario Canyon fault	<0.1	32
3	Drill Hole Wash fault	<0.1	<0.1
4	Ghost Dance fault	<0.1	<0.1
5	Sundance fault	<0.1	<0.1
6	Unnamed fault west of Dune Wash	<0.1	<0.1
7	100 m east of Solitario Canyon fault		
7a	2-m small fault	<0.1	<0.1
7b	10-cm shear	<0.1	<0.1
7c	fracture	<0.1	<0.1
7d	intact rock	<0.1	<0.1
8	Between Solitario Canyon and Ghost Dance faults		
8a	2-m small fault	<0.1	<0.1
8b	10-cm shear	<0.1	<0.1
8c	fracture	<0.1	<0.1
8d	intact rock	<0.1	<0.1
9	Midway Valley	<0.1	0.1

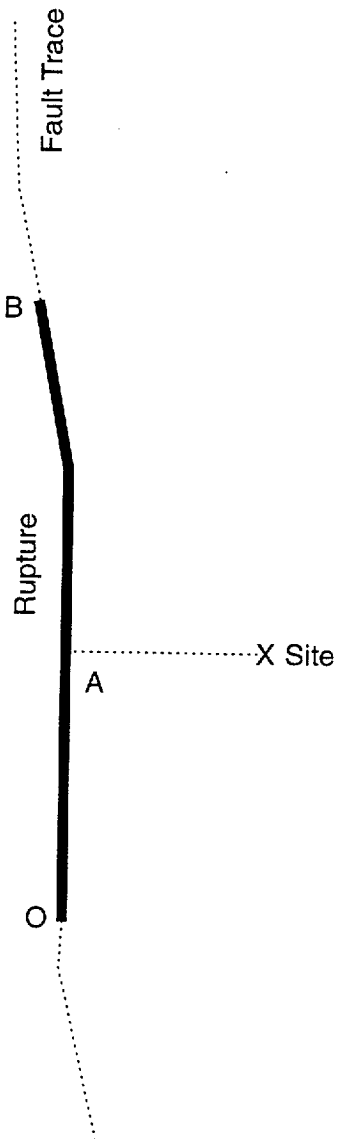

Figure 8-1 Definition of the along-strike location x/L (plane view). OX is the shortest distance from the site to the rupture. x/L is defined as OA/OB or AB/OB, whichever is smallest.

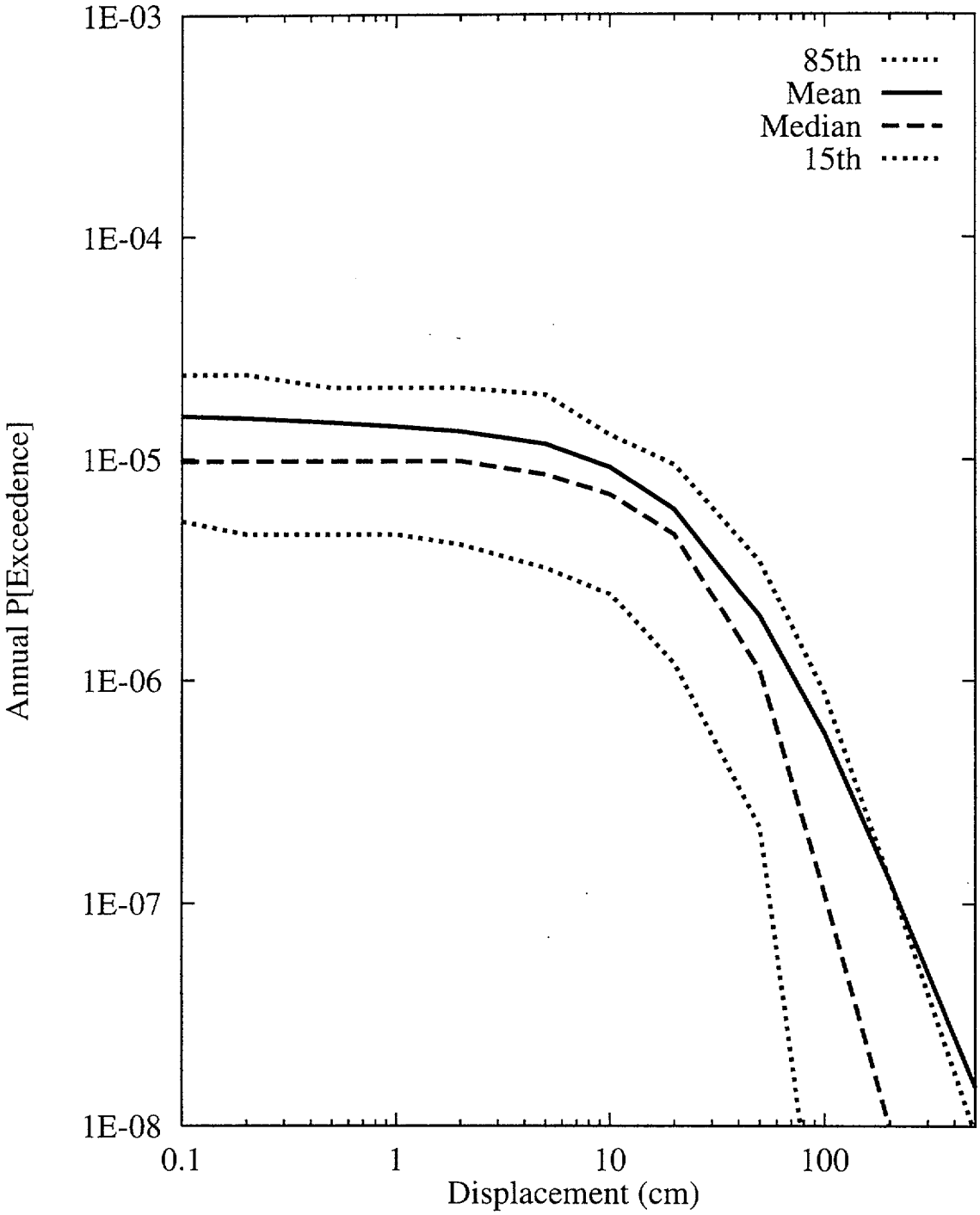

Figure 8-2 Integrated seismic hazard results: summary hazard curves for Site 1, Bow Ridge fault

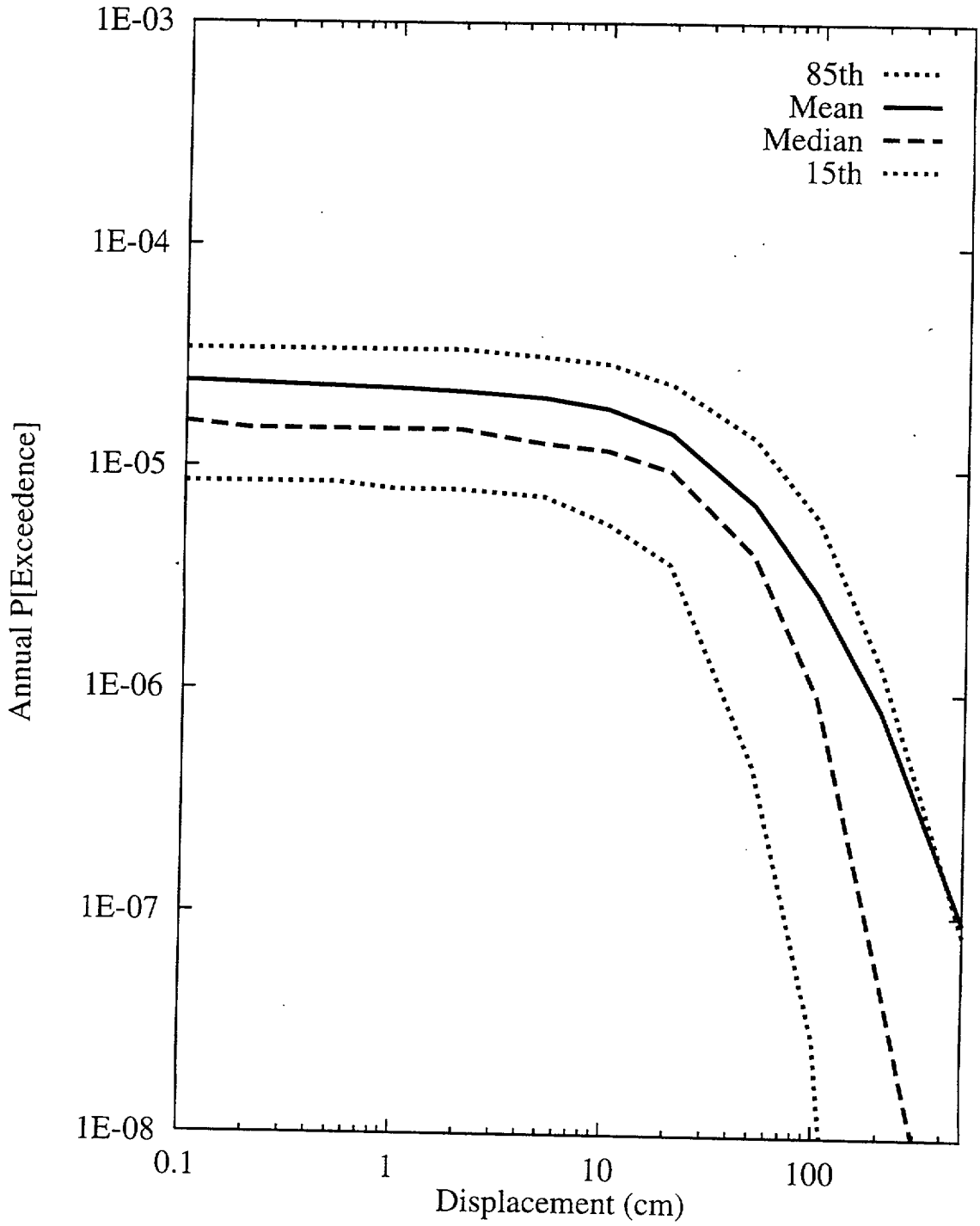

Figure 8-3 Integrated seismic hazard results: summary hazard curves for Site 2, Solitario Canyon fault

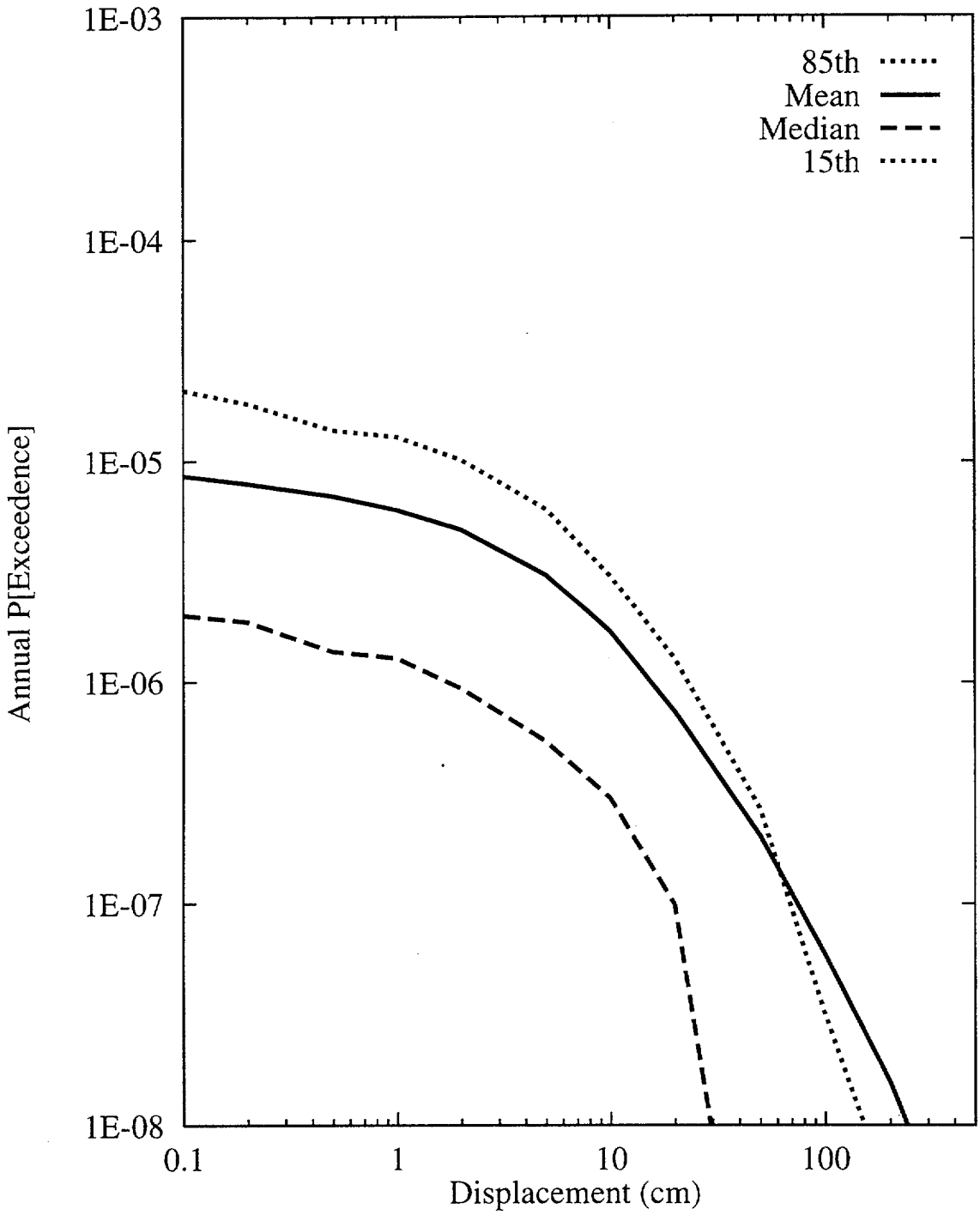

Figure 8-4 Integrated seismic hazard results: summary hazard curves for Site 3, Drill Hole Wash fault

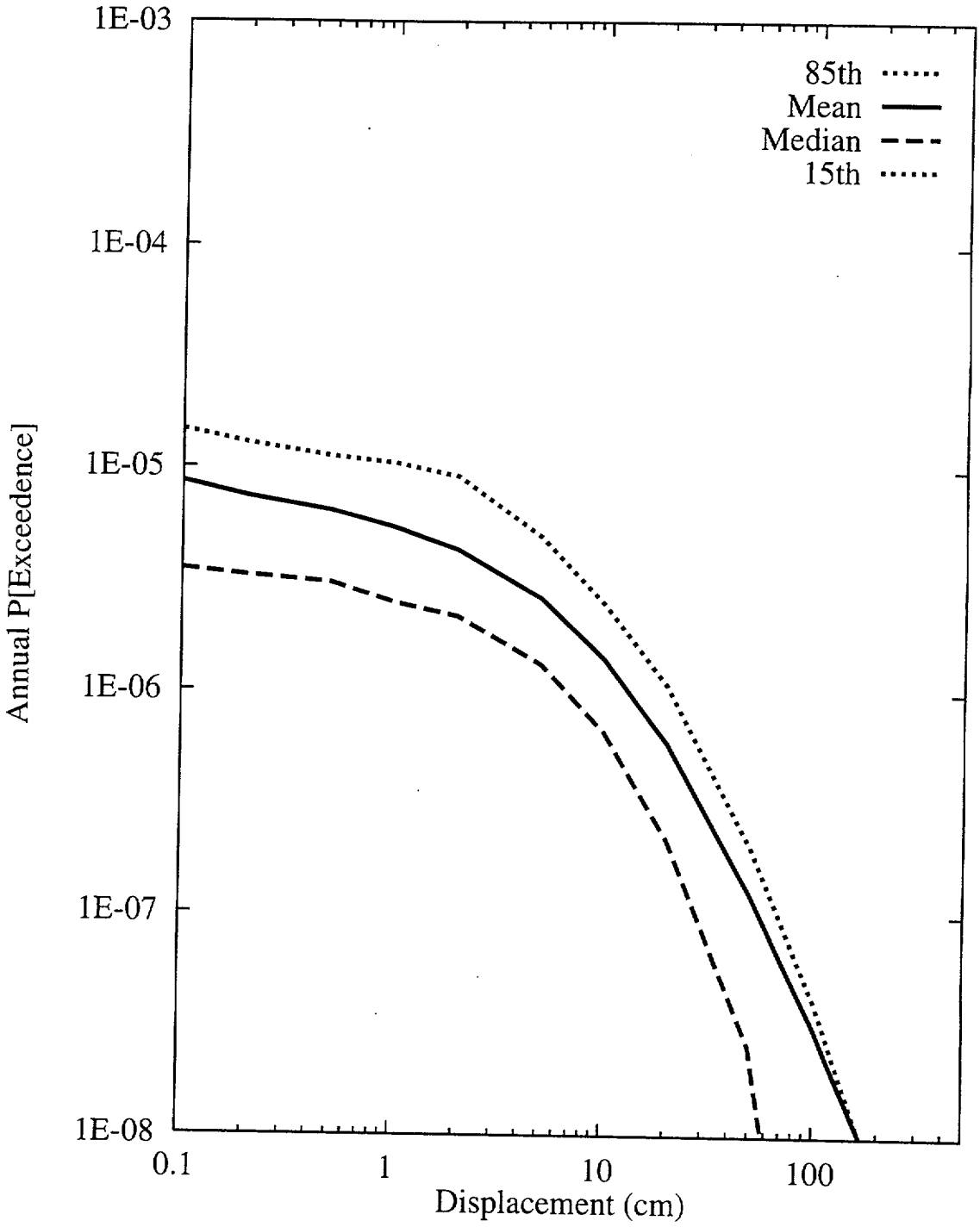

Figure 8-5 Integrated seismic hazard results: summary hazard curves for Site 4, Ghost Dance fault

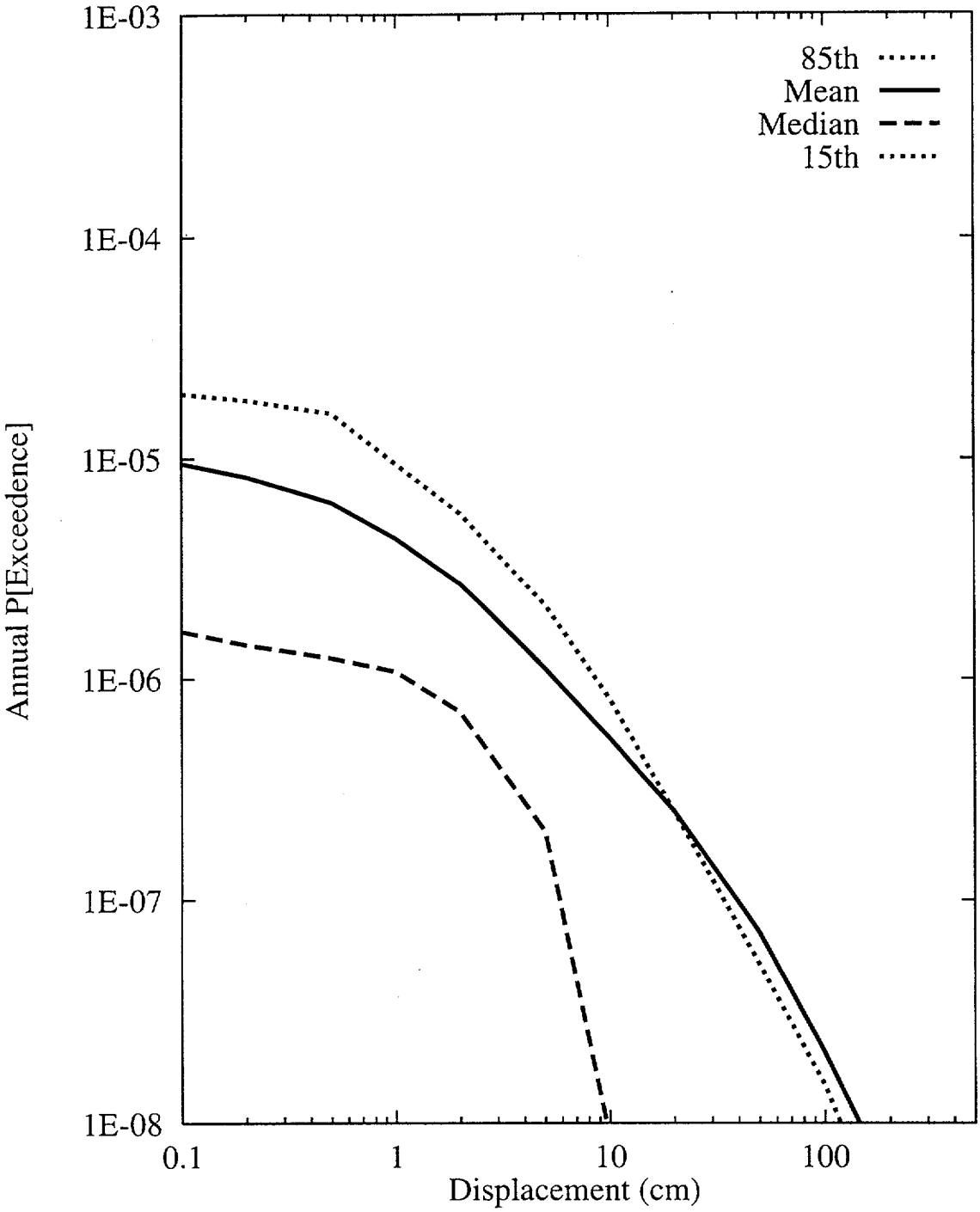

Figure 8-6 Integrated seismic hazard results: summary hazard curves for Site 5, Sundance fault

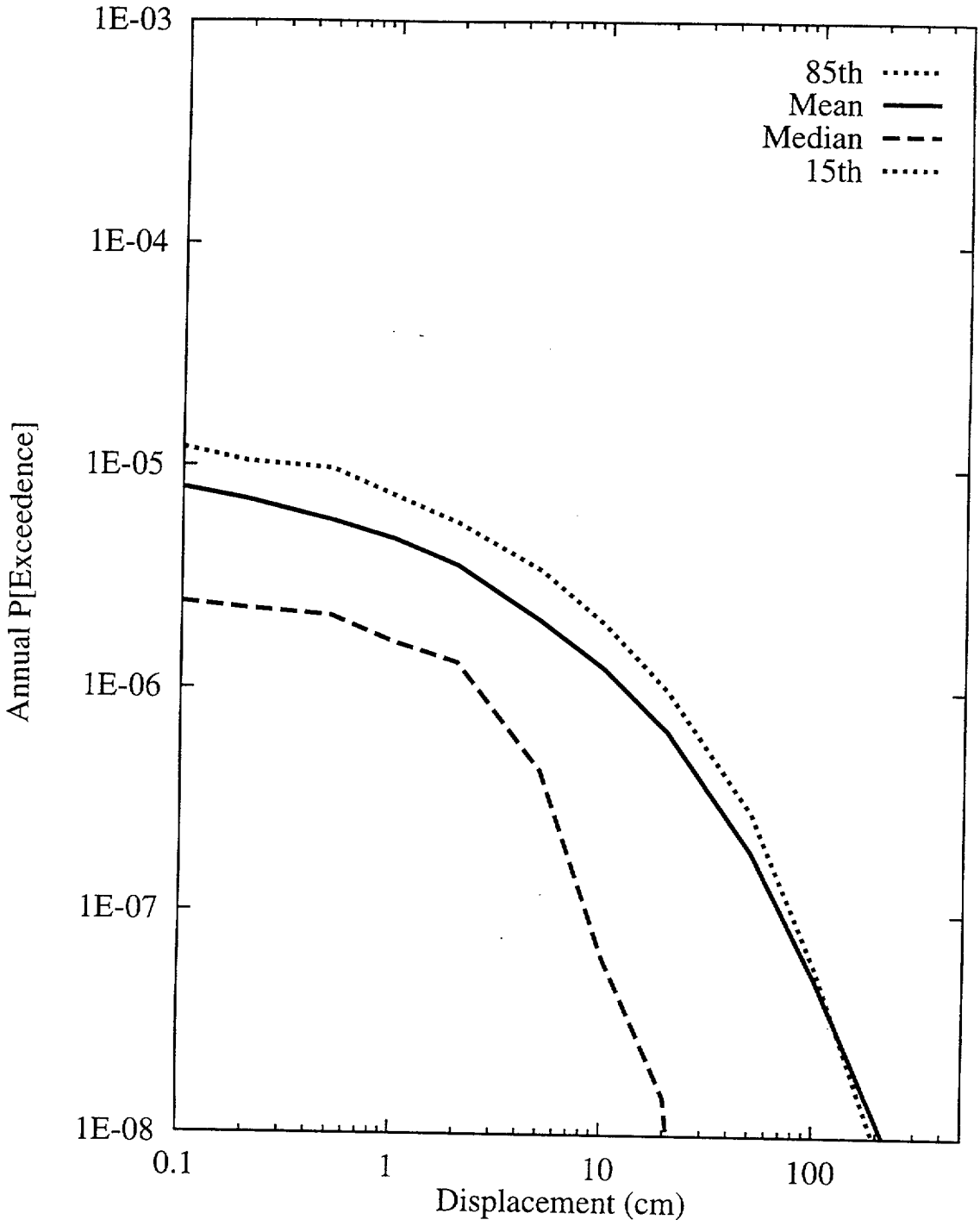

Figure 8-7 Integrated seismic hazard results: summary hazard curves for Site 6, unnamed fault west of Dune Wash

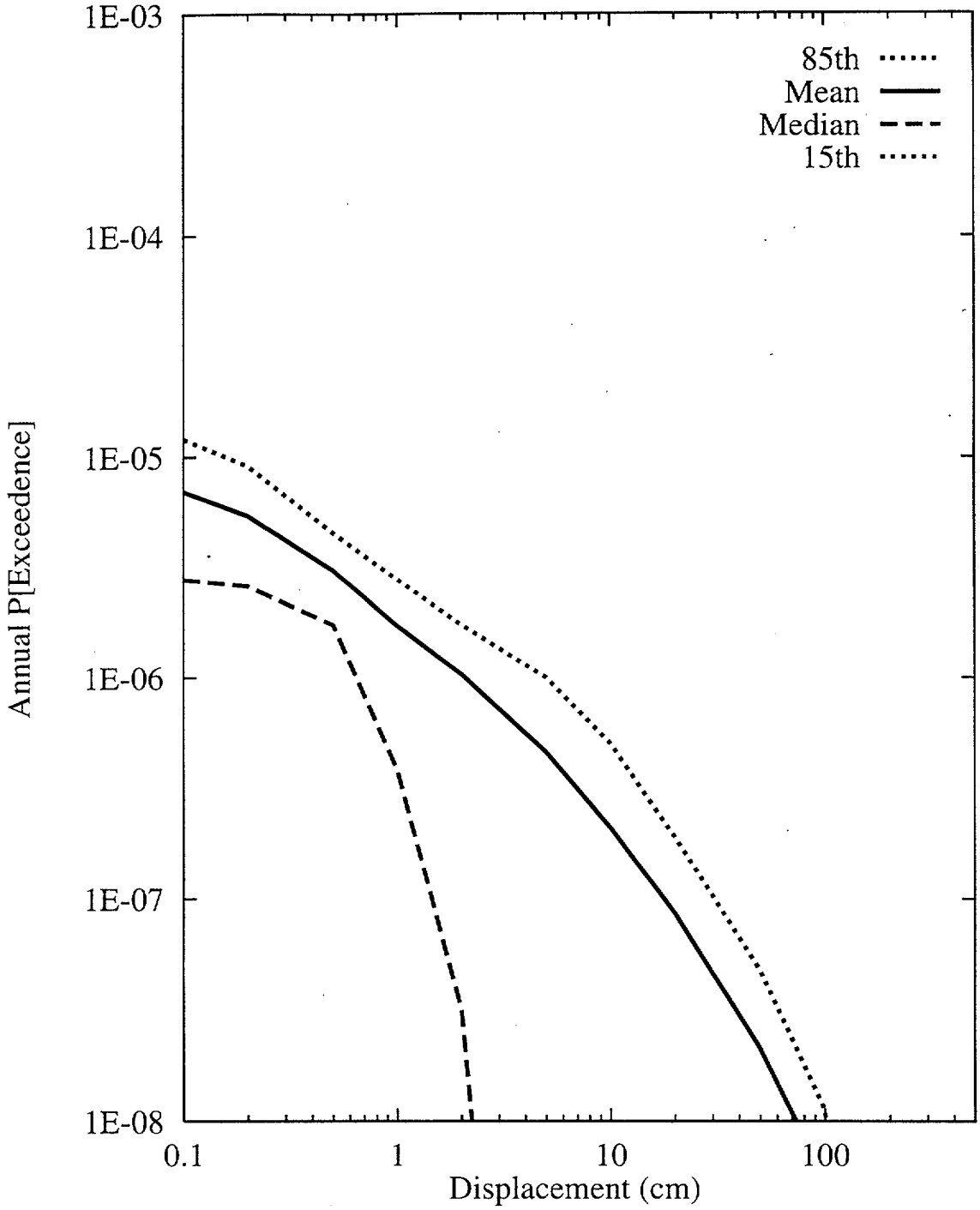

Figure 8-8 Integrated seismic hazard results: summary hazard curves for Site 7a, 100m east of Solitario Canyon fault (2m cumulative displacement)

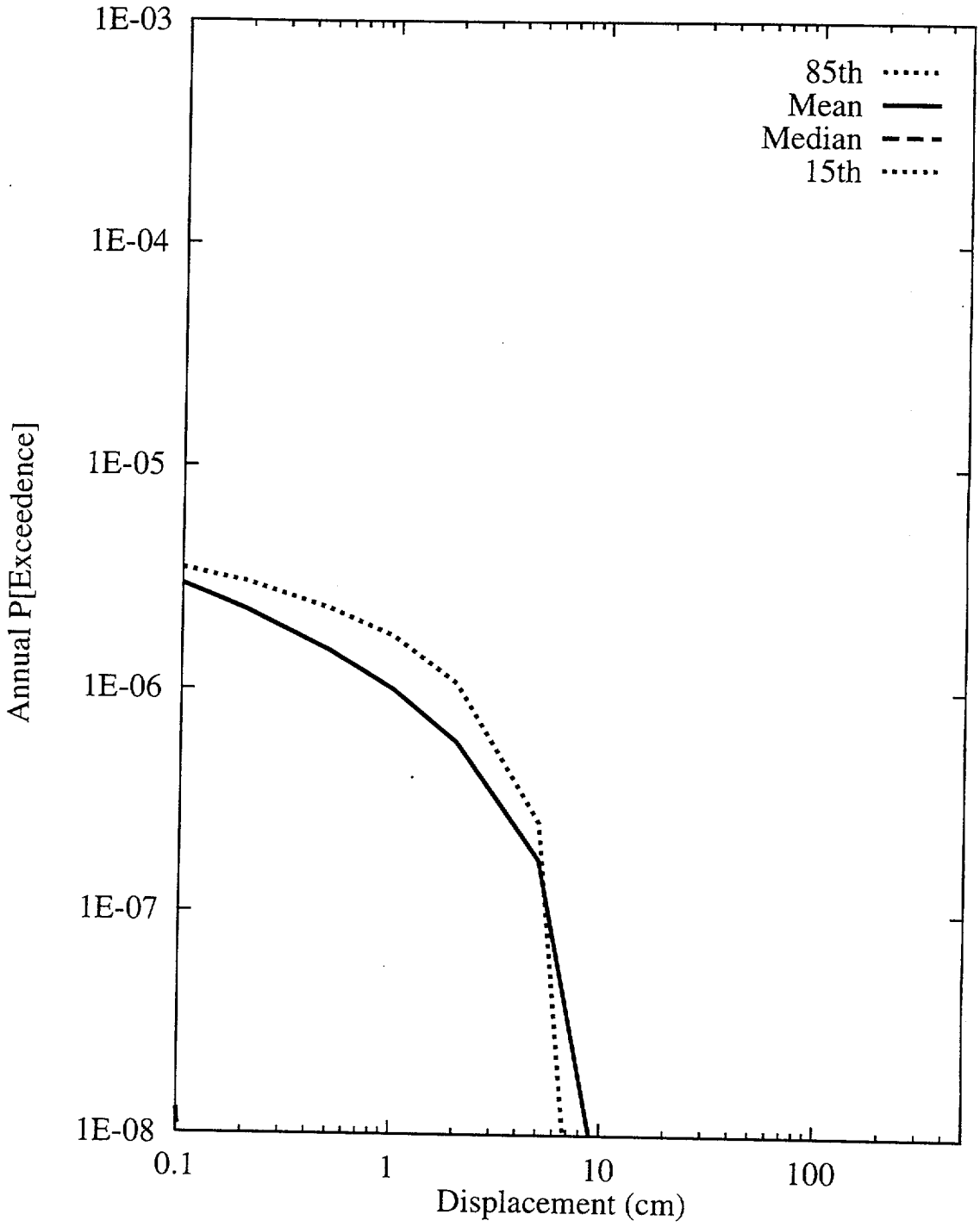

Figure 8-9 Integrated seismic hazard results: summary hazard curves for Site 7b, 100m east of Solitario Canyon fault (10cm cumulative displacement)

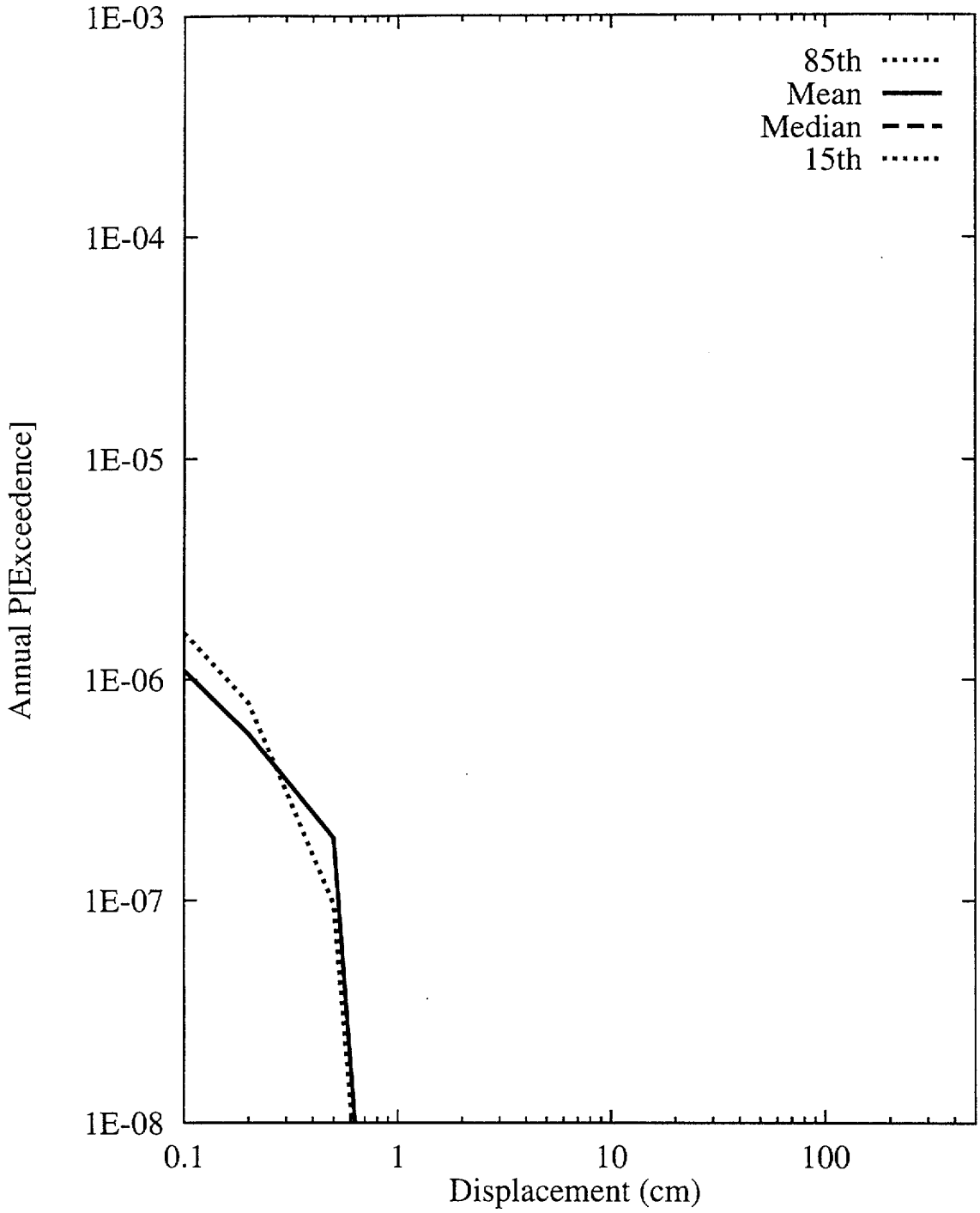

Figure 8-10 Integrated seismic hazard results: summary hazard curves for Site 7c, 100m east of Solitario Canyon fault (no measurable cumulative displacement)

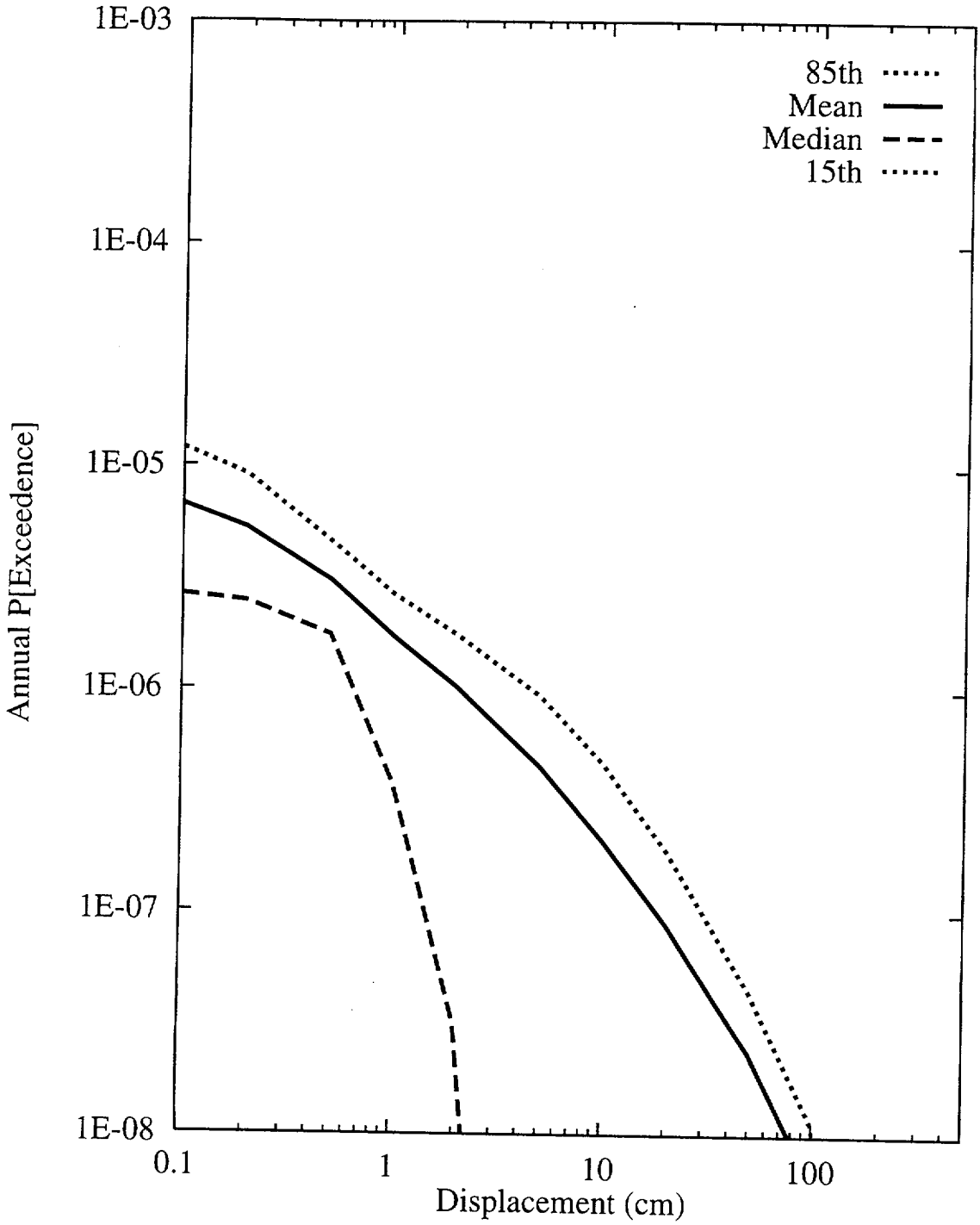

Figure 8-11 Integrated seismic hazard results: summary hazard curves for Site 8a, midway between the Ghost Dance and Solitario Canyon faults (2m cumulative displacement)

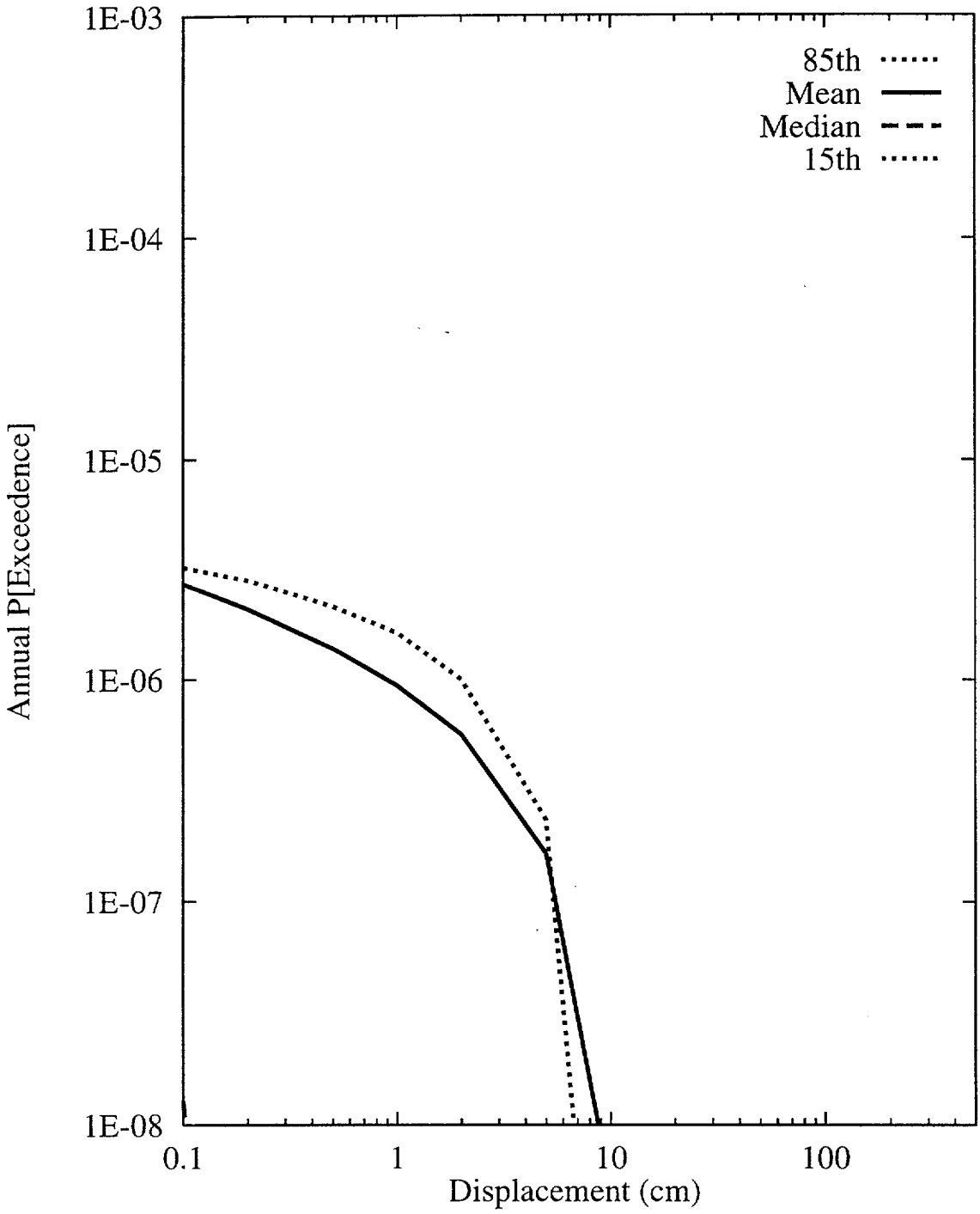

Figure 8-12 Integrated seismic hazard results: summary hazard curves for Site 8b, midway between the Ghost Dance and Solitario Canyon faults (10cm cumulative displacement)

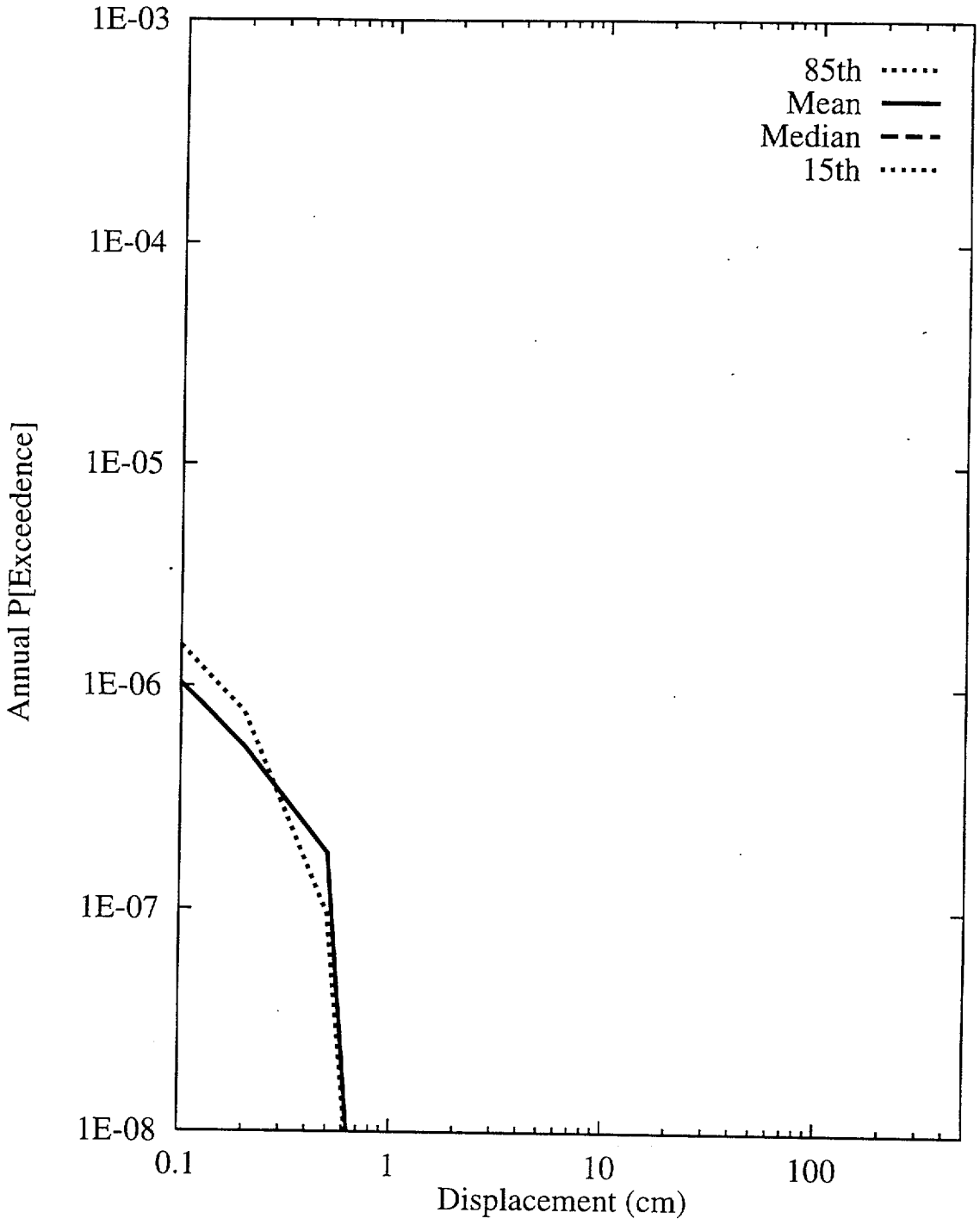

Figure 8-13 Integrated seismic hazard results: summary hazard curves for Site 8c, midway between the Ghost Dance and Solitario Canyon faults (no measurable cumulative displacement)

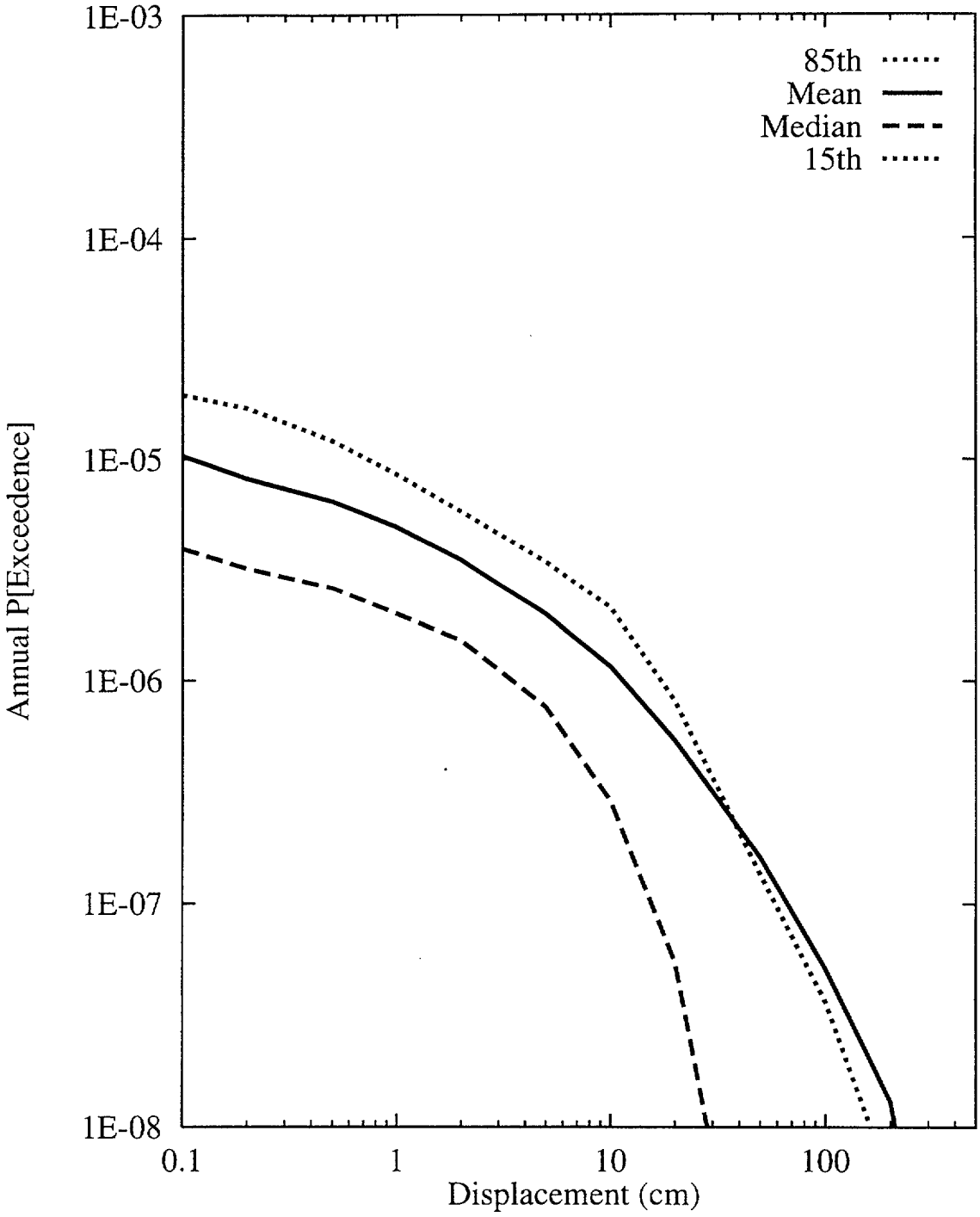

Figure 8-14 Integrated seismic hazard results: summary hazard curves for Site 9, Midway Valley

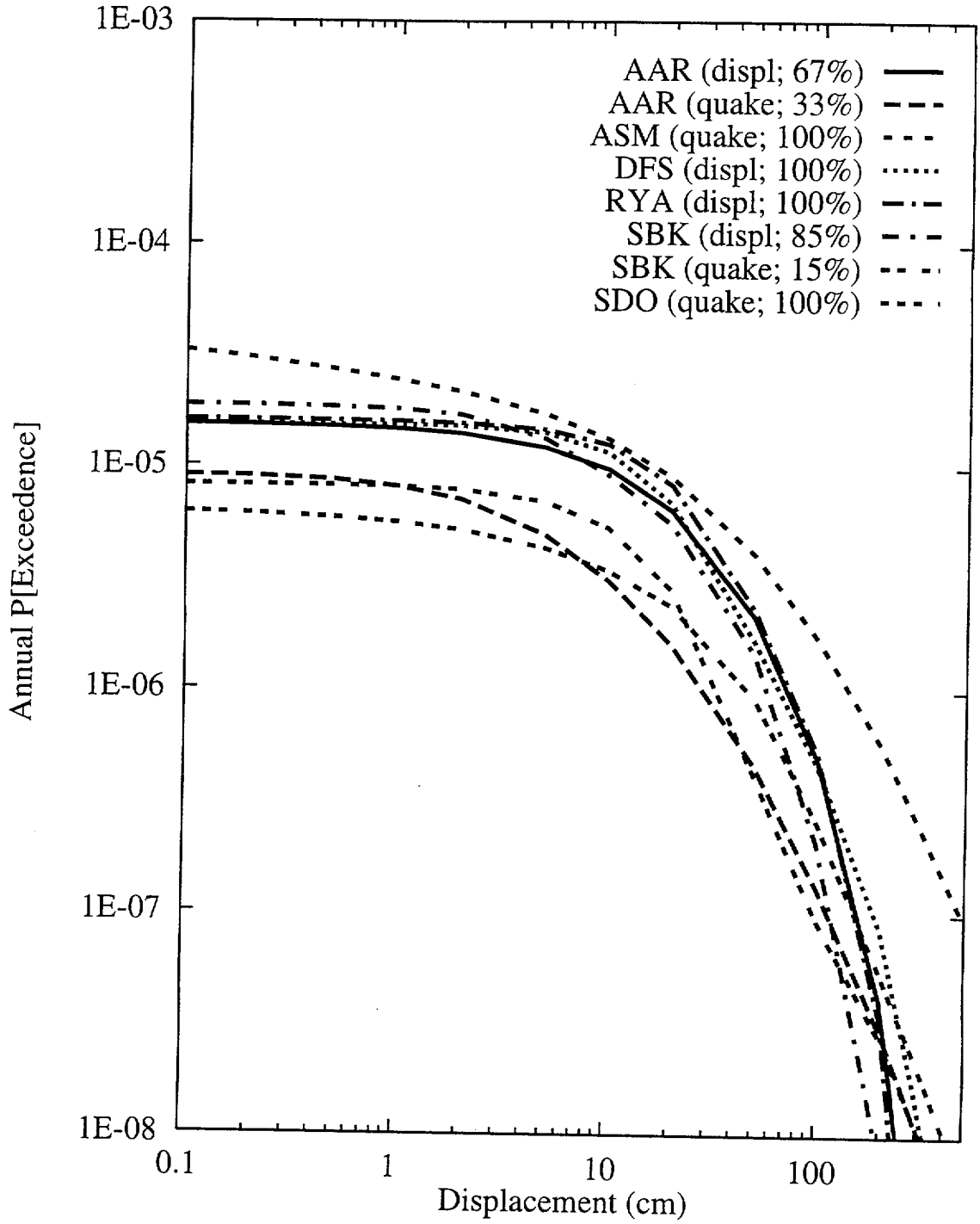

Figure 8-15 Mean hazard by teams and approaches for Site 1, Bow Ridge fault

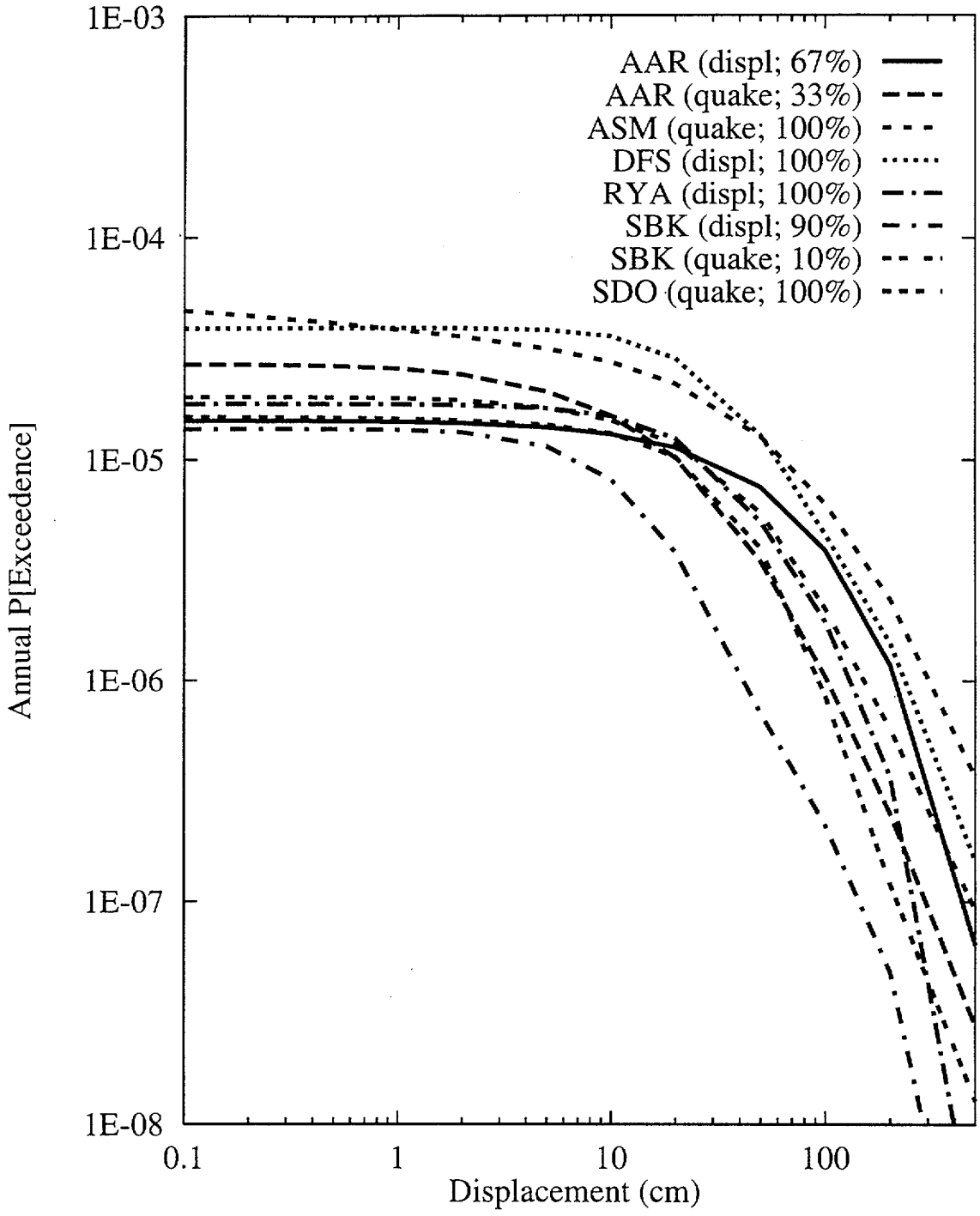

Figure 8-16 Mean hazard by teams and approaches for Site 2, Solitario Canyon fault

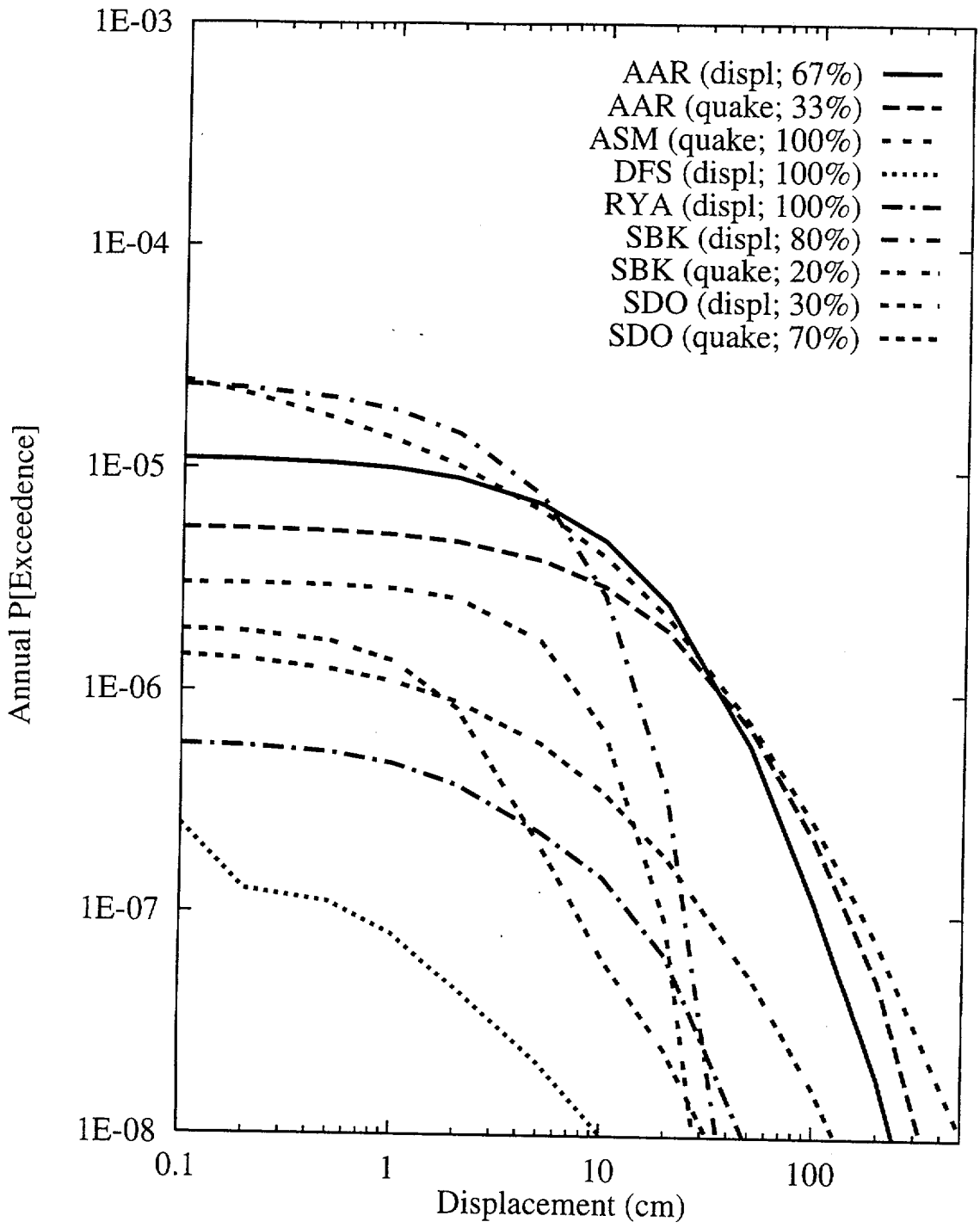

Figure 8-17 Mean hazard by teams and approaches for Site 3, Drill Hole Wash fault

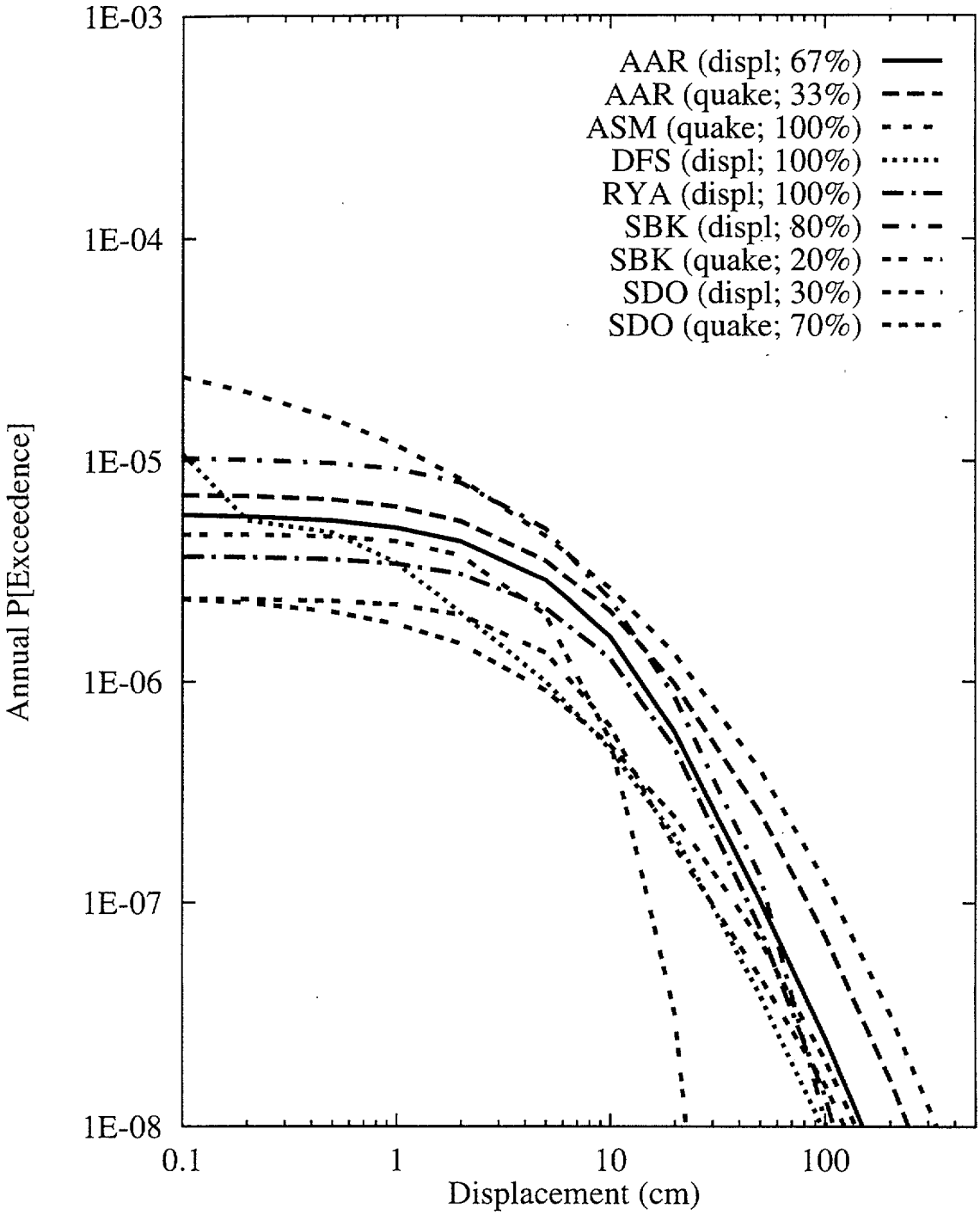

Figure 8-18 Mean hazard by teams and approaches for Site 4, Ghost Dance fault

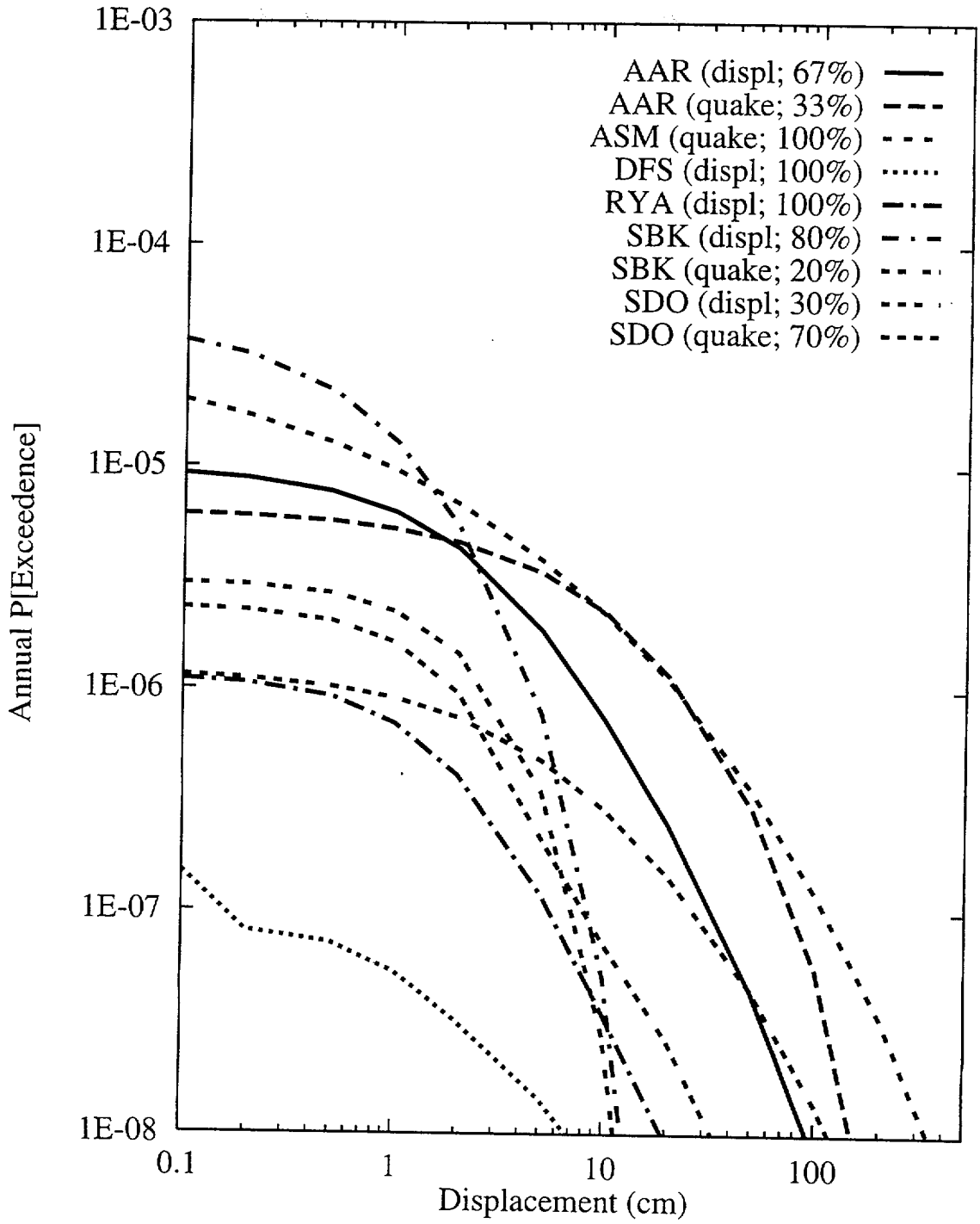

Figure 8-19 Mean hazard by teams and approaches for Site 5, Sundance fault

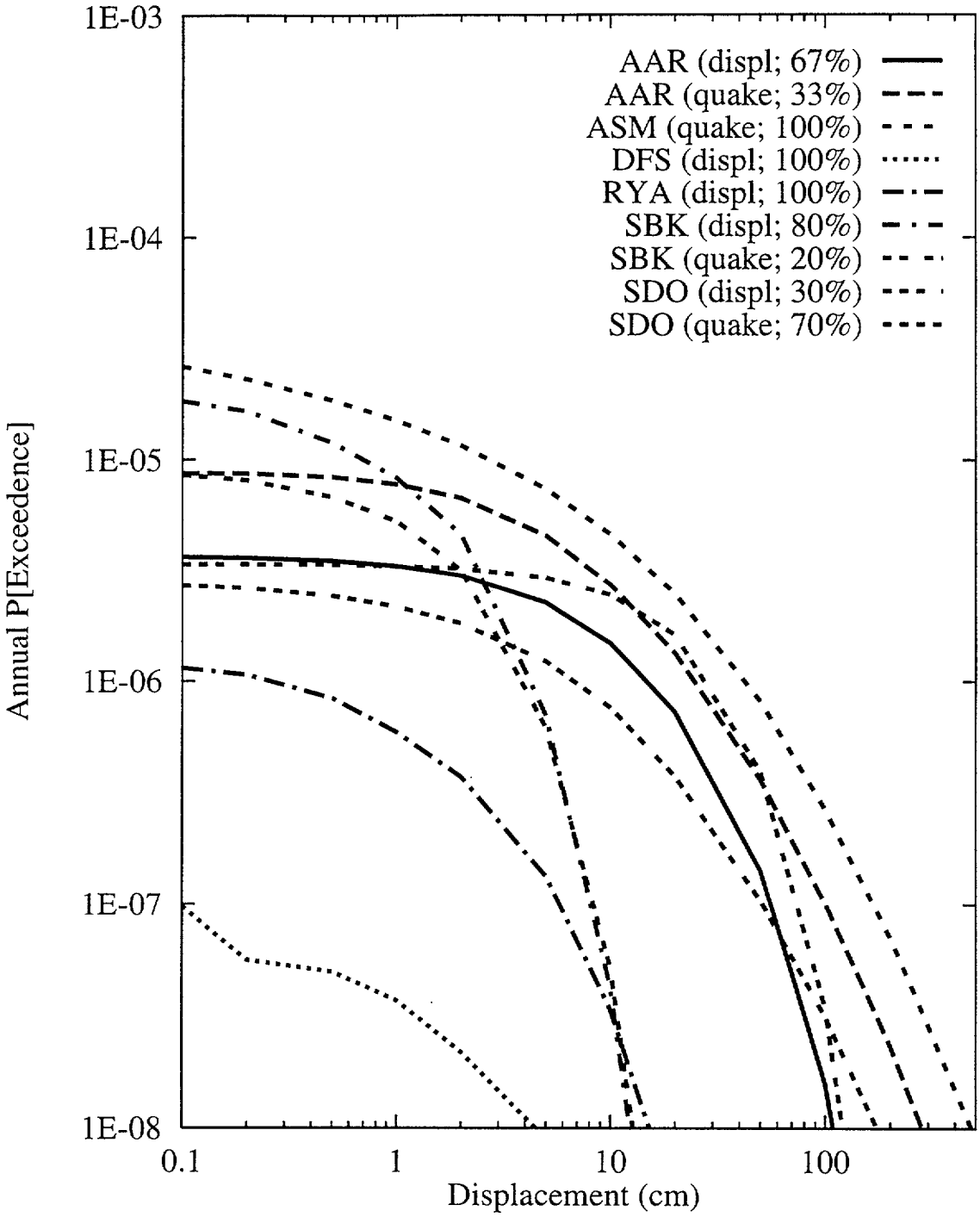

Figure 8-20 Mean hazard by teams and approaches for Site 6, unnamed fault west of Dune Wash fault

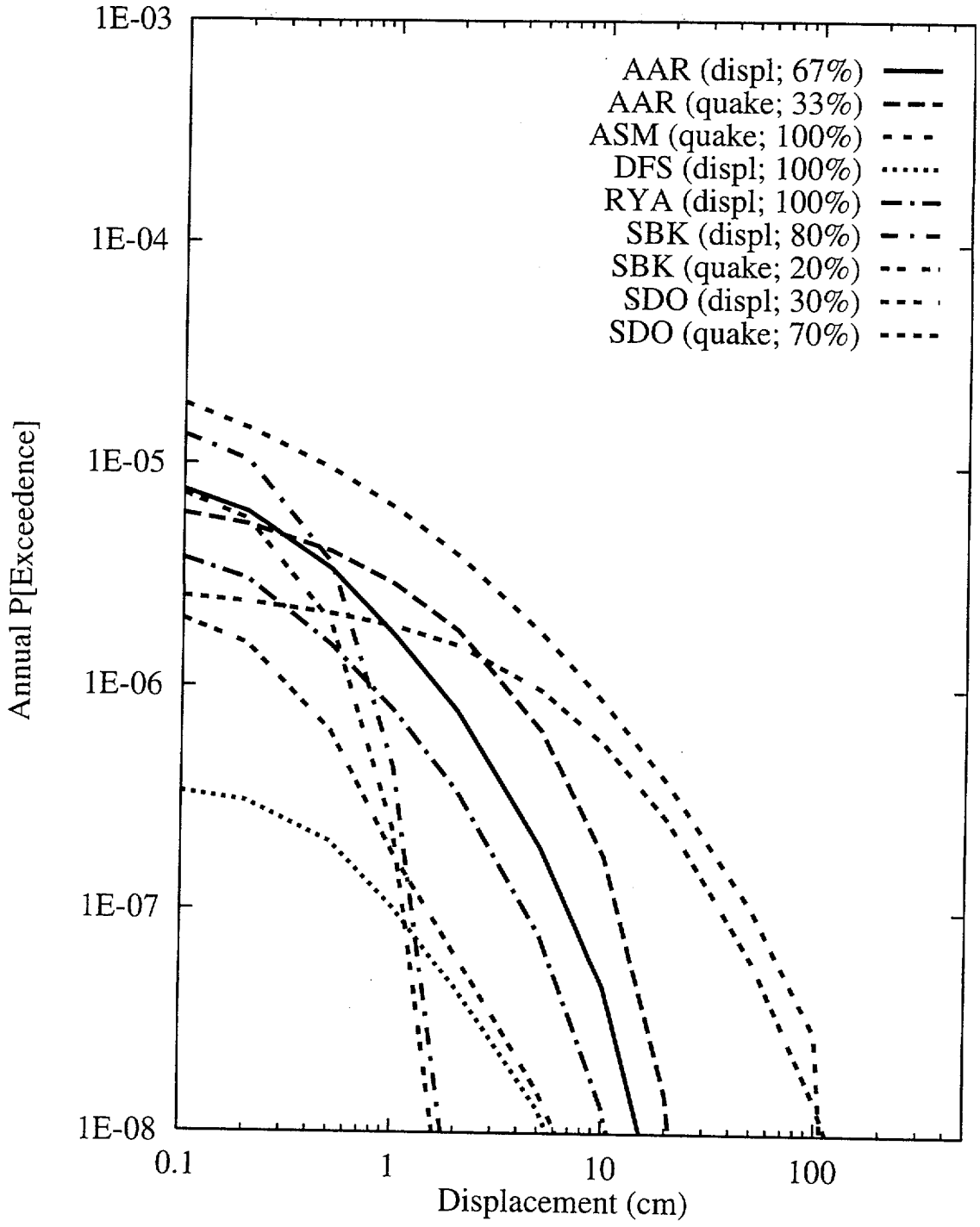

Figure 8-21 Mean hazard by teams and approaches for Site 7a, 100m east of Solitario Canyon fault (2m cumulative displacement)

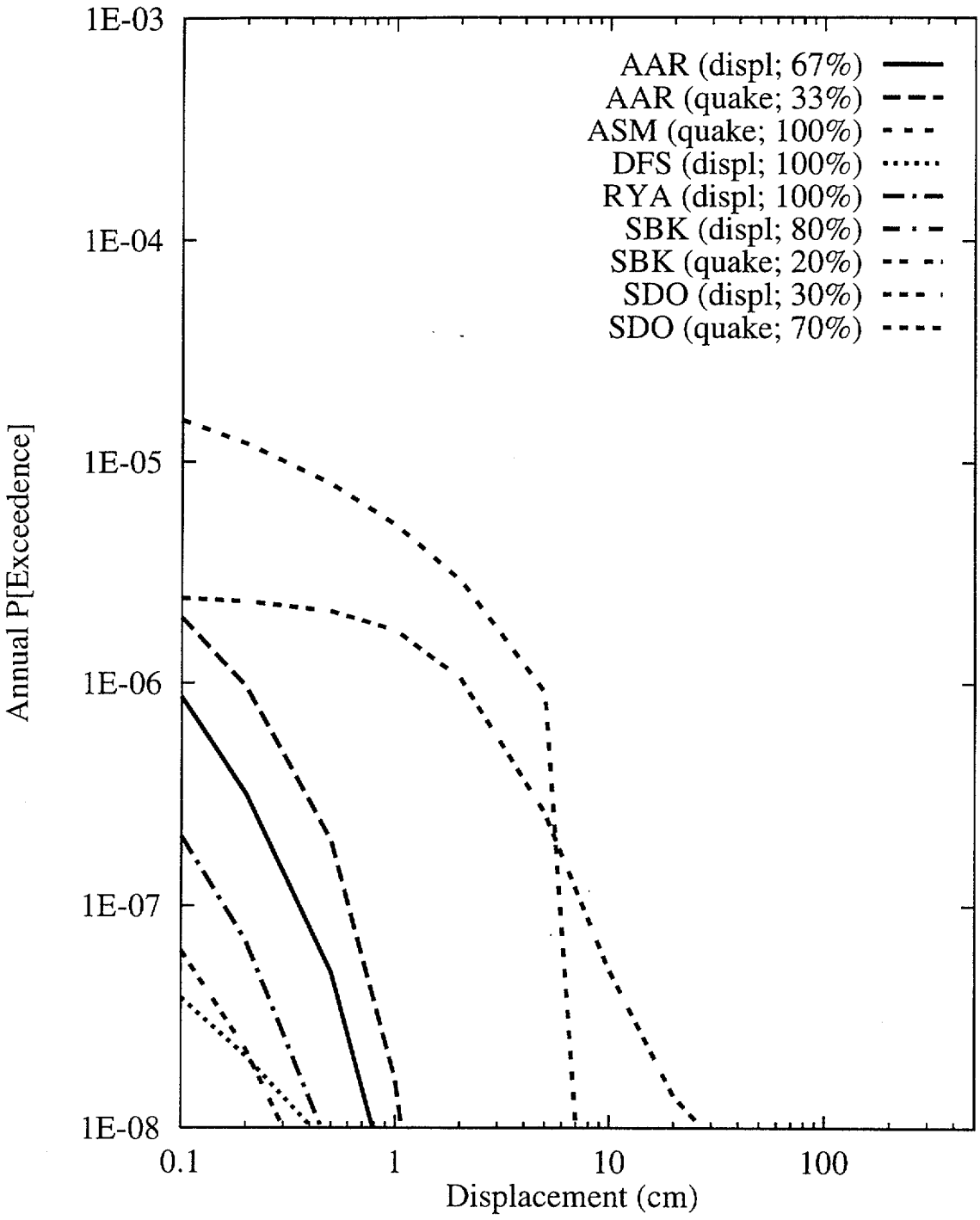

Figure 8-22 Mean hazard by teams and approaches for Site 7b, 100m east of Solitario Canyon fault (10cm cumulative displacement)

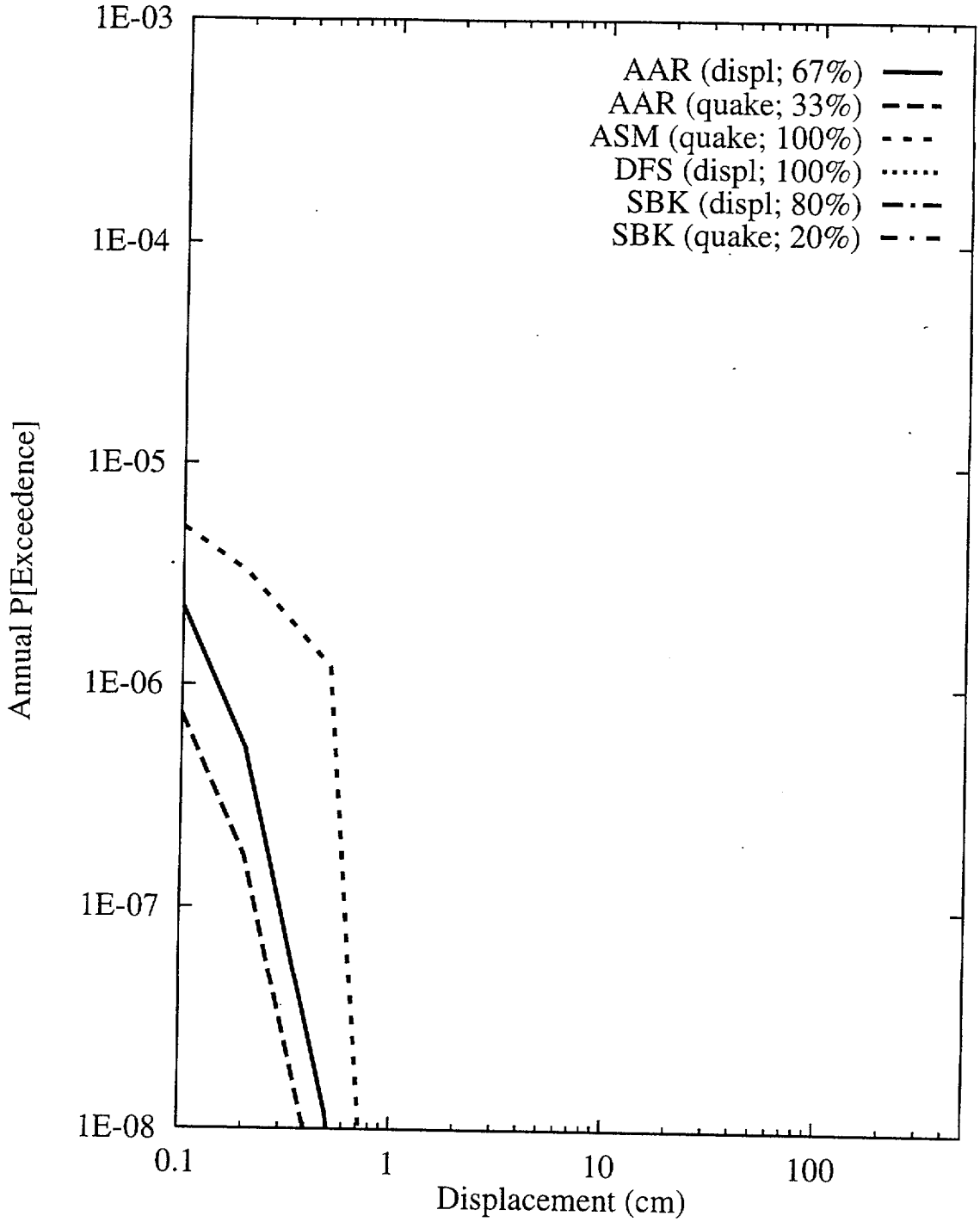

Figure 8-23 Mean hazard by teams and approaches for Site 7c, 100m east of Solitario Canyon fault (no measurable cumulative displacement)

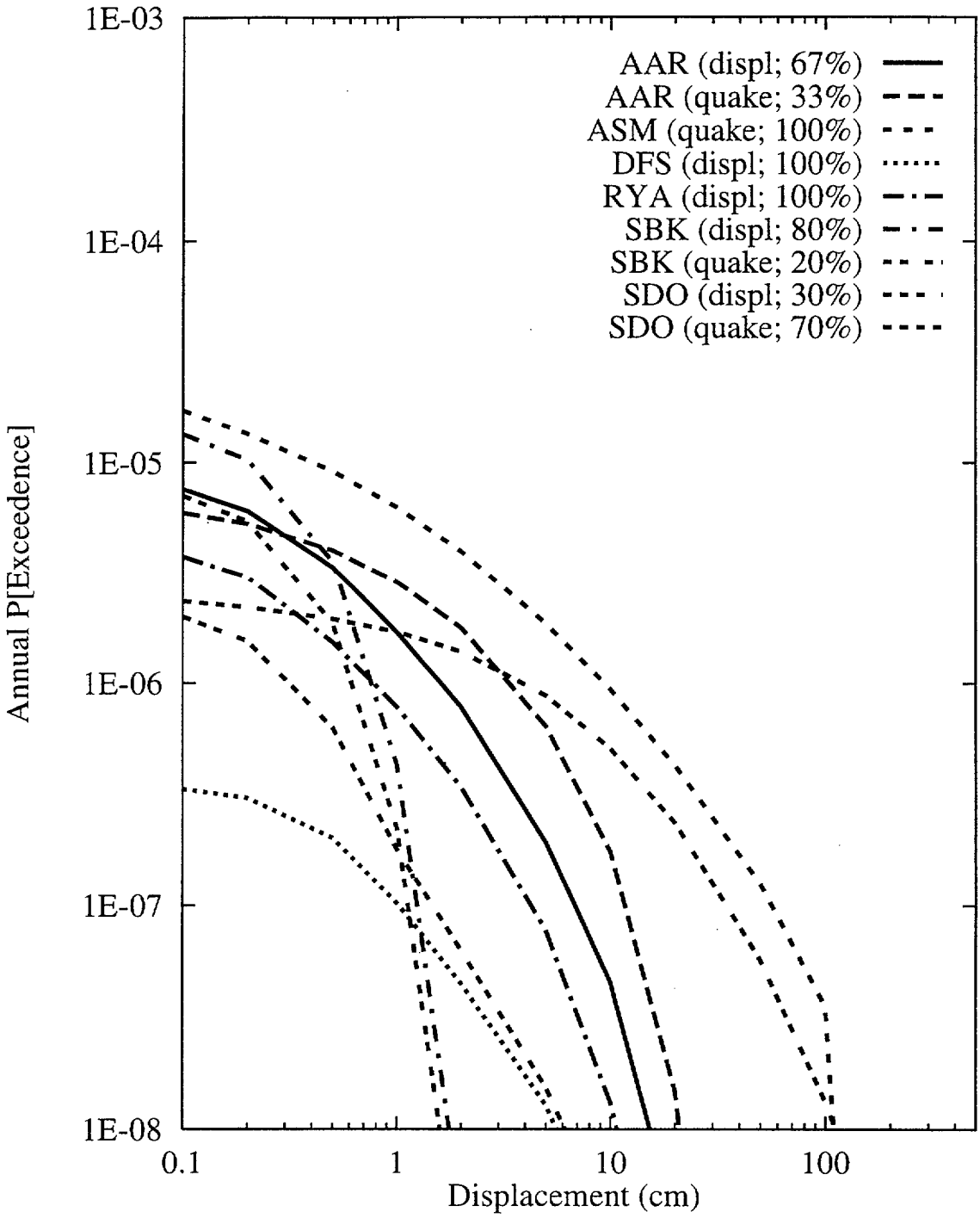

Figure 8-24 Mean hazard by teams and approaches for Site 8a, midway between the Ghost Dance and Solitario Canyon faults (2m cumulative displacement)

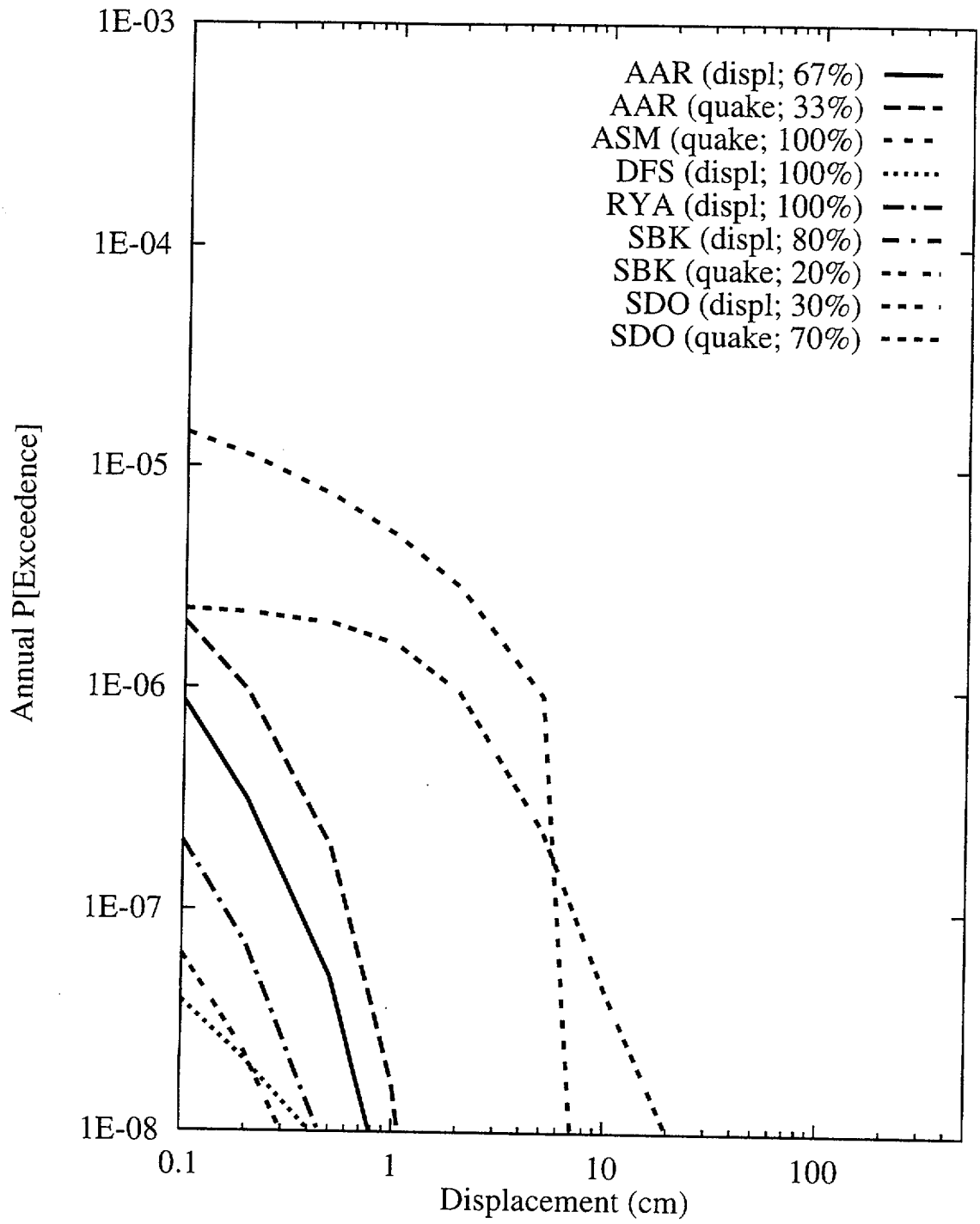

Figure 8-25 Mean hazard by teams and approaches for Site 8b, midway between the Ghost Dance and Solitario Canyon faults (10cm cumulative displacement)

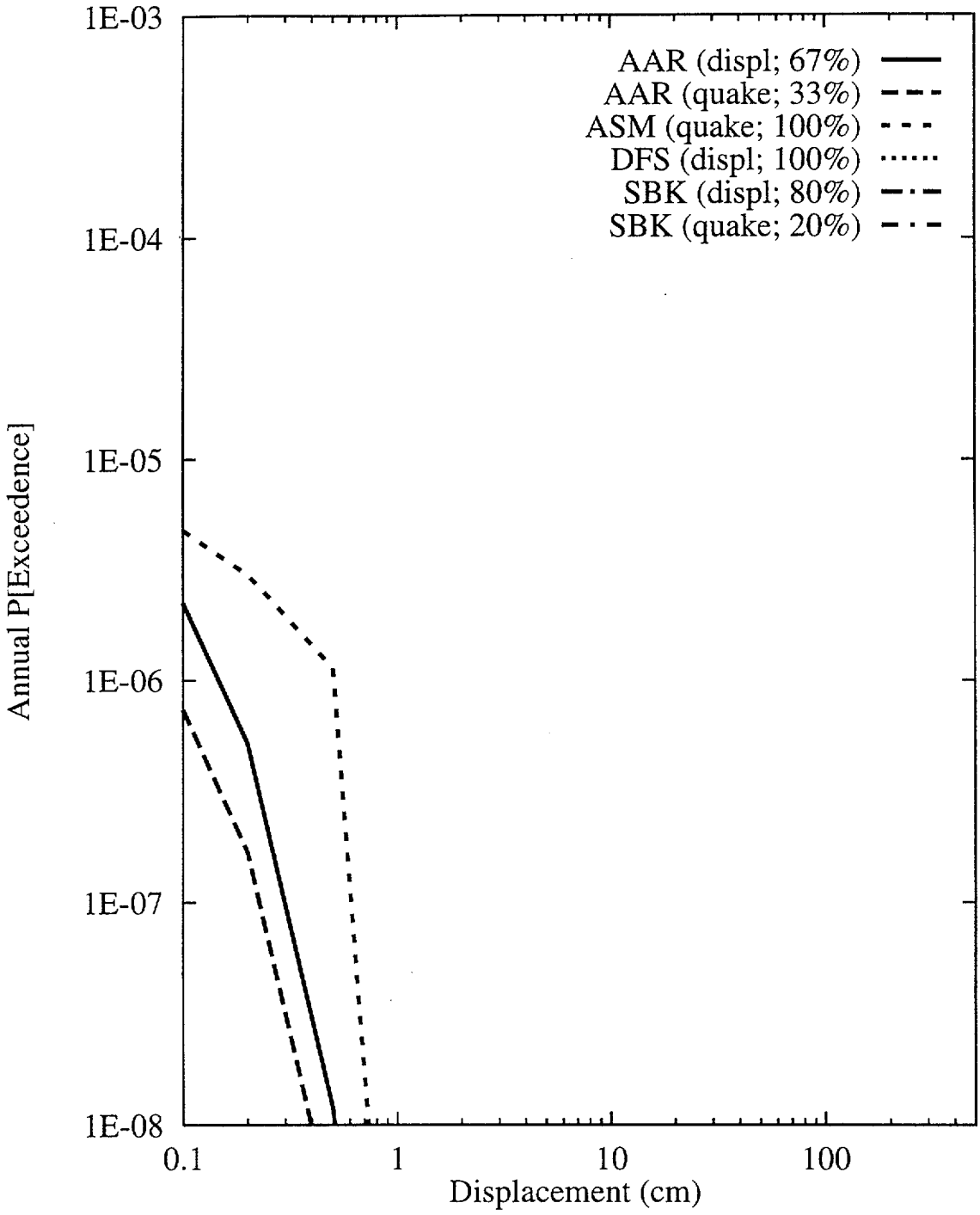

Figure 8-26 Mean hazard by teams and approaches for Site 8c, midway between the Ghost Dance and Solitario Canyon faults (no measurable cumulative displacement)

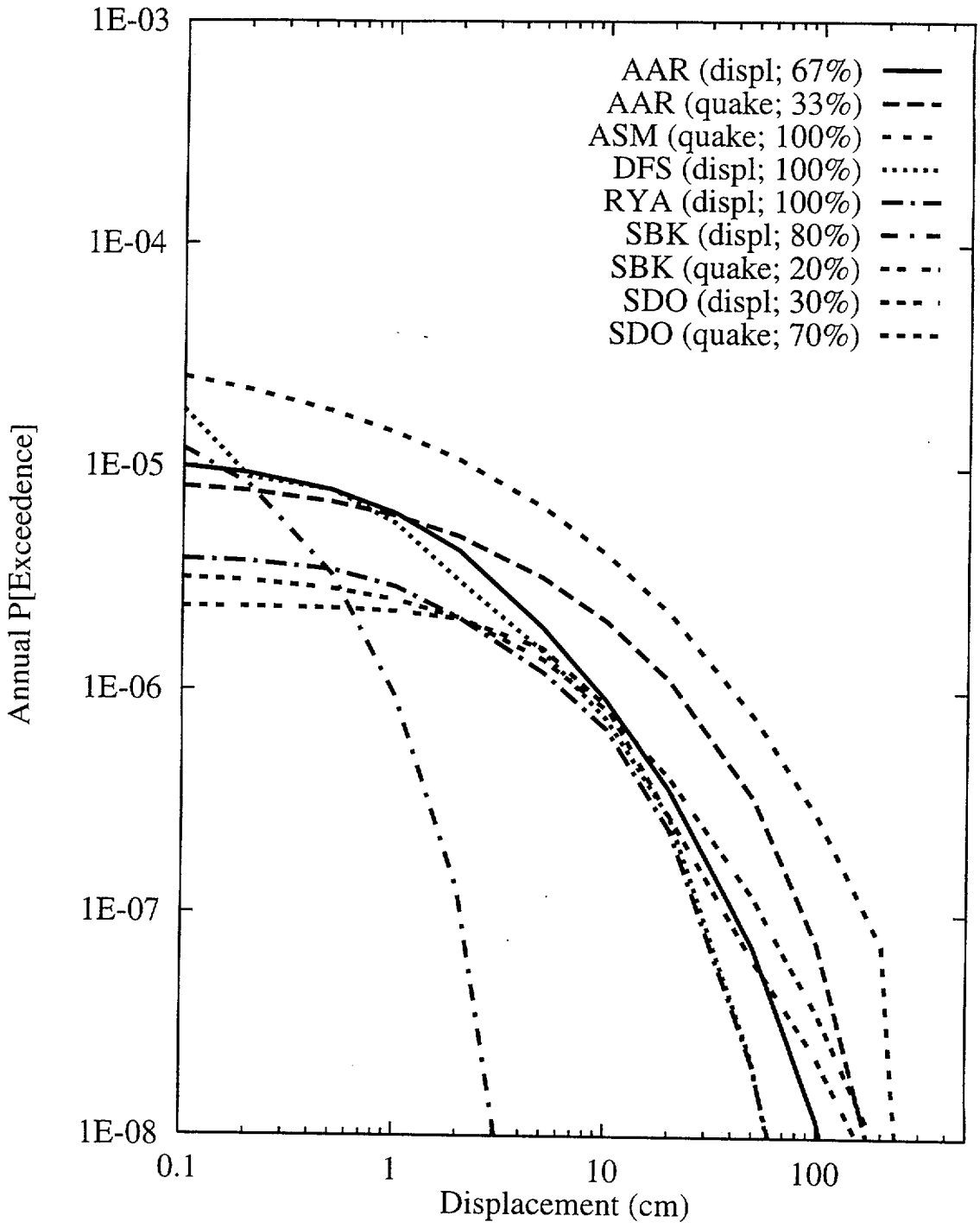

Figure 8-27 Mean hazard by teams and approaches for Site 9, Midway Valley

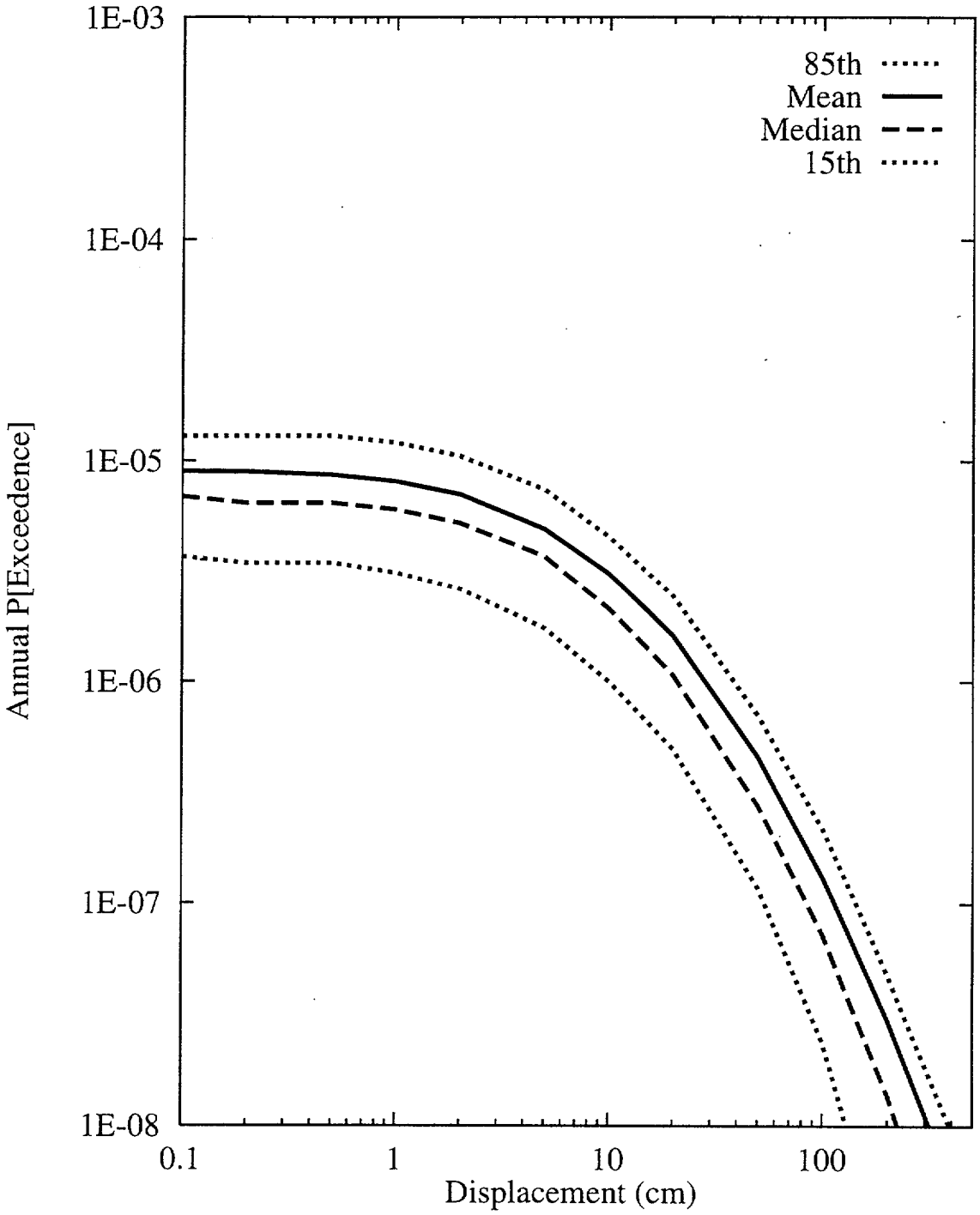

Figure 8-28 Summary hazard curves for Site 1: AAR team, earthquake approach

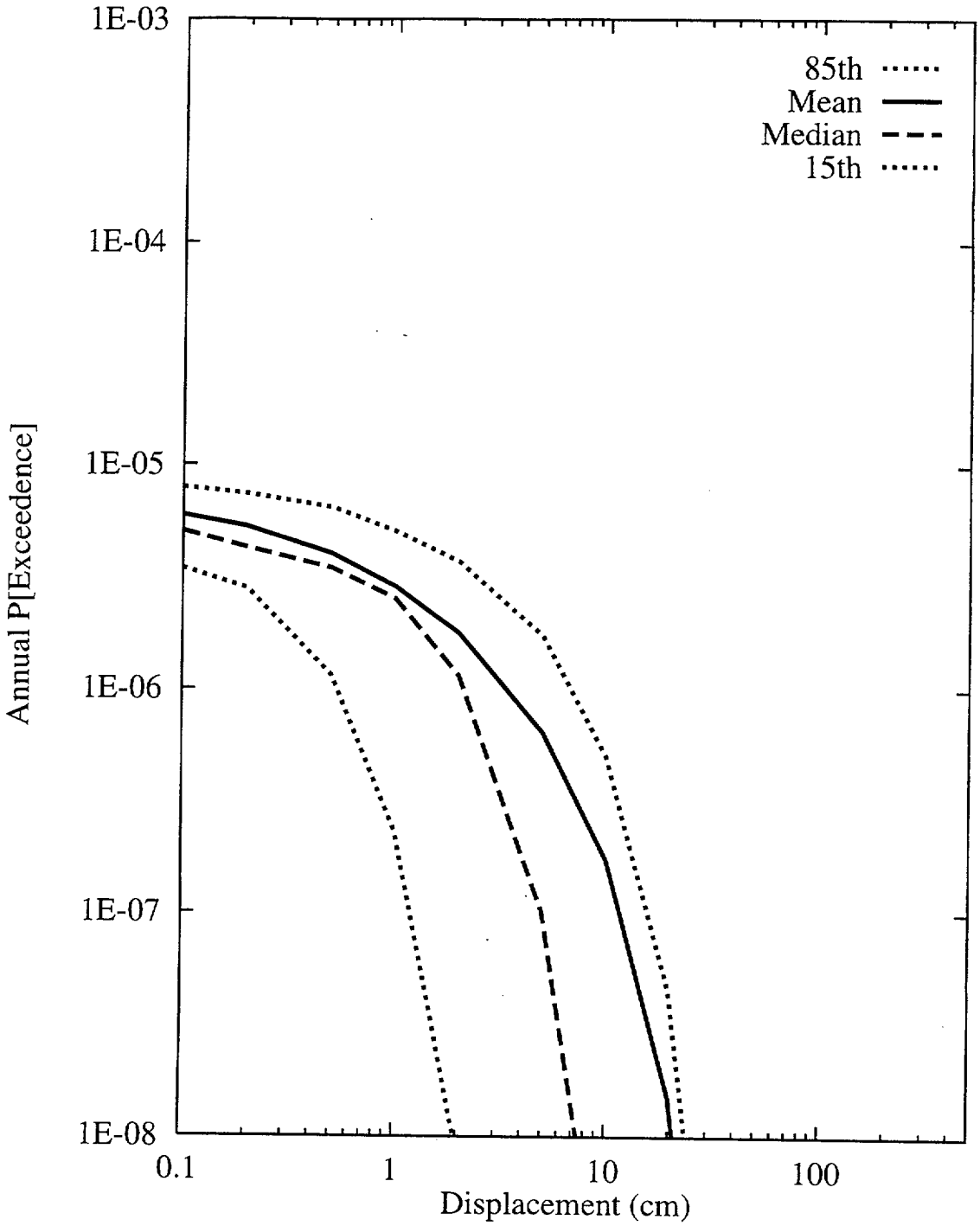

Figure 8-29 Summary hazard curves for Site 7a: AAR team, earthquake approach

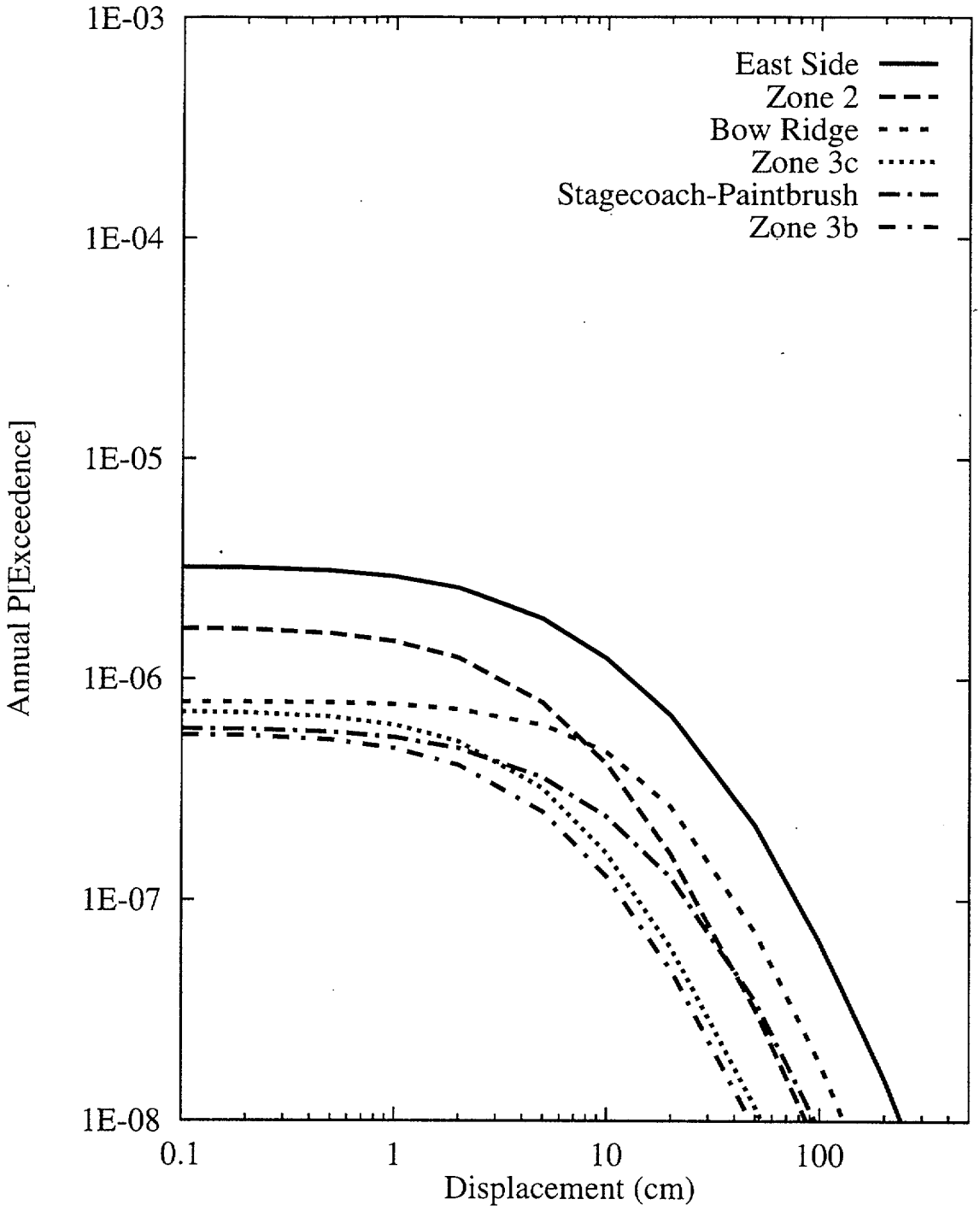

Figure 8-30 Mean hazard curves by source for Site 1: AAR team, earthquake approach

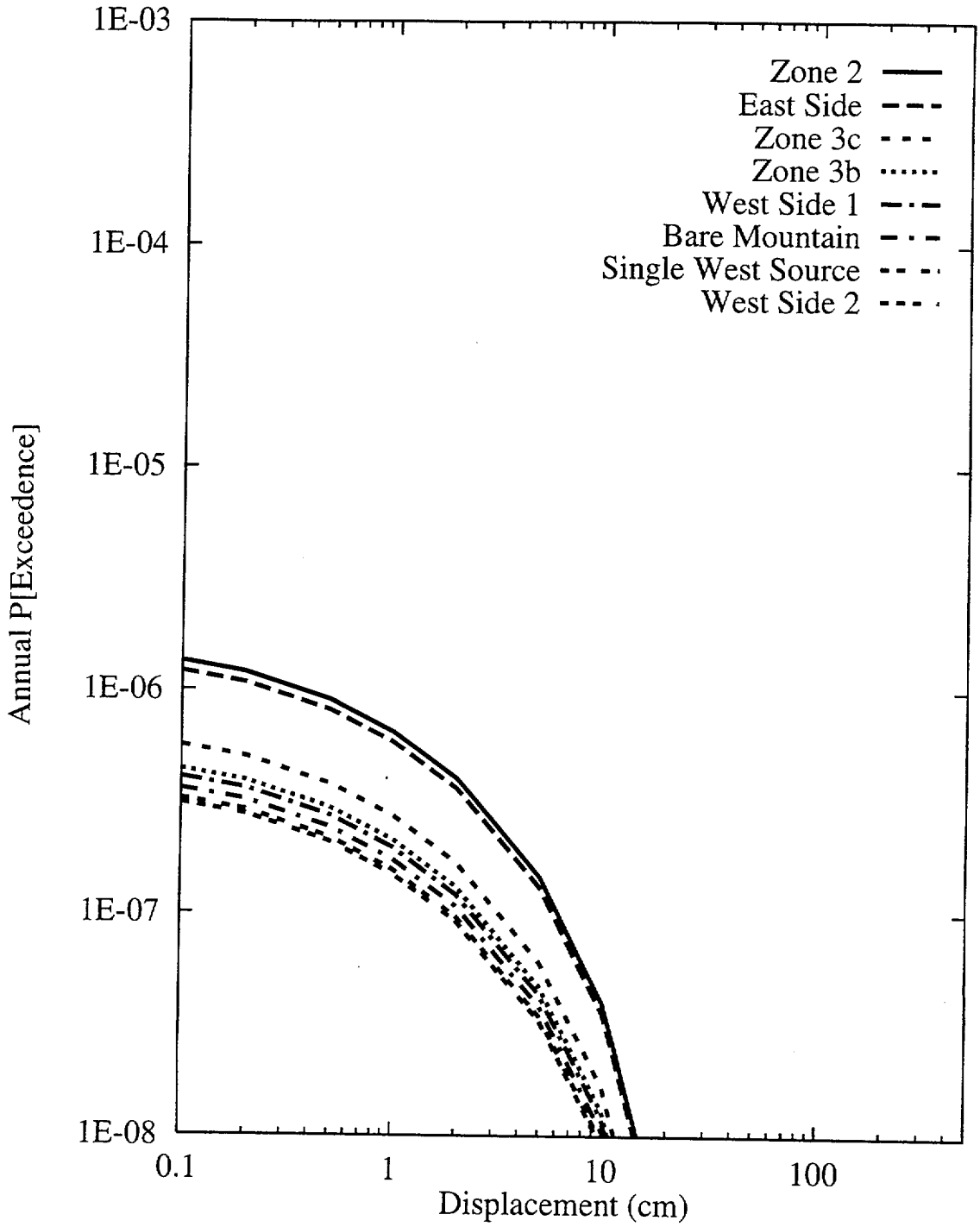

Figure 8-31 Mean hazard curves by source for Site 7a: AAR team, earthquake approach

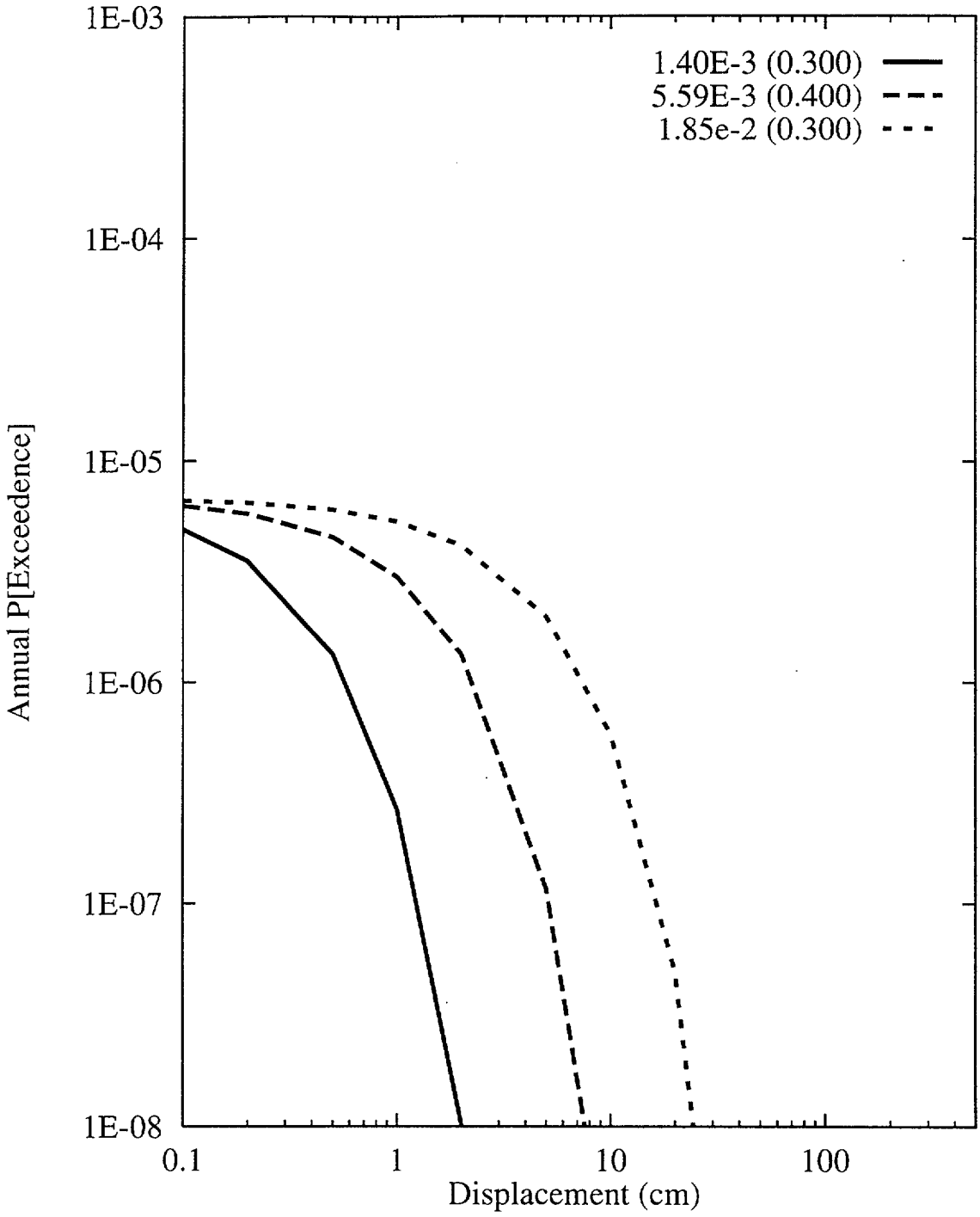

Figure 8-32 Sensitivity of displacement hazard for Site 1 to parameter beta: AAR team, earthquake approach

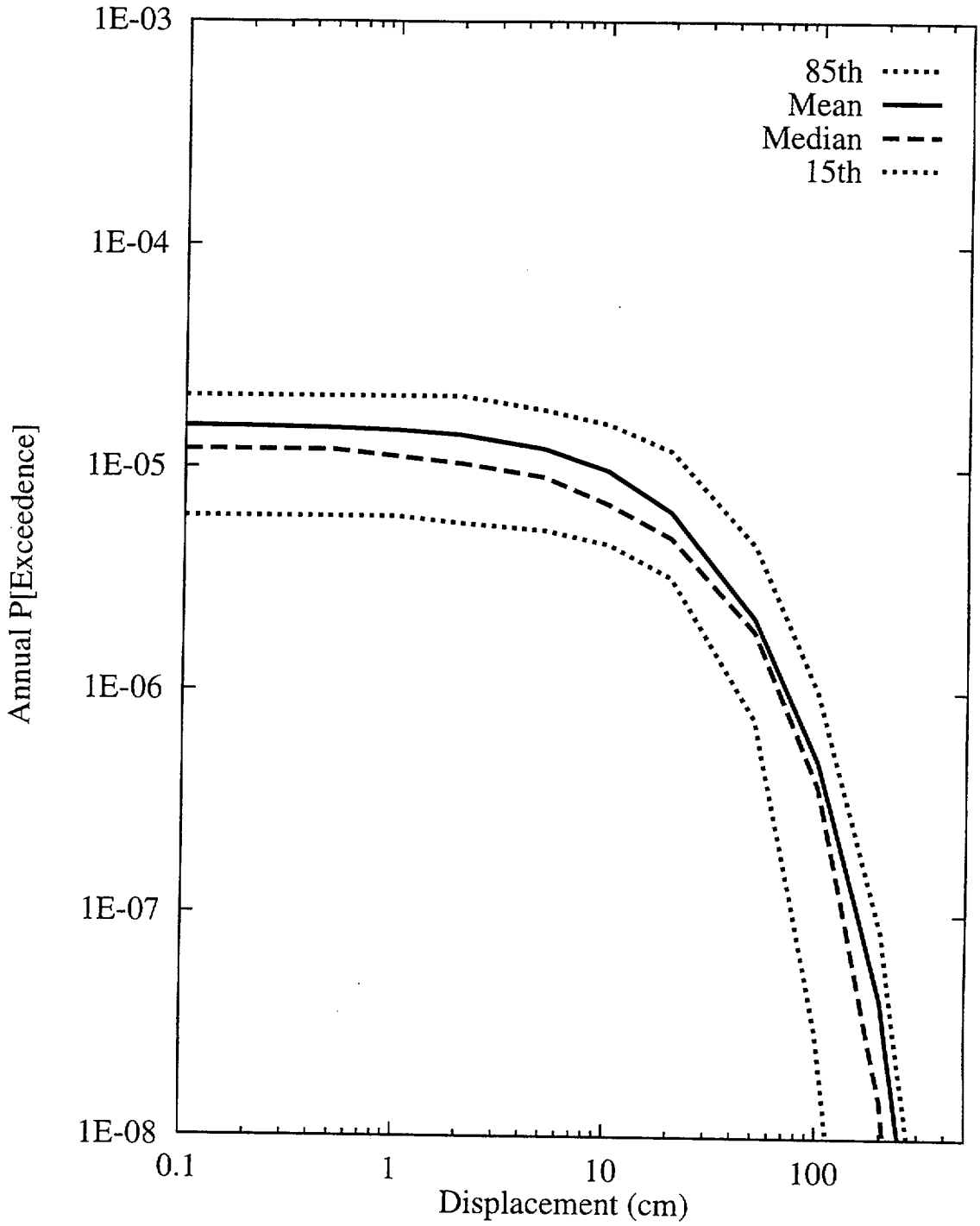

Figure 8-33 Summary hazard curves for Site 1: AAR team, displacement approach

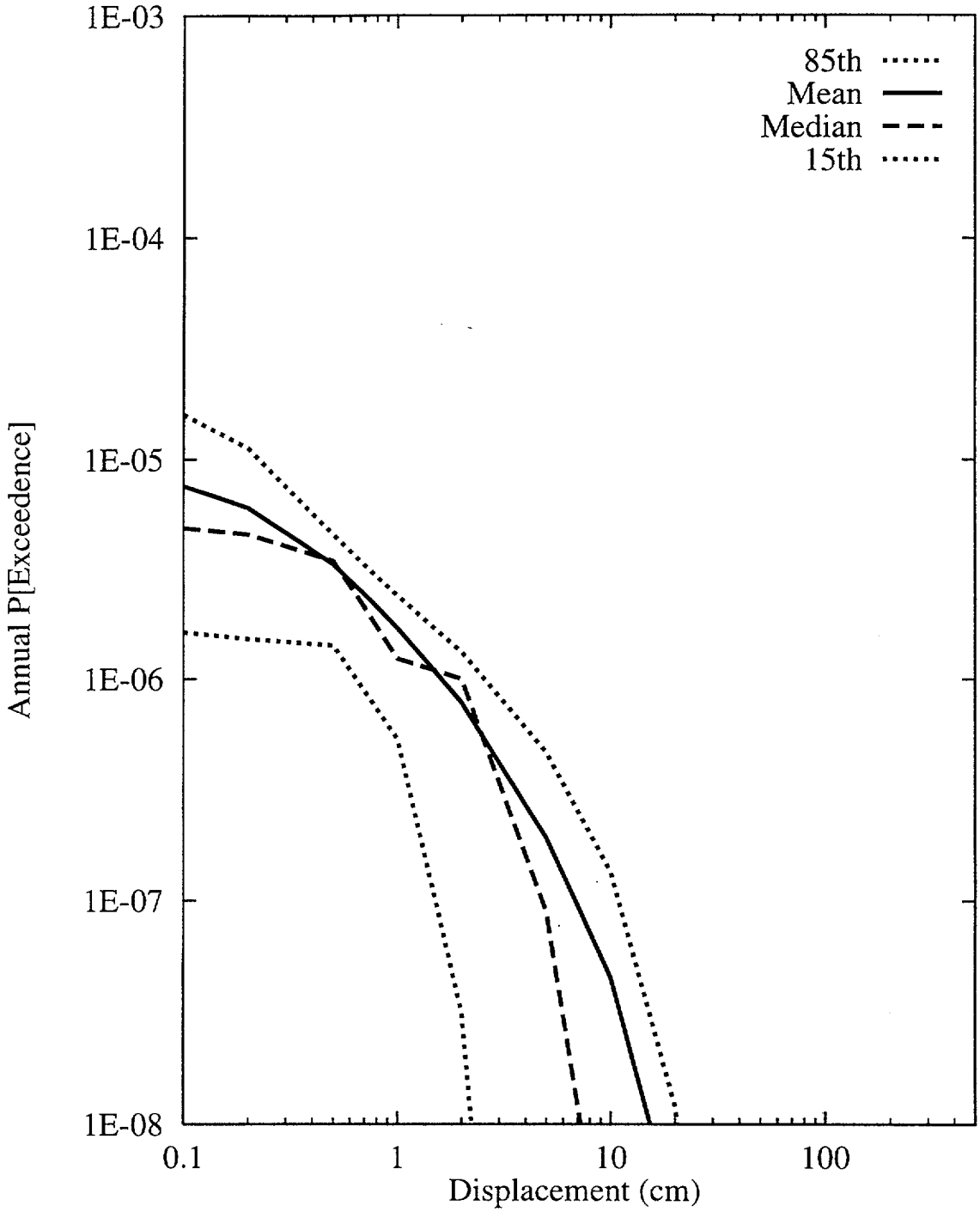

Figure 8-34 Summary hazard curves for Site 7a: AAR team, displacement approach

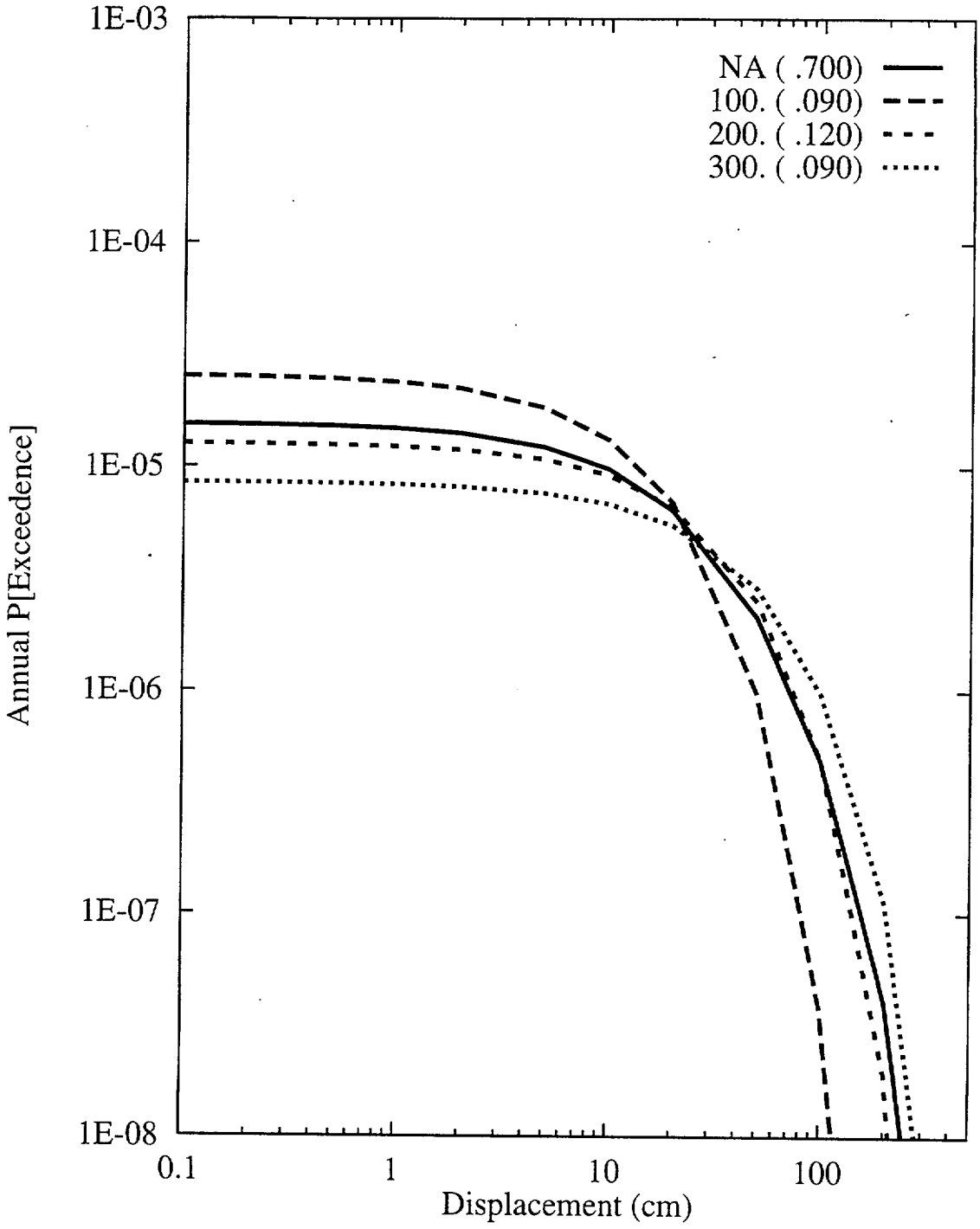

Figure 8-35 Sensitivity of displacement hazard for Site 1 to cumulative displacement: AAR team, displacement approach

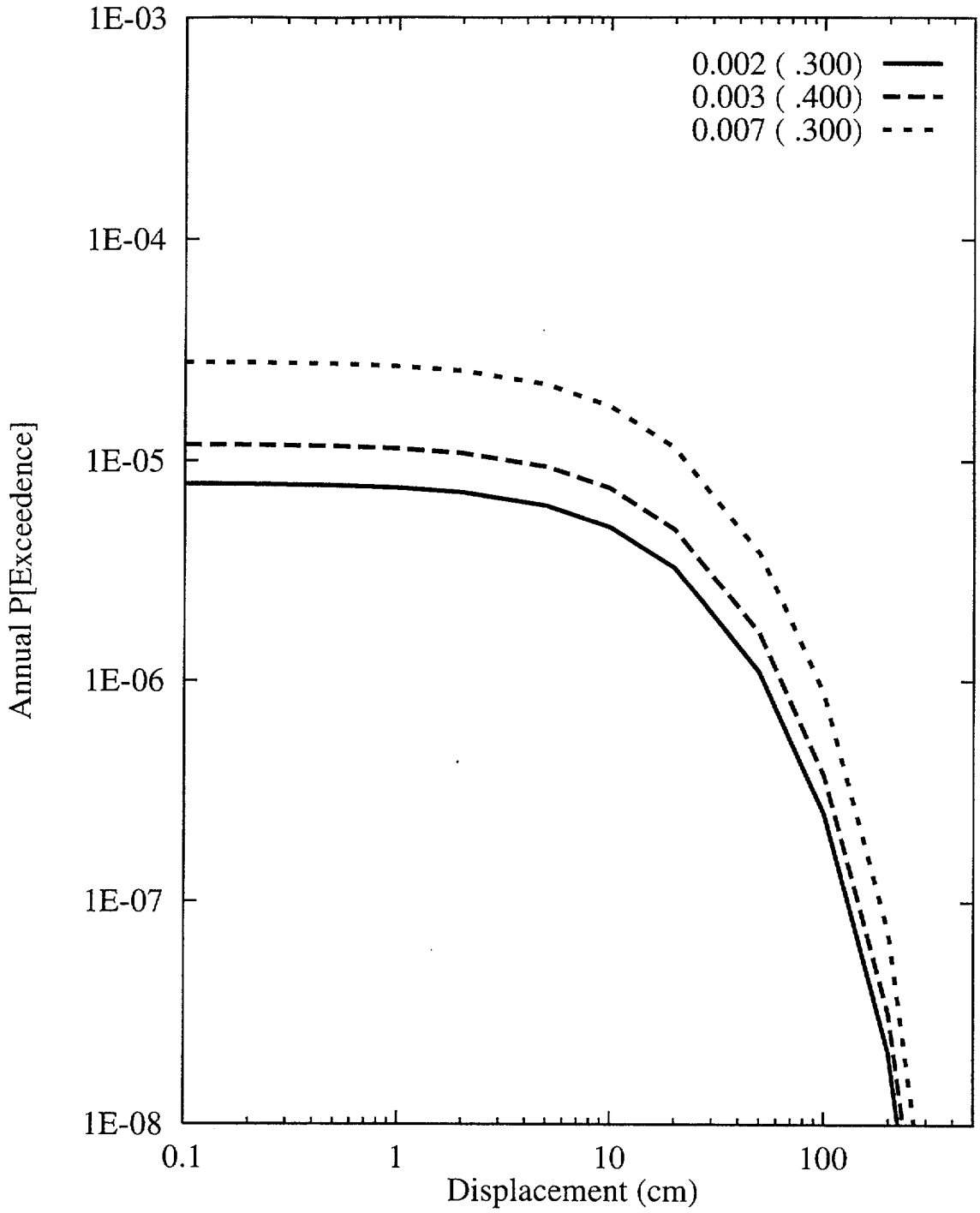

Figure 8-36 Sensitivity of displacement hazard for Site 1 to slip rate: AAR team, displacement approach

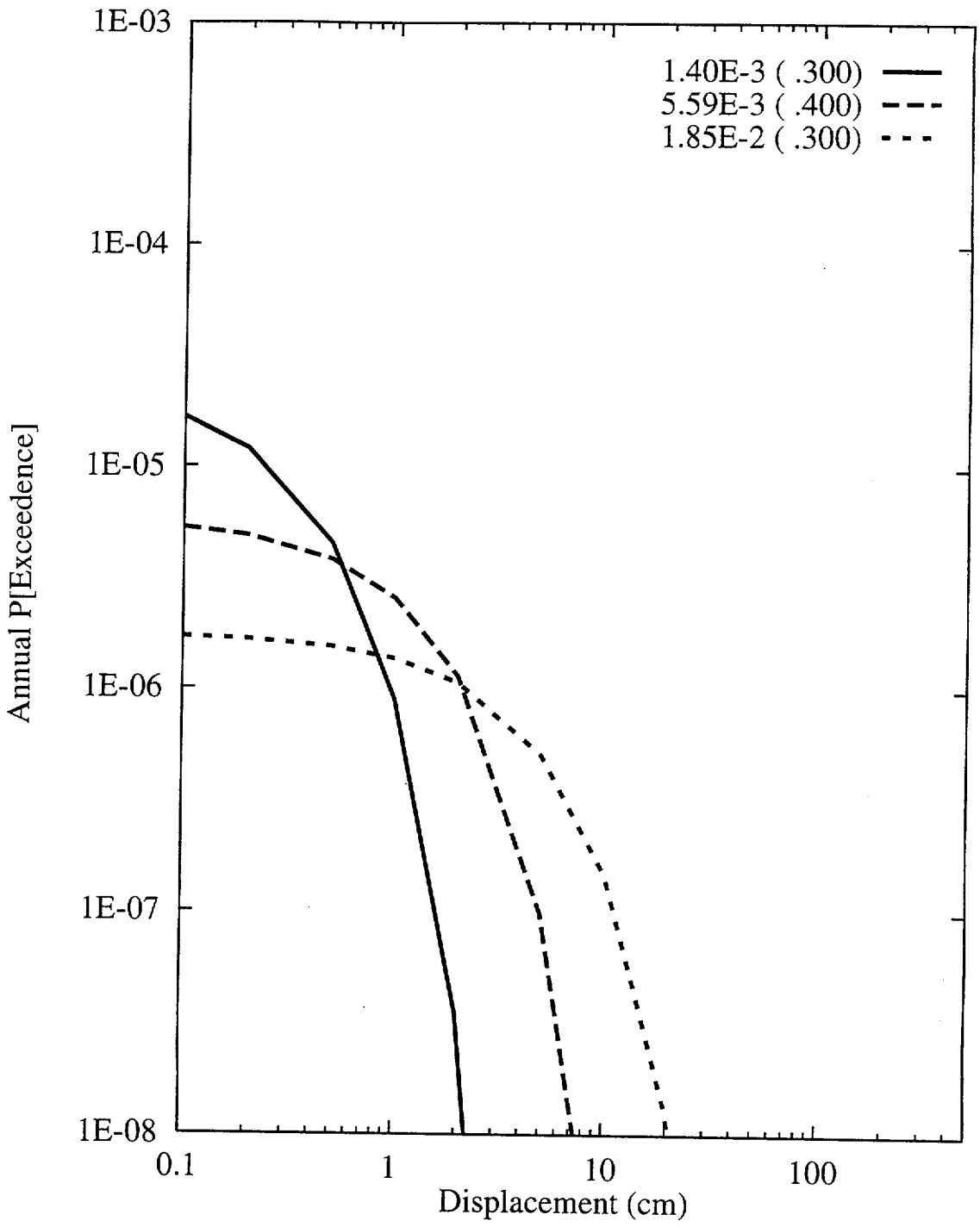

Figure 8-37 Sensitivity of displacement hazard for Site 7a to parameter beta: AAR team, displacement approach

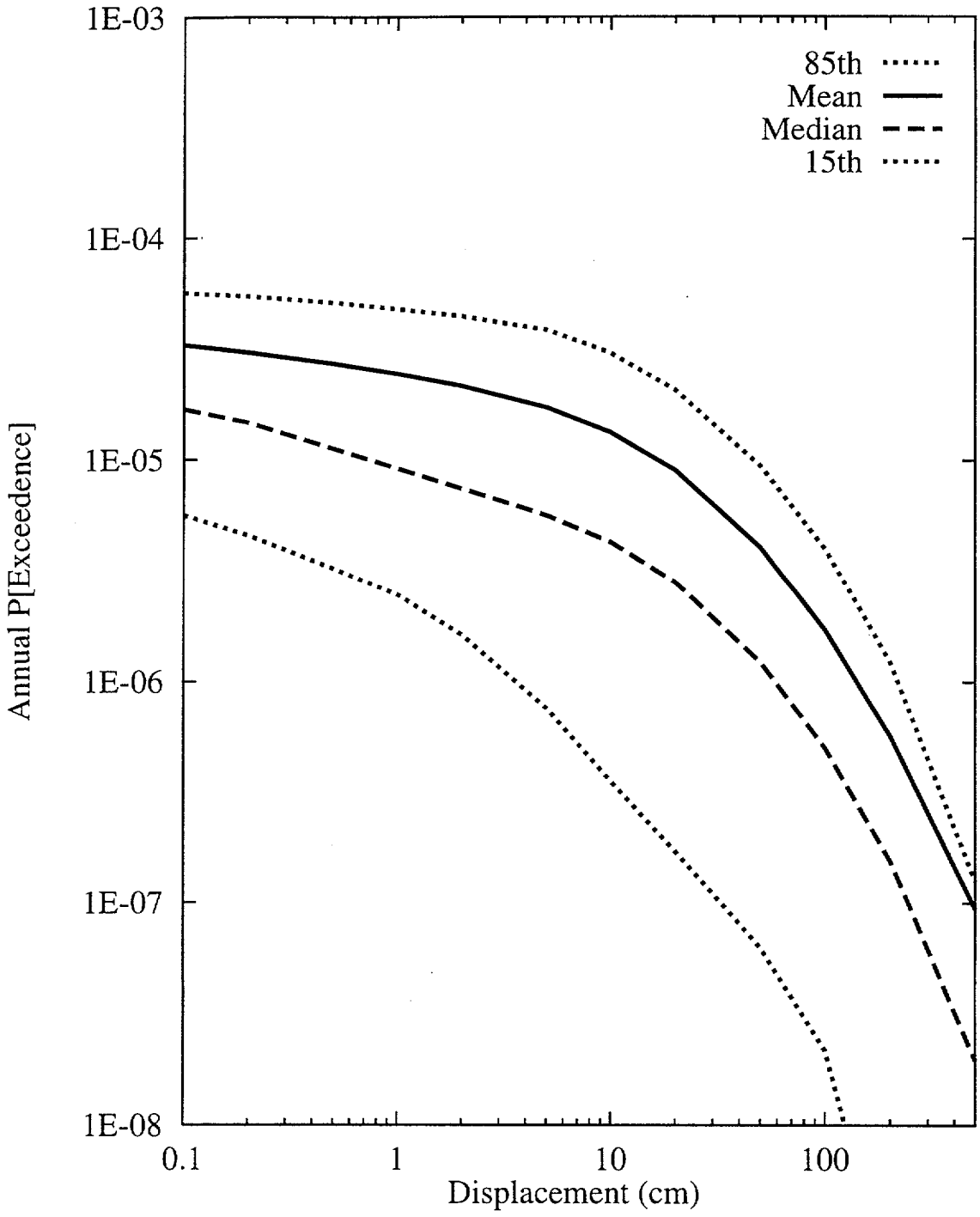

Figure 8-38 Summary hazard curves for Site 1: ASM team, earthquake approach

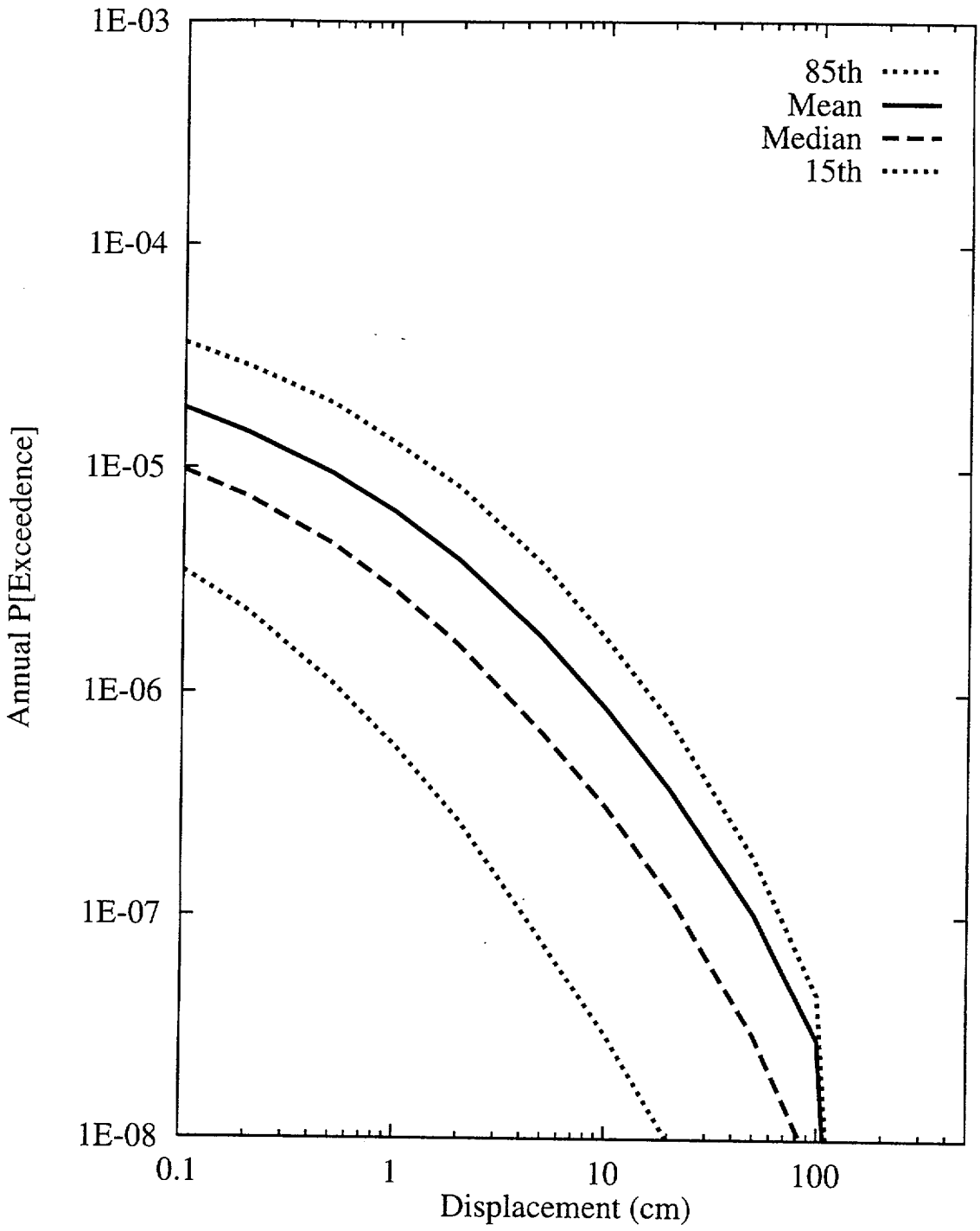

Figure 8-39 Summary hazard curves for Site 7a: ASM team, earthquake approach

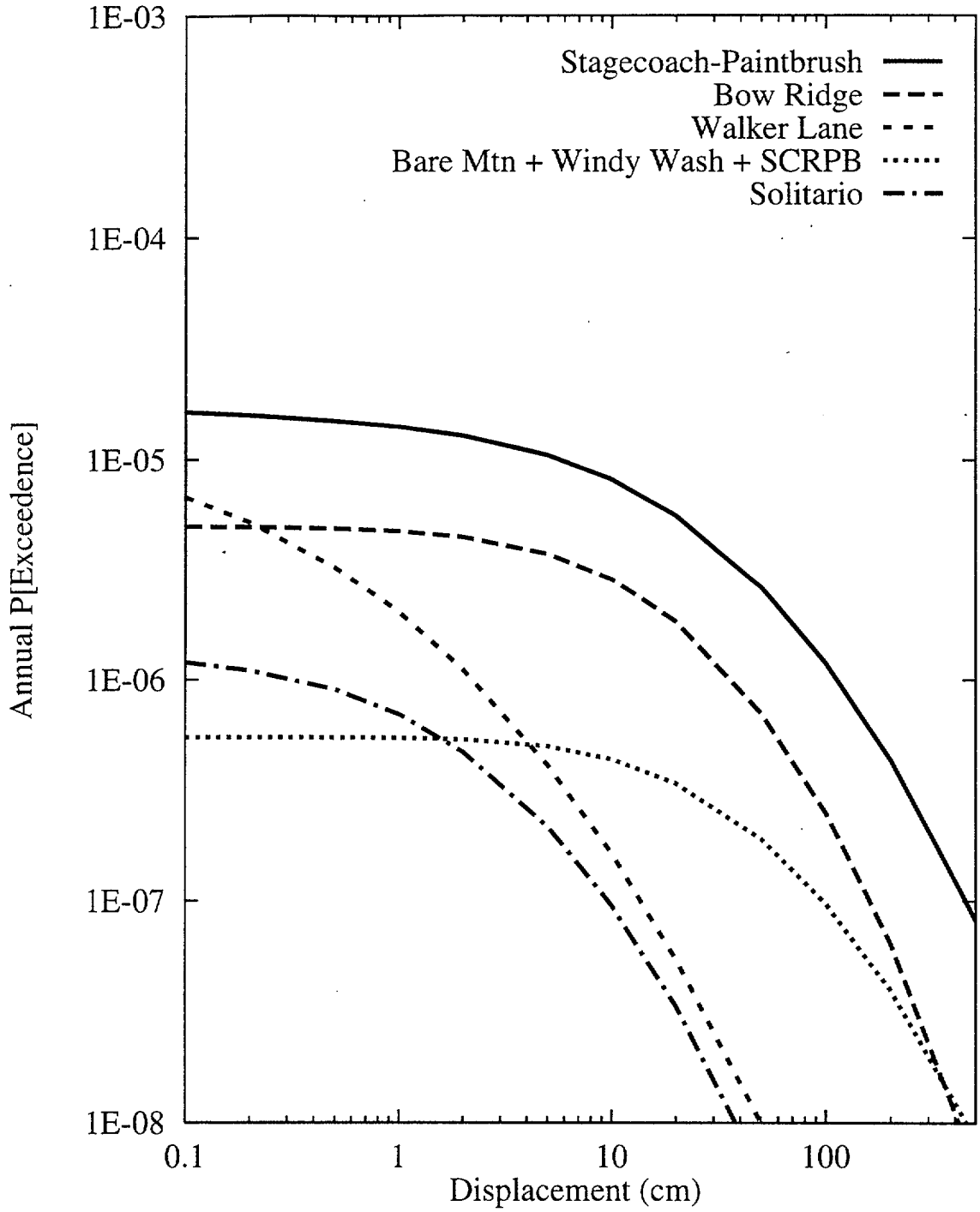

Figure 8-40 Mean hazard curves by source for Site 1: ASM team, earthquake approach

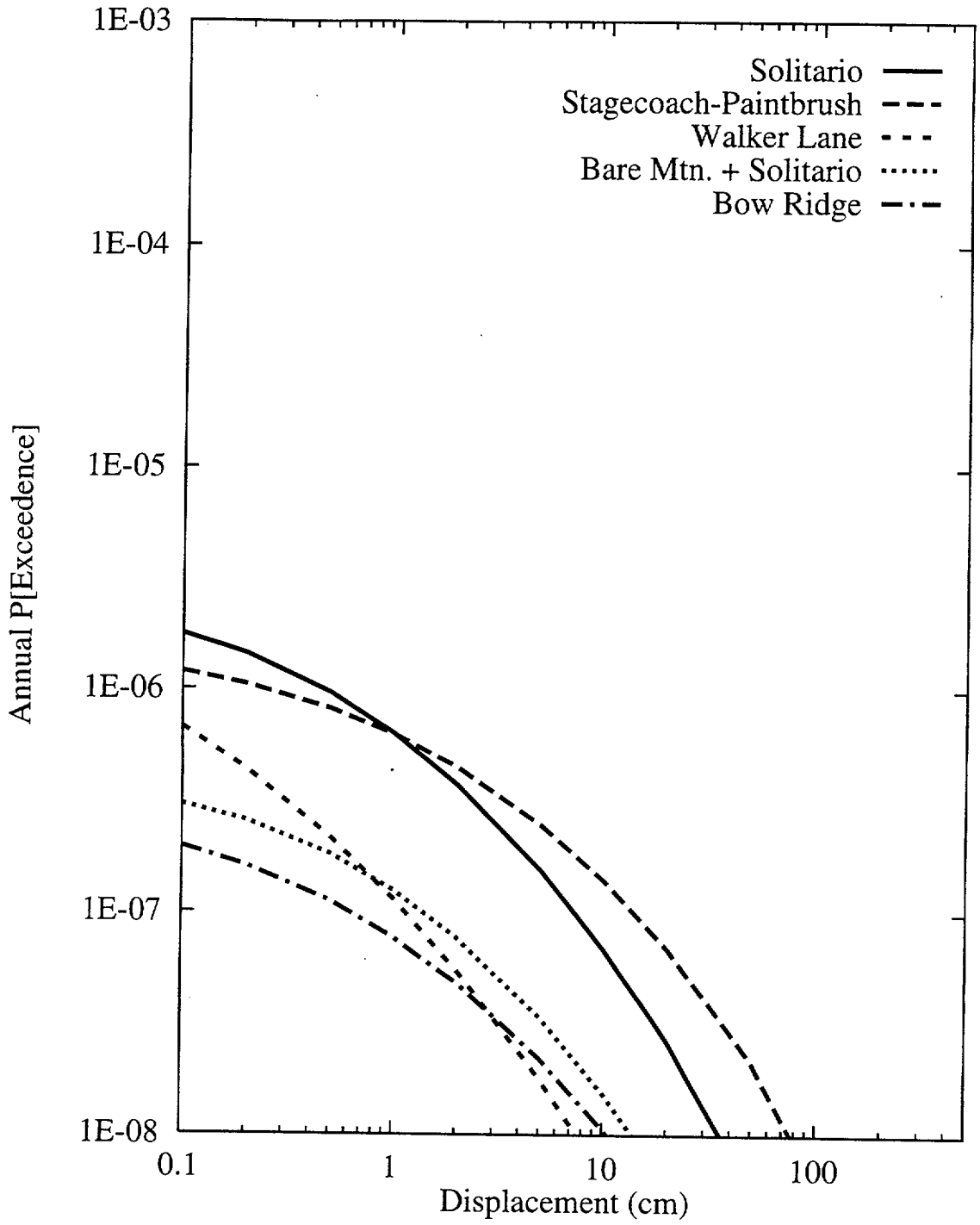

Figure 8-41 Mean hazard curves by source for Site 7a: ASM team, earthquake approach

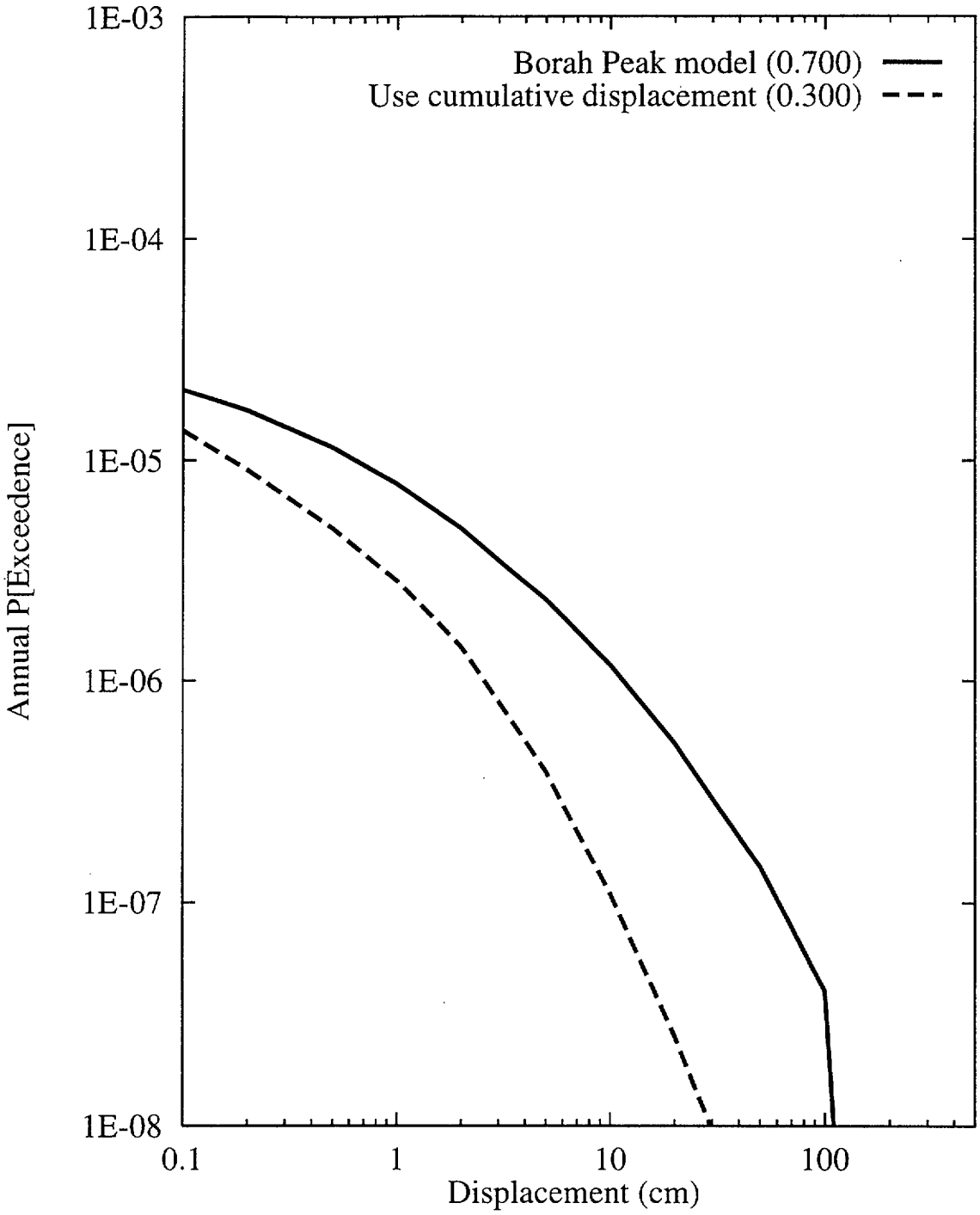

Figure 8-42 Sensitivity of displacement hazard for Site 7a to scaling of principal to distributed faulting: ASM team, earthquake approach

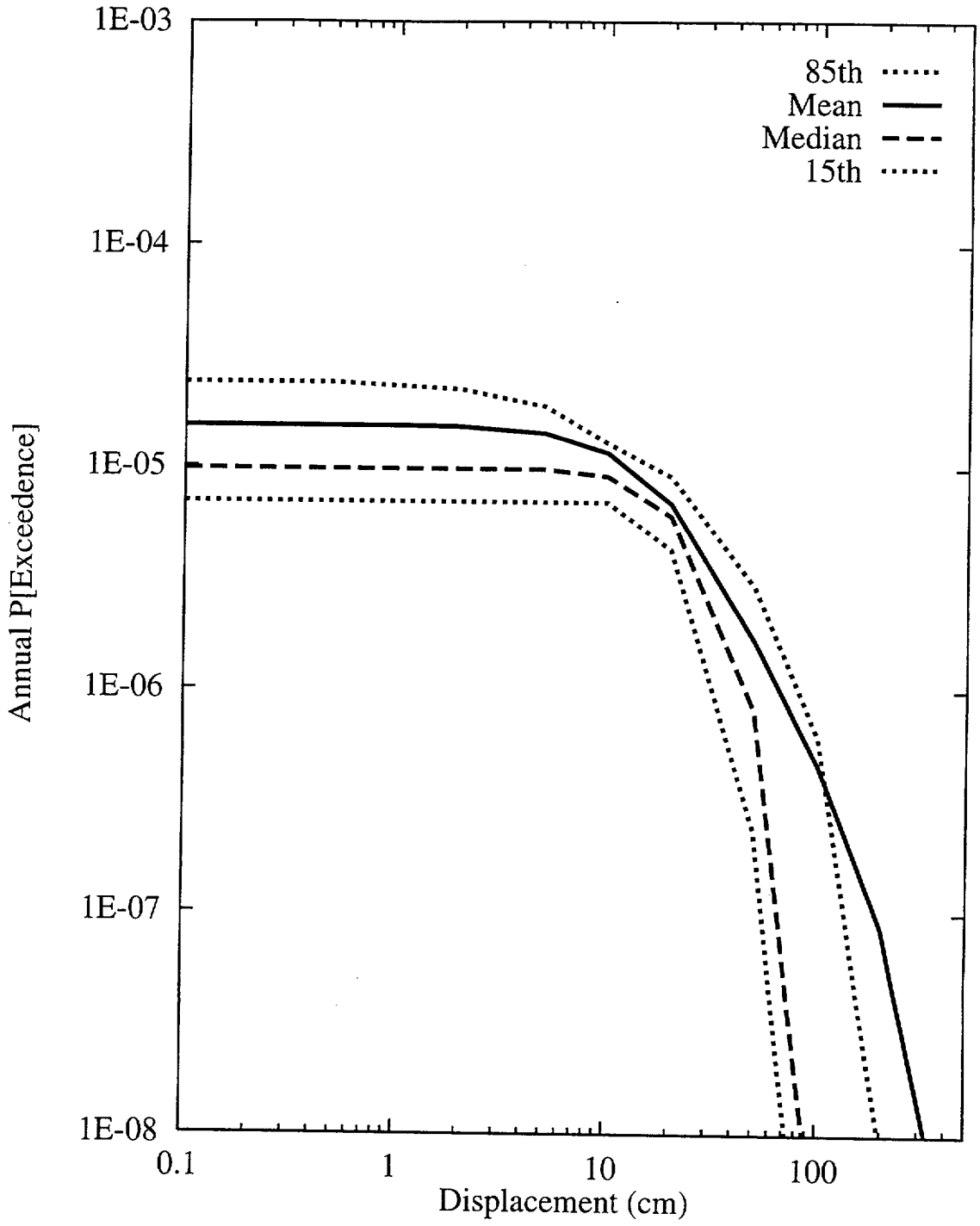

Figure 8-43 Summary hazard curves for Site 1: DFS team, displacement approach

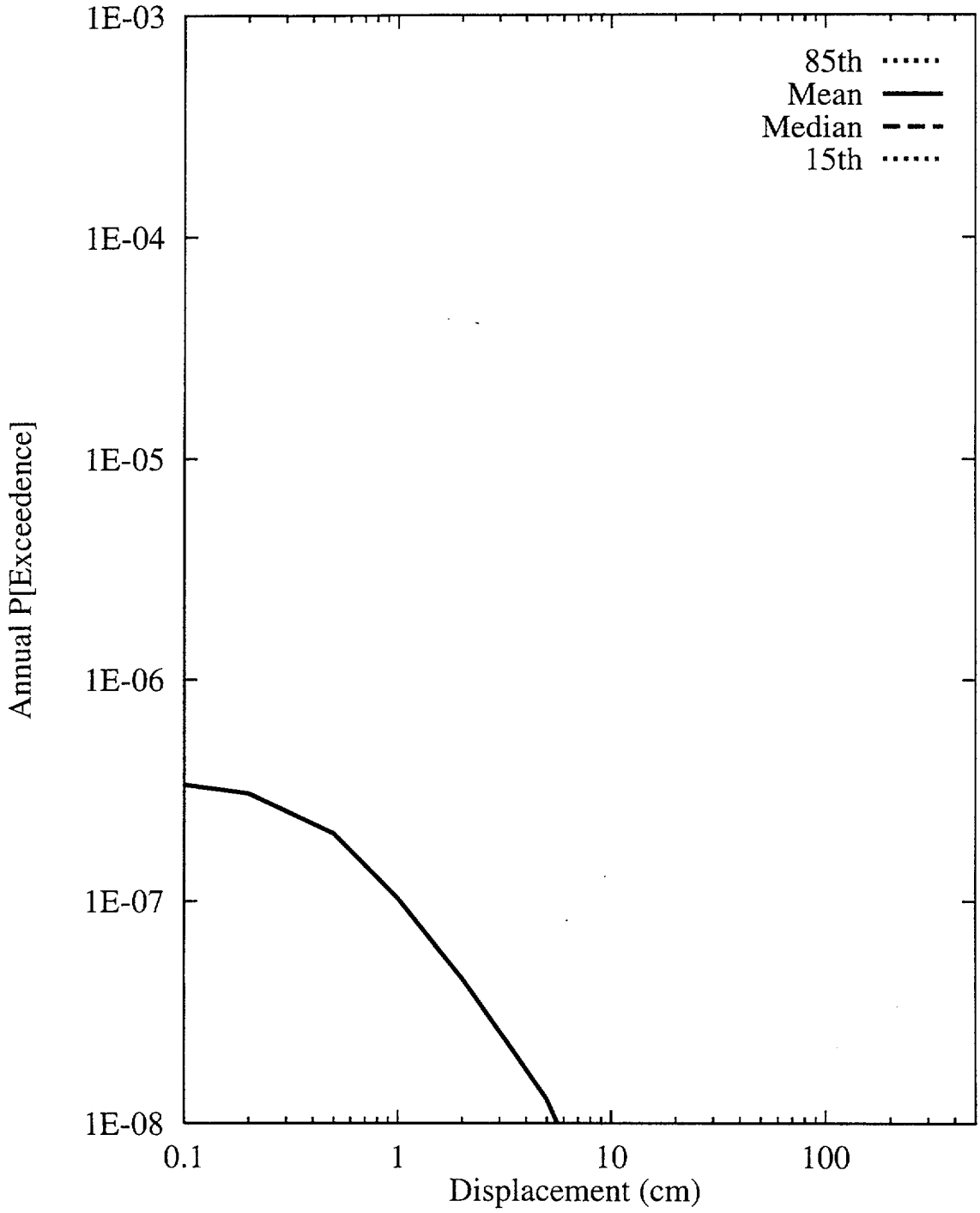

Figure 8-44 Summary hazard curves for Site 7a: DFS team, displacement approach

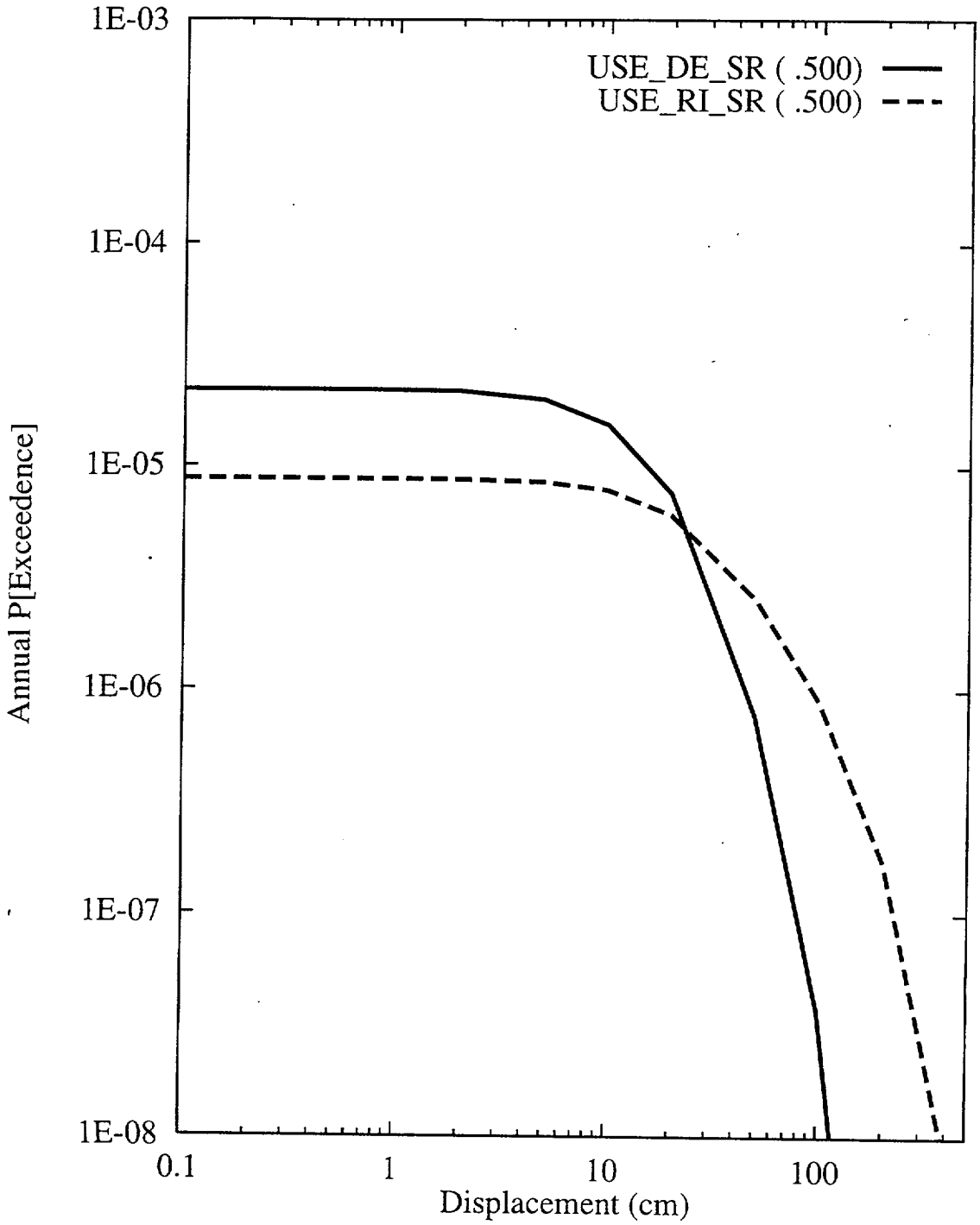

Figure 8-45 Sensitivity of displacement hazard for Site 1 to calculation option: DFS team, displacement approach

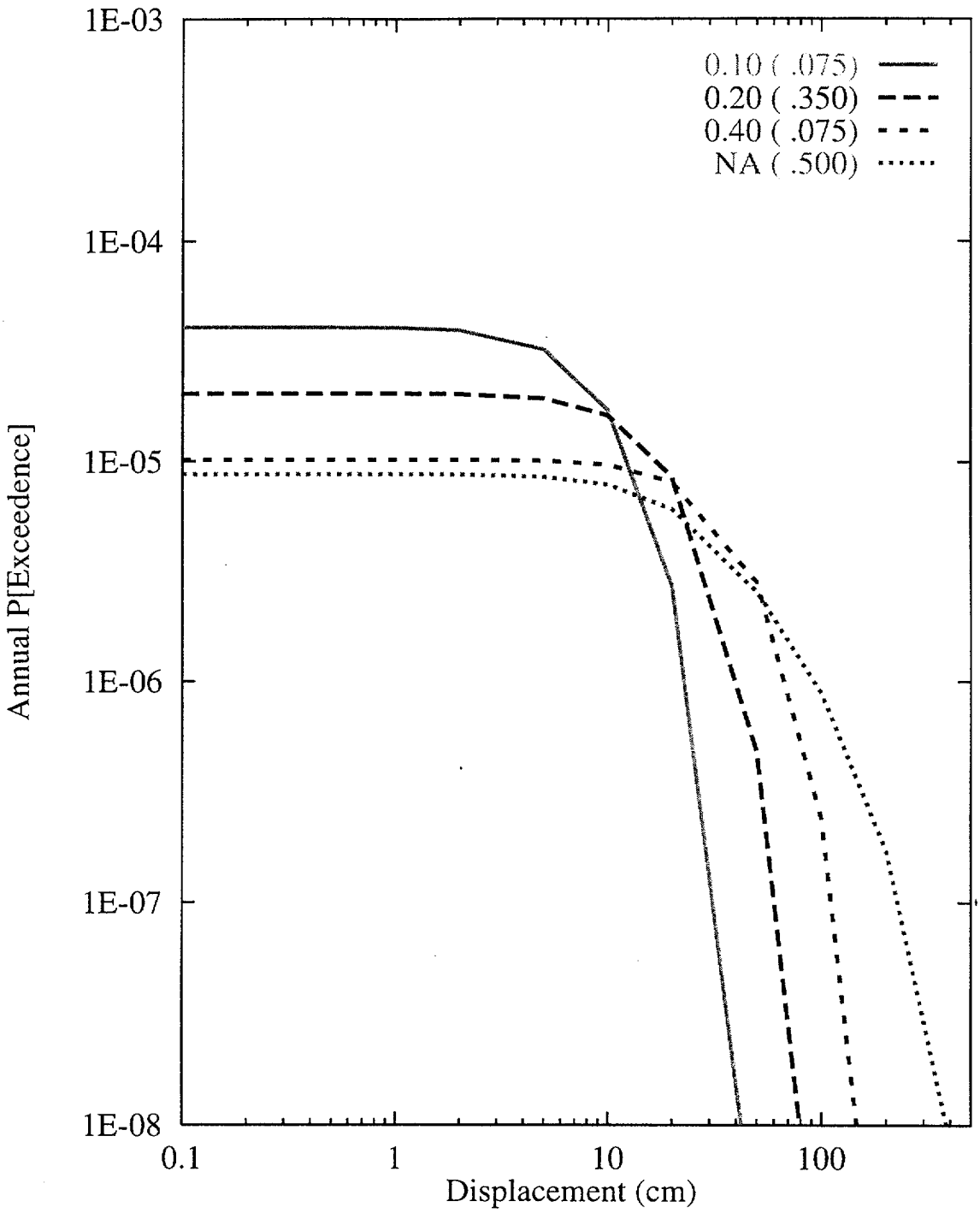

Figure 8-46 Sensitivity of displacement hazard for Site 1 to average displacement per event (m): DFS team, displacement approach

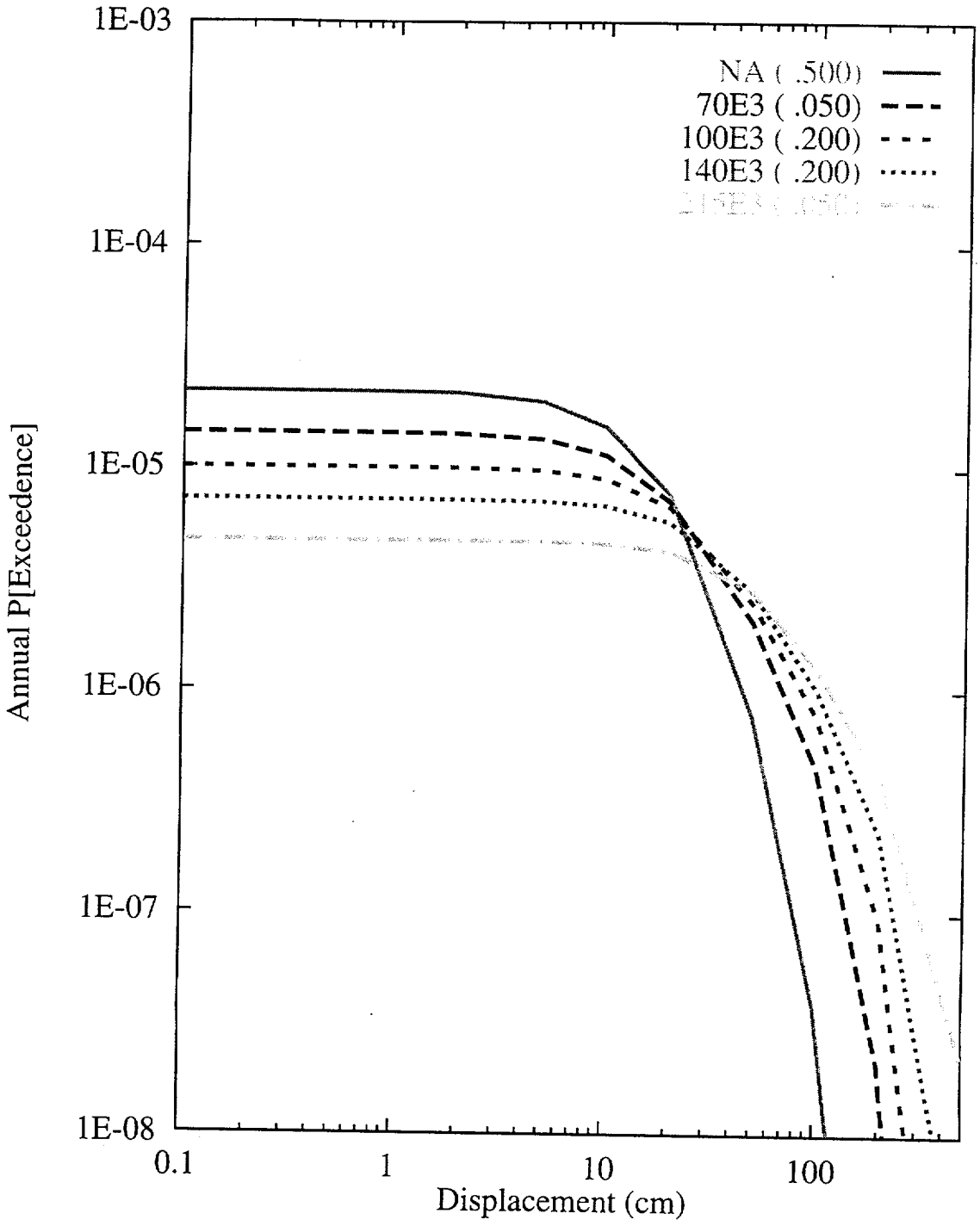

Figure 8-47 Sensitivity of displacement hazard for Site 1 to recurrence interval: DFS team, displacement approach

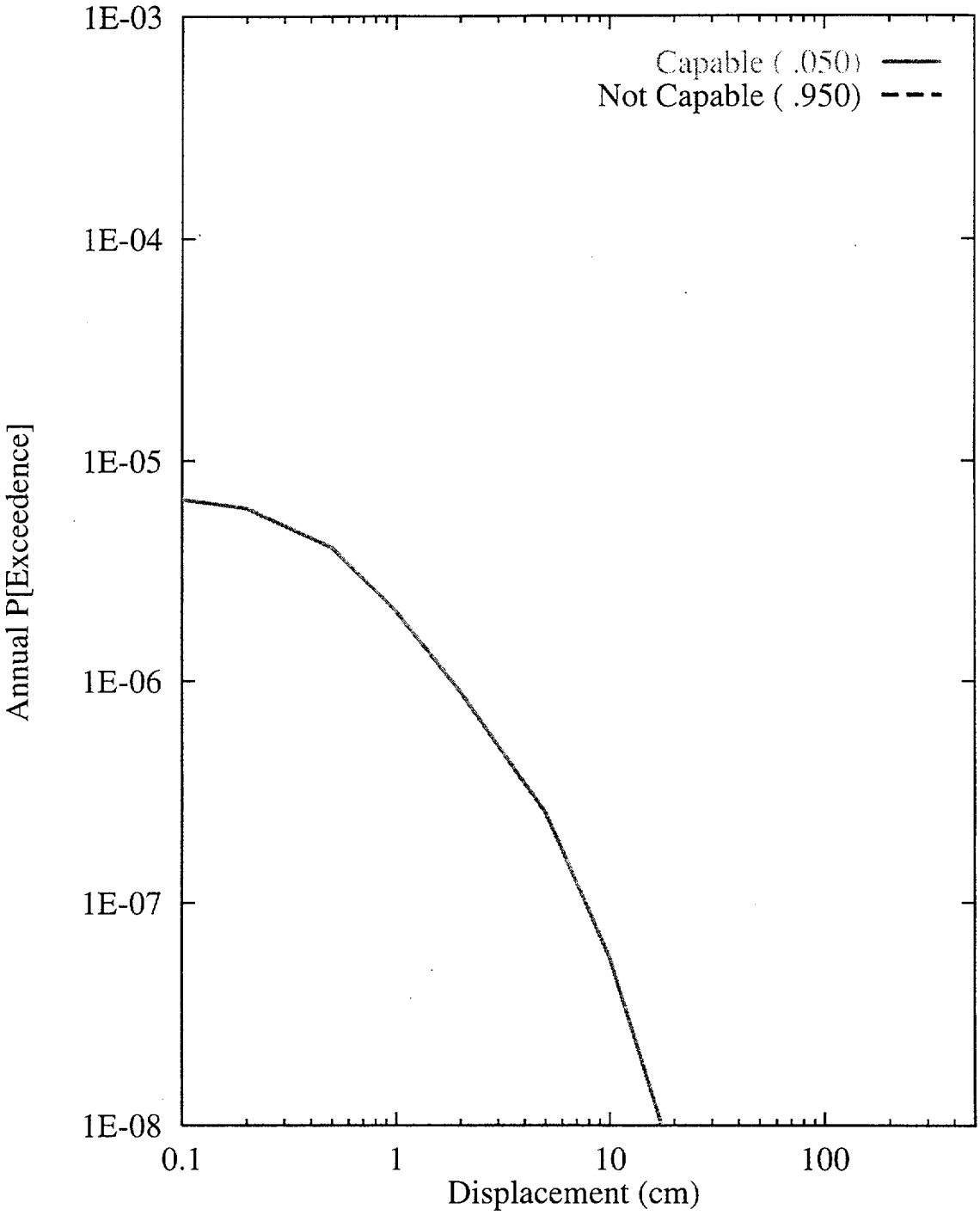

Figure 8-48 Sensitivity of displacement hazard for Site 7a to capability for fault displacement: DFS team, displacement approach

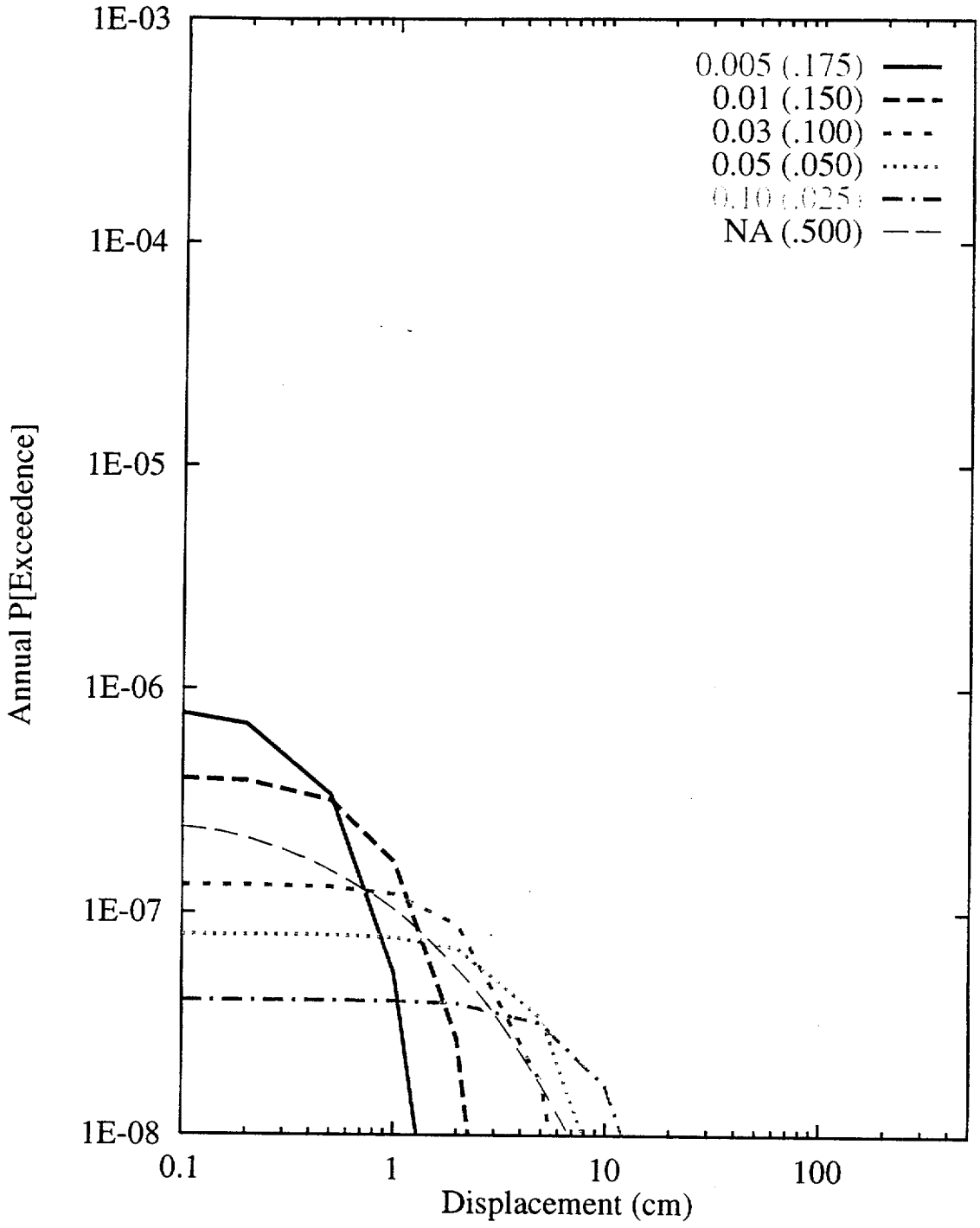

Figure 8-49 Sensitivity of displacement hazard for Site 7a to average displacement per event (m): DFS team, desplacement approach

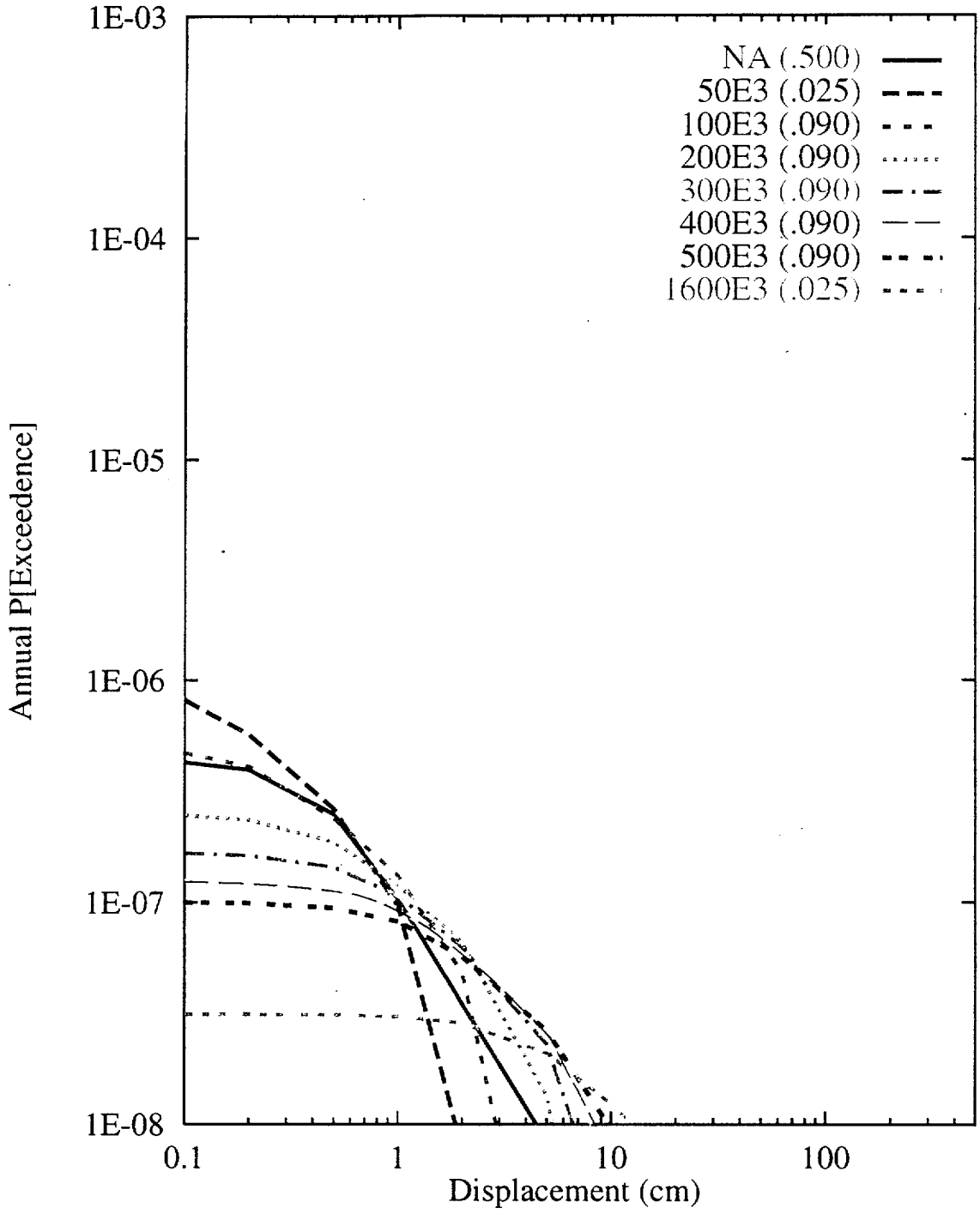

Figure 8-50 Sensitivity of displacement hazard for Site 7a to recurrence interval: DFS team, displacement approach

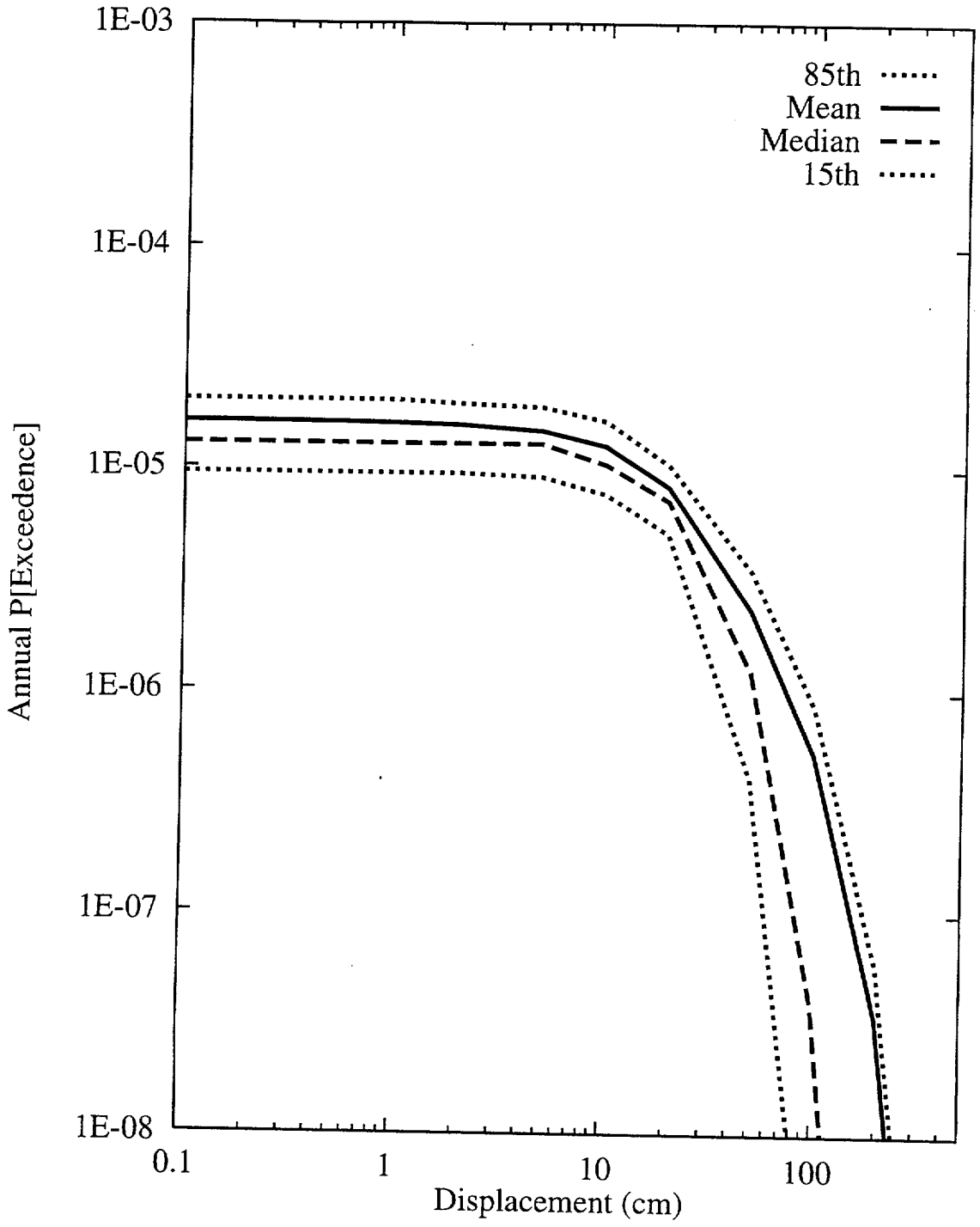

Figure 8-51 Summary hazard curves for Site 1: RYA team, displacement approach

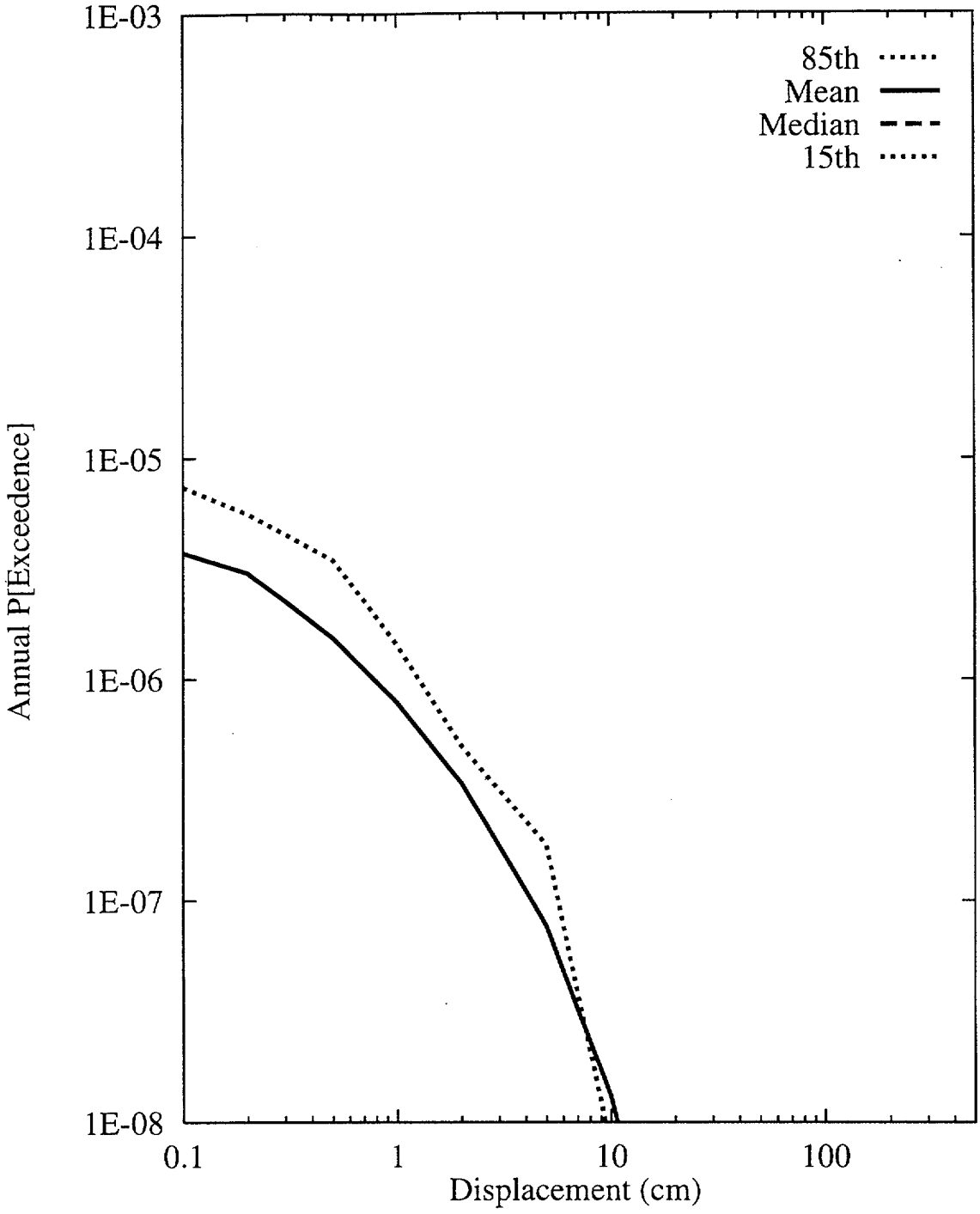

Figure 8-52 Summary hazard curves for Site 7a: RYA team, displacement approach

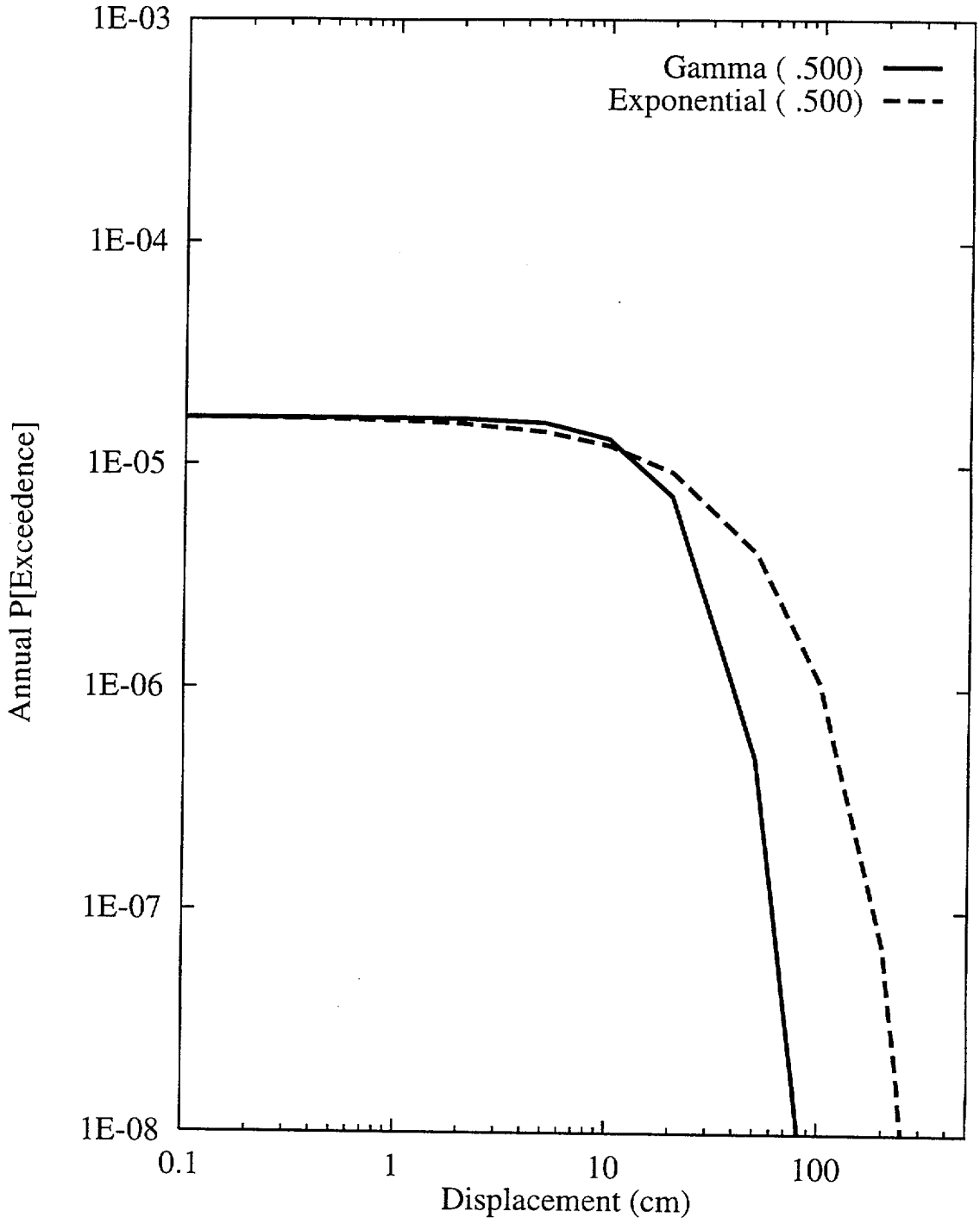

Figure 8-53 Sensitivity of displacement hazard for Site 1 to distribution shape: RYA team, displacement approach

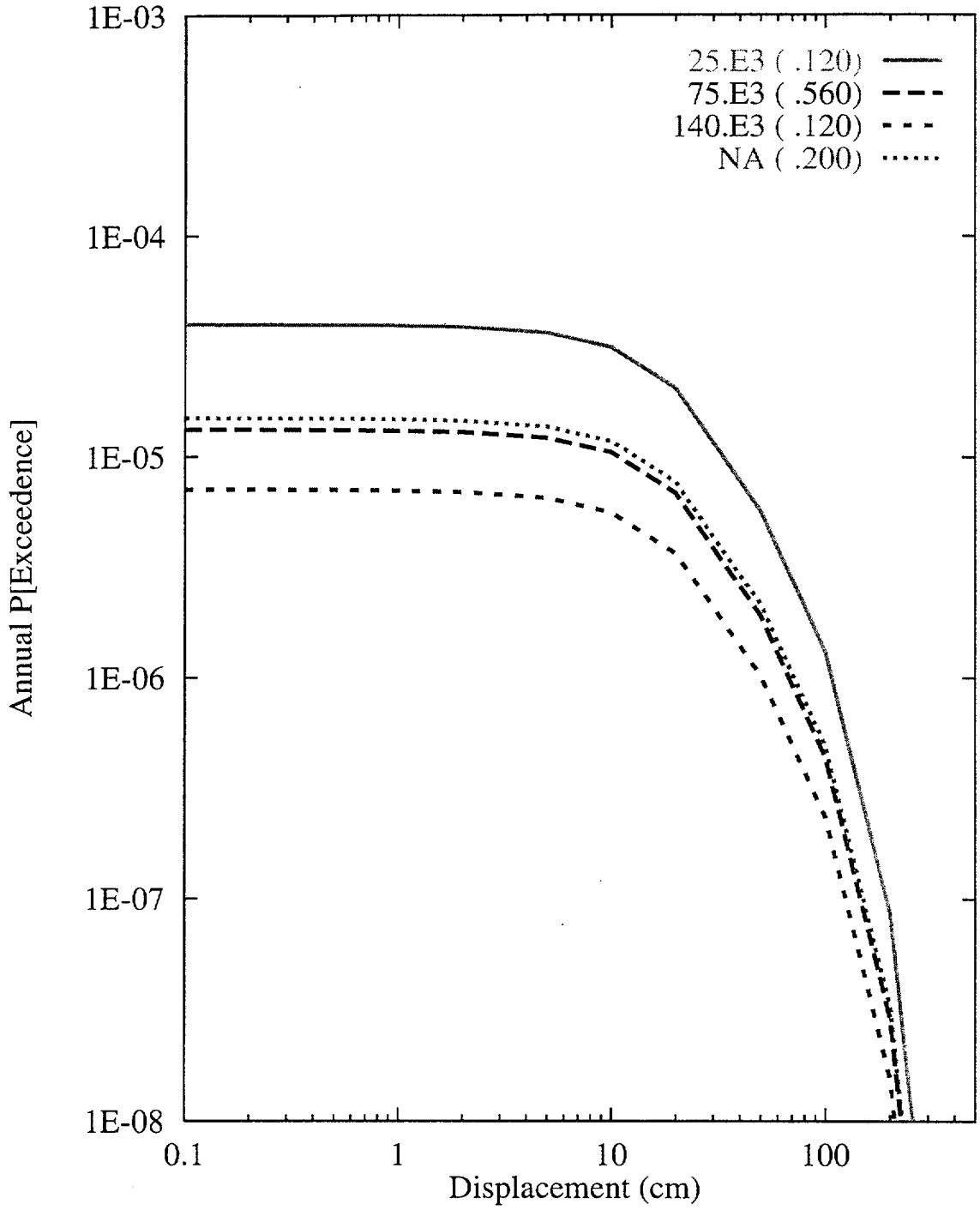

Figure 8-54 Sensitivity of displacement hazard for Site 1 to recurrence interval: RYA team, displacement approach

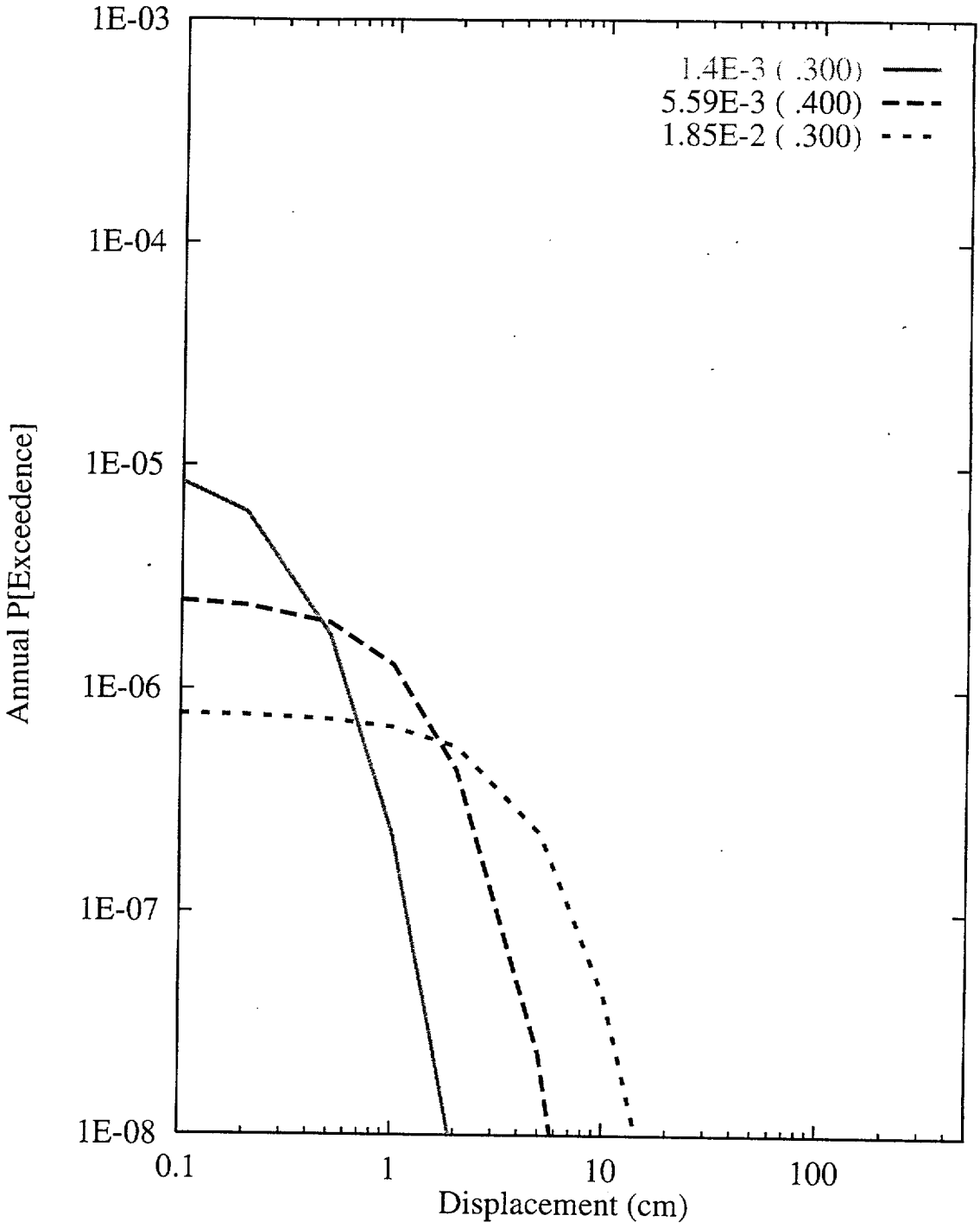

Figure 8-55 Sensitivity of displacement hazard for Site 7a to parameter beta: RYA team, displacement approach

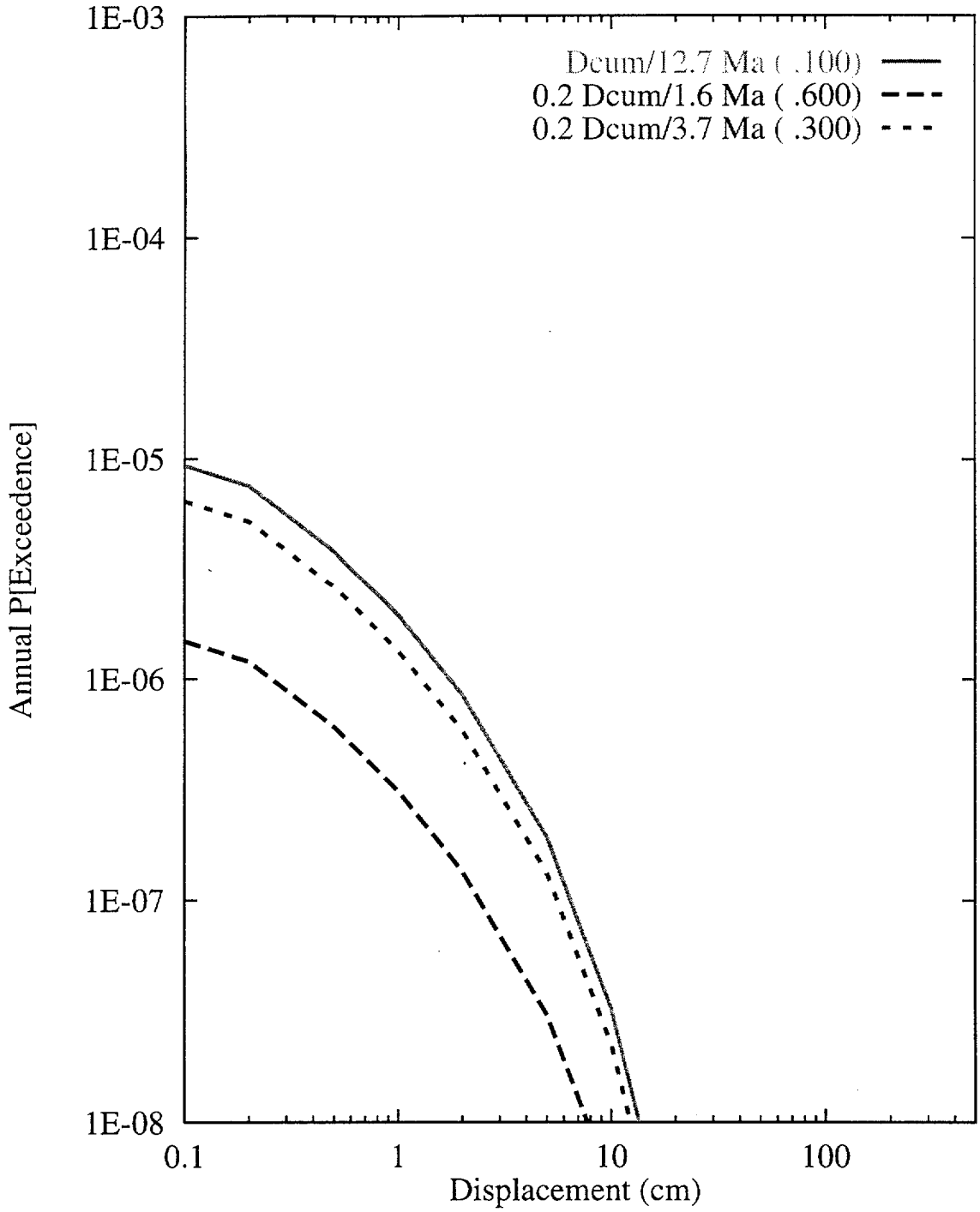

Figure 8-56 Sensitivity of displacement hazard for Site 7a to calculation of slip rate: RYA team, displacement approach

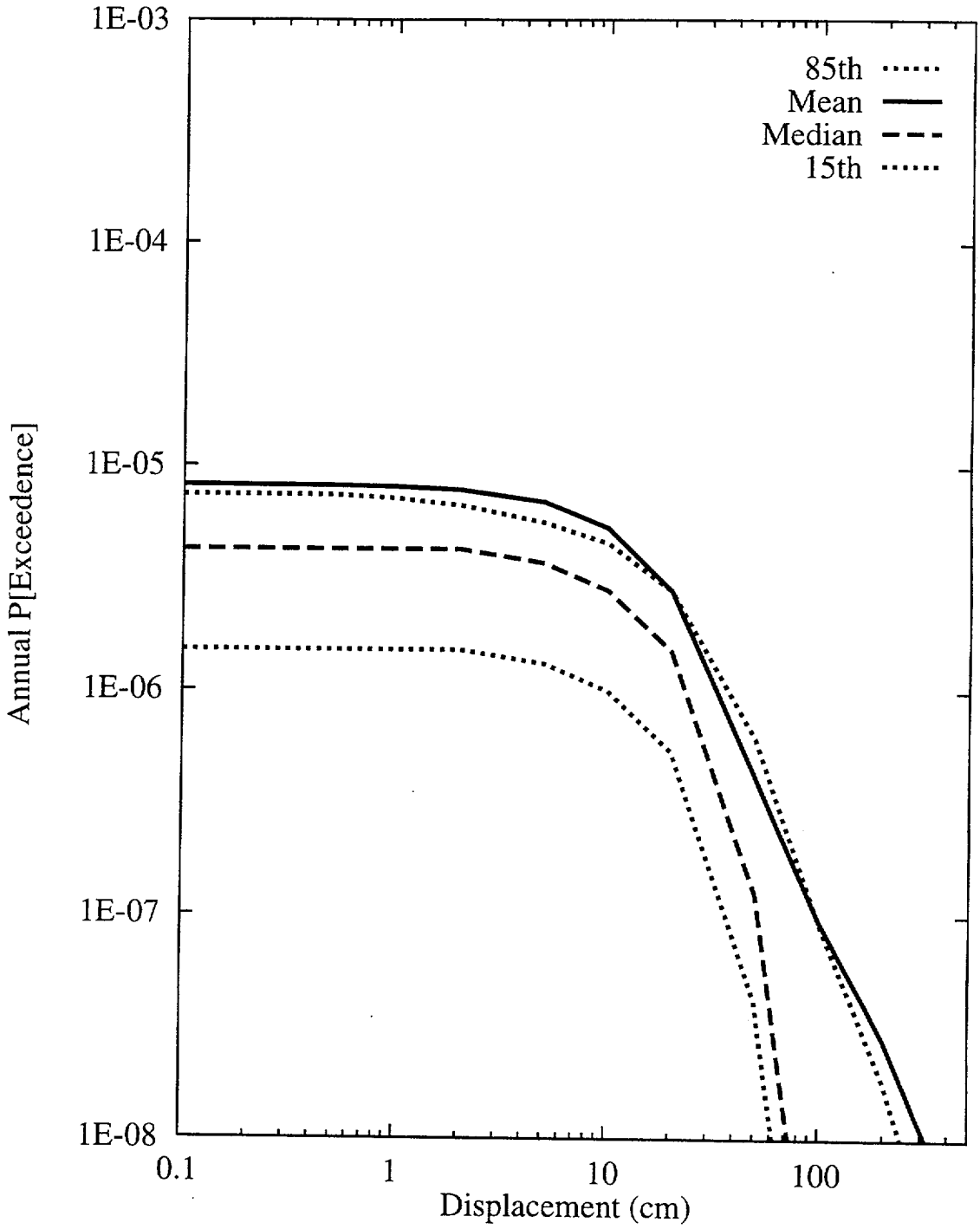

Figure 8-57 Summary hazard curves for Site 1: SBK team, earthquake approach

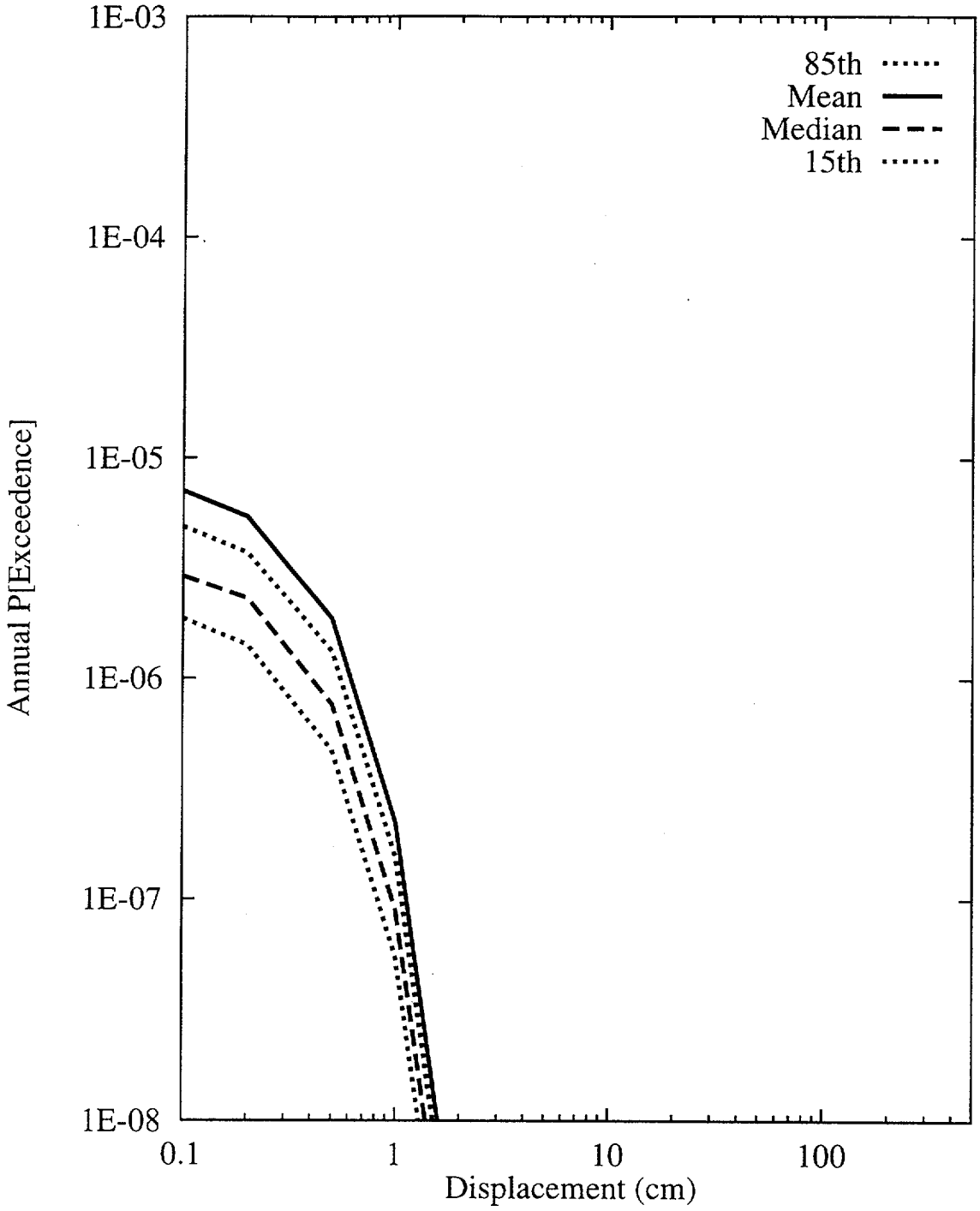

Figure 8-58 Summary hazard curves for Site 7a: SBK team, earthquake approach

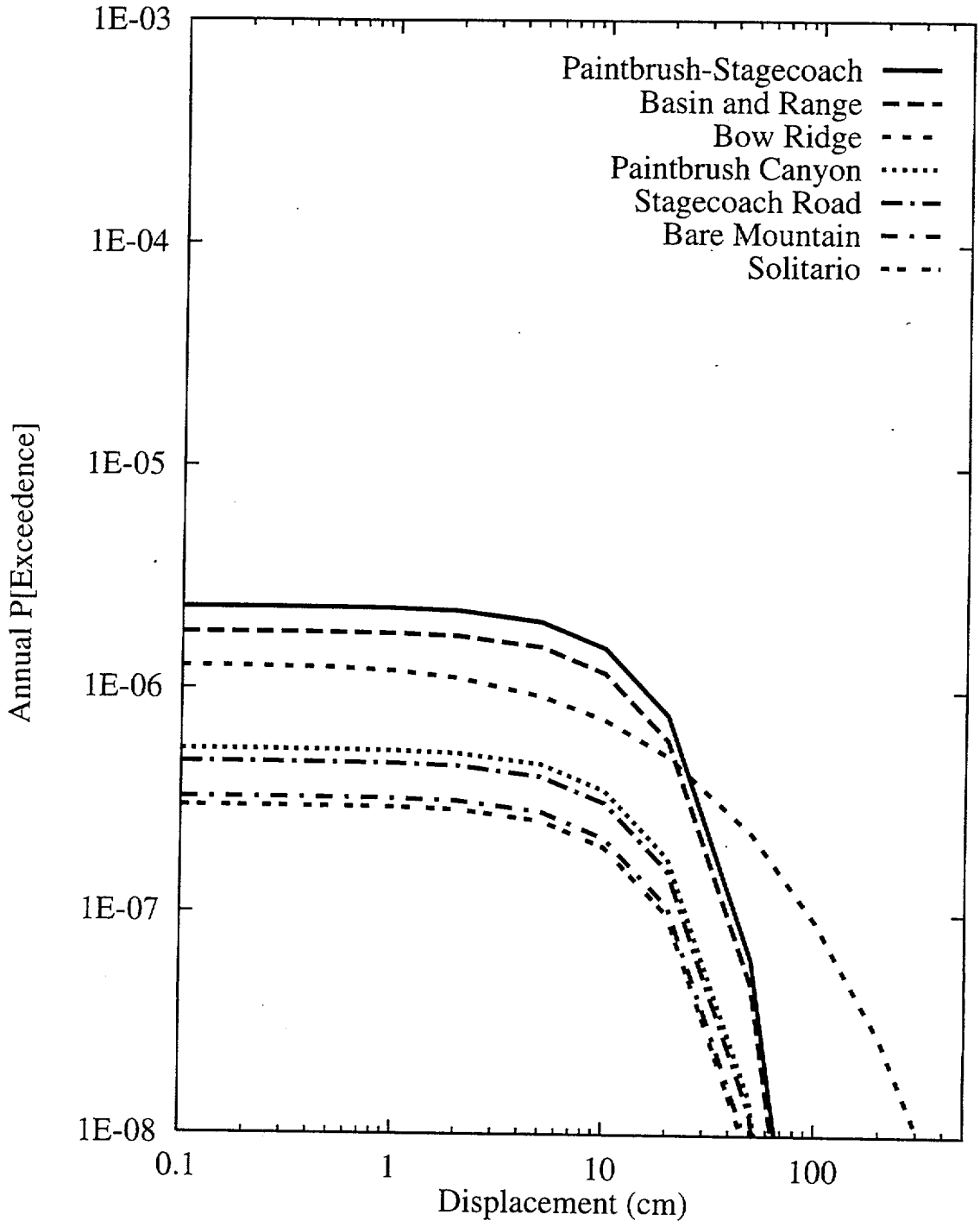

Figure 8-59 Mean hazard curves by source for Site 1: SBK team, earthquake approach

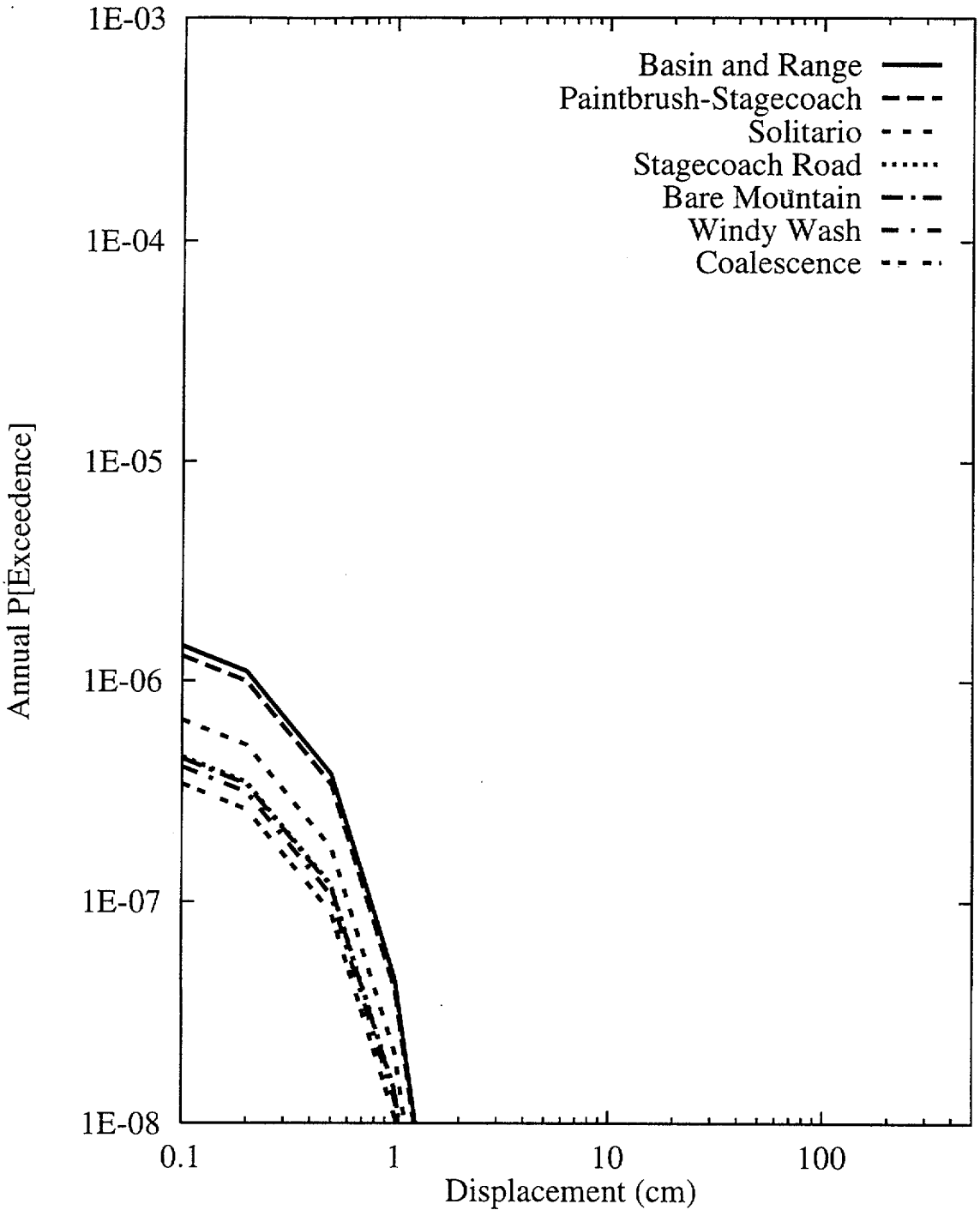

Figure 8-60 Mean hazard curves by source for Site 7a: SBK team, earthquake approach

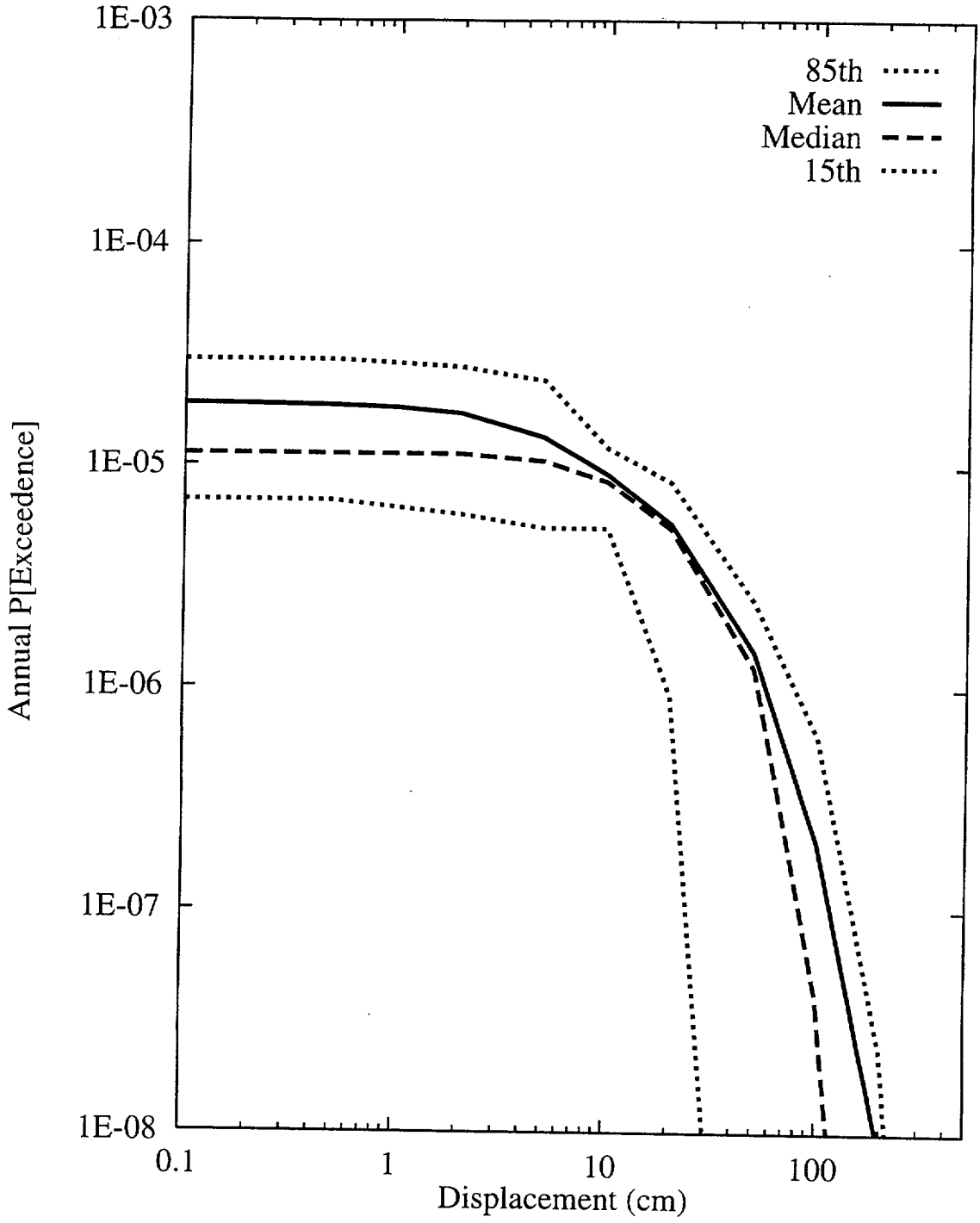

Figure 8-61 Summary hazard curves for Site 1: SBK team, displacement approach

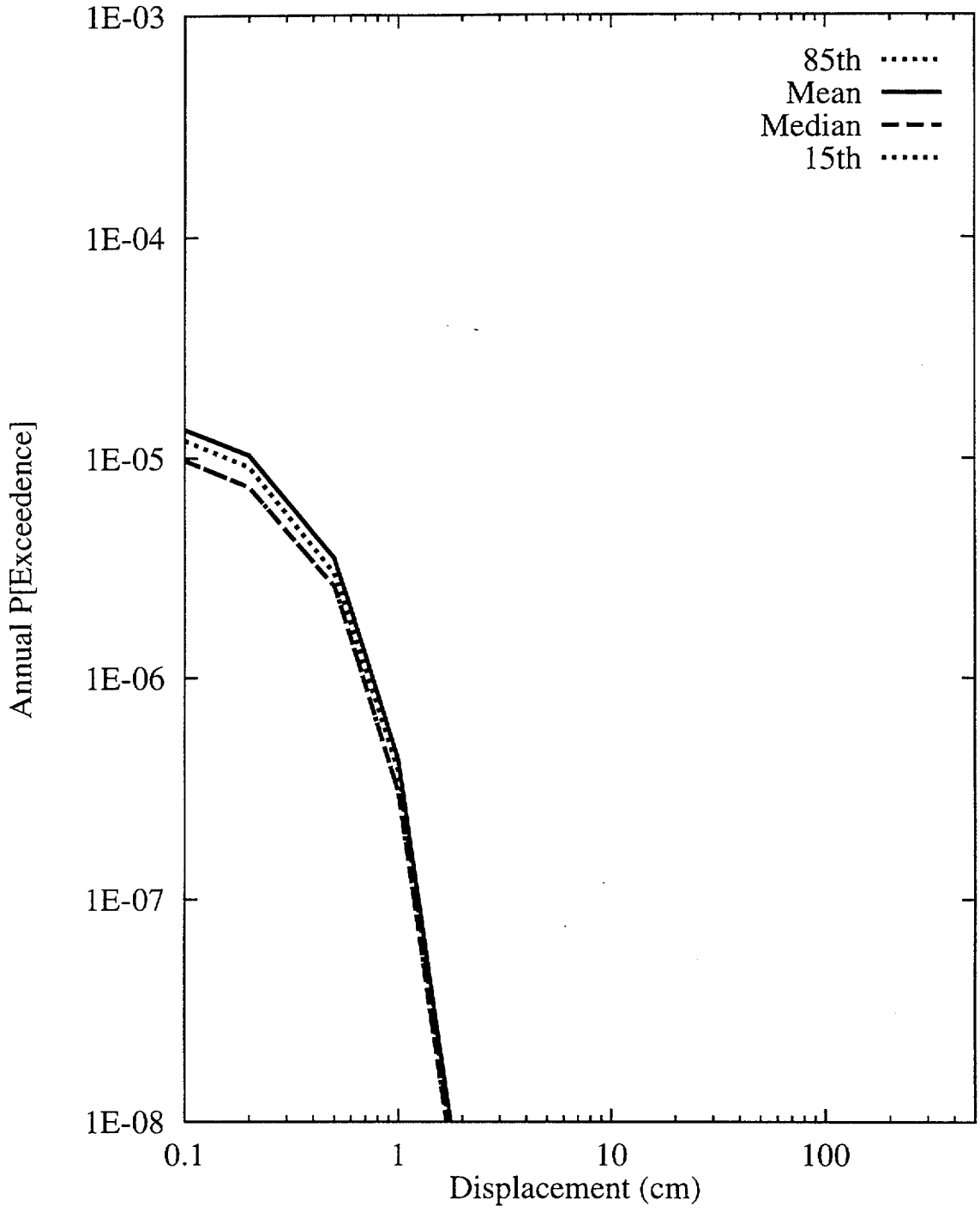

Figure 8-62 Summary hazard curves for Site 7a: SBK team, displacement approach

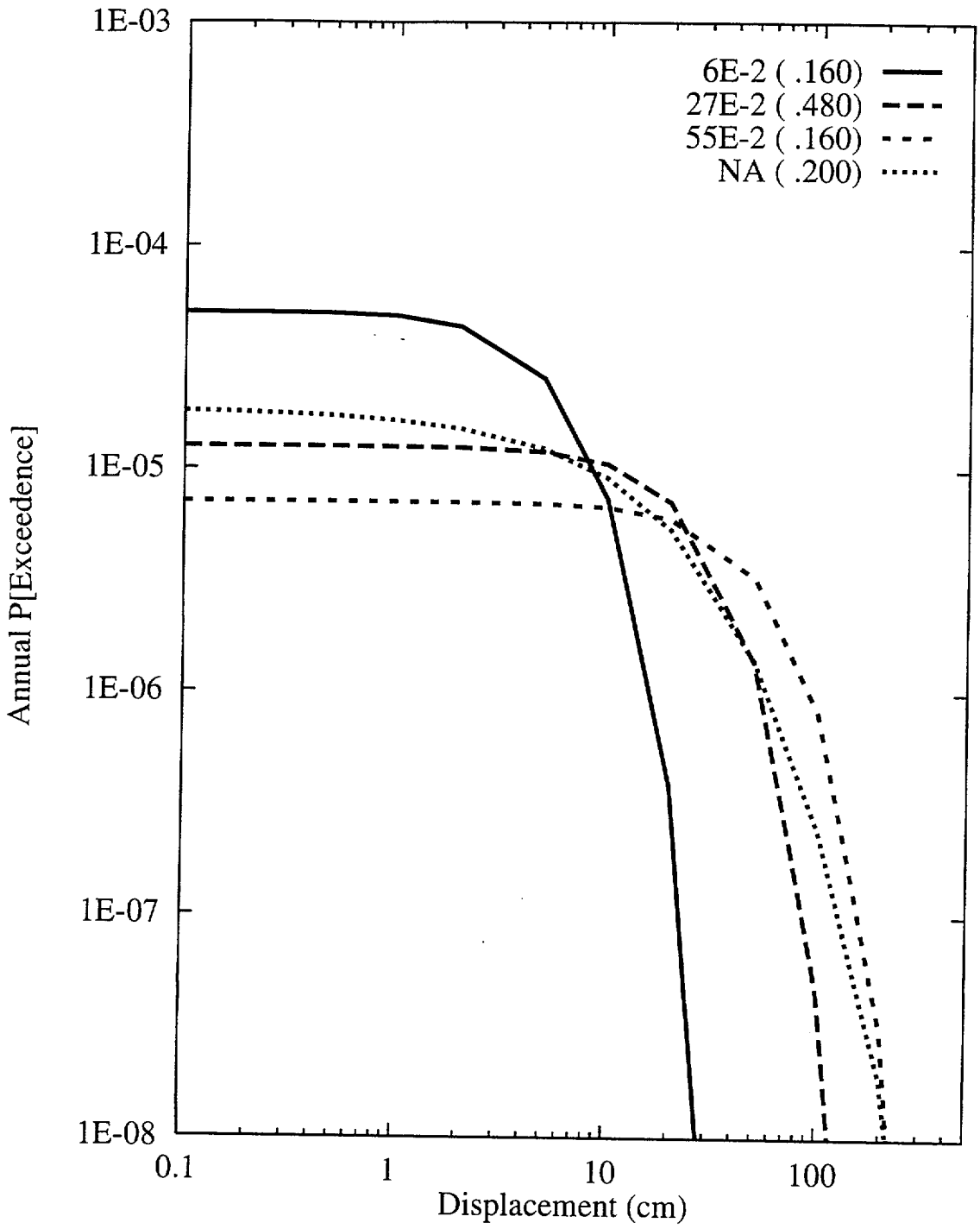

Figure 8-63 Sensitivity of displacement hazard for Site 1 to average displacement per event (m): SBK team, displacement approach

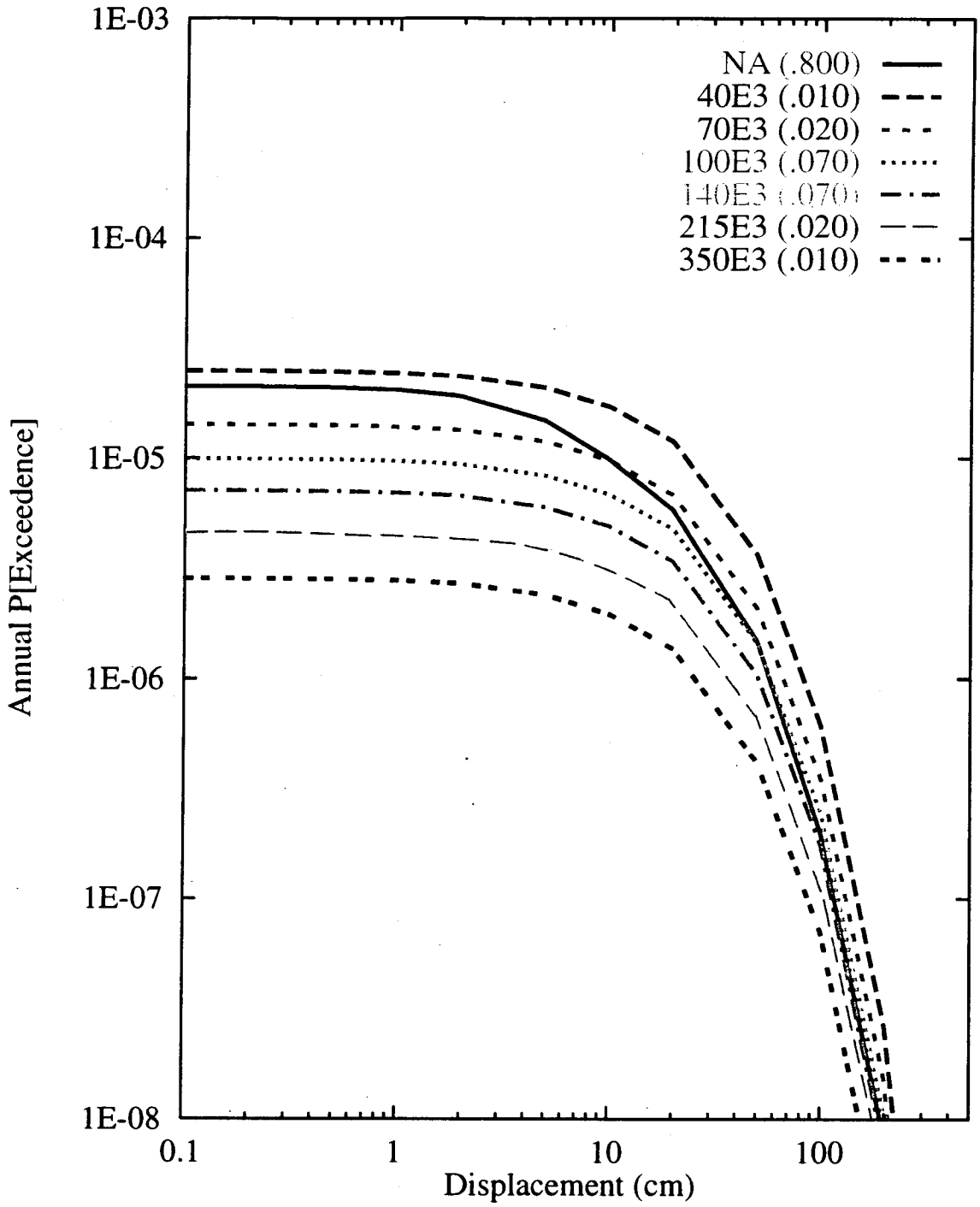

Figure 8-64 Sensitivity of displacement hazard for Site 1 to recurrence interval (yr): SBK team, displacement approach

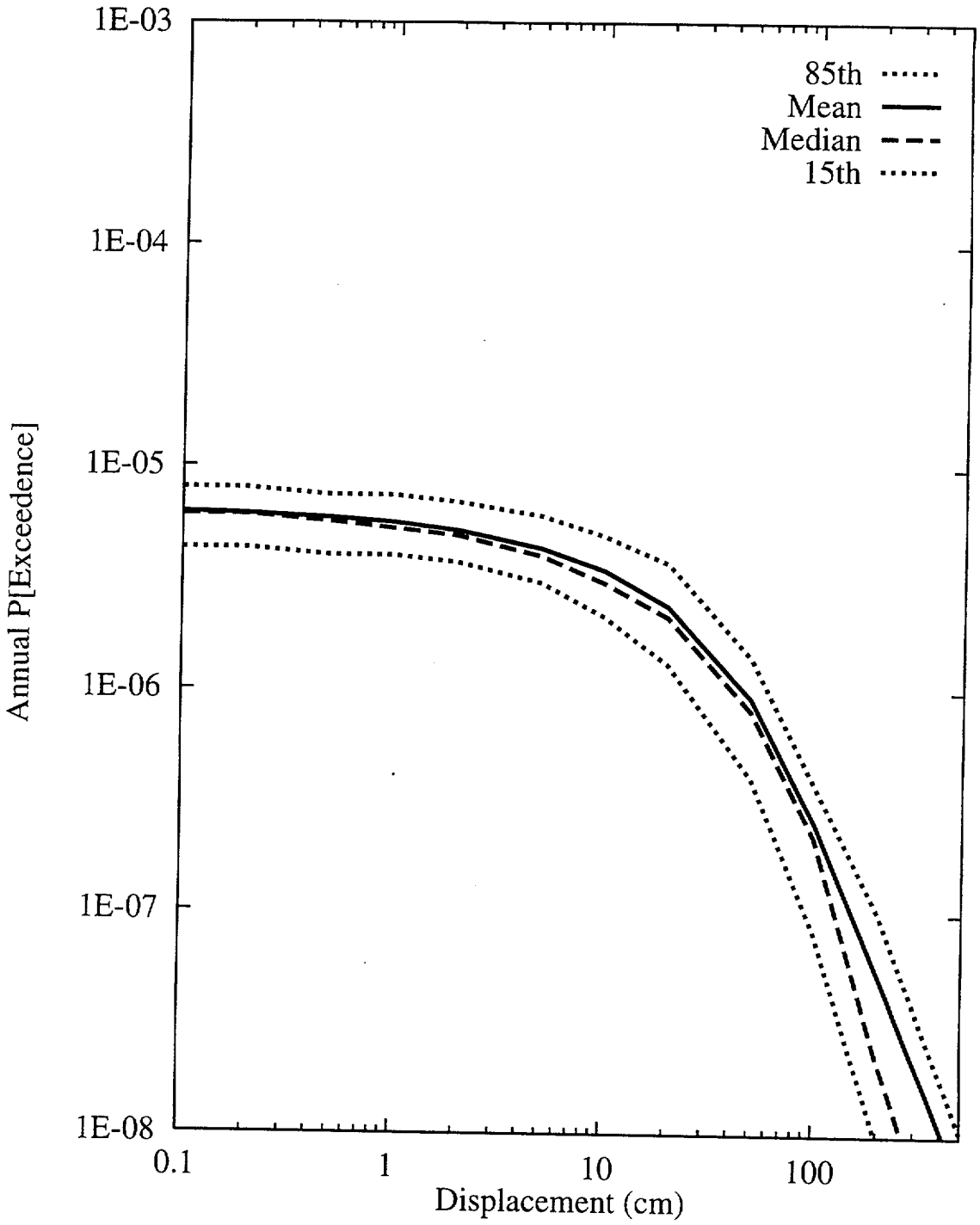

Figure 8-65 Summary hazard curves for Site 1: SDO team, earthquake approach

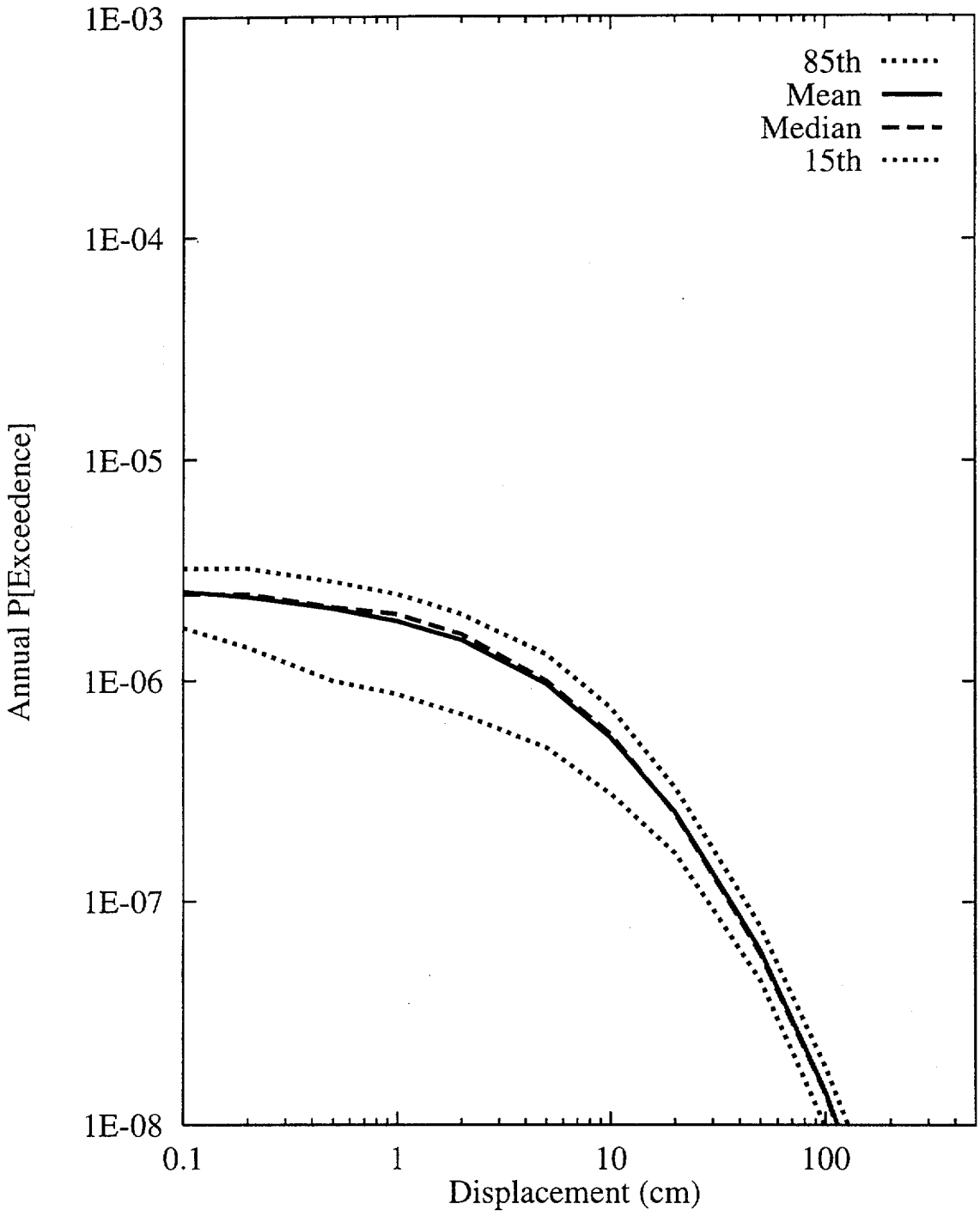

Figure 8-66 Summary hazard curves for Site 7a: SDO team, earthquake approach

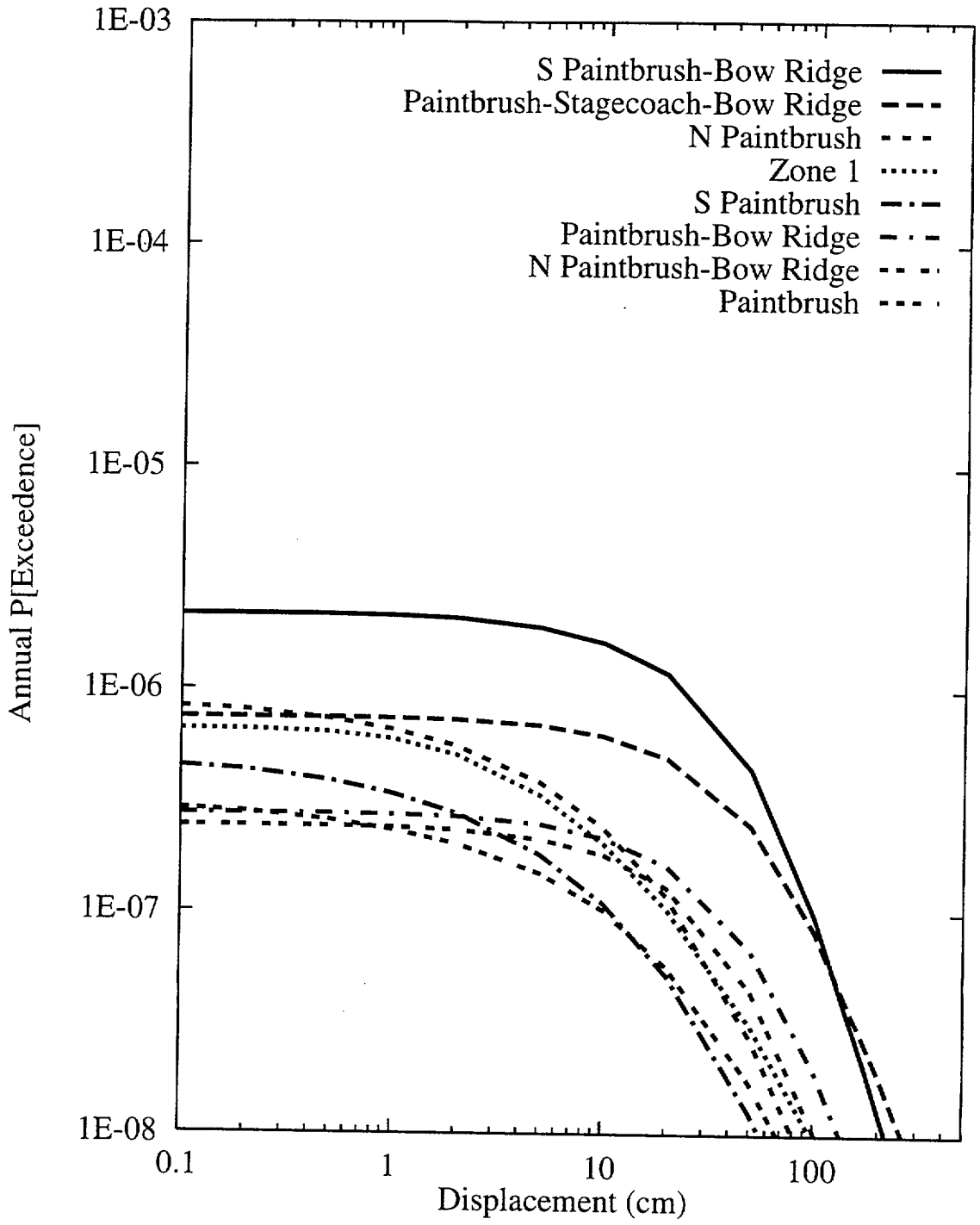

Figure 8-67 Mean hazard curves by source for Site 1: SDO team, earthquake approach

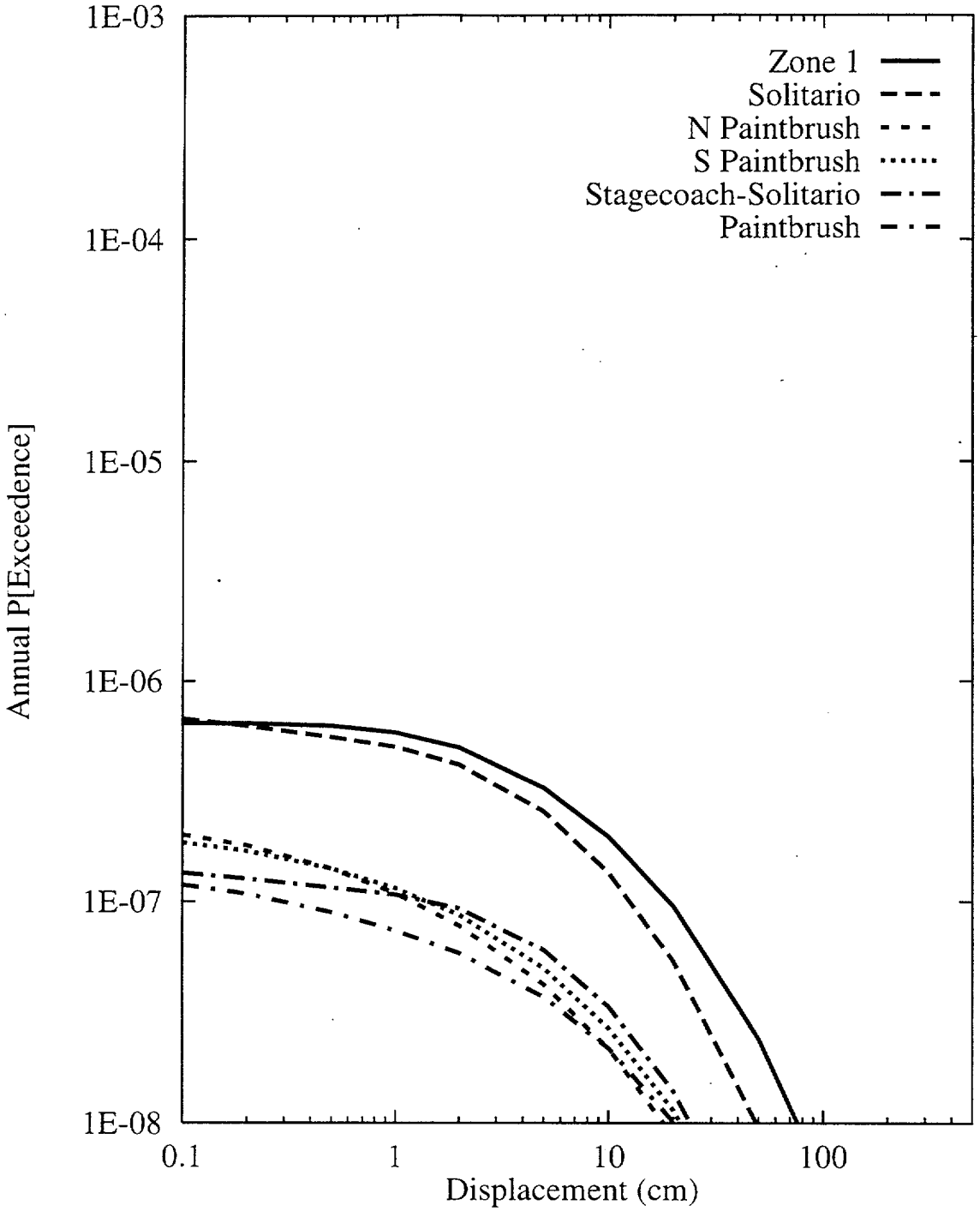

Figure 8-68 Mean hazard curves by source for Site 7a: SDO team, earthquake approach

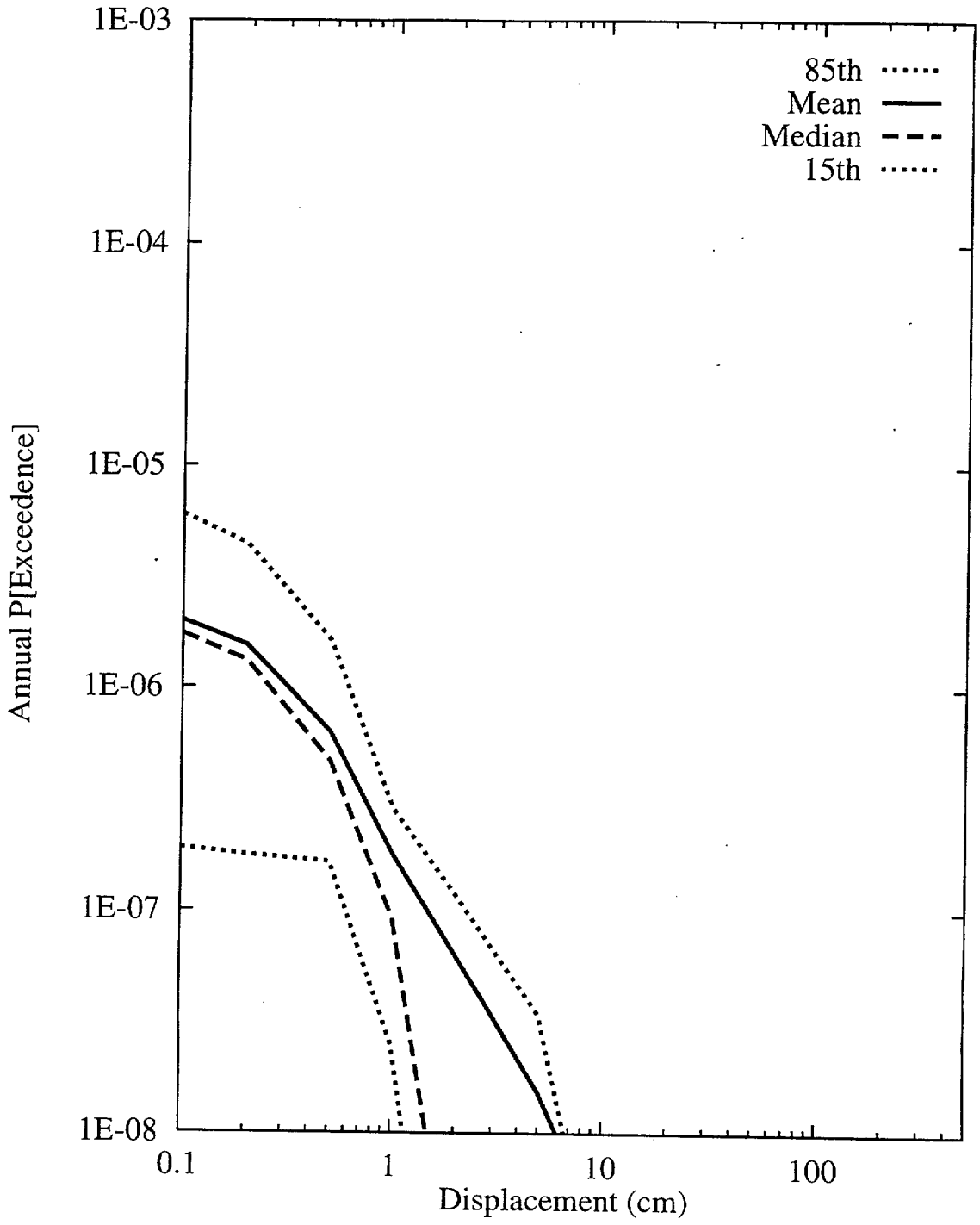

Figure 8-69 Summary hazard curves for Site 7a: SDO team, displacement approach

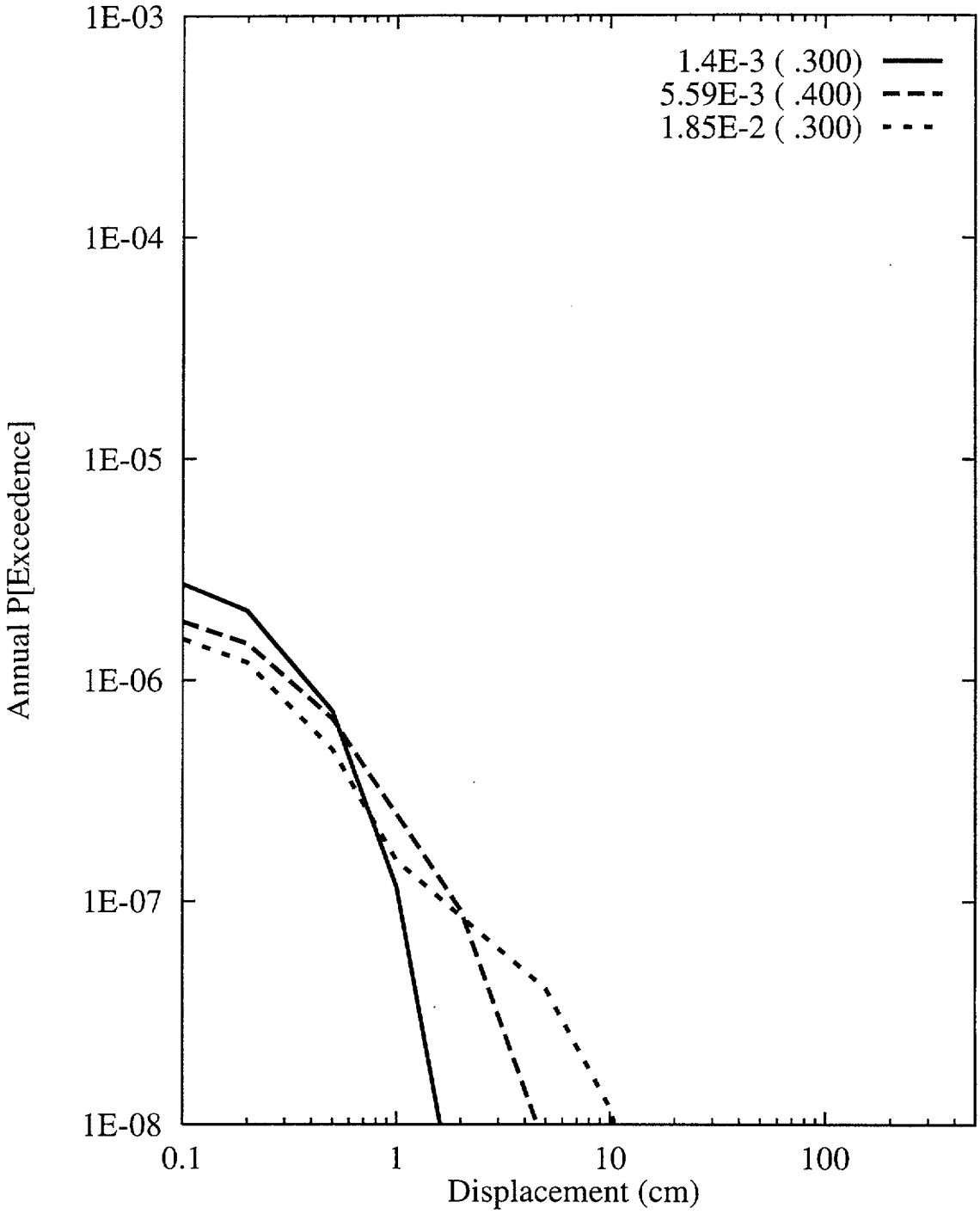

Figure 8-70 Sensitivity of displacement hazard for Site 7a to parameter beta: SDO team, displacement approach

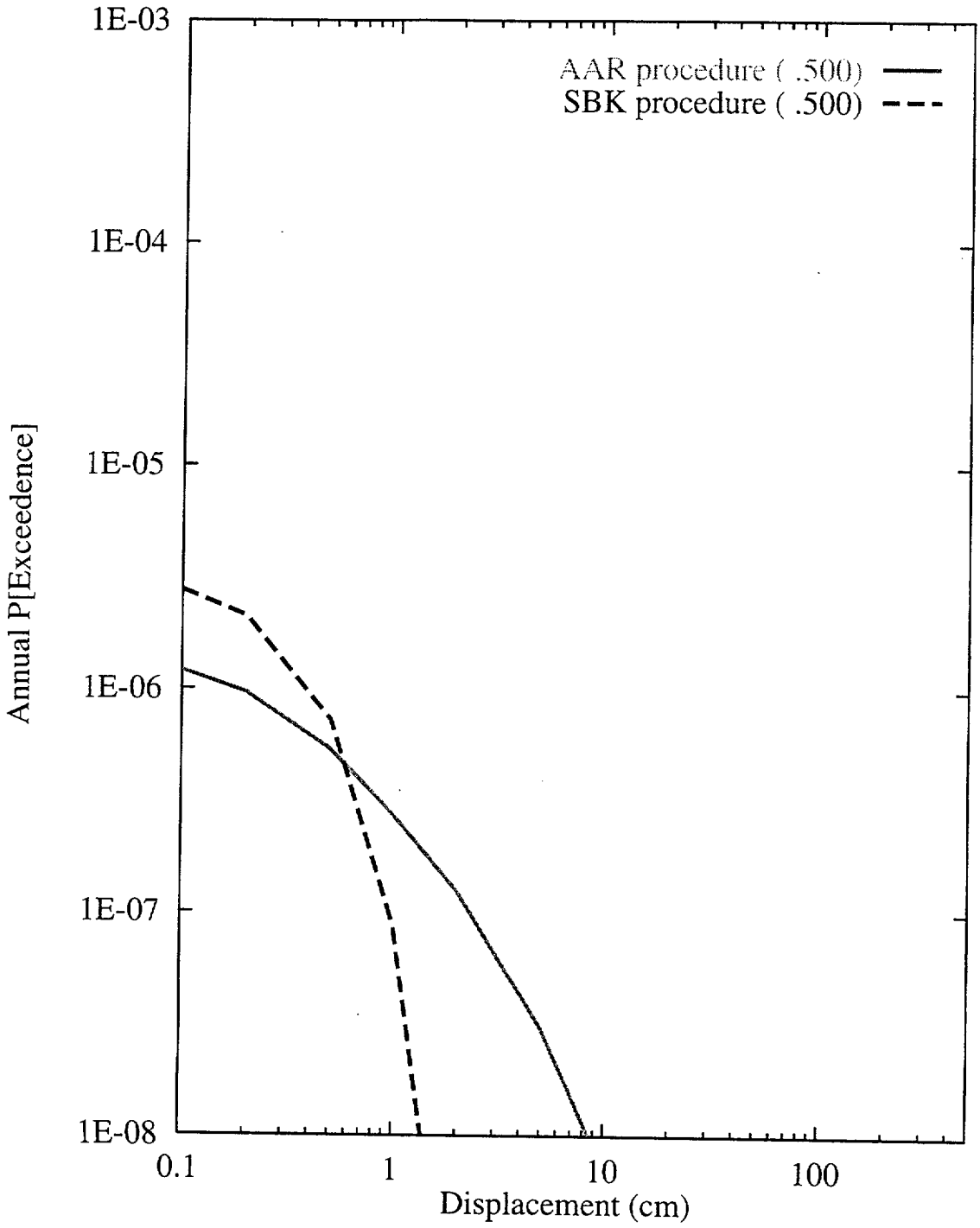

Figure 8-71 Sensitivity of displacement hazard for Site 7a to calculation of average displacement per event: SDO team, displacement approach

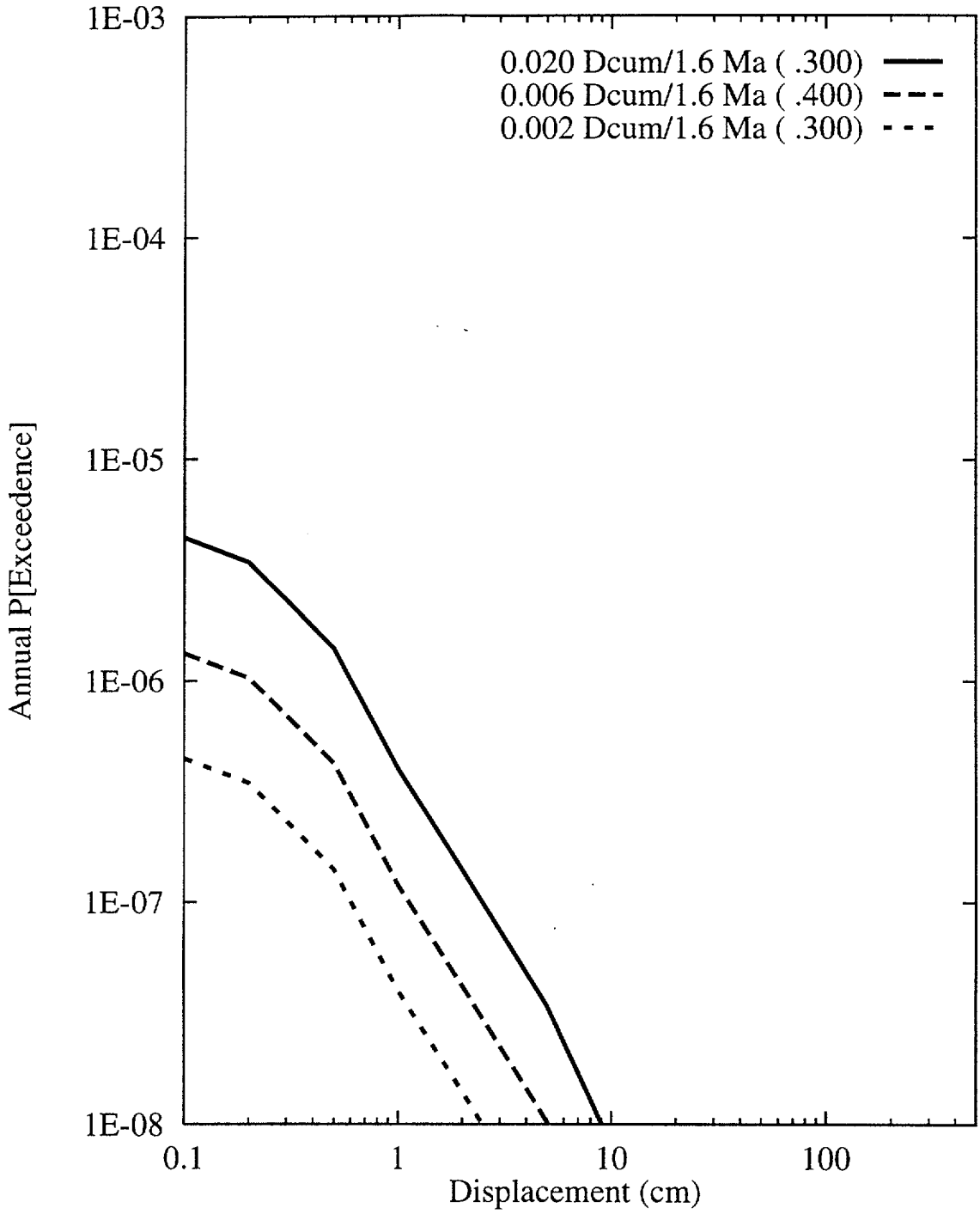

Figure 8-72 Sensitivity of displacement hazard for Site 7a to calculation of slip rate: SDO team, displacement approach

9.0

REFERENCES

Abrahamson, N.A., and Silva, W.J., 1997, Empirical response spectral attenuation relations for shallow crustal earthquakes: Seismological Research Letters v. 68, p. 94-127.

Anderson, J.G., 1979, Estimating the seismicity from geological structure for seismic risk studies: Bulletin of the Seismological Society of America, v. 69, p. 135-158.

Anderson, R.E., Buckman, R.C., Crone, A.J., Haller, K.M., Machette, M.N., Personius, S.F., Barnhard, T.P., Cecil, M.J., and Dart, R.L., 1995a, Characterization of Quaternary and suspected Quaternary faults, regional studies, Nevada and California: U.S. Geological Survey Open-File Report 95-599, 56 p. plus appendices.

Anderson, R.E., Crone, A.J., Machette, M.N., Bradley, L.A., and Diehl, S.F, 1995b, Characterization of Quaternary and suspected Quaternary faults, Amargosa area, Nevada and California: U.S. Geological Survey Open-File Report 95-613, 41 p. plus appendices.

Anderson, J.G., Wesnousky, S.G., and Stirling, M.W., 1996, Earthquake size as a function of fault slip rate: Bulletin of the Seismological Society of America, v. 86, p. 683-690.

Boore, D.M., Joyner, W.B., and Fumal, T.E., 1994, Estimation of response spectra and peak accelerations from western North American earthquakes: An interim report, part 2: U.S. Geological Survey Open-File Report 94-127, 40 p.

Boore, D.M., Joyner, W.B., and Fumal, T.E., 1997, Equations for estimating horizontal response spectra and peak acceleration from western North American earthquakes: A summary of recent work: Seismological Research Letters, v. 68, p.128 - 153.

Campbell, K.W., 1981, Near-source attenuation of peak horizontal acceleration: Bulletin of the Seismological Society of America, v. 71, p. 2039-2070.

Campbell, K.W., 1993, Empirical prediction of near-source ground motion from large earthquakes, *in* V.K. Gaur, ed., Proceedings, International Workshop on Earthquake Hazard and Large Dams in the Himalaya: New Delhi, India, Indian National Trust for Art and Cultural Heritage (INTACH), p. 93-103.

Campbell, K.W., 1997, Empirical near-source attenuation relationships for horizontal and vertical components of peak ground acceleration, peak ground velocity, and pseudo-absolute acceleration response spectra: Seismological Research Letters, v. 68, p. 154-179.

Campbell, K.W., and Bozorgnia, Y., 1994, Near-source attenuation of peak horizontal acceleration from worldwide accelerograms recorded from 1957 to 1993: Proceedings of the 5th U.S. National Conference on Earthquake Engineering, v. III, p. 283-292.

Coats, D.W., and Murray, R.C., 1984, Natural phenomena hazards modeling project: Seismic hazard models for U.S. Department of Energy sites: Lawrence Livermore National Laboratory Report UCRL-15910.

Coppersmith, K.J., and Youngs, R.R., 1986, Capturing uncertainty in probabilistic seismic hazard assessment within intraplate tectonic environments, *in* Proceedings, Third U.S. National Conference on Earthquake Engineering: v. 1, p. 301-312.

Cornell, C.A., 1968, Engineering seismic risk analysis: Bulletin of the Seismological Society of America, v. 58, p. 1583-1606.

Cornell, C.A., 1971, Probabilistic analysis of damage to structures under seismic loads, *in* Howells, D.A., Haigh, I.P., and Taylor, C., eds., Dynamic Waves in Civil Engineering: London, John Wiley.

Cornell, C.A., and Van Marke, E.H., 1969, The major influences on seismic risk, *in* Proceedings, Third World Conference on Earthquake Engineering, Santiago, Chile: v. A-1, p. 3-14.

dePolo, C.M., 1994, The maximum background earthquake in the Basin and Range: Bulletin of the Seismological Society of America, v. 84, p. 466-472.

Eckel, E.B., 1968, Nevada Test Site: Geological Society of America Memoir 110, 290 p.

Electric Power Research Institute (EPRI), 1986, Seismic hazard methodology for the central and eastern United States: NP-4726, v. 1-10.

Electric Power Research Institute (EPRI), 1988, Seismic hazard methodology for the Central and Eastern United States: NP-4726-A (revised), v. 1-10.

Electric Power Research Institute (EPRI), 1989, Probabilistic seismic hazard evaluations at nuclear plant sites in the Central and Eastern United States, Resolution of the Charleston Earthquake Issue: NP-6395-D.

Electric Power Research Institute (EPRI), 1993, Guidelines for determining design basis ground motions: TR-102293, v. 1-5.

Frankel, A., 1995, Mapping seismic hazard in the central and eastern United States: Seismological Research Letters, v. 66, p. 8-21.

Frankel, A., Mueller, C., Barnhard, T., Perkins, D., Leyendecker, E.V., Dickman, N., Hanson, S., and Hopper, M., 1996, National seismic-hazard maps—documentation: U.S. Geological Survey Open-File Report 96-532, 110 p.

Gauthier, J. H., Wilson, M. L., Borns, D. J., and Arnold, B.W., 1995, Impacts of seismic activity on long-term repository performance at Yucca Mountain: Proceedings, FOCUS "95, Methods of Seismic Hazards Evaluation: American Nuclear Society, Inc., p. 159-168.

Gutenberg, B., and Richter, C.F., 1954, Seismicity of the earth and associated phenomena: Princeton, New Jersey, Princeton University Press, 310 p.

Gutenberg, B., and Richter, C.F., 1956, Earthquake magnitude, intensity, energy, and acceleration: Bulletin of the Seismological Society of America, v. 46, p. 105-145.

Hanks, T.C., and Kanamori, H., 1979, A moment-magnitude scale: Journal of Geophysical Research, v. 84, p. 2348-2350.

Hosmer, D.W. Jr., and Lemeshow, S., 1989, Applied logistic regression: New York, John Wiley & Sons, 307 p.

Johnston, A.C., Coppersmith, K.J., Kanter, L.R., and Cornell, C.A., 1994, The earthquakes of stable continental regions, v. 1—Assessment of large earthquake potential: Report prepared for the Electric Power Research Institute (EPRI), TR-102261-V1.

Joyner, W. B., and Boore, D. M., 1988, Measurement, characterization, and prediction of strong ground motion, *in* Von Thun, J.L., ed., Proceedings of the Conference on Earthquake Engineering and Soil Dynamics: Recent Advances in Ground Motion Evaluation, American Society of Civil Engineers, p. 43-103.

Joyner, W. B., and Boore, D. M., 1993, Methods for regression analysis of strong-motion data: Bulletin of the Seismological Society of America. v. 83, p. 469-487.

Joyner, W. B., and Boore, D. M., 1998, Measurement, characterizations, and prediction of strong ground motion, *in* Proceedings, Conference on Earthquake Engineering and Soil Dynamics II: GT Div./ASCE, Park City, Utah, 27-30 June, p. 43-102.

Keefer, D.L., and Bodily, S.E., 1983, Three-point approximations for continuous random variables: Management Science, v. 29, p. 595-609.

Kulkarni, R.B., Youngs, R.R., and Coppersmith, K.J., 1984, Assessment of confidence intervals for results of seismic hazard analysis, *in* Proceedings, Eighth World Conference on Earthquake Engineering: v. 1, p. 263-270.

McGarr, A., 1984, Scaling of ground motion parameters, state of stress, and focal depth: Journal of Geophysical Research, v. 89, p. 6969-6979.

McGuire R.K., 1976, FORTRAN Computer Program for Seismic Risk Analysis: U.S. Geological Survey Open-File Report 76-67.

McGuire R.K., 1978, FRISK: Computer program for seismic risk analysis using faults as earthquake sources: U.S. Geological Survey Open-File Report 78-1007.

McGuire, R.K., and Arbasz, W.J., 1990, An introduction to probabilistic seismic hazard analysis, *in* S.H. Ward, ed., Special Publication on Environmental Geophysics: Society of Exploratory Geophysics.

Meyer, M.A., and Booker, J.M., 1991, Eliciting and analyzing expert judgment: A practical guide: San Diego, California, Academic Press Inc., 452 p.

Miller, A., and Rice, T., 1983, Discrete approximations to probability distributions: Management Science, v. 29, p. 352-362.

Morris, A., Ferrill, D.A., and Henderson, D.B., 1996, Slip-tendency analysis and fault reactivation: Geology, v. 24, p. 275-278.

Parzen, E., 1962, Stochastic processes: San Francisco: Holden-Day.

Piety, L., 1995, Compilation of known or suspected Quaternary faults within 100 km of Yucca Mountain, Nevada and California: U.S. Geological Survey Open-File Report 94-112, variously paginated, 2 plates, scale 1:250,000.

Rogers, A.M., Woulett, G.M., and Covington, P.A., 1977, Seismicity of the Pahute Mesa area, Nevada Test Site, 8 October 1975 to 30 June 1976: U.S. Geological Survey Report 474-184.

Sabetta, F., and Pugliese, A., 1996, Estimation of response spectra and simulation of nonstationary earthquake ground motions: Bulletin of the Seismological Society of America, v. 86, p. 337-352.

Sadigh, K., Chang, C-Y., Abrahamson, N.A., Chiou, S.J., and Power, M.S., 1993, Specification of long-period ground motions: Updated attenuation relationships for rock site conditions and adjustment factors for near-fault effects, *in* Proceedings, ATC-17-1 Seminar on Seismic Isolation, Passive Energy Dissipation, and Active Control: v. 1, p. 59-70.

Sadigh, K., Chang, C.-Y., Egan, J.A., Makdisi, F., and Youngs, R.R., 1997, Attenuation relationships for shallow crustal earthquakes based on California strong motion data: Seismological Research Letters, v. 68, p. 180-189.

Senior Seismic Hazard Analysis Committee (SSHAC), 1997, Recommendations for probabilistic seismic hazard analysis: Guidance on uncertainty and use of experts: U.S. Nuclear Regulatory Commission (NRC) NUREG/CR-6372, Washington, D.C.

Silverman, B.W., 1986, Density estimation for statistics and data analysis: Monographs on Statistics and Applied Probability 26, Chapman and Hall, New York.

Spudich, P., Fletcher, J.B., Hellweg, M., Boatwright, J., Sullivan, C., Joyner, W.B., Hanks, T.C., Boore, D.M., McGarr, A., Baker, L.M., and Lindh, A.G., 1996, Earthquake ground motions in extensional tectonic regimes: U.S. Geological Survey Open-File Report 96-292, 351 p.

Spudich, P., Fletcher, J.B., Hellweg, M., Boatwright, J., Sullivan, C., Joyner, W.B., Hanks, T.C., Boore, D.M., McGarr, A., Baker, L.M., and Lindh, A.G, 1997, SEA96 -- a new predictive relation for earthquake ground motions in extensional tectonic regimes: Seismological Research Letters, v. 68, p. 190-198.

Su, F., Anderson, J.G., Brune, J.N., and Zeng, Y., 1996, A comparison of direct S-wave and Coda-wave site amplification determined from aftershocks of the Little Skull Mountain earthquake: Bulletin of the Seismological Society of America, v. 86, p. 1006-1018.

Toro, G.R., Abrahamson, N.A., and Schneider, J.F., 1997, A model of strong ground motions from earthquakes in Central and Eastern North America: Best estimates and uncertainties: Seismological Research Letters, v. 68, p. 41-57.

U.S. Nuclear Regulatory Commission (NRC), 1988, Safety evaluation review of SOG/EPRI report, "Seismic Hazard Methodology for the Central and Eastern United States": Washington, DC.

U.S. Nuclear Regulatory Commission (NRC), 1991, Individual Plant Examination of External Events (IPEEE): Generic Letter No. 88-20, Supplement 4.

U.S. Nuclear Regulatory Commission (NRC), 1992, Staff technical position on investigations to identify fault displacement hazards and seismic hazards at a geologic repository: NUREG-1451.

U.S. Nuclear Regulatory Commission (NRC), 1994, Staff technical position on consideration of fault displacement hazards in geologic repository design: NUREG-1494.

U.S. Nuclear Regulatory Commission (NRC), 1996, Branch technical position on the use of expert elicitation in the high-level radioactive waste program: NUREG-1563, Washington, D.C.

U.S. Nuclear Regulatory Commission (NRC), 1997a, Recommendations for probabilistic seismic hazard analysis: Guidance on uncertainty and use of experts: NUREG/CR-6372, Washington, DC.

U.S. Nuclear Regulatory Commission (NRC), 1997b, Identification and characterization of seismic sources and determination of safe shutdown earthquake ground motion: Regulatory Guide 1.165.

Veneziano, D., and van Dyck, J., 1985, Statistical discrimination of "aftershocks" and their contribution to seismic hazard, *in* Seismic hazard methodology for nuclear facilities in the eastern United States: EPRI Research Project No. P101-29, Appendix A-4, p. A121-A186.

Weichert, D.H., 1980, Estimation of the earthquake recurrence parameters for unequal observation periods for different magnitudes: Bulletin of the Seismological Society of America, v. 70, p. 1337-1346.

Wells, D.L., and Coppersmith, K.J., 1993, Likelihood of surface rupture as a function of magnitude: Seismological Research Letters, v. 64, p. 54.

Wells, D.L., and Coppersmith, K.J., 1994, New empirical relationships among magnitude, rupture length, rupture width, rupture area, and surface displacement: Bulletin of the Seismological Society of America, v. 84, p. 974-1002.

Wesnousky, S.G., Scholz, C.H., Shimazaki, K., and Matsuda, T., 1983, Earthquake frequency distribution and the mechanics of faulting: Journal of Geophysical Research, v. 88, p. 9331-9340.

Westaway, R., and Smith, R.B., 1989, Strong ground motion in normal-faulting earthquakes: Geophysical Journal, v. 96, p. 529-559.

Wheeler, R.L., 1989, Persistent segment boundaries on Basin-Range normal faults, *in* Proceedings, Conference XLV-Fault Segmentation and Controls on Rupture Initiation and Termination, D.P., Schwartz and R.H. Sibson, eds.: U.S. Geological Survey Open-File Report 89-315, p. 432-444.

Wong, I.G., Pezzopane, S.K., Abrahamson, N.A., Green, R.K., Sun, J.I., and Quittmeyer, R.C., 1998, A preliminary assessment of earthquake ground shaking hazard at Yucca Mountain, Nevada, and implications to the Las Vegas region, *in* Proceedings, Seismic Hazards in the Las Vegas Region Conference: Nevada Bureau of Mines and Geology Special Publication (in press).

Wong, I.G., Pezzopane, S.K., Menges, C.M., Green, R.K., and Quittmeyer, R.C., 1996, Probabilistic seismic hazard analysis of the Exploratory Studies Facility at Yucca Mountain, Nevada, *in* Proceedings, Methods of Seismic Hazards Evaluation, Focus '95: American Nuclear Society, p. 51-63.

Youngs, R.R., and Coppersmith, K.J., 1985, Implications of fault slip rates and earthquake recurrence models for probabilistic seismic hazard estimates: Bulletin of the Seismological Society of America, v. 75, p. 939-964.

Youngs, R.R., Swan, F.H. III, Power, M.S., Schwartz, D.P., and Green, R.K., 1987, Probabilistic analysis of earthquake ground-shaking along the Wasatch front, Utah, *in* Hays, W.W., and Gori, P.L., eds., Assessment of Regional Earthquake Hazards and Risk Along the Wasatch Front, Utah: U.S. Geological Survey Open-File Report 87-585, v. II, p. M-1 through M-110.

PROBABILISTIC SEISMIC HAZARD ANALYSES FOR FAULT DISPLACEMENT AND VIBRATORY GROUND MOTION AT YUCCA MOUNTAIN, NEVADA

FINAL REPORT
VOLUME 2 APPENDICES

Prepared for the

U.S. Geological Survey

by the

Civilian Radioactive Waste Management System
Management & Operating Contractor

Ivan G. Wong and Carl Stepp
Report Coordinators

A report to the U.S. Department of Energy
that fulfills Level 3 Milestone SP32IM3
WBS Number 1.2.3.2.8.3.6

Prepared in cooperation with the
U.S. Department of Energy under
Interagency Agreement DE-AI08-97NV12033
Contract DE-AC04-94AL8500

Oakland, California
23 September 1998

APPENDIX A

BIOGRAPHIES OF EXPERTS

BIOGRAPHIES OF SEISMIC SOURCE AND FAULT DISPLACEMENT EXPERTS

Dr. Jon P. Ake is a seismologist whose recent research interests have been focused primarily on seismic hazard analyses, engineering seismology, and induced seismicity. He received his undergraduate degree in 1979 in geology and physics from Western State College. He then worked at the New Mexico Engineering Research Institute where he conducted research dealing with strong ground motions generated by explosions, the dynamic response of earth media, and the applications of signal analysis techniques to ground shock problems. From 1983 to 1987, Dr. Ake attended graduate school at the New Mexico Institute of Mining and Technology where he received a Ph.D. in geophysics in 1987. His research dealt with the analysis of microearthquake data applied to studies of crustal structure, seismic sources, and near-station effects. From 1987 to 1989 he had responsibility for operating a seismic network focused on assessing seismic hazard in the Colorado Front Range for Denver Water Department facilities. His research involved probabilistic seismic hazard analyses and application of inversion procedures. From 1989 to the present Dr. Ake has been employed by the U.S. Bureau of Reclamation (USBR) as a senior seismologist in the Seismotectonic and Geophysics Group. His duties include seismologic and tectonic fault assessments, estimation of strong ground motions by several techniques, and consultation on engineering geophysics. He has been responsible for review and coordination of seismic hazard and risk analyses and review of contract seismotectonic studies. Additional duties include operation, maintenance, and data analysis from two seismic monitoring networks in western Colorado. Current research involves application of finite source ground motion modeling to engineering analyses, risk-based seismic hazard assessment, and studies of induced seismicity.

Dr. R. Ernest Anderson received his Ph.D. from Washington University, St. Louis in 1962 after which he spent 11 years working on Atomic Energy Commission-sponsored geologic studies (mostly mapping at various scales) in and around the Nevada Test Site (NTS). This NTS background gives him a valuable perspective on a broad range of geologic problems in the Yucca Mountain area. Equally important, he has built on that background to become an expert on the structure and tectonics of the Basin and Range province by his mapping and topical studies in more than 40 mountain ranges throughout the province. For more than 20 years, his studies have dovetailed a broad range of regional and site-specific investigations bearing on seismicity and paleoseismicity including (1) mapping Quaternary fault scarps in

western Utah and developing some of the first quantitative relations of the time dependence of scarp degradation, (2) coordinating U.S. Geological Survey (USGS) paleoseismic studies of the Wasatch fault in Utah, (3) developing an understanding of integrated focal mechanism and fault-slip data in central Utah, (4) evaluating hazards aspects of basaltic volcanism in southern Utah and adjacent Arizona, and (5) advising other agencies such as the USBR and U.S. Soil Conservation Service on seismic hazards aspects of dams in central and southwestern Utah. Dr. Anderson has a strong interest in paleohydrology and has authored papers on the paleohydrology of areas in Clark and Lincoln counties, Nevada, and a paper interpreting the impoundment-related seismicity at Lake Mead in terms of geographic contrasts in hydraulic continuity. His strongest current research interest is in improving understanding of the 3-D aspects of the deformation field in the Basin and Range province and the role of plutonism in shaping that deformation field – two subjects of potentially great importance to understanding the seismotectonics of Yucca Mountain.

Mr. Larry W. Anderson is a geologist with over 17 years of experience in the identification, evaluation, and seismic hazard analysis of active and potentially active faults as applied to engineered facilities. Born in San Francisco, California, Mr. Anderson attended Brigham Young University and the University of Colorado. He received an M.S. degree from the University of Colorado in 1976. From 1977 to 1980, Mr. Anderson was employed by Fugro, Inc., where he worked on geotechnical investigations for major facilities including fault-related studies for several existing or planned nuclear power plants in the western U.S. While at Fugro, he compiled the first Quaternary fault map of the state of Utah. In 1981, Mr. Anderson began work with USBR's Seismotectonic Group. Since that date, Mr. Anderson has personally conducted or been responsible for numerous seismic hazard studies for USBR dams and facilities throughout the western U.S. Many of these studies included detailed fault evaluations such as those for the Ortigalita fault in California, the Pyramid Lake fault zone in Nevada, and the Horseshoe fault in Arizona. Results of these studies have been published in several publications. Since 1992, Mr. Anderson has been the Principal Investigator on the study of "Quaternary Faulting within 100 km of Yucca Mountain, Including the Walker Lane" for the Yucca Mountain Project. The major emphasis for this study has been on evaluating the Quaternary paleoseismic history of the Death Valley-Furnace Creek fault zone and the Bare Mountain fault.

Dr. Walter J. Arabasz graduated summa cum laude from Boston College in 1964 with a B.S. in Geology. He obtained an M.S. and Ph.D. in geology at the California Institute of Technology in 1966 and 1971, respectively (with a minor in geophysics). He was also a Post-Doctoral Research Fellow at the Department of Scientific and Industrial Research in New Zealand (1970-73). He has more than 27 years of experience in conducting research in seismology and tectonics, with current interests focusing on network seismology, earthquake hazard analysis, tectonics and seismicity of the intermountain area, and statistical patterns of earthquake occurrence. He has been the director of the University of Utah Seismograph Stations since 1985 and research professor at the University of Utah since 1983. He is Chair of the Utah Seismic Safety Commission and recently served as Chair of the Council of the National Seismic System (1995-97), as a member of the Board of Directors of the Seismological Society of America (1994-97), and as a member of the National Research Council's Panel on Seismic Hazard Evaluation (1992-96). His experience with regard to Yucca Mountain is extensive, including (1) member of the Peer Review Group for Early Site Suitability Evaluation of the Potential Repository Site at Yucca Mountain (1991), (2) member of the Specialist Panel for the Earthquakes and Tectonics Expert Judgment Elicitation Project (1991-92), and (3) technical reviewer for reports on seismic hazards methodology for Yucca Mountain and on seismic design inputs for the Exploratory Studies Facility (1993-94). He was also a member of the Seismic Hazard Methodology Team for the Electric Power Research Institute's (EPRI) Seismic Hazards Research Program (1984-87).

Dr. Ronald Bruhn received his B.A. in geology from Alaska Methodist University in 1971. He received his Ph.D. in geology from Columbia University in 1976. He is a Professor of Geology in the Department of Geology and Geophysics at the University of Utah, where he has worked since 1976. He teaches courses in physical geology, structural geology, engineering geology, and tectonics. Dr. Bruhn's expertise includes structural geology and tectonics, and the application of structural geology to problems in mining and petroleum geology, and seismic hazards. In earthquake hazards studies, he specializes in the applications of structural geology to infer rupture characteristics, including segmentation of fault zones, fluid flow in fault zones, and earthquake mechanics. He has conducted seismic hazards projects in strike-slip, normal, and reverse faulting regimes in the western U.S., Alaska, Israel, South America, and South Korea. He has extensive experience with both regional and detailed studies of faulting in the Basin and Range province, including the

tectonic evolution of the Mesozoic and Cenozoic Cordillera. He has also completed studies on the seismogenic properties of faults in the Central Nevada Seismic Belt. Currently he is developing new methods to date paleo-earthquakes using cosmogenic isotopes. His research and consulting work is supported by the National Earthquake Hazards Reduction Program, the National Science Foundation (NSF), the Norwegian Petroleum Directorate, the U.S. Department of Energy (DOE), and private firms.

Mr. Craig dePolo received his B.S. degree in geology from California State University, Sacramento and his M.S. degree in geology from University of Nevada, Reno. He is presently a Research Geologist for the Nevada Bureau of Mines and Geology and has been involved with seismic hazard characterization and research for the past 18 years, 12 of which have been studying the Basin and Range province. He has been involved with the seismic hazard characterization of Yucca Mountain, Nevada for the last 9 years. Mr. dePolo has conducted aerial reconnaissance and photographic missions of active faults and historical earthquake ruptures, worked on logging and interpreting trenches, and has, to date, characterized the seismic hazard of several hundred faults. He has worked on fault segmentation theory using historical earthquakes as a data base and a fault slip-rate theory using fault data from Nevada and California. He has mapped out the surface ruptures from the 1932 Cedar Mountain earthquake, and worked on trench studies along these breaks. Recent research has included an analysis of the maximum background earthquake for the Basin and Range province and studies of multiple segment and distributed surface ruptures. He is currently involved in devising and managing an earthquake scenario project in the Reno-Carson City urban corridor. Mr. dePolo is an active participant in the Nevada Earthquake Safety Council, and is the past Chairman and currently serves on the Executive Committee of the Western States Seismic Policy Council.

Dr. Diane Irene Doser obtained her B.S. in applied geophysics from Michigan Technical University. She obtained her M.S. and Ph.D. in geophysics from the University of Utah. She was a Post-Doctoral Fellow at the California Institute of Technology. She has been at the University of Texas at El Paso since 1986 where she now is a professor and the director of the Kidd Memorial Seismic Observatory. Her experience related to seismic sources in the western U.S. is extensive. Both her M.S. and Ph.D. work related to earthquakes of the intermountain west. She has published 16 papers related to source processes of U.S.

intermountain earthquakes, including 4 papers on Nevada earthquakes. She has also published papers on the source processes of earthquakes in other continental rifts (Baikal, east Africa), on southern California-northern Baja California earthquakes, and on papers related to induced seismicity in west Texas oil fields. Additionally, since 1987, Dr. Doser has been Co-Principal Investigator on numerous grants from the Texas Low-Level Radioactive Waste Authority to assess seismic hazards associated with two proposed disposal sites in west Texas, and to operate seismic monitoring networks in these regions.

Dr. Christopher J. Fridrich obtained both his doctorate and masters degrees in geology from Stanford University where he conducted research on the petrology and structure of the Grizzly Peak caldera in Colorado. He also has a bachelor's degree in geological engineering from Michigan Technical University. Dr. Fridrich has extensive mapping experience throughout the western U.S., particularly investigating volcanic deposits. He has been working on the Yucca Mountain project since 1988, including both research, oversight, and coordination duties. He is responsible for geologic mapping of the Crater Flat basin and structural analysis of the map data for the purpose of developing constraints on tectonic models to be used in seismic hazard assessments of the Yucca Mountain site. He is also principal investigator for studies of tectonic effects on the hydrology of Yucca Mountain, which includes hydrogeologic studies, surface and subsurface mapping, and evaluation of several types of geological, geophysical, and hydrologic data. Prior to working on the Yucca Mountain project, Dr. Fridrich was a Research Fellow for the American Museum of Natural History and has several years of experience working in the mineral and oil industries.

Dr. Peter L.K. Knuepfer has worked on paleoseismic and geomorphic studies of active faults in the Basin and Range of the western U.S. throughout his professional career. He received his B.S. in 1976 and his M.A. in 1977 from Stanford University, after which he spent 4 years with Woodward-Clyde Consultants. He was a member of the Woodward-Clyde Consultants team that pioneered trenching of normal faults for paleoseismic analysis along the Wasatch fault in the late 1970s. As a graduate student at the University of Arizona in the early 1980s, he assisted in trenching studies of a low-slip-rate fault, the Santa Rita Piedmont fault, south of Tucson, Arizona, and he worked with Prof. William B. Bull and other students on studies of the 1887 surface rupture and previous breaks along the Pitaycachi fault in northern Sonora, Mexico. He completed his Ph.D. there in 1984. Since joining the faculty of Binghamton

University in 1986, Dr. Knuepfer has studied the paleoseismicity of the Lemhi fault in Idaho with a group of students (jointly with Woodward-Clyde Federal Services and personnel at the Idaho National Engineering Laboratory) and more recently has been a team member and/or reviewer of trenching studies along the southern Lemhi and Lost River faults. This work led to Dr. Knuepfer's inclusion in an expert panel solicitation regarding earthquake hazards at the Idaho National Engineering Labotatory (INEL), under the direction of Lawrence Livermore National Laboratory. Further work in Idaho, in early stages of research, focuses on the temporal relationship and possible strain partitioning between basaltic volcanic eruptions in the Eastern Snake River Plain and faulting on the Lemhi and Lost River faults. Dr. Knuepfer has other extensive experience in active tectonics and paleoseismic studies in California and overseas in Taiwan and New Zealand. Recent research in New Zealand and Taiwan has focused on studies of terraces formed by river incision to deduce rates and styles of uplift during active mountain-building.

Dr. James P. McCalpin is President of GEO-HAZ Consulting, Inc., and is also Research Associate Professor of Geology at Utah State University and Special Graduate Faculty at the University of Colorado, Boulder. He has been performing neotectonic studies since 1976. Dr. McCalpin has developed an international reputation for trenching faults and using numerical dating techniques to reconstruct the magnitude and timing of paleoseismic events. He recently edited the first reference book in paleoseismology ("Paleoseismology," Academic Press, 1996) along with 10 coauthors from government and academia. Between 1982 and 1992, Dr. McCalpin was the Principal Investigator on 10 research grants, funded by the USGS and NSF, to decipher the Quaternary history of faulting on various large normal faults in the western U.S. During these studies, he developed (along with Dr. S.L. Forman) a technique for combined radiocarbon and thermoluminescence dating of fault zone sediments that provides the best dating control yet achieved for many tectonic and climatic settings. His synthesis of the Holocene paleoearthquake history of the Wasatch fault zone, Utah, is the basis for the most up-to-date estimates of future earthquake probability (work with USGS collaborator S.P. Nishenko).. More recently he has been an expert reviewer for seismic hazards assessments of two DOE facilities, the Rocky Flats Plant, Colorado, and Los Alamos National Laboratory, New Mexico. His current research involves statistical analysis of paleoseismic data for application to logic trees and probabilistic seismic hazard analyses, particularly with reference to normal faults and the western USA.

Dr. Dennis W. O'Leary has been a research geologist with the USGS since 1972 when he received a Ph.D. in geology from Penn State University. Dr. O'Leary has taken on a wide variety of research tasks in various geologic settings. He has performed bedrock and surficial geologic quadrangle mapping at scale of 1:24,000 in Massachusetts and Connecticut, and conducted remote sensing investigations in the Tonopah, Nevada area, eastern Missouri, the Mississippi embayment, the Paradox Basin in Utah, and eastern Maine, in order to analyze fault and fracture patterns relevant to seismicity, ore mineralization, and bedrock integrity for nuclear waste storage site evaluation. Dr. O'Leary also conducted marine seismic and sidescan sonar surveys (GLORIA) along the U.S. Atlantic coast in order to assess seafloor stability and geological processes within the U.S. Exclusive Economic Zone. Since 1992, Dr. O'Leary has conducted tectonics evaluation studies for the USGS Yucca Mountain Project Branch. Principal tasks include evaluation and formulation of tectonic models for Yucca Mountain and its geologic setting, and characterization of northeast-striking strike-slip faults (chiefly the Rock Valley fault zone). Dr. O'Leary has also consulted on a variety of other tectonic-related problems, including seismic hazards analysis, performance assessment, and history of Neogene and Quaternary faulting in the Yucca Mountain area. His current research specializes in tectonic processes and tectonic effects in the Yucca Mountain region, structural geology of extensional terranes, morphotectonic phenomena, and Neogene and Quaternary tectonostratigraphy.

Mr. Alan R. Ramelli received his B.S. and M.S. degrees in geology from the University of Nevada, Reno. He has held a position as Research Geologist with the Nevada Bureau of Mines and Geology since 1986. He has been involved in research studies of active faulting and paleoseismology in the Basin and Range province and issues related to high-level nuclear waste storage since 1983. From 1983 to 1986, on a consulting basis, Alan conducted active-fault evaluations and reviews of environmental assessments and other documents for the Yucca Mountain, Deaf Smith, Hanford, and Davis Canyon proposed high-level nuclear waste storage sites. From 1986 to 1991, he conducted document reviews and original studies of the Yucca Mountain area, including planning of low-sun-angle aerial photography missions and mapping of faults and Quaternary geology, as part of studies conducted by the State of Nevada. From 1992 to present, under contract to the USGS, he has conducted paleoseismic studies, including exploratory trenching, of the Yucca Mountain area and has held primary

responsibility for studies of the Solitario Canyon fault. Other recent projects involve paleoseismic studies, including exploratory trenching, of the Carson Range fault system in western Nevada and studies of the 1994 Double Spring Flat earthquake.

Dr. Albert M. Rogers is a Director of GeoRisk Associates, Inc., a geological hazards assessment corporation. Dr. Rogers has over 30 years of research experience, scientific publication, and professional project activities in both government and industry that are related to earthquake hazard assessment. He received a Ph.D. in geophysics in 1970 and a B.S. in 1965, both from Saint Louis University. He has conducted research related to earthquake hazard assessment in Nevada, Utah, the west Texas/southern New Mexico region, and the Pacific Northwest. Dr. Rogers was a Senior Scientist at Environmental Research Corporation and Technical Manager at EQE International. In these capacities, he was responsible for ground motion prediction research, site-specific probabilistic seismic hazard assessments of nuclear power plant sites in Finland and Slovokia, and at offshore oil platform sites in Venezuela, Trinidad, Java, and Sumatra. Dr. Rogers has conducted seismicity network studies to assess the seismic hazard to nuclear waste sites at the Waste Isolation Pilot Project in New Mexico, and at the proposed Yucca Mountain site in Nevada; he also led a study of induced seismicity at Lake Mead, Nevada. Dr. Rogers conducted a probabilistic seismic hazard assessment for DOE for the initial proposal for high-level nuclear waste site at NTS, termed the Retrievable Surface Storage Facility. He was an Expert Panel member for the first Tectonics Expert Judgment Elicitation Project for Yucca Mountain in 1991-92. His current research interest concerns earthquake strong motion prediction; this research focuses on prediction of the effect of geologic conditions on earthquake shaking levels, including current studies of vertical strong motion array data in Los Angeles. Dr. Rogers has had colloborative or advisory roles with scientists at the University of Roorkee, India, the Earthquake Engineering Research Institute in Skopje, Macedonia, the University of Costa Rica, and the Engineering Research Institute in Harbin, China. Dr. Rogers served as Branch Chief of the USGS Branch of Geologic Risk Assessment from 1984 to 1988 and during that time was also responsible, as Program Coordinator, for both the internal and external USGS Regional Earthquake Hazards Assessments Programs.

Dr. D. Burton Slemmons has published numerous papers, abstracts, and edited volumes dealing with neotectonics, earthquake hazard evaluation, and paleoseismicity. Dr. Slemmons

received his Ph.D. in geology from the University of California, Berkeley in 1953. While a professor at the University of Nevada-Reno, he supervised more than two dozen theses of graduate students including studies in the Yucca Mountain region, covering Owens, Panamint, Saline, Death, Fish Lake, Amargosa, and Pahrump valleys. He assisted the Lawrence Livermore National Laboratory as a consultant in making high-level nuclear waste assessments of the 11 sites considered by the DOE. From 1985 to 1989, he directed the Yucca Mountain Project of the University of Nevada-Reno. He was one of the seven expert technical specialists selected by Geomatrix Consultants in the EPRI Earthquakes and Tectonics Expert Judgment Elicitation Project for the high-level waste repository at Yucca Mountain. He has consulted for Woodward-Clyde Federal Services in support of TRW from January 1992 to present on the Yucca Mountain Project, including activity as a member of the technical assessment team that prepared the report "Seismic Design Inputs for the Exploratory Studies Facility at Yucca Mountain" in 1994. During the past 25 years, he has also been an expert consultant for the U. S. Nuclear Regulatory Commission (NRC) or industry at more than 12 power plants in the U.S. Since 1984, he has been a technical expert for the International Atomic Energy Agency (IAEA) on missions to assess earthquake hazards at nuclear power plant sites in Armenia, Brazil, Croatia, and Indonesia.

Dr. Kenneth D. Smith obtained his Ph.D. from the University of Nevada in 1991. He holds bachelors degrees in geophysics from Boise State University and in geology from Indiana University. Dr. Smith has been involved in studies of the seismotectonics of the western Basin and Range province for over 10 years. During this time, he has had extensive experience in seismic network operations, portable seismic experiments, and seismic network data management for western Great Basin earthquake activity. Since 1992, these efforts have focused on evaluating the seismicity in and around the Yucca Mountain area. He was a primary author of a study of the source parameters and faulting behavior of the 1992 Little Skull Mountain earthquake and of a study of recent earthquake activity on the Rock Valley fault zone. He participated in the data collection for the Little Skull Mountain earthquake, the 1993 Rock Valley earthquake sequence, and the 1993 Non-Proliferation Experiment refraction survey. Other research activities in the western Basin and Range province have included determining the source parameters and complex faulting geometry of mainshock-aftershock sequences near Mammoth Lakes, California. Currently, he is involved in the

operations and development of the digital upgrade for the southern Great Basin seismic network.

Dr. Robert B. Smith received his B.S. and M.S. in geology from Utah State University in 1960 and 1965, respectively. He received his Ph.D. in geophysics from the University of Utah in 1967. He is a Professor of Geophysics in the Department of Geology and Geophysics where he has worked since 1967. He has also served as a Visiting Professor at the Swiss Federal Institute of Technology and at Cambridge University. Most recently he has taught courses in tectonophysics/elastic waves, earthquake seismology, theoretical seismology, and inverse theory. He has supervised 53 graduate students. Dr. Smith's expertise includes mechanics and processes of earthquakes, the relationship between seismicity and active tectonics, wave propagation, seismicity of the Intermountain seismic belt, Global Positioning satellite measurements of crustal deformation, numerical modeling of fault and volcano processes, and analyses of earthquake hazards. In earthquake hazard, he has specifically worked on geometry and mechanics of normal faulting, scaling relations of surface fault parameters to magnitude, strong ground motion and attenuation of normal faulting earthquakes, and general seismotectonics. He has worked on seismic hazards projects in the Pacific Northwest, the Basin and Range province, and the Intermountain seismic belt. Dr. Smith has been Director and Associate Director of the University of Utah Seismograph Stations and he recently directed studies on the neotectonics of the Teton fault and paleoseismicity of the Intermountain seismic belt. His research and consulting work is supported by the NSF, the USGS National Earthquake Hazards Reduction and the Volcano Hazards programs, the National Park Service, as well as petroleum and mining companies. Smith has served as the President of the Seismology section of the American Geophysical Union, on the NSF Panel on Geophysics, on the NSF Advisory Board in Earth Sciences, on the Advisory Committee of the Southern California Earthquake Center, on the NRC Committee on Seismology, on the Executive Committee of the Seismological Society of America, and was a founding member of Incorporated Research Institutes of Seismology.

Since 1973, ***Dr. Frank H. (Bert) Swan*** has participated in and directed projects for seismic hazard evaluations for critical facilities, including more than 15 nuclear power plants, and other nuclear-related facilities. He has conducted fault studies in the eastern and western U.S., Alaska, Central and South America, North Africa, the Middle East, Southeast Asia, and

Eastern Europe. From 1978 to 1985, Dr. Swan was the principal investigator for a series of research projects funded by the USGS to investigate recurrence of moderate to-large-magnitude earthquakes associated with past surface faulting along the Wasatch fault zone in Utah and to make a probabilistic assessment of the potential ground motion levels for selected urban areas along the Wasatch Front. From 1987 to 1993, Dr. Swan was Project Manager and principal investigator for a detailed paleoseismic investigation of the Meers fault, Oklahoma for the NRC's Research Division. In 1992, he was a member of IAEA's Geological and Seismic Hazards Safety Review Mission for the Crimea Nuclear Power Plant in the former Soviet Union. In 1993, Dr. Swan provided technical review of a probabilistic seismic hazard analysis of the Krsko Nuclear Power Plant in the Republic of Slovenia. He was principal investigator for studies conducted at NTS in Nevada to assess the potential for surface faulting at the proposed site for the waste-handling facilities where high-level nuclear wastes will be received and packaged prior to their permanent burial in the proposed underground repository beneath Yucca Mountain. From 1990 to 1993, Dr. Swan was a member of the Nuclear Management and Resources Council's Ad Hoc Advisory Committee to review and propose revisions to the NRC guidelines for seismic and geological siting criteria for nuclear power plants. From 1990 to 1994, Dr. Swan was a member of the American Society of Civil Engineers Working Group on Dynamic Analysis and Design Considerations for High Level Nuclear Waste Repositories where he had the primary responsibility for preparing guidelines for investigations to assess the seismic potential of active faults and to assess the potential for fault rupture. Dr. Swan is currently a member of their Subcommittee on Design and Analysis for Seismic Fault Displacements.

Mr. James C. Yount has conducted research in tectonics with the USGS since 1975. He worked on the delineation of the seismotectonic framework of the Puget Sound region, including research on liquefaction phenomena in Seattle area, and identification of youthful faults in offshore regions of Puget Sound from 1975 to 1983. He has been investigating active faulting in the NTS area since 1983. These studies included mapping and trench description of faulting features along the Rock Valley fault system and mapping of youthful faulting features along the Solitario Canyon fault system, the Wahmonie fault, the Mine Mountain fault, and the Cane Spring fault system. Past studies related to neotectonics include investigation of faulting along the Mohawk Valley fault system, northeast California, mapping of ground rupture following the 1979 Imperial Valley earthquake, and mapping of

ground rupture following the 1980 Mammoth earthquake. Mr. Yount obtained his B.S. from the University of Washington in 1968 and his M.S. from the University of Colorado in 1970.

BIOGRAPHIES OF GROUND MOTION EXPERTS

Dr. John G. Anderson is a seismologist and the Associate Director of the Seismological Laboratory at the University of Nevada, Reno. His undergraduate degree was earned in physics from Michigan State University. He received his Ph. D. degree in geophysics from Columbia University in 1976, where he specialized in seismology, and carried out research at the Lamont Doherty Earth Observatory. After earning his degree, Dr. Anderson held positions on the research faculty at the California Institute of Technology, the University of Southern California, and the University of California at San Diego. In 1988, he accepted a position of teaching and research at the University of Nevada. Dr. Anderson's research has included a broad range of studies relating to seismic hazards. He has installed strong motion accelerograph networks in the eastern U. S., in the Los Angeles metropolitan region, and in Guerrero, Mexico. He has carried out a wide variety of analyses of strong motion data: data processing, interpretation of the seismic source, describing and understanding site effects, developing attenuation relations, and preparing complete synthetic seismograms. These studies, combined, have helped to develop an understanding of the dominant effects that control the strong motion seismogram. Dr. Anderson has also been involved in research and applications of probabilistic seismic hazard analysis. One of the critical input parameters to hazard analysis is the seismic activity rate, and Dr. Anderson has studied how this rate can be developed from geological observations. Among other studies, he is currently involved in state-of-the-art studies in ground motion attenuation for the Southern California Earthquake Center. Dr. Anderson has published over 125 research articles and reports describing results of this research. He has some personal experience with the Yucca Mountain project originating from studies of the Little Skull Mountain aftershock sequence and site effects in Midway Valley and the region around the southeastern portion of the NTS. Professional relationships have included membership on two panels for the National Academy of Science (Seismic Risk, and Base Isolation), member and Chair of the Nevada Earthquake Safety Council, and Associate Director and Acting Director of the Seismological Laboratory of the University of Nevada. He has served on advisory panels organized by the USGS and the NSF and the National Earthquake Hazard Reduction Program.

Dr. David M. Boore is a geophysicist with the USGS. He earned his B.S. and M.S. degrees in geophysics from Stanford University and his Ph.D. in geophysics from M.I.T. He is internationally known for his work in developing empirical attenuation relations from strong ground motions. He has acted as an expert consultant to the Lawrence Livermore National Laboratory panels on seismic strong ground motion estimation in the eastern U. S. and on the Senior Seismic Hazard Analysis Committee (SSHAC). Dr. Boore currently also serves as a consultant to the DOE's Tank Seismic Expert Panel and on the Peer Review Panel for the NRC's Ground Motion Guidelines Project. He has chaired and acted as a member of the International Association of Seismology and Physics of the Earth's Interior Commission on Strong Motion Seismology, and is a member of the Panel on Wind and Seismic Effects for the U. S. - Japan Cooperative Program in Natural Resources. Dr. Boore has published over 130 papers, most of which deal with predicting ground motion.

Dr. Kenneth Campbell has professional experience in strong ground motion, seismic hazard evaluation, and engineering seismology, gained in his more than 20 years of research and consulting practice. He obtained his Ph.D. in 1977 in geotechnical and earthquake engineering from the University of California at Los Angeles. Since 1972, he has worked as an earthquake engineering consultant for several engineering firms and has served as a research civil engineer with the National Oceanic and Atmospheric Administration and the USGS. His experience lies in technical management, consulting, and research in the areas of engineering seismology, strong ground motion, seismic hazards evaluation, and geotechnical and lifeline earthquake engineering. He has directed projects throughout the world to develop deterministically and probabilistically defined seismic design and evaluation criteria for the nuclear, oil, utility, and construction industries. He has developed strong ground motion attenuation relationships from empirical data and has evaluated ground motions and seismic hazards for nuclear power plants, nuclear waste repositories, DOE facilities, and other critical facilities. Dr. Campbell has also served as an engineering seismology consultant to the NRC. He has participated on two expert panels for ground motion – for the NRC's seismic hazard estimates of the eastern U. S. and on the SSHAC. Currently, he is a member of the Earth Science Advisory Committee for the Savannah River site and is reviewing ground motion and seismic hazard estimates. He has estimated ground motions and provided testimony for the proposed low-level radioactive waste repository in Hudspeth County, Texas, which is regulated by the NRC. He participated on the seismic hazard

evaluation for the Rocky Flats, Colorado nuclear arsenal performed by Risk Engineering, Inc. Dr. Campbell has also estimated ground motions for the IPEEE at the Palo Verde nuclear power plant in Arizona and at California's San Onofre Nuclear Generating Station and Diablo Canyon Nuclear Power Plant. He testified on his work at San Onofre at a hearing conducted by the Atomic Safety Licensing Board. Using regional strong motion data bases, Dr. Campbell has developed attenuation relationships appropriate for specific regions including Utah in the Basin and Range province and the source region for the 1989 Loma Prieta, California earthquake, among others. He is a recognized expert in this field and has developed near-source relationships for use in specifying seismic design criteria for critical and noncritical facilities. He has published widely on his attenuation studies in various scientific journals and presented his work at professional and technical conferences.

Dr. Arthur F. McGarr, geophysicist, is currently Chief of the Earthquake Geology and Geophysics Section, Earthquake Hazards Team, USGS, Menlo Park, California. His undergraduate degree was earned in physics followed by a M.S. in geophysics from the California Institute of Technology. He received his Ph.D. degree in geology from Columbia University in 1968, having specialized in seismology there. In late 1968, Dr. McGarr accepted the position of Senior Research Officer at the Bernard Price Institute of Geophysics, University of the Witwatersrand, Johannesburg, South Africa. During the next 9 years, he led a team of technical support staff and graduate students in numerous investigations of earthquakes induced by the deep-level gold mining operations of the Witwatersrand. Most of these studies entailed running underground networks of seismic and strain monitoring instrumentation. Broad-band, wide-dynamic range acceleration recorded in boreholes within several hundred meters of the hypocenters of mining-induced earthquakes yielded novel insights about the source processes that give rise to the strong ground motion as well as the response of the nearby mine excavations, at typical depths of 3 kilometers, to these vibrations. In 1978, Dr. McGarr accepted a research position at the USGS in Menlo Park where his primary efforts have included the analysis of strong ground motion in the western U.S., the state of stress in the lithosphere, and further studies of induced and triggered earthquakes. In 1990, for example, he determined the design seismic ground motion for the Sudbury Neutrino Observatory, Ontario, Canada, due to nearby mining-induced earthquakes. Of particular interest here, Dr. McGarr demonstrated how the state of crustal stress and focal depth influence ground motion parameters. In this latter study, a result of key interest for the

Yucca Mountain project is the finding that earthquakes in extensional tectonic regimes yield lower levels of ground motion than their counterparts in compressional regimes, for similar recording circumstances. Dr. McGarr's personal experience with the Yucca Mountain project includes participation in the study that led to the development of the ground motion attenuation model SEA 96 for earthquakes in extensional tectonic regimes, one of the empirical proponent models utilized by the Expert Panel.

Dr. Walter J. Silva is President and Senior Seismologist at Pacific Engineering and Analysis. He holds a B.A. degree in geophysics, an M.A. in geophysics, and a Ph.D. in geophysics all from the University of California, Berkeley. He has over 20 years of experience in seismology with particular emphasis on strong ground motion estimation using both numerical modeling and empirical approaches. He has developed and thoroughly validated a numerical modeling methodology that accurately models strong ground motions at any distance (0-500 km) from small or large magnitude earthquakes. In addition to source modeling, Dr. Silva also specializes in quantifying the effects of site conditions on strong ground motions using empirical and 1- and 2-dimensional modeling techniques. In this context, he has evaluated a number of nonlinear approaches as well as the widely used equivalent-linear methodology in applications to recorded motions. To augment his finite fault modeling to accommodate nonlinear site response in an accurate and computationally attractive manner, he developed and validated a frequency domain random vibration theory equivalent-linear formulation. Dr. Silva has provided ground motion evaluations on a number of both large and small projects on a worldwide basis. He has provided site response predictions for over 30 nuclear power plants and numerous small projects. He has applied strong motion modeling techniques at four DOE facilities and at the Exploratory Studies Facility for the proposed high-level nuclear repository at Yucca Mountain, Nevada. Similar projects include numerous USBR dams. He has developed region-specific attenuation relations for eastern and central North America, Colorado, Idaho, New Mexico, and Spain using the stochastic ground motion model. He has been a state-of-the-art speaker on site effects and continues to do applied research on source modeling and site effects for such agencies as National Earthquake Hazards Reduction Program and DOE.

Dr. Paul G. Somerville received his doctoral degree in geophysics from the University of British Columbia in 1976. He spent 2 years as a Visiting Research Fellow at the Earthquake

Research Institute, Tokyo University, during 1977 and 1978, and since then has participated in post-earthquake reconnaissance activities in Japan, most recently in the 1996 Kobe earthquake. He has 18 years of experience as an engineering seismologist with Woodward-Clyde and is manager of the Pasadena office. He is a member of the National Research Council's Seismology Committee and is a member of the Earthquake Engineering Research Institute and an affiliate member of the Structural Engineers Association of California. Dr. Somerville has participated in earthquake hazard evaluations for a large number and variety of engineering projects in many parts of the world. During the past 10 years, he has developed and applied seismological methods for estimating ground motions for the seismic design of engineered structures, including the use of strong motion simulation procedures to generate realistic ground motion time histories close to large earthquakes, which include near-fault effects such as those due to rupture directivity. These procedures have been used to simulate ground motion time histories for structures such as the California Department of Transportation bridges in Northern and Southern California, and the Metropolitan Water District's Domenigoni Valley Reservoir in Southern California. Dr. Somerville is currently participating with the FEMA/SAC Steel Project by providing ground motion time histories to represent the ground motions experienced by steel moment frame buildings during the Northridge earthquake as well as other possible events. Multiyear projects that Dr. Somerville has directed include a program of numerical ground motion studies for the Long Term Seismic Program for PG&E's Diablo Canyon Power Plant, evaluation of earthquake source and ground motion characteristics in eastern North America for EPRI and NRC, estimation of strong ground motions in the Pacific Northwest from large subduction earthquakes on the Cascadia subduction zone for the USGS, analysis of the characteristics of near-fault ground motions for the USGS, and analysis of the ground motion characteristics of the 1989 Loma Prieta and 1994 Northridge earthquakes for the NSF.

Dr. Marianne C. Walck has been evaluating local-to-near-regional recordings of NTS underground nuclear explosions (UNEs) since 1984. She obtained her A.B. degree in geology-physics from Hope College, Michigan, and both an M.S. and Ph.D. in geophysics from California Institute of Technology, Pasadena, California. Currently the Manager of the Geophysics Department at Sandia National Laboratories, Dr. Walck is a seismologist whose career has focused on seismic array analysis of the structure of the upper mantle. She has used seismic array data to model attenuation parameters and acceleration anomalies using ray

tracing and synthetic seismograms. She has sited acceleration stations on Jackass Flats, analyzed the resulting data for travel times and relative amplitude patterns, and modeled the shallow crustal structure at NTS using both 2-D ray tracing and finite difference synthetic seismogram techniques. Her involvement with the Yucca Mountain project began in 1988 with a study of 2-D crustal structure for three paths at NTS between nuclear testing areas and Yucca Mountain. Using UNE source, she successfully reproduced absolute travel time, relative amplitude, and waveshape data for the three paths, documenting significant crustal structure differences at shallow depths near Yucca Mountain. She has recently been employing propagator matrix techniques to model the very shallow structure at Yucca Mountain using UNE records from four borehole/surface pairs in order to develop a predictive capability at depth near the site of the potential repository. She has also conducted and published research using recordings of nuclear explosion sources at teleseismic and regional distances. The latter used NTS explosions recorded at high-frequency stations in Nevada and California; the former used Soviet Explosions recorded at NORESS to deduce path attenuation. She has published her work on spectral estimates of P-wave attenuation (teleseismic recordings), path attenuation (northern Europe, regional recordings), and attenuation of Asian explosions (teleseismic recordings) in refereed journals and conference proceedings.

APPENDIX B

DATA PACKAGES DISTRIBUTED TO EXPERTS

SEISMIC SOURCE AND FAULT DISPLACEMENT CHARACTERIZATION DATA PACKAGES DISTRIBUTED TO EXPERTS

Anderson, J.G., and Brune, J.N., 1996, Methodology for using precarious rocks in Nevada to test seismic hazard models: Bulletin of the Seismological Society of America (in press).

Anderson, J.G., Wesnousky, S.G., and Stirling, M.W., 1996, Earthquake size as a function of fault slip rate: Bulletin of the Seismological Society of America, v. 86, p. 683-690.

Anderson, L.W., and Klinger, R.E., 1996, The Beatty Scarp in Nye County, Nevada - An important late Quaternary morphologic datum: Bulletin of the Seismological Society of America, v. 86, p. 1650-1654.

Anderson, L.W., Klinger, R.E., and Anderson, D.S., 1996, Comment to Quaternary slip history of the Bare Mountain fault (Nevada) from the morphology and distribution of alluvial fan deposits: Geology (in press).

Biasi, G.P., UNR, written communication,1996.

Bodin, P., and Brune, J.N., 1996, On the scaling of slip with rupture length of shallow strike-slip earthquakes: Quasi-static models and dynamic rupture propagation: Bulletin of the Seismological Society of America, v. 86, p.1292-1299.

Bott, J.D.J., WCFS, written communication, 1997.

Brocher, T.M., Hart, P.E., Hunter, W.C., and Langenheim, V.E., 1996a, Hybrid-source seismic reflection profiling across Yucca Mountain, Nevada: regional lines 2 and 3: U.S. Geological Survey Open-File Report 96-28, 97 p.

Brocher, T.M., Hunter, W.C., and Langenheim, V.E., 1996b, Structural framework of Yucca Mountain, Nevada, based on crustal-scale seismic reflection profiles and potential field data: Geological Society of America Bulletin (in press).

Brocher, T.M., Hunter, W.C., and Langenheim, V.E., USGS, written communication, 1997.

Brune, J.N., UNR, written communication, 1996.

Carr, M.D., and Yount, J.C., eds., 1988, Geologic and hydrologic investigations of a potential nuclear waste disposal site at Yucca Mountain, southern Nevada: U.S. Geological Survey Bulletin 1790, 152 p.

Carr, W.J., 1990, Styles of extension in the Nevada Test Site region, southern Walker Lane Belt; an integration of volcano-tectonic and detachment fault models, *in* Wernicke, B.P., ed., Basin and Range Extensional Tectonics near the Latitude of Las Vegas, Nevada: Geological Society of America Memoir 176, p. 283-303.

Center for Neotectonic Studies, Mackay School of Mines, University of Nevada, Reno, written communication, 1995.

Civilian Radioactive Waste Management System Management and Operating Contractor, written communication, 1997.

Coates, M.M., and Whitney, J.W., USGS, written communication, 1995.

Connor, C.B., Stamatakos, J.A., Ferrill, D.A., and Hill, B.E., 1996, Integrating structural models into probabilistic volcanic hazard analyses: an example from Yucca Mountain, Nevada: Geological Society of America Abstracts with Programs, v. 28, p. A-192.

Coppersmith, K.J., and Youngs, R.R., 1992, Modeling fault rupture hazard for the proposed repository at Yucca Mountain, Nevada, *in* Proceedings of the Third International Conference on High-Level Radioactive Waste Management: American Nuclear Society and the American Society of Civil Engineers, v. 1, p. 1,142-1,150.

Crowe, B. M. *et al.,* LANL, written communication, 1995.

Day, W.C., Potter, C.J., Sweetkind, D.S., and Dickerson, R.P., 1996, Detailed bedrock geologic map of the central block area, Yucca Mountain--implications for structural development of the potential high-level radioactive waste repository area in Nye County, Nevada: Geological Society of America Abstracts with Program, v. 28, p. A-248.

Day, W.C., Potter, C.J., Sweetkind, D.S., Dickerson, R.P., and San Juan, C.A., USGS, written communication, 1996.

Dickerson, R.P., 1996, Geologic and geophysical evidence for normal faulting in Yucca Wash, Yucca Mountain, Nevada: Geological Society of America Abstracts with Programs, v. 28, p. A-191.

Dickerson, R.P., and Drake, R.M., 1995, Source of the rhyolite of Comb Peak, southwest Nevada volcanic field: Geological Society of America Abstracts with Program, v. 27, p. 8.

Ferrill, D.A., Sims, J., Stamatakos, J.A., and Rahe, B., 1997, Role of ductile detachment horizon in the development of pull-apart basins in physical analog models: EOS, Transactions of the American Geophysical Union (in press).

Ferrill, D.A., Stamatakos, J.A., and Morris, A.P., 1996, Structural controls on progressive deformation of the Yucca Mountain (Nevada) region: Geological Society of America Abstracts with Programs, v. 28, p. A192.

Ferrill, D.A., Stamatakos, J.A., Jones, S.M., Rahe, B., McKague, H.L., Martin, R.H., and Morris, A.P., 1996, Quaternary slip history of the Bare Mountain fault (Nevada) from the morphology and distribution of alluvial fan deposits: Geology, v. 24, p. 559-562.

Ferrill, D.A., Stirewalt, G.L., Henderson, D.B., Stamatakos, J.A., Morris, A.P., Spivey, K.H.C., and Wernicke, B.P.C., 1996, Faulting in the Yucca Mountain region: critical review and analyses of tectonic data from the central Basin and Range: Center for Nuclear Waste Regulatory Analyses Report CNWRA 96-007 or NUREG/CR-6401, San Antonio, Texas, Rev. 01, variously paginated.

Fridrich, C.J., 1996, Tectonic evolution of the Crater Flat basin, 1996, *in* Wright, L., and Troxel, B., eds., Cenozoic Basins of the Death Valley Region: Geological Society of America Special Paper (in press).

Fridrich, C.J., Whitney, J.W., Hudson, M.R., and Crowe, B.M., 1996, Tectonic evolution of the Crater Flat basin: field data and quantitative analysis of Late Cenozoic extension, vertical-axis rotation, and volcanism, *in* Wright, L., and Troxel, B. eds., Cenozoic Basins of the Death Valley Region: Geological Society of America Special Paper (in press).

Frizzell, V.A. Jr., and Shulters, J., 1990, Geologic map of the Nevada Test Site, southern Nevada: U.S. Geological Survey Miscellaneous Investigations Map I-2046, scale 1:100,000.

Hanks, T.C., and Cornell, C.A., 1997, Probabilistic seismic hazard analysis: A beginner's guide: Earthquake Spectra (in press).

Harmsen, S.C., 1994, The Little Skull Mountain, Nevada, earthquake of 29 June 1992—aftershock focal mechanisms and tectonic stress field implications: Bulletin of the Seismological Society of America, v. 84, p. 1484-1505.

Harmsen, S.C., and Rogers, A.M., 1986, Inferences about the local stress field from focal mechanisms—applications to earthquakes in the southern Great Basin of Nevada: Bulletin of the Seismological Society of America, v. 76, p. 1560-1572.

Jackson, S.M., INEL, written communication, 1994.

Janssen, R., and King, G., USGS, written communication, 1995.

Koseluk, R.A., and Bischke, R.E., 1991, An elastic rebound model for normal fault earthquakes: Journal of Geophysical Research, v. 86, p. 1081-1090.

Lundstrom, S., EG&G, written communication, 1994a.

Lundstrom, S., EG&G, written communication, 1994b.

Mason, D.B., 1996, Earthquake magnitude potential of the Intermountain seismic belt, USA, from surface-parameter scaling of late Quaternary faults: Bulletin of the Seismological Society of America, v. 86, p. 1,487-1,506.

McCalpin, J.P., and Berry, M.E., 1996, Soil catenas to estimate ages of movements of normal fault scarps, with an example from the Wasatch fault zone, Utah, USA: Catena, v. 27, p. 265 -286.

McCalpin, J.P., and Nishenko, S.P., 1996, Holocene paleoseismicity, temporal clustering and probabilities of future large (M>7) earthquakes on the Wasatch fault zone, Utah: Journal of Geophysical Research, v. 101, p. 6233-6253.

McKague, H.L. *et al.,* CNWRA, written communication, 1996.

Menges, C.M., Wesling, J.R., Whitney, J.W., Swan, F.H., Coe, J.A., Thomas, A.P., and Oswald, J.A., 1994, Preliminary results of paleoseismic investigations of Quaternary faults on eastern Yucca Mountain, Nye County, Nevada, *in* Proceedings of the 5th International Conference on High-Level Radioactive Waste Management, v. 4, p. 2373-2390.

Morris, A., Ferrill, D.A., and Henderson, D.B., 1996, Slip-tendency analysis and fault reactivation: Geology, v. 24, p. 275-278.

Nicol, A., Watterson, J., Walsh, J.J., and Childs, C., 1996, The shapes, major axis orientations and displacement patterns of fault surfaces: Journal of Structural Geology, v. 18, p. 235-248.

Ofoegbu, G.I., Ferrill, D.A., Smart, K.J., and Stamatakos, J.A., 1997, Effects of source geometry and hypocenter depth on earthquake ground motion patterns from finite element modeling: American Geophysical Union Abstracts with Programs, v. 77, p. 54.

Oliver, H.W., Ponce, D.A., and Hunter, W.C., Major results of geophysical investigations at Yucca Mountain and vicinity, southern Nevada: U.S. Geological Survey Open-File Report 95-74, 235 p.

Paces, J.B., Menges, C.M., Widmann, B., Wesling, J.R., Bush, C.A., Futa, K., Millard, N.T., Matt, P.B., and Whitney, J.W., 1994, U-series disequilibrium and thermoluminescence ages of paleosols associated with Quaternary faults, east side of Yucca Mountain, *in* Proceedings of the International Topical Meeting, High Level Nuclear Waste Management: American Nuclear Society, Inc., Las Vegas, Nevada, p. 2391-2401.

Pezzopane, S.K., Menges, C.M., and Whitney, J.W., 1994, Quaternary paleoseismology and Neogene tectonics at Yucca Mountain, Nevada: U.S. Geological Survey Open-File Report 94-568, p. 149-151.

Piety, L., 1995, Compilation of known or suspected Quaternary faults within 100 km of Yucca Mountain, Nevada and California: U.S. Geological Survey Open-File Report 94-112, variously paginated, 2 plates, scale 1:250,000.

Potter, C.J., Day, W.C., and Sweetkind, D.S., 1996, Structural evolution of the potential high-level nuclear waste repository site at Yucca Mountain, Nevada: Geological Society of America Abstracts with Program, v. 28, p. A-191.

Potter, C.J., Day, W.C., Sweetkind, D.S., and Dickerson, R.P., 1996, Fault styles and strain accommodation in the Tiva Canyon Tuff, Yucca Mountain, Nevada: EOS, Transactions of the American Geophysical Union, v. 77, p. S265.

Ramelli, A.R., and Bell, J.W., Nevada Bureau of Mines and Geology, written communications, 1991 (in preparation).

Reilinger, R., 1986, Evidence for postseismic viscoelastic relaxation following the 1959 *M*=7.5 Hebgen Lake, Montana, earthquake: Journal of Geophysical Research, v. 91, p. 9488-9494.

Rogers, A.M., and Harmsen, S.C., 1991, The seismicity of Nevada and some adjacent parts of the Great Basin, *in* The Geology of North America, Decade Map Volume 1: Geological Society of America, p. 153-184.

Sandia National Laboratories, written communication, 1997.

Sass, J.H., Dudley, W.W. Jr., and Lachenbruchm, A.H. 1995, Regional thermal setting, *in* Oliver, H.W., Ponce, D.A., and Hunter, W.C., eds., Major Results of Regional Geophysical Investigations of Yucca Mountain and Vicinity, Nevada: U.S. Geological Survey Open-File Report 95-74, 235 p. (in press).

Savage, J.C., Lisowski, M., Gross, W.K., King, N.E., and Svarc, J.L., 1994, Strain accumulation near Yucca Mountain, Nevada, 1983-1993: Journal of Geophysical Research, v. 99, p. 18,103-18,107.

Scott, R.B., 1990, Tectonic setting of Yucca Mountain, southwest Nevada, *in* Wernicke, B.P., ed., Basin and Range Extensional Tectonics near the Latitude of Las Vegas, Nevada: Geological Society of America Memoir 176, p. 251-282.

Scott, R.B., and Bonk, J., 1984, Preliminary geologic map of Yucca Mountain, Nye County, Nevada, with geologic sections: U.S. Geological Survey Open-File Report 84-494, 9 p., scale 1:12,000.

Seismic Source Characterization (SSC) Facilitation Team, written communication, 1997.

Simonds, W.F., Whitney, J.W., Fox, K.F., Ramelli, A., Yount, J., Carr, M.D., Menges, C.M., Dickerson, R., and Scott, R.B., 1996, Map of fault activity of the Yucca Mountain area, Nye County, Nevada: U.S. Geological Survey Miscellaneous Investigations Series Map I-2520, 30 p., scale 1:24,000.

Spengler, R.W., and Fox, K.F., 1989, Stratigraphic and structural framework of Yucca Mountain, Nevada, *in* Radioactive Waste Management and the Nuclear Fuel Cycle, v. 13, p. 21-36.

Stamatakos, J.A., and Ferrill, D.A., 1996, Paleomagnetism of Ordovician Pogonip Group carbonates in southwestern Nevada: Implications to tectonism of the Yucca Mountain region: American Geophysical Union Abstracts with Program, v. 77, p. F173.

Stamatakos, J.A., and Ferrill, D.A., 1997, Kinematic constraints of central Basin and Range tectonism from paleomagnetic and fission track studies at Bare Mountain, Nevada: EOS, Transactions of the American Geophysical Union (in press).

State of Nevada, written communication, 1996.

Stock, J.M., and Healy, J.H., 1988, Stress field at Yucca Mountain, Nevada, *in* Carr, M.D., and Yount, J.C., eds., Geologic and Hydrologic Investigations of a Potential Nuclear Waste Disposal Site at Yucca Mountain, Southern Nevada: U.S. Geological Survey Bulletin 1790, p. 87-93.

Swan, F.H., 1995, Approaches for characterizing fault-displacement hazard at Yucca Mountain, *in* Topical Meeting on Methods of Seismic Hazard Evaluation Focus '95, Las Vegas, Nevada: American Nuclear Society, p. 13-21.

Swan, F.H., Stepp, J.C., and McGuire, R.K., 1992, Assessment of the potential for tectonic fault rupture for high-level nuclear waste repositories, *in* Hossain, Q.A., ed., Proceedings of the Symposium on Dynamic Analysis and Design Considerations for High-Level Nuclear Waste Repositories: American Society of Civil Engineers, New York, p. 55-74.

Sweetkind, D.S., and Williams-Stroud, S., 1995, Controls on the genesis of fracture networks, Paintbrush Group, Yucca Mountain, Nevada: EOS, Transactions of the American Geophysical Union, v. 76, p. F-597.

Sweetkind, D.S., Beason, S.C., Potter, C.J., Lung, R., Day, W.C., and Barr, D., 1996, Correlation between surface and subsurface features at Yucca Mountain, Nye County, Nevada: Geological Society of America Abstracts with Program, v. 28, p. A-521.

Sweetkind, D.S., Potter, C.J., and Verbeek, E.R., 1996, Interaction between faults and the fracture network at Yucca Mountain, Nevada: EOS, Transactions of the American Geophysical Union, v. 77, p. S266.

Sweetkind, D.S., Williams-Stroud, S.C., and Coe, J.A., 1996, Characterizing the fracture network in the unsaturated zone at Yucca Mountain, Nevada, Part 1--Collection and interpretation of geologic data—case studies, *in* Hoak, T.E., Klawitter, A.L., and Blomquist, P.K., eds., Fractured Reservoirs: Characterization, and Modeling: Rocky Mountain Association of Geologists, Denver, Colorado (in press).

Toro, G.R., 1992, Probabilistic analysis of faulting associated with earthquakes for nuclear waste repositories, *in* Hossain, Q.A., ed., Proceedings of the Symposium on Dynamic Analysis and Design Considerations for High-Level Nuclear Waste Repositories: American Society of Civil Engineers, New York, p. 75-96.

U.S. Department of Energy (DOE), written communication, 1997a.

U.S. Geological Survey (USGS), written communication, 1996.

von Seggern, D.H., and Brune, J.N., 1997, Seismicity in the southern Great Basin, 1868-1992, *in* Tectonic Characterization of Yucca Mountain—a Potential Geologic Repository for Nuclear Waste: Geological Society of America Special Volume (in press).

Wong, I.G., Pezzopane, S.K., Abrahamson, N.A., Green, R.K., Sun, J.I., and Quittmeyer, R.C., 1997, Table of completeness intervals for background source zone, *in* Development of Seismic Design Criteria for the Waste Handling Building at Yucca Mountain, Nevada (in press).

Miscellaneous:

Aerial photograph of the Yucca Mountain area.

Index to orthophotos, Yucca Mountain area.

GROUND MOTION CHARACTERIZATION DATA PACKAGES

Vol. 1 Reference material for proponent models

Vol. 1B Additional reference material for proponent models

Vol. 2 Spectral plots of proponent models

Vol. 3 Individual plots of proponent models and expert estimates
Horizontal component, Rev 1

Vol. 4 Individual plots of proponent models and expert estimates
Vertical component, Rev 1

Vol. 5 Spectral plots of expert point estimates, Rev 1

Vol. 6A* Regression model fits to experts point estimates, Rev 1
Anderson, Boore, Campbell

Vol. 6B* Regression model fits to experts point estimates, Rev 1
McGarr, Silva, Somerville, Walck

Vol. 7 Individual plots of proponent models and expert estimates
Horizontal component, Rev 2

Vol. 8 Individual plots of proponent models and expert estimates
Vertical component, Rev 2

Vol. 9 Spectral plots of expert point estimates, Rev 2

Vol. 10A Regression model fits to experts point estimates
Expert: Anderson, Rev 2

Vol. 10B Regression model fits to experts point estimates
Expert: Boore, Rev 2

**

Vol. 10D Regression model fits to experts point estimates
Expert: McGarr, Rev 2

Vol. 10E Regression model fits to experts point estimates
Expert: Silva, Rev 2

Vol. 10F Regression model fits to experts point estimates
Expert: Somerville, Rev 2

Vol. 10G Regression model fits to experts point estimates
Expert: Walck, Rev 2

Vol. 11A Regression model fits to experts point estimates
Expert: Anderson, Rev 3

Vol. 11B Regression model fits to experts point estimates
Expert: Boore, Rev 3

Vol. 11C Regression model fits to experts point estimates
Expert: Campbell, Rev 3

Vol. 11D Regression model fits to experts point estimates
Expert: McGarr, Rev 3

Vol. 11E Regression model fits to experts point estimates
Expert: Silva, Rev 3

Vol. 11F Regression model fits to experts point estimates
Expert: Somerville, Rev 3

Vol. 11G Regression model fits to experts point estimates
Expert: Walck, Rev 3

Vol. 12 Spectral plots of expert point estimates, Rev 3

* The full set was not sent to the experts. Each expert only received plots for his/her own model.

** No Volume 10C.

APPENDIX C

SUMMARIES OF SEISMIC SOURCE AND FAULT DISPLACEMENT CHARACTERIZATION WORKSHOPS

SUMMARIES OF SSFDC WORKSHOPS

Note: Workshop summaries were prepared after each workshop and then distributed to workshop participants. See the project files for all figures and attachments referred to in these summaries, including agendas and copies of information distributed to workshop participants both during and after the workshops.

WBS: 1.2.3.2.8.3.6
QA: L

Civilian Radioactive Waste Management System
Management & Operating Contractor

Summary of Data Needs Workshop on Seismic Source Characterization at Yucca Mountain

SSC Workshop 1

Salt Lake City, UT
April 17-19,1995

May 25,1995

Prepared for:

U.S. Geological Survey
Box 25046, MS-425
Denver Federal Center
Denver, CO 80225

Prepared by:

Woodward-Clyde Federal Services of
Civilian Radioactive Waste Management System
Management & Operating Contractor
101 Convention Center Drive
Suite P-110
Las Vegas, NV 89109

I. INTRODUCTION

The United States Geological Survey (USGS) is carrying out a probabilistic seismic hazards analysis (PSHA) for Yucca Mountain, Nevada as part of the Department of Energy's (DOE) project to characterize this site as a potential geologic repository for high-level radioactive waste. The aim of this study is to provide the annual probability with which various levels of vibratory ground motion and fault displacement will be exceeded at the site. These results will be used as a basis for developing seismic design inputs and in assessing the performance of the site.

The PSHA process involves development by two panels of experts of input interpretations and assessments of uncertainties required by the hazards calculations. One panel addresses characterization of seismic sources and fault displacement, while the other deals with vibratory ground motion. Development of interpretations is being facilitated through a series of structured workshops to evaluate available data, to explore the range of interpretations allowed by the data, to examine critically the interpretations proposed by the experts, and to provide feedback on the implications of various interpretations for the seismic hazard at the site. The goal of this process is to have differences in experts' interpretations be the results of true differences in judgment and not differences in access to data, differences in definition, or differences resulting from a lack of understanding each others' interpretations. This report summarizes the first in the series of structured workshops for characterization of seismic sources and fault displacement: the Data Needs Workshop.

The primary goal of the workshop was to discuss and develop a specification of the data required to characterize seismic sources for vibratory ground motion and fault displacement hazards at Yucca Mountain. This includes both data that are presently available and data that are not yet available. A secondary goal was to provide information to participants, particularly the Expert Panel, on the overall study, the products to be developed, the project schedule, the roles of various participants, basic approaches to probabilistic analyses and expressing uncertainties, and ground-rules regarding communication and interaction throughout the study.

To accomplish these goals, the workshop included a series of presentations and discussion sessions, which are summarized chronologically below. Copies of overhead transparencies shown by presenters were distributed to participants during the workshop and are included with this summary as Attachment 3. The basic approach of the workshop was to: 1) identify technical issues of most significance to seismic hazards at Yucca Mountain; 2) link these issues with the data that are most important to addressing the issues; 3) specify the available relevant data for the Yucca mountain region; and 4) identify the data that are required by the Expert Panel to characterize seismic sources for the PSHA.

MONDAY, APRIL 17, 1995

A welcome and introductory presentations were given by: 1) the Project Representative for DOE, Tim Sullivan; 2) the Project Director, J. Carl Stepp of Woodward-Clyde Federal Services; and 3) the Team Leader of the Seismic Source Characterization and Fault Displacement Facilitation Team (SSC-FT), Kevin J. Coppersmith of Geomatrix Consultants. Table 1 shows the list of workshop attendees.

Because the DOE has the responsibility of evaluating Yucca Mountain as a potential repository site for the permanent disposal of spent nuclear fuel and high-level radioactive waste, Mr. Sullivan provided an overview of the overall Yucca Mountain Project. His overview included a brief description of proposed facilities and background on the DOE's program approach and general objectives for the PSHA. He emphasized that although the DOE's position was that the database was adequate to begin assessment, data would continue to be gathered, and that this PSHA will provide seismic design parameters for the preclosure period (100 years). The project will also provide seismic hazard estimates that have potential application in evaluating the performance of the repository system during the postclosure period. Dr. Stepp more specifically defined PSHA project objectives and outlined the project plan. including the basic approach, organization, and schedule for the project.

Dr. Coppersmith introduced members of the Expert Panel and SSC-FT, further explained their roles and responsibilities, and specified the guidelines used for selecting experts. He defined ground rules for experts and emphasized their role as informed "evaluators" of various interpretations, rather than "proponents" of a single model, in an intensely interactive but nonhostile process whereby a common understanding of the issues and available data is achieved. He also discussed forthcoming workshops and the project deliverables, including milestones and the final report. Four workshops are scheduled through January 1996, followed by the elicitation process through March, a workshop to provide feedback, final assessments by experts in June, and a final report delivered in September 1996. In addition to the workshops, two field trips were tentatively planned for November.

Dr. Coppersmith also provided background on multiple-expert probabilistic hazard assessments, including an ongoing study of volcanic hazards at Yucca Mountain. He highlighted important aspects of this PSHA, such as: 1) results of the source characterization component of the project will be used to evaluate the probabilities of exceeding both certain levels of vibratory ground motions and certain amounts of fault displacement through the proposed repository; 2) ground motions will be used for design purposes and fault displacements will be used for performance assessment; 3) this project is a hazard rather than risk analysis, although results could become an integral part of a risk analysis; 4) resulting probability distributions should incorporate various types of uncertainties (including expert-to-expert diversity of interpretation, modeling uncertainties, parameter uncertainties, aleatory and epistemic uncertainties); 5) probabilistic treatment should allow for full consideration of alternative models and parameters that reflect true differences of interpretation and

uncertainties rather than perceptions of conservatism, as conservatism will subsequently be more explicitly adopted by others in choices of acceptable risk; and 6) conducting the PSHA does not indicate that all applicable data have been collected, but it is vital that the present level of knowledge and uncertainty is adequately captured in the analysis. Dr. Coppersmith also answered questions from the Expert Panel, clarifying that the experts will be grouped into six teams of three, and each team will be asked to reach consensus on probability distributions for the source characterization.

Peter A. Morris of Applied Decision Analysis, Inc., initiated the second session of the day with a presentation on the treatment of uncertainties and the expert elicitation process. He compared aleatory and epistemic uncertainties and emphasized focusing on those most significant to seismic hazards at Yucca Mountain. Dr. Morris highlighted advantages and potential pitfalls of the elicitation process. He specified responsibilities of the SSC-FT, emphasizing their role in promoting interaction among experts to identify areas of unintended disagreement. He described the different "hats" experts will wear during the course of the study, including proponent, evaluator, and technical facilitator, but ultimately they must act as experts during the elicitation process. The intent in the process is not to develop one "best" model and achieve consensus but rather to preserve true diversity in the outcome and only remove unintended outcomes that result from lack of understanding.

Walter J. Arabasz of the University of Utah then gave the first of three presentations on technical issues significant to evaluating seismic hazards at Yucca Mountain. He focused on the role of historical and instrumental seismicity analysis, covering basic concepts, highlighting general and specific issues significant to characterizing seismic sources in the Yucca Mountain region, and interjecting insights on lessons learned from previous multiple-expert PSHAs. He emphasized the importance of rates in the analysis and encouraged experts to give them appropriate consideration during the investigation. He identified many of the subtle but significant caveats in compiling, processing, and analyzing the earthquake catalog for use in hazard analysis.

The first day of the workshop closed with questions and statements from observers. Dr. Stepp clarified that the focus of the project is on tectonic events and not mining-induced, or thermally induced seismicity, which are beyond the scope of this project. Bakr Ibrahim of the U.S. Nuclear Regulatory Commission (NRC) asked whether the group might be reconvened if results were found during the ongoing site characterization that impacted the PSHA, and Mr. Sullivan answered yes, if the findings would significantly impact the results of the PSHA.

TUESDAY, APRIL 18, 1995

Frank (Bert) H. Swan of Geomatrix Consultants started the morning session with a presentation on technical issues significant to characterizing fault sources at Yucca Mountain. He covered basic concepts and provided insights into both general and site-specific issues for

Yucca Mountain, particularly in regard to distributive and secondary faulting that is important to characterizing fault displacements. He also highlighted caveats in using the present geologic database, such as likely subsurface differences and complexities in geometry, absence of Quaternary cover, the incomplete paleoseismic record, and differences between average net slip and observed displacements.

Next, one of the Deputy Directors of the project, Ivan G. Wong of Woodward-Clyde Federal Services, presented technical issues found to be most significant during the preliminary PSHA done for the Exploratory Studies Facility (ESF) at Yucca Mountain. For their preliminary study of vibratory ground motions only and not fault displacement, they considered 24 faults and one background seismic source zone. They found that the background source was the most significant contributor to seismic hazard at the ESF for return periods up to 100,000 years. This finding underscores the importance of how the earthquake catalog is processed and analyzed for use in characterizing background sources at Yucca Mountain. They also found that three local faults, the Paintbrush Canyon, Solitario Canyon, and Fatigue Wash faults, became significant contributors to the peak acceleration hazard at return periods greater than 20,000 years. When asked whether this project should just focus on local faults, Mr. Wong emphasized the limitations of his study, which was not comprehensive and used simple tectonic and fault segmentation models. He cautioned the experts to use the preliminary findings from the ESF study only as guidelines for prioritizing time spent on characterizing sources.

The morning session concluded with a discussion of the significant technical issues highlighted by Drs. Arabasz, Swan, and Mr. Wong, which are shown in Table 2. Also shown in Table 2 are the data identified by project participants as being particularly important to addressing each issue. Dr. Coppersmith facilitated the discussion and Dr. Arabasz served as scribe. Many members of the Expert Panel, Oversight Panel and Project Management Team actively contributed to the discussion.

Mary-Margaret Coates of the USGS began the afternoon session with a brief explanation of the introductory data package sent out to experts prior to the workshop (Table 3) and the data that are scheduled to be forthcoming from the USGS during this, and the next, fiscal years. She described the role of the Data Management Team as a resource to the experts with the objective of providing a consistent database to all experts in a timely fashion that is as comprehensive and up-to-date as reasonably possible. In regard to timeliness, many experts expressed an interest in electronic access to digital data files, such as placing earthquake catalogs on a home page on the World-Wide Web or providing access to Silvio K. Pezzopane's (USGS) digital compilation of focal mechanism data.

Presentations on available data sets for the Yucca Mountain region began with a joint presentation on seismicity data by Kenneth D. Smith and James N. Brune of University of Nevada at Reno (UNR). Dr. Smith identified the various seismic networks operating in the region at different time periods, including monitoring networks of NTS blasts and the Non-

Proliferation Experiment. He also identified corresponding earthquake catalogs and specialized data sets available, including a forthcoming study of the 1992 Little Skull Mountain earthquake sequence. Six catalogs of historical earthquakes in the region were compiled into a comprehensive report by Gross and Jaume at UNR. In contrast, although numerous other compilations and reports exist for the instrumental record, this data set has not yet been compiled and processed into a single comprehensive and consistent catalog. Dr. Brune elaborated on some of the caveats in using the present database, such as inconsistencies and systematic errors among assigned magnitudes, some catalogs contain numerous sonic events, and it may be difficult to distinguish induced events.

The next presentation on available data for regional faults within 100 km of Yucca Mountains (except studies conducted by the State of Nevada) was primarily given by Larry W. Anderson of the USBR and supplemented by R. Ernst (Ernie) Anderson of the USGS. Mr. L. Anderson identified three types of studies: 1) general geologic; 2) regional compilations of suspected Quaternary faults; and 3) fault-specific paleoseismic studies. He also listed available data sources for each type of study and emphasized the number of fault-specific paleoseismic studies was limited; however, existing studies do help provide a Quaternary tectonic framework. He also summarized a compilation by Dr. Pezzopane showing magnitude and distance relations for known and suspected Quaternary faults in the Yucca Mountain region. Dr. R. Anderson summarized data being collected for ongoing studies of regional faults by the USGS, which are scheduled to be available before the end of this fiscal year.

John W. Bell of the Nevada Bureau of Mines and Geology (NBMG) gave the final presentation of the day, providing a summary of data from geologic studies for Yucca Mountain conducted by NBMG and UNR. Regional studies by NBMG have provided extensive data on fault zones with historical surface ruptures in the Basin and Range, particularly in the Central Nevada seismic belt and Walker Lane regions. In particular, distributive faulting of the 1932 Cedar Mountain earthquake was studied in detail by Craig M. dePolo and others to provide possible analog data for Yucca Mountain. Regional NBMG studies also include analog investigations of historical aseismic and seismic cracks in eastern Nevada to better understand the nature of prehistoric cracks found extensively in trenches at Yucca Mountain. Regional studies by UNR include a variety of data for the surrounding region, such as mapping, trenching and geochronological data that have been used to develop tectonic models. Local fault studies by NBMG have included detailed mapping using low-sun-angle photography, chronostratigraphic studies (which include soils, rock varnish, and series data), and some trenching. The day concluded with the opportunity for questions and comments from observers.

WEDNESDAY, APRIL 19,1995

The Project Chief, John W. Whitney of the USGS, opened the last day of the workshop with a presentation on available data for local Quaternary faults at Yucca Mountain. He

summarized data on geometry, kinematics, and paleoseismic behavior for the seven to eight faults closest to the proposed repository block. He focused on mapping and trenching data and emphasized the closely-spaced, complex trace geometry and the long, but incomplete, paleoseismic record preserved for most of the faults. He also identified data that are scheduled to be available this and next fiscal year, including cooperative studies with the State of Nevada being conducted by Alan R. Ramelli of NBMG and Dr. Brune of UNR.

James B. Paces of the USGS gave the next presentation on available and forthcoming geochronological data for Yucca Mountain. He gave an overview of the multiple-purpose, extensive scope, general problems, and integrated approach for the geochronology program at Yucca Mountain. Although a variety of methods have been applied, including cosmogenic, radiocarbon, tephrochronology, U-series, and thermoluminescence, the effort has been most concentrated toward applying the latter two methods. Dr. Paces then identified new developments in U-series dating that are expanding application opportunities at Yucca Mountain. He also identified extensive problems with U-trend methods such that U-trend ages are no longer deemed reliable by most geochronologists. Finally, he stated that the USGS plans to have a trench-by-trench summary of geochronology data for Yucca Mountain that will be available to the Expert Panel by this autumn.

Christopher J. Potter of the USGS summarized available and forthcoming data from structural geology studies of the proposed repository block. He summarized previous and ongoing work involving geologic mapping, paleomagnetic studies, borehole investigations, fracture studies and 3-D modeling. Fracture studies include 2-D and 3-D mapping of surface fracture networks in cleared pavements, outcrop studies of general orientations and crosscutting relations, and stratigraphic studies of vertical continuity of fractures. Many experts expressed an interest in obtaining map data of the ESF and the ongoing 3-D modeling study, which integrates stratigraphic and structural data and uses a surface handling method. Dr. Potter also highlighted some of the issues surrounding the Sundance fault and ongoing studies to address these issues.

Victoria E. Langenheim of the USGS gave the final presentation on available and forthcoming geophysical databases for Yucca Mountain. She specified available data from numerous potential field, seismic, electrical, borehole, heat flow, geodetic, and hydrofracture studies. Potential field studies included gravity and magnetic data, and seismic studies included reflection, refraction, and tomography data. Dr. Lamgenheim also highlighted good overview and summary references for geophysical data.

Dr. Coppersmith facilitated a final wrap-up discussion. No other data were identified that had not been previously discussed in the workshop. It was decided that the SSC-FT would develop a list of needed data specified during the workshop. This list will be distributed to the Expert Panel for them to specify which data they would like sent to them. A Working Group to develop criteria for a project earthquake catalog will be formed including seismologists on the Expert Panel, Mr. Wong, and Dr. Brune. A Working Group on surface

displacement methodology, including Drs. Swan, Pezzopane, and David P. Schwartz (USGS), will complete their deliberations before the next workshop and will keep the Project Management informed as to their progress. Working Groups on empirical rupture dimensions and deep structures will also be considered. Drs. Pezzopane, Whitney, and Chris J. Fridrich (USGS), will develop a preliminary itinerary for the field trip scheduled for this autumn.

The discussion was followed by a training session on Quality Assurance procedures for the project given by Martha Mustard of the USGS. After statements and questions by observers, Dr. Coppersmith adjourned the workshop.

TABLE 1
SEISMIC SOURCE CHARACTERIZATION AND FAULT DISPLACEMENT WORKSHOP

17-19 APRIL 1995
Attendance List

Name	Affiliation
Norm Abrahamson	Consultant
Jon Ake	U.S. Bureau of Reclamation
Ernie Anderson	U.S. Geological Survey
Larry Anderson	U.S. Bureau of Reclamation
Walter Arabasz	University of Utah
Ann Becker	Woodward-Clyde Federal Services
John Bell	University of Nevada at Reno
Ron Bruhn	University of Utah
Jim Brune	University of Nevada at Reno
Bob Budnitz	Future Resources Associates Inc.
Tom Chaney	U.S. Geological Survey
Mary-Margaret Coates	U.S. Geological Survey
Kevin Coppersmith	Geomatrix Consultants
Allin Cornell	Consultant
Tony Crone	U.S. Geological Survey
Craig dePolo	University of Nevada at Reno
Diane Doser	University of Texas at El Paso
Chris Fridrich	U.S. Geological Survey
Tom Hanks	U.S. Geological Survey
Robert Harpster	SAIC
Bakr Ibrahim	U.S. Nuclear Regulatory Commission
Dick Keefer	U.S. Geological Survey
Jerry King	SAIC
Vicky Langenheim	U.S. Geological Survey
Martha Mustard	U.S. Geological Survey
Jim McCalpin	GEO-HAZ Consulting
Steve McDuffie	U.S. Nuclear Regulatory Commission
Robin McGuire	Risk Engineering

TABLE 1 (Continued)

Name	Affiliation
Chris Menges	U.S. Geological Survey
Peter Morris	Applied Decision Analysis
Susan Olig	Woodward-Clyde Federal Services
Jim Paces	U.S. Geological Survey
Sue Penn	Woodward-Clyde Federal Services
Roseanne Perman	Geomatrix Consultants
Silvio Pezzopane	U.S. Geological Survey
Paul Pomeroy	Advisory Committee on Nuclear Waste
Chris Potter	U.S. Geological Survey
Rich Quittmeyer	Woodward-Clyde Federal Services
Alan Ramelli	University of Nevada at Reno
A1 Rogers	U.S. Geological Survey
Jean Savy	Lawrence Livermore National Laboratory
John Schneider	Woodward-Clyde Federal Services
David Schwartz	U.S. Geological Survey
Burt Slemmons	Woodward-Clyde Federal Services
Robert Smith	University of Utah
Ken Smith	University of Nevada at Reno
Carl Stepp	Woodward-Clyde Federal Services
Bill Sublette	SAIC
Tim Sullivan	U.S. Department of Energy
Bert Swan	Geomatrix Consultants
David Elllson	Nevada Agency for Nuclear Projects
Gabriel Toro	Risk Engineering
Engelbrecht von Tiesenhausen	Clark County Nuclear Waste Division
John Whitney	U.S. Geological Survey
Ivan Wong	Woodward-Clyde Federal Services
Bob Youngs	Geomatrix Consultants
lim Yount	U.S. Geological Survey
Mary Lou Zoback	U.S. Geological Survey

TABLE 2
SIGNIFICANT TECHNICAL ISSUES AND ASSOCIATED DATA NEEDS FOR CHARACTERIZING SEISMIC SOURCES IN THE YUCCA MOUNTAIN REGION

Note: This list of issues was not intended to be exhaustive. Rather, it was developed to focus discussion and thought on the types of data that could be used to address several key SSC issues.

Issue 1. What are the candidate seismic sources for the background earthquake and what is the relative importance of volcanic earthquakes.

Data Needed:

- Spatial and temporal relation of volcanic-related events and background seismicity
- Suzette Jackson's compilation of volcanic-related seismicity (analog information)
- Heat flow data
- Comparison of the temporal and spatial patterns of paleoseismic events and volcanic-related events
- Stress field and relation to volcanic features, such as dike injection
- Recurrence information on volcanism near Yucca Mountain

Issue 2. What is size of maximum background earthquake?

Data Needed:

- Compilation by Craig dePolo of minimum magnitudes for surface-faulting earthquakes
- Other evidence of deformation besides surface faulting
- Stability of rupture dimensions with magnitude
- Maximum magnitude of non-surface-faulting earthquakes in other extensional tectonic environments (analog information)

Issue 3. Are rates of earthquake occurrence significantly affected by remotely triggered and "encouraged" mainshocks or are the effects insignificant when averaged over long periods?

Data Needed:

- UNR's data on decay of aftershocks and triggered events
- Information on blasting induced earthquakes, including depths
- Catalog of focal mechanisms
- Dislocation modeling of "encouraged" mainshocks

Issue 4. Relative weighting of exponential versus characteristic versus maximum magnitude earthquake recurrence models for fault-specific sources.

Data Needed:

- Distribution of displacements in paleoseismic data base
- Worldwide analogs on displacement per event
- Information on scaling relations of displacement versus fracture dimension (e.g., UK conference)
- Patience Cowie's Ph.D. dissertation (Lamont) and oil company information relating length and displacement

Issue 5. Developing fault segmentation models that define likely rupture segments

Data Needed:

- Paleoseismic data including timing, displacements, rupture lengths
- Analog earthquakes

Subsurface geometry (see below)

Issue 6. Characterizing fault geometry and kinematics.

Data Needed:

- Mapping
- Subsurface data including drill hole, seismic reflection and refraction, and gravity
- Cross-sections
- Focal mechanisms, focal depths, and aftershock patterns
- Kinematic indicators (distinguish those in bedrock from those in Quaternary deposits)
- Aftershocks of normal-faulting earthquakes worldwide (analog information)

Issue 7. Characterizing distributive faulting.

Data Needed:

- Literature on hangingwall versus footwall deformation
- Analogs of normal-faulting earthquakes and their aftershocks and focal mechanisms
- Historical faulting in the Basin and Range Province
- Mapping of tunnel for superconducting supercollider in Texas
- Oil industry data on normal faults in subsurface
- Geoff King's 3-D boundary element model of Yucca Mountain
- Ron Bruhn's preprint on splay faulting and evolution of normal faults
- Mining industry data to calibrate models

Issue 8. Non-stationary and possible temporal clustering of large earthquakes

Data Needed:

(Data Needs added by SSC-FT after workshop)

- Paleoseismic data on timing and recurrence of events

- Jim McCalpin's compilation and analysis on variation of slip rates in the Basin and Range (analog information)

TABLE 3

CONTENTS OF THIS PACKAGE

BACKGROUND INFORMATION ON YUCCA MOUNTAIN SEISMIC SOURCES AND FAULT DISPLACEMENT

FIRST MAILING TO EXPERTS / APRIL 7, 1995

Cover letter from John Whitney and Mary-Margaret Coates

Preliminary table of contents: Tectonic characterization studies of Yucca Mountain, Nevada--A potential geologic repository for high-level nuclear waste, U.S. Geological Survey Circular (based on talks presented at a workshop in January 1994)

Summaries, reports, bibliographies, and other material as listed below, by topic. Note that the enclosed U.S. Geological Survey Bulletin 1790 contains several referenced papers.

Faults and Seismic Sources

Summary: Faults and seismic sources

Bibliographies: Detachment faulting
Faulting at Yucca Mountain
Quaternary faulting
Surface faulting

Carr, M.D., and Yount, J.C., eds., 1988, Geologic and hydrologic investigations of a potential nuclear waste disposal site at Yucca Mountain, southern Nevada: U.S. Geological Survey Bulletin 1790, 152 p.

Menges, C.M., Wesling, J.R., Whitney, J.W., Swan, F.H., Coe, J.A., Thomas, A.P., and Oswald, J.A., 1994, Preliminary results of paleoseismic investigations of Quaternary faults on eastern Yucca Mountain, Nye County, Nevada, *in* Proceedings, 5th International Conference, High-Level Radioactive Waste Management, v. 4, p. 2373-2390.

Pezzopane, S.K., Menges C.M., and Whitney, J.W., 1994, Quaternary paleoseismology and Neogene tectonics at Yucca Mountain, Nevada: U.S. Geological Survey Open-File Report 94-568, p. 149-151.

Piety, L.A., 1995, Appendices 2, 3, 4, and 5 of Compilation of known or suspected Quaternary faults within 100 km of Yucca Mountain; Nevada and California: U.S. Geological Survey Open-File Report 94-112, text to accompany map, 331 p. (in press).

Simonds, W.F., Whitney, J.W., Fox, K.F., Ramelli, A., Yount, J., Carr, M.D., Menges, C.M., Dickerson, R., and Scott, R.B., 1995, Map of fault activity of the Yucca Mountain area, Nye County, Nevada: text to accompany map, 30 p. (in press).

Geochronology of Surficial Stratigraphy

Summary: Geochronology of Quaternary stratigraphy

Bibliography: Geochronology of Quaternary stratigraphy

Lundstrom, Scott, 1994, Map unit descriptions for the preliminary surficial deposits of the southern half of the Topopah Spring quadrangle and northern half of the Busted Butte quadrangle, Nye County, Nevada: Prepared by EG&G, scale 1:12,000.

Paces, J.B., Menges, C.M., Widmann, B., Wesling, J.R., Bush, C.A., Futa, K., Millard, N.T., Matt, P.B., and Whitney, J.W., 1994, U-Series disequilibrium and thermoluminescense ages of paleosols associated with Quaternary faults, east side of Yucca Mountain: Proceedings, International Topical Meeting, High Level Nuclear Waste Management: American Nuclear Society, Inc., Las Vegas, Nevada, p. 2391-2401.

Geodetic Leveling

Summary: Geodetic leveling

Bibliography: Geodetic leveling

Savage, J.C., Lisowski, M., Gross, W.K., King, N.E., and Svarc, J.L., 1994, Strain accumulation near Yucca Mountain, Nevada, 1983-1993: Journal of Geophysical Research, v. 99, p. 18,103-18,107.

Geologic Mapping

Summary: Geologic mapping

Bibliography: Geologic maps

Index to orthophotos, Yucca Mountain area

Viewgraph of the Yucca Mountain Area

Frizzell, V.A., Jr., and Shulters, J., 1990, Geologic map of the Nevada Test Site, southern Nevada: U.S. Geological Survey Miscellaneous Investigations Map I-2046, scale 1:100,000.

Scott, R.B., and Bonk, J., 1984, Preliminary geologic map of Yucca Mountain, Nye County, Nevada with geologic sections: U.S. Geological Survey Open-File Report 84-494, scale 1:12,000, 9 p.

Geophysical Data

Summary: Geophysical data

Bibliographies: Gravity
Magnetic
Seismic reflection and refraction

Carr, M.D., and Yount, J.C., eds., 1988, Geologic and hydrologic investigations of a potential nuclear waste disposal site at Yucca Mountain, southern Nevada: U.S. Geological Survey Bulletin 1790, p. 3-21. Several articles.

Hildenbrand, T.G., Rogers, A.M., Oliver, H.W., Harmsen, S.C., Nakata, J.K., Aitken, D.S., Harris, R.N., and Carr, M.D., 1988, Regional geologic and geophysical maps of the southern Great Basin, *in* Carr, M.D., and Yount, J.C., eds., Geologic and hydrologic investigations of a potential nuclear waste disposal site at Yucca Mountain, southern Nevada: U.S. Geological Survey Bulletin 1790, p. 3-21.

Oliver, H.W., Ponce, D.A., and Hunter, W.C., 1995, Major results of geophysical investigations at Yucca Mountain and vicinity, southern Nevada: U.S. Geological Survey Open-File Report 95-74, 235 p., (in press).

Heat Flow

Summary: Heat flow

Bibliography: Heat flow

Sass, J.H., Dudley, W.W., Jr., and Lachenbruchm, A.H., Regional thermal setting, 1995, *in* Oliver, H.W., Ponce, D.A., and Hunter, W.C., eds, Major results of regional geophysical investigations of Yucca Mountain and vicinity, Nevada: U.S. Geological Survey Open-File Report 95-74, 235 p. (in press).

Seismicity

Summary: Historical and current seismicity

Bibliography: Seismicity

Harmsen, S.C., 1994, The Little Skull Mountain, Nevada, earthquake of 29 June 1992--Aftershock focal mechanisms and tectonic stress field implications: Bulletin Seismological Society America, v. 84, p. 1484-1505

Rogers, A.M., and Harmsen, S.C., 1991, The seismicity of Nevada and some adjacent parts of the Great Basin, *in* The Geology of North America, Decade Map: Volume 1, p 153-184

Stress Analysis

Summary: Stress analysis

Bibliography: Stress analysis

Harmsen, S.C., and Rodgers, A.M., 1986, Inferences about the local stress field from focal mechanisms--Applications to earthquakes in the southern Great Basin of Nevada: Bulletin of the Seismological Society of America, v. 76, p. 1560-1572.

Stock, J.M., and Healy, J.H., 1988, Stress field at Yucca Mountain, Nevada, *in* Carr, M.D., and Yount, J.C., eds., Geologic and hydrologic investigations of a potential nuclear waste disposal site at Yucca Mountain, southern Nevada: U.S. Geological Survey Bulletin 1790, p. 87-93.

Tectonic Models

Summary: Tectonic models

Bibliography: Tectonic models

Carr, W.J., 1990, Styles of extension in the Nevada Test Site region, southern Walker Lane Belt; an integration of volcano-tectonic and detachment fault models, *in* Wernicke, B.P., ed., Basin and Range extensional tectonics near the latitude of Las Vegas, Nevada: Geological Society of America Memoir 176, p. 283-303.

Crowe, B., Perry, F., Geissman, J., McFadden, L., Wells, S., Murrell, M., Poths, J., Valentine, G.A., Bowker, L., and Finnegan, K., 1995, Status of volcanism studies for the Yucca Mountain site characterization project: Los Alamos National Laboratory Report LA-12908-MS.

Scott, R.B., 1990, Tectonic setting of Yucca Mountain, southwest Nevada, *in* Wernicke, B.P., ed., Basin and Range extensional tectonics near the latitude of Las Vegas, Nevada: Geological Society of America Memoir 176, p. 251-282.

Spengler, R.W., and Fox, K.F., 1989, Stratigraphic and structural framework of Yucca Mountain, Nevada, *in* Radioactive Waste Management and the Nuclear Fuel Cycle: v. 13, p 21-36.

Civilian Radioactive Waste Management System
Management & Operating Contractor

Summary of Seismic Source Characterization Hazard Methodologies Workshop

SSC Workshop 2

Salt Lake City, UT
October 16-18, 1996

Prepared for:

U.S. Geological Survey
Box 25046, MS-425
Denver Federal Center
Denver, CO 80225

Prepared by:

Woodward-Clyde Federal Services of the
Civilian Radioactive Waste Management System
Management & Operating Contractor
101 Convention Center Drive
Suite P-110
Las Vegas, NV 89109

November 11, 1996

1. INTRODUCTION

The United States Geological Survey (USGS) is carrying out a probabilistic seismic hazards analysis (PSHA) for Yucca Mountain, Nevada as part of the Department of Energy's (DOE) project to characterize this site as a potential geologic repository for high-level radioactive waste. This study was initiated in April 1995 and resumed in June 1996. The aim of the analysis is to provide the annual probability with which various levels of vibratory ground motion and fault displacement will be exceeded at the site. These results will be used as a basis for developing design inputs and in assessing the performance of the site.

The PSHA process involves development by two panels of experts of input interpretations and assessments of uncertainties required by the hazards calculations. One panel addresses characterization of seismic sources and fault displacement (SSFD), while the other deals with vibratory ground motion. Development of interpretations is being facilitated through a series of structured workshops to evaluate available data, to explore the range of interpretations allowed by the data, to examine critically the interpretations proposed by the experts, and to provide feedback on the implications of various interpretations for the seismic hazard at the site. The goal of this process is to have differences in experts' interpretations be the results of true differences in judgment and not differences in access to data, differences in definitions, or differences resulting from a lack of understanding each others' interpretations. This report summarizes the second in the series of structured workshops for characterization of seismic sources and fault displacement: the Hazard Methodologies Workshop.

The workshop had two principal goals: to review the newly available data for the Yucca Mountain region, and to identify available methodologies for characterizing seismic sources for the Yucca Mountain seismic hazard analysis. The first goal is a follow-on to the first SSFD workshop held in April of 1995, because additional data have become available and/or synthesized in summary reports since that time. The workshop also served as a second kick-off meeting for restarting the project, and participants were advised on revisions to the project plan and schedule.

To accomplish the above goals, the workshop included a series of presentations and discussion sessions, which are summarized chronologically below. Copies of overhead transparencies shown by presenters were distributed to participants during the workshop and are included with this summary as Attachment 1. Also included in Attachment 1 are copies of manuscripts distributed during the workshop. Table 1 is a bibliography of all of the reference material distributed, including oversize maps and cross-sections.

The basic approach of the workshop was to divide seismic source characterization (SSC) into two parts: SSC related to vibratory ground motion hazard analysis and related to fault

displacement hazard analysis. SSC is then divided into three components: seismic source location and geometry, maximum earthquake magnitude, and earthquake recurrence assessment. Each of these topics is first introduced by overview presentations that focus on the *methods and approaches* that are available to characterize them. These talks are then followed by a series of talks that describe the available *data bases and data interpretations* that relate to these topics. Although the presentations will undoubtedly entail some interpretations, the next workshop (Workshop #3 Alternative Models and Interpretations) will provide a forum for debating alternative interpretations of the available data.

WEDNESDAY, OCTOBER 16, 1996

Introductory presentations were given by: 1) the Project Representative for DOE, Tim Sullivan; 2) the Project Director, J. Carl Stepp; and, 3) the Team Leader of the SSFD Facilitation Team, Kevin J. Coppersmith. Table 2 shows the list of workshop attendees and their affiliations.

Mr. Sullivan provided an update and overview of developments in the Yucca Mountain program since April 1995. He emphasized that the objectives for the PSHA to provide seismic design parameters for the 1998 Viability Assessment remained the same, and that the viability assessment is a interim step to site recommendation in 2001. He also pointed out that the DOE Topical Report "Methodology to Assess Fault Displacement and Vibratory Ground Motion Hazards at Yucca Mountain" has been accepted by the U.S. Nuclear Regulatory Commission (NRC) pending review of the final results of the PSHA.

Dr. Stepp reviewed changes in the PSHA schedule and project plan. The plan remains mainly the same with one difference being in the change of the Oversight Panel to a Peer Review Panel. This panel will consist of four members, reviewing different project areas according to expertise, and the process will be structured as a participatory peer review.

Dr. Coppersmith outlined the goals and approach of the workshop. He also discussed ground rules for the workshops, roles of project participants, major milestones and key aspects for the SSC component of the project, guidelines used in selecting experts, ground rules for experts and expert teams, and the goal of having a defensible basis for combining team assessments into the final analysis with equal weights. With the aid of hats as props, he emphasized that although the experts are encouraged to play the role of proponent occasionally during the process, their overall role and the role they must ultimately play when they develop their assessment is that of an evaluator.

Following the introductory session, the rest of the day consisted of presentations focusing on seismic source characterization for assessing vibratory ground motions. Dr. Walter Arabasz started out with an overview, pointing out key issues and personal insights from past experiences, including examples dealing with the processing of earthquake catalogues. A question was raised about defining the size of the area for detailed characterization, resulting in discussion about the need to be comprehensive but not to waste limited resources. Therefore, some guidance will be sought on this issue from the ground motion expert panel.

Dr. Ronald Bruhn next discussed methods for assessing the location and geometry of fault seismic sources. He pointed out significant issues regarding fault segmentation, inferring down-dip geometry from limited subsurface data, and long-term vs. short-term fault behavior. He highlighted many approaches and tools that are available for assessing the geometry and kinematics of fault systems such as: standard map and cross-section techniques, fault scaling relations, models of hanging and footwall rotation and flexure, thermal and rheologic constraints, implications from fracture mechanics and lab experiments, and kinematic and dynamic analyses to assess fault interactions and fault segmentation. He cited many examples from the February/March 1996 issue of the Journal of Structural Geology.

Following the lunchbreak, Dr. Christopher Menges summarized Quaternary fault studies in the immediate vicinity of Yucca Mountain, emphasizing results from trenching and mapping studies on fault location and geometry. Quaternary faults show a complex, anastomosing, intersecting pattern that can be separated into two fault systems: an east and west side that may possibly interconnect. Fault traces are relatively short (< 12 km), discontinuous, and densely spaced (< 1 to 5 km). Slip is dominantly normal oblique (left-lateral) on faults that dominantly strike N to NE and dip steeply to the W. These faults show small to moderate bedrock displacements and very small Quaternary displacements.

Presentations on newly available data for regional Quaternary faults were given by Mr. Larry Anderson and Dr. R. Ernst (Ernie) Anderson. Mr. L. Anderson discussed studies of the Bare Mountain, Death Valley and Furnace Creek fault zones. He emphasized information on slip rates, recurrence, and fault segmentation, particularly differences with previous and ongoing studies. Dr. E. Anderson presented results from reconnaissance mapping and scarp profiling studies of 15 different faults in the region. Theses studies focused on using fault scarp morphology to assess age of most recent activity and fault length.

Next Dr. Thomas Brocher presented newly available results from a deep seismic reflection study conducted by the U.S. Geological Survey. He also distributed preprints of manuscripts in review or in press. The two new lines extend from the Amargosa Desert to Jackass Flats, overlapping at Yucca Mountain. Dr. Brocher also presented gravity and aeromagnetic data that were used to help constrain interpretations of the seismic lines. These interpretations

suggest a series of east-dipping faults buried in Crater Flat, west of Yucca Mountain and a series of west-dipping faults that are chiefly east of and include the Solitario Canyon fault. All of those faults show relatively minor total offsets and are in the hanging wall of the larger Bare Mountain fault. Beds in the hanging wall overall step down to the west, forming a slight rollover and suggesting a listric geometry for the Bare Mountain fault. However, the Bare Mountain fault appears planar to 6-7 km depth and dips roughly 65° to the east in the seismic lines. Dr. Brocher also emphasized the large uncertainties in the data and models.

Dr. Kenneth Smith presented results from recent studies of seismicity in the vicinity of Yucca Mountain, focusing on location, depth, focal mechanisms, and spatial distributions of sequences. He discussed the 1992 Little Skull Mountain earthquake sequence, the 1993 Rock Valley earthquake sequence, and other small events in the region including the 1995 M 4.2 Timber Mountain earthquake and a sequence of small events south of Lathrop cones. He also discussed 15 very small earthquakes ($M < 1$) detected by the new network at Yucca Mountain that occurred since May 1995, and moment-magnitude scaling relations for the region.

Dr. Coppersmith then wrapped-up the day by asking for questions and comments from observers. Dr. Clarence Allen commented on the increased importance of the PSHA and the SCC due to changes in canister design and emplacement. Dr. Phil Justus presented a list of issues including points of clarification, and themes that needed further consideration, and important aspects of the SCC from the NRC's perspective.

THURSDAY, OCTOBER 17, 1996

Topics on SSC for evaluating ground motions continued to be the focus for Thursday's presentations. Dr. Coppersmith started the day with a presentation on methods for assessing maximum magnitudes, focusing on using fault rupture dimensions to estimate maximum magnitude. He pointed out some of the common pitfalls in determining maximum magnitudes and introduced methods for incorporating uncertainties using logic trees and continuous distributions.

Dr. Silvio Pezzopane gave the next presentation on data (fault length and displacement per event) for determining maximum magnitudes on Yucca Mountain faults. This included using paleoseismic data to assess fault segmentation and fault interdependence so that rupture scenarios could be developed. Surface-faulting earthquake parameters for these rupture scenarios can then be used to estimate maximum magnitudes. These rupture scenarios are discussed in more detail in the seismotectonic synthesis report by the U.S. Geologic Survey.

After the break, Dr. John Anderson discussed a new empirical relation that also incorporates fault slip rate to estimate maximum magnitude in addition to the typical fault parameters. He distributed reprints of his recent paper on this relation, which yields relatively higher magnitudes for lower slip rate faults. He also discussed possible reasons for why magnitude may be slip rate dependent.

Next, Dr. James McCalpin discussed methods for assessing earthquake recurrence on faults, emphasizing uncertainties, pitfalls, and the limitations and interdependence of paleoseismic data sets. He stressed the use of different types of probability distributions (e.g., Gaussian versus Weibull) is significant in terms of interpreting lower- and upper-bound values.

Dr. John Whitney followed with a presentation on slip rate and recurrence data for Yucca Mountain faults, summarizing information that is discussed in more detail in the seismotectonic synthesis report by the U.S. Geological Survey. Slip rates and the left-lateral component of slip generally increase to the south. However, all slip rates are relatively low (< 0.027 mm/yr) and generally have decreased through time. Depending on the recurrence model assumed, average recurrence intervals vary from about 5,000 (for < 150 ka) to 54,000 (for < 500 ka) years, with the uncertainties primarily due to ambiguities in correlating events between trench sites, ambiguities in interpreting the origin of cracking events, and uncertainties in the dating of deposits.

Mr. Alan Ramelli presented recent results from paleoseismic studies at four trench sites along the Solitaro Canyon fault. These results show variable displacements and rates of activity through time (temporal clustering) and a possible temporal association of faulting with basaltic volcanism.

Next, Dr. John Stamatakos presented results from studies of the Crater Flat area and the Bare Mountain fault that were conducted by the Center for Nuclear Waste Regulatory Analyses (CNWRA). These studies used a variety of data including: paleomagnetic, gravity, magnetic, geodetic, structural, geomorphic, and geochronologic. Based on geological and geophysical studies, they infer a possible spatial association between volcanism and faulting. They also interpret slip rates on the Bare Mountain fault to increase to the south and to be much higher than the rates of < 0.01 mm/yr reported by Mr. L. Anderson based on paleoseismic trenching studies. Dr. Stamatakos reported long-term uplift rates for the Bare Mountain fault of 0.19 mm/yr and short-term uplift rates as high as 5.0 ± 3.5 mm/yr based on geodetic data.

After the break, Dr. Thomas Channey distributed copies of the Quality Management Procedure for scientific expert elicitation (YMP-USGS-QMP-3.16, RO) to each of the experts, and Facilitation and Management Team members

Following Dr. Stamatakos, Dr. Pezzopane discussed results from geodetic studies conducted by the U.S. Geological Survey. He emphasized the questionable data quality of the earlier leveling surveys, particularly the 1907 survey. He pointed out that in contrast to the CNWRA's results, Savage *et al.* (1994 JGR) found no detectable deformation above the error limits of the network except for a negative elevation change ($\approx$ 2 cm at the surface) associated with the 1992 Little Skull Mountain earthquake.

Mr. Ivan Wong presented results on development of the historical earthquake catalogue for the Yucca Mountain PSHA. He discussed the data sources and statistics of the catalogue and highlighted significant issues related to its use. Dr. Pezzopane then gave a short unscheduled presentation on his analysis of relevant fault sources for Yucca Mountain that is summarized in Chapter 11 of the seismotectonic synthesis report, and follows guidance given by NRC in their report NUREG-1451. Mr. Wong also provided input on faults found to be most significant during their preliminary PSHA for the ESF.

Dr. Coppersmith then announced the SSC teams. Teams were selected by a random process that would ensure that each team contains a seismologist, a regional geologist, and a local geologist/paleoseismologist.

Dr. Coppersmith then closed the day with statements from observers. Dr. Allen commented on the change of the location and shape of the proposed repository block (it now lies entirely west of the ESF and the Ghost Dance fault). Dr. Jerry King commented on his role as providing regulatory oversight to ensure that the needs of the NRC are met. He discussed seismic design parameters of interest from his perspective, including dual design basis earthquakes (with return periods of 1,000 and 10,000 years) and periods of interest (up to 1 second) for the types of facilities being designed. Leon Reiter asked a question regarding the time frame in considering maximum magnitudes and Dr. Coppersmith clarified that these are independent of time with respect to the current tectonic regime. Dr. Stamatakos commented that the CNWRA's report on Type I faults will be available soon.

FRIDAY, OCTOBER 18, 1996

Dr. Robert Youngs gave the first presentation on SSC for fault displacement analysis. He discussed methods for assessing the fault displacement hazard, pointing out differences with assessments for ground motions and differences between fault hazard analysis for design purposes and performance assessments. He outlined the necessary components and various approaches to determining input for characterizing fault displacement. He emphasized characterizing uncertainty in rupture distributions and gave examples of specific applications.

Next, Dr. Warren Day presented results from detailed surface mapping of the bedrock geology at Yucca Mountain. He distributed copies of a manuscript, including maps and cross-sections, and several abstracts. He compared new results with earlier mapping , discussed accuracies, highlighted new results, and concluded by summarizing the characteristics of the principal types of bedrock faults at Yucca Mountain: block-bounding, intrablock, and northwest-striking faults (the latter including both intrablock and bridging faults). He also suggested a possible fault classification scheme based on offsets observed over certain along-strike distances.

After the break, Dr. Robert Lung presented preliminary results of detailed subsurface mapping of fractures and faults in the ESF. At the time of his report, roughly 6,600 m of the tunnel had been drilled, 6,400 m had been mapped, and 5,400 m of mapping had been cleared through quality assurance. He described the type and format of data available from their studies. He highlighted "notable" structural features observed in the ESF to date and discussed some differences and similarities between subsurface and surface mapping.

Dr. Mark Feighner then presented results from geophysical studies of Yucca Mountain conducted by Lawrence Berkeley National Laboratory. These studies involved collection of seismic, gravity, magnetic, and magnetotelluric data. He presented first order preliminary interpretations for many of these studies. He also highlighted differences between their models and those developed by the U.S. Geological Survey (previously presented by Dr. Brocher), emphasizing the assumptions made and the uncertainties in their data and models.

Dr. Whitney gave the next presentation on paleoseismic displacement data for the Ghost Dance fault. He summarized data from both geomorphic studies, which included cosmogenic dating of surfaces along Whaleback and Antler Ridges, and trenching studies. He highlighted issues related to interpreting the genesis and significance of cracking events.

After lunch Dr. Burt Slemmons discussed the advantages and disadvantages of using average and maximum fault displacements compared to using surface rupture lengths to estimate maximum magnitudes. Using examples from historic earthquakes, he highlighted issues related to assessing magnitude for complex rupture patterns, such as uncertainties in fault segmentation and distributive fault ruptures.

Dr. Pezzopane gave the final presentation of the workshop on displacement data from historic surface-rupturing earthquakes in the Basin and Range. The purpose of his study was to help characterize secondary displacement by analyzing along-strike and across-strike fault displacement distributions. He described the data set, including its uncertainties and limitations. He discussed large variations in the shape of along-strike slip distributions, variations in the width of surface ruptures, the relation between lengths of primary and secondary components of surface-rupturing events, the relation between displacements on

primary and secondary faults, and the relation between secondary rupture lengths and secondary displacements.

Dr. Coppersmith wrapped up the workshop by discussing plans for the next workshop and field trip. He then opened up the meeting to comments from observers. Dr. Allen commented on the observations of fracturing in the ESF opening up more issues. Dr. Daniel Soeder clarified the status of availability for certain data sets. Dr. Reiter commented on the difficulty of characterizing fault displacement without a more specific minimum threshold, and he encouraged design engineers to give as much guidance as possible to the SSC experts to help focus their efforts. The workshop was adjourned at about 3:00 pm.

TABLE 1
BIBLIOGRAPHY OF MATERIAL DISTRIBUTED AT HAZARD METHODOLOGIES WORKSHOP (SSC WORKSHOP #2)*

Anderson, J.G., Wesnousky, S.G., and Stirling, M.W., 1996, Earthquake size as a function of fault slip rate: Bulletin of the Seismological Society of America, v. 86, no. 3, p. 683-690.

Anderson, J.G., and Brune, J.N., 1996, Methodology for using precarious rocks in Nevada to test seismic hazard models: Bulletin of the Seismological Society of America (in press).

Biasi, G.P., 1996, Teleseismic tomographic imaging of the Yucca Mountain region: administrative report satisfying YMP activity number 8.3.1.1.7.4.1.2, 42 p.

Bodin, P., and Brune, J.N., 1996, On the scaling of slip with rupture length of shallow strike-slip earthquakes: quasi-static models and dynamic rupture propagation: Bulletin of the Seismological Society of America, v. 86, p.1292-1299.

Brocher, T.M., Hunter, W.C., and Langenheim, V.E., 1996, Structural framework of Yucca Mountain, Nevada, based on crustal-scale seismic reflection profiles and potential field data: Geological Society of America Bulletin (in press).

Brocher, T., Hart, P.E., Hunter, W.C., and Langenheim, V.E., 1996, Hybrid-source seismic reflection profiling across Yucca Mountain, Nevada: Regional Lines 2 and 3: United States Geological Survey Open-File Report 96-28, 97 p.

Brune, J.N., 1996, Dynamic wave effects on particle motions in thrust, normal, and strike-slip faulting: unpublished abstract.

*Center for Neotectonic Studies, Mackay School of Mines, University of Nevada, Reno, 1995, Evaluation of the geologic relations and seismotectonic stability of the Yucca Mountain area, Nevada nuclear waste site investigation (NNWSI), Progress Report, variously paginated.

Connor, C.B., Ferrill, D.A., Hill, B.E., Magsino, S.B.L., LaFemina, P., and Martin, R.H., 1996, Integrating structural models into volcanic hazard assessments: an example from Yucca Mountain, Nevada: American Geophysical Union Abstracts with Program, Fall 1996 (in press).‡

* Includes material distributed to SSC Experts in a November 1996 mailing following Workshop #2.

TABLE 1 (Cont.)
BIBLIOGRAPHY OF MATERIAL DISTRIBUTED AT HAZARD METHODOLOGIES WORKSHOP (SSC WORKSHOP #2)

Day, W.C., Potter, C.J., Sweetkind, D.S., and Dickerson, R.P., 1996, Detailed bedrock geologic map of the central block area, Yucca Mountain - implications for structural development of the potential high-level radioactive waste repository area in Nye County, Nevada: Geological Society of America Abstracts with Program, v. 28, no. 7, p. A-248.

Day, W.C., Potter, C.J., Sweetkind, D.S., Dickerson, R.P., and San Juan, C.A., 1996, Bedrock geologic map of the central block area, Yucca Mountain, Nye County, Nevada: U.S. Geological Survey Administrative Report, prepared in cooperation with the Nevada Operations Office, U.S. Department of Energy.

Dickerson, R.P., and Drake, R.M., 1995, Source of the rhyolite of Comb Peak, southwest Nevada Volcanic Field: Geological Society of America Abstracts with Program.

Dickerson, R.P., 1996, Geologic and geophysical evidence for normal faulting in Yucca Wash, Yucca Mountain, Nevada: unpublished abstract.

Ferrill, D.A., Stamatakos, J.A., Jones, S.M., Rahe, B., McKague, H.L., Martin, R.H., and Morris, A.P., 1996, Quaternary slip history of the Bare Mountain fault (Nevada) from the morphology and distribution of alluvial fan deposits: Geology, v. 24, no. 6, p. 559-562 (abstract only).

Ferrill, D.A., Sims, J., Stamatakos, J.A., and Rahe, B., 1996, Role of ductile detachment horizon in the development of pull-apart basins in physical analog models: American Geophysical Union Abstracts with Programs, (in press).

Ferrill, D.A., and Stamatakos, J.A., 1996, Structural controls on progressive deformation of the Yucca Mountain (Nevada) region: American Geophysical Union Abstracts with Programs, (in press).

*Ferrill, D.A., Stirewalt, G.L., Henderson, D.B., Stamatakos, J.A., Morris, A.P., Spivey, K.H.C., and Wernicke, B.P.C., 1996, Faulting in the Yucca Mountain region: Critical review and analyses of tectonic data from the central Basin and Range: Center for Nuclear Waste Regulatory Analyses NUREG/CR-6401, or CNWRA 96-007, Rev.01.

Morris, A., Ferrill, D.A., and Henderson, D.B., 1996, Slip-tendency analysis and fault reactivation: Geology, v. 24, no. 3, p. 275-278 (abstract only).

TABLE 1 (Cont.)
BIBLIOGRAPHY OF MATERIAL DISTRIBUTED AT HAZARD METHODOLOGIES WORKSHOP (SSC WORKSHOP #2)

Ofoegbu, G.I., Ferril, D.A., Smart, K.J., and Stamatakos, J.A., 1996, Effects of source geometry and hypocenter depth on earthquake ground motion patterns from finite element modeling: American Geophysical Union Abstracts with Program (in press).

Ofoegbu, G.I., Ferrill, D.A., Smart, K.J., and Stamatakos, J.A., 1996, Effects of source geometry and hypocenter depth on earthquake ground motion patterns from finite element modeling: American Geophysical Union Abstracts with Program, (in press).

Potter, C.J., Day, W.C., and Sweetkind, D.S., 1996, Structural evolution of the potential high-level nuclear waste repository site at Yucca Mountain, Nevada: Geological Society of America Abstracts with Program, v.28, no.7, p. A-191.

Potter, C.J., Day, W.C., Sweetkind, D.S., and Dickerson, R.P., 1996, Fault styles and strain accommodation in the Tiva Canyon Tuff, Yucca Mountain, Nevada: EOS, v. 77, no. 17, S265.

Stamatakos, J.A., and Ferrill, D.A., 1996, Paleomagnetism of Ordovician Pogonip Group carbonates in southwestern Nevada: Implications to tectonism of the Yucca Mountain region: American Geophysical Union Abstracts with Program, (in press).

Stamatakos, J.A., and Ferrill, D.A., 1996, Kinematic constraints of central Basin and Range tectonism from paleomagnetic and fission track studies at Bare Mountain, Nevada: American Geophysical Union Abstracts with Programs, (in press).

Sweetkind, D.S., and Williams-Stroud, S., 1995, Controls on the genesis of fracture networks, Paintbrush Group, Yucca Mountain, Nevada: EOS, v. 76, F597.

Sweetkind, D.S., Williams-Stroud, S.C., and Coe, J.A., 1996, Characterizing the fracture network in the unsaturated zone at yucca Mountain, Nevada, Part 1 Collection and interpretation of geologic data: Case Studies (1996 Guidebook ed.): Fractured Reservoirs: Detection, Characterization, and Prediction: Denver, Colorado, Rocky Mountain Association of Geologists, (in press).

Sweetkind, D.S., Beason, S.C., Potter, C.J., Lung, R., Day, W.C., and Barr, D., 1996, Correlation between surface and subsurface features at Yucca Mountain, Nye County, Nevada: Geological Society of America Abstracts with Program, v.28, no.7, p. A-521.

TABLE 1 (Cont.)
BIBLIOGRAPHY OF MATERIAL DISTRIBUTED AT HAZARD METHODOLOGIES WORKSHOP (SSC WORKSHOP #2)

Sweetkind, D.S., Potter, C.J., and Verbeek, E.R., 1996, Interaction between faults and the fracture network at Yucca Mountain, Nevada: EOS, v. 77, no. 17, p. S266.

*U.S. Geological Survey, 1996, Seismotectonic framework and characterization of faulting at Yucca Mountain, Nevada: U. S. Geological Survey Administrative Report to the U.S. Department of Energy that fulfills Level 3 Milestone 3GSH100M WBS Number 1.2.3.2.8.3.6, variously paginated.

TABLE 2
YUCCA MOUNTAIN SEISMIC SOURCE CHARACTERIZATION
WORKSHOP #2 - HAZARD METHODOLOGIES

Attendance List
OCTOBER 16-18, 1996

Name	Affiliation
1. Ake, Jon	U.S. Bureau of Reclamation (USBR)
2. Allen, Clarence	Nuclear Waste Technical Review Board (NWTRB)
3. Anderson, Ernie	U.S. Geological Survey (USGS)
4. Anderson, John	University of Nevada at Reno (UNR)
5. Anderson, Larry	USBR
6. Arabasz, Walter	University of Utah (UU)
7. Bell, John	UNR
8. Brocher, Tom	USGS
9. Bruhn, Ron	UU
10. Brune, James	UNR
11. Chaney, Tom	USGS
12. Coppersmith, Kevin	Geomatrix
13. Cornell, Allin	Consultant
14. Day, Warren	USGS
15. dePolo, Craig	UNR
16. Doser, Diane	University of Texas, El Paso
17. Feighner, Mark	Lawrence Berkeley National Laboratory
18. Fridrich, Chris	USGS
19. Hanks, Tom	USGS
20. Justus, Phil	U.S. Nuclear Regulatory Commission (NRC)
21. Kimball, Jeff	U.S. Department of Energy (DOE)
22. King, Jerry	M&O/SAIC
23. Knuepfer, Peter	State University of New York at Binghamton
24. Lui, Christiana	NRC
25. Lung, Rob	USBR
26. McCalpin, Jim	GEO-HAZ Consulting, Inc.
27. McGuire, Robin	Risk Engineering
28. Menges, Chris	USGS
29. O'Leary, Dennis	USGS
30. Olig, Susan	Woodward-Clyde Federal Services (WCFS)

TABLE 2 (Cont.)
YUCCA MOUNTAIN SEISMIC SOURCE CHARACTERIZATION
WORKSHOP #2 - HAZARD METHODOLOGIES

Attendance List
OCTOBER 16-18, 1996

Name	Affiliation
31. Perman, Roseanne	Geomatrix
32. Pezzopane, Silvio	USGS
33. Pomeroy, Paul	Advisory Committee on Nuclear Waste
34. Potter, Chris	USGS
35. Quittmeyer, Richard	WCFS
36. Ramelli, Alan	UNR
37. Reiter, Leon	NWTRB
38. Robert Smith	UU
39. Rogers, Al	EQE International
40. Savy, Jean	Lawrence Livermore National Laboratory
41. Schwartz, David	USGS
42. Slemmons, Burt	WCFS
43. Smith, Ken	UNR
44. Soeder, Daniel	USGS
45. Stamatakos, John	CNWRA
46. Stepp, Carl	WCFS
47. Sullivan, Tim	DOE
48. Swan, Bert	Geomatrix
49. Tillson, David	Nevada Agency for Nuclear Projects
50. Toro, Gabe	Risk Engineering
51. Whitney, John	USGS
52. Wong, Ivan	WCFS
53. Youngs, Robert	Geomatrix
54. Yount, Jim	UNR

Civilian Radioactive Waste Management System
Management & Operating Contractor

Summary of Seismic Source Characterization Field Trip and Workshop on Alternative Models and Interpretations

SSC Workshop 3

Amargosa Valley, NV
November 18-21, 1996

Prepared for:

U.S. Geological Survey
Box 25046, MS-425
Denver Federal Center
Denver, CO 80225

Prepared by:

Woodward-Clyde Federal Services of the
Civilian Radioactive Waste Management System
Management & Operating Contractor
101 Convention Center Drive
Suite P-110
Las Vegas, NV 89109

December 18, 1996

1. INTRODUCTION

The U.S. Geological Survey (USGS) is carrying out a probabilistic seismic hazards analysis (PSHA) for Yucca Mountain, Nevada as part of the Department of Energy's (DOE) project to characterize this site as a potential geologic repository for high-level radioactive waste. This study was initiated in April 1995 and resumed in June 1996. The aim of the analysis is to provide the annual probability with which various levels of vibratory ground motion and fault displacement will be exceeded at the site. These results will be used as a basis for developing seismic design inputs and in assessing the performance of the site.

The PSHA process involves development by two panels of experts of input interpretations and assessments of uncertainties required by the hazards calculations. One panel addresses characterization of seismic sources and fault displacement, while the other deals with vibratory ground motion. Development of interpretations is being facilitated through a series of structured workshops to evaluate available data, to explore the range of interpretations allowed by the data, to examine critically the interpretations proposed by the experts, and to provide feedback on the implications of various interpretations for the seismic hazard at the site. This report summarizes the third in the series of structured workshops for characterization of seismic sources and fault displacement: the Field Trip and Workshop on Alternative Models and Interpretations.

The primary goal of the field trip and workshop was to discuss alternative models, hypotheses, and interpretations that are important to the characterization of seismic sources for vibratory ground motion hazard and fault displacement hazard. The discussions allowed for all of the members of the panel to gain a better understanding of the technical bases for each model, to hear the pros and cons of the alternatives, and to better understand the uncertainties associated with each model. In addition, the field trip allowed experts to observe both surface and subsurface exposures at many key sites, providing first-hand insights into the limits on resolution and uncertainties associated with the field data and interpretations.

To accomplish the above goals, the approach taken was to provide a forum, both in a meeting setting and a field-trip setting, for structured debate of the alternative models and interpretations of importance to the seismic source characterization (SSC). Various individuals, including some members of the expert panel, played the role of "proponents" in presenting arguments in favor of a particular model or interpretation. The experts on the panel, as "evaluators", were encouraged to probe and technically challenge the proponent positions in an effort to better understand the positions, the available supporting data for each

position, and the associated uncertainties. The field trip included 2½ days of field review and discussion focusing on: 1) the behavior of faults in the Yucca Mountain vicinity; 2) the nature of faulting in the potential repository block; and 3) the behavior of the Bare Mountain fault. The workshop discussions entailed presentations and discussions centered around five key issues of importance to the ground motion and fault displacement hazard: tectonic models, three-dimensional geometry of faults, definition and synchroneity of faulting events, characterization of faulting in the repository, and maximum background earthquakes.

The agenda is included as Attachment 1 and it contains a map showing general locations of most field trip stops. Copies of overhead transparencies shown by presenters and additional material distributed during the workshop are included as Attachment 2. Table 1 is a list of participants and their affiliations.

MONDAY, NOVEMBER 18, 1996

The first day of the field trip covered faults on the west side of Yucca Mountain in Crater Flat. The first stop was at Steve's Pass at the southern end of Crater Flat. Dr. John Whitney, the field trip coordinator, gave a brief introduction and outline of the trip. The itinerary was constructed to highlight major issues in interpreting field data and provide a representative sampling of the range and variability of the data. At all of the sites with trench or natural exposures, excavations were still accessible and participants were given the opportunity to observe exposures first hand throughout the trip. Next, Dr. Christopher Fridrich provided a brief overview of the geology of Yucca Mountain, Crater Flat, Bare Mountain, and Black Marble Hill, including eruption of the nearby Timber Mountain and Silent Canyon calderas.

The second stop was at a trench site along the southern Crater Flat fault. Dr. Emily Taylor presented results from Trenches SCFF1 and SCFF1a, including evidence for three surface-faulting events that caused 24 to 65 cm of total vertical slip during the past 250,000 years. Dr. Taylor pointed out uncertainties and alternative interpretations, particularly for Trench SCFF1. Dr. Whitney pointed out possible structural relationships and coseismic rupture between the southern Crater Flat and Windy Wash faults. He also pointed out that deposits associated with the penultimate event on the southern Crater Flat fault contain basaltic ash and this fault may have ruptured with other faults at Yucca Mountain in addition to the Windy Wash fault, as outlined for Scenario U of the rupture scenarios presented in Chapter 5 of the Seismotectonic Synthesis Report.

The third stop was at the Windy Wash fault where Dr. Whitney discussed long-term net slip rates (with 5:1 vertical to horizontal slip ratios) of 0.027 mm/yr derived from offset of a 3.7 Ma basalt flow. He compared these to shorter-term vertical slip rates determined at trench site CF2, to the north, for the past 300 ka that are 0.011 mm/yr. The differences imply that either rates of activity have decreased through time, or perhaps the Windy Wash fault merges

down-dip with the Fatigue Wash and Solitario Canyon faults and extension on the Windy Wash fault to the south is accommodated by all three faults to the north. He also pointed out the coincidence of renewed extension with basaltic volcanism in Crater Flat.

The fourth stop was at trenches CF2 and CF3 on the Windy Wash fault. Dr. Whitney discussed evidence for 7 to 10 faulting events during the past 400,000 years. He clarified that offsets measured were vertical separations and not net slip values. However, geomorphic relations suggest any component of late Quaternary horizontal slip is small. Regardless, he believes the slip rates to be fairly robust and the greatest uncertainties in the paleoseismic record at this site to be in possibly missing small events and the ages of events, particularly older events.

Next, an unscheduled stop was made where the road crossed a fault scarp of the Fatigue Wash fault, so that the SSC experts could observe the relatively subtle geomorphic expression of most faults at Yucca Mountain. Dr. Daniel Soeder provided a brief overview of the stratigraphy of the Paintbrush Canyon Tuff visible in a nearby ridge.

After lunch, at the sixth stop, Mr. Alan Ramelli presented results from Trench T3 on the Solitario Canyon fault. Two large fissure fills provide evidence for two surface-faulting events in the past 700,000 to 900,000 years, with a very long hiatus in activity for about 500,000 years. The younger fissure fill contains a thick section of basaltic ash and Mr. Ramelli emphasized the possibility that the Solitario Canyon fault may have ruptured with the Windy Wash and Southern Crater Flat faults during this "ash event", as discussed previously by Dr. Whitney.

The seventh stop was at Trench T8, north of Trench T3, on the Solitario Canyon fault. Participants split into two groups. Dr. James Brune led one group to the top of a nearby ridge to observe a precariously balanced rock in the footwall, and very close to the trace, of the Solitario Canyon fault. Precariously balanced rocks along the fault suggest that although there is equivocal evidence for Holocene events on the Solitario Canyon fault, if these events occurred, they must have been fairly small. Mr. Ramelli presented his results for Trench T8 to the other group. The paleoseismic record at Trench T8 is similar to that at Trench T3, with suggestive evidence for two possible additional events at T8.

The next stop was an unscheduled stop at a precariously balanced rock north of Trench T8. Dr. Brune discussed results from his studies that suggest that north-south directed horizontal ground accelerations in the area have not exceeded 0.2 g during the past 10,000 to 20,000 years, based on ^{14}C-dating of rock varnish on rock pedestals and measurements of the force required to topple balanced rocks.

The last stop of the day was at Trench T4 on the Solitario Canyon fault. Mr. Ramelli first discussed the trench exposure. Of the two fault traces at this site, only the westernmost trace shows evidence for Quaternary activity, with two fissure fills that are similar to, but smaller than those in Trench T8, indicating that displacement is dying out to the north. Drs. Christopher Potter and Warren Day discussed some of the results of their bedrock mapping along the Solitario Canyon fault. They discussed deformation patterns of block-bounding, intrablock and bridging faults.

After dinner, an evening workshop session on tectonic models and their implications was convened. Dr. Christopher Fridrich presented his data and interpretations on the Late Cenozoic tectonic evolution of the Crater Flat basin. He distributed preprints of two related papers. He defined structural domains in the region and described chronologically the tectonic development of the Crater Flat basin from 13 Ma to the present. He estimated the percent of extension for two tectonic models: a tilted-block model and combination listric fault and tilted-block model. He discussed spatial and temporal patterns of extension rates, and implications for tectonic models from observed deformation patterns.

Next, Dr. Rich Schweickert presented his model for a major strike-slip fault system in the Yucca Mountain region. He proposed that a 250-km-long zone of dextral simple shear extends from Amargosa Valley, through Crater Flat and Yucca Mountain, continuing northwest of the Timber Mountain caldera. He described the fault system and outlined the evidence for it, emphasizing the caveat that the data are only permissive for his model. He proposed a geometry for the fault system after a model originally proposed by Hardyman and Oldow (1991), that kinematically links normal and oblique-normal faults at the surface with a detachment and strike-slip fault at depth. He then highlighted some of the tectonic implications of his model that are relevant to seismic hazards in the region.

The third speaker was Dr. Warren Hamilton, who presented a rolling hinge tectonic model for Yucca Mountain. He first described the model in general, emphasizing that the model explains how low-angle normal faults cutting steeply-dipping beds can evolve from initially high-angle normal faults cutting flat-lying beds. He provided examples of low-angle normal faults in the surrounding region (the Funeral and Whipple Mountains), highlighting characteristics of these fault systems that fit the rolling hinge model. Finally, he described how the rolling hinge model may apply to the Yucca Mountain region and highlighted structural features and aspects of the tectonic history that fit the rolling hinge model.

Next, Dr. John Stamatakos gave Dr. David Ferrill's presentation on their tectonic studies of Bare Mountain and Crater Flat, as Dr. Ferrill was absent on jury duty. Dr. Stamatakos first presented data and interpretations on the uplift and tilting history of Bare Mountain. He then summarized their interpretation of significant Tertiary tectonic events at Bare Mountain,

highlighting tilting to the northeast, no observed vertical axis rotation, greater uplift to the south, and some differences in the timing of uplift with previous presentations. He then presented data and interpretations in the geometry and structural style of the Bare Mountain fault and faults in Crater Flat, culminating in two models represented by balanced cross-sections. In both models, the Bare Mountain fault is listric, but one model shows a detachment fault cut-off by the Bare Mountain fault at about 5 km whereas in the other model, the Bare Mountain fault soles into a detachment fault at about 10 km. He noted that he would discuss the models and their key points further in his presentation on Wednesday.

Dr. Mark Tynan wrapped up the evening session with a brief introduction and overview of the Exploratory Studies Facilities (ESF) to prepare everyone for the trip into the tunnel the next day (Tuesday).

TUESDAY, NOVEMBER 19, 1996

The field trip on Tuesday focused on faulting in the Yucca Mountain block and on the east side. It consisted of two main components: a trip into the ESF tunnel to view subsurface exposures of the Yucca Mountain block, and visits to various surficial exposures along the Ghost Dance, Bow Ridge, and Paintbrush Canyon faults. Because of logistical constraints on the ESF trip, participants split into two groups. Group 1 visited surficial exposures in the morning while Group 2 visited the ESF tunnel. In the afternoon, Group 2 visited surficial exposures while Group 1 visited the ESF tunnel.

The ESF trip began with an introduction by Dr. Steve Beason who distributed handouts including maps and some summary data. After safety training and an introductory video, participants were outfitted with safety gear and proceeded into the tunnel. The excursion was led by Dr. Beason who was assisted by Dr. Robert Lung. Stops were made at key exposures of faults, fractures, cooling joints, and tilted beds, to allow direct observations and discussion of the exposures.

Some highlights of the trip included: 1) the 2-m-wide Bow Ridge fault; 2) smaller intrablock reverse and normal faults, some of which are identified at the surface and some of which are not; 3) cooling joints and small faults accommodating settling during cooling; 3) breccia in the imbricate fault zone at station 5+50 m; 4) the Drill Hole Wash fault; and, 5) the Ghost Dance fault. Throughout the trip, discussions focused on the character and style of deformation; density, distribution and origin of structural features; correlations with observations of structures at the surface; and the tectonic and seismogenic significance of the features. The ESF visit ended at about station 42+50 m due to respirator requirements beyond this point.

Visits to surficial exposures on Yucca Mountain started at Trench 14D on the Bow Ridge fault. For Group 2, Dr. Christopher Potter and Dr. Whitney presented results of paleoseismic investigations for Dr. Christopher Menges, who was in the ESF tunnel with Group 1. They presented evidence for at least two, probably three surface-faulting events since before 250,000 to 340,000 years ago, with a total net slip of 60-70 cm, resulting in a slip rate of 0.003 mm/yr. Slickensides rake 47° to 67° SW and displacements are 20 to 25 cm for each event. The most recent event occurred before ~50 ka and the penultimate event occurred between 140 and 150 ka. Dr. Potter also described nearby along-strike variations in the character of the Bow Ridge and small subsidiary faults that they had observed during their mapping.

The next stop was where Split Wash crosses the Ghost Dance fault. Dr. Potter discussed their detailed bedrock mapping in the area, emphasizing differences with previous interpretations by Spengler and others, particularly that Dr. Potter and his colleagues do not interpret the Sundance fault to be a through-going fault that offsets the Ghost Dance fault based on nearby continuous exposures of volcanic tuff beds. Dr. Whitney then presented results from Trenches 4a, 4b and 4c, located in Split Wash across the projection of the Ghost Dance fault. These trenches were excavated to see if older, buried Quaternary deposits in the wash were faulted. Dr. Whitney pointed out that no faults were exposed in Trenches 4b and 4c, only unfaulted late Quaternary alluvium and colluvium; whereas some bedrock fractures that are probably not part of the Ghost Dance fault were exposed in Trench 4a. Uncertainties in interpreting faulting history from the exposures were discussed.

The next stop was at the Antler Ridge pavement, an excavated bedrock surface which exposes the Ghost Dance fault. Dr. Potter described how this exposure in the Tiva Canyon Tuff was made and the characteristics of the Ghost Dance fault. Next, Dr. Whitney presented findings in two nearby trenches (Trench 5 and 5a) excavated in alluvium burying the Ghost Dance fault. Although suggestive evidence for a possible Quaternary fracturing event was found in Trench 5, they found no evidence for Quaternary fracturing in Trench 5a.

The next stop was at a trench exposure on the Ghost Dance fault in bedrock at the top of Whaleback Ridge. Dr. Potter described characteristics of the Ghost Dance fault determined from mapping and next Dr. Whitney presented results from cosmogenic isotope studies of the ridge surface, which suggests that the ridge morphology is about 500,000 years old. He also discussed Dr. Emily Taylor's interpretation of the faulting history based on the trench exposure. They found no evidence for any Quaternary events on the Ghost Dance fault at this site, in contrast to work at this site by Dr. John Bell, who next presented his interpretation. Dr. Bell found suggestive evidence for a possible Quaternary fracturing or small faulting event that occurred after 400 to 500 ka. Just south of Whaleback Ridge, we visited another

bedrock exposure of the Ghost Dance fault at the UZ 7a drill pad. Dr. Potter pointed out the distinct breccia zones that are probably related to different periods of faulting.

At the end of the day, the two groups rendezvoused at the top of Yucca Crest. Dr. Potter described characteristics of the Paintbrush Canyon fault and associated faults, visible to the east along Fran Ridge. For those who had not visited the exposure of the Paintbrush Canyon fault at Busted Butte, Dr. Whitney described this exposure and summarized the paleoseismic record, which is one of the longest and most complete faulting records in the Basin and Range province. (Note: some of Group 1 had split off to visit the Busted Butte exposure before meeting at Yucca Crest.) Finally, using the global vantage point, Dr. Whitney briefly recapped the field trip.

WEDNESDAY, NOVEMBER 20, 1996

Wednesday was divided into a morning workshop session on constraints on tectonic models, and an afternoon field trip to Bare Mountain.

Dr. Dennis O'Leary set the stage for the morning workshop by generally discussing structural constraints on tectonic models. He outlined four general constraints: 1) the extent of knowledge relative to the complexity of the object one is attempting to model; 2) the model should account for observed physical phenomena; 3) the model should contain key structural features with certain properties and histories; and 4) the model should contain realistic material properties and mechanical behavior. Throughout his presentation, he elaborated on aspects of these constraints particularly relevant to Yucca Mountain and highlighted caveats in developing various tectonic models. This included key points (with pros and cons for Yucca Mountain) for: detachment, pull-apart, strike-slip, and caldera tectonic models.

Next, Dr. Stamatakos presented fundamental geological observations from their studies and key points of their finite-element modeling and balanced cross-sections of the Bare Mountain fault. Dr. Stamatakos also distributed summary material and excerpts from their Type 1 fault study, but he did not discuss this material as their final report is still forthcoming. Key points to their tectonic models include: 1) listric faults (depth for curvature on the Bare Mountain fault is 5 to 15 km); 2) dominantly dip slip; 3) displacements and fault dip increasing to the south; and 4) minimum depth of 5 km for any detachment fault. His presentation concluded with questions from the experts and discussions of specific constraints and assumptions in the models. He emphasized that the surficial mapping data they used for the Yucca Mountain area was outdated (Scott and Bank, 1984) and that it would be beneficial to revise the cross-sections, incorporating new mapping data by Day and others (in press; distributed at the last workshop).

Dr. Thomas Brocher gave the next presentation on implications from seismic reflection data for high angle faulting in the shallow crust at Yucca Mountain. He re-emphasized that based on distinctive zones of truncated reflectors, the Bare Mountain fault appears planar to a depth of 6 to 7 km, dipping 65°E. He also emphasized that west-dipping faults at Yucca Mountain appear relatively planar and high-angle, which is in general agreement with interpretations by Lawrence Berkeley National Laboratories (LBNL) in their seismic reflection studies. He then reiterated that a major difference between the USGS and LBNL interpretations was the USGS proposes large offsets of the Tertiary-Paleozoic contact along the Ghost Dance and Solitario Canyon faults based on their interpretation of the seismic data, whereas LBNL interprets the Tertiary-Paleozoic contact to be fairly smooth with only small offsets across these faults based largely on gravity models. Finally, Dr. Brocher discussed implications for a ~12-km depth of the seismogenic crust based on seismic data, seismicity data, thermal constraints, and rheologic models.

After the break, Dr. John Bell presented results and tectonic implications from recent and ongoing fault studies conducted by the Nevada Bureau of Mines and Geology. He discussed the newly recognized east Lathrop Cone fault, the poorly understood West Dune Wash fault and several, small, down-to-the-east faults. He also pointed out how some of their interpretations for the paleoseismic history of the Ghost Dance, Bare Mountain and southern Solitario Canyon-Windy Wash faults differed from other investigators (these differences were discussed in more detail during the field trip). Finally, he highlighted aspects of the 1932 Cedar Mountain earthquake that are significant to seismic source characterization at Yucca Mountain.

Next, Dr. Robert Smith presented his insights into seismotectonic issues for normal faults, focusing on examples from the Basin and Range province and the Intermountain seismic belt. These included: 1) the caveat that many big earthquakes nucleate below the brittle-ductile transition and so we could be underestimating rupture area and seismic moment; 2) the need to consider viscoelastic deformation and long-term behavior because a significant component of the surface deformation we observe may not be coseismic; 3) the need to better understand relationships between volcanism and extensional tectonism; 4) observations of contagion behavior and triggered slip; 5) the need to consider both historic seismicity and geodetic data as contemporary strain indicators; and 6) some issues in using scaling relationships to estimate earthquake magnitudes. He provided abstracts for many references and also gave a brief introduction to application of finite and boundary element modeling to investigate normal fault interactions. This stimulated discussion among the experts of triggered slip on faults.

Next, Dr. Coppersmith facilitated a discussion of the implications of tectonic models to seismic source characterization. Discussion centered around: 1) what are the major earthquake sources at Yucca Mountain?; 2) what is the current role of Yucca Mountain faults (are they seismogenic and is activity waxing or waning)?; 3) issues of fault-rupture continuity, segmentation and distributive faulting; and 4) issues of slip rates and earthquake recurrence.

The afternoon was devoted to a field trip to Bare Mountain. The first stop was at the Tarantula Canyon trench site on the northern Bare Mountain fault. Mr. Larry Anderson presented results from their mapping and trench studies, providing an overview of the fault and the site geology, discussing their paleoseismic interpretations, and highlighting differences with previous studies. Mr. Anderson provided handouts, including a paper on the Beatty scarp and a comment paper on work by Ferrill *et al.* (1996) submitted to GEOLOGY. Next, Dr. Bell discussed their unpublished interpretations of the paleoseismic record at this site, which includes two surface-faulting events that occurred post-Q2 (post roughly 150 ka), in contrast to the one event interpreted by Mr. Anderson. In both interpretations, 1.5 m of vertical slip occurred during this time so the differences do not affect slip rate, only paleomagnitude estimates, recurrence intervals and rupture behavior.

The next stop was at the southern end of the Bare Mountain fault at the Sterling site and trench BMT-3. Mr. Anderson presented evidence for two late Pleistocene surface-faulting events, vertical slip rates of 0.01 mm/yr, and near-surface fault dips of 60° to 65°. Next, Dr. Bell discussed how their interpretations differed for this site, with an additional post-Q2 surface-faulting event, similar to the Tarantula Canyon site. Finally, Dr. Stamatakos discussed evidence for long-term uplift rates on the Bare Mountain fault that are higher by at least a factor of 3 than the shorter-term slip rates determined from the paleoseismic record, including 30 m of subsidence of a surface at the southern end of the fault thought to be about 1 Ma.

The last stop of the day was at an exposure near the Gold Ace Mine on the west side of Bare Mountain. Dr. Stamatakos pointed out that although the Gold Ace Mine fault is pre-Miocene, exposures like this provide analogues for what Paleozoic rocks might look like under Yucca Mountain. Their studies indicate that a dominant set of northeast-striking faults have a high slip tendency in the present stress regime and these faults may be prime candidates for non-surface faulting earthquakes in the region.

THURSDAY, NOVEMBER 21, 1996

The workshop sessions on Thursday focused on three issues: the synchroneity of faulting events, the characterization of future faulting in the repository, and the maximum background earthquake. Mr. Ramelli began the session on synchroneity of faulting events with a

presentation on basaltic ash exposures and evidence for a distributed late Quaternary surface-faulting event at Yucca Mountain. He discussed the location, character, age, interpretations and implications of ash exposures at several localities along many of the faults (southern Windy Wash, Fatigue Wash, Solitario Canyon, Bow Ridge, Stagecoach Road, and Paintbrush Canyon). He pointed out problems with absolute dating, and uncertainties in interpreting certain exposures and the potential involvement of corresponding faults. He also discussed the implied association of volcanism and faulting, and suggested possible explanations for the interaction of volcanism and faulting. A discussion then followed on any evidence for faulting south of Lathrop Wells and Mr. Ramelli pointed out that he and Dr. Bell were planning to finalize their fault map by the January workshop (a draft map was included with Dr. Bell's presentation package).

Next, Dr. Whitney discussed event rupture scenarios presented in the Seismotectonic Synthesis Report and implications to earthquake recurrence, maximum magnitudes and slip rates. Dr. Whitney outlined nine reasons in favor of distributive faulting at Yucca Mountain. He discussed the effects of various rupture scenarios on the slip rate data, which are generally negligible due to the long-term nature of the data. He also discussed the effect on recurrence and magnitude estimates, highlighting the trade-off between decreasing recurrence values and increasing maximum magnitudes for distributive faulting, depending on how magnitudes are calculated.

Dr. David Schwartz then gave the first presentation in the session on characterization of future faulting in the repository. He discussed various coseismic slip models and various issues in generally characterizing fault displacement, including: 1) observations of slip at a point versus along-strike slip distributions for a fault; 2) precision and uncertainties of surface and trench data; 3) whether single-event displacement measurements at the surface are representative of the slip at depth; 4) complexity of displacement patterns near segment boundaries and where faults overlap; and, 5) variations in displacements at a point for successive events. In regards to the last issue, he presented preliminary findings from a worldwide database that indicate characteristic behavior is dominant but not universal.

Next, Dr. Potter discussed the nature of fault interactions at Yucca Mountain. He first described characteristics and displacement histories for block-bounding faults, focusing on the Bow Ridge and Solitario Canyon faults. He next described interactions between block-bounding faults and northwest-striking faults. He also noted that many of the faults post-dated most of the tilting. Finally, he summarized key points on deformation in the potential repository area.

Dr. Donald Sweetkind gave the next presentation on the fracture network at Yucca Mountain and correlation between surface and subsurface structures. He described joint networks and

discussed how discontinuous faulting is accommodated on pre-existing cooling joints. He explained that correlations are generally good between surface and subsurface mapping of structures, giving many examples. He also pointed out a few examples where correlations were poor and discussed factors affecting correlations. He noted that isotope studies indicate a connected structural pathway of cooling joints and small-scale faults, corroborating the complex interactions observed in mapping studies.

Next, Dr. Frank (Bert) Swan presented results from their fault studies in Midway Valley and discussed implications for fault displacement at Yucca Mountain. He first discussed intrablock faults in Exile Hill. He then discussed characteristics, origin and history of fractures exposed in trenches in Midway Valley. Key points included: 1) fractures show a variety of orientations, but those extending into Quaternary alluvium dominantly strike north-northeast; 2) no detectable displacements were observed; 3) fractures could be tectonic or nontectonic; 4) fractures associated with the Exile Hill fault do not extend into Quaternary deposits; and, 5) evidence exists for repeated fracturing events on some features but all fractures terminate below Qa4 alluvium (estimated to be 30 to 100 ka). Finally, based on intrablock fault analogies, he highlighted possible implications for the faulting and fracturing history of the Ghost Dance fault.

Next, Dr. Silvio Pezzopane presented results from additional work on his study of historic surface-faulting earthquakes in the Basin and Range province. This work was stimulated by discussion at SSC Workshop #2. He reviewed the data and approach and described various scaling relations. These included scaling between: 1) moment magnitude and maximum surface-rupture width; 2) moment magnitude and the ratio of maximum primary displacement to maximum secondary displacement; 3) moment magnitude and the ratio of average primary to maximum secondary displacement; 4) maximum lengths of primary and distributed surface ruptures; 5) moment magnitude and maximum length of distributed rupture; and, 6) maximum lengths of distributed and principal rupture. He also analyzed the along-strike location of maximum fault parameters and the spatial relation of the length of distributed faulting to the principal rupture. He also described relations among maximum secondary rupture length, displacement, and moment magnitude. Finally, he concluded with miscellaneous ideas on various tectonic and paleoseismic issues.

After lunch, Dr. Coppersmith outlined what is next for the SSC experts, emphasizing what is expected of them by the next SSC workshop in January 1997. This included preliminary evaluations of five key issues, which were detailed in a handout.

Next, Dr. Pezzopane gave a presentation on minimum faulting earthquakes and maximum background earthquakes in the Great Basin. He analyzed the geologic effects (except liquefaction) associated with 100 historic earthquakes, including the frequency of surface-

faulting and cracking as a function of magnitude. He also developed a model for the average and maximum background earthquake that is dependent on rupture area (both shape and size).

Dr. Coppersmith gave the next presentation for Dr. Robert Youngs on some skeletal advice from the Fault Displacement Working Group regarding methodologies for characterizing fault displacement. He described required products, necessary data and interpretations, possible approaches, and differences between SSC for fault displacement and ground motion. He discussed models for characterizing the length of rupture and amount of displacement within the repository. He also discussed considerations for characterizing displacement at various designated points. Dr. Swan clarified how the Working Group envisioned this might be done to allow assessments for different teams to be easily compared.

The next presentation was by Mr. Wong on assessing the contributions from background earthquakes at Yucca Mountain. He pointed out that his assessment of the background earthquake for the ESF study conflicts with results from studies of precariously-balanced rocks and their assessment may be too conservative due to assumptions and simplifications made in modeling the background earthquake. He highlighted the significant issues and presented results from a recent study for the Waste Handling Building, including sensitivity analyses of recurrence of maximum background earthquakes.

Next, Dr. Allin Cornell gave a brief unscheduled presentation on background earthquakes and uncertainties in the Yucca Mountain region. He discussed problems with using the "standard background model" typically used in western U.S. hazard studies at Yucca Mountain where faults are better known, without consideration as to the resolution and detail of available information. He emphasized considering resolution of the data in developing background earthquake zones for Yucca Mountain.

Mr. Craig dePolo gave the final presentation of the workshop on determining the size of the maximum background earthquake. He clarified his definitions of primary and secondary faulting and discussed magnitudes for some historic Basin and Range earthquakes. He highlighted the observed overlapping magnitude ranges for non-surface rupturing, secondary surface-rupturing, and primary surface-rupturing events.

Finally, Dr. Coppersmith opened the floor to observers for comments and questions. Dr. Leon Reiter had several comments, including: 1) given the new configuration proposed for the repository block, the Nuclear Waste Technical Review Board is concerned with the need for additional subsurface data, and consequently, they believe that an E-W drift in the ESF would be very valuable; 2) he hopes that the SSC experts give due attention to the northeast splay of the Solitario Canyon fault that extends into the proposed repository block; 3) the importance of avoiding inconsistencies (including with other project data and models) in

developing SSC assessments; and 4) a useful approach in evaluating models is to try and disprove them. Dr. Bakr Ibrahim commented that he appreciated the extensive efforts made in discussing uncertainties and he thought that the geophysical data needed to be better incorporated with the geologic mapping data in developing structural models for the repository block. Next, Dr. Thomas Hanks commented that there was a lot of discussion about the size of background earthquakes but what about rates of recurrence? He also emphasized that characterizations of background and fault-related earthquakes need to be consistent with each other and given careful consideration as to how they are integrated. Dr. Richard Parizek asked about the significance of the apparent randomness of seismicity around the site and Dr. Coppersmith clarified that it is up to the experts to make any determination about this. Dr. Parizek also wondered if the issue of the southern extent of Quaternary faults at Yucca Mountain would be one of the issues covered by the experts and Dr. Coppersmith explained that this would be covered as part of the issue related to defining geometry of earthquake sources. Finally, Dr. Mark Tynan commented that the Geophysical Synthesis Report, the synthesis report on surface fracture data, and some of the ESF mapping and subsurface fracture data are available for the SSC experts. He also mentioned that Dr. Day would be producing cross-sections from the 3-D structural model of the repository block that will be made available to the expert panel. The workshop was adjourned around 4:00 pm.

TABLE 1. YUCCA MOUNTAIN SEISMIC SOURCE CHARACTERIZATION FIELD TRIP AND WORKSHOP ON ALTERNATIVE MODELS AND INTERPRETATIONS

November 18-21, 1996

Attendance List

Name	Affiliation
1. Abrahamson, Norm	Consultant
2. Ake, Jon	U.S. Bureau of Reclamation (USBR)
3. Anderson, Ernie	U.S. Geological Survey (USGS)
4. Anderson, Larry	USBR
5. Arabasz, Walter	University of Utah (UU)
6. Bell, John	UNR
7. Biggar, Norma	WCFS
8. Brocher, Tom	USGS
9. Bruhn, Ron	UU
10. Brune, James	UNR
11. Coppersmith, Kevin	Geomatrix
12. Cornell, Allin	Consultant
13. Day, Warren	USGS
14. dePolo, Craig	UNR
15. Doser, Diane	University of Texas, El Paso
16. Fridrich, Chris	USGS
17. Hamilton, Warren	Colorado School of Mines
18. Hanks, Tom	USGS
19. Ibrahim, Bakr	U.S. Nuclear Regulatory Commission (NRC)
20. Justus, Phil	NRC
21. King, Jerry	M&O/SAIC
22. Knuepfer, Peter	State University of New York at Binghamton
23. McCalpin, Jim	GEO-HAZ Consulting, Inc.
24. McGuire, Robin	Risk Engineering
25. Menges, Chris	USGS
26. O'Leary, Dennis	USGS
27. Olig, Susan	Woodward-Clyde Federal Services (WCFS)
28. Parizek, Richard	Technical Review Board
29. Penn, Sue	WCFS
30. Perman, Roseanne	Geomatrix
31. Pezzopane, Silvio	USGS
32. Pomeroy, Paul	Advisory Committee on Nuclear Waste

TABLE 1 (CONT). YUCCA MOUNTAIN SEISMIC SOURCE CHARACTERIZATION FIELD TRIP AND WORKSHOP ON ALTERNATIVE MODELS AND INTERPRETATIONS

November 18-21, 1996

Attendance List

Name	Affiliation
33. Potter, Chris	USGS
34. Quittmeyer, Richard	WCFS
35. Ramelli, Alan	UNR
36. Reiter, Leon	NWTRB
37. Rogers, Al	EQE International
38. Savino, John	SAIC
39. Savy, Jean	Lawrence Livermore National Laboratory
40. Schwartz, David	USGS
41. Schweickert, Rich	UNR
42. Slemmons, Burt	WCFS
43. Smith, Ken	UNR
44. Smith, Robert	UU
45. Soeder, Daniel	USGS
46. Stamatakos, John	CNWRA
47. Stepp, Carl	WCFS
48. Stuckless, John	USGS
49. Sullivan, Tim	DOE
50. Swan, Bert	Geomatrix
51. Sweetkind, Don	USGS
52. Taylor, Emily	USGS
53. Toro, Gabe	Risk Engineering
54. Tynan, Mark	DOE
55. Engelbrecht von Tiesenhausen	Clark County Nuclear Waste Division
56. Whitney, John	USGS
57. Wong, Ivan	WCFS
58. Yount, Jim	UNR

Civilian Radioactive Waste Management System
Management & Operating Contractor

Summary of Seismic Source Characterization Preliminary Interpretations Workshop

SSC Workshop 4

Salt Lake City, Utah
January 6-8, 1997

Prepared for:

U.S. Geological Survey
Box 25046, MS-425
Denver Federal Center
Denver, CO 80225

Prepared by:

Woodward-Clyde Federal Services of the
Civilian Radioactive Waste Management System
Management & Operating Contractor
1180 Town Center Drive
Las Vegas, NV 89134-6363

January 31, 1997

INTRODUCTION

The U.S. Geological Survey (USGS) is carrying out a probabilistic seismic hazards analysis (PSHA) for Yucca Mountain, Nevada as part of the Department of Energy's (DOE) project to characterize this site as a potential geologic repository for high-level radioactive waste. This study was initiated in April 1995 and resumed in June 1996. The aim of the analysis is to provide the annual frequency with which various levels of vibratory ground motion and fault displacement will be exceeded at the site. These results will be used as a basis for developing seismic design inputs and in assessing the waste isolation and containment performance of the site.

The PSHA involves development by two panels of experts of input interpretations and assessments of uncertainties required by the hazards calculations. One panel (consisting of six teams of three experts) addresses characterization of seismic sources and fault displacement, while the other (consisting of seven individual experts) deals with vibratory ground motion. Development of interpretations is being facilitated through a series of structured workshops to evaluate available data, to explore the range of interpretations allowed by the data, to examine critically the interpretations proposed by the experts, and to provide feedback on the implications of various interpretations for the seismic hazard at the site. This report summarizes the fourth workshop in the characterization of seismic sources and fault displacement: the Seismic Source Characterization (SSC) Preliminary Interpretations Workshop.

The primary goals of the workshop were to: (1) provide an opportunity for the expert teams to present and discuss their preliminary interpretations regarding key issues in SSC; (2) train the expert teams on the process of elicitation and uncertainty characterization; and (3) present and discuss additional information and interpretations of importance to SSC at Yucca Mountain. To accomplish these goals, a series of presentations (primarily made by the SSC expert panel members) and group discussion sessions were conducted, with emphasis on interaction among the SSC experts. Five key SSC issues were identified: (1) tectonic models; (2) potential seismic sources; (3) maximum magnitudes; (4) earthquake recurrence; and (5) fault displacement methodology. For each of these issues, two teams of experts were assigned to present their preliminary interpretations. These presentations were followed by group discussion of each issue, during which time the other teams were given the opportunity to present their preliminary interpretations. The focus of the presentations and discussions was on understanding the interpretations, their technical bases, their consistency or inconsistency with data, and the expression of uncertainty. Discussion was facilitated to ensure that each team understood the interpretations of others, including the degree to which

they were supported by earthquake and faulting process models and observed data, and could then more knowledgeably re-evaluate their own team interpretations. The overall goal is for interpretations given at the upcoming elicitation interviews to be well-reasoned, technically-supported, and complete.

The workshop agenda is included as Attachment 1. Copies of overhead transparencies shown by presenters and additional material distributed during the workshop are included as Attachment 2. Table 1 is a list of participants and their affiliations.

MONDAY, JANUARY 6, 1997

The first day of the workshop included a series of presentations to provide additional information on a variety of specific issues outstanding from previous workshops. Kevin Coppersmith gave an introduction, describing the purpose and approach, and outlining the workshop agenda. He emphasized the overall goal was to prepare for the SSC elicitations such that the expert panel's interpretations were well-reasoned, technically-supported and complete. He also emphasized that team interpretations were still preliminary and experts should: feel free to explore the issues thoroughly, ask questions that will help them during the elicitations, and continually keep in mind the characterization of uncertainties. Miscellaneous questions about developing team assessments, scheduling elicitations, and the status of the historical seismicity catalogue were then discussed.

Next, Christopher Potter gave a presentation on the Sundance fault, reviewing previous studies from a historical perspective and discussing the evolution of interpretations as additional data were collected. In particular, he compared studies by Spengler et al. (1994) with those of Potter *et al.* (1995), describing in detail differences in scope, approach, products and results. He explained many differences in interpretations with site-specific examples from maps, highlighting one of the most significant differences was that although Spengler *et al.* (1994) interpreted the Ghost Dance fault to be offset by the Sundance fault by as much as 52 m, Potter *et al.* (1995) concluded that the Sundance fault did not even intersect the Ghost Dance fault based on mapping of continuous volcanic subunits. He pointed out probable causes for differences in interpretations, including the broader area covered by Potter *et al.* (1995), their emphasis on a geologic-based rather than engineering-based approach to defining rock units, and their mapping of several zones in the upper Tiva Canyon Tuff that provided good marker beds, which were not identified in the mapping used by Spengler *et al.* (1994).

Ernie Majer gave the next presentation on geophysical interpretations of the Yucca Mountain vicinity developed by Lawrence Berkeley National Laboratories (LBNL). Due to scheduling conflicts, Dr. Majer had not been able to attend earlier workshops to discuss the LBNL interpretation of these data. He described the data they used, including seismic reflection,

gravity, magnetics, magnetotellurics, and vertical-seismic-profile well data. He pointed out that their studies were summarized in the Geophysical Synthesis Report, which has been made available to the experts. He reviewed the LBNL interpreted cross-sections, laid out seismic lines for the experts to review, and highlighted key differences with geophysical interpretations developed by Thomas Brocher and his colleagues at the USGS. Dr. Majer had met with Dr. Brocher during the last month to discuss these differences, and he had concluded that alternative interpretations are permitted by the data depending on the data sets emphasized and the approach to modeling. After extensive discussion during several meetings with USGS personnel, Dr. Majer still believes that smaller offsets of the top of Paleozoic rocks across the Ghost Dance fault are more reasonable based on the LBNL modeling of the gravity data and considering the data from a 3-D perspective. He pointed out, some ways that processing of seismic data could be improved, and discussed the uncertainties associated with each type of data. He emphasized the difficulties inherent in applying geophysical methods at Yucca Mountain and concluded that without additional drill-hole data, or perhaps simultaneous inversion of gravity and seismic data, multiple geophysical interpretations are permitted by the data and should be considered by the experts when they express their uncertainties.

John Stuckless gave the next presentation on some hydrological and geochemical considerations for evaluating movement on the Ghost Dance, Solitario Canyon, and Paintbrush Canyon faults. He discussed how spatial variations in temperatures, oxygen isotopes, and carbon isotopes of aquifers at Yucca Mountain suggest that block-bounding faults (such as the Solitario and Paintbrush Canyon faults) may be acting as conduits between aquifers, but the Ghost Dance fault does not. He pointed out that the relief on Paleozoic basement rocks, as interpreted from gravity data, has a northeast trend and probably is not related to offset on the Ghost Dance fault, but could be related to "sealed" pre-Miocene faults or erosional paleotopography and may not even be fault-related. He concluded that the hydrological and geochemical data suggests that offsets of the top of Paleozoic rocks across the Ghost Dance fault are not significant and are smaller than offsets across the Solitario and Paintbrush Canyon faults.

Next, Dennis O'Leary discussed the Yucca Mountain faults in a regional context, focusing on the southern extent of faults and their relation to surrounding tectonic features. He reviewed characteristics of the four classes of faults and constraints on spatial and temporal patterns of extension. He discussed the southern extent of the Bare Mountain fault, the southern margin of the Crater Flat basin, and the extent and role of the inferred fault, based on the Bouguer gravity field gradient, that strikes north-south along the eastern margin of the Amargosa trough. He also discussed the Spotted Range-Mine Mountain fault system, the caldera complex, the Kawich Range faults to the north of the caldera, and a faulted block of rocks on the southern flank of Mid Valley that may be an appropriate structural analog for Yucca

Mountain. Dr. O'Leary's presentation stimulated much group discussion, including input from Burt Slemmons, John Whitney, Chris Fridrich, and Alan Ramelli on the southern extent of Yucca Mountain faults and faults east, west, and south of Bare Mountain.

The next presentation was given by Brian Wernicke on whether or not shallow-dipping normal faults (SDNF) generate significant earthquakes. He said his talk would largely follow the outline of a paper he recently published on this topic, and he provided reprints of the paper (Attachment 2). He described the apparent paradox about SDNF, that they are prominent and prevalent crustal-scale features that have accommodated significant amounts of brittle extension, and yet historical seismicity patterns and mechanical considerations suggest that SDNF are not seismically active and are not even capable of producing large earthquakes. He reviewed the limited number of historic, large normal-faulting earthquakes observed worldwide and presented kinematic and mechanical arguments as to why SDNF would have very long recurrence intervals. Thus, he argued that perhaps the general lack of observed large earthquakes on SDNF may be due to the historical record being too short. He also presented paleothermal interpretations for some SDNF in the Basin and Range province that suggest the faults initiated at a shallow dip, implying that they were active at a shallow dip and have not evolved from an active high-angle normal fault to an inactive SDNF. Dr. Wernicke then switched topics to review results from geodetic studies he worked on for the Center for Nuclear Waste Regulatory Analyses, which John Stamatakos had also presented at Workshop #2. At the end of Dr. Wernicke's presentation, there was discussion about the general lack of background seismicity on SDNF and the nature of a possible detachment under Yucca Mountain, which Dr. Wernicke believes is no longer active.

The final presentation of the afternoon was given by James Brune on studies of precarious rocks conducted by him, John Whitney, and associates at UNR, and their implications to paleoseismicity. He presented results from studies in southern California and Nevada of the spatial distribution of precarious rocks and their relation to (i.e. away from) major active faults and the area affected by NTS blasts. He showed examples of the many (~100) precarious rocks they had identified in the Yucca Mountain area and discussed age data that indicates all of the rocks they dated have likely been precariously balanced for longer than 10,000 years. He emphasized that these results have implications for longer recurrence of background earthquakes and the need to allocate some historical seismicity to faults in the area. He pointed out some new developments in thinking about ground motions since their report on precarious rocks was written, which was distributed to SSC experts (Attachment 2). He also presented results from a study of precarious rocks and ground motions from the Little Skull Mountain earthquake.

There were no comments from observers at the end of the day. Finally, the seismologists on the expert panel met to discuss issues related to the status of the seismicity catalogue. Ivan

Wong distributed handouts on preliminary magnitude conversions and completeness intervals for the catalogue (Attachment 2).

TUESDAY, JANUARY 7, 1997

Tuesday was devoted to team presentations and discussion of four of the key SSC issues: tectonic models, potential seismic sources, maximum magnitudes and earthquake recurrence. Dr. Coppersmith gave an introduction, outlining the issues.

Jim McCalpin gave the first presentation on tectonic models, representing the team of Jon Ake, Burt Slemmons, and himself. He said the models they considered were primarily based on Chapter 8 of the Yucca Mountain Seismotectonic Synthesis Report, which included caldera, detachment, volcanic, planar fault-block, and lateral shear models. He described the models, discussed their strengths and weaknesses based on tectonic processes, tectonic development of Yucca Mountain, and observed data; highlighted implications; and gave the team's preliminary assigned weights to the various models. He also discussed their preferred composite tectonic model which is based primarily on the planar fault model with integrated components of the lateral-shear and volcanic models. This stimulated discussion about one problem with the planar fault model; normal dip-slip on north-south striking faults does not appear to be consistent with strike-slip focal mechanisms and northwest-directed extension determined from historical seismicity data.

Robert Smith gave the next presentation, discussing his team's preliminary tectonic models. His other team members are Craig dePolo and Chris Menges. He outlined four classes of models prioritized by their preferability: half-graben (including planar and curved faults), detachment (not likely to be shallow), volcanism, and strike-slip. He highlighted relevant features of the Tertiary tectonic setting and relative variations in strain rates through time. He discussed necessary characteristics and considerations of seismotectonic models for Yucca Mountain, emphasizing constraints from geophysical and structural data, such as low contemporary strain rates (10^{-16}/s to 10^{-17}/s); seismogenic depths of 12 to 16 km; elastic thicknesses of 5 to 15 km, normal and strike-slip focal mechanisms that indicate northwest extension; and the closely-spaced complex, interconnecting nature of faults, many of which likely merge at depth and may be truncated by the Bare Mountain fault. He also discussed the transient aspects of the tectonic regime, which may be related to asperities in the lower crust causing transient loading rates on upper crustal faults. He also noted that stress-field rotations could lock-up structures, stimulating discussion about whether the stress-field is understood well enough to reliably conclude such structures are inactive.

During the discussion session that followed, Ernie Anderson presented a tectonic model, first proposed by Al Rogers to explain observed seismicity patterns, that relates oblique-slip on north-south-striking fault blocks to southward-directed translation of the blocks rather than

dextral shear. As many teams seemed to favor the half-graben/planar fault block model, John Whitney next brought up some information relevant to a question raised earlier regarding whether the sum of late Pleistocene slip rates on Yucca Mountain faults was comparable to the late Pleistocene slip rate observed on the Bare Mountain fault. Dr. Whitney, Dennis O'Leary, and Alan Ramelli all discussed indirect geomorphic and geophysical evidence for additional buried traces of the Bare Mountain fault to the one that is visible and was trenched at the surface. Thus, although this trace has definitely been the most active during the late Quaternary, slip rates determined solely from this trace may still be minimums for the entire fault zone. David Ferrill then reiterated the higher longer-term slip rates that he and his associates have interpreted along the southern Bare Mountain fault based on 30 m of subsidence of a basalt flow inferred to be one million years old. Finally, Dr. Coppersmith reviewed the tectonic models presented and some of the key points that were discussed.

Chris Fridrich gave the first presentation on potential seismic sources, representing the team of Diane Doser, Bert Swan and himself. Dr. Fridrich described five types of seismic sources they had considered: 1) background sources; 2) regional fault sources based on mapped Quaternary faults identified in the Seismotectonic Synthesis Report; 3) local Quaternary faults, including a three-fault segment rupture model; 4) a strike-slip shear zone, which may truncate the southern end of some Yucca Mountain faults; and 5) a detachment fault. They defined seven domains for the background sources within 300 km and three domains within 100 km: the northeastern Walker Lane, the southeastern Walker Lane, and the northern Basin and Range. Bert Swan asked if there were any additional faults other teams had considered and Craig dePolo mentioned the buried fault inferred from the Bouguer gravity gradient bounding the Amargosa trough and buried faults in Crater Flat. Dr. Swan clarified that they considered the latter to be included with background sources and explained that they would zone the maximum magnitude for the background domains using a lower magnitude centered around Yucca Mountain where the resolution for identifying and characterizing potential fault sources is better because of more detailed study.

Jim Yount gave the next presentation on potential seismic sources, representing the team of Larry Anderson, Al Rogers and himself. He began by mentioning some additional buried faults under Jackass Flats that they had wondered about either characterizing explicitly or including them implicitly in the background source. Kevin Coppersmith said that the former approach was probably better for all nearby faults because the specific geometry of a source can be significant to the hazard, whereas details of geometry become less significant as sources become more distant. Dr. Yount then described the three types of seismic sources that his team considered: fault, hidden/background, and volcanic. He defined the criteria they used for considering faults as potential sources and then listed potential fault sources with their assigned probabilities of being sources and the bases for the probabilities. Next, he discussed whether volcanic sources need to be considered as potential sources of earthquakes.

He pointed out that although previous volcanic studies by Crowe *et al.* (1995) concluded that there is not a causative relation between structure and volcanism, paleoseismic evidence for the "ash event" (Event U in Chapter 5 of the Seismotectonic Synthesis Report) indicates some faulting events are synchronous with volcanism, suggesting that volcanic seismic sources may need to be considered.

Next, Larry Anderson presented another approach to characterizing potential sources that they were also considering in addition to the fault-specific approach. This approach was motivated by the apparent random pattern of paleoseismic events on faults through time. It would treat Yucca Mountain as a faulted volume with a composite recurrence of earthquakes uniformly distributed on faults. Finally, Al Rogers discussed the team's two models for background source zones, both of which include three zones. One model determines recurrence solely based on the historical seismicity in each zone and the other model attempts to first remove some seismicity that may be associated with mapped faults before calculating recurrence for each zone.

Peter Knuepfer started the discussion session off with questions about the Ghost Dance and Sundance faults as potential seismic sources, which stimulated discussion about general criteria for defining sources and the specific characteristics of these faults. Allin Cornell reiterated his concern about misusing the background earthquake as a crutch in characterizing sources and Burt Slemmons pointed out that it may be worthwhile to specifically consider some buried sources such as possible Quaternary faults in Crater Flat that are indicated on seismic lines. Dr. Cornell further stated that the background zone should be considered as the expression of a team's uncertainty in its seismic source interpretations; that is, its uncertainty that all sources have been included in the interpretation.

Jon Ake gave the first presentation on maximum magnitudes, representing the team of Slemmons, McCalpin and himself. He pointed out that maximum magnitudes are dependent on tectonic models and definition of seismic sources. For estimating maximum magnitudes on fault sources, his team chose to use regression relations by Wells and Coppersmith (1994) that relate average displacement, maximum displacement, or surface-rupture length to maximum magnitude. He discussed some assumptions and prejudices, and the reasoning behind their approach. He said they had only looked at closer fault sources so far, which had raised some questions about characterizing uncertainties and concerns about some possible inconsistencies. This initiated discussion about the shortcomings of using their approach for closely-spaced, short faults with long recurrence intervals. Difficulties in assessing displacements with limited data were also discussed, along with apparent discrepancies between short fault lengths and larger than expected displacements. Kevin Coppersmith pointed out that of the three sources of uncertainty (statistical, process, and parameter), the latter was probably the greatest, but all need to be considered.

Craig dePolo gave the next presentation on maximum magnitudes, representing the team of Robert Smith, Chris Menges, and himself. He outlined the different approaches his team would use to estimate maximum magnitudes depending on the type of data available for each seismic source. Types of data included surface and possibly subsurface rupture length, average and maximum displacement, down-dip width (to determine area), and slip rate. He discussed many different regression relations they might use and the factors they would consider in weighting the different relations. Next, he discussed their approach to assessing the maximum background earthquake, which would likely be about M_w 6.3 (+0.3, -0.1). He also discussed the problem of potentially double-counting seismic moment when characterizing fault and background sources in the same area. Finally, Robert Smith brought up concerns about uncertainties in magnitude conversions to M_w, and possible systematic biases introduced during declustering of the seismicity catalogue.

Next, two unscheduled presentations were given by David Ferrill and James Brune. Dr. Ferrill presented results of laboratory deformation studies used as a physical analog for the development of pull-part basins. He discussed similarities and differences of features in the lab experiments to those observed at Yucca Mountain. He also reiterated results from their slip-tendency analysis of Yucca Mountain faults (presented by John Stamatakos at Workshop #2), emphasizing implications for a low-slip tendency on shallow-dipping faults. Dr. Brune also discussed results from laboratory modeling experiments. He pointed out that implications from his foam rubber models are that SDNF are much more mechanically stable than shallow-dipping reverse faults because of different dynamic effects, implying that SDNF are not likely seismogenic. Following the presentations was considerable discussion about complexities in using displacement data to estimate maximum magnitudes.

Diane Doser gave the first presentation on earthquake recurrence, representing the team of Chris Fridrich, Bert Swan and herself. She discussed how they planned to use the seismicity catalogue to calculate earthquake recurrence for their background source zones. She emphasized that there were many issues in preparing the catalogue and making the calculations and she highlighted some of these. Bert Swan then discussed how their team would characterize recurrence for fault sources. He said they would use a seismic moment rate approach, explaining how they would estimate slip rates for each of three different structural/behavioral models. He pointed out that they would try to calculate average net slip rates, using ratios of vertical to net slip of between 1:1 and 1:1.4. He also noted they would use three different recurrence models: models developed by Wesnousky *et al.* (1983), Schwartz and Coppersmith (1984), and an exponential model. Paleoseismic data on recurrence intervals would only be used as a "sanity check."

Larry Anderson gave the next presentation on recurrence, representing the team of Rogers, Yount, and himself. He focused on fault sources and had compiled a space-time diagram of

paleoseismic events on Yucca Mountain faults to assist in evaluating synchroneity of rupture behavior and estimating earthquake recurrence. He discussed estimated recurrence intervals for different structural and behavioral models, pointing out ambiguities and associated uncertainties in the paleoseismic record. Al Rogers then discussed their approaches to estimating earthquake recurrence for each of their two background earthquake models, outlining the steps they used in processing the seismicity catalogue and explaining how they would allocate seismicity to faults for one of the models.

During the following discussion session, Allin Cornell asked if any team had considered using a real-time approach, stimulating discussion about advantages and disadvantages of doing so and the data needed. Next, Tom Hanks expressed concern that some of the maximum magnitudes assigned to sources would result in forcing high stress-drop events to occur in a low stress-drop regime. He urged the experts to at least keep implications for stress drop in mind when developing their characterizations. Finally, Kevin Coppersmith asked for comments from observers. Clarence Allen pointed out that the relation of historical seismicity to mapped faults is problematic in many other areas in addition to Yucca Mountain. He also cautioned experts about the uncertainties in extrapolating observations of small earthquakes to make inferences about large earthquakes. Bakr Ibrahim expressed concern about whether triggered events were adequately being considered. Leon Reiter suggested to confirm whether or not results will be used for both pre-closure design and post-closure performance assessments, the latter making it especially important that low probability scenarios be included and carried through the analysis. Jerry King suggested that additional guidance regarding which faults at what distance needed to be considered would help the experts.

WEDNESDAY, JANUARY 8, 1997

The entire morning session was devoted to addressing the last SSC issue, developing methodologies for characterizing the fault displacement hazard. Walter Arabasz gave the first presentation on their approach to characterizing fault displacement, representing the team of Ernie Anderson, Alan Ramelli, and himself. He outlined premises to their approach and discussed their two types of sources, primary and non-primary. Their approach is to directly use displacement per event data wherever it exists and for other faults to use various scaling relations to estimate slip per event. He pointed out how fault aspect ratios generally observed for moderate to large earthquakes have implications for expected fault rupture lengths at Yucca Mountain, given a certain depth of rupture penetration and vice versa. He discussed scaling relations to estimate slip per event from length and cumulative slip, including some examples developed specifically for Yucca Mountain faults. He said they were considering both recurrence interval and slip rate approaches to incorporate the frequency of displacement events into the assessment. Finally, he mentioned how scaling

relations from Chapter 9 of the Seismotectonic Report can be incorporated into the methodology developed by Coppersmith and Youngs (1992) to assess displacement within the repository, particularly various characteristics of secondary displacement.

Next, Alan Ramelli discussed the spatial distribution of faulting within the proposed repository. He focused on issues of how does the potential for secondary faulting vary and what areas of different potential can be defined. Both he and Ernie Anderson described similarities of the Clover Mountain area, which they believe provides a structural analog to Yucca Mountain and may have implications for the shallow depth of penetration of some faults, particularly non-primary faults. Discussion followed about possible problems with using some of the scaling relations in an area where deformation rates are transient and much of the total throw occurred during the Miocene. Finally, Kevin Coppersmith emphasized that the methodologies developed by the experts need to be appropriate for the entire Controlled Area, not just the proposed repository.

Ron Bruhn gave the next presentation on their team's fault displacement methodology, representing the team of Ken Smith, Peter Knuepfer, and himself. He said that there would be two parts to their presentation, he would focus on the displacement aspects and Ken Smith would discuss assessing rates using historical seismicity and paleoseismic data. Dr. Bruhn then outlined the conceptual framework of their approach, which is based on statistical analyses used in mining engineering. He emphasized that their goal was to develop an algorithm for estimating the probability of exceedance of a specified displacement at a point within a rock mass without prior knowledge of the point, but given that certain statistical and structural properties of observed faults in the rock mass are known or can be estimated. He provided details of the technical description of his method in a handout. He outlined the general steps in his talk, highlighting assumptions and the data needed for each of the three steps. He discussed application to an analog repository in Leagerdorf, Germany. Finally, he emphasized they were still working on incorporating recurrence into the assessment and he discussed some of the issues and considerations related to both direct and indirect approaches. David Schwartz offered suggestions on using paleoseismic data from primary faults to provide maximum constraints on recurrence rates. Ken Smith then discussed their preliminary analysis of the seismicity catalogue and resulting recurrence curves both with and without the incorporation of paleoseismic data for Yucca Mountain faults.

After the break, Jim McCalpin presented an approach to characterizing fault displacement that entails developing probability density functions for fault density. He discussed issues and considerations in using available data to construct the curves for Yucca Mountain faults. Next, Robert Youngs, representing the Fault Displacement Working Group, presented what he referred to as the earthquake approach to characterizing fault displacement, which uses a displacement attenuation function for secondary faulting. He discussed how scaling relations

and data presented in Chapter 9 of the Seismotectonic Synthesis Report could be used to perform this type of analysis.

Throughout the morning session, there were questions raised about more specifically defining the fault displacement objective. During the discussion session, Carl Stepp emphasized that the primary need from the SSC teams is a methodology to predict fault displacement at any point in the Controlled Area given that a particular feature exists. Kevin Coppersmith elaborated by listing four things that the Seismic Design Team were looking for regarding fault displacement: (1) fault displacement hazard curves at selected locations; (2) fault dip and sense of slip; (3) the width over which displacement occurs on a fault; and (4) recommended methodologies for assessing displacements at other locations. Silvio Pezzopane presented a "strawman" selection of points and classes of features that should be represented by the points. John Whitney suggested adding a point in Midway Valley. After some discussion, it was decided that a list of the classes of features and a map of the selected points would be distributed to the experts shortly after the workshop (Attachment 2). Other topics discussed included aspect ratios of fault ruptures at Yucca Mountain, available displacement data for tunnels and mines elsewhere in the world, availability and access to ESF fault and fracture data, and the likelihood of future displacement on intrablock and other Tertiary bedrock faults which show no evidence for Quaternary faulting but for which Quaternary movement cannot be precluded. Also discussed were problems in predicting slip for future events based on a long-term displacement record (in some cases Miocene) in an area where displacement rates have varied significantly through time.

Just before lunch, Kevin Coppersmith outlined upcoming steps in the SSC elicitation process, which had already begun with each team's preparation of preliminary interpretations for this workshop. Next would be the elicitation interview and follow-up, with draft assessments due to the Calculations Team by March 10. Preliminary results would be presented at the Feedback Workshop, which was originally scheduled for April 16-18 but was moved up to April 14-16. After this last workshop, elicitation summaries would be finalized. Dr. Coppersmith emphasized that elicitations and development of the team's interpretations were an ongoing process that would continue until the final summary was written. He then asked for comments from observers. Leon Reiter commented on the need to know the resolution for all types of data and the importance of considering this in the assessments. He also reiterated a point he had made earlier that it would be helpful to the experts if a minimum threshold of engineering concern for displacement could be defined at some level above 0 cm. He believed this would help experts to better focus on characterizing the displacements of main concern to design. Carl Stepp responded that the Management Team advised against doing this because they wanted to avoid any possible conditioning of the experts' interpretations. Kevin Coppersmith then added that in terms of guidance on the distance of interest for SSC characterization for ground motion hazard, experts needed to characterize

sources out to 100 km, with detailed characterization of sources out to 50 km from Yucca Mountain.

The final afternoon session was devoted to elicitation training, conducted by Peter Morris. Ivan Wong introduced members of the ground motion panel, who had arrived to also participate in the elicitation training (participants in the Ground Motion Workshop on Methods and Models are not included in Table 1, but will be included in a separate report on the Ground Motion Workshop). Peter Morris referred to the training as a workshop in probability assessment. The topics covered included using probability to quantify uncertainty, representing and manipulating probabilities, and assessing probabilities. The information presented followed his handout closely (Attachment 2), with the addition of many real-life examples and interactive exercises with the experts. The workshop was adjourned after the elicitation training, at about 5:00 pm.

TABLE 1. YUCCA MOUNTAIN SEISMIC SOURCE CHARACTERIZATION WORKSHOP #4 - PRELIMINARY INTERPRETATIONS

January 6 to 8, 1997

Attendance List

Name	Affiliation
1. Ake, Jon	U.S. Bureau of Reclamation (USBR)
2. Allen, Clarence	Nuclear Waste Technical Review Board (NWTRB)
3. Anderson, Ernie	U.S. Geological Survey (USGS)
4. Anderson, Larry	USBR
5. Arabasz, Walter	University of Utah (UU)
6. Bell, John	UNR
7. Bruhn, Ron	UU
8. Brune, James	UNR
9. Chaney, Tom	USGS
10. Coppersmith, Kevin	Geomatrix
11. Cornell, Allin	Consultant
12. dePolo, Craig	UNR
13. Doser, Diane	University of Texas, El Paso
14. Ferrill, David	Center for Nuclear Waste Regulatory Analyses
15. Fridrich, Chris	USGS
16. Hanks, Tom	USGS
17. Ibrahim, Bakr	U.S. Nuclear Regulatory Commission (NRC)
18. Justus, Phil	NRC
19. King, Jerry	M&O/SAIC
20. Knuepfer, Peter	State University of New York at Binghamton
21. Lui, Christiana	NRC
22. Majer, Ernie	Lawrence Berkeley National Laboratory
23. McCalpin, Jim	GEO-HAZ Consulting, Inc.
24. McGuire, Robin	Risk Engineering
25. Menges, Chris	USGS
26. Morris, Peter	Applied Decision Analysis, Inc.
27. O'Leary, Dennis	USGS
28. Olig, Susan	Woodward-Clyde Federal Services (WCFS)
29. Parks, Bruce	USGS
30. Penn, Sue	WCFS
31. Perman, Roseanne	Geomatrix
32. Pezzopane, Silvio	USGS

TABLE 1 (CONT). YUCCA MOUNTAIN SEISMIC SOURCE CHARACTERIZATION WORKSHOP #4 - PRELIMINARY INTERPRETATIONS

January 6 to 8, 1997

Attendance List

Name	Affiliation
33. Pomeroy, Paul	Advisory Committee on Nuclear Waste
34. Potter, Chris	USGS
35. Quittmeyer, Richard	WCFS
36. Ramelli, Alan	UNR
37. Reiter, Leon	NWTRB
38. Rogers, Al	EQE International
39. Savy, Jean	Lawrence Livermore National Laboratory
40. Schwartz, David	USGS
41. Sheaffer, Patricia	USGS
42. Slemmons, Burt	WCFS
43. Smith, Ken	UNR
44. Smith, Robert	UU
45. Stamatakos, John	CNWRA
46. Stepp, Carl	WCFS
47. Stuckless, John	USGS
48. Sullivan, Tim	DOE
49. Swan, Bert	Geomatrix
50. Toro, Gabriel	Risk Engineering
51. Wernicke, Brian	Cal Tech
52. Whitney, John	USGS
53. Wong, Ivan	WCFS
54. Youngs, Robert	Geomatrix
55. Yount, Jim	UNR

Civilian Radioactive Waste Management System
Management & Operating Contractor

Summary of Seismic Source Characterization Feedback Workshop

SSC Workshop 5

Salt Lake City, Utah
April 14-16, 1997

Prepared for:

U.S. Geological Survey
Box 25046, MS-425
Denver Federal Center
Denver, CO 80225

Prepared by:

Woodward-Clyde Federal Services of the
Civilian Radioactive Waste Management System
Management & Operating Contractor
1180 Town Center Drive
Las Vegas, NV 89134-6363

May 16, 1997

INTRODUCTION

The U.S. Geological Survey (USGS) is carrying out a probabilistic seismic hazards analysis (PSHA) for Yucca Mountain, Nevada as part of the Department of Energy's (DOE) project to characterize this site as a potential geologic repository for high-level radioactive waste. This study was initiated in April 1995 and resumed in June 1996. The aim of the analysis is to provide the annual frequency with which various levels of vibratory ground motion and fault displacement will be exceeded at the site. These results will be used as a basis for developing seismic design inputs and in assessing the waste isolation and containment performance of the site.

The PSHA involves development by two panels of experts of input interpretations and assessments of uncertainties required by the hazards calculations. One panel (consisting of six teams of three experts) addresses characterization of seismic sources and fault displacement, while the other (consisting of seven individual experts) deals with vibratory ground motion. Development of interpretations is being facilitated through a series of structured workshops to evaluate available data, to explore the range of interpretations allowed by the data, to examine critically the interpretations proposed by the experts, and to provide feedback on the implications of various interpretations for the seismic hazard at the site. This report summarizes the fifth workshop in the characterization of seismic sources and fault displacement: the Seismic Source Characterization (SSC) Feedback Workshop.

The primary goals of the workshop were to: (1) provide an opportunity for the expert teams to discuss the first round of their interpretations; (2) allow each team to understand and ask questions about the interpretations made by other teams; (3) provide information on the derivative products of their first-round assessments (i.e., seismic source characteristics); and (4) provide sensitivity analyses that show the relative impact of various assessments on the calculated results. To accomplish these goals, a series of presentations and group discussion sessions were conducted, with emphasis on interaction among the SSC experts and feedback from the Facilitation and Calculation Teams. For each of six key issues, two or three teams presented their interpretations with all of the teams subsequently discussing the issue and their interpretations. These six key issues, identified by the Facilitation Team from the preliminary results, included: (1) characterization of areal seismic source zones; (2) geometry of local faults; (3) synchronous ruptures of local faults; (4) maximum magnitudes and recurrence on local faults; (5) characterization of other seismic sources, such as buried strike-slip shear zones, detachments, volcanic zones and other buried or postulated structures; and (6) methodologies for evaluating fault displacement. The focus of the presentations and discussion was on understanding the interpretations of others, their technical bases,

consistency with data, and expression of uncertainty. Preliminary results and sensitivity analyses were presented for five of the teams, highlighting the most significant sources and parameters to the analyses. Assumptions and simplifications of the teams' assessments that were made for the analyses were clarified and discussed. As interpretations will be finalized shortly after this workshop, emphasis was on the experts gaining a common understanding of each other's interpretations and clarification of any outstanding questions regarding their own assessments.

The workshop agenda is included as Attachment 1. Copies of overhead transparencies shown by presenters and additional material distributed during the workshop are included as Attachment 2. Table 1 is a list of participants and their affiliations.

MONDAY, APRIL 14, 1997

Kevin Coppersmith opened the workshop with an introduction, describing the purpose and approach, and outlining the workshop agenda. He highlighted significant aspects of the key issues to be addressed, encouraged technical challenge and debate during the workshop, and emphasized that the experts need to have been exposed to and consider all of the various proponent views. He also stressed that preliminary seismic hazard results are provided only for sensitivity and information on relative importance, and are not intended as hazard results for any other purpose. He reviewed three issues relevant to the seismic source characterization for Yucca Mountain which were raised in the Nuclear Regulatory Commission's 1996 Annual Progress Report (Chapter 3 of NUREG/CR-6513, No. 1). These include questions regarding: (1) adequate consideration and incorporation of alternative tectonic models in the SSC team interpretations; (2) adequate consideration by the teams of all 52 Type I faults, identified by the NRC, as potential seismic sources that may affect repository design or performance; and (3) possible explanations for the apparent anomalous lengths of certain faults (Bare Mountain, Windy Wash, and Ghost Dance) as suggested by scaling relations between fault length and cumulative throw.

The rest of the afternoon was devoted to covering the issues of characterizing areal seismic source zones and the geometry of local faults. Al Rogers made the first presentation on his team's (Rogers, Yount, Anderson - [RYA]) interpretations of seismic source zones. They defined three zones primarily based on structural domain considerations (Yucca Mountain-Bare Mountain, Basin and Range, Death Valley-Furnace Creek), all with the same maximum moment magnitude (M_{max}) of 6.3 $\pm$ 0.3 for background earthquakes (they referred to as background faults). Recurrence rates for background faults were calculated for each zone using declustered versions of the historical seismicity catalog and uncertainties in a- and b-values were included, particularly those resulting from assessing catalog completeness. Discussions followed about observations by Walter Arabasz of an apparent systematic bias of

lower magnitudes (and resulting higher b-values) for the catalog than previous M_L-based catalogs for the Basin and Range province. Also discussed were issues relating to smoothing and systematic differences in b-values from east to west within 100 km of Yucca Mountain, observed by Diane Doser.

Robert Smith made the next presentation on his team's (Smith, dePolo, O'Leary- [SDO]) interpretations of areal seismic source zones. He explained that their interpretations were not as complete as others due to changes resulting from replacing one of their team members (Christopher Menges was replaced because of health problems by Dennis O'Leary). Dr. Smith said they had defined 5 source zones, including: a host zone (Yucca Mountain-Crater Flat); the Goldfield-Spring Mountain section of Walker Lane; the Death Valley section of Walker Lane; the central Basin and Range; and a zone defined by seismicity associated with the 1992 Little Skull Mountain earthquake. Seismogenic depths of 14, 17, and 19 km were respectively weighted 0.2, 0.6, and 0.2, primarily based on maximum focal depths for earthquakes within 100 km. These large seismogenic depths stimulated lots of discussion among the experts due to resulting effects on M_{max} and moment rates. Based on historical analog earthquakes in the Basin and Range province, the SDO Team developed a probability density function of M_{max} for background earthquakes occurring in each of the zones within 100 km of Yucca Mountain (M_w 6.2, 6.4, and 6.6 for the 3rd, 50th, and 97th percentiles, respectively). Finally, he discussed their methods for processing the seismicity catalog (including declustering, completeness assessments, magnitude conversions and uncertainties, and smoothing), and estimating recurrence rates for each source zone.

Dr. Coppersmith subsequently summarized general characteristics of all of the teams' assessments of areal source zones and asked Dr. Doser to discuss her team's characterization. She explained that even though they originally defined their zones primarily based on geologic and tectonic considerations, they observed systematic seismological differences between zones (such as shallower focal depths and a greater lateral component of slip from east to west), giving them further confidence in their definition of zones. Other teams then discussed their various bases for defining zones, particularly why some of them did or did not define a "host" or local zone, and their various approaches to characterizing this zone.

After the break, Christopher Fridrich gave a presentation on his team's (Doser, Fridrich, Swan- [DFS]) interpretations of the geometry of local faults. Dr. Fridrich described their approach to developing subsurface geometric models of local faults and characterizing uncertainties in fault length, dip, and downdip extent. He showed a series of cross-sections and structure contour maps, highlighting differences between interpretations for their two basic tectonic models (domino and detachment), and for variations within the domino tectonic model (with from one to three groups of coalescing faults). He discussed their rules of assessing downdip extent, summarized what their preferred interpretations were, and

highlighted some geometries that the cross-sections either preclude or suggest are less likely (e.g., coalescence of the Windy Wash, Solitario Canyon and Paintbrush Canyon into one fault). Discussion then followed about how they handled uncertainties in fault dips and calculated slip rates for the various models.

Peter Knuepfer gave the last presentation of the day, discussing his team's (K. Smith, Bruhn, Knuepfer - [SBK]) interpretations of local fault geometry. As their characterization of fault geometry is dependent on their tectonic models, he began with an overview of their models and the resulting influences or constraints on local fault dips, downdip extent, and lengths. He presented many arguments in favor of steeply to moderately dipping planar faults, including geophysical data, seismicity data, and arguments from stress-drop considerations and slip-length scaling relations. Based on the latter considerations and relations, and the Mammoth Lakes earthquake sequence as an analog for "the ash event" (Scenario U of Pezzopane, 1996), they favor interpreting the ash event as a sequence of multiple event ruptures that were not actually synchronous from a ground-motion viewpoint, but were separate events, on individual faults, that were tightly clustered in time. The expert panel discussed the uncertainties with this interpretation. Next, Dr. Knuepfer explained how his team characterized uncertainties in downdip extent and fault length. Except for the Bare Mountain fault, they interpreted the maximum southern extent of Yucca Mountain faults to be around Lathrop Wells.

This stimulated discussion about how other teams interpreted the southern termination of local faults, given the observed increase of total slip and slip rates to the south. Some had interpreted the Highway 95 (or Carrara) fault as truncating local faults, whereas others had terminated faults at the southern end of the Crater Flat basin structural domain. The panel also discussed implications for uncertainty in some fault lengths (i.e., Bare Mountain, Ghost Dance and Windy Wash faults) from scaling relations between length and total throw. Finally, discussion followed about the evidence both for and against listric fault geometries, and how fault segmentation was variously considered in the analyses.

Dr. Coppersmith asked for comments from observers and Clarence Allen asked for clarification about how the teams had considered the Ghost Dance fault in their assessments. Dr. Coppersmith explained that all teams had included the Ghost Dance fault as a possible source for secondary fault slip in their preliminary fault displacement analyses, but none, so far, had included it as a seismogenic source (an independent generator of earthquakes) in their characterizations for the vibratory ground motion analysis. Leon Reiter asked for clarification on the time frame being considered by the experts. Some had considered both long (10,000 years) and short (100 years) periods in developing their assessments, some had not thought about it, and others were still trying to resolve how to address possible non-stationarity of seismicity in both time and space. Ralston Barnard clarified that results from

this project will be used for performance assessments that consider periods as long as 10,000 years and longer. Carl Stepp suggested that the experts consider two questions: (1) how to best represent long-term behavior with the available data?; and (2) what type of long-term changes (if any) can be expected for earthquake and fault slip behavior in the region? Dr. Coppersmith further encouraged the teams to think about how considering a longer time period (10,000 or 100,000 years) might change their assessment.

TUESDAY, APRIL 15, 1997

The workshop continued with a series of presentations and discussion on the remaining key issues: synchronous ruptures on local faults, M_{max} and recurrence on local faults, other types of seismic sources, and methodologies for fault displacement. Alan Ramelli gave the first presentation on his team's (Arabasz, E. Anderson, Ramelli - [AAR]) interpretations of synchronous ruptures for local faults. He described their reasons for considering synchronous ruptures, their approach to developing 11 structural model categories, and how their interpretation of local fault behavior and geometry was dependent on these model categories. They distinguished linked faults (along-strike fault connections) from coalesced faults (downdip fault connections) and defined four different models for coalescence of local faults. Thus, they considered linked, independent, and coalesced behavior for possibly linked faults (e.g., Paintbrush Canyon and Solitario Canyon faults) and only coalesced and independent behavior for other local faults (e.g., Bare Mountain fault which can either rupture independently or together with many other local faults, comprising a single coalesced system). He described their bases for: favoring independent behavior of the Bare Mountain fault, fault length distributions, and preferred dips of 60°. He said they had previously favored some degree of coalesced behavior but would be reconsidering their weights given the insights provided by Dr. Fridrich's structural analysis presented on Monday. Finally, the panel discussed the distribution of moment release during synchronous ruptures and the questions that might be raised to the Ground Motion Experts regarding information that they might require in this regard for their models.

Jon Ake gave the next presentation on his team's (Ake, Slemmons, McCalpin - [ASM]) interpretations of synchronous ruptures on local faults. He prefaced his presentation with the comment that they would be revisiting some important aspects of their assessment given some of the insights they had gained during the workshop. He said they based their models of synchronous fault rupture on both temporal and geometrical considerations. He clarified that their definition of synchronous (or simultaneous) earthquake rupture was two or more faults rupturing within 10 seconds of each other. He presented the general structure of their logic tree for local faults, gave examples of simultaneous ruptures considered, and discussed their original basis for assigning a low weight to simultaneous ruptures, although they may re-evaluate this based on geometrical considerations. This stimulated discussion among the

panel about the geometries, settings, and characteristics of possible analog earthquakes that have exhibited distributive rupture on multiple faults. Examples discussed included both simultaneous rupture (according to the ASM team definition) and non-simultaneous rupture. Discussion also followed about: considering buried dike systems as a possible source, considering the Yucca Mountain faults as aseismic and dependent on the Bare Mountain fault, expanding uncertainties for synchronous rupture models and the need to clarify how teams are defining terms (such as synchronous rupture, distributive rupture, linked faults, etc.).

Craig dePolo gave the first presentation on M_{max} and recurrence on local faults, representing the SDO Team. His team's approach to characterizing M_{max} included using many different regression relations to scale earthquake size from multiple fault parameters such as length, area, maximum surface displacement, slip rate and seismic moment. He clarified how they would determine certain parameters for different scenarios in their assessment, what relations they would use, and how they would be combined. He reported some preliminary values which ranged greater than M_w 7 for certain scenarios with extreme geometries (e.g., 45° dip and 19 km depth). In terms of earthquake recurrence, he said they were considering using geodetic data, in addition to paleoseismic data, to estimate moment rates. They would also use a recurrence interval approach and he discussed how they were using the available paleoseismic data to determine average recurrence intervals for different rupture scenarios in their assessment.

Walter Arabasz gave the next presentation on M_{max} and recurrence on local faults, representing the AAR Team. He began by pointing out they had considered seismogenic depths in two different ways in their assessment because they were considering depths for Yucca Mountain that were generally larger than the depths included in the development of the empirical relations they were using to estimate M_{max} (Wells and Coppersmith, 1994). Thus, they used seismogenic depths to constrain their physical models (D_{max2}) that did not necessarily equal the seismogenic depths used to estimate M_{max} (D_{max1}), indeed D_{max2} was often greater than D_{max1}. He said they considered flexural rigidity to be a better indicator of seismogenic depth than heat flow and presented their rules for constraining downdip fault widths for their various tectonic models and structural categories. He presented the four empirical relations they had used, how they were weighted and the basis for the weights. Next, he discussed their approaches to estimating recurrence, which included both slip rate (weighted 0.6) and recurrence interval (weighted 0.4) methods, whenever data for the latter were available. They used both characteristic (weighted 0.7) and truncated exponential (weighted 0.3) models. He discussed their estimated b-values, reiterating his previous comment that 50th percentiles were surprisingly higher for Yucca Mountain than for previous Basin and Range catalogs he had analyzed. Discussion followed about their maximum magnitude distributions and how broad their uncertainties were due to the large variety of

geometries considered in their various tectonic models and structural categories. The general dependence of the slip-rate method on M_{max} and geometry was also discussed. Dr. Coppersmith then summarized all of the teams approaches to estimating M_{max} and recurrence on local faults, pointing out similarities and differences. He explained the importance of choosing recurrence models and adequately incorporating uncertainty in M_{max} and recurrence parameters. He told the teams that they would each be getting their M_{max} distributions and recurrence curves shortly after the workshop.

After lunch, there was continued discussion about recurrence, particularly about declustering the catalog, other methods of processing the catalog, and the resulting effects on recurrence curves. Jim Yount then gave the first presentation on other seismic sources that his team (RYA) had considered in their assessment. He started with a buried detachment fault, explaining why they assigned a zero probability to it being an independent seismogenic source even though it may exist. He also discussed a potential volcanic source zone that they had included. To this buried source, they assigned: a seismogenic probability of 0.7, an M_{max} of 5.5 $\pm$ 0.5 based on historical analogs for basaltic events elsewhere, and a return period of 200,000 to 1.9 million years based on the PVHA report for Yucca Mountain. He also discussed their reasons for considering a buried vertical shear zone as a source that may be decoupled from local surface faults. Their assigned probability to this buried zone being an independent seismic source was model dependent, ranging from 0.05 to 0.1. Finally, Dr. Yount described their characterization of the geometry, M_{max}, and recurrence parameters for this source, also providing the bases for their assessment.

Ernie Anderson gave the next presentation on other types of seismic sources, representing the AAR Team. He started with an overview of their four tectonic models and their influence on the inclusion of various types of seismic sources. He discussed their reasons for considering any detachment faults that may exist as accommodation zones and not as independent seismic sources. He also explained that although they believe that volcanic sources may also exist, that the expected M_{max} for these sources (M_w 5-5½) is well below that for their areal source zones and any volcanic-related earthquakes are accounted for within these zones. Finally, he discussed two types of buried sources they had included for some of their structural models: cross-basin and basin-bounding faults, and a large strike-slip shear zone. The former are assumed to exist as part of a pull-apart basin model suggested by small-scale laboratory deformation experiments conducted by the Center for Nuclear Waste Regulatory Analyses. The latter is suggested by the work of Richard Schweickert and his colleagues. Dr. Anderson discussed how they characterized these buried sources, the bases, and the uncertainties.

Silvio Pezzopane mentioned that their cross-basin faults may be geomorphically expressed as the down-to-the-east faults of Ramelli and Bell (1996). Discussion followed about the geomorphic and paleomagnetic evidence for possible basin-bounding and cross-basin faults.

As part of this discussion, Burt Slemmons then gave an overview of geomorphic and geophysical evidence supporting a fault origin for the Carrara or Highway 95 scarp. He showed slides from his aerial reconnaissance and explained that the fault could not only be important as another potential seismic source but it could truncate the Bare Mountain and Yucca Mountain faults (as for example the AAR Team had interpreted in their pull-apart basin model).

Next, Dr. Coppersmith asked the teams why they had not included either the Ghost Dance or Sundance faults as independent seismic sources. Reasons given included no definitive evidence for Quaternary displacement, too short of length (events would be small and fall into "background" or areal seismic zones), and rates of activity are too low. Craig dePolo said that they may include a low-weighted scenario where the Abandoned Wash and Ghost Dance faults are linked and seismogenic, particularly to account for the uncertainty in possible early Quaternary shearing at Whaleback Ridge. Finally, the issue of why vertical slip rates on the Bare Mountain fault are apparently much lower than total vertical slip rates for Yucca Mountain faults, and what significance this may have to tectonic models, was discussed.

After the break, Frank (Bert) Swan gave a presentation on his team's (DFS) fault displacement methodology. He reviewed their general logic tree, describing their overall approach for faults, and fractures/intact rock. Their methodology uses slip rate, displacement per event, recurrence intervals (wherever available), and an event-to-event displacement variability function to characterize the displacement hazard at a location. They use Quaternary slip rates (weighted 0.7) wherever possible and also use Tertiary slip rates with three different models for behavior. These models include: a uniform slip rate since 12.7 Ma, a uniform slip rate since 11.6 Ma with only 20% of the post-Tiva Canyon slip having occurred since 11.6 Ma, and a decreasing rate such that the Quaternary rate is between 0.3 and 3.9% of the late Miocene rate. He discussed how reduction factors and resulting rates were determined for this last model. He presented the bases for all the models and all the resulting slip rates for each of the structures at the nine specified test locations. Next, he discussed their displacement per event and recurrence estimates. He then explained how they used paleoseismic data to develop a relationship between average and maximum displacement at a point along a fault to characterize expected event-to-event variability in displacement. Finally, he explained how they characterized the probability of displacement along fractures and in intact rock using three deformation models analogous to their Tertiary slip rate models.

James McCalpin gave the next presentation on fault displacement methodology, representing the ASM Team. Their approach separates primary fault displacement on seismogenic (block-bounding) faults from distributed faulting on secondary, non-seismogenic faults. First, he

discussed various ways of using paleoseismic data to predict displacement per event at a point along a primary fault, given the along-strike-variability in slip, the event-to-event variability in slip, and the likely greater variability of slip in unconsolidated sediments than in bedrock. Given the displacement distributions on primary faults, the potential displacement on secondary faults is estimated based on their distance from the primary fault and using a bending beam model. He described this model, constrained by geodetic data from the 1983 Borah Peak earthquake, and highlighted some of the uncertainties in applying it to Yucca Mountain faults. He also described an alternative ratio approach to estimating secondary displacement and gave an example comparison for the two methods.

Ronald Bruhn gave the last presentation on fault displacement methodology, representing the SBK Team. He prefaced by saying that their approach was similar in many respects to the approach of the DFS Team. Their methodology is broken into two main parts: estimating slip per event at a point along the fault, and estimating recurrence of that event. He explained how they were using scaling relations between fault size and displacement to estimate displacement per event. He discussed the various relations and their uncertainties. He also presented results from a fractal analysis to characterize along-strike-variability in slip, but he said they may also use the approach developed by the ASM Team. He then discussed how they would use slip rates and recurrence intervals (wherever possible) to constrain the probability of displacement events.

Considerable discussion followed about the methodologies presented. Dr. Coppersmith encouraged the experts to be sure to capture uncertainty in the input parameters. Dr. Pezzopane discussed his progress on developing separate hanging wall and footwall probability density functions for secondary faulting during historical Basin and Range earthquakes. Concerns were raised about whether an elastic bending beam model was appropriate and that care should be taken in all of the assessments not to violate observations of the total slip on any of the faults, particularly where slip on secondary faults is predicated based on slip on primary faults. Dr. Coppersmith urged experts to be sure fault assessments were internally consistent, and consistent with their source characterizations for the ground motion evaluations.

Finally, Dr. Coppersmith asked for comments from observers. Dr. Allen mentioned evidence from historical earthquakes in California supporting characteristic behavior along faults. Dr. Schwartz added that evidence along the Borah Peak earthquake rupture also supported characteristic behavior. Bakr Ibrahim asked how focal depth distributions were being incorporated into fault displacement assessments and Dr. Coppersmith clarified that these were only relevant for principal faults and were included in the ground motion evaluation. Dr. Reiter urged experts to appropriately match the level of complexity of their models to the available data as simplified models that encompass the data are most defensible. He also

encouraged them to consider using multiple methodologies in evaluating fault displacement. Discussion then followed as to whether the present schedule afforded the time necessary for adequate consideration of multiple methodologies.

WEDNESDAY, APRIL 16, 1997

Dr. Coppersmith opened the discussion to miscellaneous issues that had been raised over the past two days. Dr. Brune pointed out many issues related to using a quasi-static fault mechanics approach to evaluating the displacement hazard at Yucca Mountain. These included uncertainties in: the absolute deviatoric stresses in and below the repository, pore pressures at seismogenic depths and how these affect the earthquake cycle, the heat flow paradox, and partial versus total stress drops and the large differences in general between the quasi-static models considered and the actual dynamic conditions of the earthquake rupture process. Speaking as a proponent, he believed that fault displacement methods based on total slip or the more traditional earthquake approach, coupled with empirical relations to characterize distributive faulting, were more credible than any fault mechanics approach that can be developed given our current state-of-knowledge. Next, the difference between the probability of seismogenic slip versus non-seismogenic slip on the Ghost Dance fault was discussed.

Next, Gabriel Toro presented the preliminary results for the probabilistic seismic hazard analysis (PSHA). He prefaced his talk with some assumptions made in the modeling of the site and source geometries. Starting with the AAR Team, he gave an overview of their input (in the form of logic trees and maps), presented preliminary hazard curves for 5 and 20 Hz (without many regional fault sources), and discussed some implications from the analysis of variance for the most significant sources. He also presented the ground motion curves used, explaining the significance of the uncertainties in the curves and generally how they were combined with the SSC input to calculate the hazard curves. Following this same format of input, results, and sensitivity analyses, Dr. Toro presented feedback for each team except the SDO Team because he had just received their input. Throughout his presentation, various questions were discussed by the teams, Dr. Toro, and Bob Youngs; clarifying how some of the finer complexities of the teams' characterizations were modeled in the assessment and resolving questions about some inconsistencies and gaps. Dr. Toro concluded by summarizing that: (1) both areal source zones and local faults are important at high frequencies; (2) the Death Valley and Furnace Creek faults are the dominant contributor to hazard at lower frequencies; (3) the modeling of synchronous rupture scenarios for local faults is important; and (4) overall uncertainty is in the. typical expected range for the analyses.

Next, Dr. Coppersmith reviewed the significant aspects of the key issues discussed during the workshop including: (1) the areal source zone for Yucca Mountain (the host zone); (2) M_{max} on local faults; (3) slip rate and recurrence on local faults; (4) synchronous rupture models for local faults; and (5) M_{max} and recurrence on the Death Valley-Furnace Creek fault system. He reminded the teams that they needed to provide guidance to the Calculations Team on focal depth distributions.

After the break, Dr. Youngs presented preliminary results for four of the teams' fault displacement evaluations. He grouped the methodologies into two types: point estimate methods (including the DFS and RYA Teams), and principal-distributed faulting models (including the ASM & AAR Teams). For each team, he reviewed the input, presented hazard curves for test points 2 and 8a, and discussed the results. During his presentation, assumptions about the models were clarified and questions about various aspects of the input were resolved. Of particular concern was the assumption in some cases that, given an event on a seismogenic fault, the probability of triggered slip was assumed to be 1, which can yield too high of slip rates and total slip on secondary features. Dr. Fridrich also pointed out why he believes much of secondary faulting occurred between 12.7 and 11.6 Ma, when the primary faults first formed and had the greatest amount of movement. There was also discussion about how slip rate may be dependent on fault size, changing and perhaps decreasing with time as faults grow in size and can store more strain energy.

After lunch, Dr. Coppersmith asked for discussion about whether the team's assessments would vary if they were used for a 100-year versus a 10,000-year time frame. Possible changes included using time-dependent models, increasing uncertainties, and increasing smoothing of historical seismicity in areal source zones. Dr. Barnard then provided an overview of how the PSHA results may be used in the upcoming Total System Performance Assessment being conducted by DOE. He explained that scenarios for both volcanism and tectonism were required to analyze the impact on canisters and the consequences in terms of radionuclide release from: (1) earthquake ground motions and fault displacements; (2) the combination of seismic and volcanic events; and (3) the changes in hydrology and groundwater flow resulting from seismic and volcanic events. The performance assessors will be using results from the PSHA to judge the probability of occurrence of such scenarios over 10,000-year, to 100,000-year, to multiple-100,0000 year periods.

Next, Carl Stepp gave the experts guidance, from a regulatory perspective, on the documentation required in their elicitation summaries so that their assessments will be complete. He also discussed the revised schedule, which would allow more time for the experts to develop their fault displacement methodologies and evaluate the methodologies used by others. He said to provide more feedback and interaction on fault displacement methodologies, another one-day workshop would be scheduled for early June. The date

would depend on the availability of the experts, and additional funds would be provided for associated travel costs and time.

After the break, Dr. Coppersmith and Norm Abrahamson initiated the joint session between the Ground Motion and SSC Experts. For the benefit of the Ground Motion Panel, Dr. Coppersmith reviewed the SSC issues that were covered over the last three days, emphasizing questions particularly relevant to the ground motion issues. Dr. Abrahamson prefaced his overview with the caveat that much of the SSC models are generalized by the ground motion experts to develop their source models. He then reviewed key aspects of the ground motion characterization, including: types of faults considered, magnitudes and distances that calculations were done for, the ground motion parameters calculated, and how the special cases of detachment faults and synchronous (multiple) rupture of local faults were modeled. Discussion among the panel members centered around what, if any, additional parameters the SSC experts might need to provide (such as directivity of rupture, sense of slip, and primary versus secondary rupture planes for multiple fault ruptures), and if model simplifications made by the ground motion experts were reasonable and most appropriate given the actual geologic conditions at Yucca Mountain. In regard to the latter, the geometries of detachments and synchronous ruptures of multiple local faults were of particular interest. Some discrepancies between the panels' characterizations were also highlighted, such as ground-motions models only extended to a depth of 14 km, but many SSC characterizations included deeper seismogenic depths (as deep as 22 km).

Finally, Dr. Coppersmith asked for comments from observers. Dr. Reiter commented that it would be useful to learn from experts what might occur down the road (new data or event) that would cause them to change their assessment. Responses included: (1) the occurrence of a large earthquake on a low-angle detachment anywhere worldwide; (2) occurrence of observable non-tectonic slip on local faults; (3) occurrence of a Cedar Mountain-type earthquake at Yucca Mountain; (4) obtaining additional along-strike slip data for the Solitario and/or Paintbrush Canyon faults; and (5) obtaining definitive data on deep, downdip fault geometry. Dr. Ibrahim asked how much weight was given to each of the two seismic line interpretations and how it affected their analyses. The consensus response was that the differences between the interpretations did not impact the analyses, generally because more recent markers were used to characterize rates of activity on the Ghost Dance fault. Finally, Art McGarr provided an overview of how to calculate static stress drop and insights about triggered slip from studies of mines in South Africa. Dr. Coppersmith adjourned the workshop at about 4:30 pm.

TABLE 1. YUCCA MOUNTAIN SEISMIC SOURCE CHARACTERIZATION
WORKSHOP #5 - FEEDBACK
April 14-16, 1997
Attendance List

Name	Affiliation
1. Ake, Jon	U.S. Bureau of Reclamation (USBR)
2. Allen, Clarence	Nuclear Waste Technical Review Board (NWTRB)
3. Anderson, Ernie	U.S. Geological Survey (USGS)
4. Anderson, Larry	USBR
5. Arabasz, Walter	University of Utah (UU)
6. Barnard, Ralston	Sandia National Laboratory
7. Bruhn, Ron	UU
8. Brune, James	UNR
9. Coppersmith, Kevin	Geomatrix Consultants
10. Cornell, Allin	Consultant
11. dePolo, Craig	University of Nevada, Reno (UNR)
12. Doser, Diane	University of Texas, El Paso
13. Fridrich, Chris	USGS
14. Golos, Joyce	USGS
15. Hanks, Tom	USGS
16. Harrington, Charles	Los Alamos National Laboratory
17. Hinze, William	Advisory Committee on Nuclear Waste
18. Ibrahim, Bakr	U.S. Nuclear Regulatory Commission (NRC)
19. Justus, Phil	NRC
20. King, Jerry	M&O/SAIC
21. Knuepfer, Peter	State University of New York at Binghamton
22. Lui, Christiana	NRC
23. McCalpin, Jim	GEO-HAZ Consulting, Inc.
24. McGuire, Robin	Risk Engineering
25. O'Leary, Dennis	USGS
26. Olig, Susan	Woodward-Clyde Federal Services (WCFS)
27. Parks, Bruce	USGS
28. Penn, Sue	WCFS
29. Perman, Roseanne	Geomatrix Consultants
30. Pezzopane, Silvio	USGS
31. Pomeroy, Paul	Advisory Committee on Nuclear Waste

TABLE 1. YUCCA MOUNTAIN SEISMIC SOURCE CHARACTERIZATION WORKSHOP #5 - FEEDBACK

April 14-16, 1997

Attendance List

Name	Affiliation
32. Quittmeyer, Richard	WCFS
33. Ramelli, Alan	UNR
34. Reiter, Leon	NWTRB
35. Rogers, Al	GeoRisk Associates, Inc.
36. Savino, John	Golder Associates
37. Savy, Jean	Lawrence Livermore National Laboratory
38. Schwartz, David	USGS
39. Sheaffer, Patricia	USGS
40. Slemmons, Burt	WCFS
41. Smith, Ken	UNR
42. Smith, Robert	UU
43. Soeder, Daniel	USGS
44. Stamatakos, John	Center for Nuclear Waste Regulatory Analyses
45. Stepp, Carl	WCFS
46. Stuckless, John	USGS
47. Sullivan, Tim	DOE
48. Swan, Bert	Geomatrix Consultants
49. Toro, Gabe	Risk Engineering
50. Whitney, John	USGS
51. Wong, Ivan	WCFS
52. Youngs, Robert	Geomatrix Consultants
53. Yount, Jim	UNR
54. Zurflueh, Ernest	NRC

Civilian Radioactive Waste Management System
Management & Operating Contractor

Summary of Seismic Source Characterization Fault Displacement Workshop

SSC Workshop 6

Salt Lake City, Utah
June 3, 1997

Prepared for:

U.S. Geological Survey
Box 25046, MS-425
Denver Federal Center
Denver, CO 80225

Prepared by:

Woodward-Clyde Federal Services of the
Civilian Radioactive Waste Management System
Management & Operating Contractor
1180 Town Center Drive
Las Vegas, NV 89134-6363

June 24, 1997

INTRODUCTION

The U.S. Geological Survey (USGS) is carrying out a probabilistic seismic hazards analysis (PSHA) for Yucca Mountain, Nevada as part of the Department of Energy's (DOE) project to characterize this site as a potential geologic repository for high-level radioactive waste. This study was initiated in April 1995 and resumed in June 1996. The aim of the analysis is to provide the annual frequency with which various levels of vibratory ground motion and fault displacement will be exceeded at the site. These results will be used as a basis for developing seismic design inputs and in assessing the waste isolation and containment performance of the site.

The PSHA involves development by two panels of experts of input interpretations and assessments of uncertainties required by the hazards calculations. One panel (consisting of six teams of three experts) addresses characterization of seismic sources and fault displacement, while the other (consisting of seven individual experts) deals with vibratory ground motion. Development of interpretations is being facilitated through a series of structured workshops to evaluate available data, to explore the range of interpretations allowed by the data, to examine critically the interpretations proposed by the experts, and to provide feedback on the implications of various interpretations for the seismic hazard at the site. This report summarizes the sixth workshop in the characterization of seismic sources and fault displacement: the Seismic Source Characterization (SSC) Fault Displacement Workshop.

This workshop addressed the various fault displacement evaluation approaches of the SSC experts' teams. The purpose of the workshop was threefold: (1) to review and discuss alternative methods and models for assessing fault displacement; (2) to discuss uncertainties in parameter values and models; and (3) to facilitate the expert teams' discussion of the pros and cons of alternative approaches, models and submodels. Prior to the workshop, a working paper summarizing the fault displacement evaluation approaches developed by the SSC teams was distributed to the SSC experts. During the workshop, the alternative approaches taken by each team to evaluate displacement at the nine demonstration points were reviewed in more detail. This was followed by extensive open discussion and technical challenge about the strengths and weaknesses of all of the alternative approaches, data required to apply them, and uncertainties in model parameters.

The workshop agenda is included as Attachment 1. Copies of overhead transparencies shown by presenters and additional material distributed during the workshop are included as Attachment 2. Table 1 is a list of participants and their affiliations.

TUESDAY, JUNE 3, 1997

Kevin Coppersmith opened the workshop with an introduction, describing the purpose and approach for the one-day meeting. He reviewed the workshop ground rules and the key characteristics of the nine demonstration points chosen for analysis of the fault displacement hazard.

Next, Robert Youngs explained the purpose of the fault displacement working paper that was sent out for review before the workshop, and he distributed revised copies of the paper with some minor corrections (see Attachment 2). He emphasized that, as a summary of the alternative approaches being used by the expert teams, the paper was intended to provide the teams with a common understanding of the approaches. He also emphasized that the teams needed to consider and evaluate all the available tools in developing their final fault displacement assessments. He reiterated the input needed, the basic hazard formulation, what the final hazard curves portray, and definitions for various terms. This initiated extensive discussion about the meaning and use of "triggered" slip; it was generally agreed that this term may be problematic for describing distributed slip that occurs on secondary faults associated with (geologically coeval to) principal faulting (where principal faulting is seismogenic slip on the fault with the primary moment-release during an earthquake).

Dr. Youngs then discussed each component of the various approaches in more detail, elaborating with specific examples from the team's assessments and making comparisons between various models and submodels. Throughout his presentation, there was extensive discussion, and experts often contributed responses, explanations, and comments about their individual assessments. Of particular interest were the methods used for estimating displacement event frequency and average displacement per event at locations where faults or fractures are present in Tertiary rocks, but Quaternary paleoseismic data is lacking. Frank (Bert) Swan described how his team estimated recurrence intervals when fault-specific paleoseismic data was lacking and Ronald Bruhn explained how his team used data from the Exploratory Studies Facility (ESF) to constrain curves relating fault length and cumulative displacement. Extensive discussion also focused on the use of data from historical surface-faulting events to develop relations for the likelihood of distributive faulting.

After a break, Dr. Youngs continued his presentation, describing two approaches to estimating the probability of a displacement exceeding a given value, given that a displacement event had occurred. He emphasized that variability in fault slip has two components: along-strike, and event to event variations. Dr. Swan, Alan Ramelli, and James Yount all discussed how they had used displacement data to characterize both types of variations for Yucca Mountain faults. James McCalpin described his fault displacement curves, derived from averaging slip along five normal surface-faulting events in the western

U.S. Dr. Bruhn described how he simulated generic displacement profiles using fault roughness characterized by the fractal dimension of the fault. Using typical earthquake recurrence models, such as characteristic and truncated exponential distributions, to characterize variability between displacement events was also discussed. Throughout the discussion, the strengths and weaknesses of each approach were explored by the expert teams, particularly in regard to applying the approaches to site-specific conditions at Yucca Mountain.

Next, Dr. Youngs described how one team had used geodetic data from the 1983 Borah Peak earthquake to estimate the potential for distributive faulting at a given distance from a principal fault at Yucca Mountain. Next, Robert Smith described a somewhat similar approach his team was considering that assumes that the distribution of distributive faulting is related to the strain energy, which is proportional to the second derivative of the strain measured from geodetic data. James Brune pointed out that this model assumes that secondary strains trigger secondary faulting, whereas ground shaking may actually be the cause of secondary faulting. John Stuckless asked how differences in lithologies and mechanical behavior were being considered. Dr. McCalpin responded that this was difficult to address with the available data and Dr. Coppersmith suggested that uncertainties should be used to incorporate possible lithologic effects.

After lunch, Dr. Coppersmith initiated discussion about application of the various fault displacement tools to evaluate the hazard at specific points in the Controlled Area of Yucca Mountain. Point #2 on the Solitario Canyon fault, representing a point along a principal block-bounding fault, was the first discussed (for point locations see Attachment 2, Figure 2 in "Summary of Fault Displacement Hazard Methodologies Developed for the Yucca Mountain Site"). The experts discussed what approaches were available for estimating the frequency and amount of displacement given the conditions and available data for the Solitario Canyon fault. They also talked about the weightings they would assign to these approaches and why. Preference was generally voiced for using methods based on Quaternary paleoseismic data that was as site-specific as possible whenever it was available. Dr. Swan commented how the variability in displacement along strike of the Stage Coach Road and Paintbrush Canyon faults was similar to the variability in displacement among events for all the faults. Finally, the treatment of uncertainties was discussed, and Dr. Youngs clarified that experts needed to include the probability that a rupture of a certain magnitude reaches the surface in their assessment.

The next group of demonstration points discussed were those on various intrablock faults, including points #3 through #6. These points are on Tertiary bedrock faults where Quaternary paleoseismic data is generally lacking and so available evaluation methods are more limited and indirect. Methods for estimating displacement frequency were evaluated

and discussed, such as how teams addressed the problems in applying the slip-rate approach when the parameters may have significantly changed as the fault and tectonic regime have evolved through time. The weighting of potential activity was also discussed, including consideration of the slip-tendency of faults in the present stress regime. The advantages and disadvantages of using distributive fault models were also discussed. Dr. Bruhn then described one model his team is considering in which the probability of damage and displacement is assumed to be a function of peak particle velocity at a point. He discussed general constraints on displacement probability provided by observations in underground mining studies. Dr. Brune then urged the experts to consider that the recent stress differences determined from hydrofracture tests implied that appropriately-oriented normal faults at Yucca Mountain may be on the verge of slipping.

Characterizing the frequency and amount of displacement on fractures with no measurable displacement was discussed next. Some experts commented that defendably estimating displacements on such small features is at or beyond the limit of resolution of available data and knowledge, considering the likely small size of the displacement events. Other experts commented that if a fracture showed no measurable offset in 12 million-year-old rock, the probability it would slip in the future was so low as to be negligible in the analysis. Different properties and likely behavior of different types of fractures (such as cooling, tension, shear, open, and sealed) were discussed, along with approaches used to constrain upper bounds of frequency and amounts of slip.

Next, Tim Sullivan provided an update on the ESF excavation. He stated that the tunnel boring machine reached the south portal on April 25, 1997 and provided preliminary cross-sections showing the stratigraphy and larger faults in the last part of the tunnel. Next, John Whitney showed a video of the exposure of the Ghost Dance fault at Alcove #6 in the ESF. He also distributed a one-page summary on the exposure. The exposure revealed a 0.6- to 1.0-m-wide breccia zone with isotropic fabric. There was no apparent mineralization, marker horizons, shear fabric, slickensides or other kinematric indicators. Fracture density did increase significantly within 4 m of the zone, especially in the hanging wall. The west edge of the zone appeared more open and less coherent; otherwise, there was no other evidence of repeated or different age movements. Dr. Whitney pointed out that despite the paleoseismic evidence for three to four late-Quaternary surface-faulting events on nearby faults, there is no evidence for associated secondary slip on the Ghost Dance fault. After the video, Mr. Sullivan explained that DOE plans to excavate another drift next year that will trend southeast from the ESF, intersecting the Solitario Canyon fault. The purpose of the drift is to get a better sample of the repository block to confirm constructability and investigate hydrologic parameters.

Dr. Coppersmith then gave a wrap-up presentation, discussing the process of integrating assessments, documentation requirements, and the upcoming schedule. He then reviewed the importance of the expert's elicitation summaries and described how these reports need to be complete and clearly present the logic used in developing their assessments. He discussed the key components of the summaries in detail and answered questions about the summaries and schedule.

Next, Tim Sullivan thanked the experts for their hard work on the project and assured them that results would be put to full use in upcoming performance assessments and facility design. Dr. Coppersmith added his thanks to the experts, Review Panel, and Management Team. He then asked for comments from observers. Richard Parizek urged the Management Team to get information on the project and results out into the technical community quickly. Leon Reiter asked how may experts changed their views on detachment faults as a result of discussions during the SSC workshops; the general response was interpretations had not changed significantly. The workshop was adjourned at 4:45 pm.

TABLE 1. YUCCA MOUNTAIN SEISMIC SOURCE CHARACTERIZATION
WORKSHOP #6 - FAULT DISPLACEMENT
June 3, 1997
Attendance List

Name	Affiliation
1. Ake, Jon	U.S. Bureau of Reclamation (USBR)
2. Allen, Clarence	Nuclear Waste Technical Review Board (NWTRB)
3. Anderson, Ernie	U.S. Geological Survey (USGS)
4. Anderson, Larry	USBR
5. Arabasz, Walter	University of Utah (UU)
6. Bruhn, Ron	UU
7. Brune, James	University of Nevada, Reno (UNR)
8. Coppersmith, Kevin	Geomatrix Consultants
9. dePolo, Craig	UNR
10. Doser, Diane	University of Texas, El Paso
11. Harrington, Charles	Los Alamos National Laboratory
12. Hinze, William	Advisory Committee on Nuclear Waste
13. Justus, Phil	U.S. Nuclear Regulatory Commission
14. King, Jerry	M&O/SAIC
15. Knuepfer, Peter	State University of New York at Binghamton
16. McCalpin, Jim	GEO-HAZ Consulting, Inc.
17. Nelson, Priscilla	NWTRB
18. O'Leary, Dennis	USGS
19. Olig, Susan	Woodward-Clyde Federal Services (WCFS)
20. Parizek, Richard	NWTRB
21. Parks, Bruce	USGS
22. Penn, Sue	WCFS
23. Perman, Roseanne	Geomatrix Consultants
24. Pezzopane, Silvio	USGS
25. Quittmeyer, Richard	WCFS
26. Ramelli, Alan	UNR
27. Reiter, Leon	NWTRB
28. Rogers, Al	GeoRisk Associates, Inc.
29. Savy, Jean	Lawrence Livermore National Laboratory
30. Schwartz, David	USGS
31. Slemmons, Burt	WCFS
32. Smith, Ken	UNR

TABLE 1. YUCCA MOUNTAIN SEISMIC SOURCE CHARACTERIZATION
WORKSHOP #6 - FAULT DISPLACEMENT
June 3, 1997
Attendance List

Name	Affiliation
33. Smith, Robert	UU
34. Soeder, Daniel	USGS
35. Stamatakos, John	Center for Nuclear Waste Regulatory Analyses
36. Stepp, Carl	WCFS
37. Stuckless, John	USGS
38. Sullivan, Tim	DOE
39. Swan, Bert	Geomatrix Consultants
40. Toro, Gabe	Risk Engineering
41. Whitney, John	USGS
42. Wong, Ivan	WCFS
43. Youngs, Robert	Geomatrix Consultants
44. Yount, Jim	UNR

Civilian Radioactive Waste Management System
Management & Operating Contractor

Probabilistic Seismic Hazard Analyses
Final Results Meeting

Las Vegas, Nevada
April 6, 1998

Prepared for:

U.S. Geological Survey
Box 25046, MS-425
Denver Federal Center
Denver, CO 80225

Prepared by:

Geomatrix Consultants, Inc.
100 Pine Street, 10th Floor
San Francisco, CA 94111

April 27, 1998

INTRODUCTION

The U.S. Geological Survey (USGS) recently completed a probabilistic seismic hazard analysis (PSHA) for Yucca Mountain, Nevada, as part of the Department of Energy's (DOE's) project to characterize this site as a potential geologic repository for high-level radioactive waste. The aim of the analysis is to provide the annual frequency with which various levels of vibratory ground motion and fault displacement will be exceeded at the site. These results will be used as a basis for developing seismic design inputs and for assessing the waste isolation and containment performance of the site.

This summary describes the last meeting of project team members and observers, at which the final results of the project were presented. Members of the project management team outlined the PSHA project and described the major results in seven presentations. Three additional presentations described how the results of the PSHA are being used for seismic design inputs and are being incorporated into the total system performance assessment (TSPA) for the Yucca Mountain project. The two panels of experts who provided interpretations and assessments of uncertainties for the PSHA (the seismic source and fault displacement [SSFD] panel and the ground motion panel) attended the meeting, as did the four-member Review Panel.

The workshop agenda is included as Attachment 1. Copies of overhead transparencies shown by presenters and material distributed at the workshop are included as Attachment 2. Table 1 is a list of participants and their affiliations.

MONDAY, APRIL 6, 1998

Tim Sullivan opened the meeting by welcoming participants. He noted that members of the two expert panels were interspersed in the audience (in contrast to previous meetings, where the focus of the meeting was on the panel members seated at the front of the room). He also noted that the audience included representatives of the Nuclear Regulatory Commission (NRC), Nuclear Waste Technical Review Board, and the Affected Units of Government. He stated that the objective of the meeting was to review the results of the PSHA study.

Carl Stepp reviewed the agenda for the meeting. He described the overall PSHA project objective to assess probabilistic hazards of ground shaking and fault displacement for determining design bases for preclosure ground shaking and fault displacement, and for assessing post-closure waste isolation and containment. He described the process followed in the study, including the formal selection of experts and the formal process for developing expert evaluations, including workshops, facilitation meetings, and feedback to all expert panel members. He discussed the guidance documents followed for the study, including NRC regulation 10CFR60, NRC staff technical positions, and the Senior Seismic Hazard Analysis Committee (SSHAC) guidance. He noted that the project emphasized equal weighting of the

expert interpretations both in the expert selection and in implementation of the elicitation process.

In the second presentation, John Whitney gave a project history of the Yucca Mountain site studies and an overview of the activities performed for the USGS tectonics program and the publications produced. The USGS will place all USGS reports referred to in the PSHA in an open-file, digital format that will be available to the general public. It is anticipated that the PSHA will have USGS Director's approval for publication by this summer, and will be available for distribution as a CD ROM late in 1998. Dr. Whitney closed his presentation by thanking the many individuals who participated in the PSHA project, noting that the project was a good example of how government agencies, academic institutions, and other organizations can work together.

Kevin Coppersmith, the technical leader for the seismic source characterization and fault displacement (SSFD) activities, summarized the seismic source models developed by the six SSFD expert teams to assess vibratory ground motion and fault displacement hazards at the site. He briefly described the tectonic models considered by all of the teams, the types of seismic sources included, and the characterization of the source parameters for the various types of sources considered. He emphasized that each team considered the range of seismic sources that have been postulated (e.g., seismogenic detachment faults, volcanic sources, regional and buried strike-slip faults, and various structural and behavioral models for local fault sources). In this overview, he highlighted the similarities as well as differences in the way alternative models were treated by the various teams and showed comparison recurrence curves for the different types of sources and for all sources across the various teams.

Norm Abrahamson, the technical leader for ground motion characterization, followed with a summary of the methods, models, and estimates developed by the ground motion characterization panel members. Dr. Abrahamson reviewed key aspects of the ground motion characterization, including: types of seismic sources considered (magnitudes and distances used in calculations, and how the special cases of detachment faults and synchronous (multiple) rupture of local faults were modeled); site conditions (including the estimate for kappa and location of reference rock outcrop at the repository elevation with the top 300 m stripped off); and the expert estimates for median, aleatory variability, epistemic uncertainty in the median, and epistemic uncertainty in aleatory variability. He noted that there generally was more variability in the epistemic uncertainty than the aleatory uncertainty expressed by the panel member's estimates. He noted that the Facilitation Team conducted the calculations of attenuation relations to enable the experts to focus on the weights for different models and results. He presented evaluations for epistemic uncertainty (sigma -mu) as a function of rupture distance; examples of median attenuation of horizontal peak ground acceleration (PGA) and T=1.0 sec spectral acceleration that showed the greatest variability at close distances; and examples of aleatory variability in PGA and epistemic uncertainty in median horizontal and vertical PGA. He also showed a viewgraph for approximate scale factors (not presented in the PSHA report) to estimate ground motions at a point on the

ground surface 300 m above the proposed repository elevation, that could be constructed from data in the PSHA report.

Gabriel Toro then summarized the hazard results for ground motion related to the following topics: methodology, the integrated results for all SSFD teams, de-aggregation of hazard, comparisons across SSFD teams, sensitivity results for each SSFD team, and sensitivity results for ground-motion experts. The de-aggregation of hazard by magnitude-distance-epsilon shows that the most important contributors to hazard for high-frequency motions (e.g., 10 Hz) are the Paintbrush Canyon and Solitario Canyon faults (or coalesced systems containing one or both of these faults) and the host area source. For longer-period motion (1 to 2Hz), the Death Valley/Furnace Creek fault source also is important. The results of the mean hazard show that although there was great variety in the models developed by the different teams, there was not a large difference in the mean PGA (horizontal). In general the sensitivity results by the SSFD team showed that recurrence parameters (slip rate, recurrence interval, and recurrence model) were the most significant contributors to uncertainty, and that detachments and buried strike-slip faults contributed little to total hazard.

Robert Youngs summarized the models and approaches used to characterize fault displacement hazard at the site, noting the large effort required because of the relatively undeveloped state of fault displacement hazard analysis. He started by defining displacement hazard terminology and describing the basic hazard formulation, then showed an example of a fault displacement hazard curve. Next he described the two approaches to faulting hazard used by the teams for both principal faulting and distributed faulting: the displacement approach and the earthquake approach. He discussed in more detail each component of the two approaches, elaborating with examples from the team's assessments and comparing various models and submodels. The presentation ended with a discussion of the application of the team's models to nine demonstration points selected to represent the range of conditions that may be encountered. Dr. Youngs noted that more complete descriptions of the team's assessments were provided in tables distributed in the handout package.

After a lunch break, Gabriel Toro gave the first presentation of the afternoon with a discussion of results of the fault displacement analyses. He started with a general description of the methodology and demonstration sites. He then presented integrated results from all sites, comparisons across SSFD teams for all sites, and selected sensitivity results. He noted that the mean hazard results for sites 1 and 2, which lie on recognized faults, were fairly consistent among the teams. There is considerably wider scatter in the results for sites 3 through 9, none of which are located along principal faults. This difference is expected given the greater uncertainty in evaluating the likely small size of such distributed surface rupture events. At the end of Dr. Toro's presentation there was discussion about the sites included in the demonstration points; Buck Ibrahim commented on the large difference between the median and mean results for some demonstration points and questioned the implications for the hazard results; and Peter Kneupfer noted that information regarding Quaternary displacement and activity had significant impact on the assessments.

Robin McGuire next presented an overview of the development of seismic design inputs. He began by presenting flow charts that showed: (1) the steps in preparing seismic design inputs and the appropriate reference documents that define procedures and/or input data (i.e., Topical Reports and the PSHA report); and (2) the roles of the expert panels in preparing input for seismic hazard analysis. He showed a schematic diagram of the repository vicinity, indicating points at which ground motions are calculated. He noted that the ground motions calculated for free field rock conditions at the repository elevation (Point A) should not change, but ground motions at Points B and C can be revised as new data and information on the properties of rocks in the 300 m above the repository become available. He presented results of uniform hazard spectra (UHS) for horizontal and vertical motions at the reference rock outcrop (Point A). Based on the results of the PSHA vibratory ground motion assessment for a 10^{-4}-year exceedance frequency, two design events were determined—a M6.3 at a distance of 5 km, and a M7.7 at a distance of 52 km. Dr. McGuire then discussed the sensitivity of the ground motion results to the velocity models for the upper 300 m of tuff overburden, and showed results for the horizontal design spectra for the repository interface (Point B) and at the top of the tuff overburden (Point C) for both design events for 10^{-4}- and 10^{-3}-year exceedance frequencies. His summary of the fault displacement hazard results for design consideration focussed on two sites (2 and 7a) that are most significant to the site. He noted that the finite displacement hazard at 1E-05 at site 2 on the Solitario Canyon fault would have to be considered in design. In contrast, the results for site 7a indicate that fault displacement hazard will not have to be considered in design. He concluded with a table summarizing the calculated displacements for identified faults for 10^{-4}- and 10^{-5}-year exceedance frequencies. Following Dr. McGuire's presentation was a discussion of the procedures followed to obtain the seismic design inputs and how they will be used.

Rick Nolting provided an overview of the use of the seismic design inputs in both subsurface and surface design. Design data from the PSHA included vibratory ground motions, fault displacement hazard curves, and dynamic strain assessments. He presented revised values for ground motion inputs currently being used in design. Both quasi-static and dynamic analyses are being used. For fault displacement hazard, the primary approach will be to avoid faults. Where this cannot be reasonably achieved, structures are being designed based on hazard values that are an order of magnitude more conservative than for vibratory ground motions. Some types of structures that will cross the Bow Ridge and Solitario Canyon faults (e.g., the North Ramp) should be designed to accommodate displacements of 12 cm and 30 cm, respectively; other structures will not need to be designed for fault displacement. Where faults are crossed, contingency requirements will be employed for maintenance and repair. Dr. Nolting next discussed dynamic strain, noting that dynamic strains and curvatures are given as a function of depth. In his discussion of the use of seismic data for surface design, he listed structural design inputs that include soil/rock foundation investigations, ground/structure interaction dynamic analysis, FEM static and dynamic analyses, and combined load cases. As an example, for the Waste Handling Building (the most important surface facility at the site), the structural flexibility, roof slab design, and equipment design

(e.g., overhead crane and equipment anchorages) are being analyzed. Dr. Nolting answered questions from observers on design values and how they would be used for specific facilities.

Next Ralston Barnard summarized the seismic disturbance calculations being conducted for the TSPA-VA. He noted that the PSHA results were being used to model rockfall, faulting (both inside and outside the repository), alterations of groundwater flow near the repository, and seismically induced transient rises in water-table. He focussed on the rockfall analysis, which includes thermo-mechanical as well as seismic triggering events. He noted that modeling being conducted by John Kemeny updates an Electric Power Research Institute model with current site data and PSHA results. Faulting hazard is not expected to have any direct PA impact on waste-package disruption if backfill is used. Potential alterations in groundwater flow path and head structure resulting from faulting outside the repository block are being considered. Questions from observers led to further discussion of disturbed events scenarios, such as the rock fall analysis, and their use in the TSPA.

Carl Stepp then summarized the project's plan for evaluating new data in accordance with regulatory requirements for the various phases of repository design, licensing, construction, and emplacement of the waste. He requested that PSHA project participants send new information that may be relevant to Ivan Wong, the designated responsible PSHA project person. He noted that when new data are determined to be potentially relevant, sensitivity analysis will be performed to assess the impact on the PSHA results, and the results of these analyses will be made part of the annual reporting. Also, the PSHA documentation will be updated as required by regulations to provide complete information for various license applications. He then summarized uses of the PSHA results, which include development of values for preclosure seismic design bases ground shaking and fault displacement; input to waste isolation and containment performance assessment; and input to the Safety Analysis Report supporting the application for a construction license.

Carl Stepp then opened the meeting to comments from the audience and to general discussion. Clarence Allen requested comments on the recent *Science* article by B. Wernicke *et al.* (Vol. 279, March 27, 1998). Dr. Stepp noted that there are several lines of evidence for strain rates in the Great Basin and that new interpretations must be considered in that context. John Whitney summarized the primary results of the study, which suggest that a strain rate of ~1 mm/yr, an order of magnitude greater than geologic slip rates. He noted that the USGS (through Jim Savage and his group) is preparing a formal written response to this paper that notes issues relating to: the small number of monuments, the dependence of the results on a single monument, monument stability, Jim Brune's calculated moment from the Little Skull Mountain earthquake and the need to examine aseismic aftereffects of this earthquake, recent work that shows increased strain rates across the Wasatch fault zone in Utah, basic research questions about what this strain means, and evidence of high velocity material under Crater Flat. He noted that the USGS is considering plans to rerun the Global Positioning System (GPS) network (which will include a station on Bear Mountain), rerun a vertical levelling

line, conduct a Synthetic Aperature Radar Interferometry analysis, and/or install laser strain monuments.

Jim Brune noted that the historical seismicity strain rate based on summing the moments of historical seismicity is minimal. Tests should be designed to see whether this is a transient effect related to the Little Skull Mountain earthquake. He also noted that Wernicke *et al.* (1998) did not mention evidence for high velocity under Crater Flat as recently reported by G. Bias.

Frank Perry stated that the postulated order-of-magnitude increase in the volcanic hazard as implied by the article was simplistic. He noted that Lathrop Wells, the most recent event in the region, occurred 80 ka ago, and that the tectonic setting of the region to the south was more active than the repository site. Tom Hanks noted that the expert teams heard about Wernicke's preliminary data at an earlier PSHA project workshop. At that time, the movement was largely confined to one station, with little movement indicated by the other stations.

The NRC was asked about their view of the Wernicke *et al.* paper. Phil Justus replied that in light of the investigations John Whitney mentioned the USGS is considering, new data that may be obtained will be to the benefit of the project. The NRC agrees that the Wernicke *et al.* observations may be explained by the hypothesis presented in their paper. He noted that any scientific paper that presents anomalous data will receive attention. He was gratified by the ability of the PSHA to address new data and hypotheses, stating that this project is unique in that it has pioneered a process to deal with such situations. He offered congratulations on the completion of the PSHA Final Report and stated that the NRC will independently evaluate and scrutinize the data. Dr. Justus noted that there is a high likelihood of questions, comments, and future interactions. He questioned how disruption event scenarios and insights from these analyses will be included in the TSPA-VA. During the rest of this fiscal year, the NRC will use the PSHA to resolve as many issues as possible, although many issues may not be resolved this year. Next fiscal year they will prepare written responses to seismic issues. He noted that a guidance document for PSHA (CFR Part 60) will be revised.

Leon Reiter commented that he hoped the final report for the PSHA will be clear and readable enough to be suitable to a range of audiences. He presented the following questions/comments to the audience: (1) it would be useful to receive comments on the Wernicke article from expert panel members, as well as from the CNWRA who reviewed it prior to publication; (2) he would like to hear from Review Panel members regarding their views of the PSHA process; (3) he questioned why peak ground motion values developed by Ivan Wong and others for an early study for the Exploratory Studies Facility (ESF) were lower than the values derived during the PSHA project; and (4) he questioned Carl Stepp's earlier statement that expert panel members hold sole ownership of their results, which is inconsistent with the position of the Senior Seismic Hazard Analysis Committee (SSHAC) that ownership should be shared with the technical facilitator/integrator (TFI) for the project.

In response to the fourth question, Carl Stepp stated that there had been considerable discussion of this issue at the beginning of the project; it had been decided that sole ownership by the experts was needed to sustain the integrity of the interpretations for NRC licensing purposes. Kevin Coppersmith noted that the TFIs maintain ownership in the process/procedures, but the expert panel members independently own their interpretations. Bob Budnitz stated that the SSHAC process considers ownership to reside in two places: the experts own their own interpretations, and the aggregate results are owned by the individuals who developed the algorithms for the analysis. Dr. Coppersmith stated that the goal throughout the project was to apply equal weights to all experts, and that he was prepared to defend this process.

In response to Dr. Reiter's first question, Bob Smith discussed the differences between the data and results for geodetic strain measured across the Wasatch Fault in Utah (many instruments were installed throughout a large area) and the data for the Yucca Mountain region presented in the Wernicke *et al.* article. He noted that although the Utah results also show strain rates higher than the seismologic- or geologic-based rates, the data are based on two independent determinations (GPS as well as triangulation and trilateration data). He noted that the results are a measure of an integrated effect with depth and that the question remains whether to distribute that strain aseismically or to assign it to faults. Such data provide a new source of information for areas having low strain rates, but the networks must be monitored for longer periods to obtain sufficient data to verify the anomalous rates, particularly in such a low-slip environment. Dr. Reiter asked whether the experts would have modified their models if the Wernicke *et al.* article had been published earlier. Dr. Smith responded that the data are so sparse that they probably would not make much difference, but without performing an analysis he could not say how the data would affect loading.

In response to Dr. Reiter's third comment, Ivan Wong noted that a very simple model was used to characterize local faults in the ESF study. The principal difference in ground motion values for the ESF study and the PSHA is that the kappa for the ESF study was based on empirical data from California. If the value of kappa used in the PSHA was applied in the ESF study, ground motion values would increase by approximately 40 percent, consistent with the values obtained from the PSHA. Norm Abrahamson noted that the derivation of kappa for the PSHA included information from the Little Skull Mountain earthquake.

Next John Stamatakos summarized the CNWRA review of the Wernicke *et al.* paper. He noted that Dr. Wernicke's research had been supported in part by the CNWRA, but that it was considered an independent study. The CNWRA had two GPS reviewers look at the data and calculations of errors; they were not asked to comment on the hypotheses themselves. Wernicke and others responded to the comments made by these reviewers, as well as the reviewers for *Science*. The CNWRA staff have since looked in more detail at the hypotheses presented in the published paper, and plan to submit a written response to *Science*. Dr.

Stamatakos reiterated the point made by Phil Justus that it is important that new hypotheses are put forth and challenged.

As a member of the Review Panel, David Schwartz made the following statements. He noted that the process of completing the PSHA project was interesting, but that more time was needed. He stated that seismic source characterization was relatively straightforward, and that there is a robust history to that part of the analysis. The fault displacement analysis, however, was a large and difficult undertaking that required venturing into new territory. He noted the site's complexity in the low degree of fault activity, small displacements, and complex rupture patterns. Given the data and time available, he believes the experts provided a good "first cut" at characterizing fault displacement potential for hazard assessment. He also addressed the readability of the report, stating that it could be improved so that the document would be more useful to the general public.

Allin Cornell commented that he believed the probabilistic analyses went well. He sees the fault displacement analysis as ground-breaking work that was conducted in a credible manner, with results that reflect broad uncertainty but low values. He noted that the process followed the SSHAC methodology, emphasizing the importance of experts adopting an evaluator role, and that the team approach smoothed out the edges of individual expertise and provided more robust results. He commended the TFIs (Kevin Coppersmith and Norm Abrahamson) for their efforts and noted that they were willing to address potential difficulties (such as significant outlier positions) that might have arisen. Fortunately, such problems did not arise, and equal weighting was appropriate. Dr. Stepp commented that he agreed with Drs. Coppersmith and Budnitz about ownership of the process and defense of the equal weights assigned to team assessments, but stressed again the importance of the expert's ownership of their evaluations. Dr. Abrahamson added that the process of feedback and technical challenge eliminated significant outlying positions and contributed to the success of the project.

Tom Hanks noted that staggering quantities of data were brought to the attention of the experts and that these data were successfully incorporated into manageable and coherent results. He noted that available data were generally well understood, and that new data and interpretations (e.g., inputs to kappa; the Wernicke *et al.* paper) would be dealt with by the project as they become available. He also noted that the results of the PSHA can be constructed from the information contained in the final report, having confirmed for himself that it is not necessary to use a computer to verify the results of the study.

In his summary statements, Jim Brune, expressed agreement with the general comments of the three other Review Panel members. He stated that because he and the other reviewers were involved in the entire PSHA process, they likely would find the final report more readable than would an outsider. He added that he had looked at the expert's interpretations of fault physics and concluded that they are reasonable. However, he believes that some of

the final results are too conservative when projected to the surface, based primarily on his analysis of unstable rocks in the region.

Carl Stepp closed the meeting by acknowledging the tremendous work of all the project participants, specifically noting the contributions of Ivan Wong in managing the project schedule and Sue Penn in organizing workshops and maintaining project communication. Tim Sullivan added his thanks to all, and expressed his enthusiasm that the project was complete. The meeting was adjourned by Carl Stepp.

ATTACHMENT 1

YUCCA MOUNTAIN PSHA FINAL RESULTS MEETING
Monday, April 6, 1998, AmeriSuites Hotel, Las Vegas

Final Agenda

Times	Topic	Speaker
from 6:00 am	Continental Breakfast (free to overnight guests; $6/person otherwise)	
8:30 to 8:35	Introduction	Tim Sullivan
8:35 to 8:50	Project Overview (Process and Roles, Structure of this Meeting)	Carl Stepp
8:50 to 9:00	Project Reports	John Whitney
9:00 to 9:30	Seismic Source Characterization	Kevin Coppersmith
9:30 to 10:00	Ground Motion Characterization	Norm Abrahamson
10:00 to 10:15	Break	
10:15 to 11:15	Ground Motion Hazard Results	Gabe Toro
11:15 to 11:45	Fault Displacement Characterization	Bob Youngs
11:45 - 1:00	Lunch	
1:00 to 2:00	Fault Displacement Hazard Results	Gabe Toro
2:00 to 2:30	Overview of Seismic Design Inputs Development	Robin McGuire
2:30 to 3:00	Use of Seismic Inputs in Design	Rick Nolting
3:00 to 3:15	Break	
3:15 to 3:45	Use of Seismic Hazard Results in PA	Ralston Barnard/George Barr
3:45 to 4:15	Where Do We Go From Here (New data issue, Seismic Topical Report #3)	Carl Stepp
4:15 to 5:00	Comments from Observers	
5:00	Closing Remarks	Tim Sullivan/Carl Stepp

TABLE 1. YUCCA MOUNTAIN PROBABILISTIC SEISMIC HAZARDS ANALYSES FINAL RESULTS MEETING
April 6, 1998
Attendance List

Name	Affiliation
1. Abrahamson, Norm	Consultant
2. Ake, Jon	U.S. Bureau of Reclamation (USBR)
3. Allen, Clarence	California Institute of Technology
4. Anderson, Ernie	U.S. Geological Survey (USGS)
5. Anderson, John	University of Nevada, Reno (UNR)
6. Anderson, Larry	USBR
7. Arabasz, Walter	University of Utah (UU)
8. Barnard, Ralston	Sandia National Laboratory (SNL)
9. Becker, Ann	Woodward-Clyde Federal Services (WCFS)
10. Bruhn, Ron	UU
11. Brune, James	UNR
12. Burnitz, Roby	--
13. Campbell, Ken	EQE International
14. Chen, Rui	Southwest Research Institute
15. Coppersmith, Kevin	Geomatrix
16. Cornell, Allin	Consultant
17. dePolo, Craig	UNR
18. Duan, Fei	Morrison-Knudsen
19. Dunn, Tom	Morrison-Knudsen
20. Echols, Stan	Winston & Strawn
21. Firth, Jim	U.S. Nuclear Regulatory Commission (NRC)
22. Fridrich, Chris	USGS
23. Frishman, Steve	State of Nevada
24. Gamble, Bob	Booz, Allen & Hamilton
25. Gil, April	U.S. Department of Energy (DOE)
26. Glenn, Chad	NRC
27. Greenberg, Harris	MTS/S&W
28. Gregor, Nick	Consultant
29. Hanks, Tom	USGS
30. Hanson, Kathryn	Geomatrix Consultants

TABLE 1. YUCCA MOUNTAIN PROBABILISTIC SEISMIC HAZARDS ANALYSES FINAL RESULTS MEETING

April 6, 1998

Attendance List

Name	Affiliation
31. Hawe, Tim	DOE
32. Ibrahim, Bakr	NRC
33. Justus, Phil	NRC
34. Knuepfer, Peter	State University of New York at Binghamton
35. McCalpin, Jim	GEO-HAZ Consulting, Inc.
36. McGuire, Robin	Risk Engineering
37. McKague, Larry	Center for Nuclear Waste Regulatory Analyses (CNWRA)
38. Menges, Chris	USGS
39. Nataraja, Mysore	NRC
40. Nolting, Rick	Morrison-Knudsen
41. O'Leary, Dennis	USGS
42. Orvis, Doug	Morrison-Knudsen
43. Parks, Bruce	USGS
44. Penn, Sue	WCFS
45. Perman, Roseanne	Geomatrix
46. Pezzopane, Silvio	USGS
47. Quittmeyer, Richard	WCFS
48. Ramelli, Alan	UNR
49. Reiter, Leon	Nuclear Waste Technical Review Board
50. Rogers, Al	EQE International
51. Savy, Jean	Lawrence Livermore National Laboratory
52. Schwartz, David	USGS
53. Seddon, Bill	DOE
54. Sheaffer, Patricia	Pacific Western Technologies
55. Slemmons, Burt	WCFS
56. Smith, Ken	UNR
57. Smith, Robert	UU
58. Somerville, Paul	WCFS
59. Stamatakos, John	CNWRA
60. Stellavato, Nick	Nye County, NV
61. Stepp, Carl	WCFS

TABLE 1. YUCCA MOUNTAIN PROBABILISTIC SEISMIC HAZARDS ANALYSES FINAL RESULTS MEETING
April 6, 1998
Attendance List

Name	Affiliation
62. Sullivan, Tim	DOE
63. Swan, Bert	Geomatrix
64. Toro, Gabe	Risk Engineering
65. Tynan, Mark	State of Nevada
66. von Tiesenhausen, Engelbrecht	Clark County Nuclear Waste Division
67. Walck, Marianne	Sandia National Laboratory
68. Whitney, John	USGS
69. Wong, Ivan	WCFS
70. Yount, Jim	Geomatrix
71. Yount, Jim	USGS

APPENDIX D

SUMMARIES OF GROUND MOTION WORKSHOPS

SUMMARIES OF GROUND MOTION WORKSHOPS

Civilian Radioactive Waste Management System
Management & Operating Contractor

Summary of Data Needs Workshop on Ground Motion at Yucca Mountain

Salt Lake City, UT
April 20 and 21, 1995

May 25, 1995

Prepared for

U. S. Geological Survey
Box 25046, MS-425
Denver Federal Center
Denver, CO 80225

Prepared by

Woodward-Clyde Federal Services of
Civilian Radioactive Waste Management System
Management & Operating Contractor
101 Convention Center Drive
Suite P-110
Las Vegas, NV 89109

Under Contract Number
DE-AC01-91RW00134

INTRODUCTION

The United States Geological Survey (USGS) is carrying out a probabilistic seismic hazards analysis (PSHA) Yucca Mountain, Nevada as part of the Department of Energy's (DOE) project to characterize this site as a potential geologic repository for high-level radioactive waste. The aim of this study is to provide the annual probability with which various levels of vibratory ground motion and fault displacement will be exceeded at the site. These results will be used as a basis for developing seismic design inputs and in assessing the performance of the site.

The PSHA process involves development by two panels of experts of input interpretations and assessments of uncertainties required by the hazards calculations. One panel addresses characterization of seismic sources and fault displacement, while the other deals with vibratory ground motion. Development of interpretations is being facilitated through a series of structured workshops to evaluate available data, to explore the range of interpretations allowed by the data, to examine critically the interpretations proposed by the experts, and to provide feedback on the implications of various interpretations for the seismic hazard at the site. The goal of this process is to have differences in experts' interpretations be the results of true differences in judgment and not differences in access to data, differences in definition, or differences resulting from a lack of understanding each others' interpretations. This report summarizes the first in the series of structured workshops for characterization of ground motion: the Data Needs Workshop.

The Workshop began with introductory comments including an overview of the DOE's Yucca Mountain project and specifically the PSHA project. Team experts were next briefed on several issues of relevance to the ground motion characterization and existing data bases. This information provided the grounds for a discussion by the experts of additional data required to perform a comprehensive assessment of ground motion attenuation at Yucca Mountain. Each speaker has provided a brief summary of his presentation. These summaries and copies of overhead transparencies are included as an Attachment to this Summary.

The Workshop was attended by a representative of the DOE, Tim Sullivan, and the Project Management Team, John Whitney, Carl Stepp, Ivan Wong, and Jean Savy All Ground Motion Team experts were present: John Anderson, David Boore, Kenneth Campbell, Art McGarr, Walter Silva, Paul Somerville, and Marianne Walck. Members of the Ground Motion Facilitation Team in attendance were Norman Abrahamson, Ann Becker, and John Schneider. Several members of other Teams organized for the PSHA project were also present: James Brune, Allin Cornell, and Tom Hanks (Project Oversight Panel), Robin McGuire and Richard Quittmeyer (Seismic Design Basis Team), Gabriel Toro (PSHA Calculations Team), and Mary-Margaret Coates (Data Management).

THURSDAY, APRIL 20, 1995

Introductory comments were made by Tim Sullivan, Carl Stepp, and Norman Abrahamson. The DOE Yucca Mountain Project (YMP), its objectives and background, the proposed facilities, and the project regulatory framework were summarized by Tim Sullivan. The PSHA study will consider surface ground motions on a hypothetical rock outcrop and surface ground motions on the alluvium in Midway Valley. Ground motions at the repository depth will not be considered in this study. Results of the study will be described in a report that will form part of the last in a series of three Topical Reports regarding the seismic assessment of Yucca Mountain. The Topical Report is scheduled for release in FY 1997. The findings are primarily to address the preclosure period (100 yrs), but will also be used to evaluate the postclosure (10,000 yrs) performance of the site. As outlined by Carl Stepp, the primary goal of the PSHA study is to provide input to development of seismic design parameters. The project objectives necessarily include documenting the process for regulatory review. An essential technical element is the incorporation of scientific uncertainty. This will be accomplished by considering the interpretations of a group of individual experts who will themselves incorporate uncertainty in their individual hypotheses. Norman Abrahamson, the Ground Motion Facilitation Team Leader, detailed the criteria for selection of the ground motion experts and the criteria for participation in the project. The experts must be "evaluators" of the various ground motion models. He emphasized that failure to act in a manner consistent with the criteria, particularly the endorsement of any single ground motion model without due consideration of other models would be unacceptable to the required role of evaluator expert. Dr. Abrahamson also itemized the ground motion estimates which are required for the analysis (see attached statement) and summarized the results of a preliminary assessment of the Exploratory Studies Facility as a point of reference to the PSHA project.

Because the experts must incorporate uncertainty in their ground motion predictions, the means by which uncertainty is characterized were discussed (Gabriel Toro). Total variability is composed of uncertainty and randomness, each of which can be partitioned into parametric or modeling variability. Several examples of the partitioning were cited and explained. The practical implications of large and small uncertainties were also presented and the tradeoffs inherent in categorizing uncertainty.

The elicitation process and experts' roles within the process were laid out (Jean Savy). Consensus among the experts is <u>not</u> the aim of the process. Although each expert must ultimately act as an evaluator of all models, each may also be asked to function as a proponent of a particular model in subsequent Workshops for the benefit of the other experts. Each is responsible for forming, defending, and documenting his final ground motion estimates. The project schedule was presented and the formal elicitations are planned for February and March of 1996.

The remaining briefings on the first day covered various technical issues and available seismologic data. Silvio Pezzopane discussed the tectonic and seismologic setting. He shoed

known and suspected Quaternary faults and provided a comprehensive table summarizing their characteristics. A second table listed a preliminary evaluation of "relevant" (DOE specification) and Type I (U. S. Nuclear Regulatory Commission specification) faults. Data on source parameters, crustal structure (velocity profiles) and attenuation (Q), and site effects were summarized by John Schneider. Variations in stress drop and Q were noted in the results of various studies. Within 5 to 10 km of the planned repository, a variety of geophysical data are available and two current studies will provide information local to the site. The DOE is measuring velocities in several bore holes in the immediate vicinity to depths of 1500 ft and the USGS is evaluating shallow and deep crustal profiles from a seismic refraction and reflection survey. Walter Silva summarized the effect of site conditions on spectra using empirical and theoretical data. The latter were also used to illustrate the potential influence of the uncertainty in the site properties as compared to the potential influence of variability of source properties in terms of the resulting variability of the ground motion.

A key set of seismological data near Yucca Mountain was recorded in the 29 June 1992 Little Skull Mountain main shock (m_b 5.6) and aftershock sequence (Kenneth Smith). The data shown include focal mechanisms and depth sections of aftershocks. Main shock accelerograms were recorded at an array maintained by URS/John A. Blume & Associates for the DOE with epicentral distances of 15 km to 232 km from the main shock. Records are also available from portable arrays of instruments deployed by the USGS and the University of Nevada-Reno (UNR) for the aftershock sequence. A second data set was obtained from the 1993 Rock Valley sequence and an event in Rock Valley triggered by the Little Skull Mountain (LSM) earthquake. This set includes focal mechanisms, event locations, and seismograms. Site response in Midway Valley and Yucca Mountain was assessed by UNR (John Anderson) using a number of earthquakes. Kappa and relative site amplification (as a function of frequency) were estimated at 12 stations from the LSM main shock and various other earthquakes.

Site response effects were also examined by Marianne Walck using underground nuclear explosion (UNE) data. The UNE data indicate strong azimuthal dependence on amplification. The more relevant data were recorded at various sites since 1977. These data have been evaluated for 2-dimensional crustal structure to explain the amplification and transfer functions have been developed for three uphole/downhole station pairs within about 3 m of the perimeter of the planned repository.

The special case of near fault ground motions was presented by Paul Somerville. Few earthquake data are available within about 5 to 10 km a fault rupture. Empirical and synthetic data show a levelling off of ground motion in these distances. Other issues summarized include the effects of rupture directivity, the difference between vertical and horizontal spectra shapes, and the effect of the style of faulting.

The final presentation was a quality assurance (QA) training by Martha Mustard. The experts were briefed on the project QA requirements for which the overriding philosophy is that the level of QA detail must ensure the reproducibility of the results. The expert elicitation process is currently being incorporated into a QA procedure.

FRIDAY, APRIL 21, 1995

There are two current USGS projects with direct relevance to the ground motion methodology activities. The first activity, described by Paul Spudich, is to evaluate empirical ground shaking models for extensional tectonic regimes. Currently the USGS is assembling a worldwide data set from normal and strike-slip faulting in these regions. The goal is to first evaluate several empirical attenuation relationships and, if they do not adequately describe the data, to develop correction factors for the relationships or alternatively produce a new relationship based on the extensional data. The evaluation of existing relationships should be completed by October, 1995. The second activity is the ground motion modeling of scenario earthquakes at Yucca Mountain. John Schneider outlined the project which is aimed at estimating ground motion (response spectra and time histories) with uncertainty for six realistic earthquake faulting scenarios. Six different modeling methods will be used. These procedures will first be calibrated against the Little Skull Mountain records.

The existing ground motion estimation methods were then reviewed by Norman Abrahamson. They comprise empirical (earthquake and underground nuclear blast data), numerical, and hybrid empirical-numerical schemes. The input required by each model was summarized and it was noted that some additional work is needed to determine the appropriate source parameters for the different models (particularly, the numerical simulation models).

DATA NEEDS

Throughout the Workshop, the Team discussed various technical issues which must be resolved and data which are required for a thorough assessment of the ground motion estimates. Following the last formal presentation, Dr. Abrahamson led a discussion summarizing the issues which must be resolved. Six principle issues were identified for further study and were prioritized as to importance by the experts. Most of the Issues are self-explanatory and arise from a lack of detailed information or from a need to further evaluate an available data set. The issues are:

Issue 1: What are the site response characteristics specific to Yucca Mountain?

Issue 2: What is the range of values of source parameters for earthquakes in this region of the Basin and Range? (These are model dependent.)

Issue 3: What is the explanation for the apparent aseismic slip in the uppermost few kilometers of crust for earthquakes with rupture that reaches the surface?

Issue 4: What is the Yucca Mountain specific ground motion attenuation predicted by various numerical ground motion simulations?

Issue 5: What is the basis for apparent discrepancies in the literature regarding regional attenuation (combined effect of Q and geometrical spreading)?

Issue 6: What is the explanation for the reported large amplification of motions at Yucca Mountain compared to other NTS sites?

Issues 1, 2, and 6 will be satisfied by obtaining new data or evaluating existing data. Issue 3 arises from Workshop discussions regarding numerical modeling procedures. Numerical models are typically implemented with no slip assigned to the uppermost few kilometers of the rupture surface. This assumption is attributed to two possible physical constraints which the Team believes must be investigated: either low shear modulus characterizes materials in this zone or a long source rise time. Numerical simulations specific to the proposed repository conditions (Issue 4) will be used by the experts to evaluate ground motion predictions by the various models and methods. An investigation into regional attenuation (Issue 5) is required to resolve conflicting research results on geometrical spreading and Q.

During their deliberation, the experts identified data or analyses required to resolve these issues. These specific Data Needs are discussed in detail below and are summarized in Table D-1.

Site Response

To evaluate the site response requires the shear wave velocity profile on rock and alluvium (Midway Valley). Ideally, this profile should extend to 1500' depth, but shallower profiles will also be useful.

In addition to the low strain velocity profiles, standard geotechnical information, in terms of strain dependence of the shear modulus and damping, are also needed for both rock and alluvium.

Action:
Summarize the existing velocity profile and high strain data and identify additional data collection and/or analyses that are needed. These data needs will be addressed by the DOE through their existing program.

Source Parameters

The main source parameter required for numerical simulation models is the stress-drop. The "stress-drop", however, has different meanings for the different models. For example, the stochastic needs the "high frequency stress-parameter" whereas the composite source model needs the sub-event stress-drop.

A key event is the Little Skull Mountain earthquake because it was located close to Yucca Mountain. Because these data are so important, they require special attention including a site visit to determine the geologic site conditions.

Action:
Estimate the distribution (mean and standard deviation) of the stress-drop appropriate for each model appropriate for the Basin and Range using the USGS extensional data stet as well as the aftershocks of the Little Skull Mountain and Rock Valley earthquakes. Some of this work will be done as part of the ground motion scenario earthquake exercise being run by the USGS or as part of the ground motion studies by UNR. the stress-drop for the stochastic point source model will not be addressed by these other studies and needs to be developed as part of the PSHA study.

Aseismic Shallow Slip

The faulting at Yucca Mountain clearly shows that the fault ruptures to the surface, however, if large surface slip is used with the current numerical models, they drastically overpredict the high frequency ground motion near the fault as well as produce large long period surface waves. Because these effects have not been observed in empirical recordings close to faults with shallow slip, users of the models have interpreted the shallow slip to be aseismic. By not modeling the observed shallow slip, the numerical simulation models appear to be deficient. The models have not considered using long rise-times for shallow slip which may help resolve this apparent deficiency. The impact of the shallow rupture has been partially considered in the recent Southern California Earthquake Consortium (SCEC) study. These results will be summarized in a SCEC report in June 1995. Additional insight can be gained by a detailed study of the few earthquakes that have had significant shallow slip as well as nearby recordings on rock. Two events that meet these criteria are the 1987 superstition Hills and 1992 Landers earthquakes.

Action:
Perform a sensitivity study to determine the range of rise-times for shallow slip that can be used and still give reasonable agreement with the recorded data. This will provide a means for including the shallow slip without generating unrealistic ground motions. This work may be performed as part of the scenario ground motion study.

Numerical simulations

Because there is little strong motion data in the Basin and Range, and in particular at Yucca Mountain, numerical simulations will be used to provide the experts with region- and site-specific estimates of the ground motion attenuation.

The stochastic point source should be run at all magnitudes and distances for which the experts will be asked to predict the ground motion. The stochastic point source will serve as a reference model and is selected for this purpose because it is simple and well understood by the experts.

Because the site is located close to the faults, finite-source models should also be used to estimate the ground motion for the larger magnitudes (M 6-7). The following models should be considered:

Stochastic finite-fault model
Composite source model
Empirical source function model
Hybrid empirical model

All of these models except for the hybrid empirical are being used as part of the scenario ground motion study to predict the ground motion for magnitude 6.4 normal faulting events and magnitude 7.0 strike-slip faults. this study will not consider magnitude 7.0 normal faulting events.

Action:
Compare ground motions for the following cases:

Stochastic point source model for magnitudes 5 to 7 for distances of 1 to 100 km
Finite-fault model for a magnitude 7 normal faulting event for distances less than 10 km

Regional Attenuation

Different studies have come to apparently inconsistent conclusions about Q (inelastic attenuation) in the Basin and Range. Some structures have found lower attenuation than in California whereas other studies have found similar attenuation as in California. some of this discrepancy may be due to different assumptions about the geometrical spreading. Because the net attenuation of ground motion depends on both the Q and the geometrical spreading, there is a trade-off between these two parameters.

Action
Compare the net attenuation (combined effect of Q and geometrical spreading) for the different studies to determine if the results are really inconsistent.

Yucca Mountain Site Amplification

Previous studies by Sandia have found anomalously large site amplification at Yucca Mountain from UNE data. However, this anomalous amplification may result only from shallow sources (such as explosions) and may not be applicable to ground motions from earthquakes that tend to be from much greater depths. UNR has recorded several aftershocks of the Little Skull Mountain and Rock Valley earthquakes that can be used to estimate the site response for earthquakes. UNR is already developing site-response estimates for this data set.

Action

Evaluate the Sandia study (Philips) and determine if the results are applicable to the earthquake ground motions at Yucca Mountain.

Identify the geologic site conditions for the strong motion stations that recorded the Little Skull Mountain earthquake. This task will be addressed by the DOE/USGS.

TABLE D-1
GROUND MOTION ESTIMATION DATA NEEDS

ISSUE 1: SITE RESPONSE CHARACTERISTICS

Data Needed:
Site profile information
Shear velocity of rock and soil (geophysical)
Geotechnical properties (soil and rock)

ISSUE 2: SOURCE PARAMETERS

Data Needed:
Evaluate distribution of stress drop (for each model)
Main shocks and significant aftershocks (USGS data)
Aftershocks (Little Skull Mountain and rock Valley earthquakes)
(Site conditions for Little Skull Mountain main shock recordings)

ISSUE 3: NON-SEISMOGENIC SHALLOW SLIP

Data Needed:
Evaluate research related to effects of shallow slip
SCEC summary
Detailed study of Superstition Hills and Landers (Lucerne records) earthquakes

ISSUE 4: NUMERICAL SIMULATIONS

Data Needed:
Perform numerical simulations
Stochastic point source model (set as reference; run for all distance-magnitude pairs)
Stochastic finite fault model (run for distances less than 10 km at magnitude 7)
Composite source model (run for distances less than 10 km at magnitude 7)
Empirical source function model (run for distances less than 10 km at magnitude 7)
Hybrid empirical model (run for distances less than 10 km at magnitudes 6.4 ant)

ISSUE 5: REGIONAL ATTENUATION

Data Needed:
Investigate regional attenuation (existing studies and new data)
Methodological differences in studies on geometrical attenuation and Q?
Investigate Little Skull Mountain data (require instrument site conditions, kappa, processing)

ISSUE 6: YUCCA MOUNTAIN AMPLIFICATION

Data Needed:

Compare additional data with previous study

Summary of amplitude variation with distance for blast data and earthquakes (M>3) from Upgraded UNR network data

Summary of Little Skull Mountain amplitude variation with distance

Evaluate Sandia study (Phillips) for applicability

Civilian Radioactive Waste Management System
Management & Operating Contractor

Summary of Methods, Models, and Preliminary Interpretations Workshop on Ground Motion at Yucca Mountain

Salt Lake City, UT
January 9 and 10, 1997

Prepared for

U. S. Geological Survey
Box 25046, MS-425
Denver Federal Center
Denver, CO 80225

Prepared by

Woodward-Clyde Federal Services of
Civilian Radioactive Waste Management System
Management & Operating Contractor
101 Convention Center Drive
Suite P-110
Las Vegas, NV 89109

February 4, 1997

INTRODUCTION

The United States Geological Survey (USGS) is currently performing a probabilistic seismic hazards analysis (PSHA) of the proposed high-level radioactive waste repository at Yucca Mountain, Nevada. The study is an element of the Department of Energy's (DOE) site characterization activities. The PSHA will result in the annual probability of exceedance of various levels of vibratory ground motion and fault displacement.

Input to the PSHA is being developed by two panels of experts: one characterizes seismic sources and fault displacement and the second estimates vibratory ground motion. Their interpretations are being facilitated in a series of structured workshops. The goal of the process is to have differences in experts' interpretations result from true differences in judgment and not differences in access to data, definition, or lack of full understanding of each other's interpretations. This report summarizes the second in the series of workshops for characterizing ground motion: the Methods, Models, and Preliminary Interpretations Workshop.

The Workshop proceedings included discussions of Yucca Mountain and site-specific issues as they relate to ground motion modeling. An understanding of these issues is necessary to evaluate whether and to what extent existing models of ground motion may require modification to adequately estimate motions at the proposed repository. Several models have been developed or revised since the first Workshop (Data Needs, April 1995) and these were presented in detail. Finally, results of a preliminary modeling exercise (posed to the Experts in advance of the Workshop) was discussed. Each speaker provided copies of presentation materials and these are included as an Attachment to this Summary.

The Workshop was attended by a representative of the DOE, Tim Sullivan, and members of the Project Management Team, John Whitney, Carl Stepp, Ivan Wong, and Richard Quittmeyer. All Ground Motion Team Experts were present: John Anderson, David Boore, Kenneth Campbell, Art McGarr, Walter Silva, Paul Somerville, and Marianne Walck. Members of the Ground Motion Facilitation Team in attendance were: Norman Abrahamson and Ann Becker. Also present were Robin McGuire, Seismic Design Team Leader; Gabriel Toro, PSHA Calculations Team Leader; and Review Panel members Allin Cornell, Tom Hanks, and James Brune. Technical Observers included representatives from the NRC, NWTRB, ACNW, and the CNWRA.

THURSDAY, JANUARY 9, 1997

The full scope of the Experts' involvement was detailed by Norman Abrahamson, the Ground Motion Facilitation Team Leader. They must develop ground motions as a series of point estimates for specified magnitudes and source - site geometries. Both strike-slip faulting on a vertical surface and normal slip on a moderately dipping fault are to be considered. The site

is representative rock with dynamic properties equivalent to the existing conditions at repository level (called "repository outcrop"). The repository outcrop is based on the velocity profile with the top 300 m removed. Horizontal and vertical motions will be estimated for peak ground acceleration, peak ground velocity, and spectral acceleration at frequencies of 0.5, 1, 2, 5, 10, and 20 Hz. The Experts must document in detail the reasoning underlying their interpretations. The median ground motion, aleatory uncertainty, and the epistemic uncertainties of both are to be provided. The importance of quantifying uncertainty was discussed in the context of the elicitation process by an expert in these techniques (Peter Morris, Wednesday joint session with Seismic Source Characterization Team). This was elaborated on (Gabriel Toro, Thursday) and the partitioning of uncertainty as parametric or modeling and (orthogonally) as aleatory or epistemic was discussed. Several relevant examples of the partitioning as it relates to ground motion modeling were presented to thoroughly inform the Experts of the process.

A fundamental question which the Experts must address is whether ground motions at Yucca Mountain differ from the motions represented by the data set which forms the basis for empirical models. Differences could be caused by source effects (extensional vs. compressional regimes and normal vs. strike-slip faulting), path effects (crustal differences), or site effects (site response). It was shown that significant differences in near fault ground motions for normal and reverse faults are observed in foam rubber models (James Brune). The propagating wavefront in dip-slip faulting is greatly affected by normal stresses. In reverse faulting, the surface reflected wave is dilatational and reduces normal stress on the slip surface. Foam rubber models show the reflected wave destabilizes the fault and results in increased particle motions in the hanging wall and at the fault tip. In normal faulting, the reflected wave is compressional, which stabilizes the fault and results in weak motions. Additionally, weak surficial layers were shown to significantly reduce the ground motion from near-surface slip due to increased rise-time. This supports ground motion modeling experience which consistently shows reduced high frequency motion radiated from near-surface layers.

The USGS (Paul Spudich) has compiled a data base of strong ground motion records in extensional tectonic regimes. The criteria for inclusion were that the data were: (1) available in digital form; (2) recorded in the free field or in structures less than 3 stories high; (3) triggered before the S-wave arrival; (4) resulted from earthquakes with moment magnitude at least 5; and (5) recorded at distances no greater than 105 km. Nine normal faulting events in the data base were inverted for stress drop and kappa using a Brune ω^2 spectral form with a single corner frequency (Ann Becker). The median stress drop was about 30 bars for several cases using site transfer functions developed by Silva and about 60 bars using site transfer functions by Boore and Joyner. The median kappa obtained was about 0.04 to 0.06 sec for all sites and the inversion results confirmed that the Little Skull Mountain recording sites have particularly low kappas (about 0.015 sec). This compares with stress drops for western North American events of 70 to 100 bars (Boore-Joyner, using Boore-Joyner amplifications) and for six California earthquakes of about 37 bars (Silva, using Silva's amplifications).

The faults in the Yucca Mountain region are generally characterized by low slip rates. However, slip rate has not been included in regressions of fault length on magnitude (John Anderson). Comparisons between regressions including and excluding slip rate show that ignoring slip rate may underestimate the magnitude. Or, for a given rupture length, larger earthquakes occur on faults with lower slip rates than on faults with high rates implying a larger static stress drop for low slip-rate faults. Anderson also presented the composite source model and showed how it can be used to estimate energy and several stress parameters. The key stress parameters for ground motion are dynamic stress drops, not the static stress drop. Anderson noted that lower ground motions from extensional regimes can be modeled by lower than average dynamic stress drops even if the static stress drop is larger than average. Anderson also briefly summarized the Dinar, Turkey M 6.4 normal faulting earthquake (1 Oct 1995) which caused surface rupture. Records were obtained at close distances to the fault plane and an analysis of the event has been initiated. The results should be available in February.

Site response issues were discussed in terms of measured nonlinear response of tuff samples obtained from Yucca Mountain (Kenneth Stokoe). Resonant column and dynamic torsional shear testing was performed on two welded and one unwelded tuff specimens. The specimens are not homogeneous and results of the resonant column testing are robust whereas the torsional shear tests are less so. The modulus degradation with increasing shear strain is less nonlinear than granular samples, but the low-strain modulus is significantly greater than granular soils. Similarly, material damping is low. Measured low-strain shear wave velocities are 4200, 5800, and 8100 fps (1300, 1800, 2500 m/sec) for the unwelded and welded tuffs, much greater than the approximately 600 m/sec measured in-situ (Schneider et al., Ground Motion Modeling of Scenario Earthquakes at Yucca Mountain, Final Report for Activity 8.3.1.17.3).

The effect of source, site, and regional crustal differences was evaluated using the point-source Band-Limited-White-Noise (BLWN) source model combined with Random Vibration Theory (RVT) (Kenneth Campbell). Ratios of synthetic motions (horizontal motion; response spectra ratios) for California- and Yucca Mountain-type sites showed the largest sensitivity to site kappa at frequencies higher than about 10 Hz and to stress drop at all frequencies. Regional effects other than event stress drop also cause significant amplification at high frequency for Yucca Mountain-type sites. At high frequencies, significant differences between Campbell's results and a similar analysis by Silva were noted. These differences were primarily due to different site amplifications models developed by Boore and Silva. Differences in Q models also contributed to the differences. Campbell and Silva are working to resolve these differences.

The empirical data base at Yucca Mountain consists of data recorded from underground nuclear tests. The records have been interpreted by Walck (Workshop #1) for two-dimensional crustal structure. The very shallow blasts result in large surface waves. There

are also unusual wave propagation effects observed at some locations in NTS (not Yucca Mountain) which are not well understood (Paul Somerville). Confined shallow sources, such as the blasts, are not common in large earthquakes so the variability from typical earthquake depths may be much less than observed in the blast data.

Existing empirical relationships were next examined. The USGS extensional regime study (Paul Spudich) focused on calculating correction factors for empirical relations to better fit the extensional data, and on developing a new predictive relation derived from the extensional data. The factors include a bias correction and a standard deviation correction for all distances and also for distances less than 20 km. Many of the factors show a period dependence. Spudich also presented the new attenuation relation developed using extensional regime data only. This model should be applicable to Yucca Mountain without changes to the source.

FRIDAY, JANUARY 10, 1997

The second day of the Workshop continued with discussions of proponent models arising from empirical data. The Abrahamson and Silva (1996) relationship was not available at the time of the USGS study; style-of-faulting modification factors were provided (Norman Abrahamson) as well as a discussion of the regression procedure.

An advantage to numerical simulations is the ability to modify input parameters to evaluate the sensitivity of ground motions to the parameters (and thus uncertainties) and compute scaling factors. Walter Silva presented results using the point source RVT model, and Kenneth Campbell for the hybrid empirical model. (The attached notes for Dr. Silva's presentation are not complete; much of his work was performed under separate contract to the DOE and was not authorized for release in print form.) Silva has calibrated the point source model using data from 16 earthquakes. This calibration exercise also provides estimates of the modeling uncertainty term. Silva's point source model will be presented to the experts with variable stress-drop so the experts can select their own estimate of the stress drop in applying the model.

Campbell's approach is to estimate ground motions by scaling existing empirical relationships. He develops the scaling factors from comparisons of California motion estimates to Yucca Mountain motion estimates, both developed using the BLWN RVT point source model. The examples he presented correspond to a postulated M 6.5 earthquake at 10 km distance and considered both strike-slip and normal faulting. The correction factors for peak ground acceleration were presented for three discrete values of stress drop and ranged from 1.053 to 1.832. Campbell will provide a complete set of estimates for other magnitudes, distances, and periods as part of his proponent model.

A third class of proponent models arises from the blast data base consisting of thousands of recordings at NTS (T. Joseph Bennett). Three alternative methods were presented for defining the attenuation relationship using information from the blast data. The first model uses the NTS data directly with a conversion from explosion yield to earthquake magnitude. The second model uses the attenuation rates from the blast data but with the spectral shape defined by California empirical attenuation models. This second method addresses the issue of different spectral content in explosions and earthquakes. The third method uses the attenuation rate from explosions but with a spectral shape from the Little Skull Mt. earthquake.

Because of the lack of an empirical earthquake ground motion data base at Yucca Mountain, the relevance and applicability of numerical models was the focus of the USGS report Ground Motion Modeling of Scenario Earthquakes at Yucca Mountain (J. F. Schneider *et al.*, WCFS, written communicaiton, 1996). Predictions from six methods were included in the study (Abrahamson) which covered the range of modeling methods commonly used in ground motion estimation. In the Scenario exercise, the investigators calibrated their models to data recorded in the 1992 Little Skull Mountain event and then computed motions for scenario earthquakes occurring on tectonic sources which could potentially affect Yucca Mountain. The suite of scenario earthquakes consist of five normal faulting sources and two strike-slip. The simulated motions for the normal faulting case were higher than attenuation relations derived from western U. S. data by about 60% at distances less than about 5 km and by about 20% at 15 km. The variation at short distance was attributed to differences in kappa and at longer distance due to crustal amplification and directivity. For the strike-slip event, the computed motions exceeded existing attenuation relationship predictions by about 30 % at 25 km, again attributed to kappa, but were consistent with predictions at 50 km distance.

Recent results from finite element modeling of a postulated rupture on the Bare Mountain fault beneath the repository region was presented (David Ferrill). The model assumes the regional faults are connected at depth along a subhorizontal detachment. Slip on an initially rupturing segment is transferred up-dip towards the surface and down-dip to the detachment. The modeling indicates that the rupture can trigger slip on other faults and result in higher accelerations than if it were confined to a single faulting surface. At distances approximating the location of the proposed repository, peak horizontal ground accelerations at the surface may exceed predicted values from empirical attenuation relationships by about 50%.

Although the Yucca Mountain region has not experienced a major earthquake in historic times, the western boundary of the Basin and Range has and clues to ground motion attenuation may be found in studies of the numerous precariously balanced rocks found region-wide (James Brune). The distance of balanced rocks from the ruptures combined with the acceleration required to topple these rocks provide physical evidence of the attenuation of motion surrounding an historic earthquake. This information is currently being collated to provide a constraint on ground motion attenuation in the region. Near the repository itself, balanced rocks could be toppled by about 0.3 g accelerations, and semiprecarious rocks by

about 0.4 g. Age-dating the rock varnish indicates that they have been precariously positioned for about 40,000 to 80,000 years, suggesting a bound on these acceleration levels.

At the conclusion of the Workshop, the Experts presented trial estimates of median ground motion (and uncertainties) for a M 6.5 earthquake occurring 10 km from both strike-slip and normal faulting earthquakes. The purpose of this exercise was to familiarize the experts with the process and the form of the estimates that they will have to provide. Several of the experts only presented proponent models rather than evaluating the suite of alternative models. As a result there was a large variability in their estimates; their estimates of the median peak ground acceleration varied by about a factor of 2 for the strike-slip case, up to 3 for the hanging wall of the normal case, and over 3 for the footwall.

In the comments by observers, Jerry King indicated that the seismic design will include tall structures whose natural periods are beyond 1.0 sec. It was decided that this observation needed to be verified given the fact that the planned period range to be characterized by the Experts only went to 2.0 sec (0.5 Hz). Attached is a memorandum addressing this issue; the requested period range extends to 3.0 seconds.

Civilian Radioactive Waste Management System
Management & Operating Contractor

Summary of Feedback on Ground Motion Interpretations Workshop on Ground Motion Characterization at Yucca Mountain

Salt Lake City, UT
April 16, 17 and 18, 1997

Prepared for

U. S. Geological Survey
Box 25046, MS-425
Denver Federal Center
Denver, CO 80225

Prepared by

Woodward-Clyde Federal Services of
Civilian Radioactive Waste Management System
Management & Operating Contractor
1180 Town Center Drive
Las Vegas, NV 89134

May 12, 1997

INTRODUCTION

The United States Geological Survey (USGS) is currently performing a probabilistic seismic hazards analysis (PSHA) of the proposed high-level radioactive waste repository at Yucca Mountain, Nevada. The study is an element of the Department of Energy's (DOE) site characterization activities. The PSHA will result in the annual probability of exceedance of various levels of vibratory ground motion and fault displacement.

Input to the PSHA is being developed by two panels of experts: one characterizes seismic sources and fault displacement and the second estimates vibratory ground motion. Their interpretations are being facilitated in a series of structured workshops. The goal of the process is to have differences in experts' interpretations result from true differences in judgment and not differences in access to data, definition, or lack of full understanding of each other's interpretations. This report summarizes the third in the series of workshops for characterizing ground motion: the Feedback on Ground Motion Interpretations Workshop.

The Workshop began with a joint session with the Seismic Source Characterization Team in which the preliminary models developed by each team were discussed. The remainder of the Workshop proceedings focused solely on the experts' preliminary ground motion interpretations and the proponent models on which they were based. Each speaker provided copies of presentation materials and these are included as an Attachment to this Summary.

The Workshop was attended by a representative of the DOE, Tim Sullivan, and members of the Project Management Team, John Whitney, Carl Stepp, Ivan Wong, Jean Savy, and Richard Quittmeyer. All Ground Motion Team Experts were present: John Anderson, David Boore, Kenneth Campbell, Art McGarr, Walter Silva, Paul Somerville, and Marianne Walck. Members of the Ground Motion Facilitation Team in attendance were Norman Abrahamson and Ann Becker. Also present were Robin McGuire, Seismic Design Team Leader; Gabriel Toro, PSHA Calculations Team Leader; and Review Panel members Allin Cornell, Tom Hanks, and James Brune. Technical Observers included representatives from the NRC, NWTRB, ACNW, and the CNWRA.

WEDNESDAY, APRIL 16, 1997

In this joint session held together with the Seismic Source Characterization Team, Kevin Coppersmith and Norman Abrahamson summarized the preliminary models developed by the experts. Although the source characterization teams are developing models with numerous fault geometries, the ground motion experts are developing motion estimates for specified fault geometries. These specified geometries are representations of 'average' geometries in the models, and fault geometry variation within a range is incorporated as added uncertainty in the motion estimates. Source characteristics which introduce additional uncertainty in the motion estimates include deviations from the specified fault dip and depth extent, multiple

ruptures on parallel faults, and a subhorizontal detachment fault. The latter two faulting cases may deviate too far from the average models to be covered by aleatory variation. These cases were discussed subsequently during the 3-day meeting. The experts will develop simple scaling rules to make the models applicable to these multiple rupture cases.

THURSDAY, APRIL 17, 1997

Because the focus of the Workshop was feedback and discussion among the experts, the experts each outlined their approach to developing their ground motion estimates. Generally, most experts developed weighting schemes for the proponent models, applied the weights, and evaluated the output. Two experts used approaches different from the other five experts. Marianne Walck developed a method to identify outlier points within the proponent values and eliminated these from consideration. John Anderson implemented three schemes which he then weighted to develop estimates. In the first, he accommodated all relevant proponent models and developed a uniform distribution between the maxima and minima. In the second scheme he emphasized a preferred empirical proponent model, and in the third he emphasized a preferred numerical proponent model. Norman Abrahamson presented results of regression analyses on the experts' preliminary estimates and facilitated discussions of the regressed models.

Preliminary hazard computations were presented by Gabriel Toro. The computations were based on the preliminary models developed by the source characterization teams and the regressions based on the preliminary ground motion point estimates. Large magnitude earthquakes on distant faults dominate the hazard at long period and the contribution from faults and areal sources more local to the site dominates at all other periods. Significant hazard arises from multiple ruptures on parallel faults (faults which coalesce at depth) in those models which incorporate this style of rupture. In general, the results show that the largest contribution to uncertainty in the hazard is the uncertainty in the ground motion models.

Each of the experts employed some means of weighting mean values to compute their estimates. They developed several methods of combining weighted values and some developed different objective schemes to obtain weights, all of which were discussed. Because of the importance of uncertainty, its partitioning as epistemic or aleatory and as parametric or modeling was reiterated by Norman Abrahamson. A standard statistical procedure for evaluating the epistemic uncertainty was agreed to by the experts.

FRIDAY, APRIL 18, 1997

To facilitate comparisons between the individual experts' point estimates, Norman Abrahamson showed a series of plots of these estimates and the proponent model estimates on which they are based. For a given earthquake magnitude and distance, and at a given response frequency, the proponent model estimates are bimodally distributed. Empirical estimates are generally tightly grouped separately from the numerical estimates, which are less closely clustered. Because the experts weighted both empirical and numerical proponent estimates, in general their point estimates lie between the two distributions. The experts discussed differences in the numerical proponent models at length to determine if differences in modeling would require further adjustments (changes in weighting) in their point estimates.

James Brune summarized his study of precarious rocks. At four locations near large historic earthquakes, he computed the motion required to topple the rocks and compared it to motions for a magnitude 6.5 earthquake estimated by the experts. In general, the expert estimates exceeded the toppling motions suggesting that the estimates were in turn larger than the motions which actually had occurred. However, because the study evaluated only rocks which had not toppled, and not those which had, and because the effects of motion duration, frequency content, and location in a possible shadow zone could not be quantified in the case of the precarious rocks, the consensus of opinion among the experts was that it could not be incorporated in their studies in its current form.

Ann Becker updated work presented in Workshop #2 on stress drops in normal faulting earthquakes. The earlier computations were updated to include the Dinar, Turkey earthquake and the distance measure was revised to reflect the equivalent point source distance. The median stress drops are about 10 bars higher than those previously reported, largely due to the inclusion of the Dinar event.

Two sources have been defined by the seismic source characterization teams which are significantly different than the strike-slip and normal faulting cases the ground motion experts have evaluated. The two rupture scenarios are (1) multiple ruptures on parallel faults, perhaps coalescing at depth and (2) rupture on a low-angle detachment zone. The multiple rupture scenario has a large contribution to the hazard computation whereas the contribution from a low-angle rupture has had little effect. The first scenario has been investigated in numerical modeling studies by Paul Somerville and by Walter Silva. For multiple ruptures on parallel faults, whether or not they coalesce at depth, the results suggest that the rate of attenuation is approximately the same whether several faults rupture or whether only the central fault ruptures. Issues which pertain to estimating these motions include: moment partitioning among the rupture planes, the relative timing of the ruptures, and the distances of each plane to the site. Regarding rupture on a low-angle detachment fault, issues which affect ground motions include the stress drop of these events, and the geometry. Because

these issues cannot be determined a priori, the experts will address any changes to their point estimates by incorporating additional uncertainty.

Following these discussions, Carl Stepp provided guidance on the level of detail the experts are required to provide to document their work. Data sources and all references must be thoroughly documented.

At the close of the Workshop, each expert briefly described potential changes to their point estimates based on the presentations in the Workshop. None anticipated major modifications to their procedures, but rather refinements based on closer evaluations of various proponent models.

ELICITATION SUMMARY

JON AKE, BURT SLEMMONS, AND JIM McCALPIN

TABLE OF CONTENTS

TABLE OF CONTENTS

TABLES

FIGURES

TABLE OF CONTENTS

TABLE OF CONTENTS

APPENDICES

ELICITATION SUMMARY
JON AKE, BURT SLEMMONS, JIM McCALPIN

1.0
INTRODUCTION

This document describes the authors' seismic sources for seismic hazard assessment and characterization of fault displacement hazard at the Yucca Mountain site. These evaluations relied on available data (either provided by the Yucca Mountain hazards management team or literature known and available to us). No additional data were gathered and only limited analyses were performed as part of this assessment.

The evaluations incorporate uncertainties through the use of logic trees. Some elements of the logic trees portray objective, statistical weights. However, for many elements of the tree no objective data were available, and subjective weights had to be applied. We attempted to follow a simple set of rules to aid in applying weights to those more subjective elements. If we considered a model or parameter was virtually certain, we applied a weight of 0.99 (or 0.01 if virtually unbelievable). If we considered a model or parameter strongly supported or strongly unsupported, we applied a subjective weight of 0.9 or 0.1. If we evaluated two competing models to be equally likely or we had a high degree of uncertainty between them, we applied a weight of 0.5 to each. Likewise, if three models or parameters were considered equally likely, we applied a weight of 0.333 to each. For regional seismic sources where the likelihood of the preferred interpretation was greater than the maximum and minimum values, the preferred interpretation was assigned a value of 0.6 and the extreme values were weighted as 0.2. If uncertainties were available in the form of standard deviations (usually assumed as Gaussian), we weighted the results of median ± one standard deviation as 0.15, 0.7, and 0.15. For a few elements we attempted to capture the uncertainty by defining a preferred value and then ninetieth and tenth percentile values.

This summary begins with a discussion of tectonic models, followed by a description of the local seismic sources implied by the permissible tectonic models and then a summary of the

regional and areal sources considered in this evaluation. The final part of the summary describes the team's characterization of fault displacement hazard.

2.0
TECTONIC MODELS

We considered several alternative tectonic models (as we presented in SSC Workshop 4) to explain the observations and data of the Yucca Mountain region. Our interpretations are summarized in this section. Of the seven tectonic models proposed by others in SSC Workshops 1 through 3, we assigned the greatest credibility to the planar fault blocks model, followed by the detachment model, the lateral shear model, and the volcanic-tectonic model.

In Section 2.1, we discuss each tectonic model in turn, first defining what we mean by the model, then listing the strengths and weaknesses of the model compared to available field evidence (both from Yucca Mountain and from similar extensional provinces worldwide) and theoretical considerations of seismicity and tectonics. Based on the ratio of strengths to weaknesses, we assign each model a subjective degree of belief. This rating expresses our consensus that the model correctly explains the seismotectonic setting of the Yucca Mountain region. These subjective probabilities form our basis for weighting the existence of critical structures (e.g., the detachment fault, buried strike-slip fault, planar faults) that appear in our logic tree for seismic source characterization. In Section 2.2 we discuss our preferred model that incorporates those aspects of the alternative tectonic models that we feel best explain the seismotectonic setting of the Yucca Mountain region.

2.1 COMPARISON OF TECTONIC MODELS

2.1.1 Caldera Model

Definition: Crustal blocks are sliding into a structural depression beneath Crater Flat. This depression was made by Tertiary caldera collapse or by westward detachment faulting. This model includes the caldera-detachment model of Carr (1990).

Strengths:

(1) The caldera complex is centered on a deep north-south trough or rift (Amargosa Desert rift); however, it is not clear whether the calderas are a result of the rift, or the reverse.

(2) Crater Flat/Yucca Mountain faults make a distributed fault system that mirrors the faults north of the caldera complex. This symmetry about the calderas suggests a causal connection.

Weaknesses: (USGS, written communication, 1996, p. 8-61)

(1) The calderas have been inactive since 14 Ma, so how could they affect current faulting?

(2) The calderas don't explain the change from rhyolitic to basaltic eruptions in Crater Flat in the past 3 Ma.

(3) The model doesn't explain vertical axis rotations.

(4) The model doesn't explain post-10 Ma uplift of Bare Mountain block.

Conclusion: Weaknesses much more compelling than strengths, model unlikely.

2.1.2 Volcanic-Tectonic Model

Definition: Surface-rupturing earthquakes in Crater Flat are accompanied by dike injection.

Strengths:

(1) With continuing Quaternary eruptions in Crater Flat and south, some connection between volcanic and tectonic processes is likely.

(2) Yucca Mountain faulting is widely distributed, like faulting in other volcanic-tectonic areas such as Mammoth Lakes. If USGS scenario earthquakes (USGS, written communication, 1996, Chapter 5) are single events, then such distributed rupture is also characteristic of volcanic-tectonic events.

(3) The ash event at 70 ka (see USGS, written communication, 1996, Chapter 5) appears to be connected with basaltic eruptions.

Weaknesses:

(1) Most of the 12 large (or 35 total) paleoearthquakes in the past 500 ka at Yucca Mountain are not associated with episodes of volcanic eruption.

(2) There is no direct evidence that the rift beneath Crater Flat was formed by volcanic action. Other possible origins: (1) a deep graben created by east-west tectonic extension, (2) a more northerly trending part of an Amargosa Desert rift, which thinned the crust until subcrustal magma was tapped, or (3) a northerly jog in the N50W-trending Amargosa River-Pahump-Stewart Valley strike-slip fault zone.

Conclusion: Some volcanic-tectonic connection may operate some of the time, the calderas do not appear to control currently active faulting.

2.1.3 Detachment Model

Definition: A major low-angle, west-dipping detachment fault underlies Yucca Mountain and Crater Flat, at a mid- to low-crustal position. This detachment truncates all high-angle faults observed at the surface.

Strengths:

(1) A detachment fault would explain the many narrow, parallel fault blocks as domino-style blocks above a detachment.

(2) Tertiary detachment faults exist in the region surrounding Yucca Mountain.

(3) Normal faults may utilize parts of older detachments, as in the Overthrust Belt (Smith and Arabasz, 1992).

Weaknesses: (USGS, written communication, 1996, p. 8-74)

(1) General:

(a) Historical earthquakes show planar faulting (e.g., the Little Skull Mountain event of 1992); no evidence of low-angle seismicity has been recorded, either in southwest Nevada, or in any other extensional terranes of the western US.

(b) The known detachments to the east and west are old (> 6 Ma).

(c) Basaltic volcanism requires deeply penetrating structures.

(2) Applies to shallow detachments:

(a) No shallow (< 5 to 6 km) reflectors that could be interpreted to be a detachment are seen on the seismic line (T. Brocher, SSC Workshop 2).

(b) Elsewhere in the region, there is no detachment at the boundary between Tertiary and Paleozoic rocks (that contact is an unconformity).

(c) Movement on the Bare Mountain Fault would have truncated any detachment.

(3) Applies to deep detachments:

(a) A deep (6 to 15 km) detachment could not produce the observed dip rollovers and opposed slip on some faults.

(b) A deep detachment requires tensile behavior at the base of the individual dominos, which is unlikely.

Conclusion: Weaknesses are compelling, however, a deep (>6 km) detachment cannot be ruled out by geophysics.

2.1.4 Planar Fault Blocks Model (Pure Shear)

Definition No. 1: East-west Basin and Range-type extension, with diffuse dextral shear in the south part of Crater Flat.

Strengths:

(1) The Amargosa Desert rift and all north-south-trending parallel faults suggest an east-west horst and graben system.

(2) The largest historical earthquakes in the local area (e.g., Little Skull Mountain) show planar faulting to depth.

(3) Seismic lines show no detachments within the upper 5 to 6 km.

(4) Rifting can explain basaltic volcanism.

(5) Boundary element modeling can replicate the seismic section using planar faults.

(6) Diffuse dextral shear can explain the increasing vertical axis rotation of fault blocks in southern Crater Flat.

Weaknesses:

(1) Pure horizontal extension does not explain the vertical axis rotations.

(2) Net slip (and slip rate) on the Bare Mountain fault (the supposed master fault to which Yucca Mountain faults are antithetic) must be greater than the sum of all the slips (and slip rates) on all the antithetic (Yucca Mountain) faults. This does not appear to be the case. However, some of the faults in the Bare Mountain fault zone may be buried by Holocene and late Quaternary alluvium up to 150k years old.

(3) Boundary element models show that, to produce a slip event on antithetic faults, multiple slip events on the main (Bare Mountain) fault are required. This does not appear to be the case.

(4) Planar faulting doesn't explain the ash event, which may have involved coeval rupture on six to seven parallel faults.

Conclusion: Strengths more compelling than weaknesses, model plausible.

Definition No. 2: Crater Flat is a transtensional rhombochasm (pull-apart) due to a right step in the Walker Lane. The east, south, west, and north boundaries of the rhombochasm are the Paintbrush Canyon/Stagecoach Road fault, the Carrara feature, the Bare Mountain fault, and a fault near Yucca Wash, respectively.

Strengths:

(1) The model explains the inferred oblique component of normal faulting in/near Yucca Mountain.

(2) The model explains the oblique nature of focal mechanisms observed in the instrumental seismicity (Rogers *et al.*, 1991 and K. Smith, SSC Workshop 2).

(3) The model may explain why fault behavior in the past 500 ka does not match the results of boundary element models, which assume pure east-west extension.

(4) The extreme northern limit on the main Yucca Mountain faults is at or near the linear northwest-trending Yucca Wash on the north. The faults have displacements that decrease toward this geophysical lineament, which has no known fault origin in the shallower units, and does not appear to be a seismic source. [Only the Paintbrush Canyon fault clearly crosses this feature, and it may change in character across Yucca Wash.] The extreme southern limit to Crater Flat and Yucca Mountain faults is near the linear northeast-trending inferred fault shown by Fridrich and Price (1992). The orientation of N45W suggests that it may be a right-lateral oblique fault.

Weaknesses:

(1) There is ambiguity about the existence of the required dextral faults at the north and south ends of the rhomboid.

Conclusion: Strengths more compelling than weaknesses, model plausible.

2.1.5 Lateral Shear Models

Definition No. 1: The transtensional nappe model applies (Hardyman and Oldrow, 1991).

Strengths:

(1) The model explains how Walker Lane shear could produce observed fault blocks.

(2) The Cedar Mountain earthquake of 1932 displayed distributed faulting having a high oblique component.

Weaknesses: (USGS, written communication, 1996, p. 8-80)

(1) "None of the criteria or geometry required for Hardyman's model exist at Yucca Mountain." Hardyman originally proposed this model for the Gillis Range-Cedar Mountain area, for a well-bedded pyroclastic sequence above a sheared unconformity with Mesozoic rocks that is cut by a lateral fault. We find no evidence for this type of mechanism at Yucca Mountain.

Conclusion: Compelling weaknesses, questionable applicability of model to Yucca Mountain area, model unlikely.

Definition No. 2: There is a buried, 250-km-long strike-slip fault beneath Yucca Mountain; it is a buried subvertical dextral fault, such as that proposed by R. Schweickert at SSC Workshop 3.

Strengths:

(1) The model would explain the observed vertical axis rotations in southern Crater Flat.

Weaknesses: (USGS, written communication, 1996, p. 8-84)

(1) There is no surface evidence of strike-slip faults at Yucca Mountain/Crater Flat, nor of any single, continuous strike-slip fault southeast of Crater Flat along the state line.

(2) Vertical axis rotations in the area are variable in time and space. They would be expected to be uniform if there was only one, long strike-slip fault.

(3) There is no evidence for a 25-km dextral offset of volcanics in Crater Flat.

Conclusion: Weaknesses more compelling than strengths, model unlikely.

2.2 PREFERRED TECTONIC MODEL

Our preferred tectonic model for Yucca Mountain is a composite based primarily on the Planar Fault Model, which has the following characteristics.

(1) Generally, the fault azimuth may be a first-order control on the type of fault, with conjugate relationships (a la Wright, 1976). Regionally northwest-trending faults are right-lateral; northerly-trending faults are normal; and northeast-trending are left-lateral. By far the most active faults are the strike-slip faults; normal faults have slip rates of 1% to 10% of the strike-slip faults. Most of the Yucca Mountain faults expressed at the surface are northerly-trending, normal faults.

(2) Major, block-bounding faults are planar (or weakly curved) to seismogenic depths.

(3) Faults that are closely spaced in plan view may merge above seismogenic depths. For those that are so closely spaced that they may merge above 15 km,

we calculate maximum magnitudes as if they were separate faults with aspect ratios consistent with their lengths. (Further discussion in sections on maximum magnitudes and synchronous rupture). Alternative dips and aspect ratios are considered for Yucca Mountain faults in the assessment of their downdip extent.

(4) Given the local faults may have merging geometries, for multi-fault-rupture scenarios we compute the fault area as the sum of areas for all faults that ruptured. Note, however, that unless the separate faults ruptured simultaneously (i.e., within about 30 seconds of each other in our definition), we interpret that these scenario earthquakes to be separate earthquakes spaced a few hours to decades apart, with correspondingly lower magnitudes than a large simultaneous rupture.

(5) Fault slip is dominantly dip slip in the northern part of the area; southward, the horizontal component increases via vertical axis rotation. It is not known whether this is due to a local effect at the southeast edge of Crater Flat, or to a subordinate tectonic rotation induced by a right-lateral fault zone in Amargosa Valley.

In addition to the above, our model must include the following elements from the Detachment and Lateral Shear Models:

(6) The possibility of a deep detachment (>6 km) cannot be ruled out by the existing geophysics. Therefore, we allow some probability to the existence of such a detachment (P=0.15) and an even lower weight to it being seismogenic. The likelihood that faults merge at depth is dependent, in part, on the depth of the inferred detachment.

(7) The oblique component of slip on Yucca Mountain faults and the clockwise vertical axis rotation are related to dextral strain (bending) transmitted from the Walker Lane. However, it is unclear whether discrete northwest-striking dextral faults exist north and south of Yucca Mountain (defining a rhombochasm), or whether lateral strain is diffuse. This model utilizes recognized faults as the eastern and western margins of the rhombochasm (Bare Mountain fault, Paintbrush Canyon/Stagecoach Road fault) and an inferred fault (Carrara feature) as the southern margin. These three faults are already characterized on the SSC logic tree, so no further additions to the logic tree are required for this tectonic model. The northern margin of the rhombochasm is approximately coincident with the Yucca Wash fault, to which we assign a 0% probability of being seismogenic, based on its lack of evidence for Quaternary displacement.

(8) The probability that a buried, strike-slip fault exists is dependent on the probability of a detachment. If a detachment fault exists (probability = 15%), then we consider that there is a 20% probability that a buried strike-slip fault exists (net probability = 3%). If no detachment exists (probability = 85%), then there is only a 5% chance that the buried strike-slip fault exists (net probability = 4%). The sum of the two net probabilities that the buried fault exists is thus 7%. The probability that the buried strike-slip fault is seismogenic is dependent on the depth of the detachment.

Although a volcano-tectonic source is not explicitly included as a separate source model, we include one element from the Volcanic-Tectonic Model. This element does not require a caldera source, but depends on the simultaneous basaltic volcanic eruption and the extensive tectonic, seismogenic rupturing of several faults that extend northward from a Lathrop Cone volcanic source. The possibility of such a scenario is accounted for in the simultaneous rupture portion of the local fault model.

(1) Some surface-rupturing paleoearthquakes (e.g., Scenario U) probably have accompanied episodes of basalt eruption and dike injection.

(2) Although there may be some volcanic-tectonic connection, the possibility of volcanic earthquakes does not affect our estimates of earthquake magnitude and recurrence. Therefore, we do not include a separate volcanic earthquake branch on our seismic source characterization logic tree, for two reasons. First, the maximum magnitude of volcanic earthquakes associated with dike injection (M = 5.5) and calderas (M = 4.5± 1.2) (Hackett *et al.*, 1996) are much smaller than our estimated maximum magnitudes for tectonic earthquakes, either on individual faults or for background seismic zones. Second, the recurrence interval of volcanic eruptive events is estimated to be ca. 200 to 300 ka by the experts in volcanic hazards assessment for Yucca Mountain. Thus, any volcanic contribution to earthquake hazard is insignificant compared to the rates of background seismicity in and near Yucca Mountain (see Section 3.6).

Behavioral aspects such as distributed, multi-fault earthquakes, could occur in any of the tectonic models. However, simultaneous faulting on parallel normal faults may be more easily explained by the Volcanic-Tectonic Model (which we have not included as a separate source model) than by the Lateral Shear Model (a variant of which we weight at 20%), and least by the Planar Block Model (which we give the highest weight at 80%). Thus, our

weighting of tectonic models reflects our interpretation that simultaneous multi-fault ruptures (i.e., within a ~30- second time span) have a low probability.

3.0 SEISMIC SOURCES

The characterization of fault-specific sources in the Yucca Mountain region is based on our preferred tectonic model as summarized on Figure ASM-1. In addition to these fault sources, our seismic source model also includes more regional faults (i.e., those outside the immediate vicinity of Yucca Mountain/Crater Flat) and areal source zones.

The seismogenic potential of potential sources in the Yucca Mountain region is partly a function of the depth of the brittle (seismogenic) crust. Therefore, we first consider the assessment of the thickness of the seismogenic crust.

3.1 THICKNESS OF THE SEISMOGENIC CRUST

The depth of the brittle/seismogenic crust is assessed to be 12 km (0.1), 15 km (0.6), and 17 km (0.3). These depths and their relative weights are based on the distribution of focal depths for instrumental earthquakes in the southern Great Basin, as given in von Seggern and Brune (1997), and Harmsen and Bufe (1991), the focal depths in the Yucca Mountain region summarized by K. Smith at SSC Workshop 2, and discussions presented by Robert Smith at SSC Workshop 5. The nucleation depths of M > 6 earthquakes in the Basin and Range province in general (Rogers *et al.*, 1991), and in southwestern Nevada in particular (e.g., the Little Skull Mountain earthquake; Smith *et al.*, 1997) are near the base of the seismogenic crust. This fact will be important in evaluating the existence of detachments deep in the crust.

3.2 DETACHMENT AS SEISMIC SOURCE

For this analysis, a detachment fault is defined as a regionally extensive, low-angle (< 15-20 degree) surface that truncates high-angle faults and lies within the brittle crust. A detachment would lie within the upper 6 to 15 km of the crust. A subhorizontal surface lying beneath the

brittle-ductile transition would not be considered a detachment within this terminology. The assessment of a detachment as a seismic source will evaluate seismogenic potential, depth of the structure, geometry, maximum magnitude and recurrence. Figure ASM-2 contains the logic tree detailing our assessment of this source.

3.2.1 Seismogenic Potential

The seismogenic potential for a detachment is judged to be a function of its existence, geometry and extent. This dependency is shown in the following logic tree (Figure ASM-2).

The first assessment is whether a detachment exists. The weight assigned to the existence of a detachment is 0.15 and to no detachment is 0.85. The following evidence supports the existence of a detachment: a detachment would explain the many narrow, parallel fault blocks as dominos above a detachment; Tertiary detachment faults exist in the region surrounding Yucca Mountain; and normal faults may utilize parts of old detachments, such as those in the Overthrust Belt (Smith and Arabasz, 1992; Arabasz *et al.*, 1992). The arguments against a detachment are: a lack of evidence for low-angle faulting from the seismicity, including the Little Skull Mountain earthquake; the known detachments east and west of Yucca Mountain are old (> 6 Ma); basaltic volcanism requires deep penetrating structures; elsewhere in the region, there is no detachment at the Tertiary/Paleozoic boundary; movement on the Bare Mountain fault would have truncated the detachment; and, a deep detachment could not produce the observed dip rollovers and opposed slip on some faults (C. Fridrich, SSC Workshop 3).

The second assessment is the depth of the detachment, conditional on its existence. Three depths are considered, which depend on the depth of the brittle crust. The minimum depth is 6 km, which is below the depth observed in the seismic reflection profile presented by T. Brocher (SSC Workshop 2). There is no evidence for a low-angle detachment fault on the seismic reflection profile, although such a structure should have been obvious if it existed. Therefore, if a detachment fault exists beneath Crater Flat, it must lie at or below 6 km. The maximum depth for a detachment beneath Crater Flat is the depth of the brittle-ductile transition (which, as discussed above, is assumed to lie between 12 and 17 km depth). An intermediate depth of the detachment is considered, halfway between the depth of the brittle-ductile transition and 6 km. This would place the detachment toward the base of the

seismogenic crust, which is the most common nucleation point for large earthquakes in the region (Rogers *et al.*, 1991). The relative weights assigned to the three alternative depths are 6 km (0.25), (BD-6)/2 + 6 (0.5), and BD (0.25), where BD is the depth of the brittle-ductile transition. The weights assigned to the three interpretations are based on the following observations: (1) A shallow depth for the detachment conflicts with the geometry of the Bare Mountain fault. The Bare Mountain fault would be truncated at a shallow depth that is a significant fraction of the total offset on the fault; lack of analogs to this situation suggest a low weight for this interpretation. (2) The observed opposed dips on some of the Crater Flat faults are inconsistent with normal faulting caused by extension above a subjacent detachment. This scenario also receives a low weight.

- The next conditional assessment is whether the detachment is seismogenic, that is, capable of generating significant ($M > 5$) earthquakes in the present tectonic regime. This assessment is independent of the depth of the detachment. The possibility that a detachment (if it exists) is seismogenic is given a very low weight (0.01) based on both theoretical reasoning and empirical data. First, according to Mohr-Coulomb theory of brittle failure, given a horizontal least-principal stress and rocks having internal friction angles of 30 ± 10 degrees, the most likely dip for active normal faults is 60 ± 10 degrees (see extended discussion by Sibson, 1985). A fault dipping only 10 to 20 degrees would be in a very unfavorable orientation for slip, compared to the multitude of faults having dips closer to 60 degrees at Yucca Mountain. [Forsyth (1992) rebuts this argument, saying that if the low-angle fault had sufficiently lower strength than the high-angle faults, slip might be accommodated.] These higher-angle faults have demonstrated Quaternary slip, proving that they have accommodated Quaternary extension, as would be predicted by theory. The existence of a low-angle detachment beneath Crater Flat is merely conjectural; there is no evidence that it exists, much less that it has accommodated any Quaternary slip.

Second, although low-angle detachments have been widely described in the southwest United States (e.g., Wernicke, 1995), even after 15 years of research only one of these detachments shows evidence of Quaternary activity. The sole exception (Johnson and Loy, 1992) is a case where Quaternary fault scarps exist on the trace of the Santa Rita (Arizona) fault, which has a dip determined from seismic reflection data of 19 degrees to a depth of at least 6 km. To our knowledge this is the only documented instance of Quaternary fault scarps overlying a

low-angle normal fault; although in other areas (e.g., the Overthrust Belt of Wyoming) Quaternary fault scarps commonly overlie faults interpreted as having listric geometry (McCalpin, 1991).

Third, published summaries of focal mechanisms of earthquakes in extensional regimes show few or no cases of seismogenic rupture on low-angle normal faults (Jackson, 1987; Jackson and White, 1989; Doser and Smith, 1989; Wernicke, 1995). We estimate that there are several hundred documented focal mechanisms of significant ($M > 4$) normal-faulting earthquakes worldwide. Only two of those events (the Papua New Guinea earthquake [Abers, 1991], and the 1946 Ancash, Peru earthquake [Doser, 1987]) appear to have possibly occurred on low-angle faults. [As in any double-couple energy release, inversion for a focal mechanism can only resolve two nodal planes, one of which is the true nodal plane]. The interpretation of the true nodal plane in the New Guinea event is equivocal, and the Ancash event probably occurred on a reactivated thrust. Thus, despite the acknowledged existence of low-angle detachment faults in many extensional terranes, there are only two instances of those faults possibly generating earthquakes, compared to hundreds of instances of high-angle normal faults generating earthquakes. In the Yucca Mountain region, the historical record shows earthquakes only on higher-angle faults (e.g., the Little Skull Mountain earthquake and focal mechanism compilations of Gomberg *et al.*, 1991a; Rogers *et al.*, 1991).

Based on the scarcity (or absence) of earthquakes generated by detachment faults, we weight the probability that a sub-Yucca Mountain detachment is seismogenic as 0.01. The possibility for a seismogenic detachment is included in the analysis, despite its very low weight, to allow for the slight chance that the hypothesis proposed by Wernicke (1995) might apply to the Yucca Mountain region. Wernicke proposes that the paucity of earthquakes on low-angle normal faults is caused by long recurrence intervals on this type of fault, compared to recurrence intervals on high-angle normal faults that have the same strain rate. Given the short period for which we have reliable focal mechanism data (roughly since 1960), Wernicke (1995) argued that the period of observation is too short to capture many earthquakes on detachments that have very long recurrence intervals.

Hypotheses that claim the period of observation is too short to capture a particular observation usually are tested through the ergodic substitution of space for time (Hunter and Mann, 1995). However, in this case we are already analyzing a worldwide data set, so expanding the area over which data were collected is not possible. Given that Wernicke's (1995) hypothesis is not directly testable, but claims very large earthquake magnitudes for long-recurrence detachment faults, we decided to assign a nonzero (but small) probability for the seismic potential of a sub-Yucca Mountain detachment fault.

3.2.2 Geometry

Typical dimensions of detachment faults elsewhere in the world (summarized by Wernicke, 1995, p. 20,170) are: strike lengths of 60 to 180 km and downdip lengths of 60 to 70 km. Based on these dimensions, a detachment, if it were to exist, would underlie the entire Crater Flat/Yucca Mountain region, which is only about 20 x 20 km. The break-away for the detachment (its eastern extent) would be in the middle of Jackass Flat and would extend beneath Bare Mountain on the west. By analogy to the Bullfrog Hills (the nearest detachment fault to the site), and to the typical dips of detachment faults cited by Wernicke (1995), the detachment is assumed to dip 15 to 20 degrees to the west. The north-south extent of the detachment underlying the Crater Flat region is assumed to be the same as the extent of the north-south normal faults. This extent (about 25 km) is considerably smaller than that cited by Wernicke. Our reasoning is as follows. First, if the north-south-trending normal faults around Crater Flat are the surface expressions of an underlying detachment, then the detachment should not extend far beyond that surface expression. It is possible that the Timber Mountain caldera north of Crater Flat, and the Walker Lane south of Crater Flat, could somewhat obscure this structural relationship. Thus, the north-south extent of normal faults near Yucca Mountain (25 km; probability 0.25) sets a minimum along-strike distance for a detachment, with a preferred value of 60 km (0.5) and a maximum value of 120 km (probability 0.25). Downdip extent (based on a dip of 10 to 20 degrees and a crustal thickness of 12 to 17 km; all values equally likely) ranges from 35 km (probability 0.25) to 48 km (0.25), 69 km (0.25), or 98 km (0.25). The resulting area of the hypothesized detachment thus would average about 4000 km^2, with a standard deviation of about 2000 km^2.

3.2.3 Maximum Magnitude

The maximum magnitude of a detachment-fault earthquake would arise from rupture of the entire 4000 ± 2000 km^2 surface area estimated for the detachment. A rupture of this dimension, using the empirical relationship between rupture area and magnitude for all slip types of Wells and Coppersmith (1994) results in a mean estimated earthquake magnitude of 7.6 (+0.2, -0.3). Adding the uncertainty from the Wells and Coppersmith (1994) empirical regression (0.24 magnitude unit), our estimated magnitude for the maximum detachment earthquake is 7.6 (+ 0.4, -0.5) at a 1-sigma range. We assign weights of 0.15, 0.7, and 0.15 to these values.

3.2.4 Recurrence

Because of the absence of earthquakes having low-angle focal mechanisms in the historical record in this area, it is impossible to associate earthquakes with a detachment and use the rate of those events to constrain recurrence rates. A method for constraining recurrence is to resolve the Quaternary slip rates (using the weights arrived at for the those values as discussed in a later section) of all Yucca Mountain faults along three equally spaced east-west transects. We use the same transects as shown in L. Anderson's presentation at SSC Workshop 3. We then consider the largest of those three values to be equal to the slip rate of the detachment. Our reasoning is thus: If the surface faults are expressions of extension on the underlying detachment, their combined slip rate cannot be greater than the slip rate on the detachment. However, the combined surface slip rate could be smaller than that on the detachment, if there is any component of nonelastic deformation above the detachment, or if there is any elastic deformation on faults that do not reach the surface. Therefore, the surface slip rate is a minimum value for the detachment slip rate.

The results are:
Slip Rate = 0.05 mm/yr; Probability = 0.6
Slip Rate = 0.013 mm/yr; Probability = 0.2
Slip Rate = 0.12 mm/yr; Probability = 0.2

Displacement per event is calculated from the magnitude-vs.-average displacement regression of Wells and Coppersmith (1994, all fault types), assuming that Mmax = 7.6 (+ 0.4, - 0.5). This yields mean values for average displacement of 1.3 m (0.2), 2.8 m (0.6), and 5.2 m (0.2). Mean recurrence is then calculated as mean displacement per event divided by mean slip rate. This procedure yields a mean recurrence of 75 kyr for the maximum earthquake, with

1-sigma limits of about +125 kyr and -50 kyr. The recurrence model we prefer is characteristic (weighted 100%).

3.3 BURIED STRIKE-SLIP FAULT SOURCE

Two lateral shear models were considered in our analysis of tectonic models, neither model is given much credibility based on data from the Yucca Mountain region. For the reasons discussed in Section 2, we give no weight to the transtensional nappe model. We apply a low, but non-zero, weight to the buried strike-slip fault (definition #2 in Section 2.1.5) as a seismic source. In general, the arguments in favor of a buried strike-slip fault include being in the region of the Walker Lane and invoking buried strike-slip faulting to explain the lateral component of slip on Yucca Mountain area faults. Arguments against such a fault include: lack of surface evidence for strike slip faults in the Yucca Mountain region, nor of any single, continuous strike-slip fault southeast of Crater Flat along the state line; vertical axis rotations in the area are variable in time and space and can be explained by normal faulting without any strike slip (C. Fridrich, SSC Workshop 3); and there is no evidence for large-scale offset (e.g., 25 km as suggested by Schweikert, at SSC Workshop 3) of volcanic rocks in Crater Flat.

Based on the above arguments, we consider it unlikely that a buried strike-slip fault exists. As shown in the logic tree in Figure ASM-1, whether such a fault exists is evaluated conditional on whether a detachment exists (as assessed previously). This is because, if a detachment exists, it would be more difficult to identify a strike-slip fault at depth. The detachment could serve to decouple the deeper lateral deformation from that occurring above the detachment. Assuming that a detachment does exist, the probability that a buried strike-slip fault exists is assessed to be 0.2; assuming that a detachment does not exist, the probability that a buried strike-slip fault exists is assessed to be only 0.05. This is because it is judged very unlikely that surface evidence for such a fault would have escaped detection during the field investigations in the region, especially assuming there is no detachment. Assuming that such a buried strike-slip fault exists, it could follow down-on-the-east segments along the west side of Crater Flat shown by John Bell (SSC Workshop 3) as part of a regional wrench system, or it could follow the location R. Schweikert designates—from Timber Mountain caldera to the south end of Crater Flat down the center of Crater Flat

(Schweikert, SSC Workshop 3). The hypothesized location of the buried strike-slip fault is shown on Figure ASM-3.

3.3.1 Seismogenic Potential

The next assessment is whether a buried strike-slip fault is seismogenic, given that it does exist. This assessment is judged to be conditional on the depth of the detachment lying structurally above the assumed strike-slip fault. (See discussion in Section 3.2.1 for the range of detachment depths as a function of the depth of the brittle crust). If the detachment is shallow, the probability that the strike-slip fault is seismogenic is relatively high (0.8); if the detachment is at moderate depth, the probability is 0.6; and if it is deep, the probability is 0. This assessment is based primarily on the observation that significant earthquakes on very long, thin (high aspect ratio) faults are not observed unless those faults penetrate the entire seismogenic crust.

3.3.2 Maximum Magnitude

Two estimates of rupture length are proposed to estimate maximum magnitude for a potential buried strike-slip fault. For the first approach, a 1932 Cedar Mountain earthquake-type rupture is assumed. The length of this rupture was about 60 km (Gianella and Callahan, 1934). Second, the length of Bell's down-to-the-east faults is assumed to represent a possible rupture segment for a strike-slip fault that is about 25 km long. Because the 25-km rupture length is based on local observations rather than a regional analogy, it is given higher weight (0.7) than the 60-km estimate (0.3). The magnitude associated with the 60-km rupture is 7.1 and with the 25-km rupture is 6.7, using the empirical relations between rupture length and magnitude of Wells and Coppersmith (1994).

Fault area also has an effect on maximum magnitude. Down-dip width of the buried strike-slip fault is conditional on the existence of the detachment. If the detachment exists, the range of possible widths of the buried strike-slip fault is based on combinations of estimated values of the detachment depth and thickness of the seismogenic crust. If no detachment exists, the upper limit of the buried strike-slip fault is assumed to be 7 km (just below the depth imaged on the seismic reflection profiles).

3.3.3 Recurrence

Earthquake recurrence is assessed based on the assumption that, if a buried strike-slip fault exists, its strain rate would be reflected at the surface by slip on the observed Yucca Mountain faults. Thus, we assumed the slip on this fault can be evaluated (or at least constrained) by using a geometrical relationship to the east-west extension associated with the Yucca Mountain faults. We resolve the total east-west extension (slip rates) for the faults of Yucca Mountain (i.e., Solitario Canyon, Windy Wash, Northern and Southern Crater Flat, Paintbrush Canyon/Stagecoach Road) onto a northwest-trending plane that has a pure lateral sense of motion. We assume three possible strike values for this plane (N20W, N35W, and N50W) with equal probability. A strike of approximately N35W appears to be the value indicated in Schweikert and Lahren (1997). There is uncertainty in this strike value. Hence we allowed a ± 15-degree variation in the strike of this source and assigned equal weights. This variation seemed permissible when compared to the somewhat general figures presented by Schweikert. The resulting values are:

Slip Rate = 0.1 mm/yr; Probability = 0.6
Slip Rate = 0.025 mm/yr; Probability = 0.2
Slip Rate = 0.24 mm/yr; Probability = 0.2

Given no constraints based on data for the behavior of this source, the characteristic recurrence model (Schwartz and Coppersmith, 1984; Youngs and Coppersmith, 1985) was assumed to be appropriate. This model has been shown to be appropriate for many individual faults.

3.4 LOCAL FAULT SOURCES

This section describes the local (i.e. within Crater Flat/Yucca Mountain/Bare Mountain area) fault sources considered in our preferred seismic source model (see discussion in Section 2.4). The description and characterization of the more regional faults (those outside the Crater Flat/Yucca Mountain/Bare Mountain area) is independent of the choice of local tectonic model. The more regional sources are described in Sections 3.5 and 3.6. The faults included in our evaluation (regional and local) are a subset of those identified in Piety (1995) and H. L. McKague *et al.* (CNWRA, written communication, 1996). Some faults in those compilations were omitted from consideration based on a lack of Quaternary activity in Chapter 11 of the

summary report (USGS, written communication, 1996), or those more regional faults that Anderson *et al.* (1995a,b) considered to lack evidence for Quaternary activity.

The regional and local faults are evaluated according to the probability that they are seismogenic. Given that they have some probability of being seismogenic, their location and extent are evaluated, behavioral aspects assessed, maximum magnitudes defined and recurrence evaluated.

3.4.1 Seismogenic Potential

The evaluation of which mapped faults to include as seismic sources is a function of the interpretation of the seismogenic potential (probability of activity) of each fault. The criteria we used to evaluate whether a fault is seismogenic are: (1) the recency of slip on the fault; this is the strongest criterion but is difficult to determine in this area because of long recurrence intervals; and (2) the length of the fault, which should be long enough to generate magnitude 5 to 52 earthquakes (approximate length of 5 km); and (3) the interpreted average late Quaternary displacement. Other observations that are potentially important include evidence of brittle slip in the geologic past and involvement in development of throughgoing structures. If a fault was active in the geologic past but is truncated downdip, we consider it will not become active as an independent source again.

Northwest-Trending Faults. The mapped northwest-trending faults in the site area (i.e., Drillhole Wash fault, Sever Wash fault, Pagany Wash fault, and Yucca Wash fault) are assessed to be nonseismogenic based on their short lengths (3 to 5 km), no evidence for Quaternary displacement, and a slip tendency that is not favorable within the present stress regime (Stamatokos and Ferrill, SSC Workshops 3 and 4; H. L. McKague *et al.*, CNWRA, written communication, 1996). We consider the regional seismic source zone to incorporate the hazard from small faults of these dimensions.

Ghost Dance Fault. The Ghost Dance fault is oriented favorably for slip but there is no evidence that it is active or seismogenic. Within a resolution of less than 0.5 m, slip in the past approximately 300 ka is precluded by the lack of displacement of a bedrock paleosurface (E. M. Taylor *et al.*, written communication, 1996a). During the same time, multiple paleoearthquakes are recorded along the nearby Solitario Canyon fault. The northern

terminus of the fault is identified from detailed mapping, and it appears to be truncated by a structure to the south. Therefore, the length of the fault is comparable to that of the northwest-trending faults. Further, its geologic history does not suggest that it was a zone of significant localized slip. On the basis of these arguments, the Ghost Dance fault is assessed to have a probability of zero that it is seismogenic.

Sundance Fault. The 700-m-long Sundance fault is too short to be an independent seismic source. There is also no evidence for Quaternary slip.

North-Trending Faults. We have identified nine local faults as seismic sources near Yucca Mountain (Figure ASM-4). Four of these faults (Bare Mountain, Windy Wash, Solitario Canyon, and Paintbrush Canyon/Stagecoach Road) are termed major, block-bounding faults and are interpreted to penetrate the entire seismogenic crust. {Note: we characterize the Paintbrush Canyon/Stagecoach Road faults as a single fault.} The remaining north trending faults (Northern and Southern Crater Flat, Fatigue Wash, Iron Ridge, Bow Ridge) are termed minor or secondary faults; they likely merge with the major, block-bounding faults within the seismogenic crust. Our characterization of the local Crater Flat Group (CFG) faults is summarized on Figure ASM-5. We interpreted all the major, block-bounding faults listed above to be seismogenic (probability = 1.0). The probabilities that minor faults are seismogenic are based on the sizes of per-event displacements inferred from trenches (see Section 3.4.3.1 and Table ASM-1). The mean and maximum of $D_{preferred}$ values and the probability that the fault is NOT seismogenic are as follows: Bow Ridge fault (24, 44 cm, and 0.3); Northern Crater Flat fault (47, 50 cm, and 0.2); Southern Crater Flat fault (20, 20 cm, and 0.5); Fatigue Wash fault (61, 105 cm, and 0.1); and Iron Ridge fault (80, 100 cm, and 0.1).

3.4.2 Geometry Models

Fault Rupture Lengths. For the nine local faults that we characterized in detail, we made three estimates of maximum surface rupture length to evaluate the maximum earthquakes (Table ASM-2). The minimum length equals the along-strike distance between the farthest-apart points on the fault that display Quaternary displacement indicated on the map of Simonds *et al.* (1995). The preferred length is the along-strike distance between the ends of the obvious mapped fault (irrespective of age of displacement) as shown on the fault map

of Simonds *et al.* (1995). The maximum length is the along strike distance between the maximum inferred limits of mapped bedrock fault(s), as shown on the Simonds *et al.* (1995) map. On the north, most of the faults are interpreted to be truncated by the northwest-trending faults (Yucca Wash, etc.).

Because we want the length of surface rupture during the maximum earthquake, we considered it unlikely that such a rupture would be limited to a minimum length defined by distance between trenches as postulated in Table 5.1 of the synthesis report (USGS, written communication, 1996), for two reasons: (1) the distance between trenches showing Quaternary offset is a minimum estimate for the length of Quaternary faulting, and the maximum earthquake should have a maximum (rather than a minimum) rupture length; and (2) depending on how the trenches were sited (e.g., some are clustered near roads), their spacing may show only a small extent of the Quaternary surface rupture. We give this interpretation a zero weight. We consider that the maximum earthquake would cause rupture at least equivalent to the extent of faulted Quaternary deposits. The longest possible surface rupture length in the maximum earthquake is constrained by the mapped length of the fault in bedrock. We estimate a 30 percent probability that the maximum earthquake could rupture the entire mapped extent of the fault and at least some distance beyond on along-strike structures inferred as faults on the Simonds *et al.* (1995) map.

Downdip Extent of Faults. To compute downdip width (and hence fault area), dips on the major, block-bounding local faults were interpreted to range from 45 to 70 degrees. These values are based on observed surface dips in the Basin and Range, theoretical considerations for normal faulting (Sibson, 1985), surface dips in the Yucca Mountain area (C. Fridrich, SSC Workshop 2), the seismic reflection profiles (presented by T. Brocher, SSC Workshop 2), and the observations of seismicity from the Little Skull Mountain sequence (K. Smith, SSC Workshop 2).

As described above, our assessment divides the local faults into two categories: major, block-bounding faults (which include the Bare Mountain, Solitario Canyon, Paintbrush Canyon/Stagecoach Road, and Windy Wash faults), and secondary faults (which include the Northern and Southern Crater Flat, Fatigue Wash, Iron Ridge, and Bow Ridge faults). The block-bounding faults are of sufficient length that they may fully penetrate the seismogenic

crust. This interpretation is based on the overall length of the block-bounding faults, reasonable aspect ratios given those lengths, and total displacement across the faults. Hence the area for these faults is conditional on the seismogenic crustal thickness or existence of a detachment, fault dip, and maximum rupture length. For the secondary faults, downdip width was assessed assuming an aspect ratio (AR) for the fault (horizontal/vertical) in the range of 0.91 to 2.2 based on data presented in Nicol *et al.* (1996). Dip values for the secondary local faults were assumed to be in the range of 65 to 75 degrees. These values for dip of the secondary faults are based simply on the observation from structural cross sections and seismic reflection data from normal faulting terranes that secondary faults that merge with more significant faults (in terms of structural offset) commonly have steeper dips than the associated major fault. Hence we characterize a slightly steeper dip for the secondary faults.

Our evaluation of the downdip geometry considers two basic alternatives, one with many of the faults merging at depths above the brittle-ductile transition and one with individual, planar faults that do not intersect (Figure ASM-5). Based upon the spatial proximity and anastamosing pattern of the local faults in map view, we assign a high probability (0.95) that the faults merge within the seismogeneic crust. Conditional on the existence of a detachment we assign 1.0 probability that the faults merge down dip. Note that for the interpretation that a detachment exists, then all of the local faults are limited in their depth extent by the detachment depth.

A number of geometries are considered possible for the merging case, the major, block-bounding faults (Bare Mountain, Paintbrush Canyon/Stagecoach Road, Solitario Canyon, and Windy Wash) are evaluated for likelihood of interrelationships with the secondary faults and with each other based on aspect ratio and geometry (as discussed by C. Fridrich in SSC Workshops 2 and 6). As indicated on Figure ASM-6, a large number of possible geometries were considered based on ranges of dip and aspect ratio for the secondary faults and dips for the primary faults. Cross-sections for both northern and southern transects were constructed with weights for aspect ratios and dips as described above.

The result was the development of four representative cross-sections that define the uncertainty in downdip geometry of the block bounding and secondary faults (Figures ASM-5 and ASM-7). If the faults merge down dip, then three alternative geometries are defined: a

shallow model, a preferred model, and a deep model. These models reflect the depth at which merging takes place. The dip of the faults is assumed to increase as the depth of merging increases (see Figure ASM-7). Based on the weights assigned to fault dips and aspect ratios, the weights assigned to the shallow, preferred and deep merging models are 0.1, 0.6, and 0.3 respectively. For the nonmerging case, only one model is considered because steep fault dips are required to maintain fault separation throughout the seismogenic crust. In the nonmerging case, the downdip extent of the secondary faults is limited by the preferred AR value of 1.55 (the central value of the range quoted earlier).

3.4.3 Behavioral Models

Our evaluation of the behavioral aspects of the Yucca Mountain faults focused on displacement and temporal attributes.

Maximum and Average Displacements in the Maximum Earthquake. Several procedures were utilized to estimate average and maximum displacements for each local fault source from the Yucca Mountain trench data. (Note: All data to develop these parameters is from Table 5.1 of the synthesis report (USGS, written communication, 1996). By using the several methods we intend to capture the uncertainty in models (methods) as well as sampling and interpretation uncertainties.

Average Displacement- One method to estimate the average displacement, D_{avg}, is simply to average the preferred values of displacement, D_{pref}, from all events in all trenches along each fault. An alternative is to average the D_{pref} values from the largest event on each fault. We have computed true D_{avg} using each of these techniques and assigned a weight of 0.5 to each result. The results are contained in Table ASM-1.

Maximum Displacement- One technique is to simply take the largest value of D_{pref} in any trench on the fault to represent the maximum displacement in the earthquake, true D_{max} (we distinguish true D_{max} from the maximum estimates of displacement for each event in each trench). However, based on the Borah Peak results, only 2-3% of the fault trace exhibits displacements within 80-90% of the true maximum displacement value. Hence, it is unlikely that even three randomly placed trenches would sample within 80-90% of the true maximum

displacement. We give this technique for estimating true D_{max} a weight of 0.25. An alternative method to estimate true D_{max} is to consider choose the largest displacement value from Table 5.1 for each fault. This incorporates the uncertainty in interpretation/evaluation of displacements within the trenches. We have assigned a weight of 0.5 to this technique. Another way to estimate true D_{max} is to consider it a multiple of true D_{avg}. This is a technique suggested by Mason (1996). At Borah Peak, the ratio of true D_{max}/D_{avg} is ~3.37 for the entire 33.8 km of the surface rupture, for the central portion of the fault it is ~2.59. Our alternative technique is then to take each of the true D_{avg} values described above and multiply them by 2.59 to arrive at values for D_{max}. We have assigned a subjective weight of 0.125 to each of the resulting values. Using this procedure we attempt to reduce the uncertainty due to sampling bias (i.e. trench location). The results for true D_{max} also are contained in Table ASM-1.

Simultaneous Rupture of Fault Sources. For this analysis, "simultaneous rupture" is defined as ruptures on two or more faults occurring within 30 seconds of each other. Hence, simultaneous rupture increases the magnitude of the earthquake. In effect, the *areas* of the faults involved are combined to contribute to a larger magnitude. We take this rather strict definition because the purpose of this characterization is to evaluate vibratory ground motion hazard. If two or more faults rupture more than ~30 seconds apart (i.e. strong motion from the second fault begins arriving at the site after shaking from the first event has stopped) the two earthquakes (occurrence) can be characterized as independent events. The logic tree that defines the structure and uncertainties in this assessment is given on Figure ASM-5 and is described below.

The potential for simultaneous rupture is dependent upon whether or not the faults merge down dip. If the faults do not merge, then it is assumed that simultaneous ruptures do not occur (Figure ASM-5). In addition, the probability that simultaneous ruptures occur is assessed based on the likelihood of temporal overlap during past events. Based on the results presented in the synthesis report (as presented by Pezzopane and Whitney, SSC Workshop 3) and as summarized by L. Anderson (in SSC Workshop 4) the potential simultaneous ruptures considered are listed on Figure ASM-8. We assigned probabilities to the scenarios listed in Table 5-3 of the synthesis report as follows: high confidence cited in Table 5-3 received a

P=0.9, moderate confidence received a weight of 0.5, and low-moderate confidence received a weight of 0.25. Then for each fault pair, these values were multiplied times the fractional number of total events on the two faults that were inferred to be in common to compute a probability of temporal overlap for the fault pair. The ultimate probability of simultaneous rupture (under our definition) is then the linked probability of the geometry and temporal overlap branches. This result is a probability of 0.3 that simultaneous ruptures occur, given that the faults merge down dip (Figure ASM-5).

3.4.4 Maximum Magnitude

Maximum earthquake magnitudes for the independent fault sources were assessed using maximum rupture dimensions (surface rupture length, displacement, area) for individual maximum events, as discussed above. Our parameters included surface rupture length, maximum and average displacement per event, rupture area, and displacement times length vs. magnitude (Mason (1996); see Table ASM-3). For the local faults, the subjective weights for each of the above methods used to compute magnitude estimates was applied individually, i.e., was given a fault-specific set of weights. We gave the highest weights to the surface rupture length (SRL) relationship of Wells and Coppersmith (1994) and SRLxD method of Mason (1996), each assigned a weight of 0.3. Weights of 0.15 were applied to the average and maximum displacement methods, and a weight of 0.1 was applied to the rupture area method (all from Wells and Coppersmith, 1994).

These general rules were modified on a fault-specific basis (Table ASM-3) for several reasons. First, on some faults no average displacement values could be calculated, because there was only one trench for which displacements were reported. In such a case, we could not estimate magnitude based on average displacement. Second, if the displacements in individual trenches ranged greatly from event to event, we had a low confidence that a computed average displacement was meaningful. Given the large variability of displacement along strike in historical normal surface ruptures (e.g., Wheeler, 1989; McCalpin, 1996), we generally had low confidence that a few randomly sited trenches would fortuitously sample either the maximum or average displacement for each paleoearthquake. Thus, magnitude estimates based on displacements usually were assigned lower weights than estimates derived by other methods. Third, if faults were so proximal at the surface that they could merge downdip within the crust, we acknowledged greater uncertainty in their downdip extent, and

thus lowered the weight on estimates based on rupture area. Finally, for faults that possess short lengths with respect to their observed per-event displacements, we generally assumed that: (1) the faults must fully penetrate the crust to explain such large coseismic displacements; (2) if the faults fully penetrate the crust, they must have a downdip dimension of 14 to 20 km (assuming a 60-degree dip and 12 to 17 km depth); (3) it would be very unusual for a fault having a 14- to 20-km downdip extent to be shorter than 14 km, because that would imply an aspect ratio of less than 1.0; therefore, (4) those faults were considered to have longer ruptures than the mapped fault length, by linking with other mapped faults; and thus (5) the large displacements considered were more representative of the maximum earthquake than the short lengths of the mapped faults. [We note that the definition and naming of separate faults in an anastomozing network of faults, such as exists at Yucca Mountain, is somewhat arbitrary. This is the reason we have chosen to consider the Stagecoach Road/Paintbrush Canyon system as a single fault. Based on the large reported displacements, short length and along strike geometry of the Stagecoach Road fault we infer it to be connected at depth with the Paintbrush Canyon fault].

For each fault, we evaluated the quality of the data on fault dimensions and then altered the weighting outlined above to reflect our assessment of believability in the measurements.

3.4.5 Recurrence

Fault Slip Rates. Slip rates were assessed using data in Table 5.1 of USGS (written communication, 1996). First, the long-term mean slip rate for each fault was computed (including data uncertainties), and a normalized-grouped cumulative density function (CDF) was generated, after the technique of McCalpin (1995). Examples of this technique are provided in Appendices ASM-1 and ASM-2. This technique considers the variation of slip rates among many faults over a short period to mimic the variation on a single fault over a longer period. The mean long-term slip rate is applied to the CDF to produce a fault-specific CDF of slip rate. Values of the 20-percentile, median, and 80-percentile are listed in Table ASM-4. The full CDF was used in the analysis.

Earthquake Recurrence. Two alternative approaches were used to characterize earthquake recurrence relationships for independent fault sources. In the first approach, the inter-event times from Table 5.1 of the USGS (written communication, 1996) are used, along with the

errors cited for the "preferred, maximum, and minimum" estimates, to calculate the times between characteristic paleoearthquakes. The cited values are considered to represent only measurement error for a given interval, and not the stochastic variability between successive events in a given trench.

To account for the stochastic variability, we again used the McCalpin (1995) approach. Normalizing all recurrence data by setting the long-term mean recurrence of each fault to 100 ka. We then grouped all normalized recurrence intervals for all faults and plotted the cumulative density function (CDF). Probability density functions and cumulative distributions for this technique are contained in Appendices ASM-3 and ASM-4, respectively. (This same approach was used for slip rate; see McCalpin [1995] for explanation of the technique.) We then input the long-term interevent time for each fault (which contains only measurement errors) into the CDF to produce a new CDF that incorporates both measurement error and stochastic variability, as contained within the normalized-grouped data set (Appendix ASM-5). These values are listed in Table ASM-5. This approach is given a weight of 0.5, which reflects our evaluation that it is an equally valid approach to the slip rate approach described below. This approach yields only the recurrence times between maximum (or characteristic) earthquakes; frequency of smaller earthquakes is derived from the recurrence models described below.

In the second approach, the slip rate distributions described above are used to develop recurrence relationships using a moment rate approach (e.g. Youngs and Coppersmith, 1985). This approach was also given a weight of 0.5.

The application of the slip rates and recurrence intervals to develop recurrence rates for the local faults depended upon the behavior model. Under the condition that simultaneous ruptures do not occur, the individual faults are assumed to act independently, and the assessed slip rates and recurrence intervals for each fault are used to define the recurrence relationship for the fault. Under the condition that simultaneous ruptures can occur, then the slip rates and recurrence intervals are partitioned between individual fault ruptures and simultaneous fault ruptures as follows.

Listed on Figure ASM-8 are the assessed percentage of fault ruptures on the individual block-bounding faults that are considered to be simultaneous ruptures with other faults and the relative frequency of various fault rupture combinations. The slip rate that is released in multiple-fault rupture is set equal to the assessed fault slip rate times the percentage of times the fault ruptures simultaneously with other faults. This slip rate is further partitioned among the various multiple-fault rupture scenarios by the relative frequencies listed on Figure ASM-8. For example, under the condition that simultaneous ruptures occur, 90% of major ruptures on the Bare Mountain fault are assumed to be simultaneous ruptures and 1/3 of these are in combination with the Solitario Canyon fault. Similarly, 70% of ruptures on the Solitario Canyon fault are assumed to be simultaneous ruptures and 1/2 of these are in combination with the Bare Mountain fault. The assessed slip rate used to define the recurrence of simultaneous ruptures of the Bare Mountain and Solitario Canyon faults is set equal to 30% of the Bare Mountain slip rate plus 35% of the Solitario Canyon slip rate.

The assessed recurrence rates for individual faults are similarly partitioned; 30% of the rate for Bare Mountain events are assumed to be simultaneous ruptures with Solitario Canyon and 35% of the rate for Solitario Canyon events are assumed to be simultaneous ruptures with Bare Mountain. Because these assessments are approximate, the computed frequencies were not identical, and an average of the two values was used to define the recurrence rate for the simultaneous ruptures.

Under the condition that simultaneous ruptures can occur, the slip rates and recurrence intervals for individual fault ruptures are set equal to the assessed values for the individual faults times the percentage of times that individual fault ruptures occur (e.g. for Bare Mountain 10% of the ruptures are assessed to be independent ruptures of the Bare Mountain fault).

For the local faults, three recurrence models were used. The highest weight was given to the characteristic model of Schwartz and Coppersmith (1984) (as described by Youngs and Coppersmith, 1985), weight = 0.7; the exponential recurrence model was assigned a weight of 0.2; and the "maximum magnitude" model (similar to Wesnousky *et al.*, 1983) was assigned a weight of 0.1

In constructing the recurrence relationships we assume that the maximum magnitude assessments described in Section 3.4.4 are the central value for the characteristic magnitude interval (e.g. Youngs *et al.*, 1987). For the characteristic and maximum moment recurrence models, the characteristic events are uniformly distributed in the magnitude range M_{max}±¼, such that the upper limit of the recurrence relationship is M_{max}+¼. For the exponential recurrence model the upper limit is also set at M_{max}+¼. When the recurrence relationship is specified by the recurrence interval of surface-rupturing earthquakes, this recurrence rate was assumed to apply to earthquakes of magnitude greater than or equal to M_{max}-¼.

Under the condition that simultaneous ruptures can occur, the above three recurrence models were used to assess the relative frequency of various magnitude earthquakes for individual fault ruptures only. Multiple fault ruptures were assumed to be additional, larger events and the assessed maximum magnitude earthquakes were assumed to be the only events occurring.

3.5 REGIONAL FAULT SOURCES

Regional fault sources include regional faults (i.e., those outside the immediate Yucca Mountain/Bare Mountain/Crater Flat area) within 15 to 100 km from the site that are judged to be relevant earthquake sources. The locations of these regional fault sources are shown on Figure ASM-9. Most of the faults are listed in Table 11-1 in chapter 11 of USGS (written communication, 1996). We include, in addition:

(1) Carrara (or U. S. Highway 95) fault,
(2) East Specter Range fault,
(3) a 12 km northern extension of the West Spring Mountains fault,
(4) Middle Death Valley fault, and
(5) West Death Valley fault.

Regional geologic, seismologic, and geophysical studies, and evaluation of these faults suggest that they are steeply- to moderately-dipping faults and exhibit conjugate relationships as discussed in Section 2.2. The northwest-trending faults are generally right-lateral and lie within the Walker Lane (Stewart, 1987) west of Yucca Mountain. Regional fault sources in the Basin and Range province east of the Death Valley-Furnace Creek-Fish Lake Valley fault zone have slip rates that are about one or more orders of magnitude lower than the faults within the Walker Lane.

Several other regional faults were excluded from our analysis based on: (1) data presented by Anderson *et al.* (1995a) that showed little evidence for middle to late Quaternary activity (e.g., Keane Wonder, Oasis Valley, Rocket Wash/Beatty Wash, and the Toliche Peak faults); or (2) sparse documentation of Quaternary activity (e.g., the Tin Mountain, Tikaboo, Stonewall Mountain, and Racetrack faults). The Kawich Range fault was excluded based on the discussion in Anderson *et al.* (1995a) and consideration of the short length of known Quaternary faulting. An estimated Mw 6.82 earthquake (based on SO = 1.5 m displacement at profile KRW-3) on this fault at about 72 km from the site would not be a relevant event on Figure 11-3 of Pezzopane in USGS, (written communication, 1996).

Table ASM-6 summarizes the earthquake source characteristics for the 24 active regional faults that are included in our source model. This table is revised from the table in the memorandum from the ASM team of 13 May 1997, titled A Revised Source Data for Regional Faults (ASM Team). With the exception of the Carrara fault, all sources are assigned a probability of 1.0 of being seismogenic based mainly from paleoseismic evidence summarized in Anderson *et al.* (1995a, b), R. E. Klinger and L. A. Piety (USBR, written communication, 1996), Piety (1995), and various chapters of USGS (written communication, 1996). The Carrara fault is judged to be seismogenic with a high probability (0.85) for the reasons cited in Appendix ASM-6, but because the fault has not been fully characterized, some probability (0.15) is given to the possibility that it is not seismogenic. A generalized planar fault geometry to seismogenic depth was assumed for all the regional fault sources. Predominantly strike-slip faults are modeled as having a dip of 90 degrees. Predominantly normal or dip-slip faults are modeled as having dips of 60 degrees.

3.5.1 Estimation of Quaternary Ages

The ages of fault activity of Table 2 in Anderson *et al.* (1995a, b) were used as a starting point. Our evaluation considered that: (1) the Pleistocene/Holocene boundary may be nearer 12 than 10 ka; (2) many references use 125 or 130 ka for the boundary between late and middle Pleistocene (128-770 ka); (3) the boundary between middle and early Pleistocene is 770 ka, and early Pleistocene is 770 to 1650 ka, which strongly skews the middle Pleistocene toward the present, and the middle Pleistocene is already skewed toward the present based on a start at 1650 ka bp, or more than 2000 to 2400 ka based on some recent dating. The

terminology may be misleading as the middle Pleistocene includes the most recent 8-47 percent of the Pleistocene (using 1650 ka), and does not include even the middle of the Pleistocene. It is however, the most widely used classification, and is required for comparative purposes. Accordingly, the following approximate dates are used in our analysis:

(1)	Holocene/late Pleistocene boundary =	10 ka
(2)	latest Pleistocene (avg. of 10 ka and 28 ka) =	19 ka
(3)	latest Pleistocene (avg. of 10 ka and 69 ka) =	39 ka
(4)	mid-late Pleistocene (avg. of 10 ka and 128 ka) =	69 ka
(5)	late Pleistocene/middle Pleistocene boundary =	128 ka
(6)	middle Pleistocene = (avg. of 128 and 770 ka) =	449 ka
(7)	middle Pleistocene/early Pleistocene boundary =	770 ka
(8)	beginning of Pleistocene =	1650 ka

3.5.2 Maximum Magnitude

Maximum magnitudes were calculated using an empirical relation that relates surface rupture length (SRL) to magnitude (Wells and Coppersmith, 1994, for all fault types). The relationship for all fault types was used because the data base is more robust, has a lower standard deviation, and higher correlation coefficient than for normal faults, and the relationship for strike slip, normal slip, and all fault types are almost coincident as shown on Figure 9 (b), and Table 2A of Wells and Coppersmith (1994). The uncertainty in maximum magnitudes is represented by the range of minimum, preferred, and maximum SRL. This uncertainty is approximately +/- 0.2-0.4 magnitude unit for 9 of 26 faults, and is lower for the other faults where SRL is constrained by intersection or connecting faults, or consistent magnitude values are obtained from maximum displacement or average displacement values.

3.5.3 Slip Rate

Two approaches were used to estimate slip rates for regional faults. For well- to moderately well-studied faults (designated by italic font in Table ASM-6) reported slip rates were used, with most preferred values assigned a weighting of 0.6 to 0.8, and maximum or minimum values of 0.1 to 0.2. For faults that have poor or incomplete characterization data (designated by normal font in Table ASM-6), slip rate was estimated from surface rupture length as described below. The weightings for these values have greater uncertainty than for the relatively well-studied cases. We thus assigned equal weight (approximately 0.33) to the preferred, maximum, and minimum values.

Slip Rate Estimated From Surface Rupture Length. The average slip rate for the faults that have relatively good SRL or length estimates and the approximate age of disturbed geomorphic surfaces as summarized in Piety (1995) were made as follows:

1. Maximum displacement (MD) for each event is estimated from surface rupture length (SRL) using the following relationship from Wells and Coppersmith (1994): log (MD) =-1.38 + 1.02 log (SRL). This relationship is based on a robust worldwide database of 95 events, and has a good coefficient of correlation of 0.75 and a standard deviation of 0.41. The regressions in Wells and Coppersmith (1994) generally are based on the maximum observed horizontal, oblique, and/or vertical surface displacement.

2. MD is multiplied by 0.38 to obtain AD, the average displacement (in mm). The multiplier value used is based on the average of values presented in Mason (1996) for Basin and Range normal faulting events, Slemmons (unpublished data for all fault types, and Basin and Range events), and Strom and Nikonov (unpublished data for normal faulting events) as summarized in Table ASM-7.

3. An assumed number of surface rupture events is inferred. Based on field data and observations for better studied regional faults (Table ASM-8) a value of 3 events is used in the analysis for the average number of surface faulting events.

4. Cumulative displacement is estimated by multiplying the estimated AD by 3 (the inferred number of surface rupture events).

5. An estimated slip rate is calculated using the cumulative displacement divided by the estimated ages for the geomorphic surfaces that are displaced by the fault. The displaced surfaces generally are assumed to be late to middle Pleistocene and equal weight is assigned three ages (69 ka, 128 ka, and 449 ka) (see Section 3.5.1 for discussion of estimated ages). The interval of time used is truncated at 10 ka, since mid-Holocene events appear to be absent from the faults, but early Holocene, or late Pleistocene events are present on some of the faults. Therefore, values of 59, 118, and 449 years were used to calculate maximum, preferred, and minimum slip rates.

3.5.4 Recurrence Intervals

C. M. dePolo and D. B. Slemmons (Nevada Bureau of Mines and Geology, written communication, 1997) previously examined the ten largest surface rupture areas in the Basin and Range province for earthquakes of Mw = 6.3 to 7.5, including (Owens Valley; Sonora, Mexico; Pleasant Valley; Hansel Valley; Cedar Mountain; Rainbow Mountain; Fairview

Peak; Dixie Valley; and Borah Peak earthquakes. All areas showed prominent Holocene and late Pleistocene paleoseismologic features along most scarps. Approximately 90 percent of the historical surface faults coincided with paleoscarps. This recurrent activity also is reported for most of the Yucca Mountain Quaternary faults, with all of the larger fault scarps showing geomorphic evidence for multiple events on at least parts of the fault zone. This multi-event relationship is better expressed in the exploratory trenches, and for the higher slip rate, most recently active faults, than by faults that have low slip rates and extremely long recurrence intervals (e.g., > ~ 100 kyr). Based on these observations, we assumed multiple events in our assessment of recurrence intervals for regional fault sources.

Two approaches were used to estimate recurrence intervals for regional faults: (1) for well-studied faults (designated by italic font in Table ASM-6) estimates of recurrence interval were obtained from paleoseismic data reported in the references provided and from personal observations by D. B. Slemmons as discussed in Appendix ASM-6; and (2) for faults with little or no paleoseismic data (designated by normal font) the recurrence intervals were estimated as follows.

The scarps observed in middle to late Pleistocene surfaces (based on data in Piety, 1995 and observations of D. B. Slemmons as discussed in Appendix ASM-6) are assumed to result from multiple surface faulting earthquakes. An assumed number of surface rupture events is inferred. Based on field data and observations for better studied regional faults (Table ASM-8) a value of 3 is used in the analysis for the average number of surface faulting events.

Three values (69 ka, 128 ka, and 449 ka) are used for the estimated age of the displaced geomorphic surfaces. As noted in the previous section, 10 kyr have been subtracted from these ages to estimate the pre-Holocene duration of time during which the inferred three events occurred.

The estimated duration periods of 59, 118, and 439 years are divided by 3 (the assumed number of surface rupture events) to provide the following estimated values and weights for recurrence interval: 20 kyr (0.33), 39 kyr (0.34), and 146 kyr (0.33).

In some cases (e.g., the Emigrant/Towne Pass and Grapevine faults) additional data that are available to constrain the timing of the most recent event, or possibility of connecting with

other fault extensions, also were incorporated into the assessment of recurrence interval as described in Appendix ASM-6.

3.5.5 Recurrence Models

Two recurrence relations were used to characterize the regional fault sources: the maximum moment recurrence model (Wesnousky, 1986) and the characteristic earthquake recurrence model (Youngs and Coppersmith, 1985). The maximum moment recurrence model was derived by Wesnousky (1986) from paleoseismic data for faults in southern California region, and this method, which was deemed most appropriate for our regional fault evaluations, was given a weighting of 0.8. The Youngs and Coppersmith model is widely used, but is more appropriate for earthquake catalog data. Since it is a widely used method, we felt it should be considered but assigned it a lower weighting of 0.2. The recurrence models are applied in the same manner as was done for the local sources.

The characteristic model requires estimates of the b-value associated with specific faults. The b-values used varied from fault to fault depending on the values assigned to the areal source zone in which the individual fault lies (see below).

3.6 REGIONAL SOURCE ZONES

Six regional source zones were defined within 300 km of the Yucca Mountain site for this evaluation: a Basin and Range zone, a Walker Lane zone (which contains the Yucca Mountain site), a Colorado Plateau zone, a Mojave block zone, a San Andreas zone, and a Sierra Nevada/Basin and Range zone (see Figure ASM-10). These zones are based on tectonic characteristics, style of faulting, and observed seismicity rates. From west to east the 300 km radius of the Yucca Mountain site) is divided into the following source zones:

Sierra Nevada/Basin and Range Boundary Zone. This en echelon zone includes the Mw=7.5 Owens Valley earthquake of 1872 (Beanland and Clark, 1994), that accommodates a significant fraction of the inferred activity of the Eastern California Shear Zone (Savage *et al.*, 1990) and high seismic activity rate of the southern portion of the Central Nevada Seismic Zone (Rogers *et al.*, 1991).

Walker Lane. This zone, defined by (Stewart, 1987), includes the Basin and Range Province of highest activity from Owens Valley to Death Valley, and a narrow eastern Walker Lane of lower tectonic and seismic activity from Death Valley to Yucca Mountain.

Yucca Mountain Subzone. A subzone of 50 km radius within the Walker Lane surrounding the Yucca Mountain site. Defined on the basis of enhanced geological investigations.

Basin and Range Province. The Basin and Range Province northeast of Walker Lane, which at the Yucca Mountain latitude has a much lower rate of activity than the Walker Lane. Dominated by north-trending normal faults and moderate to high seismic activity rate.

Colorado Plateau. The relatively stable block along the southeast boundary of the Basin and Range Province, more than 200 km east-southeast of Yucca Mountain.

Mojave Block. A relatively stable block generally south of the Garlock fault (about 100 km south of Yucca Mountain), which forms a boundary between the Walker Lane and Sierra Nevada/Basin and Range Province, and the Colorado Plateau Zone.

San Andreas Fault System. The highly active right-lateral fault system, which accommodates about 75 percent of the differential movement between the North American and North Pacific plates.

For characterization of seismic sources we used those source zones that extend within 100 km of the site as shown on Figure ASM-11 (these are the Walker Lane and Basin and Range Province).

3.6.1 Recurrence

For each zone, the recurrence is assessed to follow a truncated exponential form with probability of one. Although individual faults may follow a characteristic or maximum moment recurrence relationship, regions (i.e., source zones) generally are well represented by the truncated exponential model of earthquake recurrence (Youngs and Coppersmith, 1985; Richter, 1958).

The recurrence for each zone is computed using the appropriate subset of the 300-km catalog, declustered using the Veniziano and van Dyke (1985) (as described in McGuire, 1985) (weight =0.7) and Youngs *et al.* (1987) (weight=0.3) techniques (see Appendix D of the main report). The catalog declustered using the Veniziano and van Dyke approach is referred to as Version 7, the catalog declustered using the Youngs *et al.* approach is referred to as Version 5. Based on comparisons of the space-time plots, the Veniziano and Van Dyke (1985) technique appears to be more successful at declustering the catalog and has been weighted higher. Additional attempts at declustering were made using the technique of Reasenberg (1985). This technique was significantly less successful at declustering the catalog (see example space-time diagrams in Figure ASM-12). As a result, the Reasenberg algorithm was not utilized to develop recurrence statistics for the source zones. Data after 1950 from the region within the Nuclear Test Site (Figure ASM-11) where nuclear testing was performed was removed from the recurrence computations to remove the influence of induced events. Completeness intervals were estimated using existing literature (Gomberg, 1991b), comparisons of "Stepp-plots" (Stepp, 1972) (example shown in Figure ASM-13) from the catalog along with consideration of the operational history and sensitivity of instrumentation in the area (personal communication, 1997; A. Rogers, J. Brune, K. Smith). The assessed completeness intervals for the 100 km radius around Yucca Mountain are summarized below.

M 2.0-2.5	1983-present
M 2.5-3.0	1979-present
M 3.0-3.5	1961-present
M 3.5-5.0	1932-present
M 5.0-6.0	1900-present
M 6.0-6.5	1880-present

3.6.2 Maximum Magnitude

Within the broader Walker Lane zone, a subzone (the Yucca Mountain subzone) is defined by a 50-km radius around the Yucca Mountain site. Given the extensive investigations in this area, it seems unlikely that any significant (in terms of slip rate), young, potentially surface rupturing faults have escaped detection within this zone. Hence we assign a lower maximum magnitude to this part of the Walker Lane zone. We assign a maximum magnitude of 6.3 +/- 0.3 to this source. We consider this value to represent the approximate upper limit magnitude for non-surfacing rupturing earthquakes in this sub-zone. Based upon the work of C.M. dePolo, University of Nevada, Reno (written communication, 1996, and as presented in SSC

Workshop 4) and considerations of physically reasonable fault area/displacement/stress drop considerations (as presented by J. Ake at SSC Workshop 4). The logic tree used to characterize the regional source zones that lie within a 100-km radius of the site is shown on Figure ASM-14.

Estimates of maximum magnitudes for source zones (other than the Yucca Mountain source subzone) were assigned based either on the inferred surface rupture length of the largest fault not explicitly characterized with the regional faults or the maximum magnitude event inferred to have occurred historically in that zone. It is our assessment that some potentially seismogenic faults are not represented in the list of regional faults specifically included in the source model (Table ASM-6 and discussed in Section 3.5). Some of these faults lack recurrence information. We used the maximum magnitude suggested by either: the approximate maximum length of those faults or the largest earthquake in the zone, to constrain the maximum magnitude for the zone in question. The maximum magnitudes for each of the seven source zones are summarized below:

Basin and Range	Mmax = 7.2
Walker Lane	Mmax = 6.8
Yucca Mountain subzone	Mmax = 6.3
Colorado Plateau	Mmax = 7
Mojave Block	Mmax = 7.7
San Andreas	Mmax = 8
Sierra Nevada/Basin and Range	Mmax = 7.6

Uncertainty in the maximum magnitude was assumed to be ±0.3 units at the 90 percent confidence interval.

3.6.3 Stationarity of Seismicity

When characterizing the seismic hazard within a source zone, two alternative hypotheses are commonly used. One considers earthquake occurrence to be equally likely at each point within the zone and frequency is determined by the recurrence statistics developed for the zone as a whole. This is the Poisson spatial model. Alternatively, non-uniform patterns of seismicity observed in the historical record may be considered the best predictor for future earthquake occurrence within the broader zone (McGuire and Barnhard, 1981). To represent this interpretation, various types of spatial smoothing models may be applied, such as kernel

density estimation. A procedure of this type has been applied to construct the recent generation of national earthquake hazard maps (Frankel, 1995). This procedure results in a heterogeneous hazard function within any given zone. It is our view that the choice between the algorithms described above (or weighting) depends on the purpose of the hazard evaluation. If the goal is to characterize the hazard for an important facility with a relatively short economic life (say 150 years) for which a very low annual probability of exceedence for design parameters (say 10^{-4}) is desired, then a source zone characterization that mimics the observed patterns of historical seismicity should be given substantial weight in the hazard calculation. However, if the goal is to characterize seismic hazard for a much longer time span (say 10,000 years) with a reasonably low probability of exceedence, then the patterns of seismicity in the historical record may have little predictive value for occurrences on those time scales. In this case it would be appropriate to use a Poisson spatial model. It is our understanding that the performance assessors will be using results from the PSHA to judge the probability of occurrence of scenarios over 10,000-year, to 100,000-year, to multiple 100,000-year periods (SSC Workshop 5 discussion). Hence we have given a weight of 1.0 to the Poisson spatial algorithm for computation of hazard at this site.

4.0
FAULT DISPLACEMENT

4.1 INTRODUCTION

We characterize the potential for both principal and distributed fault displacement on seismogenic (block-bounding or primary) faults, and distributed faulting on five classes of secondary, nonseismogenic faults or fractures. We use generalized displacement patterns for normal faults derived from observed historical displacements. We apply the approach to characterize the potential for displacement at nine designated points within the Controlled Area at Yucca Mountain, but it can be used to evaluate the potential for displacements at any point. We do not specifically incorporate large-scale displacement patterns on the Yucca Mountain faults, specifically the Solitario Canyon fault (SC) or the Bow Ridge fault (BWR), the faults that bound the repository block. Instead, we rely on observed historical surface-rupturing on range-front faults larger than those at Yucca Mountain, related to earthquakes of M ~ 7.

There are two basic approaches for estimating the amount and timing of potential displacement on secondary faults (SSC Workshop 6). One approach is to derive all estimates from the secondary fault itself, based on its cumulative displacement, length, slip rate, or other parameters. This approach does not directly address the setting of the secondary fault, i.e., its distance to primary faults, whether it is one of many similar faults or exists alone in an otherwise unfractured block of rock, and so on; but rather assumes that these influences are reflected adequately in the fault parameters. The other approach is to examine the observed pattern of rupture in fault-bounded blocks and use this information to estimate potential displacement on distributed faults based on their position relative to principal fault rupture. This is the approach we adopted.

We consider the probability of fault displacement to be independent of depth. That is, we consider the displacement gradient between the repository level and the ground surface to be zero. Where the repository is near the surface, there is little error induced by this interpretation, because the distance over which slip would be attenuated is small. Where the repository is as much as 300 m below the surface, there is a possibility of displacement attenuation upward from the repository level to the ground surface. Whereas some data are available on slip gradients along strike in historical surface ruptures (e.g., McCalpin, 1996, p. 278, 289), few direct observations have been made on slip gradients in the dip direction during coseismic events. The observations of displacements in tunnels and mines beneath surface ruptures are too few on which to rely. Given this lack of data, our characterization of the potential for displacement applies equally to the ground surface and to the repository level (i.e., no attenuation in the dip direction).

Our approach for characterizing principal faulting hazard on seismogenic faults is based on the empirical distributions of along-strike displacement by Wheeler (1989) from the analysis of large Basin and Range earthquakes. We note that the displacement-along-strike curve for the SC fault (as described by A. Ramelli at SSC Workshop 5) is anomalous compared to historical Basin and Range ruptures, in that displacement is very high in the central 20 percent of the fault and very low elsewhere. We infer that the curve is so irregular because it only contains displacements from two faulting events; with additional events, the curve should smooth out to more resemble the Wheeler curve, or the smooth, quasi-parabolic curve of cumulative displacement along strike (J.C. Yount, SSC Workshop 6). We also note that

the most critical part of the curve is that closest to the repository, i.e., the northernmost 30 percent of the fault. In that reach the SC fault curve is almost identical to the Wheeler curve, both in mean value and upper and lower confidence limits. The rapid decrease in SC slip south of the maximum is inconsistent with other faults at Yucca Mountain, which generally increase in displacement southward. This clearly is not the case with the SC fault. The highest displacements on the SC fault occur after the Iron Ridge fault has branched off, rather than before, as one would expect if fault displacements were additive after two fault strands merged. If the SC fault displacement curve were typical of the long-term trend, Yucca Mountain would be three times higher in the vicinity of Trenches T1-T3 than elsewhere. However, the crest of Yucca Mountain does not show anomalously high elevations in the 2-km-long reach in the center. For all of these reasons, we do not use the displacements curve for the SC fault to predict the magnitude of future coseismic displacements along strike, but rather the Wheeler (1989) relationship.

Our characterization of distributed faulting rests on several interpretations about the mechanics of faulting. First, we assume that all distributed (induced) slip occurs during surface-rupturing earthquakes on primary (seismogenic) faults. It does not occur during the interseismic part of the cycle when strain is accumulating. We make this assumption because distributed faulting has been observed to occur during surface-rupturing earthquakes on normal faults. Conversely, distributed surface faulting (such as surface faulting on an intrabasin fault) without surface faulting on the adjacent primary basin-bounding fault is rare.

Secondly, we assume that during the interseismic part of the cycle, a crustal slab containing one (or more) secondary (nonseismogenic) faults in the hanging wall is strained elastically (the same is true for the foot wall). At the end of the seismic cycle, when the primary fault ruptures, the crustal rocks on either side of the fault recover through a combination of elastic rebound and inelastic deformation (fault slip) on secondary faults and discontinuities. We use the measured ground displacement profile from the 1983 Borah Peak, Idaho earthquake to characterize the variation of this displacement as a function of distance from the principal fault rupture and location in the hanging wall or foot wall of the rupture. We utilize the amplitude of this displacement profile to represent the maximum potential for ground displacement, either through elastic rebound of the rocks, or slip on secondary features, or a

combination of the two. The amount of displacement that occurs on a secondary fault, if it slips, is characterized as some fraction of this potential.

4.2 METHOD OF CHARACTERIZING THE POTENTIAL FOR FAULT DISPLACEMENT

Our method of characterizing potential fault displacement is described graphically by the logic trees shown on Figures ASM-16a and ASM-16b. We use slightly different methods for estimating the frequency and amount of slip on faults, depending on whether the fault is primary or secondary. Primary faults can experience displacement within 300 meters of the surface as principal fault rupture or as distributed fault rupture in response to principal rupture on other faults. Secondary faults can only experience distributed fault rupture.

4.2.1 Method for Principal Faulting

Figure ASM-16a shows the logic tree for characterizing the potential displacement on block-bounding, (primary) faults due to the occurrence of earthquakes on these faults. The characterization consists of the following steps.

4.2.1.1 Frequency of Potential Principal Faulting Events. The frequency of displacements occurring on a fault is estimated using the seismic source characterization developed in Section 3.0. The probability that principal faulting can occur is equal to the probability that the fault is seismogenic (see Section 3.4.1).

4.2.1.2 Probability of Principal Faulting Surface Displacement During Earthquakes. The probability that displacement will occur at or near the surface during an earthquake is computed using an empirical relationship between magnitude and the probability of surface rupture developed from the data presented in S. K. Pezzopane and T. E. Dawson (USGS, written communication, 1996). Figure ASM-17 shows these empirical relationships presented in SSC Workshop 5. Of the three regression curves in Figure ASM-17, we weight the leftmost curve (labeled 32 GB events) 0.5 and the rightmost curve (labeled 105 events EC) 0.5. (The equations defining these relationships are presented in Appendix H, Section H.4.1.) These weights reflect the fact that we have no clear preference for one extreme curve over another, and we wish to capture the full range of uncertainty. The probability that slip occurs at a point of interest on a fault, given that slip occurs near the surface, is computed by

randomizing the rupture along the fault. The length of the rupture is specified by the magnitude-rupture length relationships used in the ground motion hazard calculation.

4.2.1.3 Characterization of Displacement at a Point. The probability distribution for displacement occurring at a point of interest is computed in two steps. First, the maximum displacement on the primary fault is estimated using the Wells and Coppersmith (1994) relationship for maximum displacement (*MD*) as a function of earthquake magnitude. The variability in maximum displacement from event to event also is computed using the standard error for log(*MD*) found by Wells and Coppersmith (1994). The selected relationship is

$$\log(MD) = -5.46 + 0.82\mathbf{M}, \quad \sigma_{\log(MD)} = 0.42$$

Given a maximum displacement, we use the normalized relationships shown on Figure ASM-18 to obtain the distribution for displacement at any point on the fault rupture. Figure ASM-18 was developed using the normalized displacement distributions developed by Wheeler (1989). The data were smoothed by hand to produce curves symmetric about the midpoint of the rupture. The minimum and maximum curves on Figure ASM-18 are intended to represent low (~ 5%) and high (~95%) cumulative probabilities for the ratio of the displacement at a point to the maximum displacement. (Appendix H, Section H.3.1 presents a statistical distribution fit to these data.)

4.2.2 Method for Distributed Faulting

Figure ASM-16b shows the logic tree that characterizes the potential for distributed faulting on both primary and secondary faults and fractures. The approach consists of the following steps.

4.2.2.1 Probability Feature Can Slip. The first step in the characterization potential of the potential for distributed faulting is an evaluation of the likelihood faulting can occur on the feature of interest. This is the product of two probabilities, one based on the cumulative displacement category of the feature and one based on the strike of the feature.

Probability of distributed displacement as a function of fault displacement category. The probability of displacement depends on the cumulative displacement of the target feature. This interpretation is based on a conceptual model in which faults in extending crust evolve through time (e.g., Journal of Structural Geology, Special Issue on Fault Populations, 1996, v. 18, no. 2/3). In this model, many small faults are created during the initial phases of extension. As extension continues, some small faults coalesce to form larger faults. The larger faults become preferred loci of extension (due to their size and continuity), and thus accommodate larger displacements. With larger displacements, the fault gouge zone becomes better developed, lowering fault strength and encouraging an even greater concentration of displacement on these faults. In this progression, small-displacement faults are abandoned and larger-displacement faults accommodate more and more of the extensional strain budget.

Applying this model to Yucca Mountain implies that the smaller the displacement on a fault or fracture, the higher chance that it was abandoned in the early stages of Neogene extension and no longer experiences displacement. This concept accords with field observations by W. C. Day *et al.* (USGS, written communication, 1996b) that many fractures and small-displacement faults ceased to experience displacement between the deposition of the Tiva Canyon and Rainier Mesa tuffs. A corollary to this concept is that intact rock has a negligible probability of experiencing future fault displacement. From a mechanics standpoint, there are so many pre-existing fractures and faults in the Controlled Area that the formation of new fractures to accommodate extensional strain is not considered necessary.

We characterize the potential for distributed displacement on faults or fractures within six predefined classes of cumulative displacement (Table ASM-9). Listed in Table ASM-9 is the assessed probability that distributed faulting can occur for each class of feature. The probabilities in Table ASM-9 reflect our judgment that on the one hand, block-bounding faults (class 0) are certain to experience distributed displacement (having by definition experienced principal displacement), whereas fractures have a very small chance (P = 0.01) of experiencing future distributed displacement. The intermediate probability values for class 1-4 reflect our approximate linear subdivision between extreme probabilities of 0.01 and 1.0. These probabilities express the likelihood that there will ever be any future distributed displacement on this structure. This meaning of probability is meant to cover our estimates that

progressively smaller faults were created in an earlier stage of mechanical evolution of the crustal slab, and could be permanently abandoned now that larger, more continuous faults exist to accommodate displacement.

Probability as a function of fault/fracture orientation. Yucca Mountain faults that display evidence of Quaternary displacement all strike roughly north-south, an orientation that is compatible with the observed extension direction of approximately east-west (W. C. Day *et al.*, USGS, written communication, 1996b). Given this extension direction, distributed faults and fractures having north-south strikes are most favorably oriented to accommodate induced extension. H. L. McKague *et al.* (CNWRA, written communication, 1996) quantified the favorability of slip in the present stress field, termed slip tendency. We use slip tendency to make an estimate of the probability that induced slip can occur on a distributed fault or fracture. Based on the diminishing east-west component of displacement on faults having successively more east-west strikes, we define the probability of induced slip on a fault as the sine of the angle between its strike and east-west. Thus, for north-south-striking faults, the angle is 90 degrees, so P = 1; for N45W-striking faults, P = 0.87; and for east-west-striking faults, P = 0.

4.2.2.2 Frequency of Potential Distributed Faulting Events. Earthquakes that may induce distributed faulting can occur on any of the primary, block-bounding faults, or can be background earthquakes within the local areal source zone. Because seismicity rates for the areal source are considerably higher than for any specific fault source (see Section 3.4), we consider it critical to incorporate the effects from areal sources. Earthquake recurrence relationship for all of the sources are defined in Section 3.0.

4.2.2.3 Probability of Distributed Displacement on a Feature. The next step in the characterization of the potential for distributed faulting is an evaluation of the likelihood of faulting on the feature of interest due to the occurrence of an earthquake. This is the product of two probabilities, one based on whether the earthquake ruptures the surface on the primary fault and one based on the distance of the feature from the primary fault and the feature's location in the hanging wall or foot wall of the rupture.

Probability of secondary displacement as a function of whether surface rupture occurs. It is our interpretation that secondary faulting is only induced by surface-rupturing earthquakes. We make this assumption because: 1) most historical secondary faulting has been accompanied by surface rupture on the primary fault, and 2) the ground surface deformation data from the Borah Peak earthquake, which we use as a basis for estimating distributed faulting displacements reflects a surface-rupturing event.

The probability that an earthquake ruptures the surface, regardless of whether it occurs on a known primary fault, or on an unknown fault as a background earthquake, is a function of its magnitude. Therefore, we use the 32-event and 105-event curves from Pezzopane (as described in Sec. 4.2.1.2) to calculate the probability that a given primary earthquake will rupture the surface, and thus be able to induce distributed displacement.

Probability of distributed displacement as a function of distance to primary fault. The probability that distributed displacement will occur at a given distance from the principal rupture is assessed using an empirical relationship based on the density of distributed faulting observed for Basin and Range earthquakes. Figure ASM-19 shows the results of analysis by R.R. Youngs (presented at SSC Workshop 6) of distributed rupture patterns based on data presented in S. K. Pezzopane and T. E. Dawson (USGS, written communication, 1996). This figure shows the decreasing density of distributed faulting for historical normal faulting earthquakes with increasing distance from the primary fault. We believe that the ergodic substitution applies in this case, so that the probability of fault displacement through time on a distributed fault at a given distance from a primary fault is the same as the ratio of the area containing distributed faulting to the area containing no distributed faulting at that same distance. In other words, given enough time, the percentage of time that a given secondary fault ruptured in distributed slip would converge on the percentage of area that ruptures at that distance from the primary fault.

We use two assessments of the frequency of distributed rupture as a function of distance from the primary rupture, as shown on Figure ASM-19. The leftmost curve is an envelope of maximum frequency for earthquakes in the range of **M** 6.0 to 6.9; we weight this curve 0.6. Our slight preference for this curve over the other one is based on two considerations: (1) most of the estimated maximum earthquakes on Yucca Mountain faults are in the range of **M**

6.0 to 6.9 range, so we consider that magnitude range to be most appropriate; and (2) the maximum frequency values for this magnitude range define a relatively smooth trend that decreases with increasing distance from the primary rupture. We believe that the frequency of distributed displacement on a secondary fault should decrease with increasing distance to the seismogenic fault, based on our ergodic assumption described earlier, and the fact that for historical earthquakes, distributed faulting increases in density toward the primary fault (S. K. Pezzopane and T. E. Dawson, USGS, written communication, 1996).

We weight the right-most curve on Figure ASM-19 at 0.4, for the following reasons. First, Pezzopane (pers. comm., 1997) indicates that all the frequency values in his plot are minima, because: (1) the older points in the data set represent field reconnaissances that may have underestimated the extent of distributed faulting; and (2) although more recent investigations may be more thorough, they only record distributed faulting that broke to the surface, which is a minimum value for distributed faulting at depths as great as 300 m. Second, we wish this curve to represent the fact that the other curve is a minimum value. We accomplish this by drawing a curve parallel to the leftmost curve, through the maximum values plotted for **M** 7.0 to 7.9 earthquakes. We do not use the logistic regression fits of R.R. Youngs (presented at SSC Workshop 6), because they do not represent our interpretation that all plotted points are minimum values.

The relationships shown on Figure ASM-19 are dependent on the location of a feature within the hanging wall or foot wall of the principal rupture. This geometry is not known for earthquakes occurring within the regional source zone. Therefore, we consider it is equally likely that the point at which an assessment is made lies within the hanging wall or foot wall of the rupture.

4.2.2.4 Characterization of Distributed Displacement. The characterization of distributed displacement at a point on a feature is based on D/D_{max} defined for the principal rupture times a reduction factor (RF) that depends upon the distance and class of feature being considered. The approach is illustrated schematically on Figure ASM-20. Given the location of a point at which fault displacement hazard is being assessed with respect to a primary rupture, the distance to the rupture, x, and the location of the nearest point on the rupture, y, are defined. The distribution for displacement on the primary fault at location y, $[D(y)]$ is given by the

smoothed Wheeler curve (Figure ASM-18) once D_{max} has been specified. Two alternative approaches are used to define the values for *RF*, one based on what we term the across-strike secondary deformation (ASSD) method and one based on the relative cumulative offset on the earthquake source compared to the feature of interest.

Description of the ASSD Method. During historical normal faulting events, distributed faulting is larger and more frequent on the hanging wall near the seismogenic fault, and decreases away from the fault (S. K. Pezzopane and T. E. Dawson, USGS, written communication, 1996). The density of distributed faulting at a given distance from the fault is greater on the hanging wall than on the foot wall (Bob Smith presentation at SSC Workshop 6). This pattern is similar to the pattern of coseismic geodetic ground displacement observed following a normal faulting earthquake. We consider the amount of potential displacement on a distributed fault to be related to the amount of accumulated interseismic strain in the nearby crustal slab. This potential displacement is interpreted to have its maximum at the primary fault, where it is realized as the principal faulting displacement, and to decrease with distance from the principal rupture. This assumption lies at the heart of the ASSD method.

We first characterize the potential displacement, $DP(x)$, on secondary faults based on their distance perpendicular to the primary fault. This defines potential displacement along transects perpendicular to the seismogenic faults. $DP(x)$ is considered to be equal to or less than the predicted vertical coseismic geodetic displacement of the ground surface, which reflects the displacement of the strained crustal slab within 10 to 20 km of a seismogenic normal fault. We consider that potential (vertical) slip on any secondary fault must be equal to or smaller than the predicted vertical geodetic displacement, in order to avoid overcompensation of the elastic shape change accumulated during the previous earthquake deformation cycle.

To assess $DP(x)$ we use the geodetic profile from the 1983 Borah Peak earthquake, Figure ASM-21. We rescale the Borah Peak geodetic curve in both the vertical (z) and horizontal (x) directions. The vertical dimension is normalized by 1.44 m (the principal faulting displacement at the point of intersection of the Borah Peak geodetic profile with the fault trace). We expect the horizontal extent of distributed rupture to increase with increasing penetration of the

principal fault into the crust. Thus, the horizontal dimension is rescaled by the inverse of the ratio of the downdip extent of the primary earthquake compared to 16 km (downdip extent of the Borah Peak event). As a result, earthquakes larger than the Borah Peak earthquake will produce the same displacement potential at a greater distance from the principal rupture; earthquakes smaller than the Borah Peak earthquake will produce the same displacement potential at a smaller distance from the principal rupture.

The proportion of $DP(x)$ that is realized as distributed fault slip is difficult to estimate, thus we consider a wide distribution for defining the fraction of $DP(x)$ that is realized in distributed rupture on a single feature at the point of interest. This distribution is expressed as four discrete alternatives that are based on two considerations.

First, we consider it likely that better-developed faults accommodate a higher percentage of $DP(x)$ than less-developed faults, because they are more continuous, longer, and wider. As such, they have more cumulative displacement and better-developed fault gouge, thus weaker material properties in the fault zone, and less resistance to shear.

Secondly, there is a logarithmic increase in the number of progressively less-developed faults in any volume of rock (Nicol *et al.*, 1996). Most papers in the 1996 Journal of Structural Geology, Special Issue (v. 19, no. 2/3) cite a power law relationship between N (number of faults) and D_{cum} (the cumulative displacement on a fault), with an exponent of -0.7 to -0.8, or $\log(N) = C - 0.7 \times \log(D_{cum})$, where C is a constant. Thus, coseismic distributed faulting in the crustal slab can be accommodated by displacement on one well-developed fault, or on several less-developed faults.

Using the power law relationship given by Nicol *et al.* (1996), we compute the number of faults in all six fault classes when the number in any one class is known. For example, fault classes 0, 1, and 2 are typically mapped at the surface, but 3 through 5 are not. Thus, if we know that in a certain area there is one class 1 fault (D_{cum} = 35 m), we may predict that there are 2.2 faults that have D_{cum} = 11 m (class 2); 10.3 faults having D_{cum} = 1.25 m (class 3); and 28 faults having D_{cum} = 0.3 m (class 4). We then consider that $DP(x)$ can be partitioned among the classes of faults. We list in Table ASM-9 the expected number of faults in each class compared to one fault in class 0 with a cumulative displacement of ~100 m.

We define four possibilities for the partition of $DP(x)$ to define the displacement on an individual feature. These several approaches are necessary due to the way in which the problem of fault displacement characterization was posed by the Facilitation Team. They specified the existence and fault displacement class of the feature of interest at nine test points, but did not specify what displacement class or how many faults/fractures were in the near vicinity of the feature of interest. Our method assumes that if secondary displacement does in fact occur on the feature of interest (as determined by the preceding probability branches in the fault displacement logic tree), that it is likely that secondary displacement also occurs on some or all of the nearby faults. Thus, we desire to partition $DP(x)$ between the feature of interest and some/all of the surrounding faults, without knowing what class those other faults fall in, how many of them exist, and how far from the feature of interest they lie.

The first partition assumes that all of $DP(x)$ occurs on the fault/fracture of interest, $RF = DP(x)$. This partition defines the maximum possible distributed displacement that can occur on a feature in our method, because it assumes that: 1) 100% of $DP(x)$ is realized as distributed fault displacement, which is the limiting case, and 2) this entire displacement occurs only on the feature of interest, despite the fact that other faults and fractures may exist nearby. Given the limiting nature of this scenario we consider that it is an unlikely occurrence and assign it a probability of 5% that it occurs in an event.

The second partition assumes that 100% of $DP(x)$ occurs as distributed displacement in the vicinity of the feature of interest, but that $DP(x)$ is partitioned equally among the five classes of secondary faults. In other words, $RF = 0.2 \times DP(x)$ for each fault class. We consider this scenario to have a 20% likelihood of occurring in an event.

The third partition assumes that 100% of $DP(x)$ occurs as distributed displacement in the vicinity of the feature of interest, and that this displacement is partitioned among all faults in the same displacement class as the feature of interest. This assumption is made for the case that only faults similar to the feature of interest exist in the vicinity, so that other classes of faults may not share the displacement. Based on our examination of faults and fractures in the ESF, there are certainly some zones in the tunnel where most or all of the faults/fractures belong to the same displacement class. The number of faults in a particular class, N, is listed in Table

ASM-9. Thus, $RF = DP(x)/N$. We consider this scenario to have a 30% likelihood of occurring in an event.

The fourth partition assumes that 100% of $DP(x)$ occurs as distributed displacement, but the displacement is partitioned as 20% to each of the five secondary fault classes, and within each class, equally distributed among all faults in that class. Thus, $RF = 0.2 \times DP(x)/N$. We consider that is scenario is the most likely to occur (40%) because we consider it most plausible that, if distributed displacement does occur on the feature of interest, it would also occur on all of the nearly-identical faults/fractures nearby within the same fault displacement class.

The secondary displacement calculated for the feature of interest during a principal faulting event cannot exceed the cumulative displacement (D_{cum}) on that feature, but it may equal D_{cum}. The latter situation would arise if D_{cum} was all created in a single event, i.e., distributed faulting occurred only once during the lifetime of the secondary fault. Such a possibility cannot be ruled out. Therefore, we place an upper limit on the distributed displacement equal to D_{cum} of the feature.

The ASSD method utilizes the Borah Peak geodetic curve, which distinguishes between the hanging wall and foot wall consider to define $DP(x)$. When assessing the hazard from earthquakes occurring in the local source zone, we consider that it is equally likely that the feature of interest is located in the hanging wall or in the foot wall. We also consider that the assessment point is located normal to the midpoint of the earthquake rupture ($y/L = 0.5$).

Ratio of Cumulative Slips Approach. The alternative approach for assessing RF utilizes the ratio of the cumulative slip on the feature of interest to that on the fault where the principal rupture occurs. The concept of this approach is best explained in an simplified manner.

We consider the distributed faulting hazard at point 3 located on the Drill Hole Wash fault and assume for the moment that all of the cumulative displacement at point 3 resulted from the occurrence of characteristic earthquakes on only the Solitario canyon (SC) or Bow Ridge (BWR) faults. Because point 3 is located in the hanging wall of the BWR fault, it is likely that most of the distributed displacement resulted from earthquakes occurring on the BWR

fault because of the higher frequency of distributed rupture in the hanging wall (Figure ASM-19) and a larger displacement potential (Figure ASM-21). For the sake of illustration, we assume that 75% of the cumulative slip at point 3 occurred as a result of earthquakes occurring on the BWR fault and 25 % occurred as a result of earthquakes occurring on the SC fault. Over the lifetime of the BWR fault, n characteristic earthquakes have occurred, where $n = D_{cum}(\text{BWR})/D_{ch}(\text{BWR})$, where $D_{ch}(\text{BWR})$ is the displacement of the principal rupture of characteristic events on the fault. The fraction of these events that also produced distributed rupture at point 3 is $n \times P(\text{slip on 3}|\text{event on BWR})$, where $P(\text{slip on 3}|\text{event on BWR})$ is the probability of distributed slip at point 3 due to a characteristic earthquake on the BWR fault. Therefore, the expected displacement in a distributed slip at point 3 induced by a BWR characteristic earthquake is defined as the cumulative slip at point 3 due to earthquakes occurring on the BWR fault divided by the number of BWR events that induce distributed slip:

$$D(\text{point 3}) = 0.75 \times D_{cum}(\text{point 3})/[n \times P(\text{slip}|\text{event})]$$

The ratio of displacement on the feature at point 3 to displacement on the BWR fault defines the reduction factor, RF, and is given by:

$$RF(\text{BWR}) = \frac{D(\text{point 3})}{D_{ch}(\text{BWR})} = \frac{0.75 \times D_{cum}(\text{point 3})}{D_{cum}(\text{BWR}) \times P(\text{slip on 3}|\text{event on BWR})}$$

Similarly, the reduction factor for earthquakes occurring on the SC fault is given by:

$$RF(\text{SC}) = \frac{D(\text{point 3})}{D_{ch}(\text{SC})} = \frac{0.25 \times D_{cum}(\text{point 3})}{D_{cum}(\text{SC}) \times P(\text{slip on 3}|\text{event on SC})}$$

To apply this approach to the assessment of fault displacement hazard we must account for the distribution of earthquake magnitude that may occur on a seismic source and the contributions of multiple sources to the cumulative displacement at a point. To do this, we assume that the results of applying the ASSD approach provide a good assessment of the relative contribution of individual seismic sources to the distributed faulting displacement at the point of interest. As described in Section 4.2.2 of the main text, the displacement hazard curve can be used to

compute an effective slip rate that integrates the effects of all earthquakes occurring on all sources, designated as *TESR*. If a displacement hazard curve is computed for each source, then it can be used to compute the effective slip rate, *ESR*, due to earthquakes occurring on that source. Thus, the fraction of the cumulative slip induced by earthquakes on a particular source is estimated by the ratio of the effective slip rate for earthquakes on that source to the total effective slip rate. The result is that the reduction factor to apply to displacement on the BWR fault to estimated distributed displacement on the feature at point 3 is given by:

$$RF(\text{BWR}) = \frac{ESR(\text{BWR})}{TESR} \times \frac{D_{cum}(\text{point 3})}{D_{cum}(\text{BWR}) \times P(\text{slip on 3} | \text{event on BWR})}$$

The calculation of the effective slip rate using this approach still requires an evaluation of the probability that an earthquake on the primary fault will induce distributed rupture on the secondary fault. We assess this probability for the maximum event on the primary fault using the factors described in Section 4.2.2.3 because the maximum events on the various earthquake sources are expected to produce most of the distributed slip on any secondary feature.

Application of this method requires an assessment of the cumulative displacement on each of the seismic sources in the Yucca Mountain region. These values are as follows:

Fault	D_{cum}* (m)
	2600
BARE MOUNTAIN	
Bow Ridge	125
N. Crater Flat	00
S. Crater Flat	50
Fatigue Wash	72
Iron Ridge	215
Paintbrush Canyon	500
Solitario Canyon	700
Stagecoach Road	600
Windy Wash	500

*data from Table 4.2.1 in C. M. Menges and J. W. Whitney, (USGS, written communication, 1996a) and Chris Potter (personal communication, 1997).

As indicated in the logic tree shown on Figure ASM-16b, we assign a weights of 0.7 to the ASSD approach and 0.3 to the relative cumulative displacement approach. We favor the ASSD approach because it explicitly accounts for the effect of distance in the assessment of *RF* for each earthquake and does not assume that all of the faults have evolved in a parallel manner through time. It should be noted that only the ASSD approach can be used to assess the distributed faulting hazard from earthquakes occurring in the regional source zone because the cumulative slip on the sources is unknown. However, we do not believe that this is a significant detriment because these earthquakes are generally smaller than those occurring on the faults and are unlikely to produce principal faulting surface rupture. Thus their contribution to the total displacement hazard on a feature should be a small fraction of the total.

5.0
REFERENCES

Abers, G.A., 1991, Possible seismogenic shallow-dipping normal faults in the Woodlark-D'Entrecasteaux extensional province, Papua, New Guinea: Geology, v. 19, p.1205-1208.

Anderson, R.E., Bucknam, R.C. Crone, A.J., Haller, K.M., Machette, M.N., Personius, S.F., Barnhard, T.P., Cecil, M.J. and Dart, R.L., 1995a, Characterization of Quaternary and suspected Quaternary faults, regional studies, Nevada and California: U. S. Geological Survey Open-File Report 95-599, 56 p.

Anderson, R.E., Crone, A.J., Machette, M.N., Bradley, L., and Diehl, S.F., 1995b, Characterization of Quaternary and suspected Quaternary faults, Amargosa Area, Nevada and California: U. S. Geological Survey Open-File Report 95-613,41 p.

Arabasz, W.J., Pechmann, J.C., and Brown, E.D., 1992, Observational seismology and evaluation of earthquake hazards and risk in the Wasatch Front area, Utah, *in* Gori, P.L., and Hays, W.W., eds., Assessment of regional and earthquake hazards and risk along the Wasatch Front, Utah: U.S. Geological Survey Professional Paper 1500-D, p. D1-D36.

Beanland, S., and Clark, M.M., 1994, The Owens Valley Fault Zone, eastern California, and surface faulting associated with the 1872 earthquake: U. S. Geological Survey Bulletin 1994, 29 p. and 4 pls.

Brogan, G.E., Kellogg, L.S., Slemmons, D.B., and Terhune, C.L., 1991, Late Quaternary faulting along the Death Valley-Furnace Creek fault system, California and Nevada: U. S. Geological Survey Bulletin, map scale 1:62,500, 23 p., 4 pls.

Carr, W.J., 1990, Styles of extension in the Nevada test Site region, southern Walker Lane Belt; an integration of volcano-tectonic and detachment fault models, *in* Wernicke, B.P. (ed.), Basin and Range extensional tectonics at the latitude of Las Vegas, Nevada: Geological Society of America Memoir 176, p. 283-303.

Dohrenwend, J.C., Menges, C.M., Schell, B.A., and Morning, B.C., 1992a, Reconnaissance photogeologic map of young faults in the Las Vegas 1 x 2 quadrangle, Nevada, California, and Arizona: U. S. Geological Survey Miscellaneous Field Studies Map MF-2182, scale 1:250,000.

Dohrenwend, J. C., Schell, B. A., McKittrick, M. A., and Morning, B. C., 1992b, Reconnaissance photogeologic map of young faults in the Goldfield 1 x 2 degree quadrangle, Nevada and California: U. S. Geological Survey Miscellaneous Field Studies Map MF- 2183, scale 1:250,000.

Doser, D.I., 1987, The Ancash, Peru earthquake of 1946 November 10: evidence for low-angle normal faulting in the High Andes of Peru: Geophysical Journal of the Royal Astronomical Society, v. 91, p. 57-71.

Doser, D.I., and Smith, R.B., 1989, An assessment of source parameters of earthquakes in the Cordillera of the western United States: Bulletin of the Seismological Society of America, v. 79, p. 1393-1409.

Forsyth, D.W., 1992, Finite extension and low-angle normal faulting: Geology, v. 20, p. 27-30.

Frankel, A., 1995, Mapping seismic hazard in the central and eastern United States: Bulletin of the Seismological Society of America, v. 66, p. 8-21.

Fridrich, C., and Price, J., 1992, Tectonic framework of Crater Flat Basin, adjacent to Yucca Mountain, Nevada: A preliminary report: Geological Society of America, Abstracts with Programs, v. 24, no. 7, p. 189-190.

Gianella, V.P. and Callaghan, E., 1934, The earthquake of December 20, 1934 at Cedar Mountain, Nevada and its bearing on the genesis of Basin and Range structure: Journal of Geology, v. 42, p. 1-22.

Gomberg, J., 1991a, Seismicity and shear strain in the southern Great Basin of Nevada and California: Journal of Geophysical Research, v. 96, p. 16,383-16,399.

Gomberg, J., 1991b, Seismicity and detection/location threshold in the southern Great Basin Seismic Network, Journal Geophysical Research, v. 96, No. B10, P. 16401-16414.

Hackett, W.R., Jackson, S.M., and Smith, R.P., 1996, Paleoseismology of Volcanic Environments, *in* McCalpin, J.P., ed., Paleoseismology: San Diego, CA, Academic Press, Chapter 4.

Hardyman, R.F. and Oldow, J.S., 1991, Tertiary tectonic framework and Cenozoic history of the central Walker Lane, Nevada, *in* Raines, G.L., Lisle, R.E., Schafer, R.W., and Wilkinson, W.H., eds., Geology and ore deposits of the Great Basin: Geological Society of America, Nevada Symposium Proceedings, v. 1, p. 279-301.

Harmsen, S.C., and Bufe, C., 1991, Seismicity and focal mechanisms for the southern Great Basin of Nevada and California, 1987-1989: U.S. Geological Survey Open-File Report No. 91-572, 208 p.

Hunter, R.L., and Mann, C.J., eds., 1992, Techniques for determining probabilities of geologic events and processes: International Association for Mathematical Geology, Studies in Mathematical Geology, no. 4, Oxford University Press, Oxford, UK, 364 p.

Jackson, J.A., 1987, Active normal faulting and crustal extension, *in* Coward, M.P., Dewey, J.F., and Hancock, P.L. eds., Continental Extensional Tectonics: Geological Society of London Special Publication 28, p. 3-17.

Jackson, J.A., and White, N.J., 1989, Normal faulting in the upper continental crust; observations from regions of active extension: Journal of Structural Geology, v. 11, p. 15-36.

Johnson, R.A., and Loy, K.L., 1992, Seismic reflection evidence for seismogenic low-angle faulting in southeastern Arizona: Geology, v. 20, p. 597-600.

Mason, D.B. 1996, Earthquake magnitude potential of the intermountain seismic belt, USA, from surface-parameter scaling of late Quaternary faults: Bulletin of the Seismological Society of America, v. 86, n. 5, p. 1,487-1,506.

McCalpin, J.P., 1991, Quaternary surface-faulting earthquakes in the Overthrust Belt; did they occur on listric faults?: Geological Society of America, Abstracts with Programs, v.23, n. 7, p.140.

McCalpin, J.P., 1995, Frequency distribution of geologically determined slip rates for normal faults in the western USA: Bulletin of the Seismological Society of America, v. 85, n. 6, p. 1867-1872.

McCalpin, J.P. ed., 1996, Paleoseismology: Academic Press, New York, 583 p.

McGuire, R.K., 1985, Seismic hazard methodology for nuclear facilities in the eastern United States: EPRI Research Project Number P101-29, Dames and Moore, Golden, Colorado, Vol. 2, Appendix A.

McGuire, R.K., and Barnhard, T.P., 1981, Effects of temporal variations in seismicity on seismic hazard: Bulletin of the Seismological Society of America, v. 71, p. 321-334.

Nicol, A., Watterson, J., Walsh, J. J., and Childs, C., 1996, The shapes, major axis orientations and displacement patterns of fault surfaces: Journal of Structural Geology, v. 18, no. 2/3, p. 235-248.

Nicol, A., Walsh, J.J., Watterson, J., and Gillespie, P.A., 1996, Fault size distributions—are they really power-law?: Journal of Structural Geology, v. 18, no. 2/3, p. 191-198.

Nichols, W.D., 1987, Geohydrology of the unsaturated zone at the burial site for Low-Level Radioactive Waste near Beatty, Nye County, Nevada: U. S. Geological Survey Water-Supply Paper 2312.

Piety, L.A., 1995, Compilation of known and suspected Quaternary faults within 100 km of Yucca Mountain, Nevada and California: U. S. Geological Survey Open-File Report Number 94-112, 404 p.

Quade, J., Mifflin, M.D., Pratt, W.L., and Burkle, L., 1995, Fossil spring deposits in the southern Great Basin and their implications for changes in water-table levels near Yucca Mountain, Nevada during Quaternary time: Bulletin of the Geological Society of America, v. 107, n. 2, p. 213-230.

Reasenberg, P., 1985, Second order moment of central California seismicity, 1969-1982: Journal of Geophysical Research, v. 90, p. 5479-5495.

Reheis, M.C., 1992, Aerial photographic interpretation of lineaments and faults in late Cenozoic deposits in the Cactus Flat and Pahute Mesa 1:100,000 quadranges and the western parts of the Timpahute Range, Pahranagat Range,.Indian Springs and Las Vegas 1:100,000 quadrangles, Nevada: U. S. Geological Survey-Open File Report 92-193, scale 1:100,000, 14 p., 3 pls.

Reheis, M.C., and Noller, J.S., 1991, Aerial photographic interpretation of lineaments and faults in late Cenozoic deposits in the eastern part of Benton Range 1:100,000 quadrange and the Goldfield, Last Chance Range, Beatty, and Death Valley Junction 1:100,000 quadrangles, Nevada and California: U. S. Geological Survey-Open File Report 90-41, scale 1:100,000, 9 p., 4 pls.

Reheis, M.C., and Sawyer, T.L., 1997, Late Cenozoic history and slip rates of the Fish Lake Valley, Emigrant Peak, and Deep Springs fault zones, Nevada and California: Geological Society of America Bulletin, v. 109, n. 3, p. 280-299.

Richter, C.F., 1958, Elementary Seismology: William Freeman and Co., San Francisco, California, 300 p.

Rogers, A.M., Harmsen, S.C., Corbett, E.J., Preistly, K. and dePolo, D., 1991, The seismicity of Nevada and some adjacent parts of the Great Basin, *in* Slemmons, D.B. *et al.*, eds., Neotectonics of North America: Geological Society of America, Decade Map Volume, p. 153-184.

Savage, J.C., Lisowski, M., and Prescott, W.H., 1990, An apparent shear zone trending north-northwest across the Mojave Desert into Owens Valley, eastern California: Geophysical Research Letters, v. 17, p. 2113-2116.

Schwartz, D.P., and Coppersmith, K. J., 1984, Fault behavior and characteristic earthquakes: Examples from the Wasatch and San Andreas faults: Journal of Geophysical Research, v. 89, 5681-5698.

Schweickert, R.A., and Lahren, M.M., 1997, Strike-slip fault system in Amargosa Valley and Yucca Mountain, Nevada: Tectonophysics, v. 272, p. 25-41.

Sibson, R.H., 1985, A note on fault reactivation: Journal of Structural Geology, v. 7, p. 751-754.

Simonds, W.F., Whitney, J.W., Fox, K.F., Ramelli, A., Yount, J., Carr, M.D., Menges, C.M., Dickerson, R., and Scott, R.B., 1995, Map of fault activity of the Yucca Mountain area, Nye County, Nevada: U.S. Geological Survey Miscellaneous Investigations Series Map I-2520, scale 1:24,000.

Smith, K.D., Brune, J.N., Savage, M.K., Anooshepoor, R. and Sheehan, A.F., 1997, Main shock parameters and aftershock relocations of the 29 June 1992 Little Skull Mountain earthquake sequence: U.S. Geological Survey Circular on Yucca Mountain Tectonics, 42 p. (in press).

Smith, R. B., and Arabasz, W. J., 1992, Seismicity of the Intermountain Seismic Belt, *in* Slemmons, D. B., Engdahl, E.R., Zoback, M.D., and Blackwell, D.D., eds., Neotectonics of North America: Geological Society of America Decade Map, v. 1, Boulder, Colorado.

Stepp, C., 1972, Analysis of completeness of the earthquake sample in the Puget Sound area and its effects on statistical estimates of earthquake hazard, *in* Proceedings, First Microzonation Conference: Seattle, Washington, p. 987-909.

Stewart, J.H., 1987, Tectonics of the Walker Lane belt, western Great Basin—Mesozoic and Cenozoic deformation in a zone of shear, *in* Ernst, W.G., ed., Metamorphism and Crustal Evolution of the Western United States: Rubey Volume VII, Prentice-Hall Inc., New Jersey, p. 683-713.

Veniziano, D., and van Dyck, J., 1985, Statistical discrimination of "aftershocks" and their contribution to seismic hazard, Appendix A-4, *in* Seismic Hazard Methodology for Nuclear Facilities in the Eastern United States: EPRI Research Project No. P101-29, p. A121-A186.

von Seggern, D.H., and Brune, J.N., 1997, Seismicity in the southern Great Basin, 1968-1992, *in* Tectonic Characterization of Yucca Mountain—a Potential Geologic Repository for Nuclear Waste: Geological Society of America Special Volume (in press).

Wells, D.L., and Coppersmith, K.J., 1994, New empirical relationships among magnitude, rupture length, rupture width, rupture area, and surface displacement: Bulletin of the Seismological Society of America, v. 84, n. 4, p. 974-1002.

Wernicke, B., 1995, Low-angle normal faults and seismicity; a review: Journal of Geophysical Research, v. 100 (B10), p. 20,159-20,174.

Wesnousky, S.G., 1986, Quaternary faults and seismic hazards in California: Journal of Geophysical Research, v. 91, p. 12587-12632.

Wesnousky, S.G., Scholz, C.H., Shimazaki, K., and Matsuda, T., 1983, Earthquake frequency distribution and the mechanics of faulting: Journal of Geophysical Research, v. 88, p. 9331-9340.

Wheeler, R.L., 1989, Persistent segment boundaries on basin-range normal faults, *in* Schwartz, D.P. and Sibson, R.H. eds., Fault segmentation and controls of rupture initiation and termination: U.S. Geological Survey Open-File Report 89-315, p.432-444.

Wright, L.A., 1976, Late Cenozoic fault patterns and stress fields in the Great Basin and westward displacement of the Sierra Nevada block: Geology, v. 4, p. 489-494.

Youngs, R.R., and Coppersmith, K.J., 1985, Implications of fault slip rates and earthquake recurrence models to probabilistic seismic hazard estimates: Bulletin of the Seismological Society of America, v. 75, no. 4, p. 939-964.

Youngs, R.R., Swan, F.H. III, Power, M.S., Schwartz, D.P., and Green, R.K.,1987, Probabilistic analysis of earthquake ground shaking along the Wasatch Front, Utah, *in* W.W. Hays, and P.L. Gori, eds., Assessment of Regional Earthquake Hazards and Risk along the Wasatch Front: U. S. Geological Survey Open-File Report No. 87-585, v. II, p. 1-110.

Zhang, P., Ellis, M., Slemmons, D.B., and Mao, F., 1990, Right-lateral displacements and Holocene slip rate associated with prehistoric earthquakes along the southern Panamint Valley fault zone: implications for southern Basin and Range tectonics and coastal California deformation: Journal of Geophysical Research, v. 95, p. 4857-4872.

TABLE ASM-1
AVERAGE AND MAXIMUM DISPLACEMENTS FOR YUCCA MOUNTAIN FAULTS

Fault	Davg : Dpref Largest Event	Davg : Dpref All Events	Dmax : Largest Dpref	Dmax : Largest Dmax	Dmax : 2.59* Dpref Largest Event	Dmax : 2.59* Dpref All Events
Weights:	**0.5**	**0.5**	**0.25**	**0.5**	**0.125**	**0.125**
Bare Mountain (BM)	150	127	150	300	389	329
Bow Ridge (BWR)	44	24	44	80	114	62
N. Crater Flat (NCF)	50	47	50	50	130	122
S. Crater Flat (SCF)	13	20	20	32	34	52
Fatigue Wash (FW)	105	61	105	105	272	158
Iron Ridge (IR)	100	80	100	130	260	208
Paintbrush Canyon/ Stagecoach Road (SR-PBC)	167	51	167	205	433	132
Solitario Canyon (SC)	75	54	120	140	195	140
Windy Wash (WW)	58	44	88	98	150	114
Rock Valley (RV)	362	291	362	451	940	755

* Data was taken from all trenches, displacements are in cm.

TABLE ASM-2
SURFACE RUPTURE LENGTHS FOR YUCCA MOUNTAIN FAULTS

Fault	Minimum Length (km)	Preferred Length (km)	Maximum Length (km)
Weights:	**0.1**	**0.6**	**0.3**
Bare Mountain	17.5	20.6	24
Bow Ridge	6.7	7.6	9.4
N. Crater Flat	10.6	11.6	15.1
S. Crater Flat	6.1	7.8	8.8
Fatigue Wash	6.6	12.5	15.2
Iron Ridge	5.5	8.5	9.2
Paintbrush Canyon/ Stagecoach Road	18.0	24.0	28.5
Solitario Canyon	11.3	18.7	20.9
Windy Wash	15.6	21.6	24.6

TABLE ASM-3
WEIGHTING CRITERIA FOR MAXIMUM MAGNITUDES FOR YUCCA MOUNTAIN FAULTS

Fault	Msrl	Mra	Mmas	Mdmax	Mdavg
Bare Mountian	0.4	0.1	0.2	0.1	0.2
Bow Ridge	0.45	0.1	0.3	0.15	0
N. Crater Flat	0.3	0.2	0.3	0.2	0
S. Crater Flat	0.3	0.1	0.3	0.15	0.15
Fatigue Wash	0.35	0.25	0.3	0.1	0
Iron Ridge	0.4	0.2	0.2	0.2	0
Paintbrush Canyon/ Stagecoach Road	0.3	0.15	0.3	0.1	0.15
Solitario Canyon	0.3	0.1	0.3	0.15	0.15
Windy Wash	0.3	0.1	0.3	0.15	0.15

Methods: Msrl—surface rupture length (Wells and Coppersmith, 1994)
Mra—rupture area (Wells and Coppersmith, 1994)
Mmas—surface rupture length*displacement (Mason, 1996)
Mdmax—maximum displacement (Wells and Coppersmith, 1994)
Mdavg—average displacement (Wells and Coppersmith, 1994)

TABLE ASM-4
SLIP RATES FOR YUCCA MOUNTAIN FAULTS

Fault	20-percentile (mm/yr)	Median (mm/yr)	80-percentile (mm/yr)
Weights:	**0.2**	**0.6**	**0.2**
Bare Mountain	0.008	0.025	0.07
Bow Ridge	0.0008	0.002	0.0047
N. Crater Flat	0.0011	0.0025	0.0048
S. Crater Flat	0.001	0.0024	0.0047
Fatigue Wash	0.0038	0.009	0.0162
Iron Ridge	0.0015	0.0036	0.0068
Paintbrush Canyon/ Stagecoach Road	0.0065	0.016	0.029
Solitario Canyon	0.005	0.0125	0.024
Windy Wash	0.003	0.007	0.0128

TABLE ASM-5
RECURRENCE FOR YUCCA MOUNTAIN FAULTS

Fault	20-percentile (kyr)	Median (kyr)	80-percentile (kyr)
Weights:	**0.2**	**0.6**	**0.2**
Bare Mountain	42	87	143
Bow Ridge	71	120	188
N. Crater Flat	135	212	330
S. Crater Flat	65	107	165
Fatigue Wash	99	161	249
Iron Ridge	83	137	220
Paintbrush Canyon/ Stagecoach Road	17	27	42
Solitario Canyon	31	51	78
Windy Wash	31	50	79

TABLE ASM-6
REGIONAL FAULT DATA
(Page 1 of 2)

No.	FAULT [1]	MAP DESIGNATION	CLOSEST DIST. TO SITE [2] (km)	SLIP RATE (SR) [3] (mm/yr) MINIMUM	SLIP RATE (SR) [3] (mm/yr) PREFERRED	SLIP RATE (SR) [3] (mm/yr) MAXIMUM	RECURRENCE INTERVAL (RI) [4] (yr) MINIMUM	RECURRENCE INTERVAL (RI) [4] (yr) PREFERRED	RECURRENCE INTERVAL (RI) [4] (yr) MAXIMUM	SURFACE RUPTURE LENGTH (SRL) [5] (km) MINIMUM	SURFACE RUPTURE LENGTH (SRL) [5] (km) PREFERRED	SURFACE RUPTURE LENGTH (SRL) [5] (km) MAXIMUM	TYPE [6]	DIP (DEG./ DIRECTION)
1	*Carrara*[7]	*H95*	15 DBS*	0.013 (0.2)	0.05 (0.6)	0.12 (0.2)	10000 (0.2)	19000 (0.6)	69000 (0.2)	10 (0.1) 10 (0.5)	20 (0.8) 20 (0.5)	42 (0.1)	SS	60-90/SW
2	Mine Mountain	MM	19 P1	0.006 (0.33)	0.03 (0.34)	0.06 (0.33)	20000 (0.33)	39000 (0.34)	146000 (0.33)	10 (0.5)	20 (0.5)		SS	VERT/SW
3	Wahmonie	WAH	22 P1	0.01 (0.33)	0.04 (0.34)	0.08 (0.33)	20000 (0.33)	39000 (0.34)	146000 (0.33)		14.5 (1.0)		OS	?/SE
4	*Ash Meadows*	*AM*	22 DBS	0.01 (0.2)	0.02 (0.6)	0.03 (0.2)	10000 (0.2)	35000 (0.5)	128000 (0.3)	10 (0.1)	38 (0.8)	40 (0.1)	N	60/W
5	*Rock Valley*	*RV*	25 Ch 4.13	0.02 (0.2)	0.06 (0.6)	0.09 (0.2)	34325 (0.2)	58333 (0.6)	175000 (0.2)	32.6 (0.2)	62.1 (0.6)	72 (0.2)	SS	VERT
6	*W Specter Range*	*WSR*	28 DBS	0.004 (0.3)	0.01 (0.4)	0.02 (0.3)	10000 (0.1)	25000 (0.6)	>128000 (0.3)	18 (0.8)		25 (0.2)	N	60/W
7	Cane Spring	CS	26 P1	0.007 (0.33)	0.03 (0.34)	0.07 (0.33)	20000 (0.33)	39000 (0.34)	146000 (0.33)	21 (0.5)		26 (0.5)	SS	VERT
8	*Amargosa River*	*AR*	34 DBS	0.01 (0.2)	0.05 (0.6)	0.09 (0.2)	10000 (0.1)	69000 (0.6)	128000 (0.3)	12.4 (0.2)	24.8 (0.6)	48 (0.2)	SS	VERT
9	Yucca Lake	YCL	36 P1	0.002 (0.33)	0.02 (0.34)	0.034 (0.33)	20000 (0.33)	39000 (0.34)	146000 (0.33)	16.3 (0.5)		20.6 (0.5)	SS?	VERT/?
10	Eleana Range	ER	37 P1	0.00006 (0.33)	0.00024 (0.34)	0.0003 (0.33)	20000 (0.33)	39000 (0.34)	146000 (0.33)	10.6 (0.5)		12.7 (0.5)	N	60/E
11	*E Specter Range*	*ESR*	37 DBS	0.004 (0.33)	0.012 (0.34)	0.021 (0.33)	10000 (0.33)	25000 (0.34)	128000 (0.33)	9 (0.5)		15 (0.5)	N	60/E
12	Yucca Fault	YC	40 P1	0.008 (0.33)	0.04 (0.34)	0.08 (0.33)	20000 (0.33)	39000 (0.34)	146000 (0.33)	23 (0.5)		33 (0.5)	SS?	VERT/?
13	*W Spring Mountains*	*WSM*	45 DBS	0.02 (0.2)	0.05 (0.6)	0.07 (0.2)	20000 (0.2)	69000 (0.6)	128000 (0.2)	14.6 (0.2)	43.5 (0.6)	50 (0.2)	N	60/W
14	*Furnace Creek*	*FC*	52 DBS	4 (0.2)	5 (0.6)	8 (0.2)	600 (0.2)	700 (0.6)	800 (0.2)	70 (0.2)	105 (0.6)	120 (0.2)	SS	VERT
15	*E Death Valley*	*EDV*	52 P1	3.46 (0.2)	4.62 (0.6)	5.77 (0.2)	500 (0.2)	875 (0.6)	1000 (0.2)	34 (0.2)	60 (0.6)	75 (0.2)	N	60/W
16	*Belted Range*	*BLR*	55 P1	0.02 (0.33)	0.04 (0.34)	0.1 (0.33)	20000 (0.33)	39000 (0.34)	69000 (0.33)	21 (0.6)		49 (0.4)	N	60/W
17	*M Death Valley*	*MDV*	57 DBS	1 (0.2)	2 (0.6)	3 (0.2)	1000 (0.2)	2000 (0.6)	5000 (0.2)	32 (0.2)	60 (0.6)	72 (0.2)	SS	VERT
18	Grapevine	GV	58 P1	0.003 (0.33)	0.01 (0.34)	0.02 (0.33)	20000 (0.33)	39000 (0.34)	146000 (0.33)		29 (1.0)		N	60/W
19	W Death Valley	WDV	61 DBS	0.009 (0.33)	0.05 (0.34)	0.16 (0.33)	20000 (0.33)	39000 (0.34)	146000 (0.33)	25 (0.3)	39 (0.5)	62 (0.2)	N	60/E
20	Emigrant/Towne Pass	EM-TP	<65 DBS	0.003 (0.33)	0.01 (0.34)	0.03 (0.33)	10000 (0.33)	20000 (0.34)	69000 (0.33)	14.6 (0.2)	17 (0.6)	47 (0.2)	N	60/NW
21	*N Pahrump-Stewart Valley*	*PRP*	69 DBS	0.03 (0.2)	0.06 (0.6)	0.14 (0.2)	10000 (0.2)	39000 (0.6)	69000 (0.2)	20 (0.5)		40 (0.5)	SS, OS?	VERT/?
22	*W Pintwater Range*	*WPR*	76 P1	0.005 (0.2)	0.01 (0.6)	0.06 (0.2)	10000 (0.33)	39000 (0.34)	69000 (0.33)	18 (0.33)	37 (0.34)	56 (0.33)	N	60/W
23	*Panamint Valley-Hunter Mountain*	*PAN-HM*	95 P1	1.57 (0.1)	2.36 (0.8)	3.15 (0.1)	700 (0.1)	1610 (0.8)	2360 (0.1)	40 (0.2)	70 (0.6)	120 (0.2)	SS	VERT
24	*S Pahrump-Stateline*	*SPRP*	107 DBS	0.002 (0.33)	0.05 (0.34)	0.1 (0.33)	20000 (0.2.)	39000 (0.6)	69000 (0.2)	31 (0.5)		65 (0.5)	OS	60?/W

TABLE ASM-6
(Page 2 of 2

Notes for Table ASM-6:

1 Fault number, name, and map designation (Figure ASM-9). The 15 faults with names shown in *italic font* have substantial field data, or correlate with faults that have substantial field data, for estimating slip rates (SR), recurrence intervals (RI), and approximate surface rupture length (SRL). The 9 faults with names shown with normal font have sparse characterization data. Data and observations supporting the characterization of regional fault sources are provided in Appendix ASM-6.

2 Approximate distance from Yucca Mountain; from Piety, 1995 (P1), or observations of D.B. Slemmons (DBS).

3 Slip rates for well studied (*italic font*) faults generally are based on paleoseismic data as reported in available literature (see references cited on Piety, 1995). Slip rates for other faults (normal font) are estimated from SRL data using the approach described in Section 3.5.3.1.

4 Field observations of historical Basin and Range surface faulting for events of Mw> 6.2, YM trench data and personal observations of southern Nevada faults show that more than 90 percent of Quaternary scarps are formed by recurrent events, generally having similar magnitudes and displacements, so nearly all of the tabulated faults are assumed to reflect recurrent activity. Recurrence interval (RI) for well studied faults (*italic font*) are based on references in Piety (1995) or personal observations. They are considered to have fixed age values that show the range of uncertainty; for faults that have a better database, a preferred value is given. The assigned weights are 0.2 for the extreme values and 0.6 for the preferred value. Recurrence intervals for other faults are estimated using the approach described in Section 3.5.4 in which an assumed number of surface rupturing earthquakes (3) is represented by the scarps in middle to late Pleistocene surfaces that are estimated to be middle to late Pleistocene in age (equal weight assigned to ages of 69 ka, 128 ka, and 449 ka) and have recurrence intervals estimated at 20, 39, and 146 kyr, respectively.

5 Surface rupture length (SRL). The maximum SRL is generally limited by connections on strike to other faults, major irregularities at the ends of rupture zones, or to terminations or truncations by other faults. The length is approximately expressed by the minimum, preferred, and maximum SRL interpreted from the pattern of the 24 faults and character and size of the surface rupture patterns from historical events in the Basin and Range Province. The lengths include a minimum of about 10 km, and a maximum of 40-75 km, which is within the range of longer historical surface faulting events for normal faults in the Basin and Range Province. Faults with special relationships (e.g., having lengths that appear to be controlled by truncations or connections with other faults) generally have only one, preferred SRL. Only one value is given for cases in which the length is supported by one map, generally Piety (1995).

6 SS = strike slip, OS = oblique slip, N = normal.

7 A high probability (0.85) is assigned to the Carrara fault being seismogenic based on the evidence summarized in Appendix ASM-6. However, because the fault has not been thoroughly characterized, some probability (0.15) is given to the fault being non-seismogenic. Two alternative total lengths of 20 km and 42 km are given equal weight in the source model.

TABLE ASM-7
RATIO OF AVERAGE TO MAXIMUM DISPLACEMENT

Worker	Number Of Events	Ad/Md Ratio	Range In Values
W&C (1994)	56, all fault types	0.5	0.2-0.8
Mason (1996)	15 normal faulting events using data from W&C (1996)	0.42	0.2-0.8
Mason (1996)	3 Basin and Range events	0.33	0.3-0.6
Slemmons, in preparation	5 Basin and Range events	0.39	
Slemmons, in preparation	15, all fault types	0.37	0.2-
Strom & Nikonov, unpublished manuscript	10 normal faulting events	0.38	0.21-0.58, standard deviation = 0.11

TABLE ASM-8
INFERRED NUMBER OF EVENTS

Seismic Source	Inferred Number Of Events	Data
Ash Meadows	2	Anderson *et al.*, (1995b)
Bare Mountain	Ca. 4	USGS (written communication, 1996), Anderson (SSC Workshop Presentation)
Belted Range	4 or possibly 5, using 1-1.5m maximum per event and SO up to 4.9 m. The anomalous value of 11.3 is assumed to be an older surface.	Anderson (1995a)
East Nopah	2 or 3	Anderson *et al.* (1995a) and DBS photographs
Kawitch Range	2, profile 2 appears to be on an older, but less than 100 ka surface.	Anderson *et al.* (1995a)
West Spring Mountains	3-5	
West Specter Range	2	Anderson *et al.* (1995a)

Average=20.7/7=~3

TABLE ASM-9
FAULT CLASSES FOR DISPLACEMENT POTENTIAL.

Class	Description	Seismogenic ?	Cumulative Displacement	Probability of Slip	Number of Feature, *N*
0	block-bounding (primary)	yes	>50 m	1.0	1
1	NW-trending (secondary)	no	20-50 m	0.75	2
2	Larger Intrablock (secondary)	no	2-20 m	0.5	4.4
3	Smaller Intrablock (secondary)	no	0.5-2 m	0.25	20.6
4	Small shear (secondary)	no	0.1-0.5 m	0.05	56
5	Fracture (secondary)	no	<<0.1 m	0.01	1000

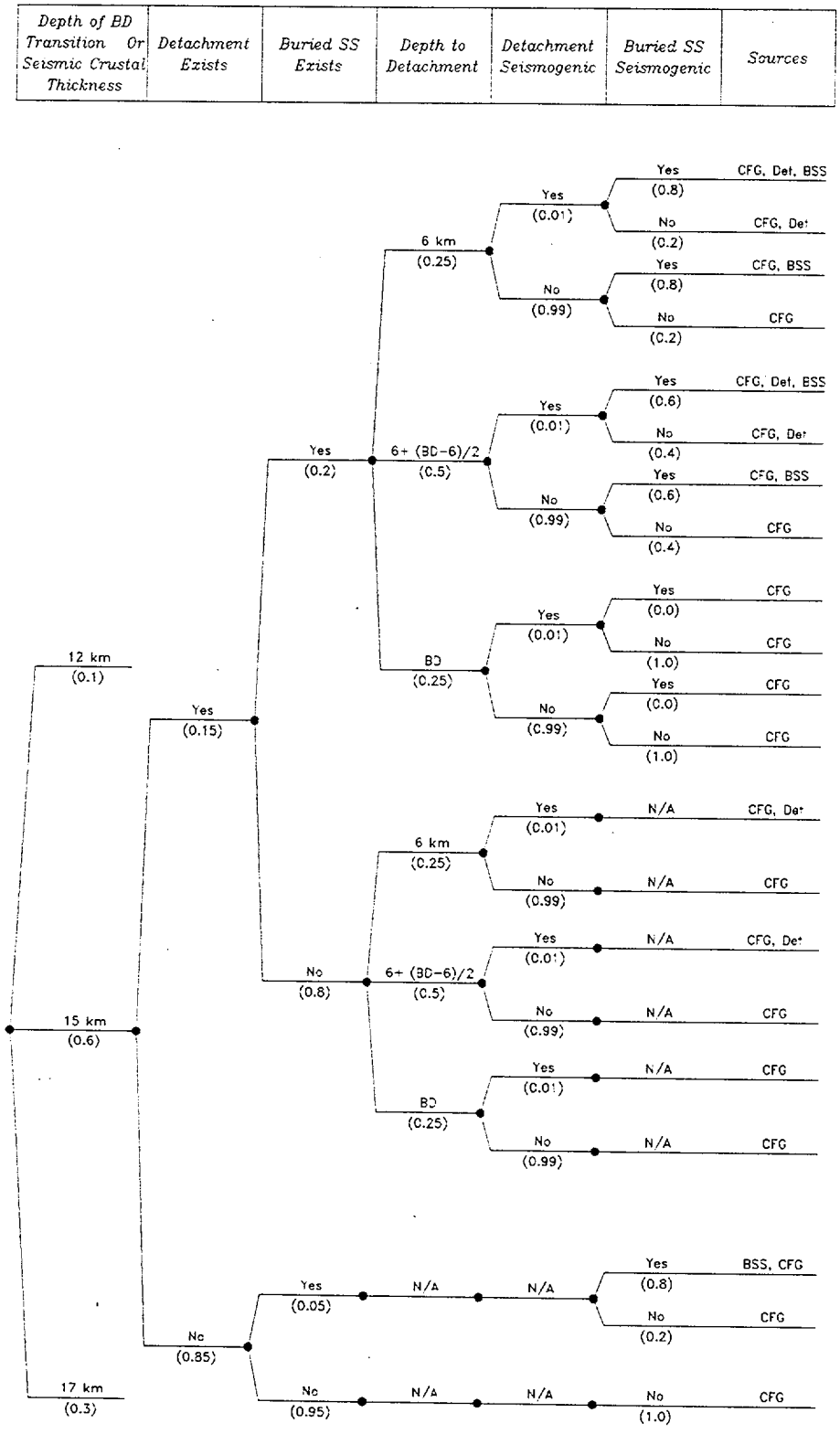

Figure ASM-1 Logic tree for local sources

Depth of Brittle Crust (BDT)	*Detachment Exists?*	*Depth of Detachment*	*Detachment Seismogenic*	*Detachment Geometry (area) (km^2)*

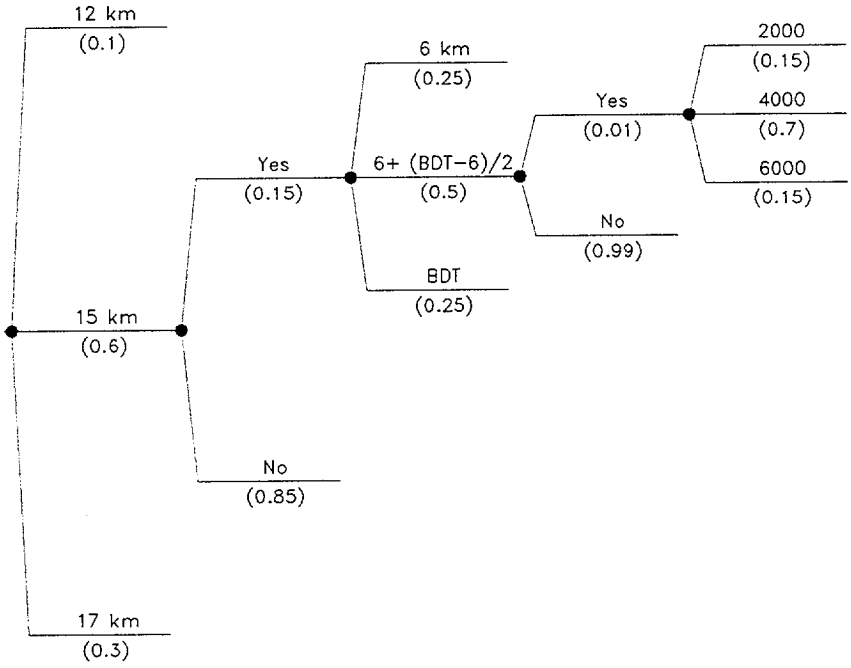

Figure ASM-2 Details of logic tree for detachment model

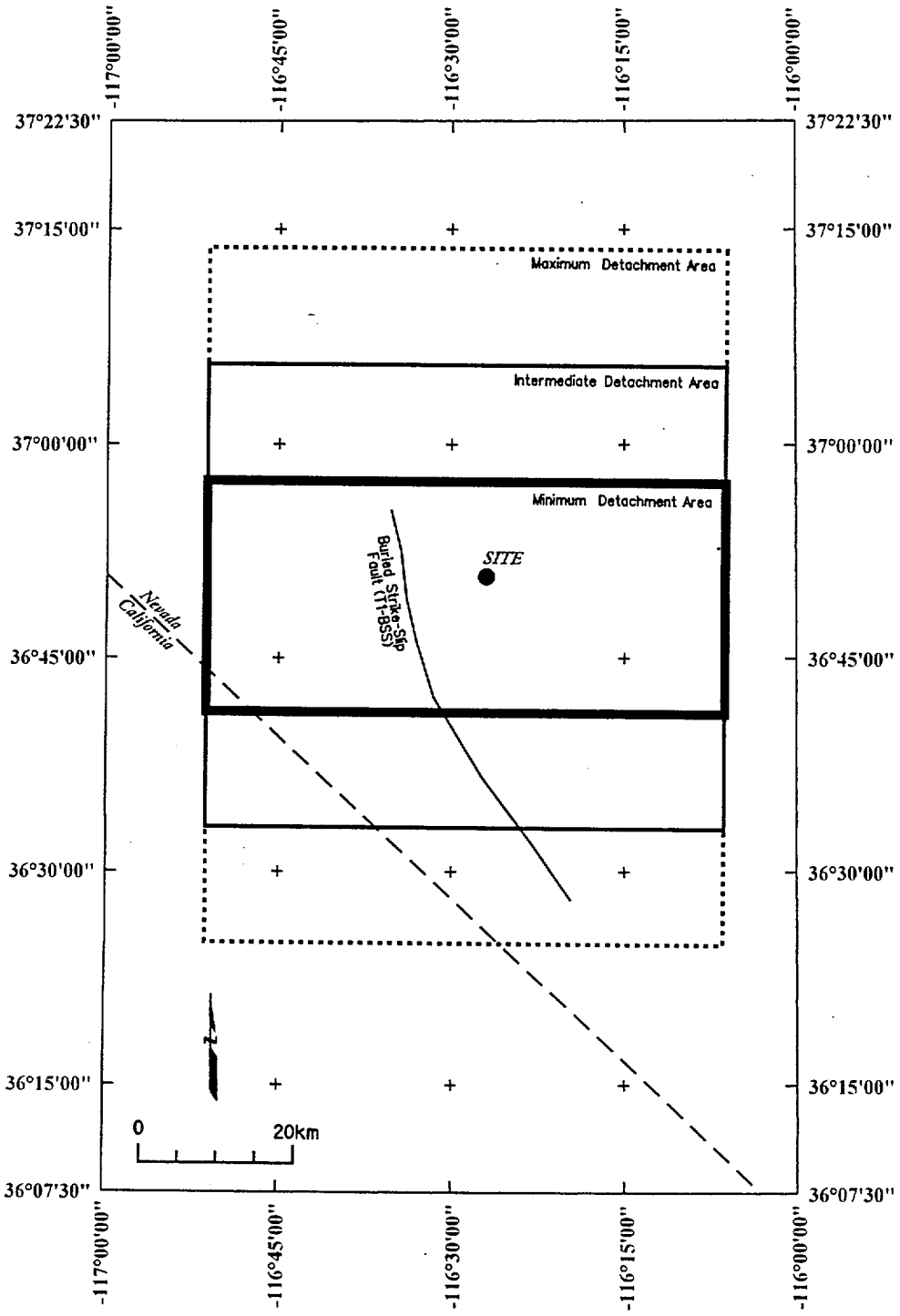

Figure ASM-3 Map showing hypothetical buried strike-slip fault and detachment fault in the vicinity of Yucca Mountain included in the seismic source model

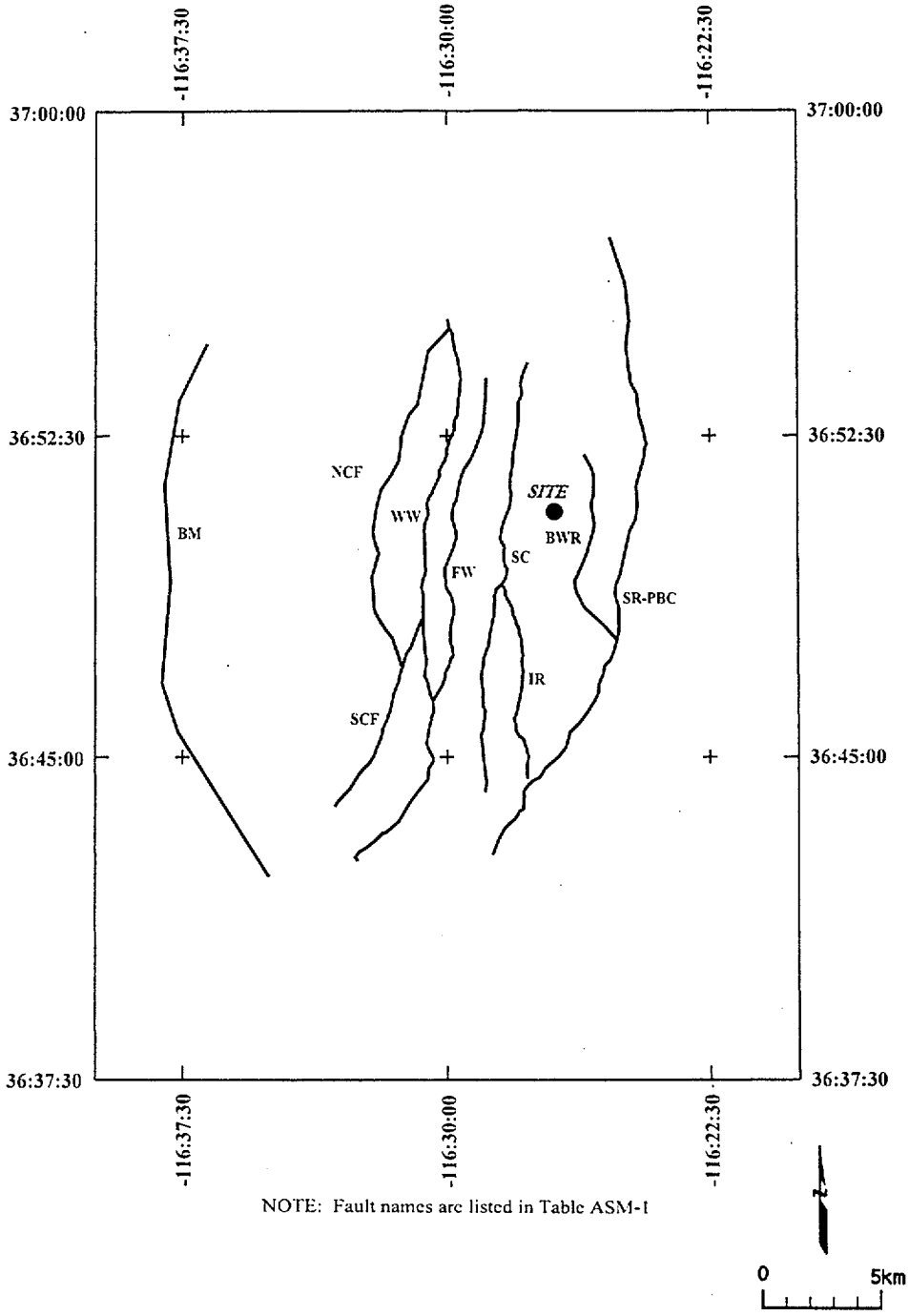

NOTE: Fault names are listed in Table ASM-1

Figure ASM-4 Map showing local fault sources included in the seismic source model

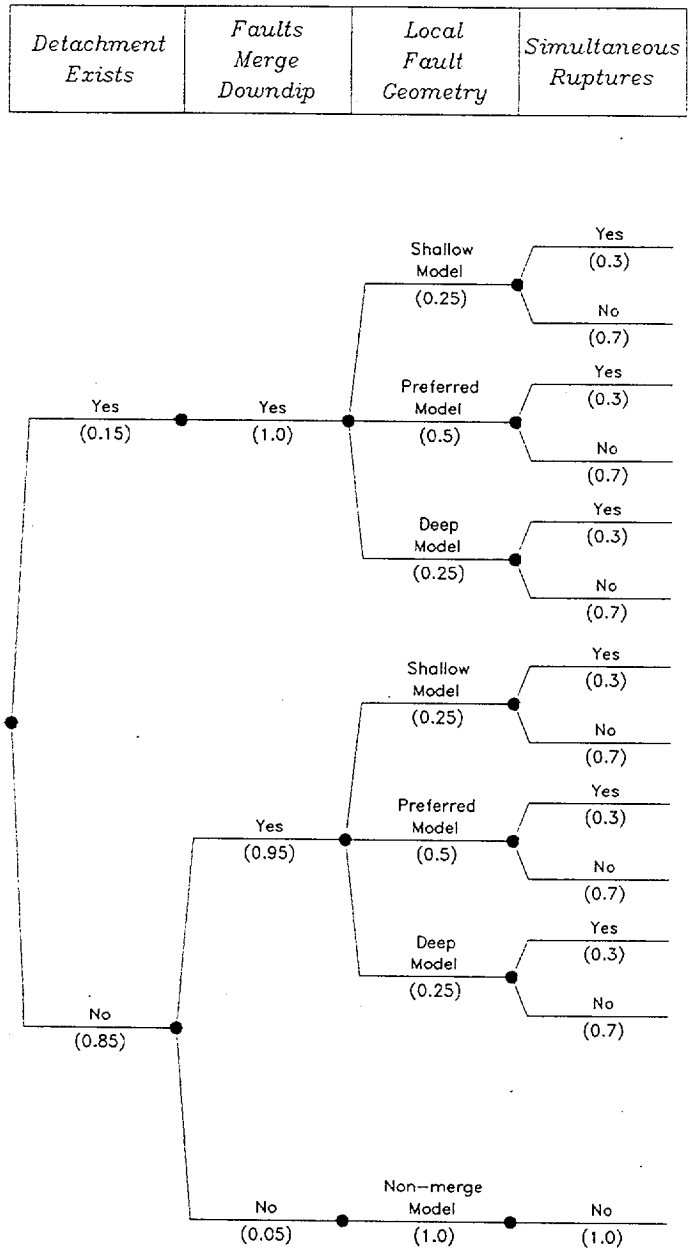

Figure ASM-5 Logic tree for Crater Flat group (CFG) behavior

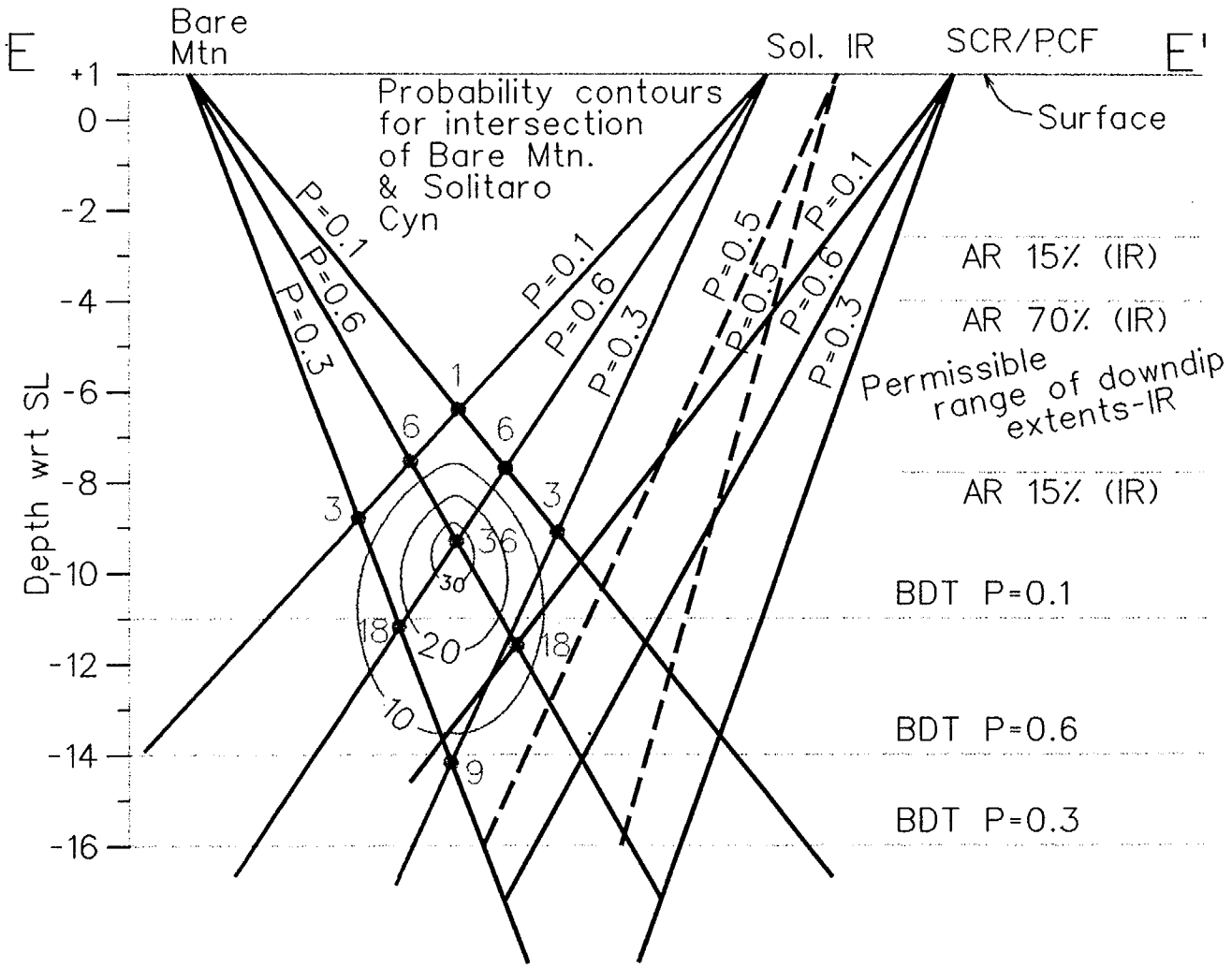

Figure ASM-6 Schematic of method used to develop downdip geometries of local faults

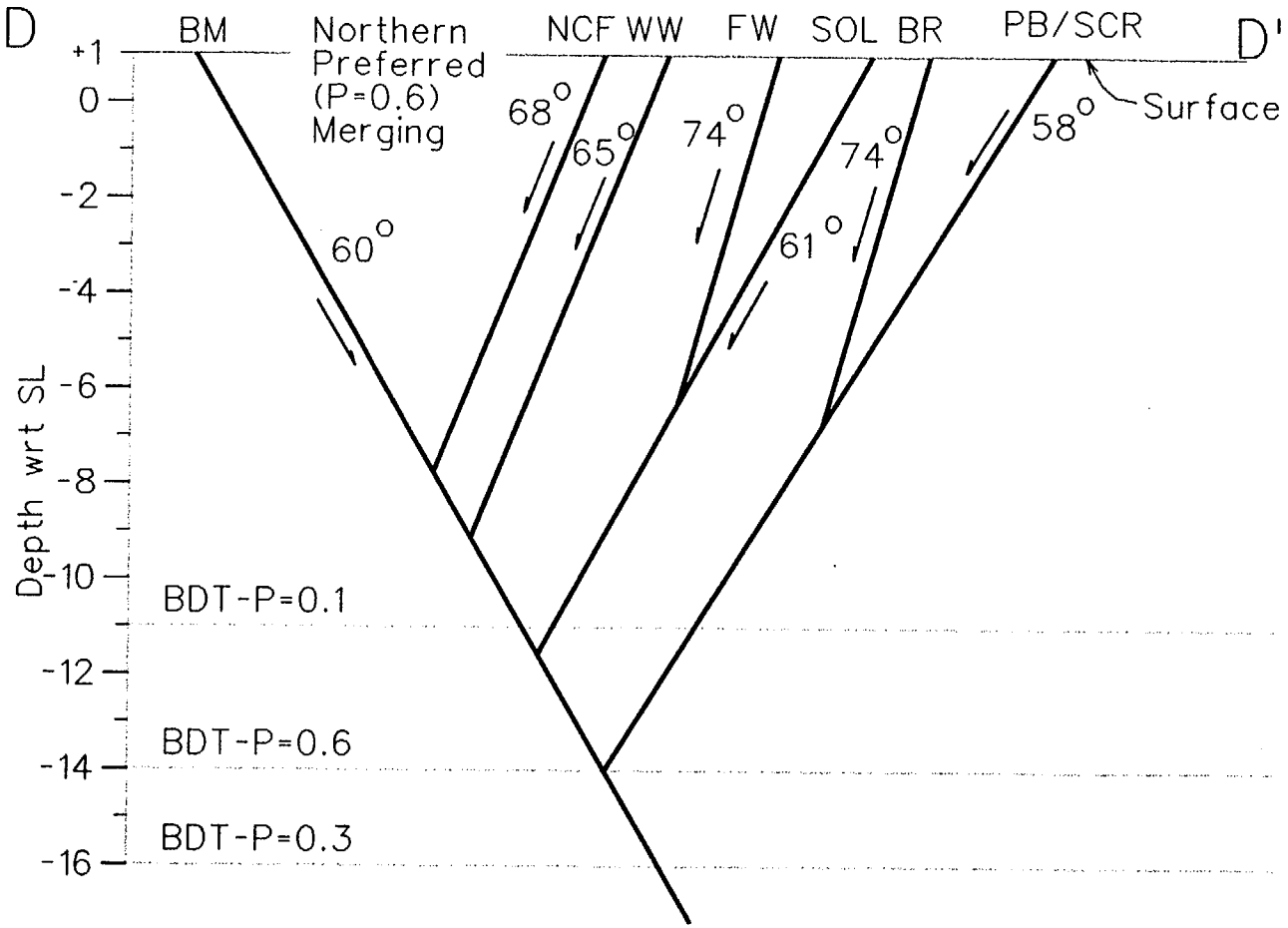

Figure ASM-7a Schematic cross section of preferred merging geometry, northern transect

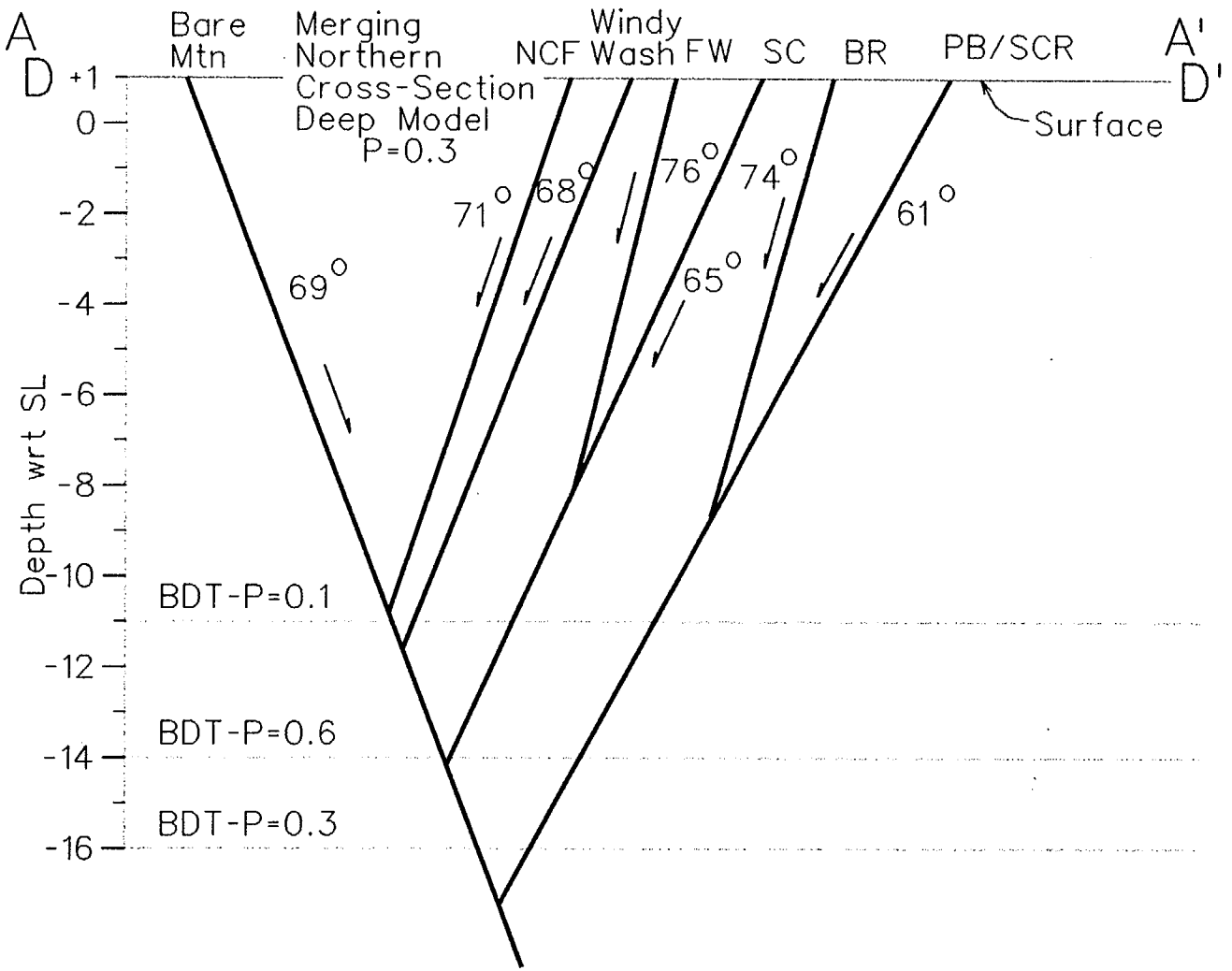

Figure ASM-7b Schematic cross-section of deep, merging geometry. Depth of secondary faults constrained by aspect ratio

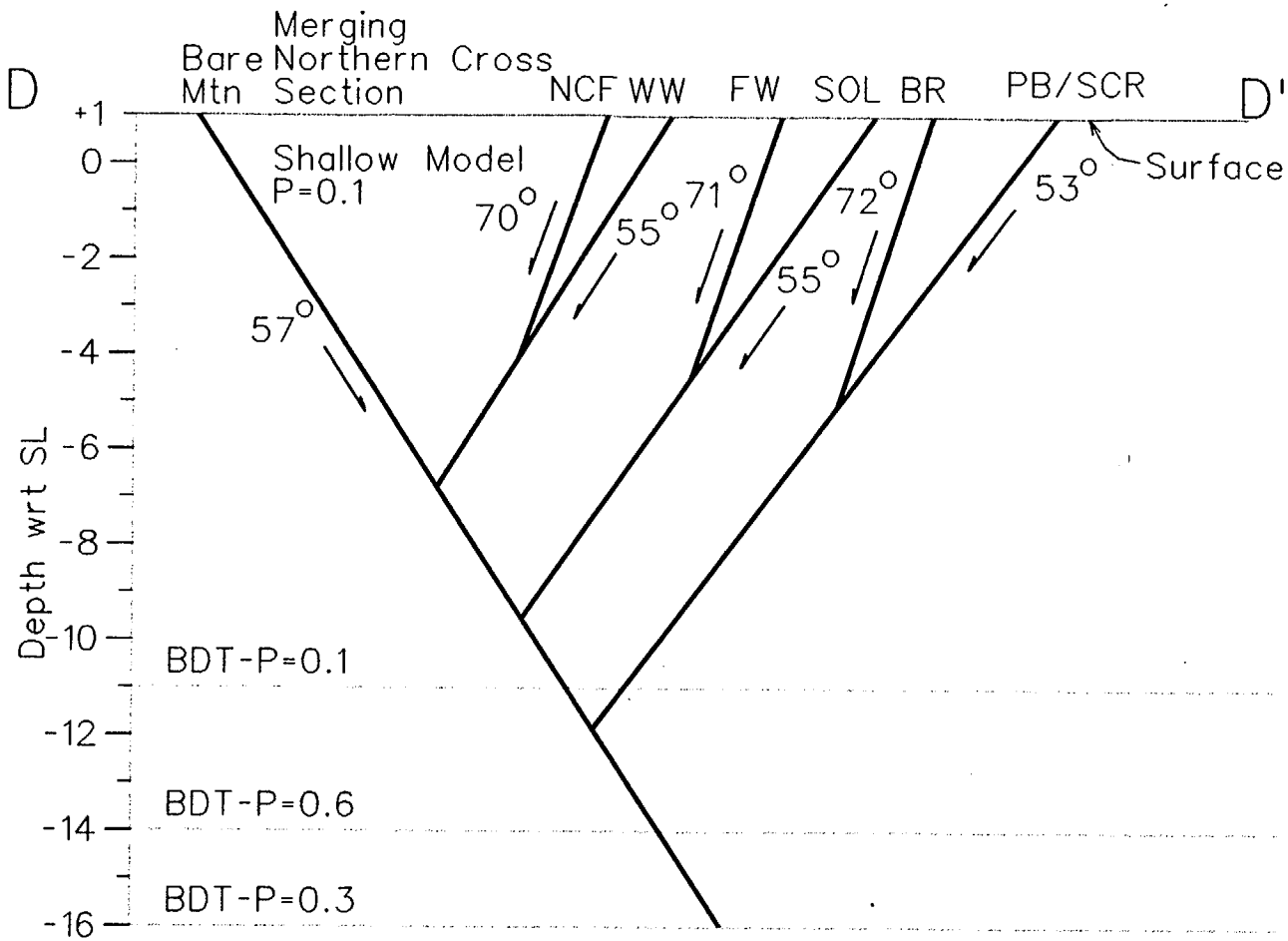

Figure ASM-7c Schematic cross-section of shallow, merging geometry, northern transect. Depth of secondary faults constrained by aspect ratio

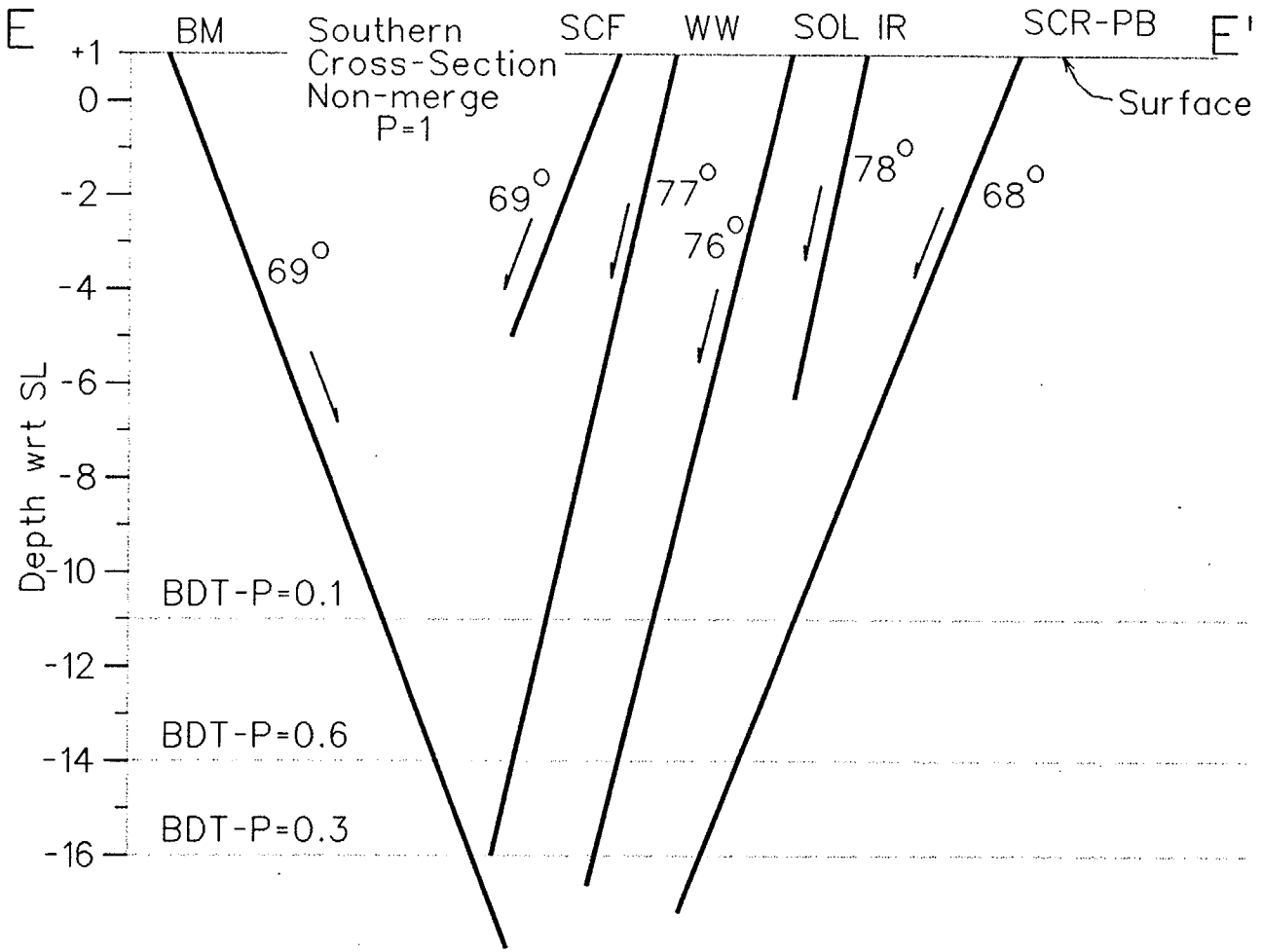

Figure ASM-7d Schematic cross-section of non-merging geometry. Depth of secondary faults constrained by aspect ratio

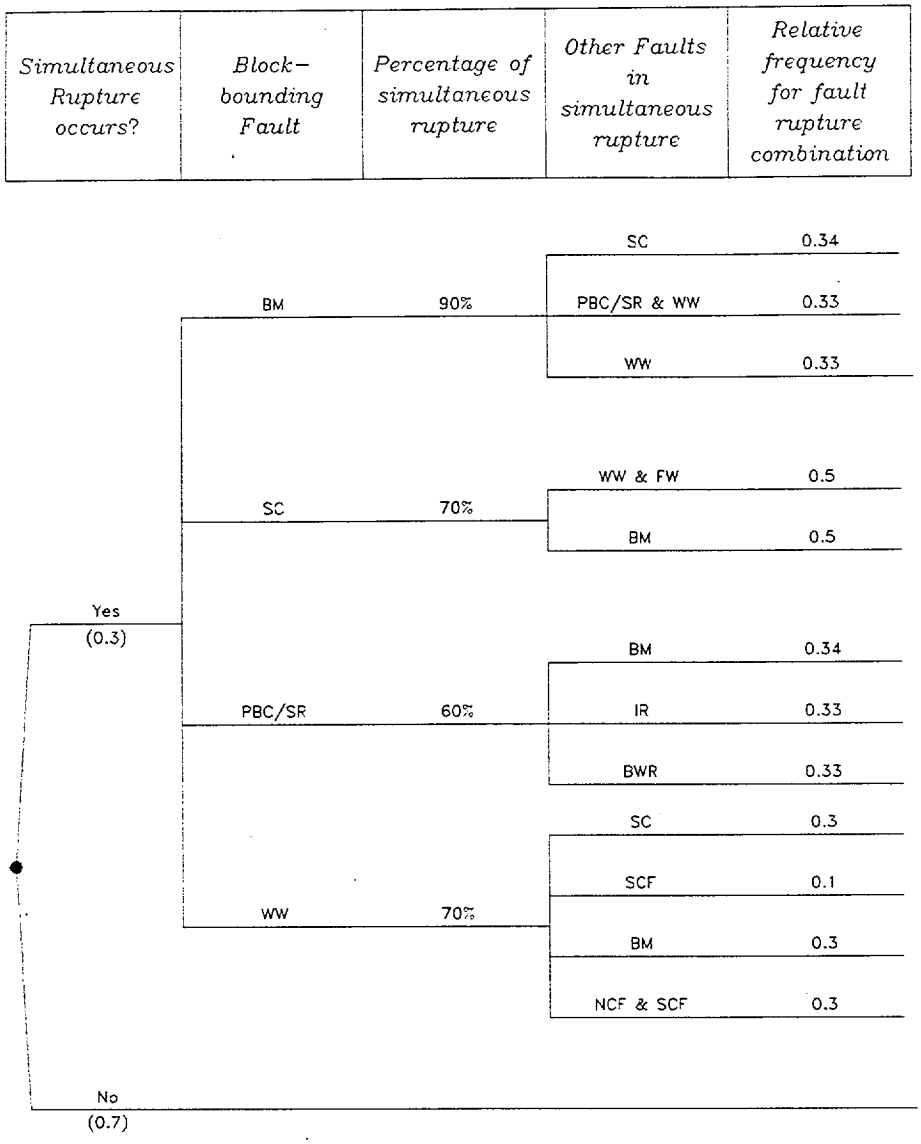

Explanation:

BM – Bare Mountain
SC – Solitario Canyon
PBC/SR – Paintbrush Canyon/Stagecoach Road
WW – Windy Wash
FW – Fatigue Wash
IR – Iron Ridge
BWR – Bow Ridge
SCF – South Crater Flat
NCF – North Crater Flat

Figure ASM-8 Simultaneous rupture scenarios and relative frequencies

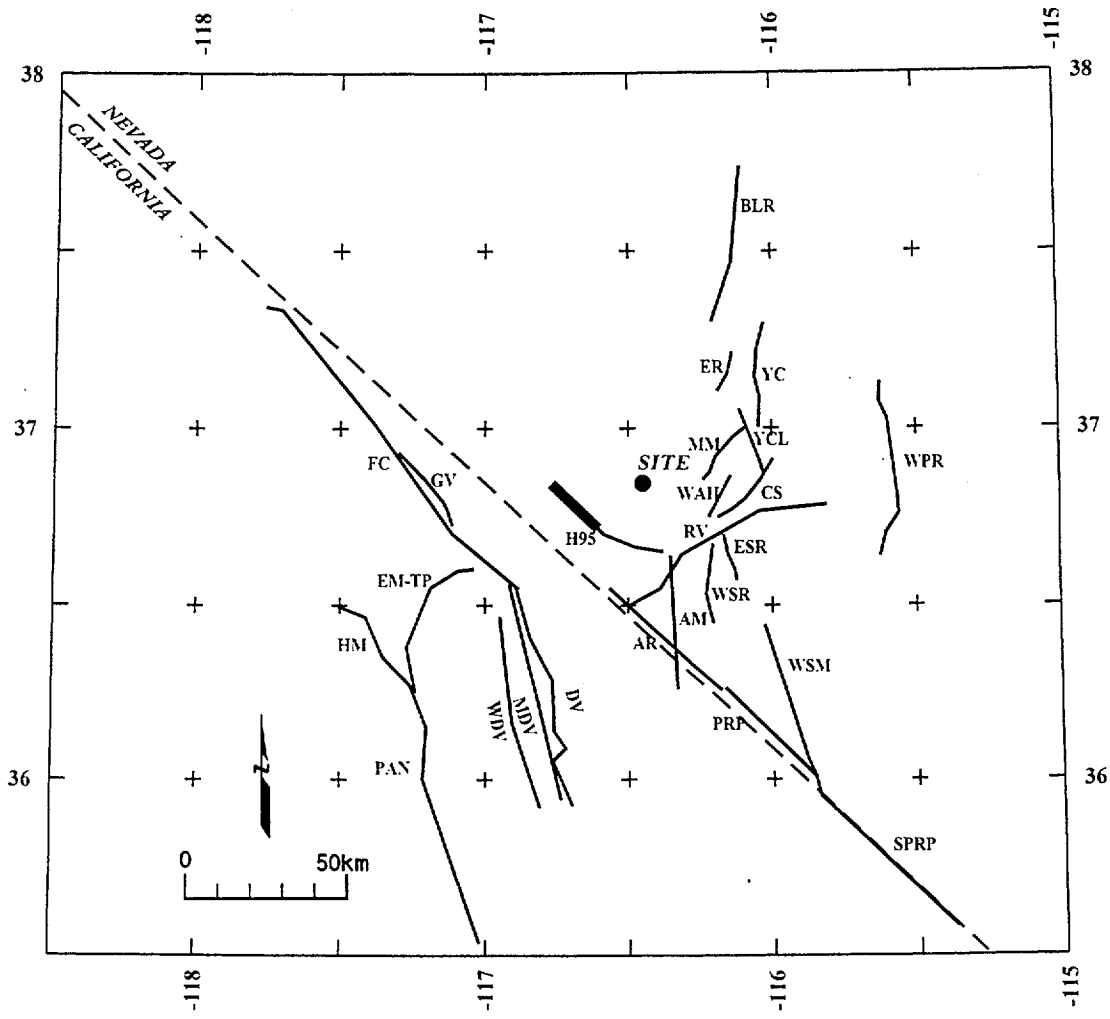

EXPLANATION

NOTE: Fault names are listed in Table ASM-6

Fault Lengths:

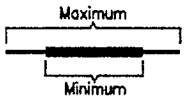

Figure ASM- 9 Map showing regional faults included in the seismic source model

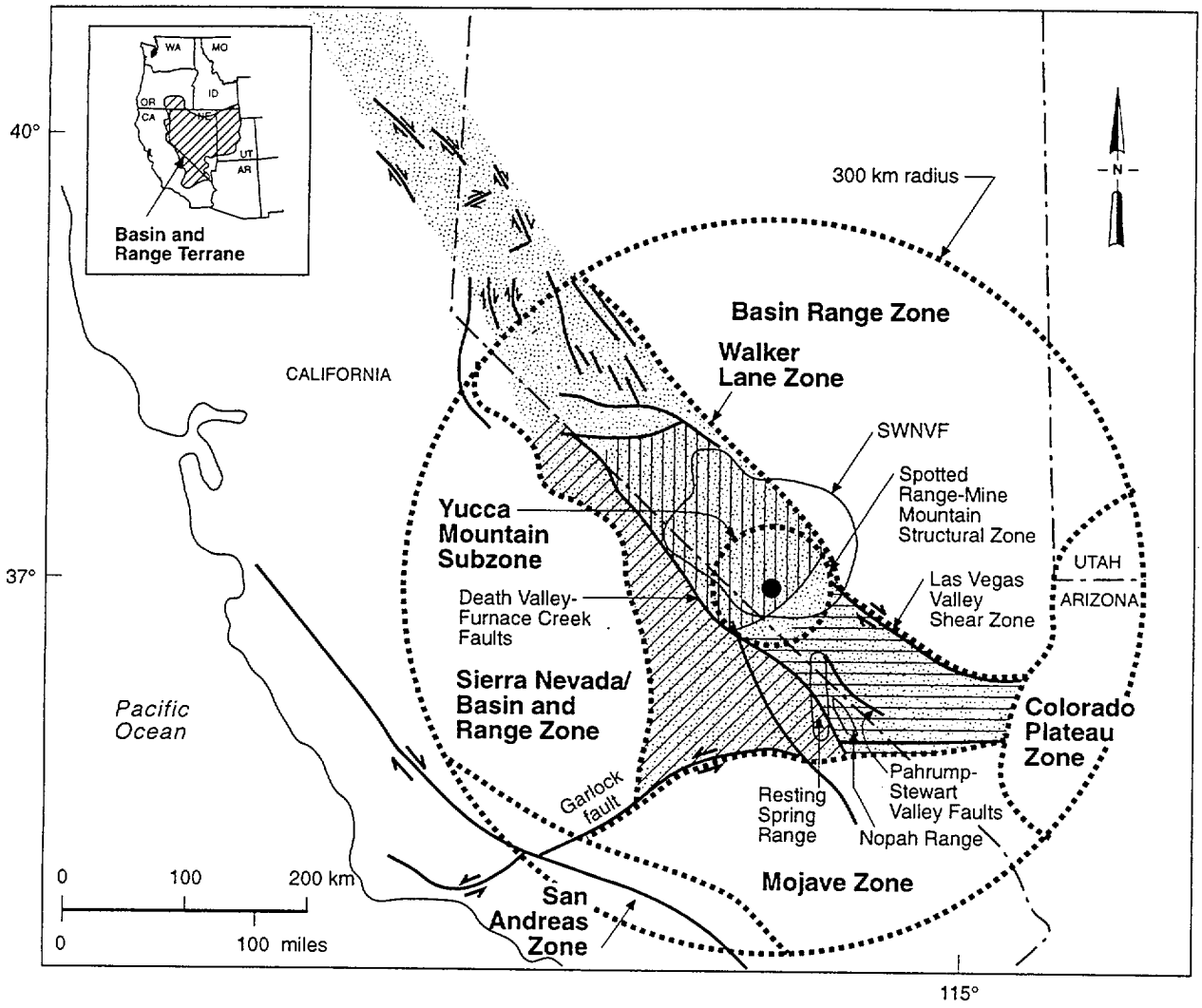

LEGEND

- Fault: arrows indicate direction of relative offset; tick on hanging wall of normal fault; dashed where inferred
- Location of Yucca Mountain
- SWNVF — Southwest Nevada volcanic field
- State boundary
- Seismic source zones
- Spring Mountains section
- Inyo-Mono Terrane
- Goldfield section
- Walker Lane

Figure ASM-10 Map of regional seismic source zones within 300 km

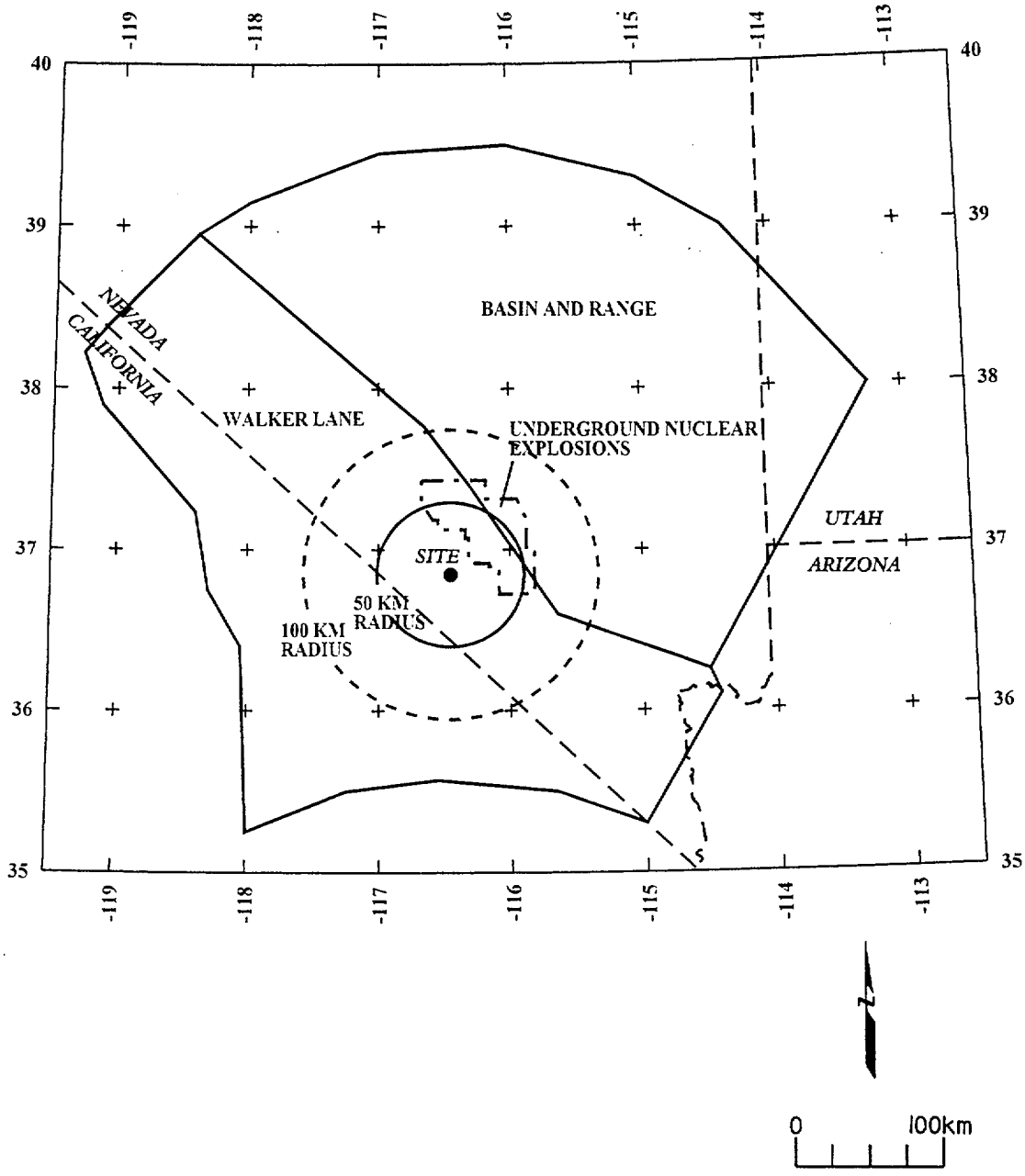

Figure ASM-11 Map showing the boundaries of zones used in the seismic source model

h:\prj\yucca_mt\dgn\1097\plate_tl_reg_zone.dgn 27-OCT-1997 14:26

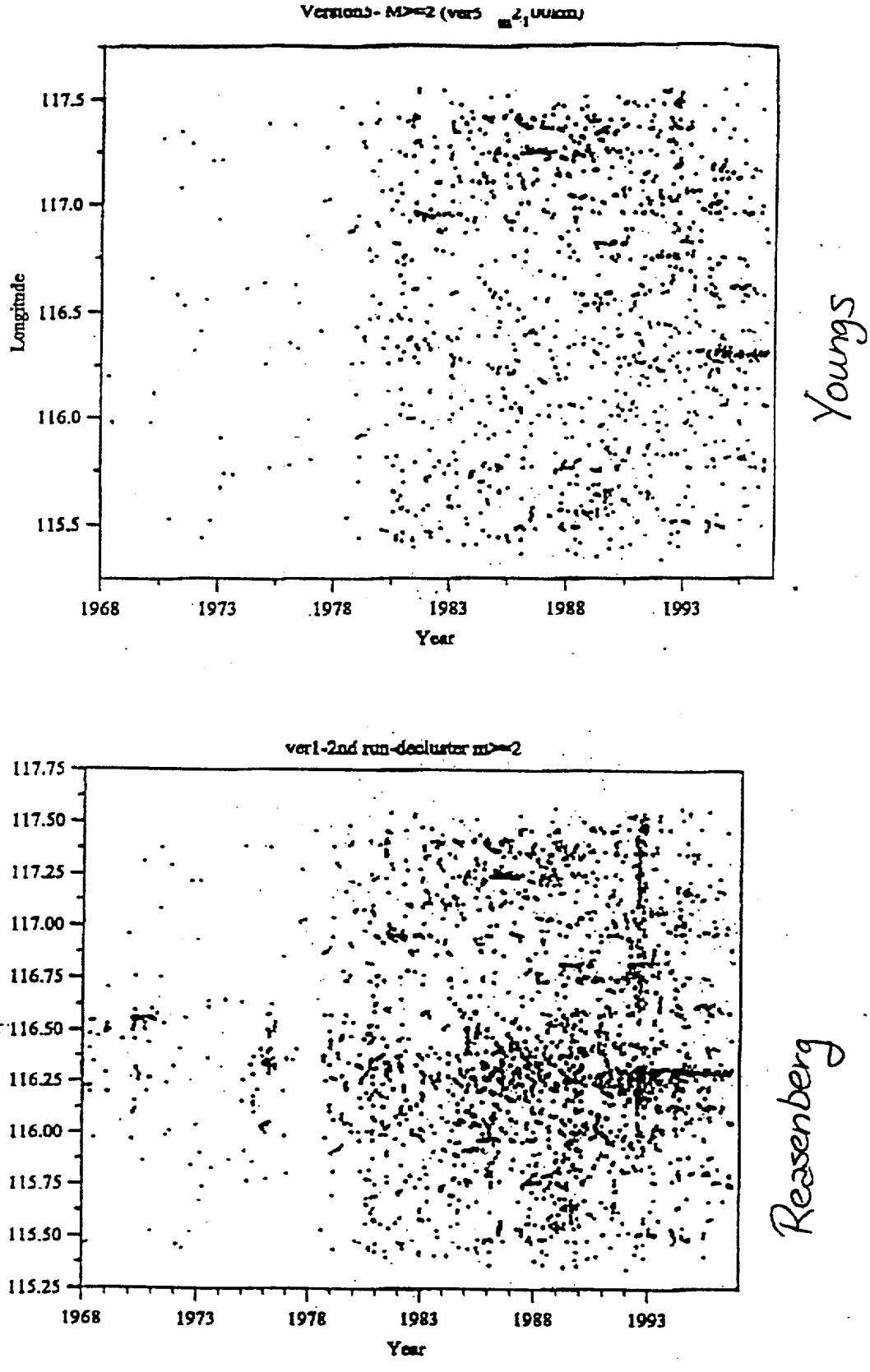

Figure ASM-12 Space-time diagrams comparing Youngs and Reasenberg declustering methods

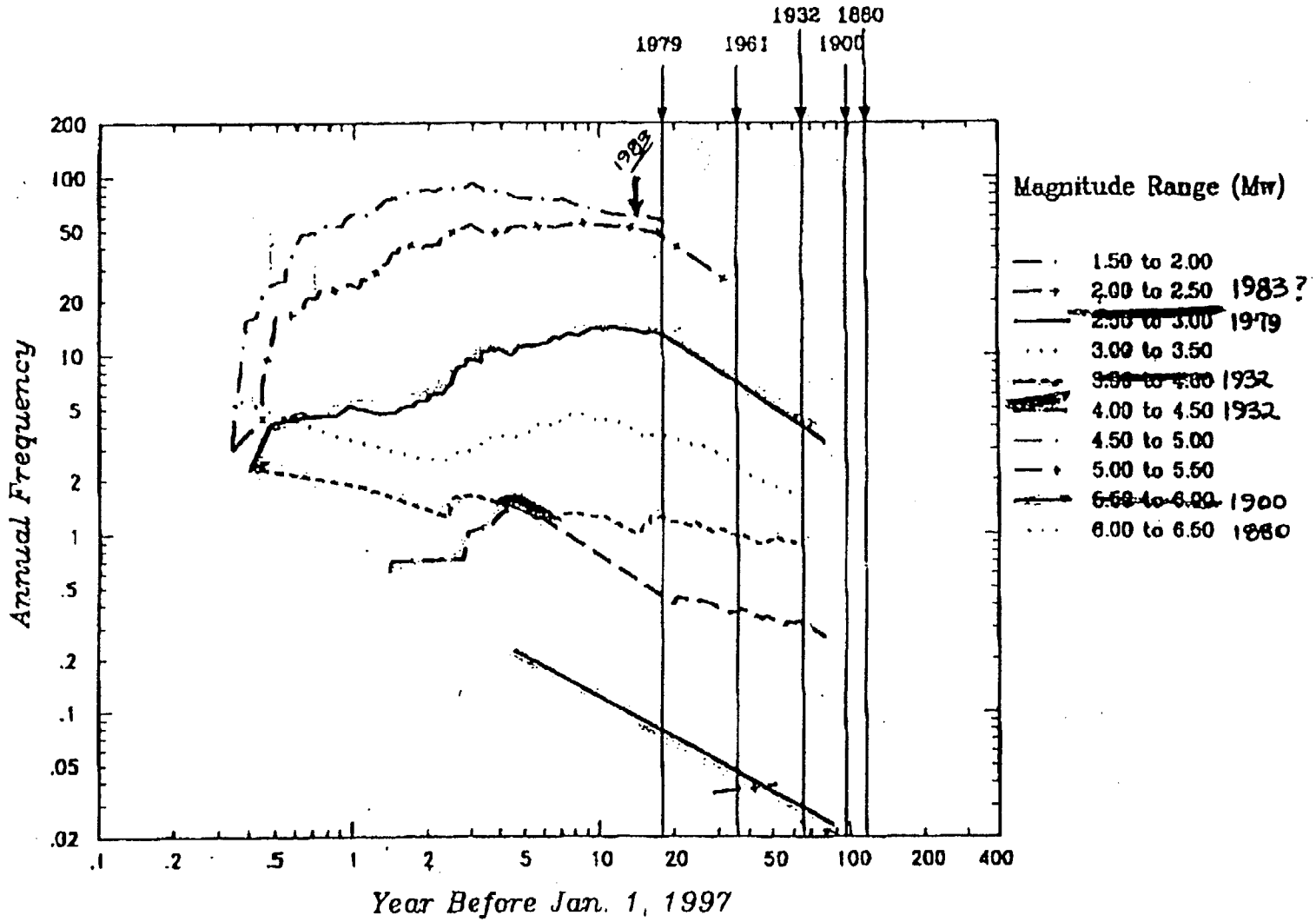

Figure ASM-13 Annual frequency of earthquake recurrence as a function of time before Jan. 1, 1997, based on the catalog declustered by approach of Youngs et al.

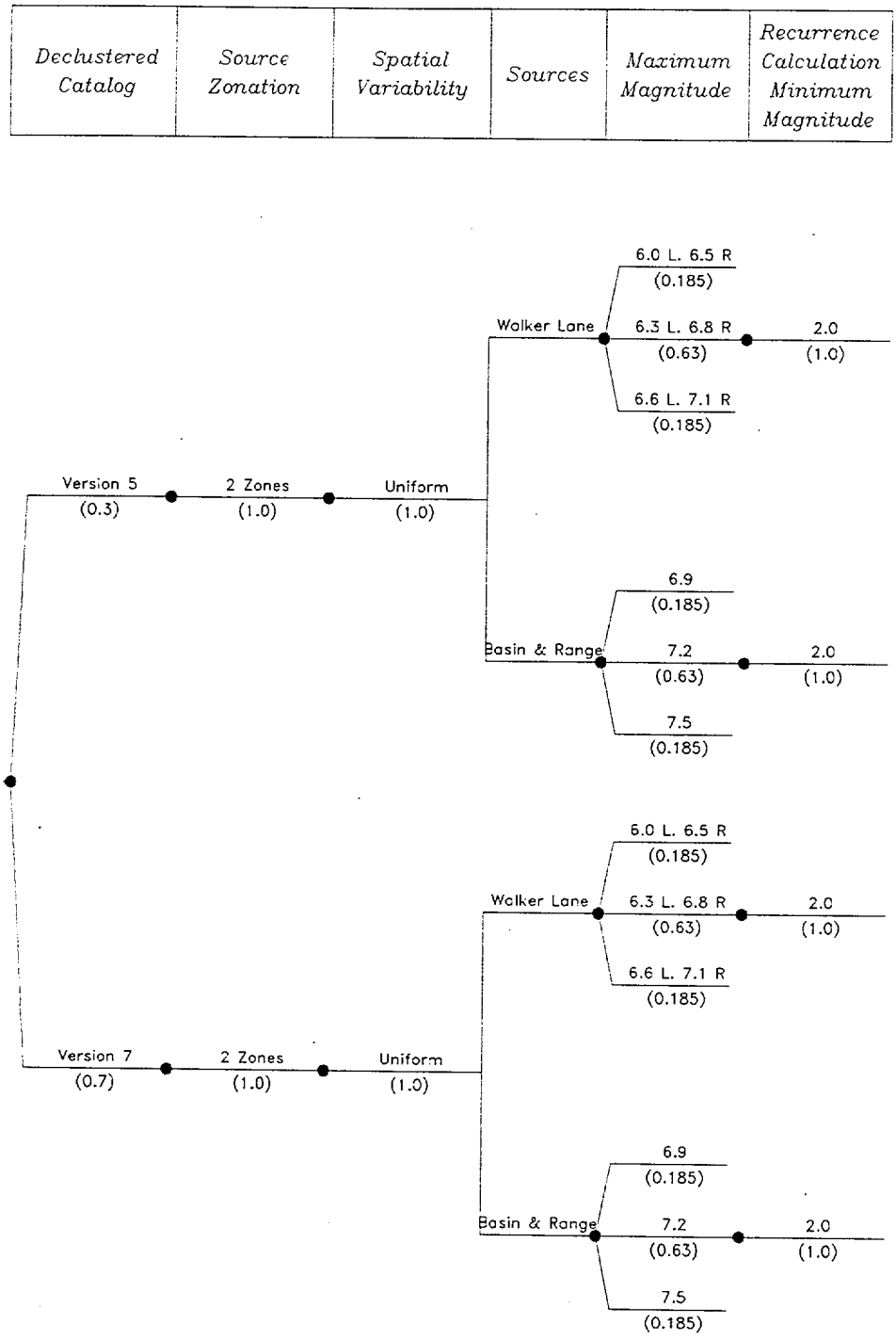

Figure ASM-14 Logic tree used to characterize seismic source zones

Principal Faulting Capability	*Earthquake Frequency*	*Probability of Surface Rupture*	*Maximum Displacement*	*Displacement Distribution*

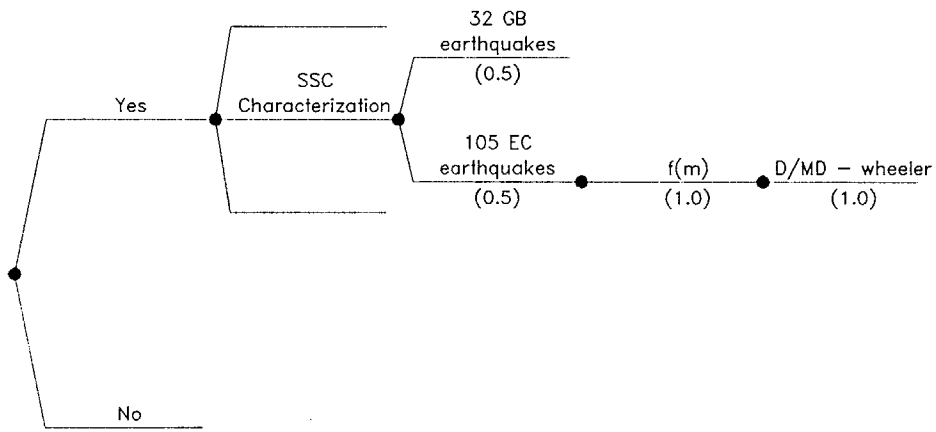

Figure ASM-16a Logic tree for principal faulting hazard

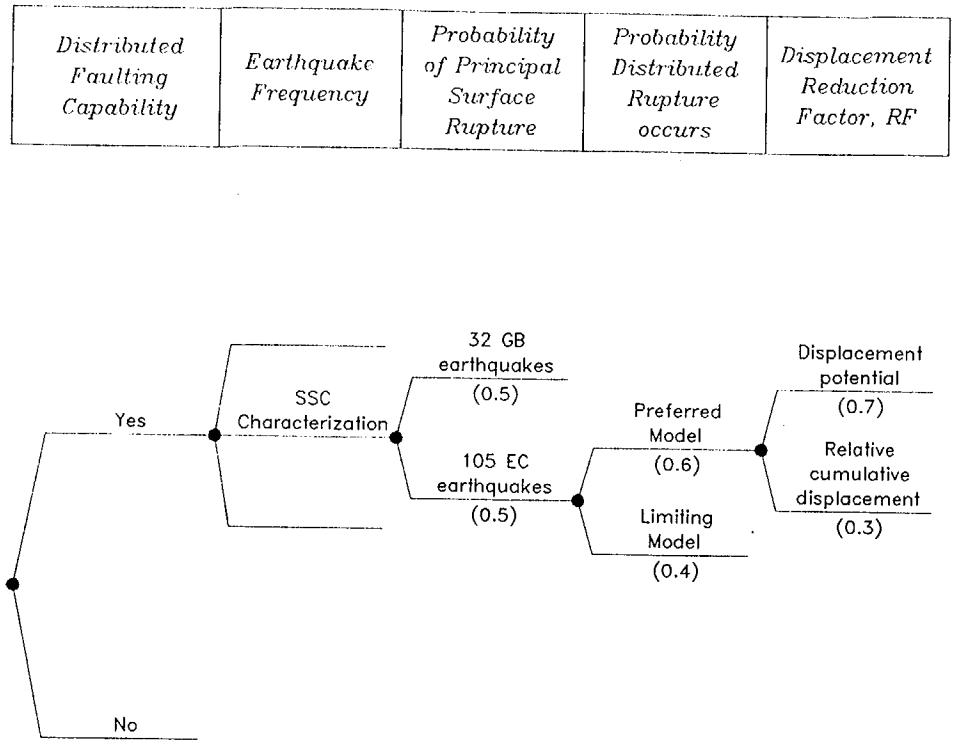

Figure ASM-16b Logic tree for distributed faulting hazard

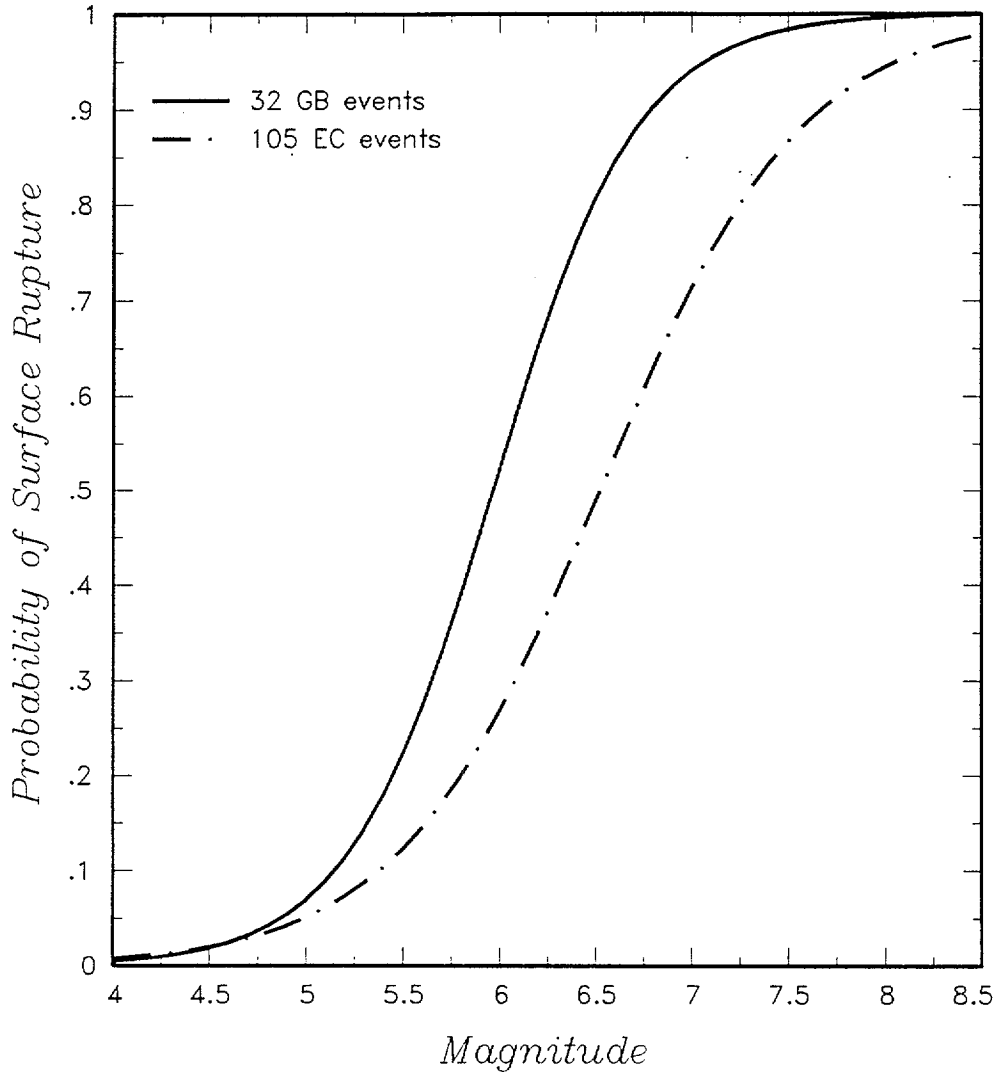

Figure ASM-17 Relationships between earthquake magnitude and probability of surface rupture

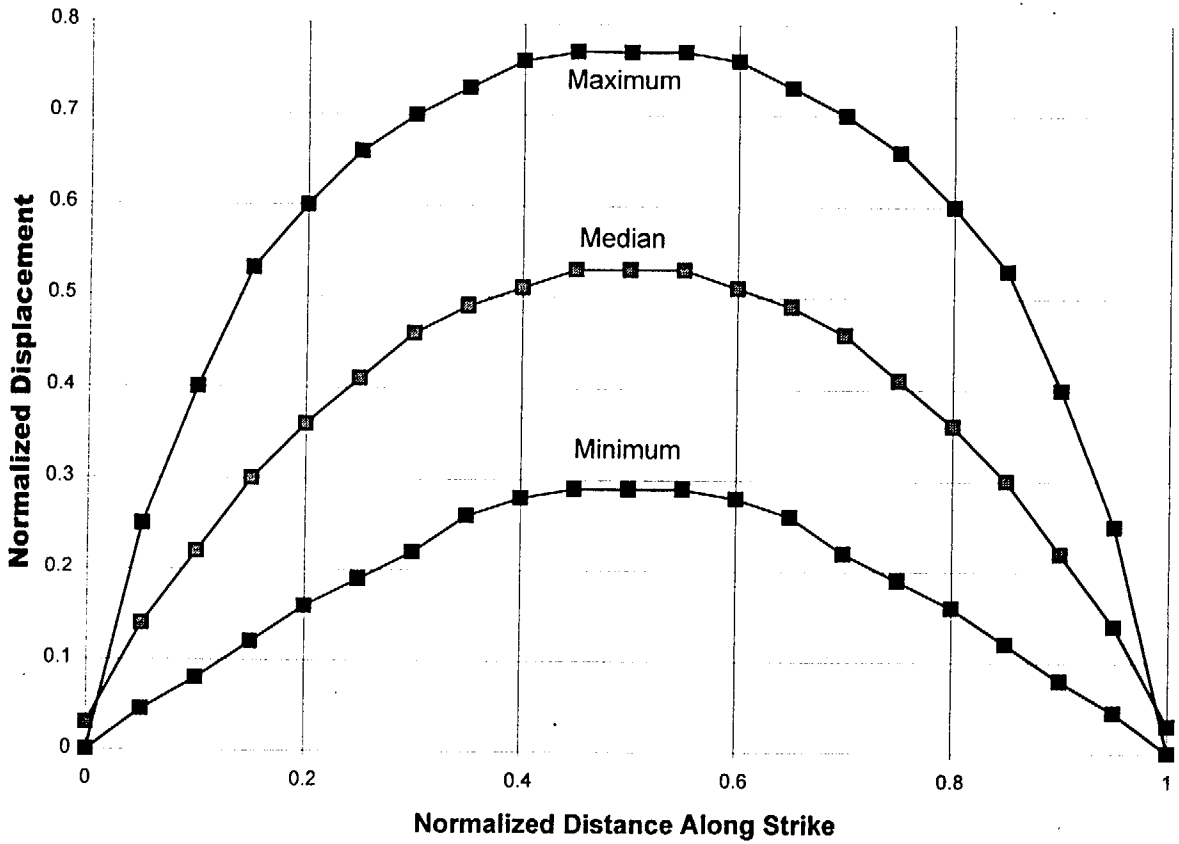

Figure ASM-18 Normalized "Wheeler" curve (adapted from Wheeler, 1989)

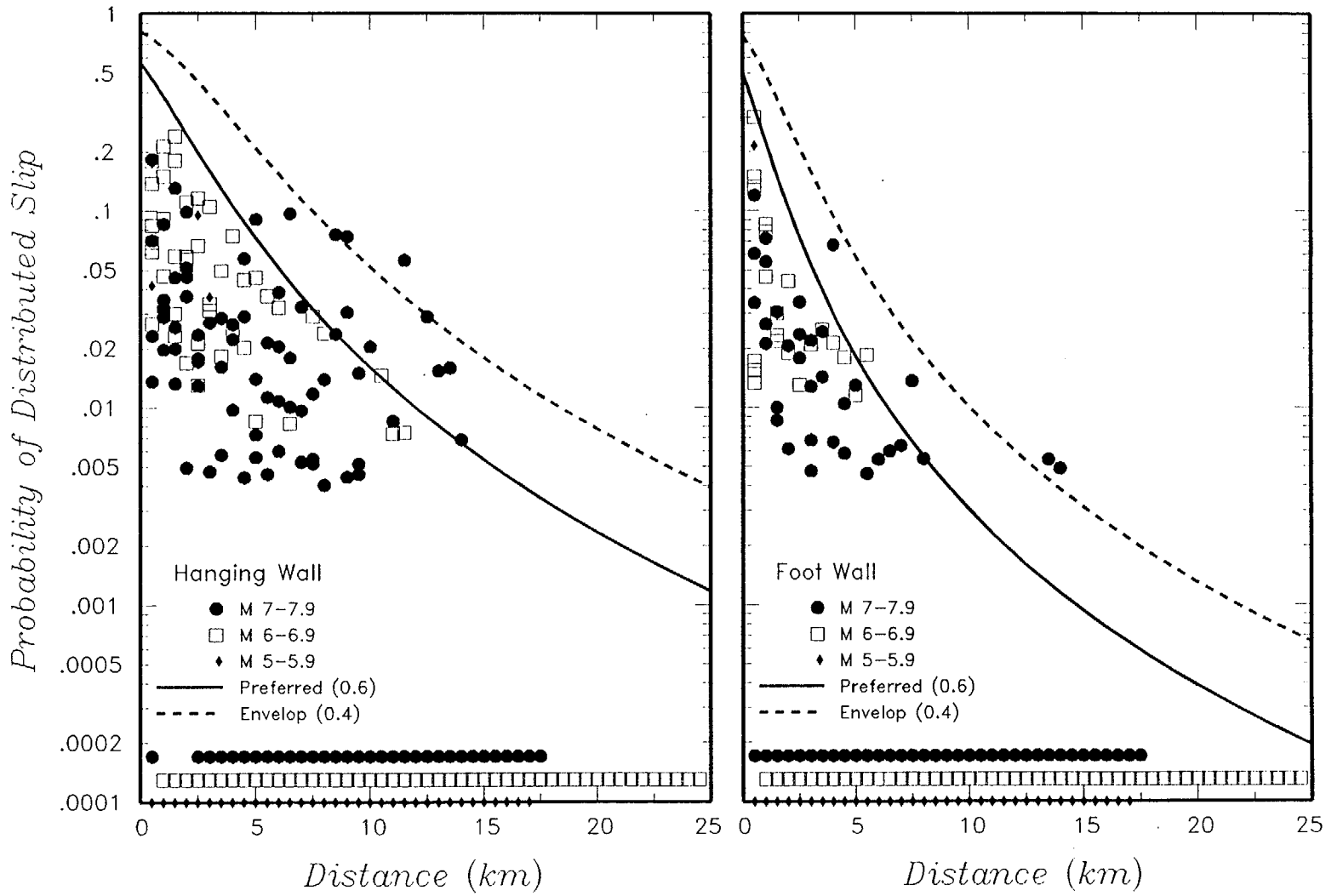

Figure ASM-19 Probability (frequency) of distributed slip as a function of distance from rupture

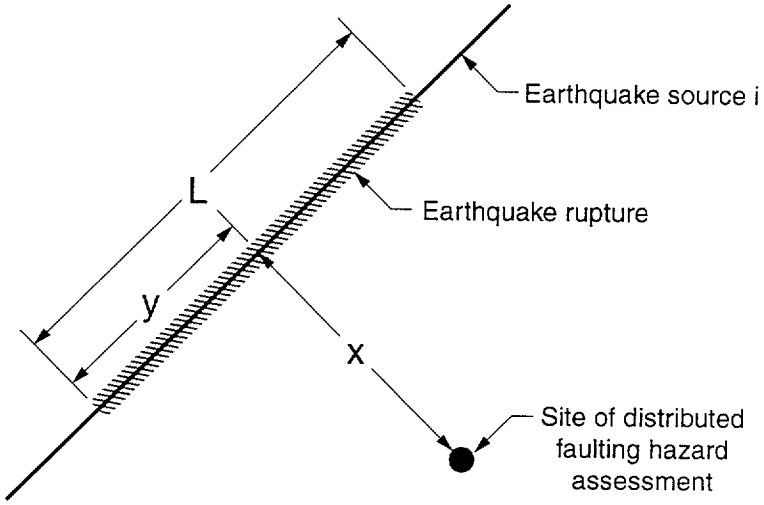

x = distance from rupture to site measured from fault normal point

y = location of fault normal point within rupture

L = length of earthquake rupture

Figure ASM-20 Schematic illustration of ASSD method

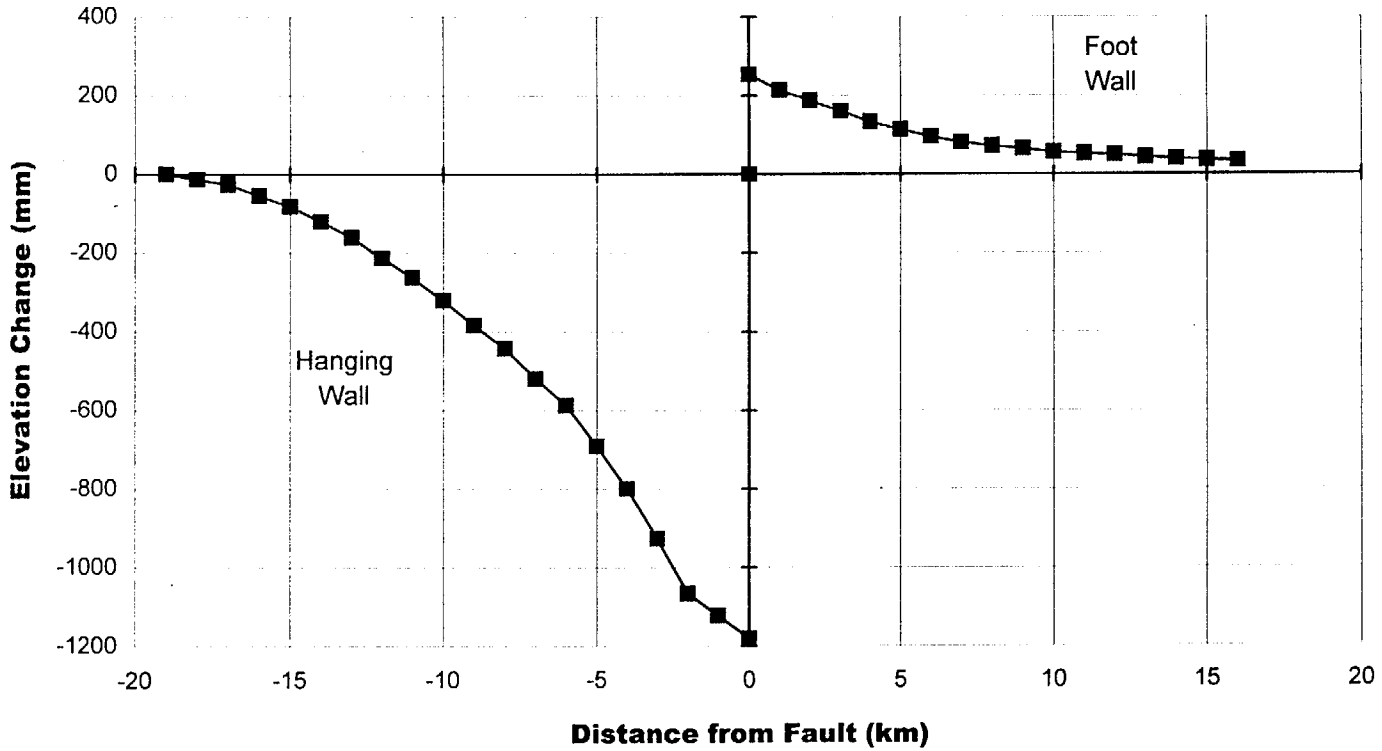

Figure ASM-21 Borah Peak geodetic curve

APPENDIX ASM-1

Graphs showing the cumulative frequency of long-term slip rates for 10 local Yucca Mountain faults.

Note: These CDFs were computed from permutations of cumulative displacement and age of deposits/soils from Table 5-1 in USGS (written communication, 1996).

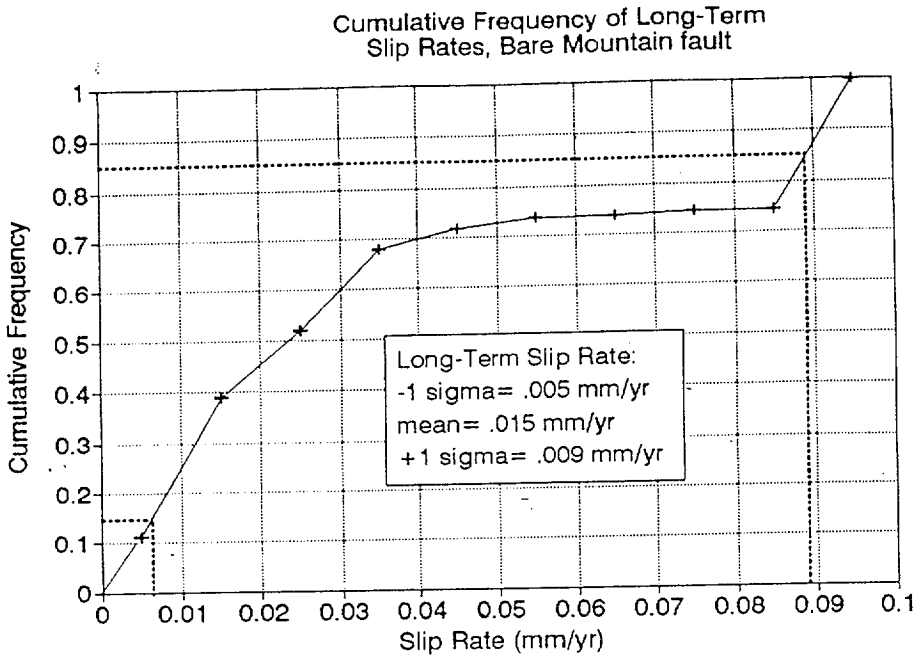
Cumulative Frequency of Long-Term Slip Rates, Bare Mountain fault
Cumulative Frequency
Slip Rate (mm/yr)
Long-Term Slip Rate:
-1 sigma= .005 mm/yr
mean= .015 mm/yr
+1 sigma= .009 mm/yr
0
0.1
0.2
0.3
0.4
0.5
0.6
0.7
0.8
0.9
1
0.01
0.02
0.03
0.04
0.05
0.06
0.07
0.08
0.09
0.1

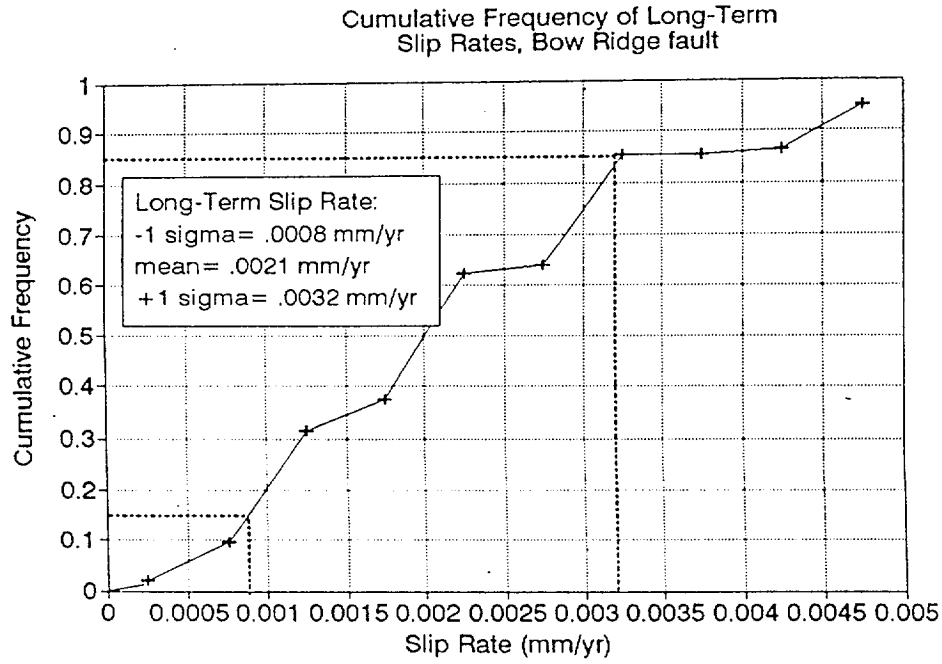
Cumulative Frequency of Long-Term Slip Rates, Bow Ridge fault
Cumulative Frequency
Slip Rate (mm/yr)
Long-Term Slip Rate:
-1 sigma= .0008 mm/yr
mean= .0021 mm/yr
+1 sigma= .0032 mm/yr
0
0.1
0.2
0.3
0.4
0.5
0.6
0.7
0.8
0.9
1
0.0005
0.001
0.0015
0.002
0.0025
0.003
0.0035
0.004
0.0045
0.005

ASM-AI-2

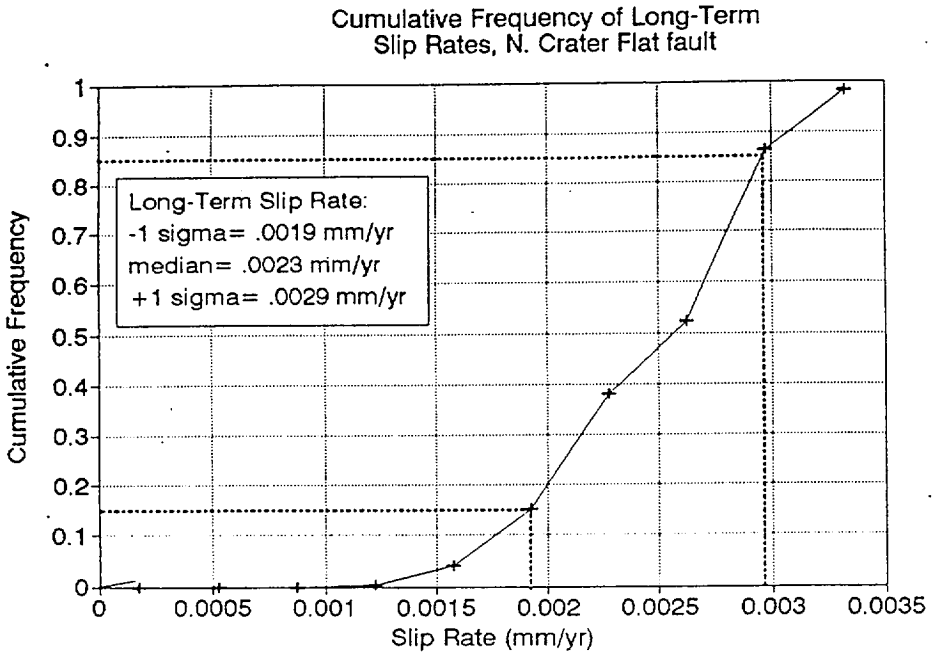
Cumulative Frequency of Long-Term Slip Rates, N. Crater Flat fault
Long-Term Slip Rate:
-1 sigma= .0019 mm/yr
median= .0023 mm/yr
+1 sigma= .0029 mm/yr
Cumulative Frequency
Slip Rate (mm/yr)
0
0.1
0.2
0.3
0.4
0.5
0.6
0.7
0.8
0.9
1
0.0005
0.001
0.0015
0.002
0.0025
0.003
0.0035

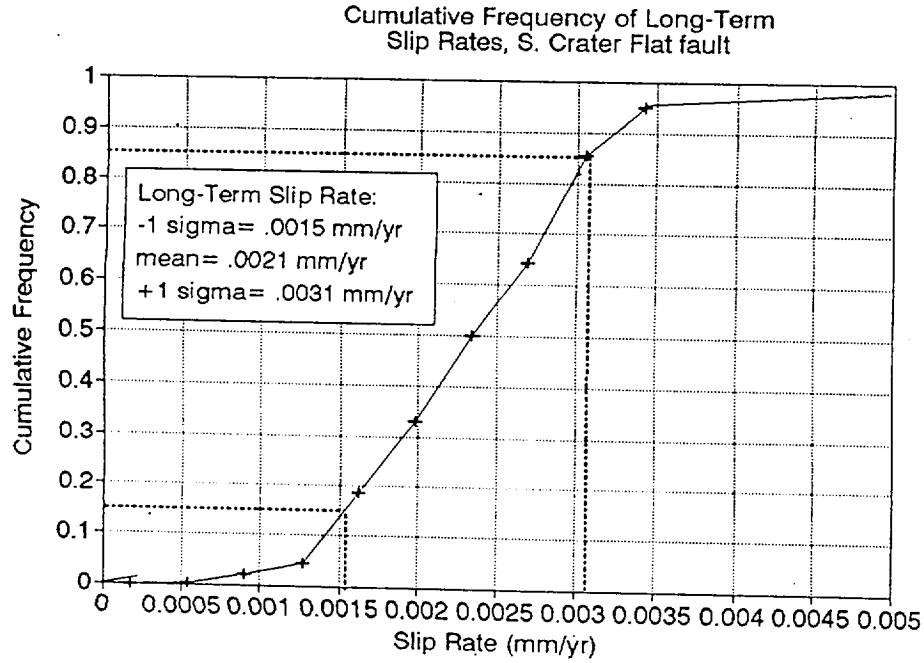
Cumulative Frequency of Long-Term Slip Rates, S. Crater Flat fault
Long-Term Slip Rate:
-1 sigma= .0015 mm/yr
mean= .0021 mm/yr
+1 sigma= .0031 mm/yr
Cumulative Frequency
Slip Rate (mm/yr)
0
0.1
0.2
0.3
0.4
0.5
0.6
0.7
0.8
0.9
1
0.0005
0.001
0.0015
0.002
0.0025
0.003
0.0035
0.004
0.0045
0.005

ASM-A1-3

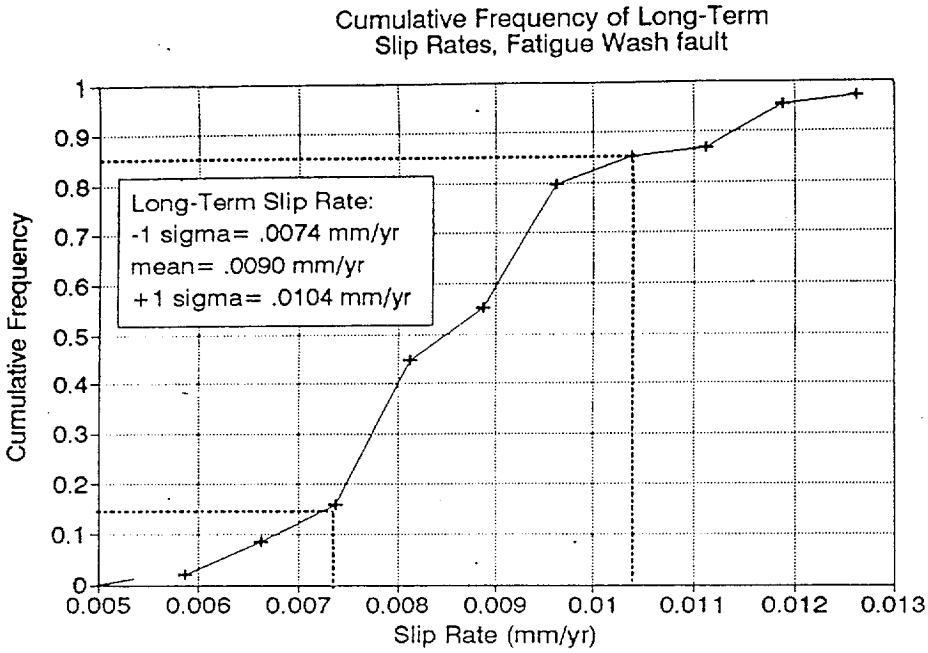
Cumulative Frequency of Long-Term Slip Rates, Fatigue Wash fault
Long-Term Slip Rate:
-1 sigma= .0074 mm/yr
mean= .0090 mm/yr
+1 sigma= .0104 mm/yr
Cumulative Frequency
Slip Rate (mm/yr)
0
0.1
0.2
0.3
0.4
0.5
0.6
0.7
0.8
0.9
1
0.005
0.006
0.007
0.008
0.009
0.01
0.011
0.012
0.013

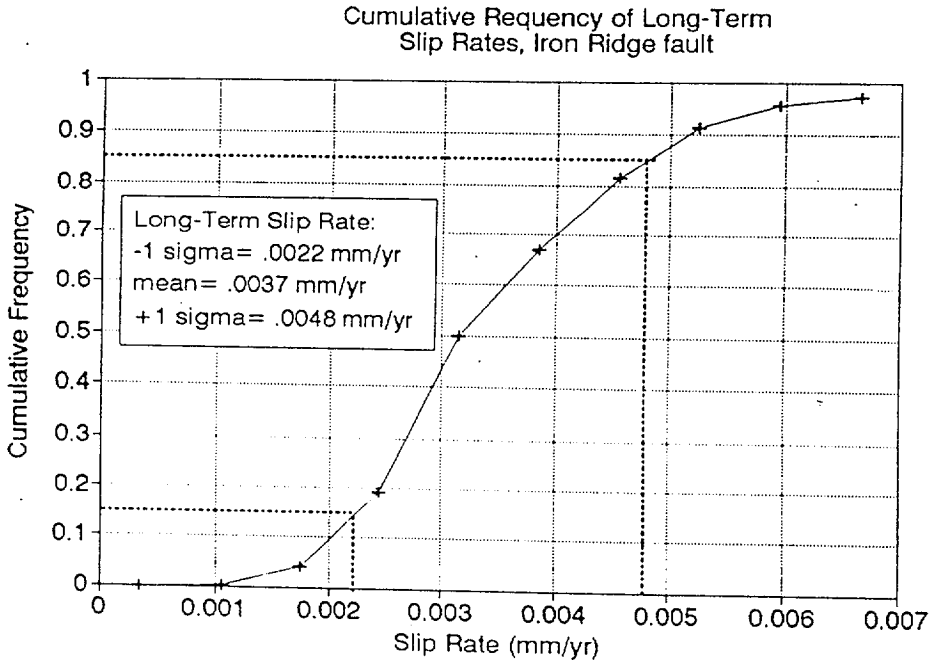
Cumulative Requency of Long-Term Slip Rates, Iron Ridge fault
Long-Term Slip Rate:
-1 sigma= .0022 mm/yr
mean= .0037 mm/yr
+1 sigma= .0048 mm/yr
Cumulative Frequency
Slip Rate (mm/yr)
0
0.1
0.2
0.3
0.4
0.5
0.6
0.7
0.8
0.9
1
0
0.001
0.002
0.003
0.004
0.005
0.006
0.007

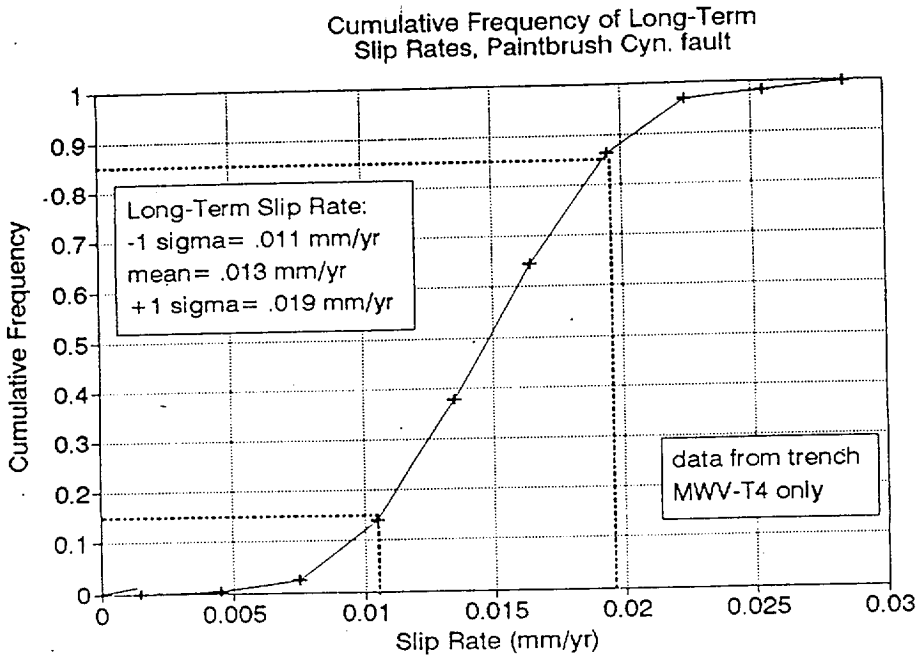
Cumulative Frequency of Long-Term Slip Rates, Paintbrush Cyn. fault
Long-Term Slip Rate:
-1 sigma= .011 mm/yr
mean= .013 mm/yr
+1 sigma= .019 mm/yr
data from trench MWV-T4 only
Cumulative Frequency
Slip Rate (mm/yr)
0
0.1
0.2
0.3
0.4
0.5
0.6
0.7
0.8
0.9
1
0.005
0.01
0.015
0.02
0.025
0.03

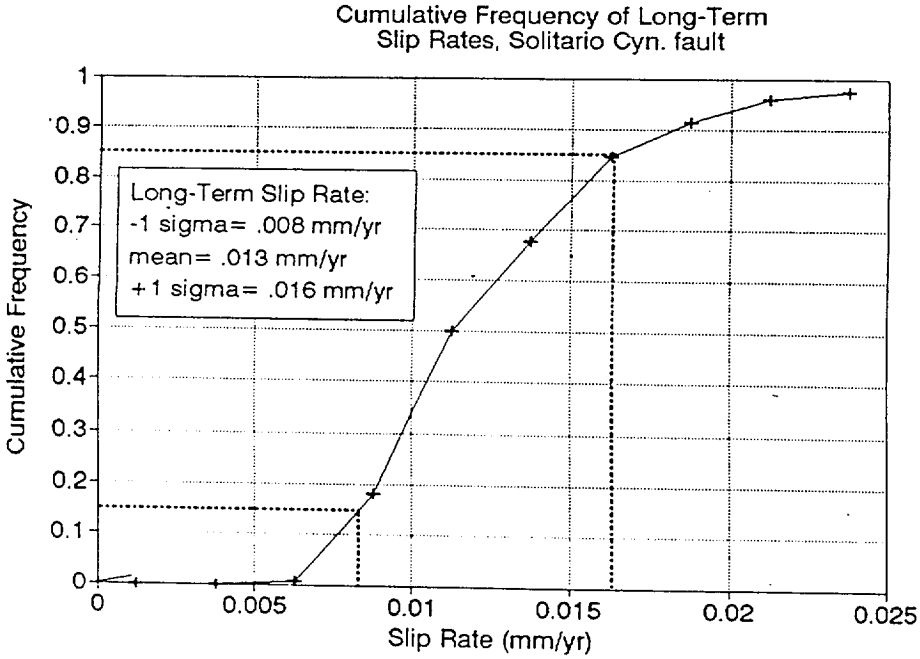
Cumulative Frequency of Long-Term Slip Rates, Solitario Cyn. fault
Long-Term Slip Rate:
-1 sigma= .008 mm/yr
mean= .013 mm/yr
+1 sigma= .016 mm/yr
Cumulative Frequency
Slip Rate (mm/yr)
0
0.1
0.2
0.3
0.4
0.5
0.6
0.7
0.8
0.9
1
0.005
0.01
0.015
0.02
0.025

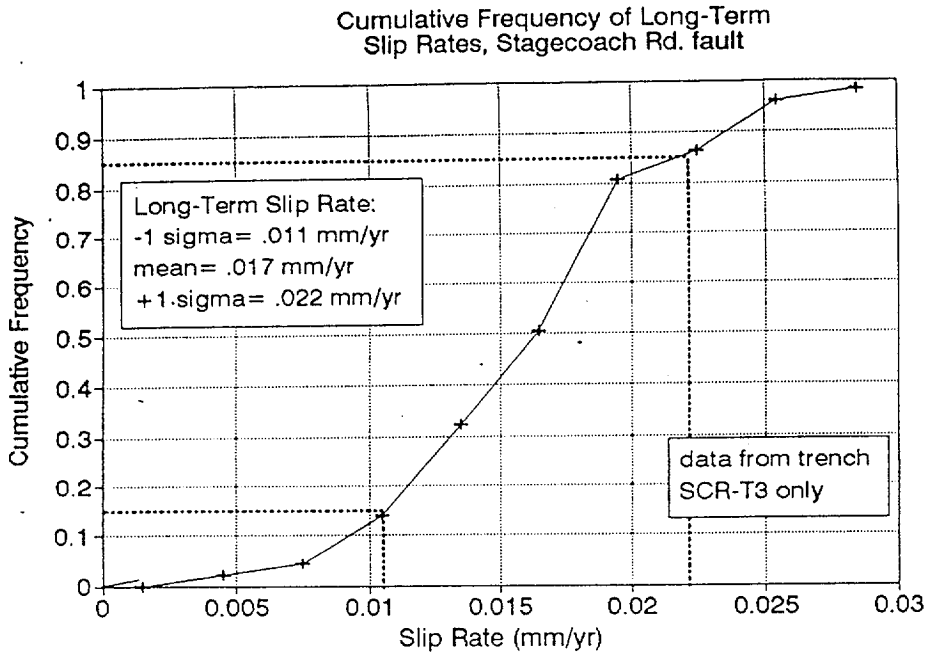
Cumulative Frequency of Long-Term Slip Rates, Stagecoach Rd. fault
Long-Term Slip Rate:
-1 sigma= .011 mm/yr
mean= .017 mm/yr
+1 sigma= .022 mm/yr
data from trench SCR-T3 only
Cumulative Frequency
Slip Rate (mm/yr)
0
0.1
0.2
0.3
0.4
0.5
0.6
0.7
0.8
0.9
1
0.005
0.01
0.015
0.02
0.025
0.03

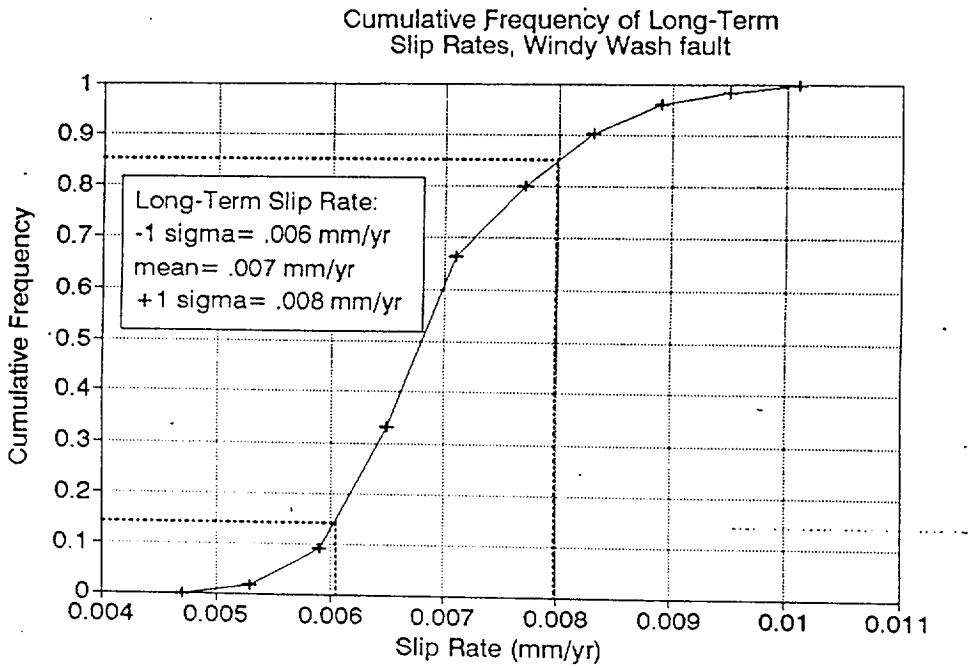
Cumulative Frequency of Long-Term Slip Rates, Windy Wash fault
Long-Term Slip Rate:
-1 sigma= .006 mm/yr
mean= .007 mm/yr
+1 sigma= .008 mm/yr
Cumulative Frequency
Slip Rate (mm/yr)
0
0.1
0.2
0.3
0.4
0.5
0.6
0.7
0.8
0.9
1
0.004
0.005
0.006
0.007
0.008
0.009
0.01
0.011

APPENDIX ASM-2

Graphs showing the cumulative frequency of interval slip rates for 10 local Yucca Mountain faults.

Note: these CDFs were computed by creating a normalized-grouped dataset of all interval slip rates on all Yucca Mountain faults, using the method of McCalpin (1995). Then for each of the 10 faults, that CDF was scaled to the long-term slip rate (from Appendix ASM-1) to yield these CDFs.

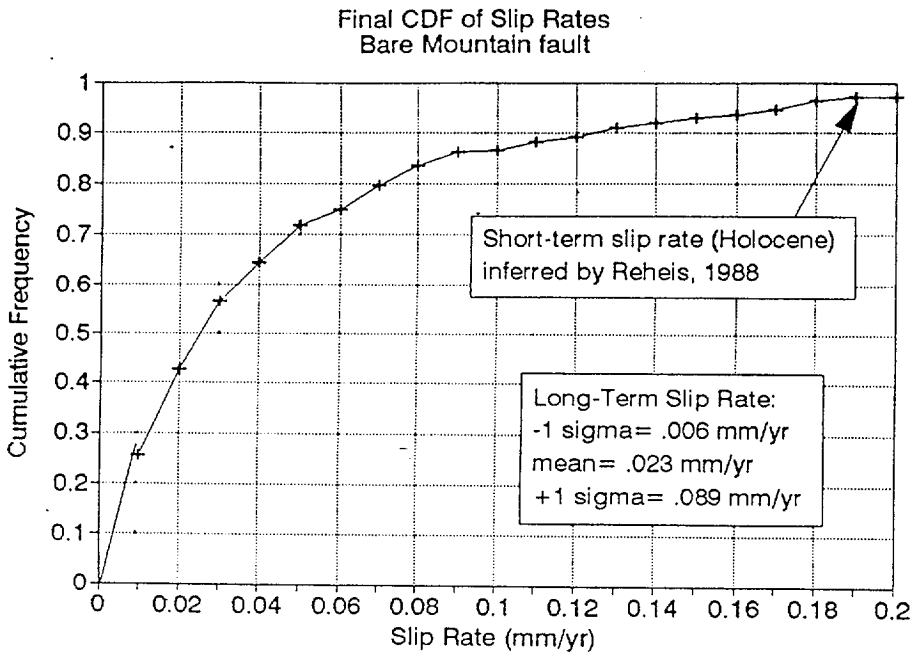
Final CDF of Slip Rates
Bare Mountain fault
Cumulative Frequency
Slip Rate (mm/yr)
Short-term slip rate (Holocene)
inferred by Reheis, 1988
Long-Term Slip Rate:
-1 sigma= .006 mm/yr
mean= .023 mm/yr
+1 sigma= .089 mm/yr

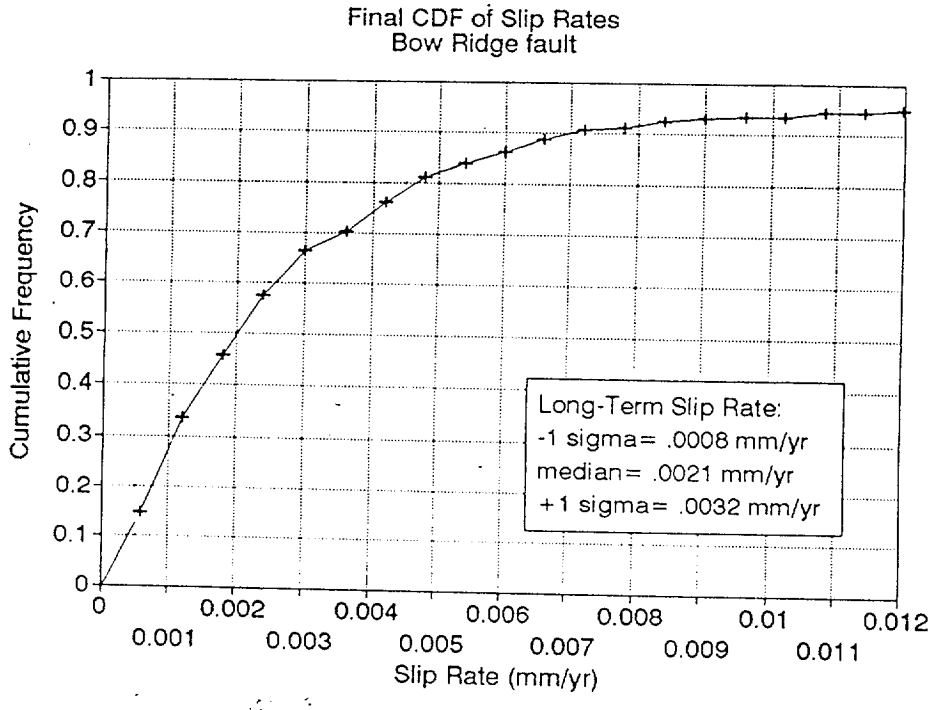
Final CDF of Slip Rates
Bow Ridge fault
Cumulative Frequency
Slip Rate (mm/yr)
Long-Term Slip Rate:
-1 sigma= .0008 mm/yr
median= .0021 mm/yr
+1 sigma= .0032 mm/yr

ASM-A2-2

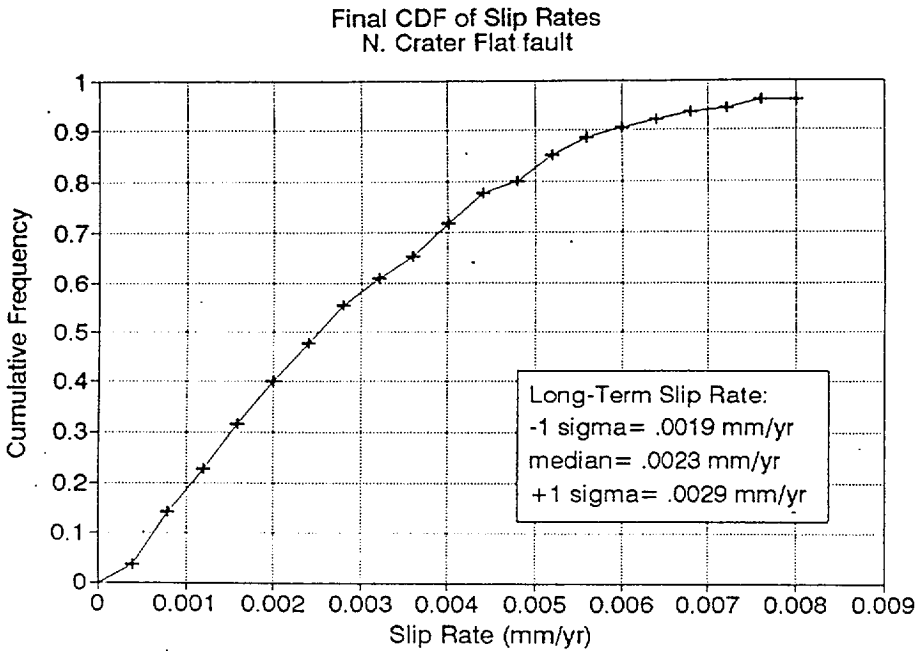
Final CDF of Slip Rates
N. Crater Flat fault
Cumulative Frequency
Slip Rate (mm/yr)
Long-Term Slip Rate:
-1 sigma= .0019 mm/yr
median= .0023 mm/yr
+1 sigma= .0029 mm/yr

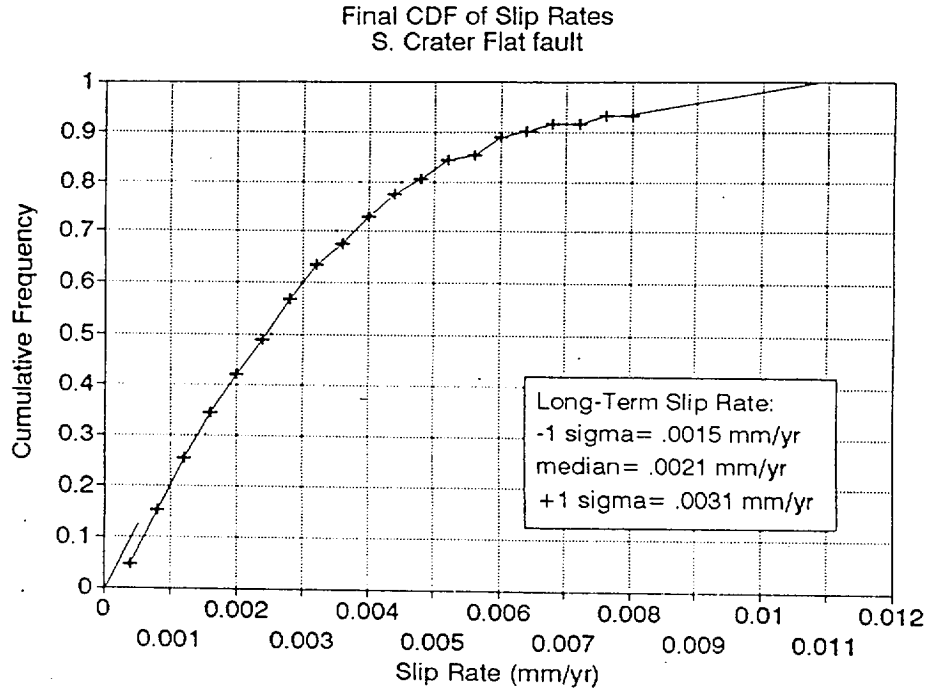
Final CDF of Slip Rates
S. Crater Flat fault
Cumulative Frequency
Slip Rate (mm/yr)
Long-Term Slip Rate:
-1 sigma= .0015 mm/yr
median= .0021 mm/yr
+1 sigma= .0031 mm/yr

ASM-AZ-3

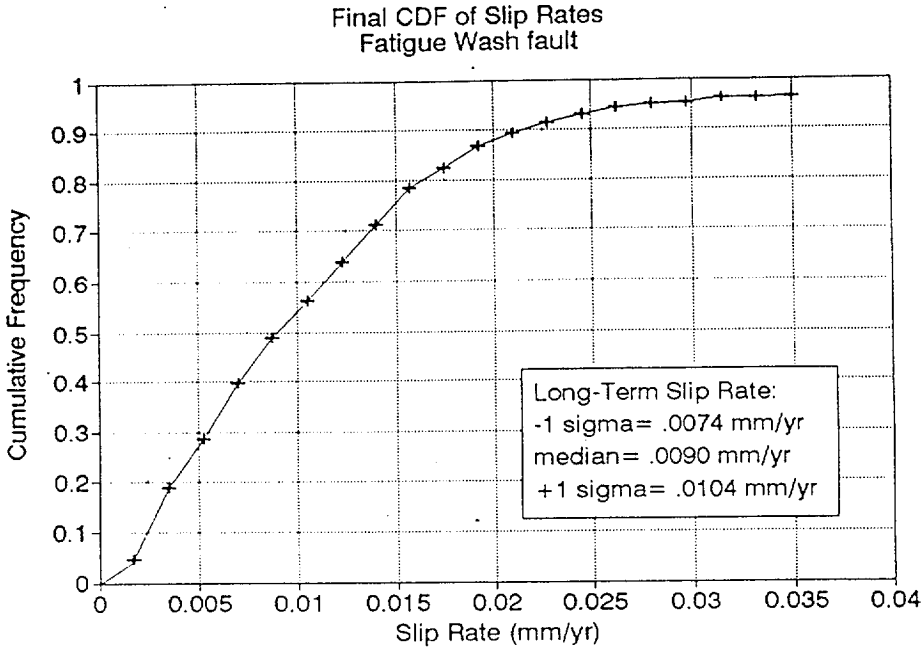
Final CDF of Slip Rates
Fatigue Wash fault
Cumulative Frequency
Slip Rate (mm/yr)
Long-Term Slip Rate:
-1 sigma= .0074 mm/yr
median= .0090 mm/yr
+1 sigma= .0104 mm/yr

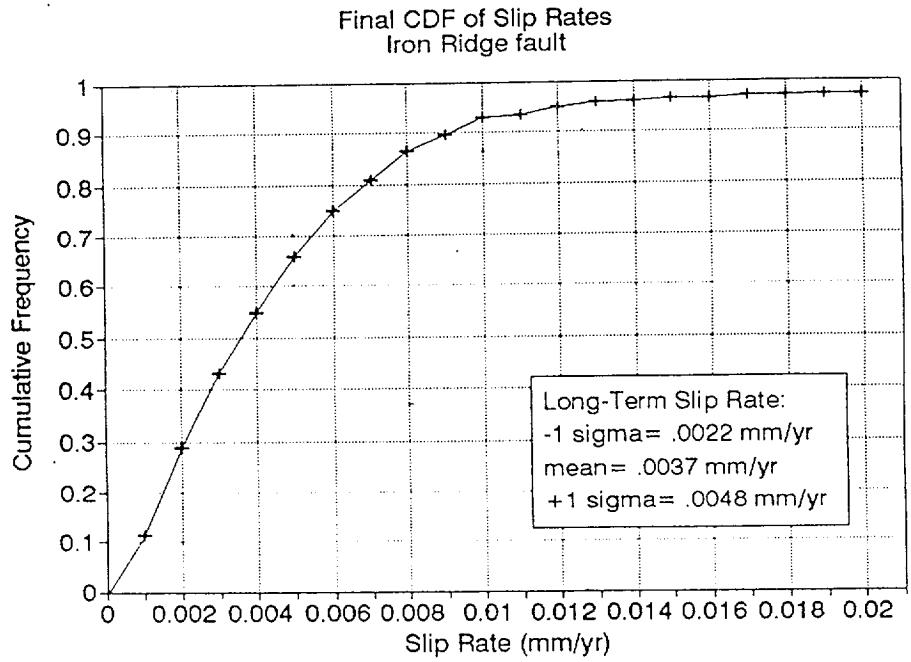
Final CDF of Slip Rates
Iron Ridge fault
Cumulative Frequency
Slip Rate (mm/yr)
Long-Term Slip Rate:
-1 sigma= .0022 mm/yr
mean= .0037 mm/yr
+1 sigma= .0048 mm/yr

ASM-A2-4

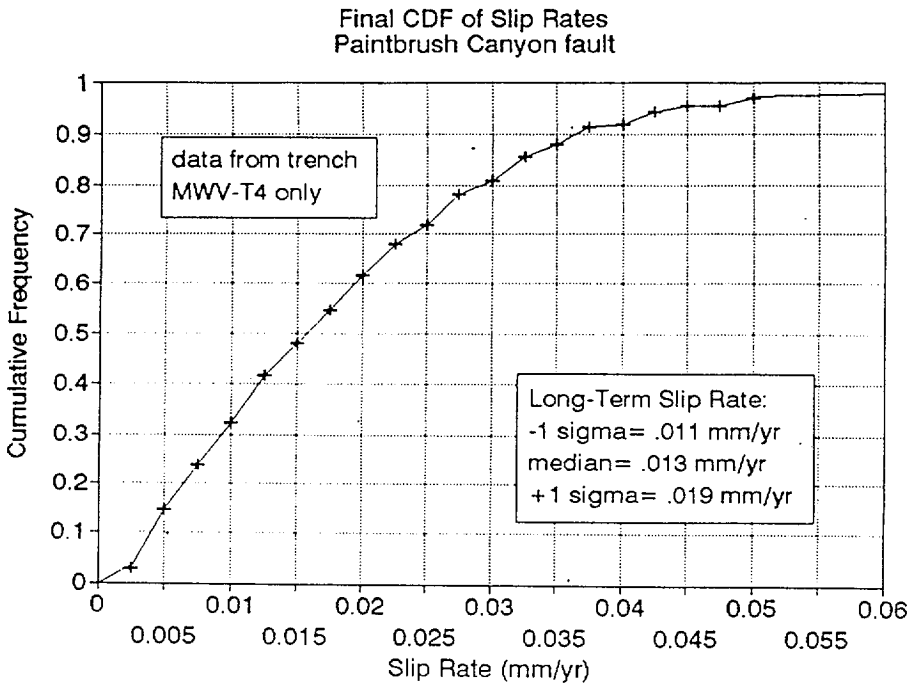
Final CDF of Slip Rates
Paintbrush Canyon fault
data from trench
MWV-T4 only
Long-Term Slip Rate:
-1 sigma= .011 mm/yr
median= .013 mm/yr
+1 sigma= .019 mm/yr
Cumulative Frequency
Slip Rate (mm/yr)
0
0.1
0.2
0.3
0.4
0.5
0.6
0.7
0.8
0.9
1
0.005
0.01
0.015
0.02
0.025
0.03
0.035
0.04
0.045
0.05
0.055
0.06

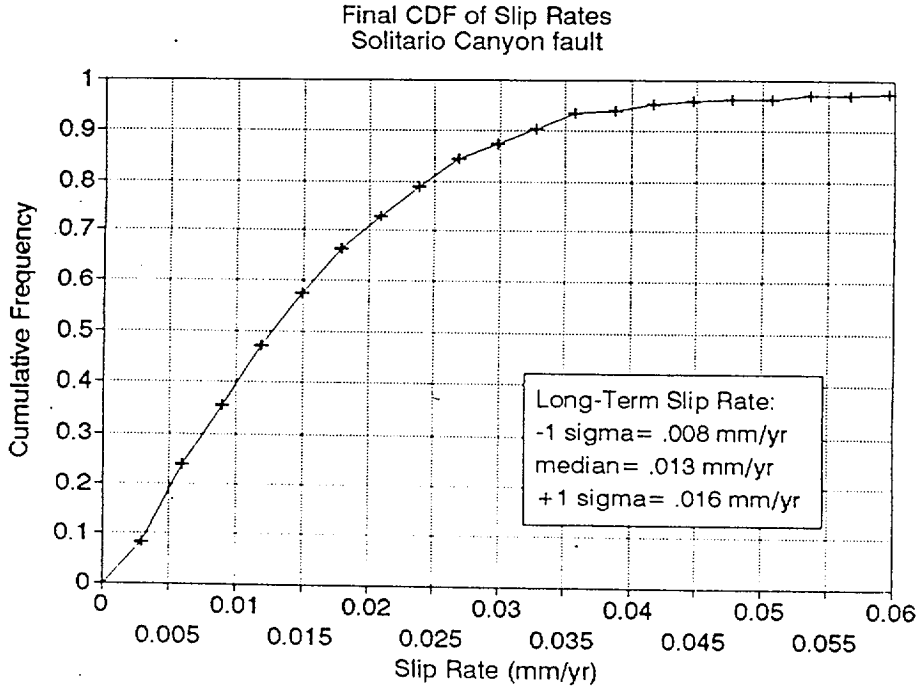
Final CDF of Slip Rates
Solitario Canyon fault
Long-Term Slip Rate:
-1 sigma= .008 mm/yr
median= .013 mm/yr
+1 sigma= .016 mm/yr
Cumulative Frequency
Slip Rate (mm/yr)
0
0.1
0.2
0.3
0.4
0.5
0.6
0.7
0.8
0.9
1
0.005
0.01
0.015
0.02
0.025
0.03
0.035
0.04
0.045
0.05
0.055
0.06

ASM-A2-5

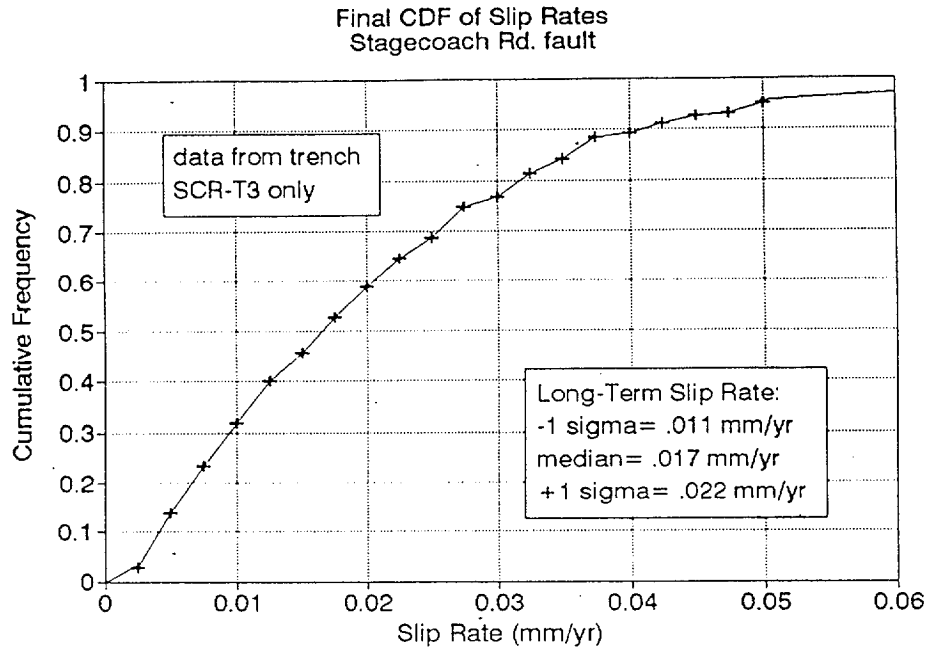
Final CDF of Slip Rates
Stagecoach Rd. fault
data from trench
SCR-T3 only
Long-Term Slip Rate:
-1 sigma= .011 mm/yr
median= .017 mm/yr
+1 sigma= .022 mm/yr
Cumulative Frequency
Slip Rate (mm/yr)
0
0.1
0.2
0.3
0.4
0.5
0.6
0.7
0.8
0.9
1
0.01
0.02
0.03
0.04
0.05
0.06

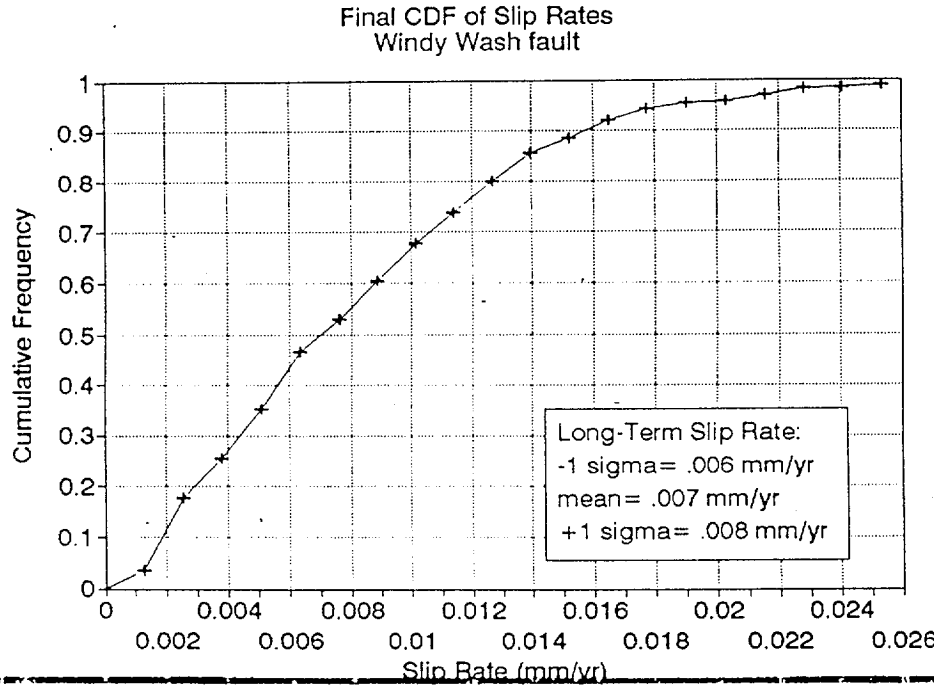
Final CDF of Slip Rates
Windy Wash fault
Long-Term Slip Rate:
-1 sigma= .006 mm/yr
mean= .007 mm/yr
+1 sigma= .008 mm/yr
Cumulative Frequency
Slip Rate (mm/yr)
0
0.1
0.2
0.3
0.4
0.5
0.6
0.7
0.8
0.9
1
0.002
0.004
0.006
0.008
0.01
0.012
0.014
0.016
0.018
0.02
0.022
0.024
0.026

ASM-A2-6

APPENDIX ASM-3

Graphs showing frequency histograms of long-term mean recurrence interval for 10 local Yucca Mountain faults.

Note: these histograms show 36 permutations of long-term mean recurrence interval, based on 6 estimates each of the age of the oldest and youngest dated paleoearthquakes, and the number of seismic cycles between those dates. We assumed that the minimum, preferred, and maximum ages for paleoearthquakes in Table 5-1 of USGS (written communication, 1996) represented ± 1 sigma limits. We then split these age values up into a six-part frequency distribution (with symmetrical probabilities of 0.025, 0.125, and 0.35) by linear interpolation (see spreadsheet RI-[fault name].WQZ for actual calculations.)

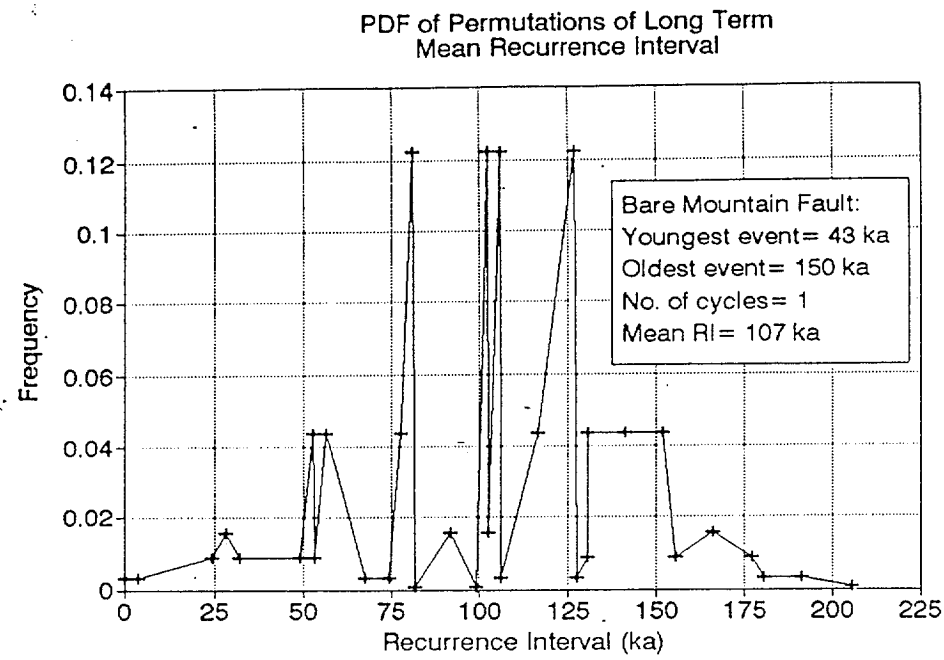
PDF of Permutations of Long Term
Mean Recurrence Interval
Frequency
Recurrence Interval (ka)
Bare Mountain Fault:
Youngest event= 43 ka
Oldest event= 150 ka
No. of cycles= 1
Mean RI= 107 ka
0.14
0.12
0.1
0.08
0.06
0.04
0.02
0
0 25 50 75 100 125 150 175 200 225

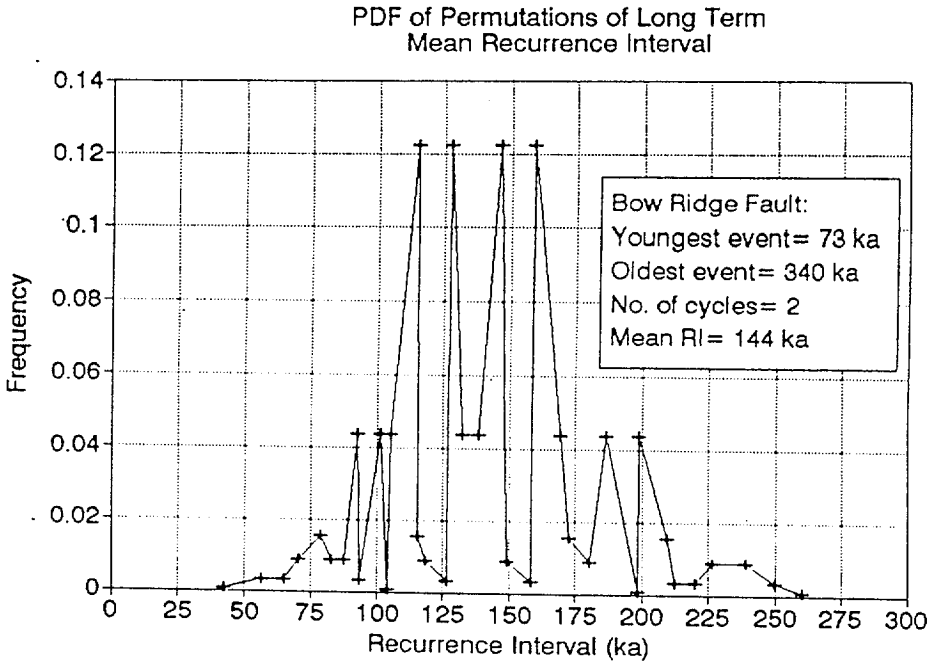
PDF of Permutations of Long Term
Mean Recurrence Interval
Frequency
Recurrence Interval (ka)
Bow Ridge Fault:
Youngest event= 73 ka
Oldest event= 340 ka
No. of cycles= 2
Mean RI= 144 ka
0.14
0.12
0.1
0.08
0.06
0.04
0.02
0
0 25 50 75 100 125 150 175 200 225 250 275 300

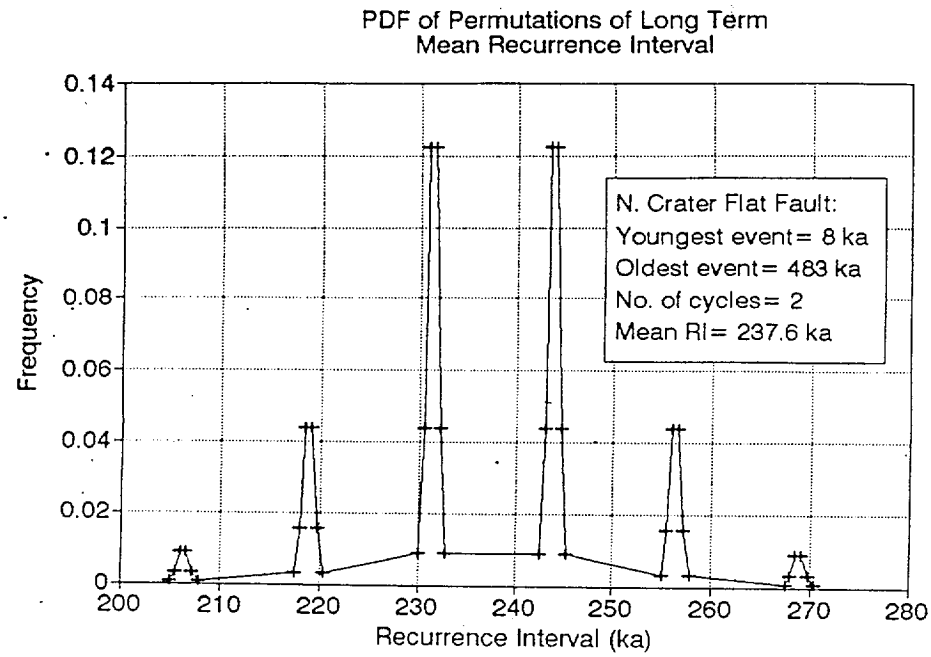
PDF of Permutations of Long Term
Mean Recurrence Interval
Frequency
0.14
0.12
0.1
0.08
0.06
0.04
0.02
0
200
210
220
230
240
250
260
270
280
Recurrence Interval (ka)
N. Crater Flat Fault:
Youngest event= 8 ka
Oldest event= 483 ka
No. of cycles= 2
Mean RI= 237.6 ka

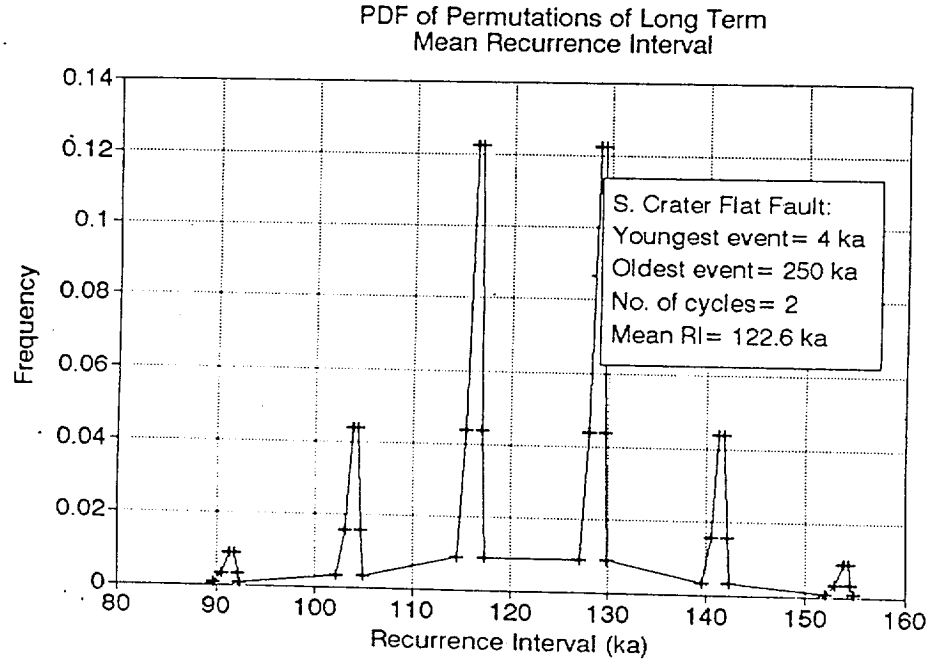
PDF of Permutations of Long Term
Mean Recurrence Interval
Frequency
0.14
0.12
0.1
0.08
0.06
0.04
0.02
0
80
90
100
110
120
130
140
150
160
Recurrence Interval (ka)
S. Crater Flat Fault:
Youngest event= 4 ka
Oldest event= 250 ka
No. of cycles= 2
Mean RI= 122.6 ka

ASM-A3-3

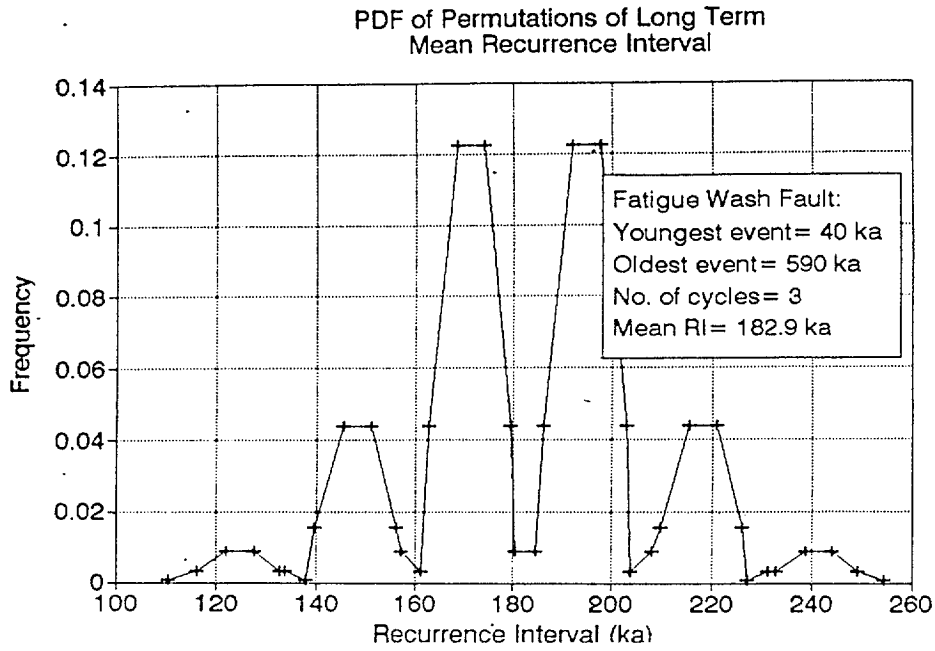
PDF of Permutations of Long Term
Mean Recurrence Interval
Frequency
Recurrence Interval (ka)
Fatigue Wash Fault:
Youngest event= 40 ka
Oldest event= 590 ka
No. of cycles= 3
Mean RI= 182.9 ka
0.14
0.12
0.1
0.08
0.06
0.04
0.02
0
100
120
140
160
180
200
220
240
260

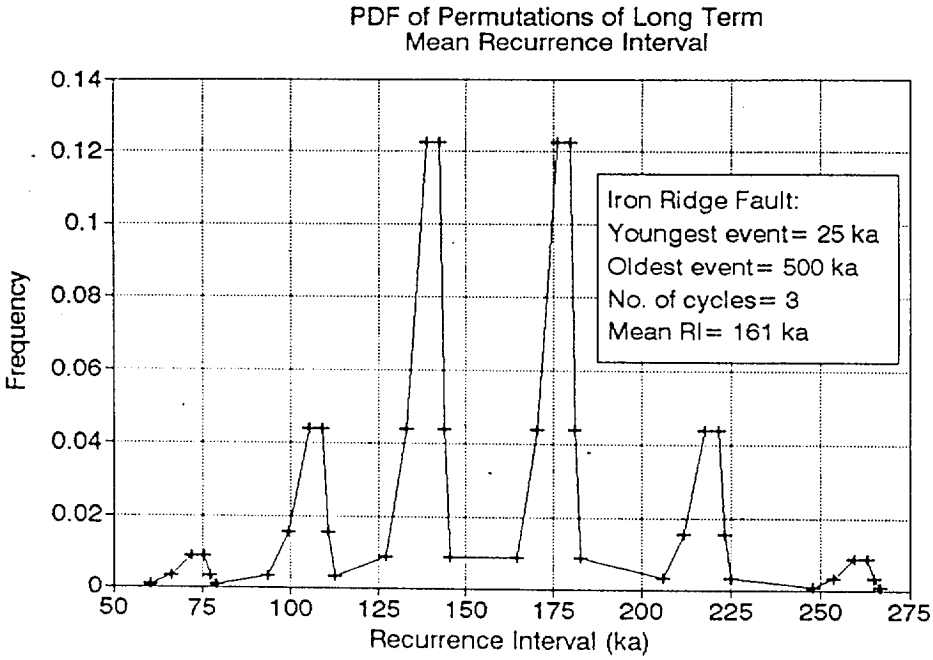
PDF of Permutations of Long Term
Mean Recurrence Interval
Frequency
Recurrence Interval (ka)
Iron Ridge Fault:
Youngest event= 25 ka
Oldest event= 500 ka
No. of cycles= 3
Mean RI= 161 ka
0.14
0.12
0.1
0.08
0.06
0.04
0.02
0
50
75
100
125
150
175
200
225
250
275

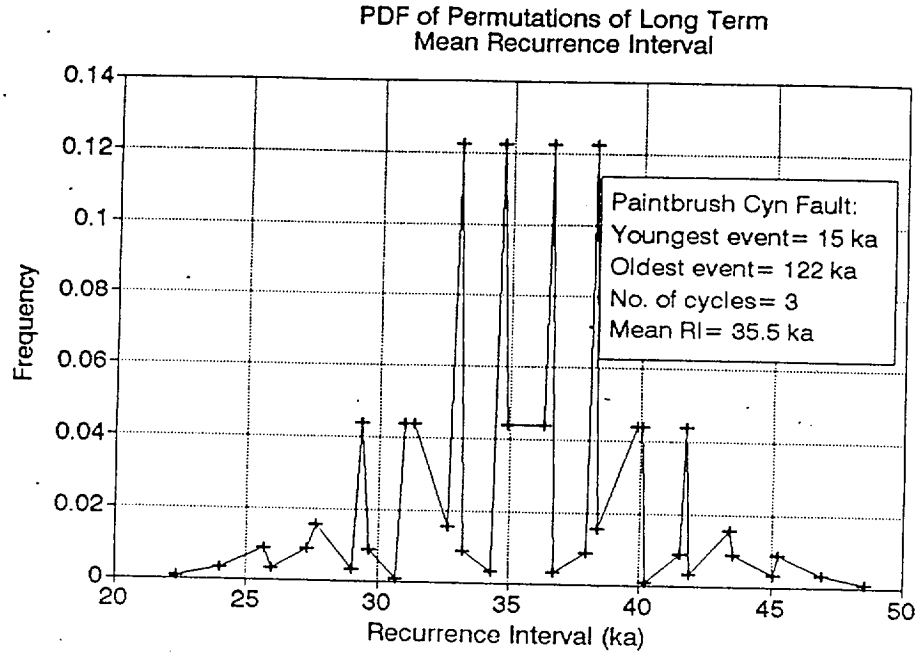
PDF of Permutations of Long Term
Mean Recurrence Interval
Frequency
Recurrence Interval (ka)
Paintbrush Cyn Fault:
Youngest event= 15 ka
Oldest event= 122 ka
No. of cycles= 3
Mean RI= 35.5 ka

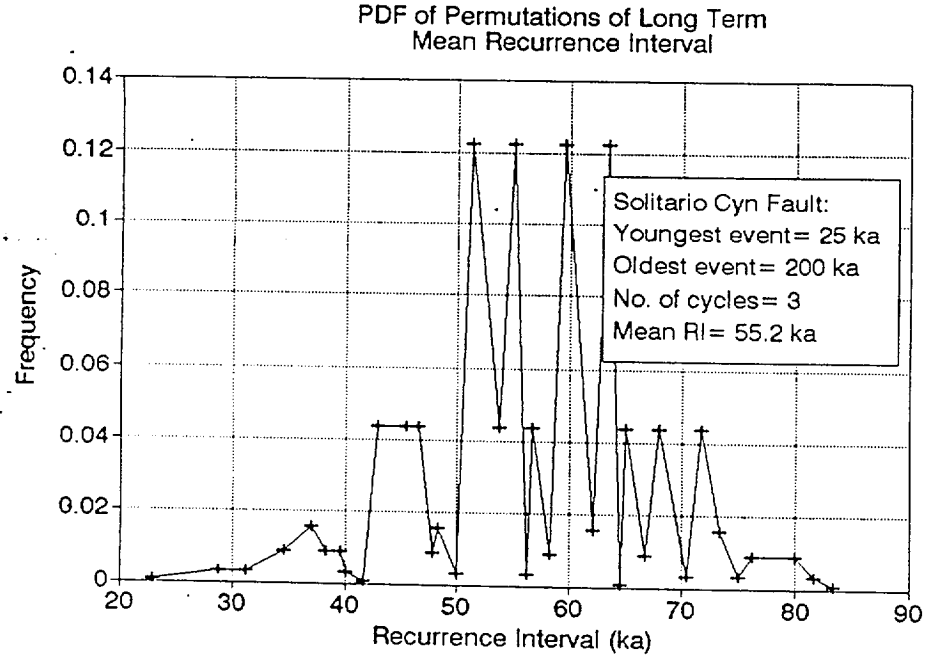
PDF of Permutations of Long Term
Mean Recurrence Interval
Frequency
Recurrence Interval (ka)
Solitario Cyn Fault:
Youngest event= 25 ka
Oldest event= 200 ka
No. of cycles= 3
Mean RI= 55.2 ka

ASM-A3-5

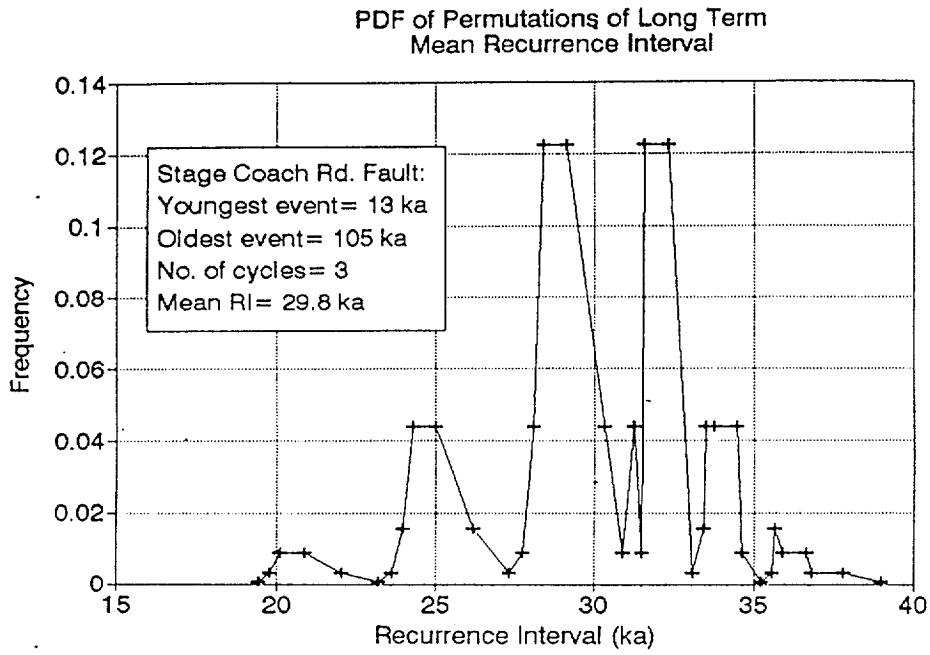
PDF of Permutations of Long Term
Mean Recurrence Interval
Stage Coach Rd. Fault:
Youngest event= 13 ka
Oldest event= 105 ka
No. of cycles= 3
Mean RI= 29.8 ka
Frequency
0.14
0.12
0.1
0.08
0.06
0.04
0.02
0
15
20
25
30
35
40
Recurrence Interval (ka)

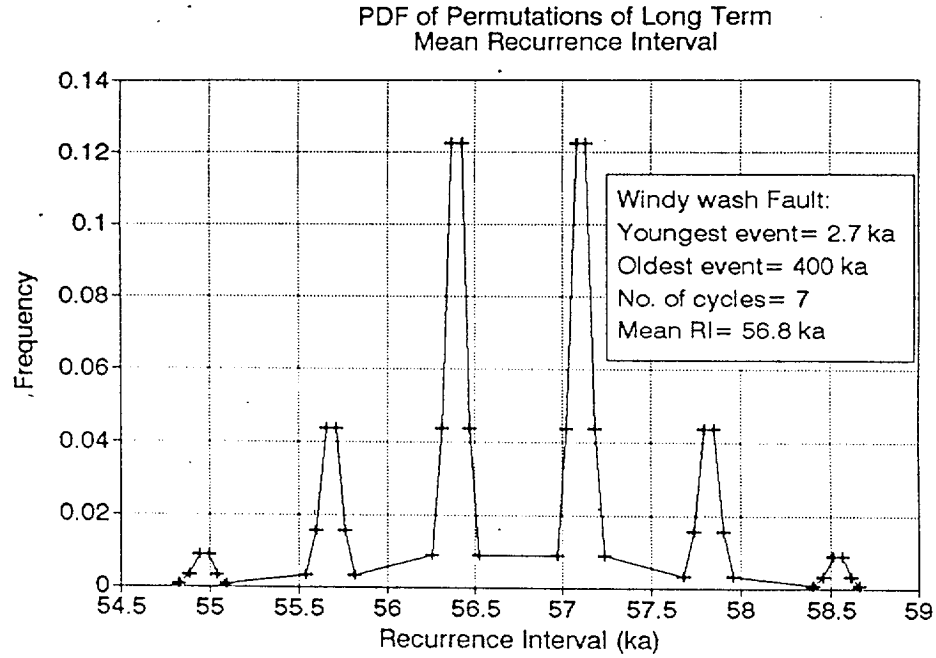
PDF of Permutations of Long Term
Mean Recurrence Interval
Windy wash Fault:
Youngest event= 2.7 ka
Oldest event= 400 ka
No. of cycles= 7
Mean RI= 56.8 ka
Frequency
0.14
0.12
0.1
0.08
0.06
0.04
0.02
0
54.5
55
55.5
56
56.5
57
57.5
58
58.5
59
Recurrence Interval (ka)

ASM-A3-6

APPENDIX ASM-4

Graphs showing cumulative frequency distributions of long-term mean recurrence interval for 10 local Yucca Mountain faults.

Note: these CDFs were derived from the PDFs of Appendix ASM-3.

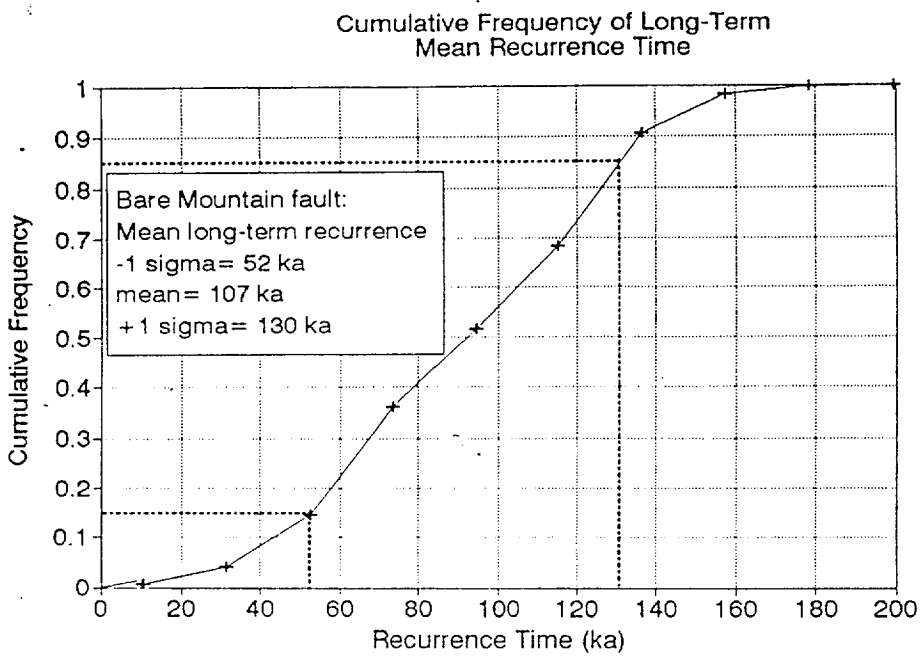
Cumulative Frequency of Long-Term
Mean Recurrence Time
Bare Mountain fault:
Mean long-term recurrence
-1 sigma= 52 ka
mean= 107 ka
+1 sigma= 130 ka
Cumulative Frequency
Recurrence Time (ka)
0
0.1
0.2
0.3
0.4
0.5
0.6
0.7
0.8
0.9
1
0
20
40
60
80
100
120
140
160
180
200

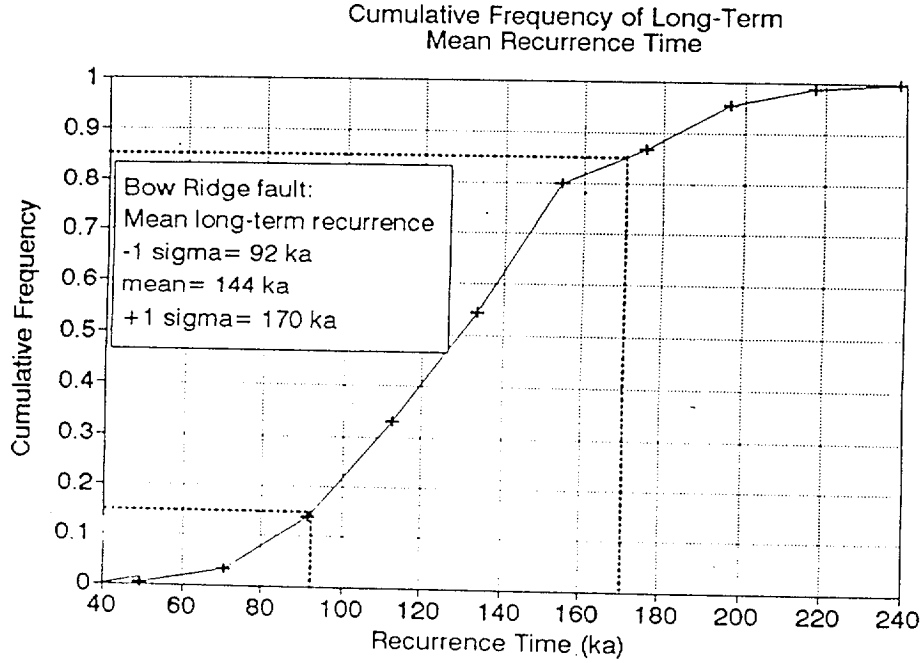
Cumulative Frequency of Long-Term
Mean Recurrence Time
Bow Ridge fault:
Mean long-term recurrence
-1 sigma= 92 ka
mean= 144 ka
+1 sigma= 170 ka
Cumulative Frequency
Recurrence Time (ka)
0
0.1
0.2
0.3
0.4
0.5
0.6
0.7
0.8
0.9
1
40
60
80
100
120
140
160
180
200
220
240

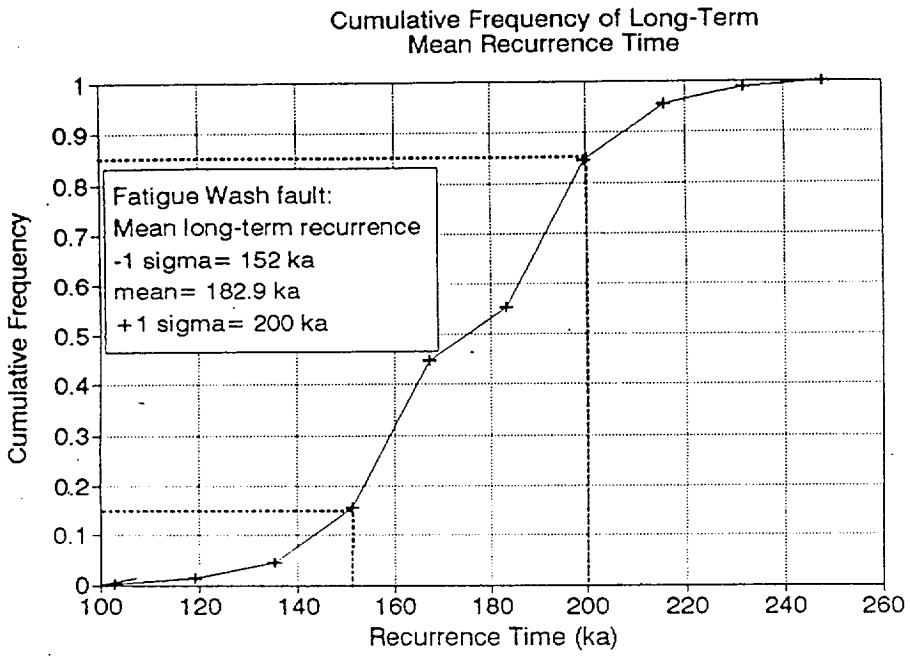
Cumulative Frequency of Long-Term
Mean Recurrence Time
Fatigue Wash fault:
Mean long-term recurrence
-1 sigma= 152 ka
mean= 182.9 ka
+1 sigma= 200 ka
Cumulative Frequency
Recurrence Time (ka)
0
0.1
0.2
0.3
0.4
0.5
0.6
0.7
0.8
0.9
1
100
120
140
160
180
200
220
240
260

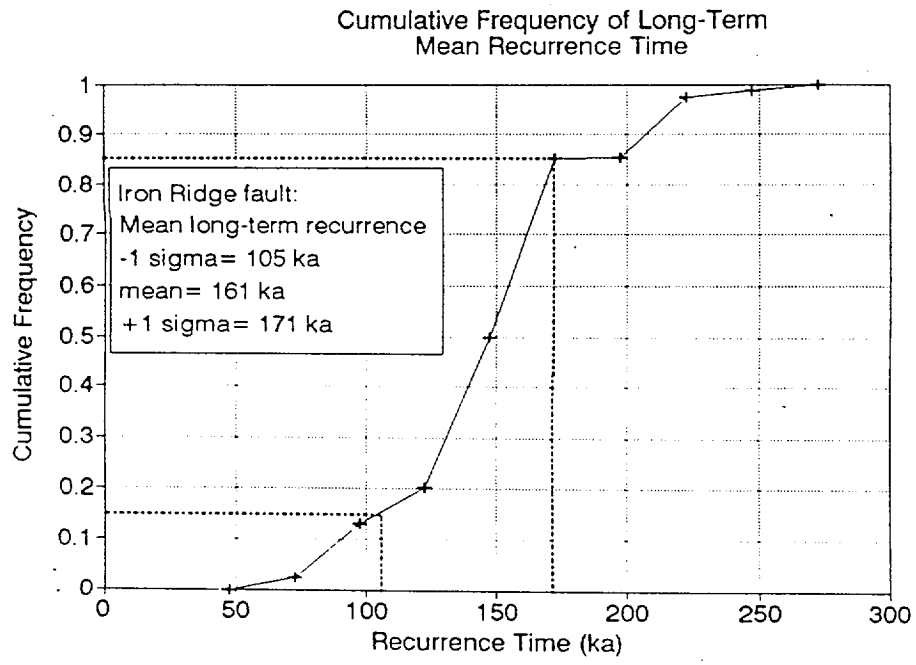
Cumulative Frequency of Long-Term
Mean Recurrence Time
Iron Ridge fault:
Mean long-term recurrence
-1 sigma= 105 ka
mean= 161 ka
+1 sigma= 171 ka
Cumulative Frequency
Recurrence Time (ka)
0
0.1
0.2
0.3
0.4
0.5
0.6
0.7
0.8
0.9
1
0
50
100
150
200
250
300

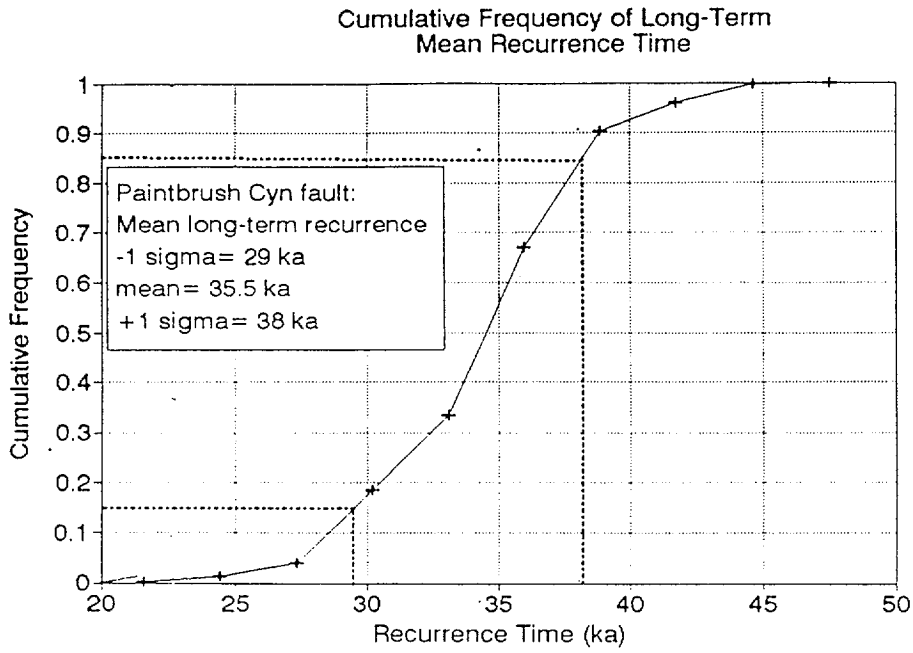
Cumulative Frequency of Long-Term
Mean Recurrence Time
Paintbrush Cyn fault:
Mean long-term recurrence
-1 sigma= 29 ka
mean= 35.5 ka
+1 sigma= 38 ka
Cumulative Frequency
Recurrence Time (ka)
0
0.1
0.2
0.3
0.4
0.5
0.6
0.7
0.8
0.9
1
20
25
30
35
40
45
50

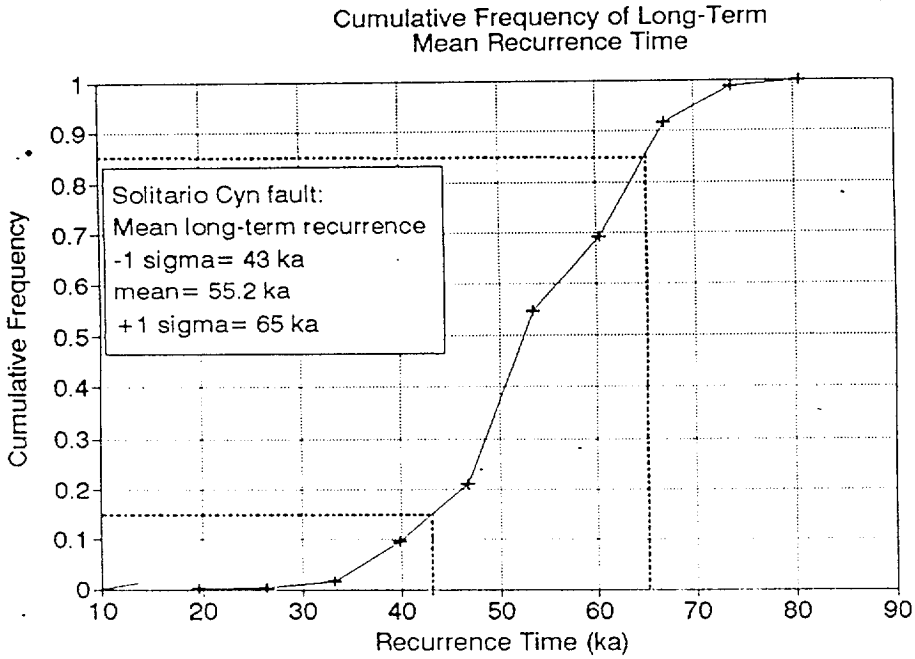
Cumulative Frequency of Long-Term
Mean Recurrence Time
Solitario Cyn fault:
Mean long-term recurrence
-1 sigma= 43 ka
mean= 55.2 ka
+1 sigma= 65 ka
Cumulative Frequency
Recurrence Time (ka)
0
0.1
0.2
0.3
0.4
0.5
0.6
0.7
0.8
0.9
1
10
20
30
40
50
60
70
80
90

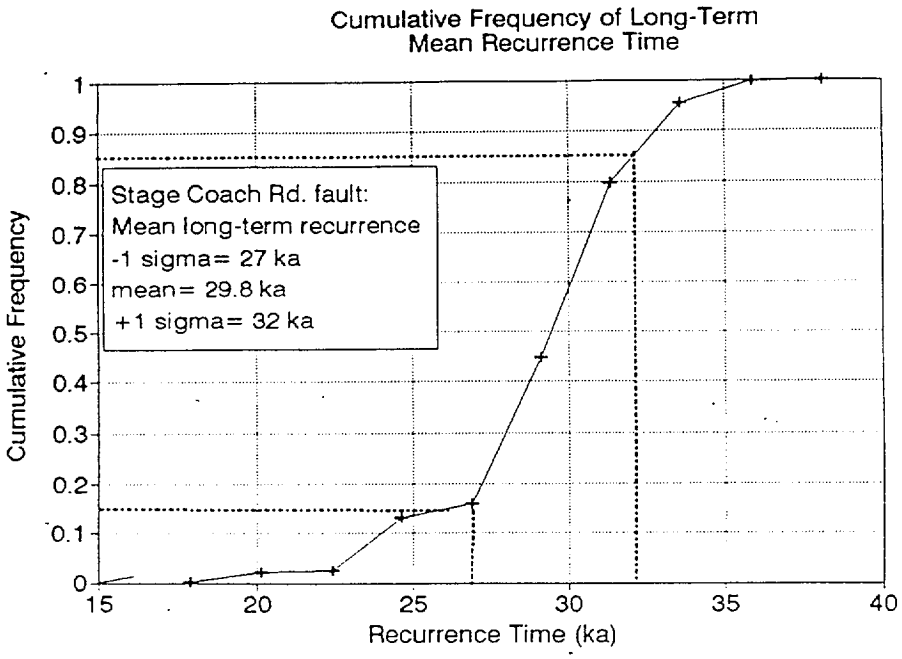
Cumulative Frequency of Long-Term
Mean Recurrence Time
Stage Coach Rd. fault:
Mean long-term recurrence
-1 sigma= 27 ka
mean= 29.8 ka
+1 sigma= 32 ka
Cumulative Frequency
Recurrence Time (ka)
0
0.1
0.2
0.3
0.4
0.5
0.6
0.7
0.8
0.9
1
15
20
25
30
35
40

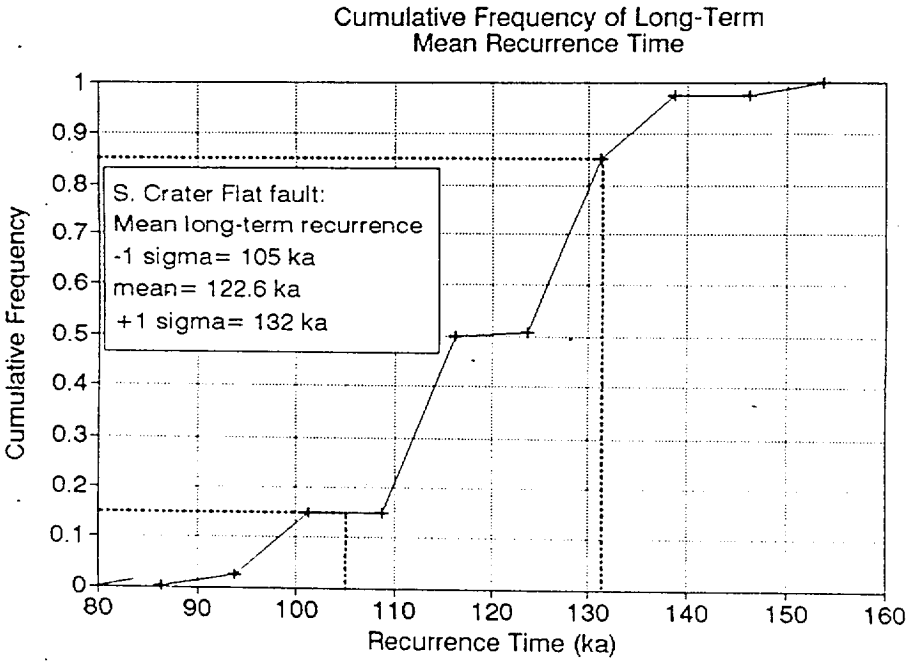
Cumulative Frequency of Long-Term
Mean Recurrence Time
S. Crater Flat fault:
Mean long-term recurrence
-1 sigma= 105 ka
mean= 122.6 ka
+1 sigma= 132 ka
Cumulative Frequency
Recurrence Time (ka)
0
0.1
0.2
0.3
0.4
0.5
0.6
0.7
0.8
0.9
1
80
90
100
110
120
130
140
150
160

ASM-A4-5

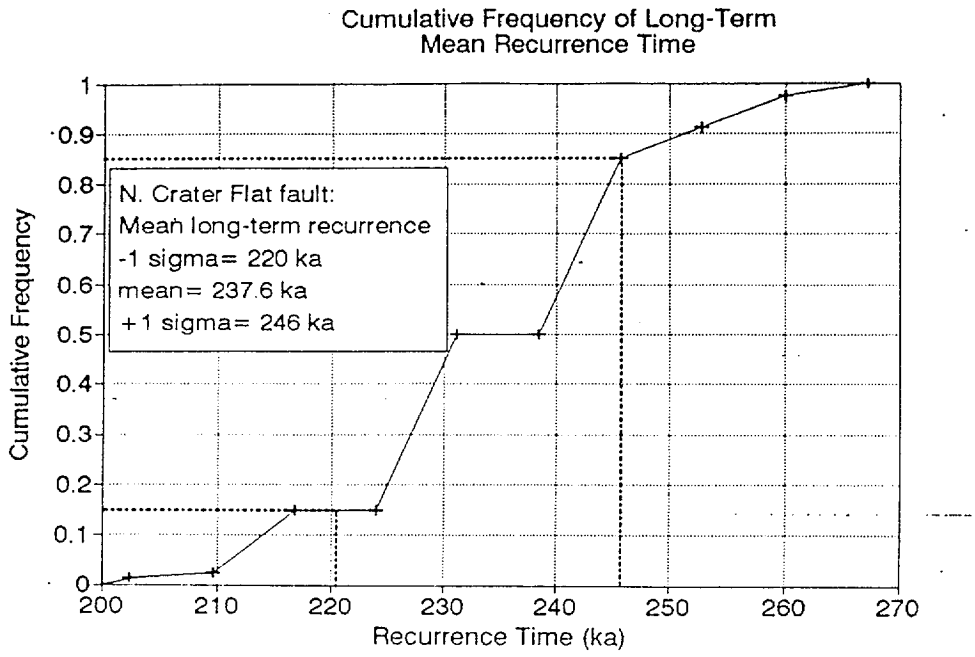
Cumulative Frequency of Long-Term
Mean Recurrence Time
N. Crater Flat fault:
Mean long-term recurrence
-1 sigma= 220 ka
mean= 237.6 ka
+1 sigma= 246 ka
Cumulative Frequency
Recurrence Time (ka)
0
0.1
0.2
0.3
0.4
0.5
0.6
0.7
0.8
0.9
1
200
210
220
230
240
250
260
270

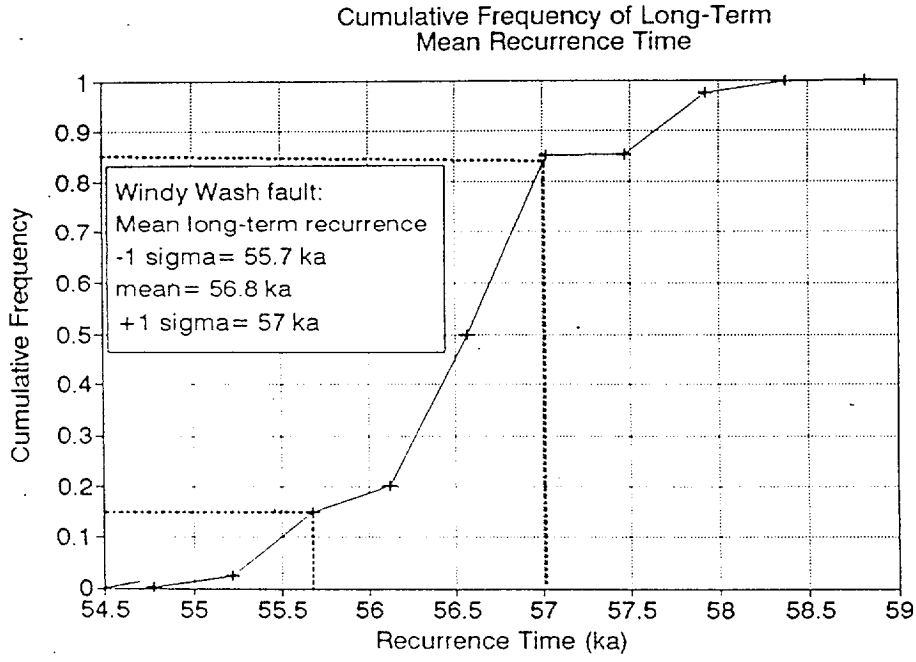
Cumulative Frequency of Long-Term
Mean Recurrence Time
Windy Wash fault:
Mean long-term recurrence
-1 sigma= 55.7 ka
mean= 56.8 ka
+1 sigma= 57 ka
Cumulative Frequency
Recurrence Time (ka)
0
0.1
0.2
0.3
0.4
0.5
0.6
0.7
0.8
0.9
1
54.5
55
55.5
56
56.5
57
57.5
58
58.5
59

APPENDIX ASM-5

Graphs showing cumulative frequency distributions of individual recurrence intervals for 10 local Yucca Mountain faults.

Note: these CDFs were created by scaling the normalized-grouped CDF of recurrence to the long-term mean recurrence interval of each fault, in the same manner as done for slip rates (Appendix ASM-2).

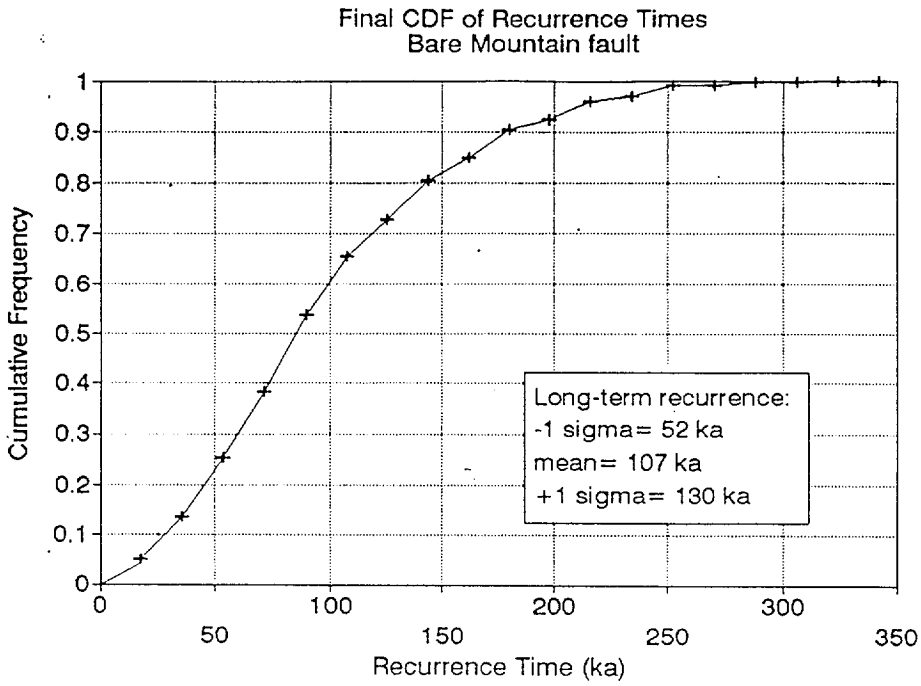
Final CDF of Recurrence Times
Bare Mountain fault
Cumulative Frequency
Recurrence Time (ka)
Long-term recurrence:
-1 sigma= 52 ka
mean= 107 ka
+1 sigma= 130 ka

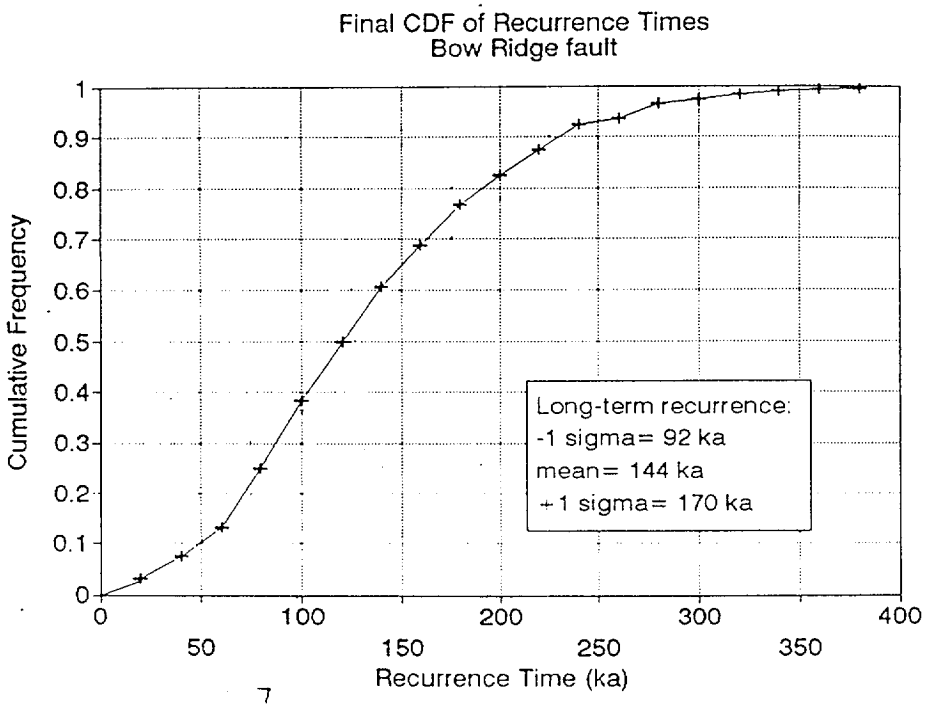
Final CDF of Recurrence Times
Bow Ridge fault
Cumulative Frequency
Recurrence Time (ka)
Long-term recurrence:
-1 sigma= 92 ka
mean= 144 ka
+1 sigma= 170 ka

ASM-AS-2

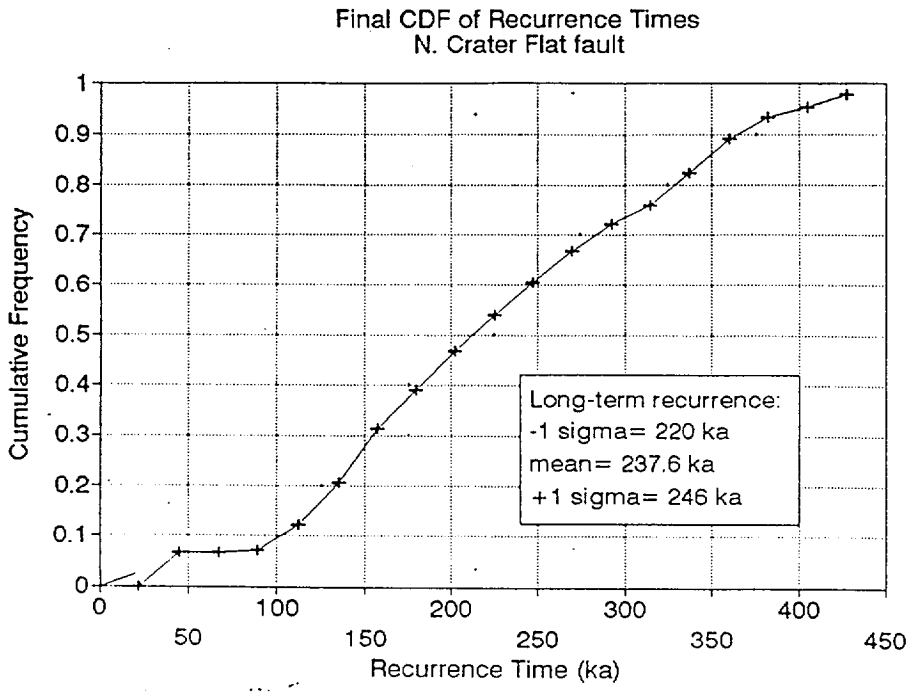
Final CDF of Recurrence Times
N. Crater Flat fault
Cumulative Frequency
Recurrence Time (ka)
Long-term recurrence:
-1 sigma= 220 ka
mean= 237.6 ka
+1 sigma= 246 ka

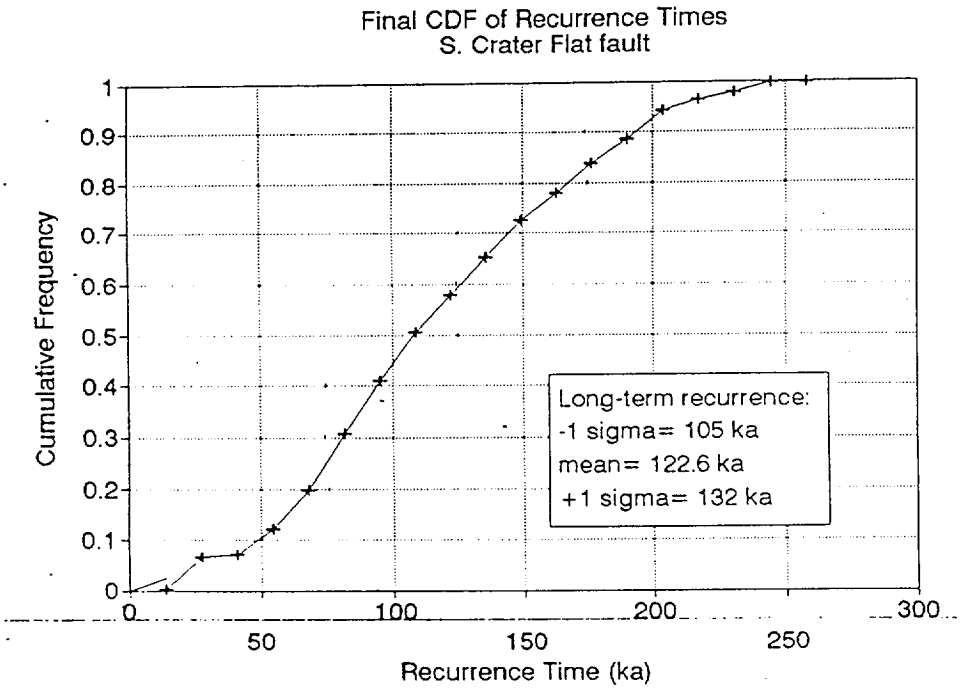
Final CDF of Recurrence Times
S. Crater Flat fault
Cumulative Frequency
Recurrence Time (ka)
Long-term recurrence:
-1 sigma= 105 ka
mean= 122.6 ka
+1 sigma= 132 ka

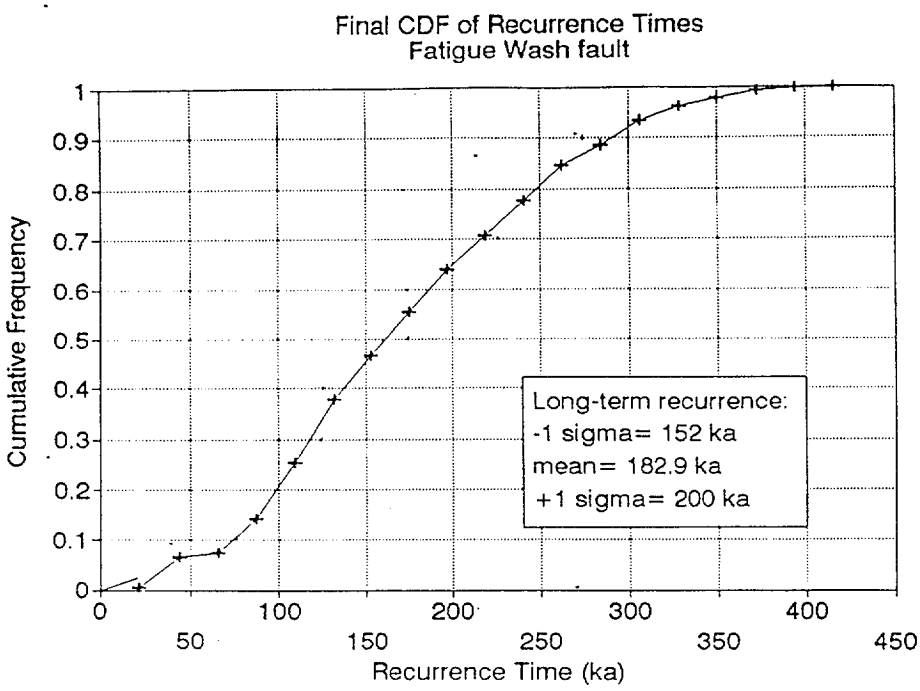
Final CDF of Recurrence Times
Fatigue Wash fault
Cumulative Frequency
Recurrence Time (ka)
Long-term recurrence:
-1 sigma= 152 ka
mean= 182.9 ka
+1 sigma= 200 ka

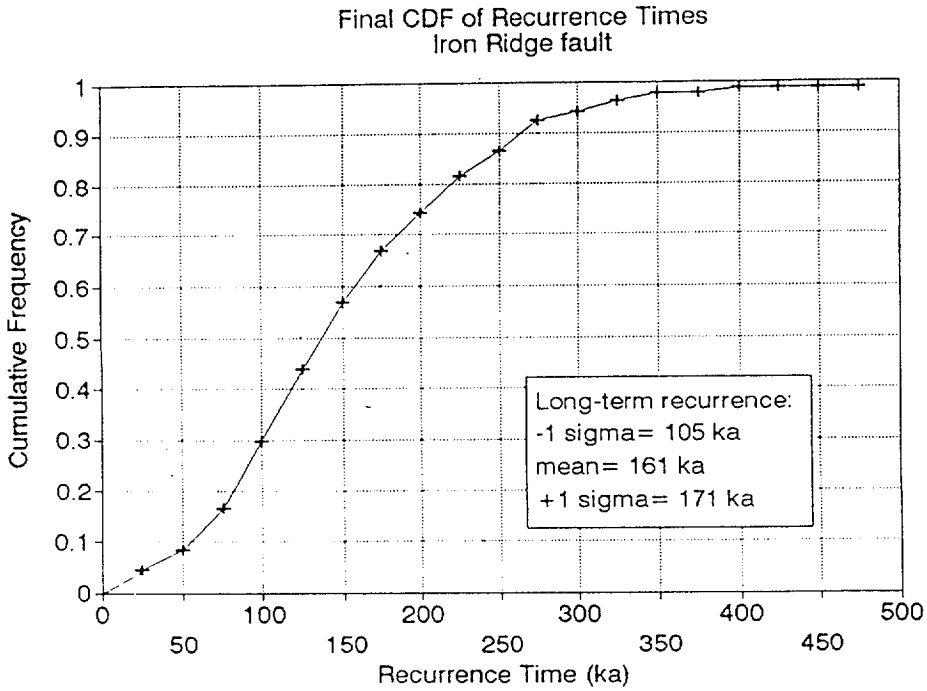
Final CDF of Recurrence Times
Iron Ridge fault
Cumulative Frequency
Recurrence Time (ka)
Long-term recurrence:
-1 sigma= 105 ka
mean= 161 ka
+1 sigma= 171 ka

ASM-AS-4

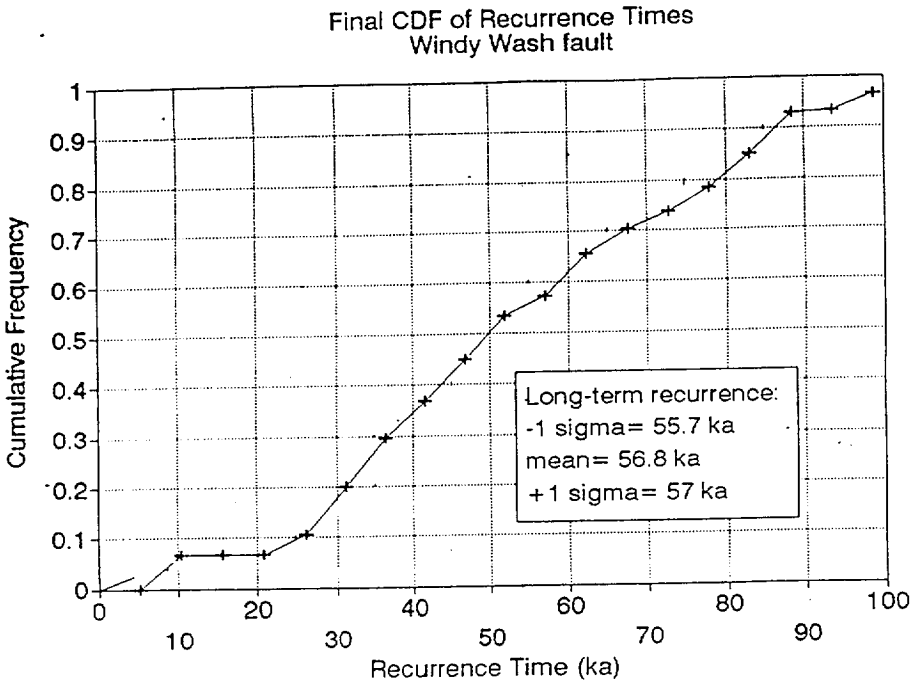
Final CDF of Recurrence Times
Windy Wash fault
Cumulative Frequency
Recurrence Time (ka)
Long-term recurrence:
-1 sigma= 55.7 ka
mean= 56.8 ka
+1 sigma= 57 ka

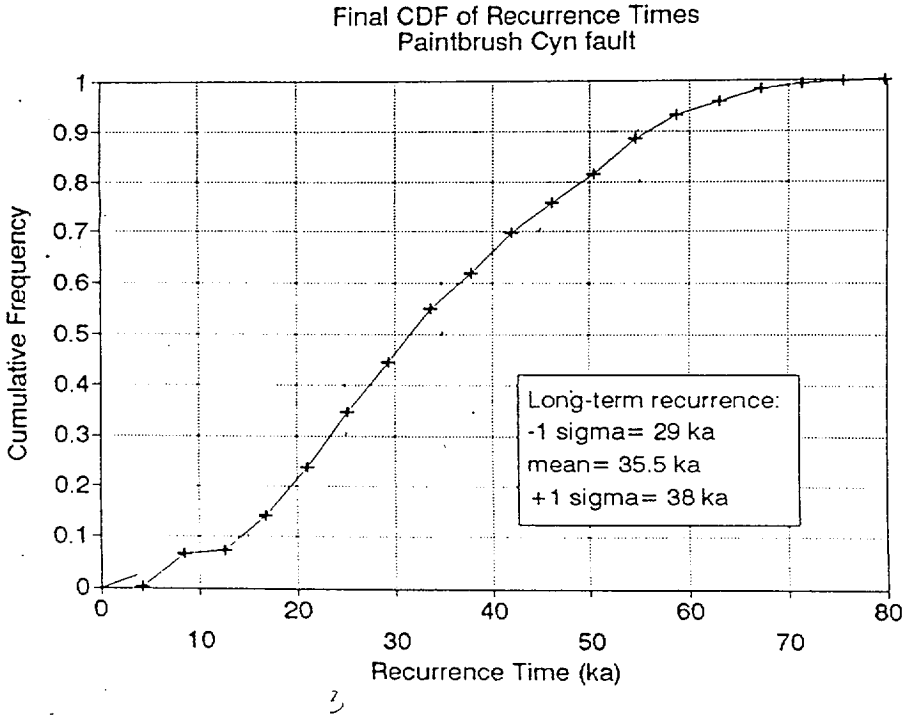
Final CDF of Recurrence Times
Paintbrush Cyn fault
Cumulative Frequency
Recurrence Time (ka)
Long-term recurrence:
-1 sigma= 29 ka
mean= 35.5 ka
+1 sigma= 38 ka

ASM-A5-5

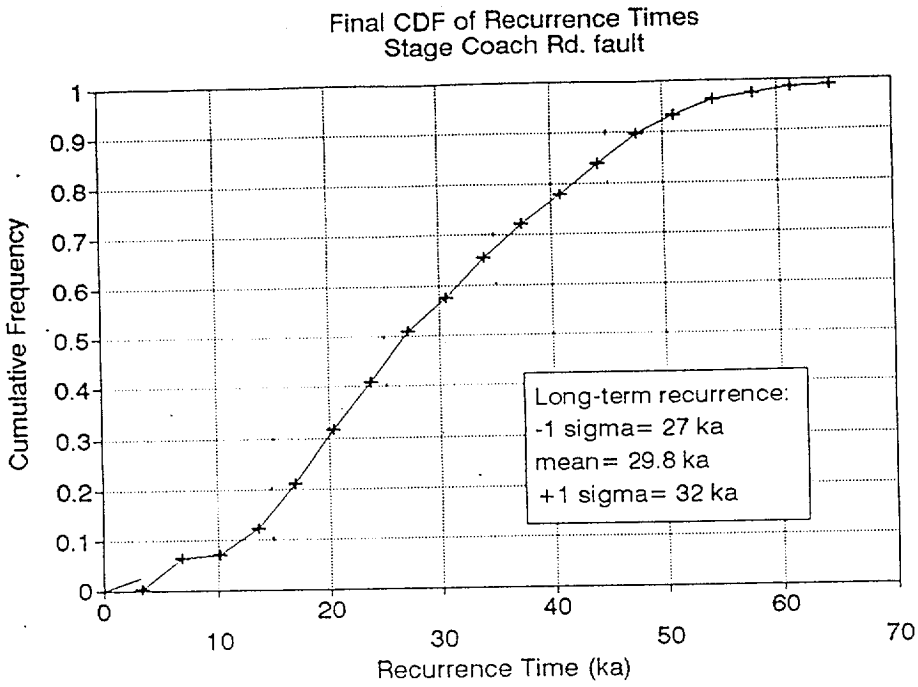
Final CDF of Recurrence Times
Stage Coach Rd. fault
Cumulative Frequency
Recurrence Time (ka)
Long-term recurrence:
-1 sigma= 27 ka
mean= 29.8 ka
+1 sigma= 32 ka

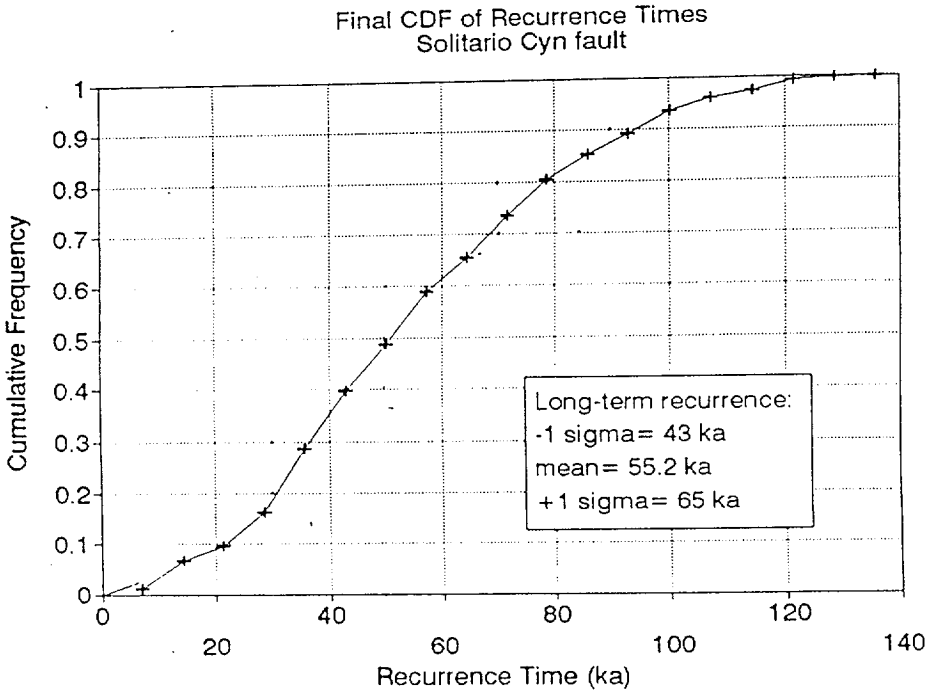
Final CDF of Recurrence Times
Solitario Cyn fault
Cumulative Frequency
Recurrence Time (ka)
Long-term recurrence:
-1 sigma= 43 ka
mean= 55.2 ka
+1 sigma= 65 ka

ASM - AS - 6

APPENDIX ASM-6
REGIONAL SEISMIC SOURCE CHARACTERIZATION

The following notes document decisions on the fault characteristics and probabilities for 24 faults listed in Table ASM-6, which summarizes the relevant regional earthquake sources for the Yucca Mountain region. The 15 faults having names shown in *italic font* have substantial field data, or correlate with faults that have substantial field data, for estimating slip rate (SR), recurrence interval (RI), and approximate surface rupture length (SRL). The 9 faults having names shown in normal font have sparse characterization data; for these we use the method described in Sections 3.5.3 and 3.5.4 to estimate SR from SRL and RI from the estimated age of the faulted geomorphic surfaces summarized in Piety (1995), Reheis (1992), Reheis and Noller (1991), and Dohrenwend *et al.* (1992a,b).

1. H95, Carrara, or U.S. 95. The Carrara fault (also referred to as the Highway 95 fault) is informally characterized. It is not referred to in the main documentation available to the team, but is described briefly in the letter of David B. Slemmons (DBS) to Richard Quittmeyer of February 3, 1997. This document lists geologic, geomorphologic, and geophysical features that indicate that it is a Quaternary fault, including the following.

   (1) W.D. Nichols' (1987) description of drill holes and geophysical surveys indicates Pleistocene fault deformation along an unnamed northwest structure.

   (2) Low-angle aerial reconnaissance by DBS showed many features that appeared to result from Quaternary faulting.

   (3) The horizontal gravity gradients shown at SSC Workshop 3 exhibit a linearity that appears to be fault-controlled.

   (4) The feature is within 2 km of the Lathrop Cone.

   (5) The feature may explain vertical axis rotation at the south end of Yucca Mountain, and Bullfrog Hills.

   (6) Gilmore's geodetic profile as summarized by Pezzopane (SSC Workshop 2) shows an anomalous segment of the Beatty-Las Vegas geodetic level line that coincides with the Carrara feature.

(7) Ken Smith (SSC Workshop 2) showed that it is aligned along a belt of higher seismicity.

(8) Brocher *et al.* (SSC Workshop 3) showed a seismic reflection profile, aeromagnetic map, and isostatic gravity map had a NW-trending fault at U.S. Highway 95.

(9) The M&O Geophysics Synthesis Report (1996) showed a prominent arcuate structure along the Carrara feature, which appears to curve into the Rock Valley structural zone near Skull Mountain.

(10) Fridrich and Price (1992) inferred this fault south of Bare Mountain and Yucca Mountain on the basis of geologic and geophysical data.

(11) Quade *et al.* (1995) and oral discussions with Quade indicate the Carrara/Highway 95 feature is at the 13,100 ^{14}C yr (and earlier Quaternary) diatomaceous spring deposits, which appear to be from deeply circulating groundwater that emerged at a Pleistocene groundwater barrier just west of the southward extension of the Crater Flat fault.

We assign a high probability (0.85) for the Carrara fault being seismogenic based on these factors. We assign a low probability (0.15) of the fault being non-seismogenic, since the fault has not been thoroughly characterized. The abrupt truncation of all of the seismogenic, NS-trending faults between the Bare Mountain fault and the southeast end of Yucca Mountain at the Carrara fault also suggests that it is an active Quaternary fault. Two total fault lengths (20 and 42 km) are considered with equal weight. The shorter length of 20 km represents the northwest part of the fault (from the Amargosa River to U.S. Highway 95 and the southward projection of Windy Wash fault) that exhibits greater geomorphic expression. Extension of the fault an additional 22 km to east of Lathrop Wells (Amargosa Valley) is less certain. A lower probability of 0.5 is assigned to the 42-km length, which extends the fault eastward from the 20-km section that has geomorphic expression. The 10-km-long extension at the south end of Yucca Mountain lacks documented geomorphic evidence of Quaternary activity, but is marked by the abrupt truncation of Yucca Mountain. The change to a more east-west trend east of the Windy Wash intersection could indicate a decrease in rate of activity. The additional 12-km extension east of Yucca Mountain is an assumed feature that is based on the geophysical map showing depth to bedrock. The Mwmax values depend on SRL and are:

Mwmax=6.94 (for SRL= 42 km), Mwpref=6.64 (SRL=20 km, with a high probability of 0.7), and Mwmin=6.24 (SRL=10 km, with a low probability of 0.2). Although there is a component of vertical slip, the Carrara fault is characterized as a strike-slip fault. The uplifted block has a relief of about 22 m at U.S. Ecology, where Jim Yount reports that the upper surface appears to have a late Pleistocene soil (128 ka), which corresponds to a vertical separation rate >0.1 mm/yr. The estimates for the horizontal component of SR of 0.013 (0.2), 0.05 (0.6), and 0.12 (0.2) mm/yr are from the Crater Flat subparallel extension rate used for our detachment model.

2. MM, Mine Mountain. This fault is characterized as a strike-slip fault. This fault is truncated by Yucca Lake fault (YCL) and possibly by a fault at the boundary with Jackass Flat. Mw=6.64 for SRL= 20 km (based on Plate 1 of Piety (1995). Based on the northern truncation by YCL and an inferred fault along the northern edge of Jackass Flat, a total fault length of 20 km is used. Two SRL values (10 and 20 km) are given equal weight. Reheis and Noller (Y-238) list the 3-km segment as "a weakly to moderately expressed lineament or scarp on surfaces of Quaternary deposits and as a topographic lineament along a range front or in bedrock." SR and RI are inferred from SRL and assumption of three pre-Holocene surface rupturing earthquakes.

3. WAH, Wahmonie. This fault is characterized as an oblique-slip fault. Mw=6.42 for SRL=14.5, based on Plates 1 and 2 in Piety (1995). Data primarily from Plate 1. Based on the truncation by the Cane Springs fault (CS), a single value of SRL (14.5) is used (weight 1.0). Reheis and Noller (1991) report "weakly expressed to prominent scarps and lineaments." Oral discussions with Jim Yount indicate late Pleistocene activity at the north end of the fault. SR and RI are inferred from SRL and assumption of three pre-Holocene surface rupturing earthquakes.

4. AM, Ash Meadow. This fault is characterized as a west-dipping normal fault. Mw=6.24, 6.91, and 6.94, respectively for SRLs=10, 38, and 40 km. This fault was at a shallow water table during Pleistocene, and the surface effects may be by partly plastic behavior. Revised on Figure 13 of Anderson *et al.* (1995b). Preferred length is 38 km from north end near Amargosa River (AR); scarp about 14 km SE of Nevada Highway 373 and Stateline, which Anderson *et al.* (1995b) notes may be a northern extension of West

Resting Spring Range (WRSR) fault. The fault has fair, but incomplete, characterization data. Although the original mapping of Donovan shows three segments, the displacement values tabulated in Anderson *et al.* (1995b) suggest that there is no segmentation. The average surface offset values from Table 5 of Anderson *et al.* (1995b) for the three fault segments are similar, which suggests that average displacement (AD) = 0.8 m; MS = 2 m; and for 35,000 years the average slip rate = 0.02 mm/yr. This corresponds to M = 6.91. The report of Anderson *et al.* includes a series of more active ruptures along the west side of Resting Springs Range, which could make the length too long, the slip rate too high, and recurrence interval too short for the entire zone. On the other hand, the late Quaternary surface fault shown by Anderson *et al.* (1995b) north of U.S. Highway 95 was verified by observations of DBS during a recent aerial flight, which is suggested by the surface scarp pattern. Their data do not clearly show whether there was one or more than one event.

5. RV, Rock Valley. This appears to be one of the most important strike-slip faults near Yucca Mountain. This fault appears to be truncated on the west end by the Amargosa River fault, and on the east end by the Buried Hills and/or Spotted Range faults, and to the southeast by distributed northeast-trending short faults. Data were derived from Piety (1995) and Chapter 4.13 of USGS (written communication,1996). The maximum earthquake is Mw=7.1+/-0.4 from Mw=6.69+0.74 MD, or Mw=7.23 from Mw=5.08 + log 72. Exploratory Studies Facility (ESF) dip is 70, 80, or 90 with left oblique. SRL is based on Plate 1 of Piety (1995); SR and RI are from Chapter 6.12 of USGS (written communication, 1996).

6. WSR, West Specter Range. This fault is characterized as a west-dipping normal fault. Based on shadows observed along this fault during low-sun-angle (LSA) aerial reconnaissance in early morning and late afternoon illumination, D.B. Slemmons (DBS) estimated that the maximum slope of the scarps in alluvium are approximately 15 to 18 degrees. Scarps with similar slopes normally indicate that the most recent displacement was early Holocene or late Pleistocene. The activity rates observed by Anderson *et al.* (1995b) appear to be correct, although DBS observations at Amargosa Flat indicate that there may be one or two Holocene to late Quaternary events. The fault probably is truncated by the Rock Valley fault and may cross the valley on the west side of West

Specter Range. No surface trace is visible toward the Last Chance Range fault. The fault appeared to connect northward with ESR (Anderson *et al.*, 1995b), and may extend northward to join or terminate against the Rock Valley fault zone for a maximum length of 25 km. DBS observed that the scarp extends south for a total length of about 18 km from north of Highway 95 to the south edge of Amargosa Flat. Several aerial observations with low-sun angle illumination did not show any offsets in active alluvial fans to the south toward Last Chance. DBS observed this zone several times with LSA, and observed a 15-km gap in late Quaternary faulting south of Amargosa Flat in bedrock and recent alluvium. There also is a possibility that it connects southward under young alluvium and bedrock units to the Last Chance Range fault discussed in Anderson *et al.* (1995a), to Y- 938, and to the North Pahrump fault zone at the northeast end of the Stewart Valley Playa. The ASM team did not characterize the Last Chance fault because it has a low rate of activity, is a short segment with a low rate of activity, and an interconnection to the West Specter Range fault would require faulting across a 20-km gap with no known Quaternary faulting. Anderson *et al.* (1995a) estimate a slip rate of 0.004 mm/yr and a recurrence interval of at least 113 ka, based on one event. Their descriptions suggest two events, which concurs with an observation of DBS for the scarp in Amargosa Flat. The observation of DBS of about 2 m of Holocene and late Quaternary offset led to higher SR estimates of 0.004, 0.01, and 0.02 mm/yr.

7. CS. Cane Springs. This fault is characterized as a strike-slip fault. Mw= 6.61 for SRL=21 and Mw=6.68 for 26 km based on interpretation of Plate 1 of Piety (1995). The fault appears to merge with three splays at the southwest end, and truncates against the curving end of Yucca Lake fault at the northeast end; accordingly, the length has a small uncertainty range. SR and RI are inferred from SRL and assumption of three pre-Holocene surface rupturing earthquakes.

8. AR, Amargosa River. This fault is characterized as a strike-slip fault. This fault has unresolved relations to other faults. Map revised from Fig. 8 of Anderson *et al.* (1995b) and Piety (1995), Mw=6.34 for SRL=12.4 km (Anderson *et al.*, 1995a), and Mw=6.70 for SRL=24.8 km (Anderson *et al.*, 1995a) and D.B. Slemmons field and LSA aerial observations of a late Quaternary fault scarp at location noted on map, and L=48 km from +north end of Y-238 to NE corner of Stewart Valley playa. DBS observations of two

other unmapped Quaternary scarps between the scarp noted above and Stewart playa. SR is poorly constrained from the small 1.1-m surface offset (Anderson *et al.*, 1995b) /12 to 128 ka, with preferred value at 0.05 mm/yr. The values, higher than those implied in Anderson *et al.* (1995b), are based on aerial reconnaissance. The RIs are estimated at >10 ka, 128 ka, and preferred value at a mid-value of 69 ka. Most of the fault zone is at or near the water-table level, and the surface deformation appears to be partly from warping. RI data are not available. The proposed maximum length of 48 km is from the northeast end of Stewart Valley playa to Y-238 on Plate 2 of Piety (1995) to the southeast of Big Dune, but a more likely scenario is segmentation into two segments. The latter possibility could include the activation of the northwest edge of Montgomery Range and springs including Devil's Hole. DBS has several LSA Ektachrome slides, and the 1:24,000 scale quadrangle map suggests that there are at least three active Quaternary faults in the 10- to 20-km gap between Stewart Valley and the south end of AR as suggested in Anderson *et al.* (1995b). However, the faults are distributed over a width of several kilometers, which appears to preclude a simple throughgoing fault. These short (2- to 3-km-long) oblique fault scarps are between the east edge of Stewart Valley, the Devil's Hole spring area, and the Grapevine Spring area. Their presence suggests that there is no gap between Amargosa River (AR) and Ash Meadow (AM) and N Pahrump-Stateline fault zones, and that the two zones may be connected by a complex, segmented zone.

9. YCL, Yucca Lake. This fault is characterized as a strike-slip fault. Mw=6.49 from SRL= 16.3 km based on extension to the south as mentioned in Piety (1995); Mw=6.63 from SRL=20.6 includes Y-238 (Plate 1, Piety, 1995) near CS. Comment in Piety (1995), "only youthful-appearing...fault." SR and RI are inferred from SRL and assumption of three pre-Holocene surface rupturing earthquakes.

10. ER, Eleana Range. This fault is characterized as an east-dipping normal fault. Length=10.6 and 12.7, based on Piety (1995, Plate 1). The database has ambiguous late to mid-Pleistocene dating and no displacement data. Piety (1995) reports that one unit with scarps is 160 to 800 ka, and one date suggests that the faulting is post-128 ka. SR and RI are inferred from SRL and assumption of three pre-Holocene surface rupturing earthquakes.

11. ESR, East Specter Range. This fault is characterized as an east-dipping normal fault. SRL=9 km (minimum) and 15 km (maximum) based on Plate 2 of Piety (1995). The length is defined by scattered scarps in alluvium and by the topography. Anderson *et al.* (1995a) and observations noted in the letter of DBS to Richard Quittmeyer of February 3, 1997, suggested similar characteristics to West Specter Range fault (WSR) when viewed with LSA. The appearance is similar, and the West Specter Range does not appear to be tilted from long-term paleoseismic activity, so parameters similar to WSR are used. SR and RI are inferred from SRL and assumption of three pre-Holocene surface rupturing earthquakes.

12. YC, Yucca. This fault is characterized as a strike-slip fault. Mw=6.66 and 6.83 for SRL=23 and 33 km, respectively. SR lengths are based on the estimated total length of distributed surface rupture. No significant measurements of displacement from multiple events is reported. Oblique slip is suggested by en echelon pattern. SR and RI are inferred from SRL and assumption of three pre-Holocene surface rupturing earthquakes.

13. WSM, West Spring Mountains. This fault is characterized as a west-dipping normal fault. Fault extends northward from Hidden Hills Ranch to scarp near Grapevine Springs, and probably to near U.S. Highway 95 at the northwest corner of Spring Mountains (LSA aerial reconnaissance and tilted Pliocene/Pleistocene surfaces). Slip rate and recurrence interval data are from Anderson *et al.* (1995a). The Wells and Coppersmith (1994) regressions suggest that the large displacements noted by Anderson *et al.* (1995a) are from multiple offsets of >2.2 m. Smaller offsets suggest an average for 17 measurements of SO of 1.33 m, or using AD/MD =0.38, the MD should be 3.5 m, and M=7.05. This is similar to M=7.09 for a rupture length from Grapevine Springs scarps to the PVFZ at Hidden Hills along a narrow and linear N17W eastern boundary of the 3- to 4-km-thick Pahrump Tertiary half-graben. Anderson *et al.* (1995b) estimate of AD=1.8-2.0 may be somewhat too high (40%). Anderson *et al.* (1995a) estimated the RI and SR at more than 28 ka to as much as 120 ka, and less than 0.02 mm/yr to as much as 0.07 mm/yr. They suggest that there were two, or possibly three, events.

14. FC, Furnace Creek. This fault is characterized as a strike-slip fault. Mw=7.49 (based on >120 km length and similarity to M=7.5 Owens Valley fault scarp of 1872). The south end is defined as the abrupt change in strike at the north end of EDV, and extends northward without apparent segmentation to the north end of the Fish Lake Valley fault (Piety [1995] and Reheis and Sawyer [1996]). FC had average displacements (ADs) of about 2.5 to 3.5 m per event along several fault strands. Table 5 of K. E. Klinger and L. A. Piety (USBR, written communication, 1996) indicates AD=4.5 m of strike-slip offset. Owens Valley is assumed to be an analogous event with M=7.5, Dmax=9+/-2 m, Davg=~4-5 m, slip rate ~2.0 m, 0.45+/- 0.75. The unpublished data of Strom and Nikonov and of Slemmons show the AD = 0.38, or approximately 0.4 x Dmax, which gives an AD of about 3.4 m for M=7.5. This is reasonably close to the 4.5 value estimated by R. E. Klinger and L. A. Piety (USBR, written communication, 1996). Accordingly, the values of R. E. Klinger and L. A. Piety (USBR, written communication, 1996) will be used. The slip rate is approximately two to four times higher than that of Owens Valley fault, and about two to three times higher than the 2.42+/-0.7 m in Panamint Valley.

15. EDV, East Death Valley. This fault is characterized as a west-dipping normal fault. Mw=7.21 (based on L=75 km, scaled from maps of Brogan *et al.* [1991]). The maximum net displacement (5.0 m at mileage 38.1 of Table A1 in R. E. Klinger and L. A. Piety, USBR, written communication, 1996) corresponds to Mw=7.21, using the regression of Wells and Coppersmith (1994). These values are consistent with the somewhat higher magnitude 1872 Owens Valley earthquake of Mw=7.5, which had a length of 100 to 108 km and MD=9.1 ± 2 m (Beanland and Clark [1994]). The north end of the fault zone is shown on Plate 2 of Piety (1995) as an abrupt strike change of Holocene scarps at California Highway 190 near Salt Springs in the middle of Section 21 of T28E, R1E. The south end is truncated by the Southern Death Valley (SDV) fault system at Shoreline Butte. The vertical component for surface fault slip rate and RI data are based on R. E. Klinger and L. A. Piety (USBR, written communication, 1996). Klinger and Piety, Tables 4 and 5, indicate a mainly vertical separation of 3 to 5 mm/yr, which should be increased by 15.5% for a 60-degree dip for use of the Wells and Coppersmith (1994) regressions. The Tertiary extension direction is about N60W in a N12S-trending Death Valley graben, as suggested by striae on fault surfaces in the bedrock (oral

communication by Martin Miller, University of Wisonsin-Eau Claire). Only a few strike-slip offsets are shown in Figure 5 of R. E. Klinger and L. A. Piety (USBR, written communication, 1996); their report did not include deformation at Cinder Hill. Accordingly, our analysis characterizes the EDV as a normal fault that is assumed to dip 60 degrees westward, and places the strike-slip component to a subparallel outboard fault, the inferred MDV, which is assumed to be a vertical strike-slip fault about 3 to 5 km west of EDV. A vector analysis of EDV of N12W orientation, and a vertical slip rate of 4 mm/yr for N50W extension (parallel to the FC and SDV right-slip faults), would be 4.62 mm/yr net normal-slip component on a frontal fault dipping 60 degrees. The dip-slip component for a normal fault dipping 60 degrees (EDV) would have net components 3.46, 4.62, and 5.77 mm/yr, for vertical separation rates of 3, 4, and 5 mm/yr, respectively. The AD (average displacement) from R. E. Klinger and L. A. Piety (USBR, written communication, 1996) is 2.5 to 3.5 m; using a 1/0.38=2.63 multiplier suggests AD=3.0 m, MD=7.9 m, or from Wells and Coppersmith (1994), Mw=7.35.

16. BLR, Belted Range. This fault is characterized as a west-dipping normal fault. Mw=7.04 for SRLmax=49 km and Mw=6.61 for SRLmin=21 km as reported in Anderson *et al.* (1995a) and Piety (1995). The scarps that Anderson *et al.* (1995a) studied are in the middle segment of BLR (Piety, 1995) opposite the highest part of the range; they did not evaluate the activity rates of the other parts of the fault. Anderson *et al.* (Table 3, 1995a) infer an AD=0.675 m based on profiles of single-event scarps at four data points; this corresponds to MD=1.8, which is close to the 1.5 m observed value. Multiple-event scarps average 2.7 m in height, which suggests four events in 118 ka. Displacements are as great as 2.5 m; they estimated SR of 0.01-0.1 mm/yr on a fault with a long-term SR of about 0.05 since 12.5 to 11.5 Ma. Examination of the data in Figures 7 and 8 (Anderson *et al.*, 1995a) indicates steep scarp slopes of 11 to 19 degrees, which suggests that for all but one profile, there were two, three, or four faulting events, with MD= 1 to 2 m and Mw=6.6-6.9 during the last 128 ka. Anderson *et al.* (1995a) report that the RI is poorly constrained. They suggest that it is greater than 10 ka, but with multiple events in less than 100 ka, perhaps much less than 100 ka. Based on multiple events (2 to 4) during the past approximately 128 ka, a range of RI (20 to 69 kyr) is used in this analysis.

17. MDV, Mid Death Valley. This fault is characterized as a strike-slip fault. The fault length is assumed to be 72 km from near Cinder Hill to an intersection with the southern segment of the Furnace Creek fault zone (DBS): Mmax=7.23 (based on L=72 km, and the regression for all fault types of Wells and Coppersmith, 1994). A mid-valley fault zone includes all of the strike-slip component of EDV as shown by vector diagrams from the striation direction shown in places along the frontal fault plane, the extension direction shown in bedrock by the Miocene and Pliocene extension in Black Mountains, and geometry of extension from the valley opening, which is subparallel to the N50W Furnace Creek and Southern Death Valley strike-slip faults. MDV is demonstrated geologically by the Cinder Hill right-lateral offset, which is variously reported to be 80 m and 100 to 200 m (as reported by Larry Anderson at Stop 5 in DOE/Participant Management Field Trip Guide Book, dated January 28-31, 1992). The earlier radiometric date of Cinder Hill is 680 ka, but a new radiometric date is reported to be 100 ka to no more than 200 ka. This suggests a geologic strike-slip rate at Cinder Hill that is about 0.15 to 2 mm/yr, with a preferred rate of about 1 mm/yr, which is the minimum value in Table ASM-6. At the north end of the EDV near Salt Creek, a strike-slip fault with associated folded Quaternary to Pliocene sediments was mapped by Lauren Wright and Bennie Troxel. Martin Miller (telephone conversation of 4/24/97) reports that the Miocene (~15 Ma) to Pliocene direction of extension for the basement rocks of Black Mountains was N60W. The slip vector diagrams indicate that the strike-slip component is about 40 percent of the rate observed for the frontal fault. The minimum slip rate is based on the ca. 1 mm/yr rate observed at Cinder Hill; the maximum rate of 3 mm/yr is based on a vector diagram for the N50W extension of the valley noted under discussion of the East Death Valley fault (EDV); and the preferred slip rate is the average of the minimum and maximum values.

18. GV, Grapevine. This fault is characterized as a strike-slip fault. Mw=6.72 for SRL=29 km, which is similar to the 23 km estimated by Reheis (1992). It appears to extend 8 km on Piety (1995), Plate 1, and 17 km on Plate 2 to a possible connection with FC, or a similar distance on strike to Y-239. The low uncertainty in length is the apparent connection at both ends to the more active Furnace Creek fault zone. Quaternary displacements are implied by topographic lineaments (subtle to prominent) on surfaces of

Quaternary deposits. SR and RI are inferred from SRL and assumption of three pre-Holocene surface rupturing earthquakes.

19. WDV, West Death Valley. This fault is characterized as an east-dipping normal fault. Mw=7.13 (based on L=62 km as mapped by Brogan *et al.* [1991] in Death Valley). The minimum and preferred SRLs of 25 and 39 km are based on the two shorter groupings. This zone appears to have a very low slip rate, demonstrated by tilted fans that appear to be middle to early Pleistocene (oral comments at SSC Workshop 5 by Charles D. Harrington) along the Panamint Mountains and that have a thin veneer of younger Quaternary alluvium. Brogan (telephone conversation) reported that the scarps are only a few meters high, and the longest continuous zone is only about 3 km long. SR and RI are inferred from SRL and assumption of three pre-Holocene surface rupturing earthquakes.

20. EM-TP, Emigrant/Towne Passe. This fault is characterized as a northwest-dipping normal fault. Mw=7.02 for the maximum SRL=47. These values are revised from Plate 2 and discussion in Piety (1995). The Stovepipe Wells fault is included with EM. One early Holocene to latest Pleistocene offset of about 1 m, observed in the field by USGS staff, is also suggested in an oblique aerial photo by D.B. Slemmons (DBS), which shows about 1 to 2 m offset of a large Pleistocene or Holocene alluvial cone at Tucki Mountain. The date of the most recent event appears to be >10 ka, approximately RI=19 ka for latest Pleistocene, or 69 ka for late Pleistocene. The fault is not relevant unless it is coupled with the Towne Pass fault, which is shown in the longest fault option.

21. PRP, North Pahrump-Stewart Valley. This fault is characterized as a strike-slip fault. Mw=6.94 (based on SRL=40 km): Piety (1995) map. The 40-km-long fault joins the south end of the Amargosa River fault (AR) or Ash Meadows fault (AM) and the north end of the South Pahrump-Stateline fault system (SPRP); the earthquake scenarios include possibilities of either a single 40-km rupture, or two segments with half that length. Our interpretation is based partly on the conclusions of J. L. Hoffard (University of Nevada, Reno, written communication, 1991) and observations by DBS during many low-sun-angle aerial reconnaissance flights over the area. Hoffard showed the North Pahrump fault extending into the Stewart Valley half-graben, and observations and photographs by DBS indicate a distributed pattern of at least three Quaternary faults

extending into Amargosa Valley. The irregularities of faulting between Stewart Valley and the Amargosa River fault suggest that they may be strongly segmented and can be considered separate sources. The assessment partly is based on the prevalence of surface warping along faults that cross areas of shallow water table and late Pleistocene activity at paleosprings. There are Holocene scarps and vegetation lineaments. The youngest scarp of early Holocene age is 5 m high (just south of Highway 52). Aerial examination with LSA shows discontinuous Holocene or late Pleistocene scarps in the valley, partly from concealment by the extensive sand dunes along the fault escarpment; deformed terraces (late Wisconsin?) and tilted spring deposits also are observed along the fault traces. The activity includes an early Holocene event and two or three events assumed since 128 ka. If the fault is primarily strike-slip or oblique-slip, as would be expected from this orientation, the horizontal component should be greater than the vertical. Louie *et al.* (in press) obtained geophysical data that suggest a lateral offset of 18 m at 24 m depth, having no more than 1 m of vertical offset. They estimate a horizontal slip rate of 0.1 mm/yr for 100 to 150 ka, and a possible higher 1.8 mm/yr rate if the offset is 10 ka old. We judge the latter rate as too high, but the relationships strongly indicate that the fault is a strike-slip fault, with a high ratio of 10:1 or 20:1 for strike-slip to vertical-slip component.

22. WPR, West Pintwater. This fault is characterized as a west-dipping normal fault. M=71 based on L=56 km (Piety, 1995). Piety (1995) reports that Reheis (1992) notes "weakly expressed to prominent lineaments and scarps on surface of Quaternary (primarily) and Tertiary deposits and as faults that are in Quaternary and Tertiary (primarily) deposits and that were identified from previous mapping." The source model assumes that the 56-km-long fault can be subdivided into three segments; there is equal likelihood of rupturing as one, two, or three segments; and rupture is equally likely to occur at any part of the zone. We have no displacement data. Fault may extend north from the tectonically active Las Vegas Valley at Indian Springs.

23. PAN-HM, Panamint Valley-Hunter Mountain. This fault is characterized as a strike-slip fault. PAN fault zone is truncated on the south end by the Garlock fault (which has SR of about 8 mm/yr) and continues north to the Hunter Mountain fault zone and Saline fault zone: Note the interconnection with Hunter Pass fault, which makes it a relevant source,

and frontal faults along the west side of Saline Valley. The seismic source parameters used in our model are based on Zhang *et al.* (1990), as summarized in Piety (1995).

24. SPRP, South Pahrump-Stateline. This fault is characterized as a strike-slip fault. Total fault length of ca. 65 km is from U.S. I-15 to Hidden Hills Ranch near the intersection of California Valley and Pahrump Valley. The north end connects with the south end of North Pahrump-Stateline and West Spring Mountains fault (WSM). The south end appears to terminate near U.S. I-15, since the adjoining Ivanpah fault does not appear to displace middle Pleistocene alluvial deposits. A full rupture length leads to Mw=7.18 and AD=1.127 m (based on MD determined from Wells and Coppersmith [1994] regression; MD, multiplied by 0.38, determines AD). The preferred RI=39 ka and SR=0.05 mm/yr, as the fault appears to be nearly linear and unsegmented. Aerial reconnaissance suggests that this section is less active than the North Pahrump/West Spring Mountains fault zones. However, the weak geomorphic expression may be due to mainly strike-slip offsets, and there may be two or more events in the past 128 ka. If the fault is primarily strike-slip or oblique-slip, as would be expected from this orientation, the horizontal component should be greater than the vertical. This fault was considered to have a low rate of activity in our first assessment, but the recent study by Louie *et al.* (in press) shows "almost purely strike-slip motion at scarp 1" near the Old Spanish Trail Highway, south of Hidden Hills Ranch. The weightings of one-third each include a high SR model, based on about 0.1 mm/yr (J. Louie *et al.*, University of Nevada, Reno, written communication, 1997), a 0.05 mm/yr rate that is intermediate, and a very low rate of 0.002 mm/yr.

APPENDIX E

SEISMIC SOURCE AND FAULT DISPLACEMENT EXPERT ELICITATION SUMMARIES

The following seismic source and fault displacement team expert interpretations have received review by PSHA Review Panel members in accordance with quality assurance approved PSHA Project Plan requirements but have not been reviewed for conformity with Department of the Interior, U.S. Geological Survey standards.

ELICITATION SUMMARY

WALTER J. ARABASZ, R. ERNEST ANDERSON, AND ALAN R. RAMELLI

TABLE OF CONTENTS

TABLE OF CONTENTS

TABLES

FIGURES

TABLE OF CONTENTS

ELICITATION SUMMARY
WALTER J. ARABASZ, R. ERNEST ANDERSON, AND ALAN R. RAMELLI

1.0
TECTONIC MODELS

No single tectonic model yet proposed can serve as a predictive template for seismic hazards assessments at Yucca Mountain. The region comprises several tectonic domains, each having distinctive (and, in most areas, complex) internal structure and contrasting bounding structures (D. W. O'Leary, USGS, written communication, 1996). In our evaluation of tectonic models, we accept that Yucca Mountain is located in a specific tectonic domain, to which we attach fundamental tectonic importance. Following D. W. O'Leary (USGS, written communication, 1996), we refer to it as the Crater Flat domain (CFD). Any viable tectonic model must explain the structural development of the CFD, especially its Quaternary structural history. It must also be consistent with contemporary regional tectonics, especially with those of the domains adjacent to the CFD.

Before determining the appropriate tectonic models, we evaluate the processes that control the contemporary tectonics of the CFD. In particular, we distinguish between pure shear and simple shear processes, evaluate whether magmatism should be considered a controlling process, and, similarly, whether regional detachment faulting is a controlling process. We recognize that fault-related tilting is pervasive in the CFD, and that in much of the domain the tilting is complicated by steep-axis rotation. These tilts and rotations are incompatible with pure (irrotational) shear, leaving simple (rotational) shear as the only option leading into the front end of our logic tree (Figure AAR-1).

We recognize that silicic magmatism, and especially caldera-forming processes, may have played an important role in the early development of the CFD. But we conclude that contemporary deformation in the CFD is not controlled by caldera-forming magmatic processes, because there is no evidence that events related to such processes continued into the latest Tertiary and Quaternary. Because there is evidence for both Quaternary basaltic

volcanism in the CFD and a temporal association of faulting and volcanism, we recognize that future earthquakes could be associated with basaltic volcanic processes. In a separate section, we assess that likelihood. Based on the estimated low frequency of basaltic volcanic events and the relatively low magnitude of earthquakes typically associated with basaltic volcanism, we do not include in our logic tree a tectonic model controlled by basaltic volcanic processes.

A separate but related question concerns the percentage of extension across the CFD that might be accommodated by volcanic intrusion. Basaltic intrusions occurring as dike injections, rather than rising along vertical pipes, should accommodate some extension and reduce the occurrence of earthquakes (cf., Parsons and Thompson, 1991). Estimates of Quaternary extension across the CFD come from evidence of surface faulting, so the question is whether surface faulting is caused by extensional stresses induced by intruding dikes (if not, then any extension accommodated by volcanism would occur in addition to that accommodated by earthquakes). Paleoseismic data for the Yucca Mountain faults typically span time frames of hundreds of thousands of years. Over these periods, most faults show evidence of several earthquake cycles (recurrence intervals for the principal faults average about 50 ka). The only evidence of volcanism over this same time span is the Lathrop Wells basalt cone, which formed within a relatively narrow time window (possibly primarily during a single eruptive episode). We do not consider accommodation of extension by volcanism for two reasons: (1) surface faulting occurs much more frequently than volcanism; and (2) surface faulting occurs over a widespread area, with little direct spatial association with the Lathrop Wells cone. If basaltic intrusions that did not reach the surface occurred much more frequently and over a broader area than suggested by the Lathrop Wells cone, this interpretation could bear revision.

We conclude that contemporary deformation in the CFD is not controlled by a regional detachment fault of the type envisioned by Scott (1990) because: (1) extensive geologic mapping of Miocene and pre-Miocene rocks has failed to reveal it; (2) there is no evidence that Miocene volcanic features or cells of Miocene hydrothermal activity have been shifted laterally from their roots; and (3) no detachment-related breakaway zone and tectonically denuded footwall have been identified in areas east of the domain. Also, we do not consider a tectonic model controlled by a deep (12 to 15 km) detachment fault because extensive

geologic evidence (geobarometry on mylonitic rocks) indicates that yielding in subhorizontal high-strain zones at those depths is accommodated by crystal-plastic recrystallization processes. In such cases, seismicity is considered to be generated only from the higher-angle faults feeding into the ductile accommodation zone.

We consider deformation in the CFD to be controlled by a stress field created by superposed stresses of uncertain relative influence, chiefly: (1) WNW-ESE Basin and Range extension, along with possible combinations of (2) NW-SE dextral shear related to Pacific-North American relative plate motion and (3) general N basal traction and/or horizontal compression related to southerly mass movement from an elevated northern Great Basin lithosphere. We conclude that all viable tectonic models for the CFD must include an element of extension.

1.1 DEXTRAL SHEAR STRUCTURES

The first node of our logic tree (Figure AAR-1) addresses whether a NW-SE dextral shear influence is manifested by significant unrecognized or poorly characterized dextral shear structure(s). The branch for "no significant NW-SE dextral shear structure(s)" does not preclude an influence by regional dextral shear. The branch simply indicates that if there is such an influence, it is not manifested by right-slip faults of a size that would produce earthquakes having maximum magnitudes greater than that of our background source zone. We weight the two possibilities equally because the issue is unresolved. Hypothesized dextral shear structures are plausible (in particular, a fault paralleling Highway 95, as proposed by Slemmons, or a cross-basin fault as supported in a presentation by Pezzopane), but (1) their existence has not been established, and (2) they are not characterized sufficiently to conclude that they are potential sources of strong ground motion above a background source.

The nature of plausible NW-SE dextral shear structure(s) is treated at the second node of our logic tree. Here three branches consider the possibility of unrecognized or poorly characterized sources in addition to the CFD faults: a throughgoing regional dextral shear zone, a right-stepping shear zone that produces a pull-apart basin, and a right-stepping shear zone in which the pull-apart basin is underlain by a cross-basin, right-slip fault. We assign

the greatest weight to a pull-apart basin containing one or more bounding dextral faults, because the Highway 95 fault is the only proposed dextral shear structure for which evidence has been described (Slemmons, information distributed to SSC teams by R. Quittmeyer dated 3/4/97). We assign less weight to the existence of a cross-basin fault; such a structure could explain the structural discontinuity of CFD faults, but its existence is based on indirect evidence. We assign a very low weight to the existence of a throughgoing regional shear zone because no direct evidence for such a feature exists and we know of no analogs.

In the absence of significant dextral shear structures, the CFD faults accommodate extension independently, but such accommodation can be accompanied by both dextral shear and southerly directed tectonic displacement. The evidence for such accompanying deformation comes from the earthquake record (Rogers *et al.*, 1991) and the geologic record of strike-slip faulting and steep-axis bending (Fridrich *et al.*, SSC Workshop 3, handout dated 11/1/1996). This model has as its analog the Gale Hills north of Lake Mead, where N- to NE-striking, left-normal faults and the blocks bounded by them bend clockwise as they are traced southward toward the adjacent right-slip Las Vegas Valley shear zone (Sonder *et al.*, 1994). Rather than having formed by drag associated with dextral shear, the faulting and bending are best interpreted as resulting from south-directed tectonic collapse and to have involved distributed basal traction (Anderson *et al.*, 1996).

1.2 LOCAL DETACHMENT

The third node of our logic tree (Figure AAR-1) addresses the existence of a local detachment and outlines credible models in which a local detachment is conditionally favored or permissible. In no case is a detachment fault considered to be a controlling structural element. As interpreted by us, a local detachment fault could be a reactivated thrust or a gently dipping accommodation zone.

The depth of a local detachment is addressed at the fourth node of the logic tree where, conditional on its existence, we consider the probability that the detachment lies at a depth < 3 km, 3 to 10 km, or > 10 km. Based on the geophysical data, we preclude a depth less than 3 km. We give greatest credibility to the 3- to 10-km depth range, because narrow fault blocks such as the 3- to 5-km-wide major blocks of the CFD are more likely to maintain their

structural integrity to depths 1 to 2 times their width than to 3 to 4 times their width. Our assigned distribution for the depth (and relative weighting) of a detachment in the 3- to 10-km depth range is:

4.5 km (0.185), 7.0 km (0.63), 9.0 km (0.185).

Throughout, when we assess a three-point distribution, we follow Keefer and Bodily (1983) in assigning relative weights. Following their guidance for three-point distributions, we consistently attempt to estimate the median (i.e., 50th percentile value) together with either the 5th and 95th percentile values or the 10th and 90th percentile values. The appropriate weights then are 0.185, 0.63, and 0.185 to approximate the 5th, 50th, and 95th percentile values, respectively, and 0.3, 0.4, and 0.3 for 10th, 50th, and 90th percentile values. Thus, our use of these combinations of weights in any three-point distribution implicitly indicates the estimated percentiles to which the weighted values correspond.

If the detachment is deeper than 10 km, we consider its depth to have a uniform probability of being anywhere between 10 km and the maximum depth of the seismogenic crust (discussed in the next section).

We conclude that a local detachment, if it exists, has a low-likelihood of being seismogenic, because the data provide no evidence for earthquakes on such faults in the Basin and Range. Accepting the agreed use of this term in this PSHA project, "seismogenic" is defined as capable of generating earthquakes significant to ground motions ($M \geq 5$). For convenience, we use the notation P[S] for "Probability [Seismogenic]." For a local detachment fault, we attach a low probability, P[S] = 0.05, to such a fault being seismogenic.

We concluded that any local detachment beneath the CFD would not be active over the entire domain. It would, for example, be constrained in extent by the downdip projection of the Bare Mountain fault on the west and the downdip projection of the Paintbrush Canyon fault on the east. Our evaluation is the following: In the unlikely case that a local detachment were seismogenic, we account sufficiently for its rare earthquake by our local background source zone, which has a maximum magnitude of 6.3 ± 0.3. This range would encompass seismic slip on a detachment having a maximum rupture of 200 km^2 and a larger than normal

average displacement of 1 m. Accordingly, we do not include a local detachment in our inventory of seismic source zones.

2.0
DEPTH OF THE SEISMOGENIC CRUST

In assessing the maximum depth of the seismogenic crust, we distinguish between (1) the maximum thickness of the seismogenic layer as a control on downdip width (and hence area) of rupture, particularly for use with regressions of Wells and Coppersmith (1994), and (2) the maximum depth to which seismic rupture (and seismic energy release) may physically reach during larger earthquakes. The latter depth becomes important in estimating rupture area, RA, for use in the moment equation, $M_0 = : * RA * ®$ (see, for example, Youngs and Coppersmith, 1985, equation 2), where : is the rigidity or shear modulus (assigned the value 3×10^{11} dyne cm^{-2}), and ® is the average (subsurface) displacement over the slip surface.

Our assessed distribution for the maximum thickness (and relative weighting) of the seismogenic layer, called DMAX1, in the Yucca Mountain region is:

11 km (0.185), 15 km (0.63), 17 km (0.185).

We base our assessment of DMAX1 on the depth distribution of seismicity in the southern Great Basin (K.D. Smith presentation at SSC Workshop 2), the aftershock sequence of the 1992 Little Skull Mountain earthquake (Harmsen, 1994), and a review of how Wells and Coppersmith (1994) measured downdip rupture width, including values for the largest historical normal-faulting earthquakes in the Western United States.

Taking into account the tectonophysics of rupture dynamics (e.g., Yeats *et al.*, 1997, p. 49ff, and references therein) and observational studies of the coseismic slip distribution for the Borah Peak and Landers earthquakes (Mendoza and Hartzell, 1988; Wald and Heaton, 1994; Cohee and Beroza, 1994), we assess a separate distribution, called DMAX2, for the maximum depth of seismic rupture during some larger earthquakes in the Yucca Mountain region. The depths and their relative weights are:

14 km (0.185), 18 km (0.63), 22 km (0.185).

Simply put, the rupture surfaces of large earthquakes can "reach down" below the seismogenic layer into the brittle-plastic transition zone, resulting in greater rupture width (and area). We interpret descriptions of this phenomenon as implying that seismic moment (and high-frequency seismic radiation) is released from the part of the rupture surface that extends into the transition zone. There, material that behaves plastically at low strain rates fails in a brittle mode at the high strain rates that accompany the dynamic rupture of a large earthquake.

We apply DMAX2 in cases where the expected rupture length is 25 km or greater (discussed presently) and where we also intend to estimate maximum magnitude through rupture area, RA, by using only the moment equation. In our evaluation, there is an important distinction between an estimate of RA for use in the moment equation and one for use in the regression equation of Wells and Coppersmith (1994). In the first case, RA can appropriately be estimated by the product of rupture length and downdip width, constrained by DMAX1 or DMAX2. In the second case, however, Wells and Coppersmith (1994) based the use of RA as an estimator of moment magnitude primarily on the spatial extent of aftershock hypocenters, inherently reflecting the thickness of the seismogenic layer. Thus, when applying their regression equation for moment magnitude using RA, we use DMAX1 as the depth constraint on area, regardless of rupture length.

Our consideration of a buried regional strike-slip fault beneath the CFD was an important factor leading to our evaluation of DMAX2. We chose a rupture length of 25 km as the threshold for applying DMAX2 based on (1) the 26.5-km surface rupture length of the 1959 Hebgen Lake normal-faulting earthquake (M_W = 7.3) (Wells and Coppersmith, 1994), and (2) our reasoning that candidate ruptures for penetrating deeper than 15 km would have an aspect ratio of length to width that exceeded 1.5, whether for a vertical strike-slip fault or a 60°-dipping normal fault. Coincidentally, 25 km corresponds to a low point in our density distribution of expected rupture lengths for local fault sources. Ultimately, DMAX2 is applied to only two local fault sources, each of them a major dextral shear structure (the buried regional strike-slip fault and the Highway 95 fault, discussed in a later section).

3.0
REGIONAL FAULT SOURCES

The surface traces of 19 regional faults having known or suspected histories of Quaternary surface displacement, and trace lengths great enough to classify them as relevant to ground motion considerations at Yucca Mountain, are shown on Figure AAR-2. Fault acronyms correspond to those used by S. K. Pezzopane (USGS, written communication, 1996). With the exception of the West Specter Range fault, map traces are generalized from Piety (1996). The trace of the West Specter Range fault is generalized from Anderson *et al.* (1995a). Also, the southeast limit of the Pahrump fault is extended about 43 km beyond that shown by Piety (1996).

3.1 TABULATED PARAMETERS

Parameters for the seismic source characterization of each regional fault source are given in Table AAR-1. Note that the table includes parameters for two linked regional faults, the Death Valley-Furnace Creek and the Amargosa River-Pahrump. On the basis of a highly preferred rhombochasm tectonic model for Death Valley, where these faults are intimately related, we assign a probability of 0.8 to the linked configuration of the Death Valley-Furnace Creek faults versus 0.2 that they behave independently. For the Amargosa River-Pahrump faults, the probabilities are 0.1 for the linked configuration and 0.9 for independent behavior. This low probability of linkage for the AR/PSV faults is based on a lack of evidence for Quaternary faulting in the 15- to 20-km-long gap between Stewart Valley and the Amargosa Desert (Anderson *et al.*, 1995b).

Where three values for any parameter are entered in Table AAR-1, these indicate estimates corresponding to 10th, 50th, and 90th percentile values, with appropriate weights of 0.3, 0.4, and 0.3, respectively. Further explanation of the table follows.

Total Fault Length

Tabulated values for minimum, preferred, and maximum total fault length (TFL) are scaled from trace lengths on Figure AAR-2. Values for minimum, preferred, and maximum maximum rupture length (MRL) for 14 of the regional faults are the same as the values for

TFL. For the remaining five faults, the Rock Valley, West Spring Mountains, Belted Range, Kawich Range, and Pahrump faults, the MRLs are less than the TFLs because the faults are considered segmented. Because little or no paleoseismologic data pertaining to segmented behavior exist, we assume that the maximum rupture length can occupy any portion of the total fault length.

The MRL on the linked Death Valley-Furnace Creek fault is less by about 30 km than the combined TFLs of those two faults because the two faults overlap. If these two faults rupture together, the rupture would likely bypass the southeastern part of the Furnace Creek fault which extends beyond the Death Valley fault. If the overlap area did rupture, we interpret that displacements would be relatively minor and would not significantly contribute to the size of the event. Also, in the Last Chance Canyon area between the Fish Lake Valley fault and the Furnace Creek fault, there is little evidence of Quaternary faulting (R. E. Klinger and L. A. Piety, USBR, written communication, 1996) despite the high rates of activity along the major faults that lead away from that area. We interpret this relatively inactive zone as a persistent segment boundary and do not link the Fish Lake Valley fault with the Furnace Creek fault.

Minimum Distance to Repository

Tabulated values were taken from S.K. Pezzopane (USGS, written communication, 1996) or measured from Figure AAR-2.

Documented Quaternary Displacement

Quaternary displacement is documented for 14 of the 19 regional faults (indicated by y). Our decision to include some faults that lack documented Quaternary displacement (indicated by y?) is based on various criteria and reasoning. The Mine Mountain and Cane Spring faults are included because they form part of a northeast-trending zone of coherent, active deformation that includes: (1) the Rock Valley fault, which has the highest slip rate of any fault located closer to Yucca Mountain than 50 km (the distance to the Death Valley/Furnace Creek fault system); and (2) the epicenter of the Little Skull Mountain earthquake. The Keane Wonder fault is included because it is a range-bounding structure at the east margin of the highly active Death Valley region (R. E. Klinger and L. A. Piety, USBR, written communication, 1996). The Yucca Lake fault is included because it appears to form the

northeast margin of the potentially active Mine Mountain-Wahmoni-Cane Spring fault group. The Oasis Valley fault is included because it is the only fault Anderson *et al.* (1995a) studied within the relatively stable Goldfield sector of the Walker Lane, for which they equivocated about Quaternary displacement over a significant length of trace.

Style of Faulting

N = normal, L = left lateral, R = right lateral, O = oblique.

Fault Dip

There are no specific subsurface data (such as from mines, drill holes, or aftershock distributions) to constrain the overall dip of any of the regional faults. Minimum, maximum, and preferred dip values are assigned mainly on the basis of known or inferred fault slip characteristics with steep dips assigned to strike-slip faults, and moderate dips to dip-slip faults. For example, preferred dips of 90 degrees are assigned to the Rock Valley, Cane Springs, Amargosa, Pahrump, and Furnace Creek strike-slip faults whereas all of the major range-front normal faults are assigned preferred dips of 65 degrees. Maximum and minimum values are assigned on the basis of reasonable ranges of overall dip of faults typical of each slip-sense category.

Slip Rate and Recurrence Data

Published slip rate and recurrence data are available for only two of the nineteen regional faults: the Death Valley and Furnace Creek faults (R. E. Klinger and L. A. Piety, USBR, written communication, 1996). These parameters were estimated for the Rock Valley fault from data in Piety (1996) augmented by more recent thermoluminescence ages (Shannon Mahan, USGS, written communication, 2/20/97). For the west Spring Mountains fault, the parameters are estimated by assuming that events equivalent in displacement to the estimated displacement of the most recent surface faulting event were responsible for forming the largest scarp and by estimating an age range for alluvium on which the largest scarp is formed (Anderson *et al.*, 1995a). For the other regional faults, slip rates are estimated, but recurrence intervals are not.

Some estimates of slip rate are based on geomorphic data (primarily scarp-profile data) combined with an estimate of the age of the surficial deposits or alluvial surfaces that are

offset by the fault. An example is the Belted Range fault. Other slip rates are estimated by qualitative comparison of the fault orientation, location, fault-trace geomorphology, and tectonic setting to the faults in the region that have provided constraints on slip rate. For the Mine Mountain and Cane Spring faults, for example, maximum slip rates were taken to be α to 2, respectively, of the conspicuously more active Rock Valley fault. The Pahrump fault may have tectonic affinities with the strike-slip faults of the Death Valley system, but reconnaissance paleoseismic study shows that it is significantly less active than that system. It was assigned a maximum slip rate twice that of the relatively active Rock Valley fault because of its potential affinity to the Death Valley faults.

Probability of Being Seismogenic, P[S]

All the regional faults having documented Quaternary displacement are considered seismogenic, with P[S] = 1. These include the linked regional faults. For faults that lack documented Quaternary displacement, probabilities are assigned based on their orientation, tectonic setting, and relation to other seismogenic faults.

3.2 M_{max} APPROACH

For the regional fault sources, we use three approaches to estimate M_{max} in terms of moment magnitude M: (a) M estimated from surface rupture length SRL, using the relation from Wells and Coppersmith (1994) for all slip types; (b) M estimated from rupture area RA (SRL x downdip rupture width) using the relation from Wells and Coppersmith (1994) for all slip types; and (c) M estimated from SRL and slip rate S, using the relation from Anderson *et al.* (1996). We assign the following weights to the three approaches:

(a) (0.4), (b) (0.2), (c) (0.4).

Although M and RA are well correlated, we downweight approach (b) because the data Wells and Coppersmith (1994) used for RA were based on aftershock hypocenters; they are not a product of rupture length and width (see earlier section on "Depth of the Seismogenic Crust"). We also recognize the uncertainty in using SRL to estimate subsurface rupture length for calculating RA. Regarding approach (c), most of the preferred slip rates tabulated

for the regional faults in Table AAR-1 lie within the range of data regressed by Anderson *et al.* (1996), and the relation is straightforwardly applicable.

In Table AAR-1, total fault length is the length of the fault that is active, meaning the length along which seismic moment should be distributed given the slip-rate approach to recurrence (discussed below). The parameter used to estimate M_{max} is maximum rupture length (a measure of SRL), estimated in terms of minimum (mi), preferred (p), and maximum (m) values. When either the preferred or minimum value is selected for total fault length, weights for allowable maximum rupture length are renormalized.

3.3 RECURRENCE APPROACH

For the regional fault sources, we use two approaches for recurrence modeling: (1) a slip-rate approach and (2) a recurrence-interval approach. Weighting of these approaches is 0.6 and 0.4, respectively, for all the regional fault sources for which both slip-rate and recurrence-interval data are provided in Table AAR-1. Otherwise, the slip-rate approach is weighted fully.

Fault-specific recurrence relationships are generated from the slip rates using the methodology of Youngs and Coppersmith (1985) assuming constant moment rate. Whether using the slip-rate or recurrence-interval approach, we adopt the characteristic earthquake model with a weight of 0.7 and the "modified exponential" model (Youngs *et al.*, 1987) with a weight of 0.3. The exception is for the Death Valley and Furnace Creek faults. Because of their high slip rates the exponential model would lead us to expect many more moderate-magnitude earthquakes than have been observed. Given this, and the fact that the characteristic model was developed from observations for faults having high rates of activity, we give 1.0 to the characteristic model for the Death Valley and Furnace Creek faults. For both the characteristic and "modified exponential" models, M_{max} evaluated for a fault is assumed to be uniformly distributed in the range $M_{max} \pm 3$ magnitude unit, with $M_{max} + 3$ being the upper-bound magnitude, m^u.

Where recurrence intervals are provided, we use the method of Youngs and Coppersmith (1985) that assumes a constant frequency of earthquakes above some specified size. Given

M_{max} for a fault, the cumulative frequency for earthquakes of M_{max} - 3 is set equal to the inverse of the tabulated recurrence interval, which is interpreted to represent the frequency of characteristic-size events for the fault.

Based on seismicity recurrence calculations provided (Section 3.1 contains a description of the methodology used to calculate seismicity parameters) from diverse regional sources within 300 km of Yucca Mountain, our assessed distribution for the b-value (and relative weighting) for applying the methodology of Youngs and Coppersmith (1985) is:

0.80 (0.3), 1.00 (0.4), 1.20 (0.3).

4.0
LOCAL FAULT SOURCES

4.1 FAULTS CONSIDERED IN LOCAL ANALYSIS

The following faults are considered potential seismic sources within 20 km of Yucca Mountain, and are referred to in our analysis as local faults. Figures AAR-3 and AAR-4 show local faults included in our coalesced and independent models (discussed later in this section).

Paintbrush Canyon Fault (PBC)

PBC connotes the fault zone that bounds the west sides of Alice and Fran Ridges and Busted Butte. Activity extends at least from near Yucca Wash, where PBC has no obvious geomorphic expression (but where trench A1 reveals minor Quaternary offsets), to southwest of Busted Butte, where Holocene alluvium truncates a subtle scarp. Some map depictions (e.g., Simonds *et al.*, 1995) indicate a left step of about 0.7 km at Fran Ridge, suggesting possible segmentation. We do not segment PBC here because other depictions suggest greater continuity, and data do not require it; in any case, we would give this a low weight and consider it for only some events. Displacement and recurrence parameters for PBC are derived from chapter 4.4 of the Tectonics Synthesis Report (USGS, written communication,1996). With multiple exposures and an extensive record (~700 ka) at Busted

Butte, a value was calculated for the average displacement per event (Davg) that is less than the maximum displacement per event (Dmax).

Stagecoach Road Fault (SR)

As delineated on most maps, SR has a short length (about 4 km), despite prominent geomorphic expression and a relatively high rate of activity. SR commonly is considered linked as a single fault with PBC, with the intervening area masked by young alluvium; we favor this interpretation. At least one depiction suggests that SR could connect with the Mine Mountain fault to the northeast (Maldonado, 1985); this interpretation is not considered here because mid to late Quaternary alluvial surfaces east of Yucca Mountain lack geomorphic evidence of such a connection. The uncertainties in trench data possibly are larger for SR than for other Crater Flat Domain (CFD) faults because of: (1) the predominant loose sand encountered in the trenches, which are difficult materials to work with; (2) dating results that were inconsistent; and (3) significant hanging wall deformation in the trenches. Unless age estimates are grossly in error, which rough agreement suggests is not the case, SR is one of the most active CFD faults during the late Quaternary, although this is based on a relatively short record. Correlation of an 8 Ma tephra across SR (J.W. Whitney presentation at SSC Workshop 2) indicates substantial post-Rainier Mesa offset.

Bow Ridge Fault (BWR)

BWR has weak geomorphic expression of Quaternary activity for < 1 km along Exile Hill, and all data come from one cluster of trenches. Length and displacement thus are poorly constrained, but do not appear significantly underestimated given the lack of geomorphic expression elsewhere. The northward projection of BWR has been depicted alternatively as continuing with a northerly strike to near Yucca Wash (Scott and Bonk, 1984; Day *et al.*, 1996a) or curving to the northwest and connecting with the Sever Wash fault (Simonds *et al.*, 1995). We favor the former interpretation because BWR appears to control a north-trending linear drainage between Exile Hill and Yucca Wash. Trench A/BWR-3, excavated across the projection of BWR north of Exile Hill, showed no evidence of displacement in Q3 gravels (est. 100 to 200 ka), supporting a low rate of activity. BWR commonly is depicted as having a steep dip and connecting with PBC at a depth of a few km; however, projection to the Exploratory Studies Facility (ESF) (cross-section, R.C. Lung presentation at SSC Workshop

2 and handouts at SSC Workshop 3) indicates a dip of about 60 degrees, similar to that of the other block-bounding faults.

Ghost Dance Fault (GD)

There is evidence of minor Quaternary activity on GD, but the evidence is nondefinitive, geomorphic evidence constrains offset to be minor (at a detection threshold), and the possible displacements could be secondary. Map depictions suggest that GD connects with the Abandoned Wash fault, but considering them as a single fault indicates an extremely high aspect ratio (i.e., a long, small displacement fault), and the Abandoned Wash fault shows no evidence of Quaternary activity. GD is considered in the analysis because of its location, but we assign a low weight to the probability that it is seismogenic (P[S]=0.1), because activity is unproven and the possible small displacements could reflect secondary slip.

East Lathrop Cone Fault (ELC)

This is a NE-striking fault south of SR and east of the Lathrop Wells basalt cone (A. R. Ramelli and J. W. Bell, Nevada Bureau of Mines and Geology, written communication, 1996). It displays a small scarp (< 0.5 m high) in late Quaternary alluvial deposits (A.R. Ramelli presentation at SSC Workshop 3). The fault has not been studied in detail, so estimated parameters are poorly constrained. However, its small scarp, its moderate post-Tiva offset (Frizzell and Shulters, 1990), and its apparent short length all indicate that ELC is a minor fault. The fault is located well south of the controlled area. If considered part of a PBC/SR system (our preferred interpretation), ELC slightly increases the overall length of the system.

Solitario Canyon Fault (SC)

SC is taken to extend along a nearly continuous scarp projecting toward Lathrop Wells cone and the southern end of SR. A possible NE-striking connection between SC and SWW is not directly included here because of its weak geomorphic expression and unproven activity, but is included in the single west-side coalesced model. The southern end of SC is buried by young alluvium. SC has the longest continuous late Quaternary scarp of any Yucca Mountain fault, but trench results indicate a lower long-term rate of activity than for the other block-bounding faults (e.g., PBC, SR, SWW, SCF). Displacement and rate estimates are based on late Quaternary activity, which is considered more likely to be representative of the next 10^4

to 10^5 years. Our estimate for Davg is less than that for Dmax, based on the multiple trench sites and the fact that relatively large displacements are confined to a short section of the fault.

Iron Ridge Fault (IR)

IR strikes subparallel to SC, and is therefore considered a SC splay that obliquely connects to SR. IR has a nearly continuous bedrock scarp along much of its length. Results from a single trench site (SCF-T2) indicate Quaternary activity. The trench revealed massively cemented gravels (mid-Pleistocene in age) juxtaposed against bedrock, with permissible minor late Quaternary extensional opening. The lack of definitive late Quaternary offset indicates a low rate of activity and precludes significant rupture associated with late Quaternary events on SC or SR.

Fatigue Wash Fault (FW)

The FW scarp originally was referred to as part of the Windy Wash fault but actually connects with Scott and Bonk's (1984) Fatigue Wash fault. FW lies close to and interconnects with the Windy Wash fault, and the two are considered likely to make up a single fault system. This likelihood is incorporated in our linked and coalesced models (discussed below). The northernmost mapped extent of FW has minor bedrock offset and no evidence of Quaternary activity; it therefore is not considered in the analysis. Estimates for FW are based largely on a single, poorly sited trench (CF-1), one of the original trenches excavated for the Yucca Mountain program. CF-1 is adjacent to a drainage that flows parallel to the fault (perpendicular to the trench), providing a cross-sectional view of channelized deposits that form poor stratigraphic markers. The estimate of slip rate is adjusted to account for surface separations where FW crosses the Crater Flat road, as discussed in USGS (written communication, 1996).

South Windy Wash Fault (SWW)

This fault is considered to be separate from the North Windy Wash fault because the two are not directly connected. To the north, SWW abruptly terminates against the Central Windy Wash fault; its southern end is less well constrained. Paleoseismic data are derived from a trench site at the extreme north end of SWW. Displacements are assumed to be somewhat larger along its central part (south of FW splay), based on a 100-m offset of 3.7 Ma basalt.

The trench site is the best along SWW with respect to Quaternary stratigraphy. The best long-term rate for a principal Yucca Mountain fault is provided by offset of 3.7 Ma basalt. Total displacement along the central part of SWW is unknown.

North Windy Wash Fault (NWW)

This is the original Windy Wash fault of Scott and Bonk (1984). A small, nearly continuous bedrock scarp likely reflects some Quaternary activity, but field relations indicate this is largely a fault-line scarp formed by erosion of deposits on the downthrown side of the fault. Late Quaternary activity is minor at most. There are no trench data or other good constraints on activity, which is therefore assumed to be similar to northern SC and the Northern Crater Flat fault.

South Crater Flat Fault (SCF)

Offset of 3.7 Ma basalt on this fault is much smaller than that on SWW (about one-third). The fault projects toward CWW, and is considered a splay of the Windy Wash system. SCF is the best candidate for having activity that extends through the hills south of Crater Flat. Trench data are complicated by uncertain correlations across the fault, but they show progressively downthrown and buried soils, indicating repeated activity.

North Crater Flat Fault (NCF)

As described by the USGS (written communication, 1996), this fault is a system that includes at least three closely spaced, subparallel faults, each having probable small Quaternary scarps. Two trenches were located across its westernmost trace. Quaternary activity is documented at trench CFF-T2a, but late Quaternary activity is constrained to be minor based on lack of faulting in trench CFF-T2 (USGS, written communication, 1996).

Central Windy Wash Fault (CWW)

This down-to-the-east fault is distinguished from the down-to-the-west faults of the Windy Wash system (SWW and NWW); it abruptly truncates the north end of SWW and terminates near the south end of NWW. The scarp of CWW is modified along its central part because of drainage deflection, but unmodified scarps are present along both ends. Displacement and rate estimates are based on vertical separations of late Quaternary alluvial surfaces.

Central Crater Flat (CCF)

This down-to-the-east fault has a similar extent and position as CWW, although it is not as directly connected to down-to-the-west faults. Displacement and rate estimates are the same as for CWW, based on similar surface separations of the same alluvial surfaces.

Black Cone Fault (BC)

This down-to-the-east fault displays a system of NW-trending, mostly down-to-the-east scarps northeast of Black Cone, indicating minor late Quaternary activity. BC is inferred to connect with a north-striking fault southeast of Black Cone. The north-striking fault has a 0.5- to 1-m scarp in alluvium that deflects drainage and possibly offsets 3.7 Ma basalt near drillhole VH-2 (Simonds *et al.*, 1995; A. R. Ramelli and J. W. Bell, Nevada Bureau of Mines and Geology, written communication, 1996). Displacement and rate estimates are the same as for CWW and CCF, based on similar surface separations and provide the basis for our preferred rate.

Bare Mountain Fault (BM)

This down-to-the-east fault forms the western boundary of Crater Flat. Its southern end is poorly defined, with bedrock offset extending south into Amargosa Desert, but Quaternary activity apparently is confined to north of Black Diamond. BM has a slightly longer continuous Quaternary trace than does SC. It was the most active fault and had the largest throw within CFD during the Miocene. Its Quaternary rate is similar to the Yucca Mountain faults, suggesting reactivation under different conditions. The postulated higher rate for BM based on alluvial fan size (Ferrill *et al.*, 1996) is incorporated in our upper bound on slip rate, but trench data and surficial mapping are considered better constraints and provide the basis for our preferred rate.

Midway Valley (MWV)

MWV is a north-striking fault inferred from geophysical surveys and shallow borehole data. It is buried by unfaulted mid to late Quaternary alluvium. Estimates for this fault are based on activity at the threshold of resolution.

West Dune Wash #1 (WD1)

WD1 is a left step of about 0.3 km from the Ghost Dance fault. McKague *et al.* (1996) list it as a Type I fault, and Quaternary activity is suggested by bedrock scarps, vertical CaCO3-filled fractures, and linear drainage (Simonds *et al.*, 1995). Estimates for this fault are based on activity at the threshold of resolution.

West Dune Wash #2 (WD2)

WD2 is a north-northwest-striking fault listed as a Type I fault by H. L. McKague *et al.* (CNWRA, written communication, 1996), and Quaternary activity is suggested by bedrock scarps (Simonds *et al.*, 1995). Estimates for this fault are based on activity at the threshold of resolution.

East Busted Butte (EB)

EB is a down-to-the-east fault bounding the eastern sides of Busted Butte and Fran Ridge. Quaternary activity is indicated by arcuate, subtle scarps flanking Busted Butte (Simonds *et al.*, 1995; A. R. Ramelli and J. W. Bell, Nevada Bureau of Mines and Geology, written communication, 1996). Estimates for EB are based on small mid to late Quaternary offset reflected in its scarp. Topographic relief suggests extension of this fault along the east side of Fran Ridge, although no evidence of Quaternary activity has been described at that location.

4.2 NOTES ON LOCAL FAULT ESTIMATES (TABLE AAR-4)

Total Active Length

This is the surface length over which a fault has apparent Quaternary activity. It is scaled from mapped depictions and cross-checked against low-sun-angle aerial photographs: mininum = distance over which Quaternary fault scarps or other evidence of activity can be traced; preferred = preferred value from considerations of topography, mapped depictions, and burial by younger deposits; maximum = upper bound considering map depictions, fault intersections, topographic expression, and relative cumulative displacements.

Style

In the nomenclature used, ln = left-normal (dominantly normal with a left-oblique component). Slip vector is poorly defined for most faults, but available constraints (fault

striations, apparent offsets) suggest that most faults are dominantly normal with a left-oblique component. Where not documented, slip is assumed to be related to fault strike.

Fault Dip

For most faults, 60 degrees is the preferred estimate of dip based variously on well-constrained cross sections (e.g., the projection of BWR to the ESF), bedrock fault exposures (e.g., trench exposures along central SC), or geophysical data (e.g., BM). Reported dips from fault trenches and other surface exposures are consistently 10 to 15 degrees steeper and therefore are not used.

Total Displacement

In most cases, this measure is made from offset of the top of the Tiva Canyon member of the Paintbrush Tuff, which is estimated from cross sections or geologic maps (or topographic maps, where necessary). It was estimated for the part of a given fault where it appears largest. It generally is well constrained for faults in the north part of the basin, and less constrained in the southern part, where hanging walls are buried by thicker alluvium.

Displacement Per Event

Using data reported in individual chapters of the Tectonics Synthesis Report (USGS, written communication, 1996), the maximum displacement per event (Dmax) and the average displacement per event (Davg) are estimated for the part of a given fault where displacement appears largest (generally the central part of the fault). Maximum observed displacements, in some cases averaged for multiple events, are taken as best estimates of average displacement for faults for which there are single trench sites or multiple sites in nonrepresentative locations. Averages are derived from the largest displacements along a given fault for which there are multiple trenches deemed to be in representative locations, and/or from records of several events.

Slip Rate

Slip rates are based on data reported in individual chapters of the Tectonics Synthesis Report (USGS, written communication, 1996) and are estimated for the part of a given fault where they appear largest. For example, trenches CF-2 & CF-3 (Simonds *et al.*, 1995) are located at the extreme northern end of SWW and north of the intersection of SWW & FW, so a slip rate

derived from offset of basalt along the central part of the fault is assumed to be more representative.

Recurrence Interval

This is the average interseismic interval derived from paleoseismic data reported in individual chapters of the Tectonics Synthesis Report (USGS, written communication, 1996).

4.3 UNCERTAINTIES IN LOCAL FAULT ESTIMATES

Estimates of activity on local faults at Yucca Mountain involve large epistemic uncertainties. Estimates of length involve difficulties in recognizing remnants of small surface offsets, especially at the ends of ruptures, and they are sometimes complicated by burial by younger deposits. Measuring displacements is uncertain because there is a general lack of piercing points (and hence poorly constrained slip vectors), poor stratigraphic markers, uncertain correlation of units across a fault zone, and the common need to project geomorphic surfaces or stratigraphic units across a broad zone of deformation. Activity rates (slip rates and recurrence intervals) are highly uncertain because they depend on age estimates, which incorporate uncertainties in such things as analytical errors, unknown errors related to poorly understood processes and the experimental nature of most dating techniques, and indirect control (i.e., events typically are bracketed and not directly dated).

Subsurface fault geometry is poorly constrained because depths of fault penetration are unknown and fault dips are uncertain. Interpreting the number of events within the paleoseismic record is complicated by several factors: (1) The nature of fault interactions is uncertain (i.e., distributed events seem likely, but it is beyond our resolution to determine which faults rupture during individual events and how consistent such events have been). (2) Some displacements may have secondary or nontectonic origins. (3) Some events—especially small, older events—likely are unrecognized, as suggested by plots of event timing (e.g., S. K. Pezzopane *et al.*, USGS, written communication, 1996a). (4) Events are not necessarily recognizable at all sites because of factors such as variable offsets, bioturbation, and carbonate overprinting. (5) Not all fault traces have been studied.

Despite these many sources of uncertainty, our estimates of activity of the CFD faults appear to be reasonable and adequately accurate, and are internally consistent and in accord with generally low rates of regional strain. For example, comparing the minimum distances over which fault activity can be traced to conservative upper bounds on length suggests that length estimates are unlikely to be off by as much as a factor of two; displacement measurements are probably rarely off by more than 20% to 30%; and comparisons based on soils and geomorphology suggest that age estimates likely are accurate within factors of two to three.

We consider that current estimates of parameters for the CFD faults are reasonable approximations. To portray their approximate nature, most estimates are rounded to a single significant digit, and no adjustments are made that introduce additional significant digits. For example, cumulative displacements and numbers of events could be reduced to account for possible secondary or nontectonic offsets. However, we would expect such nonprimary displacements to occur as fracturing or small offsets, which generally are difficult to recognize. In no cases have fracturing events lacking discernable offset been factored into earthquake frequency. We estimate the contribution of small offsets to be less than 20% to 25%, and some small offsets may represent primary faulting associated with moderate-sized events or distributed rupture, so a correction factor would be no more than 10% to 15%. Current interpretations include more frequent occurrence of small offsets within relatively recent time periods, strongly suggesting that older small offsets have been obscured and are unrecognizable. To a first approximation, unrecognized small offsets might balance out consideration of a few secondary or nontectonic offsets as seismogenic events. In either case, any adjustment we might make would be a minor fraction of the one-significant-figure estimates.

4.4 NOTES ON ESTIMATES FOR BURIED/BOUNDING FAULTS

Postulated buried or bounding fault sources associated with dextral shear across the CFD (Figure AAR-5) are model-driven; no direct evidence of activity is available. Estimates are thus hypothetical, with bounds deemed to cover reasonable possibilities.

Total Active Length

The following subsurface lengths were deemed reasonable for the postulated structures. For the throughgoing, regional strike-slip fault, min = dimension required to extend beyond CFD and thus qualify as a throughgoing structure; pref = midpoint between min and max; max = approximate comparison to the longest historical strike-slip ruptures in the Basin and Range province (specifically 1872 Owens Valley). For the "Highway 95 fault," length estimates are based on a general comparison to historical Basin and Range surface-faulting events (e.g., 1932 Cedar Mountain) and on constraints posed by postulated segment boundaries (i.e., intersection with the Rock Valley fault and the extensional bend at Oasis Valley). For the cross-basin fault, min = approximate dimension required for a seismic event above the background source; pref = midpoint between min and max; max = constrained by dimensions of the CFD. The north-bounding strike-slip fault is inferred to have similar dimensions and activity as the cross-basin fault.

Style and Fault Dip

As conceptualized, all buried and bounding sources are strike-slip faults assumed to be nearly vertical.

Displacement per Event/Slip Rate

These parameters are based on historical analogs and comparisons to the CFD faults. For the throughgoing, regional strike-slip fault, the slip rate was estimated as that required to be a driving fault (i.e., approximately equal to the sum of slips on CFD faults). For the "Highway 95 fault," we estimated rates required for the fault to be a partially driving fault (i.e., somewhat less than the summed slip on CFD faults). For the cross-basin and north-bounding faults, we used historical analogs and comparison to CFD faults (i.e., approximately equal to CFD faults).

4.5 NOTES ON THE 52 FAULTS THAT NRC CONSIDERS IMPORTANT

The faults listed below, which H. L. McKague *et al.* (CNWRA, written communication, 1996) included as Type I faults, either were not considered or have designations that could lead to confusion. Reasons for not considering these faults and/or clarifications as to fault designation are given below.

Simonds #1 Fault

Included on Simonds *et al.* (1995) as a bedrock fault having an unknown age of movement; lack of geomorphic expression in bedrock is unsupportive of significant Quaternary activity; estimated Mw 5.6 (H. L. McKague *et al.*, CNWRA, written communication, 1996) is less than M_{max} for our background source zone.

Simonds #2 Fault

Included on Simonds *et al.* (1995) as a bedrock fault having an unknown age of movement; lack of geomorphic expression in bedrock is unsupportive of significant Quaternary activity; estimated Mw 7.28 (H. L. McKague *et al.*, CNWRA, written communication, 1996) is unsupportably high given the fault's 7-km length and is inferred to be a typographical error; estimated Mw should be less than M_{max} for our background source zone.

Simonds #3 Fault

Included on Simonds *et al.* (1995) as a bedrock fault having an unknown age of movement; lack of geomorphic expression in bedrock is unsupportive of significant Quaternary activity; estimated Mw 5.9 (H. L. McKague *et al.*, CNWRA, written communication, 1996) is less than M_{max} for our background source zone.

Simonds #4 Fault

Included on Simonds *et al.* (1995) as a bedrock fault having an unknown age of movement; lack of geomorphic expression in bedrock is unsupportive of significant Quaternary activity; estimated Mw 5.9 (H. L. McKague *et al.*, CNWRA, written communication, 1996) is less than M_{max} for our background source zone.

Simonds #5 Fault

Included on Simonds *et al.* (1995) as a bedrock fault having an unknown age of movement; lack of geomorphic expression in bedrock is unsupportive of significant Quaternary activity; estimated Mw 5.9 (H. L. McKague *et al.*, CNWRA, written communication, 1996) is less than M_{max} for our background source zone.

Simonds #7 Fault

Included on Simonds *et al.* (1995) as a bedrock fault having an unknown age of movement; lack of geomorphic expression in bedrock is unsupportive of significant Quaternary activity; estimated Mw 5.9 (H. L. McKague *et al.*, CNWRA, written communication, 1996) is less than M_{max} for our background source zone.

Simonds #8 Fault

Included on Simonds *et al.* (1995) as a bedrock fault having an unknown age of movement; lack of geomorphic expression in bedrock is unsupportive of significant Quaternary activity; estimated Mw 6.1 (H. L. McKague *et al.*, CNWRA, written communication, 1996) is less than M_{max} for our background source zone.

Simonds #9 Fault

Included on Simonds *et al.* (1995) as a bedrock fault having an unknown age of movement; lack of geomorphic expression in bedrock is unsupportive of significant Quaternary activity; estimated Mw 5.8 (H. L. McKague *et al.*, CNWRA, written communication, 1996) is less than M_{max} for our background source zone.

Simonds #10 Fault

Included on Simonds *et al.* (1995) as a bedrock fault having an unknown age of movement; lack of geomorphic expression in bedrock is unsupportive of significant Quaternary activity; estimated Mw 5.9 (H. L. McKague *et al.*, CNWRA, written communication, 1996) is less than M_{max} for our background source zone.

Simonds #11 Fault

Figure 1-2 of H. L. McKague *et al.* (CNWRA, written communication, 1996) depicts this fault as one we include as part of the No. Crater Flat fault system, whereas their Appendix A describes this as the Black Cone fault of Piety (1996), which we include as a separate fault.

Simonds #12 Fault

We include this fault as part of the North Crater Flat fault system, consistent with chapter 4.11 of the Tectonics Synthesis Report (USGS, written communication, 1996).

Boomerang Point Fault (BP)

Included on Simonds *et al.* (1995) as a bedrock fault having an unknown age of movement; lack of geomorphic expression in bedrock is unsupportive of significant Quaternary activity; estimated Mw 5.9 (H. L. McKague *et al.*, CNWRA, written communication, 1996) is less than M_{max} for our background source zone.

Note: For Simonds #13 to #19 faults, there is a discrepancy between Figure 1-2 and Appendix A of H. L. McKague *et al.* (CNWRA, written communication, 1996), with all faults apparently shifted one number (e.g., fault #13 on Figure 1-2 is fault #14 in Appendix A). The following fault names refer to their Figure 1-2.

Simonds #13 Fault

Simonds *et al.* (1995) depict evidence of possible Quaternary activity along the fault's southern part; as depicted, it is located within the controlled area; we include this fault as our West Dune Wash #1 fault (WD1).

Simonds #14 Fault

Geomorphic expression suggests possible Quaternary activity on this fault (Simonds *et al.*, 1995; Bell *et al.*, 1996), and it is located within the controlled area; we include this fault as our West Dune Wash #2 fault (WD2).

Simonds #15 Fault

Included on Simonds *et al.* (1995) as bedrock fault having an unknown age of movement; lack of geomorphic expression in bedrock is unsupportive of significant Quaternary activity; estimated Mw 5.8? (H. L. McKague *et al.*, CNWRA, written communication, 1996) is less than M_{max} for our background source zone.

Simonds #16 Fault

We include most of the depicted length of this fault as part of our South Windy Wash fault (SWW). North of where it merges with SWW, it has a length of about 4 km and has geomorphic expression (bedrock scarps) permissive of Quaternary activity. We interpret this as a secondary fault connecting the SWW and Solitario Canyon faults; we do not include it as a separate source.

Simonds #17 Fault

Included on Simonds *et al.* (1995) as bedrock fault having an unknown age of movement; lack of geomorphic expression in bedrock is unsupportive of significant Quaternary activity; estimated Mw 5.6? (H. L. McKague *et al.*, CNWRA, written communication, 1996) is less than M_{max} for our background source zone.

Simonds #18 Fault

This is the South Crater Flat fault, which we include.

4.6 COMPARISON OF QUATERNARY AND MIOCENE DEFORMATION

The plausible tectonic models we consider relevant to Quaternary activity within the CFD (Figure AAR-1) hinge in part on the similarities between Quaternary and Miocene deformation. For example, we consider it likely that an active detachment surface may have existed at shallow depths (i.e., less than 10 km) during the Miocene, when heat flow associated with the caldera systems likely reduced the effective brittle thickness of the crust. The relative deformations of the Paintbrush Tuff (primarily the broadly exposed Tiva Canyon member) and the Timber Mountain Tuff (primarily the Rainier Mesa member) clearly indicate that Quaternary faulting within the CFD generally has occurred along structures that were more active during the Miocene. However, stratigraphic constraints are insufficient to demonstrate whether Quaternary activity represents the waning stages of Miocene activity, as has been suggested by Fridrich (1996), or whether it represents reactivation of preexisting zones of weakness within the past 5 Ma or so (the period marking significant changes in Basin and Range tectonics, including rapid uplift of the Sierra Nevada and formation of Death Valley). Wholesale differences in Miocene and Quaternary deformation in the Sliver Peak area about 100 km northwest of the CFD were documented by Stewart and Diamond (1990), who found no relation between the Miocene Esmeralda basin and the current basin configuration. Although they describe differences between Miocene and Quaternary deformation that are much greater than in the CFD, both areas lie just east of the Death Valley/Owens Valley region within the Nevada Walker Lane and are likely to have some affinities.

Although difficult to prove, reactivation of Miocene faults during the past 5 Ma seems plausible given the regional tectonic changes, especially onset of major activity in the adjacent Death Valley region, and renewal of basaltic volcanism in the CFD. Aside from rate, Quaternary deformation appears generally similar to Miocene deformation, but several lines of evidence indicate potentially significant differences.

(a) **Relative activity of the Bare Mountain and Yucca Mountain faults.** Cumulative throw clearly is much larger on the Bare Mountain fault (BM) than on any of the Yucca Mountain (YM) faults, and estimated uplift rates suggest that BM was considerably more active during the primary phase of Miocene deformation. Paleoseismic data, on the other hand, suggest that at least two YM faults (SWW and SR) have higher Quaternary rates than does BM, and the estimated summed slip across the YM faults is several times that on BM. The apparent discrepancy in Miocene versus Quaternary rates is significantly larger than what we consider reasonable bounds on estimates of Quaternary activity for these faults.

(b) **Contrast in deformation of Miocene tuffs and 3.7 Ma basalts along So. Windy Wash fault.** Deformation of the tuffs involved extensive and highly variable tilting, including broad-scale, low-amplitude north-south warps, whereas the basalts are uplifted uniformly. This difference is compatible with the notion of a warmer, thinner, more-ductile crust during the main phase of deformation; it also begs the question as to what extent tilting and displacements are coeval.

(c) **Age of formation of hills bounding the south end of Crater Flat.** Parts of these hills are capped by slide blocks, which rest on 10.5 Ma basalts; therefore the hills have entirely formed post-10.5 Ma. This contrasts with the topography of Yucca Mountain, which must have largely formed before eruption of the Timber Mountain Tuff (assuming that tilts and major fault displacements were coeval).

(d) **Difference in state of stress.** From populations of fault striations, extension is interpreted to have rotated in a clockwise direction; it is inferred that during the primary phase of Miocene deformation it was WSW-ENE to nearly east-west, whereas during the Plio-Quaternary it has been NW-SE (H. D. Ander, Rice University, written communication, 1984; Frizzell and Zoback, 1987).

(e) **Relative activity of NE-striking and NW-striking bridging faults.** Northeast-striking, connecting faults show Quaternary activity in several locations, whereas northwest-striking ones rarely do. In one case (the northeast-striking connection between the Fatigue Wash and southern Windy Wash faults), Quaternary scarps

trend over a bedrock ridge, producing only minor bedrock offset, which suggests that they are post-Miocene features.

4.7 SYNCHRONOUS RUPTURES

To account for possible distributed (or synchronous) ruptures involving multiple faults, we define various models that group closely spaced and/or interconnected faults into coalesced or linked fault systems. In these models, slip at depth on a defined principal structure results in distributed and/or secondary surface rupture on the faults included in a given system. Linked faults imply along-strike connection of separately defined faults (e.g., a combined Paintbrush/Stagecoach Road fault). Aside from considering combined lengths, linked faults are treated the same as independent faults. Coalesced faults imply upward-splaying fault systems, with interconnection between subparallel faults.

At the outset, we make the following points regarding our consideration of synchronous ruptures.

- Completely independent behavior of the CFD faults (with the exception of the Bare Mountain fault) seems highly unlikely, given their similarities, close cross-strike spacing (generally < 2 km), and high degree of plan-view interconnection.

- The presence of basaltic ash within extensional openings along several faults is possible indication of synchronous rupture. Without such evidence, synchronous ruptures would be more speculative.

- Similarities in timing indicated by paleoseismic data are suggestive, but not compelling, evidence for synchronous ruptures, given many uncertainties.

- Synchroneity of paleo-ruptures is ultimately unprovable. Even under ideal circumstances (e.g., tightly-constrained events based on C14 dating or dendrochronology), synchroneity cannot be distinguished from occurrences close in time, as might occur from short-term triggering.

Two methods for grouping the CFD faults into "predicted" distributed ruptures during future surface-faulting earthquakes are: (1) defining scenarios (as done by S. K. Pezzopane *et al.*, USGS, written communication, 1996a) for past ruptures, allowable within the constraints of

paleoseismic data; and (2) defining distributed systems that incorporate the principal faults and a surrounding halo of lesser faults. Both methods capture a range of behavior.

Scenarios (S. K. Pezzopane *et al.*, USGS, written communication, 1996a) allow the most direct input of paleoseismic data. Assuming that distributed behavior occurs, the data can be viewed as documenting the minimum extent of events if one includes only those faults for which evidence has been described. As defined by Pezzopane (USGS, written communication, 1996), the scenarios can generally be divided into east- and west-side rupture events.

Defined distributed systems, in our judgment, have distinct advantages. They (1) allow grouping of the most directly connected faults; (2) allow inclusion of all faults; (3) are stable (i.e., they don't jump around, thus avoiding open-ended complexity); and (4) are controlled by parameters of the principal structures, with small contributions to displacement by lesser structures.

Methodology for Treating Possible Synchronous Behavior

First, we assign weights (Table AAR-5) to the likelihood of independent versus coalesced behavior (Figure AAR-6) for each of our 11 defined tectonic models depicted on Figure AAR-1. In summary, the tectonic model designations are based on the following structure of our logic tree: A = buried, throughgoing right-slip fault beneath CFD; B = shear couple across CFD with bounding structure(s), but no buried cross-basin fault; C = shear couple with bounding structure(s) and buried cross-basin fault; D = basin extension without significant dextral shear structures; 1 = shallow (3 - 10 km) detachment; 2 = deep (> 10 km) detachment; 3 = no detachment.

Notes:

(1) Examples: In Model B-1 there is a shear couple with no buried fault and there is a shallow detachment; in Model D-3 there is basin extension with no significant dextral shear structure(s) and without any detachment.

(2) "Detachment" implies a subhorizontal zone of decoupling, but not necessarily a seismogenic structure.

(3) For buried sources, we consider only those deemed potential sources of earthquakes larger than the maximum background earthquake of M 6.3 ± 0.3.

(4) Exception to detachment numbering: Model C-2 involves a buried cross-basin fault without a detachment. (Given a detachment >10 km, we exclude the possibility that a buried cross-basin fault would generate an earthquake larger than the maximum background earthquake.)

With one exception (model C2), the CFD faults are considered much more likely to rupture during distributed (coalesced) events than as completely independent faults (Table AAR-5) for several reasons, including the close fault spacing, anastomosing nature, similar event timing, and historical analogs. In model C2, higher weighting is assigned to independent behavior based on reasoning that an overlapping cross-basin fault likely would segment the CFD faults. Coalesced behavior is considered more likely in models containing a 3- to 10-km detachment, because such a feature would provide a straightforward mechanism for interconnection of overlying steep faults. Because most CFD faults appear to have similar dips, coalesced behavior is considered less likely with increasing depth of penetration; however, no distinction is made between models having $\geq$ 10 km detachment or no detachment because at those depths ruptures have extended through most of the seismogenic layer and possible mechanisms of interconnection are poorly understood.

We exclude the possibility of a third west-side system associated with an inferred major fault in central Crater Flat, because we have no evidence of Quaternary activity. We also exclude additional coalesced options on a "diminishing-returns" basis; additional options would quickly magnify the complexity of the interpretation without adding to its credibility.

Second, we define various linked and coalesced fault systems. The following CFD faults are considered in our linked and coalesced models:

WEST-SIDE FAULTS	EAST-SIDE FAULTS
SC - Solitario Canyon	PBC - Paintbrush Canyon
IR - Iron Ridge	SR - Stagecoach Road
SWW - So. Windy Wash	ELC - E. Lathrop Cone
FW - Fatigue Wash	MWV - Midway Valley
NWW - No. Windy Wash	BWR - Bow Ridge
SCF - So. Crater Flat	WD1 - West Dune Wash #1
NCF - No. Crater Flat	WD2 - West Dune Wash #2
CWW - Central Windy Wash	EB - E. Busted Butte
CCF - Central Crater Flat	
BC - Black Cone	
BM - Bare Mountain	

For cases of independent fault behavior, we make a further distinction whether some faults may be connected along strike (i.e., linked faults). Based on map patterns, we define two plausible linked systems, PBC/SR and WW/FW (Table AAR-6). PBC/SR is considered a somewhat more likely linked system than WW/FW because PBC/SR involves faults that are on line with each other, there is no obvious discontinuity in the possible linked trace, and coincident rupture during multiple events is suggested by paleoseismic data. WW/FW involves faults that do not have the same continuity, but are closely spaced and have direct splaying relations. In models that include 3- to 10-km detachment, relatively less weighting is assigned to linked behavior because a shallow detachment would result in unusually high aspect ratios (i.e., long ruptures, given their depth of penetration). In model C2, an overlapping cross-basin fault provides a mechanism for segmenting the faults, especially WW/FW, so lower weighting is assigned to linked behavior.

For cases of coalesced behavior, we divide the CFD faults into four coalesced systems (Figure AAR-4) as follows.

- **E-side**: Coalesced system including all faults on the east side of Yucca Mountain. The PBC/SR linked fault, with a slight extension to the south along ELC, forms the principal structure of the system, with all other faults secondary.

- **W-side #1**: Simple coalesced system comprising SC and IR: SC forms the principal structure, and IR is secondary. Paleoseismic studies indicate relatively low long-term rates on these two faults, so this system is the least significant in a three-system model; however, the late Quaternary rate for SC compels inclusion at a similar level.

- **W-side #2**: Coalesced system including all faults on the west side of Yucca Mountain except SC and IR. The linked SWW/FW/CWW/NWW fault forms the principal structure of the system, with all other faults secondary.

- **Bare Mountain fault (BM)**: Mostly a singular fault trace, but also includes some possible distributed faulting along its northern part. BM is considered more likely to behave independently because it lacks the close spacing and interconnection of the YM faults.

We then distinguish and assign weights to four models involving rupture of different combinations of the defined coalesced systems (Table AAR-7). The principal structures of the three Yucca Mountain systems appear to have similar fault dips, and therefore are interpreted to extend to sufficient depths to be considered separate seismogenic structures. For models in which multiple coalesced systems rupture synchronously (for example, in response to external forces), they are treated as simultaneous rupture of separate structures.

Weights are assigned on a relative basis, with a higher probability of comprising fewer systems (increased coalescence) assigned to models including: first, a buried dextral fault spanning the CFD (i.e., throughgoing or cross-basin fault), because displacement on such a structure should affect all of the overlying area; and second, a 3- to 10-km detachment, because such a feature would provide a straightforward mechanism for interconnection of steep, overlying faults. Coalescence is thus considered most likely given a buried dextral fault AND 3- to 10-km detachment, less likely given a buried throughgoing fault AND >10-km detachment or no detachment, even less likely given deep or no detachment AND no buried dextral fault, and least likely given a cross-basin fault AND no detachment (i.e., A1>C1>A2=A3>B1=D1>B2=B3=D2=D3>C2).

- **One system**—CFD faults, including BM, comprise a single coalesced system; this possibility is considered only in models that include BOTH a 3- to 10-km detachment AND a buried strike-slip fault (i.e., models A1 and C1).

- **Two system**—All YM faults comprise a single coalesced system, and BM is independent; again, this possibility is considered only in models including BOTH a 3- to 10-km detachment AND a buried strike-slip fault (i.e., models A1 and C1).

- **Three systems (E-W)**-PBC/SR/ELC/BWR/MWV/GD/WD1/WD2/EB comprise an east-side system; SC/IR/SWW/FW/NWW/SCF/NCF/CWW/CCF/BC comprise a single west-side system; and BM is independent.

- **Four systems (E-2W)**-PBC/SR/ELC/BWR/MWV/GD/WD1/WD2/EB comprise an east-side system; SC/IR comprise one west-side system; SWW/FW/NWW/SCF/NCF/CWW/CCF/BC comprise a second west-side system; and BM is independent.

Geometry of Coalesced Systems

The following factors are considered.

- The overall geometry is controlled by the geometries of principal structures,

- In general, we consider 60 degrees our best estimate of dip for the principal structures, as suggested by well-constrained cross sections (e.g., Bow Ridge), bedrock fault exposures (e.g., Solitario Canyon), or geophysical data (e.g., Bare Mountain),

- If fault curvature is considered, deeper penetration would equate to shallower dip, but we eliminate this because of uncertainties (i.e., uncertainty in amount of curvature and insensitivity, given range of estimates),

- Depth of penetration is model-dependent (truncation at detachment, fault intersection, or base of seismogenic zone).

Slip Rates of Coalesced Systems

To assess slip rates for the coalesced systems, we use a simple summation of rates across strike.

4.8 M_{max} DIMENSIONS

For the local fault sources, maximum rupture dimensions basically are constrained by rupture length and downdip rupture width, RW. In some cases, RW is constrained not only from below, but also from above. Measures of maximum rupture length are provided in Table AAR-4 under the heading "active length," meaning the total length along which either (a) rupture may extend during a single event or (b) seismic moment should be distributed as

part of the slip-rate approach to recurrence (discussed below). For each fault source, the three entries for active length represent 10th, 50th, and 90th percentile values, for which corresponding weightings are 0.3, 0.4, and 0.3. When either the 10th or 50th percentile value is selected for fault length, allowable maximum rupture length follows accordingly, and weighting is renormalized.

Constraints on RW for the local fault sources include DMAX1 or DMAX2, aspect ratio (fault length/downdip width), and scenarios of truncation by either a local detachment (if one exists), by the Bare Mountain fault, or by a W-dipping fault in the case of E-dipping faults considered antithetic. For the CFD faults (Table AAR-3), the first general rule is that RW is not allowed to exceed twice the maximum rupture length (i.e., the minimum allowable aspect ratio is 0.5), based on data for earthquake slip-surface aspect ratios (Nicol *et al.*, 1996). The second general rule for these faults is that their downdip extent is limited by a detachment, if one exists; otherwise, the lower limit is DMAX1 or DMAX2—or the plane of the Bare Mountain fault. Rules for the other local fault sources listed in Table AAR-2, including special cases, are described below.

For the "Highway 95 fault," RW is independent of any detachment, and limits on lower and upper depth are provided by DMAX2 and the Earth's surface, respectively. RW for the "No. bounding strike-slip (ss) fault" is also independent of any detachment. For this fault, we allow RW to extend from DMAX1 up to 3 km below the surface, based on the fault's lack of clear surface expression.

Four of the down-to-the-east faults listed in Table AAR-4 are considered to be antithetic to, and hence would have downdip projections truncated by, a nearby west-dipping fault. Specifically, the Black Cone (BC), Central Crater Flat (CCF), and Central Windy Wash (CWW) faults would be truncated by the Fatigue Wash (FW) fault. Similarly, the West Dune Wash 2 (WD2) fault would be truncated by the Paintbrush Canyon (PBC) fault.

Scenarios A-1, A-2, A-3

For the regional ss fault, the lower depth limit of RW, in all cases, is constrained by DMAX2. Its uppermost limit—and the lowermost limit of the other CFD faults—is either the depth of

the detachment (scenarios A-1 and A-2) or, where no detachment exists (scenario A-3), a decoupling level for which we assign a depth distribution (and relative weighting) as follows:

4.5 km (0.185), 7.0 km (0.63), 9.0 km (0.185).

Scenarios C-1, C-2

For the cross-basin fault, the lower depth limit of RW is constrained by DMAX1. In scenario C-1, its upper-most limit—and the lowermost limit of the other CFD faults—is the depth of the detachment. In scenario C-2 we allow RW for the cross-basin fault to extend up to 3 km below the surface, based on the fault's lack of clear surface expression. In this scenario, DMAX1 or other general truncating rules constrain the lower depth limit of RW for the CFD faults. We accept the possibility of intersections between the cross-basin fault and the other CFD faults as the former develops under the shear couple.

Multiple-structure Coalesced Systems

In the cases of "multiple-structure coalesced systems" (Table AAR-4), that is, coalesced systems of the local faults that are allowed to rupture simultaneously in parallel, RW is constrained by DMAX1 in all cases. Although the tabulated lengths for these sources is greater than 25 km, we use DMAX1 because the expected value of rupture length for any of the individual coalesced systems is less than 25 km.

4.9 M_{max} APPROACH

For the local fault sources, using the data in Table AAR-4, we use four approaches to estimate M_{max} in terms of moment magnitude M: (a) M estimated from the "active length" of a fault, using either the relation for surface rupture length SRL or subsurface rupture length RLD (more below) from Wells and Coppersmith (1994) for all slip types; (b) M estimated from rupture area RA ("active length" x downdip rupture width) using the relation from Wells and Coppersmith (1994) for all slip types; (c) M estimated from fault length and slip rate S, using the relation from Anderson *et al.* (1996); and (d) M calculated from seismic moment M_o, determined from the moment equation. Note that approach (d) was not used for the regional fault sources because necessary information for single-event displacement was not available.

We refer the reader to the section on "Depth of the Seismogenic Crust" for an explanation of the moment equation and other relevant background such as DMAX1, DMAX2, and our perspective on using RA in the moment equation and in the regression equation of Wells and Coppersmith (1994).

In approach (a), we take the "active length" of the local faults (Table AAR-4) to be equivalent to estimates of subsurface rupture length (RLD) in the case of the buried or bounding strike-slip faults and to surface rupture length (SRL) for all the other cases involving the CFD faults in Table AAR-4. The correspondingly appropriate regression relation from Wells and Coppersmith (1994) is then applied. For the moment-equation approach in which RLD must be estimated for the CFD faults, data of Wells and Coppersmith (1994, their Figures 2 and 3) can be used to relate "active length" (i.e., SRL) to RLD, which is expected to have a slightly larger value. For the range of ruptures being considered, we use their mean value of 0.75 for the ratio of SRL to RLD. We consider the extra length in the subsurface (RLD - SRL) to extend symmetrically from the surface trace lengths depicted in Figures AAR-3 and AAR-4.

In approach (b), DMAX1 is used in all cases for the maximum depth constraint on downdip rupture width. In approach (d), we estimate ®, the average (subsurface) displacement over the slip surface, by (MD + AD)/2, where MD and AD are the maximum and average surface displacements per event, respectively, tabulated in Table AAR-4.

Table AAR-8 outlines our weighting used for the M_{max} approaches. The weighting depends on expected rupture length and on the subsurface structure involved in some of the tectonic models. In the case of rupture length, we assign 25 km to be the threshold for large earthquakes whose downdip rupture may extend to DMAX2. Whereas the RA regression of Wells and Coppersmith (1994) is used (along with DMAX1) when expected rupture length is less than 25 km, it is not used when expected rupture length is 25 km or greater, and its weight is redistributed to the moment-equation approach. We downweight the rupture-length/slip-rate approach because many of the local faults have slip rates lower than the range of data regressed by Anderson *et al.* (1996). Given a local detachment at 3 to 10 km depth, we downweight the rupture-length approaches and redistribute weight to the moment-equation approach. For the cases of multiple-structure coalesced systems, for which slip-rate

information is not available, weight for the rupture-length/slip-rate approach is redistributed to the rupture-length approach.

4.10 RECURRENCE APPROACH

For the local sources, we use two approaches for recurrence modeling: (1) a slip-rate approach and (2) a recurrence-interval approach. These approaches are assigned weights of 0.6 and 0.4, respectively, for all the local fault sources for which both slip-rate and recurrence-interval data are provided in Table AAR-4. Where only slip-rate or recurrence-interval data are provided, the corresponding approach is weighted fully.

Fault-specific recurrence relationships are generated from the slip rates using the methodology of Youngs and Coppersmith (1985) and assuming constant moment rate. Whether using the slip-rate or recurrence-interval approach, we assign the characteristic earthquake model a weight of 0.7 and the "modified exponential" model (Youngs *et al.*, 1987) a weight of 0.3. For both the characteristic and "modified exponential" models, M_{max} for a fault is assumed to be uniformly distributed in the range $M_{max} \pm 3$ magnitude unit, with $M_{max} + 3$ being the upper-bound magnitude, m^u.

Where recurrence intervals are provided, we use the method of Youngs and Coppersmith (1985) that assumes a constant frequency of earthquakes above some specified size. Given M_{max} for a fault, the cumulative frequency for earthquakes of M_{max} - 3 is set equal to the inverse of the tabulated recurrence interval, which is interpreted to represent the frequency of characteristic-size events for the fault.

Based on seismicity recurrence calculations provided (Section 3.1 contains a description of the methodology used to calculate seismicity parameters) from diverse regional area sources within 300 km of Yucca Mountain, our assessed distribution for the b-value (and relative weighting) in applying the methodology of Youngs and Coppersmith (1985) are:

0.80 (0.3), 1.00 (0.4), 1.20 (0.3).

5.0
REGIONAL SOURCES AND LOCAL BACKGROUND SOURCE ZONES

5.1 CATALOG

For all calculations, we place full weight on Version 7 of the Yucca Mountain earthquake catalog, which consists of primary events derived using the declustering algorithm of Veneziano and Van Dyck (1985). We believe their algorithm is statistically rigorous and far superior to declustering approaches that use fixed space-time windows as a function of mainshock size, given that mainshocks are known to generate clusters having characteristics that differ greatly in space, time, and size—even in the same general area. Our judgment here is guided by substantial experience of one team member with the practical problems of declustering earthquake catalogs (W.J. Arabasz presentation at SSC Workshop 2).

Completeness intervals adopted for the 100-km-radius declustered catalog are those proposed by I.G. Wong (handout to team seismologists at SSC Workshop 4), based on the completeness technique of J. C. Stepp (NOAA, written communication, 1973). We examined "Stepp" plots specifically for the Version 7 catalog before adopting the intervals. The completeness intervals are: 2.5-2.99 (1979 to date), 3.0-3.49 (1979 to date), 3.5-3.99 (1961 to date), 4.0-4.49 (1934 to date), 4.5-4.99 (1934 to date), 5.0-5.49 (1924 to date), 5.5-5.99 (1924 to date), and 6.0-6.49 (1914 to date). Where seismicity is sampled from regions extending beyond 100 km, we gave approval to use the same completeness intervals, recognizing that any incompleteness at the lower magnitude end would simply require selecting a higher minimum magnitude in the recurrence modeling. For the 100-km-radius area, the minimum magnitude we accepted for recurrence modeling was 2.5, with a weight = 0.3, and 3.0, with a weight = 0.7.

To delimit seismicity induced by underground nuclear explosions (UNEs) in the Nevada Test Site, we eliminate from the catalog all seismic events that lie within a zone defined by Rogers *et al.* (1987, their Figure 2) that occurred post 1950.

5.2 BACKGROUND SOURCE ZONES COUPLED TO REGIONAL SOURCES

We define our background source zones to lie within a radius of 100 km of the repository site. Three alternatives in which background source zones are coupled to regional area sources are depicted on Figures AAR-7 to AAR-9. A fourth alternative, based on spatially smoothed seismicity, is discussed in the next section. For the first three scenarios, large regional sources are defined for capturing seismicity. Seismicity is first gathered from the entirety of each regional source (except the area of exclusion for UNEs and associated seismicity). It is then normalized per unit time and unit area and assigned to the corresponding sector of the area source that lies within 100 km of the repository site—including the 20-km-radius "host zone" (explained below).

In scenario I (Figure AAR-7), we depict three background source zones that form parts of an eastern California shear zone (1), a Nevada Walker Lane belt (2), and the northern Basin and Range (3A), respectively. In scenario II (Figure AAR-8), the Walker Lane belt is not considered distinct from the northern Basin and Range (3B). In scenario III (Figure AAR-9), the southern Nevada transverse zone (3C) (e.g., Rogers *et al.*, 1991) is taken as a distinct subarea of the northern Basin and Range, parts of which lie both to its north and south (forming zone 3D).

5.3 BACKGROUND SOURCE ZONE BASED ON SPATIALLY SMOOTHED SEISMICITY

Given the spatial variability of epicentral density in the declustered Yucca Mountain catalog, we also consider a background source zone based on spatial smoothing of declustered seismicity within 100 km of the repository site. Values for the kernel width, h (i.e., 2 the distance seismicity effectively can be smoothed away from its location), and corresponding weighting are as follows: 5 km (0.25), 10 km (0.5), 20 km (0.25) (Figure AAR-10b). Where a prior b-value is used, we use the same distribution (and weighting) described for the recurrence modeling of our regional and local fault sources: 0.80 (0.3), 1.00 (0.4), 1.20 (0.3).

5.4 HOST ZONE

We define a local background source region, with an M_{max} of 6.3 ± 0.3, as extending in a 20-km radius from the repository site, within which we are confident that we have identified all fault-specific sources capable of generating earthquakes larger than the background. This "host zone" is defined only for assigning its own M_{max}. Recurrence rates derive from the applicable scenario for the background source zone within which the host zone is embedded. We use data and the results of modeling presented by S. K. Pezzopane and T. E. Dawson (USGS, written communication, 1996) for the maximum background earthquake to assess the following distribution for M_{max} of the host zone (with corresponding weighting):

6.0 (0.3), 6.3 (0.4), 6.6 (0.3).

5.5 M_{max} FOR BACKGROUND SOURCE ZONES > 20 km

Beyond 20 km—and out to 100 km—we admit the possibility that there may be faults (buried, unrecognized, or not included in our inventory of fault sources because of an interpreted lack of Quaternary slip) that may be capable of generating earthquakes larger than M = 6.3 ± 0.3. An example would be the Gravity fault, for which a Quaternary displacement history is not established and which we interpret to be distinct from, but possibly related to, the Ash Meadows fault. Accordingly, we assign a higher M_{max} to our background source zones from 20 to 100 km radial distance from the repository site to account for these potential sources. The distribution also is used to model seismicity rates for the regional sources.

For our assessment of this M_{max} we used data from Table AAR-1 for regional fault sources within 100 km of Yucca Mountain (excluding the Death Valley and Furnace Creek faults and the linked case for the Amargosa River/Pahrump faults). From these data we constructed cumulative distributions of maximum rupture lengths (using preferred and maximum values only) and slip rates. Simply put, we use what can be seen as representative of what cannot be seen or has been missed. (Simultaneously, we considered dimensional arguments for possibly unrecognized intra-basin faults.)

Using the above data and the same weighted M_{max} approaches used for the regional faults, our resulting distribution for the generic M_{max} for all background sources > 20 km (with corresponding weighting) is:

6.6 (0.3), 6.9 (0.4), 7.3 (0.3).

5.6 WEIGHTING OF ALTERNATIVES FOR BACKGROUND SOURCE ZONES

Our weighting scheme for alternative background source zones takes into account the stationarity of seismicity vis-à-vis a 10,000-yr time frame. We give higher weight to scenarios in which seismicity rates near the site are similar to those in distinct regional zones in which regional seismicity (mainshocks per unit time and area) is interpreted to be representative of a stationary pattern over thousands of years. Thus, spatially smoothed seismicity, which reflects localization of seismicity from the short instrumental time sample, is down-weighted. In our section on Tectonic Models, we discuss the uncertain relative influence on the regional stress field of WNW-ESE Basin and Range extension, NW-SE dextral shear, and general N-S basal traction and/or horizontal compression. This uncertainty leads us to give equal weight to the three scenarios based on regional seismotectonics. Our weights, then, are:

0.3: Scenario I (Zones 1, 2, 3A)
0.3: Scenario II (Zones 1, 3B)
0.3: Scenario III (Zones 1, 3C, 3D)
0.1: Spatially Smoothed Seismicity.

5.7 NON-INCLUSION OF A VOLCANIC ZONE

We considered the need to account for seismicity associated with episodic volcanism in the Crater Flat domain and concluded that it is unnecessary to include a volcanic source zone in addition to a spatially coincident background source zone. Our reasoning is as follows: An appropriate M_{max} for volcanic-related seismicity in the Yucca Mountain region is M 5.0 to M 5.5 (Smith *et al.*, 1995, 1996). Given that the project definition of seismogenic implies the generation of earthquakes of $M \geq 5.0$, the question becomes, "How often are volcanic-related earthquakes of M 5.0 to M 5.5 likely to occur in the Crater Flat domain?"

According to (B. M. Crowe *et al.*, LANL, written communication, 1995, p. i), postcaldera basaltic volcanism in the Yucca Mountain region represents "one of the lowest eruptive rates in a volcanic field in the southwest United States." More specifically, estimates of the maximum or worst-case recurrence (minimum interevent time) for volcanic events in the Yucca Mountain region are 8.0×10^{-6} events yr^{-1} (1/N = 125,00 yr) using homogeneous Poisson models and 8.4×10^{-6} events yr^{-1} (1/N = 119,000 yr) using nonhomogeneous Poisson models (ibid., p. 7-2f).

We examined the recurrence rates for background seismicity in the Yucca Mountain region calculated for DOE's 1994 design study for the ESF (I.G. Wong presentation at SSC Workshop 3). The cumulative annual number of events per km^2 above $M_{min} = 2.5$ and with $M_{max} = 6.5$ is given by $\log N = -1.37 - 0.83M$. (We assume equivalency between M_L and moment magnitude for the magnitude range being considered.) From the above, the expected annual number of events per km^2 in the range $5.0 \leq M < 5.5$ is 1.8×10^{-6} events yr^{-1} km^{-2}.

For comparison, we provisionally considered a volcanic source zone in the southwestern part of the CFD that has an area of approximately 1.4×10^3 km^2 smaller (and hence containing more events yr^{-1} km^{-2}) than the area of potential volcanism considered by B. M. Crowe *et al.* (LANL, written communication,1995). The number of background seismic events in the range $5.0 \leq M < 5.5$ within our volcanic source zone would be 1.8×10^{-6} events yr^{-1} km^{-2} * 1.4×10^3 km^2 or 2.52×10^{-3} events yr^{-1} (1/N = 397 yr).

From the above, we compared the rate of background seismic events within our volcanic source zone (2.52×10^{-3} events yr^{-1}) to the estimated worst-case rate of volcanic events with which earthquakes would be associated—$(8.0\text{-}8.4) \times 10^{-6}$. The rate of volcanic events is two to three orders of magnitude lower than the rate of M5.0 to M5.5 background earthquakes within our volcanic source zone—beyond the precision with which background seismicity can be estimated.

Thus, we concluded that there is no need to define a volcanic source zone in addition a spatially coincident background source zone. Background earthquakes in the range of

M5.0 to M5.5 sufficiently represent, for probabilistic vibratory ground-motion hazard, the rare episodic occurrence of volcanic-related earthquakes in the same magnitude range.

6.0
FAULT DISPLACEMENT CHARACTERIZATION

6.1 GENERAL REMARKS

Our methodology for characterizing the potential for fault displacement at Yucca Mountain has been influenced greatly by the presentations and interactions at SSC Workshops 4, 5, and 6. In order to characterize, in a probabilistic way, the amount, frequency, and variability of future fault displacements at a point, we use two basic approaches: (i) an earthquake approach that builds on our seismic source characterization for ground-motion hazard and (ii) a displacement approach in which the observed geology guides the expectation of the long-term outcome.

From the outset, we have held the view — based chiefly on empirical observations and a substantial literature in structural geology (see, for example, the February-March 1996 Special Issue of the Journal of Structural Geology) — that scaling relationships variously involving single-event slip, fault dimension, and total cumulative displacement on a fault offer a practical way to characterize fault-displacement potential. This applies particularly to a displacement approach.

We recognize that any use of scaling relationships in the context of earthquakes and faulting can be expected to invite scrutiny and concern. There is ongoing debate about the scaling of earthquake slip with source dimensions, particularly as it relates to implications for underlying mechanics and the dynamics of rupture propagation (e.g., Bodin and Brune, 1996, and references therein). Controversy about scaling relations for large earthquakes is a notable case in point (Romanowicz and Rundle, 1993).

In our final methodology we have taken care to use only scaling relations that are empirically founded and defensible from documented observations in the Yucca Mountain region and/or by supporting reference to the published literature. We specifically avoid assumptions about

the underlying physics of fault rupture, and we limit the validity of our empirical scaling relations to the size range and structural framework of faults and fractures at Yucca Mountain. We elaborate in Section 6.2.

6.2 THE ISSUE OF TRIGGERING

Another issue that warrants comment at the outset is the triggering of fault slip and the relative importance of static versus dynamic triggering, an issue raised at SSC Workshops 5 and 6 and a subject attracting considerable attention since the 1992 Landers, California, earthquake (see Gomberg *et al.*, 1997, and references therein). The question here is whether our characterization of fault-displacement potential adequately accounts for the possibility of both types of triggering.

Static triggering refers to seismic slip hypothesized to result from static-stress changes which are caused by fault slip elsewhere and which increase the stress on a fault or fault segment so as to move it closer to a threshold of frictional failure, generally specified by the Coulomb failure criterion (see King *et al.*, 1994, and Simpson and Reasenberg, 1994, for overviews). Such static-stress changes can act oppositely to retard failure, but our focus here is on triggering. Dynamic triggering, which also involves frictional instability, refers to the hypothesized initiation of seismic slip by transient stress/strain changes associated with the passage of seismic waves, either from near or distant earthquakes (e.g., Gomberg and Bodin, 1994; Gomberg, 1996; Gomberg *et al.*, 1997).

Gomberg *et al.* (1997) usefully distinguish two types of potential triggering: in the first, termed a clock-advance type, triggering (static or dynamic) simply advances the time of fault slip that would have eventually happened anyway; in the second, termed a new-seismicity type, triggering (static or dynamic) induces fault slip that would not otherwise have occurred under a constant background load. Triggering from near earthquakes (tens of kilometers) may result from either static or dynamic stress/strain changes or both, whereas triggering from remote earthquakes (hundreds to thousands of kilometers) would be attributed to dynamic triggering (Gomberg, 1996; Gomberg and Davis, 1996).

For the Yucca Mountain fault-displacement characterization, we can separately consider (a) the triggering of a primary faulting event on one of the principal faults and (b) the triggering of secondary/distributed fault slip on any fault or fracture at Yucca Mountain. For both (a) and (b), instances of clock-advance triggering (static or dynamic) would have no effect on our probabilistic characterization of fault-displacement potential over the long-term because the relative timing of displacement events would be altered, not their average frequency over the long term, and estimates of the amount of displacement would not change.

What about new-seismicity triggering? First, we emphasize that such a hypothesis is still in a formative stage. Observational evidence presented in its support includes the triggering of small-magnitude earthquakes interpreted to be in excess of background seismicity at Long Valley, California, and at The Geysers, California (see Gomberg *et al.*, 1997, p. 302). Gomberg *et al.* (1997) show qualitatively by using model studies that the new-seismicity hypothesis is plausible under conditions of dynamic triggering, but they caution against using their results to make quantitative interpretations or predictions. Further, the potential for dynamic triggering appears to depend strongly on site characteristics and response (Gomberg, 1996).

For the case of principal faulting, we ask the question, What are the effects on our fault-displacement characterization if triggering (static or dynamic) were to cause surface-rupturing events that otherwise would not have occurred? Logically, this implies surface rupture on a fault not included in our inventory of faults that have a nonzero probability of being seismogenic. Allowing, for the sake of argument, that such new-seismicity triggering is plausible, we reason that its relative long-term probability of occurrence in the future would be similar to that in the past. Because our inventory of principal faults is based on the observed geology, which reflects ample opportunity during the Quaternary epoch for dynamic or static triggering of surface-rupturing events on potential sources of principal faulting not now accounted for, we consider the probability of triggering new principal faulting to be negligible.

If one pushes the concept of new-seismicity triggering to have it add to the number of surface-rupturing events on our inventoried principal faults, we again reason that its long-term relative probability of occurrence in the future, would be similar to that in the past.

As we describe later (see Sections 6.3 and 6.6), our displacement approach to surface displacement on a principal fault effectively accounts for the average relative frequency of any surface displacement, regardless of its cause. In our lower-weighted earthquake approach to principal faulting (Section 6.5), the frequency-magnitude relation of earthquakes on a principal fault is constrained by the average recurrence interval and/or slip rate from paleoseismology, which implicitly accounts for the aggregate long-term history of all displacement events, however they are produced.

Continuing this line of questioning, we examine the case of secondary/distributed fault slip and question what effects new-seismicity triggering (static or dynamic) would have on our characterization. Here too, our displacement approach (Sections 6.3 and 6.7) effectively accounts for all displacements, however they are produced. The last case remaining to be examined is that of our earthquake approach to secondary/distributed faulting on faults and fractures that are not principal faults (Section 6.8). In this case, our method accounts for all earthquakes on identified fault sources and in background source zones out to 100 km that represent opportunities for static or dynamic triggering. Whether or not triggering ensues is assessed probabilistically using empirical approaches. Admittedly, we do not account for plausible new-seismicity triggering by remote earthquakes at distances greater than 100 km. The magnitude of such earthquakes would have to be reasonably large for dynamic stress/strain changes to exceed a triggering threshold (Gomberg and Davis, 1996). Faced with the epistemic uncertainties associated with this particular case, we downweight it in our logic tree.

6.3 ORDER OF PRESENTATION

In the following sections, we first lay the groundwork for our fault-displacement assessment by defining terms and notation, presenting scaling relations, and describing our analysis of variability of slip at a point. We then proceed to describe our separate logic trees for principal and distributed faulting, beginning with an overview followed by sequential description of (1) our earthquake approach to principal faulting, (2) our displacement approach to principal faulting, (3) our point-estimate method (a displacement approach) for distributed faulting, and (4) our principal-distributed-faulting method (an extension of our

earthquake approach) for distributed faulting. Finally, we provide the assessments for the nine test calculation sites.

In applying our logic trees, we distinguish between sites subject to principal faulting (on potentially seismogenic faults) and sites subject to distributed faulting only. Sites in the first category are subject to the hazard of both principal and distributed faulting.

6.4 NOTATION

A potential pitfall we encountered in the fault-displacement analysis is the use of ambiguous terms, so we emphasize the importance of careful notation. In the case of "average displacement," for example, there are clear physical distinctions between the average displacement over the slip surface (i.e., the area of a fault engaged in a rupture event), the average displacement at the ground surface along a rupture, and the average displacement at a point on a fault (at or near the surface) over many displacement events at that point.

In our notation, both for fault displacement and ground-shaking hazard, we try to be as consistent as possible with (1) terms defined by Wells and Coppersmith (1994), whose regression relations we frequently refer to, (2) the notation and terms used most recently by R.R. Youngs and the SSC Facilitation Team (presentations at SSC Workshop 6), and (3) notation used in citations to which we refer the reader. In some cases, however, we give preference to special notation needed to emphasize clear thinking about what is being described and analyzed. For example, we use the term $\bar{U}$ for the average displacement over the slip surface to prevent any possible confusion with other terms for displacement involving the letter D. Following usual convention, a bar over a symbol signifies an average value.

We use superscript notation for some special cases in which the largest value of a parameter has particular importance, in part to avoid confusion with the commonly used suffix "max." (Consider the term "Dmax," which has been used extensively during the SSC Workshops to indicate a maximum displacement, but variously defined.) Some scaling relations involving fault length are only valid for <u>total</u> fault length, which we emphasize by using the term L^{total}. Similarly, the value of maximum surface displacement, MD, that is estimated for the largest displacement event on a fault (generally involving L^{total}) we designate as MD^{max}.

The following is a basic outline of notation used. More complete explanation is given as the terms arise in subsequent discussion.

AD = average (surface) displacement
AR = aspect ratio (L/W)
D or d = general terms for a displacement on a fault
Dcum = total cumulative displacement (herein meaning post-Tiva Canyon Tuff)
D_E = single-event displacement on a fault at or near the surface
$\overline{D}_E$ = average value of D_E at a point on a fault over many displacement events
L = general term for the length or longest horizontal dimension of a fault or rupture (equivalent to RLD in the case of a single rupture)
L^{total} = total length of a fault
M = magnitude (herein meaning moment magnitude)
MD = maximum (surface) displacement
MD^{max} = expected value of MD corresponding to the largest displacement event on a particular fault
P[C] = probability of being capable of slip (i.e., slip susceptibility) given the contemporary stress field at Yucca Mountain
P[S] = probability of being seismogenic (i.e., of generating an earthquake of $M \geq 5.0$)
P[slip|pf] = probability of secondary/distributed faulting, given principal faulting on a nearby fault
QSR = Quaternary slip rate
RA = rupture area
RI = recurrence interval
RLD = subsurface rupture length (rupture length at depth)
RW = rupture width (downdip dimension)
SR = slip rate
$\overline{SRL}$ = surface rupture length
$\overline{U}$ = average displacement over a slip surface (i.e., the area of a fault engaged in a rupture event)
W = general term for the width or downdip dimension of a fault
λ_{DE} = frequency at which displacement events occur

6.5 SCALING RELATIONS

In this section we provide a basis for adapting scaling relations that can be used for characterizing fault-displacement potential on structures ranging from small fractures upward to the unsegmented relatively small faults ($L < 25$ km) with relatively small cumulative displacement (< 0.5 km) at Yucca Mountain.

We emphasize that we use only scaling relations that are empirically founded, reasonably robust, and which can be adopted without critical assumptions about the underlying physics of fault rupture. We recognize that some of the scatter in data distributions that control the scaling relations we use undoubtedly arise from the kind of complications in earthquake source mechanics discussed by Bodin and Brune (1996)—such as might be expected, for example, from dynamic rupture propagation with spatially varying stress drops, as opposed to quasi-static constant-stress-drop modeling.

The following logic is used to develop our scaling relations: (1) for the Yucca Mountain faults and fractures to be considered, and based on empirical observations alone, a linear approximation can be justified for the scaling of single-event slip $\overline{U}$ with fault rupture length L; (2) empirical observations over a wide range of scales show that total cumulative displacement Dcum on a fault scales linearly with total fault length L^{total}; (3) given (1) and (2), $\overline{U}$ should scale linearly with Dcum when $L = L^{total}$. We show how knowledge of Dcum on a fault or fracture can provide a practical basis for scaling the likely amount of slip on that feature during a future displacement event.

$\overline{U}$ Versus L

Abundant data summarized by Abercrombie (1995, her Figure 11), among others, provide an empirical basis for relating seismic moment to the cube of source dimension—without any assumption about stress drop—over the range from 10 m to at least 10^4m. The measurements of source dimension are based mostly on corner frequencies from shear-wave spectra, such that each represents the radius r of an equivalent circular fault. Based on the moment equation, the distribution of these data imply that $\overline{U}$, on average, scales linearly with r, and similarly $\overline{U}$ can be inferred to scale linearly with rupture length L for roughly equidimensional faults in this range of source dimensions. Thus we adopt a relation of the form, $\overline{U} = \alpha * L$, where α is the constant of proportionality.

Let us be clear. We are not arguing for a model-dependent linear scaling of $\overline{U}$ with L (a so-called L model), which we recognize to be controversial, particularly for large earthquakes (Romanowicz and Rundle, 1993; Bodin and Brune, 1996). Rather, we argue that a linear

relationship is a reasonable approximation for the fault sizes we are considering—based on the abundant earthquake source data summarized by Abercrombie (1995).

We derived an empirical value of α for the Yucca Mountain local faults using data in Table AAR-4 (preferred values for independent faults, Bare Mountain fault excluded). In order to compile consistently paired values of displacement and rupture length for regression, the data were first corrected in the following way. Values of MD, the maximum surface displacement per event along a fault (labeled Dmax in Table AAR-4), were converted to $\overline{U}$ using Wells and Coppersmith's (1994) modal value 0.76 for the ratio $\overline{U}$/MD. Also, we converted the tabulated values of total fault length (labeled active length in Table AAR-4), which were originally assessed as estimates of SRL, to RLD using Wells and Coppersmith's (1994) result that the expected ratio of SRL/RLD is 0.75. Applying the latter correction is appropriate insofar as all the SRL values for the independent faults in Table AAR-4 are within the range of data from which the expected ratio was originally estimated (see Wells and Coppersmith, 1994, p. 985).

Given paired values of $\overline{U}$ and L^{total} for 19 faults, we followed guidance from R.R. Youngs of the Facilitation Team to derive an empirical estimate of 3.69 ($\pm$1.10) x 10^{-5} m/m for α from the mean value of log ($\overline{U}/L^{total}$) (see equation 1, Table AAR-9). This procedure was followed in order to allow the Facilitation Team to estimate aleatory uncertainty in an appropriate form. For comparison, we performed similar calculations using data from S. K. Pezzopane and T. E. Dawson (USGS, written communication, 1996), who plot Quaternary displacement per event versus maximum fault length for six Yucca Mountain faults (their Figure 9-19). To convert their displacement values to $\overline{U}$, we interpreted them as estimates of average surface displacement AD and used Wells and Coppersmith's (1994) modal value 1.32 for the ratio $\overline{U}$/AD. Processing Pezzopane and Dawson's six paired values of displacement and fault length in the form of log ($\overline{U}/L^{total}$), α = their values of "maximum fault length" 3.42 ($\pm$ 1.08) x 10^{-5} m/m, taking L to be estimates of SRL.

For our logic tree, we adopt $\alpha = 3.69 \times 10^{-5}$ m/m derived from our own data—both for internal consistency and because of our larger data set. Because the data are specific to the Yucca Mountain faults, we prefer the result to other values found in the literature. Cowie and

Scholz (1992c) cite values for α ranging from ~1.5 x 10^{-5} for continental plate boundary earthquakes to ~1.0 x 10^{-4} for intraplate earthquakes, including an estimate of ~2.0 x 10^{-5} for earthquakes in the northern Basin and Range.

Dcum Versus L^{total}, General Relation

The basis for the linear scaling of cumulative displacement Dcum with total fault length are developed at length by Cowie and Scholz (1992a,b,c). More recently, rigorous statistical testing by Clark and Cox (1996) of 11 worldwide data sets of log (Dcum) versus log (L^{total}), for fault populations ranging in length from tenths of a meter to hundreds of kilometers, confirm a linear relationship between fault displacement and length within each data set. (See H. L. McKague *et al.*, CNWRA, written communication, 1996, for evidence of the linear scaling of Dcum with fault trace length for faults in the general Yucca Mountain region.)

Following the conventional analysis of Dcum versus L in log-log space, we seek an empirical relation of the form, log (Dcum) = K + log (L^{total}), where K is a constant. In terms of the alternate scaling factors P (Clark and Cox, 1996) and γ (Cowie and Scholz, 1992 b, c), $P = 10^{-K} = 1/\gamma$. We derived an empirical value of K for the Yucca Mountain faults using data in Table AAR-4 (preferred values for independent faults, Bare Mountain fault excluded). The values of Dcum (labeled total displacement in Table AAR-4) consistently represent total cumulative displacement of the Tiva Canyon Tuff. As we did in relating $\bar{U}$ to L^{total}, values of total fault length were first converted to RLD. The resulting regression of 16 available paired values of Dcum and L^{total} yielded a best-fit value of K = - 1.58 (see Table AAR-9 for regression parameters), equivalent to P = 38 or $\gamma = 2.6 \times 10^{-2}$ m/m. We examined, but decided not to regress 6 paired values of Dcum and L^{total} presented by S. K. Pezzopane and T. E. Dawson (USGS, written communication, 1996) in their Figures 9-19 and 9-20 because those data are presented as only preliminary.

Dcum Versus L^{total} for Small Faults and Fractures

Available data and well-constrained trends indicate that Dcum on small faults and fractures appears to be systematically smaller than that estimated by extrapolating the scaling with length from larger faults (Clark and Cox, 1996; Cowie and Scholz, 1992b). We accept this empirical observation.

Based on data in Clark and Cox (1996, their Figure 1) and the range of our data, we judge that our scaling constant for Dcum/L derived in the previous section can be reliably applied only for L greater than about 3 km and Dcum greater constant for than about 75 m. For smaller faults and fractures—down to the scale lengths of features possibly of engineering concern in the repository, we use the data of Clark and Cox (1996) to assess the following distribution for the scaling factors (and corresponding weights), where the minimum value of P is that observed from the data set of the Yucca Mountain faults:

$K = -1.58$ [$P = 38$; $\gamma = 2.63 \times 10^{-2}$] (weight = 0.3)
$K = -2.18$ [$P = 150$; $\gamma = 6.67 \times 10^{-3}$] (weight = 0.4)
$K = -2.70$ [$P = 500$; $\gamma = 2.00 \times 10^{-2}$] (weight = 0.3)

$\bar{U}$ (and MD^{max}) Versus Dcum

Given the relations: (1) $\bar{U} = \alpha * L^{total}$ and (2) $\log (Dcum) = K + \log (L^{total})$, straightforward substitution leads to (3) $\log \bar{U} = \log \alpha - K + \log (Dcum)$ when $L = L^{total}$. This in turn can be expressed in the form $\bar{U} = \beta * Dcum$, where $\beta = \log^{-1} (\log \alpha - K)$. For small faults and fractures, our distribution on K transforms into the following values (and weights) on β (m/m):

1.40×10^{-3} (0.3), 5.59×10^{-3} (0.4), 1.85×10^{-2} (0.3).

The restriction that $L = L^{total}$ implies that the assessed value of Dcum should be the largest value for the entire fault. Thus, the scaling we have derived is fundamentally tied to maximum values associated with a maximum displacement event, which is equivalent to a maximum-magnitude earthquake on a fault. In both circumstances, expected parameters for smaller-size events are scaled from those of the maximum event using other information.

Because we are concerned with fault-displacement characterization at or near the surface, we use the parameter MD^{max}, the value of MD corresponding to the maximum displacement event on a particular fault, instead of $\bar{U}^{max}$ for that same event. We relate the two using Wells and Coppersmith's (1994) modal value of 0.76 for the ratio $\bar{U}$/MD such that, for the relatively small-displacement faults at Yucca Mountain (Dcum <500m), $MD^{max} = 1.32 * \bar{U}^{max}$ or, by substitution, $MD^{max} = 1.32 * \beta * Dcum$.

QSR Versus Dcum

In our point-estimate method for distributed faulting, we require estimates of Quaternary slip rate QSR on a secondary fault or fracture, given an observation of Dcum. Here, we develop a regression relation between QSR and Dcum based on selected paired values in Table AAR-4 for the local Yucca Mountain faults. We use the median values listed for 11 of the 19 independent faults, excluding the Bare Mountain, E. Lathrop Cone, East Busted Butte, Midway Valley, and West Dune Wash (1 and 2) faults. The Bare Mountain fault is excluded because we judge it to be less relevant than the Yucca Mountain faults and it is an extreme outlier if used. Data for the latter five faults are excluded because their slip rates are based on relative comparisons of geomorphology, rather than on direct paleoseismic information.

Using the 11 paired values of QSR and Dcum, we performed a linear regression of QSR (mm/yr) on Dcum (m), constraining the intercept to be zero, and derived a value of 3.26 ($\pm$ 1.72) x 10^{-5} mm/yr/m for the slope coefficient. Statistical parameters for the regression are given in Table AAR-9.

6.6 DISPLACEMENT AT A POINT

A key part of the methodology for fault-displacement characterization is assessing the variability of slip at a point—both (1) as a function of position along strike of the fault, given the size of an event, and (2) variability of slip at the same point from event to event. Of the techniques presented and evaluated to date (summarized in presentations by R.R. Youngs at SSC Workshops 5 and 6), we are satisfied with available solutions for (1), but not (2).

The method developed by the Ake, Slemmons, McCalpin (ASM) team is well suited for estimating variable slip along strike, scaled to the maximum surface displacement MD for a given event (see summary of fault-displacement-hazard methodologies by SSC Facilitation Team, SSC Workshop 6, Figure 5; see also Appendix F this volume). The statistical averaging inherent in the method is realistic, and we see no reason to use an alternate approach that is more deterministic. We considered alternate shape functions to the elliptical displacement profile of the ASM model. Cowie and Scholz (1992a), for example, describe a profile predicted to taper gradually toward the fault tip; they also show normalized

displacement profiles for faults in Japan and Britain that are relatively linear from fault-center to fault-end. Nicol *et al.* (1996), on the other hand, show normalized profiles for restricted faults (i.e., those that intersect the surface or closely approach other faults) whose envelope follows the elliptical shape of the ASM profile. In the end, we determined the ASM model is sufficient for the use we make of it in our logic tree (1) in our earthquake approach to principal faulting (Figure AAR-16) and (2) in assessing distributed faulting at sites where principal faulting also occurs (Figure AAR-23). We adopt the statistical relationships to repeat the ASM model presented in Appendix H, Section H.3.1.

In analyzing the problem of variability of slip at a point from event to event, we observed that, in aggregate, the displacement measurements in the many fault trenches at Yucca Mountain, scaled to MD^{max} on each fault, reflect an exponential-like distribution. This appears to be a combined result of both temporal and spatial variability. We proceed to describe our analysis and use the results as a key basis for assessing the conditional probability for displacement exceedance.

We adapt and extend the approach used by the Doser, Fridrich, Swan (DFS) team (presentation at SSC Workshop 5; see also Appendix H this volume). The DFS team made a composite of displacement data measured in trenches throughout the Yucca Mountain region and summarized by S. K. Pezzopane *et al.* (USGS, written communication, 1996a) in their Table 5-1. Each displacement was normalized to the average from its same trench, and data were then pooled from all trenches. We note that the true average slip over many events at the same point is poorly estimated when the number of observations in a single trench is small. We reasoned that a more robust basis for normalizing the displacement measurements would be to compare them to some independent measure, and we selected MD^{max}, the expected value of MD corresponding to the largest displacement event on that fault.

First, we used the same multiple approaches specified in Figure AAR-16 of our logic tree (but using only median parameter values) to get a weighted-average estimate of MD^{max} for each of the nine faults associated with the 19 trench summaries in Table 5-1 of S. K. Pezzopane *et al.* (USGS, written communication,1996a). Second, we normalized each of 82 available displacement measurements (excluding the Rock Valley fault) to a corresponding value of MD^{max}. Third, we constructed both a probability density function (PDF) and a

cumulative distribution function (CDF) for the combined data, shown here in Figure AAR-11. We discuss these results presently. Fourth, as a test, we carefully examined the trench locations with respect to their along-strike location and used data only for nine of the 19 trenches that were unambiguously located along the central half of a fault to construct a separate PDF-CDF combination. Again, distributions similar to those in Figure AAR-11 resulted. For greater robustness, we chose to use the data from all 19 trenches. The data are listed in Table AAR-10.

Regarding Figure AAR-11, one might ask, 'how can the ratio D/MD^{max} exceed 1.0, as plotted on the abscissa?' Note, as described in the proceeding paragraph, that MD^{max} for each fault is a weighted-average from different approaches of the expected maximum displacement and that central values were used in the calculations. Thus epistemic uncertainty in the estimate and randomness in the process allows the observed values of D to exceed the expected value of MD^{max} estimated for any individual fault. As we have estimated it, MD^{max} simply provides a basis for normalizing observations for comparison from fault to fault.

The PDF shown in Figure AAR-11 was fit with the function $y = 0.09 \exp (- 0.68\ D/MD^{max})$. Regression parameters are listed in Table AAR-9. Following Benjamin and Cornell (1970), we analyze the CDF in terms of the generalized exponential distribution $\lambda e^{-\lambda x}$, whose CDF is $1-e^{-\lambda x}$. For the generalized PDF, values along the x-axis are numerically plotted as λx. The mean value of D/MD^{max}, which is 0.83 for the 82 displacement measurements, directly provides the expected value of $1/\lambda$. Hence $\lambda = 1.20$. The variance on λ is approximated by λ^2/n, and the median for the distribution is given by $0.693/\lambda$.

In the CDF in Figure AAR-11 we superpose the curve for $1-\exp (-1.20\ (D/MD^{max})$, which shows good agreement with the observed CDF. Importantly, the mean (0.83) of the observed values of D/MD^{max} gives a key piece of information—namely, a reliable estimate of $\bar{D}_E$, the average displacement at a point on a fault (at or near the surface) over many displacement events at that point.

The data of Figure AAR-11 were analyzed independently by the Facilitation Team (Appendix H, Section H.2.5), and various statistical distributions were fit to the data. As described in Appendix H, good fits to the data were obtained for an exponential distribution with a mean

of 0.83 and for a gamma distribution with two parameters; a slightly better goodness of fit for the gamma distribution is shown to be only marginally statistical significant.

In examining Figure AAR-11, note that a lower limit of resolution is implicit and inescapable. Some would argue that very small, unobserved surface displacements are greatly more numerous than observed ones, but such a hypothesis must be reconciled with observed earthquake statistics and the observed geology, particularly in terms of the cumulative offset implied by having many small unobserved displacement events. For example, if a one-centimeter displacement event is thought to be material, 100 such unobserved events require one meter of cumulative offset to be accounted for during some time period, and 1,000 such events, 10 m.

In the case of the data used in Figure AAR-11, the smallest bin is centered on 0.1 D/MD^{max}. Following conventional rules for rounding, the two smallest observed ratios of 0.04 and 0.05 (rounded to the nearest even integer) fell below the smallest bin. These ratios correspond to one displacement of 5 cm on the Solitario Canyon fault (MD^{max} =112 cm) and another of 6 cm on the Paintbrush Canyon fault (MD^{max} = 112 cm). The eleven displacement events included in the smallest bin range from 3 to 7 cm.

Based on the data shown on Figure AAR-11, together with the supporting analysis of the Facilitation Team (Appendix H), we adopt the exponential distribution as an appropriate and reasonable empirical predictor for the distribution of displacement at a point — within implied limits of resolution for the ratio of a displacement event to MD^{max}.

To summarize, MD^{max} provides a useful basis for scaling and comparing displacement measurements on the Yucca Mountain faults. The result that aggregated values of D/MD^{max} can be modeled approximately by an exponential distribution has great utility. Not only does the distribution enable a reliable estimate of the average displacement at a point, it also combines both spatial and temporal variability at that point. We interpret the distribution to be a composite effect of event-to-event variability of primary fault ruptures, along-strike variability during ruptures on the same fault, and distributed faulting triggered by static and/or dynamic stress/strain changes. We emphasize that having displacement events at a generalized point on the surface approximate an exponential distribution does not necessarily

imply that earthquakes on the primary faults also follow such a distribution. We adhere to our separate assessment of characteristic versus exponential slip events at depth on the principal faults.

6.7 OVERVIEW OF LOGIC TREES

For convenience, we construct separate logic trees for principal and distributed faulting. After evaluating various approaches proposed and discussed at SSC Workshops 4 and 5 for characterizing fault-displacement potential, we use both an earthquake and a displacement approach for principal faulting. We then assess the potential for distributed faulting using two methods described by R. Youngs (presentation at SSC Workshop 5) as a point-estimate (displacement) method and a principal-distributed faulting (earthquake) method.

For principal faulting, we give a weight of 0.67 to the displacement approach and 0.33 to the earthquake approach. We give greater weight to the former because we are persuaded that, ultimately, the size and frequency of displacements on faults and related features exposed at the surface (or in the repository) must be governed by the budget of what is observed—namely, the record of displacements at or near the surface.

When we assess the potential for distributed faulting, we take different approaches for (1) sites of distributed faulting only and (2) sites where principal faulting also occurs (Figure AAR-12). We do this because at the latter sites the displacement approach for principal faulting simultaneously accounts for distributed faulting at the same point. At such sites, conditional on using the earthquake approach to principal faulting (weight = 0.33), we then use only the principal-distributed faulting method to characterize distributed faulting.

For assessing the potential for distributed faulting at sites of distributed faulting only, we give a weight of 0.33 to our principal-distributed faulting method and 0.67 to our point-estimate method. We downweight the first method for two reasons. First, as discussed earlier in Section 6.2, it does not fully account for plausible new-seismicity triggering by dynamic stress/strain due to remote earthquakes at distances greater than 100 km. Second, we have more confidence in our point-estimate method for characterizing the frequency of slip on a specific secondary fault or fracture.

Throughout our logic tree, whenever we use a regression relation from Wells and Coppersmith (1994), we intend the use of the respective equation for the category of All Data. Our defined sources of principal faulting include those local fault sources in Table AAR-3 which have a probability of being seismogenic, P[S] > 0.

6.8 PRINCIPAL FAULTING—EARTHQUAKE APPROACH

In the earthquake approach (Figure AAR-13), our logic tree for ground-shaking hazard provides a starting point at which one is given a frequency-magnitude distribution for a subject fault. Given an event of magnitude M, we proceed to estimate rupture length L, in part as a predictor of maximum surface displacement (MD) and average surface displacement (AD). For later application, we distinguish between surface rupture length, SRL (for cases of rupture at or near the surface), and subsurface rupture length, RLD. Unless specified otherwise, L is implied to be subsurface rupture length.

Estimating RLD

We give equal weights (0.5, 0.5) to two approaches for estimating RLD (Figure AAR-14). The first is the straightforward use of a regression relation between RLD and M from Wells and Coppersmith (1994). In the second approach we follow Nicol *et al.* (1996), who review data indicating that simple normal faults have an approximately elliptical shape with a subhorizontal major axis. We constructed a cumulative distribution of aspect ratios for 54 earthquake slip surfaces using data from Nicol *et al.* (1996, their Table 2), from which we assess the following distribution for aspect ratio (and relative weighting):

0.8 (0.3), 1.4 (0.4), 2.5 (0.3).

Given M, we use the regression relation, log (RA) = -3.49 + 0.91 M (Wells and Coppersmith, 1994) to estimate rupture area RA in units of km^2. For an elliptical rupture, the major axis = L/2, from which it can be shown that L (km) = $[(4/\pi * \text{aspect ratio} * (RA)]^{1/2}$.

Estimating SRL

Our two approaches to estimating SRL (Figure AAR-14) basically parallel those just described for estimating RLD, and again we assign equal weights (0.5, 05). The first approach uses a regression relation between SRL and M from Wells and Coppersmith (1994). In the second approach, we calculate the length dimension of an elliptical rupture area as for RLD, but the difference is that for the range of lengths being considered, SRL is expected to be less than RLD, and we adopt the ratio 0.75 for SRL/RLD (Wells and Coppersmith, 1994) as a correction factor.

Estimating P[Surface Rupture]

In order to estimate the probability of surface rupture, P[surface rupture], given an event of magnitude M, we invoke a simulation approach developed for the ground-motion modeling in which the location of a rupture is randomized on the subject fault source (Figure AAR-15). The modeling uses our adopted focal depth distribution for $M \geq 5.0$ (based on one from K. Smith, presentation at SSC Workshop 2, "Depth Distribution—SGB 1979-present"). The distribution of distance from a hypocenter to the top of rupture is calculated by allowing the hypocenter location to be uniformly distributed on the lower 75% of the rupture.

In the randomization analysis, the subsurface dimensions of a rupture for an event of magnitude M are modeled by using, with equal weights, the two methods already described for estimating RLD (see Figure AAR-14). In the first, RLD is determined from a regression relation between RLD and M, and downdip rupture width W follows from an assessed distribution on aspect ratio (Figure AAR-15), which has the following distribution of values and weights, justified earlier: 0.8 (0.3), 1.4 (0.4), 2.5 (0.3). In the second method, RLD and W derive from the rupture area RA of an elliptical rupture (where RA is determined from a regression relation between RA and M) whose aspect ratio has the same distribution specified above.

For realizations of surface rupture, the weighted-average value of surface-rupture length SRL (Figure AAR-14) is used to randomize the along-strike location of surface rupture. For the general case in which SRL is less than the total trace length of a fault, the cases of surface rupture in effect become a one-dimensional randomization in which a rupture of trial length SRL is randomly located along the fault trace. This later enables one to assess the location of

any point on the fault with respect to a realized surface rupture in order to apply the ASM model for variability of slip along strike. In any application to a specific fault, the weighted-average value of SRL cannot exceed the total fault length and must be limited to the latter in such cases.

Although this simulation modeling for estimating the probability of surface rupture undoubtedly oversimplifies some complex aspects of faulting, we adopt it for the following reasons. It directly incorporates our subsurface characterization of fault sources at Yucca Mountain and it yields results that are similar to the empirical distributions for the probability of surface rupture derived from samples of historical earthquakes in the Great Basin and surrounding regions of the western U.S. (see Appendix H).

Estimating MD And Variability Along Strike

Given M, SRL, and RLD, we proceed to estimate the expected maximum surface displacement MD on a principal fault (Figure AAR-16).

We focus on estimating the expected value of MD for principal faulting because we adopt the ASM model to assess variability of slip along strike, and that method uses a distribution normalized to MD. Our logic tree outlines three approaches to estimating MD, and we give basically equal weights to each approach. The first two involve regression relations from Wells and Coppersmith (1994) which deliver MD, given SRL or M.

We do not use direct assessments of MD from paleoseismic data tabulated in Table AAR-4 because those values imply rupture of total fault length. Instead, the paleoseismic data for the Yucca Mountain local faults are incorporated into the scaling relation between $\bar{U}$ and RLD, which is our third approach to estimating MD.

6.9 PRINCIPAL FAULTING—DISPLACEMENT APPROACH

Estimating MD^{max}

In our displacement approach to principal faulting (Figure AAR-17), we use three methods to estimate MD^{max}, which provides an underpinning for the recurrence modeling: (1) a fault-

length approach (weight = 0.3), (2) a cumulative-displacement approach (weight = 0.3), and (3) a paleoseismology approach (weight = 0.4).

In the fault-length approach, we use (a) an empirical relation between MD and SRL from Wells and Coppersmith (1994) (weight = 0.4) and (b) our empirical scaling relation between $\overline{U}$ and L^{total}, from which MD^{max} is then scaled from the implicit maximum value of $\overline{U}$ (weight = 0.6). In the first relation, the maximum value of SRL is used to yield MD^{max}.

The cumulative-bedrock-displacement approach, informally referred to as the "Dcum approach" in parts of our logic tree, uses the scaling relations we developed and discussed at length in the section on Scaling Relations. The operative relation is $MD^{max} = 1.32 * \beta *$ Dcum, where the scaling factor β depends on the size of the fault being considered (see Figure AAR-19). We described earlier our reasoning for treating larger and smaller faults differently, where the threshold of larger faults is approximately $L^{total} > 3$ km and Dcum > 75 m. For the larger faults, which with few exceptions include nearly all the principal Yucca Mountain faults, $\beta = 1.40 \times 10^{-3}$ m/m. For the smaller faults, the values (and weights) for β (m/m), justified earlier (see section on Scaling Relations, $\overline{U}$ [and MD^{max}] Versus Dcum), have the following distribution

$$1.40 \times 10^{-3}\ (0.3),\ 5.59 \times 10^{-3}\ (0.4),\ 1.85 \times 10^{-2}\ (0.3).$$

In the Paleoseismology approach, we use the values tabulated in Table AAR-4 under Dmax as direct assessments of MD^{max}.

Recurrence Of Displacement Events And Variability At A Point

To estimate the frequency of fault displacement as a function of size, we rely on the exponential distribution we derived (Figure AAR-11) as a basis for recurrence modeling (Figure AAR-17). We originally considered using an approach similar to that of Youngs and Coppersmith (1985) to derive a frequency-displacement recurrence relation using slip-rate information to distribute seismic moment. With our exponential model in hand, however, we consider it appropriate to use the more direct approach of estimating λ_{DE}, the average frequency of slip events, by dividing slip rate by $\overline{D}_E$, the average displacement at a point over many events. As discussed in our section on "Variability in Displacement at a Point," $\overline{D}_E$ is

estimated by 0.83 MD^{max}. Slip-rate information for the principal faults is provided in Table AAR-4.

6.10 DISTRIBUTED FAULTING—POINT-ESTIMATE METHOD

This method has three basic steps, which we have modified from an approach proposed by the DFS Team at SSC Workshop 5: (1) estimation of slip rate at a point using alternative methods linked to an observed value of Dcum; (2) estimation of the average frequency of slip events at the same point; and (3) estimation of the variability of slip at the point.

In our application of this method (Figure AAR-18), we give zero weight to estimating what we will call Quaternary slip rate QSR by assuming uniform slip on a feature during the last 12.7 Ma (post-Tiva Canyon Tuff), based on abundant evidence for major deformation prior to 11.6 Ma (pre-Rainier Mesa Tuff). We adopt as one approach, however, the possibility of uniform slip during the past 11.6 Ma. In order to assess the fraction of Dcum that accumulated before 11.6 Ma—in a way that is completely independent of paleo-seismological slip-rate information, we did the following. We used data presented by Fridrich *et al.* (1996) for estimates of extension in Miocene bedrock (based on the amount of stratal tilting as a measure of extension) for the three time periods: 12.7 to 11.6 Ma, 11.6 to 10.5 Ma, and 10.5 Ma to present. For the Controlled Area (of most direct interest to this fault-displacement characterization), we estimated the proportion of the cumulative percent of extension post-dating the 12.7 Ma Tiva Canyon Tuff that occurred from 12.7 to 11.6 Ma. Based on conditional logic reasoning, we then assessed the following distribution for the fraction of Dcum that has occurred during the last 11.6 Ma:

60% (0.3), 40% (0.4), 20% (0.3).

The post-11.6 Ma slip rate in this approach is inferred to approximate the average QSR.

Our second approach to estimating QSR was adapted from one described by J. Yount (presentation at SSC Workshop 5) in which offsets of basalts 3.7 Ma old in the Crater Flat basin are used to estimate the fraction of Dcum post-Tiva Canyon Tuff that has occurred in the past 3.7 Ma. Based on estimated offsets of basalts across the So. Windy Wash and So.

Crater Flat faults, and offset tephra across the Stagecoach Road fault, we assessed the following percentages (and weights):

40% (0.3), 16% (0.4), 5% (0.3).

Our third approach is the use of an empirical estimate of QSR as a function of Dcum, based on paleoseismic slip-rate data. The regression relation has already been described and is summarized in Table AAR-9. We assign relative weights to the three approaches that are inversely proportional to the duration of the time interval for which uniformity of slip rate is assumed. Accordingly, the weights are 0.1 for uniformity during the past 11.6 Ma, 0.3 for the past 3.7 Ma, and 0.6 for the time span covered by paleoseismic data (approximately ranging from 0.1 to 1 Ma).

In order to estimate MD^{max} on a secondary fault or fracture, we use information on L^{total}, if available, together with Dcum (Figure AAR-19). If both length and total-displacement information are available, we give equal weight to estimating MD^{max} from: (1) the scaling relation, $MD^{max} = 1.32 * \bar{U}^{max}$, where $\bar{U}^{max}$ (m) = $3.69 \times 10^{-5} L^{total}$ (m); and (2) the Dcum approach we described above in the section, Principal Faulting—Displacement Approach, Estimating MD^{max}. We then use the same procedures described in that section to estimate λ_{DE} and variability of slip at a point (Figure AAR-20)—except that here, our estimates of QSR come not from paleoseismic information in Table AAR-4, but from the feature-specific estimates of QSR just made.

6.11 DISTRIBUTED FAULTING—PRINCIPAL-DISTRIBUTED FAULTING METHOD

In this method, principal faulting may cause the occurrence of slip on secondary/distributed faults and fractures as well as on other principal fault sources. The frequency-magnitude distribution on the primary seismogenic fault is first determined by the earthquake method for principal faulting (Figure AAR-21). Whether a secondary fault or fracture slips is judged to depend on its slip-susceptibility tendency, the size of the principal faulting event, and distance from the principal fault in either the footwall or hanging-wall direction.

We attempted to invert the magnitude and frequency of principal faulting from our displacement approach using MD^{max}, but we encountered what we judged to be a fatal flaw. Given a principal fault, we can straightforwardly determine MD^{max} for the fault, as we did, for example, in our Principal Faulting-Displacement Approach. Given MD^{max}, our exponential distribution yields the relative frequency of displacement events of size D_E/MD^{max}. However, this measure is for the displacement at a single point and cannot be transformed into some measure such as AD or MD from which the magnitude of the event can be estimated. Therefore, we assign full weight to the earthquake approach for determining the magnitude and frequency of principal faulting.

Our logic tree for handling secondary/distributed faulting includes two probability terms (Figure AAR-21). First, P[C] is the probability that a feature is capable of slip to produce secondary/distributed displacement, given the contemporary stress field at Yucca Mountain. Second, P[slip|pf] is the probability that a secondary fault or feature slips to produce secondary/distributed displacement, given principal faulting nearby. Given a principal faulting event, the potential for secondary/distributed displacement on a nearby fault or fracture directly contains the multiplicative terms, P[C] and P[slip|pf]. Rules for assessing P[C] are given in a following section.

In order to apply P[slip|pf], we invoke a probability distribution function described by R.R. Youngs (presentation at SSC Workshop 6; see also Appendix H this volume) based on data from S. Pezzopane for the density of distributed faulting accompanying historic normal-faulting earthquakes in the extensional western U.S. Cordillera—as a function both of event size and distance in the footwall or hanging-wall direction. We believe such a density function provides a suitable measure of the probability that a secondary fracture undergoes slip which is induced by principal faulting.

For application of the modeling of [P slip|pf] to our logic tree, we prefer to exclude data points for surface cracking from the 1986 Chalfant Valley, California, and the 1980 Mammoth Lakes, California, earthquakes. In both cases, the structural setting of Quaternary volcanic rocks that are affected by distributed faulting (S. K. Pezzopane and T. E. Dawson, USGS, written communication, 1996) arguably confound the composite, two-dimensional frequency-distance distribution being sought. Also, we prefer that the regression modeling of

the data impose a magnitude scaling effect on the hanging wall-footwall relations, which we consider more realistic than having magnitude-invariant relations.

Given that secondary/distributed faulting occurs, our procedures for estimating the amount of displacement and the variability of slip depend on whether the site is one of distributed faulting only (Figure AAR-22) or one where principal faulting also occurs (Figure AAR-23). In the former case, our logic tree uses the same approaches described for the point-estimate method.

At a site where principal faulting also occurs, we chose not to let MD^{max} be an estimator of the expected secondary displacement. In principle, this could result in secondary displacements on faults with large MD^{max} that are larger than the displacements on the primary faults. Instead, we use data summarized by S. K. Pezzopane and T. E. Dawson (USGS, written communication,1996, Figures 9-15 and 9-22) relating observations of maximum secondary displacement to maximum primary displacement as a function of mainshock magnitude. The data include both (1) their own compilation from a sample of surface-faulting earthquakes in the extensional Cordillera of the western U.S. and (2) an earlier compilation from Coppersmith and Youngs (1992; see Figure 9-22 in S. K. Pezzopane and T. E. Dawson, USGS, written communication, 1996). We relied on compilation (1) to estimate a cumulative distribution for the ratio of maximum secondary displacement to maximum primary displacement from which we assessed the following distribution of ratios (and weights):

0.20 (0.3), 0.45 (0.4), 0.70 (0.3).

This distribution is consistent with the assumption by Coppersmith and Youngs (1992) of a uniform distribution between 0.1 and 0.8 for the ratio of maximum secondary displacement to maximum primary displacement (see Figures 9-15 and 9-22 of S. K. Pezzopane and T. E. Dawson, USGS, written communication, 1996).

Given a mainshock of magnitude M, we first estimate the maximum primary displacement MD from the regression relation of Wells and Coppersmith (1994) (See Figure AAR-23). We use the ASM model to estimate the variability of MD on the primary fault. To do this,

we assume MD follows the distribution at the midpoint of the fault, which is the most conservative assumption. The maximum secondary displacement is then calculated from its ratio to MD on the primary fault.

6.12 SECONDARY/DISTRIBUTED FAULTING

We spell out 10 rules for characterizing secondary/distributed faulting at the nine test calculation sites. The rules are grouped under the issues of: (1) susceptibility to displacement; (2) the amount, frequency, and variability of displacement; (3) dip and sense of slip; and (4) the width of the zone of displacement. In terms of notation, recall that P[C] is the probability that a feature is capable of slip to produce secondary/distributed displacement, given the contemporary stress field at Yucca Mountain.

Susceptibility to Displacement:

Rule 1. For any fault assigned P[S] = 1.0 (Tables AAR-2, AAR-3), P[C] is also 1.0.

Rule 2. Based on slip-tendency analysis of Yucca Mountain faults (Morris *et al.*, 1996; H. L. McKague *et al.*, CNWRA, written communication, 1996), and using Figures 3-3 and 3-4 of H. L. McKague *et al.* (CNWRA, written communication, 1996) as a guide for relative scaling, we assign P[C] ranging from 1 for faults with high slip tendency to 0.5 for faults with intermediate slip tendency to 0.1 for faults with low slip tendency, such as the NW-SE striking faults. Although we assigned P[S] = 0 to the latter, we allow some possibility that NW-SE striking structures may undergo secondary/distributed displacement; local stresses may be rotated, for example, during principal faulting nearby.

Rule 3. In an underground excavation at Yucca Mountain, we assign P[C] = 1 to any shears with about 10 cm of cumulative offset or to fractures with less or no measurable offset—concluding that, in principle, they can participate in local strain accommodation, regardless of orientation. We adopt this interpretation because we think it very likely that the underground excavation disrupts the coherency of the stress field used for the slip-tendency analysis.

Rule 4. For intact rock, P[C] = 0.

Secondary displacement of intact rock could occur either by propagation of an existing fault or shear fracture into intact rock or by creation of a new fault. Studies at Yucca Mountain show that existing faults were reactivated during Quaternary deformation. The studies provide no examples of the creation of new faults or of the propagation of existing faults into unbroken rock. There is, therefore, no geologic basis for evaluating the probability that such events may occur.

We consider such displacement may be possible given a condition in which the existing fault or rock block is pre-loaded by regional stress to the point of failure and displacement occurs in response to passage of a transient dynamic stress. We consider such an occurrence at Yucca Mountain to be negligible because: (1) the strength of intact rock is commonly 5 to 10 times greater than that of fault rock (Cowie and Scholz, 1992a), (2) small shear fractures tend to propagate along existing fractures or joints (Segall and Pollard, 1983), (3) the rocks at Yucca Mountain (as revealed in the ESF) are cut by many fractures and faults, some of which (for example, the Ghost Dance fault) are marked by low-strength rock thus providing abundant opportunity for stress release adjacent to intact rock, and (4) there is no indication that the Ghost Dance fault, even with its low strength aspect, has been activated in secondary faulting through several cycles of local Quaternary faulting.

Local evidence for a difference in strength between intact and fractured rock can be interpreted from stress measurements made in the ESF (Sandia National Laboratories, written communication, 1997). Table 1 (p. 7) of that report shows a skewed distribution of critical pressures (Pc) measured at different levels in the test hole. Four values are in the range 1.6 to 1.8 and a fifth is 6.4. The high value is suggested to be typical of intact test intervals as opposed to the lower values which are ascribed to pre-fractured conditions (p. 20). Taking these results to be a crude estimate of strength contrasts between intact and fractured rock, we infer that intact rock is 3.8 times stronger than fractured rock. Although less than the factor of 5 to 10 we cite from Cowie and Scholz (1992a), this nonetheless provides local evidence that intact rock is significantly stronger than fractured rock in the ESF.

Amount, Frequency, and Variability of Displacement:

Rule 5. To estimate the expected amount, frequency, and variability of secondary/distributed faulting on any fault or fracture with measurable offset, our logic tree for "Distributed Faulting" should be followed.

Rule 6. For a fracture with no measurable offset, we adopt the logic of our scaling relation for $\overline{U}$ versus Ltotal, requiring an observer to assess a distribution for Ltotal, combined with our exponential distribution for DE/MDmax. Such a distribution for Ltotal (and weights), for example, might be: 5 m (0.3), 10 m (0.4), 20 m (0.3). For the median value of 10 m, MDmax = 1.32 × 3.69× 10-5 m/m × 10 m, yielding 4.87 ×10-4 m. The expected value of DE is 0.83 * MDmax or 4.0×10-4 m. To place a bound on λDE, the relative frequency of displacement events, one could assume (or assess a distribution otherwise) that "no measurable offset" means ≤ 10 cm for Dcum, in which case the upper bound number of displacement events would be 0.1 m divided by 4.0×10^{-4} m/event yielding 2.5×10^{2} events. Thus, λ_{DE} would be 2.5×10^{2} events divided by the age of the rock. For an age of 12.7 Ma, λ_{DE} would be 2.0×10^{-5} events/yr (recurrence interval = 50,000 yr).

Dip and Sense of Slip:

Rule 7 Begging the obvious, estimating the dip to be expected for displacement at a specific point should clearly rest on either (1) direct observation of the candidate feature and fracturing in its immediate vicinity or (2) inference from either detailed mapping of fractures and faults in the repository excavation similar to mapping in the ESF (e.g., R.C. Lung presentation at SSC Workshop 2) or detailed surface mapping (e.g., presentations by W.C. Day, C.J. Potter, and D.S. Sweetkind at SSC Workshops 3 and 4). Dips of 60° to 90° are well known to predominate.

Rule 8. The sense of slip to be expected on a fault or fracture can reasonably be estimated by relating its 3-D orientation to the 3-D orientations of the contemporary principal stresses at Yucca Mountain (e.g., Stock *et al.*, 1985; Morris *et al.*, 1996; Sandia National Laboratory, written communication, 1997). An interactive computer tool developed for application at Yucca Mountain provides a direct way to assess the "relative likelihood and direction of slip on surfaces of all orientations" (Morris *et al.*, 1996; H. L. McKague *et al.*, CNWRA, written communication, 1996). Such methodologies assume that slip will occur in the absence of strain partitioning involving other faults or fractures in the rock volume under consideration (e.g., Wesnousky and Jones, 1994).

partitioning involving other faults or fractures in the rock volume under consideration (e.g., Wesnousky and Jones, 1994).

Rule 9. For faults or fractures exposed in an underground excavation at Yucca Mountain, we consider that those with dimensions exceeding roughly twice the dimensions of the excavation will have an expected sense of slip controlled by the orientation of the contemporary principal stresses (Rule 8). We have little understanding of how stresses will be induced and modified by the excavation, so we have little confidence in assessing the sense of allowable slip on small fractures intersected by the excavation.

Width of the Zone of Displacement:

Rule 10. The width of the zone of displacement (fault zone thickness), interpreted to be the width of the deformation zone within which most of the slip across a fault or fracture has occurred (as distinct from a broader "damage zone" of deformed rock), scales linearly with fault throw (Knott *et al.*, 1996; Power *et al.*, 1988; Hull, 1988). The mean ratio of fault zone thickness to throw (Dcum) for natural faults is approximately 0.01, with individual values ranging between 0.1 and 0.001 (Power *et al.*, 1988).

The ratio of fault zone thickness to throw is observed to vary with lithology, and within the same lithology to vary greatly along an individual fault trace (Knott *et al.*, 1996). This ratio for the Yucca Mountain faults, in the absence of a compilation for the local fault population, can reasonably be assessed from global data by the following distribution of values (and weights): 0.001 (0.185), 0.01 (0.63), 0.1 (0.185). For illustration, a fault zone thickness of 0.6 to 1.0 m for the Ghost Dance fault observed in Alcove 6 of the ESF (J.W. Whitney presentation, SSC Workshop 6), divided by a throw of the order of 20 to 40 m, gives a ratio of the order of 0.01 to 0.05.

6.13 ASSESSMENTS FOR NINE TEST CALCULATION SITES

In this final section, we give specific guidance for calculating fault-displacement hazard at the Nine Test Calculation Sites.

Point 1 (Bow Ridge fault):

- Susceptibility to slip: Source of principal faulting, P[C] = P[S] = 1

- Amount/frequency/variability of displacement: Logic trees for Principal and Distributed Faulting, respectively (see Table AAR-4 under "total disp." for Dcum)

- Dip/Sense of Slip: Rules 7, 8

- Width of zone of displacement: Rule 10

Point 2 (Solitario Canyon fault):

- Susceptibility to slip: Source of principal faulting, P[C] = P[S] = 1

- Amount/frequency/variability of displacement: Logic trees for Principal and Distributed Faulting, respectively (see Table AAR-4 under "total disp." for Dcum)

- Dip/Sense of Slip: Rules 7, 8

- Width of zone of displacement: Rule 10

Point 3 (Drill Hole Wash fault):

- Susceptibility to slip: Susceptible to secondary/distributed faulting only; P[C] = 0.75 (see H. L. McKague *et al.*, CNWRA, written communication, 1996, Figure 3-4)

- Assessed distribution for L^{total}, in km (and weights): 2.0 (0.3), 5.0 (0.4), 9.0 (0.3); assessed distribution for Dcum, in m (and weights): 20 (0.3), 50 (0.4), 100 (0.3)

- Amount/frequency/variability of displacement: Logic tree for Distributed Faulting

- Dip/Sense of Slip: Rule 7 for dip; Rule 9 for sense of slip in an underground excavation, which reverts to Rule 8 because of the dimension of the fault

- Width of zone of displacement: Rule 10

Point 4 (Ghost Dance fault):

- Susceptibility to slip: Source of principal faulting, P[S] = 0.1; however, based on its high slip susceptibility (see H. L. McKague *et al.*, CNWRA, written communication, 1996, Figure 3-4), we assign P[C] = 1 for secondary/distributed faulting,

- Amount/frequency/variability of displacement: Logic trees for Principal and Distributed Faulting, respectively (see Table AAR-4 under "total disp." for Dcum)

- Dip/Sense of Slip: Rule 7 for dip; Rule 9 for sense of slip in presumed underground excavation, which reverts to Rule 8 because of the dimension of the fault

- Width of zone of displacement: Rule 10

Point 5 (Sundance fault W of ESF):

- Susceptibility to slip: Source of secondary/distributed faulting only; P[C] = 0.8 (see H. L. McKague *et al.*, CNWRA, written communication, 1996)

- Assessed distribution for L^{total}, in km (and weights): 0.5 (0.3), 0.75 (0.4), 2.0 (0.3); assessed distribution for Dcum, in m (and weights): 5 (0.3), 10 (0.4), 20 (0.3)

- Amount/frequency/variability of displacement: Logic tree for Distributed Faulting

- Dip/Sense of Slip: Rule 7 for dip; Rule 9 for sense of slip in presumed underground excavation, which reverts to Rule 8 because of the dimension of the fault

- Width of zone of displacement: Rule 10

Point 6 (Minor unnamed fault W of Dune Wash):

- Susceptibility to slip: Source of principal faulting, P[S] = 0.1; however, based on its high slip susceptibility (see H. L. McKague *et al.*, CNWRA, written communication, 1996, Figure 3-4), we assign P[C] = 0.9 for secondary/distributed faulting

- Amount/frequency/variability of displacement: Logic trees for Principal and Distributed Faulting, respectively. (For fault parameters, see Table AAR-4 for what we call the W. Dune Wash 2 fault, along which Point 6 is located.)

- Dip/Sense of Slip: Rules 7, 8

- Width of zone of displacement: Rule 10

Point 7 (feature 100 m E of Solitario Canyon fault):

(a) Assuming a small fault with 2 meters of cumulative offset not directly identifiable from surface mapping

- Susceptibility to slip: Source of secondary/distributed faulting only; P[C] = 0.9 (assuming northerly orientation similar to major fractures in that neighborhood)
- Amount/frequency/variability of displacement: Logic tree for Distributed Faulting
- Dip/Sense of Slip: Rule 7 for slip, Rule 9 for sense of slip in underground excavation, which reverts to Rule 8 because of the inferred length dimension of the fault
- Width of zone of displacement: Rule 10

(b) Assuming a shear with about 10 cm of cumulative offset

- Susceptibility to slip: Susceptible to secondary/distributed displacement only; P[C] = 1 (Rule 3)
- Amount/frequency/variability of displacement: Logic tree for Distributed Faulting
- Dip/Sense of Slip: Rule 7 for slip, Rule 9 for sense of slip (uncertain for small fracture in underground excavation)
- Width of zone of displacement: Rule 10

(c) Assuming a fracture with no measurable offset

- Susceptibility to slip: Susceptible to secondary/distributed displacement only; P[C] = 1 (Rule 3)
- Amount/frequency/variability of displacement: Rule 6
- Dip/Sense of Slip: Rule 7 for slip, Rule 9 for sense of slip (uncertain for small fracture in underground excavation)
- Width of zone of displacement: Rule 10

(d) Assuming intact rock

- Susceptibility to slip: No expected displacement (Rule 4)

- Amount/frequency/variability of displacement: N/A

Point 8 (Feature midway between Solitario Canyon and Ghost Dance faults):
[Except for not knowing the orientation of the feature, all assessments would be identical to those for Point 7 (a-d). The only factor that might change would be P[C] in assumption (a)—if the orientation implied higher or lower susceptibility than P[C] = 0.9 assigned for Point 7(a).]

Point 9 (Site on alluvium in Midway Valley E of the Bow Ridge fault):
All arguments heretofore assume accessibility to direct observations of a fault or fracture in order to assess MD^{max}. Nevertheless, we can proceed as follows:

- Susceptibility to slip: Figure 3-4 of H. L. McKague *et al.* (CNWRA, written communication, 1996) indicates faults/fractures in this vicinity with slip tendencies varying from high to low, so we assume uniform probability of P[C] between 0.1 and 1.0

Amount/frequency/variability of displacement: To assess displacement parameters, we can rule out (from earlier site characterization studies) the presence of a shallowly buried principal fault. We then assess that the most significant shallowly buried intrablock feature at that site has Dcum as follows:

2 m (5%) 10 m (50%) 20 m (95%)

- Given the above distribution for Dcum, follow the logic tree for Distributed Faulting

- Dip/sense of slip: Under the present stress field, the faults most favorably oriented for slip would have strikes of N0°E to N30°E, dips of 60° to 90°, and normal-slip motion with a sinistral component (Morris *et al.*, 1996)

- Width of zone of displacement: Rule 10

7.0
REFERENCES

Abercrombie, R.E., 1995, Earthquake source scaling relationships from -1 to 5 M_L using seismograms recorded at 2.5-km depth: Journal of Geophysical Research, v. 100, n. B12, p. 24,015-24,036.

Anderson, J.G., Wesnousky, S.G., and Stirling, M.W., 1996, Earthquake size as a function of fault slip rate: Bulletin of the Seismological Society of America, v. 86, n. 3, p. 683-690.

Anderson, R.E., Barnhard, T.P., and Snee, L.W., 1994, Roles of plutonism, midcrustal flow, tectonic rafting, and horizontal collapse in shaping the Miocene strain field of the Lake Mead area, Nevada and Arizona: Tectonics, v. 13, p. 1381-1410.

Anderson, R.E, Bucknam, R.C., Crone, A.J., Haller, K.M., Machette, M.N., Personius, S.F., Barnhard, T.P., Cecil, M.J., and Dart, R.L., 1995a, Characterization of Quaternary and suspected Quaternary faults, regional studies, Nevada and California: U.S. Geological Survey Open-File Report 95-599, 56 p.

Anderson, R.E., Crone, A.J., Machette, M.N., Bradley, L.-A., and Diehl, S.F., 1995b, Characterization of Quaternary and suspected Quaternary faults, Amargosa area, Nevada and California: U.S. Geological Survey Open-File Report 95-613, 41 p.

Bell, J.W., de Polo, C.M., Ramelli, A.R., Dorn, R.I., Sarna-Wojcicki, A.M., and Meyer, C.E., 1996, Surface faulting and paleoseismic history of the 1932 Cedar Mountain earthquake area, Central Nevada: Geological Society of American Bulletin (in press).

Benjamin, J.R., and Cornell, C.A., 1970, Probability, statistics, and decision for civil engineers: New York, McGraw-Hill Book Company, 684 p.

Bodin, P., and Brune, J.J., 1996, On the scaling of slip with rupture length for shallow strike-slip earthquakes: Quasi-static models and dynamic rupture propagation: bulletin of Seismological Society of America, v. 86, n. 5, p. 1292-1299.

Clark, R.M., and Cox, S.J.D., 1996, A modern regression approach to determining fault displacement-length scaling relationships: Journal of Structural Geology, v. 18, n. 2/3, p. 147-152.

Cohee, B.P., and Beroza, G.C., 1994, Slip distribution of the 1992 Landers earthquake and its implications for earthquake source mechanics: Bulletin of the Seismological Society of America, v. 84, n. 3, p. 692-712.

Coppersmith, K.J., and Youngs, R.R., 1992, Earthquakes and tectonics, *in* McGuire, R.K., ed., Demonstration of a Risk-Based Approach to High-Level Waste Repository Evaluation: Phase 2, Electric Power Research Institute, EPRI TR-100384, Palo Alto, California

Cowie, P. A., and Scholz, C.H., 1992a, Physical explanation for the displacement-length relationship of faults using a post-yield fracture mechanics model: Journal of Structural Geology, v. 14, n. 10, p. 1133-1148.

Cowie, P. A., and Scholz, C.H., 1992b, Displacement-length scaling relationships for faults: data synthesis and discussion: Journal of Structural Geology, v. 14, n. 10, p. 1149-1156

Cowie, P. A., and Scholz, C.H., 1992c, Growth of faults by accumulation of seismic slip: Journal of Geophysical Research, v. 97, n. B7, p. 11,085-11,095.

Ferrill, D.A., Stamatakos, J.A., Jones, S.M., Rahe, B., McKague, H.L., Martin, R.H., and Morris, A.P., 1996, Quaternary slip history of the Bare Mountain Fault (Nevada) from the morphology and distribution of alluvial fan deposits: Geology, v. 24, n. 6, p. 559-562.

Fridrich, C.J., 1996, Tectonic evolution of the Crater Flat basin, Yucca Mountain region, Nevada, *in* Wright, L. and Troxel, B., eds., Cenozoic basins of the Death Valley region: Geological Society of America Special Paper (in press).

Fridrich, C.J., Whitney, J.W., Hudson, M.R., and Crowe, B.M., 1996, Late Cenozoic extension, vertical-axis rotation, and volcanism in the Crater Flat basin, southwest Nevada, in Wright, L. and Troxel, B. eds., Cenozoic basins of the Death Valley region: Geological Society of America Special Paper (in press).

Frizzell, V.A., Jr., and Shulters, J., 1990, Geologic map of the Nevada Test Site, southern Nevada: U.S. Geological Survey Miscellaneous Investigations Map I-2046, scale 1:100,000.

Frizzell, V.A. and Zoback, M.L., 1987, Stress orientation determined from fault slip data in Hampel Wash area, Nevada, and its relation to contemporary regional stress field: Tectonics, v. 6, p. 89-98.

Gomberg, J., 1996, Stress/strain changes and triggered seismicity following the M_w7.3 Landers, California earthquake: Journal of Geophysical Research, v. 101, n. B1, p. 751-764.

Gomberg, J., Blanpied, M.L., and Beeler, N.M., 1997, Transient triggering of near and distant earthquakes: Bulletin of Seismological Society of America, v. 87, n. 2, p. 294-309.

Gomberg, J., and Bodin, 1994, Triggering of the Ms = 5.4 Little Skull Mountain, Nevada, earthquake with dynamic strains: Bulletin of the Seismological Society of America, v. 84, n. 3, p. 844-853.

Gomberg, J., and Davis, S., 1996, Stress/strain changes and triggered siesmicity at The Geysers, California: Journal of Geophysical Research, v. 101, n. B1, p. 733-749.

Harmsen, S.C., 1994, The Little Skull Mountain, Nevada, earthquake of 29 June 1992: Aftershock focal mechanisms and tectonic stress field implications: Bulletin of the Seismological Society of America, v. 84, n. 5, p. 1484-1505.

Hull, J., 1988, Thickness-displacement relationships for deformation zones: Journal of Structural Geology, v. 10, n. 4, p. 431-435.

Keefer, D.I., and Bodily, S.E., 1983, Three-point approximations for continuous random variables: Management Science, v. 26, p. 595-609.

King, G.C.P., Stein, R.S., and Lin, J., 1994, Static stress changes and the triggering of earthquakes: Bulletin of the Seismological Society of America, v. 84, n. 3, p. 935-953.

Knott, S.D., Beach, Alastair, Brockbank, P.J., Brown, J.L., McCallum, J.E., and Welbon, A.J., 1996, Spatial and mechanical controls on normal fault populations: Journal of Structural Geology, v. 18, n. 2/3, p. 359-372.

Maldonado, F., 1985, Geologic map of the Jackass Flats area, Nye County, Nevada: U.S. Geological Survey, Miscellaneous Investigations Map I-1519, scale 1:48,000.

Mendoza, C., and Hartzell, S.H., 1988, Inversion for slip distribution using teleseismic P-waveforms: North Palm Springs, Borah Peak, and Michoacan earthquakes: Bulletin of the Seismological Society of America, v. 78, n. 3, p. 1092-1111.

Morris, A., Ferrill, D.A., and Henderson, D.B., 1996, Slip-tendency analysis and fault reactivation: Geology, v. 24, n. 3, p. 275-278.

Nicol, A., Watterson, J., Walsh, J.J., and Childs, C., 1996, The shapes, major axis orientations and displacement patterns of fault surfaces: Journal of Structural Geology, v. 18, n. 2/3, p. 235-248.

Parsons, T., and Thompson, G.A., 1991, Coupled processes of normal faulting and dike intrusion in tectonically extended regions: Geological Society of America, Abstracts with Programs, v. 23, n. 2, p. 87.

Piety, L.A., 1996, Compilation of known and suspected Quaternary faults within 100 km of Yucca Mountain: U.S. Geological Survey Open-File Report 94-112, 31 p.

Power, W.T., Tullis, T.E., and Weeks, J.D., 1988, Roughness and wear during brittle faulting: Journal of Geophysical Research, v. 93, n. B12, p. 15,268-15,278.

Rogers, A.M., Harmsen, S.C., and Meremonte, M.E., 1987, Evaluation of the seismicity of the southern Great Basin and its relationship to the tectonic framework of the region: U.S. Geological Survey Open-File Report 87-408, 196 p.

Rogers, A.M., Harmsen, S.C., Corbett, E.J., Priestley, K., and dePolo, D., 1991, The seismicity of Nevada and some adjacent parts of the Great Basin, *in* Slemmons, D.B., Engdahl, E.R., Zoback, M.D., and Blackwell, D.D., eds., Neotectonics of North America: Boulder, Colorado, Geological Society of America, Decade Map Volume 1, p. 153-184.

Romanowicz, B., and Rundle, J.B., 1993, On scaling relations for large earthquakes: Bulletin of the Seismological Society of America, v. 83, n. 4, p. 1294-1297.

Scott, R.B., 1990, Tectonic setting of Yucca Mountain, southwest Nevada, *in* Wernicke, B.P., ed., Basin and Range extensional tectonics near the latitude of Las Vegas, Nevada: Geological Society of America Memoir 176, p. 251-282.

Scott, R.B., and Bonk, J., 1984, Preliminary geologic map of Yucca Mountain, Nye County, Nevada with geologic sections: U.S. Geological Survey Open-File Report 84-494, 9 p., scale 1:12,000.

Segall, P., and Pollard, D.D., 1983, Nucleation and growth of strike slip faults in granite: Journal of Geophysical Research, v. 88, n. B1, p. 555-568.

Simonds, W.F., Whitney, J.W., Fox, K.F., Ramelli, A., Yount, J., Carr, M.D., Menges, C.M., Dickerson, R., and Scott, R.B., 1995, Map of fault activity of the Yucca Mountain area, Nye County, Nevada: U.S. Geological Survey Miscellaneous Investigations Series Map I-2520, scale 1:24,000.

Simpson, R.W., and Reasenberg, P.A., 1994, Earthquake-induced static-stress changes on central California faults, *in* Simpson, R.W., ed., The Loma Prieta, California, Earthquake of October 17, 1989—Tectonic Processes and Models: U.S. Geological Survey Professional Paper 1550-F, p. F55-F89.

Smith, R.P., Jackson, S.M., and Hackett, W.R., 1995, Method for estimating the maximum magnitudes of earthquakes associated with potential dike intrusion and basaltic volcanism in the Yucca Mountain area: Implications for seismic hazards assessment, *in* Proceedings, Topical Meeting on Methods of Seismic Hazards Evaluation, Focus '95: American Nuclear Society, Inc., La Grange Park, Illinois, p. 178-184.

Smith, R.P., Jackson, S.M., and Hackett, W.R., 1996, Paleoseismology and seismic hazards evaluations in extensional volcanic terrains: Journal of Geophysical Research, v. 101, n. B3, p. 6277-6292.

Sonder, L.J., Jones, C.H., Salyards, S.L., and Murphy, K.M., 1994, Vertical-axis rotations in the Las Vegas Valley Shear Zone, southern Nevada: Paleomagnetic constraints on kinematics and dynamics of block rotations: Tectonics, v. 13, p. 769-788.

Stewart, J.H., and Diamond, D.S., 1990, Changing patterns of extensional tectonics; Overprinting of the basin of the middle and upper Miocene Esmeralda Formation in western Nevada by younger structural basins, *in* Wernicke, B.P., ed., Basin and Range extensional tectonics near the latitude of Las Vegas, Nevada: Geological Society of America Memoir 176, p. 447-475.

Stock, J.M., Healy, J.H., Hickman, S.H., and Zoback, M.D., 1985, Hydraulic fracturing stress measurements at Yucca Mountain, Nevada, and relationship to regional stress field: Journal of Geophysical Research, v. 90, n. B10, p. 8691-8706.

Veneziano, D., and Van Dyck, J., 1985, Statistical discrimination of "aftershocks" and their contribution to seismic hazard, seismic hazard, *in* Methodology for Nuclear Facilities in the Eastern United States: EPRI Research Project N. P101-29, EPRI/SOG 85-1, v. 2, Appendix A-4.

Wald, D.J., and Heaton, T.H., 1994, Spatial and temporal distribution of slip for the 1992 Landers, California, earthquake: Bulletin of the Seismological Society of America, v. 84, n. 3, p. 668-691.

Wells, D.L., and Coppersmith, K.J., 1994, New empirical relationships among magnitude, rupture length, rupture width, rupture area, and surface displacement: Bulletin of the Seismological Society of America, v. 84, n. 4, p. 974-1002.

Wesnousky, S.G., and Jones, C.H., 1994, Oblique slip, slip partitioning, spatial and temporal changes in the regional stress field, and the relative strength of active faults in the Basin and Range, western United States: Geology, v. 22, n. 11, p. 1031-1034.

Yeats, R.S., Sieh, K., and Allen, C.R., 1997, The geology of earthquakes: Oxford University Press, New York, 568 p.

Youngs, R.R., and Coppersmith, K.J., 1985, Implications of fault slip rates and earthquake recurrence models to probabilistic seismic hazard estimates: Bulletin of the Seismological Society of America, v. 75, n. 4, p. 939-964.

Youngs, R.R., Swan, III, F.H., Power, M.S., Schwartz, D.P, and Green, R.K., 1987, Probabilistic analysis of earthquake ground shaking hazard along the Wasatch Front, Utah, *in* Gori, P.L., and Hays, W.W., eds., Assessment of regional earthquake hazards and risk along the Wasatch Front, Utah: U.S. Geological Survey Open File Report 87-585, p. M-1 to M-110.

TABLE AAR-1
SEISMIC SOURCE PARAMETERS FOR REGIONAL FAULT SOURCES
(p. 1 of 2)

Fault Name	Total Fault Length [1] (km)	Max. Rupture Length [1] (km)	Min. Distance to Rep. (km)	Doc. Quaternary Displacement	Style	Dip [1] (deg.)	Slip Rate [1] (mm/yr)	Recur. Int.[1] (ka)	P[S]
Mine Mountain (MM)	20 23 37	20 23 37	11	y?	LO	50 70 90	0.002 0.015 0.03		0.6
Wahmoni (WAH)	11 14 17	11 14 17	22	y	N/L	50 65 90	0.002 0.025 0.05		1
Ash Meadows (AM)	8 42 72	8 42 72	24	y	N	50 65 80	0.001 0.01 0.1		1
Oasis Valley (OSV)	8 19 29	8 19 29	24	y?	N	50 65 80	0.001 0.005 0.01		0.4
Rock Valley (RV)	25 33 69	25 33 46	25	y	LO	65 90 90	0.02 0.06 0.1	33 50 180	1
Cane Spring (CS)	18 22 36	18 22 36	29	y?	LO?	65 90 90	0.002 0.025 0.05		0.6
West Specter R. (WSR)	7 8 22	7 8 22	33	y	N	45 60 80	0.001 0.004 0.01		1
Amargosa R./ Pahrump (AR/PRP)	75 82 134	75 82 110	34	y	R?	80 90 90	0.005 0.07 0.2		1
Amargosa R. (AR)	13 14 25	13 14 25	34	y	NR	80 90 90	0.005 0.04 0.2		1
Yucca Lake (YCL)	12 14 24	12 14 24	36	y?	N	45 60 80	0.001 0.005 0.01		0.5
Eleana Range (ER)	11 13 18	11 13 18	37	y	N	45 60 80	0.001 0.005 0.01		1

TABLE AAR-1
SEISMIC SOURCE PARAMETERS FOR REGIONAL FAULT SOURCES
(p. 2 of 2)

Fault Name	Total Fault Length [1] (km)	Max. Rupture Length [1] (km)	Min. Distance to Rep. (km)	Doc. Quaternary Displacement	Style	Dip [1] (deg.)	Slip Rate [1] (mm/yr)	Recur. Int.[1] (ka)	P[S]
Yucca Fault (YC)	20 25 31	20 25 31	40	y	N/RO	50 65 90	0.001 0.025 0.05		1
Keane Wonder (KW)	19 23 32	19 23 32	43	y?	N	50 65 85	0.001 0.005 0.01		0.6
Furnace Creek (FC)	100 118 146	100 118 146	50	y	R	80 90 90	2.3 8.0 10.0	0.5 0.7 1.0	1
Death Valley/ Furnace Creek (DV/FC)	154 178 193	125 150 165	50	y	N/R	50 82 90	2.3 8.0 10.0	0.5 0.7 1.0	1
West Spring Mts. (WSM)	37 52 66	23 37 48	53	y	N	50 65 80	0.02 0.05 0.07	28 30 124	1
Death Valley (DV)	42 57 74	42 57 74	55	y	N	50 65 90	3.0 4.0 5.0	0.5 0.75 1.3	1
Belted Range (BLR)	21 29 50	21 29 45	55	y	N	50 65 80	0.02 0.05 0.1		1
Kawich Range (KR)	20 27 76	20 27 45	57	y	N	50 65 80	0.005 0.03 0.07		1
Pahrump (PRP)	37 45 107	37 45 85	68	y	R	80 90 90	0.005 0.07 0.2		1
West Pintwater (WPR)	30 48 57	30 48 57	76	y	N	45 60 80	0.002 0.04 0.07		1

[1] Three numbers represent minimum, preferred, and maximum values

TABLE AAR-2
SOURCE INVENTORIES

Model [?]	Local Seismic Source	P[s]'
A-1, A-2, A-3	CFD faults *	*
	Highway 95 fault (H95)	0.5
	Regional ss (subjacent) (T4-SS)	1.0
	Background source zones	1.0
B-1, B-2, B-3	CFD faults *	*
	Highway 95 fault (H95)	0.8
	No. bounding ss fault (T4-PA2)	0.5
	Background source zones	1.0
C-1, C-2	CFD faults *	*
	Highway 95 fault (H95)	0.8
	No. bounding ss fault (T4-PA2)	0.5
	Cross-basin fault (T4-CB)	1.0
	Background source zones	1.0
D-1, D-2, D-3	CFD faults *	*
	Background sources	1.0

[?] Keyed to Figure AAR-1

[›] Probability of being seismogenic

[*] See Table AAR-3

TABLE AAR-3
INVENTORY OF CRATER FLAT DOMAIN (CFD) FAULTS

FAULT	P[s][1]
Bare Mountain	1.0
Bow Ridge	1.0
S. Crater Flat	1.0
N. Crater Flat	1.0
W. Dune Wash #1	0.1
W. Dune Wash #2	0.1
Ghost Dance	0.1
Fatigue Wash	1.0
Iron Ridge	1.0
E. Lathrop Cone	1.0
Midway Valley	0.1
Paintbrush Canyon	1.0
Solitario Canyon	1.0
Stagecoach Road	1.0
S. Windy Wash	1.0
N. Windy Wash	1.0
C. Windy Wash	0.6
C. Crater Flat	0.6
Black Cone	0.8
E. Busted Butte	0.4

[1] Probability of being seismogenic. P[S] for each fault is constant for all the logic tree branches outlined in Table AAR-2 and Figure AAR-1

TABLE AAR-4
ESTIMATES OF FAULT PARAMETERS FOR LOCAL FAULT SOURCES
(p. 1 OF 3)

fault name	act length [1] (km)	doc. Quat act?	styl	fault dip [1] (deg)	total disp. [1] (m)	disp./event Dmax [1] (cm)	disp./event Davg [1] (cm)	slip rate [1] (mm/yr)	rec. int. [1] (ka)
Independent down-to-west faults									
Bare Mountain (BM)	17 21 31	Y	n	50 60 70	2500 3000 4000	120 150 180	80 120 160	0.005 0.01 0.25	200 100 30
Bow Ridge (BWR)	4 8 10	Y	In	50 60 70	100 200 300	20 40 60	20 40 60	0.002 0.003 0.007	200 120 70
S. Crater Flat (SCF)	6 8 14	Y	In?	50 70 80	40 300 600	30 50 70	30 50 70	0.002 0.008 0.02	150 80 40
N. Crater Flat (NCF)	5 8 10	Y	In?	50 60 70	100 200 300	30 50 70	30 50 70	0.001 0.003 0.005	
W. Dune Wash 1 (WD1)	3 7 10	N?	In?	70 80 90	50 100 200	10 20 30	10 20 30	0.0001 0.0005 0.001	
Ghost Dance (GD)	2 2.5 7	Y?	In	60 70 80	30 40 50	5 10 15	5 10 15	0.0001 0.0005 0.001	
Fatigue Wash (FW)	6.5 9.5 14	Y	In	50 60 70	70 200 400	30 50 70	30 50 70	0.003 0.009 0.02	
Iron Ridge (IR)	4.5 6.5 9	Y	In?	50 60 70	200 250 400	10 50 80	10 50 80	0.001 0.002 0.005	
E. Lathrop Cone (ELC)	1.5 4 9	Y	In?	50 65 80	50 100 200	30 50 80	30 50 80	0.005 0.01 0.03	
Midway Valley (MWV)	3 4 8	N	In?	60 70 80	30 50 70	10 20 30	10 20 30	0.0001 0.0005 0.001	
Paintbrush Cyn (PBC)	8 12 25	Y	In	50 60 70	300 500 700	100 150 250	40 90 130	0.01 0.015 0.03	200 60 30
Solitario Cyn (SC)	13.5 16 25	Y	In	50 60 70	400 700 1000	70 100 130	50 80 110	0.005 0.01 0.02	100 60 35
Stagecoach Road (SR)	3.5 4.5 8	Y	In?	50 60 70	300 500 700	50 70 100	50 70 100	0.01 0.04 0.07	40 20 5
S. Windy Wash (SWW)	8 9 12	Y	In	50 60 70	300 500 700	50 70 90	50 70 90	0.01 0.03 0.04	60 40 20

TABLE AAR-4
ESTIMATES OF FAULT PARAMETERS FOR LOCAL FAULTS SOURCES
(P. 2 OF 3)

fault name	act length [1] (km)	doc. Quat act?	styl	fault dip [1] (deg)	total disp. [1] (m)	disp./event Dmax [1] (cm)	Davg [1] (cm)	slip rate [1] (mm/yr)	rec. int. [1] (ka)
Independent down-to-west faults (cont'd.)									
N. Windy Wash	7			50	300	30	30	0.001	
(NWW)	8	Y	ln?	60	400	50	50	0.003	
	10			70	600	70	70	0.005	
Independent down-to-east faults									
Black Cone	3.5			50		10	10	0.001	
(BC)	8	Y	rn?	65		30	30	0.003	
	12			80		50	50	0.005	
	1.5			50	200	10	10	0.0005	
E. Busted Butte	4	Y	n?	60	400	30	30	0.001	
(EB)	11			70	600	50	50	0.003	
	3			50		10	10	0.001	
C. Crater Flat	6.5	Y	n?	65		30	30	0.003	
(CCF)	8			80		50	50	0.005	
	1.5			70	100	10	10	0.0001	
W. Dune Wash 2	3	N?	n?	80	150	20	20	0.0005	
(WD2)	5			90	200	30	30	0.001	
	4			50		10	10	0.001	
C. Windy Wash	5	Y	n?	65		30	30	0.003	
(CWW)	6			80		50	50	0.005	
Linked systems									
	14			50	300	100	40	0.01	120
PBC/SR	18	Y	ln	60	500	150	90	0.04	40
	32			70	700	250	130	0.07	15
	21			50	300	50	50	0.01	60
SWW/FW/CWW/NWW	23	Y	ln	60	500	70	70	0.03	40
	28			70	700	90	90	0.04	20
Coalesced systems									
	22			50	300	100	40	0.01	120
E-side	24	Y	ln	60	500	150	90	0.04	40
	36			70	700	250	130	0.07	15
	13.5			50	400	70	30	0.005	100
W-side #1	16	Y	ln	60	700	100	60	0.01	60
	25			70	1000	130	90	0.02	35
	21			50	300	70	70	0.01	60
W-side #2	23	Y	ln	60	500	110	110	0.04	40
	29			70	700	150	150	0.06	20

TABLE AAR-4
ESTIMATES OF FAULT PARAMETERS FOR LOCAL FAULTS SOURCES
(P. 3 OF 3)

Multiple-structure coalesced systems (length & recurrence)

fault name	act leng [1] (km)	rec. int. [1] (ka)
Single	35	100
W-side	39	60
(W-side1+W-side2)	54	35
Single	57	120
YM system	63	60
(E-side+W-Side1 +W-side2)	907	35
Single	74	200
system	84	100
(YM+BM)	121	35

fault name	active length [1] (km)	doc Q actv?	style	fault dip [1] (deg.)	disp./event Dmax [1] (cm)	disp./event Davg [1] (cm)	slip rate [1] (m/ka)
Buried/bounding strike-slip (ss) faults							
	50			70	200	200	0.05
Regional ss fault	75	N	rl	90	400	400	0.1
(T4-ss)	100			90	600	600	0.2
No. bounding ss fault	10			70	30	30	0.005
(T4-PA2)	20	N	rl	90	80	80	0.01
	30			90	130	130	0.05
	20			60	50	50	0.02
Hwy.95 fault	40	N?	rl	80	150	150	0.05
(H95)	60			90	250	250	0.1
	10			70	30	30	0.005
Cross-basin fault	20	N	rl	90	80	80	0.01
(T4-CB)	30			90	130	130	0.05

[1] Three numbers represent minimum, preferred, and maximum values.

TABLE AAR-5
WEIGHTS FOR BEHAVIOR OF LOCAL FAULTS DEPENDING ON TECTONIC MODELS

Behavior	A1	A2	A3	B1	B2	B3	C1	C2	D1	D2	D3
Independent	0.1	0.2	0.2	0.1	0.2	0.2	0.1	0.6	0.1	0.2	0.2
Coalesced	0.9	0.8	0.8	0.9	0.8	0.8	0.9	0.4	0.9	0.8	0.8

TABLE AAR-6
WEIGHTS FOR LINKED OPTIONS GIVEN INDEPENDENT BEHAVIOR,

	A1	A2	A3	B1	B2	B3	C1	C2	D1	D2	D3
PBC/SR:											
Independent	0.4	0.2	0.2	0.4	0.2	0.2	0.4	0.5	0.4	0.2	0.2
Linked	0.6	0.8	0.8	0.6	0.8	0.8	0.6	0.5	0.6	0.8	0.8
WW/FW:											
Independent	0.5	0.4	0.4	0.5	0.4	0.4	0.5	0.7	0.5	0.4	0.4
Linked	0.5	0.6	0.6	0.5	0.6	0.6	0.5	0.3	0.5	0.6	0.6

- PBC/SR includes Paintbrush and Stagecoach Road faults.
- WW/FW includes So. Windy Wash, Fatigue Wash, Central Windy Wash, and No. Windy Wash faults. CWW is antithetic to the subparallel FW. Estimates for this linked system are primarily derived from SWW, the most active of the four faults.

TABLE AAR-7

WEIGHTS FOR COALESCED MODELS GIVEN COALESCED BEHAVIOR

Coalesced model	A1	A2	A3	B1	B2	B3	C1	C2	D1	D2	D3
1 system	0.2	0.0	0.0	0.0	0.0	0.0	0.1	0.0	0.0	0.0	0.0
2 systems 0.2	0.0	0.0	0.0	0.0	0.0	0.2	0.0	0.0	0.0	0.0	
3 systems 0.3	0.4	0.4	0.3	0.2	0.2	0.3	0.1	0.3	0.2	0.2	
4 systems 0.3	0.6	0.6	0.7	0.8	0.8	0.4	0.9	0.7	0.8	0.8	

TABLE AAR-8
WEIGHTS FOR M_{max} APPROACHES—LOCAL FAULT SOURCES

Expected Rupture Length <25 km:

Approach	Weight
a. Rupture length	0.3
b. Rupture area	0.2
c. Rupture length/slip rate	0.2
d. Moment equation	0.3

Expected Rupture Length ≥25 km:

Approach	Weight
a. Rupture length	0.3
b. Rupture area	0.0
c. Rupture length/slip rate	0.2
d. Moment equation	0.5

Exception #1: For scenarios A-1, B-1, C-1, and D-1 (local detachment at 3-10 km depth), use these weights for all CFD faults other than the Bare Mountain fault:

Approach	Weight
a. Rupture length	0.1
b. Rupture area	0.2
c. Rupture length/slip rate	0.1
d. Moment equation	0.6

Exception #2: For "multiple-structure coalesced systems" (which have no slip rates provided in Table AAR-4), use these weights:

Approach	Weight
a. Rupture length	0.5
b. Rupture area	0.2
c. Rupture length/slip rate	0.0
d. Moment equation	0.3

TABLE AAR-9
REGRESSION RELATIONS

Equation	Number of Data Points	Coefficients and Standard Errors a (sa)	b (sb)	Standard Deviation	Correlation Coefficient	Range of Variables Independent	Dependent
1. $\log \overline{U} = \log b + \log L^{total}$ [m/m]	19		log b = -4.433 (0.041)	0.18	n.d.	3.3 to 21.3 km	0.08 to 1.14 m
2. log (Dcum) = a + b (log L^{total}) [m/m]	16	-1.58 (1.37)	1.00*	0.32	0.61	3.3 to 21.3 km	40 to 700 m
3. QSR = a + b Dcum [mm/yr/m]	11	0*	3.26 (1.72) e-05	0.01	0.58	40 to 700 m	0.0005 to 0.04 m/yr
4. PDF = a * exp (b * D/MD^{max})	19	0.09 (0.02)	-0.68 (0.16)	1.88	-0.70	0.1 to 2.9	0.01 to 0.14
5. CDF = 1 - exp (-λ * D/MD^{max})	82	λ = 1.20 (0.13)		0.69	n.d.	0.1 to 2.9	0.14 to 1.00

* Constrained

Table AAR-10
Displacement Data Used for Figure AAR-11

FAULT	TRENCH	MD^{max} (cm)	D obs (cm)/ D/MD^{max}	D obs (cm)/ D/MD^{max}	D obs (cm)/ D/MD^{max}	D obs (cm)/ D/MD^{max}	D obs (cm)/ D/MD^{max}	D obs (cm)/ D/MD^{max}	D obs (cm)/ D/MD^{max}	D obs (cm)/ D/MD^{max}
BR	14D	40.92	44 1.08	13 0.32	14 0.34					
NCF	CFF-T2a	46.79	3 0.06	5 0.11	40 0.85	50 1.07	50 1.07			
SCF	CFF-T1a	52.77	18 0.34	10 0.19	20 0.38					
FW	CF 1	49.59	25 0.50	105 2.12	54 1.09					
IR	SCF-T2	46.98	5 0.11	70 1.49	100 2.13	70 1.49				
PB	A1	114.07	6 0.05	39 0.34	7 0.06	100 0.88				
PB	BB4	114.07	44 0.39	28 0.25	47 0.41	167 1.46	142 1.24	105 0.92	94 0.82	
PB	MWV-T4	114.07	20 0.18	62 0.54	98 0.86	40 0.35				
SC	SCF-T1	111.64	10 0.09	70 0.63						
SC	SCF-T3	111.64	10 0.09	80 0.72	35 0.31					
SC	SCF-T4	111.64	5 0.04	30 0.27	20 0.18					
SC	SCF-T8	111.64	10 0.09	120 1.07	30 0.27	50 0.45				
SCR	SCR-T1	66.21	40 0.60	42 0.63	47 0.71	51 0.77				
SCR	SCR-T3	66.21	43 0.65	59 0.89	57 0.86	67 1.01	35 0.53			
WW	CF-2 northwall	30.34	4 0.13	20 0.66	23 0.76	20 0.66	73 2.41	45 1.48	50 1.65	80 2.64
WW	CF-2 southwall	30.34	4 0.13	12 0.40	50 1.65	42 1.38	28 0.92	16 0.53	60 1.98	65 2.14
WW	CF-2.5	30.34	6 0.20	20 0.66	42 1.38	15 0.49				
WW	CF-3 northwall	30.34	4 0.13	33 1.09	87 2.87	35 1.15	65 2.14			
WW	CF-3 southwall	30.34	3 0.10	35 1.15	88 2.90					

Existing Tectonic Framework	*Significant NW–SE Dextral Shear Structure(s)?*	*Dextral–Shear Structure*	*Local Detachment Beneath Crater Flat Domain?*	*Depth of Detachment*	*SOURCE INVENTORY See Table AAR–2, Figure AAR–6*

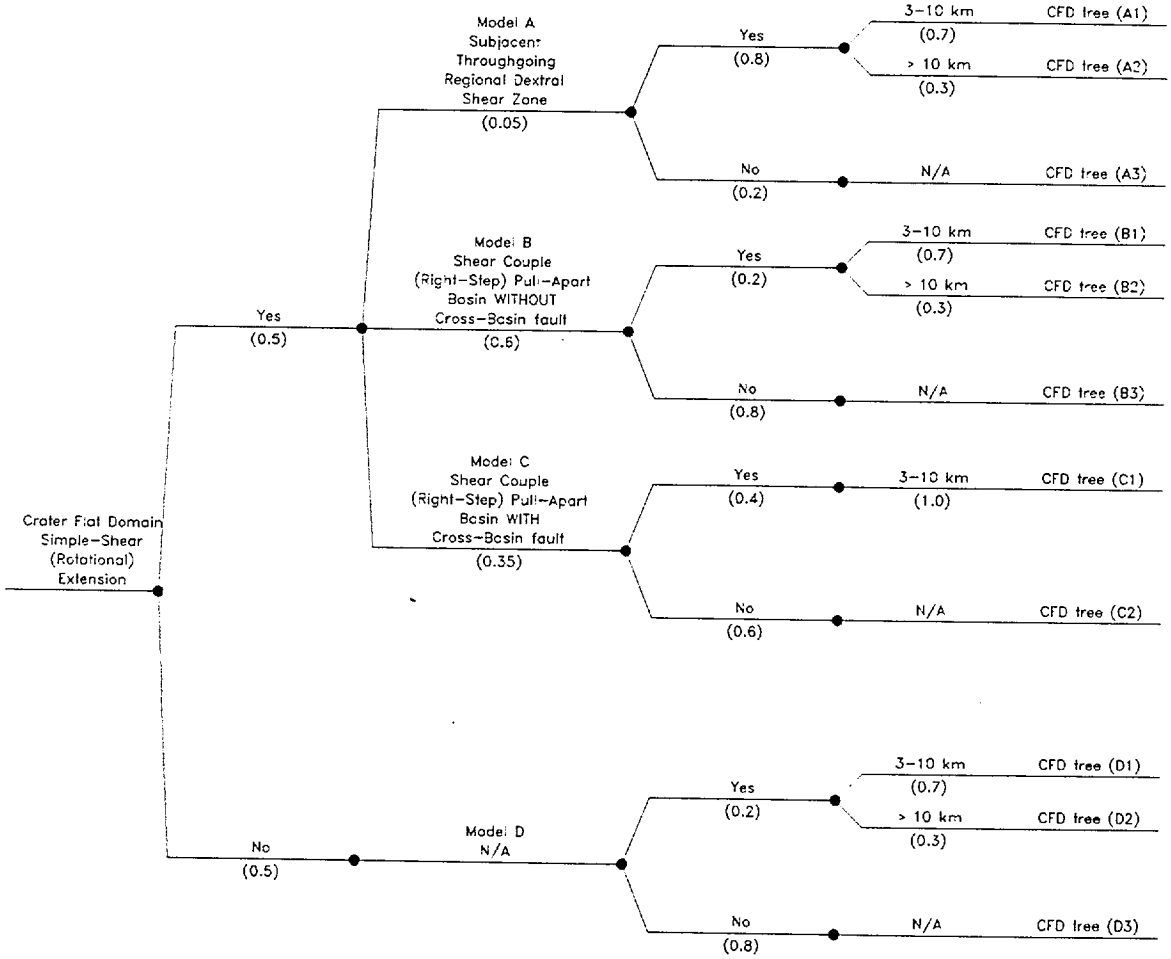

Figure AAR-1 Logic tree for tectonic models and local faults

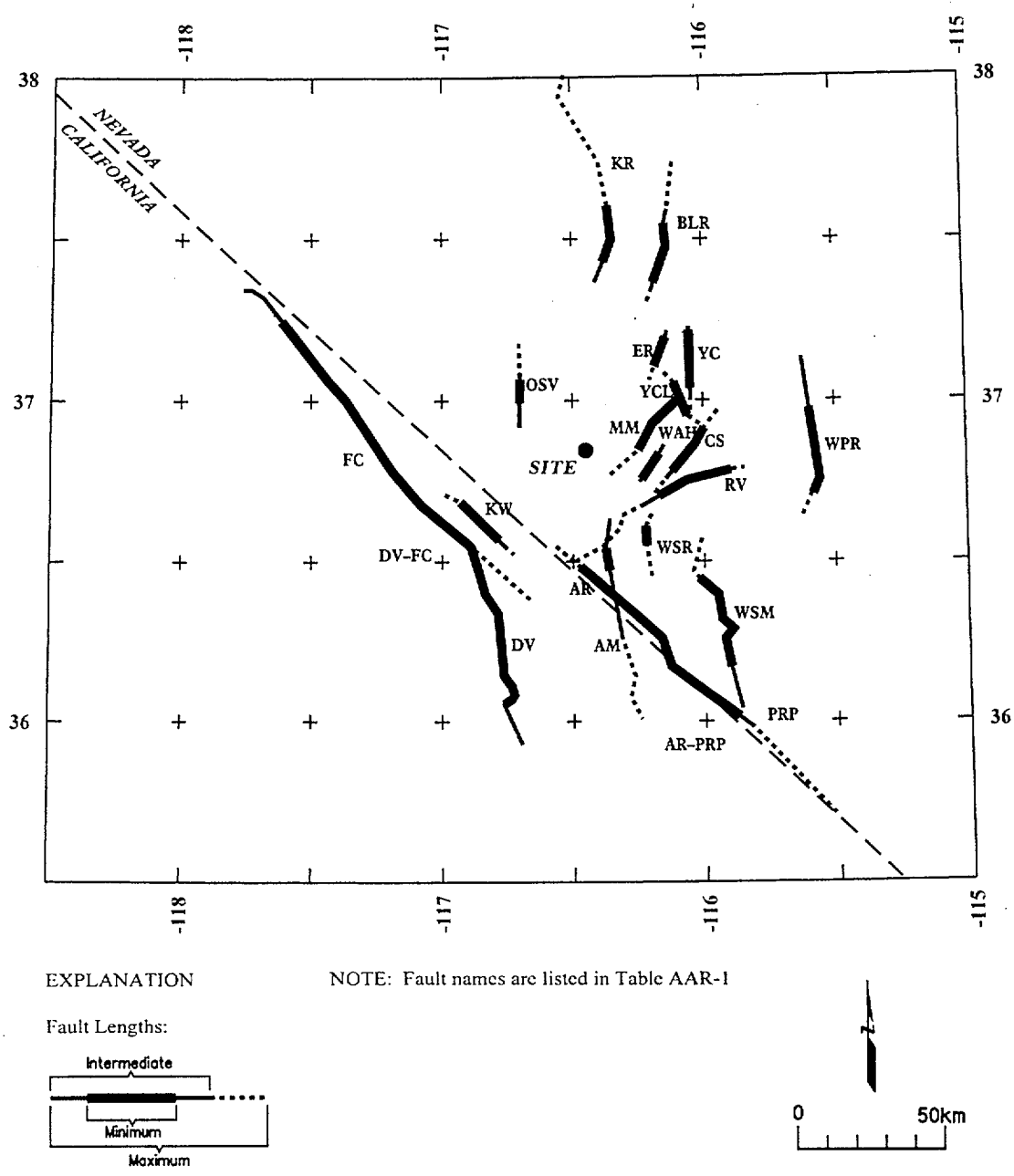

Figure AAR-2 Map showing regional faults included in the seismic source model

h:\prj\yucca_mt\dgn\1097\plate_t4_reg_fault.dgn 27-OCT-1997 15:01

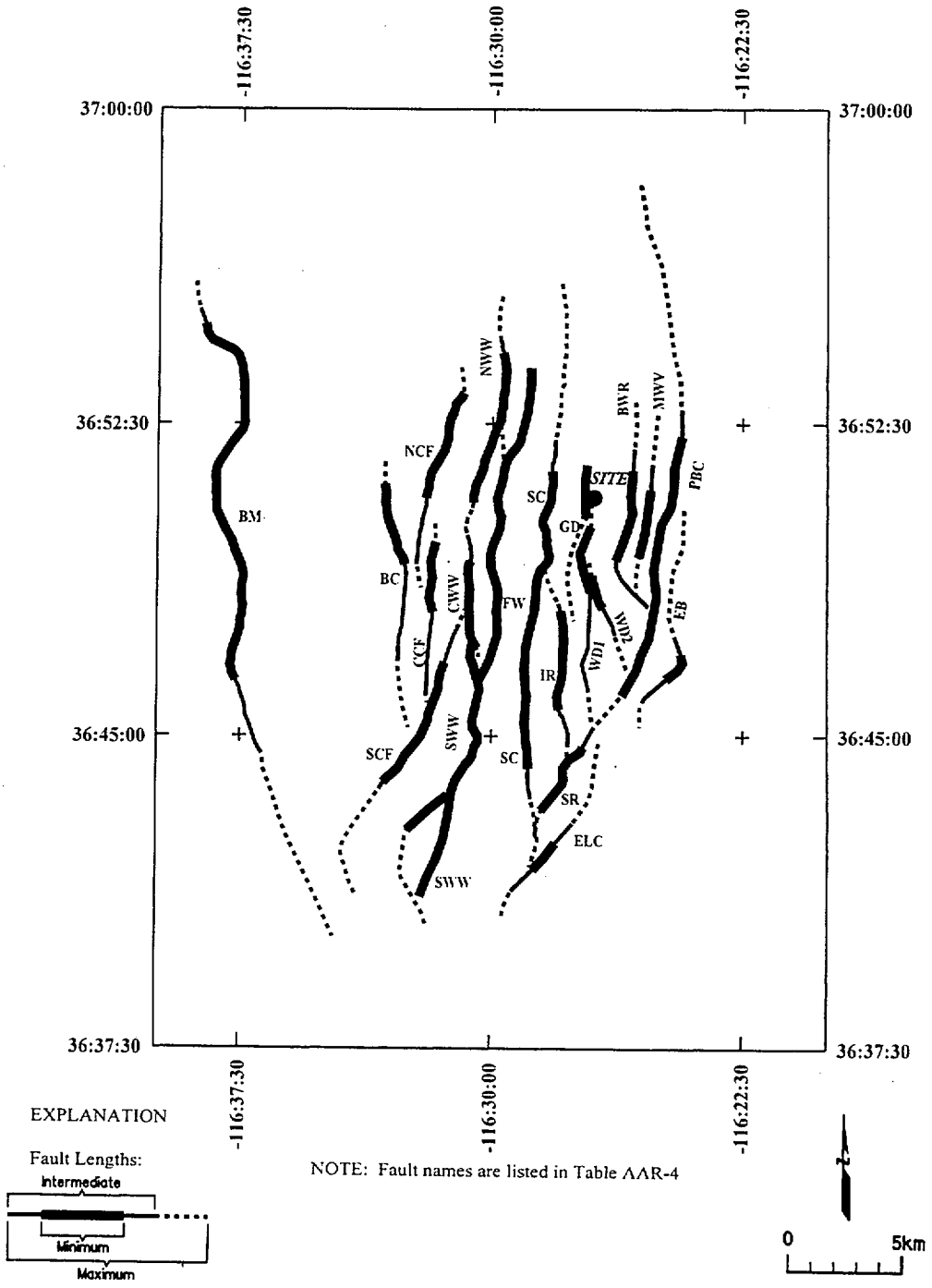

Figure AAR-3 Map showing local fault sources included in the independent model

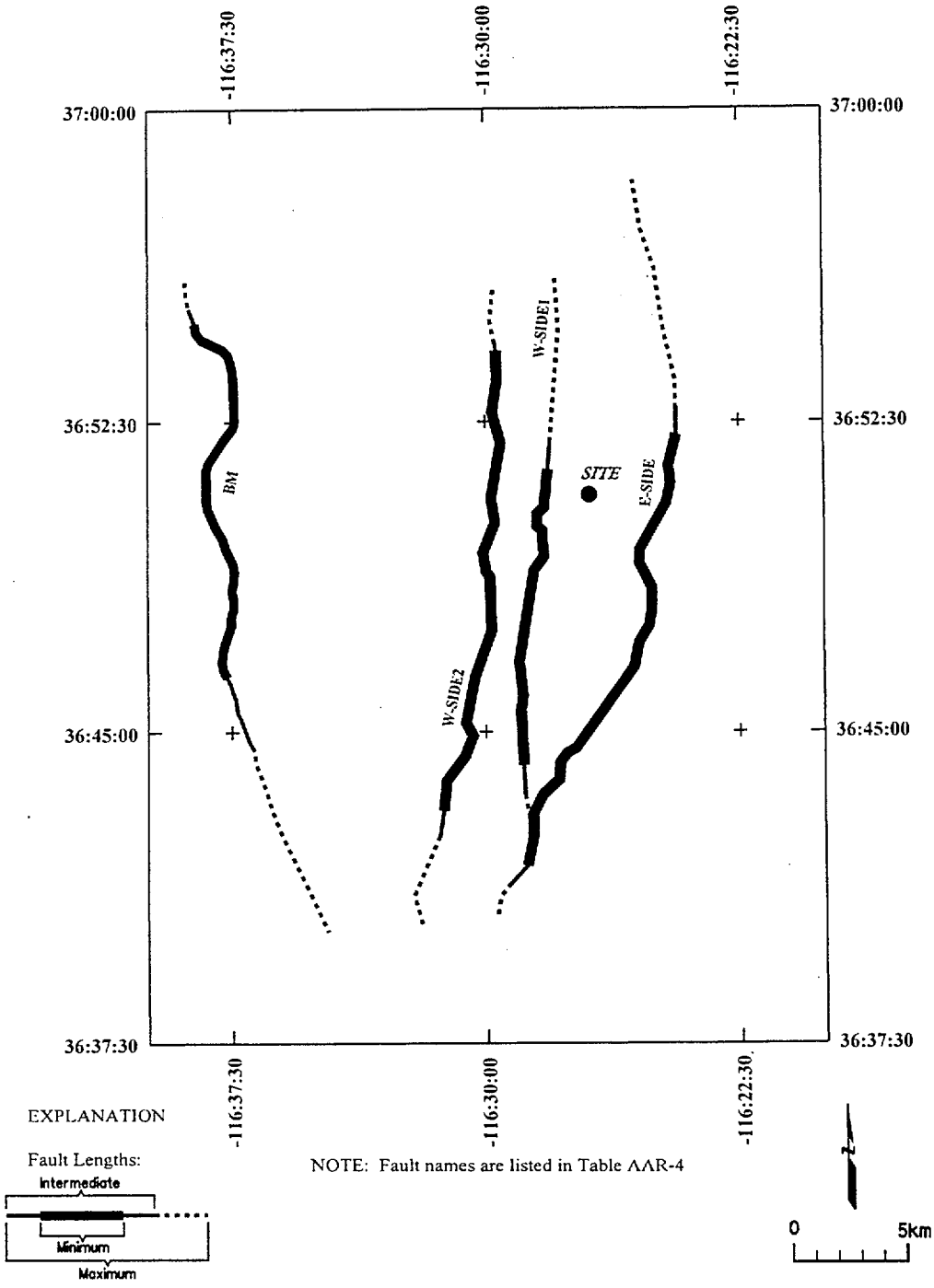

Figure AAR-4 Map showing local faults included in the coalesced model

h:\prj\yucca_mt\dgn\1097\plate_14_lcl_fault2.dgn 27-OCT-1997 15:00

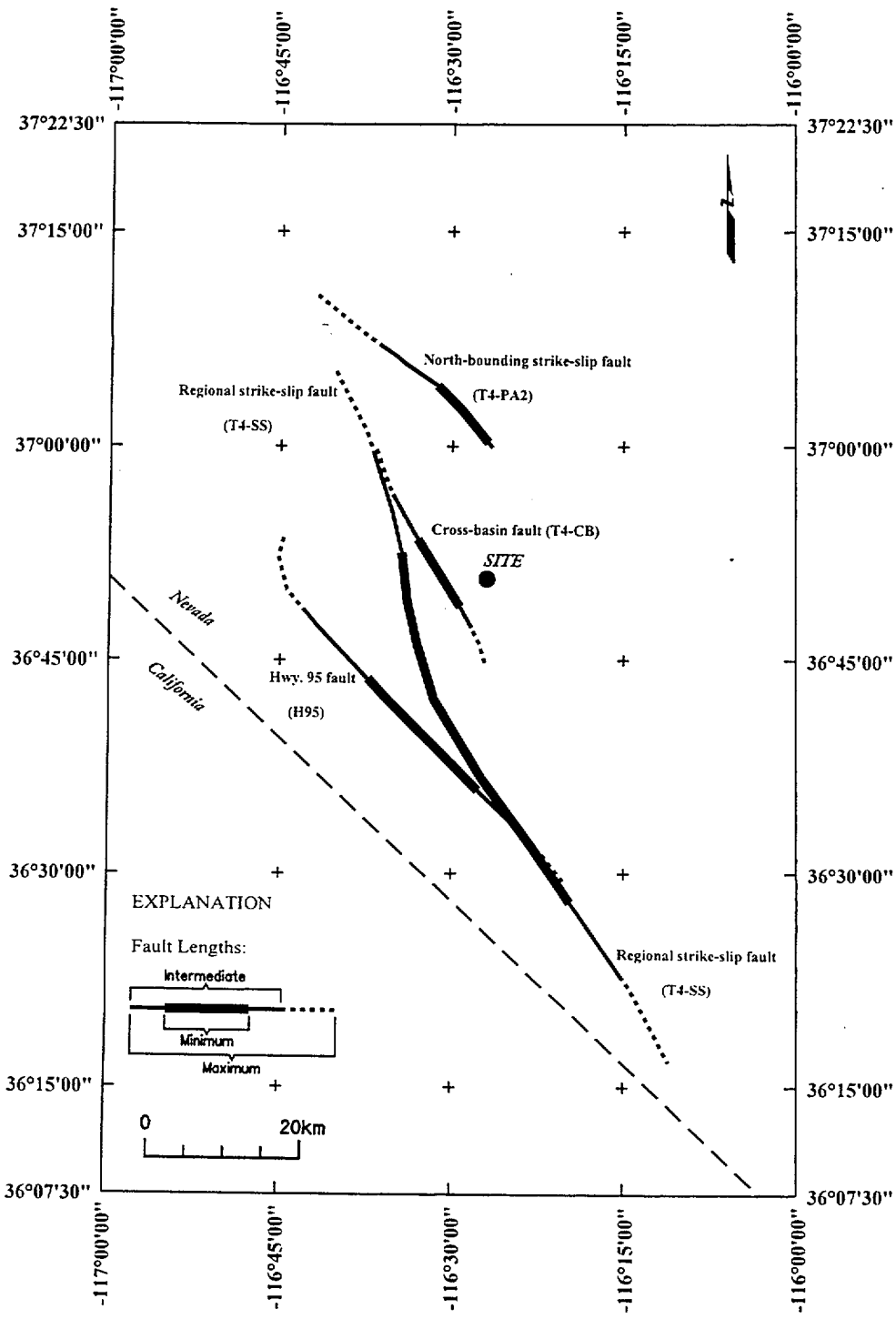

Figure AAR-5 Map showing hypothetical fault sources included in the seismic source model

h:\prj\yucca_mt\dgn\1097\plate_t4_buried_fault.dgn 27-OCT-1997 14:57

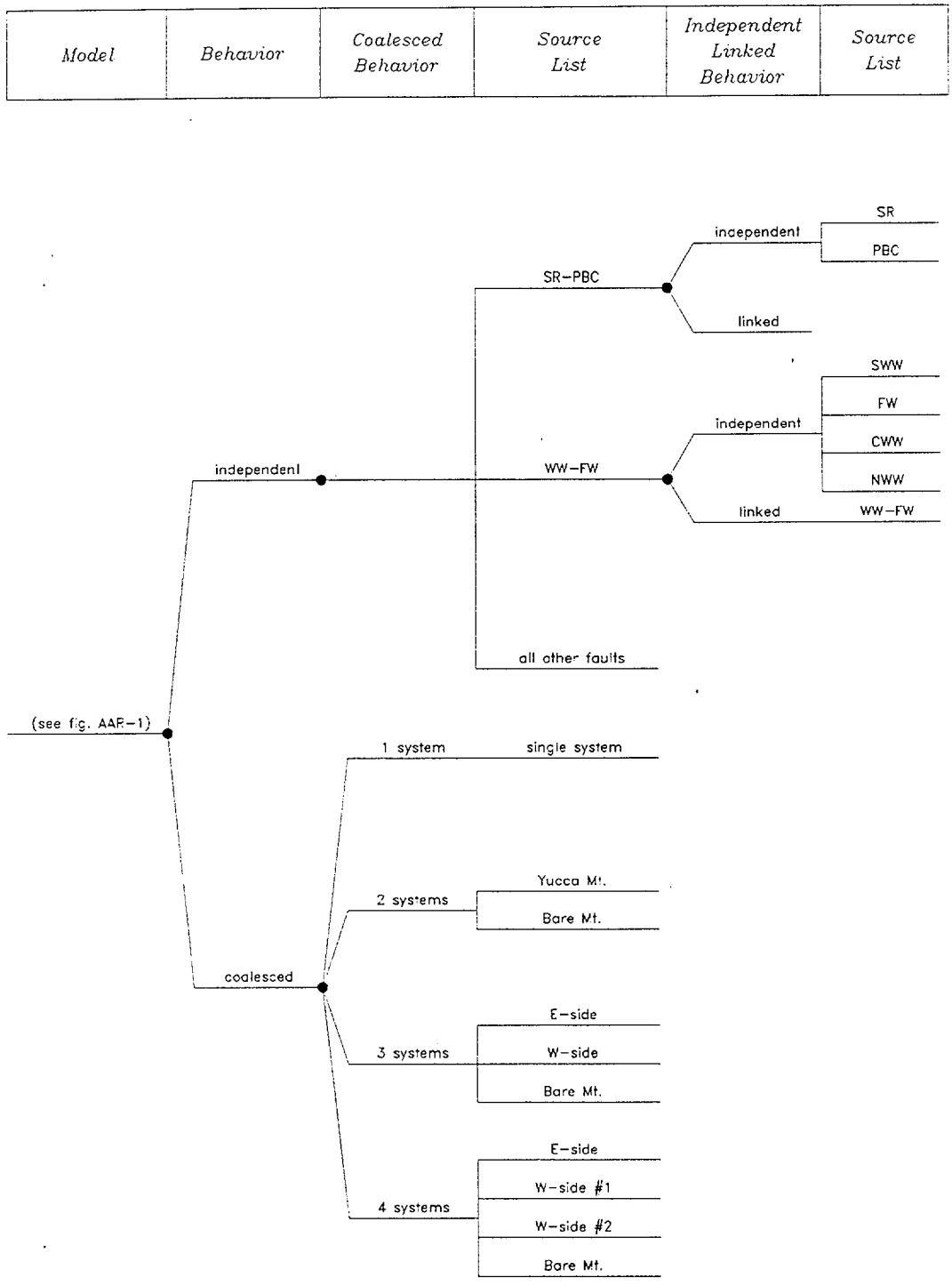

Figure AAR-6 Logic tree: behavior branches for Crater Flat domain

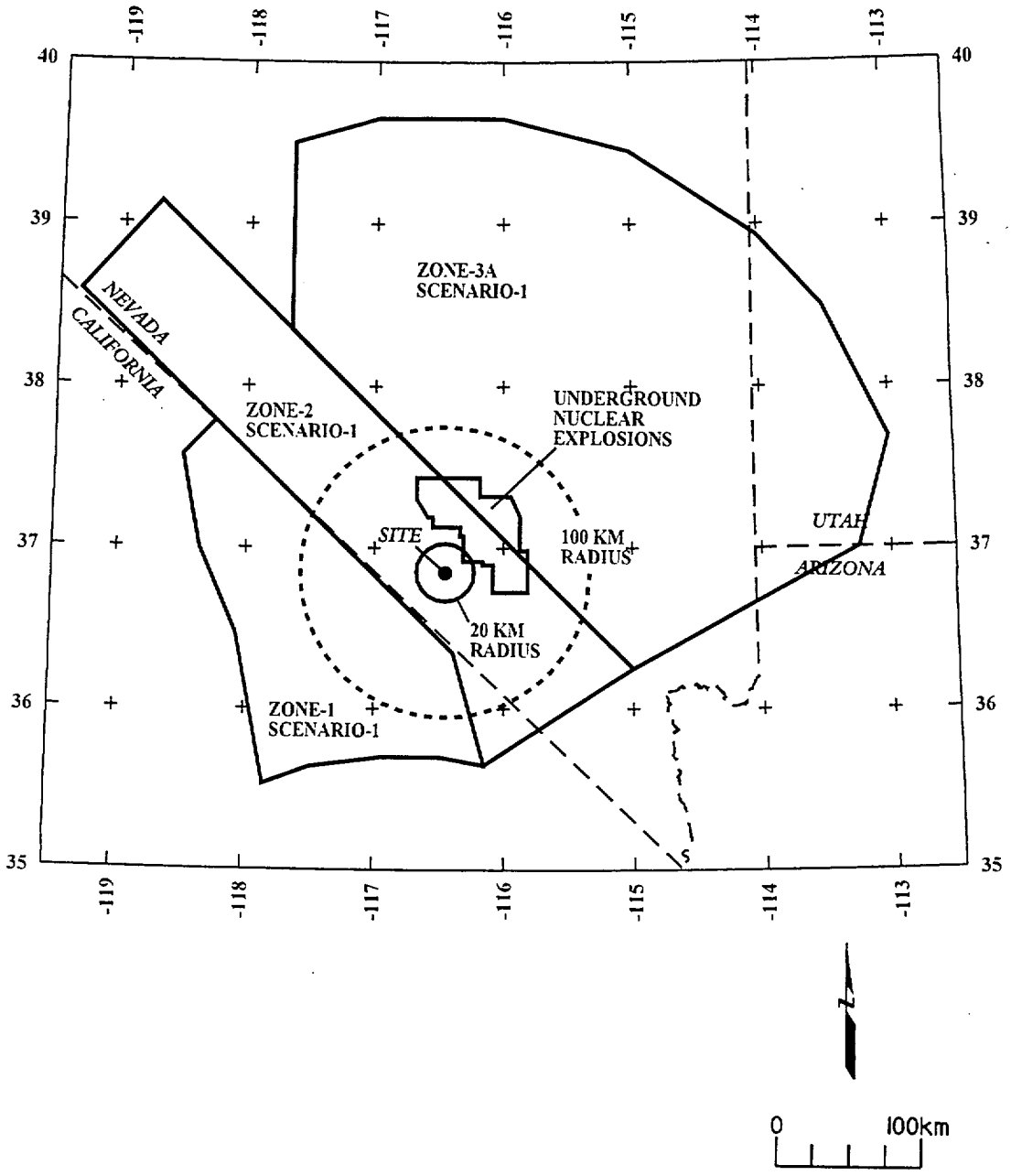

Figure AAR-7 Map showing the boundaries of seismic source zones, Scenario 1.

h:\prj\yucca_mt\dgn\1097\plate_t4_reg_zone1.dgn 27-OCT-1997 15:45

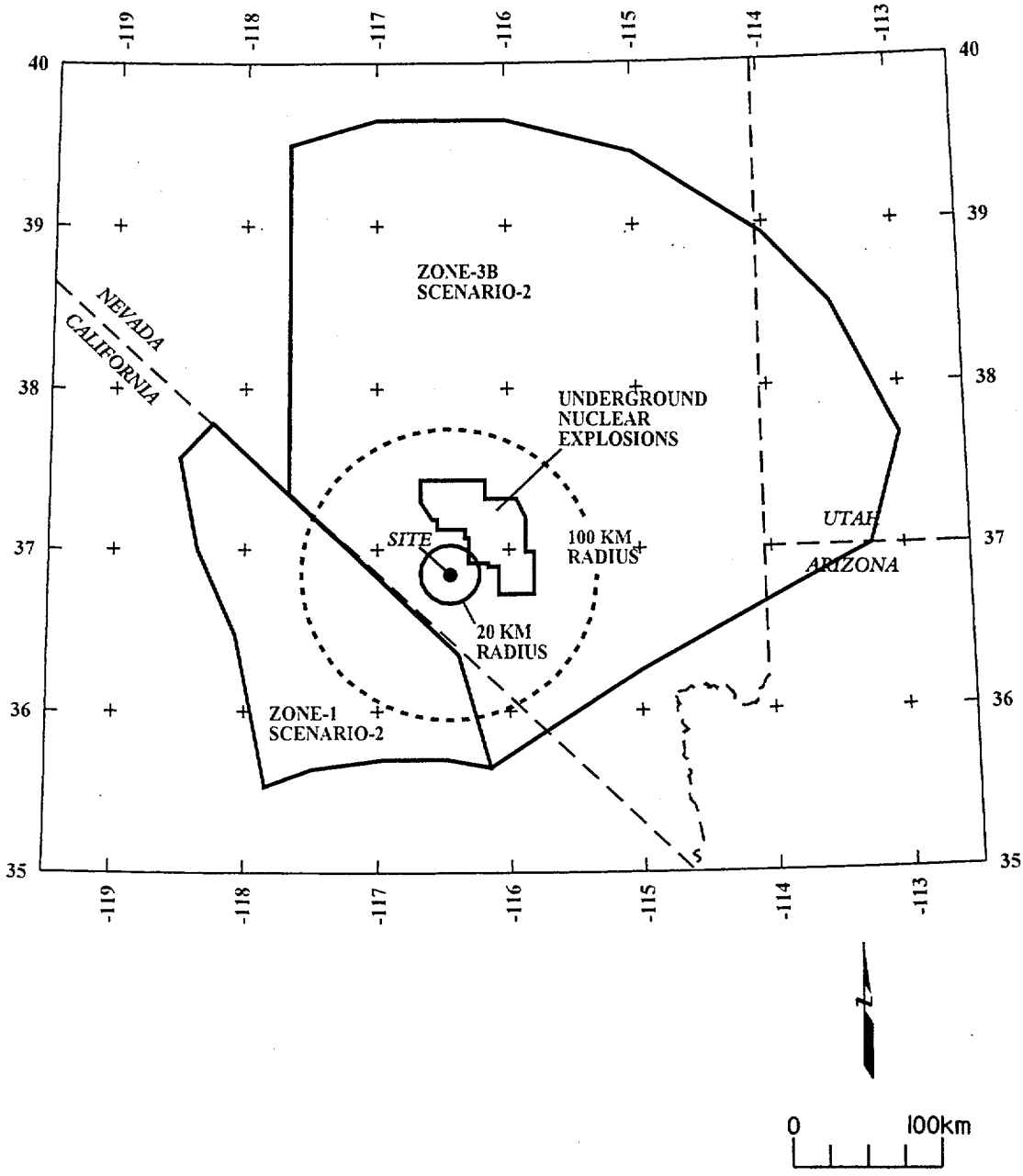

Figure AAR-8 Map showing the boundaries of seismic source zones, Scenario 2.

h:\prj\yucca_mt\dgn\1097\plate_t4_reg_zone2.dgn 27-OCT-1997 15:46

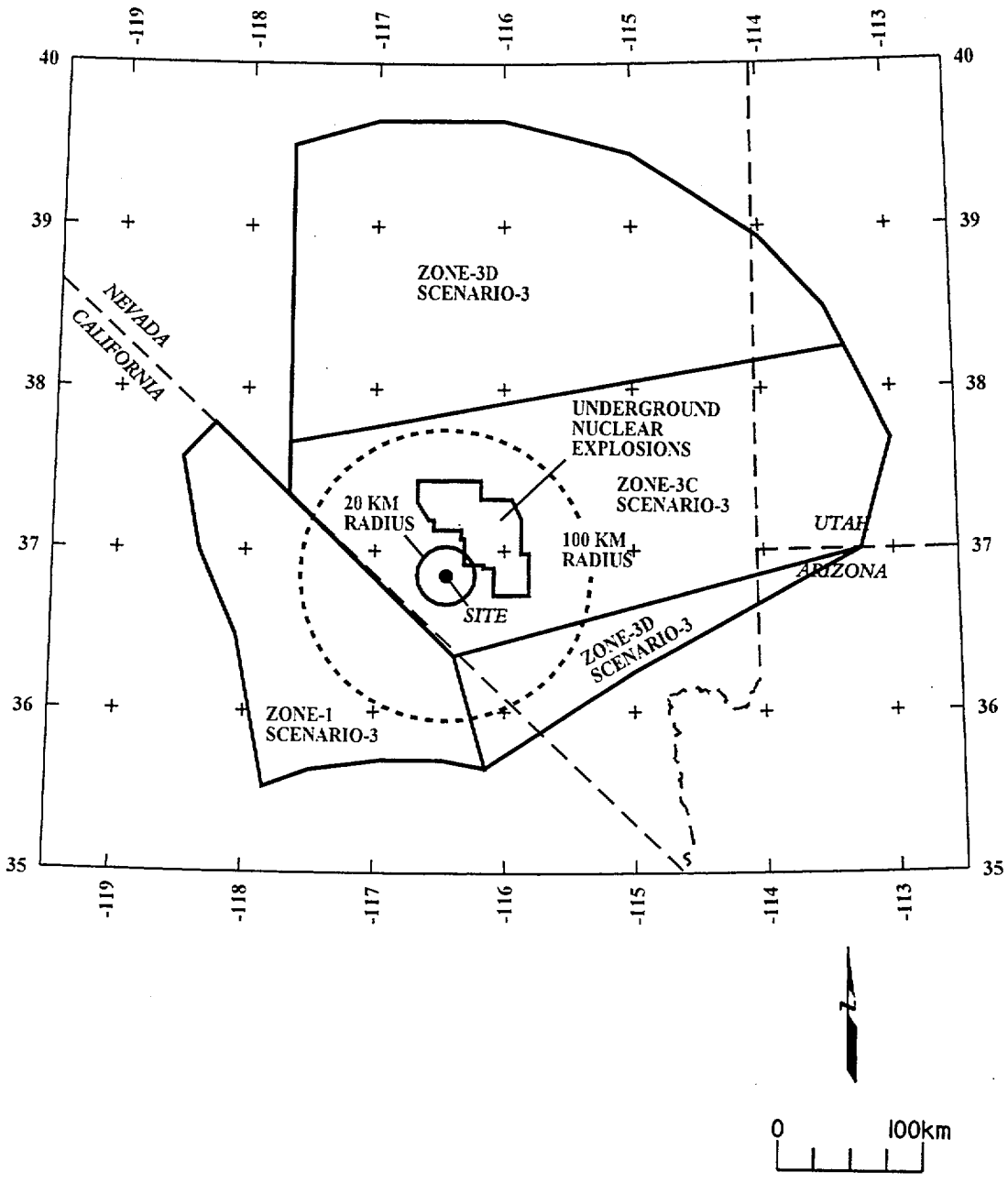

Figure AAR-9 Map showing the boundaries of seismic source zones, Scenario 3.

h:\prj\yucca_mt\dgn\1097\plate_t4_reg_zone3.dgn 27-OCT-1997 15:48

Declustered Catalog	*Source Zonation*	*Spatial Variability*	*Sources*	*Maximum Magnitude*	*Recurrence Calculation Minimum Magnitude*

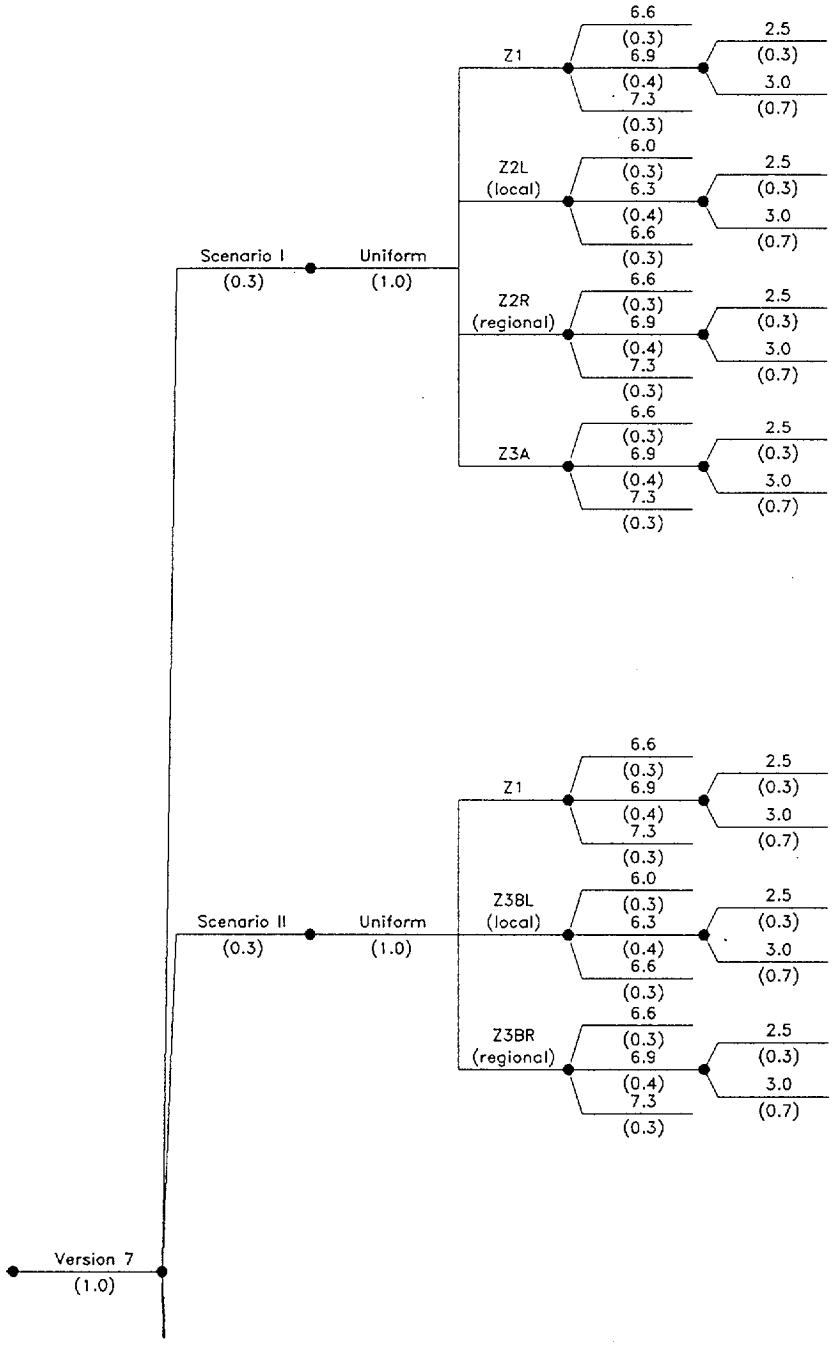

Figure AAR-10a Logic tree for source zones (top)

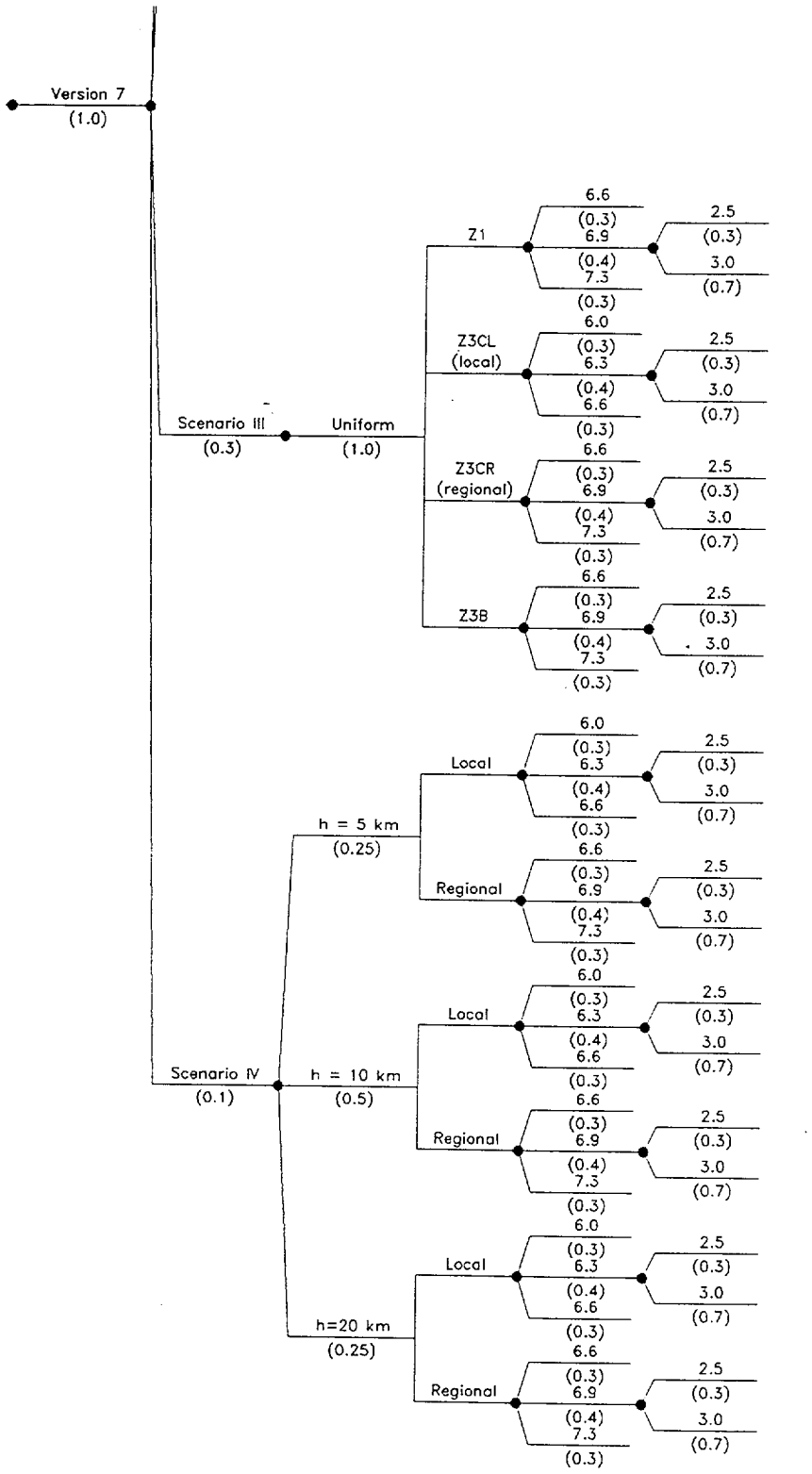

Figure AAR-10b Logic tree for source zones (bottom)

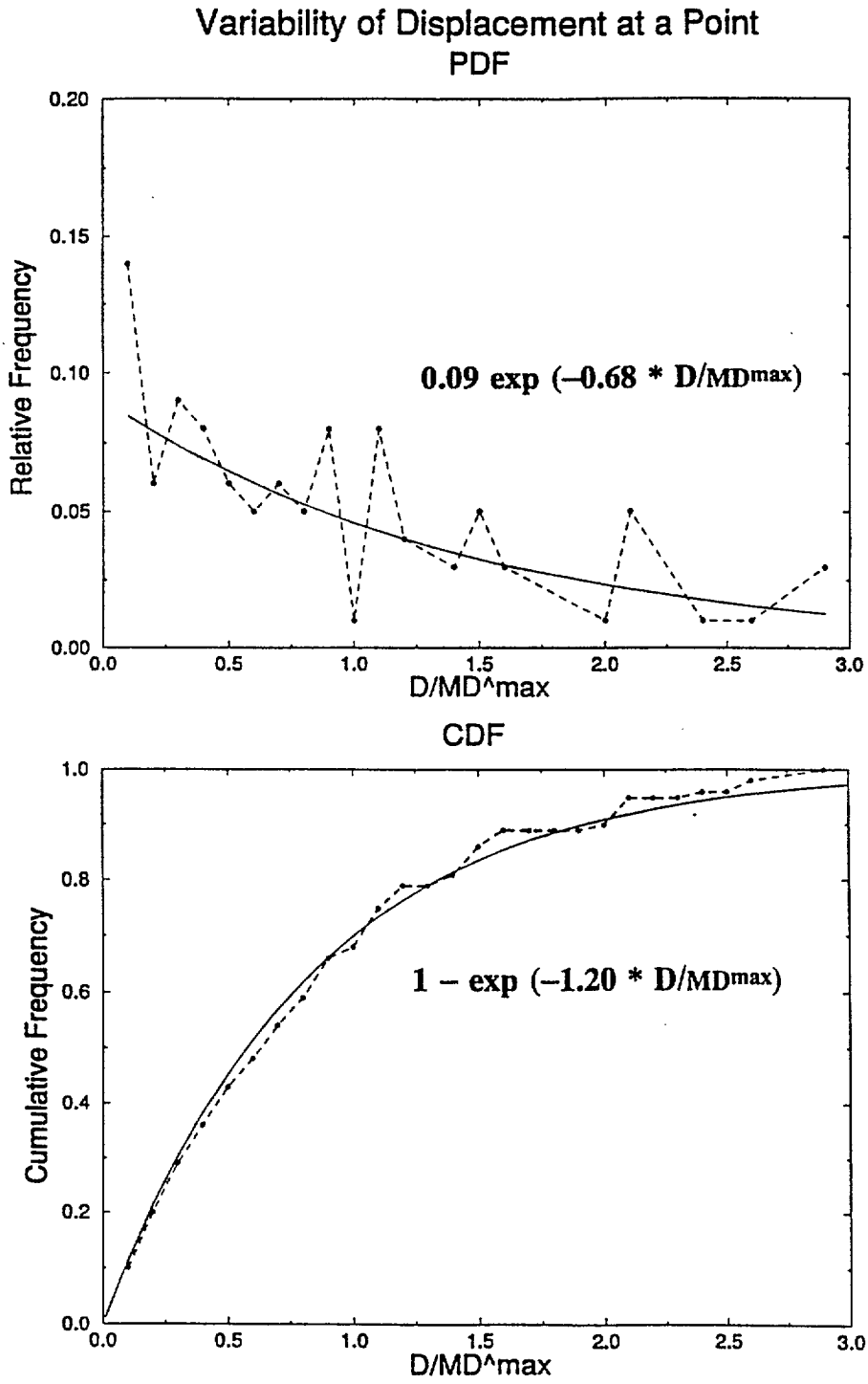

Figure AAR-11 Probability density function (PDF) and cumulative distribution function (CDF) for 80 measurements of single-event displacement, normalized to MD^{max} for the corresponding fault, from 19 trenches in the Yucca Mountain area

INITIAL BRANCHES OF SEPARATE LOGIC TREES
FOR PRINCIPAL AND DISTRIBUTED FAULTING

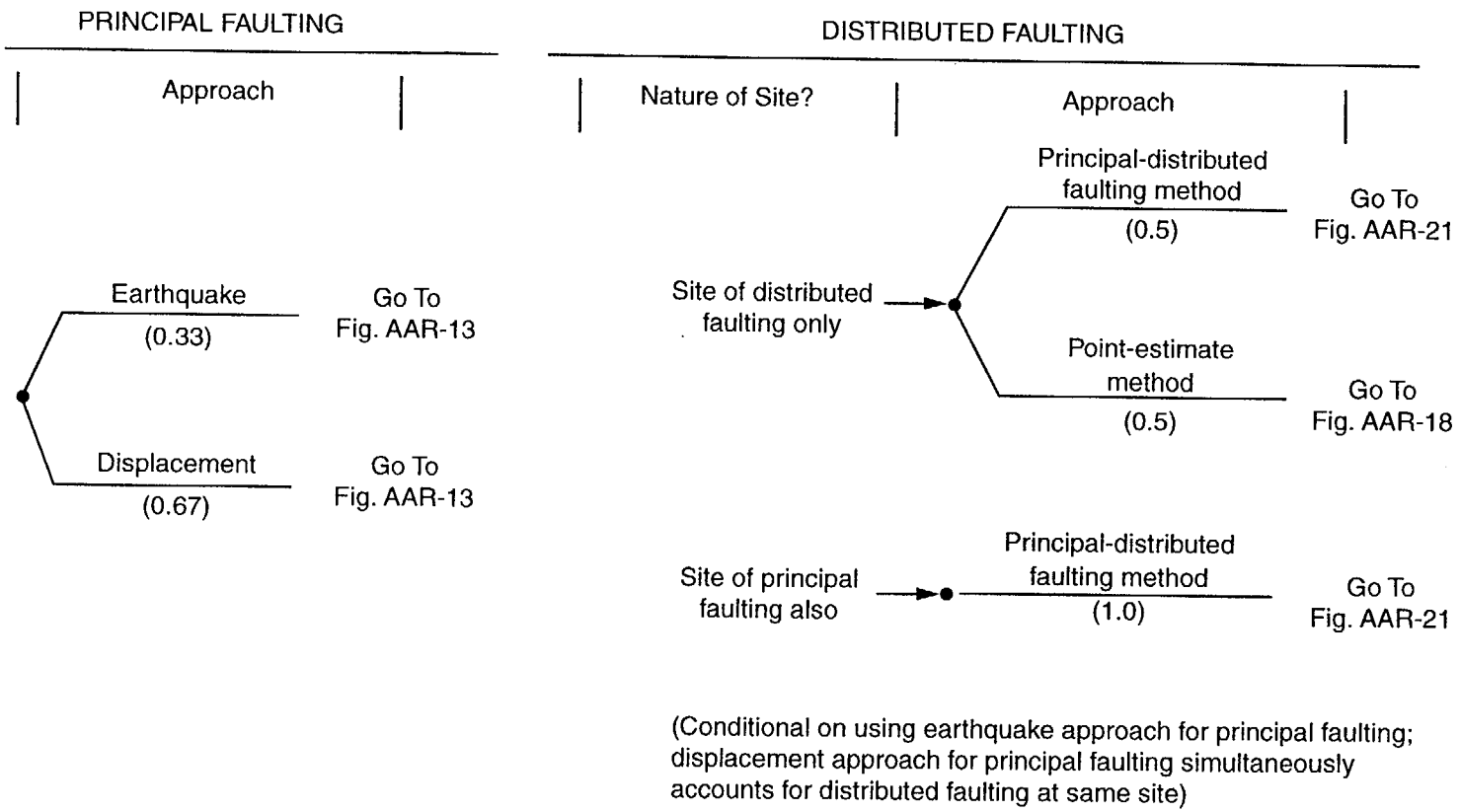

Figure AAR-12 Initial branches of separate logic trees for principal and distributed faulting

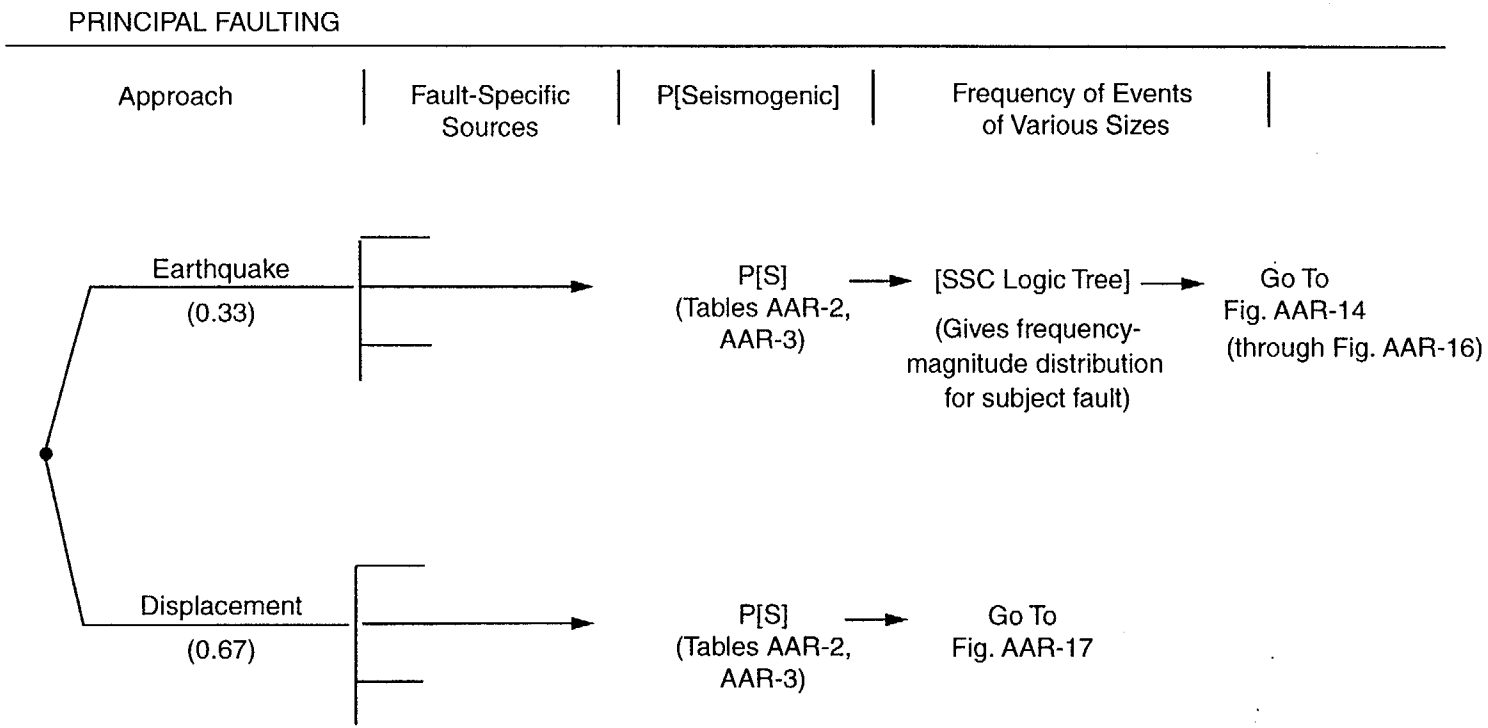

Figure AAR-13 Logic tree for principal faulting

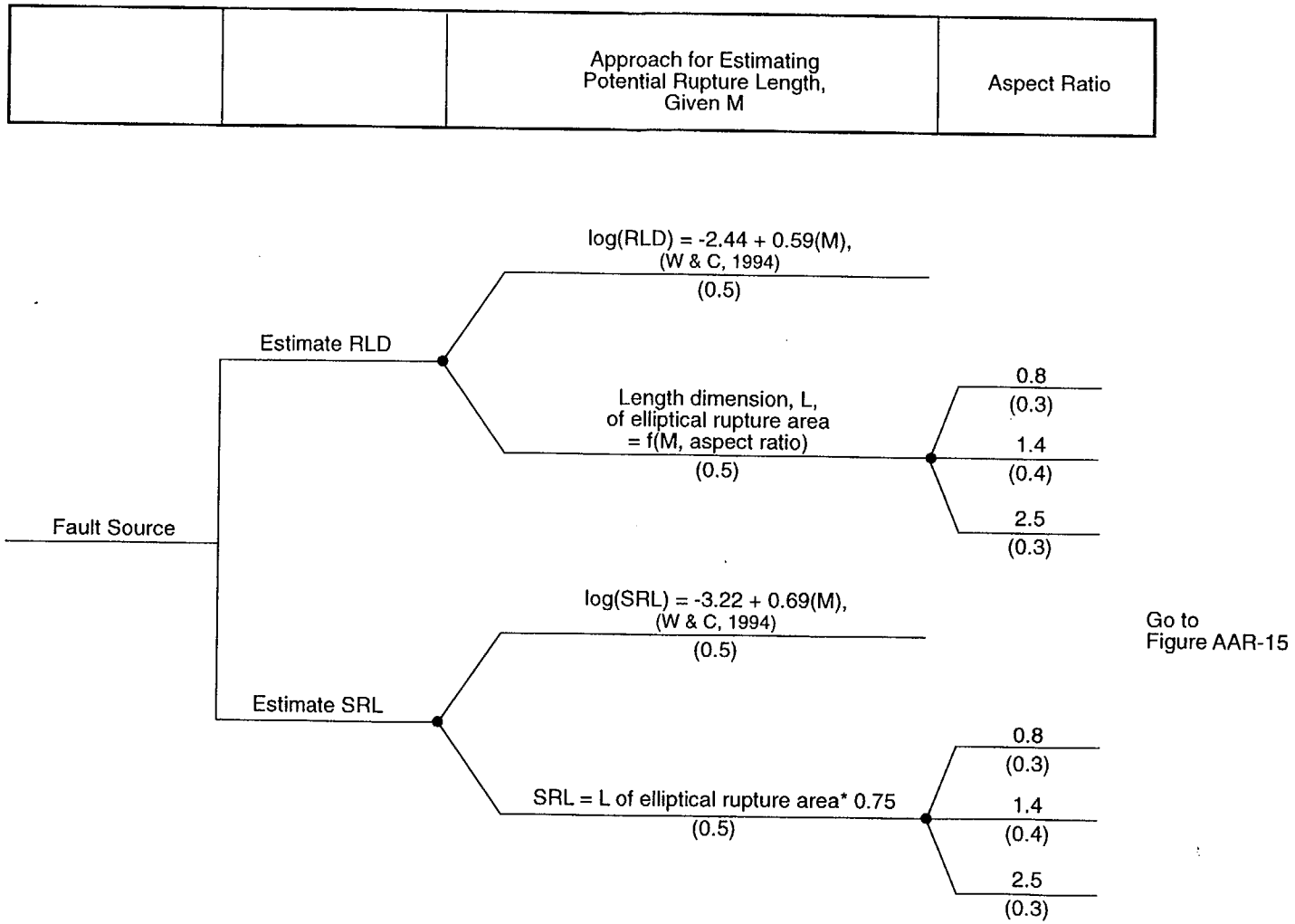

Figure AAR-14 Logic tree for principal faulting – earthquake approach (cont'd): estimating potential rupture length, given M

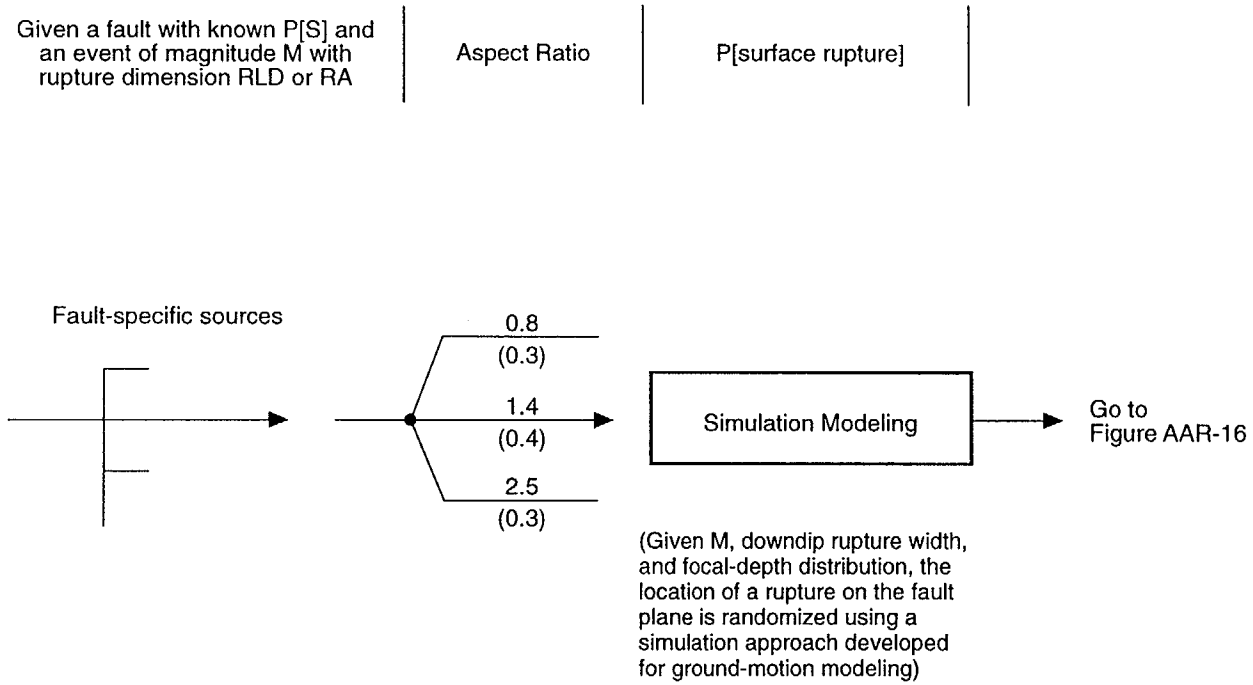

Figure AAR-15 Logic tree for principal faulting – earthquake approach (cont'd)

Given a rupture event on a fault source with known M, P[S], $\overline{RLD}$, $\overline{SRL}$, and P[surface rupture]	*Approach for Estimating Principal Fault Displacement, MD*	*Variability of Slip Along Strike*

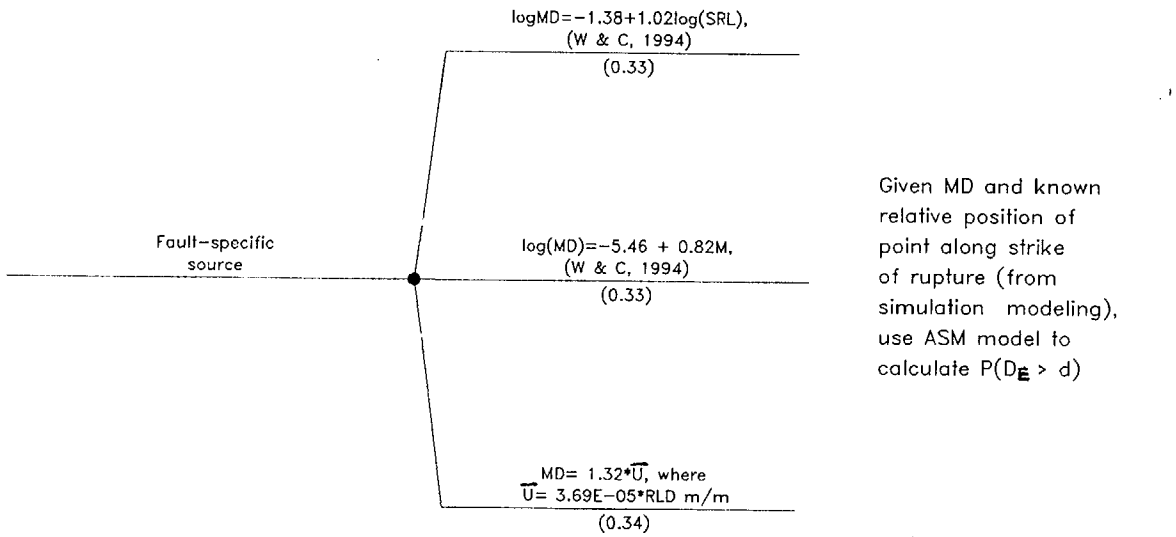

Figure AAR-16 Logic tree for earthquake approach to principal faulting (cont'd): estimating principal fault displacement, *MD*

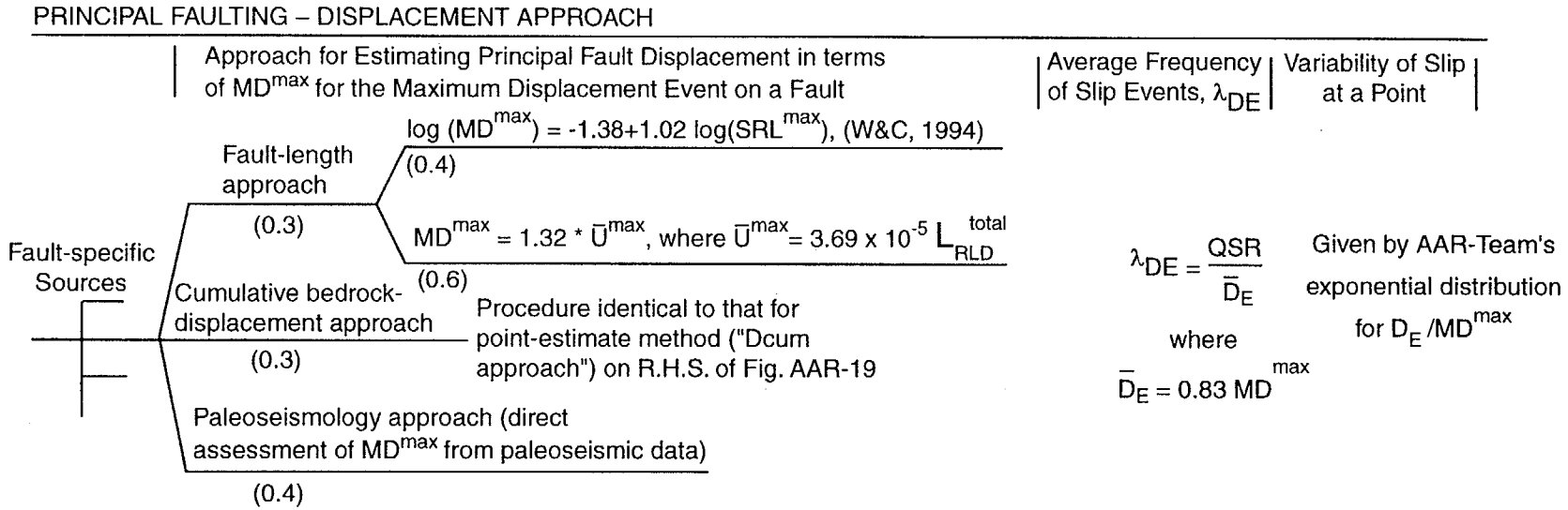

Figure AAR-17 Logic tree for principal faulting — displacement approach

DISTRIBUTED FAULTING — POINT-ESTIMATE METHOD

Secondary Fault or Fracture	P[C] (susceptibility to slip)	Total Post-Tiva Canyon Displacement, Dcum	Approach for Estimating Average Quaternary Slip Rate QSR	Portion of Dcum contributing to QSR

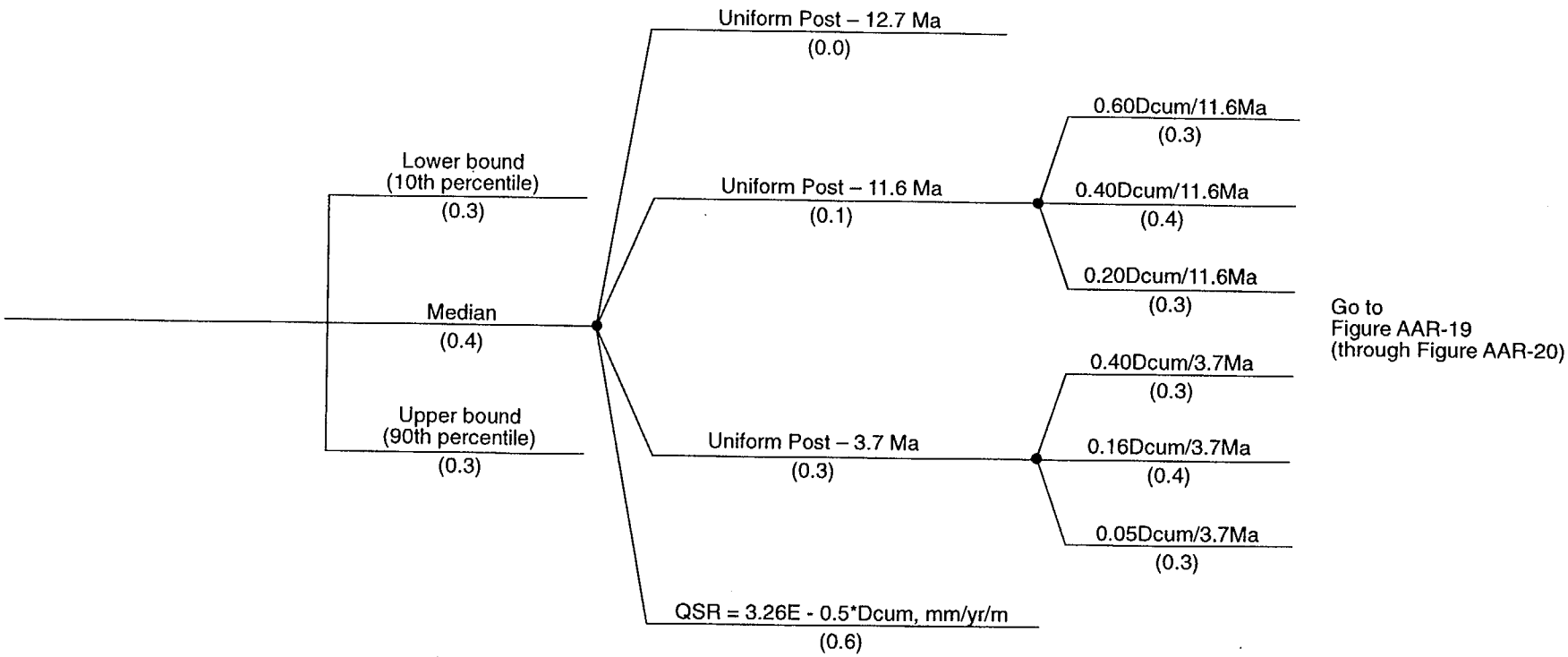

Figure AAR-18 Logic tree for distributed faulting – point estimate method

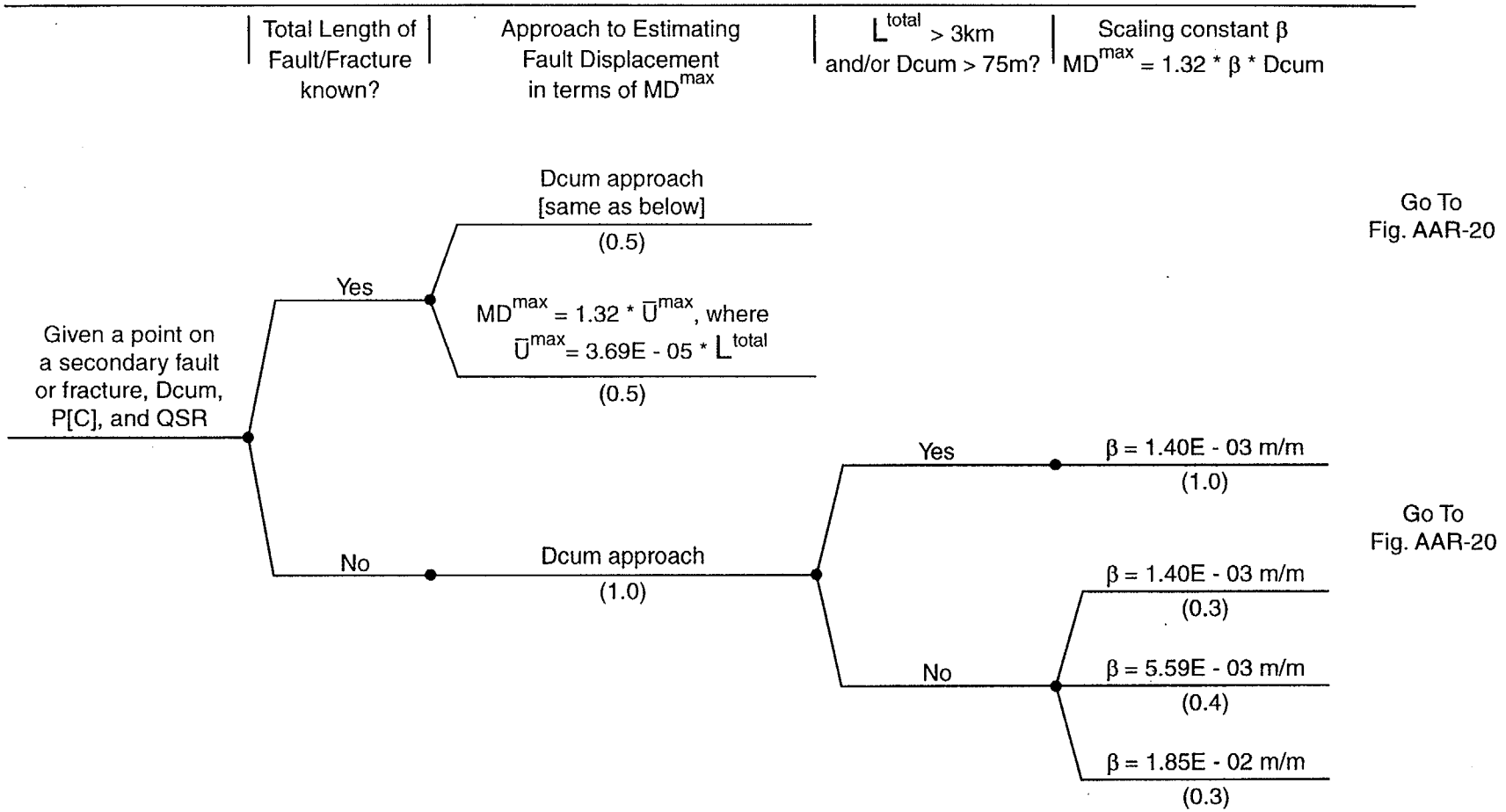

Figure AAR-19 Logic tree for distributed faulting — point-estimate method, cont'd

	Average Frequency of Slip Events, λ_{DE}	Variability of Slip at a Point
Given a point on a secondary fault or fracture, Dcum, P[C], QSR, and MD^{max}	$\lambda_{DE} = \frac{QSR}{\bar{D}_E}$ where $\bar{D}_E = 0.83\ MD^{max}$	Given by AAR-Team's exponential distribution for D_E / MD^{max}

Figure AAR-20 Logic tree for distributed faulting — point-estimate method, cont'd

DISTRIBUTED FAULTING – PRINCIPAL-DISTRIBUTED FAULTING METHOD

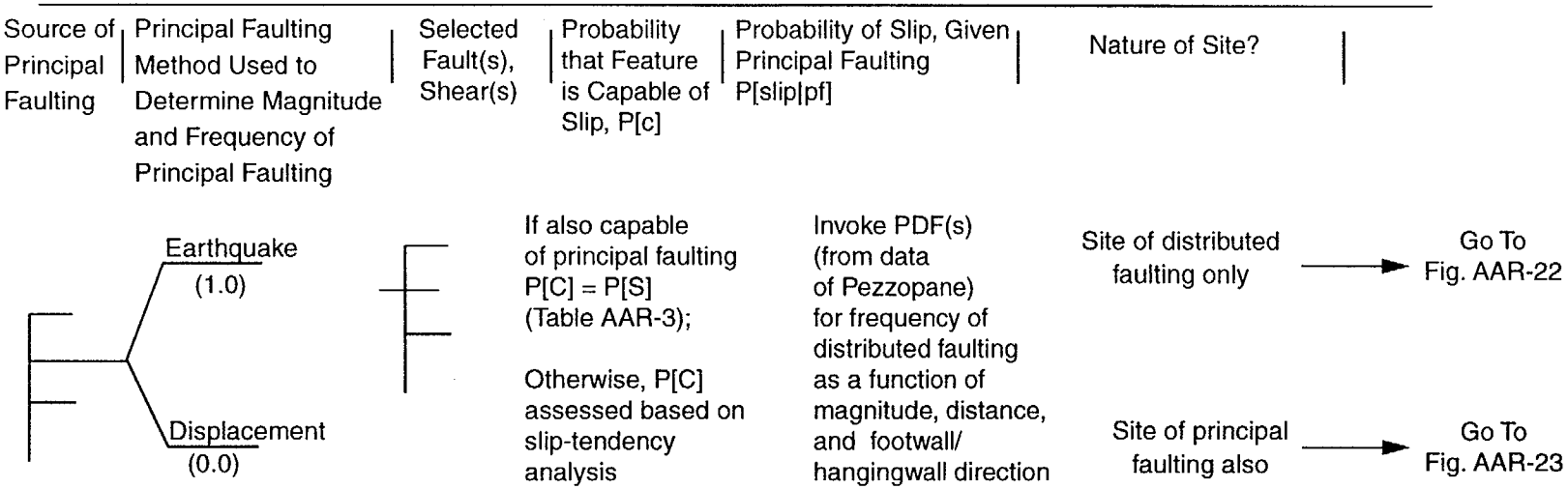

Figure AAR-21 Logic tree for distributed faulting — principal-distributed faulting method

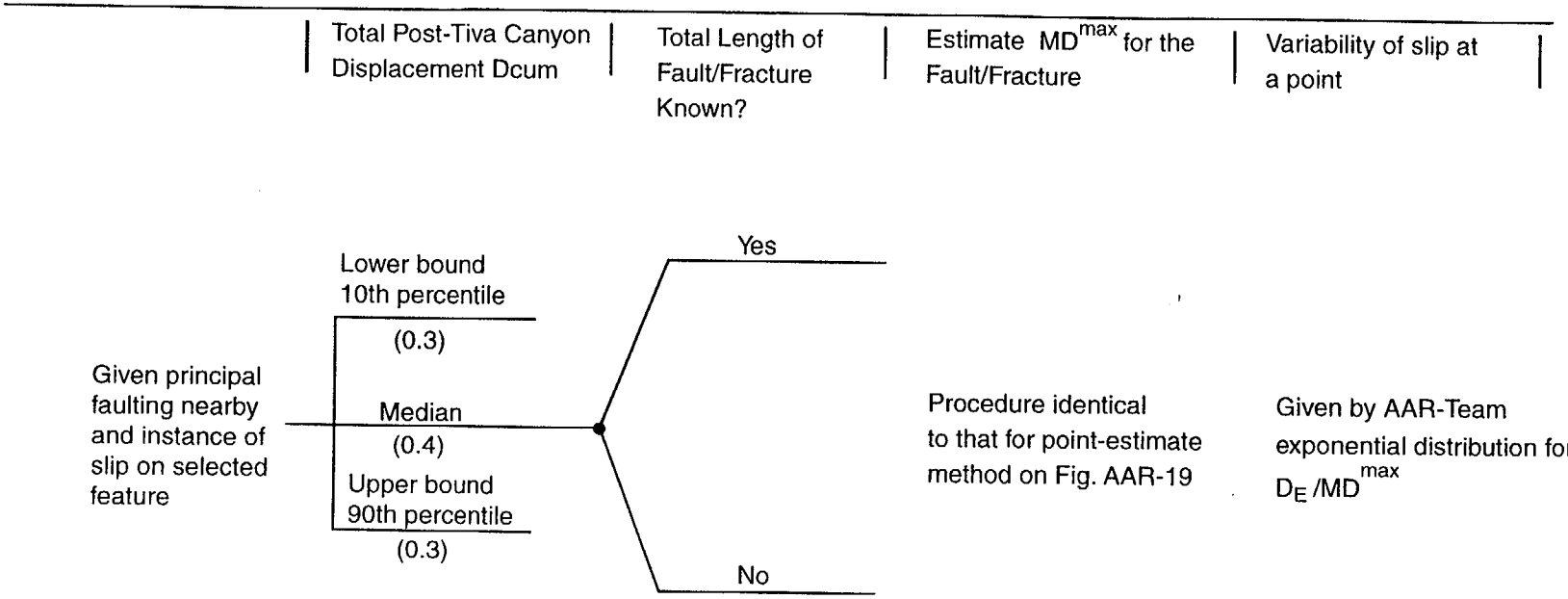

Figure AAR-22 Logic tree for distributed faulting — principal-distributed faulting method, cont'd (for site of distributed faulting only)

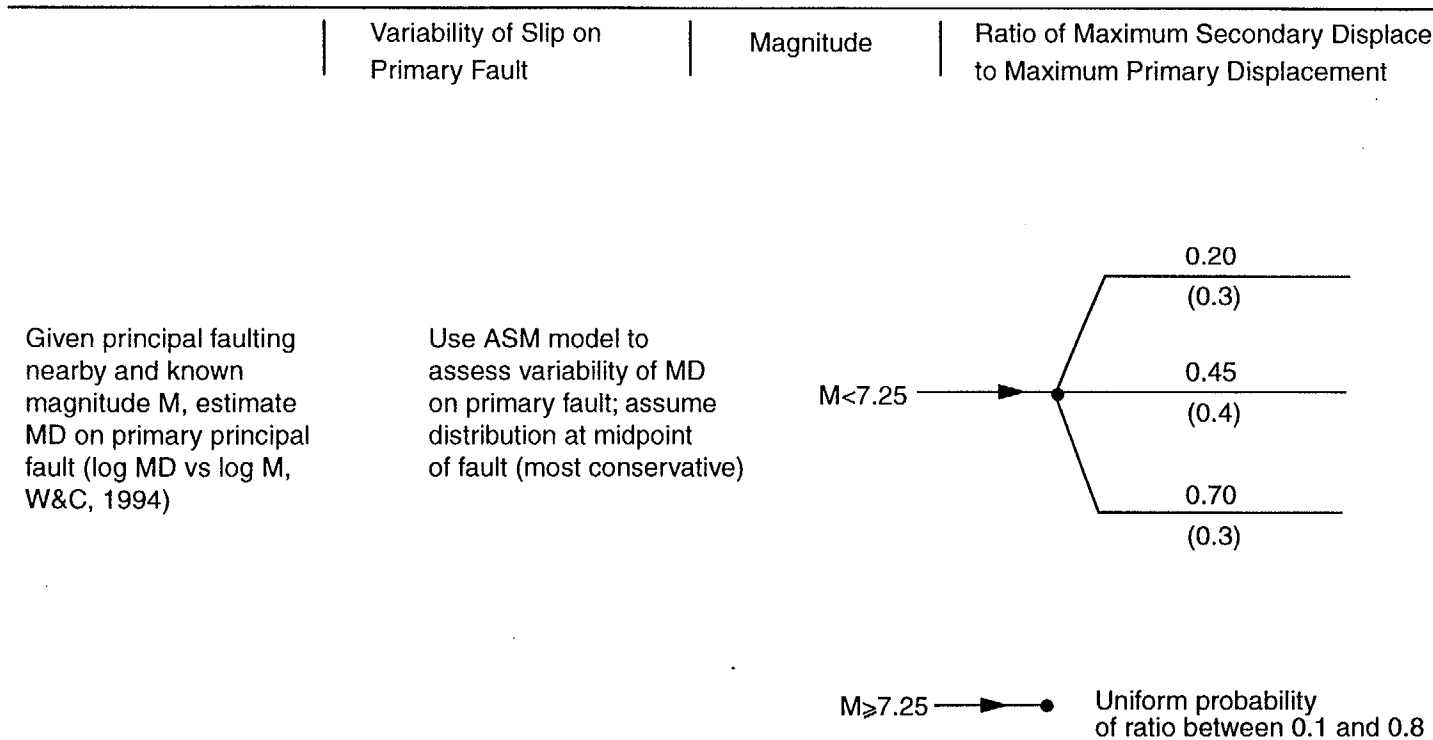

Figure AAR-23 Logic tree for distributed faulting — principal-distributed faulting method cont'd (for site of principal faulting also)

ELICITATION SUMMARY

DIANE DOSER, C.J. FRIDRICH, AND FRANK H. SWAN

TABLE OF CONTENTS

TABLE OF CONTENTS

TABLE OF CONTENTS

TABLES

TABLE OF CONTENTS

FIGURES

TABLE OF CONTENTS

ELICITATION SUMMARY
DIANE DOSER, C. J. FRIDRICH, AND FRANK H. SWAN

1.0
INTRODUCTION

Available seismic, geologic, and geophysical data are used to characterize potential earthquake hazards at Yucca Mountain. The approaches and source parameters presented here will be used by the Yucca Mountain project to develop probability functions that relate: (1) values of strong ground shaking (peak acceleration or spectral acceleration) to annual probability of exceedance; and (2) the likelihood of fault displacement at selected sites in the vicinity of the proposed underground repository.

The geologic and tectonic setting of the Yucca Mountain region and the seismicity data used in this analysis are described in Sections 2 and 3, respectively. The characterization of seismic sources for the ground motion analysis is presented in Section 4. The methods for assessing the potential for fault displacement and the characterization of tectonic features at selected localities within the controlled area at Yucca Mountain are presented in Section 5.

2.0
GEOLOGIC AND TECTONIC SETTING

Yucca Mountain is located in southwest Nevada in the eastern part of the Walker Lane belt, a 100- to 300-km-wide by 700-km-long zone of irregular topography and discontinuous strike-slip structures between the Sierra Nevada and the northern Basin and Range province (Stewart, 1988) (Figure DFS-1). Together, the northern Basin and Range and the Walker Lane belt make up the Great Basin, a region of dominantly extensional tectonism that began with back-arc spreading, at about 45 Ma, associated with subduction of the Farallon plate under the North American plate (Scholz *et al.*., 1971). During northward migration of the Mendocino triple junction, subduction along the southwest coast of North America ceased as the North American plate became juxtaposed against the Pacific plate along a strike-slip boundary, the San Andreas fault (Atwater, 1989; Oldow *et al.*., 1989). West of Yucca Mountain, this transition occurred at about 10 Ma. Since this transition, extension in the

Great Basin has been driven by the northwestward movement of the Pacific plate relative to the North American plate.

Within this framework, Yucca Mountain is a multiple-fault-block ridge in the eastern part of the Crater Flat basin, an extensional basin that formed primarily between 12.7 and 10 Ma, before the tectonic transition discussed above. The Crater Flat basin is a subbasin of the Amargosa trough, a long graben-like feature bounded on the west by the Bare Mountain range-front fault and on the east by the largely buried gravity fault (Figure DFS-2). The domain west of the Bare Mountain fault is characterized by extreme extension and by detachment faulting that terminates eastward in the vicinity of the Bare Mountain fault. The areas east of Bare Mountain fault, including the Amargosa trough, are characterized by minor to moderate extension. The domains east of the Amargosa trough are dominated by northeast-striking, left-lateral strike-slip faults and northwest-striking, right-lateral strike-slip faults. (Only the major ones are shown on Figure DFS-2.)

The Crater Flat basin lies on the south flank of the Timber Mountain caldera complex, the central eruptive source area of the southwest Nevada volcanic field. This volcanic field straddles the structural transition between the Walker Lane belt and the northern Basin and Range Province. The caldera complex has influenced the development of structures within the northernmost part of the Crater Flat basin by local modification of the stress regime associated with doming of the area around the calderas (Fridrich, 1997).

Yucca Mountain is composed of a 1.5- to 3.0-km-thick sequence of variably welded Miocene ash-flow tuffs and lesser ashfall tuffs and lavas of the southwest Nevada volcanic field overlying a complexly deformed Paleozoic and late Precambrian sequence of marine carbonates, quartzites, and argillites. The Tertiary section thickens westward within the Crater Flat basin to a maximum thickness of about 4 km, and is truncated on the western margin of the basin by the Bare Mountain fault. The Tertiary strata in the basin are tilted dominantly eastward to southeastward along a closely spaced system of mostly west- to northwest-dipping faults. Most of the intrabasin faults are thus antithetical to the range-front fault at the western margin of the basin in that they face into the range-front fault and formed coevally with it (Fridrich,1997).

Deformation in the Crater Flat basin is dominantly extensional but includes a significant component of northwest-directed right-lateral strike-slip strain. On the surface at least, the strike-slip deformation is diffuse rather than discrete—the basin evidently opened in an oblique manner, with the least extension (about 7-15 percent) and the least vertical-axis rotation (less than 5 degrees) in the northeast corner of the basin, on northern Yucca Mountain. From there, the magnitude of deformation increases to the west and south, to maximum values of 50 to 100 percent extension and at least 45 degrees clockwise rotation in the southwest corner of the basin (Fridrich *et al..*, in press). The vertical-axis rotation in the basin is accommodated by left slip on the closely spaced north- to northeast-striking normal faults that comprise the internal structure of the basin. The structural geometry of the Crater Flat basin thus resembles that of some strike-slip pull-apart basins; however, detailed mapping has failed to uncover any evidence of master strike-slip faults anywhere in, or at the margins of, this basin. As in most of the eastern Walker Lane belt, the strike-slip deformation is diffuse rather than discrete.

In the Yucca Mountain region, the 10 Ma transition in the driving force of tectonism, discussed above, coincided with a shift in the style of volcanism to much lower eruptive volumes, and a shift from dominantly silicic volcanism before 10 Ma to dominantly basaltic volcanism afterward. A significant shift in tectonic style also may have occurred during this transition; however, because of the large decrease in silicic volcanism around 10 Ma, there is poor stratigraphic constraint on the tectonic evolution of this region between 10 Ma and present.

The evidence indicates that, after 10 Ma, the locus of both volcanism and tectonism continued to migrate westward out of the Yucca Mountain vicinity toward Death Valley, as it had been doing since 12.7 Ma. In the wake of this westward migration of the focus of tectonism, tectonism rates in the Yucca Mountain region declined strongly after 10 Ma. Quaternary tectonism in the Yucca Mountain region has consisted of selective reactivation of certain faults that formed during the middle Miocene or earlier, including some of the major faults in Crater Flat basin, as well as faults in the Rock Valley fault system to the east (Figure DFS-2).

During the Quaternary, tectonism and volcanism in the Great Basin has been localized primarily along the eastern limit of the extensional province—at the Wasatch Front, and along the western limit of the province—in Death and Owen's valleys. In addition, a third and significantly lesser area of tectonism has been a north-trending zone in the center of the province. Yucca Mountain is located outside all three of these zones of major Quaternary seismic activity, and the rates of recent tectonism at Yucca Mountain are much lower than in any other part of the Great Basin where studies of Quaternary tectonism have been conducted.

In the Crater Flat basin, eight major faults show evidence of offset during the past 500,000 years, with rates of slip ranging from less than 0.001 to about 0.03 mm/yr. All of these faults formed around 12.7 Ma, and the current level of activity along these faults is very low relative to slip rates on the same structures between 12.7 and 10 Ma (Fridrich *et al.*., in press). The three largest Quaternary faults on Yucca Mountain show late Quaternary slip rates that increase southward, indicating that the oblique style of extension in the Crater Flat basin, established during the middle to late Miocene, has continued to the present.

Basalts have erupted in Crater Flat basin in four episodes, at about 10 Ma, 3.7 Ma, 1 Ma, and 70 ka, that together define a trend of progressively declining volume of magma (B.M. Crowe *et al.*, LANL, written communication, 1995). The latest eruption formed the Lathrop Wells center, a small cinder cone with associated lavas on the southern end of Yucca Mountain. The fact that ash from this eruptive center fills cracks formed during late Quaternary faulting events on Yucca Mountain has been interpreted by some workers as evidence that there may be a relationship between faulting and volcanic activity in the Crater Flat basin (J.W. Whitney *et al.*, USGS, written communication 1996a).

3.0
HISTORICAL SEISMICITY DATA

Historical seismicity catalogs available to the panel members describe seismicity within a 100- and a 300-km radius of the site, as collated by Woodward-Clyde personnel. Our calculations of recurrence parameters made exclusive use of the 300-km radius catalog, as we believe this catalog enables us to obtain better spatial averages than the smaller catalog.

Catalog magnitudes have been converted to a common moment-magnitude scale (Appendix D). We used the catalog completeness intervals defined by Woodward-Clyde Federal Services (I. Wong *et al.*, WCFS, written communication, 1997; I. Wong, SSC Workshop 3). Known nuclear explosions have been deleted from the catalog. Also, earthquakes that appear to be associated with regional fault sources have been subtracted from the catalog when estimating recurrence for the seismic source zones. These earthquakes were identified by drawing areas around each regional fault source (Section 4.2) and laying seismicity plots over the fault area map. The areas around the faults were drawn to include the area above the inclined fault plane (estimated dip projected to the base of the seismogenic zone) plus a nominal distance to allow for inaccuracies in epicentral locations.

The catalog was declustered using the algorithms of both Veneziano and van Dyck (1985) and Youngs *et al.*. (1987). The two declustered catalogs were given equal weight for calculating recurrence parameters.

A minimum magnitude of 2.5 was used to compute the recurrence parameters after considering maximum likelihood rates and b-values calculated as a function of minimum magnitude (Section 3.1 contains a description of the methods used to calculate seismicity parameters). Spatially varying a-values were included in the analysis through use of a Gaussian kernel. Details of the smoothing are discussed in Section 4.1.1

Focal mechanism data compiled by S.K. Pezzopane *et al.*. (USGS, written communication, 1996b, Table 7-3) were used for analysis of variations in focal depth and focal mechanism within the study area. Results of this analysis are discussed in Section 4.1.2.

4.0
CHARACTERIZATION OF SEISMIC SOURCES FOR GROUND MOTION ANALYSIS

Our model includes four categories of seismic sources: (1) *seismic source zones* to account for seismicity that cannot be attributed to fault-specific sources included in the model; (2) *regional fault sources,* which include mapped late Quaternary faults within about 100 km of Yucca Mountain, but not including the faults in the site vicinity; (3) *local fault sources* in the

vicinity of Yucca Mountain; and (4) *hypothetical faults* near the site. Different approaches are used to characterize each of these categories. Seismic sources that might make a significant contribution to the seismic hazard at Yucca Mountain (either because they have a relatively high rate of activity and/or because they are close to the site) are characterized in greater detail than are sources far from the site.

4.1 SEISMIC SOURCE ZONES

Seismic source zones are used to characterize volumes of the Earth's crust that are inferred to exhibit similar characteristics with respect to the magnitude and frequency of occurrence of earthquakes that cannot be attributed to fault-specific seismic sources (i.e., background seismicity). The seismicity within a given zone may be uniformly or non-uniformly distributed.

Uncertainties in the source zone geometry are incorporated in this analysis by considering different source zone models and a range of values for the depth of the seismogenic crust. Uncertainties in the magnitude frequency distribution within each zone are incorporated in the analysis by considering a range of values for the upper-bound earthquake and by considering different smoothing algorithms that provide for different levels of spatial smoothing of the earthquake epicenters in the seismicity catalog.

4.1.1 Definition

The region around Yucca Mountain commonly is divided into three major tectonic zones: the northern Basin and Range, the southwestern part of the Walker Lane belt, and the northeastern part of the Walker Lane belt. The northern Basin and Range extends from the western limit of the Colorado Plateau westward to the eastern side of the Walker Lane belt, as defined below, and from the southern boundary of the Snake River Plain southward to the gravity gradient, just north of the Hoover Dam, that separates the northern and southern parts of the Basin and Range (Saltus and Thompson, 1996). The southwestern part of the Walker Lane belt extends from the Sierra Nevada, at its western boundary, eastward to the Furnace Creek and Pahrump fault systems, and extends from the northern boundary of the Mohave Desert, namely the Garlock fault at its southern limit, about 700 km to the north-northwest. The northeastern part of the Walker Lane belt extends from the Furnace Creek and Pahrump

fault systems eastward to a line across which the topography changes from being very irregular to showing the regular N20°E pattern of basins and ranges that characterizes the northern Basin and Range.

All three provinces have been characterized by extensional tectonics from the Eocene to the present. In the northern Basin and Range, extensional structures dominate the tectonic pattern. Relatively little strike-slip deformation has occurred in this province relative to the two parts of the Walker Lane belt. The southwestern part of the Walker Lane belt is characterized by a strong northwest structural grain created by several major northwest-striking, right-slip and oblique slip faults. The northeastern part of the Walker Lane belt, in which Yucca Mountain is located, is a structural province characterized by numerous short, discontinuous strike-slip structures and by distributed strike-slip strain, including both northwest-striking right-slip structures and northeast-striking left-slip structures. This diverse structural pattern creates a very irregular topography in the northeastern Walker Lane belt.

The three provinces are structurally distinct and yet much more similar to one another than they are to any of the bordering provinces, including the Colorado Plateau to the east, the Mohave Desert to the south, and the Sierra Nevada to the west. The seismic characteristics of the Yucca Mountain region can be characterized based on the historical record of seismicity in the northern Basin and Range and the two parts of the Walker Lane belt. However, because of the structural differences between these three provinces, an even better characterization may be derived by studying the seismicity of these three provinces individually to see if they have distinct seismic characteristics. Accordingly, two seismic source zone models are considered in the logic tree (Figure DFS-3): *Model A*, which consists of one regional zone plus a site-vicinity zone (Figure DSF-4); and *Model B*, which has three regional zones plus a site-vicinity zone (Figure DFS-5). The one-zone model, three-zone model, and the site-vicinity seismic source zone are described below.

Model A - One Zone Plus Site-Vicinity Zone. In this model recurrence parameters are estimated for a single regional zone outside the local site zone (see Figure DFS-4) based on the 300-km radius historical catalog and the estimated upper-bound magnitude. This model, which is assigned a weight of 0.2, assumes that over a long period (million years), regional differences in tectonics are minimized because the region as a whole is undergoing roughly

the same rate of extension. Smoothing of the historical catalog was conducted using Gaussian kernels having different half-widths. The half-widths included in the analysis and their associated probability weights (in parentheses) are: 10 km (0.25), which is comparable to the location uncertainty for the better-located events in the region; 25 km (0.6) , which is comparable to the value used by Frankel *et al.*. (1996); and infinity (0.15), which corresponds to no smoothing.

Model B - Three Zones Plus Site Vicinity. In this model the recurrence parameters were estimated by dividing the region into three distinct zones (Figure DFS-5) in addition to a local site-vicinity zone. The zones reflect differences in fault style and orientation as well as differences in focal mechanisms and focal depths (Bellier and Zoback, 1995). The three zones are: (1) a Basin and Range zone; (2) an eastern Walker Lane zone; and (3) a western Walker Lane zone. The Basin and Range zone is characterized by extension along predominantly normal faults that trend north-south to NNE-SSW. The eastern Walker Lane zone is characterized by a mixture of normal (still dominant) and strike-slip faulting along NNW-SSE to NE-SW trending faults. In the western Walker Lane zone, strike-slip faulting predominates along NW-SE trending faults, and focal depths appear to be about 2 to 4 km shallower than surrounding regions, perhaps due to the increased regional heat flow. The three-zone model is assigned a higher weight (0.8) than the one-zone model, because in the short term (thousands of years), differences in the stress regimes in the three regions appear to have led to different styles of faulting.

Smoothing of the historical catalog was conducted in the same manner as for model A after removing earthquakes associated with specific fault sources. Half-widths for smoothing also were selected at 10 km, 25 km, and infinity, but weights were selected as 0.22, 0.53, and 0.25, respectively. Slightly more weight was given to infinity (as compared to Model A) because, if there are smaller regional zones, the spatial distribution of seismicity is more likely to be uniform within them.

Site-Vicinity Zone. The boundaries of the site-vicinity zone were drawn to include only the well-investigated part of the Yucca Mountain area that was the focus of the detailed USGS/DOE site-characterization studies. The earthquake recurrence parameters for the site-vicinity zone are estimated the same way as for Models A and B, except that a lower range of

values is considered for the upper-bound earthquake magnitude because the active faults capable of producing larger magnitude earthquakes have been identified and are included in the model as fault-specific (local) sources.

This rationale does not necessarily apply to the seismogenic part of the crust below a detachment layer, if one exists. Given a detachment zone, the potential for larger magnitude, deep events is considered by including in the hazard model a postulated hidden strike-slip fault (Section 4.4.2).

The background earthquake for the site-vicinity zone includes a potential earthquake produced by volcanic processes. Quaternary volcanic activity in the site zone has included five basaltic eruptions that formed small cinder cones and associated lava flows; four of these occurred at about 1 Ma, and the other at about 70 ka. The calculated probability of recurrence of this type of volcanic activity in the site area has been estimated at about 10E-7 per year (B.M. Crowe *et al.*, LANL, written communication, 1995). Whereas volcanic activity sometimes generates earthquakes having magnitudes > 6.0, the likely maximum magnitude earthquake associated with the formation of small cinder cones, such as formed in Crater Flat, is considerably smaller than magnitude 6.0. Given the low probability of a volcanic earthquake in Crater Flat as well as the small maximum magnitude, the upper bound earthquake for the site area source zone adequately covers this type of event.

4.1.2 Maximum Depth of Seismicity

Depth to the base of the seismogenic zone for all our models was based on studies of focal depth distributions of catalog (A quality) events and depths associated with focal mechanisms tabulated by S.K. Pezzopane *et al.* (USGS, written communication, 1996b), which also should represent high-quality hypocenters. Only 4 percent of A quality catalog events had depths ≥ 12 km; 2 percent of the events with focal mechanisms had depths ≥ 12 km. Few events had depths of greater than 16 km. The values for the depth of the seismogenic crust that were included in the analysis and their associated weights are: 12 km (0.6), 14 km (0.3), and 16 km (0.1).

4.1.3 Maximum Earthquakes

Model A (one regional source zone excluding the site-vicinity zone) regards the maximum earthquake magnitude as the largest earthquake that could occur in the region. This event could occur randomly and/or on a geologic structure that is not explicitly included in the seismic source model. For example, several Quaternary faults shown on Piety's map (1995, plates 1 and 2) but for which there is no reported evidence of late Quaternary displacement are not included in the seismic source model. These faults presumably have low slip rates; nonetheless, they could be the source of large events. Estimates of the maximum earthquake range from Mw 7.7, which corresponds to the largest earthquake considered for any of the regional fault sources (Section 4.2), down to magnitude Mw 7.0, which is believed to be a conservative estimate for the largest event that could occur without surface fault rupture. The values included in the seismic hazard analysis and their associated probability weights (in parentheses) are: Mw 7.0 (0.2), Mw 7.3 (0.6), and Mw 7.7 (0.2).

In Model B (three regional source zones excluding the site-vicinity zone), the maximum earthquake magnitude varies with the zone. The values considered for the western Walker Lane zone are the same as for Model A [i.e., Mw 7.0 (0.2), Mw 7.3 (0.6), and Mw 7.7 (0.2)]. A slightly smaller range of values is considered for the eastern Walker Lane zone and the Basin and Range zone because these zones seem to lack the major continuous structures (e.g., the Death Valley/Furnace Creek fault system) that characterize the western Walker Lane zone. The values for these zones included in the seismic hazard analysis and their associated probability weights (in parentheses) are: Mw 7.0 (0.2), Mw 7.25 (0.6), and Mw 7.5 (0.2).

Estimates of the maximum earthquake magnitude for the site-vicinity zone range from Mw 5.6 (about the size of the Little Skull Mountain earthquake) to about Mw 6, which corresponds to a rupture area of about 100 km^2 (Wells and Coppersmith, 1994). Clearly larger events have occurred in the Basin and Range that were not associated with surface fault rupture; however, given the close spacing of the local fault sources, we believe that larger events are best represented in the hazard model as occurring on the mapped faults. Selecting a cutoff magnitude of about Mw 6 also mitigates the problem of "double accounting" that can result by combining predictions of the number of large events based on observed seismicity with predictions of the number of small- to moderate-size events from paleoseismic evidence of past surface faulting events. The values included in the seismic

hazard analysis and their associated probability weights are: Mw 5.6 (0.2), Mw 5.8 (0.6), and Mw 6.0 (0.2).

4.2 REGIONAL FAULT SOURCES

Regional fault sources include the mapped late Quaternary faults that extend to within about 100 km of the site but lie outside the site vicinity (Figure DFS-6). These faults were identified based on information presented in the USGS analysis to identify relevant earthquake sources (S. K. Pezzopane, USGS, written communication, 1996), Piety's (1995) report on Quaternary faults within 100 km of Yucca Mountain, and discussions during the Seismic Source Characterization Workshops with personnel who have examined some of these faults in the field. Faults included as regional seismic sources are judged to be capable of generating magnitude 5 or larger earthquakes and, based on published reports, are inferred to have had multiple late Quaternary displacements. The regional fault sources and the seismic source parameters (and associated uncertainties) used to characterize the seismic potential of these structures are summarized in Table DFS-1.

Several faults that are known or suspected to have had Quaternary displacement, but are not reported to exhibit evidence of late Quaternary displacement, are not included as fault-specific seismic sources. The rate of slip on these faults is too low to have a significant effect on the ground motion hazard at the site, which is demonstrated by the results of previous analyses (Stepp *et al.*, 1995; I. Wong *et al.*, WCFS, written communication, 1997), which show that most of the regional fault sources have no significant effect on the overall hazard at the site. Earthquakes that occur on Quaternary faults that are not included as regional fault sources are modeled as part of the seismic source zone activity (Section 4.1).

4.2.1 Guidelines for Modeling

The logic tree used to characterize the regional fault sources is shown on Figure DFS-7. A more simplified approach is used to characterize the regional faults than is used to model the local faults (Section 4.3), particularly if the faults are more than about 50 km from the site. Generalizing the fault geometry does not have a significant effect on the source-to-site distance. It could have an effect on the calculated maximum magnitudes, but this is factored into the analysis by increasing the range of uncertainty on the estimated maximum magnitude

values. Except where noted in subsequent sections, the following guidelines were used in modeling regional fault sources.

Total Fault Length and Plan View Geometry. Discontinuous faults are generalized as a single continuous trace consisting of one or more straight line segments, so that the average source-to-site distance and total length of the modeled fault are consistent with the mapped fault. The total fault length is taken as the combined length of the straight line segments. A single, somewhat conservative, estimate of the total length is considered for most faults more than about 50 km from the site. For faults longer than about 25 km that extend to within about 50 km of the site, a range of values is assigned to account for uncertainties in total fault length.

Activity. The reported evidence for Quaternary displacement on all the regional fault sources described in this section is assumed to be associated with past seismogenic fault displacements (probability of activity = 1.0). Non-tectonic origins for some of the scarps may be possible, but are deemed to be sufficiently unlikely that their inclusion in this assessment would not significantly affect the hazard results.

Fault Dip and Downdip Width. Predominantly strike-slip faults are modeled as having a dip of 90 degrees. Predominantly dip-slip faults are modeled as having an average dip of 60 degrees. The faults are modeled as extending down to the base of the seismogenic crust, which is estimated to be between 12 and 16 km deep based on earthquake focal depths (see Section 4.1.2). The range of values for the maximum depth of faulting included in the analysis and their associated probability weights (in parentheses) are: 12 km (0.6), 14 km (0.3), and 16 km (0.1).

Maximum Earthquake Magnitude (M_{MAX}). Maximum magnitudes were calculated using an empirical relation that relates fault rupture length to magnitude (Wells and Coppersmith, 1994, relation for all fault types). Values were calculated by assuming 100 percent rupture of the longest geometrically defined fault segment and/or 100 percent rupture of the total fault length. The resulting values were considered to select a range of values for M_{MAX}. In most cases, the uncertainty associated with the preferred value for M_{max} is chosen to be about 3 of

a magnitude unit (i.e., plus or minus 0.2 to 0.3 Mw); however, as described below, somewhat wider and narrower ranges were considered in some cases.

Slip Rate. To the extent possible, estimated slip rates were based on published slip rates. Where reported rates were not available, slip rates were estimated (with wider uncertainty) based on analogy with other mapped faults and/or by inferring the likely ages and amount of displacement based on reported descriptions of the faults.

Earthquake Recurrence Models. The slip rate reflects the rate at which strain energy (seismic moment) is accumulating along a fault. The geologically derived seismic moment rate is used to translate slip rate into earthquake recurrence rate by partitioning the moment rate into earthquakes of various magnitudes according to a recurrence relationship (Cornell and Winterstein, 1986). Three general types of relationships have been proposed: (1) truncated exponential relations that mimic the behavior of recorded earthquakes in a region (e.g., Gutenberg and Richter, 1954); (2) a characteristic earthquake recurrence model (Youngs and Coppersmith, 1985) in which there is a greater tendency for earthquakes close to the maximum to occur than is predicted by seismicity-based exponential relations; and (3) relations that attribute all of the moment release on faults to earthquakes close to the maximum (Wesnousky, 1986). All three recurrence relations are considered in this hazard analysis (Figure DSF-7). The greatest weight (0.6) is assigned to the characteristic earthquake model. The results of detailed paleoseismic studies along active faults have shown repeatedly that the characteristic model is more representative of the seismicity of an individual fault than are exponential models that represent the seismicity of regions, which contain faults of various sizes. Maximum moment models assume that independent events on faults (i.e., excluding aftershocks and/or foreshocks) are always close to the maximum earthquake. This model is given less weight (0.3) than the characteristic model, but more weight than the exponential model, which is given the least weight (0.1).

The exponential and characteristic recurrence models require estimates of the b-value associated with specific faults. We used a b-value of 1.0 ± 0.1, which is based on the median value obtained for the seismic source zones plus or minus the 90-percent confidence interval. This uncertainty is about three times the uncertainty used to characterize the seismic source

zones. Greater uncertainty is warranted because there is more uncertainty in the magnitude frequency distribution associated with individual faults.

4.2.2 Parameters

Eighteen regional fault sources are included in the seismic hazard analysis (not including the hypothetical faults described in Section 4.4). The fault parameters used to characterize these sources are summarized in Table DFS-1 and described below.

Hunter Mountain/Panamint Fault Zone. The Hunter Mountain/Panamint fault zone is characterized by strike slip. Individual rupture segments are estimated to range from a minimum of about 16 km to a maximum of about 74 km. Considering the possibility of rupture along multiple segments, our preferred estimate for the maximum rupture length in the range of 45 to 98 km, suggesting a M_{MAX} in the range of Mw 7.0 to 7.4. Rupture of 146 km (the total fault length included in the model) suggests an upper bound of Mw 7.6. The values included in the analysis and their associated probability weights (in parentheses) are Mw 7.0 (0.2), Mw 7.4 (0.6), and Mw 7.6 (0.2).

The Quaternary slip rate on the Panamint Valley section of the fault is better constrained than is the rate along the Hunter Mountain section. Piety (1995, p. 383) reports that the Holocene/late Pleistocene slip rate on the Panamint Valley section is between about 1.1 and 3.2 mm per year, with a preferred estimate of about 2.5 mm per year. This range of values is used to characterize the entire fault. The values included in the analysis and their associated probability weights are 1.1 mm per year (0.2), 2.5 mm per year (0.6), and 3.2 mm per year (0.2).

Furnace Creek/Fish Lake Valley Fault Zone. This system of faults, which is characterized by strike slip, has a total combined length of at least 125 km (Piety, 1995, plates 1 and 2). Individual rupture segments are estimated to range from about 26 km to a maximum of about 87 km, with a preferred estimate for the maximum rupture length in the range of 38 to 87 km, suggesting a M_{MAX} in the range of Mw 6.9 to 7.3. Rupture of 149 km (the total fault length as shown on Figure DSF-6) suggests an upper bound of about Mw 7.6. The values included in the analysis and their associated probability weights are Mw 7.0 (0.2), Mw 7.3 (0.6), and Mw 7.6 (0.2).

There is obvious evidence of late Quaternary displacement along this fault trend, but the ages of the displaced units are not well constrained. Bryant (as cited in Piety, 1995) reports 46 m of late Pleistocene offset (right slip) along the fault. If late Pleistocene is interpreted to mean older than Holocene (10 ka) and younger than or about equal to latest Pleistocene (approximately 35 ka), the likely slip rate is in the range of ≥ 1.3 mm to < 4.6 mm per year. The values included in the analysis and their associated probability weights are 1.3 mm per year (0.2), 2.3 mm per year (0.6), and 4.6 mm per year (0.2).

Death Valley Fault Zone. The Death Valley fault zone has a mapped length of 71 km and is reported to be predominantly dip-slip (Piety, 1995). Rupture of the longest geometrically defined segment (51 km) yields an expected magnitude of Mw 7.1; rupture of the entire mapped fault suggests a magnitude of about Mw 7.2. The uncertainty associated with M_{MAX}, however, is assumed to be greater than this narrow range of values. The values included in the analysis and their associated probability weights are Mw 7.0 (0.2), Mw 7.2 (0.6), and Mw 7.5 (0.2).

Piety (1995) cites slip rates on the Death Valley fault zone ranging from as little as 0.08 mm per year to as high as 11.5 mm per year, with a best estimate of about 2.5 mm per year for the late Holocene slip rate. R.E. Klinger and L.A. Piety (USBR, written communication, 1996) report a vertical separation rate of 3 to 5 mm/yr. The values included in the analysis and their associated probability weights are 0.08 mm per year (0.2), 2.5 mm per year (0.6), and 11.5 mm per year (0.2), which gives a weighted average value of 3.96 mm/yr.

Pahrump/Stewart Valley Fault. This fault is composed of a discontinuous alignment of Quaternary fault scarps having a total length of about 41 km (Piety, 1995, plate 2). The total length of known Quaternary fault scarps is 18.5 km. The sense of Quaternary slip is inferred to be right-slip (Anderson *et al..*, 1995a). The fault can be divided into two roughly equivalent segments of about 20 km based on an apparent left step in the fault trend, suggesting a magnitude of Mw 6.6. Rupture of the entire fault suggests a magnitude of about Mw 7.0. These rupture models were considered equally likely; the values included in the analysis and their associated probability weights are Mw 6.6 (0.5) and Mw 7.0 (0.5).

The Quaternary slip rate on the Pahrump/Steward Valley fault is poorly constrained. Piety (1995) reports that the slip rate is "low," which is interpreted to mean that it is less than 1 mm per year, because faults having slip rates equivalent to or faster than this typically are well expressed geomorphically. Anderson *et al.*. (1995a, p. 12) report that the long-term vertical slip rate is "less than a few hundredths of a millimeter per year and is most likely on the order of thousandths of a millimeter per year" (less than 0.009 to 0.02 mm per year). Even allowing for a significant lateral component to the net slip, the Quaternary slip rate probably is on the order of 0.005 to 0.05 mm per year. Given the large uncertainties in the ages of the reported displacements, any slip rate within this wide range is considered to be equally likely. The values included in the analysis and their associated probability weights are 0.005 mm per year (0.5) and 0.05 mm per year (0.5).

West Spring Mountain Fault. A nearly continuous fault trace is mapped along the west flank of the Spring Mountains for about 29 km. The southern limit of the fault is uncertain; discontinuous traces (Piety, 1995, plate 2) suggest the fault might extend to its projected intersection with the Pahrump/Stewart Valley fault, for a total fault length of 51 km. Both of these options for the total length are included in the hazard analysis with equal weight. The fault may have a small oblique slip component, but is predominantly a dip-slip fault (Piety, 1995, p. 334). Values for M_{max} depend on the total fault length (Figure DFS-6). In both cases, we assumed that rupture length was equal to total fault length. The resulting values (using Wells and Coppersmith's 1994 relation for all fault types) were taken as the preferred values for M_{max} the associated uncertainty is estimated to be plus or minus about 3 of a magnitude unit (Table DFS-1).

J. L. Hoffard (University of Nevada, Reno, written communication, 1991, as cited in Piety, 1995, p. 354) reports a preferred value for the late Quaternary slip rate on the West Spring Mountains fault of 0.06 mm per year near Wheeler Wash. His maximum and minimum rates at this locality, given the uncertainty in the age of the displaced surface, are 0.2 and 0.02 mm per year, respectively. The values included in the analysis and their associated probability weights are 0.02 mm per year (0.2), 0.06 mm per year (0.6), and 0.2 mm per year (0.2).

West Pintwater Range Fault. Piety (1995, plates 1 and 2) shows a series of mapped fault traces extending nearly continuously along the west flank of the Pintwater Range for about

55 km. The faults are interpreted to be down-to-the-west normal faults. Rupture of the longest geometrically defined segment (about 41 km) suggests a magnitude of Mw 6.9; rupture of the entire fault suggests a magnitude of Mw 7.1. Accordingly, M_{max} is estimated to be Mw 7 ± 3. The values included in the analysis and their associated probability weights are Mw 6.7 (0.2), Mw 7.0 (0.6), and Mw 7.3 (0.2).

No reported slip rates were found for the West Pintwater Range fault. Piety (1995, p. 349) describes the fault as having weak geomorphic expression in late Quaternary deposits. Based on analogy to the Paintbrush Canyon fault, which is also characterized by weak geomorphic expression in late Quaternary deposits, the slip rate on the West Pintwater fault is estimated to be in the range of 0.02 to 0.2 mm per year. Having no basis for selecting a preferred value, we assumed that the actual rate is equally likely anywhere within this range. The values included in the analysis and their associated probability weights are 0.02 mm per year (0.5) and 0.2 mm per year (0.5).

Yucca Fault. The Yucca fault is predominantly dip slip (normal down-to-the-east) and has a mapped length of 25 km (Piety, 1995, plate 1). Given its short overall length, we assumed that the entire fault could rupture during the maximum earthquake, suggesting a M_{max} of 6.7 (± 3). The values included in the analysis and their associated probability weights are Mw 6.5 (0.2), Mw 6.7 (0.6), and Mw 7.0 (0.2).

No reported slip rates were found for the Yucca fault. The basis for assigning a slip rate to this fault is the same as for the West Pintwater fault. The values included in the analysis and their associated probability weights are 0.02 mm per year (0.5) and 0.2 mm per year (0.5).

Emigrant Valley North Fault. The Emigrant Valley North fault consists of a diffuse zone of north-northeast-trending fault traces having an overall length of about 27 km (Piety, 1995, plate 1). The style of faulting is uncertain. In this analysis, it is modeled as a 60 degree west-dipping normal fault having a linear surface trace centered along the zone of mapped faults. Given its short overall length, we assumed that the entire fault could rupture during the maximum earthquake, suggesting a M_{max} of 6.7 (± 3).The values included in the analysis and their associated probability weights are Mw 6.5 (0.2), Mw 6.7 (0.6), and Mw 7.0 (0.2).

No reported slip rates were found for the Emigrant Valley North fault. The basis for assigning a slip rate to this fault is the same as for the West Pintwater fault. The values included in the analysis and their associated probability weights are 0.02 mm per year (0.5) and 0.2 mm per year (0.5).

Oaks Spring Butte Fault. The Oak Springs Butte fault consists of a generally north-south zone of fault traces having an overall length of about 22 km (Piety, 1995, plate 1). Both down-to-the-east and down-to-the-west displacements occur within the zone, but the predominant displacement appears to be down-to-the east. In this analysis, it is modeled as a 60 degree east-dipping normal fault having a linear surface trace centered along the zone of mapped faults. Given its short overall length, we assumed that the entire fault could rupture during the maximum earthquake, suggesting a M_{max} of 6.7 (± ¼). The values included in the analysis and their associated probability weights are Mw 6.5 (0.2), Mw 6.7 (0.6), and Mw 7.0 (0.2).

No reported slip rates were found for the Oak Springs Butte fault. Based on published reports (Dohrenwend *et al.*, 1991, as cited in Piety, 1995, p. 256), there are "visible scarps" across surfaces that are estimated to be between 10 and 130 ka. Assuming that "visible scarps" means they are less than 1 to 2 m high, we estimated a slip rate less than about 0.01 to 0.2 mm per year. Having no basis for selecting a preferred value, we assumed that the actual rate is equally likely within this range. The values included in the analysis and their associated probability weights are 0.01 mm per year (0.5) and 0.2 mm per year (0.5).

Belted Range Fault. The Belted Range fault is a normal down-to-the-east fault that lies along the west foot of the Belted Range (eastern side of Kawich Valley). The total length of the fault is about 49 km (Piety, 1995, plate 1). Anderson *et al.* (1995b) report that scarps in Quaternary alluvium extend for only about 22 km of this length Assuming rupture lengths of between 22 and 49 km suggests a M_{MAX} in the range of Mw 6.6 to 7.0 (or about 6¾ ±¼). The values included in the analysis and their associated probability weights are Mw 6.5 (0.2), Mw 6.8 (0.6), and Mw 7.1 (0.2).

Anderson *et al.* (1995b, p. 13) report 11.3 m of displacement in surfaces that they estimate to be between 0.13 and 0.78 Ma, suggesting a slip rate between 0.01 and 0.09 mm per year.

Having no basis for selecting a preferred value, we assumed that the actual rate is equally likely within this range. The values included in the analysis and their associated probability weights are 0.01 mm per year (0.5) and 0.1 mm per year (0.5).

Kawich Range Fault. The Kawich Range fault consists of numerous subparallel normal faults and lineaments on the west side of the Kawich Range (Piety, 1995, plate 1; and Anderson *et al.*., 1995b). Most of the mapped faults occur in bedrock or at the bedrock-alluvial contact; the total length of Quaternary faulting is uncertain. The fault is divided into three line segments (Figure DFS-6), and four options are considered for the total length of the Quaternary active part of the Kawich Range fault. Most of the weight (0.68) is assigned to line segment A-B, because this is the only part of the fault having demonstrated displacements of alluvial surfaces (Anderson *et al.*., 1995b). The balance of the weight was assigned to the remaining options (Table DFS-1) based on the relative geomorphic expression of the adjacent sections of the fault. Values for M_{max} depend on total fault length (Figure DFS-6). For all four options, we assumed that the rupture length is equal to the total fault length. The resulting values (using Wells and Coppersmith's 1994 relation for all fault types) were taken as the preferred values for M_{max} and the associated uncertainty is estimated to be plus or minus about 3 of a magnitude unit (Table DFS-1).

Based on the subdued geomorphic expression of the fault and an inferred rate of scarp degradation, Anderson *et al.*. (1995b, p. 18) infer that the Quaternary slip rate on the Kawich Range fault is less than 0.01 mm per year. The values included in the analysis and their associated probability weights are 0.01 mm per year (0.5) and 0.001 mm per year (0.5).

Rock Valley Fault. The Rock Valley fault, which is inferred to be primarily a left-slip fault (Anderson *et al.*., 1995a), trends north-northeastward across alluvial fan deposits on the southeast flank of Little Skull Mountain. The continuity of this faulting with fault traces along its southwestern projection is uncertain. Three options were considered to account for uncertainty in the total length of the Rock Valley fault (Figure DFS-6 and Table DFS-1). Most of the weight (0.6) is assigned to the well-defined section of the fault (segment A-B) adjacent to Little Skull Mountain. The balance of the weight is assigned to the remaining options. The least weight (0.1) is assigned to option A-D because it seems less likely that the fault would continue west of its projected intersection with the north-south trending

Amargosa/Gravity (Ash Meadows) fault system. Values for M_{max} depend on the total fault length (Figure DFS-7). For all three options, we assumed that the rupture length is equal to the total fault length. The resulting values (using Wells and Coppersmith's 1994 relation for all fault types) were taken as the preferred values for M_{max} and the associated uncertainty is estimated to be plus or minus about ¼ of a magnitude unit (Table DFS-1).

Piety (1995, Table 6) reports vertical slip rates on the order of 0.003 to 0.01 mm per year based on observed surface displacements ranging from less than 1 m to 1.1 m. No estimate of the amount of lateral slip is presented. D. W. O'Leary *et al.* (USGS, written communication, 1996) estimate the maximum vertical displacement across the Rock Valley fault to be 0.054 mm per year (the sum across three stands of the fault). Assuming a major strike-slip component (e.g., a rake of 20 degrees) suggests that the net slip could be about three times the vertical slip, or about 0.16 mm per year. O'Leary (1996, pers. comm.) suggests the minimum slip rate (net slip) might be an order of magnitude less than the maximum. The values included in the analysis and their associated probability weights are 0.02 mm per year (0.5) and 0.16 mm per year (0.5).

Wahmonie Fault. The Wahmonie fault, which strikes northeast, has a mapped length of 14 km (Piety, 1995). The style of faulting is uncertain. The fault scarps are predominantly down-to-the-northwest according to Piety (1995, p. 346, and plate 1). In this analysis, it is modeled as a 60-degree northwest-dipping normal fault. Given its short overall length, we assumed that the entire fault could rupture during the maximum earthquake, suggesting a M_{max} of 6.4 ($\pm$¼). However, an upper-bound earthquake (M_{MAX}) of less than about 6.5 is considered unlikely for surface faulting events. The values included in the analysis and their associated probability weights are Mw 6.5 (0.8) and Mw 6.8 (0.2).

Reported scarp heights of < 1 m to 3 m on surfaces that are interpreted to be between 270 and 740 ka (Swadley and Huckins, 1990, as cited in Piety, 1995, p. 346) suggest slip rates on the order of 0.01 to 0.001 mm per year. The values included in the analysis and their associated probability weights are 0.01 mm per year (0.5) and 0.001 mm per year (0.5).

Yucca Lake Fault. The surface trace of the Yucca Lake fault measures 14 km (Piety, 1995, plate 1). The fault, which strikes northwest, appears to have predominately down-to-the-

northeast dip slip. Given its short overall length, we assumed that the entire fault could rupture during the maximum earthquake, suggesting a M_{max} of 6.4 ($\pm$3). However, an upper bound earthquake of less than about 6.5 is considered unlikely for surface faulting events. The values included in the analysis and their associated probability weights are Mw 6.5 (0.8) Mw and Mw 6.8 (0.2).

No reported slip rates were found for the Yucca Lake fault. Based on reported recognizable scarps on late Quaternary surfaces, the fault is assumed to have a slip rate on the order of 0.02 to 0.2 mm per year (see discussion for West Pintwater Range fault above). The values included in the analysis and their associated probability weights are 0.02 mm per year (0.5) and 0.2 mm per year (0.5).

Eleana Range Fault. The Eleana Range fault is a north-northeast-striking down-to-the-east normal fault having a total length of about 11 km (Piety, 1995, plate 1). Given its short overall length, we assumed that the entire fault could rupture during the maximum earthquake, suggesting an M_{max} of 6.3 ($\pm$3). However, an upper-bound earthquake of less than about 6.5 is considered unlikely for surface faulting events. The values included in the analysis and their associated probability weights are Mw 6.5 (0.8) and Mw 6.8 (0.2).

No reported slip rates were found for the Eleana Range fault. The basis for assigning slip rate values was the same as for the West Pintwater Range and Yucca Lake faults. The values included in the analysis and their associated probability weights are 0.02 mm per year (0.5) and 0.2 mm per year (0.5).

Peace Camp Fault. A series of discontinuous fault scarps have been mapped in alluvial deposits south and southwest of Mercury that are informally referred to as the Peace Camp fault (J. Yount, SSC Workshop 4). Based on its trend subparallel to the Rock Valley fault, the Peace Camp fault probably has a significant left-lateral component to the net slip. The total length of Quaternary faulting is uncertain. Estimates range from about 19 km, which includes the fairly well-expressed eastern section of the fault (segment A-B on Figure DFS-6), up to about 31 km (segment A-C) (J. Yount, SSC Workshop 4). More weight (0.7) is assigned to the better-expressed section of the fault (Table DFS-1). M_{MAX} depends on the total fault length. For both options, we assumed that the rupture length is equal to the total

fault length. The resulting values (using Wells and Coppersmith's 1994 relation for all fault types) were taken as the preferred values for M_{max} and the associated uncertainty is estimated to be plus or minus about 3 of a magnitude unit (Table DFS-1).

Half-meter-high scarps have been observed on late Pleistocene alluvial surfaces that are estimated to be between 20 ka and 130 ka (J. Yount, SSC Workshop 4), indicating vertical slip rates in the range of 0.004 to 0.025 mm per year. Allowing for a major strike-slip component, net slip might be several times vertical slip, which would be consistent with estimated slip rates on the Rock Valley fault. The values included in the analysis and their associated probability weights are the same as those assigned to the Rock Valley fault, 0.02 mm per year (0.5) and 0.16 mm per year (0.5).

Amargosa/Gravity (Ash Meadows) Fault. This fault consists of a discontinuous zone of Quaternary fault scarps and lineaments that trends north-south along the east side of Amargosa Valley. The total length of the zone is uncertain. Four options are considered, depending on how far the zone might extend to the north and/or the south. The most weight (0.56) is assigned to the 27-km-long central part of the fault (segment A-B on Figure DFS-6). It is considered equally likely that the fault extends to the north or to the south (i.e., segments B-C and A-D both have assigned weights of 0.2). The likelihood that the fault extends in both directions is equal to the products of the probabilities that it extents in either direction (0.04). M_{MAX} depends on the total fault length. For all four options, we assumed that the rupture length is equal to the total fault length. The resulting values (using Wells and Coppersmith's 1994 relation for all fault types) were taken as the preferred values for M_{max} and the associated uncertainty is estimated to be plus or minus about 3 of a magnitude unit (Table DFS-1).

Based on 155 cm vertical displacement observed in a trench across a trace of the Ash Meadows fault and an inferred age of about 40 ka, the slip rate is 0.04 mm per year (data from D.E. Donovan, University of Nevada, Reno, written communication, 1991, as cited in Piety, 1995, p. 87). Assuming that the displaced late Pleistocene deposits could be as young as about 20 ka or as old as about 89 ka suggests that the actual slip rate is probably within the range of 0.02 to 0.08 mm per year. Based on surfaces that are displaced as much as 3.4 m and an inferred minimum age of 40 ka, Anderson *et al.*. (1995a, p. 32) estimate that the slip

rate on the Ash Meadows section of the fault is no more than 0.1 mm per year and that it is likely to be an "order of magnitude less." The values included in the analysis and their associated probability weights are 0.01 mm per year (0.2), 0.04 mm per year (0.6), and 0.1 (0.2).

Bare Mountain Fault. The Bare Mountain fault is the major down-to-the-east normal fault that forms the west side of Crater Flat basin. Along the west side of Crater Flat basin, the fault is well expressed geomorphically for approximately 16 km, which is taken as the minimum total fault length. Near the southern end of the basin, the fault may bend to the southeast and continue for another 6 km. Based on the gravity data, we believe that the fault does not continue farther south as a single structure. The southernmost limit of the fault is mapped at its projected intersection with geophysical anomalies that are coincident with the proposed Highway 95 fault. M_{MAX} depends on the total fault length. A maximum rupture length of 16 km corresponds to Mw 6.5 ($\pm$ 3). However, Mw 6.5 is assumed to be the minimum upper-bound magnitude for surface faulting earthquakes. Therefore, given a rupture length of 16 km, the values included in the analysis and their associated probability weights are Mw 6.5 (0.8) and Mw 6.8 (0.2) (Table DFS-1). Similarly, a maximum rupture length of 22 km corresponds to Mw 6.6 ($\pm$ 3) and, in this case, the values included in the analysis and their associated probability weights are Mw 6.5 (0.2), Mw 6.7 (0.6), and Mw 7.0 (0.2).

Various slip rates have been reported for the Bare Mountain fault. Reheis (1988) reports 1.75 m of vertical displacement in deposits estimated to be 9 ka, suggesting a slip rate of 0.19 mm per year (Piety, 1995). However, if this represents displacement from a single event, the slip rate is unconstrained. Based on the results of mapping and of trench investigations at three locations along the Bare Mountain fault, L.W. Anderson and R.E. Klinger (USBR, written communication, 1996b) conclude that the slip rate is "quite low," about 0.01 mm per year or less. Based on uplift rates calculated from apatite fission-track thermochronometry and interpretation of alluvial fan sedimentation, Ferrill *et al.*. (1996, p. 2-28 to 2-30) argue that the slip rate increases toward the south and suggest that it could be as high as 0.28 mm per year. Structural cross sections of the faults in the site vicinity (Section 4.3.5) indicate that the local west-dipping faults intersect the Bare Mountain fault at depth and, presumably, are truncated by the Bare Mountain fault because it has a much greater

throw than the local faults. In this model, the slip rate on the Bare Mountain fault should be equal to or greater than the sum of the slip rates on the west-dipping (antithetic) faults (i.e., ≥ approximately 0.05 mm per year). Clearly, there is still considerable uncertainty in the slip rate on the Bare Mountain fault. In our judgment, the most likely value is in the range of 0.05 to 0.1 mm per year. The values included in the analysis and their associated probability weights are 0.01 mm per year (0.1), 0.05 mm per year (0.4), 0.1 mm per year (0.4), and 0.28 mm per year (0.1).

4.3 LOCAL FAULT SOURCES

Local faults having recognized Quaternary displacement are included as fault-specific seismic sources in the seismic source model. The Ghost Dance fault also is included because it is the largest fault within the footprint of the proposed repository. The locations of the principal Quaternary faults included in this analysis are based primarily on the mapping of Simonds *et al.*. (1995). The principal local faults included in the seismic source model are shown on Figure DFS-8.

Other mapped faults in the site vicinity (e.g., the Exile Hill fault, the Midway Valley fault, the Iron Ridge fault, and the northwest-trending faults such as the Yucca Wash, Sever Wash, and Pagany Wash faults) are not included as seismic sources because there is no evidence of Quaternary displacement along any of these bedrock faults. Structural models (e.g., the vertical axis block-rotation model) suggest that these faults might move in response to movements along the principal block-bounding faults. However, with the possible exception of minor fractures in calcite-silica-cemented regolith at the bedrock/alluvial-colluvial contact, the available information (USGS, written communication, 1996) indicates there have been no displacements on any of these faults younger than middle to late Quaternary. Data from numerous trenches indicate there have been repeated surface faulting events on the block-bounding faults during this same interval. The cumulative displacements on these faults in the Tertiary bedrock are small, not more than a few tens of meters. These small intrablock faults represent secondary accommodation structures that probably are related primarily to late Miocene deformation. If the intrablock faults can produce earthquakes, we assumed they would be small, having magnitudes less than or equal to the maximum random earthquake for the site-vicinity source zone (see Section 4.1).

4.3.1 Activity

There is documented Quaternary displacement on all the local fault sources except for the Ghost Dance fault (USGS, written communication, 1996; Simonds *et al.*, 1995). The Quaternary offsets are assumed to be associated with past seismogenic fault displacements, so the probability of activity is assumed to be 1.0. Non-seismogenic mechanisms might account for some of the "paleoseismic events" identified in the fault trenches. For example, a mudflow layer due to a storm event might be misinterpreted as a scarp-derived colluvial wedge from a faulting event. Alternatively, paleoseismic events may be missing from the record because of erosion or the absence of diagnostic characteristics for recognizing individual events. Regardless of the problems associated with the interpretation of individual events, we believe that the Quaternary slip rates derived from the Yucca Mountain trenches provide a reliable indicator of the seismic potential of the faults (assuming that the uncertainties in the amount, sense, and age of the displacement have been correctly factored into the assessment).

In contrast to the other local fault sources, no direct evidence of Quaternary displacement has been observed on the Ghost Dance fault, and the available evidence suggests that there has been no displacement since at least the middle Pleistocene (E.M. Taylor *et al.*, USGS, written communication, 1996). Analogies to other north-south-trending intrablock faults such as the Midway Valley fault and the Exile Hill fault indicate that Quaternary displacements on the block-bounding faults have created only minor adjustments such as fracturing on the larger intrablock faults (Wesling *et al.*, 1993; F.H. Swan *et al.*, Geomatrix Consultants, written communication, 1995; and E.M. Taylor *et al.*, USGS, written communication, 1996). Therefore, we consider it unlikely that the fault is active and capable of generating significant earthquakes; the assigned probability weights are "active" (0.05), and "not active" (0.95). The potential for fault displacement on the Ghost Dance fault is addressed separately in Section 5.

4.3.2 Distributed Faulting Versus Independent Fault Sources

A Quaternary volcanic ash deposit occurs as infilling in fractures and/or along the fault plane in several fault exploration trenches in the Yucca Mountain vicinity. Based on the occurrence of this ash, it has been suggested that there may have been simultaneous rupture

on subparallel faults, including faults on either side of Yucca Mountain (S.K. Pezzopane *et al.*, USGS, written communication, 1996a). Because of the limitations in geologic dating techniques, it cannot be demonstrated that the displacements associated with the so-called "ash event" occurred during a single earthquake. Nonetheless, the physical evidence is sufficiently compelling to warrant consideration in the hazard model.

Simultaneous rupture on two faults does not require that they be physically connected at depth. Distributed fault behavior could occur with both of the structural (end-member) models that are considered in this assessment (Section 4.3.5). Accordingly, whether the faults exhibit distributive fault behavior or behave independently has no major effect on the overall geometry of the local fault sources. It does, however, affect the assessment of the length of the maximum single-event fault rupture. Given distributed fault behavior, the maximum rupture length is not constrained by the length of an individual fault.

Figure DFS-9 is a logic tree showing the dependence of the local fault model on distributive versus independent fault behavior. Relatively low weight is assigned to the distributive fault behavior model (0.05) because of the lack of convincing historical analogs for the postulated "ash-event."

Figures DSF-10 and DSF-11 are logic trees that outline the approaches used to characterize the local fault sources given independent and distributive fault behavior, respectively. The components of the logic tree are described in the following sections.

4.3.3 Total Length

The Quaternary fault scarps are short, rarely more than a kilometer or two long, and discontinuous (Simonds *et al.*., 1995). This may, in part, be due to the character of the fault displacements, but it is largely due to the effects of erosion and deposition since the scarps were formed. In this assessment, we assumed that the generally north-south-trending faults are linked together along strike. For example, the Paintbrush Canyon and Stage Coach Road faults are modeled as a single 20- to 30-km-long fault. The uncertainty in the overall length is due to uncertainties in how far the Quaternary faulting extends to the north and/or the south. The total length of faulting is considered two ways. First, given that the local faults are independent seismic sources, uncertainties in the total length of the individual faults are

considered. Second, given the possibility of distributive faulting, the uncertainty in the total combined length of the local faults that could be involved in a distributive faulting event is considered.

Total Fault Length (Independent Fault Behavior). Figure DFS-8 and Table DFS-2 present alternatives for the total fault length and the assigned probability weights for each of the local fault sources.

Paintbrush Canyon/Stagecoach Road Fault. Four alternatives are considered, as follows.

1. Quaternary faulting is limited to the reach of the fault having evidence of Quaternary displacement, as shown on Simonds *et al.*. (1995), i.e., fault segment B-E on Figure DFS-8. This option is given the greatest weight (0.68).

2. Quaternary faulting extends about 1.5 km farther north along the mapped bedrock fault splay that has the same strike as the fault south of Yucca Wash. This option corresponds to fault segment A-E on Figure DFS-8. This is given a low weight (0.2) because: the observed Quaternary displacements die out at the north end of Alice Ridge; no evidence for Quaternary displacement has been found on the Paintbrush Canyon fault north of Yucca Wash; and the projected intersection between the buried Yucca Wash fault would be a reasonable place for the Quaternary faulting to terminate.

3. Quaternary faulting extends about 7.5 km farther south to the projected intersection between the Stagecoach Road and proposed Highway 95 faults. This alternative, which corresponds to fault segment B-F on Figure DFS-8, is also given low weight (0.1) because there is no evidence for Quaternary displacement.

4. Quaternary faulting extends both north and south (fault segment A-F on Figure DFS-8). The probability of this is equal to the combined probability of options 2 and 3 above (0.02).

Bow Ridge Fault. The southern end of the Bow Ridge fault is taken at its projected intersection with the Paintbrush Canyon fault (location K on Figure DSF-8). Two alternatives are considered for the northern extent of Quaternary faulting; either the north end of Exile Hill (location H on Figure DFS-8), or its projected intersection with the Yucca Wash fault (location G). It is unlikely that Quaternary faulting extends much beyond the northern end of Exile Hill. Alluvial surfaces have been mapped across the northward projection of the

fault that are equivalent to and older than the youngest faulted colluvial deposits on the west side of Exile Hill (J.R. Wesling *et al.*., Geomatrix Consultants, written communication, 1992; Swan *et al.*., Geomatrix Consultants, written communication, 1995). Therefore, the greatest weight (0.8) is assigned to segment KH (Table DSF-2).

Solitario Canyon Fault. The northern end of the Solitario Canyon fault is well constrained by bedrock mapping. It is unlikely that the fault extends any farther north than its projected intersection with the Yucca Wash fault (Scott and Bonk, 1984; Day *et al.*, 1996c). The southern end of the fault is less certain, and two alternatives are considered (Table DFS-2). It is likely that the limit of Quaternary faulting coincides with the southernmost extent of the mapped Quaternary traces, as shown on the fault activity map by Simonds *et al.*. (1995). This alternative (segment L-M on Figure DFS-8) is assigned a weight of 0.7. It is unlikely that the Solitario Canyon fault extends farther south than its projected intersection with the Stagecoach Road fault. This alternative (segment L-N on Figure DFS-8) is assigned a weight of 0.3 (Table DSF-2).

Windy Wash/Fatigue Wash Faults. The Northern Windy Wash, Fatigue Wash, and Southern Windy Wash faults are assumed to be linked along strike and are treated as a single fault zone. The Quaternary faulting is discontinuous, and the total length of the fault system is uncertain. Four alternatives are considered in the model (Table DFS-2).

1. Quaternary faulting is limited to the reach of the fault having evidence of Quaternary displacement, as shown on Simonds *et al.*. (1995), i.e., fault segment P-R on Figure DFS-8. This option is given the greatest weight (0.57).

2. Quaternary faulting extends about 1.5 km farther north, ending at the projected intersection of the Northern Windy Wash fault with the Yucca Wash fault. This option corresponds to fault segment O-R on Figure DFS-8. This is given a relatively low weight (0.3) because no evidence for Quaternary displacement has been found along section O-P.

3. Quaternary faulting extends about 3.5 km farther south to the projected intersection between the Southern Windy Wash fault and the proposed Highway 95 fault. This alternative, which corresponds to fault segment P-S on Figure DFS-8, is also given low weight (0.1) because there is no evidence for Quaternary displacement.

4. Quaternary faulting extends both north and south (fault segment O-S on Figure DFS-8). The probability of this is equal to the combined probability of options 2 and 3 above (0.03).

Northern and Southern Crater Flat Faults. Based on the geologic cross sections and structure contour maps described in Section 4.3.5, the Northern and Southern Crater Flat faults intersect the Bare Mountain fault at a relatively shallow depth, and it is unlikely that they are linked along strike. The narrow down-dip width of the fault is consistent with the short mapped surface traces. Therefore, the total fault lengths are taken as the mapped fault lengths shown on the fault activity map by Simonds *et al.*. (1995).

Ghost Dance Fault. Based on the detailed mapping within the controlled area (Simonds *et al.*, 1995; Day *et al.*, 1996c), the Ghost Dance fault is well defined for a distance of about 3 km (segment Y-Z, Figure DSF-8). Bedrock mapping indicates that the fault dies out at its northern end and that it does not extend north of location YY on Figure DSF-8. The southern termination of the fault is less distinct. The maximum length of the Ghost Dance fault is about 9 km if one assumes that the fault extends from location YY southward and includes the Abandoned Wash fault (i.e., segment YY-ZZ on Figure DSF-8). The geologic evidence for a continuous 9-km-long fault is not strong. Nonetheless, we assign a relatively high weight to a total fault length of 9 km because this assessment is conditional on the fault being an active seismogenic feature. A 3-km-long fault extending to seismogenic depths and acting as an independent seismic source is not very likely. A total fault length of 3 km (segment X-Y on Figure DSF-8) is assigned a weight of 0.3; a total length of 9 km (segment XX-ZZ) is given a weight of 0.7 (Table DSF-2).

Total Fault Length (Distributive Fault Behavior). Given the uncertainty in the total lengths of the individual faults described above, the sum of their lengths (total combined length) could be as long as 101.2 km, or as short as 84.5 km.[1] If the Northern and Southern Crater Flat faults are only minor features, the minimum combined total length is 69.9 km.

[1] NOTE: These totals were calculated based on the distributed fault model, so that fault segment M-N of the Solitario Canyon fault was assumed to exist. The Ghost Dance fault was not included because, unlike the other local fault sources, there is a very low probability that it is an active fault.

Three scenarios are defined to account for the uncertainty in the total length of faulting given the distributed fault model (Figure DSF-10). These are:

Scenario A - the minimum value for the total length, minus the Northern and Southern Crater Flat faults, which in this scenario are inferred to represent minor secondary features;

Scenario B - the maximum value for the total fault length minus the Northern and Southern Crater Flat faults; and

Scenario C - the maximum value for the total fault length including the Northern and Southern Crater Flat faults.

The fault segments as shown on Figure DFS-8, total length, and assigned probability weight for each of these scenarios are presented in Table DFS-3.

4.3.4 Maximum Fault Rupture Length

Estimates of the rupture length associated with the maximum earthquake depend on whether the local faults behave independently or whether multiple traces rupture simultaneously (distributive faulting) (Figure DSF-9). The maximum rupture length per event on the local faults is discussed below for each type of fault behavior.

Maximum Rupture Length for Independent Fault Behavior. If the local faults behave independently, the maximum rupture length depends on the total fault length and on the length of the longest part of the fault that is expected to rupture during a single event. Given the range of total fault lengths presented in Table DFS-2, the following alternatives were considered:

- Rupture of 100 percent of the total fault length. For long faults, such as the Paintbrush Canyon/Stagecoach Road fault, this was given a low weight. For short faults such as the Northern Crater Flat and Southern Crater Flat faults, 100 percent rupture of the total fault length is assigned a probability of 1.

- Rupture of the longest geometrically defined fault segment. Depending on the strength of the evidence for defining fault segments, this approach was generally given the most weight.

- Rupture of two or more geometrically defined fault segments.

The basis for the alternative maximum rupture lengths considered for each of the local fault sources (assuming independent fault behavior) and the assigned probability weights are given in Table DSF-4.

Maximum Rupture Length for Distributive Fault Behavior. Based primarily on paleoseismic data from trenches, S.K. Pezzopane *et al.* (USGS, written communication, 1996a) propose nine rupture scenarios, Z through R, that are consistent with our distributed fault model. That is, the inferred rupture scenarios suggest the possibility of simultaneous rupture on multiple fault traces in the vicinity of Yucca Mountain. These rupture scenarios are used to evaluate the range of values for single-event fault ruptures associated with the distributed fault model. We used a somewhat different approach to define the rupture lengths associated with each scenario. S.K. Pezzopane *et al.* (USGS, written communication, 1996a) constrain the minimum and maximum rupture length for each scenario based on the spatial distribution of the trenches. We used the trench data and geometrically defined fault segments to assess the length of surface fault rupture associated with each scenario. If the trench data suggest that two fault segments could have ruptured at the same time, we assumed that 100 percent of each segment ruptured unless trench data suggest otherwise. Our approach also incorporates the uncertainty in the total mapped length of the site-vicinity faults. Therefore, in some cases, we derive rupture lengths longer than the maximum values interpreted by S.K. Pezzopane *et al.* (USGS, written communication, 1996a). Given below are the rupture length estimates—both ours and those of S.K. Pezzopane *et al.*—associated with each rupture scenario.

RUPTURE SCENARIO	RUPTURE LENGTH IN KM (PEZZOPANE, *et al.*., 1996B, TABLE 5-3)	RUPTURE LENGTH IN KM (THIS STUDY)
Z	8.5 to 22	23.4 to 36.4
Y	18.5 to 25.5	25
X	15 to 24	18.9 to 24.9
W	10 to 22	30.6
V	9 to 15.5	14.8
U	10.5 to 23	55.5 to 59
T	14 to 20	< 15
S	9.5 19.5	< 15
R	8.5 to 22	< 15

The ranges indicated above are permitted by the data. The timing of paleoseismic events is imprecise, and the data do not necessarily indicate that single-event ruptures that are this long have occurred. Given a distributed faulting event, there is a great deal of uncertainty in the rupture length that would be associated with the maximum earthquake. The scenario earthquakes summarized above suggest values from less than 15 km up to about 60 km. Fifteen km is judged to be the minimum value that should be considered for the maximum rupture length given the distributed fault model. Using our approach to define the rupture lengths associated with the scenario earthquakes, and considering only those events having values greater than about 15 km, the average rupture is about 30 km. Using values proposed by S.K. Pezzopane *et al.* (USGS, written communication, 1996a, Table 5-3), the average is closer to 20 km.

The range of values for the surface fault rupture length associated with the maximum earthquake (given the distributed fault model) and the assigned probability weights are:

Maximum Rupture Length ***(Distributed Fault Model)***	
15 km	(0.2)
20 km	(0.35)
30 km	(0.35)
60 km	(0.1)

Pattern of Fault Rupture for Distributive Fault Behavior. The following procedures were used to model the pattern of fault rupture based on the distributive fault behavior model.

- Earthquakes associated with ruptures $\leq$ 10 km long are assumed to occur as a single rupture randomly distributed on the mapped Quaternary faults (i.e., the local fault sources).

- Earthquakes associated with ruptures > 10 km and $\leq$ 25 km long are assumed to occur as two parallel ruptures of equal length that occur randomly on local fault sources. Earthquakes associated with ruptures > 25 km and $\leq$ 45 km long are assumed to occur as three parallel ruptures of equal length that occur randomly on local fault sources.

- Earthquakes associated with ruptures > 45 km long are assumed to occur as four parallel ruptures of equal length that occur randomly on local fault sources.

The selection of the cutoff points (10 km, 25 km, and 45 km) between single, double, triple, and quadruple parallel ruptures was somewhat arbitrary. They were chosen to minimize unreasonably short ruptures while permitting simultaneous rupture on all four principal local faults during the largest events. Alternative values could be used to test the sensitivity of the results to these postulated values. We did not propose alternative values because we believe they will have no significant impact on the overall hazard results.

4.3.5 Downdip Fault Geometry (Dip and Width)

Structural models were used to estimate the down-dip geometry of the locals faults. Our understanding of the tectonics of the Yucca Mountain region is influenced by the tectonic interpretations of this region developed during the past 30 years of detailed studies. The first generation of these studies led to the proposal that Crater Flat basin formed as a caldera complex (Carr *et al.*, 1986). Carr's work was followed by more detailed mapping of the east side of Crater Flat basin (Yucca Mountain) by Scott (1990), who proposed that the faults exposed on the surface in Crater Flat basin sole into a shallow detachment fault at the Paleozoic-Tertiary contact. At about the same time, Schweickert (1989) proposed that a regional, northwest-striking, right-slip fault extends under Crater Flat basin and is concealed under a detachment fault. In the latest generation of work, the detailed mapping started by Scott has been extended across the western half of the basin and beyond (Faulds *et al.*, 1994; Fridrich, 1997), and the surface geology and trench exposures of the Quaternary faults in the basin have been mapped (Simonds *et al.*, 1995; J.W. Whitney *et al.*, USGS, written communication, 1996a). This latest work has led to a proposal that Crater Flat is a pull-apart

basin that formed in response to the combined extensional and strike-slip strain regime of the Walker Lane belt (Fridrich, 1997), as originally advocated by Wright (1989).

The latest generation of tectonic studies at Yucca Mountain (e.g., J.W. Whitney *et al.*, USGS, written communication, 1996a) largely have rejected the detachment fault hypothesis proposed by Scott (1990). Southwest Research Institute scientists (Young *et al.*, 1993) suggested that the Paleozoic-Tertiary contact is too shallow for a detachment fault under Yucca Mountain, based on computer modeling of the proposed structure in balanced cross sections. Gravity and reflection surveys (Snyder and Carr, 1984; Brocher *et al.*, 1996) across Crater Flat basin provide evidence that the Paleozoic-Tertiary contact is offset by several large, high-angle features, which is difficult to reconcile with this contact being a detachment fault of the sort invoked by Scott. Scott's model predicts that the Tertiary rocks were transported westward relative to the underlying Paleozoic rocks before the uplift of Bare Mountain. However, recent mapping has shown that the uplift of Bare Mountain was roughly coeval with formation of the extensional faults in Crater Flat basin and that a linear swarm of 14 Ma dikes is not offset significantly (if at all), as predicted at the Tertiary/Paleozoic contacts at the northeast and southeast corners of Bare Mountain (Fridrich, 1997). Scott invoked the widely accepted model in which the detachment fault allows lateral translation of extensional strain between the zone of brittle extensional faulting in the upper plate and the zone of ductile extension in the lower plate. Because any detachment fault under the Crater Flat basin would be truncated by the Bare Mountain range-front fault, it would be a rootless structure that would lack any kinematic impetus to move in Scott's model. For these reasons, our analysis gives Scott's detachment model a very low weight (Figures DSF-10 and DSF-11).

Carr *et al.*'s (1986) hypothesis, that the Crater Flat basin formed as a caldera complex, has been rejected by nearly all ensuing workers for the following reasons. (1) The structures of the Crater Flat basin are products of northwest-directed extension and right-slip strain (Scott, 1990; Minor *et al.*, 1996; Fridrich, 1997). They thus are consistent with patterns of late Cenozoic tectonism in the Great Basin as a whole. In contrast, the structures formed by calderas accommodate principally vertical strain (tumescence, collapse, and resurgence) over the subcaldera magma body and radial and concentric strain peripheral to the magma

chamber (Smith and Bailey, 1968). (2) If a caldera complex is buried under Crater Flat basin, it must be older than 13.1 Ma because the sources for all of the younger major ash-flow sheets of the southwest Nevada volcanic field have been identified (Sawyer *et al.*, 1994). In that the Crater Flat basin formed at about 12.7 Ma, any buried caldera under the basin was a fossil structure when the basin formed and, therefore, is irrelevant to the formation of this basin. We give the caldera model zero weight in our analysis for the reasons stated above and because this model provides no explanation for the Quaternary faulting in this basin.

The rapid succession of different tectonic interpretations of the Crater Flat basin during the past 30 years is an indication of the level of scientific uncertainty involved. Because of the large uncertainty, we consider a range of hypotheses. The strongest weight is assigned to the simplest, most conventional approach. The alternative models, which are assigned relatively low weights, are included primarily to facilitate assessment of the effect these models have on the overall seismic hazard at Yucca Mountain.

Domino Model. Our preferred model assumes that the faults exposed at the surface in Crater Flat basin extend as high-angle, planar faults to seismogenic basement (12 to 16 km), except where the geometry dictates that they run into another, larger-throw fault before they reach that depth, as discussed below. We call this the Domino model. The theoretical basis and supporting evidence for the Domino model consists of the following points.

(1) The 1992 Little Skull Mountain earthquake (Mw 5.7), which had its epicenter about 10 km east of Yucca Mountain, provides the only ground-truth evidence on the subsurface geometry of faults and on the relationship between faulting and earthquakes in the Yucca Mountain region.

(2) The foci of the main Little Skull Mountain shock and aftershocks defined a planar, high-angle fault that extends from the upper crust down to at least 12 km (Harmsen, 1994; Smith *et al.*, 1996).

(3) The nature of this earthquake is consistent with the majority of data on historical earthquakes in the Great Basin in that most significant (greater or equal to magnitude 5) earthquakes in this province are due to movement on normal faults that are high-angle, planar, and extend to depths of 10 to 15 km (the brittle-ductile transition).

(4) Moreover, the lack of evident ground breakage associated with the Little Skull Mountain quake is consistent with the fact that most quakes in this province having a magnitude of less than 6 have no associated ground breakage.

(5) If we can use the Little Skull Mountain quake as an analogue for what to expect at Yucca Mountain, then the Quaternary ground breakage along distances of several kilometers and more on Yucca Mountain faults having slips in individual events of as much as 1 m suggests that the Quaternary faulting events on Yucca Mountain were associated with large earthquakes (greater than magnitude 6). By inference, we believe it is valid to take the relationship of earthquake magnitude to fault rupture length (and other parameters) developed using the historical data from the Great Basin as a whole and use them to predict the potential magnitude of earthquakes at Yucca Mountain, based on the Quaternary record of surface fault rupture there.

The Domino model represents the simplest, most conventional approach because it assumes that Yucca Mountain is not seismically anomalous relative to the rest of the Great Basin. This is our preferred model because, although it is possible that Yucca Mountain may be seismically anomalous relative to the rest of the Great Basin, we believe that arguments suggesting that it is are scientifically weak. Therefore, the Domino model is assigned a very high weight (0.8) relative to the Detachment model (0.2) in the hazard analysis (Figures DSF-10 and DSF-11).

An optional feature we placed within our Domino model is the Highway 95 fault (discussed below), based on an interpretation of Slemmons (personal communication, 1997). Slemmons invoked this fault, based on airphoto lineament patterns, to explain a structural geometry problem. The Quaternary faults in Crater Flat basin show a pattern of southward increase in slip rates, with maximum rates documented near the southern terminations of recent activity. This geometric pattern is highly anomalous and suggests that the faults may be abruptly terminating against another structure, such as a northwest-striking right-slip fault along the southern boundary of the basin.

Detachment Model. A detachment layer at depths of 5 to 8 km below the surface may be used to satisfy the geometry arguments advanced by Southwest Research Institute (Young *et al.*, 1993) and to be consistent with gravity and reflection data. We used this basic fault geometry to characterize the proposed detachment models, which include:

- Scott's model in which the detachment acts as the master fault in the basin that all of the intrabasin faults sole into;

- Wernicke's (1995) model in which a master detachment fault is considered a separate seismic source; and

- Schweickert's model in which a regional-scale strike-slip fault that is a potential seismic source extends under Crater Flat basin under a shallow detachment fault.

Also considered were the ideas advanced principally by O'Leary (personal communication, November 20, 1996 Workshop), who proposed that the large difference in the mechanical behavior of the Tertiary volcanic and Paleozoic sedimentary rocks under Yucca Mountain may result in an abrupt, downward change in the style of faulting across the Paleozoic-Tertiary contact. This contact would be a passive zone of detachment that accommodates an upward change in structural behavior in the rocks. The predominantly northeast-striking, left-oblique normal faults that cut the volcanic rocks have allowed a large component of distributed right-slip strain across the basin (Fridrich *et al.*, 1997). The major point of this passive detachment model is that the distributed strike-slip strain in the volcanic surface rocks could reflect motion along a discrete strike-slip fault at seismogenic depths under Crater Flat basin. Unlike the model proposed by Schweickert, the concealed strike-slip fault would be confined to Crater Flat basin. Such a fault has been postulated beneath the Crater Flat basin, and was informally referred to as the cross-basin fault (I. Stamatakos, SSC Workshop 2). The potential for a hidden strike-slip fault beneath Crater Flat basin is addressed in Section 4.4.2.

Estimated Downdip Geometry of Local Faults. To develop defensible interpretations of subsurface fault geometry under Crater Flat basin, we constructed a suite of cross sections and structural contour maps of the exposed Quaternary faults using two geometric styles, which we view as end-member geometries: (1) a planar fault geometry, and (2) a strongly listric geometry that merges with a detachment layer. We then used these maps and sections to develop the downdip widths of the faults, listed below. For this exercise, we used the measurements of fault attitudes of Simonds *et al.* (1995) as a starting constraint and assumed that the fault planes exposed on the surface represented the steepest parts of the faults. In theory, normal faults form at an angle of 50 to 70 degrees in most rocks because this is the

angle of maximum shear stress, assuming that the principal compressive stress is vertical. As these faults approach the surface, however, they tend to steepen to attitudes approaching vertical because there is no shear stress at the surface of the Earth. Another assumption we made is that fault dip decreases smoothly with depth. In our planar sections and maps, the decrease in fault dip with depth is very small; in the listric model, the faults sole into a subhorizontal detachment fault at about 6 km below the surface.

We used a trial-and-error approach in constructing our maps and sections to arrive at subsurface geometries that we consider most credible. For example, we joined the two segments of the Paintbrush fault and the Stagecoach Road fault as a single fault at shallow depths because: (1) these three mapped fault segments are roughly coplanar; (2) if not joined, these three fault segments had length-to-width ratios in the planar model that are inconsistent with established aspect ratios of faults in the Great Basin based on historical seismic and paleoseismic data; and (3) the documented single-event slip on the Stagecoach Road fault segment is too large for a fault as short as this, based on historical fault data, suggesting that this segment is part of a longer fault. We joined the northern and southern segments of the Windy Wash fault with the Fatigue Wash fault at shallow depth for the same reasons. The two other major faults in our maps and sections are the Solitario Canyon and Bare Mountain faults, both of which were mapped as single segments.

Having made the above assumptions, we found that the Paintbrush Canyon/Stagecoach Road fault, the Solitario Canyon fault, and the Windy Wash/Fatigue Wash fault cannot come together at shallow depth; the most credible geometry appears to be that they are independent faults. The projections of the other faults in the basin (i.e., the Bow Ridge and Northern and Southern Crater Flat faults) all intersect one of the four major faults at depths much shallower than the brittle-ductile transition. These faults thus either may be splays of the Paintbrush Canyon/Stagecoach Road or Solitario Canyon faults, or, in the case of the Northern and Southern Crater Flat faults, may be minor faults that are antithetic to the Bare Mountain fault. In the Domino (planar) model, the three major intrabasin faults (the Paintbrush Canyon/Stagecoach Road fault, the Solitario Canyon fault and the Windy Wash/Fatigue Wash fault) are antithetic faults to the Bare Mountain fault because they project into the Bare Mountain fault at depths that are near or above the brittle-ductile transition. In the Detachment (listric) model, the Paintbrush Canyon/Stagecoach Road fault is the master

Crater Flat faults, which run into the Bare Mountain fault first. In the hazard analysis, given the Detachment model, the Paintbrush Canyon/Stagecoach Road fault is modeled as a shallow-dipping, seismogenic source that extends beneath the Crater Flat Basin (Table DSF-5).

In the Domino (planar) fault model, the faults probably are not truly planar. They probably are slightly curved, which would explain the observed regions of roll-over in stratal dips in the hanging walls of these faults. Minimal curvature was used in constructing the cross sections. However, in the hazard analysis, the faults are modeled as planar features, and the average dip was used. To account for uncertainties in the actual dip and downdip width of the faults, the analysis includes a range of values represented by the alternative geometries (Alternatives A and B) shown on Table DSF-5 for the Domino model.

4.3.6 Quaternary Slip Rates (Seismic Moment Rates)

Quaternary slip rates are used in conjunction with fault areas (including the uncertainties in total fault lengths and downdip fault widths) to compute a range of values for the average seismic moment rate for each local fault source. Except for the Ghost Dance fault, the Quaternary slip rates for the local faults are based on the reported results of detailed paleoseismic investigations. In general, these reported slip rates are reasonably well constrained by the available data; nonetheless, there are uncertainties in the amount of cumulative displacement, the age of the displaced units and, in some cases, the relation between the apparent vertical displacements measured in the trenches to the net slip on the fault (i.e., where there may be a significant component of lateral slip). To account for these uncertainties, a range of values is considered for each local fault. In most cases, the range is represented by three values: the maximum and minimum slip rates indicated by the data, and a preferred value, which were assigned subjective probability weights of 0.2, 0.2, and 0.6, respectively. Where preferred values were not reported, maximum and minimum slip rates are given, and a subjective probability weight of 0.5 is assigned to both values.

The range of values assigned to the Ghost Dance fault is based on the amount of post-Tiva Canyon displacement, using the procedures described in Section 5.0 (Fault Displacement Hazard). The preferred value, which we assigned a subjective probability of 0.6, is the weighted average from the three approaches used in the fault displacement assessment. The

minimum and maximum values calculated using these techniques are each assigned a subjective probability of 0.2.

Table DFS-6 presents the range in values, assigned weights, and sources of data for the reported slip rates. In several cases the slip rates presented in Table DFS-6 indicate a greater range of uncertainty than the reported slip rates either because data from several closely spaced trenches have been generalized and/or we believe that there is greater uncertainty than represented by the reported values (e.g., in some case we made allowances for a greater amount of lateral slip).

There appears to be a systematic increase from north to south in both the amount of cumulative bedrock displacement and in the Quaternary slip rates on the local faults. To preserve this spatial variability in the rate of seismic moment release, the longer faults are divided into segments characterized by different slip rates. These fault segments do not necessarily represent rupture boundaries. We assumed that single-event ruptures may extend across these boundaries.

4.3.7 Maximum Magnitude

Given the range of fault geometries, we used two methods to calculate earthquake magnitude. We used empirical relations that relate maximum rupture length to magnitude and similar relations that relate maximum rupture area to magnitude (Wells and Coppersmith, 1994, relations for all fault types). In addition to the uncertainty in the fault rupture parameters (length and downdip width), which is addressed by the range of values included in the logic trees, there also is uncertainty associated with the data sets used in formulating the empirical relations themselves. This uncertainty was included in the analysis by calculating $M_{MAX} \pm 1\sigma$.

Several other approaches and empirical relations are available for estimating earthquake magnitudes (e.g., Slemmons, 1982; Bonilla *et al.*, 1984; Wyss, 1979; dePolo and Slemmons, 1990). We concluded that by incorporating the uncertainty ($\pm 1\sigma$) in the Wells and Coppersmith (1994) relations, we would adequately capture the uncertainty associated with estimation techniques in general.

The rupture-area-versus-magnitude approach is given more weight than the rupture-length-versus-magnitude approach because it incorporates more of the parameters that affect the size of an earthquake and because the rupture-length-versus-magnitude relation is insensitive to significant variations in possible downdip geometries. The rupture area approach is assigned a weight of (0.6), the rupture length approach is assigned a weight of (0.4).

4.3.8 Recurrence Models

The same earthquake recurrence models used to characterize the regional fault sources also were used to characterize the local fault sources (i.e., an exponential recurrence model, a characteristic earthquake recurrence model, and a maximum moment model; see Section 4.2). However, we believe that there is greater potential for variability in the size of earthquakes based on distributed fault behavior than there would be if the faults behave independently. Therefore, the probability weights assigned to each earthquake recurrence model depend on the fault behavior model for the local fault sources (Figure DFS-12). Regardless of the fault behavior model, the greatest weight (0.6) was assigned to the characteristic earthquake model because the results of detailed paleoseismic studies along active faults have shown that the characteristic model is more representative of the seismicity of an individual fault than are exponential models that represent the seismicity of regions, which contain faults of various sizes. Given distributive fault behavior, more emphasis is given to the exponential model (Figure DFS-12).

4.4 HYPOTHETICAL FAULT SOURCES

In addition to the known regional and local fault sources, we included two hypothetical fault sources in the seismic hazard model. These are: the Highway 95 fault that has been proposed by Slemmons (1977), and a buried strike slip-fault that has been postulated based on proposed tectonic models (Schweikert, 1989). The existence of these faults and rate of Quaternary activity, if they exist, are uncertain. The locations of these features (as modeled in this analysis) are shown on Figure DFS-13. The seismic source parameters used to characterize the hypothetical fault sources are presented in Table DFS-7.

4.4.1 Proposed Highway 95 Fault

Slemmons (1977) proposes a fault zone, which he refers to as the "Carrara feature," along U.S. Highway 95 between the fluvial Beatty scarp near the Amargosa River to the south end of Yucca Mountain. Based on its strike (subparallel to the Furnace Creek fault), the predominant sense of slip would likely be left-lateral strike-slip.

The approach used to model the proposed Highway 95 fault is the same as the approach used to model the regional fault sources except that a low weight (0.1) is assigned to the probability that this feature is an active structure. We assigned a low probability of activity because no evidence has been found for faulting along this trend. The suspected fault-related features that have been investigated (e.g., the Beatty scarp) were found to be erosional/depositional in origin and not due to Quaternary faulting.

Because of the lack of evidence for faulting, the total length of the feature is uncertain. Two lengths are considered in the analysis: 11 km, which corresponds to the section of the lineament adjacent to the southwest flank of Bare Mountain; and 27 km, which assumes that faulting could extend southeastward to its projected intersection with the north-south-trending Amargosa/Gravity (Ash Meadows) fault. Based on the gravity data, we believe it unlikely that strike-slip faulting extends any farther southeast. The two values for the total fault length are given equal weight (maximum uncertainty). M_{MAX} depends on total fault length. A maximum rupture length of 11 km corresponds to Mw 6.3 ($\pm$ ¼). However, Mw 6.5 is considered the minimum upper-bound magnitude for surface faulting earthquakes. Therefore, given a rupture length of 11 km, the values included in the analysis and their associated probability weights are Mw 6.5 (0.7) and Mw 6.8 (0.3) (Table DFS-7). Similarly, a maximum rupture length of 27 km corresponds to Mw 6.7 ($\pm$ ¼). In this case, the values included in the analysis and their associated probability weights are Mw 6.5 (0.2), Mw 6.7 (0.6), and Mw 7.0 (0.2).

There are no reported slip rates for the proposed Highway 95 fault. Slip rates are estimated here based on the inferred rate of extension in the southern part of the Crater Flat basin. The sum of the vertical slip rates on the Quaternary faults in the southern part of the basin is approximately 0.05 to 0.1 mm per year (C.J. Fridrich *et al.*, USGS, written communication, 1996, Figure 2-9). Depending on the average dip of the north-south faults, the rate of

extension could be equivalent to, or about half of, the vertical rate (i.e., 45 degrees versus about 65 degrees). By assuming that all the extension is being taken up on the proposed Highway 95 fault, we estimated the slip rate to be in the range of 0.01 to 0.05 mm per year, with a preferred value of about 0.027 mm per year (based on preferred dips of 55 to 60 degrees). The values and associated probability weights included in the analysis are: 0.01 mm per year (0.3), 0.03 mm per year (0.4), and 0.05 mm per year (0.3). Nearly equal weights were given to all three values to reflect the high degree of uncertainty in the slip rate.

4.4.2 Postulated Hidden Strike-Slip Fault Beneath Crater Flat Basin

Given a detachment zone model, there could be hidden strike-slip faults below the detachment layer (e.g., Schweickert, 1989). The hidden strike-slip faulting could be local (restricted to Crater Flat basin) or regional. There is little physical evidence to support the existence of a hidden strike-slip fault (Section 1.0). The probability that there is an active hidden strike-slip source is given even less weight than the activity assessment for the Highway 95 fault (0.05 versus 0.1). The primary reason for including a postulated strike-slip fault in the analysis (given the detachment model) is to enable us to test the sensitivity of the results to this hypothesis.

The location of such a fault is unknown. For this analysis, we assumed that the fault strikes parallel to, and lies 40 to 50 km east of, the Death Valley/Furnace Creek fault system. To model uncertainty in location, equal weight was given to a strike-slip fault having a 90 degree dip that is either along the northeastern margin, southwestern margin, or down the center of the zone shown on Figure DFS-13. To model uncertainty in the length of the zone, two alternatives were considered. If the fault is restricted to Crater Flat basin, it has a total length of about 30 km (segment A-B on Figure DFS-13). If the fault is regional, it was assumed to extend about 100 km in either direction from Cater Flat basin and to have a total length of about 200 km (segment C-D). These alternatives were given equal weight (i.e., maximum uncertainty).

We used different approaches to estimate the maximum earthquake magnitude depending on the structural model (local strike-slip faulting restricted to Crater Flat basin versus regional strike-slip faulting). Given the local strike-slip model, the maximum rupture dimensions are constrained by the length of the basin, the depth of the detachment zone, and the maximum

depth of the seismogenic crust. The same methods used to calculate earthquake magnitudes for the local fault sources (Section 4.3.7) were used for the hypothetical buried strike-slip faults, except that more weight was given the area-versus-magnitude relation, because the structural model significantly restricts the fault width and the length-versus-magnitude relation is insensitive to this parameter. Given the local strike-slip model, the area-versus-magnitude technique is assigned a weight of 0.8, and the length-versus-magnitude technique is assigned a weight of 0.2 (Table DFS-7).

Given the regional strike-slip model, the maximum fault rupture length is unconstrained. In this case, the maximum earthquake magnitude is based on our judgment regarding the largest events that would be consistent with the lack of surface evidence for a throughgoing strike-slip fault. The threshold for surface fault rupture is generally in the range of magnitude 6 to 62, but larger historical events have occurred without producing surface fault rupture. It is unlikely that repeated events larger than about magnitude 7 could occur without producing surface evidence. Given the regional strike-slip model, the values included in the analysis and their associated probability weights are Mw 6.0 (0.3), Mw 6.5 (0.5), and Mw 7.0 (0.2).

There are no reported slip rates for a postulated hidden strike-slip fault beneath Crater Flat basin. For this analysis, we assumed that all the horizontal extension on the Quaternary faults at the surface occurs as strike slip on a northwest-trending fault at depth. Accordingly, the range of slip rates estimated for the Highway 95 fault also was used for the postulated hidden strike-slip fault (Table DFS-7).

5.0
FAULT DISPLACEMENT

The objective of the fault displacement characterization is to develop general procedures and perform evaluations for input to assess the probability of fault displacement (hazard curves that relate annual probability to amount of displacement) for any location within the controlled area at Yucca Mountain, given the structural characteristics at the specified location. Nine test calculations sites were identified during Seismic Source Characterization (SSC) Workshop 4 to represent the range of expected fault conditions within the Controlled

Area. At two locations, four alternative fault conditions are considered. The locations of the nine test calculation sites are shown on Figure DFS-14. They include:

(1) the Bow Ridge fault where it crosses the Exploratory Studies Facility (ESF);

(2) the Solitario Canyon fault where it trends toward the repository block;

(3) the Drill Hole Wash fault where it crosses the ESF;

(4) a point along the Ghost Dance fault near the center of the controlled area;

(5) a point along the Sundance fault west of the ESF;

(6) a minor unnamed fault west of Dune Wash;

(7) a point 100 m east of the Solitario Canyon fault that has:
   (a) a small fault having 0.5 to 2 m cumulative displacement,
   (b) a shear having about 10 cm cumulative displacement,
   (c) a fracture having no measurable displacement, or
   (d) intact rock;

8) a point midway between the Solitario Canyon and Ghost Dance faults that has:
   (a) a small fault having 0.5 to 2 m cumulative displacement,
   (b) a shear having about 10 cm cumulative displacement,
   (c) a fracture having no measurable displacement, or
   (d) intact rock;

9) a point along the Exile Hill fault in Midway Valley where fractures having no measurable offset have been observed in Quaternary alluvium.

5.1 GENERAL APPROACH FOR CHARACTERIZING FAULT DISPLACEMENTS

The underlying basis for assessments of fault displacement hazard is that future fault slip will recur at the same locations and in the same manner as geologically recent displacements (ASCE, 1997). Future fault displacements are most likely to occur on pre-existing faults, and the likelihood of future displacements is related to the frequency of most recent displacements. Accordingly, the most reliable assessments of the potential for fault

displacement are based on direct geologic evidence regarding the recent history (Quaternary) of past displacements.

Quaternary deposits that would enable direct assessment of recent faulting are not present over most of the Controlled Area. Also, many of the features encountered at the level of the proposed repository cannot be related directly to observed surface faults. Therefore, the analysis must rely on indirect methods that relate the character of the displacements observed in the repository host rock (late Miocene Tiva Canyon Tuff) to the probable Quaternary displacement history on these features based on our knowledge of the geologic evolution of Yucca Mountain. The methods used are calibrated using data from selected locations for which we have data on fault displacement in both the Tiva Canyon Tuff and the overlying Quaternary deposits.

Fault slip rate is the basic parameter used in this analysis to characterize the potential for the fault displacement. It is a useful parameter for: (1) assessing the fault displacement history (e.g., for comparing late Miocene faulting to Quaternary faulting on a given structure); (2) for comparing the relative hazard posed by different faults; and (3) for constraining the recurrence and/or the slip per event on a given fault. The following relation between slip rate (SR), average recurrence interval (RI), and average displacement per event (D) is important because the slip rate effectively constrains the hazard (amount of displacement and likelihood of occurrence):

$$SR = \frac{D}{RI}$$

Given the low slip rates on faults at Yucca Mountain, the average displacements must be small, or the average recurrence intervals must be long. Based on estimates of slip rate, one can use information on the average recurrence interval to calculate the average displacement per event. Alternatively, one can use information on displacement per event to calculate recurrence interval. Both approaches are used in this analysis to assess the fault displacement hazard on features for which we have slip rates (i.e., features having a measurable cumulative displacement). If the features have no detectable cumulative offset (no slip and, therefore, no slip rate), a different approach is required. The displacement characterization based on fault-

slip rate are presented in Section 5.2. The potential for displacement along fractures and in unbroken rock is discussed in Section 5.3.

5.2 POTENTIAL FOR DISPLACEMENT ON IDENTIFIED FAULTS

The logic tree used to characterize the fault displacement on the identified faults in the controlled area is shown on Figure DFS-15. The parameters used to characterize the fault displacement include:

- fault activity,
- the cumulative displacement on post-Tiva Canyon Tuff,
- the average Quaternary slip rate,
- the average displacement per event,
- the average recurrence interval, and
- the event-to-event variability in the displacement per event at a point along a fault.

Each of these factors is discussed below.

5.2.1 Fault Activity

In the context of assessing fault displacement hazard, the activity of a fault is the likelihood that the feature has undergone movement (slip) in response to tectonic forces during the present tectonic regime (the Quaternary). It includes all types of fault slip (primary and secondary faulting), except displacements due to near-surface gravitational effects such as landslides, effects of liquefaction, and effects of differential compaction.

If the fault at a test calculation site has had Quaternary displacement, we assigned it a probability of activity of 1.0 (unless there is evidence that suggests the displacements were not tectonic). Only the north-south block-bounding faults at Yucca Mountain have demonstrated evidence of Quaternary displacement. These include the Bow Ridge fault (Test Calculation Site #1) and the Solitario Canyon fault (Test Calculation Site #2). These faults are assigned a probability of activity of 1.0 (Table DFS-8).

Two zones of fractures having no detectable slip have appeared at least twice in the Quaternary alluvial and colluvial deposits that overlie north-northeast-trending bedrock faults

along the east side of Exile Hill in Midway Valley (Test Calculation Site #9; F.H. Swan *et al.*, Geomatrix Consultants, written communication, 1995; W. R. Keefer and J. W. Whitney, USGS, written communication, 1996). The fracturing occurred repeatedly (at least twice) during stratigraphically distinct episodes. Non-tectonic mechanisms for the formation of these fractures cannot be ruled out, but it seems unlikely given the consistent orientation of the fractures, the continuity of the zones along strike, the coincidence of the western zone of Quaternary fractures with the Exile Hill fault, and the fact that individual fractures in the Quaternary deposits can be traced into faults in the underlying Tertiary bedrock. The Exile Hill fault is assigned a probability of activity of 0.8.

In Section 4.3.1, we assigned a very low probability (0.05) that the Ghost Dance fault (Test Calculation Site #4) is active and capable of generating significant earthquakes. In addition to the lack of evidence for Quaternary displacement, the low weight reflects our interpretation that the small-displacement intrablock faults probably represent secondary accommodation structures rather than primary, earthquake-generating structures. Because the fault displacement hazard assessment includes the effects of both primary and secondary faulting, the probability that a fault can move is not necessarily the same as the probability that it can generate significant earthquakes. The evidence suggests there has been no displacement on the Ghost Dance fault since at least the middle Pleistocene (E.M. Taylor *et al.*, USGS, written communication, 1996a). However, very small movements similar to the fractures observed along the Exile Hill fault cannot be precluded. Based on analogy to the Exile Hill fault and consideration of structural models that suggest that the Ghost Dance fault could move in response to displacements on the block-bounding faults, we give a low but significant probability that the Ghost Dance fault has experienced a small amount of Quaternary displacement. That the fault is active and capable of displacement is assigned a probability of 0.4.

There is no evidence that any of the northwest-trending faults in the vicinity of Yucca Mountain have experienced Quaternary displacement. These include the Drill Hole Wash fault (Test Calculation Site #3) and the Sundance fault (Test Calculation Site #5). Middle Pleistocene and older deposits overlie northwest-trending faults exposed in trenches on the east side of Exile Hill, providing direct evidence of no displacement during the period of repeated displacements along the north-south block-bounding faults (F.H. Swan *et al.*,

Geomatrix Consultants, written communication, 1996). This strongly suggests that the faults are not kinematically linked under the present tectonic regime. However, Quaternary displacement cannot be precluded at Test Calculation Sites #3 and #5. Right-slip movement on northwest-striking faults is compatible with some structural models for Yucca Mountain (e.g., vertical axis rotation of the structural blocks). Day *et al.* (1996c, p. 2-6) present evidence that the north-striking and northwest-striking faults have been kinematically linked sometime during their displacement history. Movement on the northwest-striking faults is compatible with the inferred orientation of the present stress field. Considering these factors, we assign a very low probability that there has been Quaternary displacement on Drill Hole Wash and Sundance faults. The probability of activity assigned to these structures is 0.01.

The activity of the unnamed fault west of Dune Wash is more uncertain. Its north-south trend and position relative to the block-bounding faults suggest a potential for slip similar to that of the Ghost Dance fault. We assigned it the same probability of activity (0.4).

Test Calculation Sites #7 and #8 contain very small faults, fractures, or unbroken rock at two locations within the proposed repository area: one 100 m east of the Solitario Canyon fault, the other midway between the Solitario Canyon and Ghost Dance faults. The activity of fractures and unbroken rock is addressed in Section 5.3.1. Small-displacement faults (less than about 3 m) are common throughout the Controlled Area. The following factors should be considered when assessing the activity of these features.

- **Orientation.** Paleoseismic evidence of Quaternary displacement has been found only along the north-south-trending faults. Faults having other trends presumably have a much lower probability of being active (perhaps an order of magnitude or more).

- **Faults that die out during the Miocene.** Many of the small-displacement faults die out upward within the Tertiary section and are pre-latest Miocene in age, precluding any Quaternary displacement. Where this can be demonstrated, the probability of future displacement should be assessed using the approach outlined in Section 5.3.

- **Position relative to active block-bounding faults.** Secondary deformation is more likely to occur on the hanging wall than on the footwall; the zone of deformation typically is much narrower on the footwall of normal faults.

- **Distance from the active block-bounding faults.** Secondary deformation typically is most concentrated immediately adjacent to and within a few meters of a fault. It can, however, occur tens, hundreds, and even thousands of meters from the primary fault trace. There is no relation that reliably predicts the amount or likelihood of secondary faulting related to distance from a primary fault trace. Nonetheless, based on historical earthquakes, it is reasonable to infer that the probability of secondary faulting decreases significantly (by an order of magnitude or greater) at distances more than a few meters to a few tens of meters from a primary fault.

The only information given about Test Calculation Sites #7 and #8 is their location (distance from the active block-bounding faults) and the cumulative displacement of the Tertiary bedrock. Both locations are thousands of meters from the Bow Ridge fault. Secondary (hanging wall) deformation at these locations caused by slip on the Bow Ridge fault is unlikely. Test Calculation Site #7 is 100 m east of the main trace of the Solitario Canyon fault (i.e., in the footwall), but it is about the same distance west of a northeast-trending splay of the Solitario Canyon fault. Test Calculation Site #8 is more than 800 m east of the Solitario Canyon fault. The probability that there has been Quaternary displacement at either of these locations is judged to be extremely low. Based on its closer proximity to one of the active block-bounding faults, Test Calculation Site #7 is assigned a higher probability of activity than site #8. The probability of activity assigned to small faults (either 10 cm or 2 m cumulative slip) at sites #7 and #8 are 0.05 and 0.01, respectively.

5.2.2 Cumulative Displacement and Age of the Tiva Canyon Tuff

At most of the test calculation sites, the only basis for estimating fault slip rate is the cumulative net slip of the faulted bedrock. At the proposed repository level, this is the 12.7 $\pm$ 1.3 Ma Tiva Canyon Tuff. Table DFS-8 gives the cumulative net slip of the Tiva Canyon Tuff at the nine test calculation sites. The reported values are specific to the individual sites and do not represent average values along the length of the fault. The cumulative displacements are based on: geologic maps and geologic cross sections of Yucca Mountain (Scott and Bonk, 1984; W.C. Day *et al.*, USGS, written communication, 1996c,d), and geologic reports (J.D. Gibson *et al.*, SNL, written communication, 1992, Tables 4-1 and 4-2;

F.H. Swan *et al.*, Geomatrix Consultants, written communication, 1995, Table 9). Values shown may differ somewhat from previously published values because, in some cases, adjustments were made for a lateral component to net slip, and/or allowances were made for more uncertainty in the range of values.

Except for test calculation sites 7b, 7c, 8b, and 8c, where the displacements are inferred to be known based on direct observation, the displacements are reported as a range of values to include uncertainties related to:

- measurement errors (associated with measurement of dip slip from geologic cross sections and measurement of stratigraphic throw across the fault from geologic maps having 10- to 20-foot contour intervals);
- extrapolations of the dip slip along the strike of the fault in cases where the measured bedrock displacements are not coincident with the test calculation site; and/or
- uncertainties in the lateral slip component of the net slip.

The range of values and assigned probability weights for the cumulative displacement of the Tiva Canyon Tuff are presented in Table DFS-8.

The age of the Tiva Canyon Tuff used in this analysis, 12.7 $\pm$ 1.3 Ma, is based on the range of values presented in tables compiled by J.D. Gibson *et al.* (1990, and SNL, written communication, 1992, Table 4-1).

5.2.3 Average Quaternary Slip Rate

Four approaches were used to estimate the average Quaternary slip rate. Where paleoseismic data are available on the amount and timing of Quaternary displacements, these data were used to calculate the slip rate directly. In most cases, however, there is little or no geologic information to directly assess the Quaternary slip rate. Therefore, estimates also are made based on site-specific assessments of cumulative net slip of the Tiva Canyon Tuff and three different structural/historical interpretations of the late Cenozoic evolution of faulting at Yucca Mountain. Locations for which there are data on both the post-late Miocene and Quaternary displacements (e.g., Test Calculation Sites #1, #2, and #9) provide a means for

calibrating the reliability of the methods based on the post-Tiva Canyon Tuff cumulative net slip. The basis for each approach is described below.

Quaternary Slip Rates Based on Paleoseismic Data. Where possible, the rate of deformation is based on the amount of displacement and ages of Quaternary deposits, soils, and/or geomorphic features overlying the faults. The Quaternary slip rates (and the associated uncertainty) for the Bow Ridge and Solitario Canyon faults are based on the results of detailed paleoseismic investigations at or near Test Calculation Sites #1 and #2. The Quaternary slip rate on the Ghost Dance fault is based on the absence of evidence for Quaternary displacement, inferences about the threshold of detection and analogy to the Exile Hill fault (F.H. Swan *et al.*, Geomatrix Consultants, written communication, 1995). The range of values and the corresponding probability weights used in the fault displacement hazard analysis are presented in Table DFS-9.

Uniform Slip Rate, Post-Tiva Canyon Tuff. In this interpretation, the average post-Tiva Canyon slip rate is assumed to be approximately equal to the average late Quaternary slip rate. Slip rates are calculated by dividing the post-Tiva Canyon Tuff cumulative net slip by 12.7 ± 1.3 Ma.

Uniform Slip Rate, Post-Rainier Mesa. J.D. Gibson *et al.* (SNL, written communication, 1992, p. 72) suggest that an abrupt decrease in the slip rate on the block-bounding faults at Yucca Mountain may have occurred prior to 7 Ma (dashed line on Figure DFS-16). This abrupt decrease in slip rate may correlate to the marked decrease in silicic volcanic activity. Structural data (Scott and Bonk, 1984) indicate that most (70 to 80 percent) of the displacement on the Bow Ridge and Paintbrush Canyon faults predates the deposition of the Rainier Mesa member of the Timber Mountain Tuff (11.6 ± 1 Ma). In this interpretation, 80 percent of the post-Tiva Canyon displacement is interpreted to have occurred prior to deposition of the Rainier Mesa, and the average post-Rainier Mesa slip rate is inferred to be approximately equal to the average late Quaternary slip rate. Slip rates are calculated by dividing 20 percent of the post-Tiva Canyon Tuff cumulative displacement by 11.6 ± 1 Ma.

Decreasing Slip Rate Model. J.D. Gibson *et al.* (1990 and SNL, written communication,1992) suggest an alternative interpretation of the slip rates on the Bow Ridge

and Paintbrush Canyon faults in which the slip rates have decreased continuously since the late Cenozoic (solid line on Figure DFS-16). W.C. Day *et al.* (USGS, written communication, 1996b) present data that indicate that the rate of crustal extension in the Crater Flat basin has been decreasing since the middle Miocene, when the rate of extension is estimated to have been between 18 and 40 percent, to the Quaternary (Figure DFS-17). Their estimates of the Quaternary rate of extension range from 0.1 percent to 0.7 percent. This suggests that Quaternary slip rates could be between 0.3 percent and 3.9 percent of the late Miocene rate.

In this interpretation, the Quaternary slip rate is estimated by multiplying the late Miocene slip rate by a reduction factor. The late Miocene (i.e., post-Tiva Canyon, pre-Rainier Mesa) slip rate is calculated by dividing 80 percent of the post-Tiva Canyon displacement by the interval between the deposition of these units. The duration of this interval is uncertain. The difference between the preferred ages for the two units (i.e., 12.7 Ma and 11.6 Ma) suggests an interval of 1.1 Ma. Considering the reported uncertainties in the ages of the two units yields a maximum age of 4.4 Ma, which is unreasonably long, and a minimum age difference of - 0.5 Ma, which is geologically impossible because the Rainier Mesa is not older than the Tiva Canyon Tuff. The interval between the deposition of the Tiva Canyon Tuff and the deposition of the Rainier Mesa member of the Timber Mountain Tuff is probably within the range of 1.1 ± 0.6 Ma.

Accordingly, the average Quaternary slip rate (SR) is:

$$SR = \frac{0.8\ Dtc}{1.1. \pm 0.6\ Ma} RF$$

where Dtc is the cumulative net slip on the Tiva Canyon Tuff and RF is the reduction factor, which is in the range of 0.3% to 3.9%.

Slip rates calculated using this approach are compared to rates based on paleoseismic information in Table DFS-10 to assess the reliability of the interpretation. Reduction factors of 2.1 % (the midpoint of the range) to 3.9% (the minimum reduction based on Fridrich *et al.* data; Figure DFS-17) yield rates that are in general accord with the estimates based on

paleoseismic information. A reduction factor of 0.3 % (the maximum reduction suggested by Fridrich *et al.* data) yielded values that are considered too low (Table DFS-10). Based on this comparison, the probability weights assigned to the values for the reduction factor are: 0.3 % (0.04), 2.1 % (0.48), and 3.9 % (0.48) (Figure DFS-18).

Relative Weights Assigned to Techniques for Estimating Slip Rate. Quaternary slip rates based on paleoseismic data are not available for all the test calculation sites. Therefore, the relative weights assigned to the four techniques described above are dependent on the availability of paleoseismic data (Figure DFS-18). Slip rates based on the amount of displacement and ages of faulted Quaternary units provide the most reliable indication of the current slip rate and are given the greatest weight (0.7) if these data are available. There is not a strong consensus among geologists as to which of the three models for the late Cenozoic evolution of faulting at Yucca Mountain is most likely. Therefore, the three slip rate models based on the cumulative net slip of the Tiva Canyon Tuff are assigned equal weights.

5.2.4 Potential for Fault Rupture

The approaches described above are used to calculate the probability distribution for the Quaternary slip rate at each of the nine test calculation sites. Given the slip rate, the average interval between displacement events can be calculated by dividing the average displacement per event by the slip rate. Alternatively, the average displacement per event can be calculated by multiplying the slip rate times the average recurrence interval. Both methods are given equal weight in the fault displacement hazard analysis (Figure DFS-15).

Site-specific assessments of the average displacement per event and the average recurrence interval are made for each of the faults at the nine test calculation sites based on the available information (Table DFS-11). To the extent possible, these assessments are based on fault specific data on the size and timing of Quaternary faulting events. Where there are no data on the size and/or timing of Quaternary displacements (e.g., due to the absence of evidence of displacement, or due to the lack of suitable Quaternary strata), the displacement per event and recurrence interval are characterized based on analogy to similar faults.

#1 Bow Ridge Fault

Average Displacement Per Event. C.M. Menges and J.W. Whitney (USGS, written communication, 1996b, Table 4.4.3) report a maximum range of from 1 to 80 cm for the net slip associated with past surface faulting events on the Bow Ridge fault at Trench 14D, which is at the same latitude as the ESF-Bow Ridge fault crossing. If 80 cm is taken as the upperbound displacement, this suggests an average slip per event of about 46 cm (i.e., 80 cm/1.73; see Table DFS-13).[1] Menges and Whitney's preferred values for individual events identified in this trench are: 13 cm, 14 cm, and 44 cm. If 44 cm represents the maximum displacement at this location, one would expect the average displacement to be about 25 cm (44 cm/1.73), which is close to the numerical average of their preferred values (i.e., 24 cm). Based on these observations, the range of values for the average slip per event where the Bow Ridge fault crosses the ESF is considered to be 10 cm (0.15); 20 cm (0.7); and 40 cm (0.15).

Average Recurrence Interval. C.M. Menges and J.W. Whitney (USGS, written communication, 1996b, Table 4.4.5) report a range of 70 ka to 215 ka for the average recurrence interval on the Bow Ridge fault at this location (Trench 14D). Their preferred range is between 100 ka and 140 ka. Based on these data, we considered the following range of values for the average slip rate: 70 ka (0.1); 100 ka (0.4); 140 ka (0.4); and 215 ka (0.1).

#2 Solitario Canyon Fault

Average Displacement Per Event. Site #2 is located on the Solitario Canyon fault approximately midway between trenches SCF-T4 and T8. The Quaternary fault displacement data reported by A.R. Ramelli *et al.* (Nevada Bureau of Mines and Geology, written communication, 1996, Table 4.7.3) indicate that the cumulative displacement and the average displacement per event increase to the south. Accordingly, one would expect the average displacement at site #2 to be greater than the values obtained at trench SCF-T4 and less than those at T8.

The values reported from trench SCF-T4 (A.R. Ramelli *et al.*, Nevada Bureau of Mines and Geology, written communication, 1996, Table 4.7.3) range from fractures having no movement up to 40 cm. If 40 cm is the maximum at this location, it suggests an average

[1] The relation between maximum and average displacement used here is based on analysis of the variability in the single event displacements observed in the Yucca Mountain trenches. (See Section 5.2.5 for details.)

displacement per event of about 23 cm (40 cm/1.73). The average displacement for the three most recent events is about 20 cm.

The maximum values reported from trench T-8 range from 10 cm to 130 cm. If 130 cm is the upperbound displacement for a single event at this location, it suggests an average displacement per event of $\leq$ 75 cm (i.e., 130 cm/1.73). Averaging the reported values from the four most recent events yields an average displacement per event of about 50 cm.

Extrapolating these data suggests the average displacement per event at site #2 probably is in the range of 35 to 45 cm. Because of the uncertainty inherent in such an extrapolation, a wider range of values is considered. The range of values considered in the fault displacement hazard analysis for the average displacement per event at site #2 on the Solitario Canyon fault is: 20 cm (0.2); 40 cm (0.6); and 60 cm (0.2).

Average Recurrence Interval. Based on the results of paleoseismic investigations, A.R. Ramelli *et al.*. (Nevada Bureau of Mines and Geology, written communication, 1996, p. 4.7-48) suggest that the minimum recurrence interval on the Solitario Canyon fault is about 35 ka and the maximum is about 100 ka. Based on the occurrence of three or four events during about the past 200 ka, they estimate that the average recurrence interval ranges from 50 to 70 ka. The values included in the fault displacement hazard analysis and the assigned probability weights are: 35 ka (0.2); 50 ka (0.3); 70 ka (0.3); and 100 ka (0.2).

#4 Ghost Dance Fault

Average Displacement Per Event. With the possible exception of fractures, there is no evidence of Quaternary movement on the Ghost Dance fault (E.M. Taylor *et al.*, USGS, written communication, 1996a). However, we assign a low probability that movement can occur in the future. Three approaches were used to characterize the possible average displacement per event.

(1) If the Ghost Dance fault is considered to be an independent seismogenic source, which is judged to be very unlikely (see Section 4.3.1), the Wells and Coppersmith (1984) relation between average displacement and fault rupture length can be used to calculate the average displacement along strike associated with rupture of the entire length of the fault. The data set of historical earthquakes

on which this relation is based is only marginally applicable to faults as short as the Ghost Dance fault, which has a mapped length of about 3 km (Day *et al.*, 1996b, p. 2-6). If the Ghost Dance fault is combined with the Abandoned Wash fault, the total fault length is about 9 km. Using this approach, rupture lengths of 3 to 9 km suggest a maximum value for the average displacement in the range of 8 to 22 cm.

(2) If displacement on the Ghost Dance fault occurs as secondary deformation in the hanging wall of either the Bow Ridge or Paintbrush Canyon faults, the maximum displacement on the Ghost Dance fault would be significantly less than the slip per event on either of these faults. Based on displacement per event data summarized by S.K. Pezzopane *et al.* (USGS, written communication, 1996a, Table 5-1), the average displacement per event on the Bow Ridge and Paintbrush Canyon faults (i.e., at about the same latitude as Test Calculation Site #4 on the Ghost Dance fault) is about 24 cm and 55 cm, respectively. If the secondary displacements scale in proportion to the cumulative bedrock displacement on these faults, the average slip per event on the Ghost Dance fault is about 5 cm (25m/130m x 24 cm per event for the Bow Ridge fault; or 25m/300m x 55 cm per event for the Paintbrush Canyon fault).

(3) Considering the Quaternary displacement history on the Ghost Dance fault to be similar to the small north-south intrablock faults in Midway Valley, suggests that Quaternary movements have been limited to fractures having slip amounts that are less than the threshold of detection. The threshold of detection on the fracturing events in Midway Valley ranges from a few millimeters or less (essentially zero displacement) to not more than 5 cm (F.H. Swan *et al.*, Geomatrix Consultants, written communication, 1995).

(4) Considering all three approaches, the range of values included in the hazard characterization for the average displacement per event at site #4 on the Ghost Dance fault is: 0.05 cm (almost zero displacement) (0.3); 1 cm (0.25); 3 cm (0.2); 5 cm (0.15); 10 cm (0.07); and 15 cm (0.03).

Average Recurrence Interval. The available data indicate there has been no displacement on the Ghost Dance fault for approximately the past 100 ka (no displacements since the late Pleistocene). If the Ghost Dance fault can move in the present tectonic regime, the recurrence interval is presumably longer than about 100 ka. In the context of neotectonic studies, average recurrence intervals longer than half a million years probably are not meaningful. Given the lack of any evidence suggesting a particular recurrence interval, we assumed that, if the fault can move, the average recurrence interval is essentially equally

likely to be anywhere in the range of 100 to 500 ka with a slight chance that the recurrence interval could be as short as 50 ka. The range of values included in the fault displacement hazard analysis and the assigned probability weights are: 50 (0.005); 100 ka (0.1); 200 ka (0.25); 300 ka (0.25); 400 ka (0.25); and 500 ka (0.145).

#3 Drill Hole Wash Fault and #5 Sundance Fault

No evidence of Quaternary displacement has been discovered along any of the northwest-striking faults in the Yucca Mountain area. If the faults are capable of movement in the present tectonic regime, the movement probably occurs in response to movement on the more active north-striking Quaternary faults. The average displacement per event is certainly less than that along the north-south block-bounding faults and probably is less than the Ghost Dance fault. For the purpose of the fault displacement hazard analysis, the same displacement and recurrence parameters used to characterize the average displacement per event and average recurrence interval on the Ghost Dance fault also were used to characterize the Drill Hole Wash and Sundance faults.

#6 Unnamed Fault West of Dune Wash

There are no data on the Quaternary displacement history of this fault. Its orientation and location within the Yucca Mountain block are similar to the Ghost Dance fault, but it has a shorter total fault length and smaller cumulative displacement. Except for the difference in slip rate, site #6 is considered to have a potential for displacement that is similar to that of site #4 on the Ghost Dance fault (Table DFS-8). The same parameters used to characterize the average displacement per event and average recurrence interval on the Ghost Dance fault also were used to characterize the unnamed fault at Test Calculation Site #6.

Test Calculation Sites #7a, #7b, #8a, and #8b

The fault displacement hazard at these sites was treated the same except that sites #7b and #8b have lower slip rates due to their smaller cumulative displacement (10 cm versus 2 m), and site #7 is assigned a higher potential for activity (Table DFS-8) than site #8 because it is closer to an active block-bounding fault (Section 5.2.1).

Average Displacement Per Event. If movement can occur on these small intrablock faults, the average displacement per event would be less than or similar to that of Exile Hill fault

(see below). The same range of values included in the analysis for the Exile Hill fault is used to characterize the 2-m faults. In characterizing the 10-cm faults, the range is extended to include a minimum value of 0.05 cm and more weight is assigned to the low end of the range (Table DFS-11).

Average Recurrence Interval. There are no data that suggest how these short, small-displacement faults and shears behave during repeated faulting events. Therefore, a wide range of behavior is considered. If these features are capable of movement, the minimum recurrence is a single event during the present tectonic regime. For the purpose of this analysis, the period of the present tectonic regime is considered to be the Quaternary, or approximately the past 1.6 ma. The maximum recurrence rate would occur if minute displacements occurred every time there is a large-magnitude local earthquake in the immediate vicinity (e.g., on the block-bounding faults). The results of paleoseismic investigations (USGS, written communication, 1996) suggest that surface faulting events on the block-bounding faults might occur as frequently as about once every 50,000 years. This is judged to be an upper bound for the average recurrence interval for events large enough to produce secondary displacement within the Yucca Mountain block. Given the lack of evidence for a particular recurrence interval, we judge that the average recurrence interval is more or less equally likely to be anywhere in the range of 100 to 500 ka (the same as for the Ghost Dance fault) and that there is a small chance that the recurrence interval could be as long as 1.6 ma or as short as 50 ka. The range of values included in the fault displacement hazard analysis and the assigned probability weights are: 50 ka (0.05); 100 ka (0.18); 200 ka (0.18); 300 ka (0.18); 400 ka (0.18); 500 ka (0.18); and 1600 ka (0.05).

#9 Exile Hill Fault in Midway Valley

Average Displacement Per Event. Except for two zones of fractures identified in trenches, the evidence indicates that there has been no Quaternary displacement (within the limits of detection) on the Exile Hill fault in Midway Valley (F.H. Swan *et al.*, Geomatrix Consultants, written communication, 1995; W.R. Keefer and J.W. Whitney, USGS, written communication, 1996). Considering the resolution for detecting displacements, some small displacement can not be ruled out. Three approaches were used to characterize the average displacement per event.

1. The total length of the Exile Hill fault is between < 2 km and 4.4 km. Using these values and the Wells and Coppersmith (1984) relation between average displacement and fault rupture length, we obtained displacements of < 5 cm to 11 cm.

2. If the Exile Hill fault represents secondary deformation in the footwall of the Bow Ridge fault or in the hanging wall of the Paintbrush Canyon fault, the maximum displacement on the Exile Hill fault would be significantly less than the slip per event on either of these faults. Based on displacement per event data summarized by S.K. Pezzopane *et al.* (USGS, written communication, 1996a, Table 5-1), the average displacement per event on the Bow Ridge and Paintbrush Canyon faults is about 24 cm and 55 cm, respectively. Scaling the secondary displacements in proportion to the cumulative bedrock displacement on these faults, suggests the average slip per event on the Exile Hill fault is about 2 cm (10m/130m x 24 cm per event for the Bow Ridge fault, or 10m/300m x 55 cm per event for the Paintbrush Canyon fault).

3. The results of the fault exploration trenches on the east side of Exile Hill indicate that the Quaternary displacements have been less than the threshold of detection. The threshold of detection on the fracturing events in Midway Valley ranges from a few millimeters or less (essentially zero displacement) to not more than 5 cm (F.H. Swan *et al.*, Geomatrix Consultants, written communication, 1995).

Considering these approaches, the range of values included in the hazard analysis for the average displacement per event at site #9 on the Exile Hill fault is: 0.05 cm (almost zero displacement) (0.35); 1 cm (0.3); 3 cm (0.2); 5 cm (0.1); and 10 cm (0.05).

Average Recurrence Interval. The data indicate there has been no detectable displacement on the Exile Hill fault since the Middle Pleistocene or longer. Given the lack of evidence suggesting a particular recurrence interval, we consider that, if the fault can move, the average recurrence interval is more or less equally likely (i.e., maximum uncertainty) to be anywhere in the range of 100 to 500 ka. The range of values included in the fault displacement hazard analysis and the assigned probability weights are: 100 ka (0.1); 200 ka (0.25); 300 ka (0.25); 400 ka (0.25); and 500 ka (0.15).

5.2.5 Event-to-Event Variability

The procedures described above provide a means for assessing the probability of average displacements at a specified fault crossing. It is also important to know how much

displacements are likely to vary from the average displacement. The event displacement data from Yucca Mountain paleoseismic investigations were compiled to assess: (1) the relationship between average displacement and the maximum displacement during successive events at a point along the fault; and (2) the variability in the amount of displacement during successive events at a point along the fault (not to be confused with the variability in displacement along strike during a single event).

S.K. Pezzopane *et al.* (USGS, written communication, 1996a, Table 5-1) compiled the event displacement data from the Yucca Mountain paleoseismic investigations. Table DFS-12 is a summary of the event displacement data for all localities where displacements for three or more events were reported. The average of the reported events is calculated for each locality. The ratio between the size of each event and the average displacement at that locality is also calculated. The maximum reported displacement at each locality ranges from 1.03 to 2.63 times the average displacement; on average (based on 19 localities), the maximum displacement is 1.73 times the average displacement (Table DFS-13).

Figure DFS-19 is a frequency plot showing event-to-event variability in displacement based on the displacement data (ratio of the reported displacement for an event, D, to the average displacement at the same location, AD) presented on Table DFS-12. A generalization of this frequency distribution (i.e., the dashed line on Figure DFS-19) was used to define a triangular distribution for the ratio D/AD. The Facilities Team analyzed the data in Table DFS-12 and found that a better fit is obtained with a gamma distribution (see Appendix H, Section H.2.1). We adopt the distribution given in Appendix H for characterizing the distribution of displacement at a point.

5.3 POTENTIAL FOR DISPLACEMENT ON FRACTURES AND UNBROKEN ROCK

Fractures and unbroken rock have no cumulative displacement and, therefore, no slip rate. Consequently, the slip-rate approach used above to assess the potential for displacement on faults must be modified to assess the potential for displacement on fractures or in unbroken rock. The approach adopted for this analysis is based on the premise that, given the non-

occurrence of an event and a long observation period, the annual probability of the event occurring must be less than 1 divided by the duration of the observation period.

The logic tree for characterizing the displacement hazard on fractures and unbroken rock is presented in Figure DFS-20. The elements considered in assessing displacement hazard at Test Calculation Sites #7c, #7d, #8c, and #8d include:

- the potential for activity,
- relative probabilities associated with the different deformation history models,
- age of the host rock, and
- constraints on the size of an event based on the threshold of detection for fault displacement.

Uncertainties in the age of the host rock were discussed in Section 5.2.2. The other elements are discussed below.

5.3.1 Potential for Activity

If one applies the definition of activity as used to characterize faults (Section 5.2.1), fractures and unbroken rock would be classified as not active (i.e., they have had no displacement during the present tectonic regime), which implies that they have no potential for displacement during future periods of concern for repository performance. From a practical standpoint, this is true. Experience based on observations of historical surface faulting events and on detailed paleoseismic investigations of Quaternary fault movements shows that future fault movements can best be defined by recent past history and that the likelihood of new faulting is negligible (ASCE, 1997, p. 99). However, new faults must form some time. In the context of assessing fault displacement at locations where there has been no detectable displacement, the concept of activity, or potential for activity, is used to mean the relative likelihood that there could be displacement in the future. It is a relative approach whereby faults having known recent displacements would be assigned the highest weight (probability of 1), and intact rock far from active faults would have the lowest potential for activity (at least two or three orders of magnitude less likely). The factors for evaluating fault activity described in Section 5.2.1 were considered in our assessment of the potential for activity on fractures and in unbroken rock. In addition, information on the morphology of the fracture itself, such as degassing tracks that indicate formation during lithification of the tuff, may

provide clues to the origin and potential activity of a fracture. Table DFS-14 gives the subjective probability weights for potential for activity assigned to fractures and unbroken rock at Test Calculation Sites #7 and #8 and describes the basis for the assigned weights.

5.3.2 Probability of an Event Associated with Different Deformation History Models

In Section 5.2.3, three models were presented for characterizing the deformation history at Yucca Mountain. In one model, the rate of deformation has been uniform since deposition of the Tiva Canyon Tuff. In this interpretation, the annual probability of a displacement event, given no prior displacement, is less than 1 over the age of the host rock, which at the repository level is the Tiva Canyon Tuff. This corresponds to an annual probability of $<1x10^{-7}$ (Table DFS-15).

In the other two models, the present rate of deformation is significantly less than the average long-term (post-Tiva Canyon Tuff) rate. If other factors such as the stress field have remained the same, the potential for deformation (movement on existing faults and/or formation of new faults) should be less now than they were during the late Miocene, when the rate is interpreted to have been much higher.

Considering the potential for displacement to be directly proportional to the rate of deformation, the probability of an event relative to the uniform deformation model can be expressed as the ratio between the inferred present rate and the average long-term post-Tiva Canyon rate times the probability of an event for the uniform deformation model. The range of probability values for the different deformation history models is given in Table DFS-15.

As discussed in Section 5.2.3, the three deformation history models are assigned equal weight (Figure DFS-20).

5.3.3 Threshold of Detection

Where there is no apparent displacement, it could be assumed that there has been a displacement too small to be detected. The size of the displacement is constrained by (less than) the threshold of detection. What is, the largest displacement that could have occurred at the location under consideration that could have gone undetected?

The threshold of detection depends on location-specific conditions. Are there sharp, well-defined marker horizons that record/preclude offsets? Is the rock massive or extensively fractured and/or sheared? What is the quality of the exposure? How extensive and detailed were the investigations to detect offsets? For the purpose of this analysis, we infer that the conditions would be typical of those parts of the ESF where the Tiva Canyon Tuff is well exposed and has been mapped in detail. Conditions may vary locally.

Investigations can more confidently preclude small displacements in unbroken rock than along a fracture. Therefore, the threshold of displacement detection is conditional on whether the rock is fractured or unbroken (Figure DFS-20).

Given the characteristics of the Tiva Canyon Tuff, we consider offsets larger than about 10 cm to be recognizable as observable stratigraphic offsets. Displacements smaller than a millimeter would be difficult to preclude, but smaller displacements obviously can occur; nominally we selected half a millimeter as the lower bound displacement. 10 cm and 0.05 cm were taken as the end members for the displacements on fractures. More commonly displacements in the range of 1 to 5 cm can be precluded. The range of values and assigned weights included in the fault displacement hazard analysis for the threshold of detection on well exposed fractures in the Tiva Canyon Tuff are: 0.05 cm (0.145); 0.1 cm, (0.2); 0.5 cm, (0.3); 1.0 cm, (0.2); 3 cm, (0.1); 5 cm, (0.05); and 10 cm, (0.005). The range of values for unbroken rock are: 0.05 cm (0.195); 0.1 cm, (0.3); 0.5 cm (0.25); 1.0 cm, (0.1); 3 cm, (0.1); 5 cm, (0.05); and 10 cm (0.005).

5.4 ESTIMATION OF FAULT DISPLACEMENT

The approach and hazard parameters described above are used to quantitatively assess the probability of fault displacement (hazard curves that relate annual probability to amount of displacement) for the nine test calculations sites. Because the approach used to characterize the hazard on faults is different from the approach used for fractures and unbroken rock, caution should be used when comparing or combining the results. If the input parameters and their uncertainties have been appropriately characterized, the slip-rate based approach used to assess the potential for displacement on faults should yield a realistic assessment of the actual hazard. However, the approach used to assess the displacement hazard on fractures or in

unbroken rock only constrains the upper bound for the hazard; it does not necessarily define the actual hazard. The actual hazard is likely to be less than the resultant values. The threshold of detection parameter gives maximum displacement values and the age of the host rock gives the minimum period for the non-occurrence of an event. The potential for activity parameter may compensate for the conservatism that is inherent in the other parameters, but we suspect the probability of future displacement may be much lower than indicated. This parameter is largely subjective and we have probably been overly conservative in assigning probability weights to potential for activity on fractures and in unbroken rock. Despite these limitations, we feel the results are useful because they indicate the hazard is extremely low.

The nine Test Calculation Sites that were selected to represent the range of conditions expected within the control area. Application of the evaluations of these sites to other parts of the control area is straightforward. However, one important substitution may need to be made depending on the application. Here we have used the displacement data that are location-specific to characterize the potential for displacement at that location. To characterize the potential for fault displacement along the length of a fault, one should use the average post-Tiva Canyon Tuff displacement (or average Quaternary slip rate) along the plane of the fault that intersects the Control Area instead of the average displacement at a specific location along the fault.

6.0
REFERENCES

American Society of Civil Engineers (ASCE), 1997, Seismic and dynamic analysis and design considerations for high level nuclear waste repositories: A report by the Subcommittee on Dynamic Analysis and Design of High Level Nuclear Waste Repositories of the TA Committee on Dynamic Effects of the Technical Activities Division of the Structural Engineering Institute , J. Carl Stepp, ed., ASCE, New York, 185 pp., plus Appendices A through F.

Anderson, R.E., Bucknam, R.C., Crone, A.J., Haller, K.M., Machette, M.N., Personius, S.F., Barnhard, T.P., Cecil, M.J., and Dart, R.L., 1995b, Characterization of Quaternary and suspected Quaternary faults, regional studies, Nevada and California: U.S. Geological Survey Open-File Report 95-599.

Anderson, R.E., Crone, A.J., Machette, M.N., Bradley, L., and Diehl, S.F., 1995a, Characterization of Quaternary and suspected Quaternary faults, Amargosa area, Nevada and California: U.S. Geological Survey Open-File Report 95-613, 41 p.

Atwater, T., 1989, Plate tectonic history of the northeast Pacific and western North America: Geological Society of America, The Geology of North America, v. N, p. 21-72.

Bellier, O., and Zoback, M.L., 1995, Recent state of stress in the Walker Lane zone, western Basin and Range provinces, United States: Tectonics, v. 14, n. 3, p. 564-593.

Bonilla, M.G., Mark, R.K., and Lienkaemper, J.J., 1984, Statistical relations among earthquake magnitude, surface rupture length, and surface fault displacement: Bulletin Seismological Society of America, v. 74, p. 2379-2411.

Brocher, T. M., Hart, P. E., Hunter, W. C., and Langenheim, V. E., 1996, Hybrid-source seismic reflection profiling across Yucca Mountain, Nevada: regional lines 2 and 3: U. S. Geological Survey Open-File Report 96-28.

Broxton, D.E., Warren, R.G., Byers, F.M., Jr., and Scott, R.B., 1989, Chemical and mineralogical trends within Timber Mountain-Oasis Valley caldera complex, Nevada: Evidence for multiple cycles of chemical evolution in a long-lived silicic magma system: Journal of Geophysical Research, v. 94, n. B5, p. 5961-5986.

Burchfiel, B.C., Hamill, G.S., IV, and Wilhelms, D.E., 1983, Structural geology of the Montgomery Mountains and the northern half of the Nopah and Resting Springs ranges, Nevada and California: Geological Society of America Bulletin, v. 94, p. 1359-1376.

Carr, W. J., Byers, F: M., Jr., and Orkild, P.P., 1986, Stratigraphic and volcano-tectonic relations of Crater Flat Tuff and some older volcanic units, Nye County, Nevada: U. S. Geological Survey Open-File Report 82-457, 23 p.

Cornell, C.A., and Wintestein, S.R., 1986, Seismic hazard assessment: Chapter 5, in Hunter, R.L., and Mann, C.J., eds., Techniques for Determining Probabilities of Events and Processes Affecting the Performance of Geologic Repositories: NUREG/CR-3964, 1, P. 127-172, U.S. Nuclear Regulatory Commission, Washington, D.C.

Cornwall, H.R., 1972, Geology and mineral deposits of southern Nye County, Nevada: Nevada Bureau of Mines and Geology Bulletin 77, 49 p., 1 plate.

de Polo, C.M., and Slemmons, B.D., 1990, Estimation of earthquake size for seismic hazards, *in* Krimitzsky, E.L. and Slemmons, B.D. eds., Neotectonics in Earthquake Evaluation: Reviews in Engineering Geology, v. VII, Chapter 1, Boulder, CO, Geological Society of America.

Dohrenwend, J.C., Menges, C.M., Schell, B.A., and Morning, B.C., 1991, Reconnaissance photogeologic map of young faults in the Las Vegas 1o X 2o quadrangle, Nevada, California, and Arizona: U.S. Geological Survey Miscellaneous Field Studies map MF-2182, scale 1:250,000.

Ekren, E.B., Orkild, P.P., Sargent, K.A., and Dixon, G.L., 1977, Geologic map of the Tertiary rocks, Lincoln County, Nevada: U.S. Geological Survey Miscellaneous Investigations Series Map I-1041, scale 1:250,000.

Faulds, J. E., Bell., J. W., Feuerbach, and Ramelli, A. R., 1994, Geologic map of the Crater Flat area, Nye County, Nevada: Nevada Bureau of Mines and Geology Map 101, 1:24,000 scale.

Ferrill, D.A., Stirewalt, G.L., Henderson, D.B., Stamatakos, J.A., Morris, A.P., Spivey, K.H.C., and Wernicke, B.P.C., 1996, Faulting in the Yucca Mountain region: Critical review and analyses of tectonic data from the central Basin and Range: Center for Nuclear Waste Regulatory Analyses Report CNWRA 96-007 or NUREG/CR-6401, San Antonio, Texas, Rev. 01, variously paginated.

Frankel, A., Mueller, C., Barnhard, T., Perkins, D., Leyendecker, E.V., Dickman, N., Hanson, S., and Hopper, M., 1996, National seismic-hazard maps; documentation June: U.S. Geological Survey Open-File Report 96-532, 110 p.

Fredrich, C.J., 1997, Tectonic evolution of the Crater Flat basin, Yucca Montain region, Nevada, in Wright, L.A. and Troxel B. W. (eds.), Cenozoic Basins of the Death Valley Region, California and Nevada: Geological Society of America Special Paper (in press).

Fridrich, C. J., Whitney, J. W., Hudson, M. R., and Crowe, B. M., 1997, Space-time patterns of late Cenozoic extension, vertical-axis rotation, and volcanism in the Crater Flat basin, Nevada, in Wright, L. A. and Troxel B. W. (eds.) Cenozoic Basins of the Death Valley Region, California and Nevada: Geological Society of America Special Paper (in press).

Frizzel, V.A., Jr., and Schulters, J., 1990, Geologic map of the Nevada Test Site, southern Nevada: U.S. Geological Survey Miscellaneous Investigations Series Map I-2046, scale 1:100,000.

Gibson, J.D., Shephard, L.E., Swan, F.H., Wesling, J.R., and Kerl, F.A., 1990, Synthesis of studies for potential for fault rupture at the proposed surface facilities, Yucca Mountain, Nevada: Proceedings of International Topical Meeting, High Level Radioactive Waste Management, April 8-12, v. 1, p. 109-116.

Gutenberg, B., and Richter, C.F., 1954, Seismicity of the Earth: Princeton University Press, 2nd edition.

Harmsen, S. C., 1994, The Little Skull Mountain earthquake of 29 June, 1992: Aftershock focal mechanisms and tectonic stress field implications: Bulletin of Seismological Society of America, v. 84, n. 5, p. 1484-1505.

Jenkins, O.P., 1962, Geologic map of California, Trona Sheet: California Division of Mines and Geology, scale 1:250,000.

Keefer, W.R., and Pezzopane, S.K., 1996, Quaternary faults in the Yucca Mountain region: Chapter 3, in U.S. Geological Survey (Whitney, J.W., Coordinator), Seismotectonic Framework and Characterization of Faulting at Yucca Mountain, Nevada: U.S. Geological Survey report to the Department of Energy that fulfills Level 3 Milestone 3GSH100M WBS Number 1.2.3.2.8.3.6, variously paginated.

Longwell, C.R., Pampeyan, E.H., Bowyer, B., and Roberts, R.J., 1965, Geology and mineral deposits of Clark County, Nevada: Nevada Bureau of Mines and Geology Bulletin 62, 218 p., 16 plates.

Minor, S. A., Hudson, M. R., and Fridrich, C. J., 1996, Fault-slip data bearing on the tectonic development of northern Crater Flat basin, southern Nevada [abs.]: Geological Society of America Abstracts with Programs, v. 28, no. 7., p. A192.

Oldow, J.S., Bally, A.W., Av'e Lallmont, H.G., and Leeman, W.P., 1989, Phanuajoic evolution of the North American Cordillera—United States and Canada: Chapter 8 in the geology of North America: Geological Society of America, v. A., p. 139-232.

Piety, L.A., 1993, Compilation of known and suspected Quaternary faults within 100 km of Yucca Mountain: U.S. Geological Survey Open-File Report 94-112, 404 p., 2 plates.

Piety, L.A., 1995, Compilation of known and suspected Quaternary faults within 100 km of Yucca Mountain: Technical Report prepared by U.S. Bureau of Reclamation in cooperation with the Nevada Operations Office, U.S. Department of Energy under Interagency Agreement DE-A108-92NV10874; U.S. Geological Survey Open-File Report 94-112.

Reheis, M.C., 1988, Preliminary study of Quaternary faulting on the east side of Bare Mountain, Nye County, Nevada, in Carr, M.D., and Yount, J.C., eds., Geologic and hydrologic investigations of a potential nuclear waste disposal site at Yucca Mountain, southern Nevada: U.S. Geological Survey Bulletin 1790, p. 103-111.

Saltus, R. W., and Thompson, G. A., 1996, Why is it downhill from Tonopah to Las Vegas: A case for mantle plume support of the high northern Basin and Range: Tectonics, v. 14, n. 6, p. 1235-1244.

Sawyer, D.A., Fleck, R.J., Lanphere, M.A., Warren, R.G., Broxton, D.E., and Hudson, M.R., 1994, Episodic caldera volcanism in the Miocene southwest Nevada volcanic field: Revised stratigraphic framework, 40Ar/39Ar geochronalogic framework, and implications for magmatism and extension: Geologic Society of America Bulletin, v. 106, n. 10, p. 1304-1318.

Scholz, C.H., Barazangi, M., and Sbar, M.L., 1971, Late Cenozoic evolution of the Great Basin, western United States, as an ensialic interarc basin: Geological Society of America Bulletin, v. 82, p. 2979-2990.

Schweickert, R. A., 1989, Evidence for a concealed strike-slip fault beneath Crater Flat, Nevada: Geological Society of America Abstracts with Programs, v. 21, n. 9, p. A90.

Scott, R. B., 1990, Tectonic setting of Yucca Mountain, southwest Nevada, in Wernicke, B. P., ed., Basin and Range tectonics at the latitude of Las Vegas, Nevada: Geological Society of America Memoir 176, p. 251-282.

Scott, R.B., and Bonk, J., 1984, Preliminary geologic map of Yucca Mountain, with geologic sections: U.S. Geological Survey Open-File Report 84-494, scale 1:12,000.

Simonds, F.W., Whitney, J.W., Fox, K.F., Ramelli, A.R., Yount, J.C., Carr, M.D., Menges, C.M., Dickerson, R.P., and Scott, R.B., 1995, Map showing fault activity in the Yucca Mountain area, Nye County, Nevada: U.S. Geological Survey Miscellaneous Investigations Series, Map I-2520, scale 1:24,000.

Slemmons, D.B., 1997, Faults and earthquake magnitude, *in* State of the art for assessing earthquake hazards in the United States, Report 6: U.S. Army Engineers Waterways Experiment Station Miscellaneous Paper S-73-1, 129 p.

Slemmons, 1982, Determination of design earthquake magnitudes for microzonation, in Proceedings, Third International Earthquake Microzonation Conference, Seattle, Washington: Earthquake Engineering Research Institute, v. 1, p. 110-130.

Smith, K.D., Brune, J.N., Savage, M.K., Anooshehpoor, R., dePolo, D, and Sheehan, A.F., 1996, The 1992 Little Skull Mountain earthquake sequence, Southern Nevada Test Site: Bulletin of the Seismological Society of America (in press).

Smith, R. L., and Bailey, R. A., 1968, Resurgent cauldrons: Geological Society of America Memoir 116, p. 613-662.

Snyder, D. B., and Carr, W J., 1984, Interpretation of gravity in a complex volcano-tectonic setting, southwestern Nevada: U. S. Geological Survey Open-File Report 81-1349, 50 p.

Stepp, C., Whitney, J., Wong, I.G., Savy, J., Coppersmith, K., Abrahamson, N., Quittmeyer, R., and Sullivan, T., 1995, A probabilistic analysis of fault displacement and vibratory ground motion and the development of seismic design criteria for Yucca Mountain, Nevada, in Topical Meeting on Methods of Seismic Hazards Evaluation Focus '95: Las Vegas, Nevada, American Nuclear Society, p. 35-42.

Stewart, J.H., 1988, Tectonics of the Walker Lane belt, western Great Basin-Mesozoic and Tertiary deformation in a zone of shear, in Ernst, W.G., ed., Metamorphism and crustal evolution of the western United States, Rubey Volume VII: Englewood Cliffs, New Jersey, Prentice Hall, p. 683-713.

Streitz, R., and Stinson, M.C., 1974, Geologic map of California, Death Valley Sheet: California Division of Mines and Geology, scale 1:250,000.

Swadley, W.C., and Huckins, H.E., 1990, Geologic map of the surficial deposits of the Skull Mountain quadrangle, Nye County, Nevada: U.S. Geological Survey Miscellaneous Investigations Series Map I [1972], scale 1:24,000.

Veneziano, D., and Van Dyck, J., 1985, Statistical discrimination of "aftershocks" and their contribution to seismic hazard, in Seismic Hazard Methodology for Nuclear Facilities in the Eastern United States: EPRI Res. Project No. P101-29, EPRI/SOG 85-1, v. 2, Appendix A-4.

Wells, D.L., and Coppersmith, K.J., 1994, New empirical relationships among magnitude, rupture length, rupture width, rupture area, and surface displacement: Bulletin of the Seismological Society of America, v. 84, p. 974-1002.

Wernicke, B., 1995, Low-angle normal faults and seismicity—A review: Journal of Geophysical Research, v. 10, p. 201,159-20,174.

Wesling, J.R., Swan, F.H., Thomas, A.P., and Angell, M.M., 1993, Preliminary results of trench mapping at the site of prospective surface facilities for the potential Yucca Mountain repository, Nevada [abs.]: Geological Society of America, Abstracts with Programs, v. 25, n. 5, p. 162.

Wesnousky, S.G., 1986, Earthquakes, Quaternary faults, and seismic hazard in California: Journal Geophysical Research, v. 91, p. 12,587-12,631.

Wright, L. A., 1989, Overview of the role of strike-slip and normal faulting in the Neogene history of the region northeast of Death Valley, California-Nevada, in, Ellis, M. A., ed., Late Tertiary evolution of the southern Great Basin, Nevada: Nevada Bureau of Mines and Geology Open-File Report 89-1, p. 1-11.

Wyss, M., 1979, Estimating maximum expectable magnitude of earthquakes from fault dimensions: Geology, v. 7, p. 336-340.

Young, S.R., Morris, A.P., and Stirewalt, G., 1993, Geometric analysis of alternative models of faulting at Yucca Mountain, Nevada, in High level radioactive waste management: Proceedings of the Fourth Annual International Conference, Las Vegas, Nevada, American Nuclear Society, La Grange Park, Illinois, v. 2, p. 1,818-1,825.

Youngs, R.R., and Coppersmith, K.J., 1985, Implications of fault slip rates and earthquake recurrence models to probabilistic seismic hazard estimates: Seismological Society of America Bulletin, v. 75, p. 939-964.

Youngs, R.R., Swan, F.H., III, Power, M.S., Schwartz, D.P., and Green, R.K., 1987, Probabilistic analysis of earthquake and ground shaking hazard along the Wasatch Front, Utah, in Gori, P.O., and Hays, W.W., eds., Assessment of Regional Earthquake Hazards and Risk Along the Wasatch Front, Utah: U.S. Geological Survey Open File Report 87-585, p. M-1 to M-100.

TABLE DSF-1
SEISMIC SOURCE PARAMETERS FOR REGIONAL FAULT SOURCES
(Page 1 of 2)

Fault (Designation on Fig. DSF-6)	Activity	Length (km)	Dip	Slip Rate (mm/yr)			Maximum Magnitude
				Preferred	Maximum	Minimum	
1 Hunter Mt./Panamint (HM-PAN)	1	146 [1]	90	2.5 [.6]	3.2 [.2]	1.1 [.2]	7.0 7.4 7.6 [.2] [.6] [.2]
2 Furnace Creek/Fish Lake Valley (FC-FLV)	1	149 [1]	90	2.3 [.6]	4.6 [.2]	1.3 [.2]	7.0 7.3 7.6 [.2] [.6] [.2]
3 Death Valley (DV)	1	71 [1]	60W	2.5 [.6]	11.5 [.2]	0.08 [.2]	7.0 7.2 7.5 [.2] [.6] [.2]
4 Pahrump/Stewart Valley (PRP)	1	41 [1]	90		0.05 [.5]	0.005 [.5]	6.6 7.0 [.5] [.5]
5 West Springs Mt. (WSM)	1	AB-29 km [.5]	60W	0.06 [.6]	0.2 [.2]	0.02 [.2]	6.6 6.8 7.0 [.2] [.6] [.2]
		AC-51 km [.5]		"	"	"	6.7 7.0 7.3 [.2] [.6] [.2]
6 West Pintwater Range (WPR)	1	55 [1]	60W		0.2 [.5]	0.02 [.5]	6.7 7.0 7.3 [.2] [.6] [.2]
7 Yucca (YC)	1	25 [1]	60E		0.2 [.5]	0.02 [.5]	6.5 6.7 7.0 [.2] [.6] [.2]
8 Emigrant Valley North (?) (EVN)	1	27 [1]	60W		0.2 [.5]	0.02 [.5]	6.5 6.7 7.0 [.2] [.6] [.2]
9 Oaks Spring Butte (OAK)	1	22 [1]	60E		0.2 [.5]	0.01 [.5]	6.5 6.7 7.0 [.2] [.6] [.2]
10 Belted Range (BLR)	1	50 [1]	60E		0.1 [.5]	0.01 [.5]	6.5 6.8 7.1 [.2] [.6] [.2]
11 Kawitch Range (KR)	1	AB-24 km [0.68]	60W		0.01 [.5]	0,001 [.5]	6.5 6.7 7.0 [.2] [.6] [.2]
		BC-33 km [0.1]			"	"	6.5 6.8 7.1 [.2] [.6] [.2]
		AD-65 km [0.2]			"	"	6.9 7.2 7.5 [.2] [.6] [.2]
		CD-74 km [0.02]			"	"	6.9 7.2 7.5 [.2] [.6] [.2]
12 Rock Valley (RV)	1	AB-33 km [.6]	90		0.16 [.5]	0.02 [.5]	6.5 6.8 7.1 [.2] [.6] [.2]
		AC-47 km [.3]			"	"	6.7 7.0 7.3 [.2] [.6] [.2]
		AD-64 km [.1]			"	"	6.9 7.2 7.5 [.2] [.6] [.2]
13 Wahmonie (WAH)	1	15 [1]	60NW		0.01 [.5]	0.001 [.5]	6.5 6.8 [.8] -- [.2]

TABLE DSF-1
SEISMIC SOURCE PARAMETERS FOR REGIONAL FAULT SOURCES
(Page 2 of 2)

Fault (Designation on Fig. DSF-6)	Activity	Length (km)	Dip	Slip Rate (mm/yr)			Maximum Magnitude
				Preferred	Maximum	Minimum	
14 Yucca Lake (YCL)	1	13 [1]	60NE		0.2 [.5]	0.02 [.5]	6.5 6.8 [.8] -- [.2]
15 Eleana Range (ER)	1	11 [1]	60NE		0.2 [.5]	0.02 [.5]	6.5 6.8 [.8] -- [.2]
16 Peace Camp (PC)	1	AB-19 km [.7] AC-31 km [.3]	90		0.16 [.5] "	0.02 [.5] "	6.5 6.6 6.9 [.2] [.6] [.2] 6.5 6.8 7.1 [.2] [.6] [.2]
17 Amargosa/Gravity (Ash Meadows (AM)	1	AB-27 km [0.56] BC-43 km [0.2] AD-34 km [0.2] DC-51 km [0.04]	60W	0.04 [.6] " " "	0.1 [.2] " " "	0.01 [.2] " " "	6.5 6.7 7.0 [.2] [.6] [.2] 6.7 7.0 7.3 [.2] [.6] [.2] 6.6 6.9 7.2 [.2] [.6] [.2] 6.8 7.1 7.4 [.2] [.6] [.2]
18 Bare Mountain (BM)	1	AB-16 km [.3] AC-22 km [.7]	60E	0.1 0.05 [.4] [.4] "	0.28 [.1] "	0.01 [.1] "	6.5 6.8 [.8] -- [.2] 6.5 6.7 7.0 [.2] [.6] [.2]
19 Highway 95 (H95)	0.1	AB-11 km [.5] AC-27 km [.5]	90	0.03 [.4] "	0.05 [.3] "	0.01 [.3] "	6.8 6.5 [.3] -- [.7] 7.0 6.7 6.5 [.2] [.6] [.2]

MAXIMUM DEPTH OF FAULTING = 12 km, [.6]; 14 km, [.3], 16 km, [.1]

s:\yuccamtn\dfs-t1.xls

TABLE DFS-2
TOTAL FAULT LENGTHS FOR LOCAL FAULT SOURCES ASSUMING INDEPENDENT FAULT BEHAVIOR

FAULT (Map Designation, Fig. DFS-8)	Alternative Lengths (Figure DFS-8)	Total Fault Length (km)	Probability
Paintbrush Canyon/Stagecoach Road (PBC)	BE	19.4	(0.68)
	AE	20.9	(0.2)
	BF	26.9	(0.1)
	AF	28.4	(0.02)
Bow Ridge (BWR)	KH	7.6	(0.8)
	GK	10.3	(0.2)
Solitario Canyon (SC)	LM	16.5	(0.7)
	LN	20.6	(0.3)
Windy Wash/Fatigue Wash (WWF)	PR	22.3	(0.57)
	OR	23.8	(0.3)
	PS	25.8	(0.1)
	OS	27.3	(0.03)
Northern Crater Flat (NCF)	LU	6.5	(1)
Southern Crater Flat (SCF)	VX	8.1	(1)
Ghost Dance (GD)	YZ	3.0	(0.3)
	YY-ZZ	9.0	(0.7)

TABLE DFS-3
TOTAL FAULT LENGTHS FOR LOCAL FAULT SOURCES ASSUMING DISTRIBUTIVE FAULT BEHAVIOR

RUPTURE SCENARIO [1]	TOTAL LENGTH	PROBABILITY
Scenario A = BE + HK + LN + PR	69.9 km	(0.2)
Scenario B = AF + GK +LN + OS	86.6 km	(0.6)
Scenario C = AF + GK + LN + OS + TU + VX	101.2 km	(0.2)

[1] Fault segments correspond to the line segments shown on Figure DFS-8

TABLE DFS-4
MAXIMUM FAULT RUPTURE LENGTHS FOR LOCAL FAULT SOURCES ASSUMING INDEPENDENT BEHAVIOR
(Page 1 of 2)

FAULT TOTAL LENGTH (km/PROBABILITY)	MAXIMUM RUPTURE LENGTH (km)		PROBABILITY
Paintbrush Canyon/Stagecoach Road			
19.4 / 0.7	19.4	(1)	0.1
	11.1	(2)	0.7
	6.7	(3)	0.2
20.9 / 0.2	20.9	(1)	0.1
	11.1	(2)	0.7
	6.7	(3)	0.2
26.9 / 0.05	26.9	(1)	0.05
	19.7	(4)	0.4
	11.1	(2)	0.4
	6.7	(3)	0.1
28.4 / 0.05	28.4	(1)	0.05
	19.7	(4)	0.5
	11.1	(2)	0.3
	6.7	(3)	0.1
Bow Ridge			
7.6 / 0.8	7.6	(1)	0.7
	4.9	(5)	0.3
10.3 / 0.2	10.3	(1)	0.7
	4.9	(5)	0.3
Solitario Canyon			
16.5 / 0.7	16.5	(1)	0.8
	8.2	(6)	0.2
20.6 / 0.3	20.6	(1)	0.2
	15.4	(7)	0.6
	10.3	(6)	0.2

TABLE DFS-4
MAXIMUM FAULT RUPTURE LENGTHS FOR LOCAL FAULT SOURCES ASSUMING INDEPENDENT BEHAVIOR
(Page 2 of 2)

FAULT TOTAL LENGTH (km/PROBABILITY)	MAXIMUM RUPTURE LENGTH (km)	PROBABILITY
Windy Wash/Fatigue Wash		
22.3 / 0.7	22.3 (1)	0.2
	10 (6,8)	0.8
23.8 / 0.2	23.8 (1)	0.2
	10. (6,8)	0.8
25.8 / 0.05	25.8 (1)	0.1
	17.8 (9)	0.2
	10 (8)	0.7
27.3 / 0.05	27.3 (1)	0.1
	17.8 (9)	0.2
	10. (8)	0.7
Northern Crater Flat		
6.5 / 1	6.5 (1)	1.0
Southern Crater Flat	8.1 (1)	1.0
8.1 / 1		
Ghost Dance		
3.0 / 0.3	3.0 (1)	1.0
9.0 / 0.7	9.0 (1)	1.0

NOTES: (1) 100% of total fault length; (2) combined length of Alice Ridge and Fran Ridge segments; (3) length of longest segment, the Alice Ridge segment; (4) combined length of Alice Ridge, Fran Ridge, and Busted Butte segments; (5) length of well-defined north-south section of Bow Ridge fault; (6) approximately 50% of total fault length; (7) length of well-defined north-south section of Solitario Canyon fault adjacent to Yucca Crest; (8) approximate length of either the southern Windy Wash segment or the Fatigue Wash segment; (9) length of the north-south-trending section of the Windy Wash/Fatigue Wash fault system.

TABLE DFS-5
DOWNDIP GEOMETRY OF LOCAL FAULT SOURCES

FAULT	DOMINO (PLANAR) FAULT MODEL (0.8)		DETACHMENT FAULT MODEL (0.2)
	ALTERNATIVE A DIP / WIDTH (0.5)	ALTERNATIVE B DIP / WIDTH (0.5)	DIP / WIDTH (1.0)
❶ Paintbrush Canyon/Stagecoach Road Fault:			
Northern Segment, Paintbrush Canyon Fault	60° / 15 km	50° / 17 km	20° /18 km
Central Segment, Paintbrush Canyon Fault	60° / 15 km	50° / 17 km	20° /18 km
Southern Segment, Paintbrush Canyon Fault	60° / 15 km	50° / 17 km	20° /18 km
Stagecoach Road Fault	60° / 15 km	50° / 17 km	20° /13 km
❷ Bow Ridge Fault	70° / 8 km	60° / 9 km	48° / 7 km
❸ Solitario Canyon Fault	55° / 13 km	50° / 14 km	42° / 9 km
❹ Windy Wash/Fatigue Wash Fault:			
Northern Windy Wash Fault	60° / 12 km	55° / 13 km	° / 8.5 km
Fatigue Wash Fault	60° / 12 km	55° / 13 km	45° / 8.5 km
Southern Windy Wash Fault	55° / 10 km	55° / 13 km	45° / 8.5 km
❺ Northern Crater Flat Fault	60° / 9 km	55° / 9.5 km	47° / 8.6 km
❻ Southern Crater Flat Fault	71° / 10 km	60° / 11 km	52° / 8 km
❼ Ghost Dance Fault	90° / 10 km	70° / 11 km	45° / 8 km

TABLE DFS-6
QUATERNARY SLIP RATES ON LOCAL FAULT SOURCES
(Page 1 of 2)

FAULT	FAULT SEGMENT	SLIP RATE—mm/yr (PROBABILITY)			SOURCES OF DATA
		PREFERRED	MINIMUM	MAXIMUM	
Paintbrush Canyon/Stagecoach Road Fault					
Northern Segment PCF	A-B	0.002 (0.6)	0.001 (0.2)	0.004 (0.2)	Modified from: C. M. Menges and J. W. Whitney, USGS, written communication, 1996b, Tables 4.4.5 and 4.4.6 (Trench A1).
Central Segment PCF	B-B1	0.017 (0.6)	0.013 (0.2)	0.025 (0.2)	F. H. Swan *et al.*, Geomatrix Consultants, written communication, 1995, Table C-8 (Trench MWV-T4).
Southern Segment PCF	B1-C	0.01 (0.6)	0.004 (0.2)	0.016 (0.2)	Modified from: C. M. Menges and J. W. Whitney, USGS, written communication, 1996b, Tables 4.4.5 and 4.4.6 (Busted Butte exposures).
Stagecoach Road	C-F	0.04 (0.6)	0.01 (0.2)	0.07 (0.2)	Modified from: C. M. Menges and J. W. Whitney, USGS, written communication, 1996b, Tables 4.4.5 and 4.4.6 (Trenches SCR-T1 and SCR-T3).
Bow Ridge Fault	G-K	0.003 (0.6)	0.002 (0.2)	0.007 (0.2)	C. M. Menges and J. W. Whitney, USGS, written communication, 1996b, Tables 4.4.6.
Solitario Canyon Fault	L-N	0.01 to 0.03 (0.3) (0.3)	0.002 (0.2)	0.04 (0.2)	A. R. Ramelli *et al.*, Nevada Bureau of Mines and Geology, written communication, 1996, p. 4.7-49.

TABLE DFS-6
QUATERNARY SLIP RATES ON LOCAL FAULT SOURCES
(Page 2 of 2)

FAULT	FAULT SEGMENT	SLIP RATE—mm/yr (PROBABILITY)			SOURCES OF DATA
		PREFERRED	MINIMUM	MAXIMUM	
Windy Wash/Fatigue Wash Fault					
Northern Windy Wash	O-P1	0.003 (0.45)	0.001 (0.45)	0.03 (0.1)	Assumed to be similar to Southern Windy Wash segment, but with greater uncertainty.
Fatigue Wash	P1-Q	0.002 (0.6)	0.001 (0.2)	0.015 (0.2)	J. A. Coe *et al.*, USGS, written communication, 1996, p. 4.8-24.
Southern Windy Wash	Q-S	0.011 (0.6)	0.009 (0.2)	0.027 (0.2)	Reported slip rate available for one of two splays; J. W. Whitney *et al.*., USGS, written communication, 1996b, p. 4.9-31 to 4.9-32.
Northern Crater Flat Fault	T-U		0.001 (0.5)	0.002 (0.5)	Maximum rate reported to be less than 0.002 mm/yr, J.A. Coe *et al.*, USGS, written communication, 1996, P.4.11-12 (Trench TR CFF T-2).
Southern Crater Flat Fault	V-X		0.001 (0.5)	0.002 (0.5)	Maximum rate reported to be less than 0.002 mm/yr, E. M. Taylor *et al.*, USGS, written communication, 1996a, P.4.10-12 (trenches TR CFF T-1 and TR CFF T-1a).
Ghost Dance Fault	YY-ZZ	0.001 (0.6)	0.0001 (0.2)	0.0024 (0.2)	Preferred value equals the weighted average from all these displacement history models described in Section 5.2.3.

TABLE DFS-7
SEISMIC SOURCE PARAMETERS FOR HYPOTHETICAL FAULTS

Hypothetical Fault Source	Activity	Length (km)	Dip (deg.)	Depth to Detachment (km)	Slip Rate (mm/yr) Preferred	Slip Rate (mm/yr) Maximum	Slip Rate (mm/yr) Minimum	Maximum Magnitude		
Highway 95 Fault (H-95)	(0.1)	11 (0.5)	90	na	0.03 (0.4)	0.05 (0.3)	0.01 (0.3)	6.5 (0.7)		6.8 (0.3)
		27 (0.5)	90	na	" "	" "	" "	6.5 (0.2)	6.7 (0.6)	7.0 (0.2)
Postulated Hidden Strike-Slip Fault (T2-HSS)	(0.05)	30 (0.5)	90	5 to 16 (0.2) 6.5 to 14 (0.6) 8 to 12 (0.2)	" "	" "	" "	L vs. M (0.2)		A vs. M (0.8)
		200 (0.5)		5 to 16 (0.2) 6.5 to 14 (0.6) 8 to 12 (0.2)	" "	" "	" "	6.0 (0.3) " " " "	6.5 (0.5) " " " "	7.0 (0.2) " " " "

Maximum depth of faulting same as for regional fault sources [12 km (0.6), 14 km (0.3), 16 km< (0.1)].

TABLE DFS-8
FAULT ACTIVITY AND CUMULATIVE DISPLACEMENT, POST-TIVA CANYON TUFF, AT TEST CALCULATION SITES FOR FAULT DISPLACEMENT HAZARD ASSESSMENT

	Test Calculation Site	Probability of Activity	Cumulative Displacement Post-Tiva Canyon Tuff (Net Slip in m)		
1)	Bow Ridge Fault	1.0	125 (0.2)	130 (0.6)	135 (0.2)
2)	Solitario Canyon Fault	1.0	350 (0.2)	500 (0.6)	580 (0.2)
3)	Drill Hole Wash Fault	0.01	5 (0.2)	15 (0.6)	25 (0.2)
4)	Ghost Dance Fault	0.4	20 (0.2)	25 (0.6)	30 (0.2)
5)	Sundance Fault	0.01	6 (0.2)	8.5 (0.6)	11 (0.2)
6)	Unnamed Fault West of Dune Wash	0.4	3 (0.2)	5 (0.6)	7 (0.2)
7)	100 M East of Solitario Canyon Fault				
	a) Small fault	0.05	0.5 (0.2)	0.85 (0.6)	2.0 (0.2)
	b) Shear	0.05	0.1 (1.0)	--	--
8)	Midway Between Solitario Canyon and Ghost Dance Faults				
	a) Small fault	0.01	0.5 (0.2)	0.85 (0.6)	2.0 (0.2)
	b) Shear	0.01	0.1 (1.0)	--	--
9)	Exile Hill Fault (Midway Valley)	0.8	5 (0.2)	10 (0.6)	15 (0.2)

TABLE DFS-9
QUATERNARY SLIP RATES
BASED ON PALEOSEISMIC DATA

Test Calculation Site	Slip Rate (mm per yr)			Basis
1) Bow Ridge Fault	0.002 (0.2)	0.003 (0.6)	0.007 (0.2)	C. M. Menges and J. W. Whitney, USGS, written communication, 1996b, Table 4.4.6
2) Solitario Canyon Fault	0.01 (0.2)	0.02 (0.6)	0.04 (0.2)	Data from trenches SCF-T4 and T8, A. R. Ramelli *et al.*., Nevada Bureau of Mines and Geology, written communication, 1996 Table 4.7.3
3) Drill Hole Wash Fault	not available			
4) Ghost Dance Fault	less than 0.0005			(See text, Section 5.2.3)
5) Sundance Fault	not available			
6) Unnamed Fault West of Dune Wash	not available			
7) 100 M East of Solitario Canyon Fault	not available			
8) Midway Between Solitario Canyon and Ghost Dance Faults	not available			
9) Exile Hill Fault (Midway Valley)	less than 0.0005			F. H. Swan *et al.*., Geomatrix Consultants, written communicaiton, 1995

TABLE DFS-10
SLIP RATES CALCULATED USING DECREASING SLIP RATE MODEL WITH DIFFERENT REDUCTION FACTORS (RF) COMPARED TO SLIP RATES BASED ON PALEOSEISMIC DATA

FAULT	SLIP RATE (mm PER YR) [*1]			
	DECREASING SLIP RATE MODEL (REDUCTION FACTORS AS A PERCENT OF THE LATE MIOCENE SLIP RATE)			SLIP RATE BASED ON PALEOSEISMIC DATA
	2.1 %	3.9 %	0.3 %	
Paintbrush Canyon Fault (Trench MWV T4)	0.0057±	0.011±	0.0008±	0.017±
Bow Ridge Fault (Test Calculation Site #1)	0.0025±	0.0046±	0.0004±	0.003±
Solitario Canyon Fault (Test Calculation Site #2)	0.0095±	0.0177±	0.0014	0.02±
Ghost Dance Fault (Test Calculation Site #4)	0.0005±	0.0009±	0.0001	<0.0005
Exile Hill Fault (Test Calculation Site #9)	0.0002±	0.0004±	0.0003±	<0.0005

[*1] Slip rates shown here are based on preferred values for displacement and age; the uncertainties in these values were incorporated in the fault displacement hazard analysis.

TABLE DSF-11 (Page 1 of 2)
DISPLACEMENT PER EVENT AND RECURRENCE PARAM TERS FOR
FAULT DISPLACEMENT HAZARD ASSESSMEN

Displacement Approach		Rec rence Approach	
Average Displacement Per Event (cm)	Probability	Avera e Recurrence nterval (X 100 ars)	Probability
#1 BOW RIDGE FAULT			
40	0.15	2 5	0.1
20	0.7	1 0	0.4
10	0.15	1 0	0.4
		7	0.1
#2 SOLITARIO CANYON FAULT			
60	0.2	10	0.2
40	0.6	7	0.3
20	0.2	5	0.3
		3	0.2
#3 DRILLHOLE WASH FAULT			
15	0.03	50	0.145
10	0.07	40	0.25
5	0.15	30	0.25
3	0.2	20	0.25
1	0.25	10	0.1
0.05	0.3	50	0.005
#4 GHOST DANCE FAULT			
15	0.03	500	0.145
10	0.07	400	0.25
5	0.15	300	0.25
3	0.2	200	0.25
1	0.25	100	0.1
0.05	0.3	50	0.005
#5 SUNDANCE FAULT			
15	0.03	500	0.145
10	0.07	400	0.25
5	0.15	300	0.25
3	0.2	200	0.25
1	0.25	100	0.1
0.05	0.3	50	0.005

TABLE DSF-11 -(Page 2 of 2)
DISPLACEMENT PER EVENT AND RECURRENCE PARAMETERS FOR ASSESSMENT OF FAULT DISPLACEMENT HAZARD

Displacement Approach		Recurrence Approach	
Average Displacement Per Event (cm)	Probability	Average Recurrence Interval (X 1000 Years)	Probability
#6 UNNAMED FAULT WEST OF DUNE WASH			
15	0.03	500	0.145
10	0.07	400	0.25
5	0.15	300	0.25
3	0.2	200	0.25
1	0.25	100	0.1
0.05	0.3	50	0.005
#7 100 M EAST OF SOLITARIO CANYON FAULT			
(A) 2 m Displacement			
10	0.05	1600	0.05
5	0.1	500	0.18
3	0.2	400	0.18
1	0.3	300	0.18
0.5	0.35	200	0.18
		100	0.18
		50	0.05
(B) 10 cm Displacement			
10	0.005	1600	0.05
5	0.05	500	0.18
3	0.2	400	0.18
1	0.35	300	0.18
0.5	0.3	200	0.18
0.05	0.095	100	0.18
		50	0.05
#8 MIDWAY BETWEEN SOLITARIO CANYON AND GHOST DANCE FAULTS			
(A) 2 m Displacement			
10	0.05	1600	0.05
5	0.1	500	0.18
3	0.2	400	0.18
1	0.3	300	0.18
0.5	0.35	200	0.18
		100	0.18
		50	0.05
(B) 10 cm Displacement			
10	0.005	1600	0.05
5	0.05	500	0.18
3	0.2	400	0.18
1	0.35	300	0.18
0.5	0.3	200	0.18
0.05	0.095	100	0.18
		50	0.05
#9 MIDWAY VALLEY (EXILE HILL FAULT)			
10	0.05	500	0.15
5	0.1	400	0.25
3	0.2	300	0.25
1	0.3	200	0.25
0.5	0.35	100	0.1

TABLE DSF-12
SUMMARY OF DISPLACEMENT PER EVENT DATA FROM YUCCA MOUNTAIN PALEOSEISMIC INVESTIGATIONS
(Page 1 of 2)

Locality Site	Average Displacement	EVENT (Reported Displacement in cm -- Pezzopane et al. 1995, Table 5-1) [Ratio: Event Displacement / Average Displacement]							
		Z	Y	X	W	V	U	T	S
Tr 14D	23.67	44 1.86	13 0.55	14 0.59	0.00	0.00			
Tr CFF-T2A	29.60	3 0.10	5 0.17	40 1.35	50 1.69	50 1.69			
Tr CFF-T1A	19.33	18 0.93	20 1.03	20 1.03	0.00	0.00			
Tr CF 1	61.33	0.00	25 0.41	105 1.71	54 0.88	0.00			
Tr SCF-T2	61.25	5 0.08	70 1.14	100 1.63	70 1.14	0.00			
Tr A1	38.00	6 0.16	39 1.03	7 0.18	100 2.63	0.00			
BB4	89.57	44 0.49	28 0.31	47 0.52	167 1.86	142 1.59	105 1.17	94 1.05	
MWV-T4	55.00	20 0.36	62 1.13	98 1.78	40 0.73	0.00	0.00	0.00	
RV3	290.75	267 0.92	362 1.25	204 0.70	330 1.13	0.00	0.00	0.00	

TABLE DSF-12
SUMMARY OF DISPLACEMENT PER EVENT DATA FROM YUCCA MOUNTAIN PALEOSEISMIC INVESTIGATIONS
(Page 2 of 2)

Locality Site	Average Displacement	EVENT (Reported Displacement in cm -- Pezzopane et al. 1995, Table 5-1) [Ratio: Event Displacement / Average Displacement]							
		Z	Y	X	W	V	U	T	S
SCF-T3	41.67	10	80	35					
		0.24	1.92	0.84	0.00	0.00	0.00	0.00	
SCF-T4	18.33	5		30	20				
		0.27	0.00	1.64	1.09	0.00	0.00	0.00	
SCF-T8	52.50	10	120	30	50				
		0.19	2.29	0.57	0.95	0.00	0.00	0.00	
SCR-T1	45.00	40	42	47	51				
		0.89	0.93	1.04	1.13	0.00	0.00	0.00	
SCR-T3	52.20	43	59	57	67	35			
		0.82	1.13	1.09	1.28	0.67	0.00	0.00	
Tr CF-2 [north wall]	39.38	4	20	23	20	73	45	50	80
		0.10	0.51	0.58	0.51	1.85	1.14	1.27	2.03
Tr CF-2 [south wall]	34.63	4	12	50	42	28	16	60	65
		0.12	0.35	1.44	1.21	0.81	0.46	1.73	1.88
Tr CF2.5	20.75	6	20	42	15				
		0.29	0.96	2.02	0.72	0.00	0.00	0.00	
Tr CF-3 [north wall]	44.80	4	33	87	35	65			
		0.09	0.74	1.94	0.78	1.45	0.00	0.00	
Tr CF-3 [south wall]	42.00	3	35	88					
		0.07	0.83	2.10	0.00	0.00	0.00	0.00	

TABLE DSF-13
RELATIONSHIP BETWEEN AVERAGE DISPLACEMENT AND MAXIMUM DISPLACEMENT AT A POINT ALONG A FAULT
(Event -to-Event Variability)

LOCALITY	$D_{max}/D_{average}$ **
Tr 14D	1.86
Tr CFF-T2A	1.69
Tr CFF-T1A	1.03
Tr CF 1	1.71
Tr SCF-T2	1.63
Tr A1	2.63
BB4	1.86
MWV-T4	1.78
RV3	1.13
SCF-T3	1.92
SCF-T4	1.64
SCF-T8	2.29
SCR-T1	1.13
SCR-T3	1.28
Tr CF-2 [north wall]	1.85
Tr CF-2 [south wall]	1.44
Tr CF2.5	2.02
Tr CF-3 [north wall]	1.94
Tr CF-3 [south wall]	2.1
RANGE	**1.03 to 2.63**
AVERAGE	**1.73**

** From Table DSF-12

TABLE DFS-14
POTENTIAL FOR ACTIVITY
ON FRACTURES AND IN INTACT BEDROCK

Test Calculation Site	Potential Activity	Basis
#7 100 m East of Solitario Canyon Fault		
c) Fracture	< 0.05	Likelihood of occurrence judged to be less than the probability of activity on a fault that has displacement at the same location (Table 7.2-1)
d) Intact Bedrock	< 0.005	Likelihood of occurrence judged to be at least an order of magnitude less than the probability of activity on a fault or fracture at the same location.
#8 Midway Between Solitario Canyon and Ghost Dance Faults		
c) Fracture	< 0.01	Likelihood of occurrence judged to be less than the probability of activity on a fault that has displacement at the same location (Table 7.2-1)
d) Intact Bedrock	< 0.001	Likelihood of occurrence judged to be an order of magnitude less than the probability of activity on a fault or fracture at the same location.

TABLE DFS-15
PROBABILITY OF DISPLACEMENT "EVENTS" (Pe)
ACROSS FRACTURES IN UNBROKEN ROCK
GIVEN DIFFERENT MODELS OF DEFORMATION HISTORY

- **(A) Uniform Deformation Post Tiva-Canyon (Ttc).**

$$\Pr obability of\ "Event" \leq \frac{1}{Age of\ Host Rock}$$

$$Pe \leq \frac{1}{(12.7 \pm 1.3) x 10^{6}}$$

$$Pe \leq 1 x 10^{-7}$$

- **(B) Uniform Deformation Rate Post-Rainier Mesa.**

$$Pe \leq \frac{post - Rainier\ Mesa\ deformation\ rate}{post - Tiva\ Canyon\ deformation\ rate} (Pe\ \ Model\ \ A)$$

$$Pe \leq \left(\frac{0.2 / 11.6 \pm 1.0\ Ma}{1 / 12.7 \pm 1.3\ Ma} \right) \left(1 x 10^{-7} \right)$$

$$Pe \leq 1.8 x 10^{-8}\ to \leq 2.6 x 10^{-8}$$

- **(C) Decreasing Deformation Rate.**

$$Pe \leq \frac{(late\ Miocene\ deformation\ rate)(reduction\ factor)}{post - Tiva Canyon\ deformation\ rate} (Pe\ \ Model\ \ A)$$

$$Pe \leq \left(\frac{\left(0.8 / 1.1 \pm 0.6 ma\right)(0.021 \pm 0.018)}{1 / 12.7 \pm 1.3 Ma} \right) \left(1 x 10^{-7} \right)$$

$$Pe \leq 2.1 x 10^{-9}\ to \leq 5.9 x 10^{-8}$$

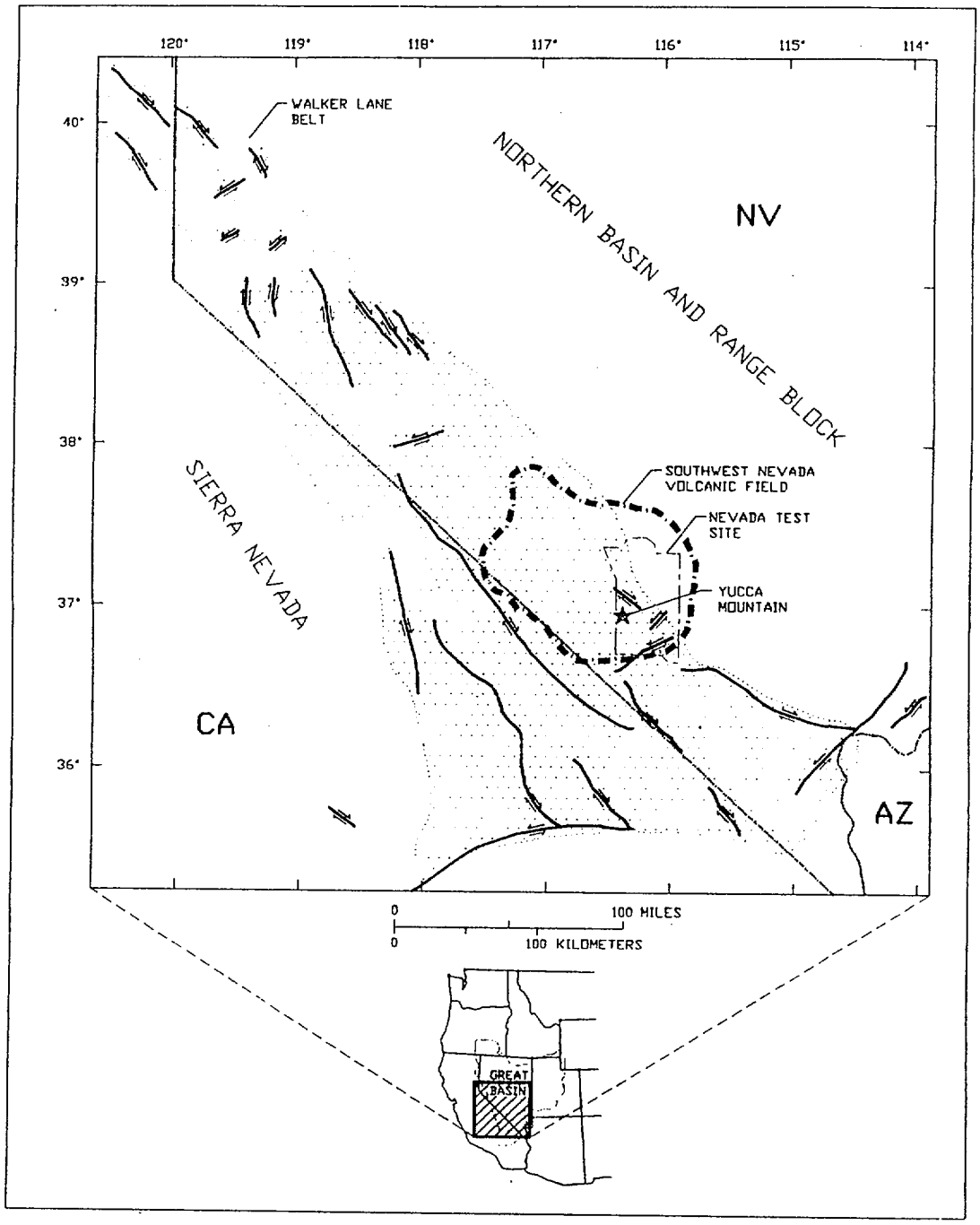

Figure DFS-1 Map showing location of Yucca Mountain (star) in the southwest Nevada volcanic field (Broxton et al., 1989, of the western Great Basin, with schematic representations of faults of the Walker Lane Belt that have strike-slip components of offset (dip-slip offsets not shown). Modified from Stewart (1988)

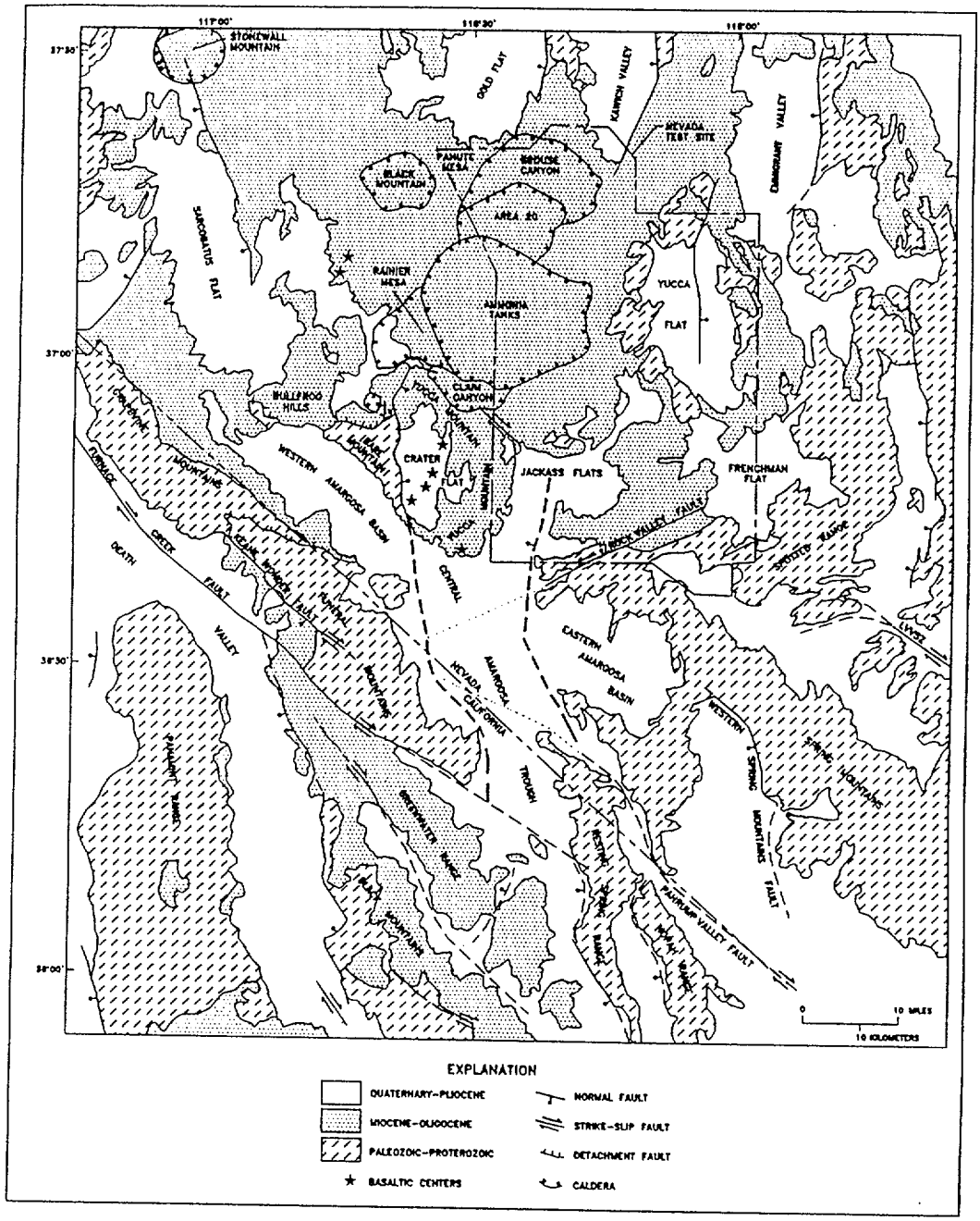

Figure DFS-2 Generalized map of the Yucca Mountain region showing major physiographic features and faults. Compiled from Jenkins, 1962; Longwell et al., 1965; Cornwall, 1972; Streitz and Stinson, 1974; Ekren et al., 1977, Burchfield et al., 1983; Wright, 1989; Frizzell and Schulters, 1990; Piety, 1993; Sawyer et al., 1994

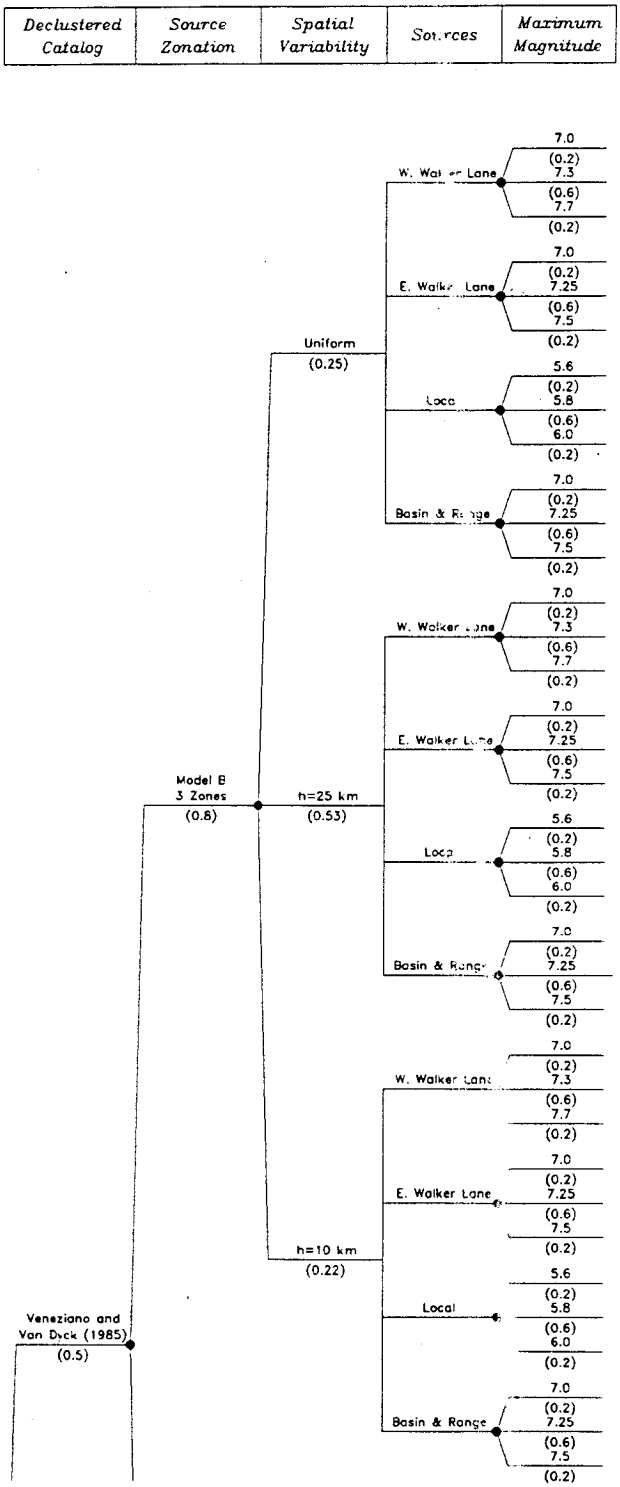

Figure DFS-3 Logic tree defining seismic source zones associated with two alternative models

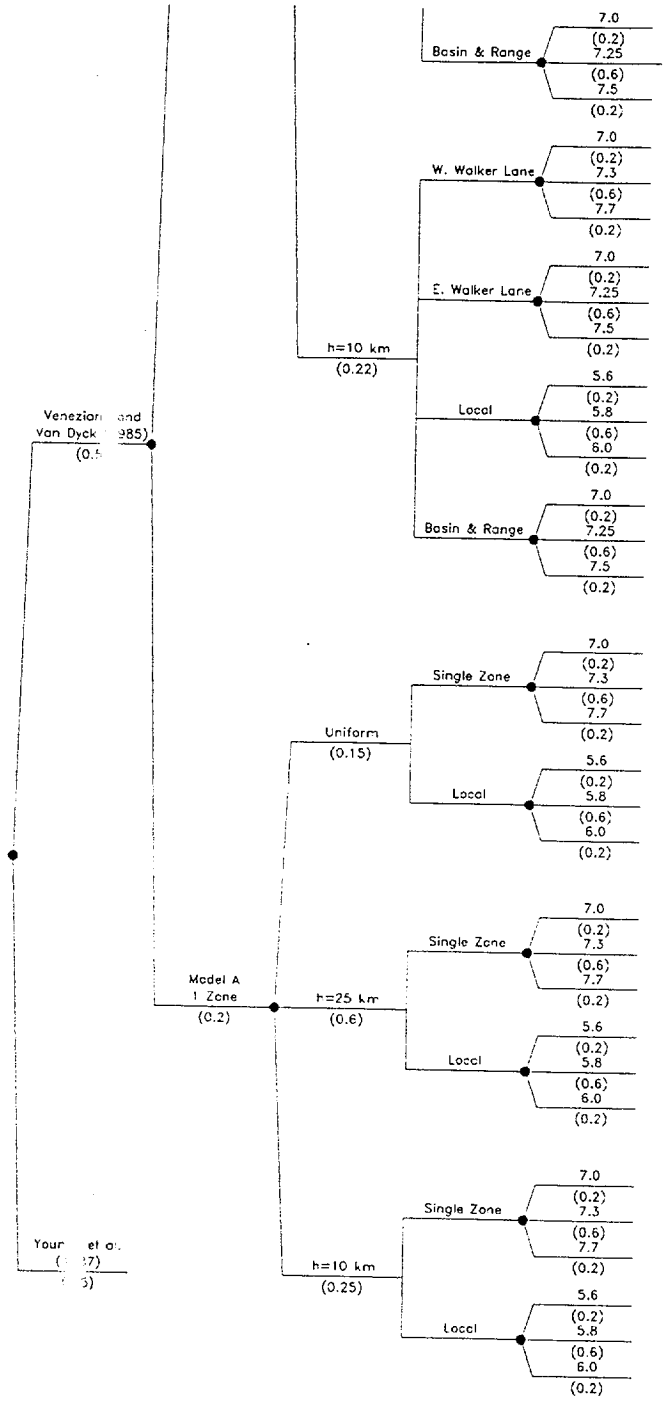

Figure DFS-3 (Cont'd) Logic tree defining seismic source zones associated with two alternative models

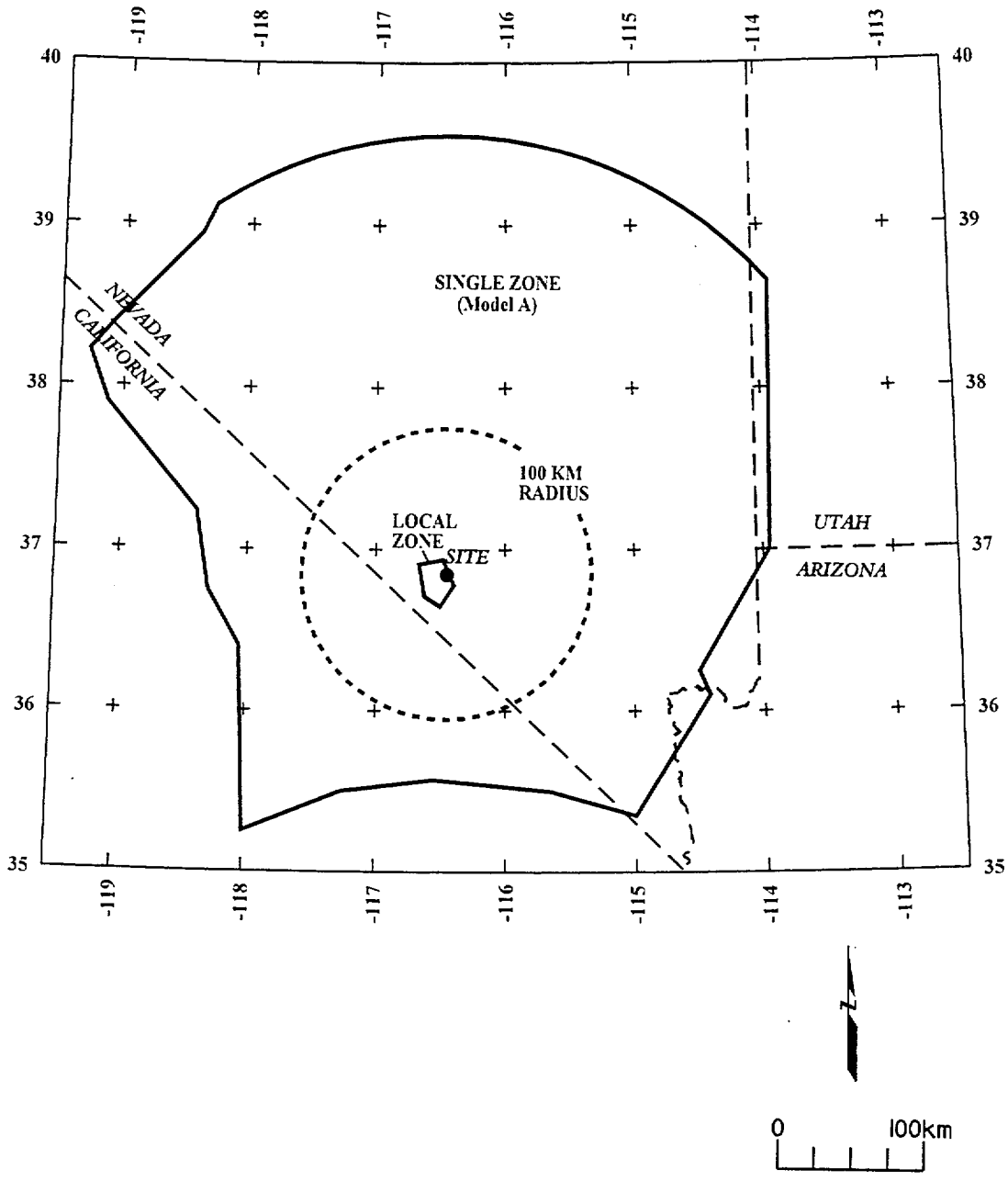

Figure DFS-4 Map showing boundaries of seismic source zones, Model A (one zones plus site vicinity).

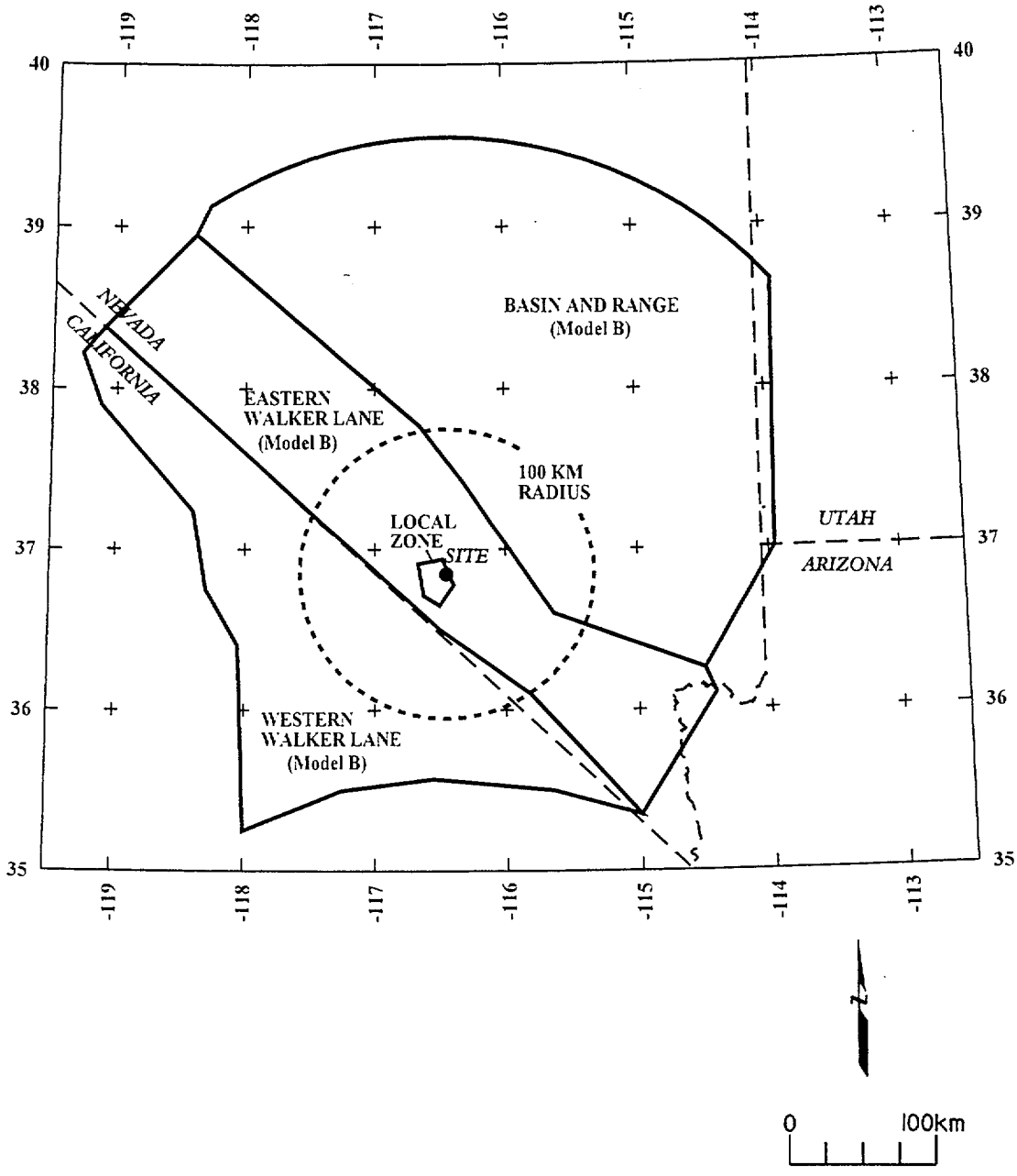

Figure DFS-5 Map showing boundaries of seismic source zones, Model B (three zones plus site vicinity).

h:\prj\yucca_mt\dgn\1097\plate_t2_reg_zone1.dgn 07-NOV-1997 10:13

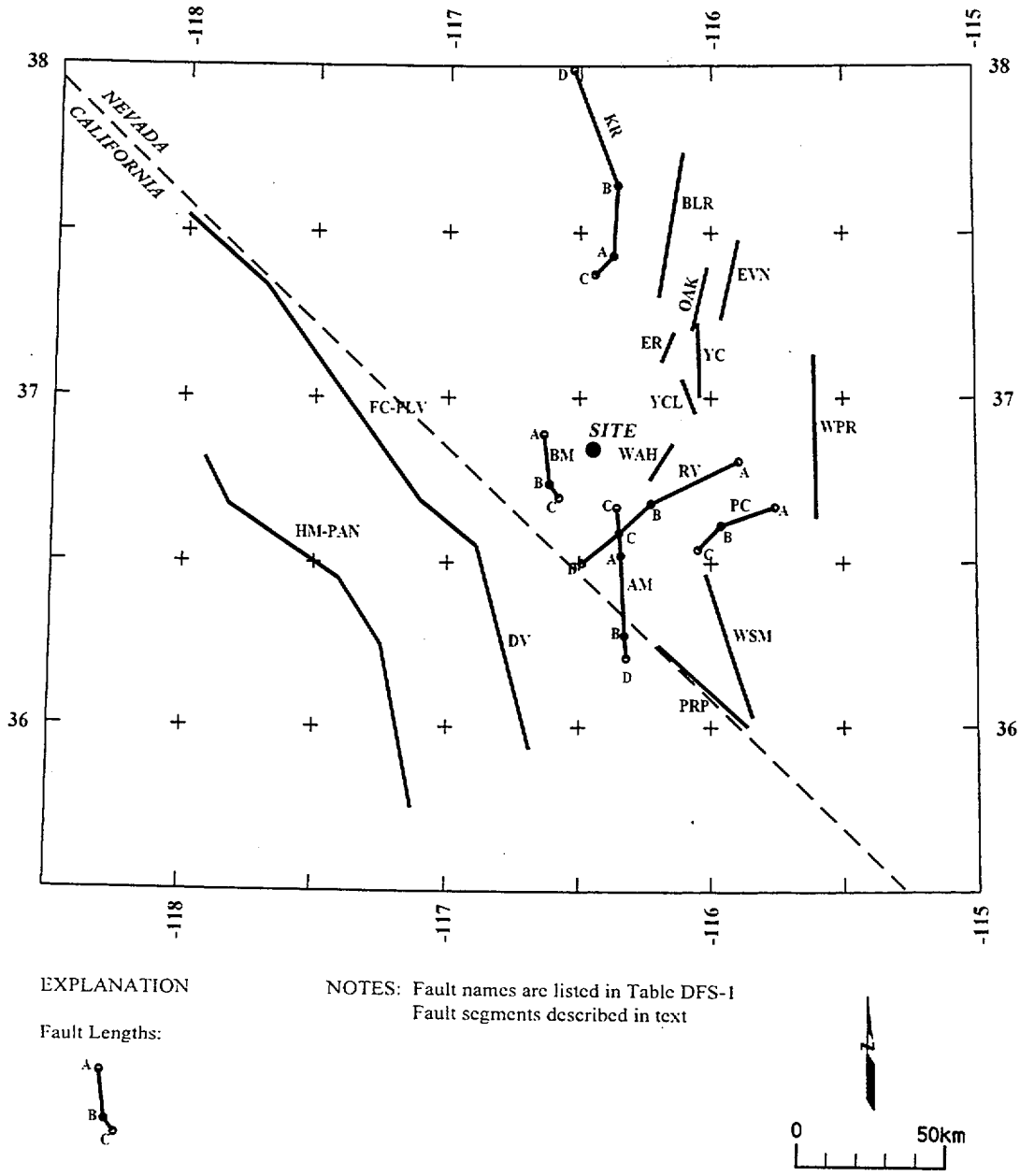

Figure DFS-6 Map showing identified late Quaternary faults included as regional fault sources in the seismic source model

Regional Fault Source	*Fault Dip*	*Maximum Depth Of Faulting*	*Total Fault Length*	*Maximum Magnitude (Mw)*	*Slip Rate (mm/yr)*	*Earthquake Recurrence Model*

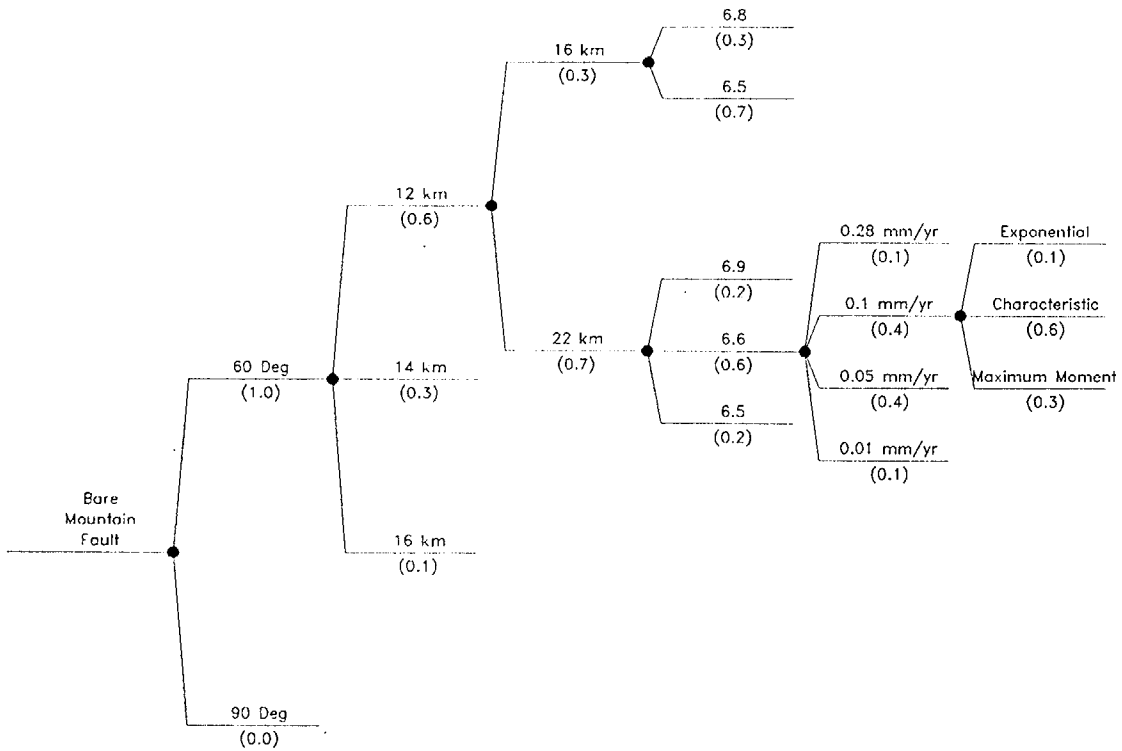

Figure DFS-7 Example of the logic tree used to characterize regional fault sources

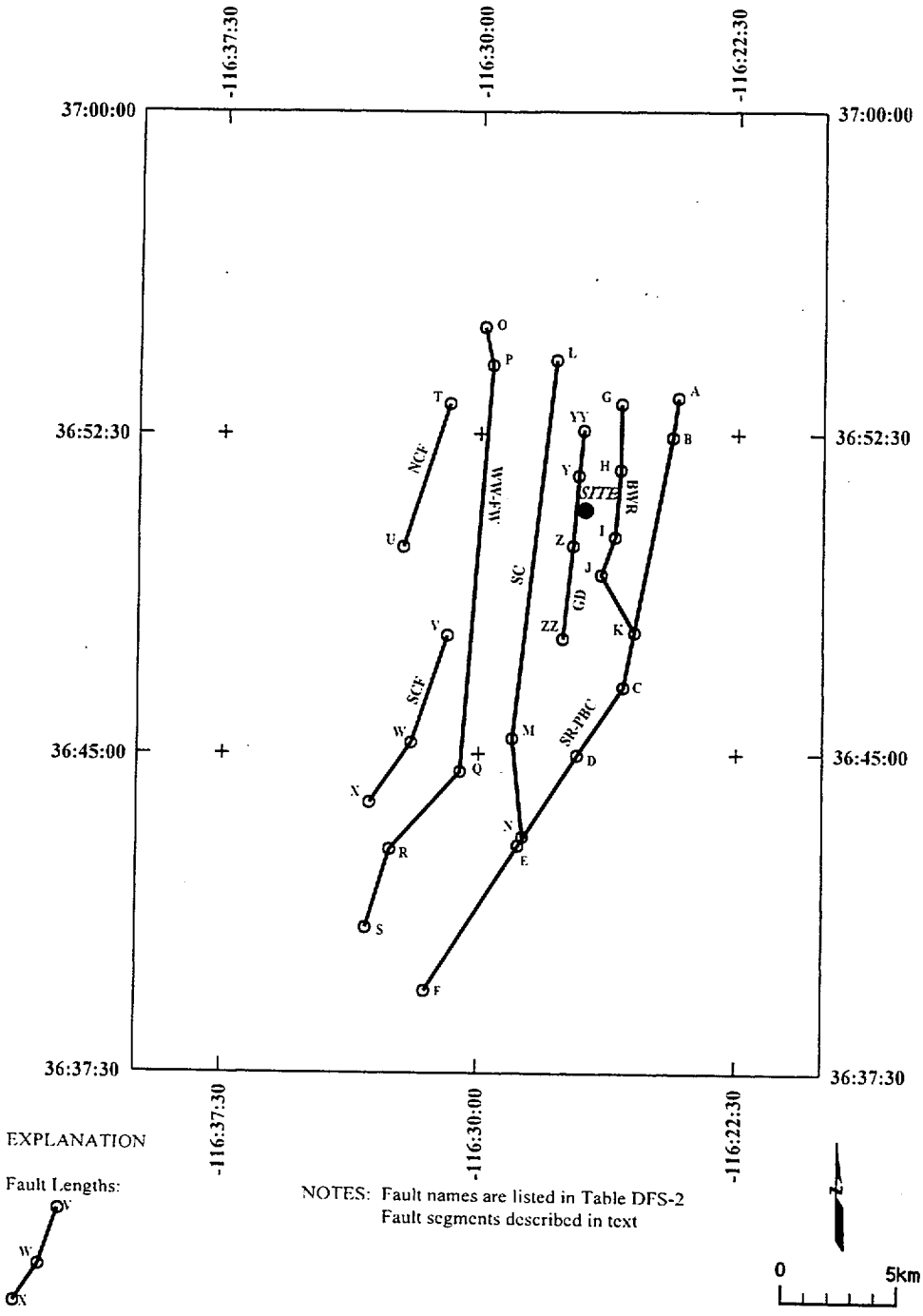

Figure DFS-8 Map showing local fault sources included in the seismic source model

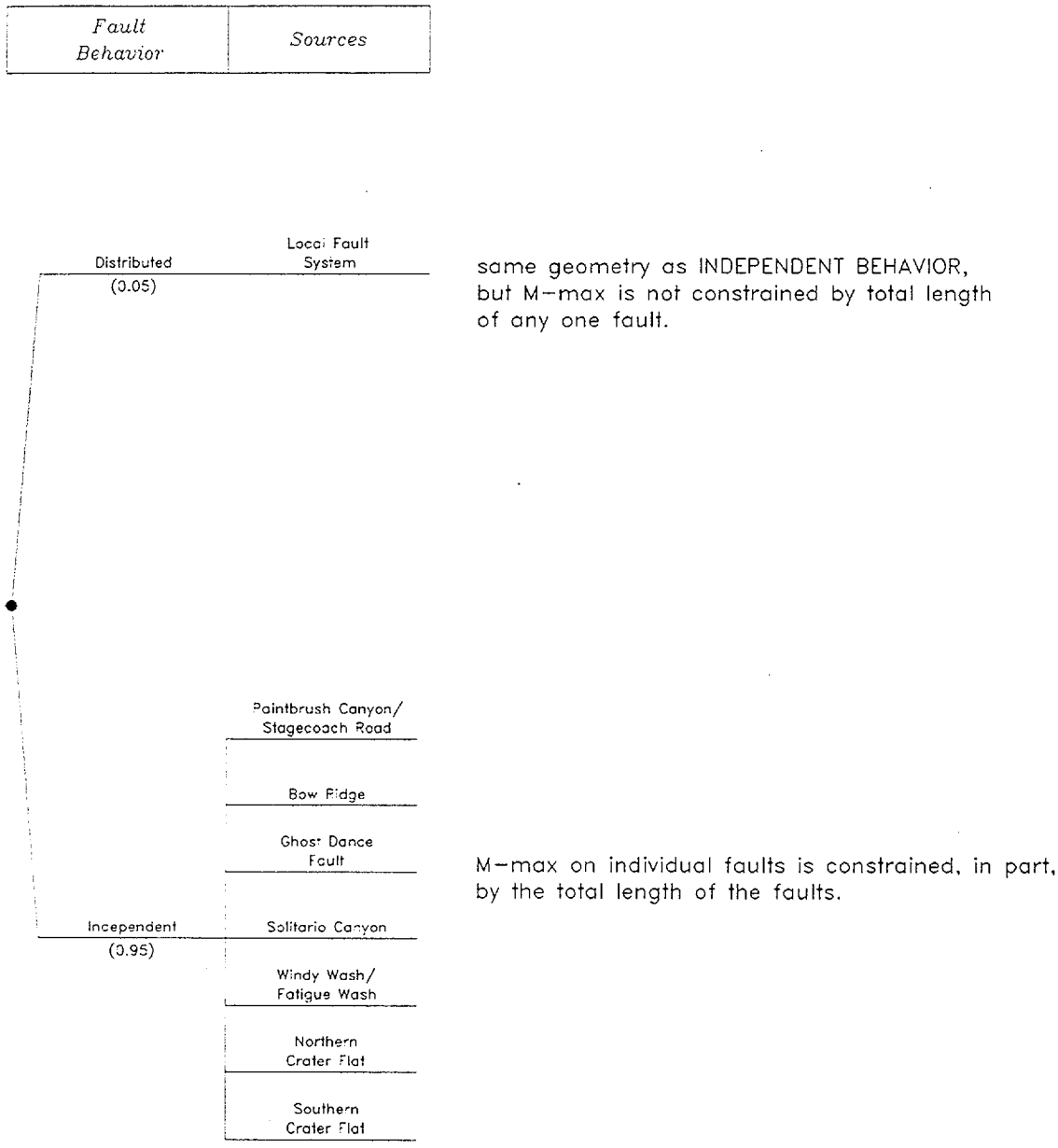

Figure DFS-9 Logic tree showing dependence of local fault model on distributive versus independent fault-behavior models

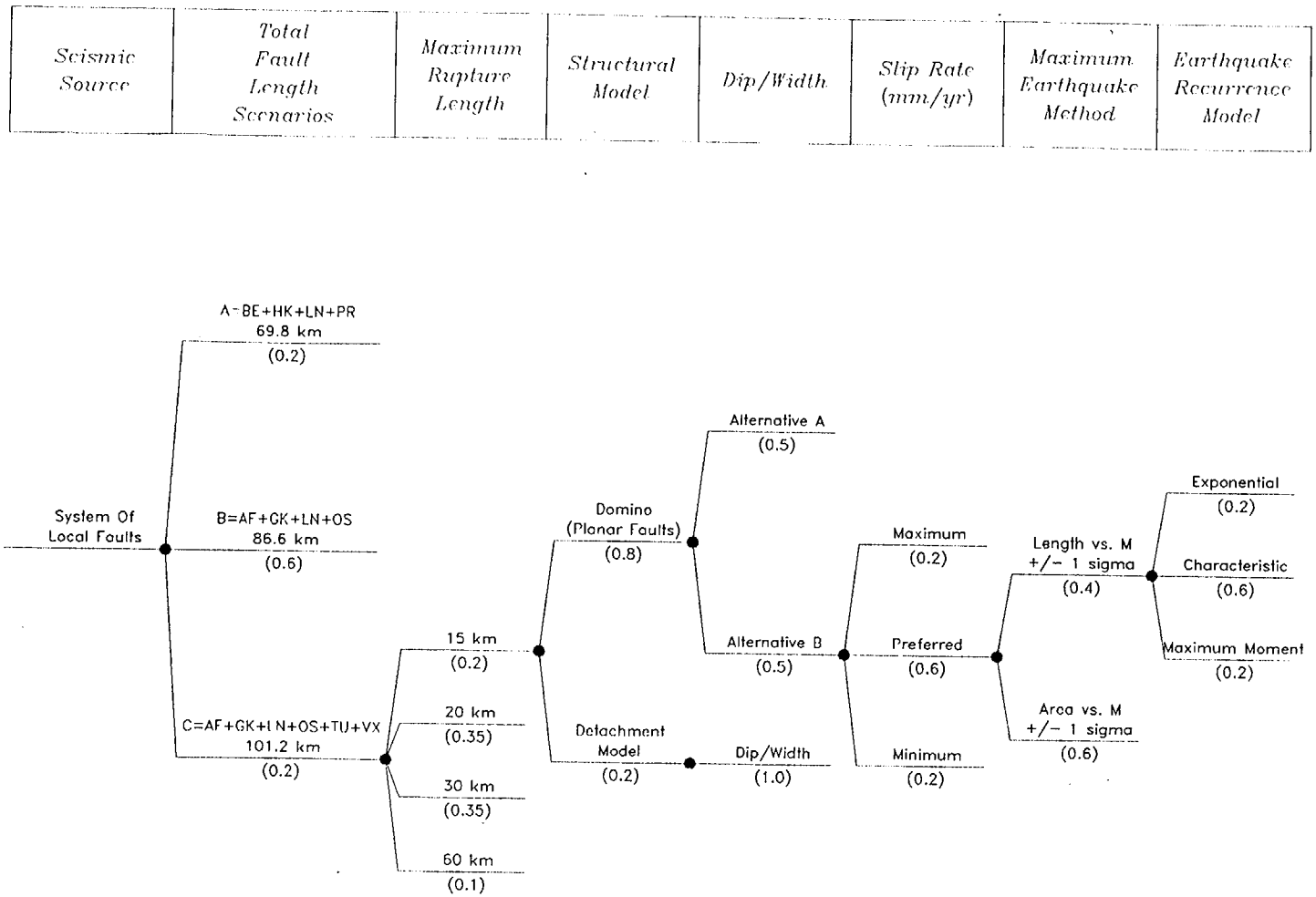

Figure DFS-10 Example logic tree used to characterize fault sources given distributed fault behavior

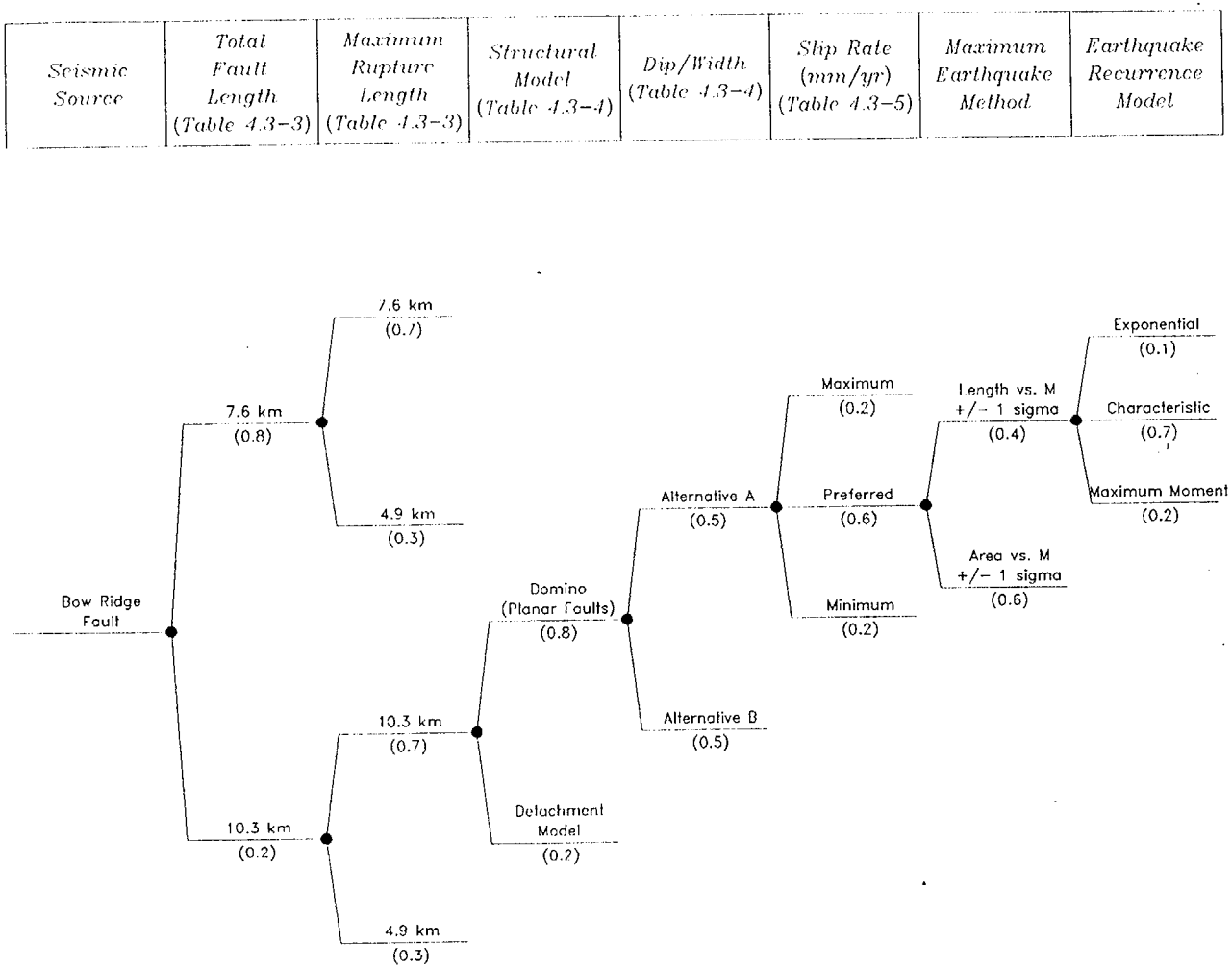

Figure DFS-11 Example logic tree used to characterize local fault sources given independent fault behavior

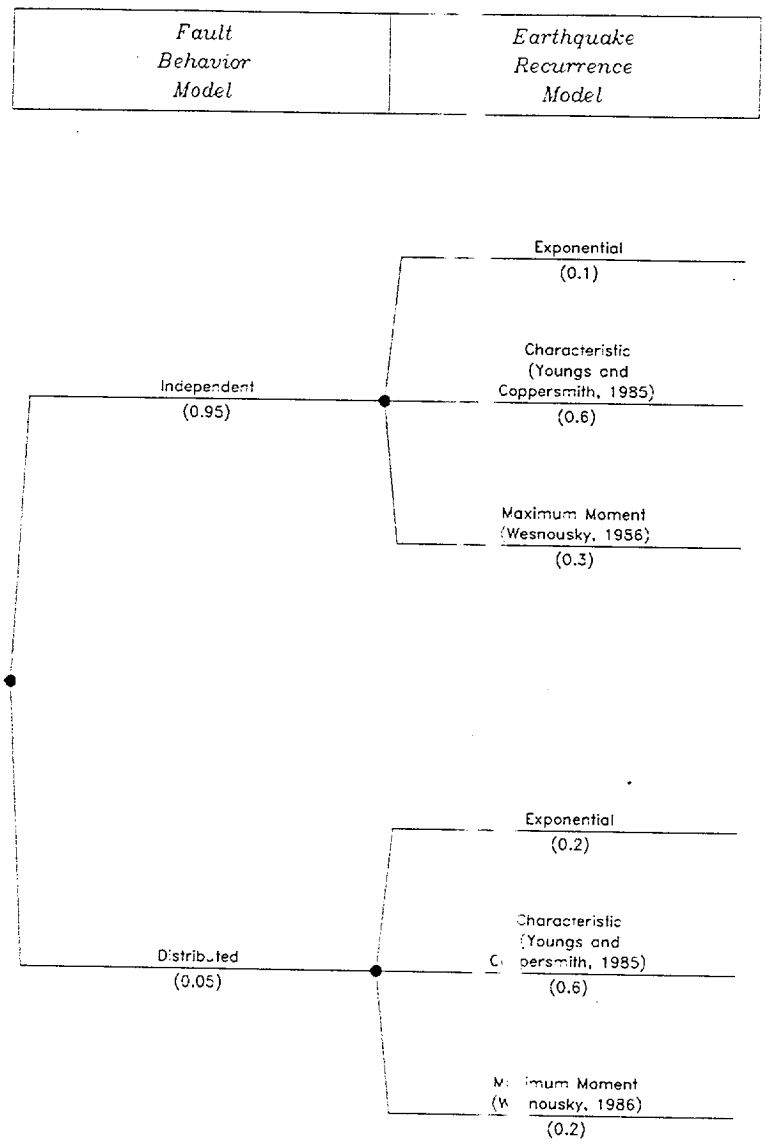

Figure DFS-12 Logic tree for conditional probability weights assigned to earthquake recurrence models

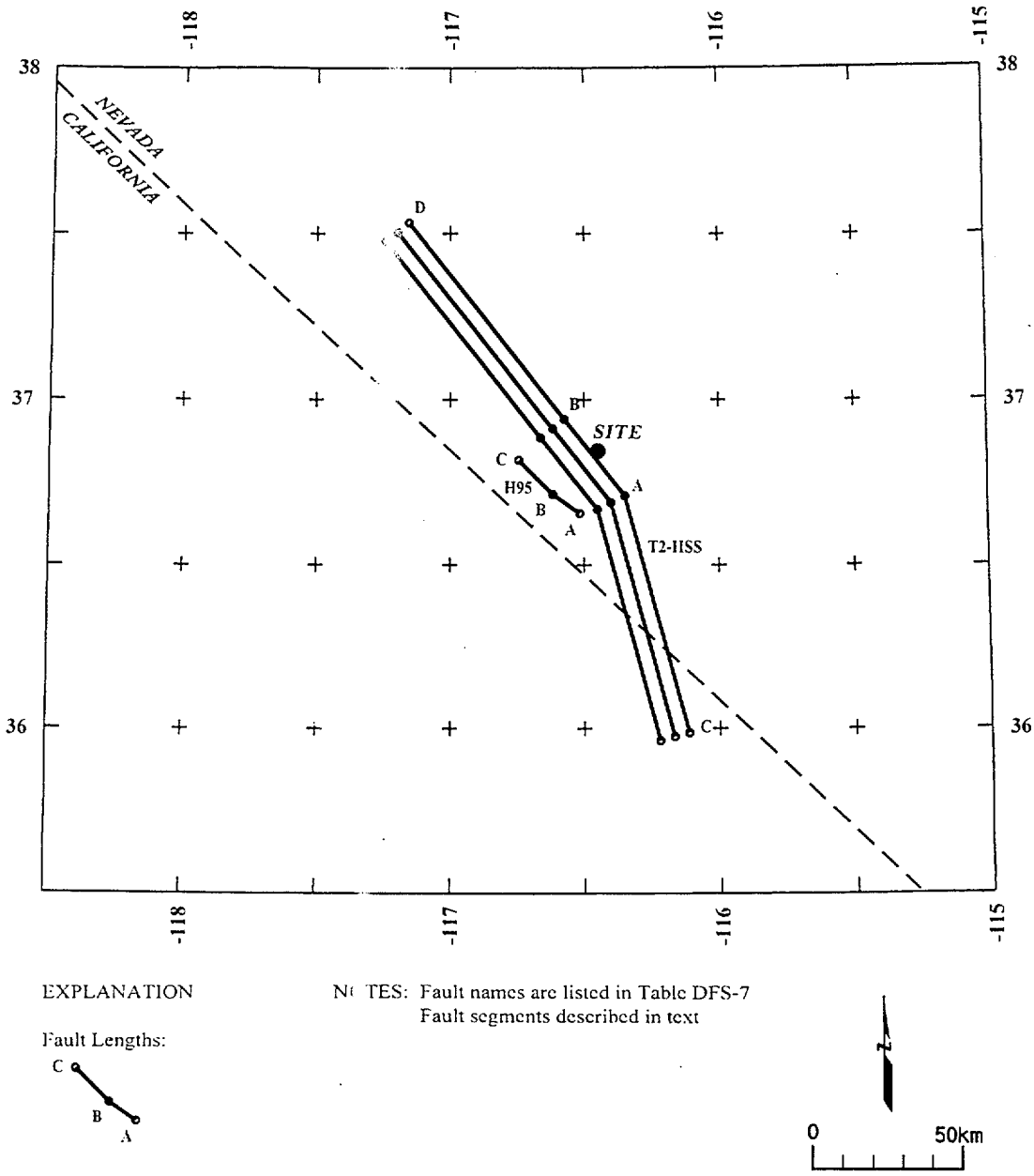

Figure DFS-13 Map showing hypothetical fault sources included in the seismic source model

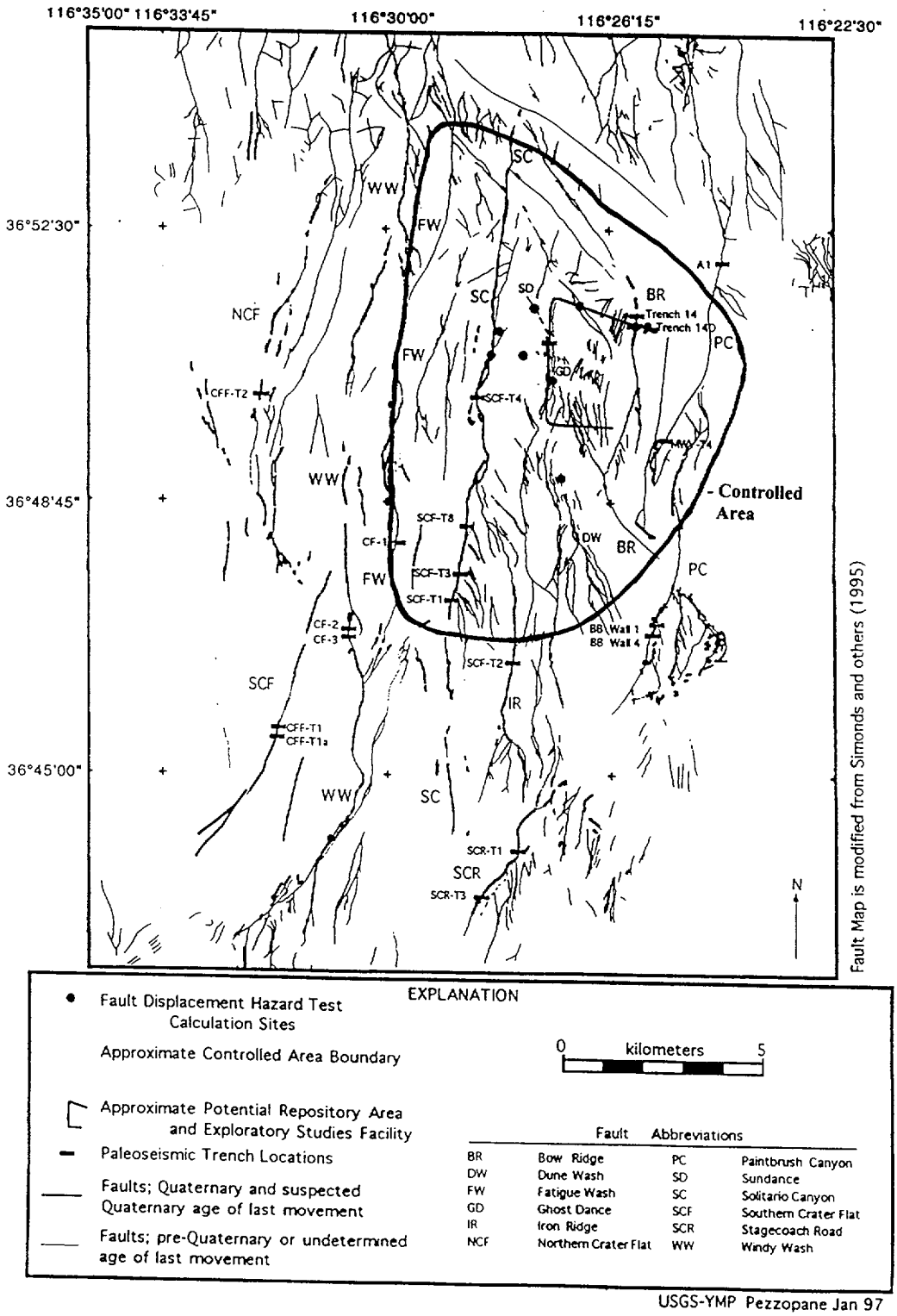

Figure DFS-14 Map showing fault displacement hazard test calculation sites.

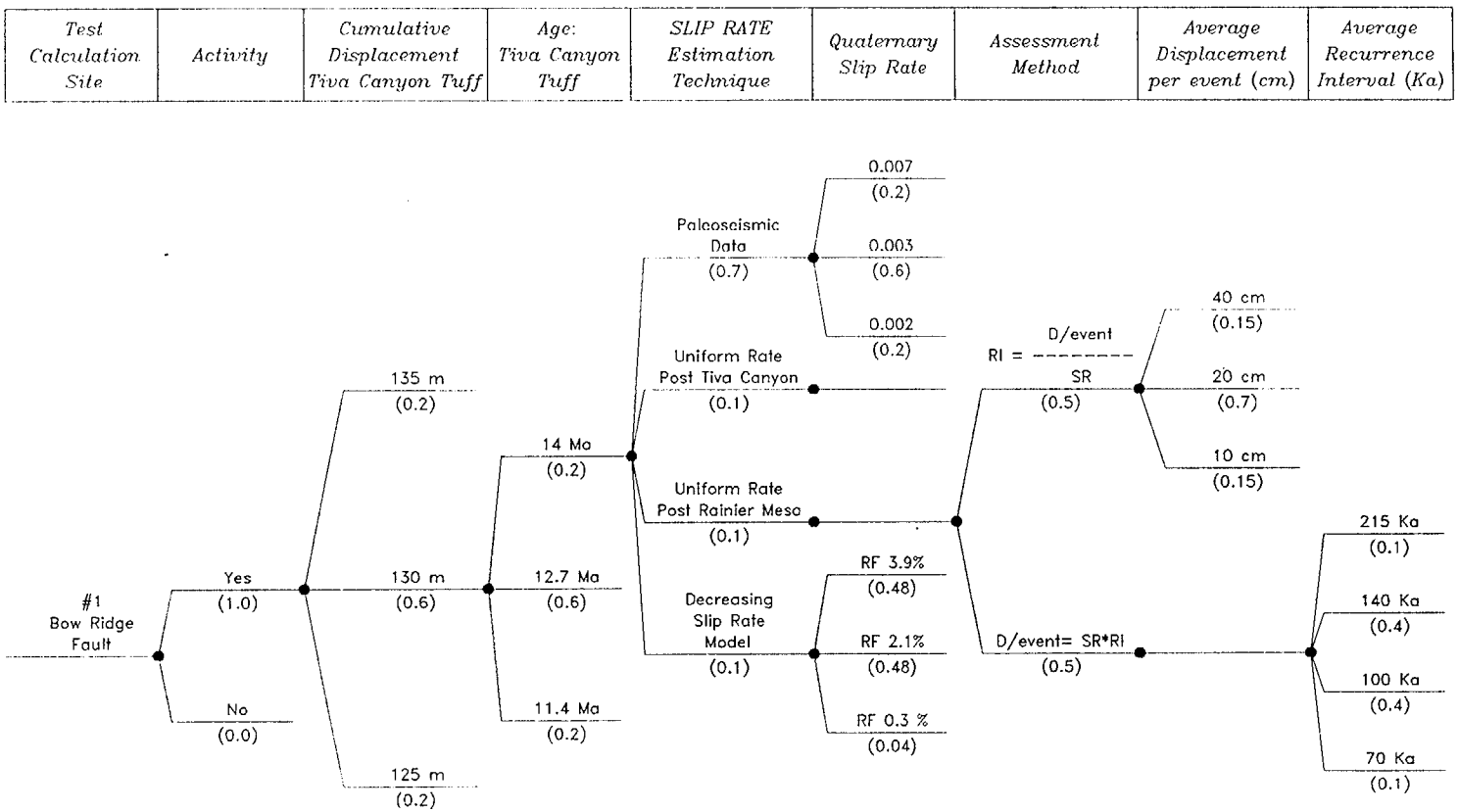

Figure DFS-15 Logic tree used to characterize the fault displacement hazard based on fault slip rates

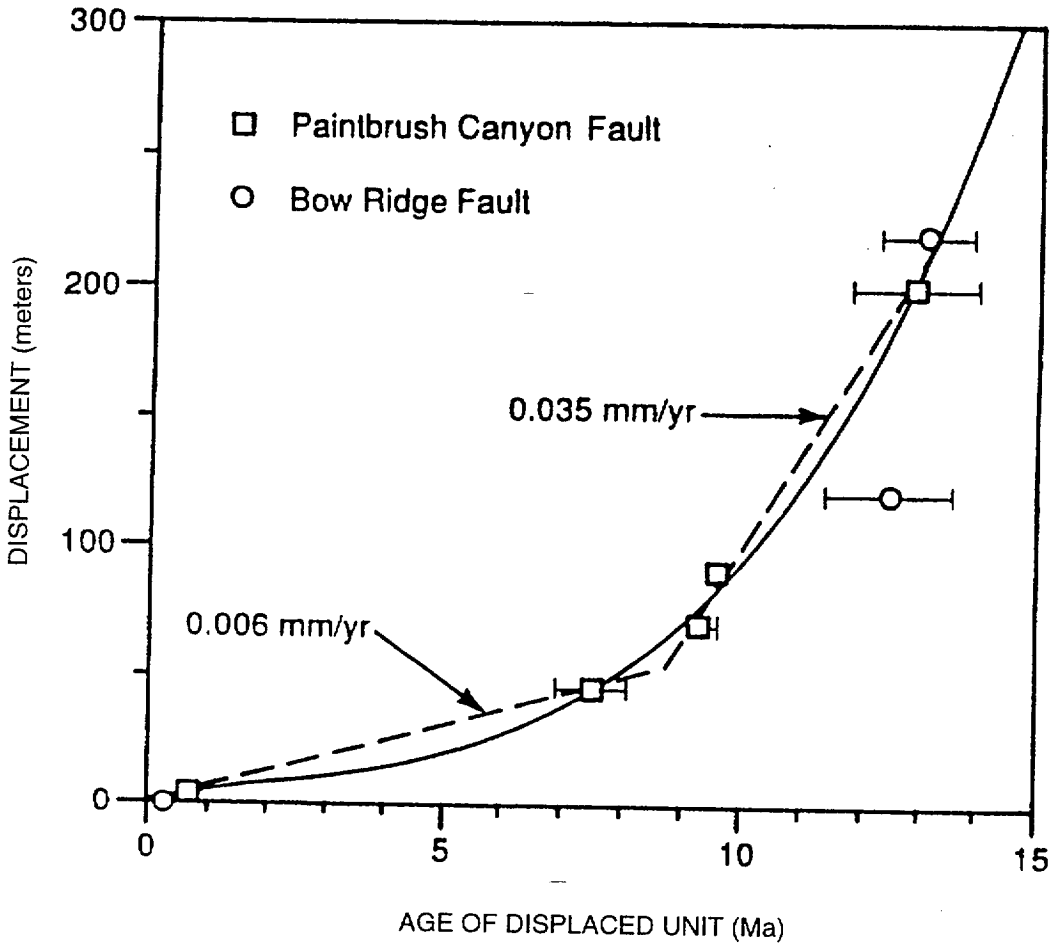

Source: Gibson and others (1990)

Figure DFS-16 Graph showing displacement versus age of displaced unit for the Paintbrush Canyon and Bow Ridge faults (From: J.D. Gibson *et al.*, SNL, written communication, 1992)

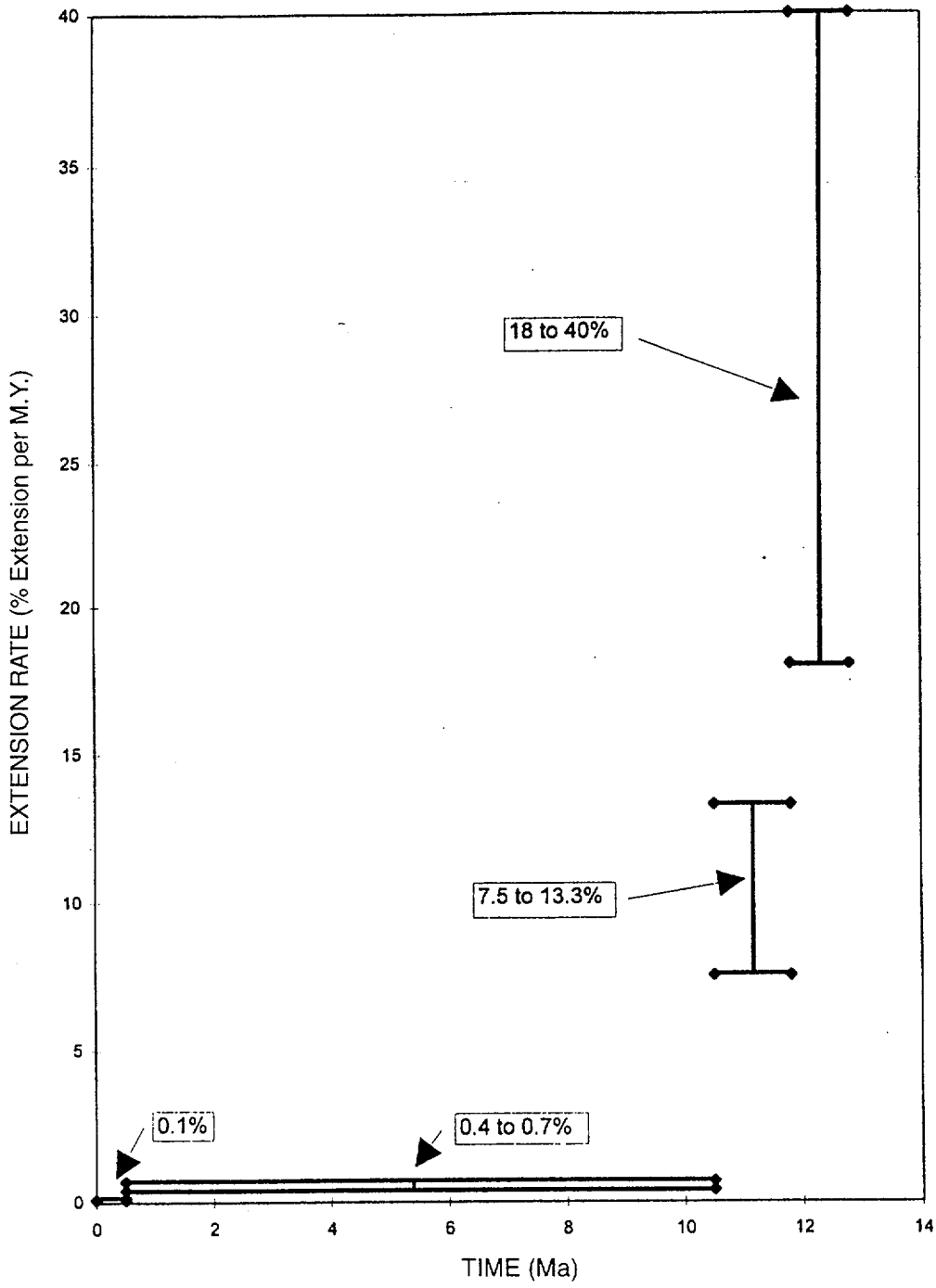

Figure DFS-17 Graph of estimated extension rates in Crater Fault basin from middle Miocene to the present (From C. J. Fridrich *et al.*, USGS, written communication, 1996)

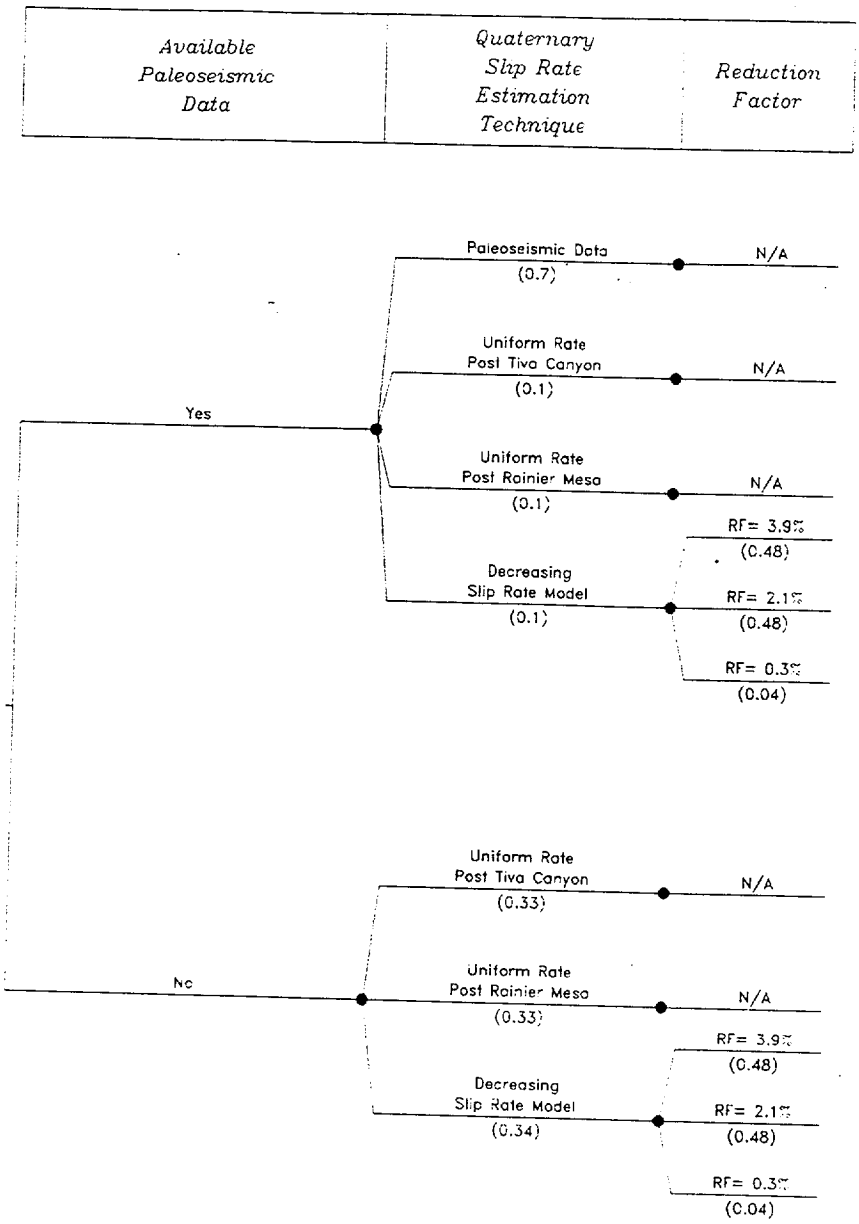

Figure DFS-18 Logic tree showing probability weights assigned to the different Quaternary-slip-rate-estimation techniques depending on the availability of site-specific paleoseismic information.

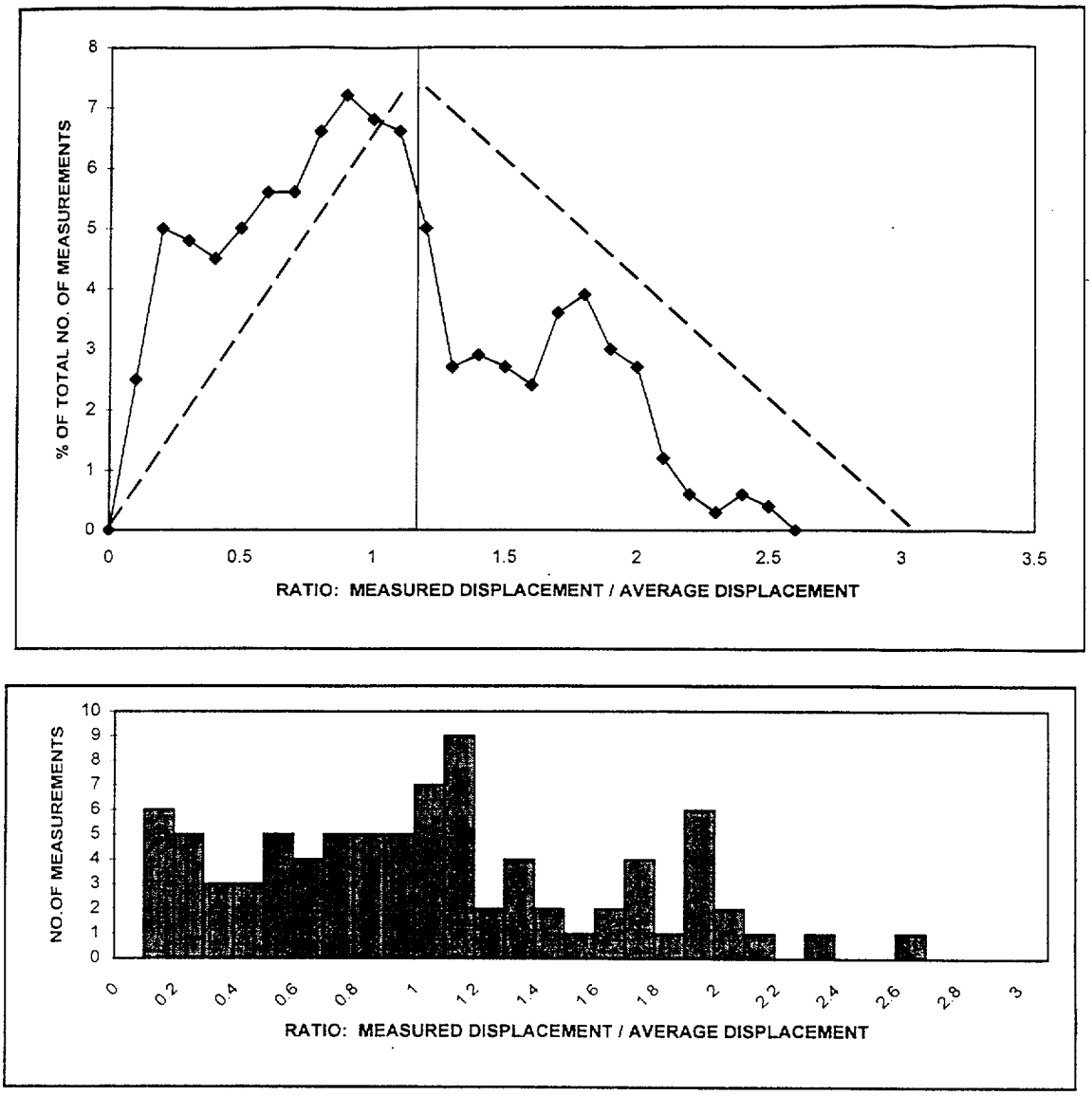

Figure DFS-19 Plots showing event-to-event variability in displacement relative to average displacement per event at a location along a fault based on data from paleoseismic investigations in the Yucca Mountain area.

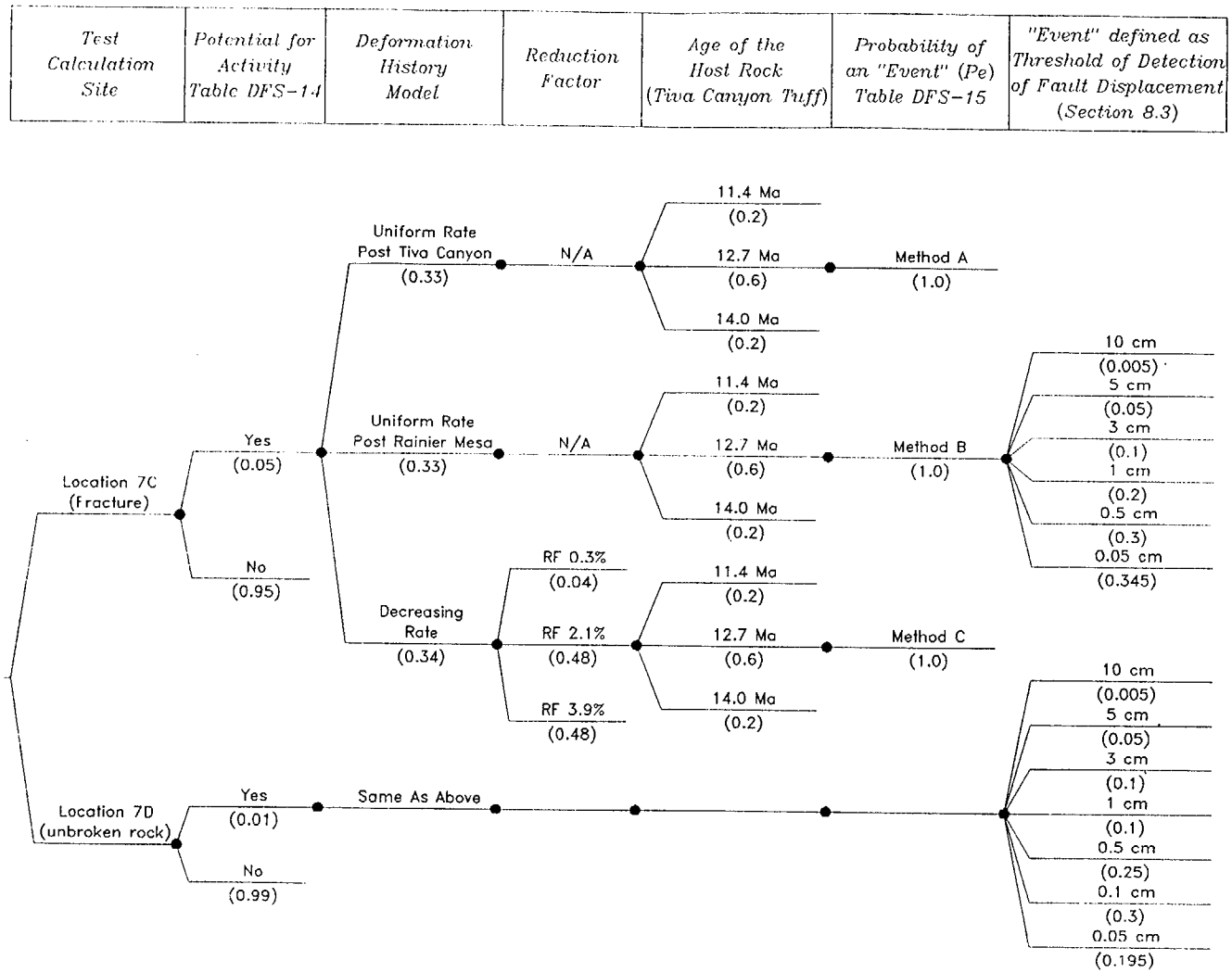

Figure DFS-20 Logic tree for assessing potential fault displacement hazard across a fracture or in unbroken rock.

ELICITATION SUMMARY

ALBERT M. ROGERS, JAMES C. YOUNT, AND LARRY W. ANDERSON

TABLE OF CONTENTS

TABLES

FIGURES

ELICITATION SUMMARY
ALBERT M. ROGERS, JAMES C. YOUNT, LARRY W. ANDERSON

1.0
INTRODUCTION

Yucca Mountain is located in the southern Great Basin of Nevada. The physiography and tectonic setting of this area are the product of late Cenozoic crustal extension and silicic volcanism that occurred primarily between 17 and 9 million years ago. This deformation created a complex structural setting that presents significant interpretational difficulties. A number of tectonic models, developed to explain this structural diversity, were presented and discussed at the Yucca Mountain Workshops held between October 1996 and April 1997. For example, see Carr (1982, 1990); Carr *et al.* (1986); Scott (1990); and Hamilton (1988). D. W. O'Leary (USGS, written communication, 1996) provides an extensive review of models and references, as well as a preferred interpretation. These models each have unique merit in explaining certain aspects of the structural evolution and present-day seismotectonic setting of the Yucca Mountain area. Although tectonic models can be useful tools, none of the models presented provide a complete, unified explanation of all the seismic, geologic, and geophysical data for Yucca Mountain and the larger Walker Lane-western Great Basin-Death Valley regions. Therefore, our approach was first to examine what appear to be the primary potential seismogenic sources, and then to use geologic and geophysical constraints to define the source properties. We find that a coalescing fault model best fits the Yucca Mountain structural domain. A question raised at several workshops was whether the Yucca Mountain faults are capable of generating earthquakes. For our assessment, faults in the Bare Mountain-Yucca Mountain area are treated as potential seismic sources. We include the following seismic sources in our assessment of the earthquake hazard at Yucca Mountain: (1) background seismicity not associated with mapped faults; (2) Yucca Mountain faults, which we interpret to have varying degrees of lateral and vertical coalescence; (3) the Bare Mountain fault; (4) volcanic activity; and (5) large, regional, late Quaternary faults.

Our analysis is based on the following fundamental interpretations: (1) the Bare Mountain fault is a planar seismogenic fault that penetrates to mid-crustal depths; (2) the faults at Yucca Mountain are planar to listric and coalesce into one, two, or three master faults at

unknown depths above or at the Bare Mountain fault; the depth at which this coalescence occurs is considered an uncertain variable (see D. W. O'Leary, USGS, written communication, 1996, for a summary of the geologic and geophysical data that support these assumptions; theoretical modeling also provides support for steeply dipping and coalescing faults); and (3) other faults, not mapped at the surface, exist in the region that can produce earthquakes below the threshold magnitude for surface rupture.

Yucca Mountain faults are considered to behave independently and/or truncate downdip in a detachment fault or a zone of decoupling. Our evaluation of Yucca Mountain faults as coalescing at variable depths implicitly includes independent rupture and truncation, although we believe that the data exclude the possibility of a seismic detachment. Because no earthquakes have been observed on detachments faults worldwide (e.g., Jackson, 1987), we do not consider them to be seismically active structures; we remain unconvinced by arguments that the historical record is too short to include earthquakes on such faults worldwide (Wernicke, 1995).

Our analysis considers regional faults that are interpreted to be steeply dipping planar faults penetrating to mid-crustal depths. Because of their distance from the site and low contribution to the hazard, these faults are modeled more simply, with little variation in downdip width. In general, we model only the larger regional faults within 100 km of Yucca Mountain, as explained below; however, we do consider background seismicity, either as uniformly distributed faults or as a smoothed historical seismicity.

2.0 SEISMIC SOURCES

The logic tree that defines our interpretations of potential seismic sources for the Yucca Mountain area is given on Figures RYA-1a and b. Various aspects of these seismic sources are discussed below. We indicate the weights assigned to the branches of the tree on the figures or in the tables that follow.

2.1 THICKNESS OF THE SEISMOGENIC CRUST

The maximum thickness of the brittle crust (with assigned probability) is interpreted to be: 12 km (0.2), 15 km (0.7), and 20 km (0.1) (Figure RYA-1b). These depths represent the limits observed for both small- and large-magnitude earthquakes (e.g., Rogers *et al.*, 1987, 1991; K. Smith, SSC Workshop 2; Harmsen and Bufe, 1991; and Doser and Smith, 1989). The largest earthquakes in the southern Great Basin occur to depths of 20 km; smaller earthquakes tend to occur above about 10 and 12 km (with some exceptions). The assessment of seismogenic crustal depth is independent of the other source interpretations, and the ensuing source characteristics for the Yucca Mountain area depend on this quantity; therefore, the depth of the brittle crustal is the first assessment on the logic tree.

2.2 AREAL OR BACKGROUND SOURCES

The region within a 100-km radius surrounding the Yucca Mountain site has been divided into three zones, which are defined by different rates of seismicity and structural characteristics (Figure RYA-2). Zone A encloses the local Yucca Mountain area. It is characterized by low seismicity; Quaternary volcanism; northerly trending, anastomosing, and branching faults that appear to belong to the same structural domain; and a basement graben structure illuminated by a gravity low that may extend south into the Amargosa trough. Zone B, which surrounds Zone A, includes the Basin and Range and parts of the Walker Lane tectonic provinces. Seismic rates in Zone B are higher than those in Zone A. Structurally, Zone B is highly complex, consisting of mixed zones of volcanism; northerly trending, block-bounding faults; and northeast-trending, left-lateral and northwest-trending, right-lateral faults. Zone C consists of the Death Valley-Furnace Creek fault zone and faults to the west, such as the Hunter Mountain and Panamint fault zones. It is characterized by long faults having higher rates of slip than the faults of Zones A or B.

2.2.1 Recurrence

In our analysis, background seismicity was interpreted to be non-uniform or uniform. In the non-uniform case, the observed seismicity was smoothed in a manner similar to that described by Frankel (1995). This method was applied to preserve the observed spatial characteristics of the historical earthquake record while including a degree of geographical

variation through spatial smoothing. Spatial seismicity smoothing is assigned a weight of 0.6, because short-term seismicity patterns are considered good predictors of future short-term seismicity (McGuire and Barnhard, 1981). A Gaussian smoothing function was applied to the cumulative gridded earthquake counts for two correlation distances: 5 and 15 km. The relatively shorter h-values were used to retain the spatial concentrations of seismicity. We assign the highest weight to the short-wavelength smoother on the basis that the accuracy of earthquake location is closer to ± 5 km than to ± 15 km, on average (K. Smith, SSC Workshop 2; Rogers *et al.*, 1987). Smoothing was conducted within the boundaries of each source zone shown on Figure RYA-2, considered a hard boundary for the spatial smoothing model. The derived rates were used with a truncated Gutenberg-Richter recurrence relationship for earthquakes below the threshold magnitude of surface faulting, discussed below.

In the uniform smoothing interpretation (weight 0.4), Zones A, B, and C are modeled as equivalent to having faults that are distributed uniformly throughout each zone. This interpretation smooths the observed seismic rate uniformly across each zone. Hence, historical seismicity is interpreted to be spatially stationary only on a zonal basis, and individual seismic clusters are assumed to be possible anywhere within the zone. The modeled faults are distributed with a uniform 1-km spacing within Zone A so that fault spacing does not artificially induce geographic variation in the computed hazard. The faults can have any length, although the rupture areas depend on the magnitude. The square rupture patches are distributed randomly on the faults. The rupture areas are constrained below the near-surface Tertiary rocks, because we assume that faults penetrating these rocks do not store significant shear strain when slip propagates from the deeper parts of the fault toward the surface; fault segments in the Tertiary sedimentary section are modeled as passive slip without significant energy release through shaking. Hence, in the model the faults are constrained below a depth of 2 km.

The seismicity rates on faults within zones A, B, and C were calculated by fitting truncated exponential relationships (e.g., Youngs and Coppersmith, 1985) to declustered catalog versions 5 and 7 within 100 km of Yucca Mountain. In this analysis, we used the Weichert maximum likelihood method (Weichert, 1980). Earthquake aftershocks were removed from the version 5 catalog using a declustering routine developed by Youngs *et al.*, 1987;

aftershocks also were removed from the version 7 catalog using a declustering technique, termed the Veneziano method, developed for EPRI (McGuire, 1985). We give equal weight to the catalogs, because we have no basis for preferring one to the other. We determined a- and b-values from the catalogs using these techniques and the following procedures. Figures RYA-3 and RYA-4 show maps of the declustered catalogs used in our analyses. Figures RYA-5 and RYA-6 show modified Stepp plots (Stepp, 1972) used to calculate the period of complete detection and reporting of earthquakes as a function of magnitude bin. If the rate of earthquake occurrence is constant over the long term, then, as the historical period increases, these curves should approach a constant annual rate; however, if detection and reporting of earthquakes becomes incomplete as the historical period increases, these curves will show a negative slope. The point at which the slope of these curves changes from zero to negative is termed the completeness time. Based on the spacing of these curves, we judged that the earthquake magnitude range of 1.5 to 2.0 is incompletely reported for all times. Although this bin could be complete for the Yucca Mountain region, it likely is incomplete for the 100-km circle. We exclude it from our calculations for this reason. Table RYA-1 shows the preferred completeness times and the ranges we inferred from these plots. We randomly selected from within these completeness ranges the corresponding annual earthquake rate from the Stepp plots. In separate trials, we used either uniform sampling or truncated normal distributions having a mean at the preferred values and a standard deviation of five years. The randomly selected annual rates were fit with a truncated Gutenberg-Richter relationship to obtain a- and b-values for each random selection. This procedure was repeated for 200 trials. Histograms of the resulting b-values are shown on Figures RYA-7, -8, -9, and -10. These figures show that the b-values have narrow distributions; modal values for catalog 5 range from 1.08 (normal distribution) to 1.09 (uniform distribution). For catalog 7, b-values of about 1.16 (normal distribution) to 1.17 (uniform distribution) were determined. We used the uniform distribution because it expresses the greatest uncertainty, as might be expected.

The consistently higher b-values for catalog 7 may be related to less complete removal of aftershocks. Typical recurrence curves for the modal b-value are shown on Figures RYA-11 (catalog 5) and RYA-12 (catalog 7). These figures show that the fitting technique weights the low- to mid-magnitude range most heavily; the largest-magnitude bin has little influence, but it also has the fewest earthquakes and, consequently, the largest expected error in the annual rate. For each b-value bin, we can assign a corresponding a-value based on the

correlation between a- and b-values observed in the Monte Carlo simulation. This correlation is shown on Figures RYA-13 and RYA-14. Based on this analysis, we used the b- and a-value pairs and their respective probabilities shown in Table RYA-2. (Note that the bin probabilities were determined using larger bins than shown on the figures.)

A proportioning process was applied to the a- and b-value pairs for the 100-km circle in each distribution above to compute corresponding distributions for each subzone. The total number of earthquakes greater than or equal to magnitude 3 in each subzone were counted in each magnitude bin over the preferred completeness time for that bin. These binned earthquake counts were summed separately for each zone and for the 100-km circle to obtain the cumulative number of earthquakes above this magnitude for the entire zone and its subzones. The ratio of counts in each zone to the total count in the 100-km circle then was computed. These ratios were used to proportion the anti-logarithm of the a-values, given above, to obtain cumulative earthquake counts for each subzone. The corresponding b-values and probability levels are carried along with their proportioned a-values. These proportioned counts and corresponding b-values were used to compute truncated recurrence relationships for each subzone.

2.2.2 Maximum Magnitude

We interpret background earthquakes to be caused by ruptures that do not intersect the Earth's surface. Based on the work of S. K. Pezzopane and T. E. Dawson (USGS, written communication, 1996), Pezzopane (SSC Workshop 3), and dePolo (1994), we consider the maximum background earthquake magnitude to be Mw = 6.3 ±0.3. We use weights (0.185, 0.63, and 0.185) to simulate the 5th percentile, mean, and 95th percentile in a normal distribution.

2.3 LOCAL FAULT SOURCES

Within Zone A (the local Yucca Mountain area), we consider three alternative structural models: pure planar faults that behave independently, faults that lie above a detachment or zone of decoupling and respond passively to slip on a buried fault, and faults that are planar to listric but that coalesce downdip. In the planar fault model, each fault identified at Yucca Mountain is considered seismogenic and is modeled as an independent seismic source that exists from the surface downdip through the entire seismogenic crust. In the detachment or

decoupled model, the surface faults could be seismic sources, but they more likely represent a relatively passive response to earthquakes occurring on buried sources below the detachment. In the coalescing fault model for Yucca Mountain, individual faults mapped at the surface are assumed to merge or coalesce downdip and along strike and, as such, to operate as a group or groups of faults in generating earthquakes. Various groups of faults, therefore, are considered synchronous seismic sources (Figure RYA-1b).

The coalescing model is our preferred model because it is the only one that appears to account for most of the spatial and temporal fault characteristics at Yucca Mountain; that is, the close fault spacing, the merging and bifurcating of faults, and the very short mapped length for some faults that have large single-event displacements. Further, the coalescing fault model explains the apparent synchroneity of faulting on multiple Yucca Mountain faults at about 70 ka (i.e., the ash event; S. K. Pezzopane *et al.*, USGS, 1996a; Figure RYA-15). In the planar fault model, this apparently synchronous event would be considered the result of the coincidental rupture of multiple, independent faults, some of which are relatively short. We do not consider this interpretation to be geologically plausible. Some investigators have discussed the possible presence in the Yucca Mountain area of a buried strike-slip fault or a seismogenic detachment fault (e.g., Wernicke, 1995; Scott, 1990; Schweickert and Lahren, 1997; J. Bell and R. Schweickert, SSC Workshop 3; Wernicke, SSC Workshop 4). In these models the faults above a detachment or zone of decoupling may be seismogenic or nonseismogenic, and the primary seismogenic source(s) lie below the detachment or zone of decoupling. Such models commonly require unlikely fault geometry, such as a long but narrow fault, produced because the fault is constrained below a detachment and above the brittle-ductile boundary. Furthermore, our coalescing sources include as end members both the independent fault treatment and the fault truncation-detachment model. Hence, we eliminated these models and included only the coalescing sources in our logic tree.

2.3.1 Coalescing Fault Structure

Seismogenic fault sources are defined as faults capable of generating earthquakes of magnitude ≥ 5. Criteria for evaluating whether a fault is seismogenic include evidence for Quaternary displacement, a minimum length of 5 km measured along scarps of equivalent age, paleoseismic displacements of at least tens of centimeters (i.e., not a cracking event), and a possible spatial association of the fault with observed seismicity. The primary independent

seismogenic sources considered for Yucca Mountain are the Windy Wash, Solitario Canyon, and Paintbrush Canyon faults (Table RYA-3). The Fatigue Wash, Iron Ridge, Bow Ridge, and Stagecoach Road faults are not considered independent sources because of their short lengths and spatial association to other nearby faults. The maximum northern extent of the Paintbrush Canyon fault is taken from the map of Frizzell and Shulters (1990). For the Solitario Canyon and Windy Wash faults, the northern extent is taken to be the bedrock ridge south of Yucca Wash (Simonds *et al.*, 1995; A. R. Ramelli and J. W. Bell, Nevada Bureua of Mines and Geology, written communication, 1997). The maximum southern extent of the Windy Wash and Stagecoach Road faults is taken from A. R. Ramelli and J. W. Bell (Nevada Bureau of Mines and Geology, written communication, 1996). The lack of Quaternary geomorphic expression in Amargosa Valley suggests that the Yucca Mountain faults do not extend south of the Lathrop Wells cone.

The Crater Flat fault system is not considered a seismic source because of the short lengths of its features and the absence of significant mid- to late Quaternary displacement on those features (see S. K. Pezzopane *et al.*, USGS, written communication, 1996a). Further, the short distance between the Crater Flat faults and the faults of the Windy Wash system suggest that the Crater Flat faults are antithetic to the Windy Wash system.

Except for the Bare Mountain (BM) fault, all the faults near Yucca Mountain are interpreted to merge downdip at relatively shallow depths (2 to 5 km) and to rupture in groups of two or more faults during individual earthquakes. The groups of faults therefore are considered to represent individual seismic sources, with the Paintbrush Canyon (PBC), Solitario Canyon (SC), and Windy Wash (WW) faults representing the primary seismogenic structures in the three-fault system (Figure RYA-16). The combinations of faults in each group are shown in the logic tree and in Tables RYA-4, RYA-5, and RYA-6.

The Bare Mountain fault always behaves independently in this model, although synchronous, secondary fault rupture could occur on some of the westernmost faults at Yucca Mountain, such as the Windy Wash. Faults in the Yucca Mountain site vicinity are considered to coalesce at depth, forming one to three groups. The branch in the logic tree that represents only one group of faults is assigned a relatively low weight (0.1 to 0.3 depending on crustal thickness) because of the large spacing between the faults (10 km across all of the mapped

faults). Given their steep dips at the surface, it appears unlikely that all the faults coalesce downdip into a single structure within the 12 to 20 km thickness of the seismogenic crust. If they did, the Paintbrush Canyon fault (PBC) would be the primary rupture source in this interpretation. The principal evidence favoring a single group of faults is the apparent contemporaneous surface rupture among several faults, which is represented by the 70-ka ash event. On the branch that has two fault groups, the east group is composed of the Paintbrush Canyon (PBC)-Stagecoach Road (SR)-Bow Ridge (BWR) faults (Paintbrush Canyon fault is primary rupture source); the west group consists of the Windy Wash (WW)-Fatigue Wash (FW)-Solitario Canyon (SC)-Iron Ridge (IR) fault systems (Solitario Canyon fault being the primary rupture source). On the branch that is composed of three groups, the east group is PBC-SR-BWR, and the west side of Yucca Mountain comprises two groups, WW-FW and SC-IR.

We consider the faults at Yucca Mountain to coalesce at variable depths. This assessment is based on the pattern of fault spacing shown on maps and geologic cross sections that suggests that many of the Yucca Mountain fault systems intersect at some depth. Coalescing faults can be modeled by allowing each mapped fault trace to intersect the master fault(s) at some depth. We assume that for magnitudes smaller than the maximum, the rupture patch is distributed uniformly on each individual fault combination. For example, a magnitude 6 rupture patch on the east fault group could occur on the Paintbrush Canyon-Stagecoach Road combination or the Paintbrush Canyon-Bow Ridge combination with equal probability; however, for the maximum magnitude (M_{max} ±1/4), we consider that all faults in a group undergo slip.

The Ghost Dance fault has no record of displacement in the past approximately 400 ka. Because of its location within the Yucca Mountain block, its short length, and its lack of Quaternary geomorphic expression, it is not considered a seismogenic source; however, the fault may experience secondary faulting or fracturing. This is discussed in Section 3.

2.3.2 Maximum Magnitude Approach

Several alternative approaches and data sets were considered to assess the maximum magnitude of each local fault source (Wells and Coppersmith, 1994; Mason, 1996; Anderson *et al.*, 1996). We used the Wells and Coppersmith regressions because: (1) the Mason data

are considered more appropriate to the longer faults of the northern Basin and Range (30 to 50 km); and (2) the approach of Anderson *et al.* is untested. In addition, many of the low slip-rate faults used in the analysis of Anderson *et al.* (1996) are thrust faults in Japan. We evaluated maximum magnitudes using rupture length (RL) and rupture area (RA) from the regressions of Wells and Coppersmith (all fault slip styles; the difference between magnitudes for all slip styles versus normal slip faults is small, and more data are used in the regressions for all slip styles), as these are the parameters that have been or can be measured with some confidence. The regressions for RA and RL have smaller standard deviations than the relationships for maximum and average displacement; the range in magnitude value for any measured displacement is approximately ± 1.0 magnitude unit. The displacement relationships also tended to produce unreasonably high stress drops for the shorter faults. For these reasons, we did not use magnitudes based on maximum and average displacement. We give weights of 0.5 each to RA and RL magnitude estimates, because we have no basis for preferring one relationship over the other.

Computation of the maximum magnitude from the fault area relationship of Wells and Coppersmith (1994) was complicated by variability in downdip fault width. Fault width is dependent on the depth of the seismogenic crust, fault dip, and the depth of intersection with the Bare Mountain fault. We calculated the extreme and preferred fault widths based on the extreme and preferred fault dips both for Bare Mountain faults (55, 60, and 65 degrees) and Yucca Mountain faults (60, 67.5, and 75 degrees), and the extreme and preferred depths for the seismogenic crust (12, 15, and 20 km). The middle of each range is the preferred value. Fault width was taken as the downdip distance to the seismogenic zone or the Bare Mountain fault, whichever was shortest. The extreme and preferred magnitudes computed from these widths are shown in Tables RYA-3, 4, and 5. (Note that the PSHA analysis uses the full distribution for fault dip, crustal thickness, and maximum rupture length to develop the distribution for maximum magnitude). Because of the uncertainties in assessing maximum magnitude, we consider the magnitudes computed from the various empirical relationships to be uncertain by ±0.5 magnitude units. The ±0.5 magnitude values are considered to represent 5- and 95-percentile values. The assigned weights are 0.63 assigned to the estimate from the empirical relationships and 0.185 assigned to the ±0.5 magnitude values, which are the appropriate weights for a three-point representation of a normal distribution (Keefer and Bodily, 1983).

2.3.3 Recurrence Approach

We assessed earthquake recurrence rates for each local fault source based on trench data (time between events) (Figure RYA-15) and on fault slip rate information and average displacement values from USGS (written communication, 1996). We give a higher weight to the slip rate (0.7) than to recurrence interval (0.3) because use of recurrence alone appears to overestimate the total slip in the Yucca Mountain area. Slip rates and their associated uncertainties are provided in Tables RYA-3, -4, -5, and -6. We consider slip of greater than 20 cm to represent earthquake occurrence at or above the threshold magnitude for surface faulting. The seismicity on mapped faults was modeled separately with both truncated-exponential (e.g., Anderson, 1979; Youngs and Coppersmith, 1985) and characteristic recurrence relationships (Schwartz and Coppersmith, 1984). The relative weights given to the two recurrence models depend on the degree to which we consider the faults to coalesce; i.e., greater coalescence suggests that the faults behave in a more exponential manner. Thus, for the one-fault system model the exponential model was given a weight of 0.9, whereas it was given 0.1 for the characteristic model. More weight was given the characteristic model in the two-fault system (0.3) and three-fault system (0.5) models. For the characteristic model, the maximum magnitude is considered to lie uniformly in the range M_{max} -1/2 to M_{max}.

2.4 POSSIBILITY OF A BURIED SEISMIC SOURCE

Within the resolution of the data, we consider it possible that a seismic source (possibly strike-slip), buried beneath cover rocks and with no direct surface manifestation, exists within Zone A; however, we conclude that this source is incapable of generating an earthquake larger than the background earthquake, or an earthquake larger than that produced by any other source

considered. Such a buried source, if it exists, is decoupled from surface faults, in that faults at depth may behave differently from faults near the surface, and the boundary between these different faulting styles may be anything from a simple low-angle fault to a zone of transition between passive and active faulting. This region of decoupling, whether a simple plane or a thicker zone, is not considered a seismic source. The surface faults above the decoupled boundary, thought to be seismic sources in the coalescing model discussed above, here are considered nonseismogenic, responding passively to earthquakes generated along a buried, near-vertical source.

The principal evidence for the decoupled structural model is the discrepancy between the earthquakes recorded in the Yucca Mountain region that have normal focal mechanisms at shallow crustal levels and those that have the more common strike-slip mechanisms recorded at depth. Further, megaton nuclear tests at Pahute Mesa produced normal faulting at the ground surface (Bucknam, 1969; McKeown and Dickey, 1969; Maldonado, 1977a, b; Orkild *et al.*, 1969; Snyder, 1971, 1973; Morris, 1971), but modeling of the ground motions from these tests (Aki and Tsai, 1972; Aki *et al.*, 1969; Lay *et al.*, 1984; Wallace *et al.*, 1983, 1985, 1986) indicated energy release consistent with right-lateral slip on north-trending faults at depth. Additional evidence is provided by geologic mapping in the Specter Range east of Yucca Mountain (Burchfiel, 1965), which shows a structural style in the Paleozoic cover that is interpreted as deformation above a buried strike-slip fault.

Two depths of decoupling (5 and 10 km) are considered. The shallower depth is considered a minimum for decoupling, because the seismic reflection data indicate that upper crustal, high-angle faults penetrate beneath the Paleozoic-Tertiary contact at least to this level. Also, the upper depth limit of aftershocks from the Little Skull Mountain earthquake was approximately 5 km (K. Smith, SSC Workshop 2). The greater decoupling depth is considered the maximum that might produce a significant buried earthquake, given the thicknesses considered for the seismogenic crust.

Estimates of M_{max} for the buried source are derived from the rupture area versus maximum magnitude relationship developed by Wells and Coppersmith (1994). Length of the buried source is considered to be 30 km. Thirty kilometers, which is slightly greater than the maximum fault lengths for the main faults at Yucca Mountain, is approximately the length of the north-trending gravity gradients that bound either side of the Amargosa trough. Fault width is estimated by the limits set by the various combinations of seismogenic crustal thickness at depth of decoupling (Table RYA-7). The buried source is considered to have vertical dip.

A 30-km-long buried source would produce an earthquake having a magnitude at or above the background magnitude of 6.3 ±0.3 only for a decoupling depth of 5 km and a thick (20-

km) seismogenic crust. We conclude, therefore, that a buried source is adequately included in our interpretation of the background source and the coalescing fault sources.

2.5 VOLCANIC SOURCE

The eruption of basaltic volcanoes in the site vicinity may be associated with seismicity. Based on observed eruptions within similar volcanic fields, we assess the probability that a volcanic source exists to be 0.7. This seismic source is assessed to be independent of the other seismic sources. The spatial location of future volcanic seismic sources and the recurrence rate are taken from the results of B. M. Crowe *et al.* (LANL, written communication, 1995). Of the numerous results described by B. M. Crowe *et al.* (LANL, written communication, 1995), return periods of 2×10^{-5} to 2×10^{-6} are preferred. The maximum magnitude associated with a volcanic eruption is assessed based on the studies by S. M. Jackson (INEL, written communication, 1994), which consider the largest observed earthquakes associated with the intrusion and eruption of small- to moderate-volume basaltic magmas. An upper limit of $M_{max} = 5.5$ is used based on this work.

2.6 REGIONAL FAULT SOURCES

Eleven regional fault sources in Zones B and C (Figure RYA-17) are identified primarily through our analysis of the data in Piety (1994) and Anderson *et al.* (1995a, b; See Table RYA-8). The eleven sources we identified are considered relevant due to their distance to Yucca Mountain, their length, high slip rates, evidence for late Quaternary surface rupturing earthquakes, or because they have not been studied in enough detail to preclude or adequately characterize their Quaternary activity (i.e., Wahmonie or Cane Spring faults). Several of the faults that H. L. McKague *et al.* (CNRWA, written communication, 1996) consider Type I faults (for example, Keane Wonder, Oasis Valley, Rocket Wash-Beatty Wash, Sarcobatus Flat, and Kawich Range) are not considered relevant to our analysis because of their short length, distance from Yucca Mountain, and studies such as those by Anderson *et al.* (1995a, b) that show that some of these faults either have no significant Quaternary displacement or are much shorter than previously thought. In addition, the so-called Carrara fault (memoranda from D.B. Slemmons, February 3 and 16, 1997, to R. Quittmeyer) is not considered a potential seismic source. Interpretation of aerial photographs and

reconnaissance geologic mapping by L.W. Anderson (unpub. mapping) found no evidence of late Quaternary fault activity in the area of the suspected fault. Our interpretation is that the features cited as evidence for Quaternary fault activity are instead normal fluvial terraces and terrace scarps produced by the southeast-flowing streams that drain the south flank of Bare Mountain (also see mapping of Swadley and Carr, 1987).

Faults within Zones B and C are considered to have the simple planar shape, with downdip widths that penetrate to mid-crust. The faults are assumed to be either near vertical (faults that display primarily strike-slip displacement) or steeply dipping (~60°; faults that display primarily normal or dip-slip displacement). For computing fault rupture areas, we have assumed a 15 km thick seismogenic crust. Estimates of surface rupture length, maximum displacement per event (if available), and slip rate are from the work of Piety (1994), Anderson *et al.* (1995a, b), R. E. Klinger and L. A. Piety (USBR, written communication, 1996), and J. A. Coe *et al.* (USGS, written communication, 1996).

2.6.1 Maximum Magnitude Approach

Empirical relationships developed by Wells and Coppersmith (1994) between magnitude and fault length, fault area, and maximum fault displacement (if available) were used to estimate the maximum magnitudes for the regional faults (Table RYA-8). Equal weights were applied to the computed magnitudes. That is, when three magnitudes were computed, weights of about 1/3 were used and when two magnitudes were computed, weights of 1/2 were used. As was done for the local faults, we consider the magnitudes computed from the various empirical relationships to be uncertain by ±0.5 magnitude units, representing 5- and 95-percentile values.

2.6.2 Recurrence Approach

The slip rates in Table RYA-8 were converted to estimated seismic recurrence rates using estimated displacement per event [the methods indicated by Anderson (1979) and Youngs and Coppersmith (1985)], and using an average b-value from the two catalogs of 1.12 (0.63), with 5 percent and 95 percent distribution values of 1.07 (0.185) and 1.20 (0.185), respectively, based on the distributions developed above.

3.0
FAULT DISPLACEMENT CHARACTERIZATION

3.1 INTRODUCTION

Two types of fault displacement are of potential concern to the Yucca Mountain Controlled Area (the proposed repository block and the associated access and waste handling facilities): (1) **principal** (or primary) faulting and (2) **distributed** (or secondary) faulting. Principal faulting is defined as the displacement along the main fault plane (or planes) responsible for the release of seismic energy during an earthquake. When the fault rupture extends to or near the ground surface, displacement may be represented by a zone of deformation up to several meters wide with measured amounts of fault offset (slip) ranging from several tens of centimeters to several meters. The amount of slip is dependent on the location along the fault and the magnitude of the earthquake. Within the site area, two possible sources of primary faulting have been identified, the Solitario Canyon-Iron Ridge fault system and the Paintbrush Canyon-Stagecoach Road-Bow Ridge fault system (Figure RYA-16 and Table RYA-4).

Distributed faulting is defined as displacement (measured slip as opposed to fracturing; based on our personal experience in the Yucca Mountain area, with the presence of suitable stratigraphic horizons, the uncertainty in the measurement of displacement or non-displacement is about $\pm$ 2.5 cm - anything less than that is essentially zero) that occurs on adjacent or nearby faults (or fractures) in response to an earthquake on another fault. If it occurs at all, distributed faulting is by nature discontinuous and can occur up to several kilometers from the principal fault rupture. Several factors influence the occurrence or non-occurrence of secondary faulting along a pre-existing fault or fracture (S. K. Pezzopane and T. E. Dawson, USGS, written communication, 1996; H. L. McKague *et al.*, CNWRA, written communication, 1996). Among them are: (1) location with respect to the principal fault rupture (hanging wall verses foot wall; (2) fault orientation; (3) sense of previous slip; and, (4) distance to the principal fault rupture or earthquake epicenter. A primary fault also can

undergo distributed displacement or fracturing in response to a nearby earthquake. Paleoseismic trench data probably cannot differentiate between principal and distributed faulting except by size of the measured displacement. However, we believe that displacement from a distributed event will always be smaller than that from a primary event. In our team's review of the Yucca Mountain paleoseismic data (Figure RYA-15), we considered all events in the trenches with less than 20 cm of displacement to represent "cracking" events. Thus, our interpretation is that most of these cracking events are the probable surface representation of distributed faulting events due to strong ground shaking.

The teams were asked to characterize fault displacement potential at nine sites within the controlled area of Yucca Mountain. The nine sites are located:

(1) Along the Bow Ridge fault where it crosses the ESF;

(2) Along the Solitario Canyon fault near the proposed repository block;

(3) Along the Drill Hole Wash fault where it crosses the ESF;

(4) Along the Ghost Dance fault;

(5) Along the Sundance fault west of the ESF;

(6) On a minor unnamed fault west of Dune Wash;

(7) 100 m east of the Solitario Canyon fault that has:

a. a small fault with 2.0 m cumulative slip;
b. a shear with about 10 cm of cumulative displacement;
c. a fracture having no measurable displacement; and
d. intact rock;

(8) Midway between the Solitario Canyon and Ghost Dance faults that has:

a. a small fault with 2.0 m cumulative slip;
b. a shear with about 10 cm of cumulative displacement;
c. a fracture having no measurable displacement; and
d. intact rock; and

(8) Along the Exile Hill fault in Midway Valley.

Two of the study sites (1 and 2) are on faults which are considered to be primary fault sources in our assessment of seismic sources. For the other 7 sites, all are considered to be potential sites for secondary displacement because of their location within an area of Quaternary faulting. However, the relative probability of activity is weighted depending on whether there is evidence for Quaternary (past 1.6 million years) activity associated with the feature, the known length of the feature, amount of total post-Tiva Canyon bedrock displacement, the orientation of the feature, whether there is an existing fault or fracture, or whether the site is on intact bedrock.

3.2 APPROACH

For either primary or secondary displacement, an assessment of the probability of fault displacement requires an assessment of the frequency of occurrence and the amount of displacement if it occurs. The fault displacement hazard at any location can be characterized in terms of the expression:

$$\nu(d) = P(C) \cdot \lambda_{DE} \cdot P(D_E > d) \qquad (1)$$

where $P(C)$ is the probability that the feature can slip in the present tectonic regime, δ_{DE} is the frequency of occurrence of displacement events on the feature, and $P(D_E > d)$ is the probability that a displacement event will exceed a slip of d. The general logic structure for characterizing the parameters of Equation (1) is shown on Figures RYA-18 and RYA-19. Figure RYA-18 shows the approaches appropriate for sites where Quaternary data are available for frequency and size of displacement events and Figure RYA-19 shows the approaches appropriate for sites where paleoseismic data are absent. The components of these approaches are discussed below.

3.2.1 Probability Slip can Occur

The probability that slip can occur on a feature in the present tectonic regime is assessed based on the evidence for recency of slip on the feature and its relationship to the structural elements of Yucca Mountain.

3.2.2 Frequency of Displacement Events

Two approaches are considered for the assessment of the frequency of displacement events: the paleoseismic recurrence intervals and the long-term fault slip rate. For sites where paleoseismic data are available, we believe that the displacement hazard at any of the various sites within the Controlled Area can best be assessed using paleoseismic data for recurrence rates (intervals) (Figure RYA-18). The alternative approach for such locations is to use the estimates of Quaternary slip rates and compute the frequency of displacement events using the expression:

$$\lambda_{DE} = SR / \bar{D}_E \qquad (2)$$

where SR is slip rate and $\bar{D}_E$ is the average displacement per event. This approach is given a weight of 0.2. The procedures used to assess the average displacement per event are described below in Section 3.2.4.

For those sites where direct paleoseismic data is lacking, a slip rate approach is used with a weight of 1.0 (Figure RYA-19). The slip rates are estimated from the total slip of the fault since eruption of the Tiva Canyon Tuff (12.7 ± 1.3 Ma).

Without paleoseismic data or total slip information; i.e., for sites located on fractures showing no displacement or for sites located in unfractured rock, a negligibly low probability of displacement is considered. We consider that: (1) displacement from a future earthquake will be in the same sense as shown by slip indicators from the last displacement event; and (2) displacement on a fault will be confined to the fault's present length; that is, faults do not generally increase in length with each new event.

3.2.3 Estimation of Slip Rate

For those locations where data are available to estimate Quaternary slip rates, these rate estimates are used to assess displacement event frequency (Figure RYA-18). For bedrock faults that either lack specific evidence for Quaternary slip or have no specific paleoseismic data, but that show post-Miocene (post-Tiva Canyon Tuff) displacement, three alternative approaches are considered for assessing the fault slip rate (Figure RYA-19). In the first approach, the total measured cumulative post-Miocene slip is divided by the age of the Miocene rocks (12.7 Ma) . This assumes a uniform slip rate through time. However, the tectonic history of the region suggests that the assumption of uniform rate over time is incorrect. Many data indicate that extensional deformation in the region has waned with time. Therefore, the assumption of uniform slip rate is given a low weight of 0.1. A second alternative is to develop a slip history that follows Fridrich *et al.*'s (1997) regional extensional history. Their analysis suggests that nearly all the regional extension was accomplished in the Crater Flat region by 11 Ma, leaving only small additional extension during Quaternary time. We estimate that 2 percent of the regional extension occurred during the past 1.6 Ma, which is consistent with Fridrich *et al.*=s interpretation. Using this approach, a slip rate for the Quaternary period is calculated on representative faults, applying 2 percent of the observed cumulative slip to estimate the Quaternary rates. This approach is given a weight of 0.6, because it accounts for what appears to be the waning tectonic activity in the region. In a third approach, the time history of Fridrich *et al.* is modified to account for the onset of volcanism in Crater Flat beginning at about 3.7 Ma. This volcanic episode may indicate an increase in tectonic rates in the region since mid-Pliocene. We allow for 20 percent of the measured fault slip to occur within the past 3.7 Ma (weight of 0.3).

3.2.4 Estimation of Average Slip Per Event

For sites where paleoseismic data are available, the average slip per event is estimated from these data (Figure RYA-18). For faults without direct paleoseismic data, analogies to other faults both locally and world wide must be made. The AAR Team at Workshop 6 (June

1997) presented data relating average displacement, $\bar{D}_E$, to total fault length, L or cumulative fault displacement D_{cum} . The AAR Team reanalyzed the data and developed new relations in their draft summary in terms of parameter MD^{max} (the expected maximum displacement in a maximum event). These relationships are:

$$MD^{max} = 1.32 \times 3.69 \times 10^{-5} \times L \text{ (in m)} \quad \textbf{(3)}$$

and

$$MD^{max} = 1.32 \times \beta \times D_{cum} \text{ (m)} \quad \textbf{(4)}$$

where β is a constant that varies for smaller faults (L < 3 km and Dcum < 75 m) between 1.40×10^{-3} (weight of 0.3) and 1.85×10^{-2} (weight of 0.3) with their preferred value of 5.59×10^{-3} (weight of 0.4). For faults with L >3 km and Dcum > 75 m, $B = 1.40 \times 10^{-3}$. We find these results to be reasonable and adopt them to characterize the uncertainty in estimating MD^{max}. They also find that the mean value of $\bar{D}_E / MD^{max} = 0.83$. Thus, to find an estimate of $\bar{D}_E$ simply multiply relations (3) and (4) by 0.83.

$$\bar{D}_E = 0.83 \times 1.32 \times 3.69 \times 10^{-5} \times L \text{ (in m)} \quad \textbf{(5)}$$

and

$$\bar{D}_E = 0.83 \times 1.32 \times \beta \times D_{cum} \text{ (m)} \quad \textbf{(6)}$$

We adopt these approaches for our assessment of sites without paleoseismic data (Figure RYA-19) and give equal weight to the assessments based on the length of the fault, (5) and the cumulative offset (6).

3.2.5 Distribution for Displacement Per Event

Trenching data from Yucca Mountain indicate that displacement per event on a fault varies greatly both at individual sites and along strike (see Figure RYA-15). Recurrence intervals between earthquakes or displacement events also vary greatly. We consider two approaches for assessing the distribution for slip per event. Both approaches are based on analyses of data from trenching studies at Yucca Mountain.

The Doser-Fridrich-Swan (DFS) team developed a distribution for the ratio of $D/\bar{D}_E$ by normalizing data from each trenching site by the average displacement at that location. Figure RYA-20 shows the resulting empirical distribution. The Facilitation Team analyzed these data and indicate that a good fit is obtained by a gamma distribution (see Appendix H, Section H.2.1). We adopt the distribution given in Appendix H for $D/\bar{D}_E$. The Arabasz-Andreson-Ramelli (AAR) team normalized the displacement data by the estimate of MD^{max} for each fault and observed that the ratio of D/MD^{max} could be represented by the exponential distribution shown on Figure RYA-21. We consider these two approaches to be equally applicable to assessing the variability in displacement from event to event and give them equal weight (Figures RYA-18 and RYA-19).

3.3 DATA FOR CHARACTERIZATION OF DISPLACEMENT HAZARD AT THE NINE TEST CALCULATION SITES

Site 1 - Bow Ridge fault where it crosses the ESF

The Bow Ridge fault is about 7 km long and is both a site for primary and secondary faulting as the fault is interpreted to be a splay of the Paintbrush Canyon- Stagecoach Road fault system. Given the evidence for Quaternary displacement, the probability of activity is considered 1.0. Cumulative slip estimated at site 1 is about 100 m (USGS, written communication, 1996, chapter 2). Paleoseismic information (Figure RYA-15) from trenches near site 1 indicate that the average recurrence for surface rupturing, displacement events is

about 75 ka (Table RYA-3) and the Quaternary slip rate for the fault is estimated to be 0.003 mm/yr. Using the Quaternary slip rate and recurrence information yields a average displacement value of 22.5 cm which is just larger than the 20 cm value we use as a break between faulting and cracking events (Table RYA-5). The trench data also indicate that the average displacement is about 21 cm, but the largest measured displacement is 44 cm in one trench (T-14D) and there was only fracturing observed in another nearby trench (T-14). The 44 cm value is our preferred maximum displacement from paleoseismic data. Relation (4) suggests that the maximum displacement for the Bow ridge fault could be about 18 cm whereas relation (3) indicates 34 cm. Relation (7) using the 1.73 factor indicates 49 cm, and relation (6) using the 1.73 factor suggests 26 cm for maximum displacement. The resulting parameters are

$P(C) = 1.0$
$SR = \{0.001 \text{ mm/yr } (0.15), 0.003 \text{ mm/yr } (0.7), 0.006 \text{ mm/yr } (0.15)\}$
$RI_{DE} = \{25 \text{ ka } (0.15), 75 \text{ ka } (0.7), 140 \text{ ka } (0.15)\}$
$\bar{D}_E = \{21 \text{ cm } (1.0)\}$
$MD^{max} = \{44 \text{ cm } (1.0)\}$

Site 2 - Solitario Canyon fault near the proposed repository block

The Solitario Canyon fault is one of the major block bounding faults at Yucca Mountain and is both a primary and a secondary fault displacement source because of the evidence for Quaternary displacement events. Therefore, the probability of activity is considered 1.0. Paleoseismic information (Figure RYA-15) indicates that the recurrence for surface rupturing events (displacement > 20 cm) ranges between 50-130 ka with a preferred value of 75 ka (Table RYA-3). However, a fracturing event that could be the result of secondary faulting apparently occurred on the fault about 25 ka. The paleoseismic Quaternary slip rate for the fault is estimated to be 0.01 mm/yr, and the post-Tiva Canyon cumulative slip estimated at site 2 is 230 m (estimated from cross section of W.C. Day *et al.*, USGS, written communication, 1996a). Although we generally prefer the 2% rule for calculating the Quaternary slip rate, the Solitario Canyon fault is the one fault we know of for which a large difference exists between the paleoseismic Quaternary slip rate estimate and the calculated

Quaternary rate. This suggests, at least for the Solitario Canyon fault, that there has been an increase in activity in the last 2-4 Ma. Be that as it may, we have used the paleoseismic Quaternary slip rate and recurrence information to calculate an average displacement value of 75 cm. Also, our analysis of data in U.S.Geological Survey (written communication, 1996) and shown in Figure RYA-15 indicates that the average displacement is about 75 cm from four trenches. However, at T-4, just to the south of the test site, the displacement during the last event was 30 cm. Since site 2 is near the northern end of the fault where displacement appears to be dying out, one would expect the average slip per event to be less than it is to the south. In addition, the slip rate also is probably less than the 0.01 mm/yr used in the calculations. Relation (4) suggests a maximum displacement of 43 cm, and relation (3) suggests 88 cm. The resulting parameters are:

$P(C) = 1.0$
SR = {0.005 mm/yr (0.15), 0.01 mm/yr (0.7), 0.02 mm/yr (0.15)}
RI_{DE} = {50 ka (0.15), 75 ka (0.7), 130 ka (0.15)}
$\bar{D}_E$ = {30 cm (1.0)}
MD^{max} = {75 cm (1.0)}

Site 3 - Drill Hole Wash fault where it crosses the ESF

The Drill hole Wash fault is considered a possible source for secondary fault displacement only. Although there is no direct paleoseismic information for the fault, given the apparent lack of evidence for Quaternary activity and the northwest strike , the probability of future slip is considered low (0.1). Available information (W. C. Day *et al.*, USGS, written communication, 1996a) indicates that the fault is about 4 km long with maximum displacement of 15 m. Thus, the estimated Quaternary (2%) slip rate is about 0.0002 mm/yr. Using relations (5) and (6) suggests that the average displacement per event could be in the range of 9 to17 cm. These values appear large in comparison to those for other short faults. However, using these displacement values and the slip estimate of 0.0002, the recurrence for such displacement events is on the order of 650 ka. Maximum displacement values are 11 and 20 cm using relations (3) and (4) and they increase to 16 and 29 cm using relations (7) and (8) and the 1.73 factor. The resulting parameters are:

$P(C) = 0.1$
D_{cum} = {5 m (0.15), 15 m (0.7), 25 m (0.15)}
L = {3 km (0.15), 4.2 km (0.7), 5.5 km (0.15)}

Site 4 - Ghost Dance fault

The Ghost Dance fault is considered a source for secondary fault displacement only. Although paleoseismic data indicates that the fault has not experienced unequivocal (>5 cm) surface rupture since the middle Quaternary, the north-south strike of the fault, the same as active faults in the site area indicates that the fault could have potential for future slip. We believe the probability of activity is 0.5. Total length of the fault is about 3 km (W. C. Day *et al.*, USGS, written communication, 1996) and the total displacement at the site is about 25 m. The Quaternary paleoseismic slip rate for the fault has been estimated to be <0.0005 mm/yr, which agrees well with the Quaternary (2%) bedrock slip estimate of 0.0003. The age of the last displacement event appears to be at least 200 ka and may be over 1 Ma (E. M. Taylor *et al.*, USGS, written communication, 1996a). Using the 200 ka age as an average recurrence and a slip rate of 0.0005 suggests average displacements of about 10 cm and 20 cm for maximum displacement (weight of 0.8; Figure RYA-18). Using relations (3) and (4) suggests slightly higher displacement values. The resulting parameters are:

$P(C) = 0.5$
D_{cum} = {20 m (0.15), 25 m (0.7), 30 m (0.15)}
L = {2.5 km (0.15), 3 km (0.7), 5 km (0.15)}

Site 5 - Sundance fault west of the ESF

The Sundance fault is a source for secondary fault displacement only. However, given its northwest strike, short length, and the lack of evidence for Quaternary activity the probability of activity is considered low (0.1). Total mapped length of the fault is only about 600 m (W.C., Day *et al.,* USGS, written communication, 1996) and total displacement is about 8.5 m (E. M. Taylor *et al.*, USGS, written communication, 1996a). Use of relations (5) and (6) suggests that the average displacement for this fault should be on the order of 2-5 cm. This value, in conjunction with an estimated Quaternary (2%) slip rate of 0.00001 yields a recurrence of 3.5 Ma. The resulting parameters are:

$P(C) = 0.1$
D_{cum} = {6 m (0.15), 8.8 m (0.7), 11 m (0.15)}
L = {0.2 km (0.15), 0.6 km (0.7), 1.0 km (0.15)}

Site 6 - Minor unnamed fault west of Dune Wash

Any unnamed fault west of Dune Wash is considered a source for secondary fault displacement only. Without site specific paleoseismic data and without knowing the strike, sense of slip for the fault, and length, the probability of activity is considered to be 0.2. We have assumed total slip at the site to be about 4 m (slightly less than the tunnel diameter) and an unknown length of about 1 km. Our preferred slip rate for the fault is 0.00005 mm/yr. Using relations (5) and (6) suggest an average displacement of 2-4 cm. This yields a recurrence of about 600 ka. The resulting parameters are:

$P(C) = 0.2$
D_{cum} = {2 m (0.15), 4 m (0.7), 6 m (0.15)}
L = {0.5 km (0.15), 1.0 km (0.7), 1.5 km (0.15)}

Site 7 - 100 m east of the Solitario Canyon fault

Four situations or conditions are evaluated for site 7. (a) A small fault with 2.0 m cumulative slip, (b) a shear with about 10 cm of cumulative displacement, (c) a fracture having no measurable displacement, and (d) intact rock. For example 7a adjacent to the Solitario Canyon fault, the potential for activity is considered higher than for site 8a (0.5 verses 0.3). For example 7a and the purpose of our analysis, we have assumed that the total displacement at the site is 1.25 m, yielding a preferred Quaternary (2%) slip rate of 0.00002 mm/yr. We do not know the length of the fault but comparison to site 6 and the Ghost Dance fault suggests the length is probably less than 1 km. From this, we estimate the average displacement to be about 1cm. This would equate to a recurrence of 500 ka. For example 7b, the fault length is probably insignificant given a total displacement of 10 cm. The Quaternary (2%) slip rate for this feature would be 0.000001 mm/yr. We assume displacement per event of 1 cm (essentially at or below the level of detection). This would indicate a recurrence of 1 Ma. For examples (c) and (d) there is an essentially 0 probability of displacement. The resulting parameters are:

Point 7a: cumulative offset 2 m
$P(C) = 0.5$
D_{cum} = {2 m (1.0)}
L not known

Point 7b: cumulative offset 10 cm
$P(C) = 0.3$
D_{cum} = {0.1 m (1.0)}
L not known

Point 7c: fracture with no measurable cumulative offset
$P(C) = 0$

Point 7d: intact rock
$P(C) = 0$

Site 8 - Midway between the Solitario Canyon and Ghost Dance faults

The same four situations used for site 7 were evaluated for site 8. The only difference between this site and site 7 is the increased distance to a potentially active fault. Thus, we have given this fault a low activity weight. The resulting parameters are:

Point 8a: cumulative offset 2 m

$P(C) = 0.3$
D_{cum} = {2 m (1.0)}
L not known

Point 8b: cumulative offset 10 cm
$P(C) = 0.1$
D_{cum} = {0.1 m (1.0)}
L not known

Point 8c: fracture with no measurable cumulative offset
$P(C) = 0$

Point 8d: intact rock
$P(C) = 0$

Site 9 - Along the Exile Hill fault in Midway Valley

The Exile Hill fault is an approximately 3 km long, north-south striking fault in Midway Valley. Work by F. H. Swan *et al.* (Geomatrix Consultants, written communication, 1995) indicates that essentially no detectable displacement has occurred on the fault in the middle to late Quaternary (limits of detection essentially 0-5 cm) although at least two fracturing events may have occurred. Because Quaternary fracturing may have been associated with this fault, the probability of activity is considered 0.7. Slip rate has been estimated to be similar to the Ghost Dance fault, <0.0005, although total slip is less than half that of the Ghost Dance (10 m). Considering the evidence for no measurable displacement in at least the last several hundred thousand years and the limited amount of total slip, the average slip per event must be small. Thus, the estimate of about 5 cm for average slip per event which is near the detection level. This leads to an estimate of >100 ka for displacement events. Using relations (5) and (6) suggests 6 and 13 cm for average displacements. Relations (3) and (4) suggest 7 and 16 cm for maximum displacement and (5) and (6) and the 1.73 factor suggest 10 and 22 cm for maximum displacement. The resulting parameters are:

$P(C) = 0.7$
D_{cum} = {5 m (0.15), 10 m (0.7), 15 m (0.15)}
L = {2 km (0.15), 3.2 km (0.7), 4.4 km (0.15)}

REFERENCES

Aki, K., Reasenberg, P., DeFazio, T., and Tsai, Y., 1969, Near-field and far-field seismic evidences for triggering of an earthquake by the Benham explosion: Seismological Society of America Bulletin, v. 59, p. 2197-2207.

Aki, K., and Tsai, Y., 1972, Mechanism of long-wave excitation by explosive sources: Journal of Geophysical Research, v. 77, p. 1452-1475.

Anderson, J.G., 1979, Estimating the seismicity from geological structure for seismic risk studies: Bulletin of the Seismological Society of America, v. 69, p. 135-158.

Anderson, R.E., Bucknam, R.C., Crone, A.J., Haller, K.M., Machette, M.N., Personius, S.F., Barnhard, T.P., Cecil, M.J., and Dart, R.L., 1995a, Characterization of Quaternary and suspected Quaternary faults, regional studies, Nevada and California: U.S. Geological Survey Open-File Report 95-599, 56 p.

Anderson, R.E., Crone, A.J., Machette, M.N., Bradley, L., and Diehl, S.F., 1995b, Characterization of Quaternary and suspected Quaternary faults, Amargosa area, Nevada and California: U.S. Geological Survey Open File Report 95-613, 41 p.

Anderson, J.G., Wesnousky, S.G., and Stirling, M.W., 1996, Earthquake size as a function of fault slip rate: Bulletin of the Seismological Society of America, v. 86, p. 683-690.

Bucknam, R.C., 1969, Geologic effects of the Benham underground nuclear explosion: Bulletin of the Seismological Society of America, v. 59, p. 2209-2220.

Burchfiel, B.C., 1965, Structural geology of the Specter Range quadrangle, Nevada, and its regional significance: Geological Society of America Bulletin, v. 76, p. 175-192.

Carr, W.J., 1982, Volcano-tectonic history of Crater Flat, southwestern Nevada, as suggested by new evidence from Drill Hole USW-VH-1: U.S. Geological Survey Open-File Report 82-457, 53 p.

Carr, W.J., 1990, Styles of extension in the Nevada Test Site region, southern Walker Lane Belt—an integration of volcano-tectonic and detachment fault models, *in* Wernicke, B.P., ed., Basin and Range Extensional Tectonics Near the Latitude of Las Vegas, Nevada: Geological Society of America Memoir 176, p. 283-303.

Carr, W.J., Byers, F.M.J., and Orkild, P.P., 1986, Stratigraphic and volcano-tectonic relations of Crater Flat tuff and some older volcanic units: U.S. Geological Survey Professional Paper 1321, 23 p.

DePolo, C.M., 1994, The maximum background earthquake for the Basin and Range province, western North America: Bulletin of the Seismological Society of America, v. 84, p. 466-472.

Doser, D.I., and Smith, R.B., 1989, An assessment of source parameters of earthquakes in the Cordillera of the Western United States: Bulletin of the Seismological Society of America, v. 79, p. 1383-1409.

Frankel, A., 1995, Mapping seismic hazard in the Central and Eastern United States: Bulletin of the Seismological Society of America, v. 66, p. 8-21.

Fridrich, C. J., Whitney, J. W., Hudson, M. R., and Crowe, B. M., 1997, Space-time patterns of late Cenozoic extension, vertical-axis rotation, and volcanism in the Crater Flat basin, Nevada, *in* Wright, L. A. and Troxel B. W., eds., Cenozoic Basins of the Death Valley Region, California and Nevada: Geological Society of America Special Paper 1996 (in press).

Frizzell, V.A. Jr., and Shulters, J., 1990, Geologic map of the Nevada Test Site, southern Nevada: U.S. Geological Survey Miscellaneous Investigations Map I-2046, scale 1:100,000.

Hamilton, W.B., 1988, Detachment faulting in the Death Valley region: U.S. Geological Survey Bulletin 1790, p. 51-85.

Harmsen, S.C., and Bufe, C., 1991, Seismicity and focal mechanisms for the southern Great Basin of Nevada and California, 1987 through 1989: U.S. Geological Survey Open-File Report 91-572, 208 p.

Jackson, J.A., 1987, Active normal faulting and crustal extension, *in* Coward, M.P., Dewey, J.F., and Hancock, P.L., eds., Continental-Extensional Tectonics: Geological Society of London Special Publication No. 28, p. 3-17.

Keefer, D.L., and S.E. Bodily, 1983, Three-point approximations for continuous random variables: Management Science, v 29, p 595-609.

Lay, T., Wallace, T.C., and Helmberger, D.V., 1984, The effects of tectonic release on short-period P-waves from NTS nuclear explosions: Bulletin of the Seismological Society of America, v. 74, p. 819-842.

Maldonado, F., 1977a, Composite postshot fracture map of Pahute Mesa, Nevada Test Site, June 1973 through March 1976, Nevada Operations Office, U.S. Energy Research and Development Administration: U.S. Geological Survey, Denver, USGS-474-243, 11 p.

Maldonado, F., 1977b, Results from fault-monitoring stations on Pahute Mesa, Nevada Test Site, from July 1973 through December 1976, Nevada Operations Office, U.S. Energy Research and Development Administration: U.S. Geological Survey, Denver, USGS-474-242, 32 p.

Mason, D.B., 1996, Earthquake magnitude potential of the Intermountain seismic belt, USA, from surface-parameter scaling of late Quaternary faults: Bulletin of the Seismological Society of America, v. 86, p. 1487-1506.

McGuire, R.K., 1985, Seismic hazard methodology for nuclear facilities in the Eastern United States: Dames and Moore, Golden, Vol. 2, Appendix A, EPRI Research Project Number P101-29.

McGuire, R.K., and Barnhard, T.P., 1981, Effects of temporal variations in seismicity on seismic hazard: Bulletin of the Seismological Society of America, v. 71, p. 321-334.

McKeown, F.A., and Dickey, D.D., 1969, Fault displacements and motion related to nuclear explosions: Bulletin of the Seismological Society of America, v. 59, p. 2253-2269.

Morris, R.H., 1971, Geologic effects, *in* Geologic and Hydrologic Effects of the Handley Event, Pahute Mesa, Nevada Test Site: U.S. Geologic Survey USGS-474-95, Denver, Colorado, p. 7-26.

Orkild, P.P., Sargent, K.A., and Snyder, R.P., 1969, Geologic map of Pahute Mesa, Nevada Test Site and vicinity, Nye County, Nevada: U.S. Geological Survey Miscellaneous Geologic Investigations Map I-567, scale 1:48,000.

Piety, L.A., 1994, Compilation of known and suspected Quaternary faults within 100 km of Yucca Mountain, Nevada and California: U.S. Geological Survey Open-File Report 94-112.

Rogers, A.M., Harmsen, S.C., Corbett, E.J., Priestley, K., and dePolo, D., 1991, The seismicity of Nevada and some adjacent parts of the Great Basin, *in* Slemmons, D.B., Engdahl, E.R., Zoback, M.D., and Blackwell, D.D., eds., Neotectonics of North America: Geological Society of America, p. 153-184.

Rogers, A.M., Harmsen, S.C., and Meremonte, M.E., 1987, Evaluation of the seismicity of the southern Great Basin and its relationship to the tectonic framework of the region: U.S. Geological Survey Open-File Report 87-408, 196 p.

Schwartz, D.P., and Coppersmith, K.J., 1984, Fault behavior and characteristic earthquakes—examples from the Wasatch and San Andreas fault zones: Journal of Geophysical Research, v. 89, p. 5681-5698.

Schweickert, R.A., and Lahren, M.M., 1997, Strike-slip fault system in Amargosa Valley and Yucca Mountain, Nevada: Tectonophysics, v. 272, p. 25-41.

Scott, R.B., 1990, Tectonic setting of Yucca Mountain, southwest Nevada, in Basin and Range extensional tectonics near the latitude of Las Vegas, Nevada: Geological Society of America Memoir 176, p. 251-282.

Simonds, F.W., Fridrich, C.J., Hoisch, T.D., and Hamilton, W.B., 1995, A synthesis of detachment fault studies in the Yucca Mountain region, *in* Topical Meeting on Methods of Seismic Hazards Evaluation—Focus '95, Las Vegas, Nevada: American Nuclear Society, p. 107-114.

Snyder, R.P., 1971, Composite postshot fracture map of Pahute Mesa, Nevada Test Site; Energy Research Development Administration, U.S. Geologic Survey, Denver, USGS-474-100, 17 p.

Snyder, R.P., 1973, Recent fault movement on Pahute Mesa, Nevada Test Site, from May 1970 through June 1973: Energy Research and Development Administration, U.S. Geological Survey, Denver, USGS-474-137, 32 p.

Stepp, J.C., 1972, Analysis of completeness of the earthquake sample in the Puget Sound area and its effects on statistical estimates of earthquake hazard: Proceedings, First Microzonation Conference, Seattle, Washington, p. 897-909.

Swadley, W.C., and Carr, W.J., 1987, Geologic map of the Quaternary and Tertiary deposits of the Big Dune quadrangle, Nye County, Nevada, and Inyo County, California: U.S. Geological Survey Miscellaneous Investigations Series Map I-1767.

Wallace, T.C., Helmberger, D.V., and Engen, G.R., 1983, Evidence of tectonic release from underground nuclear explosions in long-period P-waves: Bulletin of the Seismological Society of America, v. 73, p. 593-613.

Wallace, T.C., Helmberger, D.V., and Engen, G.R., 1985, Evidence of tectonic release from underground nuclear explosions in long-period S-waves: Bulletin of the Seismological Society of America, v. 75, p. 157-174.

Wallace, T.C., Helmberger, D.V., and Lay, J., 1986, Reply to comments by A. Douglas, J.B. Yolong, and N.S. Lyman and a note on the revised moments for Pahute Mesa tectonic release: Bulletin of the Seismological Society of America, v. 76, p. 313-318.

Weichert, D.H., 1980. Estimation of the earthquake recurrence parameters for unequal observation period for different magnitudes: Bulletin of the Seismological Society of America, v. 70, p. 1337-1346.

Wells, D.L., and Coppersmith, K.J., 1994, New empirical relationships among magnitude, rupture length, rupture width, rupture area, and surface displacement: Bulletin of the Seismological Society of America, v. 84, p. 974-1002.

Wernicke, B., 1995, Low-angle normal faults and seismicity—a review: Journal of Geophysical Research, v. 100, p. 20,159-20,174.

Youngs, R.R., and Coppersmith, K.J., 1985, Implications of fault slip rates and earthquake recurrence models for probabilistic seismic hazard estimates: Bulletin of the Seismological Society of America, v. 75, p. 939-964.

Youngs, R.R., Swan, F.H., III, Power, M.S., Schwartz, D.P., and Green, R.K., 1987, Probabilistic analysis of earthquake and ground shaking hazard along the Wasatch Front, Utah, *in* Gori, P.O., and Hays, W.W. eds., Assessment of Regional Earthquake Hazards and Risk Along the Wasatch Front, Utah: U.S. Geological Survey Open File Report 87-585, p. M-1 to M-100.

TABLE RYA-1
COMPLETENESS TIMES

VERSION 5 CATALOG (YEARS)			
MW Magnitude Bin	**Lower Limit**	**Preferred Value**	**Upper Limit**
1.5-2.0	2.6	2.8	7.7
2.0-2.5	1.4	8.3	12.0
2.5-3.0	9.3	11.2	18.9
3.0-3.5	7.4	8.2	12.9
3.5-4.0	8.2	16.6	29.7
4.0-4.5	19.6	26.1	44.6
4.5-5.0	empty	Empty	Empty
5.0-5.5	51.2	85.8	85.8
5.5-6.0	85.8	85.8	85.8
VERSION 7 CATALOG (YEARS)			
1.5-2.0	3.0	6.0	6.0
2.0-2.5	6.0	8.0	16.0
2.5-3.0	6.5	11.0	17.0
3.0-3.5	9.5	25.0	37.0
3.5-4.0	15.7	37.0	40.0
4.0-4.5	35.4	47.0	55.0
4.5-5.0	57.2	62.0	62.0
5.0-5.5	empty	Empty	empty
5.5-6.0	85.6	85.6	85.6

TABLE RYA-2
INTERVAL RECURRENCE PARAMETERS

VERSION 5 CATALOG		
b-Value	**a-Value**	**Probability**
-1.088	4.13	0.020
-1.065	4.15	0.065
-1.075	4.17	0.215
-1.085	4.22	0.215
-1.095	4.24	0.285
-1.105	4.26	0.155
-1.115	4.28	0.040
-1.125	4.32	0.005
VERSION 7 CATALOG		
-1.125	4.24	0.010
-1.135	4.36	0.020
-1.145	4.38	0.060
-1.155	4.41	0.125
-1.165	4.44	0.175
-1.175	4.46	0.167
-1.185	4.48	0.167
-1.195	4.51	0.125
-1.205	4.53	0.075
-1.215	4.56	0.075
-1.225	4.58	0.005

TABLE RYA-3
FAULT SOURCES PARAMETERS, AREA A

Fault [1]	Fault Length (km) [2]	Max.; Average Disp./Event (cm) [3]	Maximum Magnitude (Mw) [4]	Age Most Recent Event (ka) [5]	Estimated Recurrence (kyr) [6]	Late Quaternary Slip Rate (mm/yr) [7]
BM	11-40; 23	150; 100	(6.3, 6.6., 6.9) (RL) (6.2, 6.6, 7.1) (RA)	40 ± 20	80-150 100	0.01
PBC	13-28; 13	100; 50	(6.4, 6.4, 6.8) (RL) (6.2, 6.4, 6.8) (RA)	13 ± 3 (c)	37-75 50	0.005-0.013
SR	4-9; 7	67; 55	(5.8, 6.1, 6.2) (RL) (5.7, 6.1, 6.3) (RA)	13 ± 3	15-40; 25	0.02
BWR	4-10; 7	44; 21?	(5.8, 6.1, 6.2) (RL) (5.7, 6.1, 6.4) (RA)	75 ± 10	75?	0.003
WW	12-26; 23	88; 50	(6.3, 6.7, 6.7) (RL) (6.1, 6.5, 6.6) (RA)	6 ± 4 (c) 40 + 20	30-100; 46	0.01
FW	7-16; 11	105; 61	(6.1, 6.3, 6.5) (RL) (6.0, 6.3, 6.6) (RA)	40 ± 20 (c) 75 ± 10	30-100; 46	0.002
SC	12-21; 18	120; 75	(6.3, 6.5, 6.6) (RL) (6.2, 6.5, 6.7) (RA)	25 ± 10	50-130; 90	0.01
IR	6-9; 8	130; 100	(6.0, 6.1, 6.2) (RL) (5.9, 6.1, 6.3) (RA)	25 ± 10	?	?

[1] Named faults that comprise the fault systems are: BM, Bare Mountain; PBC, Paintbrush Canyon; SR, Stagecoach Road; BWR, Bow Ridge; WW, Windy Wash; FW, Fatigue Wash; SC, Solitario Canyon; and IR, Iron Ridge. Bare Mountain fault data from L. W. Anderson and R. E. Klinger (USBR, written communication, 1996a), all other fault data (displacement, age of most recent event, recurrence, and slip rate) based on review and analysis of data in USGS (written communication, 1996). Bare Mountain fault assumed to dip 55, 60, or 65 degrees to the east; Yucca Mountain faults assumed to dip 60, 67.5, or 75 degrees to the west. Faults are assumed to have pure normal to normal-oblique slip.

[2] Minimum and maximum fault lengths; preferred estimate. Distance measured along strike of fault system, primarily from Simonds *et al.* (1995). Maximum lengths from A. R. Ramelli and J. W. Bell (Nevada Bureau of Mines and Geology, written communication, 1996) and Frizzell and Shulters (1990). Maximum fault areas can be calculated by multiplying fault length by fault width (fault width calculated using dip of fault and seismogenic depth of 12, 15, or 20 km).

[3] Maximum displacement is largest single-event displacement measured or calculated from trench exposure. Average displacement represents average of all displacement values from the various trenches on the specific fault.

[4] (RL) indicates magnitudes calculated from the "all faults" Mw-fault length relationship of Wells and Coppersmith (1994). The three magnitudes given are computed from the minimum, preferred, and maximum fault length values. (RA) indicates magnitudes calculated from the "all faults" Mw-fault area relationship of Wells and Coppersmith (1994). The three magnitudes given are computed from the smallest, preferred, and largest areas for a fault given that the Yucca Mountain faults may dip between 60 and 75 degrees; Bare Mountain may dip between 55 and 65 degrees; and the thickness of the seismogenic crust is 12, 15, or 20 km (see text for a discussion of the magnitudes and weights used in the PSHA). Relative weights are 0.5 for RL and 0.5 for RA.

[5] "Cracking" event (displacement less than 20 cm) indicated by (c).

[6] Upper numbers represent elapsed time between faulting events as interpreted from trench data (USGS, written communication, 1996; Figure RYA-15). Lower number is an estimate of average recurrence using slip rate and average displacement per event. Preferred recurrence model is the "characteristic model" of Schwartz and Coppersmith (1984), assigned a relative weight of 0.9, and applied to the estimate of average recurrence only.

[7] Uncertainty probably ± 0.005 mm/yr.

TABLE RYA-4
COALESCING FAULT SOURCE MODEL, AREA A
THREE YUCCA MOUNTAIN FAULT SYSTEMS

Fault System [1]	Max. Fault Length (km) [2]	Max. Combined Disp/Event (m) [3]	Maximum Magnitude (Mw) [4]	Age Most Recent Event (ka)	Estimated Avg. Recurrence (kyr) [6]	Late Quaternary Slip Rate (mm/yr) [7]
BM (planar)	11-40; 23	1.5; 1.0	(6.3, 6.6, 6.9) (RL) (6.2, 6.6, 7.1) (RA)	40 ± 20	80-150; 100	0.01
PBC-SR-BWR	7-35; 20	1.0; 0.5	(6.1, 6.5, 6.8) (RL) (6.0, 6.5, 6.9) (RA)	13 ± 3	15-75; 25	0.005-0.02; 0.01
WW-FW	11-25; 23	1.13; 0.46	(6.3, 6.7, 6.7) (RL) (6.0, 6.5, 6.6) (RA)	6 ± 4; [5] 40 ±20	30-100; 46	0.01
SC-IR	8-21; 20	1.2; 0.75	(6.1, 6.6, 6.6) (RL) (6.0, 6.5, 6.7) (RA)	25 ± 10	50-130; 75	0.01

TABLE RYA-5
COALESCING FAULT SOURCE MODEL, AREA A
TWO YUCCA MOUNTAIN FAULT SYSTEMS

Fault System [1]	Max. Fault Length (km) [2]	Max. Combined Disp/Event (m) [3]	Maximum Magnitude (Mw) [4]	Age Most Recent Event (ka)	Estimated Avg. Recurrence (ka) [8]	Late Quaternary Slip Rate (mm/yr) [7]
BM (planar)	11-40; 23	1.5; 1.0	(6.3, 6.6, 6.9) (RL) (6.2, 6.6, 7.1) (RA)	40 ± 20	80-150; 100	0.01
East Side (SR-PBC-BWR)	7-35; 20	1.0; 0.5	(6.1, 6.5, 6.8) (RL) (6.0, 6.5, 6.9) (RA)	13 ± 3	15-75 50	0.005-0.02; 0.01
West Side (WW-FW-SC-IR)	8-26; 23	2.3; 1.8	(6.1, 6.7, 6.7) (RL) (5.9, 6.5, 6.6) (RA)	6 ± 4; [5] 40 ± 20	30-130 90	0.02-0.03; 0.025

---

[1] Named faults that comprise the fault systems are: BM, Bare Mountain; SR, Stagecoach Road; PBC, Paintbrush Canyon; BWR, Bow Ridge; WW, Windy Wash; FW, Fatigue Wash; SC, Solitario Canyon; and IR, Iron Ridge. Bare Mountain fault data from L. W. Anderson and R. E. Klinger (USBR, written communication, 1996a); all other fault data (displacement, age of most recent event, recurrence, and slip rate) based on review and analysis of data in USGS (written communication, 1996). Bare Mountain fault assumed to dip 55, 60, or 65 degrees to the east; Yucca Mountain faults assumed to dip 60, 67.5, or 75 degrees to the west. In this model, all sources are considered seismogenic. Bare Mountain fault is always an independent source. Faults are assumed to have pure normal to normal-oblique slip.

[2] Minimum and maximum rupture lengths; preferred estimate. Distance measured along strike of fault system, primarily from Simonds *et al.* (1995). Minimum rupture length assumes rupture only of preferred length of shortest part of fault system. Maximum rupture includes possible southern projections from A. R. Ramelli and J. W. Bell (Nevada Bureau of Mines and Geology, written communication, 1996) and northern bedrock projections from Frizzell and Shulters (1990). Probabilities for each rupture scenario are minimum (0.15), maximum (0.15), and preferred (0.7).

Notes for Tables RYA-4 and RYA-5 (Cont'd.):

[3] Maximum displacement is largest single-event displacement measured or calculated from trench exposure. Because the Windy Wash and Fatigue Wash fault systems are parallel, the maximum is the sum of the maximum displacement values for each fault. Average displacement represents the average of all displacement values from the various trenches on the specific fault.

[4] (RL) indicates magnitudes calculated from the all faults" Mw-fault length relationship of Wells and Coppersmith (1994). The three magnitudes given are computed from the minimum, preferred, and maximum fault length values. (RA) indicates magnitudes calculated from the "all faults" Mw-fault area relationship of Wells and Coppersmith (1994). The three magnitudes given are computed from the smallest, preferred, and largest areas for a fault given that the Yucca Mountain faults may dip between 60 and 75 degrees; Bare Mountain may dip between 55 and 65 degrees; and the thickness of the seismogenic crust is 12, 15, or 20 km (see text for a discussion of the magnitudes and weights used in the PSHA). Relative weights are 0.5 for RL and 0.5 for RA.

[5] 6 ± 4 ka age is for 6-cm "cracking" event on Windy Wash fault. 40 ± 20 ka age is for penultimate 35-cm displacement event also on Windy Wash fault.

[6] Upper numbers represent time between faulting events as interpreted from trench data (USGS, written communication, 1996; Figure RYA-15). Lower number is an estimate of average recurrence for maximum magnitude events using slip rate and average displacement per event. No preferred recurrence model. The "characteristic model" of Schwartz and Coppersmith (1984) is given a weight of 0.5, and the exponential magnitude distribution model also is given a weight of 0.5. This applies to the average recurrence only.

[7] Ranges and preferred slip rate. Relative weights are 0.15 for maximum and minimum and 0.7 for preferred estimate. Uncertainty in slip rate estimates probably ± 0.005 mm/yr.

[8] Upper numbers represent elapsed time between faulting events as interpreted from trench data. Lower number is an estimate of average recurrence for maximum magnitude events using slip rate and average displacement per event. Preferred recurrence model is the exponential magnitude distribution, using the average recurrence estimates, and is assigned a weight of 0.7.

TABLE RYA-6
COALESCING SOURCE MODEL, AREA A
ONE FAULT SYSTEM[1]

Fault System [1]	Maximum Fault Length (km) [2]	Maximum Combined Disp./Event (m) [3]	Age Most Recent Event (ka)	Estimated Average Recurrence (kyr) [4]	Slip Rate (mm/yr) [5]	Maximum Magnitude (M_W) [6]
BM (planar)	11-40; 23	1.5; 1.0	40 ± 20	80-150; 100	0.01	(6.3, 6.6, 6.9) (RL) (6.2, 6.6, 7.1) (RA)
PBC/SR (master fault)	25	3.3	75 ± 10	73.3-94.3; 82.5	0.35-0.45; 0.4	6.7 (RL) (6.1, 6.6, 6.9) (RA)

1 Bare Mountain fault remains independent source. (See Table RYA-3 or RYA-4.) The Paintbrush Canyon/Stagecoach Road (PBC/SR), fault is the master fault. Other named faults within the fault system are the Bow Ridge, Windy Wash, Fatigue Wash, Solitario Canyon, and Iron Ridge. All fault data (displacement, age of most recent event, recurrence, and slip rate) based on review and analysis of data in USGS (written communication, 1996). Faults are assumed to have pure normal to normal-oblique slip.

2 Distance measured along strike of Windy Wash-Solitario Canyon fault system, primarily from Simonds *et al.* (1995). Maximum rupture includes possible southern projections from A. R. Ramelli and J. W. Bell (Nevada Bureau of Mines and Geology, written communication, 1996).

3 Maximum displacement for the fault system is the sum of the largest single-event displacements measured or calculated from all the trench exposures of all the faults.

4 Recurrence estimate (range and preferred) for maximum magnitude events calculated from maximum displacement and slip rate estimates. Preferred recurrence model is the exponential magnitude distribution, assigned a weight of 0.9. The characteristic earthquake recurrence model is given a weight of 0.1.

5 Range and preferred slip rates. Based on the sum of late Quaternary slip rates for the major parallel faults; uncertainty probably ±0.02 mm/yr.

6 (RL) indicates magnitudes calculated from the "all faults" Mw-fault length relationship of Wells and Coppersmith (1994). The three magnitudes given are computed from the minimum, preferred, and maximum fault length values. (RA) indicates magnitudes calculated from the "all faults" Mw-fault area relationship of Wells and Coppersmith (1994). The three magnitudes given are computed from the smallest, preferred, and largest areas for a fault given that the Yucca Mountain faults may dip between 60 and 75 degrees; Bare Mountain may dip between 55 and 65 degrees; and the thickness of the seismogenic crust is 12, 15, or 20 km (see text for a discussion of the magnitudes and weights used in the PSHA). Relative weights are 0.5 for RL and 0.5 for RA. Historical analogs may be the 1932 Cedar Mountain earthquake of M7.2 and the 1959 Hebgen Lake earthquake of M7.4.

TABLE RYA-7
M_{max} FOR HYPOTHESIZED BURIED SEISMIC SOURCE 30 KM LONG
(M_{max} DERIVED FROM M = 4.04+0.98 LOG [RUPTURE AREA])
(WELLS AND COPPERSMITH, 1994)

Decoupled Depth (km)	Thickness of Seismic Crust (km)	Rupture Area (km^2)	M_{max}
5	12	210	6.3
5	15	300	6.5
5	20	450	6.7
10	12	60	5.8
10	15	150	6.2
10	20	300	6.5

TABLE RYA-8
SIGNIFICANT REGIONAL FAULT SOURCE PARAMETERS, AREAS B and C

FAULT[1]	Fault Rupture Length (km); Max. Disp/Event (m)[2] Dip (deg.) & Direction	Maximum Magnitude (M_w)[3]	Age Most Recent Event (ka)	Estimated Recurrence (ka)[4, 5]	Slip Rate (mm/yr)[5]	Reference[6]
Wahmonie (WAH; 22)	15; ? 90	6.4 (RL) 6.3 (RA)	<180	90?	0.02	1, 6
Rock Valley (RV; 25)	30 (20-40); 2.5-3.9 90	6.8 (RL) 7.3 (MD) 6.7 (RA)	<10	25-195	0.02-0.1	1, 5
Cane Spring (CS; 28)	20 (14-27); ? 90	6.6 (RL) 6.5 (RA)	<1.8 Ma ?	?	0.02	1
Ash Meadows (AM; 30)	40 (34-47); 1.8 90	6.9 (RL) 6.9 (MD) 6.8 (RA)	>10	>120-180	< 0.01	1, 3
Yucca Flat (YC; 40)	25; ? 90	6.7 (RL) 6.6 (RA)	<10	?	0.08	1, 6
Furnace Creek (FC; 52)[7]	105 (100-111); 4.5 90	7.4 (RL) 7.2 (MD) 7.2 (RA)	>0.2	0.6 - 0.8	4-8	4
Death Valley (DV; 54)[7]	60 (45-76); 3.5 60 W	7.2 (RL) 7.1 (MD) 7.0 (RA)	>0.2	0.5-1.0	3-5	4
West Spring Mts (WSM; 56)	36 (30-56); 2.0 60 W	6.9 (RL) 6.9 (MD) 6.8 (RA)	10	28-124	0.02-0.07	1, 2
Belted Range (BLR; 64)	30 (20-51); 0.9 60 W	6.8 (RL) 6.7 (MD) 6.7 (RA)	<10	9-90	0.01-0.1	1, 2
Pahrump-Stewart Valley (PSV; 65)	35 (18-42); 2.0 90	6.9 (RL) 6.9 (MD) 6.7 (RA)	<10	100-167	0.009-0.02	1, 3
West Pintwater (WPR; 76)	55 (55-60); ? 60 W	7.1 (RL) 7.0 (RA)	>10	?	0.01-0.1	1

Notes for Table RYA-8

[1] Letters and numbers in parentheses are fault abbreviations and distance in kilometers to Yucca Mountain; distance measured from Piety (1994).

[2] Preferred estimate of surface fault rupture length based on review and analysis of mapped scarp and fault length from cited references (weight 0.7). Numbers in parentheses indicate minimum and maximum values (weight 0.15 each). Where no range given, assumes rupture of entire mapped trace. Displacement estimates are from profile or trench data in cited reference. 90 degree dip assumes sense of displacement primarily strike-slip, 60 degree assumes displacement primarily dip-slip.

[3] Magnitudes estimated from regressions of Wells and Coppersmith (1994) for all faults using preferred estimated surface rupture length (RL), maximum displacement (MD), and rupture area (RA). Relative weights are 0.35 for SRL, 0.35 for RA, and 0.3 for MD or 0.5 for RL and 0.5 for RA depending on available data. Magnitudes estimated to be $\pm$ 0.5 magnitude units for RL and RA.

[4] Recurrence estimates calculated from displacement and slip rate estimates. Characteristic recurrence model given weight of 0.9; truncated exponential recurrence model is given weight of 0.1.

[5] Where a range of values is given, equal weight is assigned to end member values.

[6] References:

(1) Piety (1994).
(2) Anderson (1995a).
(3) Anderson (1995b).
(4) R. E. Klinger and L. A. Piety, USBR, written communication, 1996.
(5) J. A. Coe *et al.* USGS, written communication, 1996.
(6) Yount, J., unpub. mapping.

Simultaneous rupture of Death Valley and Furnace Creek faults would result in M_W 7.7 earthquake; however, the probability of this event is low, 10%.

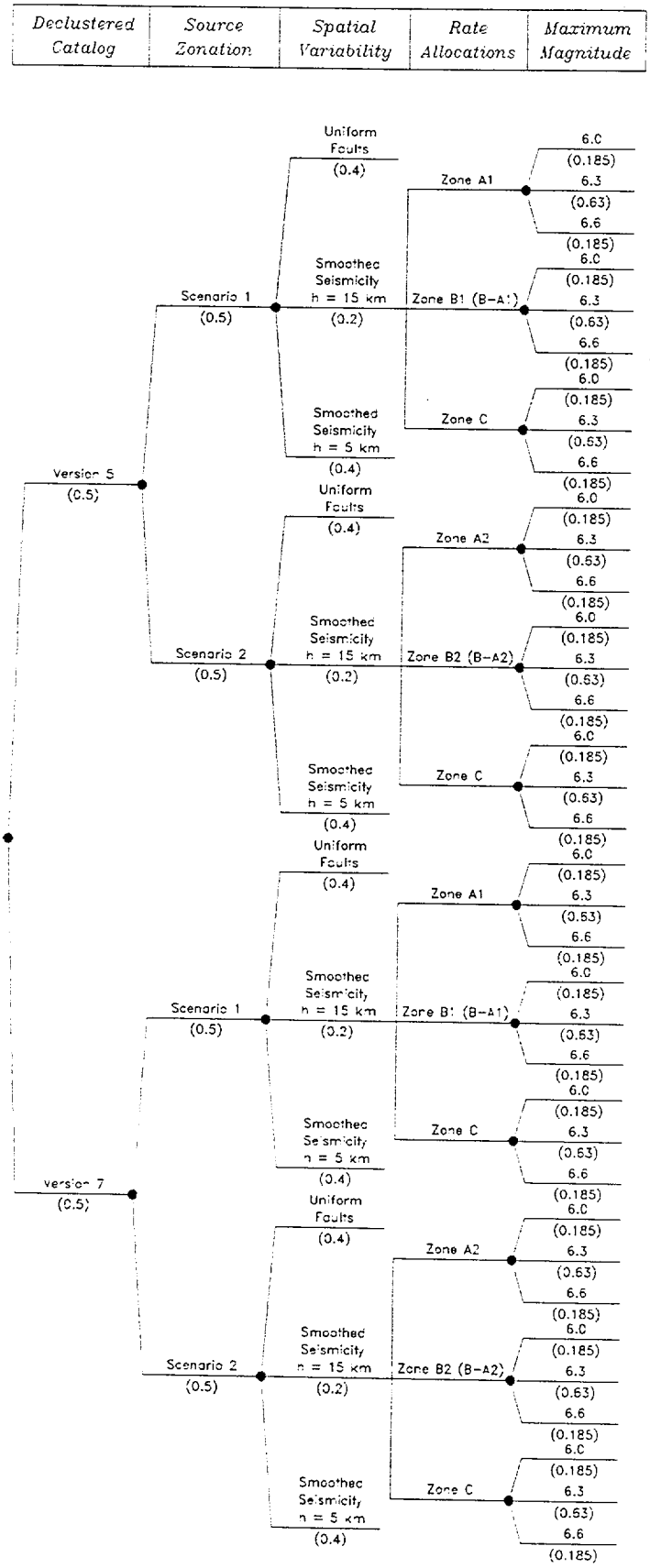

Figure RYA-1a Logic tree for background source zones

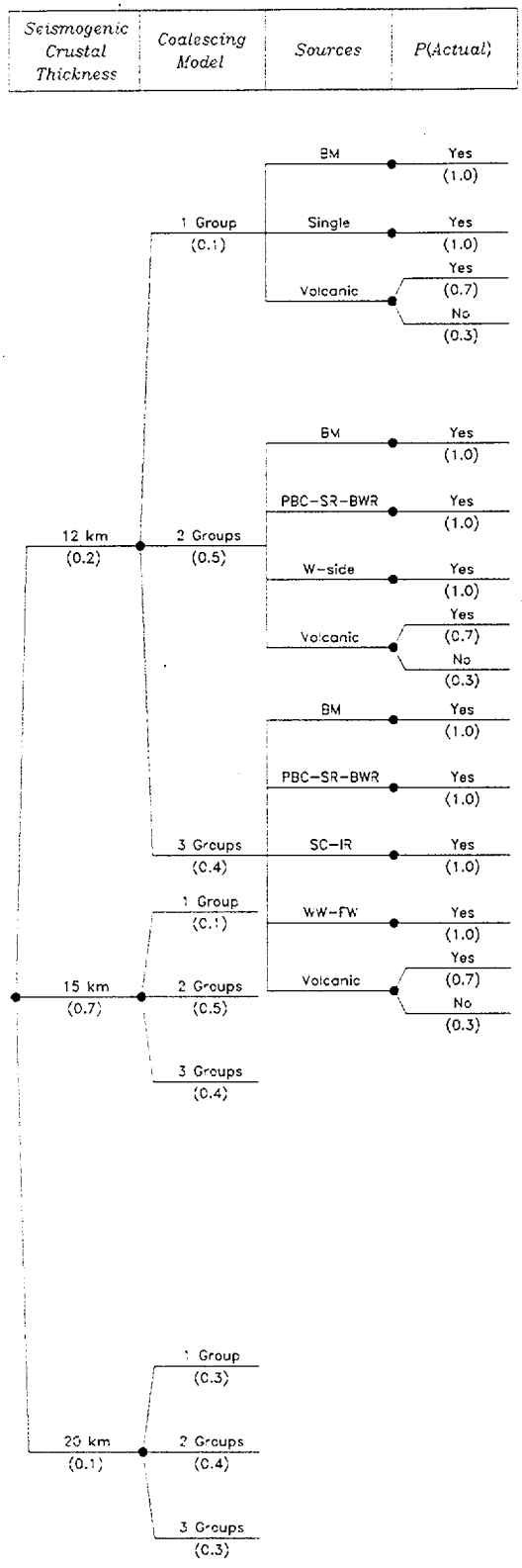

Figure RYA-1b Logic tree for local fault sources

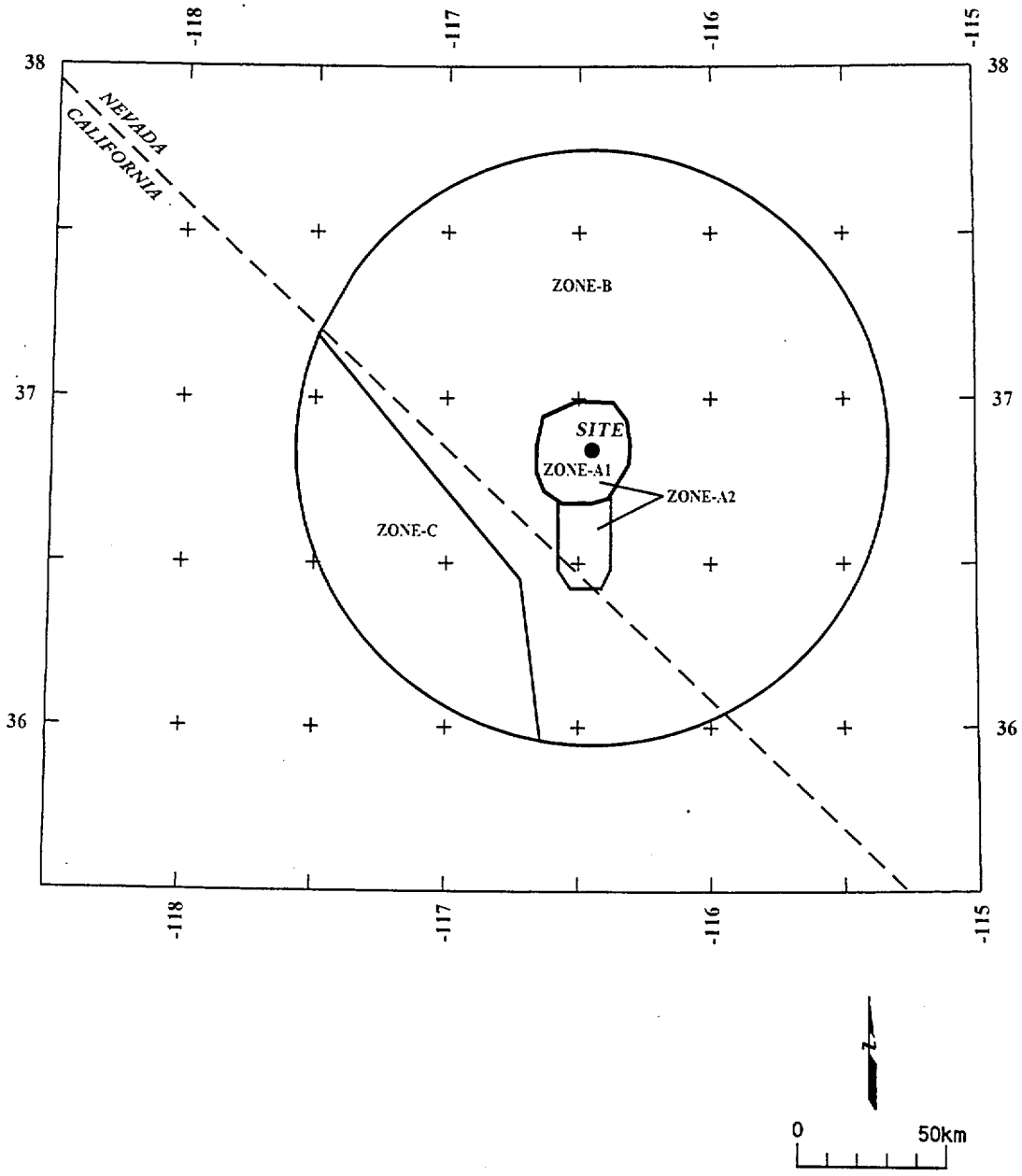

Figure RYA-2 Map showing boundaries of zones used in the seismic source model

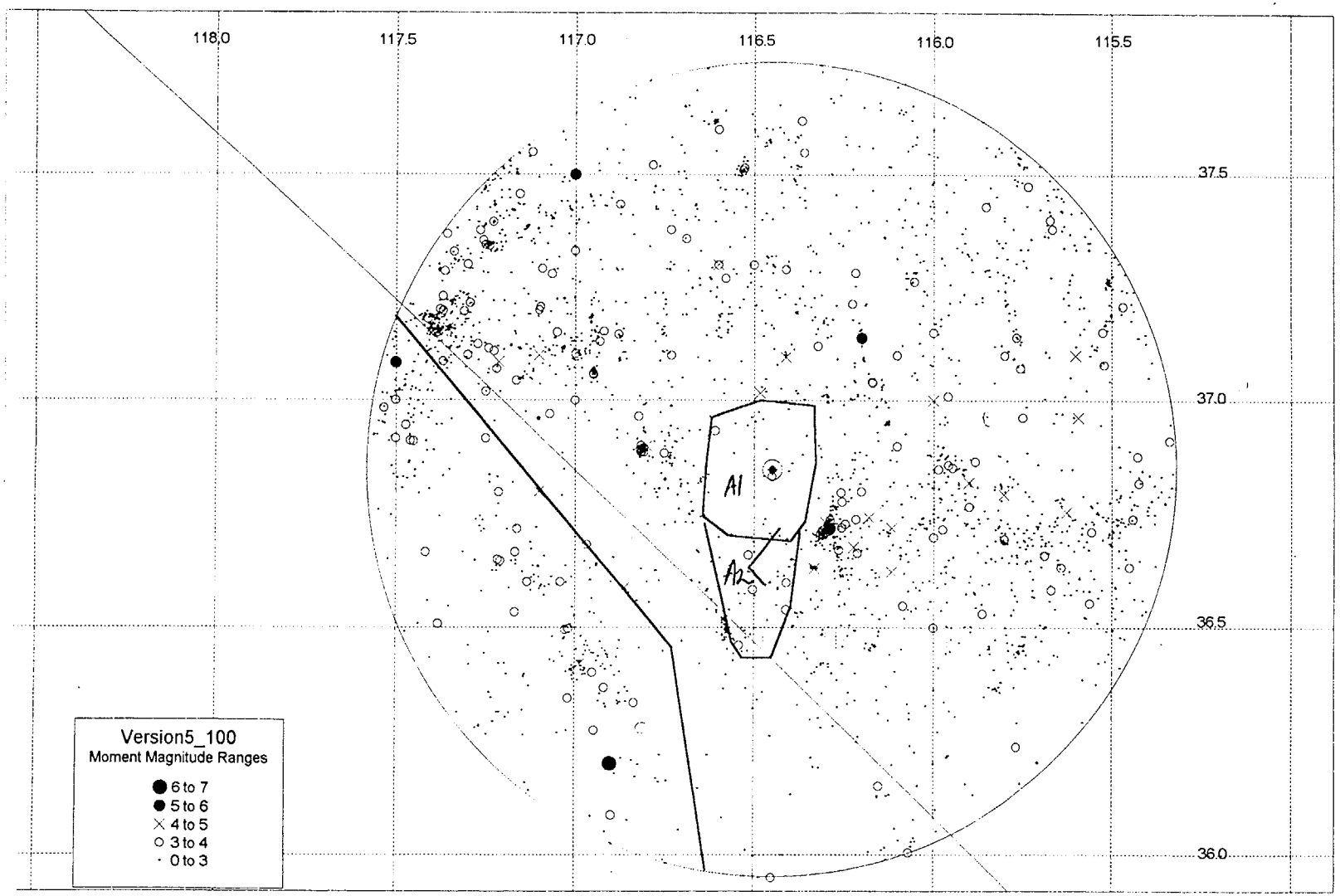

Figure RYA-3 Map showing earthquakes from the version 5 catalog and the background source zones

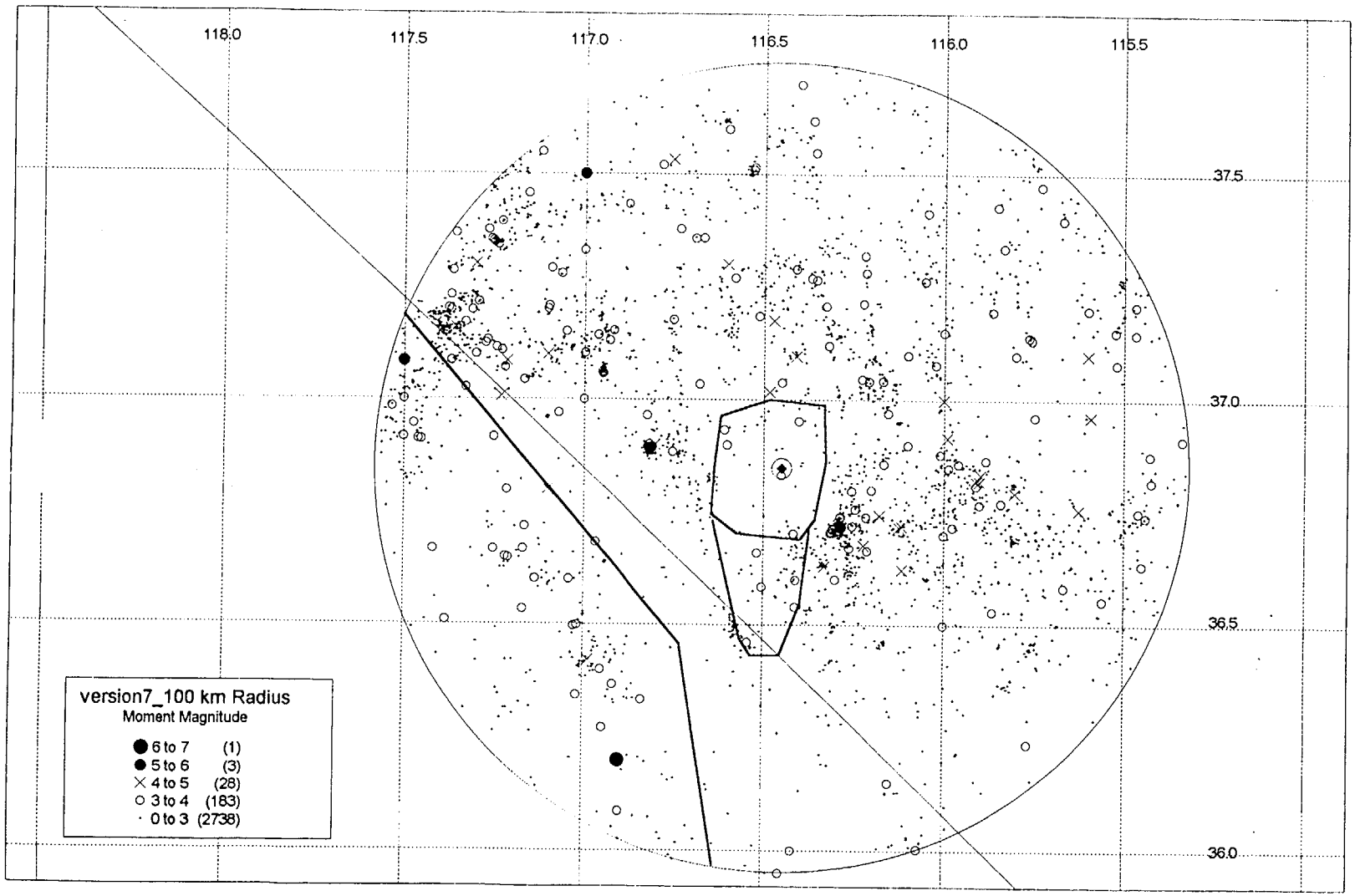

Figure RYA-4 Map showing earthquakes from the version 7 catalog and the background source zones

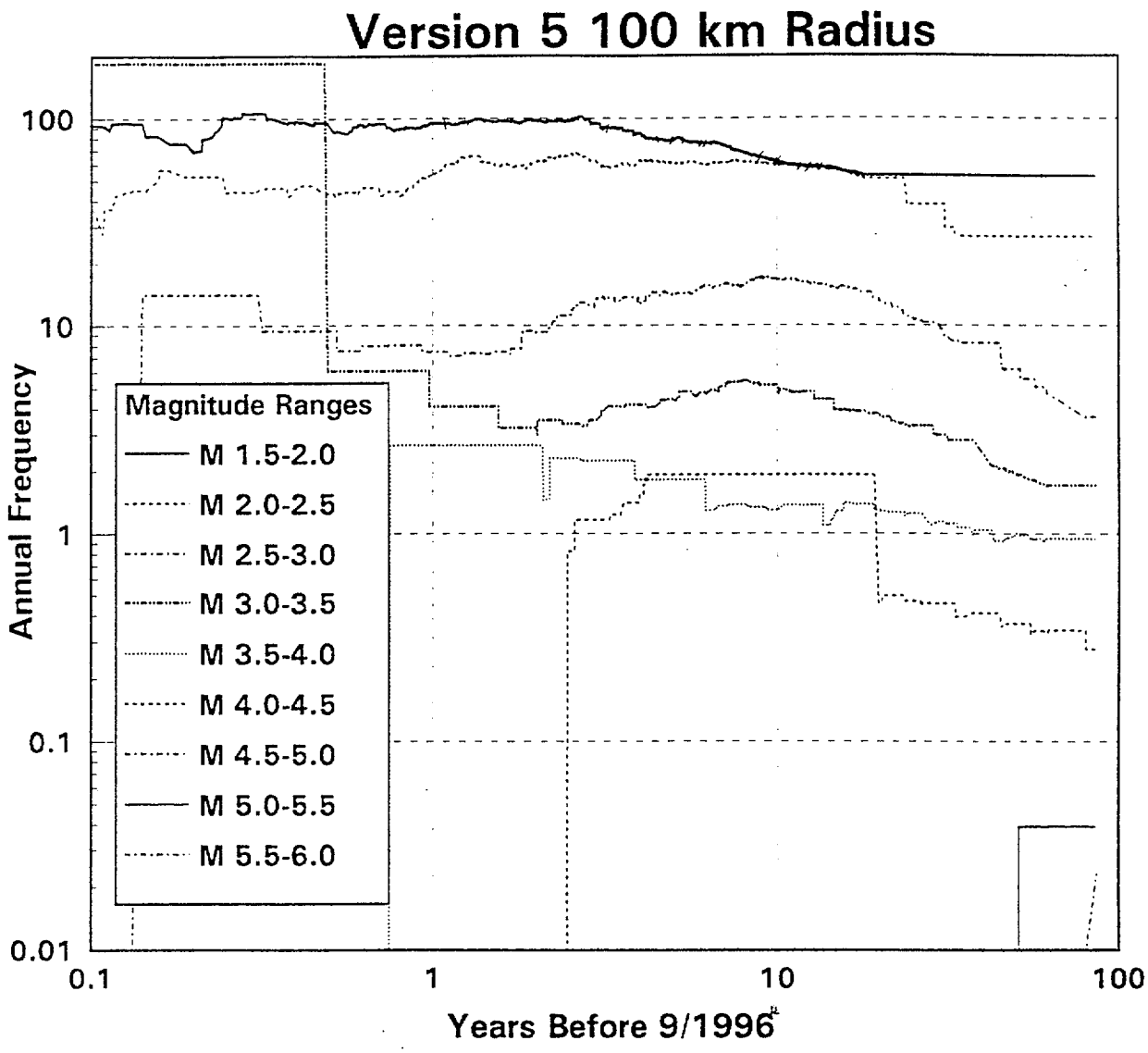

Figure RYA-5 Stepp plot of annual frequency versus years before 9/1996 for individual magnitude bins and the version 5 catalog

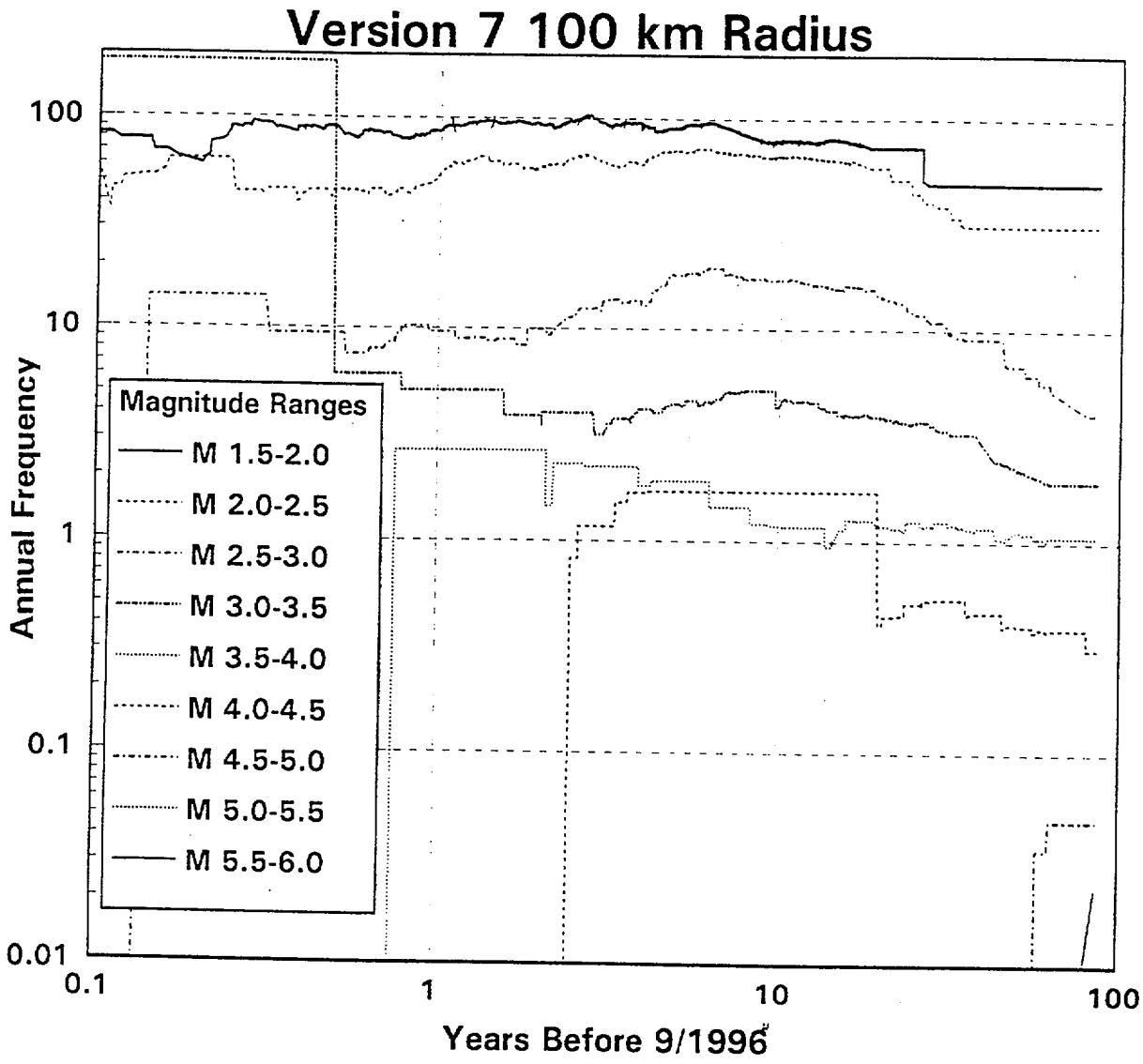

Figure RYA-6 Stepp plot of annual frequency versus years before 9/1996 for individual magnitude bins and the version 7 catalog

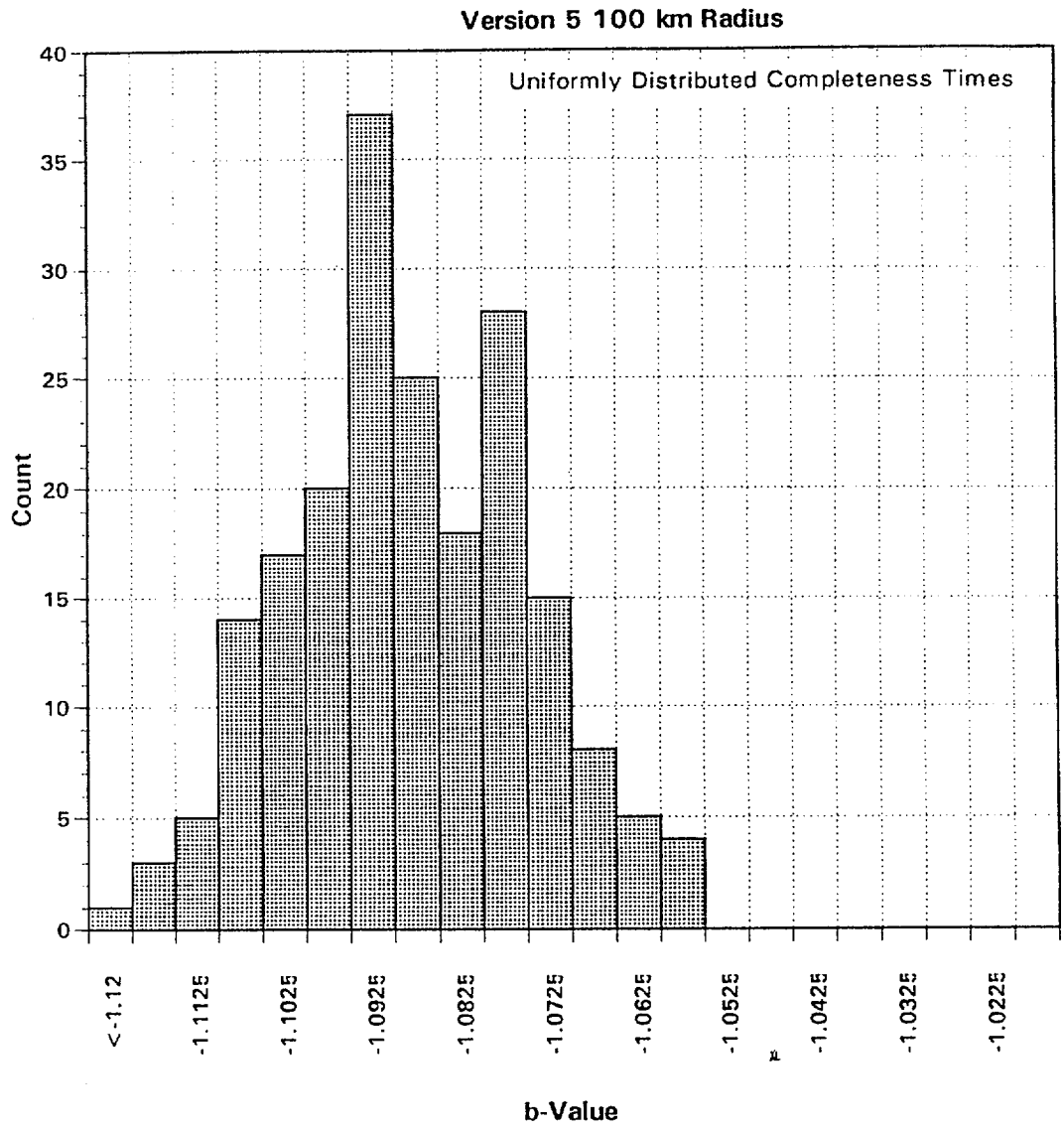

Figure RYA-7 Histogram showing b-values obtained for the version 5 catalog given uniform sampling of completeness times

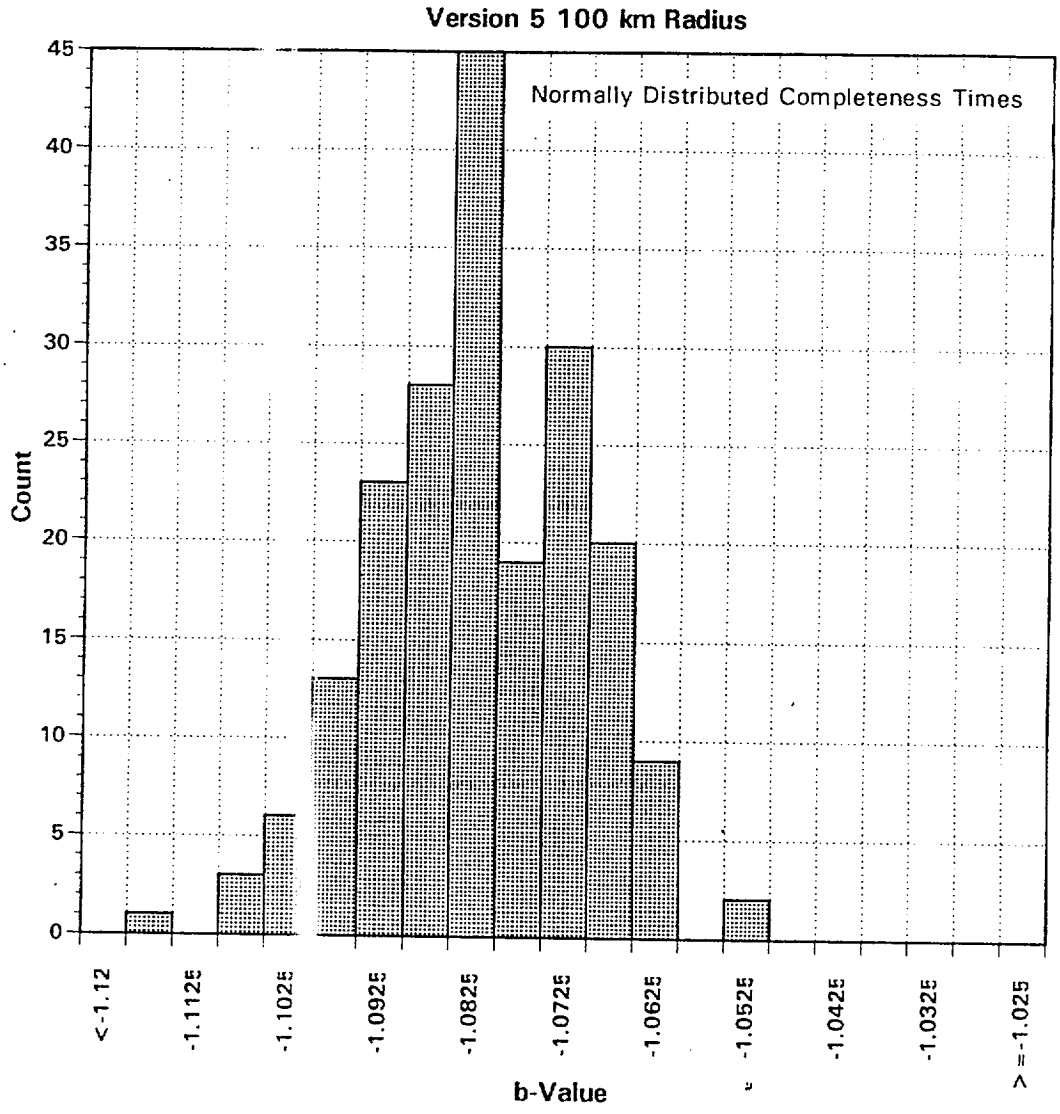

Figure RYA-8 Histog m showing b-values obtained for the version 5 catalog given normal sampli of completeness times

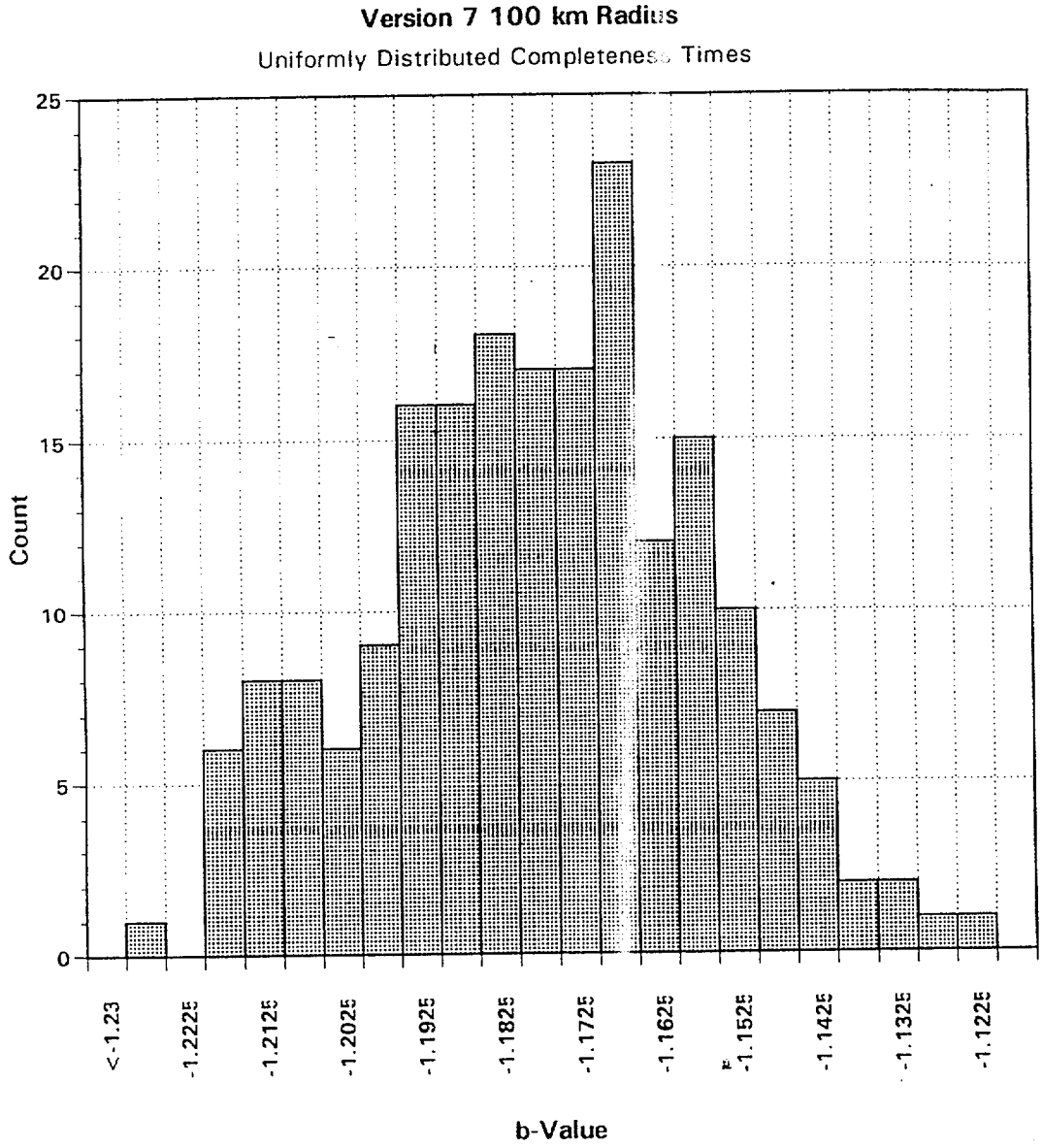

Figure RYA-9 Histogram showing b-values obtained for the version 7 catalog given uniform sampling of completeness times

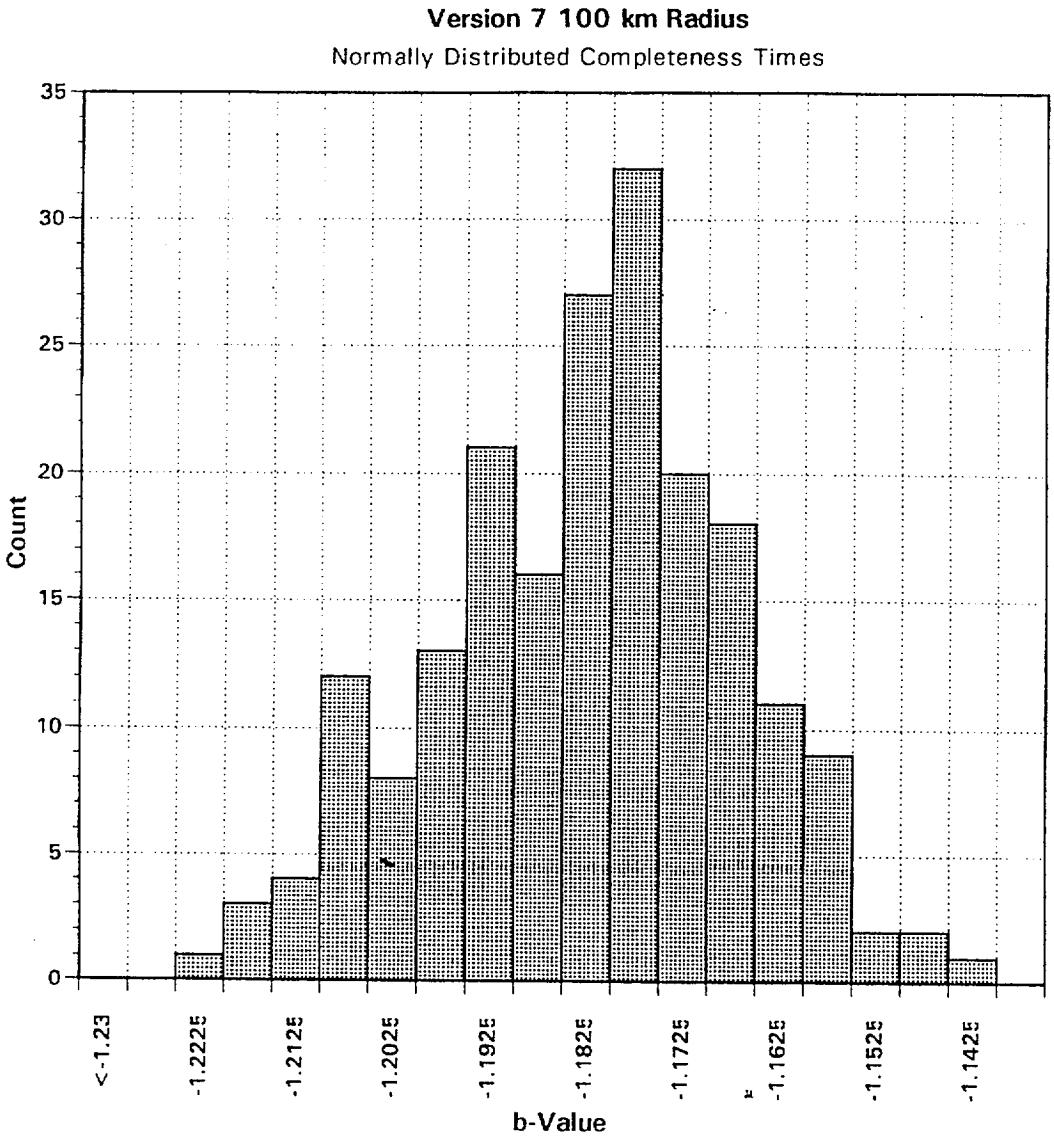

Figure RYA-10 Histogram showing b-values obtained for the version 7 catalog given normal sampling of completeness times

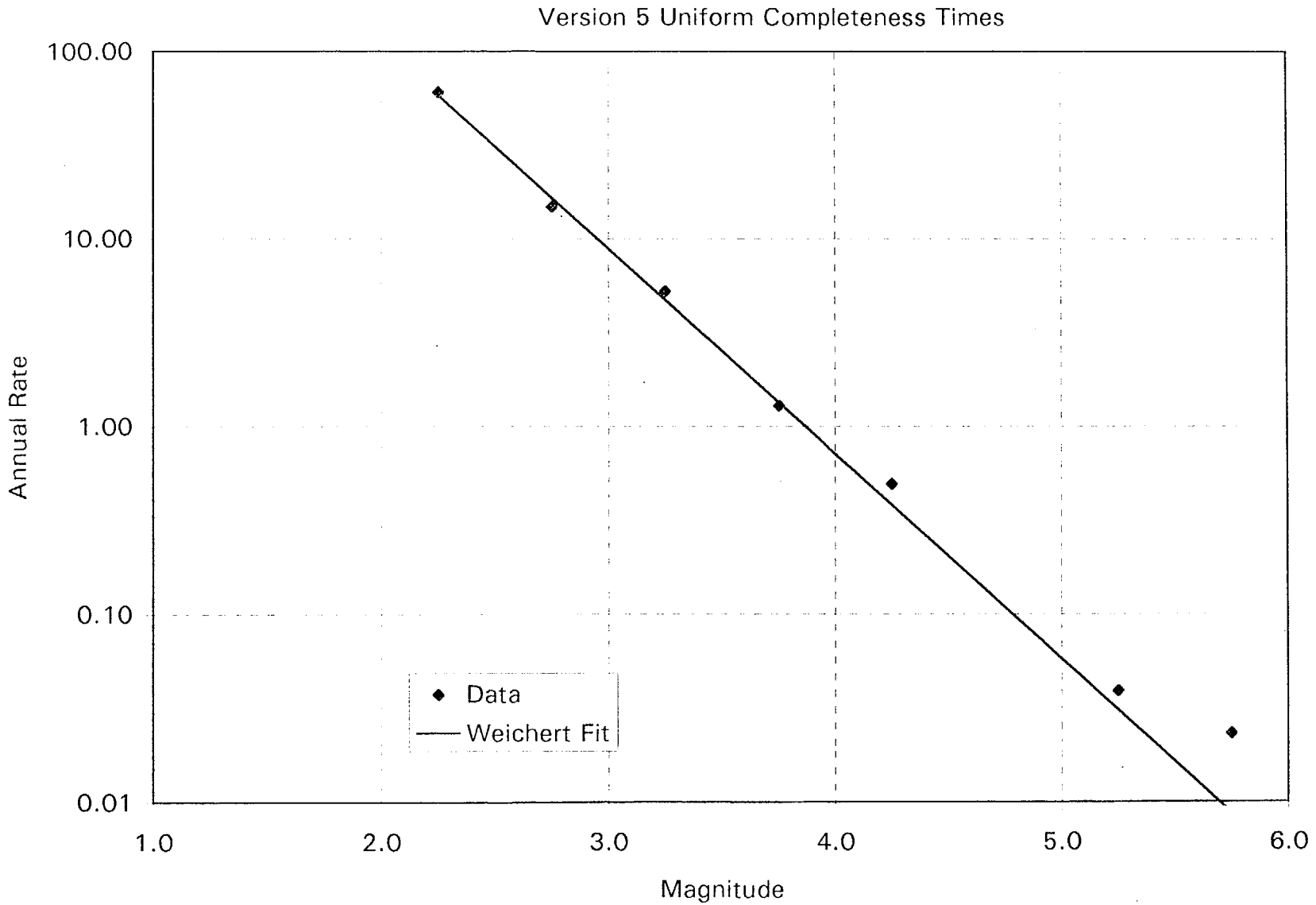

Figure RYA-11 Interval rates for the version 5 catalog that produced the modal b-value 1.09 (Figure RYA-7) and the fit to these data using the Weichert maximum likelihood method

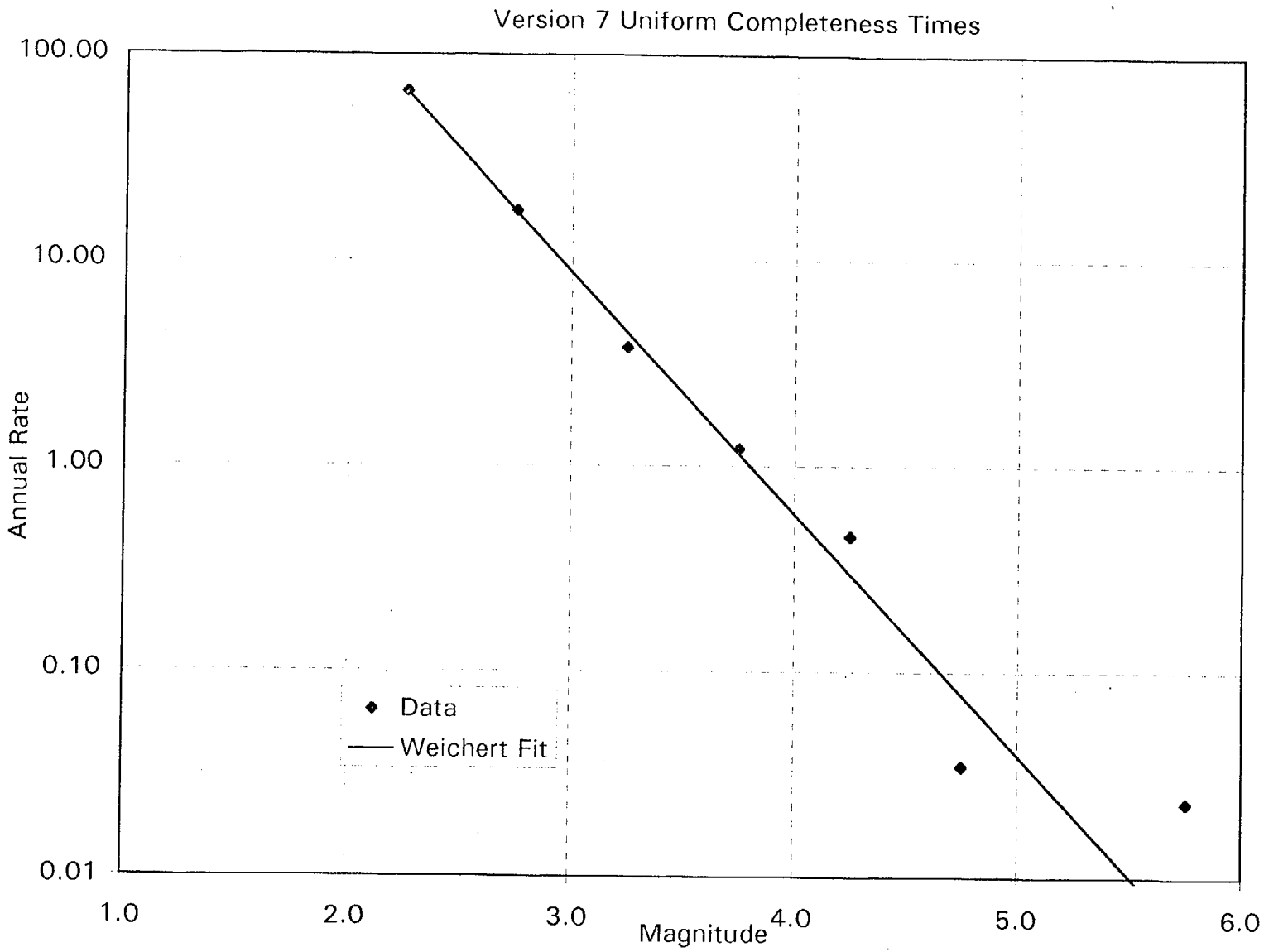

Figure RYA-12 Interval rates for the version 7 catalog that produced the modal b-value 1.17 (Figure RYA-9) and the fit to the data using the Weichert maximum likelihood method

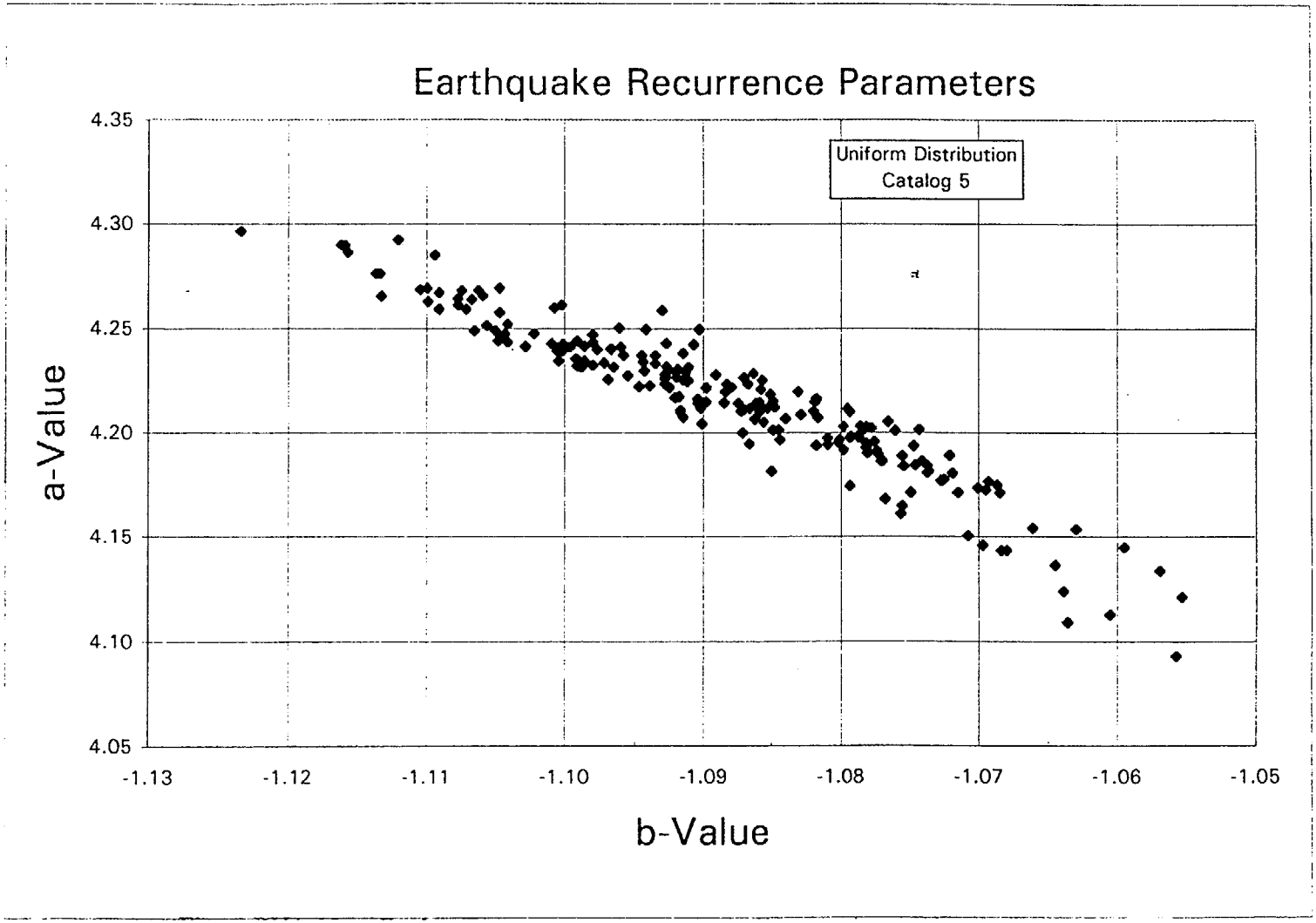

Figure RYA-13 Earthquake recurrence parameters. The paired a- and b-values calculated by uniform sampling from the range of likely completeness times and associated annual rates in the version 5 catalog. This plot shows the correlation between a- and b-values.

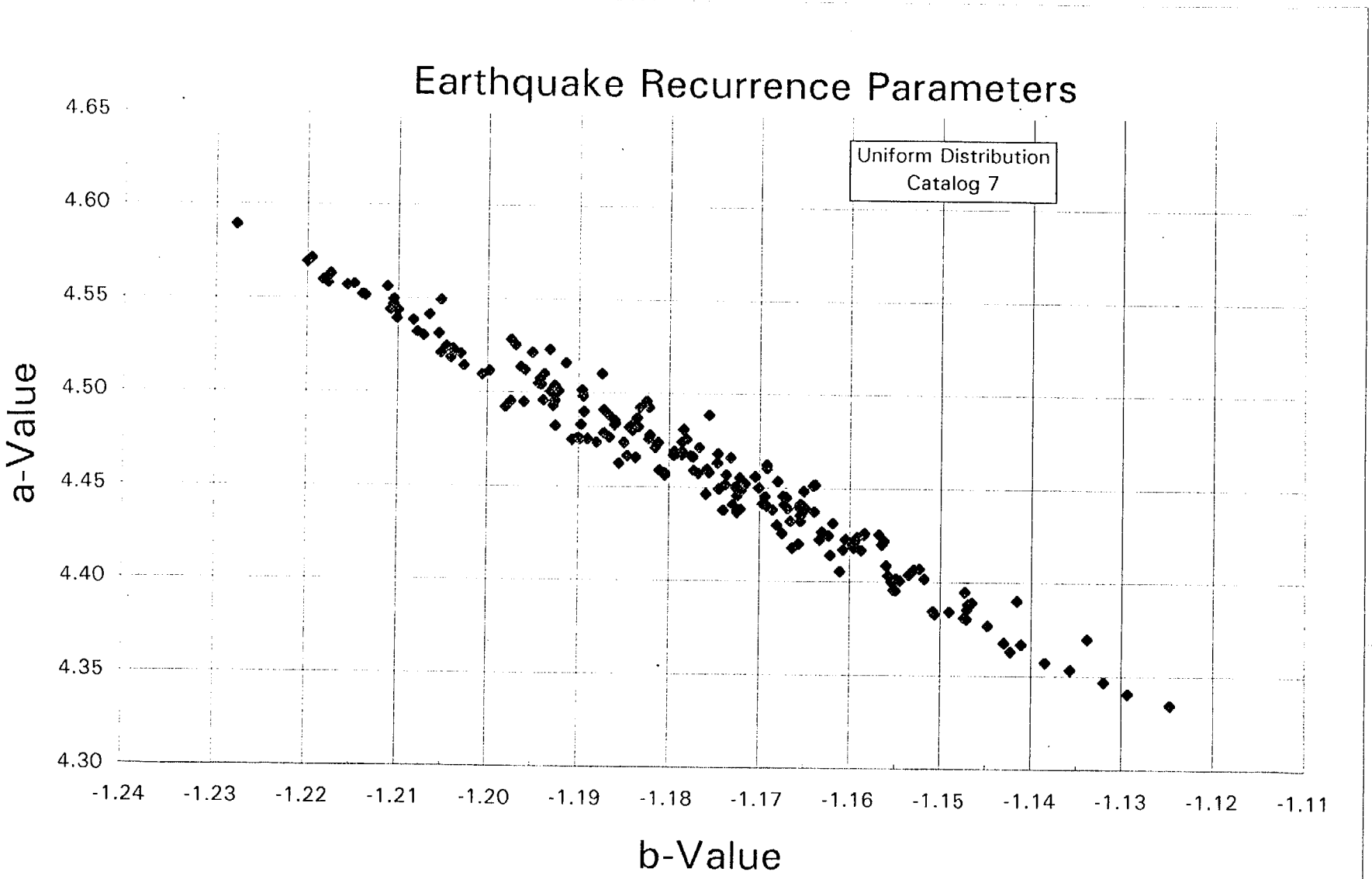

Figure RYA-14 Earthquake recurrence parameters. The paired a- and b-values calculated by uniform sampling from the range of likely completeness times and associated annual rates in the version 7 catalog. This plot shows the correlation between a- and b-values.

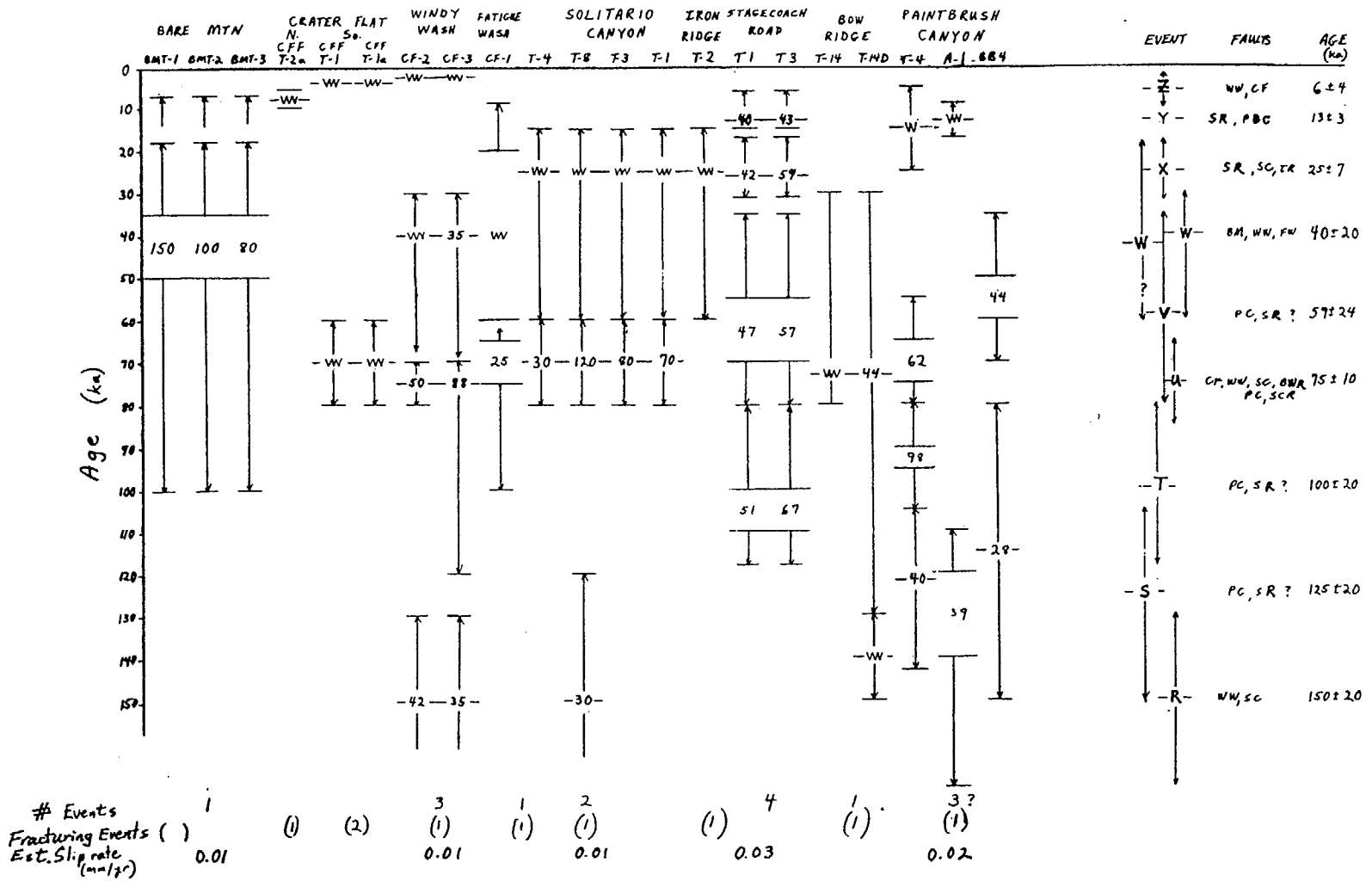

Figure RYA-15 Estimated age and amount (in cm) of late Quaternary displacement for faults in the Yucca Mountain area based on data in USGS (written communication, 1996). Faults are arranged from west to east; trench numbers under each fault are arranged from north to south. Bars and arrows show full uncertainties in estimated age of faulting event at each trench. "w" r represnts fracturing event (displacement < 20 cm). Age on far right of chart shows our best estimate for age of grouped event. See text and tables for fault abbreviations.

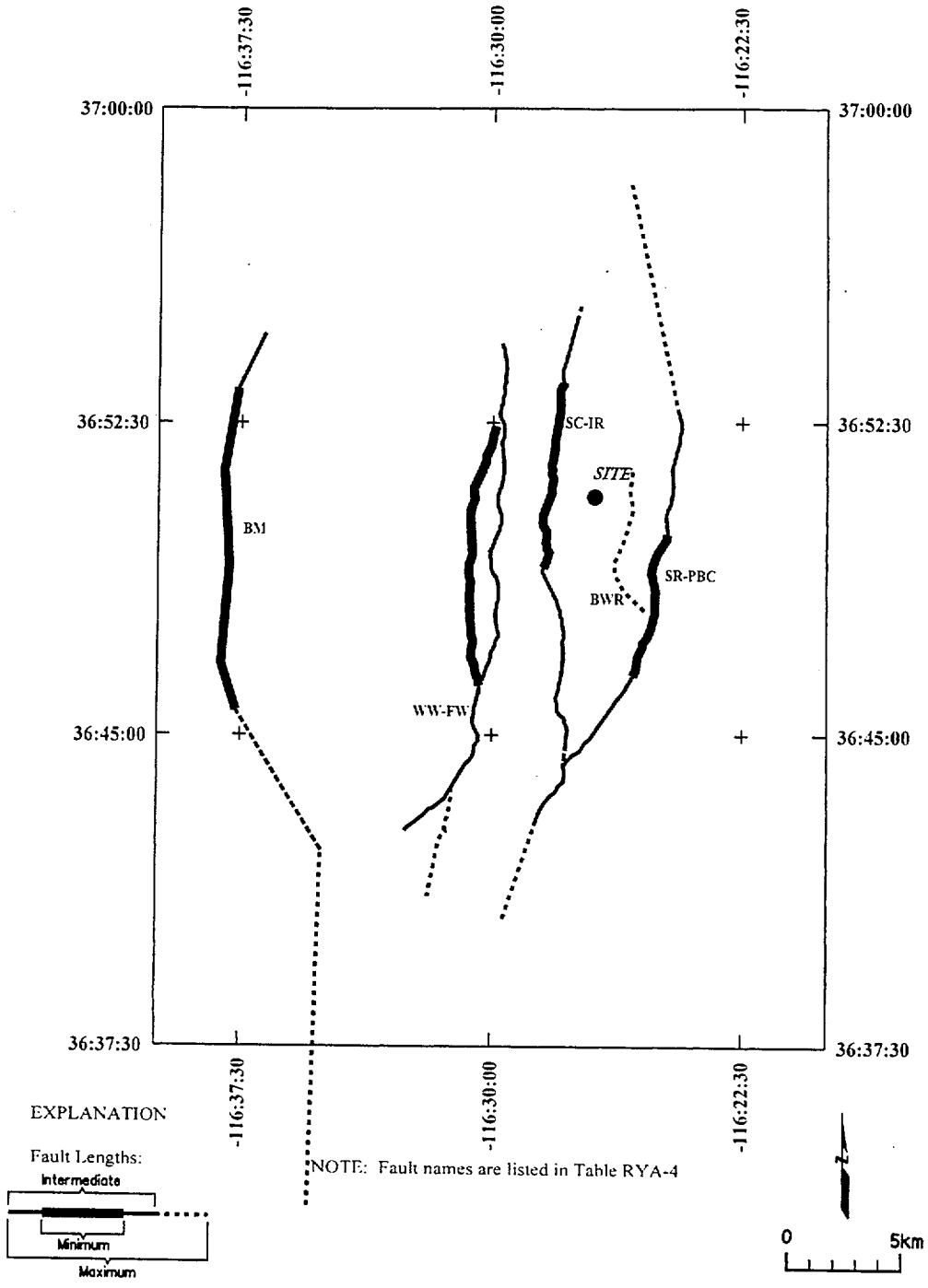

Figure RYA-16 Map showing local fault sources included in the seismic source model

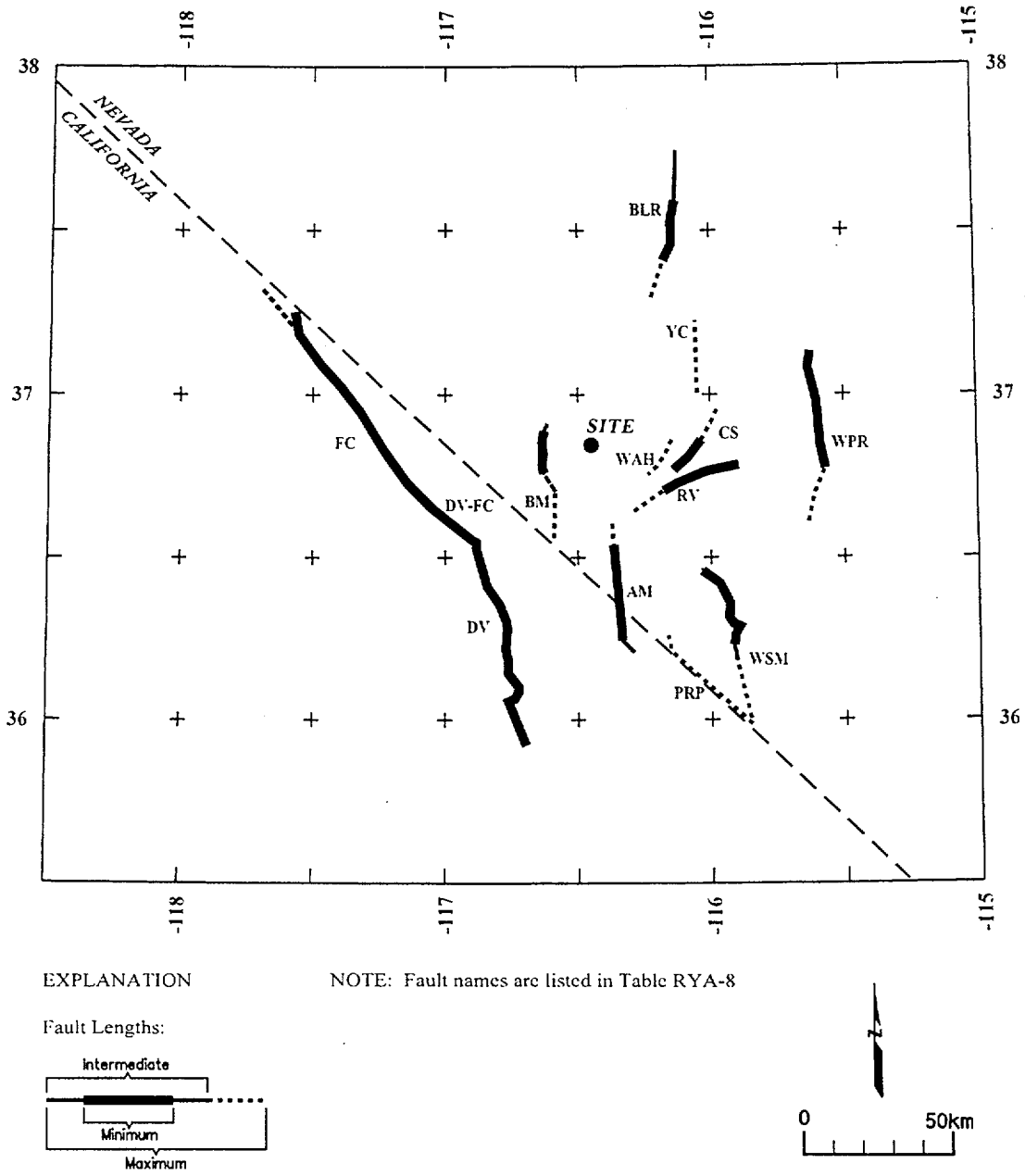

Figure RYA- 17 Map showing regional faults included in the seismic source model.

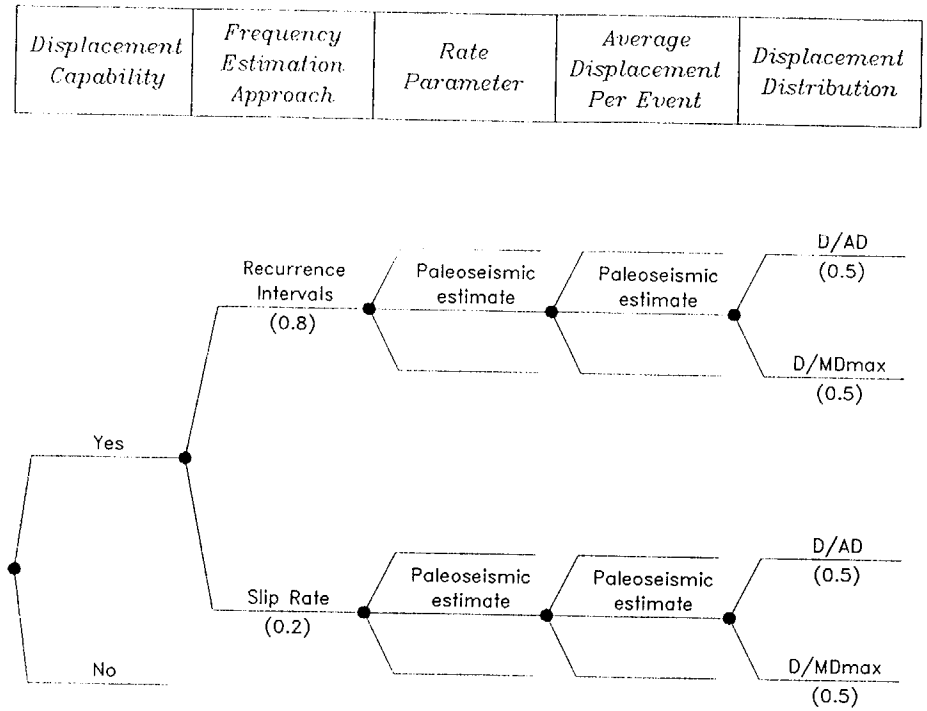

Figure RYA-18 Logic tree used to characterize fault displacement at sites with Quaternary data

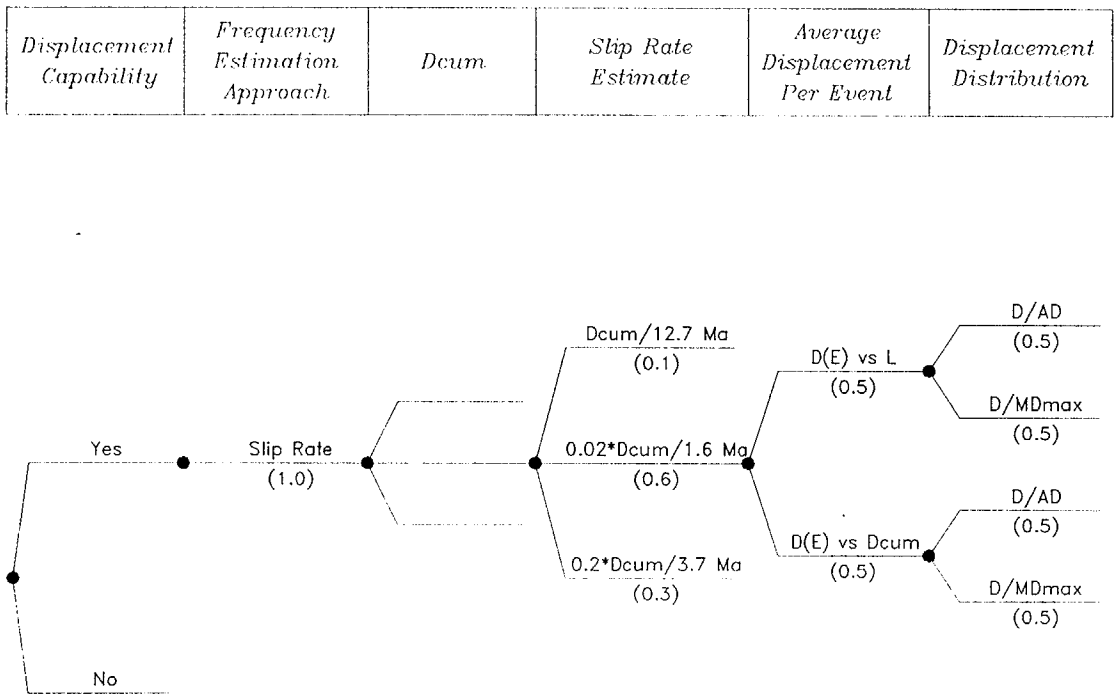

Figure RYA-19 Logic tree used to characterize fault displacement at sites without Quaternary data

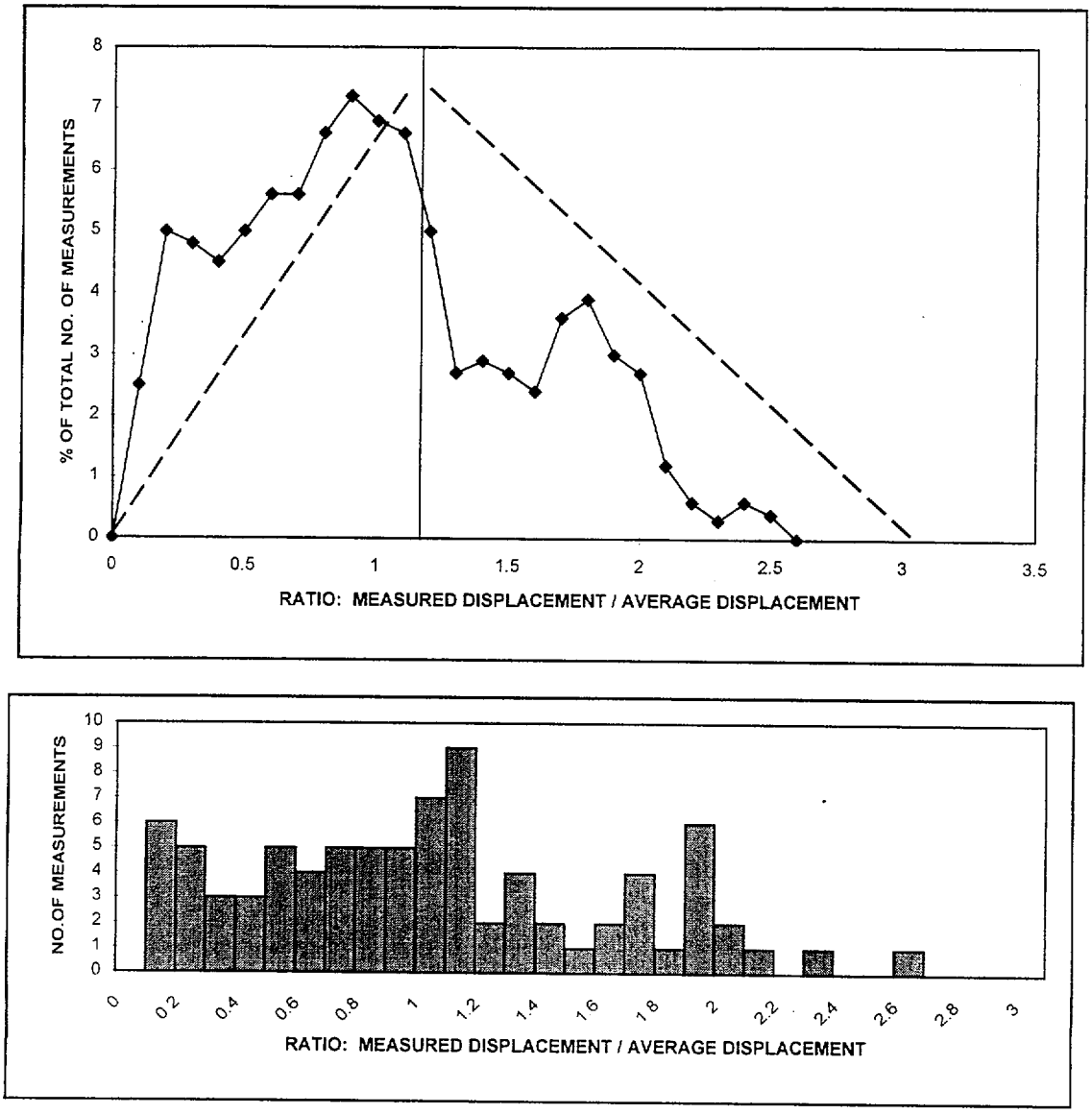

Figure RYA-20 Plots developed by DFS showing event-to-event variability in displacement relative to average displacement per event at a location along a fault based on data from paleoseismic investigations in the Yucca Mountain area

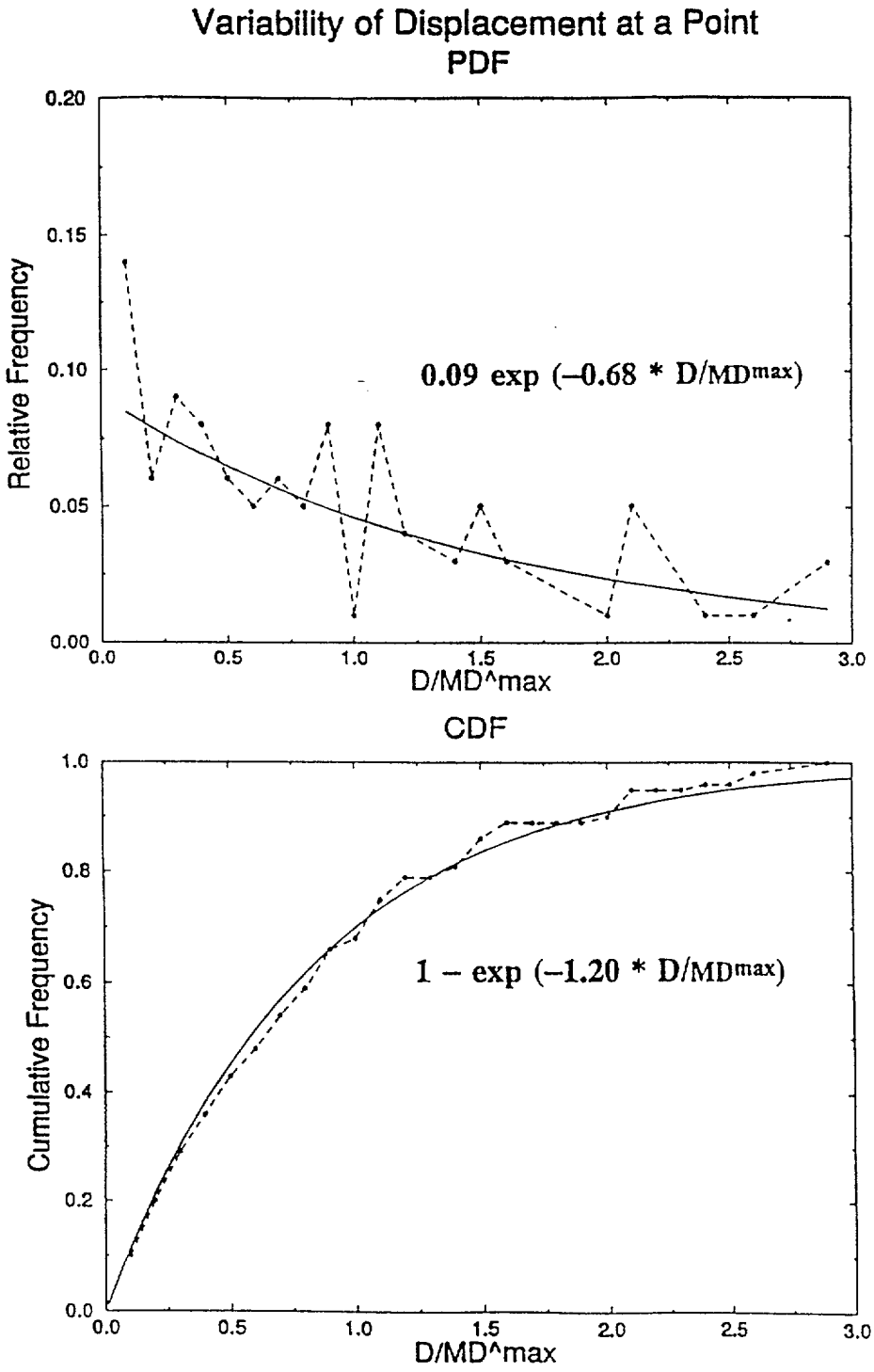

Figure RYA-21 Probability density function (PDF) and cumulative distribution function (CDF) for 80 measurements single-event displacement, normalized to Md^{max} for the corresponding fault, from 19 trenches in the Yucca Mountain area as developed by the AAR team

ELICITATION SUMMARY

KENNETH D. SMITH, RONALD L. BRUHN, AND PETER L.K. KNUEPFER

TABLE OF CONTENTS

TABLE OF CONTENTS

TABLES

FIGURES

TABLE OF CONTENTS

APPENDICES

ELICITATION SUMMARY
KENNETH D. SMITH, RONALD L. BRUHN, and PETER L.K. KNUEPFER

1.0 TECTONIC SETTING AND MODELS

1.1 TECTONIC SETTING

The Yucca Mountain site lies within the Walker Lane tectonic domain (Wright, 1976, 1989; Stewart, 1988) of the southern Great Basin of the Basin and Range province. The site area is slightly more than 300 km (200 miles) from the nearest tectonic plate boundary, the San Andreas fault. The San Andreas fault is the primary structure for strain accommodation between the Pacific and North American tectonic plates. Whereas the San Andreas fault is a transform system, the Basin and Range forms an extensional tectonic regime west of the plate boundary (Wright, 1976, 1989; Stewart, 1978). The extension in the Basin and Range, which began in the late Oligocene and culminated in the Miocene, has been expressed in a variety of deformation mechanisms involving high-angle strike-slip and normal faulting and low-angle normal faulting. Along with Miocene extension came episodes of widespread ignimbrite deposition and associated basaltic volcanism. Little evidence is available in the Yucca Mountain area to evaluate whether low-angle normal faulting remains a primary mechanism for deformation; however, all large historical Basin and Range earthquakes have occurred on moderately to steeply dipping faults (R. Smith, SSC Workshop 4).

Seismogenic faulting, which is distributed throughout the western United States, partly accommodates the relative motion between the North American and Pacific Plates. Global geodetic data and kinematic models indicate that about two-thirds of the total plate motion strain budget of about 48 mm/yr is accounted for on the San Andreas fault system in California and other offshore faults (Minster and Jordan, 1987; Ward, 1990; DeMets *et al.*, 1990; Humphreys and Weldon, 1994). The remaining one-third of the Western United States strain budget is accounted for east of the Sierra Nevada and west of the Colorado Plateau and Rocky Mountains, in the Basin and Range province.

The Sierra Nevada block moves northwestward at a rate of about 12.1 ± 1.2 mm/yr relative to fixed North America east of the Rocky Mountains (Minster and Jordan, 1987; Argus and Gordon, 1991; Dixon *et al.*, 1995). Movements on active faults in the Basin and Range province accommodate this portion of the overall strain budget through a variety of mechanisms. A significant component of lateral slip on faults in the eastern California shear zone is required in these kinematic models and has been measured in geologic and geodetic studies (e.g., Minster and Jordan, 1987; Argus and Gordon, 1991; Dixon *et al.*, 1995). This strain is also accounted for from faulting in the Central Nevada and Intermountain seismic belts (Minster and Jordan, 1987; Argus and Gordon, 1991; Dixon *et al.*, 1995; Smith and Sbar, 1974). Some of these estimates, especially geodetic and Quaternary fault studies, are based on very recent deformation and may not be representative of the total Cenozoic deformation.

The most active fault zones in the Holocene within a 300-km radius of Yucca Mountain mostly are farther than 100 km from the site itself. These faults are located within the Eastern California shear zone (Dokka and Travis, 1990). The Eastern California shear zone is a northwest-trending zone of faults that accommodate right-lateral motion along a north-northwest-trending zone through the Mojave Desert that connects with right-lateral and normal faults along the eastern Sierra Nevada. Geologic and geodetic data from the Mojave Desert indicate a rate of from 5 to more than 8 mm/yr of regional dextral shear that has been active since middle Miocene time (Dokka and Travis, 1990; Savage *et al.*, 1990; Richard, 1992).

East of the Sierra Nevada and north of the Mojave block, the Eastern California shear zone is defined by three major northwest-trending right-lateral fault zones: the Death Valley-Furnace Creek-Fish Lake Valley, the Hunter Mountain-Panamint Valley, and the Owens Valley fault zones. Geologic studies indicate an average late Quaternary slip rate of 1 to 4 mm/yr on the Hunter Mountain-Panamint Valley and Owens Valley fault zones (Burchfiel *et al.*, 1987; Lubetkin and Clark, 1988; Zhang *et al.*, 1990; Beanland and Clark, 1994), and as much as 4 to 8 mm/yr for the Death Valley-Furnace Creek-Fish Lake Valley fault zones (R. E. Klinger and L. A. Piety, written communication, 1996; Reheis and Dixon, 1996; Reheis and Sawyer, 1997). Thus, the Eastern California shear zone accounts for most of the strain budget of the plate boundary system east of the Sierra Nevada, leaving a small portion to be allocated to

faults in central Nevada and western Utah. Known and suspected Quaternary faults east of the Death Valley-Furnace Creek-Fish Lake Valley fault zone and in the Yucca Mountain vicinity have slip rates on the order of 0.001 to 0.01 mm/yr (J. W. Whitney *et al.*, USGS, written communication, 1996b); this is as much as three orders of magnitude less than slip rates on the faults in the Eastern California shear zone (Piety, 1995; W. R. Keefer and S. K. Pezzopane, USGS, written communication, 1996).

1.2 TECTONIC MODELS

Tectonic models are used to constrain fault geometry and behavior and to estimate the characteristics of buried seismogenic sources. First the tectonic model classification scheme of D. W. O'Leary (USGS, written communication, 1996) is discussed and evaluated for completeness. We then modify O'Leary's approach and evaluate the likelihood that each model exists and controls the behavior of active seismic sources. We evaluate the potential for activity of known and inferred faults, and the manner in which the dimensions of these seismic sources may be controlled by structures inherited from geologic history, or formed under the current tectonic regime. We partly follow the terminology of D. W. O'Leary (USGS, written communication, 1996) for clarity and convenience. However, the terms 'pure shear' and 'simple shear' as used by O'Leary to classify tectonic models do not accurately describe the regional tectonics, because these terms are restricted to descriptions of two-dimensional strain fields whereas the strain field at Yucca Mountain is three-dimensional.

1.2.1 Volcanic Models

Several models have been proposed in the literature that relate the development and continuing activity of faults in the Yucca Mountain area (the site fault area discussed later) to volcanic processes. We review the completeness of these models in the following sections. However, we conclude that none of these models explains the nature of active tectonism in the study area.

Caldera Model. Calderas in the Yucca Mountain region formed during Miocene tectonism. Their principal importance today could be in providing insight into the relationship between

the current stress field and the orientation of Miocene structures, which could influence geometry of active faults or help localize background seismicity. Many of these structures that formed in the Miocene also display evidence of Quaternary movement (Fridrich, 1997). The Timber Mountain-Oasis Valley caldera complex in the northern Nevada Test Site (NTS) is the primary source area for the volcanic tuffs that form Yucca Mountain (D. W. O'Leary, USGS, written communication, 1996; written communication, W.C. Day *et al.*, USGS, written communication, 1996e). Carr (1990) proposed that these Miocene calderas extended south of the Timber Mountain complex into Crater Flat. His interpretation was based in part on the presence of basaltic volcanism in Crater Flat, but this volcanism has been shown since to have occurred much later than the Miocene (Geomatrix Consultants, written communication, 1996). Also, faults at Yucca Mountain interpreted by Carr (1990) as caldera ring fracture systems have since been identified as tectonic faults rather than volcanic features (Fridrich, 1997; D. W. O'Leary, USGS, written communication, 1996). Furthermore, Crater Flat has been interpreted from gravity profiling (Langenheim, SSC Workshop 1), magnetic studies (Stamatakos *et al.*, 1997), and geologic investigation (Fridrich, 1997) to be a pull-apart basin filled with interbedded volcanics and sediments. Given this history, we conclude that calderas do not control the active structures in the Yucca Mountain area and assign zero weight to this caldera model.

Rift Model. The north-south-trending Kawich-Greenwater trough (Carr, 1984, 1990) is an older (originated pre-10 Ma) rift structure that likely established most of the regional faulting patterns and may provide the tectonic framework for current activity (Carr, 1990, Figure 8). As proposed by Carr (1984), this rift zone is identified by a nearly north-south-striking gravity low that extends from the northern NTS and the calderas of the Timber Mountain-Black Mountain-Oasis Valley complex, through Yucca Mountain and eastern Amargosa Valley, to end southwest of Death Valley in the Greenwater volcanic center of the Greenwater Range. This rift includes a number of older (15 Ma) silicic volcanic centers as well as younger basaltic cones and flows, including the Crater Flat basalts of Pliocene and Quaternary age. Aeromagnetic data (Majer, SSC Workshop 4) show several additional buried basaltic sources in the proposed rift south of Yucca Mountain near Highway 395 and near Lathrop Wells (Geomatrix Consultants, written communication, 1996; Langenheim *et al.*, 1993; Stamatakos *et al.*, 1997). Other buried volcanic sources south of Lathrop Wells may also be interpreted from the aeromagnetic data (Langenheim *et al.*, 1993). Evidence for

a throughgoing structure associated with these potential field anomalies is also shown by the near similarity in behavior of north to east-northeast faults mapped in Miocene tuffs in the Pahute Mesa area north of Timber Mountain and the faults at Yucca Mountain south of the Miocene caldera complex.

The isostatic gravity data (Ponce, 1993; Majer, SSC Workshop 4; D. W. O'Leary, USGS, written communication, 1996) show a north-south-striking, buried graben structure extending south of Yucca Mountain into Amargosa Valley. This southern part of the Kawich-Greenwater rift zone is named the Amargosa trough by D. W. O'Leary (USGS, written communication, 1996). This graben, which is about 40 km long and about 20 km wide, forms a boundary between regional tectonic domains in southern Nevada (D. W. O'Leary, USGS, written communication, 1996). Quaternary scarps of the Ash Meadows fault system (Piety, 1995) define the east side of the graben. The west edge extends north along the east margin of Bare Mountain and western Crater Flat. The southwest end of the graben parallels the Death Valley fault system, and the southeast end abuts the northern Pahrump Valley fault system near Stewart Valley. The Rock Valley fault zone appears to be truncated along the east margin of the graben, where the north-trending gravity gradient (the so-called Gravity fault) extends into Jackass Flat. The concentration of recent and historical seismicity that parallels the Rock Valley fault zone also is interrupted at this locality (K. Smith, SSC Workshop 2). However, additional northeast-trending scarps in Amargosa Valley to the southwest may be related to the Rock Valley fault (Anderson *et al.*, 1995b). We suggest that in the Miocene the graben structure accommodated strain transferred from the Las Vegas Valley shear, to the east, through the southern Great Basin. From this evidence it can be interpreted to represent a failed rift system. This is one in a family of oblique rift models that we consider to be an integral part of the Yucca Mountain tectonic setting (Figure SBK-1).

Dike Injection. As an alternative to faulting, injection of basaltic dikes may accommodate extension and strain in Crater Flat (Parsons and Thompson, 1991a, b). Thus, periods of volcanism may retard normal faulting in Crater Flat. Given this mechanism of accommodating extension, the strain rates estimated from the fault slip data would tend to underestimate the total local tectonic strain rate. Alternatively, volcanic processes may trigger faulting. For the Scenario U (ash event) of S. K. Pezzopane *et al.* (USGS, written communication, 1996a), several faults in the Crater Flat basin and at Yucca Mountain have

been interpreted to have ruptured concurrently with volcanic activity at about 70 ka. Evidence includes volcanic ash in several trench sites on the Solitario Canyon, Windy Wash, Fatigue Wash, South Crater Flat, and Bow Ridge faults. Elsewhere, subsurface movement of volcanic material has been associated with a series of moderate-sized earthquakes in the Mammoth Lakes-Bishop area of California (Appendix SBK-3). These earthquakes have generated secondary and possibly primary surface faulting and most likely local ground motions on the order of 0.5 g. The presence of Pliocene and Quaternary volcanics in Crater Flat indicates that dike injection accommodates some of the extensional strain in the Yucca Mountain area. A dike injection model may be a mechanism to passively account for strain through emplacement of basaltic material in the lower crust, and it may further trigger, or at least be associated with, earthquakes by movement of volcanics into the shallow (brittle) crust. In our evaluation of tectonic models, we consider it very likely that dike injection affects strain rates (Figure SBK-1); the principal effect of this on seismic source characterization is our treatment of volcanically related sources separately from primary faulting on local sources, as discussed in Section 2.4.1.

1.2.2 Low-Angle Fault Models

All of the low-angle fault models suggested for the Yucca Mountain region include a detachment of some kind. It is possible that an old (Oligocene-Miocene?), currently inactive and deformed, detachment structure underlies the region, with the Bare Mountain fault offsetting it beneath Crater Flat (Scott, 1990; Fridrich, 1997). Large detachments structures most likely operated in the Miocene, as evidenced by the Florspar Canyon fault system (Hamilton, SSC Workshop 3); the evidence of the unroofing of Bare Mountain (Ferrill *et al.*, 1996a); and the presence of middle to lower crustal rocks in metamorphic core complexes. Possible locations of detachments could occur beneath Crater Flat and Yucca Mountain at the Paleozoic-Tertiary contact, the Precambrian-Paleozoic contact, or the mid-crustal brittle-ductile transition (i.e., base of the seismogenic crust).

Wernicke (1995) suggests that detachment faults may be independent seismogenic sources of large lateral extent, and are capable of generating significant earthquakes. However, we do not consider detachment faults to be independent seismic sources at Yucca Mountain because: (1) geologic mapping indicates that the Paleozoic-Tertiary contact in the Yucca

Mountain vicinity is not a regional detachment (Fridrich, 1997; Simonds *et al.*, 1995); (2) there is no evidence for shallow detachments on seismic lines (Brocher, SSC Workshops 2 and 3) or in drill holes; (3) background seismicity in the vicinity shows no evidence for activity on low-angle faults; (4) although detachments occur in the surrounding regions and throughout the Basin and Range, most of these are old (Tertiary); (5) evidence shows that large normal-faulting earthquakes in continental crust occur only on high-angle faults throughout the world (Jackson and White, 1989); and (6) the Little Skull Mountain earthquake occurred on a steeply dipping (60 to 65 degrees) structure (Appendix SBK-2). The evidence indicates that even if a detachment exists under Yucca Mountain, it has a negligible probability of being seismogenic. Thus, we do not model a detachment as a seismogenic source capable of producing earthquakes above the background. In considering the possibility that one or more detachments exist, we use such structures only to constrain down-dip width and fault areas. Specific detachment geometries are discussed in the context of the assessment of dip and area of local faults.

1.2.3 Lateral Shear Models

Lateral shear models propose regional dextral shear along either a buried throughgoing shear zone in the crust or discrete, transcurrent fault populations that are characteristic of the Walker Lane belt (Wright 1976, 1989; Stewart, 1988). In this model, the primary deformation in the southern Great Basin is ultimately driven by the large throughgoing right-slip faults of the Death Valley-Furnace Creek-Fish Lake Valley, Hunter Mountain-Panamint Valley, and Owens Valley fault systems. These latter faults account for most of the approximately 12 mm/yr of the plate motion strain budget in the western Basin and Range of southern Nevada and eastern California. Slip rates on structures east of the Eastern California shear zone are significantly less than those on the primary transcurrent faults. Indeed, the small strain budget east of the high-angle faults of the Eastern California shear zone can be accommodated readily by a combination of high-angle transcurrent, normal, and oblique-normal slip faults, as supported by paleoseismic and seismicity data. This provides further evidence that it is not necessary to invoke low-angle faulting to support our conclusion that no large-area, low-angle normal faults or detachments are active.

Schweickert (SSC Workshop 3) proposed a buried regional shear zone in the Crater Flat area that had some components of the transtensional nappe model of Hardyman and Oldow (1991). This model is given an extremely low weight because: (1) conclusive evidence for offset geologic features along the postulated shear zone is lacking; (2) a 240-km-long shear zone with kilometers of offset should have scarps or other direct evidence at the surface for most of its length, and no such evidence exists.

1.2.4 High-Angle Faulting Model

The tectonic model that we consider best explains present tectonism in the Yucca Mountain region includes a component of lateral shear related to deformation through the Walker Lane belt (Stewart, 1988). The Death Valley-Furnace Creek-Fish Lake Valley fault system accommodates most of the regional strain through a slip rate of 4 to 8 mm per year (R. E. Klinger and L. A. Piety, USBR, written communication, 1996; Reheis and Sawyer, 1997). Slip rates on faults east of the Furnace Creek fault system are 2 to 3 orders of magnitude less. Short-period focal mechanisms (Rogers *et al.*, 1991) show a predominance of high-angle strike-slip faulting (S. K. Pezzopane *et al.*, USGS, written communication, 1996b), although normal mechanisms form a significant percentage of the database. The best evidence for high-angle faulting from a moderate-sized event in which the causative fault plane can be isolated is the 1992 M 5.6 Little Skull Mountain earthquake. It occurred on a steeply dipping structure (60 to 65 degrees; K. Smith, SSC Workshop 2), which is consistent with teleseismic, short-period, and regional faulting mechanisms for the event (K. Smith, SSC Workshop 2). Also, detailed aftershock relocations support the interpretation of faulting on a high-angle structure (K. Smith, SSC Workshop 2). Well-constrained short-period focal mechanisms for earthquakes in the Rock Valley fault zone in 1993, which incorporated supplemental portable instrument data, show high-angle strike-slip faulting, which is consistent with mapping and trenching studies of J. A. Coe *et al.* (USGS, written communication, 1996). Mapping of faults and dips of surface exposures for faults in the Yucca Mountain area also suggest that these are high-angle structures (Simonds *et al.*, 1995).

In the high-angle fault model, structures in the vicinity of Yucca Mountain are interpreted to be planar, and the Rock Valley fault and a buried structure near Highway 95 within the Amargosa trough to the west act as an accommodation zone, which truncates the local Yucca

Mountain faults at their south ends. The Yucca Mountain faults in this model are part of a half-graben, which is bound on the west side by the Bare Mountain fault. The faults are predominantly normal-slip structures having a left-lateral component of displacement that accommodates transtensional strain.

1.3 EVALUATION OF TECTONIC MODELS

The logic tree (Figure SBK-1) simplifies the tectonic models described above, focusing on those elements that may affect the geometric characteristics of other faults or may act as independent seismic sources. We categorize the models of O'Leary (as discussed above) into two classes: (1) oblique rifting and (2) regional dextral shear. The oblique rifting class is preferred (probability 0.99; Figure SBK-1), because it is more encompassing of volcano-tectonic structures in the Yucca Mountain region and includes the possibility of discrete strike-slip faults in addition to oblique-normal-slip and normal-slip faults.

1.3.1 Oblique Rift Models

Oblique rift models focus on the inferred presence or absence of low-angle faults (detachments, and the possibility of rolling-hinge tectonism [Hamilton, SSC Workshop 3]). All of these models include steeply to moderately dipping faults. The logic tree is structured to consider the presence of a detachment fault in two ways: (1) as a structural discontinuity that may control the depth, extent, or geometry (listric or planar) of steeply dipping faults; and (2) as a separate seismic source (active or inactive) to be considered in the seismic sources analysis. Given the lack of evidence for one or more detachment faults acting as a controlling structure in the present tectonic environment, as noted above, we apply extremely low weights (total of 0.01 to the three) to the likelihood of single or multiple detachments or Hamilton's rolling hinge model. In addition, as discussed above, we assign a likelihood of zero that a detachment structure can behave as an independent seismic source.

1.3.2 Regional Dextral Shear Models

These models are divided into two types: those with and those without a low-angle transtensional detachment. Steeply dipping faults are included in both types, but in the

former model (transtensional nappe) there is a large-area, horizontal to subhorizontal detachment fault that transfers strike-slip movement into the middle to upper crust. Given the lack of evidence for the transtensional nappe model of Schweickert (SSC Workshop 3), we assign an extremely low weight (0.01) to this possibility.

1.3.3 Effects of Igneous Dike Injection

Quaternary volcanism may accommodate some of the extension in Crater Flat, and therefore decrease the slip rates on the Bare Mountain and other faults (Parsons and Thompson, 1991a, b). Thus we include dike injection as an element in tectonic models. We do not consider the dike injection model as a separate branch on the logic tree for tectonic models (Figure SBK-1); instead, it is included as an option in both the oblique rift and dextral shear zone models. Given that dike injection has occurred in the Crater Flat area during the Quaternary, it clearly plays a role in any tectonic model. We assign a high likelihood (0.95) that dike injection affects slip rates on the local faults, as we discuss further when considering the seismic potential of volcanic sources. We further consider the significance of volcanic dikes in explaining the low late Quaternary slip rates on the Bare Mountain and possibly the local Yucca Mountain faults as well as acting as a trigger for simultaneous fault ruptures. We also address the question of whether fractures that produce aligned dikes, such as the Crater Flat cones, are also separate seismic sources, perhaps capable of generating earthquakes during magma injection at depth (see discussion of Mammoth Lakes area sequence Appendix SBK-3).

1.3.4 Utilization of Logic Tree for Tectonic Models

We have interpreted a most likely tectonic model—steep to moderately dipping faults in an oblique rift system—consistent with the tectonic history of the Yucca Mountain area and the kinematics of currently active structures. Most other models are given negligible or extremely low weights as descriptors of the active tectonic regime. Furthermore, we consider that the tectonic models principally control down-dip geometry of the local faults. For example, all of the detachment models (single detachment, multiple detachment, rolling hinge) imply that site faults merge at shallow or intermediate crustal depths; the interpretation affects the likelihood that faults coalesce down dip, as well as the width of individual and coalesced faults. Given that this is the only kind of effect we consider credible for the

nonplanar-fault tectonic models (i.e., we do not add additional seismic sources for different models, as discussed below), we do not explicitly incorporate different tectonic models as branches of a logic tree. Instead, our weighting of tectonic models provides a framework for our evaluation of the geometry of local fault sources.

2.0 SEISMIC SOURCES

Seismic source zones are identified throughout the 100-km-radius surrounding the site, as shown on Figures SBK-2 and -3. Regional and local fault sources are identified (Figures SBK-5 and -6); areal seismic source zones (Figures SBK-2 and -3) serve as background zones to these fault sources. The maximum magnitude associated with each seismic source zone is a function of several variables. Within 100 km, the regional and local fault sources that can produce potential maximum earthquakes above the maximum background were identified and are characterized separately. Assigning the maximum background magnitudes for the areal source zones is based on the observations of the largest earthquakes in the Basin and Range that did not have reported primary surface faulting. The largest of these events occurred in Montana in 1925. This event is less relevant to the Yucca Mountain area because of the thinner seismogenic crust in southern Nevada. In the local site vicinity, extensive geologic mapping has identified small-displacement events—as small as cracking events. Because of the enhanced resolution in the local site area (including Yucca Mountain and Bare Mountain), it is interpreted that a fault source comparable to those mapped has not remained undetected. Therefore, a smaller maximum magnitude is assessed for the areal source zone in the local site vicinity. Earthquake recurrence relationships were developed for each areal source zone based on observed seismicity data. For areal sources containing regional and local fault sources, seismicity associated with these fault sources was removed before calculating recurrence parameters for the source zone. Recurrence relationships for regional and local fault sources were developed from fault-specific geologic data.

2.1 THICKNESS OF SEISMOGENIC CRUST

The thickness of the seismogenic crust in the southern Great Basin is assessed both on the depth distribution of seismicity from the earthquake catalog and the record of estimated hypocentral depths for main shocks in the Basin and Range Province (SDO Team, SSC Workshop 4). We use the depth distribution of main shocks in the Basin and Range, an extensional environment, rather than considering California analogs because of the clear difference between the tectonic regimes. We also recognize that there is some variation in the tectonic styles and crustal thickness within the Basin and Range itself (Smith and Sbar, 1974). For example, deformation in the southern Great Basin, dominated by the strike-slip systems of the Death Valley-Furnace Creek-Fish Lake Valley, Hunter Mountain-Panamint Valley, and Owens Valley fault zones (Dixon *et al.*, 1995; Piety, 1995), may be quite different from the tectonics of the Central Nevada Seismic Belt in north-central Nevada and the extension associated with the basaltic volcanics of the Eastern Snake River Plain in the northern Basin and Range. Also, there is some evidence that large main shocks in the Basin and Range ($M > 6.8$) may initiate at greater depth than may be indicated purely by analyzing the depth distribution of earthquakes in the recent period of seismic monitoring (SDO Team, SSC Workshop 5).

Doser and Smith (1989), Doser (1986, 1988), and the SDO Team (SSC Workshops 4 and 5) analyzed the depth of initiation and rupture of the historical, $M > 6.5$ earthquakes in the Basin and Range. These analyses show that earthquakes in this magnitude range may initiate as deep as 20 km. For example, modeling the rupture processes of the Borah Peak earthquake from teleseismic and regional seismograms indicates seismic energy radiating from the fault plane at depths as great as 22 km, whereas the Borah Peak hypocenter has been determined to be at about 16 ± 4 km (R. Smith, SSC Workshop 4). Many of the hypocentral depths for Basin and Range events were calculated from teleseismic recordings (exclusively for the older events), using techniques that require good velocity information in the middle crust to reduce uncertainties in the estimate. Clearly, of the large events in the Basin and Range, the Borah Peak event of October 1983 would provide the best data for evaluating the depth distribution of faulting, yet there were no near-source recordings (< 20 km) for this earthquake.

In contrast, recent moderate-sized earthquakes in the Basin and Range, in particular in the central and southern Great Basin, have shown a shallower depth distribution of aftershock activity and initiation of main shock rupture. The resolution of the estimates of hypocenter depth for many of these sequences is provided by high-quality regional and local data that were not available for the large historical Basin and Range events. Recent moderate-sized earthquakes in the central and southern Basin and Range include the June 1992, M 5.6 Little Skull Mountain, Nevada (Harmsen, 1993; K. Smith, SSC Workshop 3); May 1993, M 6.1 Eureka Valley, California (Peltzer and Rosen, 1995; Massonnet and Feigl, 1995); and July 1986, M 6.3 Chalfant Valley, California, earthquakes (Appendix SBK-3). A sequence of moderate-sized earthquakes in the Mammoth Lakes area of California in the 1980s was well recorded, but its association with the active Long Valley caldera makes it questionable with respect to evaluating seismogenic depth estimates in nonvolcanic areas. The refined hypocentral depths for these moderate sized earthquakes are: Little Skull Mountain, 11.7 km (K. Smith, SSC Workshop 3; Harmsen, 1993; Meremonte *et al.*, 1995); Eureka Valley, 11.8 km (Loper *et al.*, 1993); Chalfant Valley, 12 km (Smith and Priestley, 1997). All of these earthquakes initiated near the base of the local seismogenic zone. This conclusion is based on the assumption that the maximum depth of the well-located aftershock activity defines the local base of the seismogenic zone in these areas.

Earthquakes in the southern Great Basin occur primarily between 5 and 15 km in depth (Appendix SBK-1). The distribution is dominated by the Little Skull Mountain sequence, which represents about 20 to 30 percent of the seismicity catalog for the southern Great Basin in the NTS area (Appendix SBK-1). This sequence was confined primarily between 12 and 6 km depth; the deep distribution peaks near the lower edge of the seismogenic zone. The sequence was particularly well recorded, and depth constraints are good. Rogers *et al.* (1987) showed that seismicity in the southern Great Basin was distributed between about 15 and 2 km, with a gap in activity at about 4 km. This observation has not continued through the period of digital data recording, 1995 through 1997, and may represent mislocations resulting from the misidentification of S-wave arrivals on vertical-component records. Shallow activity has been rare in the recent period but has been observed. The 1993 Rock Valley sequence, an unusually shallow cluster of earthquakes (K. Smith, SSC Workshop 3; Smith and Brune, 1997), generally was confined to less than 3 km depth. These shallow hypocentral depths were confirmed with the installation of near-source (less than one focal

depth), three-component digital recorders. Hypocentral depths of about 2 km from the surface were identified in the Shields *et al.* (1995) study for the 1993 Rock Valley sequence.

Rogers *et al.* (1987) show that most of the seismic energy released in the southern Great Basin occurs at depths less than 12 km, but this observation is based on data from a period (1978-1987) when there was minimal moment release throughout the southern Great Basin. Occasional larger-magnitude earthquakes reportedly nucleated deeper than 15 km; however, many of these events occurred early in the instrumental record, and their hypocenters probably are not well constrained. Nucleation depths of about 16 km have been reported for several major earthquakes in the Basin and Range province: the 1954 Dixie Valley, Nevada; 1959 Hebgen Lake, Montana; and 1983 Borah Peak, Idaho (all from R. Smith, SSC Workshop 4); all were M 7+ range-bounding, normal-faulting events. Critical to the estimation of maximum moment from a structure is whether rupture can propagate to these depths, which would not necessarily have to correlate with hypocentral depth. Also, slip at these depths may not contribute significant ground motion at the surface.

Our weighting of maximum seismogenic thickness allows us to account for the possibility that larger earthquakes may rupture below the depths indicated by the distribution of well-located regional seismicity and the maximum depth of the seismogenic thickness indicated for the three central and southern Great Basin earthquake sequences listed above. Rupture may extend below the brittle seismogenic zone, because the dynamic strain rate during rupture propagation may be high enough to overcome the frictional conditions in the-brittle-to-ductile transition zone that exists in the mid-crust near the base of the seismogenic zone. Under these conditions, rupture propagation may be acceptable in dynamic rheologies that physically do not allow for the initiation of the small- to moderate- sized earthquakes ($M < 6$), which comprise the bulk of the regional seismic catalogs.

The ranges and weightings of seismogenic thickness are interpreted to be the same for all source zones throughout the study area. We define the base of the seismogenic zone as: 12 km, wt. 0.3; 15 km, wt. 0.6; and 17 km, wt. 0.1.

2.2 AREAL SOURCE ZONES

Four primary source zones were delineated for non-fault-specific seismic sources within 100 km of the site (Model A - Figure SBK-2). These are the West Walker Lane, the East Walker Lane the Basin and Range, and a Local Zone within the site area that was not characterized by local faults. These source zones were chosen based on a review of the seismicity reports for the southern Great Basin (Appendix SBK-1) and an interpretation of the seismotectonic implications of the distribution of seismicity in the historical catalog (Appendix SBK-2). These seismotectonic interpretations also affected our evaluation of tectonic models, particularly with regard to neotectonic deformation (Appendix SBK-2). These zones represent those areas that remain after the areas of regional fault sources have been removed. These areas include the location of potential maximum background and other earthquakes not associated with particular fault sources. The maximum background earthquake and the rate of recurrence for this event are assessed from the activity rates estimated from the recurrence rates of the declustered seismicity in these areas.

In addition, a subregion in the East Walker Lane (Rock Valley) is defined to account for regional variability in seismicity (Model B - Figure SBK-3). The region is defined on the bases of tectonic, geologic, and seismicity rate criteria, as described below. The branch of the logic tree that includes this subregion is assigned a weight of 0.3 (Figure SBK-4), with 0.7 assigned with the interpretation of no subregion.

The Death Valley-Furnace Creek-Fish Lake Valley fault zone defines the boundary between the West Walker Lane and East Walker Lane areal source zones. Defining the western zone as the West Walker Lane is not strictly correct, as it is more appropriately termed the Eastern California shear zone, but we use this terminology. This area includes the active faults and deformation west of the Furnace Creek system. Given that seismic network coverage in this region has been sparse throughout the history of seismic monitoring, we cannot rely on the quality of earthquake locations and hypocentral depth estimates as much as we can for other areas that have denser network coverage and thereby more accurate hypocenter locations.

The East Walker Lane zone is defined on the west by the Furnace Creek system and on the east by a change in tectonic style to a dominantly range-bounding, normal-fault environment

(Figures SBK-2 and -5). We include the generally northeast-striking faults of the Sarcobatus Flat region within this source zone, although this particular fault is characterized separately (Figure SBK-5). We attribute the high level of seismicity in this zone to deformation associated with the high slip rate on the Death Valley-Furnace Creek-Fish Lake Valley fault system. Also included in this source zone is the seismicity and northeast-striking faults in the southern and central NTS region, as well as the extension of the Rock Valley fault zone east into the Spotted Range east of NTS. This zone continues south in a general northwest-southeast orientation, with its eastern border defined by the Las Vegas Valley shear zone. We also defined this zone to include only tectonic, or tectonically triggered, earthquakes, avoiding the seismicity catalog problems related to the Basin and Range source zone to the east, where nuclear testing has been isolated. The East Walker Lane zone accounts for much of the seismicity that trends outboard, to the east, from the Furnace Creek system, as well as most of the northeast-striking fault systems that we interpret to represent neotectonic deformation most likely driven by the strain in the Eastern California shear zone. The most prominent concentration of seismicity in this zone is that associated with the Rock Valley fault zone (Appendix SBK-2). We have also defined the Death Valley area as a subzone within the East Walker Lane zone in our optional configuration (Figure SBK-3). We believe that this subzone may be more likely to produce earthquakes that may cause ground motion on the order of 0.1 g at Yucca Mountain; this is evidenced by the 1992 Little Skull Mountain earthquake. Also, several $M > 3.5$ events have taken place in the Rock Valley fault zone during the past several years, and a general concentration of seismicity is associated with the fault zone. Given this difference in activity during the past tens of years in this subzone as compared to the East Walker Lane zone as a whole, the separation as a subzone enables us to address the possible stationarity of seismicity, although we cannot establish whether this subzone will be a persistent source of activity during a 10,000-year interval.

The Basin and Range zone was established to capture the north- to north-northeast-striking, predominantly low strain rate, range-bounding fault systems within 100 km of the site. We also included the nuclear testing areas of the northern and eastern NTS in this areal source in order to contain explosion-triggered recurrence bias exclusively to the Basin and Range source zone. A subzone was established around Pahute Mesa and Yucca Flat to account for the fundamental problem of separating tectonic earthquakes from explosion-triggered seismicity. These nuclear testing areas may tend to overestimate the hazard by including

seismicity that is directly triggered by explosions. Although the triggered earthquakes ultimately may have occurred without underground testing, including them could overestimate the long-term activity rate. That is, the seismicity in this subzone during the period of nuclear testing may not be representative of the long-term tectonic strain rate in the area. To account for this interpretation, we computed activity and b-values only for the periods that preceded nuclear testing. We consider any increase in seismicity in this region during the recent period of testing to be directly related to the testing, but we also recognize that any attempt to remove all of the dependent events would not be representative of the activity rate. Indeed, attempts were made to separate natural from explosion-triggered seismicity in the catalog compilation, yet we are unconvinced that this can be done adequately. Furthermore, the explosion-triggered seismicity could be a manifestation of tectonic strain, with the explosions representing a triggering stress just as the Landers earthquake was a trigger for the Little Skull Mountain earthquake. To address the uncertainty of adequately accounting for the effect of explosion-triggered seismicity in the NTS we consider two options. The first option is that the aftershock removal process has adequately removed seismicity triggered by the NTS explosions and no adjustment is necessary. This option is assigned a weight of 0.6 (Figure SBK-4). The second alternative is to adjust for the effect of the NTS explosions by removing seismicity within the NTS region post 1950 from the calculation of seismicity rates within the Basin and Range Province. A Pahute Mesa-Yucca zone was defined (Figure SBK-3) that encompasses the area of NTS explosions. All seismicity post 1950 was removed from this area in the calculation of the seismicity rate. This option was assigned a weight of 0.4 (Figure SBK-4).

We also consider the possibility of a background earthquake within the local (site) area. This Local Zone includes the volume not characterized by the recurrence estimates for the local faults themselves: central Crater Flat and the footwalls of the Bare Mountain and Paintbrush Canyon faults. Because the local faults account for most of this volume, we consider the size of the maximum background earthquake in the Local Zone to be less than that for the other areal source zones. This is based simply on the observation, particularly from the distribution of faulting and aftershock activity for the 1986 M 6.3 Chalfant earthquake (our model background earthquake; Appendix SBK-3), that earthquakes of only a limited size could occur in the remaining volume without being accounted for in the recurrence estimates for the local faults. It would be double counting to apply the same magnitude distribution for the

maximum background earthquake from the other areal source zones. The weighting for the maximum background earthquake for the Local Zone is: M 6.2, wt. 0.2; M 6.0, wt. 0.6; M 5.6, wt. 0.2.

2.2.1 Catalogs and Declustering

We have used the 100-km catalog developed for this project to assess recurrence (a- and b-values) for areal source zones. Two declustering algorithms were applied to the 100-km combined catalog. Weighting was applied relevant to the stability of the b-value estimates for the subregions. The algorithms, from Veneziano and van Dyck (1985) and Youngs *et al.* (1987), apply different assumptions in determining the definition of a foreshock or aftershock and therefore behave differently for different regions. The Veneziano and van Dyck (1985) method establishes a baseline activity rate within a given distance from a main shock, then uses this baseline activity to define the local rate. The Youngs *et al.* (1987) method removes dependent events based on several time and distance criteria. The activity rates and completeness levels range significantly within the 100-km region. We consider that earthquakes within the 100-km region follow a power-law distribution in magnitude. The declustering algorithm that returned a distribution that better represented this power-law scaling was considered more efficient in removing dependent events for that region. The Veneziano and van Dyck algorithm appeared to be more stable when applied to the Little Skull Mountain aftershock zone and therefore was weighted higher in the East Walker Lane zone, whereas the Youngs and others method generated smoother recurrence curves when applied to sparse background regions. The weighting listed below and shown in Figure SBK-4 reflects our assessment of the b-value estimates. For the West Walker Lane zone, we weight the Youngs and others declustering algorithm at 0.7, assigning 0.3 weight to the Veneziano and van Dyck algorithm. Our weighting is the opposite for the East Walker Lane zone, for reasons noted above. However, we weight the Youngs and others approach more heavily for the Rock Valley subzone (Youngs *et al.*, 0.7; Veneziano and van Dyck, 0.3). The Basin and Range zone receives weights of 0.4 for the Youngs and others algorithm and 0.6 for the Veneziano and van Dyck approach; identical weights are assigned in the Pahute Mesa-Yucca Flat subzone.

The catalog completeness intervals that we have adopted for assessing earthquake recurrence parameters are based on review of those developed by I.G. Wong (handout to team seismologists at SSC Workshop 4) and on examining the seismicity of the region. The adopted intervals are: **M** 2.5 to <3.5, 1979 to date; **M** 3.5 to <4, 1961 to date; **M** 4 to <5, 1934 to date; **M** 5 to <6, 1900 to date; **M** ≥ 6, 1880 to date. Furthermore, we considered earthquakes that occurred in close proximity to the regional faults to be associated with those faults. These events were not counted in computing the seismicity rate for the regional zones.

A truncated exponential fit using the maximum likelihood method of Wiechert (1980) was applied to all magnitude distributions. A minimum magnitude of 2.5, where this magnitude was above the completeness level, was used to determine the b-values and activity rates, otherwise the minimum completeness level was applied.

2.2.2 Maximum Background Earthquake

We define a background earthquake as any earthquake in a non-fault-specific zone that does not display primary surface rupture. Primary surface rupture is defined as surface faulting taking place on the actual fault plane that radiated the seismic energy at depth. DePolo (1994) reported on the maximum background earthquake for the Basin and Range. There is a range of earthquake magnitudes over which primary fault rupture has been observed in the Basin and Range (S. K. Pezzopane and T. E. Dawson, USGS, written communication, 1996). Distinguishing primary from secondary faulting from the historical data base (S. K. Pezzopane and T. E. Dawson, USGS, written communication, 1996) is difficult because of the variability of instrumental seismicity throughout the historical period and the details of the observations following many of these earthquakes. Actually, isolating the fault plane at depth may require a detailed analysis of the aftershock zone. Also, some interpretation is involved in distinguishing primary from secondary surface faulting based on field data.

The principal factor that affects the development of primary surface faulting is the distribution of seismic moment release with depth. For example, primary surface displacement was observed for the 1950 M 5.6 Fort Sage, California, earthquake, but no primary or secondary surface faulting was mapped following the 1992 M 5.6 Little Skull Mountain earthquake; events of the same magnitude. Although no instrumental record of

sufficient quality to resolve the moment release at depth was available for the Fort Sage event, we consider that faulting must have been shallow, based on its surface expression. This is in contrast to the 1992 Little Skull Mountain earthquake, for which faulting was confined to between 12 and 6 km depth (K. Smith, SSC Workshop 2). It is not surprising for such depth ranges that there was no expression of surface faulting for this earthquake. Therefore, there is a range of earthquake magnitudes over which primary faulting may occur, but above which primary faulting will always be seen. If primary rupture has occurred on faults of Quaternary age, then we assume that these structures have been identified in our assessment of specific fault sources described below, and listed in Tables SBK-2 and -4. Our weighting of the magnitude of the maximum background event is developed to account for the distribution of magnitudes over which no primary surface rupture is observed and for the incompleteness of the historical record and the subjectivity in the interpretation of primary versus secondary surface faulting.

The largest earthquake exhibiting no primary surface faulting in the historical record in the Western United States was the 1925 M 6.6 Clarkston, Montana, event (dePolo, 1994). This earthquake, which occurred in an area having a greater crustal thickness than does the southern Great Basin, is anomalous in the compiled record of background earthquakes (dePolo, 1994). We have taken the possibility for this event into account by assigning a low probability for an M 6.6 maximum event for our areal source zones, although we consider the tectonic and structural environment of the Montana area to be quite different from that of the southern Great Basin. We further consider that the 1986 M 6.3 Chalfant Valley earthquake is a better analog for a maximum background earthquake in the southern Great Basin (Appendix SBK-3). This earthquake produced significant surface faulting, but none that can be considered to have occurred on an extension of the causative fault plane from seismogenic depth to the surface; we interpret that no primary faulting occurred. Although right-lateral offsets of as much as 10 cm were observed along the White Mountains fault zone, a major Holocene fault zone (Lienkaemper *et al.*, 1987), the Chalfant main shock rupture did not occur on this fault. Some of the fault slip, particularly small-event slip, seen in trench data for the local site faults at Yucca Mountain, may represent this type of secondary faulting.

Another moderate-sized earthquake in the southern Great Basin that we consider an analog for the background earthquake is the M 6.1 May 1993 Eureka Valley, California, earthquake.

Although smaller than the Chalfant event, it also produced surface displacements that were most likely not primary surface faulting. In contrast to strike-slip faulting during the Chalfant earthquake, the Eureka Valley earthquake showed nearly pure normal slip on a structure oriented north-south (Peltzer and Rosen, 1995; Massonnet and Feigl, 1995). Given the similarity in faulting style, this earthquake is considered more representative of the surface expression of moderate-sized, normal-faulting earthquakes ($M < 6.5$) that may occur in the site area.

The maximum background earthquakes for the West Walker Lane, East Walker Lane, Basin and Range, Rock Valley, and Pahute Mesa-Yucca Flat zones and subzones are: M 6.6, wt. 0.1; M 6.4, wt. 0.2; M 6.3, wt. 0.5; and M 6.2, wt. 0.2. The maximum background earthquake for the Local Zone is: M 6.2, wt. 0.2; M 6.0, wt. 0.6; M 5.6, wt. 0.2.

2.3 REGIONAL FAULT SOURCES

Fault sources within 100 km of Yucca Mountain were identified based on Piety (1995), Anderson *et al.* (1995a, b), H. L. McKague *et al.* (CNWRA, written communication, 1996), W. R. Keefer and S. K. Pezzopane (USGS, written communication, 1996), and S. K. Pezzopane (USGS, written communication, 1996). Of the faults identified as relevant to ground shaking hazard (S. K. Pezzopane, USGS, written communication, 1996), potentially seismogenic faults were identified as those showing evidence of displacement since mid-Quaternary time (730 ka) or associated with historical seismicity (Table SBK-1). In many cases, only a small part of a potentially seismogenic fault is identified as having middle or late Quaternary slip; however, in assessing maximum magnitude, we treat the entire mapped fault as a seismogenic zone. We did not characterize as seismic fault sources a number of structures identified as Type I faults (H. L. McKague *et al.*, CNWRA, written communication, 1996). These are summarized in Table SBK-2, along with our bases for not including them. The areal extent of a fault source was estimated based on the uncertainties of the fault dip (see below) and the potential combinations of related local structures that may be included in the recurrence for that source. For example, we combined the Buried Hills and Emigrant Valley South faults for analysis. We also consider multiple combinations of behavior of the Death Valley-Furnace Creek-Fish Lake Valley faults, as discussed below.

The uncertainty in the length and down-dip width of the regional fault sources was established to account for any uncertainty in the locations of small-magnitude earthquakes in the regional catalog, which could be removed before estimating the background seismicity rates.

The location and extent of each fault source are given on Figure SBK-5; data on each fault source are compiled in Table SBK-1, with sources and annotations to clarify the bases for interpretations included in the table. Uncertainties in fault extent are included in the fault lengths in Table SBK-1. One example of a fault length that involves considerable uncertainty is the northern extent of the Ash Meadows fault zone. The fault is shown by Piety (1995) as extending north to the vicinity of the Rock Valley fault. However, the Ash Meadows fault is collinear with the so-called Gravity fault (Fridrich, 1997) to the north, and the inferred sense of downthrow is consistent, suggesting continuity of the structures. North of the Rock Valley fault the gravity anomaly continues, but the scarps that characterize the Ash Meadows fault are not present. Therefore, two alternative models for the northern extent of the Ash Meadows fault are considered in the analysis, with the longer fault (100 km) incorporating the Gravity fault north of the Rock Valley fault. Given the lack of evidence for Quaternary slip on this part of the possible fault, we assign a low weight (0.1) to this total fault length.

Approaches to evaluating maximum magnitude and recurrence for these regional fault sources follow. Detailed notes regarding individual faults are included with Table SBK-1. Many long faults, such as the Death Valley and Furnace Creek sources, probably rupture only in part during individual earthquakes (i.e., are segmented, either in a persistent or non-persistent manner). However, we find insufficient data to adequately characterize or model segmentation explicitly on these structures. The Southern Death Valley, Death Valley, Furnace Creek, and Fish Lake Valley faults form a nearly continuous zone of right-lateral shear with a total length on the order of 300 km. It is possible that the fault system behaves as a coherent unit, comparable to portions of the San Andreas fault, although it is much more likely that the constituent faults rupture independently. In considering the combined faults, we recognize the Death Valley normal fault as a pull-apart structure within a right-lateral shear system (which we will call the Death Valley system for simplicity). We assess possible combinations of faults explicitly in our analysis. Although there is mapped continuity among all of the faults of the Death Valley system (e.g. Jennings, 1994), it is extremely unlikely that

they rupture together (R. E. Klinger and L. A. Piety, USBR, written communication, 1996). First, the faults have distinct structural and geomorphic signatures (R. E. Klinger and L. A. Piety, USBR, written communication, 1996); second, the connection between the Furnace Creek and Fish Lake Valley faults has not ruptured in the Holocene (Reheis and Sawyer, 1997), suggesting these two faults have not ruptured continuously; and third, there is no historical analog where a strike-slip fault has ruptured through a major pull-apart of the dimensions of Death Valley. Thus we assign a probability of 0.01 to a single linked fault system. We next consider possible sub-linkages, including the Death Valley-Southern Death Valley fault (0.05 likelihood the faults rupture together, again because of lack of historical analogs and distinct geomorphic signature) and the Furnace Creek-Fish Lake Valley system (0.05 likelihood they rupture together, given the large step-over between them and the apparent difference in timing of paleoseismic events, from studies of Reheis and Sawyer, 1997, and R. E. Klinger and L. A. Piety, USBR, written communication, 1996). These two linked fault zones are not conditional; that is, Death Valley and Southern Death Valley can behave as linked faults in our model regardless of the behavior of the Furnace Creek and fish Lake Valley faults, and vice versa. Most weight (0.94 for each fault), however, is assigned to the faults rupturing independently. Details of assessments for each fault are shown in Table SBK-1.

2.3.1 Maximum Magnitude

For regional fault sources, we used various approaches for estimating maximum magnitudes based on various fault rupture parameters (Table SBK-1). These included regression relations based on surface rupture length, surface rupture area, maximum displacement, and average displacement (Wells and Coppersmith, 1994). Approaches were weighted on a fault-specific basis depending on the input needed and the data available for each fault.

Fault length is based principally on the total mapped length of a fault. In many cases, only part of the fault has documented Quaternary slip (e.g., Pahrump fault has Quaternary slip on about 18.5 km of a 50- to 65-km-long fault; Table SBK-1). We treat these faults by placing a low weight on the Quaternary section and a higher weight on the total fault length, reasoning that the *maximum* magnitude would be produced by a rupture of the entire fault, even if that apparently has not happened in the middle to late Quaternary. For the Pahrump fault, then,

we assign a weight of 0.3 to the short, Quaternary fault length, and a weight of 0.7 to the longer, total fault length (which is uncertain between 50 and 65 km).

Fault area is computed by multiplying fault length by down-dip width. We compute down-dip width from the fault dip and the thickness of the seismogenic zone. We lack specific information on dip for most of the regional faults. Thus, we assign fault dip based on type of faulting: normal faults (45 degrees weighted 0.1, 60 degrees weighted 0.8, and 70 degrees weighted 0.1); strike-slip faults (70 degrees weighted 0.2, 90 degrees weighted 0.8); and oblique-slip faults (60 degrees weighted 0.2, 70 degrees weighted 0.6, and 90 degrees weighted 0.2). Our assessment of the thickness of the seismogenic crust was discussed in section 2.1.

We obtain displacement values from surface fault studies appropriate to the individual faults. In general, we use data from paleoseismic studies (trenches, mapping) to identify the largest single-event displacement reported along a fault in estimating maximum (surface) displacement. Given that the regressions used to compute magnitude from displacement are based on surface observations (Wells and Coppersmith, 1994), use of surface data is appropriate. Although one cannot be certain that trenches have identified the true maximum coseismic surface displacement on a fault, the fact that trenches generally are sited at locations that show evidence of large displacement supports our use of these data. Average displacement is obtained from the along-fault variations in slip during a particular event, rather than from measurement of average displacement during repeated ruptures at a site, because it is the former that is the basis of the regression equations. We require at least 5 points, preferably more, along a fault to estimate average displacement, following the observations of Hemphill-Haley and Weldon (1996).

2.3.2 Recurrence

Earthquake recurrence for fault sources is assessed based on the slip rate on the fault as converted to seismic moment rate using fault area and from estimates of paleoseismic return times when available. The slip rate approach generally is preferred because of significant uncertainties in interval data, both because of dating uncertainties and because the paleoseismic events documented on each of the faults for which we can adequately assess

return periods are not all equal in size. For example, one event may have an interpreted displacement of 1.5 m, whereas others at the same trench site show 0.2 to 0.5 m. It is quite likely that not all of these paleoseismic events are the size of the maximum earthquake (*characteristic earthquakes* in the sense of Schwartz and Coppersmith, 1984). In particular, the return periods may overestimate the frequency of occurrence of maximum earthquakes. Quaternary slip rates are preferred over longer-term Tertiary slip rates because the stress regime has changed for many of the structures, especially at and near Yucca Mountain. However, even slip-rate data are unavailable for some of the faults, such as the Buried Hills-Emigrant Valley South fault. In these cases, we constrain the order of magnitude of the slip rate by comparing the topography of the range along which the fault is found with the topography of other ranges in the Basin and Range for which slip rates of bounding faults are known. We further constrain the slip rate if information is available that alluvial geomorphic surfaces of a certain age (for example, middle Quaternary) are or are not displaced. All slip rate estimates are applied to the fault as a whole, even if the estimate comes from a single point; in general, we have insufficient data to characterize the regional faults in more detail.

Both the characteristic (Youngs and Coppersmith, 1985) and truncated exponential (Berrill and Davis, 1980) recurrence models are used to model the relative frequency of various size earthquakes for a given slip rate. We assign a higher weighting to the characteristic type of distribution for range-bounding faults, reasoning that these faults are most analogous to the Wasatch fault and other major faults that fit characteristic distributions. We apply a higher weighting to the truncated exponential distribution for faults that comprise numerous, discontinuous surface traces, reasoning that these are not the continuous kinds of structures on which characteristic earthquakes generally have been recognized. We assign the weighted average b-value obtained for the areal source in which a fault is located to the recurrence curves derived for faults, as there are insufficient earthquakes associated with individual regional fault sources to compute meaningful local b-values. These assessments are listed in Table SBK-1.

In developing recurrence relationship for the local sources we assume that the maximum magnitude assessments described in Section 2.3.1 are the central value for the characteristic magnitude interval (e.g. Youngs *et al.*, 1987). The characteristic events are assumed to be uniformly distributed in the magnitude range M_{max}±¼, such that the upper limit of the

recurrence relationship is M_{max}+¼. For the exponential recurrence model the upper limit is also set at M_{max}+¼. When the overall rate of earthquake occurrence is specified by the recurrence interval of surface-rupturing earthquakes, this recurrence rate was assumed to apply to earthquakes of magnitude greater than or equal to M_{max}-¼.

2.4 LOCAL FAULT SOURCES

We consider faults within the Crater Flat domain of D. W. O'Leary (USGS, written communication, 1996) separately. Data are summarized in Table SBK-3 for all faults and fault combinations to which we assign non-zero weights as being independent seismogenic structures. These include Bare Mountain, North Crater Flat, South Crater Flat, Windy Wash, Fatigue Wash, Solitario Canyon, Iron Ridge, Bow Ridge, Paintbrush Canyon, and Stagecoach Road faults as well as the hypothesized Highway 95 fault (we refer to all but the Bare Mountain and hypothesized Highway 95 faults as the Yucca Mountain—YM—faults).

One issue concerning the Bare Mountain fault that emerged during the PSHA workshops is that the late Quaternary slip rate is less than the summed slip rates across the YM faults. If the Bare Mountain fault is the master structure, and the YM faults are antithetic or secondary, then the slip rate on the Bare Mountain fault should equal or exceed the sum of slip rates on the YM faults. This is a paradox only if one assumes that the 120-kyr of record on the Bare Mountain fault is representative of the average slip rate during the 500 kyr or more of record on the YM faults. However, additional events on the Bare Mountain fault during a 100-kyr period would increase its slip rate to a level comparable to or even greater than the YM faults. With faults such as these, which have extremely long recurrence intervals, one may need 500 kyr or more of paleoseismic record to represent the average slip rate; this is not available for the Bare Mountain fault. Second, some percentage of the extension across the master fault in this area may be accommodated by volcanism and dike injection in the lower crust in Crater Flat, which we consider a very likely scenario (as discussed in the section on tectonic models). This would reduce the slip rate across the master fault, although it may not reduce the slip rate across the antithetic faults. Clearly, several Quaternary volcanic events have accommodated extension in this area. Third, much of the slip on the YM faults occurred during the "ash event," which apparently did not rupture the Bare Mountain fault. If

it was, indeed, tied to volcanism, which we interpret as the most likely explanation, then perhaps this unique event should be subtracted from the tectonic strain rate represented by the YM faults for comparison with the Bare Mountain fault. In that case, the slip rates are comparable.

We also evaluated the following mapped faults in terms of the likelihood they generate independent seismic events: Abandoned Wash (no Quaternary displacement, although some secondary cracking possible); Drill Hole Wash (no Quaternary slip); Dune Wash (no Quaternary slip); Ghost Dance (no primary Quaternary slip); Midway Valley (no primary Quaternary slip); Sundance (no Quaternary slip); and Yucca Wash (no evidence for existence). In several cases we interpret faults as having produced no primary Quaternary slip. The Ghost Dance fault is particularly important in this regard. E. M. Taylor *et al.* (USGS, written communication, 1996a) describe paleoseismic studies along the Ghost Dance fault, and additional information was made available to us during SSC Workshops 2, 3, and 4. We interpret the results of these studies as follows: evidence for ground cracking during the Quaternary is equivocal along the Ghost Dance fault: if there has been ground cracking, it produced minimal or zero surface displacement; net displacement across the fault in the middle and late Quaternary has been undetectable, based on the detailed mapping by W. C. Day *et al.* (USGS, written communication, 1996a), which shows no surface scarps or offsets, and the evidence from surface-exposure dating of Whaleback Ridge that indicates exceptionally low rates of surface erosion. Thus we believe that the likelihood is negligible that the Ghost Dance fault produces independent seismic events above the maximum magnitude assigned to the Local Zone. Our arguments regarding other mapped faults not included in Table SBK-3 are similar.

Several other structures are hypothesized to exist in the Yucca Mountain vicinity; these were discussed by various experts during SSC Workshop 5. We evaluated each of these possible structures, and concluded either that the hypothesized structure does not exist, or that the maximum earthquake would be within the range of activity defined for the areal source zones. These include a volcanic seismic source (except for the possible link between volcanism and the ash event, considered below); a buried fault that aligns along the cones of Crater Flat; and a cross fault trending northwest across Crater Flat. The former involves earthquakes directly caused by basaltic fissure development and extensional events. We use

the evidence of Smith *et al.* (1996) to argue that such volcanic sources produce maximum earthquakes (M ~5.5) below the maximum magnitude we have assigned to the Local Zone. There is no evidence that a buried fault controls the alignment of Black, Red, and Little Cones in Crater Flat. Given the detailed mapping that has been carried out to describe tectonic activity and identify Quaternary fault scarps in Crater Flat, we would expect that if a north-northeast-trending fault existed and were active it would be recognized. No such fault has been recognized, although it is hypothesized in the Rift Model discussed above. We conclude that it cannot be any more active than the cones themselves, indicating no activity in middle or late Quaternary (post the ca. 1 Ma age of the cones). Finally, no evidence supports a hidden or buried strike-slip fault trending northwest across Crater Flat. Little space is available for this or any other structure to be hidden among or beneath the Yucca Mountain faults. Lacking surface expression, such a fault, if it exists, must produce earthquakes below the threshold of surface faulting. We conclude that we have captured all such earthquakes within the magnitude distribution for the Local Zone, and by including a smaller maximum background earthquake to account for such an event in the site area.

2.4.1 Fault Combinations and Simultaneous Ruptures

The possibility that some faults are linked or coalesce at depth and could rupture together during individual earthquakes is considered for the local fault sources based on similarities in rupture behavior or deformation patterns and possible along-strike or down-dip linkages. These are shown on Figure SBK-6 (Table SBK-3). The possible ruptures of the Yucca Mountain faults with each other and with the Bare Mountain fault constitute one group of such linkages. The chance that all local faults (Bare Mountain and YM faults) rupture together is considered, but given a negligible weight, because there is no paleoseismic evidence for simultaneous events involving the Yucca Mountain faults and the Bare Mountain fault. Indeed, the available stratigraphic and geochronologic evidence is inconsistent with simultaneous ruptures on Bare Mountain and all the other faults. Because of likely down-dip structural linkages among the faults, a rupture linkage cannot be precluded, and we note that at least one Bare Mountain rupture also may have involved minor movement on two or more of the block-bounding faults (event W of S. K. Pezzopane *et al.*, USGS, written communication, 1996a). However, combinations of Bare Mountain and other faults are not explicitly assessed in our analysis, because the rupture of other faults appears to

have been secondary, and we consider the simultaneous rupture of all local faults to be a negligible possibility.

We define terms as follows.

A. Coalesced faults. These are faults that branch upward from a common master fault at seismogenic depths. The geometries of coalescence were summarized by Fridrich during SSC Workshop 5; we adopt his approach with minor modifications. We consider a single coalesced master fault for simplicity; we deal with other combinations through our analysis of down-dip area.

B. Linked faults. These are faults mapped as independent structures (with distinct names) and separated by generally short intervals without mapped surface traces, yet having sufficient geometric continuity to make it reasonable to infer that they are linked below the surface as throughgoing structures. We consider three combinations: Paintbrush Canyon + Stagecoach Road + Bow Ridge; Solitario Canyon + Iron Ridge; and South Crater Flat + Windy Wash + Fatigue Wash. Another interpretation of the Solitario Canyon fault is that it can be linked with the Stagecoach Road fault for a few events (within S. K. Pezzopane *et al.* [USGS, written communication, 1996a] scenarios), but the potential seismic contribution already is encompassed by other combinations considered explicitly.

C. Simultaneous rupture. This is a rupture on more than one fault (as mapped at the surface) that occurs either as the result of a single earthquake or, more likely, as subevents during an earthquake that teleseismically would be considered a single event. In effect, a simultaneous event is one in which ground motion is contributed by the subevents, but they are spaced so closely in time as to be contained within the same seismogram. In our analysis this concept is applied principally to the so-called ash event, Scenario U.

Having resolved that all the YM faults and Bare Mountain fault do not rupture simultaneously in an earthquake, we next address fault coalescence and simultaneous ruptures. First, we consider whether all local faults (except Bare Mountain) are cut off by an active detachment. The evaluation is dependent on the tectonic model. We assign zero weight to the possibility of a shallow detachment as an active seismogenic structure and to a deeper detachment as an active seismogenic structure, even though one or both of these may exist within the present tectonic regime. Our reasoning is that, Wernicke's (1995) argument notwithstanding, all major earthquakes in the Basin and Range have occurred on crustal-penetrating faults, even if shallow structures were inferred in the vicinity from seismic

reflection profiling. Thus, in our evaluation, these hypothesized detachment structures affect only down-dip fault extent, which we address separately.

Next we evaluate the likelihoods that all the YM block-bounding faults are coalesced, linked, or independent (Figure SBK-7). The first possibility is that all sole into a detachment between 5 km and the base of the seismogenic crust, a model-driven possibility to which we assign a likelihood of 0.01, in keeping with our evaluation of tectonic models discussed above. Although the seismic reflection data of lines YMP-1 and -2 do not resolve structure at that depth (Brocher *et al.*, 1996), and the best substantiation for a moderate-depth detachment comes from the cross sections produced by Ferrill *et al.* (1996a), the geophysical data provide little evidence to support such a structure.

The second possibility is that all of the YM block-bounding faults are planar or near-planar but coalesce at depth, in either one or two master faults. This is more allowable than the detachment models, given surface fault geometries and dips. However, lacking any direct evidence of fault coalescence, we consider this possibility still very unlikely; we assign it a weight of 0.09.

We distribute the remaining likelihood between two end members--four linked block-bounding planar faults (assigned a weight of 0.4) and planar faults behaving independently (assigned a weight of 0.5). For each fault considered individually, we further assess whether the fault acts as an independent primary source. We assign likelihoods less than 1 for both the Iron Ridge (assigned a weight of 0.1 as an independent seismic source) and Bow Ridge (assigned a weight of 0.4 as an independent seismic source) faults, as discussed in Table SBK-3. In evaluating the alternatives of linked or independent faults, our preferred approaches were to consider fault geometries and the history of linked ruptures (i.e., is it possible that two colinear faults, such as Paintbrush Canyon and Stagecoach Road, have ruptured together some or all of the time?). Most of the scenarios described by S. K. Pezzopane *et al.* (USGS, written communication, 1996a) argue for complex interactions among faults in terms of overlapping ages of rupture events. Many combinations of behavior are possible, and independent activity is the most likely behavior (although complex linkages are considered). We simplify the possibilities by restricting ourselves to the two end members and assigning a slightly higher weight to independent fault ruptures. The front part

of the logic tree for our local fault models is shown on Figure SBK-7; remaining steps follow from the data in Table SBK-3.

Finally, we consider the likelihood that ruptures on all the faults or combinations of faults have been simultaneous. Given the uncertainties in the dating available from the paleoseismic studies (an inherent aspect of working with infrequent surface faulting events in an arid environment), it is possible to use the rupture scenarios of S. K. Pezzopane *et al.* (USGS, written communication, 1996a) as one extreme, and independence of every paleoseismic event as the other extreme. The intimate stratigraphic association of Scenario Event U with ash, apparently derived from an eruption of the Lathrop Wells Cone, perhaps about 70 ka, suggests one possible simultaneous rupture that is tied to volcanic eruptions in the Crater Flat area. We find it unlikely that even this "ash event" represents a true simultaneous rupture: some exposures show reworked ash, whereas others seem to have direct airfall, which suggests that not all ash-filled fractures opened simultaneously; even if events are closely spaced in time sufficiently to appear simultaneous form a stratigraphic point of view, it is highly unlikely that the events were simultaneous from a seismic point of view, given numerous examples such as the Mammoth Lakes earthquakes of 1980 or the Dixie Valley and Fairview Peak earthquakes of 1954. It nonetheless is a possibility for the maximum-magnitude earthquake that has been (and could be) experienced within the site area. We apply low weighting to this possibility and tie recurrence of such an event principally to the recurrence of Crater Flat volcanism as described in the Probabilistic Volcanic Hazard Analysis (Geomatrix Consultants, written communication, 1996). We also apply an unusual recurrence curve to this event, as explained further below. Given these unique circumstances, we treat this kind of simultaneous event in the logic tree as an additional source. Thus, we add a maximum magnitude event to the data on maximum magnitude otherwise developed for the faults (independent, linked, or coalesced).

We believe that a simultaneous rupture is more likely to occur on faults that are coalesced than on faults that are linked or independent. Accordingly, our weighting of such an event differs depending on the branch of the logic tree. For the branch in which all faults sole into a detachment, we assign a weight of 0.5 to a combination of simultaneous ruptures tied principally to volcanic events in the Crater Flat area and non-simultaneous events on the faults, and a weight of 0.5 to having all events be non-simultaneous. For the model in which

all faults coalesce at depth, we apply the same weights to simultaneous and non-simultaneous events. However, for the models of linked or independent faults, we apply a weight of 0.1 to the combination of simultaneous and non-simultaneous events, with a weight of 0.9 to having all events be non-simultaneous.

2.4.2 Maximum Magnitudes

Our approach to calculating maximum magnitude for the local faults is similar to that taken for the regional faults. However, we add another branch by using stress drops to constrain average displacement, and the fault areas are more sensitive to the details of the down-dip width as estimated from fault intersection analysis and combinations of coalesced and linked faults.

We evaluated fault length based on mapped surface traces. Some teams discussed the possibility that the local faults continue south of their mapped surface traces into the subsurface beneath the Amargosa Valley (SSC Workshop 5), but we conclude that data do not support this interpretation. The Highway 95 fault provides a termination to the YM faults as well as the Bare Mountain fault. Given the lack of evidence and a model for fault termination, we see no reason to speculate that the faults extend any farther south than they are mapped at the surface. The northern extent of some faults is less certain. Faults have been mapped north of the main Yucca Mountain block into bedrock, but without Quaternary displacement. We use the maximum mapped fault length, from Simonds *et al.* (1995), and consider that these pre-Quaternary fault extensions have a lower likelihood of contributing to the maximum magnitude earthquake than do the Quaternary sections of the faults (Figure SBK-6).

Treatment of fault length for coalesced and linked faults is an important consideration. For the models in which faults sole into a detachment and for coalesced faults, we interpret the fault length as that of the longest fault involved in coalescence: the combined South Crater Flat + Windy Wash + Fatigue Wash fault for the shorter length of 27 km (wt. 0.6), and the combined Paintbrush Canyon + Stagecoach Road fault for the longer length of 35 km (wt. 0.4).

Fault coalescence in the subsurface, the maximum depth of penetration of faults into the crust, and fault area were evaluated using a combination of structure contour maps and trigonometric calculations. Structure contour maps were constructed as overlays to the Quaternary fault map of A. R. Ramelli and J. W. Bell (Nevada Bureau of Mines and Geology, written communication, 1996). The structure contour overlay maps were drawn for the local fault sources (YM faults and Bare Mountain fault), as well as for the Ghost Dance fault. Fault strike was constrained by the surface trace on the map of A. R. Ramelli and J. W. Bell (Nevada Bureau of Mines and Geology, written communication, 1996), and the angle of fault dip was constrained primarily by outcrop measurements annotated on the map of Simonds *et al.* (1995). We investigated a range of fault dips, considering the common observation that the dip angle of normal faults often is steeper at the surface than at depth. Average fault dip angles between 45 and 75 degrees were considered, with subsurface dip angles between 45 and 70 degrees considered most likely. The Bare Mountain fault was assumed to be the master structure, with other faults either intersecting one another above the Bare Mountain fault, or being truncated against the Bare Mountain fault surface at depth. We do not consider it credible that one of the YM faults truncates the Bare Mountain fault at depth. The depth and orientations of fault intersections were found either by connecting points of equal depth on structure contour maps of two fault surfaces, or by direct trigonometric calculation of the depth of intersection. The trigonometric calculation was done using the dip angle of the two faults of interest and the horizontal distance between the fault surface traces as measured normal to strike. The calculated intersection depths in combination with fault lengths were used to constrain the down-dip widths of faults to estimate area for computing the maximum earthquake magnitude. The maximum seismogenic width was limited by the intersection of a fault either with the Bare Mountain fault surface or with the base of the seismogenic crust, whichever was shallower.

The following is a summary of the weighting for down-dip width for the local faults based on a Bare Mountain/YM fault dip scenario. Using minimum dip combinations for Bare Mountain and YM faults of 45 degrees/50 degrees preferred, 60 degrees/60 degrees, and a steep limit (70 degrees/70 degrees) for both, the down-dip width in km is listed for each independent YM fault. The first dip in the (aa/bb) pair is that on the Bare Mountain fault (aa); the second is the dip on the YM fault (bb). To capture all uncertainty, the base of the

seismogenic crust is interpreted to be at 17 km. The only scenario controlled by a 17-km seismogenic thickness is the case of 70 degrees/70 degrees.

	BM/YM DIPS (°)	BM/YM DIPS (°)	BM/YM DIPS (°)
	45 /50	60 /60	70 /70
Weight	0.2	0.7	0.1
DOWN-DIP WIDTH OF FAULTS IN KM			
Paintbrush Canyon	14	17	18
Bow Ridge	14	17	18
Stagecoach Road	10	15	18
Solitario Canyon	10	14	18
Windy Wash	8	11	17
Fatigue Wash	8	11	17
N Crater Flat	6	9	13
S Crater Flat	5	6	7

These estimates of down-dip fault width are multiplied by fault lengths to compute areas of individual faults. For the coalescing faults model, we compute fault area for a simultaneous rupture by summing all the contributing fault areas; we compute fault area for non-simultaneous ruptures by considering the maximum fault area for an individual contributor to the coalescing faults (i.e., the Stagecoach Road + Paintbrush Canyon combination). A similar approach is used with the model in which faults sole into a detachment.

These estimates of down-dip width also are used to compute average slip from static stress-drop weighting to establish another estimate of maximum magnitude. Stress-drop weighting was established by taking into account the distribution of static stress drops for the normal faulting regimes (Becker and Abrahamson, 1997; GMC Workshop 3), and the stress-drop estimates for the Little Skull Mountain earthquake (Becker and Abrahamson, 1997).

Weight	0.2	0.5	0.25	0.05
σ (bars)	30	35	50	100

Stress drop is calculated from (Kanamori and Anderson, 1975)

$$\sigma = 8/(3 * \pi) * \mu * [u/ W]$$

where, μ = $3x10^{11}$ dyne-cm (rigidity), **u** = average fault slip (cm), **W** = down-dip fault width (cm).

For the local faults, then, we use five methods to compute maximum magnitude. These are: fault length, fault area, maximum displacement from surface studies, average displacement from surface studies, and average displacement from stress-drop analysis. These are weighted for individual faults and combinations (Table SBK-3) based on availability and quality of data.

2.4.3 Recurrence

Calculation of earthquake recurrence parameters for the local faults followed the guidelines discussed for the regional fault sources. Considerably more data are available to constrain fault slip rate for the local faults than for most of the regional fault sources. In addition, we have repeat-time information available from paleoseismic trench studies for all of the local fault sources. These repeat times are defined in the field for events having different displacements, however, so they probably do not all represent the repeat time of the maximum earthquake for that source. Accordingly, we weight paleoseismic repeat-time data much lower (generally weighted 0.2 to 0.3) than slip-rate information.

Again, special consideration must be given to assessing repeat times for coalesced faults and the model of faults that sole into a detachment. In both cases, we summed slip rates computed at the surface on east-west transects across the faults (e.g., slip rate for coalesced faults = slip rate on Paintbrush Canyon + slip rate on Solitario Canyon + slip rate on Windy Wash + slip rate on North Crater Flat). We use these slip rate calculations exclusively to define recurrence for non-simultaneous ruptures for these fault models. Our model of simultaneous ruptures ties these events closely to the recurrence of volcanic eruptions in the Crater Flat tectonic domain. Thus, we weight the recurrence of simultaneous events heavily by recurrence of volcanic eruptions (0.75 weight) and less by fault slip rate (0.25 weight), regardless of fault model (same weighting for soling faults, coalesced faults, linked faults, and individual faults when they rupture simultaneously).

We weight the choice between characteristic and truncated exponential recurrence models differently for the local faults, depending on whether we consider individual faults or combinations. The Bare Mountain fault is a range-bounding fault, so we weight the characteristic model more strongly (0.6 weight). The YM faults are not, so we weight the truncated exponential model more strongly (0.7 weight). The behavior of the fault combinations is less well resolved, so we weight the two models equally.

Finally, we consider the case of simultaneous ruptures, as represented by the "ash event," the recurrence of which we tie strongly to volcanic eruptions in the Crater Flat area. We consider these to be unusual events, whose frequency is not as much related to conventional fault models as it is tied to volcanic eruptions. Therefore, we treat these events as single contributors to moment release within the study area, reasoning that all other earthquakes are captured either by the distributions otherwise assigned to the faults or by the maximum earthquake and distribution of seismicity for the Local Zone. They are added events, which contribute only their own moment, not a full range of moment distribution as occurs with a characteristic or truncated exponential model. Thus we assign a maximum moment distribution to this kind of event, with the recurrence constrained by a combination of fault slip rate and volcanic-event rate (Table SBK-3), and the only magnitudes given by the range of the maximum magnitude distribution (i.e., all $M < M_{max}$ give no contribution to moment for this source).

As described in Section 2.3.2 for regional faults, we assume that the characteristic and maximum moment events are uniformly distributed in the magnitude range $M_{max}\pm¼$, such that the upper limit of the recurrence relationship is $M_{max}+¼$. For the exponential recurrence model the upper limit is also set at $M_{max}+¼$. When the overall rate of earthquake occurrence is specified by the recurrence interval of surface-rupturing earthquakes, this recurrence rate was assumed to apply to earthquakes of magnitude greater than or equal to $M_{max}-¼$.

3.0
FAULT DISPLACEMENT CHARACTERIZATION

3.1 INTRODUCTION

Our characterization of fault displacement is designed to permit estimates of fault displacement potential on two general classes of faults in the Yucca Mountain Controlled Area: (1) those for which we have specific data concerning the Quaternary rupture history; and (2) those faults and fractures for which data indicate no Quaternary rupture, or for which no data on Quaternary displacement are available. The first class of faults includes the major block-bounding faults, particularly the Solitario Canyon and Bow Ridge faults, that are considered potential earthquake sources (demonstration points 1 and 2); we also include structures such as the fractures in Midway Valley that have no measurable displacement in Quaternary alluvium (demonstration point 9). The second class of faults includes intrablock faults (such as the Drill Hole Wash, Ghost Dance, Sundance, and Dune Wash faults, demonstration points 3-6) as well as small faults, shears, and fractures (demonstration points 7-8). Potential fault displacement in intact rock can be assessed using the characterizations applied to this second group.

For either class of faults, we address two questions: (1) How often might displacement events occur? and (2) How large might these events be? Responding to the first question involves assessing event frequency. Our assessment involves two approaches. In the first, frequency is estimated from analysis of fault slip rate. The second uses direct (fault- or site-specific) information on frequency of displacement or cracking events. Response to the second question involves assessing the range of displacements that might characterize the events defined during the first part of the analysis. This may include fault- or site-specific data regarding prehistoric displacement events, information on variability of displacement along a fault (which may be general or fault-specific), scaling relationships for fault displacements, and data on secondary fault ruptures.

The procedures and methods for characterizing fault displacement presumably will change with improvements in our understanding of the mechanical and statistical characteristics of

fault displacement on both individual faults and fault systems. Our approach is to use several alternative procedures for estimating the frequency and magnitude of fault displacement, which we consider in combination make the best use of available data and capture the uncertainty in characterization of fault displacement at this time. We discuss our general approaches for the two classes of faults, then apply the approaches to the demonstration points.

3.2 FAULTS HAVING DOCUMENTED QUATERNARY DISPLACEMENT

Our characterization of fault displacement potential for faults within the Controlled Area for which data on Quaternary displacement are available incorporates two approaches: one based on the frequency of earthquake occurrence, the earthquake approach; and the other based on assessments of the frequency and size of events from trenching data, the displacement approach (Figure SBK-8). The relative weights assigned to these two approaches depend on the data available for the site of interest.

3.2.1 Earthquake Approach

The earthquake approach to the assessment of fault displacement hazard considers two sources of earthquake induced displacements: principal faulting from earthquakes occurring on the feature of interest, and distributed faulting induced by earthquakes centered on other sources.

3.2.1.1 Characterization of Principal Faulting Potential. The steps involved in characterizing potential displacement due to principal faulting on a fault are shown on Figure SBK-8.

Frequency of Principal Faulting Events. Section 2.0 presents our characterization of the frequency of occurrence of earthquakes as a function of magnitude, $\lambda(m)$, on each seismic source. The frequency of displacement events, λ_{DE} at a point of interest is given by

$$\lambda_{DE} = \lambda(m) \cdot P_R(m) \cdot P(\text{intersection}) \qquad (1)$$

where $P_R(m)$ is the probability that an earthquake of magnitude m will rupture the surface and P(intersection) is the probability that the along-strike location of the rupture will pass through

the site of interest. The probability of surface rupture is assessed using the logistic probability model presented by R.R Youngs (Appendix H, Section H.4.1) in SSC Workshop 5 based on data presented in S. K. Pezzopane and T. E. Dawson (USGS, written communication, 1996). We chose to use the assessment based on recent western Basin and Range earthquake ruptures (Figure SBK-9). The assessment of the probability that the along strike location of the rupture will pass through the site is obtained by randomizing the location of the rupture along the fault in the same manner as is done for ground motion hazard assessment.

Distribution of Principal Faulting Displacement at a Point. The probability distribution for the amount of displacement at a point is defined based on the concept presented by the ASM team in SSC Workshop 5. The first step is an estimate of the maximum displacement, *MD,* in the earthquake. We use the empirical relationship between *MD* and moment magnitude developed by Wells and Coppersmith (1994) to define a lognormal distribution for *MD* in each earthquake.

Given a maximum displacement, we assess the distribution for displacement at a point using normalized distributions for *D/MD* as a function of location along the rupture. We use two approaches, one based on the ASM evaluation of historical rupture patterns presented in Wheeler (1989) (Figure SBK-10; Appendix H, Section H.3.1) and one based on our fractal model of fault surface roughness presented in SSC Workshop 5 (Figure SBK-11; Appendix H, Section H.3.2). We give equal weight to the historical rupture and fractal interpolation approaches.

The fractal model is based on the assumption that variability in displacement along the length of a fault rupture scales with the roughness of the rupture surface. This variability is modeled using a two-dimensional fractal interpolation function in which an arbitrary displacement is located at random within the length of a synthetic rupture (length = -1 to +1). Displacement at 99 additional points are then interpolated between the initial displacement point and the end points of the rupture using fractal interpolation (Barnsley, 1988). The variability in displacement between points is controlled by the fractal dimension (Df) of the interpolation function, which is set at $Df = 1.3$, a value determined by Lee and Bruhn (1996) for natural fault surfaces with Quaternary and older rupturing history. One hundred ruptures were

simulated using the fractal interpolation algorithm of Barnsley (1988). The displacements at 100 points along the length of the simulated ruptures were then normalized to the maximum displacement in each simulated rupture, and then collected as an ensemble from which the average and variability in displacement at each point was calculated to produce the results presented in Figure SBK-11. More details of the simulation procedure are included in documentation presented by the SBK team at Workshop 5.

3.2.1.2 Characterization of Distributed Faulting Potential. The steps involved in characterizing the potential for distributed faulting from earthquakes on other sources are the same regardless of whether the fault has documented Quaternary displacement or not. These methods are discussed below in Section 3.3.1.

3.2.2 Displacement Approach

The displacement approach to the characterizing fault displacement potential combines the effects of principal and distributed faulting into a single assessment. The steps involved in this approach are shown on Figure SBK-8.

3.2.2.1 Frequency of Displacement Events. The frequency of displacement events is computed using two approaches: one involving estimates of fault slip rate and average displacement per event; and the other involving event frequency estimated from trenching data. In general, the slip-rate approach is weighted higher than the event-frequency approach for the demonstration points consistent with our weighting of these types of data in the assessment of local fault seismic sources (Table SBK-3). However, weights will differ for other faults depending on the type and quality of information available concerning their Quaternary rupture history.

Slip Rate Evaluation. Slip rate is either determined directly at the point of interest or interpolated along the strike of the fault between trenches or other survey localities, where fault offsets and the age of offset horizons are known from measurements and dating. We consider these two conditions in structuring our logic tree for fault displacement hazard (Figure SBK-8).

Detailed mapping of Quaternary geomorphic surfaces and faults, along with the large number of paleoseismic trenches excavated across Yucca Mountain faults, has yielded considerable information about slip rate, and its variability, along major faults such as the Solitario Canyon and Paintbrush Canyon faults. Thus, slip rate can be estimated directly at numerous locations. The slip rate at a point of interest can be estimated by measuring the cumulative offset of a Quaternary horizon of known age, which may be measured in a trench or on a geomorphic surface in the landscape. Slip rate (*SR*) is estimated from the equation:

$$SR = \text{Offset} / (\text{Horizon Age}) \qquad (2)$$

Minimum, preferred, and maximum slip rates are calculated using the estimated range of minimum, maximum, and preferred magnitude of offset of a geologic horizon and its age. No along-strike interpolation is necessary in these cases. At demonstration point #1 on the Bow Ridge fault, for instance, slip rate can be estimated directly.

More commonly, the point of interest is located between trenches or other points along a fault where the slip rate has been calculated from site-specific geologic data. One or more methods of slip rate interpolation must be applied. We apply two methods, the first using data on Quaternary displacements along the fault of interest, the second using cumulative displacement along the fault. The slip rate at a point of interest is scaled between two points of known displacement; we use linear interpolation unless sufficient data are available to more accurately characterize the variation in displacement along strike. The first method requires data on Quaternary displacement at two points that bracket (along strike) a point of interest. For example, this approach is used for the Solitario Canyon fault at demonstration point #2, because along-strike changes in the offset of middle to late Quaternary geomorphic surfaces are known from detailed mapping and trenching (Ramelli, SSC Workshop 6). The slip rate at the point of interest is interpolated from those obtained at trench SC-T4 and the north end of Quaternary faulting using Ramelli's curve of along-strike variability in the offset of mid- to late-Quaternary geomorphic surfaces. Such an approach can be used for any point on a fault that is between two locations of known Quaternary displacement (even if one of those is a location of known zero displacement).

Along-strike variation in fault displacement also may be measured using displaced bedrock horizons of known age. Yount (SSC Workshop 6) presented curves estimating the along-strike variability in cumulative bedrock offset along both the Solitario Canyon and Bow Ridge faults, for example. We apply a linear interpolation for this method also, unless a sufficiently large data set is available to more accurately characterize the along-strike variation in fault slip.

Given an assessment of slip rate, *SR* on a feature, the frequency of displacement events, λ_{DE}, is given by the expression:

$$\lambda_{DE} = SR / \overline{D}_E \qquad (3)$$

where $\overline{D}_E$ is the average displacement per event. The approaches used to assess $\overline{D}_E$ are discussed below.

Direct Evaluation of Event Frequency. Our interpretation of the frequency of events from fault trenching data includes both those events for which we have measured shear offset and fracturing events having no measured shear offset, as both kinds of events have broken the surface. The number of events divided by the age of the youngest horizon that predates the oldest faulting or fracturing event is an estimate of the frequency (number of events / annum). Event frequency is expressed as minimum, preferred, and maximum values based on the range of estimated ages of geologic horizons and uncertainty in the number of events interpreted from the trench logs. We use the compilation (Table 5.1) of S. K. Pezzopane *et al.* (USGS, written communication, 1996a) as our principal source in estimating event frequency.

Some faults have near-surface or surface fractures that developed by cracking in Quaternary soils, but across which there is no measurable shear offset to prove Quaternary surface faulting; a good example is the Midway Valley structure at demonstration point #9. These fractures may have undergone only opening or may have been sheared less than can be detected in the paleoseismic studies (we estimate up to 10 cm). Alternatively, opening-mode or mixed shear- and opening-mode cracks may have developed at or near the surface in response to shear displacement on the fault at depth. Bruhn and Schultz (1996) provided theoretical support for this kind of surface-crack development. They investigated the nature

of near-surface fracturing caused by sliding on part of a normal fault patch at depth and found that mixed opening- and shear-mode cracking is expected at or near the Earth's surface. These features could also develop during strong ground shaking, as discussed below. Thus, surface cracking could be indicative of fault displacement at depth, even at shallow crustal depths such as those at the potential repository.

The maximum frequency of occurrence of cracking events is estimated by dividing the number of cracking events by the age of the youngest soil that is affected by the oldest cracks; the minimum is estimated by dividing the number of events by the age of the oldest deposits. The amount of displacement is estimated from the thickness of calcite or silica laminae filling the cracks following each event. Data on these events is summarized by S. K. Pezzopane *et al.* (USGS, written communication, 1996a) and recorded in detailed trench logs. We assess a 50% chance that surface cracking having no measurable shear offset reflects deformation above a slip patch on the fault at depth. This implies that not all surface cracking is directly related to shearing on the fault at depth, even if the cracks are located directly on a fault that extends to the surface.

3.2.2.2 Characterization of Amount of Displacement. Characterizing the amount of fault displacement, given a displacement event, involves estimating maximum or average displacement per event on the fault. These values can be computed from paleoseismic data (preferred, given that we have data available) or from regressions of displacement versus magnitude from historical ruptures elsewhere (Wells and Coppersmith, 1994). Paleoseismic values are obtained from S. K. Pezzopane *et al.* (USGS, written communication, 1996a) and Table SBK-3; weighting is fault-specific. As with computation of slip rate, displacement data may be available at a particular site, or it may have to be interpolated from nearby locations along the fault. Again, we use linear interpolation, and we assign greatest weighting to Quaternary displacement data.

Three approaches are used to compute the average displacement at the point of interest, two based on empirical relationships between rupture length and maximum and average displacements. Each of these, in turn, is used to characterize the variability in displacement per event.

Paleoseismic Estimates of Average Displacement. We calculate the variability of displacement about an assessment of the average displacement from paleoseismic data through three steps. Step 1: For each trench for which we have three or more offset measurements, compute the average slip, U_{ap}.

$$U_{ap} = 1/n \, \Sigma U_i \qquad (4)$$

where U_i is a single event fault slip (offset) at a site with three or more offsets, and n is the number of measurements at the site. This assessment is then used as an estimate of the average displacement per event, $\bar{D}_E$. Step 2: Divide each offset measurement (U_i) by U_{ap}. Step 3: Accumulate the U/U_{ap} samples from all trenches on all local faults, except the Rock Valley and Bare Mountain faults in Table 5.1 of S. K. Pezzopane *et al.* (USGS, written communication, 1996a). This provides an estimate of $P(U/U_{ap})$, the probability density function of a displacement U given an average displacement U_{ap} at a site. This approach is applicable directly at trench sites where at least three events have been recorded, and we interpolate between known points to calculate $P(U/U_{ap})$ when the site of interest is not at a trench location. Figure SBK-13 shows the resulting data and the fitted gamma distribution (Appendix H, Section H.2.2) used to characterize the probability distribution for U/U_{ap}. The data for this distribution is listed in Table SBK-6.

Empirical Estimates of Average Displacement. We apply a slightly different approach to estimate the distribution of displacement events about the average slip from the Wells and Coppersmith (1994) empirical relationships between rupture length and average displacement. Here, our approach involves four steps. Step 1: Determine the maximum, preferred, and minimum fault lengths for all local faults with trench data for Quaternary offset (Table 5.1 of S. K. Pezzopane *et al.*, USGS, written communication, 1996a), except the Rock Valley and Bare Mountain faults. We use the values we assessed in the seismic source characterization (Table SBK-3). Step 2: Calculate the average slip, U_a for each fault:

$$\log(U_a) = -1.99 + 1.24 \log(FL) \qquad (5)$$

where FL is the fault length used to estimate the maximum magnitude earthquake in Section 3.0. This assessment is then used as an estimate of the average displacement per event, $\bar{D}_E$. Equation (5) is from Table C2 of Wells and Coppersmith (1994). Step 3: Divide the offset measurement U_i from each trench on a fault by U_a for that fault. Do this for each local fault except the Rock Valley and Bare Mountain faults listed in Table 5.1 of S. K. Pezzopane *et al.* (USGS, written communication, 1996a). Step 4: Plot the frequency histogram of U/U_a as an estimator of $P(U/U_a)$. Figure SBK-13 shows the resulting data and the fitted gamma distribution (Appendix H, Section H.2.3) used to characterize the probability distribution for U/U_a. The data for this distribution is listed in Table SBK-6.

Empirical Estimates of Maximum Displacement. The alternative is to compute U_m from the Wells and Coppersmith (1994) regression for maximum displacement from fault length:

$$\log(U_m) = -1.98 + 1.51(FL) \quad \textbf{(6)}$$

where appropriate ranges of fault length are obtained from Table SBK-3. The estimate of average displacement per event, $\bar{D}_E$, is set equal to $0.69\times U_m$. We divide each offset measurement (U_i) from the trenches on each Yucca Mountain fault by U_m for that fault. The result is a frequency histogram of U/U_m as an estimator of $P(U/U_m)$, the probability distribution of displacement U given U_m for a site. Figure SBK-14 shows the resulting data and the fitted gamma distribution (Appendix H, Section H.2.4) used to characterize the probability distribution for U/U_m. The data for this distribution is listed in Table SBK-6.

In each case we compute a cumulative probability density function from the integrals of the probability density functions. The results are expressed as the probability of exceeding a normalized displacement if fault rupture occurs at a site of interest.

3.3 FAULTS WITHOUT DOCUMENTED QUATERNARY DISPLACEMENT

Many faults in the Controlled Area lack evidence for Quaternary displacement because they are inactive, have exceedingly long recurrence intervals, are located in areas that lack Quaternary cover, or are embedded in the rock mass beneath the surface. Our approach to characterize potential displacement on these faults follows the same principles as described

above, using either an earthquake approach to estimate the frequency of induced slip events or the displacement approach using direct assessment of slip rate and event size based on data for the feature. However, these are modified to account for the types of data available for the characterization. The generalized logic tree for this class of faults is diagrammed on Figure SBK-15.

3.3.1 Earthquake Approach for Distributed Faulting

The steps involved are assessment of the probability that slip can occur, evaluation of the frequency of distributed ruptures, and evaluation of the distribution of displacements.

3.3.1.1 Fault Orientation Weighting. Maps of distributed ruptures formed during historical earthquakes and nuclear test blasts (Covington, 1987; S. K. Pezzopane and T. E. Dawson, USGS, written communication, 1996), and simple rock mechanics theory (e.g., Ferrill *et al.*, 1996a), suggest that the likelihood of fault activation is a strong function of the orientation (strike and dip) of a fault surface with respect to the principal stresses. We develop an orientation index for evaluating the likelihood of fault activation. This index is based either on stress ratios between a most favorably oriented reference fault and the fault of interest, or by comparison to the orientations of distributed rupturing generated by historical, surface faulting earthquakes (based on diagrams in S. K. Pezzopane *et al.*, USGS, written communication, 1996a). By most favorably oriented fault, we mean that fault which would have the greatest slip tendency, or ratio of shear to normal traction, in the ambient stress field within the Controlled Area.

Use of Fault Slip Tendency. The orientation (strike and dip) of a fault surface relative to the contemporary stress field is an important measure of the likelihood of fault activation (Ferrill *et al.*, 1996a). Faults most likely to be active and slip in the contemporary stress field have the largest ratio of shear (*Ts*) to normal stress (*Tn*), which defines their slip tendency. Faults having lower shear-to-normal stress ratios are less likely to be active and slip as distributed or secondary ruptures under dynamic and static stress perturbations caused by an earthquake in the surrounding area. We extend this analysis by defining the fault activation factor (*AF*) as the ratio of the slip tendency on the fault of interest to that on the most favorably oriented fault in the contemporary stress field. The activation factor (*AF*) will range between 1.0 and 0. *AF* is a weight that reduces the expectation of failure on less favorably oriented faults.

The shear stress state on a fault or fracture is defined as:

$$\boldsymbol{Ts} = \text{magnitude } (\boldsymbol{T} - \boldsymbol{Tn}) \tag{7}$$

where $\boldsymbol{T}$ is the traction vector across the fault of interest induced by the ambient stress tensor, $\boldsymbol{Tn}$ is the normal stress acting across the fault surface, and the bracketed term implies vector subtraction. We assume that the orientation of the fault is known to within ± 10 degrees, an angular variation that captures uncertainty in measurement by the geologist or mapper, and accounts for most natural undulations of the fault surfaces. Traction vector components of $\boldsymbol{T}$ and $\boldsymbol{Tn}$ are found using standard vector and tensor operations:

$$T_i = S_{ij}\, n_j \qquad \text{and} \qquad Tn_i = [S_{ij}\, n_i\, n_j]\, n_i \tag{8}$$

where $\boldsymbol{n} = \langle n_1, n_2, n_3 \rangle$ is the unit vector parallel to the pole of the fault surface, S is the stress tensor, and summation is implied over repeated indices in the equations (Einstein Summation Convention).

The ambient stress in the ESF was determined by hydrofracture measurements in Testhole ESF-AOD-HDFR#1 at a depth of 244 m (Sandia National Laboratories, written communication, 1997). The three principal stresses are: Sv = 4.69 MPa, vertical; SH = 2.9 ± 0.4 MPa, N15°±14°E; and Sh = 1.7 ± 0.1 MPa, N75°±14°W, where Sv is the vertical compressive stress, SH is the maximum horizontal compressive stress, and Sh is the minimum horizontal compressive stress. The ESF stress tensor may originate partly by tectonic and partly by topographically induced loading. Regardless of its origin, this stress tensor indicates a normal faulting stress regime in the ESF facility, with vertical maximum compressive stress, and least horizontal compressive stress oriented approximately normal to the block-bounding faults. Notably, the orientation and magnitude of the stress tensor are compatible with other hydrofracture measurements in the Yucca Mountain block and at the Nevada Test Site, which indicate a normal faulting regime and similar horizontal stress orientations to depths of approximately 1 km (e.g. Stock and Healy, 1988).

We conclude that the most favorably oriented fault dips between 60 and 65 degrees and strikes parallel to SH. The ratio $|Ts/Tn|$ on this fault is 0.54. We use this value to normalize the ratio $|Ts/Tn|$ on faults of interest that have different orientations. The ratio of the orientation of the fault of interest to the most favorably oriented fault defines the AF factor, which we multiply by the slip rate or event frequency to compute a revised rate or frequency.

This method neglects the role of fault interactions, which may rotate and concentrate the local stress field to cause slip on adjacent faults that are not favorably oriented for failure in the ambient stress field. We acknowledge this limitation, but we consider it of secondary importance in the evaluation of displacement hazard.

Use of Orientation Histogram. An activation factor (weight) can also be derived from empirical data on the pattern of distributed rupturing generated during historical earthquakes (S. K. Pezzopane and T. E. Dawson, USGS, written communication, 1996). This method requires construction of an azimuth (fault trend) frequency distribution of secondary ruptures generated during historical earthquakes (Appendix H, Section H.4.3; S. K. Pezzopane and T. E. Dawson, USGS, written communication, 1996; diagram presented by Pezzopane, SSC Workshop 4) and following nuclear test blasts at the Nevada Test Site (Covington, 1987). The objective is to estimate the chance that secondary rupturing will occur on faults orientated at various angles to the primary rupture zone. We expect secondary rupturing to be most common on faults that parallel the primary rupture, and least common on other faults. The underlying physical principle is that secondary rupturing is most likely on those faults favorably oriented for failure under the ambient stress field, and that other, less favorably oriented faults are less likely to rupture. Visual inspection of rupture maps in S. K. Pezzopane and T. E. Dawson's (USGS, written communication, 1996) compilation shows that secondary ruptures are concentrated along the azimuth of the primary rupture trace in most earthquakes, and that the frequency and length of secondary rupturing decrease significantly for other orientations.

3.3.1.2 Frequency of Distributed Faulting Events. Section 2.0 presents our characterization of the frequency of occurrence of earthquakes as a function of magnitude,

$\lambda_n(m)$, on each seismic source, n. The frequency of distributed faulting ruptures, $_{DE}$, is computed by the relationship

$$\lambda_{DE} = \lambda_n(m) P_n(\text{Slip}|\text{Event}) \quad (9)$$

where P_n(Slip|Event) is the probability that an earthquake on source n will induce slip on the feature of interest. We employ two approaches to characterize the frequency of events by earthquake triggering (Figure SBK-15). The first approach uses the earthquake recurrence on independent seismic sources, along with empirical functional relationships for distributed ruptures on hanging and foot wall (S. K. Pezzopane and T. E. Dawson, USGS, written communication, 1996; Pezzopane, SSC Workshops 2 and 3; R.R. Youngs, SSC Workshop 6). The second approach uses empirical observations of secondary fracturing and faulting in underground workings caused by strong ground shaking (Brady, 1990).

Historical Rupture Approach. The probability that a secondary or distributed displacement event will occur on a fault away from the seismic source is computed based on distance from the source (Appendix H, Section H.4.2). Pezzopane (SSC Workshop 3) showed the relationship between width of secondary or distributed rupture zone and earthquake magnitude derived from the S. K. Pezzopane and T. E. Dawson (USGS, written communication, 1996) database of historical Basin and Range earthquakes. R.R. Youngs (SSC Workshop 6) showed the frequency of occurrence of displacement events with distance from the fault as a function of magnitude in both hanging-wall and foot wall positions. Figure SBK-16 shows the resulting relationship for the probability that distributed rupture will occur at a point as a function of earthquake magnitude, distance to rupture, and location in the hanging wall and foot wall. For earthquakes occurring in the local areal source, we consider that it is equally likely the point of interest lies in the hanging wall or the foot wall. We assign a weight of 0.5 to this approach.

Ground Shaking Approach. This approach makes use of peak particle velocity (PPV) induced by strong ground motion and transient seismic strain (Hanks and McGuire, 1981; McGarr, 1984) to estimate the probability of triggering displacement on faults and fractures in the Yucca Mountain block. The method is based on observations of damage in underground tunnels and openings (Brady, 1990), and is only applied if the point under

consideration is located within an underground excavation (See Excavated Fault, or Excavation Site decision columns in Figures SBK-9 and SBK-17).

The approach is applicable for evaluating displacement on fractures that are either located adjacent to, or intersect, an underground working. Rock excavations create stress concentrations that can either destabilize or stabilize faults and joints in the vicinity of an underground excavation. Displacements may occur, but the likelihood depends on the geometry of the excavation, the orientation of the fractures, and the ambient principal stresses (Brady, 1990; Galybin, 1997). The approach presented here reflects our evaluation that, although it is important to incorporate the effects of strong ground motion on fault displacement hazard, techniques for implementing such an analysis are not well established.

The annual probability of exceedance of a specified peak particle velocity (PPV) at the surface is a ground motion parameter that is calculated as part of the PSHA analysis. F(PPV) is the annual frequency of exceedance of a PPV at the surface above a point of interest. This is computed directly from the PSHA parameters. We define P(DamagelPPV) as the probability that joint or fault movement (damage) will occur in a subsurface excavation given a specified PPV. The function is based on the correlation between observed damage in underground excavations in jointed rock, and the PPV measured at the surface (Brady, 1990). Figure SBK-17 shows our evaluation of the probability function P(DamagelPPV). We weight this approach 0.5.

3.3.1.3 Distribution of Distributed Faulting Displacement at a Point. We lack information about average or maximum displacement during individual rupture events on faults that lack Quaternary displacement. However, cumulative (late Cenozoic) displacement generally is known on faults for which we can measure offset of marker horizons in excavations or at the surface.

Our preferred approach for estimating displacement variability on a fault where only cumulative slip is known involves comparing the cumulative slip on the fault of interest with the cumulative slips on all Yucca Mountain faults. First, we use the maximum, preferred, and minimum estimates of cumulative fault displacement, D_m, for each Yucca Mountain fault (principally from Simonds *et al.*, 1995). For each trench site on the Yucca Mountain faults,

we divide the single-event displacement by the total to develop a frequency histogram of U/D_m (see Table SBK-7), which specifies a probability density function $P(U/D_m)$ (Appendix H, Section H.3.2; U/D_m, Figure SBK-18). The cumulative slip at the site or fault of interest is then multiplied by this function to obtain the distribution of single-event displacements for the fault of interest.

3.3.2 Displacement Approach for Distributed Faulting

The steps involved are assessment of the probability that slip can occur, evaluation of the frequency of displacement events, and evaluation of the distribution of displacements.

3.3.2.1 Frequency of Displacement Events. The frequency of displacement events is evaluated using Equation (3). This assessment requires estimating the slip rate and average displacement per event.

Evaluation of Slip Rate. In the absence of data to characterize the Quaternary slip history of a fault, our use of slip rate relies on long-term, fault-specific slip data and/or on scaling of slip on one fault based on slip rates for better-studied faults in the Yucca Mountain area. We describe first the geohistorical approach, which is our preferred method because it takes into account the history of slip on a particular fault (although the weighting varies from point to point). Then we describe the fault scaling approach.

Geohistorical Method. This approach provides estimates of fault slip rate based on the cumulative displacement of a horizon of known age. The approach, which was outlined in detail by the DFS Team during SSC Workshop 5, involves not only the assessment of total displacement at a point on the fault, but also weighting of three models of slip history. The approach is applicable only to those points for which total displacement can be measured.

In the first model, we compute an average long-term slip rate. Displacement of the Tiva Canyon tuff (Ttc), with an estimated age of 12.5 Ma, is used to determine the long-term slip rate. In this model we assume that slip has been uniform during the past 12.5 Ma. Given the arguments summarized below that slip has <u>not</u> been uniform in the Yucca Mountain area during the past 12.5 Ma, we assign a weight of 0.1 to slip rates calculated using this model.

The second model assumes a change in slip rate at the close of tuff deposition. Fridrich (1997) suggests that approximately 80 percent of the post-Tiva Canyon tuff displacement on faults in the Yucca Mountain area occurred prior to deposition of the Rainier Mesa tuff (Trm) at 11.6 Ma. With this model, we calculate slip rates by dividing 20 percent of the post-Ttc displacement by 11.6 Ma. Here we assume that slip has been uniform during the past 11.6 Ma, although it was much more rapid from 12.5 to 11.6 Ma. We consider that this model accounts for the geologic evidence for changes in late Cenozoic slip better than the first model, so we weight it higher (0.3).

The third model is based on geologic observations and interpretation by Day *et al.* (USGS, written communication, 1996e, Fig. 2-10) that the rate of crustal extension in the region encompassing Yucca Mountain has continued to decrease since the middle Miocene. The late Miocene slip rate is calculated by dividing 80 percent of the post-Tiva Canyon displacement by the estimated age difference between the Rainier Mesa and Tiva Canyon tuffs (about 900 ka). Then we compute the Quaternary slip rate by multiplying this late Miocene rate by a reduction factor of 0.021±0.018, which is the ratio of Quaternary to late Miocene extension estimated by Day *et al.* (USGS, written communication, 1996e). This model most fully incorporates evidence for the changes in late Cenozoic slip history; thus we weight it the highest of the three methods for computing Quaternary slip rate from long-term slip (0.6). We note that an estimate of a long-term slip rate can be defined in principle by dividing the age of any geologic horizon into the cumulative fault offset of that horizon, so one is not restricted to offsets of the Tiva Canyon or Rainier Mesa tuff horizons. However, the displacements of Ttc or Trm are the most common measurements available on the Yucca Mountain faults.

Fault Scaling Methods. Fault scaling methods are based on the observation that the slip rates on two different faults scale with their relative surface areas (Cowie and Scholz, 1992b). That is, the larger fault presumably has the higher slip rate. If fault area is not known, then ratios of cumulative displacement or fault length may be substituted for surface area based on the scaling relationships between cumulative fault displacement and fault length, and between fault length and fault surface area (Walsh and Watterson, 1987, 1992; Cowie and Scholz, 1992a, b; Clark and Cox, 1996). Because cumulative displacement either is known or can be estimated from geologic mapping on block-bounding faults at Yucca Mountain, and

this is the most likely data available for fractures and shears mapped in the subsurface, we give highest weight to the use of the cumulative displacement ratio (however, weighting varies with each case). The displacement ratio method proposed here is supported by both observational (Nicol *et al.*, 1997) and mechanical modeling (P.A. Cowie, Lamont-Doherty, written communication, 1998) studies which indicate that the slip rates of normal faults with larger cumulative displacement are consistently greater than those of smaller faults with less cumulative displacement in the same region. Nicol *et al.*'s (1997) study is based on observations of normal faulting from six rift basins located in different parts of the world, and is applicable to terrains like those in the Controlled Area. We therefore consider the slip rates of two faults to be proportional to the ratio of their cumulative displacement:

$$Sr_i = [Dcum_i / Dcum_r] \times SR_r \qquad \textbf{(10)}$$

where *Dcum* is cumulative displacement and *SR* is slip rate. Index "*i*" refers to the fault of interest, and index "*r*" refers to a fault with known slip rate. One or more of the block-bounding faults at Yucca Mountain with known SR_r may be used as the reference fault. If more than one fault is used to calibrate slip rate, then the slip rate for the reference fault must be expressed as an average value, and the reference cumulative displacement must also be averaged over the reference faults. The fault of interest may be located in the repository block or elsewhere in the Controlled Area; it has known cumulative displacement at one or more points but no definitive geologic evidence for Quaternary slip rate.

Average Displacement Per Event. We use three probability distributions ($P(U/D_m)$, $P(U/U_a)$, and $P(U/U_m)$) for displacement per event at points on faults where both fault length and cumulative displacement are known (Figure SBK-15, displacement logic tree branch). However, for those points where only cumulative fault displacement is known we use just one function, $P(U/D_m)$.

3.3.2.2 Distribution of Distributed Faulting Displacement. The distribution function described in Section 3.3.1.3 and shown on Figure SBK-18 is used to characterize the distribution of displacements in faulting events.

4.0
REFERENCES

Anderson, L.W., and Klinger, R.E., 1996, The Beatty scarp in Nye County, Nevada—an important Late Quaternary morphologic datum: Bulletin of the Seismological Society of America, v. 86, p. 1650-1654.

Anderson, R.E., Bucknam, R.C., Crone, A.J., Haller, K.M., Machette, M.N., Personius, S.F., Barnhard, T.P., Cecil, M.J., and Dart, R.L., 1995a, Characterization of Quaternary and suspected Quaternary faults, regional studies, Nevada and California: U.S. Geological Survey Open-File Report 95-599, 56 p. plus app.

Anderson, R.E., Crone, A.J., Machette, M.N., Bradley, L.A., and Diehl, S.F, 1995b, Characterization of Quaternary and suspected Quaternary faults, Amargosa area, Nevada and California: U.S. Geological Survey Open-File Report 95-613, 41 p. plus appendices.

Argus, D.F., and Gordon, R.G., 1991, No-net-rotation model of current plate velocities incorporating plate motion model NUVEL-1: Geophysical Research Letters, v. 18, p. 2038-2042.

Barnsley, M.F., 1988, Fractals Everywhere: Boston, Academic Press, 394 p.

Beanland, S., and Clark, M.M., 1994, The Owens Valley fault zone, eastern California, and surface faulting associated with the 1872 earthquake: U.S. Geological Survey Bulletin 1982, 29 p.

Becker, A., and Abrahamson, N., 1997, Stress drops in normal faulting earthquakes [abs.]: Seismological Research Letters, v. 68, p. 322.

Berrill, J.B., and Davis, R.D., 1980, Maximum entropy and the magnitude distribution: Bulletin of the Seismological Society of America, v. 70, p. 1823-1831.

Brady, B.H., 1990, Dynamic performance and design of underground excavations in jointed rock, *in* Brummer, R. ed., Static and Dynamic Considerations in Rock Engineering: Rotterdam, A.A. Balkema, p. 1-11.

Brocher, T.M., Hart, P.E., Hunter, C.W., and Langenheim, V.E., 1996, Hybrid-source reflection profiling across Yucca Mountain, Nevada: regional lines 2 and 3: U.S. Geological Survey Open-File Report 96-28, 110 p.

Bruhn, R.L., and Schultz, R.A., 1996, Geometry and slip distribution in normal fault systems; implications for mechanics and fault-related hazards: Journal of Geophysical Research, v. 101, p. 3401-3412.

Burchfiel, B.C., Hodges, D.V., and Royden, L.M., 1987, Geology of Panamint Valley-Saline Valley pull apart system, California; palinspastic evidence for low-angle geometry of a Neogene range-bounding fault: Journal of Geophysical Research, v. 92, p. 10,422-10,426.

Carr, W. J., 1984, Regional structural setting of Yucca Mountain, Southwestern Nevada, and late Cenozoic rates of tectonic activity in part of the Southwestern Great Basin, Nevada and California: U. S. Geological Survey Open-File Report 84-854, 114 p.

Carr, W. J., 1990, Styles of extension in the Nevada Test Site region, Southern Walker Lane Belt; An integration of volcano-tectonic and detachment fault models, in Wernicke, B.P., ed., Basin and Range Extensional Tectonics near the Latitude of Las Vegas, Nevada: Geological Society of America Memoir 176, p. 283-303.

Clark, R.M, and Cox, S.J.D., 1996, A modern regression approach to determining fault displacement-length scaling relationships: Journal of Structural Geology, v. 16, p. 147-152.

Covington, H.R., 1987, Map showing surface features induced by underground nuclear explosions at Pahute Mesa, Nevada Test Site, Nye County, Nevada, April 1976 through November 1983: U.S. Geological Survey Miscellaneous Investigations Series Map I-1872, scale 1:48,000.

Cowie, P.A., and Scholz, C.H., 1992a, Physical explanation for the displacement - length relationship of faults using a post-yield fracture mechanics model: Journal of Structural Geology, v. 14, p. 1133-1148.

Cowie, P.A., and Scholz, C.H., 1992b, Displacement-length scaling relationship for faults: data synthesis and discussion: Journal of Structural Geology, v. 14, p. 1149-1156.

DeMets, C., Gordon, R.G., Argus, D.F. and Stein, S., 1990, Current plate motions: Geophysical Journal International, v. 101, p. 425-478.

dePolo, C.M., 1994, The maximum background earthquake in the Basin and Range: Bulletin of the Seismological Society of America, v. 84, p. 466-472.

Dixon, T.H., Robaudo, S., Lee, J., and Reheis, M., 1995, Constraints on present-day Basin and Range deformation from space geodesy: Tectonics, v. 14, p. 755-772.

Dokka, R.K., and Travis, C.J., 1990, Role of the Eastern California shear zone in accommodating Pacific-North American plate motion: Geophysical Research Letters, v. 17, p. 1323-1326.

Doser, D.I., 1986, Earthquake processes in the Rainbow Mountain-Fairview Peak-Dixie Valley, Nevada, region (1954-1959): Journal of Geophysical Research, v. 91, p. 12,572-12,586.

Doser, D.I., 1988, Source parameters of earthquakes in the Nevada seismic zone (1915-1943): Journal of Geophysical Research, v. 93, p. 15,001-15,016.

Doser, D.L., and Smith, R.B., 1989, As assessment of source parameters of earthquakes in the Cordillera of the western United States: Bulletin of the Seismological Society of America, v. 79, p. 1383-1409.

Ferrill, D.A., Stirewalt, G.L., Henderson, D.B., Stamatakos, J.A., Morris, A.P., Spivey, K.H., and Wernicke, B.P., 1996a, Faulting in the Yucca Mountain region: NUREG/CR-6401, CNWRA 95-017, variously paginated.

Ferrill, D.A., Stamatakos, J.A., Jones, S.M., Rahe, B., McKague, H.L., Martin, R.H., and Morris, A.P., 1996b, Quaternary slip history of the Bare Mountain fault (Nevada) from the morphology and distribution of alluvial fan deposits: Geology, v. 24, p. 559-562.

Fridrich, C.J., 1997, Tectonic evolution of the Crater Flat basin, in Wright, L., and Troxel, B., eds., Cenozoic Basins of the Death Valley Region: Geological Society of America Special Paper (in press).

Frizzell, V.A. Jr., and Shulters, J., 1990, Geologic map of the Nevada Test Site, southern Nevada: U.S. Geological Survey Miscellaneous Investigations Series Map I-2046, scale 1:100,000.

Galybin, A.N., 1997, A model of mining induced fault sliding: Proceedings of the 36th U.S. Rock Mechanics Symposium, Columbia University, June 29 - July 2.

Hanks, T.C., and McGuire, R.K., 1981, The character of high frequency strong ground motion: Bulletin of the Seismological Society of America, v. 71, p. 2071-2095.

Hardyman, R.F., and Oldow, J.S., 1991, Tertiary tectonic framework and Cenozoic history of the central Walker Lane, Nevada, in Raines, G.L., Lisle, R.E., Schafer, R.W., and Wilkinson, W.H., eds, Geology and Ore Deposits of the Great Basin: Geological Society of Nevada Symposium Proceedings, v. 1, p. 279-301.

Harmsen, S.C., 1993, Preliminary seismicity and focal mechanisms for the southern Great Basin of Nevada and California-January 1992 through September 1992: U.S. Geological Survey Open-File Report 93-369, 213 p.

Hemphill-Haley, M.A., and Weldon, R.J. II, 1996, Estimating prehistoric earthquake magnitude from point displacements instead of surface rupture length [abs.]: EOS, Transactions of the American Geophysical Union, v. 77, no. 46 supplement, p. F512.

Humphreys, E.D., and Weldon, R.J., 1994, Deformation across the western United States: a local estimate of Pacific-North America transform deformation: Journal of Geophysical Research, v. 99, p. 19,975-20,010.

Jackson, J.A., and White, N.J., 1989, Normal faulting in the upper continental crust: observations from regions of active extension: Journal of Structural Geology, v. 11, p. 15-36.

Jennings, C.W., 1994, Fault activity map of California and adjacent areas with locations and ages of recent volcanic eruptions: California Division of Mines and Geology, California Geologic Data Map Series, Map No. 6, scale 1:750,000.

Kanamori, H., and Anderson, D.L., 1975, Theoretical basis of some empirical relations in seismology: Bulletin of the Seismological Society of America, v. 65, p. 1073-1095.

Langenheim, V.E., Kirchoff-Stein, K.S., and Oliver, H.W., 1993, Geophysical investigations of buried volcanic centers near Yucca Mountain, southwestern Nevada, in Fourth International Conference on High-Level Radioactive Waste Management: La Grange Park, Illinois, American Nuclear Society, p. 1840-1846.

Lee, J-J., and Bruhn, R.L., 1996, Characterization of the structural anisotropy of normal fault surfaces: Journal of Structural Geology, 18, p. 1043-1059.

Lienkaemper, J.J., Pezzopane, S.K., Clark, M., and Rymer, M.J., 1987, Fault fractures formed in association with the 1986 Chalfant Valley, California, earthquake sequence; preliminary report: Bulletin of the Seismological Society of America, v. 77, p. 297-305.

Loper, S., Pasyanos, M., Dreger, D., and Romanowicz, B., 1993, Broadband source study of the 1993 Eureka Valley, California, earthquake sequence [abs.]: EOS, Transactions of the American Geophysical Union, v. 74, no. 43 supplement, p. 397.

Lubetkin, L.D.C., and Clark, M., 1988, Late Quaternary activity along the Lone Pine fault, eastern California: Geological Society of America Bulletin, v. 100, p. 755-766.

Massonnet, D., and Feigl, F.L., 1995, Satellite radar interferometric map of the coseismic deformation field of the M 6.1 Eureka Valley, California earthquake of May 17, 1993: Geophysical Research Letters, v. 22, p. 1541-1544.

McGarr. A., 1984, Some applications of seismic source mechanism studies to assessing underground hazard, *in* Gay, N.C., and Wainwright, eds., Proceedings of the First International Congress on Rock Bursts and Seismicity in Mines: South African Institute of Mining and Metallurgy, Johannesburg, p. 198-208.

Meremonte, M. E., Gomberg, J., and Cranswick, E., 1995, Constraints on the 29 June 1992 Little Skull Mountain sequence provided by robust hypocentral estimates: Bulletin of the Seismological Society of America, v. 85, p. 1039-1049.

Minster, J.B., and Jordan, T.H., 1987, Vector constraints on western U.S. deformation from space geodesy, neotectonics and plate motions: Journal of Geophysical Research, v. 92, p. 4798-4804.

Nicol, A., Walsh, J.J., Waterson, J., and Underhill, J., 1997, Displacement rates of normal faults. Nature (in press).

Parsons, T., and Thompson, G.A., 1991a, Coupled processes of normal faulting and dike intrusion in tectonically extended regions [abs.]: Seismological Research Letters, v. 62, p. 26.

Parsons, T., and Thompson, G.A., 1991b, The role of magma overpressure in suppressing earthquakes and topography: worldwide examples: Science, v. 253, p. 1399-1402.

Peltzer, G., and Rosen, P., 1995, Surface displacement of the 17 May 1993 Eureka Valley, California earthquake observed by SAR interferometry: Science, v. 268, p. 1333-1336.

Piety, L.A., 1995, Compilation of known and suspected Quaternary faults within 100 km of Yucca Mountain, Nevada and California: U.S. Geological Survey Open-File Report 94-112, 404 p.

Ponce, D.A., 1993, Geophysical investigations of concealed faults near Yucca Mountain, southwest Nevada, *in* High Level Radioactive Waste Management: Proceedings, Fourth Annual International Conference, v. 1, p. 168-174.

Reheis, M.C, and Dixon, T.H., 1996, Kinematics of the Eastern California shear zone: evidence for slip transfer from Owens and Saline Valley fault zones to Fish Lake Valley fault zone: Geology, v. 24, 339-342.

Reheis, M.C., and Sawyer, T.L., 1997, Late Cenozoic history and slip rates of the Fish Lake Valley, Emigrant Peak, and Deep Springs fault zones, Nevada and California: Geological Society of America Bulletin, v. 109, p. 280-299.

Richard, S.M. ed., 1992, Deformation associated with the Neogene, Eastern California shear zone, southeastern California and southwestern Arizona: Proceedings, San Bernardino County Museum Association, Special Publication 92-1, 78 p.

Rogers, A.M., Harmsen, S.C., Corbett, E.J., Priestly, K.F. and dePolo, D., 1991, The seismicity of Nevada and some adjacent parts of the Great Basin, in Slemmons, D.B., Engdahl, E.R., Zoback. M.D., and Blackwell, D.D., eds., Neotectonics of North America: Geological Society of America, Decade Map Volume 1, p. 153-184.

Rogers, A. M., Harmsen, S.C., and Meremonte, M.E., 1987, Evaluation of the seismicity of the Southern Great Basin and its relationship to the tectonic framework of the region: U.S. Geological Survey Open-File Report 87-408.

Savage, J.C., Lisowski, M., and Prescott, W.H., 1990, An apparent shear zone trending north-northwest across the Mojave Desert into Owens Valley, California: Geophysical Research Letters, v. 17, p. 2113-2136.

Schwartz, D.P., and Coppersmith, K.J., 1984, Fault behavior and characteristic earthquakes: examples from the Wasatch and San Andreas faults: Journal of Geophysical Research, v. 89, p. 5681-5698.

Scott, R.B., 1990, Tectonic setting of Yucca Mountain, southwest Nevada, in Wernicke, B.P., ed., Basin and Range Extensional Tectonics Near the Latitude of Las Vegas, Nevada: Geological Society of America Memoir 176, p. 251-282.

Shields, G., Smith, K.D., and Brune, J.N., 1995, Source parameters of a sequence of very shallow earthquakes in the Rock Valley fault zone, southern Nevada Test Site [abs.]: EOS, Transactions of the American Geophysical Union, v. 76, p. F426.

Simonds, W.F., Whitney, J.W., Fox, K., Ramelli, A., Yount, J., Carr, M., Menges, C.M., Dickerson, R., and Scott, R.B., 1995, Map of fault activity of the Yucca Mountain area, Nye County, Nevada: U.S. Geological Survey Miscellaneous Investigations Series Map I-2520, scale 1:24,000.

Smith, K.D., and Brune, J.N., 1997, A sequence of very shallow earthquakes in the Rock Valley fault zone, southern Nevada Test Site: U.S. Geological Survey Circular on Yucca Mountain Tectonics (in press).

Smith, K.D., and Priestley, K.F., 1997, The 1986 Chalfant, California earthquake sequence, earthquake relocations and source parameters: Bulletin of the Seismological Society of America (in press).

Smith, R.B., and Sbar, M.L., 1974, Contemporary tectonics and seismicity of the western United States with emphasis on the Intermountain seismic belt: Geological Society of America Bulletin, v. 85, p. 1205-1218.

Smith, R.P., Jackson, S.M., and Hackett, W.R., 1996, Paleoseismology and seismic hazards evaluations in extensional volcanic terrains: Journal of Geophysical Research, v. 101, p. 6277-6292.

Stamatakos, J.A., Connor, C.B., and Martin, R.H., 1997, Quaternary basin evolution and basaltic volcanism of Crater Flat, Nevada from detailed ground magnetic surveys of the Little Cones: Journal of Geology, v. 105, p. 319-330.

Stewart, J.H., 1978, Basin-range structure in western North America: a review, in Smith, R.B., and Eaton, G.P., eds., Cenozoic Tectonics and Regional Geophysics of the Western Cordillera: Geological Society of America Memoir 152, p. 1-31.

Stewart, J.H., 1988, Tectonics of the Walker Lane belt, western Great Basin--Mesozoic and Cenozoic deformation in a zone of hear, in Ernst, W.G., ed., Metamorphism and Crustal Evolution of the Western United States, Rubey Volume VII: Englewood Cliffs, NJ, Prentice Hall, p. 683-713.

Stock, J.M., and Healy, J.H., 1988, Stress field at Yucca Mountain, Nevada: U.S. Geological Survey Bulletin 1790, p. 87-93.

Veneziano, D. and van Dyck, J., 1985, Statistical discrimination of "aftershocks" and their contribution to seismic hazard, Appendix A-4, in Seismic Hazard Methodology for Nuclear Facilities in the Eastern United States: EPRI Research Project Number P101-29, p. A121-A186.

Walsh, J.J, and Waterson, J., 1987, Distribution of cumulative displacement and of seismic slip on a single normal fault surface: Journal of Structural Geology, v. 9, p. 1039-1046.

Walsh, J.J., and Waterson, J., 1992, Populations of faults and fault displacements and their effects on estimates of fault related regional extension: Journal of Structural Geology, v. 14, p. 701-712.

Ward, S.H., 1990, Pacific-North America plate motions: new results from very long baseline interferometry: Journal of Geophysical Research, v. 95, p. 21,965-21,981.

Wells, D.L., and Coppersmith, K.J., 1994, New empirical relationships among magnitude, rupture length, rupture width, rupture area, and surface displacement: Bulletin of the Seismological Society of America, v. 84, p. 974-1002.

Wernicke, B., 1995, Low-angle normal faults and seismicity: a review: Journal of Geophysical Research, v. 100, p. 20,159-20,174.

Wheeler, R.L., 1989, Persistent segment boundaries on basin-range normal faults, *in* Schwartz, D.P. and Sibson, R.H., eds., Fault segmentation and controls of rupture initiation and termination: U.S. Geological Survey Open-File Report 89-315, p.432-444.

Wiechert, D.H., 1980, Estimation of the earthquake recurrence parameters for unequal observation periods for different magnitudes: Bulletin of the Seismological Society of America, v. 70, p. 1337-1346.

Wright, L., 1976, Late Cenozoic fault patterns and stress fields in the Great Basin and westward displacement of the Sierra Nevada block: Geology, v. 4, p. 489-494.

Wright, L.A., 1989, Overview of the role of strike-slip and normal faulting in the Neogene history of the region northeast of Death Valley, California-Nevada, in Ellis, M.A., ed., Later Tertiary Evolution of the Southern Great Basin: Nevada Bureau of Mines and Geology Open File 89-1, p. 1-11.

Youngs, R.R., and Coppersmith, K.J., 1985, Implications of fault slip rates and earthquake recurrence models to probabilistic seismic hazard estimates: Bulletin of the Seismological Society of America, v. 75, p. 939-964.

Youngs, R.R., Swan, F.H., Power, M.S., Schwartz, D.P., and Green, R.K., 1987, Probabilistic analysis of earthquake ground shaking hazard along the Wasatch Front, Utah: U.S. Geological Survey Open-File Report 87-585, v. II, p. M1-M110.

Zhang, P., Ellis, M., Slemmons, D.B., and Mao, F., 1990, Right-lateral displacements and the Holocene slip rate associated with prehistoric earthquakes along the southern Panamint Valley fault zone; implications for southern Basin and Range tectonics and coastal California deformation: Journal of Geophysical Research, v. 95, p. 4857-4872.

TABLE SBK-1
REGIONAL FAULT SOURCES

Fault Name	Ind. Source	Type and Dip Direction	Maximum Magnitude Approach				Recurrence Approach			Recurrence Model
			Length (km)	Area	Max. Offset (m)	Av. Offset (m)	Long-term Slip Rate (m/kyr)	Quat Slip Rate (m/kyr)	Interval (kyr)	
Amargosa River	Y (0.8) N (0.2)	RL (0.6) N (0.4) East (1.0)	**(0.35)** 12 (0.7) 15 (0.3)	**(0.35)**	**(0.3)** 2.5 (0.2) 1.6 (0.8)			**(0.9)** 0.02 (0.5) 0.03 (0.5)	**(0.1)** 10 (1.0)	C (0.4). TE (0.6)
Ash Meadows	Y (0.8) N (0.2)	N (1.0) West (1.0)	**(0.35)** 30 (0.3) 40 (0.6) 100 (0.1)	**(0.35)**	**(0.3)** 1.4 (0.2) 1.8 (0.8)		**(0.1)** 0.016 (1.0)	**(0.9)** 0.01 (0.2) 0.04 (0.7) 0.1 (0.1)		C (0.6) TE (0.4)
Belted Range	Y (0.9) N (0.1)	N (1.0) West (1.0)	**(0.25)** 22 (0.4) 38 (0.2) 50 (0.4)	**(0.25)**	**(0.3)** 1.0 (1.0)	**(0.2)** 0.8 (1.0)	**(0.2)** .0.05 (1.0)	**(0.8)** 0.01 (0.1) 0.09 (0.7) 0.2 (0.2)		C (0.6) TE (0.4)
Buried Hills – Emigrant Valley South	Y (0.01) N (0.99)	N (1.0) West (1.0)	**(0.5)** 51 (0.8) 57 (0.2)	**(0.5)**				**(1.0)** 0.01 (0.5) 0.001 (0.5)		C (0.6) TE (0.4)

TABLE SBK-1
REGIONAL FAULT SOURCES
(Continued)

Fault Name	Ind. Source	Type and Dip Direction	Maximum Magnitude Approach				Recurrence Approach			Recurrence Model
			Length (km)	Area	Max. Offset (m)	Av. Offset (m)	Long-term Slip Rate (m/kyr)	Quat Slip Rate (m/kyr)	Interval (kyr)	
Southern Death Valley – Death Valley – Furnace Creek - Fish Lake Valley	Y (0.01) N (0.99)	RL (1.0) West (1.0)	**(0.25)** 340 (1.0)	**(0.25)**		**(0.5)** 2.5 (0.3) 3.5 (0.3) 4.5 (0.4)		**(0.8)** 4.0 (0.4) 5.0 (0.4) 8.0 (0.2)	**(0.2)** 0.40 (0.5) 0.80 (0.5)	C (0.9) TE (0.1)
Death Valley – Southern Death Valley	Y (0.05) N (0.95)	N (0.2) RL (0.8) West (1.0)	**(0.15)** 115 (0.7) 140 (0.3)	**(0.15)**		**(0.7)** 2.5 (0.5) 3.5 (0.5)	**(0.2)** .2.0 (0.5) .3.0 (0.5)	**(0.4)** 1.5 0.2) 3.0 (0.4) 5.0 (0.4)	**(0.4)** 0.50 (0.2) 0.70 (0.3) 1.00 (0.3) 1.30 (0.2)	C (0.9) TE (0.1)
Furnace Creek – Fish Lake Valley	Y (0.05) N (0.95)	RL (1.0) West (1.0)	**(0.2)** 230 (0.5) 240 (0.5)	**(0.2)**	**(0.2)** 3.0 (0.5) 6.0 (0.5)	**(0.4)** 2.5 (0.1) 4.5 (0.9)		**(0.8)** 2.0 (0.1) 4.0 (0.4) 8.0 (0.4) 10.0 (0.1)	**(0.2)** 0.60 (0.4) 0.80 (0.2) 1.70 (0.4)	C (0.9) TE (0.1)
Fish Lake Valley	Y (0.94) N (0.95)	RL (1.0) West (1.0)	**(0.5)** 50 (0.4) 75 0.6)	**(0.5)**			**(0.4)** .3 0 (0.3) .5 0 (0.7)	**(0.6)** 2 (0.2) 3 (0.5) 4 (0.3)		C (0.9) TE (0.1)

TABLE SBK-1
REGIONAL FAULT SOURCES
(Continued)

Fault Name	Ind. Source	Type and Dip Direction	Maximum Magnitude Approach				Recurrence Approach			Recurrence Model
			Length (km)	Area	Max. Offset (m)	Av. Offset (m)	Long-term Slip Rate (m/kyr)	Quat Slip Rate (m/kyr)	Interval (kyr)	
Southern Death Valley	Y. (0.94) N (0.06)	RL (1.0) West (1.0)	**(0.5)** 45 (0.2) 75 (0.7) 85 (0.1)	**(0.5)**			**(0.8)** .2.0 (0.5) .3.0 (0.5)	**(0.2)** 0.3 (1.0)		C (0.9) TE (0.1)
Death Valley	Y. (0.94) N (0.06)	N (0.5) 0bl (0.5) West (1.0)	**(0.35)** 45 (0.4) 51 (0.2) 68 (0.4)	**(0.35)**		**(0.3)** 2.5 (0.5) 3.5 (0.5)		**(0.6)** 1.5 (0.2) 3.0 (0.4) 5.0 (0.3) 7.0 (0.1)	**(0.4)** 0.5 (0.2) 0.7 (0.3) 1.0 (0.3) 1.3 (0.2)	C (0.9) TE (0.1)
Furnace Creek	Y. (0.94) N (0.06)	RL (1.0) West (1.0)	**(0.2)** 105 (0.7) 115 (0.1) 160 (0.2)	**(0.4)**	**(0.2)** 6.0 (1.0)	**(0.2)** 4.5 (1.0)	**(0.1)** 4.0 (0.2) 8.0 (0.4) 10.0 (0.4)	**(0.6)** 4.0 (0.4) 8.0 (0.5) 10.0 (0.1)	**(0.3)** 0.60 (0.5) 0.80 (0.5)	C (0.9) TE (0.1)
Kawich Range	Y (0.04) N (0.6)	N (1.0) West (1.0)	**(0.35)** 74 (0.1) 78 (0.3) 84 (0.6)	**(0.35)**	**(0.3)** 1.5 (1.0)			**(1.0)** 0.01 (0.3) 0.002 (0.7)		C (0.6) TE (0.4)

TABLE SBK-1
REGIONAL FAULT SOURCES
(Continued)

Fault Name	Ind. Source	Type and Dip Direction	Maximum Magnitude Approach				Recurrence Approach			Recurrence Model
			Length (km)	Area	Max. Offset (m)	Av. Offset (m)	Long-term Slip Rate (m/kyr)	Quat Slip Rate (m/kyr)	Interval (kyr)	
Pahrump	Y (0.9) N (0.1)	Obl (0.8) RL (0.2) West (1.0)	**(0.45)** 18.5 (0.33) 50 (0.33) 65 (0.34)	**(0.45)**	**(0.1)** 0.7 (1.0)		**(0.8)** (RL) .1.1 (0.5) .1.9 (0.5)	**(0.2)** (V) 0.009 (0.5) 0.02 (0.5)		C (0.4) TE (0.6)
Rock Valley	Y (1.0)	LL-N (0.3) LL (0.7) SE (1.0)	**(0.2)** 19 (0.1) 32 (0.5) 65 (0.4)	**(0.2)**	**(0.3)** 5.2 (0.2) 5.7 (0.8)	**(0.3)** 1.7 (0.5) 3.9 (0.5)		**(0.8)** 0.003 (0.1) 0.02 (0.8) 0.05 (0.1)	**(0.2)** 6 (0.1) 12 (0.2) 20 (0.2) 100 (0.5)	C (0.4) TE (0.6)
Sarcobatus Flat	Y (0.01) N (0.99)	N (1.0) West (1.0)	**(0.5)** 27 (0.2) 49 (0.8)	**(0.5)**				**(1.0)** 0.01 (0.1) 0.001 (0.6) 0.0001 (0.3)		C (0.4) TE (0.6)
West Pintwater Range	Y (0.5) N (0.5)	N (1.0) West (1.0)	**(0.5)** 60 (0.3) 82 (0.7)	**(0.5)**				**(1.0)** 0.01 (0.6) 0.001 (0.4)		C (0.6) TE (0.4)

TABLE SBK-1
REGIONAL FAULT SOURCES
(Continued)

Fault Name	Ind. Source	Type and Dip Direction	Maximum Magnitude Approach				Recurrence Approach			Recurrence Model
			Length (km)	Area	Max. Offset (m)	Av. Offset (m)	Long-term Slip Rate (m/kyr)	Quat Slip Rate (m/kyr)	Interval (kyr)	
West Spring Mountains	**(0.9)** Y (0.9) N (0.1)	**(1.0)** N (1.0) West (1.0)	**(0.3)** 30 (0.2) 47 (0.5) 54 (0.3)	**(0.3)**		**(0.4)** 1.7 (0.5) 2.0 (0.5)		**(0.7)** 0.02 (0.5) 0.07 (0.5)	**(0.3)** 28 (0.2) 120 (0.8)	**(1.0)** C (0.6) TE (0.4)
Yucca	**(0.9)** Y (0.9) N (0.1)	**(1.0)** N (0.8) Obl (0.2) East (1.0)	**(0.5)** 20 (0.2) 32 (0.5) 45 (0.3)	**(0.5)**			**(0.2)** .0.03 (0.5) .0.07 (0.5)	**(0.8)** 0.03 (0.20) 0.09 (0.79) 0.5 (0.01)		**(1.0)** C (0.4) TE (0.6)

Notes and Sources - Table SBK-1:
Each column contains a weighting in parenthesis (**bold**) for that variable within the overall grouping (e.g., weight of 0.3 for fault length as an estimator for maximum magnitude) as well as weightings of individual values for that variable (e.g., 60-km length weighted 0.3; 82-km length weighted 0.7). Ind. Source: likelihood that fault behaves as an independent source, generating a maximum magnitude earthquake that is larger than that of regional seismic source in which it is located. Type: RL - right lateral; LL - left lateral; Obl - oblique; N - normal. Area: computed from down-dip width of fault (fault dip and maximum seismogenic depth) times length; down-dip width depends on fault type, as noted in text. Seismogenic depth derived from regional source zone in which fault is embedded. Interval: average time between surface rupture events. Recurrence Model: shape of recurrence curve; C - characteristic; TE - truncated exponential.

Amargosa River Anderson *et al.*, 1995b; Piety, 1995. Discontinuous strike-slip fault; fault length of 12 km from Anderson *et al.*, 15 km from Piety. 100-ka scarps according to Anderson *et al.*; single-event ruptures interpreted from their scarp data. Slip Rate from 2.5 to 3 m offset in ca. 100 ka as best data.

TABLE SBK-1
REGIONAL FAULT SOURCES
(Continued)

Notes and Sources - Table SBK-1 (Continued):

Ash Meadows Anderson *et al.*, 1995b; Piety, 1995; Carr; 1990; regional gravity data. Discontinuous normal fault zone, up to 8 km wide. Longest length is obtained by including the so-called "gravity fault" recognizable in regional gravity gradient data along the east side of Fortymile Wash in Jackass Flat. Rock Valley fault, however, may terminate active fault zone at north, cutting off connection to "gravity fault." We consider this the more likely case, given lack of surface expression for "gravity fault," especially compared to expression of Ash Meadows fault in Amargosa Valley. Likely age of youngest event varies substantially along mapped fault traces; probably a segmented fault, but insufficient data to constrain segments.

Belted Range Piety, 1995; Anderson *et al.*, 1995a. Relatively short length (21 km according to Anderson and others) has Quaternary offset; however, maximum length set as equal to mapped fault length, which is uncertain depending on source. Limited evidence for Quaternary slip leads to conclusion that earthquakes above those defined for regional source zone are very unlikely on this fault. Slip rate estimated by using 11.3 m in about 50 ka from scarp morphology reported by Anderson and others

Buried Hills-Emigrant Valley South S. K. Pezzopane, USGS, written communication, 1996; Piety, 1995. Possible fault combination; neither fault zone considered capable of producing larger earthquake than regional maximum magnitude. Slip rate based on comparison with other Basin-Range faults, thus has low certainty. No actual evidence that these faults have ruptured together; thus low weighting as independent source.

Combined Southern Death Valley – Death Valley - Furnace Creek - Fish Lake Valley Jennings, 1994; R. E. Klinger and L. A. Piety, USBR, written communication, 1996; Piety, 1995; Reheis and Sawyer, 1997. Formed by combining all four faults. Total length measured from Jennings map. Average offset taken from data compiled by R. E. Klinger and L. A. Piety, USBR, written communication, 1996. Slip rate based on best constrained slip rates for the four constituent faults. Treats Death Valley fault as a pull-apart along the shear zone. Little likelihood that all faults rupture together, given size of pull-apart basin and discontinuous traces.

Combined Death Valley and Southern Death Valley Piety, 1995; R. E. Klinger and L. A. Piety, USBR, written communication, 1996; Jennings, 1994. Rupture length reported as 45 to 60 km, although total length is 115 km if both faults are considered together. Note that Southern Death Valley fault is strike-slip, Death Valley fault normal (pull-apart). Long-term rate for Southern Death Valley, Quaternary rate for Death Valley.

Combined Furnace Creek-Fish Lake Valley Reheis and Sawyer, 1997; Piety, 1995; R. E. Klinger and L. A. Piety, USBR, written communication, 1996; Jennings, 1994. Some chance that Furnace Creek and Fish Lake Valley faults are continuous and can rupture together, within uncertainties of the data. However, available data are insufficient to prove (within overlaps on dating) that paleoseismic events could have been simultaneous on the two faults. Note that restraining bend between them has no Holocene slip.

Fish Lake Valley Reheis and Sawyer, 1997; Piety, 1995; Jennings, 1994. Northern termination of fault poorly shown on maps of Jennings or Reheis and Sawyer, producing uncertainty in maximum fault length. Slip rate data well constrained by Reheis and Sawyer.

Southern Death Valley Piety, 1995; Jennings, 1994. Southern extent of fault uncertain. Most likely southern termination at Garlock fault. Late Quaternary slip rate poorly constrained.

Death Valley R. E. Klinger and L. A. Piety, USBR, written communication, 1996; Jennings, 1994; Piety, 1995. Shorter fault length based on older scarps in northern third of fault, suggesting rupture length less than total fault length.

Furnace Creek Piety, 1995; R. E. Klinger and L. A. Piety, USBR, written communication, 1996; Jennings, 1994. Maximum surface rupture length reported as 105 km by Klinger and Piety, so this is considered most likely maximum rupture length. Fault shown by Jennings possibly continuing as much as 20 km farther southeast into Amargosa Valley; however, no evidence for this continuation, and remainder of southern Furnace Creek fault is well expressed along the range front. Thus we consider any greater length to the fault exceedingly unlikely, and it is given zero weight.

TABLE SBK-1
REGIONAL FAULT SOURCES
(Continued)

Notes and Sources - Table SBK-1 (Continued):

Kawich Range S. K. Pezzopane, USGS, written communication, 1996, Piety, 1995; Anderson *et al.*, 1995a. Same as Kawich Range West fault zone of Anderson and others. Only a short section (3.6 to 7.4 km) is indicated by Anderson and others to have Quaternary slip; were this the entire source, it would produce earthquakes no larger than those accounted for in the regional source zone. Assessment is based on assuming entire fault could break in a single event, which is extremely unlikely, given evidence this apparently has not happened in Quaternary. Anderson and others argue that slip rate must be very low given lack of recurrent Quaternary slip and embayed range front. Most likely slip rate from approximately 2 m slip in alluvium of Quaternary age, possibly 1 Ma.

Pahrump Piety, 1995; Anderson *et al.*, 1995b. Likely length 50 to 70 km; Quaternary activity may be only along 18.5 km. Maximum vertical offset 5 m on late Quaternary deposits; no constraints on Quaternary right-lateral displacement rate.

Rock Valley Piety, 1995; Anderson *et al.*, 1995b; J. A. Coe *et al.*, USGS, written communication, 1996; unpubl preliminary TL ages from Mahan, 2/20/97. Main fault zone 32 km long, SS; youngest event post 2.45 ka at one site, >10 cm; prior event > 20km rupture ca. 7.2 ka. 14.2 m slip in that and two prior events from trench data constrain offset per event and Quaternary slip rate. Offsets of 3.2, 5.2, and 5.7 m if horiz:vert ratio remains constant. Maximum length taken by including southwest extension as mapped by Anderson and others, others; however, this section may be older than main Rock Valley fault zone, so is weighted less as defining maximum length.

Sarcobatus Flat Anderson *et al.*, 1995a; Piety, 1995. Almost no evidence for any Quaternary displacement according to Anderson and others, so slip rate must be extremely low. Rate constrained by similar low slip-rate faults in regional and local area.

West Pintwater Range Piety, 1995. Longer fault length includes North Desert Range fault. Apparently there is a lack of repeated Quaternary displacement. Slip rate constrained by comparisons with other regional and local faults.

West Spring Mountains Piety; 1995; Anderson *et al.*, 1995a. More than 20 m late Quaternary displacement. Possibly 12 m on 120-ka surface. Length uncertain principally based on how far south past range front fault is continued, as well as northern termination. Maximum length includes all of range front to north and a southern termination at the Pahrump fault. Minimum distance based on Anderson and others' mapping of scarps.

Yucca Piety, 1995. Scarp at least 20 km long; longer lengths from combining with other faults to the north, despite lack of evidence for linked ruptures. Fault shows explosion-related offsets; also reported to be youngest prehistoric scarp in test site region, as cited by Piety. 0.3-0.6 km total displacement post tuff 11 to 8.5 Ma; Quaternary slip rates computed assuming 15 m slip in middle to late Quaternary, as summarized by Piety, and the slight chance that historical explosion-related ruptures are releasing tectonic strain.

TABLE SBK-2
OTHER REGIONAL FAULTS
(Page 1 of 3)

FAULT NAME	SOURCES	NOTES
Area Three	W. R. Keefer and S. K. Pezzopane, USGS, written communication, 1996; Piety, 1995	Within regional source magnitudes
Bullfrog Hills	W. R. Keefer and S. K. Pezzopane, USGS, written communication, 1996; Piety, 1995	No convincing Q displ
Cane Spring	W. R. Keefer and S. K. Pezzopane, USGS, written communication, 1996; Piety, 1995	No convincing Q displ
Carpetbag	W. R. Keefer and S. K. Pezzopane, USGS, written communication, 1996; Piety, 1995	Largely concealed; no convincing late Q displacement
Checkpoint Pass	W. R. Keefer and S. K. Pezzopane, USGS, written communication, 1996; Piety, 1995	Little if any Quat offset proven
Crossgrain Valley	W. R. Keefer and S. K. Pezzopane, USGS, written communication, 1996; Piety, 1995	Little data on age; prob. Q scarps along 20% of mapped fault; within regional source magnitudes
Eleana Range	W. R. Keefer and S. K. Pezzopane, USGS, written communication, 1996; Piety, 1995	6-9 km likely length, but not all late Q; within regional source magnitudes
Emigrant Valley North	W. R. Keefer and S. K. Pezzopane, USGS, written communication, 1996; Piety, 1995	Within regional source magnitudes
Grapevine	W. R. Keefer and S. K. Pezzopane, USGS, written communication, 1996; Piety, 1995	Within regional source magnitudes
Hunter Mtn-Panamint Valley	Piety, 1995	Not a linked structure
Hunter Mtn	Piety, 1995	Within regional source magnitudes
Kawich Valley	W. R. Keefer and S. K. Pezzopane, USGS, written communication, 1996; Piety, 1995	Not likely middle-late Q displ

TABLE SBK-2
OTHER REGIONAL FAULTS
(Page 2 of 3)

FAULT NAME	SOURCES	NOTES
Keane Wonder	Piety, 1995; Anderson *et al.*, 1995a	Not likely middle-late Q displ; within regional source magnitudes
Mercury Ridge	W. R. Keefer and S. K. Pezzopane, USGS, written communication, 1996; Piety, 1995	Within regional source magnitudes
Mine Mountain	W. R. Keefer and S. K. Pezzopane, USGS, written communication, 1996; Piety, 1995	Not likely middle-late Q displ
North Desert Range	W. R. Keefer and S. K. Pezzopane, USGS, written communication, 1996; Piety, 1995	Within regional source magnitudes
Oak Spring Butte	W. R. Keefer and S. K. Pezzopane, USGS, written communication, 1996; Piety, 1995	Combined with Yucca fault
Oasis Valley	Piety, 1995; Anderson *et al.*, 1995a	Not likely middle-late Q displ
Pahute Mesa	W. R. Keefer and S.K. Pezzopane, USGS, written communication, 1996; Piety, 1995	Not likely middle-late Q displ; within regional source magnitudes
Panamint Valley	Piety, 1995	Paleoseismic event 25-30 km long, so within regional source magnitudes
Plutonium Valley	W. R. Keefer and S. K. Pezzopane, USGS, written communication, 1996; Piety, 1995	Within regional source magnitudes
Ranger Mountains	W. R. Keefer and S. K. Pezzopane, USGS, written communication, 1996; Piety, 1995	Within regional source magnitudes
Rocket Wash-Beatty Wash	Anderson *et al.*, 1995b; Anderson and Klinger, 1996; Piety, 1995	Not a fault
South Ridge	W. R. Keefer and S. K. Pezzopane, USGS, written communication, 1996; Piety, 1995	Within regional source magnitudes
Spotted Range	W. R. Keefer and S. K. Pezzopane, USGS, written communication, 1996; Piety, 1995	Within regional source magnitudes

TABLE SBK-2
OTHER REGIONAL FAULTS
(Page 3 of 3)

FAULT NAME	SOURCES	NOTES
Tolicha Peak	Anderson *et al.*, 1995a; W. R. Keefer and S. K. Pezzopane, USGS, written communication, 1996; Piety, 1995	Within regional source magnitudes
Wahmonie	W. R. Keefer and S. K. Pezzopane, USGS, written communication, 1996; Piety, 1995	Within regional source magnitudes
West Specter Range	Anderson *et al.*, 1996b	Within regional source magnitudes
Yucca Lake	W. R. Keefer and S. K. Pezzopane, USGS, written communication, 1996; Piety, 1995	Within regional source magnitudes

Note - Table SBK-2:
"Within regional source magnitudes" indicates that maximum magnitude on this fault would be within the range of magnitudes incorporated into the regional source zone of which this fault is a part.

TABLE SBK-3
LOCAL FAULTS

Fault Name	Ind. Source	Type	Maximum Magnitude Approach					Recurrence Approach			Recurrence Model
			Length (km)	Area	Max Offset (m)	Av Offset (m)	Offset from Stress Drop	Long-term Slip Rate (m/kyr)	Quat Slip Rate (m/kyr)	Interval (kyr)	
Hwy. 95 fault (0.8 likelihood of existence)	Y (0.4) N (0.6)	LL (0.5) N (0.5)	**(0.5)** 30 0.5 49 0.5	**(0.5)**					**(1.0)** 0.002 0.9 0.02 0.1		C **(0.1)** TE **(0.9)**
Bare Mountain	Y (1.0)	N (1.0)	**(0.2)** 15.5 0.1 20 0.5 23 0.4	**(0.5)**	**(0.3)** 0.80 0.2 1.50 0.8			**(0.05)** 0.13 0.1 0.20 0.6 0.24 0.3	**(0.65)** 0.01 0.7 0.02 0.3	**(0.3)** 20 0.05 40 0.05 100 0.45 200 0.45	C **(0.6)** TE **(0.4)**
South Crater Flat		N-LL (1.0)	**(0.2)** 6.1 0.5 8.2 0.3 10 0.2	**(0.4)**	**(0.1)** 0.20 0.5 0.50 0.5	**(0.1)** 0.05 0.3 0.10 0.6 0.20 0.1	**(0.2)**		**(0.7)** 0.001 0.1 0.002 0.8 0.003 0.1	**(0.3)** 60 0.7 70 0.2 180 0.1	C **(0.3)** TE **(0.7)**
North Crater Flat		N (0.5) Obl (0.5)	**(0.2)** 10 0.3 13.3 0.7	**(0.5)**	**(0.1)** 0.40 0.4 0.60 0.6		**(0.2)**		**(0.7)** 0.002 0.5 0.003 0.5	**(0.3)** 120 0.5 160 0.5	C **(0.3)** TE **(0.7)**
Windy Wash		N-LL (1.0)	**(0.2)** 25 0.2 27 0.5 28 0.3	**(0.4)**	**(0.2)** 0.96 0.5 0.98 0.5	**(0.1)** 0.30 0.5 0.50 0.5	**(0.1)**	**(0.1)** 0.025 0.2 0.027 0.8	**(0.7)** 0.01 0.2 0.011 0.6 0.016 0.2	**(0.2)** 35 0.1 40 0.4 45 0.4 100 0.1	C **(0.3)** TE **(0.7)**
Fatigue Wash		N (0.7) Obl (0.3)	**(0.2)** 7.5 0.2 12.5 0.5 18.5 0.3	**(0.4)**	**(0.1)** 0.50 0.9 1.50 0.1	**(0.1)** 0.25 0.2 0.30 0.4 0.50 0.4	**(0.2)**		**(0.7)** 0.002 0.2 0.009 0.8	**(0.3)** 50 0.05 120 0.1 185 0.7 250 0.15	C **(0.3)** TE **(0.7)**
Solitario Canyon		N-LL (1.0)	**(0.2)** 13 0.2 18 0.8	**(0.5)**	**(0.2)** 1.10 0.1 1.20 0.6 1.30 0.3		**(0.1)**	**(0.05)** 0.002 0.5 0.003 0.5	**(0.75)** 0.007 0.2 0.01 0.6 0.02 0.2	**(0.2)** 40 0.3 60 0.3 100 0.1 180 0.3	C **(0.3)** TE **(0.7)**

TABLE SBK-3
LOCAL FAULTS
(Continued)

Fault Name	Ind. Source	Type	Maximum Magnitude Approach					Recurrence Approach			Recurrence Model
			Length (km)	Area	Max Offset (m)	Av Offset (m)	Offset from Stress Drop	Long-term Slip Rate (m/kyr)	Quat Slip Rate (m/kyr)	Interval (kyr)	
Iron Ridge	Y (0.1) N (0.9)	N (1.0)	**(0.3)** 7.2 0.8 8.5 0.2	**(0.5)**	**(0.1)** 1.00 0.7 1.30 0.3		**(0.1)**		**(1.0)** 0.002 0.5 0.004 0.5		C **(0.3)** TE **(0.7)**
Bow Ridge	Y (0.4) N (0.6)	N (0.5) Obl (0.5)	**(0.2)** 6.7 0.7 12.2 0.3	**(0.6)**	**(0.1)** 0.40 0.2 0.45 0.6 0.80 0.2		**(0.1)**		**(0.7)** 0.002 0.2 0.003 0.6 0.007 0.2	**(0.3)** 40 0.05 70 0.1 100 0.35 140 0.35 215 0.1 350 0.05	C **(0.3)** TE **(0.7)**
Paintbrush Canyon		N-LL (1.0)	**(0.2)** 12 0.5 18 0.2 23 0.3	**(0.4)**	**(0.2)** 1.42 0.1 1.67 0.7 2.05 0.19 2.57 0.01	**(0.1)** 0.20 0.1 0.45 0.5 0.5 0.4	**(0.1)**		**(0.7)** 0.002 0.1 0.007 0.3 0.015 0.5 0.02 0.09 0.03 0.01	**(0.3)** 20 0.01 50 0.19 65 0.2 100 0.3 115 0.2 270 0.1	C **(0.3)** TE **(0.7)**
Stagecoach Road		N-LL (1.0)	**(0.2)** 8 0.7 12 0.3	**(0.4)**	**(0.2)** 0.5 0.15 0.67 0.8 0.99 0.05	**(0.1)** 0.40 0.7 0.60 0.3	**(0.1)**		**(0.7)** 0.006 0.1 0.03 0.4 0.05 0.4 0.07 0.1	**(0.3)** 5 0.05 10 0.2 35 0.5 50 0.2 75 0.05	C **(0.3)** TE **(0.7)**

TABLE SBK-3
LOCAL FAULTS
(Continued)

Fault Name	Ind. Source	Type	Maximum Magnitude Approach					Recurrence Approach			Recurrence Model
			Length (km)	Area	Max Offset (m)	Av Offset (m)	Offset from Stress Drop	Long-term Slip Rate (m/kyr)	Quat Slip Rate (m/kyr)	Interval (kyr)	
Paintbrush Canyon + Stagecoach Road + Bow Ridge		N-LL (1.0)	**(0.1)** 23 0.7 34 0.3	**(0.6)**	**(0.2)** 0.79 0.29 0.84 0.5 1.0 0.2 1.4 0.01		**(0.1)**		**(0.8)** 0.015 0.2 0.03 0.4 0.05 0.4	**(0.2)** 10 0.05 20 0.2 40 0.6 45 0.1 75 0.05	C **(0.5)** TE **(0.5)**
So. Crater Flat + Windy Wash + Fatigue Wash		N-LL (1.0)	**(0.1)** 25.5 0.3 27.2 0.4 28.3 0.3	**(0.6)**	**(0.1)** 0.50 0.3 0.98 0.7	**(0.1)** 0.30 0.5 0.50 0.5	**(0.1)**		**(0.8)** 0.011 0.5 0.016 0.5	**(0.2)** 50 0.2 185 0.8	C **(0.5)** TE **(0.5)**
Solitario Canyon + Iron Ridge		N-LL (1.0)	**(0.2)** 13 0.2 18 0.8	**(0.5)**	**(0.2)** 1.10 0.1 1.20 0.6 1.30 0.3		**(0.1)**		**(1.0)** 0.009 0.2 0.012 0.3 0.014 0.4 0.024 0.2		C **(0.5)** TE **(0.5)**
Simultaneous Rupture of Linked Faults		N-LL (1.0)	**(0.1)** 82 0.8 95 0.2	**(0.6)**	**(0.3)** 2.50 0.5 3.30 0.5				**(1.0)** 0.04 0.2 0.06 0.6 0.09 0.2		C **(0.5)** TE **(0.5)**
Coalesced Faults		N-LL (1.0)	**(0.1)** 27 0.6 34 0.4	**(0.6)**	**(0.3)** 2.50 0.5 3.30 0.5				**(0.25 to 1.0)** 0.04 0.2 0.06 0.6 0.09 0.2	**(0 to 0.75)** Same as volcanic eruption freq.	Max Moment 1.0 for volcanic otherwise C 0.5 TE 0.5

TABLE SBK-3
LOCAL FAULTS
(Continued)

Notes and Sources - Table SBK-3 (Continued):

Each column contains a weighting in parenthesis **(bold)** for that variable within the overall grouping ,as well as weightings of individual values for that variable. Both Hwy. 95 fault and Bare Mountain fault are treated as independent sources in analysis. Other local faults can rupture in various combinations, as detailed in text. Unless otherwise noted, maximum displacements obtained from trench data; average displacement used when at least four points available for a single event along strike of the fault, from trench data and/or mapping. Southern termination of each fault taken from A. R. Ramelli and J. W. Bell, Nevada Bureau of Mines and Geology, written communication, 1996, except for Hwy. 95 fault, which may truncate all of the others considered here.

Hwy. 95 fault Data interpreted from Memorandum by D.B. Slemmons, 3 February 1997. Likelihood of existence 0.8; if it exists, likelihood it ruptures as an independent seismogenic structure 0.5 (lacking any definitive evidence of offset in the Quaternary, yet there are sufficient indicators of possible activity to convince us we can't favor one conclusion over the other). Arguments in favor of existence and activity: apparent uplift of bedrock across feature, truncation of faults of Crater Flat/Yucca Mountain block, irregular subdued scarps as described by Slemmons, left-lateral deflection of gravity gradient at south end of Bare Mountain fault plus deflection of subsurface horizons as reported by Slemmons, April 1997 SSC Workshop. Arguments against existence and activity: irregular subdued scarps along regional gradient suggest fluvial activity.

Bare Mountain fault Sources of data: L. W. Anderson and R. E. Klinger, USBR, written communication, 1996b; Piety, 1995; Ferrill *et al.*, 1996a, b; S. K. Pezzopane *et al.*, 1996a; A. R. Ramelli and J. W. Bell, Nevada Bureau of Mines and Geology, written communication, 1996. Length of fault confined to that mapped by previous workers at surface along Bare Mountain. Although a gravity gradient is approximately aligned with Bare Mountain fault to south, no Quaternary faulting is associated with it, so we do not include it. There may be some secondary rupture on Yucca Mountain faults associated with primary events on the Bare Mountain fault, based on Pezzopane and others' compilation; however, no evidence of simultaneous ruptures, and the "ash event" is not recorded in Bare Mtn. rupture stratigraphy; thus we consider this an independent structure. Displacement data based on assuming that Anderson and Klinger's single late Quaternary event is in fact two events. Long-term slip rate from 2 to 3 km; total displacement in 15 Ma.

South Crater Flat fault Sources of data: A. R. Ramelli and J. W. Bell, Nevada Bureau of Mines and Geology, written communication, 1996; E. M. Taylor, USGS, written communication, 1996; Simonds *et al.*, 1995; S. K. Pezzopane *et al.*, USGS, written communication, 1996a. Three-dimensional fault geometry consistent with possible linkage to Windy Wash fault. Late Quaternary slip rate estimated from total displacement from trenches divided by age of offset deposits.

North Crater Flat fault Sources of data: A. R. Ramelli and J. W. Bell, Nevada Bureau of Mines and Geology, written communication, 1996; J. A. Coe *et al.*, USGS, written communication, 1996; Simonds *et al.*, 1995; S. K. Pezzopane *et al.*, 1996a. Three-dimensional fault geometry consistent with lack of connection to South Crater Flat fault. Late Quaternary slip rate estimated from displacement in trenches, although ages of offset deposits not well constrained.

Windy Wash fault Sources of data: A. R. Ramelli and J. W. Bell, Nevada Bureau of Mines and Geology, written communication, 1996; J. W. Whitney *et al.*, USGS, written communication, 1996b; Simonds *et al.*, 1995; S. K. Pezzopane *et al.*, USGS, written communication, 1996a. Northern extension of fault from Simonds and others; however, northernmost portion of fault has no convincing evidence of Quaternary displacement, so given lower weighting. Slip rate estimated from trench data.

TABLE SBK-3
LOCAL FAULTS
(Continued)

Notes and Sources - Table SBK-3 (Continued):

Fatigue Wash fault Sources of data: A. R. Ramelli and J. W. Bell, Nevada Bureau of Mines and Geology, written communication, 1996; Coe *et al.*, USGS, written communication, 1996; Simonds *et al.*, 1995; S. K. Pezzopane *et al.*, 1996a. Most likely geometry is splaying from Windy Wash fault at both north and south; second possible geometry is that Fatigue Wash fault continues north, parallel to Windy Wash fault. All Fatigue Wash paleoseismic events are permissibly same timing as some of the Windy Wash events, although equally well they could be independent earthquakes. Slip rate estimated from trench data.

Solitario Canyon fault Sources of data: A. R. Ramelli and J. W. Bell, Nevada Bureau of Mines and Geology, written communication, 1996; A. R. Ramelli *et al.*, Nevada Bureau of Mines and Geology, written communication, 1996; Simonds *et al.*, 1995; W.C. Day *et al.*, USGS, written communication, 1996a; S. K. Pezzopane *et al.*, USGS, written communication, 1996a. Fault mapped in detail by Simonds and others and Day and others, yielding little uncertainty on fault length. Surface breakage events are extremely variable in displacement, including minor cracking events as well as a major displacement (the maximum event noted in table) as part of the "ash event." It is likely that at least some of the surface breaks are secondary in nature. South end of fault could link with Stagecoach Road fault, although we have not addressed this possibility explicitly in our analysis. Slip rate estimated from trench data.

Iron Ridge fault Sources of data: A. R. Ramelli and J. W. Bell, Nevada Bureau of Mines and Geology, written communication, 1996; A. R. Ramelli, *et al.*, Nevada Bureau of Mines and Geology, written communication, 1996; Simonds *et al.*, 1995; S. K. Pezzopane *et al.*, USGS, written communication, 1996a. Given geometry and timing of rupture event, it is very unlikely that this structure ruptures independently of the Solitario Canyon fault. Slip rate estimated from trench data.

Bow Ridge fault Sources of data: A. R. Ramelli and J. W. Bell, Nevada Bureau of Mines and Geology, written communication, 1996; E. M. Taylor *et al.*, USGS, written communication, 1996b; C. M. Menges and J. W. Whitney, USGS, written communication, 1996b; Simonds *et al.*, 1995; S. K. Pezzopane *et al.*, USGS, written communication, 1996a. Fault may link north end of Solitario Canyon fault with Paintbrush Canyon fault, although the most likely geometry is as a splay of the Paintbrush Canyon fault. Given this geometry and the short length of the fault, we consider it less likely to behave as an independent seismogenic structure than to slip in response to other faults. Northern continuation of fault uncertain; we used the Pagany Wash fault mapped by Simonds and others as the most likely continuation, although given the lack of Quaternary displacement on this structure it is considered a less likely geometry than the Bow Ridge fault as shown by Ramelli and Bell. Slip rate based on trench data; complicated options for return periods based on uncertainties in dating from trench studies and variability in repeat times of events inferred from the trenches.

Paintbrush Canyon fault Sources of data: A. R. Ramelli and J. W. Bell, Nevada Bureau of Mines and Geology, written communication, 1996; C. M. Menges and J. W. Whitney, 1996; Simonds *et al.*, 1995; Frizzell and Shulters, 1990; S. K. Pezzopane *et al.*, USGS, written communication, 1996a. Northern extent of fault from Frizzell and Shulters map; however, no evidence of Quaternary slip along north half of fault, so given lower weight in assessment of length. Slip rate and displacement data obtained principally from Busted Butte paleoseismic data.

Stagecoach Road fault Sources of data: A. R. Ramelli and J. W. Bell, Nevada Bureau of Mines and Geology, written communication, 1996; C. M. Menges and J. W. Whitney, USGS, written communication, 1996b; Simonds *et al.*, 1995; S. K. Pezzopane *et al.*, USGS, written communication, 1996a. Connection between Stagecoach Road fault and Paintbrush Canyon fault is uncertain, and we interpret the Stagecoach Road fault *sensu stricto* to extend as shown by Simonds and others. Displacement, slip rate, and repeat-time data all obtained from trench studies.

TABLE SBK-3
LOCAL FAULTS
(Continued)

Notes and Sources - Table SBK-3 (Continued):

Linked faults As discussed in text, we consider one set of models in which four "block-bounding" faults behave as either independent structures or rupture simultaneously. The former case involves three linked structures--Paintbrush Canyon + Stagecoach Road + Bow Ridge; South Crater Flat + Windy Wash + Fatigue Wash; and Solitario Canyon + Iron Ridge--along with the North Crater Flat fault. Fault lengths for each linked system are estimated by taking the longest along-strike fault zone; parallel and branch faults that are part of a linked system do not contribute to fault length. Maximum displacement and slip rate data are obtained from any part of the total linked fault system, using data from events that are in common for any given set of faults as summarized by S. K. Pezzopane *et al.*, USGS, written communication, 1996a. The latter case assumes that all linked faults may have ruptured simultaneously during one or more surface faulting events. The principal example of this is the "ash event." For this scenario, the fault length is the sum of the various linked faults, and the maximum displacement is estimated from the maximum displacement on each constituent linked fault. The return time of the event can be estimated either from the sum of the slip rates on each fault, or (given the unique nature of the "ash event" and its apparent tie to volcanism) from the frequency of occurrence of volcanic eruptions in the Crater Flat area.

Coalesced faults As discussed in text, we consider a set of models in which all of the YM faults (excluding Hwy. 95 and Bare Mountain) coalesce at depth. Should all these faults rupture at the surface in a single event, as may have been the case for the "ash event," the fault length would be that of the longest ("master") fault, in this case the Paintbrush Canyon-Stagecoach Road linked fault or the Solitario Canyon-Iron Ridge linked fault. An alternative is that during any given event on a master fault at depth, any combination of the surface faults may rupture, depending on the pathway the rupture takes between the hypocenter and the surface. Recurrence estimate for the former case is tied strongly to volcanic eruption frequency (0.75 likelihood); recurrence for the latter case is tied exclusively to the summed slip rates determined from the surface faults.

TABLE SBK-4
FAULT DISPLACEMENT HAZARD CHARACTERIZATION DATA, POINTS 1, 2, AND 9

Point	Slip Rate (mm/yr) weight 0.8			Event Frequency weight 0.2		Displacement (m)			
	Site-Specific	Interpolated Quaternary	Interpolated Cumulative	Paleoseismic Data	EQ Recur.	Uave Paleo	Uave W&C	Umax Paleo	Umax W&C
1 (Bow Ridge fault)	1.0 wt. 0.002, 0.2 wt. 0.003, 0.6 wt. 0.007, 0.2 wt.			0.5 wt. Details in Table SBK-3	0.5 wt.	0.4 wt. 0.06, 0.2wt 0.27, 0.6wt 0.55, 0.2wt	0.1 wt	0.4 wt Table SBK-3	0.1 wt
2 (Solitario Canyon fault)		1.0 wt 0.0006 to 0.00355 (see notes)		0.5 wt. 4 events 0.5 wt 3 events 0.5 wt	0.5 wt.	0.25 wt.	0.25 wt	0.25 wt 0.3, 0.4 0.4, 0.6	0.25 wt
9 (Midway Valley fractures)	1.0 wt. 0.0, 0.2 wt. $6.6x10^{-5}$, 0.4 $1.4x10^{-4}$, 0.4			Event frequnecy not used for point 9			0.3 wt.	0.4 wt. 0.05, .8 0, 0.2	0.3 wt.

Notes, Table SBK-4

EQ Recur.: earthquake recurrence distribution computed in ground shaking hazard analysis for SBK Team; **Uave Paleo:** average displacement per rupture event from paleoseismic data; **Uave W&C:** average displacement computed from Wells and Coppersmith regression; **Umax Paleo**: maximum displacement from trench-specific data; **Umax W&C**: maximum displacement computed from Wells and Coppersmith regression.

Bow Ridge fault: Slip rate approach given 0.7 weight for computation of occurrence frequency, event frequency approach given 0.3 weight. Site-specific data from Trench 14D, as compiled by S. K. Pezzopane *et al.*, USGS, written communication, 1996a.

Solitario Canyon fault: Slip rate approach given 0.7 weight for computation of occurrence; event frequency approach given 0.3 weight. Slip rate calculated by interpolating slip rate from known point, Trench 4, along strike; demonstration point is between this trench and a point of known zero displacement (Ramelli, SSC Workshop 6). Slip rate at Trench 4, based on data from A. R. Ramelli *et al.*, USGS, written communication, 1996: 0.0012 (0.2 wt.), 0.0024 (0.3 wt.), 0.004 (0.2 wt.), 0.0053 (0.3 wt.). Reduction factor, computed based on distance between points and uncertainty in interpolation: 0.67 (0.2 wt.), 0.59 (0.6 wt.), 0.5 (0.2 wt.). Final slip-rate results: 0.0006 (0.04 wt.), 0.00071 (0.12 wt.), 0.0084 (0.04 wt.), 0.0012 (0.06 wt.), 0.00142 (0.18 wt.), 0.00161 (0.06 wt.), 0.002 (0.04 wt.), 0.00236 (0.12 wt.), 0.00265 (0.06 wt.) 0.00268 (0.04 wt.), 0.00313 (0.18 wt.), and 0.00355 (0.06 wt.). Data on paleoseismic event frequency from

TABLE SBK-4
FAULT DISPLACEMENT HAZARD CHARACTERIZATION DATA, POINTS 1, 2, AND 9
(Continued)

A. R. Ramelli *et al.*, USGS, written communication, 1996: 4 events in 150 ka (0.2 wt.), 200 ka (0.6 wt.), or 250 ka (0.2 wt.) is assigned weight of 0.5; 3 events in same time periods assigned weight of 0.5. Average and maximum displacements computed by interpolating between Trench SCF-T4 and zero displacement point, the position of which was shown by Ramelli (SSC Workshop 6). Displacement values for Uave are dependent on number of events (3 or 4) assumed to have occurred. For 4 events

Notes, Table SBK-4 (cont.)

(weight 0.5), Uave weighted 0.075 m (0.2 wt.), 0.1375 m (0.6 wt.), and 0.2 m (0.2 wt.). For 3 events (weight 0.5), Uave weighted 0.1 m (0.2 wt.), 0.183 m (0.6 wt.), and 0.267 m (0.2 wt.). Umax is not sensitive to number of events.

Midway Valley fractures: Data from Swan, SSC Workshop 3. Event frequency constrained only by slip rate. Fractures on the Exile Hill fault have maximum net displacement of 5 cm in deposits 350-760 ka in age, producing extremely low slip rates. Yet the displacement may be zero. Displacement amount constrained using maximum slip of 5 cm for fractures. Fault length 0.4 km for computation of maximum and average displacement from Wells and Coppersmith regressions.

TABLE SBK-5
FAULT DISPLACEMENT HAZARD CHARACTERIZATION DATA, POINTS 3-8

Point	Slip Rate (mm/yr) 0.8 weight		Event Frequency 0.2 weight		Activation Factor	
	Geologic History	Fault Parameter	Distributed Rupture	PPV Frequency	Slip Tendency	Angular Histogram
3 (Drill Hole Wash)	0.75 wt. Model 1 (0.1) 0.0041 (0.2) 0.0033 (0.6) 0.0025 (0.2) Model 2 (0.3) 0.0009 (0.2) 0.0007 (0.6) 0.0005 (0.2) Model 3 (0.6) 0.0009 (0.2) 0.0007 (0.6) 0.0006 (0.2)	0.25 wt. 0.0036 (0.2) 0.0009 (0.6) 0.0004 (0.2)	0.5 wt.	0.5 wt.	(0.4 wt.) 0.6 (0.1 weight) 0.5 (0.8) 0.4 (0.1)	(0.6 wt.)
4 (Ghost Dance fault)	0.75 wt. Model 1 (0.1) 0.0029 (0.2) 0.0025 (0.6) 0.0021 (0.2) Model 2 (0.3) 0.0006 (0.2) 0.0005 (0.6) 0.0004 (0.2) Model 3 (0.6) 0.0007 (0.2) 0.0006 (0.6) 0.0005 (0.2)	0.25 wt. 0.0026 (0.2) 0.00072 (0.6) 0.00034 (0.2)	0.5 wt.	0.5 wt.	(0.4 wt.) 0.8 (0.1) 0.7 (0.8) 0.3 (0.1)	(0.6 wt.)
5 (Sundance fault)	0.75 wt. Model 1 (0.1) 0.0017 (0.2) 0.0013 (0.6)	0.25 wt. 0.0014 (0.2) 0.00036 (0.6) 0.00008 (0.2)	1.0 wt.		(0.4 wt.) 0.6 (0.1) 0.56 (0.8) 0.48 (0.1)	(0.6 wt.)

TABLE SBK-5
FAULT DISPLACEMENT HAZARD CHARACTERIZATION DATA, POINTS 3-8
(Continued)

Point	Slip Rate (mm/yr) 0.8 weight		Event Frequency 0.2 weight		Activation Factor	
	Geologic History	Fault Parameter	Distributed Rupture	PPV Frequency	Slip Tendency	Angular Histogram
	0.0005 (0.2) Model 2 (0.3) 0.0003 (0.2) 0.0003 (0.6) 0.0001 (0.2) Model 3 (0.6) 0.0004 (0.2) 0.0003 (0.6) 0.0001 (0.2)					
6 (west of Dune Wash fault)	0.75 wt. Model 1 (0.1) 0.0017 (0.2) 0.0009 (0.6) 0.00017 (0.2) Model 2 (0.3) 0.00035 (0.2) 0.00019 (0.6) 0.00003 (0.2) Model 3 (0.6) 0.00037 (0.2) 0.00021 (0.4) 0.00004 (0.2)	0.25 wt. 0.0014 (0.2) 0.00027 (0.6) 0.000026 (0.2)	0.5 wt.	0.5 wt.	1.0 (1.0 weight)	(not implemented)
7a Fault (2 m)	0.75 wt. Model 1 (0.1) 1.7e-4 (1.0) Model 2 (0.3) 5.2e-5 (1.0)	0.25 wt. 1.4e-4 (0.2) 4.8e-5 (0.6) 2.6e-5 (0.2)	0.5 wt.	0.5 wt.	1.0 (1.0 weight)	(not implemented)

TABLE SBK-5
FAULT DISPLACEMENT HAZARD CHARACTERIZATION DATA, POINTS 3-8
(Continued)

Point	Slip Rate (mm/yr) 0.8 weight		Event Frequency 0.2 weight		Activation Factor	
	Geologic History	Fault Parameter	Distributed Rupture	PPV Frequency	Slip Tendency	Angular Histogram
	Model 3 (0.6) 5.2e-5 (1.0)					
7b Shear (10 cm)	0.75 wt. Model 1 (0.1) 8e-6 (1.0) Model 2 (0.3) 2e-6 (1.0) Model 3 (0.6) 2e-6 (1.0)	0.25 wt. 7.0e-6 (0.2) 2.4e-6 (0.6) 1.3e-6 (0.2)	0.5 wt.	0.5 wt.	1.0 (1.0 weight)	(not implemented)
7c Fracture (<10 cm)	0.75 wt. [uniform between 0 & maximum of 7b]	0.25 wt. [uniform between 0 & maximum of 7b]	0.5 wt.	0.5 wt.	1.0 (1.0 weight)	(not implemented)
7d Intact Rock	notes below					
8a Fault (2 m)	0.75 wt. Model 1 (0.1) 1.7e-4 (1.0) Model 2 (0.3) 5.2e-5 (1.0) Model 3 (0.6) 5.2e-5 (1.0)	0.25 wt. 1.4e-4 (0.2) 4.8e-5 (0.6) 2.6e-5 (0.2)	0.5 wt.	0.5 wt.	1.0 (1.0 weight)	(not implemented)
8 bShear (10 cm)	0.75 wt. Model 1 (0.1) 8e-6 (1.0) Model 2 (0.3) 2e-6 (1.0)	0.25 wt. 7.0e-6 (0.2) 2.4e-6 (0.6) 1.3e-6 (0.2)	0.5 wt.	0.5 wt.	1.0 (1.0 weight)	(not implemented)

TABLE SBK-5
FAULT DISPLACEMENT HAZARD CHARACTERIZATION DATA, POINTS 3-8
(Continued)

Point	Slip Rate (mm/yr) 0.8 weight		Event Frequency 0.2 weight		Activation Factor	
	Geologic History	Fault Parameter	Distributed Rupture	PPV Frequency	Slip Tendency	Angular Histogram
	Model 3 (0.6) 2e-6 (1.0)					
8c Fracture (<10 cm)	0.75 wt. [uniform between 0 & maximum of 7b]	0.25 wt. [uniform between 0 & maximum of 7b]	0.5 wt.	0,1 overall	1.0 (1.0 weight)	(not implemented)
8d Intact Rock	see notes below					

Notes, Table SBK-5:

Fault Parameter Method: Total displacement and slip rate of the Bow Ridge fault are the reference parameters for this trial set of calculations. We could use an average of the Solitario Canyon and Bow Ridge fault parameters, but the slip rates of the two faults are similar, and Bow Ridge fault slip rate is well defined by trench #4 near the entrance to the repository ESF. Bow Ridge fault displacement is estimated as 100 m minimum, 125 m preferred value, and 150 m maximum value based on Day *et al.* (USGS, written communication, 1996b) and our judgement of maximum error in estimating total slip from mapping. Slip rate estimates for the Bow Ridge fault and weights are given in Table SBK-4. We report three estimated slip rates for the fault parameter method which are the preferred, the most minimum and most maximum values estimated using all combinations of the reference fault (Bow Ridge fault) parameters (displacement and slip rate) and subject fault parameters (displacement). Application of displacement variability (probability) functions is described in Section 3.3.4.

Drill Hole Wash Fault: Slip rate methods - Geologic History weighted 0.6, Model 1,2 & 3 as described in manuscript. Fault Parameter method weighted 0.2, Event Frequency - Distributed Rupture method weighted 0.1, Peak Particle Velocity method weighted 0.1). Fault parameter slip rates found by ratio of maximum estimated displacement on Drill Hole Wash to Bow Ridge Fault. Displacement estimates are (30 m, 40m, 50 m) from Day *et al.*, 1996. Stress activation factor computed using ESF stress tensor and orientation of Drill Hole Wash fault reported by Day *et al.* (USGS, written communication, 1996b). Fault pole trends 045°, plunges 05° with an assumed variation of ± 10° in both trend and plunge.

Ghost Dance Fault: Slip rate methods - Geologic History weighted 0.6, Model 1,2 & 3 as described in manuscript. Fault Parameter method weighted 0.2, Event Frequency - Distributed Rupture method weighted 0.1, Peak Particle Velocity (PPV) method weighted 0.1. Fault parameter slip rates found by ratio of maximum estimated displacement on Ghost Dance to Bow Ridge Fault. Displacement estimates are (25 m, 30 m , 35 m) from Day *et al.* USGS, written communication, 1996b).

TABLE SBK-5
FAULT DISPLACEMENT HAZARD CHARACTERIZATION DATA, POINTS 3-8
(Continued)

Stress activation factor computed using ESF stress tensor and orientation of Ghost Dance fault reported by Day *et al.* (USGS, written communication, 1996b). Fault pole trends 090°, plunges 15° with an assumed variation of ± 10° in both trend and plunge.

Sun Dance Fault: Slip rate methods - Geologic History weighted 0.6, with application of Modelsl 1,2 & 3 as described in manuscript. Fault Parameter method weighted 0.2., Event Frequency - Distributed Rupture method weighted 0.2. Fault parameter slip rates found by ratio of maximum estimated displacement on Sun Dance to Bow Ridge Fault multiplied. Displacement estimates are (6 m, 15 m, 20 m) from Day *et al.* (USGS, written communication, 1996b). Stress activation factor computed using ESF stress tensor and orientation of Sun Dance fault reported by Day *et al.* (USGS, written communication, 1996b). Fault pole trends 050°, plunges 00° with an assumed variation of ± 10° in both trend and plunge.

Point 6 west of Dune Wash: The amount of displacement on this fault is assumed to be between 2 and 20 meters. We assume a minimum of 2 m, a maximum of 20 m and a preferred value of 11 m (the average of the minimum and maximum displacement estimates for this type of intrablock fault (SSC Facilitation Team memo of January 16, 1997 entitled 'Fault Displacement Hazard Guidance). Geohistory (0.6), Fault Parameter (0.2), Distributed Rupture (0.1) and Peak Particle Velocity (PPV) (0.1) methods are all implemented with appropriate weigthing in closed brackets (wt).

Points 7 and 8: Value of 10 cm slip is used for both geohistory and fault parameter methods. No fault orientation is specified, so we assume that slip tendency is 1.0. Slip of less than 10 cm is not specified, so we assume that slip rates are less than those calculated using the geohistory and fault parameter methods for slip of 10 cm. Geohistory (0.6), Fault Parameter (0.2), Distributed Rupture (0.1) and Peak Particle Velocity (PPV) (0.1) methods are all implemented with appropriate weigthing in ( ).

Intact Rock: We use a n event frequency approach by assuming that the annual probability of fracturing is less than 1 / (age of intact rock). Consider an unfractured wall of Tiva Canyon Tuff in the repository. The chance of fracuring is less than 1 / (1.2e7 years) = 8.3e-8 yr^{-1}. We assume that if new fracturing does occur, the maximum amount of shear offset will be less than 10 cm, and use the event frequency displacement variability function P(U/Dm) to estimate the probability of the amount of slip.

TABLE SBK-6
TRENCHING DATA USED TO DEVELOP DISTRIBUTIONS FOR DISPLACEMENT PER EVENT

Fault	Trench	Event	U (cm)			U/Uap*			U/Ua**			U/Um***		
			min.	pref.	max.	min	pref.	max	min	pref	max	min.	pref	max
Bow Ridge	T-14D	Z	1	1	5	0.19	0.06	0.12	0.092	0.092	0.220	0.054	0.054	0.109
		Z	15	44	80	2.86	2.44	1.88	1.386	4.066	3.516	0.810	2.377	1.749
		Y	4	13	45	0.76	0.72	1.06	0.370	1.201	1.978	0.216	0.702	0.984
		X	1	14	40	0.19	0.78	0.94	0.092	1.294	1.758	0.054	0.756	0.874
N. Crater Flat	CFFT2-a	Z	1	3	5	0.04	0.10	0.15	0.056	0.114	0.190	0.030	0.055	0.092
		Y	1	5	5	0.04	0.17	0.15	0.056	0.190	0.190	0.030	0.092	0.092
		X	35	40	45	1.38	1.35	1.36	1.968	1.522	1.713	1.033	0.734	0.826
		W	45	50	55	1.77	1.69	1.67	2.531	1.903	2.093	1.328	0.917	1.009
		V	45	50	55	1.77	1.69	1.67	2.531	1.903	2.093	1.328	0.917	1.009
S. Crater Flat	CFFT1	Z	7.5	8	10				0.795	0.575	0.562	0.479	0.319	0.295
		Y	7.5	10	10				0.795	0.719	0.562	0.479	0.398	0.295
	CFFT1-a	Z	2	18	18	0.25	1.13	0.83	0.212	1.295	1.012	0.128	0.717	0.531
		Y	5	10	15	0.63	0.63	0.69	0.530	0.719	0.844	0.319	0.398	0.443
		X	17	20	32	2.13	1.25	1.47	1.801	1.438	1.799	1.085	0.796	0.944
Fatigue Wash	CF-1	Z	0	1	5	0.00	0.02	0.10	0.000	0.043	0.131	0.000	0.021	0.058
		Y	15	25	35	0.37	0.54	0.67	1.205	1.066	0.918	0.684	0.527	0.408
		X	100	105	110	2.44	2.27	2.11	8.034	4.477	2.885	4.557	2.212	1.282
		W	49	54	59	1.20	1.17	1.13	3.937	2.303	1.547	2.233	1.138	0.688
Iron Ridge	SCF-T2	Z	1	5	10	0.02	0.08	0.13	0.085	0.423	0.688	0.048	0.242	0.377
		Y	50	70	90	1.17	1.14	1.13	4.225	5.916	6.191	2.423	3.393	3.395
		X	70	100	130	1.64	1.63	1.63	5.916	8.451	8.943	3.393	4.846	4.904
		W	50	70	90	1.17	1.14	1.13	4.225	5.916	6.191	2.423	3.393	3.395
Stagecoach Rd	SCR-T1	Z	40	40	82	1.51	0.89	1.01	2.966	2.966	3.678	1.653	1.653	1.838
		Y	28	42	70	1.06	0.93	0.86	2.076	3.115	3.140	1.157	1.736	1.569
		X	14	47	99	0.53	1.04	1.22	1.038	3.486	4.441	0.579	1.943	2.219

TABLE SBK-6
TRENCHING DATA USED TO DEVELOP DISTRIBUTIONS FOR DISPLACEMENT PER EVENT
(Continued)

Fault	Trench	Event	U (cm)			U/Uap*			U/Ua**			U/Um***		
			min.	pref.	max.	min	pref.	max	min	pref	max	min.	pref	max
		W	24	51	74	0.91	1.13	0.91	1.780	3.782	3.319	0.992	2.108	1.658
	SCR-T3	Z	25	43	66	1.04	0.76	0.84	1.854	3.189	2.960	1.033	1.777	1.479
		Y	20	59	77	0.83	1.04	0.98	1.483	4.375	3.454	0.827	2.439	1.726
		X	25	57	84	1.04	1.01	1.07	1.854	4.227	3.768	1.033	2.356	1.882
		W	26	67	87	1.08	1.19	1.11	1.928	4.969	3.902	1.075	2.770	1.950
Solitario Cyn	SCFT-1	Z	1	10	20				0.041	0.249	0.498	0.020	0.109	0.219
		Y	10	70	90				0.406	1.742	2.240	0.199	0.765	0.984
	SCFT-3	Z	1	10	20				0.041	0.249	0.498	0.020	0.109	0.219
		W	20	35	50				0.812	0.871	1.244	0.397	0.383	0.547
	SCFT-T4	Z	1	5	20	0.10	0.27	0.67	0.041	0.124	0.498	0.020	0.055	0.219
		Y	20	30	40	1.94	1.64	1.33	0.812	0.747	0.995	0.397	0.328	0.437
		W	10	20	30	0.97	1.09	1.00	0.406	0.498	0.747	0.199	0.219	0.328
	SCFT-8	Z	5	10	20	0.13	0.19	0.30	0.203	0.249	0.498	0.099	0.109	0.219
		Y	100	120	140	2.58	2.29	2.07	4.062	2.986	3.484	1.986	1.312	1.531
		X	20	30	40	0.52	0.57	0.59	0.812	0.747	0.995	0.397	0.328	0.437
		W	30	50	70	0.77	0.95	1.04	1.219	1.244	1.742	0.596	0.547	0.765
Paint Brush C.	Trench A-1	Z	5	6	10	0.43	0.35	0.41	0.224	0.157	0.200	0.112	0.070	0.084
		Y	29	39	49	2.48	2.25	2.01	1.301	1.023	0.981	0.650	0.455	0.411
		X	1	7	14	0.09	0.40	0.58	0.045	0.184	0.280	0.022	0.082	0.117
		W	100						4.486	0.000	0.000	2.241	0.000	0.000
	Trench BB4	Z	1	44	72	0.03	0.49	0.47	0.045	1.154	1.441	0.022	0.513	0.604
		Y	16	28	56	0.49	0.31	0.36	0.718	0.734	1.121	0.359	0.326	0.470
		X	35	47	69	1.07	0.52	0.45	1.570	1.233	1.381	0.784	0.548	0.579

TABLE SBK-6
TRENCHING DATA USED TO DEVELOP DISTRIBUTIONS FOR DISPLACEMENT PER EVENT
(Continued)

Fault	Trench	Event	U (cm)			U/Uap*			U/Ua**			U/Um***		
			min.	pref.	max.	min	pref.	max	min	pref	max	min.	pref	max
		W	88	167	205	2.70	1.86	1.33	3.947	4.379	4.104	1.972	1.947	1.720
		V	1	142	222	0.03	1.59	1.44	0.045	3.724	4.444	0.022	1.655	1.863
		U	12	105	257	0.37	1.17	1.66	0.538	2.754	5.145	0.269	1.224	2.156
		T	75	94	201	2.30	1.05	1.30	3.364	2.465	4.024	1.681	1.096	1.687
	MWV-T4	Z	15	20	25	0.53	0.36	0.26	0.673	0.524	0.500	0.336	0.233	0.210
		Y	44	62	77	1.56	1.13	0.80	1.974	1.626	1.542	0.986	0.723	0.646
		X	53	98	143	1.88	1.78	1.49	2.377	2.570	2.863	1.188	1.142	1.200
		W	1	40	140	0.04	0.73	1.45	0.045	1.049	2.803	0.022	0.466	1.175
Windy Wash	T-CF2	Z	1	4	10	0.03	0.10	0.20	0.018	0.066	0.157	0.007	0.026	0.062
		Y	14	20	24	0.44	0.51	0.47	0.253	0.328	0.376	0.104	0.132	0.150
		X	20	23	30	0.63	0.58	0.59	0.361	0.377	0.471	0.148	0.151	0.187
		W	18	20	25	0.56	0.51	0.49	0.325	0.328	0.392	0.133	0.132	0.156
		V	70	73	83	2.19	1.85	1.62	1.264	1.198	1.302	0.518	0.481	0.517
		U	30	45	60	0.94	1.14	1.17	0.542	0.738	0.941	0.222	0.296	0.374
		T	38	50	78	1.19	1.27	1.52	0.686	0.821	1.224	0.281	0.329	0.486
		S	65	80	100	2.03	2.03	1.95	1.173	1.313	1.569	0.481	0.527	0.623
		Z	1	4	10	0.03	0.11	0.23	0.018	0.066	0.157	0.007	0.026	0.062
		Y	8	12	18	0.28	0.34	0.41	0.144	0.197	0.282	0.059	0.079	0.112
		X	45	50	53	1.56	1.43	1.22	0.812	0.821	0.831	0.333	0.329	0.330
		W	38	42	52	1.32	1.20	1.20	0.686	0.689	0.816	0.281	0.277	0.324
		V	24	28	30	0.83	0.80	0.69	0.433	0.459	0.471	0.178	0.184	0.187
		U	15	19	24	0.52	0.54	0.55	0.271	0.312	0.376	0.111	0.125	0.150
		T	55	60	65	1.90	1.71	1.50	0.993	0.985	1.020	0.407	0.395	0.405
		S	45	65	95	1.56	1.86	2.19	0.812	1.067	1.490	0.333	0.428	0.592
	TCF-3	Z	4	6	10	0.27	0.29	0.34	0.072	0.098	0.157	0.030	0.040	0.062
		Y	10	20	32	0.68	0.96	1.10	0.181	0.328	0.502	0.074	0.132	0.199

TABLE SBK-6
TRENCHING DATA USED TO DEVELOP DISTRIBUTIONS FOR DISPLACEMENT PER EVENT
(Continued)

Fault	Trench	Event	U (cm)			U/Uap*			U/Ua**			U/Um***		
			min.	pref.	max.	min	pref.	max	min	pref	max	min.	pref	max
		X	33	42	54	2.24	2.02	1.86	0.596	0.689	0.847	0.244	0.277	0.337
		W	12	15	20	0.81	0.72	0.69	0.217	0.246	0.314	0.089	0.099	0.125
		Z	1	4	6	0.03	0.10	0.12	0.018	0.066	0.094	0.007	0.026	0.037
		Y	25	33	42	0.82	0.83	0.87	0.451	0.542	0.659	0.185	0.217	0.262
		X	71	87	96	2.33	2.19	1.98	1.282	1.428	1.506	0.525	0.573	0.598
		W	25	35	50	0.82	0.88	1.03	0.451	0.574	0.784	0.185	0.231	0.312
	T?	Z	1	3	6	0.03	0.07	0.12	0.018	0.049	0.094	0.007	0.020	0.037
		Y	25	35	45	0.72	0.83	0.91	0.451	0.574	0.706	0.185	0.231	0.281
		X	78	88	98	2.25	2.10	1.97	1.408	1.444	1.537	0.577	0.580	0.611

Notes

* Uap is the average of measurements for fault. Minimum, preferred, and maximum values are obtained by averaging min., pref., and max. columns, respectively for U.

** Ua is computed using minimum, preferred, and maximum lengths of faults from Table SBK-3 and relationship

$\log(Ua)=-1.99+1.24\times\log(L)$

*** Um is computed using minimum, preferred, and maximum lengths of faults from Table SBK-3 and relationship

$\log(Ua)=-1.98+1.51\times\log(L)$

TABLE SBK-7
DATA USED TO DEVELOP DISTRIBUTION FOR U/D_m

Fault	Trench	Displacement, U (cm)	Cumulative Displacement D_m (cm)	U/D_m
Solitario Canyon	SCF-T1	10	45313	2.21E-04
		70		1.54E-03
	SCF-T3	10		2.21E-04
		80		1.77E-03
		35		7.72E-04
	SCF-T4	5		1.10E-04
		30		6.62E-04
		20		4.41E-04
	SCF-T8	10		2.21E-04
		120		2.65E-03
		30		6.62E-04
		50		1.10E-03
Bow Ridge	Trench 14D	44	7500	5.87E-03
		13		1.73E-03
		14		1.87E-03
Paintbrush	Trench A1	6	35000	1.71E-04
		39		1.11E-03
		7		2.00E-04
	BB-4	44		1.26E-03
		28		8.00E-04
		47		1.34E-03
		167		4.77E-03
		142		4.06E-03
		105		3.00E-03
		94		2.69E-03
	MWV-T4	20		5.71E-04
		62		1.77E-03
		98		2.80E-03
		40		1.14E-03
Stagecoach Road	SCR-T1	40	25625	1.56E-03
		42		1.64E-03
		47		1.83E-03
		51		1.99E-03
	SCR-T3	43		1.68E-03
		59		2.30E-03
		57		2.22E-03
		67		2.61E-03
Windy Wash	CF-2nwall	4	20000	2.00E-04
		20		1.00E-03
		23		1.15E-03
		20		1.00E-03
		73		3.65E-03
		45		2.25E-03
		50		2.50E-03
		80		4.00E-03
	CF-2swall	4		2.00E-04
		12		6.00E-04
		50		2.50E-03

TABLE SBK-7
DATA USED TO DEVELOP DISTRIBUTION FOR U/D_m
(Continued)

Fault	Trench	Displacement, U (cm)	Cumulative Displacement D_m (cm)	U/D_m
		42		2.10E-03
		28		1.40E-03
		19		9.50E-04
		60		3.00E-03
		65		3.25E-03
	CF-3nwall	4		2.00E-04
		33		1.65E-03
		87		4.35E-03
		35		1.75E-03
	CF-3swall	3		1.50E-04
		35		1.75E-03
		88		4.40E-03

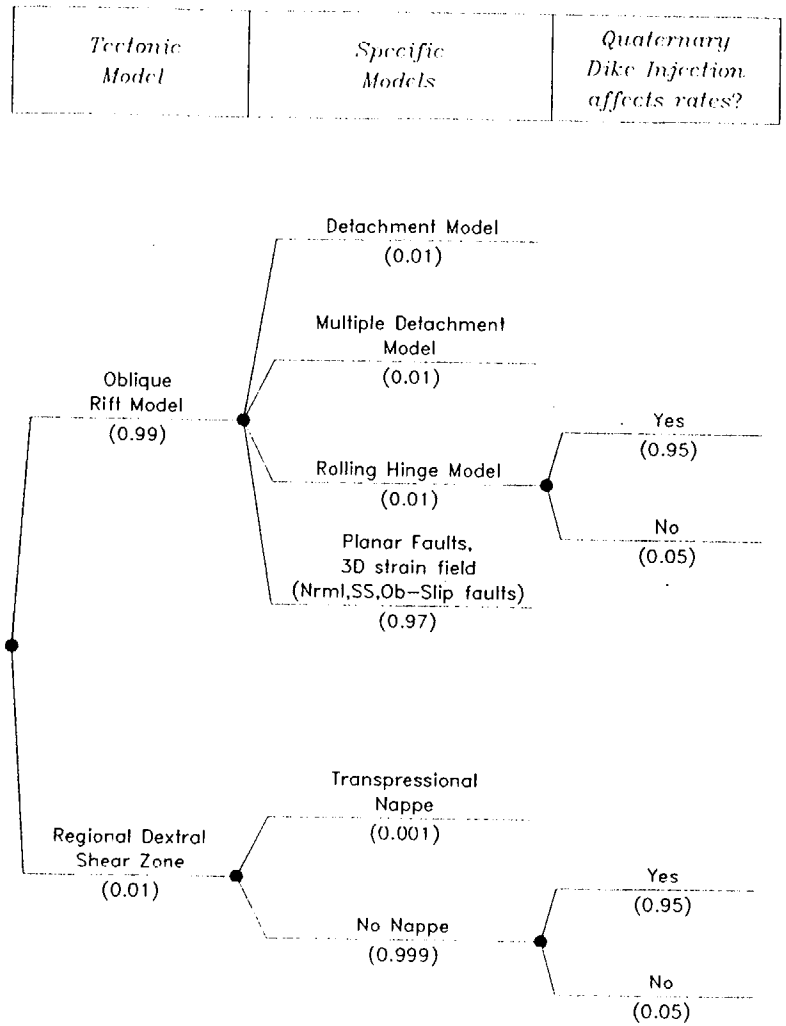

Figure SBK-1 Logic tree for tectonic models

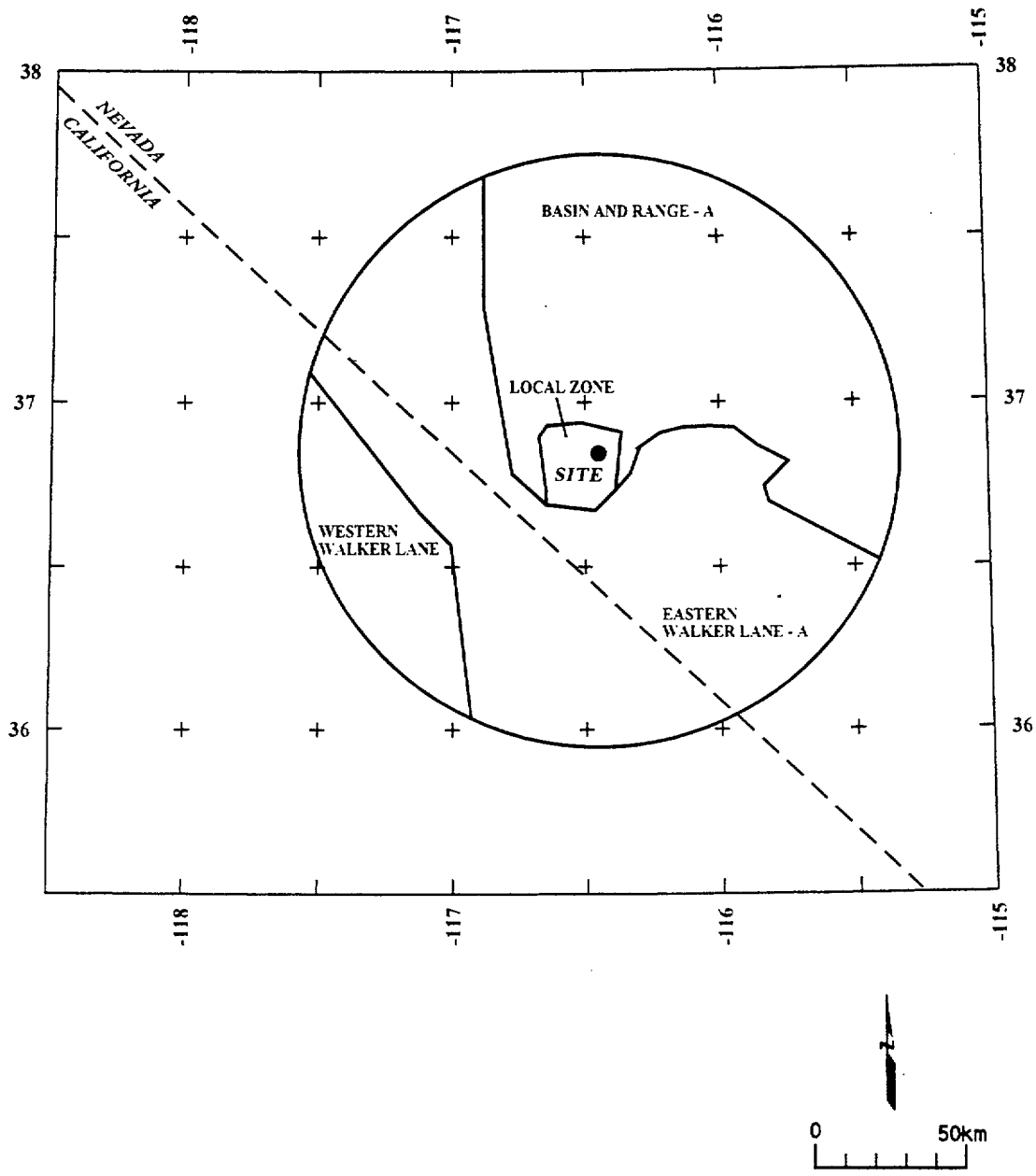

Figure SBK-2 Map showing boundaries of seismic source zones, Model A.

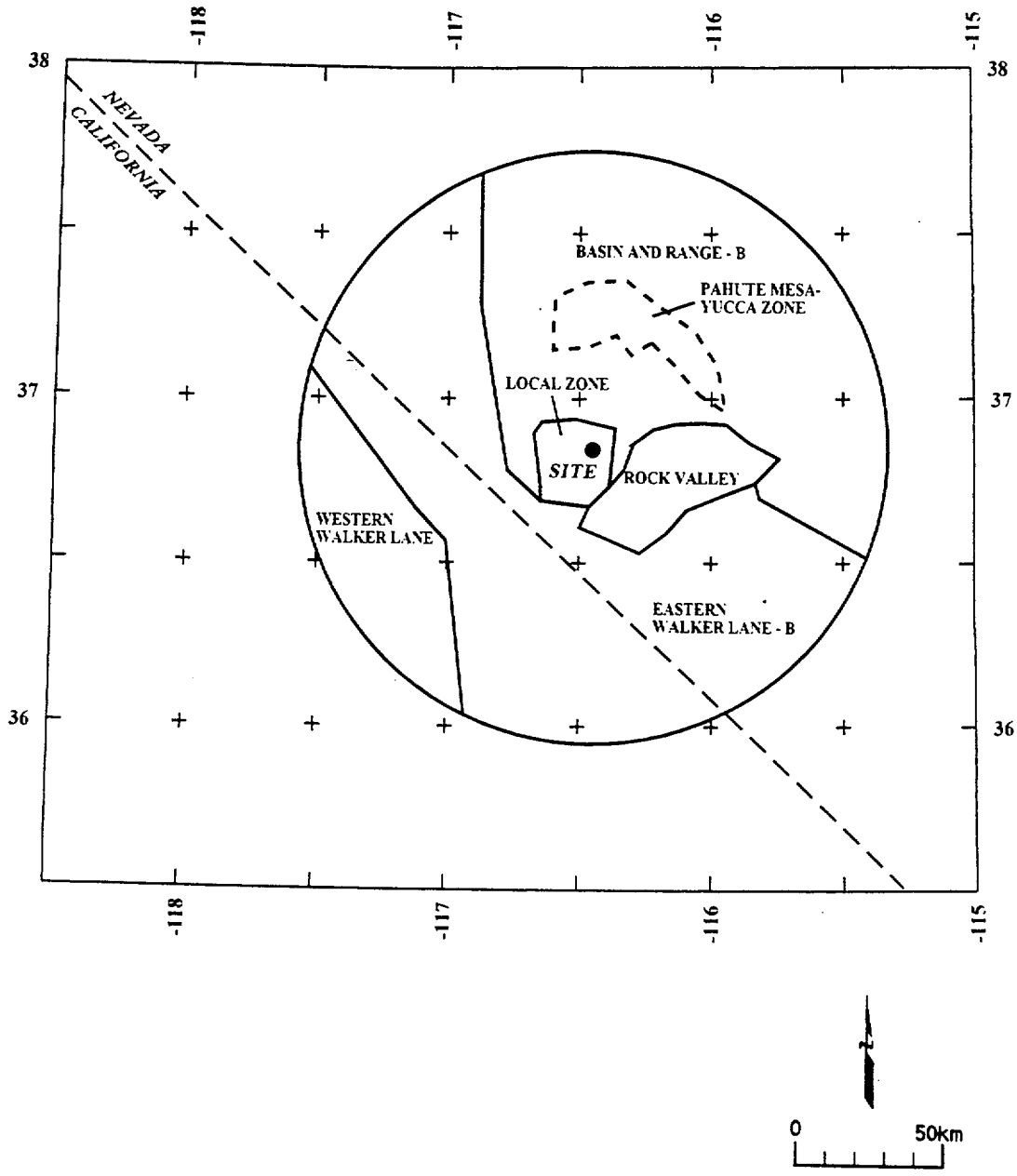

Figure SBK-3 Map showing the boundaries of seismic source zones, Model B.

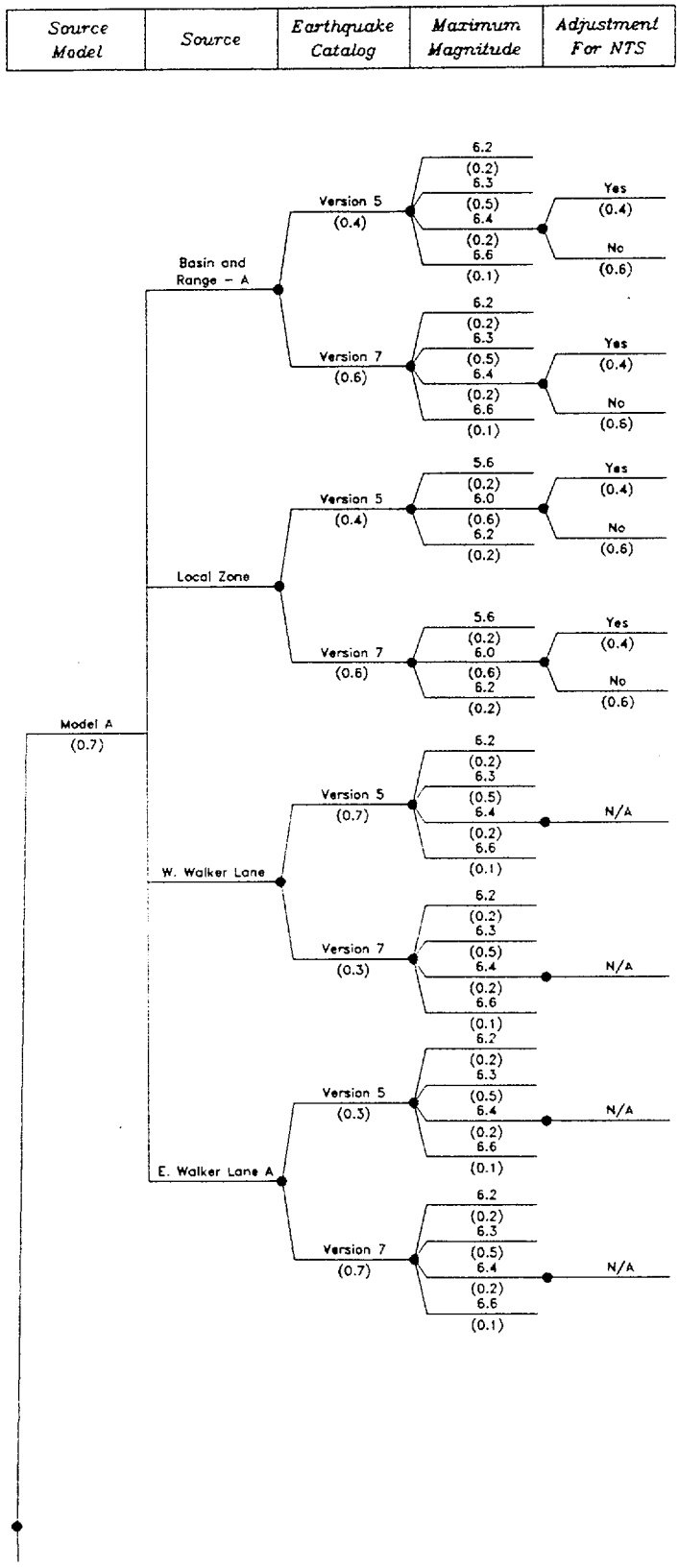

Figure SBK-4 Logic tree for characterizing areal source zones

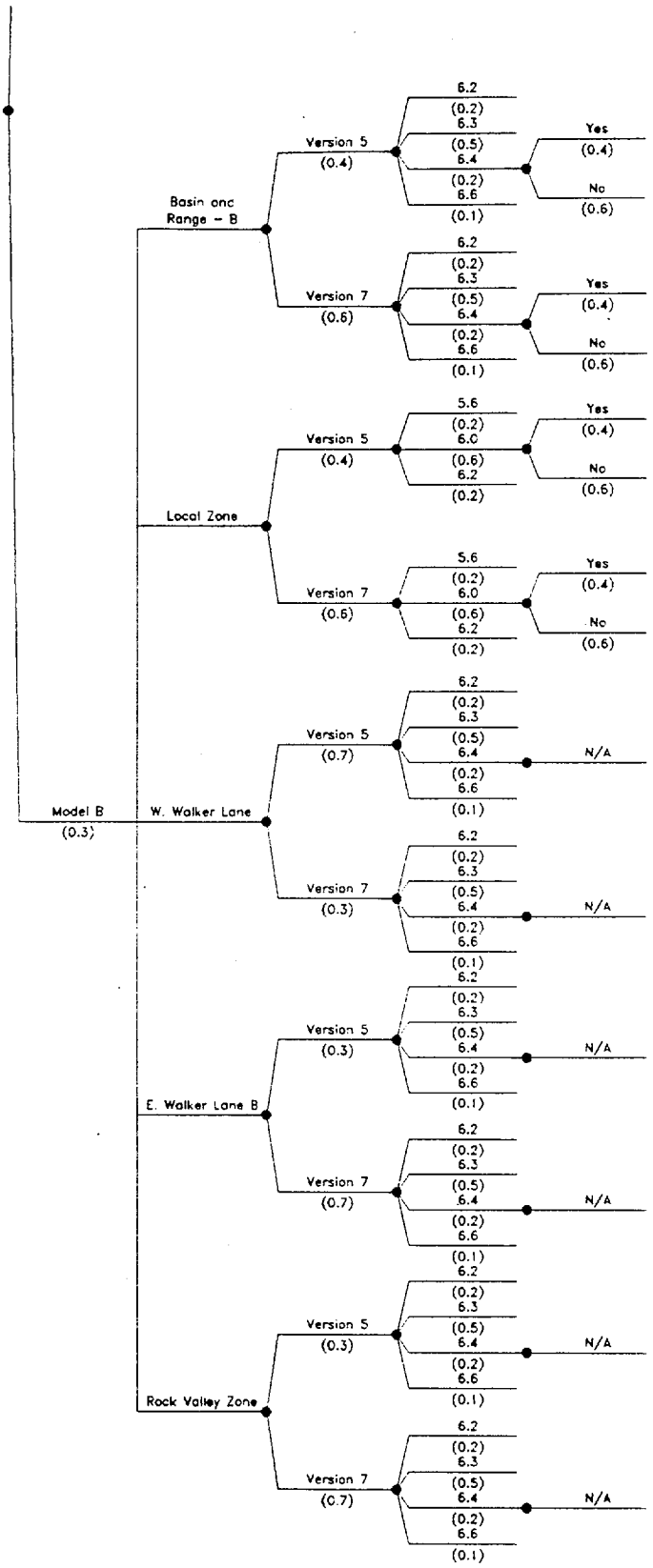

Figure SBK-4 (Cont'd.) Logic tree for characterizing areal source zones

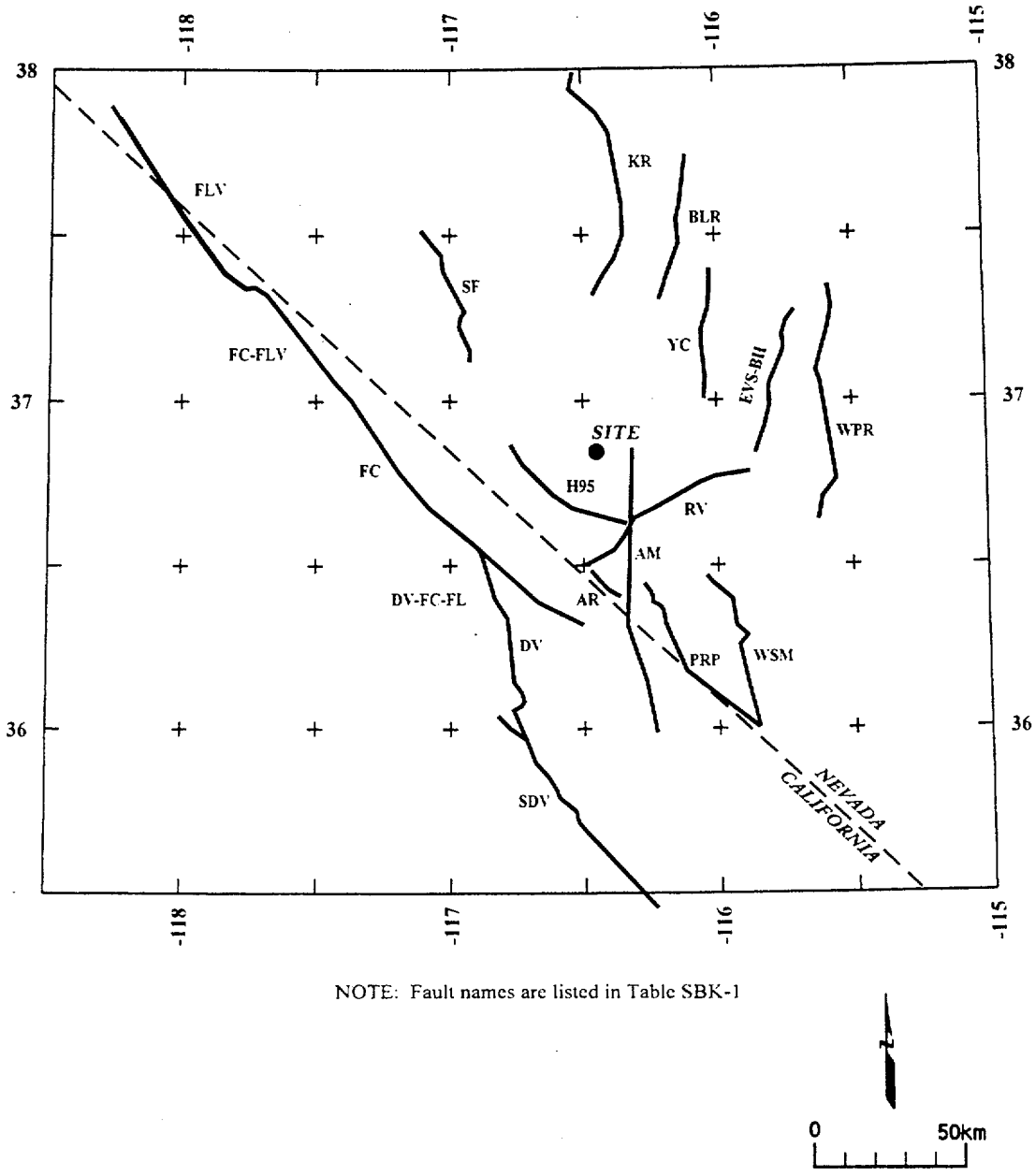

NOTE: Fault names are listed in Table SBK-1

Figure SBK-5 Map showing regional faults included in the seismic source model

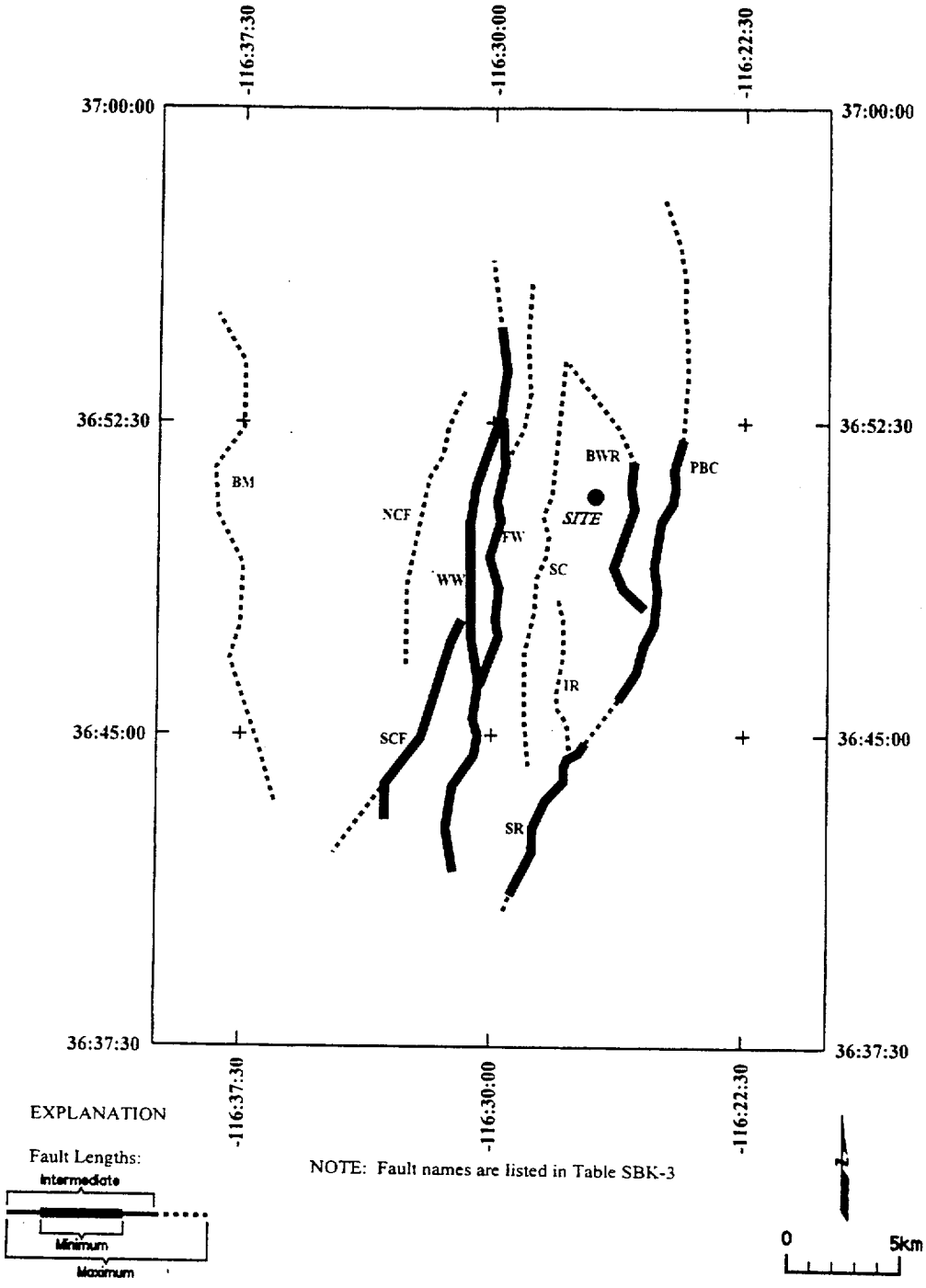

Figure SBK-6 Map showing local fault sources included in the seismic source model

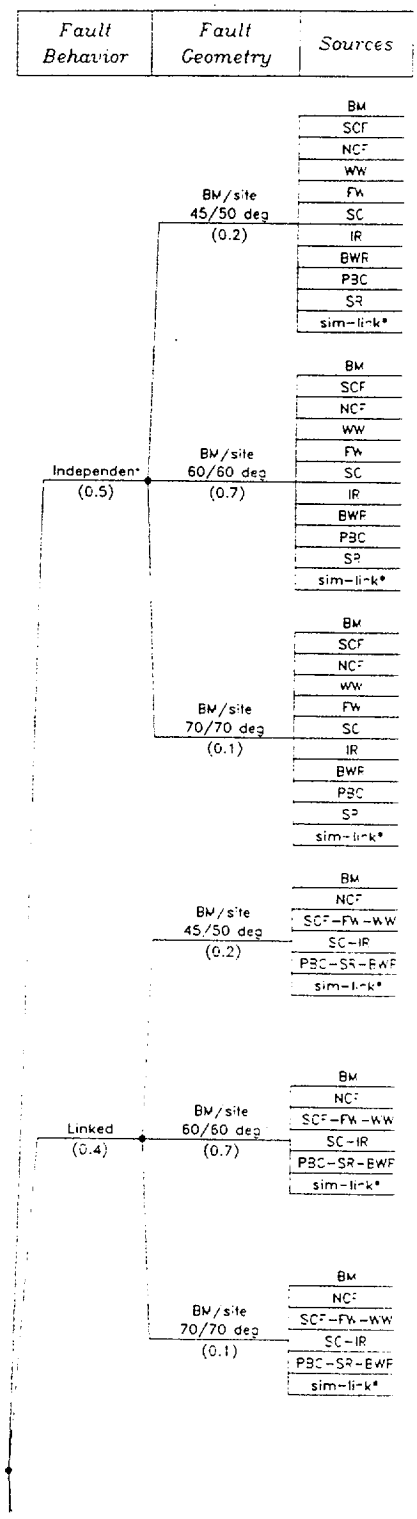

Figure SBK 7 Logic tree for local faults

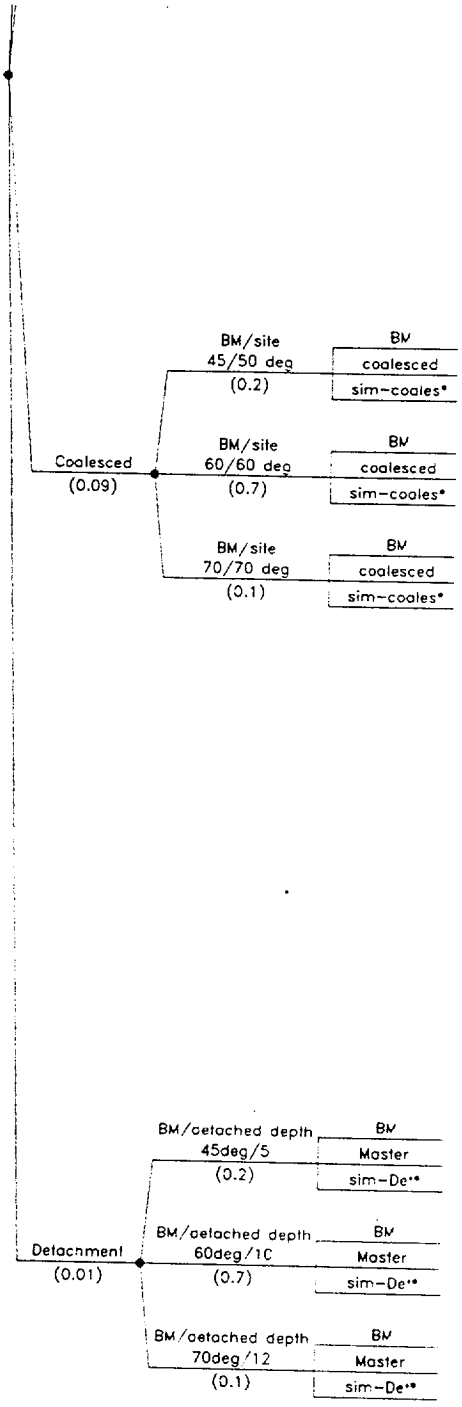

* sim-link, sim-coales and sim-det are synchronous rupture scenarios that act as additional sources of large events

Figure SBK 7 (Cont'd.) Logic tree for local faults

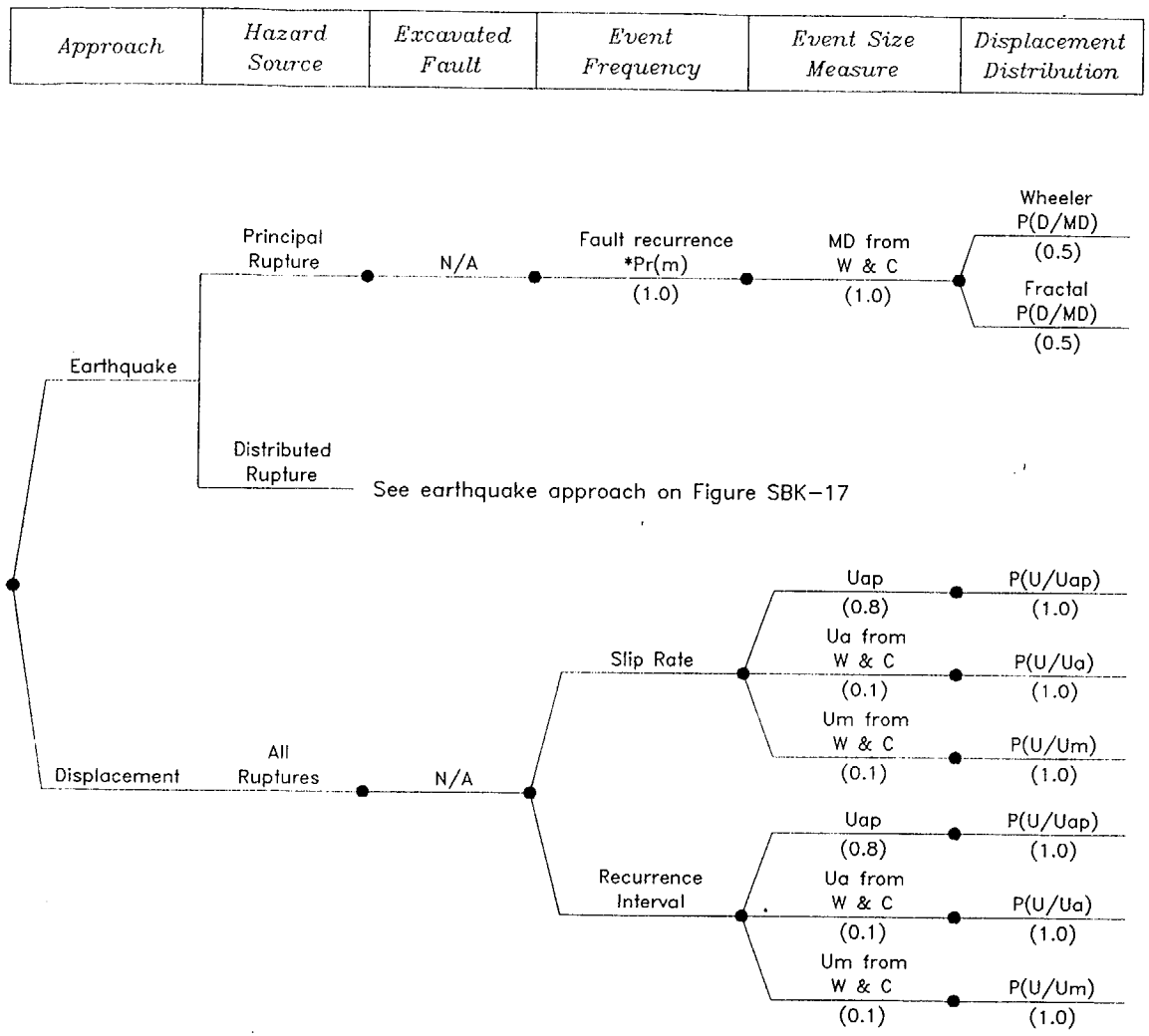

Figure SBK-8 Logic tree to characterize site with Quaternary displacement

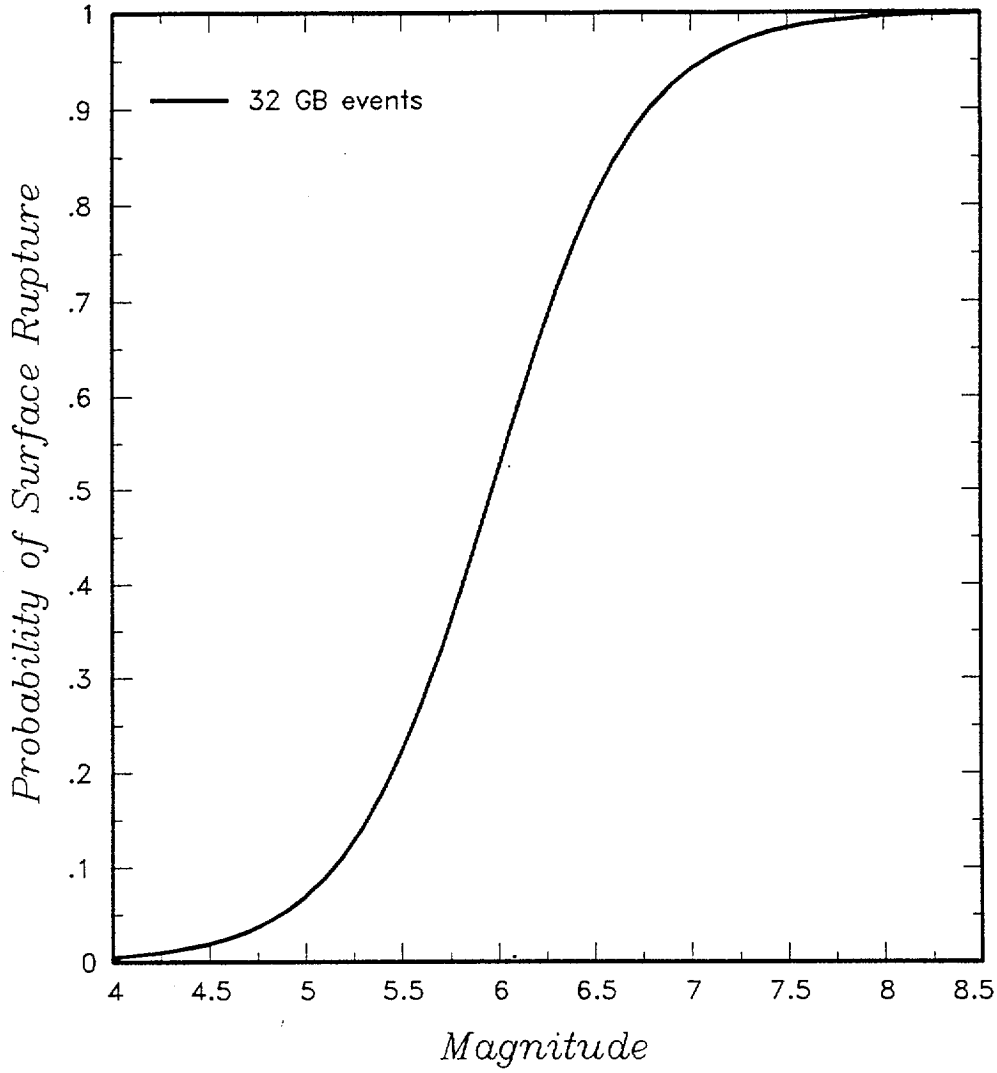

Figure SBK-9 Probability of surface rupture versus magnitude computed from data presented in S.K. Pezzopane and T.E. Dawson (USGS, written communication, 1996)

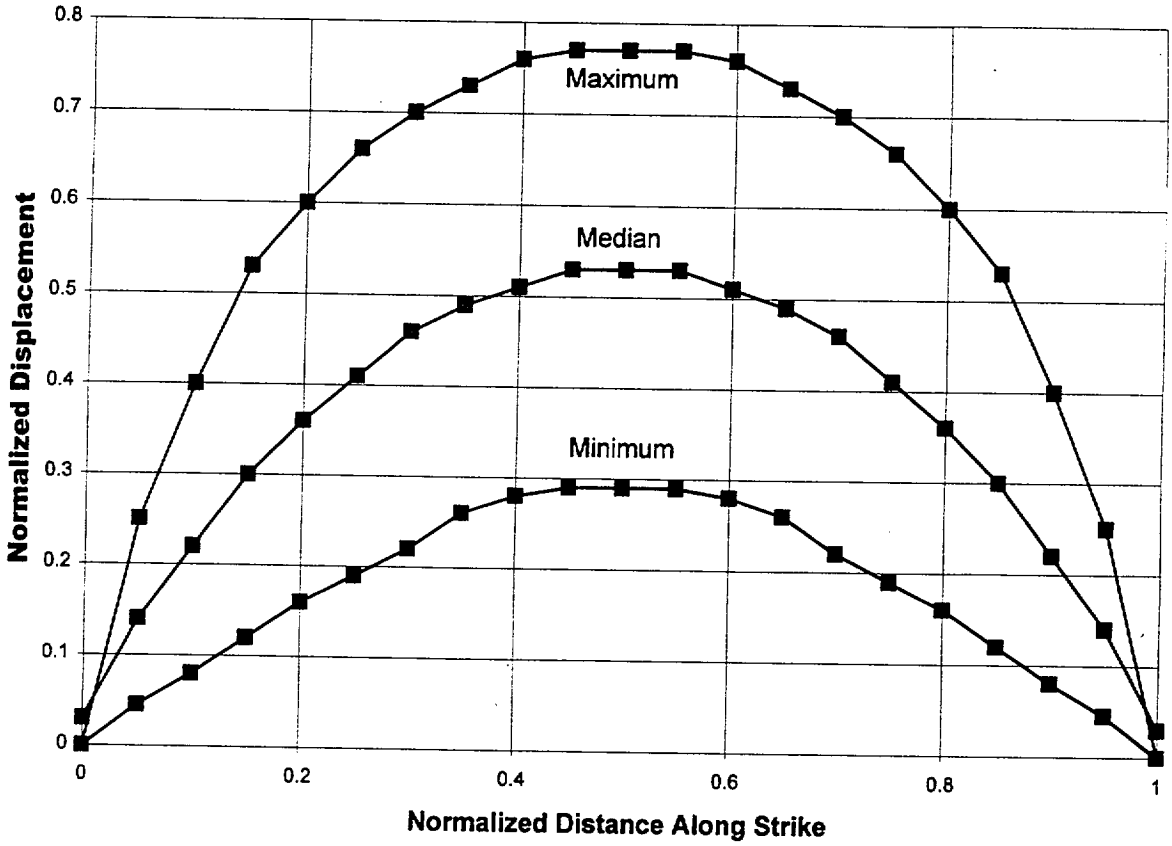

Figure SBK-10 Normalized slip along strike from five normal fault ruptures developed by ASM team from data in Wheeler (1989)

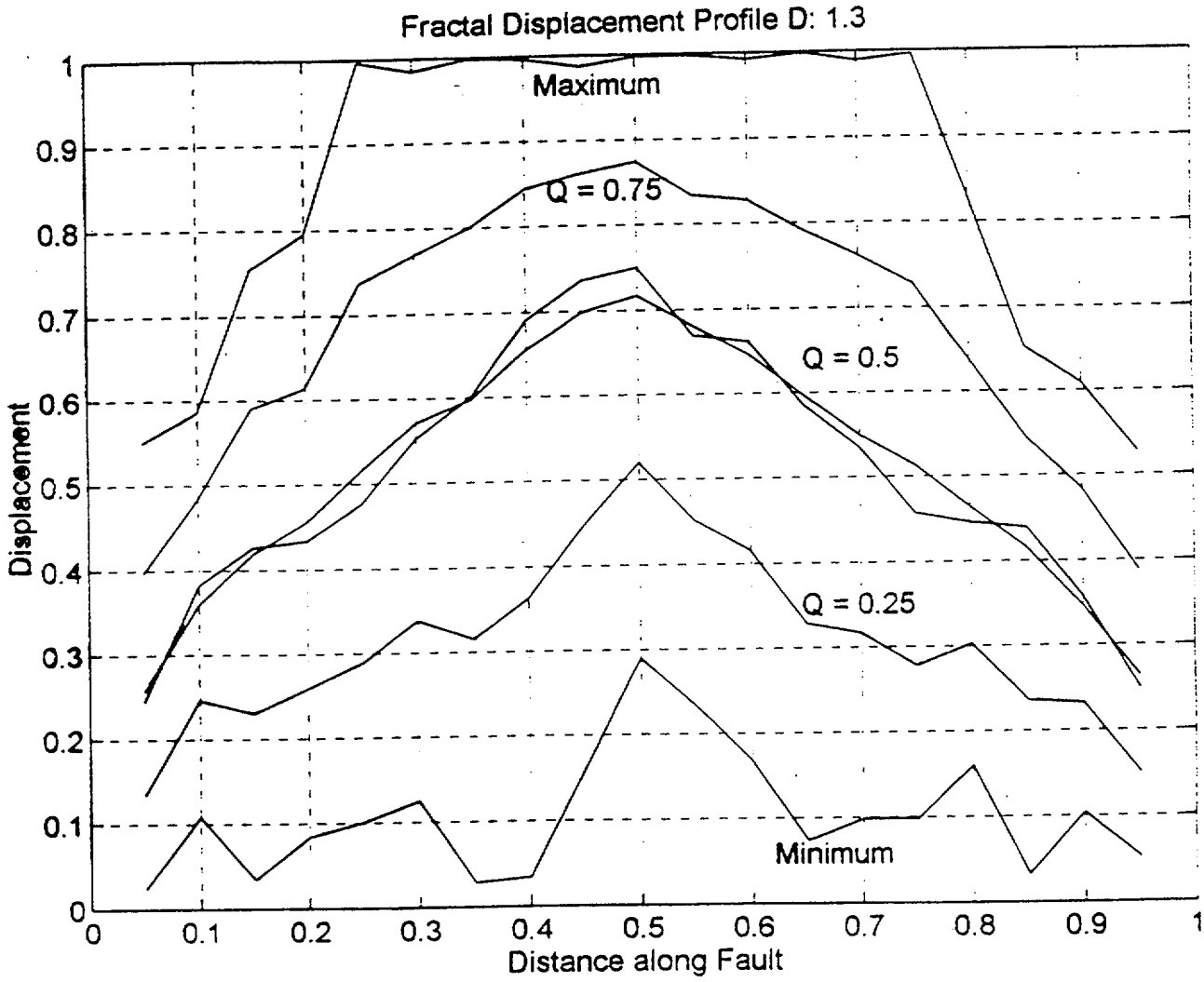

Figure SBK-11 Fractal displacement profiles developed by R. Bruhn (SBK) to predict distribution for the ratio of displacement at a point to the maximum displacement in an earthquake

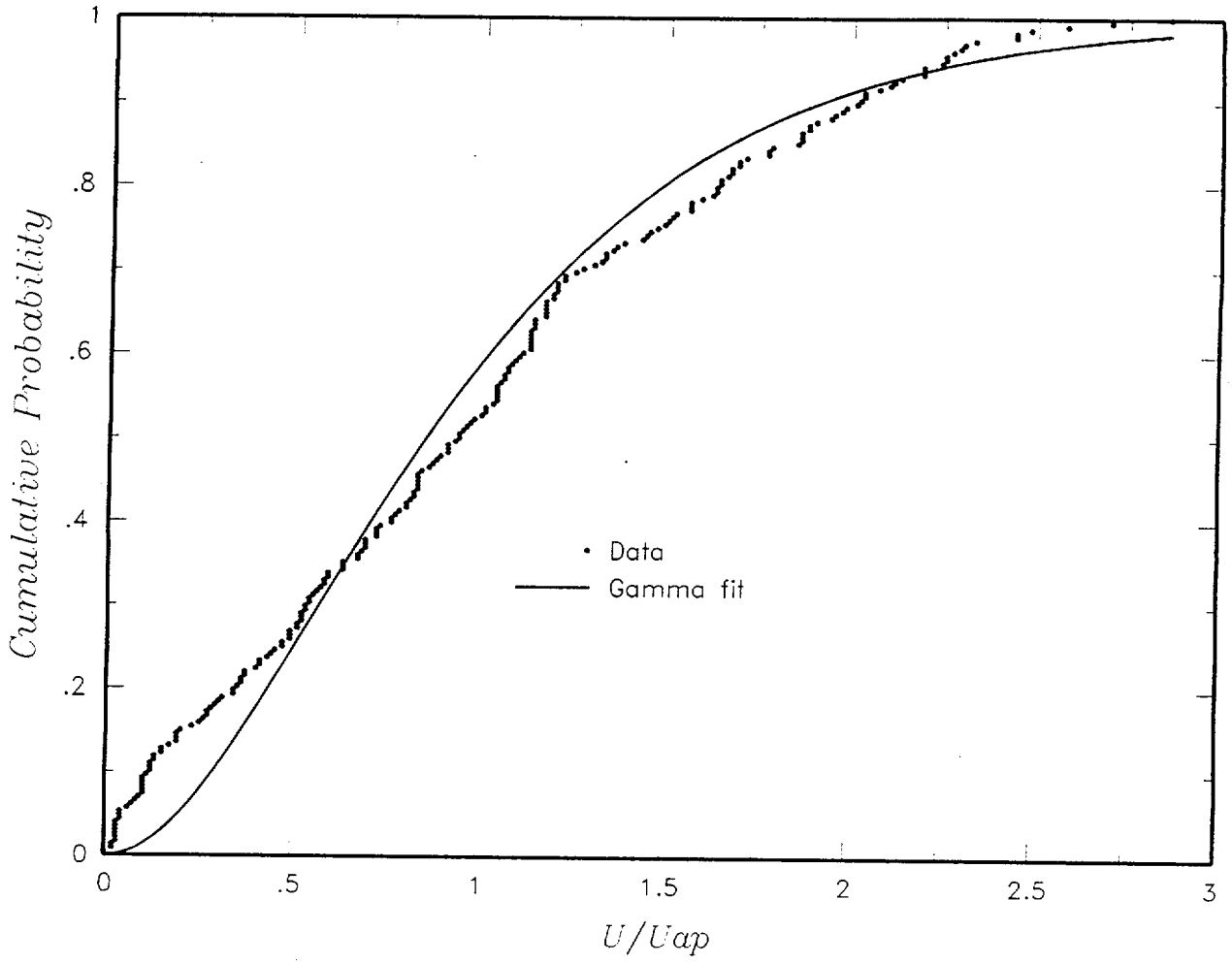

Figure SBK-12 Distribution of U/Uap

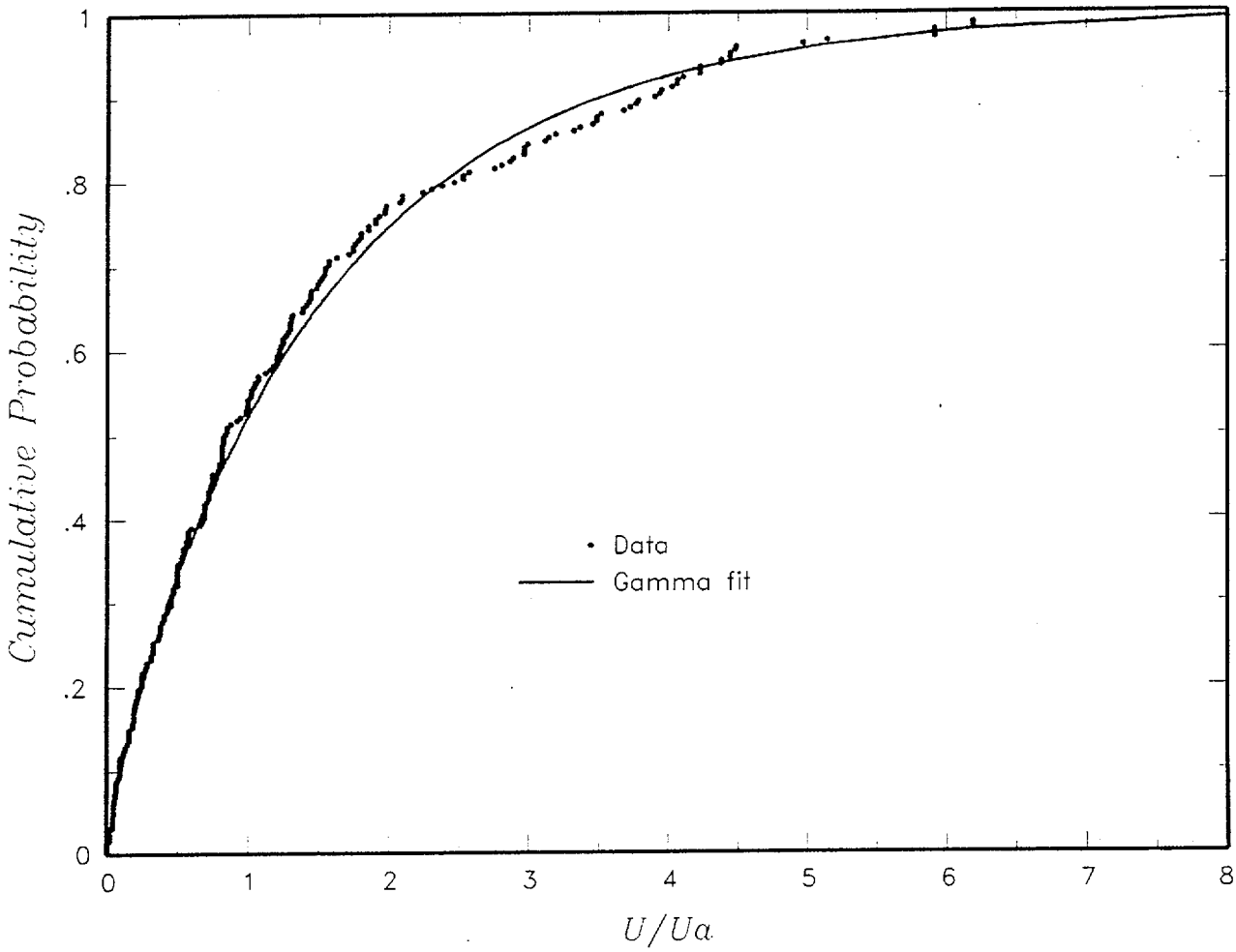

Figure SBK-13 Distribution of U/Ua

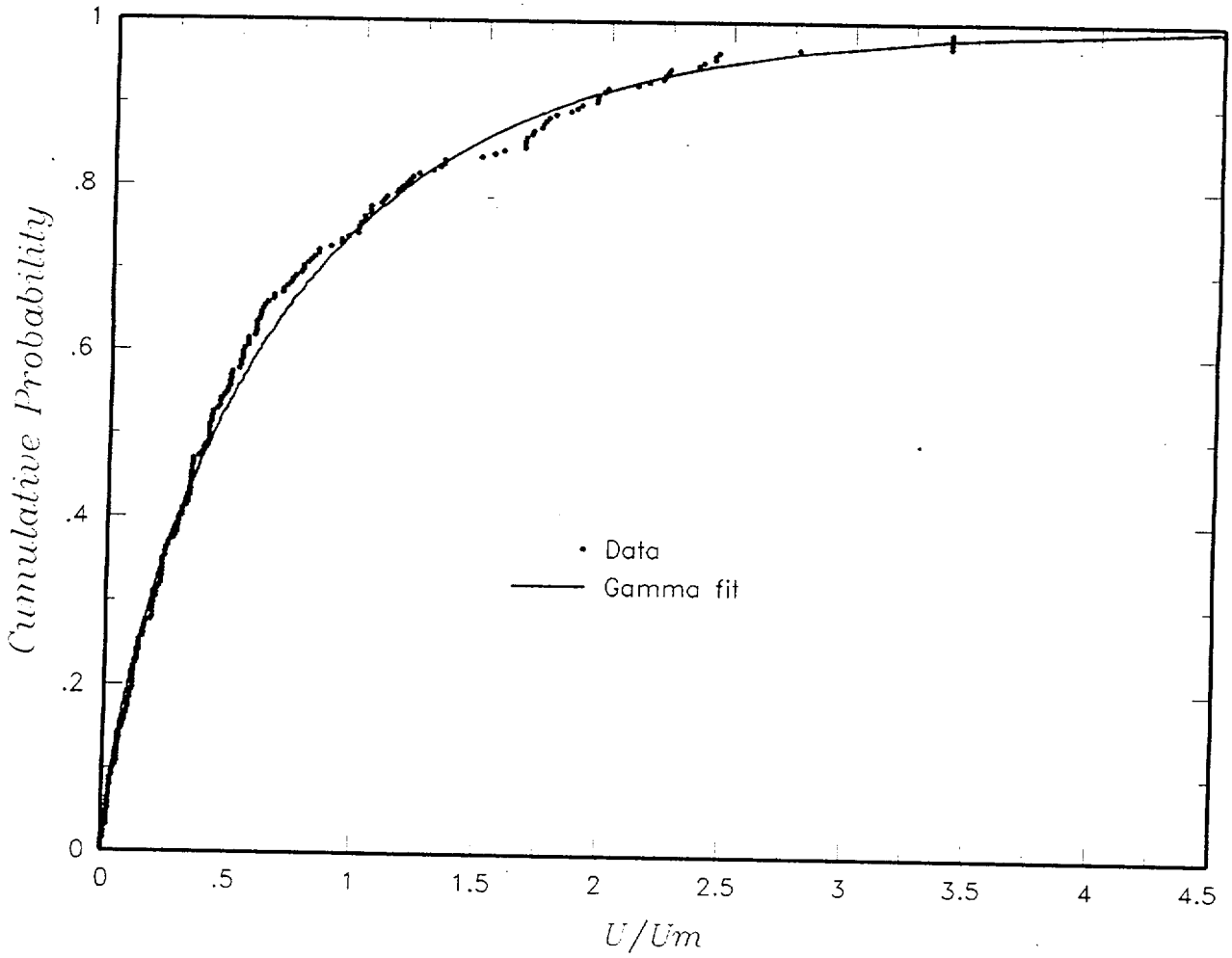

Figure SBK-14 Distribution of U/Um

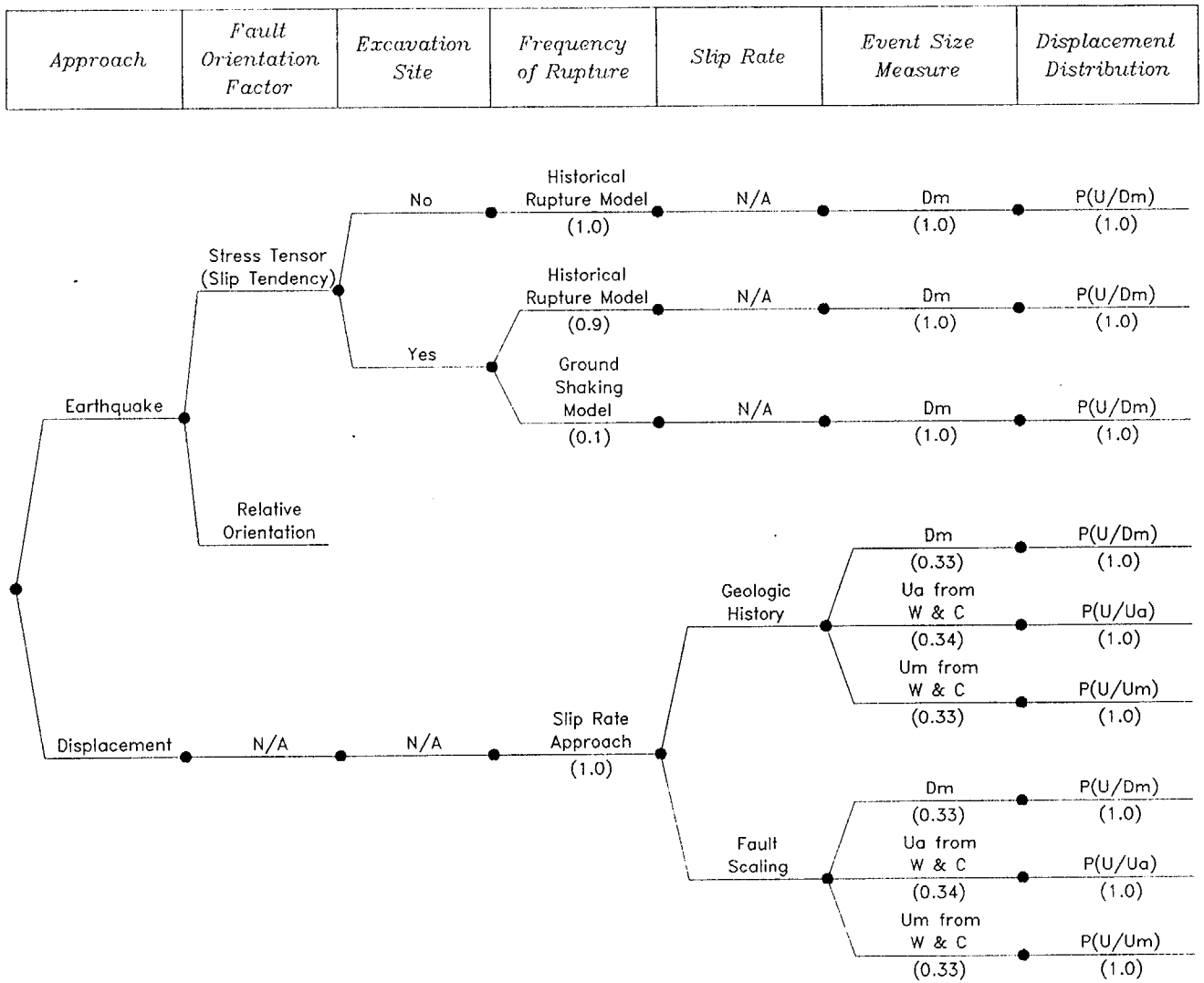

Figure SBK-15 Logic tree to characterize sites without Quaternary displacement

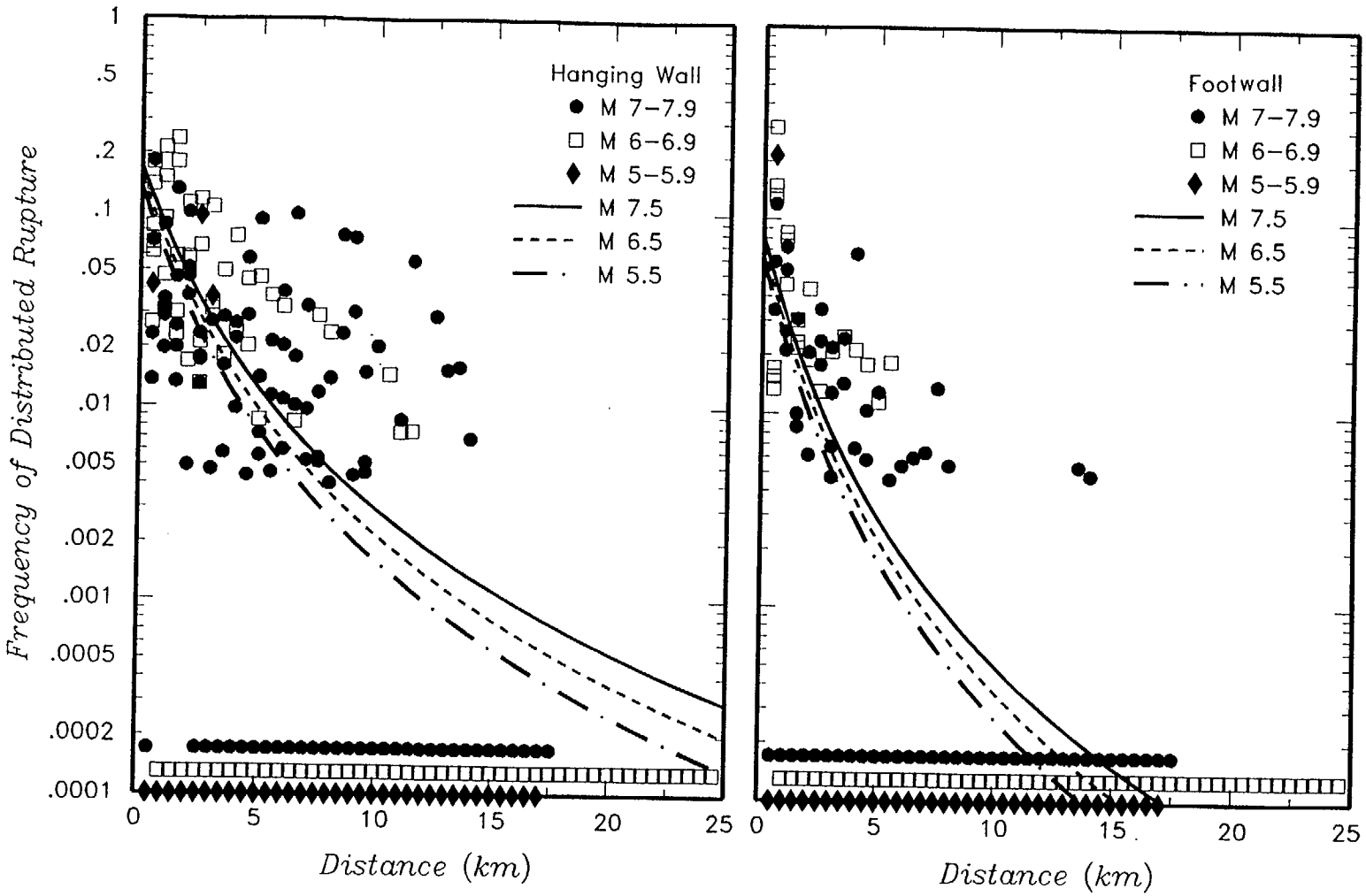

Figure SBK-16 Probability of induced distributed slip as a function of distance from the rupture and hanging wall/footwall location computed from the data presented in S.K. Pezzopane and T.E. Dawson (USGS, written communication, 1996). Curves show logit regression fits to data.

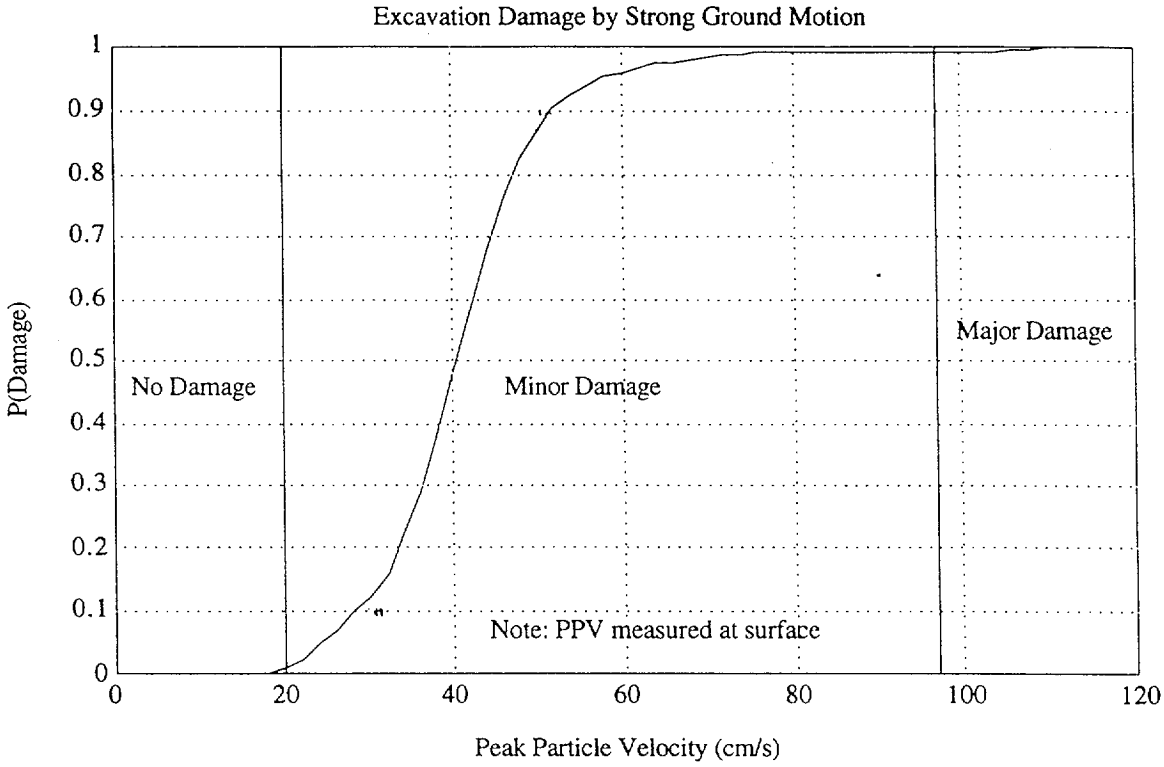

Figure SBK-17 Probability density function (sketched) for probability of initiating joint or fault displacement in an underground excavation. PDF is based on data summarized in Figure 2, page 2 of Brady (1990).

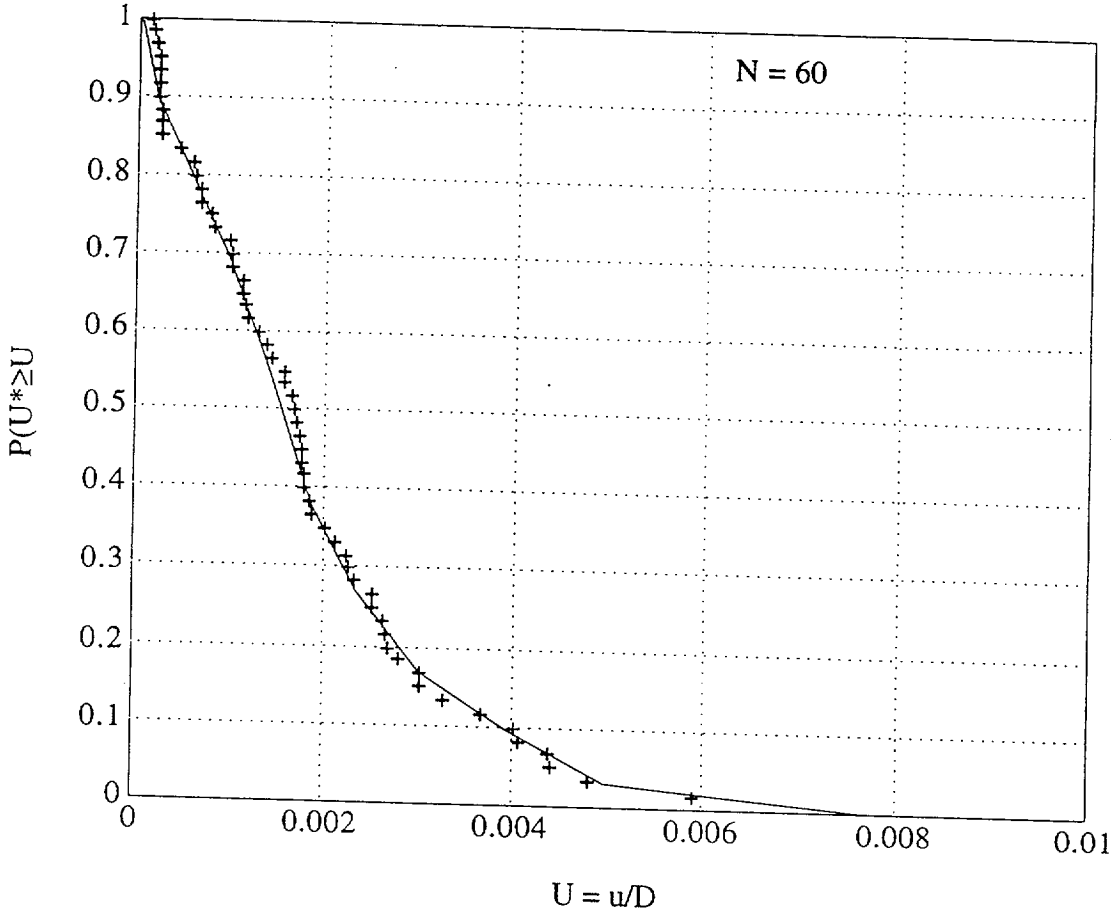

Figure SBK-18 Cumulative Probability Function P(U/Dm). See Section 3.3.1.3 for discussion of derivation and use. Crosses represent date points from Yucca Mountain faults, solid line is a sketched fit to the data values.

APPENDIX SBK-1
SUMMARY OF SEISMICITY REPORTS

Our decisions and weightings for the particular locations of background source regions and the behavior of seismicity were based on published reports on seismicity in the southern Great Basin. These reports have varied in their focus and scope: There are periods of time for which minor sequences are discussed in some detail, whereas other time periods are covered only by being represented in the historical earthquake catalog. Detailed reports of the seismicity in selected regions near Yucca Mountain began with the Nuclear Testing program in the 1960s, in particular, with reports on the explosion-triggered seismicity in the Pahute Mesa area (Hamilton *et al.*, 1969a).

Meremonte and Rogers (1987) have compiled a catalog of historical earthquakes in the southern Great Basin from 1868 through 1978. This established the historical catalog to the time of the installation of the southern Great Basin regional seismic network in 1978; Meremonte and Rogers (1987) provide a full bibliography of sources for that historical compilation. In the 1930s, instrumental records of small- to moderate-sized earthquakes in the southern Great Basin were compiled for the first time by the Californian Institute of Technology; prior to that, catalog entries were primarily based on felt reports.

From 1910 through 1939, all entries in the 100 km catalog are M > 3, and all but one of these events is located west of Yucca Mountain. These earthquakes generally are associated with the northwest-trending Death Valley-Furnace Creek (DVFC) fault zone. From 1940 through 1949, with the increase in instrumental recording and a corresponding decrease in the magnitude detection threshold, earthquakes were located throughout the 100-km region. During this time period, the region adjacent and within DVFC fault zone is the dominant source of seismic energy release. The largest event between 1940 and 1949 was an M 4.8 in 1944.

King *et al.* (1971) provide maps and some discussion of notable earthquakes within 100 km of the central Nevada Test Site (NTS) from 1950 through 1971. Many of the earthquakes reported by King *et al.* (1971) are not assigned magnitudes and are considered to be smaller than M 3. Several M 4 events are reported for the NTS, including several felt events, during

this 20-year period. The most significant earthquake during this time period was the August 5, 1971, M 4.5 Massachusetts Mountain event. Portable instruments were deployed in the epicentral area of the Massachusetts Mountain sequence: 612 aftershocks were counted in the 72 hours following the earthquake (King *et al.*, 1971). They note that the 1971 Massachusetts Mountain event took place near the location of an M 4.3 earthquake in 1957, although the locations of the two earthquakes are clearly separated in their published maps. From 1971 through the late-1970s, earthquakes were reported in monthly reports for the Atomic Energy Commission by the Earth Sciences Laboratories, a division of NOAA (Las Vegas, Nevada). The other significant earthquake sequence in the 1970s was the February, 1973, Ranger Mountains swarm. This sequence was unusual in that it produced eight earthquakes greater than M 3.5 during a three-week period, including two events greater than M 4. Also, the seismicity was distributed over a 10 x 10 km area (Earth Sciences Laboratories, 1973).

In the region south and east of the Massachusetts Mountain earthquake and within the 100-km region, approximately 75 percent of an estimated total moment release of 4.1 x 10^23 dyne-cm (estimated from the historical catalog) is represented by the Massachusetts Mountain and Ranger Mountain sequences. Only 5 percent of the total moment release is from the pre-1971 period. Another 12 percent is accounted for in a cluster in January 1993. In the 10-year period 1980 through 1990, the moment release rate for this region was about 2 x 10^21 dyne-cm/yr. The 1993 cluster occurred during a general increase in seismicity in the Rock Valley fault zone following the Little Skull Mountain earthquake, although this small sequence was east of the Rock Valley system.

In 1978, the USGS installed a regional analog telemetered seismic network and began reporting on the seismicity in the southern Great Basin for Yucca Mountain Site Characterization. These reports covered the years 1978 through 1991 (Rogers *et al.*, 1981, 1983; Harmsen and Rogers, 1987; Harmsen, 1991, 1993a). Seismicity reports from 1992 to the present have been generated by the University of Nevada Reno Seismological Laboratory (von Seggern and dePolo, 1995; von Seggern *et al.*, 1996, von Seggern and Smith, 1997). A report by Rogers *et al.* (1987a) on the relationship of the seismicity to the regional tectonic framework summarized the initial years of comprehensive seismic monitoring with the regional network. That study included detailed discussions of the seismicity and focal

mechanisms of specific source regions, descriptions of the development of the various magnitude scales in use, an analysis of the regional stress field, and proposed models of regional deformation. Conclusions regarding the seismicity and tectonic framework of the Yucca Mountain region from the Rogers *et al.* (1987a) are summarized as follows (Priestley, written communication, 1991).

- Seismic activity in the southern Great Basin is generally expressed in clusters of earthquakes distributed in an east-west belt between latitude 36 and 38 degrees north, referred to here as the southern Nevada seismic zone (Figure 7-1). The earthquake clusters are diffusely distributed around mapped faults, covering areas larger than the surface projections of the rupture (Figure. 7-2). Most events are not readily associated with the surface traces of known faults. These clusters may align with local structural grain; composite and single-event focal mechanisms suggest that nodal planes correlate with regional stress directions.

- Earthquakes tend to distribute in vertical tubular-shaped clusters rather than along planar fault zones. Rogers *et al.* (1987a) interpret this geometry to represent activity at the intersections of faults. These vertically distributed, localized clusters of seismicity stretch to 10 to 15 km deep. Most seismicity is within the upper 15 km of the crust, but some earthquakes may occur below 15 km. The depth distribution of seismicity is bimodal, with maxima at 1.5 and 9 km, and a minimum of activity at 4 km.

- Focal mechanisms and hypocenter alignments indicate that right-lateral slip on northerly trending faults is the predominant mode of stress release near the site (Figures 7-3, 7-4, and 7-5). Subordinate faulting on east-northeast (left-lateral) and northeast (normal) faults has been observed, as has oblique slip on structures of intermediate orientation with the appropriate dip angles. The inferred principal stress orientations are NW for the extensional (minimum compression) axis, and angles between NE and vertical for the maximum compressional axis (Harmsen and Rogers, 1986). The style of faulting determined from the focal mechanisms is not a function of depth.

- The comparison of energy release maps for the pre-1978 and post-1978 periods show that, averaged over decades, the seismically active zones appear to be releasing moment at about the same rates. Rogers *et al.* (1991) show that the historical rate of occurrence of the largest earthquakes (M 7) in the central Nevada seismic belt west and northwest of Yucca Mountain is larger by an order of magnitude than would be expected from geologic evidence. Wallace (1987) notes evidence that the occurrence of active periods lasting hundreds to thousands of years is followed by quiescent periods of 10,000 to 30,000 years. On a larger

distance but shorter time scale, Bufe and Toppozada (1981) describe a period of relative quiescence encompassing both California and western Nevada from 1960 to 1980. The current active period for M 6 encompasses the same large region, as characterized by Bufe and Toppozada (1981).

- Yucca Mountain lies within a region of relatively low historic seismic energy release.

- Focal mechanisms indicate that the maximum (P-axis) and minimum (T-axis) compressive stresses are roughly horizontal, although there is more variation in the P-axis, implying a preponderance of strike-slip faulting mechanisms. The T-axis has a consistent orientation throughout the region.

- Regional stress orientations indicate north-south and east-west orientations for high angle fault planes, with dextral slip on the north striking and sinistral slip on the east-west-striking surfaces. Normal and oblique slip are preferred on fault surfaces with orientation intermediate to these directions.

Gross and Jaume (1995) compiled a historical catalog of the southern Great Basin and discussed intensity based magnitude scales (Modified Mercalli) and levels of shaking experienced at Yucca Mountain in the historical period. After compiling a list of events within 200 km of Yucca Mountain, they concluded that the strongest shaking experienced at Yucca Mountain in historic time has been during the 1992 Little Skull Mountain earthquake. They also determined a revised location for the M 6.1, 1916 earthquake, the largest event within the 100km region, by comparing waveforms recorded during the Little Skull Mountain earthquake with a heliocorder record of the 1916 event from the Reno Seismograph Station. The revised location suggests that the event may have taken place in the Death Valley fault zone. Von Seggern and Brune (1997) relocated two M 3.5 earthquakes from 1948 that previously were reported as being located at Yucca Mountain. The initial locations of these two events were constrained by first-motion data at California seismic stations. The waveforms and S minus P times at the regional stations operating in 1948 were more consistent with a source near the Rock Valley fault zone rather than one at Yucca Mountain. By comparing waveforms from Little Skull Mountain aftershocks and heliocorder records from the Caltech station for one more well-located 1948 Rock Valley area event, they concluded that the two 1948 events most likely occurred in the Rock Valley area and not at Yucca Mountain. Von Seggern and Brune (1997) concluded that events were most likely part of one localized earthquake sequence in the Rock Valley area. Nevertheless, the quality

of locations for earthquakes in the Yucca Mountain area in the 1940s would be expected to be poor at best because of the lack of station coverage.

A report by Rogers *et al.* (1987b) initiated some controversy by concluding that the attenuation in the southern Great Basin was lower than that in California. Therefore, earthquake magnitudes would be lower for an equivalent amplitude recorded at the same distance in the California region. This meant that the Ao curve of Richter (1958) was not appropriate for Nevada. These conclusions have a direct effect on recurrence estimates, moment-magnitude scales, and estimates of moment release rate for the southern Great Basin. In contrast, Chavez and Priestly (1985) and Savage and Anderson (1995) concluded that the Richter curve was in fact applicable to Nevada. In support of these results, von Seggern and Smith (1997), from an analysis of three-component digital seismograms, have shown that the Richter curve is generally appropriate for the southern Great Basin, in contrast to the Rogers *et al.* (1987b) study. They note that the Hanks and Kanamori (1979) moment magnitude relationship is acceptable for the Basin and Range province, and that at small magnitudes, moment-magnitude relations determined from the modern three-component digital records are not consistent with the Rogers *et al.* (1987b) results. Chavez and Priestly (1985) also determined a moment-magnitude relationship that was different from the Hanks and Kanamori (1979) relation, at intermediate magnitudes, for the western Great Basin.

Other published reports on the seismotectonics of the southern Great Basin have applied the historical seismicity data set to constrain models of regional deformation. Gomberg (1991b) developed regional strain models that incorporated slip rates on active faults and comparisons with regional seismicity, then tested these models using a boundary element method. They concluded that the seismicity is associated with the local strain field near more active faults and that Yucca Mountain was geometrically situated such that strain accumulation in the Yucca Mountain block was minimal. Also, they interpreted the general lack of seismicity at Yucca Mountain as reflecting the presence of an isolated block or zone of low strain accumulation. In another study, Harmsen and Rogers (1986) analyzed the stress field from a set of regional focal mechanisms. The presence of both strike-slip and dip-slip mechanisms in particular localities was explained as most likely resulting from an axially symmetric stress field, in which the intermediate and maximum compressive stresses are nearly equal (Harmsen and Rogers, 1986). They suggested that because no large earthquakes were present

in the data set, that movement along a variety of fault plane orientations was accommodated by an ample number of small, preferably oriented faults.

Rogers *et al.* (1991) proposed a model in which right-lateral strike-slip faulting on north-striking planes is indicative of north-south crustal shortening. Anderson *et al.* (1993) suggest a crustal shortening mechanism for deformation in the Lake Mead area, consistent with the model proposed by Rogers *et al.* (1991). Interpreting models of regional deformation from the focal mechanism database is problematic because of the limited number of small earthquakes that account for only a small portion of moment release; the record of historical seismicity does not span the complete seismic cycle of faults in the region, which can be on the order of 10s to 100s of thousands of years in most cases.

REFERENCES

See reference list that follows main SBK text.

APPENDIX SBK-2
SUMMARY OF SEISMICITY

This appendix presents a discussion of the seismicity in the Nevada Test Site (NTS) region. The discussion focuses on specific issues regarding the behavior of earthquake sequences, earthquake clusters, and focal mechanisms and issues related to observations of earthquake triggering. The observations of the behavior of earthquake activity contributed to the weightings we assigned to background source zones, thickness of the seismogenic crust, relationship between seismicity and mapped Quaternary faults, and the problem of discriminating between true tectonic earthquakes and earthquakes triggered or potentially triggered by underground nuclear testing. This appendix includes some of the team's interpretations of the distribution of historical seismicity.

Northern Nevada Test Site

The northern region of the NTS includes the Timber Mountain caldera, Pahute Mesa, Rainier Mesa, and Yucca Flat. These areas have been the focus of considerable seismic activity, either directly or indirectly associated with nuclear testing. In contrast, most of the seismicity that extends across the south part of the NTS, within and adjacent to the Rock Valley, Mine Mountain, and Cane Springs fault zones (including the 1992 M 5.6 Little Skull Mountain earthquake), and activity around the southern boundary of the Timber Mountain caldera is, we believe, most likely tectonic in origin. We draw this conclusion primarily because this area is somewhat distant from the testing areas.

Determining what earthquake activity is related to underground nuclear explosions (UNEs), either through cavity collapse or the stresses induced by the explosions, is problematic. A study to determine the relative number of artificial and induced seismic events in the testing area suggests that the natural seismicity of the region reflects the background activity generally found in the southern Basin and Range province (Vortman, 1991). In 1979 and 1983, several swarms of micro-seismicity apparently unrelated to the UNEs occurred in the region. Two sequences that occurred during the period of active testing took place in the vicinity of Dome Mountain and Thirsty Canyon (Rogers *et al.*, 1981, 1987a). Focal mechanisms indicate primarily right-lateral strike-slip faulting on north-trending structures and normal faulting on northeast-trending structures (Rogers *et al.*, 1987a).

Southern Nevada Test Site

The south part of the NTS is a seismically active region relative to some other areas in the southern Great Basin. Most of the seismicity that stretches across the south part of the NTS, within and adjacent to the Rock Valley, Mine Mountain, and Cane Springs fault zones (including the 1992 M 5.6 Little Skull Mountain earthquake), and activity around the southern boundary of the Timber Mountain caldera, is not in areas of underground nuclear testing. Some of the activity near the eastern NTS boundary, particularly the 1971 Massachusetts Mountain earthquake and 1973 Ranger Mountain swarms, may have been triggered following the initiation of testing in the Yucca Flat area; however, there seem to be considerable numbers of small earthquakes related to natural tectonic strain release (Gomberg, 1991a, b). The largest event in this region is the 1992 ML 5.6 Little Skull Mountain earthquake, which most likely was triggered by a larger regional earthquake (Anderson *et al.*, 1993a, b).

Focal mechanisms from Rogers *et al.* (1987a) indicate sinistral slip on northeast structures and (or) dextral slip on northerly striking structures in the southern Great Basin. A prominent concentration of seismicity that includes the 1992 Little Skull Mountain earthquake occurs within a wide northeast-trending zone centered on the Rock Valley fault zone. This area includes the 1970 M 4.5 Massachusetts Mountain earthquake, the 1973 Range Mountains sequence, the 1992 M 5.6 Little Skull Mountain earthquake (Harmsen, 1993; Meremonte *et al.*, 1995; Smith *et al.*, 1997), the 1993 Rock Valley sequence (Shields *et al.*, 1995), and other relatively minor earthquake clusters and alignments. Also, spatial patterns in the seismicity within this wider Rock Valley zone extend both north along the Mine Mountain system (Rogers *et al.*, 1987) and south subparallel to the South Specter Range fault.

A general lack of seismicity characterizes the vicinity of Yucca Mountain. An analysis of the earthquake detection threshold for the Southern Great Basin Seismic Network (SGBSN) suggests that this zone of quiescence is real (Gomberg, 1991b). An experiment in high-resolution monitoring of seismicity at the potential site by Brune *et al.* (1992) confirms the existence of the quiescent zone. Modeling of the strain field in southern Nevada by Gomberg (1991a) suggests that this area is not accumulating significant strain, and that

Yucca Mountain is an isolated block within the structural framework of the southern Great Basin.

Northern Amargosa Valley-Sarcobatus Flat

The northern Amargosa Valley-Sarcobatus Flat encompasses the areas west and northwest of the Bare Mountain fault, 25 to 90 km from the site. Seismicity in the northern Amargosa Valley is diffusely distributed in the vicinity of Beatty, Nevada, and the Bullfrog Hills mining district. In Sarcobatus Flat, earthquakes have occurred in four clusters since the advent of instrumental monitoring (Rogers *et al.*, 1983, 1987a). These clusters are spaced roughly 10 to 20 km apart in a northerly trend along the length of the valley. Focal mechanisms for the three southern clusters suggest dextral slip along north- to north-northeast-trending structures.

Northern Death Valley Region

Seismicity along the Furnace Creek fault zone in northern Death Valley is diffusely distributed over an area much larger than the mapped surface traces of the primary fault system. A concentration of activity extends northeast from northern Death Valley at the north end of the Furnace Creek fault through the Gold Mountain-Mount Dunfee region. The largest event in this area in the modern era was an ML 4 event at Gold Mountain. A cluster of events occurred in a northeast alignment near Mount Dunfee in 1983. A composite focal mechanism from several of these earthquakes suggests left-oblique normal faulting on a northeast-striking fault plane (Rogers *et al.*, 1987a). The seismicity appears to be occurring at a low rate for such a high-slip system of faults, suggesting that the moment release in the region is concentrated on the main structures.

Explosions and Seismicity Triggered by Non-Tectonic Events

Seismicity analyses attempt to distinguish between underground nuclear explosions (UNEs), their collapses and aftershocks, chemical explosions associated with testing and mining, seismicity associated with the filling and subsequent changes in level of Lake Mead, and the natural seismicity in the region. The historical catalog of southern Great Basin earthquakes for the period 1868 to 1978, compiled by Meremonte and Rogers (1987a), labels seismic events that are attributed to UNEs. The triggering of earthquakes by UNEs presents a difficulty in interpreting the distribution of seismicity within the context of a seismotectonic framework for the NTS area.

The most active regions within the southern Great Basin are the north and southeast sections of the NTS, the area west of the Bare Mountain fault, the region at the north end of the Death Valley-Furnace Creek fault system, and the Pahranagat Shear Zone (Rogers *et al.*, 1987a). The level of seismic activity may reflect tectonic release following explosions in the region surrounding the NTS. Mining-related explosions have occurred in the Bullfrog Hills west of the Bare Mountain fault and various other mining sites around the region (Vortman, 1991).

Underground Nuclear Explosions

Extensive aftershock sequences followed several UNEs in the Pahute Mesa area from 1968 through 1970 (Hamilton *et al.*, 1971). These sequences were not confined to the test locations, but were distributed along several mapped faults as far as 15 km from the shot points. Portable instruments deployed in the late 1960s following the Benham shot recorded about 2500 earthquakes greater than M 2.0 from December 1968 through December 1970. This period included several explosions. Hamilton *et al.* (1971) reported that 94 percent of the events with well-constrained focal mechanisms were shallower than 5 km; some of the events were as deep as 8 km. Focal mechanisms show dominantly normal slip on northeast- to north-northeast-striking fault planes, and fault planes generally align with the fabric of mapped normal faults in the Tertiary tuffs. This correlation would imply a predominantly down-to-the-west/northwest sense of motion for most of the earthquakes.

Aftershocks of UNEs also appear in the Yucca Flat and Raineer Mesa areas in the eastern NTS, although they are not as prolific or as distributed as the triggered seismicity in the Pahute Mesa area. The earthquake locations and depth distributions of these earthquakes have not been studied in the detail Hamilton *et al.* (1971) applied to the Pahute Mesa area. There are also complications in resolving the relationship of UNEs to triggered earthquakes in the southeastern NTS south and east of Yucca Flat, wherein a notable increase in seismicity occurred in the 1970s following the initiation of underground testing in that area. All UNEs in Yucca Flat were reported at or below 150 kilotons, whereas some explosions at Pahute Mesa had reported yields as great as 1 megaton (Mt).

Large UNEs (~1 Mt) have been known to trigger release of natural tectonic strain (Wallace *et al.*, 1983, 1985). Thus, the potential exists that future testing may induce displacements on

faults in the Yucca Mountain site vicinity and adjacent region; although coseismic tectonic release has not been observed far from the UNEs. The relations between UNEs and natural seismic activity near the NTS have been discussed by Aki *et al.* (1969); Bucknam (1969); Dickey (1968, 1969, 1971); Dickey *et al.* (1972); McKeown and Dickey (1969); Hamilton and Healy (1969); Hamilton *et al.* (1969, 1972); Smith *et al.* (1972); Rogers *et al.* (1987a); and Vortman (1991). These studies observed that strain release and related effects become difficult to find beyond 5 to 10 km from surface ground zero of even the largest events (1 Mt). The Buckboard area is the nearest historical or proposed UNE testing area to Yucca Mountain, and is approximately 25 km northeast.

The relationship between UNEs and seismicity has been discussed by Rogers *et al.* (1987a), Vortman (1991), and Hamilton *et al.* (1971). Vortman's (1991) analysis of the seismicity of the NTS and vicinity deleted those events interpreted as human-made, but considered the number and location of earthquakes triggered by UNEs. Vortman (1991) proposed that considerable numbers of small-magnitude earthquakes apparently are induced by dynamic stresses of the seismic energy generated during the explosion, whereas other small events seem to occur in response to the altered static-stress field resulting from the explosion. Some events are triggered by the arrival of the UNE phase; others appear to be in response to changes in an altered stress field caused by the explosion. A UNE may cause a stress change on the order of several bars, a fraction of the lithostatic stress in the hypocentral region. Some areas of the southern Great Basin may be in a state of critical stress, in which a small perturbation in the load on a fault, such as UNE-induced stress changes, can cause the release of accumulated tectonic strain.

Triggered Earthquakes

The triggering of aftershocks by UNEs at the Nevada Test Site near Yucca Mountain (Hamilton and Healy, 1969; Hamilton *et al.*, 1972, Rogers *et al.*, 1983) and the continued occurrence of induced seismicity following the impoundment of Lake Mead (Carder, 1945; Rogers and Lee, 1976) are evidence that a number of fault segments in the southern Great Basin may be near failure. There is strong evidence that the June 29, 1992, Little Skull Mountain earthquake was triggered by the June 28, 1992, Landers, California, earthquake (Ms 7.6, Mw 7.3). The Landers earthquake also apparently triggered smaller earthquakes at locations throughout a large region of the western United States, extending as far as the

Yellowstone Caldera at a distance of 1250 km (Hill *et al.*, 1993). The Little Skull Mountain earthquake occurred about 225 km north of the Landers rupture. An increase in microseismic activity in the vicinity of Little Skull Mountain was observed beginning in the coda of the Landers event (Anderson *et al.*, 1994). This was recorded by the Yucca Mountain microearthquake array (instrumentation described in Brune *et al.*, 1992). The activity accelerated over the next 23 hours, culminating in the M 5.6 Little Skull Mountain main shock. This pattern may indicate that the Little Skull Mountain region was near failure prior to the Landers earthquake, which in turn may have advanced the time of rupture.

The specific mechanism of triggering of the Little Skull Mountain earthquake is uncertain, but a consensus appears to be that the dynamic strains associated with the propagation of long-period surface waves from the Landers earthquake (Anderson *et al.*, 1994; Gomberg and Bodin, 1994) initiated a failure process possibly involving fluids (Hill *et al.*, 1993) or sympathetic slip or creep (Bodin and Gomberg, 1994). Following the Landers main shock, Johnston *et al.* (1995) observed a transient strain change associated with an increase in seismicity at the Long Valley Caldera. The Landers earthquake produced an unprecedented increase in seismicity in the eastern California shear zone (Roquemore and Simila, 1994) and in the Sierra Nevada-Great Basin boundary zone (Anderson *et al.*, 1994).

Historical Seismicity near Yucca Mountain

Throughout the southern Great Basin and including the site area, seismicity generally is distributed in a broad belt that trends east-west from the Utah border to California. Earthquakes generally have strike-slip and normal faulting mechanisms and focal depths ranging from near-surface to 12 to 15 km deep. The number of resolved focal mechanisms indicates that approximately half of the solutions are strike-slip and half are dip-slip (Rogers *et al.*, 1992). In this region, as elsewhere in the Great Basin, there is a general lack of correlation between the distribution of epicenters and Quaternary faults.

The focal mechanisms of earthquakes closer to Yucca Mountain are strike slip to normal oblique slip along moderately to steeply dipping fault planes. The nodal planes are consistent with right-lateral faulting on north- to north-northwest-striking planes or normal-left oblique slip on northeast- to east-striking faults. These directions of inferred faulting are consistent with the style of Quaternary faulting and the orientations of principal stresses in the region.

Rogers *et al.* (1987a, 1991) and Bellier and Zoback (1995) analyze the modern stress field in regions of Nevada near Yucca Mountain.

A zone of quiescence centered on Yucca Mountain is apparent in all studies that describe seismicity in the southern Great Basin. Brune *et al.* (1992) and Gomberg (1991a, b) have shown that this zone is a real feature of the seismicity and not an artifact of network design. The largest earthquake to occur under Yucca Mountain from the inception of the SGBSN in 1978 was an ML 2.1 event that occurred on November 18, 1988, located 12 km north-northwest of the proposed repository at a depth of 11 km (Harmsen and Bufe, 1992). The inferred tension axis for this event is rotated about 25 degrees counterclockwise from the average tension axis observed in the region. The observed relatively aseismic character of the site area may result because the principal faults in the Yucca Mountain block are unfavorably oriented with respect to the present stress field. In other words, in the present regional stress field, north-striking faults would be expected to accommodate a portion of right-lateral motion and not pure normal slip.

RECENT SEISMICITY

The 1992 M 5.6 Little Skull Mountain Earthquake

The largest and most significant earthquake recorded in the vicinity of Yucca Mountain since the regional seismic network was established in 1979 was the June 29, 1992, M 5.6 Little Skull Mountain (LSM) earthquake (Lum and Honda, 1992; Harmsen, 1994; Walter, 1993; Meremonte *et al.*, 1995; Smith *et al.*, 1997). Origin Time: June 29, 1992; 1014 22.47 UTC; Latitude: 36 N 43.1'; Longitude: 116 W 17.16'; depth 11.8 km; ML 5.8 UNRSL; ML 5.6 NEIC. The event occurred approximately 20 km southeast of the proposed repository. The highest ground acceleration was 0.206 g recorded at a strong-motion station a Lathrop Wells, Nevada, at about 11 km epicentral distance (Blume and Honda, 1992). The earthquake caused some minor damage to the Yucca Mountain Field Operations Center in Jackass Flat, which was almost directly on the surface projection of the buried fault plane. The event was widely felt throughout the region.

The LSM earthquake initiated at a depth of 11.7 km, and nearly the entire sequence, main shock rupture surface and aftershock sequence, was confined to between 5 and 12 km depth.

Fault rupture propagated unilaterally from southwest to northeast for about 6 km; the epicenter of the main shock plots near the southwest end of the aftershock zone. There was no evidence of primary or secondary surface faulting. Rockfalls along the south-facing cliffs of Little Skull Mountain were observed shortly after the earthquake. The distribution of rockfalls, which was found to be consistent with the ground shaking predicted from the source model, provided a means of calibrating the distribution of ground shaking in the epicentral region (Brune and Smith, 1996). The earthquake occurred on a northeast-striking fault plane dipping steeply to the southeast (Harmsen, 1993; Meremonte *et al.*, 1995; Smith *et al.*, 1997) and involved nearly pure normal slip with a small left-slip component. The following table is a compilation of short-period and waveform-based focal mechanisms and reported seismic moments for the LSM earthquake.

THE 1992 LITTLE SKULL MOUNTAIN MAIN SHOCK SOURCE PARAMETERS *

Information Source	Strike	Dip	Rake	Mo x10^24 dyne-cm
Smith *et al.* (1997)	60±15	70±13	-70±10	-
Meremonte *et al.* (1995)	55	56	-72	-
Romanowicz *et al.* (1993)	43	66	-73	3.5
Romanowicz *et al.* (1993)	34	44	-70	2.6
Zhao and Helmberger (1994)	45	55	-60	3.0
Walter (1993)	35	54	-87	4.1
Harmsen (1994)	55	56	-72	-

There were three aftershocks of M > 4; none occurred on the main shock fault plane, but rather on adjacent "off-fault" structures that most likely accommodated the stress change from main shock rupture. These larger aftershocks also triggered near-source stations of the Blume strong motion network (Lum and Honda, 1992). The first M 4 aftershock occurred in the coda of the main shock; its location could be constrained only as being east of the main shock epicenter. Focal mechanisms and quality locations could be determined for the following two M 4+ events: M 4.4 July 5th, 0654 13.27 UT; Latitude: 36 N 43.55'; Longitude: 116 W 16.46'; depth 9.39 km; (Fault Plane Parameters: Strike: N75°E, Dip: 70°SE, Rake: -20°); M 4.5 September 13th, 1146 20.87 UT; Latitude: 36 N 43.41'; Longitude: 116 W 18.28'; depth 8.93 km (Fault Plane Parameters: Strike: N20°E, Dip: 45°SE, Rake: -80°).

* Source parameters strike, dip, and rake are in degrees using the convention of Aki and Richards (1980); seismic moment, Mo, is in units of 10^24 dyne-cm. Modified from Schneider *et al.* (1996).

The LSM earthquake could not be correlated with any mapped faults, although Harmsen (1993) and Meremonte *et al.* (1993) suggested that it may have taken place on a southern extension of the Mine Mountain fault zone. Smith *et al.* (1997) point out that the LSM sequence is situated where the Wahmonie, Caine Springs, as well as the Mine Mountain fault systems project into the Rock Valley fault zone. Some earthquakes within the LSM aftershock zone that occurred off the main shock fault plane align along a southern projection of the Wahmonie fault zone as well.

The LSM earthquake occurred in an area of persistent recent seismicity throughout the recording period of the network. This may be a zone of stress concentration, accommodating strain throughout the fault systems in the southcentral NTS area. The Rock Valley fault zone is the primary Quaternary system in this group and shows the most associated seismicity. The LSM main shock epicenter plots directly along the crest of LSM, which would place it, at hypocentral depth, at the base of the seismogenic zone, potentially near an intersection with the Rock Valley fault system. Whether the Mine Mountain fault was the causative structure for the LSM earthquake, it is clear that there is a direct relationship with the Rock Valley system.

Earthquakes in the Rock Valley Region in the Post-LSM Period

Following the Little Skull Mountain earthquake, there has been a notable increase in earthquake activity in the southern Rock Valley fault zone (Smith and Brune, 1997; Shields *et al.*, 1995; O'Leary, 1996). Only two M 3+ earthquakes adjacent to the Rock Valley fault zone in the southern NTS region are included in the SGBSN earthquake catalog from 1979 to prior to the LSM sequence. Since LSM, three M 3.5+ earthquakes, and an unusual sequence of very shallow earthquakes in mid-1993 (Smith *et al.*, 1997, written communication; Shields *et al.*, 1995), have taken place in Rock Valley; these M 3.5+ earthquakes occurred at various locations in southern Rock Valley near the LSM sequence. This activity appears to be diminishing (at the time of this report - October 1997), suggesting that indeed the LSM event may have had a role in triggering the increased activity along the Rock Valley fault.

The shallow sequence of earthquakes in 1993 (main event M 3.8) was recorded on a near-source portable digital instrument. This station recorded more than 500 earthquakes, of which only 140 triggered the regional seismic network and could be located. S minus P times

for the events averaged about 0.5 sec at this station; relocations of the earthquakes place them about 2 km from the surface. The largest event of the sequence, M 3.8, was also reported at a 2-km depth. Stress drops determined from modeling the S-wave spectra and using an empirical Green's function were on the order of 10 bars for all the larger events. A cluster of earthquake activity also occurred southeast of the Rock Valley fault zone in the Spotted Range in late 1993. This was the most active cluster of seismicity in the region east of the NTS since the 1973 Ranger Mountain sequence. In contrast to the Ranger Mountain and 1971 Massachusetts Mountain sequences, the 1992 cluster was confined to a small volume and included only one earthquake greater than M 3.

Micro-Earthquakes at Yucca Mountain: 1995 and 1996

From May 1995 through September 1996, 15 micro-earthquakes were located in and around the Yucca Mountain block (Smith *et al.*, 1996; Brune and Anooshepoor, 1996). Depths ranged from 5 to 10 km; magnitudes ranged from M -0.76 to M 0.72 (Brune and Anooshepoor, 1997). Short-period focal mechanisms were determined for four of the events, and although there was not enough information from the focal mechanism data to unequivocally correlate the earthquake with mapped faults, one event may have occurred on or near the Stage Coach Road Fault, and another three events may have taken place on or near the Paintbrush Canyon Fault. Gross and Jaume (1995) reviewed the archived waveform data to analyze a number of small events that were in the catalog and reported to be in the Yucca Mountain block after 1978 and before 1992. Their report lists some events that were incorrectly identified as earthquakes.

TABLE: SMALL-MAGNITUDE EARTHQUAKES AT YUCCA MOUNTAIN

#	Date	Origin Time		Lat	Lon	Depth	M
1.	*95 5 5	1321	33.12	36N50.66	116W24.08	6.15	0.58
2.	95 7 1	1526	56.69	36N40.84	116W30.88	8.65	
3.	95 7 7	759	-0.33	36N49.67	116W24.85	6.02	-0.27
4.	95 728	618	51.42	36N54.10	116W30.52	4.80	-0.48
5.	*95 9 4	1239	47.11	36N44.43	116W30.02	4.45	0.72
6.	95 1119	2215	84.91	36N50.80	116W23.59	6.46	-0.25
7.	95 1120	226	57.44	36N50.81	116W23.67	5.95	-0.43
8.	95 12 6	2327	15.90	36N43.74	116W29.06	7.80	0.29
9.	96 129	1020	32.32	36N44.23	116W29.44	9.90	
10.	96 330	1957	28.63	36N48.60	116W27.98	7.24	-0.59
11.	96 4 8	714	49.64	36N49.96	116W25.21	8.23	-0.58
12.	96 6 2	1645	75.18	36N49.11	116W29.44	9.61	-0.69
13.	*96 6 2	1015	33.29	36N49.23	116W29.55	9.87	0.01
14.	96 731	357	37.30	36N45.91	116W34.54	8.55	-0.76
15.	96 812	422	50.68	36N48.48	116W23.09	5.02	-0.62

- referenced on figure of Smith, SSC Workshop 3.
Origin Time: Year-Month-Day-Hour-Minute-Second (UTC). Depth: event depth referenced to surface elevation. M - ML
* - triggered; the older analog seismic network.

REFERENCES

See reference list that follows main SBK text.

APPENDIX SBK-3
POTENTIAL ANALOGS TO FUTURE SITE AREA ACTIVITY

This appendix includes a discussion of earthquakes related to volcanic activity in the Mammoth Lakes, California, area as an analog to potential volcanic earthquakes in Crater Flat and a discussion of the 1986 M 6.3 Chalfant Valley, California, earthquake and aftershock sequence, which we believe represents the most likely analog to the maximum background earthquake for the southern Great Basin.

Analog to Yucca Mountain Volcanic Earthquakes

The Mammoth Lakes, California, volcanic area, within and adjacent to the Long Valley caldera, has been the location of a recent series of moderate-sized (M 5 to 6) earthquakes, aftershock sequences, and volcanic-related earthquake swarms (1940 to the present) (Hill *et al.*, 1985). We believe that this area may represent an analog to potential earthquake activity associated with the emplacement of volcanic materials in Crater Flat and to activity that contributed to the structural features present in the northern Nevada Test Site (NTS), which formed during emplacement of the Timber Mountain Caldera. Several late Pleistocene and younger eruptions (> 750 ka) of the Long Valley caldera have shaped the physiography of the Mammoth Lakes-Chalfant Valley-Bishop area of California (Bailey *et al.*, 1976). Deformation in the caldera (1980 to the present) has been directly associated with most of the foreshock-mainshock-aftershock sequences (main shocks M > 6) and volcanic earthquake swarms (Hill *et al.*, 1990). These sequences have been prolific, producing tens of thousands of earthquakes in and adjacent to the caldera.

Before the recent increase in seismicity, activity in the area had been at a low level since the 1940s (Gumper and Scholz, 1971; Pitt and Steeples, 1975; VanWormer and Ryall, 1980). But in the 1940s, two M 5 earthquakes coincided with the filling of Crowley Lake in the western part of the caldera. The recent series of moderate-sized earthquakes that began in October 1978 culminated with four M 6+ earthquakes during a 48-hour period from May 25 to May 27, 1980 (Cramer and Toppazada, 1980; Lide and Ryall, 1985). The sequence continued with the 1984 M 5.8 Round Valley earthquake (Priestley *et al.*, 1988) and 1986 M 6.4 Chalfant Valley earthquake. Swarm-like earthquake activity (Savage and Cockerham, 1984; Cockerham and Pitt, 1984; Hill *et al.*, 1990) and occasional tremors (Ryall and Ryall,

1983; Aki, 1984) within and adjacent to the caldera were accompanied by inflation of the caldera's resurgent dome (Savage and Clark, 1982; Rundle and Whitcomb, 1984; Denlinger and Bailey, 1984).

An energetic earthquake swarm under Mammoth Mountain near the town of Mammoth Lakes in 1989 included a number of deep, long-period earthquakes that may be associated with deep magma movement (Pitt and Hill, 1994; Langbein *et al.*, 1993). There is some controversy regarding the possibility of non-double-couple source mechanisms, possibly associated with dike injection, determined for some of the earthquakes in and around the caldera (Julian, 1983; Julian and Sipken, 1985; Wallace, 1984). Although none of the moderate earthquakes have shown a significant component of dip-slip motion, Holocene faulting with predominantly normal offsets bound the Sierra Nevada and White Mountains (Bryant, 1984). The recent series of moderate-sized earthquakes have shown predominantly strike-slip motion.

The 1986 M 6+ Chalfant Valley Earthquake Sequence

The Chalfant Valley sequence occurred adjacent to the White Mountains beneath the volcanic Tableland, 15 km east of the Long Valley caldera (Smith and Priestly, 1988; dePolo and Ramelli, 1987; Lienkaemper *et al.*, 1987). We believe that this sequence of earthquakes represents the best analog to the maximum background earthquake for the southern Great Basin. The sequence is a composite of three distinct faulting events (M 6.3, M 5.8, and M 5.5) that occurred over a period of 11 days (Smith and Priestly, 1988). All three earthquakes showed predominantly strike slip-motion, with the main shock occurring within the hanging wall block of the White Mountains fault zone. The main shock, M 6.3, was the largest event in the western Nevada seismic region since the 1954 Fairview Peak-Dixie Valley earthquakes.

The Chalfant sequence produced surface ruptures along the White Mountains fault zone and within the Tableland fault system west of the White Mountains (dePolo and Ramelli, 1987; Lienkaemper *et al.*, 1987). Surface ruptures along the White Mountains fault zone stretched for a distance of 12 ± 2 km, with scattered cracks within the volcanic Tableland. The M 6.3 Chalfant earthquake may be the model event for the maximum background earthquake (MBE) in the western Basin and Range (dePolo, 1994; Pezzopane and Dawson, 1996). The

MBE is defined as the largest magnitude earthquake that does not produce primary displacement on faults at the surface. Although extensive fracturing occurred at the surface along mapped Holocene faults in the volcanic Tableland area, it is arguable whether any of that is primary rupture (Lienkaemper *et al.*, 1987).

Smith and Priestly (1997) have performed a detailed relocation of the earthquakes of the first three months of the sequence and determined the source parameters of the primary events. Static stress drops determined from the teleseismic moment and rupture areas estimated from the extent of the aftershock activity for the three primary events (M 5.8, M 6.3, and M 5.5) are 87, 26, and 23 bars, respectively. Uncertainties in these estimates are shown in that report. The primary characteristic of the sequence is the conjugate fault geometry resulting from the first two moderate-sized events: left-lateral strike-slip motion for the initial M 5.8 event, followed 24 hours later by right-lateral slip during the M 6.3 main shock (Smith and Priestley, 1997; Savage and Gross, 1995). Main shock rupture extended 12 to 15 km on a northwest-striking, southwest-dipping (55 degrees) fault plane. Surface fracturing in the volcanic Tableland area was confined to the hanging wall of the main shock fault plane (Smith and Priestley, 1997). A peak acceleration of 0.46 g was recorded on an accelerometer record of horizontal component at a sediment site on an alluvial fan about 12 km northeast of the main shock epicenter.

REFERENCES

See reference list that follows main SBK text.

ELICITATION SUMMARY

ROBERT SMITH, CRAIG DEPOLO, AND DENNIS O'LEARY

TABLE OF CONTENTS

TABLE OF CONTENTS

TABLES

FIGURES

TABLE OF CONTENTS

TABLE OF CONTENTS

APPENDICES

ELICITATION SUMMARY
ROBERT SMITH, CRAIG DEPOLO, AND DENNIS O'LEARY

1.0
INTRODUCTION

To properly represent expert epistemic uncertainty, the Yucca Mountain Probabilistic Seismic Hazard Analysis (PSHA) input evaluations were carried out by six expert teams free to choose their own methodologies, but also free to share or combine approaches. The team Smith, DePolo, O'Leary followed the evaluation structure provided to all of the teams at the PSHA workshops. We attempted to be impartial and objective in our evaluations, taking into account our different levels and areas of expertise. We amassed the data that were freely available to all participants, we attended the Yucca Mountain field trip to observe local faults and the Bare Mountain fault, and we obtained guidance from the expert presentations. We then developed our own interpretations based on the evidence, and developed our own scenarios and evaluations, then put the information and the models into a PSHA context. Team Smith, DePolo, and O'Leary shared a number of hypotheses and premises with other teams, but we adopted a fundamentally reductionist and epistemic approach to the analysis. We realized that the issue of earthquake hazard has a historical component inherent in the paleoseismic data that could not be accounted for by numerical or theory-based techniques. Accordingly, we relied as much as possible on data for Pleistocene events. Our first step was to evaluate tectonic models on the basis of field evidence or tectonic history, especially Quaternary history. The tectonic model we consider best supported by the data (a planar fault model) and its variants guided our evaluations of fundamental fault behavior, and set bounds on the key seismic parameters of magnitude and displacement. Field data from trench studies guided our estimates of recurrence and slip rates for local faults.

2.0
TECTONIC MODELS

A useful tectonic model provides an explanation for the origin, mechanical behavior, and resulting structure (deformation) of some volume of the Earth's crust. A tectonic model integrates: (1) geometry and spatial relations among structures; (2) mechanisms by which structures interact and respond to regional stress; and (3) the succession, duration, and evolution of deformation events (i.e., the history of strain). We look to tectonic models to help (1) guide understanding of present (and future) seismotectonics; (2) relate observable structure to inferences concerning fault parameters (e.g., width, distribution, extent, linkage); (3) provide bounding estimates or boundary conditions for fault behavior; and (4) identify hidden structure and behavior at seismogenic depths. Because our model must account for fault displacement hazard, it is specifically a model for Yucca Mountain. Therefore, the model incorporates Quaternary fault activity, basaltic volcanism, and other tectonic phenomena that provide evidence for seismogenic behavior at Yucca Mountain during late Pleistocene.

The model we use is conceptual and primarily kinematic. Three fundamental concepts constrain our evaluation of a model, the first of which is the domain concept. This concept holds that the crust of the southern Great Basin is an assemblage of structurally bounded slabs or blocks in various states of destruction and activity. Observed at sufficiently small scale, the domains evince regional strain patterns; taken individually they reveal local histories of deformation that complicate a regional pattern. We term the second concept "inheritance". In evaluating a tectonic model, a certain degree of idealization is necessary. However, our model does not assume pristine, ideal components; we consider that Yucca Mountain formed in a hybrid tectonic environment having a complex stress history, that the structural components reflect the processes that have varied with time and place, and that some processes are more tectonic than others. To a greater or lesser degree, present-day deformation follows ancient strain patterns. Our third concept focuses on history. The pattern and amplitude of deformation were set millions of years ago; although the style of deformation may be inherited, ancient deformation may have nothing to do with present rates and distributions of strain. Therefore, our analyses and probabilities rely on evidence of Quaternary, not Miocene, events.

An important aspect of the tectonic setting of Yucca Mountain (that is, the structural and stratigraphic assemblage of rocks within a radius of about 100 km of the mountain) is the current strain rate. Strain rate is assessed based on the moment rate of observed seismicity, geodetic data, and paleoseismology. All indications are that the current strain rate is very low--on the order of 10^{-16}/yr to 10^{-17}/yr (Eddington *et al.*, 1987; data from Chapter 6 of the Seismotectonic Framework report [USGS, written communication, 1996]). This is an order of magnitude lower than strain rates in the more active areas of the nearby Basin and Range province. This low rate constrains the loading rate of active faults and hence our deductions about the potential for activity and seismogenic depths.

Our preferred model for Yucca Mountain is that of an asymmetric graben, or a half graben, partly filled by a collapsed volcanic carapace. There are two fundamental components to this model. First is the half graben itself, represented by Crater Flat basin. The USGS seismic reflection profile (Brocher *et al.*, 1996) shows clearly the structural asymmetry of the half graben, of which Bare Mountain represents the relatively uplifted footwall. Second is the volcanic carapace. Yucca Mountain is the emergent part of a faulted, extended slab of volcanic rock about 2.5 to 3 km thick that has subsided into the half graben. We call this the carapace because it forms a resistant shield that completely covers the Paleozoic bedrock beneath Yucca Mountain. Most block-bounding faults at Yucca Mountain dip westward toward Bare Mountain and show a history of extension antithetic to the Bare Mountain fault.

The half graben model requires that the Bare Mountain fault be the master fault and that the strata to the east (the hanging wall) subside against it, as a group of antithetic fault blocks. This mechanical model has two limitations which affect uncertainty in our analysis: (1) the cumulative Pleistocene dip slip on the Bare Mountain fault is less than that measured across Yucca Mountain; and (2) some faults at Yucca Mountain and in Crater Flat have a down-to-the east offset. The latter observations can be explained by local keystone faulting in the volcanic carapace, but the former observation is less readily explained. Nevertheless, the asymmetry of Crater Flat basin, the structural relief of Bare Mountain (several kilometers), the overall sense of slip on the main block-bounding faults of Yucca Mountain, the profound (about 30 mgal) gravity gradient along the Bare Mountain fault, and the evidence that the Bare Mountain front was the source of large slab slides into Crater Flat in late Miocene time

indicate that the early history of the Bare Mountain fault was that of a master, range-front fault.

The pre-Pleistocene slip history of the Bare Mountain fault lies buried beneath the pediment cover in Crater Flat. The steep part of the gravity gradient, which lies a kilometer or more east of the present range front, indicates that the fault generally dips east at less than 50 degrees. Our model, and the seismic reflection profile (Brocher *et al.*, 1996), permit the interpretation that the Bare Mountain fault consists of an imbricate zone of several more steeply dipping fault planes, variously banked at depth by colluvial wedges or mass movement deposits. The Pleistocene fault trace sampled for this study may be the most recently active of several synthetic fault planes, and may have the least cummulative displacement (see, for example, Hancock and Barka, 1987, Figure 10).

The half graben model works well only near the central latitudinal axis of Crater Flat basin. Viewed longitudinally, the basin is plugged at its north end by the emergent caldera complex from which a population of radial faults extends through generally south-dipping strata into Crater Flat (S. Minor, USGS, written communication, 1995). The Bare Mountain fault loses throw near the caldera rim area and transitions northward into a minor normal fault, the Tram Ridge fault, which dies out within the Rainier Mesa caldera rim zone (C.J. Fridrich, USGS, written communication, 1995). To the south, the Crater Flat basin abruptly narrows and shallows. The Bare Mountain fault has not been traced south of Steve's Pass (Figure SDO-1), and the faults of Yucca Mountain are abruptly terminated, or at least are not traceable south of a dissected escarpment along Highway 95 at the southern margin of the basin. The strata of the escarpment are the same volcanic units that form Yucca Mountain, but dip northward into the basin. The eastern margin of Crater Flat basin is well defined by an arcuate gravity gradient concave to the west, which closely parallels the trace of the combined Paintbrush Canyon-Stagecoach Road fault. On this basis, we infer that the Paintbrush Canyon-Stagecoach Road fault is a major bounding fault for Yucca Mountain, the fault that defines the basin rim and most likely descends to the base of the seismogenic crust.

The form of Crater Flat basin and its association with the caldera complex led Carr (1990) to interpret it as a sector graben, an area of subsidence caused by evacuation of an apophysis of magma from the base of the crust during or shortly following eruption of the Topopah Spring

Tuff. This interpretation accords well with the timing and magnitude of initial faulting of Yucca Mountain as well as with the shape and position of the basin. Brun *et al.* (1994) effectively simulated the structure, in cross section, with a sandbox model that utilized deformation of a low-density viscous mass at the base of the crust.

If the location and longitudinal axis of Crater Flat basin indicate that it originated as a sector graben, they also imply that it is a flaw within the larger rift-like Amargosa trough (i.e., the Kawich-Greenwater rift of Carr [1988, 1990] or the Amargosa Desert rift zone of Wright [1989]); that is, it is a rift within a rift. As such, crustal extension within Crater Flat basin reflects the structural orientation of the trough and perhaps is linked to basement faulting of greater extent. Carr (1990) noted the similarity between the faults at Yucca Mountain and a fault population in Pahute Mesa north of the caldera complex and on strike with Yucca Mountain (Minor *et al.*, 1993), and surmised that both fault sets reflect extension fundamentally tied to the evolution of the Amargosa trough. Accordingly, Crater Flat basin can be understood as the southern part of a deeper, narrower flanking rift along the western flank of the Amargosa trough; or perhaps even a basin that projects from the Basin and Range terrane southward into the Walker Lane. This rift-like aspect of the model downplays the notion of the Bare Mountain fault as a conventional range-front fault. It implies that Pleistocene extensional faulting at Yucca Mountain is not a function of antithetic slip controlled by the Bare Mountain fault, but is instead controlled by axial fractures within the deepest part of the Amargosa trough.

But casting Crater Flat basin and Yucca Mountain in the context of a trough controlled (at least during its Middle Miocene phase) by dominantly east-west extension raises two questions relevant to faulting at Yucca Mountain: (1) what becomes of Bare Mountain fault at and beyond the south end of Yucca Mountain, and (2) what is the nature of the fault that bounds the east side of the Amargosa trough near Yucca Mountain?

The southward projection of the Bare Mountain fault is problematic. We infer that the fault is not traceable south of Steve's Pass (Figure SDO-1) because there it loses its identity, including its expression as a pronounced gravity gradient (Snyder and Carr, 1984), among a distributed set of small right-lateral fault segments within a shear zone that steps to the southeast for about 4 km across the dissected escarpment that marks the southern end of

Crater Flat (C.J. Fridrich, USGS, written communication, 1995). The fault then regains its identity as a unified structure, gains dip displacement, and strikes south as the boundary between the Funeral Mountains and the Amargosa trough. Although the fault is a major domain-bounding feature south of Bare Mountain, its projection along a relatively subdued gravity gradient and its weak expression as a physiographic feature indicates that the fault has played little part in the late Neogene and Quaternary history of the Amargosa trough.

The eastern margin of the Amargosa trough is bounded by faults of seismogenic significance. Especially significant for model evaluation is the so-called gravity fault (Figure SDO-1). The gravity fault was defined by Winograd and Thordarson (1975) on the basis of a gravity gradient (hence their term "gravity fault") that extends along the spring line in Ash Meadows north to Highway 95 (Figure SDO-1) and the west end of the Skeleton Hills. Down-to-the-west displacement of Paleozoic bedrock is estimated to range from about 150 m at the north end to several hundred meters at the south end. Brocher *et al.* (1993), on the basis of seismic profile data, confirmed that the gravity fault forms the structural boundary of the east side of the trough at about 36°35'N. Brocher *et al.* (1993) interpreted the gravity fault as being listric to a reflector (K) at about 2 s. (5.5 km) depth. Although Brocher *et al.* (1993) did not offer a preferred interpretation of reflector K, they emphasized the role of ductile flow in the lower crust at a depth of about 6 s. below the Amargosa trough. Reflector K may represent an abandoned, pre-late Oligocene detachment that controlled extension of the Specter Range.

A concident gravity and aeromagnetic gradient aligned with the gravity fault implies that the fault can be carried northward past the west end of Little Skull Mountain (Chapter 8, Seismotectonic Framework report [USGS, written communication, 1996])). The fault trace passes through the magnetic anomaly that marks the position of the 4.4-Ma buried volcano south of Highway 95. North of this point, a high magnetic anomaly along the gradient suggests that the hanging wall of the gravity fault contains considerable basalt or volcaniclastic sediment. There are sparse surface expressions of the gravity fault. At the west end of the Striped Hills, bedrock exposures indicate strike-slip displacement, but the western flank of Little Skull Mountain is marked by toreva blocks that indicate down-to-the-west collapse. Reheis and Noller (1991) mapped a 2.5-km-long Pleistocene scarp along the fault trace between the Striped Hills and the Skeleton Hills. The scarp is clear in large-scale

aerial photos, which show that the most recent drainage courses have been influenced by the fault. The scarp probably represents displacement within the last 10 ka.

The gravity fault is an important domain boundary; it separates dominantly east-striking structures associated with the Rock Valley fault system to the east from the north-striking structures of the Amargosa trough-Crater Flat domain to the west. North of Little Skull Mountain, the trace of the gravity fault and the eastern margin of the trough are obscure. We infer that the eastern border of the trough trends roughly due north, as expressed by a set of down-to-the west, post-12.7 Ma faults along the west side of the Calico Hills dome (F.W. Simonds and R.B. Scott, USGS, written communication, 1996).

If formation of the Bare Mountain fault and one or more crustal faults at Yucca Mountain were driven by a deep master fracture zone in the axis of Crater Flat basin, they may be largely independent of each other in terms of slip budget. This modification of our basic model is based on a mechanism proposed by Okaya and Thompson (1985) and demonstrated by boundary element modeling done for Crater Flat basin by King and Janssen (Chapter 8, Seismotectonic Framework report [USGS, written communication, 1996]). The interpretation is consistent with the localization of basaltic volcanism near the axis of the basin: extensional stress is focused along one or more axial fractures or fault intersections at the base of the seismogenic crust. Such intersections can focus dilational strain, even at depths of 15 to 20 km, and thereby facilitate the ascent of basaltic magma to higher crustal levels. The Bare Mountain fault and the Paintbrush Canyon-Stagecoach Road fault likely would be the primary intersecting faults at the deepest crustal level; interaction of these faults at a sufficient stress threshold could be accompanied by basaltic intrusion. We consider such events would cause most faults at Yucca Mountain to slip, including those that might be antithetic to Bare Mountain fault, and that some fault crevasses might receive basaltic ash fill. G.A. Thompson (Stanford University., written communication, 1994) proposed that basaltic dike intrusion would compensate for local extensional stress and significantly reduce deviatoric stress. This would cause the stress threshold for post-intrusive faulting at Yucca Mountain to be reset to some higher level. However, as regional extensional stress continues to be applied to the mountain, small stress thresholds are exceeded and weaker faults slip from time to time. Ultimately, the maximum basinal stress threshold is exceeded, at which point the basin may experience widespread faulting associated with basaltic intrusion. This

aspect of the model holds that not all faulting at Yucca Mountain is accompanied by volcanism, but that volcanism is always associated with faulting.

2.1 DEXTRAL SHEARING AND BURIED STRIKE-SLIP FAULTS

The alignment of basaltic cones and vents in Crater Flat follows a northeast trend, oblique to the axis of the basin. Volcanism is clustered in the southwest quadrant of the basin, the area of most recent subsidence and deposition. These facts indicate a distinct tectonic asymmetry linked to processes active within the past 4 m.y. Tectonic asymmetry is also indicated by paleomagnetic evidence for clockwise vertical axis rotation of fault-bounded blocks across the south end of the mountain. The rotation, which is about 30 percent, is considered to have occurred following deposition of the Tiva Canyon Tuff at about 12.7 Ma (S. Minor, written communication, 1995). These data led C.J. Fridrich (USGS, written communication, 1995) to infer that Crater Flat basin has evolved as a sphenochasm, opening at its southern end but fixed at its northern end.

This motion is compatible with a northwest-oriented zone of dextral shear at the southern end of the basin, and with a general N50°W-oriented transtensional stress throughout the Walker Lane. In terms of our model, the question is whether oblique dextral shear is confined to Crater Flat basin (i.e., the basin itself is becoming distorted because of distributed, regional shear), or whether shear is imposed by a buried regional right-lateral fault that passes through Crater Flat basin. The latter case has been argued by Schweickert and Lahren (1997) and modeled as a pull-apart basin in sandbox experiments by the Center for Nuclear Waste Regulatory Analyses (presentation by D. Ferrill at Workshop 4). The question is important because a hidden throughgoing fault could generate an earthquake comparable in magnitude and mechanism to the 1932 Cedar Mountain earthquake.

Nonsystematic distributions of vertical axis rotations in time and space within the southwest Nevada volcanic field, as reported by Hudson *et al.* (1994), imply that individual basins have responded uniquely to distributed northwest-oriented dextral shear typical of the Walker Lane setting. This observation, plus the lack of evidence for transcurrent dextral fault offset of Pleistocene age though Crater Flat basin, supports the interpretation that dextral shear is restricted to the basin itself. The only hint of a discrete dextral shear feature within the basin

is a N25°W-striking alignment known informally as the hingeline (C.J. Fridrich, written communication, 1995). The hingeline separates paleomagnetic rotations of 10 degrees or less to its north from rotations of 20 degrees or more to its south. The boundary is more strongly indicated by the divergence of aeromagnetic gradient alignments across the mountain, and by landform terminations along the trace of the hingeline. The hingeline is considered to define a structural boundary that concentrates dextral shear between it and the southern end of the mountain. A possible second indication of a buried strike-slip fault are the scarps and lineaments along the Black Cone fault, shown on Faulds *et al.* (1994).

Despite painstaking investigation, researchers have identified no expression of any feature comparable to the hingeline along its strike northwest of Crater Flat. However, a strong structural alignment does exist to the southeast of Crater Flat. The structural alignment extends along Stewart Valley and along the trace of the Pahrump-Stewart Valley fault zone for a distance of about 120 km. At least 4 km of dextral offset is shown along the alignment between the Resting Spring Range and the Montgomery Mountains.

The alignment is expressed by isostatic gravity anomalies that include the gradients that form the western flank of Pahrump Valley basin and (farther north) the eastern flank of Ash Meadows basin. In general, the alignment defines the eastern margin of a large crustal block that is expressed by the Amargosa Range on the west, and by Bare Mountain, the Resting Spring Range, and the Nopah Range on the east. Structurally, the alignment is comparable to the subparallel Death Valley and Panamint faults farther west. The alignment is less well expressed by aeormagnetic anomalies except for the local gradients along the hingeline through Yucca Mountain.

We consider the structural alignment, which includes the Yucca Mountain hingeline, to be a projection of the Pahrump-Stewart Valley fault zone into, but not through, Crater Flat basin thus accounting for clockwise vertical axis rotation at Yucca Mountain, northeast alignment of basaltic volcanic centers in Crater Flat, dextral shear at the south end of Crater Flat basin, and a dextral slip component toward the southern end of Bare Mountain fault. Additionally, shear stress concentrated at the edge of the basin is considered have contributed to uplift of Bare Mountain and Calico Hills within the past 9 m.y. In light of these features, we include a buried fault source among our regional seismic fault sources and assign a 40% probability to

a model that contains a strike-slip earthquake within or proximal to Crater Flat basin along the hingeline-Pahrump-Stewart Valley fault zone alignment (Figure SDO- 1). Such an earthquake could have a magnitude as great as the 1932 Cedar Mountain earthquake. Basaltic volcanism could be associated with such an event.

2.2 DETACHMENT FAULTS

Detachment fault models of varied geometries and crustal depths have been applied to Yucca Mountain solely on the basis of the succession of rotated, west-facing normal faults that form the mountain. Each detachment mechanism invariably is referred to a single latitudinal cross section that emphasizes the rotated normal fault blocks but ignores the structural complications at the northern and southern ends of Crater Flat basin. A detachment fault model has important implications. Because all rotated normal faults of the upper plate are rooted in a common slip plane (the detachment), all faulting necessarily is distributed, and (if the detachment is deep enough) all rooted normal faults are equally seismogenic. Because the subhorizontal detachment plane is of wide lateral extent and separates structures of radically different ages and attitudes, a major seismogenic feature such as a strike-slip fault could be hidden beneath the detachment.

The most recent attempts to fit a detachment model to Yucca Mountain are provided by D.A. Ferrill *et al.* (CNWRA, written communication,1995), who describe two model variants based on syntheses of previous proposals. Model 1 of D.A. Ferrill *et al.* (CNWRA, written communication, 1995) assumes that the faults of Yucca Mountain developed from the headwall of the Bullfrog Hills detachment system, which is thought to accommodate as much as 275 percent of local extension (D.A. Ferrill *et al.*, CNWRA, written communication, 1995). According to this model, Yucca Mountain faults were isolated from the Bullfrog Hills system by rise of the Bare Mountain block along the Bare Mountain fault, which truncated the Yucca-Bullfrog detachment. Continued motion of the Bare Mountain fault formed a deeper, east-directed detachment plane. According to this model, the older, shallower, west-directed detachment accounts for the imbricate faulting at Yucca Mountain; the younger, deeper, east-directed detachment accounts for hanging wall collapse of the carapace into Crater Flat basin. Model 2 of D.A. Ferrill *et al.* (CNWRA, written communication, 1995) accounts directly for the hanging wall rollover and imbricate faulting at Yucca Mountain by

assuming that the Bare Mountain fault is the driving listric (detachment) fault and that Yucca Mountain faults are simply antithetic to the deep, master, east-directed Bare Mountain detachment. However, in this model, faults antithetic to the Bare Mountain listric fault are simultaneously listric faults synthetic to a breakaway fault located somewhere to the east in Jackass Flats. The result is a curious "bathtub" profile having listric faults at each end that merge at a common plane of detachment (D.A. Ferrill *et al.*, CNWRA, written communiction, 1995). It is not clear how slip is partitioned between the two apparently competing listric faults and along the common detachment surface.

These detachments are presumed to operate in the 6 to 8 km depth range. Shallow detachment at the Tertiary/Paleozoic contact can be ruled out. Numerous exposures throughout the area, as well as the Crater Flat seismic profile (Brocher and Hunter, 1996), combine to show that the Paleozoic contact is an unconformity locally cut by high-angle faults. We leave open the question of deep detachment within the brittle-ductile lower crust transition. Much geologic evidence, such as high-grade metamorphic facies and mylonite in lower plates exposed elsewhere, indicates that detachments typically occur in the ductile transition zone, and theoretical and experimental rheological considerations (e.g., Melosh, 1990) support the mechanism in this setting. However, the occurrence of normal fault earthquakes at depths of 19 km or greater (see section 3.1) indicates that strain at these depths is not effectively assimilated by detachment. And because most of our inferences of fault behavior rely on processes that involve the brittle part of the crust, we consider whatever is meant or envisioned by "detachment" in the lower crust to be simply part of poorly understood, quasi-viscous flow deformation.

The oldest deformation that can be attributed plausibly to detachment is block faulting of the Topopah Spring Tuff at about 12.7 Ma. At that time, Bare Mountain was already an elevated range that was shedding debris into Crater Flat basin. In fact, Yucca Mountain field work revealed evidence that Bare Mountain was shedding metamorphic rock debris prior to deposition of the Crater Flat Tuff and that Crater Flat was an aggrading alluvial plain prior to 14 Ma. The Bare Mountain fault was active well before deposition of the Paintbrush Group C.J. Fridrich, USGS, written communication, 1995). This means that uplift of Bare Mountain cannot have terminated a detachment at Yucca Mountain, and that there was no tectonic association of Yucca Mountain extension with the formation of the Bullfrog Hills.

In fact, the Bullfrog Hills formed from 2 to 3 m.y. after the initial phase of Yucca Mountain faulting, in a completely different tectonic setting. The Bullfrog Hills originated from a breakaway fault along the west side of Tram Ridge beginning about 12.7 Ma (C.J. Fridrich, USGS, written communication, 1995; Hoisch *et al.*, 1997). The transport vector of the Bullfrog Hills projects eastward to the Rainier Mesa caldera, diverging some 20 degrees counterclockwise from the orientation of the transport vector of Yucca Mountain.

The style and direction of deformation in Crater Flat clearly are diachronous, having shifted from mountain-wide imbricate block faulting around 11.4 Ma primarily to subsidence at the southwest corner of the basin beginning around 9 Ma. Beginning around 11 Ma, sporadic basaltic volcanism became an important component of tectonism in this area. The basaltic volcanism implies that fracturing and faulting in the upper crust repeatedly connected with deep mantle sources. If a detachment plane existed in this area, it was not an effective barrier for fractures that penetrated through the crust.

Exposed detachment faults typically show slices of the upper plate resting at a high dip angle (65°) against the detachment plane. The geometric relations among the steeply dipping faults in a moderately extended domain, especially one that has no clearly identified breakaway fault, such as Yucca Mountain, are highly idealized. Detachment model 2 of D.A. Ferrill *et al.* (CNWRA, written communication, 1995) requires severe curvature of the fault planes as they merge into the detachment fault at about 8 km depth. No explanation for this "special case" geometry is offered; it is a precondition of a listric model that is never seen in exposed detachment systems.

The domino mechanism of imbricate faulting is unable to resolve this geometry problem. If the block-bounding faults at Yucca Mountain are controlled by deep detachment, they cannot behave like dominos. The domino model requires rigid behavior and completely distributed simple shear; there can be no variable rollover or opposed slip. It is clear, however, that the big blocks at Yucca Mountain have some rollover and that there is local reversal of offset along strike on some of the bounding faults. Furthermore, domino rotation presumes uniform frictional slip across the entire width of the slip plane, unrealistic expectations to depths of 8 km at Yucca Mountain, even given extreme pore pressure. Nevertheless, a domino model is a more satisfactory explanation of hanging wall collapse against the Bare Mountain fault

than is the quasi-listric geometry called for in model 2 of D.A. Ferrill *et al.* (CNWRA, written communication, 1995), which requires a listric geometry as a consequence of a competing breakaway fault at the east side of Yucca Mountain.

A major shortcoming of the detachment model is that no breakaway zone has been identified for the imbricate faults of Yucca Mountain. For example, no such fault has been reasonably shown in the vicinity of Fortymile Wash. On the contrary, a good case can be made, both from seismic reflection profile data and stratigraphy in well UE25J#13, for a down-to-the-east fault near Fortymile Wash (Carr, 1984). The gravity fault is inferred by D.A. Ferrill *et al.* (CNWRA, written communication, 1995) to be a candidate breakaway fault for Yucca Mountain. However, despite the array of small down-to-the-west normal faults (post-9 Ma) that cut Little Skull Mountain, the primary structure here is a north-dipping block, which indicates that structural rotations are referred to east-northeast-striking rotation axes. This geometry is even more pronounced in the Striped Hills, but totally absent from Yucca Mountain.

The Little Skull Mountain earthquake demonstrated that a seismogenic normal fault beneath Little Skull Mountain dips southeast and would project to the surface west of the inferred breakaway fault for Yucca Mountain. The aftershocks occurred up to nearly 5 km from the surface (K.D. Smith *et al.*, University of Nevada, Reno, written communication, 1995), suggesting that the hypocentral projection of this fault (cf. Meremonte *et al.*, 1995) can be projected across a west-dipping breakaway fault. Additional constraints on the cross-sectional geometry of the detachment model are the lack of any expression of listric geometry or a detachment plane in the USGS seismic reflection profile (Brocher and Hunter, 1996). A detachment plane would have a seismic reflection in Crater Flat basin as in other areas of the Basin and Range Province (Smith *et al.*, 1989). Another geometric constraint for any model is the elevation of Yucca Mountain. It is difficult to restore the fault blocks (W. B. Hamilton, written communication, 1995) unless the detachment plane mimics the elevation profile, or we appeal to depositional thickening or to displacements outside the plane of the section.

In fact, displacements outside the plane of the section must be factored into the model geometry because field data show that the block-bounding faults have a left-oblique component of slip. But when we consider the overall planimetric aspect of the structure of

Yucca Mountain, the detachment model faces its most serious problems. Among these problems is the fact that Yucca Mountain faulting is tied exclusively to the geometry of a subjacent basin. Left-lateral bounding accommodation zones are not indicated at the margin of this basin, nor does the model offer any explanation of vertical axis rotation in the basin. Indeed, an important function of the detachment model is to isolate the upper plate extensional structure from influence of a lower plate structure, such as a strike-slip fault that could impose a dextral torque on the surface fault pattern. To continue to operate as an extensional mechanism into Pleistocene time, a detachment plane must be a chronic locus of slip or of strain-decoupling; this is the fundamental meaning of the word detachment. It cannot behave this way and transmit shear stress from the lower crust to the upper plate. In other words, if a detachment fault were present, there could be no possibility of a 1932 Cedar Mountain type earthquake at Yucca Mountain: seismic slip below 6 to 8 km depth could never break ground.

If an inferred detachment system has operated at least intermittently for the past 12 m.y., we find it to be a contradiction that the geophysical signature of intrusive bodies such as the basalts in Crater Flat and even the calderas show no systematic offset. If the fault set at Pahute Mesa (Minor *et al.*, 1996) were genetically related to faults of Yucca Mountain, then the detachment model must be extended north though the caldera complex. This model does not explain how a detachment could operate within or near a volume of crust subject to large-scale magma flux during nearly 7 m.y.

In terms of mechanics, the detachment model must operate on assumptions that present difficult and even intractable problems concerning dynamics. Among these is the assumption that the ductility and vertical strength profile in the crust is the same today as it was in mid-Miocene time. Models that require shifts from east-directed to west-directed detachment or invoke uplift of Bare Mountain by several kilometers during a tectonic event that terminates one episode of detachment and initiates another are unconstrained by available data and understanding of tectonic processes that have been active in the southern Great Basin.

G.I. Ofoegbu and D.A. Ferrill (CNWRA, written communication, 1995) applied finite-element modeling to the problem of detachment-related fault slip. A five-layer linear elastic model was used, and the initial stress state included previous fault slip on simulated Yucca

Mountain fault planes. For the model to work, each fault was treated as a weakly cohesive or cohesionless layer at least 150 m thick and decoupled from confining rock. Slip was forced to occur on a selected fault by reducing its coefficient of static friction. Under applicable confining stress, a friction angle of 0.93 degrees is required. The model implies also that a significant proportion of fault displacement is taken up by deformation of the hanging wall and footwall. G.I. Ofoegbu and D.A. Ferrill *et al.* (CNWRA, written communication, 1995) found that slip rates in the detachment fault and in the steep, off-branching perturbed fault differed by six orders of magnitude. They concluded that a detachment fault is likely to slip aseismically in response to slip events that may occur at seismic rates on the off-branching steep faults. To reach this conclusion, however, the modeled mechanism appears to violate the concept of detachment faulting: steep fault perturbation is not supposed to generate strain in a detachment fault. Rather, the detachment is the master slip plane, and motion along it is supposed to generate slip along the faults of the upper plate and distribute strain among them by virtue of independent motion. In other words, the model did not demonstrate how detachment is supposed to control fault slip in the upper plate.

It is clear from the model, however, that detachment can work only along a weak layer that has an unusually low angle of friction and low cohesive strength. This is why detachments are common as slump mechanisms (undrained failure) in saturated sediments and in the marine environment (leaving apart the issue of low effective stress). It also explains why exposed detachments typically show evidence of ductile deformation in the lower plate. Given the present structure and physical conditions of the upper crust near Yucca Mountain, we consider it highly unlikely that there is a throughgoing subhorizontal weak layer having the required properties and thickness at mid-crustal levels beneath Yucca Mountain and Crater Flat. Observed focal mechanism data from the Basin and Range (Doser and Smith, 1989) do not reveal nodal plane populations that would be consistent with low-angle, listric faulting. The fact that focal mechanisms of normal to oblique slip normal faulting earthquakes in extensional regimes from a global record (Jackson and White, 1989) show no low-angle (detachment) slip further supports our conclusions. Therefore, detachment models do not figure in our analysis of local faults and they are not incorporated into the seismic source characterization model.

2.3 HALF GRABEN MODEL—CARAPACE EFFECT

The collapsed carapace model (actually a submodel, hereafter termed the *carapace effect*, of the half graben model) of Yucca Mountain defines two layers. Yucca Mountain is the morphological expression of a faulted layer about 2.5 km thick of volcanic rock (the carapace) that rests unconformably on a thicker crustal layer (15 to 20 km thick) of Paleozoic and Precambrian marine sedimentary and metasedimentary rocks. This configuration is important because the layers differ greatly in bulk material properties and have radically different stress histories. The sub-carapace structure is revealed at Bare Mountain, the Specter Range, and the core of the Calico Hills. We emphasize that the fault characteristics, including slip history, that we measure in the carapace may have little or no relationship to seismogenic faults in the Paleozoic substrate. If we discount the carapace effect, then all of the faults we characterize at Yucca Mountain are potentially seismogenic and each can be projected as continuous fault planes to seismogenic depth as an end-member idealization of the half-graben model. If we strongly weight the carapace effect, then perhaps only one, two, or three Yucca Mountain faults project deep into the crust. The others are confined to the carapace, or link to faults having different attitudes and aspect ratios below the unconformity. According to this interpretation, the bulk of the faults in the volcanic carapace either are postseismic strain adjustments, or reflect strain that originates within or at the base of the carapace. To understand such processes we must regard the carapace as behaving like a huge, fragmented, incipient slab slide, much like an arrested slab slide or avalanche. This structure requires a basal weak layer or some form of decoupling from the substrate.

Arrested slab slides typically are broken by anastamosing faults that are broadly concave-facing downslope and have high length-to-width ratios. In cross section the fault slices show a general slump-like sense of hanging wall rotation, but along strike they are variably tilted. Much of the fault pattern at Yucca Mountain has the structural characteristics of an arrested slab slide. The abundance of toreva blocks and graben-like splays, the presence of footwall slices that are only a kilometer or two wide and that pinch out and change elevation along strike, faults that die out or fray out along strike, that are better described as breccia zones than faults (such as the Ghost Dance fault), all constitute a pattern of local tearing, spreading, and extensile damage within which the traces of deep-seated faults that span the length of the mountain are not apparent (the trace of the Solitario Canyon fault being an exception).

The closest structural analog to Yucca Mountain is the faulted volcanic carapace exposed along the south and west flanks of Mid Valley, about 22 km to the northeast. There, the faulted blocks of Timber Mountain Group and Paintbrush Group tuffs closely resemble those at Yucca Mountain, except they are about half the scale. The carapace rests unconformably on an eroded substrate of well-exposed 13-Ma Wahmonie dacite flows that do not reflect the structural attitude of the overlying tilted slices. The Wahmonie volcanic substrate is analogous to the Paleozoic carbonate substrate beneath Yucca Mountain. Two features are important here: (1) the Mid Valley carapace has subsided and partly extended into Mid Valley basin; and (2) deep stream erosion has isolated the blocks, facilitating some local faulting and tilting. These features suggest that the fault pattern in the carapace is a local, slope-controlled phenomenon rather than one controlled by a system of deep-seated faults.

How could such a system be accounted for at Yucca Mountain? It could work only by way of a weak layer beneath the carapace. Strata beneath the volcanic carapace in Crater Flat basin are equivalent to Rocks of Pavits Spring, a pre-14-Ma unit well exposed near Pavits Spring in Rock Valley (Hinrichs, 1968). The Rocks of Pavits Spring include weakly consolidated volcaniclastic silts and fine-grained sands. Layers of the requisite compositions could include fine-grained, altered airfall tuffs. In a saturated state (normal hydrostatic stress), such sediment could be susceptible to undrained failure or abrupt loss of shear strength. The mechanism might be driven by cumulative seismic strain ("hydraulic jacking" and grain redistribution) during times of high groundwater flux (Castro and Poulos, 1977; Seed and Idriss, 1982). We emphasize that the mechanism involves transient reductions of effective stress, not wholesale grain repacking from a metastable condition as in liquefaction or quick behavior. For example, soft-sediment faults are exposed below the volcanic section at the base of the south flank of Skull Mountain. Extensive failure of this type is considered to have facilitated the collapse of the south flank of Skull Mountain into Rock Valley. Deformation of this type is well documented in the extensively collapsed Eocene lower Absaroka Volcanic Supergroup, Wyoming (Decker, 1990).

In Crater Flat, the extent of an inferred weak layer is unknown. The model assumes that the sediments form a continuous deposit that thins and perhaps pinches out against the Paleozoic rock that forms the relatively elevated eastern rim of Crater Flat basin. This distribution

implies that the eastern margin of Yucca Mountain (east of the Paintbrush Canyon-Stagecoach Road fault) is anchored directly on the Paleozoic substrate, leaving the carapace to the west susceptible to deformation of the inferred weak layer.

The bulk movement we expect from weak layer failure is chiefly translational. Such motion could explain the relatively minor offset accompanied by extensive damage along some of the faults. For example, the Bow Ridge fault as seen in the Exploratory Surface Facility (ESF) is a zone about 2 m wide that dips 60 degrees west and contains sand- and gravel-size crush material. Likewise, the Drill Hole Wash fault, as projected into the ESF, is a breccia zone about 2 m wide that contains rotated blocks as much as a meter in diameter. The characteristic breccia that defines the Ghost Dance fault could also be of oblique extensional origin. We consider an early stage of failure and collapse in which the entire volcanic carapace pulled away from the caldera rim, like a shattered ice floe on a gelid stream, the various fault blocks extending, colliding, and subsiding upon the weak layer as Crater Flat basin widened and deepened to the southwest (cf. Fossen and Gabrielsen, 1996). Such motion explains Yucca Wash as a minor extensional structure, and accounts for the odd down-to-the-east offsets along the west side of the mountain. Extension of the carapace to the west is limited by the footwall of the Bare Mountain fault. In-situ stress measurements by Stock *et al.* (1985) reveal that the least compressive stress at Yucca Mountain is at the limit of normal fault slip, implying that the carapace may be held together by the strength of the strata on which it rests.

The carapace effect means that most or all of the faults at Yucca Mountain are distributed. It means that Yucca Mountain is high not because of footwall uplift, but because of original deposition. It implies that any buried fault in the Paleozoic substrate could have been overridden repeatedly and broken through the carapace in more than one place, thus explaining complex fault zone structure. It also implies that some of the slip budget can be attributed to creep or postseismic adjustment to weak layer deformation. It finally implies that exogenous effects, such as high groundwater flux, may be more important here, at least locally, than tectonic effects; that unknown aspects of high pore pressure and time-dependent seismic strain weakening could be significant controls on recurrent fault slip.

The carapace effect does not explain the long, throughgoing, nearly rectilinear trace of the Solitario Canyon fault, nor the major block-bounding aspect of fault segments such as the Windy Wash fault. Accordingly, our preferred interpretation is that the large block-bounding faults (the Paintbrush Canyon-Stagecoach Road fault, the Solitario Canyon, and Windy Wash faults) are through-the-crust seismogenic faults, and that many intrablock faults such as the Ghost Dance fault, probably are confined to the carapace.

The tectonic model for Yucca Mountain best supported by the data is that of a half graben that includes both axial faults in Crater Flat basin and faults antithetic to Bare Mountain. This model posits the block-bounding faults of Yucca Mountain and the Bare Mountain fault as discrete, single plane faults that descend to the base of the seismogenic crust. It also provides a mechanism for one or more of the block bounding faults to interact with the Bare Mountain fault at the deepest seismogenic level where basaltic magma intrusion may be facilitated by fault displacement or dilation, thus providing a mechanism for coupled volcano-seismic events. All or some of the faults west of the Solitario Canyon fault may be antithetic to the Bare Mountain fault, a structural configuration that reduces the capability of large-scale faulting with widths of the scale of the seismogenic crust thickness, thereby reducing maximum magnitude. This fundamental model provides for individual fault scenarios as well as linked and distributed fault scenarios.

We do not find evidence to support an active detachment fault, which is a form of special pleading for mechanisms that are not reasonably demonstrable at Yucca Mountain. In other words, the data set do not require these models; their only purpose is to explain a "hidden" structure or some hypothetical mechanism that could act at any time but that has no manifest or unequivocal history at Yucca Mountain.

We consider two modifications to our basic model that do take into account buried faults, however: the collapsed carapace effect and a dextral strike-slip fault external to Crater Flat that projects from the southeast into Crater Flat beneath the carapace. These modifications are not exclusive and they are supported by some data. They support linked and distributed fault scenarios as well as a buried seismic source. We do not weight these modifications; their physical presence accounts for seismic sources the activity of which is assessed

separately. Because specific tectonic models are not explicitly weighted, we have no tectonic models logic tree; all our local seismic structural sources are referred to in our favored model.

3.0 SEISMIC SOURCES

Three kinds of seismic sources are considered in our analysis, in order of increasing scale and specificity: seismic source zones, regional faults, and local faults. Seismic source zones are geographic regions discriminated on the basis of tectonic style and the structural nature of the seismogenic faults contained therein. As seismic sources, these regions are noted for the maximum background earthquake each is capable of hosting. Regional faults are specific, identified structural sources within these zones that, on the evidence of past surface rupture, are capable of generating earthquakes of some estimable magnitude greater than background. We also include discussion of a possible buried strike-slip fault source with regional faults. Local faults are structural sources confined to Yucca Mountain. Because of their proximity to the potential repository, local faults are analyzed for both ground shaking and displacement hazard. The local faults are all close to each other relative to depth of the seismogenic crust so linking and distributed motion are important considerations. The potential dynamic interactions among local faults constrains estimates of earthquake magnitude and fault mechanics; for this reason, a tectonic model constitutes an important rationale for our estimates of local fault parameters.

3.1 FOCAL DEPTH DISTRIBUTION AND DEPTH OF THE SEISMOGENIC CRUST

The maximum depth distribution of earthquakes in the Yucca Mountain area was determined by analyzing focal depth data on well recorded earthquakes recorded by seismic networks within the region as well as checking this information against rheologic models of the seismogenic crust that constrain the depth to the brittle-ductile transition. We studied the focal depth distribution using filtered focal-depth plots determined by our own study employing the ZMAP (S. Weimer, Univerity of Alaska, Fairbanks, written communication, 1996, seismicity analysis program) and by focal depth data provided by Woodward-Clyde Federal Services from the Yucca Mountain catalog filtered to our specifications.

The composite Yucca Mountain earthquake catalog, encompassing a 300 km radius sort from the Yucca Mountain site, is the same catalog that was distributed by Woodward-Clyde Federal Services to all Yucca Mountain teams after revisions for removal of multiple events and non-tectonic events. Focal depths were filtered by focal-depth accuracy, assumed to be related to the hypocenter parameter, DMN. DMN is the distance to the nearest station and is the standard statistical parameter used in the seismograph network community for analyzing focal depth accuracies. DMN is generally an indicator of the depth for which the eigenvalue for a particular hypocenter is within a single solution space whose major and minor axes represent a source volume ellipsoid and are a measure of the error ellipse for the specified standard error of picking the appropriate phase, such as the first P wave arrival.

The Yucca Mountain earthquake catalog was first evaluated for important non-earthquake contributions such as nuclear explosions as well as mislocated epicenters. After finalizing the most complete catalog, the hypocenter files were filtered for earthquakes for most accurate focal depths in two categories: 1) with DMN equal to or less than 1, and 2) DMN equal to or less than 1.5. We finally used the focal depth constraint to be DMN equal to or less than 1.5 to constrain the depths as it gave a larger population necessary for the best statistical treatment and still retained accurately determined focal depths. We used the ZMAP seismicity analysis package (S. Weimer, University of Alaska Fairbanks, written communication, 1996) to sort the hypocenter data for the various source areas in the 300 km wide catalog window. We used the Woodward-Clyde focal mechanism data to check against ours using the same DMN criteria.

We first considered the local Yucca Mountain area, encompassing the site and the nearby faults from the Bare Mountain fault on the west to the Gravity fault on the east and from the south edge of the Timber Mountain caldera to approximately the Highway 95 (Figure SDO-1). However using this area only provided a limited number of accurate focal depths; and we expanded our window to include the region of Source Zone 1 (Figure SDO-2).

The sorting process provided data for epicenter maps, recurrence plots for the filtered data for a given DMN value, and focal depth distributions. For completeness and to compare our data, we also asked Woodward-Clyde to provide the same data which revealed reasonably the

same distributions. We then proceeded to sort the earthquake data into bins that we consider representative of the region: 1) the Yucca Mountain site, 2) a zone which included the Yucca Mountain site and extended across the California-Nevada border on the south on a NW trending line that extended across the NTS site and extended ~150 km NW and 150 km SE, 3) a zone that extended southwest from California-Nevada border ~90 km and 120 km E-W, and 4) a zone that extended ~ 200 NE into the Basin-Range. We also made epicenter plots for various depths of the distribution to examine if the distribution characteristics varied across the zones. Note these are a little different from our final three seismic source zones within 100 km of the site, but were used to assess enough good focal depth data to give statistically useful distributions.

The filtered focal depth data revealed Gaussian shaped distributions, centered at depths of ~ 8 to 10 km, with a scarcity of hypocenters from 0 to 2 km and an exponential decay to maximum depths of ~ 19 km (Figure SDO-3). We note the scarcity of data in the 0-2 km depth range, a depth range that we consider to be incapable of radiating strong ground motion because of the reduced stress state.

Alternate Evaluations--As alternate evaluations we examined focal distributions for areas around the Yucca Mountain site out to distances of 300 km, but we use data primarily from an area with a radius of 100 km from the site, because we wanted the data as representative as possible for this area which constitutes the Yucca Mountain geologic setting. We did not consider seismic sources beyond 100 km in our source models as beyond this distance the peak ground accelerations would not be significant at the site for earthquakes in this region.

We based our final maximum-depth of earthquakes on the focal depth distributions (rather than a 80 to 90% focal depth cut-off as suggested in rheological arguments) with consideration to the uncertainties in focal depth. We define a distribution for the maximum depth of earthquakes weighted as follows:

Depth (km)	Weight
14 km	0.2
17 km	0.7
19 km	0.1

We assigned the minimum focal depth as the depth with the largest (minimum) error for depth in the distribution considering ± 2 km for well resolved focal depths. The average maximum depth is near 17 km (Figure SDO-4). This depth also is consistent with the observed M 7+ normal faulting distribution of the Basin-Range (Smith and Arabasz, 1991).

A maximum focal depth of 19 km was chosen by our team as the depth of the largest well recorded earthquakes in the Basin and Range. This depth was as determined from the top of the maximum depth source zone that was modeled to depths of 25 km for a dynamic source by Mendoza and Hartzel (1988) for the M 7.3, 1983, Borah Peak normal faulting earthquake. We recognize that it is deeper than 95% of the depths of background seismicity, but it was taken as an upper bound of depths that could plausibly occur in the Basin Range province.

Our focal depth distributions were also compared with idealized rheological models for the southern Basin-Range area considering the hypothesis that the focal depth distribution relates to the thickness of the seismogenic crust (the brittle layer). This depth has been shown to correlate with background seismicity at about the 80 percentile depth and was taken as indicator for the bottom of the background seismicity (Smith and Bruhn, 1984). It corresponds to Smith and Bruhn's (1984) model for extensional normal-faulting regimes in the Basin-Range, where the maximum focal depths of large normal-faulting earthquakes correlate approximately with the 80th percentile of focal depths for smaller background earthquakes. We followed the use of such indicators, which since the mid-1970s, have revealed that accurate hypocenter data acquired by regional and portable seismic networks in the Basin-Range region permit the construction of reliable focal-depth histograms (Sibson, 1982; Smith and Bruhn, 1984).

Seismogenic models based on theoretical depths were hypothesized for peaks in maximum shear stress at the boundary between the brittle upper crust and a quasi-plastic layer (Scholz, 1990). These models in a general way account for the maximum depths of nucleation of large normal faulting earthquakes and for the maximum depths of background seismicity, corresponding to the base of the seismogenic layer. The models involve a temperature-dependent, depth-varying power law for creep combined with a linear brittle-behavior criterion. Scholz (1990) predicts the thickness of the seismogenic layer, and hence the

maximum focal depths of earthquakes, using both a similar temperature criterion as that described above and additional fault-velocity constraints.

Qualitative arguments of Sibson (1982) and Smith and Bruhn (1984) suggested that the theoretically derived transition depth from brittle to quasi-plastic flow for silica-rich rocks is controlled primarily by a critical temperature of approximately 350 °C to 450 °C and occurs at or near the depth of maximum shear stress. At this depth, short-term strain rates greater than 10^{-3} to 10^{-4}/sec are necessary to achieve brittle failure during earthquakes within the more ductile, intermediate-depth crustal material. In theory, this is the critical depth for nucleation of the largest magnitude earthquakes. For the Yucca Mountain site the critical depth or depth to the brittle-ductile transition is taken to be 10 to 15 km for a quartz to dry quartzite composition and for the relatively low regional strain rate of 10^{-17} per second (Eddington *et al.*, 1987).

Comparison of background focal depth data (Smith and Arabasz, 1991) for three of the best studied, scarp-forming normal faulting earthquakes of the Basin-Range (the 1959 M7.5 Hebgen Lake, the 1971 M7.1 Dixie Valley, and the 1983 M7.3 Borah Peak earthquakes) supports our evaluation of depth of nucleation of large, M7+ events at a few kilometers beneath the idealized brittle-ductile transition depth.

3.2 SEISMIC SOURCE ZONES

Seismic source zones are defined on the basis of tectonic style, structural pattern, and rates of deformation. On this basis, the source zones are equivalent to tectonic subprovinces or regional domains of the southern Great Basin. Three of these regional domains fall within a 100-km radius of Yucca Mountain and therefore qualify as source zones of potential ground shaking hazard at and near the mountain.

We determined three seismic source zones that include most, or large areas of, (1) the Walker Lane, (2) the Inyo-Mono terrane (or the Death Valley Zone), and (3) the Basin and Range Province. Figure SDO-2 shows the source zones in relation to the 100 km radius centered on Yucca Mountain.

Zone 1 comprises the Goldfield-Spring Mountain sections of the Walker Lane (Stewart 1988). It is characterized by a complex structural pattern that includes north-south-striking Basin-and-Range style normal faults, local basins, and Walker Lane style structures (northwest-striking dextral faults and northeast-striking sinistral faults). The northern part of the zone is dominated by volcanic rocks (tuffs of Miocene age); the southern part (Spring Mountains section) consists chiefly of little-extended Paleozoic rock. It is bounded on the west by the Furnace Creek-Death Valley fault zone and the Pahrump-Stewart Valley fault zone, and on the east by the Las Vegas Valley shear zone. North of Indian Springs, the eastern margin of the zone is structurally diffuse, but generally is distinguished by northwest-striking dextral faults.

Zone 2 is the Death Valley section (or the Inyo-Mono terrane), which is characterized by active strike-slip faulting. The zone extends west from the Furnace Creek fault to the Sierra Nevada block. The Mammoth Lakes area to the north is purposely excluded from this zone because recent high levels of seismicity are associated with the Long Valley caldera and potentially localized volcano-tectonic activity. The southern boundary is marked by the Garlock fault.

Zone 3 is the central Basin and Range zone, which is bounded on the south by the Intermountain Seismic Belt that extends westward from Utah at about 36 degrees latitude and on the north by the 300-km cut-off distance from the site.

Alternative zones - Our initial categorization identified the Yucca Mountain site as a separate source zone having its own fault and seismicity characteristics. This area was bounded on the west by the Bare Mountain fault and on the east by the gravity fault. The north boundary was defined by Yucca Wash and the rim zone of the Claim Canyon caldera; the south side was at the southern termination of the Solitario and Stagecoach Road faults (Figure SDO-1). Plots of the historical seismicity from the project catalog (Appendix D of the main report) reveal only about 30 local earthquakes in this zone. Because of the sparcity of earthquakes, we chose not to identify this as a discrete seismic source zone, but included it in our regional source Zone 1 that would be characterized by its historic seismicity data.

We also considered as a separate seismic source zone an area defined by the Little Skull Mountain earthquake and its aftershock distribution. We made this interpretation based on the length of the aftershock zone (~ 30 km), which would correspond to the lower bound of our maximum background earthquake distribution for the lowest standard of error with a corresponding magnitude 6.3. However, after considering how to sort the historical data in both time and space, and considering that this location has been the site of smaller earthquakes that reflect ongoing seismicity characterized by our Zone 1 seismicity, we ultimately chose not to identify this as a discrete source area.

3.2.1 Maximum Background Earthquake

The maximum background earthquake, or MBE, is a critical parameter for the Yucca Mountain site PSHA. For our seismic source zones we consider the MBE to mean the largest earthquake that reasonably could occur in each seismic source zone without producing a distinguishable shear displacement of the ground surface (although there could be considerable ground cracks, fissures, etc. such as those that occurred with the M 6.2, 1986 Chalfant Valley, Nevada-California border earthquake). MBE was evaluated by comparing the seismicity characteristics of the Yucca Mountain area with the Quaternary tectonics (faults, fault lengths, relations to other structures, etc.) of the region and other extensional tectonic regimes. We considered that the seismic sources vary as a function of the faults that lie within them.

We used the data from Doser and Smith (1989) and the USGS fault data from Pezzopane (Seismotectonic Framework report [USGS, written communication, 1996]) to assess the maximum background earthquake distribution. We constructed our own distribution of Basin-Range earthquakes according to the following criteria: for magnitudes of $M_S > 5.5$, and for all ground breaking events.

We identified the maximum magnitude for each source zone, but also qualified that parameterization for a source radius of 100 km to ensure completeness for the Yucca Mountain site (Table SDO-1, Figure SDO-5).

Using the analogy of no tectonic fracturing associated with the Chalfant Valley earthquake and the largest earthquake in the Basin and Range province without surface rupture, the 1925 Clarkston Valley, Montana, M 6.6 (Doser and Smith, 1989; C.M. dePolo, written communication, 1997, from field mapping) a density distribution was defined from magnitude 6.2 to 6.6 for the MBE. We define a M_{max} of 6.4 ± 0.2 within 100 km with a cumulative lognormal distribution of:

Magnitude (MBE)	Cumulative distribution
6.2	0.03
6.4	0.50
6.6	0.97

Allowing for uncertainty in the magnitude of the Clarkston Valley earthquake, the maximum magnitude may be somewhat higher, as large as 6.8.

Our magnitude distribution is in accordance with a compilation of data on the occurrence of surface rupture for normal faulting earthquakes from (Doser and Smith, 1989) that revealed a similar distribution of MBE for a range of $5.3 < M < 7.5$ earthquakes. They showed that 8 events in the Doser and Smith (1989) data set revealed rupture beginning as small as M 6.1 and that all events above 7.1 experienced rupture. These data support our MBE distribution.

3.2.2 Recurrence Rates

Recurrence models describe the relative frequency of large- and small-magnitude earthquakes. The exponential model is considered to be appropriate for seismic source zones. However, for fault sources, it is not clear whether an exponential model or a characteristic earthquake model (Youngs and Coppersmith, 1985) is appropriate. We chose a truncated exponential recurrence model for our recurrence rate determination using the maximum-likelihood method of calculating the recurrence values (see Section 3.1 of the main report). We used all of the earthquake data in the catalog from the smallest to the largest magnitudes in the Yucca Mountain catalog. The choice of the entire magnitude range was made to provide as complete as possible a range of recorded

earthquakes in the region. We discuss the treatment of historical seismicity for calculation of earthquake recurrence rates for the seismic source zones in section 4.0.

3.3 REGIONAL FAULT SOURCES

Regional faults within 100 km of Yucca Mountain were reviewed for inclusion in the ground motion analysis. Potential regional fault sources (Figure SDO-6) were identified first from among the following data sources: Slemmons (1967); Dohrenwend *et al.* (1991, 1992); Piety (1995); Chapters 5 and 11 of the Seismotectonic Framework report (USGS, written communication 1996); Jennings (1994); Reheis (1992); and Reheis and Noller (1991). Candidate faults were screened on the basis of evidence of Quaternary displacement. The faults were further screened according to whether they are assessed to equal or exceed 0.05g in the analysis by Pezzopane (Seismotectonic Framework report, Chapters 8 and 11 [USGS, written communication, 1996]). All identified and possible Quaternary faults capable of magnitudes 6.4 ± 0.2 within 50 km were included. In the range of 50 to 100 km from Yucca Mountain, only faults with lengths equal to or greater than 20 km were included. This criterion was based on the potential peak ground accelerations estimated in chapter 11 of the Seismotectonic Framework report (USGS, written communication, 1996). A few faults having slightly lower ground motion potential also were included to account for potential uncertainties that could increase their ground motion, or because long-period ground motions from earthquakes along these faults may be important to the site. Two faults that generally lie beyond 100 km were included: the Panamint Valley fault zone and the Ash Hill fault zone (Figure SDO-6). These were included for their potential contribution to long-period ground motions. Most of the faults show clear evidence of Quaternary activity, such as fault scarps. For a few faults, the existence of Quaternary activity or the fault itself is equivocal. For these faults, a probability of Quaternary activity is assessed based on the degree of belief of fault activity (e.g., how likely the scarps observed along the Oasis Valley fault are from fault movement in the Quaternary).

In general, regional fault sources are characterized only on the basis of fault length for maximum magnitude and slip rate for earthquake recurrence, although a few have a maximum surface displacement as well. Maximum magnitudes were estimated using the

scaling relations shown in Table SDO-2 and discussed further in Section 3.3.2. Each regional fault source is characterized according to the parameters in Table SDO-3.

Regional faults were compiled to a mylar overlay of Piety's (1995) map. Fault length estimates were measured on the mylar overlay. Faults were weighted as to whether or not they had Quaternary activity, by evaluating published studies of the individual faults. Maximum surface displacement measurements were taken from the published literature, such as the Seismotectonic Framework report (USGS, written communication, 1996). Fault dips for the regional faults are largely unknown. For the normal-slip faults, 60° was used; for strike-slip faults, 90° was used. Because the regional faults occur within three different seismic source zones, there is an implication that faults within each source zone should mirror a distinct tectonic framework, or structural geometry. However, the Gaussian distribution of epicenters through the seismogenic crust suggests that dynamic distinctions in fault behavior throughout the region are not significant enough to require a models-based explanation. Therefore, we use a simple, universal model for all the faults: they are planar fractures that descend to seismogenic depths, the depths to a maximum of 19 km being directly proportional to fault length.

3.3.1 Description

The Gravity Fault

Because of its tectonic significance as a domain-bounding structure, the "gravity fault" (Winograd and Thordarson, 1975, p. C85) was described in the section on tectonic models. Surface expression along this fault is meager, but available data suggest chiefly normal slip. A subtle fault scarp segment on an alluvial fan was recognized by Reheis and Noller (1991); thus, there is indication of Quaternary activity along it. The lack of fault scarps suggests slip rates on the order of 0.0005 to 0.005 m/ky, but the subtle scarp may support a slip rate of 0.005 to 0.05 m/kyr (see Section 3.3.3 on recurrence justification of slip rate estimates for faults where data is lacking). Thus, the potential range of slip rate is 0.0005 to 0.05 m/kyr, with a preferred median value of 0.005 m/kyr. The minimum and preferred length is estimated to be 45 km, from the hills in the middle of Jackass Flats where the gravity anomaly diminishes, south to the end of the scarps that are on a southerly projection in the Ash Meadows area. The gravity gradient is essentially continuous along this extent. The maximum length extends south about 55 km to where

many scarps are at an angle to the gravity fault. Although the Ash Meadows fault zone continues on strike to the south of the gravity fault on the basis of surficial expression, we do not extend it southward because the defining gravity gradient becomes indistinct (Winograd and Thordarson, 1975).

Amargosa River Fault

The Amargosa River fault was mapped by D.E. Donovan (University of Nevada, Reno, written communication, 1991) as a series of fault scarps and lineaments in southwest Amargosa Valley that are considered related to a strike-slip fault. Anderson *et al.* (1995a) confirm Quaternary activity along this fault, suggesting that it is a reactivated Miocene and Pliocene? strike-slip fault. The minimum and preferred lengths are the distance of the fault scarps mapped by Donovan. This length can be measured from the east-northeast-trending scarps in Amargosa Valley, which may be a westward extension of the Rock Valley fault zone at the north end, to a near-intersection with the Ash Meadows fault along the south end. This is a distance of 16 km. The maximum length pushes the south end to an intersection with the Ash Meadows fault and continues north along a lineament, for a total distance of 29 km. Further extension to the north is plausible. No slip rate is reported for the Amargosa River fault; thus, a comparative methodology is employed to estimate the slip rate (see section 3.3.1.3).

Furnace Creek Fault Zone (Northern Death Valley Fault Zone)

The Furnace Creek fault zone is part of the Death Valley fault system, the largest and most active system in the Basin and Range province. The length, single-event displacements, and slip rate of this fault, as determined by R.E. Klinger and L.A. Piety (USBR, written communication, 1996), support this notion. The preferred length of the Furnace Creek fault zone is given by Klinger and Piety as 105 km as measured from the intersection with the central Death Valley fault zone to the Last Chance Canyon area. They suggest that this represents a single rupture segment, an impression supported by the conspicuous scarp trace lineament seen in the USGS Death Valley 1:250,000 SLAR image composite. The minimum length for the maximum event is estimated to be 85 km based on the nearly continuous scarps represented by Piety (1995). If the Furnace Creek fault is continuous with the northern Death Valley fault the length is 120 km by our estimate, and this is our preferred value. The maximum fault length includes both the

Furnace Creek and Fish Lake Valley fault zones, 195 km. Research by T.L. Sawyer and M.C. Reheis (Piedmont Consultants, written communication, 1997) suggests that a small restraining step in the system may control the total rupture length along the Fish Lake Valley fault. The restraining step through Last Chance canyon, which lies between the Fish Lake Valley and Furnace Creek fault zones, is the basis for considering the failure of both of these faults consecutively. The Last Chance restraining step apparently has not ruptured during the Holocene, while both the Furnace Creek and Fish Lake Valley fault zones had multiple displacements. Yet, if this restraining step were to fail when both faults zones are mature in their seismic cycles, it could create a cascading double-fault zone rupture. R.E. Klinger and L.A. Piety (USBR, written communication, 1996) measured the maximum single-event displacement as 6 m of lateral displacement, and an average single-event displacement of 4.5 m, but report no uncertainties for these. We infer a maximum surface displacement to range from 5.5 m to 6.5 m, with an estimated measurement uncertainty of 0.5 m. R.E. Klinger and L.A. Piety (USBR, written communication, 1996) estimated two slip rates for the Furnace Creek fault zone, one near Ubehebe Crater and one near Red Wall Canyon. The Ubehebe Crater site, located on the main strand of the Furnace Creek fault zone, is distinguished by an anticline that includes the Bishop Tuff (~ 760 ka). The anticline is offset, yielding a slip rate of 8 to 10 m/kyr . The slip rate estimate from the Red Wall Canyon site is 4 to 8 m/kyr. We use the overlapping value of the reported ranges (8 m/kyr) for the preferred rate (a decision suggested by R.E. Klinger, written communication, 1997), and use the reported range (4 to 10 m/kyr) for the minimum and maximum values. A good analog for earthquakes along the Furnace Creek fault zone is the 1872 Owens Valley earthquake, which had average surface displacements of 6 m and was about 110 km long (dePolo *et al.*, 1991). That earthquake had a moment magnitude of about 7.8.

Central Death Valley Fault Zone

The Central Death Valley fault zone is a right-normal, oblique-slip fault. The fault zone is part of a right step in the right-lateral Death Valley fault system. Recent work by R.E. Klinger and L.A. Piety (USBR, written communication, 1996) concluded that the Central Death Valley fault zone is the most active, dominantly normal-slip fault in the Basin and Range province. Klinger and Piety measured a minimum surface rupture length of 45 km along the Central Death Valley fault zone, and a total length of about 60 km. Our

estimate of 75 km extends this rupture to the south. Because of the rate and the potential size of offsets during paleoevents, we use 75 km for the preferred length, considering that the surface expression is poor along the northern part of the fault zone. The maximum and preferred values are identical, because the fault is structurally intersected at either end. For maximum surface displacement, RE. Klinger and L.A. Piety (USBR, written communication, 1996) measure surface separations (which in this case are essentially equal to vertical displacements because of steep near-surface fault dips and shallowly dipping offset surfaces) of 2.5 to 3.5 m; we adopt these values as the minimum and preferred maximum surface displacement values. Our maximum value adds 1 m to the preferred value to cover surficial noise and possible local poor preservation. Thus, the maximum surface displacement considered is 4.5 m. The minimum, preferred, and maximum slip rates are 2.6, 3.8, and 7.4 m/kyr, respectively. These are based on late Holocene offsets and age estimations of alluvial fan deposits made by R.E. Klinger and L.A. Piety (USBR, written communication, 1996).

Rock Valley Fault Zone

The Rock Valley fault zone comprises at least three major strike-slip faults and numerous bridging oblique faults in a zone that extends from Frenchman Flat west through Rock Valley, and possibly to Jackass Flats south of the Striped Hills, although there is evidence that the faults veer south into the Specter Range. The major faults strike N65°-80°E, are dominantly left-slip to slightly oblique, transtensional faults expressed geomorphically as a series of intermittent fault scarps and vegetation lineaments. Late Pleistocene to possible Holocene faulting has been documented through surficial mapping and trenching studies (Chapter 4, Seismotectonic Framework report [USGS, written communication, 1996]). Fault lengths for the Rock Valley fault zone were measured from the compilation by Piety (1995). The minimum length is 32 km, based on the faults mapped in Frenchman Flat to the west end of the scarps in Rock Valley. The preferred length is 47 km, measured between the faults mapped in Frenchman Flat and faults that pass immediately south of Skeleton Hills (Chapter 4, Seismotectonic Framework report [USGS, written communication, 1996]). The maximum length, 68 km, is measured from faults east of Frenchman Flat to the west end of the north-northeast-trending scarps and lineaments that cross Amargosa Valley. Individual fault strands, as mapped and indicated by lineaments, are about 15 to 17 km long. The Rock Valley fault zone has some of the

largest single-event displacements measured in the Yucca Mountain area (Chapter 4, Seismotectonic Framework report [USGS, written communication, 1996]). Paleoseismic events have produced a minimum displacement of 1.14 m to a maximum of 4.51 m. Preferred displacements range from 2.04 to 3.62 m. The second largest preferred displacement is 3.30 m. Because natural variations in surficial expression from earthquakes can be comparable to the difference between the two largest displacement values, we consider it reasonable to use the maximum value as the maximum surface displacement for maximum earthquakes along the Rock Valley fault. Slip rates along Rock Valley fault strands range from 0.05 m/kyr to < 0.002 m/kyr. Yount *et al.* (1987) estimate 0.02 m/kyr for the medial fault strand; we adopt this value as the preferred slip rate for the entire fault zone. The Seismotectonic Framework report (USGS, written communication, 1996) reports a long-term lateral slip rate of 0.084 m/kyr over the past 30 Myr, but suggests that much of this activity may have occurred during the Miocene, when the rates of tectonic activity were higher.

Mine Mountain Fault

The Mine Mountain fault is defined by a 3-km-long fault contact at Mine Mountain that sets Miocene tuff against Paleozoic limestone (Maldonado, 1985). The fault can be projected 3.8 km to the northeast and 26 km to the southwest, based on scattered outcrop evidence and aeromagnetic anomalies. The maximum length is about 35 km (Maldonado, 1985; S.R. Young *et al.*, CNWRA, written communication, 1992). We prefer a length of 21 km, which includes the Mine Mountain segment and the segment projected along Shoshone Mountain to near Kiwi Mesa (Maldonado, 1985). The fault strikes N35°E and dips from 90 to 60 degrees southeast; it is considered planar, based on aeromagnetic gradients and focal plane mechanisms to depths of 9 km. The fault is chiefly normal along Shoshone Mountain, but has a sinistral component along its entire length. No Quaternary offsets are mapped, but colluvium offset against caliche crust in a prospect pit at the southeast corner of Shoshone Mountain amounts to about 20 cm of dip slip. Total offset of surficial material at this site is about one meter, possibly having occurred within the past 100 ky D. O'Leary, USGS, written communication, 1996). Lineaments in old fan surfaces suggest degraded scarps of perhaps mid to early Pleistocene age. Carr (1984) reported an offset of the Paintbrush and Timber Mountain tuffs of about 1 km left-lateral on the south side of Mine Mountain. Assuming that this

offset has occurred during the last 11.5 Myr, a slip rate of 0.09 km/Myr (m/kyr) can be calculated, which is considered the maximum slip rate. Because geomorphology along the Mine Mountain is more poorly expressed than along the Rock Valley fault zone, its preferred slip rate is estimated to be similar or slightly lower than for that fault zone, or about 0.01 m/kyr or less; we use a lower limit of 0.005. Recurrent clustered earthquakes beneath the hanging wall of the Mine Mountain fault and along Mine Mountain indicate overall transtension and a low strain threshold. The Mine Mountain fault is considered to be susceptible to normal-oblique, southeast-side-down slip at this time. All of these features suggest that the Little Skull Mountain earthquake was generated by the Mine Mountain fault zone. However, the Mine Mountain fault strikes consistently N35°E rather than N55°E (the strike of the Little Skull Mountain slip plane); therefore, we believe that the Little Skull Mountain earthquake was generated within the Wahmonie fault zone or represents a fault in the hanging wall of the Mine Mountain fault.

Cane Spring Fault

The Cane Spring fault is expressed as a well-defined fault-line scarp that strikes N50°-40°E along a hillslope (Poole *et al.*, 1965). The fault is a single-plane structure that evidently controls the location and flow of Cane Spring. The fault line scarp is only about 6 km long. Frizzell and Shulters (1990) show an additional inferred 5 km extending into Barren Wash, and 2 km projected to the south side of Skull Mountain. The fault is traceable as a lineament into Skull Mountain, but is truncated by and breaks down into a complex of more northeast-striking normal faults. Field examination by O'Leary found no evidence for Quaternary offsets at Skull Mountain, and no evidence that the Cane Spring fault connects with the Rock Valley fault zone. Northeast of Cane Spring ,the fault projects into an alluvial basin. Gross landforms suggest that the fault extends, buried, a considerable distance toward Yucca Flat; therefore our preferred length estimate is 26 km, following the interpretation of Cornwall (1972). The maximum cumulative lateral offset is about 1 km (Poole *et al.*, 1965). The cumulative vertical offset, if any, is unknown because latest movement on the fault is nearly pure strike-slip. The youngest offset unit is about 9.5 Ma which gives a slip rate as high as 0.105 m/kyr. Overall geomorphic character implies very low Pleistocene activity. Thus, the minimum, preferred, and maximum slip rates assigned to the Cane Spring fault are 0.005, 0.01, and 0.05 m/kyr, respectively. In light of its tectonic isolation, lack of late Quaternary

expression, and weak correlation with significant slope breaks or boundaries, we rank its probability of activity as 0.8.

Wahmonie Fault Zone

The Wahmonie fault zone is represented by degraded scarp segments in alluvial fans along the north flank of Skull Mountain, which faces Jackass Flats, and as a zone of complex faults exposed in bedrock in the divide between Little Skull Mountain and Skull Mountain (Frizzell and Shulters, 1990). The zone projects directly toward the Striped Hills, which have left-lateral offset as great as 1.4 km along the projection. The projection can be carried even farther south, across Rock Valley and along the flanks of the Specter Range. The Wahmonie fault zone either truncates or intersects the Rock Valley fault zone in a relationship not understood. The structural interaction, which is considered to be related to the recurrent, clustered seismicity at the western end of Rock Valley. Quaternary activity is indicated by fault scarps and lineaments in deposits dated 270-740 ka, and by concealment beneath Holocene deposits (Swadley and Huckins, 1990). Possible Holocene movement is suggested by cracked and slightly offset caliche pavement (observed by O'Leary), and by a conspicuous dearth of precarious rocks at the east end of Little Skull Mountain (J. Brune, oral commun. PSHA workshop). The minimum length of the Wahmonie fault is 9 km. The preferred and maximum lengths are 15 km, which include the discontinuous series of scarps and lineaments in eastern Jackass Flats, just north of Skull Mountain (Swadley and Huckins, 1990). The minimum, preferred, and maximum slip rates assigned to the Wahmonie fault are 0.005, 0.01, and 0.05 m/kyr, respectively. Despite hints of late Pleistocene activity, evidence for significant Pleistocene offset for any appreciable distance along strike has not been noted. On this basis we rank the probability of activity as 0.8.

South Silent Canyon Fault

The South Silent Canyon fault (herein named) lies in the structural system north of the Timber Mountain caldera that is remarkably similar to the Yucca Mountain fault system (described in the section on Tectonic Models). This is only one of several faults in Pahute Mesa that are suspected to have Quaternary activity (i.e., Quaternary alluvium in fault contact with rhyolitic tuffs), but for which we have little information. Maps, such as that of Frizzell and Shulters (1990), show several of these faults bounding local

Quaternary alluvial deposits. The South Silent Canyon fault ruptured following an underground nuclear explosion and/or earthquakes that occurred following the blast. The minimum length is 10 km. A preferred distance of 14 km includes the entire fault zone; a maximum distance of 17 km includes faults in the tuffs farther north. Slip rate estimates are poorly constrained; on the basis of structural similarity to the Yucca Mountain faults, minimum, preferred, and maximum slip rates are assumed to be 0.001, 0.005, and 0.01 m/kyr, respectively. These rates suggest that the South Silent Canyon fault is more active than the Bow Ridge fault, but that the minimum value might be lower. The maximum value approaches the slip rate of the Solitario Canyon fault. Little is known about the Quaternary history of the South Silent Canyon fault. Because of sparse data and uncertainty, we rank its probability of activity 0.8.

Pahute Mesa #1 Fault

The Pahute Mesa #1 fault (herein named) lies just west of the South Silent Canyon fault and is part of the same system. Also similar to the South Silent Canyon fault, the Pahute Mesa #1 fault ruptured in association with an underground nuclear explosion. This fault has a few kilometers of fault-bounded Quaternary alluvium along it (Orkild *et al.*, 1969). The minimum length of the Pahute Mesa #1 fault is about 10 km, the distance of the fairly continuous single-plane trace. The preferred length of 13 km includes the entire fault zone. The maximum length of 16 km includes faults in tuffs farther north. The weak slip rate estimates are based on structural similarities to the Yucca Mountain faults. Thus, minimum, preferred, and maximum slip rates are interpreted to be 0.001, 0.005, and 0.01 m/kyr, respectively. These rates suggest that the Pahute Mesa #1 fault is more active than the Bow Ridge fault, but that the minimum value might be lower. The maximum value approaches the slip rate of the Solitario Canyon fault. The fault-bounded Quaternary alluvium indicates a likelihood that the Pahute Mesa #1 fault has experienced some Quaternary activity, but otherwise we rank its probability of activity the same as for the South Silent Canyon fault, for the same reasons..

Yucca-Butte Fault Zone

The Yucca-Butte fault zone is a down-to-the-east, normal-slip fault that extends across the middle of Yucca Flat (Yucca fault) into the hills north of the flat (Butte fault). Because of the continuity between the Yucca and Butte faults, they are treated here as a

structurally linked fault zone. The minimum length of the Yucca-Butte fault zone is 26 km, the distance of the Yucca fault portion. The preferred value is 34 km, which includes the small range-front portion (the Butte fault) north of Yucca Flat. The maximum value, 41 km, includes scarps and lineaments north of the Butte fault. Fault scarps clearly indicate Quaternary activity (Swadley and Hoover, 1990). Fernald *et al.* (1968) measure a surface displacement of 15 m in the Quaternary alluvium. Using ages for surfaces mapped by Swadley and Hoover (1990) and correlations with surfaces that have been studied in the Yucca Mountain area, slip rates for the Yucca-Butte fault range from 0.015 to 0.053 m/kyr, with a preferred value of 0.026 m/kyr.

Peace Camp Fault

The Peace Camp fault has been mapped by Dohrenwend *et al.* (1991) as a northeast-trending, fault-controlled lineament; by Reheis (1992) as a prominent scarp or lineament in Quaternary deposits; and by Yount (unpublished mapping) as a fault in older Quaternary alluvial deposits. Its strike and location suggest that the Peace Camp fault may be a left-slip fault, part of a small system that includes the South Ridge Faults" of Piety (1995). This structural association apparently would require a left step of about 2 km. The minimum and preferred length for the Peace Camp fault, 12 km, represents its clear expression in Quaternary alluvium. The maximum length of 30 km includes the South Ridge faults. Although Dohrenwend *et al.* (1991) show the South Ridge faults as juxtaposing Quaternary alluvium against bedrock, lack of geomorphic expression along this eastern extension suggests that earthquakes likely are restricted to half of this maximum length (15 km). Extension of the Peace Camp fault to the west would require another left step and a change to a more northerly orientation. A westward extension would bring the Peace Camp fault into structural association with the West Spring Mountains fault.

Slip rates from the Mine Mountain fault are adopted for the Peace Camp fault, on the basis of similar geomorphic expression. Thus, the minimum, preferred, and maximum slip rates assigned to the Peace Camp fault are 0.005, 0.01, and 0.09 m/kyr, respectively.

West Spring Mountains Fault

The West Spring Mountains fault is a west-side-down, normal-slip fault that bounds the northwest side of the Spring Mountains. The fault has been mapped and studied by J. L. Hoffard (University of Nevada, Reno, written communication,1991). Quaternary activity is evidenced by fault scarps. The minimum length of a continuous fault is 30 km. The preferred length of 37 km accounts for a south scarp that is on strike, but separated by a small gap in surficial expression. The maximum length of the West Spring Mountains fault is 56 km, which includes the Eastern Pahrump Valley fault zone southward to an intersection with the Pahrump Valley fault zone. This south reach may have a right-lateral component, given its relatively linear nature and left-stepping patterns. Based on geomorphology, the north 30 to 37 km of the West Spring Mountains fault appears to be a single earthquake segment. J. L. Hoffard (University of Nevada, Reno, written communication, 1991) measured a vertical surface separation of 12 m, which has been corrected to a vertical offset of 13.2 m to account for the surface slope and fault dip. Different projections of the profile made by Hoffard yield potential uncertainties of - 2 and + 4 m. Hoffard estimates the age of this offset surface to be 200 ka, with a range of 130 to 500 ka. These data yield a range of slip rates from 0.02 to 0.2 m/kyr, with a preferred rate of 0.09 m/kyr.

Oasis Valley Fault Zone

The Oasis Valley fault zone is a normal-slip fault that lies along a steep north-south gravity gradient (Anderson *et al.*, 1995b). This fault zone lacks evidence for late Quaternary faulting (Anderson *et al.*, 1995b). A prominent lineament, however, may be evidence of minor early Pleistocene displacement (Anderson *et al.*, 1995b). The minimum length of 5 km represents the bold faults from Piety's (1995) map. The preferred length of 8 km accounts for other faults and/or lineaments on strike. The maximum length of 20 km is the total possible expression of this fault zone, including projected faulting in Oasis Valley. Overall lack of geomorphic expression suggests that the slip rate likely is low, perhaps similar to that of the Bow Ridge fault. A range of 0.0005 to 0.003 m/kyr is assigned to the Oasis Valley fault zone, with a preferred value of 0.001 m/kyr. The very weak evidence for Quaternary activity leads us to assign a probability of activity of 0.8.

Pahrump Valley Fault Zone

The Pahrump Valley fault zone is made up of a series of discontinuous, northwest-trending scarps, spring alignments, and lineaments that indicate a right-slip fault zone (J. L. Hoffard, University of Nevada, Reno, written communication, 1991; Anderson *et al.*, 1995b; and Louie *et al.*, University of Nevada, Reno, written communication, 1997). The fault zone lies along the center of Pahrump Valley (essentially along the Nevada/California state line); it extends from Black Butte at the south end to an apparent pull-apart basin, Stewart Valley, at the north. The minimum length (25 km) is the distance of continuous geomorphic features in north Pahrump Valley, extending into south Stewart Valley. The preferred and maximum lengths (61 and 67 km, respectively) extend the zone down to Black Butte, with a maximum rupture length that traverses all of Stewart Valley. To estimate slip rate, we compare this fault zone with the Rock Valley fault zone, which has a similar, zone-like, geomorphic expression, but sharper geomorphic features. We assign a preferred slip rate of 0.01 m/kyr, with a range of 0.005 to 0.1 m/kyr.

Bare Mountain Fault

The Bare Mountain fault is poorly exposed, probably because in Quaternary time erosion and deposition have far outweighed tectonic activity along the fault. Gravity and seismic reflection data indicate that the fault plane stands at least a kilometer out from the eroded range front at the north end of the mountain, and converges more closely to the range front toward the south. Younger activity of the fault is also indicated to the south. The fault (or faults, if several planes are involved) dips east at 50 to 70 degrees; displacement is chiefly normal, with an oblique dextral component prominent to the south (Reheis, 1988; Monsen *et al.*, 1992). The fault is at least 18 km long. At the northeast corner of Bare Mountain, the Bare Mountain fault loses throw and breaks into a group of faults that extend across tuffs of the caldera rim assemblage. The easternmost fault is the Tram Ridge fault; it extends about 10 km to the Rainier Mesa caldera. A smaller, less clearly defined fault 8 km long, east side down, bounds the tuffs and the alluvium of Crater Flat. This fault apparently is post-8 Ma (C. Fridrich, USGS, written communication). At the south end, near Steves Pass, the Bare Mountain fault abruptly loses throw and ceases to be a range-front fault. It becomes lost in a distributed zone that includes faults traceable to Yucca Mountain itself; although a set of northwest-striking, dextral oblique faults

appears to dominate the fault structure in this area. Within this plexus, the Bare Mountain fault is not a single-plane structure and probably is not a major tectonic influence. Because it surfaces within surficial deposits for most of its length, there is no direct indication of total bedrock displacement. The fault does not appear to be segmented; surface rupture has occurred along a relatively linear, narrow zone on all or most of its (preferred) 23-km length. Surface-rupturing earthquakes on the fault occur infrequently. The recurrence of moderate- to large-magnitude, surface-rupturing earthquakes appears to be on the order of tens of thousands to a hundred thousand years or more. The most recent surface-rupturing event occurred no more recently than about 14 to 24 ka and could be as old as 100 ka (Seismotectonic Framework report [USGS, written communication, 1996]). Maximum surface displacement ranges from 1.2 m to 1.8 m; we adopt a preferred value of 1.5 m which is the value reported in the Seismotectonic Framework report (USGS, written communication, 1996). An uncertainty of ± 0.3 m is considered to encompass a potential range of measurements (projection uncertainties or variability of datums). The minimum slip rate (0.006g m/ky) is taken from a minimum offset measured by L. W. Anderson and R. E. Klinger (USBR, written communication, 1996a) of 2.2 m taken over their maximum estimated age of 400 ka. The preferred value of 0.01 m/ky is the value estimated from L. W. Anderson and R. E. Klinger (USBR, written communication, 1996a). Ferrill *et al.* (1996) suggest a higher slip (0.2 m/ky) based on indirect evidence; we adopt this as our maximum slip rate.

Keane Wonder Fault

The Keane Wonder fault is a west-side-down, normal-slip fault that bounds the southeast side of north Death Valley and part of the west side of the Grapevine Mountains. The minimum, preferred, and maximum lengths are 19, 27, and 29 km, respectively. The minimum length is the continuous central part mapped by Piety (1995); the preferred length extends this to the north and south along a range front. The maximum length extends the fault farther south along a fault trace that bounds a range front for some distance before trending into the range. Lack of a faceted range front and of fault scarps indicates a relatively low rate of activity. The preferred slip rate estimate is the approximate threshold of faults having fault scarps of 0.005 m/kyr. The fault appears to lack late Quaternary activity (Anderson *et al.*, 1995b); but an abrupt, rectilinear range front indicates possible early to mid-Quaternary activity. Given that deposition along the

range front is fairly uniform at the front, some Quaternary activity is considered likely. Thus, we consider a minimum slip rate of 0.001 m/kyr. The maximum rate is 0.05 m/kyr, just a little higher than the maximum rate of the Solitario Canyon fault. We make it slightly higher to reflect our uncertainty, because the Keane Wonder fault is untrenched.

Eleana Range Fault

The Eleana Range fault is an east-side-down, normal-slip fault that bounds the northwest side of Yucca Flat and the east side of part of the Eleana Range. This fault is about 5 km west of, and is synthetic to, the Carpetbag fault. The Eleana Range fault appears to bound a small subbasin within Yucca Flat, just west of the Carpetbag fault (Frizzell and Shulters, 1990). Fault scarps along the Eleana Range fault are indicated by Swadley and Hoover (1990) and Dohrenwend *et al.* (1992); the latter authors indicate some of these scarps are in late Pleistocene deposits. The Eleana Range fault is considered to be limited to its range-front expression, 15 km. This value is used for both the preferred and maximum values. A minimum value of 11 km represents the central part of the fault that has scarps. No direct slip rates are available for the Eleana Range fault, so we used comparisons. Because fault scarps are present, we assigned a minimum value of 0.003 m/kyr. The preferred value is difficult to ascertain, but we consider it be comparable to the Solitario Canyon fault, about 0.01 m/kyr. The maximum value assigned to the Eleana Range fault is the approximate maximum value for the Yucca-Butte fault zone, 0.05 m/kyr.

Yucca Lake Fault

The Yucca Lake fault is a down-to-the-northeast, normal-slip fault that bounds a short section of the west side of Yucca Flat. The fault is shown to offset the buried upper surface of pre-Cenozoic rocks in the subsurface, and a potential right-lateral component is indicated by McKeown *et al.* (1976). No fault scarps are identified along the Yucca Lake fault, and Quaternary activity is uncertain, although Cornwall (1972) shows the fault in Quaternary deposits. Given the information at hand, this fault is given a 50% chance of having Quaternary activity. The minimum length is the trace portrayed by Piety (1995), 12 km. The preferred length, 20 km, considers an inferred extension to the northwest and southeast of the trace shown on Piety's map; and the maximum length, 23 km, includes an extension southward that intersects the Cane Springs fault. Slip rate estimates for the

Yucca Lake fault are based on the interpretation that the fault is active and lacks scarps. The minimum rate is estimated to be 0.001 m/kyr; the preferred rate is assigned at the approximate threshold of faults that have scarps, 0.005 m/kyr. The maximum rate is similar to the preferred rate of the Solitario Canyon fault, about 0.01 m/kyr.

Carpetbag Fault

The Carpetbag fault is part of the down-to-the east system of normal faults in Yucca Flat, including the Yucca-Butte fault zone and the Eleana Range fault. At the surface, the Carpetbag fault manifested as faulting induced by nuclear testing. This exposed a fault zone that apparently has a Quaternary history of fracturing, but that had no natural surface expression prior to nuclear testing (Shroba *et al.*, 1988). Subsurface work has further defined the extent of the Carpetbag fault by following an offset of the floor of the Yucca Flat basin (Carr, 1984). The fault is composed of two traces south of the induced surface expression; these are synthetic normal faults separated by about 1.5 km (Frizzell and Shulters, 1990). The minimum length of the Carpetbag fault, 18 km, is based on a simple geometric segment interpretation of the subsurface projection. The preferred length is the extent of the fault indicated by the extent of offset of the basin floor to the north margin of Yucca Flat and, in the south, to an intersection with the Yucca Lake fault. The maximum length, 37 km, includes some rupture along the southeast part of Quartzite Ridge, and some rupture along the south part of the fault, parallel to the Yucca Lake faults. Slip rate estimates for the Carpetbag fault are based on assuming that the fault is active and lacks scarps. The minimum rate is estimated to be 0.001 m/kyr; the preferred rate is assigned at the approximate threshold of faults with fault scarps, 0.005 m/kyr. The maximum rate is similar to the preferred rate of the Solitario Canyon fault, about 0.01 m/kyr.

Oak Spring Butte Fault

The Oak Spring Butte fault is a down-to-the-east, normal-slip fault that bounds the easternmost part of the Belted Range and forms the west side of Emigrant Valley. The fault is expressed as a zone of scarps and lineaments. Several of the faults offset rhyolitic volcanic flows, creating expressions similar to those of the Yucca Mountain faults. Several of these faults are considered to have possible Quaternary displacement (Reheis, 1992; Dohrenwend *et al.*, 1992). The orientation, sense-of-displacement, and position

suggest that the Oak Spring Butte fault is an overlapping extension of the Yucca-Butte fault zone. The length of the Oak Spring Butte fault is difficult to assess, since it is part of a large fault swarm within the east part of the Belted Range and Emigrant Valley. The minimum length (9 km) is taken from a straight, central part of the fault. The preferred length, 16 km, extends this to the north and south, the north part along the physiographic expression of the Belted Range range front. The maximum length, 19 km, includes a small projection to the north and south. With the possible exception of some weak lineaments and/or scarps reported by Reheis (1992) along the north end, no Quaternary scarps are identified along the Oak Spring Butte fault. Slip rate estimates for the fault are based on assuming that the fault is active and lacks scarps. The minimum rate is estimated to be 0.001 m/kyr; the preferred rate is assigned at the approximate threshold of faults with fault scarps, 0.005 m/kyr. The maximum rate is similar to the preferred rate of the Solitario Canyon fault, about 0.01 m/kyr.

Belted Range Fault

The Belted Range fault is a down-to-the-west, normal-slip fault that bounds the west side of the Belted Range and the east side of Kawich Valley. This fault, which has been mapped by Reheis (1992) and Anderson *et al.* (1995b), shows evidence of latest Pleistocene to earliest Holocene faulting. The minimum length of the Belted Range fault is 22 km; this is the length of surface scarps mapped by Anderson *et al.* (1995b). The preferred length of 35 km includes much of the topographic expression of the fault. The maximum length is 47 km, which includes projections of the fault into the mountains along the south end of the fault and a north projection along weak lineaments or fault scarps in alluvium mapped along Lava Ridge by Reheis (1992). Slip rate estimates were assigned following Anderson *et al.* (1995b), who estimate a Holocene slip rate of 0.1 m/kyr (1 m of offset in 10 kyr) and a Pleistocene slip rate of 0.01 to 0.09 m/kyr (11.3 m total offset in 130 to 780 kyr). From this information, we adopt minimum and maximum slip rates of 0.01 and 0.1 m/kyr. A mid-range value of 0.05 m/kyr was adopted as the preferred rate, which is the same rate as indicated by the long-term offset of the 11.5- to 12.5-Ma Timber Mountain Tuff (Anderson *et al.*, 1995b).

Kawich Range Fault

The Kawich Range fault is a down-to-the-west, normal-slip fault that bounds the west side of the Kawich Range and the east side of Gold Flat. Anderson *et al.* (1995b) found latest Pleistocene fault scarps over only a small percentage of the length of this fault, but this confirms Quaternary activity. The minimum length is 23 km, as indicated by Piety (1995) and Anderson *et al.* (1995b). The preferred value, 33 km, includes much of the topographic expression of the fault. The maximum value, 46 km, extends the fault to the south along faults mapped by Reheis (1992) and to the north to intersect the next major strand of the Kawich fault. The total length of the Kawich Range system is not reported here. Slip rate estimates for the Kawich Range fault are based on the interpretation that the fault is active but lacks scarps. The minimum rate is estimated to be 0.001 m/kyr; the preferred rate is assigned at the approximate threshold of faults that have scarps, 0.005 m/kyr. The maximum rate is similar to the preferred rate of the Solitario Canyon fault, about 0.01 m/kyr. Although the Kawitch fault is a substantial range front fault, lack of Quaternary expression leads us to assess a low probability of activity of 0.8.

Western Pintwater Range Fault

The Western Pintwater Range fault is a west-side-down, range-bounding, normal-slip fault that bounds the west side of the Pintwater Range and the east side of Indian Spring Valley. Dohrenwend *et al.* (1991) indicate that this fault is likely early to mid-Quaternary in age. The minimum fault length is 33 km, considering only the most prominent central part that bounds Indian Spring Valley. The preferred length, 54 km, includes the entire western side of the Pintwater Range. The maximum length, 75 km, includes a north extension of the fault that bounds the west side of the north Desert Range. Dohrenwend *et al.* (1991) identify some fault scarps along the Western Pintwater Range, but they are generally short, discontinuous scarps in mid- to early Pleistocene deposits (J. Yount, written communication, 1996). Yount finds no evidence for faulting along much of the fault, including apparently faceted portions, limiting the potential slip rate estimate. The minimum slip rate of the Western Pintwater Range is 0.005 m/kyr, near the lowest slip rate for normal faults that have fault scarps. The maximum estimated rate is 0.05 m/kyr, the approximate threshold slip rate for faults that have fault facets. The preferred slip rate is estimated to be between these two, or 0.008 m/kyr.

Grapevine Mountains Fault

The Grapevine Mountains fault is a west-side-down, normal-slip fault that bounds the north side of the Grapevine Mountains (Reheis and Noller, 1991; Dohrenwend *et al.*, 1992). The fault is made up of two principal strands, a range-front trace and a piedmont trace that bounds some small hills along its east end. The fault is represented as a single trace for analysis purposes. The minimum and preferred lengths of the Grapevine Mountains fault are 25 km, which represents most of the easternmost part of the fault shown by Piety (1995). The maximum length, 32 km, includes a south extension of the fault that strikes into the Grapevine Mountains. Fault scarps in Quaternary alluvium are present along the piedmont trace of the Grapevine Mountains fault, but fault facets are not present. The minimum slip rate estimate, 0.003 m/kyr, is the lowest rate for a fault that has a fault scarp; the preferred slip rate, 0.01 m/kyr, is the middle of the range for faults having alluvial scarps but no fault facets; and the maximum slip rate, 0.05 m/kyr, is approaching the maximum rate of faults that lack fault facets.

Panamint Valley Fault Zone

The Panamint Valley fault zone is a major strike-slip fault that bounds the west side of the Panamint Range and the east side of Panamint Valley and has a normal-right-lateral sense of displacement. The fault zone has been discussed or mapped by several individuals (W. A. Bryant, CDMG, written communication, 1989; Zhang *et al.*, 1990). The minimum length of the Panamint Valley fault zone is 82 km, which is its extent from the south part of Panamint Valley north to a small reentrant in the range front. The preferred length, 90 km, extends the north part of the fault to the more westerly-trending Hunter Mountain fault. The maximum length, 104 km, considers an additional extension to the southmost part of Panamint Valley. A Holocene slip rate was determined by Zhang *et al.* (1990) from offset alluvial features. Their slip rate estimate is 2.36 ± 0.79 m/kyr; we round this off to 2.4 ± 0.8 m/kyr.

Hunter Mountain Fault Zone

The Hunter Mountain fault zone is basically a northward extension of the Panamint Valley fault zone, but its strike is 25 degrees more westerly, and it is separated by a gap in fault scarps (see W. A. Bryant, CDMG, written communication, 1989). The fault zone has a minimum length of about 46 km and a maximum length of 65 km. Our preferred

length, 64 km, is close to the maximum value. The Hunter Mountain fault zone exhibits one of the finest series of right-laterally offset stream channels in the Basin and Range province, on the southwest flank of Hunter Mountain. The fault zone is a normal-right-oblique fault, with alternating downthrown sides, down-to-the-west in the south and down-to-the-east in the north. Slip rates for the Hunter Mountain fault zone are relatively high, ranging from 1.3 m/kyr to 2.7 m/kyr. Our preferred value is 2 m/kyr, comparable to the rate for the Panamint Valley fault. Slip rates for this fault were taken from Piety (1995), Schweig (1989), and Burchfiel *et al.* (1987).

Ash Hill Fault Zone

The Ash Hill fault zone is a right-slip fault zone that runs up the west side of Panamint Valley. W. A. Bryant (CDMG, written communication, 1989) provides the most detailed description of this fault. The Ash Hill fault zone appears to alternate downthrown sides along strike, being down-to-the-east along the south part and down-to-the-west along the north part. The Ash Hill fault zone appears to coincide with the western margin of Panamint Valley; if so, it apparently has a much stronger normal component than the north part. The minimum length estimated for the fault zone is 33 km, which is the minimum length of the relatively continuous "backfacing-scarp appearance." The preferred length, 55 km, extends the Ash Hill fault zone slightly on the north and substantially along the south. The south end is extended along the northeast flank of the Slate Range as a buried fault (only probable liquefaction grabens are portrayed by W. A. Bryant (CDMG, written communication, 1989) along this projection). A buried fault is inferred primarily because this range front is on strike with the mapped surficial expression, and some active tectonism along the range front is considered to account for its youthful appearance. The maximum length, 90 km, includes a small increase in length on the north and, again, a substantial increase in length to the south. This is to account for the continued on-strike potential southward, along the west side of Panamint Valley, to just north of Wingate Pass. The slip rate of the Ash Hill fault has been investigated by Densmore and Anderson (1994). They map an olivine basalt K/Ar dated at 4.05±0.15 Ma that is offset right laterally by 1.2 ±0.3 km, indicating minimum, preferred, and maximum slip rates of 0.21, 0.3, and 0.38 m/kyr, respectively.

West Specter Range Fault

The West Specter Range fault is a west-side-down, normal-slip fault just west of the Specter Range (Anderson *et al.*, 1995b). The north part of the West Specter Range fault is expressed as "small scarps and conspicuous lineaments on alluvial deposits"; the south part is made up of "discontinuous but prominent scarps on alluvial deposits and by lineations in Tertiary(?) bedrock" (Anderson *et al.*, 1995b). Anderson *et al.* indicate that fault scarps have as much as 1.4 m of surface offset in deposits of probable middle Pleistocene age. Small scarps along the north part have 0.3 to 0.5 m of surface offset on deposits that likely are latest Pleistocene in age (Anderson *et al.*, 1995b). The minimum length given to the West Specter Range fault is 10 km, which is the extent of faulting mapped by Anderson *et al.* (1995b). The preferred length, 19 km, extends this fault north across a small wash and south across Amargosa Valley. The maximum length, 25 km, extends the fault farther north up a crude linear valley and completely across the valley in the south. The slip rate is based on Anderson and *et al.*'s estimated maximum of 0.004 m/kyr. We adopt this as the preferred value and estimate 0.001 to 0.01 m/kyr for the minimum and the maximum slip rates. These values are identical to the values Anderson currently is using for his team's analysis (1997, this report).

Spotted Range Fault Zone

The Spotted Range fault zone represents a swarm of faults around the Spotted Range, the primary one of which was culled to represent the zone. This is the longest, most continuous fault of the group identified by Reheis (1992) and Piety (1995). This fault is a down-to-the-west, normal-slip fault that bounds the west side of a central ridge in the Spotted Range. Quaternary fault scarps and lineaments are indicated by Reheis (1992), supporting Quaternary activity. The minimum length of 17 km represents the central part of the fault, roughly the continuous expression mapped by Reheis. The preferred length, 30 km, extends the minimum to the south across a small wash and to the north along a series of discontinuous fault traces shown by Piety (1995). The maximum length is the same as the preferred because it is difficult to push the fault in either direction reasonably. Slip rates for this fault are difficult because of limited information. The minimum rate estimated, 0.001 m/kyr, is below the range of faults having no fault facets; the preferred value, 0.01 m/kyr, is typical of faults that have fault scarps and fault facets in the Great Basin; and the maximum value is 0.05 m/kyr.

Buried Hills Fault Zone

The Buried Hills fault zone generally bounds the west side of the Buried Hills and is a down-to-the-west, normal-slip fault (Reheis, 1992; Piety, 1995). The minimum length, 15 km, represent the central part of the fault zone as mapped by Reheis. The preferred length, 18 km, extends the minimum to the north and south along discontinuous fault traces. The maximum length, 25 km, extends the fault farther north along the southeast side of Papoose Lake flat. Slip rate estimates for this fault are difficult because of limited information. The Buried Hills themselves lack fault facets and have a relatively laid-back range front. Quaternary fault scarps and lineaments shown by Reheis (1992) are weakly to moderately expressed (Piety, 1995). The minimum slip rate estimated, 0.001 m/kyr, is below the range for faults having no fault facets; the preferred value, 0.01 m/kyr, is typical of faults that have fault scarps and fault facets in the Great Basin; and the maximum value is more than 0.05 m/kyr.

Northern Emigrant Valley Fault Zone

The Northern Emigrant Valley fault zone is made up of a swarm of more than 75 Quaternary fault scarps in the western part of an alluvial valley. The nature of the tectonism that gives rise to this pattern is uncertain, but it seems to be related or interconnected to adjacent faults in the surrounding hills. A few right-lateral offsets have been identified by Reheis (1992), suggesting that the pattern could represent the distributed expression of a lateral-slip fault. Because this system is more than 50 km from the site area, the exact mechanism of the fault is of lesser importance; thus, a right-lateral fault is assumed. The minimum length, 18 km, is the length of the main part of the fault swarm shown by Reheis (1992). The preferred length, 37 km, includes the fault scarps to the north and south. The maximum length, 45 km, considers possible extensions of the fault in the Papoose Lake area, and a small extension to the north. Evaluating the slip rate of this swarm is difficult. The slip rate was assumed to be similar to the Rock Valley fault zone; we adopt the Rock Valley fault zone's slip rates, 0.01, 0.02, and 0.08 m/kyr, for the Northern Emigrant Valley fault zone.

Eastern Pintwater Range Fault Zone

The Eastern Pintwater Range fault zone is an east-side-down, normal-slip fault on the east side of the Pintwater Range (Dohrenwend *et al.*, 1991; Reheis, 1992). Geomorphic expression along the Eastern Pintwater Range fault zone appears to be subtle, consisting of short fault scarps, lineaments, and abrupt alluvium/bedrock contacts. The minimum length, 28 km, is the central part of the fault zone. The preferred length of 36 km includes most of the range front that seems to be related to the fault. The maximum length, 57 km, includes the entire range front. The Eastern Pintwater Range fault zone appears to be near the threshold of geomorphic expression, specifically as regards fault scarps. The minimum slip rate, 0.001 m/kyr, is less than that for faults that have little expression. The preferred rate is 0.005 m/kyr, the middle value for faults with and without scarps. The maximum slip rate is 0.01 m/kyr, close to the rate of the Solitario Canyon fault.

Towne Pass Fault Zone

The Towne fault zone is a northwest-side-down, normal-slip fault that bounds the west side of the Panamint Range. This fault reportedly has weak Quaternary expression (W. A. Bryant, CDMG, written communication, 1989; Reheis, 1991; Piety, 1995), although W. A. Bryant (CDMG, written communication, 1989) suggests that two beheaded drainages indicate latest Pleistocene to Holocene displacement. The Towne Pass fault locally is a prominent west-facing scarp in dolomite (W. A. Bryant, CDMG, written communication, 1989) and may have some small fault facets. These, if they are facets, are highly eroded and occur only along small parts of the fault zone. The minimum length of the Towne Pass fault zone is 33 km, from the north end of the Panamint Range to the south end of the Holocene or latest Pleistocene activity indicated by Piety (1995). The preferred length of 38 km extends the fault a little farther south, to a point where the fault bifurcates, and most of the range-front expression is gone. The maximum length of 50 km includes the total mapped geologic fault, with some minor inferred faulting off the north end. There was little information for estimating slip rate, so we used a broad range, 0.005 to 0.1 m/kyr. This rate places the fault zone between the threshold of faults that generally lack fault scarps and the point at which fault facets may be expected. The preferred value is 0.03 m/kyr.

3.3.2 Maximum Earthquake Estimates

Maximum earthquakes were estimated for the regional faults using empirical magnitude versus length, magnitude versus length and slip rate, and, in a few cases, magnitude versus maximum surface displacement relationships (Table SDO-2). All fault lengths given are the estimated maximum earthquake segment lengths for these faults. For regional faults that have multiple earthquake segments, only the closest segment was analyzed; in all these cases the other segments were too far away to have a significant impact on Yucca Mountain. A distribution of earthquake magnitudes also is considered for these faults down to the maximum background earthquake; these events are distributed randomly along the maximum earthquake segment. Different relations for magnitude versus length and magnitude versus maximum displacement were used for normal-slip versus strike-slip faults. All relationships are weighted equally, except that of Anderson *et al.* (1996). A concern about how well the data used by Anderson *et al.* compares to the southern Great Basin caused us to give this relationship a weight of one-third that of the other relations. A more extensive discussion of scaling relations for estimating maximum magnitudes and the associated input fault parameters in general is included in Section 3.4.2

The maximum magnitude evaluation assumed a similarity of structural style and expected geometry of regional faults throughout the areas within the same part of the southern Basin and Range province. Therefore, we assumed that they nucleated under similar stress field of extension. We considered, for example, unless there were contradictory data, that the faults have planar geometries from the surface to the depth of the maximum focal depths discussed earlier.

3.3.3 Recurrence

The occurrence of the maximum earthquake along regional faults is expressed by estimating the strain accumulation interval for the maximum event. The minimum, preferred, and maximum fault lengths are associated with an average surface displacement using relationships from Wells and Coppersmith (1994). This average displacement is divided by the fault slip rate, providing the slip accumulation time, which is considered to be the average recurrence interval. This is then inverted for annual earthquake occurrence rate. Since there is significant uncertainty in making these kinds of estimations, the final weighting of the average earthquake recurrence intervals are set at the 10^{th} and 90^{th} percentiles for the

minimum and maximum values, and hence a "0.3, 0.4, 0.3" weighting is used in a three-point discrete distribution. Slip rates were taken from or derived from the published literature where possible. Estimates generally were made by comparing faults having unknown slip rates with the structural and geomorphic characteristics of faults having known slip rates, and thereby making a comparative estimate of the potential slip rate for the former. For example, faults that have alluvial fault scarps but do not have facets tend to have rates around 0.01 m/kyr, whereas faults that have neither facets or scarps tend to have rates of 0.001 m/kyr or less (dePolo, written communication, 1997). Although a more rigorous approach is desired, most of these faults have moderate to low slip rates and their impacts on the final ground motion values at Yucca Mountain are likely small. Slip rates are similar to the local faults at Yucca Mountain and, thus, can be compared with these relatively well-studied local faults. For the more active faults, results from field studies generally were available.

Earthquake occurrence rates for events smaller than the maximum earthquake are estimated by assuming a combination of characteristic and a truncated exponential distributions, weighted 0.7 and 0.3, respectively. For both of these models, it is assumed that the occurrence of earthquakes smaller than the MBE (magnitude 6.2) is addressed by the regional source zones. Therefore, the size of earthquakes occurring on the regional faults is limited to magnitudes greater than or equal to **M** 6.2.

The approaches used to evaluate maximum magnitude and recurrence for other regional fault sources were used to evaluate both the possible buried strike-slip faults and the Carrara fault. Fault parameters used to characterize these faults are provided in Table SDO-3.

3.3.4 Buried Strike-Slip Fault Sources

The question of a buried strike-slip fault in Crater Flat or beneath Yucca Mountain was introduced in Section 2.0 on Tectonic Models. Although there is direct evidence that dextral strike-slip has influenced the structural development of Yucca Mountain, there is insufficient data to characterize a single-plane strike-slip fault source, particularly one active in Quaternary time. There are two ways we dealt with the issue: one was to assume that a strike-slip fault (after Schweickert and Lahren, 1997) passes beneath Yucca Mountain and that it will be undetectable until it generates an earthquake. We do not consider this a well-founded proposition; it precludes the use of many of the rational tools developed for the

present evaluation, such as estimation of slip rate, estimation of recurrence, or parametric evaluation of magnitude. We have no means of assessing the likelihood that it could happen. Thus it cannot be treated the way we treat all the other fault sources.

A second way we deal with the issue of a buried strike-slip fault source is to build on the meager evidence we have. The pattern and history of deformation at the southern end of Crater Flat, including the alignment of basaltic volcanoes, the structure along the rampart that forms the southern end of Yucca Mountain and Crater Flat north of Highway 95, evidence of vertical axis rotation at Yucca Mountain, alignment and changes of fault and fault block geometry south of the hingeline, all suggest a zone of distributed dextral faulting. The hingeline represents a structural border to this zone, albeit a poorly defined one. It could indicate a buried fault or fault zone, or a series of linked faults of relatively small local displacement that die out to the northwest. We plausibly can characterize the hingeline as a strike-slip fault trace approximately 20 km long, having as much as a kilometer of cumulative offset. We plausibly can consider the hingeline as the northwest extension of the Pahrump Valley fault zone and, therefore, infer a maximum length of about 120 km and a cumulative lateral offset of at least 4 km for the inferred fault trace. However, our preferred length for such a fault projection is limited to its possible extent beneath Yucca Mountain and Crater Flat, 27 km.

The Pahrump Valley fault shows some evidence of Quaternary activity (Piety, 1995) but the hingeline projection does not. Therefore, we assign a slip rate to the inferred buried fault projection (0.005 m/kyr) and a probability of activity of 0.4. The important point about this buried fault is that it could generate a large earthquake external to Crater Flat that could propagate focused ground motion along strike into Crater Flat, perhaps triggering any number of faults at Yucca Mountain that are susceptible to slip. Because of the large degree of assertion and speculation involved in a multiple-fault scenario, we model only a single buried strike-slip fault. The hingeline seems to be the only candidate for a buried fault (in the sense that there is no recognized fault trace at the surface) that can be characterized by at least some of the basic fault parameters established for this analysis.

We assign a probability of 0.2 to the likelihood of a fault extending along the southwest side of Bare Mountain in Amargosa Wash (the Carrara fault proposed by D.B. Slemmons, oral

commun.)(Figure SDO-6). No measurable evidence for such a fault is available; much of the area is covered by latest Quaternary alluvium. Plausible lengths range from 12 to 24 km. With no physical features on which to base an estimate of earthquake magnitude or recurrence, we have no means of arguing for either the existence of a fault or any seismogenic characteristics. We assign a provisional slip rate of 0.001 m/kyr to this hypothetical fault. This rate is so slow that surficial evidence, such as fault scarps, are generally lacking in the Great Basin.

3.4 LOCAL FAULT SOURCES

Local faults are those at Yucca Mountain and in Crater Flat. These faults are considered to be potential seismic sources on the evidence of Quaternary displacement; a number of these faults have been trenched to determine the amounts, recurrence, and ages of the Quaternary offsets. Local faults that have a history of Quaternary displacement are all normal to steeply left-lateral oblique (primarily west-dipping) faults. The faults are categorized, on the basis of length and cumulative offset, as block-bounding faults and intrablock faults. The block-bounding faults, which are the largest and most likely seismogenic, are inferred to descend through the seismogenic crust as more or less uniformly dipping, single plane faults, in keeping with our tectonic model. The intrablock faults tend to be curvilinear in plan, segmented or distributed, and only locally follow large slope breaks (i.e. have small paleo-offsets). This distinctive structural pattern is one of the primary reasons for invoking a carapace collapse effect in our preferred model. These latter faults may be confined to the volcanic carapace or linked to the block-bounding faults at relatively shallow depths. Of the numerous interconnected faults at Yucca Mountain (Figures SDO-7a, b), six are long enough to warrant consideration as penetrating the Paleozoic substrate. These six Quaternary faults are:

Paintbrush Canyon fault
Stagecoach Road fault
Solitario Canyon fault
Iron Ridge fault
Fatigue Wash fault
Windy Wash fault

Local fault parameters are listed in Table SDO-4, event scenarios are listed in Table SDO-5. All principal faults considered but the Iron Ridge and Fatigue Wash faults are considered block-bounding faults—faults that define major tilted panels of the carapace, and that are considered to penetrate to significant seismogenic depth without intersection. The Fatigue Wash and Iron Ridge faults are less confidently interpreted; the interpretations are discussed below. All local faults are considered 100 percent active, but some may be involved only in linked or distributed event scenarios (see Section 3.4.1 for further discussion of event scenarios).

Paintbrush Canyon Fault

Paintbrush Canyon fault is the easternmost block-bounding fault that cuts Yucca Mountain. It is distinguished by: (1) it coincides with the northern part of the gravity gradient that defines the eastern structural margin of Crater Flat basin; (2) it is the only Yucca Mountain fault that is continuously traceable north of Yucca Mountain, deep into the unextended caldera rim terrane (a maximum distance of about 12 km north of Yucca Wash); and (3) the footwall consists of segmented, variably tilted and dissected buttes or ridges, rather than the more or less coherent rotated panel typical of Yucca Mountain to the west, and the hanging wall is broken by horsts and graben and numerous splay faults. Despite this evidence of major fault displacement and a broad zone of fault damage, the Paintbrush Canyon fault is poorly exposed south of Paintbrush Canyon. Along Yucca Mountain, it lies buried along the east side of Midway Valley; it is questionable whether the main break has been observed or is anywhere exposed south of Yucca Wash. Estimates of down-to-the-west displacement of Tertiary volcanic strata range from 250 to 500 m (Lipman and McKay, 1965; Scott and Bonk, 1984). Average dip on the fault plane is about 70 degrees west, and slip along it has been left oblique (Simonds *et al.*, 1995). We divide the Paintbrush Canyon fault into two segments, a segment that extends along Paintbrush Canyon north of Yucca Wash (PC(N)), and a segemnt that extends along the east side of Midway Valley south of Yucca Wash (PC(S)). The preferred length of PC(N) is 6 km, and of PC(S) is 12 km. We add 2 km from the south end of Busted Butte to establish linkage with the Stagecoach Road fault, for a total maximum length of 20 km (the maximum total length is 26.3 km if we carry PC(N) as far north as seems reasonable). Paleoseismic studies at three sites--natural exposures of sand ramps on the west side of Busted Butte and one trench each at Fran Ridge and Alice Ridge--indicate that multiple Quaternary displacements have occurred. As many as five faulting episodes

may have occurred during earlier Quaternary time (Seismotectonic Framework report [USGS, written communication, 1996]). Measurements of net slip displacements vary widely among individual events and from one study site to another, with values ranging from 28 to 167 cm for a single Quaternary event. Cumulative Quaternary displacement ranges from 1.7 to 7.8 m locally. Age determinations for the various events differ from one site to another, with the most recent event ranging from 5 to 90 ka and the next youngest ranging from 70 to 150 ka. Values of recurrence intervals based on the combined age data for all three study sites range from 21 to 118 ky. Our preferred slip rate for the entire fault is 0.008 m/kyr. The slip rate is a mid-Pleistocene rate inferred from the exposures at Busted butte. Menges (Seismotectonic Framework report [USGS, written communication, 1996]) estimates the offset at the base of the strata there as 5.22 m to 7.62m; an approximate mean value of 6.4 m is used for the preferred value. The age of the base of these sediments is interpreted to be about 740 ka, based on exposure of the Bishop ash.

Stagecoach Road Fault

The minimum fault length, as mapped by Simonds *et al.* (1995) from Stagecoach Road south, is 4.5 km. However, if we extend it north to join the Paintbrush Canyon fault near the south end of Busted Butte, and extend it south to the dissected escarpment near Wells Cone, the maximum inferred length is 11 km. We take it to the most southerly mapped fault scarp for a preferred distance of 9 km. The minimum segment is expressed as discontinuous scarps in mid-Pleistocene alluvium; the south end of this trace is concealed by undeformed Holocene sediment. Alluvium of late Quaternary age is displaced 1.0 to 2.3 m; slickensides indicate chiefly dip slip. Bedrock displacement is estimated to be 400 to 600 m down-to-the-west (Scott, 1990). Average dip is 73 degrees west. Trench excavations display evidence for three to seven episodes of Quaternary faulting (Seismotectonic Framework report [USGS, written communication, 1996]). The two youngest events have been dated at 5 to 15 ka and 20 to 30 ka, respectively. Two earlier events may have occurred in late Pleistocene time, the oldest about 110 ka. The age relationships indicate preferred values of recurrence intervals in the range of 10 to 35 ky, and slip rates of 0.0057 to 0.028 m/kyr. The slip rates are calculated from data reported in the Seismotectonic Framework report (USGS, written communication, 1996) for trench SCR-T3. Here, our inferred range of dip-slip offset is 0.67 m to 2.7 m, corrected for hanging wall rollover. The offset unit, G2, has a U-series date of 108±10 ka.

Solitario Canyon Fault

The Solitario Canyon fault is a block-bounding fault that defines the west side of the potential repository block. Displacement along most of the fault trace is down-to-the-west, with offsets of more than 500 m. Average dip of the fault plane is 72 degrees west. At the north end, the fault dips east, and displacement is 61 m down-to-the-east (Scott and Bonk, 1984). From a north terminus on the south flank of Yucca Wash on south to the hingeline, it is a well-defined fault zone 14.8 km long. Farther south, it loses topographic definition and splays into three or more faults that distribute the total displacement (W. C. Day, USGS, written communication, 1997). South of the hingeline, the main fault trace may regather and strike west of south to join up with the Windy Wash fault (W. C. Day *et al.*, unpub. map); or it may trend east of south and merge with the Stagecoach Road fault. On the basis of aeromagnetic data, we infer that it becomes a buried fault--possibly a graben-bounding fault--that continues south, parallel to the Stagecoach Road fault, for a maximum length of 21.5 km. Our preferred length is 18.5 km for Stagecoach Road fault linkage option, based on mapping by Simonds *et al.* (1995). The fault appears to become more shallow in dip and more zonal in general as it extends south from the elevated area of the Prow, exposing more footwall on strike. Opposite the potential repository block, the footwall includes an attenuated slice 3.5 km long and about 200 m wide broken by complex scarps and local faults. The slice is sampled by trenches T4 and T5. The character of the main fault trace is unclear along this segment. Eleven trenches and one natural wash exposure have been excavated across or near the Solitario Canyon fault, exposing evidence that suggests as many as four paleoseismic events dated at 20 to 30, 70 to 80, 120 to 250, and 150 to 250 ka, respectively, took place along the fault (Seismotectonic Framework report [USGS, written communication, 1996]). There is also indication that two episodes of fracturing postdate the most recent event; these fracturing episodes are interpreted as being associated with moderate-sized earthquakes on the Solitario Canyon fault or with earthquakes on nearby or regional faults. Characteristics of the affected surficial deposits suggest that the fractures developed in Holocene and/or latest Pleistocene time. A recurrence interval of 35 ky is considered a minimum (two events within the past 70 to 80 ka and four within the past 150 ka). Estimates of cumulative displacement over 150 to 250 ky range from 1.8 m (from scarp measurements and trench logs) to 2.6 m (from trench logs). Our preferred average slip rate for the fault is 0.015 m/kyr, based on a preferred soil correlation age of 200 ka.

Iron Ridge Fault

The Iron Ridge fault is what Day *et al.* (written commun.) term a relay fault. Its minimum (and preferred) length of 8.3 km spans the distance between its juncture with the Solitario and Stagecoach Road faults. However, the Iron Ridge fault is well defined only along the western edge of Iron Ridge. The north and south termini are frayed out for a kilometer or more along strike; and it is possible that, at the south end, the main trace projects south to merge with the (buried) Solitario Canyon fault. If so, this gives a maximum length of 10 km. However, Iron Ridge is terminated at the hingeline, where the fault jogs east for a kilometer, around the nose of the truncated ridge, bringing the ridge-bounding fault trace within 500 m of the Stagecoach Road fault. For half its length, the Iron Ridge fault forms a bedrock-alluvial contact with prominent scarps. Displacement is chiefly dip-slip, down to the west on a fault plane that dips 70 degrees. At least one locality shows multiple late-Quaternary faulting (Simonds *et al.*, 1995). The Iron Ridge fault is a complex and damaged zone of normal faults that have numerous splays and flare-off fractures (including the Abandoned Wash fault). As such, it simply may be the most prominent of a wide zone of linked-bridging faults that have formed in response to extension and left-lateral shear between the Solitario and Stagecoach Road faults. Its seismogenic significance is questionable; it may be confined to the carapace (minimum width of about 2 km) or at least not extend deeply into the Paleozoic substrate as a single-plane (about 5 km). A.R. Ramelli (written communication, 1996) estimates 2 m of offset has occurred since mid-Quaternary, but considering erosion over this time, the offset could range from 1.7 m to 2.2 m. Ramelli correlates the offset unit with deposits that make up the Solitario surface of Peterson *et al.* (1995). This surface ranges in age from 433 ka to 730 ka. To calculate our preferred slip rate (0.0033m/kyr) we chose a mid-point age of 600 ka. Smaller displacements (0.5, 0.7, 1 m; Table SDO-5) are reported from trench SCF-T2 observations (Seismotectonic Framework report [USGS, written communication, 1966]).

Fatigue Wash Fault

The Fatigue Wash fault is a north- to northeast-striking, down-to-the-west normal to steep oblique fault located about 3.5 km west of the potential repository. From its south merger with the Windy Wash fault to a possible northern merger with the Windy Wash fault at the south end of West Ridge, it has a minimum length of 12 km. It also could be carried north along a deep notch that defines the east side of West Ridge to the Prow, where it frays out in a plexus of normal faults and graben. The longest trace through this area takes it into the

caldera rim zone, for a maximum length of 22 km. We prefer 18 km because of uncertainty in the north termination. The Fatigue Wash fault is remarkably parallel to the Windy Wash fault, which lies only about a kilometer to the west, along the west flank of West Ridge. It probably is not a major fault despite its considerable length. Its geometry and association with bridge faults to the Windy Wash fault suggests that the Fatigue Wash fault is either: (1) one or more linked slices of the footwall of the Windy Wash fault, formed in response to Windy Wash faulting, or (2) a parallel subsidiary fault that merges with the Windy Wash fault beneath the carapace. The fact that Fatigue Wash fault merges with the south Windy Wash fault strongly implies that the Northern and Southern Windy Wash faults are indeed a single continuous fault, or at least linked faults, the middle (linking) part of which is buried but which apparently forms a graben in association with the Fatigue Wash fault in the vicinity of the hingeline. Average dip of the fault plane is 73 degrees, and displacement is about 72 m (Scott and Bonk, 1984). Three to six paleoseismic events (five being the preferred number) are documented by the stratigraphic and structural relations exposed in two trenches excavated in Quaternary deposits along the fault trace. Four of the preferred events occurred after 730 ka. The two most recent events probably took place between 20 to 70 ka, suggesting a late-Quaternary clustering of earthquakes. An estimate of the long-term average recurrence interval ranges from 120 to 250 ky, with a preferred value of 185 ky. Two meters of cumulative vertical displacement during the last four events indicate a Quaternary slip rate of 0.002 ± 0.0001 m/kyr. Data from measurements on scarps outside the trenches indicate a greater Quaternary slip rate of 0.009 ± 0.006 m/kyr (Seismotectonic Framework report, [USGS, written communication, 1996]). Offsets at trench SP5 were measured by projection of intact correlative surfaces to give values of 2.8 and 3.9 m of nomal displacement. A minimum value of 2.5 m of vertical separation is estimated based on uncertainties of scarp measurement and surface projection. The fault scarp is developed in the Solitario surface of Peterson *et al.* (1995) which is estimated to have and age range of 433 ka to 739 ka, with a preferred age of 600 ka.

Windy Wash Fault

We consider the north-striking Windy Wash fault to be a segmented or linked block-bounding fault. The north strand extends from the Prow south for 9 km. It can be carried north of the Prow into the caldera rim zone an additional 2 km, but we prefer a length of 9 km to accommodate the uncertainties. The south strand extends south from trench CF2 for

8 km as a well-defined fault trace (Simonds *et al.*, 1995). It can be carried farther south by linking scarp segments for a preferred length of 11.5 km. If we carry it north of trench CF2 (along an east-facing scarp; Simonds *et al.*, 1995), we obtain a maximum length of 12.5 km. The total maximum length of the linked north and south segments is about 24 km. Apart from the central, down-to-the-east scarp in alluvium, the fault has down-to-the-west displacement of a few hundred meters (Scott, 1990). Average dip of the fault is 63 degrees to the west, and offset is chiefly dip slip; but locally both right and left oblique slip have occurred. Evidence of Quaternary displacement is limited to subtle scarps in alluvium and to fractures in hanging walls of fault line scarps. Three trenches were excavated across scarps in alluvium along the central part of the fault (USGS, written communication, 1996). One trench displays evidence of eight coseismic surface ruptures during Quaternary time; the other two display evidence of five ruptures. Mid- to late-Pleistocene gravel in one trench is displaced about a meter down-to-the-west, and Holocene silt above the main fault plane is ruptured. Dating of soils and fine silt deposits indicates that the surface faulting along the Windy Wash fault took place about 3, 40, 75, 150, 200, 240, 340, and 400 ka (preferred values or mid-points of the ranges of event timing). The recurrence interval of faulting for the last four events is about 40 to 50 ky, and between 50 to 57 ky for the longer record; the preferred recurrence interval is 40 ky. Total net displacement on the oldest hanging wall deposit is 3.67 m with an uncertainty of ± 0.3 m. U-series ages constrain the offset unit to be at least 300 ka old, and as much as 400 ka (USGS, written communication, 1996), indicating a long-term average slip rate ranging from 0.009 to 0.017 m/kyr. Displacements measured in trench CF-2 are 0.6 m to a maximum value of 0.88 m (USGS, written communication, 1996). A 1 m offset is proposed on the basis that the trench may not be sited at a point of maximum displacement.

In addition to the faults described above, several other faults at the site may penetrate the carapace, but in our evaluation these are capable of generating maximum earthquakes only at or below MBE levels of moment magnitude 6.4 ± 0.2; thus, these faults are considered to be covered by the background seismicity. Several of these faults are used in the linked and distributed event scenarios developed for this analysis. These include the Bow Ridge, Ghost Dance, Abandoned Wash, Northern Crater Flat, and Southern Crater Flat faults. Although these faults are considered not capable of individually generating an earthquake larger than

the maximum background, by virtue of linkage or distributed connections they may make a small contribution to some of the earthquake scenario parameters.

Bow Ridge Fault

The Bow Ridge fault has been called a block-bounding fault (W. C. Day, written communication, 1998), but little is known about it except that it is a largely alluvium-covered, north-striking, west-dipping normal fault that lies along the east side of the potential repository block for a length of 7 km. It is exposed only along the west side of Bow Ridge and Exile Hill (site of trench 14) and in the ESF. Structure at Bow Ridge is complex, marked by breccia and small graben; a throughgoing fault that defines the arcuate scarp face of Bow Ridge is strongly suggested. Its shape and bounding structure imply that the Bow Ridge fault, as an inferred single-plane fault, arcs abruptly east to merge with the Paintbrush Canyon fault. However, the Bow Ridge fault may simply represent an assemblage of variously striking fault segments, all part of hanging wall damage associated with the Paintbrush fault. The fault is defined in places along the west side of Exile Hill by a fault line scarp and a bedrock-colluvium contact (Simonds *et al.*, 1995). Here, Tertiary volcanic rocks show about 125 m of down-to-the-west displacement along a 65- to 75-degree, west-dipping, left-oblique fault plane. North of Isolation Ridge, the Bow Ridge fault has east-side-down displacement. A series of trenches has been excavated to reveal a complex fault zone developed in highly fractured Tertiary volcanic rock and Quaternary colluvial deposits. Several faulting events are evident in the surficial units, the oldest more than 700 ka and two younger events 130 to 150 ka and 30 to 130 ka, respectively. A minimum age of 48 ± 20 ka is established for the youngest displacement. Cumulative dip-slip displacement of the Quaternary deposits ranges from 30 to 45 cm (considering an oblique slip component, net slip is 33 to 70 cm). Preferred values for average recurrence intervals of faulting events range from 100 to 140 ky. Slip rates range from 0.002 to 0.007 m/kyr, with a preferred value of 0.003 m/kyr.

Ghost Dance Fault

The Ghost Dance fault strikes north through the central part of the repository block between Wren Wash on the north and Abandoned Wash on the south, a distance of 3.7 km. The fault is not exposed as a single-plane feature, but consists of three right-stepping segments. The north segment is 660 m long; it extends south to Split Wash, is 2 to 4 m wide, and has as

much as 6 m displacement down-to-the-west. The central segment is 450 m long; it extends from Live Yucca Ridge to Antler Ridge, forms a zone of breccia-filled splays from 1 to 2 m thick over a zone as much as 150 m wide, and has as much as 20 m down-to-the-west displacement. The south segment is 830 m long; it extends to Broken Limb Ridge, forms a breccia zone as much as 55 m wide, and has about 27 m of down-to-the-west displacement. Near Broken Limb Ridge, the fault bifurcates, the most prominent and continuous branch extending southwest for 1.5 km to apparently link with the Abandoned Wash fault of Scott and Bonk (1984) at Abandoned Wash. The Ghost Dance fault does not physically connect with the Abandoned Wash fault; it more or less comes into alignment with the local slip planes that comprise the north extent of the Abandoned Wash fault (W. C. Day, USGS, written communication, 1996).

The amount of brecciation and offset along the Ghost Dance fault decrease in the vicinity of the ESF and Ghost Dance Wash (a 2- to 15-m wide breccia zone; 3 to 6 m of offset); but displacement increases with proximity to the Abandoned Wash fault (as much as 17 m). Throughout its length, the Ghost Dance fault ranges in dip from vertical to 75 degrees west and is characterized by one or more breccia zones of variable thickness. The breccia typically is uncemented or an open fretwork that shows little or no evidence of size or shape segregation or milling due to shear. The Ghost Dance fault has no aeromagnetic signature and only small, low-amplitude gravity lows along the hanging wall (C. J. Potter *et al.*, written commun.).

Four trenches have been excavated in Quaternary sediment across projected traces of the Ghost Dance fault, but no offset of any of these deposits has been observed. In one trench, for example, 40 to 50 cm of unfaulted latest Pleistocene to early Holocene (age 82.8 ± 1.9 to 9.6 ±0.1 ka) slope-wash colluvium and fine-grained eolian deposits can be seen to overlie faulted and fractured tuff. A discontinuous fracture, however, was observed in a highly calcified horizon draped over bedrock in one trench; but it does not extend upward through the overlying units. Age relations suggest that the fracturing must have occurred at least 82 ka; the fracture may have resulted from a seismic event on any number of faults in the area. The non-integration of the fault segments along strike; the brecciated, zonal character and the poorly defined, fayed fault terminations; and the lack of shear tooling or shear segregation within and along the fault breaks, all indicate that the rock broke with minor

offset during a single, short-lived failure event and has not undergone subsequent deformation that might have modified the initial damage.

We interprete the Ghost Dance fault as a tear fault confined to the carapace. It is considered to have resulted from clockwise torque and bending applied to the central block during the initial to peak phase of vertical axis rotation. C. J. Potter *et al.* (written commun.) deduce that the right steps may be controlled by pre-existing sets of closely spaced, northwest-striking cooling joints. Because the Ghost Dance fault is a relic of ancient tensile failure and has virtually no cohesive strength, it is a locus of tensile strain for overlying cohesive strata and likely will remain so as long as extension dominates the stress regime at Yucca Mountain.

Abandoned Wash Fault

The Abandoned Wash fault is essentially a 6-km-long zone of small normal faults and horsts and graben of negligible offset that connects the Ghost Dance and the Solitario Canyon faults. It probably is structurally and genetically akin to the Ghost Dance fault and is confined to the carapace. Its presence is marked by deep erosion. Where it crosses ridge divides and especially at its junction with the Solitario Canyon fault, there is little geomorphic indication of offset.

Northern Crater Flat Fault

The Northern Crater Flat fault is a poorly defined structure that appears to consist of aligned horsts and graben in a zone about 600 m wide. Dominant displacement is down-to-the-west normal or normal oblique. It trends north to northeast along the east side of Crater Flat, about 5 km west of the potential repository. As mapped (Simonds *et al.*, 1995), the maximum length is about 12 km. It terminates to the south at the hingeline and frays out to the north among normal faults within the caldera rim zone. Its location implies that it is antithetic to Bare Mountain fault; hence, we infer a relatively small fault width. Only one of the two trenches excavated across the center of the projected trace of the fault intersected the fault. Stratigraphic and structural evidence for as many as five paleoearthquake events was observed in this trench. On the basis of a minimum age of 500 ka for the oldest exposed Quaternary unit and an estimate of less than 10 ka (preliminary age date of 5.46 ± 1.4 ka) for the most recent faulting event, a possible range in average recurrence interval is 120 to

160 ky. Cumulative displacement for all five events is about 160 cm, indicating a slip rate of 0.003 m/kyr since the earliest event.

Southern Crater Flat Fault

The Southern Crater Flat fault is a north- to northeast-striking, normal fault that is down to the west, and has a left-slip component. It is defined by a basalt-alluvium contact, fractured carbonate-cemented alluvium, subtle scarps in alluvium, and a linear stream channel (Simonds *et al.*, 1995). North of trench CFFT1, the fault trace is subtle. It projects toward convergence with the north end of the Southern Windy Wash fault. Alternatively, the north end of the Southern Crater Flat fault could be offset 1.5 km east of the Northern Crater Flat fault by slip along the hingeline. The Southern Crater Flat fault can be traced south for a maximum of about 15 km. The minimum length, as mapped by Simonds *et al.* (1995), is 6 km. The amount of offset is unknown; slickensides on a plane that dips 70 degrees indicate left-oblique movement. Two trenches were excavated across the Southern Crater Flat fault, exposing alluvial gravel deposits that contain accumulations of fine-grained aeolian material. There is evidence that at least three paleoseismic events occurred during the Quaternary, for a total measured offset of 24 to 65 cm. Preliminary age determinations of the alluvial materials and of opaline silica collected from the inner rinds of clasts indicate that the oldest event occurred 130 to 250 ka, the next 10 to 60 ka, and the youngest 2 to 6 ka. Minimum recurrence intervals are in the range of 5 to 60 ky; the estimated maximum vertical slip rate is 0.002 m/kyr.

3.4.1 Event Scenarios: Single Faults, Linked Faults, and Distributed Faults

For local faults, three types of maximum earthquake models, or scenarios, are considered: single fault, linked fault, and distributed fault scenarios. Single-fault scenarios are given for the six local (i.e., Yucca Mountain) faults identified for this analysis (Figure SDO-7a). Linked-fault scenarios were developed by considering direct structural linkages and indications of potential event correlation between adjacent faults (Figure SDO-7b). Earthquake lengths are based on the end-to-end length of the combined fault plane segments. Distributed-fault scenarios involve parallel faults that slip together. For distributed fault scenarios, maximum surface displacements are combined in a cross-strike fashion, and lengths may or may not be increased over single-fault scenarios. All event scenarios, individual fault, linked faults, and distributed faults, are presented in Appendix SDO-1. Six

faults are involved, and one (Paintbrush Canyon) has two earthquake segment alternatives. Thus, there can be seven individual fault scenarios. Nine combinations of faults are modeled for the linked scenarios (Figure SDO-7b), and eight combinations of faults are modeled for the distributed fault scenarios. The relative weighting of each scenario is expressed in the occurrence rates given in Appendix SDO-1; the generation of these occurrence rates is discussed in section 3.3.3 on earthquake recurrence.

3.4.2 Fault Source Parameters for Maximum Magnitude

Fault source parameters are the basic, quantitative components needed to estimate the maximum earthquake a mapped fault is capable of generating. We estimate maximum earthquake magnitudes on the basis of as many parameters as possible to mitigate the uncertainties inherent in any individual parameter. An attempt is made to capture the uncertainties of the input values by using minimum and maximum values along with preferred values; various observational uncertainties are considered to be accounted for in empirical relationships relating fault parameters to magnitude. We consider the fault parameters we measure at the surface to be representative of the seismogenic structure at depth. For each scaling parameter, either an empirical relationship or an equation is used to scale magnitude from the input parameters. For the final value, we averaged the results for our magnitude estimates.

Using multiple magnitude estimation techniques provides the epistemic uncertainty to the final value. To characterize some of the aleatory uncertainty that also exists, each final value is considered to have an uncertainty of $\pm$ 0.25 magnitude units. This is a comparable value to the standard deviations of the regressions used to scale earthquake magnitude.

A logic tree (Figure SDO-8) was designed on the simplest sequence of parameter decisions necessary and justified by the data. The sizes of potential maximum earthquakes were scaled using fault length, fault width, maximum surface displacement, length times maximum surface displacement, fault area, length and slip rate, and calculations of seismic moment. Measured values are ordered in our assessments (Table SDO-4) and weighted on the basis of the uncertainties we assess for each parameter. The bases of the various input parameters are discussed in the respective subsections that follow.

Geometry of Planar Normal Faulting

We recognized the sparcity of data on the geometry of active normal faults for the Yucca Mountain region and decided to use data from studies of normal faulting earthquakes from other areas of the Basin-Range province as well as the focal mechanism data provided at the YMPHSA workshops by Ken Smith (1996, 1997) of the University of Nevada and the earlier research on the seismicity of southern Great Basin, including the Yucca Mountain area (Rogers *et al.*, 1991). We also studied the data of Doser and Smith (1989) who summarized the geometry of historic normal faults and used focal mechanism data for both short and long period arrivals, source mechanisms from seismic moments and from geologic and related geodetic information.

We also referred to published working models of large Basin and Range-type normal faulting earthquakes from Smith and Arabasz (1991). These include three of the largest earthquakes in the western U.S. that had dominantly normal-faulting slip: Ms 6.8 Dixie Valley, Nevada, earthquake of 1954; the Ms 7.5 Hebgen Lake, Montana, earthquake of 1959; and the Ms 7.3 Borah Peak, Idaho, earthquake of 1983.

The primary characteristics of these large earthquakes include rupture on planar normal faults, dipping 40° to 60°, nucleation at mid-crustal depths of about 15 km, and no evidence from the seismic data of non-planar geometries.

Estimates of fault dip are based on studies of the most modern (since 1954, when well-recorded seismic data became available) historical, scarp-forming nomal-faulting earthquakes as analogs. We chose 50°, 60° and 75° as our distribution of likely dips. Our rationale for these values is based on the minimum dip of 49° for one of the 1959 Hebgen Lake, Montana, main shock segments, including an error of 10°. We assigned 60° the greatest weight because this is a typical mid-value for the dips of earthquakes in the Basin and Range province (e.g., Doser and Smith, 1989, their Figure 4) and it is commonly measured surface dip throughout the province. It was determined using the most modern methodology and with the widest variety of instrumentation, short-and long-period data; several authors found a similar geometry (Richins *et al.*, 1985; Doser and Smith, 1985; Stein and Barrientios, 1985; Nablek *et al.*, Oregon State University, written communication, 1990). The upper bound value of 75° was used because it is considered a bound of the steepest dips of historical

earthquakes from seismic data, such as the 78±5° dip of the 1954 Rainbow Mountain, Nevada, earthquake. Also, this highest value is near that for steeper normal surface faulting of these normal-faulting events of approximately 90°. The estimates of dip are also closely constrained by field measurements made during mapping of Yucca Mountain and observations made from logging the ESF. Data from fault mechanism solutions for nearby earthquakes, notably from that of the 1992 Little Skull Mountain earthquake, also guided our estimates. Our observation, supported by regional data, is that steep dips measured in outcrop tend to decrease to moderate dips at seismogenic depths.

Alternative Models

We considered low angle and listric fault geometries as possible seismogenic structures. But because of the global lack of unequivocal data on focal mechanisms of large, scarp forming normal faulting earthquakes having dips less than ~40°, we did not consider the shallower fault dips for earthquake source at Yucca Mountain. That is not to say that low angle and listric faults do not exist in the Yucca Mountain region, but we consider that if they are present, they are not now seismogenic and were generated in an earlier tectonic regime. Hence, we do not appeal to detachment faulting as a tectonic model for fault behavior.

Fault width refers to the downdip dimension of a fault. Unless otherwise noted, we consider the width to be the seismogenic depth, taking into account the fault dip (i.e., the seismogenic depth divided by the sine of the fault dip).

Magnitude versus fault length. Estimating magnitudes on the basis of fault length is a conventional approach for all fault sources. Three lengths are estimated: the minimum, preferred, and maximum. Because many of the faults at Yucca Mountain are short relative to depth of the seismogenic crust, these lengths are considered to correspond to earthquake segments. Two regressions are used as scaling relations to estimate moment magnitudes: Mason (1996) and Wells and Coppersmith (1994). These relations are shown in Table SDO-2. Mason's relationship is based on earthquakes from extensional environments; Wells and Coppersmith (1994) use a worldwide data set of normal to oblique-slip earthquakes.

Magnitude versus maximum surface displacement. Because single-event surface displacements are available from the many trenches involved with this project, the

opportunity exists for estimating earthquake magnitude based on surface diplacement. Many of the displacements are small (less than a meter). Several trenches appear to be located such that the maximum surface displacement would have been recorded, but this is speculation, and local situations that would diminish surface rupture could prevail. There generally were only a few points of information along any one fault, and information commonly varied at each site. Only a few faults appeared to have documentable modes of rupture that might be inferred as average surface displacements. Many of the paleoevents at the sites have displacements of a few decimeters to a meter, and surface manifestation, after such rupture works its way through the volcanic carapace, may be attenuated up dip, broken up and discontinuous at the surface, and/or widely distributed between faults. Estimates of maximum surface displacement could be made and bracketed, however, using maximum single-event displacements from the trenches, or the maximum displacements for an event from different trenches. For distributed ruptures, displacements for the same event are added in a cross-strike manner to obtain a maximum surface displacement of the event.

As with fault length, two regressions are used to scale earthquake size as a function of displacement, one by Mason (1996), and one by Wells and Coppersmith (1994). These relations are shown in Table SDO-2. Mason's relationship is based on a data set using earthquakes from extensional envionments. Wells and Coppersmith use a worldwide data set. Mason's regression uses surface-wave magnitude, which is assumed to be equal to moment magnitude (see discussion in Wells and Coppersmith, 1994). Wells and Coppersmith's regression is in moment magnitude.

Magnitude versus fault length x maximum surface displacement. Mason (1996) developed a regression for magnitude versus fault length times maximum surface displacement, which provides a parameter that more closely estimates seismic moment than either of the base parameters individually. Both fault length and maximum surface displacement are determined as discussed above and simply are multiplied. Mason's regression uses surface-wave magnitude, which is assumed to be equal to moment magnitude (see discussion in Wells and Coppersmith, 1994).

Magnitude versus fault area. Fault area is estimated from two parameters, fault length and downdip width. Fault area also affords a closer estimate of seismic moment than does a

single parameter. However, the fault areas used in magnitude-scaling relationships typically are derived from aftershock data, so there is a large uncertainty in the resulting values. For example, many of the minimum downdip widths of faults are significantly limited by intersections with other faults. This limitation was added to the information constraining earthquake sizes by using the magnitude versus fault area relationship and by calculating seismic moments. Fault areas are calculated using the estimated fault lengths and downdip widths, and magnitudes are scaled using Wells and Coppersmith's (1994) regression, acknowledging the error produced by the lack of internal consistency (fault area versus aftershock area). Downdip widths were estimated considering maximum dynamic seismogenic depth, ranges in fault dips, and possible structural intersections.

Magnitude versus length and slip rate. Anderson *et al.* (1996) developed a magnitude-scaling relationship that includes fault slip rate and fault length. Their approach is based on observations that, for a given length, faults having lower slip rates or faults having longer recurrence intervals tend to have larger earthquakes. Although the method is controversial, it builds on the previously established observation that earthquake size has a dependency on earthquake return time (e.g., Kanamori and Allen, 1986) and tectonic environment (Scholz and Aviles, 1986). Wesnousky (1986) sorted magnitude versus fault length data into high and low slip-rate categories and regressed them separately to account for the potential effects on slip rate. Unfortunately, several of the faults in the Yucca Mountain area have slip rates lower than the data used in Anderson *et al.*; thus, the overall technique is given a third of the weight of other, more established, approaches.

Magnitude versus seismic moment. Seismic moments are estimated using fault area times average subsurface displacement times shear rigidity. Shear rigidity for the seismogenic zone is taken to be 3×10^{11} dynes/cm^2. Average subsurface displacements are considered to be half the maximum surface displacement. This ratio was chosen after examination of Figures 6 and 7 of Wells and Coppersmith (1994) and considerations that D.B. Slemmons articulated during the January 1997 Probabilistic Sesimic Hazards Analysis Workshop. Slemmons suggested that new studies will indicate that average subsurface displacements will be found to be about 38 percent of maximum surface displacements. Wells and Coppersmith (1994) find a mode of this ratio from 44 earthquakes to be 0.76. We use the rough average of these two ratios, 50 percent.

3.4.3 Recurrence

The assessment of earthquake recurrence for the local fault sources is based on the interpretation that all three types of rupture scenarios (individual ruptures, linked ruptures, and distributed ruptures) can occur. These data are interpreted to define the frequency of maximum events for each type of rupture behavior. The recurrence rates for "maximum" earthquakes are defined using the procedure described below. In constructing the recurrence relationships we follow the convention of Youngs *et al.* (1987) and consider that the maximum magnitude earthquake assessed above is the central estimate of a "characteristic" magnitude interval. For the characteristic and maximum moment recurrence models discussed below, the characteristic events are uniformly distributed in the magnitude range M_{max}±¼, such that the upper limit of the recurrence relationship is M_{max}+¼. For the exponential recurrence model the upper limit is also set at M_{max}+¼. Thus, the frequency of "maximum" earthquakes is interpreted to be the frequency of earthquakes of magnitude greater than or equal to M_{max}-¼. This frequency is interpreted to be the frequency of earthquakes within 1/2 magnitude unit of the maximum magnitude earthquake defined for each type of rupture behavior. For the individual fault rupture scenarios, the frequency of earthquakes smaller than the maximum magnitude minus 1/2 magnitude units are estimated using either a characteristic or truncated exponential recurrence model, weighted 0.7 and 0.3, respectively. Our preference for a characteristic model is based on the observation that paleoearthquake displacements exposed in the trenches at Yucca Mountain demonstrate repeated offsets of about a meter. However, we do not discount the observation that the historical seismicity of the southern Great Basin may have a truncated exponential distribution. The linked and distributed rupture scenarios are interpreted to be larger earthquakes that occur in addition to the individual rupture scenarios. Thus we allow for only these events to occur. As was the case for the regional sources, the size of earthquakes occurring on the local faults is limited to magnitudes of 6.2 and larger. The occurrence of smaller earthquakes is addressed by the regional source zones.

The relative frequency of each type of rupture behavior is estimated from the recorded paleoseismic data. If there have been n paleoearthquakes on fault x, then we have n observations of the fault's behavior. The number of times that it has ruptured as a single fault versus the number as a linked or distributed fault define the relative frequency of these types of behavior. Because of the uncertainty in assessing what type of behavior actually occurred

in each paleoevent, we assess the relative likelihood (or probability) of the various types of behavior that might have occurred for each event. Averaging these over all of the paleoevents provides an assessment of the expected relative frequency of each type of event. These relative frequencies are then multiplied by the overall frequency of events on the fault to define the actual frequency of occurrence of each type of behavior.

This type of analysis is motivated by the desire to incorporate as much of the extensive paleoseismic data set that has been developed at the Yucca Mountain site as possible. To be as clear as possible about this analysis, we have broken it up into steps, which are described individually in the following subsections, and an example is illustraded in Figure SDO-9. This analysis tracks earthquake occurrence rate (events/year) rather than recurrence intervals.

Analysis step 1 determines the occurrence rates of earthquakes along the principal local faults. Three techniques were used to determine the occurrence rates for the faults, a moment rate technique, an average earthquake recurrence interval technique, and an average interseismic interval technique.

The moment rate technique uses the various fault lengths, down-dip widths, and slip rates to generate a moment rate ($MR = LWS\mu$, where MR = moment rate, L = length, W= downdip width, S = slip rate, and μ = shear rigidity [3×10^{11} dyne/cm^2]). Slip rates were determined using total offsets from trench logs and the estimated time since those offsets (S=O/T; S=slip rate, O = offset, T = time). Uncertainties in slip rates are calculated by cross multiplying the range in possible offset and dating uncertainties. The seismic moment was calculated using preferred values. Using the full range in moment estimations produced unreasonable results for occurrence rate. Thus, the maximum and minimum values were obtained by use of the preferred parameters, but considering the maximum and minimum displacement values. The seismic moment estimated for the fault is divided by the moment rate to obtain the recurrence interval for events. This interval is inverted to get occurrence rate.

The average earthquake recurrence interval technique is estimated by taking the age of the oldest reported paleoseismic event and dividing the age by the number of events that have occurred since, minus the most recent event. Since the elapsed time since the last event is an

incomplete interseismic interval, the last event and the time since the last event are removed from the calculation.

The average interseismic interval technique averages the preferred interseismic intervals determined for each fault. The maximum and minimum interseismic intervals are adopted directly for the maximum and minimum values. Five of the six principal faults have at least four or more paleoseismic events to consider for interseismic intervals. The other fault (the Iron Ridge fault) has two to three events.

In general the preferred values of the average and interseismic interval techniques are similar as we might expect. The most significant difference comes from the estimation of the maximum and minimum values. For the average earthquake recurrence interval technique, the uncertainty that is translated into maximum and minimum values is determined from the uncertainty in the age of the oldest event and the number of events since. The uncertainty in the interseismic interval technique comes from the variation of the interseismic intervals themselves.

These three estimates, moment rate, average recurrence interval, and interseismic interval, are averaged for estimating the occurrence rates ascribed to the fault. We weight these three methods equally because the uncertainty in the methods is roughly the same.

Analysis step 2 is an empirical approach that uses data from the Yucca Mountain trenches to identify paleoseismic events. These are listed in Appendix SDO-2 for each fault, with a nominal age of each event listed as well. Then a single and perhaps multiple possible event histories are determined for a fault. If multiple possible event histories exist, the relative likelihood of these histories is assessed, and a relative weight is assigned to each history. For example, if there was uncertainty as to whether a particular paleoseismic event occurred, two models of paleoseismic history can be used, one with the uncertain event and one without.

Analysis step 3. Each paleoseismic event is considered an observation or sampling of a fault's behavior (whether it might behave as an individual, linked, or distributed fault during an earthquake event). Each paleoseismic event is considered an equally valuable piece of information, and is given a weight in the analysis of $1/n$, where n is the number of

paleoevents in the history. This is not a "relative weight" in the classic sense; thus we call this a relative frequency. The series of paleoevents thus define the relative frequency of different rupture patterns.

Analysis step 4 divides paleoseismic events into event scenarios and relatively weights these scenarios. Three main models of event scenarios are considered, (1) single fault, (2) linked faults, and (3) distributed faults. The potential event scenarios are determined considering potential correlations of events from trenching data on different faults and structural linkages.

Because of the small cross-strike distances, the highly interconnected nature of the faults, empirical information from historical Basin and Range province earthquakes, and the apparent similarities in age of paleoseismic events along different faults within the relatively small area of Yucca Mountain, we considered the occurrence of multiple fault scenarios to be a likelihood in some cases. The weighting between different event scenarios was based on the uncertainties in the age estimates of events, secondary correlation evidence (e.g., same volcanic ash found within the fault zone or in an event horizon), representations of event scenarios given in Chapter 5 of the Seismotectonic Framework report (USGS, written communication, 1996). Most of the weights are 50/50 or 30/70 between the single faults and multiple fault scenarios dependent on age uncertainties and number of correlating factors, or are equal weights across all event scenarios reflecting similar uncertainties in dates and high degrees of structural connectivity.

Earthquake lengths are based on the end-to-end length of the combined faults for the linked scenarios. Distributed fault scenarios involve parallel faults that fail together. For distributed scenarios, maximum surface displacements are combined in a cross-strike fashion, and lengths may or may not be increased over single fault scenarios. All events scenarios are presented in Appendix SDO-1 as a listing of all events, and under each of the six principal faults considered.

Analysis step 5 calculates the occurrence rate of the event scenarios for each paleoseismic event. This is done by multiplying the occurrence rate from each fault times the relative weight of the paleoseismic histories times the relative frequency of a specific paleoseismic

event ($1/n$, where n is the number of events) times the relative weighting of the specific event scenario (based on age uncertainties and structural connectivity).

Analysis step 6 adds up the occurrence rates for each event scenario with that from multiple paleoseismic events along a fault. The occurrence rates for each event scenario involved in multiple paleoseismic events are added together. This now represents the occurrence rate of a specific scenario per fault. These results are displayed in the beginning of Appendix SDO-1 by principal fault. Note that there are different occurrence rates for some of the same event scenarios for different faults. These are resolved in the next step.

Analysis step 7 combines the occurrence rates from event scenarios common to multiple principal faults. A simple averaging of the occurrence rates from different faults is done to accomplish this. These final values are the occurrence rates then used for the different event scenarios.

3.5 VOLCANIC SOURCES

Our team recognized the importance of volcanic-related seismicity in light of the Quaternary basaltic volcanoes near the Yucca Mountain site. We used the data from the Yucca Mountain volcanic hazard analysis (Geomatrix Consultants, written communication, 1996). We considered several sources that could be activated along the northeast alignment of approximately 1-million-year-old volcanic vents across Crater Flat, as well as those that might be associated with the Lathrop Wells vent at the south end of Crater Flat.

One volcanic source (Figure SDO-10) is taken to represent volcanism along the alignment of vents within an area determined by a spatial smoothing of the average distance between volcanic vents, that average defining a perimeter around each vent to make up a northeast-aligned source zone. We assumed two to three volcanic events per million years. The potential activity of this source was weighted 0.25.

Our second volcanic source is at the south end of the vent alignment that encompasses the 70,000-year-old Lathrop Wells volcanic vent (Figure SDO-10). We weighted the potential activity of that source 0.75.

The maximum magnitude for a volcanic earthquake was assigned on the basis of Smith and Jackson (1996), a study of volcanic-related earthquakes worldwide, as well as the recently completed Yucca Mountain Probabilistic Volcanic Hazard Assessment and its documentation (Probabilistic Hazard Analysis for Yucca Mountain, Nevada, Civilian Radioactive Waste Management System, Management and Operating Contract, BA00000-01717-2200-00082, Rev.0).

We characterize the distribution for volcanic-related earthquakes magnitudes as follows.

Magnitude	Weight
6.0 ± 0.2	0.1
5.8 ± 0.4	0.6
5.5 ± 0.4	0.3

Smith and Jackson (1996) found a maximum magnitude of M 4.5 for basaltic vents. We choose a preferred Mmax of 5.8 for volcanic source zones in the Yucca Mountain area on that basis, with the most likely occurrence along our northeast alignment.

4.0
HISTORICAL SEISMICITY: EVALUATION AND TREATMENT OF RECORD PARAMETERS

Spatial Smoothing

The final earthquake catalog data were treated by a smoothing algorithm as a means of distributing the seismic moment uniformly across the source zones.

Our smoothing parameters were choosing from three zones:

(a) Uniform smoothing with fixed boundaries of the source areas were chosen to approximate the long term windows (thousands to hundreds of thousands of years) that would encompass seismotectonic potential of our identified source areas.

Weight = 0.50

(b) We considered shorter time frames of tectonic processes (a few hundred years), we assigned a weight to Frankel's (1995) smoothing algorithm for a 10 km radius of the Gaussian kernel (with a 1 s standard error) and with magnitude 3 and 5 cutoffs. This radius was assumed to take into account the events with a 10 km aftershock length that generally are consistent with a few tens to a few hundred year return period for the Basin-Range.

Weight =0.25

(c) We addressed a wider geographic window (several hundred years) by assigning a wider aperture of 20 km to Frankel's (1995) smoothing algorithm for the Gaussian kernel for a 1 s standard error for his radii specifications for magnitude 3 and 5 cutoffs. This considers aftershock distributions that correspond to larger and less frequent earthquakes of several hundred years for the Basin-Range.

Weight = 0.25

Alternate Model—We initially attempted to smooth the earthquake catalog data by developing a weighting algorithm that would have as its smoothing kernel a radius determined by first searching a grid up to 50 km, then assigning a window with a radius on the basis of the aftershock length vs. magnitude (using the relationship of Wells and Coppersmith, 1994). However, because of the low background historical seismicity of the Yucca Mountain area, this method produced a very small effective search radius of ~5 km or less and was not used.

Relationships Between Magnitude Scales

We studied the magnitude scales for various catalog contributions that were done by Woodward-Clyde Federal Services. After examining these conversions we chose to use them as described in the Woodward-Clyde Federal Services Yucca Mountain PHSA unpublished report (I. Wong, WCFS, written communication, 1996).

Magnitude Uncertainties

We assessed magnitude uncertainties by comparing the catalog period with the Woodward-Clyde Federal Services Yucca Mountain PHSA unpublished report on the Yucca Mountain composite catalog (I. Wong *et al.*, WCFS, written communication, 1996) as follows:

Time Period	Estimate of Magnitude Uncertainty
1900-1930	± 0.8
1931-1961	± 0.6
1962-1970	± 0.5
1971-1978	± 0.2
1978-present	± 0.2

Declustering Parameters

We used a distribution for declustering of our earthquake catalog as follows.

(a) We used Youngs *et al.* (1987) declustering parameters (updated Geomatrix version 5) for the four weighting parameter sets.

Weight = 0.6

(b) We used the Veneziano and van Dyke (1985) approach but downweighted the method as it is not yet fully accepted. It used a variable radius-dependent spatial smoothing window to acquire sufficient numbers of earthquakes to determine if a single event was independent either in time or space to the previous event. Parameters are dynamic and not stationary over the study area.

Weight = 0.2

(c) Our team, SDO, also developed a modified time-distance window based upon Youngs *et al.* (1987) declustering parameters. These were patterned after the Wasatch Front seismicity and are as follows:

Weight = 0.2

Mag.	Time (hours)	Distance (km)
2.5	20	20
3.5	30	30
4.5	100	40
5.5	300	60
6.5	600	200
7.25	2000	300

Catalog Completeness

Catalog completeness is a parameter that captures the idea of a minimum magnitude cutoff above which the earthquake catalog is complete such that a recurrence curve will not deviate from an exponential decay with an assumed constant slope. We estimated the completeness by examining the temporal distribution of earthquakes using the method of Stepp (1972) to each of the catalogs. Our team's estimate of the completeness from our own time-space windows are:

Magnitude Completeness	Period
M 6+	1900 present
M 5.0 - 5.9	1924 present
M 4.0 - 4.9	1934 present
M 3.5 - 3.9	1950 present
M 3.0 - 3.5	1962 present
M 2.5 - 2.9	1972 present
M 2.0 - 2.4	1979 present

The catalog completeness intervals for the catalogs declustered using the Youngs *et al.* (1987) and the Veneziano and van Dyke (1985) approaches are based on those presented by Ivan Wong in SSC Workshop 3 and on review of the data. The completeness intervals are:

Completeness Magnitude	Period
M 7.0+	1880-present
M 6.0-6.9	1900-present
M 5.0-5.9	1914-present
M 4.0-4.9	1934-present
M 3.5-3.9	1961-present
M 2.5-3.5	1979-present

Recurrence parameters were estimated using the maximum likelihood method described in Section 3.1 of the main report. The minimum magnitude was set at 2.0 except for Zone 2. For this zone, the minimum magnitude was set at 2.5 because the catalog appeared to be incomplete at magnitude 2.

5.0
FAULT DISPLACEMENT

5.1 INTRODUCTION

In dealing with fault displacement hazard, our team considered that the level of our scientific knowledge of the subject and technique is less certain than that applicable to seismic source characterization. There are a number of reasons for this, but a prime consideration is that idealizations that can be applied to rock behavior at seismogenic depth are not as readily applicable to the upper one or two kilometers of the earth's crust where the repository site is located. At seismogenic depths (~ 4 to 19 km) rock is under high confining stress and is assumed to behave as an elastic, isotropic medium; the strength of fractures is high ($0.6 < \mu < 0.8$) and exhibits essentially frictional behavior. At depths less than about 4 km the crustal carapace consists of a variety of rock types ranging from pristine rock, to weathered or altered rock, to consolidated and unconsolidated alluvium; here, fracture strength may be appreciably different than the shear strength of the host material.

Because of these differences in properties and conditions, strain release (stress drop) considered as seismogenic slip along deep-seated faults may not efficiently be propagated to the surface as a fault displacement. Accordingly, we followed closely working models and data presented at the Yucca Mountain Fault Displacement workshops that extend our teams concept of the problem, and gave weight to the cogency and reasoning of alternate approaches. Our basic premise, however, was to use, where possible, observational data on principal and distributed faulting appropriate for the Basin and Range extensional regime, and especially to use data from the Yucca Mountain area. This is not to say that the problems of fault displacement are not amenable to epistemic solution, though we emphasize that uncertainties in the interpretation of the data may be large. We also note that it is important to the user of our characterization to understand that we downplayed research-oriented approaches and attempted to understand the uncertainties of observational data, and hence dealt with them in a probabilistic sense.

There are three major questions that we considered:

First, there is the problem of what constitutes principal surface displacement. Ideally, principal surface displacement is systematically proportional to the source-depth displacement of the causative earthquake. In practice, the primary displacement is smaller to a greater or lesser degree for the following reasons:

- Anti-clustering and roll-over effects in the hanging wall.
- Material and fault damage differences in hanging wall versus foot wall.
- Strain diffusion associated with local fracturing, reconsolidation, and fissuring.

Second, there is the complication of secondary faulting: How can we discriminate secondary from primary faulting on a genetic basis?

- Time-dependent strain release involves reconsolidation, compaction, groundwater phenomena, foot-wall degradations, subsidence, stress history, "effective elastic thickness" phenomena, etc. These factors contribute to well-defined criteria for defining the extant of these ruptures.

Third, there is a time and spatial sampling problem.

- Degradation of sample sites with time.
- Sample technique: authoritative vs. random/systematic sampling.

To address these problems we approached the analysis at two levels: one for ruptures on the primary faults, i.e., those considered to be seismogenic (at depth), and one for distributed rupturing on secondary faults (near the ground surface). There is a general logic tree for each. The methodology for displacement along the seismogenic faults is largely an extension of our teams (SDO) approach to the seismic source characterization analysis, using the magnitudes of earthquakes and their frequency of occurrence developed in Sections 3 and 4. We considered distributed or secondary displacements to be diffusely scattered and discontinuous ruptures that mostly occur in the hanging wall of normal-slip faults. These are interpreted to result from local strain release distributed along and across the hanging wall, triggered by a nearby earthquake or by non-tectonic mechanisms such as thermal contraction, ground slumping, localized ground subsidence due to ground water withdrawal, etc.

Most of the methods we used for estimating the potential for distributed faulting lack the refinement of seismic source characterization. However, we considered them reasonable

given the relatively small data base, the precision of the data, the generally limited knowledge of the normal faulting process and the relationships of primary to secondary fault triggering. To span the variety of methodologies, we used several approaches that we judged applicable to the Yucca Mountain environment to overcome the large uncertainties or potential bias of any one approach.

5.2 PRINCIPAL FAULTING DISPLACEMENT CHARACTERIZATION

The logic tree for characterizing the potential for principal fault displacement (Figure SDO-11) is divided into five parts: (1) type of event, (2) frequency of occurrence of events, (3) approach for estimating fault displacement, (4) scaling techniques, and (5) distribution for displacement at a point. The following discussion expands these topics.

5.2.1 Type of Event

We considered two levels of principal rupture size along seismogenic faults: maximum displacement events and events smaller than the maximum earthquake. The characterization of displacement hazard from events associated with distributed displacements is described in Section 5.3. Defining the size and frequency of maximum earthquakes (those within ½ magnitude unit of the upper bound earthquake for the fault) are a focus of the earthquake source characterization for assessment of ground motion hazard. The frequency and size distribution of smaller earthquakes down to the maximum background earthquake are assessed using the earthquake recurrence models described in Sections 3.0 and 4.0 We consider that secondary displacement is possible in response to earthquakes along other faults, including aftershock sequences. The characterization of these faults is discussed in Section 5.3. In that part of the analysis, the seismogenic fault is treated in the distributed faulting as the larger end of the fractal distribution of faults.

5.2.2 Frequency of Occurrence of Principal Faulting Events

We utilize the earthquake approach for characterizing principal faulting displacement hazard. The frequency of earthquakes along the seismogenic faults is developed in our (team SDO) earthquake source characterization study (Sections 3 and 4). This is based on three approaches: (1) averaging of moment rates; (2) using an average recurrence interval; and (3) using the interseismic time interval. Events that have magnitudes distributed between the maximum earthquake and the maximum background earthquake have their occurrence rates

developed using the characteristic and truncated exponential models. These models are weighted 0.7 and 0.3, respectively.

The probability of seismogenic rupture at or near the surface is computed using an empirical relationship between the probability of surface rupture and earthquake magnitude developed from data presented by S. K. Pezzopane and T. E. Dawson (USGS, written communication, 1996). Figure SDO-12 shows the results of fitting a logistic probability model to the data sets presented by S. K. Pezzopane and T. E. Dawson (USGS, written communication, 1996) for recent Basin and Range earthquakes (see Appendix H, Section H.4.1). We assign equal weight to these two treatments. The probability of surface rupture at any given point along a fault is computed by randomizing the location of the rupture along the length of the fault.

5.2.3 Approach for Estimating Fault Displacement

The approaches used for estimating fault displacement include empirical regressions of observations of faults that produce normal-faulting earthquakes, data from single-event paleoearthquake displacements, and an along-strike displacement plot for the Solitario Canyon fault determined by Allan Ramelli (Nevada Bureau of Mines and Geology, written communication, 1997) as part of the Yucca Mt. earthquake hazard assessment.

Four types of empirical regressions are used: (1) average displacement versus moment magnitude; (2) average displacement versus length; (3) maximum surface displacement versus moment magnitude; and (4) maximum surface displacement versus length. These are taken from Wells and Coppersmith (1994) and an analysis by the AAR Team of Yucca Mountain data. Both the average and maximum surface displacements are considered because both can be used for assessing the distribution for displacement at a point in an event.

Fault parameter data were taken from the trenching studies of Quaternary faults in the Yucca Mountain area and are the interpreted maximum surface displacements that have been reported in the earthquake seismic source characterization analysis. Average surface displacements were scaled from maximum surface displacements using scaling relationships of Wells and Coppersmith (1994) judged appropriate for an extensional, normal faulting stress regime. Wells and Coppersmith's (1994) Figure 5 plots the ratio of average surface

displacement to maximum surface displacement and shows a distribution between 0.2 and 0.8. We used the approximate average value of these data and take the ratio between average and maximum displacement to be 0.5.

The Ramelli fault displacement data for the Solitario Canyon fault is a combination of trench observations and measurements from the scarp observed along the Solitario Canyon fault trace (Figure SDO-13). It shows some of the ambiguities involved in assessing surface data from both random (field reconnaissance) and authoritative sampling (trench measurements). The curve is useful, however, because it uses direct information from the fault that is in close proximity to the Yucca Mountain site and therefore judged as a good proxy for conditions at the repository.

5.2.3.1 Scaling Techniques. The scaling techniques we used (Table SDO-6) are the regressions aforementioned and a theoretical relationship presented at the SSC workshop #4 and based on a rock mechanics approach (see Bruhn, 1997, SSC Workshop #5). The Wells and Coppersmith (1994) regressions are those for normal faults; the analysis by the AAR Team (presented at SSC workshop #4, Jan. 8, 1997) is developed using data from the Yucca Mountain area. Values from these regressions were used to scale the displacement diagrams presented in the next section.

5.2.3.2 Distributions for Displacement at a Point. Because engineered structures are designed for site specific locations, we need to be able to estimate the potential scale of local fault displacement. Typically, displacement at a surface rupture can range from large values along a single scarp, to smaller values across a broader stepped-scarp distribution. We attempt to model the distribution for the amount of displacement that occurs at a point on a principal rupture by employing a variety of displacement distributions (some named after their developers): (1) a compilation of five large Basin and Range historical earthquakes compiled by Wheeler (1989), called here the five-earthquake curves (Figure SDO-14),;(2) a fault-roughness curve (Figure SDO-15) which is developed in more of a rock mechanics sense by R. Bruhn; (3) a Yucca Mountain site-specific, trench-displacement distribution developed by the DFS Team (Figure SDO-16); and (4) for the Solitario Canyon fault, the displacement plot (Figure SDO-13) developed by Alan Ramelli of the Nevada Geological Survey.

The Wheeler five-earthquake curves (presented at SSC Workshop #5, April 15, 1997) are based on data from five large, scarp-forming Basin and Range province earthquakes. The ASM Team smoothed the data presented in Wheeler (1989) to derive, symmetric curves that define the median and range of the ratio of displacement at a point to the maximum displacement associated with an earthquake, *D/MD*, as a function of location along the principal fault rupture (Figure SDO-14). The Facilitation team developed a statistical model to represent this distribution (see Appendix H, Section H.3.1). The fault roughness curve is based on the consideration that surface roughness along a fault plane is related to amount of displacement, as noted by Ronald Bruhn (SSC Workshop #5). The SBK Team developed a model that represents the theoretical surface roughness along a fault and predicts a distribution for the ratio of displacement at a point to the maximum displacement associated with earthquake magnitude (Figure SDO-15). This distribution is analogous to the empirical distribution developed by the ASM Team (Figure SDO-14) and presented at SSC Workshop # 5, April 15, 1997. Although Bruhn's model is considered to portray real displacement variation along strike, we note that it is an untested theoretical model and should be weighted accordingly. The Facilitation team developed a statistical model to represent this distribution (see Appendix H, Section H.3.2).

The Yucca Mountain trench-displacement distribution, developed by the DFS Team and presented at SSC Workshop # 5, April 15, 1997, examines the event-to-event variability in displacement at a point on a fault about the average historical displacement (Figure SDO-16). This distribution was originally specified as a triangular distribution by the DFS team. However, the Facilitation team determined that a gamma distribution provided a better fit to the data (see Appendix H, Section H.2.1) and we adopt that distribution.

The longitudinal displacement profile for the Solitario Canyon fault offered by Ramelli (Figure SDO-13) shows a large "bump" in fault displacement created entirely by measured offsets in trenches T1 and T8. Elsewhere along the fault, displacement determined by trenching is compatible with scarp heights. Why are the T1 and T8 offsets on the fault anomalously large? The answer seems to be fault segmentation (Ramelli, SSC Workshop #5 information transmittal, May 5, 1997). But we are cautious when asked to compare scarp heights cited by Simonds *et al.* (1995) from field reconnaissance with displacements

measured in four trenches. Two of the trenches, T1 and T3, give displacement values that are twice as great as the range of all other measurements. This leads us to ask what is actually being measured in these two trenches that returns such anomalously large mid- to late-Quaternary displacements? If we project a line through the span of displacements of all the other data sources we get a broad convex longitudinal profile along the fault, a curve similar to that obtained by Jim Yount (SSC Workshop # 6, June 1, 1997), who measured cumulative displacement with reference to a single Miocene horizon the observed length of the fault.

5.2.3.3 Assessment of the Distribution for Amount of Displacement at a Point on a Principal Rupture. The procedures to assess the distribution of potential amount of displacement at a point are shown on Figure SDO-11. There are two approaches: one based on assessment of the maximum displacement, *MD*, associated with an earthquake; and one based on an assessment of the average surface displacement, *AD*, that occurs during an earthquake. These two approaches are given equal weight in the analysis because of the uncertainties we describe in the Introduction.

The estimation of *MD* and *AD* depends upon the size of the earthquake. For magnitudes smaller than m^U - ½ the estimation is based solely on the relationships given in Table SDO-6 for *MD* and *AD* as a function of earthquake magnitude. For the maximum events (m^U - ½ ≤ m ≤ m^U), we also estimate *MD* and *AD* using scaling relationships based on the assessment of rupture length using the relationships in Table SDO-6, and directly from the paleoseismic data. The weights assigned to these various approaches are 0.2 to assessment based on magnitude, 0.4 to assessments based on rupture length, and 0.4 on the paleoseismic displacement data. These weights reflect the relative importance we place on empirical data. For assessment of *AD* as a function of rupture length, equal weight is given to the Wells and Coppersmith (1994) regression and the regression developed by the AAR team (Table SDO-6).

The displacement plot for the Solitario Canyon fault (Figure SDO-13) allowed us to consider a different treatment for displacement along this fault. The displacement at any point of interest is read from the displacement curve and is taken to be the average displacement at that point during maximum earthquakes. This estimate is given a weight of 0.7 and all of the above assessments are given a combined weight of 0.3. We have not been able to determine

whether the displacement peak along the Solitario Canyon fault is a segmentation phenomenon or a sampling alias; we consider the data with due caution, in light of possible interpretations that may significantly bias analytical conclusions.

Given an assessment of *MD* from the various scaling relationships, the probability of exceeding a specified displacement at a point is computed as follows: The uncertainty in MD in a single event is considered to be lognormally distributed about the assessed value, with a standard deviation of log (*MD*) equal to that obtained by Wells and Coppersmith (1994) from regression analysis of empirical data. This lognormal distribution is used to assess the value of *MD* in a single earthquake. Given *MD* for an individual earthquake, the probability of exceeding a specified displacement is computed using the distributions for *D/MD* shown on Figures SDO-14 and SDO-15. The empirical distribution developed by the ASM team (Figure SDO-14) is weighted 0.8 and the theoretical distribution developed by the SBK team (Figure SDO-15) is weighted 0.2 for the reasons discussed above in Section 5.2.3.2.

Given an assessment of *AD*, the probability of exceeding a specified displacement at a point is computed as follows. The estimate of *AD* is considered to represent the average displacement over multiple earthquakes. The distribution for the ratio of the displacement in a single event to the average over multiple events, *D/AD*, developed by the Facilitation team from the data presented by the DFS team (Figure SDO-16), is used to assess the probability of exceeding a specified displacement.

5.3 DISTRIBUTED FAULTING DISPLACEMENT CHARACTERIZATION

Modeling the potential displacements from distributed faulting involves: (1) evaluating the characteristics of faults not directly part of the primary fault trace; (2) estimating the cumulative magnitude of the distributed fault displacements and the probability of occurrence of subsequent displacements; and (3) evaluating the affect of the free surface on fault propagation from the repository depth to the surface. Figure SDO-7 shows the logic structure used to characterize distributed faulting hazard. Two approaches were used. One is based on assessment of the frequency at which earthquakes on the various seismic sources induce distributed slip on the feature of interest. This is termed the earthquake approach. The second approach uses the cumulative slip at the point of interest to estimate the slip rate and displacement per event. This is termed the displacement approach. Both approaches are

used for features that are subject to only distributed faulting hazard, with the earthquake approach given a weight of 0.8 and the displacement approach given a weight of 0.2. The earthquake approach is given a higher weight because it has a stronger theoretical basis and a more complete database. It is also favored because it is ties to our paleoearthquake analysis. The displacement approach has not been studied in as much detail and has limited data. For those features that are also subject to principal faulting hazard, only the earthquake approach is used. Again, the large uncertainties associated with near-surface phenomena and widely variable material properties of media in the upper few hundred meters lead us to give a relatively low weight to the displacement approach.

5.3.1 Earthquake Approach to Distributed Faulting Hazard

The steps in the earthquake approach are: (1) assessment of the probability that distributed faulting can occur on the feature (activation probability); (2) an assessment of the probability of slip in an individual earthquake; and (3) an assessment of the distribution relative to the amount of potential total displacement.

5.3.1.1 Activation Probability. The probability that an individual fault can be activated among many during a distributed faulting event is estimated using an analysis of slip tendency of faults with respect to the regional stress field (Morris *et al.*, 1996). The slip tendency technique considers the ratio of shear to normal stresses imposed on a fault within a regional stress field. Slip tendency, T_S, reduces to μ, the coefficient of static friction which, according to Byerlee's law (Byerlee, 1978), is 0.85 from ground surface to seismogenic depths (10 km). H. L. McKague *et al.* (CNWRA, written communication, 1996) present an analysis of the slip tendency of faults in the Yucca Mountain region. Their analysis of the local faults (their Figure 3-5b) indicates the north-south trending faults have the highest slip tendency (~0.7). Because most of the larger north-south trending faults show evidence of Quaternary slip, we utilize a value of T_S of 0.7 to correspond to a probability that slip can occur, $P(C)$ of 1.0. For faults and features with other orientations, we define $P(C)$ as the ratio T_S /0.7. For northwest-southeast trending structures, T_S read from Figure 3-5b of H. L. McKague *et al.* (CNWRA, written communication, 1996) is approximately 0.55, resulting in $P(C) = 0.8$.

5.3.1.2 Probability of Slip Per Event. The frequency of occurrence of earthquakes on each of the seismic sources is defined by our seismic source characterization described in Sections 3.0 and 4.0. The probability of distributed slip on a feature in an individual earthquake is assessed using an analysis of the density of distributed rupture based on the mapped patterns of rupture presented in S. K. Pezzopane and T. E. Dawson (USGS, written communication, 1996). The logistic regression model presented by R. R. Youngs (Yucca Mountain SSC Workshop #6) was adopted (Figure SDO-18) (see also Appendix H, Section H.4.2). We excluded the data for hanging wall cracking from the 1988 Chalfant Valley earthquake and data from the 1980 Mammoth earthquake because these earthquakes are considered background type earthquakes. The curves show the probability of secondary rupture occurring at a point as a function of earthquake magnitude, distance from the principal rupture, and location in the hanging wall or foot wall of the rupture. For earthquakes occurring on the regional areal source, it is considered equally likely that the point of interest lies in either the hanging wall or the foot wall of the rupture.

We further modify the probability of distributed rupture in an event by a factor related to the orientation of the feature relative to the principal fault rupture. The distribution of the orientation of distributed ruptures with respect to the principal rupture provides an assessment of the likelihood that distributed faulting occurs on a feature with a given orientation with respect to the strike of the earthquake-generating fault. Maps of historical ruptures presented in S. K. Pezzopane and T. E. Dawson (USGS, written communication, 1996) were used to assess the relative frequency of distributed ruptures in increments of 5° of the angle θ between the strike of the principal rupture and the strike of the distributed rupture (see Appendix H, Section H.4.3). This relative frequency was used to define the likelihood of rupture as a function of relative strike between the principal rupture and the feature of interest. We selected the assessment based on a minimum of three points defining the distributed rupture trace because the process used to digitize the fault maps produced a distribution of two-point rupture traces with modes in the north-south and east-west directions, suggesting poor estimation of the strike azimuth distribution.

The strike azimuth for earthquakes occurring in the regional source zone is not known. Examination of the orientation of nodal planes of Yucca Mountain region earthquakes presented in Chapter 7 of USGS (written communication, 1996) indicates a nearly random

pattern. Therefore, we assume that the strike azimuth of these earthquakes is uniformly distributed from 0° to 360° and compute an average value of the orientation probability of 0.34 to apply to these earthquakes.

5.3.1.3 Probability Distribution for Displacement at a Point. Two approaches are used to assess the distribution of possible displacements at a given point along a fault scarp induced by slip on an earthquake source: one based on the ratio of cumulative displacements; and one based on maximum potential displacement computed from earthquake magnitude.

Cumulative Displacement Ratio Approach. In this approach, we consider the ratio of displacement on the principal rupture to displacement on the secondary rupture to be equal to the ratio of their cumulative displacements. We define a factor, *RF*, that is used to scale the principal rupture displacement to the distributed rupture displacement. The scaling factor *RF* is set equal to the ratio of the cumulative displacement on the fault of interest to the cumulative displacement on the earthquake source fault. We impose an upper limit of 0.8 to *RF* based on the maximum ratio of secondary to primary slip reported by Coppersmith and Youngs (1992). The procedures described in Section 5.2.3.3 are used to assess the distribution for slip on the principal rupture at its closest approach and this slip is scaled by *RF* to the point of interest. This approach is given a weight of 0.2. The low weight takes into account the uncertainties associated with origin, mechanics, displacements, and slip histories of shallow distributed faults compared to the seismogenic faults.

The application of this approach requires an assessment of the average cumulative displacement for each of the seismic sources in the vicinity of Yucca Mountain. The assessed values are:

Source	Average Cumulative Displacement (m)
Paintbrush Canyon	380
Bow Ridge	244
Solitario Canyon	457
Fatigue Wash	396
Windy Wash	380
N. Crater Flat	244
S. Crater Flat	<244
Iron Ridge	350
Stagecoach Road	457
Bare Mountain	500-900

When simultaneous fault ruptures are considered, the largest cumulative displacement among the individual faults is used to define *RF*.

Displacement Potential Approach. As an empirical data set, secondary (or distributed) faults include numerous, difficult to discriminate strain phenomena along with true fault displacements. We consider that distributed displacement represents an upper limit of stain, i.e., failure in the rock mechanics sense, but that all the strain effects measurable as geodetic displacement normal to the rupture are consequences of main fault plane seismogenic rupture. The displacement potential approach simply acknowledges the reality that surficial materials are not classic elastic media and cannot be expected to behave (strain and fail) the same way a seismogenic fault does at depth.

For this approach we used a distribution ratio of secondary to primary slip empirically observed in historical, ground-breaking earthquakes in the Basin and Range province: (1) the **M** 7.1 1954 Fairview Peak, Nevada, earthquake and associated Stingaree Valley rupture; (2) the M_s 7.5 1959, Hebgen Lake, Montana, earthquake; and (3) the M_s 7.3 1983 Borah Peak earthquakes recognizing there are many more data points in the hanging wall than in the foot wall. Figure SDO-19 shows maximum distributed fault displacements normalized to the maximum principal fault rupture, *MD*, plotted versus distance from the principal rupture, and distinguishes displacement in the hanging wall from the foot wall side of the fault. We define an approximate envelope of the observed data on the hanging wall side of the rupture and fit an exponential curve to these data, as shown on Figure SDO-19. An exponential

curve is used because it is a simple parametric model that allows for a gradual decay of amplitude with distance. The resulting curve for the hanging wall displacement potential is

$$D(\text{distributed in hanging wall})/MD(\text{principal}) = 0.35 \times \exp(-0.091r)$$

where r is the distance from the principal rupture. Examination of data presented in S. K. Pezzopane and T. E. Dawson (USGS, written communication, 1996) and Coppersmith and Youngs (1992) indicates that the distributed faulting zones on the foot wall side of normal fault ruptures are much narrower that those on the hanging wall side of the rupture. Consequently, we assume that the rate of decay of distributed displacement amplitude is 50 percent greater on the foot wall side than on the hanging wall side, and using the single foot wall data point define a foot wall displacement potential as:

$$D(\text{distributed in foot wall})/MD(\text{principal}) = 0.16 \times \exp(-0.137r)$$

The displacement potential is interpreted to represent the 95th-percentile of the distribution of possible displacements, with the lower limit of this distribution equal to 0. We use a distribution with a similar degree of skewness as exhibited by the distribution for *D/AD* shown on Figure SDO-16 and impose an upper limit to the displacement potential equal to the cumulative displacement on the feature. As described in Appendix H, the various normalized displacement data sets developed by the expert teams can be modeled by gamma distributions with the shape parameter, a, of about 2.5. For $a = 2.5$, the 95 th-percentile of a gamma distribution occurs at $5.535b$, where b is the normalizing parameter of the distribution. Thus, we define a gamma distribution for the distribution of D(distributed)/MD(principal) at a distance r from a principal rupture with a equal to 2.5 and b equal to the displacement potential defined by the above relationships divided by 5.535. The computation of the distribution for the displacement is completed by utilizing a lognormal distribution for *MD* on the principal rupture about the values given by the various scaling relationships defined in Section 5.2.3.1.

We weight the displacement potential approach 0.8. In assessing the potential for fault displacement from earthquakes occurring in the areal source zone only the displacement

potential approach can be used because the cumulative displacement on the earthquake source is not known.

5.3.2 Displacement Approach to Distributed Faulting Hazard

The steps in the displacement approach are: (1) assessment of the probability that distributed faulting can occur on a fault (activation probability); (2) assessment of the rate of slip on the feature; (3) assessment of the average slip per event; and (4) assessment of the distribution for the amount of displacement. In the displacement approach the location, size, and orientation of the faults that generate earthquakes inducing the distributed slip are unknown.

5.3.2.1 Activation Probability. The probability that an individual fault can be activated during a distributed faulting event is estimated using the analysis of slip tendency of faults with respect to the regional stress field, as discussed in Section 5.3.1.1.

5.3.2.2 Assessment of Slip Rate. The Quaternary slip rate on the feature of interest is assessed by estimating the fraction of the cumulative slip that has occurred in the past 1.6 Ma, and dividing that slip by 1.6 Ma. Based on review of the various proposed slip histories for the Yucca Mountain faults, the following distribution is assessed for the percentage of cumulative slip that has occurred in the Quaternary, 0.2% (0.3), 0.6% (0.4), 2% (0.3).

5.3.2.3 Assessment of Average Displacement per Event. We utilize two approaches for estimating the average slip per event, $\bar{D}_E$. The first is based on the scaling relationships between cumulative offset and average offset developed by the AAR Team (SSC Workshop # 4, Jan. 8, 1997). The second is based on an analysis of the fault offset data from Yucca Mountain normalized by the cumulative offset on the fault. This empirical distribution was developed by the SBK Team (SSC Workshop #6, June 1, 1997) (see Figure SDO-20). These two alternatives are given equal weight. The frequency of faulting events is equal to the fault slip rate divided by the average slip per event.

5.3.2.4 Distribution for Displacement at a Point. The approach for assessing the distribution for the displacement in an event is tied to the approach used for estimating the average slip per event. If the AAR scaling relationships are used, then the exponential distribution for D/MD^{max} developed by AAR is used to calculate the probability distribution

for D, with $MD^{max} = \bar{D}_E$ /0.83 based on the scaling relationship developed by the AAR team. If the approach developed by the SBK team is used, then the empirical distribution shown on Figure SDO-20 is used to assess the probability distribution for displacement. This distribution was modeled by the Facilitation team by a gamma distribution (see Appendix H, Section H.2.6).

5.4 DATA FOR NINE CALCULATION SITES

The following summarizes the data required to characterize the displacement hazard at each of the nine demonstration sites.

Point 1 Bow Ridge fault

Site of potential principal faulting , use the methods described in Sections 5.2 and 5.3.1. For distributed faulting , P(C) = 1.0. The paleoseismic MD = 44 cm, with assumed lognormal distribution, and $\sigma_{\log(MD)}$ = 0.42 based on empirical models. The assessed cumulative displacement at Point 1 is 200 m. The distribution for the length of the feature is {7 (0.3), 8 (0.4), 10 (0.3)} km.

Point 2 Solitario Canyon fault

Site of potential principal faulting , use the methods described in Sections 5.2 and 5.3.1. For distributed faulting , P(C) = 1.0. The paleoseismic MD = 0.7 m, with assumed lognormal distribution, and $\sigma_{\log(MD)}$ = 0.42 based on empirical models. The paleoseismic AD estimated from the profile developed by Alan Ramelli is 25 cm. The assessed cumulative displacement at Point 2 is 700 m. The distribution for the length of the feature is {16 (0.3), 18.5 (0.4), 21.5 (0.3)} km

Point 3 Drill Hole Wash fault

Site of distributed faulting, use the methods described in Section 5.3. $P(C)$ = 0.8 from slip tendency. The cumulative displacement is assessed to be 12 m.

Point 4 Ghost Dance fault

Site of distributed faulting, use the methods described in Section 5.3. $P(C)$ = 1.0 from slip tendency. The cumulative displacement is assessed to be 40 m.

Point 5 Sundance fault

Site of distributed faulting , use the methods described in Section 5.3. $P(C) = 0.8$ from slip tendency. The cumulative displacement is assessed to be 11 m.

Point 6 Unnamed fault west of Dune Wash

Site of distributed faulting , use the methods described in Section 5.3. $P(C) = 1.0$ from slip tendency. The cumulative displacement is assessed to be 150 m.

Point 7 Point 100 m east of Solitario Canyon

Site of distributed faulting, use the methods described in Section 5.3. For point 7a, $P(C) = 1.0$ from slip tendency and the cumulative displacement is 2 m. For point 7b, $P(C) = 1.0$ from slip tendency and the cumulative displacement is 10 cm. It is judged that the probability of displacement in intact rock (point 7d) is essentially negligible because the Yucca Mountain block is highly faulted and fractured at a wide range of scales and displacement within the block will likely occur along these pre-existing zones of weakness rather than break intact rock. Fractures with no displacement (point7c) are either small features or are on the fringe of a larger feature. In both cases, secondary displacement will probably be negligible.

Point 8 Point midway between Ghost Dance and Solitario Canyon faults

Use the same set of parameters defined above for Point 7.

Point 9 Midway Valley

Site of distributed faulting , use the methods described in Section 5.3. $P(C) = 1.0$ from slip tendency. The cumulative displacement is assessed to be 50 m.

6.0
REFERENCES

Anderson, J.G., Wesnousky, S.G., and Stirling, M.W., 1996, Earthquake size as a function of fault slip rate: Bulletin of the Seismological Society of America, v. 86, n. 3, p. 683-690.

Anderson, R.E., Bucknam, R.C., Crone, A.J., Haller, K M., Machette, M.N., Personius, S.F., Barnhard, T.P., Cecil, M.J., and Dart, R.L., 1995b, Characterization of Quaternary and suspected Quaternary faults, regional studies, Nevada and California: U. S. Geological Survey Open-File Report 95-599, 56 p.

Anderson, R.E., Crone, A.J., Machette, M.N., Bradley, L.-A., and Diehl, S.F., 1995a, Characterization of Quaternary and suspected Quaternary faults, Amargosa area, Nevada and California: U. S. Geological Survey Open-File Report 95-613, 41 p.

Brocher, T.M., Carr, M.D., Fox, K.F., J., and Hart, P.E., 1993, Seismic reflection profiling across Tertiary extensional structures in the eastern Amargosa Desert, southern Nevada, Basin and Range province: Geological Society of America Bulletin, v. 105, p. 30-46.

Brocher, T.M., Hart, P.E., Hunter, W.C., and Langenheim, V.E., 1996, Hybrid-source seismic reflection profiling across Yucca Mountain, Nevada: regional lines 2 and 3: , U.S. Geological Survey Open-File Report 96-28, 110 p.

Brocher, T.M., and Hunter, W.C., 1996, Seismic reflection evidence against a shallow detachment beneath Yucca Mountain, Nevada: High-Level Radioactive Waste Management Proceedings of the Seventh International Conference, Las Vegas, Nevada, American Nuclear Society, La Grange Park, Illinois, p. 148-150.

Brun, J.-P., Sokoutis, D., and Van Den Driessche, J., 1994, Analogue modeling of detachment fault systems and core complexes: Geology, v. 22, p. 319-322.

Burchfiel, B.C., Hodges, D.V., and Royden, L.M., 1987, Geology of Panamint Valley-Saline Valley pull apart system, California; palinspastic evidence for low-angle geometry of a Neogene range-bounding fault: Journal of Geophysical Research, v. 92, p. 10,422-10,426.

Byerlee, J. D., 1978, Friction of rocks: Pure and Applied Geophysics, v. 116, p. 615-626.

Carr, W. J., 1984, Regional structural setting of Yucca Mountain, southwestern Nevada, and late Cenozoic rates of tectonic activity in part of the southwestern Great Basin, Nevada and California: U.S. Geological Survey Open-File Report 84-854, 109 p.

Carr, W.J., 1988, Volcano-tectonic setting of Yucca Mountain and Crater Flat, southwestern Nevada: U.S. Geological Survey Bulletin 1790, p. 35-85.

Carr, W.J., 1990, Styles of extension in the Nevada Test Site region, southern Walker Lane Belt; an integration of volcano-tectonic and detachment fault models, *in* Wernicke, B. P., ed., Basin and Range extensional tectonics near the latitude of Las Vegas, Nevada: Geological Society of America Memoir 176, p. 283-303.

Castro, G., and Poulos, S., 1977, Factors affecting liquefaction and cyclic mobility: American Society of Civil Engineers, Journal of the Geotechnical Engineering Division, v. 103, n. GT6, p. 501-516.

Coppersmith, K.J., and Youngs, R.R., 1992, Earthquakes and tectonics: in McGuire, R.K., ed., Demonstration of a Risk-Based Approach to High-Level Waste Repository Evaluation: Phase 2, Electric Power Research Institute, EPRI TR-100384, Palo Alto, California

Cornwall, H.R., 1972, Geology and mineral deposits of southern Nye County, Nevada: Nevada Bureau of Mines and Geology, Bulletin 77, 49 p.

Cowie, P. A., and Scholz, C.H. 1992, Growth of faults by accumulation of seismic slip: Journal of Geophysical Research, v. 97, p. 11085-11095.

Decker, P.L., 1990, Style and mechanics of liquefaction-related deformation, lower Absaroka Volcanic Supergroup (Eocene), Wyoming: Geological Society of America Special Paper 240, 71 p., 8 plates.

Densmore, A. L., and Anderson, R. S., 1994, Recent tectonic geomorphology of Panamint Valley, California: American Geophysical Union, EOS, Fall Meeting Abstracts with Programs, p. 296.

dePolo, C.M., Clark, D.G., Slemmons, D.B., and Ramelli, A.R., 1991, Historical surface faulting in the Basin and Range province, western North America—Implications for fault segmentation: Journal of Structural Geology, v. 13, n. 2, p. 123-136.

Dohrenwend, J.C., Menges, C.M., Schell, B A., and Moring, B.C., 1991, Reconnaissance photogeologic map of young faults in the Las Vegas 1° x 2° quadrangle, Nevada, California, and Arizona: U. S. Geological Survey, Miscellaneous Field Studies Map MF-2182, 1:250,000.

Dohrenwend, J.C., Schell, B.A., McKittrick, M.A., and Moring, B.C., 1992, Reconnaissance photogeologic map of young faults in the Goldfield 1°x2° quadrangle, Nevada and California: U. S. Geological Survey Miscellaneous Field Studies Map MF-2183, 1:250,000.

Doser, D.D., and Smith, R.B., 1985, Source parameters of the October 28, 1983 Borah Peak, Idaho earthquake from body wave analysis: Bulletin of the Seismological Society of America, v. 75, p. 1041-1051.

Doser, D.D., and Smith, R.B., 1989, An assessment of source parameters of earthquakes in the Intermontane region of the United States: Bulletin of the Seismological Society of America, v. 79, p. 1383-1409.

Eddington, P.J., Smith, R.B., and Renggli, C., 1987, Kinematics of Basin-Range intraplate extension, *in* Coward, M.P., Dewey, J.F., and Hancock, P.L., eds., Continental Extension: London Geological Society, Special Publication 28, p. 371-392.

Fauld, J. E., Bell, J. W., Feuerbach, D. L., and Ramelli, A. R. 1994, Geologic map of the Crater Flats area: Nevada Bureau of Mines & Geology Map 101, scale 1:24,000.

Fernald, A.T., Corchary, G.S., Williams, W.P., and Colton, R.B., 1968, Surficial deposits of Yucca Flat area, Nevada Test Site, *in* Eckel, E. B., eds., Nevada Test Site: Geological Society of America, Memoir 110, p. 49-55.

Ferrill, D.A., Stamatakos, J.A., Jones, S.M., Rahe, B., McKague, H.L., Martin, R.H., and Morris, A.P., 1996, Quaternary slip history of the Bare Mountain Fault (Nevada) from the morphology and distribution of alluvial fan deposits: Geology, v.24, n. 6, p.559-562.

Fossen, H., and Gabrielsen, R.H., 1996, Experimental modeling of extensional fault systems by use of plaster: Journal of Structural Geology, v. 18, n. 5, p. 673-687.

Frankel, A., 1995, Mapping seismic hazard in the Central and Eastern United States: Bulletin of the Seismological Society of America, v. 66, p. 8-21.

Frizzell, V.A., Jr., and Shulters, J., 1990, Geologic map of the Nevada Test Site, southern Nevada: U.S. Geological Survey Miscellaneous Investigations Series Map I-2046, 1 plate (1:100,000).

Hancock, P.L., and Barka, A.A., 1987, Kinematic indicators on active normal faults in western Turkey: Journal of Structural Geology, v. 9, n. 5/6, p. 573-584.

Hanks, T.C., and Kanamori, H., 1979, A moment magnitude scale: Journal of Geophysical Research, v. 84, p. 2348-2350.

Hinrichs, E.N., 1968, Geologic map of the Camp Desert Rock quadrangle, Nye County, Nevada: U. S. Geological Survey Geologic Quadrangle Map GQ-726, 1:24,000.

Hoisch, T.D., Heizler, M.T., and Zartman, R.E., 1997, Timing of detachment faulting in the Bullfrog Hills and Bare Mountain area, southwest Nevada: inferences from 40Ar/39Ar, K-Ar, U-Pb and fission-track thermochronology: Journal of Geophysical Research, v. 102, n. B2, p. 2815-2833.

Hudson, M.R., Sawyer, D.A., and Warren, R.G., 1994, Paleomagnetism and rotation constraints for the middle Miocene southwestern Nevada volcanic field: Tectonics, v. 13, n. 2, p. 258-277.

Jackson, J., and White, N., 1989, Normal faulting in the upper continental crust: observations from regions of active extension: Journal of Structural Geology, v. 11, p. 15-36.

Jennings, C. W., 1994, Fault activity map of California and adjacent areas with locations and ages of recent volcanic eruptions: California Division of Mines and Geology, California Geologic Data Map Series, Map No. 6, scale 1:750,000.

Kamamori, H., and Allen, C.R., 1986, Earthquake repeat time and average stress drop, *in* Das, S., Boatwright, J., and Scholz, C.H., eds. Earthquake Source Mechanics: Geophysical Monograph 37, Maurice Ewing v. 6, Washington, D.C., American Geophysical Union.

Lipman, P.W., and McKay, E.J., 1965, Geologic map of the Topopah Spring SW quadrangle, Nye County, Nevada: U. S. Geological Survey Quadrangle Map GQ-439, scale 1:24,000.

Maldonado, F., 1985, Geologic map of the Jackass Flats area, Nye County, Nevada: U.S. Geological Survey, Miscellaneous Investigations, Map I-1519, 1 plate (1:48,000).

Mason, D.B., 1996, Earthquake magnitude potential of the Intermountain seismic belt, USA, from surface-parameter scaling of late Quaternary faults: Bulletin of the Seismological Society of America, v. 86, p. 1487-1506.

McKeown, F.A., Healey, D.L., and Miller, C.H., 1976, Geologic map of the Yucca Lake Quadrangle, Nye County, Nevada: U. S. Geological Survey Geologic Quadrangle Map GQ-1327, scale 1:24,000.

Melosh, H.J., 1990, Mechanical basis for low-angle normal faulting in Basin and Range province: Nature, v. 343, p. 331-335.

Mendoza, C., and Hartzell, S.H., 1988, Inversion for slip distribution using teleseismic P-waveforms: North Palm Springs, Borah Peak, and Michoacan earthquakes: Bulletin of the Seismological Society of America, v. 78, p. 1092-1111.

Meremonte, M., Gomberg, J., and Cranswick, E., 1995, Constraints on the 29 June 1992 Little Skull Mountain, Nevada, earthquake sequence provided by robust hypocenter estimates: Bulletin of the Seismological Society of America, v. 85, n. 4, p. 1039-1049.

Minor, S.A., Sawyer, D.A., Wahl, R.R., Frizzel, V.A., Jr., Schilling, S.P., Warren, R.G., Orkild, P.P., Coe, F.A., Hudson, M.R., Fleck, R.J., Lanphere, M.A., Swadley, WC, and Cole, J.C., 1993, Preliminary geologic map of the Pahute Mesa 30'x60' quadrangle, Nevada: U.S. Geological Survey Open-File Report 93-299, 39 p.

Minor, S. A., Hudson, M. R., and Fridrich, C. J., 1996, Fault-slip data bearing on the tectonic development of northern Crater Flat basin, southern Nevada [abs.]: Geological Society of America Abstracts with Programs, v. 28, n. 7., p. A192.

Monsen, S.A., Carr, M.D., Reheis, M.C., and Orkild, P.P., 1992, Geologic map of Bare Mountain, Nye County, Nevada: U.S. Geological Survey Miscellaneous Investigations Series Map I-2201, 1:24,000 scale.

Morris, A., Ferrill, D. A., and Henderson, D. B., 1996, Slip-tendency analysis and fault reactivation: Geology, v. 24, p. 275-278.

Nicol, A., Walsh, J.J., Watterson, J., and Gillespie, P.A., Fault size distributions-are they really power-law?, , Journal of Structural Geology, v. 18, p. 191-197.

Okaya, D.A., and Thompson, G.A., 1985, Geometry of Cenozoic extensional faulting, Dixie Valley, Nevada: Tectonics, v. 4, n. 1, p. 107-125.

Orkild, P.P., Sargent, K.A., and Snyder, R.P., 1969, Geologic map of Pahute Mesa, Nevada Test Site and vicinity, Nye County: U.S. Geological Survey, Miscellaneous Geologic Investigations Map I-567, 1 plate (1:48,000).

Peterson, F.F., Bell, J.W., Dorn, R.I., Ramelli, A.R., and Ku, T.-L., 1995, Late Quaternary geomorphology and soils in Crater Flat, Yucca Mountain, southern Nevada: Geological Society of America Bulletin, v. 107, n. 4, p. 379-395.

Piety, L. A., 1995, Compilation of known and suspected Quaternary faults within 100 km of Yucca Mountain, Nevada and California: U.S. Geological Survey Open-File Report 94-112, 404 p.

Poole, F.G., Elston, D.P., and Carr, W.J., 1965, Geologic map of the Cane Spring Quadrangle, Nye County, Nevada: U.S. Geological Survey Geologic Map GQ-455, scale 1:24,000.

Reheis, M.C., 1988, Preliminary study of Quaternary faulting on the east side of Bare Mountain, Nye County, Nevada, *in* Carr, M.D., and Yount, J.C., eds., Geologic and hydrologic investigations of a potential nuclear waste disposal site at Yucca Mountain, southern Nevada: U.S. Geological Survey Bulletin 1790, p. 103-111.

Reheis, M.C., 1991, Aerial photographic interpretation of lineaments and faults in late Cenozoic deposits in the eastern parts of the Saline Valley 1:100,000 Quadrangle, Nevada and California, and the Darwin Hills 1:100,000 Quadrangle, California: U.S. Geological Survey Open-File Report 90-500, 6 p., 2 plates.

Reheis, M.C., 1992, Aerial photographic interpretation of lineaments and faults in late Cenozoic deposits in the Cactus Flat and Pahute Mesa 1:100,000 quadrangles and the western parts of the Timpahute Range, Pahranagat Range, Indian Springs, and Las Vegas 1:100,000 Quadrangles, Nevada: U.S. Geological Survey Open-File Report 92-193, 14 p., 3 plates.

Reheis, M.C. and Noller, J.S., 1991, Aerial photographic interpretation of lineaments and faults in late Cenozoic deposits in the eastern part of the Benton Range 1:100,000 Quadrangle and the Goldfield, Last Chance Range, Beatty, and Death Valley Junction 1:100,000 Quadrangles, Nevada and California: U.S. Geological Survey Open-File Report 90-41, 9 p., 4 plates.

Richins, W.D., Smith, R.B., Langer, C.J., Zollweg, J.E., King, J.J., and Pechmann, J.C., 1985, The 1983 Borah Peak, Idaho earthquake: Relationship of aftershocks to the mainshock, surface faulting, and regional tectonics, Workshop XXVIII on "The Borah Peak Earthquake": U.S. Geological Survey Open-File Report, 85-290, p. 285-310.

Rogers, A. M., Corbett, E.J, Priestley, K., and dePolo, D, 1991, The seismicity of Nevada and some adjacent part of the Great Basin, *in* Slemmons, D.B., Engdahl, E.R., Zoback, M.L. and Blackwell, D.D., eds., Neotectonics of North America: Geological Society of America, SMV V-1, Decade Map v. 1, p. 153-184.

Scholz, C. H., 1990, The Mechanics of Earthquakes and Faulting: New York, Cambridge University Press, 439 p.

Scholz, C.H., and Aviles, C.A., 1986, The fractal geometry of faults and faulting, *in* Das, S., Boatwright, J., and Scholz, C.H., eds., Earthquake Source Mechanics: American Geophysical Union Monograph 37, p. 147-155.

Schweickert, R.A., and Lahren, M.M., 1997, Strike-slip fault system in Amargosa Valley and Yucca Mountain, Nevada: Tectonophysics, v. 272, n. 1, p. 25-42.

Schweig, E.S., III, 1989, Basin-Range tectonics in Darwin Plateau, southwestern Great Basin, California: Geological Society of America Bulletin, v. 101, n. 5, p. 652-662.

Scott, R.B., 1990, Tectonic setting of Yucca Mountain, southwest Nevada, *in* Wernicke, B. P., ed., Basin and Range extensional tectonics near the latitude of Las Vegas, Nevada: Boulder, Colorado ,Geological Society of America Memoir 176, p. 251-282.

Scott, R.B., and Bonk, J., 1984, Preliminary geologic map of Yucca Mountain, Nye County, Nevada with geologic sections: U. S. Geological Survey Open File Report 84-494, 9 p., map scale 1:12,000.

Seed, H.B., and Idriss, I.M., 1982, Ground motions and soil liquefactions during earthquakes: Berkeley, California, Earthquake Engineering Research Institute, 134 p.

Shroba, R.R., Muhs, D.R., and Rosholt, J.N., 1988, Uranium-trend and uranium-series age estimates of surficial and fracture-fill deposits on the Carpetbag fault system, Nye County, Nevada: Geologic Society of America, Abstracts with Programs, v. 20, p. 231.

Sibson, R.H., 1982, Fault zone models, heat flow, and the depth distribution of earthquakes in the continental crust of the United States: Bulletin of the Seismological Society of America, v. 72, p. 151-163.

Simonds, F.W., *et al.*, 1995, Map showing fault activity of the Yucca Mountain area, Nye County, Nevada: U.S. Geological Survey Miscellaneous Investigations Series Map I-2520, 30 p., scale 1:24,000.

Slemmons, D.B., 1967, Pliocene and Quaternary crustal movements of the Basin and Range Province, USA: Journal of Geoscience, Osaka City University, v. 10, p. 91-103.

Smith, R.B. and Arabasz, W.J., 1991, Seismicity of the Intermountain Seismic Belt, *in* D.B. Slemmons, E.R. Engdahl, M.L. Zoback and D. D. Blackwell, eds., Neotectonics of North America: Geological Society of America, SMV V-1, Decade Map Volume 1, p. 185-228.

Smith, R.B. and Bruhn, R.L., 1984, Intraplate extensional tectonics of the western U.S. Cordillera: Inferences on structural style from seismic reflection data, regional tectonics and thermal-mechanical models of brittle-ductile deformation: Journal of Geophysical Research, v. 89, p. 5733-5762.

Smith, R.B., Nagy, W.C., Julander, K.A., Viveiros, J.J., Barker, C.A., and Gants, D.G., 1989, Geophysical and tectonic framework of the eastern Basin and Range-Colorado Plateau-Rocky Mountain transition, *in* Pakiser, L.C. and Mooney, W.C., eds., Geophysical Framework of the Continental U.S.: Geological Society of America Memoir 172, p. 205-233.

Smith, R.P., and Jackson, S.M., 1996, Paleoseismology and seismic hazards evaluations in extensional volcanic terrains: Journal of Geophysical Research, v. 10, p. 6,277-6,292.

Snyder, D.B., and Carr, W.J., 1984, Interpretation of gravity data in a complex volcano-tectonic setting, southwestern Nevada: Journal of Geophysical Research, v. 89, n. B12, p. 10,193-10,206.

Stein, R.S., and Barrientos, S.E., 1985, Planar high-angle faulting in the Basin and Range: geodetic analysis of the 1983 Borah Peak, Idaho, earthquake: Journal of Geophysical Research, v. 90, no. B13, p. 11,355-11,366.

Stepp, J. C., 1972, Analysis of completeness of the earthquake sample in the Puget Sound area and its effects on statistical estimates of earthquake hazard: Proceedings, First Microzonation Conference, Seattle, Washington, p. 897-909.

Stewart, J.H., 1988, Tectonics of the Walker Lane Belt, western Great Basin-Mesozoic and Tertiary deformation in a zone of shear, *in* Ernst, W.G., ed., Metamorphism and crustal evolution of the western United States, Rubey Volume VII: Englewood Cliffs, New Jersey, Prentice Hall, p. 683-713.

Stock, J.M., Healy, J.H., Hickman, S.H., and Zoback, M.D., 1985, Hydraulic fracturing stress measurements at Yucca Mountain, Nevada, and relationship to the regional stress field: Journal of Geophysical Research, v. 90, n. B10, p. 8691-8706.

Swadley, W.C., and Hoover, D.L., 1990, Geologic Map of the surficial deposits of the Yucca Flat area, Nye County, Nevada: U.S. Geological Survey, Miscellaneous Investigations Series Map I-2047, 1 plate (1:48,000).

Swadley, W.C., and Huckins, H.E., 1990, Geologic map of the surficial deposits of the Skull Mountain Quadrangle, Nye County, Nevada: U.S. Geological Survey, Miscellaneous Investigation Series, Map I-1972, 1 plate (1:24,000).

Veneziano, D., and Van Dyck, J., 1985, Statistical discrimination of *aftershocks* and their contribution to seismic hazard: Seismic Hazard Methodology for Nuclear Facilities in the Eastern United States: EPRI Res. Project No. P101-29, EPRI/SOG 85-1, v. 2, Appendix A-4.

Wells, D.L., and Coppersmith, K.J., 1994, New empirical relationships among magnitude, rupture length, rupture width, rupture area, and surface displacement: Bulletin of the Seismological Society of America, v. 84, n. 4, p. 974-1002.

Wesnousky, S. G., 1986, Earthquakes, Quaternary faults, and seismic hazard in California: Journal of Geophysical Research, v. 91, p. 12,587-12,631.

Wheeler, R.L., 1989, Persistent segment boundaries on basin-range normal faults, *in* Schwartz, D.P. and Sibson, R.H., eds., Fault segmentation and controls of rupture initiation and termination: U.S. Geological Survey Open File Report 89-315, p.432-444.

Winograd, I.J., and Thordarson, W., 1975, Hydrogeologic and hydrochemical framework, south-central Great Basin, Nevada-California, with special reference to the Nevada Test Site: U. S. Geological Survey Professional Paper 712-C, 126 p.

Wright, L.A., 1989, Overview of the role of strike-slip and normal faulting in the Neogene history of the region northeast of Death Valley, California-Nevada, *in* Ellis, M. A., ed., Late Cenozoic evolution of the southern Great Basin: Nevada Bureau of Mines and Geology Open File Report 89-1, p. 1-11.

Youngs, R.R., and Coppersmith, K.J., 1985, Implications of fault slip rates and earthquake recurrence models for probabilistic seismic hazard estimates: Bulletin of the Seismological Society of America, v. 75, p. 939-964.

Youngs, R.R., Swan, F.H., III, Power, M.S., Schwartz, D.P., and Green, R.K., 1987, Probabilistic analysis of earthquake and ground shaking hazard along the Wasatch Front, Utah, *in* Gori, P.O., and Hays, W.W., eds., Assessment of Regional Earthquake Hazards and Risk Along the Wasatch Front, Utah: U.S. Geological Survey Open File Report 87-585, p. M-1 to M-100.

Yount, J.C., Shroba, R.R., McMasters, C.R., Huckins, H.E., and Rodriguez, E. A., 1987, Trench logs from a strand of the Rock Valley fault system, Nevada Test Site, Nye County, Nevada: U.S. Geological Survey, Miscellaneous Field Studies Map MF-1824, 1 plate.

Zhang, P., Ellis, M., Slemmons D. B., and Moa, F., 1990, Right-lateral displacements and the Holocene slip rate associated with prehistoric earthquakes along the southern Panamint Valley fault zone: Implications for southern basin and range tectonics and coastal California deformation: Journal of Geophysical Research, v. 95, p. 4857-4872.

TABLE SDO-1
MAXIMUM MAGNITUDES FOR SOURCE ZONES

Zone	Maximum Magnitude [1]	Name of Zone and Comments
1		**Goldfield-Spring Mountain Zone including Yucca Mountain site:**
	6.4 ± 0.2 MBE	a) within 100 km of the site
		b) outside 100 km
	Ms 7.1 ± 0.2	South, Frenchman Mtns. Fault
	Ms 7.0 ± 0.2	North, Emigrant Peak fault
2		**Death Valley Zone**
	6.4 ± 0.2 MBE	a) within 100 km
		b) outside 100 km
	Ms 7.4 ± 0.2	White Mountain fault system
3		**Basin-Range Zone**
	6.4 ± 0.2 MBE	a) within 100 km
		b) outside 100 km
	Ms 7.4 ± 0.2	Railroad Valley fault system

[1] Ms should be equivalent to Mw (Hanks and Kanamori, 1979).

TABLE SDO-2
MAGNITUDE SCALING RELATIONSHIPS USED

Magnitude versus Length	
Mason (1996)	
Mw = 5.08 + 1.16 log L	extensional environments; all displacement types
Wells and Coppersmith (1994)	
Mw = 4.86 + 1.32 log L	All environments (excl. subduction zones)
Mw = 5.16 + 1.12 log L	normal-slip faults
Mw = 5.08 + 1.16 log L	strike-slip faults
	all displacement types
Magnitude versus Maximum Surface Displacement	
Mason (1996)	
Ms = 6.81 + 0.74 log D	extensional environments; all types
Wells and Coppersmith (1994)	
Mw = 6.61 + 0.71 log D	All environments (excl. subduction zones)
Mw = 6.81 + 0.78 log D	normal-slip faults
Mw = 6.69 + 0.74 log D	strike-slip faults
	all displacement types
Magnitude versus Fault Area	
Wells and Coppersmith (1994)	
Mw = 3.93 + 1.02 log A	all environments (excl. subduction zones)
Mw = 3.98 + 1.02 log A	normal-slip faults
Mw = 4.07 + 0.98 log A	strike-slip faults
	all displacement types
Magnitude versus Length x Displacement	
Mason (1996)	
Ms = 5.95 + 0.55 log LD	extensional environments; all displacement types
Magnitude versus Length and Slip Rate	
Anderson *et al.* (1996)	
Mw = 5.12 + 1.16 log L - 0.20 log SR	15-20 km maximum seismogenic depth
	all displacement types
Magnitude via Seismic Moment	
Hanks and Kanamori (1979)	all environments
Mw = 2/3 log Mo - 10.7	all displacement types
Average Displacement versus surface length	
Wells and Coppersmith (1994)	
log (AD) = -0.99 + 1.24 log L	all environments (excl. subduction zones) normal-
log (AD) = -0.70 + 1.04 log L	slip faults
log (AD) = -1.43 + 0.88 log L	strike-slip faults
	all faults

TABLE SDO-3
PARAMETERS FOR REGIONAL FAULT SOURCES
(Page 1 of 2)

Fault (map designation)		Sense of Displacement	Length			Maximum Surface Displacement Per Event			Slip Rate			Quaternary Activity Relative Weighting	
			Minimum	Preferred	Maximum	Minimum	Preferred	Maximum	Minimum	Preferred	Maximum	Yes	No
Amaragosa River	(AR)	rl	17	17	28				0.001	0.01	0.05	1	0
Ash Hill	(AH)	rl	33	55	90				0.21	0.3	0.38	1	0
Bare Mountain	(BM)	n	18	23	30	1.2	1.5	1.8	0.006	0.01	0.2	1	0
Belted Range	(BLR)	n	22	34	46				0.01	0.05	0.1	1	0
Buried Hills	(BH)	n	15	18	25				0.001	0.01	0.05	1	0
Buried Strike-slip	(T6-SS)	rl	20	27	120				0.001	0.005	0.02	0.4	0.6
Cane Spring	(CS)	ll	19	26	30				0.005	0.01	0.05	0.8	0.2
Carpetbag	(CB)	n	17	28	39				0.001	0.005	0.01	0.8	0.2
Carrara (Highway 95)	(H95)	rl	11	26	41				0.0005	0.001	0.005	0.2	0.8
Central Death Valley	(DV)	rn	41	61	75	2.5	3.5	4.5	2.6	3.8	7.4	1	0
E. Pintwater Range	(EPR)	n	28	36	58				0.001	0.005	0.01	1	0
Eleana Range	(ER)	n	11	15	15				0.003	0.01	0.05	1	0
Furnace Creek	(FC)	rl	85	105	195	5.5	6	6.5	4	8	10	1	0
Grapevine Mountains	(GM)	n	26	26	32				0.003	0.01	0.05	1	0
Hunter Mountain	(HM)	nrl	46	64	65				1.3	2	2.7	1	0
Jackass Flats "Gravity"	(JFG)	n	26	34	44				0.0005	0.005	0.05	0.9	0.1
Kawich Range	(KR)	n	22	32	45				0.001	0.005	0.01	1	0
Keane Wonder	(KW)	n	19	27	29				0.001	0.005	0.05	0.8	0.2
Mine Mountain	(MM)	ll	21	21	35				0.005	0.01	0.09	1	0
N. Emigrant Valley	(EVN)	rl?	18	37	45				0.01	0.02	0.08	1	0
Oak Spring Butte	(OAK)	n	9	16	19				0.001	0.005	0.01	0.8	0.2
Oasis Valley	(OSV)	n	5	8	19				0.0005	0.001	0.003	0.8	0.2
Pahrump Valley	(PRP)	rl	24	61	66				0.005	0.01	0.1	1	0
Pahute Mesa #1	(PMI)	n	11	13	15				0.001	0.005	0.01	0.8	0.2
Panamint Valley	(PAN)	rl	82	90	105				1.6	2.4	3.2	1	0
Peace Camp	(PC)	nl	12	12	30				0.005	0.01	0.09	1	0
Rock Valley	(RV)	ll	33	48	68	1.1	3.6	4.5	0.01	0.02	0.08	1	0

TABLE SDO-3
(Page 2 of 2)

Fault (map designation)	Sense of Displacement	Length			Maximum Surface Displacement Per Event			Slip Rate			Quaternary Activity Relative Weighting	
		Minimum	Preferred	Maximum	Minimum	Preferred	Maximum	Minimum	Preferred	Maximum	Yes	No
South Silent Canyon (SSC)	n	11	14	17				0.001	0.005	0.01	0.8	0.2
Spotted Range (SPR)	n	17	30	30				0.001	0.01	0.05	1	0
Towne Pass (TP)	n	33	38	50				0.005	0.03	0.1	1	0
Wahmonie (WAH)	II	9	15	15				0.005	0.01	0.05	0.8	0.2
West Specter Range (WSR)	n	10	19	25				0.001	0.004	0.01	1	0
West Spring Mountains(WSM)	n	31	36	58				0.02	0.09	0.2	1	0
Western Pintwater Range (WPR)	n	33	54	76				0.005	0.008	0.05	1	0
Yucca Lake (YCL)	n	12	19	23				0.001	0.005	0.01	0.5	0.5
Yucca-Butte (YB)	n	26	34	49				0.015	0.026	0.053	1	0

TABLE SDO-4
PARAMETERS FOR LOCAL FAULT SOURCES

FAULT	TOTAL LENGTH	WEIGHTING	FAULT DIP	DOWNDIP WIDTH	WEIGHTING	MAXIMUM SURFACE DISPLACEMENT	WEIGHTING	SLIP RATE	WEIGHTING	MOMENT RATE	EVENT MOMENT	MOMENT MAGNITUDE
	Km		degrees	km		(m)		m/kyr		dyne-cm/yr	dyne-cm	
Solitario Canyon fault	16	0.3	55	11.1	0.2	0.7	0.3	0.009	0.3	4.436e+20	1.72494e+25	6.2
(SC)	18.5	0.4	55	13.3	0.4	1.2	0.4	0.015	0.4	1.107e+21	4.42890e+25	6.6
	21.5	0.3	55	17.6	0.4	1.5	0.3	0.022	0.3	2.497e+21	8.51400e+25	6.9
Iron Ridge fault	8.3	0.3	55	11.5	0.2	0.5	0.3	0.0023	0.3	6.586e+19	7.15875e+24	5.9
(IR)	8.3	0.4	55	14.5	0.6	0.7	0.4	0.0033	0.4	1.191e+20	1.26368e+25	6.1
	9	0.3	55	19	0.2	1	0.3	0.0051	0.3	2.907e+20	2.85000e+25	6.4
Fatigue Wash fault	16	0.3	55	9.7	0.2	1	0.3	0.003	0.3	1.048e+20	1.74600e+25	6.2
(FW))	17	0.4	55	11.6	0.6	1.25	0.4	0.005	0.4	3.132e+20	3.91500e+25	6.6
	20	0.3	75	17.6	0.2	1.5	0.3	0.009	0.3	1.045e+21	8.71200e+25	6.9
Southern Windy Wash fault	9	0.3	45	8.5	0.2	0.6	0.3	0.009	0.3	2.066e+20	6.88500e+24	5.9
(SWW)	11.5	0.4	55	10.5	0.6	0.88	0.4	0.011	0.4	3.985e+20	1.59390e+25	6.2
	15	0.3	75	17.6	0.2	1	0.3	0.017	0.3	1.122e+21	3.30000e+25	6.5
Paintbrush Canyon fault	12	0.3	55	14.5	0.3	0.4	0.3	0.007	0.3	3.654e+20	1.04400e+25	6.0
(PC(N) + PC(S))	17.5	0.4	55	17.3	0.6	1.7	0.4	0.008	0.4	7.266e+20	7.72013e+25	6.8
	26.2	0.3	55	23	0.1	2.6	0.3	0.011	0.3	1.989e+21	2.35014e+26	7.3
Paintbrush Canyon (North)	7	0.3	55	14.5	0.3	0.4	0.3	0.007	0.3	2.132e+20	6.09000e+24	5.8
(PC(N))	12.3	0.4	55	17.3	0.6	1	0.4	0.008	0.4	5.107e+20	3.19185e+25	6.5
	18.7	0.3	55	23	0.1	1.45	0.3	0.011	0.3	1.419e+21	9.35468e+25	6.9
Paintbrush Canyon (South)	9	0.3	55	14.5	0.3	0.3	0.3	0.007	0.3	2.436e+20	5.22000e+24	5.8
(PC(S)	11	0.4	55	17.3	0.6	1.7	0.4	0.008	0.4	4.567e+20	4.85265e+25	6.6
	11	0.3	55	23	0.1	2.6	0.3	0.011	0.3	8.349e+20	9.86700e+25	6.9
Stagecoach Road fault	4.5	0.3	55	11.5	0.2	0.6	0.3	0.0057	0.3	8.849e+19	4.65750e+24	5.7
(SCR)	10	0.4	55	14.5	0.6	0.8	0.4	0.017	0.4	6.656e+20	1.56600e+25	6.2
	12	0.3	55	19	0.2	1.2	0.3	0.028	0.3	1.756e+21	376200e+25	6.5

TABLE SDO-5
MULTIPLE-FAULT EVENT SCENARIOS AND EVENT MOMENTS FOR LOCAL FAULTS
(Page 1 of 2)

FAULT[1]	TOTAL LENGTH	WEIGHTING	FAULT DIP	DOWNDIP WIDTH	WEIGHTING	MAXIMUM SURFACE DISPLACEMENT	WEIGHTING	EVENT MOMENT	MOMENT MAGNITUDE
	km		degrees	km		(cm)		dyne-cm	
PC(N) + BR	8	0.3	55	14.5	0.3	33	0.3	5.742e+24	5.8
	14	0.4	55	17.3	0.6	52	0.4	1.889e+25	6.3
	19.7	0.3	55	23.2	0.1	94	0.3	6.444e+25	6.8
PC(N) + PC(S) + BR + SCR	18.6	0.3	55	14.5	0.3	33	0.3	1.335e+25	6.1
	28.8	0.4	55	17.3	0.6	53	0.4	3.961e+25	6.6
	34.4	0.3	55	23.2	0.1	185	0.3	2.215e+26	7.2
PC(N) + PC(S) + BR	12	0.3	55	14.5	0.3	33	0.3	8.613e+24	6.0
	17.5	0.4	55	17.3	0.6	53	0.4	2.407e+25	6.4
	26.2	0.3	55	23.2	0.1	185	0.3	1.687e+26	7.1
SC + SWW	22	0.3	55	11.1	0.2	20	0.3	7.326e+24	5.9
	24.8	0.4	55	13.3	0.4	35	0.4	1.732e+25	6.2
	25	0.3	55	17.6	0.4	50	0.3	3.300e+25	6.5
FW + SWW + SCF	18.8	0.3	55	9.7	0.2	47	0.3	1.286e+25	6.1
	26	0.4	55	11.6	0.6	105	0.4	4.641e+25	6.6
	31	0.3	75	17.6	0.2	165	0.3	1.333e+26	7.0
SWW + SCF	9	0.3	45	8.5	0.2	55	0.3	6.311e+24	5.8
	12.3	0.4	55	10.5	0.6	62	0.4	1.201e+25	6.1
	14.4	0.3	75	17.6	0.2	84	0.3	3.193e+25	6.5
SWW + SCF + NCF	19.8	0.3	45	8.5	0.2	7.5	0.3	1.893e+24	5.4
	22.2	0.4	55	10.5	0.6	12	0.4	4.196e+24	5.7
	23	0.3	75	17.6	0.2	20	0.3	1.214e+25	6.1
ash event	18.6	0.3	55	14.5	0.3	115	0.3	4.652e+25	6.6
	28.8	0.4	55	17.3	0.6	145	0.4	1.084e+26	7.0
	34.4	0.3	55	23.2	0.1	175	0.3	2.095e+26	7.2
PC(N) +PC(S) + SCR	18.6	0.3	55	14.5	0.3	26	0.3	1.052e+25	6.0
	28.8	0.4	55	17.3	0.6	40	0.4	2.989e+25	6.5
	34.4	0.3	55	23.2	0.1	140	0.3	1.676e+26	7.1

[1] Fault names are given in Table SDO-4

TABLE SDO-5
(Page 2 of 2)

FAULT[1]	TOTAL LENGTH	WEIGHTING	FAULT DIP	DOWNDIP WIDTH	WEIGHTING	MAXIMUM SURFACE DISPLACEMENT	WEIGHTING	EVENT MOMENT	MOMENT MAGNITUDE
	km		degrees	km		(cm)		dyne-cm	
PC(S) + SCR	15.2	0.3	55	14.5	0.3	25	0.3	8.265e+24	5.9
	19.8	0.4	55	17.3	0.6	57	0.4	2.929e+25	6.4
	19.8	0.3	55	23.2	0.1	84	0.3	5.788e+25	6.7
PC(S) + BR	11	0.3	55	14.5	0.3	88	0.3	2.450e+25	6.4
	12.8	0.4	55	17.3	0.6	167	0.4	4.767e+25	6.6
	15.6	0.3	55	23.2	0.1	205	0.3	1.113e+26	7.0
SCR + SC	20.4	0.3	55	11.1	0.2	28	0.3	9.510e+24	6.0
	25.6	0.4	55	13.3	0.6	59	0.4	3.013e+25	6.5
	25.6	0.3	55	17.6	0.2	77	0.3	5.204e+25	6.7
IR + AW	9.7	0.3	55	11.1	0.2	50	0.3	8.075e+24	5.9
	9.7	0.4	55	13.3	0.6	70	0.4	1.355e+25	6.1
	11	0.3	55	17.6	0.2	100	0.3	2.904e+25	6.4
IR + AW + GD	13.2	0.3	55	11.1	0.2	50	0.3	1.099e+25	6.1
	13.2	0.4	55	13.3	0.6	70	0.4	1.843e+25	6.3
	13.7	0.3	55	17.6	0.2	100	0.3	3.643e+25	6.5
FW + SWW	18.8	0.3	55	9.7	0.2	30	0.3	8.206e+24	5.9
	26	0.4	55	11.6	0.6	105	0.4	4.604e+25	6.6
	31	0.3	75	17.6	0.2	165	0.3	1.307e+26	7.0
SWW + FW + NWW	22.8	0.3	55	9.7	0.2	14	0.3	4.644e+24	5.7
	26	0.4	55	11.6	0.6	20	0.4	9.048e+24	6.0
	27.4	0.3	75	17.6	0.2	24	0.3	1.736e+25	6.2
SWW + CWW	12.6	0.3	55	8.5	0.2	38	0.3	6.105e+24	5.8
	15.4	0.4	55	10.5	0.6	73	0.4	1.771e+25	6.2
	18	0.3	75	17.6	0.2	83	0.3	3.944e+25	6.6

[1] Fault names are given in Table SDO-4

Table SDO-6
Regressions Used for Estimating Displacement
Note that the regressions assumed *AD* and *MD* as the independent variable.

Regression	**Reference**
$\log AD = 0.63\ \mathbf{M} - 4.45$	Wells and Coppersmith (1994)
$\log AD = 1.24 \log L - 1.99$	Wells and Coppersmith (1994)
$\log AD = \log L - 1.43$	AAR Team (SSC workshop #4, Jan. 8, 1997)
$\log MD = 0.89\ \mathbf{M} - 5.90$	Wells and Coppersmith (1994)
$\log MD = 1.51 \log L - 1.98$	Wells and Coppersmith (1994)

where *AD* = average surface displacement in meters; *MD* = maximum surface displacement in meters; **M** = moment magnitude; and *L* = surface rupture length in kilometers.

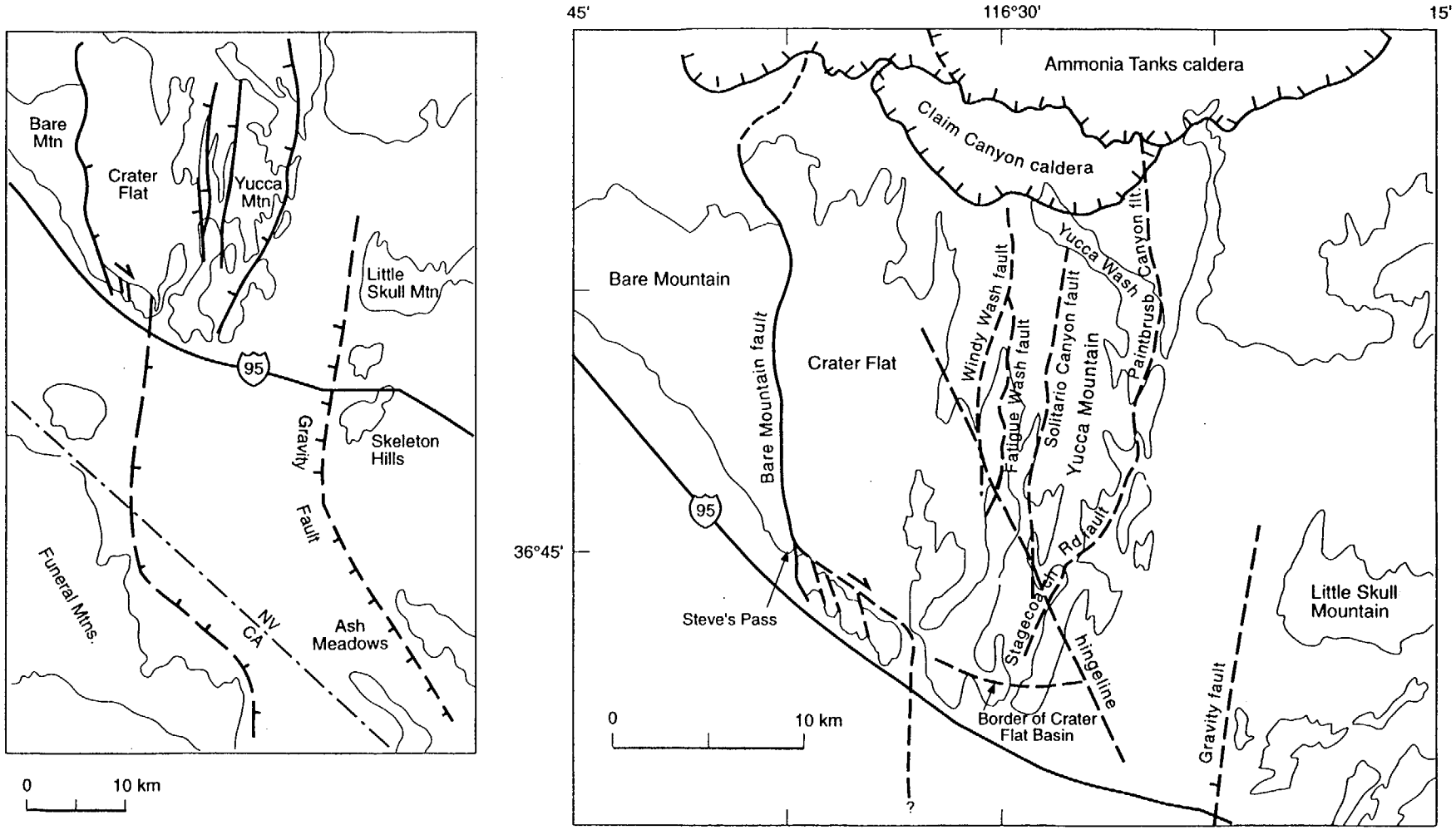

Figure SDO-1 Map showing location and features of Yucca Mountain and Crater Flat

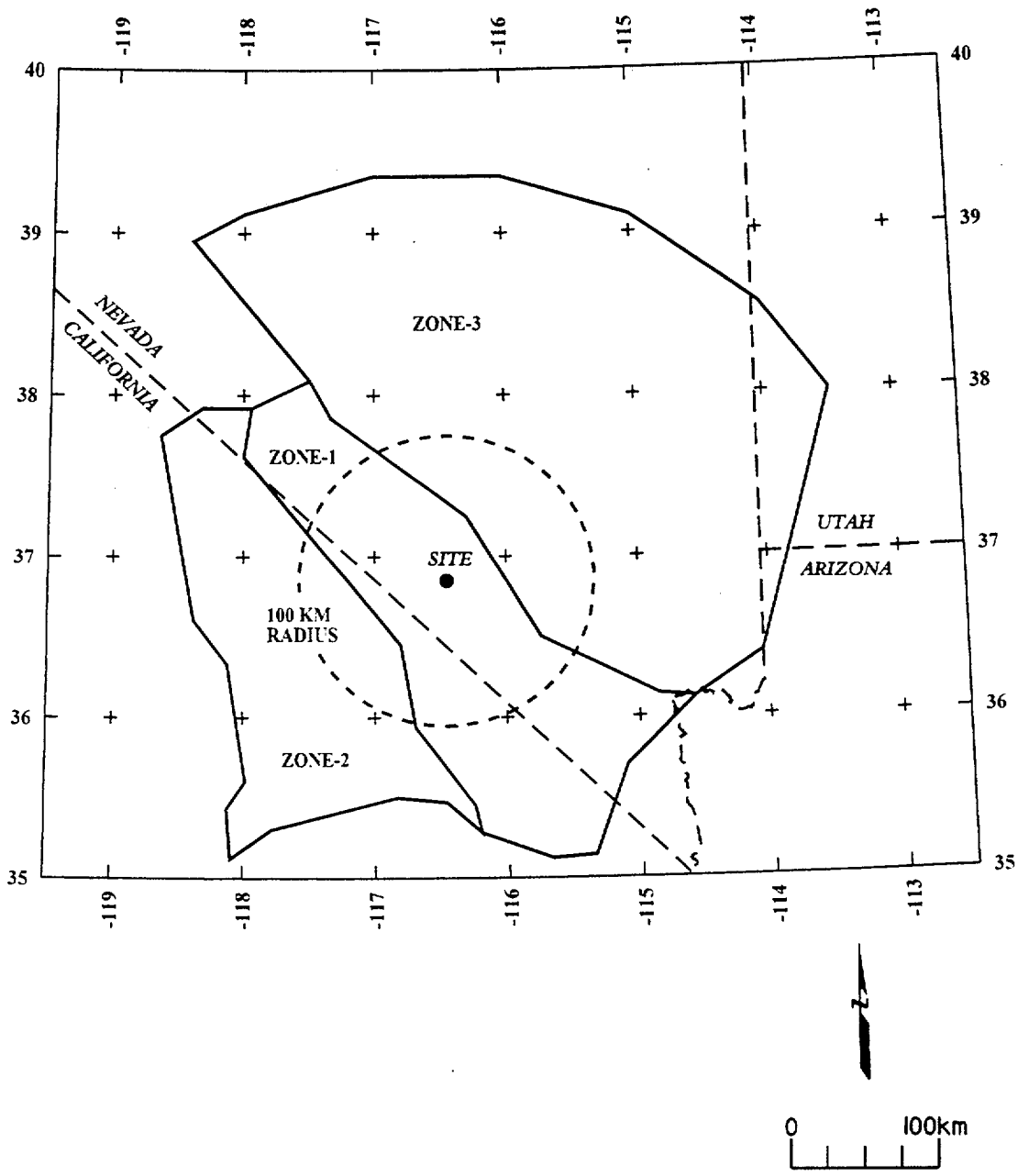

Figure SDO-2 Map showing the boundaries of zones used in the seismic source model

h:\prj\yucca_mt\dgn\1097\plate_16_reg_zone.dgn 07-NOV-1997 10:16

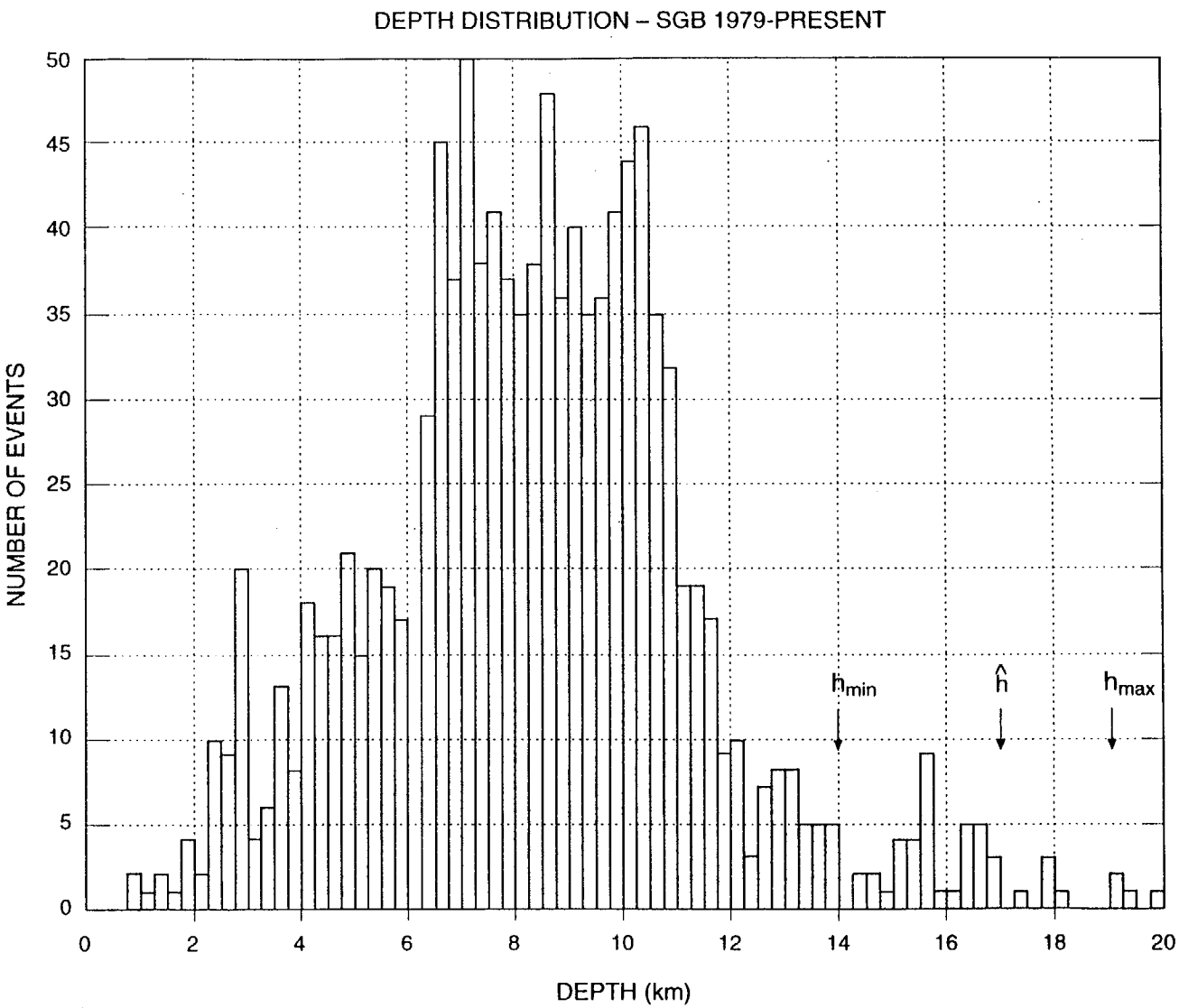

Figure SDO-3 **Depth distribution of hypocenters (focal depth distribution) of earthquakes in the southern Great Basin (SGB)**

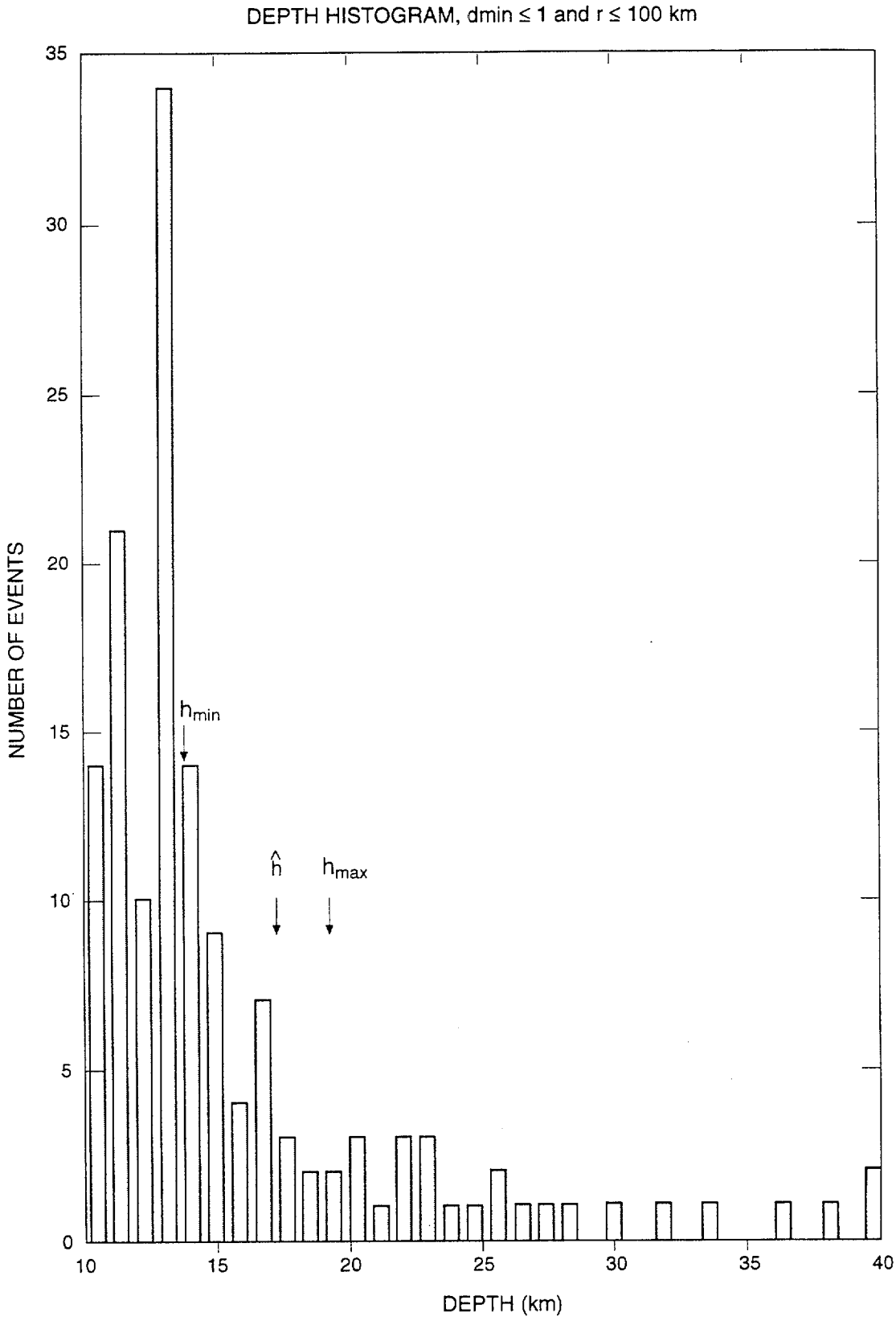

Figure SDO-4 Focal depth distribution of deep earthquakes in the area within r<100 km of Yucca Mountain

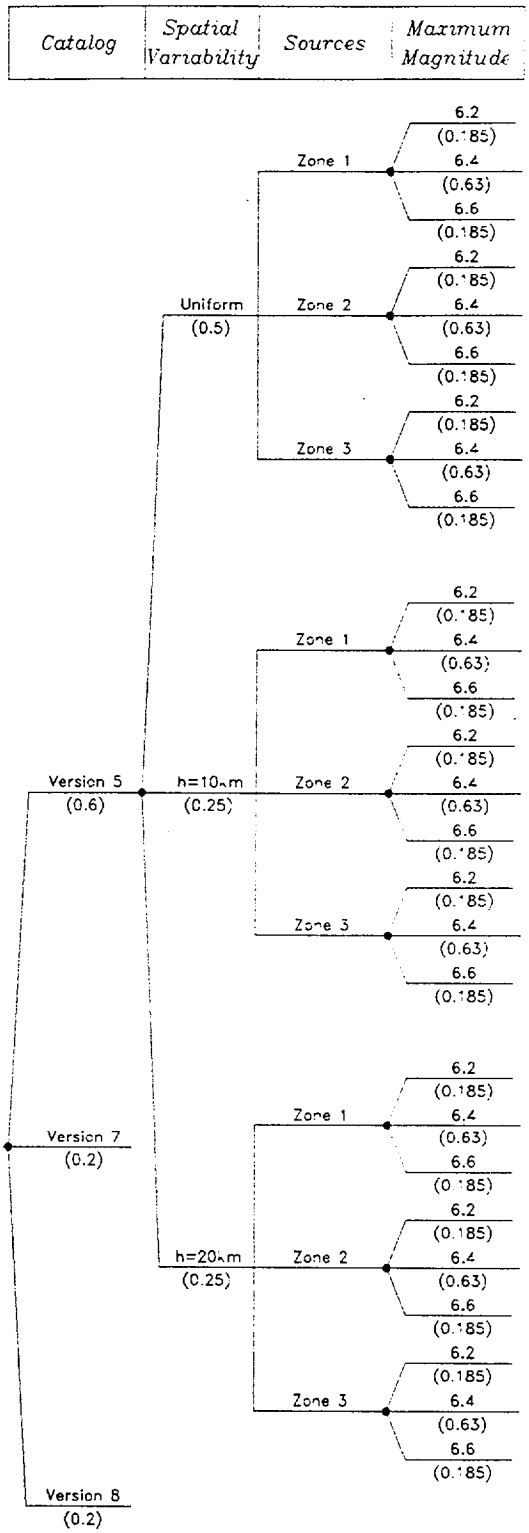

Figure SDO-5 Logic tree for regional source zones

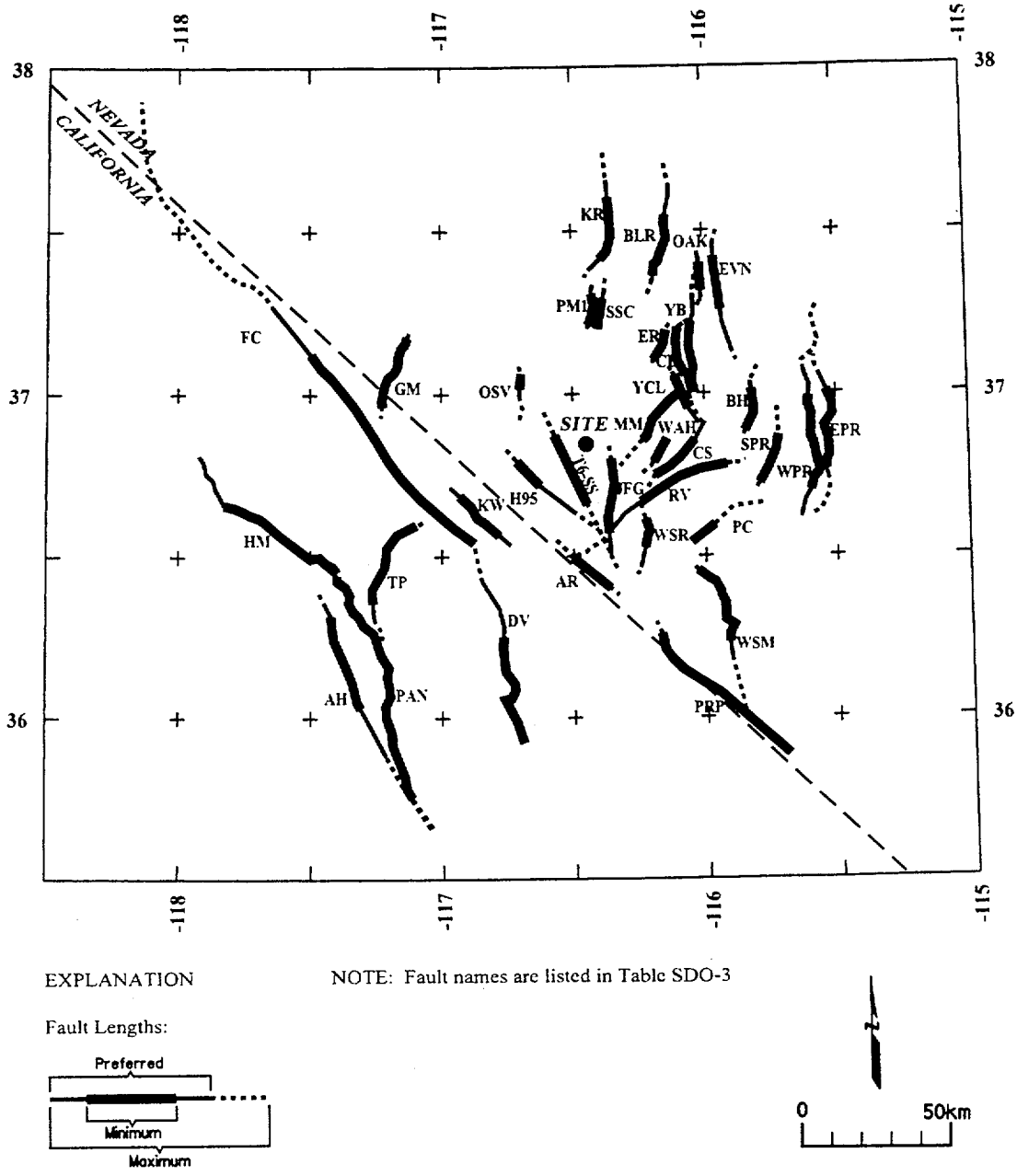

Figure SDO- 6 Map showing regional faults included in the seismic source model.

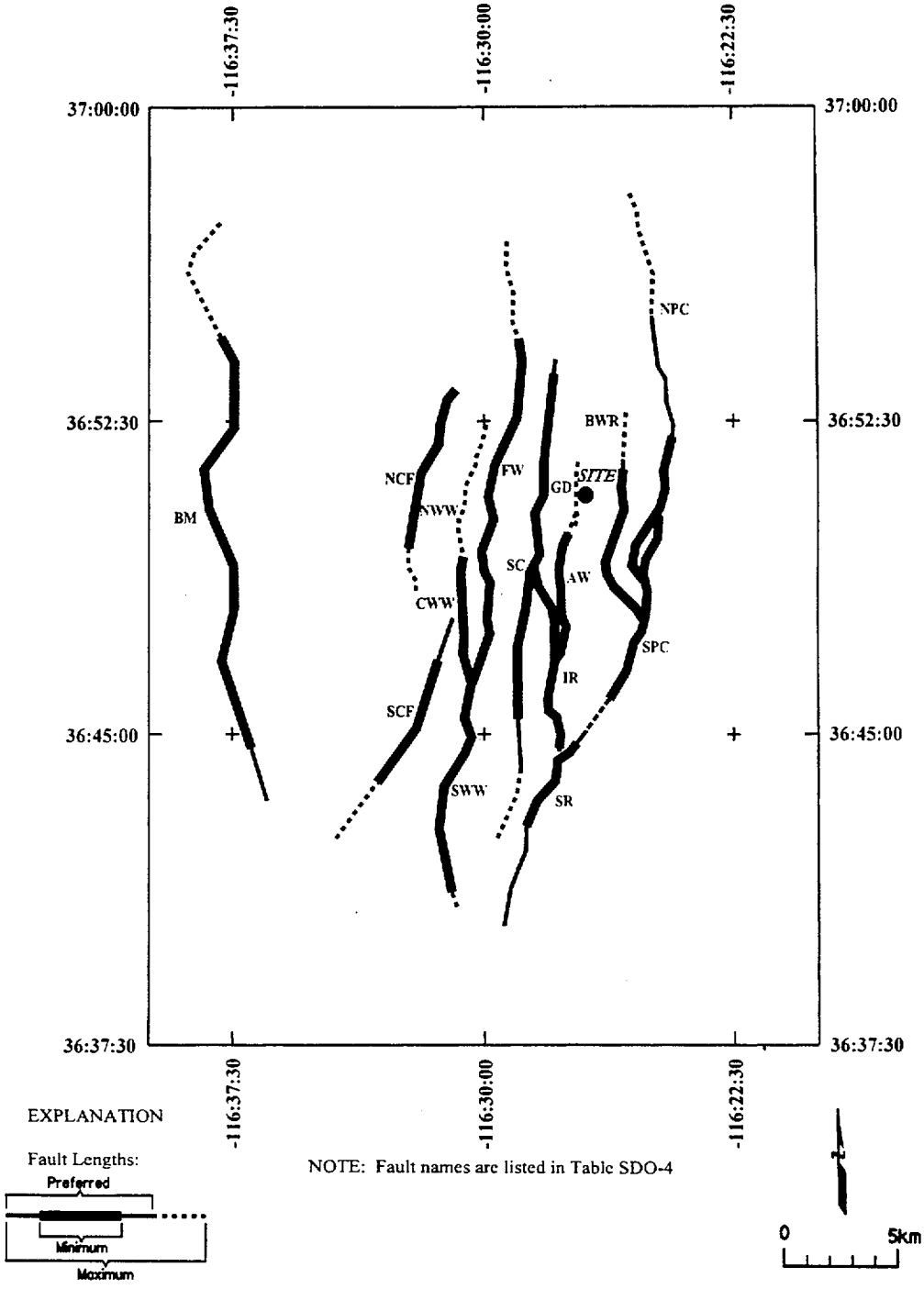

Figure SDO- 7a Map showing local fault sources included in the independent seismic source model

h:\prj\yucca_mt\dgn\1097\plate_t6_ici_fault.dgn 07-NOV-1997 10:43

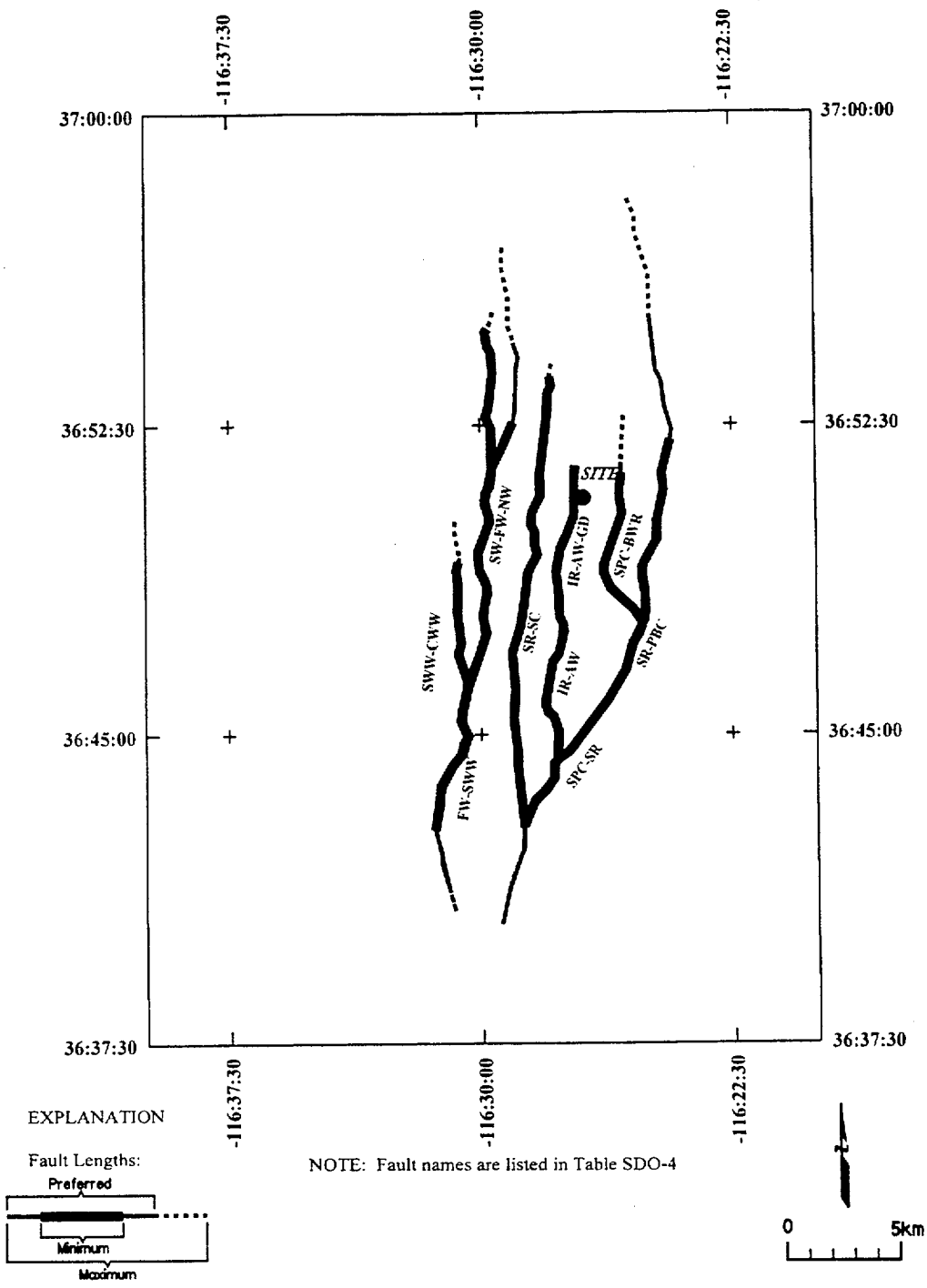

Figure SDO-7b Map showing local fault sources included in the linked seismic source model

h:\prj\yucca_mt\dgn\1097\plots_16_lcl_linked.dgn 07-NOV-1997 10:29

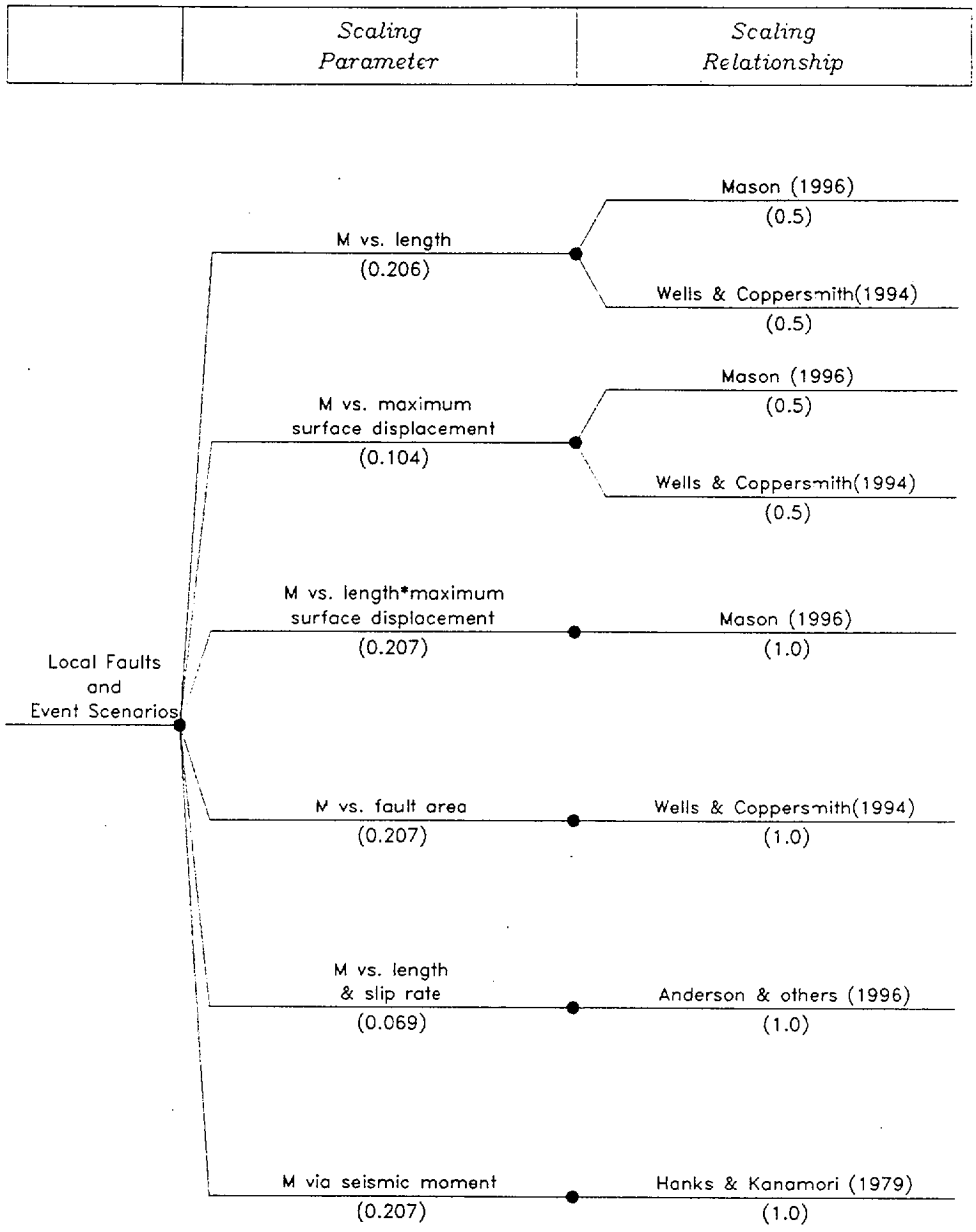

Figure SDO-8 Scaling parameters and relationships used to estimate maximum magnitudes for local faults

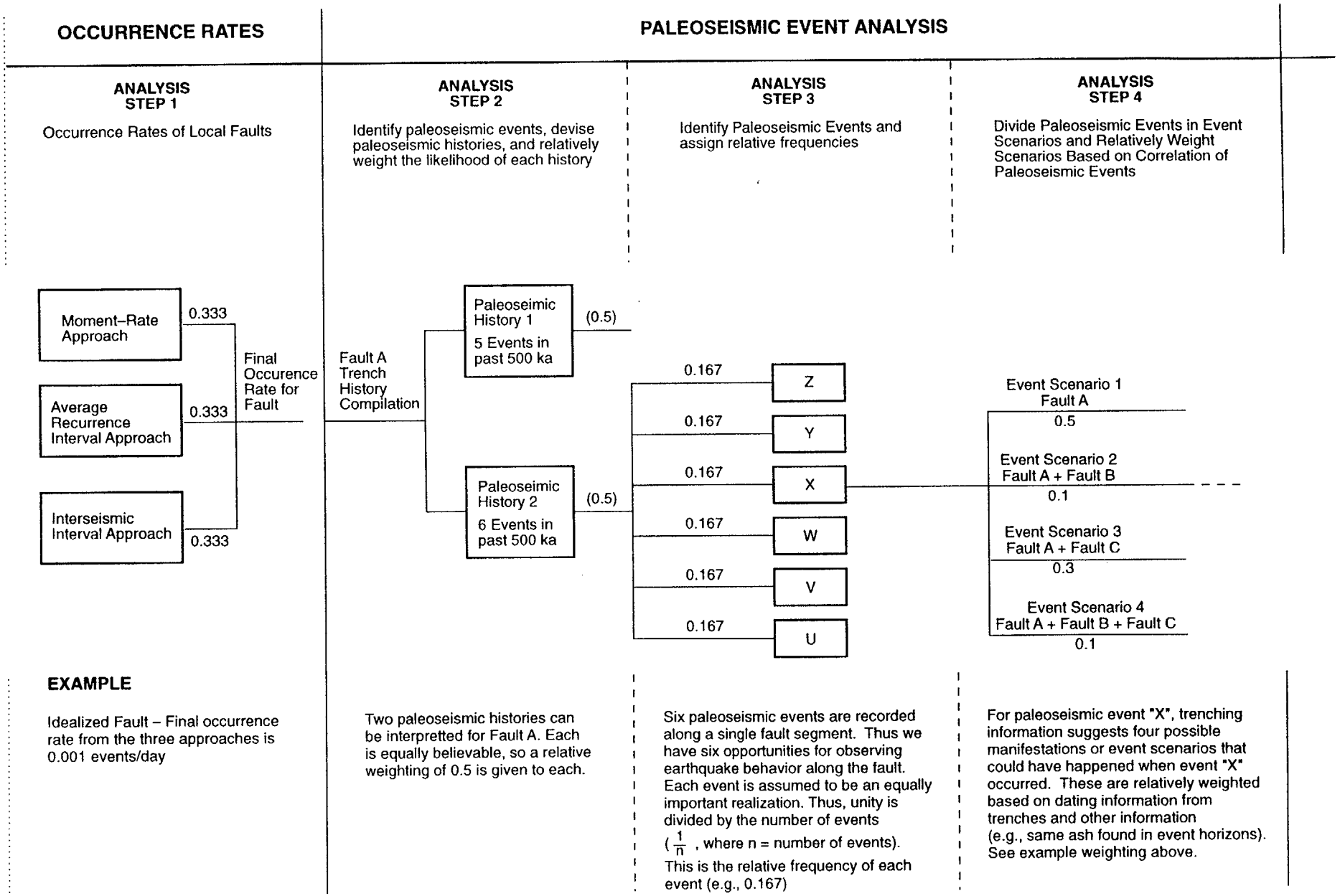

Figure SDO-9 Example calculation of occurrence rates for local faults

EVENT SCENARIO OCCURRENCE RATES

ANALYSIS STEP 5

Calculate Occurrence Rate of Event Scenarios Relative to Individual Paleoseismic Events

ANALYSIS STEP 6

Add Up Occurrence Rates for Each Event Scenario from All Paloseismic Events from a Fault that Includes It

ANALYSIS STEP 7

Combining Occurrence Rates from Linked and Distributed Event Scenarios

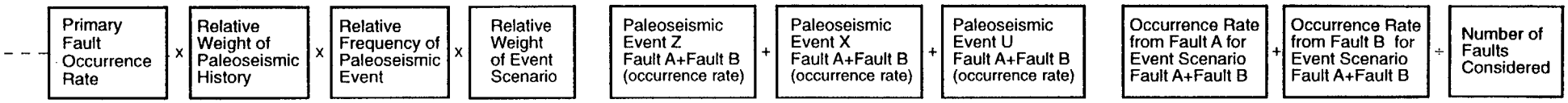

Event X

0.001 x 0.5 x 0.167 x 0.1 ⇒ 8.35E–6

3.34E–5 + 8.35E–6 + 1.67E–5 ⇒ 5.85E–5

5.85E–5 + 7.32E–6 = 6.58E–5 ÷ 2 ⇒ 3.29E–5

Figure SDO-9 Example calculation of occurrence rates for local faults (continued)

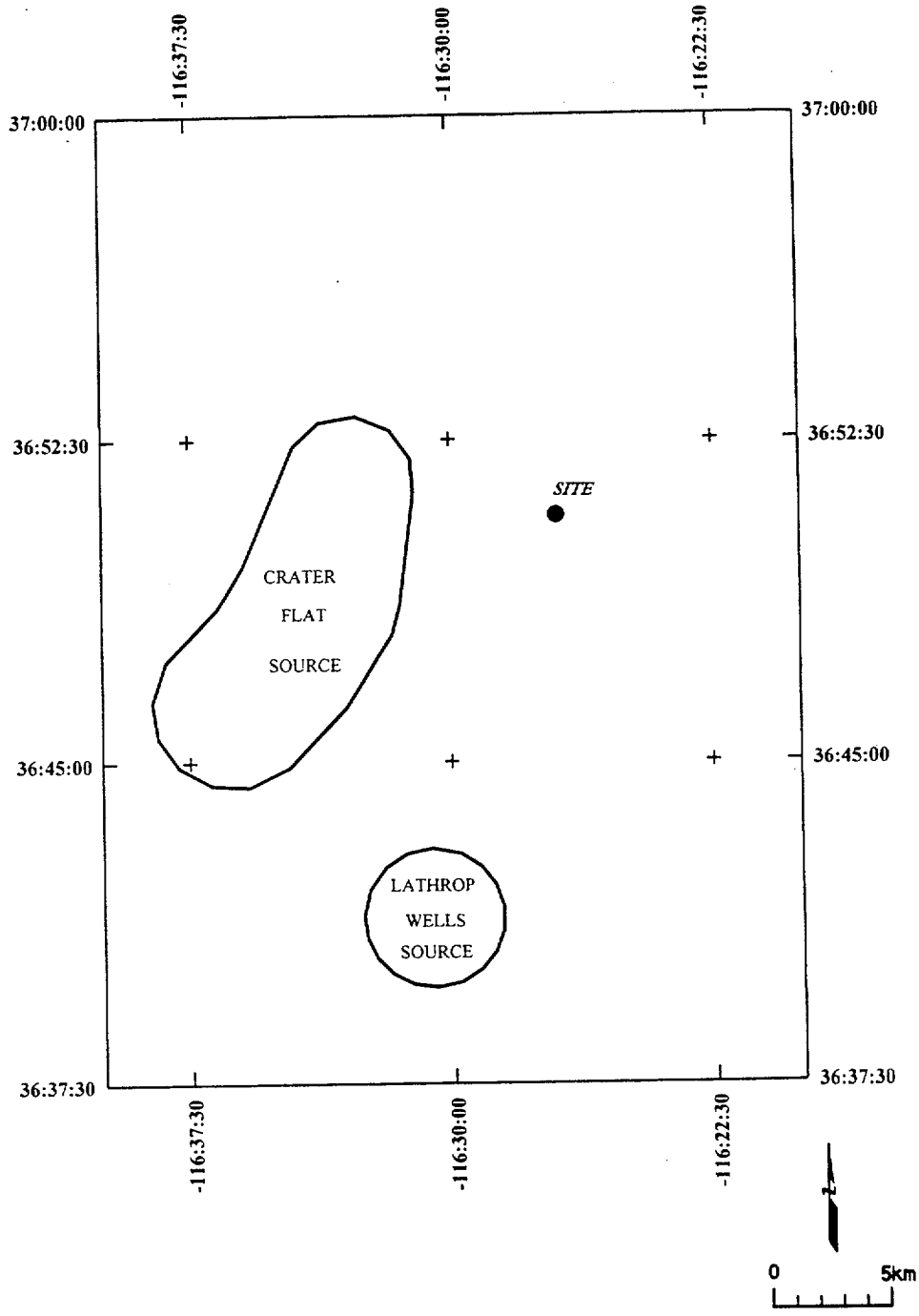

Figure SDO-10 Map showing volcanic zones included in the seismic source model

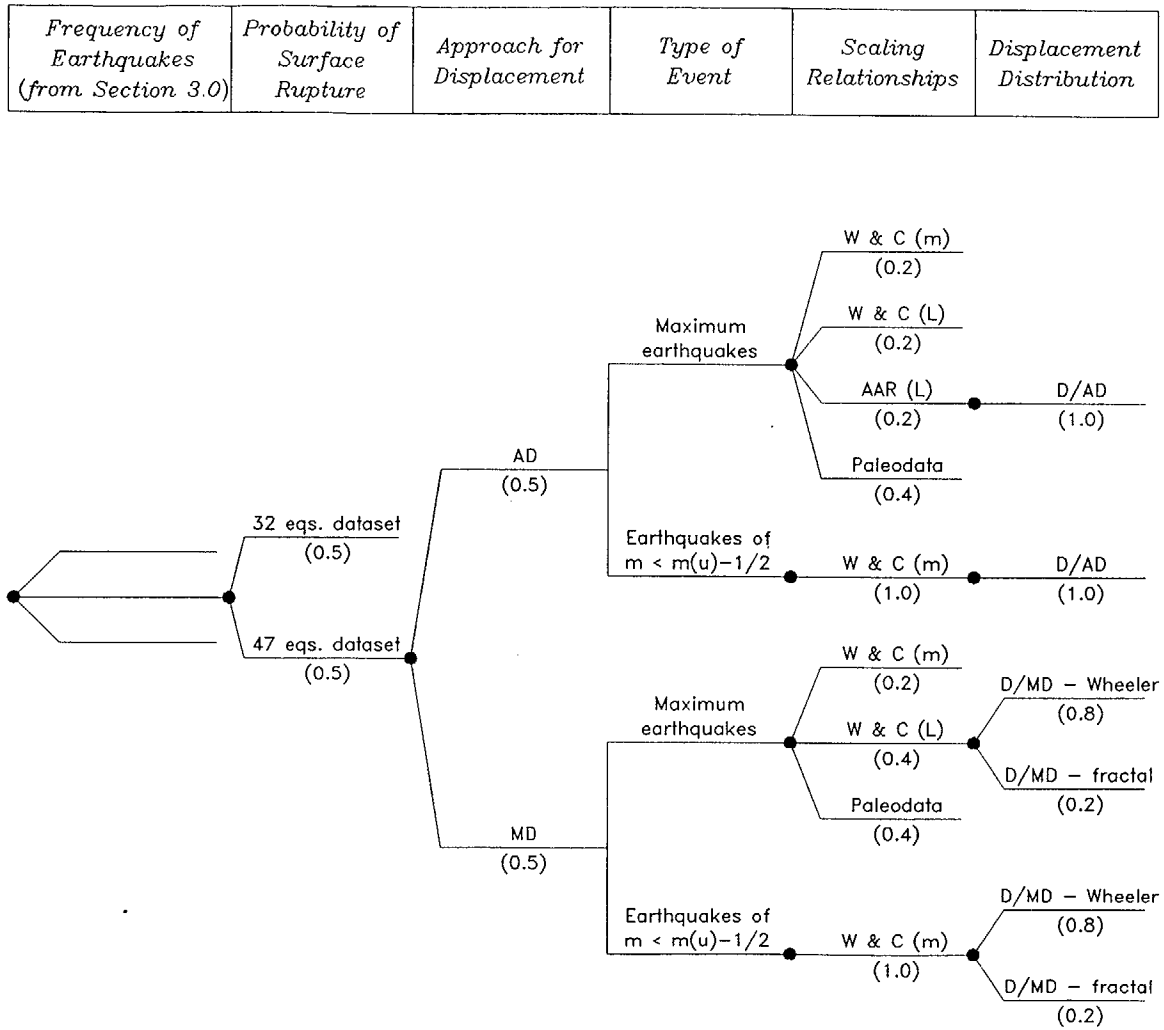

Figure SDO-11 Logic tree used to characterize principal faulting displacement hazard.

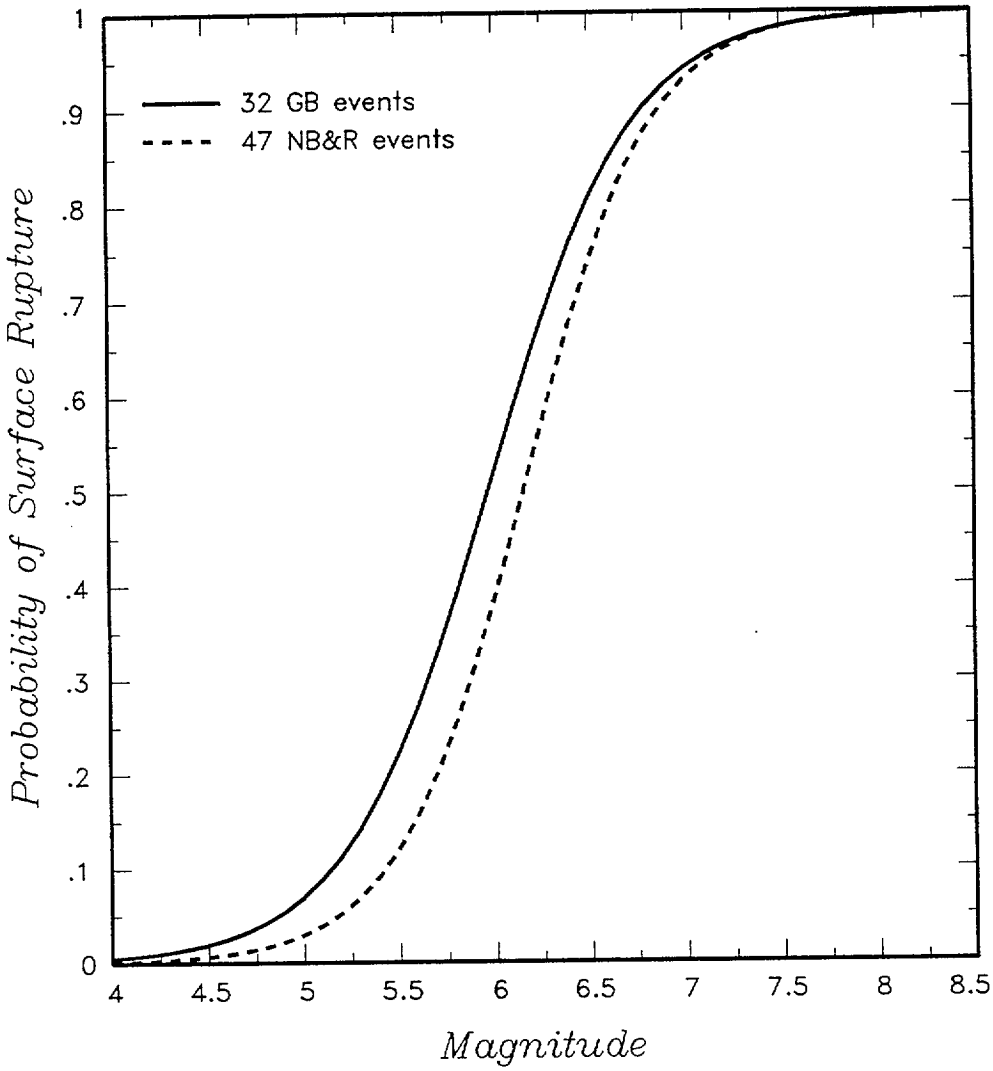

Figure SDO-12 Probability of surface rupture as a function of earthquake magnitude computed from various data sets given in S.K. Pezzopane and T.E. Dawson (USGS, written communication, 1996)

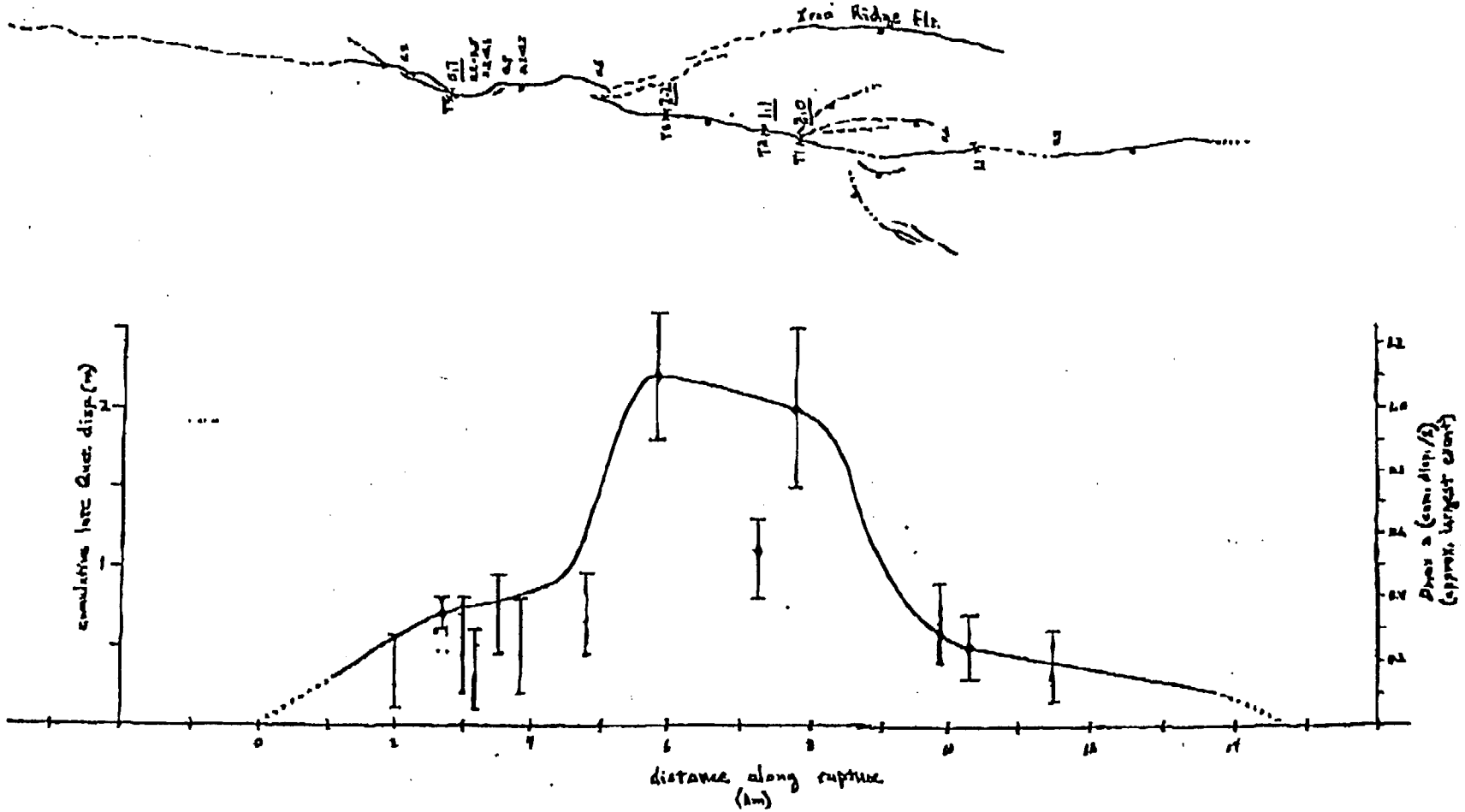

Figure SDO-13 Estimated mid- to late-Quaternary displacement along the Solitario Canyon fault. Strip map depicts displacement data from trench studies (Chap. 4.7 of U.S. Geological Survey, written communication, 1996) and scarp heights from Simonds *et al.* (1995). Graph depicts trench data (large dots) and scarp heights converted to estimated displacements (small dots). Left axis scales cumulative mid- to late-Quaternary displacement, and right axis scales *MD* based on 1/2 of the cumulative offset (a close approximation of the largest event).

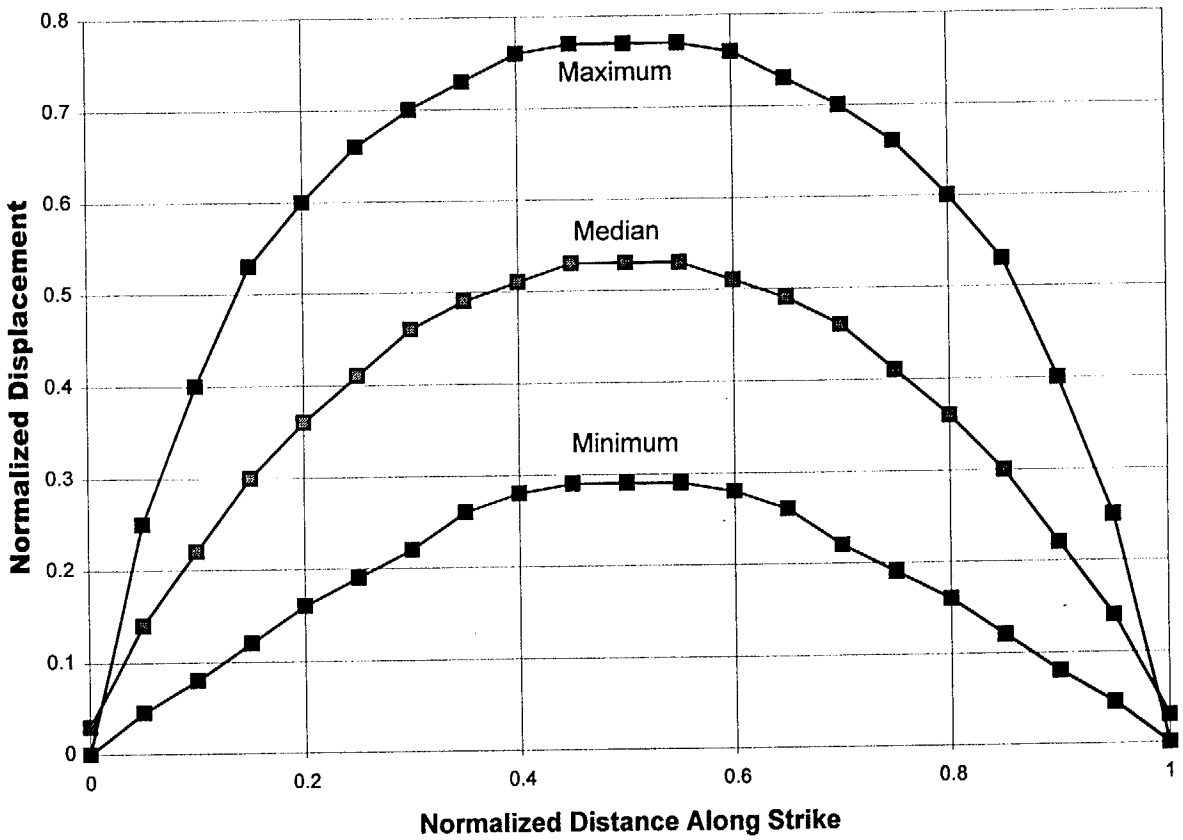

Figure SDO-14 Normalized slip along strike from five Basin and Range historic normal fault earthquake ruptures developed by the ASM team from data presented in Wheeler (1989).

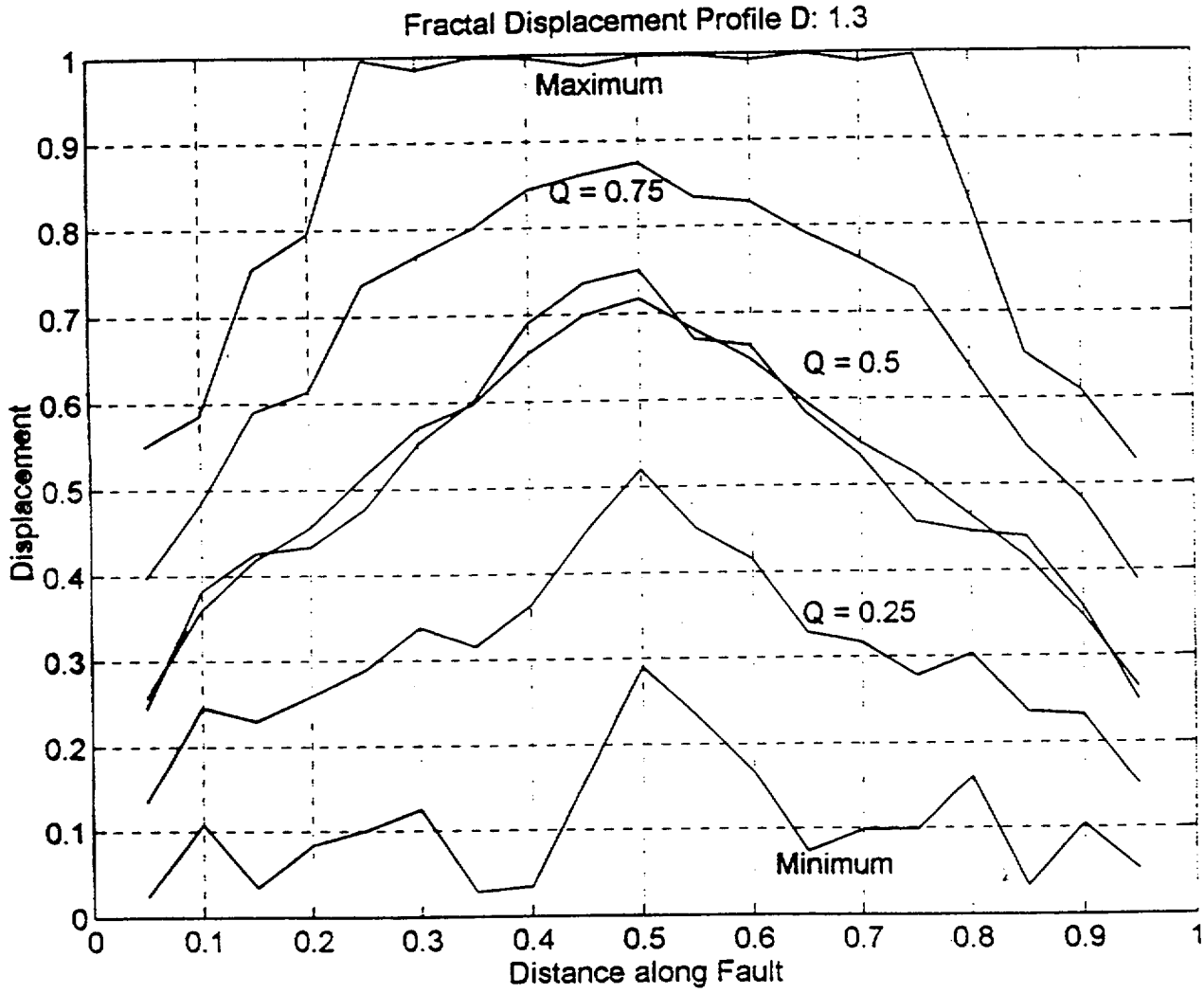

Figure SDO-15 Fractal displacement profiles developed by Ron Bruhn, University of Utah, to predict distribution for the ratio of displacement at a point to the maximum displacement in an earthquake.

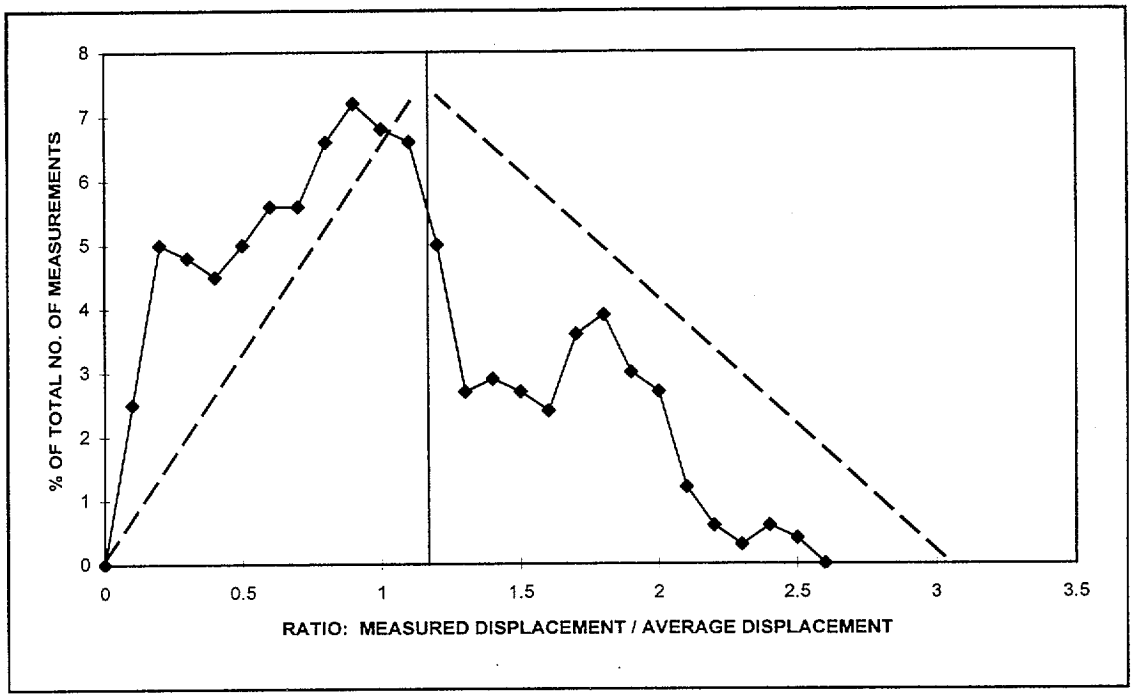

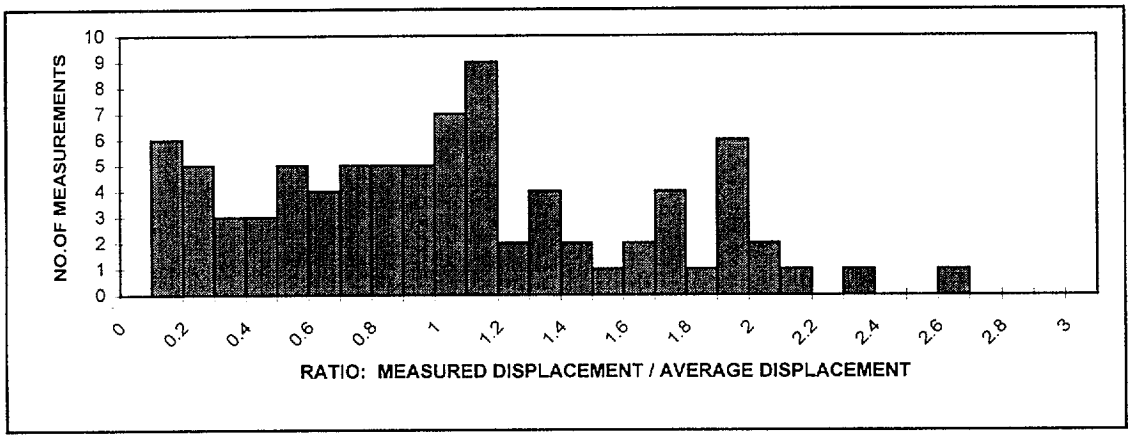

Figure SDO-16 Plots showing event-to-event variability in displacement relative to average displacement per event at a location along a fault based on data from paleoseismic investigations in the Yucca Mountain area.

Distributed Faulting Approach	*Activation Probability*	*P(Slip|event)*	*Slip Rate*	*Average Displacement per Event*	*Distribution of Slip per Event*

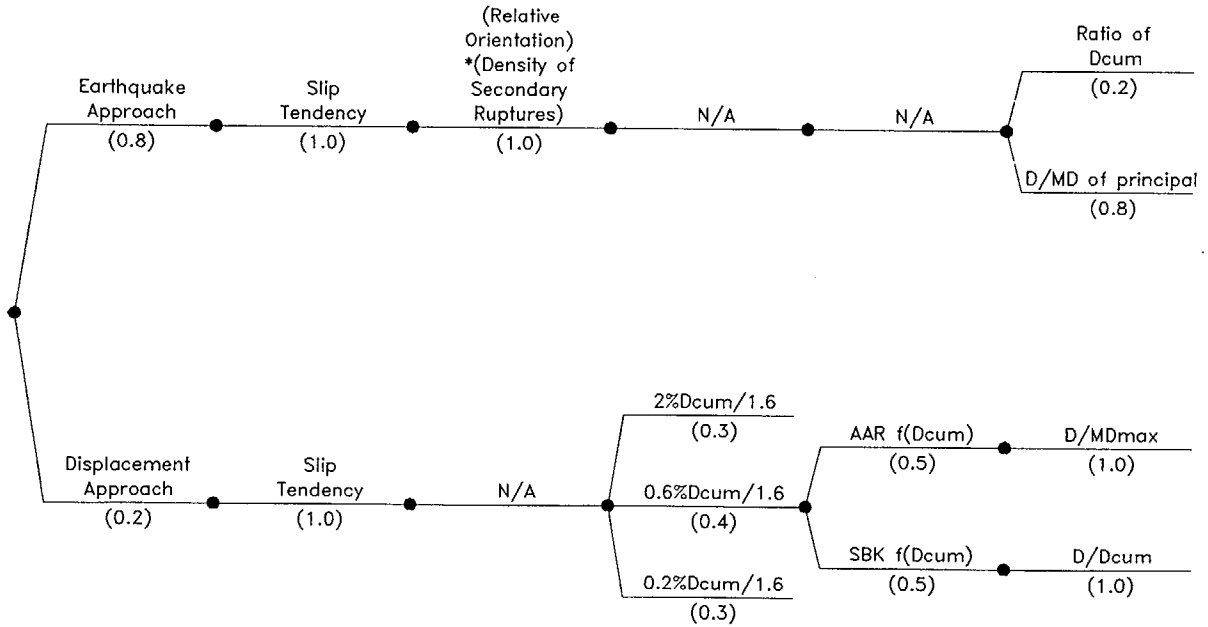

Figure SDO-17 Logic tree used to characterize distributed faulting displacement hazard.

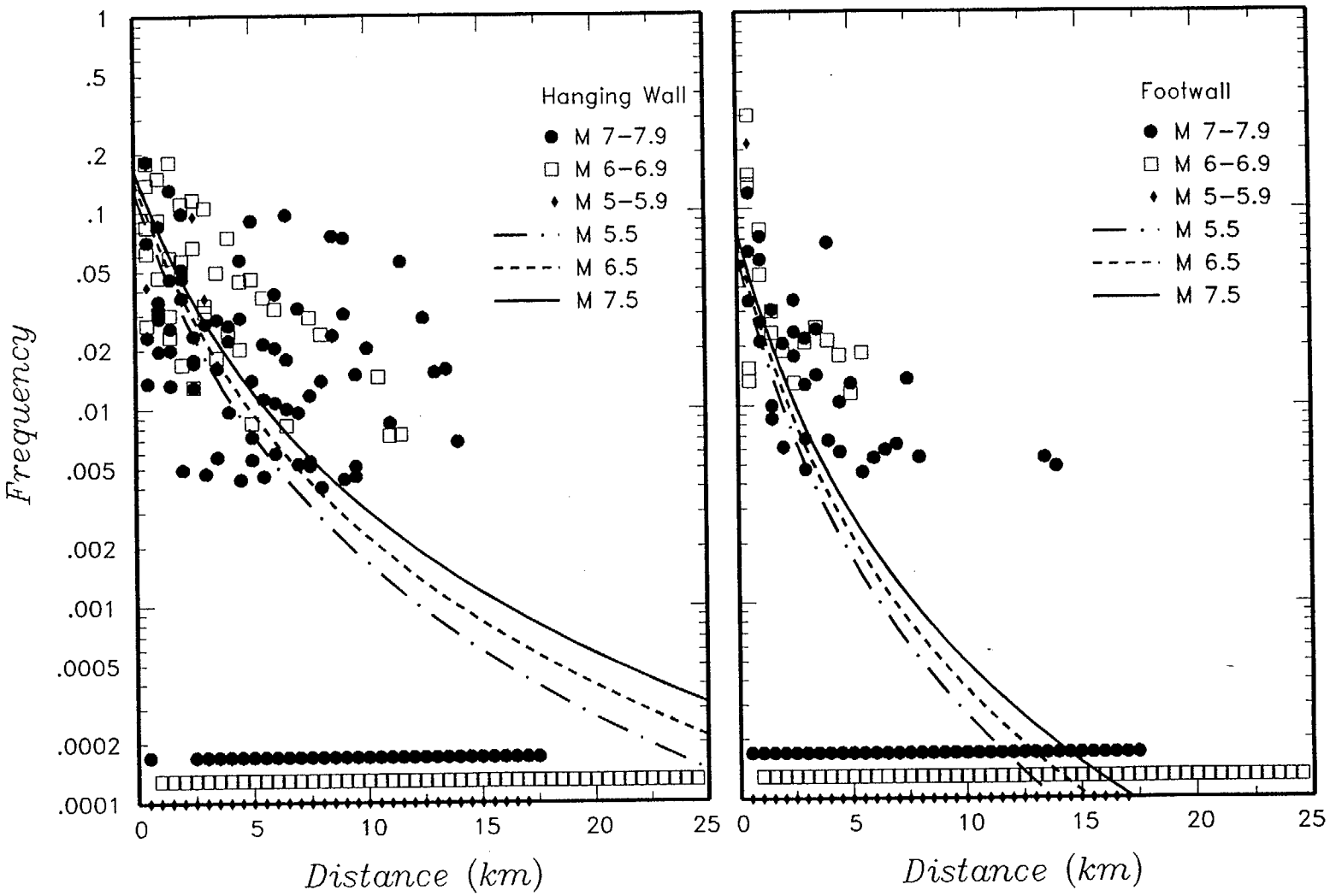

Figure SDO-18 Probability of induced distributed slip as a function of distance from the rupture and hanging wall/footwall location computed from the data presented in S.K. Pezzopane and T.E. Dawson (USGS, written communication, 1996). Curves show logistic regression fits to data.

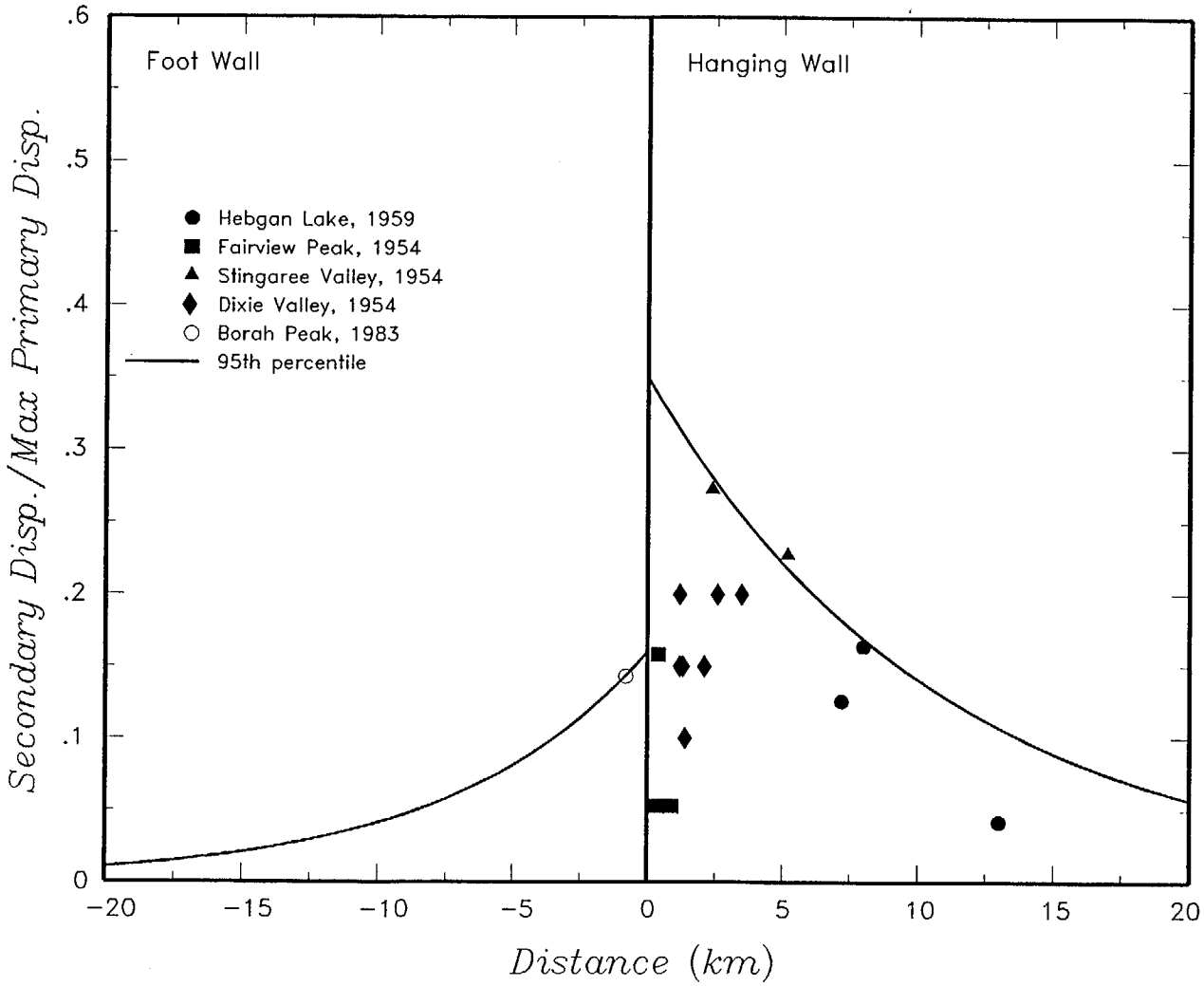

Figure SDO-19 Observed secondary faulting distribution normalized to main fault displacement for large scarp -forming, historic normal faulting earthquakes in the Basin and Range province.

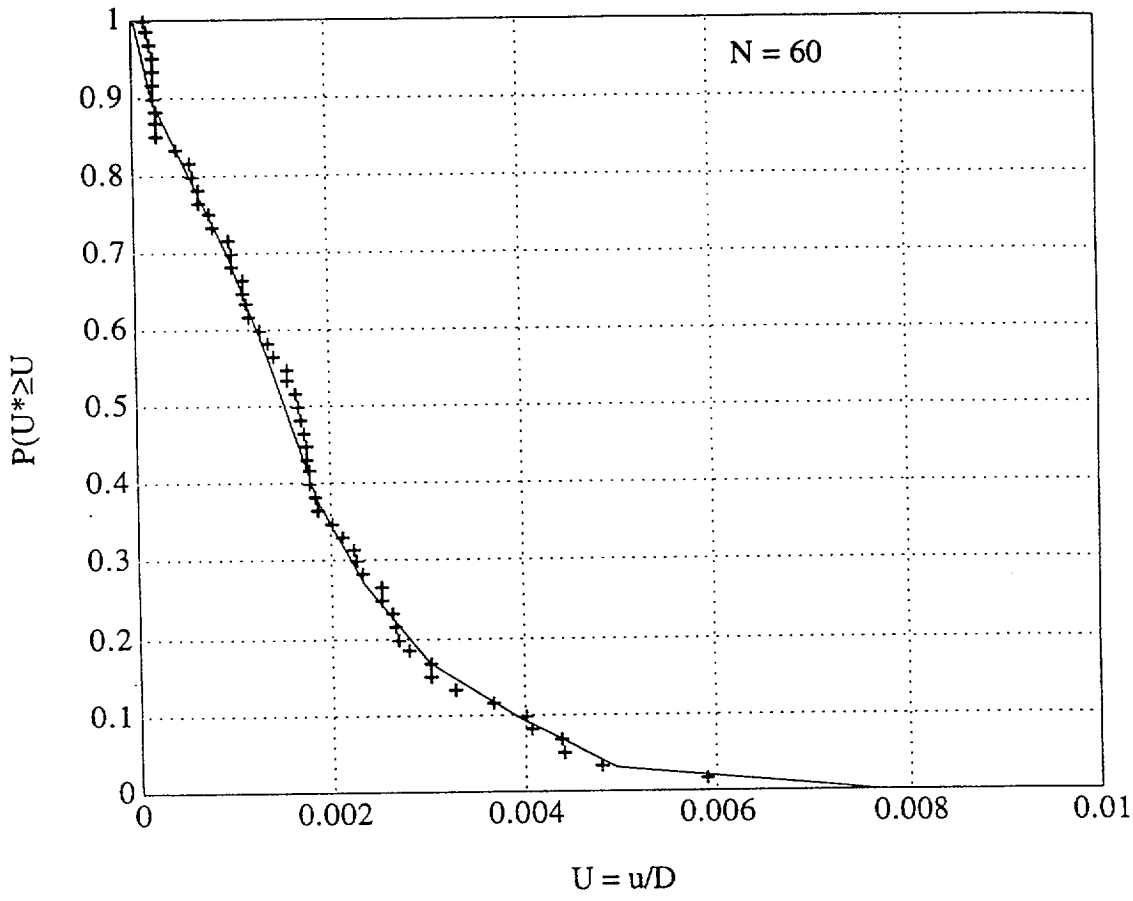

Figure SDO-20 Cumulative probability graph of D/D_{cum}, where D is fault slip per event and D_{cum} is the cumulative displacement on the fault surface at the point of interest. Function is derived from Yucca Mountain fault data synthesis of S.K. Pezzopane and T.E. Dawson (USGS, written communication, 1996) and discussions of Cowie and Scholz (1992) by SBK team.

APPENDIX SDO-1
EVENT SCENARIOS FOR LOCAL FAULTS
(Page 1 of 3)

Event Scenarios	Occurrence Rates (events/yr)		
	Minimum	Preferred	Maximum
Paintbrush	1.96E-005	3.13E-005	7.174E-005
PC(N)	7.98E-006	1.27E-005	2.91E-005
PC(S)	4.63E-006	7.39E-006	1.69E-005
PC(N+S)	1.88E-006	3.00E-006	6.85E-006
PCN+BR	1.76E-007	2.82E-007	6.43E-007
PC(S)+BR	1.45E-006	2.32E-006	5.28E-006
PC+BR	1.76E-007	2.82E-007	6.43E-007
PC+SCR	1.88E-006	3.00E-006	6.85E-006
PC(S)+SCR	8.23E-007	1.31E-006	3.00E-006
PC+BR+SCR	1.76E-007	2.82E-007	6.43E-007
PC+ash event	4.31E-007	6.89E-007	1.57E-006
Stagecoach Road	2.44E-005	3.33E-005	5.00E-005
SCR	1.22E-005	1.67E-005	2.50E-005
SCR+PC(S)	2.24E006	3.06E-006	4.60E-006
SCR+PC	4.07E-006	5.56E-006	8.35E-006
SCR+ash event	1.83-006	2.50E-006	3.75E-006
SCR+SC	3.05E-006	4.16E-006	6.25E-006
SCR+PC+BR	1.02E-006	1.40E-006	2.10E-006
Solitario Canyon	1.47E-005	1.92E-005	2.7E-005
SC	8.45E-006	1.10E-005	1.55E-005
SC+SCR	1.84E-006	2.40E-006	3.38E-006
SC+ash event	2.57E-006	3.36E-006	4.73E-006
SC+SWW	1.84E-006	2.40E-006	3.38E-006
Iron Ridge	3.91E-006	4.98E-006	6.99E-006
IR	3.52E-006	4.48E-006	6.29E-006
IR+AW	2.61E-007	3.32E-007	4.66E-007
IR+AW+GD	1.30E-007	1.66E-007	2.33E-007

APPENDIX SDO-1
EVENT SCENARIOS FOR LOCAL FAULTS

Event Scenarios	Occurrence Rates (events/yr)		
	Minimum	Preferred	Maximum
Fatigue Wash	3.46E-006	6.06E-006	1.16E-005
FW	2.22E-006	3.98E-006	7.45E-006
FW+SWW	3.71E-007	6.49E-007	1.24E-006
FW+SW+NW	1.24E-007	2.16E-007	4.14E-006
FW+SW+SCF	2.47E-007	4.33E-007	8.29E-007
FW+ash event	4.94E-007	8.66E-007	1.65E-006
S. Windy Wash	1.3E-005	1.96E-005	2.78E-005
SWW	8.16E-006	1.23E-005	1.75E-005
SWW+SCF	1.08E-006	1.63E-006	2.31E-006
SWW+FW	6.76E-007	1.02E-006	1.45E-006
SWW+SC	4.03E-007	6.08E-007	8.62E-007
SWW+CW	8.06E-007	1.22E-006	1.72E-006
SWW+SCF+NCF	4.03E-007	6.08E-007	8.62E-007
SWW+FW+NWW	4.03E-007	6.08E-007	8.62E-007
SWW+FW+SCF	2.73E-007	4.12E-007	5.84E-007
SWW+ash event	8.19E-007	1.23E-006	1.75E-006
Individual Faults			
PC (N + S)	2.24E-006	2.91E-006	8.3E-006
PC (N)	7.98E-006	1.27E-005	2.91E-005
PC (S)	4.63E-006	7.39E-006	1.69E-005
SCR	1.22E-005	1.67E-005	2.50E-005
SC	8.45E-006	1.10E-005	1.55E-005
IR	3.52E-006	4.48E-006	6.29E-006
FW	2.22E-006	3.89E-006	7.45E-006
SWW	8.16E-006	1.23E-005	1.75E-005
Linked Faults		Scenarios:	
PC+SCR	2.98E-006	4.28E-006	7.60E-006
PC(S)+SCR	1.53E-006	2.19E-006	3.80E-006
PC(S)+BR	1.45E-006	2.32E-006	5.28E-006
SCR+SC	2.45E-007	3.28E-006	4.82E-006
IR+AW	2.61E-007	3.32E-007	4.66E-007
IR+AW+GD	1.30E-007	1.66E-007	2.33E-007
FW+SWW	5.24E-007	8.35E-007	1.35E-006
SWW+FW+NWW	2.64E-007	4.12E-007	6.38E-007
SWW+CW	4.03E-007	6.08E-007	8.62E-007

APPENDIX SDO-1
EVENT SCENARIOS FOR LOCAL FAULTS
(Page 3 of 3)

Event Scenarios	Occurrence Rates (events/yr)		
	Minimum	Preferred	Maximum
Distributed Faults			
PC(N)+BR	1.76E-007	2.82E-007	6.43E-007
PC+BR+SCR	5.98E-007	8.41E-007	1.37E-006
PC+BR	1.76E-007	2.82E-007	6.43E-007
SC+SWW	1.12E-006	1.50E-006	2.12E-006
FW+SWW+SCF	2.60E-007	4.23E-007	7.07E-007
SWW+SCF	1.08E-006	1.63E-006	2.31E-006
SWW+SCF+NCF	4.03E-007	6.08E-007	8.62E-007
ash event	1.22E-006	1.73E-006	2.69E-006

REPRESENTATIVE AGES

Representative or nominal ages were ascribed to the paleoseismic data to make the use of this information more tractable (especially, given the time frame for the analysis) and transparent. There are, however, large uncertainties associated with these age data; we handle these in the relative weighting of event scenarios. Most of the ages and displacements used for the local faults at Yucca Mountain came from the Seismotectonic Framework Report produced by the U.S. Geological Survey. In particular, Table 5-1, "Event Displacements and Timing Data from Paleoseismic Studies of Yucca Mountain Faults", was used extensively.

PAINTBRUSH CANYON FAULT

Paleoseismic Earthquake Recurrence Information:

Six to nine events in the last 300 to 410 ka along the Paintbrush Canyon fault have been revealed by trenching. However, four to six of these events have occurred in the last 100 to 150 ka. Either paleoevents prior to 100 to 150 ka have been erased or left no record where the fault has been examined, or earthquake occurrence is becoming more frequent post 100 to 150 ka. In either case, it makes the most sense to calibrate earthquake recurrence for future predictions of the next earthquakes on the last 100 to 150 ka. The preferred number of events is five, the midpoint, and the preferred age is 120 ka. The most recent event occurred at 15 ka.

	Raw Average Earthquake Recurrence Intervals	Corrected Average Earthquake Recurrence Intervals - Most Recent Event and Elapsed Time Removed
Min.	17 kyr	17 kyr
Pref.	24 kyr	26 kyr
Max.	38 kyr	45 kyr

Similar to the average recurrence interval, the interseismic intervals examined are for the last 100 to 150 ka. Considering the preferred ranges presented in Chapter 5 of the U. S. Geological Survey Synthesis Report, interseismic intervals were estimated by subtracting the extreme

values. The range of values for the interseismic intervals is 15 to 60 kyr. The average of all the estimates, 38 kyr, is taken as the preferred value.

	Moment Rate Recurrence	Average Earthquake Recurrence	Preferred Interseismic Interval	Averaged Earthquake Recurrence	Maximum Earthquake Occurrence Rate (events/yr)
Min.	8.6 kyr	17 kyr	15 kyr	14 kyr	7.14×10^{-5}
Pref.	31 kyr	26 kyr	38 kyr	32 kyr	3.13×10^{-5}
Max.	47 kyr	45 kyr	60 kyr	51 kyr	1.96×10^{-5}

Relative Frequency	Nominal Age of the Event	Surface Displacement	Possible Event Scenarios
(0.167)	15 ka	0.05/0.2/0.2	PC(N) + PC(S.?, poss. erased) + SCR or PC(N)
(0.167)	50-75 ka	0.44/0.62/0.77	PC(N) + "ash event" or PC(S) + SCR or PC(N) and PC(S)
(0.167)	90-95 ka	0.53/0.98/1.43	PC(N)
(0.167)	115-140 ka	0.29/0.4/1.40	PC(N) + PC(S) + BR + SCR or PC(N) +PC(S) PC(N) + PC(S) + BR or PC(N) + PC(S) + SCR PC (N) + BR or PC(S) + BR PC(N) and PC(S)
(0.167)	225-250 ka	0.35/0.47/0.69	PC(N) + PC(S) or PC(N) and PC(S)
(0.167)	335 ka	0.88/1.67/2.05	PC(S) + BR

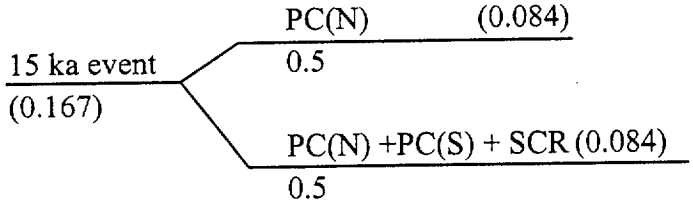

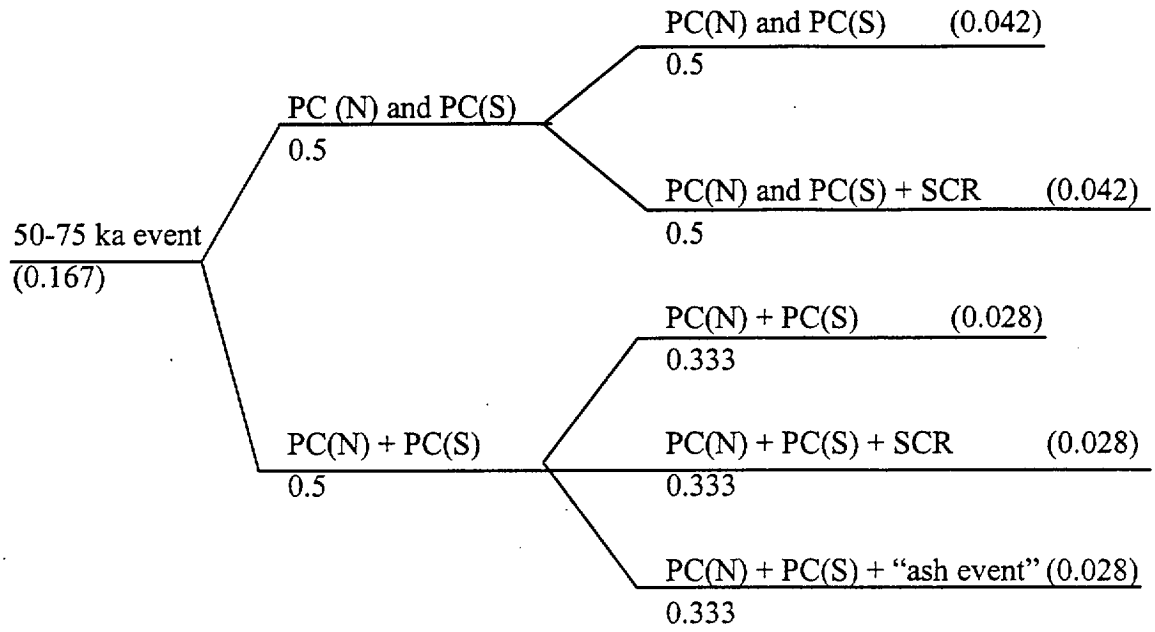

90-95 ka event PC(N) (0.167)
(0.167)

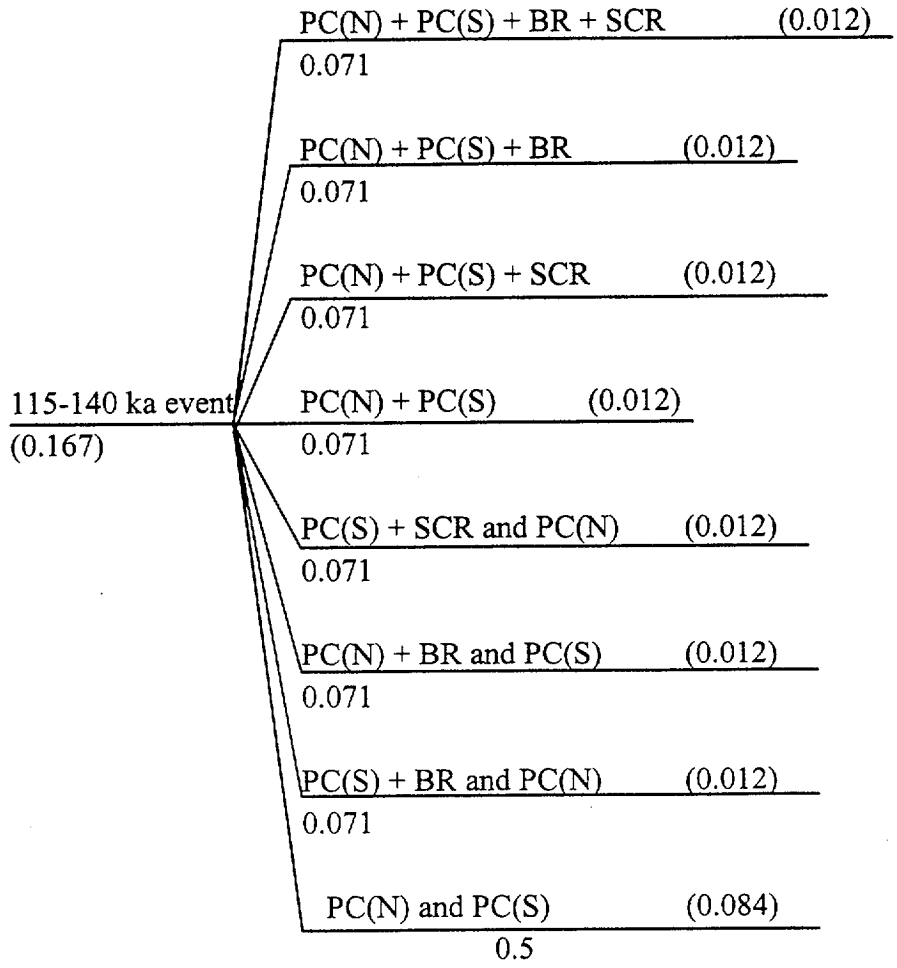
115-140 ka event
(0.167)
PC(N) + PC(S) + BR + SCR (0.012)
0.071
PC(N) + PC(S) + BR (0.012)
0.071
PC(N) + PC(S) + SCR (0.012)
0.071
PC(N) + PC(S) (0.012)
0.071
PC(S) + SCR and PC(N) (0.012)
0.071
PC(N) + BR and PC(S) (0.012)
0.071
PC(S) + BR and PC(N) (0.012)
0.071
PC(N) and PC(S) (0.084)
0.5

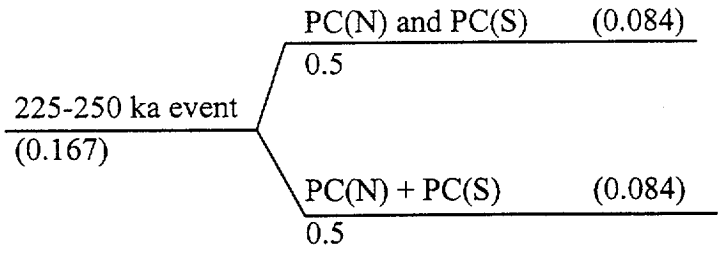
225-250 ka event
(0.167)
PC(N) and PC(S) (0.084)
0.5
PC(N) + PC(S) (0.084)
0.5

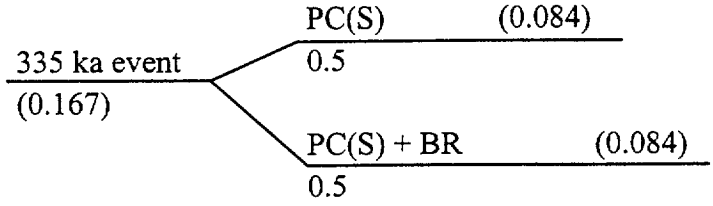
335 ka event
(0.167)
PC(S) (0.084)
0.5
PC(S) + BR (0.084)
0.5

Final Relative Weighting:

(0.407)	PC(N)
(0.236)	PC(S)
(0.096)	PC(N) + PC(S)
(0.009)	PC(N) + BR
(0.074)	PC(S) + BR
(0.009)	PC(N) + PC(S) + BR
(0.096)	PC(N) + PC(S) + SCR
(0.042)	PC(S) + SCR
(0.009)	PC(N) + PC(S) + BR + SCR
(0.022)	PC(N) + PC(S) + "ash event"

STAGECOACH ROAD FAULT

Paleoseismic Earthquake Recurrence Information:
Four events have occurred in the last 98 to 118 ka, with a preferred value of 108 ka. The most recent event was 6 to 15 ka, with a preferred value of 13 ka.

	Raw Average Earthquake Recurrence Intervals	Corrected Average Earthquake Recurrence Intervals Most Recent Event and Elapsed Time Removed
Min.	25 kyr	28 kyr
Pref.	27 kyr	32 kyr
Max.	30 kyr	34 kyr

Considering the preferred ranges presented in Chapter 5 of the U. S. Geological Survey Synthesis Report, interseismic intervals were estimated by subtracting the extreme values. Preferred value interseismic intervals ranged from 13 kyr to 55 kyr; the average interseismic interval is 34 kyr.

	Moment Rate Recurrence	Average Earthquake Recurrence	Preferred Interseismic Interval	Averaged Earthquake Recurrence	Maximum Earthquake Occurrence Rate (events/yr)
Min.	18 kyr	28 kyr	13 kyr	20 kyr	5×10^{-5}
Pref.	24 kyr	32 kyr	34 kyr	30 kyr	3.33×10^{-5}
Max.	35 kyr	34 kyr	55 kyr	41 kyr	2.44×10^{-5}

Relative Frequency	Nominal Age of the event	Surface Displacement	Poss. Event Scenarios
(0.25)	13 ka	0.4/0.43/0.82 m	SCR or SCR + PC(S.?, poss erased) + PC(N)
(0.25)	26 ka	0.28/0.59/0.77 m	SCR or SCR + SC
(0.25)	55-70 ka	0.25/0.57/0.99 m	SCR + "ash event" or SCR + PC(S) or SCR
(0.25)	100-110 ka	0.26/0.67/0.87 m	SCR + PC(S) + PC(N) or SCR

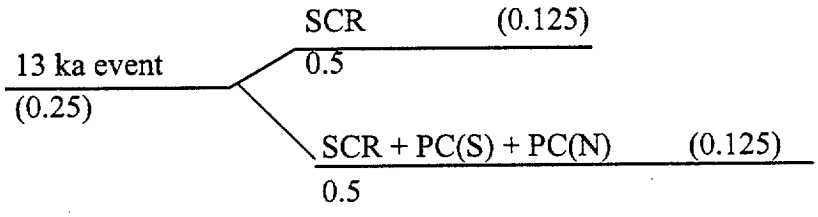

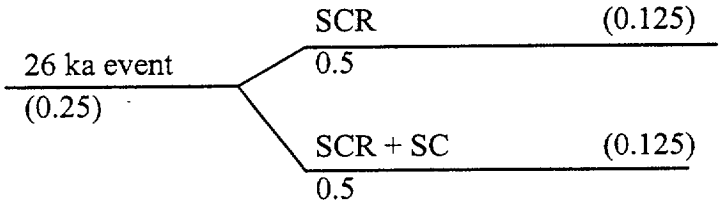

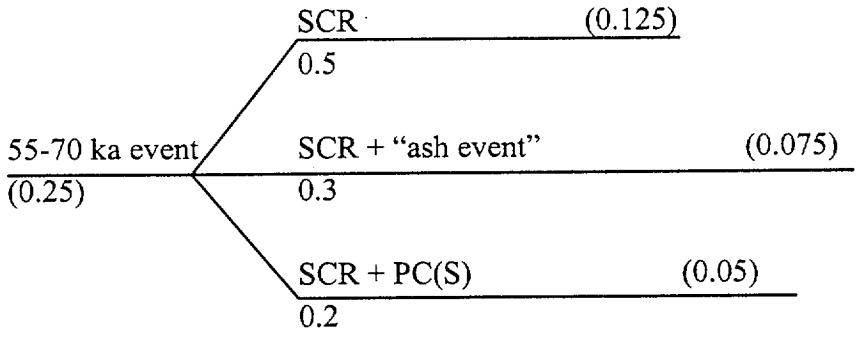

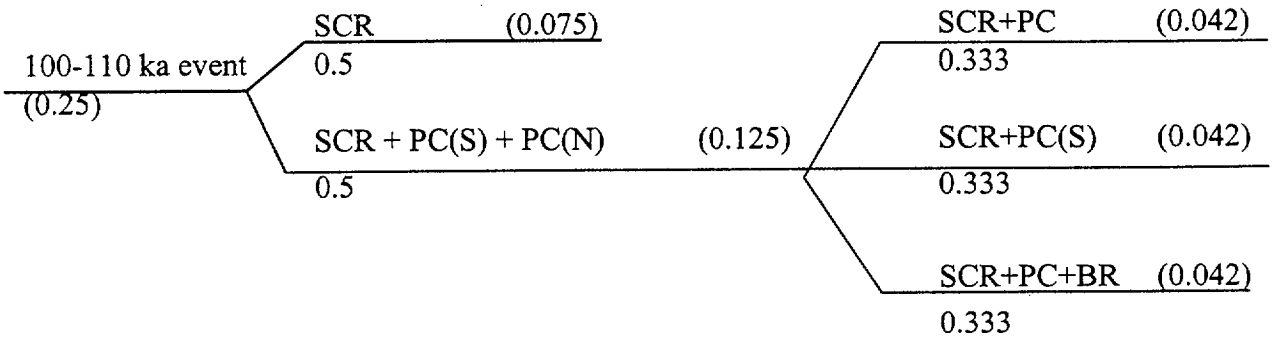

Final Relative Weighting:

(0.5)	SCR
(0.092)	SCR + PC(S)
(0.167)	SCR + PC(S) + PC(N)
(0.075)	SCR + "ash event"
(0.125)	SCR + SC
(0.042)	SCR+PC+BR

SOLITARIO CANYON FAULT

Paleoseismic Information:

Four events have occurred over the last 150 to 250 ka (preferred 200 ka). The most recent event occurred at about 25 ka.

	Raw Average Earthquake Recurrence Intgervals	Corrected Average Earthquake Recurrence Interval Most Recent Event and Elapsed Time Removed
Min.	38 kyr	42 kyr
Pref.	50 kyr	58 kyr
Max.	63 kyr	75 kyr

Interseismic intervals of preferred values are 45, 50, and 80 kyr, with an average of 58 kyr.

	Moment Rate Recurrence	Average Earthquake Recurrence	Preferred Interseismic Recurrence	Average Earthquake Recurrence	Maximum Earthquake Occurrence Rate (EVENTS/YR)
Min.	23 kyr	42 kyr	45 kyr	37 kyr	2.7×10^{-5}
Pref.	40 kyr	58 kyr	58 kyr	52 kyr	1.92×10^{-5}
Max.	50 kyr	75 kyr	80 kyr	68 kyr	1.47×10^{-5}

Relative Frequency	Nominal Age of the event	Surface Displacement	Poss. Event Scenarios
(0.25)	25 ka	0.05/0.1/0.2 m	SC or SC + SCR
(0.25)	70 ka	1.00/1.20/1.40 m	SC + "ash event"
(0.25)	150 ka	0.2/0.3/0.4 m	SC
(0.25)	200 ka	0.3/0.5/0.7 m	SC + SWW or SC

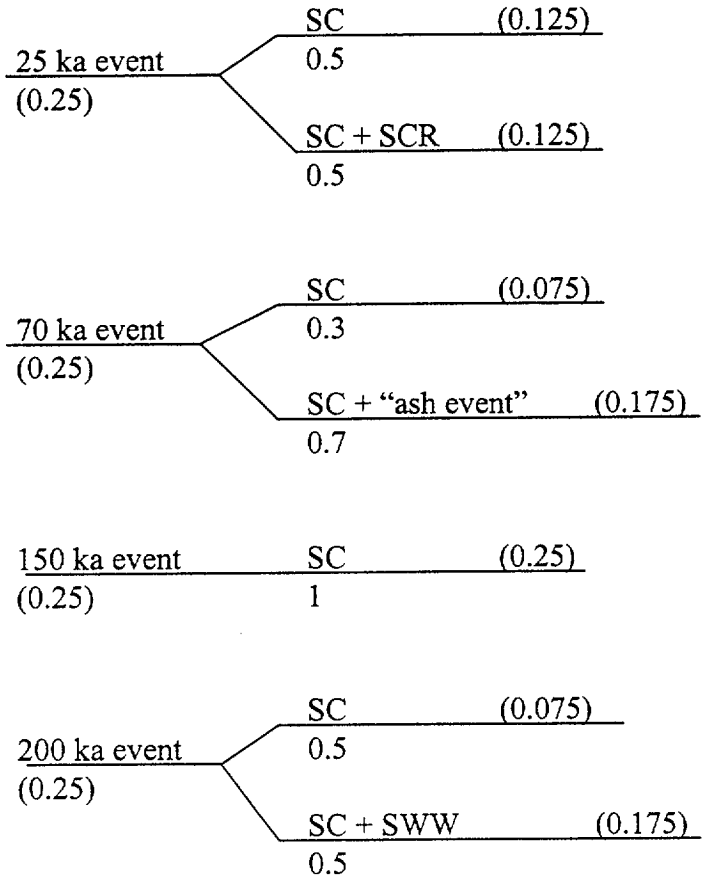

Final Relative Weighting:

(0.575)	SC
(0.125)	SC+SCR
(0.175)	SC + "ash event"
(0.125)	SC + SWW

FATIGUE WASH FAULT

Paleoseismic Information:

Three to four events (four preferred) have occurred within the last 450 to 730 ka (assume 600 ka for preferred value. The most recent event was 20 to 60 ka ago (the midpoint, 40 ka is used for preferred).

	Raw Average Earthquake Recurrence Intervals	Corrected Average Earthquake Recurrence Intervals Most Recent Event and Elapsed Time Removed
Min.	113 kyr	130 kyr
Pref.	150 kyr	187 kyr
Max.	243 kyr	237 kyr

Interseismic intervals of the preferred values range from 28 to 480 kyr, with an average of 183 kyr. A possible other minimum interseismic interval can be calculated from comparing the extremes of 65-60=5 kyr, but this is deemed wholly unreasonable given the trench information available along and geomorphic expression of the Fatigue Wash fault.

	Moment Rate Recurrence	Average Earthquake Recurrence	Preferred Interseismic Interval	Averaged Earthquake Recurrence	Maximum Earthquake Occurence Rate (events/yr)
Min.	100 kyr	130 kyr	28 kyr	86 kyr	1.16×10^{-5}
Pref.	125 kyr	187 kyr	183 kyr	165 kyr	6.06×10^{-6}
Max.	150 kyr	237 kyr	480 kyr	289 kyr	3.46×10^{-6}

Relative Frequency	Nominal Age of the Event	Surface Displacement	Poss. Event Scenarios
(0.143)	20-60 ka	large fractures	FW + SWW + NWW or FW + SWW or FW
(0.286)	65-75 ka	0.15/0.25/0.35 m	FW + "ash event"
(0.286)	250-300 ka	/1.25/ m	FW + SWW + SCF or FW + SWW or FW
(0.286)	450-730 ka	/0.54/ m	FW

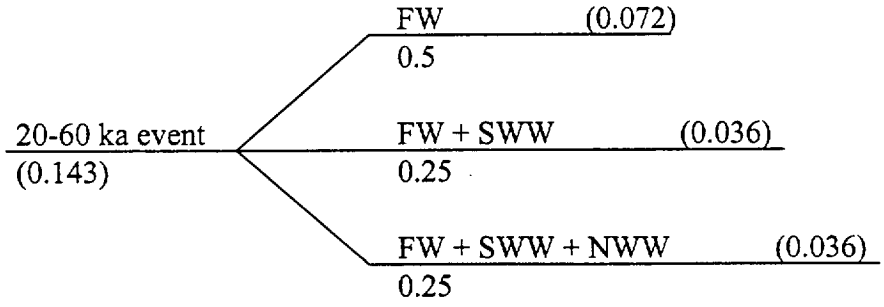

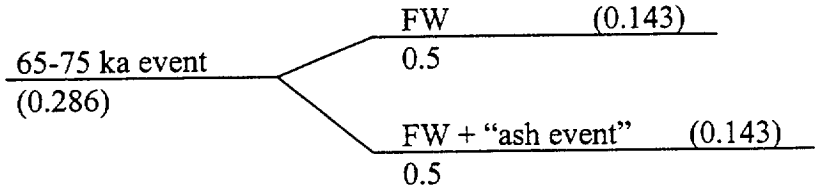

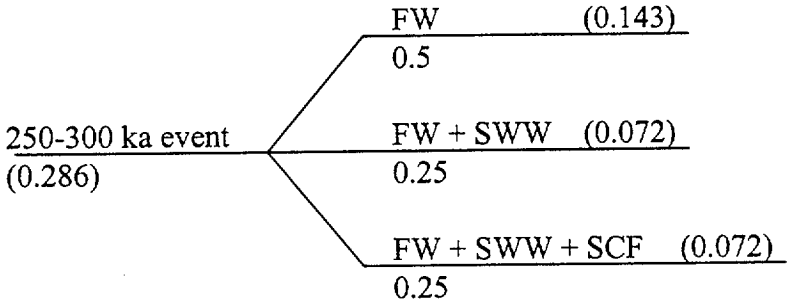

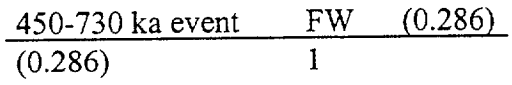

Final Relative Weighting:

(0.643)	FW
(0.107)	FW + SWW
(0.036)	FW + SWW + NWW
(0.071)	FW + SWW + SCF
(0.143)	FW + "ash event"

SOUTHERN WINDY WASH FAULT

Paleoseismic Information:

Eight events have occurred in the last 390 to 450 ka (preferred 400 ka). The most recent event occurred about 2.7 ka age.

	Raw Average Earthquake Recurrence Intervals	Corrected Average Earthquake Recurrence Intervals Most Recent and Elapsed Time Removed
Min.	49 kyr	55 kyr
Pref.	50 kyr	57 kyr
Max.	56 kyr	64 kyr

Interseismic intervals of the preferred values range from 30 kyr to 130 kyr, with an average of 62 kyr.

	Moment Rate Recurrence	Average Earthquake Recurrence	Preferred Interseismic Interval	Averaged Earthquake Recurrence	Maximum Earthquake Occurrence Rate (events/yr)
Min.	22 kyr	55 kyr	30 kyr	36 kyr	2.78×10^{-5}
Pref.	33 kyr	57 kyr	62 kyr	51 kyr	1.76×10^{-5}
Max.	37 kyr	64 kyr	130 kyr	77 kyr	1.3×10^{-5}

Relative Frequency	Nominal Age of the Event	Surface Displacement	Poss. Event Scenarios
(0.125)	2.7 ka	0.04/0.06/0.1 m	SWW + SCF + NCF or SWW + SCF or SWW
(0.125)	40 ka	0.14/0.20/0.45 m	SWW + FW + NWW or SWW + FW or SWW
(0.125)	75 ka	0.78/0.88/0.98 m	SWW + "ash event" or SWW
(0.125)	150 ka	0.38/0.42/0.52 m	SWW + CWW or SWW + SCF or SWW
(0.125)	200 ka	0.70/0.73/0.83 m	SWW + SC or SWW + CWW or SWW
(0.125)	240 ka	0.30/0.45/0.60 m	SWW + FW + SCF or SWW + FW or SWW + SCF or SWW
(0.125)	340-370 ka	0.55/0.60/0.78 m	SWW
(0.125)	400 ka	0.65/0.80?/1.00? m	SWW

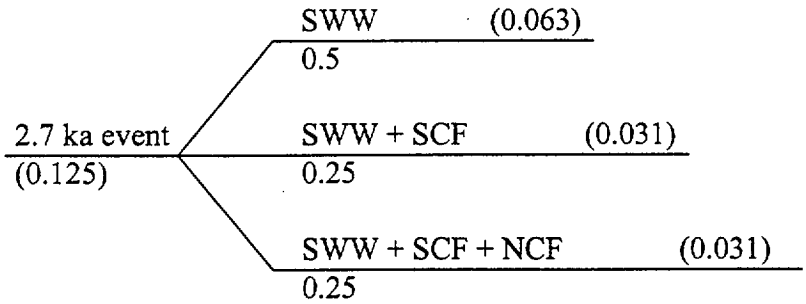

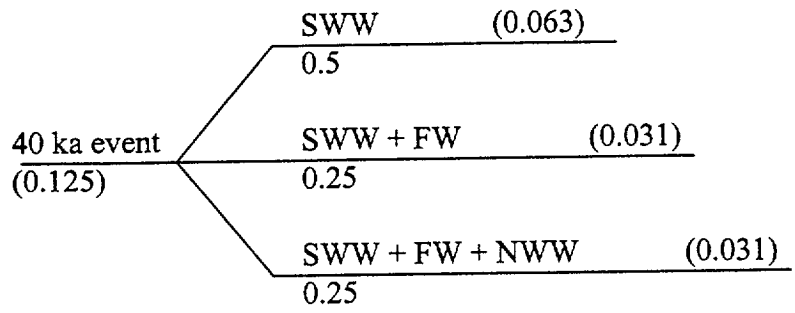
40 ka event
(0.125)
SWW (0.063)
0.5
SWW + FW (0.031)
0.25
SWW + FW + NWW (0.031)
0.25

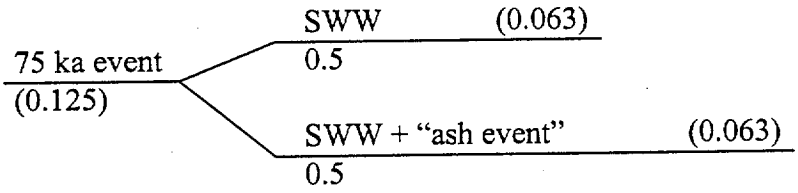
75 ka event
(0.125)
SWW (0.063)
0.5
SWW + "ash event" (0.063)
0.5

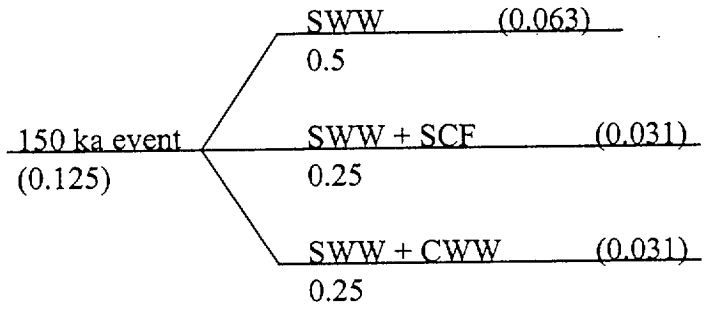
150 ka event
(0.125)
SWW (0.063)
0.5
SWW + SCF (0.031)
0.25
SWW + CWW (0.031)
0.25

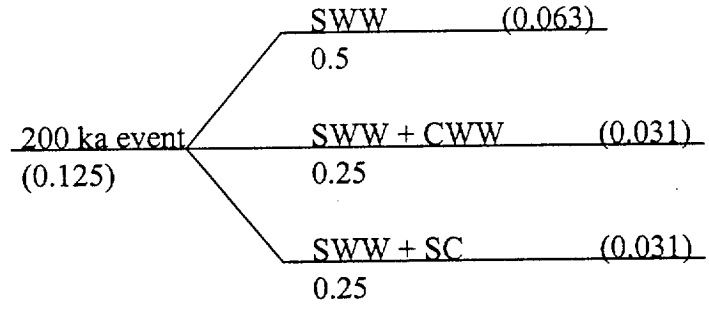
200 ka event
(0.125)
SWW (0.063)
0.5
SWW + CWW (0.031)
0.25
SWW + SC (0.031)
0.25

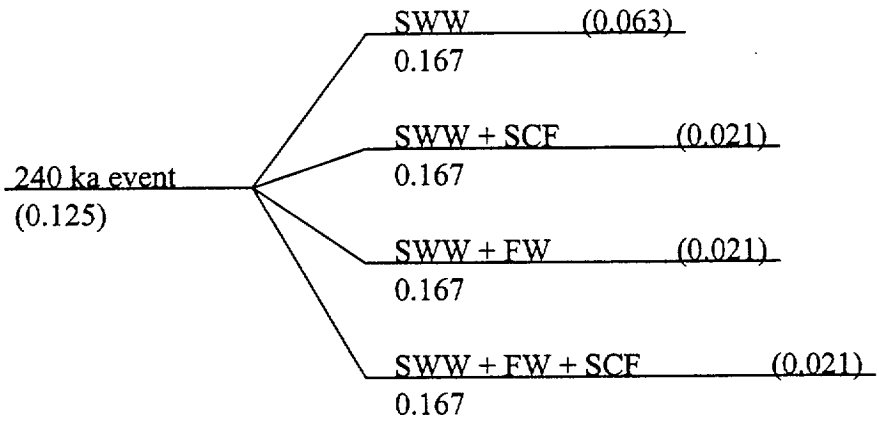

340 ka event	SWW	(0.125)
(0.125)	1	

400 ka event	SWW	(0.125)
(0.125)	1	

Final Relative Weighting:

(0.625)	SWW
(0.083)	SWW + SCF
(0.052)	SWW + FW
(0.031)	SWW + SC
(0.063)	SWW + CWW
(0.031)	SWW + SCF + NCF
(0.031)	SWW + FW + NWW
(0.021)	SWW + FW + SCF
(0.063)	SWW + "ash event"

IRON RIDGE FAULT

Paleoseismic Information:

Three events have occurred along the Iron Ridge fault since 430 to 730 kyr (600 kyr pref.). The most recent event was at 5 to 10 ka and was small in offset (<0.1 m) with some question to its existence. Because of the lack of information, this event is assumed to occur for estimating corrected average earthquake recurrence intervals.

	Raw Average Earthquake Recurrence Intervals	Corrected Average Earthquake Recurrence Intervals Most Recent Event and Elapsed Time Removed
Min.	143 kyr	210 kyr
Pref.	200 kyr	295 kyr
Max.	243 kyr	360 kyr

Interseismic intervals are poorly constrained along the Iron Ridge fault.

	Moment Rate Recurrence	Average Earthquake Recurrence	Preferred Interseismic Interval	Averaged Earthquake Recurrence	Maximum Earthquake Occurrence Rate (events/yr)
Min.	76 kyr	210 kyr	none	143 kyr	6.99×10^{-6}
Pref.	106 kyr	295 kyr	none	201 kyr	4.98×10^{-6}
Max.	152 kyr	360 kyr	none	256 kyr	3.91×10^{-6}

Relative Frequency	Nominal Age of the Event	Surface Displacement	Poss. Event Scenarios
(0.333)	5-10 ka	0/0.05/0.1 m	IR
(0.333)	430-730 ka	0.5/0.7/1.0 m	IR or IR + AW or IR + AW + GD
(0.333)	430-730 ka	0.5/0.7/1.0 m	IR or IR + AW or IR + AW + GD

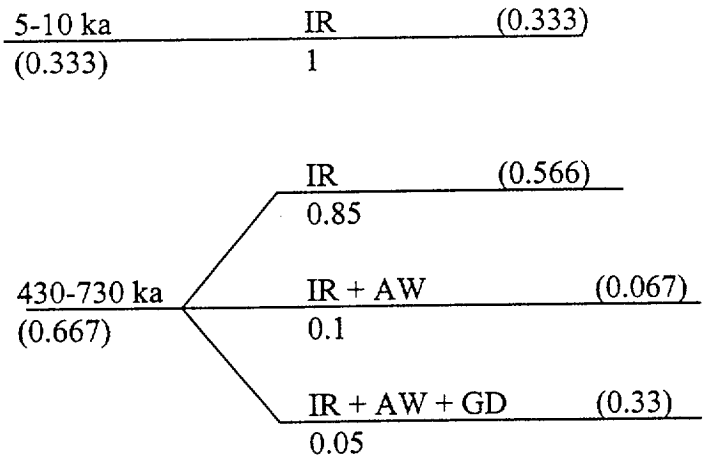

Final Relative Weighting:

(0.900)	IR
(0.067)	IR + AW
(0.033)	IR + AW + GD

PROBABILISTIC SEISMIC HAZARD ANALYSES FOR FAULT DISPLACEMENT AND VIBRATORY GROUND MOTION AT YUCCA MOUNTAIN, NEVADA

FINAL REPORT
VOLUME 3 APPENDICES

Prepared for the

U.S. Geological Survey

by the

Civilian Radioactive Waste Management System
Management & Operating Contractor

Ivan G. Wong and Carl Stepp
Report Coordinators

A report to the U.S. Department of Energy
that fulfills Level 3 Milestone SP32IM3
WBS Number 1.2.3.2.8.3.6

Prepared in cooperation with the
U.S. Department of Energy under
Interagency Agreement DE-AI08-97NV12033
Contract DE-AC04-94AL8500

Oakland, California
23 September 1998

APPENDIX F

GROUND MOTION EXPERT ELICITATION SUMMARIES

The following ground motion expert interpretations have received review by PSHA Review Panel members in accordance with quality assurance approved PSHA Project Plan requirements, but have not been reviewed for conformity with Department of the Interior, U.S. Geological Survey standards.

APPENDIX F1

GROUND MOTIONS FOR THE YUCCA MOUNTAIN VICINITY, SOUTHERN NEVADA

John G. Anderson

APPENDIX F1
TABLE OF CONTENTS

APPENDIX F1

GROUND MOTIONS FOR THE YUCCA MOUNTAIN VICINITY, SOUTHERN NEVADA

John G. Anderson

F1-1 INTRODUCTION

In Fall, 1994, I was selected to be on a panel of "ground motion experts" with the responsibility to develop estimates of ground motions needed to prepare a licensing application for the proposed nuclear waste repository at Yucca Mountain, in southern Nevada. The panel met once in the spring of 1995, then due to funding and political considerations took a year off during FY 1996. The panel became active again early in 1997. Altogether, we met three times in Salt Lake City and twice in Oakland to compare approaches and share information. My stack of paper associated with this panel, if organized onto a single bookshelf, would take at least 1.3 meters of space, and the page count would be on the order of 6000 pages.

Ultimately, the panel was asked to prepare estimates of ground motions for 51 specified combinations of earthquake source and station location. The earthquake source was specified by moment magnitude, using Hanks and Kanamori (1979) as a definition to relate moment magnitude to seismic moment. The fault orientation and mechanism were given. The station location was also given. For each of these 51 combinations, each member of our panel was asked to provide his best estimate of nine ground motion parameters. These parameters were to be specified for both a random horizontal component and a vertical component. The ground motion parameters for each of these components were to be given together with three uncertainty values. To be specific, the mean estimate will be called 'mu', μ, the standard deviation of the data relative to this mean is 'sigma', σ, the uncertainty on the mean value is 'sigma-mu', σ_μ, and the uncertainty on the standard deviation is 'sigma-sigma', σ_σ. Thus the number of numbers to be specified by each expert is:

51 cases x 2 components/case x 9 parameters / component x 4 numbers / parameter
= 3672 numbers.

Information supplied to each expert included several "proponent models", in which people who have studied ground motions at Yucca Mountain provided the predictions of their model. Some of these models are empirical regressions, and some are physical models. To make the problem more tractable, I began by developing my estimates from weighted averages of some of these "proponent models". After the implications of these weighted averages were studied, I modified the input to some of the weighted averages, and then the point values themselves.

This report contains my personal evaluation of various proponent models, followed by my weighting scheme. I discuss reasons for modifying my weighting scheme and then my point estimates in some cases to produce my final point estimates.

F1-2 WEIGHTING SCHEME

The weighting scheme used to develop the preliminary point estimates is given in this section. I used the approach of first dividing the proponent models into model classes and then assigning weights to each class and to each model within a class consistent with the methodology described in Section 3.3.

F1-2.1 Model Classes

I divided the proponent models into two classes. My weighting scheme by class is as follows:

Synthetic models: 0.65
Empirical regressions: 0.35

My reasoning for this weighting is as follows:
First, I consider that the synthetic models are successful in fitting observations of ground motions where there are adequate data. Thus for these situations, it should make little difference whether one uses regressions or synthetic models. However, for some combinations of magnitudes and distances, we are using a regression or synthetic seismogram

model to extrapolate beyond the reaches of abundant data. In these situations, I trust the synthetics more for extrapolation than I trust regressions. While I recognize that the physical models for the synthetics are incomplete, there is no physical model at all behind the empirical regressions. Thus I have no reason at all to trust them for extrapolation.

Second, there is another type of extrapolation in our problem, and that is the extrapolation to a very specific site condition. For the regressions, it is necessary to make a very complicated set of adjustments to obtain those conditions. The regressions are dominantly developed for strike-slip and thrust earthquakes in a compressional environment, while the Yucca Mountain region has strike-slip and normal earthquakes in an extensional environment. The difference between a horizontal and vertical orientation for the maximum compressive stress is not explicitly taken into account in any of the models. However, our panel was presented with one study (Becker and Abrahamson 1997) indicating that on average the stress drop (defined in a special way) is smaller in extensional environments. Thus the panel was given the option to adjust regressions for this difference in average stress drops. There is a second adjustment to the regressions for the difference between the specific site condition in our project and the "average site condition" for the stations used to develop the regressions. This adjustment includes Q. Yet another adjustment for the regressions comes from the shortage of regressions for peak velocity or vertical components. One "fix" is to use ratios of these parameters to horizontal components, combined with a "trustworthy" horizontal regression. I am not aware of any documented studies which demonstrate that these adjustments are successful, although I do not see any major flaws in the physical reasoning behind them. Still, every time another adjustment is applied, more uncertainties are introduced. In contrast, the physical models do not require adjustments to calculate ground motions because the source and site condition can be input directly. Thus, the physical models are two or more steps more direct, a feature that I appreciate.

F1-2.2 Model Weights - Horizontal Component

I specified a weighting approach designed to include the full range of all of the models, and also put more emphasis on one or more preferred models. This approach is used for both the empirical regressions and the numerical simulation models.

To include the full range of the models, the probability distribution is considered to be a uniform distribution between the smallest (Ymin) and largest (Ymax) proponent model that I considered to be "qualified" as discussed below. (The uniform distribution is on the natural logarithm of the ground motion.) The median for this approach is given by the geometric mean of the largest and smallest proponent models. The epistemic uncertainty is computed from the standard deviation of the "boxcar" shaped probability distribution which is given by 0.29 ln(Ymax/Ymin). The second approach is based on my preferred model or models and is intended to give additional weight to the models that I believe to be most applicable.

The same weights are used for both the median (μ) and the aleatory uncertainty (σ).

F1-2.2.1 Empirical Models. In evaluating the empirical regressions, I look for models that are as consistent as possible with the physics of earthquakes as I understand it. My own studies indicate that the shape of regression curves ought to change with magnitude: large events ought to have a less rapid decay with distance than small events. The interaction of fault size and duration, and complexity in the Green's function, can cause varying rates of decay with distance that defy any simplistic $R^{-\gamma}$ model. Saturation is expected at short distances as magnitude increases, but it is not expected at large distances. I also expect regressions to show some nonlinear behavior in their relationship between soil and rock ground motions, although I consider this to be a weaker constraint. We are predicting motions on rock. The way soil/rock behavior is built in, however, is of the highest consequence because the majority of the available data constraining these regressions is recorded on soft sites. Thus the regressions will tend to follow the available soil data more closely, and misfit on the few rock sites can be difficult to distinguish from natural variability.

Abrahamson and Silva (1997) regression. This regression model is generally consistent with my expectations, both for magnitude-distance behavior, and in its ratio of soil/rock motions. In our tests on southern California data, it performs very well at all periods, although at 1 sec and 3 sec, its fit to the data is not as impressive as for PGA and SA at 0.3 Hz. I consider this model to be qualified. It is also my preferred model for the second approach.

Boore, *et al.* (1997); Spudich *et al.* (1997) regressions. These "USGS class" regressions do a very good job of fitting the data also. However, they do not allow for a variable ratio between soil and rock, or for a magnitude-dependent shape. The unusual definition of distance may in part compensate for the lack of magnitude-dependent shape, but I do not see a physical justification for using it. Thus, although I consider that it is crucial to take their predictions into account within my range of uncertainties, I feel less confident in using any of these to extrapolate to situations where there are little data. I consider these models to be qualified but not as preferred models.

Campbell regressions (1990, 1993, 1994, 1997). These use a lot of data for short distances. Using the distance to "seismogenic rupture" instead of the fault is conceptually good, although I consider it a little ambiguous in its implementation. They are not constrained at larger distances which, although arguably less important, are distances for which we need to make estimates of motions. Thus, I feel I cannot assign the method as much weight as the other methods above. I consider these models to be qualified but not as preferred models.

Idriss (University of California, Davis, written communication, 1997), Sadigh *et al.* (1997), Sabetta and Pugliese (1996). I have a high respect for each of these regressions, and consider that they all have some merit. I consider these models to be qualified but not as preferred models.

McGarr (1984) regression: Only the peak velocity model is recommended by McGarr as a proponent model applicable to Yucca Mountain. I consider that the physical assumptions behind this model are a little overly simplified. Therefore, I do not consider this model to be "qualified" and it is not included in defining the range of model estimates.

Weights:

I specified a relative weight of 0.1 for the boxcar model and a relative weight of 0.25 for the preferred model. (This sums to the total weight of 0.35 for the empirical models)

I considered the following empirical models to be qualified: Abrahamson and Silva (1997) with the normal faulting factor included; Boore *et al.* (1997); Campbell (1997) for soft rock; Idriss (University of California, Davis, written communication, 1997) with Idriss (University

of California, Davis, written communication, 1993) for spectral shape; Sadigh *et al.* (1997); Sabetta and Pugliese (1996); and Spudich *et al.* (1996). The preferred empirical model is Abrahamson and Silva (1997).

F1-2.2.2 Numerical Simulations.

Zeng and Anderson synthetics. This model has the least amount of empiricism of any of the synthetic approaches. The source is described in a way that has been shown to include a plausible amount of complexity. Wave propagation from source to station is computed for a layered medium, so it includes body and surface waves, and scattering is incorporated. The disadvantage of this approach would be related to sensitivity of the results to Q and velocity models, which are uncertain. Still, having an approach that is predominantly a model of the physical phenomena that are involved gives me confidence in its ability to extrapolate to situations where there are little or no data. In spite of the model's successes, I recognize that there is still some physics that is not modeled properly, so I cannot give it a full weight.

Silva synthetics. This approach has the greatest amount of empiricism and the least amount of physics of any of the synthetic approaches. The spectrum of a M=5 subevent is specified, the attenuation with distance is greatly simplified, and wave propagation is not thoroughly incorporated. The advantage of this approach is that vagaries of wave propagation are "averaged out", i.e. it is less sensitive to uncertainties in regional velocity models for instance because this information is not used.

Somerville synthetics. This model is between the Zeng and Anderson approach and the Silva approach. The source is described with an empirical time function. However, wave propagation is modeled for a layered medium.

Point source model:

The point source proponent model was provided with the median and uncertainties in the point source stress drop to be specified by each expert. The following values are used:

median stress drop = 40 bars
standard deviation of stress drop = 0.5 (natural log units)
standard error of the median stress drop = 0.2 (natural log units)
standard error of the standard deviation of stress drop = 0.05

These values of the standard deviation and epistemic uncertainties are based on Ann Becker's evaluations of the normal faulting data.

Weights:

I consider all four of the numerical simulation models to be qualified. The three finite-fault synthetics are all preferred models, but the point source model is not preferred. I assigned a relative weight of 0.15 to the boxcar model and a relative weight of 0.50 to the preferred models. (This sums to the total weight of 0.65 for the numerical simulations).

Due to the differences in the finite fault simulations discussed above, I have given the following relative weights to the preferred models:

Silva finite fault	0.10
Somerville	0.15
Zeng and Anderson	0.25

More weight is given to the models with less empiricism. In some of the cases, I elected to deviate from the above approach to weighing the various models. These special cases are described below with the explanations.

F1-2.2.3 Weighting Scheme for Uncertainties. There are three types of uncertainties that need to be estimated: sigma, sigma-mu, and sigma-sigma, as defined above.

To estimate sigma, I recommend a weighted average of the values of sigma from each of the proponent models as the starting point. The weighting scheme was to be exactly the same as the scheme used to estimate the median value.

To estimate sigma-mu, I specified values of sigma-mu that I believe are reasonable to apply to each of the regressions and the synthetics as given below: These values replace the proponent model estimates of sigma mu. The total sigma-mu is computed by combining this proponent model sigma-mu with the variability of the weighted median ground motions computed using the weights described earlier.

To estimate sigma-sigma, the statistical estimates from the weighted averages are used. The magnitude 5 cases produced lower estimates of sigma-sigma than for the other magnitudes. I do not think that there should be a lower value of sigma-sigma for the lower magnitudes, so I used a constant value for all magnitudes computed from the average for magnitudes greater or equal to 5.8.

F1-2.2.4 Blast Models. The source for a blast is so different from the source of an earthquake that, in spite of all adjustments, I did not have much confidence in these models. Therefore, I gave zero weight to this class of models.

F1-2.2.5 Horizontal Component Variability. he proponent models for the horizontal component all predict the average of the two horizontal components. This project is using the random horizontal component, so the component-to-component variability needs to be added to the aleatory uncertainty. The average component-to-component variability is well determined from empirical models. The two proponent models are Boore *et al.* (1997) and Spudich *et al.* (1997). These two models are very similar. I selected the horizontal component to component variability from the Boore *et al.* (1997) model.

F1-2.3 Model Weights - Vertical Component

The weighting scheme described for the horizontal component is also used for the vertical component. For models without a vertical component, a zero weight is used. No scaling based on vertical/horizontal ratios is used.

F1-3 ADJUSTMENTS TO WEIGHTED POINT ESTIMATES

The weighting scheme described in Section F1-2 is used to develop preliminary point estimates for each of the 918 required estimates of the median and aleatory uncertainty. I reviewed these point estimates and made some adjustments for particular cases for which the weighted estimates were not consistent with my judgments.

The changes to the point estimates are listed below: for cases 22, 23, and 24, Spudich *et al.* (1997), Boore *et al.* (1997), and Sabetta and Pugliese (1996) were excluded. I consider that

the inflexible distance dependence and magnitude form used in these models will tend to cause these models to overestimate the ground motions for M=5 at 50 and 160 km distances.

F1-4 EPISTEMIC UNCERTAINTY

Based on my weighting scheme and proponent model sigma-mu (Table F1-1), the epistemic uncertainties (σ_μ and σ_σ) were computed by the facilitation team. I made the following modifications to these statistical estimates of the epistemic uncertainty:

I set a minimum value of 0.2 natural log units for the epistemic uncertainty to cover the cases in which the statistical estimate was low due to chance agreement of the various proponent models or few proponent models being available for some particular cases.

Table F1-1. Values of Sigma-Mu to be used for the Proponent Models

	X Distance			
M Range	**1,5 km**	**10 km**	**50 km**	**100,160 km**
5, 5.8	0.6	0.4	0.4	0.5
6.5	0.65	0.3	0.3	0.60
70, 7.5, 8.0	0.70	0.4	0.4	0.60

F1-5 FINAL POINT ESTIMATES

After making the adjustments to the weighted estimates as described above, my final point estimates of μ, σ, σ_μ, and σ_σ for the horizontal component for the 51 cases are given in Tables F1-2 to F1-10 for the nine ground motion parameters. The corresponding point estimates for the vertical component are given in Tables F1-11 to F1-19.

F1-6 EVALUATION OF REGRESSION MODELS

The facilitation team developed regression models to parameterize my point estimates in terms of the dependence on magnitude, distance, and style-of-faulting. I reviewed the final regression models given in Volume 11A of the data package. These regression models

adequately model my point estimates of the median, aleatory uncertainty, epistemic uncertainty in the median, and epistemic uncertainty in the aleatory uncertainty.

F1-7 SPECIAL CASES

The ground motion models developed in this study are for " typical" events that cover the majority of the source models developed by the source experts. There are two source models that have geometries significantly different from those considered in developing the base models. These are simultaneous rupture of multiple parallel faults (local events) and a low angle fault. These two cases are discussed below.

F1-7.1 Multiple Parallel Faults

Some of the experts on describing sources have hypothesized that it is possible for more than one fault to rupture in a single earthquake. The question then is what the ground motion would be. What is needed is some approach that is simple to implement for a probabilistic seismic hazard assessment.

In order to discuss options, some terminology is needed. Suppose that there are J faults that are involved in a single earthquake. I characterize the moment, moment magnitude, and rupture distance to the jth fault as M_o^j, M_w^j, and R^j. The total moment and moment magnitude for the event are $M_o = \sum_{j=1}^{J} M_o^j$, and $M_w = \frac{2}{3}(\log(M_o - 16)$. Finally, let the ground motion parameter that we are seeking to predict be $Y = GM(M,R)$, and designate the ground motion from each of the subevents as Y_1, Y_2, ...

While any number of possibilities exist, I considered the following alternatives:

A1. Choose Y = max(Y_1, Y_2,...). This treats each subfault as an independent event, and acts as if the ruptures are sufficiently separated in time that the peak is controlled by the one causing the largest motions. However, having multiple ruptures on either side of the station could lead to multiple sources of energy that are all contributing at the same time. Thus, intuitively we might expect something larger than the prediction in this approach.

A2. Define $R^m = \min\{R^1,...,R^J\}$. Use $Y = GM(M_w, R^m)$. If we had any strong motion data, this is the way that it would be entered into the regression. It does not model the physics correctly, but the ground motion it predicts will be greater than the approach A1. Some preliminary calculations by Paul Somerville, supplied to our panel, suggested that the predictions using this approach are smaller than his model. However, it should be clear that we do not know what input to a physical rupture model is appropriate for this situation.

A3. Let R^e be an "effective distance" defined as $\frac{1}{R^e} = \sum_{j=1}^{J} \frac{1}{R^j}$. Use $Y = GM(M_w, R^e)$.

This is strictly an "engineering fix" which adjusts to a closer distance, and thus predicts a larger ground motion than approach A1 or A2.

A4. Choose $Y = \{\sum_{j=1}^{J} Y_j^2\}^{1/2}$. This approach would rest on the physical assumption that the peak values of Y from all of the subfaults arrive at the same time, but interfere randomly.

A5. Choose $Y = \sum_{j=1}^{J} Y_j$. This approach would rest on the physical assumption that the peak values of Y from all of the subfaults arrive at the same time, and that they add constructively.

A6. Considering that subevent 1 causes the largest motions of any of the subevents, choose $Y = \{Y_1^2 + \sum_{j=2}^{J} (kY_j)^2\}^{1/2}$. This approach would rest on the physical assumption that the peak values of Y from all of the subfaults interfere randomly. It is modified from A4 with a judgmental assumption that ground motions from other subevents will be below their peak values at the time that the peak from the largest subevent arrives. The factor k is obviously arbitrary within the range $0 \le k \le 1$. Case A1 is the special case of this one in which *k=0*. Case 4 is a special case of this one where *k=1*. A value of *k=2/3* seems plausible to me.

Considering these six alternatives, I think A1, A3, and A5 are least likely since they do not match the physics of the situation. A2 may match the practice of regression analysis, but

actual recordings for this situation may tend to have positive residuals because of the special geometry. I prefer approach A6 with *k=2/3* ; however, if this gives values of ground motions that are smaller than A2, then replace those values with the estimate using method A2.

F1-7.2 Low Angle Fault

The second difficult case is one of a detachment fault beneath the site. The hypothesis is that there could be some "normal" faulting detachment, potentially large, on a very shallow dipping fault. There are no data available to predict how such a fault could behave. One physical hypothesis is that an event of this type would be much like any other event. A second hypothesis is that such an event could have a longer rise time, looking more like a creep event. Defense of this hypothesis would rest on the lack of observations of any well documented events of this type. The reasoning would be that the lack of observations is caused by these events mostly occurring by creep, but once in a while they accelerate more to be an actual earthquake. To my mind, the most reasonable approach for this case is to assume that if there should be such an event, the ground motions that it causes will be similar to the ground motions caused by other earthquakes in the region. It is plausible that there have been some detachment events, but they have not been recognized as such; failure to recognize them would be more likely if they are otherwise typical. Lacking any other better information, for this type of event, my recommendation is to use the regressions we have without modification.

F1-8 REFERENCES

Abrahamson, N. A., and Silva, W. J. 1997, Empirical response spectral attenuation relations for shallow crustal earthquakes: Seismological Research Letters, v. 68, n. 1, p. 94-127.

Becker, A. M., and Abrahamson, N. A., 1997, Stress drops in normal faulting earthquakes (abstract): Seismological Research Letters, v. 68, n. 2, p. 322.

Boore, D. M., Joyner, W. B., and Fumal, T. E., 1997, Equations for estimating horizontal response spectra and peak acceleration from western North American earthquakes, a summary of recent work: Seismological Research Letters v. 68, n. 1, p. 128-153.

Campbell, K.W., 1993, Empirical prediction of near-source ground motion from large earthquakes, *in* V.K. Gaur, ed., Proceedings, International Workshop on Earthquake Hazard and Large Dams in the Himalaya: Indian National Trust for Art and Cultural Heritage (INTACH), New Delhi, India, p. 93-103.

Campbell, K. W., 1997, Empirical near-source attenuation relationships for horizontal and vertical components of peak ground acceleration, peak ground velocity, and pseudo-absolute acceleration response spectra: Seismological Research Letters, v. 68, n. 1, p. 154-179.

Campbell, K.W., and Bozorgnia, Y., 1994, Near-source attenuation of peak horizontal acceleration from worldwide accelerograms recorded from 1957 to 1993: 5th U.S. National Conference. on Earthquake Engineering, Chicago, IL.

Hanks, T.C., and Kanamori, H., 1979, A moment-magnitude scale: Journal of Geophysical Research, v.84, p. 2348-2350.

McGarr, A. 1984, Scaling of ground motion parameters, state of stress, and focal depth: Journal of Geophysical Research, v. 89, p. 6969-6979.

Sabetta, F., and Pugliese, A., 1996, Estimation of response spectra and simulation of nonstationary earthquake ground motions: Bulletin of the Seismological Society of America, v. 86, p. 337-352.

Sadigh, K., Chang, C.-Y., Egan, J. A., Makdisi, F., and Youngs, R. R., 1997, Attenuation relationships for shallow crustal earthquakes based on California strong motion data: Seismological Research Letters, v. 68, n. 1, p. 180-189.

Somerville, P.G., Smith, N.F., Graves, R.W., and Abrahamson, N.A., 1997, Modification of empirical strong ground motion attenuation relations to include the amplitude and duration effects of rupture directivity: Seismological Research Letters, v. 68, p. 199-222.

Spudich, P., Fletcher, J.B., Hellweg, M., Boatwright, J., Sullivan, C., Joyner, W.B., Hanks, T.C., Boore, D.M., McGarr, A., Baker, L.M., and Lindh, A.G., 1996, Earthquake ground motions in extensional tectonic regimes: U.S. Geologic Survey Open-File Report 96-292, 351 p.

Spudich, P., Fletcher, J. B., Hellweg, M., Boatwright, J., Sullivan, C. Joyner, W. B., Hanks, T. C., Boore, D. M., McGarr, A., Baker, L. M., and Lindh, A. G., 1997, SEA96 -- a new predictive relation for earthquake ground motions in extensional tectonic regimes: Seismological Research Letters 68, no. 1., p. 190 - 198.

Zeng, Y., Anderson, J. G., and Yu, G., 1994, A composite source model for computing realistic synthetic strong ground motions: Geophysical Research Letters, v. 21, p. 725-728.

TABLE F1-2
J. G. ANDERSON: HORIZONTAL POINT ESTIMATES
PEAK GROUND ACCELERATION

CASE NO.	MAGNITUDE	DISTANCE (KM)	MU	SIGMA	SIGMA MU	SIGMA SIGMA
1	5.00	1	0.12411	0.65861	0.60000	0.09940
2	5.00	1	0.21635	0.66848	0.60000	0.09751
3	5.00	5	0.04459	0.66354	0.60000	0.09838
4	5.00	5	0.07861	0.66848	0.60000	0.09751
5	5.80	10	0.09918	0.60246	0.40000	0.11865
6	5.80	20	0.07996	0.60163	0.40000	0.11873
7	6.50	1	0.49138	0.57948	0.65000	0.11251
8	6.50	1	0.58235	0.58496	0.65000	0.11615
9	6.50	1	0.49031	0.58159	0.65000	0.11337
10	6.50	5	0.40357	0.57561	0.65000	0.11103
11	6.50	5	0.27324	0.58284	0.65000	0.11404
12	6.50	50	0.03178	0.57500	0.30000	0.11091
13	6.50	50	0.03063	0.57469	0.30000	0.11086
14	7.00	10	0.28433	0.54940	0.40000	0.12564
15	7.50	50	0.06512	0.55389	0.40000	0.13012
16	7.50	50	0.06628	0.55029	0.40000	0.12811
17	5.00	1	0.05417	0.67286	0.60000	0.05269
18	5.80	5	0.16911	0.60316	0.60000	0.11862
19	5.80	5	0.09635	0.60271	0.60000	0.11863
20	5.00	10	0.06634	0.66354	0.40000	0.09838
21	5.00	10	0.08545	0.65861	0.40000	0.09940
22	5.00	50	0.00580	0.65861	0.40000	0.09940
23	5.00	50	0.00555	0.65369	0.40000	0.10058
24	5.00	160	0.00076	0.64878	0.50000	0.10190
25	5.80	1	0.27500	0.60477	0.60000	0.11932
26	5.80	5	0.23217	0.60200	0.60000	0.11868
27	5.80	5	0.13897	0.60223	0.60000	0.11866
28	5.80	10	0.12399	0.61010	0.40000	0.12100
29	5.80	10	0.17957	0.60223	0.40000	0.11866
30	5.80	10	0.07494	0.60440	0.60000	0.11936
31	5.80	50	0.01290	0.60631	0.40000	0.06216
32	5.80	50	0.01273	0.61383	0.40000	0.06304
33	6.50	5	0.35218	0.57646	0.65000	0.11124
34	6.50	10	0.22425	0.57921	0.30000	0.11243
35	6.50	10	0.33871	0.57876	0.30000	0.11230
36	6.50	10	0.16640	0.57583	0.65000	0.11108
37	6.50	20	0.11192	0.57507	0.30000	0.11092
38	6.50	20	0.16599	0.57966	0.30000	0.11257
39	6.50	20	0.08065	0.57239	0.65000	0.10990
40	6.50	100	0.01559	0.57652	0.60000	0.11190
41	6.50	160	0.00544	0.59316	0.60000	0.12156
42	7.00	1	0.50377	0.55133	0.60000	0.12653
43	7.00	10	0.38880	0.55458	0.40000	0.12835
44	7.00	10	0.20551	0.54700	0.60000	0.12475
45	7.00	50	0.04945	0.54715	0.40000	0.12480
46	7.00	50	0.04857	0.54926	0.40000	0.12559
47	7.50	1	0.54649	0.57853	0.60000	0.14692
48	5.00	10	0.29788	0.56966	0.40000	0.14041
49	5.00	10	0.39649	0.55316	0.40000	0.12968
50	8.00	50	0.07505	0.58503	0.40000	0.07992
51	8.00	160	0.02345	0.57622	0.60000	0.07396

TABLE F1-3
J. G. ANDERSON: HORIZONTAL POINT ESTIMATES
SPECTRAL ACCELERATION AT 0.05 SEC PERIOD

CASE NO.	MAGNITUDE	DISTANCE (KM)	MU	SIGMA	SIGMA MU	SIGMA SIGMA
1	5.00	1	0.21962	0.66700	0.60000	0.07622
2	5.00	1	0.36309	0.67199	0.60000	0.07449
3	5.00	5	0.08181	0.67199	0.60000	0.07449
4	5.00	5	0.12701	0.67699	0.60000	0.07296
5	5.80	10	0.16346	0.61190	0.40000	0.11023
6	5.80	20	0.12482	0.60578	0.40000	0.10898
7	6.50	1	0.78883	0.58479	0.65000	0.10645
8	6.50	1	0.89820	0.58975	0.65000	0.11012
9	6.50	1	0.76665	0.58320	0.65000	0.10570
10	6.50	5	0.67474	0.58136	0.65000	0.10581
11	6.50	5	0.45286	0.58163	0.65000	0.10514
12	6.50	50	0.04361	0.57927	0.30000	0.10469
13	6.50	50	0.04262	0.57887	0.30000	0.10466
14	7.00	10	0.44758	0.54791	0.40000	0.12662
15	7.50	50	0.09058	0.55293	0.40000	0.13241
16	7.50	50	0.09298	0.54901	0.40000	0.13032
17	5.00	1	0.10922	0.67982	0.60000	0.04674
18	5.80	5	0.26202	0.60503	0.60000	0.10813
19	5.80	5	0.15036	0.60649	0.60000	0.10881
20	5.00	10	0.12213	0.69203	0.40000	0.06961
21	5.00	10	0.16206	0.67199	0.40000	0.07449
22	5.00	50	0.00921	0.66711	0.40000	0.05695
23	5.00	50	0.00869	0.66711	0.40000	0.05695
24	5.00	160	0.00109	0.65221	0.50000	0.06686
25	5.80	1	0.47736	0.60699	0.60000	0.10872
26	5.80	5	0.40567	0.61356	0.60000	0.11139
27	5.80	5	0.23371	0.61142	0.60000	0.11033
28	5.80	10	0.20626	0.61684	0.40000	0.11236
29	5.80	10	0.29213	0.60651	0.40000	0.10881
30	5.80	10	0.12417	0.60413	0.60000	0.10826
31	5.80	50	0.01881	0.61804	0.40000	0.03868
32	5.80	50	0.01822	0.62182	0.40000	0.03960
33	6.50	5	0.57701	0.57538	0.65000	0.10302
34	6.50	10	0.37664	0.58812	0.30000	0.10868
35	6.50	10	0.56006	0.58070	0.30000	0.10490
36	6.50	10	0.27161	0.58483	0.65000	0.10717
37	6.50	20	0.17553	0.58611	0.30000	0.10852
38	6.50	20	0.25800	0.58596	0.30000	0.10735
39	6.50	20	0.12533	0.57872	0.65000	0.10465
40	6.50	100	0.01850	0.57817	0.60000	0.10465
41	6.50	160	0.00726	0.57862	0.60000	0.10465
42	7.00	1	0.85798	0.55091	0.60000	0.12790
43	7.00	10	0.65565	0.55480	0.40000	0.13006
44	7.00	10	0.33873	0.54622	0.60000	0.12607
45	7.00	50	0.07000	0.54543	0.40000	0.12584
46	7.00	50	0.06948	0.54814	0.40000	0.12671
47	7.50	1	0.89060	0.57994	0.60000	0.15113
48	5.00	10	0.48541	0.57051	0.40000	0.14410
49	5.00	10	0.63775	0.55230	0.40000	0.13204
50	8.00	50	0.10072	0.58885	0.40000	0.08569
51	8.00	160	0.02545	0.57608	0.60000	0.07834

TABLE F1-4
J. G. ANDERSON: HORIZONTAL POINT ESTIMATES
SPECTRAL ACCELERATION AT 0.10 SEC PERIOD

CASE NO.	MAGNITUDE	DISTANCE (KM)	MU	SIGMA	SIGMA MU	SIGMA SIGMA
1	5.00	1	0.27826	0.72629	0.60000	0.09707
2	5.00	1	0.48422	0.71610	0.60000	0.09652
3	5.00	5	0.10119	0.72629	0.60000	0.09707
4	5.00	5	0.18575	0.72119	0.60000	0.09671
5	5.80	10	0.20065	0.63353	0.40000	0.12796
6	5.80	20	0.16039	0.63396	0.40000	0.12801
7	6.50	1	1.01411	0.61305	0.65000	0.12920
8	6.50	1	1.25153	0.61461	0.65000	0.13042
9	6.50	1	1.03999	0.61199	0.65000	0.12864
10	6.50	5	0.81889	0.60378	0.65000	0.12470
11	6.50	5	0.57148	0.60757	0.65000	0.12634
12	6.50	50	0.05993	0.60472	0.30000	0.12501
13	6.50	50	0.05698	0.60203	0.30000	0.12366
14	7.00	10	0.56552	0.56009	0.40000	0.13217
15	7.50	50	0.11973	0.57033	0.40000	0.14153
16	7.50	50	0.12691	0.56279	0.40000	0.13713
17	5.00	1	0.12606	0.68511	0.60000	0.05783
18	5.80	5	0.35628	0.63468	0.60000	0.12811
19	5.80	5	0.19970	0.63161	0.60000	0.12695
20	5.00	10	0.14936	0.72629	0.40000	0.09707
21	5.00	10	0.19680	0.70592	0.40000	0.09670
22	5.00	50	0.01241	0.71610	0.40000	0.09652
23	5.00	50	0.01174	0.70592	0.40000	0.09670
24	5.00	160	0.00140	0.69069	0.50000	0.09831
25	5.80	1	0.55892	0.63821	0.60000	0.12947
26	5.80	5	0.50366	0.63422	0.60000	0.12804
27	5.80	5	0.28199	0.63986	0.60000	0.13073
28	5.80	10	0.23985	0.63929	0.40000	0.13071
29	5.80	10	0.35203	0.63389	0.40000	0.12800
30	5.80	10	0.15166	0.62657	0.60000	0.12560
31	5.80	50	0.02490	0.65456	0.40000	0.07141
32	5.80	50	0.02364	0.65835	0.40000	0.07331
33	6.50	5	0.72848	0.60678	0.65000	0.12591
34	6.50	10	0.46044	0.60837	0.30000	0.12684
35	6.50	10	0.70615	0.60734	0.30000	0.12650
36	6.50	10	0.34014	0.60774	0.65000	0.12662
37	6.50	20	0.22633	0.60070	0.30000	0.12316
38	6.50	20	0.31735	0.60326	0.30000	0.12424
39	6.50	20	0.15737	0.60418	0.65000	0.12483
40	6.50	100	0.02506	0.60004	0.60000	0.12296
41	6.50	160	0.00918	0.60035	0.60000	0.12305
42	7.00	1	1.05676	0.56497	0.60000	0.13511
43	7.00	10	0.79509	0.57010	0.40000	0.13808
44	7.00	10	0.41749	0.56023	0.60000	0.13192
45	7.00	50	0.09343	0.55857	0.40000	0.13120
46	7.00	50	0.09229	0.56109	0.40000	0.13286
47	7.50	1	1.07643	0.59466	0.60000	0.15928
48	5.00	10	0.59081	0.58555	0.40000	0.15206
49	5.00	10	0.77500	0.56822	0.40000	0.14024
50	8.00	50	0.13350	0.63443	0.40000	0.10837
51	8.00	160	0.02994	0.61071	0.60000	0.09424

TABLE F1-5
J. G. ANDERSON: HORIZONTAL POINT ESTIMATES
SPECTRAL ACCELERATION AT 0.20 SEC PERIOD

CASE NO.	MAGNITUDE	DISTANCE (KM)	MU	SIGMA	SIGMA MU	SIGMA SIGMA
1	5.00	1	0.21253	0.75048	0.60000	0.08726
2	5.00	1	0.36713	0.76045	0.60000	0.08706
3	5.00	5	0.07666	0.74055	0.60000	0.08821
4	5.00	5	0.13967	0.73559	0.60000	0.08897
5	5.80	10	0.19290	0.67167	0.40000	0.12614
6	5.80	20	0.16291	0.65818	0.40000	0.12219
7	6.50	1	0.97252	0.63718	0.65000	0.12026
8	6.50	1	1.17980	0.65105	0.65000	0.12674
9	6.50	1	1.02196	0.65803	0.65000	0.13015
10	6.50	5	0.80188	0.64246	0.65000	0.12287
11	6.50	5	0.56675	0.63835	0.65000	0.12050
12	6.50	50	0.06656	0.63731	0.30000	0.12030
13	6.50	50	0.06494	0.63044	0.30000	0.11766
14	7.00	10	0.56999	0.59392	0.40000	0.13309
15	7.50	50	0.15030	0.59980	0.40000	0.13938
16	7.50	50	0.15874	0.59278	0.40000	0.13557
17	5.00	1	0.09982	0.71644	0.60000	0.05958
18	5.80	5	0.31328	0.66445	0.60000	0.12392
19	5.80	5	0.20028	0.66170	0.60000	0.12302
20	5.00	10	0.11445	0.74055	0.40000	0.08821
21	5.00	10	0.14818	0.73559	0.40000	0.08897
22	5.00	50	0.01303	0.75048	0.40000	0.08726
23	5.00	50	0.01051	0.72570	0.40000	0.09100
24	5.00	160	0.00201	0.73559	0.50000	0.08897
25	5.80	1	0.50600	0.66414	0.60000	0.12391
26	5.80	5	0.43848	0.66353	0.60000	0.12392
27	5.80	5	0.25975	0.66463	0.60000	0.12392
28	5.80	10	0.22186	0.66860	0.40000	0.12500
29	5.80	10	0.32185	0.65864	0.40000	0.12223
30	5.80	10	0.15099	0.67076	0.60000	0.12612
31	5.80	50	0.02556	0.68556	0.40000	0.06030
32	5.80	50	0.02720	0.68514	0.40000	0.06040
33	6.50	5	0.70065	0.63179	0.65000	0.11813
34	6.50	10	0.42825	0.64154	0.30000	0.12203
35	6.50	10	0.65041	0.63582	0.30000	0.11971
36	6.50	10	0.34349	0.62979	0.65000	0.11725
37	6.50	20	0.22125	0.63987	0.30000	0.12151
38	6.50	20	0.33881	0.63629	0.30000	0.12002
39	6.50	20	0.17088	0.63492	0.65000	0.11933
40	6.50	100	0.03070	0.63597	0.60000	0.11994
41	6.50	160	0.01278	0.64211	0.60000	0.12281
42	7.00	1	1.02238	0.59574	0.60000	0.13386
43	7.00	10	0.80487	0.59900	0.40000	0.13591
44	7.00	10	0.44746	0.59163	0.60000	0.13176
45	7.00	50	0.11076	0.59190	0.40000	0.13190
46	7.00	50	0.11222	0.59254	0.40000	0.13227
47	7.50	1	1.17143	0.62217	0.60000	0.15375
48	5.00	10	0.65887	0.61950	0.40000	0.15180
49	5.00	10	0.83377	0.59386	0.40000	0.13627
50	8.00	50	0.16681	0.65700	0.40000	0.09999
51	8.00	160	0.04360	0.64045	0.60000	0.09158

TABLE F1-6
J. G. ANDERSON: HORIZONTAL POINT ESTIMATES
SPECTRAL ACCELERATION AT 0.50 SEC PERIOD

CASE NO.	MAGNITUDE	DISTANCE (KM)	MU	SIGMA	SIGMA MU	SIGMA SIGMA
1	5.00	1	0.09182	0.81772	0.60000	0.07969
2	5.00	1	0.17663	0.79323	0.60000	0.08046
3	5.00	5	0.03461	0.81281	0.60000	0.07943
4	5.00	5	0.06542	0.79811	0.60000	0.07990
5	5.80	10	0.10844	0.72136	0.40000	0.13195
6	5.80	20	0.10151	0.72685	0.40000	0.13418
7	6.50	1	0.62512	0.69297	0.65000	0.13291
8	6.50	1	0.72492	0.69748	0.65000	0.13511
9	6.50	1	0.62977	0.70147	0.65000	0.13678
10	6.50	5	0.50364	0.69308	0.65000	0.13277
11	6.50	5	0.34712	0.69310	0.65000	0.13297
12	6.50	50	0.05285	0.69814	0.30000	0.13484
13	6.50	50	0.05828	0.69137	0.30000	0.13230
14	7.00	10	0.42692	0.64534	0.40000	0.14039
15	7.50	50	0.13294	0.65082	0.40000	0.14673
16	7.50	50	0.13968	0.64518	0.40000	0.14279
17	5.00	1	0.04782	0.76695	0.60000	0.06060
18	5.80	5	0.18569	0.72762	0.60000	0.13448
19	5.80	5	0.10197	0.72540	0.60000	0.13321
20	5.00	10	0.04771	0.79323	0.40000	0.08046
21	5.00	10	0.06542	0.78350	0.40000	0.08216
22	5.00	50	0.00671	0.79064	0.40000	0.06722
23	5.00	50	0.00796	0.79552	0.40000	0.06614
24	5.00	160	0.00163	0.78092	0.50000	0.07001
25	5.80	1	0.29543	0.71784	0.60000	0.13144
26	5.80	5	0.26108	0.72073	0.60000	0.13230
27	5.80	5	0.14513	0.71364	0.60000	0.13035
28	5.80	10	0.14499	0.72699	0.40000	0.13423
29	5.80	10	0.21267	0.72216	0.40000	0.13265
30	5.80	10	0.08279	0.72160	0.60000	0.13250
31	5.80	50	0.01904	0.74592	0.40000	0.06706
32	5.80	50	0.01898	0.75642	0.40000	0.06982
33	6.50	5	0.46682	0.69192	0.65000	0.13249
34	6.50	10	0.31615	0.69644	0.30000	0.13441
35	6.50	10	0.46655	0.69592	0.30000	0.13419
36	6.50	10	0.21889	0.69184	0.65000	0.13246
37	6.50	20	0.15813	0.69313	0.30000	0.13298
38	6.50	20	0.24457	0.70130	0.30000	0.13668
39	6.50	20	0.12575	0.69227	0.65000	0.13262
40	6.50	100	0.03114	0.69300	0.60000	0.13292
41	6.50	160	0.01463	0.70174	0.60000	0.13703
42	7.00	1	0.73935	0.64696	0.60000	0.14155
43	7.00	10	0.62325	0.64772	0.40000	0.14220
44	7.00	10	0.30515	0.64527	0.60000	0.14035
45	7.00	50	0.09002	0.64567	0.40000	0.14069
46	7.00	50	0.09322	0.64853	0.40000	0.14275
47	7.50	1	0.83194	0.67418	0.60000	0.16209
48	5.00	10	0.47527	0.66602	0.40000	0.15619
49	5.00	10	0.60988	0.64994	0.40000	0.14625
50	8.00	50	0.15882	0.71713	0.40000	0.10679
51	8.00	160	0.05723	0.70921	0.60000	0.10354

TABLE F1-7
J. G. ANDERSON: HORIZONTAL POINT ESTIMATES
SPECTRAL ACCELERATION AT 1.00 SEC PERIOD

CASE NO.	MAGNITUDE	DISTANCE (KM)	MU	SIGMA	SIGMA MU	SIGMA SIGMA
1	5.00	1	0.03848	0.83470	0.60000	0.07295
2	5.00	1	0.07157	0.82983	0.60000	0.07357
3	5.00	5	0.01459	0.82497	0.60000	0.07440
4	5.00	5	0.02649	0.82497	0.60000	0.07440
5	5.80	10	0.05332	0.78390	0.40000	0.12761
6	5.80	20	0.04668	0.77780	0.40000	0.13073
7	6.50	1	0.32531	0.75929	0.65000	0.13322
8	6.50	1	0.33897	0.75905	0.65000	0.13728
9	6.50	1	0.29366	0.75099	0.65000	0.13450
10	6.50	5	0.26459	0.75485	0.65000	0.13543
11	6.50	5	0.16689	0.74962	0.65000	0.13387
12	6.50	50	0.03369	0.75189	0.30000	0.13086
13	6.50	50	0.03060	0.74996	0.30000	0.13399
14	7.00	10	0.22092	0.72545	0.40000	0.14131
15	7.50	50	0.08143	0.73839	0.40000	0.13724
16	7.50	50	0.08248	0.73188	0.40000	0.13754
17	5.00	1	0.01923	0.80619	0.60000	0.04866
18	5.80	5	0.08099	0.79699	0.60000	0.13633
19	5.80	5	0.04612	0.79288	0.60000	0.13484
20	5.00	10	0.01851	0.82013	0.40000	0.07543
21	5.00	10	0.02390	0.82013	0.40000	0.07543
22	5.00	50	0.00251	0.81501	0.40000	0.07523
23	5.00	50	0.00272	0.82955	0.40000	0.07216
24	5.00	160	0.00087	0.82469	0.50000	0.07298
25	5.80	1	0.13518	0.79064	0.60000	0.12931
26	5.80	5	0.11623	0.77322	0.60000	0.12975
27	5.80	5	0.06390	0.78821	0.60000	0.13368
28	5.80	10	0.06662	0.78645	0.40000	0.12831
29	5.80	10	0.10017	0.77485	0.40000	0.12996
30	5.80	10	0.04015	0.78745	0.60000	0.13335
31	5.80	50	0.01000	0.78801	0.40000	0.08169
32	5.80	50	0.01057	0.79829	0.40000	0.08448
33	6.50	5	0.22618	0.76405	0.65000	0.13487
34	6.50	10	0.16864	0.75653	0.30000	0.13220
35	6.50	10	0.25515	0.75155	0.30000	0.13453
36	6.50	10	0.11253	0.74926	0.65000	0.13376
37	6.50	20	0.08329	0.75034	0.30000	0.13031
38	6.50	20	0.12713	0.75584	0.30000	0.13575
39	6.50	20	0.06423	0.75055	0.65000	0.13420
40	6.50	100	0.02102	0.75253	0.60000	0.13101
41	6.50	160	0.01007	0.75449	0.60000	0.13177
42	7.00	1	0.34756	0.72444	0.60000	0.14096
43	7.00	10	0.30195	0.72178	0.40000	0.14501
44	7.00	10	0.17011	0.71521	0.60000	0.14153
45	7.00	50	0.04970	0.72526	0.40000	0.14124
46	7.00	50	0.04579	0.71639	0.40000	0.14205
47	7.50	1	0.43714	0.74001	0.60000	0.15057
48	5.00	10	0.27341	0.73851	0.40000	0.14979
49	5.00	10	0.33899	0.72074	0.40000	0.14591
50	8.00	50	0.10819	0.75977	0.40000	0.12039
51	8.00	160	0.04934	0.76032	0.60000	0.12097

TABLE F1-8
J. G. ANDERSON: HORIZONTAL POINT ESTIMATES
SPECTRAL ACCELERATION AT 2.00 SEC PERIOD

CASE NO.	MAGNITUDE	DISTANCE (KM)	MU	SIGMA	SIGMA MU	SIGMA SIGMA
1	5.00	1	0.00967	0.91473	0.60000	0.09834
2	5.00	1	0.01766	0.90503	0.60000	0.09833
3	5.00	5	0.00429	0.89054	0.60000	0.09949
4	5.00	5	0.00722	0.89054	0.60000	0.09949
5	5.80	10	0.01764	0.86291	0.40000	0.14263
6	5.80	20	0.01324	0.85159	0.40000	0.15310
7	6.50	1	0.14955	0.84202	0.65000	0.15042
8	6.50	1	0.14694	0.83226	0.65000	0.15898
9	6.50	1	0.12619	0.83308	0.65000	0.15927
10	6.50	5	0.10994	0.83285	0.65000	0.15946
11	6.50	5	0.08031	0.83409	0.65000	0.15992
12	6.50	50	0.01482	0.84269	0.30000	0.15107
13	6.50	50	0.01245	0.82926	0.30000	0.15709
14	7.00	10	0.09530	0.81592	0.40000	0.15893
15	7.50	50	0.04246	0.84784	0.40000	0.15496
16	7.50	50	0.03945	0.82720	0.40000	0.14887
17	5.00	1	0.00529	0.93024	0.60000	0.03541
18	5.80	5	0.03223	0.84236	0.60000	0.14847
19	5.80	5	0.01781	0.84938	0.60000	0.15168
20	5.00	10	0.00620	0.89054	0.40000	0.09949
21	5.00	10	0.00689	0.89536	0.40000	0.09894
22	5.00	50	0.00097	0.88665	0.40000	0.07855
23	5.00	50	0.00079	0.88665	0.40000	0.07855
24	5.00	160	0.00051	0.88665	0.50000	0.07855
25	5.80	1	0.05348	0.87420	0.60000	0.14729
26	5.80	5	0.04402	0.84245	0.60000	0.14833
27	5.80	5	0.02789	0.84705	0.60000	0.15045
28	5.80	10	0.02181	0.86939	0.40000	0.14679
29	5.80	10	0.02737	0.85828	0.40000	0.15678
30	5.80	10	0.01554	0.84433	0.60000	0.14919
31	5.80	50	0.00377	0.87408	0.40000	0.11319
32	5.80	50	0.00355	0.87403	0.40000	0.11837
33	6.50	5	0.10674	0.84274	0.65000	0.15044
34	6.50	10	0.06854	0.84455	0.30000	0.15122
35	6.50	10	0.08816	0.83175	0.30000	0.15931
36	6.50	10	0.04899	0.82984	0.65000	0.15742
37	6.50	20	0.03960	0.84732	0.30000	0.15266
38	6.50	20	0.04725	0.82660	0.30000	0.15579
39	6.50	20	0.02678	0.82769	0.65000	0.15634
40	6.50	100	0.01006	0.84426	0.60000	0.15142
41	6.50	160	0.00501	0.85388	0.60000	0.15625
42	7.00	1	0.21678	0.81592	0.60000	0.15893
43	7.00	10	0.12529	0.79484	0.40000	0.16543
44	7.00	10	0.07081	0.79876	0.60000	0.16891
45	7.00	50	0.02427	0.81633	0.40000	0.15916
46	7.00	50	0.02062	0.79152	0.40000	0.16282
47	7.50	1	0.24029	0.82688	0.60000	0.16830
48	5.00	10	0.11234	0.81701	0.40000	0.16160
49	5.00	10	0.13137	0.78776	0.40000	0.16196
50	8.00	50	0.06787	0.86100	0.40000	0.16242
51	8.00	160	0.03689	0.86532	0.60000	0.16370

TABLE F1-9
J. G. ANDERSON: HORIZONTAL POINT ESTIMATES
SPECTRAL ACCELERATION AT 3.33 SEC PERIOD

CASE NO.	MAGNITUDE	DISTANCE (KM)	MU	SIGMA	SIGMA MU	SIGMA SIGMA
1	5.00	1	0.00348	0.98219	0.60000	0.10129
2	5.00	1	0.00584	0.96740	0.60000	0.09676
3	5.00	5	0.00152	0.96740	0.60000	0.09676
4	5.00	5	0.00264	0.96740	0.60000	0.09676
5	5.80	10	0.00826	0.89185	0.40000	0.14181
6	5.80	20	0.00526	0.87786	0.40000	0.15200
7	6.50	1	0.07200	0.88468	0.65000	0.16220
8	6.50	1	0.06817	0.85442	0.65000	0.15369
9	6.50	1	0.05983	0.86099	0.65000	0.15885
10	6.50	5	0.05654	0.86581	0.65000	0.16260
11	6.50	5	0.04285	0.86895	0.65000	0.16557
12	6.50	50	0.00737	0.88514	0.30000	0.15858
13	6.50	50	0.00550	0.86360	0.30000	0.16081
14	7.00	10	0.04539	0.84914	0.40000	0.17006
15	7.50	50	0.02694	0.88919	0.40000	0.12968
16	7.50	50	0.02115	0.87418	0.40000	0.12221
17	5.00	1	0.00155	0.97729	0.60000	0.06387
18	5.80	5	0.01386	0.88358	0.60000	0.15653
19	5.80	5	0.00702	0.88264	0.60000	0.15561
20	5.00	10	0.00233	0.95757	0.40000	0.09449
21	5.00	10	0.00238	0.96248	0.40000	0.09555
22	5.00	50	0.00050	0.95267	0.40000	0.09359
23	5.00	50	0.00041	0.95267	0.40000	0.09359
24	5.00	160	0.00015	0.95267	0.50000	0.09359
25	5.80	1	0.02297	0.89964	0.60000	0.14690
26	5.80	5	0.02023	0.88146	0.60000	0.15537
27	5.80	5	0.01397	0.87741	0.60000	0.15163
28	5.80	10	0.01126	0.89500	0.40000	0.14368
29	5.80	10	0.01062	0.87660	0.40000	0.15088
30	5.80	10	0.00667	0.88068	0.60000	0.15386
31	5.80	50	0.00189	0.92592	0.40000	0.09874
32	5.80	50	0.00145	0.91665	0.40000	0.09830
33	6.50	5	0.05655	0.88682	0.65000	0.16167
34	6.50	10	0.03491	0.88393	0.30000	0.15842
35	6.50	10	0.03733	0.86239	0.30000	0.16017
36	6.50	10	0.02277	0.86639	0.65000	0.16356
37	6.50	20	0.01790	0.87865	0.30000	0.15357
38	6.50	20	0.01737	0.86969	0.30000	0.16634
39	6.50	20	0.01238	0.85816	0.65000	0.15649
40	6.50	100	0.00363	0.87205	0.60000	0.14893
41	6.50	160	0.00257	0.88894	0.60000	0.16201
42	7.00	1	0.12545	0.84476	0.60000	0.16560
43	7.00	10	0.06112	0.82039	0.40000	0.17091
44	7.00	10	0.03272	0.81881	0.60000	0.16914
45	7.00	50	0.01213	0.84134	0.40000	0.16246
46	7.00	50	0.00978	0.82097	0.40000	0.17157
47	7.50	1	0.15876	0.85261	0.60000	0.17609
48	5.00	10	0.05928	0.84187	0.40000	0.16559
49	5.00	10	0.07190	0.81800	0.40000	0.17039
50	8.00	50	0.04513	0.92864	0.40000	0.15902
51	8.00	160	0.02424	0.93020	0.60000	0.15859

TABLE F1-10
J. G. ANDERSON: HORIZONTAL POINT ESTIMATES
PEAK GROUND VELOCITY

CASE NO.	MAGNITUDE	DISTANCE (KM)	MU	SIGMA	SIGMA MU	SIGMA SIGMA
1	5.00	1	5.95368	0.77651	0.60000	0.09377
2	5.00	1	11.94466	0.77651	0.60000	0.09377
3	5.00	5	2.33973	0.77651	0.60000	0.09377
4	5.00	5	4.82999	0.76681	0.60000	0.08963
5	5.80	10	6.58281	0.73789	0.40000	0.10574
6	5.80	20	5.77092	0.73518	0.40000	0.10859
7	6.50	1	37.87487	0.73826	0.65000	0.12078
8	6.50	1	42.64674	0.73784	0.65000	0.12504
9	6.50	1	36.03432	0.73784	0.65000	0.12504
10	6.50	5	33.90291	0.73015	0.65000	0.12098
11	6.50	5	21.35413	0.72875	0.65000	0.12033
12	6.50	50	2.66481	0.72948	0.30000	0.11687
13	6.50	50	2.62790	0.72653	0.30000	0.11911
14	7.00	10	25.61209	0.71950	0.40000	0.13054
15	7.50	50	6.65118	0.71862	0.40000	0.13758
16	7.50	50	7.08289	0.70574	0.40000	0.13552
17	5.00	1	2.88039	0.75041	0.60000	0.04856
18	5.80	5	12.21397	0.73389	0.60000	0.10805
19	5.80	5	6.47582	0.73304	0.60000	0.10765
20	5.00	10	2.98180	0.76197	0.40000	0.08776
21	5.00	10	4.17823	0.76681	0.40000	0.08963
22	5.00	50	0.32234	0.75714	0.40000	0.08604
23	5.00	50	0.35921	0.76197	0.40000	0.08776
24	5.00	160	0.06889	0.74751	0.50000	0.08307
25	5.80	1	17.18409	0.74141	0.60000	0.10711
26	5.80	5	16.05410	0.72978	0.60000	0.10614
27	5.80	5	9.52540	0.73245	0.60000	0.10741
28	5.80	10	7.80374	0.74290	0.40000	0.10765
29	5.80	10	12.21401	0.73521	0.40000	0.10860
30	5.80	10	5.11692	0.73209	0.60000	0.10727
31	5.80	50	0.92102	0.74839	0.40000	0.08574
32	5.80	50	0.95812	0.75016	0.40000	0.08729
33	6.50	5	26.39163	0.73692	0.65000	0.12027
34	6.50	10	17.90324	0.73584	0.30000	0.11974
35	6.50	10	26.67163	0.73044	0.30000	0.12114
36	6.50	10	12.92577	0.72822	0.65000	0.12012
37	6.50	20	8.97351	0.73337	0.30000	0.11854
38	6.50	20	12.96219	0.73093	0.30000	0.12141
39	6.50	20	6.85566	0.72373	0.65000	0.11777
40	6.50	100	1.47121	0.73356	0.60000	0.11890
41	6.50	160	0.53372	0.74577	0.60000	0.12519
42	7.00	1	50.85425	0.71709	0.60000	0.12918
43	7.00	10	36.90607	0.71115	0.40000	0.13164
44	7.00	10	18.94126	0.70719	0.60000	0.12915
45	7.00	50	4.43288	0.71535	0.40000	0.12848
46	7.00	50	4.50998	0.70723	0.40000	0.12917
47	7.50	1	61.70474	0.73257	0.60000	0.14612
48	5.00	10	32.23119	0.72249	0.40000	0.14002
49	5.00	10	39.51812	0.70725	0.40000	0.13646
50	8.00	50	11.39069	0.74528	0.40000	0.12715
51	8.00	160	4.17337	0.75030	0.60000	0.12935

TABLE F1-11
J. G. ANDERSON: VERTICAL POINT ESTIMATES
PEAK GROUND ACCELERATION

CASE NO.	MAGNITUDE	DISTANCE (KM)	MU	SIGMA	SIGMA MU	SIGMA SIGMA
1	5.00	1	0.06378	0.65949	0.60000	0.12094
2	5.00	1	0.09231	0.66794	0.60000	0.12009
3	5.00	5	0.02423	0.65949	0.60000	0.12094
4	5.00	5	0.03063	0.66530	0.60000	0.12031
5	5.80	10	0.05316	0.65523	0.40000	0.14238
6	5.80	20	0.06651	0.63641	0.40000	0.13725
7	6.50	1	0.29684	0.62878	0.65000	0.12843
8	6.50	1	0.34868	0.63915	0.65000	0.13192
9	6.50	1	0.35225	0.62724	0.65000	0.12800
10	6.50	5	0.30597	0.62302	0.65000	0.12693
11	6.50	5	0.22112	0.62724	0.65000	0.12800
12	6.50	50	0.01982	0.62417	0.30000	0.12720
13	6.50	50	0.02435	0.62148	0.30000	0.12658
14	7.00	10	0.18926	0.62894	0.40000	0.13031
15	7.50	50	0.04332	0.63855	0.40000	0.13414
16	7.50	50	0.05311	0.63778	0.40000	0.13381
17	5.00	1	0.02533	0.64999	0.60000	0.12236
18	5.80	5	0.07798	0.63372	0.60000	0.13678
19	5.80	5	0.06272	0.64448	0.60000	0.13907
20	5.00	10	0.03258	0.67375	0.40000	0.11974
21	5.00	10	0.06918	0.64312	0.40000	0.12368
22	5.00	50	0.00410	0.65474	0.40000	0.12159
23	5.00	50	0.00365	0.64101	0.40000	0.12413
24	5.00	160	0.00045	0.65738	0.50000	0.12121
25	5.80	1	0.14869	0.63948	0.60000	0.13787
26	5.80	5	0.16475	0.63372	0.60000	0.13678
27	5.80	5	0.09909	0.63948	0.60000	0.13787
28	5.80	10	0.06674	0.64601	0.40000	0.13948
29	5.80	10	0.12768	0.63795	0.40000	0.13755
30	5.80	10	0.05887	0.64102	0.60000	0.13822
31	5.80	50	0.00621	0.63641	0.40000	0.13725
32	5.80	50	0.00755	0.64255	0.40000	0.13858
33	6.50	5	0.24213	0.62148	0.65000	0.12658
34	6.50	10	0.14657	0.63031	0.30000	0.12888
35	6.50	10	0.28602	0.63531	0.30000	0.13051
36	6.50	10	0.13342	0.62417	0.65000	0.12720
37	6.50	20	0.07673	0.62724	0.30000	0.12800
38	6.50	20	0.14856	0.63723	0.30000	0.13120
39	6.50	20	0.06182	0.62148	0.65000	0.12658
40	6.50	100	0.00823	0.63185	0.60000	0.12936
41	6.50	160	0.00205	0.62417	0.60000	0.12720
42	7.00	1	0.37990	0.63663	0.60000	0.13331
43	7.00	10	0.34283	0.63778	0.40000	0.13381
44	7.00	10	0.16806	0.63317	0.60000	0.13190
45	7.00	50	0.02878	0.63240	0.40000	0.13160
46	7.00	50	0.03869	0.63240	0.40000	0.13160
47	7.50	1	0.69730	0.65737	0.60000	0.14381
48	5.00	10	0.23206	0.63855	0.40000	0.13414
49	5.00	10	0.39478	0.64738	0.40000	0.13835
50	8.00	50	0.06157	0.63912	0.40000	0.09000
51	8.00	160	0.01270	0.64124	0.60000	0.09134

TABLE F1-12
J. G. ANDERSON: VERTICAL POINT ESTIMATES
SPECTRAL ACCELERATION AT 0.05 SEC PERIOD

CASE NO.	MAGNITUDE	DISTANCE (KM)	MU	SIGMA	SIGMA MU	SIGMA SIGMA
1	5.00	1	0.13347	0.67393	0.60000	0.06680
2	5.00	1	0.18731	0.67393	0.60000	0.06680
3	5.00	5	0.04507	0.67129	0.60000	0.06812
4	5.00	5	0.05963	0.68343	0.60000	0.06245
5	5.80	10	0.09997	0.67209	0.40000	0.12087
6	5.80	20	0.11158	0.65903	0.40000	0.11773
7	6.50	1	0.60196	0.64703	0.65000	0.11350
8	6.50	1	0.69029	0.65202	0.65000	0.11562
9	6.50	1	0.71534	0.64396	0.65000	0.11232
10	6.50	5	0.61004	0.64396	0.65000	0.11232
11	6.50	5	0.42481	0.64089	0.65000	0.11124
12	6.50	50	0.02887	0.64549	0.30000	0.11290
13	6.50	50	0.03687	0.64703	0.30000	0.11350
14	7.00	10	0.33989	0.64818	0.40000	0.11581
15	7.50	50	0.06402	0.65467	0.40000	0.11847
16	7.50	50	0.07822	0.65543	0.40000	0.11889
17	5.00	1	0.04883	0.67604	0.60000	0.06578
18	5.80	5	0.14738	0.66709	0.60000	0.11946
19	5.80	5	0.11678	0.67593	0.60000	0.12212
20	5.00	10	0.06320	0.70297	0.40000	0.05591
21	5.00	10	0.13313	0.67393	0.40000	0.06680
22	5.00	50	0.00682	0.67129	0.40000	0.06812
23	5.00	50	0.00696	0.68343	0.40000	0.06245
24	5.00	160	0.00058	0.67604	0.50000	0.06578
25	5.80	1	0.30288	0.67593	0.60000	0.12212
26	5.80	5	0.30355	0.66517	0.60000	0.11898
27	5.80	5	0.19563	0.66517	0.60000	0.11898
28	5.80	10	0.12937	0.67785	0.40000	0.12280
29	5.80	10	0.22267	0.66364	0.40000	0.11863
30	5.80	10	0.10612	0.66210	0.60000	0.11831
31	5.80	50	0.00987	0.66210	0.40000	0.11831
32	5.80	50	0.01181	0.67401	0.40000	0.12147
33	6.50	5	0.48935	0.64549	0.65000	0.11290
34	6.50	10	0.27891	0.65740	0.30000	0.11817
35	6.50	10	0.52724	0.65049	0.30000	0.11495
36	6.50	10	0.25454	0.64857	0.65000	0.11413
37	6.50	20	0.13869	0.64857	0.30000	0.11413
38	6.50	20	0.26216	0.65740	0.30000	0.11817
39	6.50	20	0.10770	0.64242	0.65000	0.11177
40	6.50	100	0.01080	0.64857	0.60000	0.11413
41	6.50	160	0.00316	0.63973	0.60000	0.11086
42	7.00	1	0.79242	0.65855	0.60000	0.12113
43	7.00	10	0.63653	0.66239	0.40000	0.12333
44	7.00	10	0.31664	0.65356	0.60000	0.11845
45	7.00	50	0.04579	0.65125	0.40000	0.11729
46	7.00	50	0.05981	0.65010	0.40000	0.11672
47	7.50	1	1.35242	0.67925	0.60000	0.13410
48	5.00	10	0.42535	0.65390	0.40000	0.11806
49	5.00	10	0.74040	0.66465	0.40000	0.12430
50	8.00	50	0.09158	0.66378	0.40000	0.07215
51	8.00	160	0.01473	0.65955	0.60000	0.06882

TABLE F1-13
J. G. ANDERSON: VERTICAL POINT ESTIMATES
SPECTRAL ACCELERATION AT 0.10 SEC PERIOD

CASE NO.	MAGNITUDE	DISTANCE (KM)	MU	SIGMA	SIGMA MU	SIGMA SIGMA
1	5.00	1	0.14358	0.72387	0.60000	0.08768
2	5.00	1	0.21911	0.73443	0.60000	0.08924
3	5.00	5	0.05581	0.73443	0.60000	0.08924
4	5.00	5	0.07690	0.74605	0.60000	0.09187
5	5.80	10	0.12015	0.68991	0.40000	0.15612
6	5.80	20	0.14451	0.67802	0.40000	0.14957
7	6.50	1	0.69039	0.66357	0.65000	0.13438
8	6.50	1	0.84340	0.66972	0.65000	0.13824
9	6.50	1	0.87979	0.66972	0.65000	0.13824
10	6.50	5	0.69046	0.66357	0.65000	0.13438
11	6.50	5	0.52342	0.66664	0.65000	0.13628
12	6.50	50	0.03783	0.66357	0.30000	0.13438
13	6.50	50	0.04730	0.66511	0.30000	0.13532
14	7.00	10	0.39644	0.67336	0.40000	0.14211
15	7.50	50	0.08229	0.68253	0.40000	0.14900
16	7.50	50	0.09791	0.67793	0.40000	0.14547
17	5.00	1	0.05885	0.72387	0.60000	0.08768
18	5.80	5	0.18801	0.67954	0.60000	0.15036
19	5.80	5	0.15102	0.67954	0.60000	0.15036
20	5.00	10	0.07559	0.74288	0.40000	0.09106
21	5.00	10	0.16114	0.71648	0.40000	0.08709
22	5.00	50	0.00825	0.74024	0.40000	0.09044
23	5.00	50	0.00797	0.72123	0.40000	0.08742
24	5.00	160	0.00081	0.72915	0.50000	0.08836
25	5.80	1	0.35533	0.67493	0.60000	0.14804
26	5.80	5	0.37619	0.67954	0.60000	0.15036
27	5.80	5	0.22244	0.67340	0.60000	0.14730
28	5.80	10	0.14317	0.68607	0.40000	0.15391
29	5.80	10	0.29315	0.68607	0.40000	0.15391
30	5.80	10	0.12861	0.67493	0.60000	0.14804
31	5.80	50	0.01286	0.68801	0.40000	0.15500
32	5.80	50	0.01375	0.68607	0.40000	0.15391
33	6.50	5	0.54287	0.66664	0.65000	0.13628
34	6.50	10	0.33094	0.66818	0.30000	0.13725
35	6.50	10	0.63894	0.66818	0.30000	0.13725
36	6.50	10	0.31466	0.66511	0.65000	0.13532
37	6.50	20	0.15833	0.66511	0.30000	0.13532
38	6.50	20	0.31703	0.67471	0.30000	0.14156
39	6.50	20	0.13572	0.66088	0.65000	0.13277
40	6.50	100	0.01408	0.65743	0.60000	0.13078
41	6.50	160	0.00427	0.66242	0.60000	0.13368
42	7.00	1	0.90562	0.67950	0.60000	0.14663
43	7.00	10	0.74908	0.68911	0.40000	0.15405
44	7.00	10	0.37997	0.67336	0.60000	0.14211
45	7.00	50	0.05691	0.67067	0.40000	0.14020
46	7.00	50	0.07430	0.67413	0.40000	0.14267
47	7.50	1	1.54266	0.69406	0.60000	0.15826
48	5.00	10	0.49762	0.67985	0.40000	0.14693
49	5.00	10	0.89378	0.68791	0.40000	0.15325
50	8.00	50	0.11464	0.70386	0.40000	0.10366
51	8.00	160	0.01686	0.70492	0.60000	0.10448

TABLE F1-14
J. G. ANDERSON: VERTICAL POINT ESTIMATES
SPECTRAL ACCELERATION AT 0.20 SEC PERIOD

CASE NO.	MAGNITUDE	DISTANCE (KM)	MU	SIGMA	SIGMA MU	SIGMA SIGMA
1	5.00	1	0.09530	0.68923	0.60000	0.06986
2	5.00	1	0.12766	0.71035	0.60000	0.07419
3	5.00	5	0.04435	0.70718	0.60000	0.07330
4	5.00	5	0.05031	0.70190	0.60000	0.07199
5	5.80	10	0.09233	0.65049	0.40000	0.15539
6	5.80	20	0.12191	0.64396	0.40000	0.15180
7	6.50	1	0.53242	0.65116	0.65000	0.14171
8	6.50	1	0.55432	0.64770	0.65000	0.13937
9	6.50	1	0.58307	0.64616	0.65000	0.13835
10	6.50	5	0.55121	0.64271	0.65000	0.13613
11	6.50	5	0.38906	0.63964	0.65000	0.13421
12	6.50	50	0.03658	0.63272	0.30000	0.13015
13	6.50	50	0.04760	0.64271	0.30000	0.13613
14	7.00	10	0.34350	0.65794	0.40000	0.13770
15	7.50	50	0.08702	0.65982	0.40000	0.13890
16	7.50	50	0.10808	0.66328	0.40000	0.14150
17	5.00	1	0.04324	0.70718	0.60000	0.07330
18	5.80	5	0.13677	0.63897	0.60000	0.14924
19	5.80	5	0.11382	0.64550	0.60000	0.15262
20	5.00	10	0.04595	0.71299	0.40000	0.07500
21	5.00	10	0.12379	0.70190	0.40000	0.07199
22	5.00	50	0.00883	0.70892	0.40000	0.06851
23	5.00	50	0.00750	0.67723	0.40000	0.06238
24	5.00	160	0.00100	0.69783	0.50000	0.06526
25	5.80	1	0.24693	0.64051	0.60000	0.15001
26	5.80	5	0.28649	0.65241	0.60000	0.15650
27	5.80	5	0.17210	0.64550	0.60000	0.15262
28	5.80	10	0.11572	0.66009	0.40000	0.16115
29	5.80	10	0.23704	0.65625	0.40000	0.15878
30	5.80	10	0.10260	0.64051	0.60000	0.15001
31	5.80	50	0.01217	0.65049	0.40000	0.15539
32	5.80	50	0.01658	0.65049	0.40000	0.15539
33	6.50	5	0.41027	0.63964	0.65000	0.13421
34	6.50	10	0.25199	0.63272	0.30000	0.13015
35	6.50	10	0.49643	0.64616	0.30000	0.13835
36	6.50	10	0.25521	0.63964	0.65000	0.13421
37	6.50	20	0.13948	0.64271	0.30000	0.13613
38	6.50	20	0.28301	0.65846	0.30000	0.14687
39	6.50	20	0.13011	0.64117	0.65000	0.13516
40	6.50	100	0.01762	0.64924	0.60000	0.14040
41	6.50	160	0.00601	0.64424	0.60000	0.13711
42	7.00	1	0.65462	0.65794	0.60000	0.13770
43	7.00	10	0.64684	0.67100	0.40000	0.14753
44	7.00	10	0.33569	0.66024	0.60000	0.13937
45	7.00	50	0.05831	0.65371	0.40000	0.13472
46	7.00	50	0.08283	0.65487	0.40000	0.13552
47	7.50	1	1.10802	0.67518	0.60000	0.15089
48	5.00	10	0.45521	0.66750	0.40000	0.14476
49	5.00	10	0.73504	0.67134	0.40000	0.14779
50	8.00	50	0.11738	0.70993	0.40000	0.09915
51	8.00	160	0.02268	0.69937	0.60000	0.09117

TABLE F1-15
J. G. ANDERSON: VERTICAL POINT ESTIMATES
SPECTRAL ACCELERATION AT 0.50 SEC PERIOD

CASE NO.	MAGNITUDE	DISTANCE (KM)	MU	SIGMA	SIGMA MU	SIGMA SIGMA
1	5.00	1	0.03461	0.70674	0.60000	0.05557
2	5.00	1	0.05549	0.70938	0.60000	0.05658
3	5.00	5	0.01312	0.72258	0.60000	0.06250
4	5.00	5	0.02005	0.70674	0.60000	0.05557
5	5.80	10	0.05091	0.64925	0.40000	0.15674
6	5.80	20	0.07600	0.65269	0.40000	0.15880
7	6.50	1	0.28059	0.65246	0.65000	0.14631
8	6.50	1	0.35104	0.64900	0.65000	0.14379
9	6.50	1	0.34972	0.65054	0.65000	0.14490
10	6.50	5	0.30222	0.64132	0.65000	0.13846
11	6.50	5	0.24210	0.64593	0.65000	0.14162
12	6.50	50	0.02860	0.63863	0.30000	0.13667
13	6.50	50	0.03920	0.63748	0.30000	0.13592
14	7.00	10	0.23688	0.65572	0.40000	0.14267
15	7.50	50	0.07639	0.66105	0.40000	0.14682
16	7.50	50	0.08323	0.65644	0.40000	0.14308
17	5.00	1	0.01561	0.74899	0.60000	0.07761
18	5.80	5	0.07051	0.65768	0.60000	0.16189
19	5.80	5	0.05091	0.64348	0.60000	0.15347
20	5.00	10	0.02033	0.70198	0.40000	0.05393
21	5.00	10	0.04626	0.69776	0.40000	0.05268
22	5.00	50	0.00385	0.72115	0.40000	0.05793
23	5.00	50	0.00435	0.70055	0.40000	0.04796
24	5.00	160	0.00063	0.71059	0.50000	0.05237
25	5.80	1	0.10383	0.65076	0.60000	0.15764
26	5.80	5	0.14270	0.67268	0.60000	0.17197
27	5.80	5	0.09774	0.64769	0.60000	0.15585
28	5.80	10	0.06844	0.66115	0.40000	0.16411
29	5.80	10	0.13211	0.66459	0.40000	0.16640
30	5.80	10	0.05844	0.66651	0.60000	0.16770
31	5.80	50	0.00723	0.64769	0.40000	0.15585
32	5.80	50	0.01101	0.65576	0.40000	0.16068
33	6.50	5	0.24617	0.65745	0.65000	0.15004
34	6.50	10	0.17192	0.65400	0.30000	0.14744
35	6.50	10	0.32681	0.65246	0.30000	0.14631
36	6.50	10	0.17436	0.64593	0.65000	0.14162
37	6.50	20	0.09853	0.65246	0.30000	0.14631
38	6.50	20	0.19322	0.65937	0.30000	0.15151
39	6.50	20	0.08057	0.64593	0.65000	0.14162
40	6.50	100	0.01513	0.64747	0.60000	0.14270
41	6.50	160	0.00603	0.64593	0.60000	0.14162
42	7.00	1	0.41676	0.67339	0.60000	0.15720
43	7.00	10	0.43246	0.66726	0.40000	0.15200
44	7.00	10	0.22559	0.65917	0.60000	0.14541
45	7.00	50	0.04310	0.65572	0.40000	0.14267
46	7.00	50	0.06536	0.65687	0.40000	0.14358
47	7.50	1	0.57789	0.67488	0.60000	0.15856
48	5.00	10	0.28605	0.65915	0.40000	0.14525
49	5.00	10	0.45321	0.66414	0.40000	0.14936
50	8.00	50	0.11083	0.70875	0.40000	0.09052
51	8.00	160	0.02744	0.71245	0.60000	0.09346

TABLE F1-16
J. G. ANDERSON: VERTICAL POINT ESTIMATES
SPECTRAL ACCELERATION AT 1.00 SEC PERIOD

CASE NO.	MAGNITUDE	DISTANCE (KM)	MU	SIGMA	SIGMA MU	SIGMA SIGMA
1	5.00	1	0.01569	0.71898	0.60000	0.02452
2	5.00	1	0.02295	0.74274	0.60000	0.03950
3	5.00	5	0.00552	0.72795	0.60000	0.02956
4	5.00	5	0.00828	0.71528	0.60000	0.02282
5	5.80	10	0.02151	0.68143	0.40000	0.13285
6	5.80	20	0.02740	0.67595	0.40000	0.13874
7	6.50	1	0.13121	0.68518	0.65000	0.13981
8	6.50	1	0.16387	0.67576	0.65000	0.14189
9	6.50	1	0.14674	0.67230	0.65000	0.13950
10	6.50	5	0.15014	0.67422	0.65000	0.14082
11	6.50	5	0.11533	0.66347	0.65000	0.13372
12	6.50	50	0.01272	0.67980	0.30000	0.13613
13	6.50	50	0.02246	0.66078	0.30000	0.13206
14	7.00	10	0.10488	0.69653	0.40000	0.14760
15	7.50	50	0.04057	0.68614	0.40000	0.14004
16	7.50	50	0.05275	0.68017	0.40000	0.14371
17	5.00	1	0.00531	0.71686	0.60000	0.02351
18	5.80	5	0.03241	0.67902	0.60000	0.14061
19	5.80	5	0.02735	0.68401	0.60000	0.14378
20	5.00	10	0.00597	0.70789	0.40000	0.02036
21	5.00	10	0.01285	0.71528	0.40000	0.02282
22	5.00	50	0.00121	0.71543	0.40000	0.01850
23	5.00	50	0.00195	0.71755	0.40000	0.01992
24	5.00	160	0.00029	0.72230	0.50000	0.02326
25	5.80	1	0.05133	0.70985	0.60000	0.15191
26	5.80	5	0.06535	0.68747	0.60000	0.14606
27	5.80	5	0.04567	0.67441	0.60000	0.13783
28	5.80	10	0.02959	0.68758	0.40000	0.13654
29	5.80	10	0.05575	0.67172	0.40000	0.13628
30	5.80	10	0.03640	0.68555	0.60000	0.14478
31	5.80	50	0.00359	0.69795	0.40000	0.14334
32	5.80	50	0.00655	0.67441	0.40000	0.13783
33	6.50	5	0.10873	0.68326	0.65000	0.13847
34	6.50	10	0.08182	0.68172	0.30000	0.13742
35	6.50	10	0.11766	0.65809	0.30000	0.13046
36	6.50	10	0.09168	0.66462	0.65000	0.13444
37	6.50	20	0.03949	0.68326	0.30000	0.13847
38	6.50	20	0.07980	0.66078	0.30000	0.13206
39	6.50	20	0.04988	0.65809	0.65000	0.13046
40	6.50	100	0.00766	0.67097	0.60000	0.13048
41	6.50	160	0.00315	0.68172	0.60000	0.13742
42	7.00	1	0.17045	0.70613	0.60000	0.15506
43	7.00	10	0.19912	0.68401	0.40000	0.14655
44	7.00	10	0.12073	0.68401	0.60000	0.14655
45	7.00	50	0.02385	0.68424	0.40000	0.13871
46	7.00	50	0.03566	0.67518	0.40000	0.14014
47	7.50	1	0.26612	0.73763	0.60000	0.18206
48	5.00	10	0.13927	0.68808	0.40000	0.14140
49	5.00	10	0.22823	0.68209	0.40000	0.14512
50	8.00	50	0.05822	0.73901	0.40000	0.10757
51	8.00	160	0.02017	0.72950	0.60000	0.10109

TABLE F1-17
J. G. ANDERSON: VERTICAL POINT ESTIMATES
SPECTRAL ACCELERATION AT 2.00 SEC PERIOD

CASE NO.	MAGNITUDE	DISTANCE (KM)	MU	SIGMA	SIGMA MU	SIGMA SIGMA
1	5.00	1	0.00535	0.74083	0.60000	0.05673
2	5.00	1	0.00814	0.73027	0.60000	0.05138
3	5.00	5	0.00162	0.73766	0.60000	0.05504
4	5.00	5	0.00244	0.73133	0.60000	0.05188
5	5.80	10	0.00814	0.72890	0.40000	0.15389
6	5.80	20	0.00863	0.72174	0.40000	0.17478
7	6.50	1	0.07747	0.73163	0.65000	0.17064
8	6.50	1	0.10304	0.69927	0.65000	0.16982
9	6.50	1	0.08477	0.69503	0.65000	0.16666
10	6.50	5	0.09284	0.70386	0.65000	0.17335
11	6.50	5	0.06191	0.69503	0.65000	0.16666
12	6.50	50	0.00630	0.71818	0.30000	0.16036
13	6.50	50	0.01372	0.69773	0.30000	0.16866
14	7.00	10	0.04800	0.72129	0.40000	0.16589
15	7.50	50	0.01992	0.73051	0.40000	0.17307
16	7.50	50	0.03657	0.70863	0.40000	0.17920
17	5.00	1	0.00130	0.73502	0.60000	0.05368
18	5.80	5	0.01722	0.70023	0.60000	0.15884
19	5.80	5	0.00893	0.70638	0.60000	0.16317
20	5.00	10	0.00160	0.73027	0.40000	0.05138
21	5.00	10	0.00484	0.72710	0.40000	0.04996
22	5.00	50	0.00029	0.73238	0.40000	0.05238
23	5.00	50	0.00102	0.72710	0.40000	0.04996
24	5.00	160	0.00004	0.75351	0.50000	0.06411
25	5.80	1	0.02833	0.75847	0.60000	0.17745
26	5.80	5	0.03583	0.71521	0.60000	0.16972
27	5.80	5	0.02316	0.72174	0.60000	0.17478
28	5.80	10	0.00982	0.72736	0.40000	0.15277
29	5.80	10	0.01829	0.72673	0.40000	0.17875
30	5.80	10	0.01544	0.71675	0.60000	0.17089
31	5.80	50	0.00126	0.71622	0.40000	0.14503
32	5.80	50	0.00350	0.71982	0.40000	0.17327
33	6.50	5	0.05427	0.72471	0.65000	0.16525
34	6.50	10	0.03856	0.72779	0.30000	0.16762
35	6.50	10	0.06147	0.71617	0.30000	0.18318
36	6.50	10	0.04818	0.71425	0.65000	0.18161
37	6.50	20	0.01914	0.72471	0.30000	0.16525
38	6.50	20	0.03821	0.70580	0.30000	0.17485
39	6.50	20	0.02393	0.69773	0.65000	0.16866
40	6.50	100	0.00282	0.72279	0.60000	0.16379
41	6.50	160	0.00163	0.72779	0.60000	0.16762
42	7.00	1	0.08861	0.72705	0.60000	0.17033
43	7.00	10	0.09911	0.71439	0.40000	0.18395
44	7.00	10	0.05745	0.71286	0.60000	0.18267
45	7.00	50	0.01144	0.72052	0.40000	0.16530
46	7.00	50	0.02570	0.70172	0.40000	0.17365
47	7.50	1	0.11571	0.75240	0.60000	0.19136
48	5.00	10	0.06462	0.74741	0.40000	0.18705
49	5.00	10	0.13770	0.74128	0.40000	0.20746
50	8.00	50	0.04427	0.78063	0.40000	0.14388
51	8.00	160	0.01940	0.78538	0.60000	0.14718

TABLE F1-18
J. G. ANDERSON: VERTICAL POINT ESTIMATES
SPECTRAL ACCELERATION AT 3.33 SEC PERIOD

CASE NO.	MAGNITUDE	DISTANCE (KM)	MU	SIGMA	SIGMA MU	SIGMA SIGMA
1	5.00	1	0.00172	0.79952	0.60000	0.07516
2	5.00	1	0.00294	0.78790	0.60000	0.06615
3	5.00	5	0.00057	0.79212	0.60000	0.06941
4	5.00	5	0.00117	0.78473	0.60000	0.06372
5	5.80	10	0.00441	0.76674	0.40000	0.16974
6	5.80	20	0.00479	0.74345	0.40000	0.17920
7	6.50	1	0.04079	0.77565	0.65000	0.19693
8	6.50	1	0.06270	0.74021	0.65000	0.19293
9	6.50	1	0.05420	0.73521	0.65000	0.18854
10	6.50	5	0.06335	0.74136	0.65000	0.19395
11	6.50	5	0.03295	0.73293	0.65000	0.18654
12	6.50	50	0.00330	0.77222	0.30000	0.19376
13	6.50	50	0.00665	0.75672	0.30000	0.20789
14	7.00	10	0.03026	0.79220	0.40000	0.21535
15	7.50	50	0.01281	0.78183	0.40000	0.20546
16	7.50	50	0.01975	0.75343	0.40000	0.20678
17	5.00	1	0.00043	0.79793	0.60000	0.07392
18	5.80	5	0.01097	0.74461	0.60000	0.18017
19	5.80	5	0.00580	0.74038	0.60000	0.17662
20	5.00	10	0.00053	0.79582	0.40000	0.07228
21	5.00	10	0.00197	0.78473	0.40000	0.06372
22	5.00	50	0.00011	0.79793	0.40000	0.07392
23	5.00	50	0.00050	0.78526	0.40000	0.06412
24	5.00	160	0.00003	0.81959	0.50000	0.09098
25	5.80	1	0.01266	0.77135	0.60000	0.17377
26	5.80	5	0.02133	0.74729	0.60000	0.18247
27	5.80	5	0.01036	0.74115	0.60000	0.17726
28	5.80	10	0.00466	0.76290	0.40000	0.16642
29	5.80	10	0.00880	0.74845	0.40000	0.18345
30	5.80	10	0.00739	0.75459	0.60000	0.18880
31	5.80	50	0.00061	0.76175	0.40000	0.16544
32	5.80	50	0.00177	0.75690	0.40000	0.19083
33	6.50	5	0.03717	0.76453	0.65000	0.18681
34	6.50	10	0.01879	0.75071	0.30000	0.17472
35	6.50	10	0.03036	0.75175	0.30000	0.20330
36	6.50	10	0.02208	0.74291	0.65000	0.19532
37	6.50	20	0.01017	0.77913	0.30000	0.20013
38	6.50	20	0.01555	0.74405	0.30000	0.19635
39	6.50	20	0.01502	0.75019	0.65000	0.20189
40	6.50	100	0.00121	0.76453	0.60000	0.18681
41	6.50	160	0.00086	0.76453	0.60000	0.18681
42	7.00	1	0.05217	0.77645	0.60000	0.20042
43	7.00	10	0.05235	0.76649	0.40000	0.21916
44	7.00	10	0.03337	0.75573	0.60000	0.20894
45	7.00	50	0.00745	0.78452	0.40000	0.20801
46	7.00	50	0.01359	0.76649	0.40000	0.21916
47	7.50	1	0.08370	0.80411	0.60000	0.22692
48	5.00	10	0.03555	0.77837	0.40000	0.20222
49	5.00	10	0.07235	0.77378	0.40000	0.22620
50	8.00	50	0.03412	0.84048	0.40000	0.16943
51	8.00	160	0.01277	0.84418	0.60000	0.17227

TABLE F1-19
J. G. ANDERSON: VERTICAL POINT ESTIMATES
PEAK GROUND VELOCITY

CASE NO.	MAGNITUDE	DISTANCE (KM)	MU	SIGMA	SIGMA MU	SIGMA SIGMA
1	5.00	1	2.80810	0.65924	0.60000	0.08546
2	5.00	1	4.29556	0.66083	0.60000	0.08648
3	5.00	5	0.90284	0.66083	0.60000	0.08648
4	5.00	5	1.48331	0.65924	0.60000	0.08546
5	5.80	10	2.94654	0.63290	0.40000	0.12525
6	5.80	20	3.73412	0.61474	0.40000	0.11732
7	6.50	1	17.20402	0.63012	0.65000	0.11997
8	6.50	1	25.50247	0.62147	0.65000	0.11992
9	6.50	1	21.73553	0.62415	0.65000	0.12255
10	6.50	5	24.66848	0.61595	0.65000	0.11400
11	6.50	5	14.60814	0.61993	0.65000	0.11843
12	6.50	50	1.22950	0.61990	0.30000	0.10950
13	6.50	50	2.44010	0.61772	0.30000	0.11600
14	7.00	10	13.23987	0.64282	0.40000	0.13144
15	7.50	50	4.39409	0.63815	0.40000	0.13276
16	7.50	50	7.06752	0.63410	0.40000	0.13639
17	5.00	1	0.99430	0.65924	0.60000	0.08546
18	5.80	5	5.57618	0.61282	0.60000	0.11554
19	5.80	5	3.61064	0.61743	0.60000	0.11985
20	5.00	10	1.07860	0.66716	0.40000	0.09061
21	5.00	10	2.89521	0.65343	0.40000	0.08181
22	5.00	50	0.17204	0.66294	0.40000	0.08784
23	5.00	50	0.23777	0.63548	0.40000	0.07137
24	5.00	160	0.02367	0.67667	0.50000	0.09700
25	5.80	1	7.57530	0.62714	0.60000	0.11978
26	5.80	5	10.35665	0.61474	0.60000	0.11732
27	5.80	5	5.78659	0.61013	0.60000	0.11279
28	5.80	10	3.55716	0.62982	0.40000	0.12232
29	5.80	10	7.32232	0.61627	0.40000	0.11876
30	5.80	10	3.82405	0.61743	0.60000	0.11985
31	5.80	50	0.34628	0.62829	0.40000	0.12086
32	5.80	50	0.68701	0.61743	0.40000	0.11985
33	6.50	5	14.87275	0.63165	0.65000	0.12144
34	6.50	10	9.29801	0.62345	0.30000	0.11320
35	6.50	10	16.00772	0.62569	0.30000	0.12406
36	6.50	10	10.05691	0.61329	0.65000	0.11105
37	6.50	20	4.60363	0.61931	0.30000	0.10890
38	6.50	20	8.79620	0.61772	0.30000	0.11600
39	6.50	20	5.39304	0.61595	0.65000	0.11400
40	6.50	100	0.59426	0.62743	0.60000	0.11743
41	6.50	160	0.18813	0.62167	0.60000	0.11133
42	7.00	1	22.74919	0.64512	0.60000	0.13366
43	7.00	10	25.58826	0.63837	0.40000	0.13490
44	7.00	10	14.56536	0.63299	0.60000	0.12954
45	7.00	50	2.53180	0.63706	0.40000	0.12596
46	7.00	50	4.69880	0.63299	0.40000	0.12954
47	7.50	1	38.22290	0.66313	0.60000	0.15761
48	5.00	10	17.87472	0.64124	0.40000	0.13575
49	5.00	10	32.33877	0.64370	0.40000	0.14617
50	8.00	50	9.00461	0.68372	0.40000	0.14362
51	8.00	160	2.67731	0.70749	0.60000	0.16129

APPENDIX F2

MY RULES (FOR COMPUTING GROUND MOTIONS FOR PSHA OF YUCCA MOUNTAIN WASTE REPOSITORY)

David M. Boore

APPENDIX F2
TABLE OF CONTENTS

APPENDIX F2

MY RULES (FOR COMPUTING GROUND MOTIONS FOR PSHA OF YUCCA MOUNTAIN WASTE REPOSITORY)

David M. Boore

U.S.G.S.
345 Middlefield Road
Menlo Park, CA 94025

F2-1 INTRODUCTION

Because of the huge number of ground motion values that I am to provide (Tables F2-1 to F2-18), I have decided that the only practical way to provide the numbers is to first specify weights used in combining the proponent estimates and then review the resulting weighted ground motions. These weights are specified in this documentation. Included are very brief discussions of the reasons for the various weights. It should be understood that the actual weights are based on my judgment; my comments regarding the weights will not attempt to justify the precise numerical values, but rather will dwell more on the relative weights of the various proponent models.

F2-2 WEIGHTING SCHEME

F2-2.1 Distances

The distances are computed assuming Wells & Coppersmith (1994) width as a function of M, centered at the depth (shallow) or with bottom edge at greatest depth (deep). The point source calculations should use a distance as per Walt Silva's suggestion (rps = sqrt(rjb**2 + h**2), where rps = equivalent point source distance, rjb = "Joyner-Boore" distance, and h = depth to midpoint of rupture surface on fault).

F2-2.2 Classes Of Proponent Models

I divide the proponent models into three classes: 1) empirical, 2) point source simulations, and 3) finite fault simulations.

F2-2.3 Between-Class Weights

When combining the various proponent models, the weights should be normalized so that various classes have the following relative weights:

Type of Motion	Class	Weight
Horizontal	Empirical	2
Horizontal	Pt. Source	1
Horizontal	Finite Fault	1
Vertical	Empirical	4
Vertical	Pt. Source	1
Vertical	Finite Fault	1

For the horizontal component motions I decided that the empirical and the simulated motions should be given equal weight. I further decided that the point source and finite simulations should be given equal weight. The point source is a well-established model that has been well tested; in particular, it has been shown to provide good predictions of ground motions close to large earthquakes, where it would seem that the point source approximation is not valid. The use of some variant of closest distance to the fault in applying the point source model may overcome the apparent deficiency of the point source model at close distance to faults. The finite fault models are not as well validated and require the estimation of a number of parameters. The motions can be sensitive to such things as radiation pattern if adequate randomization is not included. The computation of motions at high frequencies using the finite source models must be done with care if a propagating rupture is to be properly modeled. On the other hand, what is needed may not be the proper mathematical modeling of the idealized rupture; randomness probably should be included to account for the complexities of the real world. In this sense the finite-fault models take on the flavor of the point source stochastic model.

For vertical motions it is my opinion that the numerical simulations have not been adequately validated, and for this reason I have downweighted them relative to the empirical models (giving them 1/2 the weight of the empirical models).

F2-2.4 Within-Class Weights

F2-2.4.1 Empirical Model Weights. Fourteen empirical models were considered. Six models were given zero weight (see below). The remaining eight models were separated into two categories based on the distance measure used, those using the Joyner-Boore" distance and those using any other distance measure.

For spectral acceleration, the weights were evenly balanced between these two distance groups. For the relations using a distance measure different from Joyner-Boore, I gave most weight to AS97 as I feel that it is the most current and complete study. With respect to peak velocity, few proponent models are available; I gave equal weight to all models providing peak velocity, with the exception of those proponent models receiving no weight for any ground motion estimates. The weights applied to the empirical models are summarized below.

Models used in analysis:

- BJF 97: weight = 1 except weight = 0.5 for M = 5 and weight = 0 for pga
- SEA97: weight = 1
- AS97: weight = 1
- Campbell 97 (soft rock): weight = 0.6
- Idriss 97 (University of California, Davis, written communication): weight = 0.2
- JB88: weight = 0 except for pgv, for which weight = 1
- Sadigh 97: weight = 0.2
- McGarr 84: weight = 1 (this is for pgv only)

Models given zero weight:

- BJF94, site class A and B: more recent relations in terms of shear-wave velocity are available.

- Blast-Based Models: I expect that the attenuation from a surface source differs from an earthquake source.
- Campbell's early models: more recent models are available
- Campbell's hard rock model: other relations are for "soft" rock; few hard rock data are available.
- Idriss, University of California, Davis, written communicaiton, 93 (pga): more recent relation is available
- Sabetta & Pugliese 96: not up-to-date; uses S triggered data

	Proponent Model	Model Weight	
		Spectral Acceleration, PGA	PGV
Joyner-Boore Distance	BJF94	1.0 (0.5 for M=5); 0 for PGA	–
	SEA96	1.0	–
	JB88	0.0	1.0
All Other Distance Measures	AS97	1.0	–
	C97	0.6	1.0
	Idriss 97	0.2	–
	Sadigh 97	0.2	–
	McGarr 84	0.0	1.0

F2-2.4.2 Point Source Weights. The validations for the point source model show that there is a significant bias (over prediction) for this model at long periods ($T \geq 2$ sec). Since no correction was made for this bias, I gave the point source model zero weight for periods greater than or equal to 2 sec. At periods less than 1 sec, there is not a significant bias so I gave the point source model full weight for short periods.

- $T \geq 2.0$ sec: weight = 0.0 (because of uncorrected bias)
- $T = 1.0$ sec: weight = 0.5 (transition to periods with no bias)
- $T < 1.0$ sec: weight = 1.0

F2-2.4.3 Finite Fault Weights. I consider all three finite fault models to be equally credible so I gave equal weight to all three. Only Zeng and Anderson provided estimates at M = 5. To avoid giving much larger weight to this model for magnitude 5 events, I gave it zero weight. This ensures that all models have equal impact on the estimates.

- Zeng and Anderson: weight = 1, except = 0 for M = 5 (the only finite fault model for M = 5)
- Silva: weight = 1
- Somerville: weight = 1

F2-2.5 Conversions

Use same source and path corrections for horizontal and vertical motions.

F2-2.5.1 Empirical Models.

- Source differences: all empirical except Abrahamson & Silva (1997) and SEA96 need corrections for differences in source. Use Silva's corrections.
- Site differences: Campbell CA-->YM300
- pgv: For those proponent models lacking pgv use pgv/Sa(T=1.0s) from the point source model to scale the Sa(T=1.0s) estimates. Apply the conversion to the Sa(T=1.0s) AFTER conversions to YM300 and normal fault source.
- Sa(T=0.05s): For those proponent models lacking Sa at T = 0.05 s (20 Hz), use the following factor: Sa(T=0.05s)/Sa(T=0.10s) = 0.7 See the Appendix F2-A for the derivation of this factor. Apply the conversion factor to the Sa(T=0.1s) results before applying the source and YM300 conversion factors.
- Point source model: use stress = 45 bars, sigma(lnStress) = 0.5 (these numbers will probably be updated after receiving the new Becker results).

F2-2.5.2 Finite Fault Models.

- Source differences: apply the source correction, as in the empirical proponent models.
- Site differences: the simulations accounted for the YM site condition, so no corrections are needed.

F2-3 SIGMAS

F2-3.1 Aleatory

Find the average of the sigma from the empirical proponent models, using the same in-class weights used for finding the median ground motions. Include component-to-component

variance (square root of the sum of the squares) for those models giving values for the geometric mean horizontal motion rather than the random horizontal component of motion. Use the BJF factors for the component-to-component variance for the random horizontal.

F2-3.2 Sigma_Sigma

Sigma-sigma has not been well studied. Use 0.1 natural log units based on my judgment.

F2-3.3 Sigma_Mu

Use the standard deviation of the median value of the weighted ground motion based on the weights given in section F2-2 combined with the weighted average proponent model epistemic uncertainty (square root of the sum of the squares), with a lower limit of 0.2 natural log units.

F2-4 REGRESSION MODELS

The facilitation team developed regression models to parameterize my point estimates in terms of the dependence on magnitude, distance, and style-of-faulting. The regression models given in Volume 11B of the data package adequately model my point estimates of mu, sigma, sigma-mu, and sigma-sigma.

F2-5 SPECIAL CASES

F2-5.1 Multiple Fault Scenarios

Compute the motions as the square root of the sum of the squares of the motions from the individual faults. This assumes that the motions from each fault overlap in time at the site, and that the motions from each fault are uncorrelated.

F2-5.2 Low Angle Fault Scenarios

The empirical models account for this case. Do not make a change for this model.

F2-6 REFERENCES

Abrahamson, N. A., and Silva, W. J., 1997, Empirical response spectral attenuation relations for shallow crustal earthquakes: Seismological Research Letters, v. 68, n. 1, p. 94-127.

Boore, D.M., 1996, SMSIM -- FORTRAN Programs for Simulating Ground Motions from Earthquakes--Version 1.0: U.S. Geological Survey Open-File Report 96-80-A, 73 p.

Boore, D.M., Joyner, W.B., and Fumal, T.E., 1994, Estimation of response spectra and peak accelerations from western North American earthquakes--an interim report, part 2: U.S. Geological Survey Open-File Report 94-127, 40 p.

Boore, D. M., Joyner, W. B., and Fumal, T. E. 1997, Equations for estimating horizontal response spectra and peak acceleration from western North American earthquakes, a summary of recent work: Seismological Research Letters, v. 68, n. 1, p. 128 - 153.

Campbell, K. W., 1997, Empirical near-source attenuation relationships for horizontal and vertical components of peak ground acceleration, peak ground velocity, and pseudo-absolute acceleration response spectra: Seismological Research Letters, v. 68, n. 1, p. 154-179.

Joyner, W. B. and Boore, D. M., 1988, Measurement, characterization, and prediction of strong ground motion, *in* Procedures, Conference on Earthquake Engineering and Soil Dynamics II: GT Div/. ASCE, Park City, UT, 27-30 June 1988, p. 43-102.

McGarr, A., 1984. Scaling of ground motion parameters, state of stress, and focal depth: Journal of Geophysical Research, v. 89, p. 6969-6979.

Sabetta, F., and Pugliese, A., 1996, Estimation of response spectra and simulation of nonstationary earthquake ground motions: Bulletin of the Seismological Society of America, v. 86, p. 337-352.

Sadigh, K., Chang, C.-Y., Egan, J. A., Makdisi, F., and Youngs, R. R., 1997, Attenuation relationships for shallow crustal earthquakes based on California strong motion data: Seismological Research Letters, v. 68, n. 1, p. 180 - 189.

Spudich, P., Fletcher, J.B., Hellweg, M., Boatwright, J., Sullivan, C., Joyner, W.B., Hanks, T.C., Boore, D.M., McGarr, A., Baker, L.M., and Lindh, A.G., 1996, Earthquake ground motions in extensional tectonic regimes: U.S. Geological Survey Open-File Report 96-292, 351 p.

Spudich, P., Fletcher, J. B., Hellweg, M., Boatwright, J., Sullivan, C., Joyner, W. B., Hanks, T. C., Boore, D. M., McGarr, A., Baker, L. M., and Lindh, A. G., 1997, SEA96 -- a new predictive relation for earthquake ground motions in extensional tectonic regimes: Seismological Research Letters, v. 68, n. 1, p. 190-198.

Wells, D.L., and Coppersmith, K.J., 1994, New empirical relationships among magnitude, rupture length, rupture width, rupture area, and surface displacement: Bulletin of the Seismological Society of America, v. 84, p. 974-1002.

APPENDIX F2-A: Deriving the Sa(T=0.05s)/Sa(T=0.10s) Factor

I used the stochastic model point source model (using the computer program SMSIM, Boore, 1996) for a coastal California, rock site ground motion model (Appendix G in Boore, 1996). I computed the motions for T = 0.10 and 0.05 sec oscillators for M = 5, 6.5, 7.5 and R = 5, 15, and 50. I formed the ratios of the response spectra at the two periods and plotted the ratios vs magnitude (Fig. D1). I then fit curves to these ratios, with the result:

$$Sa(T=0.05s)/Sa(T=0.10s) = 0.9327 - 0.05047*M + 0.00245*M**2 - 0.00263*Rps + 0.0003303*M*Rps$$

where Rps = point source distance. As can be seen in Fig. D1, the range of factors in my simulations over a set spanning M = 5 to 7.5 and Rps = 5 to 50 km is only 0.68 to 0.74. For this reason and to simplify the procedure I recommend that

$$Sa(T=0.05)/Sa(T=0.1) = 0.7$$

TABLE F2-1
D. M. BOORE: HORIZONTAL POINT ESTIMATES
PEAK GROUND ACCELERATION

CASE NO.	MAGNITUDE	DISTANCE (KM)	MU	SIGMA	SIGMA MU	SIGMA SIGMA
1	5.00	1	0.14919	0.63260	0.31234	0.10000
2	5.00	1	0.14319	0.63260	0.32244	0.10000
3	5.00	5	0.05679	0.63260	0.24565	0.10000
4	5.00	5	0.06240	0.63260	0.33435	0.10000
5	5.80	10	0.08957	0.58371	0.20000	0.10000
6	5.80	20	0.07154	0.58371	0.22390	0.10000
7	6.50	1	0.38525	0.54186	0.39468	0.10000
8	6.50	1	0.41908	0.54186	0.49926	0.10000
9	6.50	1	0.39064	0.54186	0.44869	0.10000
10	6.50	5	0.36702	0.54186	0.42916	0.10000
11	6.50	5	0.25808	0.54186	0.35909	0.10000
12	6.50	50	0.02821	0.54186	0.23269	0.10000
13	6.50	50	0.02942	0.54186	0.20118	0.10000
14	7.00	10	0.23292	0.51275	0.32608	0.10000
15	7.50	50	0.05789	0.50601	0.22828	0.10000
16	7.50	50	0.06540	0.50601	0.24984	0.10000
17	5.00	1	0.06659	0.63260	0.29977	0.10000
18	5.80	5	0.14647	0.58371	0.25451	0.10000
19	5.80	5	0.08812	0.58371	0.24928	0.10000
20	5.00	10	0.05755	0.63260	0.20000	0.10000
21	5.00	10	0.07746	0.63260	0.24277	0.10000
22	5.00	50	0.00704	0.63260	0.33711	0.10000
23	5.00	50	0.00758	0.63260	0.34169	0.10000
24	5.00	160	0.00114	0.63260	0.62439	0.10000
25	5.80	1	0.25631	0.58371	0.38706	0.10000
26	5.80	5	0.23127	0.58371	0.37947	0.10000
27	5.80	5	0.14330	0.58371	0.29328	0.10000
28	5.80	10	0.11035	0.58371	0.24831	0.10000
29	5.80	10	0.15939	0.58371	0.32389	0.10000
30	5.80	10	0.08385	0.58371	0.27738	0.10000
31	5.80	50	0.01303	0.58371	0.41328	0.10000
32	5.80	50	0.01379	0.58371	0.43780	0.10000
33	6.50	5	0.28566	0.54186	0.35783	0.10000
34	6.50	10	0.18238	0.54186	0.31601	0.10000
35	6.50	10	0.28517	0.54186	0.40414	0.10000
36	6.50	10	0.16104	0.54186	0.29979	0.10000
37	6.50	20	0.09142	0.54186	0.25699	0.10000
38	6.50	20	0.12788	0.54186	0.32974	0.10000
39	6.50	20	0.07954	0.54186	0.22867	0.10000
40	6.50	100	0.01231	0.54186	0.31929	0.10000
41	6.50	160	0.00560	0.54186	0.41771	0.10000
42	7.00	1	0.43824	0.51275	0.34602	0.10000
43	7.00	10	0.35682	0.51275	0.35833	0.10000
44	7.00	10	0.20232	0.51275	0.29417	0.10000
45	7.00	50	0.04249	0.51275	0.23329	0.10000
46	7.00	50	0.04774	0.51275	0.23704	0.10000
47	7.50	1	0.52288	0.50601	0.37962	0.10000
48	5.00	10	0.28542	0.50601	0.33668	0.10000
49	5.00	10	0.42367	0.50601	0.43496	0.10000
50	8.00	50	0.07589	0.50601	0.24963	0.10000
51	8.00	160	0.02045	0.50601	0.27435	0.10000

TABLE F2-2
D. M. BOORE: HORIZONTAL POINT ESTIMATES
SPECTRAL ACCELERATION AT 0.05 SEC PERIOD

CASE NO.	MAGNITUDE	DISTANCE (KM)	MU	SIGMA	SIGMA MU	SIGMA SIGMA
1	5.00	1	0.27749	0.65243	0.47990	0.10000
2	5.00	1	0.26627	0.65243	0.46670	0.10000
3	5.00	5	0.09988	0.65243	0.20539	0.10000
4	5.00	5	0.10966	0.65243	0.20095	0.10000
5	5.80	10	0.15678	0.60300	0.22342	0.10000
6	5.80	20	0.12083	0.60300	0.23553	0.10000
7	6.50	1	0.69824	0.56066	0.36691	0.10000
8	6.50	1	0.75877	0.56066	0.44831	0.10000
9	6.50	1	0.70642	0.56066	0.42981	0.10000
10	6.50	5	0.67739	0.56066	0.44334	0.10000
11	6.50	5	0.47179	0.56066	0.39667	0.10000
12	6.50	50	0.04023	0.56066	0.28649	0.10000
13	6.50	50	0.04228	0.56066	0.28720	0.10000
14	7.00	10	0.39682	0.53118	0.31447	0.10000
15	7.50	50	0.07644	0.52488	0.34229	0.10000
16	7.50	50	0.08728	0.52488	0.35951	0.10000
17	5.00	1	0.11740	0.65243	0.20626	0.10000
18	5.80	5	0.25572	0.60300	0.25114	0.10000
19	5.80	5	0.15205	0.60300	0.27090	0.10000
20	5.00	10	0.10241	0.65243	0.31947	0.10000
21	5.00	10	0.14022	0.65243	0.35767	0.10000
22	5.00	50	0.00989	0.65243	0.27148	0.10000
23	5.00	50	0.01075	0.65243	0.25534	0.10000
24	5.00	160	0.00124	0.65243	0.49432	0.10000
25	5.80	1	0.47286	0.60300	0.41930	0.10000
26	5.80	5	0.42889	0.60300	0.41648	0.10000
27	5.80	5	0.25852	0.60300	0.37976	0.10000
28	5.80	10	0.19544	0.60300	0.28478	0.10000
29	5.80	10	0.28447	0.60300	0.34648	0.10000
30	5.80	10	0.14844	0.60300	0.37851	0.10000
31	5.80	50	0.01869	0.60300	0.47960	0.10000
32	5.80	50	0.01974	0.60300	0.51750	0.10000
33	6.50	5	0.51807	0.56066	0.33519	0.10000
34	6.50	10	0.32746	0.56066	0.29644	0.10000
35	6.50	10	0.52056	0.56066	0.41803	0.10000
36	6.50	10	0.28588	0.56066	0.33884	0.10000
37	6.50	20	0.15273	0.56066	0.26047	0.10000
38	6.50	20	0.21861	0.56066	0.33041	0.10000
39	6.50	20	0.13236	0.56066	0.29967	0.10000
40	6.50	100	0.01488	0.56066	0.36799	0.10000
41	6.50	160	0.00652	0.56066	0.43117	0.10000
42	7.00	1	0.78691	0.53118	0.35714	0.10000
43	7.00	10	0.63346	0.53118	0.40336	0.10000
44	7.00	10	0.34912	0.53118	0.34442	0.10000
45	7.00	50	0.05913	0.53118	0.28924	0.10000
46	7.00	50	0.06771	0.53118	0.29887	0.10000
47	7.50	1	0.89134	0.52488	0.44879	0.10000
48	5.00	10	0.46672	0.52488	0.39777	0.10000
49	5.00	10	0.70051	0.52488	0.51238	0.10000
50	8.00	50	0.09159	0.52488	0.45833	0.10000
51	8.00	160	0.02018	0.52488	0.41281	0.10000

TABLE F2-3
D. M. BOORE: HORIZONTAL POINT ESTIMATES: SPECTRAL ACCELERATION AT 0.10 SEC PERIOD

CASE NO.	MAGNITUDE	DISTANCE (KM)	MU	SIGMA	SIGMA MU	SIGMA SIGMA
1	5.00	1	0.27334	0.66967	0.51247	0.10000
2	5.00	1	0.26227	0.66967	0.50386	0.10000
3	5.00	5	0.10524	0.66967	0.20000	0.10000
4	5.00	5	0.11524	0.66967	0.20000	0.10000
5	5.80	10	0.17942	0.61967	0.22441	0.10000
6	5.80	20	0.14208	0.61967	0.28452	0.10000
7	6.50	1	0.79034	0.57665	0.41582	0.10000
8	6.50	1	0.87456	0.57665	0.55378	0.10000
9	6.50	1	0.81287	0.57665	0.49375	0.10000
10	6.50	5	0.75019	0.57665	0.47093	0.10000
11	6.50	5	0.53348	0.57665	0.38946	0.10000
12	6.50	50	0.05189	0.57665	0.30028	0.10000
13	6.50	50	0.05419	0.57665	0.26218	0.10000
14	7.00	10	0.46251	0.54654	0.37293	0.10000
15	7.50	50	0.09772	0.54009	0.38246	0.10000
16	7.50	50	0.11191	0.54009	0.39768	0.10000
17	5.00	1	0.12290	0.66967	0.20000	0.10000
18	5.80	5	0.29680	0.61967	0.28173	0.10000
19	5.80	5	0.17682	0.61967	0.30078	0.10000
20	5.00	10	0.10616	0.66967	0.34157	0.10000
21	5.00	10	0.14322	0.66967	0.40097	0.10000
22	5.00	50	0.01209	0.66967	0.24420	0.10000
23	5.00	50	0.01310	0.66967	0.24568	0.10000
24	5.00	160	0.00143	0.66967	0.48470	0.10000
25	5.80	1	0.51495	0.61967	0.44929	0.10000
26	5.80	5	0.47605	0.61967	0.43665	0.10000
27	5.80	5	0.28721	0.61967	0.36107	0.10000
28	5.80	10	0.21673	0.61967	0.30052	0.10000
29	5.80	10	0.31551	0.61967	0.39188	0.10000
30	5.80	10	0.16647	0.61967	0.32546	0.10000
31	5.80	50	0.02405	0.61967	0.40117	0.10000
32	5.80	50	0.02509	0.61967	0.45991	0.10000
33	6.50	5	0.59017	0.57665	0.38351	0.10000
34	6.50	10	0.37351	0.57665	0.34577	0.10000
35	6.50	10	0.59127	0.57665	0.46083	0.10000
36	6.50	10	0.32752	0.57665	0.32565	0.10000
37	6.50	20	0.18310	0.57665	0.30784	0.10000
38	6.50	20	0.25242	0.57665	0.35936	0.10000
39	6.50	20	0.15634	0.57665	0.27577	0.10000
40	6.50	100	0.01908	0.57665	0.41850	0.10000
41	6.50	160	0.00775	0.57665	0.46690	0.10000
42	7.00	1	0.89674	0.54654	0.40089	0.10000
43	7.00	10	0.71549	0.54654	0.43065	0.10000
44	7.00	10	0.40556	0.54654	0.34398	0.10000
45	7.00	50	0.07534	0.54654	0.33072	0.10000
46	7.00	50	0.08630	0.54654	0.33524	0.10000
47	7.50	1	1.00818	0.54009	0.47314	0.10000
48	5.00	10	0.54374	0.54009	0.44256	0.10000
49	5.00	10	0.81113	0.54009	0.52174	0.10000
50	8.00	50	0.11757	0.54009	0.48252	0.10000
51	8.00	160	0.02191	0.54009	0.50496	0.10000

TABLE F2-4
D. M. BOORE: HORIZONTAL POINT ESTIMATES
SPECTRAL ACCELERATION AT 0.20 SEC PERIOD

CASE NO.	MAGNITUDE	DISTANCE (KM)	MU	SIGMA	SIGMA MU	SIGMA SIGMA
1	5.00	1	0.21108	0.71148	0.47764	0.10000
2	5.00	1	0.20419	0.71148	0.47402	0.10000
3	5.00	5	0.08710	0.71148	0.20000	0.10000
4	5.00	5	0.09458	0.71148	0.20000	0.10000
5	5.80	10	0.16670	0.66268	0.21601	0.10000
6	5.80	20	0.13622	0.66268	0.28724	0.10000
7	6.50	1	0.70273	0.62098	0.44388	0.10000
8	6.50	1	0.77052	0.62098	0.55652	0.10000
9	6.50	1	0.72490	0.62098	0.51070	0.10000
10	6.50	5	0.67225	0.62098	0.47485	0.10000
11	6.50	5	0.49154	0.62098	0.38296	0.10000
12	6.50	50	0.05644	0.62098	0.31300	0.10000
13	6.50	50	0.05941	0.62098	0.23931	0.10000
14	7.00	10	0.44347	0.59199	0.38485	0.10000
15	7.50	50	0.11227	0.58586	0.40840	0.10000
16	7.50	50	0.12879	0.58586	0.40367	0.10000
17	5.00	1	0.09971	0.71148	0.20000	0.10000
18	5.80	5	0.25726	0.66268	0.29793	0.10000
19	5.80	5	0.16651	0.66268	0.26740	0.10000
20	5.00	10	0.08817	0.71148	0.26949	0.10000
21	5.00	10	0.11673	0.71148	0.35655	0.10000
22	5.00	50	0.01211	0.71148	0.22459	0.10000
23	5.00	50	0.01315	0.71148	0.24498	0.10000
24	5.00	160	0.00187	0.71148	0.49051	0.10000
25	5.80	1	0.43814	0.66268	0.43825	0.10000
26	5.80	5	0.40232	0.66268	0.42095	0.10000
27	5.80	5	0.25602	0.66268	0.31384	0.10000
28	5.80	10	0.19673	0.66268	0.29418	0.10000
29	5.80	10	0.28038	0.66268	0.37636	0.10000
30	5.80	10	0.15672	0.66268	0.26049	0.10000
31	5.80	50	0.02516	0.66268	0.42483	0.10000
32	5.80	50	0.02794	0.66268	0.36462	0.10000
33	6.50	5	0.53378	0.62098	0.39471	0.10000
34	6.50	10	0.34289	0.62098	0.33411	0.10000
35	6.50	10	0.52469	0.62098	0.43798	0.10000
36	6.50	10	0.31252	0.62098	0.32013	0.10000
37	6.50	20	0.17702	0.62098	0.29717	0.10000
38	6.50	20	0.25202	0.62098	0.37550	0.10000
39	6.50	20	0.15930	0.62098	0.25913	0.10000
40	6.50	100	0.02329	0.62098	0.41560	0.10000
41	6.50	160	0.01041	0.62098	0.47419	0.10000
42	7.00	1	0.80724	0.59199	0.42424	0.10000
43	7.00	10	0.66441	0.59199	0.42823	0.10000
44	7.00	10	0.39809	0.59199	0.34559	0.10000
45	7.00	50	0.08503	0.59199	0.35492	0.10000
46	7.00	50	0.09664	0.59199	0.33360	0.10000
47	7.50	1	0.95971	0.58586	0.51975	0.10000
48	5.00	10	0.54633	0.58586	0.47689	0.10000
49	5.00	10	0.77038	0.58586	0.51445	0.10000
50	8.00	50	0.13491	0.58586	0.48046	0.10000
51	8.00	160	0.02927	0.58586	0.55333	0.10000

TABLE F2-5
D. M. BOORE: HORIZONTAL POINT ESTIMATES
SPECTRAL ACCELERATION AT 0.50 SEC PERIOD

CASE NO.	MAGNITUDE	DISTANCE (KM)	MU	SIGMA	SIGMA MU	SIGMA SIGMA
1	5.00	1	0.11369	0.77480	0.29740	0.10000
2	5.00	1	0.11098	0.77480	0.30212	0.10000
3	5.00	5	0.04705	0.77480	0.20000	0.10000
4	5.00	5	0.05393	0.77480	0.31695	0.10000
5	5.80	10	0.10305	0.72795	0.20315	0.10000
6	5.80	20	0.08760	0.72795	0.24544	0.10000
7	6.50	1	0.51137	0.68803	0.27261	0.10000
8	6.50	1	0.55262	0.68803	0.36393	0.10000
9	6.50	1	0.51806	0.68803	0.32801	0.10000
10	6.50	5	0.48170	0.68803	0.30903	0.10000
11	6.50	5	0.33849	0.68803	0.29283	0.10000
12	6.50	50	0.04628	0.68803	0.25221	0.10000
13	6.50	50	0.04998	0.68803	0.24380	0.10000
14	7.00	10	0.34437	0.66034	0.32042	0.10000
15	7.50	50	0.10937	0.65440	0.27702	0.10000
16	7.50	50	0.12483	0.65440	0.28724	0.10000
17	5.00	1	0.05624	0.77480	0.28491	0.10000
18	5.80	5	0.17256	0.72795	0.20068	0.10000
19	5.80	5	0.09944	0.72795	0.25597	0.10000
20	5.00	10	0.04571	0.77480	0.20272	0.10000
21	5.00	10	0.06124	0.77480	0.27953	0.10000
22	5.00	50	0.00769	0.77480	0.22496	0.10000
23	5.00	50	0.00832	0.77480	0.23430	0.10000
24	5.00	160	0.00176	0.77480	0.45601	0.10000
25	5.80	1	0.28031	0.72795	0.29396	0.10000
26	5.80	5	0.26005	0.72795	0.31403	0.10000
27	5.80	5	0.15636	0.72795	0.26923	0.10000
28	5.80	10	0.12523	0.72795	0.26526	0.10000
29	5.80	10	0.18230	0.72795	0.32405	0.10000
30	5.80	10	0.09464	0.72795	0.28288	0.10000
31	5.80	50	0.01843	0.72795	0.42581	0.10000
32	5.80	50	0.01921	0.72795	0.51552	0.10000
33	6.50	5	0.37870	0.68803	0.31405	0.10000
34	6.50	10	0.24897	0.68803	0.32784	0.10000
35	6.50	10	0.38882	0.68803	0.35972	0.10000
36	6.50	10	0.21620	0.68803	0.28905	0.10000
37	6.50	20	0.12901	0.68803	0.25969	0.10000
38	6.50	20	0.18231	0.68803	0.33941	0.10000
39	6.50	20	0.11735	0.68803	0.22388	0.10000
40	6.50	100	0.02328	0.68803	0.34779	0.10000
41	6.50	160	0.01215	0.68803	0.41708	0.10000
42	7.00	1	0.65061	0.66034	0.25222	0.10000
43	7.00	10	0.55030	0.66034	0.30902	0.10000
44	7.00	10	0.29977	0.66034	0.25931	0.10000
45	7.00	50	0.07516	0.66034	0.26618	0.10000
46	7.00	50	0.08635	0.66034	0.30425	0.10000
47	7.50	1	0.80395	0.65440	0.27804	0.10000
48	5.00	10	0.44274	0.65440	0.30808	0.10000
49	5.00	10	0.67156	0.65440	0.37559	0.10000
50	8.00	50	0.14398	0.65440	0.27050	0.10000
51	8.00	160	0.04367	0.65440	0.41657	0.10000

TABLE F2-6
D. M. BOORE: HORIZONTAL POINT ESTIMATES
SPECTRAL ACCELERATION AT 1.00 SEC PERIOD

CASE NO.	MAGNITUDE	DISTANCE (KM)	MU	SIGMA	SIGMA MU	SIGMA SIGMA
1	5.00	1	0.05077	0.82272	0.20777	0.10000
2	5.00	1	0.04829	0.82272	0.25406	0.10000
3	5.00	5	0.02078	0.82272	0.25317	0.10000
4	5.00	5	0.02418	0.82272	0.49105	0.10000
5	5.80	10	0.05295	0.77866	0.20000	0.10000
6	5.80	20	0.04446	0.77866	0.23070	0.10000
7	6.50	1	0.30479	0.74108	0.20000	0.10000
8	6.50	1	0.31933	0.74108	0.30317	0.10000
9	6.50	1	0.29622	0.74108	0.29291	0.10000
10	6.50	5	0.28605	0.74108	0.27666	0.10000
11	6.50	5	0.18743	0.74108	0.33632	0.10000
12	6.50	50	0.03051	0.74108	0.27067	0.10000
13	6.50	50	0.03068	0.74108	0.30220	0.10000
14	7.00	10	0.21027	0.71497	0.26106	0.10000
15	7.50	50	0.07767	0.70910	0.23239	0.10000
16	7.50	50	0.08638	0.70910	0.26409	0.10000
17	5.00	1	0.02589	0.82272	0.44020	0.10000
18	5.80	5	0.08945	0.77866	0.36661	0.10000
19	5.80	5	0.04973	0.77866	0.34652	0.10000
20	5.00	10	0.01977	0.82272	0.20000	0.10000
21	5.00	10	0.02570	0.82272	0.23830	0.10000
22	5.00	50	0.00375	0.82272	0.21840	0.10000
23	5.00	50	0.00393	0.82272	0.24368	0.10000
24	5.00	160	0.00105	0.82272	0.42656	0.10000
25	5.80	1	0.14475	0.77866	0.28871	0.10000
26	5.80	5	0.13368	0.77866	0.31701	0.10000
27	5.80	5	0.07648	0.77866	0.34486	0.10000
28	5.80	10	0.06291	0.77866	0.24631	0.10000
29	5.80	10	0.09209	0.77866	0.31278	0.10000
30	5.80	10	0.04838	0.77866	0.30594	0.10000
31	5.80	50	0.01060	0.77866	0.43187	0.10000
32	5.80	50	0.01119	0.77866	0.48362	0.10000
33	6.50	5	0.21308	0.74108	0.26923	0.10000
34	6.50	10	0.14595	0.74108	0.30634	0.10000
35	6.50	10	0.22857	0.74108	0.33093	0.10000
36	6.50	10	0.12285	0.74108	0.31132	0.10000
37	6.50	20	0.07628	0.74108	0.25422	0.10000
38	6.50	20	0.10393	0.74108	0.34845	0.10000
39	6.50	20	0.06771	0.74108	0.26978	0.10000
40	6.50	100	0.01644	0.74108	0.29750	0.10000
41	6.50	160	0.00922	0.74108	0.40024	0.10000
42	7.00	1	0.39166	0.71497	0.25673	0.10000
43	7.00	10	0.34312	0.71497	0.30801	0.10000
44	7.00	10	0.18397	0.71497	0.29585	0.10000
45	7.00	50	0.05090	0.71497	0.29206	0.10000
46	7.00	50	0.05535	0.71497	0.34534	0.10000
47	7.50	1	0.52693	0.70910	0.34228	0.10000
48	5.00	10	0.29289	0.70910	0.27779	0.10000
49	5.00	10	0.45647	0.70910	0.44204	0.10000
50	8.00	50	0.11008	0.70910	0.20583	0.10000
51	8.00	160	0.04045	0.70910	0.34348	0.10000

TABLE F2-7
D. M. BOORE: HORIZONTAL POINT ESTIMATES
SPECTRAL ACCELERATION AT 2.00 SEC PERIOD

CASE NO.	MAGNITUDE	DISTANCE (KM)	MU	SIGMA	SIGMA MU	SIGMA SIGMA
1	5.00	1	0.01800	0.88358	0.31131	0.10000
2	5.00	1	0.01578	0.88358	0.43214	0.10000
3	5.00	5	0.00922	0.88358	0.44283	0.10000
4	5.00	5	0.00937	0.88358	0.65892	0.10000
5	5.80	10	0.02169	0.84293	0.34180	0.10000
6	5.80	20	0.01653	0.84293	0.36987	0.10000
7	6.50	1	0.12981	0.80831	0.23913	0.10000
8	6.50	1	0.12452	0.80831	0.24498	0.10000
9	6.50	1	0.11316	0.80831	0.20000	0.10000
10	6.50	5	0.10301	0.80831	0.22319	0.10000
11	6.50	5	0.07882	0.80831	0.21401	0.10000
12	6.50	50	0.01476	0.80831	0.42250	0.10000
13	6.50	50	0.01379	0.80831	0.46915	0.10000
14	7.00	10	0.09729	0.78426	0.23511	0.10000
15	7.50	50	0.04089	0.77857	0.50374	0.10000
16	7.50	50	0.04152	0.77857	0.55522	0.10000
17	5.00	1	0.01080	0.88358	0.50814	0.10000
18	5.80	5	0.03732	0.84293	0.39597	0.10000
19	5.80	5	0.02174	0.84293	0.41406	0.10000
20	5.00	10	0.00821	0.88358	0.25718	0.10000
21	5.00	10	0.00917	0.88358	0.45640	0.10000
22	5.00	50	0.00176	0.88358	0.42797	0.10000
23	5.00	50	0.00170	0.88358	0.50730	0.10000
24	5.00	160	0.00055	0.88358	0.60523	0.10000
25	5.80	1	0.05417	0.84293	0.24750	0.10000
26	5.80	5	0.04635	0.84293	0.32645	0.10000
27	5.80	5	0.03136	0.84293	0.31191	0.10000
28	5.80	10	0.02443	0.84293	0.28419	0.10000
29	5.80	10	0.03097	0.84293	0.32879	0.10000
30	5.80	10	0.01929	0.84293	0.37921	0.10000
31	5.80	50	0.00462	0.84293	0.70473	0.10000
32	5.80	50	0.00447	0.84293	0.72100	0.10000
33	6.50	5	0.09550	0.80831	0.21019	0.10000
34	6.50	10	0.06416	0.80831	0.21903	0.10000
35	6.50	10	0.08304	0.80831	0.21251	0.10000
36	6.50	10	0.05115	0.80831	0.26189	0.10000
37	6.50	20	0.03709	0.80831	0.24300	0.10000
38	6.50	20	0.04433	0.80831	0.27320	0.10000
39	6.50	20	0.02917	0.80831	0.32362	0.10000
40	6.50	100	0.00889	0.80831	0.36221	0.10000
41	6.50	160	0.00507	0.80831	0.60176	0.10000
42	7.00	1	0.18094	0.78426	0.20000	0.10000
43	7.00	10	0.12949	0.78426	0.25827	0.10000
44	7.00	10	0.08046	0.78426	0.27746	0.10000
45	7.00	50	0.02712	0.78426	0.38658	0.10000
46	7.00	50	0.02702	0.78426	0.43312	0.10000
47	7.50	1	0.22024	0.77857	0.21250	0.10000
48	5.00	10	0.13195	0.77857	0.36065	0.10000
49	5.00	10	0.16590	0.77857	0.44999	0.10000
50	8.00	50	0.06575	0.77857	0.28822	0.10000
51	8.00	160	0.02875	0.77857	0.49552	0.10000

TABLE F2-8
D. M. BOORE: HORIZONTAL POINT ESTIMATES
SPECTRAL ACCELERATION AT 3.33 SEC PERIOD

CASE NO.	MAGNITUDE	DISTANCE (KM)	MU	SIGMA	SIGMA MU	SIGMA SIGMA
1	5.00	1	0.00811	0.86063	0.53592	0.10000
2	5.00	1	0.00644	0.86063	0.67803	0.10000
3	5.00	5	0.00301	0.86063	0.31872	0.10000
4	5.00	5	0.00261	0.86063	0.49998	0.10000
5	5.80	10	0.01085	0.79229	0.46462	0.10000
6	5.80	20	0.00670	0.79229	0.47766	0.10000
7	6.50	1	0.08046	0.73402	0.31913	0.10000
8	6.50	1	0.07180	0.73402	0.31592	0.10000
9	6.50	1	0.06592	0.73402	0.32658	0.10000
10	6.50	5	0.05763	0.73402	0.35986	0.10000
11	6.50	5	0.04756	0.73402	0.39059	0.10000
12	6.50	50	0.00876	0.73402	0.61106	0.10000
13	6.50	50	0.00724	0.73402	0.66328	0.10000
14	7.00	10	0.06135	0.69350	0.40387	0.10000
15	7.50	50	0.03049	0.68354	0.49215	0.10000
16	7.50	50	0.02611	0.68354	0.61248	0.10000
17	5.00	1	0.00334	0.86063	0.33745	0.10000
18	5.80	5	0.01541	0.79229	0.46358	0.10000
19	5.80	5	0.00921	0.79229	0.51723	0.10000
20	5.00	10	0.00325	0.86063	0.33105	0.10000
21	5.00	10	0.00318	0.86063	0.53491	0.10000
22	5.00	50	0.00060	0.86063	0.20000	0.10000
23	5.00	50	0.00054	0.86063	0.27373	0.10000
24	5.00	160	0.00018	0.86063	0.33072	0.10000
25	5.80	1	0.02971	0.79229	0.44377	0.10000
26	5.80	5	0.02229	0.79229	0.50500	0.10000
27	5.80	5	0.01605	0.79229	0.47797	0.10000
28	5.80	10	0.01311	0.79229	0.46031	0.10000
29	5.80	10	0.01284	0.79229	0.51970	0.10000
30	5.80	10	0.00873	0.79229	0.63843	0.10000
31	5.80	50	0.00222	0.79229	0.73800	0.10000
32	5.80	50	0.00188	0.79229	0.79835	0.10000
33	6.50	5	0.06118	0.73402	0.32251	0.10000
34	6.50	10	0.03893	0.73402	0.38926	0.10000
35	6.50	10	0.03958	0.73402	0.35858	0.10000
36	6.50	10	0.02773	0.73402	0.52384	0.10000
37	6.50	20	0.02117	0.73402	0.43779	0.10000
38	6.50	20	0.02083	0.73402	0.46556	0.10000
39	6.50	20	0.01567	0.73402	0.56064	0.10000
40	6.50	100	0.00454	0.73402	0.57117	0.10000
41	6.50	160	0.00313	0.73402	0.64451	0.10000
42	7.00	1	0.12015	0.69350	0.30377	0.10000
43	7.00	10	0.06358	0.69350	0.33234	0.10000
44	7.00	10	0.04587	0.69350	0.49980	0.10000
45	7.00	50	0.01789	0.69350	0.50976	0.10000
46	7.00	50	0.01568	0.69350	0.56556	0.10000
47	7.50	1	0.15112	0.68354	0.30267	0.10000
48	5.00	10	0.08531	0.68354	0.49638	0.10000
49	5.00	10	0.08400	0.68354	0.45359	0.10000
50	8.00	50	0.05201	0.68354	0.28424	0.10000
51	8.00	160	0.02336	0.68354	0.36676	0.10000

TABLE F2-9
D. M. BOORE: HORIZONTAL POINT ESTIMATES
PEAK GROUND VELOCITY

CASE NO.	MAGNITUDE	DISTANCE (KM)	MU	SIGMA	SIGMA MU	SIGMA SIGMA
1	5.00	1	5.63744	0.63355	0.30714	0.10000
2	5.00	1	5.34570	0.63355	0.32694	0.10000
3	5.00	5	2.53868	0.63355	0.30562	0.10000
4	5.00	5	3.16611	0.63355	0.51962	0.10000
5	5.80	10	5.54542	0.58682	0.23247	0.10000
6	5.80	20	4.49709	0.58682	0.26603	0.10000
7	6.50	1	32.52051	0.54723	0.22786	0.10000
8	6.50	1	33.15668	0.54723	0.31239	0.10000
9	6.50	1	30.08151	0.54723	0.26110	0.10000
10	6.50	5	28.69017	0.54723	0.20000	0.10000
11	6.50	5	18.69324	0.54723	0.20000	0.10000
12	6.50	50	2.62938	0.54723	0.34200	0.10000
13	6.50	50	2.60177	0.54723	0.29430	0.10000
14	7.00	10	22.77278	0.51988	0.22215	0.10000
15	7.50	50	8.36202	0.50040	0.37089	0.10000
16	7.50	50	8.93632	0.50040	0.37049	0.10000
17	5.00	1	3.33298	0.63355	0.44472	0.10000
18	5.80	5	10.54929	0.58682	0.36606	0.10000
19	5.80	5	5.37063	0.58682	0.34252	0.10000
20	5.00	10	2.01408	0.63355	0.20000	0.10000
21	5.00	10	2.68060	0.63355	0.22924	0.10000
22	5.00	50	0.29354	0.63355	0.21760	0.10000
23	5.00	50	0.30720	0.63355	0.26757	0.10000
24	5.00	160	0.06052	0.63355	0.46622	0.10000
25	5.80	1	15.07693	0.58682	0.28742	0.10000
26	5.80	5	13.71370	0.58682	0.25911	0.10000
27	5.80	5	7.81970	0.58682	0.20000	0.10000
28	5.80	10	6.27613	0.58682	0.25295	0.10000
29	5.80	10	9.12798	0.58682	0.25511	0.10000
30	5.80	10	4.56310	0.58682	0.20977	0.10000
31	5.80	50	0.82666	0.58682	0.46172	0.10000
32	5.80	50	0.85114	0.58682	0.45643	0.10000
33	6.50	5	22.01258	0.54723	0.20000	0.10000
34	6.50	10	14.51244	0.54723	0.24682	0.10000
35	6.50	10	21.57574	0.54723	0.20000	0.10000
36	6.50	10	11.62623	0.54723	0.20000	0.10000
37	6.50	20	7.52492	0.54723	0.26537	0.10000
38	6.50	20	10.09189	0.54723	0.26984	0.10000
39	6.50	20	6.24234	0.54723	0.22083	0.10000
40	6.50	100	1.38147	0.54723	0.40595	0.10000
41	6.50	160	0.66802	0.54723	0.65143	0.10000
42	7.00	1	46.70370	0.51988	0.23657	0.10000
43	7.00	10	36.13906	0.51988	0.28411	0.10000
44	7.00	10	18.52680	0.51988	0.24293	0.10000
45	7.00	50	4.98080	0.51988	0.32964	0.10000
46	7.00	50	5.24308	0.51988	0.31889	0.10000
47	7.50	1	65.92093	0.50040	0.40169	0.10000
48	5.00	10	33.51372	0.50040	0.34425	0.10000
49	5.00	10	49.55303	0.50040	0.54845	0.10000
50	8.00	50	14.51932	0.50040	0.37427	0.10000
51	8.00	160	5.60324	0.50040	0.64135	0.10000

TABLE F2-10
D. M. BOORE: VERTICAL POINT ESTIMATES
PEAK GROUND ACCELERATION

CASE NO.	MAGNITUDE	DISTANCE (KM)	MU	SIGMA	SIGMA MU	SIGMA SIGMA
1	5.00	1	0.11402	0.71508	0.37006	0.10000
2	5.00	1	0.09926	0.71508	0.47342	0.10000
3	5.00	5	0.03255	0.71508	0.20000	0.10000
4	5.00	5	0.03130	0.71508	0.22040	0.10000
5	5.80	10	0.05920	0.66220	0.21872	0.10000
6	5.80	20	0.04497	0.66220	0.34656	0.10000
7	6.50	1	0.34390	0.59419	0.21624	0.10000
8	6.50	1	0.34347	0.59419	0.20000	0.10000
9	6.50	1	0.33136	0.59419	0.20865	0.10000
10	6.50	5	0.28975	0.59419	0.25501	0.10000
11	6.50	5	0.21902	0.59419	0.20000	0.10000
12	6.50	50	0.01667	0.59419	0.33062	0.10000
13	6.50	50	0.01840	0.59419	0.26415	0.10000
14	7.00	10	0.18832	0.56181	0.20000	0.10000
15	7.50	50	0.03541	0.55559	0.21494	0.10000
16	7.50	50	0.03952	0.55559	0.28440	0.10000
17	5.00	1	0.03698	0.71508	0.20000	0.10000
18	5.80	5	0.09011	0.66220	0.29901	0.10000
19	5.80	5	0.05658	0.66220	0.28630	0.10000
20	5.00	10	0.03731	0.71508	0.20000	0.10000
21	5.00	10	0.04424	0.71508	0.33679	0.10000
22	5.00	50	0.00353	0.71508	0.21817	0.10000
23	5.00	50	0.00353	0.71508	0.20000	0.10000
24	5.00	160	0.00050	0.71508	0.39837	0.10000
25	5.80	1	0.20276	0.66220	0.34989	0.10000
26	5.80	5	0.16856	0.66220	0.35557	0.10000
27	5.80	5	0.10892	0.66220	0.24307	0.10000
28	5.80	10	0.07677	0.66220	0.21655	0.10000
29	5.80	10	0.10838	0.66220	0.31092	0.10000
30	5.80	10	0.06192	0.66220	0.22077	0.10000
31	5.80	50	0.00729	0.66220	0.51975	0.10000
32	5.80	50	0.00780	0.66220	0.42894	0.10000
33	6.50	5	0.24964	0.59419	0.20000	0.10000
34	6.50	10	0.14700	0.59419	0.20000	0.10000
35	6.50	10	0.23939	0.59419	0.32624	0.10000
36	6.50	10	0.12830	0.59419	0.20000	0.10000
37	6.50	20	0.06659	0.59419	0.20883	0.10000
38	6.50	20	0.10498	0.59419	0.36544	0.10000
39	6.50	20	0.05674	0.59419	0.20000	0.10000
40	6.50	100	0.00616	0.59419	0.37455	0.10000
41	6.50	160	0.00252	0.59419	0.52136	0.10000
42	7.00	1	0.40253	0.56181	0.20000	0.10000
43	7.00	10	0.29257	0.56181	0.29839	0.10000
44	7.00	10	0.16286	0.56181	0.20000	0.10000
45	7.00	50	0.02458	0.56181	0.22789	0.10000
46	7.00	50	0.02797	0.56181	0.30719	0.10000
47	7.50	1	0.52422	0.55559	0.26848	0.10000
48	5.00	10	0.23518	0.55559	0.20000	0.10000
49	5.00	10	0.35553	0.55559	0.32731	0.10000
50	8.00	50	0.05090	0.55559	0.21890	0.10000
51	8.00	160	0.01006	0.55559	0.30579	0.10000

TABLE F2-11
D. M. BOORE: VERTICAL POINT ESTIMATES
SPECTRAL ACCELERATION AT 0.05 SEC PERIOD

CASE NO.	MAGNITUDE	DISTANCE (KM)	MU	SIGMA	SIGMA MU	SIGMA SIGMA
1	5.00	1	0.29134	0.74602	0.28753	0.10000
2	5.00	1	0.25322	0.74602	0.37902	0.10000
3	5.00	5	0.07582	0.74602	0.21405	0.10000
4	5.00	5	0.07321	0.74602	0.20469	0.10000
5	5.80	10	0.12726	0.69468	0.37495	0.10000
6	5.80	20	0.09167	0.69468	0.30962	0.10000
7	6.50	1	0.81804	0.63035	0.39655	0.10000
8	6.50	1	0.81003	0.63035	0.27898	0.10000
9	6.50	1	0.78597	0.63035	0.27443	0.10000
10	6.50	5	0.68034	0.63035	0.29323	0.10000
11	6.50	5	0.49885	0.63035	0.33317	0.10000
12	6.50	50	0.02805	0.63035	0.41588	0.10000
13	6.50	50	0.03150	0.63035	0.31111	0.10000
14	7.00	10	0.41089	0.59908	0.32795	0.10000
15	7.50	50	0.05987	0.59370	0.26752	0.10000
16	7.50	50	0.06764	0.59370	0.26199	0.10000
17	5.00	1	0.08702	0.74602	0.20739	0.10000
18	5.80	5	0.19958	0.69468	0.44204	0.10000
19	5.80	5	0.12293	0.69468	0.34736	0.10000
20	5.00	10	0.08845	0.74602	0.20458	0.10000
21	5.00	10	0.10650	0.74602	0.30122	0.10000
22	5.00	50	0.00642	0.74602	0.29402	0.10000
23	5.00	50	0.00647	0.74602	0.23436	0.10000
24	5.00	160	0.00062	0.74602	0.46907	0.10000
25	5.80	1	0.48148	0.69468	0.49721	0.10000
26	5.80	5	0.38546	0.69468	0.39322	0.10000
27	5.80	5	0.24896	0.69468	0.34065	0.10000
28	5.80	10	0.16954	0.69468	0.38298	0.10000
29	5.80	10	0.23616	0.69468	0.36419	0.10000
30	5.80	10	0.13347	0.69468	0.35498	0.10000
31	5.80	50	0.01265	0.69468	0.58858	0.10000
32	5.80	50	0.01350	0.69468	0.53831	0.10000
33	6.50	5	0.57668	0.63035	0.33993	0.10000
34	6.50	10	0.32305	0.63035	0.33202	0.10000
35	6.50	10	0.53096	0.63035	0.42008	0.10000
36	6.50	10	0.28207	0.63035	0.29023	0.10000
37	6.50	20	0.13578	0.63035	0.31149	0.10000
38	6.50	20	0.21717	0.63035	0.41757	0.10000
39	6.50	20	0.11525	0.63035	0.28768	0.10000
40	6.50	100	0.00851	0.63035	0.43063	0.10000
41	6.50	160	0.00326	0.63035	0.53770	0.10000
42	7.00	1	0.95736	0.59908	0.35616	0.10000
43	7.00	10	0.64958	0.59908	0.39906	0.10000
44	7.00	10	0.35648	0.59908	0.26961	0.10000
45	7.00	50	0.04229	0.59908	0.30033	0.10000
46	7.00	50	0.04836	0.59908	0.30195	0.10000
47	7.50	1	1.24159	0.59370	0.32250	0.10000
48	5.00	10	0.51714	0.59370	0.32562	0.10000
49	5.00	10	0.79402	0.59370	0.42984	0.10000
50	8.00	50	0.08536	0.59370	0.24836	0.10000
51	8.00	160	0.01223	0.59370	0.35465	0.10000

TABLE F2-12
D. M. BOORE: VERTICAL POINT ESTIMATES
SPECTRAL ACCELERATION AT 0.10 SEC PERIOD

CASE NO.	MAGNITUDE	DISTANCE (KM)	MU	SIGMA	SIGMA MU	SIGMA SIGMA
1	5.00	1	0.24204	0.74602	0.39650	0.10000
2	5.00	1	0.22229	0.74602	0.44014	0.10000
3	5.00	5	0.06757	0.74602	0.20000	0.10000
4	5.00	5	0.06878	0.74602	0.20000	0.10000
5	5.80	10	0.12732	0.69468	0.20000	0.10000
6	5.80	20	0.09787	0.69468	0.36150	0.10000
7	6.50	1	0.78319	0.63035	0.21590	0.10000
8	6.50	1	0.81799	0.63035	0.20000	0.10000
9	6.50	1	0.79310	0.63035	0.20000	0.10000
10	6.50	5	0.66349	0.63035	0.23795	0.10000
11	6.50	5	0.50915	0.63035	0.20000	0.10000
12	6.50	50	0.03142	0.63035	0.30398	0.10000
13	6.50	50	0.03644	0.63035	0.27455	0.10000
14	7.00	10	0.40565	0.59908	0.20000	0.10000
15	7.50	50	0.06708	0.59370	0.22253	0.10000
16	7.50	50	0.07794	0.59370	0.27280	0.10000
17	5.00	1	0.07703	0.74602	0.20000	0.10000
18	5.80	5	0.20709	0.69468	0.27043	0.10000
19	5.80	5	0.12848	0.69468	0.25003	0.10000
20	5.00	10	0.07747	0.74602	0.20000	0.10000
21	5.00	10	0.09727	0.74602	0.31486	0.10000
22	5.00	50	0.00664	0.74602	0.20000	0.10000
23	5.00	50	0.00706	0.74602	0.20000	0.10000
24	5.00	160	0.00065	0.74602	0.43114	0.10000
25	5.80	1	0.45669	0.69468	0.30699	0.10000
26	5.80	5	0.38285	0.69468	0.32634	0.10000
27	5.80	5	0.24534	0.69468	0.23793	0.10000
28	5.80	10	0.16270	0.69468	0.22685	0.10000
29	5.80	10	0.24229	0.69468	0.32879	0.10000
30	5.80	10	0.13671	0.69468	0.22620	0.10000
31	5.80	50	0.01415	0.69468	0.42456	0.10000
32	5.80	50	0.01522	0.69468	0.47612	0.10000
33	6.50	5	0.55235	0.63035	0.20000	0.10000
34	6.50	10	0.32074	0.63035	0.20000	0.10000
35	6.50	10	0.53809	0.63035	0.34712	0.10000
36	6.50	10	0.29370	0.63035	0.20000	0.10000
37	6.50	20	0.13739	0.63035	0.20000	0.10000
38	6.50	20	0.22830	0.63035	0.38694	0.10000
39	6.50	20	0.12456	0.63035	0.20000	0.10000
40	6.50	100	0.00975	0.63035	0.39293	0.10000
41	6.50	160	0.00355	0.63035	0.42947	0.10000
42	7.00	1	0.92313	0.59908	0.20000	0.10000
43	7.00	10	0.66256	0.59908	0.31526	0.10000
44	7.00	10	0.37061	0.59908	0.20000	0.10000
45	7.00	50	0.04658	0.59908	0.21996	0.10000
46	7.00	50	0.05555	0.59908	0.29108	0.10000
47	7.50	1	1.20178	0.59370	0.24330	0.10000
48	5.00	10	0.51393	0.59370	0.20000	0.10000
49	5.00	10	0.82072	0.59370	0.33449	0.10000
50	8.00	50	0.09485	0.59370	0.25124	0.10000
51	8.00	160	0.01235	0.59370	0.35178	0.10000

TABLE F2-13
D. M. BOORE: VERTICAL POINT ESTIMATES
SPECTRAL ACCELERATION AT 0.20 SEC PERIOD

CASE NO.	MAGNITUDE	DISTANCE (KM)	MU	SIGMA	SIGMA MU	SIGMA SIGMA
1	5.00	1	0.12462	0.70713	0.50178	0.10000
2	5.00	1	0.12102	0.70713	0.49133	0.10000
3	5.00	5	0.03834	0.70713	0.20000	0.10000
4	5.00	5	0.04098	0.70713	0.20546	0.10000
5	5.80	10	0.08163	0.67134	0.20000	0.10000
6	5.80	20	0.06872	0.67134	0.46928	0.10000
7	6.50	1	0.47259	0.62063	0.20000	0.10000
8	6.50	1	0.49409	0.62063	0.20000	0.10000
9	6.50	1	0.48039	0.62063	0.21650	0.10000
10	6.50	5	0.42890	0.62063	0.30308	0.10000
11	6.50	5	0.32279	0.62063	0.23173	0.10000
12	6.50	50	0.02641	0.62063	0.36626	0.10000
13	6.50	50	0.03160	0.62063	0.39398	0.10000
14	7.00	10	0.27126	0.59908	0.22352	0.10000
15	7.50	50	0.05854	0.59370	0.29923	0.10000
16	7.50	50	0.06991	0.59370	0.33439	0.10000
17	5.00	1	0.04315	0.70713	0.20297	0.10000
18	5.80	5	0.13045	0.67134	0.24661	0.10000
19	5.80	5	0.08441	0.67134	0.30033	0.10000
20	5.00	10	0.04321	0.70713	0.23352	0.10000
21	5.00	10	0.05605	0.70713	0.34299	0.10000
22	5.00	50	0.00511	0.70713	0.20000	0.10000
23	5.00	50	0.00567	0.70713	0.20000	0.10000
24	5.00	160	0.00076	0.70713	0.44620	0.10000
25	5.80	1	0.26304	0.67134	0.30578	0.10000
26	5.80	5	0.23705	0.67134	0.38285	0.10000
27	5.80	5	0.15504	0.67134	0.23895	0.10000
28	5.80	10	0.10375	0.67134	0.20000	0.10000
29	5.80	10	0.15573	0.67134	0.42351	0.10000
30	5.80	10	0.09021	0.67134	0.22914	0.10000
31	5.80	50	0.01168	0.67134	0.42079	0.10000
32	5.80	50	0.01377	0.67134	0.42668	0.10000
33	6.50	5	0.33898	0.62063	0.20000	0.10000
34	6.50	10	0.20336	0.62063	0.20000	0.10000
35	6.50	10	0.34629	0.62063	0.38900	0.10000
36	6.50	10	0.19758	0.62063	0.23290	0.10000
37	6.50	20	0.09810	0.62063	0.27505	0.10000
38	6.50	20	0.16282	0.62063	0.48862	0.10000
39	6.50	20	0.09337	0.62063	0.28711	0.10000
40	6.50	100	0.01010	0.62063	0.51508	0.10000
41	6.50	160	0.00419	0.62063	0.54226	0.10000
42	7.00	1	0.56285	0.59908	0.20000	0.10000
43	7.00	10	0.44472	0.59908	0.37081	0.10000
44	7.00	10	0.25778	0.59908	0.23960	0.10000
45	7.00	50	0.04041	0.59908	0.29684	0.10000
46	7.00	50	0.04986	0.59908	0.39269	0.10000
47	7.50	1	0.73116	0.59370	0.33005	0.10000
48	5.00	10	0.35034	0.59370	0.24886	0.10000
49	5.00	10	0.55055	0.59370	0.36432	0.10000
50	8.00	50	0.08269	0.59370	0.29710	0.10000
51	8.00	160	0.01418	0.59370	0.47609	0.10000

TABLE F2-14
D. M. BOORE: VERTICAL POINT ESTIMATES
SPECTRAL ACCELERATION AT 0.50 SEC PERIOD

CASE NO.	MAGNITUDE	DISTANCE (KM)	MU	SIGMA	SIGMA MU	SIGMA SIGMA
1	5.00	1	0.05258	0.70713	0.45198	0.10000
2	5.00	1	0.05257	0.70713	0.42459	0.10000
3	5.00	5	0.01683	0.70713	0.20000	0.10000
4	5.00	5	0.01847	0.70713	0.20248	0.10000
5	5.80	10	0.04351	0.67134	0.20000	0.10000
6	5.80	20	0.03908	0.67134	0.53219	0.10000
7	6.50	1	0.25719	0.62063	0.20000	0.10000
8	6.50	1	0.28930	0.62063	0.21224	0.10000
9	6.50	1	0.27751	0.62063	0.24661	0.10000
10	6.50	5	0.23437	0.62063	0.32056	0.10000
11	6.50	5	0.18402	0.62063	0.28224	0.10000
12	6.50	50	0.02004	0.62063	0.40333	0.10000
13	6.50	50	0.02483	0.62063	0.44688	0.10000
14	7.00	10	0.16293	0.59908	0.34780	0.10000
15	7.50	50	0.04651	0.59370	0.40640	0.10000
16	7.50	50	0.05403	0.59370	0.36499	0.10000
17	5.00	1	0.01873	0.70713	0.20491	0.10000
18	5.80	5	0.06631	0.67134	0.21042	0.10000
19	5.80	5	0.04328	0.67134	0.21776	0.10000
20	5.00	10	0.01870	0.70713	0.23803	0.10000
21	5.00	10	0.02459	0.70713	0.32468	0.10000
22	5.00	50	0.00308	0.70713	0.30020	0.10000
23	5.00	50	0.00347	0.70713	0.31842	0.10000
24	5.00	160	0.00078	0.70713	0.49342	0.10000
25	5.80	1	0.12531	0.67134	0.36386	0.10000
26	5.80	5	0.11917	0.67134	0.36776	0.10000
27	5.80	5	0.08097	0.67134	0.24144	0.10000
28	5.80	10	0.05497	0.67134	0.23886	0.10000
29	5.80	10	0.08079	0.67134	0.45535	0.10000
30	5.80	10	0.04850	0.67134	0.23208	0.10000
31	5.80	50	0.00774	0.67134	0.55652	0.10000
32	5.80	50	0.00950	0.67134	0.51599	0.10000
33	6.50	5	0.18643	0.62063	0.25299	0.10000
34	6.50	10	0.11931	0.62063	0.34209	0.10000
35	6.50	10	0.19303	0.62063	0.49235	0.10000
36	6.50	10	0.11698	0.62063	0.33947	0.10000
37	6.50	20	0.06155	0.62063	0.37379	0.10000
38	6.50	20	0.09769	0.62063	0.56470	0.10000
39	6.50	20	0.05800	0.62063	0.31207	0.10000
40	6.50	100	0.00946	0.62063	0.53408	0.10000
41	6.50	160	0.00480	0.62063	0.56717	0.10000
42	7.00	1	0.33288	0.59908	0.20005	0.10000
43	7.00	10	0.25185	0.59908	0.46804	0.10000
44	7.00	10	0.15671	0.59908	0.31199	0.10000
45	7.00	50	0.03044	0.59908	0.34233	0.10000
46	7.00	50	0.03852	0.59908	0.45522	0.10000
47	7.50	1	0.41526	0.59370	0.28631	0.10000
48	5.00	10	0.20845	0.59370	0.32852	0.10000
49	5.00	10	0.30834	0.59370	0.40348	0.10000
50	8.00	50	0.06768	0.59370	0.45030	0.10000
51	8.00	160	0.01710	0.59370	0.55724	0.10000

TABLE F2-15
D. M. BOORE: VERTICAL POINT ESTIMATES
SPECTRAL ACCELERATION AT 1.00 SEC PERIOD

CASE NO.	MAGNITUDE	DISTANCE (KM)	MU	SIGMA	SIGMA MU	SIGMA SIGMA
1	5.00	1	0.02516	0.70713	0.49096	0.10000
2	5.00	1	0.02343	0.70713	0.49316	0.10000
3	5.00	5	0.00835	0.70713	0.23322	0.10000
4	5.00	5	0.00852	0.70713	0.23263	0.10000
5	5.80	10	0.02427	0.67134	0.20212	0.10000
6	5.80	20	0.02047	0.67134	0.29882	0.10000
7	6.50	1	0.15930	0.62063	0.28130	0.10000
8	6.50	1	0.17138	0.62063	0.20822	0.10000
9	6.50	1	0.15922	0.62063	0.24129	0.10000
10	6.50	5	0.13787	0.62063	0.33158	0.10000
11	6.50	5	0.10798	0.62063	0.20000	0.10000
12	6.50	50	0.01368	0.62063	0.45100	0.10000
13	6.50	50	0.01679	0.62063	0.39269	0.10000
14	7.00	10	0.10262	0.59908	0.20000	0.10000
15	7.50	50	0.03443	0.59370	0.26211	0.10000
16	7.50	50	0.03950	0.59370	0.37091	0.10000
17	5.00	1	0.00923	0.70713	0.24410	0.10000
18	5.80	5	0.03545	0.67134	0.30427	0.10000
19	5.80	5	0.02473	0.67134	0.26398	0.10000
20	5.00	10	0.00921	0.70713	0.24837	0.10000
21	5.00	10	0.01115	0.70713	0.32028	0.10000
22	5.00	50	0.00177	0.70713	0.37368	0.10000
23	5.00	50	0.00184	0.70713	0.31732	0.10000
24	5.00	160	0.00057	0.70713	0.50534	0.10000
25	5.80	1	0.07237	0.67134	0.45050	0.10000
26	5.80	5	0.06332	0.67134	0.42667	0.10000
27	5.80	5	0.04379	0.67134	0.23828	0.10000
28	5.80	10	0.03069	0.67134	0.20000	0.10000
29	5.80	10	0.04235	0.67134	0.35891	0.10000
30	5.80	10	0.02883	0.67134	0.23053	0.10000
31	5.80	50	0.00503	0.67134	0.67154	0.10000
32	5.80	50	0.00614	0.67134	0.46051	0.10000
33	6.50	5	0.11193	0.62063	0.20000	0.10000
34	6.50	10	0.07446	0.62063	0.20000	0.10000
35	6.50	10	0.10136	0.62063	0.30170	0.10000
36	6.50	10	0.07223	0.62063	0.23415	0.10000
37	6.50	20	0.03788	0.62063	0.21824	0.10000
38	6.50	20	0.05507	0.62063	0.31668	0.10000
39	6.50	20	0.03846	0.62063	0.23846	0.10000
40	6.50	100	0.00729	0.62063	0.45411	0.10000
41	6.50	160	0.00405	0.62063	0.63472	0.10000
42	7.00	1	0.20427	0.59908	0.27724	0.10000
43	7.00	10	0.14722	0.59908	0.36222	0.10000
44	7.00	10	0.10070	0.59908	0.23794	0.10000
45	7.00	50	0.02245	0.59908	0.32572	0.10000
46	7.00	50	0.02681	0.59908	0.39173	0.10000
47	7.50	1	0.27132	0.59370	0.25287	0.10000
48	5.00	10	0.13720	0.59370	0.22190	0.10000
49	5.00	10	0.18748	0.59370	0.37945	0.10000
50	8.00	50	0.04960	0.59370	0.23337	0.10000
51	8.00	160	0.01630	0.59370	0.42446	0.10000

TABLE F2-16
D. M. BOORE: VERTICAL POINT ESTIMATES
SPECTRAL ACCELERATION AT 2.00 SEC PERIOD

CASE NO.	MAGNITUDE	DISTANCE (KM)	MU	SIGMA	SIGMA MU	SIGMA SIGMA
1	5.00	1	0.00992	0.70713	0.55535	0.10000
2	5.00	1	0.00806	0.70713	0.62071	0.10000
3	5.00	5	0.00339	0.70713	0.21353	0.10000
4	5.00	5	0.00302	0.70713	0.27253	0.10000
5	5.80	10	0.01136	0.67134	0.35190	0.10000
6	5.80	20	0.00829	0.67134	0.27266	0.10000
7	6.50	1	0.09186	0.62063	0.26468	0.10000
8	6.50	1	0.09017	0.62063	0.24863	0.10000
9	6.50	1	0.08036	0.62063	0.20000	0.10000
10	6.50	5	0.06859	0.62063	0.38835	0.10000
11	6.50	5	0.05303	0.62063	0.20410	0.10000
12	6.50	50	0.00819	0.62063	0.47627	0.10000
13	6.50	50	0.00967	0.62063	0.65250	0.10000
14	7.00	10	0.05373	0.59908	0.28290	0.10000
15	7.50	50	0.02066	0.59370	0.55448	0.10000
16	7.50	50	0.02364	0.59370	0.78504	0.10000
17	5.00	1	0.00374	0.70713	0.23472	0.10000
18	5.80	5	0.01690	0.67134	0.34340	0.10000
19	5.80	5	0.01013	0.67134	0.40337	0.10000
20	5.00	10	0.00364	0.70713	0.22809	0.10000
21	5.00	10	0.00368	0.70713	0.33459	0.10000
22	5.00	50	0.00082	0.70713	0.29778	0.10000
23	5.00	50	0.00074	0.70713	0.20000	0.10000
24	5.00	160	0.00031	0.70713	0.40567	0.10000
25	5.80	1	0.03653	0.67134	0.40660	0.10000
26	5.80	5	0.02829	0.67134	0.50031	0.10000
27	5.80	5	0.01967	0.67134	0.34329	0.10000
28	5.80	10	0.01342	0.67134	0.34559	0.10000
29	5.80	10	0.01613	0.67134	0.42922	0.10000
30	5.80	10	0.01244	0.67134	0.41090	0.10000
31	5.80	50	0.00243	0.67134	0.80875	0.10000
32	5.80	50	0.00309	0.67134	0.67644	0.10000
33	6.50	5	0.05934	0.62063	0.21993	0.10000
34	6.50	10	0.03957	0.62063	0.20000	0.10000
35	6.50	10	0.04729	0.62063	0.35419	0.10000
36	6.50	10	0.03576	0.62063	0.33171	0.10000
37	6.50	20	0.02101	0.62063	0.22873	0.10000
38	6.50	20	0.02718	0.62063	0.46050	0.10000
39	6.50	20	0.01919	0.62063	0.42248	0.10000
40	6.50	100	0.00413	0.62063	0.63825	0.10000
41	6.50	160	0.00270	0.62063	0.73801	0.10000
42	7.00	1	0.11642	0.59908	0.35782	0.10000
43	7.00	10	0.07009	0.59908	0.37122	0.10000
44	7.00	10	0.04925	0.59908	0.35177	0.10000
45	7.00	50	0.01338	0.59908	0.50949	0.10000
46	7.00	50	0.01627	0.59908	0.67299	0.10000
47	7.50	1	0.13835	0.59370	0.35172	0.10000
48	5.00	10	0.07162	0.59370	0.36706	0.10000
49	5.00	10	0.09263	0.59370	0.46475	0.10000
50	8.00	50	0.03606	0.59370	0.28919	0.10000
51	8.00	160	0.01426	0.59370	0.48117	0.10000

TABLE F2-17
D. M. BOORE: VERTICAL POINT ESTIMATES
SPECTRAL ACCELERATION AT 3.33 SEC PERIOD

CASE NO.	MAGNITUDE	DISTANCE (KM)	MU	SIGMA	SIGMA MU	SIGMA SIGMA
1	5.00	1	0.00477	0.72379	0.92441	0.10000
2	5.00	1	0.00388	0.72379	1.02715	0.10000
3	5.00	5	0.00163	0.72379	0.55050	0.10000
4	5.00	5	0.00146	0.72379	0.69499	0.10000
5	5.80	10	0.00675	0.68801	0.42730	0.10000
6	5.80	20	0.00494	0.68801	0.40473	0.10000
7	6.50	1	0.05809	0.63730	0.35744	0.10000
8	6.50	1	0.06017	0.63730	0.27889	0.10000
9	6.50	1	0.05477	0.63730	0.20618	0.10000
10	6.50	5	0.04798	0.63730	0.46134	0.10000
11	6.50	5	0.03376	0.63730	0.21316	0.10000
12	6.50	50	0.00525	0.63730	0.55556	0.10000
13	6.50	50	0.00607	0.63730	0.61207	0.10000
14	7.00	10	0.03777	0.61575	0.29256	0.10000
15	7.50	50	0.01504	0.61037	0.54513	0.10000
16	7.50	50	0.01629	0.61037	0.68859	0.10000
17	5.00	1	0.00180	0.72379	0.58149	0.10000
18	5.80	5	0.01075	0.68801	0.48666	0.10000
19	5.80	5	0.00637	0.68801	0.45583	0.10000
20	5.00	10	0.00175	0.72379	0.57265	0.10000
21	5.00	10	0.00178	0.72379	0.75353	0.10000
22	5.00	50	0.00040	0.72379	0.27701	0.10000
23	5.00	50	0.00036	0.72379	0.39423	0.10000
24	5.00	160	0.00016	0.72379	0.45134	0.10000
25	5.80	1	0.02057	0.68801	0.57496	0.10000
26	5.80	5	0.01758	0.68801	0.63970	0.10000
27	5.80	5	0.01097	0.68801	0.48094	0.10000
28	5.80	10	0.00767	0.68801	0.49367	0.10000
29	5.80	10	0.00914	0.68801	0.59601	0.10000
30	5.80	10	0.00708	0.68801	0.50772	0.10000
31	5.80	50	0.00142	0.68801	0.85446	0.10000
32	5.80	50	0.00182	0.68801	0.69425	0.10000
33	6.50	5	0.04150	0.63730	0.20000	0.10000
34	6.50	10	0.02456	0.63730	0.24642	0.10000
35	6.50	10	0.02925	0.63730	0.35687	0.10000
36	6.50	10	0.02167	0.63730	0.32481	0.10000
37	6.50	20	0.01344	0.63730	0.28852	0.10000
38	6.50	20	0.01606	0.63730	0.38322	0.10000
39	6.50	20	0.01280	0.63730	0.51911	0.10000
40	6.50	100	0.00253	0.63730	0.82091	0.10000
41	6.50	160	0.00180	0.63730	0.80928	0.10000
42	7.00	1	0.08010	0.61575	0.45456	0.10000
43	7.00	10	0.04594	0.61575	0.36458	0.10000
44	7.00	10	0.03301	0.61575	0.46265	0.10000
45	7.00	50	0.00946	0.61575	0.58622	0.10000
46	7.00	50	0.01083	0.61575	0.66578	0.10000
47	7.50	1	0.10514	0.61037	0.28790	0.10000
48	5.00	10	0.04847	0.61037	0.51393	0.10000
49	5.00	10	0.06191	0.61037	0.49521	0.10000
50	8.00	50	0.02837	0.61037	0.32298	0.10000
51	8.00	160	0.01088	0.61037	0.35571	0.10000

TABLE F2-18
D. M. BOORE: VERTICAL POINT ESTIMATES
PEAK GROUND VELOCITY

CASE NO.	MAGNITUDE	DISTANCE (KM)	MU	SIGMA	SIGMA MU	SIGMA SIGMA
1	5.00	1	3.88858	0.62369	0.20000	0.10000
2	5.00	1	3.66232	0.62369	0.20000	0.10000
3	5.00	5	0.83821	0.62369	0.20000	0.10000
4	5.00	5	0.89974	0.62369	0.20000	0.10000
5	5.80	10	2.42393	0.57616	0.20000	0.10000
6	5.80	20	1.86606	0.57616	0.44090	0.10000
7	6.50	1	12.98893	0.53579	0.20000	0.10000
8	6.50	1	14.79397	0.53579	0.34837	0.10000
9	6.50	1	12.98248	0.53579	0.29288	0.10000
10	6.50	5	13.15960	0.53579	0.37869	0.10000
11	6.50	5	9.31642	0.53579	0.24233	0.10000
12	6.50	50	1.04531	0.53579	0.28273	0.10000
13	6.50	50	1.39697	0.53579	0.44049	0.10000
14	7.00	10	9.95682	0.50781	0.20000	0.10000
15	7.50	50	3.65805	0.48785	0.29944	0.10000
16	7.50	50	4.57237	0.48785	0.51247	0.10000
17	5.00	1	0.95957	0.62369	0.20000	0.10000
18	5.80	5	4.02337	0.57616	0.22159	0.10000
19	5.80	5	2.49333	0.57616	0.33395	0.10000
20	5.00	10	0.92797	0.62369	0.20000	0.10000
21	5.00	10	1.18479	0.62369	0.20000	0.10000
22	5.00	50	0.12743	0.62369	0.20000	0.10000
23	5.00	50	0.13861	0.62369	0.20000	0.10000
24	5.00	160	0.02803	0.62369	0.20000	0.10000
25	5.80	1	7.63536	0.57616	0.20000	0.10000
26	5.80	5	7.17495	0.57616	0.28243	0.10000
27	5.80	5	4.42173	0.57616	0.20000	0.10000
28	5.80	10	2.99451	0.57616	0.20000	0.10000
29	5.80	10	4.14464	0.57616	0.37371	0.10000
30	5.80	10	2.63851	0.57616	0.26694	0.10000
31	5.80	50	0.35141	0.57616	0.52035	0.10000
32	5.80	50	0.46347	0.57616	0.47054	0.10000
33	6.50	5	10.42233	0.53579	0.20000	0.10000
34	6.50	10	6.94081	0.53579	0.20000	0.10000
35	6.50	10	8.68423	0.53579	0.35642	0.10000
36	6.50	10	6.34164	0.53579	0.27235	0.10000
37	6.50	20	3.44859	0.53579	0.20000	0.10000
38	6.50	20	4.66256	0.53579	0.41189	0.10000
39	6.50	20	3.33761	0.53579	0.34932	0.10000
40	6.50	100	0.44755	0.53579	0.20000	0.10000
41	6.50	160	0.19570	0.53579	0.35343	0.10000
42	7.00	1	15.62568	0.50781	0.20000	0.10000
43	7.00	10	12.44673	0.50781	0.39138	0.10000
44	7.00	10	9.46423	0.50781	0.26956	0.10000
45	7.00	50	2.05968	0.50781	0.25237	0.10000
46	7.00	50	2.71398	0.50781	0.50666	0.10000
47	7.50	1	19.01198	0.48785	0.33017	0.10000
48	5.00	10	12.83757	0.48785	0.20000	0.10000
49	5.00	10	15.26005	0.48785	0.42082	0.10000
50	8.00	50	6.69893	0.48785	0.20000	0.10000
51	8.00	160	1.64870	0.48785	0.27705	0.10000

APPENDIX F3

EXPERT EVALUATION OF GROUND-MOTION ATTENUATION RELATIONSHIPS FOR THE PROBABILISTIC SEISMIC HAZARD ASSESSMENT OF THE YUCCA MOUNTAIN NUCLEAR WASTE REPOSITORY

Kenneth W. Campbell

APPENDIX F3
TABLE OF CONTENTS

APPENDIX F3

EXPERT EVALUATION OF GROUND-MOTION ATTENUATION RELATIONSHIPS FOR THE PROBABILISTIC SEISMIC HAZARD ASSESSMENT OF THE YUCCA MOUNTAIN NUCLEAR WASTE REPOSITORY

Kenneth W. Campbell
EQE International, Inc.
2942 Evergreen Parkway, Suite 302
Evergreen, Colorado 80439

F3-1 INTRODUCTION

This report documents the basis for my expert evaluation of ground-motion attenuation relationships for the Yucca Mountain Nuclear Waste Repository. This evaluation is based on my synthesis and analysis of data, discussions, and information obtained during a series of ground-motion characterization workshops and from a vast amount of information provided by the facilitation team in an eleven-volume Yucca Mountain Ground Motion Data Package. The methodology that I used to develop the ground-motion estimates is based on weighting several credible models for estimating ground motions in regions where empirical attenuation relationships are not available.

I was asked to provide ground-motion estimates for 51 individual combinations of earthquake magnitude, horizontal distance, faulting mechanism, location with respect to the fault trace, and rupture depth. These 51 cases are presented in Table F3-1. Earthquake magnitude was defined as moment magnitude (M_w). Horizontal distance (R_{hor}) was defined as the distance from a hypothetical site to the surface trace of the fault. Faulting mechanism was defined as strike slip on a vertical fault plane or normal on a 60° dipping fault plane. The location with respect to the fault trace was defined as a site that either lies on the hanging wall (HW) or the footwall (FW) side of the fault plane. Shallow rupture was defined as a rupture plane whose initial centroid was located at a depth of 5 km, but whose rupture plane was confined between depths of 0 and 14 km. Deep rupture was defined as a rupture plane whose down-dip edge was constrained to occur at a depth of 14 km.

I was also asked to provide a method for estimating ground motions for a parallel fault rupture scenario and for a low angle (30° dipping) fault rupture. No actual ground-motion estimates were required for these scenarios, only a procedure for making those estimates.

The ground-motion parameters for which I was asked to provide estimates were peak ground acceleration (PGA), peak ground velocity (PGV), and 5%-damped response spectral acceleration (SA) at frequencies of 0.33, 0.5, 1, 2, 5, 10, and 20 Hz. Both the horizontal and the vertical components were required. The horizontal component was defined as the random horizontal component. For each of the 51 cases in Table F3-1, I was asked to provide four quantities for each ground-motion parameter: the median value (μ), the aleatory variability (σ), the epistemic uncertainty in the median value (σ_μ), and the epistemic uncertainty in the aleatory variability (σ_σ). The hypothetical site on which these ground-motion estimates were provided was located on an outcrop of the materials found at a depth of 300 m below the top of Yucca Mountain, and is referred to as YM300 in this report.

F3-2 GROUND-MOTION MODELS

There were a number of proponent ground-motion models that were solicited by the facilitation team specifically for this study and that were subsequently documented in the Yucca Mountain Ground Motion Data Package that was provided to all experts. In addition, each expert was asked to provide additional models to the facilitation team for consideration by all experts. I did not provide the team with any additional models. The ground-motion models that I used in my expert evaluations and those that I did not are described below.

The ground-motion models that I used to develop my expert evaluations were the hybrid empirical model proposed by myself (Campbell Hybrid model), the stochastic point source simulation model proposed by Silva (Silva PS model), the stochastic finite fault simulation model proposed by Silva (Silva FF model), the semi-empirical Green's function finite fault simulation model proposed by Somerville (Somerville FF model), and the compound fractile finite fault model proposed by Zeng and Anderson (Anderson FF). These models are described in detail in the Yucca Mountain Ground Motion Data Package. All of the models were developed for the YM300 crustal profile.

The ground-motion models that I considered but did not use in my evaluation were the strong-motion empirical models developed by Sabetta and Pugliese (1996) and McGarr (1984), the blast models developed by R. J. Bennett *et al.* (S-Cubed, written communication, 1997), and the theoretical models, other than those mentioned above, that were used in the Yucca Mountain scenario ground-motion study. The empirical models were rejected as being too restricted in their geographical extent or parametric range of applicability. I did not have any confidence that the source and crustal properties associated with the Italian recordings used by Sabetta and Pugliese were appropriate to the Yucca Mountain region. McGarr's model was too restricted to be easily integrated with the other empirical models that were used in the Campbell Hybrid model. The blast models are based on seismic sources with much different source mechanisms than earthquakes and their shallow source depth and travel paths are not consistent with those expected from earthquakes. The theoretical models used for the scenario earthquake study were applied only to a very restricted subset of possible earthquake scenarios and were not generally applicable to the more generalized ground-motion estimates requested in this study.

F3-2.1 Campbell Hybrid Model

The Campbell Hybrid model uses empirical attenuation relationships developed from strong-motion recordings primarily from California to estimate the ground-motion parameters, then it adjusts these estimates using theoretical source and crustal adjustment factors to represent the region of interest. The theoretical adjustment factors are developed from a point source stochastic simulation model by taking the ratio of the theoretical estimates of the ground-motion parameters between California (CA) and YM300. The model was applied exactly as described in the Yucca Mountain Strong Motion Data Package, so a complete description will not be provided here. The more important elements of the model are described below.

The specific empirical attenuation relationships that were used with the Campbell Hybrid model are described in Table F3-2. The weights assigned to each of the empirical model classes are given in Table F3-3. Also given in this table are the values of parameters that were required to evaluate the models. The theoretical YM300/CA adjustment factors were weighted to give a median stress drop of 60 bars and an epistemic uncertainty in the natural log of this stress drop of 0.2, consistent with the value of these parameters determined for an average source mechanism in California as derived from stochastic simulations of California strong-motion recordings (W. Silva, oral comm., 1997). These weights are given in Table

F3-4. The adjustment factors were applied to the empirical ground-motion estimates for a strike-slip source mechanism, which have an average stress drop of about 45 bars (W. Silva, oral comm., 1997). The use of the strike-slip mechanism was intended to approximate the lower median stress drop expected for normal earthquakes in an extensional stress regime as estimated by Becker and Abrahamson (1997).

I have included the empirical attenuation relationship developed by Spudich *et al.* (1997) for an extensional stress environment as one member of the set of attenuation relationships included in the Campbell Hybrid model rather than as a separate model. This was done for the following reasons:

- The functional form of the Spudich relationship is identical to that proposed by Boore *et al.* (1997) and, in my judgment, is less physically based than other functional forms that are available for the western U.S.

- The magnitude scaling term in the Spudich relationship was adopted directly from Boore *et al.* (1997) and was not evaluated independently from the regression analysis of the extensional strong-motion recordings.

- The Spudich relationship includes earthquakes such as those from the Imperial Valley of California that are included in other attenuation relationships that are used in the Campbell Hybrid model.

- The aleatory variability of the Spudich relationship is much higher than that of Boore *et al.* (1997) based on western U.S. recordings, possibly indicating a statistically inferior regression model and/or a less reliable set of strong-motion parameters and supporting data than is available for the western U.S.

- The predictions of PGA from the Spudich relationship for the set of strong-motion parameters, magnitudes, and distances of interest in this study are very similar (i.e., well within one standard deviation) of those estimated for strike-slip faults in the western U.S. from the relationship of Boore *et al.* (1997), which has an identical functional form and magnitude scaling term, indicating that there is not a significant difference between these two relationships.

As part of this project, the facilitation team compared the predictions of ground motion for the strong-motion recordings compiled by Spudich *et al.* (1997) with those given by the attenuation relationship of Abrahamson and Silva (1997) for western U.S. strike-slip earthquakes. They found that the extensional recordings had amplitudes generally lower than those predicted from the Abrahamson and Silva relationship. However, I have tentatively considered these differences as insignificant because of their relatively small differences and because of the use of data from crustal environments and site conditions potentially very different from the Great Basin in general and the Yucca Mountain region in particular.

I have used the comparison of the predictions of Spudich *et al.* (1997) with those of Boore *et al.* (1997), the comparison of the extensional stress regime recordings with predictions from the Abrahamson and Silva (1997) attenuation relationship, and the independent evaluations of high-frequency stress drop from normal-faulting earthquakes in the U.S. provided by the facilitation team to tentatively conclude that the empirical attenuation relationships in the western U.S. should be evaluated for strike-slip faulting to approximate the extensional stress environment in the Yucca Mountain region. Based on this conclusion, I adjusted the predictions from the Spudich relationship with the regional adjustment factors and I combined these predictions with those from the western U.S. attenuation relationships evaluated for strike-slip faulting.

Because of its empirical nature and its reliance on multiple attenuation relationships, the Campbell Hybrid model can be used to directly estimate all of the variabilities and uncertainties required for this study (i.e., σ, σ_μ, and σ_σ). The procedure used to estimate these parameters is described in the Yucca Mountain Strong Motion Data Package.

F3-2.2 Anderson, Silva, and Somerville Finite Fault Models

These finite fault models use theoretical and in some cases empirical source and propagation models to estimate ground motions. They use a three-dimensional description of the fault to account for the kinematic effects of propagation of the rupture front along the fault plane. This allows these faults to directly incorporate important finite source characteristics such as source directivity in their theoretical estimates. All three of these finite fault models have been validated and/or calibrated to strong-motion recordings, but the Anderson FF model, because it is newer, has undergone less validation than the others. A more thorough description of these models is given in the Yucca Mountain Strong Motion Data Package.

Because of their theoretical nature, these models are best used for estimating median ground motions (i.e., μ). Some validation studies have been performed to estimate σ, but because the specific earthquake data required for these studies is fairly comprehensive, these estimates are not as reliable as those determined from empirical attenuation relationships. Estimates of σ_μ and σ_σ, although provided by some investigators, are largely based on the opinions of the proponents of these models.

F3-2.3 Silva Point Source Model

The Silva PS model uses simple stochastic simulation theory and theoretical seismological models to estimate ground motions at a given location. The source model used in these estimates is based on the ω^2 source scaling relation. The ground motions are simulated using random process theory based on the concept of band-limited white noise. The model has been calibrated with strong-motion data and with the attenuation relationship of Abrahamson and Silva (1997). Like empirical attenuation relationships, it produces estimates of the ground-motion parameters without having to generate time series. This model is described in the Yucca Mountain Strong Motion Data Package.

The facilitation team provided an attenuation relationship based on the simulations from this model that could be used to provide median ground-motion estimates at all of the magnitudes and distances of interest in this study. This relationship included stress drop as a parameter for flexibility in application to the Yucca Mountain region. The Silva PS model, being point source, is calibrated to a larger number of strong motion recordings than the finite fault versions. However, the same limitations apply with respect to the estimation σ.

F3-3 POINT ESTIMATES

Point estimates of μ, σ, σ_μ, and σ_σ were provided for all 51 cases using the selected models discussed above. These evaluations were made for both the random horizontal and the vertical components of all nine ground-motion parameters of interest by applying weights to the estimates provided by the selected models. The weighting scheme was designed to be case-specific to more heavily weight those models that in my opinion were the best for making predictions for that particular case. The weights were the same for both the random horizontal and the vertical components. The weights were adjusted through an iteration process until the desired weighted estimates were obtained. Any irregularities in the point estimates were smoothed out in the regression models developed from these point estimates. These regression models are presented in a later section.

F3-3.1 Weighting Scheme

F3-3.1.1 Median Estimates (μ). The weighting scheme used in developing the point estimates of the median ground motions (μ) is presented in Table F3-5. These weights were determined by applying a set of loosely defined rules that depended on the particular case being evaluated. In general, the greatest weight was given to the Campbell Hybrid model because of its robust empirical basis. However, this model was given relatively less weight for those cases that are not well-represented in the empirical database. These weights depended on the frequency of the ground-motion parameter and the magnitude and distance of the hypothetical site from the earthquake source in an interrelated but systematic manner.

In general, the Campbell Hybrid model was given less weight than the theoretical models at low frequencies, small magnitudes, and large distances. Of the finite source models, the Anderson FF model was given less weight than the Silva FF and Somerville FF models because of its more limited validation and its undesirable, overly strong dependence on radiation pattern and directivity. The Silva PS model was given relatively high weight at small magnitudes where there were no estimates from the Silva FF and Somerville FF models. The weight given to the Silva PS model was gradually decreased to zero at magnitude 6.5 where estimates were available from all three finite fault models.

F3-3.1.2 Variabilities (σ, σ_μ, and σ_σ). I have very little confidence in the variabilities provided with the theoretical proponent models. Therefore, I used only the Campbell Hybrid model for estimating these parameters. Any undesirable fluctuations in these parameters that resulted from using only a single model were smoothed out in the regression models used to provide continuous estimates of these parameters. Of course, the term "single model" is a misnomer here, since the Campbell Hybrid model uses up to six attenuation relationships as the basis for its estimates. The epistemic uncertainty in the median estimate of ground motion was increased to reflect the added uncertainty in the various ground motion estimates that were used to develop it.

F3-3.2 Random Horizontal Component

The point estimates of the random horizontal components of the median ground-motion parameters were derived directly from the weighted horizontal estimates of these parameters obtained from the selected ground-motion models. Consistent with the weighting scheme, the estimates of the variabilities were taken directly from the Campbell Hybrid model. A summary of the horizontal point estimates for all 51 cases is provided in Tables F3-6 through F3-14.

F3-3.3 Vertical Component

The point estimates of the vertical components was done a little differently than the horizontal components because of the lack of vertical components for the Silva FF model. The Silva PS model had both vertical and horizontal estimates of median ground motions and was based on the same source and crustal models as the Silva FF model. Because of this similarity, the vertical-to-horizontal ratio from the Silva PS model was used to estimate vertical ground motions from the horizontal component of the Silva FF model. Weighted estimates of the vertical components of the median ground motions were then derived in the same manner as the horizontal components. Consistent with the weighting scheme, the estimates of the variabilities were taken directly from the Campbell Hybrid model. A summary of the vertical point estimates for all 51 cases are given in Tables F3-15 through F3-23.

F3-4 REGRESSION MODELS

The facilitation team took my point estimates for μ, σ, σ_μ, and σ_σ and performed a regression analyses to develop a set of attenuation relationships for the ground-motion parameters of interest. These regression models were adjusted through several iterations until they provided continuous estimates for these parameters that I believed were realistic and systematic.

F3-4.1 Median Estimates (μ)

For the median ground motions, the facilitation team used the functional form and statistical procedure recommended by Abrahamson and Silva (1997). For the variabilities they used simpler models that captured the important behavior of these parameters. I recommended that the distance parameter R_{SEIS}, the closest distance to the seismogenic rupture zone, be used for these analyses. The number of parameters and functional form of these regression models were adjusted through an iterative process until they provided an acceptable predictive model for each parameter.

I first recommended that the functional form for the median estimates be adjusted to reflect the combined magnitude-distance term recommended by Campbell (1997). However, this model did not appear to model the point estimates better than the original model. Furthermore, it appeared to provide unrealistic estimates at very short distances. This behavior might have been corrected by further iteration in which the functional form of other parts of the model were changed. This, however, did not seem necessary since the original functional form appeared to fit the point estimates and provide realistic magnitude and distance scaling at near-source distances.

I first asked that the regression model for the median estimates of ground motion from dipping normal faults explicitly include a parameter that distinguished between the hanging wall and the footwall. However, including this parameter did not seem to improve the model, and in fact provided unrealistic behavior at some frequencies, so I recommended that this parameter be removed and the added randomness absorbed in the standard error of the estimate of the regression model.

F3-4.2 Variability Estimates (σ, σ_μ, and σ_σ)

The regression model for the aleatory variability (σ) was found to be a very strong and well-behaved function of magnitude and frequency. No additional adjustments were required. The regression model for the epistemic uncertainty (σ_μ) was found to be a strong function of both frequency and distance; however, the distance dependence was erratic due to the strong and erratic influence of the median estimates of the Anderson FF model. Because of this erratic behavior, I asked the facilitation team to remove the distance parameter and leave only the frequency parameter. The final model predicts higher values of σ_μ at both high and low frequencies which are consistent with my understanding of the expected behavior of this uncertainty.

The regression model for the epistemic uncertainty in the aleatory variability (σ_σ) was very nearly constant. There was a slight dependence on distance for some frequencies, but this dependence resulted in values that I considered to be too small (i.e., less than 0.08). Therefore, I recommended that a constant value of 0.1 be used for this parameter for both the random horizontal and the vertical components.

F3-5 SPECIAL CASES

I was asked to provide a recommendation on how to estimate ground motions for two special rupture scenarios that are being considered by the source characterization panel. These rupture scenarios refer to multiple parallel faults and low angle (i.e., about a 30° dipping) faults.

F3-5.1 Multiple Parallel Faults

Multiple parallel faults represent an earthquake in which multiple ruptures are triggered on closely spaced parallel faults. My recommendation for modeling this special case is based on an assumption that rupture begins on one of the faults, then triggers rupture on the other faults in what can be referred to as a cascaded rupture scenario. In my opinion, this scenario can be compared to a single earthquake in which one sub-event triggers a second sub-event which triggers and third sub-event, etc. Consistent with this analogy, I recommend that the multiple parallel fault scenario be assigned the moment magnitude that corresponds to the total seismic moment released on all of the faults that make up the rupture, and that the distance associated with this scenario be taken as the distance to the closest rupture.

I believe that the median estimates of ground motion provided by the recommended procedure will be generally conservative. Therefore, I do not recommend that the epistemic uncertainty in these estimates be increased from that estimated for a standard rupture scenario. I do, however, expect that the multiple parallel fault scenario will cause more randomness in the recorded ground motions, so I recommend that the value of σ be increased by a factor of 1.2 over that estimated from the standard rupture scenario.

F3-5.2 Low Angle Faults

I do not know of any recordings from a low angle normal fault. There are, however, recordings either directly over or very near to low-angle thrust faults, such as a subduction zone megathrust interface or a continental thrust fault. Low angle thrust faults and megathrust interfaces appear to produce near-source ground motions that are similar in amplitude to continental reverse faults unless they are unusually deep (e.g., the 1987 Whittier Narrows and 1994 Northridge earthquakes). Based on this observation, I recommend that low angle normal faults be treated as standard high angle normal faults for purposes of estimating median ground motions unless they are unusually deep. The estimates should be modified as follows depending on the depth of the bottom of the fault: (1) for depths less than 8 km, no change; (2) for depths greater than 15 km, multiply the estimates by 1.2; (3) for depths between 8 and 15 km, multiple the estimates by a factor that linearly increases from 1.0 to 1.2.

I would also expect that the values of σ and σ_μ would be greater for this scenario. The larger value for the aleatory variability is expected because of the assumption of a larger variation in stress drop and radiation pattern, although this opinion has not been confirmed with observations. The larger value for epistemic uncertainty is used to compensate for the lack of any validation. The recommended values for σ and σ_μ for this scenario should be taken to be 1.2 times higher than those estimated for a high angle normal fault.

F3-6 REFERENCES

Abrahamson, N.A., and Silva, W. J., 1997, Empirical response spectral attenuation relations for shallow crustal earthquakes: Seismological Research Letters, v. 68, n. 1, p. 94-127.

Becker, A.M., and Abrahamson, N. A., 1997, Stress drops in normal faulting earthquakes, abstract: Seismological Research Letters, v. 68, n. 2, p. 322.

Boore, D.M., Joyner, W. B., and Fumal, T. E., 1997, Equations for estimating horizontal response spectra and peak acceleration from western north american earthquakes--a summary of recent work: Seismological Research Letters, v. 68, n. 1, p.128-153.

Campbell, K.W., 1997, Empirical near-source attenuation relationships for horizontal and vertical components of peak ground acceleration, peak ground velocity, and pseudo-absolute acceleration response spectra: Seismological Research Letters, v. 68, p. 154-179.

Joyner, W. B., and Boore, D. M., 1988, Measurement, characterization, and prediction of strong groun motion, *in* Procedures, Conference on Earthquake Engineering and Soil Dynamics II: GT Div/.ASCE, Park City, UT, 27-30 June 1988, p. 43-102.

McGarr, A., 1984, Scaling of ground motion parameters, state of stress, and focal depth: Journal of Geophysical Research, v. 89, p. 6969-6979.

Sabetta, F., and Pugliese, A., 1996, Estimation of response spectra and simulation of nonstationary earthquake ground motions, *Bulletin of the Seismological Society of America*, v. 86, p. 337-352.

Sadigh, K., Chang, C-Y, Egan, J.A., Makdisi, F., and Youngs, R. R., 1997, Attenuation relationships for shallow crustal earthquakes based on California strong motion data: Seismological Research Letters, v. 68, n. 1, p. 180-189.

Spudich, P., Fletcher, J.B., Hellweg, M., Boatwright, J., Sullivan, C., Joyner, W.B., Hanks, T.C., Boore, D. M., McGarr, A., Baker, L. M., and Lindh, A. G., 1997, SEA96—A New Predictive Relation for Earthquake Ground Motions in Extensional Tectonic Regimes: Seismological Research Letters, v. 68, n. 1, p.190-198.

Spudich, P., Fletcher, J.B., Hellweg, M., Boatwright, J., Sullivan, C., Joyner, W. B., Hanks, T.C., Boore, D. M., McGarr, A., Baker, L. M., and Lindh, A. G., 1996, Earthquake ground motions in extensional tectonic regimes: U. S. Geologic Survey Open-File Report 96-292, 351 p.

TABLE F3-1
IDENTIFICATION OF CASES

CASE	DEPTH	M_w	R_{RUP} (KM)	FAULT TYPE
1	Shallow	5.0	1	SS
2	Shallow	5.0	1	HW
3	Shallow	5.0	10	SS
4	Shallow	5.0	10	HW
5	Shallow	5.0	50	SS
6	Shallow	5.0	50	HW
7	Shallow	5.0	160	SS
8	Deep	5.0	1	SS
9	Deep	5.0	5	SS
10	Deep	5.0	5	HW
11	Shallow	5.8	1	SS
12	Shallow	5.8	5	HW
13	Shallow	5.8	5	FW
14	Shallow	5.8	10	SS
15	Shallow	5.8	10	HW
16	Shallow	5.8	10	FW
17	Shallow	5.8	50	SS
18	Shallow	5.8	50	HW
19	Deep	5.8	5	HW
20	Deep	5.8	5	FW
21	Deep	5.8	10	SS
22	Deep	5.8	20	HW
23	Shallow	6.5	1	SS
24	Shallow	6.5	1	HW
25	Shallow	6.5	1	FW
26	Shallow	6.5	5	SS
27	Shallow	6.5	5	HW
28	Shallow	6.5	5	FW
29	Shallow	6.5	10	SS
30	Shallow	6.5	10	HW
31	Shallow	6.5	10	FW
32	Shallow	6.5	20	SS
33	Shallow	6.5	20	HW
34	Shallow	6.5	20	FW
35	Shallow	6.5	50	SS

TABLE F3-1
IDENTIFICATION OF CASES

CASE	DEPTH	M_w	R_{HOR} (KM)	FAULT TYPE
36	Shallow	6.5	50	HW
37	Shallow	6.5	100	SS
38	Shallow	6.5	160	SS
39	Shallow	7.0	1	SS
40	Shallow	7.0	10	SS
41	Shallow	7.0	10	HW
42	Shallow	7.0	10	FW
43	Shallow	7.0	50	SS
44	Shallow	7.0	50	HW
45	Shallow	7.5	1	SS
46	Shallow	7.5	10	SS
47	Shallow	7.5	10	HW
48	Shallow	7.5	50	SS
49	Shallow	7.5	50	HW
50	Shallow	8.0	50	SS
51	Shallow	8.0	160	SS

TABLE F3-2
SELECTED ATTENUATION RELATIONSHIPS FOR THE HYBRID EMPIRICAL MODEL

CLASS	REFERENCE	FAULT TYPE	SITE CONDITION	σ
1	Abrahamson & Silva (1997)	Strike slip	Rock	N.A.
1	Campbell (1997)	Strike slip	Soft Rock, D=2 km	$\sigma = f(\mu)$
1	Idriss (University of California, Davis, written communications, 1991, 1997)	Strike slip	Rock	N.A.
1	Sadigh et al. (1997)	Strike slip	Rock	N.A.
2	Boore et al. (1997)	Strike slip	$V_{s,30}$ = 620 m/sec	N.A.
2	Spudich et al. (1996)	N.A.	Rock	N.A.
3	Joyner & Boore (1988)	N.A.	Rock	N.A.

TABLE F3-3
WEIGHTS USED FOR THE CAMPBELL HYBRID EMPIRICAL MODEL

Model Class	Random Horizontal		Vertical
	PGV	All Others	
1	0.75	0.75	1.0
2	0	0.25	0
3	0.25	0	0

TABLE F3-4
WEIGHTS FOR THE THEORETICAL ESTIMATES OF THE REGIONAL CAMPBELL YM300/CA ADJUSTMENT FACTORS

STRESS DROP, $\Delta\sigma$ (BARS)	RANDOM HORIZONTAL COMPONENT
30	0.02
45	0.10
60	0.76
85	0.10
120	0.02
Weighted Median $\Delta\sigma = 60.4$ Weighted $\sigma_{\ln(\Delta\sigma)} = 0.199$	

TABLE F3-5
WEIGHTS FOR EVALUATING HORIZONTAL AND VERTICAL POINT ESTIMATES OF SA, PGA, AND PGV

CASE	FREQUENCY (HZ)	MODEL				
		CAMPBELL	SOMER-VILLE	SILVA PS	SILVA FF	ANDERSON
1–4	0.33	0.25	—	0.50	—	0.25
	0.50	0.33	—	0.45	—	0.22
	All others	0.50	—	0.34	—	0.16
5–6	0.33	0.17	—	0.56	—	0.27
	0.50	0.25	—	0.50	—	0.25
	All others	0.33	—	0.45	—	0.22
7	All	0	—	0.70	—	0.30
8–10	0.33	0.25	—	0.50	—	0.25
	0.50	0.33	—	0.45	—	0.22
	All others	0.50	—	0.34	—	0.16
11–16	0.33	0.33	0.22	0.11	0.12	0.22
	All others	0.50	0.17	0.08	0.09	0.16
17–18	0.33	0.25	0.25	0.12	0.13	0.25
	All others	0.33	0.22	0.11	0.12	0.22
19–22	0.33	0.33	0.22	0.11	0.12	0.22
	All others	0.50	0.17	0.08	0.09	0.16
23–36	All	0.67	0.11	0	0.11	0.11
37	All	0.50	0.17	0	0.17	0.16
38	All	0.25	0.25	0	0.25	0.25
39–49	All	0.67	0.11	0	0.11	0.11
50	All	0.50	0.17	0	0.17	0.16
51	All	0.25	0.25	0	0.25	0.25

TABLE F3-6
K. W. CAMPBELL: HORIZONTAL POINT ESTIMATES
PEAK GROUND ACCELERATION

CASE NO.	MAGNITUDE	DISTANCE (KM)	MU	SIGMA	SIGMA MU	SIGMA SIGMA
1	5.00	1	0.15683	0.63400	0.45104	0.11400
2	5.00	1	0.18764	0.63400	0.44792	0.11400
3	5.00	5	0.05466	0.65000	0.35772	0.09000
4	5.00	5	0.07114	0.64900	0.40247	0.09200
5	5.80	10	0.09729	0.58200	0.26161	0.06100
6	5.80	20	0.07793	0.59300	0.25931	0.04400
7	6.50	1	0.41902	0.53000	0.38678	0.04000
8	6.50	1	0.44992	0.53000	0.47983	0.04000
9	6.50	1	0.41243	0.53000	0.41965	0.04000
10	6.50	5	0.35617	0.53000	0.33721	0.04000
11	6.50	5	0.26314	0.53000	0.33466	0.04000
12	6.50	50	0.02985	0.55700	0.29984	0.02100
13	6.50	50	0.03135	0.55700	0.29833	0.02100
14	7.00	10	0.24540	0.49700	0.31905	0.03900
15	7.50	50	0.06139	0.50300	0.26687	0.04300
16	7.50	50	0.06838	0.49900	0.26025	0.04100
17	5.00	1	0.05620	0.64700	0.54042	0.09400
18	5.80	5	0.16290	0.57800	0.34360	0.06900
19	5.80	5	0.09740	0.58300	0.36051	0.06000
20	5.00	10	0.06533	0.64800	0.27155	0.09300
21	5.00	10	0.09075	0.64200	0.26852	0.10100
22	5.00	50	0.00635	0.66100	0.41708	0.07900
23	5.00	50	0.00683	0.66100	0.43385	0.07900
24	5.00	160	0.00078	0.66100	0.74144	0.07900
25	5.80	1	0.27385	0.57800	0.41931	0.06900
26	5.80	5	0.23766	0.57800	0.35031	0.06900
27	5.80	5	0.14912	0.57800	0.36283	0.06900
28	5.80	10	0.12083	0.57800	0.29383	0.06900
29	5.80	10	0.17246	0.57800	0.30078	0.06900
30	5.80	10	0.08461	0.58200	0.39688	0.06100
31	5.80	50	0.01084	0.60500	0.59133	0.03200
32	5.80	50	0.01131	0.60500	0.61026	0.03200
33	6.50	5	0.30413	0.53000	0.34623	0.04000
34	6.50	10	0.19854	0.53000	0.32376	0.04000
35	6.50	10	0.26996	0.53000	0.34376	0.04000
36	6.50	10	0.16982	0.53000	0.32504	0.04000
37	6.50	20	0.10078	0.53700	0.28475	0.02600
38	6.50	20	0.13497	0.53300	0.34932	0.03500
39	6.50	20	0.08533	0.53900	0.30135	0.02200
40	6.50	100	0.01341	0.55700	0.43997	0.02100
41	6.50	160	0.00498	0.55700	0.63341	0.02100
42	7.00	1	0.45944	0.49700	0.33008	0.03900
43	7.00	10	0.32809	0.49700	0.31129	0.03900
44	7.00	10	0.20863	0.49700	0.29214	0.03900
45	7.00	50	0.04567	0.52300	0.27876	0.04500
46	7.00	50	0.05049	0.51900	0.27304	0.03900
47	7.50	1	0.50690	0.48700	0.33727	0.04300
48	5.00	10	0.28319	0.48700	0.29876	0.04300
49	5.00	10	0.36567	0.48700	0.36296	0.04300
50	8.00	50	0.07877	0.49400	0.30402	0.04000
51	8.00	160	0.02277	0.51400	0.42621	0.05500

TABLE F3-7
K. W. CAMPBELL: HORIZONTAL POINT ESTIMATES SPECTRAL ACCELERATION AT 0.05 SEC PERIOD

CASE NO.	MAGNITUDE	DISTANCE (KM)	MU	SIGMA	SIGMA MU	SIGMA SIGMA
1	5.00	1	0.29995	0.64900	0.57346	0.09300
2	5.00	1	0.35387	0.64800	0.45607	0.09300
3	5.00	5	0.10104	0.66300	0.39369	0.07600
4	5.00	5	0.12677	0.66100	0.32477	0.07800
5	5.80	10	0.16352	0.59300	0.32897	0.03800
6	5.80	20	0.12542	0.60200	0.30661	0.02900
7	6.50	1	0.70488	0.53800	0.39909	0.02100
8	6.50	1	0.75240	0.53800	0.44534	0.02100
9	6.50	1	0.68863	0.53800	0.42224	0.02100
10	6.50	5	0.60759	0.53800	0.35217	0.02100
11	6.50	5	0.44634	0.53800	0.39280	0.02100
12	6.50	50	0.04107	0.56200	0.37716	0.04500
13	6.50	50	0.04319	0.56200	0.39244	0.04500
14	7.00	10	0.39506	0.50300	0.31677	0.04200
15	7.50	50	0.08132	0.50700	0.34371	0.06700
16	7.50	50	0.09054	0.50400	0.33007	0.06200
17	5.00	1	0.10433	0.66000	0.57747	0.07900
18	5.80	5	0.26683	0.58900	0.37690	0.04400
19	5.80	5	0.15869	0.59300	0.42227	0.03800
20	5.00	10	0.12180	0.66100	0.35550	0.07800
21	5.00	10	0.17284	0.65500	0.34457	0.08400
22	5.00	50	0.00992	0.67200	0.45528	0.07100
23	5.00	50	0.01061	0.67200	0.49847	0.07100
24	5.00	160	0.00105	0.67200	0.70417	0.07100
25	5.80	1	0.47645	0.58900	0.48049	0.04400
26	5.80	5	0.41923	0.58900	0.39844	0.04400
27	5.80	5	0.25297	0.58900	0.48167	0.04400
28	5.80	10	0.20304	0.58900	0.36904	0.04400
29	5.80	10	0.28661	0.58900	0.34486	0.04400
30	5.80	10	0.14227	0.59200	0.51980	0.03900
31	5.80	50	0.01533	0.61300	0.69773	0.03300
32	5.80	50	0.01569	0.61300	0.73060	0.03300
33	6.50	5	0.51185	0.53800	0.35587	0.02100
34	6.50	10	0.33468	0.53800	0.33789	0.02100
35	6.50	10	0.45448	0.53800	0.36573	0.02100
36	6.50	10	0.28242	0.53800	0.38217	0.02100
37	6.50	20	0.15973	0.54400	0.31655	0.01900
38	6.50	20	0.21588	0.54000	0.37955	0.02000
39	6.50	20	0.13424	0.54600	0.38097	0.02000
40	6.50	100	0.01552	0.56200	0.53933	0.04500
41	6.50	160	0.00647	0.56200	0.70266	0.04500
42	7.00	1	0.78445	0.50300	0.36471	0.04200
43	7.00	10	0.54715	0.50300	0.35145	0.04200
44	7.00	10	0.34037	0.50300	0.35208	0.04200
45	7.00	50	0.06198	0.52600	0.34852	0.07000
46	7.00	50	0.06921	0.52200	0.33573	0.06400
47	7.50	1	0.84839	0.49300	0.38741	0.05300
48	5.00	10	0.45321	0.49300	0.33056	0.05300
49	5.00	10	0.58293	0.49300	0.39263	0.05300
50	8.00	50	0.09828	0.49900	0.39596	0.05700
51	8.00	160	0.02392	0.51700	0.55379	0.08100

TABLE F3-8
K. W. CAMPBELL: HORIZONTAL POINT ESTIMATES
SPECTRAL ACCELERATION AT 0.10 SEC PERIOD

CASE NO.	MAGNITUDE	DISTANCE (KM)	MU	SIGMA	SIGMA MU	SIGMA SIGMA
1	5.00	1	0.31946	0.66700	0.54046	0.10500
2	5.00	1	0.38194	0.66700	0.58883	0.10500
3	5.00	5	0.11152	0.68100	0.26800	0.08700
4	5.00	5	0.14676	0.68000	0.35697	0.08900
5	5.80	10	0.19289	0.61100	0.26170	0.05500
6	5.80	20	0.15239	0.62000	0.30092	0.04500
7	6.50	1	0.81655	0.55600	0.38087	0.04100
8	6.50	1	0.89724	0.55600	0.51664	0.04100
9	6.50	1	0.81904	0.55600	0.43548	0.04100
10	6.50	5	0.68940	0.55600	0.33578	0.04100
11	6.50	5	0.51563	0.55600	0.30063	0.04100
12	6.50	50	0.05248	0.58100	0.35756	0.04800
13	6.50	50	0.05495	0.58100	0.31781	0.04800
14	7.00	10	0.46234	0.52100	0.32388	0.05200
15	7.50	50	0.10095	0.52500	0.37623	0.06900
16	7.50	50	0.11337	0.52100	0.34333	0.06600
17	5.00	1	0.11685	0.67800	0.38603	0.09000
18	5.80	5	0.32919	0.60700	0.37242	0.06000
19	5.80	5	0.19381	0.61200	0.40046	0.05400
20	5.00	10	0.13338	0.67900	0.38588	0.08900
21	5.00	10	0.18613	0.67400	0.39672	0.09500
22	5.00	50	0.01280	0.69100	0.33995	0.07900
23	5.00	50	0.01369	0.69100	0.38095	0.07900
24	5.00	160	0.00138	0.69100	0.63067	0.07900
25	5.80	1	0.54393	0.60700	0.44841	0.06000
26	5.80	5	0.49569	0.60700	0.34511	0.06000
27	5.80	5	0.29445	0.60700	0.39032	0.06000
28	5.80	10	0.23162	0.60700	0.30997	0.06000
29	5.80	10	0.33316	0.60700	0.34058	0.06000
30	5.80	10	0.16579	0.61100	0.39297	0.05500
31	5.80	50	0.02077	0.63200	0.57492	0.04300
32	5.80	50	0.02054	0.63200	0.64057	0.04300
33	6.50	5	0.59559	0.55600	0.34261	0.04100
34	6.50	10	0.38507	0.55600	0.32038	0.04100
35	6.50	10	0.53056	0.55600	0.38330	0.04100
36	6.50	10	0.32627	0.55600	0.27578	0.04100
37	6.50	20	0.19194	0.56200	0.30485	0.03700
38	6.50	20	0.25021	0.55800	0.34777	0.03900
39	6.50	20	0.15849	0.56400	0.27522	0.03600
40	6.50	100	0.02062	0.58100	0.57368	0.04800
41	6.50	160	0.00819	0.58100	0.70662	0.04800
42	7.00	1	0.90085	0.52100	0.35714	0.05200
43	7.00	10	0.62375	0.52100	0.34521	0.05200
44	7.00	10	0.39794	0.52100	0.25599	0.05200
45	7.00	50	0.07772	0.54400	0.36197	0.07000
46	7.00	50	0.08737	0.54000	0.32754	0.06500
47	7.50	1	0.94122	0.51100	0.37112	0.06000
48	5.00	10	0.51831	0.51100	0.33726	0.06000
49	5.00	10	0.67010	0.51100	0.35946	0.06000
50	8.00	50	0.12622	0.51700	0.45113	0.06300
51	8.00	160	0.02720	0.53500	0.63680	0.08100

TABLE F3-9
K. W. CAMPBELL: HORIZONTAL POINT ESTIMATES
SPECTRAL ACCELERATION AT 0.20 SEC PERIOD

CASE NO.	MAGNITUDE	DISTANCE (KM)	MU	SIGMA	SIGMA MU	SIGMA SIGMA
1	5.00	1	0.24514	0.69800	0.51382	0.10600
2	5.00	1	0.29141	0.69800	0.56237	0.10600
3	5.00	5	0.09037	0.71200	0.26798	0.08700
4	5.00	5	0.11726	0.71000	0.31413	0.08800
5	5.80	10	0.18239	0.64300	0.24869	0.06000
6	5.80	20	0.14853	0.65200	0.30883	0.04800
7	6.50	1	0.75359	0.58900	0.41983	0.05000
8	6.50	1	0.81648	0.58900	0.53010	0.05000
9	6.50	1	0.75665	0.58900	0.47442	0.05000
10	6.50	5	0.64478	0.58900	0.37454	0.05000
11	6.50	5	0.49146	0.58900	0.31927	0.05000
12	6.50	50	0.05814	0.61300	0.37635	0.05000
13	6.50	50	0.06129	0.61300	0.30588	0.05000
14	7.00	10	0.45918	0.55500	0.34805	0.06000
15	7.50	50	0.12173	0.55900	0.43356	0.07200
16	7.50	50	0.13682	0.55500	0.39847	0.07000
17	5.00	1	0.09159	0.70900	0.45519	0.09000
18	5.80	5	0.28404	0.63900	0.40519	0.06500
19	5.80	5	0.18766	0.64300	0.33587	0.05900
20	5.00	10	0.10850	0.71000	0.31132	0.08900
21	5.00	10	0.14702	0.70500	0.34044	0.09600
22	5.00	50	0.01329	0.72100	0.28452	0.07800
23	5.00	50	0.01319	0.72100	0.37125	0.07800
24	5.00	160	0.00201	0.72100	0.58304	0.07800
25	5.80	1	0.47856	0.63900	0.44745	0.06500
26	5.80	5	0.42347	0.63900	0.35604	0.06500
27	5.80	5	0.26605	0.63900	0.33556	0.06500
28	5.80	10	0.21177	0.63900	0.31216	0.06500
29	5.80	10	0.29919	0.63900	0.33753	0.06500
30	5.80	10	0.15993	0.64300	0.31039	0.06000
31	5.80	50	0.02107	0.66300	0.61995	0.04300
32	5.80	50	0.02433	0.66300	0.50886	0.04300
33	6.50	5	0.55663	0.58900	0.36255	0.05000
34	6.50	10	0.36053	0.58900	0.31343	0.05000
35	6.50	10	0.48504	0.58900	0.36053	0.05000
36	6.50	10	0.31944	0.58900	0.29063	0.05000
37	6.50	20	0.18803	0.59500	0.30149	0.04500
38	6.50	20	0.25742	0.59100	0.37609	0.04800
39	6.50	20	0.16526	0.59700	0.26956	0.04400
40	6.50	100	0.02553	0.61300	0.56153	0.05000
41	6.50	160	0.01169	0.61300	0.69349	0.05000
42	7.00	1	0.84222	0.55500	0.39185	0.06000
43	7.00	10	0.60683	0.55500	0.35290	0.06000
44	7.00	10	0.40463	0.55500	0.29277	0.06000
45	7.00	50	0.09109	0.57700	0.39949	0.07100
46	7.00	50	0.10123	0.57400	0.35501	0.06700
47	7.50	1	0.94693	0.54500	0.45621	0.06800
48	5.00	10	0.54808	0.54500	0.40912	0.06800
49	5.00	10	0.67101	0.54500	0.37280	0.06800
50	8.00	50	0.15397	0.55100	0.49137	0.06800
51	8.00	160	0.03877	0.56800	0.71848	0.08100

TABLE F3-10
K. W. CAMPBELL: HORIZONTAL POINT ESTIMATES
SPECTRAL ACCELERATION AT 0.50 SEC PERIOD

CASE NO.	MAGNITUDE	DISTANCE (KM)	MU	SIGMA	SIGMA MU	SIGMA SIGMA
1	5.00	1	0.11568	0.75700	0.42849	0.11700
2	5.00	1	0.14184	0.75700	0.45804	0.11700
3	5.00	5	0.04467	0.77100	0.33880	0.09500
4	5.00	5	0.05942	0.77000	0.40063	0.09700
5	5.80	10	0.11056	0.70400	0.26663	0.07600
6	5.80	20	0.09438	0.71300	0.26309	0.06200
7	6.50	1	0.55089	0.65200	0.27903	0.06800
8	6.50	1	0.58164	0.65200	0.36035	0.06800
9	6.50	1	0.53766	0.65200	0.31778	0.06800
10	6.50	5	0.46034	0.65200	0.24920	0.06800
11	6.50	5	0.34131	0.65200	0.26816	0.06800
12	6.50	50	0.04893	0.67500	0.30693	0.05200
13	6.50	50	0.05328	0.67500	0.31414	0.05200
14	7.00	10	0.37140	0.61800	0.32561	0.07400
15	7.50	50	0.12381	0.62200	0.34020	0.07600
16	7.50	50	0.13854	0.61900	0.34512	0.07600
17	5.00	1	0.04695	0.76800	0.54042	0.09900
18	5.80	5	0.18171	0.70100	0.27618	0.08100
19	5.80	5	0.10411	0.70400	0.35615	0.07500
20	5.00	10	0.05090	0.76900	0.24751	0.09800
21	5.00	10	0.06981	0.76400	0.28540	0.10600
22	5.00	50	0.00756	0.78000	0.30281	0.08300
23	5.00	50	0.00872	0.78000	0.27334	0.08300
24	5.00	160	0.00175	0.78000	0.57902	0.08300
25	5.80	1	0.29175	0.70100	0.33228	0.08100
26	5.80	5	0.26091	0.70100	0.32768	0.08100
27	5.80	5	0.15771	0.70100	0.32862	0.08100
28	5.80	10	0.13888	0.70100	0.28409	0.08100
29	5.80	10	0.19833	0.70100	0.31923	0.08100
30	5.80	10	0.09264	0.70400	0.37384	0.07600
31	5.80	50	0.01541	0.72300	0.62511	0.05000
32	5.80	50	0.01530	0.72300	0.74242	0.05000
33	6.50	5	0.40434	0.65200	0.31340	0.06800
34	6.50	10	0.27262	0.65200	0.33338	0.06800
35	6.50	10	0.37015	0.65200	0.33804	0.06800
36	6.50	10	0.22516	0.65200	0.30349	0.06800
37	6.50	20	0.14123	0.65800	0.28028	0.06100
38	6.50	20	0.19190	0.65400	0.34682	0.06600
39	6.50	20	0.12504	0.65900	0.26480	0.05900
40	6.50	100	0.02596	0.67500	0.45449	0.05200
41	6.50	160	0.01320	0.67500	0.63553	0.05200
42	7.00	1	0.68767	0.61800	0.27434	0.07400
43	7.00	10	0.51458	0.61800	0.31744	0.07400
44	7.00	10	0.31198	0.61800	0.27130	0.07400
45	7.00	50	0.08329	0.64000	0.31709	0.07100
46	7.00	50	0.09415	0.63700	0.35810	0.06900
47	7.50	1	0.79216	0.60900	0.28452	0.07900
48	5.00	10	0.45704	0.60900	0.29608	0.07900
49	5.00	10	0.59211	0.60900	0.34164	0.07900
50	8.00	50	0.16426	0.61500	0.38295	0.07600
51	8.00	160	0.05602	0.63100	0.60572	0.07900

TABLE F3-11
K. W. CAMPBELL: HORIZONTAL POINT ESTIMATES
SPECTRAL ACCELERATION AT 1.00 SEC PERIOD

CASE NO.	MAGNITUDE	DISTANCE (KM)	MU	SIGMA	SIGMA MU	SIGMA SIGMA
1	5.00	1	0.04731	0.79800	0.37638	0.12400
2	5.00	1	0.05820	0.79800	0.43594	0.12400
3	5.00	5	0.01850	0.81100	0.35780	0.10100
4	5.00	5	0.02500	0.81000	0.50206	0.10300
5	5.80	10	0.05395	0.74600	0.27684	0.09100
6	5.80	20	0.04636	0.75500	0.25786	0.07700
7	6.50	1	0.30772	0.69600	0.21691	0.09000
8	6.50	1	0.31859	0.69600	0.32054	0.09000
9	6.50	1	0.29143	0.69600	0.29693	0.09000
10	6.50	5	0.26238	0.69600	0.24222	0.09000
11	6.50	5	0.18199	0.69600	0.32160	0.09000
12	6.50	50	0.03129	0.71900	0.30774	0.06900
13	6.50	50	0.03182	0.71900	0.38146	0.06900
14	7.00	10	0.21434	0.66400	0.25635	0.09500
15	7.50	50	0.08372	0.66800	0.28904	0.09400
16	7.50	50	0.09308	0.66400	0.32776	0.09500
17	5.00	1	0.01924	0.80900	0.66543	0.10500
18	5.80	5	0.08693	0.74300	0.48805	0.09700
19	5.80	5	0.04984	0.74700	0.48477	0.09000
20	5.00	10	0.02033	0.80900	0.18365	0.10400
21	5.00	10	0.02758	0.80500	0.22099	0.11200
22	5.00	50	0.00313	0.82000	0.40294	0.08700
23	5.00	50	0.00352	0.82000	0.36505	0.08700
24	5.00	160	0.00095	0.82000	0.57773	0.08700
25	5.80	1	0.13803	0.74300	0.38888	0.09700
26	5.80	5	0.12638	0.74300	0.39040	0.09700
27	5.80	5	0.07274	0.74300	0.44504	0.09700
28	5.80	10	0.06566	0.74300	0.28541	0.09700
29	5.80	10	0.09740	0.74300	0.32030	0.09700
30	5.80	10	0.04700	0.74600	0.39645	0.09100
31	5.80	50	0.00820	0.76500	0.60472	0.06400
32	5.80	50	0.00877	0.76500	0.70971	0.06400
33	6.50	5	0.21495	0.69600	0.28064	0.09000
34	6.50	10	0.15359	0.69600	0.31885	0.09000
35	6.50	10	0.21413	0.69600	0.31854	0.09000
36	6.50	10	0.12467	0.69600	0.32233	0.09000
37	6.50	20	0.07990	0.70200	0.27435	0.08300
38	6.50	20	0.10688	0.69800	0.37329	0.08700
39	6.50	20	0.07013	0.70400	0.31209	0.08100
40	6.50	100	0.01715	0.71900	0.38208	0.06900
41	6.50	160	0.00859	0.71900	0.61184	0.06900
42	7.00	1	0.37706	0.66400	0.28714	0.09500
43	7.00	10	0.30690	0.66400	0.31404	0.09500
44	7.00	10	0.18551	0.66400	0.29378	0.09500
45	7.00	50	0.05381	0.68500	0.33302	0.08500
46	7.00	50	0.05819	0.68200	0.40688	0.08600
47	7.50	1	0.47539	0.65400	0.34507	0.10100
48	5.00	10	0.28707	0.65400	0.25438	0.10100
49	5.00	10	0.38674	0.65400	0.42445	0.10100
50	8.00	50	0.11479	0.66000	0.32491	0.09700
51	8.00	160	0.04590	0.67700	0.47887	0.09400

TABLE F3-12
K. W. CAMPBELL: HORIZONTAL POINT ESTIMATES
SPECTRAL ACCELERATION AT 2.00 SEC PERIOD

CASE NO.	MAGNITUDE	DISTANCE (KM)	MU	SIGMA	SIGMA MU	SIGMA SIGMA
1	5.00	1	0.01180	0.84400	0.52384	0.13400
2	5.00	1	0.01594	0.84400	0.48973	0.13400
3	5.00	5	0.00503	0.85700	0.56941	0.11100
4	5.00	5	0.00690	0.85600	0.59896	0.11300
5	5.80	10	0.01992	0.79500	0.43127	0.11100
6	5.80	20	0.01611	0.80300	0.42186	0.09800
7	6.50	1	0.13960	0.74700	0.28682	0.11500
8	6.50	1	0.14308	0.74700	0.29839	0.11500
9	6.50	1	0.12991	0.74700	0.28765	0.11500
10	6.50	5	0.11313	0.74700	0.31483	0.11500
11	6.50	5	0.08903	0.74700	0.32982	0.11500
12	6.50	50	0.01493	0.76900	0.45494	0.09400
13	6.50	50	0.01511	0.76900	0.56184	0.09400
14	7.00	10	0.10504	0.71600	0.32105	0.12200
15	7.50	50	0.04502	0.72000	0.53620	0.11900
16	7.50	50	0.04869	0.71700	0.62436	0.12000
17	5.00	1	0.00456	0.85400	0.85279	0.11500
18	5.80	5	0.03617	0.79200	0.45125	0.11600
19	5.80	5	0.02138	0.79500	0.48735	0.11000
20	5.00	10	0.00618	0.85500	0.33902	0.11400
21	5.00	10	0.00816	0.85000	0.35573	0.12200
22	5.00	50	0.00105	0.86600	0.51825	0.09600
23	5.00	50	0.00106	0.86600	0.58131	0.09600
24	5.00	160	0.00042	0.86600	0.76188	0.09600
25	5.80	1	0.05545	0.79200	0.35937	0.11600
26	5.80	5	0.05028	0.79200	0.41450	0.11600
27	5.80	5	0.03324	0.79200	0.40843	0.11600
28	5.80	10	0.02379	0.79200	0.39066	0.11600
29	5.80	10	0.03230	0.79200	0.40620	0.11600
30	5.80	10	0.01960	0.79500	0.47817	0.11100
31	5.80	50	0.00312	0.81300	0.82942	0.08400
32	5.80	50	0.00319	0.81300	0.88153	0.08400
33	6.50	5	0.10114	0.74700	0.30082	0.11500
34	6.50	10	0.06829	0.74700	0.31275	0.11500
35	6.50	10	0.08870	0.74700	0.30715	0.11500
36	6.50	10	0.05808	0.74700	0.38263	0.11500
37	6.50	20	0.03926	0.75200	0.31400	0.10900
38	6.50	20	0.04870	0.74900	0.36120	0.11300
39	6.50	20	0.03298	0.75400	0.43697	0.10600
40	6.50	100	0.00847	0.76900	0.43990	0.09400
41	6.50	160	0.00401	0.76900	0.79330	0.09400
42	7.00	1	0.19350	0.71600	0.25225	0.12200
43	7.00	10	0.13692	0.71600	0.30921	0.12200
44	7.00	10	0.09273	0.71600	0.38105	0.12200
45	7.00	50	0.02879	0.73700	0.41198	0.10800
46	7.00	50	0.03064	0.73400	0.50676	0.11000
47	7.50	1	0.23284	0.70700	0.28003	0.12700
48	5.00	10	0.14295	0.70700	0.42464	0.12700
49	5.00	10	0.17572	0.70700	0.47320	0.12700
50	8.00	50	0.07185	0.71300	0.36780	0.12300
51	8.00	160	0.03450	0.72900	0.56066	0.11600

TABLE F3-13
K. W. CAMPBELL: HORIZONTAL POINT ESTIMATES
SPECTRAL ACCELERATION AT 3.33 SEC PERIOD

CASE NO.	MAGNITUDE	DISTANCE (KM)	MU	SIGMA	SIGMA MU	SIGMA SIGMA
1	5.00	1	0.00340	0.84700	0.71550	0.13900
2	5.00	1	0.00459	0.84700	0.74832	0.13900
3	5.00	5	0.00147	0.86000	0.69703	0.11100
4	5.00	5	0.00208	0.85900	0.80285	0.11300
5	5.80	10	0.00841	0.80000	0.53073	0.11100
6	5.80	20	0.00609	0.80800	0.55284	0.09800
7	6.50	1	0.07209	0.75300	0.35350	0.11500
8	6.50	1	0.07362	0.75300	0.32531	0.11500
9	6.50	1	0.06791	0.75300	0.34277	0.11500
10	6.50	5	0.06125	0.75300	0.36731	0.11500
11	6.50	5	0.05000	0.75300	0.40127	0.11500
12	6.50	50	0.00797	0.77500	0.60584	0.09400
13	6.50	50	0.00756	0.77500	0.72195	0.09400
14	7.00	10	0.05823	0.72300	0.42429	0.12200
15	7.50	50	0.02830	0.72600	0.51711	0.11900
16	7.50	50	0.02808	0.72300	0.65830	0.12000
17	5.00	1	0.00131	0.85800	0.89531	0.11500
18	5.80	5	0.01525	0.79600	0.49342	0.11600
19	5.80	5	0.00806	0.80000	0.56937	0.11000
20	5.00	10	0.00189	0.85800	0.57155	0.11400
21	5.00	10	0.00241	0.85400	0.53519	0.12400
22	5.00	50	0.00037	0.86900	0.60821	0.09600
23	5.00	50	0.00038	0.86900	0.58191	0.09600
24	5.00	160	0.00012	0.86900	0.76686	0.09600
25	5.80	1	0.02275	0.79600	0.48024	0.11600
26	5.80	5	0.02255	0.79600	0.50198	0.11600
27	5.80	5	0.01578	0.79600	0.45116	0.11600
28	5.80	10	0.01102	0.79600	0.51758	0.11600
29	5.80	10	0.01231	0.79600	0.55565	0.11600
30	5.80	10	0.00752	0.79900	0.69946	0.11100
31	5.80	50	0.00141	0.81800	0.85972	0.08400
32	5.80	50	0.00119	0.81800	0.96615	0.08400
33	6.50	5	0.05567	0.75300	0.38091	0.11500
34	6.50	10	0.03588	0.75300	0.41885	0.11500
35	6.50	10	0.04295	0.75300	0.38912	0.11500
36	6.50	10	0.02954	0.75300	0.54536	0.11500
37	6.50	20	0.01958	0.75800	0.44232	0.10900
38	6.50	20	0.02211	0.75500	0.50389	0.11300
39	6.50	20	0.01670	0.76000	0.59572	0.10600
40	6.50	100	0.00354	0.77500	0.60831	0.09400
41	6.50	160	0.00212	0.77500	0.78530	0.09400
42	7.00	1	0.11288	0.72300	0.33501	0.12200
43	7.00	10	0.07286	0.72300	0.34848	0.12200
44	7.00	10	0.05019	0.72300	0.51401	0.12200
45	7.00	50	0.01640	0.74400	0.52213	0.10800
46	7.00	50	0.01664	0.74000	0.61464	0.11000
47	7.50	1	0.14997	0.71300	0.33329	0.12700
48	5.00	10	0.08412	0.71300	0.51248	0.12700
49	5.00	10	0.10035	0.71300	0.50394	0.12700
50	8.00	50	0.04851	0.71900	0.41432	0.12300
51	8.00	160	0.02198	0.73500	0.49377	0.11600

TABLE F3-14
K. W. CAMPBELL: HORIZONTAL POINT ESTIMATES
PEAK GROUND VELOCITY

CASE NO.	MAGNITUDE	DISTANCE (KM)	MU	SIGMA	SIGMA MU	SIGMA SIGMA
1	5.00	1	6.63860	0.73100	0.57332	0.19600
2	5.00	1	8.18581	0.73100	0.58301	0.19600
3	5.00	5	2.26876	0.73100	0.29743	0.13100
4	5.00	5	3.09310	0.73100	0.45337	0.13800
5	5.80	10	5.96975	0.66600	0.25136	0.14200
6	5.80	20	4.80004	0.66800	0.21667	0.10900
7	6.50	1	37.28022	0.61100	0.32930	0.13800
8	6.50	1	38.74037	0.61100	0.38815	0.13800
9	6.50	1	35.36159	0.61100	0.36600	0.13800
10	6.50	5	30.79080	0.61100	0.23019	0.13800
11	6.50	5	22.13452	0.61100	0.31591	0.13800
12	6.50	50	2.88233	0.61900	0.32730	0.10500
13	6.50	50	2.98282	0.61900	0.36086	0.10500
14	7.00	10	23.47610	0.57300	0.24734	0.13800
15	7.50	50	8.32337	0.56600	0.34307	0.13200
16	7.50	50	9.10473	0.56400	0.38677	0.13100
17	5.00	1	2.34005	0.73000	0.59039	0.14400
18	5.80	5	10.65910	0.66600	0.41477	0.15600
19	5.80	5	5.87083	0.66600	0.39903	0.14000
20	5.00	10	2.56407	0.73100	0.25909	0.14000
21	5.00	10	3.58413	0.73000	0.25154	0.16300
22	5.00	50	0.31756	0.73500	0.37796	0.09300
23	5.00	50	0.35317	0.73500	0.36130	0.09300
24	5.00	160	0.06570	0.73500	0.69923	0.09300
25	5.80	1	17.65386	0.66600	0.42437	0.15600
26	5.80	5	15.57512	0.66600	0.35315	0.15600
27	5.80	5	9.48561	0.66600	0.32309	0.15600
28	5.80	10	7.32386	0.66600	0.29310	0.15600
29	5.80	10	10.76958	0.66600	0.26768	0.15600
30	5.80	10	5.28294	0.66600	0.36777	0.14200
31	5.80	50	0.75865	0.67300	0.65835	0.08100
32	5.80	50	0.79487	0.67300	0.66997	0.08100
33	6.50	5	25.12508	0.61100	0.28158	0.13800
34	6.50	10	16.30602	0.61100	0.26409	0.13800
35	6.50	10	22.90958	0.61100	0.25665	0.13800
36	6.50	10	13.66907	0.61100	0.30957	0.13800
37	6.50	20	8.19863	0.61200	0.23433	0.12300
38	6.50	20	11.05582	0.61100	0.29057	0.13200
39	6.50	20	7.12903	0.61200	0.30575	0.11800
40	6.50	100	1.45679	0.61900	0.38915	0.10500
41	6.50	160	0.55795	0.61900	0.73544	0.10500
42	7.00	1	47.49108	0.57300	0.32957	0.13800
43	7.00	10	33.87643	0.57300	0.41390	0.13800
44	7.00	10	20.06264	0.57300	0.32681	0.13800
45	7.00	50	5.24521	0.58200	0.29611	0.13100
46	7.00	50	5.66115	0.58000	0.34570	0.12700
47	7.50	1	58.27975	0.56200	0.55636	0.13900
48	5.00	10	30.98703	0.56200	0.34253	0.13900
49	5.00	10	41.76862	0.56200	0.65424	0.13900
50	8.00	50	12.66615	0.56300	0.36846	0.13300
51	8.00	160	4.76428	0.57200	0.49541	0.14100

TABLE F3-15
K. W. CAMPBELL: VERTICAL POINT ESTIMATES
PEAK GROUND ACCELERATION

CASE NO.	MAGNITUDE	DISTANCE (KM)	MU	SIGMA	SIGMA MU	SIGMA SIGMA
1	5.00	1	0.10617	0.68700	0.64998	0.13000
2	5.00	1	0.12027	0.68700	0.48743	0.13000
3	5.00	5	0.03371	0.68800	0.45765	0.09000
4	5.00	5	0.04019	0.68700	0.38728	0.09200
5	5.80	10	0.05913	0.66800	0.34449	0.07500
6	5.80	20	0.05682	0.67100	0.42437	0.04400
7	6.50	1	0.31800	0.59100	0.39266	0.10900
8	6.50	1	0.34623	0.59100	0.35709	0.10900
9	6.50	1	0.32903	0.59100	0.37305	0.10900
10	6.50	5	0.28446	0.59100	0.28168	0.10900
11	6.50	5	0.20884	0.59100	0.35886	0.10900
12	6.50	50	0.01797	0.60000	0.34213	0.15600
13	6.50	50	0.02050	0.60000	0.38721	0.15600
14	7.00	10	0.17951	0.58300	0.28892	0.08500
15	7.50	50	0.03787	0.58800	0.29717	0.12000
16	7.50	50	0.04513	0.58600	0.36054	0.11000
17	5.00	1	0.03797	0.68700	0.51445	0.09400
18	5.80	5	0.09408	0.66800	0.47608	0.09000
19	5.80	5	0.06481	0.66900	0.42824	0.07300
20	5.00	10	0.03969	0.68700	0.33012	0.09300
21	5.00	10	0.06640	0.68600	0.35909	0.10500
22	5.00	50	0.00368	0.69100	0.47066	0.07900
23	5.00	50	0.00391	0.69100	0.45205	0.07900
24	5.00	160	0.00035	0.69100	0.71627	0.07900
25	5.80	1	0.18222	0.66800	0.53577	0.09000
26	5.80	5	0.18198	0.66800	0.39652	0.09000
27	5.80	5	0.10949	0.66800	0.38363	0.09000
28	5.80	10	0.07359	0.66800	0.35795	0.09000
29	5.80	10	0.12285	0.66800	0.36717	0.09000
30	5.80	10	0.06359	0.66800	0.37421	0.07600
31	5.80	50	0.00559	0.67700	0.77894	0.03200
32	5.80	50	0.00682	0.67700	0.75640	0.03200
33	6.50	5	0.22965	0.59100	0.32717	0.10900
34	6.50	10	0.13989	0.59100	0.30890	0.10900
35	6.50	10	0.21909	0.59100	0.41332	0.10900
36	6.50	10	0.12736	0.59100	0.34857	0.10900
37	6.50	20	0.06718	0.59200	0.28678	0.11500
38	6.50	20	0.10211	0.59100	0.48324	0.11100
39	6.50	20	0.05939	0.59200	0.35464	0.11800
40	6.50	100	0.00714	0.60000	0.45674	0.15600
41	6.50	160	0.00213	0.60000	0.77441	0.15600
42	7.00	1	0.37762	0.58300	0.33209	0.08500
43	7.00	10	0.27600	0.58300	0.38638	0.08500
44	7.00	10	0.16227	0.58300	0.34348	0.08500
45	7.00	50	0.02686	0.59500	0.26030	0.14900
46	7.00	50	0.03247	0.59200	0.37990	0.13600
47	7.50	1	0.48778	0.58100	0.41359	0.08500
48	5.00	10	0.21561	0.58100	0.29680	0.08500
49	5.00	10	0.31344	0.58100	0.46850	0.08500
50	8.00	50	0.04782	0.58400	0.44735	0.09800
51	8.00	160	0.01053	0.59400	0.50852	0.15200

TABLE F3-16
K. W. CAMPBELL: VERTICAL POINT ESTIMATES
SPECTRAL ACCELERATION AT 0.05 SEC PERIOD

CASE NO.	MAGNITUDE	DISTANCE (KM)	MU	SIGMA	SIGMA MU	SIGMA SIGMA
1	5.00	1	0.23760	0.71600	0.71755	0.09300
2	5.00	1	0.26754	0.71600	0.51334	0.09300
3	5.00	5	0.06958	0.71900	0.54870	0.07600
4	5.00	5	0.08429	0.71900	0.42287	0.07800
5	5.80	10	0.11491	0.69800	0.48708	0.06100
6	5.80	20	0.10453	0.70200	0.41241	0.04300
7	6.50	1	0.69233	0.62500	0.51922	0.05900
8	6.50	1	0.74236	0.62500	0.45460	0.05900
9	6.50	1	0.71168	0.62500	0.46441	0.05900
10	6.50	5	0.61465	0.62500	0.34515	0.05900
11	6.50	5	0.43725	0.62500	0.47850	0.05900
12	6.50	50	0.02888	0.63800	0.46754	0.13400
13	6.50	50	0.03344	0.63800	0.48807	0.13400
14	7.00	10	0.36565	0.61900	0.39134	0.05800
15	7.50	50	0.06053	0.62800	0.38360	0.10900
16	7.50	50	0.07270	0.62500	0.40772	0.09600
17	5.00	1	0.07961	0.71800	0.58943	0.07900
18	5.80	5	0.18554	0.69700	0.63269	0.07200
19	5.80	5	0.12725	0.69800	0.53209	0.06000
20	5.00	10	0.08320	0.71900	0.46077	0.07800
21	5.00	10	0.14144	0.71700	0.35155	0.08400
22	5.00	50	0.00638	0.72400	0.47071	0.07100
23	5.00	50	0.00725	0.72400	0.45425	0.07100
24	5.00	160	0.00045	0.72400	0.76637	0.07100
25	5.80	1	0.37779	0.69700	0.69485	0.07200
26	5.80	5	0.35869	0.69700	0.51274	0.07200
27	5.80	5	0.22185	0.69700	0.53661	0.07200
28	5.80	10	0.14582	0.69700	0.50848	0.07200
29	5.80	10	0.23265	0.69700	0.47761	0.07200
30	5.80	10	0.12109	0.69800	0.55926	0.06200
31	5.80	50	0.00907	0.70900	0.84953	0.05000
32	5.80	50	0.01073	0.70900	0.90667	0.05000
33	6.50	5	0.49007	0.62500	0.41182	0.05900
34	6.50	10	0.28680	0.62500	0.38995	0.05900
35	6.50	10	0.44913	0.62500	0.51482	0.05900
36	6.50	10	0.26088	0.62500	0.45661	0.05900
37	6.50	20	0.12930	0.62800	0.36029	0.07400
38	6.50	20	0.19884	0.62600	0.55359	0.06400
39	6.50	20	0.11330	0.62800	0.46291	0.08100
40	6.50	100	0.00938	0.63800	0.56693	0.13400
41	6.50	160	0.00294	0.63800	0.79473	0.13400
42	7.00	1	0.82482	0.61900	0.45149	0.05800
43	7.00	10	0.56933	0.61900	0.51632	0.05800
44	7.00	10	0.33153	0.61900	0.45218	0.05800
45	7.00	50	0.04445	0.63300	0.35876	0.14200
46	7.00	50	0.05378	0.63100	0.42050	0.12700
47	7.50	1	1.04288	0.61900	0.49211	0.05800
48	5.00	10	0.43691	0.61900	0.43615	0.05800
49	5.00	10	0.64200	0.61900	0.61318	0.05800
50	8.00	50	0.07128	0.62300	0.53204	0.08000
51	8.00	160	0.01164	0.63500	0.60982	0.14400

TABLE F3-17
K. W. CAMPBELL: VERTICAL POINT ESTIMATES
SPECTRAL ACCELERATION AT 0.10 SEC PERIOD

CASE NO.	MAGNITUDE	DISTANCE (KM)	MU	SIGMA	SIGMA MU	SIGMA SIGMA
1	5.00	1	0.21064	0.72400	0.67833	0.10500
2	5.00	1	0.24045	0.72400	0.55691	0.10500
3	5.00	5	0.06968	0.72700	0.34004	0.08700
4	5.00	5	0.08364	0.72600	0.27315	0.08900
5	5.80	10	0.12890	0.70500	0.30013	0.06200
6	5.80	20	0.11903	0.70900	0.44955	0.04500
7	6.50	1	0.72475	0.63100	0.38074	0.05900
8	6.50	1	0.79023	0.63100	0.33160	0.05900
9	6.50	1	0.75754	0.63100	0.36328	0.05900
10	6.50	5	0.62377	0.63100	0.27546	0.05900
11	6.50	5	0.46851	0.63100	0.33452	0.05900
12	6.50	50	0.03436	0.64200	0.38397	0.13300
13	6.50	50	0.03934	0.64200	0.39589	0.13300
14	7.00	10	0.39108	0.62400	0.26982	0.05700
15	7.50	50	0.07118	0.63200	0.34919	0.10800
16	7.50	50	0.08384	0.63000	0.35735	0.09500
17	5.00	1	0.07804	0.72600	0.39342	0.09000
18	5.80	5	0.20901	0.70400	0.41368	0.07200
19	5.80	5	0.14432	0.70500	0.36497	0.06100
20	5.00	10	0.08141	0.72600	0.37815	0.08900
21	5.00	10	0.13404	0.72500	0.46066	0.09500
22	5.00	50	0.00760	0.73100	0.33794	0.07900
23	5.00	50	0.00826	0.73100	0.33066	0.07900
24	5.00	160	0.00067	0.73100	0.69204	0.07900
25	5.80	1	0.41203	0.70400	0.47059	0.07200
26	5.80	5	0.38911	0.70400	0.41031	0.07200
27	5.80	5	0.23262	0.70400	0.38951	0.07200
28	5.80	10	0.15386	0.70400	0.36628	0.07200
29	5.80	10	0.26079	0.70400	0.40986	0.07200
30	5.80	10	0.13284	0.70500	0.39231	0.06200
31	5.80	50	0.01195	0.71500	0.68224	0.05000
32	5.80	50	0.01288	0.71500	0.79681	0.05000
33	6.50	5	0.50962	0.63100	0.28926	0.05900
34	6.50	10	0.30867	0.63100	0.27422	0.05900
35	6.50	10	0.47532	0.63100	0.41244	0.05900
36	6.50	10	0.28248	0.63100	0.31842	0.05900
37	6.50	20	0.14008	0.63300	0.27161	0.07400
38	6.50	20	0.21477	0.63200	0.47371	0.06400
39	6.50	20	0.12621	0.63400	0.31463	0.08000
40	6.50	100	0.01222	0.64200	0.52353	0.13300
41	6.50	160	0.00415	0.64200	0.67642	0.13300
42	7.00	1	0.86904	0.62400	0.31192	0.05700
43	7.00	10	0.60504	0.62400	0.38639	0.05700
44	7.00	10	0.35774	0.62400	0.30515	0.05700
45	7.00	50	0.05183	0.63700	0.31506	0.14100
46	7.00	50	0.06269	0.63500	0.35867	0.12700
47	7.50	1	1.08842	0.62400	0.40714	0.06000
48	5.00	10	0.46505	0.62400	0.31279	0.06000
49	5.00	10	0.68518	0.62400	0.45843	0.06000
50	8.00	50	0.08713	0.62700	0.50123	0.08000
51	8.00	160	0.01378	0.63900	0.63848	0.14400

TABLE F3-18
K. W. CAMPBELL: VERTICAL POINT ESTIMATES
SPECTRAL ACCELERATION AT 0.20 SEC PERIOD

CASE NO.	MAGNITUDE	DISTANCE (KM)	MU	SIGMA	SIGMA MU	SIGMA SIGMA
1	5.00	1	0.11928	0.71300	0.69994	0.10600
2	5.00	1	0.12934	0.71300	0.65252	0.10600
3	5.00	5	0.04483	0.71500	0.26598	0.08700
4	5.00	5	0.04964	0.71500	0.27857	0.08800
5	5.80	10	0.08995	0.70100	0.24905	0.07300
6	5.80	20	0.08656	0.70400	0.57827	0.07200
7	6.50	1	0.45518	0.63300	0.36983	0.06600
8	6.50	1	0.46998	0.63300	0.37398	0.06600
9	6.50	1	0.45167	0.63300	0.40249	0.06600
10	6.50	5	0.40641	0.63300	0.36599	0.06600
11	6.50	5	0.29733	0.63300	0.35891	0.06600
12	6.50	50	0.02952	0.64300	0.40872	0.14700
13	6.50	50	0.03323	0.64300	0.45699	0.14700
14	7.00	10	0.27965	0.62900	0.32990	0.07000
15	7.50	50	0.06577	0.63600	0.43973	0.11900
16	7.50	50	0.07616	0.63400	0.45761	0.10700
17	5.00	1	0.04847	0.71400	0.30686	0.09000
18	5.80	5	0.13445	0.70000	0.39023	0.07700
19	5.80	5	0.09665	0.70100	0.41715	0.07200
20	5.00	10	0.04786	0.71500	0.33256	0.08900
21	5.00	10	0.08233	0.71300	0.61085	0.09600
22	5.00	50	0.00667	0.71800	0.39161	0.07800
23	5.00	50	0.00673	0.71800	0.28190	0.07800
24	5.00	160	0.00081	0.71800	0.69006	0.07800
25	5.80	1	0.25542	0.70000	0.46322	0.07700
26	5.80	5	0.25377	0.70000	0.50751	0.07700
27	5.80	5	0.15656	0.70000	0.35465	0.07700
28	5.80	10	0.11098	0.70000	0.28802	0.07700
29	5.80	10	0.17952	0.70000	0.52898	0.07700
30	5.80	10	0.09258	0.70100	0.34330	0.07300
31	5.80	50	0.01067	0.70900	0.64581	0.09000
32	5.80	50	0.01346	0.70900	0.67833	0.09000
33	6.50	5	0.32873	0.63300	0.33642	0.06600
34	6.50	10	0.20397	0.63300	0.30833	0.06600
35	6.50	10	0.30921	0.63300	0.43675	0.06600
36	6.50	10	0.19094	0.63300	0.34353	0.06600
37	6.50	20	0.10513	0.63400	0.34800	0.08500
38	6.50	20	0.15489	0.63300	0.55000	0.07300
39	6.50	20	0.09544	0.63500	0.36308	0.09100
40	6.50	100	0.01331	0.64300	0.60613	0.14700
41	6.50	160	0.00545	0.64300	0.70300	0.14700
42	7.00	1	0.55351	0.62900	0.35046	0.07000
43	7.00	10	0.41380	0.62900	0.40295	0.07000
44	7.00	10	0.25411	0.62900	0.35382	0.07000
45	7.00	50	0.04676	0.64100	0.37306	0.15200
46	7.00	50	0.05622	0.63900	0.45840	0.13800
47	7.50	1	0.70222	0.62900	0.49575	0.07000
48	5.00	10	0.34508	0.62900	0.36290	0.07000
49	5.00	10	0.47169	0.62900	0.40407	0.07000
50	8.00	50	0.08523	0.63200	0.56350	0.09100
51	8.00	160	0.01902	0.64200	0.73033	0.15500

TABLE F3-19
K. W. CAMPBELL: VERTICAL POINT ESTIMATES
SPECTRAL ACCELERATION AT 0.50 SEC PERIOD

CASE NO.	MAGNITUDE	DISTANCE (KM)	MU	SIGMA	SIGMA MU	SIGMA SIGMA
1	5.00	1	0.04732	0.73400	0.70969	0.11700
2	5.00	1	0.05404	0.73400	0.62177	0.11700
3	5.00	5	0.01724	0.73500	0.41310	0.09500
4	5.00	5	0.02123	0.73500	0.36666	0.09700
5	5.80	10	0.04848	0.71900	0.28977	0.07600
6	5.80	20	0.04940	0.72200	0.65510	0.07700
7	6.50	1	0.24900	0.65000	0.25799	0.08000
8	6.50	1	0.27118	0.65000	0.30046	0.08000
9	6.50	1	0.25620	0.65000	0.32164	0.08000
10	6.50	5	0.22341	0.65000	0.33943	0.08000
11	6.50	5	0.16858	0.65000	0.35760	0.08000
12	6.50	50	0.02198	0.65800	0.39878	0.16100
13	6.50	50	0.02522	0.65800	0.46612	0.16100
14	7.00	10	0.17494	0.64400	0.41002	0.08500
15	7.50	50	0.05626	0.64800	0.43707	0.13400
16	7.50	50	0.06100	0.64700	0.41928	0.12200
17	5.00	1	0.02015	0.73500	0.43567	0.09900
18	5.80	5	0.07022	0.71900	0.35942	0.08100
19	5.80	5	0.04632	0.71900	0.34492	0.07500
20	5.00	10	0.02051	0.73500	0.31973	0.09800
21	5.00	10	0.03300	0.73400	0.54440	0.10600
22	5.00	50	0.00331	0.73800	0.36267	0.08300
23	5.00	50	0.00369	0.73800	0.34572	0.08300
24	5.00	160	0.00056	0.73800	0.73250	0.08300
25	5.80	1	0.11469	0.71900	0.53924	0.08100
26	5.80	5	0.12724	0.71900	0.50978	0.08100
27	5.80	5	0.08200	0.71900	0.35320	0.08100
28	5.80	10	0.06083	0.71900	0.35922	0.08100
29	5.80	10	0.09540	0.71900	0.56601	0.08100
30	5.80	10	0.04919	0.71900	0.33574	0.07600
31	5.80	50	0.00615	0.72600	0.79146	0.09900
32	5.80	50	0.00821	0.72600	0.75952	0.09900
33	6.50	5	0.18541	0.65000	0.36194	0.08000
34	6.50	10	0.12301	0.65000	0.44966	0.08000
35	6.50	10	0.18019	0.65000	0.54422	0.08000
36	6.50	10	0.11128	0.65000	0.43287	0.08000
37	6.50	20	0.06536	0.65200	0.44016	0.09900
38	6.50	20	0.09342	0.65100	0.64233	0.08700
39	6.50	20	0.05667	0.65200	0.35495	0.10600
40	6.50	100	0.01169	0.65800	0.54696	0.16100
41	6.50	160	0.00556	0.65800	0.64101	0.16100
42	7.00	1	0.34520	0.64400	0.27669	0.08500
43	7.00	10	0.25651	0.64400	0.47782	0.08500
44	7.00	10	0.15656	0.64400	0.39264	0.08500
45	7.00	50	0.03541	0.65300	0.35238	0.16600
46	7.00	50	0.04264	0.65100	0.48103	0.15200
47	7.50	1	0.43841	0.64300	0.35390	0.08500
48	5.00	10	0.22442	0.64300	0.36561	0.08500
49	5.00	10	0.30249	0.64300	0.41320	0.08500
50	8.00	50	0.07893	0.64500	0.57582	0.10700
51	8.00	160	0.02349	0.65300	0.63697	0.16800

TABLE F3-20
K. W. CAMPBELL: VERTICAL POINT ESTIMATES
SPECTRAL ACCELERATION AT 1.00 SEC PERIOD

CASE NO.	MAGNITUDE	DISTANCE (KM)	MU	SIGMA	SIGMA MU	SIGMA SIGMA
1	5.00	1	0.02026	0.75200	0.80925	0.12400
2	5.00	1	0.02277	0.75200	0.73986	0.12400
3	5.00	5	0.00739	0.75400	0.52158	0.10100
4	5.00	5	0.00928	0.75400	0.47024	0.10300
5	5.80	10	0.02231	0.73700	0.32804	0.09100
6	5.80	20	0.02249	0.73900	0.41974	0.08100
7	6.50	1	0.13963	0.66600	0.36196	0.09000
8	6.50	1	0.15511	0.66600	0.30695	0.09000
9	6.50	1	0.14029	0.66600	0.29806	0.09000
10	6.50	5	0.13124	0.66600	0.36976	0.09000
11	6.50	5	0.09490	0.66600	0.27199	0.09000
12	6.50	50	0.01322	0.67300	0.47775	0.16900
13	6.50	50	0.01636	0.67300	0.48396	0.16900
14	7.00	10	0.09994	0.65900	0.28218	0.09500
15	7.50	50	0.03887	0.66200	0.40408	0.14300
16	7.50	50	0.04535	0.66100	0.50769	0.13100
17	5.00	1	0.00817	0.75300	0.65841	0.10500
18	5.80	5	0.03616	0.73600	0.49773	0.09700
19	5.80	5	0.02516	0.73700	0.41709	0.09000
20	5.00	10	0.00774	0.75300	0.51534	0.10400
21	5.00	10	0.01229	0.75300	0.48843	0.11200
22	5.00	50	0.00130	0.75600	0.54345	0.08700
23	5.00	50	0.00171	0.75600	0.40211	0.08700
24	5.00	160	0.00027	0.75600	0.79605	0.08700
25	5.80	1	0.05834	0.73600	0.64874	0.09700
26	5.80	5	0.06360	0.73600	0.61412	0.09700
27	5.80	5	0.04166	0.73600	0.38959	0.09700
28	5.80	10	0.02840	0.73600	0.32868	0.09700
29	5.80	10	0.04645	0.73600	0.50058	0.09700
30	5.80	10	0.02896	0.73700	0.37489	0.09100
31	5.80	50	0.00325	0.74300	0.88702	0.10500
32	5.80	50	0.00517	0.74300	0.69312	0.10500
33	6.50	5	0.09974	0.66600	0.32774	0.09000
34	6.50	10	0.06945	0.66600	0.34923	0.09000
35	6.50	10	0.09262	0.66600	0.31824	0.09000
36	6.50	10	0.06611	0.66600	0.37543	0.09000
37	6.50	20	0.03497	0.66700	0.33287	0.10800
38	6.50	20	0.05072	0.66700	0.44118	0.09600
39	6.50	20	0.03620	0.66800	0.36894	0.11500
40	6.50	100	0.00711	0.67300	0.44963	0.16900
41	6.50	160	0.00298	0.67300	0.74142	0.16900
42	7.00	1	0.19275	0.65900	0.35073	0.09500
43	7.00	10	0.15377	0.65900	0.36723	0.09500
44	7.00	10	0.09917	0.65900	0.32051	0.09500
45	7.00	50	0.02388	0.66700	0.40054	0.17400
46	7.00	50	0.02872	0.66500	0.49191	0.16000
47	7.50	1	0.27419	0.65800	0.38784	0.10100
48	5.00	10	0.13951	0.65800	0.32018	0.10100
49	5.00	10	0.19678	0.65800	0.43525	0.10100
50	8.00	50	0.05113	0.65900	0.54972	0.11600
51	8.00	160	0.01782	0.66600	0.55129	0.17700

TABLE F3-21
K. W. CAMPBELL: VERTICAL POINT ESTIMATES
SPECTRAL ACCELERATION AT 2.00 SEC PERIOD

CASE NO.	MAGNITUDE	DISTANCE (KM)	MU	SIGMA	SIGMA MU	SIGMA SIGMA
1	5.00	1	0.01180	0.84400	0.52384	0.13400
2	5.00	1	0.01594	0.84400	0.48973	0.13400
3	5.00	5	0.00503	0.85700	0.56941	0.11100
4	5.00	5	0.00690	0.85600	0.59896	0.11300
5	5.80	10	0.01992	0.79500	0.43127	0.11100
6	5.80	20	0.01611	0.80300	0.42186	0.09800
7	6.50	1	0.13960	0.74700	0.28682	0.11500
8	6.50	1	0.14308	0.74700	0.29839	0.11500
9	6.50	1	0.12991	0.74700	0.28765	0.11500
10	6.50	5	0.11313	0.74700	0.31483	0.11500
11	6.50	5	0.08903	0.74700	0.32982	0.11500
12	6.50	50	0.01493	0.76900	0.45494	0.09400
13	6.50	50	0.01511	0.76900	0.56184	0.09400
14	7.00	10	0.10504	0.71600	0.32105	0.12200
15	7.50	50	0.04502	0.72000	0.53620	0.11900
16	7.50	50	0.04869	0.71700	0.62436	0.12000
17	5.00	1	0.00456	0.85400	0.85279	0.11500
18	5.80	5	0.03617	0.79200	0.45125	0.11600
19	5.80	5	0.02138	0.79500	0.48735	0.11000
20	5.00	10	0.00618	0.85500	0.33902	0.11400
21	5.00	10	0.00816	0.85000	0.35573	0.12200
22	5.00	50	0.00105	0.86600	0.51825	0.09600
23	5.00	50	0.00106	0.86600	0.58131	0.09600
24	5.00	160	0.00042	0.86600	0.76188	0.09600
25	5.80	1	0.05545	0.79200	0.35937	0.11600
26	5.80	5	0.05028	0.79200	0.41450	0.11600
27	5.80	5	0.03324	0.79200	0.40843	0.11600
28	5.80	10	0.02379	0.79200	0.39066	0.11600
29	5.80	10	0.03230	0.79200	0.40620	0.11600
30	5.80	10	0.01960	0.79500	0.47817	0.11100
31	5.80	50	0.00312	0.81300	0.82942	0.08400
32	5.80	50	0.00319	0.81300	0.88153	0.08400
33	6.50	5	0.10114	0.74700	0.30082	0.11500
34	6.50	10	0.06829	0.74700	0.31275	0.11500
35	6.50	10	0.08870	0.74700	0.30715	0.11500
36	6.50	10	0.05808	0.74700	0.38263	0.11500
37	6.50	20	0.03926	0.75200	0.31400	0.10900
38	6.50	20	0.04870	0.74900	0.36120	0.11300
39	6.50	20	0.03298	0.75400	0.43697	0.10600
40	6.50	100	0.00847	0.76900	0.43990	0.09400
41	6.50	160	0.00401	0.76900	0.79330	0.09400
42	7.00	1	0.19350	0.71600	0.25225	0.12200
43	7.00	10	0.13692	0.71600	0.30921	0.12200
44	7.00	10	0.09273	0.71600	0.38105	0.12200
45	7.00	50	0.02879	0.73700	0.41198	0.10800
46	7.00	50	0.03064	0.73400	0.50676	0.11000
47	7.50	1	0.23284	0.70700	0.28003	0.12700
48	5.00	10	0.14295	0.70700	0.42464	0.12700
49	5.00	10	0.17572	0.70700	0.47320	0.12700
50	8.00	50	0.07185	0.71300	0.36780	0.12300
51	8.00	160	0.03450	0.72900	0.56066	0.11600

TABLE F3-22
K. W. CAMPBELL: VERTICAL POINT ESTIMATES
SPECTRAL ACCELERATION AT 3.33 SEC PERIOD

CASE NO.	MAGNITUDE	DISTANCE (KM)	MU	SIGMA	SIGMA MU	SIGMA SIGMA
1	5.00	1	0.00169	0.78800	1.09920	0.13900
2	5.00	1	0.00226	0.78800	1.10327	0.13900
3	5.00	5	0.00059	0.79000	0.90037	0.11100
4	5.00	5	0.00091	0.78900	0.91120	0.11300
5	5.80	10	0.00439	0.77300	0.50030	0.11100
6	5.80	20	0.00413	0.77500	0.64680	0.09800
7	6.50	1	0.04151	0.70000	0.50066	0.11500
8	6.50	1	0.05066	0.70000	0.49276	0.11500
9	6.50	1	0.04543	0.70000	0.47348	0.11500
10	6.50	5	0.04417	0.70000	0.56552	0.11500
11	6.50	5	0.02893	0.70000	0.46797	0.11500
12	6.50	50	0.00382	0.70600	0.64162	0.17500
13	6.50	50	0.00483	0.70600	0.91242	0.17500
14	7.00	10	0.03213	0.69200	0.40550	0.12200
15	7.50	50	0.01325	0.69500	0.64421	0.14800
16	7.50	50	0.01634	0.69400	0.81930	0.13600
17	5.00	1	0.00054	0.78900	1.08609	0.11500
18	5.80	5	0.01001	0.77300	0.62674	0.11600
19	5.80	5	0.00531	0.77300	0.58721	0.11000
20	5.00	10	0.00060	0.78900	0.90635	0.11400
21	5.00	10	0.00144	0.78900	0.89639	0.12400
22	5.00	50	0.00009	0.79200	0.90668	0.09600
23	5.00	50	0.00023	0.79200	1.19029	0.09600
24	5.00	160	0.00002	0.79200	0.87387	0.09600
25	5.80	1	0.01268	0.77300	0.66035	0.11600
26	5.80	5	0.01862	0.77300	0.76270	0.11600
27	5.80	5	0.00910	0.77300	0.61134	0.11600
28	5.80	10	0.00463	0.77300	0.55539	0.11600
29	5.80	10	0.00778	0.77300	0.78351	0.11600
30	5.80	10	0.00577	0.77300	0.80086	0.11100
31	5.80	50	0.00049	0.77900	0.91297	0.09300
32	5.80	50	0.00115	0.77900	1.25032	0.09300
33	6.50	5	0.03172	0.70000	0.43275	0.11500
34	6.50	10	0.01918	0.70000	0.41740	0.11500
35	6.50	10	0.02647	0.70000	0.51492	0.11500
36	6.50	10	0.01871	0.70000	0.57109	0.11500
37	6.50	20	0.01011	0.70100	0.50449	0.11800
38	6.50	20	0.01364	0.70000	0.59397	0.11300
39	6.50	20	0.01085	0.70100	0.77483	0.12400
40	6.50	100	0.00143	0.70600	0.85496	0.17500
41	6.50	160	0.00078	0.70600	0.84026	0.17500
42	7.00	1	0.06232	0.69200	0.54459	0.12200
43	7.00	10	0.04550	0.69200	0.51633	0.12200
44	7.00	10	0.03064	0.69200	0.62588	0.12200
45	7.00	50	0.00777	0.69900	0.65102	0.17800
46	7.00	50	0.01012	0.69800	0.81504	0.16500
47	7.50	1	0.08756	0.69100	0.48247	0.12700
48	5.00	10	0.04340	0.69100	0.59736	0.12700
49	5.00	10	0.06419	0.69100	0.67377	0.12700
50	8.00	50	0.02288	0.69300	0.72047	0.12300
51	8.00	160	0.00943	0.69900	0.68016	0.18000

TABLE F3-23
K. W. CAMPBELL: VERTICAL POINT ESTIMATES
PEAK GROUND VELOCITY

CASE NO.	MAGNITUDE	DISTANCE (KM)	MU	SIGMA	SIGMA MU	SIGMA SIGMA
1	5.00	1	2.75875	0.70500	0.66526	0.19600
2	5.00	1	3.12226	0.70500	0.61871	0.19600
3	5.00	5	0.93296	0.70300	0.36223	0.13100
4	5.00	5	1.15376	0.70300	0.33082	0.13800
5	5.80	10	2.68354	0.68600	0.24056	0.14200
6	5.80	20	2.62518	0.68600	0.46480	0.10900
7	6.50	1	13.62704	0.60700	0.33457	0.13800
8	6.50	1	15.77485	0.60700	0.45385	0.13800
9	6.50	1	14.60730	0.60700	0.39073	0.13800
10	6.50	5	13.71329	0.60700	0.45010	0.13800
11	6.50	5	10.35880	0.60700	0.33822	0.13800
12	6.50	50	1.23053	0.61200	0.39295	0.15600
13	6.50	50	1.60122	0.61200	0.52679	0.15600
14	7.00	10	10.05228	0.59900	0.24932	0.13800
15	7.50	50	3.60724	0.60100	0.40119	0.13200
16	7.50	50	4.44701	0.59900	0.61452	0.13100
17	5.00	1	1.04033	0.70300	0.44087	0.14400
18	5.80	5	4.45109	0.68600	0.36802	0.15600
19	5.80	5	2.86244	0.68600	0.45573	0.14000
20	5.00	10	1.06252	0.70300	0.30357	0.14000
21	5.00	10	1.80913	0.70300	0.46217	0.16300
22	5.00	50	0.13784	0.70500	0.37517	0.09300
23	5.00	50	0.16999	0.70500	0.37906	0.09300
24	5.00	160	0.02015	0.70500	0.81692	0.09300
25	5.80	1	6.99665	0.68600	0.46941	0.15600
26	5.80	5	7.52566	0.68600	0.55111	0.15600
27	5.80	5	4.73640	0.68600	0.31977	0.15600
28	5.80	10	3.28442	0.68600	0.29801	0.15600
29	5.80	10	5.25751	0.68600	0.46819	0.15600
30	5.80	10	3.00636	0.68600	0.37030	0.14200
31	5.80	50	0.30379	0.69000	0.79816	0.08100
32	5.80	50	0.48754	0.69000	0.76283	0.08100
33	6.50	5	10.76594	0.60700	0.32741	0.13800
34	6.50	10	7.32413	0.60700	0.29354	0.13800
35	6.50	10	10.77394	0.60700	0.44162	0.13800
36	6.50	10	7.03702	0.60700	0.35924	0.13800
37	6.50	20	3.79664	0.60700	0.25600	0.12300
38	6.50	20	5.85031	0.60700	0.49843	0.13200
39	6.50	20	3.79388	0.60700	0.42516	0.11800
40	6.50	100	0.54107	0.61200	0.42789	0.15600
41	6.50	160	0.18701	0.61200	0.84403	0.15600
42	7.00	1	16.87021	0.59900	0.32449	0.13800
43	7.00	10	15.29462	0.59900	0.50730	0.13800
44	7.00	10	9.86153	0.59900	0.37831	0.13800
45	7.00	50	2.26745	0.60600	0.33159	0.14900
46	7.00	50	2.91340	0.60400	0.57051	0.13600
47	7.50	1	21.30142	0.59700	0.57685	0.13900
48	5.00	10	12.61132	0.59700	0.29534	0.13900
49	5.00	10	18.10722	0.59700	0.70412	0.13900
50	8.00	50	5.20460	0.59800	0.59487	0.13300
51	8.00	160	1.69181	0.60600	0.60372	0.15200

APPENDIX F4

EXPERT REPORT ON YUCCA MOUNTAIN GROUND MOTION ATTENUATION

A. McGarr
U.S. Geological Survey
345 Middlefield Road
Menlo Park, CA 94025

APPENDIX F4
TABLE OF CONTENTS

APPENDIX F4

EXPERT REPORT ON YUCCA MOUNTAIN GROUND MOTION ATTENUATION

A. McGarr
U.S. Geological Survey
345 Middlefield Road
Menlo Park, CA 94025

F4-1 INTRODUCTION

The ideal data set for evaluating the design ground motion at Yucca Mountain would have been a set of strong motion records from the scenario earthquakes proposed by the seismic source characterization teams. In the absence of such records, the next best data would be from earthquakes of magnitude greater than 5 within the Basin and Range Province which includes Yucca Mountain; unfortunately, such data are currently limited to records from the 1992 Little Skull Mountain earthquake of M5.7 (e.g. Spudich *et al.*, 1996). Accordingly, it was necessary to evaluate the ground motion for the 51 cases (combinations of magnitude, distance, and style of faulting) using less direct information.

The less specific data, as used here, are of four types: first, empirical ground motion relations for western North America, mostly California; second, empirical ground motion relations for earthquakes in extensional tectonic regimes worldwide; third, the point source model of Silva; fourth, finite faulting models. These four independent categories of ground motion data can all be adapted to the repository circumstances at Yucca Mountain, where we attempt to evaluate the ground motion assuming that the top 300 m of ground have been removed.

As Yucca Mountain is situated within an extensional tectonic regime, one of the background issues is whether earthquakes in extensional regimes produce less ground motion, all other factors being equal, than do earthquakes in more compressive regimes. Empirical studies (e.g., McGarr, 1984; N. A. Abrahamson, consultant, written communication, 1993; Boore *et al.*, 1994; Campbell and Bozorgnia, 1994; and most recently, Spudich *et al.*, 1996) indicate that this is the case and so the point of view taken here is that ground motion from

earthquakes in extensional regimes is, indeed, less than elsewhere (e.g., much of California). Moreover, I assume that this is primarily a source effect, which applies to both normal and strike-slip faulting earthquakes within extensional tectonic provinces. This viewpoint, then, is the basis for dividing the empirical relationships into the two categories as just described and also the source corrections discussed later.

Definitions:

μ_{med} is the geometric mean of the ground motion estimates (μ's).

σ_{al} is the geometric mean of the individual σ's for each model.

σ_{μ} is the standard deviation of the μ's.

σ_{σ} is the standard deviation of the σ's.

F4-2 WEIGHTING SCHEME FOR PROPONENT GROUND MOTION MODELS

Among the agreed-upon suite of proponent models, each expert was required to assess each model for its applicability to the various scenario earthquake, frequency, distance, component combination. To calculate weighted medians of the ground motion parameters, as well as the various measures of uncertainty, the proponent models were divided into different classes, each of which was assigned a weight. then within each class, individual models were assigned weights. A summary of the actual nonzero weights for classes and models is given in the "Summary Table of Weights" (F4-2.4).

F4-2.1 Classes Of Proponent Models

I defined four classes of proponent models: (1) Empirical (California), (2), Empirical (Extensional), (3) Point source numerical simulations, and (4) Finite fault numerical simulations. the empirical (CA) models are attenuation relations based on data primarily from California (Abrahamson and Silva, 1997; Boore *et al.*, 1997; Campbell, 1997; Idriss, University of California, Davis, written communication, 1991; and Sadigh *et al.*, 1997. The empirical (ext.) models are attenuation relations developed from ground motion recordings of earthquakes in extensional tectonic regimes (Spudich *et al.*, 1996; Abrahamson and Silva, 1997; McGarr, 1984). The Sabetta and Pugliese (1996) model, an empirical relation based on Italian earthquakes, falls into neither of the two empirical classes, but, for reasons to be

given, was considered and not used here. Models developed from nuclear explosion data at the Nevada Test Site (R. J. Bennett *et al.*, S-Cubed, written communication, 1997)) are also in the empirical category but, as will be explained, played no role in the point estimates of ground motion. For the point source simulation class the only available model was that developed by W. Silva. The finite fault simulation class includes three quite different models developed by Y. Zeng and J. Anderson, P. Somerville, and W. Silva (N. A. Abrahamson and A. M. Becker, Consultants, written communication, 1997b).

The four classes of models are weighted equally, primarily because each is unique and independent in its set of approaches to point ground motion estimates. Similar remarks apply to the corresponding weights for uncertainties. In the absence of information suggesting superiority of a particular class or classes, it seems advisable to adhere to equal class weights.

F4-2.2 Model Weights: Horizontal Component

Within each class, for a particular model, the medians and various uncertainties receive the same weights. This is because there was no reason to suppose that the strengths or weaknesses of any model of ground motion median estimates would not apply also to the associated uncertainties.

In the following sections, the discussion of models is organized according to the four classes, described before; models assigned a weight of zero are discussed afterward. Adjustments for each model are discussed at the same time.

F4-2.2.1 Empirical Models.

F4-2.2.1.1 Empirical (CA) Models

Adjustments: Campbell Table 8.3.2 (Data Package Vol. 1) for CA to YM_{300}; Silva Table 7.3 (ibid.) for stress drop, where YM/CA=42.5/57 (Becker and Abrahamson, 1997).

Models used:

Abrahamson and Silva (1997, strike-slip only). This model was assigned a weight of 1 because it is based on an up-to-date, appropriate data set. The strike-slip predictions are used for both strike-slip and normal events. The normal faulting factors presented in the Data Package Vol. 1 are not used. Rather, the source scaling from the point source model is used

instead. This model was used for all SA's and PGA's and is applicable to all magnitudes and distances under consideration.

Boore, Joyner, Fumal (1997, Vs-620m/s). Again, this model was assigned weight 1 because it is based on a very modern, appropriate data set. The velocity of 620 m/s is used to be consistent with the average rock site for California which is used as the basis for the crust/site adjustment factor. It was used for all SA's and PGA's. For f=20 Hz, I arithmetically averaged the b coefficients for PGA and f=10 Hz values to interpolate. Of the various Boore, Joyner, Fumal relations under consideration, this is the one recommended by the authors.

Campbell (1997, soft rock). This is based on an appropriate data set and is the most modern of all the Campbell models. I used it for all SA's, PGA's, and PGV's. In contrast to Campbell (1997, hard rock), the soft rock sites are deemed to be more typical of California sites. Additionally, this model is recommended by the author from amongst his various regression models and so is was assigned a weight of 1.

Idriss (University of California, Davis, written communications, 1991, 1997). Idriss used an independent method of fitting a regression curve to ground motion data recorded at rock sites. I used this model for all SA's. Idriss 97 was used for PGA's. Thus the Idriss models were assigned a weight of 1.

Sadigh et al. (1993). Sadigh used another independent method of fitting a curve to ground motion data recorded at typical California rock sites. This model, with a weight of 1, was used for all SA's and PGA's.

Joyner-Boore (1988). I used this venerable model with a weight of 1 for PGV's only because of the scarcity of trustworthy models that yield PGV. For the SA's and PGA's BJF '97 is far more up-to-date.

F4-2.2.1.2 Empirical (Extensional) Models

Adjustments: CA to YM_{300} as for F4-2.2.1.1, no stress drop correction.

Models used:

Spudich et al. (1996). This model, assigned a weight of 1, is exceptionally appropriate as it is based on ground motion data exclusively from earthquakes in extensional regimes. I used this model for all SA's and PGA's. For f=20 Hz I arithmetically averaged the b coefficients for PGA and f=10 Hz to calculate 20 Hz SA for purposes of interpolation.

Abrahamson and Silva (1997, normal faulting events). This model, also assigned weight 1, is appropriate here in that it is based on a subset of normal-faulting earthquakes from A&S '97. This was used for all SA's and PGA's.

McGarr (1984, extensional). I used this model for PGV for those cases for which epicentral distance is less than or comparable to hypocentral depth, which is taken to be at the bottom of the rupture zone. These values are tabulated on p. 4.1.4-1 of Data Package Vol. I and were calculated from equation (16a) of McGarr (1984). No adjustments are applied because the data used to develop this model are mostly from rock sites having Vs at least as high as 1900 m/s. The aleatory uncertainty is assumed to be 0.5. This relation was used partly because it is one of the few that yield PGV and is based on a very independent data set.

F4-2.2.1.3 Empirical Models Assigned Weight Zero

All Campbell models except Campbell '97 (soft rock), because these are either redundant or inappropriate. Moreover, the author recommended Campbell (1997, soft rock).

All Boore-Joyner-Fumal except BJF Vs because of redundancy, based on recommendations of the authors.

Sabetta and Pugliese because this is quite an old data set (no post-1985 data), many S wave triggers (see Spudich *et al.*, 1996) and the site characteristics are exceptionally uncertain.

F4-2.2.2 Numerical Simulations. There are two distinct types of numerical simulations, point sources and finite fault. Both are appropriate for YM300 conditions.

F4-2.2.2.1 Point Source Simulation (Silva)

This model was assigned a weight of 1 for all ground motion estimates with YM_{300} site conditions and the YM stress drop of 42.5 bars. The empirical PGV/PGA (8.6.1-1 of Data Package Vol. 1) was used to calculate PGV. Aleatory uncertainty for stress drop is taken as 0.5. For the SS and HW cases, the point source distance is the vector sum of the JB distance and the depth to the center of the rupture plane. For the FW cases, this distance is the slant distance to the center of the rupture plane.

F4-2.2.2.2 Finite Fault Simulations

The following three models were weighted equally in this class because they are all quite independent, with unique strengths and weaknesses.

Somerville Finite (Somerville *et al.*, 1997). This model was used for all ground motion estimates for M(5.8. Its main advantage is that it take rupture directivity into account. There may be some problems at low frequency, however, resulting in unrealistically low ground motion estimates. I finally elected to use these results in spite of the apparent problems that surfaced at the May 7, 1997, meeting at Woodward-Clyde.

Silva Finite. This model, an extension of his point source model, was used for all ground motion point estimates of M≥5.8.

Anderson composite finite fault (Zeng and Anderson, 1996). This model was used for all point estimates. The advertised aleatory uncertainty is unrealistically low and should be increased, perhaps by taking stress drop uncertainty into account. Some of the resulting point estimates are remarkably high suggesting possibly some instability.

Note: For all finite fault models, a YM/CA stress drop correction was applied.

F4-2.2.3 Blast Models. These models, even though they are the only models local to Yucca Mountain, were assigned zero weight because they yield results that are unrealistically large at small epicentral distances. Moreover, the Rg phase dominates the blast data in a way that would not be expected for earthquakes, unless exceptionally shallow.

F4-2.2.4 Horizontal Component Variability. For all models that yield the average horizontal component, the aleatory uncertainty is increased by vector addition of the average of the two factors given in Table 4.1.2 of Data Package Vol. 1.

F4-2.3 Model Weights - Vertical Component

The class weighting scheme is the same as for the horizontal components. Within each of the classes, as before, models are weighted equally. Fewer models are available, however.

F4-2.3.1 Empirical (CA) Models.

Models used:

Abrahamson and Silva (1997, strike-slip).

Campbell (1997, soft rock).

Sadigh.

F4-2.3.2 Empirical (Extensional) Models.

Models used:

Abrahamson and Silva (1997, normal).

F4-2.3.3 Point Source Model.

Silva. To calculate the vertical component, I used the Silva point source ratio Z/H.

F4-2.3.4 Finite Fault Models.

Models used:

Somerville for M(5.8.

Anderson.

F4-2.3.5 Adjustments. The source adjustment is the same as for the horizontal component. For the site/path adjustment, I used Walck's formula:

$$\mu_{YMZ} = \mu_{CAZ} \times (YM_H/CA_H) \times (YM_Z/YM_H) \times (CA_H/CA_Z)$$

where the first factor is the Campbell adjustment, the second is the Silva point source ratio, and the third is the empirical model H/Z. Admittedly, this may amount to over analysis inasmuch as, from a few trials, I find the product of the last two factors is close to 1.

F4-2.4 Summary Table of Weights

HORIZONTAL

Class, Model	Class Wt.	Wt.	CA to YM300	Stress Drop
Empirical (CA)	1			
A&S '97 (SS)		1	Y	Y
BJF 97 Vs=620 m/s		1	Y	Y
Campbell 97 (soft rock)		1	Y	Y
Idriss 97		1	Y	Y
JB 88 (PGV only)		1	Y	Y
Sadigh		1	Y	Y
Empirical (ext.)	1			
Spudich		1	Y	N
A&S 97 (N)		1	Y	N
McGarr 84 (PGV only)		1	N	N
Pt. Source	1			
Silva (Use V/A for PGV)		1	N	N
Finite Source	1			
Anderson		1	N	Y
Silva		1	N	Y
Somerville		1	N	Y

Adjustments: Use Campbell Table 8.3.2 (Data Package Vol. 1) for CA to YM300.
Use Silva Table 7.3 (ibid.) for stress drop, where YM/CA is 42.5 bars/57 bars.

VERTICAL

Class, Model	Class Wt.	Wt.	CA to YM300	Stress Drop	Z/H
Empirical (CA)	1				
A&S '97 (SS)		1	Y	Y	N
Campbell '97 (soft rock)		1	Y	Y	N

Class, Model	Class Wt.	Wt.	CA to YM300	Stress Drop	Z/H
Sadigh		1	Y	Y	N
Empirical (ext.)	1				
A&S 97 (N)		1	Y	N	N
Pt. source	1				
Silva		1	N	N	Y

Class, Model	Class Wt.	Wt.	CA to YM300	Stress Drop	Z/H
Finite source	1				
Somerville (M>5.79)		1	N	Y	N
Anderson		1	N	Y	N

Adjustments: For CA to YM300, use Walck's formula.
For Stress drop, same as for H.
For Silva pt. source, use Silva pt. source ratio Z/H
For Silva pt. source PGV(Z), use Silva empirical. V/A.

F4-3 ADJUSTMENTS TO WEIGHTED POINT ESTIMATES

There were none. Previously, I considered using the precarious boulder results to limit PGA but finally decided that, at this time, such an adjustment is not warranted.

F4-4 EPISTEMIC UNCERTAINTY

Based on my weighting scheme, the epistemic uncertainties (σ_μ and σ_σ) were computed by the facilitation team. These statistical estimates were not altered.

F4-5 FINAL POINT ESTIMATES

After making the adjustments to the weighted estimates as described above, my final point estimates of m, s, s_m, and s_s for the horizontal component for the 51 cases are given in Tables F4-1 to F4-9 for the nine ground motion parameters. The corresponding point estimates for the vertical component are given in Tables F4-10 to F4-18.

F4-6 EVALUATION OF REGRESSION MODELS

The facilitation team developed regression models to parameterize my point estimates in terms of the dependence on magnitude, distance, and style-of-faulting. I reviewed the final regression models given in Volume 11D of the data package.

F4-6.1 Mu

Regression fits look fine; in the case of PGA the regressions allow for magnitude saturation at small distances. No distinction was made between HW and FW for normal faults.

F4-6.2 Sigma

Regression fits look fine.

F4-6.3 Sigma mu

These regressions include distance dependence only. The point estimates did not argue persuasively for magnitude dependence. For the distance dependence the quadratic fit seems fine.

F4-6.4 Sigma sigma

The regression fits look good.

F4-7 SPECIAL CASES

The ground motion models developed in this study are for "typical" events that cover the majority of the source models developed by the source experts. There are two source models that have geometries significantly different from those considered in developing the base

models. These are simultaneous rupture of multiple parallel faults (local events) and a low angle fault. These two cases are discussed below.

F4-7.1 Multiple Parallel Faults

Parallel simultaneous ruptures:

(1) For given M, calculate M_o from $\log M_o = 16.05 + 1.5M$.

(2) Distribute M_o evenly among multiple faults, $M_o = nM_{of}$.

(3) Calculate $M_f = (\log M_{of} - 16.05)/1.5$, which is the magnitude of each individual event on a single fault.

(4) Calculate ground motion using previous rules assuming that only nearest fault contributes significantly to mu.

(5) Enlarge aleatory sigma by 20% to account for possibility of constructive or destructive interference from other ruptures.

F4-7.2 Low Angle Fault

Deep detachment surface:

(1) Treat exactly as for normal fault dip-slip cases using same rules. Assume hypocenter is at deepest part of fault plane.

(2) Enlarge epistemic sigma by 30% to account for stress drop uncertainty.

F4-8 REFERENCES

Abrahamson, N. A., and Silva, W. J., 1997, Empirical response spectral attenuation relations for shallow crustal earthquakes: Seismological Research Letters, v. 68, p. 94-127.

Becker, A. M., and N. A. Abrahamson, 1997, Stress drops in normal faulting earthquakes: Seismological Research Letters, v. 68, p. 322.

Boore, D. M., Joyner, W.B., and Fumal, T.E., 1994, Estimation of response spectra and peak accelerations from western North American earthquakes--an interim report, Part 2: U.S. Geological Survey Open-File Report 94-127, 40 p.

Boore, D. M., Joyner, W. B., and Fumal, T. E., 1997, Equations for estimating horizontal response spectra and peak acceleration from western North American earthquakes--a summary of recent work: Seismological Research Letters, v. 68, p. 128-153.

Campbell, K.W., 1997, Empirical near-source attenuation relationships for horizontal and vertical components of peak ground acceleration, peak ground velocity, and pseudo-absolute acceleration response spectra: Seismological Research Letters, v. 68, p. 154-179.

Campbell, K. W., and Bozorgnia, Y., 1994, Near-source attenuation of peak horizontal acceleration from worldwide accelerograms recorded from 1957 to 1993: 5th U.S. National Conference on Earthquake Engineering, Chicago, IL, July 10-14, 1994.

Joyner, W.B. and Boore, D.M., 1988, Measurement, characterization, and prediction of strong ground motion, *in* Procedures, Conference on Earthquake Engineering and Soil Dynamics II: GT Div./ASCE, Park City, UT, June 27-30, 1988.

McGarr, A., 1984, Scaling of ground motion parameters, state of stress and focal depth: Journal of Geophysical Research, v. 89, p. 6969-6979.

Sabetta, F., and Pugliese, A., 1996, Estimation of response spectra and simulation of nonstationary earthquake ground motions: Bulletin of the Seismological Society of America, v. 86, p. 337-352.

Sadigh, K., Chang, C.-Y., Abrahamson, N.A., Chiou, S. J., and Power, M.S., 1993, Specification of long-period ground motions: Updated attenuation relations for rock site conditions and adjustment factors for near-fault effects: Proceedings ATC-17-1, Seminar on Seismic Isolation, Passive Energy Dissipation, and Active Control, San Francisco, CA, March 11-12.

Sadigh, K., Chang, C.-Y., Egan, J.A., Makdisi, F., and Youngs, R.R., 1997, Attenuation relationships for shallow crustal earthquakes based on California strong motion data: Seismological Research Letters, v. 68, p. 180-189.

Somerville, P.G., Smith, N.F., Graves, R.W., and Abrahamson, N.A., 1997, Modification of empirical strong ground motion attenuation relations to include the amplitude and duration effects of rupture directivity: Seismological Research Letters, v. 68, p. 199-222.

Spudich, P., Fletcher, J. B., Hellweg, M., Boatwright, J., Sullivan, C., Joyner, W. B., Hanks, T. C., Boore, D. M., McGarr, A., Baker, L. M., and Lundh, A. G., 1996, Earthquake ground motions on extensional tectonic regimes: U.S. Geological Survey Open-File Report 96-292, 351 p.

Zeng, Y., and Anderson, J.G., 1996, A composite source model of the 1994 Northridge earthquake using genetic algorithms: Bulletin of the Seismological Society of America, v. 86, p. S71-S83.

TABLE F4-1
A. McGARR: HORIZONTAL POINT ESTIMATES
PEAK GROUND ACCELERATION

CASE NO.	MAGNITUDE	DISTANCE (KM)	MU	SIGMA	SIGMA MU	SIGMA SIGMA
1	5.00	1	0.12521	0.65221	0.36507	0.08907
2	5.00	1	0.16195	0.65688	0.35962	0.08844
3	5.00	5	0.04721	0.65455	0.34109	0.08867
4	5.00	5	0.06612	0.65688	0.33346	0.08844
5	5.80	10	0.08551	0.61124	0.17324	0.08753
6	5.80	20	0.06749	0.61054	0.18911	0.08769
7	6.50	1	0.38603	0.58723	0.31804	0.09205
8	6.50	1	0.41976	0.58821	0.41766	0.09326
9	6.50	1	0.32315	0.58899	0.31122	0.09278
10	6.50	5	0.35842	0.58517	0.38397	0.09139
11	6.50	5	0.20904	0.58886	0.24898	0.09277
12	6.50	50	0.02673	0.58466	0.22833	0.09132
13	6.50	50	0.02805	0.58440	0.24146	0.09129
14	7.00	10	0.22608	0.56513	0.26768	0.10192
15	7.50	50	0.05498	0.56414	0.20112	0.10674
16	7.50	50	0.06200	0.56229	0.24435	0.10568
17	5.00	1	0.04642	0.65221	0.61058	0.08907
18	5.80	5	0.13838	0.61182	0.23658	0.08744
19	5.80	5	0.07490	0.61144	0.28809	0.08750
20	5.00	10	0.05700	0.65455	0.14223	0.08867
21	5.00	10	0.07695	0.65221	0.22216	0.08907
22	5.00	50	0.00598	0.65221	0.35455	0.08907
23	5.00	50	0.00622	0.64989	0.40264	0.08966
24	5.00	160	0.00085	0.64757	0.62439	0.09042
25	5.80	1	0.25314	0.61200	0.34501	0.08777
26	5.80	5	0.22326	0.61085	0.35782	0.08761
27	5.80	5	0.12140	0.61105	0.23108	0.08757
28	5.80	10	0.10672	0.61402	0.21330	0.08838
29	5.80	10	0.15274	0.61105	0.28354	0.08757
30	5.80	10	0.07145	0.61168	0.27983	0.08784
31	5.80	50	0.01202	0.60888	0.46203	0.08747
32	5.80	50	0.01276	0.61138	0.49412	0.08751
33	6.50	5	0.28242	0.58588	0.29242	0.09153
34	6.50	10	0.17872	0.58700	0.25296	0.09198
35	6.50	10	0.27834	0.58663	0.36760	0.09189
36	6.50	10	0.13346	0.58535	0.23886	0.09142
37	6.50	20	0.08861	0.58472	0.20556	0.09132
38	6.50	20	0.12521	0.58738	0.28025	0.09210
39	6.50	20	0.06728	0.58365	0.21823	0.09100
40	6.50	100	0.01139	0.58477	0.27506	0.09165
41	6.50	160	0.00509	0.58978	0.42529	0.09537
42	7.00	1	0.43269	0.56843	0.28894	0.10330
43	7.00	10	0.34164	0.56933	0.34762	0.10381
44	7.00	10	0.16714	0.56467	0.19750	0.10182
45	7.00	50	0.04034	0.56398	0.18777	0.10157
46	7.00	50	0.04529	0.56506	0.22353	0.10189
47	7.50	1	0.50870	0.57305	0.35356	0.11543
48	5.00	10	0.27447	0.56890	0.31262	0.11172
49	5.00	10	0.40176	0.56454	0.45398	0.10676
50	8.00	50	0.07201	0.57128	0.25320	0.10191
51	8.00	160	0.01924	0.56732	0.25924	0.09901

TABLE F4-2
A. McGARR: HORIZONTAL POINT ESTIMATES SPECTRAL ACCELERATION AT 0.05 SEC PERIOD

CASE NO.	MAGNITUDE	DISTANCE (KM)	MU	SIGMA	SIGMA MU	SIGMA SIGMA
1	5.00	1	0.23293	0.66080	0.53004	0.08395
2	5.00	1	0.29505	0.66316	0.32601	0.08334
3	5.00	5	0.08674	0.66316	0.38582	0.08334
4	5.00	5	0.11470	0.66552	0.20912	0.08293
5	5.80	10	0.15173	0.61921	0.24388	0.08527
6	5.80	20	0.11579	0.61648	0.23319	0.08521
7	6.50	1	0.69176	0.59350	0.35426	0.09081
8	6.50	1	0.75147	0.59408	0.41858	0.09196
9	6.50	1	0.53598	0.59335	0.31652	0.09071
10	6.50	5	0.65316	0.59064	0.44026	0.09047
11	6.50	5	0.34934	0.59205	0.33485	0.09031
12	6.50	50	0.03900	0.59007	0.29150	0.09011
13	6.50	50	0.04112	0.58974	0.32908	0.09012
14	7.00	10	0.38444	0.56893	0.29561	0.10206
15	7.50	50	0.07665	0.56861	0.27704	0.10699
16	7.50	50	0.08700	0.56660	0.32435	0.10597
17	5.00	1	0.08549	0.66080	0.66347	0.08395
18	5.80	5	0.24437	0.61704	0.28170	0.08459
19	5.80	5	0.12224	0.61707	0.38088	0.08497
20	5.00	10	0.10528	0.67265	0.23115	0.08291
21	5.00	10	0.14528	0.66316	0.26277	0.08334
22	5.00	50	0.00928	0.65844	0.36660	0.08475
23	5.00	50	0.00956	0.65844	0.43628	0.08475
24	5.00	160	0.00109	0.65140	0.50966	0.08823
25	5.80	1	0.47237	0.61749	0.41806	0.08482
26	5.80	5	0.41845	0.61941	0.42099	0.08585
27	5.80	5	0.20604	0.61882	0.35046	0.08541
28	5.80	10	0.19151	0.62056	0.29376	0.08616
29	5.80	10	0.27510	0.61709	0.34532	0.08496
30	5.80	10	0.11927	0.61628	0.40227	0.08483
31	5.80	50	0.01813	0.61663	0.54892	0.08514
32	5.80	50	0.01913	0.61787	0.59579	0.08517
33	6.50	5	0.50520	0.58919	0.32942	0.08966
34	6.50	10	0.31751	0.59391	0.27829	0.09146
35	6.50	10	0.50069	0.59127	0.42177	0.09018
36	6.50	10	0.21820	0.59235	0.33193	0.09089
37	6.50	20	0.14804	0.59224	0.24508	0.09140
38	6.50	20	0.21267	0.59329	0.31691	0.09099
39	6.50	20	0.10410	0.58962	0.33092	0.09013
40	6.50	100	0.01417	0.58916	0.34145	0.09018
41	6.50	160	0.00617	0.58953	0.45208	0.09014
42	7.00	1	0.77515	0.57360	0.33274	0.10364
43	7.00	10	0.60359	0.57481	0.41314	0.10425
44	7.00	10	0.26677	0.56963	0.28680	0.10234
45	7.00	50	0.05781	0.56766	0.24226	0.10184
46	7.00	50	0.06584	0.56905	0.28245	0.10209
47	7.50	1	0.88934	0.57933	0.41930	0.11669
48	5.00	10	0.46035	0.57421	0.36960	0.11271
49	5.00	10	0.67955	0.56907	0.53377	0.10698
50	8.00	50	0.09587	0.57771	0.36158	0.10204
51	8.00	160	0.02048	0.57158	0.35635	0.09867

TABLE F4-3
A. McGARR: HORIZONTAL POINT ESTIMATES
SPECTRAL ACCELERATION AT 0.10 SEC PERIOD

CASE NO.	MAGNITUDE	DISTANCE (KM)	MU	SIGMA	SIGMA MU	SIGMA SIGMA
1	5.00	1	0.25255	0.69718	0.44454	0.09060
2	5.00	1	0.32633	0.69235	0.52935	0.08843
3	5.00	5	0.09517	0.69718	0.23287	0.09060
4	5.00	5	0.13543	0.69476	0.31223	0.08942
5	5.80	10	0.17258	0.63608	0.20009	0.09041
6	5.80	20	0.13523	0.63645	0.24725	0.09045
7	6.50	1	0.78402	0.61132	0.34662	0.09768
8	6.50	1	0.86727	0.61082	0.47691	0.09780
9	6.50	1	0.64324	0.61224	0.32901	0.09816
10	6.50	5	0.72461	0.60718	0.43661	0.09500
11	6.50	5	0.41271	0.61035	0.22043	0.09668
12	6.50	50	0.04951	0.60797	0.27267	0.09531
13	6.50	50	0.05196	0.60752	0.27543	0.09485
14	7.00	10	0.44550	0.58653	0.32080	0.10659
15	7.50	50	0.09464	0.58748	0.33134	0.11387
16	7.50	50	0.10794	0.58367	0.36506	0.11095
17	5.00	1	0.09623	0.68753	0.44076	0.08701
18	5.80	5	0.28199	0.63704	0.25552	0.09056
19	5.80	5	0.14624	0.63629	0.30596	0.08999
20	5.00	10	0.11520	0.69718	0.29476	0.09060
21	5.00	10	0.15661	0.68753	0.35325	0.08701
22	5.00	50	0.01123	0.69235	0.24848	0.08843
23	5.00	50	0.01160	0.68753	0.31549	0.08701
24	5.00	160	0.00126	0.68032	0.42887	0.08637
25	5.80	1	0.51208	0.63819	0.40882	0.09128
26	5.80	5	0.46240	0.63666	0.40126	0.09048
27	5.80	5	0.23657	0.63776	0.24428	0.09180
28	5.80	10	0.21123	0.63729	0.27558	0.09178
29	5.80	10	0.30405	0.63639	0.35997	0.09044
30	5.80	10	0.13817	0.63388	0.26457	0.08927
31	5.80	50	0.02273	0.63601	0.45063	0.09040
32	5.80	50	0.02374	0.63664	0.52169	0.09105
33	6.50	5	0.57705	0.60969	0.32333	0.09624
34	6.50	10	0.36264	0.60921	0.28539	0.09621
35	6.50	10	0.57040	0.60836	0.42752	0.09584
36	6.50	10	0.25955	0.60869	0.19739	0.09597
37	6.50	20	0.17680	0.60642	0.24853	0.09437
38	6.50	20	0.24544	0.60855	0.31811	0.09542
39	6.50	20	0.12707	0.60752	0.19069	0.09512
40	6.50	100	0.01796	0.60586	0.36022	0.09419
41	6.50	160	0.00723	0.60612	0.43847	0.09427
42	7.00	1	0.87781	0.58919	0.33754	0.10839
43	7.00	10	0.67820	0.59070	0.41991	0.10963
44	7.00	10	0.32068	0.58695	0.15892	0.10695
45	7.00	50	0.07216	0.58496	0.27582	0.10566
46	7.00	50	0.08242	0.58705	0.30345	0.10690
47	7.50	1	0.98266	0.59546	0.43184	0.12326
48	5.00	10	0.52439	0.59037	0.40456	0.11804
49	5.00	10	0.76957	0.58686	0.52580	0.11330
50	8.00	50	0.11603	0.60112	0.43406	0.11027
51	8.00	160	0.02186	0.59392	0.45212	0.10429

TABLE F4-4
A. McGARR: HORIZONTAL POINT ESTIMATES SPECTRAL ACCELERATION AT 0.20 SEC PERIOD

CASE NO.	MAGNITUDE	DISTANCE (KM)	MU	SIGMA	SIGMA MU	SIGMA SIGMA
1	5.00	1	0.19209	0.72598	0.41417	0.08696
2	5.00	1	0.24739	0.73070	0.50903	0.08878
3	5.00	5	0.07508	0.72127	0.26024	0.08588
4	5.00	5	0.10545	0.71892	0.27923	0.08563
5	5.80	10	0.15816	0.67162	0.18066	0.09110
6	5.80	20	0.12788	0.66737	0.24396	0.08916
7	6.50	1	0.70120	0.64193	0.37011	0.09346
8	6.50	1	0.76870	0.64650	0.47601	0.09669
9	6.50	1	0.61049	0.65056	0.36481	0.09957
10	6.50	5	0.65317	0.64284	0.42569	0.09448
11	6.50	5	0.40377	0.64394	0.22869	0.09441
12	6.50	50	0.05392	0.64204	0.28184	0.09350
13	6.50	50	0.05702	0.63967	0.24439	0.09231
14	7.00	10	0.43035	0.62164	0.32298	0.10382
15	7.50	50	0.11023	0.62069	0.33856	0.10927
16	7.50	50	0.12589	0.61824	0.34846	0.10761
17	5.00	1	0.07250	0.71657	0.52574	0.08558
18	5.80	5	0.24240	0.66910	0.27668	0.08997
19	5.80	5	0.14288	0.66855	0.23413	0.08953
20	5.00	10	0.09217	0.72127	0.24548	0.08588
21	5.00	10	0.12207	0.71892	0.32175	0.08563
22	5.00	50	0.01152	0.72598	0.20731	0.08696
23	5.00	50	0.01103	0.71423	0.35588	0.08571
24	5.00	160	0.00174	0.71892	0.40683	0.08563
25	5.80	1	0.43222	0.66884	0.39554	0.08998
26	5.80	5	0.38759	0.66833	0.38931	0.09002
27	5.80	5	0.21960	0.66925	0.20678	0.08997
28	5.80	10	0.18907	0.67081	0.26835	0.09052
29	5.80	10	0.26709	0.66775	0.34321	0.08916
30	5.80	10	0.13500	0.67086	0.19482	0.09108
31	5.80	50	0.02347	0.66950	0.46958	0.08997
32	5.80	50	0.02609	0.66923	0.41429	0.08997
33	6.50	5	0.52340	0.64079	0.32970	0.09270
34	6.50	10	0.33299	0.64382	0.27829	0.09447
35	6.50	10	0.50803	0.64253	0.40365	0.09357
36	6.50	10	0.26164	0.64028	0.19585	0.09247
37	6.50	20	0.17085	0.64243	0.24444	0.09394
38	6.50	20	0.24507	0.64119	0.31662	0.09324
39	6.50	20	0.13636	0.64179	0.16381	0.09321
40	6.50	100	0.02201	0.64092	0.34995	0.09317
41	6.50	160	0.00975	0.64254	0.42500	0.09441
42	7.00	1	0.80047	0.62368	0.35782	0.10505
43	7.00	10	0.63776	0.62357	0.39741	0.10504
44	7.00	10	0.33463	0.62047	0.18668	0.10327
45	7.00	50	0.08216	0.62060	0.28265	0.10333
46	7.00	50	0.09307	0.62093	0.28406	0.10347
47	7.50	1	0.95190	0.62808	0.45612	0.11687
48	5.00	10	0.53334	0.62652	0.41618	0.11545
49	5.00	10	0.74366	0.61879	0.49779	0.10793
50	8.00	50	0.13531	0.63335	0.42231	0.10312
51	8.00	160	0.02984	0.62857	0.48561	0.09967

TABLE F4-5
A. McGARR: HORIZONTAL POINT ESTIMATES
SPECTRAL ACCELERATION AT 0.50 SEC PERIOD

CASE NO.	MAGNITUDE	DISTANCE (KM)	MU	SIGMA	SIGMA MU	SIGMA SIGMA
1	5.00	1	0.09408	0.78921	0.35494	0.08239
2	5.00	1	0.12759	0.77760	0.40561	0.07818
3	5.00	5	0.03808	0.78688	0.33888	0.08116
4	5.00	5	0.05581	0.77991	0.32861	0.07863
5	5.80	10	0.09734	0.73214	0.18824	0.09231
6	5.80	20	0.08215	0.73295	0.21058	0.09277
7	6.50	1	0.49629	0.70629	0.23021	0.09949
8	6.50	1	0.53565	0.70663	0.32029	0.10017
9	6.50	1	0.44392	0.70995	0.23537	0.10176
10	6.50	5	0.45438	0.70738	0.30880	0.10006
11	6.50	5	0.28673	0.70640	0.19241	0.09954
12	6.50	50	0.04446	0.70948	0.24497	0.10147
13	6.50	50	0.04821	0.70496	0.25579	0.09899
14	7.00	10	0.33018	0.68942	0.26958	0.11298
15	7.50	50	0.10581	0.69089	0.22371	0.12148
16	7.50	50	0.12022	0.68679	0.25248	0.11918
17	5.00	1	0.03887	0.78921	0.58915	0.08239
18	5.80	5	0.15795	0.73360	0.18515	0.09309
19	5.80	5	0.08856	0.73374	0.24305	0.09325
20	5.00	10	0.04359	0.77760	0.19409	0.07818
21	5.00	10	0.05966	0.77298	0.26170	0.07790
22	5.00	50	0.00674	0.77529	0.26470	0.07794
23	5.00	50	0.00769	0.77760	0.22716	0.07818
24	5.00	160	0.00155	0.77068	0.41756	0.07807
25	5.80	1	0.26897	0.73044	0.28280	0.09134
26	5.80	5	0.24327	0.73129	0.31881	0.09176
27	5.80	5	0.13833	0.72709	0.21590	0.09044
28	5.80	10	0.11971	0.73307	0.22512	0.09282
29	5.80	10	0.17139	0.73077	0.29279	0.09171
30	5.80	10	0.08471	0.73030	0.26780	0.09157
31	5.80	50	0.01728	0.73081	0.47267	0.09154
32	5.80	50	0.01802	0.73239	0.56708	0.09285
33	6.50	5	0.36574	0.70542	0.26328	0.09914
34	6.50	10	0.24055	0.70747	0.26598	0.10021
35	6.50	10	0.37022	0.70704	0.33527	0.10001
36	6.50	10	0.18834	0.70535	0.21757	0.09912
37	6.50	20	0.12470	0.70642	0.21653	0.09955
38	6.50	20	0.17731	0.70980	0.29052	0.10167
39	6.50	20	0.10509	0.70571	0.17444	0.09925
40	6.50	100	0.02213	0.70631	0.29387	0.09950
41	6.50	160	0.01144	0.70845	0.40268	0.10121
42	7.00	1	0.62292	0.69025	0.22411	0.11339
43	7.00	10	0.51173	0.68994	0.30369	0.11320
44	7.00	10	0.26018	0.68938	0.17538	0.11296
45	7.00	50	0.07252	0.68813	0.21359	0.11223
46	7.00	50	0.08304	0.69105	0.27230	0.11386
47	7.50	1	0.75940	0.69782	0.28949	0.12824
48	5.00	10	0.42137	0.69464	0.29154	0.12506
49	5.00	10	0.61968	0.69063	0.40666	0.12131
50	8.00	50	0.13952	0.70611	0.25434	0.11343
51	8.00	160	0.04306	0.70202	0.36680	0.11172

TABLE F4-6
A. McGARR: HORIZONTAL POINT ESTIMATES SPECTRAL ACCELERATION AT 1.00 SEC PERIOD

CASE NO.	MAGNITUDE	DISTANCE (KM)	MU	SIGMA	SIGMA MU	SIGMA SIGMA
1	5.00	1	0.04141	0.82412	0.30516	0.07128
2	5.00	1	0.05545	0.82182	0.39650	0.07107
3	5.00	5	0.01665	0.81952	0.36408	0.07110
4	5.00	5	0.02459	0.81952	0.43752	0.07110
5	5.80	10	0.05043	0.78845	0.20197	0.08301
6	5.80	20	0.04207	0.78654	0.21934	0.08614
7	6.50	1	0.29217	0.76628	0.21096	0.09875
8	6.50	1	0.30525	0.76701	0.31509	0.10181
9	6.50	1	0.25518	0.76217	0.23163	0.09985
10	6.50	5	0.26587	0.76567	0.31860	0.10119
11	6.50	5	0.16142	0.76262	0.25448	0.09977
12	6.50	50	0.02959	0.76286	0.28559	0.09762
13	6.50	50	0.02986	0.76291	0.34876	0.09986
14	7.00	10	0.20101	0.74890	0.25864	0.11597
15	7.50	50	0.07470	0.75033	0.25503	0.12649
16	7.50	50	0.08269	0.74842	0.29251	0.12758
17	5.00	1	0.01676	0.81722	0.72014	0.07134
18	5.80	5	0.08104	0.79407	0.36904	0.09110
19	5.80	5	0.04537	0.79209	0.34173	0.08900
20	5.00	10	0.01813	0.81722	0.14918	0.07134
21	5.00	10	0.02417	0.81722	0.21981	0.07134
22	5.00	50	0.00293	0.81493	0.41534	0.07180
23	5.00	50	0.00320	0.82182	0.37162	0.07107
24	5.00	160	0.00090	0.81952	0.41360	0.07110
25	5.80	1	0.13781	0.79135	0.30971	0.08489
26	5.80	5	0.12383	0.78401	0.34350	0.08432
27	5.80	5	0.06911	0.78985	0.31612	0.08716
28	5.80	10	0.06058	0.78968	0.22683	0.08392
29	5.80	10	0.08685	0.78479	0.29479	0.08466
30	5.80	10	0.04437	0.79050	0.29278	0.08874
31	5.80	50	0.01007	0.78400	0.48317	0.08137
32	5.80	50	0.01065	0.78646	0.53086	0.08526
33	6.50	5	0.20543	0.76853	0.26516	0.09979
34	6.50	10	0.14143	0.76614	0.26065	0.09874
35	6.50	10	0.21626	0.76409	0.32505	0.10033
36	6.50	10	0.10926	0.76232	0.24306	0.09968
37	6.50	20	0.07419	0.76271	0.24685	0.09751
38	6.50	20	0.10122	0.76615	0.33036	0.10150
39	6.50	20	0.06206	0.76340	0.24613	0.10003
40	6.50	100	0.01580	0.76339	0.28697	0.09772
41	6.50	160	0.00878	0.76388	0.43595	0.09797
42	7.00	1	0.36811	0.74990	0.32675	0.11649
43	7.00	10	0.31315	0.75058	0.35191	0.11855
44	7.00	10	0.16192	0.74645	0.23605	0.11695
45	7.00	50	0.04928	0.74880	0.29796	0.11595
46	7.00	50	0.05339	0.74706	0.36957	0.11711
47	7.50	1	0.48414	0.75679	0.41763	0.12961
48	5.00	10	0.27547	0.75406	0.31417	0.12864
49	5.00	10	0.40973	0.75064	0.49681	0.12841
50	8.00	50	0.10475	0.75795	0.25976	0.12604
51	8.00	160	0.03921	0.76188	0.33445	0.12695

TABLE F4-7
A. McGARR: HORIZONTAL POINT ESTIMATES
SPECTRAL ACCELERATION AT 2.00 SEC PERIOD

CASE NO.	MAGNITUDE	DISTANCE (KM)	MU	SIGMA	SIGMA MU	SIGMA SIGMA
1	5.00	1	0.01170	0.91687	0.44990	0.07130
2	5.00	1	0.01556	0.91228	0.37888	0.07193
3	5.00	5	0.00542	0.90544	0.54983	0.07446
4	5.00	5	0.00738	0.90544	0.51380	0.07446
5	5.80	10	0.02039	0.88529	0.31735	0.10388
6	5.80	20	0.01603	0.88198	0.34426	0.11280
7	6.50	1	0.13624	0.86561	0.26294	0.12915
8	6.50	1	0.13756	0.86033	0.32083	0.13460
9	6.50	1	0.11574	0.86217	0.21271	0.13531
10	6.50	5	0.11617	0.86312	0.40839	0.13601
11	6.50	5	0.07994	0.86301	0.25717	0.13577
12	6.50	50	0.01503	0.86272	0.43598	0.12849
13	6.50	50	0.01473	0.86013	0.50787	0.13438
14	7.00	10	0.10475	0.85316	0.35852	0.15056
15	7.50	50	0.04270	0.85226	0.50795	0.16212
16	7.50	50	0.04513	0.84361	0.57992	0.16507
17	5.00	1	0.00486	0.91000	0.89805	0.07257
18	5.80	5	0.03228	0.87676	0.33589	0.11027
19	5.80	5	0.01972	0.87801	0.35255	0.11071
20	5.00	10	0.00636	0.90544	0.25571	0.07446
21	5.00	10	0.00778	0.90771	0.31558	0.07341
22	5.00	50	0.00117	0.90544	0.46521	0.07446
23	5.00	50	0.00112	0.90544	0.55630	0.07446
24	5.00	160	0.00047	0.90544	0.48000	0.07446
25	5.80	1	0.05435	0.89000	0.24463	0.10599
26	5.80	5	0.04744	0.87569	0.33961	0.10984
27	5.80	5	0.03023	0.87722	0.27912	0.11036
28	5.80	10	0.02407	0.88939	0.29054	0.10784
29	5.80	10	0.03153	0.88555	0.35098	0.11678
30	5.80	10	0.01896	0.87611	0.35654	0.11000
31	5.80	50	0.00458	0.88163	0.64329	0.10248
32	5.80	50	0.00459	0.88026	0.66741	0.11234
33	6.50	5	0.10013	0.86505	0.27767	0.12876
34	6.50	10	0.06675	0.86542	0.28345	0.12887
35	6.50	10	0.09241	0.86336	0.39798	0.13647
36	6.50	10	0.05269	0.86061	0.31857	0.13459
37	6.50	20	0.03809	0.86773	0.28966	0.12992
38	6.50	20	0.04730	0.85792	0.34860	0.13363
39	6.50	20	0.03039	0.85997	0.37785	0.13437
40	6.50	100	0.00874	0.86403	0.36371	0.12863
41	6.50	160	0.00511	0.86858	0.59103	0.13045
42	7.00	1	0.19363	0.85316	0.30861	0.15056
43	7.00	10	0.14430	0.84904	0.46045	0.15547
44	7.00	10	0.08445	0.85029	0.36053	0.15645
45	7.00	50	0.02789	0.85108	0.39784	0.14990
46	7.00	50	0.02908	0.84582	0.47628	0.15417
47	7.50	1	0.24850	0.85676	0.45266	0.16441
48	5.00	10	0.14675	0.85170	0.49999	0.16193
49	5.00	10	0.19363	0.84570	0.64907	0.16566
50	8.00	50	0.06564	0.86234	0.30079	0.16399
51	8.00	160	0.02777	0.86352	0.41672	0.16411

TABLE F4-8
A. McGARR: HORIZONTAL POINT ESTIMATES SPECTRAL ACCELERATION AT 3.33 SEC PERIOD

CASE NO.	MAGNITUDE	DISTANCE (KM)	MU	SIGMA	SIGMA MU	SIGMA SIGMA
1	5.00	1	0.00407	0.95631	0.55928	0.07796
2	5.00	1	0.00493	0.94932	0.53335	0.07431
3	5.00	5	0.00170	0.94932	0.48334	0.07431
4	5.00	5	0.00215	0.94932	0.50607	0.07431
5	5.80	10	0.00940	0.89777	0.34842	0.11603
6	5.80	20	0.00646	0.89363	0.34813	0.12481
7	6.50	1	0.07791	0.87968	0.24975	0.15548
8	6.50	1	0.07449	0.86199	0.26963	0.14763
9	6.50	1	0.06375	0.86630	0.24394	0.15104
10	6.50	5	0.06215	0.86799	0.34984	0.15240
11	6.50	5	0.04552	0.87061	0.29508	0.15501
12	6.50	50	0.00885	0.87424	0.53610	0.14787
13	6.50	50	0.00787	0.86615	0.59643	0.15083
14	7.00	10	0.06460	0.85716	0.36724	0.17276
15	7.50	50	0.03205	0.85189	0.43624	0.18038
16	7.50	50	0.02976	0.84587	0.57781	0.18362
17	5.00	1	0.00151	0.95165	0.73524	0.07532
18	5.80	5	0.01297	0.89723	0.33121	0.12813
19	5.80	5	0.00809	0.89644	0.37226	0.12728
20	5.00	10	0.00220	0.94468	0.39526	0.07290
21	5.00	10	0.00241	0.94700	0.35118	0.07349
22	5.00	50	0.00046	0.94237	0.34346	0.07252
23	5.00	50	0.00042	0.94237	0.30143	0.07252
24	5.00	160	0.00015	0.94237	0.33319	0.07252
25	5.80	1	0.02572	0.89960	0.30701	0.11755
26	5.80	5	0.02062	0.89663	0.33583	0.12785
27	5.80	5	0.01392	0.89325	0.33091	0.12448
28	5.80	10	0.01153	0.89923	0.33671	0.11707
29	5.80	10	0.01252	0.89141	0.36938	0.12303
30	5.80	10	0.00808	0.89481	0.47855	0.12568
31	5.80	50	0.00216	0.89940	0.63111	0.11716
32	5.80	50	0.00196	0.89456	0.68478	0.12568
33	6.50	5	0.05887	0.87914	0.24520	0.15359
34	6.50	10	0.03783	0.87673	0.29971	0.15063
35	6.50	10	0.04436	0.86747	0.38968	0.15216
36	6.50	10	0.02779	0.86963	0.41675	0.15418
37	6.50	20	0.02094	0.87233	0.35747	0.14617
38	6.50	20	0.02253	0.87122	0.41900	0.15569
39	6.50	20	0.01613	0.86394	0.47096	0.14906
40	6.50	100	0.00476	0.86915	0.51889	0.14370
41	6.50	160	0.00329	0.87857	0.58656	0.15219
42	7.00	1	0.12487	0.85491	0.28151	0.17065
43	7.00	10	0.07585	0.84840	0.46087	0.17388
44	7.00	10	0.04878	0.84914	0.43370	0.17437
45	7.00	50	0.01845	0.85394	0.44843	0.16989
46	7.00	50	0.01743	0.84947	0.52519	0.17476
47	7.50	1	0.17502	0.85792	0.38368	0.18555
48	5.00	10	0.09741	0.85630	0.51116	0.18411
49	5.00	10	0.11032	0.84693	0.64831	0.18444
50	8.00	50	0.05303	0.87160	0.25135	0.18110
51	8.00	160	0.02409	0.87208	0.31114	0.18150

TABLE F4-9
A. McGARR: HORIZONTAL POINT ESTIMATES
PEAK GROUND VELOCITY

CASE NO.	MAGNITUDE	DISTANCE (KM)	MU	SIGMA	SIGMA MU	SIGMA SIGMA
1	5.00	1	5.76892	0.77513	0.42153	0.07727
2	5.00	1	8.96000	0.77513	0.37607	0.07727
3	5.00	5	2.01906	0.77513	0.30275	0.07727
4	5.00	5	3.34081	0.76900	0.38084	0.07375
5	5.80	10	5.59918	0.74832	0.18514	0.09661
6	5.80	20	4.59678	0.74679	0.18488	0.09881
7	6.50	1	33.93066	0.75161	0.18533	0.11509
8	6.50	1	37.32352	0.74897	0.31358	0.11705
9	6.50	1	28.89401	0.74897	0.21364	0.11705
10	6.50	5	33.16038	0.74696	0.30885	0.11576
11	6.50	5	18.36356	0.74540	0.18142	0.11522
12	6.50	50	2.47847	0.74552	0.33705	0.11290
13	6.50	50	2.55408	0.74445	0.37580	0.11482
14	7.00	10	23.59593	0.74789	0.24704	0.12606
15	7.50	50	7.44233	0.74841	0.38578	0.13626
16	7.50	50	8.47371	0.74335	0.45892	0.13663
17	5.00	1	1.84080	0.76900	0.71942	0.07375
18	5.80	5	9.73234	0.74761	0.34306	0.09896
19	5.80	5	5.20978	0.74667	0.31641	0.09860
20	5.00	10	2.42389	0.76594	0.12511	0.07232
21	5.00	10	3.50263	0.76900	0.10771	0.07375
22	5.00	50	0.27286	0.76289	0.20093	0.07113
23	5.00	50	0.30460	0.76594	0.19567	0.07232
24	5.00	160	0.05448	0.75681	0.24571	0.06949
25	5.80	1	17.18606	0.74999	0.31394	0.09721
26	5.80	5	16.38807	0.74456	0.31007	0.09789
27	5.80	5	8.45280	0.74601	0.22597	0.09840
28	5.80	10	6.95378	0.75164	0.22147	0.09773
29	5.80	10	10.82250	0.74683	0.21336	0.09882
30	5.80	10	4.81959	0.74561	0.29965	0.09829
31	5.80	50	0.80705	0.74895	0.52645	0.09675
32	5.80	50	0.86779	0.74884	0.56224	0.09952
33	6.50	5	24.09546	0.75074	0.19797	0.11468
34	6.50	10	15.56801	0.74954	0.19304	0.11421
35	6.50	10	24.93648	0.74728	0.31349	0.11589
36	6.50	10	11.51401	0.74482	0.21603	0.11506
37	6.50	20	7.54828	0.74832	0.23254	0.11375
38	6.50	20	10.65791	0.74782	0.27492	0.11613
39	6.50	20	5.98332	0.74287	0.25458	0.11431
40	6.50	100	1.20417	0.74701	0.35479	0.11354
41	6.50	160	0.53600	0.75174	0.58288	0.11601
42	7.00	1	45.19347	0.74891	0.29994	0.12675
43	7.00	10	37.40738	0.74592	0.41376	0.12772
44	7.00	10	17.71020	0.74322	0.30764	0.12672
45	7.00	50	4.61680	0.74404	0.32868	0.12495
46	7.00	50	5.17090	0.74223	0.40715	0.12641
47	7.50	1	60.57650	0.75566	0.50900	0.14015
48	5.00	10	33.02724	0.75068	0.42410	0.13735
49	5.00	10	48.64212	0.74540	0.67888	0.13727
50	8.00	50	12.06421	0.75608	0.36087	0.13408
51	8.00	160	3.71883	0.76042	0.45514	0.13457

TABLE F4-10
A. McGARR: VERTICAL POINT ESTIMATES
PEAK GROUND ACCELERATION

CASE NO.	MAGNITUDE	DISTANCE (KM)	MU	SIGMA	SIGMA MU	SIGMA SIGMA
1	5.00	1	0.08773	0.65788	0.61424	0.07873
2	5.00	1	0.10244	0.66188	0.31600	0.07940
3	5.00	5	0.02608	0.65788	0.40156	0.07873
4	5.00	5	0.03042	0.66063	0.22121	0.07912
5	5.80	10	0.05001	0.60510	0.26502	0.09930
6	5.80	20	0.04325	0.59898	0.36240	0.09243
7	6.50	1	0.29021	0.56190	0.28457	0.11353
8	6.50	1	0.32237	0.56528	0.24609	0.11759
9	6.50	1	0.26248	0.56140	0.21735	0.11298
10	6.50	5	0.27964	0.56003	0.31306	0.11152
11	6.50	5	0.16792	0.56140	0.24414	0.11298
12	6.50	50	0.01241	0.56040	0.29642	0.11191
13	6.50	50	0.01493	0.55953	0.28418	0.11102
14	7.00	10	0.15156	0.53819	0.19367	0.14253
15	7.50	50	0.02606	0.53671	0.26060	0.15077
16	7.50	50	0.03198	0.53646	0.36468	0.15046
17	5.00	1	0.02872	0.65338	0.46575	0.07871
18	5.80	5	0.07677	0.59810	0.37503	0.09164
19	5.80	5	0.04600	0.60160	0.36352	0.09510
20	5.00	10	0.03355	0.66463	0.28174	0.08020
21	5.00	10	0.05823	0.65013	0.29962	0.07917
22	5.00	50	0.00275	0.65563	0.16842	0.07862
23	5.00	50	0.00281	0.64913	0.15459	0.07940
24	5.00	160	0.00030	0.65688	0.24926	0.07866
25	5.80	1	0.17892	0.59998	0.46725	0.09339
26	5.80	5	0.17016	0.59810	0.38014	0.09164
27	5.80	5	0.09041	0.59998	0.26397	0.09339
28	5.80	10	0.06710	0.60210	0.29646	0.09565
29	5.80	10	0.10974	0.59948	0.33714	0.09290
30	5.80	10	0.05089	0.60048	0.26298	0.09390
31	5.80	50	0.00514	0.59898	0.55375	0.09243
32	5.80	50	0.00604	0.60098	0.50851	0.09442
33	6.50	5	0.21342	0.55953	0.20921	0.11102
34	6.50	10	0.12410	0.56240	0.17870	0.11410
35	6.50	10	0.22048	0.56403	0.32217	0.11602
36	6.50	10	0.09872	0.56040	0.23381	0.11191
37	6.50	20	0.05555	0.56140	0.17455	0.11298
38	6.50	20	0.09089	0.56465	0.31443	0.11680
39	6.50	20	0.04323	0.55953	0.25315	0.11102
40	6.50	100	0.00468	0.56290	0.35610	0.11468
41	6.50	160	0.00169	0.56040	0.46202	0.11191
42	7.00	1	0.32060	0.54069	0.22876	0.14549
43	7.00	10	0.25173	0.54107	0.32693	0.14596
44	7.00	10	0.11848	0.53957	0.20036	0.14413
45	7.00	50	0.01822	0.53932	0.21504	0.14383
46	7.00	50	0.02303	0.53932	0.38217	0.14383
47	7.50	1	0.42540	0.54283	0.34844	0.15906
48	5.00	10	0.18229	0.53671	0.24519	0.15077
49	5.00	10	0.29286	0.53958	0.39797	0.15451
50	8.00	50	0.03734	0.54292	0.29347	0.14981
51	8.00	160	0.00781	0.54392	0.34952	0.15101

TABLE F4-11
A. McGARR: VERTICAL POINT ESTIMATES
SPECTRAL ACCELERATION AT 0.05 SEC PERIOD

CASE NO.	MAGNITUDE	DISTANCE (KM)	MU	SIGMA	SIGMA MU	SIGMA SIGMA
1	5.00	1	0.19611	0.66776	0.74679	0.07405
2	5.00	1	0.22714	0.66776	0.40246	0.07405
3	5.00	5	0.05487	0.66651	0.58540	0.07425
4	5.00	5	0.06538	0.67226	0.34465	0.07387
5	5.80	10	0.09962	0.61616	0.40006	0.09436
6	5.80	20	0.08278	0.61191	0.32080	0.08956
7	6.50	1	0.59513	0.57615	0.41567	0.11001
8	6.50	1	0.65188	0.57777	0.37186	0.11213
9	6.50	1	0.49860	0.57515	0.31546	0.10876
10	6.50	5	0.57174	0.57515	0.40572	0.10876
11	6.50	5	0.30783	0.57415	0.36895	0.10756
12	6.50	50	0.01997	0.57565	0.36803	0.10938
13	6.50	50	0.02442	0.57615	0.31693	0.11001
14	7.00	10	0.28825	0.55289	0.30716	0.13788
15	7.50	50	0.04088	0.55102	0.27650	0.14468
16	7.50	50	0.05064	0.55127	0.35364	0.14502
17	5.00	1	0.06152	0.66876	0.62732	0.07394
18	5.80	5	0.15471	0.61453	0.50509	0.09239
19	5.80	5	0.08652	0.61741	0.46528	0.09598
20	5.00	10	0.07164	0.68151	0.45203	0.07604
21	5.00	10	0.12523	0.66776	0.22462	0.07405
22	5.00	50	0.00513	0.66651	0.23809	0.07425
23	5.00	50	0.00560	0.67226	0.21339	0.07387
24	5.00	160	0.00039	0.66876	0.37943	0.07394
25	5.80	1	0.37618	0.61741	0.61769	0.09598
26	5.80	5	0.34437	0.61391	0.51263	0.09168
27	5.80	5	0.17400	0.61391	0.39888	0.09168
28	5.80	10	0.13601	0.61803	0.44266	0.09682
29	5.80	10	0.21540	0.61341	0.46138	0.09112
30	5.80	10	0.09348	0.61291	0.42610	0.09059
31	5.80	50	0.00893	0.61291	0.62613	0.09059
32	5.80	50	0.01039	0.61678	0.63282	0.09516
33	6.50	5	0.42971	0.57565	0.32267	0.10938
34	6.50	10	0.24185	0.57952	0.29392	0.11456
35	6.50	10	0.43085	0.57727	0.40965	0.11147
36	6.50	10	0.17916	0.57665	0.34712	0.11065
37	6.50	20	0.10371	0.57665	0.24709	0.11065
38	6.50	20	0.17143	0.57952	0.32035	0.11456
39	6.50	20	0.07476	0.57465	0.34334	0.10815
40	6.50	100	0.00624	0.57665	0.42745	0.11065
41	6.50	160	0.00213	0.57377	0.49972	0.10713
42	7.00	1	0.65060	0.55626	0.31494	0.14236
43	7.00	10	0.48672	0.55751	0.40088	0.14412
44	7.00	10	0.21085	0.55464	0.27340	0.14015
45	7.00	50	0.02975	0.55389	0.26624	0.13916
46	7.00	50	0.03755	0.55351	0.37479	0.13867
47	7.50	1	0.85022	0.55902	0.34831	0.15653
48	5.00	10	0.34681	0.55077	0.33709	0.14435
49	5.00	10	0.56548	0.55427	0.46742	0.14925
50	8.00	50	0.05744	0.56270	0.29045	0.14875
51	8.00	160	0.00856	0.56070	0.42310	0.14628

TABLE F4-12
A. McGARR: VERTICAL POINT ESTIMATES
SPECTRAL ACCELERATION AT 0.10 SEC PERIOD

CASE NO.	MAGNITUDE	DISTANCE (KM)	MU	SIGMA	SIGMA MU	SIGMA SIGMA
1	5.00	1	0.17932	0.70108	0.54242	0.08433
2	5.00	1	0.21198	0.70608	0.24608	0.08744
3	5.00	5	0.05854	0.70608	0.33249	0.08744
4	5.00	5	0.06892	0.71158	0.15364	0.09168
5	5.80	10	0.10659	0.63343	0.23175	0.11105
6	5.80	20	0.09024	0.62955	0.41739	0.10506
7	6.50	1	0.58532	0.58992	0.29588	0.11368
8	6.50	1	0.64442	0.59192	0.30262	0.11687
9	6.50	1	0.51292	0.59192	0.28156	0.11687
10	6.50	5	0.53488	0.58992	0.39294	0.11368
11	6.50	5	0.32512	0.59092	0.24212	0.11525
12	6.50	50	0.02516	0.58992	0.35971	0.11368
13	6.50	50	0.02998	0.59042	0.33795	0.11446
14	7.00	10	0.29998	0.56768	0.27498	0.14037
15	7.50	50	0.05144	0.56669	0.32701	0.14950
16	7.50	50	0.06150	0.56519	0.39521	0.14697
17	5.00	1	0.06380	0.70108	0.39876	0.08433
18	5.80	5	0.16259	0.63005	0.30390	0.10580
19	5.80	5	0.09609	0.63005	0.33024	0.10580
20	5.00	10	0.07437	0.71008	0.22507	0.09045
21	5.00	10	0.12434	0.69758	0.35532	0.08262
22	5.00	50	0.00624	0.70883	0.22066	0.08946
23	5.00	50	0.00649	0.69983	0.21479	0.08367
24	5.00	160	0.00054	0.70358	0.39052	0.08579
25	5.80	1	0.36638	0.62855	0.37523	0.10363
26	5.80	5	0.33337	0.63005	0.39968	0.10580
27	5.80	5	0.17546	0.62805	0.23318	0.10293
28	5.80	10	0.13695	0.63218	0.31612	0.10905
29	5.80	10	0.22037	0.63218	0.41889	0.10905
30	5.80	10	0.10064	0.62855	0.24779	0.10363
31	5.80	50	0.01126	0.63280	0.52392	0.11004
32	5.80	50	0.01231	0.63218	0.59821	0.10905
33	6.50	5	0.42559	0.59092	0.23559	0.11525
34	6.50	10	0.25479	0.59142	0.22340	0.11606
35	6.50	10	0.42767	0.59142	0.41362	0.11606
36	6.50	10	0.19632	0.59042	0.23794	0.11446
37	6.50	20	0.11288	0.59042	0.23139	0.11446
38	6.50	20	0.18205	0.59354	0.39339	0.11957
39	6.50	20	0.08684	0.58904	0.22634	0.11233
40	6.50	100	0.00838	0.58792	0.44726	0.11064
41	6.50	160	0.00287	0.58954	0.48917	0.11309
42	7.00	1	0.64614	0.56968	0.26616	0.14368
43	7.00	10	0.48712	0.57281	0.41971	0.14909
44	7.00	10	0.22972	0.56768	0.19058	0.14037
45	7.00	50	0.03653	0.56681	0.29672	0.13895
46	7.00	50	0.04542	0.56793	0.39735	0.14077
47	7.50	1	0.84681	0.57044	0.43931	0.15609
48	5.00	10	0.36351	0.56582	0.34873	0.14802
49	5.00	10	0.57576	0.56844	0.48598	0.15253
50	8.00	50	0.07132	0.58777	0.35881	0.15898
51	8.00	160	0.01038	0.58827	0.44070	0.15966

TABLE F4-13
A. McGARR: VERTICAL POINT ESTIMATES
SPECTRAL ACCELERATION AT 0.20 SEC PERIOD

CASE NO.	MAGNITUDE	DISTANCE (KM)	MU	SIGMA	SIGMA MU	SIGMA SIGMA
1	5.00	1	0.11264	0.69996	0.43327	0.08494
2	5.00	1	0.12451	0.70996	0.27520	0.08623
3	5.00	5	0.04017	0.70846	0.16527	0.08581
4	5.00	5	0.04299	0.70596	0.17344	0.08529
5	5.80	10	0.07777	0.63319	0.17111	0.11102
6	5.80	20	0.06835	0.63107	0.50257	0.10845
7	6.50	1	0.44086	0.59667	0.20892	0.11293
8	6.50	1	0.45906	0.59554	0.25431	0.11116
9	6.50	1	0.38845	0.59504	0.24801	0.11039
10	6.50	5	0.41591	0.59392	0.34828	0.10870
11	6.50	5	0.25808	0.59292	0.25631	0.10724
12	6.50	50	0.02274	0.59067	0.38503	0.10413
13	6.50	50	0.02725	0.59392	0.41687	0.10870
14	7.00	10	0.24849	0.57241	0.27143	0.12883
15	7.50	50	0.05116	0.56905	0.36987	0.13407
16	7.50	50	0.06091	0.57017	0.42926	0.13592
17	5.00	1	0.04230	0.70846	0.24675	0.08581
18	5.80	5	0.11510	0.62944	0.30366	0.10665
19	5.80	5	0.07245	0.63157	0.34337	0.10904
20	5.00	10	0.04468	0.71121	0.23177	0.08663
21	5.00	10	0.08317	0.70596	0.52475	0.08529
22	5.00	50	0.00520	0.70996	0.36602	0.08623
23	5.00	50	0.00505	0.69496	0.24330	0.08561
24	5.00	160	0.00059	0.70471	0.33462	0.08511
25	5.80	1	0.25224	0.62994	0.32370	0.10719
26	5.80	5	0.23759	0.63382	0.37464	0.11181
27	5.80	5	0.13329	0.63157	0.20669	0.10904
28	5.80	10	0.10175	0.63632	0.20110	0.11518
29	5.80	10	0.16022	0.63507	0.44697	0.11346
30	5.80	10	0.07741	0.62994	0.22574	0.10719
31	5.80	50	0.00957	0.63319	0.49152	0.11102
32	5.80	50	0.01146	0.63319	0.50075	0.11102
33	6.50	5	0.32166	0.59292	0.21526	0.10724
34	6.50	10	0.19259	0.59067	0.20637	0.10413
35	6.50	10	0.32625	0.59504	0.40591	0.11039
36	6.50	10	0.16182	0.59292	0.24749	0.10724
37	6.50	20	0.09331	0.59392	0.27914	0.10870
38	6.50	20	0.14895	0.59904	0.47863	0.11683
39	6.50	20	0.07684	0.59342	0.30506	0.10796
40	6.50	100	0.00916	0.59604	0.50193	0.11194
41	6.50	160	0.00362	0.59442	0.48893	0.10944
42	7.00	1	0.49837	0.57241	0.24831	0.12883
43	7.00	10	0.39984	0.57666	0.42799	0.13597
44	7.00	10	0.20125	0.57316	0.27225	0.13004
45	7.00	50	0.03542	0.57103	0.33009	0.12664
46	7.00	50	0.04434	0.57141	0.46095	0.12723
47	7.50	1	0.65472	0.57405	0.44585	0.14258
48	5.00	10	0.31265	0.57155	0.33984	0.13823
49	5.00	10	0.47565	0.57280	0.46870	0.14038
50	8.00	50	0.07163	0.59740	0.38540	0.14792
51	8.00	160	0.01378	0.59240	0.49521	0.14131

TABLE F4-14
A. McGARR: VERTICAL POINT ESTIMATES
SPECTRAL ACCELERATION AT 0.50 SEC PERIOD

CASE NO.	MAGNITUDE	DISTANCE (KM)	MU	SIGMA	SIGMA MU	SIGMA SIGMA
1	5.00	1	0.04395	0.73405	0.53915	0.08267
2	5.00	1	0.05306	0.73530	0.28672	0.08279
3	5.00	5	0.01460	0.74155	0.42222	0.08422
4	5.00	5	0.01800	0.73405	0.21245	0.08267
5	5.80	10	0.04496	0.65847	0.15653	0.11556
6	5.80	20	0.04200	0.65959	0.52128	0.11676
7	6.50	1	0.25877	0.62705	0.18034	0.11553
8	6.50	1	0.29198	0.62593	0.18759	0.11393
9	6.50	1	0.25345	0.62643	0.18413	0.11463
10	6.50	5	0.25351	0.62343	0.27599	0.11058
11	6.50	5	0.17452	0.62493	0.19850	0.11255
12	6.50	50	0.01834	0.62255	0.30791	0.10948
13	6.50	50	0.02291	0.62218	0.33268	0.10902
14	7.00	10	0.17743	0.60420	0.27592	0.12911
15	7.50	50	0.04542	0.60433	0.36211	0.13916
16	7.50	50	0.05128	0.60283	0.32687	0.13694
17	5.00	1	0.01682	0.75405	0.37923	0.09095
18	5.80	5	0.06376	0.66122	0.26159	0.11859
19	5.80	5	0.04010	0.65659	0.23231	0.11371
20	5.00	10	0.01965	0.73180	0.22403	0.08260
21	5.00	10	0.03358	0.72980	0.44269	0.08269
22	5.00	50	0.00253	0.74155	0.20988	0.08422
23	5.00	50	0.00280	0.73180	0.22509	0.08260
24	5.00	160	0.00043	0.73655	0.35657	0.08296
25	5.80	1	0.12219	0.65897	0.46511	0.11608
26	5.80	5	0.12624	0.66609	0.35400	0.12484
27	5.80	5	0.07854	0.65797	0.16988	0.11505
28	5.80	10	0.05937	0.66234	0.17839	0.11994
29	5.80	10	0.09163	0.66347	0.40558	0.12135
30	5.80	10	0.04646	0.66409	0.19000	0.12215
31	5.80	50	0.00621	0.65797	0.59425	0.11505
32	5.80	50	0.00777	0.66059	0.52415	0.11787
33	6.50	5	0.20274	0.62868	0.17454	0.11793
34	6.50	10	0.13198	0.62755	0.26996	0.11625
35	6.50	10	0.22523	0.62705	0.38873	0.11553
36	6.50	10	0.11414	0.62493	0.27476	0.11255
37	6.50	20	0.06598	0.62705	0.30271	0.11553
38	6.50	20	0.10799	0.62930	0.48456	0.11888
39	6.50	20	0.05427	0.62493	0.22832	0.11255
40	6.50	100	0.00861	0.62543	0.41112	0.11323
41	6.50	160	0.00400	0.62493	0.42565	0.11255
42	7.00	1	0.33300	0.60995	0.18651	0.13831
43	7.00	10	0.28411	0.60795	0.40194	0.13498
44	7.00	10	0.14843	0.60533	0.25427	0.13082
45	7.00	50	0.02866	0.60420	0.25382	0.12911
46	7.00	50	0.03688	0.60458	0.41774	0.12967
47	7.50	1	0.41407	0.60883	0.30230	0.14627
48	5.00	10	0.22150	0.60370	0.27594	0.13822
49	5.00	10	0.33432	0.60533	0.37385	0.14068
50	8.00	50	0.06706	0.63650	0.41892	0.14094
51	8.00	160	0.01758	0.63825	0.46570	0.14290

TABLE F4-15
A. McGARR: VERTICAL POINT ESTIMATES
SPECTRAL ACCELERATION AT 1.00 SEC PERIOD

CASE NO.	MAGNITUDE	DISTANCE (KM)	MU	SIGMA	SIGMA MU	SIGMA SIGMA
1	5.00	1	0.01926	0.75468	0.47268	0.07644
2	5.00	1	0.02190	0.76593	0.25586	0.07572
3	5.00	5	0.00632	0.75893	0.43968	0.07558
4	5.00	5	0.00756	0.75293	0.19447	0.07699
5	5.80	10	0.02214	0.69853	0.26455	0.09747
6	5.80	20	0.01985	0.69573	0.32964	0.10305
7	6.50	1	0.14190	0.67160	0.35861	0.10753
8	6.50	1	0.15766	0.66745	0.24439	0.10972
9	6.50	1	0.13288	0.66632	0.22151	0.10836
10	6.50	.5	0.13989	0.66695	0.34171	0.10910
11	6.50	5	0.09722	0.66345	0.10304	0.10519
12	6.50	50	0.01084	0.66985	0.43326	0.10539
13	6.50	50	0.01416	0.66257	0.37913	0.10432
14	7.00	10	0.10003	0.65427	0.22631	0.13014
15	7.50	50	0.02989	0.65060	0.23696	0.13700
16	7.50	50	0.03523	0.64751	0.40349	0.13880
17	5.00	1	0.00654	0.75368	0.56634	0.07674
18	5.80	5	0.03187	0.69673	0.34070	0.10398
19	5.80	5	0.02193	0.69836	0.30981	0.10562
20	5.00	10	0.00713	0.74943	0.45917	0.07844
21	5.00	10	0.01160	0.75293	0.25261	0.07699
22	5.00	50	0.00101	0.75368	0.32419	0.07674
23	5.00	50	0.00130	0.75468	0.15191	0.07644
24	5.00	160	0.00023	0.75693	0.52079	0.07589
25	5.80	1	0.06369	0.70778	0.49307	0.10816
26	5.80	5	0.06223	0.69948	0.42074	0.10685
27	5.80	5	0.04029	0.69523	0.17231	0.10260
28	5.80	10	0.02950	0.70053	0.20974	0.09936
29	5.80	10	0.04451	0.69436	0.33898	0.10186
30	5.80	10	0.02707	0.69886	0.21488	0.10616
31	5.80	50	0.00355	0.70391	0.69121	0.10311
32	5.80	50	0.00467	0.69523	0.47841	0.10260
33	6.50	5	0.10896	0.67097	0.24016	0.10675
34	6.50	10	0.07436	0.67047	0.17102	0.10614
35	6.50	10	0.10899	0.66170	0.29556	0.10349
36	6.50	10	0.06783	0.66382	0.17906	0.10558
37	6.50	20	0.03546	0.67097	0.27290	0.10675
38	6.50	20	0.05674	0.66257	0.28752	0.10432
39	6.50	20	0.03495	0.66170	0.22112	0.10349
40	6.50	100	0.00572	0.66697	0.35020	0.10223
41	6.50	160	0.00285	0.67047	0.58308	0.10614
42	7.00	1	0.17745	0.65740	0.38601	0.13460
43	7.00	10	0.15936	0.64906	0.34746	0.12935
44	7.00	10	0.09235	0.64906	0.17421	0.12935
45	7.00	50	0.01881	0.65027	0.31589	0.12501
46	7.00	50	0.02359	0.64618	0.43099	0.12572
47	7.50	1	0.24116	0.66735	0.37247	0.16095
48	5.00	10	0.13286	0.65122	0.27302	0.13771
49	5.00	10	0.19815	0.64813	0.41587	0.13954
50	8.00	50	0.04350	0.67995	0.15722	0.14612
51	8.00	160	0.01488	0.67545	0.40442	0.14211

TABLE F4-16
A. McGARR: VERTICAL POINT ESTIMATES
SPECTRAL ACCELERATION AT 2.00 SEC PERIOD

CASE NO.	MAGNITUDE	DISTANCE (KM)	MU	SIGMA	SIGMA MU	SIGMA SIGMA
1	5.00	1	0.00590	0.82151	0.39748	0.07480
2	5.00	1	0.00668	0.81651	0.35261	0.07724
3	5.00	5	0.00185	0.82001	0.47369	0.07544
4	5.00	5	0.00215	0.81701	0.22194	0.07695
5	5.80	10	0.00852	0.76922	0.31030	0.12524
6	5.80	20	0.00685	0.76425	0.34775	0.14192
7	6.50	1	0.07216	0.74340	0.22998	0.14956
8	6.50	1	0.07920	0.73013	0.30401	0.15463
9	6.50	1	0.06482	0.72875	0.15843	0.15347
10	6.50	5	0.06912	0.73163	0.44399	0.15599
11	6.50	5	0.04605	0.72875	0.21209	0.15347
12	6.50	50	0.00548	0.73903	0.35622	0.14537
13	6.50	50	0.00721	0.72963	0.73295	0.15420
14	7.00	10	0.04717	0.72099	0.38391	0.16836
15	7.50	50	0.01551	0.72417	0.58840	0.18468
16	7.50	50	0.02011	0.71422	0.86965	0.18993
17	5.00	1	0.00173	0.81876	0.76101	0.07603
18	5.80	5	0.01311	0.75725	0.32002	0.13617
19	5.80	5	0.00769	0.75925	0.41478	0.13758
20	5.00	10	0.00199	0.81651	0.55549	0.07724
21	5.00	10	0.00369	0.81501	0.36171	0.07814
22	5.00	50	0.00029	0.81751	0.56535	0.07668
23	5.00	50	0.00053	0.81501	0.55390	0.07814
24	5.00	160	0.00006	0.82751	1.13750	0.07314
25	5.80	1	0.02792	0.77885	0.27050	0.13547
26	5.80	5	0.02615	0.76212	0.46622	0.13994
27	5.80	5	0.01649	0.76425	0.33324	0.14192
28	5.80	10	0.01064	0.76872	0.32389	0.12483
29	5.80	10	0.01499	0.76587	0.49498	0.14356
30	5.80	10	0.01031	0.76262	0.47282	0.14039
31	5.80	50	0.00140	0.76510	0.65362	0.12223
32	5.80	50	0.00206	0.76362	0.74810	0.14132
33	6.50	5	0.05061	0.74115	0.23864	0.14731
34	6.50	10	0.03409	0.74215	0.16407	0.14829
35	6.50	10	0.04842	0.73563	0.48882	0.16002
36	6.50	10	0.03144	0.73500	0.37211	0.15935
37	6.50	20	0.01702	0.74115	0.23276	0.14731
38	6.50	20	0.02454	0.73225	0.54022	0.15658
39	6.50	20	0.01593	0.72963	0.48470	0.15420
40	6.50	100	0.00267	0.74053	0.51410	0.14672
41	6.50	160	0.00166	0.74215	0.63519	0.14829
42	7.00	1	0.09153	0.72286	0.40551	0.17014
43	7.00	10	0.07365	0.71591	0.52759	0.17886
44	7.00	10	0.04352	0.71541	0.39336	0.17833
45	7.00	50	0.00962	0.72074	0.49261	0.16814
46	7.00	50	0.01348	0.71179	0.75641	0.17471
47	7.50	1	0.11313	0.73129	0.49443	0.19224
48	5.00	10	0.06513	0.72967	0.51407	0.19037
49	5.00	10	0.10136	0.72484	0.66017	0.20165
50	8.00	50	0.02830	0.76211	0.29458	0.19185
51	8.00	160	0.01195	0.76436	0.52852	0.19349

TABLE F4-17
A. McGARR: VERTICAL POINT ESTIMATES
SPECTRAL ACCELERATION AT 3.33 SEC PERIOD

CASE NO.	MAGNITUDE	DISTANCE (KM)	MU	SIGMA	SIGMA MU	SIGMA SIGMA
1	5.00	1	0.00199	0.86897	0.58471	0.08812
2	5.00	1	0.00239	0.86347	0.56624	0.08745
3	5.00	5	0.00066	0.86547	0.58288	0.08758
4	5.00	5	0.00091	0.86197	0.51706	0.08744
5	5.80	10	0.00404	0.80443	0.29218	0.15407
6	5.80	20	0.00323	0.79421	0.45921	0.16547
7	6.50	1	0.03715	0.78276	0.21028	0.18037
8	6.50	1	0.04356	0.76849	0.39428	0.18396
9	6.50	1	0.03677	0.76686	0.34242	0.18232
10	6.50	5	0.04027	0.76886	0.57489	0.18435
11	6.50	5	0.02405	0.76611	0.29248	0.18159
12	6.50	50	0.00283	0.78164	0.34175	0.17903
13	6.50	50	0.00363	0.77386	0.72255	0.18998
14	7.00	10	0.02839	0.77047	0.25707	0.20706
15	7.50	50	0.00981	0.76746	0.50584	0.21467
16	7.50	50	0.01194	0.75538	0.78796	0.21833
17	5.00	1	0.00061	0.86822	0.83448	0.08797
18	5.80	5	0.00672	0.79458	0.54608	0.16581
19	5.80	5	0.00393	0.79321	0.46905	0.16459
20	5.00	10	0.00068	0.86722	0.67584	0.08780
21	5.00	10	0.00141	0.86197	0.60323	0.08744
22	5.00	50	0.00010	0.86822	0.63733	0.08797
23	5.00	50	0.00022	0.86222	0.93270	0.08744
24	5.00	160	0.00003	0.87847	0.70783	0.09164
25	5.80	1	0.01230	0.80593	0.30922	0.15559
26	5.80	5	0.01303	0.79546	0.60522	0.16663
27	5.80	5	0.00723	0.79346	0.44067	0.16481
28	5.80	10	0.00480	0.80318	0.31641	0.15287
29	5.80	10	0.00663	0.79583	0.56525	0.16698
30	5.80	10	0.00465	0.79783	0.57046	0.16897
31	5.80	50	0.00064	0.80281	0.57289	0.15252
32	5.80	50	0.00095	0.79858	0.79828	0.16976
33	6.50	5	0.02960	0.77914	0.20062	0.17617
34	6.50	10	0.01720	0.77464	0.15228	0.17157
35	6.50	10	0.02369	0.77224	0.47767	0.18807
36	6.50	10	0.01545	0.76936	0.41252	0.18488
37	6.50	20	0.00889	0.78389	0.19476	0.18176
38	6.50	20	0.01136	0.76974	0.46478	0.18528
39	6.50	20	0.00882	0.77174	0.65561	0.18749
40	6.50	100	0.00131	0.77914	0.56415	0.17617
41	6.50	160	0.00090	0.77914	0.56231	0.17617
42	7.00	1	0.05357	0.76534	0.39249	0.20056
43	7.00	10	0.03962	0.75927	0.55596	0.21178
44	7.00	10	0.02477	0.75577	0.52185	0.20744
45	7.00	50	0.00571	0.76797	0.51771	0.20381
46	7.00	50	0.00745	0.75927	0.79249	0.21178
47	7.50	1	0.07725	0.77471	0.29861	0.22386
48	5.00	10	0.03848	0.76633	0.53179	0.21336
49	5.00	10	0.05754	0.76201	0.72542	0.22623
50	8.00	50	0.02032	0.81560	0.50803	0.21526
51	8.00	160	0.00826	0.81735	0.51294	0.21677

TABLE F4-18
A. McGARR: VERTICAL POINT ESTIMATES
PEAK GROUND VELOCITY

CASE NO.	MAGNITUDE	DISTANCE (KM)	MU	SIGMA	SIGMA MU	SIGMA SIGMA
1	5.00	1	3.51791	0.65369	0.63598	0.08446
2	5.00	1	4.54194	0.65469	0.28625	0.08515
3	5.00	5	0.84525	0.65469	0.45857	0.08515
4	5.00	5	1.16534	0.65369	0.16207	0.08446
5	5.80	10	2.54933	0.62518	0.18207	0.13171
6	5.80	20	2.38133	0.61594	0.41413	0.12905
7	6.50	1	15.68956	0.61778	0.22500	0.15041
8	6.50	1	20.80833	0.61258	0.24880	0.15108
9	6.50	1	8.58214	0.61375	0.89385	0.15224
10	6.50	5	19.51708	0.60975	0.30496	0.14840
11	6.50	5	5.92469	0.61191	0.85398	0.15043
12	6.50	50	0.82693	0.61245	0.37987	0.14562
13	6.50	50	1.26487	0.61075	0.56537	0.14932
14	7.00	10	10.58788	0.61933	0.21741	0.17205
15	7.50	50	2.62447	0.61442	0.40242	0.18642
16	7.50	50	3.69140	0.61114	0.68314	0.18811
17	5.00	1	0.92577	0.65369	0.52421	0.08446
18	5.80	5	4.20172	0.61511	0.30767	0.12820
19	5.80	5	2.53698	0.61711	0.42130	0.13029
20	5.00	10	1.09262	0.65869	0.34852	0.08812
21	5.00	10	2.40898	0.65003	0.21098	0.08205
22	5.00	50	0.11739	0.65603	0.06887	0.08611
23	5.00	50	0.15247	0.63869	0.17117	0.07638
24	5.00	160	0.01701	0.66469	0.49392	0.09305
25	5.80	1	8.53003	0.62268	0.44687	0.12888
26	5.80	5	9.66733	0.61594	0.34810	0.12905
27	5.80	5	2.65836	0.61378	0.91903	0.12688
28	5.80	10	3.42054	0.62384	0.21454	0.13018
29	5.80	10	5.95535	0.61661	0.34049	0.12975
30	5.80	10	2.92209	0.61711	0.29270	0.13029
31	5.80	50	0.27576	0.62318	0.66480	0.12943
32	5.80	50	0.42276	0.61711	0.60964	0.13029
33	6.50	5	12.42783	0.61845	0.17451	0.15106
34	6.50	10	7.69370	0.61445	0.15610	0.14732
35	6.50	10	12.85128	0.61441	0.37841	0.15292
36	6.50	10	4.06735	0.60825	0.81126	0.14708
37	6.50	20	3.44543	0.61211	0.19834	0.14535
38	6.50	20	5.72157	0.61075	0.39690	0.14932
39	6.50	20	3.28365	0.60975	0.39781	0.14840
40	6.50	100	0.37168	0.61661	0.31329	0.14929
41	6.50	160	0.14707	0.61345	0.55159	0.14646
42	7.00	1	19.08100	0.62033	0.28288	0.17304
43	7.00	10	17.78589	0.61588	0.43819	0.17382
44	7.00	10	5.71387	0.61355	0.77096	0.17145
45	7.00	50	1.56797	0.61683	0.35194	0.16967
46	7.00	50	2.38716	0.61355	0.66397	0.17145
47	7.50	1	26.74642	0.62525	0.37924	0.19758
48	5.00	10	14.02704	0.61575	0.32293	0.18766
49	5.00	10	22.31861	0.61530	0.58960	0.19236
50	8.00	50	4.99881	0.64678	0.30704	0.19667
51	8.00	160	1.34581	0.66178	0.53584	0.20831

APPENDIX F5

ESTIMATION OF STRONG GROUND MOTIONS AT YUCCA MOUNTAIN

Walter Silva

APPENDIX F5
TABLE OF CONTENTS

APPENDIX F5

ESTIMATION OF STRONG GROUND MOTIONS AT YUCCA MOUNTAIN

Walter Silva

Pacific Engineering and Analysis

August 15, 1997

F5-1 INTRODUCTION

The process used to develop appropriate site-specific attenuation relations for both probabilistic and deterministic applications to Yucca Mountain is by the use of multiple expects. A total of seven strong ground motion experts were given the task of developing a suite of scaling rules and weights to apply to an expert selected suite of strong ground motion empirical and/or numerical models. Fifty-one specific cases of magnitude, source mechanism, source depth, and site distance (Table 3-3) were specified for which 4 ground motion parameters were requested: median (μ), aleatory uncertainty (σ), standard error of the median estimate (σ_μ), and uncertainty of the aleatory uncertainty (σ_σ). These estimates were requested for both horizontal (random component) and vertical components at seven frequencies: 0.33, 0.50, 1.00, 2.00, 5.00, 10.00 and 20.00 Hz as well as peak ground acceleration (PGA) and peak ground velocity (PGV). The 3,672 point estimates were then used to develop smoothed models over magnitude, source mechanism, and site location (distance and hanging wall/foot wall) for each expert. The suite of expert models then represent the expected epistemic uncertainty for strong ground motion estimation on a site specific-basis at Yucca Mountain.

The magnitude range is **M** 5.0 to 8.0 with a horizontal distance range of 1 to 160 km (Yucca Mountain Data Package, Volume 1, Table 3-3). The specific cases selected by the facilitation team were based on sources expected to be major contributors to the seismic hazard at Yucca Mountain. Both strike-slip and normal-slip mechanisms are considered with normal faults representing 25 of 51 cases in Table 3-3. In addition to the 51 cases, two additional cases or scenarios were specified: 1) nearly simultaneous (triggered) multiple ruptures on parallel or possibly sub-parallel faults; and 2) a low angle normal fault.

The evaluation, specification, and defense of appropriate empirical and numerical point estimates and their associated uncertainties for all of these cases is a formidable task, particularly in view of the relatively "new" parameters requested: $\sigma\mu$ and $\sigma\sigma$. The consideration and use of these parameters does not reflect state-of-the-practice and considerable uncertainty exists regarding appropriate methods to estimate their values. As a result they should be regarded in the context of development rather than mature and stable practice. In addition, there are several issues, site

specific and general, which were controlling factors in the selection of empirical and numerical models and their associated weights. These issues are discussed below.

F5-2 SITE-SPECIFIC ISSUES

The site-specific issues at Yucca Mountain requiring special consideration are: 1) the definition of the free-surface; 2) crustal, kappa, and Q(f) differences between California and the Yucca Mountain region of the Basin and Range province; and 3) the large contribution of normal fault sources to the seismic hazard.

F5-2.1 Free Surface At -300m

The free surface at which the ground motions are defined for Yucca Mountain was at a depth of -300m, the average depth (or horizon) of the repository. The shear-wave velocity at this depth is about 6,000 ft/sec (1.9 km/sec), much greater than shear-wave velocities of about 1,000 ft/sec which are typical of soft rock sites near the surface. Since empirical attenuation relations for rock are dominated by soft California rock, a significant ($\geq$ 20%) site-specific adjustment factor is necessary. At rock sites, over the frequency range of 0.33 to 20.00 Hz, horizontal motions are dominated by vertically propagating shear-waves (W. J. Silva *et al.*, Pacific Engineering and Analysis, written communication, 1997) and vertical motions are comprised of inclined compression- and shear-waves (EPRI, 1993; W. J. Silva *et al.*, Pacific Engineering and Analysis, written communication, 1997). As a result, separate adjustment factors are warranted for horizontal and vertical motions.

F5-2.2 Yucca Mountain Regional Crustal Structure

The differences between the regional crustal structure containing the site and those representative of the empirical strong motion database (largely California) are large and represent differences in shear-wave velocity, deep crustal damping (Q(f)), and shallow crustal damping (as expressed by kappa in the top 1 to 2 km). These parameters have large and predictable effects on strong ground motions (EPRI, 1993; Silva and Darragh, 1995; Silva, 1992; W. J. Silva *et al.*, Pacific Engineering and Analysis, written communication, 1997) and substantial ($\pm$ 20%) differences in these parameters should be accommodated in scale factors for the empirical (largely California based) attenuations relations. Both the definition of -300m outcropping as the reference point of free field motions as well as the differences in regional crustal models is accommodated in a single set of frequency-dependent scale factors for horizontal motions. For numerical simulations, use of the site and regional-specific parameters precludes the use of these adjustment factors.

F5-2.3 Normal Faulting Sources

It has long been recognized that normal faulting sources produce strong ground motions that are generally lower than those expected for reverse fault sources. More recently, evidence suggests that strong ground motions from normal fault ruptures in extensional regimes are also lower than those from comparable strike-slip ruptures in compressional regimes, suggesting that this observation should be incorporated into the Yucca Mountain ground motion point estimates.

Because of sparse normal faulting strong motion data available for WUS sources, currently available empirical attenuation relations do not distinguish between strike-slip and normal-slip mechanisms. As a result, the USGS recently acquired world-wide strong motion data from normal faulting earthquakes, added these to existing data for extensional regime strike-slip earthquakes, and developed an attenuation relation appropriate for extensional regime sources (Spudich *et al.*, 1997). They also made the data available to the Yucca Mountain project and normal fault adjustment factors to the predominately compressional strike-slip attenuation relation of Abrahamson and Silva (1997) were developed by N. Abrahamson. Because the combination of both strike-slip and normal-slip data into the relation of Spudich *et al.* (1997) makes applying their relation somewhat ambiguous, the normal-slip adjustment factors of Abrahamson for horizontal and vertical motions are applied to each empirical relation selected. As a result, each selected relation is implemented for strike-slip mechanism and the normal-slip factors applied as appropriate (see Table F5-1). Because the adjustment factors of Abrahamson are large, particularly at low frequencies, only 50% of the factors are implemented. This is a judgmental assessment since there are still too few data to unambiguously constrain the adjustment factors. Both more earthquakes and a larger number of sites, particularly at close distances ($D \leq 20$ km) are needed.

F5-3 GENERAL ISSUES

The general issues are those which are faced for most seismic hazard assessments: the magnitude and distance ranges exceed those used in developing empirical attenuation relations and exceed the magnitudes and distances used in validating the numerical models as well. To address the ranges in magnitudes and distances appropriate for implementing the empirical relations, only the ranges specified by the authors are used. The relations receive a substantially lower weight outside their respective **M** and D ranges (Table F5-1).

For the numerical simulations, a wide range in degree of validation exists between the four proponent models. The Anderson finite-fault model currently has had only limited validations ($\mathbf{M} > 5.0$) in the form of comparisons to recorded data. Formal validations resulting in statistically significant estimates of model variability are not available. The Silva point- and finite-source models have recently been validated for horizontal motions for 15 earthquakes for the finite-source (**M** 5.7 to 7.4) and 18 earthquakes for the point-source (**M** 4.2 to 7.4) at about 500 sites (W. J. Silva *et al.*, Pacific Engineering and Analysis, written communication, 1997) over the fault distance range of 1 to 218 km (460 km for the Saguenay earthquake). For vertical motions, which are only computed for the point-source model, validations to-date consist of five earthquakes (**M** 6.4 to 7.2) at about 200 sites. As a result, the modeling variability is well constrained for horizontal motions and reasonably well constrained for the vertical component.

For the Somerville finite-fault model, reasonably extensive validations have also been performed Approximately four earthquakes have model variability estimates: Loma Prieta, Nahanni, Saguenay, and Northridge but with few sites exceeding source-to-site distances of about 30 km

(EPRI, 1993; P. G. Somerville *et al.*, WCFS, written communication, 1995). As a result, the model variability estimates are most appropriate for close-in conditions. For WUS crustal conditions, model variability increases sharply for distances exceeding about 50 km (Silva *et al.*, 1997) suggesting that close-in model variability estimates may result in values which are too low for applications to larger distances.

For vertical motions, neither the Anderson nor Somerville models have validation results which produced model variability estimates. As a result, the point-source vertical component model variability estimates were applied to both the Anderson and Somerville point estimates. For the horizontal components, because the Somerville validations covered a limited distance range and the values given by Somerville appeared low compared to published results (EPRI, 1993; P. G. Somerville *et al.*, WCFS, written communication, 1995) and since no estimates were available for the Anderson model, the finite-source model uncertainty estimates of Silva were used for their simulations.

F5-4 PROPONENT GROUND MOTION MODELS AND WEIGHTING SCHEME

The proponent models were selected from two general classes: empirical and numerical.

F5-4.1 Empirical Models

The empirical models chosen were those considered to generally reflect the most recent analyses of data, represent different functional forms, be appropriate for crustal earthquakes, and use a consistent data set for soft rock site conditions. To represent empirical attenuation relations the following models were selected: Abrahamson and Silva (1997), Boore *et al.* (1997), Campbell (1997), and Sadigh *et al.* (1997). Because few of the relations specify peak ground velocity, Joyner and Boore (1988) was added for PGV only since it has the same functional form as Boore *et al.* (1997). The selected empirical relations, ground motion parameters, and magnitude and distance ranges specified by the authors are listed in Table F5-1. The class weight for the empirical is 0.4 and the within class (proponent model) weights are generally equal at 1.0 (Table F5-1). Exceptions to the weights of 1.0 are cases outside the specified ranges (weight of 0.25) and the case-specific weights which are listed in Table F5-2. These case-specific weights reflect a judgmental assessment that the ground motion point estimates were unrealistic. For the empirical relations (BJF97, CP97, and SD97), this may be an artifact of smoothing of coefficients or simply cases outside the range of applicability which are poorly constrained by little or no data.

F5-4.1.1 Scale Factors for the Empirical Models. For the empirical models up to four scale factors are used depending upon which parameters are available. The first scale factor adjusts the empirical rock (soft rock for CP97) horizontal motion estimates to Yucca Mountain crustal conditions and to a depth of 300m outcropping. This scale factor is termed "crust" in Table F5-1 and is the factor developed by Campbell. This factor is distance dependent due to the difference in Q(f) models between California and the Yucca Mountain region of the Basin and Range province. This factor is preferred to the distance independent crustal factor of Silva.

The second scale factor is the normal faulting factors of Abrahamson for horizontal and vertical motions. This is applied to normal slip (NS in Table F5-1) sources and, as previously stated, only 50% of the factor is implemented. The third scale factor is the PGV/PGA (VOA) point-source scale factor of Silva for horizontal and vertical components. The fourth factor is related to the third and is the vertical-to-horizontal (VOH) point-source scale factor of Silva. These last two factors are site-specific. Because a crustal adjustment factor is not available for vertical components, appropriate vertical component motions are estimated by applying the VOH scale factor to the horizontal motions adjusted to a 300m depth at Yucca Mountain. This approach is considered preferable to directly using the empirical vertical component estimates combined with the horizontal component crustal factor.

F5-4.2 Numerical Models

The numerical models available were the finite-fault models of Anderson, Silva, and Somerville and the point-source model of Silva. This suite of models generally reflects the range in currently viable approaches to kinematic (specification of slip) numerical simulations. The finite-source models share common features in that they sum small earthquakes to construct a large earthquake. The Silva and Somerville models use asperity slip distributions and an empirical constant rise time model which determines the number of events to sum for each subfault. Both approaches use $\mathbf{M} \approx 5$ subevents to model crustal earthquakes. The models differ in their wave propagation algorithms as well as subevent source spectra (W. J. Silva *et al.*, Pacific Engineering and Analysis, written communication, 1997; P. G. Somerville *et al.*, WCFS, written communication, 1995). The Anderson model uses a distinctly different subevent source description (Zeng *et al.*, 1994) with a wave propagation algorithm similar to that of Somerville.

The inclusion of the point-source model, which has been demonstrated over the years to reliably predict strong ground motions (Boore, 1983; 1986; Schneider *et al.*, 1993; Silva and Darragh, 1995; W. J. Silva *et al.*, Pacific Engineering and Analysis, written communication, 1997) completes the suite of numerical models. The point-source model is an important adjunct to the suite of numerical models as it has been implemented on numerous seismic hazard evaluations and is the model which forms the basis for evaluating strong ground motions in the CEUS. As a result, the point-source model provides base-case site-specific predictions.

For the numerical models, the class weight is 0.6 as compared to the class weight of 0.4 for the empirical models (Table F5-1). The higher weight for the numerical models reflects the preference in their fundamentally site-specific nature as well as the degree of validation, particularly for the Silva and Somerville models. In adjusting the empirical (i.e. California) models for Yucca Mountain, essentially doubling the parametric assumptions and model computations are necessary compared to direct site-specific simulations.

Table F5-1 also lists the **M** and D ranges of applicability for which simulations were available as well as the proponent model's weights. For the Anderson model, although simulations were available, the **M** 5.0 simulations were not used as validations were not available for $\mathbf{M} \leq 5.7$

(1992 Little Skull Mountain earthquake). Also, for this model, because model variability estimates were not available, it was given a weight of 0.7 compared to the equal weights of 1.0 assigned to the other numerical models. This lower weight is not intended to reflect the expectation that it will perform less well than the other finite-fault models in statistically significant validations over a large range in **M** and D, but simply indicates less confidence in its predictions at this time.

As with the empirical model estimates, case-specific weights are listed in Table F5-2. The **M** 5.0 exclusion of the Anderson model was addressed earlier. The case and frequency exclusions of the Somerville model reflect unreasonable values possibly due to computational errors (i.e. deterministic radiation pattern nodes).

F5-4.2.1 Scale Factors for the Numerical Models. As with the empirical models, scale factors were applied to the numerical models (Table F5-1). Because the simulations were site specific, the crustal factor is not necessary resulting in direct use of the horizontal and vertical components for strike-slip earthquakes. This also applies to the point-source model. For the latter, a constant stress drop of 60 bars was used, the appropriate average value for strike-slip earthquakes (W. J. Silva *et al.*, Pacific Engineering and Analysis, written communication, 1997). The remaining scale factors; the Abrahamson normal slip factor for vertical and horizontal components, the VOA, and the VOH factors were all applied in a manner analogous to the empirical estimates (Table F5-1).

F5-5 ESTIMATES OF UNCERTAINTY

The estimates of uncertainty provided for each median ground motion estimate include: 1) the uncertainty about the median estimate (aleatory, σ), uncertainty of the median estimate (epistemic, σ_μ), and the uncertainty of the aleatory uncertainty σ (epistemic, σ_σ). Table F5-3 summarizes the partition of uncertainty for both the empirical and numerical model.

F5-5.1 Aleatory Uncertainty

The aleatory uncertainties (σ_i) for the empirical models are given by each proponent for an average horizontal component and vertical component (if available). If the vertical component median estimate is computed using the average horizontal component estimate, the average horizontal component aleatory is increased by the σ_{VOH} factor in Table F5-3. A similar approach is applied to peak ground velocity (PGA). These increases in aleatory uncertainty were computed based on the increase in aleatory uncertainty for the vertical component over the average horizontal component for σ_{VOH} and the increase of 1 sec aleatory uncertainty for response spectral acceleration over peak ground acceleration for the σ_{VOA} (Table F5-3). For the numerical point-source aleatory uncertainty, an uncertainty in stress drop ($\sigma_{\Delta\sigma}$) of 0.5 was specified. This value is considered appropriate for the expected variability in stress drop for large (**M** $\geq$ 5) earthquakes located within a tectonic province.

The total aleatory uncertainty (σ_j^T) for the jth proponent model is computed as the vector sum of the various contributions. The σ_{MECH} is included for the potential case of higher aleatory uncertainty for normal-slip earthquakes over strike-slip earthquakes. Since not enough data are available to constrain the normal-slip aleatory uncertainty, this increase is set to zero. The σ_{CRUST} is the increase in aleatory uncertainty due to a possible larger variability in crustal structure in the Yucca Mountain region (within about 200 km of the site) than exists in California. The potential increased variability in crustal structure, evidenced by a suite of measured shear-wave velocities at Yucca Mountain, would result in a larger contribution of ground motion variations due to path and site variations than exists in California. As a result, the modeling uncertainty, based almost entirely on California data (W. J. Silva *et al.*, Pacific Engineering and Analysis, written communication, 1997) would not reflect this potentially higher uncertainty. The value of 0.2 is based on judgment from parametric analyses on the effects of variations in crustal and site parameters on estimated ground motions (C. J. Roblee *et al.*, Caltrans, written communication, 1997).

The final two aleatory component, σ_{MOD} and σ_{RANDOM}, are the modeling uncertainties estimated for the Silva finite-fault model (W. J. Silva *et al.*, Pacific Engineering and Analysis, written communication, 1997) and the increase in aleatory uncertainty for a random horizontal component (Boore *et al.*, 1997). A previously discussed, because the modeling uncertainty computed for the Silva finite-source covers a large distance and magnitude range, it is applied to both the Anderson and Somerville models. This approach is justified by direct comparisons in limited validation exercises (Northridge and Landers earthquakes at about 20 sites) which showed comparable model uncertainties and bias estimate for all three finite-source models. Interestingly, comparison exercises between the point-source model and the Somerville finite-source model also showed similar uncertainties and bias estimates for frequencies of 1 Hz and greater (EPRI, 1993). At lower frequencies, the point-source model tendency to overpredict (particularly at close distances) is reflected in negative bias estimates (EPRI, 1993; W. J. Silva *et al.*, Pacific Engineering and Analysis, written communication, 1997).

F5-5.2 Epistemic Uncertainty

For the epistemic uncertainties of each proponent model, σ_μ's of 0.1 and 0.2 were assumed for the empirical and numerical finite-source models, respectively. For the point-source model, using the law of propagation of errors combined with the sensitivity of the point-source ground motion estimates to variations in stress drop ($\sigma_{\text{ground motion}} \approx 0.7\ \sigma_{\Delta\sigma}$, Silva, 1991), estimates of $\sigma_{\sigma\Delta\sigma}$ and $\sigma_{\mu\Delta\mu}$ of 0.2 were obtained. The partition for the j^{th} model's epistemic uncertainties is listed in Table F5-3. These estimates reflect uncertainties in the median scale factors or transfer functions due to parametric uncertainties and are based on judgement. The model component is assumed to be contained in the proponent model epistemic uncertainties on the first page of Table F5-3.

F5-5.3 Median And Uncertainty Estimates

The rules for computing the point estimates are given in Table F5-3. The median estimate (lognormal) is simply the weighted median with the combined class and proponent model weights normalized to sum to unity. The aleatory uncertainty is computed in a similar manner

simply as the mean of weighted variances. For the uncertainty of the median (σ_μ), a double sum is used with the first contribution due to the weighted variance about the median and the second due to a weighted average of the proponent models epistemic uncertainties In a similar manner, the uncertainty of the aleatory uncertainty (σ_σ) is computed as a double sum: a weighted variation about the mean σ in addition to a weighted average of the proponent models total aleatory uncertainties. These relations reflect a consensus opinion at the April 1997 ground motion workshop. More development work is necessary in characterizing appropriate methods to estimate σ_μ and σ_σ and this current relation with both contributions is appealing but certainly not definitive. Tables F5-4 through F5-21 list the point estimates for all 51 cases.

F5-6 MULTIPLE RUPTURE ON PARALLEL FAULTS

Based on the results of the multiple rupture deterministic scenarios of Somerville and the incoherent or SRSS (Square Root Sum Squares) results of Silva, the recommendation is to apply the SRSS approach. The SRSS approach should be applied to the Fourier amplitude spectra and the response spectra subsequently estimated from the SRSS Fourier amplitude spectra. However, in view of all the uncertainties inherent in the multiple rupture scenario, computing the SRSS response spectra directly is a reasonable approach. Because the SRSS is most appropriate at high frequencies, it is recommended to increase the low frequency ($\leq$ 1 Hz SRSS) by 25%. This value is based on the coherent verses incoherent (SRSS) sum results presented by Silva at the April, 1997 ground motion workshop.

F5-7 LOW ANGLE FAULT

Because of the lack of empirical strong motion data from low angle normal faults and no modeling results to provide guidance, it is recommended that this scenario should be treated as a normal fault.

F5-8 REGRESSION MODEL

For the regression model, the distance metric of shortest site-to-rupture surface distance was specified. The regression model for motions was specified to reflect hanging/foot-wall effects while the regression model on aleatory uncertainty was specified to reflect effects of magnitude and period. For the epistemic uncertainties, $\sigma\mu$ and $\sigma\sigma$, the regression model was specified to be magnitude independent and to vary monotomically with distance. All four regression models (μ, σ, σ_μ, σ_σ) reflect appropriate fits to the point estimates and capture stable features of magnitude, distance, and period dependencies.

F5-9 REFERENCES

Abrahamson, N.A., and Silva, W.J., 1997, Empirical response spectral attenuation relations for shallow crustal earthquakes: Seismological Research Letters, v. 68, n. 1, p. 94-127.

Boore, D.M., 1983, Stochastic simulation of high-frequency ground motions based on seismological models of the radiated spectra: Bulletin of the Seismological Society of America, v. 73, n. 6, p. 1865-1894.

Boore, D.M., 1986, Short-period P- and S-wave radiation from large earthquakes--implications for spectral scaling relations: Bulletin of the Seismological Society of America, v. 76, n. 1, p. 43-64.

Boore, D.M., Joyner, W.B., and Fumal, T.E., 1997, Equations for estimating horizontal response spectra and peak acceleration from Western North American earthquakes--a summary of recent work: Seismological Research Letters, v. 68, n. 1, p. 128-153.

Campbell, K.W., 1983, The effects of site characteristics on near-source recordings of strong ground motion, *in* Site-Specific Effects of Soil and Rock on Ground Motion and the Implications for Earthquake-Resistant Design, Proceedings of Workshop XXII: U. S. Geological Survey Open-File Report 83-845, p. 280-309.

Campbell, K.W., 1997, Empirical near-source attenuation relationships for horizontal and vertical components of peak ground acceleration, peak ground velocity, and pseudo-absolute acceleration response spectra: Seismological Research Letters, v. 68, n. 1, p. 154-179.

Electric Power Research Institute (EPRI), 1993, Guidelines for determining design basis ground motions: Palo Alto, CA, vol. 1-5, EPRI TR-102293.
Vol. 1: Methodology and guidelines for estimating earthquake ground motion in eastern North America.
Vol. 2: Appendices for ground motion estimation.
Vol. 3: Appendices for field investigations.
Vol. 4: Appendices for laboratory investigations.
Vol. 5: Quantification of seismic source effects.

Joyner, H.B., and Boore, D.M., 1988, Measurement, characteristics and prediction of strong ground motion--State-of-the-Art Report: Proceedings, Specialty Conference on Earthquake Engineering and Soil Dynamics II--Recent Adv. in Ground Motion Evaluation, ASCE, Park City, Utah, June 27-30, p. 43-102.

Sadigh, K., Chang, C.-Y., Egan, J.A., Makdisi, F., and Youngs, R.R., 1997, Attenuation relationships for shallow crustal earthquakes based on California strong motion data: Seismological Research Letters, v. 68, n. 1, p. 180-189.

Schneider, J.F., Silva, W.J., and Stark, C.L. 1993, Ground motion model for the 1989 M 6.9 Loma Prieta earthquake including effects of source, path and site: Earthquake Spectra, v. 9, n. 2, p. 251-287.

Silva, W.J., 1991, Global characteristics and site geometry, *in* Proceedings, NSF/EPRI Workshop on Dynamic Soil Properties and Site Characterization, Palo Alto, Calif.: Electric Power Research Institute, NP-7337, Chapter 6.

Silva, W.J., 1992, Factors controlling strong ground motions and their associated uncertainties, Dynamic analysis and design considerations for high level nuclear waste repositories: ASCE 132-161.

Silva, W.J., and Darragh, R., 1995, Engineering characterization of earthquake strong ground motion recorded at rock sites: Palo Alto, CA, Electric Power Research Institute, TR-102261.

Spudich, P., Fletcher, J. B., Hellweg, M., Boatwright, J., Sullivan, C., Joyner, W. B., Hanks, T. C., Boore, D.M., McGarr, A., Baker, L. M., and Lindh, A. G., 1997, SEA96 -- a new predictive relation for earthquake ground motions in extensional tectonic regimes: Seismological Society of America, v. 68, n. 1., p. 190-198.

Zeng, Y., Anderson, J. G., and Yu, G. 1994, A composite source model for computing realistic synthetic strong ground motions: Geophysical Research Letters, v. 21, p. 725-728.

TABLE F5-1
PROPONENT MODELS, WEIGHTS, AND SCALE FACTORS

EMPIRICAL RELATIONS

Relation	Parameters	M Range	D Range (km)	WT
AS97	H,V	5 - 8	0 - 200	1.0
BJF97	H	5.5 - 7.5	0 - 80	1.0
CP97	H, V, PGV	5 - 8	3 - 60	1.0
SD97	H, V	4 - 8	0 - 100	1.0
JB88	PGV (only)	5 - 7.5	0 - 100	1.0

Class weights: Empirical 0.4
Numerical 0.6
For cases outside ranges WT = 0.25

TABLE F5-1 CONT.
EMPIRICAL SCALE FACTORS

Parameter	Scale Factor	σ_μ	σ	WT all
H Spectra	Crust	0.15	0.20	1.0
	Normal H (NS)	0.00	0.00	
H PGA	Crust	0.15	0.20	1.0
	Normal H (NS)	0.00	0.00	
H PGV (V available)	Crust	0.15	0.20	1.0
	Normal H (NS)	0.00	0.00	
H PGV (V not available use PGA)	Crust	0.15	0.20	0.5
	Normal H (NS)	0.00	0.00	
	VOA H	0.15	0.30	
V Spectra (use horizontal)	Crust	0.15	0.20	1.0
	Normal V (NS)	0.00	0.00	
	VOH	0.20	0.20	
V PGA (use horizontal)	Crust	0.15	0.20	1.0
	Normal V (NS)	0.00	0.00	
	VOH	0.20	0.20	
V PGV (use horizontal PGA)	Crust	0.15	0.00	0.5
	Normal V (NS)	0.00	0.00	
	VOA V	0.15	0.30	
	VOH	0.20	0.20	

TABLE F5-1 CONT.
NUMERICAL RELATIONS

Relation	Parameters	M Range	D Range(km)	WT
AND	H, V, PGV	5.8 - 8.0	ALL	0.7
POINT	H, VOH, VOA	ALL	ALL	1.0
SIL	H, PGV	ALL	ALL	1.0
SOM	H, V, PGV	ALL	ALL	1.0

TABLE F5-1 CONT.
NUMERICAL SCALE FACTORS

Parameter	Scale Factor	σ_μ	σ	WT all
H Spectra	Normal H (NS)	0.00	0.00	1.0
H PGA	Normal H (NS)	0.00	0.00	1.0
H PGV (V available)	Normal H (NS)	0.00	0.00	1.0
H PGV (V not available use PGA)	Normal H (NS)	0.00	0.00	0.5
	VOA H	0.15	0.30	
V Spectra (available)	Normal V (NS)	0.00	0.00	1.0
	VOH*, 0.00	0.20	0.20	
V Spectra (not available use H)	Normal V (NS)	0.00	0.00	1.0
	VOH	0.20	0.20	
V PGA (available)	Normal V (NS)	0.00	0.00	1.0
	VOH*, 0.00	0.20	0.20	
V PGA (not available use H)	Normal V (NS)	0.00	0.00	1.0
	VOH	0.20	0.20	
V PGV (available)	Normal V (NS)	0.00	0.00	1.0
	VOH*, 0.00	0.20	0.20	
V PGV (not available use H)	VOH	0.20	0.20	0.5
	VOA V	0.15	0.30	

*Use scale factor of 0.0 and σln of 0.20 to increase variability for vertical components

N.B. Normal Faulting Scale Factor: Use 0.5 of scale factor for horizontal and vertical components.

TABLE F5-2
CASE SPECIFIC WEIGHTS

Relation	Component	F (Hz)	Case
Anderson	H, V	ALL	ALL **M** 5.0
Somerville	H, V	0.3, 0.5	5, 6
	H, V	0.3, 0.5, 1.0	12, 13, 14, 15, 16, 38, 39, 40, 41
	H, V	ALL	31, 32
	H, V	1.0	42
	H, V	0.3, 0.5, 1.0	44, 45, 46, 47, 48, 49
Silva PT	H, V	ALL	51
BJF97	H	0.5	ALL
	H	ALL	24, 42, 47, 48
CMP 97	H	ALL	40, 41
SAD 97	H	ALL	40, 41

TABLE F5-3
APPROACH TO COMPUTING POINT ESTIMATES

Given μ_j, σ_j, σ_{μ_j}, WT_j for j^{th} relation

Empirical σ_j = aleatory for average component
$\sigma_\mu = 0.1$

Numerical (Point) σ_j = aleatory modeling plus parametric for average component
$\sigma_\mu = 0.2$

Numerical (Finite) σ_j = aleatory parametric for average component
$\sigma_\mu j = 0.2$

Compute Total Aleatory

$$\sigma_j^{T2} = \sigma_j^2 + \sigma_{MECH}^2 + \sigma_{CRUST}^2 + \sigma_{VOA}^2 + \sigma_{VOH}^2 + \sigma_{MOD}^2 + \sigma_{RANDOM}^2$$

Where σ_{MECH} = increase in aleatory due to mechanism
= 0

σ_{CRUST} = increase in aleatory due to YM crust at -300m
= 0.2

σ_{VOA} = increase in aleatory for larger PGV than PGA aleatory
= 0.3

σ_{VOH} = increase in aleatory for larger vertical than horizontal aleatory
= 0.2

σ_{MOD} = modeling aleatory
= $\sigma_{MOD}(f)$

σ_{RANDOM}= increase in aleatory for random component (JBF 97)

Compute Total Epistemic

$$\sigma_{\mu j}^{T2} = \sigma_{\mu j}^2 + \sigma_{\mu\, CRUST}^2 + \sigma_{\mu\, VOA}^2 + \sigma_{\mu\, VOH}^2$$

Where $\sigma_{\mu\, CRUST}$ = epistemic uncertainty in median crustal transfer function
= 0.15

$\sigma_{\mu\, VOA}$ = epistemic uncertainty in median peak velocity/peak acceleration transfer function
= 0.15

$\sigma_{\mu\, VOH}^2$ = epistemic uncertainty in median vertical/horizontal transfer function
= 0.2

Then

$$\mu' = \sum \mu_j WT_j$$

$$\sigma = \sqrt{\sum \sigma_j^{T2}\ WT_j}$$

$$\sigma_\mu^2 = \sum WT_j (\mu'_j - \bar{\mu})^2 - \sum WT_j \sigma_{\mu j}^2$$

$$\sigma_\sigma^2 = \sum WT_j (\sigma'_j - \bar{\sigma})^2 - \sum WT_j \sigma_{\sigma j}^2$$

TABLE F5-4
W. J. SILVA: HORIZONTAL POINT ESTIMATES
PEAK GROUND ACCELERATION

CASE NO.	MAGNITUDE	DISTANCE (KM)	MU	SIGMA	SIGMA MU	SIGMA SIGMA
1	5.00	1	0.18154	0.69272	0.33829	0.09780
2	5.00	1	0.16407	0.69790	0.35660	0.09664
3	5.00	5	0.05301	0.69142	0.30515	0.09733
4	5.00	5	0.05273	0.69404	0.32525	0.09694
5	5.80	10	0.09850	0.64265	0.28714	0.12739
6	5.80	20	0.07220	0.64150	0.30682	0.12754
7	6.50	1	0.44361	0.63259	0.35821	0.13041
8	6.50	1	0.44822	0.63454	0.47015	0.13169
9	6.50	1	0.40568	0.63572	0.42342	0.13101
10	6.50	5	0.38053	0.62620	0.39716	0.13056
11	6.50	5	0.25263	0.63550	0.37082	0.13102
12	6.50	50	0.03212	0.62533	0.28341	0.13052
13	6.50	50	0.02886	0.62489	0.30835	0.13051
14	7.00	10	0.25534	0.61246	0.29294	0.13619
15	7.50	50	0.06446	0.61457	0.26442	0.14042
16	7.50	50	0.06725	0.61118	0.30051	0.13935
17	5.00	1	0.05988	0.69272	0.31289	0.09780
18	5.80	5	0.14463	0.64362	0.36724	0.12730
19	5.80	5	0.08764	0.64587	0.37996	0.12697
20	5.00	10	0.06253	0.69142	0.27819	0.09733
21	5.00	10	0.08381	0.68884	0.31447	0.09788
22	5.00	50	0.00627	0.68884	0.30815	0.09788
23	5.00	50	0.00647	0.68629	0.32103	0.09860
24	5.00	160	0.00082	0.68479	0.31645	0.10058
25	5.80	1	0.28355	0.64688	0.39176	0.12727
26	5.80	5	0.23086	0.64201	0.38387	0.12747
27	5.80	5	0.13760	0.64521	0.36858	0.12706
28	5.80	10	0.12277	0.64761	0.29022	0.12838
29	5.80	10	0.16273	0.64233	0.33084	0.12742
30	5.80	10	0.07790	0.64636	0.40005	0.12735
31	5.80	50	0.01366	0.63860	0.36519	0.12722
32	5.80	50	0.01308	0.64289	0.43421	0.12736
33	6.50	5	0.32732	0.62743	0.32643	0.13068
34	6.50	10	0.20988	0.62944	0.30294	0.13110
35	6.50	10	0.28650	0.62878	0.37365	0.13102
36	6.50	10	0.15940	0.62928	0.34808	0.12992
37	6.50	20	0.10365	0.62543	0.27592	0.13052
38	6.50	20	0.13123	0.63010	0.34906	0.13119
39	6.50	20	0.07799	0.62631	0.32867	0.12961
40	6.50	100	0.01536	0.62875	0.32606	0.13088
41	6.50	160	0.00692	0.63373	0.47604	0.13417
42	7.00	1	0.50973	0.62110	0.30018	0.13682
43	7.00	10	0.34653	0.61999	0.36376	0.13793
44	7.00	10	0.19675	0.61444	0.35980	0.13565
45	7.00	50	0.04820	0.61044	0.28756	0.13590
46	7.00	50	0.05004	0.61234	0.29839	0.13617
47	7.50	1	0.53874	0.63507	0.40136	0.14863
48	5.00	10	0.31386	0.62399	0.33627	0.14593
49	5.00	10	0.37202	0.61523	0.50832	0.14039
50	8.00	50	0.08215	0.62024	0.30312	0.12008
51	8.00	160	0.02067	0.62010	0.35827	0.11416

TABLE F5-5
W. J. SILVA: HORIZONTAL POINT ESTIMATES
SPECTRAL ACCELERATION AT 0.05 SEC PERIOD

CASE NO.	MAGNITUDE	DISTANCE (KM)	MU	SIGMA	SIGMA MU	SIGMA SIGMA
1	5.00	1	0.38075	0.69545	0.33018	0.09939
2	5.00	1	0.34394	0.69805	0.34951	0.09873
3	5.00	5	0.10251	0.69548	0.29638	0.09736
4	5.00	5	0.10245	0.69812	0.30720	0.09693
5	5.80	10	0.16409	0.63976	0.30585	0.12667
6	5.80	20	0.11575	0.63497	0.31270	0.12610
7	6.50	1	0.75712	0.62015	0.35657	0.12836
8	6.50	1	0.76219	0.62146	0.43611	0.12976
9	6.50	1	0.68812	0.61987	0.43093	0.12822
10	6.50	5	0.66534	0.61581	0.42085	0.12742
11	6.50	5	0.43674	0.61751	0.43627	0.12761
12	6.50	50	0.04384	0.61474	0.31454	0.12693
13	6.50	50	0.03978	0.61417	0.36969	0.12690
14	7.00	10	0.41711	0.59704	0.31474	0.13136
15	7.50	50	0.08330	0.59945	0.31441	0.13590
16	7.50	50	0.08779	0.59570	0.36204	0.13439
17	5.00	1	0.11669	0.69545	0.29720	0.09939
18	5.80	5	0.23822	0.63580	0.38003	0.12552
19	5.80	5	0.14207	0.63612	0.41122	0.12621
20	5.00	10	0.12277	0.70626	0.29028	0.09669
21	5.00	10	0.16854	0.69548	0.33278	0.09736
22	5.00	50	0.01000	0.69028	0.30905	0.09874
23	5.00	50	0.01042	0.69028	0.32072	0.09874
24	5.00	160	0.00099	0.68274	0.40870	0.10417
25	5.80	1	0.49887	0.63682	0.42044	0.12612
26	5.80	5	0.40840	0.64025	0.41323	0.12735
27	5.80	5	0.23339	0.63927	0.46608	0.12701
28	5.80	10	0.20516	0.64232	0.33043	0.12788
29	5.80	10	0.27113	0.63597	0.36271	0.12594
30	5.80	10	0.13033	0.63472	0.49343	0.12591
31	5.80	50	0.01944	0.63522	0.40813	0.12605
32	5.80	50	0.01836	0.63740	0.50336	0.12632
33	6.50	5	0.55790	0.61308	0.32780	0.12628
34	6.50	10	0.35724	0.62170	0.30464	0.12893
35	6.50	10	0.49397	0.61682	0.40082	0.12716
36	6.50	10	0.26690	0.61819	0.40799	0.12832
37	6.50	20	0.16394	0.61881	0.29092	0.12870
38	6.50	20	0.21231	0.62052	0.36935	0.12833
39	6.50	20	0.12355	0.61327	0.40765	0.12707
40	6.50	100	0.01847	0.61249	0.30872	0.12709
41	6.50	160	0.00845	0.61438	0.33375	0.12670
42	7.00	1	0.87614	0.60436	0.35197	0.13442
43	7.00	10	0.59235	0.60776	0.41121	0.13462
44	7.00	10	0.31968	0.59715	0.43808	0.13237
45	7.00	50	0.06437	0.59479	0.30839	0.13092
46	7.00	50	0.06837	0.59726	0.33628	0.13141
47	7.50	1	0.91498	0.62010	0.47839	0.14962
48	5.00	10	0.49585	0.61084	0.39232	0.14368
49	5.00	10	0.59665	0.60023	0.58079	0.13592
50	8.00	50	0.10607	0.61548	0.37871	0.11540
51	8.00	160	0.02092	0.60722	0.42481	0.10915

TABLE F5-6
W. J. SILVA: HORIZONTAL POINT ESTIMATES
SPECTRAL ACCELERATION AT 0.10 SEC PERIOD

CASE NO.	MAGNITUDE	DISTANCE (KM)	MU	SIGMA	SIGMA MU	SIGMA SIGMA
1	5.00	1	0.39383	0.72685	0.33473	0.10557
2	5.00	1	0.35579	0.72097	0.35847	0.10343
3	5.00	5	0.11568	0.72462	0.26049	0.10507
4	5.00	5	0.11509	0.72165	0.28142	0.10385
5	5.80	10	0.19650	0.65992	0.28205	0.13387
6	5.80	20	0.14256	0.66057	0.33892	0.13396
7	6.50	1	0.90812	0.64863	0.36622	0.13818
8	6.50	1	0.94720	0.64780	0.51587	0.13834
9	6.50	1	0.85388	0.65031	0.45483	0.13872
10	6.50	5	0.77595	0.64005	0.42035	0.13486
11	6.50	5	0.52081	0.64671	0.37779	0.13702
12	6.50	50	0.05912	0.64148	0.34010	0.13524
13	6.50	50	0.05319	0.64058	0.32424	0.13469
14	7.00	10	0.51271	0.62640	0.32021	0.13898
15	7.50	50	0.11119	0.63247	0.33855	0.14576
16	7.50	50	0.11615	0.62514	0.36698	0.14221
17	5.00	1	0.13068	0.71520	0.25901	0.10197
18	5.80	5	0.29465	0.66162	0.38624	0.13415
19	5.80	5	0.17510	0.66122	0.40895	0.13372
20	5.00	10	0.13621	0.72462	0.27916	0.10507
21	5.00	10	0.18229	0.71293	0.35210	0.10121
22	5.00	50	0.01295	0.71872	0.29561	0.10280
23	5.00	50	0.01345	0.71293	0.31691	0.10121
24	5.00	160	0.00126	0.70502	0.44366	0.10370
25	5.80	1	0.57206	0.66483	0.42477	0.13536
26	5.80	5	0.48805	0.66094	0.38818	0.13402
27	5.80	5	0.27315	0.66422	0.40810	0.13591
28	5.80	10	0.23716	0.66235	0.30539	0.13556
29	5.80	10	0.31674	0.66046	0.37521	0.13395
30	5.80	10	0.15342	0.65687	0.40971	0.13262
31	5.80	50	0.02554	0.65979	0.35464	0.13385
32	5.80	50	0.02426	0.66105	0.42436	0.13466
33	6.50	5	0.67664	0.64466	0.34330	0.13634
34	6.50	10	0.42901	0.64384	0.32123	0.13631
35	6.50	10	0.59590	0.64228	0.42454	0.13587
36	6.50	10	0.32047	0.64369	0.34451	0.13621
37	6.50	20	0.20817	0.63857	0.30495	0.13410
38	6.50	20	0.26145	0.64250	0.37121	0.13537
39	6.50	20	0.15332	0.64148	0.33919	0.13520
40	6.50	100	0.02454	0.64086	0.34071	0.13350
41	6.50	160	0.01037	0.63794	0.35233	0.13329
42	7.00	1	1.05138	0.63215	0.34290	0.14156
43	7.00	10	0.69986	0.63435	0.41723	0.14262
44	7.00	10	0.39947	0.62794	0.36645	0.13986
45	7.00	50	0.08577	0.62346	0.35112	0.13785
46	7.00	50	0.09091	0.62737	0.35685	0.13936
47	7.50	1	1.09550	0.64992	0.43579	0.15738
48	5.00	10	0.61825	0.63865	0.37085	0.15098
49	5.00	10	0.74590	0.63125	0.54426	0.14507
50	8.00	50	0.14082	0.64910	0.35904	0.12581
51	8.00	160	0.02399	0.64110	0.45416	0.11630

TABLE F5-7
W. J. SILVA: HORIZONTAL POINT ESTIMATES
SPECTRAL ACCELERATION AT 0.20 SEC PERIOD

CASE NO.	MAGNITUDE	DISTANCE (KM)	MU	SIGMA	SIGMA MU	SIGMA SIGMA
1	5.00	1	0.29847	0.74854	0.33926	0.10165
2	5.00	1	0.27594	0.75429	0.35347	0.10372
3	5.00	5	0.09593	0.74013	0.26000	0.09958
4	5.00	5	0.09702	0.73735	0.27983	0.09905
5	5.80	10	0.18766	0.69017	0.27809	0.13316
6	5.80	20	0.14310	0.68225	0.34102	0.13009
7	6.50	1	0.84001	0.66866	0.35835	0.13145
8	6.50	1	0.87850	0.67736	0.48194	0.13556
9	6.50	1	0.80461	0.68506	0.43649	0.13906
10	6.50	5	0.74158	0.66924	0.40238	0.13282
11	6.50	5	0.51119	0.67238	0.34014	0.13271
12	6.50	50	0.06646	0.66760	0.35420	0.13159
13	6.50	50	0.05943	0.66320	0.30521	0.12992
14	7.00	10	0.50960	0.65322	0.31623	0.13472
15	7.50	50	0.13073	0.65530	0.35163	0.13935
16	7.50	50	0.13931	0.65062	0.34940	0.13712
17	5.00	1	0.10735	0.73740	0.26197	0.09953
18	5.80	5	0.26423	0.68548	0.41272	0.13139
19	5.80	5	0.17504	0.68595	0.34558	0.13095
20	5.00	10	0.11123	0.74013	0.27116	0.09958
21	5.00	10	0.14790	0.73735	0.33823	0.09905
22	5.00	50	0.01282	0.74578	0.29048	0.10114
23	5.00	50	0.01350	0.73188	0.30896	0.09853
24	5.00	160	0.00162	0.73894	0.40344	0.10244
25	5.80	1	0.50229	0.68656	0.39079	0.13152
26	5.80	5	0.43108	0.68415	0.36844	0.13129
27	5.80	5	0.25756	0.68728	0.34025	0.13158
28	5.80	10	0.22041	0.68861	0.31411	0.13235
29	5.80	10	0.29702	0.68292	0.35859	0.13018
30	5.80	10	0.15331	0.69036	0.33123	0.13313
31	5.80	50	0.02768	0.68619	0.31997	0.13148
32	5.80	50	0.02781	0.68572	0.35820	0.13142
33	6.50	5	0.63007	0.66524	0.32814	0.13051
34	6.50	10	0.39870	0.67092	0.29532	0.13289
35	6.50	10	0.54925	0.66848	0.38074	0.13171
36	6.50	10	0.32403	0.66557	0.31994	0.13012
37	6.50	20	0.20155	0.66839	0.29263	0.13214
38	6.50	20	0.26532	0.66606	0.35180	0.13119
39	6.50	20	0.16082	0.66835	0.29726	0.13114
40	6.50	100	0.03067	0.66895	0.34597	0.13063
41	6.50	160	0.01402	0.66932	0.35415	0.13206
42	7.00	1	0.97826	0.65818	0.31707	0.13641
43	7.00	10	0.69059	0.65687	0.39630	0.13634
44	7.00	10	0.40746	0.65219	0.32591	0.13408
45	7.00	50	0.09853	0.65130	0.37144	0.13404
46	7.00	50	0.10531	0.65191	0.35123	0.13424
47	7.50	1	1.08750	0.67163	0.40961	0.14898
48	5.00	10	0.64133	0.66709	0.35800	0.14740
49	5.00	10	0.74593	0.65166	0.49921	0.13756
50	8.00	50	0.16533	0.67096	0.32923	0.11557
51	8.00	160	0.03379	0.66753	0.51995	0.10831

TABLE F5-8
W. J. SILVA: HORIZONTAL POINT ESTIMATES
SPECTRAL ACCELERATION AT 0.50 SEC PERIOD

CASE NO.	MAGNITUDE	DISTANCE (KM)	MU	SIGMA	SIGMA MU	SIGMA SIGMA
1	5.00	1	0.13522	0.81449	0.34956	0.08523
2	5.00	1	0.12851	0.80047	0.38467	0.08003
3	5.00	5	0.04671	0.80668	0.27762	0.08473
4	5.00	5	0.04856	0.79821	0.34027	0.08112
5	5.80	10	0.11628	0.75054	0.29414	0.13229
6	5.80	20	0.09467	0.75207	0.34893	0.13297
7	6.50	1	0.58368	0.73321	0.26841	0.13433
8	6.50	1	0.60411	0.73395	0.38593	0.13521
9	6.50	1	0.55182	0.74010	0.35849	0.13733
10	6.50	5	0.50889	0.73200	0.34874	0.13580
11	6.50	5	0.34953	0.73341	0.34083	0.13440
12	6.50	50	0.05392	0.73599	0.28677	0.13772
13	6.50	50	0.05286	0.72752	0.35419	0.13421
14	7.00	10	0.37911	0.71835	0.27366	0.14163
15	7.50	50	0.12512	0.72211	0.29990	0.14947
16	7.50	50	0.13674	0.71435	0.36390	0.14608
17	5.00	1	0.05212	0.81449	0.29750	0.08523
18	5.80	5	0.17702	0.75327	0.35948	0.13344
19	5.80	5	0.10319	0.75708	0.41754	0.13324
20	5.00	10	0.05319	0.79545	0.27832	0.08032
21	5.00	10	0.07100	0.79000	0.37147	0.07933
22	5.00	50	0.00767	0.79271	0.28738	0.07972
23	5.00	50	0.00820	0.79545	0.32952	0.08032
24	5.00	160	0.00147	0.78732	0.40005	0.08107
25	5.80	1	0.31193	0.75088	0.33225	0.13058
26	5.80	5	0.27107	0.74893	0.39535	0.13150
27	5.80	5	0.15949	0.74482	0.35737	0.12900
28	5.80	10	0.14424	0.75229	0.27727	0.13305
29	5.80	10	0.20182	0.74800	0.36465	0.13134
30	5.80	10	0.09329	0.75069	0.40305	0.13084
31	5.80	50	0.01998	0.74803	0.34683	0.13116
32	5.80	50	0.01998	0.75110	0.45120	0.13298
33	6.50	5	0.44536	0.72836	0.30158	0.13445
34	6.50	10	0.29824	0.73219	0.31326	0.13599
35	6.50	10	0.42055	0.73139	0.39146	0.13570
36	6.50	10	0.22780	0.73149	0.35711	0.13380
37	6.50	20	0.14717	0.73021	0.26420	0.13507
38	6.50	20	0.19826	0.73660	0.36628	0.13799
39	6.50	20	0.12344	0.73213	0.31473	0.13399
40	6.50	100	0.02976	0.73583	0.31874	0.13449
41	6.50	160	0.01669	0.73377	0.33919	0.13607
42	7.00	1	0.71694	0.72297	0.29790	0.14164
43	7.00	10	0.56484	0.71932	0.39154	0.14196
44	7.00	10	0.30914	0.72136	0.34770	0.14104
45	7.00	50	0.08734	0.71590	0.30747	0.14054
46	7.00	50	0.09732	0.72142	0.38978	0.14289
47	7.50	1	0.77911	0.73938	0.35015	0.15766
48	5.00	10	0.47774	0.72965	0.31895	0.15448
49	5.00	10	0.61504	0.72161	0.50614	0.14922
50	8.00	50	0.15956	0.73746	0.29987	0.12457
51	8.00	160	0.04859	0.73704	0.47048	0.11943

TABLE F5-9
W. J. SILVA: HORIZONTAL POINT ESTIMATES
SPECTRAL ACCELERATION AT 1.00 SEC PERIOD

CASE NO.	MAGNITUDE	DISTANCE (KM)	MU	SIGMA	SIGMA MU	SIGMA SIGMA
1	5.00	1	0.05203	0.83787	0.33457	0.06192
2	5.00	1	0.04591	0.83512	0.35431	0.06111
3	5.00	5	0.01892	0.82674	0.27351	0.06286
4	5.00	5	0.01826	0.82674	0.33637	0.06286
5	5.80	10	0.05763	0.79957	0.31238	0.11302
6	5.80	20	0.04397	0.79678	0.32987	0.11642
7	6.50	1	0.32106	0.78624	0.25789	0.11892
8	6.50	1	0.29904	0.78822	0.39454	0.12328
9	6.50	1	0.27001	0.77927	0.38985	0.11987
10	6.50	5	0.26325	0.78181	0.32625	0.12470
11	6.50	5	0.17052	0.78005	0.40892	0.11982
12	6.50	50	0.03584	0.77602	0.26291	0.11923
13	6.50	50	0.03203	0.77663	0.29929	0.12232
14	7.00	10	0.23790	0.76702	0.27533	0.13051
15	7.50	50	0.08908	0.76888	0.25013	0.14030
16	7.50	50	0.09139	0.76585	0.29240	0.14164
17	5.00	1	0.02107	0.82972	0.31377	0.06033
18	5.80	5	0.07935	0.81109	0.50249	0.12427
19	5.80	5	0.04668	0.81133	0.52346	0.11902
20	5.00	10	0.02130	0.82403	0.25282	0.06236
21	5.00	10	0.02592	0.82403	0.31780	0.06236
22	5.00	50	0.00358	0.82135	0.25850	0.06213
23	5.00	50	0.00353	0.82948	0.28079	0.06362
24	5.00	160	0.00088	0.82812	0.34767	0.06361
25	5.80	1	0.14750	0.80923	0.41946	0.11373
26	5.80	5	0.12206	0.79191	0.43336	0.11339
27	5.80	5	0.06975	0.80703	0.46860	0.11635
28	5.80	10	0.06974	0.80192	0.29376	0.11445
29	5.80	10	0.09338	0.79338	0.35029	0.11406
30	5.80	10	0.04458	0.80848	0.41368	0.11847
31	5.80	50	0.01163	0.79135	0.30733	0.10972
32	5.80	50	0.01153	0.79645	0.32481	0.11528
33	6.50	5	0.23284	0.78651	0.28756	0.12327
34	6.50	10	0.16994	0.78207	0.28843	0.12143
35	6.50	10	0.22677	0.77882	0.33715	0.12321
36	6.50	10	0.11742	0.77950	0.37156	0.11965
37	6.50	20	0.08398	0.77574	0.27473	0.11904
38	6.50	20	0.11220	0.78272	0.37362	0.12522
39	6.50	20	0.06715	0.78147	0.34645	0.12031
40	6.50	100	0.02052	0.78236	0.28705	0.11735
41	6.50	160	0.01231	0.77855	0.33980	0.11842
42	7.00	1	0.40718	0.77270	0.29120	0.12910
43	7.00	10	0.30266	0.77069	0.36690	0.13461
44	7.00	10	0.18086	0.76678	0.36592	0.12942
45	7.00	50	0.06159	0.76684	0.26528	0.13046
46	7.00	50	0.06109	0.76410	0.30338	0.13191
47	7.50	1	0.49178	0.78510	0.36727	0.14289
48	5.00	10	0.32253	0.77606	0.32670	0.14407
49	5.00	10	0.39192	0.77000	0.54056	0.14326
50	8.00	50	0.11448	0.77401	0.32558	0.12702
51	8.00	160	0.04251	0.78754	0.40197	0.12370

TABLE F5-10
W. J. SILVA: HORIZONTAL POINT ESTIMATES
SPECTRAL ACCELERATION AT 2.00 SEC PERIOD

CASE NO.	MAGNITUDE	DISTANCE (KM)	MU	SIGMA	SIGMA MU	SIGMA SIGMA
1	5.00	1	0.01406	0.92404	0.42119	0.06278
2	5.00	1	0.01107	0.91864	0.45775	0.06215
3	5.00	5	0.00534	0.90504	0.33300	0.07094
4	5.00	5	0.00452	0.90504	0.38411	0.07094
5	5.80	10	0.02254	0.88033	0.36006	0.12220
6	5.80	20	0.01450	0.87633	0.35129	0.13360
7	6.50	1	0.15787	0.87063	0.28618	0.13191
8	6.50	1	0.13059	0.86266	0.37284	0.13922
9	6.50	1	0.11571	0.86616	0.40327	0.14100
10	6.50	5	0.10370	0.86381	0.43998	0.14671
11	6.50	5	0.07706	0.86779	0.46418	0.14204
12	6.50	50	0.01743	0.86100	0.32579	0.13444
13	6.50	50	0.01411	0.85796	0.43034	0.14294
14	7.00	10	0.12817	0.85880	0.30973	0.15059
15	7.50	50	0.05667	0.85606	0.26936	0.16020
16	7.50	50	0.05058	0.84152	0.36750	0.16231
17	5.00	1	0.00584	0.91597	0.34412	0.06224
18	5.80	5	0.02839	0.86626	0.46777	0.12729
19	5.80	5	0.01749	0.87317	0.53078	0.12467
20	5.00	10	0.00605	0.90504	0.31070	0.07094
21	5.00	10	0.00643	0.90768	0.35738	0.07062
22	5.00	50	0.00114	0.90504	0.25700	0.07094
23	5.00	50	0.00100	0.90504	0.30806	0.07094
24	5.00	160	0.00036	0.90830	0.28989	0.06864
25	5.80	1	0.06006	0.89372	0.36848	0.12242
26	5.80	5	0.04238	0.86420	0.46849	0.12606
27	5.80	5	0.02746	0.87165	0.47769	0.12376
28	5.80	10	0.02488	0.88859	0.41456	0.12971
29	5.80	10	0.02692	0.88372	0.46276	0.14089
30	5.80	10	0.01612	0.86955	0.53698	0.12268
31	5.80	50	0.00509	0.87340	0.43792	0.11835
32	5.80	50	0.00419	0.87310	0.46872	0.13212
33	6.50	5	0.11307	0.86528	0.31075	0.13578
34	6.50	10	0.07464	0.86598	0.33687	0.13610
35	6.50	10	0.08162	0.86436	0.41815	0.14753
36	6.50	10	0.04834	0.86317	0.50868	0.13930
37	6.50	20	0.04150	0.87040	0.35369	0.13861
38	6.50	20	0.04650	0.85374	0.39565	0.14080
39	6.50	20	0.02984	0.86195	0.46623	0.13871
40	6.50	100	0.01212	0.86763	0.31010	0.13130
41	6.50	160	0.00794	0.87394	0.37731	0.13736
42	7.00	1	0.21378	0.86289	0.32864	0.14619
43	7.00	10	0.12100	0.85301	0.46195	0.15766
44	7.00	10	0.08697	0.85968	0.47307	0.15572
45	7.00	50	0.03527	0.85486	0.24972	0.14881
46	7.00	50	0.03042	0.84679	0.36692	0.15434
47	7.50	1	0.25659	0.86919	0.46354	0.16075
48	5.00	10	0.18127	0.85499	0.37731	0.15969
49	5.00	10	0.17889	0.84550	0.57756	0.16411
50	8.00	50	0.07454	0.86928	0.34933	0.15550
51	8.00	160	0.03223	0.87951	0.46998	0.14636

TABLE F5-11
W. J. SILVA: HORIZONTAL POINT ESTIMATES
SPECTRAL ACCELERATION AT 3.33 SEC PERIOD

CASE NO.	MAGNITUDE	DISTANCE (KM)	MU	SIGMA	SIGMA MU	SIGMA SIGMA
1	5.00	1	0.00420	0.97945	0.70348	0.08419
2	5.00	1	0.00331	0.97092	0.70624	0.08009
3	5.00	5	0.00164	0.96419	0.62818	0.09238
4	5.00	5	0.00139	0.96419	0.64245	0.09238
5	5.80	10	0.01035	0.91179	0.41614	0.13882
6	5.80	20	0.00595	0.90654	0.45226	0.15049
7	6.50	1	0.07607	0.92510	0.39247	0.16939
8	6.50	1	0.06318	0.89224	0.40895	0.15739
9	6.50	1	0.05735	0.90074	0.44846	0.16294
10	6.50	5	0.05340	0.89866	0.43180	0.17082
11	6.50	5	0.04196	0.90939	0.50174	0.16919
12	6.50	50	0.00909	0.90816	0.41315	0.16399
13	6.50	50	0.00643	0.89498	0.62048	0.16829
14	7.00	10	0.07079	0.90413	0.34909	0.18306
15	7.50	50	0.03483	0.89336	0.30628	0.18730
16	7.50	50	0.02856	0.88420	0.39667	0.19274
17	5.00	1	0.00178	0.97374	0.64340	0.08126
18	5.80	5	0.01226	0.91376	0.48884	0.15597
19	5.80	5	0.00723	0.91824	0.57367	0.14853
20	5.00	10	0.00184	0.95857	0.59693	0.09042
21	5.00	10	0.00195	0.96137	0.56138	0.09131
22	5.00	50	0.00037	0.95580	0.49356	0.08972
23	5.00	50	0.00032	0.95580	0.51509	0.08972
24	5.00	160	0.00013	0.96222	0.39776	0.08295
25	5.80	1	0.02612	0.92146	0.46384	0.13440
26	5.80	5	0.01879	0.91262	0.49037	0.15547
27	5.80	5	0.01292	0.91193	0.50451	0.14394
28	5.80	10	0.01142	0.91462	0.51200	0.14059
29	5.80	10	0.01059	0.90217	0.55810	0.14740
30	5.80	10	0.00656	0.91498	0.72348	0.14594
31	5.80	50	0.00218	0.91495	0.52901	0.14075
32	5.80	50	0.00170	0.90841	0.61821	0.15194
33	6.50	5	0.05961	0.91832	0.38728	0.17282
34	6.50	10	0.03622	0.91329	0.45475	0.16829
35	6.50	10	0.03636	0.89769	0.48008	0.17043
36	6.50	10	0.02250	0.90745	0.65839	0.16791
37	6.50	20	0.01892	0.90435	0.51072	0.16133
38	6.50	20	0.01976	0.90529	0.48632	0.17602
39	6.50	20	0.01412	0.89605	0.60252	0.15974
40	6.50	100	0.00534	0.90352	0.47216	0.15104
41	6.50	160	0.00411	0.92051	0.44715	0.16635
42	7.00	1	0.12247	0.90447	0.41650	0.17410
43	7.00	10	0.06150	0.88952	0.50200	0.18536
44	7.00	10	0.04636	0.89592	0.55029	0.18100
45	7.00	50	0.02004	0.89763	0.29794	0.17858
46	7.00	50	0.01626	0.89166	0.40332	0.18676
47	7.50	1	0.14939	0.91067	0.51679	0.18968
48	5.00	10	0.10758	0.90229	0.44994	0.19330
49	5.00	10	0.09822	0.88634	0.66807	0.19411
50	8.00	50	0.04955	0.92324	0.37824	0.18569
51	8.00	160	0.02100	0.93330	0.38988	0.17415

TABLE F5-12
W. J. SILVA: HORIZONTAL POINT ESTIMATES
PEAK GROUND VELOCITY

CASE NO.	MAGNITUDE	DISTANCE (KM)	MU	SIGMA	SIGMA MU	SIGMA SIGMA
1	5.00	1	6.75385	0.81085	0.37484	0.06924
2	5.00	1	5.99852	0.81085	0.40353	0.06924
3	5.00	5	2.20889	0.79932	0.29676	0.07699
4	5.00	5	2.16783	0.79367	0.36090	0.07371
5	5.80	10	6.41480	0.77058	0.29603	0.12615
6	5.80	20	4.72000	0.76895	0.32184	0.12815
7	6.50	1	36.87325	0.79058	0.31082	0.13466
8	6.50	1	34.80685	0.78758	0.41903	0.13697
9	6.50	1	31.54553	0.78758	0.40525	0.13697
10	6.50	5	29.80575	0.76841	0.35401	0.14279
11	6.50	5	20.57563	0.78262	0.39351	0.13520
12	6.50	50	3.55206	0.76596	0.32155	0.13970
13	6.50	50	3.10300	0.76493	0.42666	0.14154
14	7.00	10	27.12796	0.76862	0.28271	0.15155
15	7.50	50	10.19356	0.76800	0.32316	0.16046
16	7.50	50	10.09783	0.76142	0.39706	0.16018
17	5.00	1	2.49106	0.80528	0.32710	0.06657
18	5.80	5	9.50616	0.77004	0.45049	0.12836
19	5.80	5	5.56210	0.78316	0.45409	0.12334
20	5.00	10	2.50309	0.79089	0.25802	0.07237
21	5.00	10	3.20192	0.79367	0.32364	0.07371
22	5.00	50	0.34513	0.78813	0.30167	0.07124
23	5.00	50	0.34398	0.79089	0.33098	0.07237
24	5.00	160	0.07450	0.78271	0.27826	0.06964
25	5.80	1	17.09039	0.78720	0.40421	0.12170
26	5.80	5	14.08704	0.76587	0.41538	0.12703
27	5.80	5	8.62235	0.78228	0.36726	0.12318
28	5.80	10	7.67284	0.77511	0.29585	0.12750
29	5.80	10	10.12376	0.76901	0.32817	0.12816
30	5.80	10	4.95588	0.78175	0.43091	0.12310
31	5.80	50	1.15414	0.77143	0.39779	0.12634
32	5.80	50	1.07340	0.77176	0.47901	0.12902
33	6.50	5	26.36674	0.77316	0.28155	0.14206
34	6.50	10	17.64168	0.77149	0.27097	0.14146
35	6.50	10	23.35256	0.76886	0.34837	0.14296
36	6.50	10	12.82736	0.78185	0.40468	0.13506
37	6.50	20	8.80323	0.76980	0.30778	0.14087
38	6.50	20	11.50766	0.76962	0.35509	0.14326
39	6.50	20	7.06512	0.77919	0.41324	0.13434
40	6.50	100	1.98055	0.78436	0.48392	0.13330
41	6.50	160	1.04059	0.77473	0.81491	0.14353
42	7.00	1	51.16418	0.78763	0.34450	0.14320
43	7.00	10	34.06840	0.76640	0.41122	0.15307
44	7.00	10	20.53811	0.78031	0.43224	0.14345
45	7.00	50	6.50598	0.76331	0.29957	0.14991
46	7.00	50	6.28715	0.76124	0.37082	0.15121
47	7.50	1	60.22858	0.79663	0.53296	0.15441
48	5.00	10	38.05346	0.77125	0.41266	0.16193
49	5.00	10	45.09637	0.76428	0.64673	0.16116
50	8.00	50	14.52860	0.75883	0.44569	0.15123
51	8.00	160	5.25501	0.78261	0.51865	0.14299

TABLE F5-13
W. J. SILVA: VERTICAL POINT ESTIMATES
PEAK GROUND ACCELERATION

CASE NO.	MAGNITUDE	DISTANCE (KM)	MU	SIGMA	SIGMA MU	SIGMA SIGMA
1	5.00	1	0.14263	0.71377	0.26693	0.09726
2	5.00	1	0.11105	0.71879	0.24455	0.09616
3	5.00	5	0.03515	0.71251	0.22334	0.09680
4	5.00	5	0.03051	0.71505	0.21837	0.09643
5	5.80	10	0.06150	0.66528	0.21279	0.12683
6	5.80	20	0.03778	0.66417	0.20327	0.12698
7	6.50	1	0.31936	0.65557	0.30171	0.12965
8	6.50	1	0.28471	0.65745	0.41510	0.13085
9	6.50	1	0.25684	0.65859	0.36583	0.13020
10	6.50	5	0.24171	0.64940	0.32700	0.12978
11	6.50	5	0.15153	0.65838	0.31198	0.13021
12	6.50	50	0.01385	0.64857	0.20923	0.12974
13	6.50	50	0.01107	0.64814	0.22976	0.12973
14	7.00	10	0.15922	0.63617	0.21993	0.13496
15	7.50	50	0.02709	0.63820	0.18196	0.13884
16	7.50	50	0.02581	0.63494	0.19160	0.13784
17	5.00	1	0.04034	0.71377	0.23381	0.09726
18	5.80	5	0.08192	0.66622	0.29552	0.12675
19	5.80	5	0.04689	0.66839	0.30947	0.12644
20	5.00	10	0.04276	0.71251	0.18479	0.09680
21	5.00	10	0.05266	0.71000	0.17666	0.09733
22	5.00	50	0.00290	0.71000	0.22927	0.09733
23	5.00	50	0.00266	0.70752	0.21046	0.09801
24	5.00	160	0.00035	0.70608	0.37176	0.09988
25	5.80	1	0.21469	0.66937	0.34117	0.12672
26	5.80	5	0.15049	0.66466	0.30822	0.12691
27	5.80	5	0.08290	0.66776	0.30482	0.12652
28	5.80	10	0.08075	0.67007	0.21695	0.12776
29	5.80	10	0.09919	0.66498	0.23584	0.12687
30	5.80	10	0.04324	0.66887	0.34508	0.12680
31	5.80	50	0.00606	0.66137	0.31170	0.12668
32	5.80	50	0.00515	0.66551	0.38120	0.12681
33	6.50	5	0.22548	0.65059	0.26313	0.12988
34	6.50	10	0.13380	0.65253	0.23334	0.13028
35	6.50	10	0.17455	0.65190	0.30783	0.13020
36	6.50	10	0.08781	0.65238	0.28239	0.12918
37	6.50	20	0.05811	0.64866	0.19711	0.12974
38	6.50	20	0.06808	0.65316	0.28287	0.13036
39	6.50	20	0.03766	0.64951	0.25732	0.12890
40	6.50	100	0.00541	0.65186	0.37589	0.13009
41	6.50	160	0.00213	0.65667	0.48793	0.13318
42	7.00	1	0.33592	0.64448	0.27881	0.13555
43	7.00	10	0.20452	0.64341	0.29173	0.13658
44	7.00	10	0.10528	0.63807	0.29202	0.13446
45	7.00	50	0.02045	0.63423	0.21446	0.13468
46	7.00	50	0.01939	0.63605	0.19216	0.13494
47	7.50	1	0.36054	0.65796	0.36353	0.14665
48	5.00	10	0.18868	0.64728	0.29507	0.14406
49	5.00	10	0.21813	0.63883	0.46153	0.13881
50	8.00	50	0.03435	0.64366	0.22474	0.11784
51	8.00	160	0.00753	0.64353	0.29907	0.11230

TABLE F5-14
W. J. SILVA: VERTICAL POINT ESTIMATES
SPECTRAL ACCELERATION AT 0.05 SEC PERIOD

CASE NO.	MAGNITUDE	DISTANCE (KM)	MU	SIGMA	SIGMA MU	SIGMA SIGMA
1	5.00	1	0.32913	0.72253	0.26056	0.09849
2	5.00	1	0.25614	0.72504	0.27708	0.09787
3	5.00	5	0.07623	0.72256	0.21682	0.09661
4	5.00	5	0.06638	0.72511	0.24464	0.09620
5	5.80	10	0.11650	0.66910	0.24507	0.12596
6	5.80	20	0.06895	0.66452	0.26000	0.12544
7	6.50	1	0.62225	0.65037	0.30533	0.12750
8	6.50	1	0.55190	0.65162	0.40169	0.12880
9	6.50	1	0.49672	0.65011	0.40029	0.12737
10	6.50	5	0.48176	0.64624	0.38088	0.12664
11	6.50	5	0.29948	0.64786	0.41146	0.12681
12	6.50	50	0.02167	0.64521	0.26048	0.12619
13	6.50	50	0.01750	0.64467	0.33797	0.12616
14	7.00	10	0.30078	0.62838	0.25551	0.13015
15	7.50	50	0.04026	0.63067	0.25970	0.13424
16	7.50	50	0.03888	0.62710	0.31031	0.13286
17	5.00	1	0.08802	0.72253	0.21783	0.09849
18	5.80	5	0.15295	0.66531	0.34661	0.12491
19	5.80	5	0.08643	0.66562	0.37986	0.12553
20	5.00	10	0.09387	0.73294	0.20810	0.09597
21	5.00	10	0.11758	0.72256	0.25656	0.09661
22	5.00	50	0.00527	0.71756	0.23949	0.09789
23	5.00	50	0.00487	0.71756	0.26193	0.09789
24	5.00	160	0.00042	0.71030	0.37677	0.10294
25	5.80	1	0.42365	0.66628	0.37800	0.12546
26	5.80	5	0.29851	0.66957	0.37427	0.12659
27	5.80	5	0.15870	0.66863	0.44430	0.12627
28	5.80	10	0.15300	0.67154	0.27469	0.12709
29	5.80	10	0.18635	0.66548	0.31770	0.12529
30	5.80	10	0.08210	0.66428	0.47496	0.12526
31	5.80	50	0.00986	0.66476	0.36860	0.12540
32	5.80	50	0.00827	0.66684	0.48261	0.12564
33	6.50	5	0.43965	0.64364	0.27121	0.12559
34	6.50	10	0.26128	0.65185	0.24291	0.12803
35	6.50	10	0.34379	0.64720	0.36684	0.12640
36	6.50	10	0.16864	0.64851	0.38052	0.12747
37	6.50	20	0.10572	0.64909	0.22651	0.12782
38	6.50	20	0.12654	0.65073	0.33767	0.12748
39	6.50	20	0.06861	0.64382	0.38013	0.12632
40	6.50	100	0.00685	0.64307	0.42320	0.12634
41	6.50	160	0.00257	0.64488	0.48597	0.12598
42	7.00	1	0.67555	0.63533	0.31513	0.13294
43	7.00	10	0.40369	0.63857	0.37286	0.13313
44	7.00	10	0.19781	0.62848	0.40817	0.13106
45	7.00	50	0.03137	0.62624	0.25257	0.12976
46	7.00	50	0.03049	0.62858	0.28179	0.13020
47	7.50	1	0.71179	0.65033	0.44942	0.14702
48	5.00	10	0.34660	0.64150	0.36092	0.14149
49	5.00	10	0.40781	0.63141	0.55684	0.13426
50	8.00	50	0.05108	0.64592	0.33134	0.11287
51	8.00	160	0.00762	0.63806	0.38179	0.10712

TABLE F5-15
W. J. SILVA: VERTICAL POINT ESTIMATES
SPECTRAL ACCELERATION AT 0.10 SEC PERIOD

CASE NO.	MAGNITUDE	DISTANCE (KM)	MU	SIGMA	SIGMA MU	SIGMA SIGMA
1	5.00	1	0.27664	0.75810	0.26051	0.10417
2	5.00	1	0.23919	0.75246	0.28073	0.10217
3	5.00	5	0.07494	0.75596	0.15498	0.10372
4	5.00	5	0.07184	0.75312	0.17885	0.10258
5	5.80	10	0.12440	0.69419	0.20526	0.13244
6	5.80	20	0.08505	0.69480	0.26899	0.13253
7	6.50	1	0.63025	0.68346	0.31031	0.13636
8	6.50	1	0.63765	0.68268	0.47277	0.13652
9	6.50	1	0.57386	0.68506	0.40652	0.13686
10	6.50	5	0.52237	0.67533	0.36571	0.13332
11	6.50	5	0.34010	0.68164	0.32059	0.13529
12	6.50	50	0.02888	0.67668	0.28501	0.13367
13	6.50	50	0.02558	0.67583	0.25383	0.13316
14	7.00	10	0.33041	0.66240	0.25490	0.13695
15	7.50	50	0.05352	0.66815	0.28297	0.14306
16	7.50	50	0.05632	0.66121	0.30074	0.13981
17	5.00	1	0.08537	0.74694	0.15233	0.10082
18	5.80	5	0.18414	0.69580	0.32870	0.13269
19	5.80	5	0.10588	0.69542	0.35489	0.13229
20	5.00	10	0.08969	0.75596	0.18428	0.10372
21	5.00	10	0.11857	0.74476	0.27212	0.10013
22	5.00	50	0.00658	0.75030	0.21443	0.10160
23	5.00	50	0.00669	0.74476	0.22890	0.10013
24	5.00	160	0.00058	0.73719	0.42514	0.10240
25	5.80	1	0.40122	0.69885	0.37748	0.13380
26	5.80	5	0.32775	0.69515	0.32843	0.13258
27	5.80	5	0.17644	0.69828	0.35648	0.13432
28	5.80	10	0.15473	0.69650	0.23570	0.13400
29	5.80	10	0.20583	0.69470	0.31347	0.13251
30	5.80	10	0.09478	0.69129	0.35915	0.13128
31	5.80	50	0.01268	0.69407	0.30225	0.13243
32	5.80	50	0.01183	0.69526	0.37432	0.13317
33	6.50	5	0.45851	0.67969	0.28295	0.13467
34	6.50	10	0.27799	0.67892	0.25602	0.13465
35	6.50	10	0.39243	0.67744	0.37250	0.13425
36	6.50	10	0.19935	0.67878	0.28027	0.13455
37	6.50	20	0.12420	0.67393	0.23645	0.13263
38	6.50	20	0.15674	0.67765	0.31224	0.13378
39	6.50	20	0.08766	0.67668	0.27364	0.13363
40	6.50	100	0.00957	0.67609	0.47979	0.13209
41	6.50	160	0.00343	0.67333	0.54178	0.13190
42	7.00	1	0.69735	0.66784	0.31823	0.13929
43	7.00	10	0.45750	0.66992	0.36290	0.14028
44	7.00	10	0.24611	0.66386	0.30452	0.13774
45	7.00	50	0.04151	0.65962	0.29789	0.13591
46	7.00	50	0.04428	0.66332	0.28879	0.13729
47	7.50	1	0.73641	0.68468	0.41024	0.15387
48	5.00	10	0.38802	0.67400	0.34704	0.14792
49	5.00	10	0.49067	0.66699	0.50409	0.14243
50	8.00	50	0.06758	0.68391	0.30118	0.12225
51	8.00	160	0.00973	0.67632	0.42190	0.11351

TABLE F5-16
W. J. SILVA: VERTICAL POINT ESTIMATES
SPECTRAL ACCELERATION AT 0.20 SEC PERIOD

CASE NO.	MAGNITUDE	DISTANCE (KM)	MU	SIGMA	SIGMA MU	SIGMA SIGMA
1	5.00	1	0.16623	0.76178	0.26270	0.10111
2	5.00	1	0.16199	0.76743	0.28750	0.10312
3	5.00	5	0.04871	0.75352	0.14763	0.09910
4	5.00	5	0.05230	0.75079	0.18493	0.09859
5	5.80	10	0.09349	0.70451	0.19398	0.13254
6	5.80	20	0.07421	0.69675	0.27561	0.12957
7	6.50	1	0.45824	0.68345	0.29757	0.13087
8	6.50	1	0.51346	0.69196	0.43561	0.13484
9	6.50	1	0.46945	0.69950	0.38340	0.13823
10	6.50	5	0.43343	0.68402	0.34698	0.13220
11	6.50	5	0.28962	0.68709	0.26637	0.13209
12	6.50	50	0.02649	0.68242	0.29653	0.13101
13	6.50	50	0.02560	0.67811	0.21906	0.12940
14	7.00	10	0.25797	0.66835	0.24582	0.13398
15	7.50	50	0.05175	0.67039	0.29353	0.13841
16	7.50	50	0.06070	0.66581	0.28383	0.13626
17	5.00	1	0.05500	0.75084	0.15097	0.09905
18	5.80	5	0.14346	0.69992	0.35708	0.13082
19	5.80	5	0.09197	0.70038	0.27953	0.13039
20	5.00	10	0.05748	0.75352	0.16619	0.09910
21	5.00	10	0.08345	0.75079	0.27046	0.09859
22	5.00	50	0.00520	0.75907	0.20063	0.10061
23	5.00	50	0.00588	0.74542	0.22589	0.09808
24	5.00	160	0.00068	0.75235	0.38876	0.10187
25	5.80	1	0.27852	0.70098	0.33556	0.13095
26	5.80	5	0.25274	0.69861	0.30785	0.13073
27	5.80	5	0.14472	0.70168	0.26777	0.13101
28	5.80	10	0.11315	0.70298	0.24236	0.13175
29	5.80	10	0.16797	0.69741	0.29676	0.12965
30	5.80	10	0.08228	0.70470	0.25614	0.13250
31	5.80	50	0.01111	0.70061	0.25437	0.13091
32	5.80	50	0.01206	0.70015	0.29026	0.13085
33	6.50	5	0.33549	0.68010	0.26048	0.12996
34	6.50	10	0.20322	0.68567	0.21796	0.13226
35	6.50	10	0.31385	0.68328	0.31830	0.13112
36	6.50	10	0.17502	0.68043	0.24130	0.12960
37	6.50	20	0.09519	0.68319	0.21524	0.13155
38	6.50	20	0.13839	0.68091	0.28174	0.13062
39	6.50	20	0.08034	0.68315	0.21020	0.13058
40	6.50	100	0.01036	0.68374	0.48396	0.13009
41	6.50	160	0.00434	0.68410	0.55763	0.13147
42	7.00	1	0.50485	0.67321	0.29286	0.13561
43	7.00	10	0.39013	0.67192	0.33821	0.13554
44	7.00	10	0.21771	0.66734	0.25092	0.13336
45	7.00	50	0.03909	0.66648	0.31692	0.13333
46	7.00	50	0.04598	0.66707	0.28590	0.13352
47	7.50	1	0.56438	0.68636	0.38940	0.14775
48	5.00	10	0.31461	0.68191	0.33624	0.14621
49	5.00	10	0.42183	0.66682	0.45360	0.13668
50	8.00	50	0.06538	0.68571	0.25757	0.11434
51	8.00	160	0.01310	0.68235	0.48849	0.10734

TABLE F5-17
W. J. SILVA: VERTICAL POINT ESTIMATES
SPECTRAL ACCELERATION AT 0.50 SEC PERIOD

CASE NO.	MAGNITUDE	DISTANCE (KM)	MU	SIGMA	SIGMA MU	SIGMA SIGMA
1	5.00	1	0.06918	0.80988	0.27202	0.08554
2	5.00	1	0.07209	0.79577	0.31859	0.08029
3	5.00	5	0.02158	0.80202	0.17040	0.08503
4	5.00	5	0.02479	0.79350	0.25960	0.08140
5	5.80	10	0.05260	0.74552	0.21185	0.13264
6	5.80	20	0.04638	0.74707	0.27491	0.13332
7	6.50	1	0.29052	0.72808	0.17585	0.13465
8	6.50	1	0.33587	0.72883	0.31340	0.13554
9	6.50	1	0.30622	0.73501	0.27566	0.13769
10	6.50	5	0.28293	0.72686	0.27042	0.13614
11	6.50	5	0.18792	0.72828	0.24892	0.13472
12	6.50	50	0.01939	0.73088	0.20570	0.13808
13	6.50	50	0.02140	0.72235	0.26496	0.13453
14	7.00	10	0.17407	0.71311	0.18499	0.14201
15	7.50	50	0.04474	0.71690	0.22490	0.14991
16	7.50	50	0.05605	0.70908	0.28730	0.14648
17	5.00	1	0.02431	0.80988	0.20112	0.08554
18	5.80	5	0.09107	0.74827	0.28423	0.13380
19	5.80	5	0.05126	0.75211	0.35384	0.13360
20	5.00	10	0.02504	0.79072	0.17138	0.08059
21	5.00	10	0.03811	0.78523	0.30658	0.07959
22	5.00	50	0.00280	0.78796	0.18815	0.07998
23	5.00	50	0.00335	0.79072	0.24234	0.08059
24	5.00	160	0.00056	0.78254	0.37505	0.08134
25	5.80	1	0.15843	0.74587	0.26178	0.13091
26	5.80	5	0.15162	0.74391	0.33178	0.13183
27	5.80	5	0.08515	0.73976	0.27529	0.12931
28	5.80	10	0.06737	0.74729	0.18741	0.13340
29	5.80	10	0.10850	0.74297	0.29807	0.13168
30	5.80	10	0.04740	0.74567	0.33063	0.13117
31	5.80	50	0.00723	0.74300	0.28230	0.13149
32	5.80	50	0.00813	0.74609	0.38602	0.13333
33	6.50	5	0.21599	0.72319	0.22329	0.13477
34	6.50	10	0.13806	0.72705	0.23895	0.13633
35	6.50	10	0.22819	0.72625	0.32066	0.13604
36	6.50	10	0.11640	0.72634	0.27251	0.13412
37	6.50	20	0.06291	0.72506	0.17026	0.13540
38	6.50	20	0.09765	0.73150	0.28313	0.13836
39	6.50	20	0.05813	0.72699	0.21349	0.13430
40	6.50	100	0.00937	0.73072	0.39342	0.13481
41	6.50	160	0.00491	0.72864	0.47901	0.13641
42	7.00	1	0.34965	0.71777	0.21799	0.14201
43	7.00	10	0.30226	0.71408	0.32281	0.14234
44	7.00	10	0.15601	0.71615	0.26259	0.14142
45	7.00	50	0.03128	0.71064	0.23434	0.14091
46	7.00	50	0.03995	0.71620	0.31916	0.14329
47	7.50	1	0.38815	0.73429	0.28690	0.15817
48	5.00	10	0.21752	0.72449	0.25019	0.15497
49	5.00	10	0.32892	0.71640	0.45235	0.14966
50	8.00	50	0.05702	0.73235	0.21460	0.12502
51	8.00	160	0.01737	0.73194	0.42710	0.11980

TABLE F5-18
W. J. SILVA: VERTICAL POINT ESTIMATES
SPECTRAL ACCELERATION AT 1.00 SEC PERIOD

CASE NO.	MAGNITUDE	DISTANCE (KM)	MU	SIGMA	SIGMA MU	SIGMA SIGMA
1	5.00	1	0.02745	0.82591	0.25041	0.06267
2	5.00	1	0.02465	0.82312	0.29666	0.06185
3	5.00	5	0.00898	0.81462	0.16021	0.06363
4	5.00	5	0.00889	0.81462	0.27468	0.06363
5	5.80	10	0.02642	0.78702	0.23362	0.11356
6	5.80	20	0.02020	0.78419	0.27523	0.11706
7	6.50	1	0.16186	0.77348	0.15726	0.11945
8	6.50	1	0.15613	0.77549	0.34897	0.12393
9	6.50	1	0.14069	0.76640	0.34309	0.12043
10	6.50	5	0.13744	0.76898	0.27069	0.12542
11	6.50	5	0.08595	0.76719	0.36428	0.12038
12	6.50	50	0.01262	0.76309	0.16742	0.11979
13	6.50	50	0.01181	0.76371	0.23447	0.12297
14	7.00	10	0.10983	0.75394	0.18632	0.13128
15	7.50	50	0.03101	0.75583	0.15012	0.14122
16	7.50	50	0.03399	0.75275	0.22785	0.14260
17	5.00	1	0.01010	0.81764	0.22202	0.06104
18	5.80	5	0.03841	0.79873	0.46808	0.12509
19	5.80	5	0.02177	0.79898	0.49020	0.11971
20	5.00	10	0.01032	0.81187	0.12140	0.06313
21	5.00	10	0.01330	0.81187	0.25308	0.06313
22	5.00	50	0.00131	0.80915	0.13478	0.06289
23	5.00	50	0.00134	0.81739	0.20213	0.06441
24	5.00	160	0.00033	0.81601	0.31068	0.06439
25	5.80	1	0.07637	0.79684	0.36441	0.11427
26	5.80	5	0.06448	0.77925	0.39343	0.11396
27	5.80	5	0.03511	0.79460	0.43053	0.11697
28	5.80	10	0.03308	0.78941	0.20789	0.11503
29	5.80	10	0.04734	0.78074	0.30039	0.11464
30	5.80	10	0.02130	0.79608	0.37001	0.11914
31	5.80	50	0.00416	0.77868	0.22815	0.11017
32	5.80	50	0.00431	0.78386	0.26680	0.11589
33	6.50	5	0.11422	0.77376	0.20232	0.12394
34	6.50	10	0.07933	0.76924	0.20364	0.12205
35	6.50	10	0.11541	0.76594	0.28383	0.12388
36	6.50	10	0.05606	0.76663	0.32223	0.12021
37	6.50	20	0.03594	0.76281	0.18409	0.11960
38	6.50	20	0.05149	0.76990	0.32520	0.12595
39	6.50	20	0.02933	0.76864	0.29279	0.12089
40	6.50	100	0.00649	0.76953	0.29099	0.11784
41	6.50	160	0.00365	0.76567	0.38606	0.11894
42	7.00	1	0.20248	0.75971	0.21248	0.12981
43	7.00	10	0.15152	0.75767	0.31863	0.13550
44	7.00	10	0.08502	0.75370	0.31658	0.13014
45	7.00	50	0.02152	0.75375	0.17285	0.13123
46	7.00	50	0.02280	0.75097	0.24155	0.13273
47	7.50	1	0.25246	0.77232	0.33480	0.14385
48	5.00	10	0.14744	0.76313	0.25761	0.14509
49	5.00	10	0.19612	0.75697	0.50909	0.14427
50	8.00	50	0.03984	0.76105	0.24821	0.12827
51	8.00	160	0.01464	0.77481	0.34613	0.12482

TABLE F5-19
W. J. SILVA: VERTICAL POINT ESTIMATES
SPECTRAL ACCELERATION AT 2.00 SEC PERIOD

CASE NO.	MAGNITUDE	DISTANCE (KM)	MU	SIGMA	SIGMA MU	SIGMA SIGMA
1	5.00	1	0.00704	0.89820	0.35586	0.06486
2	5.00	1	0.00509	0.89264	0.39207	0.06420
3	5.00	5	0.00239	0.87864	0.32160	0.07331
4	5.00	5	0.00189	0.87864	0.38563	0.07331
5	5.80	10	0.00965	0.85316	0.30034	0.12441
6	5.80	20	0.00572	0.84903	0.30794	0.13642
7	6.50	1	0.07311	0.84314	0.20464	0.13430
8	6.50	1	0.05694	0.83492	0.30551	0.14203
9	6.50	1	0.05042	0.83853	0.34035	0.14390
10	6.50	5	0.04624	0.83610	0.36984	0.14995
11	6.50	5	0.03248	0.84021	0.40580	0.14498
12	6.50	50	0.00549	0.83320	0.25192	0.13705
13	6.50	50	0.00419	0.83006	0.38802	0.14601
14	7.00	10	0.05412	0.83092	0.22875	0.15389
15	7.50	50	0.01735	0.82809	0.17710	0.16376
16	7.50	50	0.01506	0.81306	0.29836	0.16597
17	5.00	1	0.00266	0.88989	0.34623	0.06428
18	5.80	5	0.01192	0.83863	0.42428	0.12985
19	5.80	5	0.00691	0.84577	0.49268	0.12704
20	5.00	10	0.00274	0.87864	0.24988	0.07331
21	5.00	10	0.00282	0.88135	0.29047	0.07300
22	5.00	50	0.00038	0.87864	0.24859	0.07331
23	5.00	50	0.00031	0.87864	0.30003	0.07331
24	5.00	160	0.00012	0.88199	0.30993	0.07092
25	5.80	1	0.02889	0.86697	0.27701	0.12454
26	5.80	5	0.01925	0.83651	0.38926	0.12856
27	5.80	5	0.01166	0.84420	0.41410	0.12609
28	5.80	10	0.01095	0.86168	0.34965	0.13219
29	5.80	10	0.01178	0.85665	0.40160	0.14395
30	5.80	10	0.00647	0.84204	0.49653	0.12496
31	5.80	50	0.00169	0.84600	0.43147	0.12039
32	5.80	50	0.00131	0.84570	0.47628	0.13487
33	6.50	5	0.05096	0.83763	0.22390	0.13847
34	6.50	10	0.03167	0.83834	0.25521	0.13880
35	6.50	10	0.03564	0.83667	0.34676	0.15079
36	6.50	10	0.01906	0.83544	0.45647	0.14212
37	6.50	20	0.01595	0.84291	0.27997	0.14142
38	6.50	20	0.01762	0.82570	0.32829	0.14377
39	6.50	20	0.01061	0.83419	0.41498	0.14150
40	6.50	100	0.00317	0.84004	0.23808	0.13369
41	6.50	160	0.00195	0.84656	0.32968	0.14006
42	7.00	1	0.09830	0.83516	0.25573	0.14916
43	7.00	10	0.05294	0.82494	0.40598	0.16131
44	7.00	10	0.03390	0.83183	0.41487	0.15917
45	7.00	50	0.01090	0.82685	0.13988	0.15202
46	7.00	50	0.00913	0.81851	0.30127	0.15784
47	7.50	1	0.12076	0.84166	0.42006	0.16419
48	5.00	10	0.07745	0.82698	0.31553	0.16322
49	5.00	10	0.07944	0.81717	0.53232	0.16787
50	8.00	50	0.02283	0.84175	0.27730	0.16013
51	8.00	160	0.00975	0.85231	0.41325	0.15042

TABLE F5-20
W. J. SILVA: VERTICAL POINT ESTIMATES
SPECTRAL ACCELERATION AT 3.33 SEC PERIOD

CASE NO.	MAGNITUDE	DISTANCE (KM)	MU	SIGMA	SIGMA MU	SIGMA SIGMA
1	5.00	1	0.00199	0.95511	0.66765	0.08674
2	5.00	1	0.00143	0.94635	0.67180	0.08255
3	5.00	5	0.00067	0.93945	0.58778	0.09531
4	5.00	5	0.00053	0.93945	0.60584	0.09531
5	5.80	10	0.00407	0.88558	0.35777	0.14182
6	5.80	20	0.00210	0.88018	0.39800	0.15406
7	6.50	1	0.03373	0.89929	0.33183	0.17323
8	6.50	1	0.02626	0.86544	0.34640	0.16105
9	6.50	1	0.02377	0.87420	0.39537	0.16679
10	6.50	5	0.02219	0.87207	0.36849	0.17510
11	6.50	5	0.01666	0.88311	0.45333	0.17325
12	6.50	50	0.00256	0.88185	0.35650	0.16792
13	6.50	50	0.00172	0.86827	0.59301	0.17248
14	7.00	10	0.02800	0.87769	0.28168	0.18775
15	7.50	50	0.00966	0.86660	0.22911	0.19211
16	7.50	50	0.00771	0.85716	0.33488	0.19780
17	5.00	1	0.00074	0.94925	0.60402	0.08375
18	5.80	5	0.00463	0.88761	0.43498	0.15971
19	5.80	5	0.00260	0.89223	0.53284	0.15190
20	5.00	10	0.00078	0.93368	0.55425	0.09330
21	5.00	10	0.00080	0.93655	0.51483	0.09421
22	5.00	50	0.00011	0.93083	0.44106	0.09257
23	5.00	50	0.00009	0.93083	0.47153	0.09257
24	5.00	160	0.00004	0.93742	0.33057	0.08557
25	5.80	1	0.01201	0.89554	0.41220	0.13709
26	5.80	5	0.00795	0.88644	0.43409	0.15919
27	5.80	5	0.00513	0.88573	0.45429	0.14717
28	5.80	10	0.00469	0.88850	0.46577	0.14365
29	5.80	10	0.00425	0.87567	0.51365	0.15087
30	5.80	10	0.00244	0.88887	0.69480	0.14923
31	5.80	50	0.00063	0.88884	0.48476	0.14382
32	5.80	50	0.00046	0.88211	0.58969	0.15556
33	6.50	5	0.02551	0.89231	0.32568	0.17700
34	6.50	10	0.01455	0.88713	0.40360	0.17234
35	6.50	10	0.01462	0.87106	0.42702	0.17469
36	6.50	10	0.00833	0.88112	0.62728	0.17193
37	6.50	20	0.00680	0.87793	0.46583	0.16516
38	6.50	20	0.00696	0.87889	0.43904	0.18046
39	6.50	20	0.00467	0.86937	0.56852	0.16349
40	6.50	100	0.00128	0.87707	0.32936	0.15434
41	6.50	160	0.00092	0.89456	0.36242	0.17023
42	7.00	1	0.05271	0.87805	0.36182	0.17832
43	7.00	10	0.02417	0.86263	0.44904	0.19021
44	7.00	10	0.01681	0.86923	0.50555	0.18556
45	7.00	50	0.00558	0.87100	0.21565	0.18312
46	7.00	50	0.00441	0.86485	0.34612	0.19166
47	7.50	1	0.06418	0.88443	0.47484	0.19437
48	5.00	10	0.04243	0.87580	0.40109	0.19831
49	5.00	10	0.03853	0.85936	0.62662	0.19922
50	8.00	50	0.01373	0.89737	0.31251	0.19152
51	8.00	160	0.00575	0.90771	0.32797	0.17932

TABLE F5-21
W. J. SILVA: VERTICAL POINT ESTIMATES
PEAK GROUND VELOCITY

CASE NO.	MAGNITUDE	DISTANCE (KM)	MU	SIGMA	SIGMA MU	SIGMA SIGMA
1	5.00	1	4.02063	0.79848	0.30458	0.07021
2	5.00	1	3.63480	0.79848	0.36422	0.07021
3	5.00	5	1.14604	0.78677	0.20089	0.07814
4	5.00	5	1.15680	0.78103	0.31448	0.07480
5	5.80	10	2.95145	0.75756	0.21252	0.12718
6	5.80	20	2.16782	0.75590	0.27688	0.12924
7	6.50	1	18.33007	0.77789	0.23189	0.13585
8	6.50	1	18.03647	0.77484	0.38526	0.13822
9	6.50	1	16.30184	0.77484	0.36980	0.13822
10	6.50	5	15.44497	0.75535	0.31362	0.14426
11	6.50	5	10.16407	0.76980	0.35621	0.13641
12	6.50	50	1.12685	0.75285	0.24686	0.14109
13	6.50	50	1.03599	0.75181	0.39181	0.14298
14	7.00	10	11.70002	0.75556	0.19073	0.15328
15	7.50	50	3.04512	0.75493	0.24510	0.16241
16	7.50	50	3.25418	0.74824	0.36079	0.16211
17	5.00	1	1.30940	0.79282	0.24350	0.06750
18	5.80	5	4.66900	0.75701	0.41940	0.12945
19	5.80	5	2.60342	0.77035	0.42310	0.12426
20	5.00	10	1.33212	0.77820	0.13735	0.07344
21	5.00	10	1.82780	0.78103	0.27279	0.07480
22	5.00	50	0.13110	0.77540	0.20902	0.07228
23	5.00	50	0.13645	0.77820	0.27836	0.07344
24	5.00	160	0.02898	0.76989	0.36336	0.07066
25	5.80	1	9.22932	0.77445	0.34759	0.12257
26	5.80	5	7.76950	0.75277	0.38225	0.12809
27	5.80	5	4.45780	0.76946	0.32784	0.12410
28	5.80	10	3.68903	0.76217	0.21218	0.12857
29	5.80	10	5.28468	0.75596	0.28505	0.12925
30	5.80	10	2.39286	0.76892	0.39736	0.12401
31	5.80	50	0.39300	0.75842	0.34091	0.12738
32	5.80	50	0.38397	0.75876	0.44868	0.13013
33	6.50	5	12.63204	0.76018	0.19084	0.14352
34	6.50	10	7.91494	0.75849	0.17495	0.14290
35	6.50	10	11.68760	0.75581	0.30629	0.14443
36	6.50	10	5.89662	0.76901	0.36829	0.13626
37	6.50	20	3.53467	0.75676	0.22792	0.14229
38	6.50	20	5.02494	0.75658	0.31304	0.14474
39	6.50	20	2.89825	0.76631	0.37765	0.13552
40	6.50	100	0.56912	0.77157	0.39061	0.13445
41	6.50	160	0.27961	0.76178	0.70186	0.14502
42	7.00	1	23.17708	0.77489	0.28343	0.14461
43	7.00	10	16.27792	0.75330	0.37647	0.15483
44	7.00	10	9.02237	0.76745	0.39894	0.14486
45	7.00	50	1.98927	0.75016	0.21559	0.15158
46	7.00	50	2.07269	0.74806	0.33142	0.15292
47	7.50	1	27.14126	0.78404	0.47213	0.15608
48	5.00	10	15.80830	0.75823	0.35217	0.16392
49	5.00	10	21.18422	0.75114	0.62516	0.16312
50	8.00	50	4.29233	0.74560	0.38614	0.15378
51	8.00	160	1.47492	0.76979	0.46899	0.14528

APPENDIX F6

YUCCA MOUNTAIN PROBABILISTIC SEISMIC HAZARD ANALYSIS DOCUMENTATION OF EXPERT MODEL GROUND MOTIONS

Paul G. Somerville
Woodward-Clyde Federal Services

APPENDIX F6
TABLE OF CONTENTS

APPENDIX F6

YUCCA MOUNTAIN PROBABILISTIC SEISMIC HAZARD ANALYSIS DOCUMENTATION OF EXPERT MODEL GROUND MOTIONS

Paul G. Somerville
Woodward-Clyde Federal Services

F6-1 INTRODUCTION

This report documents the decisions that I made in developing a ground motion model for use at Yucca Mountain. The model pertains to a hypothetical rock surface that is produced by excavating the top 300 meters of overburden at the site.

F6-2 WEIGHTING SCHEME

The overall weight, W, for each model is developed by scaling four weights:

$$W = B \times M \times D \times F$$

where

B = base level weight
M = magnitude applicability weight
D = distance applicability weight
F = frequency applicability weight

The base level weights represent my general evaluation of the applicability of the models within each class to the prediction of ground motion at Yucca Mountain. The magnitude, distance, and frequency weights reflect how well the models are expected to predict ground motions at specific magnitudes, distances and frequencies, respectively

F6-2.1 Model Classes

I divided the proponent models into four classes: 1) finite fault numerical simulations, 2) explosion, 3) empirical, and 4) point source stochastic. The model classes and their base level weights are shown in Table F6-1.

The finite fault numerical simulations are generally well validated against recorded data and thus are expected to have the capacity to predict ground motions for Yucca Mountain specific conditions.

The explosion models contain region-specific distance attenuation information, however the distance attenuation has not been adjusted for differences in the source depth of explosions and earthquakes. Since the explosions are at shallower depths than are representative of earthquake source depths, they will contain more surface waves which may significantly affect the distance attenuation.

The empirical models are based on strong motion data that span the relevant ranges of magnitude, distance, and period that are considered in this study. The adjustment factors for the empirical model account for Yucca Mountain specific conditions. The empirical model class is given the largest weight.

The point source stochastic model has been extensively validated against data; however it does not include finite fault effects such as rupture directivity at low frequencies.

F6-2.2 Model Weights - Horizontal Component

Model classes 1, 2, and 3 contain multiple proponent models. The relative weights that I assigned to these models are listed in Table F6-1. The same weights are used for both the median (μ) and the aleatory uncertainty (σ) for all of the models.

F6-2.2.1 Finite Fault Models. All three finite source models have been validated against recorded data. The Silva and Somerville models have been validated against a larger number of earthquakes than the Zeng and Anderson model. The Zeng and Anderson model uses an unconventional source model. The Somerville and Zeng and Anderson models include rupture directivity effects at low frequencies, but these effects are not fully included in the Silva model. Since all three models have been validated against data, I specified equal weight for the three finite source models.

F6-2.2.2 Explosion Models. There are three proponent models based on explosion data. The first model (Blast 1) is based on an explosion source that is not relevant for earthquakes. The third model (Blast 3) is based on the Little Skull Mountain source that is not generally applicable to other earthquakes. Therefore, these two models were given zero weight.

The second model (Blast 2), uses an empirical response spectra shape that is attenuated based on the observed NTS attenuation. This model has a reasonable spectral shape and includes information on the regional attenuation. Of the three proponent explosion models, I consider this to be the only applicable model. Therefore, I assigned it a model weight of 1.0.

F6-2.2.3 Empirical Models. I included the empirical models listed below. I gave higher weight to those models that incorporate magnitude dependent attenuation rates and different attenuation rates for soil and rock sites. Models that were not based on recent data or current regression methods were down weighted. The specific models are discussed below.

Abrahamson and Silva (1997): This model includes recent data and incorporates distance dependent magnitude scaling and different attenuation rates for soil and rock. It includes near fault effects such footwall/hanging wall effects. It includes style-of-faulting factors for normal faulting earthquakes so it does not need scaling for stress drop. Due to the inclusion of near fault effects, I increased the weight on this model to 0.3.

Joyner and Boore (1988): This model is not based on recent data. It uses the same attenuation shape for rock and soil and for different magnitudes which I consider to be unrealistic. Its distance metric (Joyner-Boore distance) makes it unsuitable for use in the near source region of dipping faults. Due to these disadvantages, I down weighted this model to 0.1. This model does include peak velocity which only a few models include.

Campbell (1997), soft rock: This model includes recent data and incorporates distance dependent magnitude scaling and different attenuation rates for soil and rock. I assigned a weight of 0.2 to this model.

Idriss (University of California, Davis, written communication, 1997): This model includes recent data and incorporates distance dependent magnitude scaling and different attenuation

rates for soil and rock. It is not based on current regression methods. Due to the regression methods used in this model, I reduced the weight to 0.1.

Sadigh et al. (1997): This model includes recent data and incorporates distance dependent magnitude scaling and different attenuation rates for soil and rock. I assigned a weight of 0.2 to this model.

Spudich et al. (1997): This model is specific for events in extensional regimes so it does not require scaling for stress drop difference. The use of the same attenuation shape for rock and soil sites and for different magnitudes is unrealistic. Its distance metric (Joyner-Boore distance) makes it unsuitable for use in the near source region of dipping faults. I reduced the weight for this model to 0.1.

The following empirical models were excluded (given zero weight) for the reasons given.

McGarr (1984) : The theoretically based dependence of ground motions on faulting mechanism is not borne out in recorded data.

Sabetta and Pugliese (1996): This model is based on Italian data. The Italian data that are relevant to Yucca Mountain is included in the Spudich *et al.* (1996) model.

Campbell (Dames and Moore, written communication, 1990; Campbell, 1993; Campbell and Bozorgnia, 1994): These Campbell models have been superseded by Campbell (1997).

Boore et al. (1997): The assumption of a constant, distance-independent relation between soil and rock causes this model to underpredict rock motions at close distances.

F6-2.2.4 Point Source Stochastic Model. The point source proponent model was provided with the median and uncertainties in the point source stress drop to be specified by each expert. I specified the following values to be used:

Median stress drop = 60 bars
Standard deviation of stress drop = 0.7 (natural log units)

Standard error of the median stress drop = 0.3

Standard error of the standard deviation of stress drop = 0.3

F6-2.2.5 Magnitude Weights. The magnitude weights reflect how well the models are expected to predict ground motions as a function of magnitude; Table F6-2 summarizes these factors. The weights for the explosion model reflect the decreasing constraint on the explosion attenuation model with increasing magnitude. The weights on the point source stochastic model reflect the decreasing physical realism of the point source model with increasing magnitude.

F6-2.2.6 Distance Weights. The distance weights (Table F6-3) reflect how well the models are expected to predict ground motions as a function of distance. For the Silva models (finite source and point source), the weights are different for two frequency ranges: less than 1 Hz and greater than 1 Hz. The weights for the Silva finite fault reflect the decreasing physical realism of the homogeneous radiation pattern with decreasing distance for frequencies of 1 Hz and less. The weights for the point source stochastic model reflect the decreasing physical realism of the homogeneous radiation pattern with decreasing distance for frequencies of 1 Hz and less and of the point source model with decreasing distance. The need to calibrate the point source stochastic model against empirical models makes it more like an empirically based algorithm. The weights for the explosion model reflect the decreasing appropriateness of the attenuation function with decreasing distance.

F6-2.2.7 Frequency Weights. These weights (Table F6-4) reflect how well the models are expected to predict ground motions as a function of frequency. The weights for the point source stochastic model represent the decreasing physical realism of the point source model with decreasing frequency; it contains no physical representation of source finiteness and rupture directivity effects. The weights for the Silva finite fault stochastic model represents the decreasing physical realism of the homogeneous radiation pattern with decreasing frequency.

F6-2.2.8 Horizontal Component Variability. The proponent models for the horizontal component all predict the average of the two horizontal components. This project is using the random horizontal component, so the component-to-component variability needs to be

added to the aleatory uncertainty. The two available proponent models are Boore et al. (1997) and Spudich *et al.* (1997). These two models are very similar. I selected the horizontal component to component variability from the Boore *et al.* (1997) model.

F6-2.3 Model Weights - Vertical Component

The weighting scheme described for the horizontal component is also used for the vertical component.

F6-3 ADJUSTMENTS TO WEIGHTED POINT ESTIMATES

The weighting scheme described above assumed that predictions were available for each model in a given model class. However, for the class of numerical simulation models, predictions were available for only some of the models for the largest and smallest magnitudes (magnitude 5 and 8). In some instances, the predictions of the one or two available numerical models were quite different from those of the other classes of models and from available recorded data. In these cases, the point estimates were modified to give a lower weight to the class of numerical models.

In particular, for the magnitude 5 case, the Zeng and Anderson model was the only finite fault model that was run. I did not want to give a weight of 0.4 to that single simulation so I modified the point estimates for those cases by hand.

F6-4 EPISTEMIC UNCERTAINTY

Estimates of epistemic uncertainties in the median ground motion values and their aleatory variability were based principally on the variations among the estimates of different models. Most of the proponent models did not provide epistemic uncertainties. The exceptions were the Somerville numerical simulation and the point source stochastic model. The epistemic uncertainties from these proponent models were included in the total epistemic uncertainty. The epistemic uncertainties were computed by the facilitation team.

I made the following modifications to these statistical estimates of the epistemic uncertainty: For the epistemic uncertainty in sigma (σ_σ), I set a minimum value of 0.05 natural log units and a maximum value of 0.2 natural log units.

F6-5 FINAL POINT ESTIMATES

The final point estimates were checked for consistency and found to be mutually consistent. My final point estimates of μ, σ, σ_μ, and σ_σ for the horizontal component for the 51 cases are given in Tables F6-5 to F6-13 for the nine ground motion parameters. The corresponding point estimates for the vertical component are given in Tables F6-14 to F6-22.

F6-6 EVALUATION OF REGRESSION MODELS

The facilitation team developed regression models to parameterize my point estimates in terms of the dependence on magnitude, distance, and style-of-faulting. I reviewed the final regression models given in Volume 10F of the Data Package.

F6-6.1 Mu

The point estimates of the median ground motion are well fit by the regression fits. The point estimates for each magnitude cluster around the regression fits, and point estimates for different magnitudes are generally well separated. Based on review of residual plots (Vol. 10F of the Ground Motion Data Package), the regression fit is judged to be an appropriate representation of my point estimates.

F6-6.2 Sigma

The sigma values are well modeled by a functional form in which sigma decreases with increasing magnitude until it reaches a minimum value at magnitude 7. The sigma values vary from about 0.6 for peak acceleration to about 0.8 for 0.3 Hz spectral acceleration. This degree of variation is not very much larger than that of empirical attenuation relations derived for a specified region, and for this reason is considered to be a realistic representation of the aleatory variation of ground motion at Yucca Mountain.

F6-6.3 Sigma Mu

There are wide variations in the values of sigma mu. They have a systematic variation with distance, tending to have a minimum at a distance of about 20 km. This variation is modeled using a quadratic equation in distance. The values of sigma mu also have a magnitude dependence which is highly variable. This was fit by a linear magnitude dependence, which was allowed to vary from frequency to frequency. This variation is quite large with the magnitude dependence having a minimum at 5 Hz and larger values at both lower and higher frequencies. Based on review of the residual plots (Vol. 10F of the Ground Motion Data Package), these models were judged to be an appropriate representation of my sigma Mu estimates.

F6-6.4 Sigma Sigma

The values of sigma sigma have small variations with magnitude. They also have small variations with distance, except for the lower frequencies and for the vertical component. The regression model is judged to be an appropriate representation of my sigma sigma estimates.

F6-7 SPECIAL CASES

Adjustments for two special fault rupture cases were developed using ground motion simulations. These two scenarios are described below. The simulations used the high frequency part of Woodward-Clyde's simulation procedure (i.e. same method as Somerville simulations) to predict the ground motion for the special cases and for the base cases. The ratios of the predicted ground motions were used to guide the recommendation of adjustment factors to use for the special cases. These simulations are unbiased for frequencies above 1 Hz. At frequencies less than 1 Hz, the simulations tend to underpredict recorded data. However, as described below, the adjustments are based on the ratio of the two simulations and not on their absolute values, so I have also based my estimates on the computed ratios at frequencies less than 1 Hz.

F6-7.1 Multiple Parallel Faults

The response spectral ratios were computed for the case of three parallel faults dipping 60 degrees (separated by 2 and 3 km) rupturing simultaneously compared to a single fault

rupture. The total moment for both cases corresponds to a moment magnitude 6.82 (each of the three parallel faults had moment corresponding to magnitude 6.5). The resulting ratios are given in the Ground Motion Data Package (Vol. 1b). Based on these computed ratios, my estimates of the adjustment factors for simultaneous rupture on parallel faults are given in Table F6-23. These adjustments include additional aleatory and epistemic uncertainty.

F6-7.2 Low Angle Fault

The second case is one of a low angle fault with a dip of about 30 degrees beneath the site, together with a set of three more steeply dipping conjugate faults. The total moment for both cases corresponds to magnitude 6.8. The resulting ratios are given in the Ground Motion Data Package (Vol. 1b). Based on these computed ratios, my estimates of the adjustment factors for simultaneous rupture are given in Table F6-24. These adjustments include additional aleatory and epistemic uncertainty.

F6-8 REFERENCES

Abrahamson, N. A., and Silva, W. J., 1997, Empirical response spectral attenuation relations for shallow crustal earthquakes: Seismological Research Letters,.v. 68, n. 1, p. 94-127.

Boore, D. M., Joyner, W. B., and Fumal, T. E., 1997, Equations for estimating horizontal response spectra and peak acceleration from western North American earthquakes--a summary of recent work: Seismological Research Letters, v. 68, n. 1, p. 128 - 153.

Campbell, K.W. 1993, Empirical prediction of near-source ground motion from large earthquakes, *in* Gaur, V.K. ed., Proceedings, International Workshop on earthquake hazard and large dams in the Himalayas: Indian National Trust for Art and Cultural Heritage (INTACH), New Delhi, India, p. 93-103.

Campbell, K. W., 1997, Empirical near-source attenuation relationships for horizontal and vertical components of peak ground acceleration, peak ground velocity, and pseudo-absolute acceleration response spectra: Seismological Research Letters, v. 68, n. 1, p. 154 - 179.

Campbell, K.W., and Bozorgnia, Y., 1994, Near-source attenuation of peak horizontal acceleration from worldwide accelerograms recorded from 1957 to 1993: 5th U.S. National Conference on Earthquake Engineering., Chicago, IL, July 10-14, 1994.

Joyner, W. B., and Boore, D. M., 1988, Measurement, characterization, and prediction of strong ground motion, *in* Proceedings, Conference on Earthquake Engineering and Soil Dynamics II: GT Div/. ASCE, Park City, UT, 27-30 June 1988, p. 43-102.

McGarr, A. 1984, Scaling of ground motion parameters, state of stress, and focal depth: Journal of Geophysical Research, v. 89, p. 6969-6979.

Sabetta, F., and Pugliese, A., 1996, Estimation of response spectra and simulation of nonstationary earthquake ground motions: Bulletin of the Seismological Society of America, v. 86, p. 337-352.

Sadigh, K., Chang, C.-Y., Egan, J. A., Makdisi, F., and Youngs, R. R., 1997, Attenuation relationships for shallow crustal earthquakes based on California strong motion data: Seismological Research Letters, v. 68, n. 1, p. 180-189.

Somerville, P.G., Smith, N.F., Graves, R.W., and Abrahamson, N.A., 1997, Modification of empirical strong ground motion attenuation relations to include the amplitude and duration effects of rupture directivity: Seismological Research Letters, v. 68, p. 199-222.

Spudich, P., Fletcher, J. B., Hellweg, M., Boatwright, J., Sullivan, C., Joyner, W. B., Hanks, T. C., Boore, D.M., McGarr, A., Baker, L. M., and Lindh, A. G., 1997, SEA96 -- a new predictive relation for earthquake ground motions in extensional tectonic regimes: Seismological Society of America, v. 68, n. 1., p. 190-198.

Zeng, Y., Anderson, J. G., and Yu, G., 1994, A composite source model for computing realistic synthetic strong ground motions: Geophysical Research Letters, v. 21, p. 725-728.

TABLE F6-1
WEIGHTS FOR MODEL CLASSES
(BASE LEVEL WEIGHT B)

MODEL	CLASS	WEIGHT
Finite Fault Numerical	1	0.4
Explosion (NTS)	2	0.05
Empirical	3	0.5
Point Source Stochastic	4	0.05

TABLE F6-2
MAGNITUDE FACTORS M

MODEL	M 5.0	M 5.8	M 6.5	M 7.0	M 7.5
Zeng and Anderson	1	1	1	1	1
Silva Finite Fault	1	1	1	1	1
Somerville	1	1	1	1	1
Explosion	1	1	0.9	0.8	0.7
Empirical	1	1	1	1	1
Point Source Stochastic	1	0.9	0.8	0.7	0.6

TABLE F6-3
DISTANCE FACTORS D (APPLIED TO RUPTURE DISTANCE)

MODEL	1 KM	5 KM	10 KM	20 KM	50 KM
Zeng and Anderson	1	1	1	1	1
Silva Finite Fault	0.5 (f<1 Hz) 1.0 (f >1 Hz)	0.7 (f<1 Hz) 1.0 (f >1 Hz)	0.8 (f<1 Hz) 1.0 (f >1 Hz)	0.9 (f<1 Hz) 1.0 (f >1 Hz)	1.0 (f<1 Hz) 1.0 (f >1 Hz)
Somerville	1	1	1	1	1
Blast 2	0	0	0.75	1	1
Empirical	1	1	1	1	1
Point Source Stochastic	0.2 (f<1 Hz) 0.5 (f >1 Hz)	0.4 (f<1 Hz) 0.7 (f >1 Hz)	0.6 (f<1 Hz) 0.8 (f >1 Hz)	0.8 (f<1 Hz) 0.9 (f >1 Hz)	1.0 (f<1 Hz) 1.0 (f >1 Hz)

TABLE F6-4
FREQUENCY FACTORS F

MODEL	0.3 HZ	0.5 HZ	1.0 HZ, PGV	2-20 HZ	PGA
Zeng and Anderson	1	1	1	1	1
Silva Finite Fault	0.4	0.6	0.8	1	1
Somerville	1	1	1	1	1
Explosion	1	1	1	1	1
Empirical	1	1	1	1	1
Point Source Stochastic	0.25	0.5	0.75	1	1

TABLE F6-5
P. G. SOMERVILLE: HORIZONTAL POINT ESTIMATES
PEAK GROUND ACCELERATION

CASE NO.	MAGNITUDE	DISTANCE (KM)	MU	SIGMA	SIGMA MU	SIGMA SIGMA
1	5.00	1	0.12685	0.66211	0.34401	0.17028
2	5.00	1	0.20004	0.67019	0.46825	0.16916
3	5.00	5	0.04871	0.66711	0.32421	0.16981
4	5.00	5	0.07955	0.67110	0.39932	0.16929
5	5.80	10	0.09769	0.60725	0.22804	0.16059
6	5.80	20	0.07441	0.60700	0.27123	0.16107
7	6.50	1	0.42450	0.57421	0.30895	0.16175
8	6.50	1	0.45352	0.57590	0.44710	0.16307
9	6.50	1	0.40468	0.57327	0.35879	0.15956
10	6.50	5	0.35922	0.57225	0.31859	0.16200
11	6.50	5	0.24893	0.57305	0.23152	0.15953
12	6.50	50	0.02844	0.57185	0.29228	0.16329
13	6.50	50	0.02874	0.57143	0.25031	0.16324
14	7.00	10	0.25219	0.54359	0.27775	0.16772
15	7.50	50	0.05831	0.54086	0.24524	0.17343
16	7.50	50	0.06337	0.53782	0.23715	0.17194
17	5.00	1	0.04215	0.66211	0.61112	0.17028
18	5.80	5	0.15546	0.60692	0.30883	0.16036
19	5.80	5	0.09311	0.60105	0.31775	0.15643
20	5.00	10	0.06646	0.66987	0.21914	0.16989
21	5.00	10	0.08515	0.66605	0.27478	0.17056
22	5.00	50	0.00619	0.66772	0.33520	0.17069
23	5.00	50	0.00623	0.66399	0.38635	0.17150
24	5.00	160	0.00076	0.66028	0.53082	0.17243
25	5.80	1	0.26746	0.60578	0.30810	0.15966
26	5.80	5	0.22324	0.60528	0.27648	0.16047
27	5.80	5	0.13839	0.60036	0.23796	0.15646
28	5.80	10	0.12035	0.61178	0.23646	0.16143
29	5.80	10	0.16267	0.60694	0.28490	0.16062
30	5.80	10	0.07877	0.60147	0.29348	0.15679
31	5.80	50	0.01163	0.60503	0.48840	0.16126
32	5.80	50	0.01200	0.60901	0.50764	0.16137
33	6.50	5	0.30989	0.57347	0.27315	0.16224
34	6.50	10	0.20335	0.57463	0.26236	0.16318
35	6.50	10	0.28016	0.57401	0.32126	0.16304
36	6.50	10	0.15880	0.56687	0.23014	0.15748
37	6.50	20	0.10034	0.57119	0.23849	0.16276
38	6.50	20	0.13590	0.57548	0.30907	0.16380
39	6.50	20	0.07770	0.56387	0.20893	0.15668
40	6.50	100	0.01201	0.57202	0.41962	0.16360
41	6.50	160	0.00473	0.58008	0.48846	0.16752
42	7.00	1	0.46160	0.54927	0.29043	0.16799
43	7.00	10	0.33444	0.55053	0.31262	0.17045
44	7.00	10	0.19492	0.53863	0.20610	0.16217
45	7.00	50	0.04389	0.54249	0.27267	0.16829
46	7.00	50	0.04717	0.54425	0.25900	0.16883
47	7.50	1	0.50761	0.55646	0.34719	0.18185
48	5.00	10	0.28777	0.54833	0.28260	0.17857
49	5.00	10	0.36600	0.54105	0.38566	0.17251
50	8.00	50	0.07351	0.55289	0.25562	0.18382
51	8.00	160	0.01859	0.54634	0.42745	0.18045

TABLE F6-6
P. G. SOMERVILLE: HORIZONTAL POINT ESTIMATES
SPECTRAL ACCELERATION AT 0.05 SEC PERIOD

CASE NO.	MAGNITUDE	DISTANCE (KM)	MU	SIGMA	SIGMA MU	SIGMA SIGMA
1	5.00	1	0.23556	0.67213	0.50631	0.16613
2	5.00	1	0.35471	0.67621	0.26888	0.16530
3	5.00	5	0.08473	0.67707	0.38640	0.16543
4	5.00	5	0.12255	0.68112	0.26846	0.16472
5	5.80	10	0.16379	0.61207	0.27084	0.15854
6	5.80	20	0.11618	0.60838	0.27001	0.15864
7	6.50	1	0.74006	0.57360	0.29435	0.15886
8	6.50	1	0.77949	0.57461	0.35631	0.16011
9	6.50	1	0.69017	0.56929	0.31567	0.15548
10	6.50	5	0.62012	0.57031	0.32786	0.15909
11	6.50	5	0.42881	0.56699	0.31483	0.15471
12	6.50	50	0.03927	0.56955	0.35488	0.16028
13	6.50	50	0.03968	0.56902	0.33133	0.16022
14	7.00	10	0.40569	0.53667	0.26482	0.16408
15	7.50	50	0.07920	0.53438	0.29135	0.17008
16	7.50	50	0.08491	0.53108	0.27838	0.16836
17	5.00	1	0.07255	0.67213	0.66627	0.16613
18	5.80	5	0.25176	0.60754	0.31705	0.15754
19	5.80	5	0.15041	0.60238	0.35176	0.15407
20	5.00	10	0.12032	0.69470	0.24836	0.16328
21	5.00	10	0.15528	0.67917	0.25124	0.16544
22	5.00	50	0.00908	0.67292	0.40172	0.16738
23	5.00	50	0.00891	0.67292	0.44778	0.16738
24	5.00	160	0.00101	0.66165	0.58586	0.17105
25	5.80	1	0.49351	0.60686	0.32597	0.15681
26	5.80	5	0.40211	0.61159	0.27547	0.15891
27	5.80	5	0.24027	0.60546	0.36690	0.15478
28	5.80	10	0.20613	0.61425	0.28229	0.15942
29	5.80	10	0.26987	0.60860	0.27723	0.15810
30	5.80	10	0.13220	0.60100	0.41634	0.15381
31	5.80	50	0.01637	0.60930	0.57855	0.15902
32	5.80	50	0.01654	0.61128	0.59802	0.15913
33	6.50	5	0.53572	0.56783	0.28093	0.15797
34	6.50	10	0.34849	0.57482	0.26659	0.16122
35	6.50	10	0.46808	0.57049	0.34531	0.15949
36	6.50	10	0.26252	0.56752	0.30668	0.15539
37	6.50	20	0.15998	0.57228	0.26549	0.16135
38	6.50	20	0.21731	0.57398	0.33571	0.16119
39	6.50	20	0.12109	0.56271	0.30574	0.15380
40	6.50	100	0.01428	0.56807	0.49650	0.16014
41	6.50	160	0.00585	0.56868	0.58154	0.16019
42	7.00	1	0.80673	0.54469	0.31693	0.16514
43	7.00	10	0.54141	0.54639	0.35894	0.16810
44	7.00	10	0.31455	0.53358	0.28527	0.15887
45	7.00	50	0.06028	0.53540	0.31849	0.16472
46	7.00	50	0.06482	0.53766	0.29889	0.16542
47	7.50	1	0.85600	0.55313	0.39192	0.18094
48	5.00	10	0.46037	0.54323	0.30558	0.17678
49	5.00	10	0.55923	0.53466	0.41191	0.16909
50	8.00	50	0.09699	0.54969	0.32081	0.18063
51	8.00	160	0.02039	0.53952	0.47171	0.17578

TABLE F6-7
P. G. SOMERVILLE: HORIZONTAL POINT ESTIMATES
SPECTRAL ACCELERATION AT 0.10 SEC PERIOD

CASE NO.	MAGNITUDE	DISTANCE (KM)	MU	SIGMA	SIGMA MU	SIGMA SIGMA
1	5.00	1	0.26627	0.72587	0.30872	0.16689
2	5.00	1	0.41922	0.71752	0.56245	0.16623
3	5.00	5	0.10108	0.72620	0.23935	0.16687
4	5.00	5	0.16962	0.72206	0.46122	0.16648
5	5.80	10	0.19342	0.63565	0.24279	0.16280
6	5.80	20	0.14547	0.63668	0.31630	0.16308
7	6.50	1	0.83758	0.60363	0.34411	0.16750
8	6.50	1	0.92271	0.60277	0.52665	0.16759
9	6.50	1	0.81708	0.60185	0.41828	0.16558
10	6.50	5	0.70440	0.59789	0.35826	0.16542
11	6.50	5	0.49557	0.59853	0.23690	0.16381
12	6.50	50	0.05084	0.59820	0.34842	0.16708
13	6.50	50	0.05128	0.59748	0.26587	0.16661
14	7.00	10	0.48458	0.56810	0.31459	0.17257
15	7.50	50	0.09807	0.56838	0.35769	0.18113
16	7.50	50	0.10788	0.56212	0.32674	0.17742
17	5.00	1	0.09171	0.70918	0.44310	0.16611
18	5.80	5	0.31077	0.63703	0.35302	0.16296
19	5.80	5	0.18390	0.63153	0.37054	0.15918
20	5.00	10	0.14000	0.72669	0.29136	0.16665
21	5.00	10	0.18111	0.71089	0.34593	0.16603
22	5.00	50	0.01180	0.71936	0.30093	0.16602
23	5.00	50	0.01172	0.71165	0.34041	0.16601
24	5.00	160	0.00113	0.70011	0.57071	0.16700
25	5.80	1	0.52907	0.63783	0.34188	0.16286
26	5.80	5	0.46096	0.63638	0.28735	0.16289
27	5.80	5	0.27090	0.63412	0.26397	0.16106
28	5.80	10	0.23132	0.63761	0.25615	0.16405
29	5.80	10	0.31414	0.63614	0.32321	0.16284
30	5.80	10	0.15332	0.62729	0.28296	0.15831
31	5.80	50	0.02140	0.63652	0.46335	0.16339
32	5.80	50	0.02147	0.63753	0.51396	0.16396
33	6.50	5	0.61894	0.60216	0.31541	0.16686
34	6.50	10	0.40442	0.59967	0.29965	0.16719
35	6.50	10	0.56217	0.59827	0.39534	0.16676
36	6.50	10	0.31055	0.59561	0.21021	0.16285
37	6.50	20	0.19614	0.59505	0.28443	0.16562
38	6.50	20	0.25581	0.59849	0.32972	0.16680
39	6.50	20	0.14720	0.59356	0.20680	0.16180
40	6.50	100	0.01784	0.59481	0.56710	0.16584
41	6.50	160	0.00640	0.59523	0.68033	0.16595
42	7.00	1	0.92215	0.57375	0.35370	0.17315
43	7.00	10	0.64438	0.57500	0.37483	0.17636
44	7.00	10	0.37921	0.56626	0.20668	0.16845
45	7.00	50	0.07569	0.56589	0.36236	0.17238
46	7.00	50	0.08315	0.56929	0.32682	0.17398
47	7.50	1	0.96213	0.58391	0.38809	0.19009
48	5.00	10	0.54278	0.57316	0.33028	0.18513
49	5.00	10	0.68498	0.56732	0.40738	0.17953
50	8.00	50	0.11749	0.59142	0.37641	0.19357
51	8.00	160	0.01992	0.57948	0.75236	0.18723

TABLE F6-8
P. G. SOMERVILLE: HORIZONTAL POINT ESTIMATES
SPECTRAL ACCELERATION AT 0.20 SEC PERIOD

CASE NO.	MAGNITUDE	DISTANCE (KM)	MU	SIGMA	SIGMA MU	SIGMA SIGMA
1	5.00	1	0.20496	0.74800	0.31892	0.16234
2	5.00	1	0.32023	0.75617	0.55911	0.16285
3	5.00	5	0.07769	0.74023	0.23264	0.16235
4	5.00	5	0.12930	0.73621	0.39891	0.16258
5	5.80	10	0.18434	0.66914	0.24758	0.16336
6	5.80	20	0.14387	0.66279	0.32779	0.16157
7	6.50	1	0.79685	0.62831	0.33769	0.16327
8	6.50	1	0.86816	0.63618	0.49054	0.16704
9	6.50	1	0.78611	0.64023	0.41777	0.16880
10	6.50	5	0.68378	0.63114	0.35506	0.16510
11	6.50	5	0.49115	0.62859	0.23777	0.16257
12	6.50	50	0.05720	0.62913	0.35788	0.16484
13	6.50	50	0.05860	0.62532	0.24486	0.16344
14	7.00	10	0.49293	0.60051	0.31422	0.16971
15	7.50	50	0.12167	0.59775	0.37504	0.17575
16	7.50	50	0.13486	0.59373	0.34083	0.17351
17	5.00	1	0.06626	0.73174	0.52280	0.16294
18	5.80	5	0.27529	0.66444	0.37614	0.16241
19	5.80	5	0.17928	0.65960	0.31658	0.15977
20	5.00	10	0.11052	0.74162	0.27433	0.16224
21	5.00	10	0.14044	0.73777	0.32602	0.16249
22	5.00	50	0.01228	0.74986	0.24322	0.16206
23	5.00	50	0.01083	0.73108	0.32822	0.16335
24	5.00	160	0.00162	0.73857	0.52835	0.16245
25	5.80	1	0.47160	0.66292	0.33285	0.16185
26	5.80	5	0.40567	0.66314	0.29076	0.16241
27	5.80	5	0.25115	0.66083	0.21331	0.16028
28	5.80	10	0.21509	0.66782	0.28684	0.16280
29	5.80	10	0.29150	0.66285	0.33711	0.16146
30	5.80	10	0.15017	0.66366	0.20506	0.16151
31	5.80	50	0.02232	0.66670	0.49040	0.16261
32	5.80	50	0.02484	0.66627	0.40043	0.16260
33	6.50	5	0.59066	0.62763	0.30157	0.16310
34	6.50	10	0.38428	0.63144	0.28040	0.16537
35	6.50	10	0.52735	0.62934	0.35164	0.16437
36	6.50	10	0.31420	0.62215	0.22346	0.15992
37	6.50	20	0.19461	0.62917	0.26755	0.16497
38	6.50	20	0.27263	0.62716	0.34790	0.16416
39	6.50	20	0.15878	0.62480	0.19867	0.16097
40	6.50	100	0.02251	0.62733	0.53137	0.16439
41	6.50	160	0.00902	0.62994	0.65107	0.16573
42	7.00	1	0.88557	0.60483	0.32568	0.17012
43	7.00	10	0.65355	0.60370	0.36173	0.17132
44	7.00	10	0.40028	0.59587	0.22543	0.16537
45	7.00	50	0.09106	0.59920	0.37087	0.16977
46	7.00	50	0.09930	0.59974	0.32289	0.16998
47	7.50	1	1.01131	0.61181	0.41856	0.18346
48	5.00	10	0.59450	0.60735	0.37395	0.18268
49	5.00	10	0.71661	0.59447	0.39673	0.17323
50	8.00	50	0.14508	0.61914	0.36173	0.18322
51	8.00	160	0.02856	0.61121	0.74180	0.17934

TABLE F6-9
P. G. SOMERVILLE: HORIZONTAL POINT ESTIMATES
SPECTRAL ACCELERATION AT 0.50 SEC PERIOD

CASE NO.	MAGNITUDE	DISTANCE (KM)	MU	SIGMA	SIGMA MU	SIGMA SIGMA
1	5.00	1	0.09150	0.81820	0.35807	0.11651
2	5.00	1	0.15592	0.79811	0.54214	0.11576
3	5.00	5	0.03637	0.81384	0.29882	0.11592
4	5.00	5	0.06318	0.80192	0.39047	0.11545
5	5.80	10	0.11233	0.72973	0.26054	0.16404
6	5.80	20	0.09283	0.73164	0.29147	0.16373
7	6.50	1	0.57048	0.69005	0.23564	0.16926
8	6.50	1	0.60408	0.69062	0.35060	0.17001
9	6.50	1	0.54719	0.69347	0.29477	0.17306
10	6.50	5	0.47555	0.69307	0.26573	0.16977
11	6.50	5	0.33672	0.68723	0.22342	0.17011
12	6.50	50	0.04810	0.69664	0.31576	0.17025
13	6.50	50	0.05156	0.68937	0.30935	0.16727
14	7.00	10	0.39010	0.66504	0.30204	0.17609
15	7.50	50	0.11930	0.66328	0.32425	0.18392
16	7.50	50	0.13247	0.65656	0.32840	0.18035
17	5.00	1	0.03323	0.81820	0.55906	0.11651
18	5.80	5	0.17997	0.73100	0.27433	0.16606
19	5.80	5	0.10319	0.72866	0.34550	0.17100
20	5.00	10	0.04654	0.80005	0.22366	0.11571
21	5.00	10	0.06256	0.79249	0.26854	0.11676
22	5.00	50	0.00646	0.79687	0.24879	0.11608
23	5.00	50	0.00758	0.80057	0.24584	0.11563
24	5.00	160	0.00134	0.78950	0.52214	0.11750
25	5.80	1	0.29417	0.72485	0.28678	0.16543
26	5.80	5	0.25563	0.72709	0.31633	0.16471
27	5.80	5	0.15236	0.71695	0.25123	0.16779
28	5.80	10	0.13898	0.73125	0.25558	0.16453
29	5.80	10	0.19236	0.72750	0.32545	0.16345
30	5.80	10	0.08929	0.72259	0.30048	0.16916
31	5.80	50	0.01640	0.72856	0.52114	0.16210
32	5.80	50	0.01655	0.73108	0.61930	0.16330
33	6.50	5	0.42564	0.68972	0.27307	0.16855
34	6.50	10	0.29008	0.69268	0.29561	0.16919
35	6.50	10	0.40129	0.69197	0.34186	0.16893
36	6.50	10	0.22010	0.68538	0.26278	0.16946
37	6.50	20	0.14499	0.69118	0.24339	0.16811
38	6.50	20	0.20260	0.69663	0.31729	0.17059
39	6.50	20	0.12046	0.68600	0.20392	0.16967
40	6.50	100	0.02362	0.69155	0.47442	0.16796
41	6.50	160	0.01099	0.69499	0.62162	0.16987
42	7.00	1	0.70091	0.66658	0.26716	0.17661
43	7.00	10	0.54131	0.66590	0.34128	0.17644
44	7.00	10	0.30141	0.66167	0.21693	0.17500
45	7.00	50	0.08183	0.66354	0.30611	0.17524
46	7.00	50	0.09179	0.66829	0.35469	0.17757
47	7.50	1	0.78365	0.67552	0.28380	0.19197
48	5.00	10	0.46638	0.66913	0.28560	0.18822
49	5.00	10	0.59559	0.66245	0.36648	0.18310
50	8.00	50	0.15150	0.68582	0.35736	0.19604
51	8.00	160	0.04286	0.67904	0.70696	0.19366

TABLE F6-10
P. G. SOMERVILLE: HORIZONTAL POINT ESTIMATES
SPECTRAL ACCELERATION AT 1.00 SEC PERIOD

CASE NO.	MAGNITUDE	DISTANCE (KM)	MU	SIGMA	SIGMA MU	SIGMA SIGMA
1	5.00	1	0.03684	0.83469	0.33193	0.08148
2	5.00	1	0.06206	0.83067	0.60540	0.08165
3	5.00	5	0.01457	0.82650	0.26743	0.08192
4	5.00	5	0.02506	0.82650	0.44080	0.08192
5	5.80	10	0.05252	0.77721	0.23950	0.15479
6	5.80	20	0.04284	0.77375	0.28050	0.15604
7	6.50	1	0.29635	0.74215	0.18465	0.16585
8	6.50	1	0.29795	0.74257	0.33535	0.16913
9	6.50	1	0.26623	0.73288	0.28143	0.16849
10	6.50	5	0.24537	0.74086	0.22083	0.16696
11	6.50	5	0.16304	0.73328	0.23493	0.16839
12	6.50	50	0.02948	0.73676	0.33435	0.16061
13	6.50	50	0.02857	0.73621	0.36707	0.16286
14	7.00	10	0.21064	0.71277	0.19504	0.17229
15	7.50	50	0.07496	0.70823	0.30571	0.17979
16	7.50	50	0.08091	0.70462	0.32346	0.18029
17	5.00	1	0.01255	0.82266	0.61964	0.08275
18	5.80	5	0.08015	0.78508	0.43353	0.16412
19	5.80	5	0.04604	0.78072	0.44976	0.17009
20	5.00	10	0.01740	0.82507	0.21418	0.08270
21	5.00	10	0.02264	0.82507	0.24977	0.08270
22	5.00	50	0.00239	0.82203	0.36740	0.08359
23	5.00	50	0.00264	0.83320	0.30942	0.08132
24	5.00	160	0.00070	0.82947	0.52026	0.08183
25	5.80	1	0.13136	0.78076	0.34181	0.16064
26	5.80	5	0.11392	0.76917	0.34941	0.15745
27	5.80	5	0.06605	0.77734	0.33776	0.16841
28	5.80	10	0.06332	0.77894	0.23340	0.15560
29	5.80	10	0.08897	0.77117	0.34175	0.15610
30	5.80	10	0.04217	0.77745	0.27790	0.16945
31	5.80	50	0.00868	0.77161	0.51785	0.15059
32	5.80	50	0.00905	0.77464	0.57520	0.15439
33	6.50	5	0.21089	0.74657	0.21098	0.16627
34	6.50	10	0.15596	0.74104	0.24869	0.16352
35	6.50	10	0.21720	0.73750	0.32650	0.16479
36	6.50	10	0.11297	0.73283	0.21914	0.16824
37	6.50	20	0.07793	0.73589	0.20854	0.16093
38	6.50	20	0.10511	0.74032	0.35329	0.16554
39	6.50	20	0.06245	0.73445	0.20333	0.16883
40	6.50	100	0.01547	0.73751	0.44519	0.16081
41	6.50	160	0.00758	0.73845	0.59921	0.16123
42	7.00	1	0.34316	0.71578	0.27740	0.17388
43	7.00	10	0.29263	0.71453	0.31788	0.17550
44	7.00	10	0.16508	0.70645	0.19392	0.17339
45	7.00	50	0.04968	0.71282	0.36017	0.17192
46	7.00	50	0.05178	0.70948	0.42042	0.17260
47	7.50	1	0.41974	0.71955	0.29846	0.18445
48	5.00	10	0.27324	0.71321	0.23654	0.18272
49	5.00	10	0.35357	0.70820	0.39652	0.18182
50	8.00	50	0.10447	0.71589	0.32365	0.19499
51	8.00	160	0.03703	0.72344	0.64636	0.19765

TABLE F6-11
P. G. SOMERVILLE: HORIZONTAL POINT ESTIMATES
SPECTRAL ACCELERATION AT 2.00 SEC PERIOD

CASE NO.	MAGNITUDE	DISTANCE (KM)	MU	SIGMA	SIGMA MU	SIGMA SIGMA
1	5.00	1	0.00935	0.89172	0.49082	0.07346
2	5.00	1	0.01588	0.88361	0.57965	0.07156
3	5.00	5	0.00424	0.87199	0.42286	0.07095
4	5.00	5	0.00695	0.87199	0.45999	0.07095
5	5.80	10	0.01734	0.83440	0.34705	0.16632
6	5.80	20	0.01304	0.82725	0.31630	0.17233
7	6.50	1	0.13040	0.79967	0.29657	0.17861
8	6.50	1	0.12585	0.79124	0.31512	0.18592
9	6.50	1	0.11443	0.78346	0.24399	0.18540
10	6.50	5	0.09634	0.79442	0.30664	0.18535
11	6.50	5	0.07563	0.78346	0.22409	0.18540
12	6.50	50	0.01255	0.80184	0.49514	0.17480
13	6.50	50	0.01162	0.79359	0.51534	0.17977
14	7.00	10	0.09182	0.78090	0.31233	0.18956
15	7.50	50	0.03627	0.77257	0.61321	0.19429
16	7.50	50	0.03656	0.75720	0.67174	0.19306
17	5.00	1	0.00321	0.87957	0.81982	0.07103
18	5.80	5	0.02974	0.81767	0.42108	0.17328
19	5.80	5	0.01613	0.81468	0.43387	0.18124
20	5.00	10	0.00564	0.87375	0.32829	0.07002
21	5.00	10	0.00659	0.87757	0.34831	0.06986
22	5.00	50	0.00089	0.87503	0.40978	0.06988
23	5.00	50	0.00080	0.87503	0.43352	0.06988
24	5.00	160	0.00038	0.87503	0.67053	0.06988
25	5.80	1	0.04779	0.83937	0.29572	0.17496
26	5.80	5	0.04019	0.81765	0.38144	0.17326
27	5.80	5	0.02605	0.81267	0.33872	0.17996
28	5.80	10	0.02066	0.83756	0.32523	0.16963
29	5.80	10	0.02601	0.82820	0.35891	0.17768
30	5.80	10	0.01499	0.81065	0.36414	0.17876
31	5.80	50	0.00324	0.83232	0.70135	0.15990
32	5.80	50	0.00316	0.82608	0.68550	0.16912
33	6.50	5	0.09168	0.80289	0.28001	0.17827
34	6.50	10	0.06077	0.80252	0.29024	0.17778
35	6.50	10	0.07721	0.79323	0.32399	0.18391
36	6.50	10	0.04671	0.78145	0.24919	0.18392
37	6.50	20	0.03449	0.80536	0.31726	0.17839
38	6.50	20	0.04115	0.78951	0.36495	0.17917
39	6.50	20	0.02517	0.77944	0.35264	0.18250
40	6.50	100	0.00736	0.80333	0.49687	0.17544
41	6.50	160	0.00375	0.81024	0.71032	0.17996
42	7.00	1	0.17833	0.78134	0.28807	0.18974
43	7.00	10	0.11726	0.76955	0.34867	0.19232
44	7.00	10	0.07280	0.75719	0.31483	0.18813
45	7.00	50	0.02407	0.77831	0.47644	0.18647
46	7.00	50	0.02391	0.76752	0.52341	0.18875
47	7.50	1	0.20165	0.77358	0.25862	0.19437
48	5.00	10	0.12130	0.77014	0.46233	0.19296
49	5.00	10	0.14380	0.75932	0.51746	0.19531
50	8.00	50	0.06298	0.78669	0.41537	0.19320
51	8.00	160	0.02673	0.78818	0.71781	0.19390

TABLE F6-12
P. G. SOMERVILLE: HORIZONTAL POINT ESTIMATES
SPECTRAL ACCELERATION AT 3.33 SEC PERIOD

CASE NO.	MAGNITUDE	DISTANCE (KM)	MU	SIGMA	SIGMA MU	SIGMA SIGMA
1	5.00	1	0.00374	0.92730	0.58312	0.09756
2	5.00	1	0.00590	0.91491	0.50987	0.08801
3	5.00	5	0.00166	0.91521	0.41817	0.08808
4	5.00	5	0.00270	0.91521	0.37529	0.08808
5	5.80	10	0.00818	0.83867	0.40845	0.17568
6	5.80	20	0.00548	0.82797	0.39025	0.18281
7	6.50	1	0.06993	0.80856	0.31632	0.19199
8	6.50	1	0.06577	0.78857	0.27741	0.18916
9	6.50	1	0.06095	0.78495	0.23834	0.19035
10	6.50	5	0.05266	0.79868	0.31813	0.19668
11	6.50	5	0.04578	0.78903	0.28735	0.19460
12	6.50	50	0.00658	0.81892	0.68448	0.19413
13	6.50	50	0.00557	0.80189	0.66287	0.19465
14	7.00	10	0.04984	0.79348	0.44755	0.20000
15	7.50	50	0.02366	0.78296	0.62152	0.20000
16	7.50	50	0.02061	0.76972	0.72085	0.20000
17	5.00	1	0.00128	0.91903	0.80692	0.09107
18	5.80	5	0.01352	0.82829	0.36323	0.18747
19	5.80	5	0.00707	0.81654	0.42916	0.18526
20	5.00	10	0.00231	0.90732	0.31295	0.08259
21	5.00	10	0.00247	0.91141	0.31563	0.08528
22	5.00	50	0.00045	0.90390	0.28857	0.08035
23	5.00	50	0.00042	0.90390	0.23381	0.08035
24	5.00	160	0.00014	0.90390	0.44023	0.08035
25	5.80	1	0.02187	0.84211	0.37290	0.18271
26	5.80	5	0.01919	0.82662	0.39827	0.18624
27	5.80	5	0.01446	0.81451	0.32315	0.18351
28	5.80	10	0.01057	0.84091	0.40847	0.17743
29	5.80	10	0.01075	0.82595	0.40321	0.18302
30	5.80	10	0.00716	0.81654	0.55838	0.18526
31	5.80	50	0.00159	0.84453	0.75672	0.17671
32	5.80	50	0.00134	0.83035	0.80990	0.18290
33	6.50	5	0.05362	0.81462	0.33815	0.19526
34	6.50	10	0.03180	0.81477	0.39268	0.19346
35	6.50	10	0.03487	0.79757	0.30877	0.19399
36	6.50	10	0.02312	0.78699	0.46158	0.19245
37	6.50	20	0.01700	0.81292	0.40440	0.18977
38	6.50	20	0.01701	0.80450	0.42581	0.19931
39	6.50	20	0.01283	0.78495	0.50653	0.19035
40	6.50	100	0.00316	0.80945	0.59371	0.18525
41	6.50	160	0.00208	0.82167	0.69273	0.19709
42	7.00	1	0.11074	0.78821	0.38796	0.20000
43	7.00	10	0.05961	0.77543	0.34455	0.20000
44	7.00	10	0.03930	0.76712	0.48181	0.20000
45	7.00	50	0.01376	0.79471	0.62554	0.20000
46	7.00	50	0.01248	0.78081	0.65245	0.20000
47	7.50	1	0.14308	0.78140	0.35964	0.20000
48	5.00	10	0.07049	0.79079	0.59501	0.20000
49	5.00	10	0.07945	0.76750	0.52931	0.20000
50	8.00	50	0.04597	0.81706	0.45953	0.20000
51	8.00	160	0.01879	0.81578	0.58322	0.20000

TABLE F6-13
P. G. SOMERVILLE: HORIZONTAL POINT ESTIMATES
PEAK GROUND VELOCITY

CASE NO.	MAGNITUDE	DISTANCE (KM)	MU	SIGMA	SIGMA MU	SIGMA SIGMA
1	5.00	1	6.19240	0.75430	0.48845	0.11281
2	5.00	1	10.98591	0.75430	0.44195	0.11281
3	5.00	5	2.13188	0.75475	0.29240	0.11259
4	5.00	5	3.96052	0.74672	0.38568	0.10788
5	5.80	10	5.73685	0.70714	0.23293	0.17259
6	5.80	20	4.46827	0.70587	0.25751	0.17196
7	6.50	1	33.83729	0.69455	0.23259	0.19018
8	6.50	1	35.56729	0.69278	0.36673	0.19230
9	6.50	1	32.10643	0.68924	0.30448	0.19336
10	6.50	5	29.22446	0.69089	0.20506	0.18875
11	6.50	5	19.66437	0.68321	0.16941	0.18943
12	6.50	50	2.32895	0.69468	0.34012	0.18354
13	6.50	50	2.35763	0.69286	0.30174	0.18464
14	7.00	10	22.72798	0.68570	0.21177	0.19698
15	7.50	50	7.06813	0.68144	0.34854	0.20000
16	7.50	50	7.84944	0.67493	0.39502	0.20000
17	5.00	1	1.81194	0.74619	0.73224	0.10803
18	5.80	5	10.64026	0.70322	0.39214	0.17548
19	5.80	5	5.30738	0.69587	0.40784	0.17855
20	5.00	10	2.57144	0.74327	0.23137	0.10563
21	5.00	10	3.52047	0.74724	0.20853	0.10773
22	5.00	50	0.27154	0.74046	0.19880	0.10353
23	5.00	50	0.30210	0.74435	0.19384	0.10539
24	5.00	160	0.05051	0.73270	0.22300	0.10031
25	5.80	1	16.37890	0.70654	0.33392	0.17749
26	5.80	5	15.12992	0.69995	0.29071	0.17411
27	5.80	5	8.61951	0.69587	0.27074	0.17855
28	5.80	10	6.92135	0.71078	0.26388	0.17417
29	5.80	10	10.22196	0.70459	0.25593	0.17381
30	5.80	10	4.64371	0.69587	0.32568	0.17855
31	5.80	50	0.72668	0.71013	0.50384	0.16922
32	5.80	50	0.77207	0.70909	0.51733	0.17102
33	6.50	5	23.37201	0.69623	0.18464	0.18913
34	6.50	10	15.43033	0.69673	0.21861	0.18767
35	6.50	10	21.77278	0.69291	0.25140	0.18804
36	6.50	10	11.93642	0.68321	0.18789	0.18943
37	6.50	20	7.37069	0.69655	0.22603	0.18593
38	6.50	20	10.05950	0.69514	0.28043	0.18750
39	6.50	20	5.93595	0.67921	0.21433	0.18716
40	6.50	100	1.10247	0.69685	0.42514	0.18468
41	6.50	160	0.43038	0.70314	0.49181	0.18840
42	7.00	1	44.13552	0.68544	0.31694	0.19959
43	7.00	10	32.65550	0.68215	0.36959	0.19730
44	7.00	10	18.28486	0.67107	0.26776	0.19578
45	7.00	50	4.39625	0.68437	0.33475	0.19421
46	7.00	50	4.78176	0.68145	0.36190	0.19458
47	7.50	1	55.89795	0.67939	0.47824	0.20000
48	5.00	10	30.25994	0.68017	0.34578	0.20000
49	5.00	10	39.85450	0.67402	0.59017	0.20000
50	8.00	50	11.98477	0.68782	0.30368	0.20000
51	8.00	160	3.31111	0.69414	0.47062	0.20000

TABLE F6-14
P. G. SOMERVILLE: VERTICAL POINT ESTIMATES
PEAK GROUND ACCELERATION

CASE NO.	MAGNITUDE	DISTANCE (KM)	MU	SIGMA	SIGMA MU	SIGMA SIGMA
1	5.00	1	0.07378	0.68879	0.60833	0.16487
2	5.00	1	0.09796	0.69571	0.38181	0.16406
3	5.00	5	0.02559	0.68912	0.41014	0.16484
4	5.00	5	0.03143	0.69383	0.25717	0.16424
5	5.80	10	0.05484	0.66131	0.29139	0.16307
6	5.80	20	0.05205	0.65132	0.48094	0.15984
7	6.50	1	0.31880	0.61061	0.28922	0.16555
8	6.50	1	0.34340	0.61640	0.20069	0.16863
9	6.50	1	0.33587	0.60731	0.20631	0.16382
10	6.50	5	0.28387	0.60837	0.21197	0.16464
11	6.50	5	0.21082	0.60731	0.20044	0.16382
12	6.50	50	0.01650	0.61043	0.37978	0.16558
13	6.50	50	0.01988	0.60896	0.33968	0.16502
14	7.00	10	0.18538	0.61075	0.19717	0.17078
15	7.50	50	0.03757	0.61342	0.26064	0.17526
16	7.50	50	0.04418	0.61299	0.38933	0.17499
17	5.00	1	0.02721	0.68100	0.47680	0.16622
18	5.80	5	0.08101	0.64918	0.43419	0.15918
19	5.80	5	0.05844	0.65283	0.44034	0.15927
20	5.00	10	0.03367	0.70077	0.26507	0.16368
21	5.00	10	0.06272	0.67609	0.47126	0.16747
22	5.00	50	0.00379	0.68582	0.21681	0.16543
23	5.00	50	0.00353	0.67487	0.20705	0.16789
24	5.00	160	0.00040	0.68792	0.45153	0.16507
25	5.80	1	0.16573	0.65169	0.44521	0.15950
26	5.80	5	0.16104	0.64918	0.34511	0.15918
27	5.80	5	0.10091	0.64999	0.29685	0.15841
28	5.80	10	0.06959	0.65626	0.28642	0.16110
29	5.80	10	0.11272	0.65184	0.37393	0.15985
30	5.80	10	0.05912	0.65086	0.30619	0.15866
31	5.80	50	0.00593	0.65165	0.72426	0.16001
32	5.80	50	0.00695	0.65499	0.64679	0.16083
33	6.50	5	0.24040	0.60752	0.20043	0.16431
34	6.50	10	0.14494	0.61287	0.19855	0.16664
35	6.50	10	0.23415	0.61562	0.33336	0.16804
36	6.50	10	0.12774	0.60556	0.20593	0.16302
37	6.50	20	0.06978	0.61164	0.22117	0.16607
38	6.50	20	0.11311	0.61711	0.42433	0.16881
39	6.50	20	0.05738	0.60403	0.26757	0.16237
40	6.50	100	0.00635	0.61462	0.42089	0.16746
41	6.50	160	0.00194	0.61043	0.57122	0.16558
42	7.00	1	0.38450	0.61379	0.23054	0.17269
43	7.00	10	0.28262	0.61563	0.30664	0.17356
44	7.00	10	0.16071	0.60976	0.21314	0.17056
45	7.00	50	0.02533	0.61346	0.23752	0.17214
46	7.00	50	0.03102	0.61346	0.44565	0.17214
47	7.50	1	0.56608	0.62222	0.34497	0.18242
48	5.00	10	0.22360	0.61272	0.20075	0.17500
49	5.00	10	0.32582	0.61763	0.32960	0.17837
50	8.00	50	0.05658	0.62428	0.25618	0.18716
51	8.00	160	0.01068	0.62600	0.39057	0.18808

TABLE F6-15
P. G. SOMERVILLE: VERTICAL POINT ESTIMATES
SPECTRAL ACCELERATION AT 0.05 SEC PERIOD

CASE NO.	MAGNITUDE	DISTANCE (KM)	MU	SIGMA	SIGMA MU	SIGMA SIGMA
1	5.00	1	0.15772	0.70749	0.76790	0.16445
2	5.00	1	0.20636	0.70749	0.41530	0.16445
3	5.00	5	0.04953	0.70556	0.60813	0.16506
4	5.00	5	0.06307	0.71540	0.34975	0.16229
5	5.80	10	0.10625	0.68165	0.46289	0.16527
6	5.80	20	0.09462	0.67475	0.39269	0.16364
7	6.50	1	0.67470	0.63947	0.49673	0.15854
8	6.50	1	0.70605	0.64225	0.32958	0.15997
9	6.50	1	0.70342	0.63577	0.29604	0.15662
10	6.50	5	0.59567	0.63853	0.27704	0.15815
11	6.50	5	0.41764	0.63402	0.37116	0.15585
12	6.50	50	0.02526	0.64049	0.46268	0.15908
13	6.50	50	0.03119	0.64133	0.36746	0.15946
14	7.00	10	0.35760	0.63993	0.38624	0.16145
15	7.50	50	0.05804	0.64166	0.29617	0.16428
16	7.50	50	0.06865	0.64208	0.33342	0.16455
17	5.00	1	0.05422	0.70922	0.65489	0.16394
18	5.80	5	0.15984	0.67869	0.59931	0.16438
19	5.80	5	0.11461	0.68203	0.51714	0.16521
20	5.00	10	0.06652	0.73120	0.44195	0.15945
21	5.00	10	0.12529	0.70780	0.32486	0.16437
22	5.00	50	0.00629	0.70590	0.30308	0.16497
23	5.00	50	0.00655	0.71558	0.27563	0.16223
24	5.00	160	0.00049	0.70968	0.52859	0.16381
25	5.80	1	0.34670	0.68313	0.65271	0.16574
26	5.80	5	0.31565	0.67763	0.43895	0.16411
27	5.80	5	0.20463	0.67590	0.44077	0.16327
28	5.80	10	0.13755	0.68481	0.47950	0.16640
29	5.80	10	0.20970	0.67702	0.45211	0.16402
30	5.80	10	0.11064	0.67415	0.47794	0.16286
31	5.80	50	0.00969	0.67667	0.77705	0.16403
32	5.80	50	0.01110	0.68313	0.77305	0.16578
33	6.50	5	0.49492	0.63937	0.37995	0.15853
34	6.50	10	0.28340	0.64630	0.36624	0.16217
35	6.50	10	0.45400	0.64250	0.39416	0.16005
36	6.50	10	0.24953	0.63840	0.33306	0.15790
37	6.50	20	0.12885	0.64181	0.32264	0.15969
38	6.50	20	0.21089	0.64665	0.42316	0.16232
39	6.50	20	0.10462	0.63490	0.34463	0.15622
40	6.50	100	0.00825	0.64217	0.47322	0.15986
41	6.50	160	0.00263	0.63735	0.57091	0.15778
42	7.00	1	0.82059	0.64473	0.40287	0.16449
43	7.00	10	0.55246	0.64778	0.38121	0.16632
44	7.00	10	0.31272	0.64028	0.31713	0.16189
45	7.00	50	0.04108	0.64226	0.30352	0.16268
46	7.00	50	0.04971	0.64163	0.40652	0.16232
47	7.50	1	1.18734	0.65404	0.34735	0.17433
48	5.00	10	0.43726	0.64068	0.37812	0.16377
49	5.00	10	0.64258	0.64665	0.40857	0.16789
50	8.00	50	0.08547	0.66203	0.29039	0.17689
51	8.00	160	0.01236	0.65859	0.43773	0.17525

TABLE F6-16
P. G. SOMERVILLE: VERTICAL POINT ESTIMATES
SPECTRAL ACCELERATION AT 0.10 SEC PERIOD

CASE NO.	MAGNITUDE	DISTANCE (KM)	MU	SIGMA	SIGMA MU	SIGMA SIGMA
1	5.00	1	0.16010	0.74611	0.57763	0.16184
2	5.00	1	0.22337	0.75476	0.35306	0.16219
3	5.00	5	0.05690	0.75452	0.29900	0.16220
4	5.00	5	0.07365	0.76393	0.20953	0.16329
5	5.80	10	0.11966	0.69210	0.23728	0.17931
6	5.80	20	0.11051	0.68580	0.50707	0.17535
7	6.50	1	0.73823	0.64401	0.30713	0.16749
8	6.50	1	0.81988	0.64744	0.18027	0.17011
9	6.50	1	0.81870	0.64556	0.18794	0.16913
10	6.50	5	0.62633	0.64477	0.23455	0.16788
11	6.50	5	0.48760	0.64381	0.18300	0.16774
12	6.50	50	0.03099	0.64588	0.39884	0.16841
13	6.50	50	0.03811	0.64672	0.36705	0.16902
14	7.00	10	0.38956	0.64615	0.22586	0.17258
15	7.50	50	0.07112	0.64937	0.27952	0.17817
16	7.50	50	0.08301	0.64682	0.33218	0.17576
17	5.00	1	0.06011	0.74611	0.37151	0.16184
18	5.80	5	0.18698	0.68620	0.38200	0.17567
19	5.80	5	0.13471	0.68460	0.37525	0.17492
20	5.00	10	0.07480	0.76120	0.19357	0.16293
21	5.00	10	0.14081	0.73993	0.50731	0.16195
22	5.00	50	0.00726	0.75879	0.25986	0.16267
23	5.00	50	0.00723	0.74363	0.23044	0.16185
24	5.00	160	0.00060	0.74995	0.50419	0.16196
25	5.80	1	0.38666	0.68319	0.37642	0.17407
26	5.80	5	0.35789	0.68620	0.34186	0.17567
27	5.80	5	0.22123	0.68109	0.30115	0.17299
28	5.80	10	0.14538	0.69000	0.30249	0.17792
29	5.80	10	0.24753	0.69000	0.43017	0.17792
30	5.80	10	0.12627	0.68197	0.30673	0.17345
31	5.80	50	0.01192	0.69144	0.59903	0.17871
32	5.80	50	0.01278	0.69039	0.69742	0.17803
33	6.50	5	0.53015	0.64647	0.19864	0.16914
34	6.50	10	0.31970	0.64768	0.20723	0.16996
35	6.50	10	0.51149	0.64768	0.37936	0.16996
36	6.50	10	0.29303	0.64294	0.17847	0.16706
37	6.50	20	0.14115	0.64636	0.23173	0.16885
38	6.50	20	0.23712	0.65162	0.47233	0.17299
39	6.50	20	0.12456	0.64053	0.20182	0.16526
40	6.50	100	0.01040	0.64253	0.48776	0.16611
41	6.50	160	0.00327	0.64526	0.48243	0.16796
42	7.00	1	0.88551	0.64860	0.21343	0.17525
43	7.00	10	0.61710	0.65486	0.33202	0.18076
44	7.00	10	0.35691	0.64348	0.18161	0.17130
45	7.00	50	0.04823	0.64532	0.27453	0.17159
46	7.00	50	0.05975	0.64721	0.39348	0.17321
47	7.50	1	1.28060	0.65447	0.31953	0.18430
48	5.00	10	0.47984	0.64734	0.23851	0.17655
49	5.00	10	0.73446	0.65181	0.32953	0.18095
50	8.00	50	0.10233	0.68628	0.30746	0.19296
51	8.00	160	0.01305	0.68714	0.46111	0.19349

TABLE F6-17
P. G. SOMERVILLE: VERTICAL POINT ESTIMATES
SPECTRAL ACCELERATION AT 0.20 SEC PERIOD

CASE NO.	MAGNITUDE	DISTANCE (KM)	MU	SIGMA	SIGMA MU	SIGMA SIGMA
1	5.00	1	0.09737	0.70790	0.46283	0.15812
2	5.00	1	0.12227	0.72519	0.39050	0.15806
3	5.00	5	0.04052	0.72272	0.18015	0.15790
4	5.00	5	0.04497	0.71844	0.20833	0.15778
5	5.80	10	0.08398	0.66224	0.18203	0.18448
6	5.80	20	0.08352	0.65903	0.65002	0.18247
7	6.50	1	0.49988	0.63131	0.17124	0.17447
8	6.50	1	0.51212	0.62938	0.18859	0.17289
9	6.50	1	0.51422	0.62618	0.23132	0.17140
10	6.50	5	0.46260	0.62753	0.32639	0.17104
11	6.50	5	0.33509	0.62246	0.25549	0.16853
12	6.50	50	0.02766	0.62344	0.45348	0.16774
13	6.50	50	0.03472	0.62889	0.50463	0.17147
14	7.00	10	0.30345	0.63424	0.27424	0.17130
15	7.50	50	0.06965	0.63346	0.37064	0.17292
16	7.50	50	0.08244	0.63537	0.43457	0.17464
17	5.00	1	0.04035	0.72260	0.19173	0.15791
18	5.80	5	0.12461	0.65555	0.37005	0.18102
19	5.80	5	0.09263	0.65653	0.44917	0.18261
20	5.00	10	0.04271	0.72746	0.18553	0.15821
21	5.00	10	0.09779	0.71852	0.74214	0.15778
22	5.00	50	0.00690	0.72542	0.44304	0.15803
23	5.00	50	0.00621	0.70016	0.24477	0.15911
24	5.00	160	0.00072	0.71658	0.49537	0.15778
25	5.80	1	0.24341	0.65564	0.32974	0.18135
26	5.80	5	0.24503	0.66296	0.42537	0.18511
27	5.80	5	0.15421	0.65653	0.28785	0.18261
28	5.80	10	0.10607	0.66751	0.19628	0.18788
29	5.80	10	0.17645	0.66540	0.55566	0.18646
30	5.80	10	0.09044	0.65368	0.29935	0.18107
31	5.80	50	0.01039	0.66293	0.58305	0.18449
32	5.80	50	0.01318	0.66293	0.61210	0.18449
33	6.50	5	0.36537	0.62583	0.22202	0.16980
34	6.50	10	0.22157	0.62249	0.22821	0.16739
35	6.50	10	0.36529	0.62989	0.45026	0.17263
36	6.50	10	0.21717	0.62246	0.25934	0.16853
37	6.50	20	0.11352	0.62844	0.34263	0.17133
38	6.50	20	0.18856	0.63707	0.61682	0.17837
39	6.50	20	0.10412	0.62334	0.35721	0.16918
40	6.50	100	0.01150	0.63245	0.60045	0.17420
41	6.50	160	0.00411	0.62972	0.54124	0.17209
42	7.00	1	0.60068	0.63310	0.19069	0.17094
43	7.00	10	0.47908	0.64146	0.43190	0.17788
44	7.00	10	0.28186	0.63245	0.29635	0.17142
45	7.00	50	0.04658	0.63267	0.34077	0.16961
46	7.00	50	0.05956	0.63330	0.51532	0.17013
47	7.50	1	0.85330	0.64043	0.44020	0.18075
48	5.00	10	0.38870	0.63707	0.28920	0.17668
49	5.00	10	0.56272	0.63921	0.38650	0.17877
50	8.00	50	0.10036	0.68291	0.37053	0.18694
51	8.00	160	0.01642	0.67430	0.53252	0.18193

TABLE F6-18
P. G. SOMERVILLE: VERTICAL POINT ESTIMATES
SPECTRAL ACCELERATION AT 0.50 SEC PERIOD

CASE NO.	MAGNITUDE	DISTANCE (KM)	MU	SIGMA	SIGMA MU	SIGMA SIGMA
1	5.00	1	0.03422	0.72666	0.54012	0.10665
2	5.00	1	0.04993	0.72882	0.41620	0.10695
3	5.00	5	0.01232	0.73947	0.35201	0.10923
4	5.00	5	0.01741	0.72663	0.21465	0.10662
5	5.80	10	0.04662	0.65851	0.24269	0.18656
6	5.80	20	0.05016	0.66082	0.72138	0.18736
7	6.50	1	0.26071	0.62923	0.17557	0.18081
8	6.50	1	0.30714	0.62730	0.24440	0.17909
9	6.50	1	0.29822	0.62503	0.26336	0.18029
10	6.50	5	0.25551	0.62428	0.34690	0.17539
11	6.50	5	0.20449	0.62240	0.30592	0.17795
12	6.50	50	0.02245	0.62466	0.41703	0.17416
13	6.50	50	0.03038	0.62403	0.45203	0.17368
14	7.00	10	0.20587	0.62996	0.42429	0.17897
15	7.50	50	0.06178	0.63173	0.46813	0.18414
16	7.50	50	0.06727	0.62919	0.42753	0.18167
17	5.00	1	0.01432	0.76125	0.30912	0.11776
18	5.80	5	0.06382	0.66273	0.31794	0.19017
19	5.80	5	0.04414	0.65166	0.32333	0.18853
20	5.00	10	0.01813	0.72279	0.22900	0.10622
21	5.00	10	0.03611	0.71939	0.64392	0.10603
22	5.00	50	0.00319	0.73923	0.29197	0.10918
23	5.00	50	0.00357	0.72281	0.30218	0.10620
24	5.00	160	0.00052	0.73081	0.56655	0.10723
25	5.80	1	0.10242	0.65806	0.45303	0.18849
26	5.80	5	0.12047	0.67098	0.44117	0.19668
27	5.80	5	0.08359	0.65407	0.29963	0.19000
28	5.80	10	0.06043	0.66503	0.29652	0.19111
29	5.80	10	0.09647	0.66693	0.58754	0.19256
30	5.80	10	0.05001	0.66479	0.29310	0.19770
31	5.80	50	0.00650	0.65852	0.75795	0.18518
32	5.80	50	0.00892	0.66290	0.69756	0.18809
33	6.50	5	0.21349	0.63320	0.31690	0.18321
34	6.50	10	0.14788	0.63188	0.44315	0.18135
35	6.50	10	0.23830	0.63103	0.59458	0.18058
36	6.50	10	0.14073	0.62240	0.40740	0.17795
37	6.50	20	0.07789	0.63162	0.45983	0.18051
38	6.50	20	0.13040	0.63541	0.70133	0.18403
39	6.50	20	0.06610	0.62240	0.34585	0.17795
40	6.50	100	0.01098	0.62948	0.51170	0.17806
41	6.50	160	0.00465	0.62865	0.47417	0.17735
42	7.00	1	0.37356	0.63806	0.24628	0.18873
43	7.00	10	0.31077	0.63633	0.55801	0.18526
44	7.00	10	0.18731	0.62710	0.37192	0.17995
45	7.00	50	0.03612	0.63112	0.34425	0.17919
46	7.00	50	0.04877	0.63175	0.54639	0.17978
47	7.50	1	0.47227	0.63670	0.34192	0.19122
48	5.00	10	0.25397	0.62957	0.37017	0.18263
49	5.00	10	0.34902	0.63234	0.40330	0.18541
50	8.00	50	0.09759	0.68433	0.52539	0.19740
51	8.00	160	0.02225	0.68735	0.52815	0.19908

TABLE F6-19
P. G. SOMERVILLE: VERTICAL POINT ESTIMATES
SPECTRAL ACCELERATION AT 1.00 SEC PERIOD

CASE NO.	MAGNITUDE	DISTANCE (KM)	MU	SIGMA	SIGMA MU	SIGMA SIGMA
1	5.00	1	0.01487	0.72396	0.59915	0.06096
2	5.00	1	0.02009	0.74355	0.52136	0.06759
3	5.00	5	0.00514	0.73143	0.46037	0.06258
4	5.00	5	0.00709	0.72107	0.28922	0.06060
5	5.80	10	0.02063	0.68152	0.24850	0.16501
6	5.80	20	0.02121	0.67694	0.45973	0.16960
7	6.50	1	0.12704	0.65261	0.33598	0.17161
8	6.50	1	0.14949	0.64528	0.23075	0.17320
9	6.50	1	0.13288	0.64060	0.26323	0.17300
10	6.50	5	0.12916	0.64549	0.36728	0.17189
11	6.50	5	0.10138	0.63557	0.18932	0.16874
12	6.50	50	0.01184	0.65215	0.56161	0.16763
13	6.50	50	0.01778	0.63964	0.51927	0.16506
14	7.00	10	0.09980	0.65692	0.19090	0.17820
15	7.50	50	0.03706	0.64962	0.33361	0.17571
16	7.50	50	0.04440	0.64416	0.54776	0.17808
17	5.00	1	0.00498	0.72222	0.57960	0.06073
18	5.80	5	0.03013	0.67793	0.40827	0.17218
19	5.80	5	0.02336	0.67826	0.41718	0.18000
20	5.00	10	0.00561	0.71512	0.46046	0.06052
21	5.00	10	0.01065	0.72115	0.40098	0.06060
22	5.00	50	0.00109	0.72258	0.54108	0.06072
23	5.00	50	0.00164	0.72429	0.31752	0.06093
24	5.00	160	0.00027	0.72813	0.84266	0.06164
25	5.80	1	0.05079	0.69639	0.51719	0.17954
26	5.80	5	0.05576	0.68263	0.52813	0.17563
27	5.80	5	0.04016	0.67278	0.28952	0.17625
28	5.80	10	0.02737	0.68492	0.21740	0.16725
29	5.80	10	0.04364	0.67425	0.48164	0.16882
30	5.80	10	0.02979	0.67913	0.34723	0.18065
31	5.80	50	0.00354	0.69126	0.90359	0.17011
32	5.80	50	0.00544	0.67645	0.65565	0.16837
33	6.50	5	0.10058	0.65256	0.22116	0.17007
34	6.50	10	0.07520	0.65221	0.24430	0.16905
35	6.50	10	0.09753	0.63706	0.31782	0.16436
36	6.50	10	0.07775	0.63622	0.30979	0.16927
37	6.50	20	0.03587	0.65356	0.31777	0.16953
38	6.50	20	0.06067	0.63910	0.44461	0.16526
39	6.50	20	0.04127	0.63250	0.33262	0.16636
40	6.50	100	0.00668	0.64728	0.42363	0.16373
41	6.50	160	0.00300	0.65321	0.66840	0.16854
42	7.00	1	0.16517	0.66079	0.34362	0.18386
43	7.00	10	0.15615	0.64781	0.41130	0.17729
44	7.00	10	0.10686	0.64346	0.27268	0.17740
45	7.00	50	0.02192	0.65112	0.41624	0.17186
46	7.00	50	0.02905	0.64397	0.57490	0.17276
47	7.50	1	0.23897	0.67597	0.31835	0.20000
48	5.00	10	0.13373	0.64966	0.20006	0.17622
49	5.00	10	0.18746	0.64416	0.36136	0.17863
50	8.00	50	0.05750	0.69457	0.26407	0.20000
51	8.00	160	0.01873	0.68676	0.37409	0.19792

TABLE F6-20
P. G. SOMERVILLE: VERTICAL POINT ESTIMATES
SPECTRAL ACCELERATION AT 2.00 SEC PERIOD

CASE NO.	MAGNITUDE	DISTANCE (KM)	MU	SIGMA	SIGMA MU	SIGMA SIGMA
1	5.00	1	0.00528	0.75061	0.58970	0.05000
2	5.00	1	0.00737	0.74177	0.55608	0.05000
3	5.00	5	0.00163	0.74874	0.58722	0.05000
4	5.00	5	0.00221	0.74347	0.27709	0.05000
5	5.80	10	0.00829	0.71014	0.38829	0.17663
6	5.80	20	0.00728	0.70218	0.42240	0.19370
7	6.50	1	0.07362	0.67633	0.35637	0.19223
8	6.50	1	0.08710	0.65272	0.37668	0.19073
9	6.50	1	0.07256	0.64898	0.27299	0.18843
10	6.50	5	0.07212	0.65664	0.51043	0.19334
11	6.50	5	0.05199	0.64898	0.31616	0.18843
12	6.50	50	0.00603	0.67365	0.52647	0.18233
13	6.50	50	0.00952	0.65708	0.96688	0.18877
14	7.00	10	0.04515	0.66836	0.36952	0.18848
15	7.50	50	0.01758	0.67308	0.77941	0.19735
16	7.50	50	0.02587	0.65546	1.14281	0.20000
17	5.00	1	0.00132	0.74575	0.89256	0.05000
18	5.80	5	0.01465	0.68790	0.40234	0.18453
19	5.80	5	0.00813	0.68909	0.51553	0.19023
20	5.00	10	0.00163	0.74340	0.65642	0.05000
21	5.00	10	0.00406	0.74077	0.50402	0.05000
22	5.00	50	0.00030	0.74672	0.88321	0.05000
23	5.00	50	0.00085	0.74239	0.55950	0.05000
24	5.00	160	0.00006	0.76401	1.58506	0.05895
25	5.80	1	0.02657	0.72484	0.42309	0.19681
26	5.80	5	0.02763	0.69635	0.60058	0.19235
27	5.80	5	0.01876	0.69785	0.43628	0.19876
28	5.80	10	0.00988	0.70928	0.37559	0.17583
29	5.80	10	0.01468	0.70392	0.58568	0.19781
30	5.80	10	0.01200	0.69500	0.60653	0.19588
31	5.80	50	0.00136	0.70513	0.90701	0.16811
32	5.80	50	0.00261	0.70217	1.00268	0.19151
33	6.50	5	0.04904	0.67365	0.28416	0.18732
34	6.50	10	0.03521	0.67660	0.23218	0.18886
35	6.50	10	0.04713	0.66486	0.54750	0.20000
36	6.50	10	0.03764	0.65992	0.49680	0.20000
37	6.50	20	0.01769	0.67608	0.32514	0.18656
38	6.50	20	0.02765	0.66031	0.71023	0.19400
39	6.50	20	0.01883	0.65051	0.65120	0.19011
40	6.50	100	0.00272	0.67622	0.65840	0.18507
41	6.50	160	0.00165	0.67900	0.76614	0.18814
42	7.00	1	0.09073	0.66920	0.46200	0.19194
43	7.00	10	0.07471	0.65909	0.53847	0.20000
44	7.00	10	0.04910	0.65445	0.48829	0.20000
45	7.00	50	0.01057	0.67032	0.66237	0.18831
46	7.00	50	0.01771	0.65447	0.98430	0.19427
47	7.50	1	0.10482	0.68098	0.41106	0.20000
48	5.00	10	0.06140	0.68036	0.50301	0.20000
49	5.00	10	0.10125	0.67152	0.66516	0.20000
50	8.00	50	0.04051	0.73228	0.37460	0.20000
51	8.00	160	0.01646	0.73621	0.55947	0.20000

TABLE F6-21
P. G. SOMERVILLE: VERTICAL POINT ESTIMATES
SPECTRAL ACCELERATION AT 3.33 SEC PERIOD

CASE NO.	MAGNITUDE	DISTANCE (KM)	MU	SIGMA	SIGMA MU	SIGMA SIGMA
1	5.00	1	0.00212	0.80009	0.81491	0.08029
2	5.00	1	0.00328	0.79034	0.67230	0.06965
3	5.00	5	0.00070	0.79434	0.73290	0.07391
4	5.00	5	0.00128	0.78815	0.42549	0.06727
5	5.80	10	0.00473	0.73397	0.37989	0.19519
6	5.80	20	0.00416	0.71640	0.49586	0.20000
7	6.50	1	0.04135	0.70526	0.41153	0.20000
8	6.50	1	0.05512	0.67985	0.38815	0.20000
9	6.50	1	0.04824	0.67626	0.31782	0.20000
10	6.50	5	0.05056	0.68124	0.58873	0.20000
11	6.50	5	0.02963	0.67494	0.23803	0.20000
12	6.50	50	0.00340	0.70604	0.64597	0.20000
13	6.50	50	0.00514	0.69210	0.92433	0.20000
14	7.00	10	0.02949	0.71144	0.32946	0.20000
15	7.50	50	0.01158	0.70415	0.75431	0.20000
16	7.50	50	0.01515	0.68269	1.01080	0.20000
17	5.00	1	0.00056	0.79876	1.07275	0.07883
18	5.80	5	0.00977	0.71573	0.47570	0.20000
19	5.80	5	0.00530	0.71199	0.45211	0.20000
20	5.00	10	0.00066	0.79787	0.86940	0.07761
21	5.00	10	0.00200	0.78862	0.60788	0.06777
22	5.00	50	0.00012	0.80051	1.02821	0.08014
23	5.00	50	0.00049	0.78999	0.69468	0.06919
24	5.00	160	0.00004	0.81848	1.25153	0.09937
25	5.80	1	0.01358	0.73535	0.50251	0.19959
26	5.80	5	0.01754	0.71726	0.65394	0.20000
27	5.80	5	0.00938	0.71243	0.42227	0.20000
28	5.80	10	0.00517	0.73180	0.44532	0.19274
29	5.80	10	0.00753	0.71857	0.68221	0.20000
30	5.80	10	0.00626	0.72009	0.60544	0.20000
31	5.80	50	0.00073	0.73238	0.96513	0.19074
32	5.80	50	0.00144	0.72463	1.01649	0.20000
33	6.50	5	0.03435	0.69963	0.26675	0.20000
34	6.50	10	0.01888	0.69250	0.25079	0.19993
35	6.50	10	0.02501	0.68785	0.50129	0.20000
36	6.50	10	0.01916	0.68064	0.44058	0.20000
37	6.50	20	0.01007	0.70926	0.35489	0.20000
38	6.50	20	0.01324	0.68423	0.57333	0.20000
39	6.50	20	0.01179	0.68480	0.78724	0.20000
40	6.50	100	0.00135	0.70171	0.90168	0.20000
41	6.50	160	0.00095	0.70171	0.87878	0.20000
42	7.00	1	0.05691	0.70119	0.58391	0.20000
43	7.00	10	0.04173	0.69145	0.52428	0.20000
44	7.00	10	0.02888	0.68326	0.62865	0.20000
45	7.00	50	0.00684	0.70838	0.79110	0.20000
46	7.00	50	0.01008	0.69281	0.99900	0.20000
47	7.50	1	0.07796	0.71433	0.33975	0.20000
48	5.00	10	0.03502	0.70094	0.63890	0.20000
49	5.00	10	0.05615	0.69292	0.71565	0.20000
50	8.00	50	0.03083	0.78137	0.47685	0.20000
51	8.00	160	0.01107	0.78445	0.51313	0.20000

TABLE F6-22
P. G. SOMERVILLE: VERTICAL POINT ESTIMATES
PEAK GROUND VELOCITY

CASE NO.	MAGNITUDE	DISTANCE (KM)	MU	SIGMA	SIGMA MU	SIGMA SIGMA
1	5.00	1	2.65124	0.66362	0.39808	0.07893
2	5.00	1	3.68688	0.66494	0.17883	0.07975
3	5.00	5	0.66013	0.66561	0.26741	0.07994
4	5.00	5	0.96828	0.66430	0.21965	0.07914
5	5.80	10	2.37668	0.61922	0.17473	0.16909
6	5.80	20	2.24397	0.60845	0.60395	0.16487
7	6.50	1	13.68076	0.59985	0.23627	0.17461
8	6.50	1	18.01303	0.59288	0.45881	0.17465
9	6.50	1	15.20432	0.59298	0.39291	0.17667
10	6.50	5	16.30697	0.59062	0.49712	0.17078
11	6.50	5	10.52329	0.59058	0.33527	0.17433
12	6.50	50	0.97511	0.59841	0.41709	0.16702
13	6.50	50	1.57279	0.59607	0.62754	0.17095
14	7.00	10	10.41637	0.59929	0.21922	0.18707
15	7.50	50	3.50694	0.59006	0.45058	0.19379
16	7.50	50	4.83217	0.58567	0.75462	0.19531
17	5.00	1	0.70917	0.66362	0.32042	0.07893
18	5.80	5	3.98799	0.60486	0.34393	0.16629
19	5.80	5	2.55361	0.60488	0.50608	0.17134
20	5.00	10	0.83952	0.67145	0.18448	0.08344
21	5.00	10	1.90272	0.66019	0.60964	0.07667
22	5.00	50	0.12397	0.66922	0.17214	0.08150
23	5.00	50	0.16313	0.64709	0.30707	0.07142
24	5.00	160	0.01747	0.68029	0.51732	0.08893
25	5.80	1	6.76514	0.61360	0.27080	0.16883
26	5.80	5	7.65992	0.60594	0.42510	0.16721
27	5.80	5	4.52524	0.60051	0.27394	0.16761
28	5.80	10	3.00607	0.61751	0.21426	0.16750
29	5.80	10	4.84362	0.60806	0.52434	0.16673
30	5.80	10	2.78572	0.60488	0.40269	0.17134
31	5.80	50	0.28533	0.61897	0.71864	0.16443
32	5.80	50	0.45959	0.61114	0.69462	0.16512
33	6.50	5	11.37272	0.60207	0.27895	0.17491
34	6.50	10	7.50399	0.59826	0.26593	0.16980
35	6.50	10	10.45618	0.59804	0.48593	0.17606
36	6.50	10	7.18017	0.58576	0.37996	0.16991
37	6.50	20	3.59531	0.59663	0.25990	0.16697
38	6.50	20	5.69562	0.59471	0.55034	0.17124
39	6.50	20	3.72142	0.58773	0.50517	0.17167
40	6.50	100	0.44705	0.60370	0.23614	0.17149
41	6.50	160	0.16347	0.59968	0.46234	0.16805
42	7.00	1	16.95840	0.59794	0.28176	0.18852
43	7.00	10	15.26860	0.59464	0.52837	0.18866
44	7.00	10	10.35549	0.58749	0.39525	0.18548
45	7.00	50	1.99607	0.59869	0.38269	0.18393
46	7.00	50	3.03759	0.59432	0.72999	0.18558
47	7.50	1	23.05415	0.59902	0.42991	0.20000
48	5.00	10	13.34890	0.58922	0.22836	0.19484
49	5.00	10	18.30014	0.58844	0.59026	0.20000
50	8.00	50	7.36929	0.62780	0.24077	0.20000
51	8.00	160	1.95719	0.64728	0.35007	0.20000

TABLE F6-23
ADJUSTMENT FACTORS FOR SIMULTANEOUS RUPTURE ON PARALLEL FAULTS

FREQUENCY (HZ)	HANGING WALL SCALE FACTOR	FOOTWALL SCALE FACTOR	ADDITIONAL ALEATORY UNC.	ADDITIONAL EPISTEMIC UNC.
PGV	1.5	1.75	0.3	0.2
20	1.5	1.75	0.3	0.2
10	1.5	1.75	0.3	0.2
5	1.5	1.75	0.3	0.2
2	1.4	1.75	0.3	0.2
1	1.4	1.6	0.3	0.2
0.5	1.4	1.6	0.3	0.2
0.3	1.4	1.6	0.3	0.2
PGV	1.4	1.6	0.3	0.2

TABLE F6-24
ADJUSTMENT FACTORS FOR SIMULTANEOUS RUPTURES ON PARALLEL FAULTS AND A DEEP DETACHMENT SURFACE

FREQUENCY (HZ)	SCALE FACTOR	ADDITIONAL ALEATORY UNC.	ADDITIONAL EPISTEMIC UNC.
PGA	1.0	0.3	0.2
20	1.0	0.3	0.2
10	1.0	0.3	0.2
5	1.0	0.3	0.2
2	1.2	0.3	0.2
1	2.2	0.3	0.2
0.5	2.2	0.3	0.2
0.3	1.7	0.3	0.2
PGV	2.2	0.3	0.2

APPENDIX F7

ESTIMATION OF GROUND MOTION ATTENUATION FOR THE YUCCA MOUNTAIN PROBABILISTIC SEISMIC HAZARD ASSESSMENT

Marianne C. Walck
Geophysical Technology Department
Sandia National Laboratories
Albuquerque, NM 87185-0750

APPENDIX F7
TABLE OF CONTENTS

APPENDIX F7

ESTIMATION OF GROUND MOTION ATTENUATION FOR THE YUCCA MOUNTAIN PROBABILISTIC SEISMIC HAZARD ASSESSMENT

Marianne C. Walck
Geophysical Technology Department
Sandia National Laboratories
Albuquerque, NM 87185-0750

F7-1 INTRODUCTION

One aspect of the evaluation of Yucca Mountain, Nevada as a potential geological repository for high-level radioactive waste is assessment of seismic hazards at the site. The selected approach to probabilistic seismic hazard assessment uses two panels, seismic source characterization and ground motion evaluation, to provide expert opinion on the likely sizes and probabilities of earthquakes in the region and the ground motions that these sources would produce at Yucca Mountain. The ground motion estimates combined with the likelihood of occurrence of the various seismic sources provide information on the site seismic hazard as a function of time.

Members of the ground motion expert panel were asked to provide point estimates of ground motion for 51 different combinations of magnitude, source distance, and source mechanism. These combinations included moment magnitudes of 5.0, 5.8, 6.5, 7.0, 7.5, and 8.0. The distances considered were horizontal separations of 1, 5, 10, 20, 50, and 160 km. Strike-slip and normal faulting (both foot wall and hanging wall) source mechanisms were included. The ground motions were not calculated for all possible combinations of these parameters, but rather for those combinations selected by the ground motion facilitation team as the most appropriate for hazard at Yucca Mountain. For each of the identified seismic sources, the experts calculated spectral acceleration at 7 frequencies (0.33, 0.5, 1.0, 2.0, 5.0, 10.0, and 20.0 Hz) plus peak ground acceleration (PGA) and peak ground velocity (PGV) for both

horizontal and vertical motion components. Each ground motion estimate consists of four (4) numbers: the median ground motion (μ), the aleatory uncertainty in the median (σ), the epistemic uncertainty in the median (σ_μ) and the epistemic uncertainty in the aleatory uncertainty (σ_σ). Thus the experts have calculated a total of 3672 parameters relevant to ground motion at a site called "YM300", which is a surface site but has velocities representative of Yucca Mountain at a depth of 300 m. The ground motion facilitation team for the project regressed the point estimates using standard techniques to develop continuous models of the ground motion attenuation at Yucca Mountain as functions of magnitude and distance.

F7-2 WEIGHTING SCHEME FOR PROPONENT GROUND MOTION MODELS

The ground motion facilitation team provided the experts with a suite of proponent models that were to be considered for their applicability to ground motions at Yucca Mountain. Each expert was required to evaluate each model and decide on its applicability in each of the 918 earthquake-frequency-component combinations. The typical approach was to develop estimates based on a weighted median of the proponent models. Each expert divided the proponent models into different classes, with each class assigned a weight, and then assigned a relative weight to each candidate model within each class. The various classes of proponent models and their weights are discussed in detail in the following sections.

F7-2.1 Classes Of Proponent Models

I chose to define three classes of proponent models: empirical, point source numerical simulation, and finite fault numerical simulation. The empirical models considered include several attenuation relations based on data primarily from California (e.g., Abrahamson and Silva, 1997; Boore *et al.*, 1997; Campbell, 1997; Idriss, 1993, 1997 [University of California, Davis, written communications]; Sadigh *et al.*, 1997), the Spudich *et al.* (1996) model for extensional regime data, the Sabetta and Pugliese (1996) model based on Italian earthquakes, and the McGarr (1984) relation for peak ground acceleration and velocity for close-in, extensional data. Also in this category are the explosion models developed for the Yucca Mountain Project by R.J. Bennett *et al.* (S-Cubed, written communication, 1997) and the Campbell hybrid empirical model (N. A. Abrahamson and A. M. Becker, consultants, written

communication, 1997b). The single model of the point source numerical simulation class was developed by W. Silva. Three different approaches to finite fault simulation were also exercised for the YM300 structure; these are the work of Zeng and Anderson; P. Somerville, and W. Silva. N. A. Abrahamson and A. M. Becker (Consultants, written communication, 1997) contains information documenting all four of the numerical simulation models.

F7-2.2 Model Weights: Horizontal Components

All of the proponent models were available for making predictions of the horizontal component data. Many of the empirical models provide estimates for spectral acceleration and peak ground acceleration only, so there were only limited choices in models for the peak ground velocity estimates. A few of the empirical models (Boore *et al.*, 1997; Spudich *et al.*, 1996) did not provide high-frequency (20 Hz spectral acceleration) ground motion values.

In most cases, adjustments were made to the raw horizontal model estimates to make them applicable for the YM300 site. The adjustments that I chose to include were the effects of 1) crustal structure, 2) source differences (chiefly due to stress drop), 3) compensation for the difference between the average horizontal component (applicable for most proponent models) and the random horizontal component (the required estimate), and 4) interpolation for 20 Hz estimates when needed.

Two crustal adjustment factors were available for use by the experts: these were similar, but not identical, band-limited-white-noise-random-vibration theory estimates from Ken Campbell and Walt Silva (N. A. Abrahamson, and A. M. Becker, Consultants, written communication, 1997b). These corrections account for the difference between a "California" crust and the YM300 velocity structure. I chose to apply the Campbell crustal correction to the appropriate empirical models as detailed below. The point source model and the three finite fault simulations were calculated directly for the YM300 model and did not require crustal transfer functions.

Some recent studies (Abrahamson and Silva, 1997; Spudich *et al.*, 1996) have determined that the ground motions expected from normal-faulting earthquakes and also strike-slip earthquakes in extensional regimes may be lower than that expected for "typical" California strike slip and thrust earthquakes. The lower ground motions could be due to lower stress

drop parameters for extensional-regime earthquakes. Becker and Abrahamson (1997) studied stress drops for extensional regime earthquakes and found an average stress drop of 45 bars for a limited set of normal faulting earthquakes, and a value near 55 bars for extensional strike-slip earthquakes. These values are lower than those found for typical California events by Silva *et al.* (written communication, Pacific Engineering and Analysis, 1997). Because Yucca Mountain is in an extensional regime, and the expected earthquakes are either normal or strike slip in nature, one might expect lower stress drops for these events and therefore lower ground motions than for the equivalent California events, which have an average stress drop of about 60 bars. This source effect was included in the ground motion estimates by using a source correction based on the same theory as the crustal correction, and coded by Ken Campbell. I chose to use source corrections for all models except those developed specifically for extensional regimes (Spudich *et al.*, 1997; McGarr, 1984). Strike-slip events were assigned a stress drop parameter of 55 bars, and the normal events were assigned 45 bars. The numerical simulations were given the same source corrections as the empirical models.

Most of the empirical models and all of the numerical simulations were calculated for an average horizontal component. Because the desired attenuation relationships were for a random horizontal component, I incorporated additional aleatory uncertainty into the horizontal estimates for the appropriate models using the frequency-varying values of Boore *et al.* (1993).

Two of the empirical models do not provide coefficients applicable for calculating the spectral acceleration at 20 Hz (Boore *et al.* 1997 [BJF]; Spudich *et al.*, 1997 [SEA]). In order to avoid biasing the overall spectral shape for the event, I incorporated the interpolation scheme of Boore (N. A. Abrahamson and A. M. Becker, Consultants, written communication, 1997b) to estimate 20 Hz values for the BJF and SEA models.

F7-2.2.1 Empirical Models. In an overall sense, I favor the empirical models over the numerical simulations, thus I typically assigned a class weight of 0.6 or 0.7 (out of 1.0) to the empirical class. Slight variations occurred from case to case and even for various frequencies within each case due to different availability of applicable models. For example, there are few empirical models which provide peak ground velocity estimates, so the numerical

simulations often received a relatively higher weight for PGV estimates. Generally, however, the empirical models were always assigned a class weight of 0.5 or higher.

The general rules as applied to each model are discussed below. Models within the empirical class ordinarily receive equal weight; exceptions are noted for each model.

Abrahamson and Silva (1997) (AS97). This model is applicable for the entire range of distance (0-160 km) and magnitude (5-8) considered here. AS97 does not provide peak ground velocity estimates, therefore this model was not used for PGV. AS97 has an available adjustment for normal faulting, however for consistency among the models instead of using the AS97-specific normal faulting corrections I applied the Campbell version of the source correction discussed above. For the strike-slip earthquakes, I assigned the stress drop to be 55 bars; 45 bars was chosen for the normal events. The AS97 model was a "workhorse" as it was included in the vast majority of the calculations. It is a modern model based on a good data set using state-of-the-art regression methods.

Boore, Joyner, and Fumal (1997) (BJF). The BJF model was developed using a carefully selected data set and the two-step regression approach (Joyner and Boore, 1993) to model the data. It has few data at small magnitudes and an unusual attenuation shape for large distances. I applied the BJF model in the range recommended by Boore *et al.* (1997); magnitudes greater than or equal to 5.5 and distances less than 100 km. The BJF model also does not include any magnitude saturation at short ranges. Because I believe that some magnitude saturation does occur, I gave the BJF model a lower weight within the empirical class for large events at short distances. I applied crustal and source corrections as detailed above to the BJF model, and applied the Boore (N. A. Abrahamson and A. M. Becker, Consultants, written communication, 1997b) interpolation scheme to provide 20 Hz spectral values. The model was calculated for a shear wave velocity of 620 m/s, consistent with California 'rock'. This Vs is lower than for the YM300 site, however the crustal transfer function should account for average velocity differences between typical California rock sites and the YM300 site.

Boore, Joyner, and Fumal (1994, class A). I did not use this model in the calculations. Boore (personal communication, 1997) recommended use of the BJF 1997 model.

Boore, Joyner, and Fumal (1997, class B). I did not use this model in the calculations. Boore (personal communication, 1997) recommended use of the BJF 1997 model.

Campbell, 1997 (soft rock) (C97). This model was used for most of the events at distances of 50 km or less. This model has a large degree of magnitude saturation; I gave it a lesser weight in some cases at close distance. Also, the Campbell model predicts higher amplitudes at low frequencies than the other models. In cases where the spectral shape was significantly different from my preference, I gave it a lower weight at .33, .5, and 1. Hz. The soft rock parameters are consistent with use of the Campbell crustal transfer function described above.

Campbell, 1997 (hard rock). I did not use this model in the calculations. According to Campbell (personal communication, 1997) the soft rock 1997 model is better suited for use in this study, coupled with the crustal and source transfer functions that he developed.

Campbell, 1993-1994 (hard rock). This model was not used. Campbell (personal communication) confirmed that the more recent 1997 model is more applicable.

Campbell, 1990-1994 (soft rock). This model was not used. Campbell (personal communication) confirmed that the more recent 1997 model is more applicable.

Campbell, 1990 (Dames and Moore, written communication) (soil/soft rock). This model was not used. Campbell (personal communication) confirmed that the more recent 1997 model is more applicable.

Idriss, 1993 and 1997 (University of California, Davis, written communications) (rock/stiff soil). This model was used, in combination with the appropriate crustal and source corrections, for magnitudes of 7.0 and less and distances of less than 100 km. It was generally given equal weight with the other applicable models. Both crustal and source corrections were applied to this model.

Joyner and Boore, 1988 (JB88). This older model uses similar methodology to BJF, but with a smaller data set. It was not used for the spectral acceleration or PGA estimates, but it does

provide peak velocity predictions (PGV) and was used for PGV estimates for events in the magnitude range 5.5 to 7.5 and distances closer than 100 km.

Sadigh *et al.*, 1997 (Sa97). I used this model for spectral acceleration and PGA estimates for the events of all magnitudes. Its stated distance limit is 100 km, however I also used it for the 160 km estimates for the magnitude 6.5 and 8.0 cases, as the data distribution illustrations in Sadigh *et al.* (1997) show significant amounts of data beyond 100 km at the higher magnitudes. The Sa97 model was, however, assigned a relatively lower weight for the distant events. The usual crustal and source corrections were applied to this model.

Sabetta and Pugliese, 1996 (SP96). This model is based on data from Italy and does include some normal faulting recordings. The data set is small, however, and the regression method is not as sophisticated as for some of the California models. I used it only for peak velocity estimates. Because the data set included some normal faulting data, I did not apply the source correction to the SP96 model, however I did apply the crustal transfer function. Due to uncertainty in the comparative crustal structure of California and the Italian sites, I added an additional 0.1 of epistemic uncertainty in the median each time the SP96 model was used. Also, this model received a lower weight (typically half) within the empirical class for the peak velocity estimates. It was not used for events larger than magnitude 7.0, or for distances larger than 100 km.

Spudich *et al.*, 1997 (SEA96). This model is the first to be developed specifically for extensional regime data (strike-slip and normal faulting). The data were carefully selected and are applicable to the Yucca Mountain exercise without source correction. Because of the few data available, however, Spudich *et al.* were forced to place additional constraints on their regression that makes the shape of their model with frequency very similar to that of the BJF model. I used the SEA96 model for events from magnitude 5.5 through 7.0, and for distances less than 100 km. The crustal transfer function was applied, although its applicability to this worldwide data set is not as well known; I made the assumption that the crustal structure for the worldwide data (which included significant data from California) is similar to the generic California structure used in the transfer function. The SEA96 model did not provide 20 Hz spectral acceleration values, and the method proposed by Boore was used to interpolate a 20 Hz value for use in the point estimates.

McGarr, 1984. I used McGarr's model for horizontal PGV estimates only, in the distance range of 20 km and less and for magnitudes of 7 and less (McGarr, 1984 and McGarr, personal communication, 1997). As it was developed for extensional regime data, no source correction was applied to this model, but the crustal transfer function was applied since McGarr's data set includes several California events.

Bennett, Murphy, and Barker, 1997 (Model 1). This model was developed using the underground nuclear explosion (UNE) data from the Nevada Test Site. Because Yucca Mountain is located in the immediate vicinity, the UNE data should be appropriate for the local crustal structure. UNE sources, however, differ from earthquake sources in a number of important ways. One difference is the large amount of surface wave energy generated in UNE data as a consequence of the shallow UNE burial. I do not believe that the spectral shape for this model is appropriate for earthquakes and therefore did not incorporate it into the calculations.

Bennett, Murphy, and Barker, S-Cubed, written communication, 1997 (Model 2). Bennett *et al.*, cognizant of the potential problems associated with Model 1, provided a model that is scaled to the spectral shape of Sadigh *et al.* (1997) at 10 km. This Bennett *et al.* Model 2 also contain the NTS-appropriate crustal attenuation. I judged this model to be the most applicable of the three Bennett *et al.* UNE models and applied it to a subset of the calculations, limited to certain magnitudes that most closely match the UNE yields. Bennett *et al.* provided a yield-magnitude relation; it shows that the UNE data are applicable for magnitude range less than 6. Due to the lack of close-in data in the UNE database, I chose to apply Model 2 to only the magnitude 5.8 events at distances of 20 km or greater (while UNE data are available at 10 km, this Model 2 is identical to the Sadigh *et al.* 1997 model at 10 km, and therefore would provide only redundant data). No crustal correction was applied, but a source correction was applied to the calculations. Typically, I gave this model half of the weight of the other empirical models.

Bennett, Murphy, and Barker, S-Cubed, written communication, 1997 (Model 3). This version of the Bennett *et al.* models used the Little Skull Mountain earthquake spectrum to

scale the UNE attenuation. I chose not to use this model due to this event's small size (not much long-period energy) and somewhat unusual spectral shape.

Campbell Hybrid Empirical Model (1997). Campbell developed a methodology to combine estimates from different empirical models with varying weights, including theoretical crustal and source corrections as outlined above. I chose not to use this model directly, although the concept of weighting the empirical models within the class and applying crustal and source corrections is quite similar to this model. The hybrid empirical model does not include any models that are not outlined above, therefore no information is lost by combining the various models in the way I chose as opposed to the perhaps more elegant hybrid empirical approach.

F7-2.2.2 Numerical Simulations. There are two types of proponent models that are numerical simulations of ground motion at the YM300 site. Silva developed a stochastic point source approach which can be viewed as a baseline for comparison to the more sophisticated finite-fault simulations. My use of these models in the ground motion calculations is outlined below.

F7-2.2.2.1 Point Source Simulation. Silva (N. A. Abrahamson and A. M. Becker, Consultants, written communication, 1997b) developed a band limited white noise/random vibration theory (BLWN/RVT) stochastic point source method for calculating ground motions from a point source. The methodology combines the effects of the point source, path operator, and site operator to predict site-specific ground motion. He provided spectral accelerations, PGA, and PGV values for the full suite of 51 cases, using the YM300 crustal model. I generally assigned the stochastic point source model a class weight of about 0.1. It received a lower weight for the cases of large magnitude and short distances, where it would tend to overpredict the ground motion, and for the long period (0.33 Hz, 0.5 Hz) estimates for most cases. This model did receive weight up to 0.2, however, in cases where there were few other numerical simulations to include in the point estimate. For example, only the Zeng/Anderson finite fault model provided estimates for magnitude 5.0 earthquakes, so the point source model received a higher class weight for those cases. Because this model was the only one in its class, its relative weight within the class is always 1.0. I applied the source correction factors for stress drop to this model, but did not apply a crustal correction. This model requires a stress drop variability which I assigned to be 0.5 natural log units

based on the studies of stress drop variability by Becker (Ground Motion Data Package). The model also incorporates the epistemic uncertainties in the median stress drop and standard deviation which I assigned to be 0.2 natural log units for both based on the results from Becker and on judgment.

F7-2.2.2.2 Finite-Fault Simulations. There are three proponent models that use finite fault simulations of ground motions. In all three cases, these simulations were performed for the YM300 structure directly and no crustal correction was applied. This class of models generally received a class weight of 0.3 or 0.35, depending on the other available models and their limitations for the particular case. If only one finite fault simulation was available for a particular case, it was assigned a class weight of 0.2.

Zeng and Anderson, 1997 (ZA). The estimates from this model (described in N. A. Abrahamson and A. M. Becker, Consultants, written communication, 1997b) were developed from the composite fractal finite fault source method developed and described by Zeng *et al.* (1994). Its validation has not included any normal faulting earthquakes, and like the other finite fault models, it has also not been thoroughly validated for vertical data. Zeng and Anderson provided predictions for the full suite of events and distances. I used the results for this model in all cases, although in some instances it received a lower weight than the other finite fault simulations. If no other finite fault simulation was available for a particular case, the ZA model received a weight of 1.0 and its overall contribution was controlled by the class weight for the finite fault class. In my judgment, this model produced excessively high predictions for normal faulting events on the hanging wall, and as Anderson (personal communication, 1997) agreed that many of them seemed high and did not offer an explanation as to the cause, I weighted the ZA model at half weight for all hanging wall estimates. In other specific cases, this model also received a lower weight because it was an outlier, that is, different from all of the other model predictions by a factor of 2 or more. I applied the source corrections (stress drops of 55 and 45 bars for strike-slip and normal events, respectively) with a median stress drop uncertainty of 0.2.

Somerville (1997). This model uses a combination of theoretical (at long period) and empirical (at short periods) Green's functions to calculate ground motions from a specified finite fault (N. A. Abrahamson and A. M. Becker, Consultants, written communication,

1997b). Due to limitations on the available empirical Green's functions, Somerville provided estimates for the events of magnitudes 5.8, 6.5, 7.0, and 7.5 only. Thus his model was not included in estimates for the magnitude 5.0 or 8.0 events. This model generally was weighted equally with the others within the class with the exception of outlier predictions. For this model, some very low ground motions were obtained at low frequencies for some events. I decreased the relative weight of the Somerville model for those instances to half, or occasionally to 1/4, of the other finite fault models. In one or two cases this model was not included at all in the calculations because its prediction over the entire spectrum was extremely different from the other models (cases 31 and 32). The source corrections were applied as in the Anderson model.

Silva (1997). This model is an extension of the point-source stochastic method to finite faults (N. A. Abrahamson and A. M. Becker, Consultants, written communication, 1997b). Simulations were provided for all events except for the M5.0 cases. In general, the Silva model received a relative weight equal to the other finite fault simulations. Source corrections were also applied to this model in an analogous fashion to the other models.

F7-2.3 Model Weights: Vertical Models

The application of model weights for the vertical models was very similar to that of the horizontal models. The vertical ground motion at the desired frequency was calculated and crustal and source corrections applied. I used only models that included vertical motions and did not use vertical/horizontal motion ratios in order to include models developed only for horizontal motions. This practice resulted in a generally smaller number of models contributing to each weighted median ground motion estimate. In particular, there were often only a few models applicable for vertical PGV.

The crustal correction developed by Campbell is applicable to horizontal motions only, so I developed an alternative approach for calculating the vertical ground motions while incorporating the crustal transfer function. In this procedure, the horizontal ground motions were scaled by the crustal correction factors and then scaled by the Yucca Mountain point source vertical/horizontal ratios. This method was applied to empirical models only (because the numerical simulations were done directly for the YM300 structure), and will be described in section 2.3.1.

The class weights for the vertical motions are generally the same as for the horizontal motions. Because there are fewer available data and models, the epistemic uncertainty is typically higher for the vertical; this will be discussed below in the uncertainty section.

F7-2.3.1 Empirical Models. There are four proponent empirical models that provide vertical attenuation relations: Abrahamson and Silva (1997), Campbell (1997), Sadigh *et al.* (1997), and Sabetta and Pugliese (1996). The SP96 model was used only for peak ground velocity. The Campbell model also provides PGV but the AS97 and Sa97 models do not, thus the number of empirical models used for vertical PGV was small.

The class weight for the empirical models is typically 0.6 - 0.7.

To apply the Campbell crustal correction, developed for horizontal motions, to the vertical data, I used the following simple method. Silva provided the ground motion experts with vertical to horizontal (z/h) ratios for the stochastic point source calculations. I started with the *horizontal* prediction for the empirical model and multiplied it by the horizontal crustal correction and then the appropriate point source z/h ratio to produce a crust-corrected vertical ground motion estimate. Both the aleatory and epistemic uncertainties were increased for model estimates obtained with this procedure; more explanation is given in the uncertainty section below.

The AS97, Campbell, and Sadigh models generally received equal weights within the empirical class. Exceptions are similar to those for the horizontals as described above. Each model's range of applicability is the same for vertical motions as it is for horizontal motions.

F7-2.3.2 Numerical Simulations. Three of the four numerical simulation proponent models provided vertical ground motion estimates. These were used as the horizontals, with source corrections but no crustal corrections. The class weights were assigned in a manner analogous to the horizontal estimates.

F7-2.3.2.1 Point Source Simulation. Silva provided z/h ratios for the stochastic point source simulations to convert the horizontal to vertical estimates. The class weight for the point

source model is typically 0.1 as discussed above. This model is applicable to all of the spectral amplitudes, PGA, and PGV. Deviations from the standard weighting scheme are as for the horizontal components.

F7-2.3.2.2 Finite Fault Simulations. The Zeng and Anderson and Somerville models provided vertical component estimates, while the Silva model did not. The ZA and Somerville model weights were applied as for the horizontal estimates described above. The Somerville model is not applicable for magnitude 5.0 or 8.0 events, therefore for these event sizes the ZA model is alone in this model class. In these cases, the class weights were adjusted so that typically the empirical model class would receive a relative weight of 0.6 with the point source and ZA models assigned 0.2 each. Exceptions to the general weighting scheme are chiefly for data outliers as discussed above for the horizontal components.

F7-3 ADJUSTMENTS TO WEIGHTED ESTIMATES

Case-specific adjustments to the weighted estimates were made based on judgement.

F7-4 ESTIMATES OF UNCERTAINTIES

Three types of uncertainty were calculated for each median ground motion estimate. The FORTRAN program WT_AVE (N. A. Abrahamson and A. M. Becker, Consultants, written communication, 1997b) was used to provide statistical calculations of all three uncertainty values. The expert was provided the opportunity in the input file to WT_AVE to add additional uncertainty to that provided by the model proponent in any of the three uncertainty categories. These additions will be discussed below.

F7-4.1 Aleatory Uncertainty: σ

The aleatory uncertainty for each point estimate was calculated as a weighted average of the stated uncertainty for each model. The effect of the random horizontal component was included in this uncertainty for the appropriate model using the method recommended by Boore *et al.* (1993). The finite fault simulations include both parametric and modeling uncertainty in this term, while the empirical models typically provide a single number for uncertainty.

For the vertical component empirical and stochastic point source estimates, additional aleatory uncertainty associated with the regression fit to the point source z/h ratios was added (assuming no correlation) to the aleatory uncertainty. The proponents of the numerical simulations did not provide uncertainty estimates specific for the vertical components. To convert the horizontal aleatory uncertainty to a value appropriate for the vertical component, I used the horizontal uncertainty value (without random effect) and multiplied it by an average vertical/horizontal uncertainty ratio determined from the applicable empirical relationships.

F7-4.2 Epistemic Uncertainty For Median Point Estimate: σ_μ

The FORTRAN program WT_AVE calculates statistical values of the epistemic uncertainty on the median point estimate. For the horizontal components, I assigned epistemic uncertainty to have several components: 1) effect of uncertainty in crustal correction, 2) effect of uncertainty in source correction (as quantified by an uncertainty in median stress drop of 0.2) and 3) additional added uncertainty for some models. This additional assigned epistemic uncertainty included 0.1 for the SP97 model due to increased uncertainty in crustal structure, and 0.2 assigned to the numerical simulations that did not provide epistemic uncertainty estimates: stochastic point source, ZA, and Silva finite fault. The 0.2 value is similar to that obtained for the empirical models and is the same as Somerville value assigned from his expert judgment.

Each model thus has an epistemic uncertainty value assigned to it. In addition, the effect of the weighted deviation of each individual model from the median is included using standard statistics. The weighted individual model epistemic uncertainty estimates and the deviation effect are combined as documented by N. Abrahamson at the April, 1997 ground motion workshop. I have additionally defined a floor value for epistemic uncertainty of 0.2, such that if the calculation produces a value of less than 0.2, it is adjusted upward to 0.2.

For the vertical estimates, I included all of the above uncertainties, with some additions. I defined the σ_μ for the finite fault and point source simulations to be 0.3 rather than the 0.2 used for the horizontals, because due to lack of data and modeling efforts for vertical ground motions there is more uncertainty associated with these estimates that could be reduced given

additional information. I also assigned additional epistemic uncertainty of 0.2 above the statistical crustal and source corrections to the empirical models. This is meant to incorporate the additional uncertainty of applying the point source z/h ratio and the horizontal crustal transfer function. The deviation from the median part of the epistemic uncertainty was included in the vertical estimate as well, with a total floor of 0.3 for any vertical σ_μ value.

F7-4.3 Epistemic Uncertainty In Aleatory Uncertainty: σ_σ

The epistemic uncertainty associated with the aleatory uncertainty was also calculated via the FORTRAN program WT_AVE. Here the main component is the variability in the σ estimates from model to model. A component was also included to allow inclusion of individual σ_σ estimates for each model, however only the Somerville finite fault model provided a σ_σ estimate, so in order to avoid model bias I did not include a contribution in this term. The vertical σ_σ computations were done in a manner analogous to the horizontal σ_σ.

F7-5 FINAL POINT ESTIMATES OF GROUND MOTION FOR THE 51 CASES

Tables F7-1 to F7-9 contain my horizontal component point estimates for the 51 cases, 9 frequencies. Tables F7-10 to F7-18 contain my vertical component point estimates. For each of the 918 event-frequency-component combinations, the four ground motion parameters (median and three uncertainties) are presented.

F7-6 EVALUATION OF REGRESSION FIT TO POINT ESTIMATES

The facilitation team applied regression models to all four ground motion parameters for each case, frequency, and component and provided plots of the regression results for my approval. In general, the regression fits were very satisfactory representations of my point estimates.

F7-6.1 Median Estimate: μ

Illustrations and tables elsewhere in this report present the results of the regressions on the 918 median ground motion estimates. In general, these regression lines are a good representation of my results. The regression lines for the peak velocity values do not always fit the data as well as the other spectral points; this could reflect greater uncertainty in the

peak velocity values themselves due to fewer contributing models and less experience in predicting peak velocities.

With my approval, the effects of the hanging wall and foot wall were included in the normal faulting regressions. The hanging wall effect is a "bump" between 3 and 20 km, which increases with increasing magnitude. The foot wall effect is a more subtle trough in the regression relation at the same distance. There were no foot wall calculations for the magnitude 5.0 events. The hanging wall effect for magnitude 5.8 events is rather small and increases rapidly with size. The effect at magnitude 8.0, however, is unknown because no point estimates were made for normal faulting earthquakes at this large magnitude.

F7-6.2 Aleatory Uncertainty: σ

The facilitation team also provided regressions for the aleatory uncertainty. In all cases, the σ values decrease with increasing magnitude, and are generally tightly clustered for the horizontal estimates, with more scatter evident for the vertical estimates. In all cases the regressions provide a good representation of my σ estimates.

F7-6.3 Epistemic Uncertainty In The Median: σ_μ

The epistemic uncertainty regressions provide the most challenge in the regression process, as the statistical values are generally quite scattered. Each expert was offered the opportunity to specify σ_μ values as functions of magnitude and distance and/or to specify the functional form used in the regression. Generally, the epistemic uncertainty values are higher at small and large distance, and have a minimum around 10-20 km distance. This may reflect the larger body of data available for developing experience in the medium distance range. A magnitude dependence is not well defined therefore I chose a magnitude-independent regression. A quadratic distance dependence is appropriate for these data. In general, the σ_μ value for a given event-frequency-component combination has a fairly large uncertainty associated with it due to the large scatter around the regression curve.

F7-6.4 Epistemic Uncertainty In The Aleatory Uncertainty: σ_σ

The regressions for the uncertainty in the aleatory uncertainty are simple in form and generally have tightly clustered data that adequately define the regression line. The σ_σ values generally increase with magnitude, and, like the σ values themselves, there is considerably

more scatter in the vertical σ_σ values than the horizontal values. The effect of distance is very small on this parameter. The regression lines are a good representation of the σ_σ estimates.

F7-7 SPECIAL CASE FAULT RUPTURE SCENARIOS

The experts were asked to provide rule revisions for two special cases of fault rupture: multiple parallel faults and a low-angle normal fault.

F7-7.1 Multiple Parallel Faults

The multiple parallel fault scenario consists of three or more parallel normal faults dipping at 60 degrees that all rupture essentially simultaneously. One example would be three magnitude 6.5 events that would have a combined moment magnitude of about 6.8. Paul Somerville provided a simulation of peak ground acceleration (N. A. Abrahamson and A. M. Becker, Consultants, written communication, 1997b) using his finite fault model for evaluating the effects of the multiple fault rupture. He determined that in all cases the three faults rupturing simultaneously resulted in higher ground motions than one magnitude 6.8 at the closest equivalent distance. Unfortunately, no simulation data is available for evaluating frequencies other than PGA.

As a distance measure for parallel multiple faults, I recommend using the rupture distance modified to be the distance to the closest fault rupture of all the available faults.

For predicting ground motion amplitudes, I recommend summing the ground motions for the multiple events incoherently (square root of the sum of the squares, or SRSS). In coming to this conclusion, I examined the relative ground motions at the relevant frequencies for a multiple fault scenario using the AS97 model. I compared the SRSS for a magnitude 6.5 at 1 km (foot wall), a magnitude 6.5 at 1 km (hanging wall) and a magnitude 6.5 at 5 km (hanging wall) to a single magnitude 6.8 event at 1 km (hanging wall). I also examined coherently adding the ground motions of these three events, which resulted in very high ground motions. The PGA for the single 6.8 event is about 35% lower than the SRSS combined amplitudes. This is quite similar to the Somerville prediction for a similar situation. The difference between the single 6.8 and the SRSS of the three 6.5s decreased with decreasing frequency,

however the SRSS value is still significantly higher than that of the single 6.8 down to 0.33 Hz, by about 25-30%. Thus using the SRSS-combined events is consistent with the available modeling, and because the degree of coherency expected among the multiple faults at low frequencies is unknown and certain to vary due to interevent timing differences, the SRSS approach should provide an adequate estimate of expected ground motion amplitudes.

I also recommend increasing the epistemic uncertainty for such a calculation by 0.1 at frequencies at and above 1 Hz, and by 0.2 for frequencies below 1 Hz.

F7-7.2 Low Angle Fault

A low angle normal fault rupture could occur in an area where a detachment fault exists. Unfortunately, while there are very few actual ground motion data for normal faults in general, there are none of which I am aware for low-angle normal faults. While thrust faults have shallower dips than normal faults, they are widely known to produce higher ground motions than strike-slip events, thus it is unlikely that a thrust-fault-based estimate would be appropriate for a low-angle normal fault in an extensional regime.

I recommend using the Yucca Mountain attenuation relations as they stand for a low-angle normal fault. The distance measure can also remain the same. Due to the high level of uncertainty stemming from lack of data, it is appropriate to increase the epistemic uncertainty on the median by 0.25 for all frequencies for the case of a low-angle normal fault.

F7-8 REFERENCES

Abrahamson, N. A., and Silva, W. J., 1997, Empirical response spectral attenuation relations for shallow crustal earthquakes: Seismological Research Letters, v. 68, n. 1, p. 94-127.

Becker, A. M., and Abrahamson, N. A., 1997, Stress drops in normal faulting earthquakes (abstract): Seismological Research Letters, v. 68, n. 2, p. 322.

Boore, D., Joyner, W.B., and Fumal, T.E., 1993, Estimation of response spectra and peak accelerations from western North American earthquakes - An interim report: U. S. Geological Survey Open-File Reptort 93-509, 72pp.

Boore, D.M., Joyner, W.B., and Fumal, T.E., 1994, Estimation of response spectra and peak accelerations from western North Amercan earthquakes - An interim report, part 2: U.S. Geological Survey Open-File Report 94-127, 40 p.

Boore, D.M., Joyner, W.B., and Fumal, T.E., 1997, Equations for estimating horizontal response spectra and peak acceleration from western North American earthquakes - A summary of recent work: Seismogical Research Letters, v. 68, n. 1, p. 128-153.

Campbell, K.W., 1993, Empirical prediction of near-source ground motion from large earthquakes, *in* V.K. Gaur, ed., Proceedings, International Workshop on Earthquake Hazard and Large Dams in the Himalaya: Indian National Trust for Art and Cultural Heritage (INTACH), New Delhi, India, p. 93-103.

Campbell, K.W., 1997, Empirical near-source attenuation relationships for horizontal and vertical components of peak ground acceleration, peak ground velocity, and pseudo-absolute acceleration response spectra: Seismological Research Letters, v. 68, n. 1, p. 154-179.

Campbell, K.W., and Bozorgnia, Y., 1994, Near-source attenuation of peak horizontal acceleration from worldwide accelerograms recorded from 1957 to 1993: 5th U.S. National Conference on Earthquake Engineering, Chicago, IL, July 10-14, 1994.

Joyner, W.B. and Boore, D.M., 1988, Measurement, characterization, and prediction of strong ground motion, *in* Proceedings, Conference on Earthquake Engineering and Soil Dynamics II: GT Div/. ASCE, Park City, UT, 27-30 June 1988, p. 43-102.

Joyner, W.B., and Boore, D.M., 1993, Methods for regression analysis of strong-motion data: Bulletin of the Seismological Society of America, v. 83, p. 469-487.

McGarr, A., 1984, Scaling of ground motion parameters, state of stress, and focal depth: Journal of Geophysical Research, v. 89, p. 6969-6979.

Sabetta, F., and Pugliese, A., 1996, Estimation of response spectra and simulation of nonstationary earthquake ground motions: Bulletin of the Seismological Society of America, v. 86, p. 337-352.

Sadigh, K., Chang, C.-Y., Egan, J. A, Makdisi, F., and Youngs, R. R. ,1997, Attenuation relationships for shallow crustal earthquakes based on California strong motion data: Seismological Research Letters, v. 68, n. 1, p. 180-189.

Spudich, P., Fletcher, J. B., Hellweg, M., Boatwright, J., Sullivan, C., Joyner, W.B., Hanks, T.C., Boore, D.M., McGarr, A., Baker, L. M., and Lindh, A.G., 1997, SEA96 -- a new predictive relation for earthquake ground motions in extensional tectonic regimes: Seismological Research Letters, v. 68, n. 1, p. 190-198.

Zeng, Y., Anderson, J.G., and Yu, G., 1994, A composite source model for computing realistic synthetic strong ground motions: Geophysical Research Letters, v. 21, p. 725 - 728.

TABLE F7-1
M. C. WALCK: HORIZONTAL POINT ESTIMATES
PEAK GROUND ACCELERATION

CASE NO.	MAGNITUDE	DISTANCE (KM)	MU	SIGMA	SIGMA MU	SIGMA SIGMA
1	5.00	1	0.15747	0.69327	0.35738	0.16200
2	5.00	1	0.14893	0.69514	0.35111	0.16200
3	5.00	5	0.05358	0.68368	0.32129	0.16400
4	5.00	5	0.05457	0.68461	0.32675	0.16400
5	5.80	10	0.09241	0.59828	0.25933	0.16400
6	5.80	20	0.06166	0.59607	0.26755	0.16400
7	6.50	1	0.38852	0.57062	0.36402	0.16900
8	6.50	1	0.35251	0.56816	0.41030	0.16900
9	6.50	1	0.33806	0.57273	0.39394	0.16900
10	6.50	5	0.30374	0.56602	0.36025	0.16800
11	6.50	5	0.21798	0.57258	0.32663	0.16900
12	6.50	50	0.02796	0.56754	0.29064	0.16800
13	6.50	50	0.02521	0.56492	0.29747	0.16700
14	7.00	10	0.23732	0.53881	0.29775	0.17400
15	7.50	50	0.05798	0.53528	0.25147	0.18000
16	7.50	50	0.05518	0.53230	0.25711	0.17900
17	5.00	1	0.06367	0.68896	0.29045	0.16500
18	5.80	5	0.13394	0.59970	0.30801	0.16400
19	5.80	5	0.08310	0.60148	0.30195	0.16400
20	5.00	10	0.06425	0.67839	0.27113	0.16300
21	5.00	10	0.07225	0.68274	0.27208	0.16400
22	5.00	50	0.00604	0.69758	0.30799	0.16000
23	5.00	50	0.00591	0.70637	0.32378	0.15900
24	5.00	160	0.00073	0.69766	0.32037	0.16300
25	5.80	1	0.25740	0.59919	0.37730	0.16500
26	5.80	5	0.19424	0.59512	0.33244	0.16400
27	5.80	5	0.12500	0.59805	0.32680	0.16400
28	5.80	10	0.11239	0.60162	0.27836	0.16500
29	5.80	10	0.13403	0.59540	0.28374	0.16400
30	5.80	10	0.07770	0.59884	0.33817	0.16500
31	5.80	50	0.01418	0.61013	0.33151	0.16200
32	5.80	50	0.01352	0.61205	0.38770	0.16200
33	6.50	5	0.28357	0.56900	0.33092	0.16800
34	6.50	10	0.18387	0.57035	0.30849	0.16900
35	6.50	10	0.22646	0.56756	0.34523	0.16800
36	6.50	10	0.13907	0.56837	0.30764	0.16800
37	6.50	20	0.09308	0.56761	0.27556	0.16800
38	6.50	20	0.10799	0.56864	0.30814	0.16800
39	6.50	20	0.06954	0.56632	0.28629	0.16800
40	6.50	100	0.01204	0.57210	0.36945	0.16200
41	6.50	160	0.00530	0.57536	0.46762	0.17000
42	7.00	1	0.44383	0.53927	0.30919	0.17300
43	7.00	10	0.27758	0.54277	0.34186	0.17600
44	7.00	10	0.17595	0.53825	0.29134	0.17400
45	7.00	50	0.04299	0.53911	0.27352	0.17000
46	7.00	50	0.04130	0.54645	0.25922	0.17400
47	7.50	1	0.49124	0.53707	0.35613	0.18800
48	5.00	10	0.27890	0.52712	0.29747	0.18300
49	5.00	10	0.31205	0.52791	0.41191	0.18100
50	8.00	50	0.07557	0.54384	0.27652	0.18200
51	8.00	160	0.01943	0.53130	0.35089	0.17800

TABLE F7-2
M. C. WALCK: HORIZONTAL POINT ESTIMATES
SPECTRAL ACCELERATION AT 0.05 SEC PERIOD

CASE NO.	MAGNITUDE	DISTANCE (KM)	MU	SIGMA	SIGMA MU	SIGMA SIGMA
1	5.00	1	0.32745	0.69777	0.41292	0.16100
2	5.00	1	0.30646	0.69872	0.27924	0.16100
3	5.00	5	0.10396	0.69224	0.37626	0.16100
4	5.00	5	0.10347	0.69318	0.30920	0.16100
5	5.80	10	0.15904	0.60472	0.29881	0.16400
6	5.80	20	0.10212	0.59889	0.29471	0.16400
7	6.50	1	0.67480	0.57475	0.35986	0.16900
8	6.50	1	0.61859	0.57152	0.38692	0.16900
9	6.50	1	0.58774	0.57457	0.38506	0.16900
10	6.50	5	0.54050	0.56827	0.37543	0.16800
11	6.50	5	0.38410	0.57301	0.38250	0.16900
12	6.50	50	0.03878	0.57064	0.33608	0.16800
13	6.50	50	0.03524	0.56754	0.36609	0.16800
14	7.00	10	0.38863	0.53927	0.30178	0.17500
15	7.50	50	0.07473	0.53857	0.31567	0.17700
16	7.50	50	0.07176	0.53858	0.32265	0.17700
17	5.00	1	0.12690	0.69842	0.31469	0.16100
18	5.80	5	0.22890	0.60281	0.33491	0.16300
19	5.80	5	0.14020	0.60523	0.33843	0.16400
20	5.00	10	0.12307	0.69364	0.30121	0.16000
21	5.00	10	0.14356	0.69224	0.28780	0.16100
22	5.00	50	0.01023	0.69524	0.40966	0.16200
23	5.00	50	0.01022	0.70547	0.42930	0.16100
24	5.00	160	0.00111	0.69842	0.35969	0.16700
25	5.80	1	0.46464	0.60265	0.41041	0.16400
26	5.80	5	0.35141	0.60075	0.36053	0.16500
27	5.80	5	0.22026	0.60424	0.42546	0.16500
28	5.80	10	0.19522	0.60634	0.32292	0.16500
29	5.80	10	0.23177	0.59910	0.31638	0.16400
30	5.80	10	0.13811	0.60313	0.43254	0.16400
31	5.80	50	0.02068	0.61316	0.38131	0.16300
32	5.80	50	0.02015	0.61135	0.46664	0.16300
33	6.50	5	0.49601	0.56957	0.31995	0.16800
34	6.50	10	0.32009	0.57524	0.30129	0.17000
35	6.50	10	0.39796	0.56974	0.37291	0.16800
36	6.50	10	0.23872	0.57337	0.36340	0.16900
37	6.50	20	0.15103	0.57323	0.28855	0.16900
38	6.50	20	0.17874	0.57152	0.33335	0.16900
39	6.50	20	0.11310	0.57009	0.36390	0.16200
40	6.50	100	0.01441	0.56538	0.42257	0.16200
41	6.50	160	0.00658	0.56838	0.52760	0.16700
42	7.00	1	0.76340	0.54120	0.33536	0.17500
43	7.00	10	0.47397	0.54504	0.39241	0.17800
44	7.00	10	0.29186	0.54010	0.35777	0.17500
45	7.00	50	0.05792	0.53954	0.31750	0.17100
46	7.00	50	0.05688	0.54780	0.31097	0.17500
47	7.50	1	0.82750	0.53667	0.40126	0.18700
48	5.00	10	0.45640	0.54122	0.34733	0.18400
49	5.00	10	0.50871	0.53438	0.47077	0.17800
50	8.00	50	0.09575	0.54949	0.34048	0.18000
51	8.00	160	0.02069	0.52843	0.43869	0.17900

TABLE F7-3
M. C. WALCK: HORIZONTAL POINT ESTIMATES
SPECTRAL ACCELERATION AT 0.10 SEC PERIOD

CASE NO.	MAGNITUDE	DISTANCE (KM)	MU	SIGMA	SIGMA MU	SIGMA SIGMA
1	5.00	1	0.33655	0.71877	0.29022	0.15900
2	5.00	1	0.31895	0.71684	0.32724	0.15800
3	5.00	5	0.11180	0.71040	0.26946	0.16000
4	5.00	5	0.11507	0.70944	0.32592	0.16000
5	5.80	10	0.16513	0.62111	0.30300	0.16700
6	5.80	20	0.11928	0.61750	0.29574	0.16700
7	6.50	1	0.76878	0.59229	0.38578	0.17400
8	6.50	1	0.71468	0.58667	0.44479	0.17300
9	6.50	1	0.68548	0.59338	0.42280	0.17500
10	6.50	5	0.60124	0.58317	0.38448	0.17100
11	6.50	5	0.43719	0.59112	0.32329	0.17400
12	6.50	50	0.05011	0.58826	0.33069	0.17300
13	6.50	50	0.04542	0.58423	0.30204	0.17200
14	7.00	10	0.41550	0.55633	0.31393	0.17900
15	7.50	50	0.09523	0.55001	0.33531	0.18400
16	7.50	50	0.09276	0.54336	0.32893	0.18000
17	5.00	1	0.13085	0.70790	0.23968	0.16000
18	5.80	5	0.24562	0.62428	0.31138	0.16600
19	5.80	5	0.14893	0.62740	0.30640	0.16600
20	5.00	10	0.13666	0.71290	0.25060	0.15900
21	5.00	10	0.15192	0.70654	0.27228	0.15900
22	5.00	50	0.01282	0.72578	0.30656	0.15600
23	5.00	50	0.01252	0.72608	0.32780	0.15600
24	5.00	160	0.00135	0.72545	0.36412	0.15900
25	5.80	1	0.46931	0.62363	0.38041	0.16800
26	5.80	5	0.37000	0.61710	0.29742	0.16700
27	5.80	5	0.24561	0.62312	0.34714	0.16800
28	5.80	10	0.19745	0.62256	0.29084	0.16800
29	5.80	10	0.24013	0.61671	0.24891	0.16700
30	5.80	10	0.13956	0.61803	0.36625	0.16600
31	5.80	50	0.02105	0.64240	0.44083	0.16500
32	5.80	50	0.02420	0.63434	0.37988	0.16500
33	6.50	5	0.56819	0.59033	0.34507	0.17300
34	6.50	10	0.36498	0.58976	0.32182	0.17300
35	6.50	10	0.45543	0.58429	0.39613	0.17200
36	6.50	10	0.27384	0.58913	0.29071	0.17300
37	6.50	20	0.17989	0.58640	0.31475	0.17100
38	6.50	20	0.20550	0.58572	0.31885	0.17200
39	6.50	20	0.13300	0.58773	0.27961	0.16900
40	6.50	100	0.01894	0.58413	0.43051	0.16300
41	6.50	160	0.00783	0.58750	0.49137	0.16800
42	7.00	1	0.82210	0.55754	0.31198	0.18600
43	7.00	10	0.50176	0.55891	0.35060	0.18200
44	7.00	10	0.31152	0.55683	0.27988	0.18000
45	7.00	50	0.06652	0.55849	0.36973	0.17700
46	7.00	50	0.06517	0.56111	0.31139	0.17900
47	7.50	1	0.93462	0.55758	0.38943	0.19400
48	5.00	10	0.52804	0.55146	0.35314	0.18800
49	5.00	10	0.58427	0.54481	0.44174	0.19000
50	8.00	50	0.11668	0.56637	0.37581	0.18800
51	8.00	160	0.02374	0.55357	0.41943	0.18400

TABLE F7-4
M. C. WALCK: HORIZONTAL POINT ESTIMATES
SPECTRAL ACCELERATION AT 0.20 SEC PERIOD

CASE NO.	MAGNITUDE	DISTANCE (KM)	MU	SIGMA	SIGMA MU	SIGMA SIGMA
1	5.00	1	0.25013	0.74571	0.30485	0.15000
2	5.00	1	0.23865	0.74760	0.34933	0.15000
3	5.00	5	0.08854	0.73459	0.26480	0.15100
4	5.00	5	0.09155	0.73365	0.29509	0.15200
5	5.80	10	0.16983	0.65616	0.25248	0.16300
6	5.80	20	0.11554	0.64789	0.29625	0.16100
7	6.50	1	0.70354	0.62146	0.39807	0.17000
8	6.50	1	0.64469	0.62205	0.44509	0.17100
9	6.50	1	0.62409	0.63182	0.43766	0.17500
10	6.50	5	0.55352	0.61791	0.39052	0.17000
11	6.50	5	0.41151	0.62389	0.31071	0.17100
12	6.50	50	0.05527	0.62160	0.34725	0.17000
13	6.50	50	0.05048	0.61559	0.28077	0.16900
14	7.00	10	0.44910	0.58967	0.32624	0.17700
15	7.50	50	0.11225	0.58207	0.35640	0.17800
16	7.50	50	0.10926	0.57658	0.33698	0.17600
17	5.00	1	0.10364	0.73607	0.22682	0.15300
18	5.80	5	0.23346	0.65466	0.32112	0.16100
19	5.80	5	0.15447	0.65819	0.29528	0.16100
20	5.00	10	0.10765	0.73311	0.24164	0.15000
21	5.00	10	0.12641	0.73365	0.27240	0.15200
22	5.00	50	0.01218	0.75535	0.25559	0.14700
23	5.00	50	0.01121	0.75333	0.30631	0.14800
24	5.00	160	0.00158	0.76487	0.32903	0.15100
25	5.80	1	0.43968	0.65283	0.40415	0.16200
26	5.80	5	0.33978	0.64741	0.33800	0.16200
27	5.80	5	0.22173	0.65332	0.29380	0.16200
28	5.80	10	0.19720	0.65519	0.29763	0.16300
29	5.80	10	0.23340	0.64770	0.31001	0.16200
30	5.80	10	0.14015	0.65486	0.26688	0.16200
31	5.80	50	0.02748	0.67622	0.28952	0.15900
32	5.80	50	0.02646	0.66936	0.31769	0.15900
33	6.50	5	0.52459	0.62010	0.35504	0.16900
34	6.50	10	0.33960	0.62373	0.31006	0.17100
35	6.50	10	0.41266	0.61916	0.36050	0.17000
36	6.50	10	0.26587	0.61950	0.28059	0.16900
37	6.50	20	0.17721	0.62207	0.29211	0.17200
38	6.50	20	0.21091	0.61666	0.33768	0.16900
39	6.50	20	0.13709	0.62130	0.25582	0.17000
40	6.50	100	0.02370	0.61930	0.39592	0.16500
41	6.50	160	0.01064	0.62699	0.44743	0.16600
42	7.00	1	0.82620	0.59000	0.35074	0.17700
43	7.00	10	0.52239	0.58988	0.37419	0.17800
44	7.00	10	0.34447	0.58827	0.28105	0.17600
45	7.00	50	0.08668	0.59385	0.37181	0.17500
46	7.00	50	0.08283	0.59424	0.31205	0.17700
47	7.50	1	0.94092	0.58805	0.41872	0.18600
48	5.00	10	0.54929	0.58670	0.37104	0.18500
49	5.00	10	0.58369	0.57502	0.43161	0.17700
50	8.00	50	0.13717	0.59726	0.36255	0.18000
51	8.00	160	0.03448	0.59114	0.38604	0.17700

TABLE F7-5
M. C. WALCK: HORIZONTAL POINT ESTIMATES
SPECTRAL ACCELERATION AT 0.50 SEC PERIOD

CASE NO.	MAGNITUDE	DISTANCE (KM)	MU	SIGMA	SIGMA MU	SIGMA SIGMA
1	5.00	1	0.11039	0.80160	0.34495	0.12700
2	5.00	1	0.11046	0.79695	0.38764	0.12700
3	5.00	5	0.04213	0.78831	0.27237	0.13000
4	5.00	5	0.04489	0.78552	0.28880	0.13000
5	5.80	10	0.10526	0.71665	0.25882	0.15500
6	5.80	20	0.07631	0.71435	0.27086	0.15600
7	6.50	1	0.51424	0.68397	0.27234	0.16900
8	6.50	1	0.46582	0.67902	0.30448	0.16900
9	6.50	1	0.44663	0.68836	0.29872	0.17200
10	6.50	5	0.39892	0.68177	0.27747	0.17000
11	6.50	5	0.28652	0.68411	0.26640	0.16900
12	6.50	50	0.04598	0.68780	0.29308	0.17100
13	6.50	50	0.04260	0.67773	0.28831	0.16900
14	7.00	10	0.35757	0.65225	0.30192	0.17900
15	7.50	50	0.11236	0.64437	0.27670	0.17900
16	7.50	50	0.10653	0.63609	0.27229	0.17600
17	5.00	1	0.04925	0.78572	0.23161	0.13200
18	5.80	5	0.15782	0.72325	0.27443	0.15400
19	5.80	5	0.09331	0.72727	0.28783	0.15400
20	5.00	10	0.04873	0.78347	0.23432	0.12700
21	5.00	10	0.05659	0.78275	0.27918	0.13000
22	5.00	50	0.00661	0.80633	0.23097	0.12100
23	5.00	50	0.00677	0.81342	0.22079	0.12100
24	5.00	160	0.00141	0.80973	0.24169	0.12300
25	5.80	1	0.27984	0.71461	0.31148	0.15400
26	5.80	5	0.22026	0.71142	0.31178	0.15600
27	5.80	5	0.13672	0.71060	0.28586	0.15300
28	5.80	10	0.12722	0.71777	0.27544	0.15600
29	5.80	10	0.15738	0.71011	0.29657	0.15300
30	5.80	10	0.08649	0.71536	0.30012	0.15300
31	5.80	50	0.02041	0.74643	0.27397	0.14500
32	5.80	50	0.01931	0.74361	0.32748	0.14600
33	6.50	5	0.37861	0.68293	0.30669	0.16900
34	6.50	10	0.25004	0.69312	0.30991	0.16900
35	6.50	10	0.30967	0.68854	0.32048	0.16900
36	6.50	10	0.18707	0.68285	0.28680	0.16900
37	6.50	20	0.13079	0.68413	0.28848	0.16600
38	6.50	20	0.15485	0.68360	0.29918	0.17100
39	6.50	20	0.10309	0.68327	0.24284	0.16900
40	6.50	100	0.02357	0.68660	0.35592	0.16600
41	6.50	160	0.01203	0.68935	0.50722	0.16300
42	7.00	1	0.65664	0.65013	0.27392	0.17800
43	7.00	10	0.42928	0.64941	0.33614	0.17900
44	7.00	10	0.26343	0.65221	0.26255	0.17900
45	7.00	50	0.07800	0.65740	0.29966	0.17800
46	7.00	50	0.07419	0.66071	0.30133	0.18100
47	7.50	1	0.73800	0.64770	0.29866	0.18800
48	5.00	10	0.44275	0.64566	0.28266	0.18400
49	5.00	10	0.48336	0.63731	0.38897	0.17900
50	8.00	50	0.14844	0.66084	0.27606	0.17700
51	8.00	160	0.05004	0.66096	0.37236	0.17200

TABLE F7-6
M. C. WALCK: HORIZONTAL POINT ESTIMATES
SPECTRAL ACCELERATION AT 1.00 SEC PERIOD

CASE NO.	MAGNITUDE	DISTANCE (KM)	MU	SIGMA	SIGMA MU	SIGMA SIGMA
1	5.00	1	0.04240	0.90227	0.26394	0.12400
2	5.00	1	0.04511	0.89384	0.38188	0.12900
3	5.00	5	0.01702	0.82882	0.21964	0.10700
4	5.00	5	0.01845	0.82882	0.25495	0.10700
5	5.80	10	0.05194	0.77611	0.24690	0.13600
6	5.80	20	0.03915	0.76766	0.26170	0.14000
7	6.50	1	0.29071	0.74524	0.21867	0.16000
8	6.50	1	0.26180	0.74327	0.31514	0.16300
9	6.50	1	0.25574	0.74499	0.28978	0.16400
10	6.50	5	0.22943	0.74246	0.28014	0.16200
11	6.50	5	0.15551	0.74085	0.33034	0.16100
12	6.50	50	0.02961	0.73550	0.29476	0.16000
13	6.50	50	0.02758	0.74207	0.30795	0.16200
14	7.00	10	0.20999	0.70235	0.25464	0.17600
15	7.50	50	0.07920	0.69302	0.27814	0.17800
16	7.50	50	0.07820	0.69742	0.28205	0.18000
17	5.00	1	0.01966	0.83187	0.20000	0.11000
18	5.80	5	0.08207	0.78980	0.41204	0.14400
19	5.80	5	0.04702	0.78768	0.34359	0.14100
20	5.00	10	0.01882	0.82546	0.20000	0.10500
21	5.00	10	0.02314	0.81392	0.22509	0.11300
22	5.00	50	0.00283	0.83808	0.30103	0.09800
23	5.00	50	0.00306	0.84839	0.21956	0.09700
24	5.00	160	0.00087	0.85116	0.20000	0.09700
25	5.80	1	0.13646	0.77959	0.32270	0.13800
26	5.80	5	0.11043	0.76846	0.34796	0.13700
27	5.80	5	0.06594	0.77779	0.36178	0.14000
28	5.80	10	0.06103	0.77758	0.25363	0.13700
29	5.80	10	0.07928	0.76959	0.28937	0.13200
30	5.80	10	0.04523	0.76876	0.31707	0.14300
31	5.80	50	0.01093	0.78853	0.25215	0.12900
32	5.80	50	0.01124	0.79169	0.23834	0.13200
33	6.50	5	0.20133	0.74794	0.26541	0.16100
34	6.50	10	0.14162	0.74507	0.29900	0.16000
35	6.50	10	0.18376	0.74018	0.31947	0.16100
36	6.50	10	0.10475	0.74050	0.30865	0.16000
37	6.50	20	0.07433	0.74096	0.26036	0.15900
38	6.50	20	0.08610	0.74314	0.32253	0.16300
39	6.50	20	0.05877	0.74179	0.29597	0.16700
40	6.50	100	0.01558	0.73628	0.31868	0.16000
41	6.50	160	0.00966	0.73900	0.54121	0.14500
42	7.00	1	0.36082	0.70909	0.28703	0.17500
43	7.00	10	0.25392	0.70719	0.33867	0.17700
44	7.00	10	0.15837	0.70422	0.30564	0.17500
45	7.00	50	0.05020	0.71254	0.33456	0.17600
46	7.00	50	0.05052	0.71948	0.31899	0.17900
47	7.50	1	0.44211	0.69949	0.36243	0.18000
48	5.00	10	0.28308	0.69870	0.28780	0.18000
49	5.00	10	0.31676	0.69201	0.43455	0.17700
50	8.00	50	0.11233	0.69906	0.28918	0.18100
51	8.00	160	0.04627	0.71335	0.40257	0.17700

TABLE F7-7
M. C. WALCK: HORIZONTAL POINT ESTIMATES
SPECTRAL ACCELERATION AT 2.00 SEC PERIOD

CASE NO.	MAGNITUDE	DISTANCE (KM)	MU	SIGMA	SIGMA MU	SIGMA SIGMA
1	5.00	1	0.01223	0.90638	0.34180	0.10000
2	5.00	1	0.01321	0.89520	0.36787	0.10800
3	5.00	5	0.00528	0.88594	0.29770	0.10900
4	5.00	5	0.00570	0.89246	0.26458	0.10800
5	5.80	10	0.02067	0.85748	0.35377	0.13500
6	5.80	20	0.01499	0.85396	0.36901	0.14300
7	6.50	1	0.13034	0.82080	0.25445	0.16100
8	6.50	1	0.11916	0.80747	0.25991	0.16400
9	6.50	1	0.11032	0.81599	0.27063	0.16700
10	6.50	5	0.09622	0.81345	0.29630	0.16900
11	6.50	5	0.07555	0.81716	0.31728	0.16700
12	6.50	50	0.01519	0.82594	0.35863	0.16000
13	6.50	50	0.01340	0.82717	0.47154	0.16400
14	7.00	10	0.10179	0.78901	0.29082	0.18900
15	7.50	50	0.04994	0.76822	0.38285	0.19700
16	7.50	50	0.04513	0.75873	0.48182	0.19400
17	5.00	1	0.00641	0.88717	0.22050	0.11100
18	5.80	5	0.03367	0.84574	0.37031	0.13800
19	5.80	5	0.02093	0.85015	0.36627	0.13800
20	5.00	10	0.00617	0.88416	0.20623	0.10700
21	5.00	10	0.00719	0.87819	0.24130	0.11900
22	5.00	50	0.00104	0.90441	0.27672	0.08900
23	5.00	50	0.00104	0.91271	0.31086	0.08900
24	5.00	160	0.00046	0.91556	0.20328	0.08900
25	5.80	1	0.05259	0.85720	0.26004	0.13900
26	5.80	5	0.04239	0.83249	0.31911	0.13900
27	5.80	5	0.02943	0.83930	0.33057	0.14700
28	5.80	10	0.02336	0.85634	0.31988	0.14100
29	5.80	10	0.02839	0.84907	0.34359	0.14900
30	5.80	10	0.02035	0.84789	0.33901	0.13900
31	5.80	50	0.00455	0.86675	0.51464	0.12300
32	5.80	50	0.00495	0.87496	0.41651	0.12900
33	6.50	5	0.09457	0.82003	0.25276	0.16000
34	6.50	10	0.06361	0.82054	0.26612	0.16100
35	6.50	10	0.07657	0.81449	0.29887	0.17000
36	6.50	10	0.04914	0.82363	0.36406	0.16500
37	6.50	20	0.03670	0.82377	0.28893	0.16300
38	6.50	20	0.04119	0.81470	0.33250	0.16200
39	6.50	20	0.02837	0.82255	0.40192	0.16800
40	6.50	100	0.00822	0.81432	0.40052	0.15200
41	6.50	160	0.00593	0.82032	0.63580	0.14600
42	7.00	1	0.18443	0.78293	0.26410	0.18400
43	7.00	10	0.11318	0.77324	0.34169	0.18700
44	7.00	10	0.07903	0.78909	0.36750	0.19100
45	7.00	50	0.02956	0.80019	0.31635	0.18800
46	7.00	50	0.02724	0.79772	0.40272	0.19000
47	7.50	1	0.22501	0.76600	0.34122	0.19800
48	5.00	10	0.14676	0.76436	0.40618	0.19400
49	5.00	10	0.15075	0.76181	0.46627	0.19400
50	8.00	50	0.07127	0.76747	0.32439	0.21300
51	8.00	160	0.03580	0.78183	0.47097	0.20500

TABLE F7-8
M. C. WALCK: HORIZONTAL POINT ESTIMATES
SPECTRAL ACCELERATION AT 3.33 SEC PERIOD

CASE NO.	MAGNITUDE	DISTANCE (KM)	MU	SIGMA	SIGMA MU	SIGMA SIGMA
1	5.00	1	0.00464	0.93238	0.50526	0.10800
2	5.00	1	0.00501	0.90893	0.52239	0.11400
3	5.00	5	0.00205	0.92002	0.50603	0.11600
4	5.00	5	0.00224	0.92535	0.47386	0.11500
5	5.80	10	0.00966	0.85902	0.38489	0.13600
6	5.80	20	0.00619	0.85366	0.42506	0.14400
7	6.50	1	0.06970	0.82151	0.32286	0.18300
8	6.50	1	0.06360	0.79051	0.30294	0.16200
9	6.50	1	0.05945	0.80278	0.33343	0.17100
10	6.50	5	0.05077	0.79863	0.31533	0.17100
11	6.50	5	0.04285	0.80882	0.38311	0.17800
12	6.50	50	0.00829	0.83501	0.45752	0.17800
13	6.50	50	0.00639	0.81328	0.53040	0.17400
14	7.00	10	0.05767	0.79810	0.37422	0.20900
15	7.50	50	0.03143	0.78632	0.38707	0.22200
16	7.50	50	0.02608	0.78038	0.52036	0.22200
17	5.00	1	0.00270	0.89832	0.40974	0.11500
18	5.80	5	0.01369	0.86042	0.33063	0.15200
19	5.80	5	0.00861	0.86169	0.40556	0.14700
20	5.00	10	0.00256	0.91218	0.36592	0.11200
21	5.00	10	0.00282	0.90356	0.44487	0.12900
22	5.00	50	0.00048	0.93104	0.28253	0.08800
23	5.00	50	0.00044	0.93795	0.34788	0.09200
24	5.00	160	0.00017	0.94864	0.23141	0.08300
25	5.80	1	0.02510	0.85231	0.37156	0.13700
26	5.80	5	0.01938	0.84373	0.35537	0.15700
27	5.80	5	0.01446	0.84342	0.36839	0.14200
28	5.80	10	0.01138	0.85178	0.41367	0.13600
29	5.80	10	0.01132	0.83432	0.43811	0.13900
30	5.80	10	0.00935	0.84617	0.47177	0.14100
31	5.80	50	0.00222	0.88998	0.40918	0.12600
32	5.80	50	0.00217	0.87671	0.47531	0.12700
33	6.50	5	0.05288	0.82075	0.32841	0.18000
34	6.50	10	0.03385	0.81739	0.37672	0.17500
35	6.50	10	0.03492	0.79906	0.35211	0.17200
36	6.50	10	0.02619	0.81421	0.49206	0.17600
37	6.50	20	0.01845	0.81122	0.42856	0.16800
38	6.50	20	0.01848	0.82092	0.47534	0.18400
39	6.50	20	0.01482	0.80742	0.54931	0.16900
40	6.50	100	0.00381	0.82571	0.49493	0.15900
41	6.50	160	0.00321	0.86096	0.62653	0.16500
42	7.00	1	0.10849	0.78395	0.34419	0.19700
43	7.00	10	0.05689	0.76936	0.34807	0.19600
44	7.00	10	0.04346	0.78952	0.48616	0.20300
45	7.00	50	0.01778	0.79403	0.38366	0.20700
46	7.00	50	0.01515	0.79208	0.49211	0.21100
47	7.50	1	0.14280	0.78764	0.37969	0.21900
48	5.00	10	0.08623	0.79609	0.49034	0.22200
49	5.00	10	0.07976	0.79161	0.50733	0.21900
50	8.00	50	0.04748	0.79218	0.35157	0.24000
51	8.00	160	0.02279	0.82752	0.40694	0.22100

TABLE F7-9
M. C. WALCK: HORIZONTAL POINT ESTIMATES
PEAK GROUND VELOCITY

CASE NO.	MAGNITUDE	DISTANCE (KM)	MU	SIGMA	SIGMA MU	SIGMA SIGMA
1	5.00	1	6.41921	0.69059	0.46971	0.14800
2	5.00	1	7.17257	0.67002	0.42351	0.14200
3	5.00	5	2.72278	0.67002	0.34900	0.14200
4	5.00	5	3.22851	0.66818	0.42848	0.14000
5	5.80	10	6.37310	0.71422	0.27348	0.16100
6	5.80	20	4.74515	0.71000	0.32044	0.16100
7	6.50	1	34.15452	0.71099	0.22892	0.17600
8	6.50	1	31.37688	0.70490	0.29075	0.17500
9	6.50	1	29.34413	0.70861	0.29551	0.17600
10	6.50	5	29.49820	0.70438	0.25267	0.17500
11	6.50	5	19.29887	0.70540	0.27023	0.17500
12	6.50	50	2.52660	0.70551	0.30546	0.17300
13	6.50	50	2.29040	0.70223	0.33963	0.17400
14	7.00	10	26.38220	0.70314	0.28532	0.18300
15	7.50	50	7.79752	0.70844	0.33204	0.19300
16	7.50	50	7.81732	0.70389	0.38956	0.19200
17	5.00	1	3.37499	0.64944	0.36703	0.13300
18	5.80	5	10.67598	0.71629	0.37579	0.16200
19	5.80	5	5.97682	0.71689	0.33199	0.16200
20	5.00	10	2.65139	0.68508	0.20743	0.14300
21	5.00	10	3.39941	0.66818	0.20000	0.14000
22	5.00	50	0.33848	0.68465	0.33390	0.15200
23	5.00	50	0.35234	0.68694	0.36638	0.15300
24	5.00	160	0.07464	0.71030	0.44988	0.14600
25	5.80	1	16.54418	0.71572	0.33990	0.16800
26	5.80	5	14.28111	0.70869	0.30680	0.16000
27	5.80	5	8.32652	0.71214	0.27402	0.16100
28	5.80	10	7.22272	0.71721	0.25563	0.16200
29	5.80	10	9.66396	0.71004	0.21227	0.16100
30	5.80	10	5.15102	0.70542	0.30981	0.16400
31	5.80	50	0.97198	0.76116	0.22495	0.15400
32	5.80	50	0.96185	0.76103	0.29571	0.15700
33	6.50	5	24.71942	0.71020	0.20000	0.17500
34	6.50	10	16.56292	0.70913	0.23266	0.18100
35	6.50	10	22.35008	0.70473	0.25199	0.17500
36	6.50	10	12.19726	0.70487	0.30020	0.17400
37	6.50	20	8.44397	0.70803	0.31167	0.17400
38	6.50	20	10.15552	0.70531	0.31577	0.17500
39	6.50	20	6.44230	0.70312	0.36365	0.17400
40	6.50	100	1.17220	0.70684	0.34623	0.17300
41	6.50	160	0.53879	0.76270	0.55741	0.15700
42	7.00	1	48.69814	0.70194	0.31744	0.18200
43	7.00	10	36.54720	0.69952	0.42746	0.18300
44	7.00	10	19.71888	0.69893	0.39890	0.18200
45	7.00	50	4.65942	0.69683	0.30272	0.18000
46	7.00	50	4.57622	0.69608	0.36163	0.18100
47	7.50	1	63.97175	0.71327	0.56319	0.19600
48	5.00	10	34.96797	0.71049	0.37695	0.19400
49	5.00	10	39.83652	0.71226	0.71809	0.18700
50	8.00	50	13.10689	0.71306	0.32048	0.19300
51	8.00	160	3.43297	0.81055	0.43466	0.13300

TABLE F7-10
M. C. WALCK: VERTICAL POINT ESTIMATES
PEAK GROUND ACCELERATION

CASE NO.	MAGNITUDE	DISTANCE (KM)	MU	SIGMA	SIGMA MU	SIGMA SIGMA
1	5.00	1	0.11369	0.69558	0.53612	0.16269
2	5.00	1	0.10072	0.69861	0.40954	0.16195
3	5.00	5	0.03309	0.68234	0.42608	0.16493
4	5.00	5	0.03093	0.68631	0.37652	0.16399
5	5.80	10	0.05344	0.63373	0.38506	0.17229
6	5.80	20	0.03846	0.62149	0.45259	0.16608
7	6.50	1	0.29473	0.58699	0.35841	0.17957
8	6.50	1	0.28070	0.59398	0.33916	0.18452
9	6.50	1	0.27565	0.58956	0.34846	0.18100
10	6.50	5	0.23629	0.58800	0.35774	0.17989
11	6.50	5	0.17714	0.58956	0.34939	0.18100
12	6.50	50	0.01308	0.59100	0.44465	0.18161
13	6.50	50	0.01304	0.58519	0.41643	0.17825
14	7.00	10	0.15579	0.56803	0.33335	0.19961
15	7.50	50	0.02728	0.56205	0.41914	0.20807
16	7.50	50	0.02610	0.55440	0.34875	0.20224
17	5.00	1	0.03642	0.67848	0.45772	0.16576
18	5.80	5	0.07518	0.63065	0.45167	0.16811
19	5.80	5	0.05282	0.63597	0.44772	0.17111
20	5.00	10	0.03811	0.68934	0.39280	0.16461
21	5.00	10	0.05303	0.67942	0.37081	0.16479
22	5.00	50	0.00292	0.71091	0.35426	0.15724
23	5.00	50	0.00271	0.70601	0.33233	0.15803
24	5.00	160	0.00029	0.71185	0.38931	0.15715
25	5.80	1	0.17897	0.64061	0.49009	0.16742
26	5.80	5	0.15631	0.63065	0.40182	0.16811
27	5.80	5	0.09711	0.63350	0.38638	0.16964
28	5.80	10	0.07000	0.63673	0.38964	0.17159
29	5.80	10	0.10067	0.62598	0.39387	0.17385
30	5.80	10	0.05514	0.63426	0.37744	0.17008
31	5.80	50	0.00677	0.66025	0.34001	0.16372
32	5.80	50	0.00718	0.66480	0.38273	0.16559
33	6.50	5	0.21483	0.58743	0.32670	0.17950
34	6.50	10	0.12825	0.59070	0.32432	0.18186
35	6.50	10	0.17978	0.59255	0.41881	0.18333
36	6.50	10	0.10448	0.58843	0.33840	0.18019
37	6.50	20	0.05851	0.58956	0.34824	0.18100
38	6.50	20	0.07648	0.58908	0.44404	0.18130
39	6.50	20	0.04509	0.58743	0.36445	0.17950
40	6.50	100	0.00470	0.60003	0.51108	0.17858
41	6.50	160	0.00159	0.59461	0.51825	0.17519
42	7.00	1	0.31765	0.57089	0.33933	0.20213
43	7.00	10	0.20531	0.57132	0.41746	0.20252
44	7.00	10	0.12475	0.56960	0.34178	0.20097
45	7.00	50	0.01876	0.56932	0.38307	0.20072
46	7.00	50	0.01992	0.56753	0.46811	0.19930
47	7.50	1	0.41683	0.56908	0.49259	0.21532
48	5.00	10	0.18278	0.56205	0.34225	0.20807
49	5.00	10	0.23210	0.56535	0.44386	0.21133
50	8.00	50	0.03980	0.56913	0.44882	0.21311
51	8.00	160	0.00768	0.57462	0.52849	0.21196

TABLE F7-11
M. C. WALCK: VERTICAL POINT ESTIMATES
SPECTRAL ACCELERATION AT 0.05 SEC PERIOD

CASE NO.	MAGNITUDE	DISTANCE (KM)	MU	SIGMA	SIGMA MU	SIGMA SIGMA
1	5.00	1	0.26123	0.70187	0.58070	0.16050
2	5.00	1	0.22206	0.69952	0.45254	0.16004
3	5.00	5	0.06932	0.69299	0.49648	0.16103
4	5.00	5	0.06365	0.69575	0.43193	0.16052
5	5.80	10	0.10045	0.64158	0.46330	0.16851
6	5.80	20	0.06939	0.63017	0.43620	0.16401
7	6.50	1	0.58764	0.59623	0.44450	0.17630
8	6.50	1	0.54414	0.60327	0.41898	0.18064
9	6.50	1	0.54237	0.60024	0.41497	0.17817
10	6.50	5	0.46094	0.60024	0.40963	0.17817
11	6.50	5	0.33347	0.59909	0.43621	0.17730
12	6.50	50	0.01966	0.60579	0.46599	0.18109
13	6.50	50	0.01999	0.59623	0.44919	0.17630
14	7.00	10	0.28363	0.57958	0.38466	0.19667
15	7.50	50	0.04045	0.57321	0.41686	0.20393
16	7.50	50	0.04023	0.56036	0.39218	0.19403
17	5.00	1	0.07736	0.69004	0.51735	0.16289
18	5.80	5	0.14307	0.64724	0.53519	0.16869
19	5.80	5	0.10098	0.65166	0.47942	0.17164
20	5.00	10	0.07836	0.70283	0.47674	0.16167
21	5.00	10	0.11311	0.69347	0.34895	0.16101
22	5.00	50	0.00541	0.70938	0.36916	0.15902
23	5.00	50	0.00531	0.71376	0.36499	0.15861
24	5.00	160	0.00037	0.71109	0.50776	0.15880
25	5.80	1	0.36625	0.65418	0.61403	0.17107
26	5.80	5	0.29600	0.64628	0.47649	0.16810
27	5.80	5	0.18958	0.64628	0.47061	0.16810
28	5.80	10	0.13519	0.65262	0.47398	0.17233
29	5.80	10	0.19882	0.63719	0.46799	0.17151
30	5.80	10	0.10210	0.64474	0.48033	0.16721
31	5.80	50	0.01126	0.66486	0.37545	0.16697
32	5.80	50	0.01228	0.67379	0.40207	0.17146
33	6.50	5	0.41413	0.60082	0.38354	0.17862
34	6.50	10	0.23822	0.60529	0.37354	0.18244
35	6.50	10	0.33179	0.60269	0.44762	0.18015
36	6.50	10	0.19440	0.60197	0.39894	0.17955
37	6.50	20	0.10381	0.60197	0.37245	0.17955
38	6.50	20	0.13728	0.59883	0.45039	0.17866
39	6.50	20	0.07944	0.59967	0.40135	0.17773
40	6.50	100	0.00596	0.59813	0.57919	0.18078
41	6.50	160	0.00191	0.59482	0.61728	0.17816
42	7.00	1	0.62677	0.58348	0.38877	0.20036
43	7.00	10	0.37784	0.58492	0.43654	0.20182
44	7.00	10	0.22890	0.58160	0.37566	0.19854
45	7.00	50	0.02725	0.58073	0.40219	0.19772
46	7.00	50	0.03087	0.57669	0.47324	0.19462
47	7.50	1	0.81120	0.58247	0.46988	0.21405
48	5.00	10	0.33461	0.57292	0.38328	0.20365
49	5.00	10	0.42845	0.57697	0.45942	0.20781
50	8.00	50	0.05783	0.58663	0.43421	0.21341
51	8.00	160	0.00801	0.57451	0.61532	0.21599

TABLE F7-12
M. C. WALCK: VERTICAL POINT ESTIMATES
SPECTRAL ACCELERATION AT 0.10 SEC PERIOD

CASE NO.	MAGNITUDE	DISTANCE (KM)	MU	SIGMA	SIGMA MU	SIGMA SIGMA
1	5.00	1	0.22257	0.71774	0.45873	0.16014
2	5.00	1	0.20359	0.72606	0.34144	0.16161
3	5.00	5	0.06819	0.70912	0.35947	0.16227
4	5.00	5	0.06621	0.72128	0.31819	0.16531
5	5.80	10	0.10969	0.65167	0.33890	0.17800
6	5.80	20	0.07294	0.62565	0.44565	0.16730
7	6.50	1	0.59360	0.59764	0.39359	0.17725
8	6.50	1	0.55396	0.60904	0.38729	0.18458
9	6.50	1	0.55181	0.60904	0.41502	0.18458
10	6.50	5	0.44102	0.60671	0.40894	0.18216
11	6.50	5	0.34787	0.60788	0.37240	0.18336
12	6.50	50	0.02516	0.61579	0.50244	0.18651
13	6.50	50	0.02471	0.59802	0.45734	0.17768
14	7.00	10	0.29918	0.58552	0.36855	0.20086
15	7.50	50	0.05142	0.57999	0.46136	0.21044
16	7.50	50	0.05044	0.55033	0.41485	0.18425
17	5.00	1	0.07590	0.70214	0.39009	0.16340
18	5.80	5	0.15377	0.65987	0.38453	0.17652
19	5.80	5	0.10943	0.65987	0.42844	0.17652
20	5.00	10	0.07982	0.72012	0.33161	0.16468
21	5.00	10	0.10474	0.70583	0.39178	0.16092
22	5.00	50	0.00664	0.74176	0.33983	0.15899
23	5.00	50	0.00628	0.73478	0.32934	0.15700
24	5.00	160	0.00053	0.73769	0.49384	0.15768
25	5.80	1	0.35946	0.66184	0.40616	0.17357
26	5.80	5	0.29806	0.65987	0.40200	0.17652
27	5.80	5	0.18920	0.65676	0.36647	0.17397
28	5.80	10	0.13979	0.66317	0.36152	0.17942
29	5.80	10	0.19493	0.64487	0.45157	0.17584
30	5.80	10	0.10868	0.65754	0.37187	0.17459
31	5.80	50	0.01416	0.70133	0.35690	0.17885
32	5.80	50	0.01447	0.69987	0.37130	0.17780
33	6.50	5	0.41821	0.60788	0.34647	0.18336
34	6.50	10	0.25621	0.60846	0.35544	0.18396
35	6.50	10	0.33891	0.60846	0.49280	0.18396
36	6.50	10	0.20996	0.60730	0.36038	0.18276
37	6.50	20	0.11406	0.60730	0.37715	0.18276
38	6.50	20	0.14591	0.60045	0.50022	0.18049
39	6.50	20	0.09063	0.60570	0.36312	0.18115
40	6.50	100	0.00829	0.60479	0.57721	0.17993
41	6.50	160	0.00269	0.60669	0.59005	0.18176
42	7.00	1	0.63139	0.58786	0.37876	0.20362
43	7.00	10	0.38649	0.59151	0.47925	0.20817
44	7.00	10	0.24426	0.58552	0.36133	0.20086
45	7.00	50	0.03583	0.58450	0.44241	0.19969
46	7.00	50	0.03792	0.57709	0.47672	0.19451
47	7.50	1	0.81662	0.58438	0.56737	0.21612
48	5.00	10	0.35482	0.57897	0.39824	0.20916
49	5.00	10	0.44539	0.58204	0.50211	0.21304
50	8.00	50	0.07230	0.60438	0.48122	0.22485
51	8.00	160	0.01006	0.59918	0.57261	0.22875

TABLE F7-13
M. C. WALCK: VERTICAL POINT ESTIMATES
SPECTRAL ACCELERATION AT 0.20 SEC PERIOD

CASE NO.	MAGNITUDE	DISTANCE (KM)	MU	SIGMA	SIGMA MU	SIGMA SIGMA
1	5.00	1	0.11915	0.74433	0.46099	0.15222
2	5.00	1	0.11711	0.75668	0.35199	0.15036
3	5.00	5	0.04525	0.73523	0.31430	0.15387
4	5.00	5	0.04276	0.73607	0.31617	0.15257
5	5.80	10	0.08215	0.66781	0.31789	0.17158
6	5.80	20	0.05601	0.64832	0.48157	0.16777
7	6.50	1	0.43463	0.62042	0.35342	0.17432
8	6.50	1	0.38876	0.63068	0.36436	0.17789
9	6.50	1	0.38907	0.63011	0.39949	0.17733
10	6.50	5	0.34692	0.62883	0.43720	0.17609
11	6.50	5	0.26044	0.62769	0.39517	0.17503
12	6.50	50	0.02324	0.63441	0.54840	0.17535
13	6.50	50	0.02210	0.61833	0.51736	0.17207
14	7.00	10	0.25064	0.60924	0.41303	0.19042
15	7.50	50	0.05149	0.60135	0.53266	0.19615
16	7.50	50	0.04785	0.57198	0.42092	0.17459
17	5.00	1	0.04978	0.72934	0.34039	0.15551
18	5.80	5	0.11164	0.67566	0.39388	0.16775
19	5.80	5	0.08028	0.67889	0.47775	0.16994
20	5.00	10	0.04987	0.74005	0.33575	0.15345
21	5.00	10	0.06689	0.74659	0.48302	0.15230
22	5.00	50	0.00540	0.76547	0.45873	0.14813
23	5.00	50	0.00483	0.75416	0.34783	0.14895
24	5.00	160	0.00058	0.76150	0.44249	0.14803
25	5.80	1	0.25883	0.68229	0.35921	0.16723
26	5.80	5	0.21636	0.68819	0.44543	0.17131
27	5.80	5	0.14038	0.67889	0.35944	0.16994
28	5.80	10	0.10689	0.68612	0.31807	0.17562
29	5.80	10	0.13886	0.67016	0.47128	0.17194
30	5.80	10	0.08159	0.67642	0.37356	0.16825
31	5.80	50	0.01247	0.72315	0.38009	0.16311
32	5.80	50	0.01377	0.72315	0.49615	0.16311
33	6.50	5	0.31946	0.62769	0.36472	0.17503
34	6.50	10	0.19532	0.62514	0.36132	0.17279
35	6.50	10	0.26109	0.63011	0.52854	0.17733
36	6.50	10	0.16446	0.62769	0.38885	0.17503
37	6.50	20	0.09588	0.62883	0.44118	0.17609
38	6.50	20	0.11907	0.62223	0.57674	0.17642
39	6.50	20	0.07675	0.62826	0.44514	0.17556
40	6.50	100	0.00908	0.62450	0.56489	0.17302
41	6.50	160	0.00354	0.63396	0.55902	0.17563
42	7.00	1	0.48332	0.60924	0.39263	0.19042
43	7.00	10	0.31922	0.61411	0.55553	0.19605
44	7.00	10	0.20255	0.61010	0.42556	0.19138
45	7.00	50	0.03515	0.60767	0.50128	0.18872
46	7.00	50	0.03689	0.59903	0.55346	0.18347
47	7.50	1	0.59964	0.59538	0.56119	0.19448
48	5.00	10	0.30787	0.60421	0.45452	0.19951
49	5.00	10	0.36676	0.60565	0.55797	0.20126
50	8.00	50	0.07284	0.63330	0.54117	0.21369
51	8.00	160	0.01423	0.62612	0.55591	0.20965

TABLE F7-14
M. C. WALCK: VERTICAL POINT ESTIMATES
SPECTRAL ACCELERATION AT 0.50 SEC PERIOD

CASE NO.	MAGNITUDE	DISTANCE (KM)	MU	SIGMA	SIGMA MU	SIGMA SIGMA
1	5.00	1	0.05254	0.79817	0.49726	0.13044
2	5.00	1	0.05047	0.79709	0.39457	0.12836
3	5.00	5	0.01809	0.78444	0.40182	0.13411
4	5.00	5	0.01817	0.78201	0.32900	0.13091
5	5.80	10	0.04862	0.70898	0.32493	0.16448
6	5.80	20	0.03522	0.68355	0.49364	0.16595
7	6.50	1	0.26046	0.66311	0.31076	0.17141
8	6.50	1	0.25599	0.67514	0.32902	0.17372
9	6.50	1	0.25030	0.67570	0.34003	0.17426
10	6.50	5	0.21875	0.67234	0.37300	0.17117
11	6.50	5	0.17562	0.67402	0.34578	0.17267
12	6.50	50	0.01727	0.67899	0.40296	0.16882
13	6.50	50	0.02007	0.65947	0.47511	0.16778
14	7.00	10	0.18989	0.65343	0.42984	0.18477
15	7.50	50	0.04685	0.63512	0.49617	0.18548
16	7.50	50	0.04191	0.60962	0.35319	0.16940
17	5.00	1	0.02069	0.78229	0.39086	0.13604
18	5.80	5	0.06261	0.72751	0.37420	0.16513
19	5.80	5	0.04214	0.72060	0.37315	0.16033
20	5.00	10	0.02157	0.78034	0.33218	0.13074
21	5.00	10	0.02888	0.78008	0.44162	0.13339
22	5.00	50	0.00251	0.82298	0.34002	0.12094
23	5.00	50	0.00254	0.81573	0.34006	0.12160
24	5.00	160	0.00039	0.81926	0.44692	0.12106
25	5.80	1	0.12397	0.73377	0.46365	0.16056
26	5.80	5	0.11968	0.73483	0.43466	0.17129
27	5.80	5	0.08098	0.72265	0.34352	0.16165
28	5.80	10	0.06269	0.72920	0.32493	0.16646
29	5.80	10	0.07990	0.71914	0.44963	0.16347
30	5.80	10	0.04784	0.73182	0.34934	0.16863
31	5.80	50	0.00820	0.77517	0.35071	0.14141
32	5.80	50	0.00935	0.78105	0.49730	0.14395
33	6.50	5	0.21049	0.67822	0.34638	0.17679
34	6.50	10	0.13791	0.69044	0.40088	0.17810
35	6.50	10	0.16898	0.67096	0.47860	0.16861
36	6.50	10	0.11383	0.66152	0.38903	0.16974
37	6.50	20	0.06886	0.66311	0.43389	0.17141
38	6.50	20	0.08859	0.65348	0.53994	0.16899
39	6.50	20	0.05327	0.67402	0.37758	0.17267
40	6.50	100	0.00857	0.67613	0.51114	0.16707
41	6.50	160	0.00381	0.68825	0.52168	0.16865
42	7.00	1	0.33895	0.65991	0.35161	0.19225
43	7.00	10	0.23344	0.64425	0.51943	0.18264
44	7.00	10	0.14661	0.64228	0.38422	0.18017
45	7.00	50	0.02874	0.64144	0.40444	0.17916
46	7.00	50	0.03161	0.64172	0.51339	0.17949
47	7.50	1	0.40965	0.65294	0.43353	0.19822
48	5.00	10	0.23162	0.64716	0.40666	0.19133
49	5.00	10	0.26688	0.63587	0.45521	0.18643
50	8.00	50	0.06587	0.65451	0.52987	0.19284
51	8.00	160	0.01910	0.69134	0.52989	0.19626

TABLE F7-15
M. C. WALCK: VERTICAL POINT ESTIMATES
SPECTRAL ACCELERATION AT 1.00 SEC PERIOD

CASE NO.	MAGNITUDE	DISTANCE (KM)	MU	SIGMA	SIGMA MU	SIGMA SIGMA
1	5.00	1	0.02251	0.82804	0.46249	0.11372
2	5.00	1	0.02162	0.83488	0.36788	0.10950
3	5.00	5	0.00788	0.81083	0.40687	0.11886
4	5.00	5	0.00790	0.80683	0.32138	0.11478
5	5.80	10	0.02338	0.74780	0.38817	0.14346
6	5.80	20	0.01840	0.73324	0.40292	0.14699
7	6.50	1	0.13153	0.71625	0.41345	0.15660
8	6.50	1	0.14071	0.72165	0.32905	0.16053
9	6.50	1	0.13355	0.73078	0.35747	0.16117
10	6.50	5	0.12701	0.73171	0.39018	0.16190
11	6.50	5	0.09859	0.71721	0.31007	0.15688
12	6.50	50	0.01109	0.72501	0.45279	0.16362
13	6.50	50	0.01210	0.69576	0.42580	0.15553
14	7.00	10	0.10564	0.70855	0.32721	0.18648
15	7.50	50	0.03093	0.68810	0.37006	0.18806
16	7.50	50	0.02795	0.67171	0.36903	0.18290
17	5.00	1	0.00800	0.80548	0.53900	0.11542
18	5.80	5	0.03312	0.75813	0.43764	0.14630
19	5.80	5	0.02428	0.76054	0.42325	0.14803
20	5.00	10	0.00845	0.80315	0.45959	0.11574
21	5.00	10	0.01200	0.80507	0.32359	0.11546
22	5.00	50	0.00108	0.85685	0.33059	0.09833
23	5.00	50	0.00128	0.84866	0.30000	0.09884
24	5.00	160	0.00021	0.85072	0.52215	0.09788
25	5.80	1	0.06203	0.78386	0.51717	0.14895
26	5.80	5	0.05985	0.77411	0.46828	0.14523
27	5.80	5	0.04261	0.75590	0.33461	0.14483
28	5.80	10	0.03090	0.76114	0.34215	0.14477
29	5.80	10	0.04244	0.75289	0.38668	0.14543
30	5.80	10	0.02904	0.76129	0.35133	0.14859
31	5.80	50	0.00455	0.82066	0.30000	0.12692
32	5.80	50	0.00573	0.80867	0.44832	0.12181
33	6.50	5	0.11199	0.72668	0.33152	0.16498
34	6.50	10	0.07813	0.71656	0.32849	0.16174
35	6.50	10	0.09479	0.70703	0.35995	0.15821
36	6.50	10	0.07016	0.69993	0.32895	0.15772
37	6.50	20	0.03809	0.72668	0.36417	0.16498
38	6.50	20	0.05025	0.69901	0.40078	0.15694
39	6.50	20	0.03421	0.69836	0.34980	0.15642
40	6.50	100	0.00557	0.73882	0.42781	0.15057
41	6.50	160	0.00259	0.74653	0.59736	0.15446
42	7.00	1	0.19294	0.70481	0.38614	0.18404
43	7.00	10	0.13571	0.68314	0.40176	0.17496
44	7.00	10	0.09317	0.68314	0.33263	0.17496
45	7.00	50	0.01894	0.69873	0.38136	0.17908
46	7.00	50	0.02135	0.69583	0.48485	0.17897
47	7.50	1	0.24159	0.72152	0.38300	0.21899
48	5.00	10	0.13607	0.68880	0.33792	0.18873
49	5.00	10	0.16174	0.67551	0.42032	0.18432
50	8.00	50	0.04540	0.69122	0.32018	0.19859
51	8.00	160	0.01538	0.70538	0.47162	0.18755

TABLE F7-16
M. C. WALCK: VERTICAL POINT ESTIMATES
SPECTRAL ACCELERATION AT 2.00 SEC PERIOD

CASE NO.	MAGNITUDE	DISTANCE (KM)	MU	SIGMA	SIGMA MU	SIGMA SIGMA
1	5.00	1	0.00678	0.88549	0.46852	0.11450
2	5.00	1	0.00705	0.87631	0.42081	0.11343
3	5.00	5	0.00237	0.86803	0.47049	0.12583
4	5.00	5	0.00250	0.85719	0.36052	0.12271
5	5.80	10	0.00886	0.79801	0.46183	0.14454
6	5.80	20	0.00727	0.81344	0.33804	0.15070
7	6.50	1	0.07251	0.76337	0.33918	0.15573
8	6.50	1	0.07745	0.76214	0.36434	0.16170
9	6.50	1	0.06760	0.76037	0.30883	0.15981
10	6.50	5	0.06404	0.74678	0.44093	0.15909
11	6.50	5	0.04945	0.76037	0.33229	0.15981
12	6.50	50	0.00535	0.77626	0.38745	0.16491
13	6.50	50	0.00621	0.74366	0.65569	0.16232
14	7.00	10	0.04862	0.75534	0.41696	0.18841
15	7.50	50	0.01718	0.75305	0.66741	0.21330
16	7.50	50	0.01527	0.72573	0.46999	0.21606
17	5.00	1	0.00247	0.86758	0.63817	0.12585
18	5.80	5	0.01447	0.81085	0.39998	0.14838
19	5.80	5	0.00922	0.81158	0.41625	0.14896
20	5.00	10	0.00248	0.86179	0.56762	0.12443
21	5.00	10	0.00374	0.86622	0.35662	0.12600
22	5.00	50	0.00036	0.91215	0.46018	0.08829
23	5.00	50	0.00047	0.91124	0.42230	0.08891
24	5.00	160	0.00011	0.92172	0.38971	0.08684
25	5.80	1	0.02713	0.84228	0.38846	0.15603
26	5.80	5	0.02661	0.77117	0.49684	0.15336
27	5.80	5	0.01983	0.81219	0.42325	0.15853
28	5.80	10	0.01067	0.81180	0.47696	0.14521
29	5.80	10	0.01604	0.82565	0.46240	0.16092
30	5.80	10	0.01108	0.81283	0.40427	0.15009
31	5.80	50	0.00169	0.84566	0.45976	0.10900
32	5.80	50	0.00247	0.87637	0.61765	0.12119
33	6.50	5	0.05162	0.77992	0.34342	0.16857
34	6.50	10	0.03555	0.76717	0.32074	0.16505
35	6.50	10	0.04262	0.74065	0.48919	0.16670
36	6.50	10	0.03273	0.74970	0.42895	0.16294
37	6.50	20	0.01794	0.77992	0.34190	0.16857
38	6.50	20	0.02280	0.77295	0.43695	0.17419
39	6.50	20	0.01647	0.77198	0.40151	0.17324
40	6.50	100	0.00263	0.81180	0.51824	0.15910
41	6.50	160	0.00157	0.81300	0.64078	0.16017
42	7.00	1	0.09206	0.73172	0.43005	0.17722
43	7.00	10	0.06411	0.71896	0.48616	0.18208
44	7.00	10	0.04760	0.76282	0.44026	0.20344
45	7.00	50	0.00971	0.76625	0.49027	0.19859
46	7.00	50	0.01151	0.75081	0.66155	0.19843
47	7.50	1	0.11826	0.76896	0.47227	0.22853
48	5.00	10	0.06665	0.76261	0.49973	0.22342
49	5.00	10	0.08976	0.75221	0.58175	0.22755
50	8.00	50	0.02813	0.75332	0.43307	0.23856
51	8.00	160	0.01338	0.80370	0.66215	0.23060

TABLE F7-17
M. C. WALCK: VERTICAL POINT ESTIMATES
SPECTRAL ACCELERATION AT 3.33 SEC PERIOD

CASE NO.	MAGNITUDE	DISTANCE (KM)	MU	SIGMA	SIGMA MU	SIGMA SIGMA
1	5.00	1	0.00241	0.90833	0.66442	0.11871
2	5.00	1	0.00277	0.90426	0.55143	0.11727
3	5.00	5	0.00094	0.89903	0.57642	0.12042
4	5.00	5	0.00108	0.90315	0.46535	0.11697
5	5.80	10	0.00426	0.83225	0.40409	0.15340
6	5.80	20	0.00321	0.84909	0.40232	0.15410
7	6.50	1	0.03634	0.78356	0.35702	0.17110
8	6.50	1	0.04273	0.78651	0.43780	0.17901
9	6.50	1	0.03870	0.78438	0.37080	0.17622
10	6.50	5	0.03914	0.76508	0.59273	0.17178
11	6.50	5	0.02519	0.78340	0.32541	0.17496
12	6.50	50	0.00274	0.81220	0.41241	0.19414
13	6.50	50	0.00311	0.76463	0.63762	0.17965
14	7.00	10	0.02779	0.80165	0.37850	0.23034
15	7.50	50	0.00993	0.78826	0.63386	0.24121
16	7.50	50	0.00860	0.74546	0.45127	0.22953
17	5.00	1	0.00087	0.91422	0.76265	0.12259
18	5.80	5	0.00637	0.84923	0.49327	0.15425
19	5.80	5	0.00413	0.84872	0.43662	0.15372
20	5.00	10	0.00088	0.91044	0.70143	0.12040
21	5.00	10	0.00136	0.91191	0.52932	0.12201
22	5.00	50	0.00014	0.93455	0.54743	0.08650
23	5.00	50	0.00019	0.93234	0.61792	0.08622
24	5.00	160	0.00003	0.94559	0.67308	0.08926
25	5.80	1	0.01215	0.85398	0.44284	0.16412
26	5.80	5	0.01384	0.79933	0.57890	0.16080
27	5.80	5	0.00860	0.84047	0.45190	0.15874
28	5.80	10	0.00481	0.84917	0.45811	0.15302
29	5.80	10	0.00657	0.86264	0.50811	0.16649
30	5.80	10	0.00473	0.85045	0.45738	0.15562
31	5.80	50	0.00078	0.87094	0.44210	0.11855
32	5.80	50	0.00109	0.90785	0.69911	0.13429
33	6.50	5	0.03042	0.78883	0.35740	0.18087
34	6.50	10	0.01731	0.78293	0.34091	0.17305
35	6.50	10	0.02206	0.78088	0.52409	0.19043
36	6.50	10	0.01512	0.76552	0.44788	0.17245
37	6.50	20	0.00915	0.81616	0.34224	0.19917
38	6.50	20	0.01088	0.79579	0.39062	0.18952
39	6.50	20	0.00849	0.79654	0.47104	0.19049
40	6.50	100	0.00123	0.84113	0.58334	0.17460
41	6.50	160	0.00080	0.84113	0.60910	0.17460
42	7.00	1	0.05222	0.75311	0.49502	0.19450
43	7.00	10	0.03658	0.80251	0.49129	0.22854
44	7.00	10	0.02523	0.79074	0.51698	0.22303
45	7.00	50	0.00532	0.79930	0.53770	0.22316
46	7.00	50	0.00598	0.77920	0.67899	0.22049
47	7.50	1	0.07115	0.79929	0.39738	0.25134
48	5.00	10	0.03541	0.78628	0.55567	0.23882
49	5.00	10	0.04708	0.76023	0.56543	0.23797
50	8.00	50	0.01743	0.78519	0.58667	0.26068
51	8.00	160	0.00803	0.84737	0.65950	0.25360

TABLE F7-18
M. C. WALCK: VERTICAL POINT ESTIMATES
PEAK GROUND VELOCITY

CASE NO.	MAGNITUDE	DISTANCE (KM)	MU	SIGMA	SIGMA MU	SIGMA SIGMA
1	5.00	1	4.51356	0.66047	0.53075	0.14023
2	5.00	1	4.29438	0.67793	0.38538	0.14361
3	5.00	5	1.33613	0.66075	0.49131	0.14046
4	5.00	5	1.54938	0.67738	0.57971	0.14321
5	5.80	10	2.69191	0.65374	0.31002	0.15986
6	5.80	20	2.13480	0.63642	0.43392	0.15093
7	6.50	1	17.03227	0.63830	0.30000	0.16385
8	6.50	1	19.31325	0.64194	0.33219	0.16810
9	6.50	1	17.14802	0.64291	0.31767	0.16917
10	6.50	5	18.23540	0.63959	0.36093	0.16561
11	6.50	5	11.03472	0.64139	0.30343	0.16750
12	6.50	50	0.90034	0.64793	0.40357	0.16787
13	6.50	50	1.06003	0.63207	0.53879	0.16160
14	7.00	10	10.69709	0.64638	0.30000	0.18118
15	7.50	50	2.73714	0.61448	0.45160	0.19726
16	7.50	50	2.56927	0.59904	0.39884	0.18716
17	5.00	1	1.60177	0.67650	0.64331	0.14313
18	5.80	5	5.25829	0.65530	0.47390	0.15895
19	5.80	5	2.82126	0.65751	0.45774	0.16116
20	5.00	10	1.19757	0.68012	0.38232	0.14528
21	5.00	10	2.00067	0.65947	0.30000	0.13940
22	5.00	50	0.14050	0.68443	0.32431	0.15158
23	5.00	50	0.16511	0.67262	0.34160	0.14482
24	5.00	160	0.02683	0.69038	0.70235	0.15590
25	5.80	1	8.41111	0.66134	0.42743	0.16207
26	5.80	5	9.35552	0.65622	0.38035	0.15986
27	5.80	5	4.93251	0.65383	0.32411	0.15754
28	5.80	10	3.26196	0.66237	0.33981	0.16340
29	5.80	10	5.24598	0.65690	0.35237	0.16526
30	5.80	10	2.93759	0.65751	0.38580	0.16116
31	5.80	50	0.40833	0.70338	0.30830	0.17142
32	5.80	50	0.59621	0.73215	0.54833	0.16423
33	6.50	5	12.35000	0.64661	0.30216	0.16952
34	6.50	10	7.42157	0.64329	0.33021	0.16604
35	6.50	10	11.62291	0.64346	0.39110	0.16979
36	6.50	10	6.71575	0.63835	0.34967	0.16436
37	6.50	20	3.34907	0.64137	0.34078	0.16416
38	6.50	20	4.75040	0.63207	0.43228	0.16160
39	6.50	20	3.16873	0.63959	0.46847	0.16561
40	6.50	100	0.43082	0.67610	0.31885	0.16552
41	6.50	160	0.19098	0.70913	0.58774	0.16540
42	7.00	1	22.95208	0.65020	0.36876	0.19157
43	7.00	10	18.73886	0.64368	0.51185	0.18170
44	7.00	10	9.81755	0.64174	0.38473	0.17944
45	7.00	50	1.60028	0.64429	0.40706	0.17889
46	7.00	50	1.92625	0.64085	0.52861	0.17896
47	7.50	1	26.02660	0.65398	0.41984	0.21336
48	5.00	10	13.98912	0.64336	0.34566	0.20143
49	5.00	10	18.11451	0.64312	0.59717	0.20581
50	8.00	50	5.24948	0.65526	0.43019	0.21662
51	8.00	160	2.16459	0.86826	0.45761	0.14152

APPENDIX G

HISTORICAL SEISMICITY CATALOGUE FOR YUCCA MOUNTAIN

HISTORICAL SEISMICITY CATALOGUE FOR YUCCA MOUNTAIN

by
Jacqueline D.J. Bott, Anna Sojourner, Doug Wright,
and Ivan Wong
Woodward-Clyde Federal Services

A report to the U.S. Geological Survey
that fulfills Level 4 Milestone SPG280M4
WBS Number 1.2.3.3.8.3.6

30 October 1997

HISTORICAL SEISMICITY CATALOGUE FOR YUCCA MOUNTAIN

TABLE OF CONTENTS

LIST OF TABLES

LIST OF FIGURES

HISTORICAL SEISMICITY CATALOGUE FOR YUCCA MOUNTAIN

INTRODUCTION

A historical earthquake catalogue of all known events within a 300-km radius circular region centered on the Yucca Mountain site was compiled for use in the: (1) characterization of the regional seismicity; (2) evaluation of the seismicity for any possible associations with geologic structures, particularly late-Quaternary faults; and (3) computation of earthquake recurrence parameters for the various seismotectonic provinces that make up the Yucca Mountain region. These activities are all part of the Probabilistic Seismic Hazard Analysis Project for Yucca Mountain.

The Yucca Mountain catalogue, which covers the time period from 1868 to 1996, was compiled from all available regional and national earthquake catalogues. Two catalogues for the Yucca Mountain region compiled prior to this study were used as a basis for this work (Meremonte and Rogers, 1987; S. Gross and S. Jaume, UNR, written communication, 1995). The catalogue described in this report differs from the previous catalogues in that it covers a much larger geographical region in order to satisfy the U.S. Nuclear Regulatory Commission's regulatory standards. Also, unlike the other catalogues, the Yucca Mountain catalogue lists all known magnitudes assigned to each event to derive values using a common magnitude scale. A best-estimate moment magnitude (M_W) value was calculated for each earthquake for this project. All known Nuclear Test Site (NTS) blasts were identified and were removed along with the associated dependent events using declustering algorithms. The historical catalogue was declustered using two different approaches, the results of which were compared for their effectiveness.

DATA SOURCES

The Yucca Mountain catalogue was compiled from the following regional and national catalogues (abbreviations for each catalogue are listed in parentheses):

- Catalogue for the Southern Great Basin network for the period 1978 to 1992 (Rogers *et al.*, 1987) (SGB)
- Seismological Laboratory of the University of Nevada, Reno catalogue for Nevada, 1874 to 1994 including the Southern Great Basin network data for 1992 to 1996 (UNR)
- California Institute of Technology Seismological Laboratory and U.S. Geological Survey catalogue for southern California, 1932 to 1996 (CIT)
- University of California at Berkeley Seismographic Station catalogue for northern California, 1910 to 1972 (UCB)
- U.S. Geological Survey catalogue for northern and central California, 1969 to 1996 (USGS)
- Catalogue of Southern Great Basin earthquakes, 1868 to 1978, compiled by Meremonte and Rogers (1987) (MER)
- University of Utah Seismographic Stations catalogue for Utah, 1881 to 1996 (UUTAH)
- California Division of Mines and Geology catalogue for California, 1868 to 1932 (CDMG)
- Stover, Reagor and Algermissen state catalogues for Utah and Arizona compiled by the National Earthquake Information Center (NEIC), 1881 to 1985 (SRA)
- NEIC Preliminary Determination of Epicenters catalogue for Utah and Arizona, 1938 to 1996 (PDE)
- Northern Arizona University catalogue for Arizona, 1891 to 1992 (NAU)
- Decade of North American Geology catalogue, 1868 to 1985 (Engdahl and Rinehart, 1988) (DNAG)

CATALOGUE COMPILATION

In the compilation of the Yucca Mountain catalogue, only specific time periods of several catalogues were used due to the availability of higher quality data from other networks. For example, only data prior to 1972 was used from the UCB catalogue, because the USGS network has provided much wider and denser seismographic coverage for northern and central California since 1972. Only earthquakes prior to 1932 were extracted from the CDMG catalogue, since the CIT, UCB, and USGS catalogues are more complete for

California after 1932. All available magnitude and intensity estimates, however, were extracted from each catalogue used in the compilation.

All events from the source catalogues within the 300-km Yucca Mountain region were combined into a single catalogue. This catalogue was then subdivided into seven subregions to remove duplicate events: southwestern Utah, northwestern Arizona, north-central Nevada, southern Nevada, east-central California, Mammoth Lakes, and southeastern California (Figure G-1). Each region had a different constituent catalogue hierarchy to retain the most precise location for each earthquake (Table G-1). The seven subregions overlap to retain events that may straddle the boundaries (Figure G-1).

In each subregion catalogue, multiple entries for the same earthquake were removed. The duplicate removal procedure compares the inter-event time and distances to user-specified time and distance windows to identify multiple entries for the same earthquake. If two earthquakes from the same source catalogue (e.g., CIT) occur within the user-specified time window, the time window is automatically reduced to just less than this inter-event time. If the inter-event times and distances of earthquakes from other source catalogues are small enough (i.e., lie within the user-specified time and distance windows or the adjusted time window), the events are identified as belonging to a duplicate group. The most accurate entry for each event within the group is then selected according to the specified catalogue hierarchy for that region (Table G-1). The allowable time and distance windows are greater for the historical period (1868 to 1964), and are reduced for the instrumental period (1965 to 1996). We used a time window of 1.5 minutes and a distance window of 1° for the period 1868 to 1964 and time and distance windows of 1.25 minutes and 0.75°, respectively, for the period 1965 to 1992. For the period 1993 to date, the parameters were 1.0 minute and 0.55°, respectively.

Duplicate entries were checked visually because the computer algorithm may not always identify every duplicate. This often occurs for historical earthquakes which may have uncorrected origin times or for earthquakes which occurred on the edge of or outside a network and may have significantly different locations. In some cases, referral to the original data sources (e.g., Townley and Allen, 1939 or U.S. Earthquakes) was necessary to discern

whether the entries were duplicate sets or not. The events within each duplicate group were examined, and if a different entry was preferred to the event flagged by the computer algorithm based on azimuthal gap, minimum station distance, or standard errors, then this event was flagged manually as the preferred event. The file of flagged preferred events was then used to produce the final subregion catalogues.

The subregion catalogues were combined sequentially and duplicate events were removed for overlap regions. In the duplicate removal procedure, all available magnitudes were extracted and kept in the final catalogue, along with their associated magnitude scale and data source. The final catalogue was truncated at August 31, 1996, the end date of the component catalogue CIT, to produce uniform coverage in space and time. The resulting catalogue contains 271,223 earthquakes of approximately M 0.5 and greater, from 1868 to 1996. Figure G-2 shows the events since 1904 and Table G-2 lists all earthquakes of M_w 5 and greater in the catalogue.

MAGNITUDE ESTIMATES AND CONVERSION TO MOMENT MAGNITUDE

Since the Yucca Mountain catalogue was compiled from several source catalogues, a uniform magnitude scale for all earthquakes was required in order to properly compute the earthquake recurrence for the region. In addition, it was necessary to assign magnitudes to historical earthquakes that occurred prior to calibrated seismographic instrumentation. Such magnitude estimates are usually based on the felt area or the maximum Modified Mercalli (MM) intensity. This is particularly problematic in the Basin and Range province where settlement and population growth have been erratic and sparse due to the boom and bust nature of mining operations and the rugged environment.

For each earthquake within the Yucca Mountain catalogue, a M_W was calculated from the best available magnitude estimate. Published relationships between seismic moment (M_o) and M_W or local magnitude (M_L) (or other magnitude scale) were used when available (Table G-3), and previously determined M_w values (Stover and Coffman, 1993; Doser and Smith, 1989) were added to the catalogue. Otherwise, magnitudes were first converted to M_L, from which an M_W was derived. The M_W conversion employed depended upon the source catalogue from which the earthquake was derived and upon the type and source of the

magnitude. A hierarchy of magnitude types and sources were developed for each catalogue (Tables G-4 and G-5). The procedures used for each source catalogue are described below

We have not addressed the issue of the standard errors in converting the magnitudes to M_W, but there is uncertainty in all the relationships used that can be incorporated into the recurrence estimates. Standard errors in converting maximum MM intensity into M_W are much larger due to the larger uncertainty.

Southern Great Basin Network Catalogue

The USGS SGB catalogue lists an M_L (USGS Digital Recording; USGSDR) magnitude for the majority of earthquakes recorded by the digital network. Other magnitude types listed include M_V (USGSDR), a local magnitude derived from the vertical records, M_C (USGSDR) the coda-amplitude magnitude and M_D (USGSDR), the duration magnitude, all of which are described in detail in Rogers *et al.* (1987). Both M_C and M_D were originally calibrated to the USGS M_L. The digital network was operated by the USGS from October 1981 to September 1992, when the responsibility was relinquished to the University of Nevada, Reno (UNR). During the handover in September of 1992, M_L computed by both the USGS and UNR (CUSP), were collected and a comparison (D. von Seggern, UNR, written communication, 1996; Figure G-3) indicates that the two are essentially equivalent in the range M_L 1.5 to 4. This is the only direct comparison of the two methodologies for computing M_L within the SGB.

D. von Seggern (UNR, written communication, 1996) also compared M_o with M_L for the Southern Great Basin region (Figure G-4). The M_L's are derived from both the Southern Great Basin Seismic Network (SGBSN) from before and after 1992 and from Savage and Anderson (1995). The seismic moments are from Mayeda and Walter (1996) and other unpublished data computed by Ken Smith and Feng Su (UNR). Von Seggern concluded that above M 3, the moment-magnitude relation was essentially the same as that from Hanks and Kanamori (1979) relationship $\log M_o = {}^3/_2 M_L + 16$ (Figure G-4). For $M_L < 3$, the moment-magnitude relation has a slope of 1 and was fixed to the Hanks and Kanamori (1979) curve at M_L 3 (D. von Seggern, UNR, written communication, 1996). The relationship for $M_L < 3$ is

$\log M_o = M_L + 17.55$. The relation between M_o and M_W (Hanks and Kanamori, 1979) of $M_W = {}^2/_3 \log M_o - 10.7$ was used to calculate M_W from M_L. The relations are $M_W = M_L$ for $M_L \geq 3$ and $M_W = {}^2/_3 M_L + 1$ for $M_L < 3$.

All earthquakes recorded by the SGB digital network for the period October 1981-September 1992 assigned M_L values were converted to M_W using the above relationships. However, many earthquakes within the catalogue only have M_C, M_V and/or M_D designations. For these earthquakes, a M_L value was first estimated from regressions developed in this study (Figures G-5 to G-7; Table G-3). The magnitude conversions, which are only valid for ranges indicated by the regressions, were used in a few cases for magnitudes just outside the specified ranges. M_L estimated from M_V was considered the best estimate followed in order by M_L estimates from M_C and M_D.

For the period prior to installation of the digital network, August 1978 to September 1981, and after 1981 in the event of computer failure, a M_D was computed from develocorder records. M_D (USGS Develocorder; USGSDV) was regressed with M_D values from UNR (Figure G-8; Table G-3). UNR M_D values were calibrated to M_L from UNR and BRK. M_W was estimated assuming the same relationships between M_W and M_L as were used for the Southern Great Basin.

University of Nevada, Reno Catalogue

All M_L magnitudes from UNR prior to September 1992 were converted to M_W using the same relationships between M_W and M_L as discussed above for the Southern Great Basin. M_D is calibrated to M_L for the range $1.5 \leq M_L \leq 5.7$ and is assumed to be equivalent to M_L UNR. After September 1992, magnitudes were determined by UNR from the CUSP (Caltech USGS Processing) system for the Southern Great Basin and are mostly M_D values. The relationship between M_D and M_L from CUSP for the period 1993-1995 is $M_L = -1.244 + 1.31 M_D$ (Figure G-9), where $M_L = M_D$ at a value of 4.0 (D. von Seggern, UNR, written communication, 1996). M_D values were first converted to M_L and then to M_W using the Southern Great Basin relationships between M_W and M_L.

California Institute of Technology Catalogue

Most earthquakes from the CIT catalogue have a M_L PAS designation which was converted to M_W assuming that $M_L = M_W$ for $M_L \geq 3$ (L. Wald, USGS, personal communication, 1996). All $M_L < 3$ were converted to M_W using the relationship of Chung and Bernreuter (1981) for California (Table G-3) since no regressions have been performed for this magnitude range for the region of interest (L. Wald, USGS, K. Hutton and L. Jones, California Institute of Technology, personal communications, 1996).

University of California, Berkeley Catalogue

Most of the earthquakes from the UCB catalogue give a M_L BRK (also designated BERK and UCB) and were converted to M_W directly using a relationship developed by R. Uhrhammer (UCB, personal communication, 1996) for $3.6 \leq M_L \leq 6.8$. Below M_L 3.6 the relationship was assumed to be the same (R. Uhrhammer, UCB, personal communication, 1996).

USGS Northern California Catalogue

Most earthquake magnitudes listed in the USGS catalogue are a M_L or M_D. Relationships between M_L and M_W developed for the Mammoth region (Chavez and Priestly, 1985) were used to convert the M_L values (Table G-3). These are valid for ranges of $1 \leq M_L \leq 6$ and $½ \leq M_L \leq 3$ respectively. Since the second equation is less reliable (Chavez and Priestly, 1985), it was only used for $M_L < 1$. If M_L was not available for a particular earthquake, the preferred alternative was M_D which has been calibrated to M_L. Other magnitudes were used if necessary (Tables G-3 and G-4).

Southern Great Basin Historical Earthquake Catalogue

The Southern Great Basin historical catalogue compiled by Meremonte and Rogers (1987) lists many magnitude data sources, many of which are unknown (UK). The catalogue includes the results from several microearthquake surveys conducted in the vicinity of the NTS which were assigned M_D values. These M_D values were assumed to be the same as M_D

computed by UNR. All M_L values from UNR, PAS and BRK were converted to M_W using the appropriate relationships (Table G-3). Surface-wave magnitudes (M_S) were converted using the formula $M_W = 0.79M_S + 1.24$ (M.L. Jost and R.B. Herrmann, St. Louis University, written communication, 1990). Body-wave magnitudes (m_b) were assumed to be equivalent to M_L and then converted to M_W (Boore and Joyner, 1982) Other unspecified magnitudes were assumed to be equivalent to M_L for the Southern Great Basin and then converted to M_W. The magnitude conversion hierarchy (Table G-4) was based on the reliability of each magnitude type (Meremonte and Rogers, 1987).

University of Utah Catalogue

Most earthquakes from the University of Utah catalogue were assigned an M_L (UVUTAH, UU or SLC) and were converted to M_W directly using relationships developed by Shemeta and Pechmann (1989; unpublished work). These relationships are similar to the California relationships. Alternatively, M_D values (UVUTAH) calibrated to M_L for $M_D < 2.5$, were used when M_L was not available.

CDMG, SRA and PDE Catalogues

The CDMG, SRA, and PDE catalogues list magnitudes from a variety of sources. Relations between M_L and M_W for original sources were used where possible (i.e., UCB, CIT, UNR, and USGS). m_b or m_{bLg} magnitudes were converted to M_L using the m_b-M_L formula described in the MER catalogue section. M_L values from Arizona were assumed to be equivalent to M_L for the SGB catalogue. Any magnitudes of unknown origin from the CDMG catalogue were assumed to be equivalent to M_L from UCB.

Northern Arizona University Catalogue

A small number of earthquakes came from the NAU catalogue, which in most cases gives adopted magnitudes. M_L (AE) values were assumed to be equivalent to M_L for the Southern Great Basin. Conversions of other magnitudes used in the NAU catalogue (Table G-4) are described elsewhere in this section.

Decade of North American Geology Catalogue

Adopted magnitudes from UCB, CIT, UNR, and USGS contained in the DNAG catalogue were converted using the appropriate M_w relations. Unknown magnitudes and intensity-based magnitudes (M_I) from UCB and CIT were assumed to be equivalent to an M_L from the same institution, and UK or M_I magnitudes were assumed to be equivalent to M_L for the Southern Great Basin.

Maximum Modified Mercalli Intensity

Earthquakes with no magnitude but an assigned maximum MM intensity (I_0) were converted to M_L from I_0 depending on the location of the earthquake. For California and Nevada earthquakes, the Toppozada (1975) relation was used and for earthquakes in Arizona and Utah, the Gutenberg and Richter (1956) relation was used.

REMOVAL OF NTS EXPLOSIONS AND ASSOCIATED DEPENDENT EVENTS

For 40 years, the U.S. government conducted unannounced underground nuclear weapons tests at the Nevada Test Site (NTS) near the Yucca Mountain site. Many unannounced tests were detected by regional seismograph networks but were often not distinguished from earthquakes. A catalogue of 742 nuclear explosions conducted at or near the NTS (Figure G-10, Table G-6) was compiled and used to identify all blasts in the Yucca Mountain catalogue. The list was also used to remove events from the Yucca Mountain catalogue induced by or associated with the NTS explosions.

Underground nuclear tests were conducted at the NTS from 26 July 1957 to 23 September 1992. Atmospheric tests conducted from 1951 to 1957 were excluded from this catalogue. Testing at the NTS was halted on 2 October 1992. In 1994, DOE released data all nuclear tests conducted at the NTS (DOE, 1994).

Several data sources were combined to create a comprehensive nuclear explosion catalogue containing date and time, location, and equivalent magnitude. The most complete list of blasts came from the California Institute of Technology (Riley, CIT,

written communication, 1996). However, many tests announced by the DOE were not included in this list or did not contain pertinent information such as location or magnitude. Additional information was obtained from the Lawrence Livermore National Laboratory (LLNL) Containment Database (G. Pawloski, LLNL, personal communication, 1997) and Seismological Database (T. Hauk, LLNL, personal communication, 1997), and from the UCB Seismograph Stations (Collins and Uhrhammer, 1988; Becker *et al.*, 1990). These data sources were cross-referenced to create as complete a record as possible for each blast. The depths of burial given by the DOE were all significantly less than 1 km, so all blasts were assigned a zero depth.

To remove nuclear blast-induced aftershocks and possible cavity collapses from the Yucca Mountain catalogue, the events were removed using the Youngs *et al.* (1987) declustering algorithm described in the next section. Time and distance windows created by the declustering algorithm are a function of magnitude, so each nuclear blast with no recorded magnitude was assigned a calculated value.

Magnitudes for most of the tests were given in the original data sources, but many blasts had no magnitude, particularly blasts prior to 1963. For the approximately 225 blasts without recorded magnitudes, we calculated a magnitude based on yield (total effective energy released in a nuclear explosion), using the equation

$$M_L=3.603+0.3774\ ln W$$

where M_L is the local magnitude and W is the yield in equivalent kilotons of TNT (M. Walck, Sandia Laboratories, personal communication, 1997). Blasts with both a known magnitude and yield were used to compare the calculated M_L with recorded body-wave magnitudes. The average difference between recorded m_b and calculated M_L magnitudes was 0.29.

Although recorded blast magnitudes and magnitude-yield relationships are not classified by the U.S. government, nuclear test yields are classified information. For some tests, an exact yield has been released by the DOE and for some, no information has been released. For most events, however, yield information was released as a range of values (e.g., 12-20 kt).

For approximately 35 blasts with an exact yield released by the DOE, M_L values were calculated. Approximately 13 blasts with a yield range of 20 to 200 kt were assigned M_L 5.15, the average of the maximum (M_L 5.6) and minimum (M_L 4.7) possible magnitudes for this yield range. Approximately 160 blasts with a yield range given by the DOE as "less than 20 kt" or "12 - 20 kt" were assigned a value of M_L 4.7, which corresponds to the maximum possible yield of 20 kt. Blasts with an assigned yield value of "$\leq$ 1 kt" or for which yield was listed as "sparse" without elaboration were assigned a value of M_L 3.6, the minimum magnitude from this equation. Approximately 11 events with neither known magnitude nor listed yield range were assigned M_L 3.6.

DECLUSTERING OF THE HISTORICAL SEISMICITY CATALOGUE

To assess the hazard from "background" earthquakes, estimates of earthquake recurrence are required. The background earthquake is defined as an event that can occur without an apparent association with a known tectonic feature. Recurrence is estimated from a catalogue of independent earthquakes which are assumed to follow a Poissonian distribution of earthquake occurrence. Dependent events (foreshocks and aftershocks or smaller events within an earthquake swarm) are identified using various criteria and then removed from the catalogue.

The 300-km catalogue was declustered using procedures developed by Youngs *et al.* (1987) and Veneziano and Van Dyck (1985). In the Youngs *et al.* (1987) method, dependent events were identified using empirical criteria for the size in time and space of foreshock-mainshock-aftershock sequences developed by Arabasz and Robinson (1976), Gardner and Knopoff (1974), and Uhrhammer (1986). If an event was identified as dependent by two of the three criteria, it was deleted from the catalogue.

The Veneziano and Van Dyck (1985) procedure is more sophisticated than that of Youngs *et al.* (1987) and allows for spatial nonhomogeneities and apparent nonstationarity caused by catalogue incompleteness. The method first sorts earthquakes by size and then date. Each earthquake in turn is statistically tested from largest to smallest for clustering. To accomplish this testing, the seismicity rates of a local temporal and spatial window are compared with

that for an extended temporal and spatial window. Cluster dimensions are then estimated based on this comparison, and all identified secondary events (dependent events) within the cluster are deleted from the catalogue. The procedure is repeated iteratively until no secondary events are removed.

The declustering algorithm of Reasenberg (1985) was not used to decluster the 300-km catalogue based on discussions with M. Savage (Victoria University, written communication, 1997). The Reasenberg code uses California-specific parameters which are not suitable for Nevada, a region with lower rates of earthquake occurrence. Savage has modified the Reasenberg code as part of a study to determine foreshock probabilities for Nevada (Savage and dePolo, 1993), but met with limited success (M. Savage, Victoria University, written communication, 1997).

Only 26,250 and 31,147 earthquakes remained in the 300-km catalogue after declustering with the Youngs *et al.* (1987) and Veneziano and Van Dyck (1985) methods, respectively (see Figures G-11 and G-12 for plots of declustered catalogues within 100 km of Yucca Mountain).

Distance-time plots for the 100 km catalogue before and after declustering (Figures G-13 to G-15) were used to test the effectiveness of the declustering procedures. In addition, earthquakes in the vicinity of Little Skull Mountain were plotted as a function of time after declustering (Figures G-16a-g and G-17a-g). The Youngs *et al.* (1987) procedure appears to miss some aftershocks that occurred up to four years after the 1992 mainshock. Two of the three methods used in the Youngs *et al.* (1987) procedure were developed for California and therefore may be inappropriate for the lower rates of seismicity of the Southern Great Basin. In comparison, the more sophisticated Veneziano and Van Dyck (1985) procedure produced a more even temporal distribution without the large year-to-year differences seen in the Youngs *et al.* declustered catalogue, particularly from 1993 to 1994 (Figures G-16d-e and G-17d-e). Both approaches, however, leave in aftershocks, particularly a year after the 1992 mainshock. The Little Skull Mountain fault zone as defined by the aftershock distribution is somewhat less pronounced in the plots of the Veneziano declustered catalogue (Figures G-16a and G-17a).

LAKE MEAD RESERVOIR-INDUCED SEISMICITY

Since the early 1940's, reservoir-induced-seismicity has occurred at Lake Mead, the reservoir impounded by Hoover Dam (Rogers and Lee, 1976). One of the issues to be addressed in the Probabilistic Seismic Hazard Analysis Project is whether such seismicity will contribute to the hazard at the Yucca Mountain site in the future and if so, if it should be incorporated into the hazard analysis. The reservoir-induced earthquakes at Lake Mead were retained in the Yucca Mountain catalogue and it was left to the judgments of the experts to keep or delete the events for their analysis.

REFERENCES

Abe, K., and Noguchi, S., 1983, Determination of magnitude for large shallow earthquakes, 1898-1917: Physics of the Earth and Planetary Interiors, v. 32, p. 45-59.

Arabasz, W.J., and Robinson, R., 1976, Microseismicity and geologic structure in the northern South Island, New Zealand: New Zealand Journal of Geology and Geophysics, v. 19, p. 561-601.

Becker, A.M., Mc Kenzie, M.R., and Uhrhammer, R.A., 1990, Bulletin of the Seismographic Stations - Earthquakes and the Registration of Earthquakes from January 1, 1989 to December 31, 1989, University of California at Berkeley Seismographic Stations, v. 59, 117 p.

Boore, D.M., and Joyner, W.B., 1982, The empirical prediction of ground motion: Bulletin of the Seismological Society of America, v. 72, p. S43-S60.

Chavez, D.E., and Priestley, K.F., 1985, M_L observations in the Great Basin and M_o versus M_L relationships for the 1980 Mammoth Lakes, California earthquake sequence: Bulletin of the Seismological Society of America, v. 75, p. 1583-1598.

Chung, D.H., and Bernreuter, D.L., 1981, Regional relationships among earthquake magnitude scales: Review of Geophysics and Space Physics, v. 19, p. 649-663.

Collins, E.R., and Uhrhammer, R.A., 1988, Bulletin of the Seismographic Stations - Earthquakes and the Registration of Earthquakes from January 1 1987 to December 31, 1987, University of California at Berkeley Seismographic Stations, v. 57, 98 p.

Doser, D.I., and Smith, R.B., 1989, An assessment of source parameters of earthquakes in the Cordillera of the western U.S: Bulletin of the Seismological Society of America, v. 79, p. 1383-1409.

Eaton, J.P., 1992, Determination of amplitude and duration magnitudes and site residuals from short-period seismographs in northern California: Bulletin of the Seismological Society of America, v. 82, p. 533-579.

Engdahl, E. R., and Rinehart, W.A., 1988, Seismicity map of North America: Decade of North American Geology Catalogue, The Geological Society of America, scale 1:5,000,000.

Fisher, F.G., Papenek, P.J., and Hamilton, R.M., 1972, The Massachusetts Mountain earthquake of 5 August 1971 and its aftershocks, Nevada Test Site: U.S. Geological Survey Report USGS-474-149, NTS-238, 20 p.

Gardner, J.K., and Knopoff, L., 1974, Is the sequence of earthquakes in Southern California, with aftershocks removed, Poissonian?: Bulletin of the Seismological Society of America, v. 65, p. 1363-1367.

Gutenberg, B., and Richter, C.F., 1956, Earthquake magnitude, intensity, energy and acceleration: Bulletin of the Seismological Society of America, v. 46, p. 105-145.

Hanks, T.C., and Kanamori, H., 1979, A moment magnitude scale: Journal of Geophysical Research, v. 84, p. 2348-2350.

Mayeda, K., and Walter, W.R., 1996, Moment, energy, stress drop , and source spectra of western United States earthquakes from regional coda envelopes: Journal of Geophysical Research, v. 101, p. 11,195-11, 208.

Meremonte, M.E., and Rogers, A.M., 1987, Historical catalog of Southern Great Basin earthquakes, 1868-1978: U.S. Geological Survey Open-File Report 87-80, 204 p.

Papanek, P.J., and Hamilton, R.M., 1972, A seismicity study along the northern Death Valley-Furnace Creek fault zone, California-Nevada boundary: U.S. Geological Survey Report USGS-474-141, 41 p.

Reasenberg, P., 1985, Second-order moment of central California seismicity, 1969-1982: Journal of Geophysical Research, v. 90, p. 5479-5495.

Rogers, A.M., Harmsen, S.C., and Meremonte, M.E., 1987, Evaluation of the seismicity in the Southern Great Basin and its relationship to the tectonic framework of the region: U.S. Geological Open-File Report 87-408, 196 p.

Rogers, A.M., and Lee, W.H.K., 1976, Seismic study of earthquakes in Lake Mead: Bulletin of the Seismological Society of America, v. 66, p. 1657-1681.

Rogers, A.M., Woulett, G.M., and Covington, P.A., 1977, Seismicity of the Pahute Mesa area, Nevada Test Site, 8 October 1975 to 30 June 1976: U.S. Geological Survey Report USGS-474-184, 63 p.

Savage, M. K., and Anderson, J. G., 1995, A local magnitude scale for the Western Great Basin-Eastern Sierra Nevada from synthetic Wood-Anderson seismograms: Bulletin of the Seismological Society of America, v. 85, p. 1236-1243.

Savage, M.K., and dePolo, C.M., 1993, Foreshock probabilities in the western Great Basin, eastern Sierra Nevada: Bulletin of the Seismological Society of America, v. 83, p. 1910-1938.

Shemeta, J.E., and J.C. Pechmann, 1989, Source parameters of aftershocks of the 1983 Borah Peak, Idaho, earthquake (abstract): EOS, Transactions of the American Geophysical Union, v. 70, p. 1188.

Slemmons, D.B., Jones, A.E., and Gimlett, J.I., 1965, Catalog of Nevada earthquakes, 1852-1960: Bulletin of the Seismological Society of America, v. 55, p. 537-583.

Smith, B.E., Hamilton, R.M., and Jackson, W.H., 1971, Seismicity of the central Nevada test area, 26 September 1969 - 1 October 1970: U.S. Geological Survey Report USGS-474-109, 27 p.

Stover, C.W., and Coffman, J.L., 1993, Seismicity of the United States, 1568-1989 (Revised): U.S. Geological Survey Professional Paper 1527, 418 p.

Thatcher, W., and Hanks, T.C., 1973, Source parameters of southern California earthquakes: Journal of Geophysical Research, v. 78, p. 8547-8576.

Toppozada, T.R., 1975, Earthquake magnitude as a function of intensity data in California and western Nevada: Bulletin of the Seismological Society of America, v. 65, p. 1,223-1,238.

Townley, S.D., and Allen, M.W., 1939, Descriptive catalog of earthquakes of the Pacific Coast of the United States: 1769 to 1928: Bulletin of the Seismological Society of America, v. 29, p. 1-297.

U.S. Department of Energy (DOE), 1994, Announced United States Nuclear Tests, July 1945 through September 1992: DOE/NV 209 (Rev. 14), 96 p.

Uhrhammer, R.A., 1986, Characteristics of northern and central California seismicity (abstract): Earthquake Notes, v. 57, p. 21.

Veneziano, D., and Van Dyck, J., 1985, Statistical discrimination of "aftershocks" and their contribution to seismic hazard, Appendix A-4, *in* Seismic Hazard Methodology for Nuclear Facilities in the Eastern United States: EPRI Research Project Number P101-29, p. A121-A186.

von Seggern, D.H., and Brune, J.N., 1996, Seismicity in the Southern Great Basin, 1868-1992: Geological Society of America Special Volume: Tectonic Characterization of Yucca Mountain - A potential geologic repository for nuclear waste (in press).

Youngs, R.R., Swan, F.H., III, Power, M.S., Schwartz, D.P., and Green, R.K., 1987. Probabilistic analysis of earthquake ground-shaking along the Wasatch front, Utah, *in* W.W. Hays and P.L. Gori ,eds., Assessment of Regional Earthquake Hazards and Risk Along the Wasatch Front, Utah: U.S. Geological Survey Professional Paper (in press).

TABLE G-1
HIERARCHIES FOR REMOVAL OF DUPLICATE EVENTS IN SUBREGION CATALOGUES

SUBREGION CATALOGUES (LISTED IN ORDER OF PREFERENCE)						
North-Central Nevada	**Northwestern Arizona**	**Southern Nevada**	**Southeastern California**	**Mammoth Lakes**	**East-Central California**	**Southwestern Utah**
UNR	MER	SGB	CIT	USGS*	USGS	UUTAH
SGB	SGB	MER	CDMG	UNR	UCB	DNAG
MER	UNR	UNR	UNR	UCB	CDMG	MER
DNAG	NAU	COMG	UCB	CDMG	UNR	SGB
CDMG	SRA	DNAG	NAU	CIT	CIT	UNR
CIT	PDE	CIT	SRA	DNAG	DNAG	PDE
USGS	DNAG	UCB				SRA
UCB	UUTAH	USGS				NAU
UUTAH	CIT	PDE				CIT
	USGS	NAU				USGS
		SRA				
		UUTAH				

* The USGS location was exclusively used for all Mammoth Lakes events after 1982

TABLE G-2
EARTHQUAKES OF MAGNITUDE 5 OR GREATER IN THE YUCCA MOUNTAIN HISTORICAL SEISMICITY CATALOGUE

Cat. No.	Year	Mo.	Day	Time (GMT)			Lat.	Long.	Depth	Mag1	Scale	Mag1 Source	Mag2	Scale	Mag2 Source	Location
				Hour	Min	Sec			(km)							Source
1	1868	7	25	2	30	00.0000	36.3000	-119.3000	n c	5.28	Mw	MITOPO	-9.99			NEIC
2	1871	7	5	21	6	00.0000	36.4000	-118.0000	n c	5.13	Mw	UK DMG	5.20	UK	DMG	NEIC
3	1872	3	26	10	30	00.0000	36.7000	-118.1000	n c	7.75	Mw	STOCOF	7.80	MW	H&K	NEIC
4	1872	3	26	14	6	00.0000	36.9000	-118.2000	n c	6.63	Mw	UK DMG	6.70	UK	DMG	NEIC
5	1872	4	3	12	15	00.0000	37.0000	-118.2000	n c	6.53	Mw	UK DMG	6.60	UK	DMG	NEIC
6	1872	4	11	19	0	00.0000	37.5000	-118.5000	n c	6.53	Mw	UK DMG	7.00	MI	CDMG	NEIC
7	1872	4	18	12	0	00.0000	36.5000	-117.8000	n c	6.26	Mw	MITOPO	-9.99			NEIC
8	1872	11	12	0	0	00.0000	39.5000	-117.0000	n c	6	Mw	UK	6.00	UK		DNAG
9	1875	4	2	2	0	00.0000	39.5000	-115.8000	n c	5.5	Mw	MD UNR	5.50	MD	UNRENO	UNRENO
10	1886	4	14	3	20	00.0000	37.2000	-117.7000	n c	4.9	Mw	MD UNR	5.00	MS	BRP	UNRENO
11	1889	2	7	5	20	00.0000	34.1000	-116.7000	n c	5.23	Mw	UK DMG	5.30	UK	DMG	NEIC
12	1889	9	30	5	20	00.0000	37.2000	-118.7000	n c	5.53	Mw	UK DMG	5.60	UK	DMG	NEIC
13	1891	4	20	13	55	00.0000	37.1063	-113.5735	n c	4.83	Mw	MI UU	5.00	MI	UVUTAH	UVUTAH
14	1894	7	30	5	12	00.0000	34.3000	-117.6000	n c	5.83	Mw	UK DMG	5.90	UK	DMG	NEIC
15	1896	8	17	11	30	00.0000	36.7000	-118.3000	n c	5.83	Mw	UK DMG	5.90	UK	DMG	NEIC
16	1899	7	22	0	46	00.0000	34.2000	-117.4000	n c	5.43	Mw	UK DMG	5.50	UK	DMG	NEIC
17	1899	7	22	20	32	00.0000	34.3000	-117.5000	n c	6.35	Mw	STOCOF	6.50	UK	DMG	NEIC
18	1902	11	17	19	50	00.0000	37.3930	-113.5200	n c	6	Mw	WCFS1	6.33	MI	SRA	UVUTAH
19	1902	12	5	-1	-1	00.0000	37.3947	-113.5200	n c	4.83	Mw	MI UU	5.00	MI	SRA	UVUTAH
20	1905	1	6	14	30	00.0000	35.5000	-118.7000	n c	4.93	Mw	UK TO	5.00	UK	TO	NEIC
21	1905	12	23	22	23	00.0000	35.3000	-118.8000	n c	4.93	Mw	UK TO	5.00	UK	TO	NEIC
22	1907	9	20	1	54	00.0000	34.2000	-117.1000	n c	5.93	Mw	ML RI	6.00	ML	RI	NEIC
23	1908	11	4	8	37	00.0000	36.0000	-117.0000	n c	6.43	Mw	ML RI	6.50	ML	RI	NEIC
24	1910	5	6	16	40	00.0000	37.3300	-118.4200	n c	4.93	Mw	MICDMG	5.67	MI	BRK	UCB
25	1910	11	7	17	20	00.0000	37.5000	-117.0000	n c	5.5	Mw	MD UNR	5.70	MS	BRP	MER
26	1910	11	19	2	25	00.0000	38.0000	-118.0000	n c	5.5	Mw	MD UNR	5.70	MS	BRP	MER
27	1910	11	21	23	23	00.0000	38.0000	-118.0000	n c	6.1	Mw	MD UNR	6.33	MI	SGB	MER
28	1910	11	22	0	30	00.0000	38.0000	-118.0000	n c	4.9	Mw	MD UNR	5.00	MS	BRP	MER
29	1910	11	22	6	5	00.0000	38.0000	-118.0000	n c	5.5	Mw	MD UNR	5.70	MS	BRP	MER
30	1912	1	5	3	54	00.0000	37.3300	-118.4200	n c	4.93	Mw	MICDMG	5.67	MI	BRK	UCB
31	1915	5	29	6	46	00.0000	36.0800	-118.8200	n c	4.93	Mw	UK TO	5.00	UK	TO	NEIC
32	1916	11	10	9	11	00.0000	36.2000	-116.9000	n c	6.1	Mw	MD UNR	6.10	MD	UNRENO	UNRENO
33	1917	7	6	11	1	00.0000	36.5800	-118.0800	n c	5.28	Mw	MITOPO	-9.99			NEIC
34	1919	2	16	15	57	00.0000	35.0000	-119.0000	n c	4.93	Mw	UK TO	5.67	MI	USN	NEIC

TABLE G-2
EARTHQUAKES OF MAGNITUDE 5 OR GREATER IN THE YUCCA MOUNTAIN HISTORICAL SEISMICITY CATALOGUE

Cat. No.	Year	Mo.	Day	Time (GMT)			Lat.	Long.	Depth	Mag1	Scale	Mag1 Source	Mag2	Scale	Mag2 Source	Location
				Hour	Min	Sec			(km)							Source
35	1920	11	26	0	0	00.0000	37.1063	-113.5735	n c	4.13	Mw	MI UU	5.00	MI	USN	UVUTAH
36	1926	6	30	13	31	00.0000	35.6000	-118.8000	n c	4.93	Mw	UK TO	5.00	UK	TO	NEIC
37	1927	9	18	2	7	07.0000	37.5000	-118.7500	n c	5.93	Mw	ML BRK	6.00	ML	GR	UCB
38	1929	9	26	20	0	22.7000	34.8300	-116.5200	n c	5.03	Mw	ML RI	5.10	ML	RI	NEIC
39	1929	11	28	19	49	00.0000	36.9000	-118.1900	n c	5.43	Mw	UK TO	5.50	UK	TO	NEIC
40	1929	12	2	7	0	00.0000	37.0000	-118.1700	n c	4.93	Mw	MICDMG	5.00	MI	CDMG	UCB
41	1929	12	8	12	45	00.0000	37.0000	-118.1700	n c	4.93	Mw	MICDMG	5.00	MI	CDMG	UCB
42	1930	1	16	0	24	33.9000	34.1800	-116.9200	n c	5.13	Mw	ML EH	5.20	ML	EH	NEIC
43	1930	1	16	0	34	03.6000	34.1800	-116.9200	n c	5.03	Mw	ML EH	5.10	ML	EH	NEIC
44	1931	9	23	8	25	00.0000	37.0800	-118.1700	n c	4.93	Mw	MICDMG	5.00	MI	USN	UCB
45	1932	12	21	6	10	04.0000	38.8000	-117.9800	n c	6.8	Mw	DOSSM1	7.20	ML	PAS	UNRENO
46	1932	12	24	12	41	00.0000	38.8000	-118.0000	n c	5	Mw	MD UNR	5.00	MD	UNRENO	UNRENO
47	1932	12	25	3	55	00.0000	38.8000	-118.0000	n c	5.5	Mw	MD UNR	5.50	ML	UNW	UNRENO
48	1932	12	26	5	2	00.0000	38.0200	-117.6200	n c	5.3	Mw	MD UNR	5.30	MD	UNRENO	UNRENO
49	1932	12	29	6	21	00.0000	38.8000	-118.0000	n c	5.2	Mw	MD UNR	5.20	ML	UNW	UNRENO
50	1932	12	29	6	38	00.0000	38.8000	-118.0000	n c	5	Mw	MD UNR	5.00	MD	UNRENO	UNRENO
51	1932	12	29	6	46	00.0000	38.8000	-118.0000	n c	5	Mw	MD UNR	5.00	MI	USN	UNRENO
52	1933	1	4	1	2	00.0000	38.4000	-118.1000	n c	5.1	Mw	MD UNR	5.10	MD	UNRENO	UNRENO
53	1933	1	5	6	51	00.0000	38.7700	-117.7400	n c	5.9	Mw	MD UNR	5.90	UK	MAK	UNRENO
54	1933	1	6	13	6	00.0000	39.0000	-117.8000	n c	5.1	Mw	MD UNR	5.10	MD	UNRENO	UNRENO
55	1933	1	11	17	30	00.0000	38.9000	-117.8000	n c	5.2	Mw	MD UNR	5.20	MD	UNRENO	UNRENO
56	1933	1	29	13	52	00.0000	38.5000	-118.0000	n c	5	Mw	MD UNR	5.00	UK	RYC	UNRENO
57	1933	2	3	3	26	00.0000	37.3333	-118.8333	n c	5	Mw	ML PAS	5.00	ML	PAS	CIT
58	1933	2	13	22	9	00.0000	38.0000	-118.0000	n c	5.5	Mw	MD UNR	5.50	ML	BRP	MER
59	1933	3	12	20	45	00.0000	38.8000	-117.6000	n c	5	Mw	MD UNR	5.00	ML	UNW	UNRENO
60	1933	5	9	9	47	00.0000	38.5000	-117.9000	n c	5.1	Mw	MD UNR	5.10	UK	RYC	UNRENO
61	1933	6	4	14	9	00.0000	38.5000	-117.9000	n c	5.2	Mw	MD UNR	5.20	MD	UNRENO	UNRENO
62	1933	6	11	8	35	00.0000	38.7000	-117.7000	n c	5.2	Mw	MD UNR	5.20	UK	MAK	UNRENO
63	1933	10	27	10	59	00.0000	38.9000	-117.6000	n c	5.5	Mw	MD UNR	5.50	MD	UNRENO	UNRENO
64	1934	1	30	19	24	00.0000	38.3000	-118.4000	n c	5.6	Mw	MD UNR	5.67	MI	NEV	UNRENO
65	1934	1	30	20	16	35.0000	38.2800	-118.3700	n c	6.1	Mw	DDSSM1	6.60	ML	PAS	UNRENO
66	1934	1	30	20	30	00.0000	38.3000	-118.4000	n c	5.7	Mw	MD UNR	5.70	ML	UNW	UNRENO
67	1934	1	30	23	40	00.0000	38.1000	-118.5000	n c	5.4	Mw	MD UNR	5.40	MD	UNRENO	UNRENO
68	1934	1	31	0	25	00.0000	38.3000	-118.4000	n c	5	Mw	MD UNR	5.00	MD	UNRENO	UNRENO

TABLE G-2
EARTHQUAKES OF MAGNITUDE 5 OR GREATER IN THE YUCCA MOUNTAIN HISTORICAL SEISMICITY CATALOGUE

Cat. No.	Year	Mo.	Day	Time (GMT)			Lat.	Long.	Depth	Mag1	Scale	Mag1 Source	Mag2	Scale	Mag2 Source	Location
				Hour	Min	Sec			(km)							Source
69	1934	1	31	3	55	00.0000	38.3000	-118.4000	n c	5	Mw	MD UNR	5.00	MI	USN	UNRENO
70	1934	2	1	11	1	00.0000	38.3000	-118.4000	n c	5	Mw	MD UNR	5.00	ML	UNW	UNRENO
71	1934	2	1	11	19	00.0000	38.3000	-118.4000	n c	5.2	Mw	MD UNR	5.20	MD	UNRENO	UNRENO
72	1934	2	1	11	46	00.0000	38.3000	-118.4000	n c	5.4	Mw	MD UNR	5.40	MD	UNRENO	UNRENO
73	1934	2	9	9	21	00.0000	38.3000	-118.4000	n c	5.5	Mw	MD UNR	5.50	MD	UNRENO	UNRENO
74	1934	3	13	16	20	00.0000	37.9000	-118.5000	n c	4.7	Mw	MD UNR	5.00	ML	BRK	UNRENO
75	1934	4	15	12	9	00.0000	38.0000	-115.0000	n c	5	Mw	MD UNR	5.00	MS	BRP	MER
76	1935	10	24	14	48	07.6000	34.1000	-116.8000	n c	5.1	Mw	ML PAS	5.10	ML	PAS	CIT
77	1936	5	10	17	40	00.0000	37.5000	-118.5300	n c	4.93	Mw	ML BRK	5.00	ML	UCBMLT	UCB
78	1936	7	2	16	29	00.0000	39.2000	-117.5000	n c	4.93	Mw	ML BRK	5.00	ML	UCBMLT	UCB
79	1937	2	19	9	9	00.0000	38.3000	-118.3000	n c	5	Mw	MD UNR	5.00	ML	UCBMLT	UNRENO
80	1937	11	12	0	39	00.0000	36.0000	-114.8000	n c	3.5	Mw	UK RYC	5.00	MI	UVUTAH	MER
81	1938	12	3	17	42	00.0000	37.5000	-118.7700	n c	5.43	Mw	ML BRK	5.70	ML	PAS	UCB
82	1939	5	4	20	44	48.3600	35.7680	-114.7850	8	5	Mw	ML PAS	5.00	MI	NEV	MER
83	1939	5	11	18	40	00.0000	38.6000	-117.8000	n c	5.5	Mw	MD UNR	5.50	ML	UCBMLT	UNRENO
84	1939	6	11	19	15	00.0000	36.0000	-114.8000	n c	5	Mw	ML RWL	5.00	ML	RWL	MER
85	1939	6	13	17	15	32.0700	37.0070	-117.2290	8	4.93	Mw	ML BRK	5.00	ML	UCBMLT	MER
86	1940	3	10	18	1	53.3100	37.3890	-114.9370	8	5	Mw	ML PAS	5.00	UK	RYC	MER
87	1940	5	18	5	3	58.5000	34.0833	-116.3000	n c	5.4	Mw	ML PAS	5.40	ML	PAS	CIT
88	1940	5	18	5	51	20.2500	34.0667	-116.3333	n c	5.2	Mw	ML PAS	5.20	ML	PAS	CIT
89	1940	5	18	7	21	32.7000	34.0667	-116.3333	n c	5	Mw	ML PAS	5.00	ML	PAS	CIT
90	1940	7	8	10	57	40.0000	37.4500	-119.0000	n c	4.93	Mw	ML BRK	5.00	ML	UCBMLT	UCB
91	1941	9	14	16	43	32.0000	37.5700	-118.7300	n c	5.93	Mw	ML BRK	6.00	UK	PAS	UCB
92	1941	9	14	18	21	19.0000	37.5700	-118.7300	n c	5.43	Mw	ML BRK	5.50	ML	PAS	UCB
93	1941	9	14	18	39	12.0000	37.5700	-118.7300	n c	5.93	Mw	ML BRK	6.00	ML	PAS	UCB
94	1941	9	14	21	16	01.0000	37.5700	-118.7300	n c	4.93	Mw	ML BRK	5.00	ML	UCBMLT	UCB
95	1941	12	31	6	48	44.0000	37.5700	-118.7300	n c	5.43	Mw	ML BRK	5.50	UK	PAS	UCB
96	1942	7	11	16	41	48.0000	38.3000	-116.1000	n c	5	Mw	MD UNR	5.00	ML	PAS	UNRENO
97	1942	8	18	21	55	24.0000	38.6000	-118.5000	n c	5	Mw	MD UNR	5.00	UK		UNRENO
98	1942	9	9	5	15	00.0000	36.0000	-114.7000	n c	5	Mw	ML RWL	5.00	ML	RWL	MER
99	1943	5	31	20	16	53.0000	37.3800	-118.6000	n c	4.44	Mw	ML BRK	5.00	MI	PAS	UCB
100	1943	8	9	5	30	04.0000	38.2000	-118.2000	n c	5.5	Mw	MD UNR	5.50	ML	UCBMLT	UNRENO
101	1943	8	29	3	45	13.0000	34.2667	-116.9667	n c	5.5	Mw	ML PAS	5.50	ML	PAS	CIT
102	1943	12	22	15	50	28.0000	34.3333	-115.8000	n c	5.5	Mw	ML PAS	5.50	ML	PAS	CIT

TABLE G-2
EARTHQUAKES OF MAGNITUDE 5 OR GREATER IN THE YUCCA MOUNTAIN HISTORICAL SEISMICITY CATALOGUE

Cat. No.	Year	Mo.	Day	Time (GMT)			Lat.	Long.	Depth	Mag1	Scale	Mag1 Source	Mag2	Scale	Mag2 Source	Location
				Hour	Min	Sec			(km)							Source
103	1945	3	20	21	55	07.0000	34.2500	-116.1667	n c	5	Mw	ML PAS	5.00	ML	PAS	CIT
104	1945	6	14	3	30	13.0000	37.0833	-117.5000	n c	5	Mw	ML PAS	5.00	ML	PAS	CIT
105	1946	3	15	13	21	00.9000	35.7533	-117.9863	n c	5.2	Mw	ML PAS	5.20	ML	PAS	CIT
106	1946	3	15	13	49	35.9000	35.7252	-118.0547	22	6.06	Mw	STOCOF	6.30	ML	PAS	CIT
107	1946	3	15	14	0	35.4000	35.7148	-118.0740	n c	5.3	Mw	ML PAS	5.30	ML	PAS	CIT
108	1946	3	15	19	18	53.6000	35.7143	-117.9772	n c	5.4	Mw	ML PAS	5.40	ML	PAS	CIT
109	1946	3	15	21	54	33.4000	35.7513	-118.0290	n c	5.2	Mw	ML PAS	5.20	ML	PAS	CIT
110	1946	3	16	9	46	17.9000	35.7450	-118.0388	n c	5.1	Mw	ML PAS	5.10	ML	PAS	CIT
111	1946	3	17	14	45	53.0000	38.3000	-117.9000	n c	5	Mw	MD UNR	5.00	MD	UNRENO	UNRENO
112	1946	3	18	15	50	42.6500	35.7467	-117.9085	4.4	5.3	Mw	ML PAS	5.30	ML	PAS	CIT
113	1946	7	18	14	27	58.0000	34.5333	-115.9833	n c	5.6	Mw	ML PAS	5.60	ML	PAS	CIT
114	1947	1	11	11	57	48.0000	37.6000	-118.4300	n c	4.34	Mw	ML BRK	5.00	MI	CDMG	UCB
115	1947	4	10	15	58	06.0000	34.9833	-116.5500	n c	6.51	Mw	STOCOF	6.20	ML	PAS	CIT
116	1947	4	10	16	3	00.0000	34.9667	-116.5500	n c	5.1	Mw	ML PAS	5.10	ML	PAS	CIT
117	1947	4	10	17	18	22.0000	34.9500	-116.5333	n c	5	Mw	ML PAS	5.00	ML	PAS	CIT
118	1947	4	11	7	47	00.0000	34.9667	-116.5500	n c	5	Mw	ML PAS	5.00	ML	PAS	CIT
119	1948	11	2	16	48	08.0000	35.9830	-114.7830	n c	5	Mw	ML RWL	5.00	ML	RWL	MER
120	1949	2	11	21	5	24.0000	37.0833	-117.7500	n c	5.6	Mw	ML PAS	5.60	ML	PAS	CIT
121	1949	11	2	2	30	-01.0000	37.1063	-113.5735	n c	4.7	Mw	ML PAS	5.00	MI	PAS	UVUTAH
122	1951	12	28	2	49	27.0000	37.5700	-118.5800	n c	5.13	Mw	ML BRK	5.20	ML	PAS	UCB
123	1952	2	20	13	41	11.0000	36.0000	-114.7000	16	3.6	Mw	ML PAS	5.00	UK	RWL	MER
124	1952	5	24	4	15	15.4400	35.9390	-114.7320	8	4.9	Mw	ML PAS	5.00	MI	SGB	MER
125	1952	7	21	12	5	31.0000	35.0000	-119.0000	n c	6.27	Mw	STOCOF	6.40	ML	PAS	CIT
126	1952	7	21	12	19	36.0000	34.9500	-118.8667	n c	5.3	Mw	ML PAS	5.30	ML	PAS	CIT
127	1952	7	21	15	13	58.0000	35.1833	-118.6500	n c	5.1	Mw	ML PAS	5.10	ML	PAS	CIT
128	1952	7	21	17	42	44.0000	35.2333	-118.5333	n c	5.1	Mw	ML PAS	5.10	ML	PAS	CIT
129	1952	7	21	19	41	22.0000	35.1333	-118.7667	n c	5.5	Mw	ML PAS	5.50	ML	PAS	CIT
130	1952	7	23	0	38	32.0000	35.3667	-118.5833	n c	5.7	Mw	STOCOF	6.10	ML	PAS	CIT
131	1952	7	23	3	19	23.0000	35.3667	-118.5833	n c	5	Mw	ML PAS	5.00	ML	PAS	CIT
132	1952	7	23	7	53	19.0000	35.0000	-118.8333	n c	5.4	Mw	ML PAS	5.40	ML	PAS	CIT
133	1952	7	23	13	17	05.0000	35.2167	-118.8167	n c	5.76	Mw	STOCOF	5.70	ML	PAS	CIT
134	1952	7	23	18	13	51.0000	35.0000	-118.8333	n c	5.2	Mw	ML PAS	5.20	ML	PAS	CIT
135	1952	7	25	13	13	08.2500	35.3108	-118.4992	2.8	5	Mw	ML PAS	5.00	ML	PAS	CIT
136	1952	7	25	19	9	44.6200	35.3173	-118.4945	5.5	5.76	Mw	STOCOF	5.70	ML	PAS	CIT

TABLE G-2
EARTHQUAKES OF MAGNITUDE 5 OR GREATER IN THE YUCCA MOUNTAIN HISTORICAL SEISMICITY CATALOGUE

Cat. No.	Year	Mo.	Day	Time (GMT)			Lat.	Long.	Depth	Mag1	Scale	Mag1 Source	Mag2	Scale	Mag2 Source	Location
				Hour	Min	Sec			(km)							Source
137	1952	7	25	19	43	23.6700	35.3153	-118.5158	11.2	5.94	Mw	STOCOF	5.70	ML	PAS	CIT
138	1952	7	29	7	3	47.0000	35.3833	-118.8500	n c	6.27	Mw	STOCOF	6.10	ML	PAS	CIT
139	1952	7	29	8	1	46.0000	35.4000	-118.8167	n c	5.1	Mw	ML PAS	5.10	ML	PAS	CIT
140	1952	7	31	12	9	09.0000	35.3333	-118.6000	n c	5.8	Mw	ML PAS	5.80	ML	PAS	CIT
141	1952	8	22	22	41	24.0000	35.3333	-118.9167	n c	5.78	Mw	STOCOF	5.80	ML	PAS	CIT
142	1952	8	23	10	9	07.1500	34.5193	-118.1982	13.1	5	Mw	ML PAS	5.00	ML	PAS	CIT
143	1952	10	20	7	26	39.0000	36.0000	-114.8000	n c	4.9	Mw	MD UNR	5.00	MS	BRP	MER
144	1954	1	27	14	19	48.0000	35.1500	-118.6333	n c	5	Mw	ML PAS	5.00	ML	PAS	CIT
145	1954	5	23	23	52	43.0000	34.9833	-118.9833	n c	5.1	Mw	ML PAS	5.10	ML	PAS	CIT
146	1954	7	20	0	11	38.0000	38.2000	-116.4000	n c	5	Mw	MD UNR	5.00	MD	UNRENO	UNRENO
147	1954	12	16	11	7	11.0000	39.2800	-118.1200	15	7.1	Mw	DOSSM1	7.30	MD	UNRENO	UNRENO
148	1954	12	16	11	11	00.0000	39.6700	-117.9000	12	6.8	Mw	DOSSM1	-9.99			DOSSM1
149	1955	1	1	12	13	54.0000	39.0000	-118.0000	n c	5.1	Mw	MD UNR	5.10	MD	UNRENO	UNRENO
150	1955	1	9	9	10	50.0000	39.0000	-118.0000	n c	5	Mw	MD UNR	5.00	MI	USN	UNRENO
151	1955	6	19	19	20	00.0000	38.9700	-118.2500	n c	5.2	Mw	MD UNR	5.20	ML	UCBMLT	UNRENO
152	1955	6	19	19	25	16.0000	39.0000	-118.5000	n c	4.93	Mw	ML BRK	5.00	ML	UCBMLT	DNAG
153	1955	8	8	10	35	38.0000	38.3300	-118.6700	n c	5.2	Mw	MD UNR	5.20	ML	UCBMLT	UNRENO
154	1956	12	31	17	37	45.0000	38.2500	-118.9300	n c	5	Mw	MD UNR	5.00	MD	UNRENO	UNRENO
155	1956	12	31	17	39	24.0000	38.2800	-118.9700	n c	5.1	Mw	MD UNR	5.10	MD	UNRENO	UNRENO
156	1958	4	19	9	1	02.0000	36.0000	-114.8000	n c	4.9	Mw	MD UNR	5.00	MS	BRP	MER
157	1959	6	18	0	29	40.0000	37.5500	-118.5700	n c	4.64	Mw	ML BRK	5.00	MI	BRK	UCB
158	1959	6	23	15	4	34.0000	38.9300	-118.7700	n c	5.4	Mw	DOSSM1	5.50	UK	BRK	DNAG
159	1959	8	4	7	36	59.0000	37.3500	-118.5500	n c	5.2	Mw	MD UNR	5.20	ML	PAS	UNRENO
160	1960	1	26	4	17	36.0000	38.0000	-116.5000	n c	4.9	Mw	MD UNR	5.00	MI	SGB	UNRENO
161	1960	6	5	7	47	07.0000	37.5200	-118.7300	n c	5.13	Mw	ML BRK	5.20	ML	PAS	UCB
162	1961	1	28	8	12	46.1800	35.7782	-118.0487	5.5	5.3	Mw	ML PAS	5.30	ML	PAS	CIT
163	1961	2	2	0	4	16.0000	37.4500	-118.6300	n c	5.23	Mw	ML BRK	5.30	ML	UCBMLT	UCB
164	1961	2	2	0	7	42.0000	37.4200	-118.6700	n c	5.03	Mw	ML BRK	5.10	ML	PAS	UCB
165	1962	4	13	15	38	51.9000	38.2200	-119.4500	n c	5.03	Mw	ML BRK	5.10	ML	UCBMLT	UCB
166	1963	3	25	9	28	42.7700	36.0180	-114.7710	8	4.9	Mw	ML PAS	5.00	MS	BRP	MER
167	1963	4	13	15	38	51.9000	38.2160	-119.4330	16	5.1	Mw	MD UNR	5.10	MD	UNRENO	UNRENO
168	1963	12	6	8	34	25.7000	37.5400	-118.4200	n c	4.7	Mw	MD UNR	5.00	MI	PAS	UNRENO
169	1964	3	22	16	30	55.9000	38.7000	-118.8000	n c	5.5	Mw	MD UNR	5.50	MD	UNRENO	UNRENO
170	1964	10	23	13	57	05.0000	38.7000	-118.1000	n c	5.3	Mw	MD UNR	5.30	ML	BRK	UNRENO

TABLE G-2
EARTHQUAKES OF MAGNITUDE 5 OR GREATER IN THE YUCCA MOUNTAIN HISTORICAL SEISMICITY CATALOGUE

Cat. No.	Year	Mo.	Day	Time (GMT)			Lat.	Long.	Depth	Mag1	Scale	Mag1 Source	Mag2	Scale	Mag2 Source	Location
				Hour	Min	Sec			(km)							Source
171	1964	10	30	19	3	09.3000	37.5000	-117.8000	n c	4.44	Mw	ML BRK	5.00	MI	SGB	MER
172	1965	9	25	17	43	44.1200	34.7125	-116.5027	10.6	5.2	Mw	ML PAS	5.20	ML	PAS	CIT
173	1965	9	26	7	0	01.7500	34.7112	-116.0268	8.3	5	Mw	ML PAS	5.00	ML	PAS	CIT
174	1966	4	2	12	48	38.0000	38.7000	-118.1000	n c	4.8	Mw	MD UNR	5.00	MI	CDMG	UNRENO
175	1966	8	16	18	2	32.8500	37.4635	-114.1512	7	5.3	Mw	DOSSM1	6.10	MB	NEIC	UVUTAH
176	1966	8	17	23	8	00.1600	37.3550	-114.2070	7	5.43	Mw	ML BRK	5.50	ML	BRK	MER
177	1966	8	18	9	15	37.5000	37.3000	-114.2000	33	5	Mw	ML PAS	5.10	MB	NEIC	DNAG
178	1966	8	18	10	9	22.4000	37.3000	-114.2000	33	3.84	Mw	ML BRK	5.60	MB	DNAG	DNAG
179	1966	8	18	17	35	06.4000	37.4000	-114.2000	33	5	Mw	ML PAS	5.20	MB	NEIC	DNAG
180	1966	9	22	18	56	41.5600	37.3160	-114.2140	7	5.3	Mw	ML PAS	5.30	ML	PAS	MER
181	1966	9	22	18	57	34.0700	37.3690	-114.1830	7	5.73	Mw	ML BRK	5.80	ML	BRK	MER
182	1966	10	1	2	57	58.0000	38.1000	-118.3000	n c	3.7	Mw	MD UNR	5.50	MB	DNAG	UNRENO
183	1966	12	22	17	30	01.7000	37.3390	-116.4300	8	5	Mw	MD UNR	5.00	MD	UNRENO	MER
184	1967	5	7	18	1	36.1000	37.0000	-115.0000	20	5.1	Mw	MD UNR	5.10	ML	PDX	MER
185	1968	2	6	0	41	38.0000	38.0200	-118.3500	n c	4.9	Mw	MD UNR	5.00	MI	CDMG	UNRENO
186	1968	4	26	15	14	52.0000	37.1380	-116.1980	33	5.1	Mw	MD UNR	5.10	MD	UNRENO	MER
187	1968	12	19	22	23	26.3000	37.2170	-116.4670	4	4.5	Mw	MD UNR	5.00	MB	PDX	MER
188	1968	12	21	0	14	25.1000	37.2630	-116.4880	3.5	4.7	Mw	MD UNR	5.00	MB	DNAG	MER
189	1969	9	16	17	31	14.2000	37.3170	-116.4600	0.6	4.14	Mw	ML BRK	5.00	UK	GDY	MER
190	1970	7	30	20	16	35.4000	37.2830	-116.5600	0.6	4.4	Mw	ML PAS	5.20	MB	DNAG	MER
191	1970	9	12	14	30	52.9800	34.2698	-117.5400	8	5.4	Mw	ML PAS	5.40	ML	PAS	CIT
192	1975	6	1	1	38	49.2300	34.5157	-116.4955	4.46	5.2	Mw	ML PAS	5.20	ML	PAS	CIT
193	1975	7	1	18	14	08.1400	37.3360	-116.1780	13.5	4.74	Mw	ML BRK	5.00	MI	SGB	MER
194	1977	2	22	6	24	06.1000	38.4800	-119.2800	n c	4.74	Mw	ML BRK	5.00	MI	GS	DNAG
195	1978	10	4	16	42	47.9300	37.5350	-118.6982	22.88	5.5	Mw	DOSSM1	5.80	ML	PAS	USGS
196	1978	10	4	17	39	02.4100	37.5447	-118.6657	25.19	4.88	Mw	MDUSGS	5.30	MX	USGS	USGS
197	1979	3	15	21	7	16.5300	34.3273	-116.4448	2.48	5.52	Mw	STOCOF	5.20	ML	PAS	CIT
198	1979	10	7	20	54	40.7100	38.2550	-119.3303	5	4.32	Mw	MDUSGS	5.20	ML	BRK	USGS
199	1980	5	25	16	33	43.9300	37.5893	-118.8458	10.16	6.21	Mw	STOCOF	6.50	ML	PAS	USGS
200	1980	5	25	16	49	27.1100	37.6747	-118.9152	8.86	5.93	Mw	ML BRK	6.00	ML	BRK	USGS
201	1980	5	25	17	6	27.2100	37.4743	-118.8490	5	5.1	Mw	ML PAS	5.10	ML	PAS	CIT
202	1980	5	25	19	44	49.4500	37.4788	-118.8332	20.6	5.9	Mw	STOCOF	6.70	ML	PAS	USGS
203	1980	5	25	20	35	48.0300	37.6258	-118.8407	8.15	5.63	Mw	ML BRK	5.90	ML	PAS	USGS
204	1980	5	25	20	59	22.3800	37.6070	-118.8245	17.15	4.93	Mw	ML BRK	5.50	ML	PAS	USGS

TABLE G-2
EARTHQUAKES OF MAGNITUDE 5 OR GREATER IN THE YUCCA MOUNTAIN HISTORICAL SEISMICITY CATALOGUE

Cat. No.	Year	Mo.	Day	Time (GMT)			Lat.	Long.	Depth	Mag1	Scale	Mag1 Source	Mag2	Scale	Mag2 Source	Location
				Hour	Min	Sec			(km)							Source
205	1980	5	26	12	24	24.8400	37.5582	-118.8765	7.86	4.72	Mw	MDUSGS	5.60	ML	PAS	USGS
206	1980	5	26	18	57	55.4900	37.5150	-118.8805	4.72	5.63	Mw	ML BRK	5.70	ML	BERK	USGS
207	1980	5	27	14	50	56.7300	37.4927	-118.8132	16.06	5.86	Mw	STOCOF	6.30	ML	PAS	USGS
208	1980	5	27	19	1	07.8200	37.5927	-118.7810	6.57	4.96	Mw	MDUSGS	5.00	MD	USGS	USGS
209	1980	5	28	5	16	22.9900	37.5765	-118.8887	5.07	4.64	Mw	MDUSGS	5.30	MD	UNRENO	USGS
210	1980	5	28	5	48	23.0200	37.6257	-118.8687	6.71	4.72	Mw	MDUSGS	5.20	MD	UNRENO	USGS
211	1980	6	1	6	47	36.1300	37.4737	-118.8447	7.04	4.48	Mw	MDUSGS	5.00	UK		USGS
212	1980	6	6	14	18	17.2500	37.5072	-118.8378	6.71	3.36	Mw	MDUSGS	5.27	ML	CCN	USGS
213	1980	6	7	3	16	41.3200	37.5312	-118.7535	6.05	3.6	Mw	MDUSGS	5.49	ML	CCN	USGS
214	1980	6	8	6	11	39.8300	37.5337	-118.7680	6.48	3.36	Mw	MDUSGS	5.12	ML	CCN	USGS
215	1980	6	11	4	40	58.3200	37.5448	-118.8822	7.74	4.64	Mw	MDUSGS	5.20	UK		USGS
216	1980	6	18	18	55	37.4900	37.5275	-118.8340	7.71	3.6	Mw	MDUSGS	5.30	UK		USGS
217	1980	6	19	7	19	31.0900	37.5592	-118.9170	3.94	3.36	Mw	MDUSGS	5.00	MD	UNRENO	USGS
218	1980	6	19	14	4	29.9400	37.6358	-118.8460	9.35	3.76	Mw	MDUSGS	5.20	UK		USGS
219	1980	6	20	15	24	59.4800	37.5445	-118.8470	9.16	3.36	Mw	MDUSGS	5.30	UK		USGS
220	1980	6	28	0	58	41.8400	37.5817	-118.8205	4.29	4.24	Mw	MDUSGS	5.90	MD	UNRENO	USGS
221	1980	6	29	7	46	13.2700	38.0133	-118.6620	9.32	4.64	Mw	MDUSGS	5.00	ML	BRK	USGS
222	1980	8	1	16	38	55.9200	37.5643	-118.8742	6.21	5.04	Mw	MDUSGS	5.40	ML	PAS	USGS
223	1980	9	4	21	3	33.8000	38.0750	-118.5640	7.28	4.9	Mw	MD UNR	5.10	MB	DNAG	UNRENO
224	1980	9	7	1	30	42.6000	38.0690	-118.5780	8.31	4.9	Mw	MD UNR	5.10	ML	BERK	UNRENO
225	1980	9	7	4	36	38.1000	38.0650	-118.5900	8.4	5.3	Mw	MD UNR	5.70	ML	PAS	UNRENO
226	1980	9	7	6	47	10.4000	38.0620	-118.5890	9.62	5.2	Mw	MD UNR	5.30	ML	BERK	UNRENO
227	1980	9	7	6	48	30.6000	38.0900	-118.5700	n c	5.23	Mw	ML BRK	5.40	ML	PAS	DNAG
228	1980	12	28	22	58	09.4000	38.1640	-118.3620	6.97	4.8	Mw	MD UNR	5.00	ML	BRK	UNRENO
229	1981	9	30	11	53	26.1800	37.5852	-118.8665	5.65	5.64	Mw	STOCOF	6.10	ML	PAS	USGS
230	1981	9	30	13	5	47.8200	37.6410	-118.8485	8.49	4.84	Mw	MLUSGS	5.30	MX	USGS	USGS
231	1982	4	15	21	52	09.0000	38.0710	-118.5490	1.38	4.9	Mw	MD UNR	5.10	ML	BERK	UNRENO
232	1982	6	24	14	14	37.9600	38.8297	-115.2645	n c	5.2	Mw	ML PAS	5.20	ML	PAS	CIT
233	1982	9	24	7	40	24.4300	37.8458	-118.1572	7.46	5.34	Mw	MD UNR	5.50	ML	BERK	UNRENO
234	1982	12	28	19	6	24.7700	37.9905	-118.3917	4.75	4.59	Mw	MD UNR	5.20	ML	PAS	UNRENO
235	1983	1	7	1	38	10.3200	37.6380	-118.8988	9.75	5.22	Mw	MLUSGS	5.70	ML	PAS	USGS
236	1983	1	7	3	24	14.8100	37.6202	-118.8787	4.17	5.33	Mw	ML BRK	5.60	ML	PAS	USGS
237	1983	1	7	3	24	18.9800	37.6295	-118.9350	5.82	5.26	Mw	MLUSGS	5.40	MD	UNRENO	USGS
238	1983	7	3	18	40	07.6200	37.5598	-118.8445	11.52	5.17	Mw	MLUSGS	5.30	ML	BERK	USGS

TABLE G-2
EARTHQUAKES OF MAGNITUDE 5 OR GREATER IN THE YUCCA MOUNTAIN HISTORICAL SEISMICITY CATALOGUE

Cat. No.	Year	Mo.	Day	Time (GMT)			Lat.	Long.	Depth	Mag1	Scale	Mag1 Source	Mag2	Scale	Mag2 Source	Location
				Hour	Min	Sec			(km)							Source
239	1984	11	23	18	8	25.3300	37.4590	-118.6057	11.46	5.8	Mw	STOCOF	6.20	ML	PAS	USGS
240	1984	11	23	19	12	34.7700	37.4372	-118.6070	12.13	5.37	Mw	MLUSGS	5.51	ML	USGS	USGS
241	1984	11	26	16	21	40.8500	37.4487	-118.6475	8.94	5.18	Mw	MLUSGS	5.60	ML	BERK	USGS
242	1985	1	24	11	27	21.0100	38.1550	-118.8108	10.82	4.92	Mw	MLUSGS	5.30	ML	BRK	USGS
243	1985	3	25	16	5	12.7800	37.4545	-118.6118	7.62	5.01	Mw	MLUSGS	5.10	ML	BERK	USGS
244	1986	7	20	14	29	45.4600	37.5668	-118.4380	6.67	5.8	Mw	DOSSM1	5.90	ML	BERK	USGS
245	1986	7	21	14	42	26.0200	37.5388	-118.4425	10.48	6.25	Mw	STOCOF	6.60	MD	UNRENO	USGS
246	1986	7	21	14	51	09.0200	37.4928	-118.4280	11.78	5.45	Mw	MLUSGS	5.80	MD	UNRENO	USGS
247	1986	7	21	14	57	49.8300	37.5240	-118.4738	8.29	4.76	Mw	MLUSGS	5.00	MD	USGS	USGS
248	1986	7	21	22	7	00.7600	37.4898	-118.3762	6.68	3.52	Mw	MDUSGS	5.50	MD	UNRENO	USGS
249	1986	7	21	22	7	16.4300	37.5940	-118.3768	6.1	5.33	Mw	MLUSGS	5.60	ML	BERK	USGS
250	1986	7	22	13	48	59.1700	37.5317	-118.4692	11.89	4.92	Mw	MLUSGS	5.00	ML	BERK	USGS
251	1986	7	31	7	22	39.7400	37.4732	-118.3653	8.1	5.5	Mw	DOSSM1	5.90	MX	USGS	USGS
252	1986	8	1	14	28	18.1600	37.5158	-118.3962	9	5.06	Mw	MLUSGS	5.30	MD	USGS	USGS
253	1988	6	10	23	6	43.0500	34.9430	-118.7427	6.81	5.4	Mw	ML PAS	5.40	ML	PAS	CIT
254	1988	9	19	2	56	31.7700	38.4613	-118.3418	8.97	5	Mw	MD UNR	5.35	ML	USGS	UNRENO
255	1990	10	24	6	15	17.7700	38.1712	-119.1997	8.22	5.12	Mw	MDUSGS	5.80	ML	BERK	USGS
256	1992	6	28	11	57	34.1300	34.2005	-116.4357	1.03	7.3	Mw	CALT1	7.40	ML	PAS	CIT
257	1992	6	28	12	0	45.0000	34.1307	-116.4082	0.01	5.6	Mw	ML PAS	5.60	ML	PAS	CIT
258	1992	6	28	12	1	16.1900	34.1198	-116.3232	6	5.4	Mw	ML PAS	5.40	ML	PAS	CIT
259	1992	6	28	12	36	40.6400	34.1348	-116.4343	7.39	5.3	Mw	ML PAS	5.30	ML	PAS	CIT
260	1992	6	28	12	40	53.8200	34.3305	-116.5473	6	5.4	Mw	ML PAS	5.40	ML	PAS	CIT
261	1992	6	28	14	43	21.8500	34.1618	-116.8522	11.06	5.5	Mw	ML PAS	5.50	ML	PAS	CIT
262	1992	6	28	15	5	30.7300	34.2027	-116.8268	5.32	6.4	Mw	ML PAS	6.40	ML	PAS	CIT
263	1992	6	28	17	1	31.9200	34.1785	-116.9225	13.72	5.1	Mw	ML PAS	5.10	ML	PAS	CIT
264	1992	6	28	17	5	57.5600	34.2552	-116.9120	7.66	5	Mw	ML PAS	5.00	ML	PAS	CIT
265	1992	6	29	10	14	20.0600	36.7183	-116.2860	11.8	5.61	Mw	MD UNR	5.61	MD	UNRENO	UNRENO
266	1992	6	29	10	31	03.3900	36.7330	-116.2500	6.64	4.3	Mw	MLGSDR	5.00	MX	USGS	SGB
267	1992	6	29	14	8	37.7300	34.1045	-116.4032	10.35	5.5	Mw	ML PAS	5.50	ML	PAS	CIT
268	1992	6	29	14	13	38.7800	34.1082	-116.4038	9.88	5	Mw	ML PAS	5.00	ML	PAS	CIT
269	1992	7	1	7	40	29.9000	34.3307	-116.4627	8.28	5.3	Mw	ML PAS	5.30	ML	PAS	CIT
270	1992	7	5	21	18	27.1400	34.5825	-116.3178	0.11	5.4	Mw	ML PAS	5.40	ML	PAS	CIT
271	1992	7	11	18	14	16.1500	35.2100	-118.0657	10.69	5.7	Mw	ML PAS	5.70	ML	PAS	CIT
272	1992	8	17	20	41	52.1200	34.1947	-116.8620	11.27	5.2	Mw	ML PAS	5.20	ML	PAS	CIT

TABLE G-2
EARTHQUAKES OF MAGNITUDE 5 OR GREATER IN THE YUCCA MOUNTAIN HISTORICAL SEISMICITY CATALOGUE

Cat. No.	Year	Mo.	Day	Time (GMT)			Lat.	Long.	Depth	Mag1	Scale	Mag1 Source	Mag2	Scale	Mag2 Source	Location
				Hour	Min	Sec			(km)							Source
273	1992	9	2	10	26	19.2900	37.1650	-113.3330	9.59	5.9	Mw	MLGSDR	5.90	ML	SLC	SGB
274	1992	9	15	8	47	11.2900	34.0637	-116.3607	8.3	5.1	Mw	ML PAS	5.10	ML	PAS	CIT
275	1992	11	27	16	0	57.4900	34.3397	-116.8995	1.48	5.4	Mw	ML PAS	5.40	ML	PAS	CIT
276	1992	12	4	2	8	57.5000	34.3683	-116.8973	2.99	5.3	Mw	ML PAS	5.30	ML	PAS	CIT
277	1993	5	17	23	20	50.1000	37.1763	-117.8323	9.13	6.1	Mw	MDUNRC	6.20	ML	PAS	UNRENO
278	1993	5	17	23	35	28.4700	37.0970	-117.5790	n c	4.64	Mw	MDUSGS	5.20	MX	USGS	USGS
279	1993	5	19	14	13	23.8400	37.1383	-117.7332	6	4.9	Mw	ML PAS	5.01	MD	UNRCSP	CIT
280	1993	5	28	4	47	40.6000	35.1493	-119.1037	21.43	5.2	Mw	ML PAS	5.20	ML	PAS	CIT
281	1993	11	28	8	21	22.4000	37.6365	-118.9308	7.2	2.48	Mw	MDUSGS	5.10	ML	PAS	USGS
282	1994	4	6	19	1	03.0600	34.2245	-117.0580	0.09	4.64	Mw	MDUSGS	5.00	MX	USGS	USGS
283	1995	8	17	22	39	58.4800	35.7665	-117.6517	10.54	5.2	Mw	MDUSGS	5.80	MX	USGS	USGS
284	1995	9	20	23	27	35.9000	35.7478	-117.6422	8.32	5.28	Mw	MDUSGS	5.90	MX	USGS	USGS
285	1995	9	25	4	47	28.7000	35.8025	-117.6073	12.14	4.72	Mw	MDUSGS	5.20	MX	USGS	USGS
286	1996	1	7	14	32	52.5500	35.7603	-117.6397	10.42	4.8	Mw	MDUSGS	5.20	MX	USGS	USGS
287	1996	3	30	15	22	23.7600	37.6230	-118.8600	8.45	5.46	Mw	MLUSGS	5.62	ML	USGS	USGS

Table G-3
MAGNITUDE CONVERSIONS FOR THE YUCCA MOUNTAIN CATALOGUE (MAJOR CONTRIBUTORS)

Catalogue	Magnitude Scale	MW-ML and Other Magnitude Relationships, Their Ranges of Validity, and References
CIT	ML PAS	MW = ML for $3 \leq ML \leq 6.8$ (L. Wald, USGS, personal communication, 1996; Hanks and Kanamori, 1979; Thatcher and Hanks, 1973) MW = 0.887 ML + 0.633 for ML < 3 for California (Chung and Bernreuter, 1981)
UCB	ML BRK	MW = (0.997± 0.02) ML - 0.05 (±0.131) for $3.6 \leq ML \leq 6.8$ (R. Uhrhammer, UCB, written communication, 1996) For ML < 3.6 assume same as above (R. Uhrhammer, UCB, oral communication, 1997)
USGS_CA	ML USGS MD USGS	For Mammoth region MW = 0.8 ML + 0.96 for $1 \leq ML \leq 6$ and MW = 0.54 ML + 1.55 for $½ \leq ML \leq 3$ (Chavez and Priestly, 1985) Coda duration magnitude equivalent to ML for $0.5 \leq ML \leq 5.5$ (Eaton, 1992) so use above conversions
SGB	ML USGSDR MC USGSDR MV USGSDR MD USGSDR MD USGSDV	MW = ML for $ML \geq 3$; Use MW = 0.667 ML + 1 for ML < 3 (D. von Seggern, UNR, written communication, 1996) Coda amplitude magnitude - convert to ML using ML =1.05 MC -0.01 for $1.0 \leq MC \leq 3.0$ (Figure G-6) then to MW ML from vertical record - convert to ML using ML =1.01 MV + 0.22. Valid for $0.5 \leq MV \leq \sim 3.0$ (Figure G-5) then to MW Coda duration magnitude - convert to ML using ML =1.01 MD + 0.06 for $0.5 \leq MD \leq 2.25$ (Figure G-7) then to MW Coda duration magnitude from develocorder - convert to MD UNR using MD (UNR) = 0.82MD (USGS)+ 1.07 for $1.25 \leq$ MD (USGS)≤ 2.5 (Figure G-8) then to MW
UNR	ML UNRENO MD UNRENO MD CUSP	Using same Mo-ML relation as for SGB MW = ML for $3 \leq ML \leq 6.8$; and MW = 0.667 ML + 1.0 for ML < 3 MD calibrated to ML (UNR or UCB) for $1.5 \leq ML \leq 5.7$. Use equations above Convert to ML CUSP using ML = -1.24 + 1.31 MD for $0.5 \leq MD \leq 4$ (D. von Seggern, UNR, written communication, 1996) then to MW
MER	ML MD MB MS	Adopted from UCB, CIT or UNR - use appropriate conversion Adopted from UNR or NTS related seismic research, e.g., HSF, ROW and FPH - Assume equivalent to MD UNR mb = ML for mb < 5.5 and then convert to MW (Boore and Joyner, 1982) MW = 0.79MS + 1.24 (Jost and Herrmann, 1990)
UU	ML MD	MW = 0.8 ML + 0.5 for $2.3 \leq ML \leq 3.5$ and MW = ML - 0.17 for $3.5 \leq ML \leq 6.0$ (Shemeta and Pechmann, 1989 and unpublished work): Calibrated to ML for $1.5 \leq ML \leq 2.5$

TABLE G-4
HIERARCHIES FOR MAGNITUDE CONVERSION FOR SUB-CATALOGUES OF THE 300 KM YUCCA MOUNTAIN CATALOGUE

CATALOGUE	MAGNITUDE SCALE	MAGNITUDE CONVERSION
CIT	ML PAS	See Table G-2
UCB	ML BRK/BERK/UCB	See Table G-2
	ML PAS	See Table G-2
	MI CDMG	=ML BRK (See Table G-2)
	MI BRK	=ML BRK (See Table G-2)
	UK MAK	=ML BRK (See Table G-2)
USGS_CA	ML USGS	See Table G-2
	MD USGS	See Table G-2
	MX USGS	=ML USGS (See Table G-2)
	MD UNRCSP	See Table G-2
	ML BRK/BERK	See Table G-2
	MD UNRENO	See Table G-2
	ML PAS	See Table G-2
	ML CCN	=ML USGS (See Table G-2)
SGB	ML USGSDR	See Table G-2
	MV USGSDR	See Table G-2
	MC USGSDR	See Table G-2
	MD USGSDR	See Table G-2
	MD USGSDV	See Table G-2
	MD UNRENO	See Table G-2
	MD SGB	=MD USGSDR (See Table G-2)
UNR	ML UNRENO	See Table G-2
	MD UNRENO	See Table G-2
	MD UNRCSP	See Table G-2
	ML BRK	See Table G-2
	ML USGSDR	See Table G-2
	MV USGSDR	See Table G-2
	MD USGS	See Table G-2
	ML PAS	See Table G-2

TABLE G-4
HIERARCHIES FOR MAGNITUDE CONVERSION FOR SUB-CATALOGUES OF THE 300 KM YUCCA MOUNTAIN CATALOGUE
(CONTINUED)

CATALOGUE	MAGNITUDE SCALE	MAGNITUDE CONVERSION
MER	ML BRK	See Table G-2
	ML PAS	See Table G-2
	ML UNRENO	See Table G-2
	MD UNR	See Table G-2
	MD HSF, ROW, FPH, RWL, PHM, SHJ, RYN	=MD UNRENO (See Table G-2)
	ML KKG, RYN, PDX, RWL, NOS	=ML USGSDR (See Table G-2)
	UK ALX, RYC, KKG, ERS, PDX, GDY, ISC	=ML USGSDR (See Table G-2)
	ML ISC	=ML USGSDR (See Table G-2)
	MI UVUTAH	=ML UVUTAH(See Table G-2)
	MX UVUTAH	=ML UVUTAH (See Table G-2)
	MB	See Table G-2
	MS	See Table G-2
UVUTAH	ML UVUTAH/SLC	See Table G-2
	MD UVUTAH/SLC	See Table G-2
	ML PAS	See Table G-2
	ML UNRENO	See Table G-2
	MI UVUTAH	=ML UVUTAH (See Table G-2)
	MD UNRENO	See Table G-2
	MX UVUTAH	=ML UVUTAH (See Table G-2)
DNAG	ML BRK	See Table G-2
	ML PAS	See Table G-2
	ML GS	=ML USGSDR (See Table G-2)
	ML CCN	=ML USGSDR (See Table G-2)
	MB DNAG	See Table G-2
	MD UNRENO	See Table G-2
	MD SGB	See Table G-2
	ML UNV	=ML UNRENO (See Table G-2)
	UK BRK	=ML BRK (See Table G-2)
	UK PAS	=ML PAS (See Table G-2)
	UK	=ML USGSDR (See Table G-2)
	MI BRK, CDMG	=ML BRK
DNAG (Cont.)	MI GS	=ML USGSDR (See Table G-2)
	MI SGB	=ML USGSDR (See Table G-2)

TABLE G-4
HIERARCHIES FOR MAGNITUDE CONVERSION FOR SUB-CATALOGUES OF THE 300 KM YUCCA MOUNTAIN CATALOGUE
(CONTINUED)

CATALOGUE	MAGNITUDE SCALE	MAGNITUDE CONVERSION
NEIC - CDMG	MW H&K	No conversion needed
	ML RI	=ML BRK (See Table G-2)
	ML EH	=ML BRK (See Table G-2)
	UK TO	=ML BRK (See Table G-2)
	UK DMG	=ML BRK (See Table G-2)
NEIC - SRA	MD UU	See Table G-2
	LG AE	=mb (See Table G-2)
NEIC - PDE	ML GS	=ML USGSDR (See Table G-2)
	ML AE	=ML USGSDR (See Table G-2)
	MB NEIC	See Table G-2
NAU	ML UNRENO	See Table G-2
	ML AE	=ML USGSDR (See Table G-2)
	ML GS	=ML USGSDR (See Table G-2)
	LG AE	=mb (See Table G-2)

TABLE G-5
EXPLANATION OF MAGNITUDE DATA SOURCES IN THE YUCCA MOUNTAIN CATALOGUE

ABE1	Abe and Noguchi (1983)
ALX	U.S. Army Corps of Engineers, Alexandria Laboratories
BDA	Unknown
BRK, BERK	University of California at Berkeley, California
BRP	Basin and Range Province
CALT1	Caltech
CCN	USGS Central California Network
CDMG	California Division of Mines and Geology
CGS	U.S. Coast and Geodetic Survey
CIT	California Institute of Technology
DMG	California Department of Mines and Geology
DNAG	Decade of North American Geology
DOSSM1	Doser and Smith (1989)
DW	Dewey
DWR	California Department of Water Resources
EQH	Earthquake History of the United States
ERL	Environmental Research Laboratory 1971-1973
ERS	W.W. Hays *et al.* (USGS, written communication, 1975)
FPH	Fischer *et al.*, 1972
GDY	W. Gawthrop and J. Dewey, USGS, written communication, 1980
GTR1	Gutenberg-Richter magnitude from intensity
HSF	Hamilton *et al.* (1971)
H&K	Hanks and Kanamori
ISC	International Seismological Centre
KKG	K.W. King *et al.* (NOAA, written communication, 1971) K. Bayer *et al.* (NOAA, written communication, 1972) K. Bayer (NOAA, written communications, 1973a,b, 1974)
MAK	Unknown
MER	Meremonte and Rogers (1987)
NAU	Northern Arizona University
NEIC	National Earthquake Information Center
NOS	Unknown
OTT	Ottawa
PAS	Pasadena, California
PDE	

TABLE G-5
EXPLANATION OF MAGNITUDE DATA SOURCES IN THE YUCCA MOUNTAIN CATALOGUE
(CONTINUED)

PDX	National Oceanic and Atmospheric Administration
PHM	Papanek and Hamilton (1972)
REN	Reno, Nevada
ROW	Rogers *et al.* (1977)
RPM	Unknown
RWL	Rogers and Lee (1976)
RYC	F. Ryall, UNR, written communication, 1980
RYN	Historical catalogue data, update of Slemmons *et al.* (1965)
SGB	Southern Great Basin Network
SHJ	Smith *et al.* (1971)
SLC	Salt Lake City, Utah
SRA	Stover, Reagor, Algermissen catalogue from NEIC
STOCOFF	Stover and Coffman
TOPO	Toppozada magnitude from intensity
UCB, UCBMLT	University of California, Berkeley
USE	U.S. Earthquakes, U.S. Coast and Geodetic Survey
USGS, NEIC, GS	National Earthquake Information Center, USGS
USGSDR	USGS SGB catalogue magnitude from digital recordings
USGSDV	USGS SGB catalogue magnitude from develocorders
UNRCSP	University of Nevada, Reno, from UNRSL CUSP system
UNW	Unknown
USN	W.W. Hays *et al.* (USGS, written communication, 1975)
UU, UVUTAH	University of Utah
VSB	Von Seggern and Brune (1996)
WCFS1	Woodward-Clyde Federal Services
XXX	Unknown

TABLE G-6
CATALOGUE OF UNDERGROUND NUCLEAR BLASTS AT THE NEVADA TEST SITE, 1957 TO 1992

Explanation of abbreviations:

Cat. No. Event number

Date Date of blast, GMT year, month, day

Time Time of blast, GMT hour, minute, second

Latitude Latitude, decimal degrees

Longitude Longitude, decimal degrees

Depth Depth of event, kilometers (all were assumed to be zero)

Magnitude 1 Magnitude, two-letter magnitude scale, magnitude source

Magnitude scales:

- M_L Local magnitude
- M_B Body-wave magnitude
- M_D Coda-duration magnitude
- M_w Moment magnitude

Magnitude sources:

WCFS	Woodward-Clyde Federal Services, calculated from yield
UNRENO	University of Nevada, Reno
RIL, RILEY OPP	Riley, California Institute of Technology
ISC	International Seismological Centre
ALX	U.S. Army Corps of Engineers, Alexandria Laboratories
RYN	Historical catalogue data, update of Slemmons *et al.* (1965)
UCB	University of California, Berkeley
MVDSDR	Calculated from USGS develocorder

Magnitude 2 Secondary magnitude

Intensity (MM) Modified Mercalli intensity

Agency Source

LLNL	Data from Lawrence Livermore National Laboratory
UNRENO	Data from University of Nevada, Reno
RILEY OPP	Data from Riley, CIT, provided by David Oppenheimer, USGS (1996)
MER	Meremonte and Rogers (1987)

TABLE G-7
ANNOUNCED UNITED STATES NUCLEAR TESTS AT THE NEVADA TEST SITE

Cat. No.	Year	Mo.	Day	Time (GMT hr:min.sec	Latitude	Longitude	Depth (km)	Magnitude 1	Magnitude 2	Agency Source
1	1957	JUL	26	00:00.0	37.052	-116.03	0	3.60MLWCFS		LLNL
2	1957	AUG	27	35:00.0	37.049	-116.03	0	3.60MLWCFS		LLNL
3	1957	SEP	19	59:00.6	37.196	-116.2	0	3.80MLWCFS		LLNL
4	1957	DEC	6	15:00.0	37.05	-116.03	0	3.60MLWCFS		LLNL
5	1958	FEB	22	00:00.0	0	0	0	3.60MLWCFS		LLNL
6	1958	MAR	14	00:00.0	0	0	0	3.60MLWCFS		LLNL
7	1958	SEP	12	00:00.0	37.05	-116.03	0	4.80MLWCFS		LLNL
8	1958	SEP	17	30:00.0	37.05	-116.03	0	4.40MLWCFS		LLNL
9	1958	SEP	21	00:00.0	37.049	-116.03	0	3.76MLWCFS		LLNL
10	1958	SEP	23	00:00.0	0	0	0	3.60MLWCFS		LLNL
11	1958	SEP	26	00:00.0	37.05	-116.03	0	3.86MLWCFS		LLNL
12	1958	SEP	26	00:00.0	37.193	-116.2	0	3.86MLWCFS		LLNL
13	1958	OCT	5	15:00.0	37.049	-116.03	0	4.24MLWCFS		LLNL
14	1958	OCT	8	00:00.0	37.195	-116.2	0	5.21MLWCFS		LLNL
15	1958	OCT	14	00:00.0	37.194	-116.2	0	5.39MLWCFS		LLNL
16	1958	OCT	16	00:00.0	37.184	-116.2	0	4.21MLWCFS		LLNL
17	1958	OCT	16	00:00.0	37.18	-116.2	0	4.50MDUNRENO		UNRENO
18	1958	OCT	20	30:00.0	37.05	-116.03	0	3.60MLWCFS		LLNL
19	1958	OCT	29	00:00.0	37.195	-116.21	0	5.10MLWCFS		LLNL
20	1958	OCT	30	00:00.0	37.186	-116.2	0	3.60MLWCFS		LLNL
21	1961	SEP	15	00:00.0	37.188	-116.21	0	3.96MLWCFS		LLNL
22	1961	SEP	16	45:00.0	37.048	-116.03	0	4.70MLWCFS		LLNL
23	1961	OCT	1	30:00.0	37.048	-116.04	0	4.70MLWCFS		LLNL
24	1961	OCT	10	00:00.0	37.194	-116.21	0	4.70MLWCFS		LLNL
25	1961	OCT	29	30:00.0	37.049	-116.03	0	4.70MLWCFS		LLNL
26	1961	DEC	3	04:00.6	37.046	-116.03	0	4.60MLWCFS		LLNL
27	1961	DEC	10	00:00.0	32.264	-103.87	0	4.00MLWCFS		LLNL
28	1961	DEC	13	00:00.0	37.127	-116.05	0	3.60MLWCFS		LLNL
29	1961	DEC	17	35:00.0	37.043	-116.03	0	4.70MLWCFS		LLNL
30	1961	DEC	22	30:00.0	37.195	-116.21	0	4.70MLWCFS		LLNL
31	1962	JAN	9	30:00.0	37.045	-116.04	0	4.20MLWCFS		LLNL
32	1962	JAN	18	00:00.0	37.047	-116.03	0	4.30MLWCFS		LLNL
33	1962	JAN	30	00:00.0	37.047	-116.04	0	4.70MLWCFS		LLNL
34	1962	FEB	8	00:00.0	37.127	-116.05	0	4.00MLWCFS		LLNL
35	1962	FEB	9	30:00.0	37.044	-116.04	0	4.30MLWCFS		LLNL
36	1962	FEB	15	00:00.0	37.226	-116.06	0	4.25MLWCFS		LLNL
37	1962	FEB	19	30:00.0	37.049	-116.03	0	3.85MLWCFS		LLNL
38	1962	FEB	19	50:00.0	37.127	-116.04	0	4.70MLWCFS		LLNL
39	1962	FEB	23	00:00.0	37.129	-116.05	0	4.50MLWCFS		LLNL
40	1962	FEB	24	30:00.0	37.048	-116.03	0	4.70MLWCFS		LLNL

TABLE G-7
ANNOUNCED UNITED STATES NUCLEAR TESTS AT THE NEVADA TEST SITE

Cat. No.	Year	Mo.	Day	Time (GMT hr:min.sec	Latitude	Longitude	Depth (km)	Magnitude 1	Magnitude 2	Agency Source
41	1962	MAR	1	10:00.0	37.041	-116.03	0	4.70MLWCFS		LLNL
42	1962	MAR	5	15:00.0	37.111	-116.37	0	3.60MLWCFS		LLNL
43	1962	MAR	6	30:00.0	37.048	-116.03	0	4.70MLWCFS		LLNL
44	1962	MAR	8	00:00.0	37.122	-116.05	0	4.40MLWCFS		LLNL
45	1962	MAR	15	30:00.0	37.044	-116.03	0	4.70MLWCFS		LLNL
46	1962	MAR	28	00:00.0	37.124	-116.03	0	4.10MLWCFS		LLNL
47	1962	MAR	31	00:00.0	37.047	-116.04	0	4.70MLWCFS		LLNL
48	1962	APR	5	00:00.0	37.045	-116.02	0	4.50MLWCFS		LLNL
49	1962	APR	6	00:00.0	37.118	-116.04	0	4.70MLWCFS		LLNL
50	1962	APR	12	00:00.0	37.127	-116.05	0	4.70MLWCFS		LLNL
51	1962	APR	14	00:00.0	37.222	-116.16	0	3.84MLWCFS		LLNL
52	1962	APR	21	40:00.0	37.119	-116.03	0	4.70MLWCFS		LLNL
53	1962	APR	27	00:00.0	37.118	-116.04	0	4.70MLWCFS		LLNL
54	1962	MAY	7	33:00.0	37.047	-116.03	0	4.70MLWCFS		LLNL
55	1962	MAY	10	00:00.0	37.128	-116.05	0	4.70MLWCFS		LLNL
56	1962	MAY	12	00:00.0	37.065	-116.03	0	5.00MLWCFS		LLNL
57	1962	MAY	19	00:00.0	37.123	-116.05	0	4.70MLWCFS		LLNL
58	1962	MAY	25	00:00.0	37.125	-116.05	0	4.70MLWCFS		LLNL
59	1962	JUN	1	00:00.0	37.046	-116.03	0	4.70MLWCFS		LLNL
60	1962	JUN	6	00:00.0	37.046	-116.04	0	4.70MLWCFS		LLNL
61	1962	JUN	13	00:00.0	37.222	-116.16	0	4.70MLWCFS		LLNL
62	1962	JUN	21	00:00.0	37.043	-116.03	0	4.70MLWCFS		LLNL
63	1962	JUN	27	00:00.0	37.042	-116.04	0	5.20MLWCFS		LLNL
64	1962	JUN	28	00:00.0	37.009	-116.2	0	4.70MLWCFS		LLNL
65	1962	JUN	30	30:00.0	37.117	-116.05	0	4.70MLWCFS		LLNL
66	1962	JUL	6	00:00.0	37.177	-116.05	0	5.40MLWCFS		LLNL
67	1962	JUL	13	00:00.2	37.055	-116.03	0	5.15MLWCFS		LLNL
68	1962	JUL	27	00:00.0	37.13	-116.06	0	4.70MLWCFS		LLNL
69	1962	AUG	24	00:00.0	37.119	-116.04	0	4.70MLWCFS		LLNL
70	1962	AUG	24	00:00.0	37.046	-116.02	0	4.70MLWCFS		LLNL
71	1962	SEP	6	00:00.0	37.13	-116.05	0	4.70MLWCFS		LLNL
72	1962	SEP	14	10:00.0	37.044	-116.02	0	4.70MLWCFS		LLNL
73	1962	SEP	20	00:00.0	37.055	-116.03	0	4.70MLWCFS		LLNL
74	1962	SEP	29	00:00.0	37.117	-116.03	0	4.70MLWCFS		LLNL
75	1962	OCT	5	00:00.0	37.139	-116.05	0	5.40MLWCFS		LLNL
76	1962	OCT	12	00:00.0	37.123	-116.05	0	4.70MLWCFS		LLNL
77	1962	OCT	12	00:00.0	37.049	-116.03	0	4.70MLWCFS		LLNL
78	1962	OCT	18	00:00.0	37.129	-116.04	0	4.70MLWCFS		LLNL
79	1962	OCT	19	00:00.0	37.04	-116.02	0	4.70MLWCFS		LLNL
80	1962	OCT	27	00:00.0	37.149	-116.05	0	4.70MLWCFS		LLNL

TABLE G-7
ANNOUNCED UNITED STATES NUCLEAR TESTS AT THE NEVADA TEST SITE

Cat. No.	Year	Mo.	Day	Time (GMT hr:min.sec	Latitude	Longitude	Depth (km)	Magnitude 1	Magnitude 2	Agency Source
81	1962	NOV	9	00:00.0	37.164	-116.07	0	4.70MLWCFS		LLNL
82	1962	NOV	15	30:00.0	37.042	-116.02	0	4.70MLWCFS		LLNL
83	1962	NOV	27	00:00.0	37.123	-116.03	0	4.70MLWCFS		LLNL
84	1962	DEC	4	00:00.0	37.128	-116.05	0	4.70MLWCFS		LLNL
85	1962	DEC	7	00:00.0	37.052	-116.03	0	4.70MLWCFS		LLNL
86	1962	DEC	12	25:00.0	37.172	-116.2	0	4.70MLWCFS		LLNL
87	1962	DEC	12	45:00.0	37.046	-116.02	0	4.70MLWCFS		LLNL
88	1962	DEC	14	00:00.0	37.124	-116.04	0	4.70MLWCFS		LLNL
89	1963	FEB	8	00:00.2	37.149	-116.05	0	4.70MLWCFS		LLNL
90	1963	FEB	8	30:00.1	37.058	-116.03	0	4.70MLWCFS		LLNL
91	1963	FEB	15	00:00.0	37.049	-116.03	0	4.70MLWCFS		LLNL
92	1963	FEB	21	47:00.0	37.12	-116.05	0	4.70MLWCFS		LLNL
93	1963	MAR	1	00:00.0	37.045	-116.03	0	4.70MLWCFS		LLNL
94	1963	MAR	15	22:00.5	37.126	-116.05	0	4.70MLWCFS		LLNL
95	1963	MAR	29	49:00.0	37.042	-116.02	0	4.70MLWCFS		LLNL
96	1963	APR	5	52:00.0	37.037	-116.02	0	4.70MLWCFS		LLNL
97	1963	APR	10	01:00.3	37.049	-116.03	0	4.70MLWCFS		LLNL
98	1963	APR	11	03:00.0	37.157	-116.07	0	4.70MLWCFS		LLNL
99	1963	APR	24	09:30.1	37.121	-116.04	0	4.70MLWCFS		LLNL
100	1963	MAY	9	19:00.3	37.049	-116.02	0	4.70MLWCFS		LLNL
101	1963	MAY	17	55:00.1	37.048	-116.03	0	4.70MLWCFS		LLNL
102	1963	MAY	22	40:00.0	37.111	-116.04	0	5.15MLWCFS		LLNL
103	1963	MAY	29	03:00.3	37.128	-116.04	0	4.70MLWCFS		LLNL
104	1963	JUN	5	00:00.0	37.196	-116.21	0	4.70MLWCFS		LLNL
105	1963	JUN	6	00:00.0	37.044	-116.04	0	4.70MLWCFS		LLNL
106	1963	JUN	6	58:00.0	37.125	-116.04	0	4.70MLWCFS		LLNL
107	1963	JUN	14	10:00.0	37.046	-116.02	0	4.70MLWCFS		LLNL
108	1963	JUN	25	00:00.0	37.131	-116.07	0	4.70MLWCFS		LLNL
109	1963	AUG	12	45:00.0	37.04	-116.02	0	4.70MLWCFS		RILEY OPP
110	1963	AUG	15	00:00.0	37.15	-116.08	0	4.70MLWCFS		RILEY OPP
111	1963	AUG	23	20:00.0	37.13	-116.04	0	4.70MLWCFS		RILEY OPP
112	1963	SEP	13	53:00.0	37.16	-116.08	0	4.70MLWCFS		RILEY OPP
113	1963	SEP	13	00:00.0	37.06	-116.02	0	5.70MLWCFS		RILEY OPP
114	1963	SEP	27	20:00.0	0	0	0	3.00MBRIL		RILEY OPP
115	1963	OCT	11	00:00.0	37.037	-116.02	0	4.70MLWCFS		RILEY OPP
116	1963	OCT	11	00:00.0	37.12	-116.03	0	4.70MLWCFS		RILEY OPP
117	1963	OCT	16	00:00.0	37.2	-116.23	0	5.15MLWCFS		RILEY OPP
118	1963	OCT	26	00:00.0	39.2	-118.38	0	4.80MLWCFS		RILEY OPP
119	1963	NOV	14	00:00.0	37.04	-116.02	0	4.70MLWCFS		RILEY OPP
120	1963	NOV	15	00:00.0	37.13	-116.05	0	4.70MLWCFS		RILEY OPP

TABLE G-7
ANNOUNCED UNITED STATES NUCLEAR TESTS AT THE NEVADA TEST SITE

Cat. No.	Year	Mo.	Day	Time (GMT hr:min.sec	Latitude	Longitude	Depth (km)	Magnitude 1	Magnitude 2	Agency Source
121	1963	NOV	22	30:00.0	37.12	-116.05	0	5.15MLWCFS		RILEY OPP
122	1963	DEC	4	38:30.0	37.04	-116.03	0	4.70MLWCFS		RILEY OPP
123	1963	DEC	12	02:00.0	37.13	-116.04	0	4.70MLWCFS		RILEY OPP
124	1964	JAN	16	00:00.0	37.142	-116.05	0	5.20MBISC		LLNL
125	1964	JAN	23	00:00.0	37.126	-116.04	0	4.20MBRIL		RILEY OPP
126	1964	JAN	30	00:00.0	37.1	-115.9	0	4.10MBRIL		RILEY OPP
127	1964	FEB	12	37:59.5	37.03	-116.12	0	4.70MLWCFS		RILEY OPP
128	1964	FEB	13	30:00.0	37.2	-115.9	0	4.00MBRIL		RILEY OPP
129	1964	FEB	18	37:19.0	37.1	-116	0	4.80MBRIL	4.40MBRIL	RILEY OPP
130	1964	FEB	20	30:00.0	37.15	-116.04	0	5.10MBRIL		RILEY OPP
131	1964	MAR	12	00:07.0	37.3	-116.2	0	3.30MBRIL		RILEY OPP
132	1964	MAR	13	02:00.0	37.05	-116.01	0	4.70MLWCFS		RILEY OPP
133	1964	APR	14	40:00.0	37.129	-116.03	0	4.70MLWCFS		RILEY OPP
134	1964	APR	15	30:00.0	37.044	-116.02	0	4.70MLWCFS		RILEY OPP
135	1964	APR	24	10:00.0	37.15	-116.06	0	5.20MBRIL		RILEY OPP
136	1964	APR	29	47:00.0	37.04	-116.03	0	4.10MBRIL		RILEY OPP
137	1964	MAY	14	40:00.0	37.12	-116.04	0	4.70MLWCFS		RILEY OPP
138	1964	MAY	15	15:00.0	37.04	-116.01	0	4.70MLWCFS		RILEY OPP
139	1964	JUN	11	45:00.0	37.15	-116.08	0	4.70MLWCFS		RILEY OPP
140	1964	JUN	12	01:00.0	36.8	-116.2	0	3.60MBRIL		RILEY OPP
141	1964	JUN	18	30:00.0	37.3	-115.6	0	3.20MBRIL		RILEY OPP
142	1964	JUN	24	06:12.0	36.8	-116.7	0	3.20MBRIL		RILEY OPP
143	1964	JUN	25	30:00.0	37.11	-116.03	0	4.70MLWCFS		RILEY OPP
144	1964	JUN	30	33:00.0	37.17	-116.06	0	4.70MLWCFS		RILEY OPP
145	1964	JUL	16	15:00.0	37.18	-116.05	0	5.15MLWCFS		RILEY OPP
146	1964	JUL	17	18:30.0	37.02	-116.03	0	4.70MLWCFS		RILEY OPP
147	1964	AUG	19	00:00.0	37.16	-116.08	0	4.70MLWCFS		RILEY OPP
148	1964	AUG	22	17:00.0	37.07	-116.02	0	4.70MLWCFS		RILEY OPP
149	1964	AUG	28	06:00.0	37.07	-116.02	0	4.70MLWCFS		RILEY OPP
150	1964	SEP	4	15:00.0	37.02	-116.02	0	4.70MLWCFS		RILEY OPP
151	1964	SEP	11	00:00.0	37.2	-114.8	0	3.30MBRIL		RILEY OPP
152	1964	OCT	2	03:00.0	37.08	-116.01	0	4.00MBISC		LLNL
153	1964	OCT	9	00:00.0	37.15	-116.08	0	4.80MBRIL		RILEY OPP
154	1964	OCT	16	59:30.0	37.04	-116.02	0	4.70MLWCFS		RILEY OPP
155	1964	OCT	22	00:00.0	31.14	-189.57	0	5.30MBRIL	4.60MBRIL	RILEY OPP
156	1964	OCT	31	04:59.0	37.11	-116.03	0	4.70MLWCFS		RILEY OPP
157	1964	NOV	5	00:00.0	37.17	-116.07	0	4.80MBRIL		RILEY OPP
158	1964	DEC	5	15:00.0	37.11	-116.05	0	4.80MBRIL		RILEY OPP
159	1964	DEC	5	15:00.0	37.13	-116.07	0	5.15MLWCFS		RILEY OPP
160	1964	DEC	16	00:00.0	37.03	-116.01	0	3.70MLWCFS		RILEY OPP

TABLE G-7
ANNOUNCED UNITED STATES NUCLEAR TESTS AT THE NEVADA TEST SITE

Cat. No.	Year	Mo.	Day	Time (GMT hr:min.sec	Latitude	Longitude	Depth (km)	Magnitude 1	Magnitude 2	Agency Source
161	1964	DEC	16	10:00.0	37.18	-116.07	0	4.00MLWCFS		RILEY OPP
162	1964	DEC	18	35:00.0	37.08	-116.34	0	3.60MLWCFS		RILEY OPP
163	1964	DEC	23	43:00.0	37.3	-115.1	0	2.90MBRIL		RILEY OPP
164	1965	JAN	14	00:00.0	37.119	-116.03	0	4.70MLWCFS		RILEY OPP
165	1965	JAN	29	22:00.0	37	-116	0	3.60MBRIL		RILEY OPP
166	1965	FEB	4	30:00.0	37.131	-116.06	0	4.70MLWCFS		RILEY OPP
167	1965	FEB	12	10:30.0	37.165	-116.08	0	4.70MLWCFS		RILEY OPP
168	1965	FEB	16	30:00.0	37.052	-116.02	0	4.50MLWCFS		RILEY OPP
169	1965	FEB	18	18:47.0	36.82	-115.95	0	4.70MLWCFS		RILEY OPP
170	1965	MAR	3	13:00.0	37.065	-116.04	0	5.15MLWCFS		RILEY OPP
171	1965	MAR	20	23:50.0	37	-116.3	0	3.60MBRIL		RILEY OPP
172	1965	MAR	26	34:08.0	37.148	-116.04	0	5.15MLWCFS		RILEY OPP
173	1965	APR	5	00:00.0	37.026	-116.02	0	4.70MLWCFS		RILEY OPP
174	1965	APR	14	14:00.0	37.28	-116.52	0	4.30MBRIL		RILEY OPP
175	1965	APR	21	00:00.0	37.01	-116.2	0	5.00MBRIL		RILEY OPP
176	1965	APR	22	39:00.0	37.1	-115.9	0	3.90MBRIL		RILEY OPP
177	1965	APR	23	44:00.0	37.02	-116	0	3.70MBRIL		RILEY OPP
178	1965	MAY	7	47:11.0	37.14	-116.07	0	4.70MLWCFS		RILEY OPP
179	1965	MAY	12	15:00.0	37.24	-116.43	0	4.70MLWCFS		RILEY OPP
180	1965	MAY	14	57:52.0	36.82	-115.97	0	4.70MLWCFS		RILEY OPP
181	1965	MAY	14	32:36.0	37.06	-116.01	0	4.70MLWCFS		RILEY OPP
182	1965	MAY	21	08:52.0	37.119	-116.03	0	4.70MLWCFS		RILEY OPP
183	1965	JUN	11	45:00.0	37.043	-116.02	0	3.70MLWCFS		RILEY OPP
184	1965	JUN	11	28:38.0	37.116	-116.02	0	3.60MBRIL		RILEY OPP
185	1965	JUN	16	30:00.0	36.82	-115.96	0	4.70MLWCFS		RILEY OPP
186	1965	JUN	17	00:00.0	37.22	-116.06	0	4.70MLWCFS		RILEY OPP
187	1965	JUL	22	21:10.1	37.2	-115.98	0	2.40UKALX		MER
188	1965	JUL	23	00:00.0	37.1	-116.03	0	5.40MBRIL		RILEY OPP
189	1965	AUG	6	23:30.0	37.02	-116.04	0	4.70MLWCFS		RILEY OPP
190	1965	AUG	21	43:09.0	37.113	-116.03	0	3.40MBRIL		RILEY OPP
191	1965	AUG	27	51:13.0	37.14	-116.07	0	4.70MLWCFS		RILEY OPP
192	1965	SEP	1	08:00.0	37.02	-116.01	0	4.20MBRIL		RILEY OPP
193	1965	SEP	10	12:00.0	37.08	-116.02	0	5.10MBRIL		RILEY OPP
194	1965	SEP	17	08:23.0	37.11	-116.03	0	4.70MLWCFS		RILEY OPP
195	1965	NOV	12	00:00.0	37.05	-116.02	0	4.70MLWCFS		RILEY OPP
196	1965	NOV	23	17:33.0	37.162	-116.07	0	3.60MBRIL		RILEY OPP
197	1965	DEC	3	13:02.0	37.165	-116.05	0	5.60MBRIL		RILEY OPP
198	1965	DEC	16	39:18.0	37.14	-116.06	0	4.70MLWCFS		RILEY OPP
199	1965	DEC	16	15:00.0	37.07	-116.03	0	5.30MBRIL		RILEY OPP
200	1965	DEC	25	59:53.0	37	-116.3	0	4.10MBRIL	3.60MBRIL	RILEY OPP

TABLE G-7
ANNOUNCED UNITED STATES NUCLEAR TESTS AT THE NEVADA TEST SITE

Cat. No.	Year	Mo.	Day	Time (GMT hr:min.sec	Latitude	Longitude	Depth (km)	Magnitude 1	Magnitude 2	Agency Source
201	1966	JAN	13	37:43.0	37.12	-116.03	0	4.70MLWCFS		RILEY OPP
202	1966	JAN	18	35:00.0	37.09	-116.02	0	5.20MBRIL		RILEY OPP
203	1966	JAN	21	28:00.0	37.03	-116.02	0	4.70MLWCFS		RILEY OPP
204	1966	JAN	22	17:20.0	36.5	-114.7	0	3.20MBRIL		RILEY OPP
205	1966	FEB	3	17:37.0	37.13	-116.07	0	4.30MBRIL		RILEY OPP
206	1966	FEB	24	55:07.0	37.27	-116.43	0	4.80MBRIL		RILEY OPP
207	1966	MAR	5	15:00.0	37.17	-116.21	0	4.70MLWCFS		RILEY OPP
208	1966	MAR	7	41:00.0	37.04	-116.03	0	4.70MLWCFS		RILEY OPP
209	1966	MAR	12	04:13.0	37.14	-116.05	0	4.70MLWCFS		RILEY OPP
210	1966	MAR	18	00:00.0	37.01	-116.01	0	4.70MLWCFS		RILEY OPP
211	1966	MAR	24	55:28.0	37.11	-116.03	0	4.70MLWCFS		RILEY OPP
212	1966	APR	1	40:00.0	37.1	-116.02	0	4.70MLWCFS		RILEY OPP
213	1966	APR	6	57:17.0	37.14	-116.14	0	4.40MBRIL		RILEY OPP
214	1966	APR	7	27:30.0	37.02	-115.99	0	4.70MLWCFS		RILEY OPP
215	1966	APR	14	13:43.0	37.24	-116.43	0	5.40MBRIL		RILEY OPP
216	1966	APR	23	55:26.0	37.161	-116.08	0	3.30MBRIL		RILEY OPP
217	1966	APR	25	38:00.0	36.89	-115.94	0	4.50MBRIL		RILEY OPP
218	1966	MAY	4	32:17.0	37.14	-116.14	0	5.50MBRIL		RILEY OPP
219	1966	MAY	5	00:00.0	37.05	-116.04	0	4.20MBRIL		RILEY OPP
220	1966	MAY	6	00:00.0	37.35	-116.32	0	5.50MBRIL		RILEY OPP
221	1966	MAY	12	37:26.0	37.13	-116.07	0	4.20MBRIL		RILEY OPP
222	1966	MAY	13	30:00.0	37.09	-116.03	0	5.60MBRIL		RILEY OPP
223	1966	MAY	19	56:28.0	37.11	-116.06	0	5.80MBRIL		RILEY OPP
224	1966	MAY	27	00:00.0	37.18	-116.1	0	5.10MBRIL		RILEY OPP
225	1966	JUN	2	30:00.0	37.23	-116.06	0	5.60MBRIL		RILEY OPP
226	1966	JUN	3	00:00.0	37.07	-116.04	0	5.70MBRIL		RILEY OPP
227	1966	JUN	10	30:00.0	37.06	-116.04	0	4.70MLWCFS		RILEY OPP
228	1966	JUN	15	00:00.0	37.01	-116.2	0	4.70MLWCFS		RILEY OPP
229	1966	JUN	15	02:47.0	37.17	-116.05	0	5.15MLWCFS		RILEY OPP
230	1966	JUN	25	13:00.0	37.16	-116.07	0	4.40MLWCFS		RILEY OPP
231	1966	JUN	30	15:00.0	37.32	-116.3	0	6.10MBRIL		RILEY OPP
232	1966	JUL	28	33:30.0	37.14	-116.13	0	4.70MLWCFS		RILEY OPP
233	1966	AUG	10	16:00.0	37.17	-116.05	0	4.70MLWCFS		RILEY OPP
234	1966	SEP	12	30:00.0	36.88	-115.95	0	4.60MBRIL		RILEY OPP
235	1966	SEP	23	00:00.0	37.1	-116.04	0	4.70MLWCFS		RILEY OPP
236	1966	SEP	29	45:30.0	37.17	-116.05	0	4.10MBRIL		RILEY OPP
237	1966	NOV	5	45:00.0	37.17	-116.05	0	4.70MLWCFS		RILEY OPP
238	1966	NOV	11	00:00.0	37.13	-116.05	0	4.70MLWCFS		RILEY OPP
239	1966	NOV	18	02:00.0	37.04	-116.01	0	4.70MLWCFS		RILEY OPP
240	1966	DEC	13	50:00.0	37.035	-116.01	0	3.90MBRIL		RILEY OPP

TABLE G-7
ANNOUNCED UNITED STATES NUCLEAR TESTS AT THE NEVADA TEST SITE

Cat. No.	Year	Mo.	Day	Time (GMT hr:min.sec	Latitude	Longitude	Depth (km)	Magnitude 1	Magnitude 2	Agency Source
241	1966	DEC	13	00:00.0	36.88	-115.94	0	4.60MBRIL		RILEY OPP
242	1966	DEC	20	30:00.0	37.3	-116.41	0	6.30MBRIL		RILEY OPP
243	1967	JAN	18	55:00.0	37.165	-116.05	0	3.20MBRIL		RILEY OPP
244	1967	JAN	19	45:00.0	37.14	-116.14	0	5.40MBRIL		RILEY OPP
245	1967	JAN	20	40:04.0	37.1	-116	0	5.20MBRIL		RILEY OPP
246	1967	JAN	26	30:00.0	37.165	-116.05	0	3.80MBRIL		RILEY OPP
247	1967	FEB	8	15:00.0	37.17	-116.05	0	4.80MBRIL		RILEY OPP
248	1967	FEB	23	34:00.0	37.02	-116.02	0	4.40MBRIL		RILEY OPP
249	1967	FEB	23	50:00.0	37.13	-116.07	0	5.80MBRIL		RILEY OPP
250	1967	MAR	2	00:00.0	37.17	-116.05	0	4.20MBRIL		RILEY OPP
251	1967	MAR	3	19:00.0	37.039	-116.01	0	3.70MBRIL		RILEY OPP
252	1967	APR	7	00:00.0	37.05	-116.02	0	3.90MBRIL		RILEY OPP
253	1967	APR	21	09:00.0	37.02	-116.04	0	4.30MBRIL		RILEY OPP
254	1967	APR	27	45:00.0	37.14	-116.06	0	3.80MBRIL		RILEY OPP
255	1967	MAY	10	40:00.0	37.08	-116	0	5.00MBRIL		RILEY OPP
256	1967	MAY	20	00:00.0	37.13	-116.06	0	5.90MBRIL		RILEY OPP
257	1967	MAY	23	00:00.0	37.28	-116.37	0	5.70MBRIL		RILEY OPP
258	1967	MAY	26	00:00.0	37.25	-116.48	0	5.50MBRIL		RILEY OPP
259	1967	JUN	22	10:00.0	37.13	-116.03	0	4.70MLWCFS		RILEY OPP
260	1967	JUN	26	00:00.0	37.2	-116.21	0	5.10MBRIL		RILEY OPP
261	1967	JUN	29	25:00.0	37.03	-116.02	0	4.60MBRIL		RILEY OPP
262	1967	JUL	27	00:00.0	37.15	-116.05	0	5.00MBRIL		RILEY OPP
263	1967	AUG	4	00:00.0	37.01	-116.15	0	4.00MBRIL		RILEY OPP
264	1967	AUG	10	10:00.0	37.16	-116.05	0	4.70MLWCFS		RILEY OPP
265	1967	AUG	18	12:30.0	37.01	-116.04	0	4.60MBRIL		RILEY OPP
266	1967	AUG	24	30:00.0	37.163	-116.07	0	4.70MLWCFS		RILEY OPP
267	1967	AUG	31	30:00.0	37.18	-116.21	0	5.00MBRIL		RILEY OPP
268	1967	SEP	7	45:00.0	37.15	-116.05	0	5.00MBRIL		RILEY OPP
269	1967	SEP	21	45:00.0	37.17	-116.04	0	3.90MLWCFS		RILEY OPP
270	1967	SEP	27	00:00.0	37.1	-116.05	0	5.70MBRIL		RILEY OPP
271	1967	OCT	18	30:00.0	37.12	-116.06	0	5.70MBRIL		RILEY OPP
272	1967	OCT	25	30:00.0	37.03	-116.03	0	4.70MLWCFS		RILEY OPP
273	1967	NOV	8	00:00.0	37.09	-116.04	0	5.10MBRIL		RILEY OPP
274	1967	DEC	6	00:00.0	37.159	-116.05	0	4.70MLWCFS		RILEY OPP
275	1967	DEC	10	30:00.0	36.68	-107.21	0	4.90MLWCFS		RILEY OPP
276	1967	DEC	15	00:00.0	37.04	-116	0	4.70MLWCFS		RILEY OPP
277	1968	JAN	18	30:00.0	37.15	-116.07	0	4.40MLWCFS		RILEY OPP
278	1968	JAN	19	00:00.0	37.16	-116.05	0	5.15MLWCFS		RILEY OPP
279	1968	JAN	19	15:00.0	38.63	-116.22	0	6.30MBRIL		RILEY OPP
280	1968	JAN	26	00:00.0	37.28	-116.51	0	2.30MBRIL		RILEY OPP

TABLE G-7
ANNOUNCED UNITED STATES NUCLEAR TESTS AT THE NEVADA TEST SITE

Cat. No.	Year	Mo.	Day	Time (GMT hr:min.sec	Latitude	Longitude	Depth (km)	Magnitude 1	Magnitude 2	Agency Source
281	1968	JAN	31	30:01.0	36.89	-116.12	0	4.70MLWCFS		RILEY OPP
282	1968	FEB	21	30:00.0	37.12	-116.05	0	5.80MBRIL		RILEY OPP
283	1968	FEB	29	08:30.0	37.18	-116.21	0	5.00MBRIL		RILEY OPP
284	1968	MAR	12	04:00.0	37.01	-116.37	0	5.40MBRIL	4.00MBRIL	RILEY OPP
285	1968	MAR	14	19:00.0	37.05	-116.01	0	1.50MBRIL		RILEY OPP
286	1968	MAR	22	00:00.0	37.33	-116.31	0	5.60MBRIL		RILEY OPP
287	1968	MAR	25	44:27.0	36.87	-115.93	0	4.70MLWCFS		RILEY OPP
288	1968	APR	10	00:00.0	37.15	-116.08	0	4.60MBRIL		RILEY OPP
289	1968	APR	18	05:00.0	37.15	-116.04	0	4.90MBRIL		RILEY OPP
290	1968	APR	23	01:30.0	37.34	-116.38	0	4.10MBRIL		RILEY OPP
291	1968	APR	26	00:00.0	37.3	-116.46	0	6.30MBRIL		RILEY OPP
292	1968	MAY	3	00:01.0	37	-115.99	0	4.10MBRIL		RILEY OPP
293	1968	MAY	8	10:00.0	37.157	-116.04	0	3.90MBRIL		RILEY OPP
294	1968	MAY	17	00:00.0	37.12	-116.06	0	4.70MBRIL		RILEY OPP
295	1968	JUN	5	21:30.0	37.035	-116.02	0	4.00MBRIL		RILEY OPP
296	1968	JUN	6	30:00.0	37.17	-116.04	0	4.70MLWCFS		RILEY OPP
297	1968	JUN	15	00:00.0	37.26	-116.31	0	5.90MBRIL		RILEY OPP
298	1968	JUN	28	22:00.0	37.25	-116.48	0	5.30MBRIL		RILEY OPP
299	1968	JUL	17	00:00.0	37.001	-116	0	4.00MBRIL		RILEY OPP
300	1968	JUL	30	00:00.0	37.12	-116.08	0	5.15MLWCFS		RILEY OPP
301	1968	AUG	9	00:00.0	37.162	-116.08	0	3.50MBRIL		RILEY OPP
302	1968	AUG	15	00:00.0	37.124	-116.05	0	3.90MBRIL		RILEY OPP
303	1968	AUG	27	30:00.0	36.88	-115.93	0	4.70MLWCFS		RILEY OPP
304	1968	AUG	29	45:00.0	37.25	-116.35	0	5.90MBRIL		RILEY OPP
305	1968	SEP	6	00:00.0	37.14	-116.05	0	5.60MBRIL		RILEY OPP
306	1968	SEP	12	00:00.0	37.03	-116.01	0	4.70MLWCFS		RILEY OPP
307	1968	SEP	17	00:00.0	37.12	-116.13	0	5.10MBRIL		RILEY OPP
308	1968	SEP	24	05:00.0	37.2	-116.21	0	5.00MBRIL		RILEY OPP
309	1968	OCT	3	29:00.0	37.03	-115.99	0	4.70MLWCFS		RILEY OPP
310	1968	OCT	10	30:00.0	37.133	-116.04	0	3.90MBRIL		RILEY OPP
311	1968	OCT	29	36:01.0	37.1	-116	0	3.40MBRIL		RILEY OPP
312	1968	OCT	31	30:00.0	37.047	-116.03	0	3.90MBRIL		RILEY OPP
313	1968	NOV	4	15:00.0	37.13	-116.09	0	5.00MBRIL		RILEY OPP
314	1968	NOV	15	30:00.0	37.048	-116	0	3.90MBRIL		RILEY OPP
315	1968	NOV	15	45:00.0	37.03	-116.03	0	4.70MLWCFS		RILEY OPP
316	1968	NOV	20	00:00.0	37.01	-116.21	0	4.90MBRIL		RILEY OPP
317	1968	NOV	22	19:00.0	37.14	-116.04	0	4.70MLWCFS		RILEY OPP
318	1968	DEC	8	00:00.0	37.34	-116.57	0	4.80MBRIL		RILEY OPP
319	1968	DEC	12	10:01.0	37.12	-116.08	0	4.70MLWCFS		RILEY OPP
320	1968	DEC	12	20:00.0	37	-116.1	0	3.90MBRIL		RILEY OPP

TABLE G-7
ANNOUNCED UNITED STATES NUCLEAR TESTS AT THE NEVADA TEST SITE

Cat. No.	Year	Mo.	Day	Time (GMT hr:min.sec	Latitude	Longitude	Depth (km)	Magnitude 1	Magnitude 2	Agency Source
321	1968	DEC	19	30:00.0	37.23	-116.47	0	6.30MBRIL		RILEY OPP
322	1969	JAN	15	00:00.0	37.15	-116.07	0	4.50MLWCFS		RILEY OPP
323	1969	JAN	15	30:00.0	37.21	-116.23	0	5.15MLWCFS		RILEY OPP
324	1969	JAN	22	00:02.0	36.96	-116.03	0	4.60MBRIL		RILEY OPP
325	1969	JAN	30	00:00.0	37.05	-116.03	0	4.80MBRIL	4.90MBRIL	RILEY OPP
326	1969	FEB	4	00:00.0	37	-116	0	3.70MBRIL		RILEY OPP
327	1969	FEB	12	18:21.0	37.17	-116.21	0	4.70MLWCFS		RILEY OPP
328	1969	MAR	18	40:02.0	37.1	-116	0	4.40MBRIL	4.10MBRIL	RILEY OPP
329	1969	MAR	20	12:00.0	37.02	-116.03	0	4.60MBRIL	4.50MBRIL	RILEY OPP
330	1969	MAR	21	30:00.0	37.13	-116.09	0	4.90MBRIL	4.85MBRIL	RILEY OPP
331	1969	APR	24	04:00.0	37.1	-116.1	0	3.80MBRIL		RILEY OPP
332	1969	APR	30	00:00.0	37.08	-116.01	0	5.30MBRIL	5.25MBRIL	RILEY OPP
333	1969	APR	30	00:00.0	37.09	-116.01	0	5.15MLWCFS		RILEY OPP
334	1969	MAY	7	45:00.0	37.283	-116.5	0	5.50MBISC		LLNL
335	1969	MAY	7	45:00.0	37.28	-116.5	0	5.80MBRIL	5.75MBRIL	RILEY OPP
336	1969	MAY	15	00:00.0	37	-116	0	4.50MBRIL	4.05MBRIL	RILEY OPP
337	1969	MAY	27	15:00.0	37.08	-116	0	5.00MBRIL	4.95MBRIL	RILEY OPP
338	1969	JUN	12	00:00.0	37.01	-116.03	0	4.40MBRIL	4.50MBRIL	RILEY OPP
339	1969	JUN	26	00:00.0	37.1	-116	0	4.40MBRIL	4.10MBRIL	RILEY OPP
340	1969	JUL	16	02:30.0	37.12	-116.06	0	4.70MBRIL	4.60MBRIL	RILEY OPP
341	1969	JUL	16	55:00.0	37.14	-116.09	0	5.60MBRIL	5.55MBRIL	RILEY OPP
342	1969	AUG	14	30:00.0	37.16	-116.06	0	4.70MLWCFS		RILEY OPP
343	1969	AUG	27	45:00.0	37.02	-116.04	0	4.70MBRIL	4.75MBRIL	RILEY OPP
344	1969	SEP	10	00:00.0	39.36	-107.95	0	5.30MBRIL		RILEY OPP
345	1969	SEP	12	02:23.0	36.88	-115.93	0	4.50MBRIL	4.40MBRIL	RILEY OPP
346	1969	SEP	16	30:00.0	37.31	-116.46	0	6.20MBRIL	6.25MBRIL	RILEY OPP
347	1969	SEP	20	30:01.0	37.1	-116.1	0	4.30MBRIL	3.90MBRIL	RILEY OPP
348	1969	OCT	8	30:00.0	37.26	-116.44	0	5.50MBRIL	5.50MBRIL	RILEY OPP
349	1969	OCT	28	35:00.0	37.3	-116.4	0	3.10MBRIL		RILEY OPP
350	1969	OCT	29	30:00.0	37.12	-116.13	0	5.10MBRIL	4.80MBRIL	RILEY OPP
351	1969	OCT	29	00:00.0	37.14	-116.14	0	5.00MBRIL	4.80MBRIL	RILEY OPP
352	1969	OCT	29	01:51.0	37.14	-116.06	0	5.70MBRIL	5.65MBRIL	RILEY OPP
353	1969	NOV	13	15:00.0	37.16	-116.07	0	3.80MLWCFS		RILEY OPP
354	1969	NOV	21	52:00.0	37.03	-116	0	5.00MBRIL	4.95MBRIL	RILEY OPP
355	1969	DEC	5	00:00.0	37.18	-116.21	0	5.00MBRIL	5.00MBRIL	RILEY OPP
356	1969	DEC	10	30:00.0	37.1	-116	0	4.20MBRIL		RILEY OPP
357	1969	DEC	17	00:00.0	37.08	-116	0	5.50MBRIL	5.45MBRIL	RILEY OPP
358	1969	DEC	17	15:00.0	37.01	-116.02	0	4.80MBRIL	4.70MBRIL	RILEY OPP
359	1969	DEC	18	00:00.0	37.12	-116.03	0	5.20MBRIL	5.10MBRIL	RILEY OPP
360	1970	JAN	23	30:00.0	37.14	-116.04	0	4.60MBRIL	4.30MBRIL	RILEY OPP

TABLE G-7
ANNOUNCED UNITED STATES NUCLEAR TESTS AT THE NEVADA TEST SITE

Cat. No.	Year	Mo.	Day	Time (GMT hr:min.sec	Latitude	Longitude	Depth (km)	Magnitude 1	Magnitude 2	Agency Source
361	1970	JAN	30	00:00.0	37.03	-116.03	0	4.60MBRIL	4.55MBRIL	RILEY OPP
362	1970	FEB	4	00:00.0	37.1	-116.03	0	5.60MBRIL	5.60MBRIL	RILEY OPP
363	1970	FEB	5	00:00.0	37.16	-116.04	0	4.40MBRIL	4.75MBRIL	RILEY OPP
364	1970	FEB	11	15:00.0	37.2	-116.21	0	4.60MBRIL	4.60MBRIL	RILEY OPP
365	1970	FEB	25	28:38.0	37.04	-116	0	5.20MBRIL	5.15MBRIL	RILEY OPP
366	1970	FEB	26	30:00.0	37.12	-116.06	0	5.30MBRIL	5.20MBRIL	RILEY OPP
367	1970	MAR	6	24:01.0	37.17	-116.09	0	4.50MBRIL	4.45MBRIL	RILEY OPP
368	1970	MAR	6	00:00.0	37.14	-116.04	0	4.30MBRIL	4.00MBRIL	RILEY OPP
369	1970	MAR	19	03:30.0	37	-116.02	0	4.10MBRIL	4.30MBRIL	RILEY OPP
370	1970	MAR	23	05:00.0	37.09	-116.02	0	5.50MBRIL	5.50MBRIL	RILEY OPP
371	1970	MAR	26	00:00.0	37.3	-116.53	0	6.50MBRIL	6.50MBRIL	RILEY OPP
372	1970	APR	21	30:00.0	37.05	-115.99	0	4.60MBRIL	4.65MBRIL	RILEY OPP
373	1970	APR	21	00:00.0	37.12	-116.08	0	4.80MBRIL	4.80MBRIL	RILEY OPP
374	1970	MAY	1	13:00.0	37.06	-116.03	0	4.20MBRIL	4.10MBRIL	RILEY OPP
375	1970	MAY	1	40:00.0	37.13	-116.03	0	4.50MBRIL	4.30MBRIL	RILEY OPP
376	1970	MAY	5	30:00.0	37.22	-116.18	0	5.20MBRIL	5.00MBRIL	RILEY OPP
377	1970	MAY	12	00:00.0	37.01	-116.2	0	4.70MLWCFS		RILEY OPP
378	1970	MAY	15	30:00.0	37.16	-116.04	0	5.30MBRIL	5.15MBRIL	RILEY OPP
379	1970	MAY	21	00:00.0	37.01	-115.99	0	3.50MBRIL	3.95MBRIL	RILEY OPP
380	1970	MAY	21	15:00.0	37.07	-116.01	0	5.10MBRIL	5.00MBRIL	RILEY OPP
381	1970	MAY	26	16:00.0	37.18	-116.21	0	5.00MBRIL	4.80MBRIL	RILEY OPP
382	1970	MAY	26	00:00.0	37.11	-116.06	0	5.60MBRIL	5.60MBRIL	RILEY OPP
383	1970	MAY	28	00:00.0	37.1	-116	0	4.20MBRIL	3.90MBRIL	RILEY OPP
384	1970	JUN	26	00:00.0	37.11	-116.09	0	4.30MBRIL	4.20MBRIL	RILEY OPP
385	1970	OCT	13	05:00.0	37.1	-116.1	0	3.90MBRIL		RILEY OPP
386	1970	OCT	14	30:00.0	37.07	-116.01	0	5.50MBRIL	5.50MBRIL	RILEY OPP
387	1970	OCT	28	30:00.0	37.3	-116	0	3.90MBRIL		RILEY OPP
388	1970	NOV	5	00:00.0	37.03	-116.01	0	4.90MBRIL	4.75MBRIL	RILEY OPP
389	1970	NOV	19	00:00.0	37	-116	0	4.10MBRIL		RILEY OPP
390	1970	DEC	3	07:00.0	37.12	-116.27	0	3.10MBRIL		RILEY OPP
391	1970	DEC	16	00:00.0	37.1	-116.01	0	5.10MBRIL	5.10MBRIL	RILEY OPP
392	1970	DEC	16	00:00.0	37.14	-116.03	0	4.70MLWCFS		RILEY OPP
393	1970	DEC	17	05:00.0	37.13	-116.08	0	5.70MBRIL	5.80MBRIL	RILEY OPP
394	1970	DEC	18	30:00.0	37.17	-116.1	0	5.20MBRIL	5.05MBRIL	RILEY OPP
395	1971	APR	29	00:00.0	37.12	-116.33	0	4.70MLWCFS		RILEY OPP
396	1971	JUN	16	50:00.0	37.03	-116.01	0	4.90MBRIL	4.60MBRIL	RILEY OPP
397	1971	JUN	23	30:00.0	37.02	-116.02	0	4.80MBRIL	4.70MBRIL	RILEY OPP
398	1971	JUN	24	00:00.0	37.15	-116.07	0	5.20MBRIL	5.10MBRIL	RILEY OPP
399	1971	JUN	29	30:00.0	37.18	-116.21	0	4.90MBRIL		RILEY OPP
400	1971	JUL	1	00:00.0	37.01	-116.2	0	4.70MLWCFS		RILEY OPP

TABLE G-7
ANNOUNCED UNITED STATES NUCLEAR TESTS AT THE NEVADA TEST SITE

Cat. No.	Year	Mo.	Day	Time (GMT hr:min.sec	Latitude	Longitude	Depth (km)	Magnitude 1	Magnitude 2	Agency Source
401	1971	JUL	8	00:00.0	37.11	-116.05	0	5.50MBRIL	5.50MBRIL	RILEY OPP
402	1971	JUL	9	00:00.0	37	-116.1	0	3.40MBRIL		RILEY OPP
403	1971	JUL	21	33:00.0	0	0	0	4.70MLWCFS		RILEY OPP
404	1971	AUG	18	00:00.0	37.06	-116.04	0	5.40MBRIL	5.30MBRIL	RILEY OPP
405	1971	SEP	22	00:00.0	37.1	-116	0	3.60MBRIL		RILEY OPP
406	1971	SEP	29	00:00.0	37.01	-116.01	0	4.40MBRIL	4.10MBRIL	RILEY OPP
407	1971	OCT	8	30:00.0	37.11	-116.04	0	4.70MBRIL	4.55MBRIL	RILEY OPP
408	1971	OCT	14	30:00.0	37.2	-116.1	0	4.40MBRIL	4.15MBRIL	RILEY OPP
409	1971	NOV	24	15:00.0	36.88	-115.93	0	3.80MBRIL		RILEY OPP
410	1971	NOV	30	45:00.0	37.1	-116.1	0	4.70MBRIL	4.44MBRIL	RILEY OPP
411	1971	DEC	14	09:59.0	37.12	-116.09	0	4.70MBRIL	4.50MBRIL	RILEY OPP
412	1972	FEB	3	45:00.0	37	-115.8	0	4.10MBRIL		RILEY OPP
413	1972	FEB	17	02:00.0	37.1	-116	0	4.60MBRIL	4.25MBRIL	RILEY OPP
414	1972	MAR	30	00:00.0	37	-116	0	4.60MBRIL	4.40MBRIL	RILEY OPP
415	1972	MAR	30	00:17.8	37.684	-116.96	0	4.30MLRYN	4.30MDUNRENO	MER
416	1972	APR	19	32:00.0	37.12	-116.08	0	4.60MBRIL	4.30MBRIL	RILEY OPP
417	1972	MAY	2	15:00.0	37.21	-116.21	0	5.00MBRIL	5.05MBRIL	RILEY OPP
418	1972	MAY	11	00:00.0	37.2	-116.1	0	3.60MBRIL		RILEY OPP
419	1972	MAY	17	10:00.0	37.12	-116.09	0	4.40MBRIL	4.35MBRIL	RILEY OPP
420	1972	MAY	19	00:00.0	37.06	-116	0	4.90MBRIL	4.55MBRIL	RILEY OPP
421	1972	JUN	7	20:00.0	0	0	0	3.80MBRIL		RILEY OPP
422	1972	JUN	28	30:00.0	37.1	-116.1	0	3.70MBRIL		RILEY OPP
423	1972	JUL	20	16:00.0	37.21	-116.18	0	5.00MBRIL	5.00MBRIL	RILEY OPP
424	1972	JUL	25	30:00.0	36.9	-116	0	4.00MBRIL	3.70MBRIL	RILEY OPP
425	1972	SEP	21	30:00.0	37.08	-116.04	0	5.70MBRIL	5.60MBRIL	RILEY OPP
426	1972	SEP	26	30:00.0	37.12	-116.09	0	4.40MBRIL	4.45MBRIL	RILEY OPP
427	1972	NOV	9	15:00.0	37.2	-116.3	0	3.70MBRIL		RILEY OPP
428	1972	NOV	9	15:00.0	0	0	0	3.70MBRIL		RILEY OPP
429	1972	DEC	12	30:00.0	37.081	-116.04	0	3.30MBRIL		RILEY OPP
430	1972	DEC	21	15:00.0	37.14	-116.08	0	5.00MBRIL	5.00MBRIL	RILEY OPP
431	1973	MAR	8	10:00.0	37.1	-116.03	0	5.40MBRIL	5.40MBRIL	RILEY OPP
432	1973	MAR	23	15:00.0	0	0	0	3.30MBRIL		RILEY OPP
433	1973	APR	25	25:00.0	37	-116.03	0	4.70MBRIL	4.70MBRIL	RILEY OPP
434	1973	APR	26	15:00.0	37	-116	0	4.10MBRIL	3.80MBRIL	RILEY OPP
435	1973	APR	26	15:00.0	37.12	-116.06	0	5.60MBRIL	5.50MBRIL	RILEY OPP
436	1973	MAY	17	00:00.0	39.79	-108.37	0	5.40MBRIL		RILEY OPP
437	1973	MAY	24	30:00.0	37.2	-116.1	0	4.80MBRIL	4.35MBRIL	RILEY OPP
438	1973	JUN	5	00:00.0	37.18	-116.22	0	5.10MBRIL	5.10MBRIL	RILEY OPP
439	1973	JUN	6	00:00.0	37.25	-116.35	0	6.10MBRIL	6.20MBRIL	RILEY OPP
440	1973	JUN	21	45:00.0	37.1	-116	0	5.30MBRIL	5.40MBRIL	RILEY OPP

TABLE G-7
ANNOUNCED UNITED STATES NUCLEAR TESTS AT THE NEVADA TEST SITE

Cat. No.	Year	Mo.	Day	Time (GMT hr:min.sec	Latitude	Longitude	Depth (km)	Magnitude 1	Magnitude 2	Agency Source
441	1973	JUN	28	15:12.0	37.15	-116.09	0	4.90MBRIL	5.00MBRIL	RILEY OPP
442	1973	JUN	28	45:00.0	37.1	-116	0	4.70MLWCFS		RILEY OPP
443	1973	OCT	2	15:00.0	37.2	-115.8	0	3.90MBRIL		RILEY OPP
444	1973	OCT	12	00:00.0	37.2	-116.2	0	4.80MBRIL	4.65MBRIL	RILEY OPP
445	1973	NOV	28	30:00.0	37.01	-116.02	0	4.40MBRIL	4.40MBRIL	RILEY OPP
446	1973	DEC	12	00:00.0	36.9	-116	0	4.50MBRIL	4.45MBRIL	RILEY OPP
447	1973	DEC	19	16:01.4	37.013	-116.03	0	3.50MDUNRENO	3.20MDRYN	MER
448	1974	FEB	27	00:00.0	37.1	-116.05	0	5.80MBRIL	5.60MBRIL	RILEY OPP
449	1974	APR	23	13:00.0	37.1	-116.1	0	3.40MLRIL		RILEY OPP
450	1974	MAY	22	15:00.0	37.1	-116.1	0	4.40MBRIL	4.30MBRIL	RILEY OPP
451	1974	MAY	23	38:30.0	37.12	-116.08	0	4.80MBRIL	4.80MBRIL	RILEY OPP
452	1974	JUN	6	40:00.0	37	-116	0	4.40MBRIL	4.30MBRIL	RILEY OPP
453	1974	JUN	19	00:00.0	37.21	-116.21	0	5.00MBRIL	4.90MBRIL	RILEY OPP
454	1974	JUL	10	00:00.0	37.08	-116.03	0	5.70MBRIL	5.70MBRIL	RILEY OPP
455	1974	JUL	18	00:00.0	37.1	-116.1	0	4.10MBRIL	3.90MBRIL	RILEY OPP
456	1974	AUG	14	00:00.0	37.02	-116.04	0	4.60MBRIL	4.45MBRIL	RILEY OPP
457	1974	AUG	30	00:00.0	37.15	-116.08	0	5.80MBRIL	5.70MBRIL	RILEY OPP
458	1974	SEP	25	00:00.0	37	-116	0	4.40MBRIL	4.20MBRIL	RILEY OPP
459	1974	SEP	26	30:00.0	0	0	0	3.30MBRIL		RILEY OPP
460	1974	SEP	26	05:00.0	37.13	-116.07	0	5.60MBRIL	5.50MBRIL	RILEY OPP
461	1974	OCT	28	00:00.0	37.2	-137.2	0	4.70MLWCFS		RILEY OPP
462	1974	DEC	16	30:00.0	36.9	-116	0	4.30MBRIL		RILEY OPP
463	1975	FEB	6	30:00.0	37.259	-115.91	0	3.50MBRIL		RILEY OPP
464	1975	FEB	6	13:00.0	37	-116	0	4.50MBRIL		RILEY OPP
465	1975	FEB	28	15:00.0	37.11	-116.06	0	5.70MBRIL	5.70MBRIL	RILEY OPP
466	1975	MAR	7	00:00.0	37.13	-116.08	0	5.50MBRIL	5.60MBRIL	RILEY OPP
467	1975	APR	5	45:00.0	37.19	-116.21	0	4.80MBRIL	5.00MBRIL	RILEY OPP
468	1975	APR	24	10:00.0	37.12	-116.09	0	4.60MBRIL	4.50MBRIL	RILEY OPP
469	1975	APR	30	00:00.0	37.11	-116.03	0	5.20MBRIL	5.10MBRIL	RILEY OPP
470	1975	MAY	14	00:00.0	37.22	-116.47	0	6.00MBRIL	6.00MBRIL	RILEY OPP
471	1975	JUN	3	20:00.0	37.34	-116.52	0	5.90MBRIL	5.80MBRIL	RILEY OPP
472	1975	JUN	3	40:00.0	37.09	-116.04	0	5.70MBRIL	5.65MBRIL	RILEY OPP
473	1975	JUN	19	00:00.0	37.35	-116.32	0	6.10MBRIL	6.05MBRIL	RILEY OPP
474	1975	JUN	26	30:00.0	37.28	-116.37	0	6.20MBRIL	6.15MBRIL	RILEY OPP
475	1975	AUG	30	12:00.0	37.28	-116.21	0	3.10MBRIL		RILEY OPP
476	1975	SEP	6	00:00.0	37.02	-116.03	0	4.60MBRIL	4.65MBRIL	RILEY OPP
477	1975	OCT	24	11:26.0	37.22	-116.18	0	4.70MBRIL	4.80MBRIL	RILEY OPP
478	1975	OCT	28	30:00.0	37.29	-116.41	0	6.40MBRIL	6.30MBRIL	RILEY OPP
479	1975	NOV	18	30:00.0	37	-116	0	4.40MBRIL	4.45MBRIL	RILEY OPP
480	1975	NOV	20	00:00.0	37.22	-116.37	0	6.00MBRIL	5.85MBRIL	RILEY OPP

TABLE G-7
ANNOUNCED UNITED STATES NUCLEAR TESTS AT THE NEVADA TEST SITE

Cat. No.	Year	Mo.	Day	Time (GMT) hr:min.sec	Latitude	Longitude	Depth (km)	Magnitude 1	Magnitude 2	Agency Source
481	1975	NOV	26	30:00.0	37.12	-116.02	0	5.00MBRIL	4.35MBRIL	RILEY OPP
482	1975	DEC	20	00:00.0	37.13	-116.06	0	5.70MBRIL	5.70MBRIL	RILEY OPP
483	1976	JAN	3	15:00.0	37.3	-116.33	0	6.20MBRIL	6.25MBRIL	RILEY OPP
484	1976	FEB	4	20:00.0	37.07	-116.03	0	5.80MBRIL	5.65MBRIL	RILEY OPP
485	1976	FEB	4	40:00.0	37.11	-116.04	0	5.70MBRIL	5.65MBRIL	RILEY OPP
486	1976	FEB	12	45:00.0	37.27	-116.49	0	6.30MBRIL	6.20MBRIL	RILEY OPP
487	1976	FEB	14	30:00.0	37.24	-116.42	0	6.00MBRIL	5.85MBRIL	RILEY OPP
488	1976	FEB	26	50:00.0	37	-116	0	4.20MBRIL	4.25MBRIL	RILEY OPP
489	1976	MAR	9	00:00.0	37.31	-116.36	0	6.00MBRIL	6.05MBRIL	RILEY OPP
490	1976	MAR	14	30:00.0	37.31	-116.47	0	6.30MBRIL	6.40MBRIL	RILEY OPP
491	1976	MAR	17	15:00.0	37.26	-116.33	0	6.10MBRIL	6.05MBRIL	RILEY OPP
492	1976	MAR	17	45:00.0	37.11	-116.05	0	5.80MBRIL	5.90MBRIL	RILEY OPP
493	1976	MAY	12	50:00.0	37.21	-116.21	0	4.90MBRIL		RILEY OPP
494	1976	MAY	20	30:00.0	37.1	-116	0	3.70MBRIL		RILEY OPP
495	1976	JUL	27	30:00.0	37.08	-116.04	0	5.30MBRIL	5.40MBRIL	RILEY OPP
496	1976	AUG	26	30:00.0	37.13	-116.08	0	5.30MBRIL	5.30MBRIL	RILEY OPP
497	1976	OCT	6	30:00.0	0	0	0	3.70MBRIL		RILEY OPP
498	1976	NOV	23	15:00.0	37.17	-116.05	0	4.70MLWCFS		RILEY OPP
499	1976	DEC	8	49:30.0	37.08	-116	0	4.90MBRIL	4.70MBRIL	RILEY OPP
500	1976	DEC	21	09:00.0	37.12	-116.07	0	4.70MLWCFS		RILEY OPP
501	1976	DEC	28	00:00.0	37.1	-116.04	0	5.50MBRIL	5.45MBRIL	RILEY OPP
502	1977	FEB	16	53:00.0	37	-116	0	4.80MBRIL	4.35MBRIL	RILEY OPP
503	1977	MAR	8	24:00.0	37.2	-116.3	0	3.80MBRIL		RILEY OPP
504	1977	APR	5	00:00.0	37.12	-116.06	0	5.60MBRIL	5.65MBRIL	RILEY OPP
505	1977	APR	27	00:00.0	37.09	-116.03	0	5.40MBRIL	5.30MBRIL	RILEY OPP
506	1977	MAY	25	00:00.0	37.09	-116.04	0	5.30MBRIL	5.25MBRIL	RILEY OPP
507	1977	JUL	28	07:00.0	37.1	-115.9	0	3.70MBRIL		RILEY OPP
508	1977	AUG	4	40:00.0	37.09	-116.01	0	5.00MBRIL	5.05MBRIL	RILEY OPP
509	1977	AUG	16	41:00.0	37.2	-115.9	0	3.70MBRIL		RILEY OPP
510	1977	AUG	16	49:00.0	37.2	-116	0	4.00MBRIL		RILEY OPP
511	1977	AUG	19	32:00.0	37	-116	0	3.30MBRIL		RILEY OPP
512	1977	AUG	19	55:00.0	37.11	-116.05	0	5.60MBRIL	5.60MBRIL	RILEY OPP
513	1977	SEP	15	36:30.0	37.03	-116.04	0	4.50MBRIL	4.50MBRIL	RILEY OPP
514	1977	SEP	27	00:00.0	37.15	-116.07	0	4.80MBRIL	4.80MBRIL	RILEY OPP
515	1977	OCT	26	15:00.0	37.01	-116.02	0	4.40MBRIL	4.35MBRIL	RILEY OPP
516	1977	NOV	1	06:00.0	37.19	-116.21	0	4.70MBRIL		RILEY OPP
517	1977	NOV	9	00:00.0	37.07	-116.05	0	5.70MBRIL	5.70MBRIL	RILEY OPP
518	1977	NOV	17	30:00.0	37.02	-116.03	0	4.70MBRIL	4.70MBRIL	RILEY OPP
519	1977	DEC	14	00:00.0	37	-116.1	0	3.80MBRIL		RILEY OPP
520	1977	DEC	14	30:00.0	37.14	-116.09	0	5.70MBRIL	5.65MBRIL	RILEY OPP

TABLE G-7
ANNOUNCED UNITED STATES NUCLEAR TESTS AT THE NEVADA TEST SITE

Cat. No.	Year	Mo.	Day	Time (GMT hr:min.sec	Latitude	Longitude	Depth (km)	Magnitude 1	Magnitude 2	Agency Source
521	1978	FEB	13	53:00.0	37.13	-116.03	0	3.80MBRIL	3.95MBRIL	RILEY OPP
522	1978	FEB	23	00:00.0	37.12	-116.06	0	5.60MBRIL	5.65MBRIL	RILEY OPP
523	1978	MAR	16	00:00.0	37.1	-116.1	0	3.90MBRIL	4.05MBRIL	RILEY OPP
524	1978	MAR	23	30:00.0	37.1	-116.05	0	5.60MBRIL	5.60MBRIL	RILEY OPP
525	1978	APR	11	30:00.0	37.3	-116.33	0	5.30MBRIL	5.40MBRIL	RILEY OPP
526	1978	APR	11	45:00.0	37.23	-116.37	0	5.50MBRIL	5.50MBRIL	RILEY OPP
527	1978	JUN	1	00:00.0	37	-116	0	3.70MBRIL		RILEY OPP
528	1978	JUL	7	00:00.0	37.1	-116	0	4.00MBRIL	4.00MBRIL	RILEY OPP
529	1978	JUL	12	00:00.0	37.08	-116.04	0	5.50MBRIL	5.60MBRIL	RILEY OPP
530	1978	AUG	31	00:00.0	37.28	-116.36	0	5.60MBRIL	5.60MBRIL	RILEY OPP
531	1978	SEP	13	15:00.0	37.21	-116.21	0	4.60MBRIL	4.65MBRIL	RILEY OPP
532	1978	SEP	27	30:00.0	38.825	-115.98	0	3.40MBRIL		RILEY OPP
533	1978	SEP	27	00:00.0	37.07	-116.02	0	5.00MBRIL	5.05MBRIL	RILEY OPP
534	1978	SEP	27	20:00.0	37.08	-116.05	0	5.70MBRIL	5.80MBRIL	RILEY OPP
535	1978	NOV	2	25:00.0	37.29	-116.3	0	4.20MBRIL	4.25MBRIL	RILEY OPP
536	1978	NOV	18	00:00.0	37.13	-116.08	0	5.10MBRIL	5.20MBRIL	RILEY OPP
537	1978	DEC	1	07:30.0	37	-116	0	3.70MBRIL		RILEY OPP
538	1978	DEC	16	30:00.0	37.27	-116.41	0	5.50MBRIL	5.55MBRIL	RILEY OPP
539	1979	JAN	24	00:00.0	37.11	-116.01	0	4.50MBRIL	4.50MBRIL	RILEY OPP
540	1979	FEB	8	00:00.0	37.1	-116.05	0	5.50MBRIL	5.55MBRIL	RILEY OPP
541	1979	FEB	15	05:00.0	37.15	-116.07	0	4.80MBRIL	4.90MBRIL	RILEY OPP
542	1979	MAR	14	30:00.0	37.03	-116.04	0	4.30MBRIL	4.50MBRIL	RILEY OPP
543	1979	MAY	11	00:00.0	37	-116	0	4.40MBRIL		RILEY OPP
544	1979	JUN	11	00:00.0	37.29	-116.46	0	5.50MBRIL	5.50MBRIL	RILEY OPP
545	1979	JUN	20	00:14.0	37.11	-116.02	0	4.00MBRIL	4.15MBRIL	RILEY OPP
546	1979	JUN	28	44:00.0	37.14	-116.09	0	5.00MBRIL	5.05MBRIL	RILEY OPP
547	1979	AUG	3	07:30.0	37.08	-116.07	0	4.50MBRIL	4.55MBRIL	RILEY OPP
548	1979	AUG	8	00:00.0	37.01	-116.01	0	4.80MBRIL	4.75MBRIL	RILEY OPP
549	1979	AUG	29	08:00.0	37.12	-116.07	0	4.70MBRIL	4.90MBRIL	RILEY OPP
550	1979	SEP	6	00:00.0	37.09	-116.05	0	5.80MBRIL	5.80MBRIL	RILEY OPP
551	1979	SEP	8	02:00.0	37.16	-116.04	0	3.50MBRIL		RILEY OPP
552	1979	SEP	26	00:00.0	37.23	-116.36	0	5.60MBRIL	5.60MBRIL	RILEY OPP
553	1979	NOV	29	00:00.0	36.99	-116.02	0	3.80MBRIL	3.95MBRIL	RILEY OPP
554	1979	DEC	14	00:00.0	37.14	-116.06	0	3.70MBRIL		RILEY OPP
555	1980	FEB	28	00:00.0	37.13	-116.09	0	4.40MBRIL		RILEY OPP
556	1980	MAR	8	35:00.0	37.18	-116.08	0	3.90MBRIL		RILEY OPP
557	1980	APR	3	00:00.0	37.15	-116.08	0	4.70MBRIL		RILEY OPP
558	1980	APR	16	00:00.0	37.1	-116.03	0	5.30MBRIL		RILEY OPP
559	1980	APR	26	00:00.0	37.25	-116.42	0	5.40MBRIL		RILEY OPP
560	1980	MAY	2	46:30.0	37.06	-116.02	0	4.40MBRIL		RILEY OPP

TABLE G-7
ANNOUNCED UNITED STATES NUCLEAR TESTS AT THE NEVADA TEST SITE

Cat. No.	Year	Mo.	Day	Time (GMT hr:min.sec	Latitude	Longitude	Depth (km)	Magnitude 1	Magnitude 2	Agency Source
561	1980	MAY	22	00:00.0	37	-116.03	0	3.50MBRIL		RILEY OPP
562	1980	JUN	12	15:00.0	37.28	-116.45	0	5.60MBRIL		RILEY OPP
563	1980	JUN	24	10:00.0	37.02	-116.03	0	4.40MBRIL		RILEY OPP
564	1980	JUL	25	05:00.0	37.26	-116.48	0	5.50MBRIL		RILEY OPP
565	1980	JUL	31	19:00.0	37.01	-116.02	0	4.30MBRIL		RILEY OPP
566	1980	SEP	25	45:00.0	37.06	-116.05	0	4.60MBRIL		RILEY OPP
567	1980	SEP	25	26:30.0	37.12	-116.06	0	3.40MBRIL		RILEY OPP
568	1980	OCT	24	15:00.0	37.07	-116	0	4.40MBRIL		RILEY OPP
569	1980	OCT	31	00:00.0	37.24	-116.21	0	4.70MBRIL		RILEY OPP
570	1980	NOV	14	50:00.0	37.11	-116.02	0	4.10MBRIL		RILEY OPP
571	1980	DEC	17	10:00.0	37.32	-116.32	0	5.10MBRIL		RILEY OPP
572	1981	JAN	15	25:00.0	37.09	-116.04	0	5.60MBRIL		RILEY OPP
573	1981	FEB	5	00:00.0	37.01	-116.03	0	3.20MLRIL		RILEY OPP
574	1981	FEB	25	00:00.0	37.18	-116.08	0	3.00MLRIL		RILEY OPP
575	1981	APR	30	35:00.0	37.18	-116.08	0	3.20MBRIL		RILEY OPP
576	1981	MAY	29	00:00.0	37.1	-116	0	4.20MBRIL	4.30MBRIL	RILEY OPP
577	1981	JUN	6	00:00.0	37.303	-116.33	0	5.60MBISC		LLNL
578	1981	JUN	6	00:00.0	37.3	-116.33	0	5.50MBRIL	5.50MBRIL	RILEY OPP
579	1981	JUL	10	00:00.0	37.13	-116.03	0	4.10MBRIL		RILEY OPP
580	1981	JUL	16	00:00.0	37.09	-116.02	0	3.30MLRIL		RILEY OPP
581	1981	AUG	5	41:00.0	37.15	-116.04	0	2.80MLRIL		RILEY OPP
582	1981	AUG	27	31:00.0	37.16	-116.07	0	3.80MBRIL		RILEY OPP
583	1981	SEP	4	00:00.0	37.06	-116.05	0	3.80MBRIL		RILEY OPP
584	1981	SEP	24	00:00.0	37.01	-116.02	0	3.50MLRIL		RILEY OPP
585	1981	OCT	1	00:00.0	37.08	-116.01	0	4.90MBRIL	5.00MBRIL	RILEY OPP
586	1981	NOV	11	00:00.0	37.08	-116.07	0	4.80MBRIL	4.80MBRIL	RILEY OPP
587	1981	NOV	12	00:00.0	37.11	-116.05	0	5.30MBRIL	5.35MBRIL	RILEY OPP
588	1981	DEC	3	00:00.0	37.15	-116.07	0	4.60MBRIL	4.75MBRIL	RILEY OPP
589	1981	DEC	16	05:00.0	37.11	-116.12	0	4.40MBRIL	4.35MBRIL	RILEY OPP
590	1982	JAN	28	00:00.0	37.09	-116.05	0	5.90MBRIL	5.90MBRIL	RILEY OPP
591	1982	FEB	12	55:00.0	37.22	-116.46	0	5.40MBRIL	5.50MBRIL	RILEY OPP
592	1982	FEB	12	25:00.0	37.35	-116.32	0	5.60MBRIL	5.60MBRIL	RILEY OPP
593	1982	APR	17	00:00.0	37.02	-116.01	0	4.50MBRIL	4.50MBRIL	RILEY OPP
594	1982	APR	25	05:00.0	37.26	-116.42	0	5.40MBRIL	5.45MBRIL	RILEY OPP
595	1982	MAY	6	00:00.0	37.12	-116.13	0	4.30MBRIL	4.10MBRIL	RILEY OPP
596	1982	MAY	7	17:00.0	37.07	-116.05	0	5.70MBRIL	5.70MBRIL	RILEY OPP
597	1982	JUN	16	00:00.0	37.11	-116.02	0	3.90MBRIL		RILEY OPP
598	1982	JUN	24	15:00.0	37.24	-116.37	0	5.60MBRIL	5.70MBRIL	RILEY OPP
599	1982	JUL	29	05:00.0	37.1	-116.07	0	4.50MBRIL	4.45MBRIL	RILEY OPP
600	1982	AUG	5	00:00.0	37.08	-116.01	0	5.70MBRIL	5.70MBRIL	RILEY OPP

TABLE G-7
ANNOUNCED UNITED STATES NUCLEAR TESTS AT THE NEVADA TEST SITE

Cat. No.	Year	Mo.	Day	Time (GMT hr:min.sec	Latitude	Longitude	Depth (km)	Magnitude 1	Magnitude 2	Agency Source
601	1982	AUG	11	00:00.0	37.19	-116.05	0	3.30MLRIL		RILEY OPP
602	1982	SEP	2	00:00.0	37.02	-116.02	0	3.30MLRIL		RILEY OPP
603	1982	SEP	23	00:00.0	37.21	-116.21	0	4.90MBRIL	5.00MBRIL	RILEY OPP
604	1982	SEP	23	00:00.0	37.17	-116.09	0	4.90MBRIL	4.95MBRIL	RILEY OPP
605	1982	SEP	29	30:00.0	37.09	-116.04	0	3.80MBRIL		RILEY OPP
606	1982	NOV	12	17:00.0	37.02	-116.03	0	4.40MBRIL	4.50MBRIL	RILEY OPP
607	1982	DEC	10	20:00.0	37.03	-116.07	0	4.60MBRIL	4.70MBRIL	RILEY OPP
608	1983	FEB	11	00:00.0	37.05	-116.05	0	3.70MBRIL	4.20MLUCB	RILEY OPP
609	1983	FEB	17	00:00.0	37.16	-116.06	0	4.00MBRIL	3.90MBRIL	RILEY OPP
610	1983	MAR	26	20:00.0	37.3	-116.46	0	5.10MBRIL	5.25MBRIL	RILEY OPP
611	1983	APR	14	05:00.0	37.07	-116.05	0	5.70MBRIL	5.70MBRIL	RILEY OPP
612	1983	APR	22	53:00.0	37.11	-116.02	0	4.00MBRIL	4.00MBRIL	RILEY OPP
613	1983	MAY	5	20:00.0	37.01	-116.09	0	4.50MBRIL	4.55MBRIL	RILEY OPP
614	1983	MAY	26	30:00.0	0	0	0	4.70MLWCFS		RILEY OPP
615	1983	MAY	26	00:00.0	37.1	-116.01	0	4.40MBRIL	4.65MBRIL	RILEY OPP
616	1983	JUN	9	10:00.0	37.16	-116.09	0	4.50MBRIL	4.50MBRIL	RILEY OPP
617	1983	AUG	3	33:00.0	37.12	-116.09	0	4.20MBRIL	4.20MBRIL	RILEY OPP
618	1983	AUG	11	00:00.0	37	-116	0	4.40MBRIL	4.40MBRIL	RILEY OPP
619	1983	AUG	27	00:00.0	37.2	-116	0	4.10MBRIL		RILEY OPP
620	1983	SEP	1	00:00.0	37.27	-116.36	0	5.40MBRIL	5.45MBRIL	RILEY OPP
621	1983	SEP	21	00:00.0	37.21	-116.21	0	3.70MBRIL		RILEY OPP
622	1983	SEP	21	25:00.0	37.1	-116	0	3.70MBRIL		RILEY OPP
623	1983	SEP	22	00:00.0	37.11	-116.05	0	4.00MBRIL		RILEY OPP
624	1983	DEC	9	00:00.0	37	-116	0	4.00MBRIL		RILEY OPP
625	1983	DEC	16	30:00.0	37.14	-116.07	0	5.10MBRIL	5.10MBRIL	RILEY OPP
626	1984	JAN	31	30:00.0	37.11	-116.12	0	4.10MBRIL	4.40MBRIL	RILEY OPP
627	1984	FEB	15	00:00.0	37.22	-116.18	0	5.00MBRIL	5.05MBRIL	RILEY OPP
628	1984	MAR	1	45:00.0	37.07	-116.05	0	5.90MBRIL	5.85MBRIL	RILEY OPP
629	1984	MAR	31	30:00.0	37.15	-116.08	0	4.10MBRIL	4.35MBRIL	RILEY OPP
630	1984	MAY	1	05:00.0	37.11	-116.02	0	5.30MBRIL	5.40MBRIL	RILEY OPP
631	1984	MAY	2	50:00.0	37.2	-116	0	3.40MBRIL		RILEY OPP
632	1984	MAY	16	00:00.0	37.1	-116	0	3.80MBRIL		RILEY OPP
633	1984	MAY	31	04:00.0	37.1	-116.05	0	5.80MBRIL	5.75MBRIL	RILEY OPP
634	1984	JUN	20	15:00.0	37	-116.04	0	4.60MBRIL	4.75MBRIL	RILEY OPP
635	1984	JUL	12	00:00.0	37.2	-116.1	0	3.60MBRIL		RILEY OPP
636	1984	JUL	25	30:00.0	37.27	-116.41	0	5.30MBRIL	5.40MBRIL	RILEY OPP
637	1984	AUG	2	00:00.0	37.02	-116.01	0	4.70MBRIL	4.65MBRIL	RILEY OPP
638	1984	AUG	30	45:00.0	37.09	-115.99	0	4.50MBRIL	4.65MBRIL	RILEY OPP
639	1984	SEP	13	00:00.0	37.09	-116.07	0	5.00MBRIL	5.10MBRIL	RILEY OPP
640	1984	OCT	2	14:00.0	37.1	-116	0	4.20MBRIL		RILEY OPP

TABLE G-7
ANNOUNCED UNITED STATES NUCLEAR TESTS AT THE NEVADA TEST SITE

Cat. No.	Year	Mo.	Day	Time (GMT hr:min.sec	Latitude	Longitude	Depth (km)	Magnitude 1	Magnitude 2	Agency Source
641	1984	NOV	10	40:00.0	37	-116.02	0	4.50MBRIL	4.50MBRIL	RILEY OPP
642	1984	DEC	9	40:00.0	37.27	-116.49	0	5.50MBRIL	5.50MBRIL	RILEY OPP
643	1984	DEC	15	45:00.0	37.28	-116.31	0	5.40MBRIL	5.45MBRIL	RILEY OPP
644	1984	DEC	20	20:00.0	37	-116	0	4.20MBRIL		RILEY OPP
645	1985	MAR	15	31:00.0	37.06	-116.05	0	4.80MBRIL	4.80MBRIL	RILEY OPP
646	1985	MAR	23	30:00.0	37.18	-116.09	0	5.30MBRIL	5.35MBRIL	RILEY OPP
647	1985	APR	2	00:00.0	37.1	-116.03	0	5.70MBRIL	5.75MBRIL	RILEY OPP
648	1985	APR	6	15:00.0	37.2	-116.21	0	4.80MBRIL	4.90MBRIL	RILEY OPP
649	1985	MAY	2	20:00.0	37.25	-116.33	0	5.70MBRIL	5.65MBRIL	RILEY OPP
650	1985	JUN	12	15:00.0	37.25	-116.49	0	5.50MBRIL	5.50MBRIL	RILEY OPP
651	1985	JUN	12	30:00.0	37.01	-116.08	0	4.40MBRIL	4.30MBRIL	RILEY OPP
652	1985	JUN	26	03:00.0	37.12	-116.12	0	4.30MBRIL	4.10MBRIL	RILEY OPP
653	1985	JUL	25	00:00.0	37.3	-116.44	0	5.20MBRIL	5.25MBRIL	RILEY OPP
654	1985	AUG	14	00:00.0	0	0	0	4.70MLWCFS		RILEY OPP
655	1985	AUG	17	25:00.0	37	-116.04	0	4.60MBRIL	4.50MBRIL	RILEY OPP
656	1985	SEP	27	15:00.0	37.09	-116	0	4.60MBRIL	4.65MBRIL	RILEY OPP
657	1985	OCT	9	40:00.0	0	0	0	4.70MLWCFS		RILEY OPP
658	1985	OCT	9	20:00.0	37.21	-116.21	0	4.20MBRIL	4.30MBRIL	RILEY OPP
659	1985	OCT	16	35:00.0	37.11	-116.12	0	4.60MBRIL	4.60MBRIL	RILEY OPP
660	1985	DEC	5	00:00.0	37.05	-116.05	0	5.70MBRIL	5.65MBRIL	RILEY OPP
661	1985	DEC	28	01:00.0	37.24	-116.47	0	5.30MBRIL	5.35MBRIL	RILEY OPP
662	1986	MAR	22	15:00.0	37.08	-116.07	0	5.10MBRIL	5.25MBRIL	RILEY OPP
663	1986	APR	10	08:30.0	37.22	-116.18	0	4.90MBRIL	5.00MBRIL	RILEY OPP
664	1986	APR	20	12:30.0	37	-116	0	4.00MBRIL		RILEY OPP
665	1986	APR	22	30:00.0	37.26	-116.44	0	5.30MBRIL	5.35MBRIL	RILEY OPP
666	1986	MAY	21	59:00.0	37.13	-116.06	0	4.00MBRIL		RILEY OPP
667	1986	JUN	5	04:00.0	37.1	-116.02	0	5.30MBRIL	5.35MBRIL	RILEY OPP
668	1986	JUN	25	27:45.0	37.27	-116.5	0	5.50MBRIL		RILEY OPP
669	1986	JUL	17	00:00.0	37.28	-116.36	0	5.70MBRIL	5.70MBRIL	RILEY OPP
670	1986	JUL	24	05:00.0	37.14	-116.07	0	4.40MBRIL	4.45MBRIL	RILEY OPP
671	1986	SEP	4	09:00.0	37.2	-116.4	0	3.50MLRIL		RILEY OPP
672	1986	SEP	11	57:00.0	37.07	-116.05	0	3.20MLRIL		RILEY OPP
673	1986	SEP	30	30:00.0	37.3	-116.31	0	5.50MBRIL	5.50MBRIL	RILEY OPP
674	1986	OCT	16	25:00.0	37.22	-116.46	0	5.60MBRIL	5.60MBRIL	RILEY OPP
675	1986	NOV	14	00:00.0	37.1	-116.05	0	5.80MBRIL	5.75MBRIL	RILEY OPP
676	1986	DEC	13	50:05.0	37.26	-116.41	0	5.50MBRIL	5.55MBRIL	RILEY OPP
677	1987	FEB	3	20:00.0	37.18	-116.05	0	2.20MLRIL		RILEY OPP
678	1987	FEB	11	45:00.0	37.01	-116.05	0	4.50MBRIL	4.40MBRIL	RILEY OPP
679	1987	MAR	18	28:00.0	37.21	-116.21	0	4.30MBRIL		RILEY OPP
680	1987	APR	18	40:01.0	37.25	-116.51	0	5.50MBRIL		RILEY OPP

TABLE G-7
ANNOUNCED UNITED STATES NUCLEAR TESTS AT THE NEVADA TEST SITE

Cat. No.	Year	Mo.	Day	Time (GMT hr:min.sec	Latitude	Longitude	Depth (km)	Magnitude 1	Magnitude 2	Agency Source
681	1987	APR	22	00:00.0	36.983	-116.01	0	4.20MLUCB		UC BERK
682	1987	APR	22	00:00.0	36.98	-116.01	0	4.20MBRIL		RILEY OPP
683	1987	APR	30	30:00.0	37.23	-116.42	0	5.50MBRIL		RILEY OPP
684	1987	JUN	18	20:00.0	37.19	-116.04	0	4.70MLWCFS		RILEY OPP
685	1987	JUN	20	00:00.0	37.22	-116.18	0	3.50MLRIL		RILEY OPP
686	1987	JUN	30	05:00.0	36.99	-116.04	0	4.60MBRIL		RILEY OPP
687	1987	JUL	16	00:00.0	37.1	-116.02	0	4.80MBRIL		RILEY OPP
688	1987	AUG	13	00:00.0	37.06	-116.05	0	5.90MBRIL		RILEY OPP
689	1987	SEP	24	00:00.0	37.23	-116.38	0	5.70MBRIL		RILEY OPP
690	1987	OCT	23	00:00.0	37.14	-116.08	0	5.20MBRIL		RILEY OPP
691	1987	DEC	1	30:00.0	37	-116	0	4.70MLWCFS		RILEY OPP
692	1987	DEC	2	30:00.0	37.24	-116.16	0	4.10MBRIL		RILEY OPP
693	1988	FEB	15	10:00.0	37.31	-116.47	0	5.30MBRIL		RILEY OPP
694	1988	APR	7	15:00.0	37.01	-116.04	0	4.10MBRIL		RILEY OPP
695	1988	MAY	13	35:00.0	37.12	-116.07	0	4.80MBRIL		RILEY OPP
696	1988	MAY	21	30:00.0	37.03	-115.99	0	4.30MBRIL		RILEY OPP
697	1988	JUN	2	00:00.0	37.26	-116.44	0	5.30MBRIL		RILEY OPP
698	1988	JUN	22	00:00.0	37.17	-116.07	0	3.10MLRIL		RILEY OPP
699	1988	JUL	7	05:30.0	37.25	-116.38	0	5.60MBRIL		RILEY OPP
700	1988	AUG	17	00:00.0	37.3	-116.31	0	5.50MBRIL		RILEY OPP
701	1988	AUG	23	30:00.0	36.99	-116.01	0	4.10MBRIL		RILEY OPP
702	1988	AUG	30	00:00.0	37.09	-116.07	0	5.00MBRIL		RILEY OPP
703	1988	OCT	13	00:00.0	37.09	-116.05	0	5.90MBRIL		RILEY OPP
704	1988	NOV	9	15:00.0	36.98	-116.01	0	3.60MLRIL		RILEY OPP
705	1988	DEC	10	30:00.0	37.2	-116.21	0	5.00MBRIL		RILEY OPP
706	1989	FEB	10	06:00.0	37.08	-116	0	5.20MBRIL		RILEY OPP
707	1989	FEB	24	15:00.0	37.13	-116.12	0	4.40MBRIL		RILEY OPP
708	1989	MAR	9	05:00.0	37.14	-116.07	0	4.90MBRIL		RILEY OPP
709	1989	MAY	15	10:00.0	37.11	-116.12	0	4.40MBRIL	4.70MBRIL	RILEY OPP
710	1989	MAY	26	07:00.0	37.09	-116.06	0	3.70MLRIL	3.9	RILEY OPP
711	1989	JUN	22	15:00.0	37.28	-116.41	0	5.30MBRIL	5.60MBRIL	RILEY OPP
712	1989	JUN	27	30:00.0	37.28	-116.35	0	4.90MBRIL		RILEY OPP
713	1989	SEP	14	00:00.0	37.236	-116.16	0	4.40MLUCB		UC BERK
714	1989	SEP	14	00:00.0	37.24	-116.16	0	3.80MBRIL		RILEY OPP
715	1989	OCT	31	30:00.0	37.263	-116.49	0	5.40MLUCB		UC BERKRK
716	1989	OCT	31	30:00.0	37.26	-116.49	0	5.70MBRIL	5.70MBRIL	RILEY OPP
717	1989	NOV	15	20:00.0	37.11	-116.01	0	3.40MLRIL	3.50MBRIL	RILEY OPP
718	1989	DEC	8	00:00.0	37.23	-116.41	0	5.50MBRIL		RILEY OPP
719	1989	DEC	20	00:00.0	37.03	-116.03	0	4.70MLWCFS		RILEY OPP
720	1990	MAR	10	00:00.0	37.11	-116.06	0	5.00MBRIL	5.00MBRIL	RILEY OPP

TABLE G-7
ANNOUNCED UNITED STATES NUCLEAR TESTS AT THE NEVADA TEST SITE

Cat. No.	Year	Mo.	Day	Time (GMT hr:min.sec	Latitude	Longitude	Depth (km)	Magnitude 1	Magnitude 2	Agency Source
721	1990	APR	6	00:00.0	37	-116.05	0	3.10MBRIL		RILEY OPP
722	1990	JUN	13	00:00.0	37.26	-116.42	0	5.70MBRIL	5.80MBRIL	RILEY OPP
723	1990	JUN	21	15:00.0	36.99	-116	0	4.00MBRIL	4.50MBRIL	RILEY OPP
724	1990	JUL	25	00:00.0	37.21	-116.21	0	4.80MBRIL		RILEY OPP
725	1990	SEP	20	15:00.0	0	0	0	4.70MLWCFS		RILEY OPP
726	1990	SEP	27	02:00.0	37.004	-116.05	0	2.27MwMVGSDR		RILEY OPP
727	1990	OCT	12	30:00.0	37.25	-116.49	0	5.60MBRIL	5.70MBRIL	RILEY OPP
728	1990	NOV	14	17:00.0	37.23	-116.37	0	5.40MBRIL	5.40MBRIL	RILEY OPP
729	1991	MAR	8	02:00.0	37.1	-116.07	0	4.30MBRIL		RILEY OPP
730	1991	APR	4	00:00.0	37.3	-116.31	0	5.60MBRIL		RILEY OPP
731	1991	APR	16	30:00.0	37.24	-116.44	0	5.40MBRIL		RILEY OPP
732	1991	AUG	15	00:00.0	37.09	-116	0	4.20MBRIL		RILEY OPP
733	1991	SEP	14	00:00.0	37.23	-116.43	0	5.50MBRIL		RILEY OPP
734	1991	SEP	19	30:00.0	37.24	-116.17	0	4.00MBRIL		RILEY OPP
735	1991	OCT	18	12:00.0	37.06	-116.04	0	5.20MBRIL		RILEY OPP
736	1991	NOV	26	35:00.0	37.1	-116.07	0	4.60MBRIL		RILEY OPP
737	1992	MAR	26	30:00.0	37.27	-116.36	0	5.50MBRIL		RILEY OPP
738	1992	APR	30	30:00.0	37.2	-116.2	0	4.70MLWCFS		RILEY OPP
739	1992	JUN	19	45:00.0	37	-116.01	0	3.00MBRIL		RILEY OPP
740	1992	JUN	23	00:00.0	37.12	-116.03	0	3.90MBRIL		RILEY OPP
741	1992	SEP	18	00:00.0	37.2	-116.2	0	4.20MBRIL		RILEY OPP
742	1992	SEP	23	04:00.0	37	-116	0	4.40MBRIL		RILEY OPP
743	1993	SEP	22	01:00.0	37.2	-116.1	0	4.30MBRIL		RILEY OPP

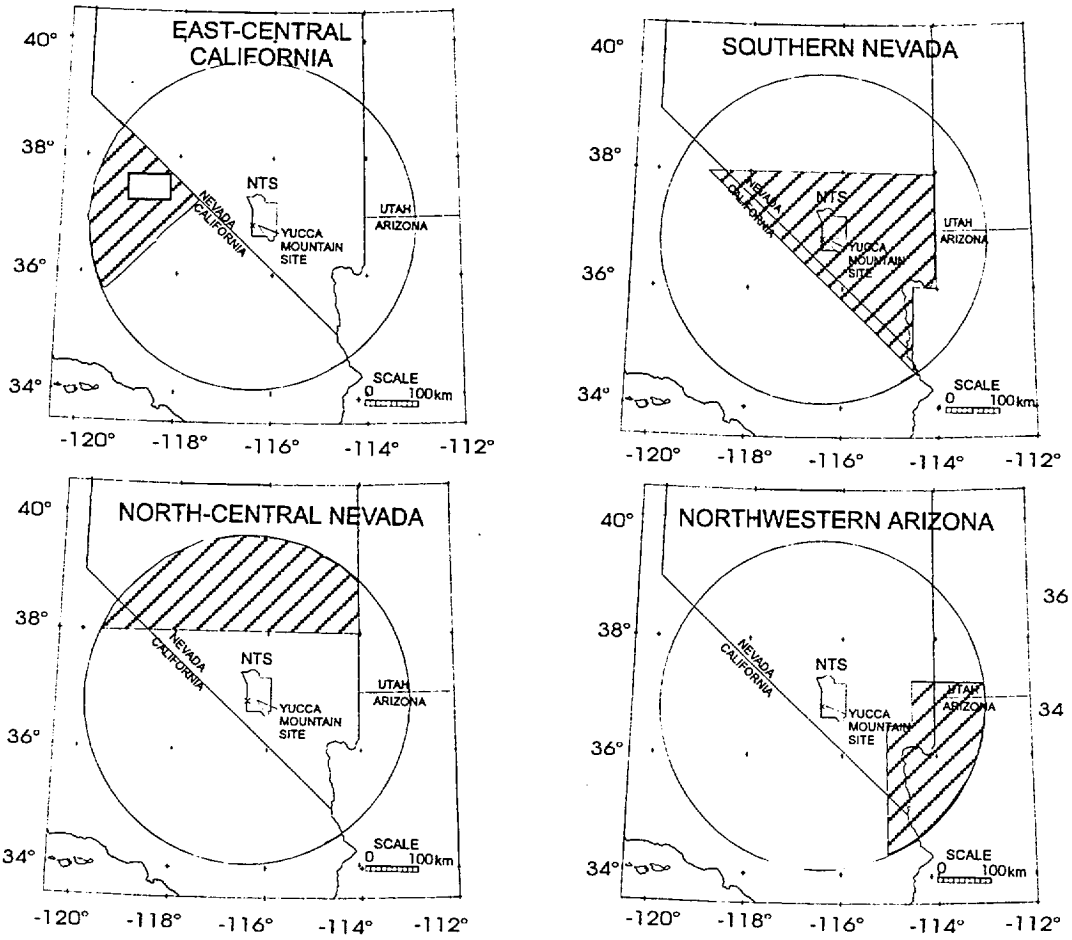

Figure G-1 Subregions that comprise the 300-km radius Yucca Mountain catalogue

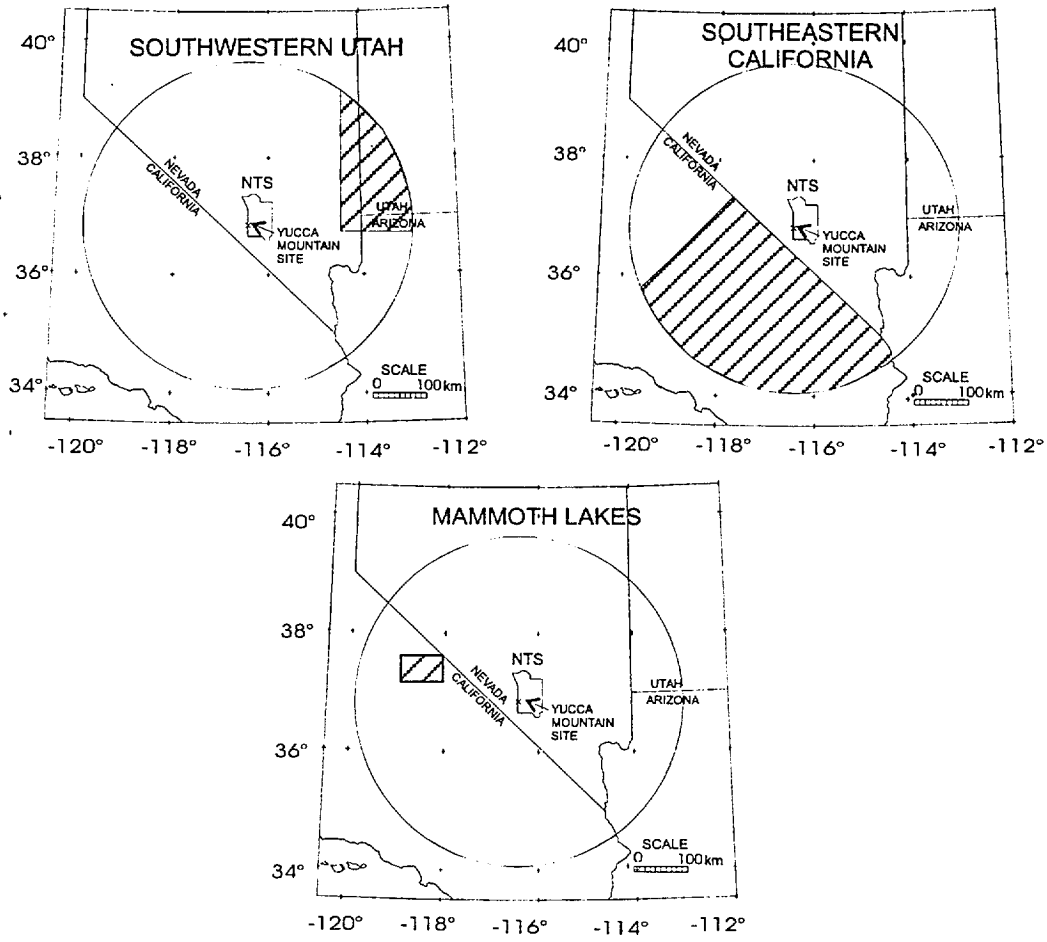

Figure G-1(continued) Subregions that comprise the 300-km radius Yucca Mountain catalogue

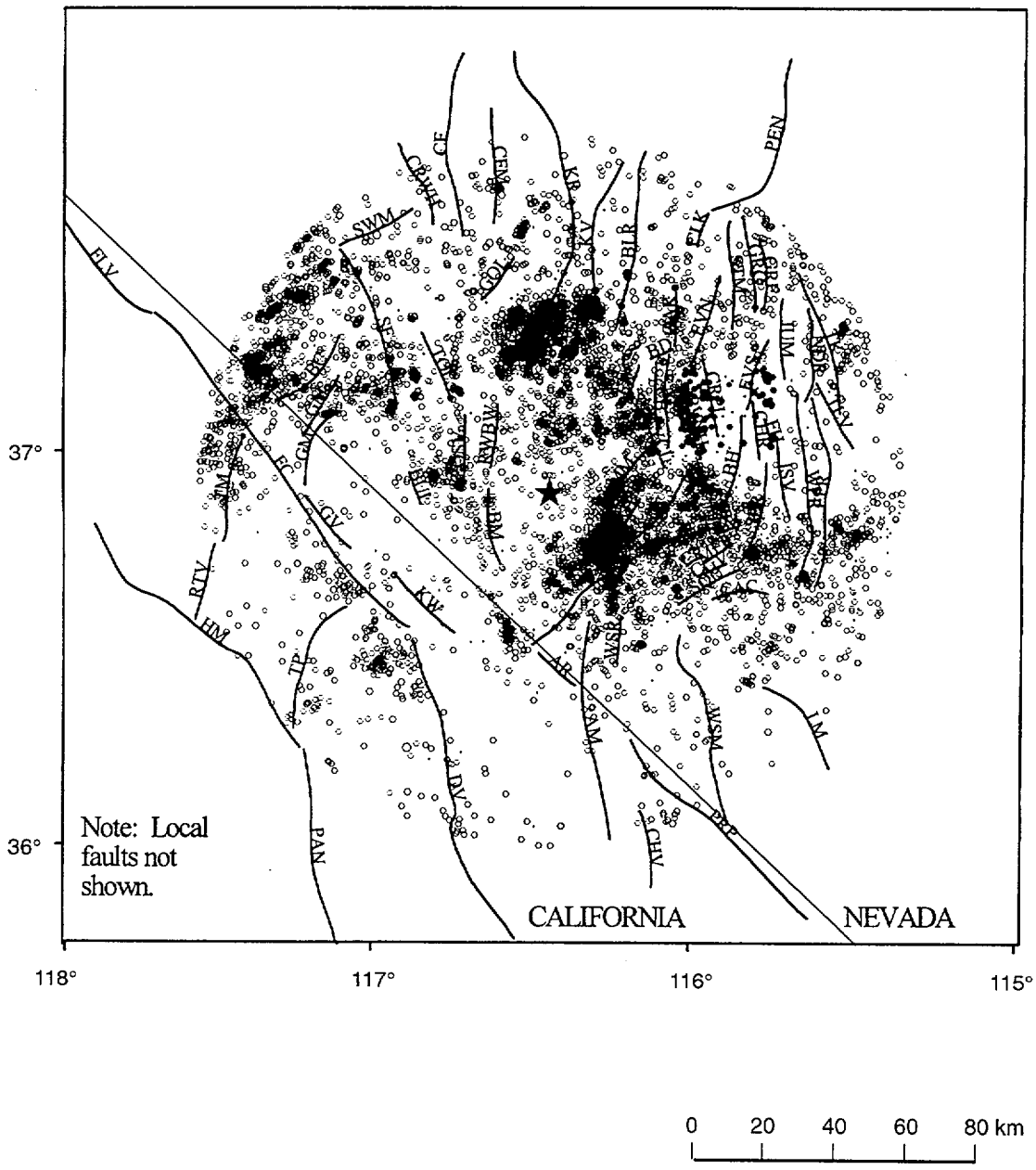

Figure G-2 Historical seismicity (1904 - 1996) and faults within the 100-km radius Yucca Mountain region

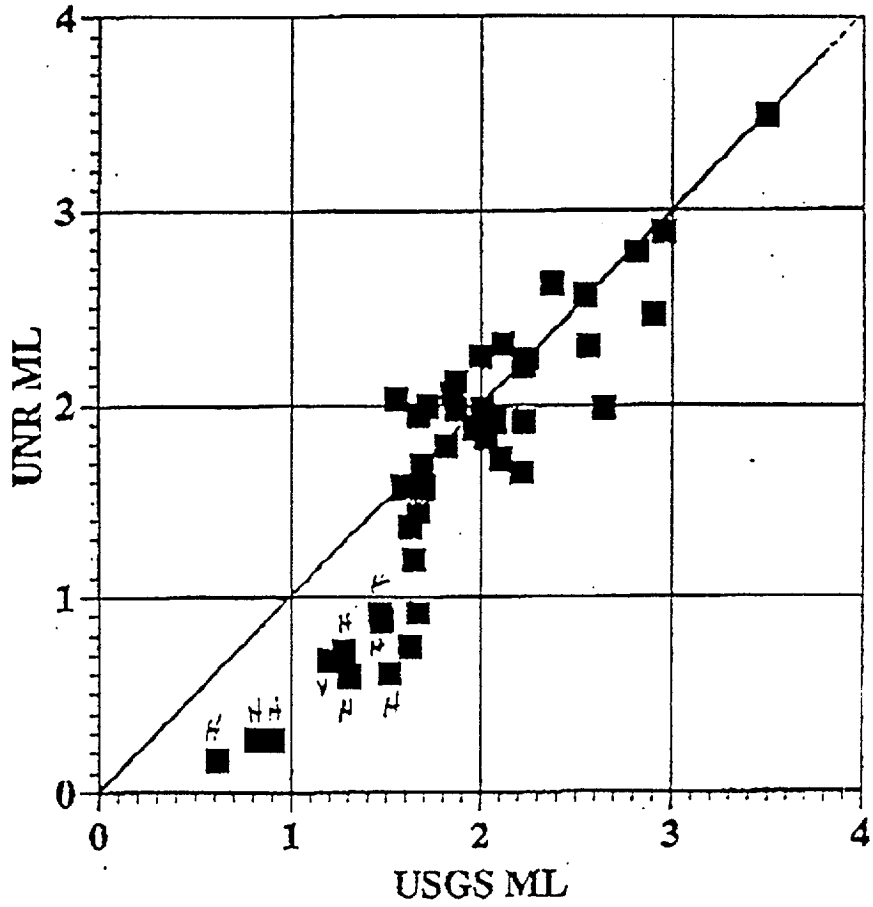

Figure G-3 M_L (UNR CUSP) vs. M_L (USGSDR) for the Southern Great Basin for common events in September 1992. From von Seggern (UNR, written communication, 1996).

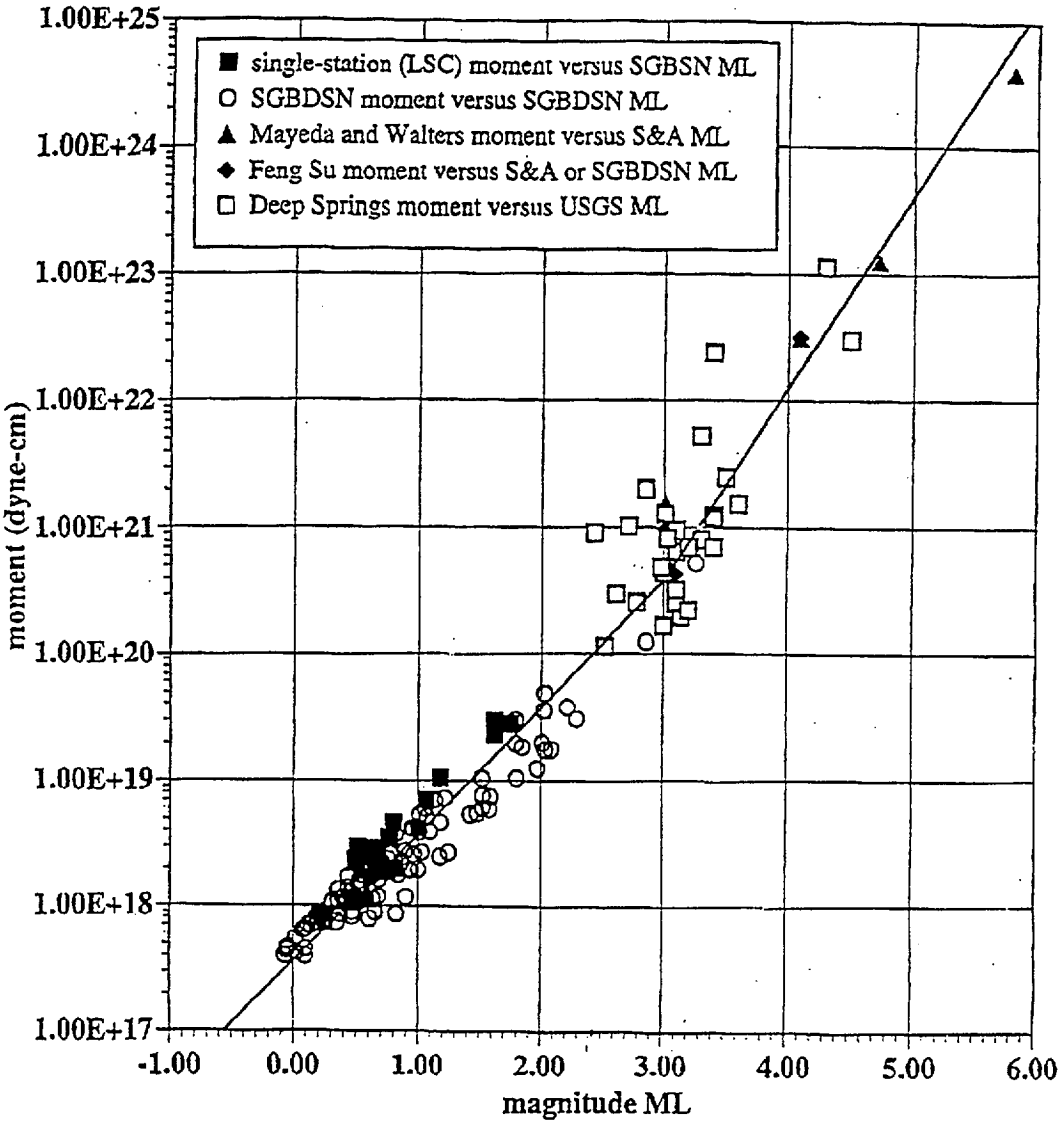

Figure G-4 Moment vs. M_L for the Southern Great Basin-selected data. From von Seggern (UNR, written communication, 1996).

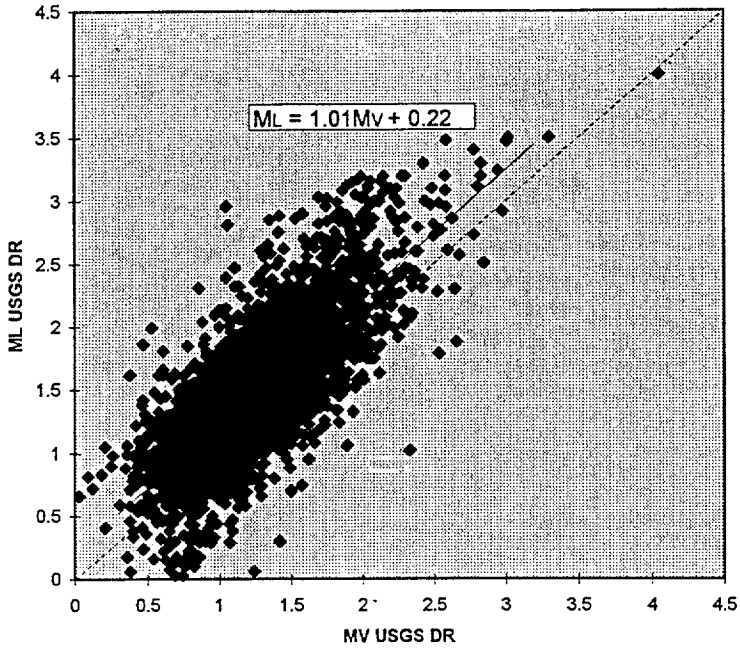

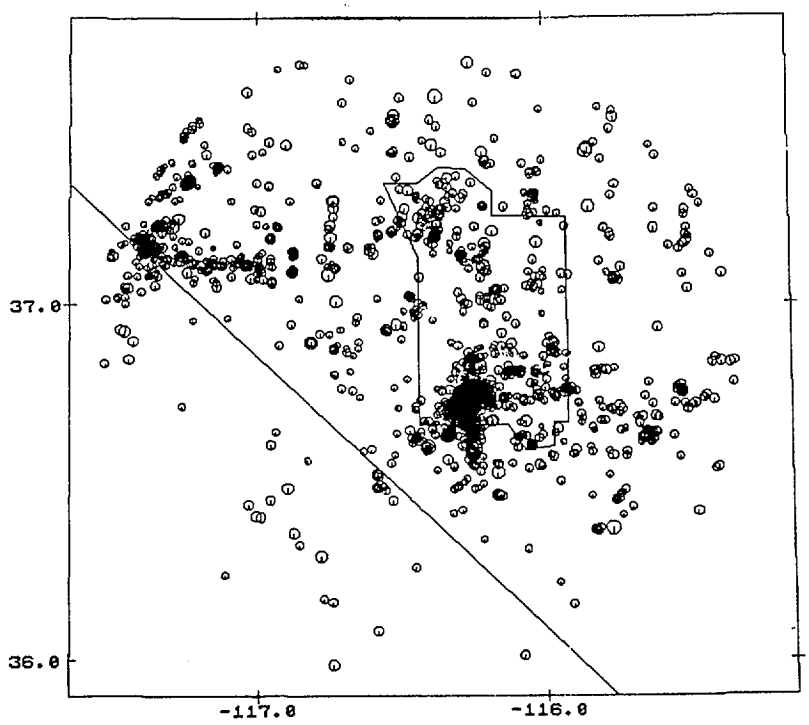

Figure G-5 Regression of M_L (USGSDR) on M_V (USGSDR) for the SGB catalogue and locations of earthquakes used (1985 to 1991)

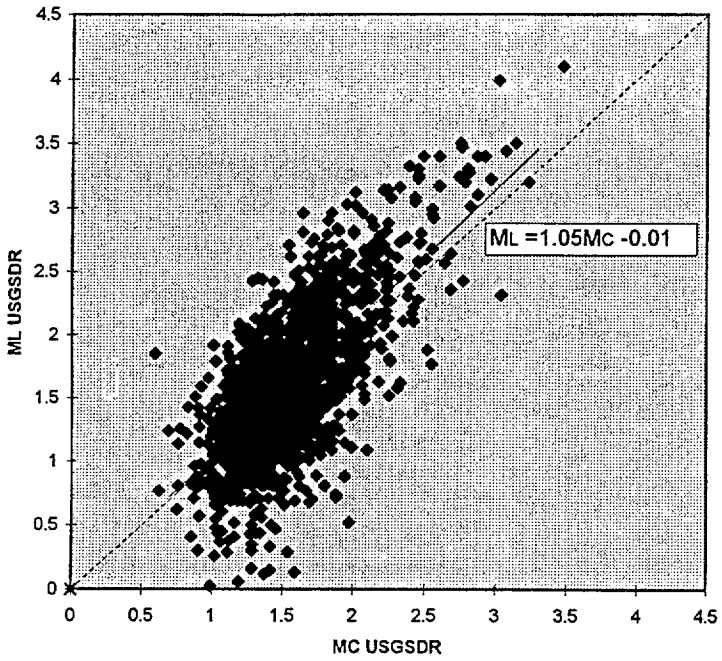

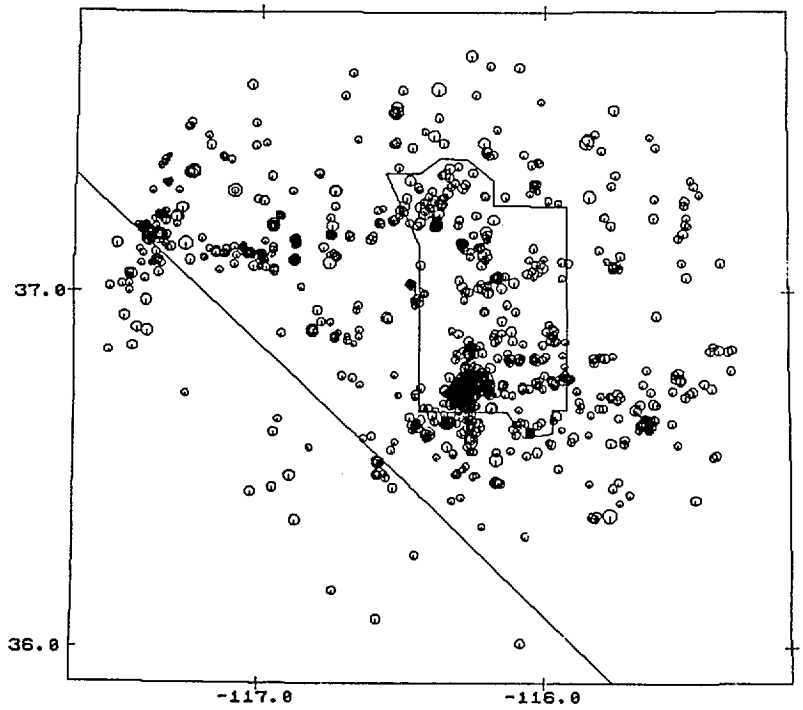

Figure G-6 Regression of M_L (USGSDR) on M_C (USGSDR) for the SGB catalogue and locations of earthquakes used (1985 to 1992)

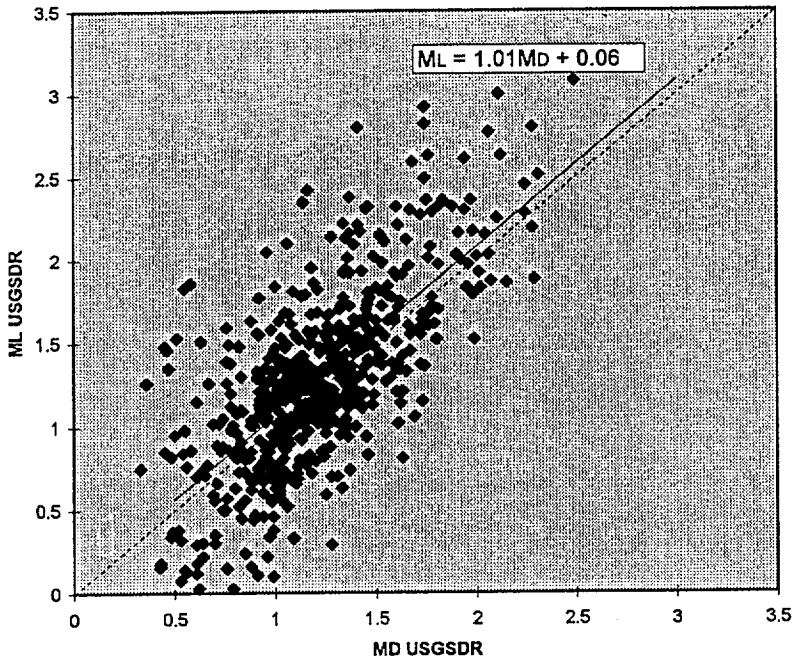

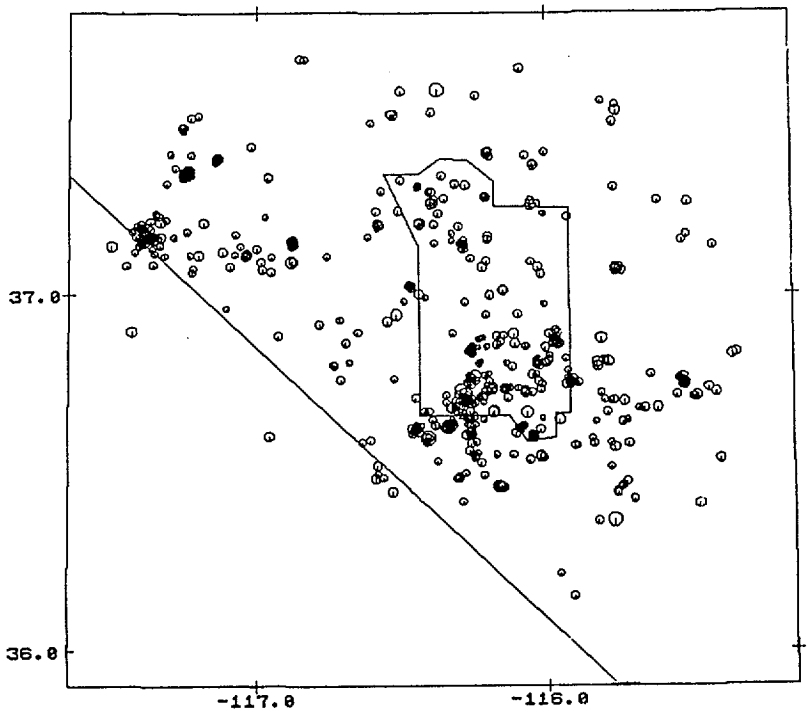

Figure G-7 Regression of M_L (USGSDR) on M_D (USGSDR) for the SGB catalogue and locations of earthquakes used (1984 to 1992)

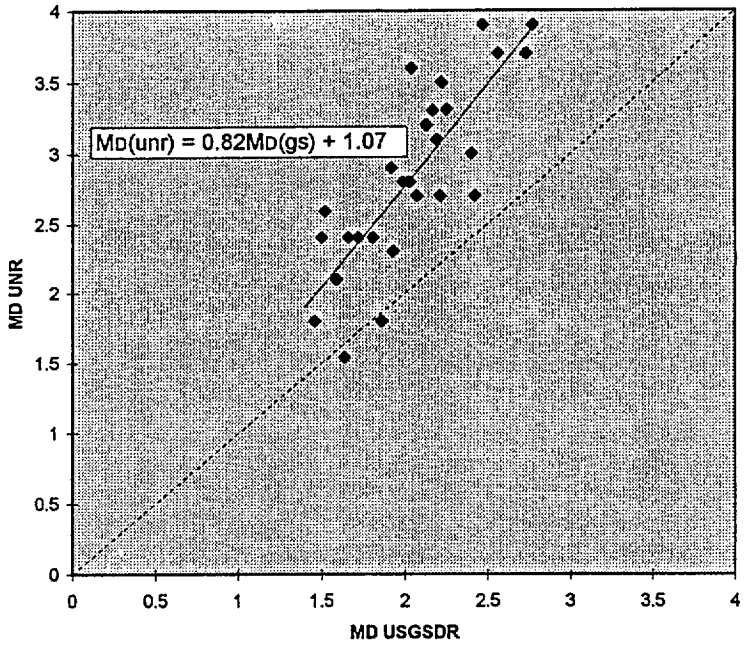

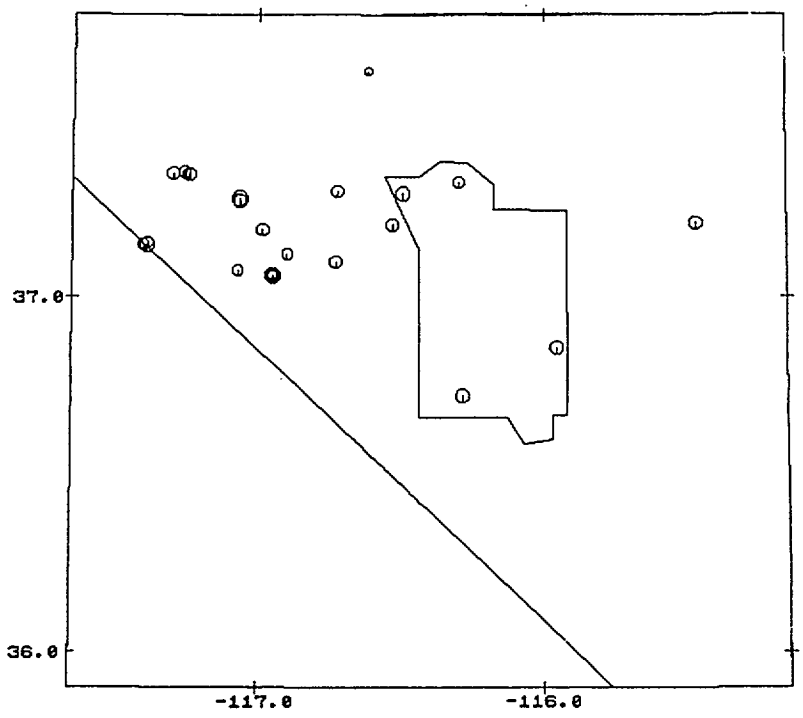

Figure G-8 Regression of M_D (UNR) on M_D (USGSDV) for the SGB catalogue and locations of earthquakes used (1978 to 1992)

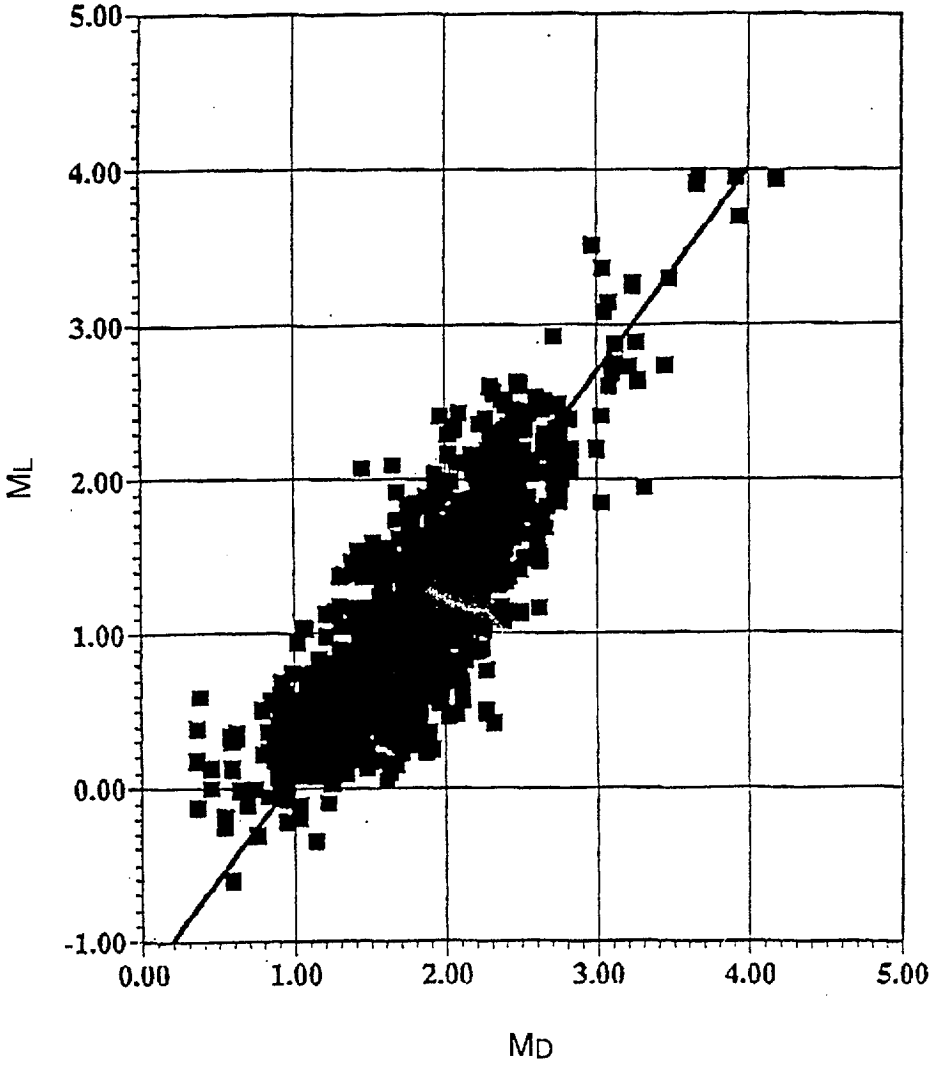

Figure G-9 M_L (CUSP) vs. M_D (CUSP) for the Southern Great Basin (1993 to 1995). From von Seggern (UNR, written communication, 1996).

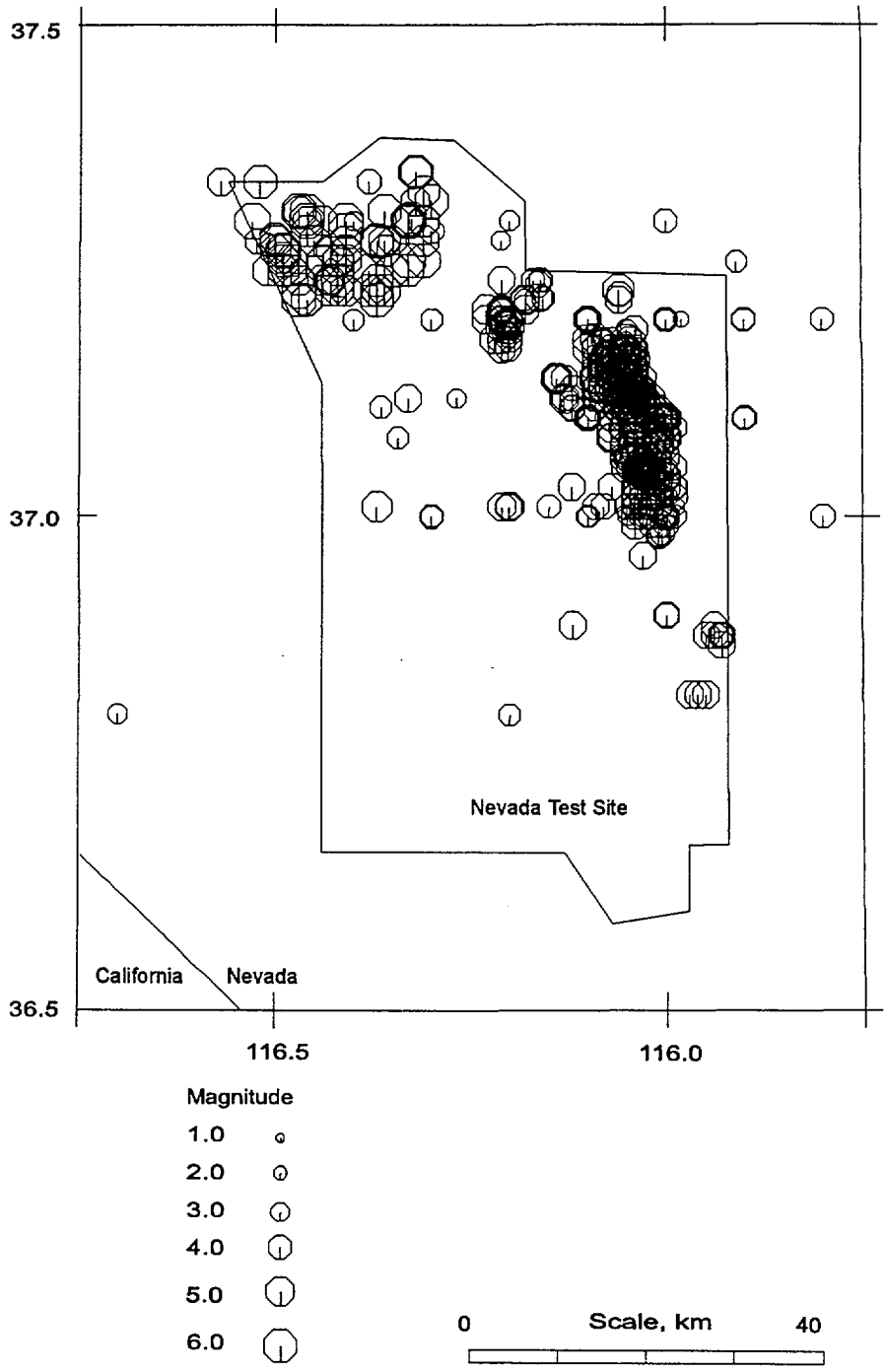

Figure G-10 Announced United States underground nuclear tests, 1957 to 1992

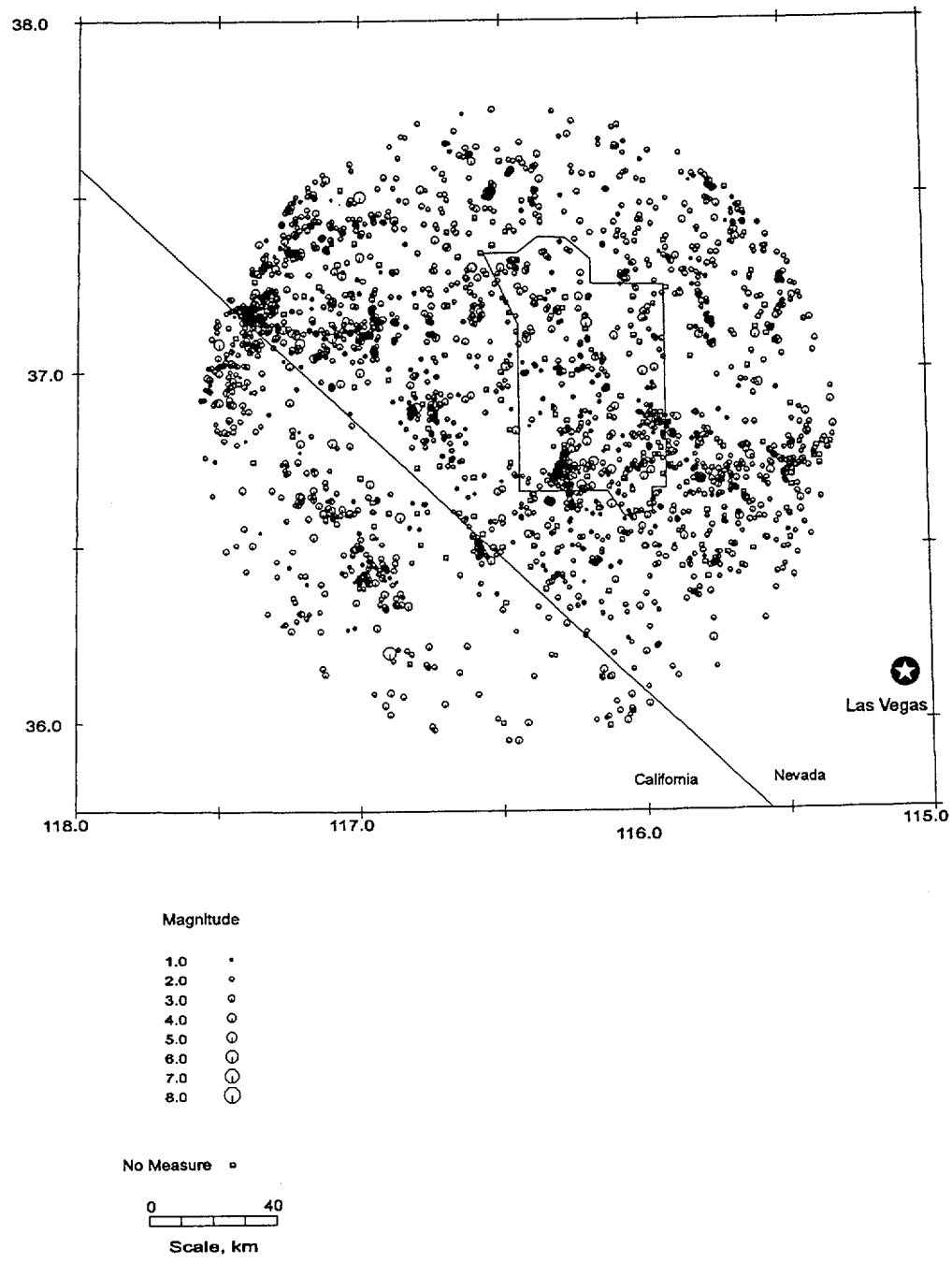

Figure G-11 Historical seismicity (1868 to 1996) after declustering with the Youngs *et al.* approach

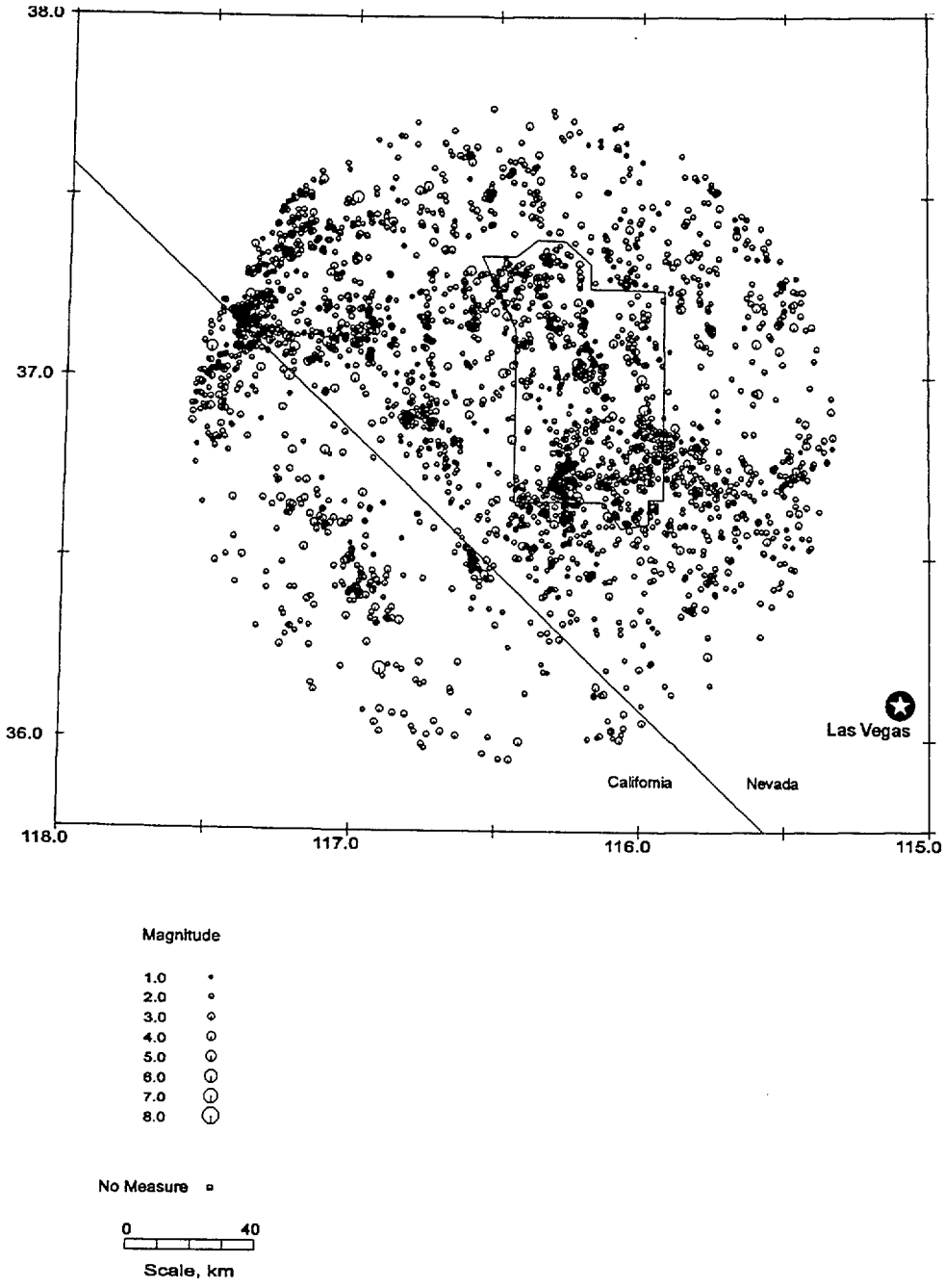

Figure G-12 Historical seismicity (1868 to 1996) after declustering with the Veneziano and van Dyck approach

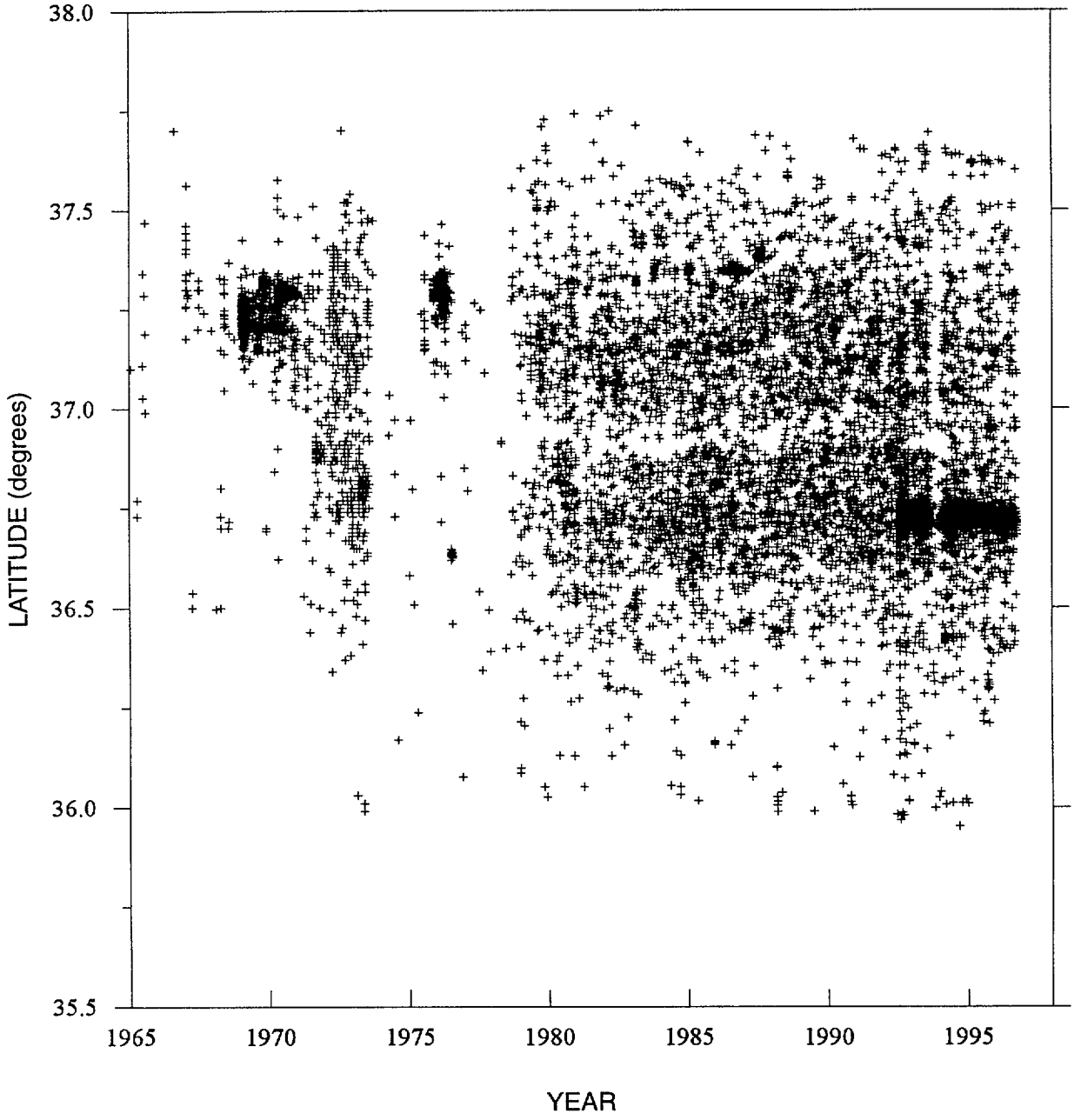

Figure G-13 Earthquakes in the 100 km catalogue as a function of latitude and time prior to declustering

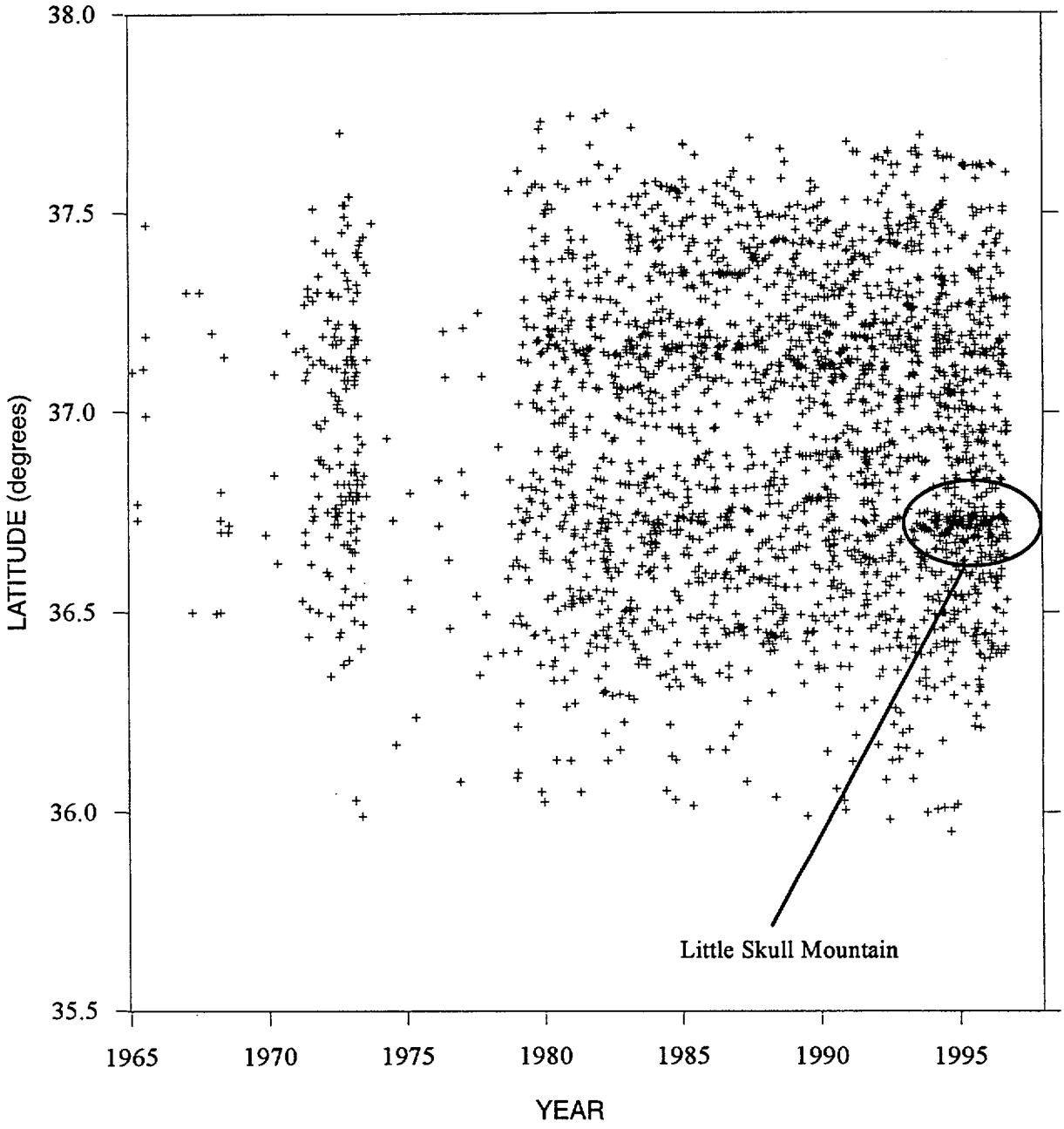

Figure G-14 Earthquakes in the 100 km catalogue as a function of latitude and time after declustering with the Youngs *et al.* approach

Figure G-15 Earthquakes in the 100 km catalogue as a function of latitude and time after declustering with the Veneziano and van Dyck approach

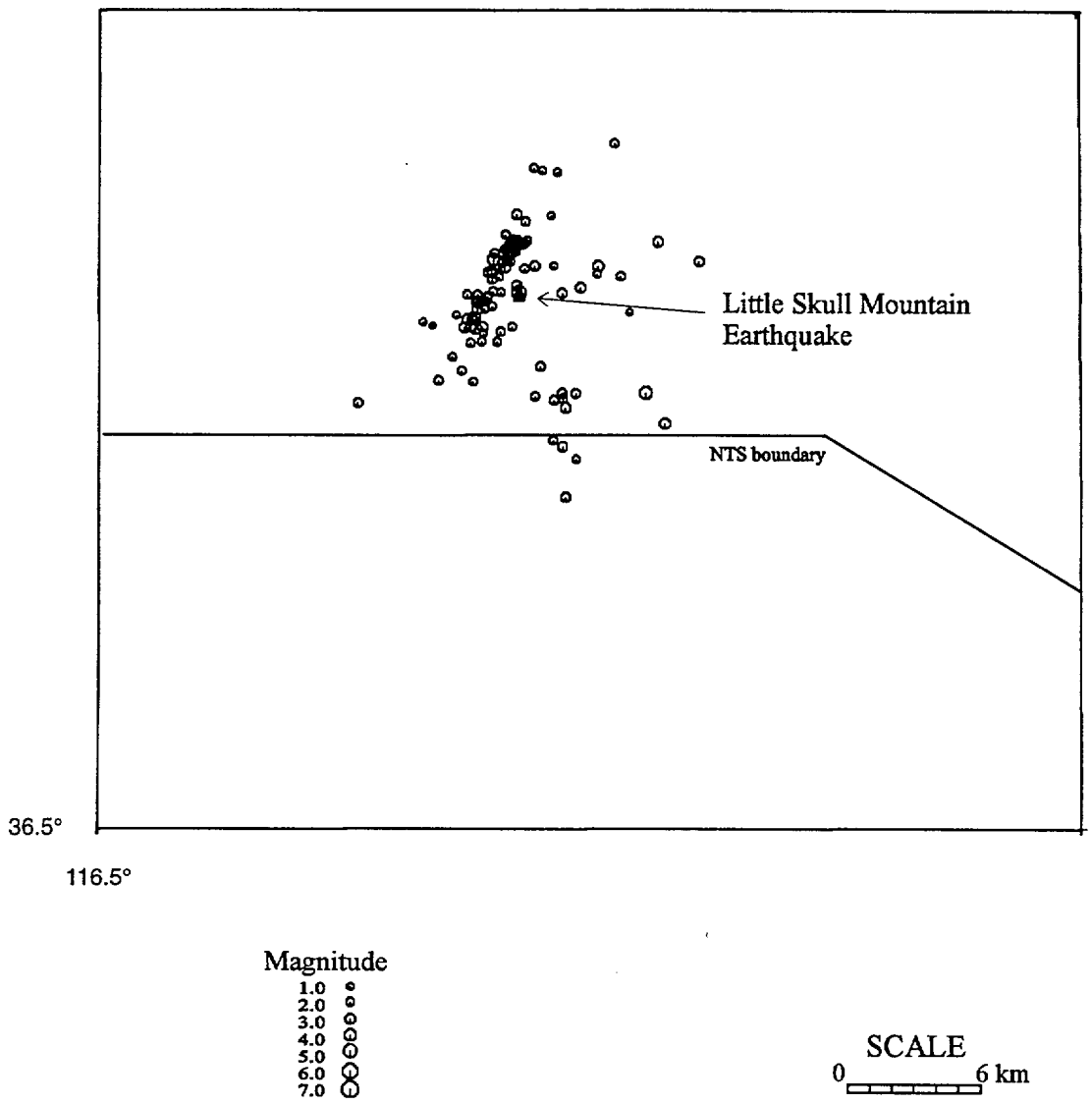

Figure G-16a Earthquakes from 1965 to 1996 within 10 km of Little Skull Mountain after declustering with the Youngs *et al.* approach

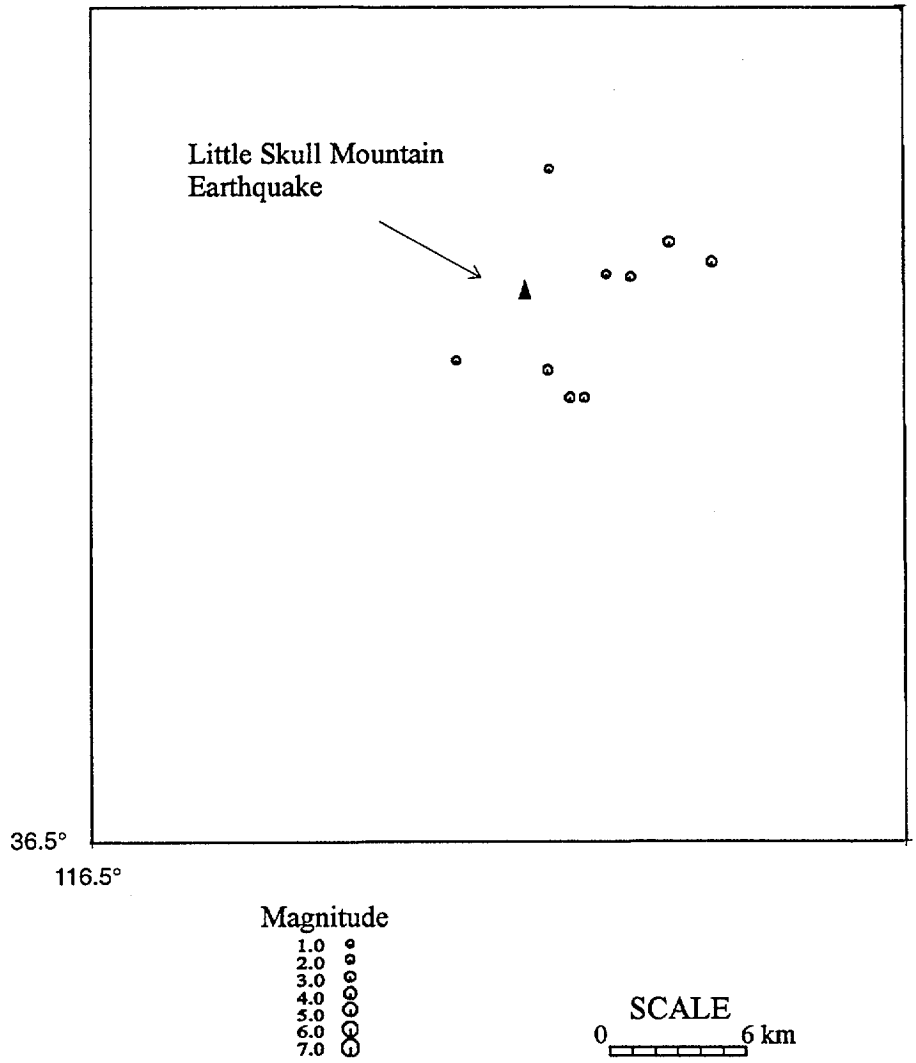

Figure G-16b Earthquakes in 1991 within 10 km of Little Skull Mountain after declustering with the Youngs *et al.* approach

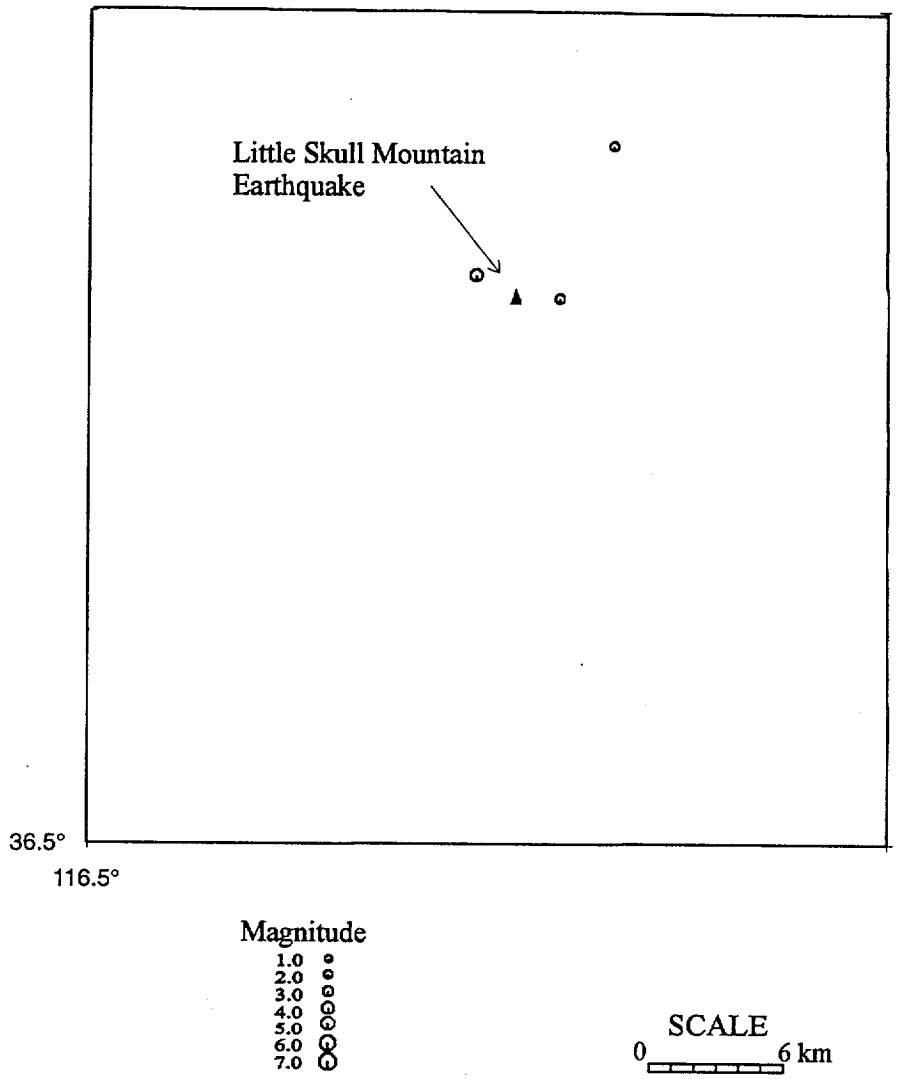

Figure G-16c Earthquakes in 1992 within 10 km of Little Skull Mountain after declustering with the Youngs *et al.* approach

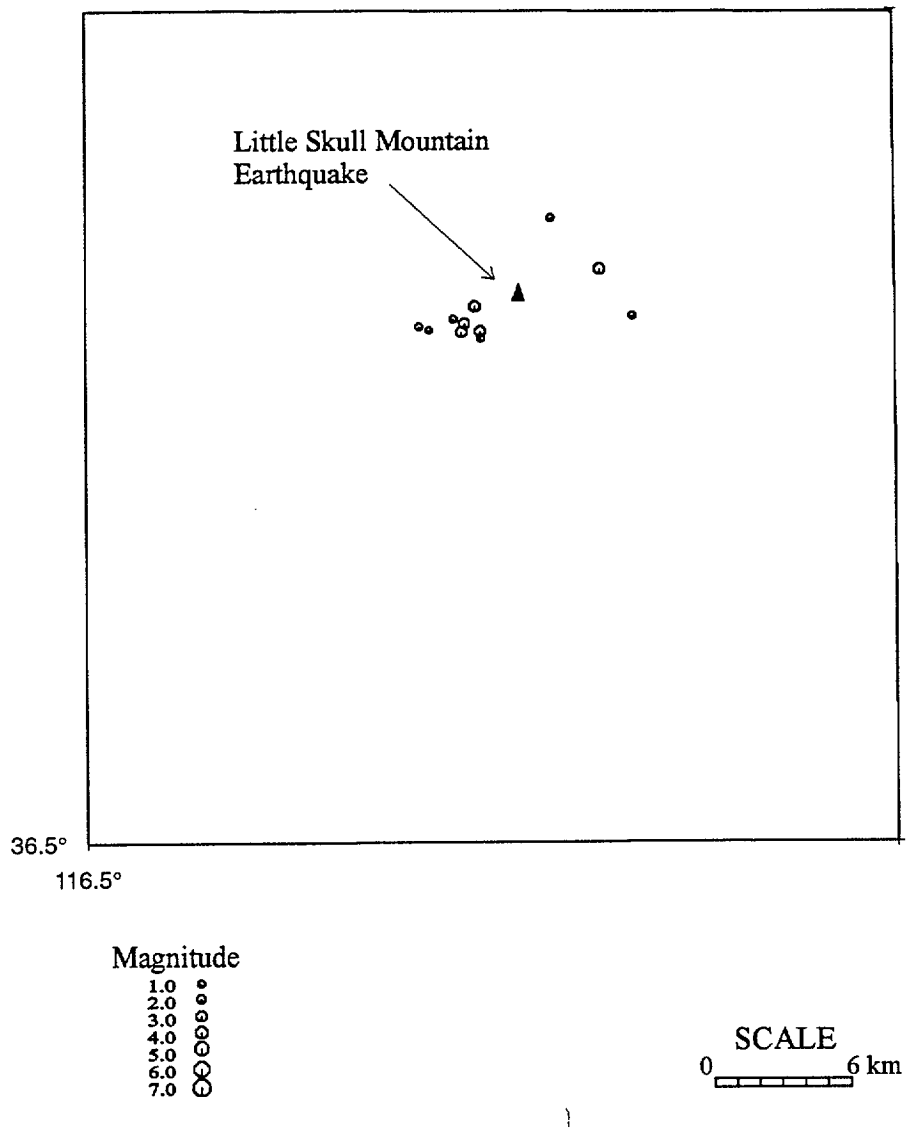

Figure G-16d Earthquakes in 1993 within 10 km of Little Skull Mountain after declustering with the Youngs *et al.* approach

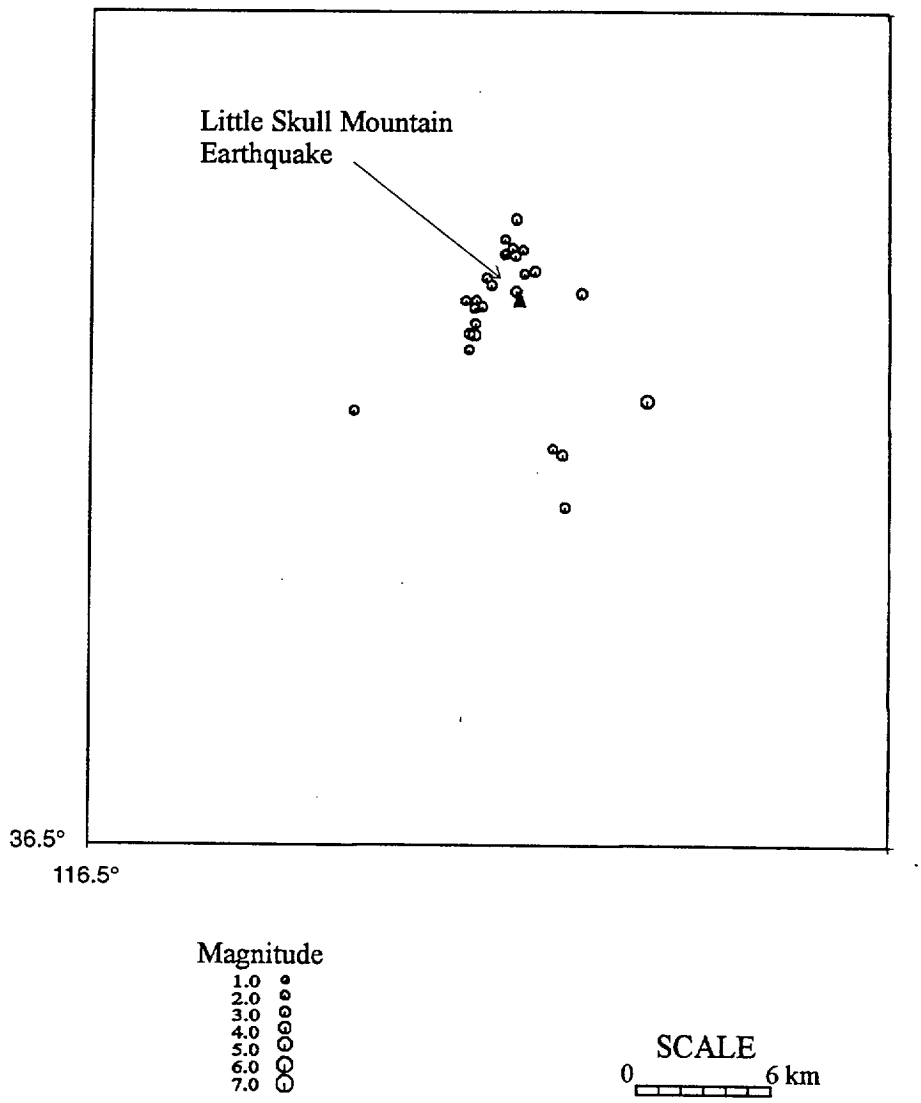

Figure G-16e Earthquakes in 1994 within 10 km of Little Skull Mountain after declustering with the Youngs *et al.* approach

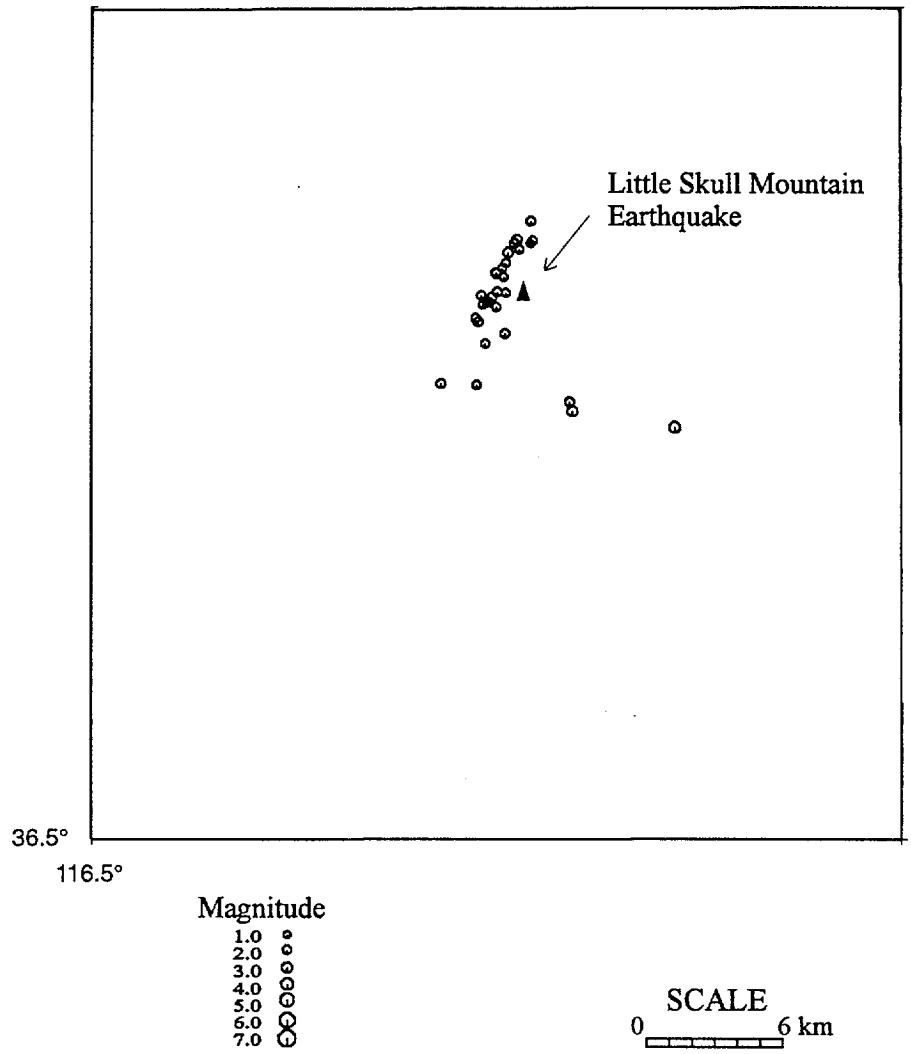

Figure G-16f Earthquakes in 1995 within 10 km of Little Skull Mountain after declustering with the Youngs *et al.* approach

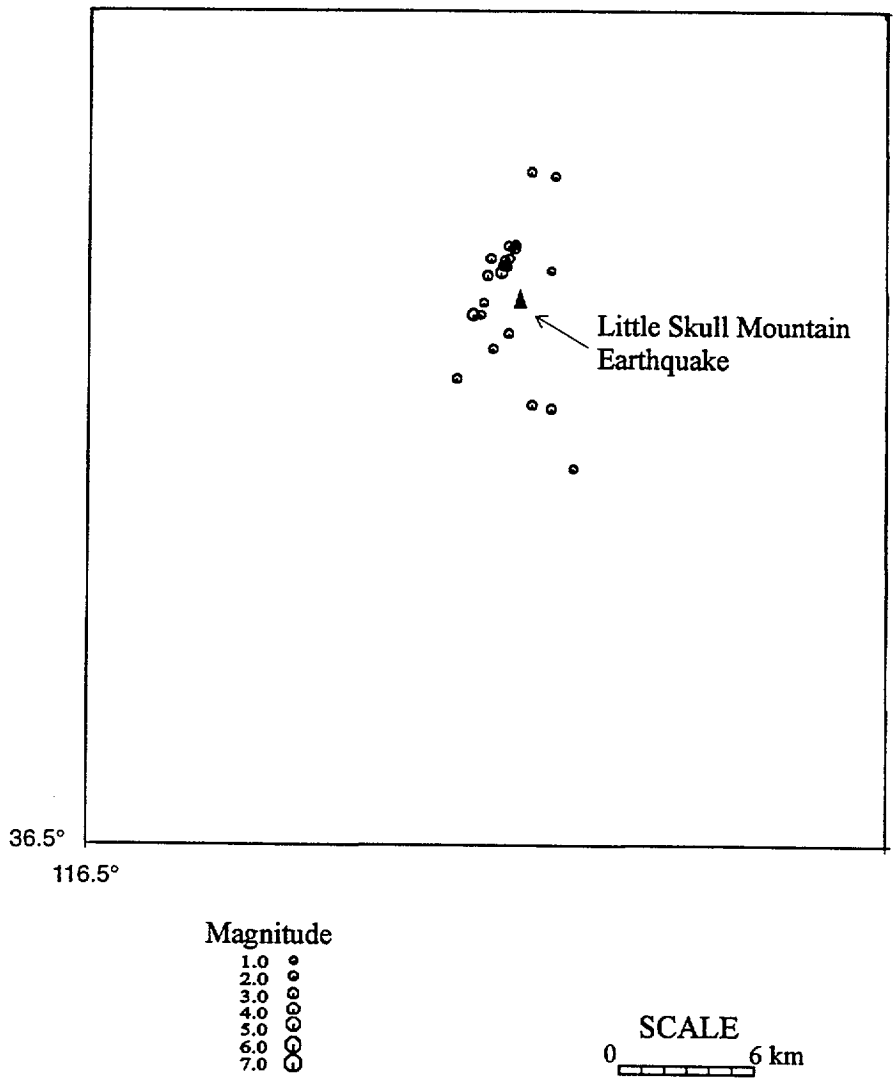

Figure G-16g Earthquakes in 1996 within 10 km of Little Skull Mountain after declustering with the Youngs *et al.* approach

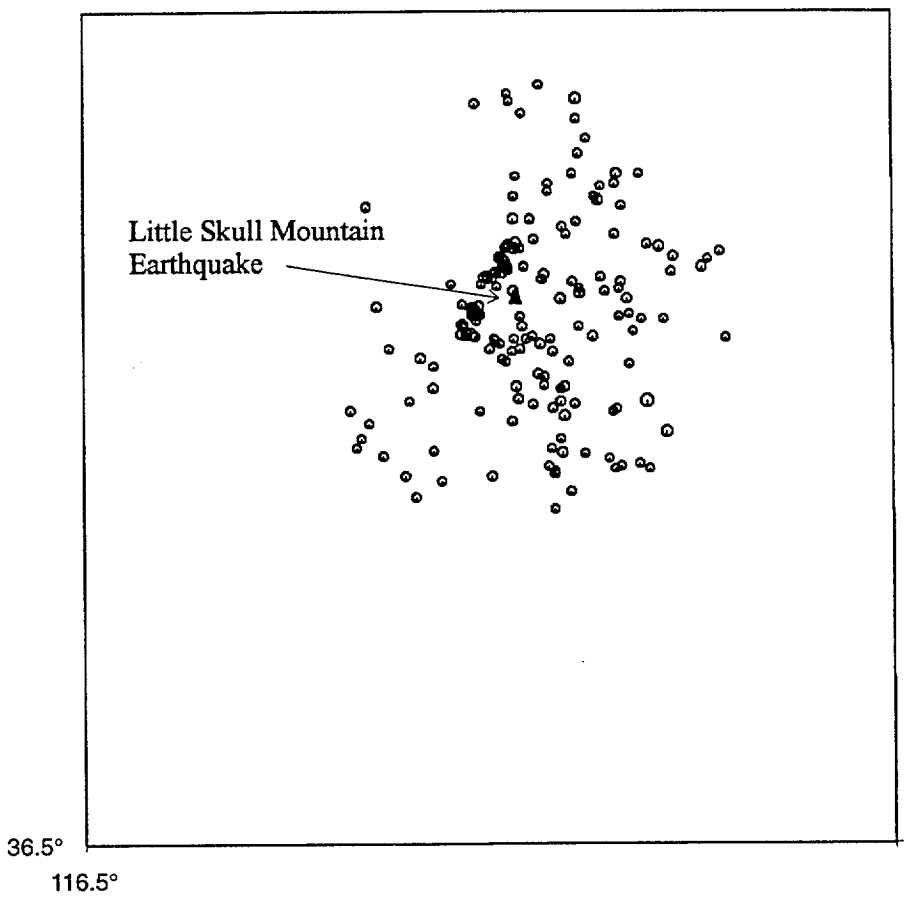

Figure G-17a Earthquakes from 1965 to 1996 within 10 km of Little Skull Mountain after declustering with the Veneziano and van Dyck approach

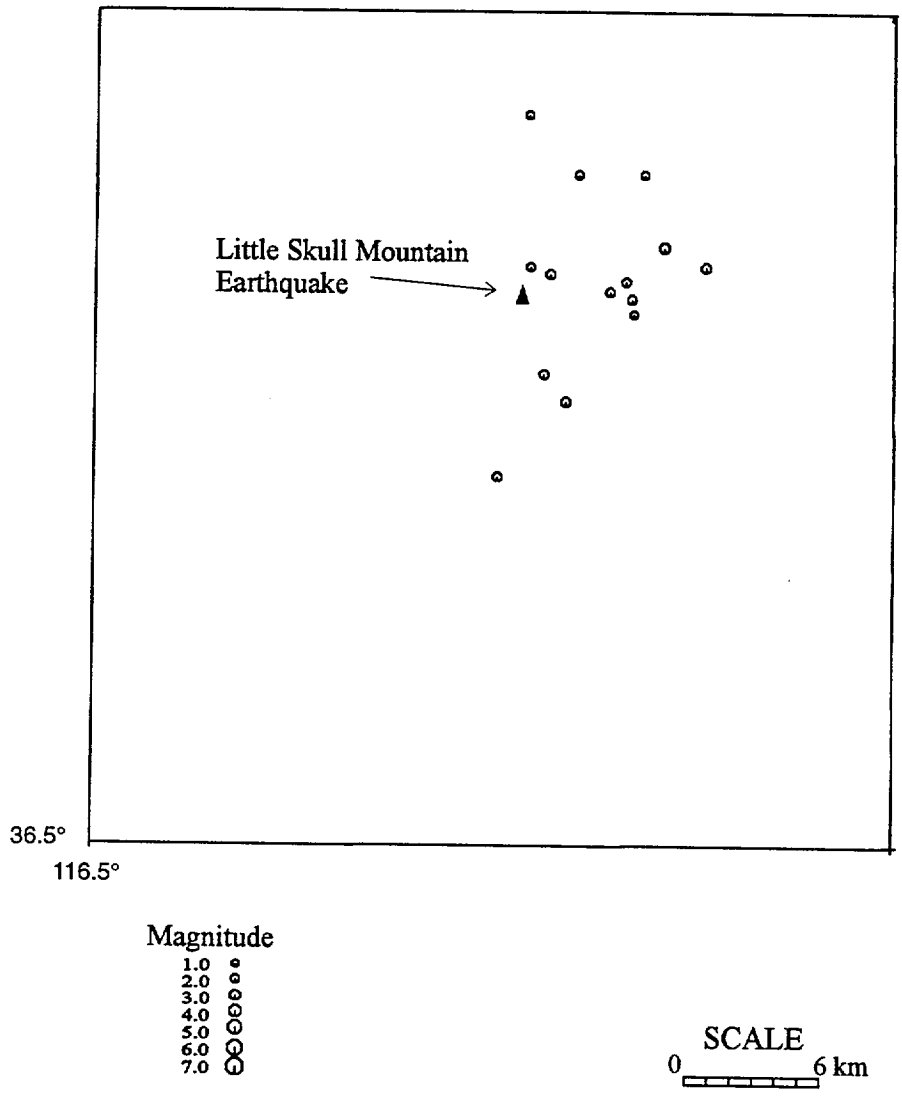

Figure G-17b Earthquakes in 1991 within 10 km of Little Skull Mountain after declustering with the Veneziano and van Dyck approach

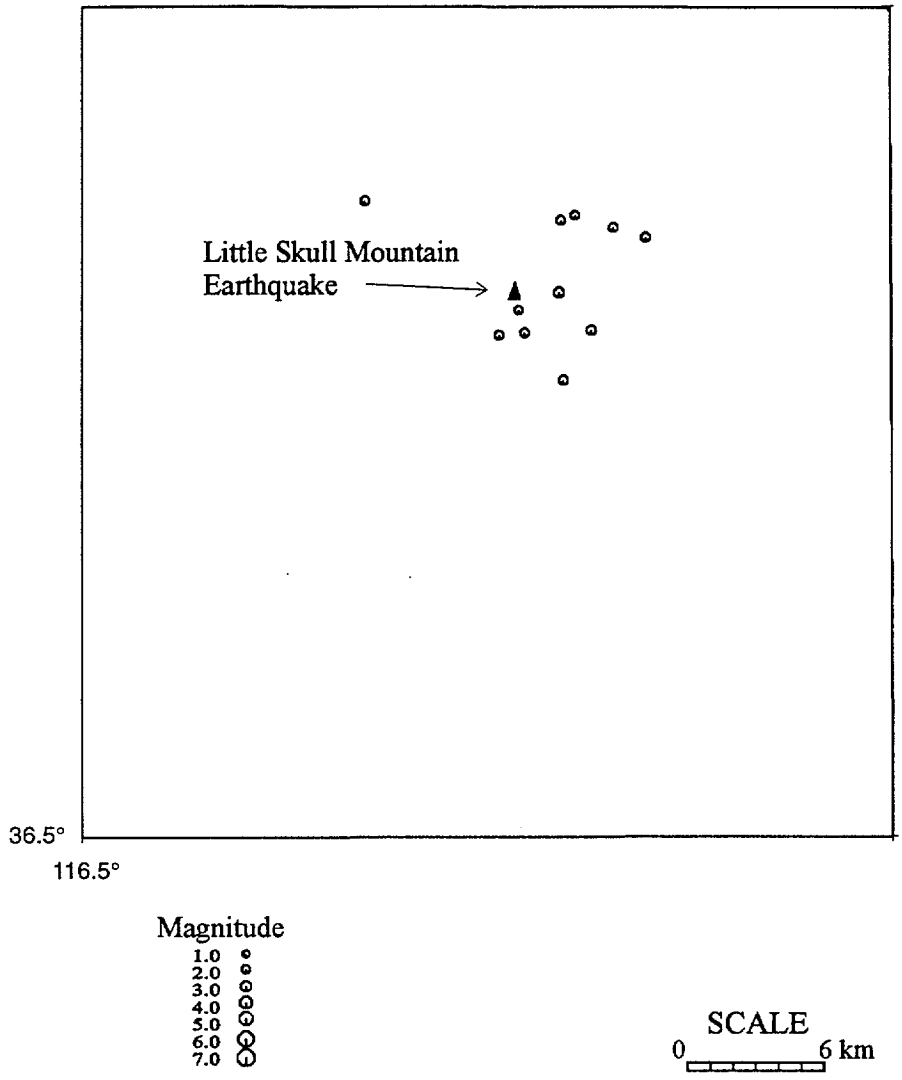

Figure G-17c Earthquakes in 1992 within 10 km of Little Skull Mountain after declustering with the Veneziano and van Dyck approach

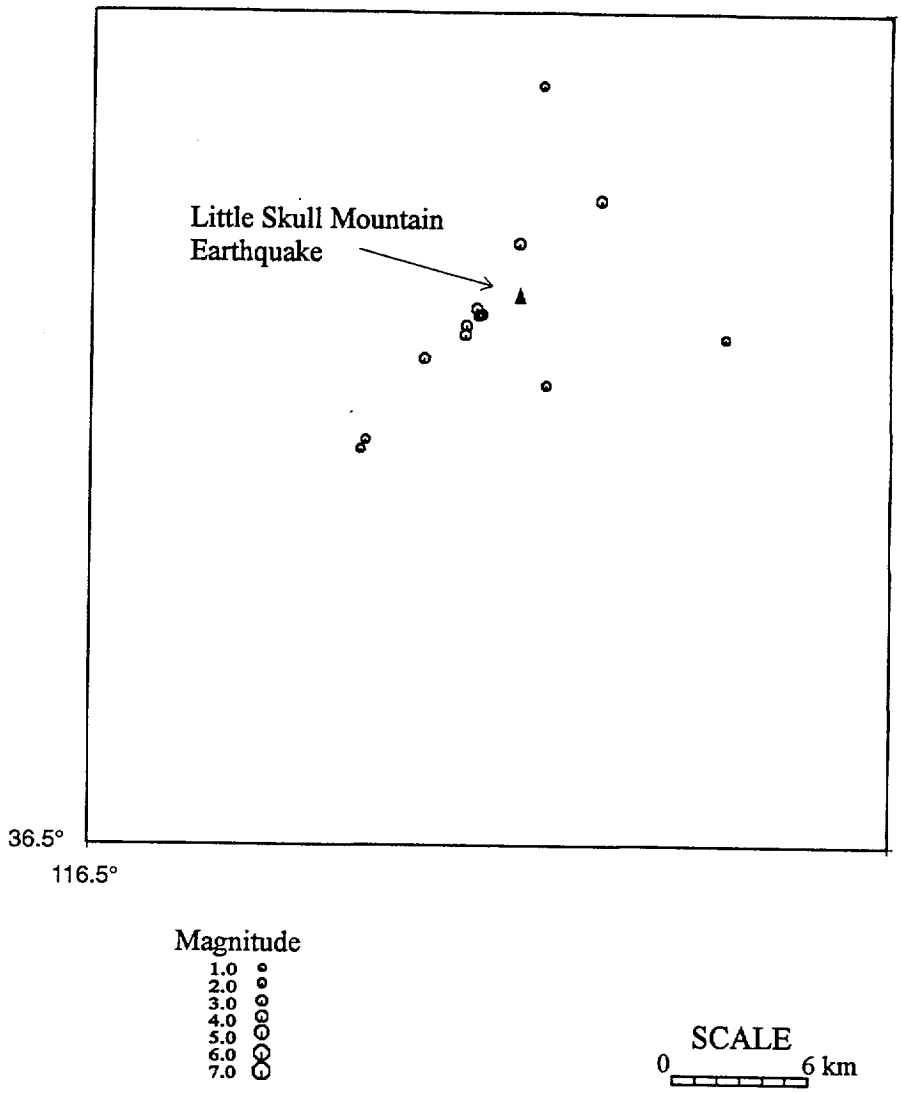

Figure G-17d Earthquakes in 1993 within 10 km of Little Skull Mountain after declustering with the Veneziano and van Dyck approach

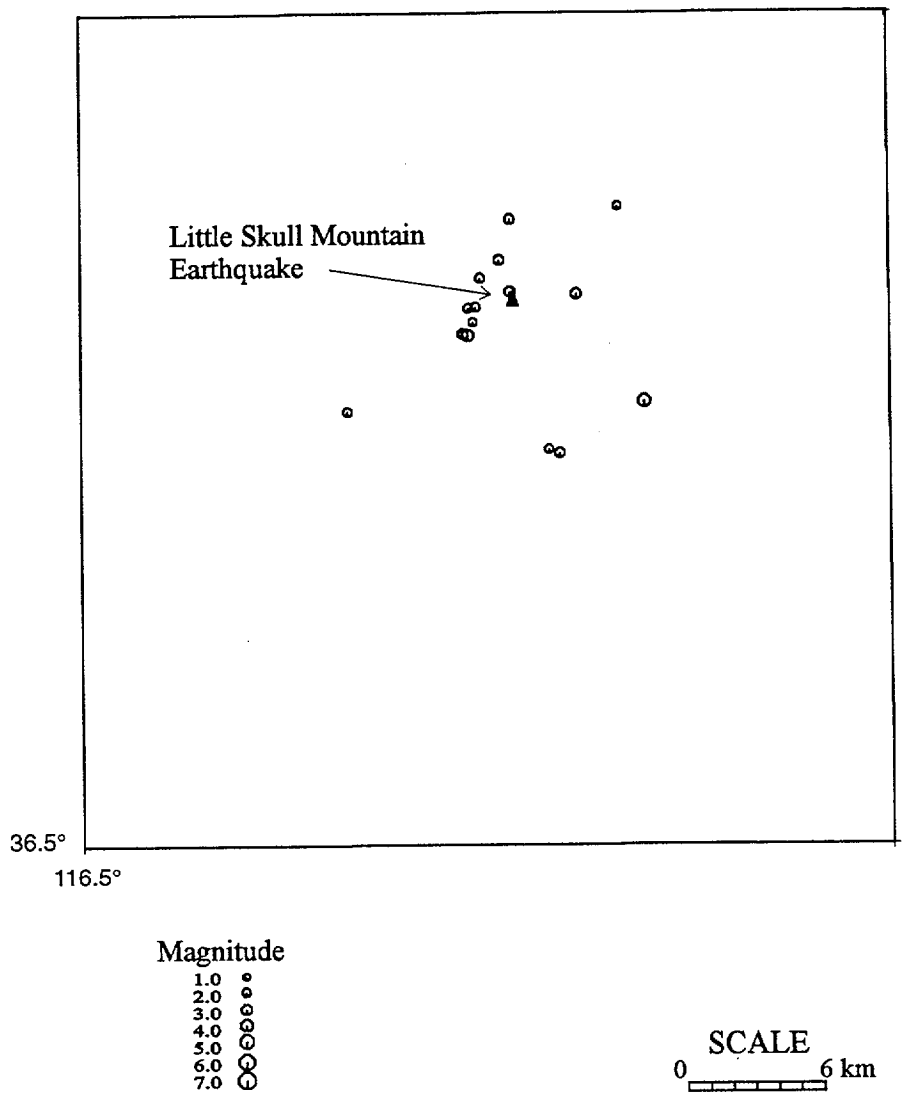

Figure G-17e Earthquakes in 1994 within 10 km of Little Skull Mountain after declustering with the Veneziano and van Dyck approach

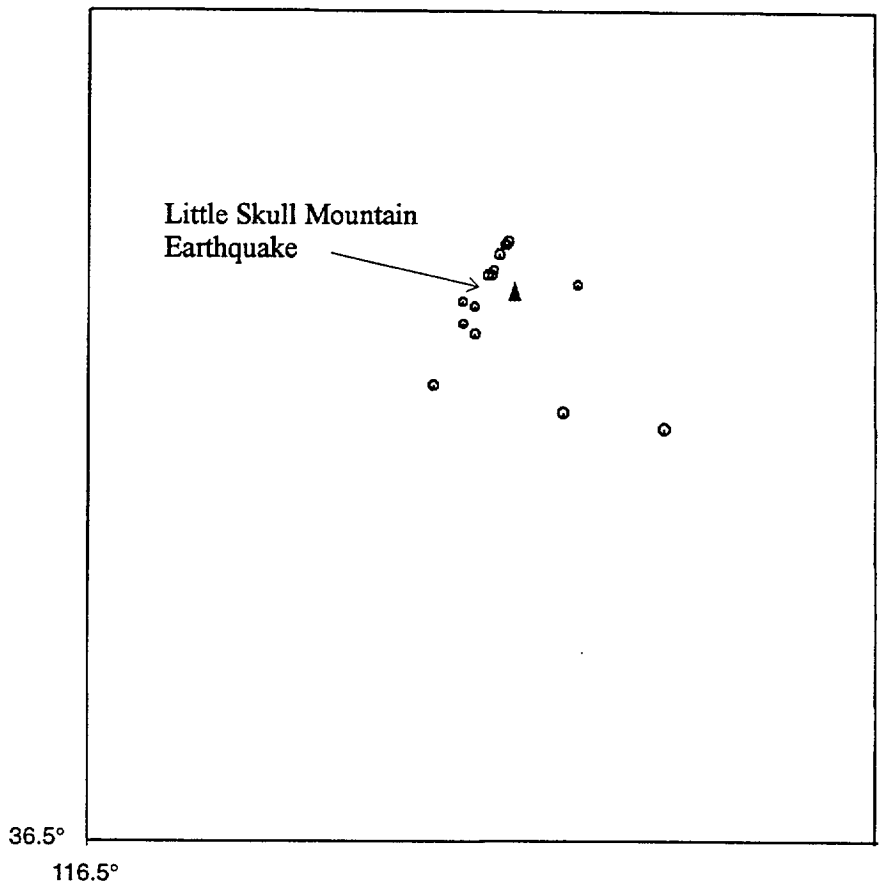

Figure G-17f Earthquakes in 1995 within 10 km of Little Skull Mountain after declustering with the Veneziano and van Dyck approach

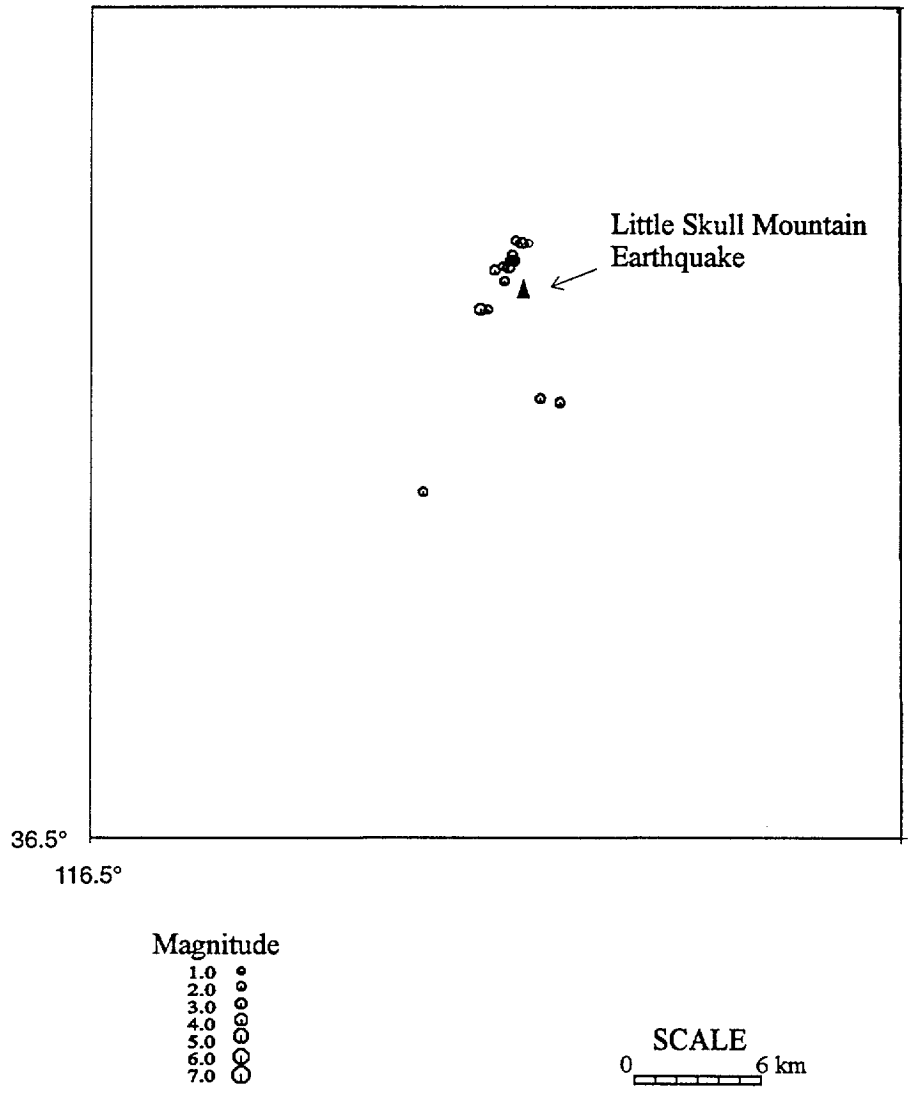

Figure G-17g Earthquakes in 1996 within 10 km of Little Skull Mountain after declustering with the Veneziano and van Dyck approach

APPENDIX H

DEVELOPMENT OF FAULT DISPLACEMENT HAZARD PARAMETER DISTRIBUTIONS

TABLE OF CONTENTS

LIST OF TABLES

LIST OF FIGURES

Figure H-13a Frequency of distributed rupture as a function of distance from principal rupture. The plot on the left shows hanging wall data; the plot on the right shows footwall data. Data include hanging wall cracking from 1988 Chalfant Valley earthquake. Points along bottom of plot represent distances for individual earthquakes where observed frequency was zero. The data for the three magnitude intervals are offset for clarity.

Figure H-13b Frequency of distributed rupture as a function of distance from principal rupture. The plot on the left shows hanging wall data; the plot on the right shows footwall data. Data do not include hanging wall cracking from 1988 Chalfant Valley earthquake. Points along bottom of plot represent distances for individual earthquakes where observed frequency was zero. The data for the three magnitude intervals are offset for clarity.

Figure H-13c Frequency of distributed rupture as a function of distance from principal rupture developed for the AAR and SDO teams. The plot on the left shows hanging wall data, the plot on the right shows footwall data. Data do not include hanging wall cracking from the 1988 Chalfant Valley earthquake or data from the 1980 Mammoth earthquake. Points along bottom of plot represent distances for individual earth quakes where observed frequency was zero. The data for the three magnitude intervals are offset for clarity.

Figure H-14 Example of fitting straight line (dashed line) to digitized rupture trace (solid points) to determine the average strike azimuth.

Figure H-15 Frequency distribution for angle between average strike of principal rupture and strike of individual distributed rupture traces. Parameter n denotes the number of digitization points along an individual rupture trace. Top plot shows the data from Table H-3 presented in terms of fraction of total ruptures. Bottom plot shows exponential fits to the data normalized to unity at a relative angle of 0°.

APPENDIX H
DEVELOPMENT OF FAULT DISPLACEMENT HAZARD PARAMETER DISTRIBUTIONS

H.1 INTRODUCTION

The approaches for assessing fault displacement hazard developed by the SSFD expert teams include a number of empirical models for the distribution of various parameters. To assist in translating the teams' assessments into quantitative methods for use in computing the fault displacement hazard, the SSFD facilitation Team fit statistical distributions to the various empirical data sets specified by the teams. This appendix documents the development of these fault displacement hazard parameter distributions.

H.2 DISTRIBUTIONS FOR NORMALIZED DISPLACEMENT DATA FROM YUCCA MOUNTAIN TRENCHING STUDIES

The assessment of fault displacement hazard requires a model for the conditional probability of exceeding a specified displacement, d, given the occurrence of a displacement event, $P(D>d)$. The SSFD expert teams developed a number of empirical models to compute this probability. These models were based on data for displacement in individual events obtained from the Yucca Mountain paleoseismic trenching studies. The data from the various trenches were typically pooled together by normalizing the data from each trench using a normalizing parameter related to the location where they were obtained. The SSFD Facilitation Team then developed a statistical model for the distribution of D/D_{norm} that can be used to compute $P(D>d)$. These various data sets and the fitted statistical models are described below.

H.2.1 Normalization by Average Displacement at a Point

The DFS team developed a pooled set of displacement data by normalizing the displacements from each trench by the average of all of the displacements measured in the trench, designated AD. They used only data from trenches with three or more displacement events. Figure H-1 shows the cumulative distribution function (CDF) of the normalized data (the data are listed in Table DFS-12 in Appendix E). The DFS team developed a triangular distribution for D/AD by setting the mode of the distribution at 1.0 and placing the lower and upper limits for D/AD at 0 and 2.6, respectively. However, the

resulting CDF does not provide a good fit to the empirical CDF, as indicated in the upper left-hand plot on Figure H-1. In addition, it was judged more appropriate to fit a statistical model to the data that does not have a fixed upper limit. Because *D/AD* is restricted to non-negative values and the data indicate that the distribution is skewed to the right, three reasonable distributions are the exponential, lognormal, and gamma distributions. The exponential distribution has the form

$$F(x) = 1 - e^{-x/\mu_x} \tag{H-1}$$

where $F(x)$ is the CDF (the probability that the variable X is less than or equal to a value x) and parameter μ_x is the mean value of x. Setting x equal to *D/AD*, the mean value of *D/AD* is 1.0.

The lognormal distribution has the form

$$F(x) = \frac{1}{\sqrt{2\pi}\sigma_{\ln(x)}} \int_{-\infty}^{\ln(x)} e^{-1/2\left(\frac{z-\mu_{\ln(x)}}{\sigma_{\ln(x)}}\right)^2} dz \tag{H-2}$$

Setting x equal to *D/AD*, the resulting parameters are $\mu_{\ln(D/AD)} = -0.267$ and $\sigma_{\ln(D/AD)} = 0.839$.

The gamma distribution has the form

$$F(x) = \frac{1}{\Gamma(a)} \int_0^{x/b} e^{-t} t^{a-1} dt \tag{H-3}$$

where $\Gamma(a)$ is the gamma function. Setting x equal to *D/AD* and using the moments of the data, the resulting parameters of the gamma distribution are $a = 2.78$ and $b = 0.36$.

Two other types of distributions that provide skewed-to-the-right density functions and a positive mode are the Type I and II extreme value distributions, although the Type I distribution is not limited to non-negative values.

The Type I distribution has the form

$$F(x) = e^{-e^{-a(x-u)}} \quad \text{(H-4)}$$

where $a = 1.282/\sigma_x$ and $u = \mu_x - 0.577/a$ (Benjamin and Cornell, 1970). Setting x equal to *D/AD* and using the moments of the data, the resulting parameters of the Type I distribution are $a = 2.11$ and $u = 0.726$.

The Type II distribution has the form

$$F(x) = e^{-(u/x)^k} \quad \text{(H-5)}$$

where $\mu_x = u\Gamma(1\text{-}1/k)$ and $\sigma^2_x = u^2[\Gamma(1\text{-}2/k) - \Gamma^2(1\text{-}1/k)]$ (Benjamin and Cornell, 1970). Setting x equal to *D/AD* and using the moments of the data, the resulting parameters of the Type II distribution are $u = 0.757$ and $k = 3.19$.

Shown on Figure H-1 are the resulting CDFs for the exponential, lognormal, gamma, Type I, and Type II distributions fit to the data for *D/AD*. The best fits are obtained using the gamma and Type I distributions. The fit of the Type I distribution (as measured by the χ^2 and Kolmogorov-Smirnov goodness of fit tests) is slightly better than the gamma distribution. However, the fitted Type I distribution has a small tail (0.01 probability) of negative values for *D/AD*. Therefore, the gamma distribution with parameters $a = 2.78$ and $b = 0.36$ is preferable to model the distribution of *D/AD*.

H.2.2 Normalization by Average Paleoseismic Displacement for a Fault

The SBK team also developed a pooled set of displacement data by normalizing the displacements from each trench by an estimate of the average displacement per event for paleoseismic events, designated $AD_{\text{-}paleo}$, for the fault on which the trench was located. These data are listed in Table SBK-6 in Appendix E. Figure H-2 shows the resulting CDFs for fits of exponential, lognormal, gamma, and Type I distributions to the $D/AD_{\text{-}paleo}$ data. The best fits are obtained using the gamma and Type I distributions, with the Type I distribution providing better goodness of fit statistics. However, as was the case for the

data shown on Figure H-1, the fitted Type I distribution has a small tail (0.02 probability) of negative values for $D/AD_{\text{-paleo}}$. Therefore, the gamma distribution with parameters a = 2.17 and b = 0.46 is preferable to model the distribution of $D/AD_{\text{-paleo}}$.

H.2.3 Normalization by Average Displacement as a Function of Fault Rupture Length

The SBK team also developed a pooled set of displacement data by normalizing the displacements from each trench by the average displacement per event based on an empirical relationship between average displacement and fault rupture length, designated $AD_{\text{-F(RL)}}$, for the fault on which the trench was located. These data are listed in Table SBK-6 in Appendix E. Figure H-3 shows the resulting CDFs for fits of exponential, lognormal, gamma, and Type I distributions to the $D/AD_{\text{-F(RL)}}$ data. The best fit is obtained using the gamma distribution with parameters a = 0.82 and b = 1.77.

H.2.4 Normalization by Maximum Displacement as a Function of Fault Rupture Length

The SBK team developed a pooled set of displacement data by normalizing the displacements from each trench by the maximum displacement per event based on an empirical relationship between maximum displacement and fault rupture length, designated $MD_{\text{-F(RL)}}$, for the fault on which the trench was located. These data are listed in Table SBK-6 in Appendix E. Figure H-4 shows the resulting CDFs for fits of exponential, lognormal, gamma, and Type I distributions to the $D/MD_{\text{-F(RL)}}$ data. The best fit is obtained using the gamma distribution with parameters a = 0.69 and b = 1.05.

H.2.5 Normalization by Expected Maximum Displacement

The AAR team developed a pooled set of displacement data by normalizing the displacements from each trench by the expected maximum displacement for a feature, designated M/MD, for the fault on which the trench was located. These data are listed in Table AAR-10 in Appendix E. Figure H-4 shows the resulting CDFs for fits of exponential, lognormal, gamma, and Type I distributions to these data. Good fits were obtained for the exponential distribution with μ_{MD}^{max} = 0.83, and for the gamma distribution with parameters a = 1.41 and b = 0.59. The goodness of fit statistics were slightly better for the gamma distribution. Because the gamma distribution has two parameters, one would expect it to provide a better fit than the single parameter exponential model. The statistical significance of the improvement in the fit can be evaluated using the likelihood ratio test (e.g. Seber and Wild, 1989, p. 196). The

likelihood of observing a particular data set, x_i (i = 1 to n), given a gamma distribution with parameters a and b is

$$L(a,b) = \prod_{i=1}^{n} \frac{(x_i/b)^{a-1} e^{-x_i/b}}{b\Gamma(a)} \qquad \text{(H-6)}$$

The likelihood ratio statistic, LR, defined as

$$LR = 2\ln[L(\hat{\theta}) / L(\theta_o)] \qquad \text{(H-7)}$$

is used to test the hypothesis that the parameters $\hat{\theta}$ are equal to specified values θ_o. In this case, the exponential distribution is a special case of the gamma distribution with a = 1.0. The hypothesis that a is different from 1.0 is tested by setting $\hat{\theta}$={1.41, 0.59} and θ_o={1.0, 0.83} (for the exponential case $b = \mu_x$). The resulting value of LR is 2.93. The LR statistic is approximately χ_r^2 distributed with the degrees of freedom, r, equal to the number of additional free parameters in going from parameter set θ_o to parameter set $\hat{\theta}$. For this case, r = 1, and $P(\chi_1^2 > 2.93) = 0.09$. Thus, the improved fit of the gamma distribution over the exponential distribution is only marginally statistically significant.

H.2.6 Normalization by Cumulative Displacement

The SBK team developed a pooled set of displacement data by normalizing the displacements from each trench by the cumulative displacement, designated D_{cum}, for the fault on which the trench was located. These data are listed in Table SBK-7 in Appendix E. Figure H-6 shows the resulting CDFs for fits of exponential, lognormal, gamma, and Type I distributions to the D/D_{cum} data. The best fits are obtained with the gamma and Type I distributions, with the fit of the Type I distribution producing better goodness of fit statistics. However, the fitted Type I distribution has a small tail (0.04 probability) of negative values for D/AD_{-paleo}. Therefore, the gamma distribution with parameters a = 1.79 and b = 0.00098 is preferable to model the distribution of D/D_{cum}.

H.3 DISTRIBUTIONS FOR DISPLACEMENT AT A POINT ALONG A PRINCIPAL RUPTURE

The SSFD expert teams developed an approach for assessing the variability of the displacement at a point along a principal rupture as a fraction of the maximum displacement on the rupture. These assessments were based on empirical data or simulations using fault roughness. The SSFD Facilitation Team then developed statistical models for the distribution of *D/MD* as a function of location along the principal rupture that can be used to compute $P(D_E>d)$. These models are described below.

H.3.1 Empirical Distribution for *D/MD* Along a Fault Rupture

Wheeler (1989) presented displacement profiles normalized by peak displacement for five large Basin and Range earthquake ruptures. The ASM team smoothed these data to develop curves defining the minimum, median, and maximum values of *D/MD* at a point as a function of normalized location along strike. The normalized point location is specified as *x/L*, where *x* is measured from one end of the rupture and *L* is the length of rupture. The data were smoothed to make the curves symmetric about $x/L = 0.5$. Shown at the left of Figure H-7 are the resulting normalized displacement curves. These curves were interpreted to represent a low percentile, the median value, and a high percentile for *D/MD*, and were used to construct a cumulative distribution function for *D/MD*.

The ratio *D/MD* is limited to the range of 0 to 1.0. A very flexible distribution form for modeling variables that have a fixed range is the beta distribution. When the variable y is limited to the range $0 \le y \le 1$, the beta distribution has the form

$$F(y) = \frac{\Gamma(a+b)}{\Gamma(a)\Gamma(b)} \int_0^y z^{a-1}(1-z)^{b-1} dz \qquad \text{(H-8)}$$

Setting y = *D/MD* and interpreting the minimum and maximum curves to be the 5th and 95th percentiles of the CDF for *D/MD*, beta distributions were developed at increments of $0.05x/L$. The resulting a and b parameters are plotted on Figure H-8. Relationships were developed for the parameters a and b as a function of *x/L*; specifically, $a = 3.73+3.98x/L$ and $b = 5.28+46.28e^{-16.7x/L}$, with $0 \le x/L \le 0.5$. The CDFs shown on the right of Figure H-7 were obtained using values of a and b from these relationships.

H.3.2 Numerical Simulations of *D/MD* Along a Fault Rupture

The SBK team presented in Workshop #5 the results of numerical simulations of the displacement pattern along a fault based on a fractal modeling of fault roughness. Figure H-9 shows the resulting CDFs for *D/MD* as a function of *x/L* computed from 100 simulations. These simulated CDFs were fit with beta distributions. The resulting values of parameters *a* and *b* as a function of *x/L* are shown on Figure H-10. Relationships were developed for the parameters *a* and *b* as a function of *x/L*; specifically, $a = \exp[0.6064+21.83x/L - 108.0(x/L)^2 + 136.6(x/L)^3]$ and $b = \exp[2.027+12.21x/L - 87.90(x/L)^2 + 115.5(x/L)^3]$, with $0 \leq x/L \leq 0.5$. Figure H-11 shows a comparison of the simulated CDFs to those obtained using values of *a* and *b* from these relationships.

H.4 DISTRIBUTIONS FOR PROBABILITY OF NEAR SURFACE RUPTURE

The SSFD teams developed approaches for assessing the probability the rupture will occur near the surface, given the occurrence of an earthquake, using data sets developed from mapping of historical ruptures. These models are described below.

H.4.1 Empirical Distribution for Probability of Principal Fault Rupture

S.K. Pezzopane and T.E. Dawson (USGS, written communication, 1996) present a data base of historical ruptures that have occurred in the extensional Cordillera of the western U.S. On their Figures 9-4A, 9-6, and 9-8A they present histograms that list the number of earthquakes that have reported principal rupture near the surface and the number of earthquakes that have no reported principal rupture near the surface. These histograms show data on 105 earthquakes from the extensional Cordillera (their Figure 9-4A), 47 earthquakes in the northern Basin and Range Province that occurred post-1930 (their Figure 9-6), and 32 earthquakes in the Great Basin province that occurred post-1930 (their Figure 9-8A). These data, summarized in Table H-1, can be used to develop a model for the probability of near-surface rupture given the occurrence of an earthquake.

Wells and Coppersmith (1994) used a *logistic regression* model to analyze these types of data. The logistic regression model (e.g., Hosmer and Lemeshow, 1989) is a commonly used model for assessing the outcome of a dichotomous variable; in this case given the occurrence of an earthquake, surface rupture either occurs or does not occur. The

probability of a positive outcome (the occurrence of principal faulting given the occurrence of the event) is given by the expression

$$P(rupture|event) = \frac{e^{f(x)}}{1+e^{f(x)}} \qquad \text{(H-9)}$$

where $f(x)$ is a function of a set of variables characterizing the event. Wells and Coppersmith (1994) used magnitude to characterize the earthquake, defining $f(x)$ to be:

$$f(x) = a + b\mathbf{M} \qquad \text{(H-10)}$$

Using this functional form, logistic regression functions were fit to the three data sets listed in Table H-1 using a maximum likelihood approach. The resulting models for the probability of principal surface faulting are shown on Figure H-12 and the parameters of the models are listed below.

Coefficients of Equation (H-10)

Data Set	a	b
32 Great Basin events	-16.02	2.685
47 Northern Basin & Range events	-18.71	3.041
105 extensional Cordillera events	-12.53	1.921

H.4.2 Empirical Distribution for Probability of Distributed Fault Rupture

S.K. Pezzopane and T.E. Dawson (USGS, written communication, 1996) present a set of maps (their Plate 21) of historical ruptures that have occurred in the extensional Cordillera of the western U.S. indicating the location of distributed (secondary) ruptures around the principal (primary) fault rupture. Silvio Pezzopane presented in Workshop #3 an analysis of these data that showed the length of distributed rupture as a function of the distance from the principal rupture. His analysis was performed by constructing a raster scan of each map with a 0.5 km pixel size. The length of distributed faulting was set equal to 0.5 km times the number of pixels containing distributed rupture at a given distance from the principal rupture.

These data were used in the assessment of the distributed faulting hazard to develop an empirical model for the probability of the occurrence of distributed faulting at a point given

the occurrence of an earthquake. Dr. Pezzopane extended his analysis of the mapping data to also count the number of pixels that did not contain distributed faulting as a function of distance from the principal rupture. These data are presented in Table H-2. Figures H-13a and H-13b show these data in terms of the frequency of occurrence of distributed faulting. The frequencies plotted for each earthquake and distance from the principal rupture were computed by dividing the number of pixels with surface rupture by the total number of pixels. The row of data plotted at the bottom of the figures represent data points for which the observed frequency is zero. Figure H-13a shows the data including the hanging wall cracking that was observed in the 1988 Chalfant Valley, California earthquake and Figure H-13b shows the data without the Chalfant Valley hanging wall cracking observations.

The data for observations of the occurrence of distributed faulting listed in Table H-2 also represent the outcome of a dichotomous variable; distributed rupture either occurs or does not occur at each point (pixel). The logistic model [Equation (H-9)] was used to compute the probability of distributed rupturing occurring at a point. The data indicate a decrease in the frequency of occurrence with increasing distance, a decrease in frequency with decreasing magnitude, and lower frequencies in the footwall than in the hanging wall. The functional form used to represent these trends is

$$f(x) = C_1 + (C_2 + C_3 m + C_4 h) \cdot \ln(r + C_5) \qquad \text{(H-11)}$$

where m is earthquake magnitude, r is the distance to the principal rupture (in km), and h = 1 for the hanging wall side of the rupture and h = 0 for the footwall side of the rupture. Equation (H-11) was fit to the data listed in Table H-2 considering the two cases shown on Figures H-13a and H-13b. The resulting maximum likelihood parameters are listed below, including a case specified by the AAR team.

Coefficients of Equation (H-11)

Data Set	C_1	C_2	C_3	C_4	C_5
Table H-2 with Chalfant Valley Cracking	-0.891	-2.93	0.0065	0.957	1.48
Table H-2 without Chalfant Valley Cracking	2.06	-4.62	0.118	0.682	3.32
Table H-2 without Chalfant Valley Cracking and Mammoth (AAR)	2.04	-4.60	0.118	0.705	3.38

Shown on Figures H-13a and H-13b are curves indicating the probability of distributed rupture at a point, give the occurrence of an earthquake of M_w 5.5, 6.5, and 7.5. These relationships indicate that when the hanging wall cracking data from the 1988 Chalfant Valley earthquake are included in the data set, the resulting relationship shows no dependence on magnitude. If these data are not considered appropriate, then a significant magnitude effect is observed. The AAR and SDO teams considered an additional case exluding the hanging wall cracking data from Chalfant Valley and data from the 1980 Mammoth earthquake. The resulting parameters of Equation (H-11) are listed above and the data and logistic regression model are shown on Figure H-13c

H.4.3 Empirical Distribution for Probability of Distributed Rupture as a Function of Fault Orientation

The SBK and SDO teams considered a model for the probability that distributed rupture could occur on a feature based on data on the relative orientation between the principal and distributed ruptures in historical earthquakes. The data used for this assessment were the maps of historical ruptures presented on Plate 21 of S.K. Pezzopane and T.E. Dawson (USGS, written communication, 1996). The digitized faulting maps were analyzed to calculate the strike azimuths of the principal faulting trace and the individual distributed faulting traces. Figure H-14 shows an example of how a straight line was fit to a digitized fault trace. The average strike line was found by minimizing the squared distance from the fault trace digitization points measured normal to the strike line. Table H-3 summarizes the data for the angle between the principal fault trace and the individual distributed fault traces in terms of the number of distributed ruptures with relative angles within 5° intervals. Figure H-15 shows the data for all of the historical ruptures in terms of frequency of ruptures in each 5° relative angle increment (the number of ruptures in each increment divided by the total number of ruptures). The data are presented in terms of the number of digitization points for each distributed rupture trace. It is expected that the average strike for traces with more digitization points are somewhat better defined.

The frequency data plotted at the top of Figure H-15 were fit with the functional form:

$$\ln(frequency) = C_1 + C_2 \,\mathrm{int}[\theta/5] + C_3 \,\mathrm{int}[\theta/5]^2 \qquad \text{(H-12)}$$

where θ is the angle between the average strike of the principal and distributed rupture and int[ ] is the integer function (i.e., int[4/5] = 0, int[7/5] = 1). The following table lists the coefficients of the individual fits to the data.

Coefficients of Equation (H-12)

Data Set	C_1	C_2	C_3
n ≥ 2	-2.09	-0.0732	-0.00546
n ≥ 3	-1.84	-0.130	-0.00415
n ≥ 4	-1.73	-0.173	-0.00226
n ≥ 5	-1.72	-0.186	-0.00132
n ≥ 6	-1.86	-0.0734	-0.0117

These relationships can be used to assess the relative likelihood of rupture by normalizing them to produce unity at θ = 0 [i.e., setting C_1 to 0 in Equation (H-12)]. The resulting relationships are shown on the bottom plot of Figure H-15.

H.5 REFERENCES

Benjamin, J.R., and Cornell, C.A., 1970, Probability, Statistics, and Decision for Civil Engineers: McGraw-Hill Book Company, 694 p.

Hosmer, D.W. Jr., and Lemeshow, S., 1989, Applied Logistic Regression: New York, John Wiley & Sons, 307 p

Seber, G.A.F., and Wild, C.J., 1989, Nonliner Regression: New York, John Wiley & Sons, 768 p.

Wells, D.L., and Coppersmith, K.J., 1994, New empirical relationships among magnitude, rupture length, rupture width, rupture area, and surface displacement: Bulletin of the Seismological Society of America, v. 84, p. 974-1002.

Wheeler, R.L., 1989, Persistent segment boundaries on Basin-Range normal faults, *in* D.P., Schwartz and R.H. Sibson, eds, Proceedings, Conference XLV-Fault Segmentation and Controls on Rupture Initiation and Termination: U.S. Geological Survey Open-File Report 89-315, p. 432-444.

Table H-1
Summary of Data Presented in S.K. Pezzopane and T.E. Dawson (USGS, written communication, 1996) For the Occurrence of Principal Faulting During Historical Ruptures

Moment Magnitude (M_w)	Extensional Cordillera		Northern Basin & Range Post-1930		Great Basin Post-1930	
	Number of Events with:		Number of Events with:		Number of Events with:	
	Surface Rupture	No Surface Rupture	Surface Rupture	No Surface Rupture	Surface Rupture	No Surface Rupture
4.5	1	0				
4.6						
4.7						
4.8						
4.9	1	0	1	0	1	0
5.0	0	1	0	1		
5.1						
5.2	1	0				
5.3	0	1	0	1	0	1
5.4						
5.5	1	17	0	7	0	4
5.6	1	4	1	4	1	2
5.7	0	4	0	3	0	2
5.8	2	3	2	2	2	1
5.9	0	3	0	3	0	1
6.0	5	23	2	2	2	2
6.1	2	6	2	5	2	3
6.2	1	3	1	0	1	0
6.3	1	3	1	1	1	0
6.4	1	1				
6.5	1	4				
6.6	3	0	2	0	2	0
6.7						
6.8	3	0	3	0	2	0
6.9						
7.0						
7.1	1	0	1	0	1	0
7.2	1	0	1	0	1	0
7.3	2	0				
7.4	3	0	1	0		
7.5						
7.6	1	0				

Table H-2
Summary of Data from S.K. Pezzopane and T.E. Dawson (USGS, written communication, 1996, Plate 21) for Frequency of Distributed Faulting

Distance from Principal Rupture (km)	Hanging Wall		Footwall	
	Number of 0.5 km² Pixels with Distributed Rupture	Number of 0.5 km² Pixels without Distributed Rupture	Number of 0.5 km² Pixels with Distributed Rupture	Number of 0.5 km² Pixels without Distributed Rupture
1992 M_w 7.4 Landers, CA				
0.5	88	396	58	426
1.0	28	300	18	310
1.5	42	281	0	323
2.0	48	439	10	477
2.5	6	332	6	332
3.0	2	422	2	422
3.5	2	347	0	349
4.0	4	407	0	411
4.5	2	452	0	454
5.0	2	357	0	359
5.5	2	435	2	435
6.0	4	366	2	368
6.5	0	474	0	474
7.0	4	411	0	415
7.5	2	383	0	385
8.0	2	494	0	496
8.5	0	464	0	464
9.0	2	449	0	451
9.5	2	436	0	438
10.0	0	412	0	412
10.5	0	525	0	525
11.0	0	482	0	482
11.5	0	481	0	481
12.0	0	465	0	465
12.5	0	534	0	534
13.0	0	493	0	493
13.5	0	479	0	479
14.0	0	540	0	540
14.5	0	489	0	489
15.0	0	562	0	562
15.5	0	506	0	506
16.0	0	485	0	485
16.5	0	521	0	521
17.0	0	546	0	546
1887 M_w 7.4 Sonora, Mexico				
0.5	0	375	0	375
1.0	6	299	0	305
1.5	4	298	0	302
2.0	2	403	0	405
2.5	4	306	0	310
3.0	0	345	0	345
3.5	0	322	0	322
4.0	0	339	0	339
4.5	0	418	0	418

Table H-2
Summary of Data from S.K. Pezzopane and T.E. Dawson (USGS, written communication, 1996, Plate 21) for Frequency of Distributed Faulting

Distance from Principal Rupture (km)	Hanging Wall		Footwall	
	Number of 0.5 km² Pixels with Distributed Rupture	Number of 0.5 km² Pixels without Distributed Rupture	Number of 0.5 km² Pixels with Distributed Rupture	Number of 0.5 km² Pixels without Distributed Rupture
5.0	0	333	0	333
5.5	0	367	0	367
6.0	0	345	0	345
6.5	0	403	0	403
7.0	0	378	0	378
7.5	0	361	0	361
8.0	6	426	0	432
8.5	10	414	0	424
9.0	12	383	0	395
9.5	6	395	0	401
10.0	0	387	0	387
10.5	0	454	0	454
11.0	0	437	0	437
11.5	0	428	0	428
12.0	0	426	0	426
12.5	0	489	0	489
13.0	0	452	0	452
13.5	0	439	0	439
14.0	0	482	0	482
14.5	0	451	0	451
15.0	0	507	0	507
15.5	0	474	0	474
16.0	0	467	0	467
16.5	0	490	0	490
17.0	0	537	0	537
1959 M_w 7.4 Hebgen Lake, MT				
0.5	14	185	12	187
1.0	4	135	10	129
1.5	6	125	4	127
2.0	10	185	0	195
2.5	0	117	4	113
3.0	0	157	2	155
3.5	0	128	0	128
4.0	0	159	0	159
4.5	0	179	0	179
5.0	2	141	0	143
5.5	4	183	0	187
6.0	6	150	0	156
6.5	20	187	0	207
7.0	6	179	0	185
7.5	2	168	0	170
8.0	0	229	0	229
8.5	16	196	0	212
9.0	16	201	0	217
9.5	0	211	0	211

Table H-2
Summary of Data from S.K. Pezzopane and T.E. Dawson (USGS, written communication, 1996, Plate 21) for Frequency of Distributed Faulting

Distance from Principal Rupture (km)	Hanging Wall		Footwall	
	Number of 0.5 km² Pixels with Distributed Rupture	Number of 0.5 km² Pixels without Distributed Rupture	Number of 0.5 km² Pixels with Distributed Rupture	Number of 0.5 km² Pixels without Distributed Rupture
10.0	4	193	0	197
10.5	0	263	0	263
11.0	2	233	0	235
11.5	14	237	0	251
12.0	0	238	0	238
12.5	8	269	0	277
13.0	4	257	0	261
13.5	4	248	0	252
14.0	2	291	0	293
14.5	0	265	0	265
15.0	0	308	0	308
15.5	0	288	0	288
16.0	0	280	0	280
16.5	0	315	0	315
17.0	0	321	0	321
1932 M_w 7.2 Cedar Mtn., NV				
0.5	4	169	0	173
1.0	6	184	4	186
1.5	4	197	2	199
2.0	14	289	0	303
2.5	4	229	0	233
3.0	0	275	6	269
3.5	4	244	6	242
4.0	6	264	18	252
4.5	10	335	2	343
5.0	2	274	0	276
5.5	0	322	0	322
6.0	6	288	0	294
6.5	6	330	2	334
7.0	0	315	2	313
7.5	0	295	4	291
8.0	0	367	2	365
8.5	0	346	0	346
9.0	0	331	0	331
9.5	0	336	0	336
10.0	0	318	0	318
10.5	0	378	0	378
11.0	0	367	0	367
11.5	0	361	0	361
12.0	0	359	0	359
12.5	0	403	0	403
13.0	0	384	0	384
13.5	0	370	2	368
14.0	0	410	2	408
14.5	0	381	0	381

Table H-2
Summary of Data from S.K. Pezzopane and T.E. Dawson (USGS, written communication, 1996, Plate 21) for Frequency of Distributed Faulting

Distance from Principal Rupture (km)	Hanging Wall		Footwall	
	Number of 0.5 km² Pixels with Distributed Rupture	Number of 0.5 km² Pixels without Distributed Rupture	Number of 0.5 km² Pixels with Distributed Rupture	Number of 0.5 km² Pixels without Distributed Rupture
15.0	0	429	0	429
15.5	0	407	0	407
16.0	0	397	0	397
16.5	0	411	0	411
17.0	0	433	0	433
1954 M_w 7.1 Fairview Peak, NV				
0.5	4	291	10	285
1.0	8	219	6	221
1.5	6	228	2	232
2.0	12	315	2	325
2.5	6	250	6	250
3.0	8	288	2	294
3.5	8	273	4	277
4.0	8	294	2	300
4.5	22	363	4	381
5.0	28	282	4	306
5.5	4	350	0	354
6.0	2	332	0	334
6.5	4	393	0	397
7.0	2	377	0	379
7.5	2	364	0	366
8.0	0	441	0	441
8.5	0	411	0	411
9.0	0	391	0	391
9.5	2	386	0	388
10.0	0	374	0	374
10.5	0	436	0	436
11.0	0	425	0	425
11.5	0	413	0	413
12.0	0	407	0	407
12.5	0	466	0	466
13.0	0	431	0	431
13.5	0	420	0	420
14.0	0	463	0	463
14.5	0	429	0	429
15.0	0	482	0	482
15.5	0	451	0	451
16.0	0	442	0	442
16.5	0	473	0	473
17.0	0	506	0	506
1954 M_w 6.8 Dixie Valley, NV				
0.5	16	243	4	255
1.0	18	178	0	196
1.5	36	164	0	200
2.0	32	257	0	289

Table H-2
Summary of Data from S.K. Pezzopane and T.E. Dawson (USGS, written communication, 1996, Plate 21) for Frequency of Distributed Faulting

Distance from Principal Rupture (km)	Hanging Wall		Footwall	
	Number of 0.5 km² Pixels with Distributed Rupture	Number of 0.5 km² Pixels without Distributed Rupture	Number of 0.5 km² Pixels with Distributed Rupture	Number of 0.5 km² Pixels without Distributed Rupture
2.5	24	183	0	207
3.0	26	220	0	246
3.5	4	215	0	219
4.0	6	236	0	242
4.5	6	290	0	296
5.0	2	232	0	234
5.5	0	269	0	269
6.0	0	246	0	246
6.5	0	295	0	295
7.0	0	277	0	277
7.5	0	260	0	260
8.0	0	325	0	325
8.5	0	308	0	308
9.0	0	300	0	300
9.5	0	299	0	299
10.0	0	286	0	286
10.5	0	346	0	346
11.0	0	330	0	330
11.5	0	332	0	332
12.0	0	325	0	325
12.5	0	373	0	373
13.0	0	348	0	348
13.5	0	340	0	340
14.0	0	379	0	379
14.5	0	352	0	352
15.0	0	394	0	394
15.5	0	374	0	374
16.0	0	367	0	367
16.5	0	394	0	394
17.0	0	417	0	417
1983 M_w 6.8 Borah Peak, ID				
0.5	14	152	22	144
1.0	6	122	10	118
1.5	4	129	4	129
2.0	12	200	4	208
2.5	2	152	2	152
3.0	6	186	4	188
3.5	8	153	4	157
4.0	14	174	4	184
4.5	10	214	4	220
5.0	8	166	2	172
5.5	8	209	4	213
6.0	6	180	0	186
6.5	2	238	0	240
7.0	0	218	0	218

Table H-2
Summary of Data from S.K. Pezzopane and T.E. Dawson
(USGS, written communication, 1996, Plate 21)
for Frequency of Distributed Faulting

Distance from Principal Rupture (km)	Hanging Wall		Footwall	
	Number of 0.5 km² Pixels with Distributed Rupture	Number of 0.5 km² Pixels without Distributed Rupture	Number of 0.5 km² Pixels with Distributed Rupture	Number of 0.5 km² Pixels without Distributed Rupture
7.5	0	202	0	202
8.0	0	266	0	266
8.5	0	252	0	252
9.0	0	246	0	246
9.5	0	243	0	243
10.0	0	230	0	230
10.5	0	295	0	295
11.0	0	276	0	276
11.5	0	276	0	276
12.0	0	271	0	271
12.5	0	314	0	314
13.0	0	297	0	297
13.5	0	287	0	287
14.0	0	320	0	320
14.5	0	299	0	299
15.0	0	344	0	344
15.5	0	323	0	323
16.0	0	315	0	315
16.5	0	338	0	338
17.0	0	372	0	372
1954 M_w 6.8 Stillwater, NV				
0.5	4	146	2	148
1.0	4	126	6	124
1.5	8	128	0	136
2.0	10	190	0	200
2.5	10	140	0	150
3.0	6	172	0	178
3.5	0	162	0	162
4.0	0	179	0	179
4.5	0	213	0	213
5.0	0	178	0	178
5.5	0	203	0	203
6.0	0	190	0	190
6.5	0	223	0	223
7.0	0	215	0	215
7.5	6	200	0	206
8.0	6	245	0	251
8.5	0	245	0	245
9.0	0	236	0	236
9.5	0	243	0	243
10.0	0	234	0	234
10.5	4	271	0	275
11.0	2	270	0	272
11.5	2	266	0	268
12.0	0	269	0	269

Table H-2
Summary of Data from S.K. Pezzopane and T.E. Dawson (USGS, written communication, 1996, Plate 21) for Frequency of Distributed Faulting

Distance from Principal Rupture (km)	Hanging Wall		Footwall	
	Number of 0.5 km² Pixels with Distributed Rupture	Number of 0.5 km² Pixels without Distributed Rupture	Number of 0.5 km² Pixels with Distributed Rupture	Number of 0.5 km² Pixels without Distributed Rupture
12.5	0	305	0	305
13.0	0	291	0	291
13.5	0	285	0	285
14.0	0	313	0	313
14.5	0	297	0	297
15.0	0	330	0	330
15.5	0	318	0	318
16.0	0	313	0	313
16.5	0	331	0	331
17.0	0	359	0	359
1954 M_w 6.6 Rainbow Mtn., NV				
0.5	12	75	26	61
1.0	12	68	0	80
1.5	2	84	2	84
2.0	2	116	0	118
2.5	0	96	0	96
3.0	0	108	0	108
3.5	0	108	0	108
4.0	0	116	0	116
4.5	0	150	0	150
5.0	0	124	0	124
5.5	0	140	0	140
6.0	0	136	0	136
6.5	0	160	0	160
7.0	0	156	0	156
7.5	0	152	0	152
8.0	0	190	0	190
8.5	0	184	0	184
9.0	0	180	0	180
9.5	0	184	0	184
10.0	0	180	0	180
10.5	0	215	0	215
11.0	0	211	0	211
11.5	0	212	0	212
12.0	0	212	0	212
12.5	0	247	0	247
13.0	0	232	0	232
13.5	0	228	0	228
14.0	0	255	0	255
14.5	0	240	0	240
15.0	0	272	0	272
15.5	0	260	0	260
16.0	0	256	0	256
16.5	0	276	0	276
17.0	0	298	0	298

Table H-2
Summary of Data from S.K. Pezzopane and T.E. Dawson (USGS, written communication, 1996, Plate 21) for Frequency of Distributed Faulting

Distance from Principal Rupture (km)	Hanging Wall		Footwall	
	Number of 0.5 km² Pixels with Distributed Rupture	Number of 0.5 km² Pixels without Distributed Rupture	Number of 0.5 km² Pixels with Distributed Rupture	Number of 0.5 km² Pixels without Distributed Rupture
1986 M_w 6.2 Chalfant Valley, CA				
0.5	12	55	10	57
1.0	0	66	0	66
1.5	0	68	0	68
2.0	0	96	0	96
2.5	0	80	0	80
3.0	0	93	0	93
3.5	0	92	0	92
4.0	0	101	0	101
4.5	0	127	0	127
5.0	0	108	0	108
5.5	0	125	0	125
6.0	0	120	0	120
6.5	0	141	0	141
7.0	0	140	0	140
7.5	0	136	0	136
8.0	0	172	0	172
8.5	0	164	0	164
9.0	0	165	0	165
9.5	0	168	0	168
10.0	0	164	0	164
10.5	0	197	0	197
11.0	0	193	0	193
11.5	0	197	0	197
12.0	0	196	0	196
12.5	0	227	0	227
13.0	0	216	0	216
13.5	0	212	0	212
14.0	0	238	0	238
14.5	0	224	0	224
15.0	0	253	0	253
15.5	0	244	0	244
16.0	0	240	0	240
16.5	0	261	0	261
17.0	0	277	0	277
17.5	0	277	0	277
18.0	0	286	0	286
18.5	0	277	0	277
19.0	0	300	0	300
19.5	0	288	0	288
20.0	0	317	0	317
20.5	0	301	0	301
21.0	0	317	0	317
21.5	0	328	0	328
22.0	0	316	0	316

Table H-2
Summary of Data from S.K. Pezzopane and T.E. Dawson (USGS, written communication, 1996, Plate 21) for Frequency of Distributed Faulting

Distance from Principal Rupture (km)	Hanging Wall		Footwall	
	Number of 0.5 km² Pixels with Distributed Rupture	Number of 0.5 km² Pixels without Distributed Rupture	Number of 0.5 km² Pixels with Distributed Rupture	Number of 0.5 km² Pixels without Distributed Rupture
22.5	0	341	0	341
23.0	0	328	0	328
23.5	0	357	0	357
24.0	0	356	0	356
24.5	0	372	0	372
1986 M_w 6.2 Chalfant Valley, CA with hanging wall cracking				
0.5	12	55	10	57
1.0	0	66	0	66
1.5	0	68	0	68
2.0	0	96	0	96
2.5	0	80	0	80
3.0	0	93	0	93
3.5	0	92	0	92
4.0	0	101	0	101
4.5	0	127	0	127
5.0	0	108	0	108
5.5	0	125	0	125
6.0	0	120	0	120
6.5	0	141	0	141
7.0	0	140	0	140
7.5	0	136	0	136
8.0	0	172	0	172
8.5	0	164	0	164
9.0	0	165	0	165
9.5	2	166	0	168
10.0	0	164	0	164
10.5	0	197	0	197
11.0	8	185	0	193
11.5	4	193	0	197
12.0	10	186	0	196
12.5	2	225	0	227
13.0	0	216	0	216
13.5	8	204	0	212
14.0	10	228	0	238
14.5	10	214	0	224
15.0	20	233	0	253
15.5	10	234	0	244
16.0	8	232	0	240
16.5	2	259	0	261
17.0	10	267	0	277
17.5	2	275	0	277
18.0	0	286	0	286
18.5	2	275	0	277
19.0	6	294	0	300

Table H-2
Summary of Data from S.K. Pezzopane and T.E. Dawson (USGS, written communication, 1996, Plate 21) for Frequency of Distributed Faulting

Distance from Principal Rupture (km)	Hanging Wall		Footwall	
	Number of 0.5 km² Pixels with Distributed Rupture	Number of 0.5 km² Pixels without Distributed Rupture	Number of 0.5 km² Pixels with Distributed Rupture	Number of 0.5 km² Pixels without Distributed Rupture
19.5	2	286	0	288
20.0	2	315	0	317
20.5	0	301	0	301
21.0	2	315	0	317
21.5	0	328	0	328
22.0	2	314	0	316
22.5	0	341	0	341
23.0	0	328	0	328
23.5	0	357	0	357
24.0	0	356	0	356
24.5	0	372	0	372
1980 M_w 6.1 Mammoth Lake, CA				
0.5	8	108	2	114
1.0	20	74	8	86
1.5	22	70	2	90
2.0	8	129	6	131
2.5	2	92	0	94
3.0	0	121	0	121
3.5	0	105	0	105
4.0	0	122	0	122
4.5	0	153	0	153
5.0	0	120	0	120
5.5	0	149	0	149
6.0	0	133	0	133
6.5	0	168	0	168
7.0	0	158	0	158
7.5	0	148	0	148
8.0	0	194	0	194
8.5	0	186	0	186
9.0	0	183	0	183
9.5	0	185	0	185
10.0	0	175	0	175
10.5	0	223	0	223
11.0	0	213	0	213
11.5	0	215	0	215
12.0	0	212	0	212
12.5	0	244	0	244
13.0	0	234	0	234
13.5	0	228	0	228
14.0	0	257	0	257
14.5	0	238	0	238
15.0	0	277	0	277
15.5	0	261	0	261
16.0	0	254	0	254
16.5	0	279	0	279

Table H-2
Summary of Data from S.K. Pezzopane and T.E. Dawson (USGS, written communication, 1996, Plate 21) for Frequency of Distributed Faulting

Distance from Principal Rupture (km)	Hanging Wall		Footwall	
	Number of 0.5 km² Pixels with Distributed Rupture	Number of 0.5 km² Pixels without Distributed Rupture	Number of 0.5 km² Pixels with Distributed Rupture	Number of 0.5 km² Pixels without Distributed Rupture
17.0	0	299	0	299
1950 M_w 5.6 Fort Sage, CA				
0.5	2	46	0	48
1.0	0	46	0	46
1.5	0	50	0	50
2.0	0	72	0	72
2.5	0	62	0	62
3.0	0	74	0	74
3.5	0	74	0	74
4.0	0	82	0	82
4.5	0	106	0	106
5.0	0	90	0	90
5.5	0	106	0	106
6.0	0	102	0	102
6.5	0	122	0	122
7.0	0	122	0	122
7.5	0	118	0	118
8.0	0	150	0	150
8.5	0	146	0	146
9.0	0	146	0	146
9.5	0	150	0	150
10.0	0	146	0	146
10.5	0	178	0	178
11.0	0	174	0	174
11.5	0	178	0	178
12.0	0	178	0	178
12.5	0	206	0	206
13.0	0	198	0	198
13.5	0	194	0	194
14.0	0	218	0	218
14.5	0	206	0	206
15.0	0	234	0	234
15.5	0	226	0	226
16.0	0	222	0	222
16.5	0	242	0	242
17.0	0	260	0	260
1979 M_w 5.5 Homestead Valley, CA				
0.5	0	28	6	22
1.0	0	26	0	26
1.5	0	30	0	30
2.0	0	52	0	52
2.5	4	38	0	42
3.0	2	53	0	55
3.5	0	54	0	54
4.0	0	63	0	63

Table H-2
Summary of Data from S.K. Pezzopane and T.E. Dawson (USGS, written communication, 1996, Plate 21) for Frequency of Distributed Faulting

Distance from Principal Rupture (km)	Hanging Wall		Footwall	
	Number of 0.5 km² Pixels with Distributed Rupture	Number of 0.5 km² Pixels without Distributed Rupture	Number of 0.5 km² Pixels with Distributed Rupture	Number of 0.5 km² Pixels without Distributed Rupture
4.5	0	87	0	87
5.0	0	70	0	70
5.5	0	87	0	87
6.0	0	82	0	82
6.5	0	107	0	107
7.0	0	102	0	102
7.5	0	98	0	98
8.0	0	128	0	128
8.5	0	130	0	130
9.0	0	127	0	127
9.5	0	130	0	130
10.0	0	126	0	126
10.5	0	163	0	163
11.0	0	155	0	155
11.5	0	159	0	159
12.0	0	158	0	158
12.5	0	187	0	187
13.0	0	178	0	178
13.5	0	174	0	174
14.0	0	200	0	200
14.5	0	186	0	186
15.0	0	219	0	219
15.5	0	206	0	206
16.0	0	202	0	202
16.5	0	223	0	223
17.0	0	242	0	242

Table H-3
Summary of Data from S.K. Pezzopane and T.E. Dawson (USGS, written communication, 1996, Plate 21) for Frequency of Angle Between Strikes of Principal and Distributed Ruptures

θ	n = 2		n = 3		n = 4		n = 5		n = 6	
	No.	Freq.	No.	Freq.	No.	Freq.	No.	Freq.	No.	Freq.
1983 M_w 6.8 Borah Peak, ID										
0 to 5	20	0.049	5	0.051	3	0.047	1	0.023	0	0
5 to 10	11	0.027	5	0.051	3	0.047	2	0.045	2	0.077
10 to 15	6	0.015	4	0.041	3	0.047	3	0.068	2	0.077
15 to 20	69	0.169	12	0.122	7	0.109	4	0.091	1	0.038
20 to 25	6	0.015	6	0.061	4	0.062	3	0.068	3	0.115
25 to 30	70	0.172	10	0.102	6	0.094	3	0.068	2	0.077
30 to 35	9	0.022	7	0.071	5	0.078	3	0.068	1	0.038
35 to 40	24	0.059	8	0.082	6	0.094	6	0.136	4	0.154
40 to 45	13	0.032	8	0.082	3	0.047	2	0.045	2	0.077
45 to 50	7	0.017	3	0.031	2	0.031	2	0.045	2	0.077
50 to 55	9	0.022	6	0.061	6	0.094	3	0.068	2	0.077
55 to 60	8	0.020	8	0.082	5	0.078	3	0.068	1	0.038
60 to 65	98	0.240	5	0.051	4	0.062	4	0.091	2	0.077
65 to 70	0	0	0	0	0	0	0	0	0	0
70 to 75	32	0.078	0	0	0	0	0	0	0	0
75 to 80	8	0.020	6	0.061	3	0.047	3	0.068	1	0.038
80 to 85	7	0.017	3	0.031	3	0.047	2	0.045	1	0.038
85 to 90	11	0.027	2	0.020	1	0.016	0	0	0	0
1932 M_w 7.2 Cedar Mtn, NV										
0 to 5	1	0.029	0	0	0	0	0	0	0	0
5 to 10	2	0.059	0	0	0	0	0	0	0	0
10 to 15	2	0.059	2	0.200	0	0	0	0	0	0
15 to 20	2	0.059	1	0.100	1	0.333	1	0.333	0	0
20 to 25	5	0.147	2	0.200	0	0	0	0	0	0
25 to 30	3	0.088	1	0.100	0	0	0	0	0	0
30 to 35	3	0.088	0	0	0	0	0	0	0	0
35 to 40	3	0.088	1	0.100	1	0.333	1	0.333	1	1.0
40 to 45	1	0.029	0	0	0	0	0	0	0	0
45 to 50	55	0.147	1	0.100	0	0	0	0	0	0
50 to 55	3	0.088	1	0.100	0	0	0	0	0	0
55 to 60	0	0	0	0	0	0	0	0	0	0
60 to 65	1	0.029	1	0.100	1	0.333	1	0.333	0	0
65 to 70	0	0	0	0	0	0	0	0	0	0
70 to 75	0	0	0	0	0	0	0	0	0	0
75 to 80	1	0.029	0	0	0	0	0	0	0	0
80 to 85	0	0	0	0	0	0	0	0	0	0
85 to 90	2	0.059	0	0	0	0	0	0	0	0
1986 M_w 6.2 Chalfant Valley, CA										
0 to 5	23	0.291	5	0.312	4	0.667	1	0.500	1	1.0
5 to 10	20	0.253	2	0.125	0	0	0	0	0	0
10 to 15	17	0.215	5	0.312	1	0.167	1	0.500	0	0
15 to 20	10	0.127	0	0	0	0	0	0	0	0
20 to 25	4	0.051	2	0.125	0	0	0	0	0	0
25 to 30	2	0.025	1	0.062	0	0	0	0	0	0
30 to 35	1	0.013	0	0	0	0	0	0	0	0
35 to 40	2	0.025	1	0.062	1	0.167	0	0	0	0

Table H-3
Summary of Data from S.K. Pezzopane and T.E. Dawson (USGS, written communication, 1996, Plate 21) for Frequency of Angle Between Strikes of Principal and Distributed Ruptures

	n = 2		n = 3		n = 4		n = 5		n = 6	
θ	No.	Freq.	No.	Freq.	No.	Freq.	No.	Freq.	No.	Freq.
40 to 45	0	0	0	0	0	0	0	0	0	0
45 to 50	0	0	0	0	0	0	0	0	0	0
50 to 55	0	0	0	0	0	0	0	0	0	0
55 to 60	0	0	0	0	0	0	0	0	0	0
60 to 65	0	0	0	0	0	0	0	0	0	0
65 to 70	0	0	0	0	0	0	0	0	0	0
70 to 75	0	0	0	0	0	0	0	0	0	0
75 to 80	0	0	0	0	0	0	0	0	0	0
80 to 85	0	0	0	0	0	0	0	0	0	0
85 to 90	0	0	0	0	0	0	0	0	0	0
1954 M_w 6.8 Dixie Valley, NV										
0 to 5	46	0.162	34	0.183	26	0.173	16	0.163	12	0.154
5 to 10	42	0.148	34	0.183	32	0.213	24	0.245	20	0.256
10 to 15	54	0.190	28	0.151	20	0.133	12	0.122	10	0.128
15 to 20	36	0.127	34	0.183	28	0.187	18	0.184	16	0.205
20 to 25	24	0.085	8	0.043	8	0.053	4	0.041	4	0.051
25 to 30	16	0.056	8	0.043	2	0.013	0	0	0	0
30 to 35	18	0.063	10	0.054	8	0.053	6	0.061	4	0.051
35 to 40	8	0.028	8	0.043	6	0.040	6	0.061	6	0.077
40 to 45	10	0.035	6	0.032	6	0.040	2	0.020	2	0.026
45 to 50	6	0.021	2	0.011	2	0.013	2	0.020	2	0.026
50 to 55	2	0.007	2	0.011	2	0.013	0	0	0	0
55 to 60	10	0.035	4	0.022	4	0.027	4	0.041	2	0.026
60 to 65	4	0.014	2	0.011	2	0.013	0	0	0	0
65 to 70	2	0.007	2	0.011	2	0.013	2	0.020	0	0
70 to 75	0	0	0	0	0	0	0	0	0	0
75 to 80	6	0.021	4	0.022	2	0.013	2	0.020	0	0
80 to 85	0	0	0	0	0	0	0	0	0	0
85 to 90	0	0	0	0	0	0	0	0	0	0
1993 M_w 6.1 Eureka Valley,CA										
0 to 5	0	0	0	0	0	0	0	0	0	0
5 to 10	2	0.020	0	0	0	0	0	0	0	0
10 to 15	2	0.020	0	0	0	0	0	0	0	0
15 to 20	1	0.010	0	0	0	0	0	0	0	0
20 to 25	1	0.010	0	0	0	0	0	0	0	0
25 to 30	7	0.070	1	0.059	0	0	0	0	0	0
30 to 35	12	0.120	2	0.118	0	0	0	0	0	0
35 to 40	20	0.200	2	0.118	1	0.167	0	0	0	0
40 to 45	8	0.080	4	0.235	2	0.333	0	0	0	0
45 to 50	14	0.140	4	0.235	1	0.167	0	0	0	0
50 to 55	19	0.190	0	0	0	0	0	0	0	0
55 to 60	4	0.040	2	0.118	0	0	0	0	0	0
60 to 65	3	0.030	0	0	0	0	0	0	0	0
65 to 70	2	0.020	0	0	0	0	0	0	0	0
70 to 75	2	0.020	1	0.059	1	0.167	0	0	0	0
75 to 80	2	0.020	0	0	0	0	0	0	0	0
80 to 85	1	0.010	1	0.059	1	0.167	1	1.000	0	0

Table H-3
Summary of Data from S.K. Pezzopane and T.E. Dawson (USGS, written communication, 1996, Plate 21) for Frequency of Angle Between Strikes of Principal and Distributed Ruptures

θ	n = 2		n = 3		n = 4		n = 5		n = 6	
	No.	Freq.	No.	Freq.	No.	Freq.	No.	Freq.	No.	Freq.
85 to 90	0	0	0	0	0	0	0	0	0	0
1954 M_w 7.1 Fairview Peak, NV										
0 to 5	25	0.181	17	0.191	13	0.197	12	0.245	9	0.231
5 to 10	35	0.254	22	0.247	17	0.258	11	0.224	10	0.256
10 to 15	12	0.087	10	0.112	9	0.136	4	0.082	4	0.103
15 to 20	18	0.130	10	0.112	7	0.106	6	0.122	5	0.128
20 to 25	19	0.138	13	0.146	8	0.121	6	0.122	5	0.128
25 to 30	8	0.058	3	0.034	3	0.045	2	0.041	2	0.051
30 to 35	6	0.043	6	0.067	4	0.061	4	0.082	1	0.026
35 to 40	9	0.065	4	0.045	2	0.030	2	0.041	2	0.051
40 to 45	0	0	0	0	0	0	0	0	0	0
45 to 50	3	0.022	2	0.022	2	0.030	2	0.041	1	0.026
50 to 55	1	0.007	0	0	0	0	0	0	0	0
55 to 60	0	0	0	0	0	0	0	0	0	0
60 to 65	1	0.007	1	0.011	0	0	0	0	0	0
65 to 70	1	0.007	1	0.011	1	0.015	0	0	0	0
70 to 75	0	0	0	0	0	0	0	0	0	0
75 to 80	0	0	0	0	0	0	0	0	0	0
80 to 85	0	0	0	0	0	0	0	0	0	0
85 to 90	0	0	0	0	0	0	0	0	0	0
1950 M_w 5.6 Fort Sage, CA										
0 to 5	1	1.0	1	1.0	0	0	0	0	0	0
5 to 10	0	0	0	0	0	0	0	0	0	0
10 to 15	0	0	0	0	0	0	0	0	0	0
15 to 20	0	0	0	0	0	0	0	0	0	0
20 to 25	0	0	0	0	0	0	0	0	0	0
25 to 30	0	0	0	0	0	0	0	0	0	0
30 to 35	0	0	0	0	0	0	0	0	0	0
35 to 40	0	0	0	0	0	0	0	0	0	0
40 to 45	0	0	0	0	0	0	0	0	0	0
45 to 50	0	0	0	0	0	0	0	0	0	0
50 to 55	0	0	0	0	0	0	0	0	0	0
55 to 60	0	0	0	0	0	0	0	0	0	0
60 to 65	0	0	0	0	0	0	0	0	0	0
65 to 70	0	0	0	0	0	0	0	0	0	0
70 to 75	0	0	0	0	0	0	0	0	0	0
75 to 80	0	0	0	0	0	0	0	0	0	0
80 to 85	0	0	0	0	0	0	0	0	0	0
85 to 90	0	0	0	0	0	0	0	0	0	0
1975 M_w 5.2 Galway Valley										
0 to 5	1	0.143	0	0	0	0	0	0	0	0
5 to 10	0	0	0	0	0	0	0	0	0	0
10 to 15	0	0	0	0	0	0	0	0	0	0
15 to 20	1	0.143	0	0	0	0	0	0	0	0
20 to 25	3	0.429	1	1.0	1	1.0	0	0	0	0
25 to 30	0	0	0	0	0	0	0	0	0	0
30 to 35	0	0	0	0	0	0	0	0	0	0

Table H-3
Summary of Data from S.K. Pezzopane and T.E. Dawson
(USGS, written communication, 1996, Plate 21)
for Frequency of Angle Between Strikes of Principal and Distributed Ruptures

	n = 2		n = 3		n = 4		n = 5		n = 6	
θ	No.	Freq.	No.	Freq.	No.	Freq.	No.	Freq.	No.	Freq.
35 to 40	0	0	0	0	0	0	0	0	0	0
40 to 45	0	0	0	0	0	0	0	0	0	0
45 to 50	0	0	0	0	0	0	0	0	0	0
50 to 55	0	0	0	0	0	0	0	0	0	0
55 to 60	0	0	0	0	0	0	0	0	0	0
60 to 65	1	0.143	0	0	0	0	0	0	0	0
65 to 70	1	0.143	0	0	0	0	0	0	0	0
70 to 75	0	0	0	0	0	0	0	0	0	0
75 to 80	0	0	0	0	0	0	0	0	0	0
80 to 85	0	0	0	0	0	0	0	0	0	0
85 to 90	0	0	0	0	0	0	0	0	0	0
1959 M_w 7.4 Hebgen Lake, MT										
0 to 5	13	0.143	8	0.151	5	0.135	5	0.156	3	0.130
5 to 10	6	0.066	5	0.094	3	0.081	3	0.094	3	0.130
10 to 15	18	0.198	12	0.226	7	0.189	6	0.187	4	0.174
15 to 20	3	0.033	1	0.019	0	0	0	0	0	0
20 to 25	0	0	0	0	0	0	0	0	0	0
25 to 30	6	0.066	5	0.094	5	0.135	5	0.156	4	0.174
30 to 35	14	0.154	3	0.057	3	0.081	2	0.062	1	0.043
35 to 40	4	0.044	4	0.075	3	0.081	2	0.062	1	0.043
40 to 45	3	0.033	0	0	0	0	0	0	0	0
45 to 50	8	0.088	6	0.113	5	0.135	3	0.094	3	0.130
50 to 55	5	0.055	4	0.075	2	0.054	2	0.062	1	0.043
55 to 60	6	0.066	4	0.075	3	0.081	3	0.094	2	0.087
60 to 65	1	0.011	1	0.019	1	0.027	1	0.031	1	0.043
65 to 70	0	0	0	0	0	0	0	0	0	0
70 to 75	1	0.011	0	0	0	0	0	0	0	0
75 to 80	1	0.011	0	0	0	0	0	0	0	0
80 to 85	1	0.011	0	0	0	0	0	0	0	0
85 to 90	1	0.011	0	0	0	0	0	0	0	0
1979 M_w 5.5 Homestead Valley, CA										
0 to 5	6	0.120	0	0	0	0	0	0	0	0
5 to 10	6	0.120	0	0	0	0	0	0	0	0
10 to 15	5	0.100	2	0.667	0	0	0	0	0	0
15 to 20	25	0.100	0	0	0	0	0	0	0	0
20 to 25	11	0.220	1	0.333	1	1.000	1	1.000	0	0
25 to 30	4	0.080	0	0	0	0	0	0	0	0
30 to 35	2	0.040	0	0	0	0	0	0	0	0
35 to 40	1	0.020	0	0	0	0	0	0	0	0
40 to 45	2	0.040	0	0	0	0	0	0	0	0
45 to 50	1	0.020	0	0	0	0	0	0	0	0
50 to 55	3	0.060	0	0	0	0	0	0	0	0
55 to 60	2	0.040	0	0	0	0	0	0	0	0
60 to 65	1	0.020	0	0	0	0	0	0	0	0
65 to 70	1	0.020	0	0	0	0	0	0	0	0
70 to 75	0	0	0	0	0	0	0	0	0	0
75 to 80	0	0	0	0	0	0	0	0	0	0

Table H-3
Summary of Data from S.K. Pezzopane and T.E. Dawson (USGS, written communication, 1996, Plate 21) for Frequency of Angle Between Strikes of Principal and Distributed Ruptures

θ	n = 2		n = 3		n = 4		n = 5		n = 6	
	No.	Freq.	No.	Freq.	No.	Freq.	No.	Freq.	No.	Freq.
80 to 85	0	0	0	0	0	0	0	0	0	0
85 to 90	0	0	0	0	0	0	0	0	0	0
1992 M_w 7.4 Landers, CA										
0 to 5	11	0.143	8	0.136	6	0.200	6	0.353	4	0.333
5 to 10	7	0.091	5	0.085	1	0.033	0	0	0	0
10 to 15	6	0.078	4	0.068	4	0.133	2	0.118	1	0.083
15 to 20	8	0.104	4	0.068	3	0.100	3	0.176	2	0.167
20 to 25	7	0.091	6	0.102	4	0.133	2	0.118	1	0.083
25 to 30	6	0.078	6	0.102	3	0.100	1	0.059	1	0.083
30 to 35	2	0.026	1	0.017	0	0	0	0	0	0
35 to 40	4	0.052	2	0.034	1	0.033	0	0	0	0
40 to 45	2	0.026	2	0.034	1	0.033	0	0	0	0
45 to 50	55	0.065	3	0.051	2	0.067	1	0.059	1	0.083
50 to 55	4	0.052	4	0.068	2	0.067	1	0.059	1	0.083
55 to 60	1	0.013	1	0.017	0	0	0	0	0	0
60 to 65	3	0.039	3	0.051	0	0	0	0	0	0
65 to 70	2	0.026	2	0.034	0	0	0	0	0	0
70 to 75	3	0.039	2	0.034	1	0.033	1	0.059	1	0.083
75 to 80	3	0.039	3	0.051	0	0	0	0	0	0
80 to 85	1	0.013	1	0.017	1	0.033	0	0	0	0
85 to 90	2	0.026	2	0.034	1	0.033	0	0	0	0
1980 M_w 6.1 Mammoth Lake, CA										
0 to 5	8	0.061	3	0.120	1	0.143	0	0	0	0
5 to 10	11	0.083	3	0.120	1	0.143	0	0	0	0
10 to 15	17	0.129	1	0.040	1	0.143	1	0.250	0	0
15 to 20	4	0.030	3	0.120	1	0.143	1	0.250	0	0
20 to 25	19	0.144	7	0.280	2	0.286	2	0.500	1	1.000
25 to 30	11	0.083	1	0.040	0	0	0	0	0	0
30 to 35	8	0.061	1	0.040	0	0	0	0	0	0
35 to 40	31	0.235	4	0.160	1	0.143	0	0	0	0
40 to 45	1	0.008	1	0.040	0	0	0	0	0	0
45 to 50	0	0	0	0	0	0	0	0	0	0
50 to 55	10	00.076	0	0	0	0	0	0	0	0
55 to 60	3	0.023	1	0.040	0	0	0	0	0	0
60 to 65	2	0.015	0	0	0	0	0	0	0	0
65 to 70	75	0.038	0	0	0	0	0	0	0	0
70 to 75	0	0	0	0	0	0	0	0	0	0
75 to 80	2	0.015	0	0	0	0	0	0	0	0
80 to 85	0	0	0	0	0	0	0	0	0	0
85 to 90	0	0	0	0	0	0	0	0	0	0
1872 M_w 7.6 Owens Valley, CA										
0 to 5	29	0.266	8	0.229	6	0.250	4	0.250	4	0.286
5 to 10	20	0.183	5	0.143	4	0.167	3	0.187	2	0.143
10 to 15	4	0.037	4	0.114	1	0.042	1	0.062	1	0.071
15 to 20	27	0.248	4	0.114	2	0.083	1	0.062	1	0.071
20 to 25	5	0.046	5	0.143	4	0.167	2	0.125	2	0.143
25 to 30	8	0.073	5	0.143	3	0.125	2	0.125	1	0.071

Table H-3
Summary of Data from S.K. Pezzopane and T.E. Dawson (USGS, written communication, 1996, Plate 21) for Frequency of Angle Between Strikes of Principal and Distributed Ruptures

	n = 2		n = 3		n = 4		n = 5		n = 6	
θ	No.	Freq.	No.	Freq.	No.	Freq.	No.	Freq.	No.	Freq.
30 to 35	8	0.073	2	0.057	2	0.083	1	0.062	1	0.071
35 to 40	45	0.046	2	0.057	2	0.083	2	0.125	2	0.143
40 to 45	1	0.009	0	0	0	0	0	0	0	0
45 to 50	1	0.009	0	0	0	0	0	0	0	0
50 to 55	1	0.009	0	0	0	0	0	0	0	0
55 to 60	0	0	0	0	0	0	0	0	0	0
60 to 65	0	0	0	0	0	0	0	0	0	0
65 to 70	0	0	0	0	0	0	0	0	0	0
70 to 75	0	0	0	0	0	0	0	0	0	0
75 to 80	0	0	0	0	0	0	0	0	0	0
80 to 85	0	0	0	0	0	0	0	0	0	0
85 to 90	0	0	0	0	0	0	0	0	0	0
1915 M_w 7.3 Pleasant Valley, CA										
0 to 5	4	0.200	1	0.111	1	0.167	0	0	0	0
5 to 10	1	0.050	1	0.111	0	0	0	0	0	0
10 to 15	1	0.050	1	0.111	1	0.167	0	0	0	0
15 to 20	1	0.050	1	0.111	1	0.167	1	0.500	1	0.500
20 to 25	1	0.050	1	0.111	0	0	0	0	0	0
25 to 30	1	0.050	1	0.111	0	0	0	0	0	0
30 to 35	6	0.300	2	0.222	2	0.333	1	0.500	1	0.500
35 to 40	2	0.100	0	0	0	0	0	0	0	0
40 to 45	0	0	0	0	0	0	0	0	0	0
45 to 50	2	0.100	0	0	0	0	0	0	0	0
50 to 55	1	0.050	1	0.111	1	0.167	0	0	0	0
55 to 60	0	0	0	0	0	0	0	0	0	0
60 to 65	0	0	0	0	0	0	0	0	0	0
65 to 70	0	0	0	0	0	0	0	0	0	0
70 to 75	0	0	0	0	0	0	0	0	0	0
75 to 80	0	0	0	0	0	0	0	0	0	0
80 to 85	0	0	0	0	0	0	0	0	0	0
85 to 90	0	0	0	0	0	0	0	0	0	0
1954 M_w 6.6 Rainbow Mtn., NV										
0 to 5	5	0.098	2	0.100	1	0.111	1	0.143	1	0.500
5 to 10	4	0.078	2	0.100	1	0.111	0	0	0	0
10 to 15	13	0.255	1	0.050	1	0.111	0	0	0	0
15 to 20	4	0.078	1	0.050	0	0	0	0	0	0
20 to 25	1	0.020	0	0	0	0	0	0	0	0
25 to 30	2	0.039	0	0	0	0	0	0	0	0
30 to 35	7	0.137	2	0.100	1	0.111	1	0.143	0	0
35 to 40	2	0.039	1	0.050	1	0.111	1	0.143	0	0
40 to 45	1	0.020	1	0.050	0	0	0	0	0	0
45 to 50	2	0.039	1	0.050	1	0.111	1	0.143	1	0.500
50 to 55	0	0	0	0	0	0	0	0	0	0
55 to 60	3	0.059	2	0.100	1	0.111	1	0.143	0	0
60 to 65	5	0.098	5	0.250	1	0.111	1	0.143	0	0
65 to 70	1	0.020	1	0.050	0	0	0	0	0	0
70 to 75	1	0.020	1	0.050	1	0.111	1	0.143	0	0

Table H-3
Summary of Data from S.K. Pezzopane and T.E. Dawson (USGS, written communication, 1996, Plate 21) for Frequency of Angle Between Strikes of Principal and Distributed Ruptures

	n = 2		n = 3		n = 4		n = 5		n = 6	
θ	No.	Freq.	No.	Freq.	No.	Freq.	No.	Freq.	No.	Freq.
75 to 80	0	0	0	0	0	0	0	0	0	0
80 to 85	0	0	0	0	0	0	0	0	0	0
85 to 90	0	0	0	0	0	0	0	0	0	0
1887 M_w 7.4 Sonora, Mexico										
0 to 5	25	0.145	18	0.161	16	0.188	8	0.154	3	0.091
5 to 10	24	0.140	16	0.143	13	0.153	12	0.231	7	0.212
10 to 15	18	0.105	14	0.125	12	0.141	6	0.115	4	0.121
15 to 20	19	0.110	15	0.134	13	0.153	8	0.154	3	0.091
20 to 25	11	0.064	9	0.080	7	0.082	5	0.096	4	0.121
25 to 30	14	0.081	7	0.062	5	0.059	5	0.096	5	0.152
30 to 35	13	0.076	7	0.062	5	0.059	2	0.038	2	0.061
35 to 40	12	0.070	8	0.071	4	0.047	1	0.019	1	0.030
40 to 45	14	0.081	8	0.071	4	0.047	2	0.038	2	0.061
45 to 50	9	0.052	5	0.045	3	0.035	2	0.038	1	0.030
50 to 55	6	0.035	2	0.018	2	0.024	1	0.019	1	0.030
55 to 60	2	0.012	2	0.018	0	0	0	0	0	0
60 to 65	2	0.012	0	0	0	0	0	0	0	0
65 to 70	1	0.006	0	0	0	0	0	0	0	0
70 to 75	1	0.006	0	0	0	0	0	0	0	0
75 to 80	0	0	0	0	0	0	0	0	0	0
80 to 85	1	0.006	1	0.009	1	0.012	0	0	0	0
85 to 90	0	0	0	0	0	0	0	0	0	0
1954 M_w 6.8 Stillwater, NV										
0 to 5	7	0.159	3	0.097	3	0.187	2	0.286	1	0.200
5 to 10	7	0.159	4	0.129	0	0	0	0	0	0
10 to 15	7	0.159	4	0.129	3	0.187	1	0.143	1	0.200
15 to 20	25	0.114	5	0.161	0	0	0	0	0	0
20 to 25	5	0.114	5	0.161	3	0.187	1	0.143	1	0.200
25 to 30	3	0.068	3	0.097	3	0.187	1	0.143	0	0
30 to 35	1	0.023	1	0.032	1	0.062	0	0	0	0
35 to 40	4	0.091	2	0.065	1	0.062	1	0.143	1	0.200
40 to 45	2	0.045	2	0.065	1	0.062	0	0	0	0
45 to 50	2	0.045	1	0.032	0	0	0	0	0	0
50 to 55	1	0.023	1	0.032	1	0.062	1	0.143	1	0.200
55 to 60	0	0	0	0	0	0	0	0	0	0
60 to 65	0	0	0	0	0	0	0	0	0	0
65 to 70	0	0	0	0	0	0	0	0	0	0
70 to 75	0	0	0	0	0	0	0	0	0	0
75 to 80	0	0	0	0	0	0	0	0	0	0
80 to 85	0	0	0	0	0	0	0	0	0	0
85 to 90	0	0	0	0	0	0	0	0	0	0
Combined Statistics										
0 to 5	225	0.125	113	0.148	85	0.166	56	0.167	38	0.160
5 to 10	198	0.110	104	0.136	75	0.147	55	0.164	44	0.186
10 to 15	182	0.101	92	0.120	63	0.123	37	0.110	27	0.114
15 to 20	213	0.119	91	0.119	63	0.123	43	0.128	29	0.122
20 to 25	122	0.068	66	0.086	42	0.082	26	0.078	21	0.089

Table H-3
Summary of Data from S.K. Pezzopane and T.E. Dawson
(USGS, written communication, 1996, Plate 21)
for Frequency of Angle Between Strikes of Principal and Distributed Ruptures

	n = 2		n = 3		n = 4		n = 5		n = 6	
θ	No.	Freq.	No.	Freq.	No.	Freq.	No.	Freq.	No.	Freq.
25 to 30	161	0.090	52	0.068	30	0.059	19	0.057	15	0.063
30 to 35	110	0.061	44	0.058	31	0.061	20	0.060	11	0.046
35 to 40	131	0.073	47	0.061	30	0.059	22	0.066	18	0.076
40 to 45	58	0.032	32	0.042	17	0.033	6	0.018	6	0.025
45 to 50	65	0.036	28	0.037	18	0.035	13	0.039	11	0.046
50 to 55	65	0.036	21	0.027	16	0.031	8	0.024	6	0.025
55 to 60	39	0.022	24	0.031	13	0.025	11	0.033	5	0.021
60 to 65	122	0.068	18	0.024	9	0.018	7	0.021	3	0.013
65 to 70	16	0.009	6	0.008	3	0.006	2	0.006	0	0
70 to 75	40	0.022	4	0.005	3	0.006	2	0.006	1	0.004
75 to 80	23	0.013	13	0.017	5	0.010	5	0.015	1	0.004
80 to 85	11	0.006	6	0.008	6	0.012	3	0.009	1	0.004
85 to 90	16	0.009	4	0.005	2	0.004	0	0	0	0

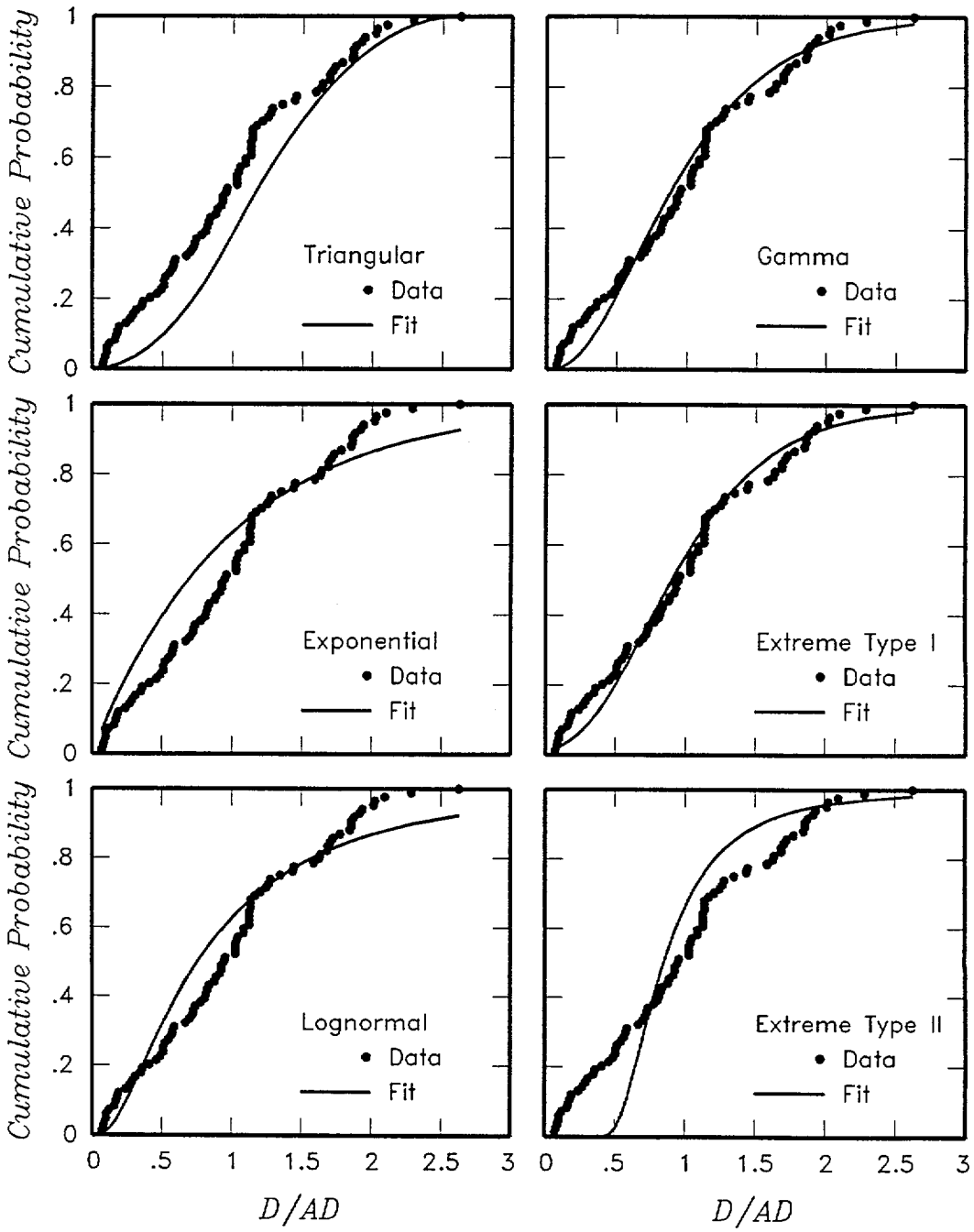

Figure H-1 Comparison of empirical CDF for the ratio D/D_{avg} developed by the DFS team with the CDFs for various statistical distributions fit to the data

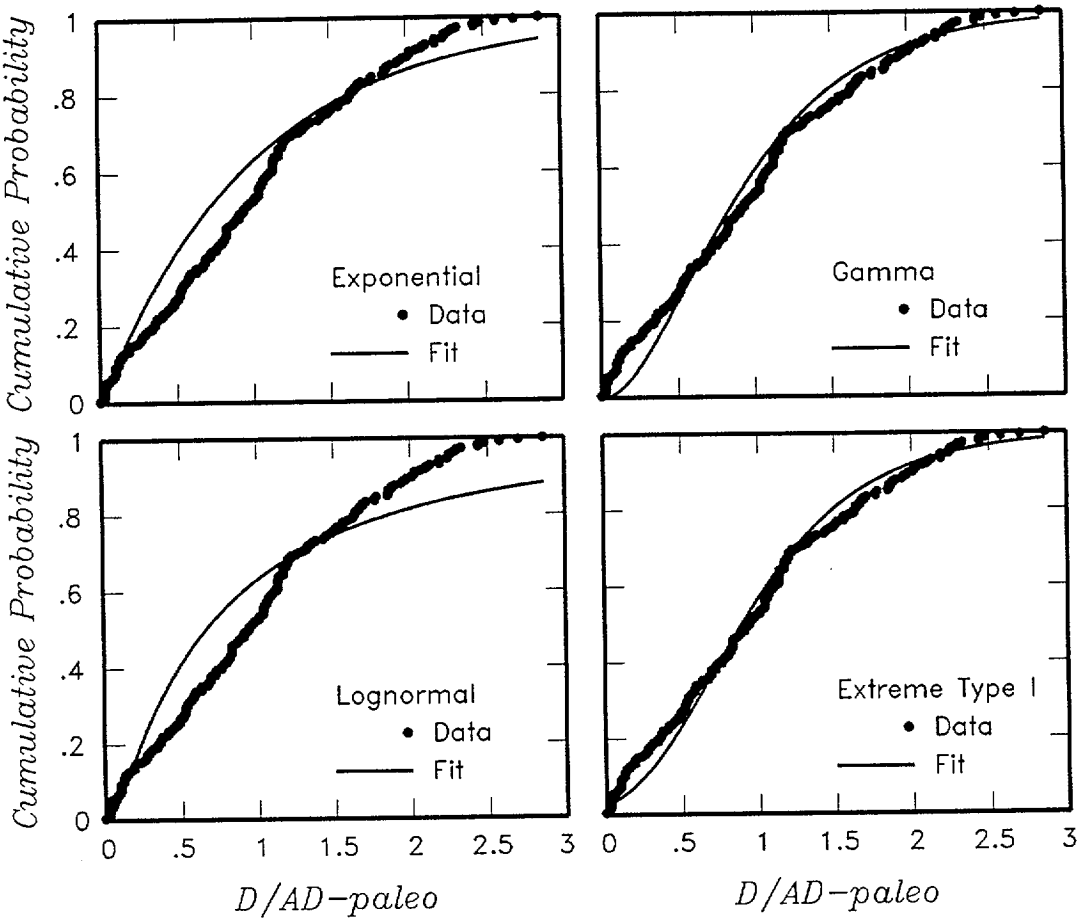

Figure H-2 Comparison of empirical CDF for the ratio $D/D_{avg\text{-}paleo}$ developed by the SBK team with the CDFs for various statistical distributions fit to the data

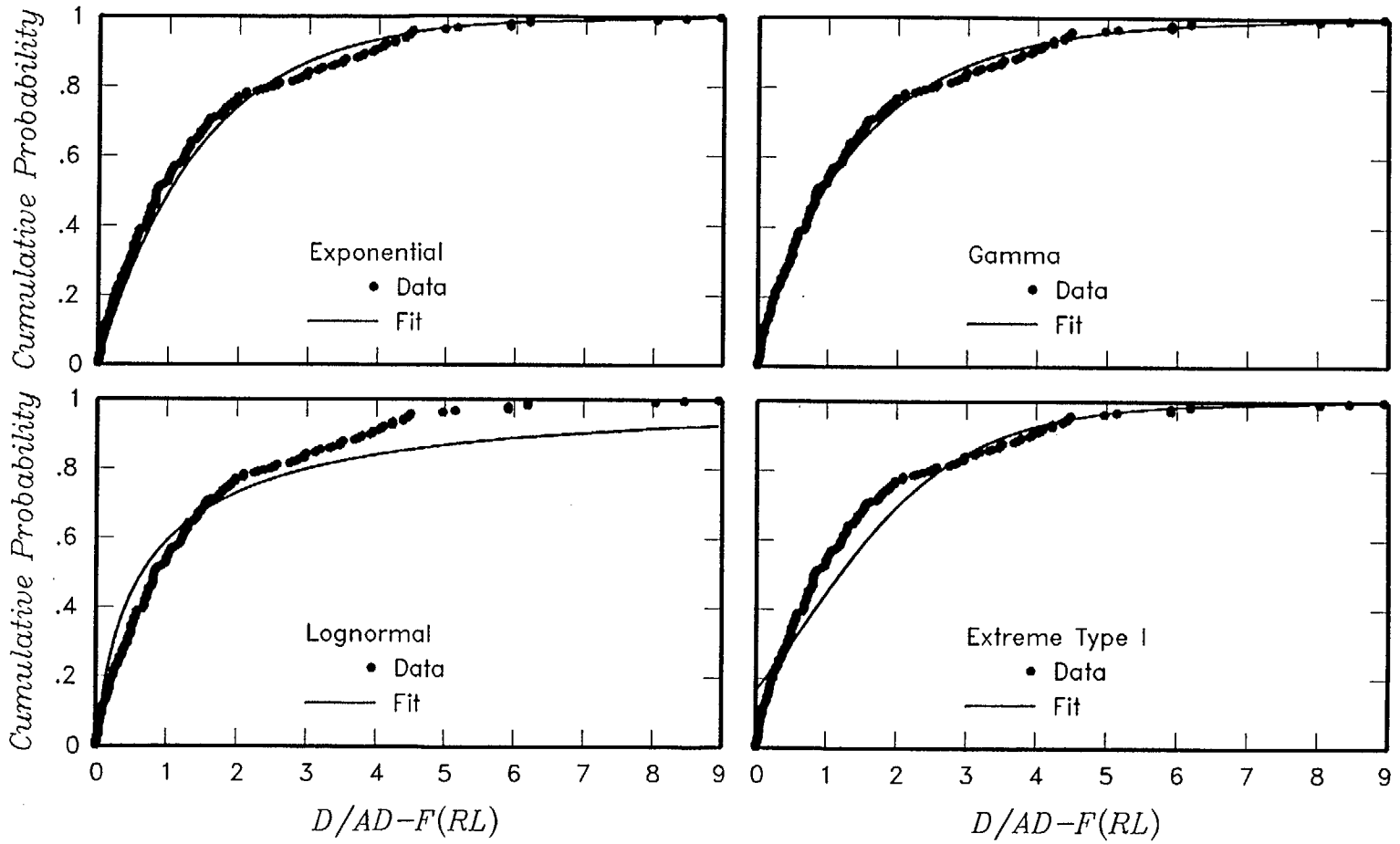

Figure H-3 Comparison of empirical CDF for the ratio $D/D_{avg\text{-}F(RL)}$ developed by the SBK team with the CDFs for various statistical distributions fit to the data

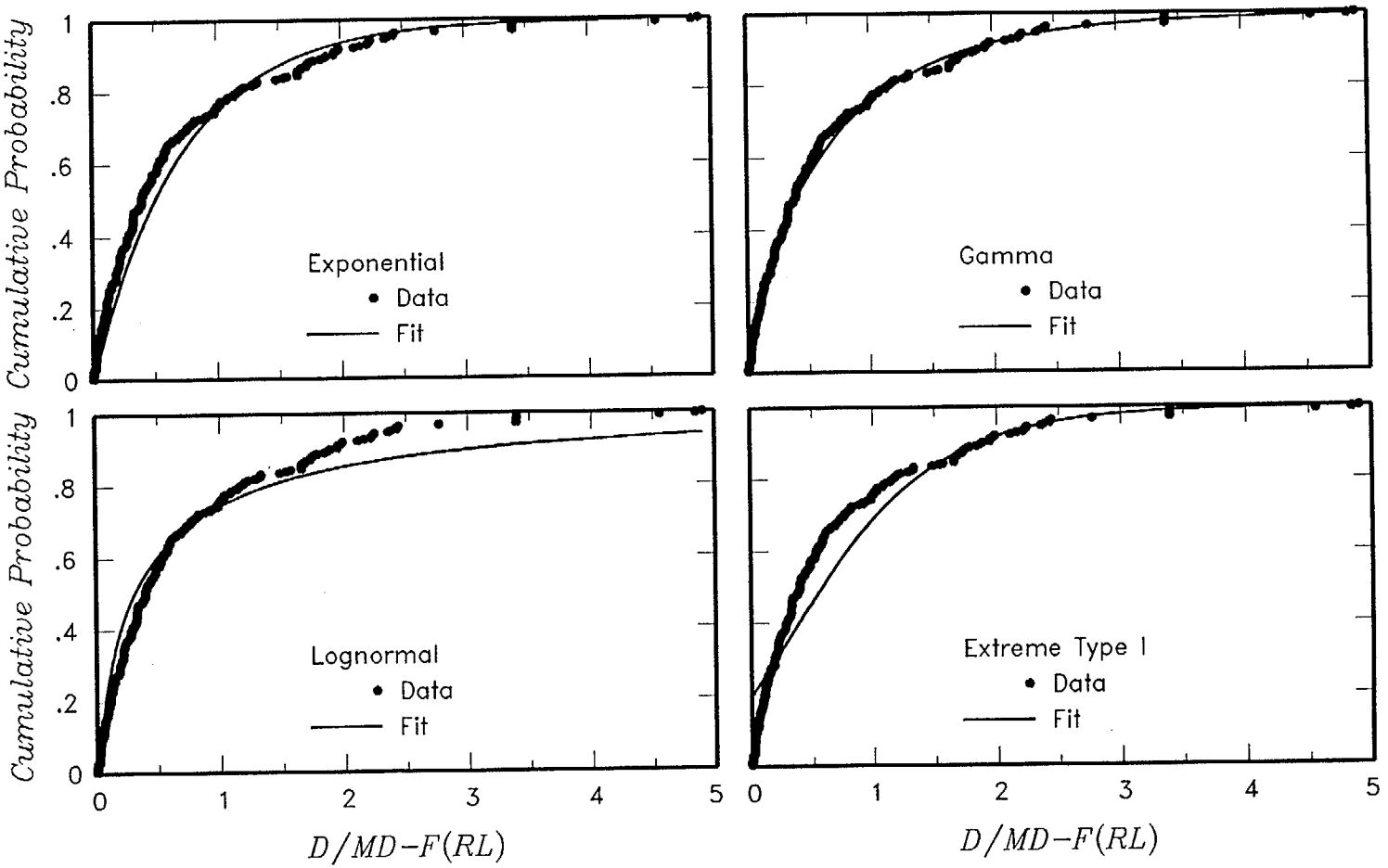

Figure H-4 Comparison of empirical CDF for the ratio $D/D_{max\text{-}F(RL)}$ developed by the SBK team with the CDFs for various statistical distributions fit to the data

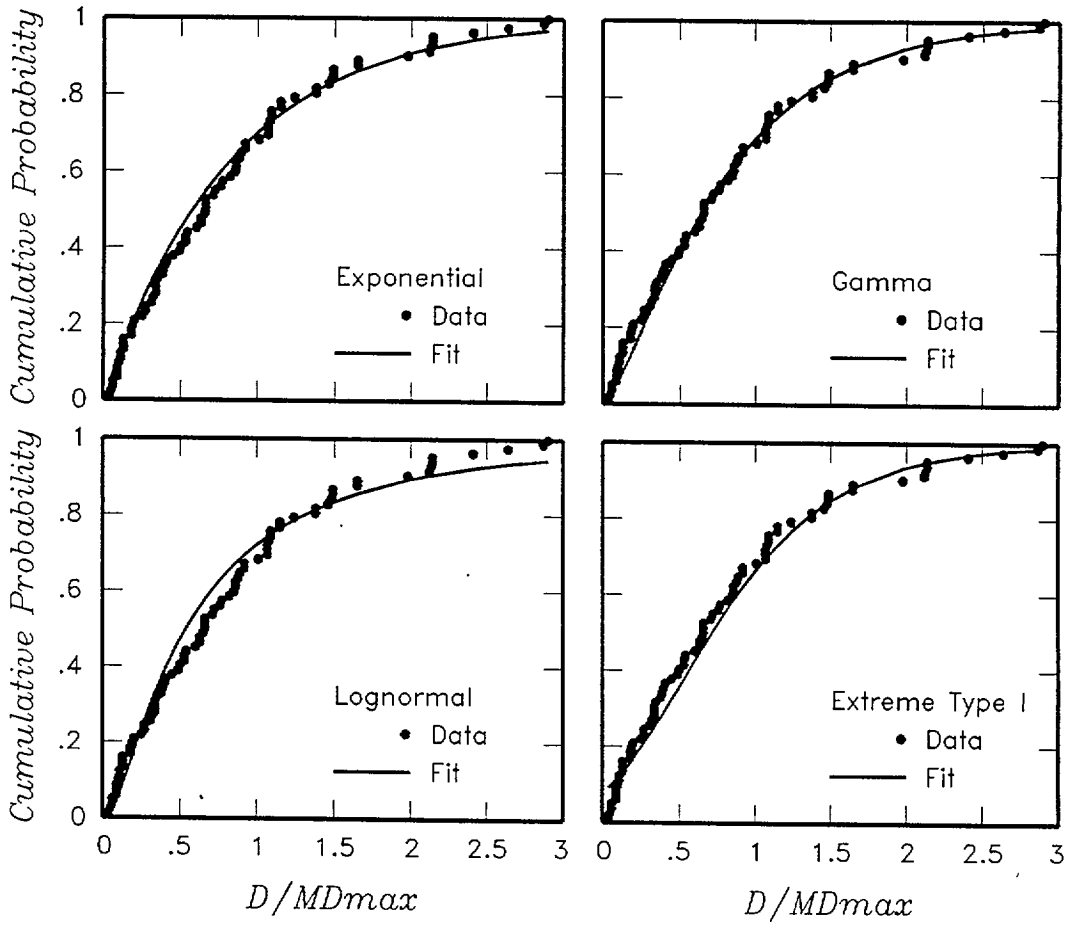

Figure H-5 Comparison of empirical CDF for the ratio D/D^{max} developed by the AAR team with the CDFs for various statistical distributions fit to the data

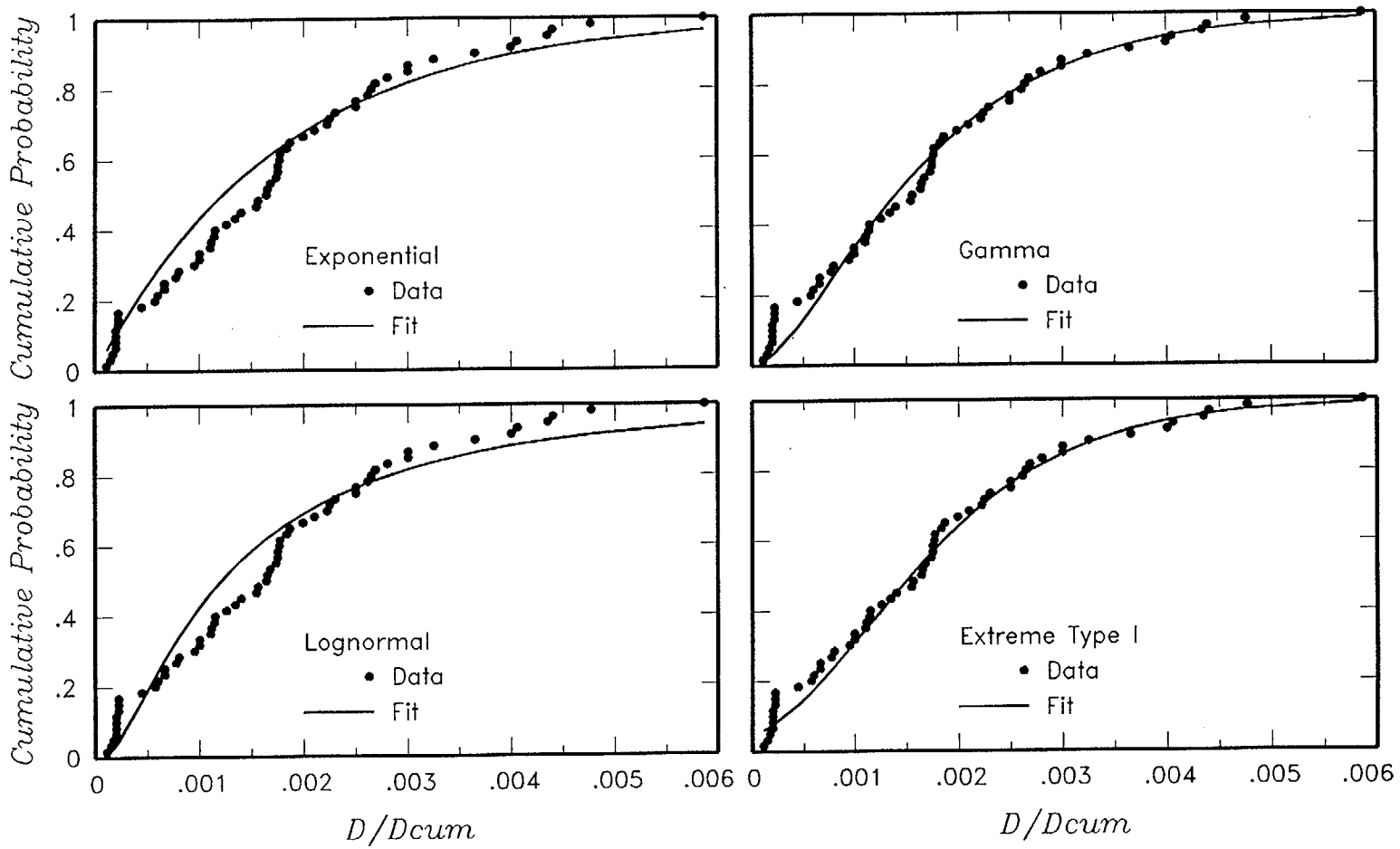

Figure H-6 Comparison of empirical CDF for the ratio D/Dcum developed by the SBK team with the CDFs for various statistical distributions fit to the data

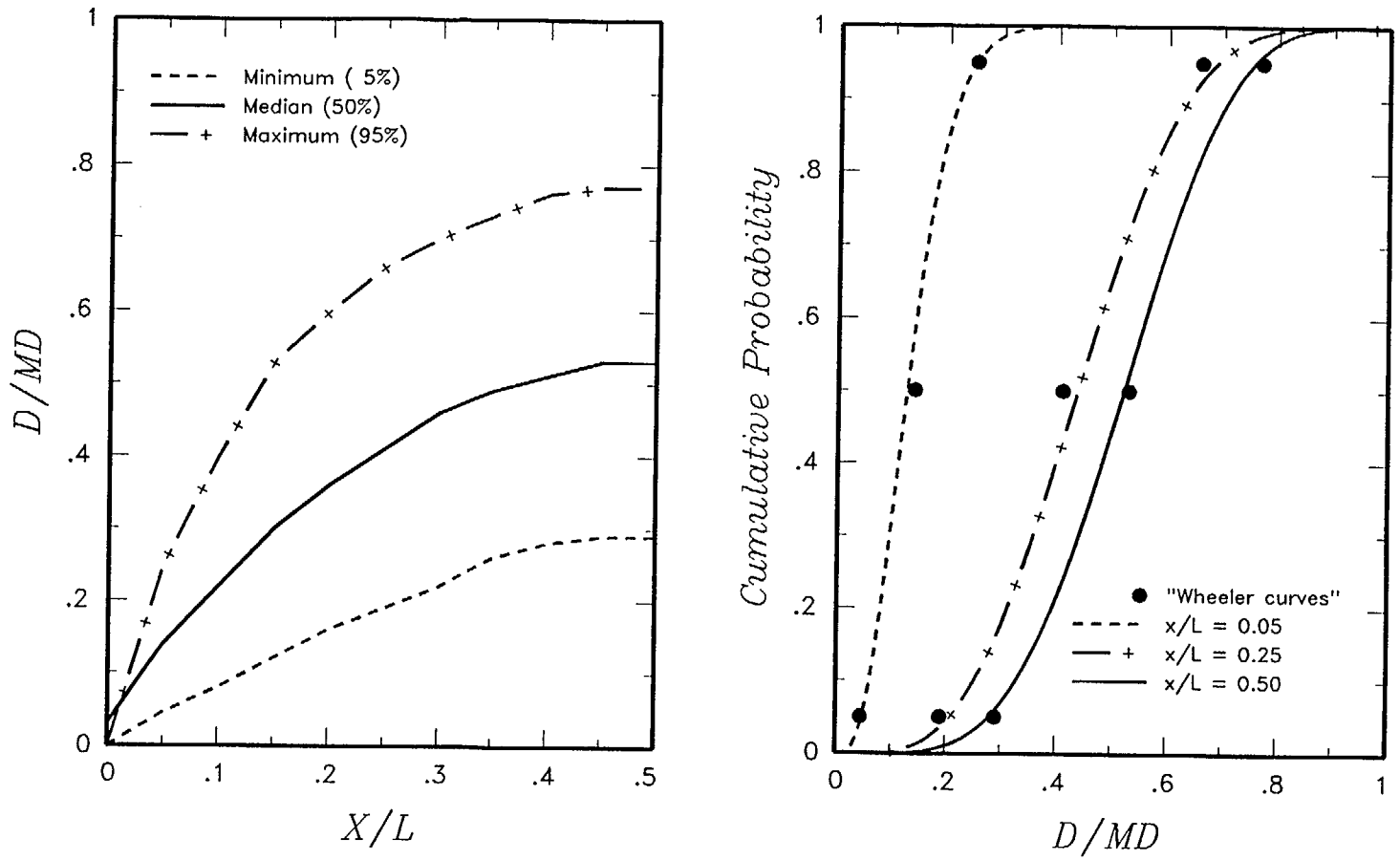

Figure H-7 Probability distributions for D/Dmax as a function of normalized location, x/L, along a principal rupture. Left, smooth curves for minimum, median, and maximum values of D/Dmax developed by the ASM team from analysis of historical ruptures presented in Wheeler (1989). Right, CDFs for beta distributions computed using the beta parameters from the smooth curves shown on Figure H-8.

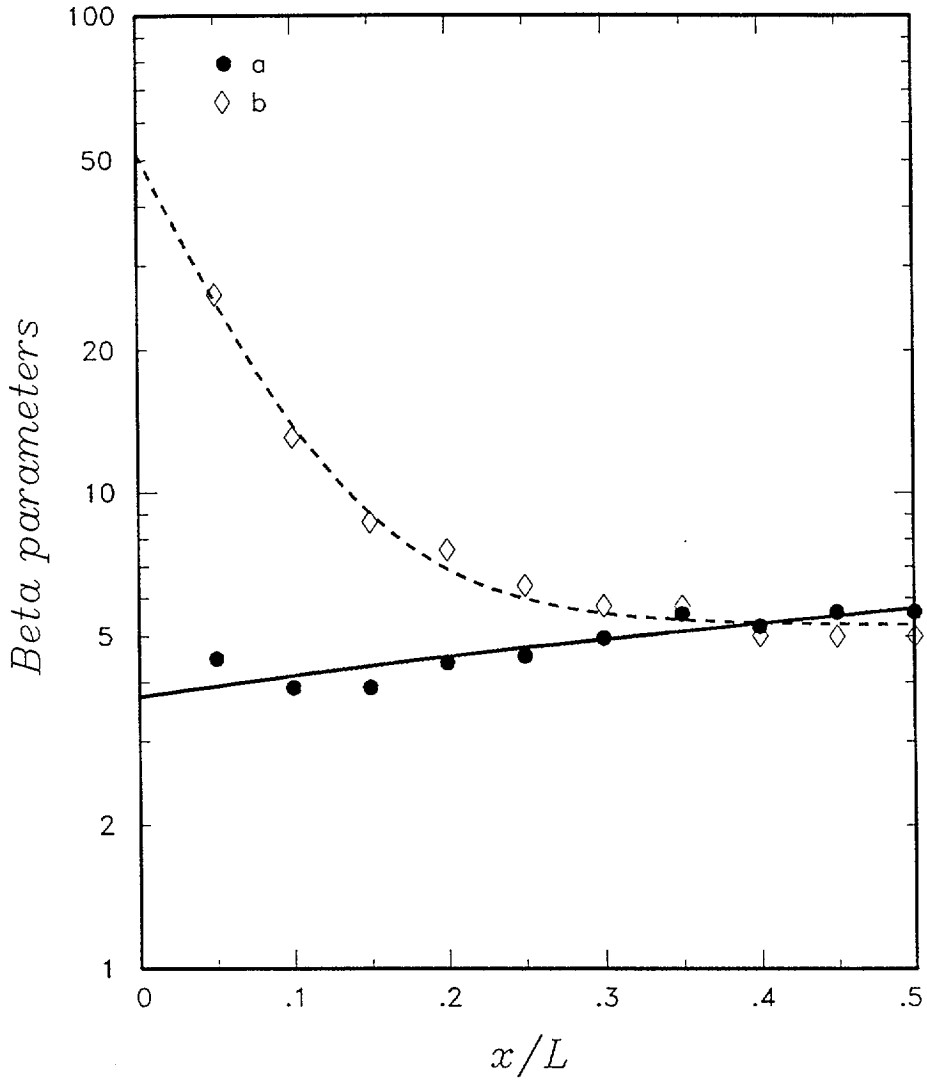

Figure H-8 Beta distribution parameters a and b developed at specific values of x/L from the "Wheeler" curves shown on the left of Figure H-7 and the smooth curves fit to these parameters

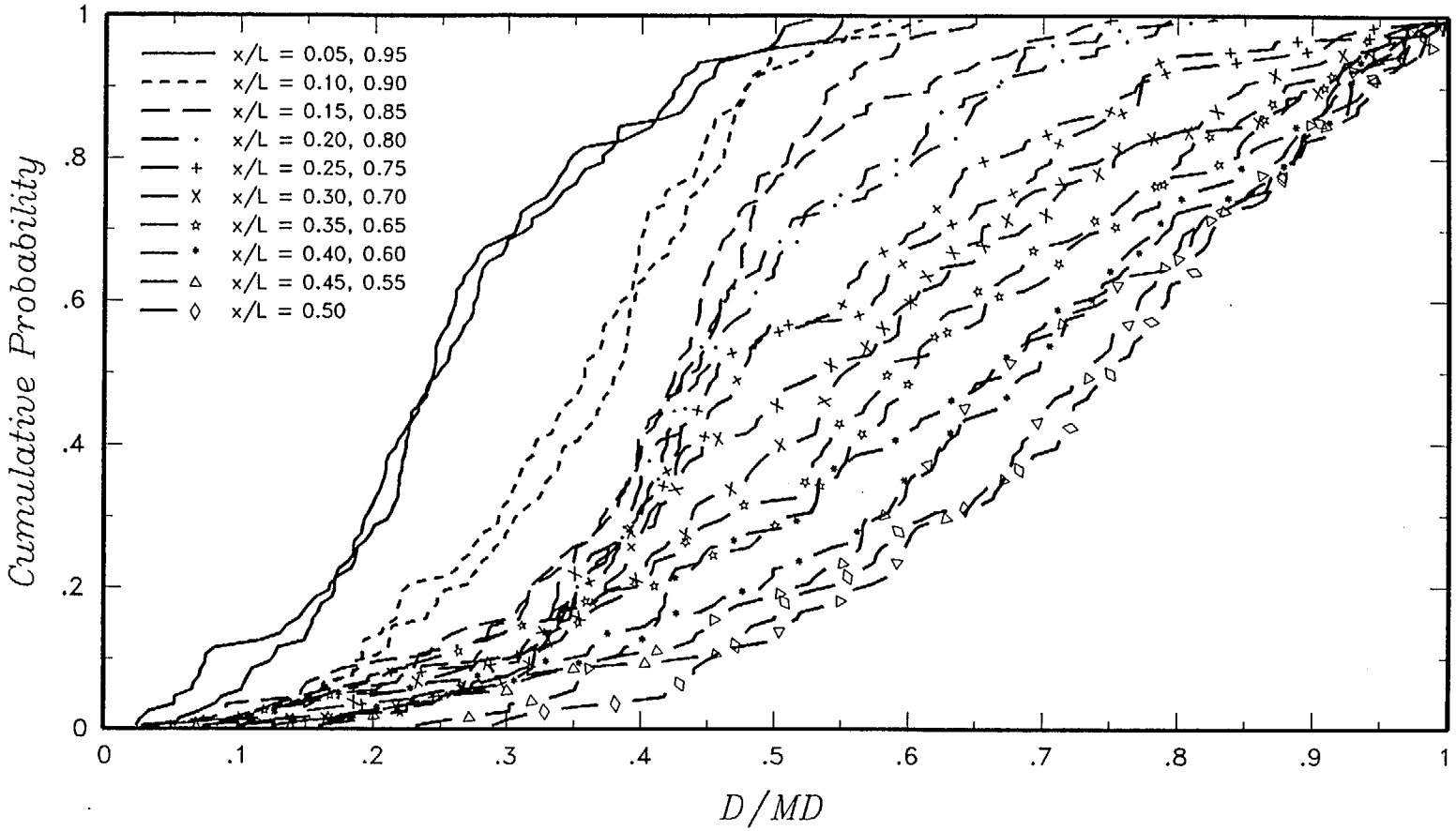

Figure H-9 Probability distributions for D/D_{max} as a function of normalized location, x/L, along a principal rupture developed by the SBK team using numerical simulations of slip with fractal fault roughness

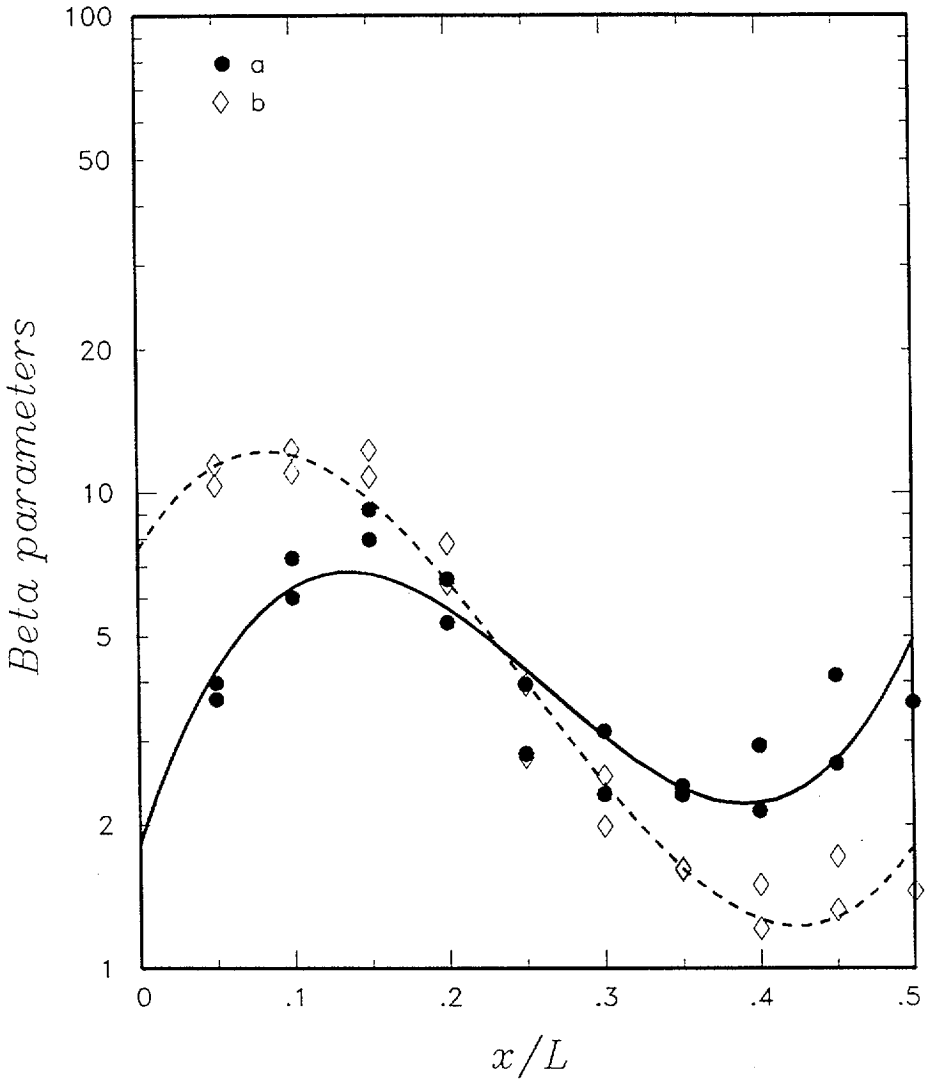

Figure H-10 Beta distribution parameters a and b developed at specific values of x/L from the simulation results shown on Figure H-9 and the smooth curves fit to these parameters

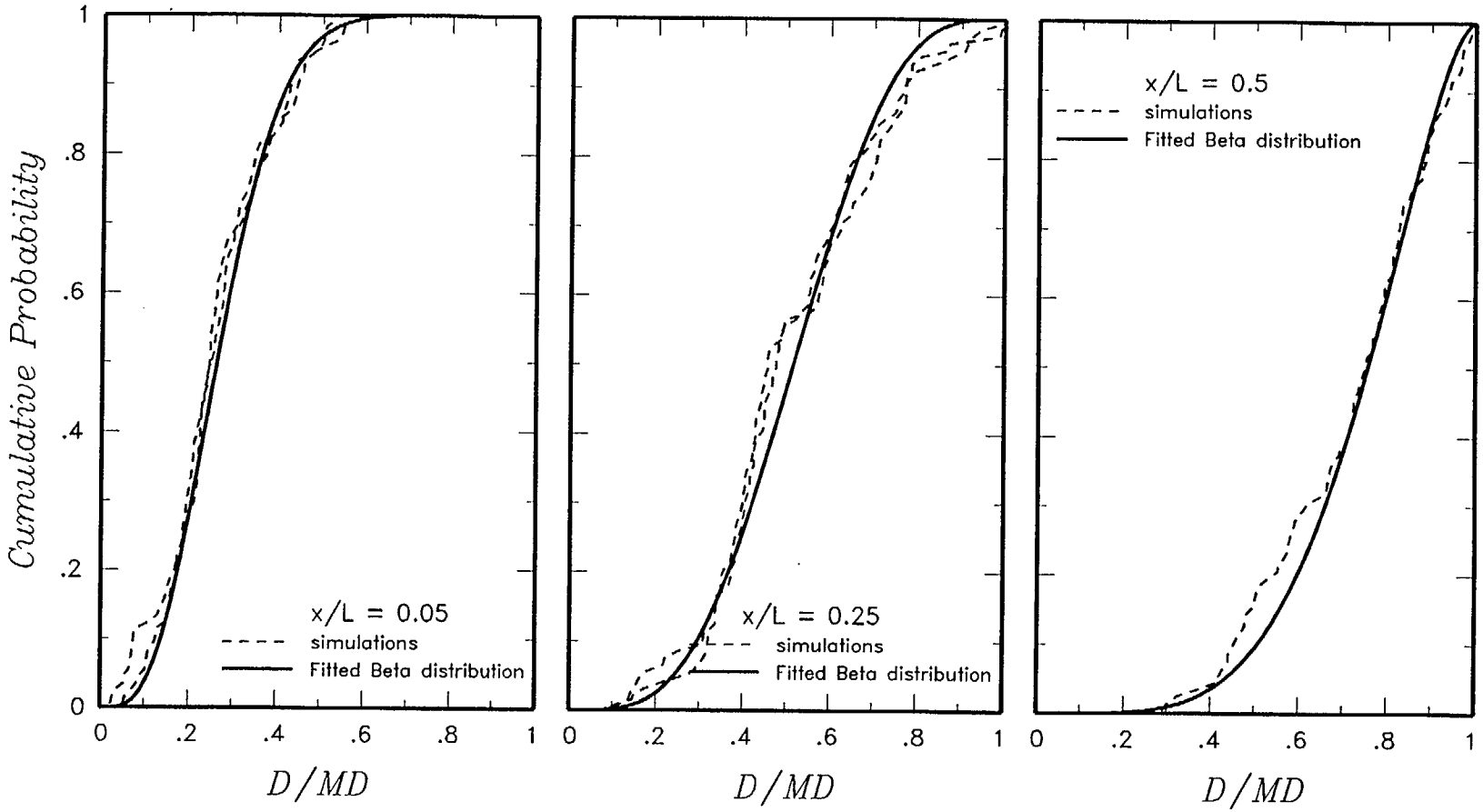

Figure H-11 CDFs for simulations of D/D_{max} as a function of normalized location, x/L, from Figure H-9 compared to CDFs for beta distributions computed using the beta parameters from the smooth curves shown on Figure H-10

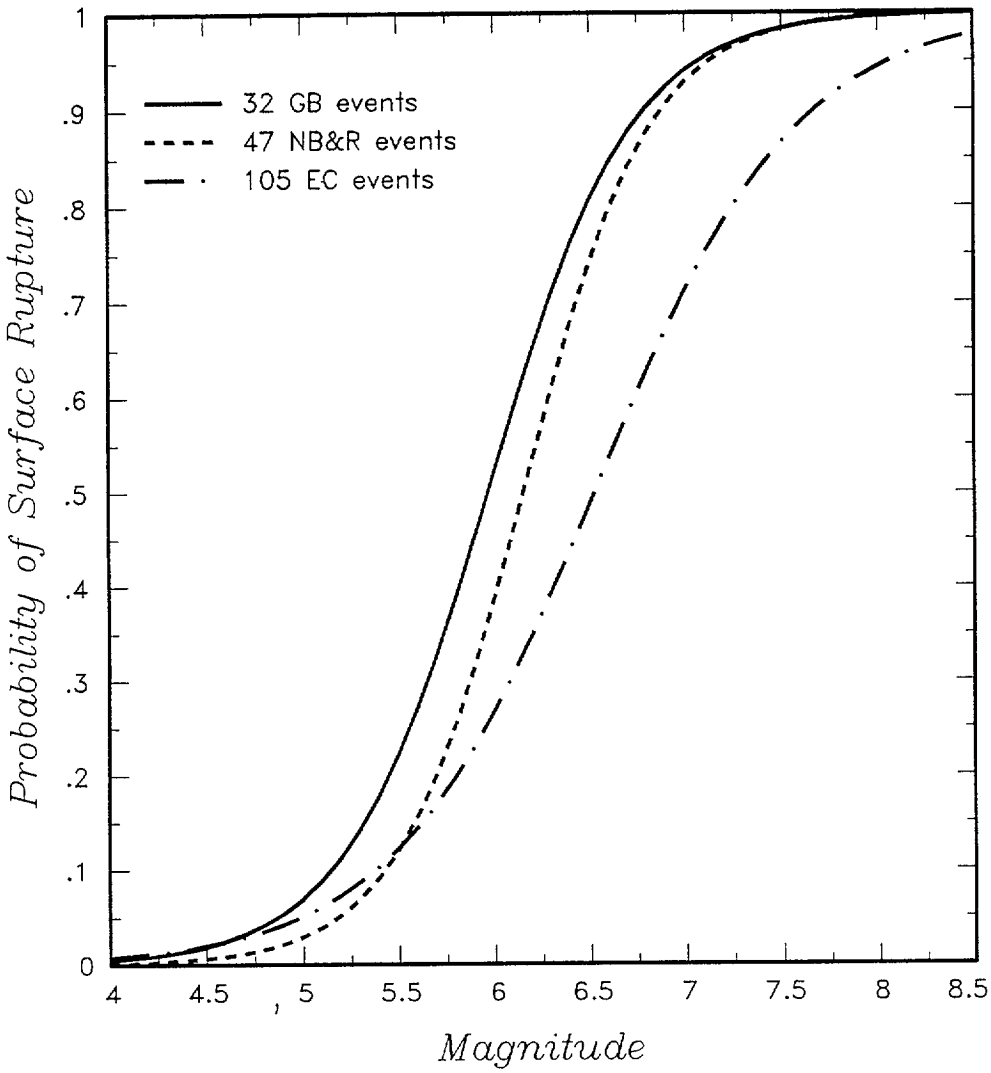

Figure H-12. Logistic regression models for the probability of surface rupture as a function of moment magnitude developed from three data sets presented in S.K. Pezzopane and T.E. Dawson (USGS, written communication, 1996). GB = Great Basin post 1930, NB&R = northern Basin and Range post 1930, and EC = extensional cordillera.

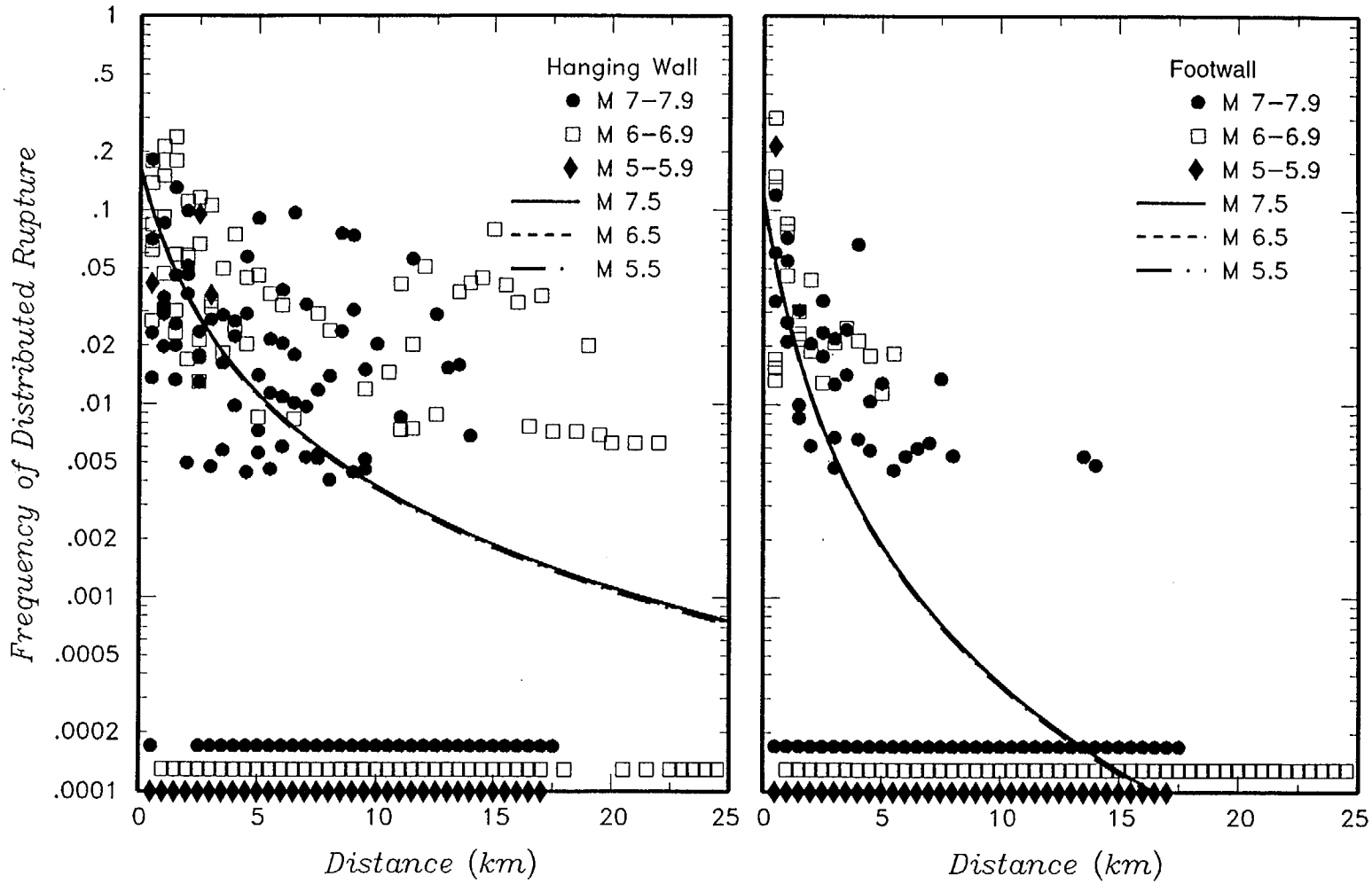

Figure H-13a Frequency of distributed rupture as a function of distance from principal rupture. Data include hanging wall cracking from 1988 Chalfant Valley earthquake. Points along bottom of plot represent distances for individual earthquakes where observed frequency was zero. The data for the three magnitude intervals are offset for clarity.

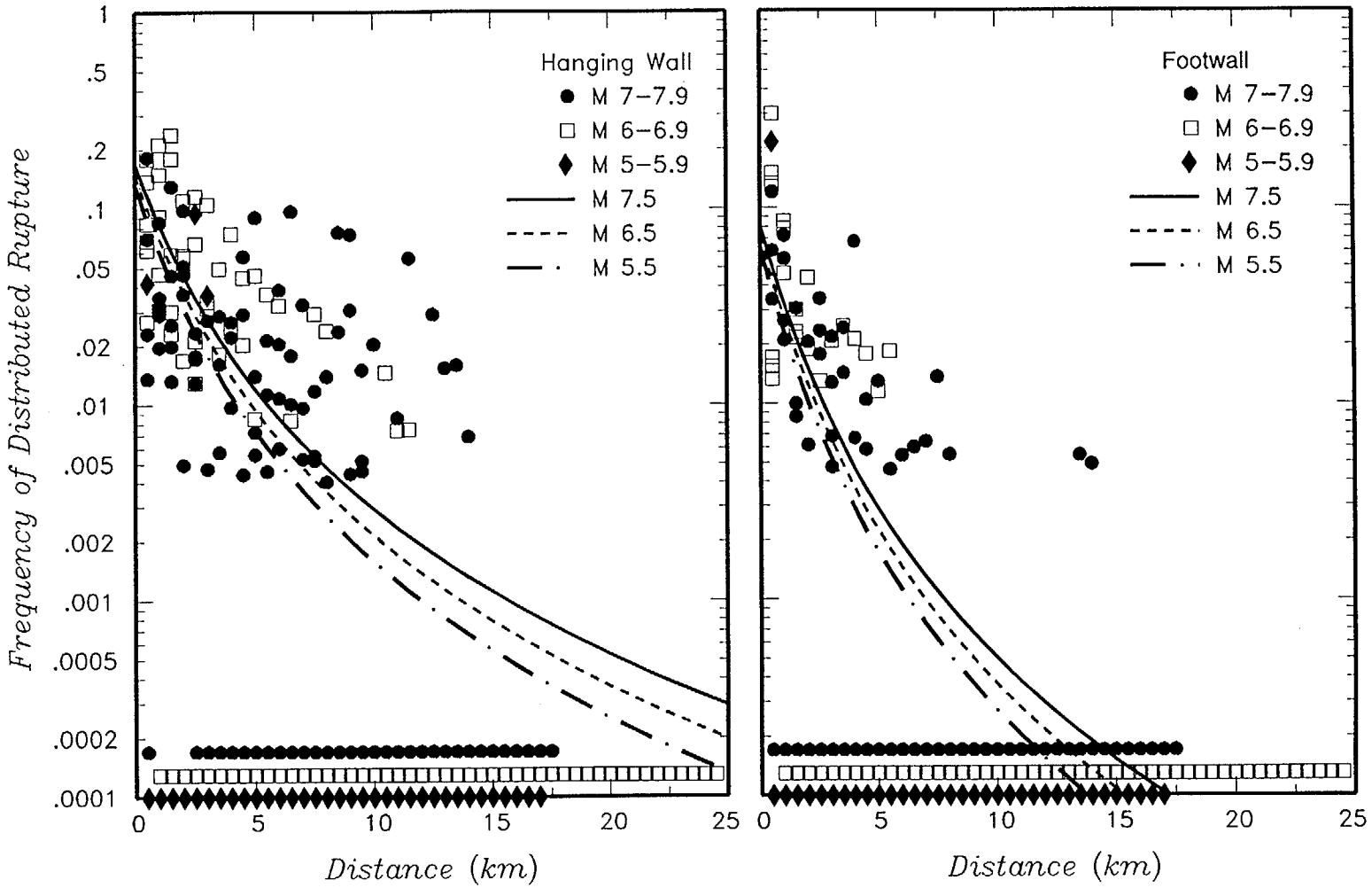

Figure H-13b Frequency of distributed rupture as a function of distance from principal rupture. Data do not include hanging wall cracking from 1988 Chalfant Valley earthquake. Points along bottom of plot represent distances for individual earthquakes where observed frequency was zero. The data for the three magnitude intervals are offset for clarity.

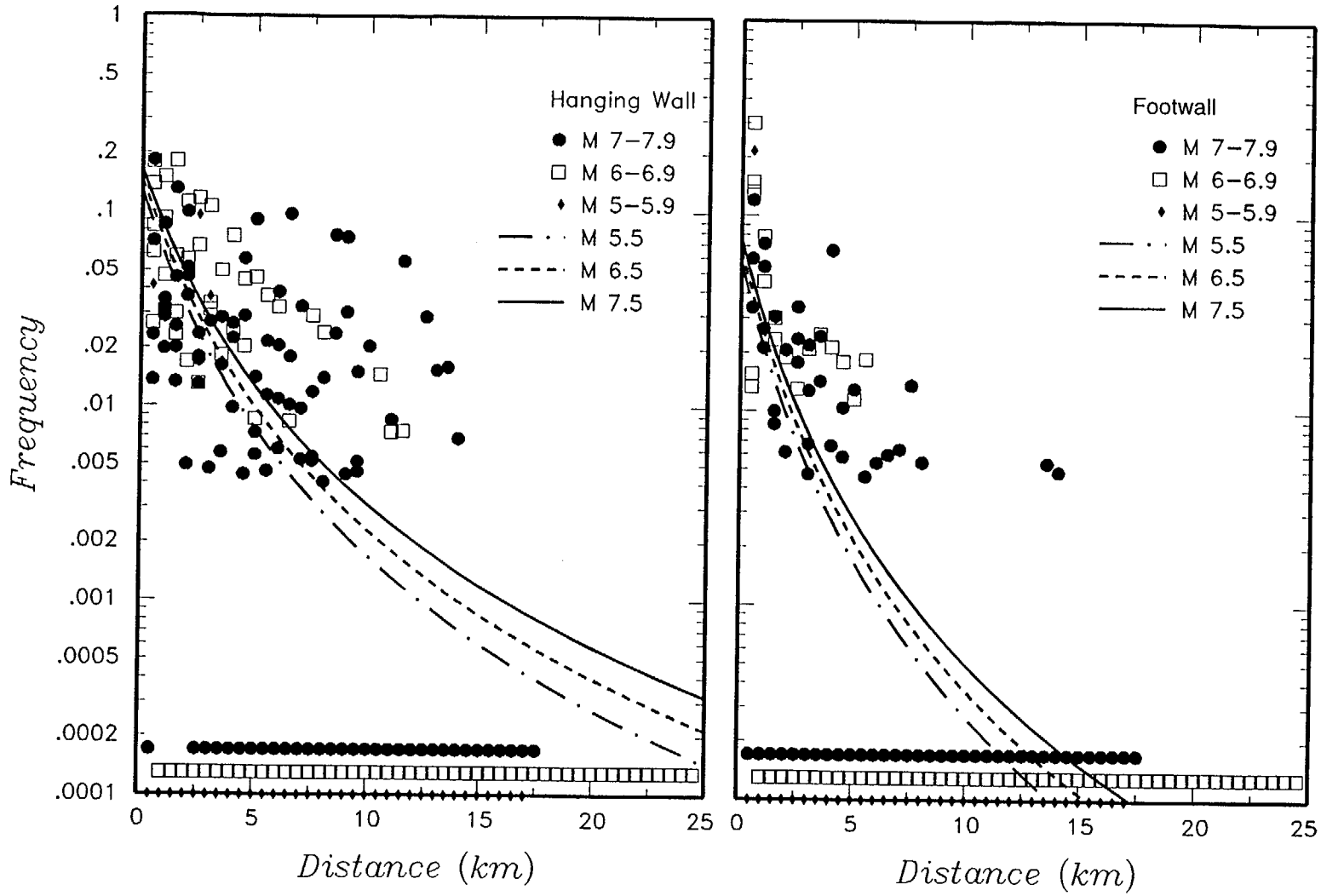

Figure H-13c Frequency of distributed rupture as a function of distance from principal rupture developed for thr AAR and SDO teams. The plot on the left shows hanging wall data, the plot on the right shows footwall data. Data do not include hanging wall cracking from the 1988 Chalfant Valley earthquake or data from the 1980 Mammoth earthquake. Points along bottom of plot represent distances for individual earthquakes where observed frequency was zero. The data for the three magnitude intervals are offset for clarity.

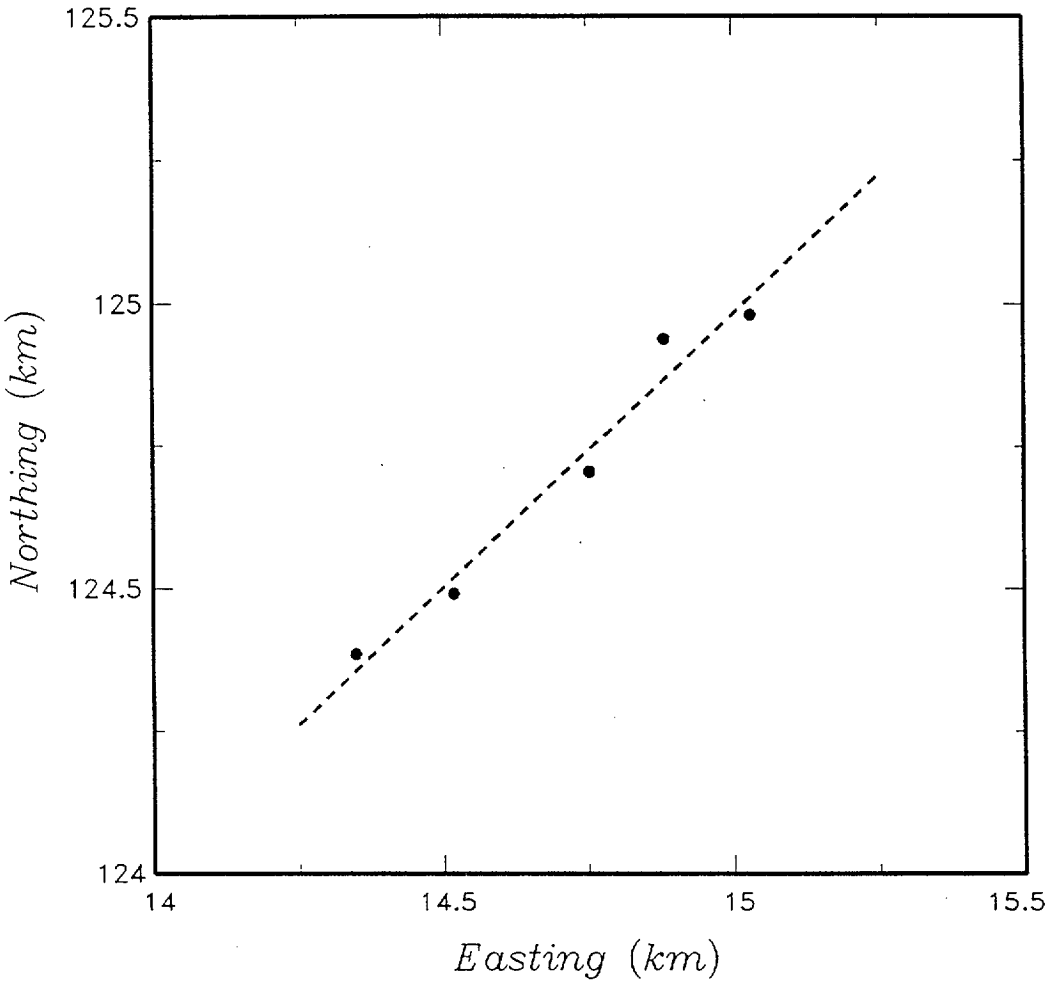

Figure H-14 Example of fitting straight line (dashed line) to digitized rupture trace (solid points) to determine the average strike azimuth

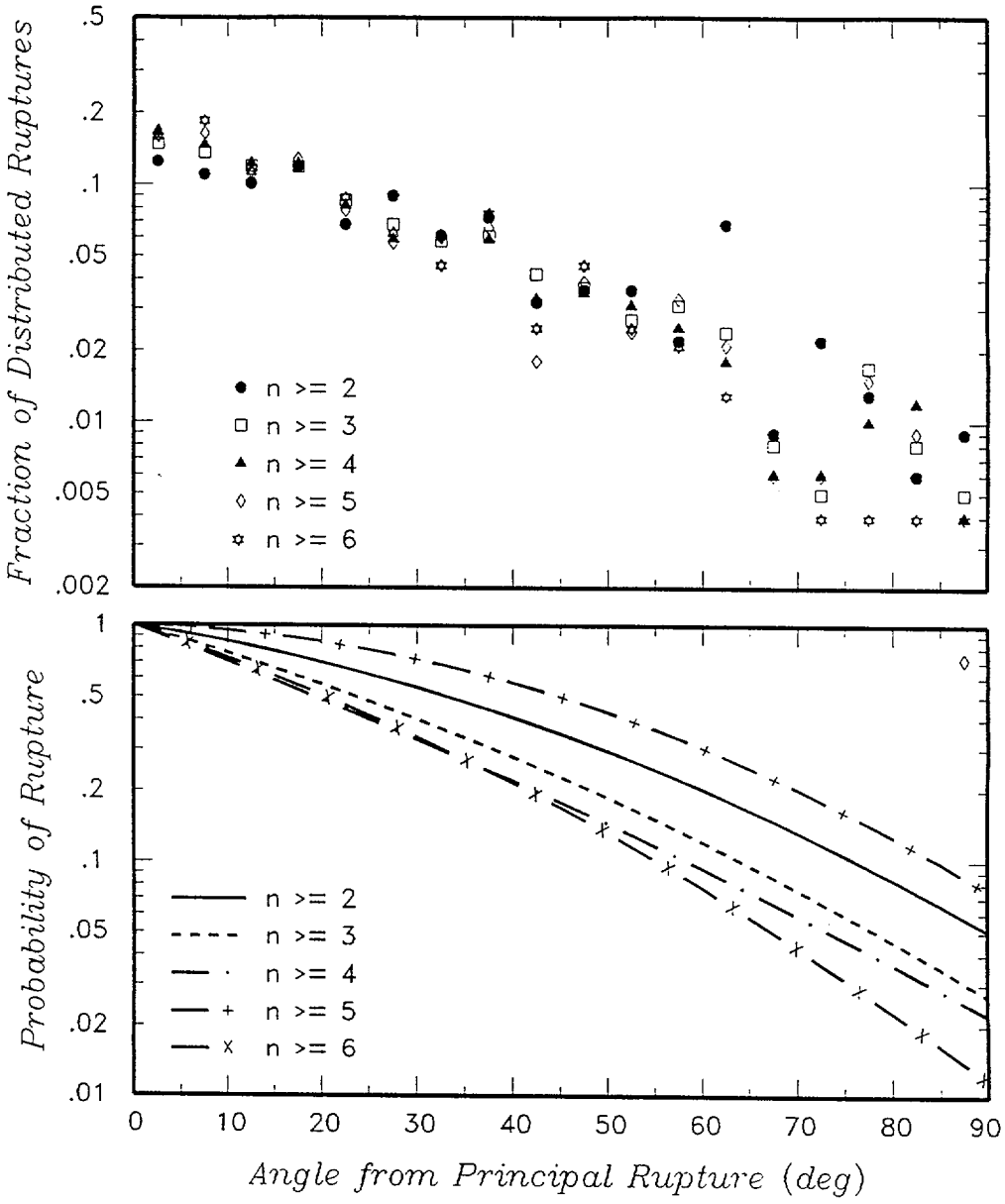

Figure H-15 Frequency distribution for angle between average strike of principal rupture and strike of individual distributed rupture traces. Parameter n denotes the number of digitization points along an individual rupture trace. Top plot shows the data from Table H-3 presented in terms of fraction of total ruptures. Bottom plot shows exponential fits to the data normalized to unity at a relative angle of 0°.

APPENDIX I

RESULTS OF REGRESSION ATTENUATION ANALYSES

APPENDIX I

RESULTS OF REGRESSION ATTENUATION ANALYSES

The following tables summarize the regression coefficients developed from each experts' point estimates. The equation forms adopted for the regressions are discussed in Chapter 6.

TABLE I-1A
J. G. ANDERSON: REGRESSION COEFFICIENTS
MEDIAN MODEL

COMPONENT	FREQUENCY (HZ)	a_1	a_2	a_3	a_4	a_5	a_6	a_7	a_8	a_9	a_{10}	a_{11}	a_{12}	SIGMA FIT
Horiz	PGA	1.9771	0.4586	-1.4197	-0.3066	0.2303	0.0000	0.0076	6.7	0.2144	-0.3545	5.2	6.0	0.1493
	20	2.8264	0.4586	-1.5590	-0.3066	0.2303	0.0136	-0.0263	7.4	0.2236	-0.3492	5.0	6.1	0.1455
	10	3.0127	0.4586	-1.5426	-0.3066	0.2303	0.0123	0.0354	7.4	0.1317	-0.3955	5.0	5.9	0.1631
	5	2.5847	0.4586	-1.3715	-0.3066	0.2303	-0.0100	0.0220	6.7	0.2009	-0.3174	5.3	6.0	0.1598
	2	1.7055	0.4586	-1.1607	-0.2628	0.2303	-0.0469	0.0382	5.8	0.2553	-0.3625	5.3	5.9	0.1521
	1	0.7983	0.4586	-1.0296	-0.2628	0.2303	-0.0803	-0.0330	5.0	0.3555	-0.2645	5.0	6.1	0.1557
	0.5	-0.5006	0.4586	-0.8625	-0.1752	0.2303	-0.1139	-0.1220	2.9	0.3861	-0.0211	5.0	6.5	0.1889
	0.3	-1.0946	0.4586	-0.8745	-0.0876	0.2303	-0.1407	-0.1366	3.0	0.2769	-0.0830	5.0	6.7	0.1992
	PGV	6.0533	0.4586	-1.2687	-0.1752	0.2303	-0.0476	0.0217	5.9	0.2551	-0.3154	5.1	6.0	0.1696
Vert	PGA	1.8132	0.7399	-1.5441	0.2825	0.1375	0.0000	0.1492	7.8	0.3229	-0.2993	5.1	6.5	0.1728
	20	2.7352	0.7399	-1.6777	0.2825	0.1375	0.0066	0.1284	7.6	0.3390	-0.2740	5.5	6.3	0.1668
	10	3.1549	0.7399	-1.6122	-0.1412	0.1375	-0.0364	0.1170	7.7	0.3135	-0.3205	5.1	6.5	0.2131
	5	2.5230	0.7399	-1.4196	-0.1695	0.1375	-0.0475	0.1274	8.2	0.3532	-0.2886	5.2	6.5	0.2079
	2	1.7173	0.7399	-1.2318	-0.1695	0.1375	-0.1003	0.1907	8.0	0.3075	-0.2739	5.0	6.2	0.2090
	1	0.5757	0.7399	-1.0973	-0.1695	0.1375	-0.1243	0.2956	6.9	0.2498	-0.1456	5.4	7.0	0.1679
	0.5	-0.0541	0.7399	-1.0697	-0.1695	0.1375	-0.1933	0.5981	5.8	-0.1117	-0.3472	5.0	5.5	0.2462
	0.3	-0.7565	0.7399	-0.9967	-0.1695	0.1375	-0.2338	0.6419	4.7	-0.1892	-0.5016	5.3	6.5	0.2554
	PGV	6.0353	0.7399	-1.3048	-0.1695	0.1375	-0.1137	0.4000	7.7	0.0160	-0.4243	5.0	5.9	0.2679

TABLE I-1B
J. G. ANDERSON: REGRESSION COEFFICIENTS
SIGMA MODEL

COMPONENT	FREQUENCY (HZ)	b_1	b_2	b_3	b_4	SIGMA FIT
Horiz	PGA	0.5590	-0.0543	0.0	6.8	0.0094
	20	0.5598	-0.0597	0.0	6.8	0.0105
	10	0.5756	-0.0680	0.0	6.9	0.0155
	5	0.6074	-0.0659	0.0	6.9	0.0148
	2	0.6603	-0.0637	0.0	7.0	0.0158
	1	0.7316	-0.0456	0.0	7.0	0.0091
	0.5	0.8199	-0.0392	0.0	6.9	0.0159
	0.3	0.8646	-0.0901	0.0	6.1	0.0224
	PGV	0.7201	-0.0202	0.0	7.0	0.0102
Vert	PGA	0.6326	-0.0205	0.0	6.2	0.0081
	20	0.6528	-0.0182	0.0	6.5	0.0082
	10	0.6742	-0.0636	0.0	5.9	0.0103
	5	0.6530	-0.0606	0.0	5.8	0.0146
	2	0.6573	-0.0691	0.0	5.8	0.0148
	1	0.6838	-0.0453	0.0	5.8	0.0169
	0.5	0.7221	-0.0156	0.0	5.8	0.0183
	0.3	0.7640	-0.0382	0.0	5.8	0.0219
	PGV	0.6299	-0.0370	0.0	5.8	0.0173

TABLE I-1C
J. G. ANDERSON: REGRESSION COEFFICIENTS
SIGMA-MU MODEL

COMPONENT	FREQUENCY (HZ)	c_1	c_2	c_3	c_4	c_5	c_6	MINIMUM	SIGMA FIT
Horiz	PGA	0.9620	0.0	-0.3323	0.0516	0.0304	6.0	0.2	0.0989
	20	0.9291	0.0	-0.2891	0.0434	0.0100	6.0	0.2	0.1008
	10	0.9696	0.0	-0.3295	0.0496	0.0386	6.0	0.2	0.0968
	5	0.9489	0.0	-0.3064	0.0457	0.0260	6.0	0.2	0.0996
	2	0.9234	0.0	-0.2859	0.0425	0.0240	6.0	0.2	0.0961
	1	0.9467	0.0	-0.3018	0.0465	0.0394	6.0	0.2	0.1025
	0.5	0.8838	0.0	-0.2370	0.0393	0.0071	6.0	0.2	0.1059
	0.3	0.8841	0.0	-0.1975	0.0327	-0.0180	6.0	0.2	0.1128
	PGV	0.9170	0.0	-0.2645	0.0412	0.0060	6.0	0.2	0.1081
Vert	PGA	0.9061	0.0	-0.2806	0.0480	0.0242	6.0	0.2	0.1220
	20	0.9655	0.0	-0.2351	0.0349	-0.0417	6.0	0.2	0.1257
	10	0.8968	0.0	-0.2670	0.0438	0.0269	6.0	0.2	0.1131
	5	0.8608	0.0	-0.2251	0.0366	0.0584	6.0	0.2	0.1058
	2	0.8496	0.0	-0.1971	0.0315	0.0232	6.0	0.2	0.1073
	1	0.9472	0.0	-0.2968	0.0551	-0.0050	6.0	0.2	0.1308
	0.5	0.8773	0.0	-0.2503	0.0602	0.0613	6.0	0.2	0.2003
	0.3	0.8719	0.0	-0.1939	0.0476	0.0375	6.0	0.2	0.1721
	PGV	0.8580	0.0	-0.2441	0.0483	0.0259	6.0	0.2	0.1412

TABLE I-1D
J. G. ANDERSON: REGRESSION COEFFICIENTS
SIGMA-SIGMA MODEL

COMPONENT	FREQUENCY (HZ)	d_1	d_2	d_3	d_4	SIGMA FIT
Horiz	PGA	0.1147	0.0	0.0	0.0	0.0
	20	0.1095	0.0	0.0	0.0	0.0
	10	0.1262	0.0	0.0	0.0	0.0
	5	0.1221	0.0	0.0	0.0	0.0
	2	0.1322	0.0	0.0	0.0	0.0
	1	0.1325	0.0	0.0	0.0	0.0
	0.5	0.1539	0.0	0.0	0.0	0.0
	0.3	0.1549	0.0	0.0	0.0	0.0
	PGV	0.1197	0.0	0.0	0.0	0.0
Vert	PGA	0.1310	0.0	0.0	0.0	0.0
	20	0.1153	0.0	0.0	0.0	0.0
	10	0.1419	0.0	0.0	0.0	0.0
	5	0.1411	0.0	0.0	0.0	0.0
	2	0.1473	0.0	0.0	0.0	0.0
	1	0.1390	0.0	0.0	0.0	0.0
	0.5	0.1702	0.0	0.0	0.0	0.0
	0.3	0.1929	0.0	0.0	0.0	0.0
	PGV	0.1240	0.0	0.0	0.0	0.0

TABLE I-2A
D. M. BOORE: REGRESSION COEFFICIENTS
MEDIAN MODEL

COMPONENT	FREQUENCY (HZ)	a_1	a_2	a_3	a_4	a_5	a_6	a_7	a_8	a_9	a_{10}	a_{11}	a_{12}	SIGMA FIT
Horiz	PGA	1.5497	0.3084	-1.3607	0.0428	0.1679	0.0000	-0.0091	6.6	0.3143	-0.1556	5.0	6.6	0.0652
	20	2.6166	0.3084	-1.5608	0.0428	0.1679	0.0060	-0.0008	7.2	0.3150	-0.1482	5.2	6.5	0.0745
	10	2.8493	0.3084	-1.5616	0.0428	0.1679	-0.0015	0.0202	7.8	0.2528	-0.1906	5.0	6.4	0.0891
	5	2.4108	0.3084	-1.4094	0.0428	0.1679	-0.0139	0.0240	7.5	0.2560	-0.1443	5.0	6.5	0.0880
	2	1.5149	0.3084	-1.1710	0.0428	0.1679	-0.0522	-0.0020	5.8	0.3720	-0.1352	5.0	6.6	0.0779
	1	0.7658	0.3084	-1.0502	0.0428	0.1679	-0.0864	-0.0353	5.0	0.4619	-0.1113	5.0	6.8	0.0812
	0.5	-0.2483	0.3084	-0.9440	0.0428	0.1679	-0.1015	-0.1290	4.8	0.3628	-0.0287	5.1	6.7	0.0939
	0.3	-0.5903	0.3084	-0.9312	0.0428	0.1679	-0.1629	-0.2092	4.1	0.1632	-0.0246	5.1	6.5	0.0825
	PGV	5.8882	0.3084	-1.1710	0.0428	0.1679	-0.1051	-0.0677	5.5	0.3161	-0.2053	5.0	6.1	0.1341
Vert	PGA	1.6973	0.5387	-1.5373	0.2029	0.1404	0.0000	-0.0580	6.4	0.3991	-0.0696	5.6	6.4	0.0707
	20	3.1350	0.5387	-1.7786	0.2029	0.1404	0.0058	-0.0629	7.0	0.3832	-0.0957	5.7	6.3	0.0799
	10	3.0993	0.5387	-1.7441	0.2029	0.1404	-0.0027	-0.0034	7.3	0.3445	-0.1193	5.6	6.4	0.0872
	5	1.9869	0.5387	-1.4854	0.2029	0.1404	-0.0142	0.0407	6.7	0.3542	-0.0831	5.6	6.3	0.0852
	2	0.6682	0.5387	-1.1881	0.2029	0.1404	-0.0404	0.0537	5.3	0.3557	-0.0107	5.5	6.4	0.0934
	1	-0.1466	0.5387	-1.0425	0.2029	0.1404	-0.0646	0.0188	4.4	0.3217	0.0840	5.5	6.5	0.0963
	0.5	-1.0320	0.5387	-0.9188	0.2029	0.1404	-0.0963	-0.0472	3.4	0.3081	0.1089	5.6	6.5	0.1120
	0.3	-1.3453	0.5387	-0.9122	0.2029	0.1404	-0.1313	-0.0431	3.3	0.2441	0.0609	5.2	6.5	0.1209
	PGV	5.0911	0.5387	-1.2405	0.2029	0.1404	-0.0725	0.1002	6.3	0.0365	-0.1530	5.0	6.2	0.1720

TABLE I-2B
D. M. BOORE: REGRESSION COEFFICIENTS
SIGMA MODEL

COMPONENT	FREQUENCY (HZ)	b_1	b_2	b_3	b_4	SIGMA FIT
Horiz	PGA	0.5060	-0.0601	0.0	7.1	0.0004
	20	0.5246	-0.0607	0.0	7.1	0.0004
	10	0.5399	-0.0616	0.0	7.1	0.0003
	5	0.5855	-0.0598	0.0	7.1	0.0004
	2	0.6540	-0.0573	0.0	7.1	0.0005
	1	0.7089	-0.0540	0.0	7.1	0.0004
	0.5	0.7786	-0.0498	0.0	7.1	0.0004
	0.3	0.6838	-0.0839	0.0	7.1	0.0006
	PGV	0.5048	-0.0588	0.0	7.2	0.0021
Vert	PGA	0.5577	-0.0807	0.0	7.0	0.0049
	20	0.5954	-0.0770	0.0	7.0	0.0044
	10	0.5954	-0.0770	0.0	7.0	0.0044
	5	0.5954	-0.0576	0.0	7.0	0.0044
	2	0.5954	-0.0576	0.0	7.0	0.0044
	1	0.5954	-0.0576	0.0	7.0	0.0044
	0.5	0.5954	-0.0576	0.0	7.0	0.0044
	0.3	0.6121	-0.0576	0.0	7.0	0.0044
	PGV	0.4924	-0.0600	0.0	7.2	0.0022

TABLE I-2C
D. M. BOORE: REGRESSION COEFFICIENTS
SIGMA-MU MODEL

COMPONENT	FREQUENCY (HZ)	c_1	c_2	c_3	c_4	c_5	c_6	MINIMUM	SIGMA FIT
Horiz	PGA	0.5471	-0.0146	-0.1968	0.0337	0.0358	6.0	0.2	0.0659
	20	0.5194	0.0186	-0.1558	0.0269	0.0384	6.0	0.2	0.0691
	10	0.5976	0.0331	-0.1950	0.0323	0.0330	6.0	0.2	0.0660
	5	0.6248	0.0482	-0.2179	0.0361	0.0192	6.0	0.2	0.0603
	2	0.3572	0.0034	-0.0872	0.0187	0.0305	6.0	0.2	0.0543
	1	0.2909	-0.0070	-0.0330	0.0090	0.0523	6.0	0.2	0.0652
	0.5	0.2121	-0.0561	0.0153	0.0123	0.0502	6.0	0.2	0.0891
	0.3	0.2584	-0.0061	0.0870	-0.0082	0.0773	6.0	0.2	0.1139
	PGV	0.3575	0.0070	-0.1036	0.0271	0.0050	6.0	0.2	0.0840
Vert	PGA	0.3162	-0.0271	-0.0839	0.0201	0.0411	6.0	0.2	0.0726
	20	0.4047	-0.0043	-0.0734	0.0157	0.0076	6.0	0.2	0.0808
	10	0.2951	-0.0211	-0.0745	0.0187	0.0451	6.0	0.2	0.0679
	5	0.3058	-0.0036	-0.0760	0.0213	0.0599	6.0	0.2	0.0858
	2	0.2463	0.0210	-0.0090	0.0123	0.0444	6.0	0.2	0.0874
	1	0.3998	-0.0363	-0.1366	0.0329	0.0324	6.0	0.2	0.0847
	0.5	0.3062	0.0196	-0.0457	0.0207	0.0741	6.0	0.2	0.1323
	0.3	0.4412	-0.0852	-0.0048	0.0092	0.0306	6.0	0.2	0.1680
	PGV	0.1711	0.0371	0.0060	0.0035	0.1135	6.0	0.2	0.0744

TABLE I-2D
D. M. BOORE: REGRESSION COEFFICIENTS
SIGMA-SIGMA MODEL

COMPONENT	FREQUENCY (HZ)	d_1	d_2	d_3	d_4	SIGMA FIT
Horiz	PGA	0.1	0.0	0.0	7.1	0.0
	20	0.1	0.0	0.0	7.1	0.0
	10	0.1	0.0	0.0	7.1	0.0
	5	0.1	0.0	0.0	7.1	0.0
	2	0.1	0.0	0.0	7.1	0.0
	1	0.1	0.0	0.0	7.1	0.0
	0.5	0.1	0.0	0.0	7.1	0.0
	0.3	0.1	0.0	0.0	7.1	0.0
	PGV	0.1	0.0	0.0	7.1	0.0
Vert	PGA	0.1	0.0	0.0	7.1	0.0
	20	0.1	0.0	0.0	7.1	0.0
	10	0.1	0.0	0.0	7.1	0.0
	5	0.1	0.0	0.0	7.1	0.0
	2	0.1	0.0	0.0	7.1	0.0
	1	0.1	0.0	0.0	7.1	0.0
	0.5	0.1	0.0	0.0	7.1	0.0
	0.3	0.1	0.0	0.0	7.1	0.0
	PGV	0.1	0.0	0.0	7.1	0.0

TABLE I-3A
K. W. CAMPBELL: REGRESSION COEFFICIENTS
MEDIAN MODEL

COMPONENT	FREQUENCY (HZ)	a_1	a_2	a_3	a_4	a_5	a_6	a_7	a_8	a_9	a_{10}	a_{11}	a_{12}	SIGMA FIT
Horiz	PGA	1.8960	0.2126	-1.4434	-0.2258	0.2412	0.0000	0.0399	6.5	0.0000	0.0000	0.0	0.0	0.1105
	20	2.7450	0.2126	-1.5910	-0.2258	0.2412	0.0132	0.0291	6.9	0.0000	0.0000	0.0	0.0	0.1168
	10	2.7735	0.2126	-1.5481	-0.2032	0.2412	0.0144	0.0483	7.0	0.0000	0.0000	0.0	0.0	0.1180
	5	2.3798	0.2126	-1.3963	-0.1806	0.2412	-0.0011	0.0574	6.8	0.0000	0.0000	0.0	0.0	0.1230
	2	1.7052	0.2126	-1.2043	-0.1671	0.2412	-0.0496	0.0483	5.7	0.0000	0.0000	0.0	0.0	0.1487
	1	1.0160	0.2126	-1.1143	-0.1671	0.2412	-0.0885	0.0519	5.2	0.0000	0.0000	0.0	0.0	0.1519
	0.5	0.1935	0.2126	-1.0324	-0.1671	0.2412	-0.1418	0.0549	4.7	0.0000	0.0000	0.0	0.0	0.1782
	0.3	-0.2184	0.2126	-1.0371	-0.1671	0.2412	-0.2034	0.0269	4.6	0.0000	0.0000	0.0	0.0	0.1910
	PGV	6.0095	0.2126	-1.2345	-0.1671	0.2412	-0.0840	0.0469	4.9	0.0000	0.0000	0.0	0.0	0.1305
Vert	PGA	1.9650	0.4014	-1.6105	0.0000	0.2009	0.0000	0.1042	6.8	0.0000	0.0000	0.0	0.0	0.1308
	20	3.2137	0.4014	-1.8135	0.0000	0.2009	0.0040	0.0972	7.3	0.0000	0.0000	0.0	0.0	0.1464
	10	3.0633	0.4014	-1.7233	0.0000	0.2009	0.0001	0.1022	7.3	0.0000	0.0000	0.0	0.0	0.1405
	5	2.0716	0.4014	-1.4754	0.0000	0.2009	-0.0101	0.0949	7.0	0.0000	0.0000	0.0	0.0	0.1262
	2	1.0862	0.4014	-1.2540	0.0000	0.2009	-0.0531	0.1019	6.1	0.0000	0.0000	0.0	0.0	0.1309
	1	0.4391	0.4014	-1.1841	0.0000	0.2009	-0.0920	0.1647	5.7	0.0000	0.0000	0.0	0.0	0.1077
	0.5	-0.2319	0.4014	-1.1386	0.0000	0.2009	-0.1564	0.2868	4.7	0.0000	0.0000	0.0	0.0	0.1118
	0.3	-0.6304	0.4014	-1.1370	0.0000	0.2009	-0.2225	0.3577	4.3	0.0000	0.0000	0.0	0.0	0.1582
	PGV	5.4130	0.4014	-1.3230	0.0000	0.2009	-0.0702	0.1917	6.7	0.0000	0.0000	0.0	0.0	0.1153

TABLE I-3B
K. W. CAMPBELL: REGRESSION COEFFICIENTS
SIGMA MODEL

COMPONENT	FREQUENCY (HZ)	b_1	b_2	b_3	b_4	SIGMA FIT
Horiz	PGA	0.4952	-0.0718	0.0	7.1	0.0107
	20	0.5000	-0.0756	0.0	7.1	0.0095
	10	0.5180	-0.0759	0.0	7.1	0.0097
	5	0.5518	-0.0743	0.0	7.1	0.0094
	2	0.6156	-0.0722	0.0	7.1	0.0090
	1	0.6611	-0.0697	0.0	7.1	0.0090
	0.5	0.7137	-0.0666	0.0	7.1	0.0087
	0.3	0.7203	-0.0649	0.0	7.1	0.0087
	PGV	0.5657	-0.0789	0.0	7.1	0.0032
Vert	PGA	0.5842	-0.0642	0.0	6.8	0.0134
	20	0.6238	-0.0628	0.0	6.7	0.0124
	10	0.6287	-0.0644	0.0	6.7	0.0124
	5	0.6327	-0.0550	0.0	6.7	0.0123
	2	0.6475	-0.0586	0.0	6.7	0.0121
	1	0.6596	-0.0584	0.0	6.8	0.0121
	0.5	0.6838	-0.0603	0.0	6.8	0.0128
	0.3	0.6929	-0.0603	0.0	6.8	0.0128
	PGV	0.5989	-0.0652	0.0	6.8	0.0137

TABLE I-3C
K. W. CAMPBELL: REGRESSION COEFFICIENTS
SIGMA-MU MODEL

COMPONENT	FREQUENCY (HZ)	c_1	c_2	c_3	c_4	c_5	c_6	MINIMUM	SIGMA FIT
Horiz	PGA	0.7267	0.0	-0.3005	0.0535	0.0173	6.0	0.2	0.0800
	20	0.7021	0.0	-0.2571	0.0486	0.0132	6.0	0.2	0.0829
	10	0.8492	0.0	-0.3861	0.0691	0.0222	6.0	0.2	0.0660
	5	0.9030	0.0	-0.4097	0.0721	0.0007	6.0	0.2	0.0601
	2	0.5303	0.0	-0.1899	0.0395	0.0131	6.0	0.2	0.0843
	1	0.4384	0.0	-0.1203	0.0273	0.0477	6.0	0.2	0.0992
	0.5	0.2665	0.0	0.0325	0.0096	0.0263	6.0	0.2	0.1223
	0.3	0.2476	0.0	0.1379	-0.0106	0.0240	6.0	0.2	0.1341
	PGV	0.7873	0.0	-0.3460	0.0620	0.0272	6.0	0.2	0.1085
Vert	PGA	0.6835	0.0	-0.2488	0.0476	0.0222	6.0	0.2	0.1022
	20	0.7763	0.0	-0.2297	0.0423	0.0085	6.0	0.2	0.1093
	10	0.7307	0.0	-0.3015	0.0569	0.0342	6.0	0.2	0.0964
	5	0.8226	0.0	-0.3631	0.0677	0.0620	6.0	0.2	0.0944
	2	0.5424	0.0	-0.1390	0.0318	0.0378	6.0	0.2	0.1164
	1	0.7375	0.0	-0.2475	0.0475	-0.0049	6.0	0.2	0.1283
	0.5	0.5831	0.0	-0.1478	0.0433	0.0501	6.0	0.2	0.1541
	0.3	0.5651	0.0	-0.0052	0.0136	0.0817	6.0	0.2	0.1910
	PGV	0.8300	0.0	-0.3837	0.0728	0.1044	6.0	0.2	0.1112

TABLE I-3D
K. W. CAMPBELL: REGRESSION COEFFICIENTS
SIGMA-SIGMA MODEL

COMPONENT	FREQUENCY (HZ)	d_1	d_2	d_3	d_4	SIGMA FIT
Horiz	PGA	0.1	0.0	0.0	7.1	0.0
	20	0.1	0.0	0.0	7.1	0.0
	10	0.1	0.0	0.0	7.1	0.0
	5	0.1	0.0	0.0	7.1	0.0
	2	0.1	0.0	0.0	7.1	0.0
	1	0.1	0.0	0.0	7.1	0.0
	0.5	0.1	0.0	0.0	7.1	0.0
	0.3	0.1	0.0	0.0	7.1	0.0
	PGV	0.1	0.0	0.0	7.1	0.0
Vert	PGA	0.1	0.0	0.0	7.1	0.0
	20	0.1	0.0	0.0	7.1	0.0
	10	0.1	0.0	0.0	7.1	0.0
	5	0.1	0.0	0.0	7.1	0.0
	2	0.1	0.0	0.0	7.1	0.0
	1	0.1	0.0	0.0	7.1	0.0
	0.5	0.1	0.0	0.0	7.1	0.0
	0.3	0.1	0.0	0.0	7.1	0.0
	PGV	0.1	0.0	0.0	7.1	0.0

TABLE I-4A
A. F. McGARR: REGRESSION COEFFICIENTS
MEDIAN MODEL

COMPONENT	FREQUENCY (HZ)	a_1	a_2	a_3	a_4	a_5	a_6	a_7	a_8	a_9	a_{10}	a_{11}	a_{12}	SIGMA FIT
Horiz	PGA	1.6594	0.2412	-1.4068	-0.1238	0.2153	0.0000	0.0166	6.8	0.0000	0.0000	0.0	0.0	0.1588
	20	2.6292	0.2412	-1.5697	-0.1238	0.2153	0.0074	-0.0037	7.3	0.0000	0.0000	0.0	0.0	0.1796
	10	2.8002	0.2412	-1.5646	-0.1238	0.2153	0.0050	0.0153	7.7	0.0000	0.0000	0.0	0.0	0.1764
	5	2.3506	0.2412	-1.4123	-0.0825	0.2153	-0.0088	0.0439	7.4	0.0000	0.0000	0.0	0.0	0.1633
	2	1.5042	0.2412	-1.1972	-0.0413	0.2153	-0.0471	0.0690	6.1	0.0000	0.0000	0.0	0.0	0.1648
	1	0.7751	0.2412	-1.0911	0.0000	0.2153	-0.0819	0.0620	5.4	0.0000	0.0000	0.0	0.0	0.1687
	0.5	-0.0836	0.2412	-0.9972	0.0413	0.2153	-0.1217	0.0304	5.1	0.0000	0.0000	0.0	0.0	0.1765
	0.3	-0.5679	0.2412	-0.9422	0.0413	0.2153	-0.1860	-0.0560	4.4	0.0000	0.0000	0.0	0.0	0.1545
	PGV	5.9472	0.2412	-1.2788	0.0413	0.2153	-0.0740	0.0723	5.7	0.0000	0.0000	0.0	0.0	0.1747
Vert	PGA	1.8472	0.3457	-1.6393	-0.1253	0.2179	0.0000	0.0630	6.8	0.0000	0.0000	0.0	0.0	0.1728
	20	3.0364	0.3457	-1.8353	-0.1253	0.2179	0.0115	0.0401	7.5	0.0000	0.0000	0.0	0.0	0.1927
	10	2.8984	0.3457	-1.7478	-0.1253	0.2179	0.0100	0.0391	7.8	0.0000	0.0000	0.0	0.0	0.1796
	5	2.2051	0.3457	-1.5680	-0.0835	0.2179	-0.0082	0.0592	7.4	0.0000	0.0000	0.0	0.0	0.1683
	2	1.3797	0.3457	-1.3725	-0.0418	0.2179	-0.0555	0.1148	6.9	0.0000	0.0000	0.0	0.0	0.1712
	1	0.5173	0.3457	-1.2524	0.0000	0.2179	-0.0879	0.1526	6.2	0.0000	0.0000	0.0	0.0	0.1494
	0.5	-0.4559	0.3457	-1.1451	0.0418	0.2179	-0.1399	0.2048	5.0	0.0000	0.0000	0.0	0.0	0.1516
	0.3	-1.0476	0.3457	-1.1063	0.0418	0.2179	-0.1827	0.2133	4.6	0.0000	0.0000	0.0	0.0	0.1560
	PGV	5.4176	0.3457	-1.4111	0.0418	0.2179	-0.0483	0.1238	6.4	0.0000	0.0000	0.0	0.0	0.2830

TABLE I-4B
A. F. McGARR: REGRESSION COEFFICIENTS
SIGMA MODEL

COMPONENT	FREQUENCY (HZ)	b_1	b_2	b_3	b_4	SIGMA FIT
Horiz	PGA	0.5670	-0.0441	0.0	6.9	0.0034
	20	0.5714	-0.0462	0.0	6.9	0.0041
	10	0.5895	-0.0543	0.0	6.8	0.0055
	5	0.6240	-0.0520	0.0	6.8	0.0053
	2	0.6939	-0.0486	0.0	6.7	0.0056
	1	0.7523	-0.0370	0.0	6.8	0.0032
	0.5	0.8528	-0.0302	0.0	6.8	0.0045
	0.3	0.8541	-0.0494	0.0	6.8	0.0070
	PGV	0.7480	-0.0256	0.0	5.8	0.0041
Vert	PGA	0.5404	-0.0636	0.0	6.8	0.0036
	20	0.5557	-0.0625	0.0	6.8	0.0036
	10	0.5716	-0.0754	0.0	6.7	0.0069
	5	0.5757	-0.0735	0.0	6.7	0.0075
	2	0.6194	-0.0986	0.0	6.2	0.0090
	1	0.6572	-0.0593	0.0	6.6	0.0074
	0.5	0.7320	-0.0665	0.0	6.3	0.0097
	0.3	0.7732	-0.0849	0.0	6.1	0.0109
	PGV	0.6176	-0.0454	0.0	5.8	0.0089

TABLE I-4C
A. F. McGARR: REGRESSION COEFFICIENTS
SIGMA-MU MODEL

COMPONENT	FREQUENCY (HZ)	c_1	c_2	c_3	c_4	c_5	c_6	MINIMUM	SIGMA FIT
Horiz	PGA	0.4361	0.0	-0.1255	0.0231	0.0170	6.0	0.2	0.0944
	20	0.4444	0.0	-0.0793	0.0147	0.0093	6.0	0.2	0.0933
	10	0.5028	0.0	-0.1443	0.0256	0.0145	6.0	0.2	0.0833
	5	0.5358	0.0	-0.1647	0.0283	-0.0043	6.0	0.2	0.0829
	2	0.3175	0.0	-0.0454	0.0106	0.0012	6.0	0.2	0.0858
	1	0.3177	0.0	-0.0251	0.0075	0.0198	6.0	0.2	0.0943
	0.5	0.2482	0.0	0.0727	-0.0044	0.0056	6.0	0.2	0.1191
	0.3	0.2057	0.0	0.1263	-0.0157	0.0154	6.0	0.2	0.1098
	PGV	0.3386	0.0	-0.0486	0.0133	0.0072	6.0	0.2	0.1265
Vert	PGA	0.3355	0.0	-0.0288	0.0061	-0.0004	6.0	0.2	0.0977
	20	0.4595	0.0	-0.0238	0.0019	-0.0302	6.0	0.2	0.1128
	10	0.3773	0.0	-0.0699	0.0165	0.0148	6.0	0.2	0.0919
	5	0.2906	0.0	-0.0434	0.0157	0.0613	6.0	0.2	0.0899
	2	0.2361	0.0	0.0213	0.0027	0.0069	6.0	0.2	0.1045
	1	0.4178	0.0	-0.0855	0.0194	-0.0507	6.0	0.2	0.1106
	0.5	0.2854	0.0	-0.0087	0.0196	0.0659	6.0	0.2	0.1487
	0.3	0.2291	0.0	0.0702	0.0018	0.1555	6.0	0.2	0.1379
	PGV	0.4553	0.0	-0.1333	0.0277	0.1640	6.0	0.2	0.1883

TABLE I-4D
A. F. McGARR: REGRESSION COEFFICIENTS
SIGMA-SIGMA MODEL

COMPONENT	FREQUENCY (HZ)	d_1	d_2	d_3	d_4	SIGMA FIT
Horiz	PGA	0.1010	0.0073	0.0	7.2	0.0045
	20	0.1015	0.0097	0.0	7.2	0.0046
	10	0.1072	0.0102	0.0	7.2	0.0046
	5	0.1040	0.0092	0.0	7.2	0.0038
	2	0.1156	0.0171	0.0	7.2	0.0035
	1	0.1207	0.0239	0.0	7.2	0.0042
	0.5	0.1620	0.0396	0.0	7.2	0.0034
	0.3	0.1818	0.0496	0.0	7.1	0.0047
	PGV	0.1347	0.0273	0.0	7.2	0.0022
Vert	PGA	0.1435	0.0324	0.0	7.2	0.0072
	20	0.1402	0.0322	0.0	7.2	0.0065
	10	0.1431	0.0271	0.0	7.2	0.0074
	5	0.1322	0.0207	0.0	7.2	0.0071
	2	0.1364	0.0215	0.0	7.2	0.0082
	1	0.1332	0.0257	0.0	7.2	0.0079
	0.5	0.1893	0.0477	0.0	7.2	0.0095
	0.3	0.2130	0.0609	0.0	6.9	0.0111
	PGV	0.1858	0.0449	0.0	7.2	0.0066

TABLE I-5A
W. J. SILVA: REGRESSION COEFFICIENTS
MEDIAN MODEL

COMPONENT	FREQUENCY (HZ)	a_1	a_2	a_3	a_4	a_5	a_6	a_7	a_8	a_9	a_{10}	a_{11}	a_{12}	SIGMA FIT
Horiz	PGA	1.8005	0.3153	-1.3837	-0.2558	0.2277	0.0000	-0.1026	6.5	0.2448	-0.2330	5.3	6.1	0.1025
	20	2.7125	0.3153	-1.5541	-0.2558	0.2277	0.0167	-0.1075	7.0	0.2384	-0.2658	5.2	6.2	0.1244
	10	2.9773	0.3153	-1.5532	-0.2558	0.2277	0.0107	-0.0789	7.5	0.1681	-0.2994	5.1	6.0	0.1266
	5	2.6009	0.3153	-1.4075	-0.2558	0.2277	-0.0054	-0.0685	7.2	0.1991	-0.2360	5.3	6.1	0.1167
	2	1.6999	0.3153	-1.1745	-0.2345	0.2277	-0.0455	-0.0619	5.9	0.3161	-0.1954	5.1	6.2	0.1026
	1	0.9533	0.3153	-1.0575	-0.2131	0.2277	-0.0823	-0.1434	5.6	0.3724	-0.1700	5.3	6.2	0.1075
	0.5	0.0547	0.3153	-0.9277	-0.2131	0.2277	-0.1430	-0.2633	4.5	0.3164	-0.0652	5.4	6.3	0.1123
	0.3	-0.4523	0.3153	-0.9075	-0.2345	0.2277	-0.2005	-0.2867	4.3	0.3268	-0.0615	5.0	7.4	0.1246
	PGV	5.9145	0.3153	-1.1166	-0.2558	0.2277	-0.0938	-0.1484	5.5	0.3349	-0.1934	5.0	6.7	0.1001
Vert	PGA	1.8504	0.2013	-1.6070	-0.3040	0.2360	0.0000	-0.2461	6.3	0.3630	-0.2009	5.1	6.5	0.1031
	20	3.1590	0.2013	-1.8481	-0.3040	0.2360	0.0138	-0.2468	7.3	0.3313	-0.2651	5.2	6.5	0.1239
	10	3.0835	0.2013	-1.7702	-0.2606	0.2360	0.0090	-0.1158	7.8	0.2430	-0.2923	5.1	6.2	0.1238
	5	2.1817	0.2013	-1.5370	-0.2606	0.2360	-0.0083	-0.0119	6.9	0.3048	-0.1845	5.2	6.5	0.1094
	2	1.1944	0.2013	-1.2980	-0.2606	0.2360	-0.0514	0.0302	5.6	0.4316	-0.1490	5.0	6.6	0.1045
	1	0.5178	0.2013	-1.1971	-0.2606	0.2360	-0.0885	-0.1312	5.4	0.4854	-0.1251	5.1	6.6	0.1141
	0.5	-0.4204	0.2013	-1.0913	-0.2606	0.2360	-0.1457	-0.3447	4.5	0.4766	-0.0200	5.2	6.7	0.1182
	0.3	-0.9693	0.2013	-1.0845	-0.2823	0.2360	-0.2036	-0.3732	4.3	0.4332	0.0053	5.0	7.2	0.1408
	PGV	5.3774	0.2013	-1.2790	-0.2823	0.2360	-0.0798	-0.1293	5.2	0.4871	-0.1266	5.0	6.9	0.1054

TABLE I-5B
W. J. SILVA: REGRESSION COEFFICIENTS
SIGMA MODEL

COMPONENT	FREQUENCY (HZ)	b_1	b_2	b_3	b_4	SIGMA FIT
Horiz	PGA	0.6246	-0.0606	0.0	6.1	0.0062
	20	0.6107	-0.0696	0.0	6.2	0.0072
	10	0.6391	-0.0722	0.0	6.1	0.0066
	5	0.6648	-0.0696	0.0	6.1	0.0071
	2	0.7288	-0.0584	0.0	6.2	0.0069
	1	0.7716	-0.0311	0.0	6.8	0.0058
	0.5	0.8620	-0.0439	0.0	6.1	0.0081
	0.3	0.9044	-0.0671	0.0	5.9	0.0098
	PGV	0.7744	-0.0278	0.0	5.8	0.0091
Vert	PGA	0.6479	-0.0586	0.0	6.1	0.0060
	20	0.6414	-0.0667	0.0	6.2	0.0069
	10	0.6744	-0.0688	0.0	6.1	0.0062
	5	0.6797	-0.0683	0.0	6.1	0.0069
	2	0.7237	-0.0588	0.0	6.2	0.0070
	1	0.7586	-0.0316	0.0	6.8	0.0059
	0.5	0.8342	-0.0453	0.0	6.1	0.0084
	0.3	0.8780	-0.0690	0.0	5.9	0.0101
	PGV	0.7614	-0.0283	0.0	5.8	0.0093

TABLE I-5C
W. J. SILVA: REGRESSION COEFFICIENTS
SIGMA-MU MODEL

COMPONENT	FREQUENCY (HZ)	c_1	c_2	c_3	c_4	c_5	c_6	MINIMUM	SIGMA FIT
Horiz	PGA	0.3235	0.0	0.0	0.0	0.0415	6.0	0.2	0.0489
	20	0.3439	0.0	0.0	0.0	0.0585	6.0	0.2	0.0567
	10	0.3432	0.0	0.0	0.0	0.0442	6.0	0.2	0.0543
	5	0.3372	0.0	0.0	0.0	0.0233	6.0	0.2	0.0532
	2	0.3141	0.0	0.0	0.0	0.0606	6.0	0.2	0.0417
	1	0.3046	0.0	0.0	0.0	0.0705	6.0	0.2	0.0580
	0.5	0.3462	0.0	0.0	0.0	0.0929	6.0	0.2	0.0610
	0.3	0.4627	0.0	0.0	0.0	0.0756	6.0	0.2	0.0959
	PGV	0.3673	0.0	0.0	0.0	0.0344	6.0	0.2	0.0954
Vert	PGA	0.2695	0.0	0.0	0.0	0.0167	6.0	0.2	0.0710
	20	0.3043	0.0	0.0	0.0	0.0591	6.0	0.2	0.0759
	10	0.3016	0.0	0.0	0.0	0.0240	6.0	0.2	0.0830
	5	0.2917	0.0	0.0	0.0	0.0012	6.0	0.2	0.0847
	2	0.2500	0.0	0.0	0.0	0.0489	6.0	0.2	0.0669
	1	0.2294	0.0	0.0	0.0	0.0945	6.0	0.2	0.0757
	0.5	0.2881	0.0	0.0	0.0	0.0996	6.0	0.2	0.0689
	0.3	0.4034	0.0	0.0	0.0	0.0888	6.0	0.2	0.1069
	PGV	0.2940	0.0	0.0	0.0	0.0700	6.0	0.2	0.0990

TABLE I-5D
W. J. SILVA: REGRESSION COEFFICIENTS
SIGMA-SIGMA MODEL

COMPONENT	FREQUENCY (HZ)	d_1	d_2	d_3	d_4	SIGMA FIT
Horiz	PGA	0.1335	0.0354	0.0	6.0	0.0050
	20	0.1298	0.0345	0.0	5.9	0.0054
	10	0.1379	0.0383	0.0	5.9	0.0054
	5	0.1326	0.0403	0.0	5.8	0.0056
	2	0.1384	0.0631	0.0	5.9	0.0059
	1	0.1275	0.0649	0.0	6.0	0.0065
	0.5	0.1469	0.0711	0.0	6.1	0.0081
	0.3	0.1855	0.0508	0.0	6.8	0.0090
	PGV	0.1454	0.0669	0.0	6.1	0.0066
Vert	PGA	0.1317	0.0383	0.0	5.9	0.0049
	20	0.1287	0.0342	0.0	5.9	0.0053
	10	0.1360	0.0375	0.0	5.9	0.0053
	5	0.1319	0.0400	0.0	5.8	0.0056
	2	0.1388	0.0632	0.0	5.9	0.0059
	1	0.1282	0.0648	0.0	6.0	0.0066
	0.5	0.1499	0.0720	0.0	6.1	0.0084
	0.3	0.1900	0.0519	0.0	6.8	0.0092
	PGV	0.1468	0.0674	0.0	6.1	0.0068

TABLE I-6A
P. G. SOMERVILLE: REGRESSION COEFFICIENTS
MEDIAN MODEL

COMPONENT	FREQUENCY (HZ)	a_1	a_2	a_3	a_4	a_5	a_6	a_7	a_8	a_9	a_{10}	a_{11}	a_{12}	SIGMA FIT
Horiz	PGA	1.9958	0.4419	-1.4672	-0.0696	0.1873	0.0000	0.0474	7.4	0.1137	-0.3247	5.2	6.0	0.1357
	20	2.8175	0.4419	-1.6032	-0.0696	0.1873	0.0088	0.0192	7.5	0.1163	-0.3085	5.0	6.1	0.1331
	10	3.2424	0.4419	-1.6657	-0.0696	0.1873	0.0115	0.0692	8.6	0.0472	-0.3688	5.1	5.9	0.1415
	5	2.7528	0.4419	-1.4804	-0.0696	0.1873	-0.0101	0.0698	7.9	0.0888	-0.3043	5.1	6.0	0.1419
	2	1.8591	0.4419	-1.2335	-0.0696	0.1873	-0.0592	0.0723	6.4	0.1728	-0.2919	5.3	5.9	0.1362
	1	0.9851	0.4419	-1.1037	-0.0696	0.1873	-0.0981	0.0358	5.7	0.2394	-0.2533	5.1	6.0	0.1408
	0.5	-0.2631	0.4419	-0.9365	-0.0696	0.1873	-0.1388	-0.0296	4.0	0.2554	-0.1006	5.0	6.2	0.1682
	0.3	-0.7669	0.4419	-0.9285	-0.0696	0.1873	-0.1725	-0.0665	3.8	0.1646	-0.1141	5.0	7.0	0.1806
	PGV	6.1419	0.4419	-1.2895	-0.0696	0.1873	-0.0818	0.0720	6.0	0.1300	-0.3366	5.2	5.9	0.1831
Vert	PGA	1.7975	0.7212	-1.5779	0.3965	0.1132	0.0000	0.0977	7.2	0.1952	-0.2478	5.1	6.5	0.1377
	20	2.9792	0.7212	-1.7716	0.3965	0.1132	0.0048	0.0938	7.6	0.1789	-0.2697	5.2	6.5	0.1366
	10	3.0338	0.7212	-1.7444	0.3965	0.1132	0.0036	0.1249	7.7	0.1519	-0.2566	5.1	6.3	0.1380
	5	2.2087	0.7212	-1.5319	0.3965	0.1132	-0.0066	0.1270	7.7	0.1861	-0.2233	5.1	6.3	0.1346
	2	1.2175	0.7212	-1.2841	0.3965	0.1132	-0.0595	0.1763	7.2	0.1857	-0.1821	5.1	6.0	0.1521
	1	0.1031	0.7212	-1.1187	0.3965	0.1132	-0.0900	0.2377	6.1	0.1295	-0.0242	5.1	6.0	0.1248
	0.5	-0.7137	0.7212	-1.0516	0.3965	0.1132	-0.1418	0.3920	4.9	0.0000	-0.3000	6.5	7.4	0.1833
	0.3	-1.3183	0.7212	-1.0035	0.3965	0.1132	-0.1706	0.4636	4.2	0.0000	-0.4000	6.2	7.4	0.2021
	PGV	5.3412	0.7212	-1.3183	0.3965	0.1132	-0.0770	0.3185	7.0	0.0000	-0.3000	5.0	7.4	0.1912

TABLE I-6B
P. G. SOMERVILLE: REGRESSION COEFFICIENTS
SIGMA MODEL

COMPONENT	FREQUENCY (HZ)	b_1	b_2	b_3	b_4	SIGMA FIT
Horiz	PGA	0.5454	-0.0613	0.0	6.9	0.0059
	20	0.5396	-0.0694	0.0	6.9	0.0071
	10	0.5714	-0.0767	0.0	6.8	0.0094
	5	0.6028	-0.0732	0.0	6.8	0.0089
	2	0.6665	-0.0721	0.0	6.8	0.0090
	1	0.7130	-0.0597	0.0	6.9	0.0046
	0.5	0.7717	-0.0538	0.0	6.9	0.0096
	0.3	0.7958	-0.1063	0.0	6.1	0.0134
	PGV	0.6876	-0.0535	0.0	6.1	0.0072
Vert	PGA	0.6137	-0.0504	0.0	6.5	0.0058
	20	0.6436	-0.0465	0.0	6.5	0.0062
	10	0.6492	-0.0785	0.0	6.3	0.0089
	5	0.6337	-0.0701	0.0	6.2	0.0109
	2	0.6336	-0.0895	0.0	6.1	0.0126
	1	0.6502	-0.0533	0.0	6.4	0.0115
	0.5	0.6701	-0.0545	0.0	6.4	0.0161
	0.3	0.7010	-0.0963	0.0	6.0	0.0197
	PGV	0.5972	-0.0676	0.0	6.0	0.0103

TABLE I-6C
P. G. SOMERVILLE: REGRESSION COEFFICIENTS
SIGMA-MU MODEL

COMPONENT	FREQUENCY (HZ)	c_1	c_2	c_3	c_4	c_5	c_6	MINIMUM	SIGMA FIT
Horiz	PGA	0.4746	-0.0453	-0.1543	0.0312	0.0132	6.0	0.2	0.0697
	20	0.4341	-0.0389	-0.1050	0.0255	-0.0082	6.0	0.2	0.0787
	10	0.5688	-0.0117	-0.2377	0.0492	0.0298	6.0	0.2	0.0746
	5	0.5514	-0.0025	-0.2143	0.0438	0.0085	6.0	0.2	0.0787
	2	0.4041	-0.0191	-0.1270	0.0315	0.0187	6.0	0.2	0.0855
	1	0.3950	-0.0398	-0.1307	0.0329	0.0502	6.0	0.2	0.0905
	0.5	0.3231	-0.0260	-0.0168	0.0179	0.0012	6.0	0.2	0.1039
	0.3	0.2431	0.0271	0.1117	-0.0081	-0.0317	6.0	0.2	0.1216
	PGV	0.3855	0.0034	-0.0656	0.0137	-0.0022	6.0	0.2	0.1132
Vert	PGA	0.3466	-0.0558	-0.0529	0.0164	0.0179	6.0	0.2	0.1088
	20	0.5132	-0.0676	-0.0360	0.0075	-0.0614	6.0	0.2	0.1086
	10	0.3193	-0.0411	-0.0549	0.0183	0.0299	6.0	0.2	0.1035
	5	0.2389	-0.0050	-0.0177	0.0155	0.1039	6.0	0.2	0.1167
	2	0.2227	0.0080	0.0725	-0.0031	0.0506	6.0	0.2	0.1237
	1	0.4351	-0.0868	-0.1008	0.0301	0.0191	6.0	0.2	0.1147
	0.5	0.4045	-0.0669	-0.0585	0.0360	0.0896	6.0	0.2	0.1836
	0.3	0.4448	-0.0947	-0.0035	0.0238	0.0291	6.0	0.2	0.1773
	PGV	0.2434	0.0309	-0.0209	0.0123	0.1925	6.0	0.2	0.1203

TABLE I-6D
P. G. SOMERVILLE: REGRESSION COEFFICIENTS
SIGMA-SIGMA MODEL

COMPONENT	FREQUENCY (HZ)	d_1	d_2	d_3	d_4	SIGMA FIT
Horiz	PGA	0.1648	-0.0070	0.0	5.8	0.0062
	20	0.1619	-0.0055	0.0	5.8	0.0062
	10	0.1748	0.0062	0.0	7.2	0.0060
	5	0.1715	0.0055	0.0	7.2	0.0043
	2	0.1759	0.0593	0.0	6.0	0.0064
	1	0.1713	0.0992	0.0	5.9	0.0078
	0.5	0.1858	0.1278	0.0	5.9	0.0055
	0.3	0.1957	0.1219	0.0	5.9	0.0044
	PGV	0.1924	0.0850	0.0	6.0	0.0048
Vert	PGA	0.1727	0.0057	0.0	7.2	0.0052
	20	0.1626	-0.0010	0.0	6.5	0.0042
	10	0.1741	0.0148	0.0	5.8	0.0056
	5	0.1763	0.0228	0.0	5.8	0.0056
	2	0.1843	0.0952	0.0	5.8	0.0060
	1	0.1741	0.1405	0.0	5.8	0.0078
	0.5	0.1919	0.1762	0.0	5.8	0.0067
	0.3	0.1995	0.1538	0.0	5.8	0.0044
	PGV	0.1805	0.1120	0.0	5.9	0.0088

TABLE I-7A
M. C. WALCK: REGRESSION COEFFICIENTS
MEDIAN MODEL

COMPONENT	FREQUENCY (HZ)	a_1	a_2	a_3	a_4	a_5	a_6	a_7	a_8	a_9	a_{10}	a_{11}	a_{12}	SIGMA FIT
Horiz	PGA	1.9092	0.2170	-1.4495	-0.1943	0.2237	0.0000	-0.1331	7.4	0.1574	-0.2079	5.1	6.3	0.0721
	20	2.7014	0.2170	-1.5881	-0.1943	0.2237	0.0216	-0.1501	7.6	0.2096	-0.1813	5.5	6.2	0.0775
	10	2.7707	0.2170	-1.5581	-0.1943	0.2237	0.0171	-0.1007	7.8	0.1045	-0.2559	5.0	6.0	0.0982
	5	2.5077	0.2170	-1.4277	-0.1943	0.2237	-0.0054	-0.1224	7.7	0.1503	-0.1854	5.0	6.4	0.0829
	2	1.6685	0.2170	-1.1947	-0.1943	0.2237	-0.0550	-0.1270	6.2	0.2306	-0.1506	5.1	6.1	0.0732
	1	0.8069	0.2170	-1.0454	-0.1943	0.2237	-0.0956	-0.1003	5.3	0.2657	-0.1260	5.3	6.0	0.0816
	0.5	-0.1650	0.2170	-0.9097	-0.1943	0.2237	-0.1406	-0.1338	4.5	0.2454	0.0210	5.0	6.0	0.1039
	0.3	-0.5989	0.2170	-0.9200	-0.1943	0.2237	-0.1764	-0.1613	4.6	0.1336	-0.0249	5.3	7.0	0.1074
	PGV	6.3192	0.2170	-1.3065	-0.1943	0.2237	-0.0782	-0.1320	6.8	0.3225	-0.2042	5.0	6.7	0.1270
Vert	PGA	2.0111	0.3076	-1.6747	-0.0548	0.1979	0.0000	-0.0856	7.2	0.2393	-0.1406	5.5	6.5	0.0876
	20	3.1584	0.3076	-1.8811	-0.0548	0.1979	0.0171	-0.0874	7.8	0.2197	-0.1740	5.6	6.3	0.1029
	10	2.9870	0.3076	-1.7765	-0.0548	0.1979	0.0118	-0.0870	8.0	0.1850	-0.1570	5.6	6.3	0.0990
	5	2.2835	0.3076	-1.5785	-0.0548	0.1979	-0.0102	-0.0954	7.7	0.2268	-0.1040	5.7	6.2	0.0838
	2	1.5135	0.3076	-1.3836	-0.0548	0.1979	-0.0632	-0.0658	7.0	0.2301	-0.0831	5.5	6.4	0.0842
	1	0.7035	0.3076	-1.2693	-0.0548	0.1979	-0.0958	-0.0031	6.5	0.2117	0.0130	5.5	6.3	0.0898
	0.5	-0.5457	0.3076	-1.0812	-0.0548	0.1979	-0.1405	0.0455	4.5	0.2538	0.1001	5.1	6.5	0.1082
	0.3	-0.9148	0.3076	-1.1201	-0.0548	0.1979	-0.1834	0.0927	4.7	0.1565	-0.0677	5.7	6.2	0.1171
	PGV	5.1786	0.3076	-1.2816	-0.0548	0.1979	-0.0599	0.0255	5.1	0.3538	-0.0906	5.0	6.8	0.1381

TABLE I-7B
M. C. WALCK: REGRESSION COEFFICIENTS
SIGMA MODEL

COMPONENT	FREQUENCY (HZ)	b_1	b_2	b_3	b_4	SIGMA FIT
Horiz	PGA	0.5377	-0.0799	0.0	6.8	0.0116
	20	0.5398	-0.0817	0.0	6.8	0.0109
	10	0.5556	-0.0842	0.0	6.8	0.0112
	5	0.5895	-0.0813	0.0	6.8	0.0116
	2	0.6509	-0.0731	0.0	6.9	0.0108
	1	0.6993	-0.0675	0.0	7.1	0.0144
	0.5	0.7753	-0.0558	0.0	7.2	0.0099
	0.3	0.7917	-0.0705	0.0	6.8	0.0152
	PGV	0.7140	0.0446	0.0	5.8	0.0204
Vert	PGA	0.5681	-0.0698	0.0	6.8	0.0086
	20	0.5793	-0.0684	0.0	6.8	0.0075
	10	0.5838	-0.0769	0.0	6.8	0.0131
	5	0.6052	-0.0784	0.0	6.8	0.0135
	2	0.6472	-0.0830	0.0	6.8	0.0176
	1	0.6921	-0.0696	0.0	6.9	0.0183
	0.5	0.7536	-0.0753	0.0	6.7	0.0221
	0.3	0.7861	-0.0813	0.0	6.6	0.0224
	PGV	0.6522	-0.0154	0.0	6.5	0.0360

TABLE I-7C
M. C. WALCK: REGRESSION COEFFICIENTS
SIGMA-MU MODEL

COMPONENT	FREQUENCY (HZ)	c_1	c_2	c_3	c_4	c_5	c_6	MINIMUM	SIGMA FIT
Horiz	PGA	0.4410	0.0	-0.1066	0.0180	0.0220	6.0	0.2	0.0342
	20	0.4270	0.0	-0.0826	0.0166	0.0273	6.0	0.2	0.0457
	10	0.4561	0.0	-0.1182	0.0225	0.0151	6.0	0.2	0.0423
	5	0.4926	0.0	-0.1386	0.0237	0.0138	6.0	0.2	0.0398
	2	0.3457	0.0	-0.0568	0.0111	0.0133	6.0	0.2	0.0430
	1	0.3454	0.0	-0.0684	0.0136	0.0424	6.0	0.2	0.0575
	0.5	0.2627	0.0	-0.0027	0.0073	0.0447	6.0	0.2	0.0684
	0.3	0.2924	0.0	0.0682	-0.0086	0.0274	6.0	0.2	0.0724
	PGV	0.4004	0.0	-0.0878	0.0184	0.0292	6.0	0.2	0.0909
Vert	PGA	0.4292	0.0	-0.0364	0.0085	-0.0061	6.0	0.2	0.0533
	20	0.5320	0.0	-0.0759	0.0148	-0.0112	6.0	0.2	0.0598
	10	0.4840	0.0	-0.0941	0.0209	0.0126	6.0	0.2	0.0555
	5	0.4053	0.0	-0.0295	0.0112	0.0358	6.0	0.2	0.0693
	2	0.3742	0.0	-0.0048	0.0054	0.0125	6.0	0.2	0.0605
	1	0.4533	0.0	-0.0666	0.0142	-0.0085	6.0	0.2	0.0592
	0.5	0.3733	0.0	0.0239	0.0027	-0.0032	6.0	0.2	0.0845
	0.3	0.4412	0.0	0.0000	0.0074	0.0124	6.0	0.2	0.0973
	PGV	0.3698	0.0	-0.0176	0.0088	0.0322	6.0	0.2	0.0902

TABLE I-7D
M. C. WALCK: REGRESSION COEFFICIENTS
SIGMA-SIGMA MODEL

COMPONENT	FREQUENCY (HZ)	d_1	d_2	d_3	d_4	SIGMA FIT
Horiz	PGA	0.1757	0.0072	0.0	7.2	0.0035
	20	0.1757	0.0075	0.0	7.2	0.0034
	10	0.1826	0.0115	0.0	7.2	0.0035
	5	0.1794	0.0131	0.0	7.2	0.0022
	2	0.1786	0.0281	0.0	6.8	0.0036
	1	0.1779	0.0343	0.0	7.0	0.0057
	0.5	0.1956	0.0423	0.0	7.2	0.0075
	0.3	0.2137	0.0505	0.0	7.2	0.0105
	PGV	0.1826	0.0202	0.0	6.9	0.0088
Vert	PGA	0.2010	0.0203	0.0	7.2	0.0066
	20	0.1990	0.0197	0.0	7.2	0.0063
	10	0.2036	0.0205	0.0	7.2	0.0077
	5	0.1933	0.0192	0.0	7.2	0.0061
	2	0.1885	0.0264	0.0	7.1	0.0075
	1	0.1877	0.0350	0.0	7.2	0.0082
	0.5	0.2058	0.0446	0.0	7.2	0.0150
	0.3	0.2305	0.0567	0.0	7.2	0.0141
	PGV	0.1860	0.0194	0.0	7.2	0.0108

APPENDIX J

HYPOCENTRAL DISTANCE METRIC: DEVELOPMENT OF MODELS FOR AREAL SOURCES

APPENDIX J
TABLE OF CONTENTS

LIST OF TABLES

LIST OF FIGURES

APPENDIX J

HYPOCENTRAL DISTANCE METRIC: DEVELOPMENT OF MODELS FOR AREAL SOURCES

J.1 INTRODUCTION

The attenuation relations developed directly from the experts' point estimates were formulated to describe ground motions from planar seismogenic sources (faults). However, most hazard models - including those proposed for the Yucca Mountain PSHA project - incorporate areal sources over which uniform seismic activity is expected. These areal sources typically model background seismic activity (activity which cannot be assigned to known faults) or activity arising from a laterally distributed source zone. In the hazard analysis, areal sources are typically treated as point sources. The distance measure for a point source is hypocentral distance as opposed to the 'closest distance to the fault' measures used by the experts in this study.

In this appendix, a conversion from hypocentral distance to "closest distance" is developed that accounts for the finite dimension of the fault rupture. This conversion affects both the median ground motion and the aleatory variability and, to a lesser extent, the epistemic uncertainty in both.

J.2 MEDIAN GROUND MOTION

We consider a fault rupture dimension as given by the Wells and Coppersmith (1994)[1] magnitude-area and magnitude-width scaling relations for all fault types. For this study, we only used the mean relations for the rupture dimension scaling relations. (This will tend to underestimate the aleatory variability impact; however, it is a small effect). For each magnitude, the hypocenter is located at various locations on the rupture plane along-strike and down-dip (Figure J-1). Since hypocenters tend to be located near the bottom of fault ruptures, a minimum depth (in terms of the fraction of the fault width) is used to constrain the depth distribution of the hypocenters. Note that this constraint is in terms of the location of the hypocenter on the rupture plane, which is not the same as the depth distribution of the hypocenters. The top of the hypocenters is defined by the parameter T, where T=0

[1] Wells, D.L. and Coppersmith, K.J., 1994, New empirical relationships among magnitude, rupture length, rupture width, rupture area, and surface displacement: Bulletin of the Seismological Society of America, v. 84, p. 974-1002.

corresponds to the top of the rupture and T=1 corresponds to the bottom of the rupture (Figure J-1).

For each hypocenter, sites were located in a circle around the hypocenter (sites with constant hypocentral distance, Figure J-2). For each site, the rupture distance was computed. The mean and standard deviation of the rupture distance for the ith hypocenter are denoted R_i and σ_{R_i}, respectively. This process was applied for both vertical faults and 60 degree dipping faults (no distinction is made for the difference due to fault dip).

The resulting correlation between hypocentral distance and mean rupture distance (R_i) for T=0.25 is shown on Figure J-3 for magnitude 6.5. Based on the trends on Figure J-3, the following functional form was adopted

For $H \le 30$ km,

$$\overline{R}(H,M,T) = H\left(1 + e_1 + \left(e_2 + e_9(T-0.25)\right)(M-5)\right) + H^2\left(e_3 + \left(e_4 + e_{10}(T-0.25)\right)(M-5)\right) \quad \text{(J-1a)}$$

and for $H > 30$ km,

$$\overline{R}(H,M,T) = H + 30\left(e_1 + \left(e_2 + e_9(T-0.25)\right)(M-5)\right) + 900\left(e_3 + \left(e_4 + e_{10}(T-0.25)\right)(M-5)\right) \quad \text{(J-1b)}$$

where $\overline{R}$ is the mean rupture distance (in km), M is moment magnitude, H is hypocentral distance (in km), and T is the top of the hypocenter zone on the fault rupture (in fraction of fault width). An ordinary least-squares regression analyses was performed. The resulting coefficients are listed in Table J-1; the standard deviation of the fit is $\sigma_{\overline{R}}$ = 1.2 km.

The mean $\overline{R}$ is plotted versus hypocentral distance on Figures J-4a, J-4b, and J-4c for magnitudes 5.0, 5.8, and 6.5, respectively. This model can be used to convert the hypocentral distance for a given magnitude to a closest-distance measure.

J.3 ALEATORY VARIABILITY

The correlation of the aleatory variability of the individual estimates of R_i with hypocentral distance is shown on Figure J-5 for M = 6.5 and T = 0.25. This correlation suggests a relation of the form

$$\sigma_{R_i}(H,M,T) = \left(e_5 + \left(e_6 + e_{11}(T-0.25)\right)(M-5)\right)\tanh\left\{H\left(e_7 + e_8(M-5)\right)\right\} \quad \text{(J-2)}$$

The estimated coefficients resulting from an ordinary least-squares regression are listed in Table J-1. The aleatory variability for magnitude 5.0, 5.8 and 6.5 are plotted versus hypocentral distance on Figures J-6a, J-6b, and J-6c, respectively.

The total aleatory variability is the combination of σ_{Ri} and the equation fitting variability of the $\overline{R}_i$

$$\sigma_R(H,M,T)=\sqrt{\sigma^2_{R_i}(H,M,T)+\sigma^2_{\overline{R}}} \tag{J-3}$$

The effect of variability of rupture distance (given H, M and T) on the resulting ground motion is computed by standard propagation of errors:

$$\sigma_{Hypo}(H,M,T)=\sqrt{\left(\frac{\partial Y}{\partial R}\right)^2\cdot\sigma^2_R(H,M,T)} \tag{J-4}$$

where Y is the natural log ground motion attenuation relation. For the functional form used in this study (Eq. 6-1 in Section 6; without hanging wall and footwall effects)

$$\frac{\partial Y}{\partial R}=\left(a_3+a_5(M-6.25)\right)\frac{R(H,M,T)}{R^2(H,M,T)+a_8^2} \tag{J-5}$$

where a_3, a_5, and a_8 are coefficients in the regression equations for each expert (Appendix I).

Substituting Equations J-5 and J-3 into Equation J-4 leads to:

$$\sigma_{Hypo}(H,M,T)=\left(\left(a_3+a_5(M-6.25)\right)\frac{R(H,M,T)}{R^2(H,M,T)+a_8^2}\right)\sqrt{\sigma^2_{R_i}(H,M,T)+\sigma^2_{\overline{R}}} \tag{J-6}$$

This additional aleatory variability should be added (using square-root-sum-squares) to the aleatory variability of the experts models (σ_{Total}) given in Equation 6-6. The σ_{hypo} is plotted on Figure J-7.

J.4 EPISTEMIC UNCERTAINTY

The epistemic uncertainty was estimated by considering the uncertainty in the model resulting from uncertainty in T given by σ_T,.

The epistemic uncertainty in the median is given by

$$\sigma_{\mu}^{Hypo}(H,M,T)=\sqrt{\left(\frac{\partial Y}{\partial T}\right)^2\cdot\sigma_T^2} \tag{J-7}$$

where

$$\frac{\partial Y}{\partial T}=\frac{\partial Y}{\partial R}\frac{\partial R}{\partial T} \tag{J-8}$$

and

$$\frac{\partial R(H,M)}{\partial T}=\begin{cases}e_9 H(M-5)+e_{10}H^2(M-5) & \text{for } H \le 30 \text{ km}\\ e_9 30(M-5)+e_{10}900(M-5) & \text{for } H > 30 \text{ km}\end{cases} \tag{J-9}$$

The epistemic uncertainty in the aleatory variability is expressed as

$$\sigma_{\sigma}^{Hypo}=\sqrt{\left(\frac{\partial \sigma_{Hypo}}{\partial T}\right)^2\sigma_T^2} \tag{J-10}$$

$$=\left|\frac{\partial Y}{\partial R}\right|\frac{\partial \sigma_R}{\partial T}\sigma_T \tag{J-11}$$

where

$$\frac{\partial \sigma_R}{\partial T}=e_{11}(M-5)\tanh\left\{H\left(e_7+e_8(M-5)\right)\right\} \tag{J-12}$$

For this study, we assumed that $\sigma_T = 0.15$ (i.e., 15% of the down-dip width).

The resulting epistemic uncertainty in the median variability is plotted on Figure J-8 for M_w 6.5 and 5.8. The epistemic uncertainty in the aleatory variability is negligible.

J.5 CONCLUSIONS

If the hypocentral distance is simply applied to the attenuation equations developed in Section 6 in place of the "closest distance to the fault rupture," the resulting median ground motion will be overestimated and the aleatory variability will be underestimated. The factors developed in this appendix provide an approximate correction for these effects so that the hazard for areal sources can be easily evaluated using the attenuation relations developed in Section 6.

TABLE J-1
REGRESSION MODEL COEFFICIENTS

COEFFICIENT	ESTIMATE
e_1	-0.207
e_2	-0.323
e_3	0.0058
e_4	0.0059
e_5	1.894
e_6	3.854
e_7	0.0116
e_8	0.0094
e_9	-0.177
e_{10}	0.0055
e_{11}	0.0111

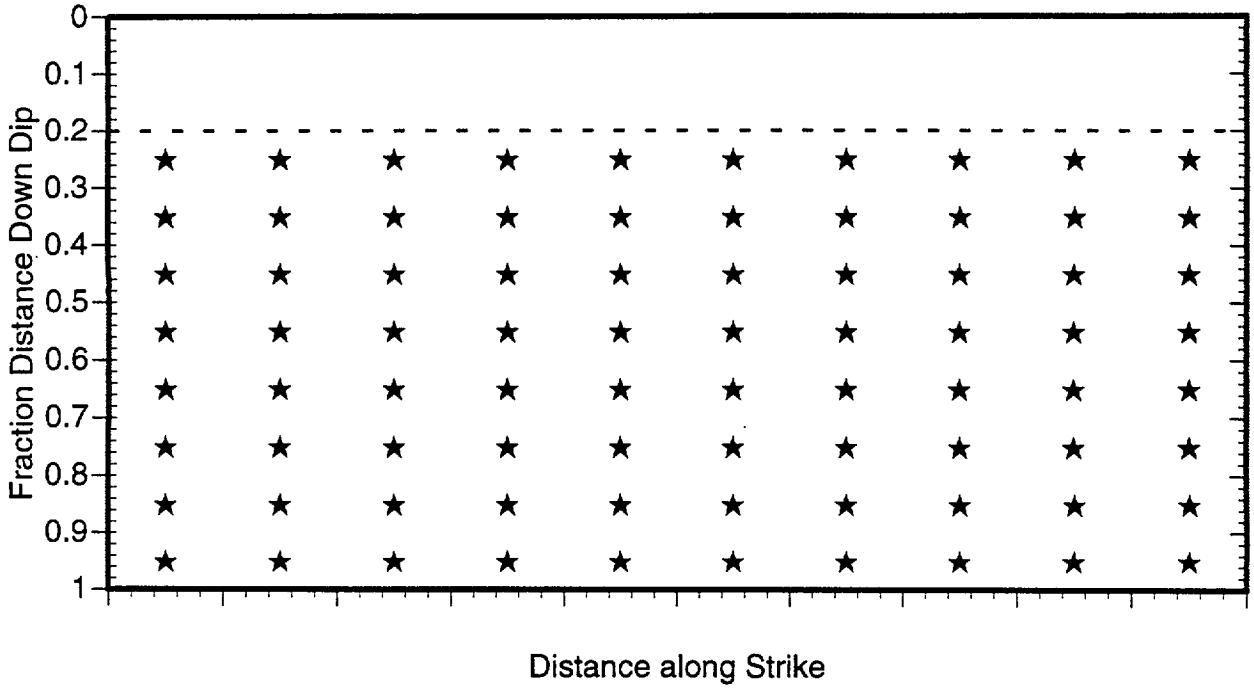

Figure J-1 Example distribution of hypocenters (stars) on the rupture plane for T = 0.2. If T = 0, then hypocenters would be uniformly distributed over the rupture plane. If T = 0.5, then the hypocenters would be uniformly distributed over the lower half of the rupture plane.

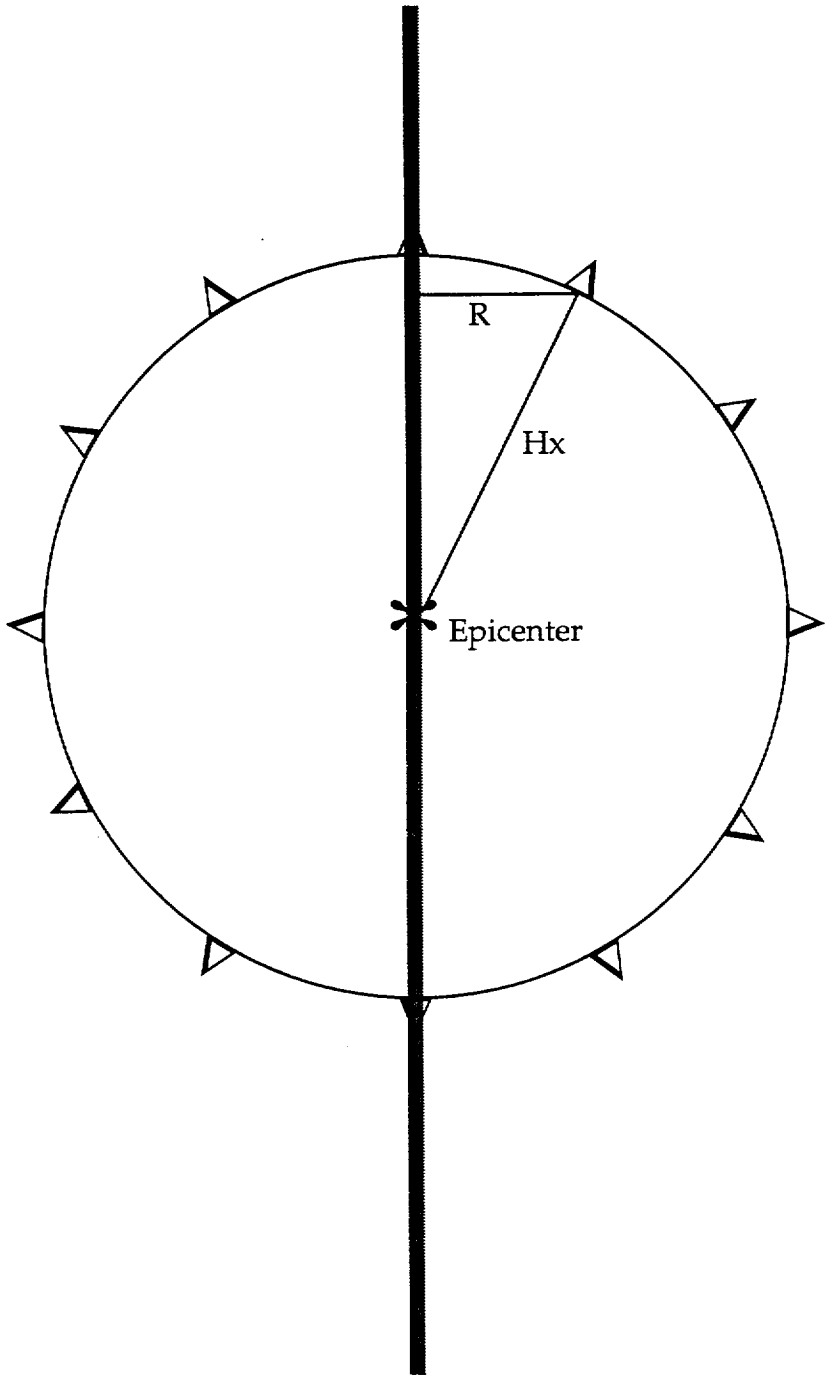

Figure J-2 Map view of a vertical fault rupture plane. For each hypocenter on the rupture plane, a suite of locations (shown by the triangles) is used for each hypocentral distance. The closest distance is then computed for each location to produce a set of hypocentral distance-rupture distance pairs.

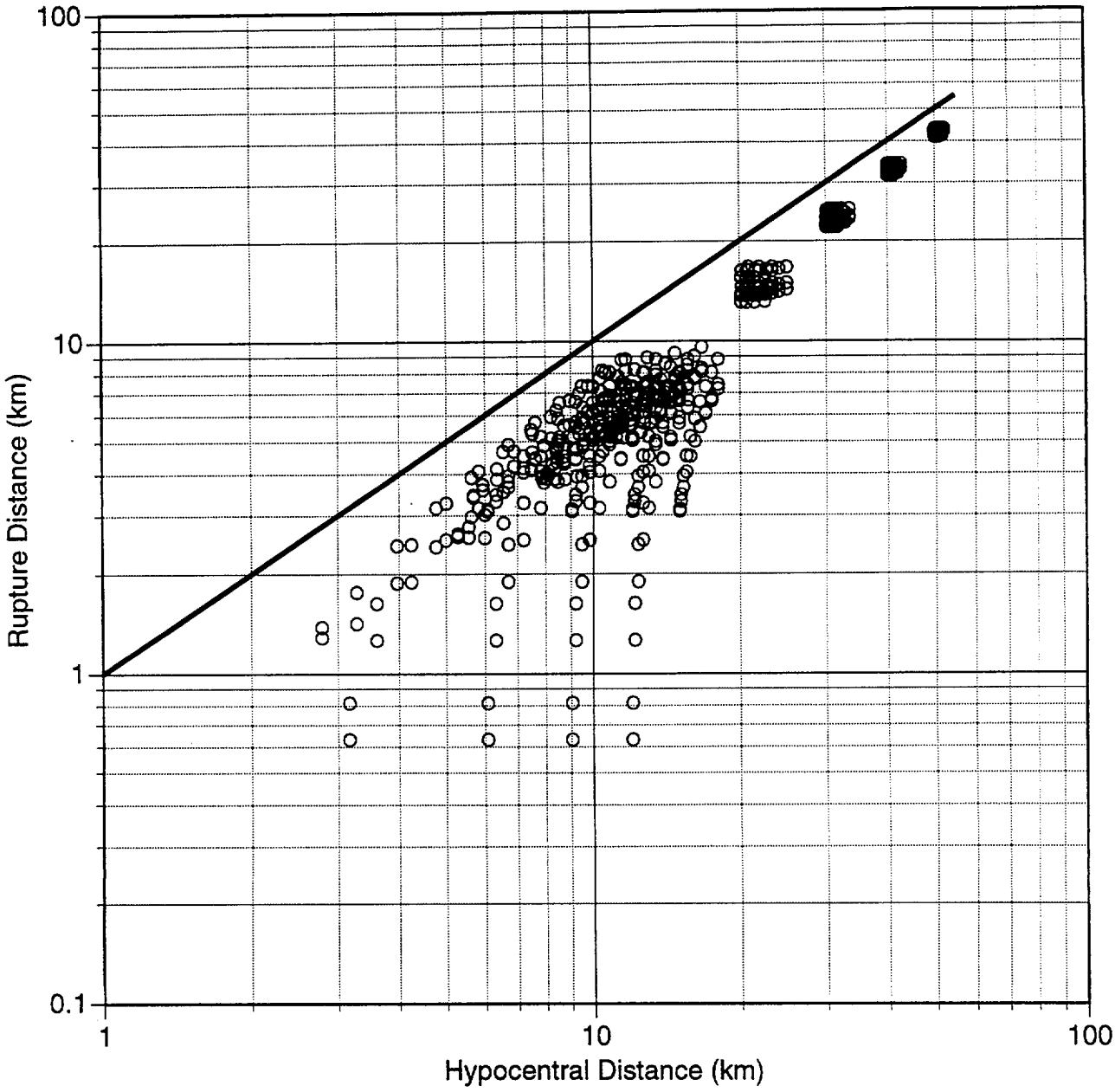

Figure J-3 Mean rupture distance versus hypocentral distance for M_W 6.5 for T = 0.25. The rupture distance is less than the hypocentral distance (the points all plot below the R = H line).

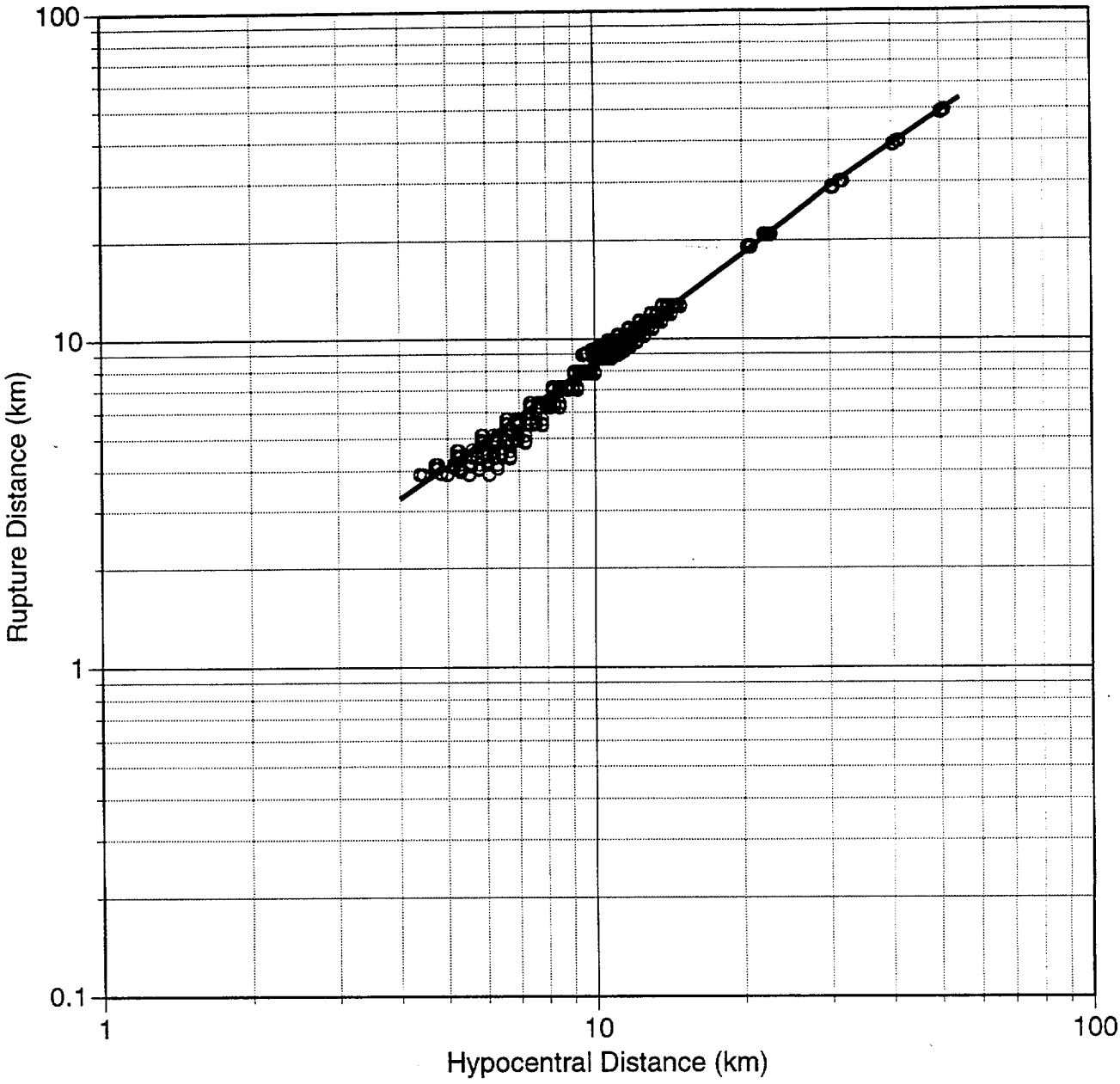

Figure J-4a Model of the mean rupture distance versus hypocentral distance for M_W 5.0 for T = 0.25

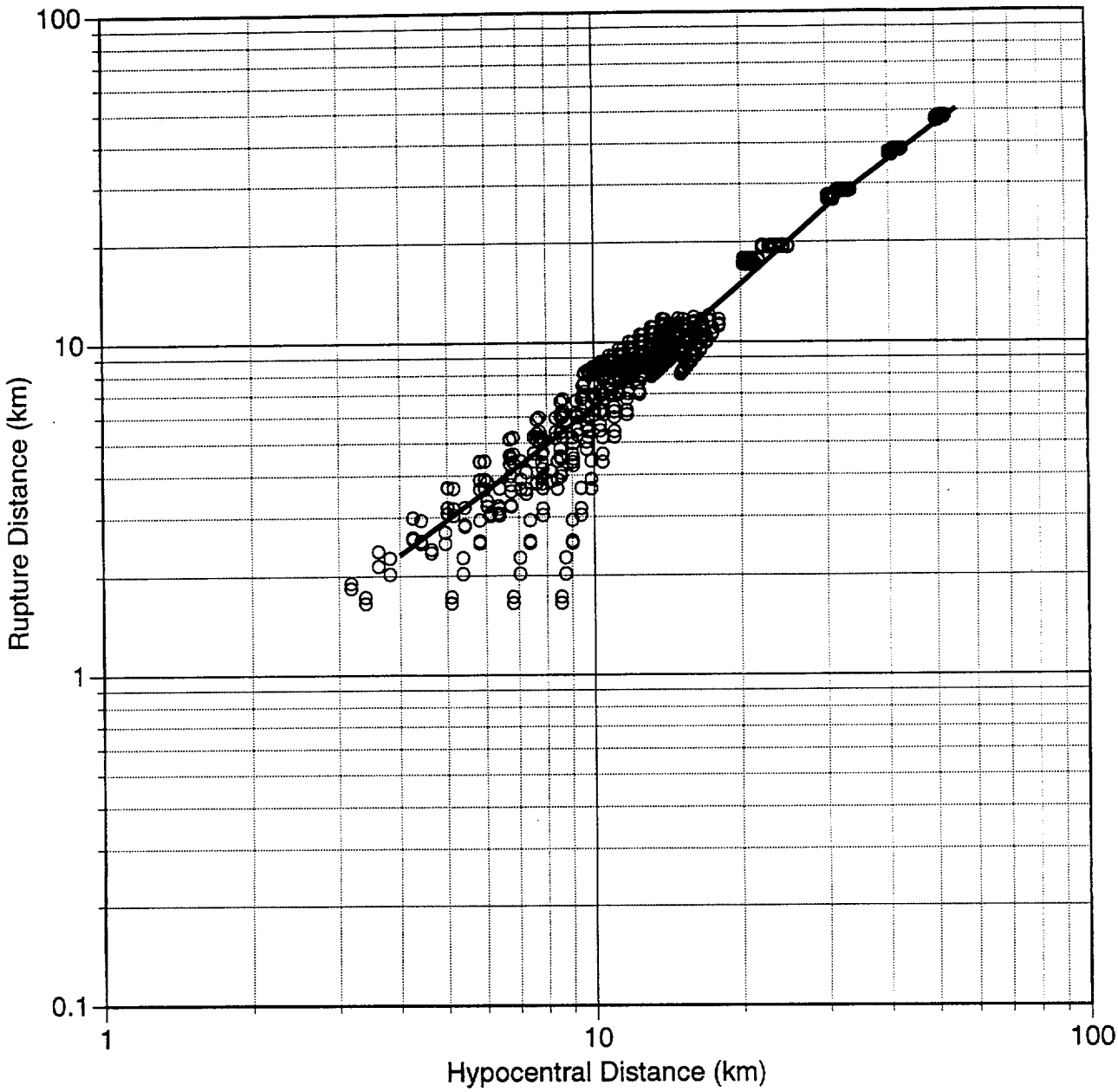

Figure J-4b Model of the mean rupture distance versus hypocentral distance for M_W 5.0 for T = 0.25

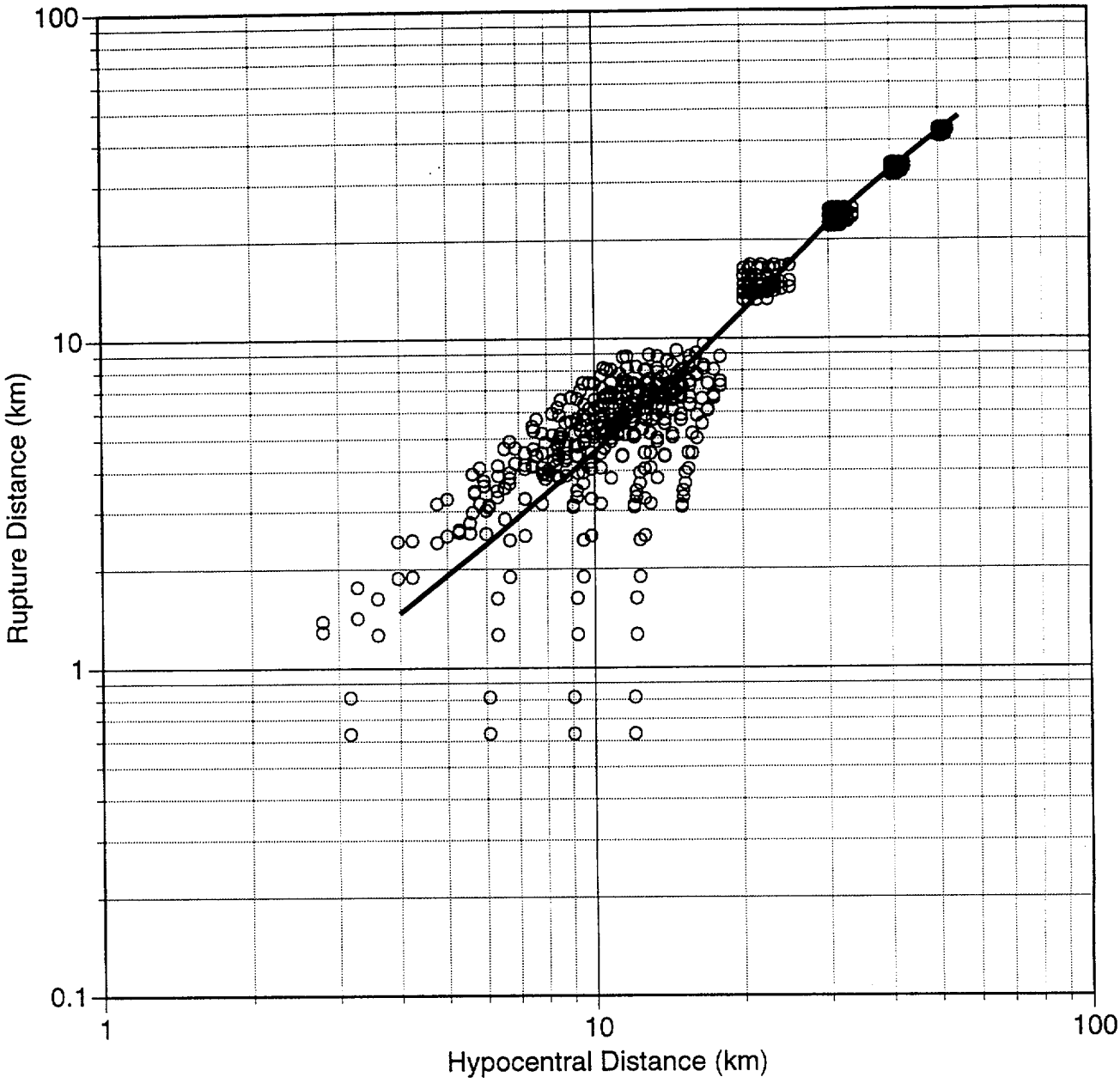

Figure J-4c Model of the mean rupture distance versus hypocentral distance for M_W 6.5 for T = 0.25

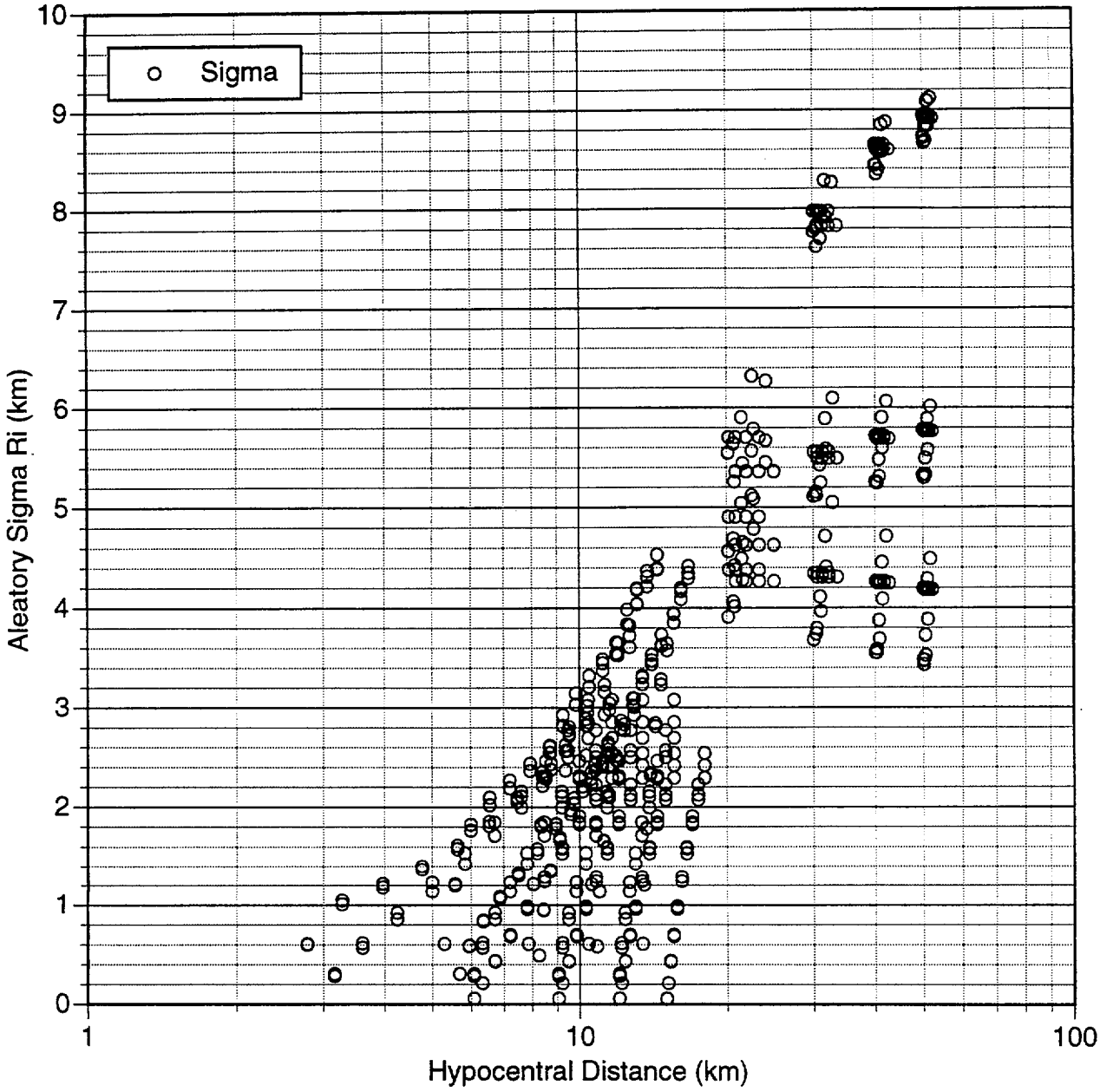

Figure J-5 Aleatory variability of the individual estimates of Ri given a hypocentral distance and M_W 6.5 and T = 0.25

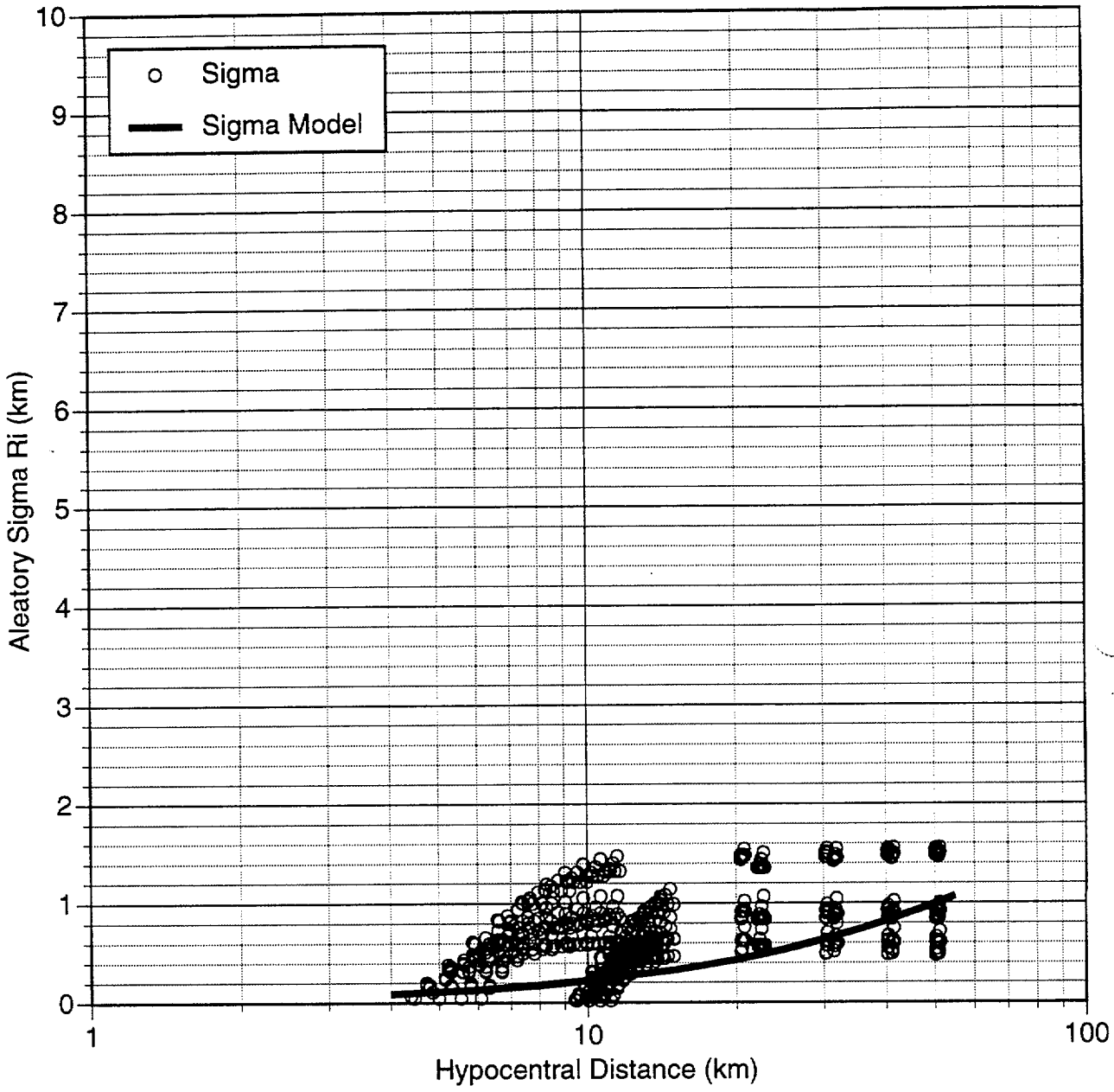

Figure J-6a Aleatory variability of the individual estimates of Ri given a hypocentral distance and M_W 5.0 and T = 0.25

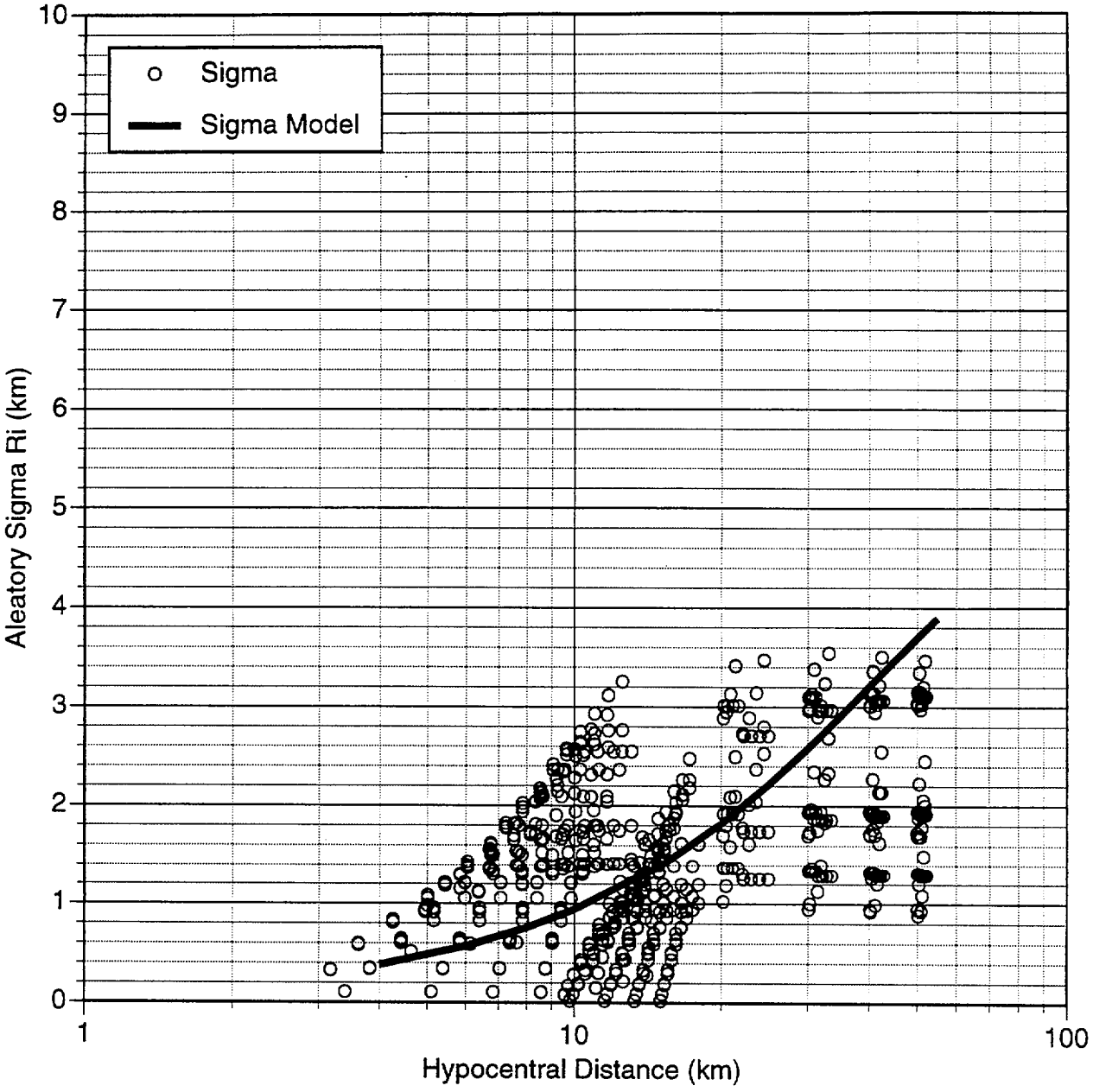

Figure J-6b Aleatory variability of the individual estimates of Ri given a hypocentral distance and M_W 5.8 and T = 0.25

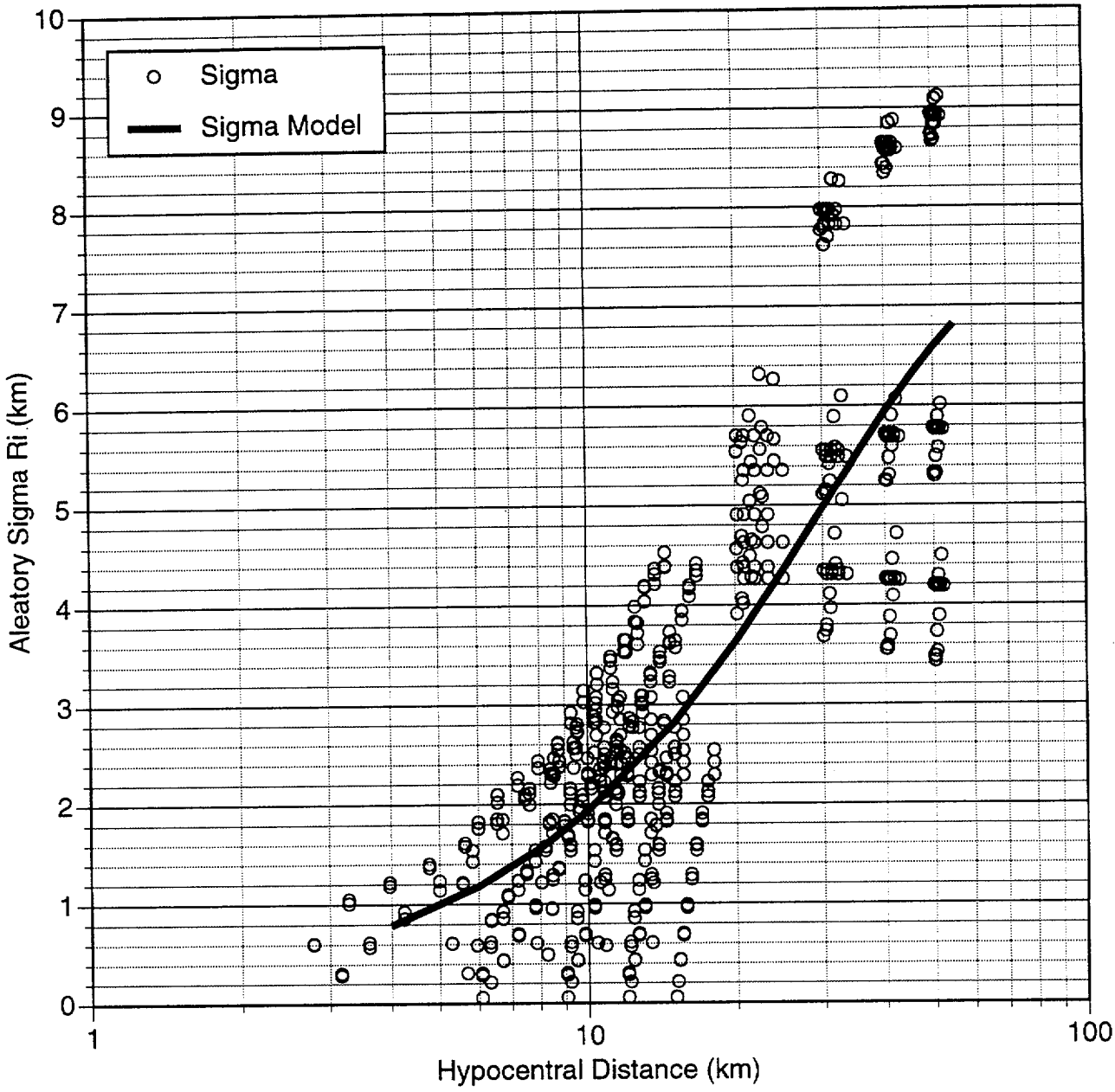

Figure J-6c Aleatory variability of the individual estimates of Ri given a hypocentral distance and M_W 6.5 and T = 0.25

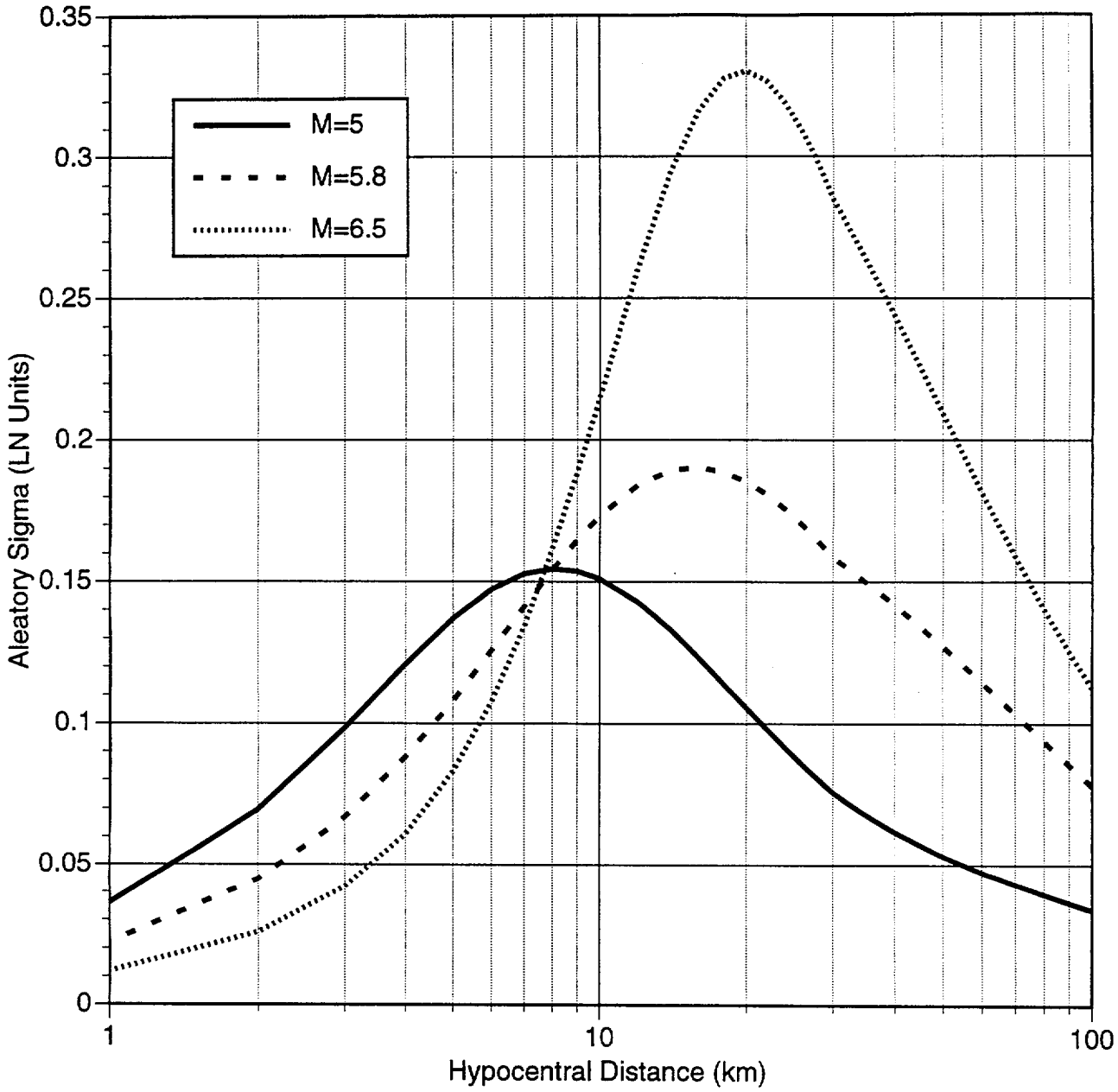

Figure J-7 Example of additional aleatory variability (Sigma hypo) in the natural log ground motion due to hypocentral distance. This is added (using SRSS) to the aleatory variability given by the experts. This example is for horizontal PGA using the Anderson model

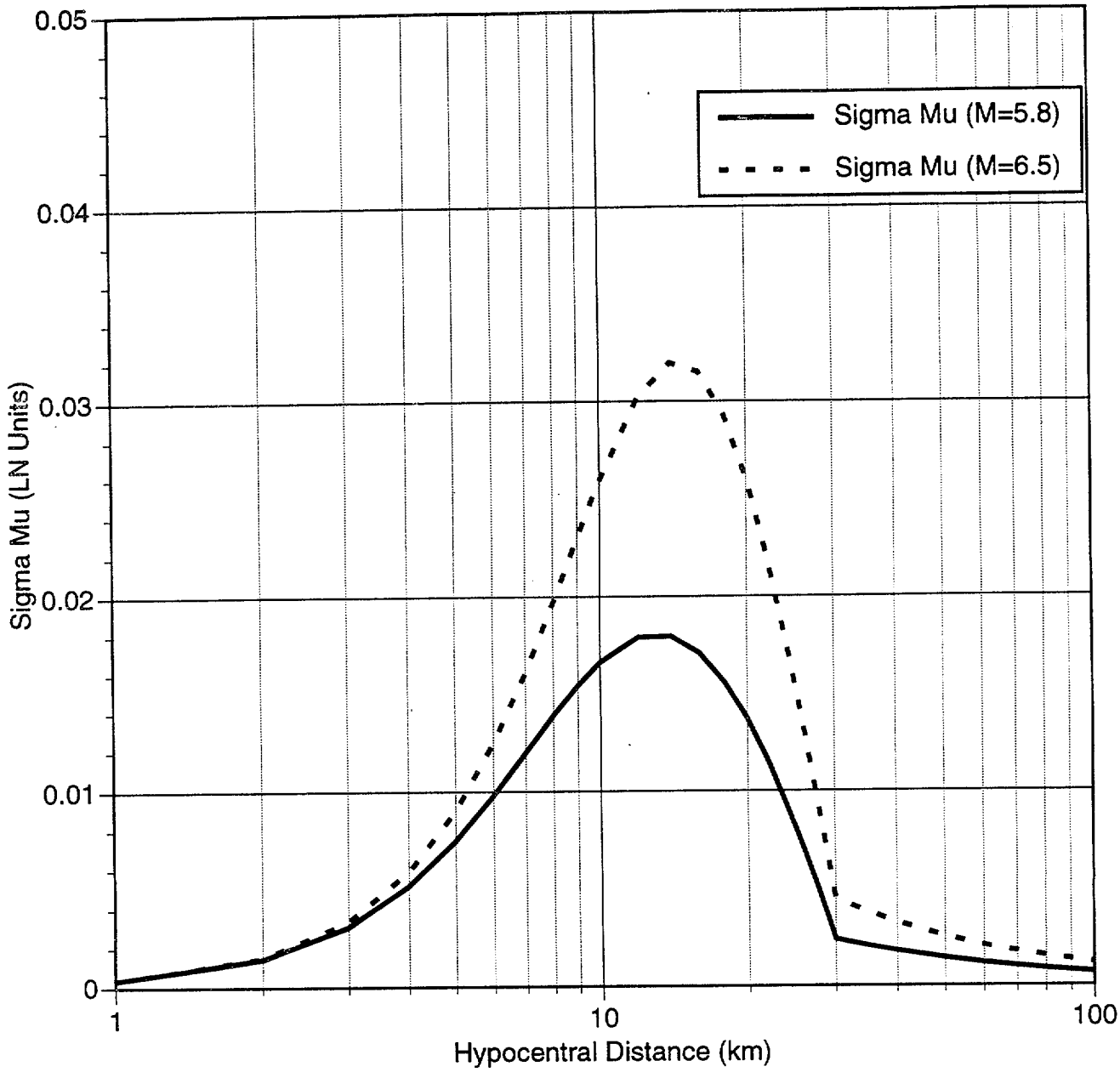

Figure J-8 Example of epistemic uncertainty in the median natural log ground motion due to uncertainty in the T value (depth distribution of hypocenters). This example is for horizontal PGA using Anderson's results. This additional epistemic uncertainty is negligible.